European Network of Fourier-Transform Ion-Cyclotron-Resonance Mass Spectrometry Centers

Grant Agreement n° 731077

Deliverable D2.10 – Course material and school proceedings for the different AUS - Iteration#2

Start date of the project: 1st January 2018
Duration: 54 months
Project Coordinator: Christian ROLANDO – CNRS-
Contact: christian.rolando@univ-lille1.fr

"This project has received funding from the European Union's Horizon 2020 research and innovation programme under grant agreement No 731077"

Document Classification

Title	Course material and school proceedings for the different AUS - Iteration#2
Authors	P3 PRAG – Petr Novak P3 PRAG – Pavla Kramlova
Work package	WP2 – NA- Training, education and networking activities
Dissemination	PU = Public
Nature	R: Document, report
Doc ID Code	20220117_EU_FT-ICR_MS_D2.10
Keywords	EU_FT-ICR_MS, Advanced Users Schools, FT-ICR

Document History

Name	Date	Comment
P3 PRAG – Petr Novak P3 PRAG – Pavla Kramlova	2021-12-28	First version (Draft)
P3 PRAG – Petr Novak P3 PRAG – Pavla Kramlova	2022-01-15	Final version

Document Validation

Project Coordinator	Date	E-mail
P1 CNRS – Christian Rolando	2022-01-17	christian.rolando@univ-lille1.fr

Neutral Reviewer	Date	E-mail
P6 ROMA - Mariaelisa Crestoni	2022-01-16	mariaelisa.crestoni@uniroma1.it

Document Abstract

The deliverable D2.10 “Course material and school proceedings for the AUS2” is part of WP2, which includes the organization of several short courses and schools (for End Users and Advanced Users). This deliverable reports the course materials and proceedings for the 2nd Advanced Users School (AUS) that took place in Prague/Vestec.

Table of Contents

1. Introduction **6**

2. Organization and programme **8**

3. School participants **15**

4. Course materials ***15***

Presentations **16**

Abbreviations:

AUS Advanced Users School

1. Introduction

One of the objectives of the EU FT-ICR-MS consortium is to provide training and advanced education in the field of FT-ICR MS. For this purpose, several courses and schools are planned with the participation of the whole EU FT-ICR MS network. These training courses aim to: i) contribute to the research work performed by graduate and postgraduate (PhD) students, post-docs and early-stage researchers, by exposing them to FT-ICR MS and its applications; ii) share newly developed state-of-the-art procedures for experiments and data analysis; iii) train qualified and highly skilled FT-ICR specialists (engineers and scientists); iv) extend and reinforce the contribution of FT-ICR MS to the current and future applications in many research fields; v) attract both FT-ICR data end-users and scientists from other disciplines required for further development of the FT-ICR technique (especially physicists, applied mathematicians and computer scientists). The Advanced User Schools (AUS) are mainly intended for researchers from both academia and industry who are already experienced in the use of FT-ICR MS and want to expand their knowledge and skills in terms of the more advanced methodology or specific applications of the technique. Thus, the main objective of AUS is to allow participants to gain a state-of-the- art expertise in FT-ICR MS and to provide incentive towards novel developments and applications.

The second AUS was organized in Prague / Vestec by Petr Novak (P3 - PRAG), between 26th and 30th September 2022, at the Institute of Microbiology of the Czech Academy of Sciences, Prague / Vestec, Czech Republic (flyer in Figure 1).

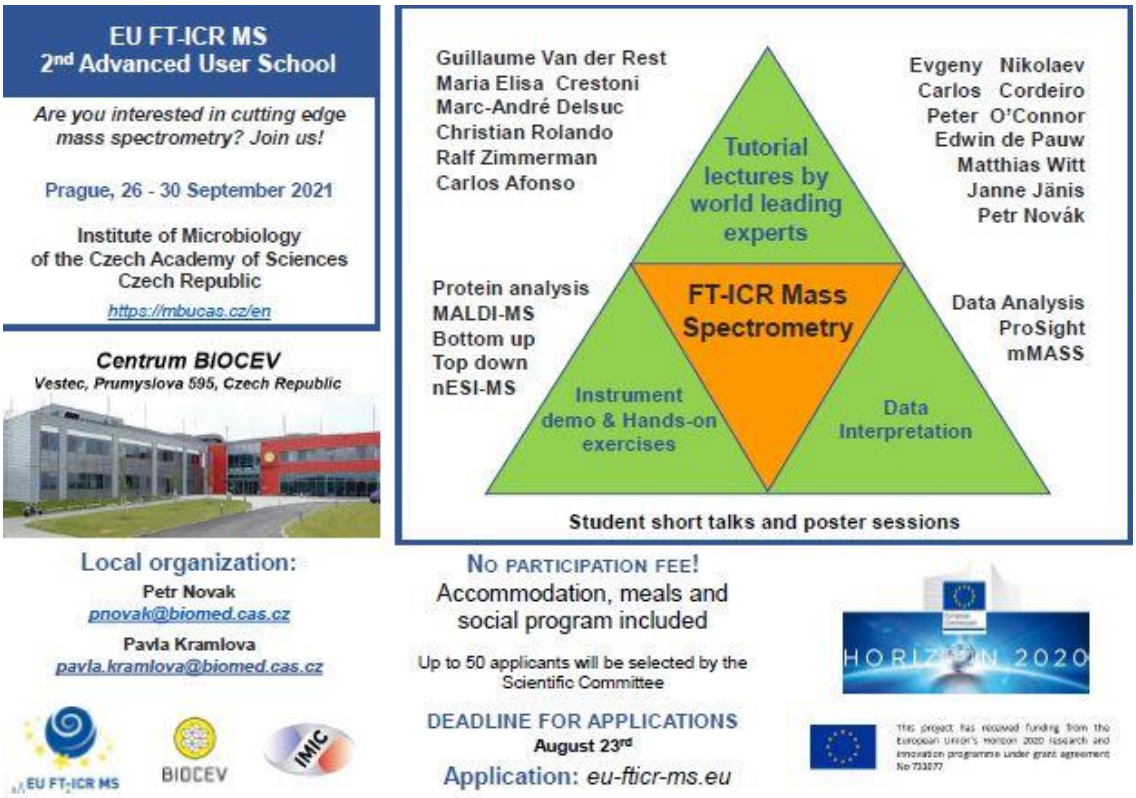

Figure 1. Flyer of the 2nd AUS of the EU_FT-ICR_MS network.

This school brought together FT-ICR experts and students eager to learn together the tricks of the trade. Training was accomplished by a blend of lectures and practice sessions, either in front of computers or in front of a real FT-ICR mass spectrometer. Students also presented their work, with posters and some selected oral presentations, which is the best way to generate fruitful discussions and to discover yet unknown ways to solve difficult problems.

2. Organization and programme

The second AUS in Prague / Vestec was organized between 26th and 30th September 2022, at the Institute of Microbiology of the Czech Academy of Sciences. It included 14 tutorial lectures, 1 computer sessions (demonstrations and data analysis) and 1 laboratory live demo sessions. There were 9 participant posters exhibited at the second AUS and 14 were selected for oral presentations (short talks). The best oral presentation and best poster were awarded with the MALDISAURUS statues printed by the Institute of Microbiology on 3D printer. There were 2 social events: Orienteering in the Kunratice forest with the welcome reception at Na ty louce zeleny and the Sightseeing tour "Karlštejn castle" followed by the Boat trip on Vltava river with the course dinner.

26th September, Sunday

12:00 – 17:30	Registration @ IMIC – hotel EMMY, Prague – see details below
17:30 – 22:00	Orienteering in Kunratice forest and Welcome reception @ Restaurant "On the green meadow/Na tý louce zelený", Prague (https://www.natyloucezeleny.cz/)

27th September, Monday

WHERE: BIOCEV Center, Průmyslová 595, 252 50 Vestec,

Transfer by private bus from hotel EMMY to BIOCEV – departure at 8:30 am from EMMY

9:00 – 9:20	Opening
9:20 – 10:40	**Carlos Afonso "The beautiful friendship of IMS and FT-ICR mass spectrometry for complex mixtures analysis"**
10:40 – 11:00	Coffee break
11:00 – 12:20	**Carlos Cordeiro "Metabolomics - Revealing the Biochemical Fingerprints of Life"** *(on-line)*
12:20 – 13:20	Lunch

13:20 – 14:40	**Guillaume Van der Rest "Combination of FT-ICR mass spectrometry and spectroscopy for the characterization of ion structures"**
14:40 – 16:00	**Maria Elisa Crestoni "Exploring the intrinsic properties of bioinorganic complexes by Ion-Molecule Reactions"**
16:00 – 16:20	Coffee break
16:20 – 17:40	**Christopher Rüger "Ionization schemes and techniques in FT- ICR MS: From commercial towards customized solutions"** *(on- line)*
17:40 – 18:30	**Short presentations of participants I**
18:30 – 21:00	Dinner and poster section

Transfer by private bus from BIOCEV to EMMY – departure at 21:15

28th September, Tuesday

WHERE: BIOCEV Center, Průmyslová 595, 252 50 Vestec

Transfer by private bus from hotel EMMY to BIOCEV – departure at 8:30 am from EMMY

9:00 – 10:00	**Petr Novák "Structural Proteomics – From protein stable covalent labeling to chemical cross-linking"**
10:00 – 11:00	**Petr Man "Structural Proteomics – Hydrogen-deuterium exchange"**
11:00 – 11:40	Coffee break and Guided tour at BIOCEV (Structural mass spectrometry and Proteomics)
11:40 – 13:00	**Petr Man, Zdeněk Kukačka and Petr Novák "Sample preparation, FT-ICR MS sample analysis / Top down of proteins / Data interpretation"**

13:00 – 14:00	Lunch
14:00 – 17:30	**Sightseeing tour "Karlštejn castle" –** transfer by private bus
19:00 – 23:00	**Boat trip and course dinner -** transfer by private bus from castle to the boat. Transfer from the boat back to the hotel EMMY by municipal transport

29th September,
Wednesday

WHERE: BIOCEV Center, Průmyslová 595, 252 50 Vestec,

Transfer by private bus from hotel EMMY to BIOCEV – departure at 8:30 am from EMMY

9:00 – 10:20	**Peter O'Connor "Current capabilities in 2DMS on FTICR mass spectrometers**" *(on-line)*
10:20 – 10:40	Coffee break
10:40 – 12:00	**Marc-André Delsuc "Elements of data analysis in 1D and 2D FTICR-MS data"**
12:00 – 12:30	**Short presentations of participants II**
12:30 – 13:30	Lunch
13:30 – 14:50	**Maria Andrea van Agthoven "The Benefits of 2D-Mass Spectrometry for Protein Structural Characterization"**
14:50 – 15:10	Coffee break
15:10 – 16:30	**Janne Janis "Principle and practice of native mass spectrometry"**
16:30 – 17:30	**Short presentations of participants III**
17:30 – 20:00	Dinner and poster section

Transport to hotel EMMY by private bus from BIOCEV – departure at 20:15

30th September, Thursday

WHERE: Institute of Microbiology of the Czech Academy of Sciences (IMIC), Vídeňská 1083, 142 20 Prague 4

9:00 – 10:20	**Evgeny Nikolaev "FT ICR cell: How to make the best"**
10:20 – 11:40	**Mathias Witt "Petroleomics – from crude oil to asphaltenes"**
11:40 – 12:00	Coffee break
12:00 – 13:20	**Christian ROLANDO "FT-ICR MS for Cultural Heritage"**
13:20 – 14:00	**Prize awards and Closing**
14:00 – 15:00	Lunch

Short presentations of participants I

Anthony Abou Dib **"Pushing the capacity of the FT-ICR MS to a higher level"**

Marc Haegelin **"Super-resolution in FT-ICR MS by non-Fourier Transform genetic evolution signal processing"**

Julie Guillemant **"Sulfur compounds characterization using FT-ICR MS: towards a better comprehension of vacuum gas oils hydrodesulfurization process"**

Davide Corinti **"Open-shell Pt(III)-containing complexes characterized by IRMPD spectroscopy and quantum chemical calculations"**

Nathaniel Terra Telles Souza **"Analysis of solid and liquid samples in the context of SWIM using LDI FT-ICR MS"**

Short presentations of participants II

David Jurnečka **"Acylation dictates the extent of activation of bacterial RTX toxins"**

Cristina Dal Lago **"Modification of Therapeutic monoclonal antibodies by Togni reagents"**

Palasser Michael **""FAST MS - An open-source software for automated and quantitative analysis of top-down mass spectra"**

Short presentations of participants III

Hynek Mácha **"Visualization of Polyamines and Amino Acids Alterations in Neonatal Brain Hypoxic-Ischemic Injury in Rats by Mass Spectrometry Imaging"**

Alessandro Maccelli **"Untargeted metabolomic profiling of Goji berries and leaves (Lycium barbarum L.) by FT-ICR MS"**

Rutuja Patil **"Freeing Aspergillus fumigatus of Polymycovirus Infection Renders It More Resistant to Competition with Pseudomonas aeruginosa Due to Altered Iron-Acquiring Tactics"**

Dominika Luptáková **"Siderophore-based differentiation of Aspergillus fumigatus colonization and invasion"**

Caterina Bordin **"Oil paints: identification of siccative oil and cross-links from museum size sample by chemical depolymerization and ultra-high resolution mass spectrometer"**

Bogdan Purcareanu **"Application of MALDI-FT-ICR-MS for nanostructured thin films characterization"**

Posters

Alpesh Thakker **"An improved semi targeted mass spectrometry approach to provide broader coverage of oxidised lipidome in inflammatory disease model"**

Kas J.Houthuijs **"Towards IR ion spectroscopy on a trapped ion mobility enabled API/MALDI dual source FT-ICR MS platform"**

Josef Dvořák **"Identification of procalcitonin in septic patients by affinity chips and mass spectrometry"**

Marek Polák **“Combination of fast photochemical oxidation of protein and top-down mass spectrometry enables structural characterization of protein/DNA complex”**

Maxime Sueur **“Characterization of organic aerosol using DIP-APCI FT-ICR MS”**

Charlotte Mase **“Molecular characterization of a mixed plastic pyrolysis oil from municipal wastes by direct infusion FTICR mass spectrometry”**

Limei Han **“FT-ICR MS hyphenated with liquid chromatography enables advanced characterization of DOM and DBPs”**

Filip Dyčka **“Studying of hexameric viral helicase by hydrogen-deuterium exchange mass spectrometry”**

Zuzana Kalaninová **“Detection of Botulinum Neurotoxin Type BoNT/A1 Using Modified MALDI Surfaces”**

3. School participants

In the second AUS participated 51 students where 4 were on line due to the SARS2 pandemic restrictions. The gender balance was 33 men / 18 women, coming from 13 different countries. Students presented their work, with posters and some selected oral presentations, which is the best way to generate fruitful discussions and to discover yet unknown ways to solve difficult problems. There were 9 participant posters exhibited at the second AUS and 14 were selected from the abstracts for oral presentations (short talks). The best oral presentation and best poster were awarded with MALDISAURUS statues printed by laboratory of structural biology and cell signaling at The Institute of Microbiology. The best oral presentation was awarded to Michael Palasser (University of Innsbruck) for his talk “FAST MS - An open-source software for automated and quantitative analysis of top-down mass spectra” and the best poster award was given to Limei Han for her poster “FT-ICR MS hyphenated with liquid chromatography enables advanced characterization of DOM and DBPs”. The winners were voted and selected by the jury comprised by the three consortium PIs. There were 2 social events: Orienteering in Kunratice forest and Welcome reception @ Restaurant “On the green meadow; the Sightseeing tour “Karlštejn castle” @ the Boat trip on Vltava river with the course dinner. Overall, the feedback was very positive. This second AUS promoted the establishment of interesting and fruitful collaborations, not only within the network, but also from people outside the consortium. Moreover, one of the participants was hired to work in a project at the Institute of Microbiology.

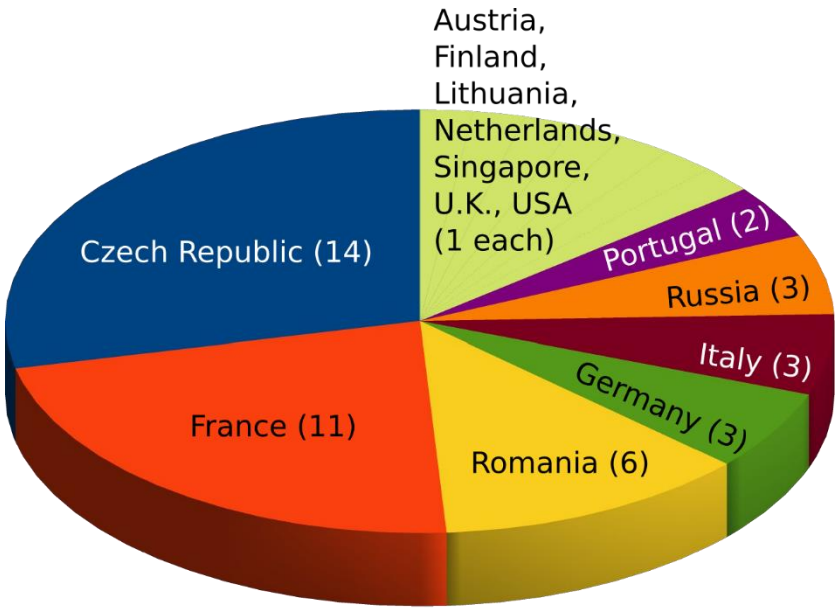

Total (49)

4. Course materials

All participants (teachers and students) received a USB pen drive containing all presentations. Additionally, all presentations are freely available at http://peterslab.org/2ndAUS/.

Monday

Laboratoire Cobra

iC2MC
INTERNATIONAL – COMPLEX MATRICES MOLECULAR CHARACTERIZATION

THE BEAUTIFUL FRIENDSHIP OF IMS AND FTICR MASS SPECTROMETRY FOR COMPLEX MIXTURES ANALYSIS

Carlos Afonso

cnrs INSA UNIVERSITE DE ROUEN

Context

Carlos AFONSO, Brice BOUYSSIERE, Ryan RODGERS, Pierre GIUSTI

Highly Complex organic mixtures

- Complex mixture analysis
  - Requires high peak capacity
  - Post-ionization separation
    - 1 dimension: ultra-high resolution
    - 2 dimensions: ion mobility coupling

WATERS SYNAPT G2

BRUKER 12T SOLARIX XR

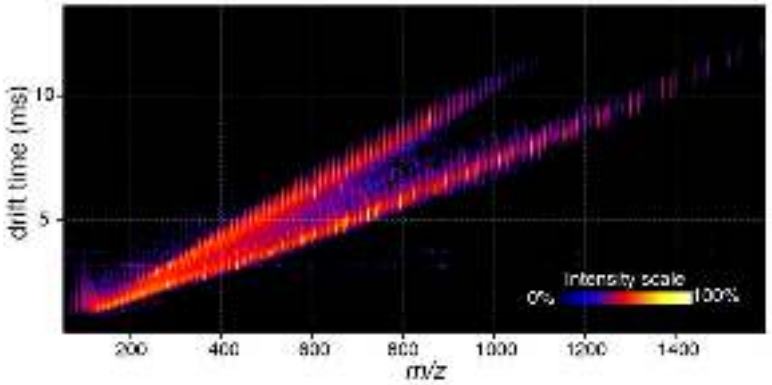

- 12 T Solarix XR
  - Highly Complex organic mixtures
  - Energy
  - Environment
  - Metabolomics

National and European infrastructure

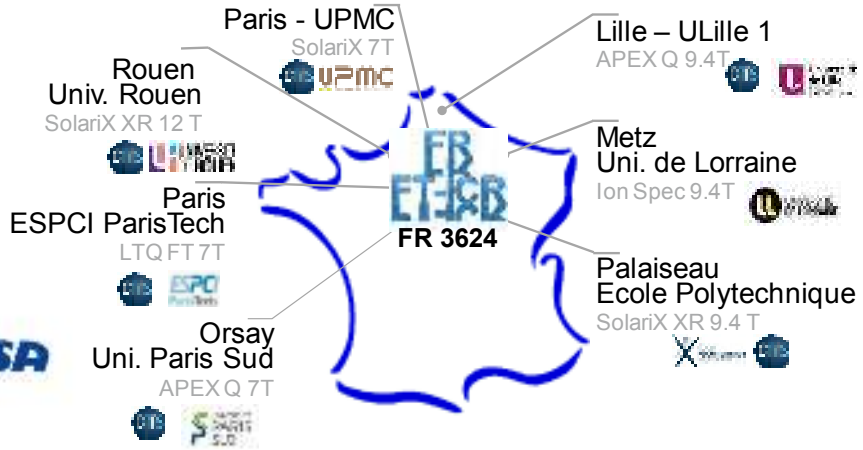

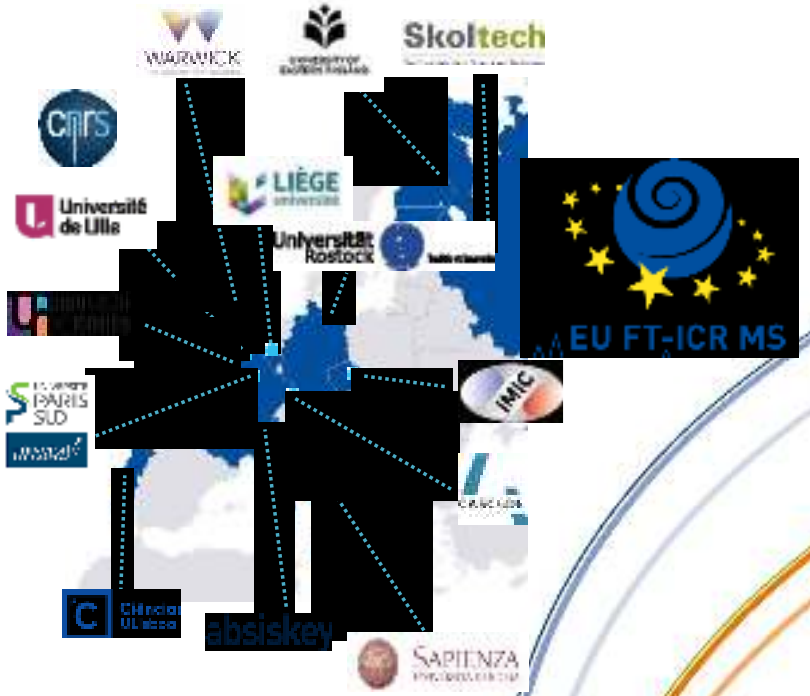

Complex mixture analysis and resolving power

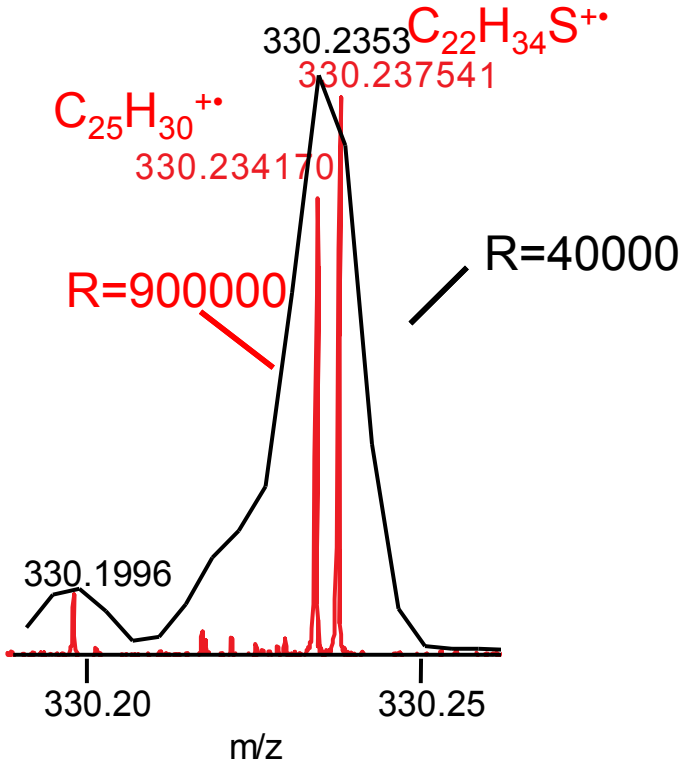

Isotopic Fine Structure

Lincomycin
($C_{18}H_{34}N_2OS$)

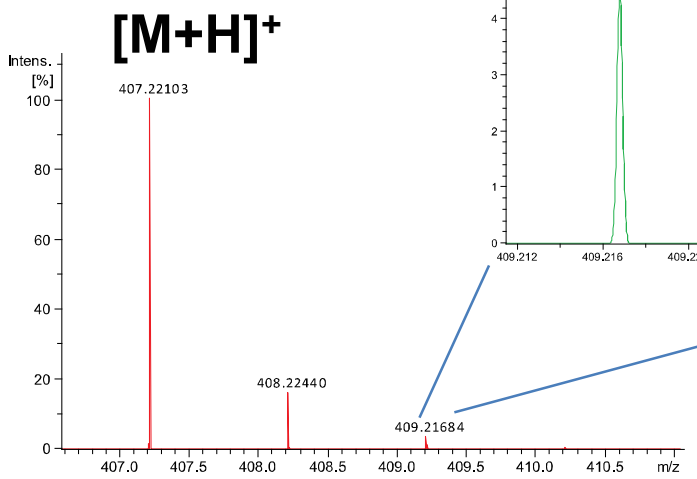

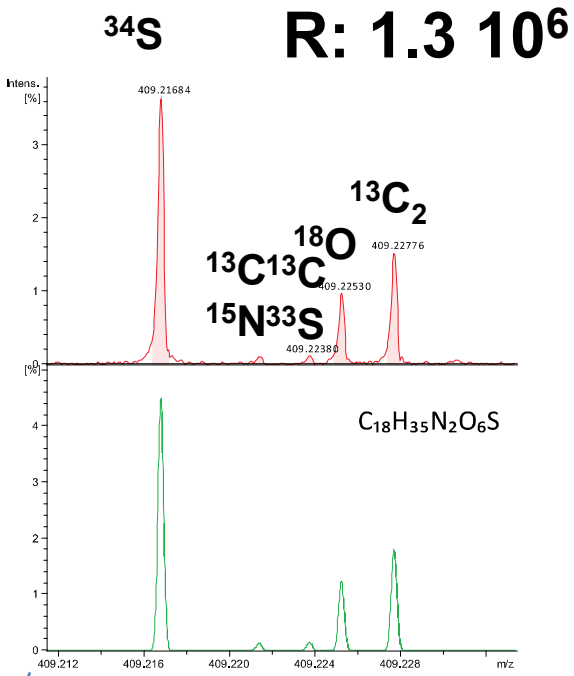

Laboratoire Cobra

iC2MC INTERNATIONAL – COMPLEX MATRICES MOLECULAR CHARACTERIZATION

TotalEnergies

Johann Le Maitre

Crude oil analysis

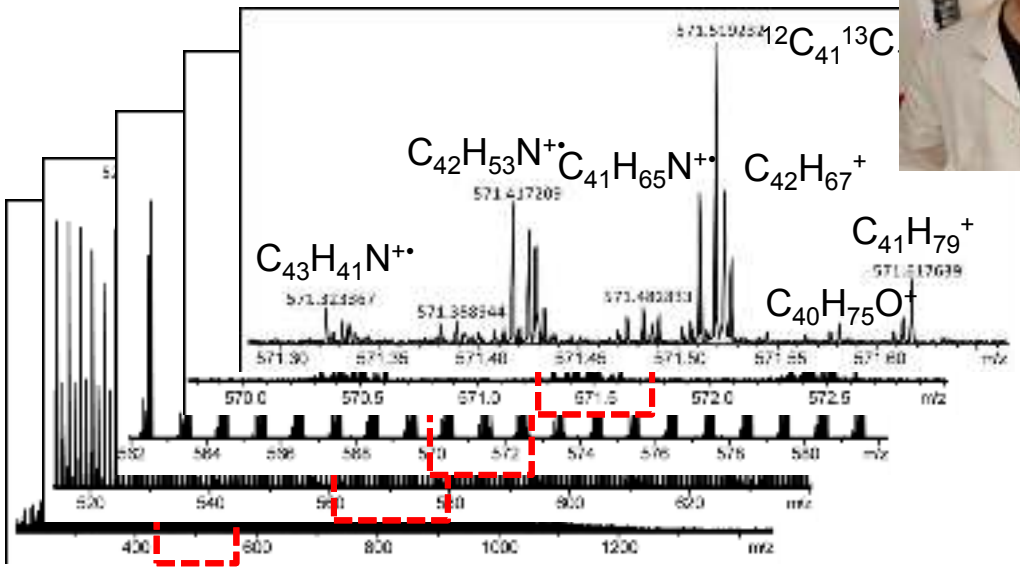

Crude Oil

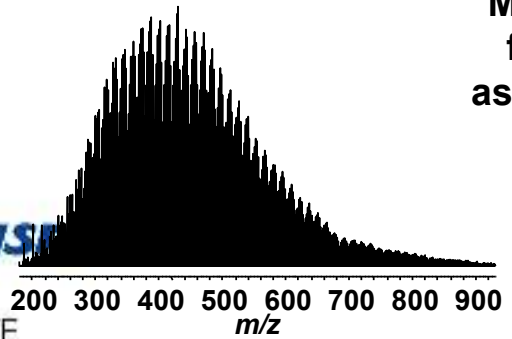

Molecular formula assignment

Molecular Formula	Measured Mass	Calculated Mass	ppm error
$C_{29}H_{42}N_1$	404.3323	404.33227	0.16
$C_{30}H_{44}N_1$	418.348	418.34792	0.18
$C_{31}H_{46}N_1$	432.3638	432.36357	0.48
$C_{32}H_{50}N_1$	446.3793	446.37922	0.15
$C_{27}H_{47}O_2$	403.3582	403.35815	0.09
$C_{28}H_{49}O_2$	417.3738	417.37380	-0.13
$C_{29}H_{51}O_2$	431.3895	431.38945	0.18
$C_{30}H_{53}O_2$	445.4052	445.40510	0.12
$C_{31}H_{55}O_2$	459.4210	459.42075	0.49
$C_{32}H_{57}O_2$	473.4364	473.43640	-0.07

Data visualization

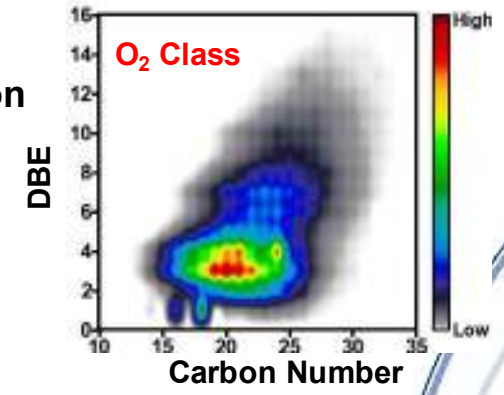

cnrs INSA UNIVERSITE DE ROUEN

Data vizualization

Crude Oil

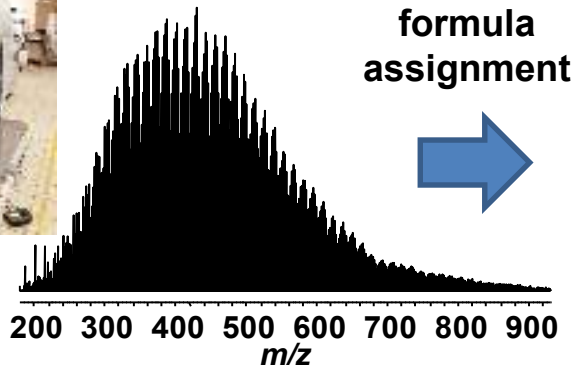

Molecular formula assignment

Molecular Formula	Measured Mass	Calculated Mass	ppm error
$C_{29}H_{42}N_1$	404.3323	404.33227	0.16
$C_{30}H_{44}N_1$	418.348	418.34792	0.18
$C_{31}H_{46}N_1$	432.3638	432.36357	0.48
$C_{32}H_{50}N_1$	446.3793	446.37922	0.15
$C_{27}H_{47}O_2$	403.3582	403.35815	0.09
$C_{28}H_{49}O_2$	417.3738	417.37380	-0.13
$C_{29}H_{51}O_2$	431.3895	431.38945	0.18
$C_{30}H_{53}O_2$	445.4052	445.40510	0.12
$C_{31}H_{55}O_2$	459.4210	459.42075	0.49
$C_{32}H_{57}O_2$	473.4364	473.43640	-0.07

Data visualization

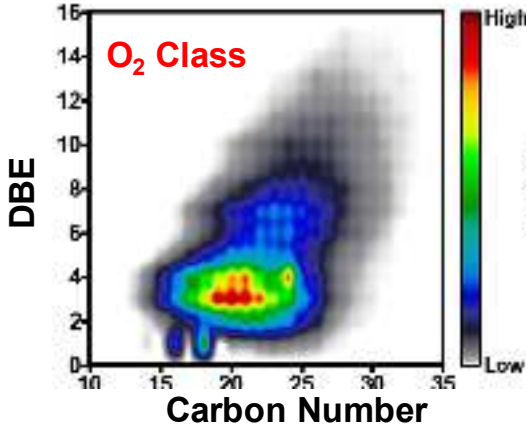

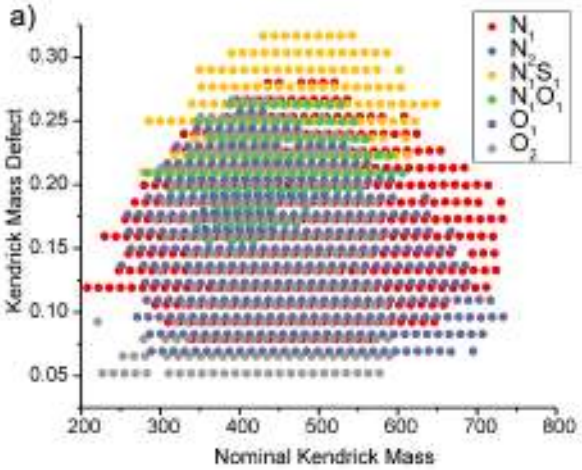

Kendrick Diagram

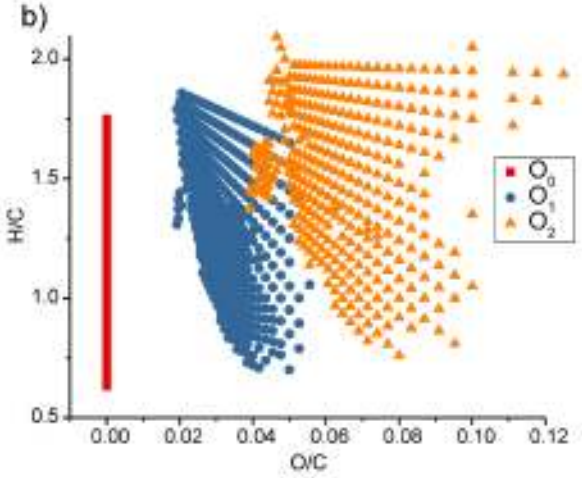

van Krevelen Diagram

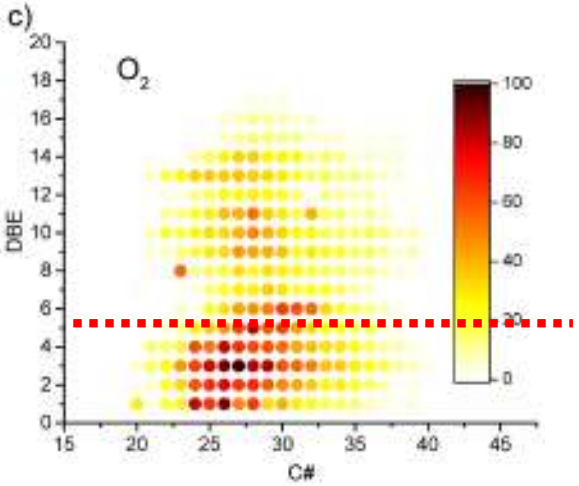

DBE vs C#

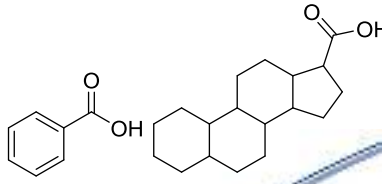

DBE =5 DBE =5

S. Gutierrez Sama et al. *Energy Fuels* **2018**.

Isomers

***m/z* 310.25293**
Molecular Formula: $C_{22}H_{32}N^+$

Many structural formulas

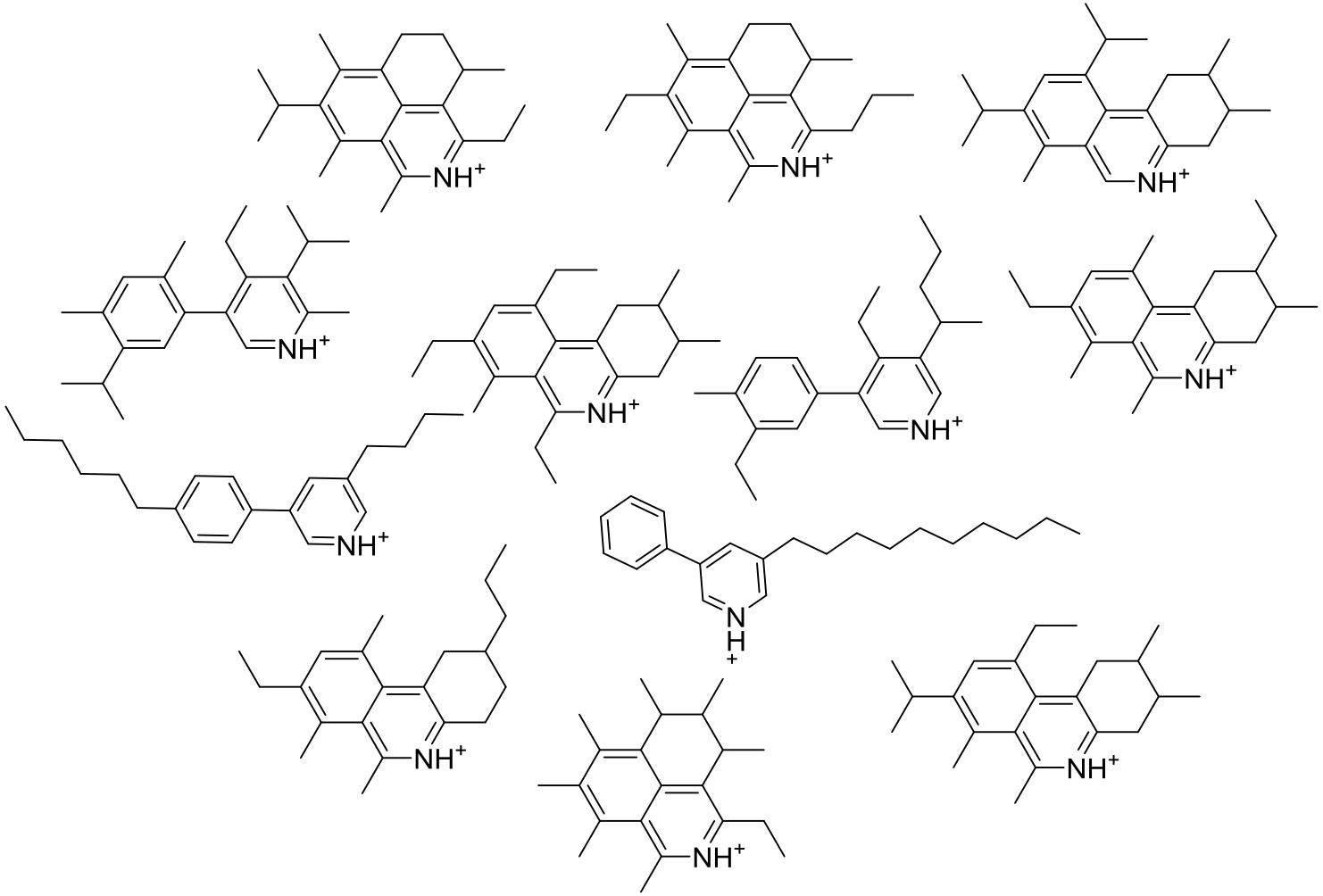

Structural information with IMS

- separation based on size and shape
  - drift time (1-30 ms)
  - access to collision cross section (CCS)
    - intrinsic property of the ion
    - predictable

- IMS-MS coupling
  - 2D separation
  - information on isomers
  - coupling with TOF
    (acquisition in µs range)

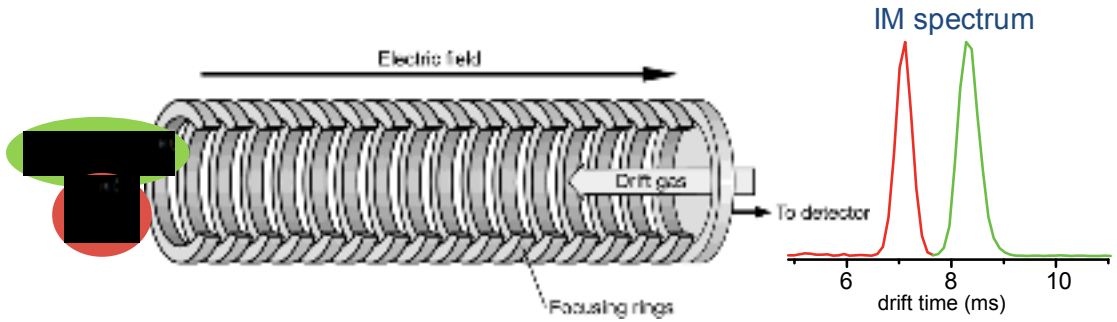

$$v_d = K \times E$$

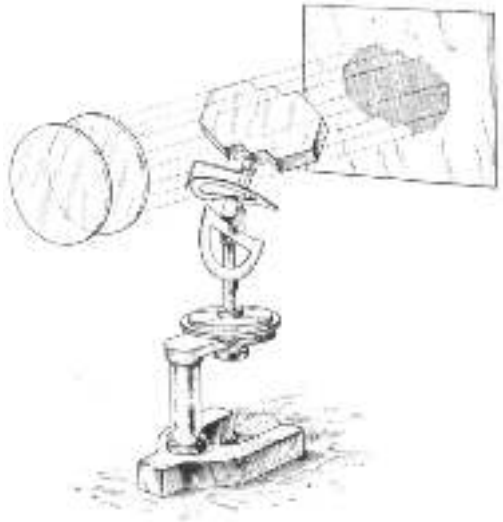

Edward Mack, Jr, *J. Am. Chem. Soc.* 1925, 47, 2468

$$\frac{\Omega_{\exp}}{z} = \left(\frac{3}{16N}\right)\left(\frac{2\pi}{\mu kT}\right)^{\frac{1}{2}}\left(\frac{e}{K}\right)$$

Drift tube IMS

- A very simple instrument
  - Uniform field
  - Atmospheric pressure
  - Cortana discharge ionization

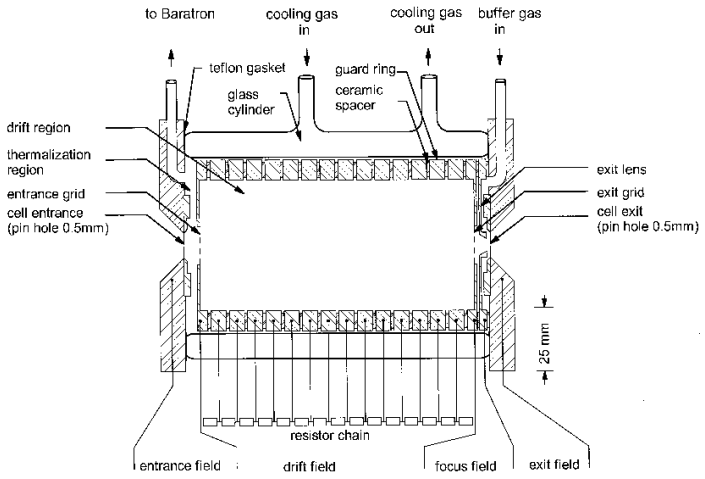

P. Weis et al./Int. J. Mass Spectrom. 216 (2002) 59–73

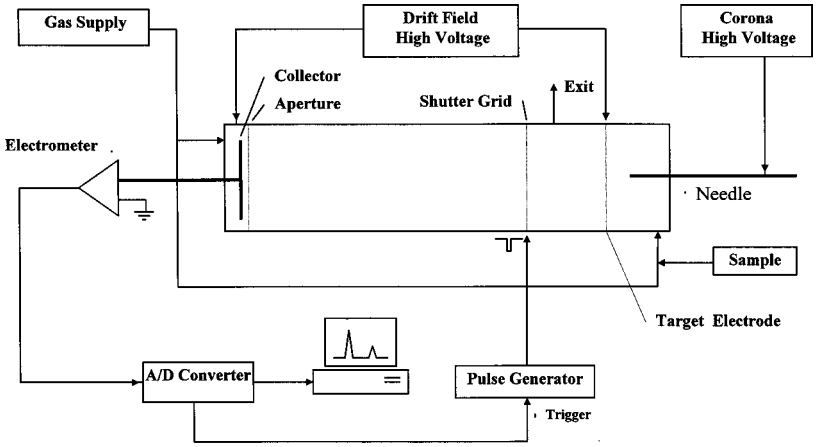

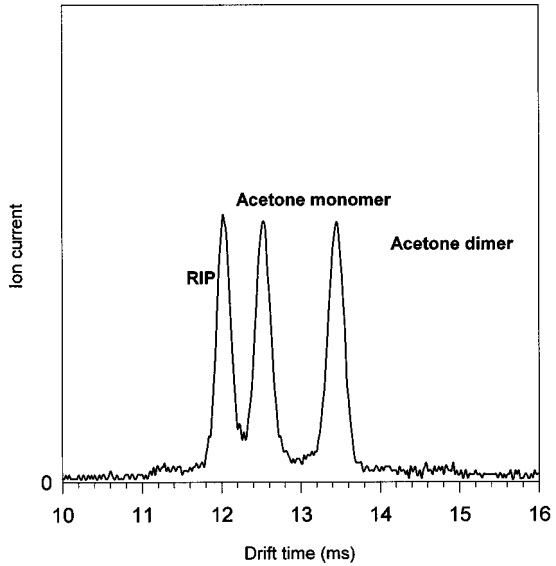

Rev. Sci. Instrum., Vol. 71, No. 6, June 2000

Portable IMS

Home land security

TR1000 Handheld Explosive Trace Detector

Smiths Detection (Ionscan 400B)

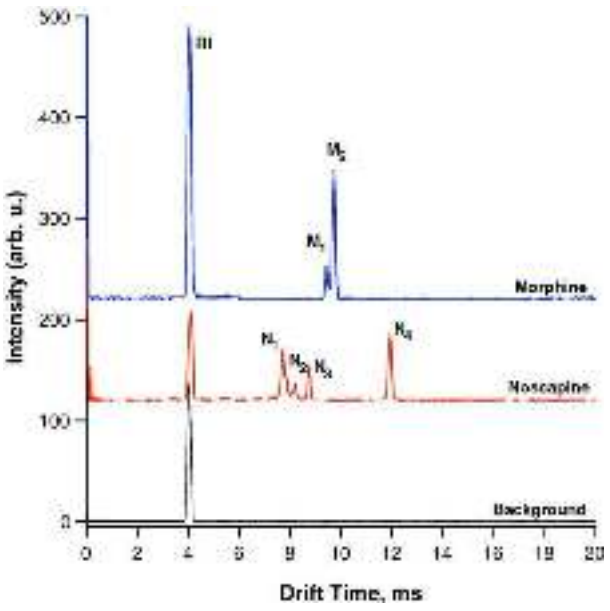

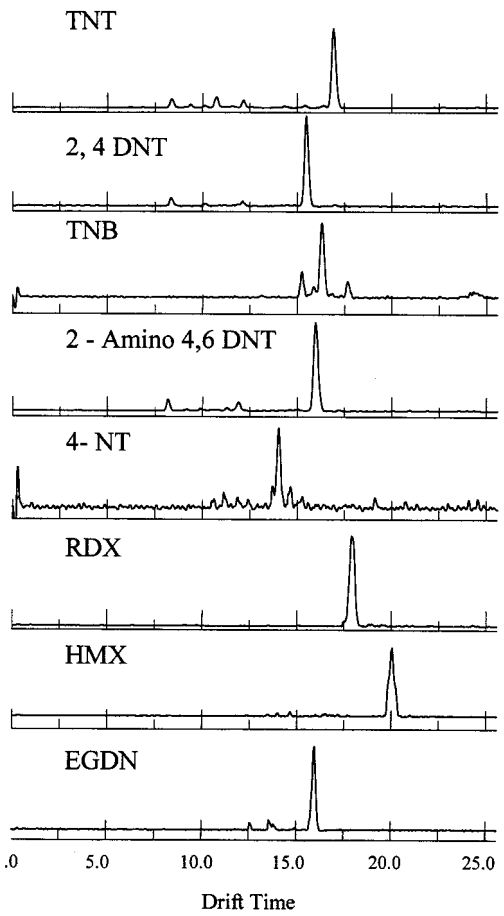

T. Khayamian et al. / Talanta 69 (2006) 795–799

G. Reid Asbury et al. / Talanta 50 (2000) 1291–1298

McKnight, Lee G., McAfee, Kenneth B., Jr. Sipler, D. P. Low-field drift velocities and reactions of nitrogen ions in nitrogen, Phys. Rev. 1067, 164, 62-70

IMS-MS coupling

- IMS separation
  - <100 ms
- Fast mass analyzer
  - TOF
- First IM-MS
  - McKnight 1967
  - Ion/molecules reactions
  - Reintroduced in 1998-1999
    - David Clemmer

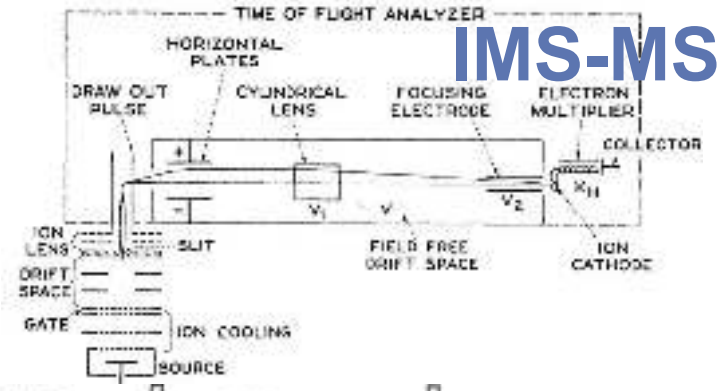

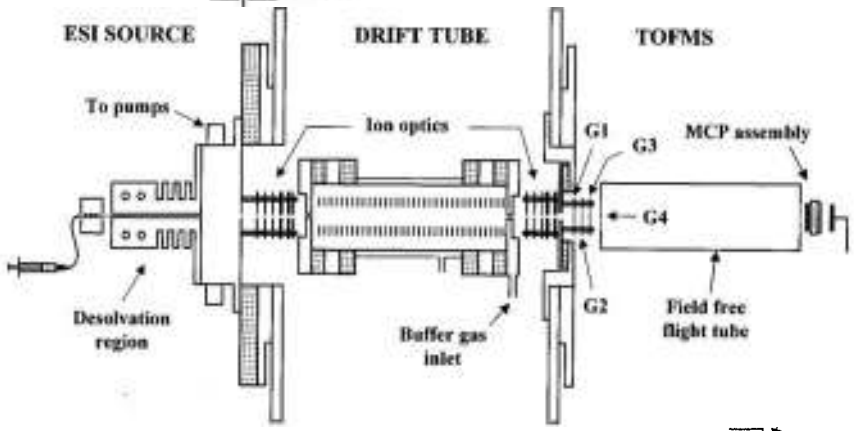

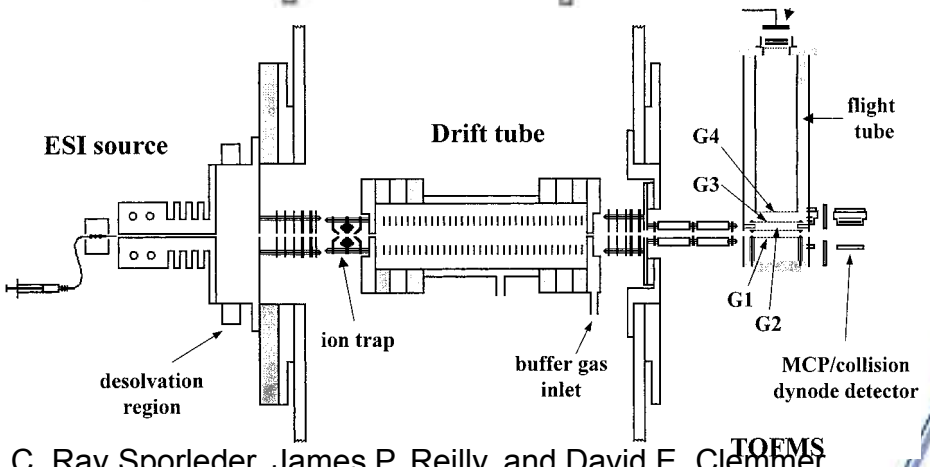

Cherokee S. Hoaglund, Stephen J. Valentine, C. Ray Sporleder, James P. Reilly, and David E. Clemmer Anal. Chem. 1998, 70, 2236-2242

Ion Mobility-Mass spectrometry

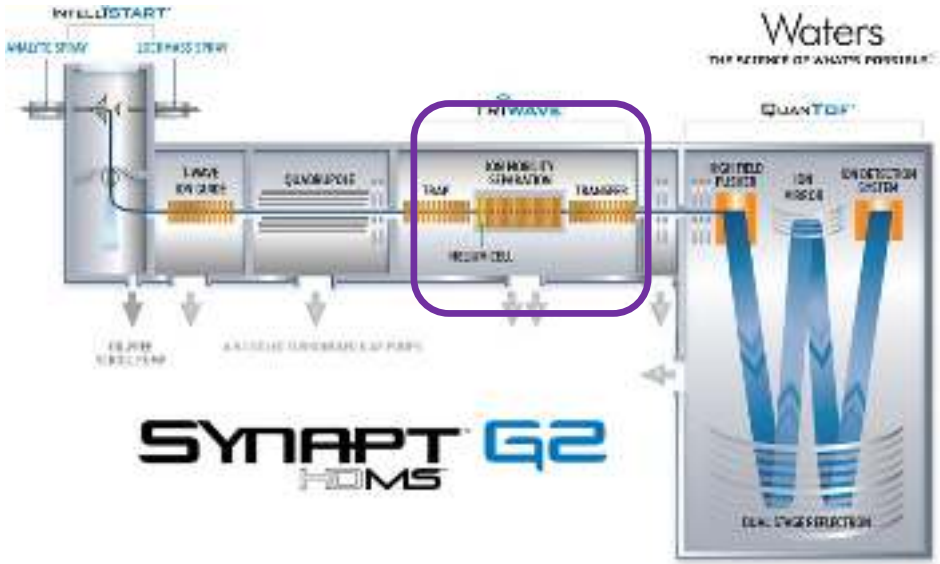

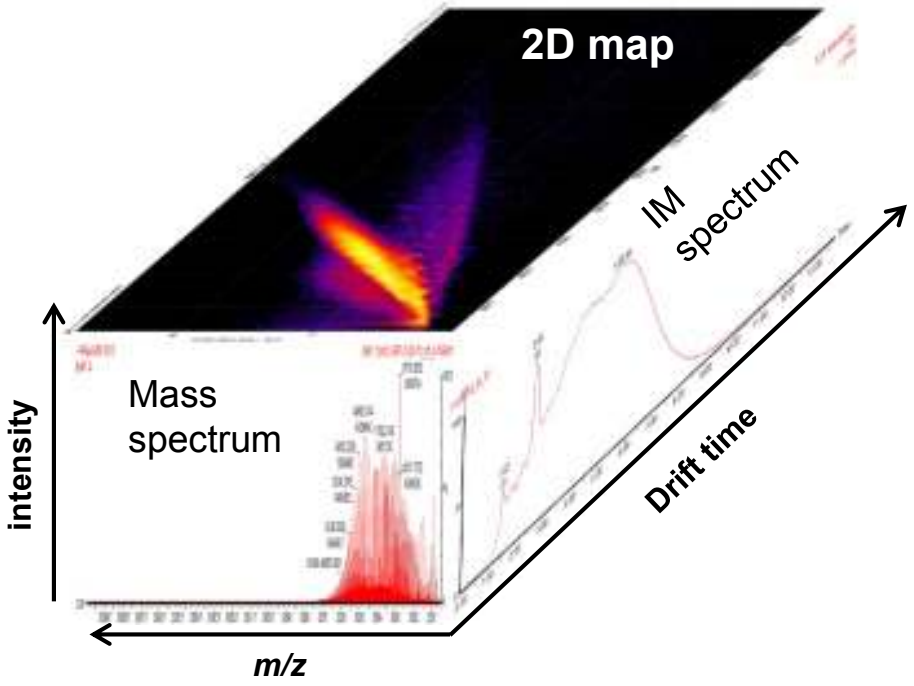

- Ion coordinats = *m/z* + drift time + intensity

Timing

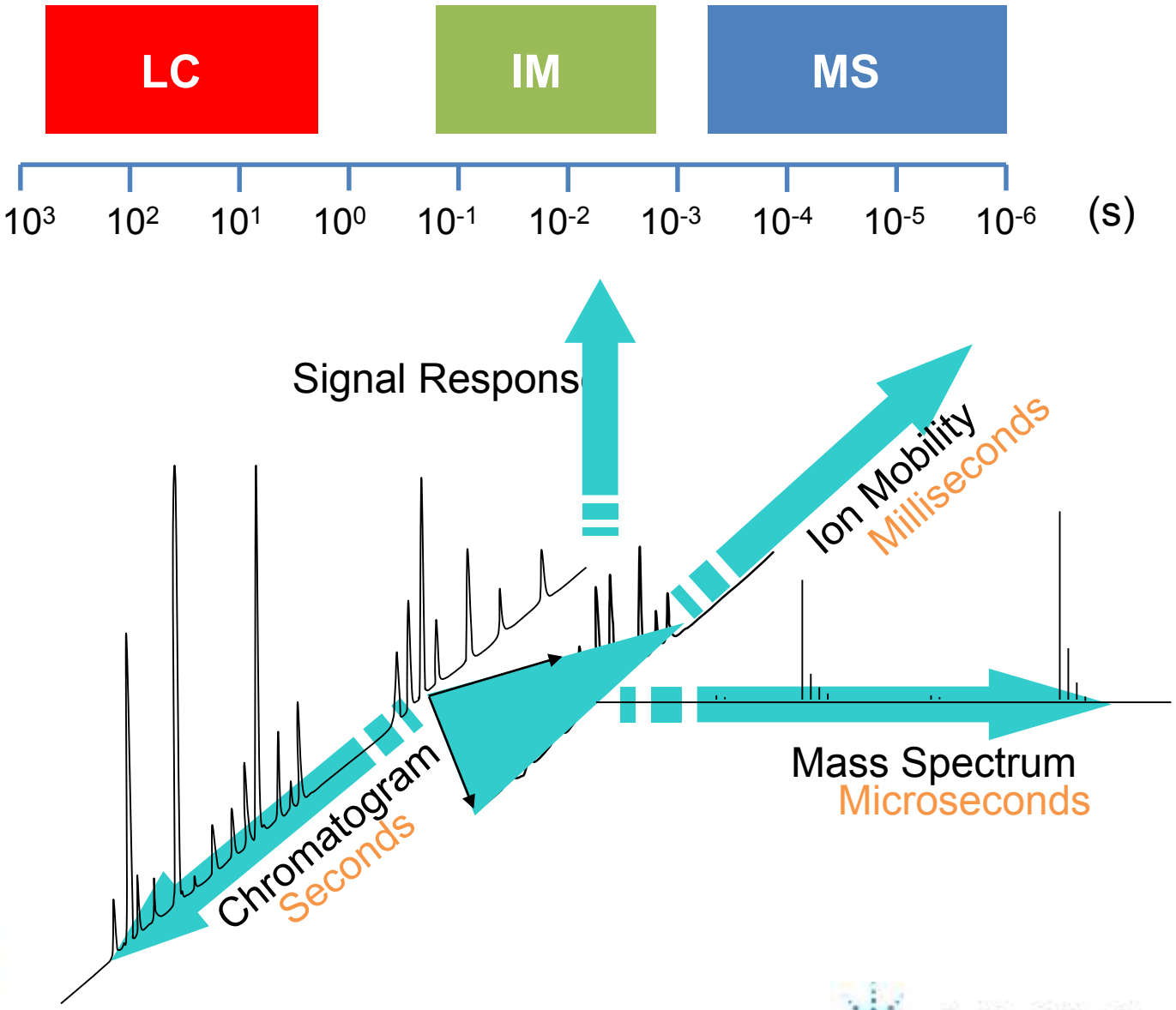
LC
IM
MS
10^3 10^2 10^1 10^0 10^{-1} 10^{-2} 10^{-3} 10^{-4} 10^{-5} 10^{-6} (s)
Signal Respons
Ion Mobility
Milliseconds
Chromatogram
Seconds
Mass Spectrum
Microseconds

2D Map

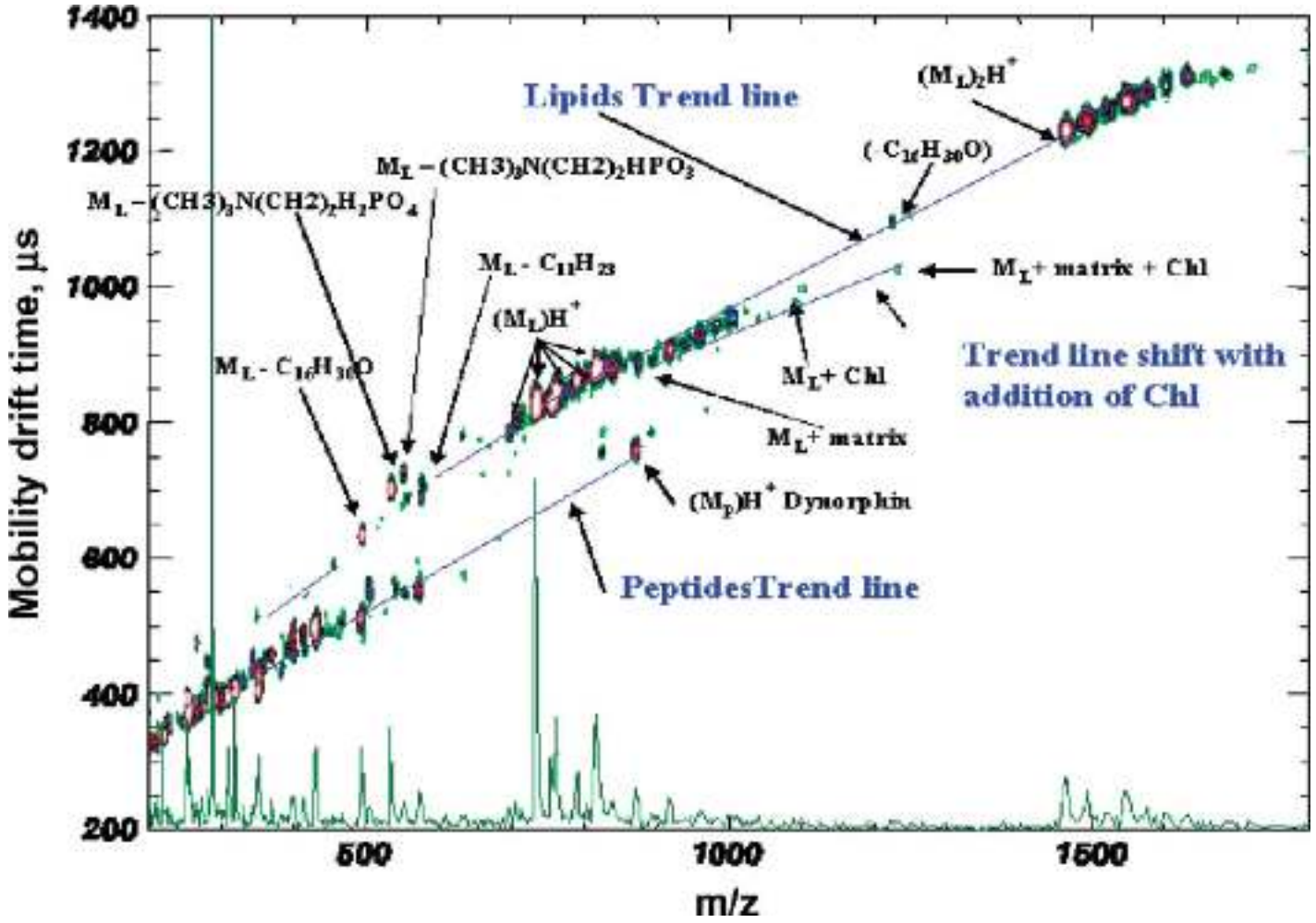

Woods A, Ugarov M, Egan T, Koomen J, Gillig KJ, Fuhrer K, Gonin M, Schultz JA. Lipid/peptide/nucleotide separation with MALDI-ion mobility-TOF MS. *Analytical Chemistry* 2004; 76: 2187–2195.

Complex mixture with TOF? Nitrogen speciation in Oil

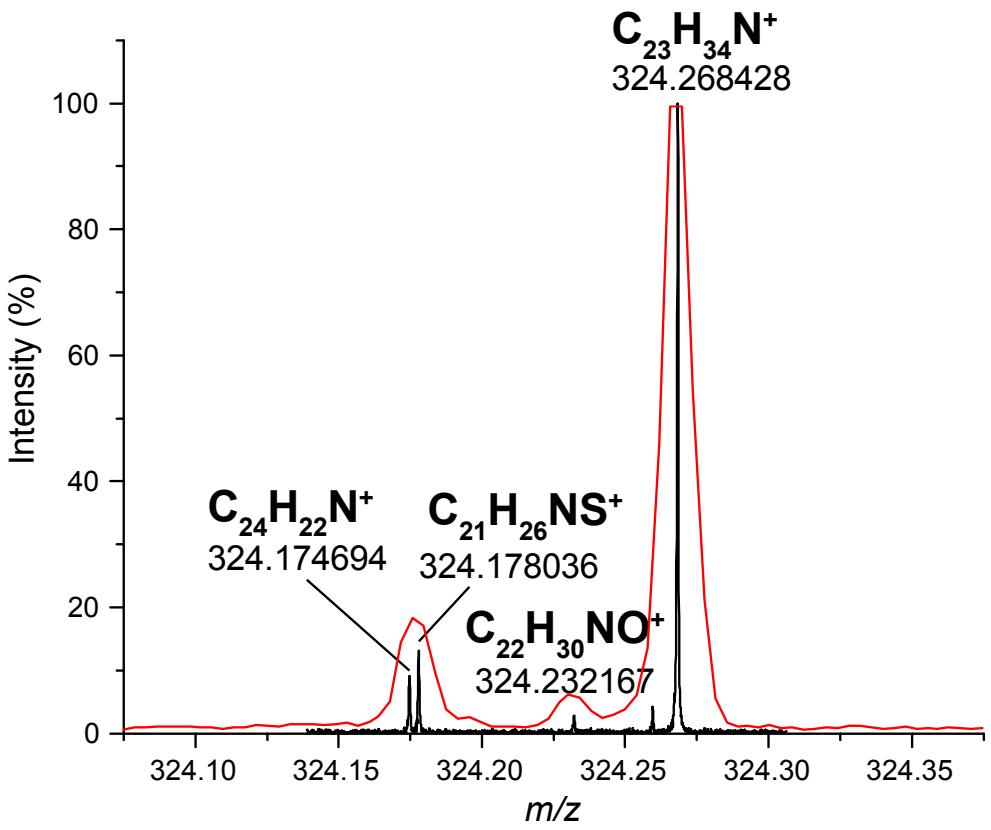

- isobaric interferences <u>not</u> resolvable (C_3 vs. SH_4) with the TOF but selected species can be investigated regarding IMS-profile
- UHRMS required for full molecular formula specification and proof for interferences

Application nitrogen speciation on a VGO

- ESI in positive mode:

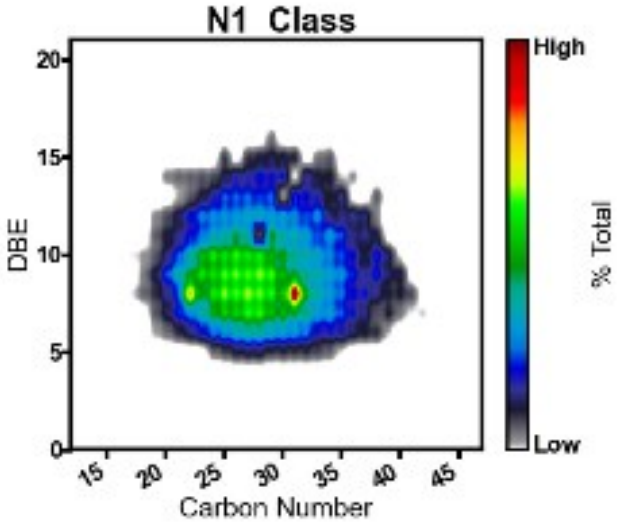

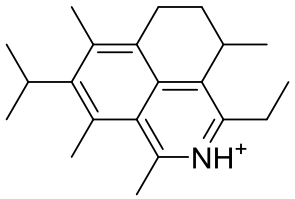

- Ion mobility display :

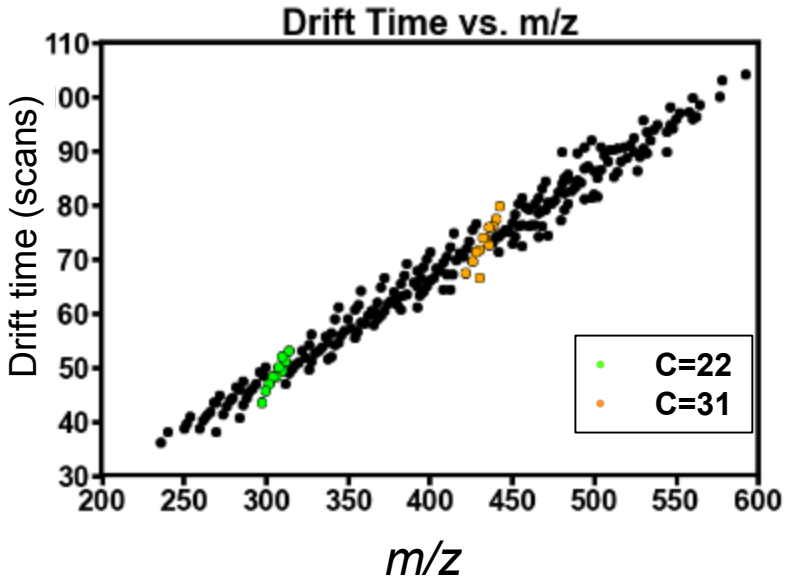

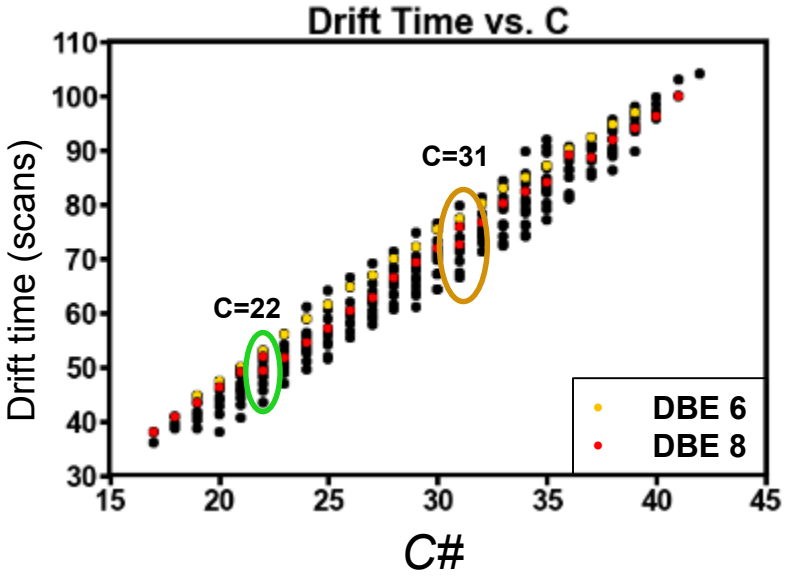

M. Farenc, Y. E. Corilo, P. M. Lalli, E. Riches, R. P. Rodgers, C. Afonso and P. Giusti, *Energy Fuels*, 2016, **30**, 8896-8903.

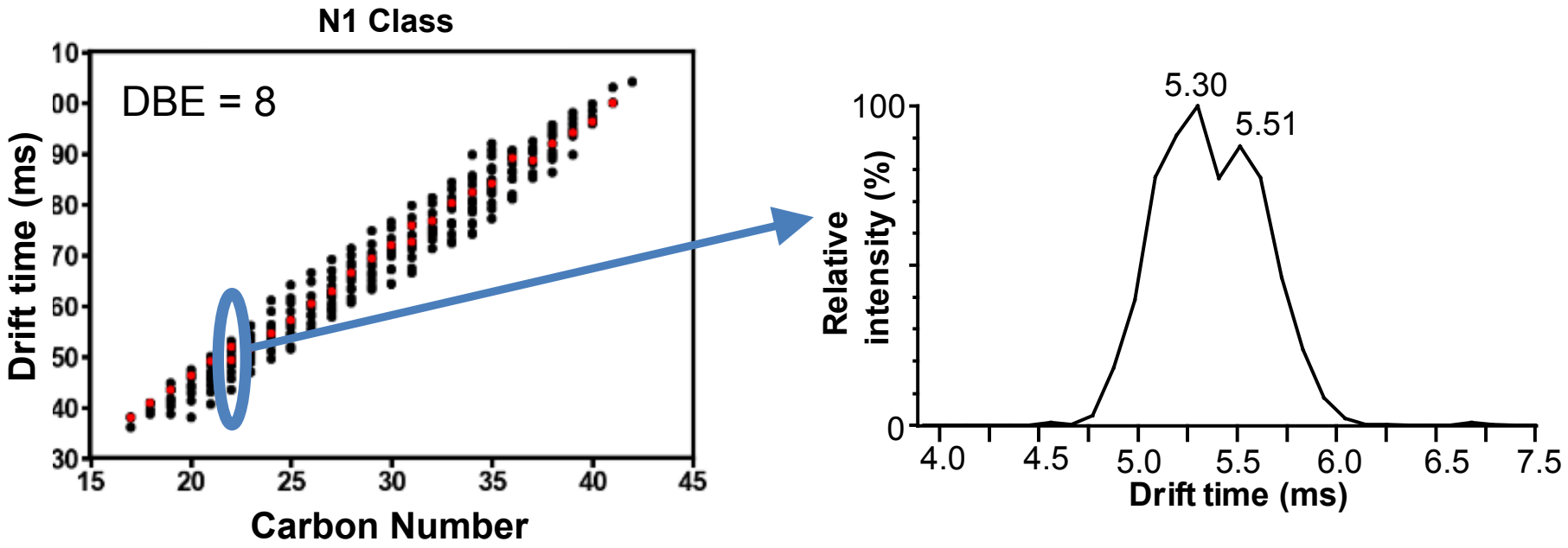
N1 Class
DBE = 8
Drift time (ms)
Carbon Number
10
00
90
80
70
60
50
40
30
15
20
25
30
35
40
45
5.30
5.51
100
0
Relative intensity (%)
4.0
4.5
5.0
5.5
6.0
6.5
7.5
Drift time (ms)

IMS profile

DBE8 N1 class

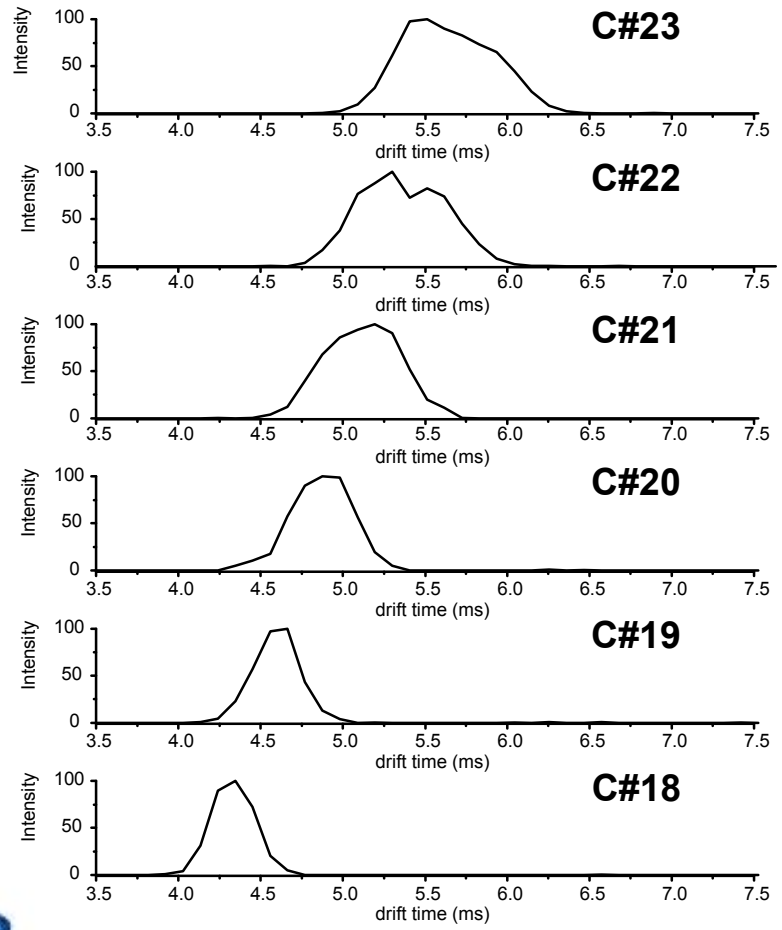

Polyalanine

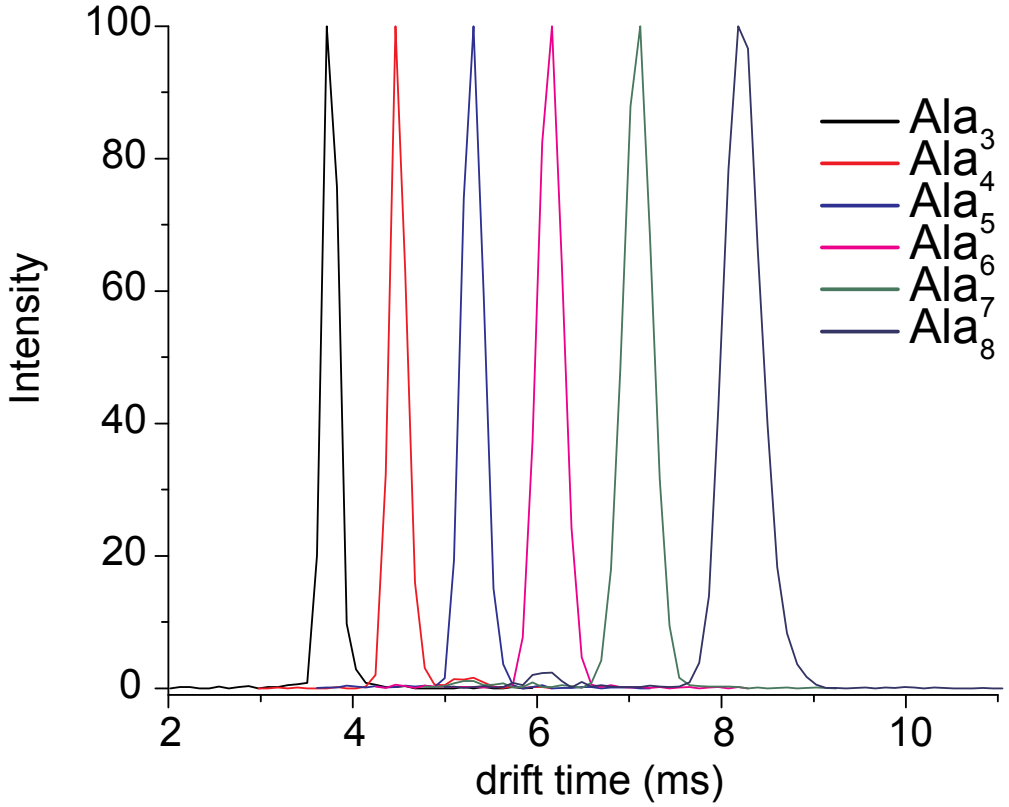

FWHM *vs* drift time

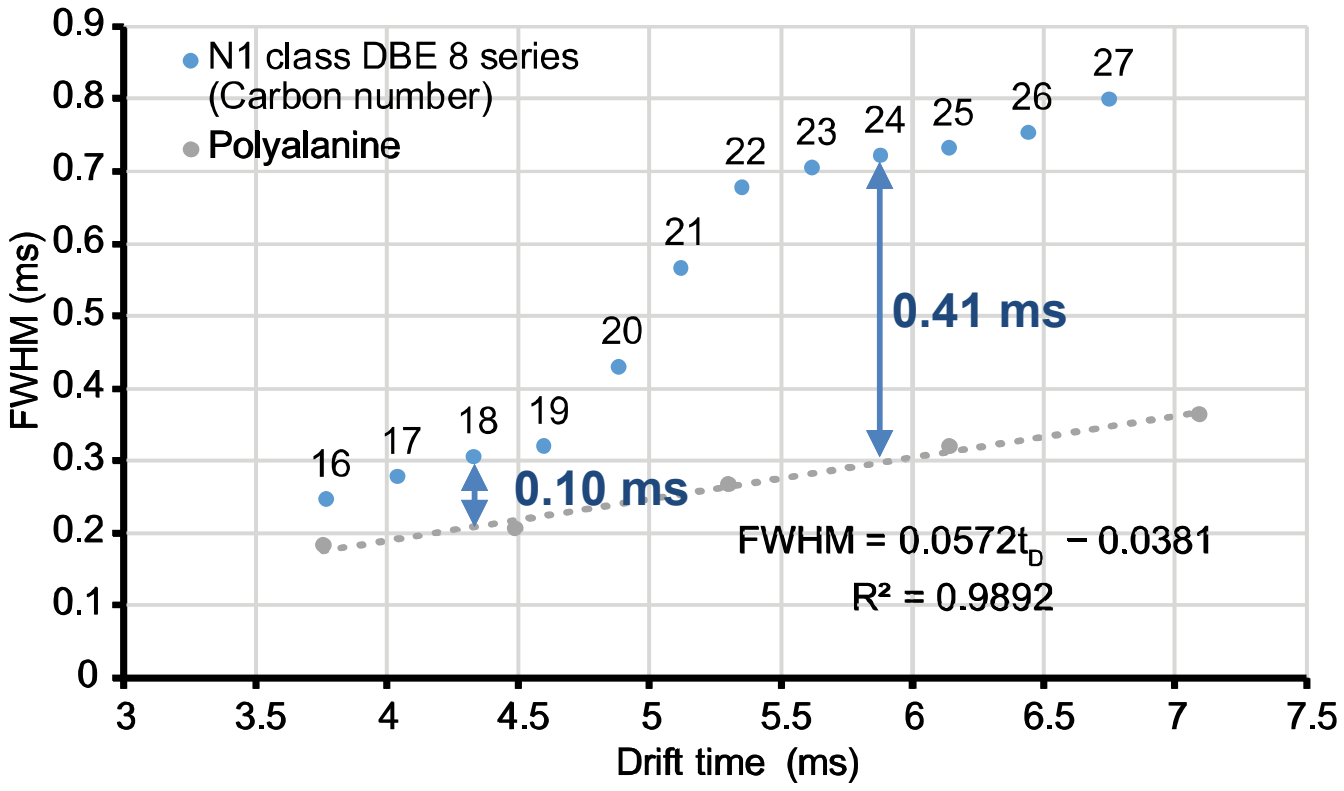

$$\mathbf{FWHM = 0.0572t_D - 0.0381}$$

Prediction of peak width

FWHM = 0.0572t_D − 0.0381 → $f(x) = ae^{\frac{(x-b)^2}{2c^2}}$

Gauss function

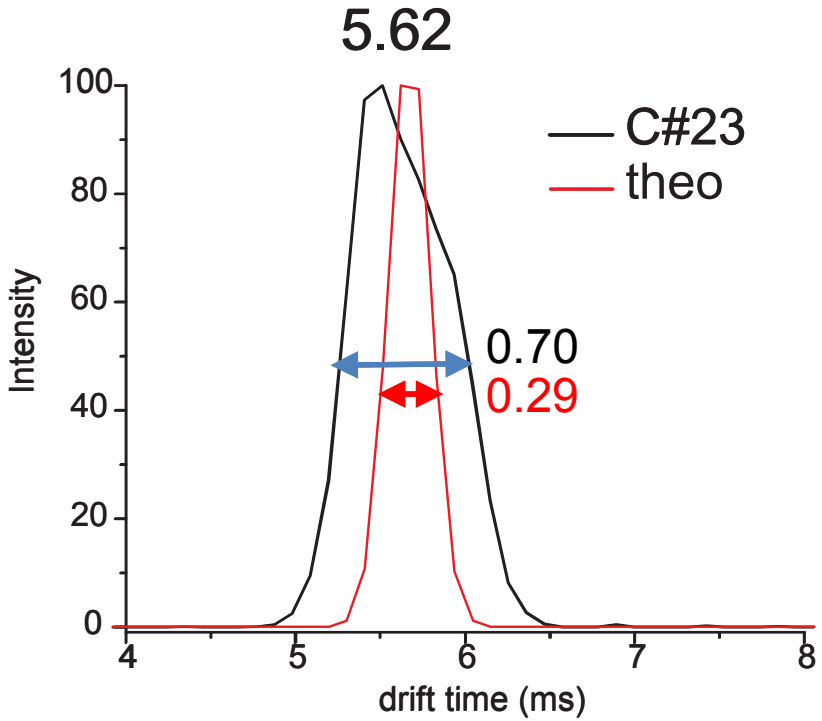

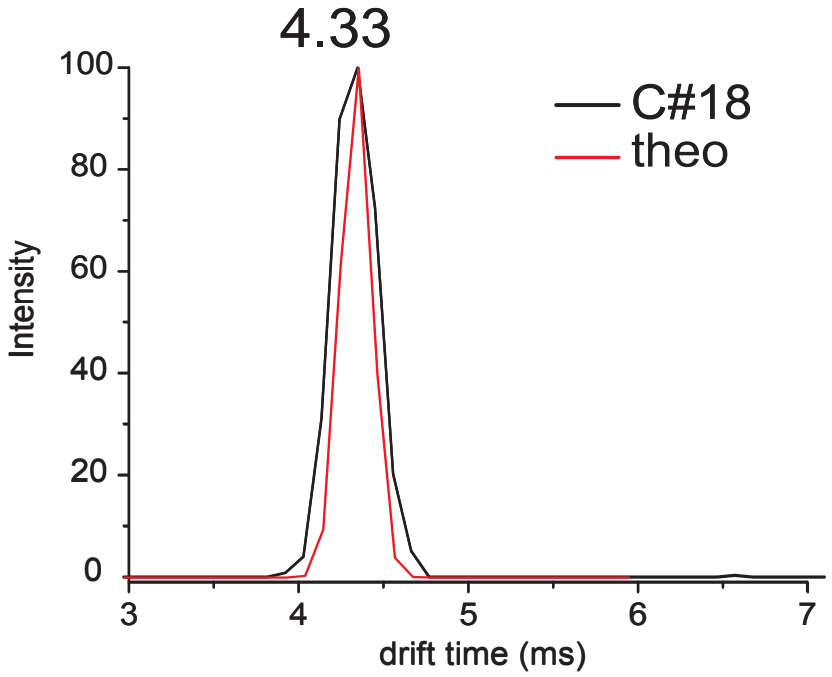

- Other way to obtain information on isomeric content?

Farenc, M., Paupy, B., Marceau, S. et al. J. Am. Soc. Mass Spectrom. (2017) 28: 2476. https://doi.org/10.1007/s13361-017-1749-1

Peak deconvolution ?

m/z 296

$C_{21}H_{30}N$

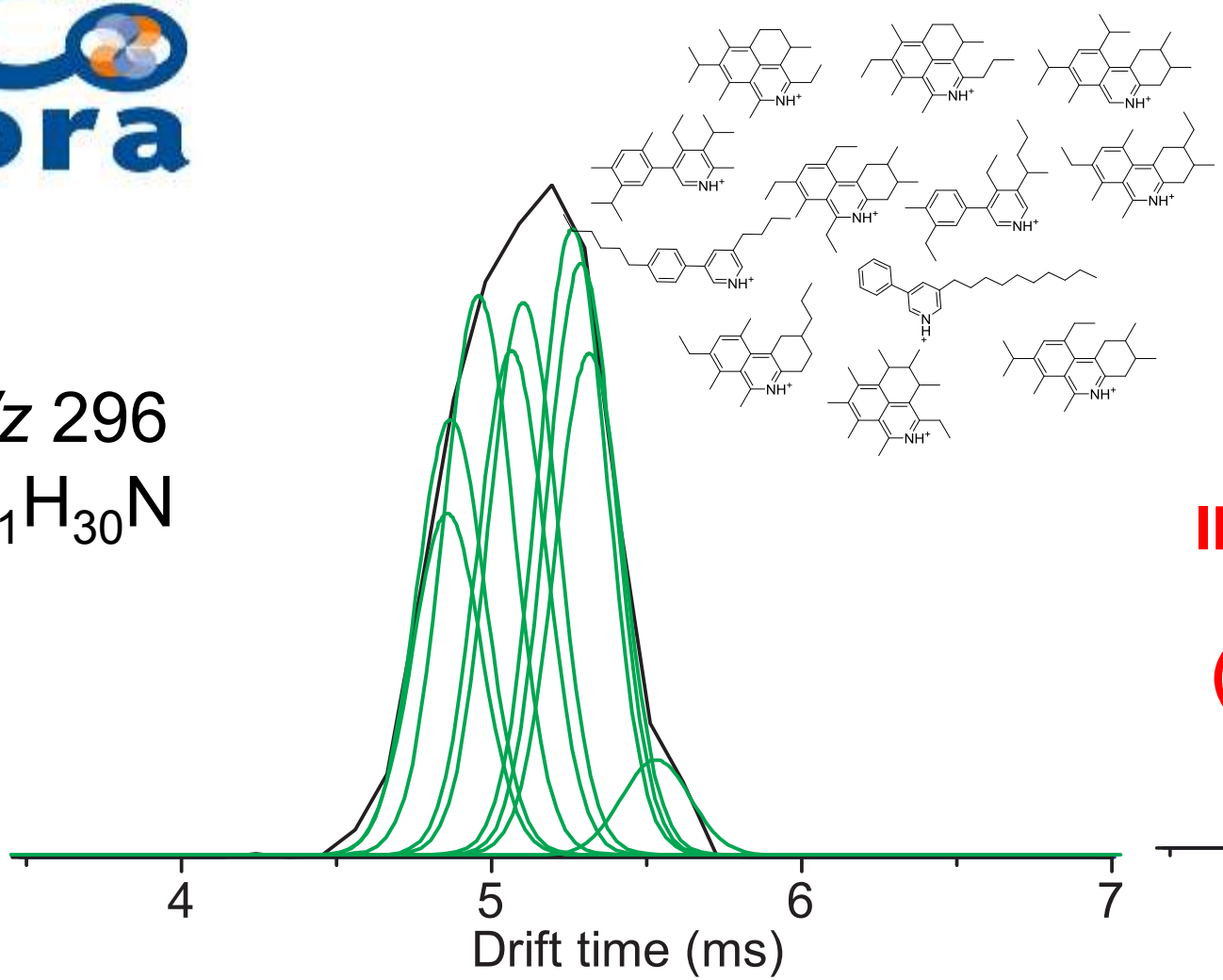

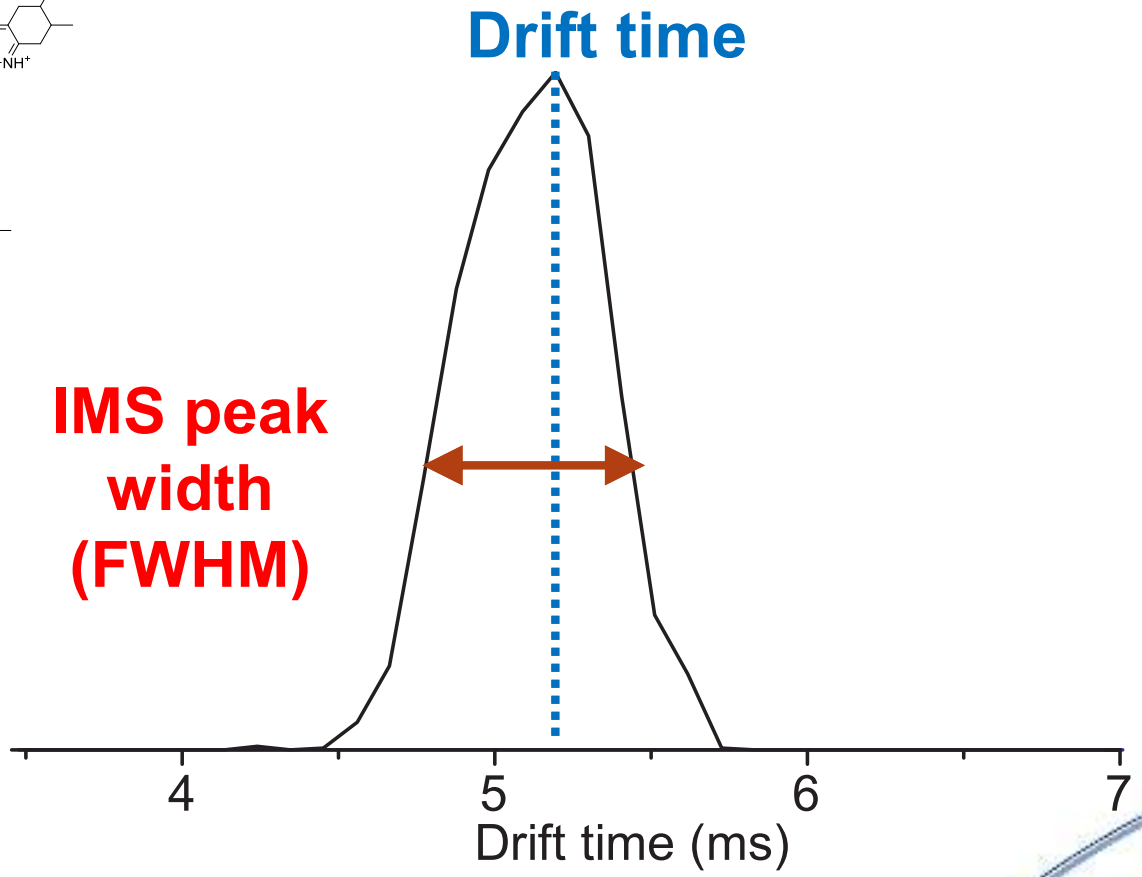

- Ion peak deconvolution on petroleum compounds not possible
- Continuum of isomeric species

Trap
IMS

Post IMS CID

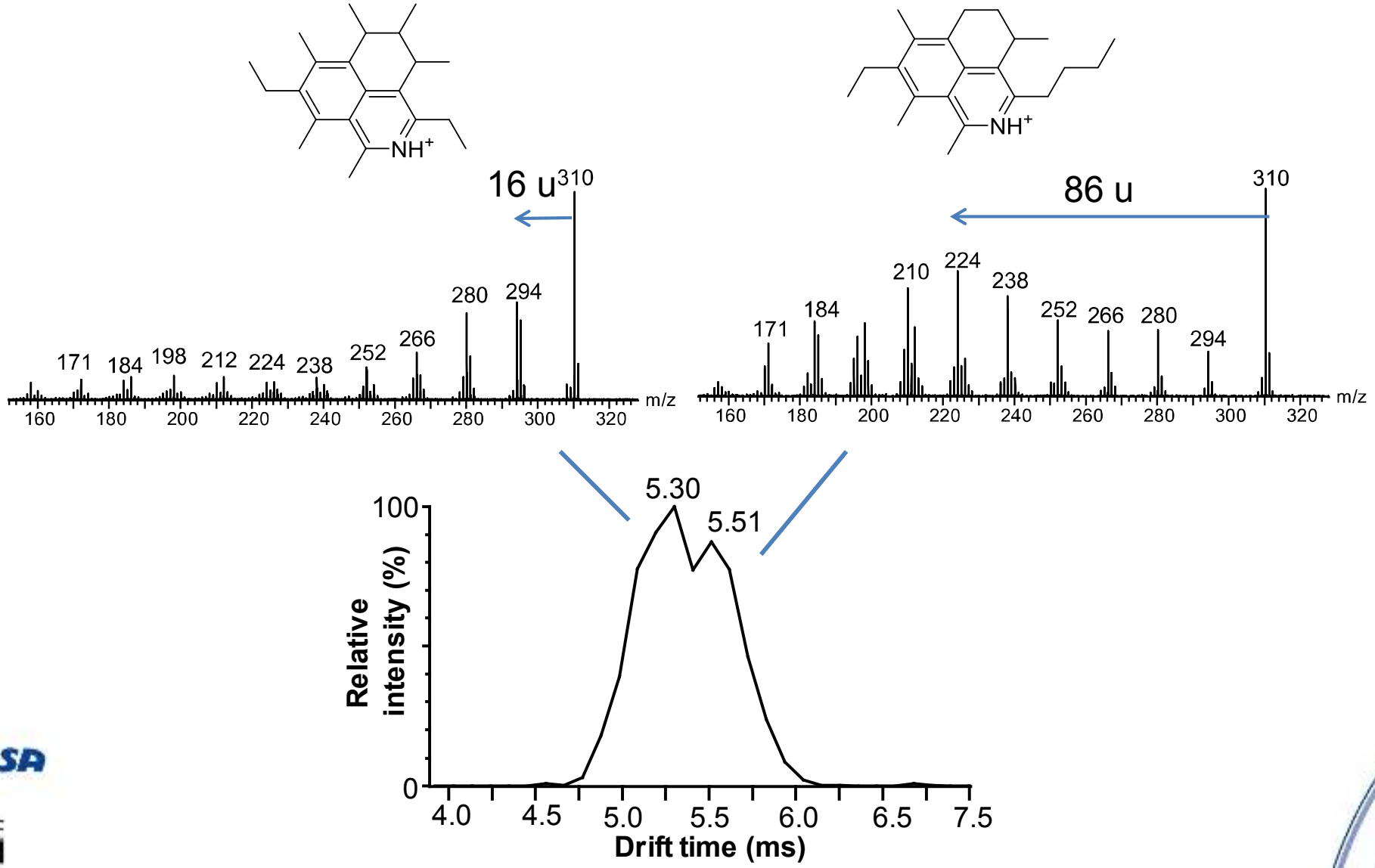
NH+
NH+
16 u
310
86 u
310
171
184
198
212
224
238
252
266
280
294
m/z
160
180
200
220
240
260
280
300
320
171
184
210
224
238
252
266
280
294
m/z
160
180
200
220
240
260
280
300
320
5.30
5.51
100
0
Relative intensity (%)
4.0
4.5
5.0
5.5
6.0
6.5
7.5
Drift time (ms)

Molecules refractory to the HDN process

HYDRODENITROGENATION OF VGO

Neutral Nitrogen

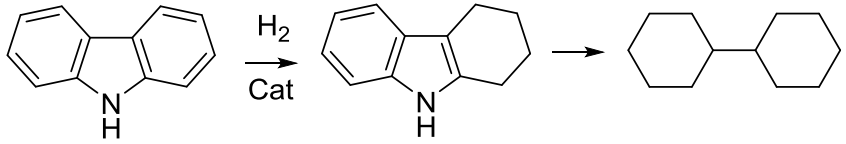

Basic Nitrogen

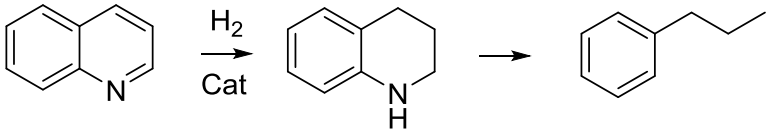

Basic Nitrogen
ESI(+)

Neutral Nitrogen
ESI(−)

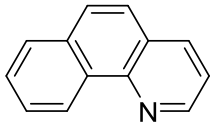

benzoquinoline

DBE=10

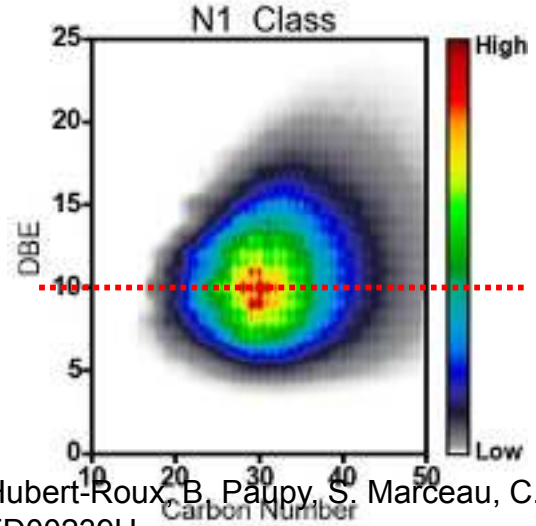

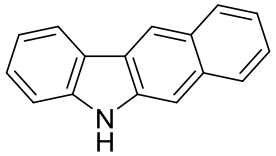

benzocarbazole

DBE=12

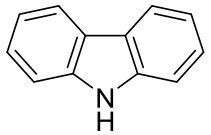

carbazole

DBE=9

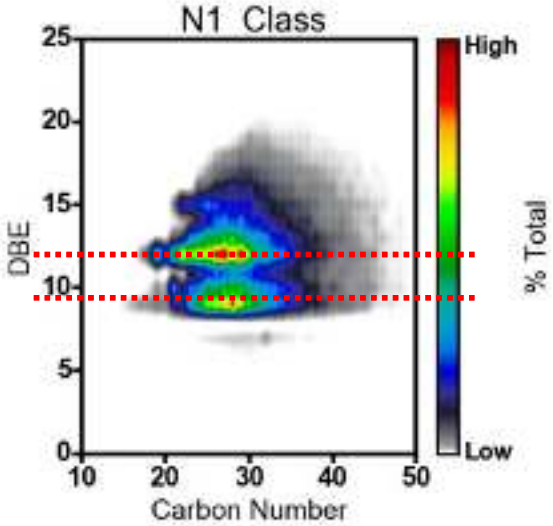

J. Le Maître, M. Hubert-Roux, B. Paupy, S. Marceau, C. Rüger, C. Afonso, P. Giusti, *Faraday Discussions*, 2019, DOI:10.1039/C8FD00239H

Faraday Discussion

Challenges in Analysis of Complex Natural Mixtures Faraday Discussion May 13, 2019 - May 15, 2019

Molecules refractory to the HDN process

Hydrodenitrogenation of VGO

(+)-ESI
12T FTICR

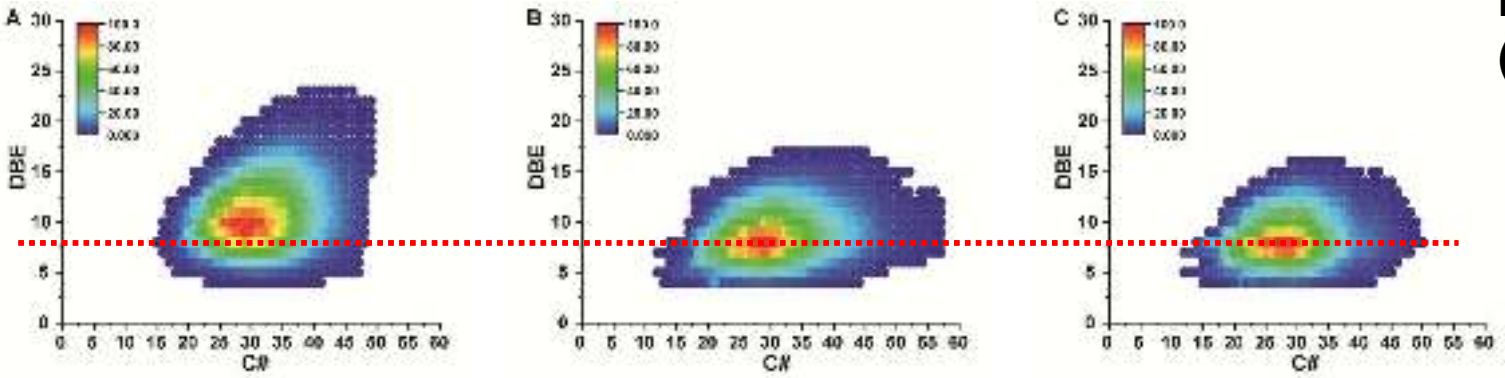

VGO | 70 ppm | 10 ppm

$DBE = c - h/2 + n/2 + 1$
(for $C_cH_hN_nO_oS_s$)

DBE 7-8-9 most refractory to HDN

(+)-ESI
IMS-QTOF

$C_{27}H_{40}N^+$ *m/z* 378.3155
DBE 9

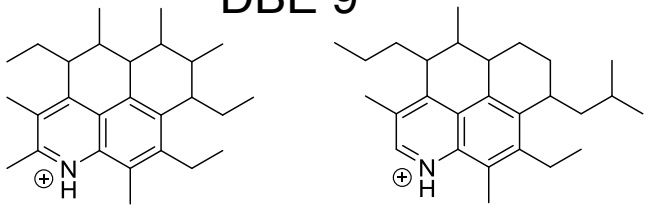

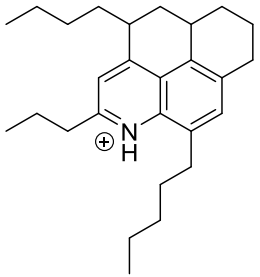

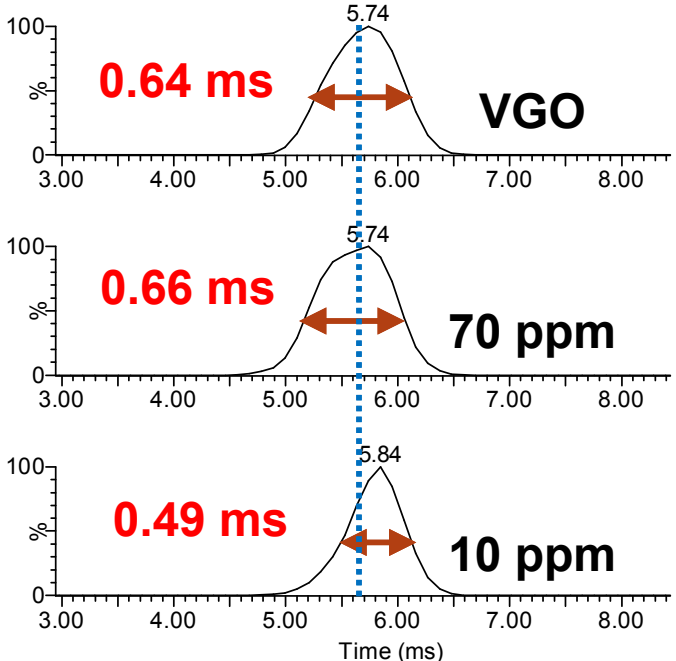

137.5 Å²

137.5 Å²

139.4 Å²

J. Le Maître, M. Hubert-Roux, B. Paupy, S. Marceau, C. Rüger, C. Afonso, P. Giusti, *Faraday Discussions*, 2019, 218 (0), 417-430.

IMS-HRTOF (-)-ESI

$C_{21}H_{18}N^-$
DBE 13

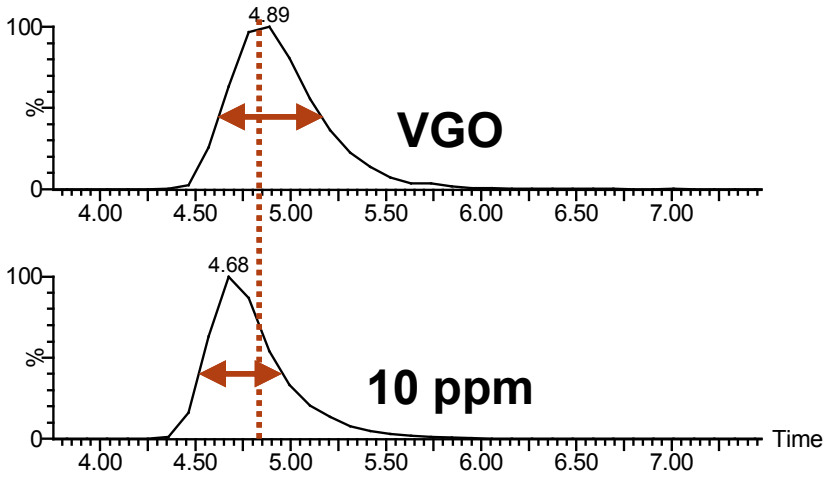

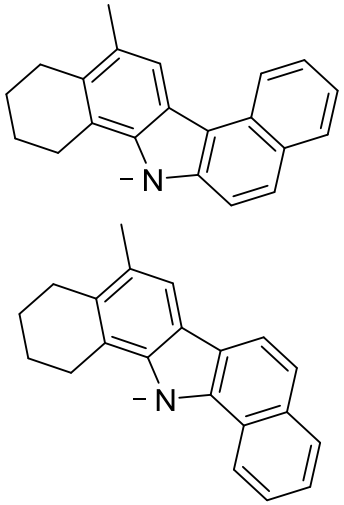

- significant shift in peak apex and FWHM also for (-)-ESI

CCS based structure prediction

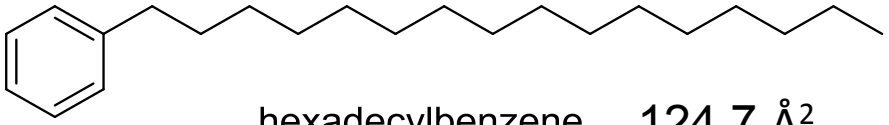

hexadecylbenzene 124.7 Å^2

Simulation and modeling of CCS for structural elucidation…

- minimization using MMFF94 Force Field
- CCS determination of all structures using Mobcal

Lowest energy structure

71.9 kJ/mol
119.6 Å^2

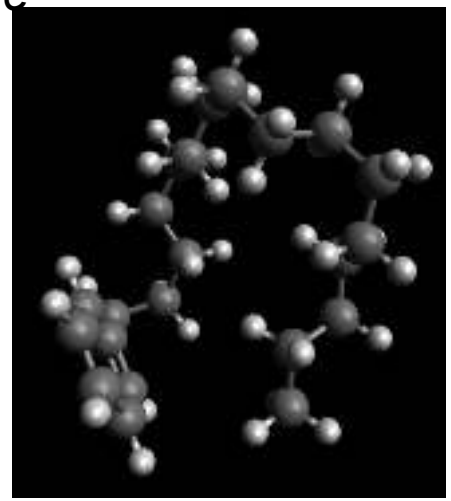

Highest energy structure

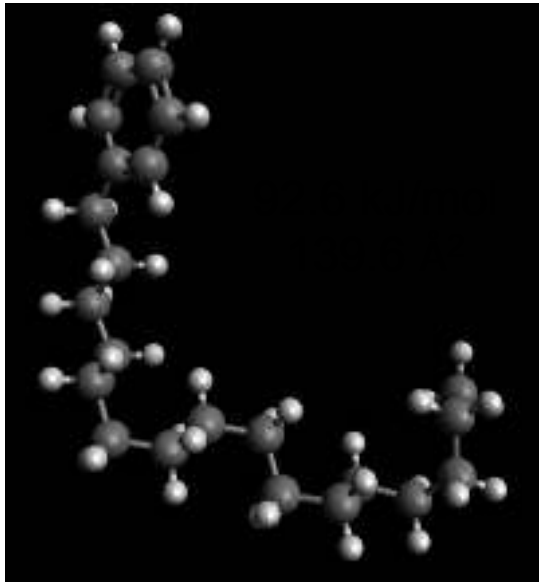

Structure prediction based on IMS-MS

Towards unsupervised polyaromatic hydrocarbons structural assignment from SA-TIMS-FTMS data

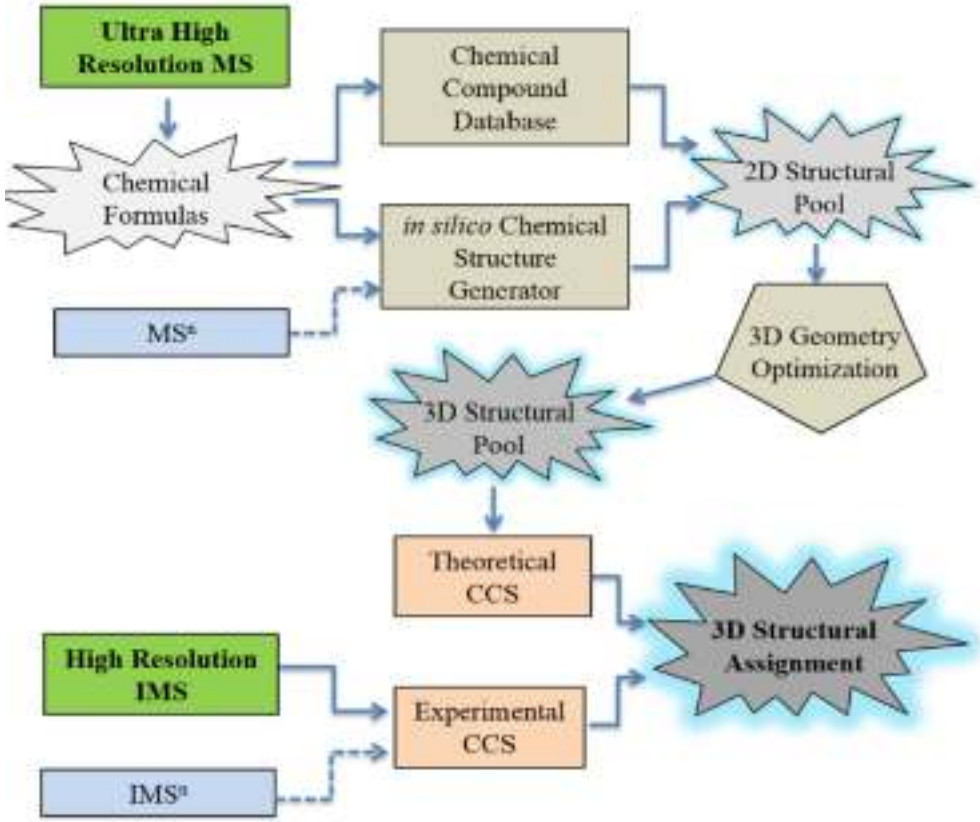

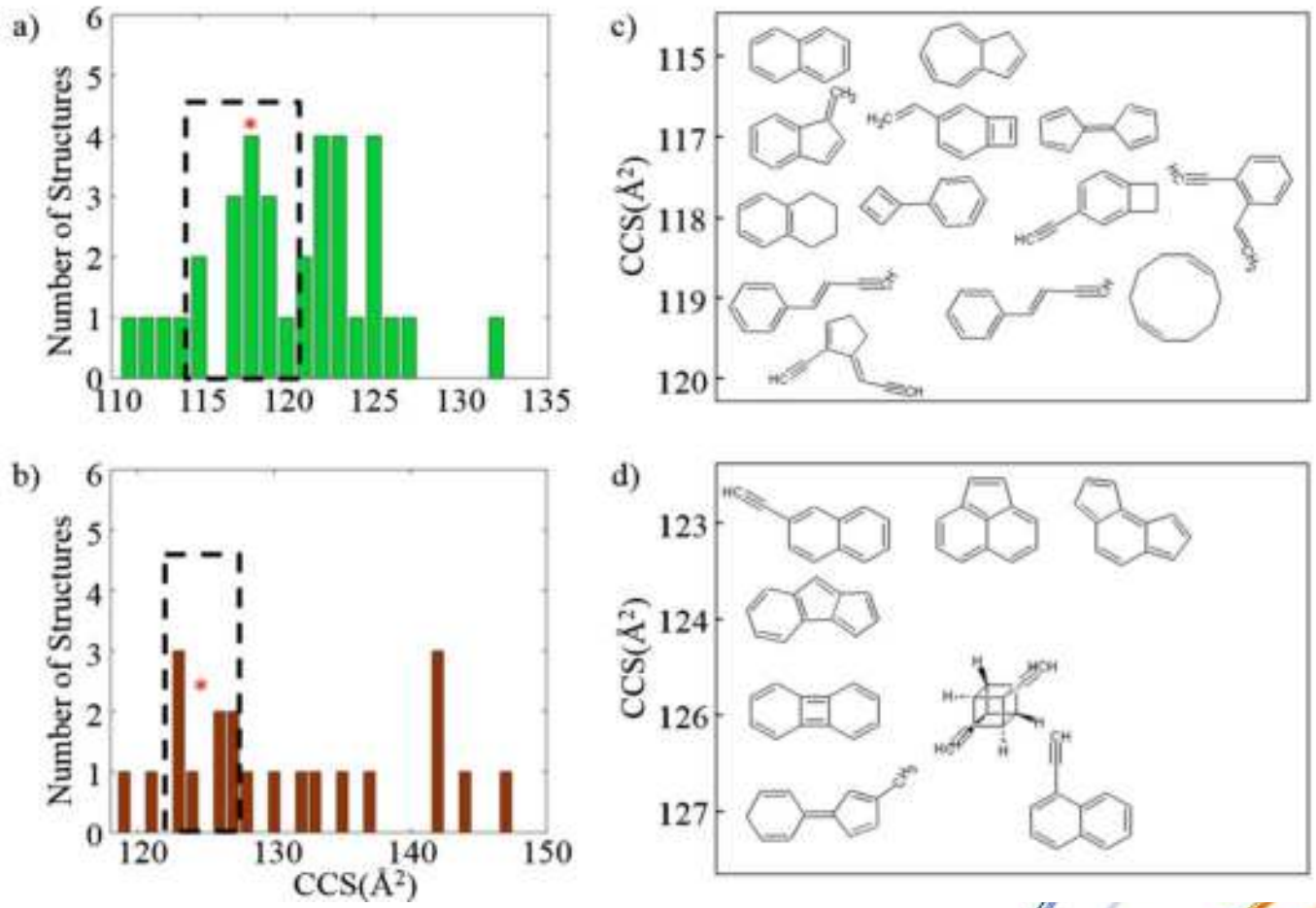

Complex mixture of polyaromatic hydocarbons coal tar in oil (SRM1597)

P. Benigni, R. Marin and F. Fernandez-Lima, *Int J Ion Mobil Spectrom*, 2015, **18**, 151-157.

CCS calculation from long alkyl chain molecules

Rigid molecule

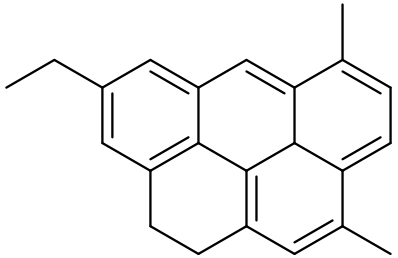

Highly floppy molecule

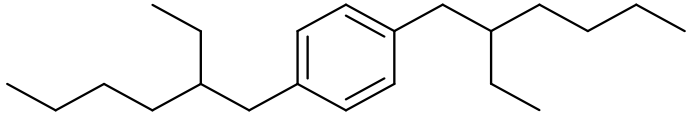

1,4-Bis(2-ethylhexyl)benzene

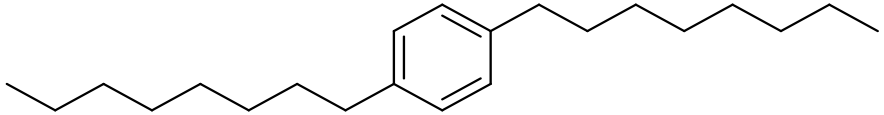

1,4-Dioctylbenzene

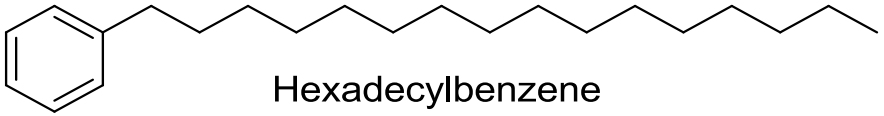

Hexadecylbenzene

Previous Work on CCS based structure prediction

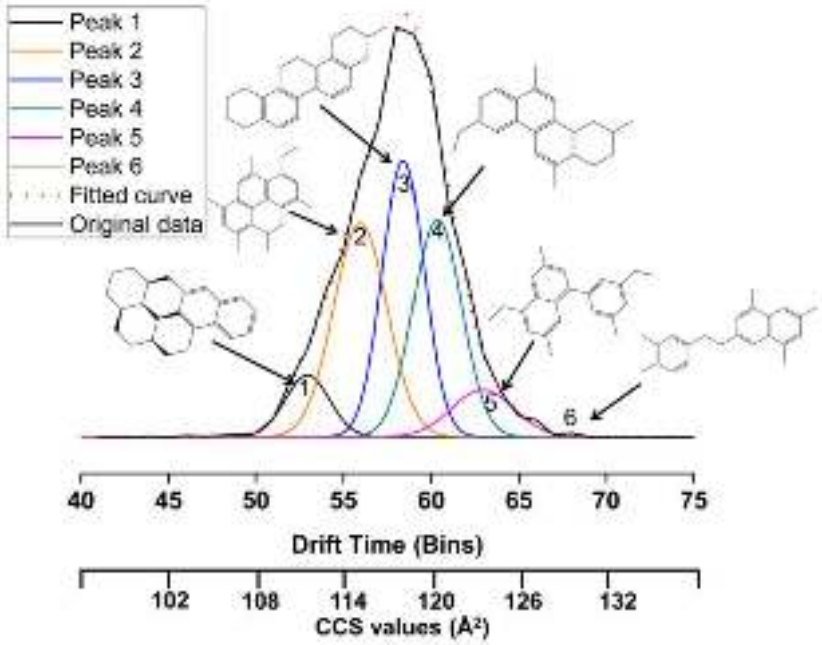

Standard compounds	Suggested structures	Experimental CCS values (Å²)	Theoretical CCS values (Å²)	$\Delta\Omega_{(exp.-theo.)\%}$
1,4-didecylnaphthalene	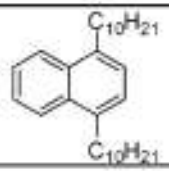	155.86	199.50	-28.0
1,6-diheptylpyrene	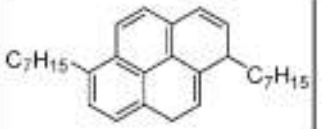	148.04	174.68	-18.0
9,10-diheptylanthracene	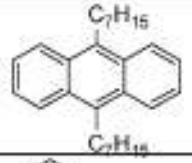	139.52	164.67	-18.0
3-octylperylene	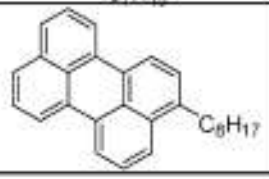	128.68	147.48	-14.6
1,4-didecylbenzene	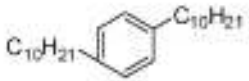	147.96	186.47	-26.0

DFT using B3LYP/6-31G(d) base set

A. Ahmed, Y. Cho, K. Giles, E. Riches, J. W. Lee, H. I. Kim, C. H. Choi and S. Kim, *Anal. Chem.*, 2014, **86**, 3300-3307.

How floppy molecules fly in the IMS cell?

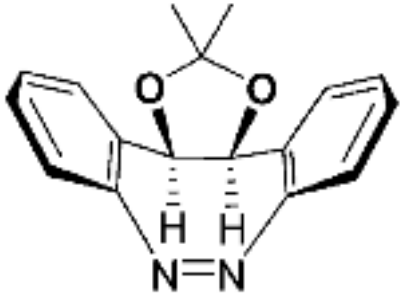

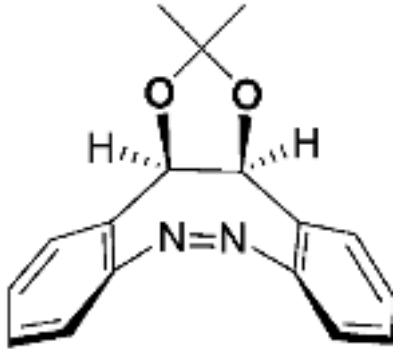

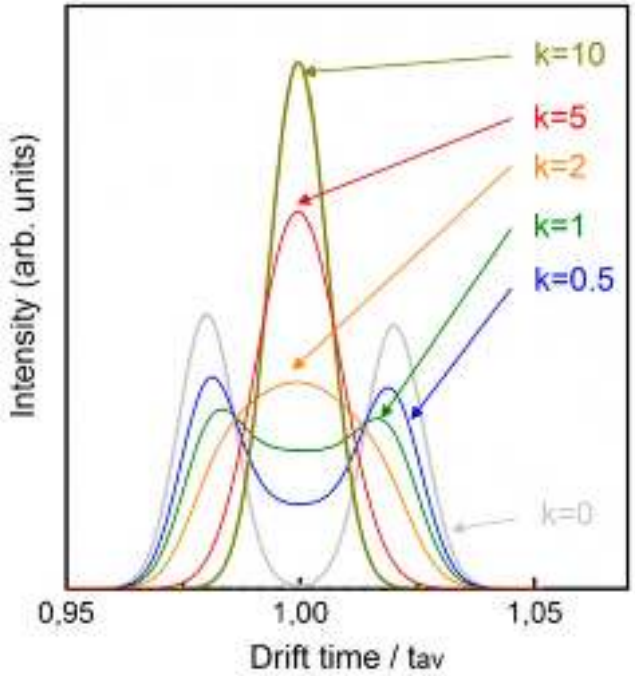

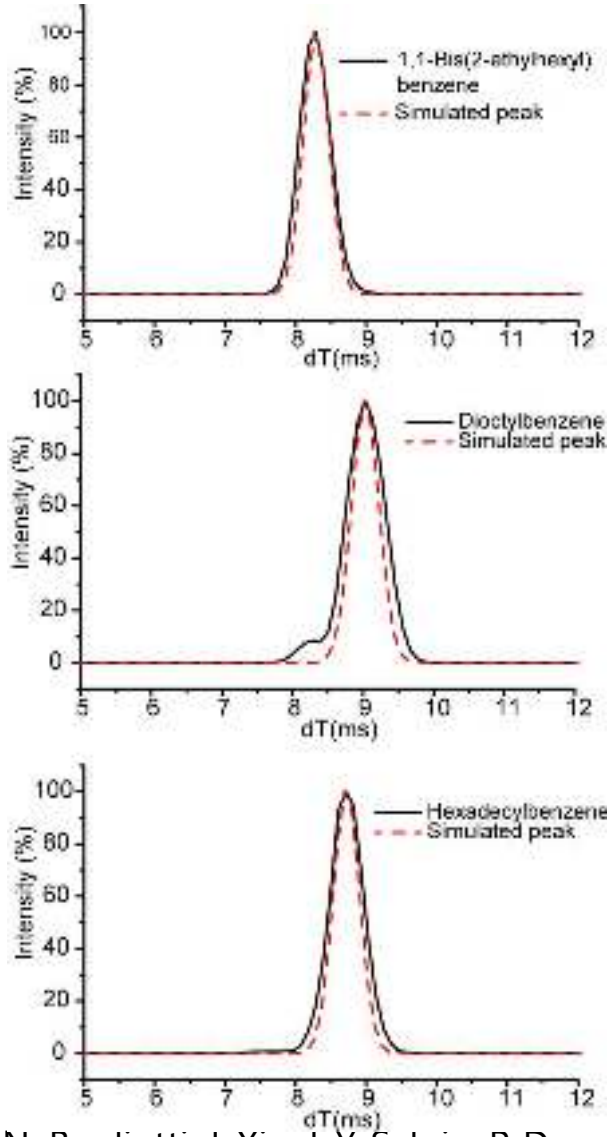

S. Poyer, C. Comby-Zerbino, C. M. Choi, L. MacAleese, C. Deo, N. Bogliotti, J. Xie, J. Y. Salpin, P. Dugourd and F. Chirot, *Anal. Chem.*, 2017, **89**, 4230-4237

CCS prediction Workflow

[redacted]

[redacted]

[redacted]

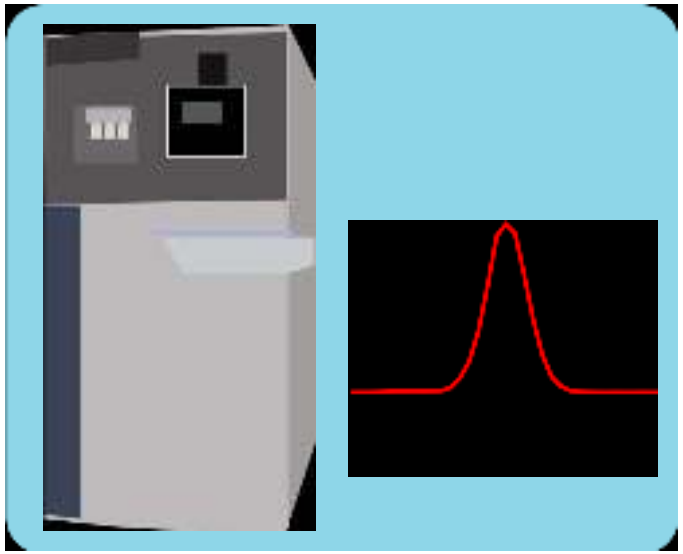

Measurement
CCS calibration

Theoretical

$^{calc}CCS_{N2}$: 201.9 Å²

$^{exp}CCS_{N2}$: 200.5 Å²

Experimental

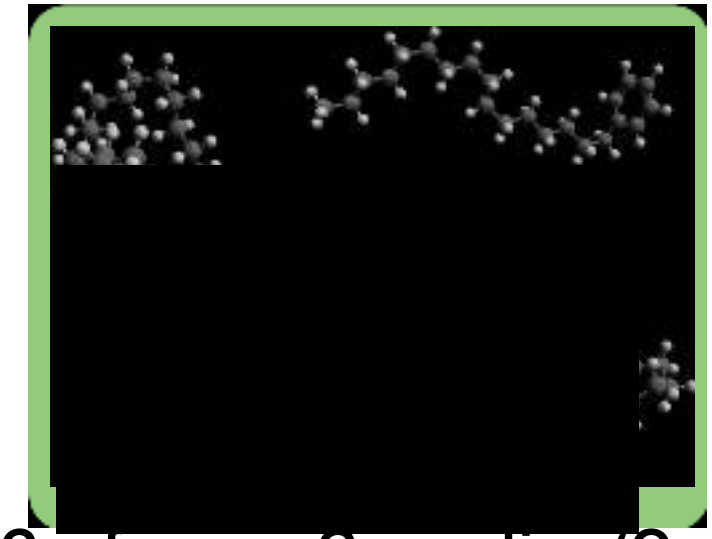

Conformers Generation (OpenBabel)
Minimization MMFF94

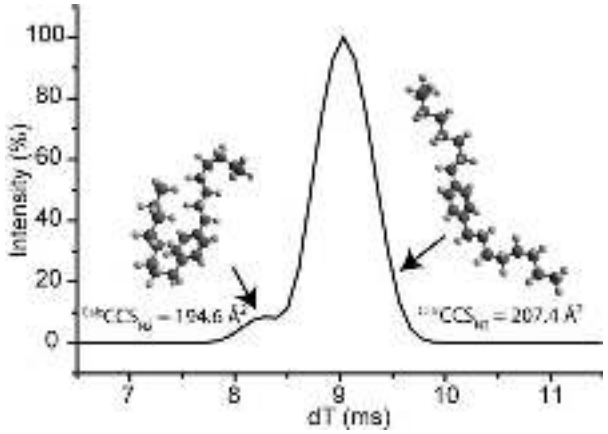

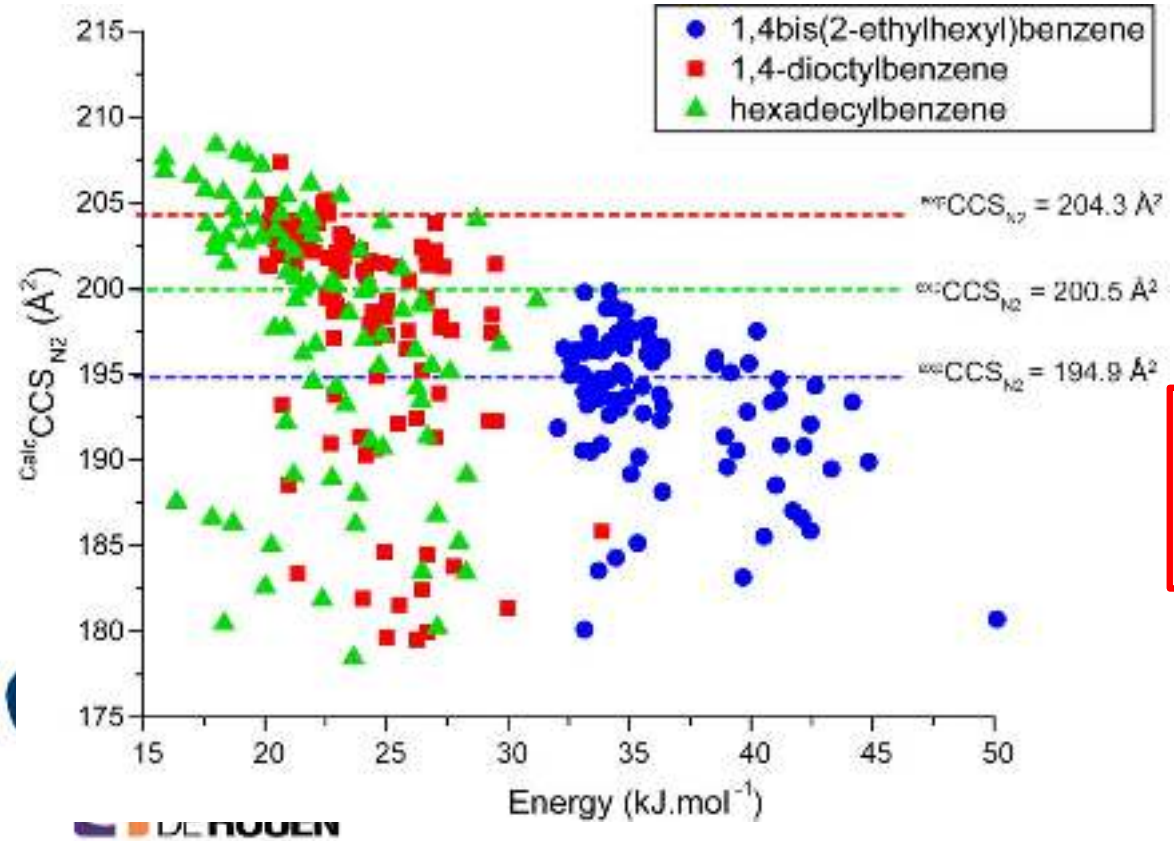

Name	1,4bis(2-ethylhexyl)benzene	1,4-dioctylbenzene	hexadecylbenzene	Average error (%)
$^{Exp}CCS_{N2}$	194.9	204.3	200.5	
1% Lowest energy (^{calc}CCS)	191.8 (1.59%)	201.4 (1.42%)	207.5 (-3.49%)	2.17
25% Lowest energy (^{calc}CCS)	193.3 (0.82%)	201.5 (1.37%)	203.9 (-1.69%)	1.29
50% Lowest energy (^{calc}CCS)	194.0 (0.46%)	200.5 (1.86%)	201.9 (-0.70%)	1.01
Average all $^{calc}CCS_{N2}$	193.3 (0.82%)	197.6 (3.28%)	198.7 (0.89%)	1.66

HDN VGO

$C_{27}H_{42}N^+$

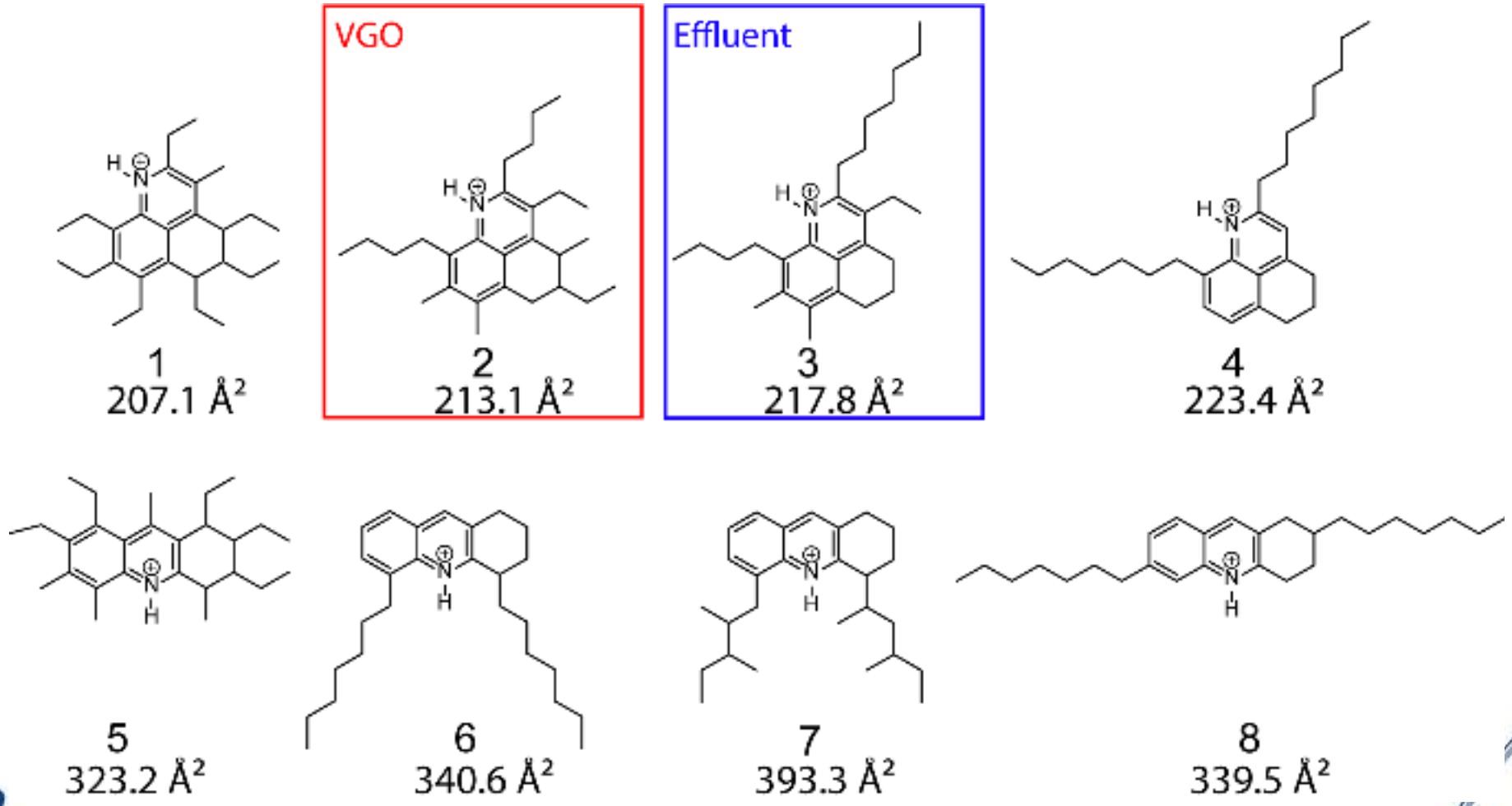

Structural Characterization of Acids in Petroleum by IMS-MS

ESI(−)
O_2 Class, DBE=5

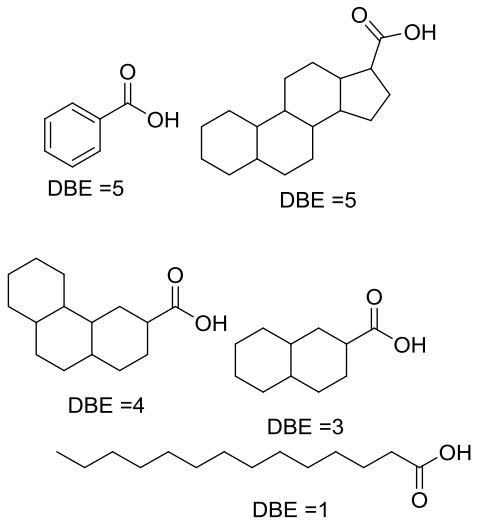

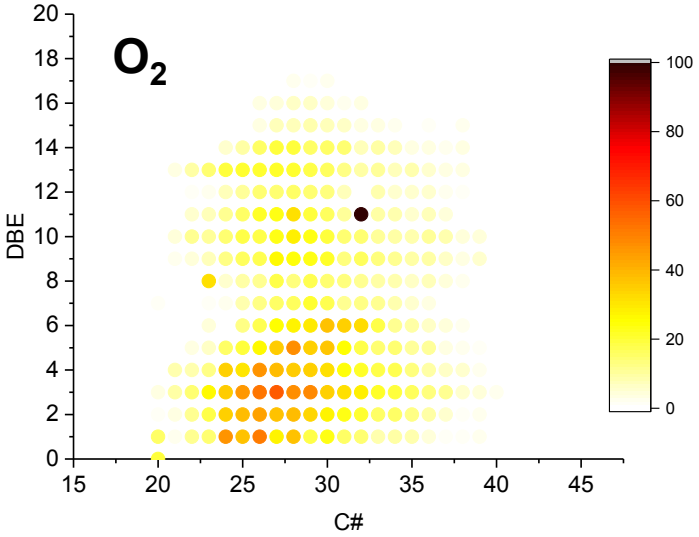

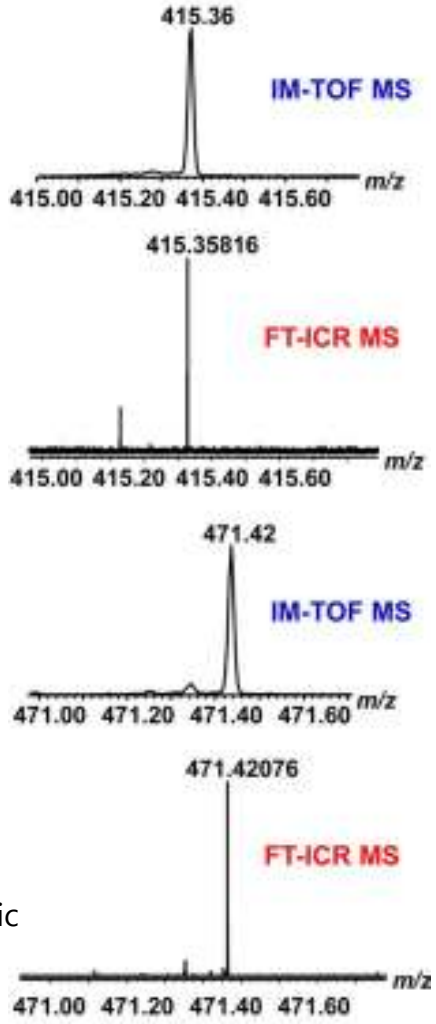

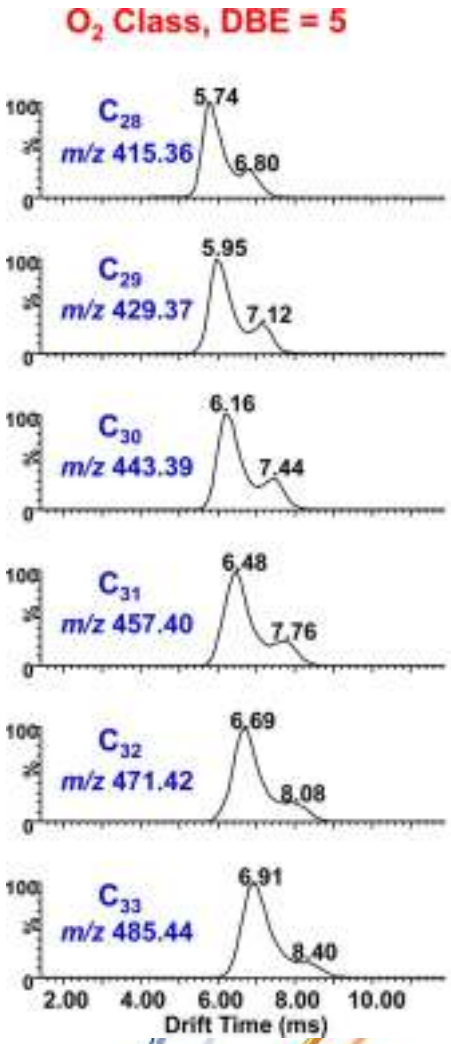

P. M. Lalli, Y. E. Corilo, S. M. Rowland, A. G. Marshall, R. P. Rodgers. Isomeric Separation and Structural Characterization of Acids in Petroleum by Ion Mobility Mass Spectrometry. *Energy Fuels* **2015**, *29*, 3626.

Comparison with standard compounds

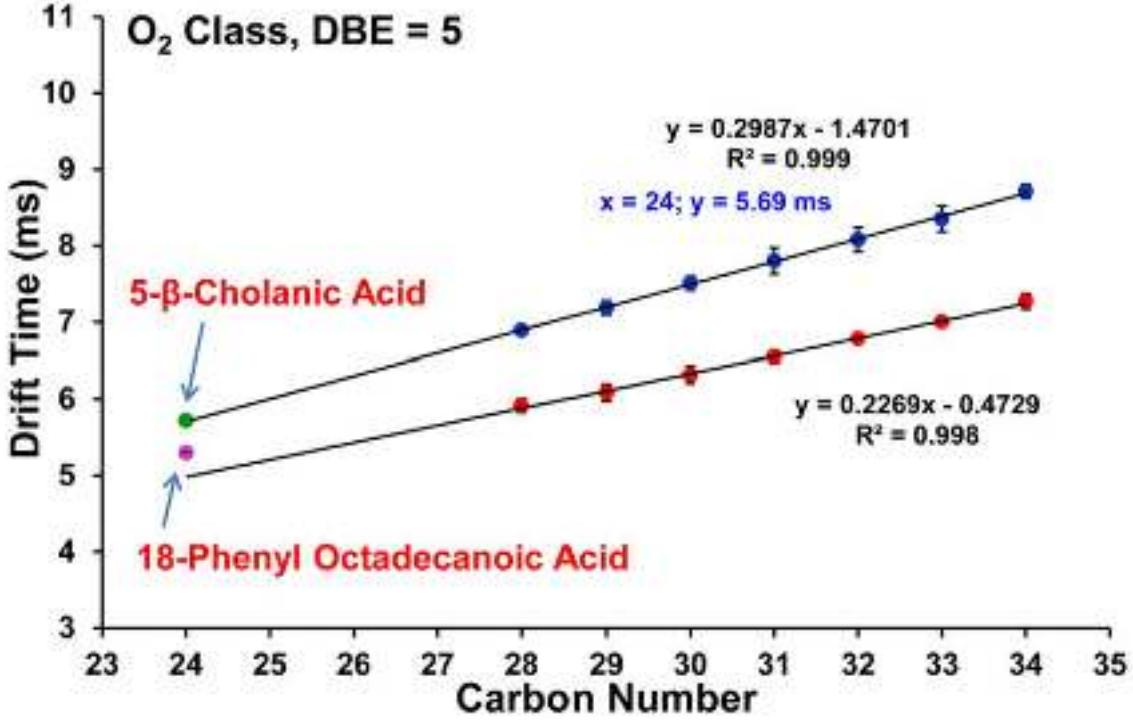

Drift time vs carbon number for the O_2 class species of DBE = 5

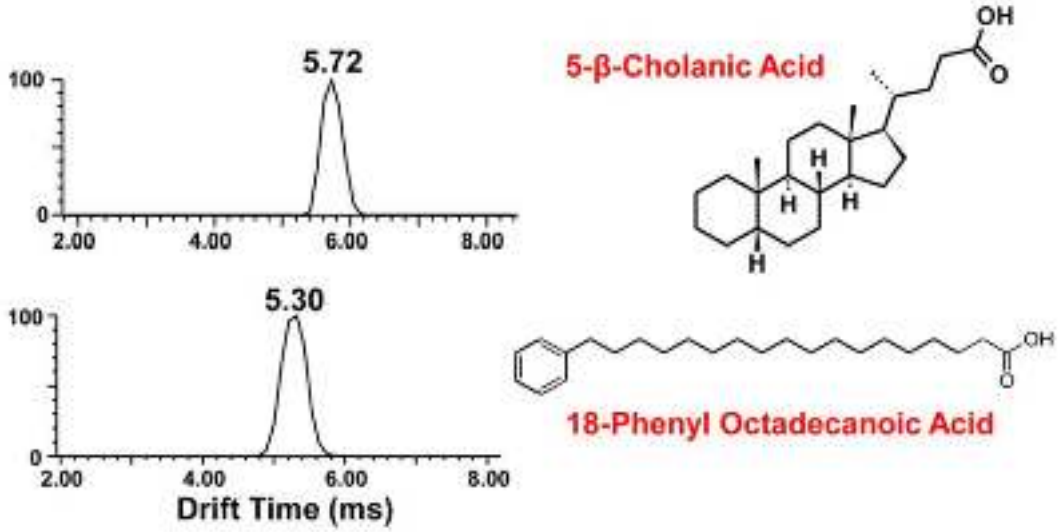

Experimental drift times for two standard compounds (both C24): 5-β-cholanic acid and 18-phenyl octadecanoic acid.

Tholins

Nathalie Carasco

Cassini-Huygens Mission

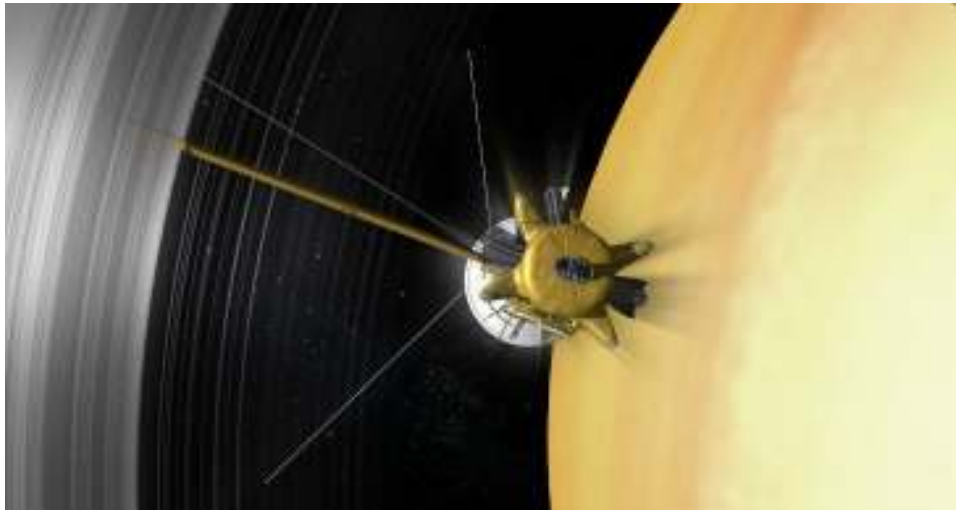

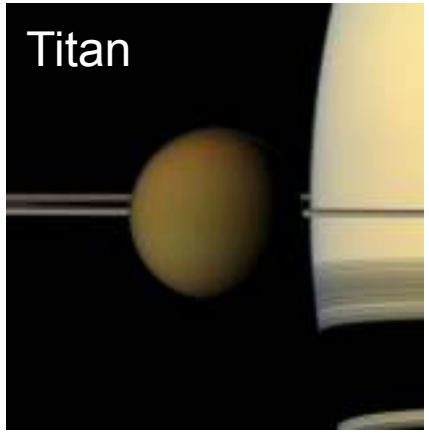

PhD of Julien Maillard

- 95 % N_2, 5 % CH_4
- Photochemistry reactions due to solar UV photons and Saturn charged particles (Khare et *al*. 1981)
  - Thick brown smog
  - Prebiotic chemistry

Earth. Planet. Sci. Lett., 2018, **495**, 185-191

PAMPRE experiment

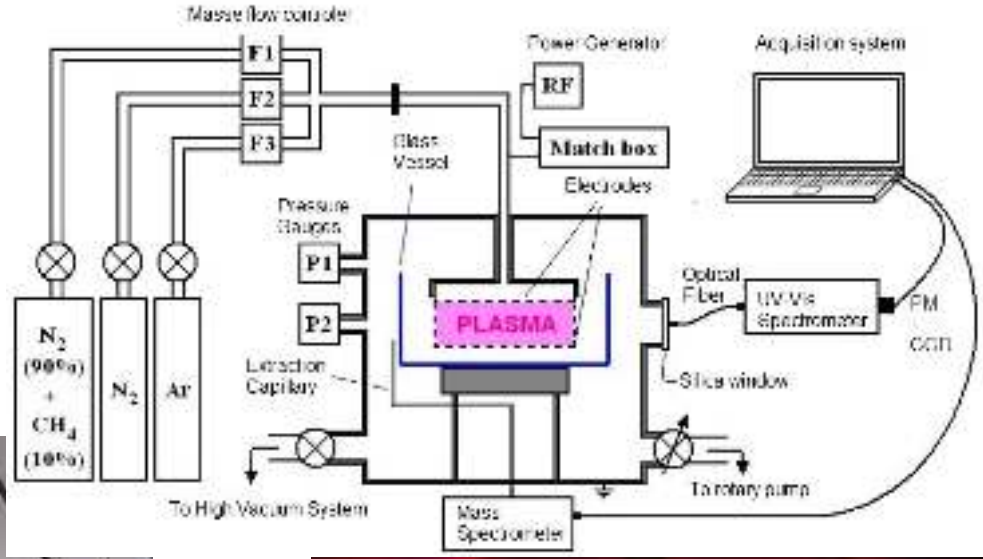

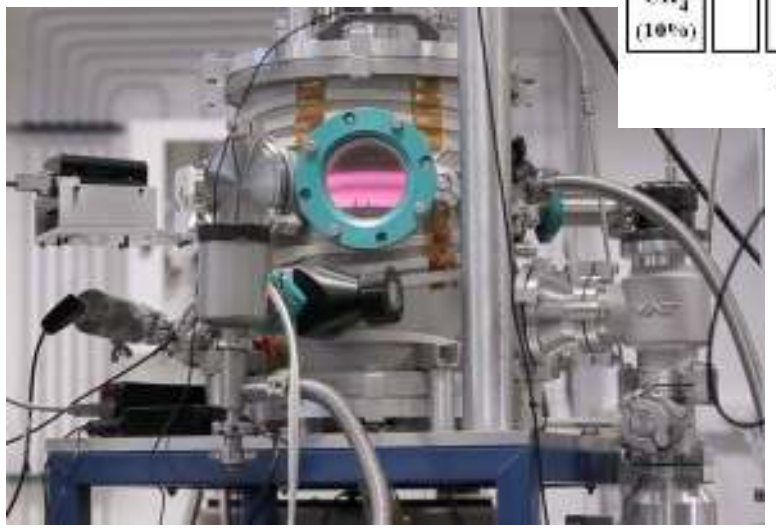

Tholins

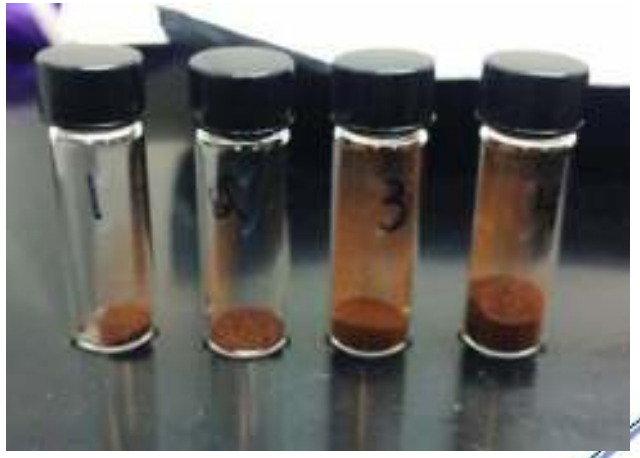

PAMPRE experiment (Szopa et al 2006)
(**P**roduction d'**A**érosols en **M**icrogravité par **P**lasma **Re**actifs)

Highly complex organic matter

How to analyse the non soluble fraction ?

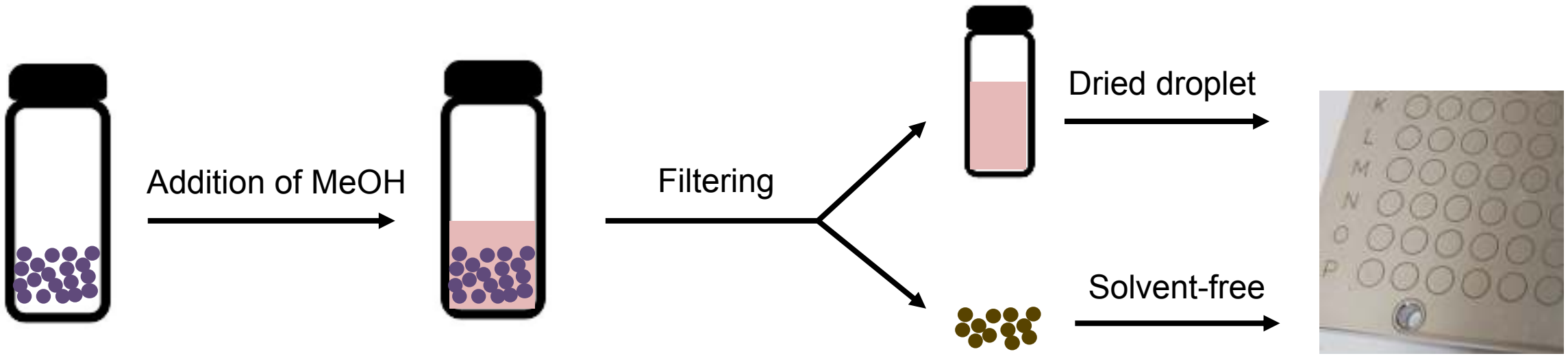

Analysis with a **Laser desorption ionisation source (LDI) coupled to a 12T FTICR**

* Barrere. C.. et *al.* (2012). "Solvent-based and solvent-free characterization of low solubility and low molecular weight polyamides by mass spectrometry: a complementary approach." Rapid Commun Mass Spectrom 26(11): 1347-1354.

Optimization for the best performances

- Optimisation of the ICR cell by a DoE
  - Resolution 4.10^6 @ *m/z* 200 (7.5 s TD, AMP mode)
  - Mean error 0.050 ppm

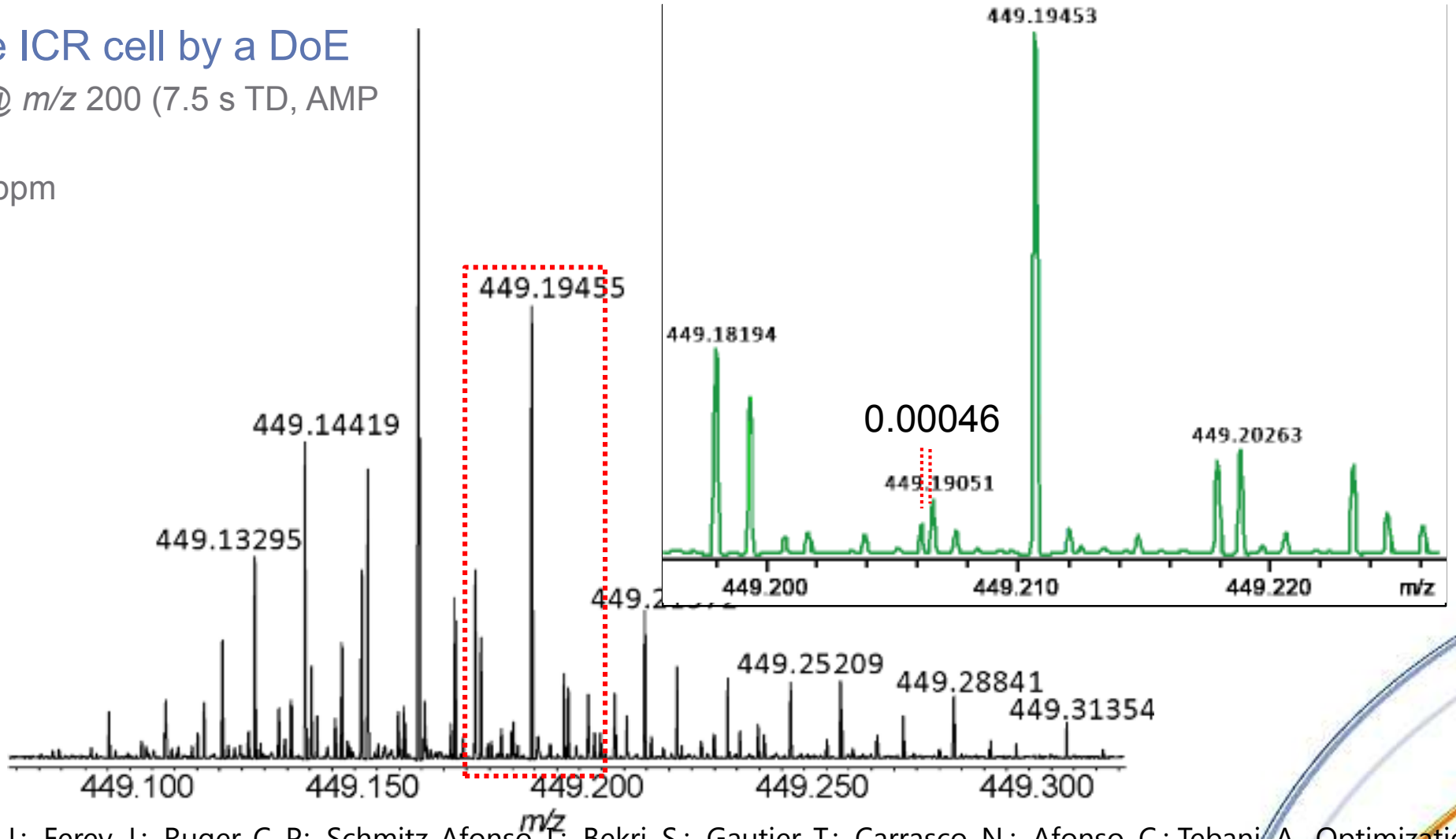

Maillard, J.; Ferey, J.; Ruger, C. P.; Schmitz-Afonso, I.; Bekri, S.; Gautier, T.; Carrasco, N.; Afonso, C.; Tebani, A., Optimization of ion trajectories in a dynamically harmonized Fourier-Transform Ion Cyclotron Resonance cell using a Design of Experiments strategy. *Rapid Commun. Mass Spectrom.* **2019**.

- Only 35 % of tholins are soluble in MeOH
- Structure of non soluble fraction is unkown

LDI-FTICR

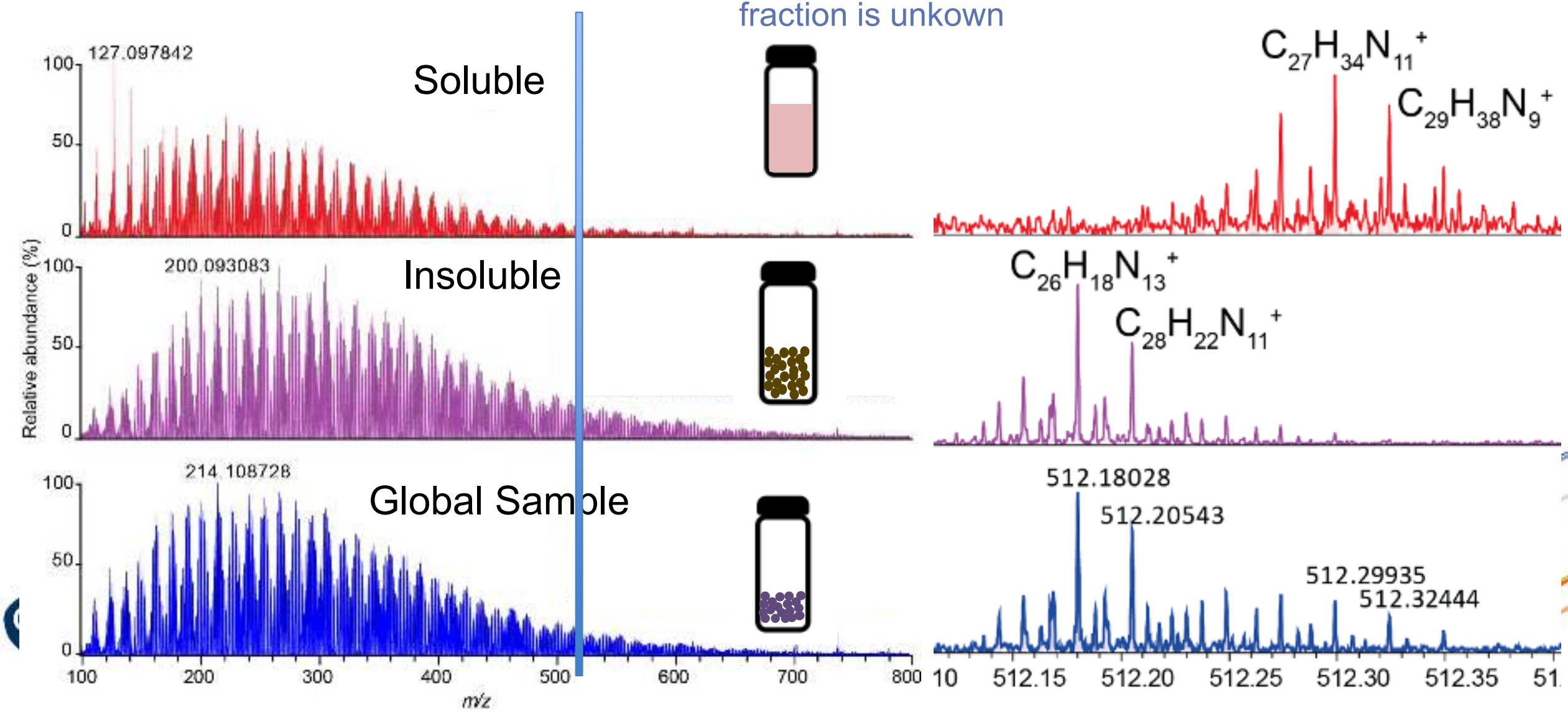

Molecular mapping: soluble and non soluble fractions

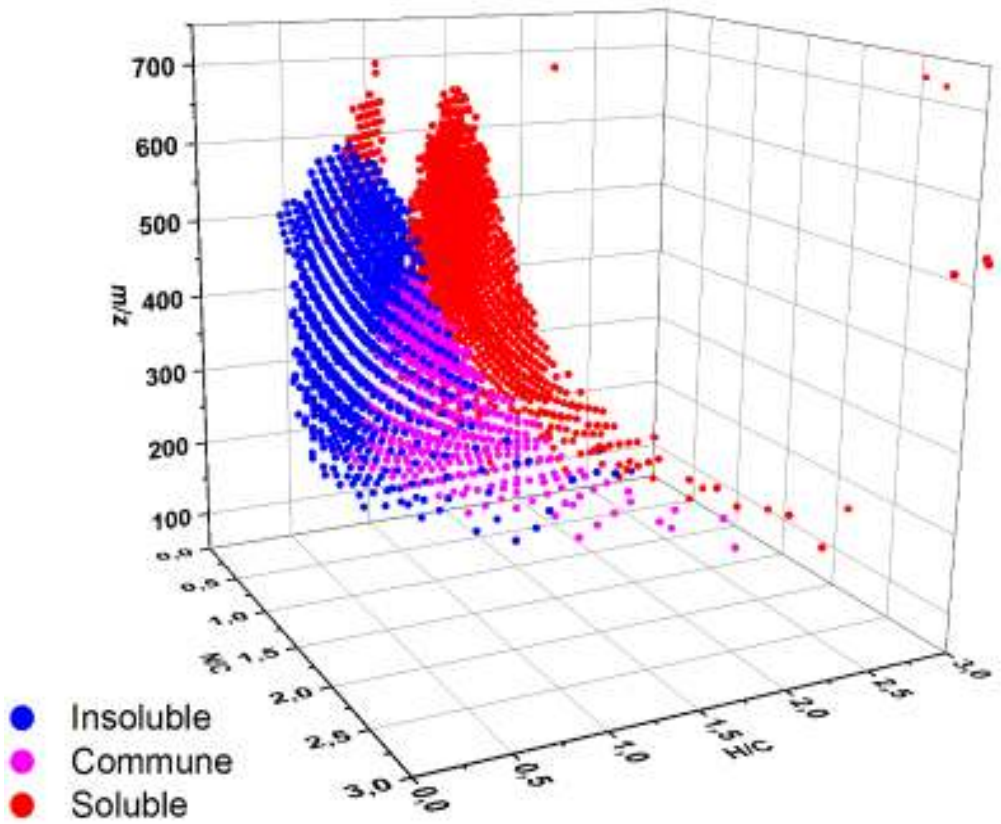

Van Krevelen diagram

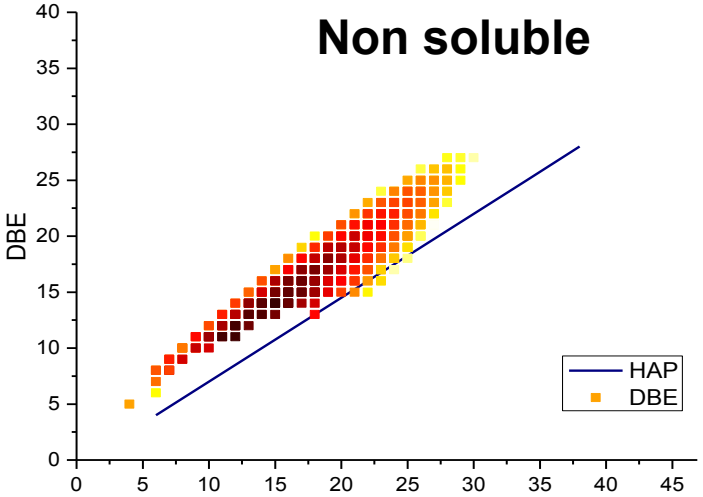

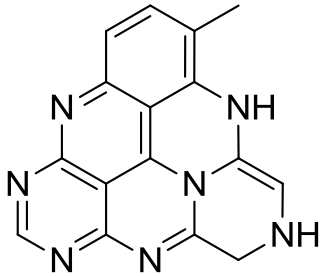

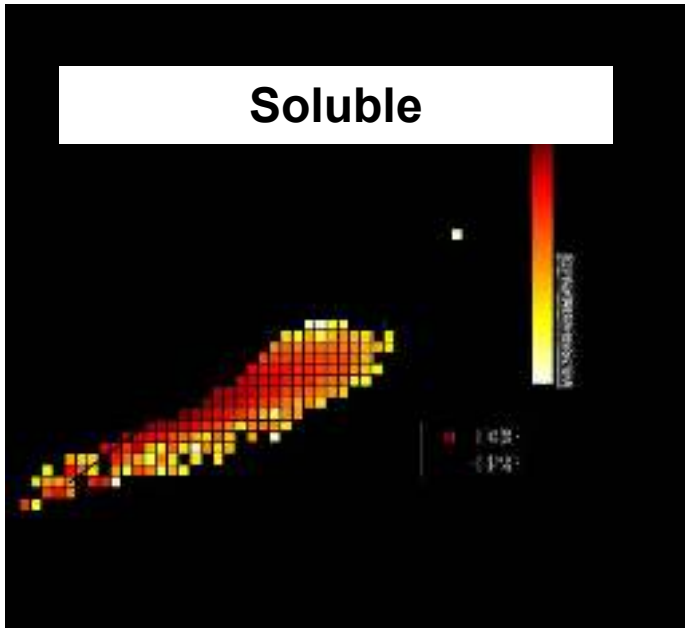

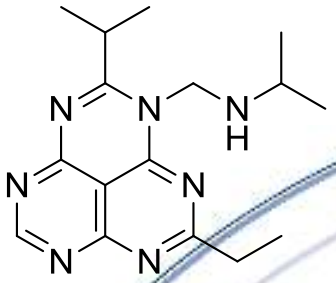

Maillard, J.; Carrasco, N.; Schmitz-Afonso, I.; Gautier, T.; Afonso, C., Comparison of soluble and insoluble organic matter in analogues of Titan's aerosols. *Earth and Planetary Science Letters* **2018,** *495*, 185-191.

IMS of Tholins?

TOF *vs* FTICR

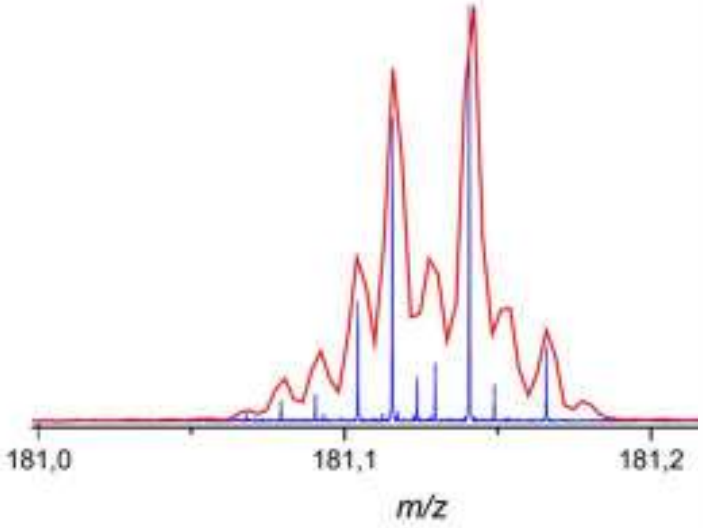

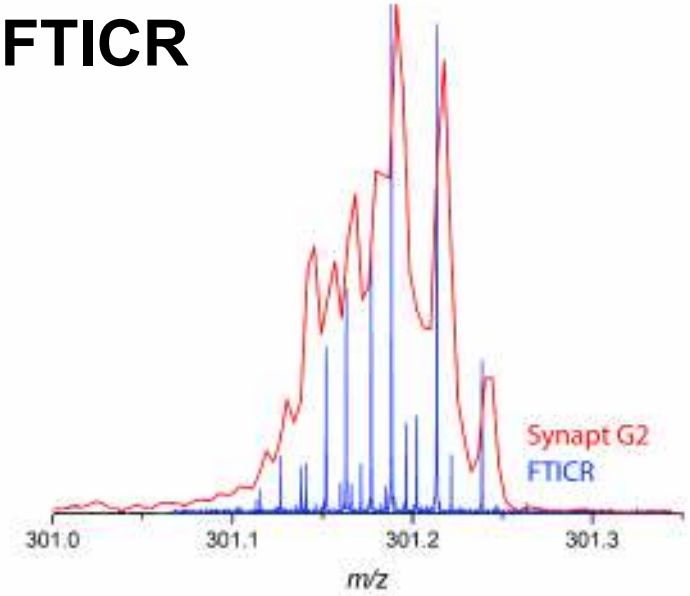

- Owing to the high complexity IMS-TOF analysis is very challenging and limited to low masses
- IMS with FTICR?
  - Drift tube IMS or TWIMS: ms time scale
  - FTICR second time scale
- Other IMS technique compatible with FTICR
  - FAIMS (High-field asymmetric waveform ion mobility spectrometry)
  - TIMS (tapped ion mobility spectrometry)
    - Low field access to

IMS-MS of Tholins

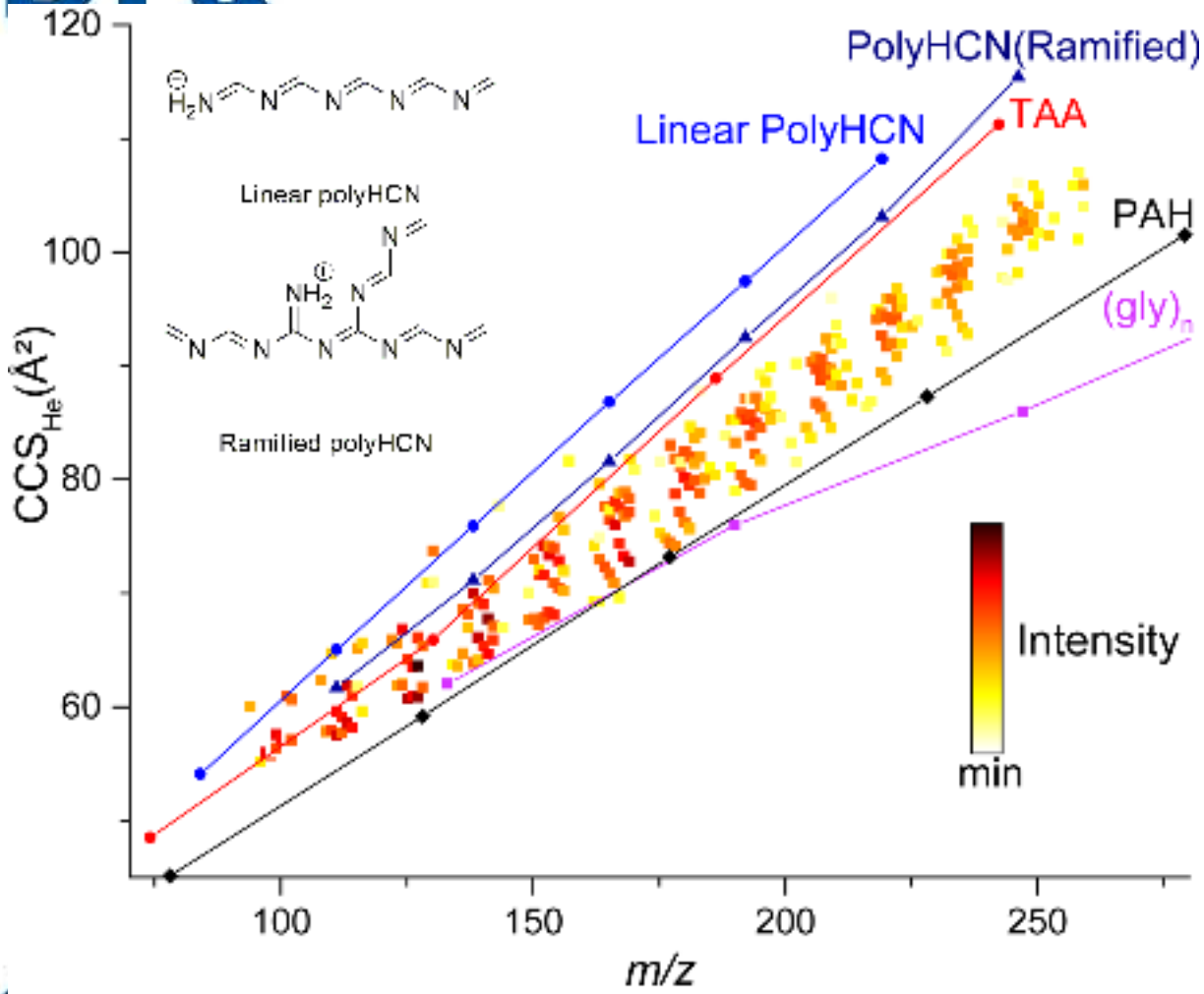

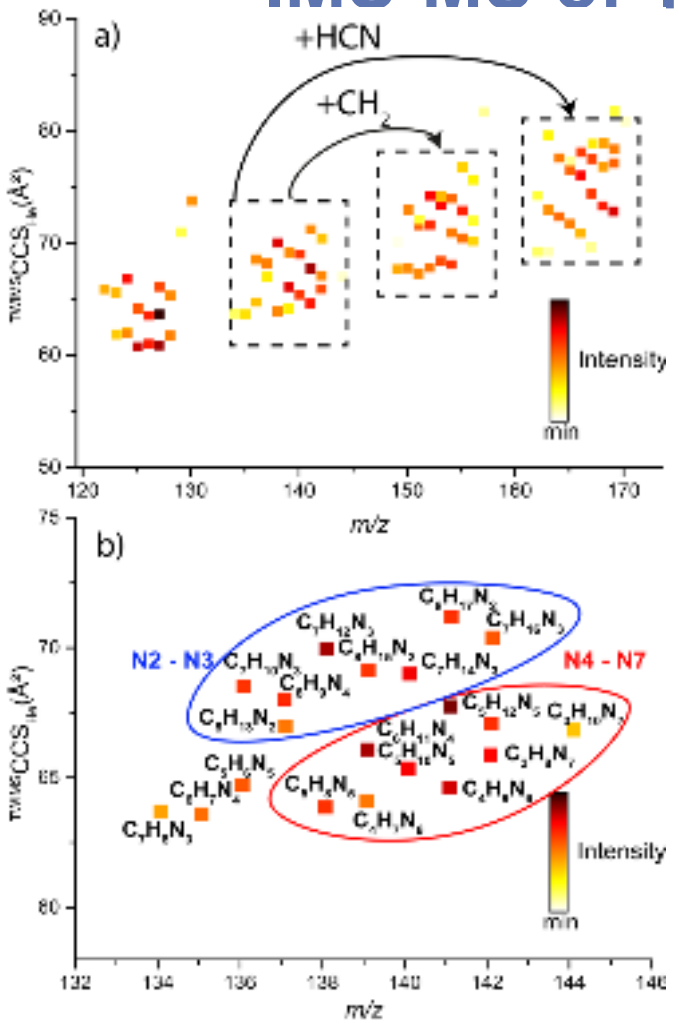

Comparison of collision cross section (A²) *vs m/z* of ions of tholins sample with polyHCN (blue), tetraalkylammonium salts (red), polyaromatics hydrocarbons (black) and polyglycan (purple).

IMS-MS of Tholins

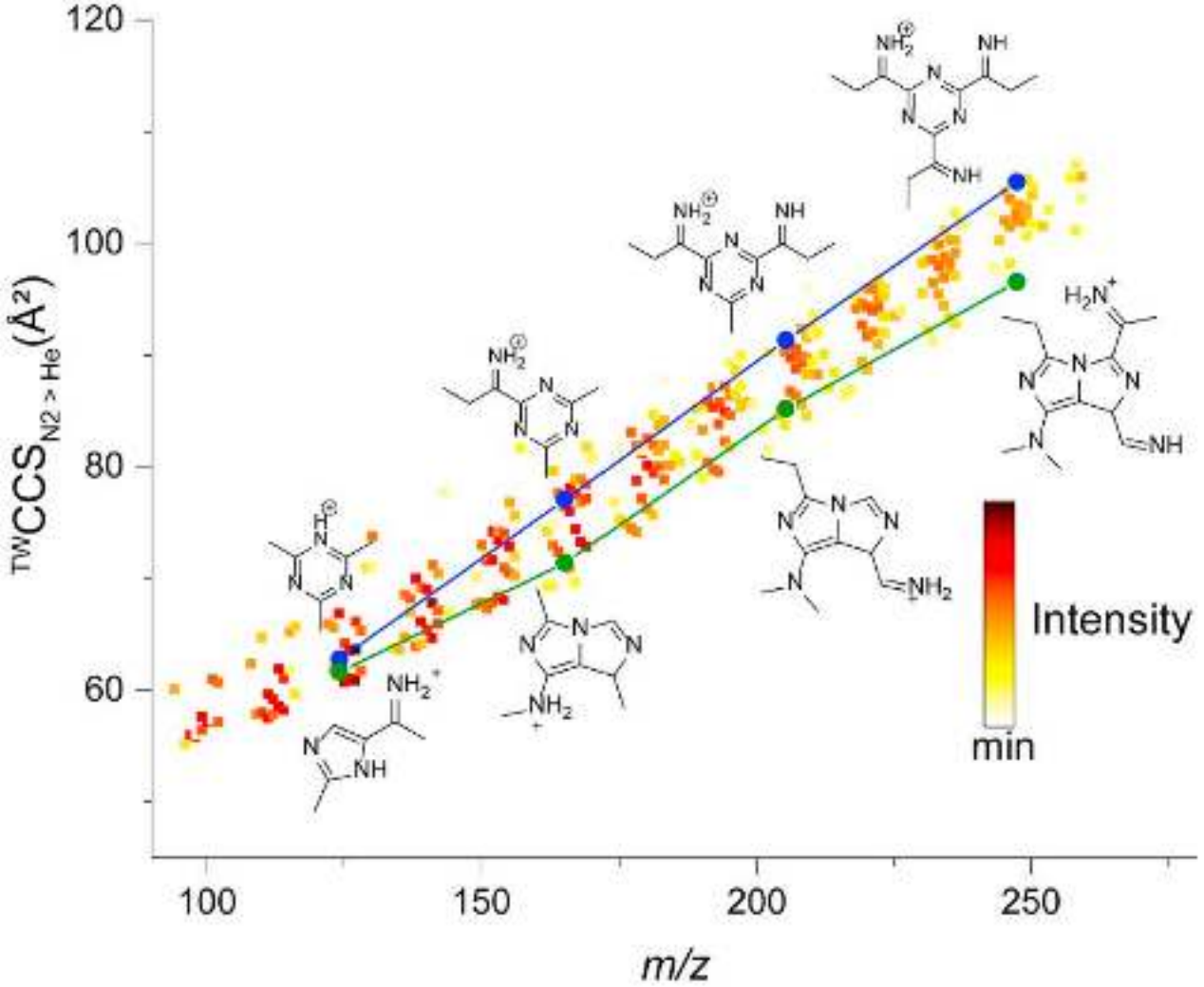

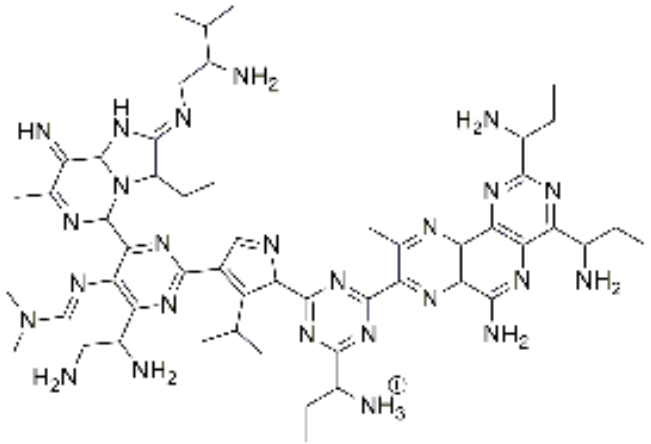

Comparison of CCS vs m/z with (blue) calculated CCS of triazine family (green) calculated CCS of pyrazole family

Maillard, J.; Hupin, S.; Carrasco, N.; Schmitz-Afonso, I.; Gautier, T.; Afonso, C., Structural elucidation of soluble organic matter: Application to Titan's haze. *Icarus* **2020**.

IMS with FTICR?

TOF *vs* FTICR

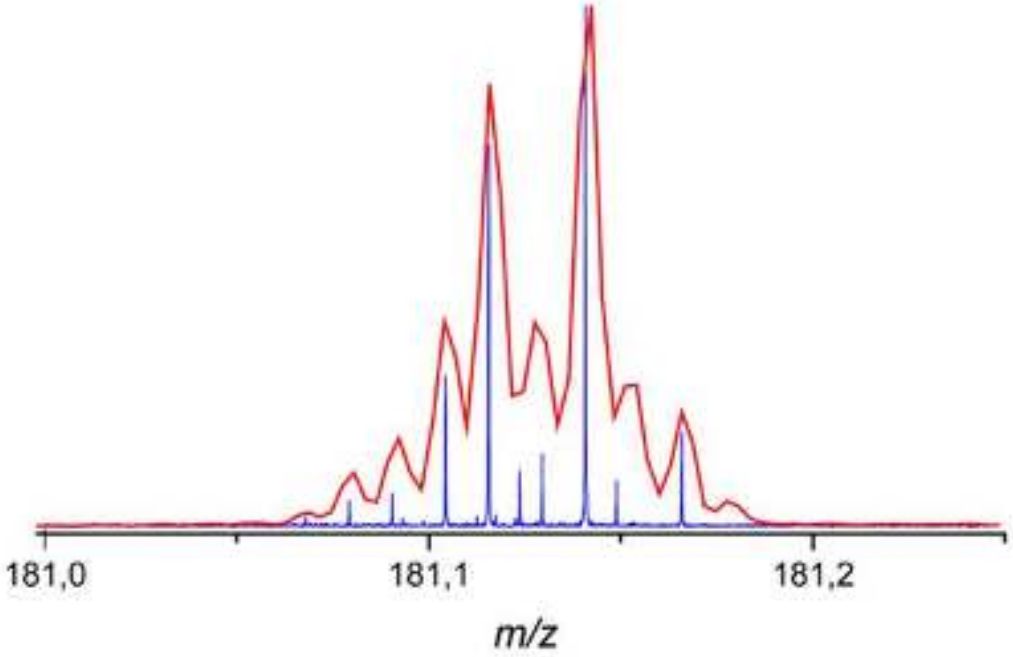

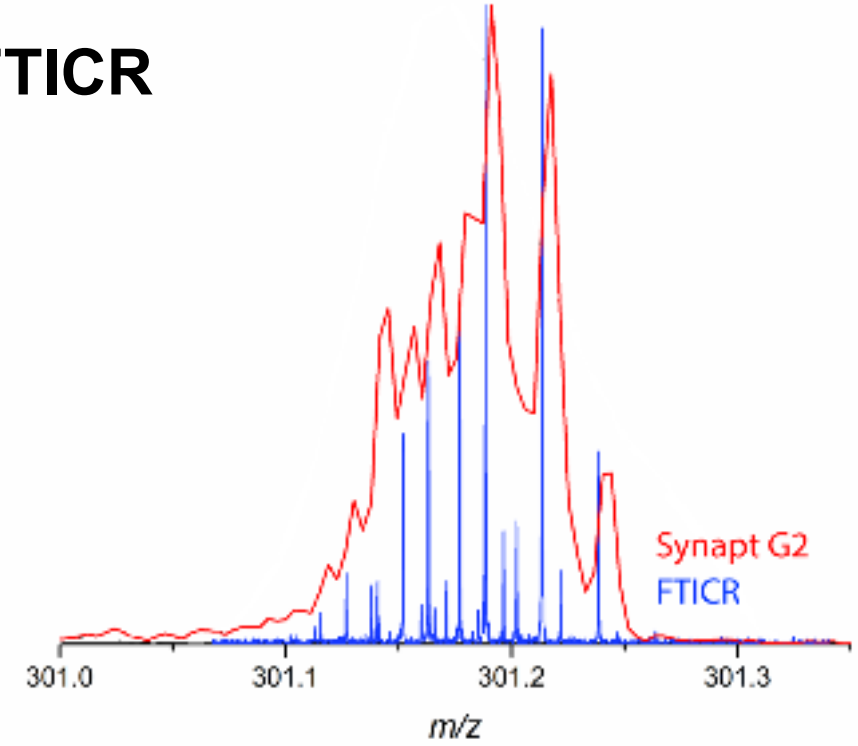

- Owing to the high complexity IMS-TOF analysis is very challenging and limited to low masses

TIMS-FTICR

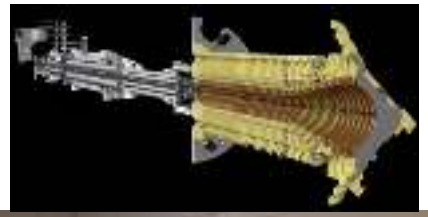

Experiments at Bruker (Summer 2018)

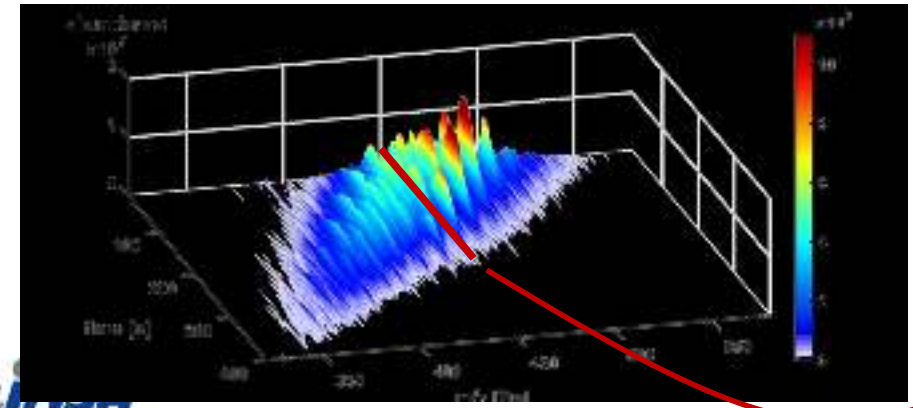

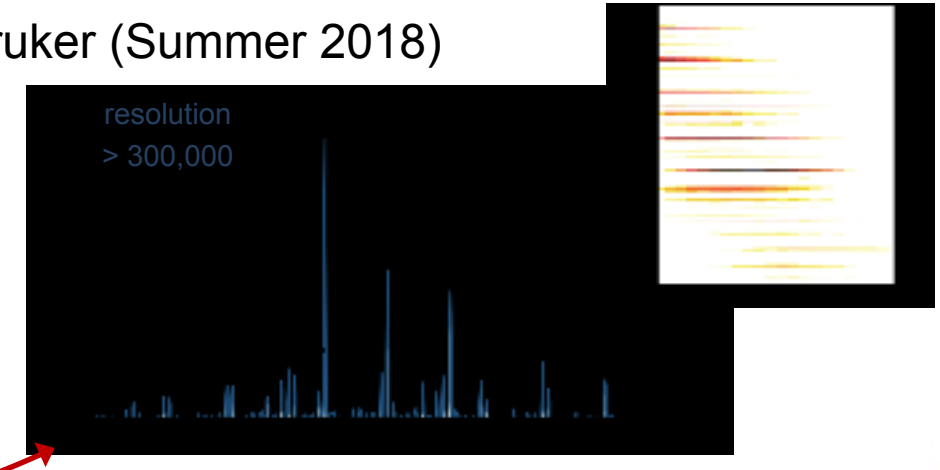

zoom-into 0.3 Da window → ultra-high resolving power needed

TIMS-FTICR

Ruger, C. P.; Maillard, J.; Le Maitre, J.; Ridgeway, M.; Thompson, C. J.; Schmitz-Afonso, I.; Gautier, T.; Carrasco, N.; Park, M. A.; Giusti, P.; Afonso, C.,. *J Am Soc Mass Spectrom* **2019,** *30* (7), 1169-1173.

Trapped Ion Mobility Spectrometry (TIMS)

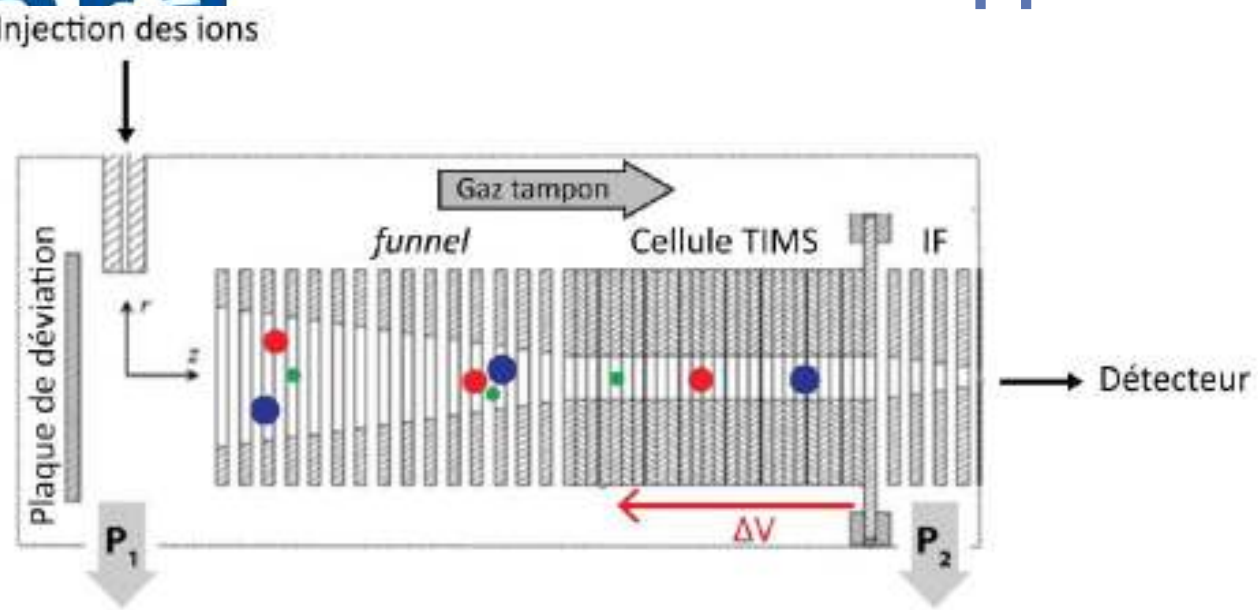

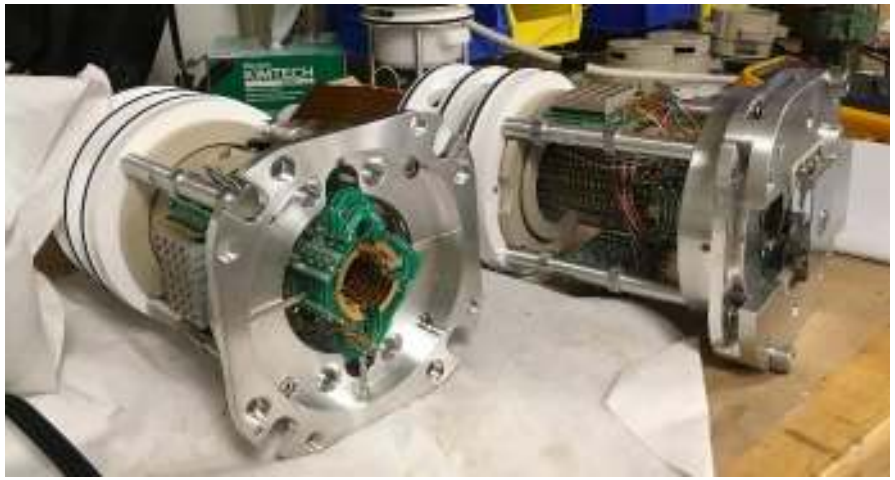

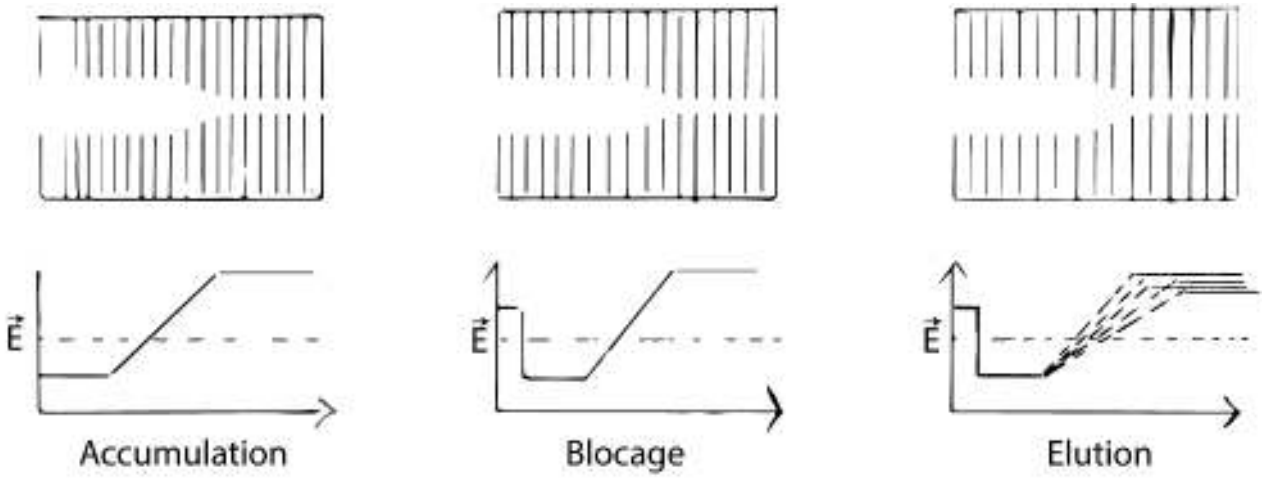

TIMS-FTICR of Tholins

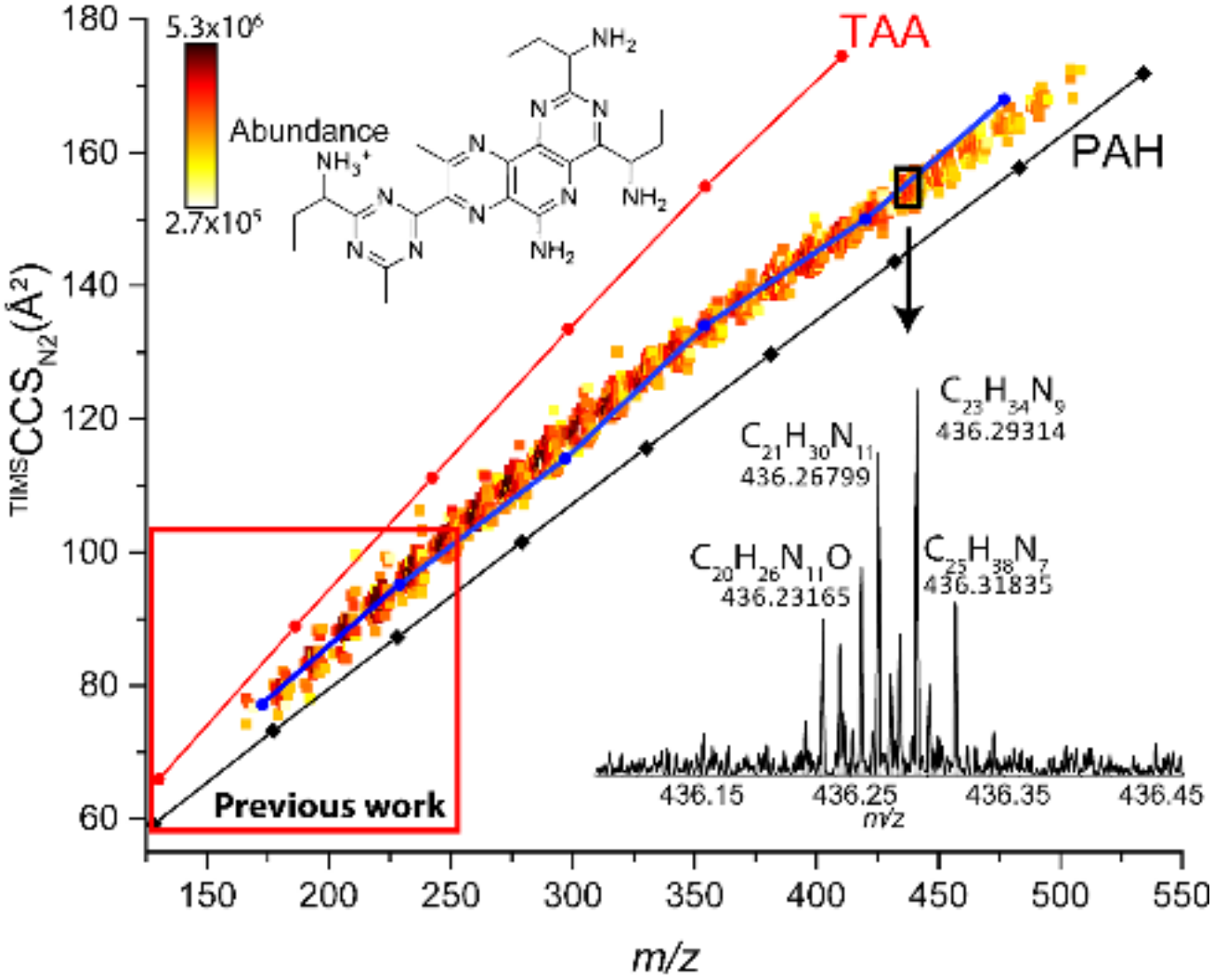

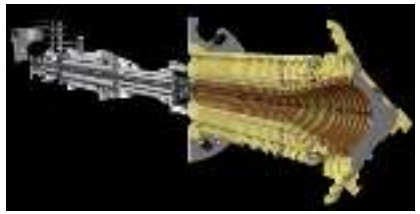

Ruger, C. P.; Maillard, J.; Le Maitre, J.; Ridgeway, M.; Thompson, C. J.; Schmitz-Afonso, I.; Gautier, T.; Carrasco, N.; Park, M. A.; Giusti, P.; Afonso, C.,. *J Am Soc Mass Spectrom* **2019,** *30* (7), 1169-1173.

AFM @ IBM

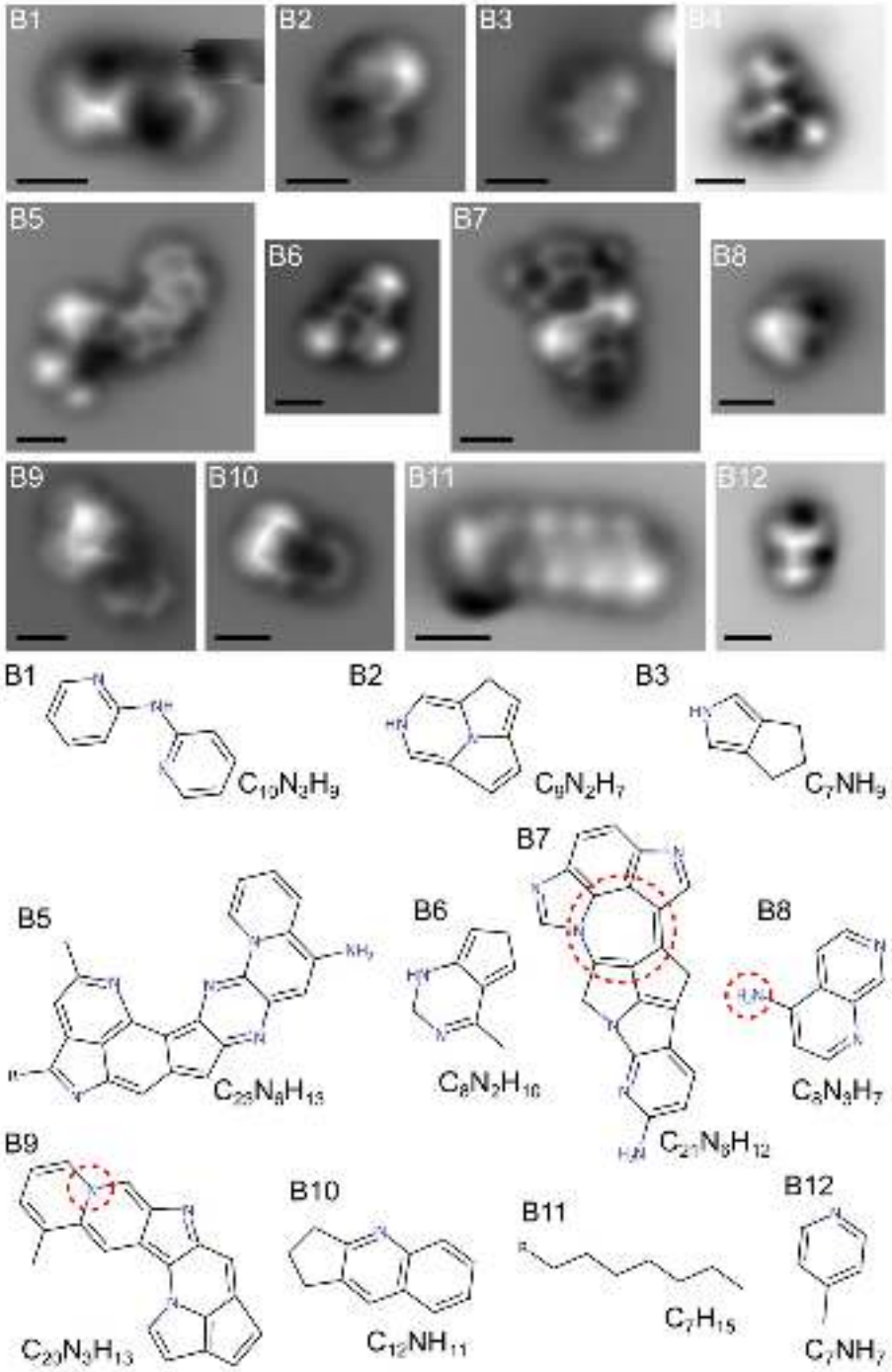

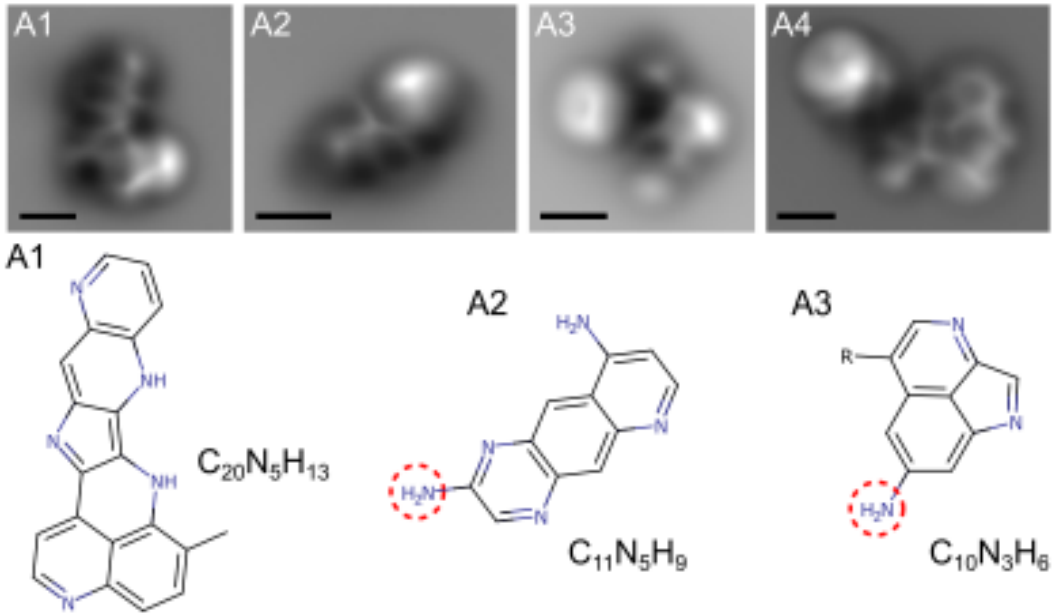

F. Schulz, J. Maillard, K. Kaiser, I. Schmitz-Afonso, T. Gautier, C. Afonso, N. Carrasco and L. Gross, The Astrophysical Journal Letters, 2021, 908.

TIMS FTICR of petrophyrins

Structural analysis

energy&fuels — Article
pubs.acs.org/EF

Analysis of Geologically Relevant Metal Porphyrins Using Trapped Ion Mobility Spectrometry–Mass Spectrometry and Theoretical Calculations

Paolo Benigni,[†] Carlos Bravo,[†] J. Martin E. Quirke,[†] John D. DeBord,[†] Alexander M. Mebel,[†] and Francisco Fernandez-Lima[*,†,‡]

[†]Department of Chemistry and Biochemistry and [‡]Biomolecular Sciences Institute, Florida International University, Miami, Florida 33199, United States

Scheme 1. Diagram Illustrating the Chemical Changes Outlined in the Treibs Hypothesis[a]

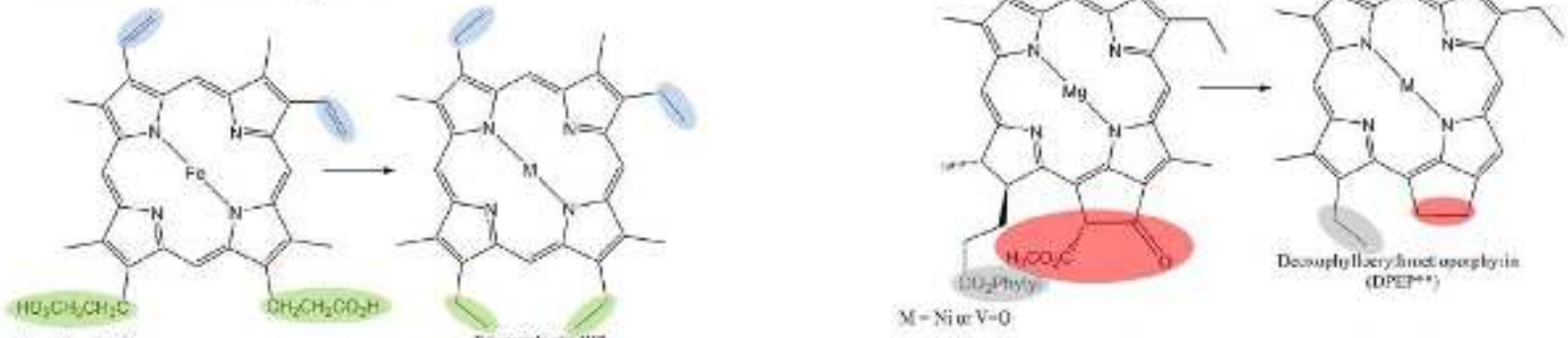

[a]Note the changes in the different functional groups observed.

What about their structure in real sample?

APPI asphaltene fraction

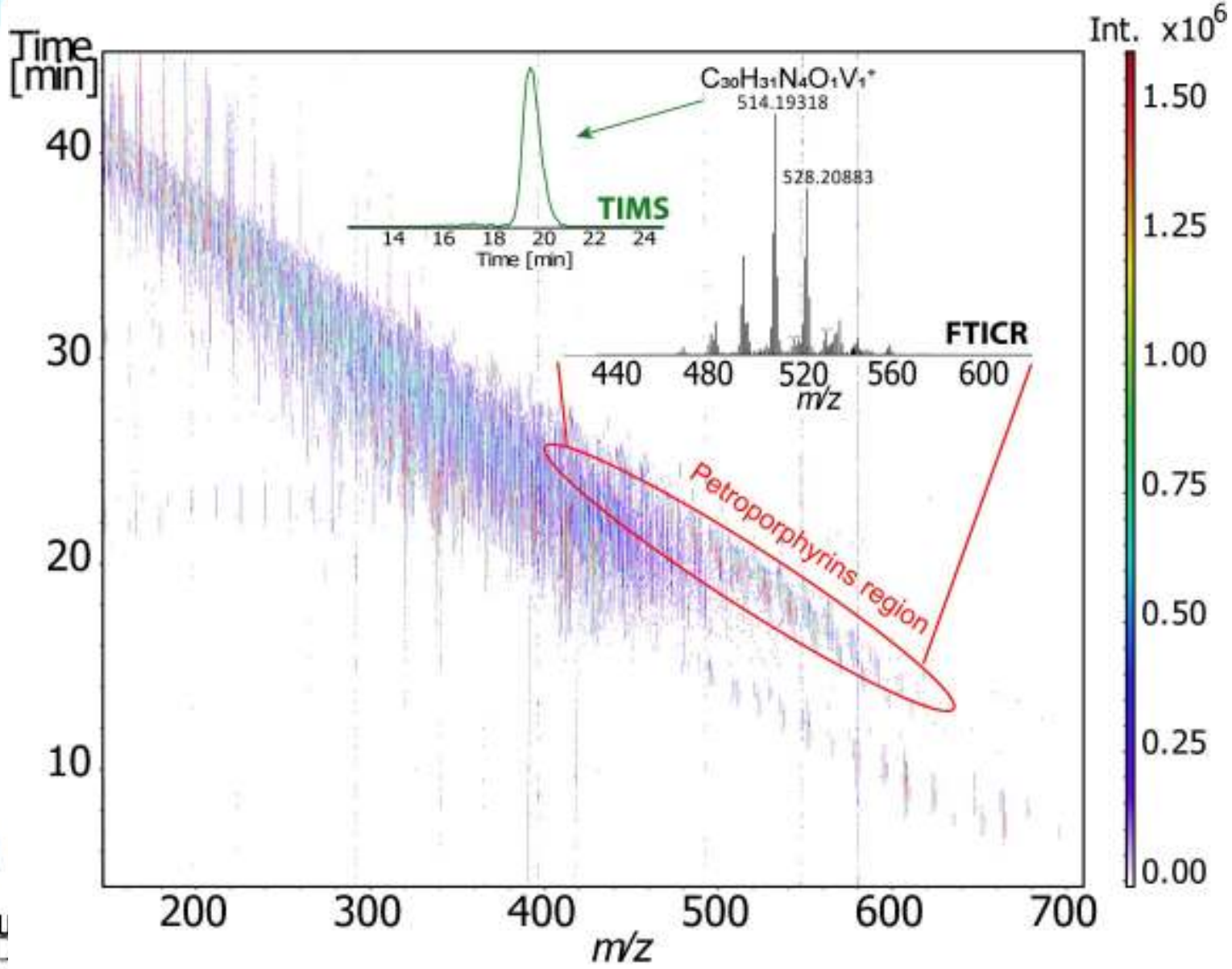

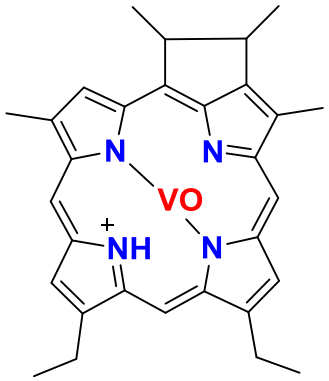

Chemical Formula: $C_{30}H_{31}N_4OV^+$

Exact Mass: 514,1932

Attribution and extraction of petroporphyrins signals

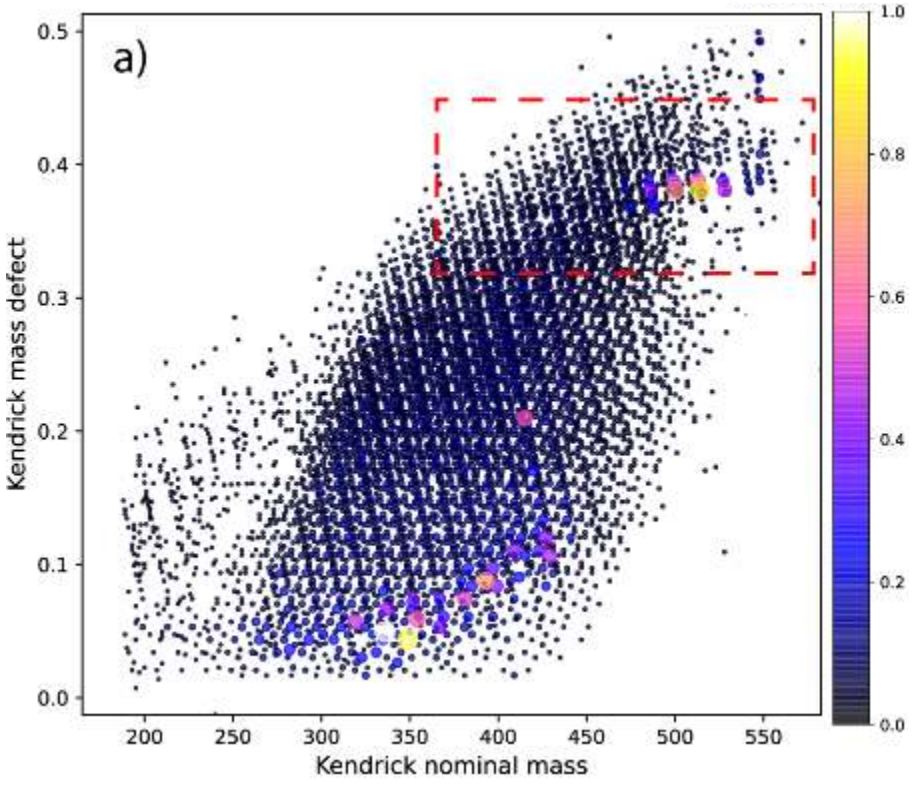

EIM generations

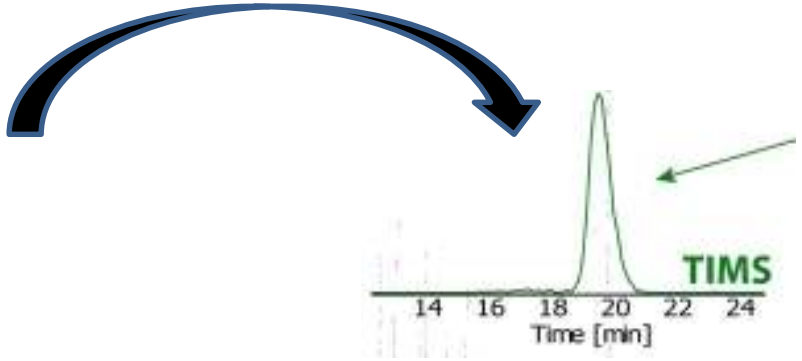

Recovering of the CCS

Attribution and extraction of petroporphyrins signals

Molecular formula $[M+H]^+$	Calculated *m/z*	Experimental *m/z*	Error (ppm)	C#	DBE	TIMS CCS_{N2} ($Å^2$)	FWHM (s)
$C_{26}H_{25}N_4O_1V_1^+$	460.14625	460.14624	0.01	26	17	199.6	27
$C_{27}H_{27}N_4O_1V_1^+$	474.1619	474.16189	0.01	27	17	205.1	29
$C_{28}H_{29}N_4O_1V_1^+$	488.17755	488.17754	0.01	28	17	210.8	32
$C_{27}H_{25}N_4O_1V_1^+$	472.14625	472.14623	0.04	27	18	201.3	34
$C_{28}H_{27}N_4O_1V_1^+$	486.1619	486.1619	-0.01	28	18	206.9	38
$C_{29}H_{29}N_4O_1V_1^+$	500.17755	500.17754	0.01	29	18	212.7	35
$C_{30}H_{31}N_4O_1V_1^+$	514.1932	514.19319	0.01	30	18	217.3	35
$C_{31}H_{33}N_4O_1V_1^+$	528.20885	528.20885	-0.01	31	18	222.8	34
$C_{28}H_{25}N_4O_1V_1^+$	484.14624	484.14626	-0.02	28	19	203.7	38
$C_{29}H_{27}N_4O_1V_1^+$	498.1619	498.16184	0.1	29	19	210.1	38
$C_{30}H_{29}N_4O_1V_1^+$	512.17755	512.17751	0.07	30	19	215.3	41
$C_{29}H_{25}N_4O_1V_1^+$	496.14625	496.14628	-0.07	29	20	208.8	39
$C_{30}H_{27}N_4O_1V_1^+$	510.1619	510.16188	0.04	30	20	214	46
$C_{30}H_{25}N_4O_1V_1^+$	508.14625	508.14629	-0.09	30	21	210.6	37
$C_{31}H_{27}N_4O_1V_1$	522.1619	522.16191	-0.04	31	21	215.9	40
$C_{32}H_{29}N_4O_1V_1^+$	536.17755	536.17754	0.01	32	21	222	39
$C_{33}H_{31}N_4O_1V_1^+$	550.1932	550.19319	0.02	33	21	226.9	44
$C_{32}H_{27}N_4O_1V_1^+$	534.1619	534.16193	-0.06	32	22	218.5	43

Information recovered using the CCS vs m/z graphic

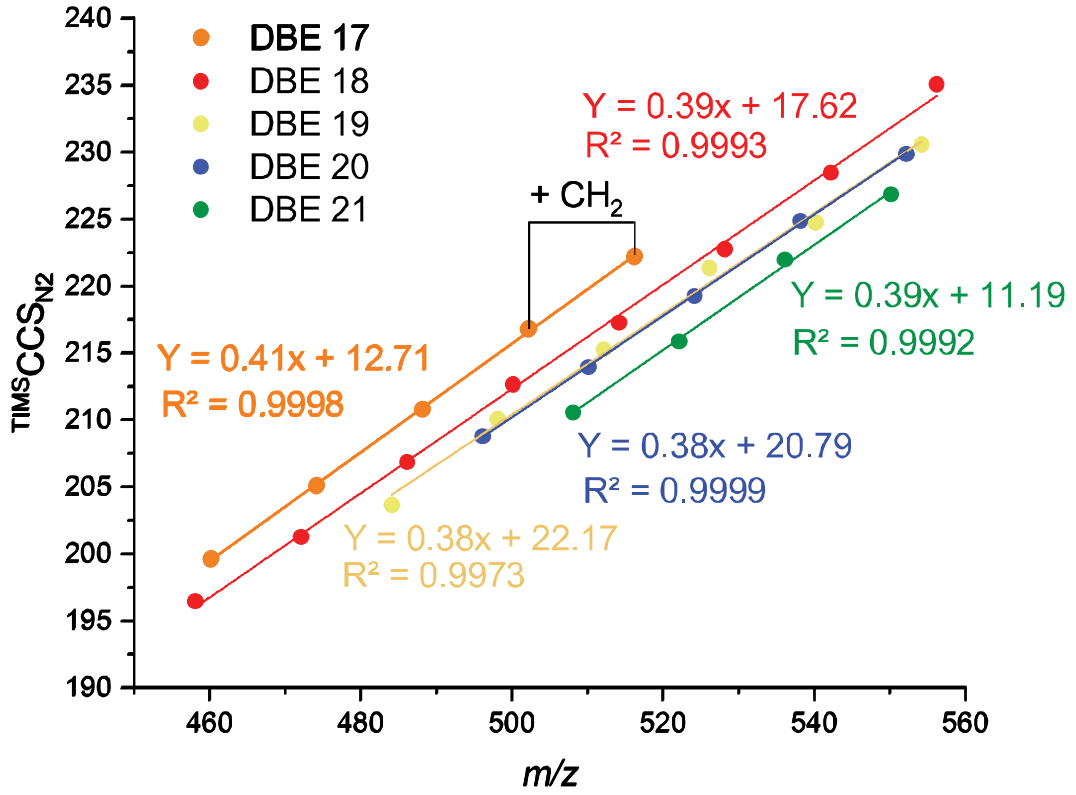

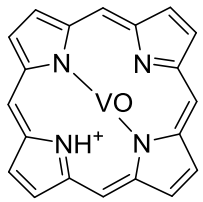

$C_{20}H_{13}N_4OV^+$
m/z 376.05235

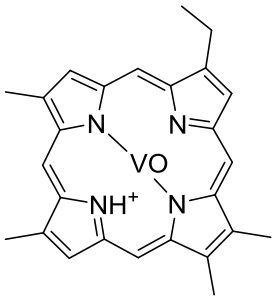

$C_{26}H_{25}N_4OV^+$
m/z 460.14625
C6

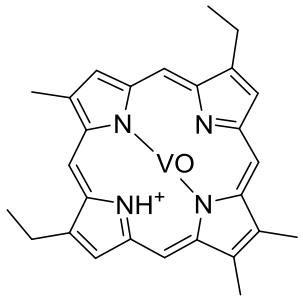

$C_{27}H_{27}N_4OV^+$
m/z 474.16190
C7

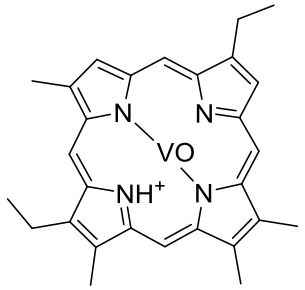

$C_{28}H_{29}N_4OV^+$
m/z 488.17755
C8

Plot of the experimental $^{TIMS}CCS_{N2}$ (Å^2) of porphyrins by DBE (DBE 17 to 21) as a function of m/z. Linear regression is given for the different homolog rows.

Drawing of all possible core structures

DBE 17

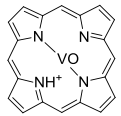

$C_{20}H_{13}N_4OV^+$
m/z 376.05235

Core 1

DBE 18

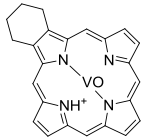

$C_{24}H_{19}N_4OV^+$
m/z 430.09930

Core 2

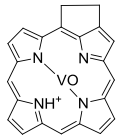

$C_{22}H_{15}N_4OV^+$
m/z 402.06800

Core 3

DBE 19

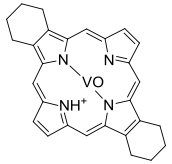

$C_{28}H_{25}N_4OV^+$
m/z 484.14625

Core 4

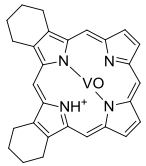

$C_{28}H_{25}N_4OV^+$
m/z 484.14625

Core 5

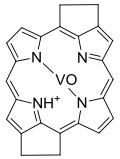

$C_{24}H_{17}N_4OV^+$
m/z 428.08365

Core 6

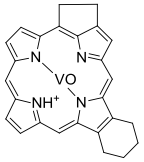

$C_{26}H_{21}N_4OV^+$
m/z 456.11495

Core 7

DBE 20

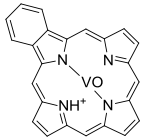

$C_{24}H_{15}N_4OV^+$
m/z 426.06800

Core 8

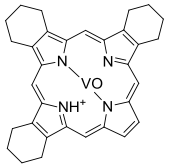

$C_{32}H_{31}N_4OV^+$
m/z 538.19320

Core 9

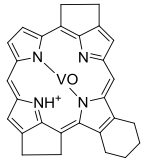

$C_{28}H_{23}N_4OV^+$
m/z 482.13060

Core 10

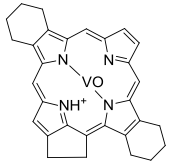

$C_{30}H_{27}N_4OV^+$
m/z 510.16190

Core 11

DBE 21

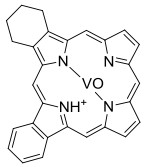

$C_{28}H_{21}N_4OV^+$
m/z 480.11495

Core 12

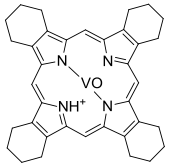

$C_{36}H_{37}N_4OV^+$
m/z 592.24015

Core 13

DBE 22

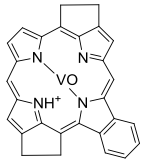

$C_{28}H_{19}N_4OV^+$
m/z 478.09930

Core 14

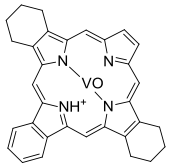

$C_{32}H_{27}N_4OV^+$
m/z 534.16190

Core 15

To CCS Calculations

Calculation of CCS for proposed core structures

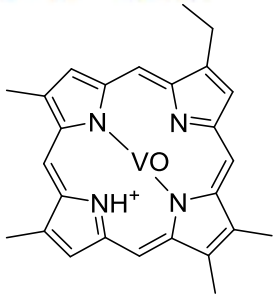

$C_{26}H_{25}N_4OV^+$
m/z 460.14625
C6

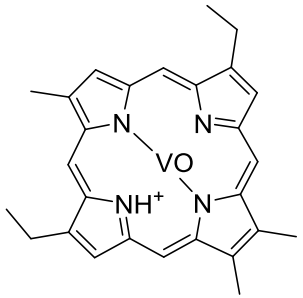

$C_{27}H_{27}N_4OV^+$
m/z 474.16190
C7

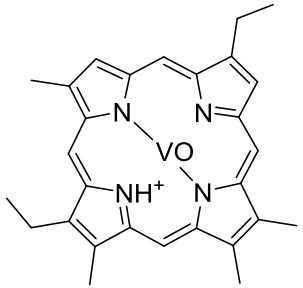

$C_{28}H_{29}N_4OV^+$
m/z 488.17755
C8

3D model of metal containing compounds

Use of DFT with Gaussian m062x/6-31g(d,p) level

CCS calculations with IMOS

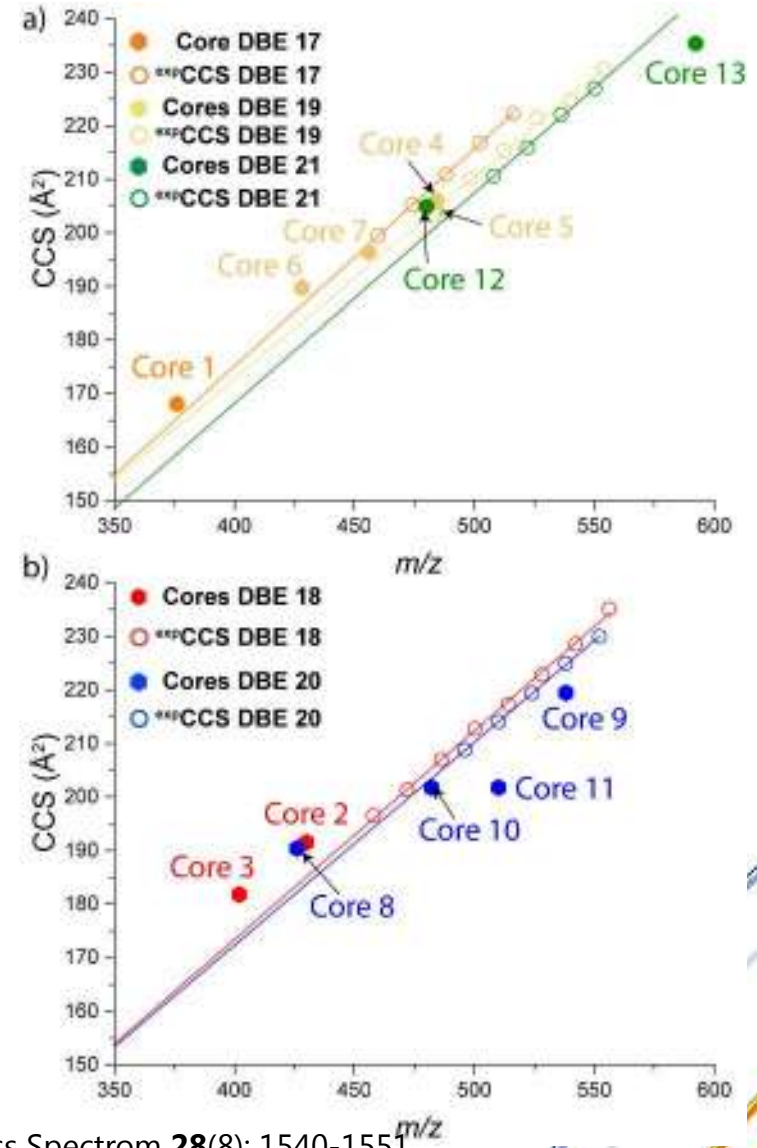

Shrivastav, V., M. Nahin, C. J. Hogan and C. Larriba-Andaluz (2017). J Am Soc Mass Spectrom **28**(8): 1540-1551.

Exclusion of several core structures

DBE 17

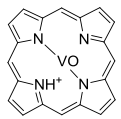

$C_{20}H_{13}N_4OV^+$
m/z 376.05235

Core 1

DBE 18

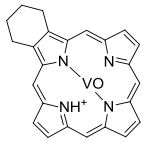

$C_{24}H_{19}N_4OV^+$
m/z 430.09930

Core 2

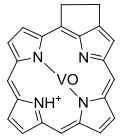

$C_{22}H_{15}N_4OV^+$
m/z 402.06800

Core 3

DBE 19

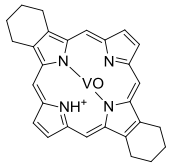

$C_{28}H_{25}N_4OV^+$
m/z 484.14625

Core 4

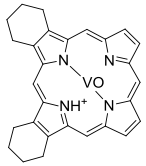

$C_{28}H_{25}N_4OV^+$
m/z 484.14625

Core 5

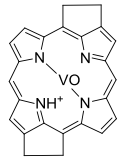

$C_{24}H_{17}N_4OV^+$
m/z 428.08365

Core 6

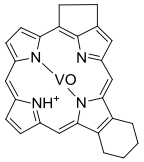

$C_{26}H_{21}N_4OV^+$
m/z 456.11495

Core 7

DBE 20

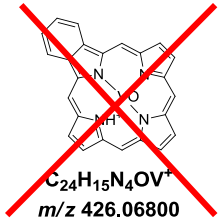

$C_{24}H_{15}N_4OV^+$
m/z 426.06800

Core 8

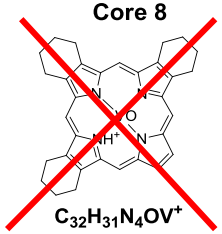

$C_{32}H_{31}N_4OV^+$
m/z 538.19320

Core 9

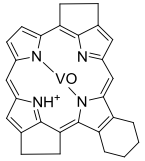

$C_{28}H_{23}N_4OV^+$
m/z 482.13060

Core 10

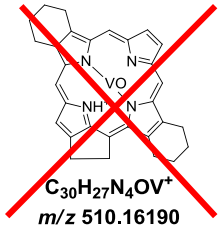

$C_{30}H_{27}N_4OV^+$
m/z 510.16190

Core 11

DBE 21

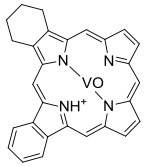

$C_{28}H_{21}N_4OV^+$
m/z 480.11495

Core 12

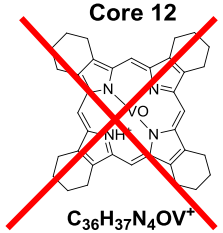

$C_{36}H_{37}N_4OV^+$
m/z 592.24015

Core 13

DBE 22

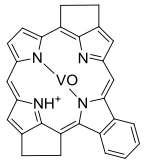

$C_{28}H_{19}N_4OV^+$
m/z 478.09930

Core 14

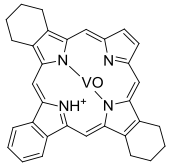

$C_{32}H_{27}N_4OV^+$
m/z 534.16190

Core 15

Calculations of putative structures

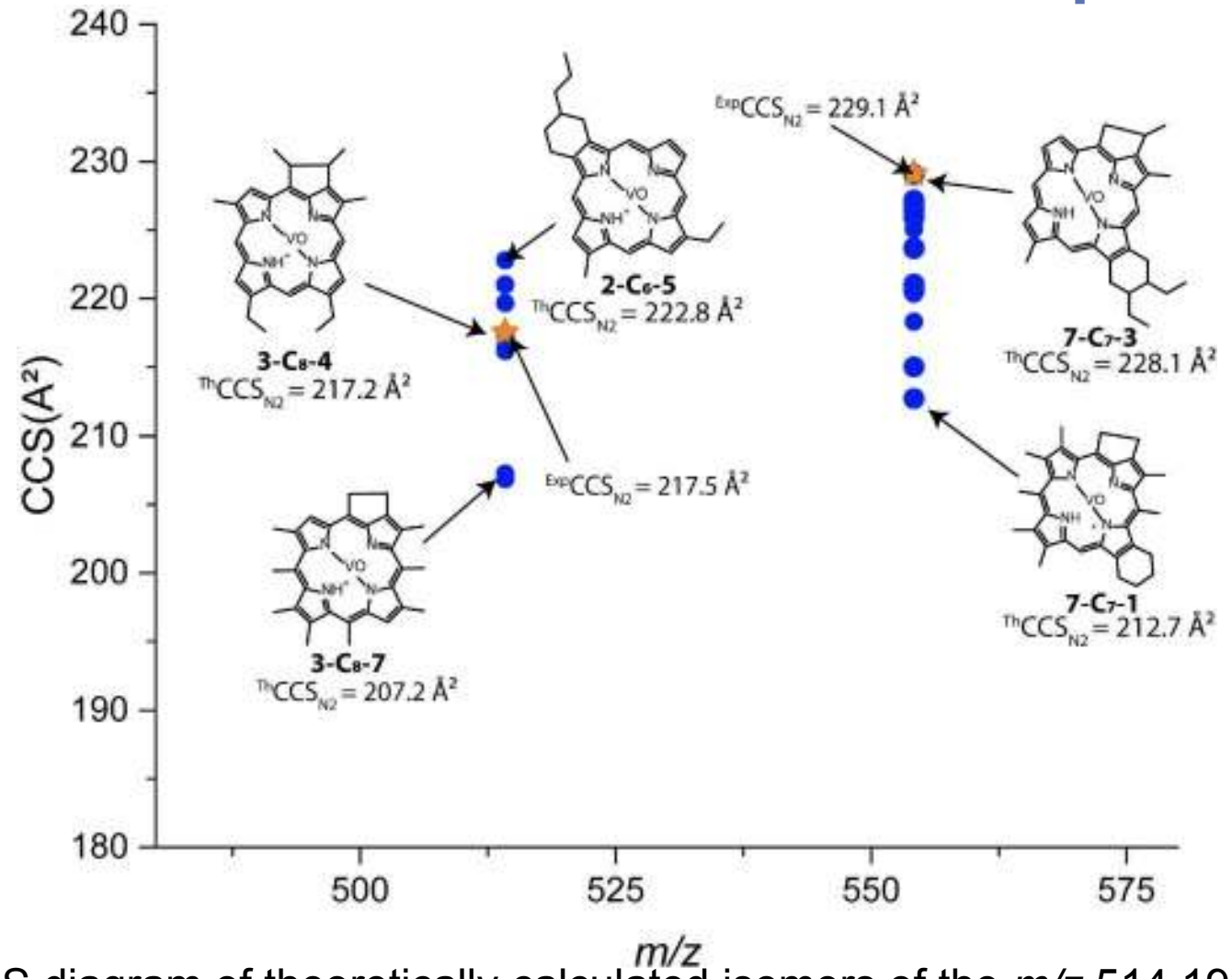

IMS-MS diagram of theoretically calculated isomers of the *m/z* 514.19320 and 554.22450 (light blue dots) and the corresponding experimental measurement (orange star). Selected isomeric structure are included visualizing unlikely (high deviation) and likely (low deviation) structures.

Conclusion

- Analysis of real petrophyrin by TIMS-FTICR
- Experimental CCS determination
- Theoretical CCS determination of petroporphyrin cores and akylated cores
- Comparison of experimental and theoretical data allowed to propose putative species with CCS in agreement with the experimental values.

cIMS Experiments in Manchester

Johann Le Maitre
Christopher Ruger

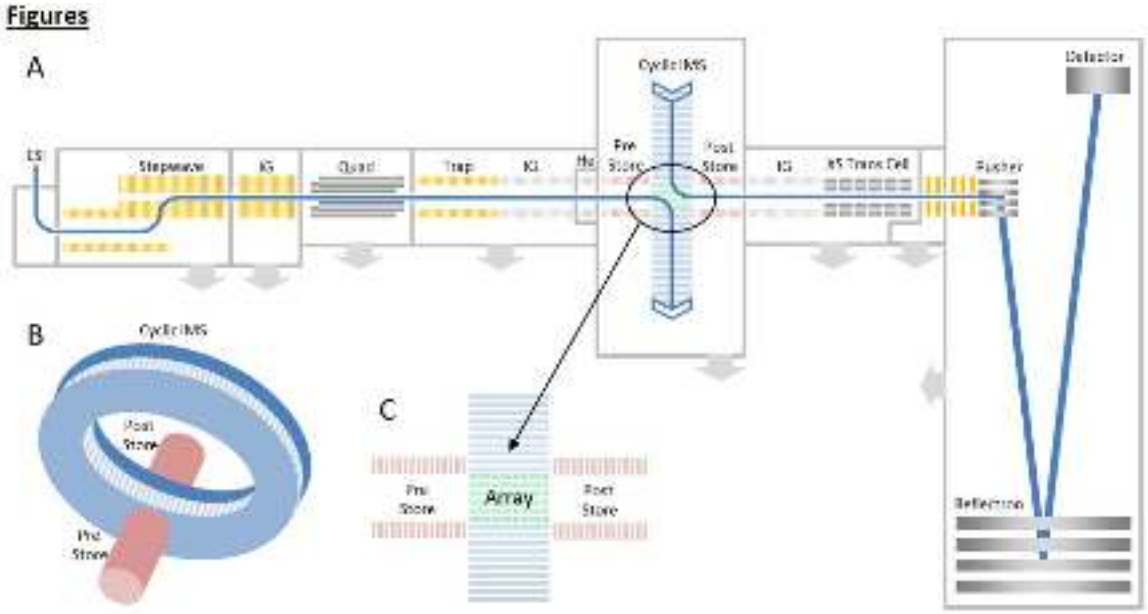

Separation of isomers

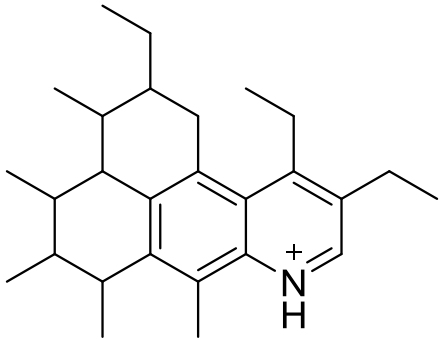

Chemical Formula: $C_{27}H_{40}N^+$
Exact Mass: 378.3155

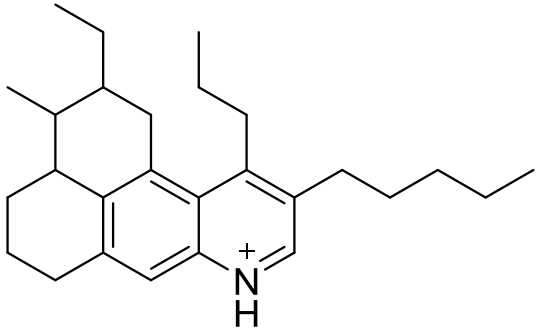

Chemical Formula: $C_{27}H_{40}N^+$
Exact Mass: 378.3155

Too many isomers !

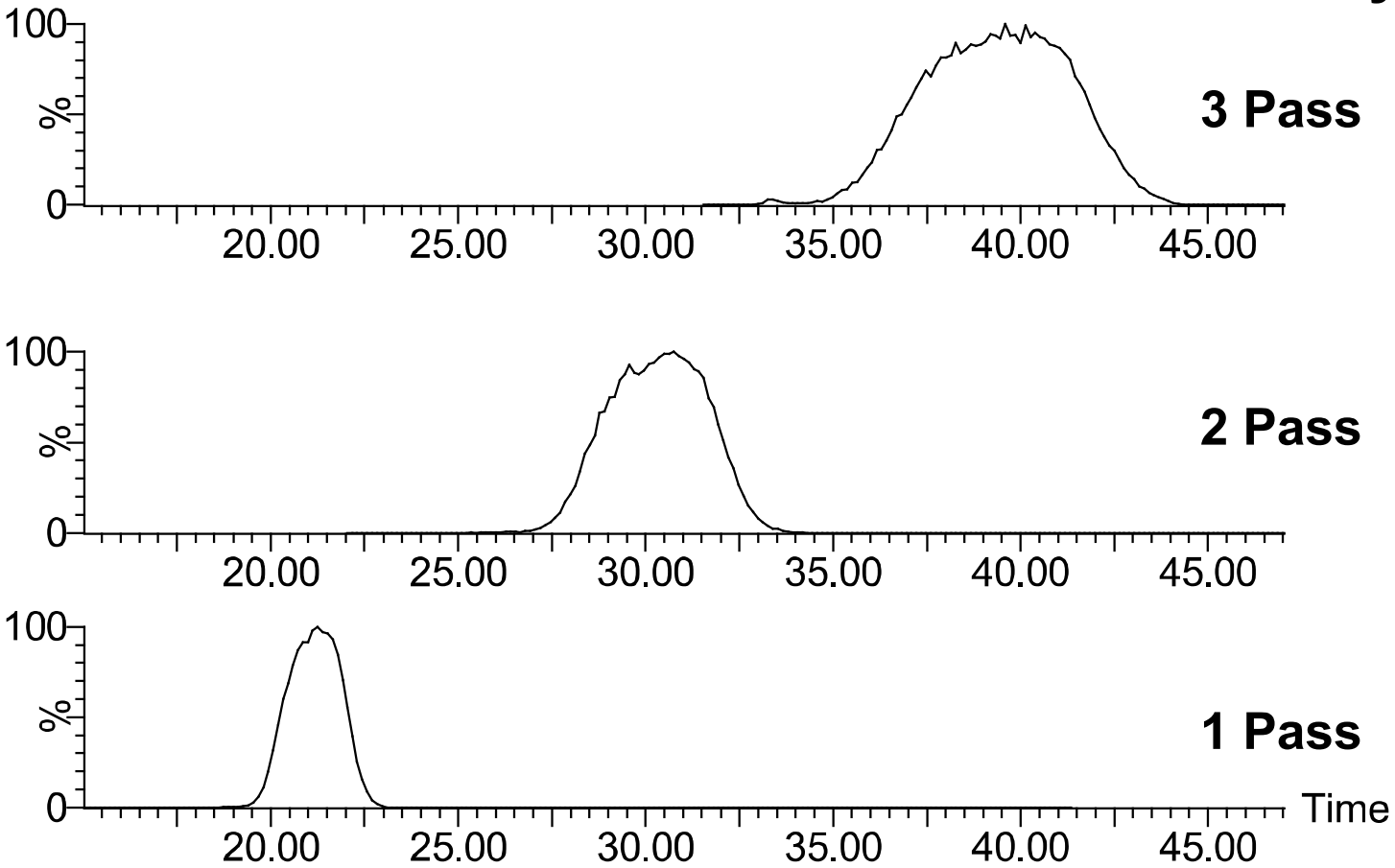

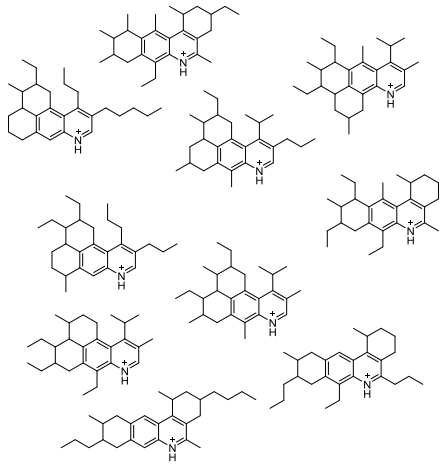

Core structure

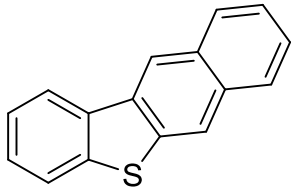

Chemical Formula: $C_{16}H_{10}S$
Exact Mass: 234.0503

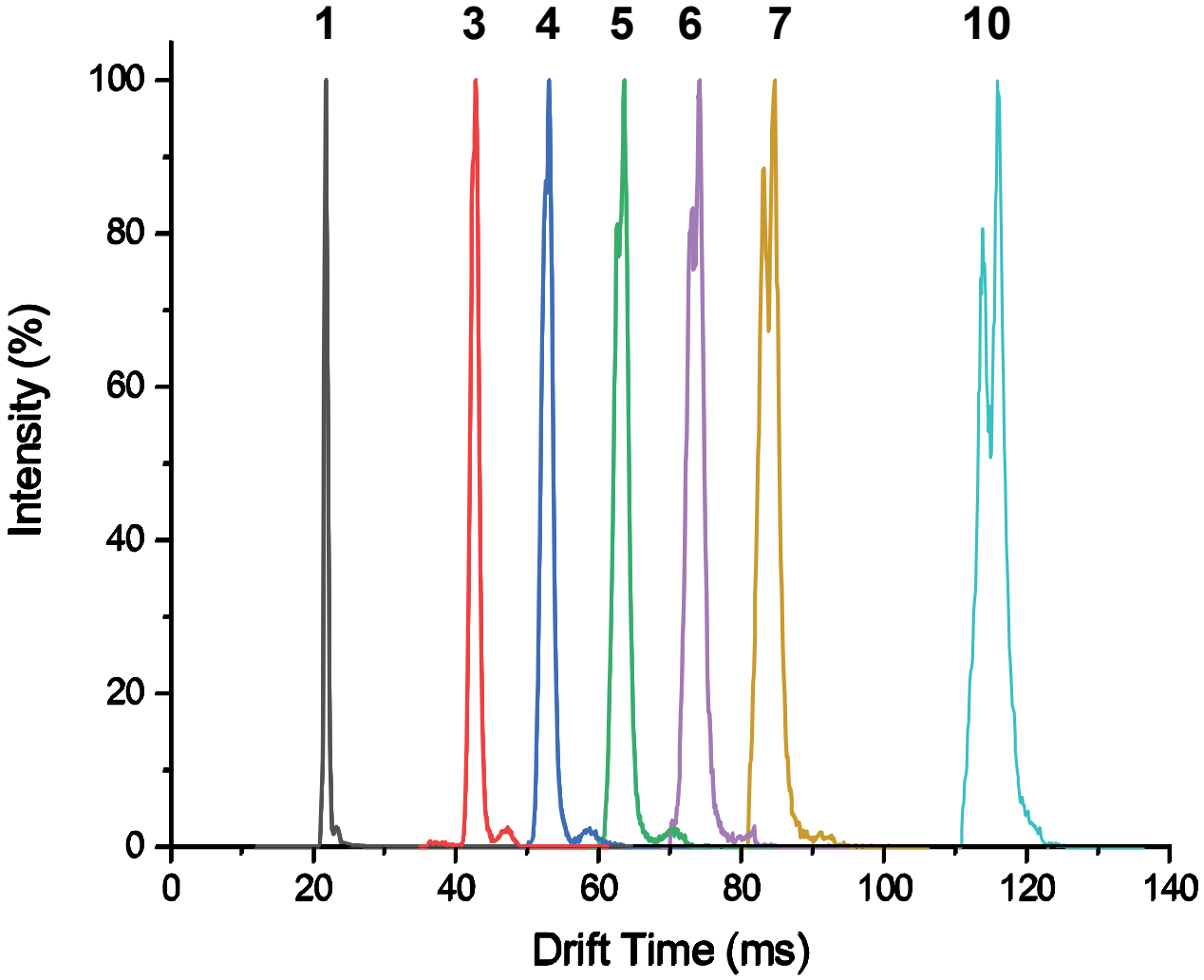

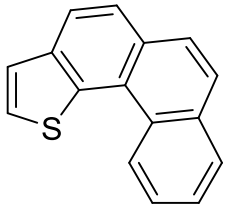

Chemical Formula: $C_{16}H_{10}S$
Exact Mass: 234.0503

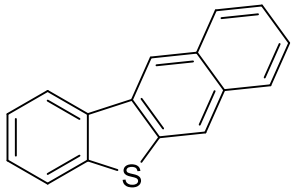

Chemical Formula: $C_{16}H_{10}S$
Exact Mass: 234.0503

C_3-SH_4 split: VGO on the cIMS-MS

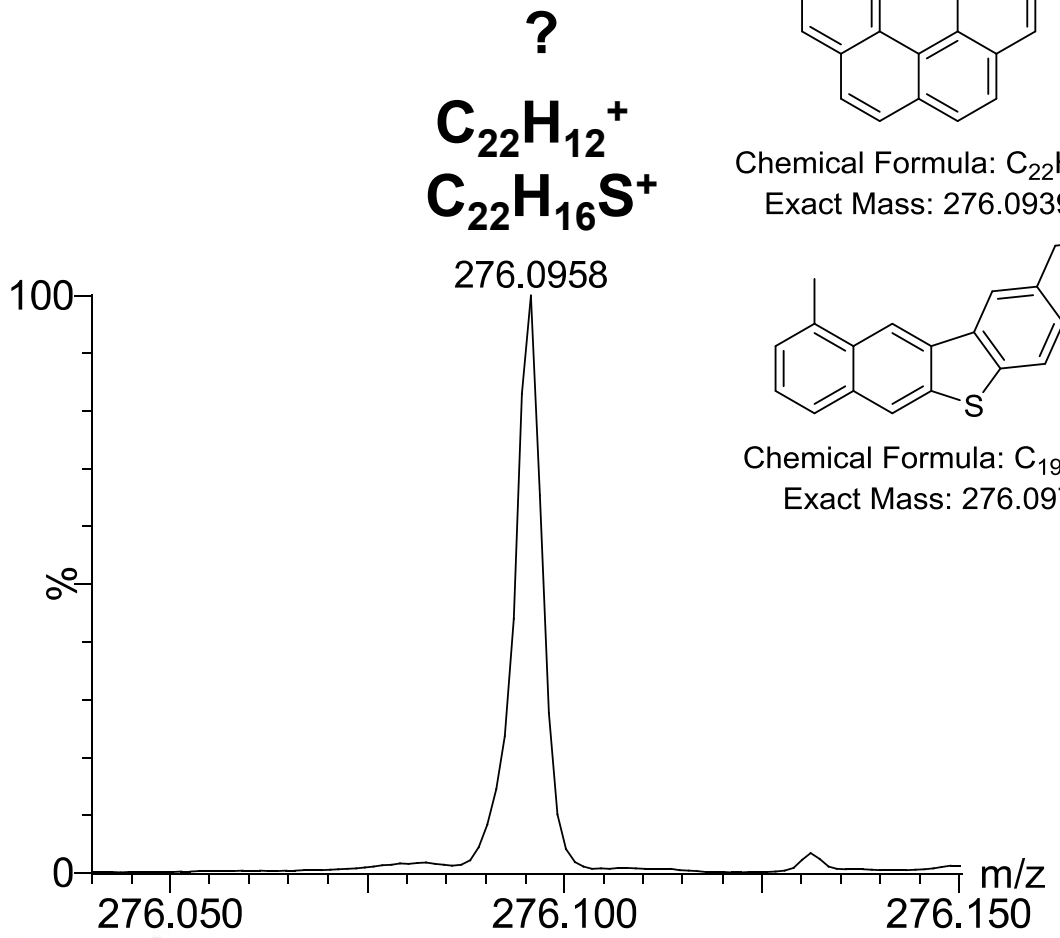

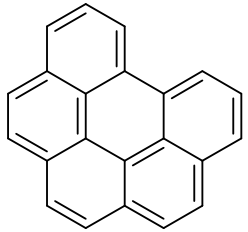

Chemical Formula: $C_{22}H_{12}$
Exact Mass: 276.0939

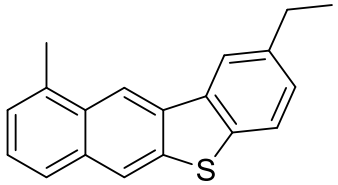

Chemical Formula: $C_{19}H_{16}S$
Exact Mass: 276.0973

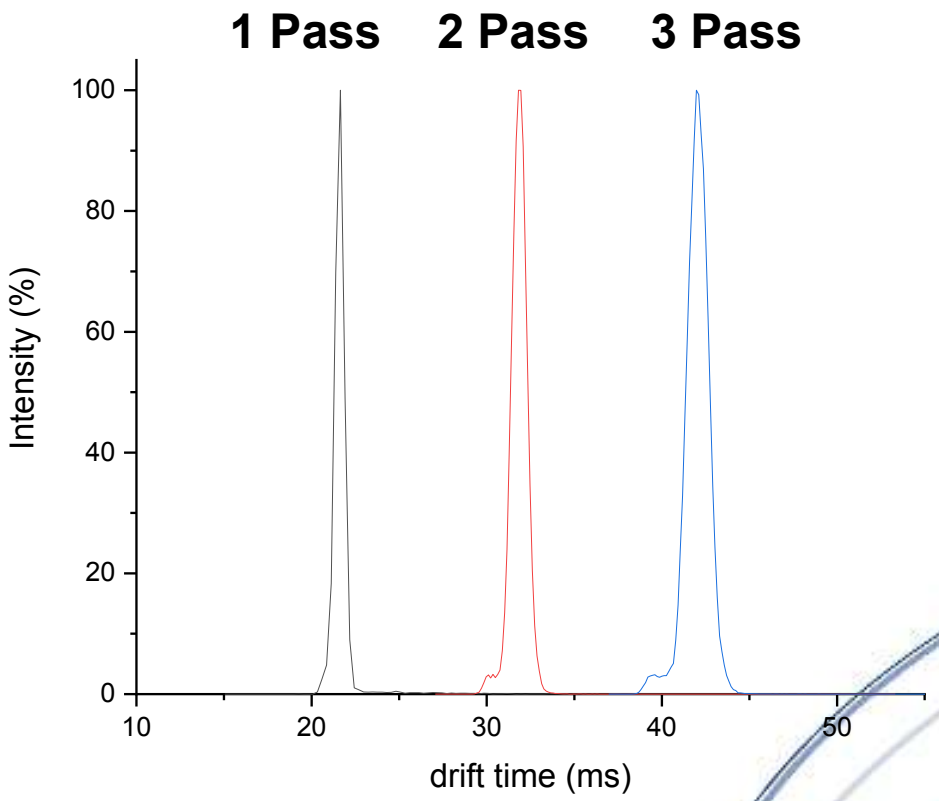

C_3-SH_4 split: VGO on the cIMS-MS

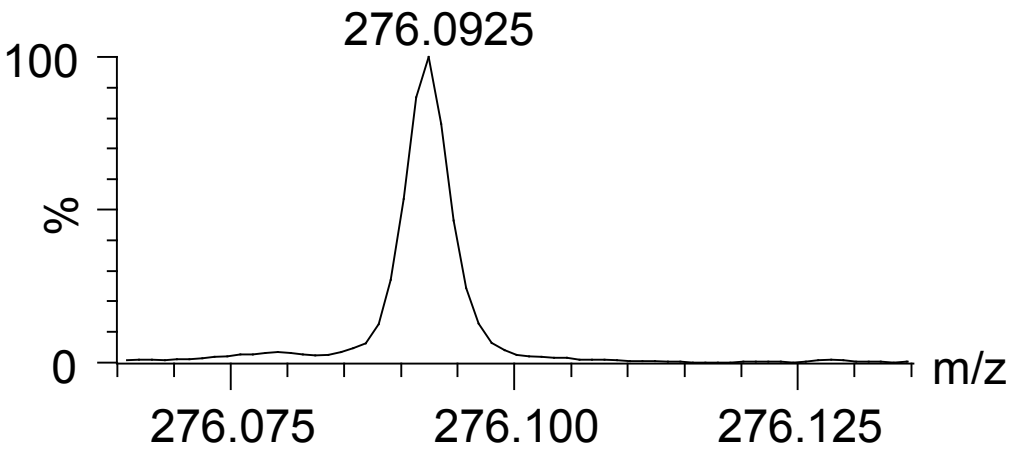

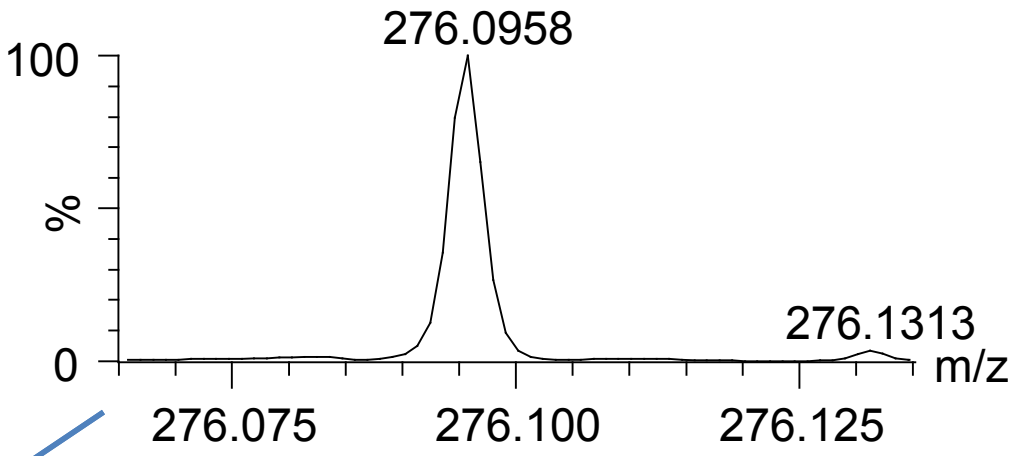

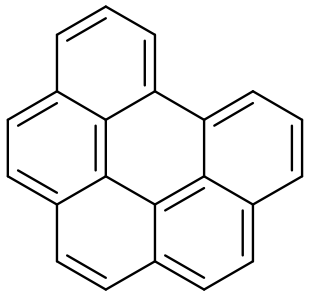

Chemical Formula: $C_{22}H_{12}$
Exact Mass: 276.0939

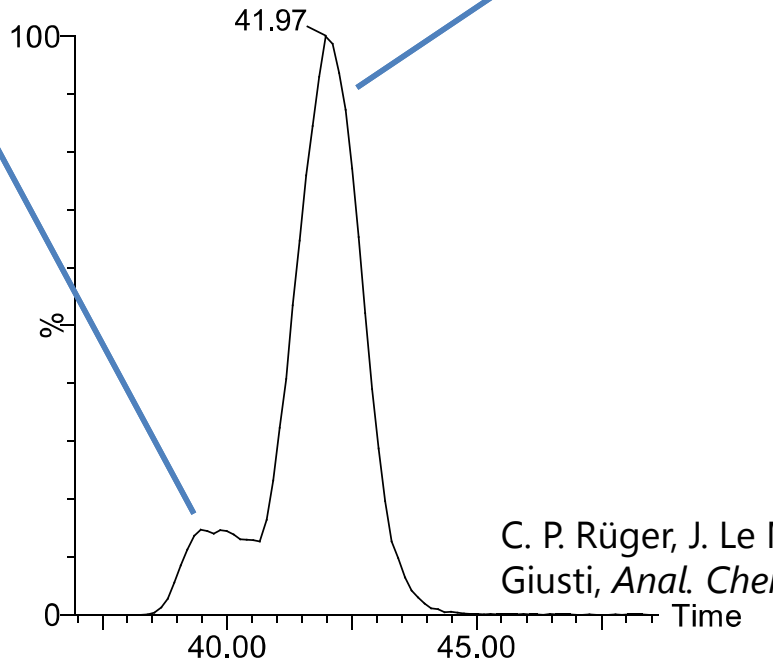

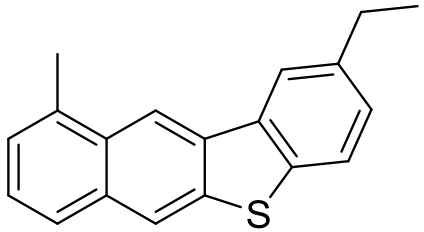

Chemical Formula: $C_{19}H_{16}S$
Exact Mass: 276.0973

C. P. Rüger, J. Le Maître, J. Maillard, E. Riches, M. Palmer, C. Afonso and P. Giusti, *Anal. Chem.*, 2021, **93**, 5872-5881.

Acknowledgments

Marie Hubert-Roux
Julien Maillard
Johann Le Maitre
Charlotte Mase

Christopher P. Rüger
Ralf Zimmermann

Pierre Giusti
Anna-Luiza Siqueira

Brice Bouyssiere
Ryan Rodgers

Mark Ridgeway
Mel Park
Christopher Thompson

Metabolomics: Revealing the Biochemical Fingerprints of Life

Carlos Cordeiro

MARE

Ciências ULisboa

EU FT-ICR MS

HOW COMPLEX IS THE METABOLOME?

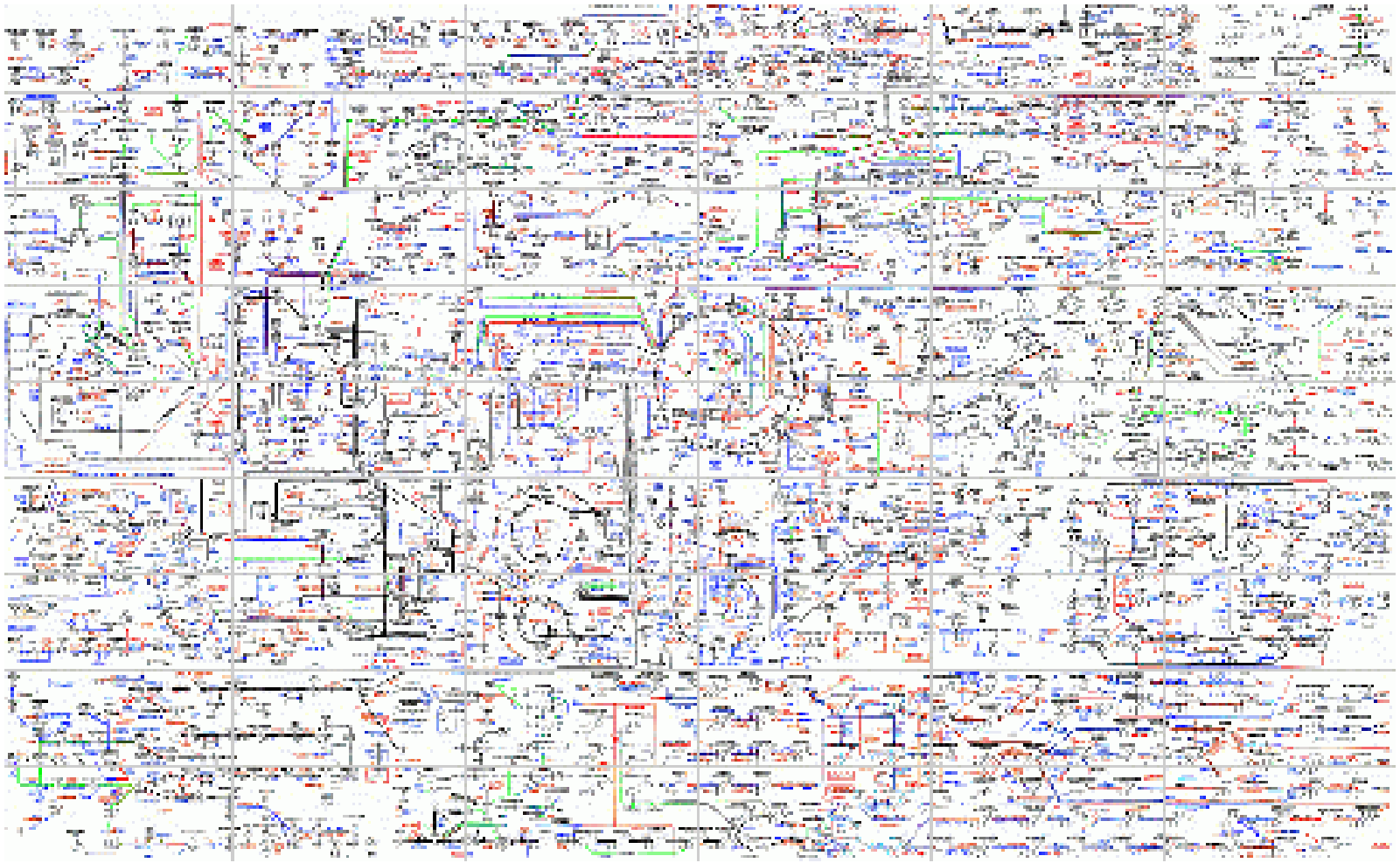

Biological model

Chemical diversity

Sample preparation

Dynamic range

Databases

Sofwtare

CHEMISTRY vs BIOLOGY

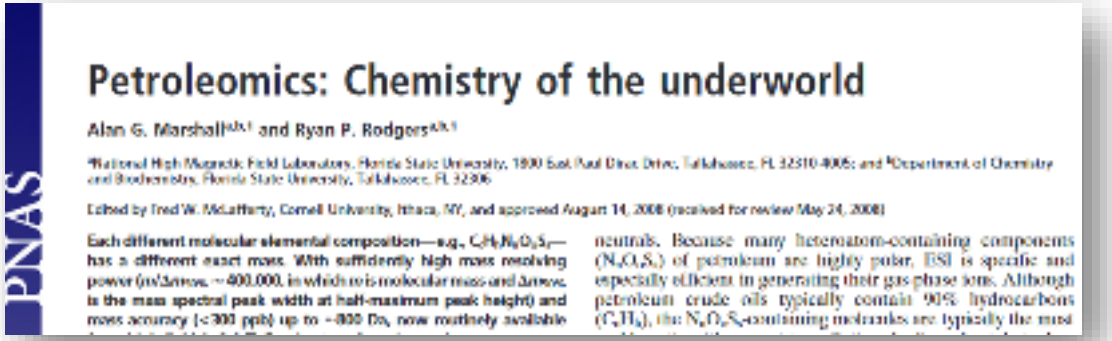

PNAS

Petroleomics: Chemistry of the underworld

Alan G. Marshall[a,b,1] and Ryan P. Rodgers[a,b,1]

[a]National High Magnetic Field Laboratory, Florida State University, 1800 East Paul Dirac Drive, Tallahassee, FL 32310-4005; and [b]Department of Chemistry and Biochemistry, Florida State University, Tallahassee, FL 32306

Edited by Fred W. McLafferty, Cornell University, Ithaca, NY, and approved August 14, 2008 (received for review May 24, 2008)

Each different molecular elemental composition—e.g., $C_xH_yN_zO_zS_z$—has a different exact mass. With sufficiently high mass resolving power ($m/\Delta m_{50\%}$ ~400,000, in which m is molecular mass and $\Delta m_{50\%}$ is the mass spectral peak width at half-maximum peak height) and mass accuracy (<300 ppb) up to ~800 Da, now routinely available

neutrals. Because many heteroatom-containing components ($N_zO_zS_z$) of petroleum are highly polar, ESI is specific and especially efficient in generating their gas phase ions. Although petroleum crude oils typically contain 90% hydrocarbons (C_xH_y), the $N_zO_zS_z$-containing molecules are typically the most

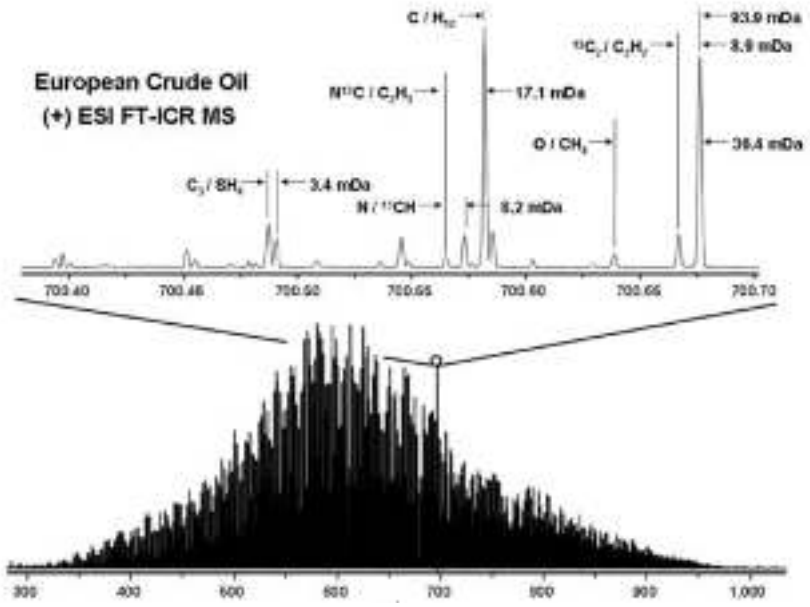

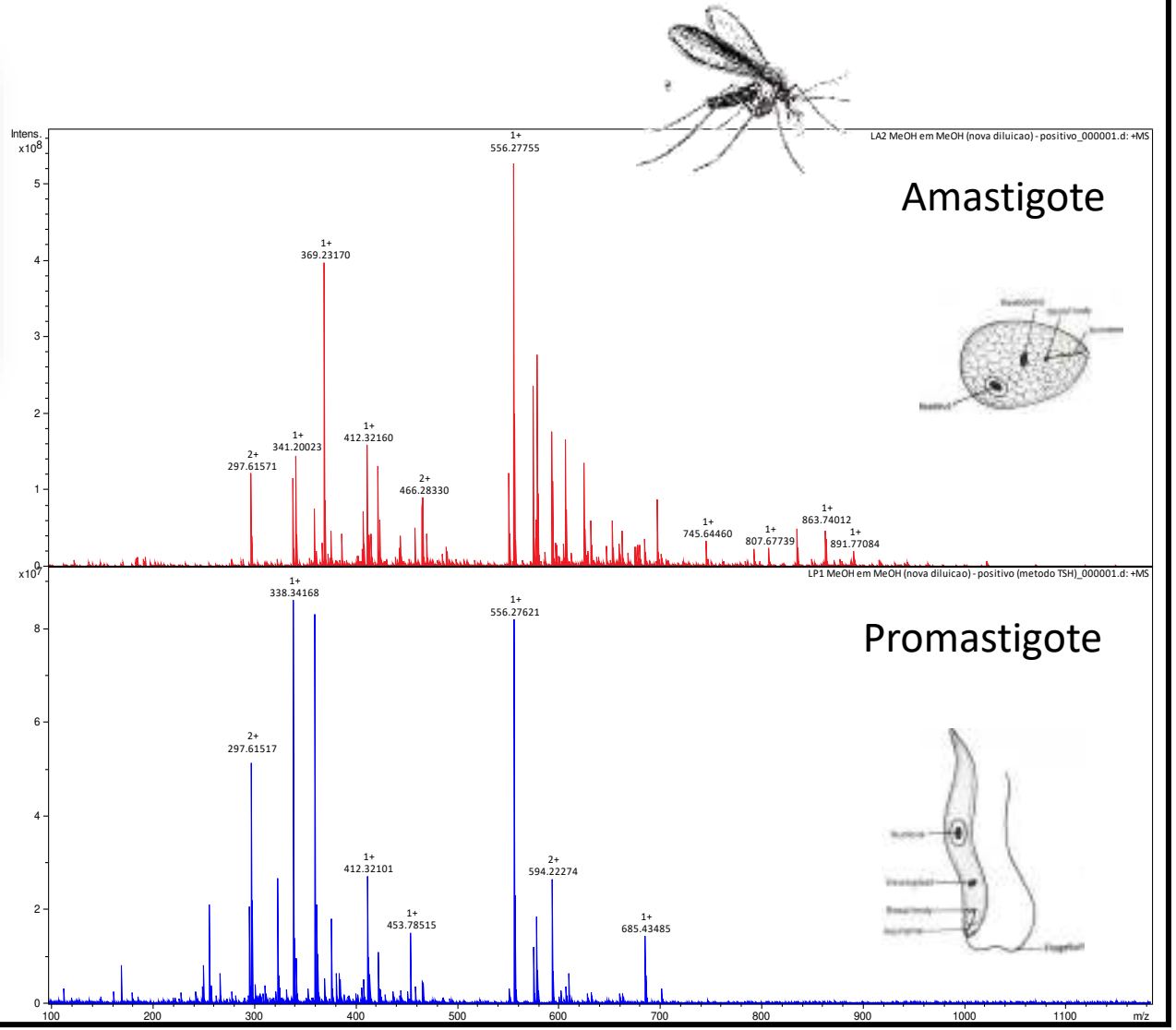

FROM SPECTRUM TO BIOCHEMISTRY

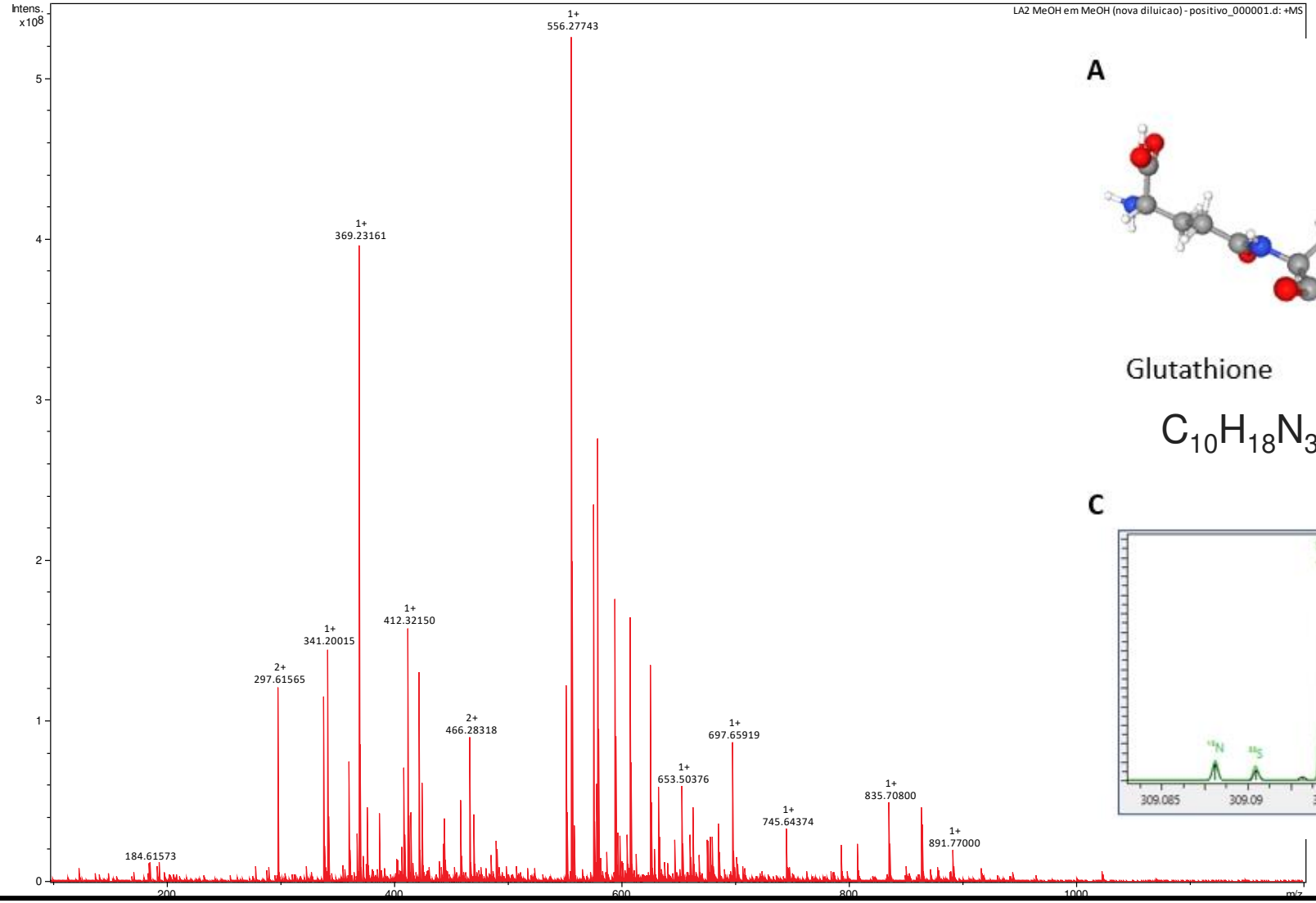

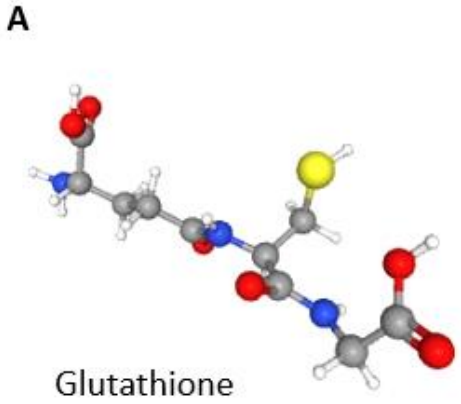

$C_{10}H_{18}N_3O_6S$

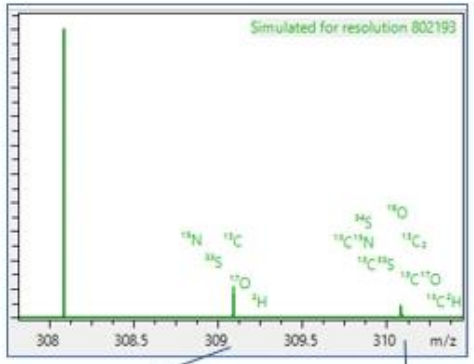

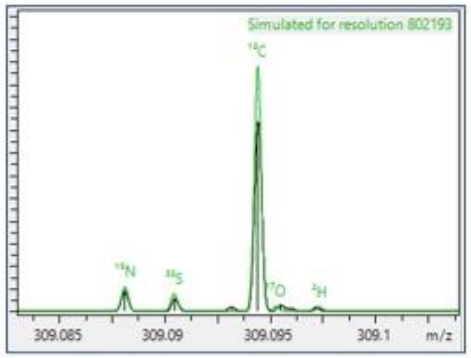

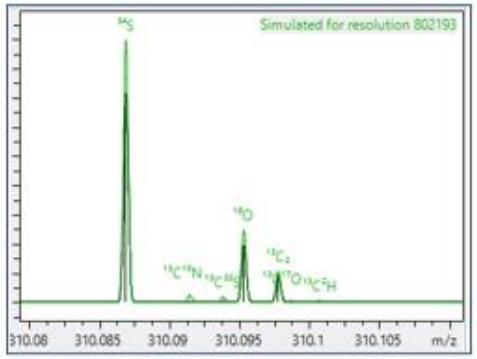

FROM SPECTRUM TO BIOCHEMISTRY

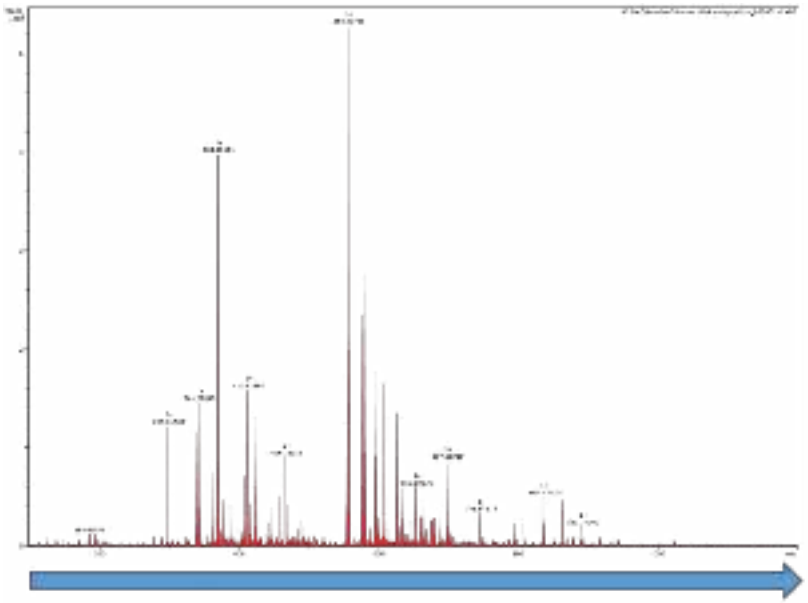

http://masstrix3.helmholtz-muenchen.de/masstrix3/

6500

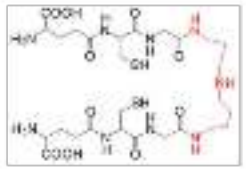

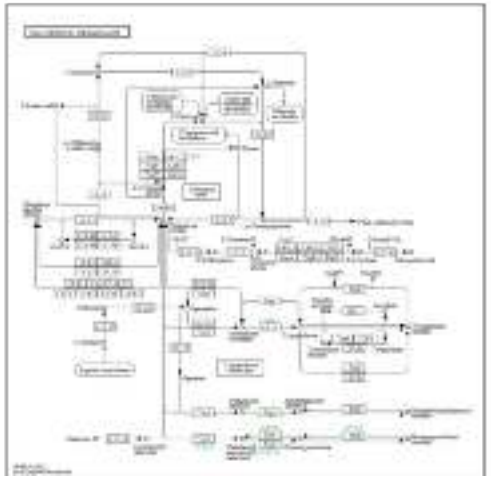

PATHWAY MAPPING

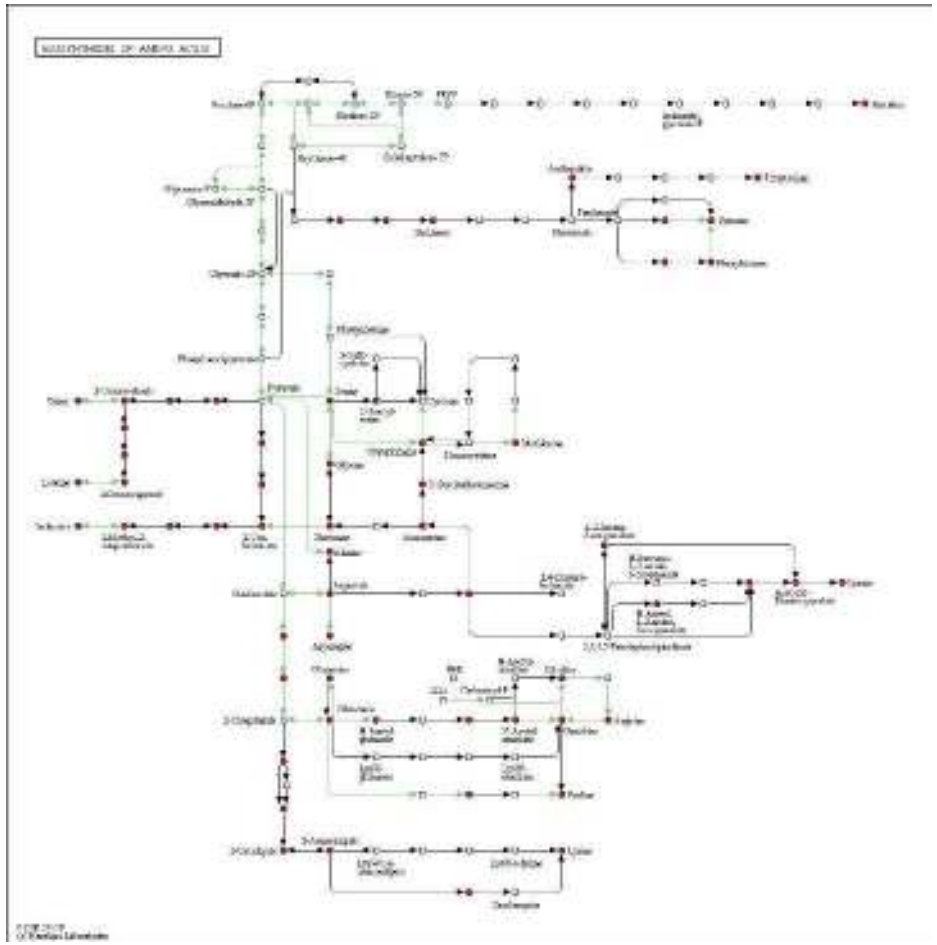

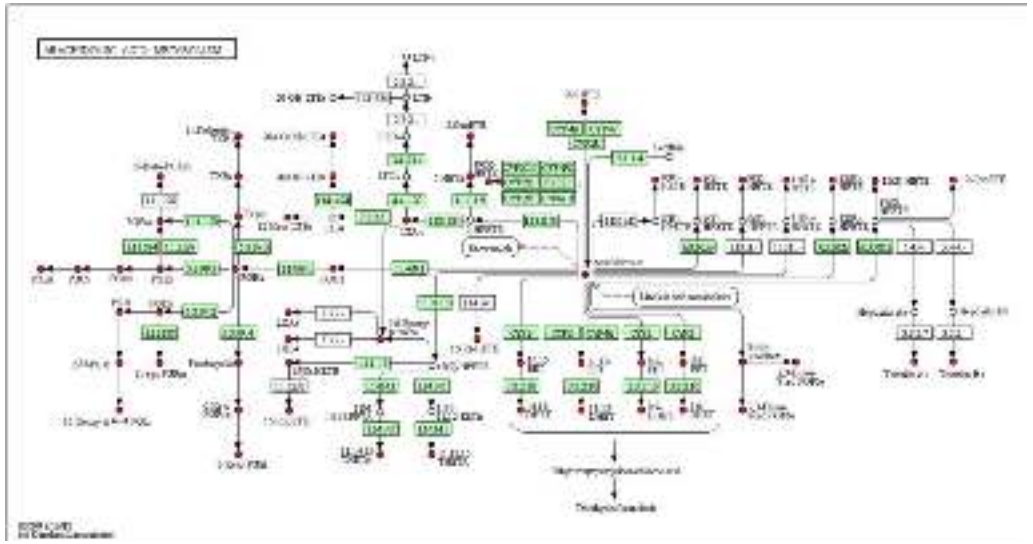

NETWORK ANALYSIS

reactome

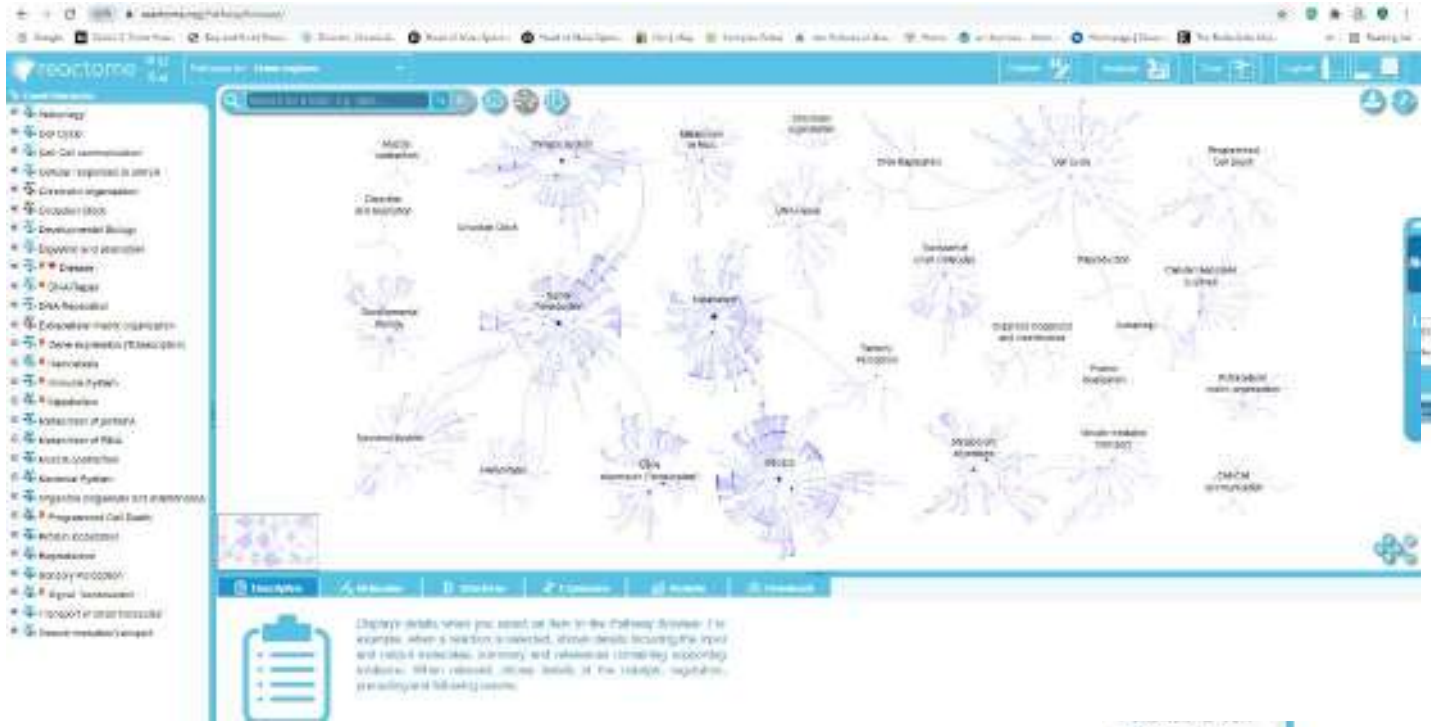

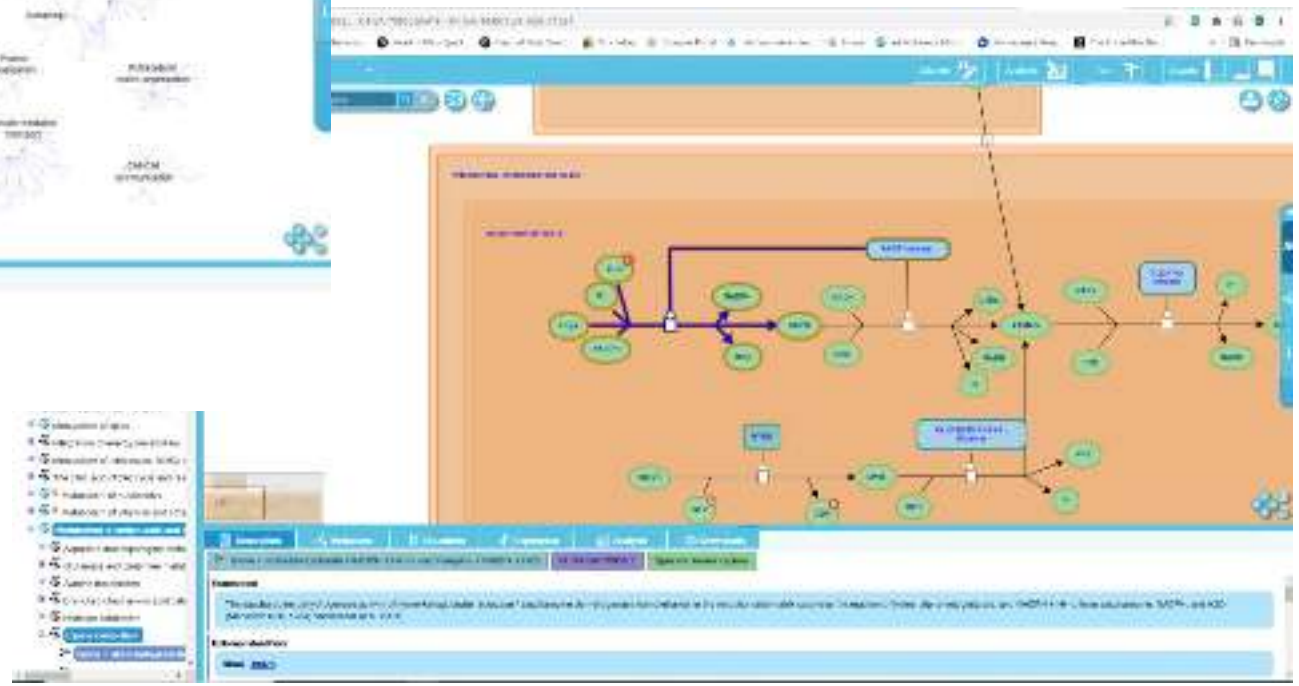

WE ARE ALL DIFFERENT

EU-FT-ICR-MS
Advanced Users School
Lisboa, April 2019

THE REAL FINGERPRINT

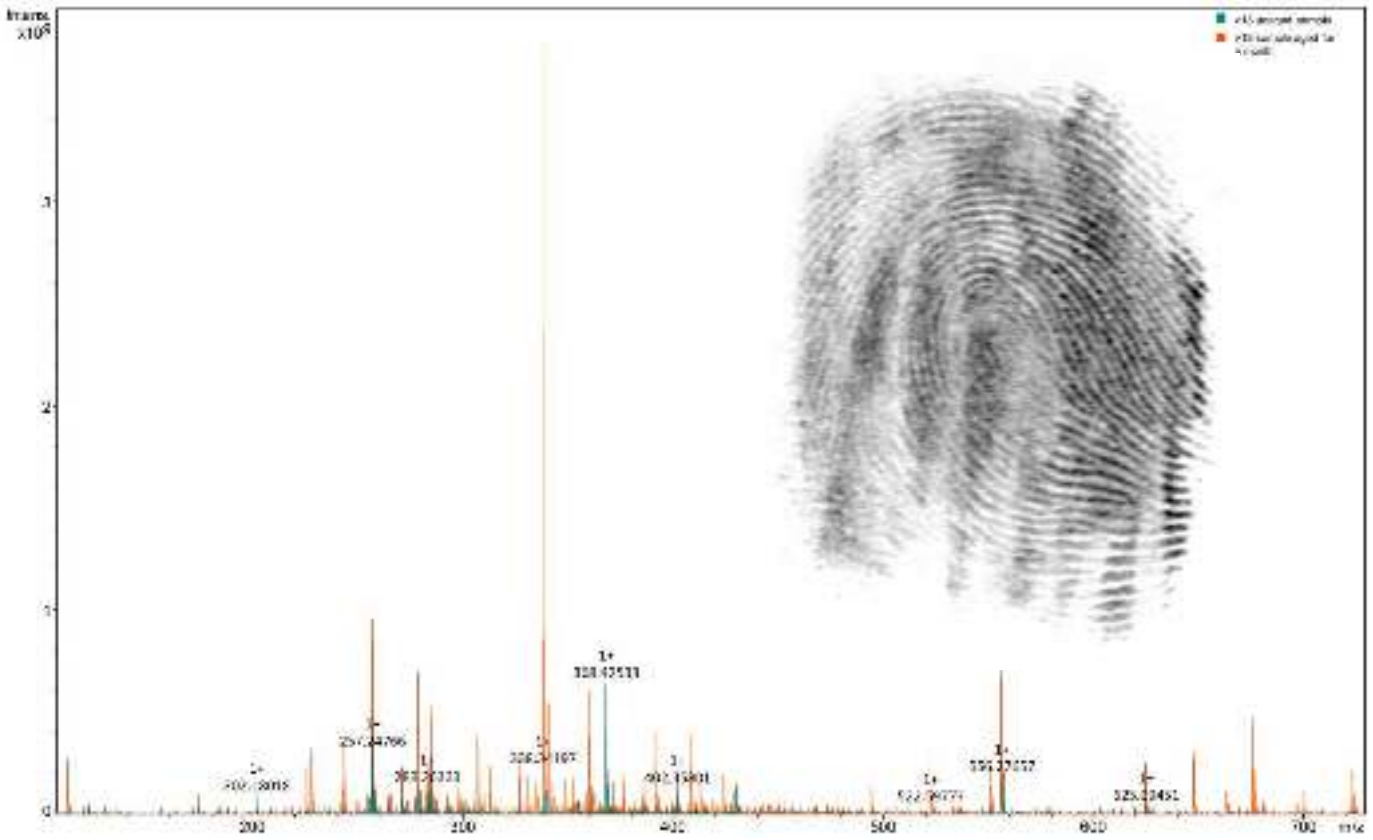

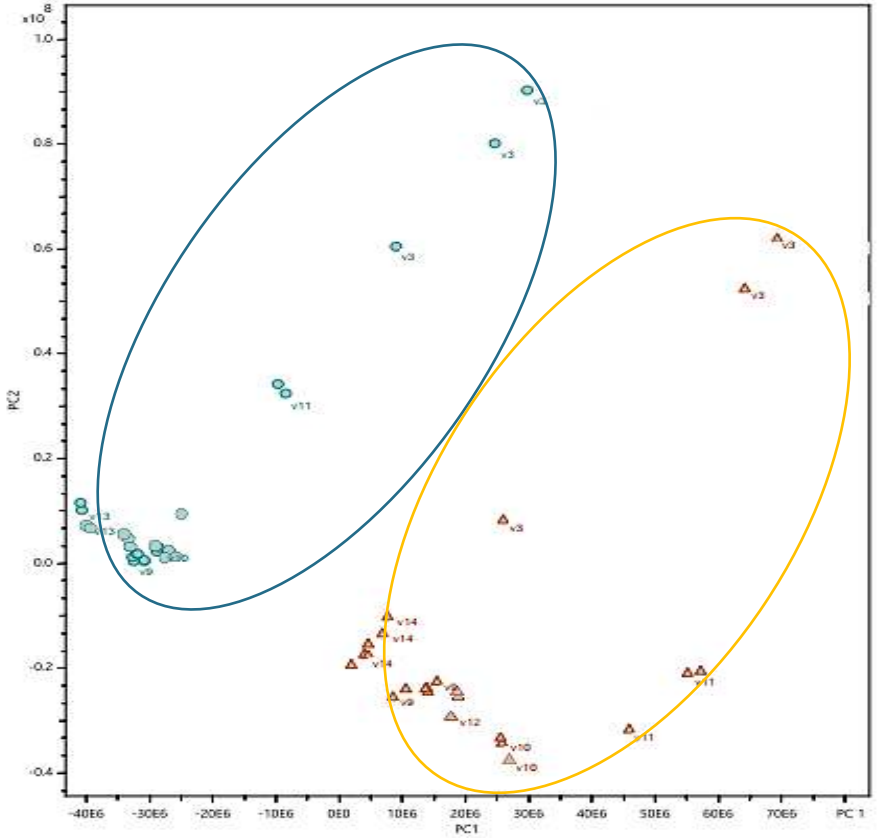

DISCRIMINATION OF GRAPEVINE GENOTYPES

SAMPLE PREPARATION

EuPA Open Proteomics 12 (2016) 4–9

Contents lists available at ScienceDirect

EuPA Open Proteomics

journal homepage: www.elsevier.com/locate/euprot

Metabolite extraction for high-throughput FTICR-MS-based metabolomics of grapevine leaves

Marisa Maia[a,b,c], Filipa Monteiro[a], Mónica Sebastiana[a], Ana Patrícia Marques[b,c], António E.N. Ferreira[b,c], Ana Ponces Freire[c], Carlos Cordeiro[b,c], Andreia Figueiredo[a,*], Marta Sousa Silva[b,c,a,1]

[a] Biosystems & Integrative Sciences Institute (BioISI), Science Faculty of Lisbon University, 1749-016 Lisbon, Portugal
[b] Laboratório de FTICR e Espectrometria de Massa Estrutural, FacuMade de Ciências da Universidade de Lisbon, Portugal

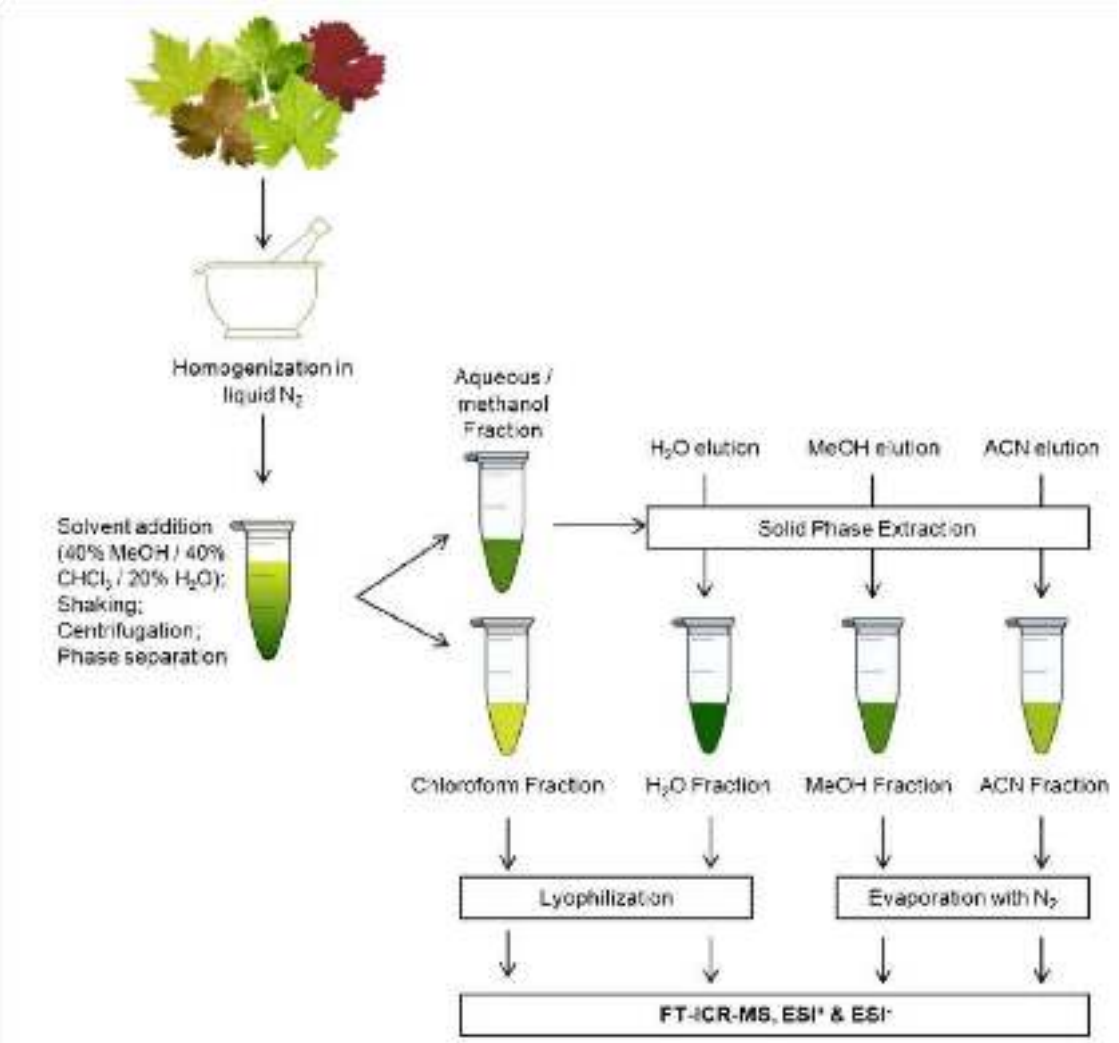

DISCRIMINATION OF RESISTANT AND SUSCEPTIBLE GRAPEVINE GENOTYPES

Wild *Vitis* (*V. riparia*)
Resistant

X

V. vinifera
Susceptible

The problem

The **screening process for disease resistance and grape quality** takes **2-3 years!**

The goal:
To shorten this time,
by uncovering **biomarkers** for downy mildew resistance

What producers want

New cultivars with good berry quality and a high degree of resistance against downy mildew

DISCRIMINATION OF RESISTANT AND SUSCEPTIBLE GRAPEVINE GENOTYPES

Wild *Vitis*, Resistant

Wild *Vitis* species

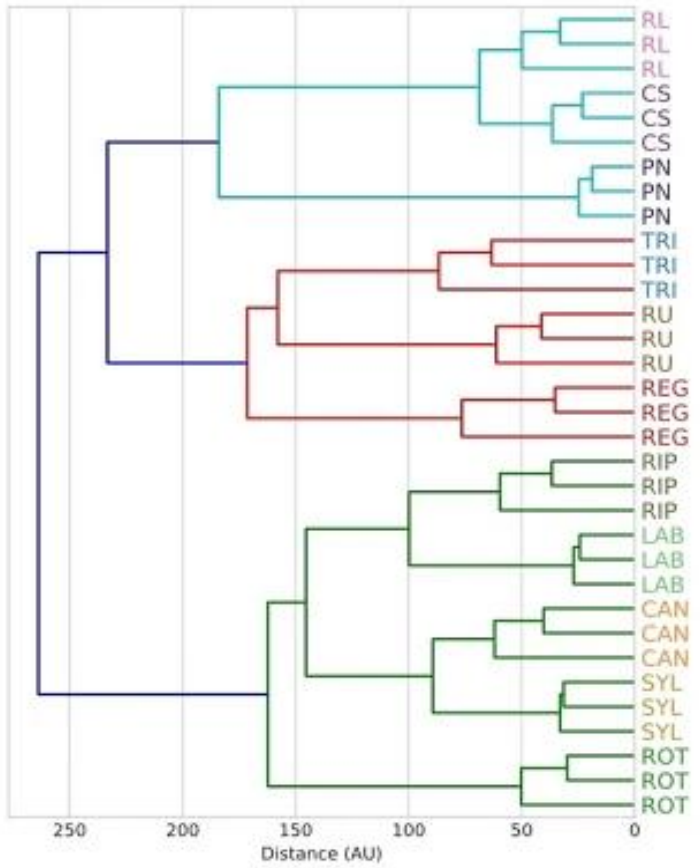

Vitis vinifera cultivars

V. vinifera, Susceptible

Separation between *V. vinifera* and wild *Vitis* only based on their metabolic composition

DISCRIMINATION OF RESISTANT AND SUSCEPTIBLE GRAPEVINE GENOTYPES

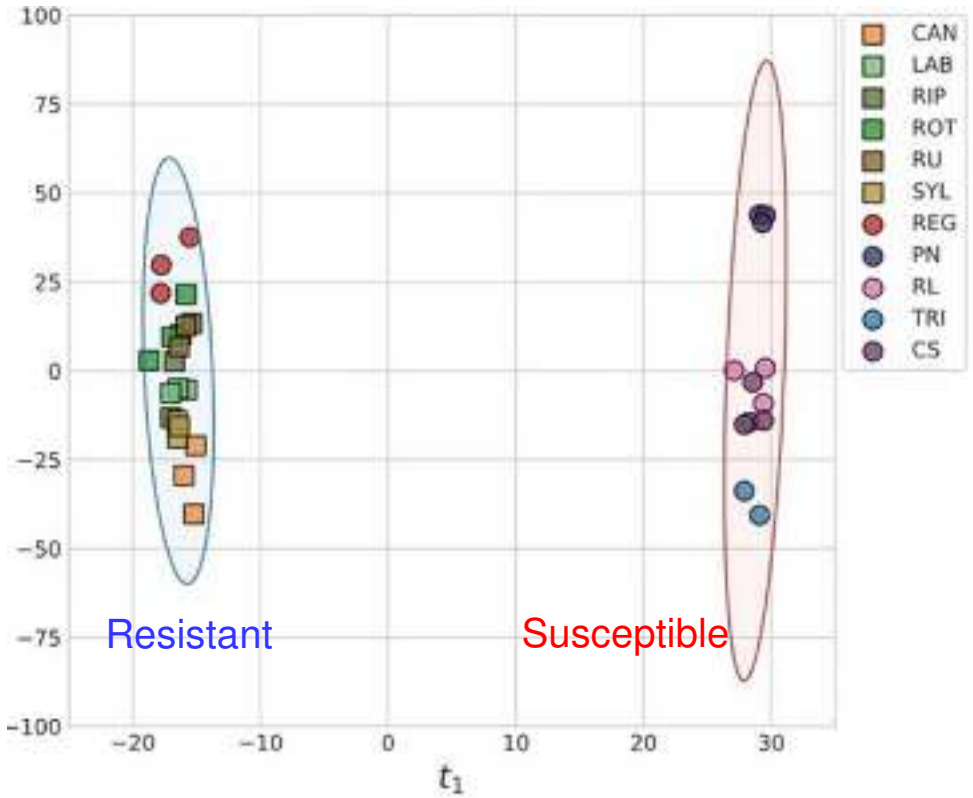

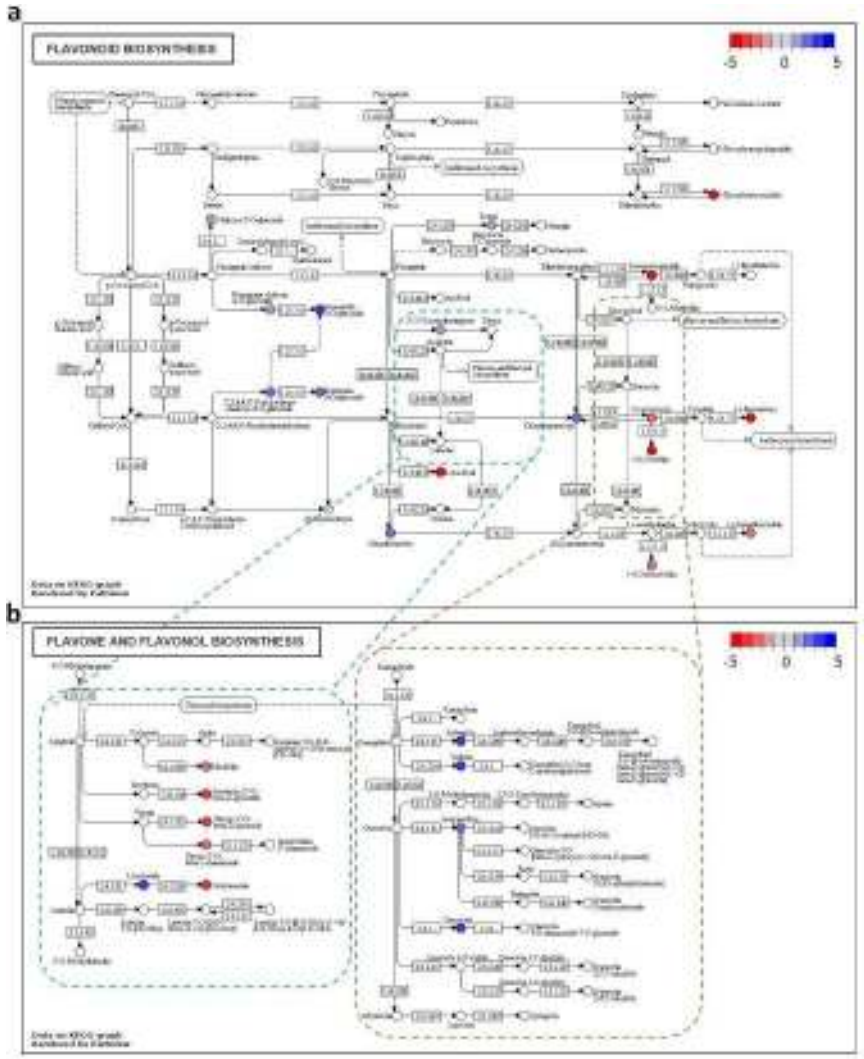

Discriminating compounds between resistant and susceptible genotypes identified

Activation of different metabolic pathways

DISCRIMINATION OF RESISTANT AND SUSCEPTIBLE GRAPEVINE GENOTYPES

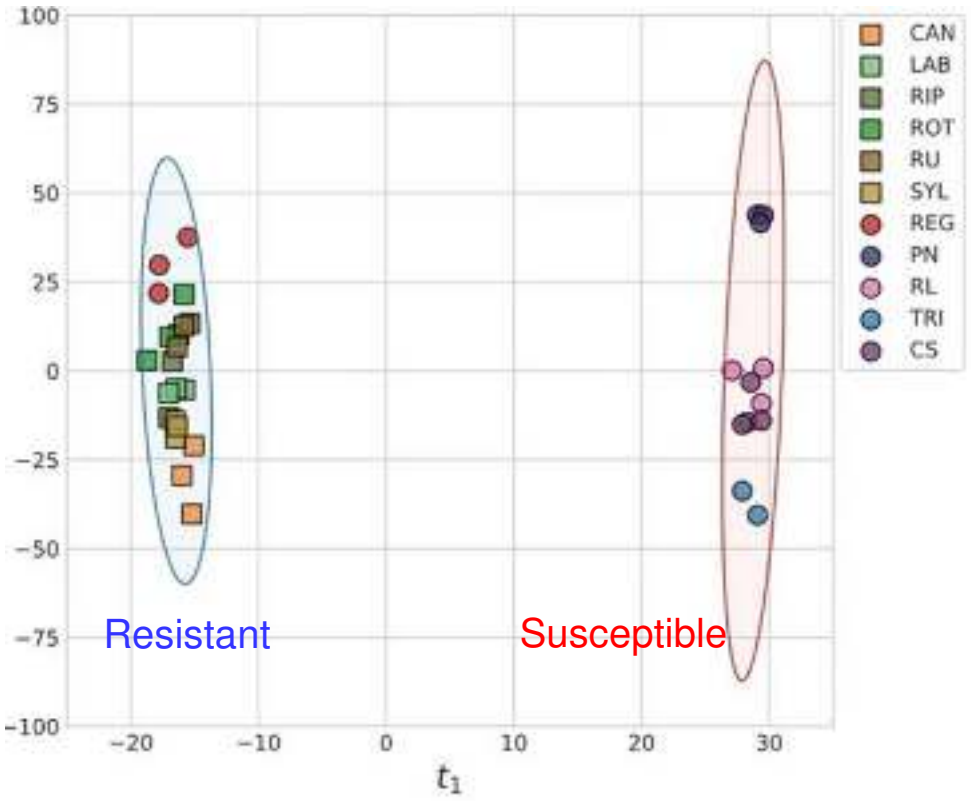

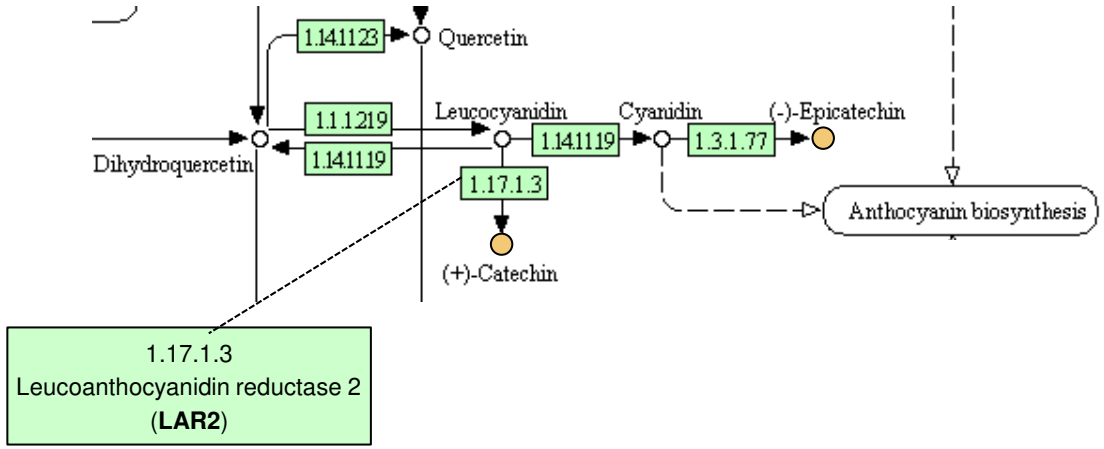

***LAR2* expression analysis by qPCR**

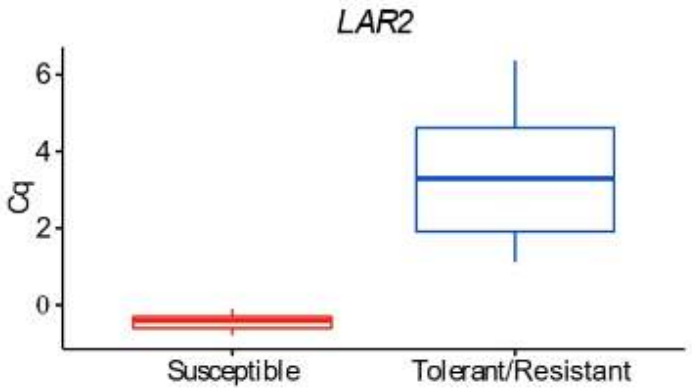

***Catechin* emerged as a promising biomarker of susceptibility**

DISCRIMINATION OF MALE AND FEMALE WILD GRAPEVINES, *VITIS SYLVESTRIS*

Vitis sylvestris

Plant images from
Scientific Reports | (2020) 10:18993
https://doi.org/10.1038/s41598-020-76012-6

Vitis vinifera

Image from:
Patty Skinkis, Oregon State University

DISCRIMINATION OF MALE AND FEMALE WILD GRAPEVINES, *VITIS SYLVESTRIS*

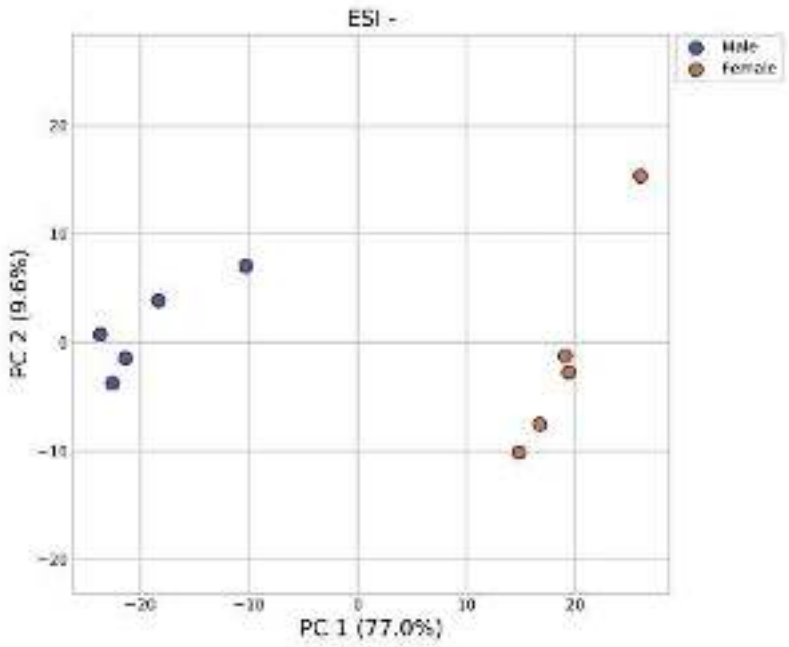

Discriminating compounds between male and female genotypes identified, before the appearance of flowers

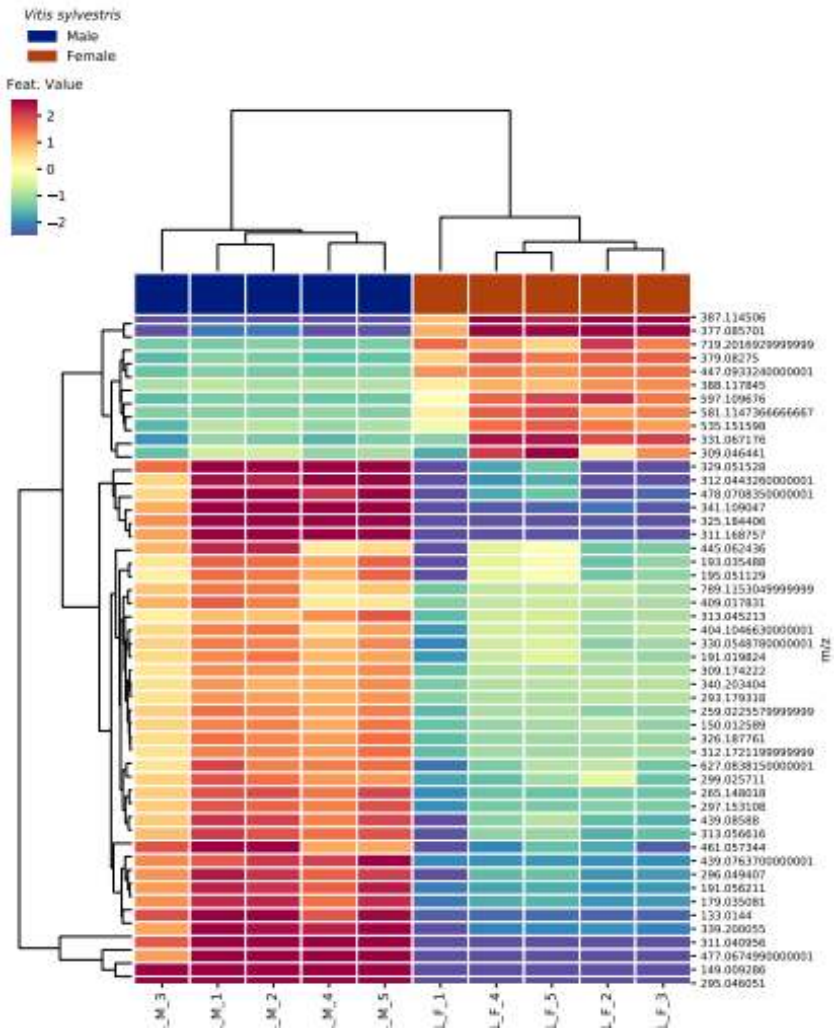

DISCRIMINATION OF SINGLE-GENE YEAST MUTANTS

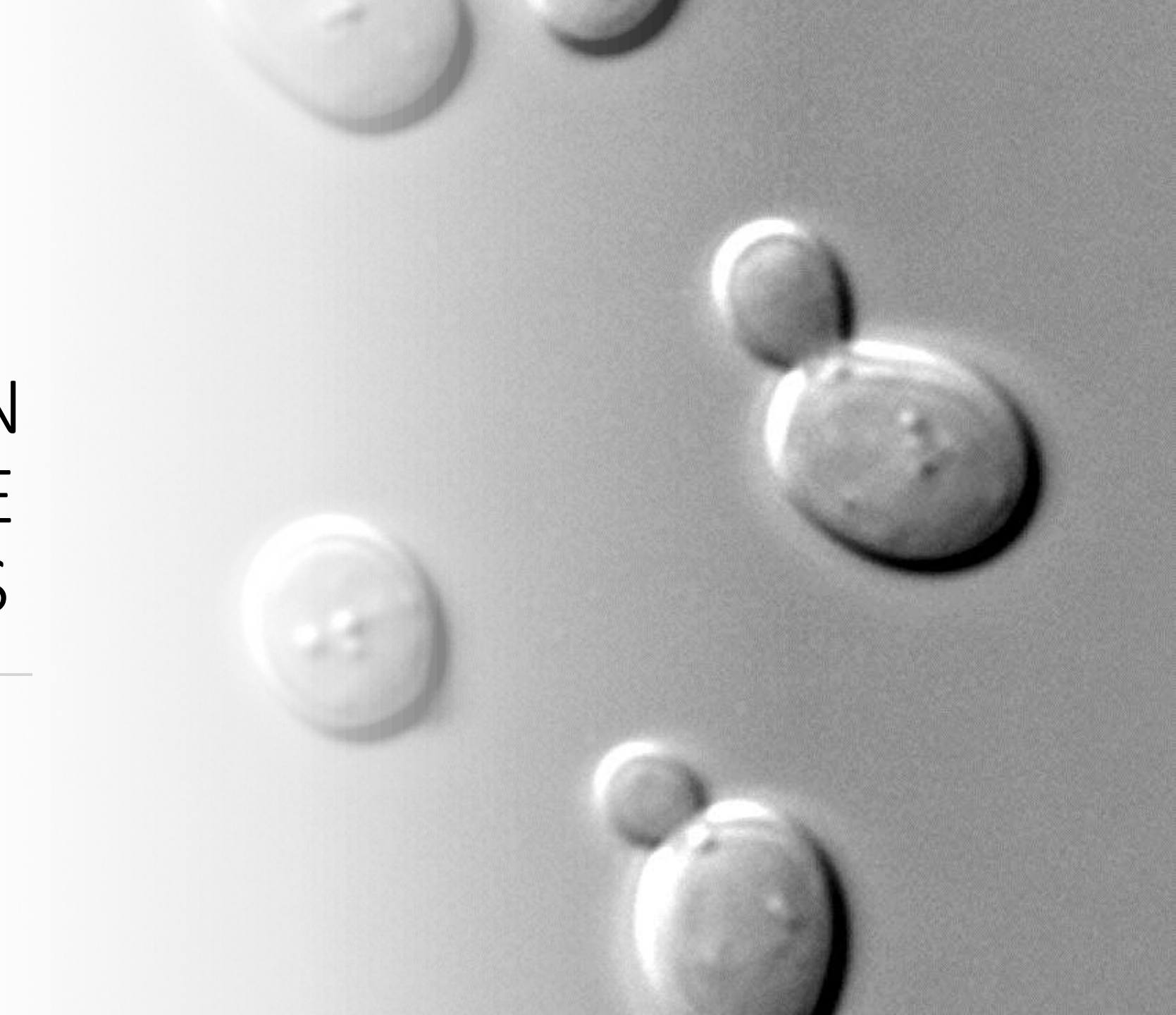

DISCRIMINATION OF SINGLE-GENE YEAST MUTANTS

BY4741
MATa; his3Δ1; leu2Δ0; met15Δ0; ura3Δ0

Genetically identical
Secondary pathway, not essential
No growth deficiency

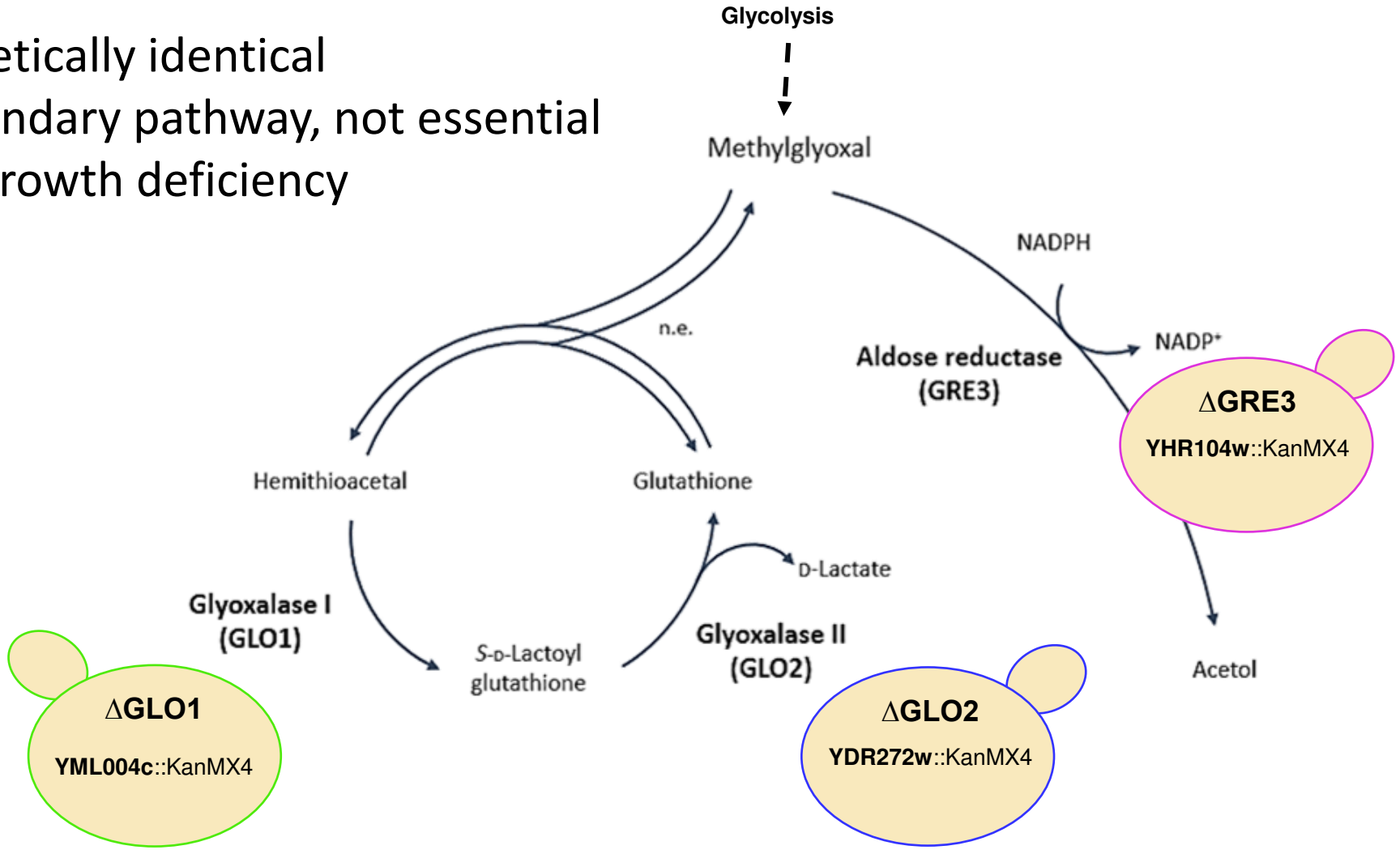

DISCRIMINATION OF SINGLE-GENE YEAST MUTANTS

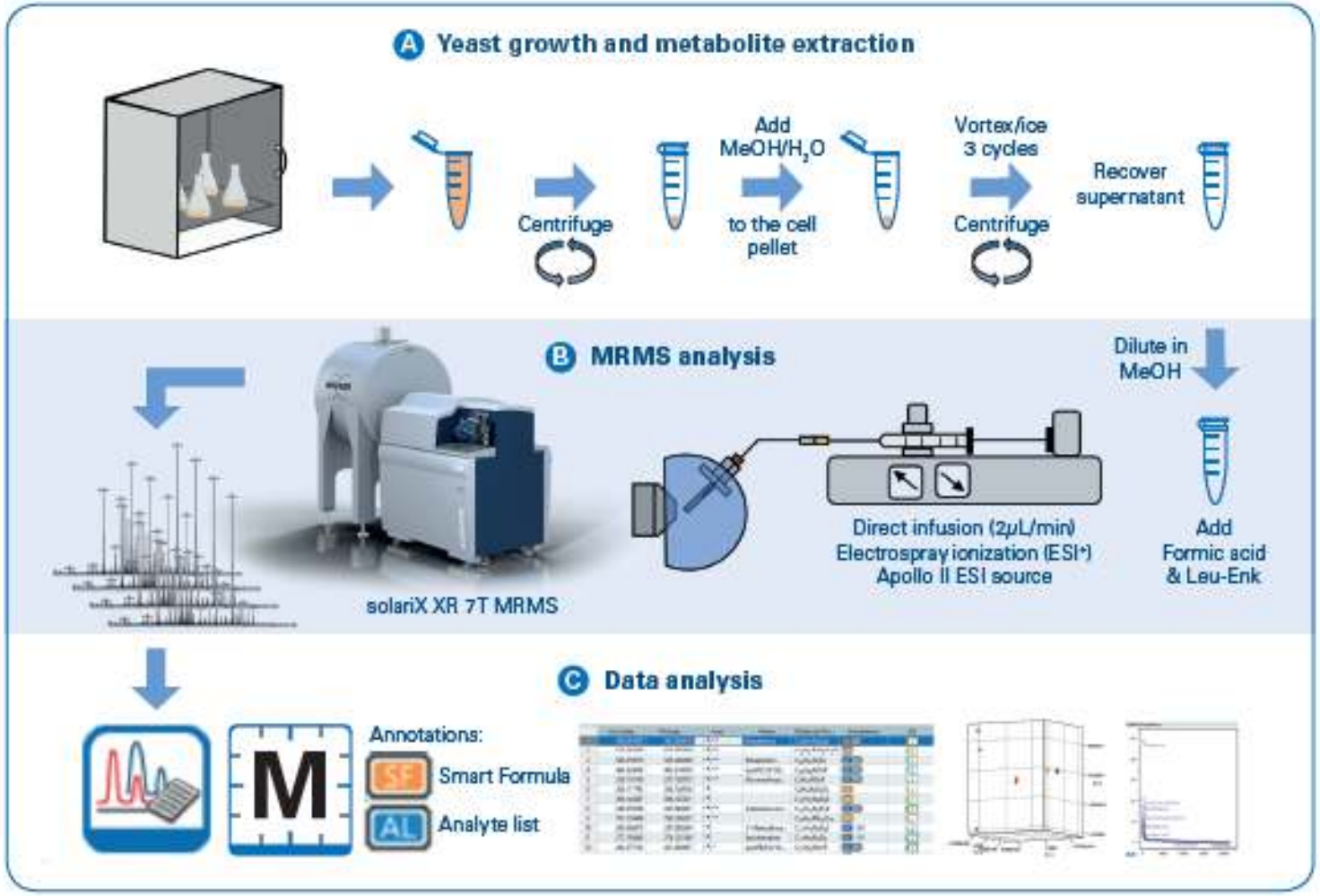

DISCRIMINATION OF SINGLE-GENE YEAST MUTANTS

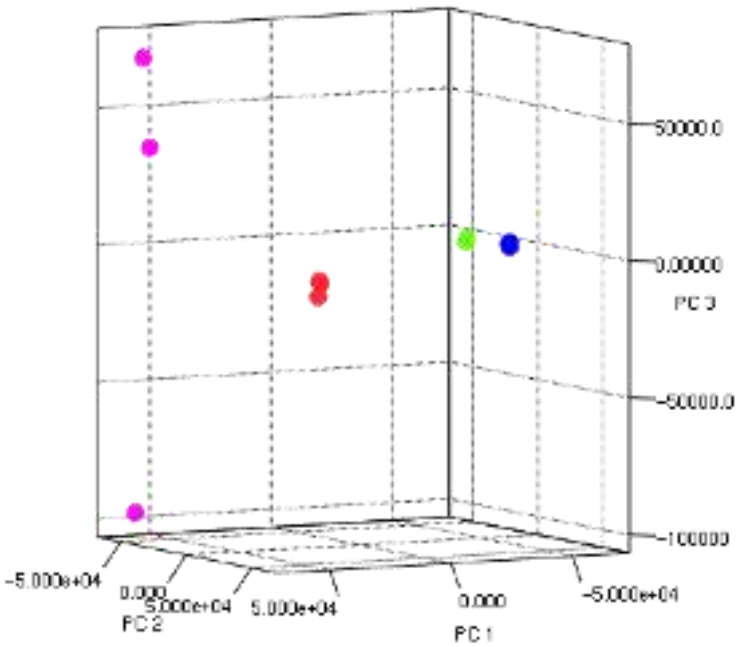

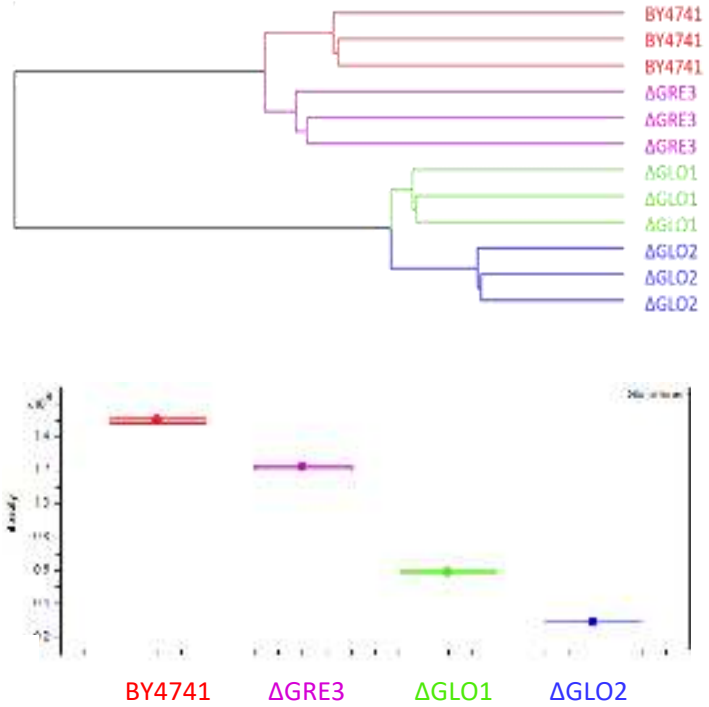

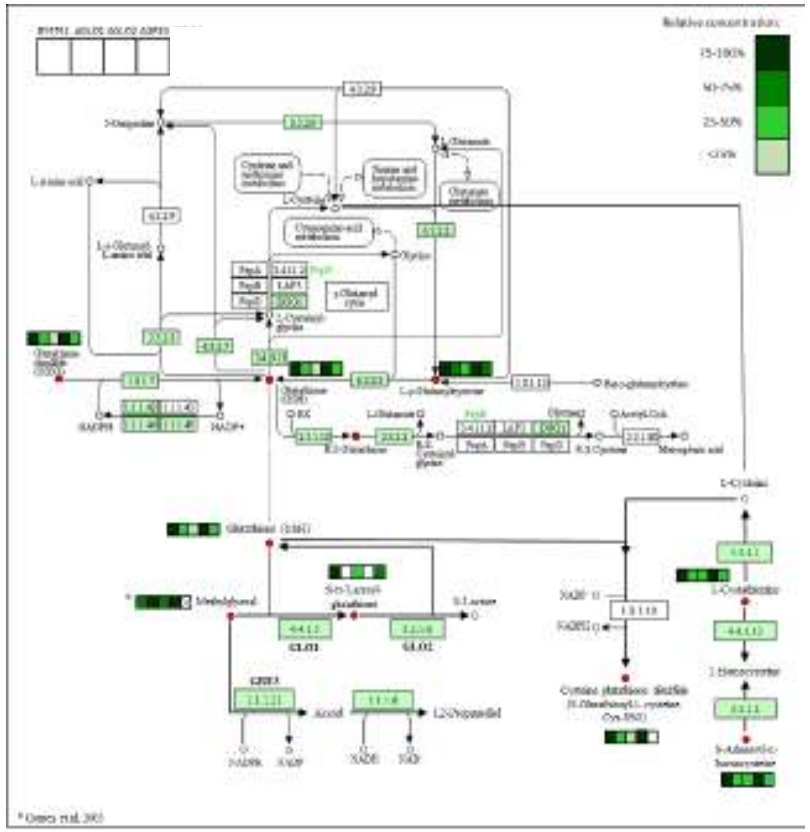

Glutathione metabolism

Discrimination only based on their metabolic composition
Glutathione was the most discriminating compound
Wider functional and cellular effects elucidated

BEYOND GLUTATHIONE

Position	Mass (Da)	Metabolite Name	Molecular Formula	VIP Score
1	307.0838	Glutathione	$C_{10}H_{17}N_3O_6S$	8.417995046
2	493.3168	PC(16:1(9Z)/0:0)	$C_{24}H_{48}NO_7P$	5.993469554
3	624.0873	N/A	$C_{14}H_{28}N_{10}O_{10}S_4$	5.587837143
4	257.1029	Glycerophosphocholine	$C_8H_{20}NO_6P$	4.837523121
5	324.1057	N/A	$C_{12}H_{20}O_{10}$	4.177424151
6	337.3345	N/A	$C_{22}H_{43}NO$	4.153906335
7	254.2246	Hypogeic acid	$C_{16}H_{30}O_2$	4.077281087
8	385.3192	Pentadecanoylcarnitine	$C_{22}H_{43}NO_4$	3.77589036
9	398.1372	N/A	$C_{15}H_{22}N_6O_5S$	3.484675636
10	451.2699	PE(16:1(9Z)/0:0)	$C_{21}H_{42}NO_7P$	3.172850261

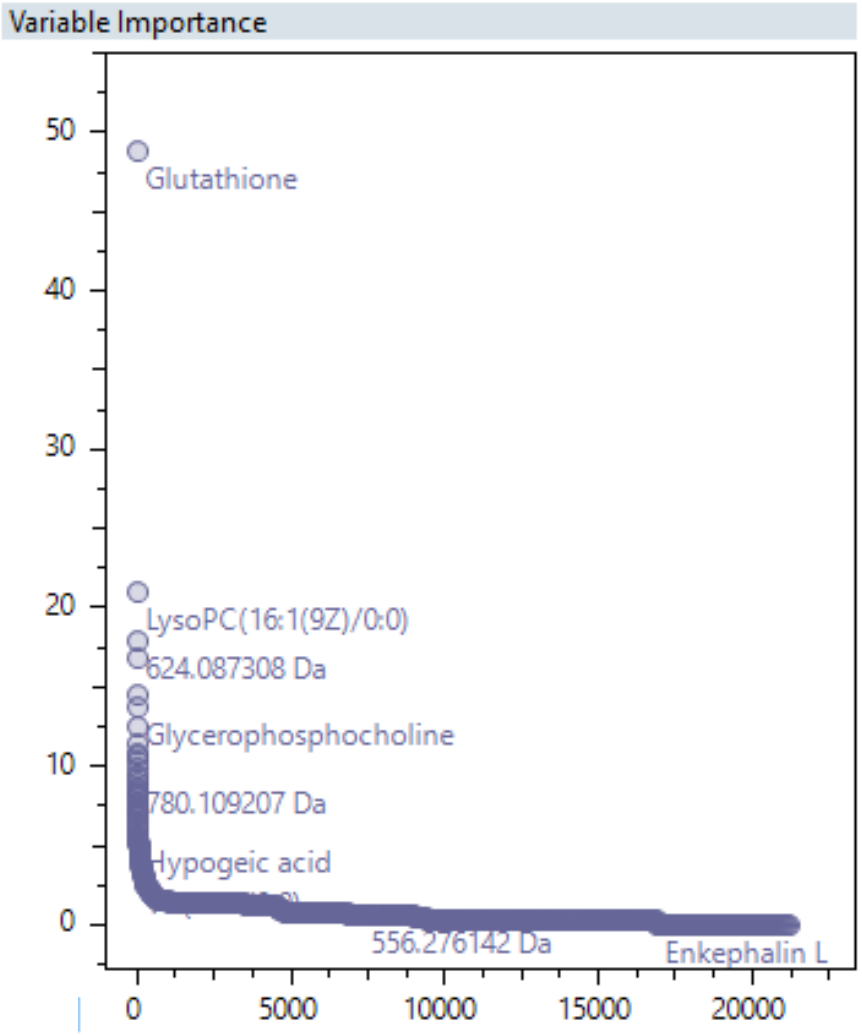

DEVELOPMENT OF NEW METHODS FOR METABOLOMICS DATA ANALYSIS

DEVELOPMENT OF NEW METHODS FOR METABOLOMICS DATA ANALYSIS

Sample Preparation
↓
Data Acquisition
↓
Data Pre-Processing
↓
Compound identification (optional)
↓
Data Pre-Treatment
↓
Statistical Analysis
↓
Data Interpretation

Binary similarity (BinSim)

Samp./ Feat.	A-1	A-2	A-3	B-1	B-2	B-3
x	163	124	189	200	176	223
y	115	108	101	-	98	-
z	-	-	-	165	126	-
w	-	98	103	879	-	-
v	-	-	-	176	215	245

Samp./ Feat.	A-1	A-2	A-3	B-1	B-2	B-3
x	1	1	1	1	1	1
y	1	1	1	0	1	0
z	0	0	0	1	1	0
w	0	1	1	1	0	0
v	0	0	0	1	1	1

Mass Difference Networks (MDiN) construction

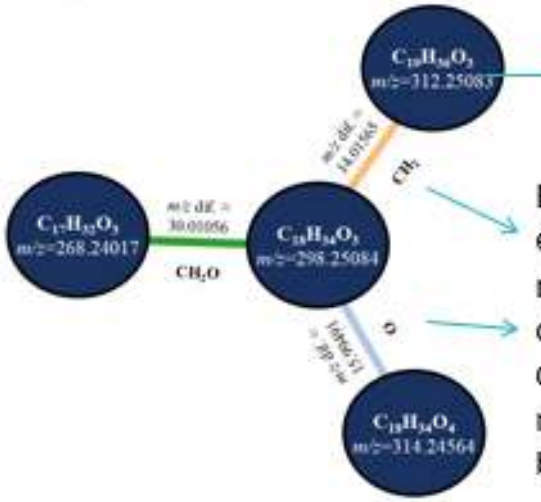

m/z peaks are nodes

Edges are established between nodes if their mass difference is very close to one of the mass different-based building blocks used

Transformations	Δ Mass (Da)	Reaction Types
O (-NH)	0.984016	Deamination
NH_3 (-O)	1.031634	Transamination
H_2	2.015650	Hydrogenations / Dehydrogenations
CH_2	14.015650	Methylations
O	15.994915	Oxygenations / Hydroxylations
H_2O	18.010565	Condensation / Dehydration / Cyclization
NCH	27.010899	Transfer of a formidoyl group
CO	27.994915	Formylation
CHOH	29.002740	Hydroxymethylation
S	31.972071	Transfer of a –SH group
C_2H_2O	42.010565	Acetylation
CONH	43.005814	Transfer of a carbamoyl group
CO_2	43.989829	Carboxylation / Decarboxylation
SO_3	79.956815	Sulphation
PO_3H	79.966331	Phosphorylation

JOIN US IN LISBON FOR THE 6TH SHORT COURSE ON FT-ICR-MS

EU FT-ICR MS

EU FT-ICR MS
6th Short Course

Mapping post-translational modifications through FT-ICR

Where and when

LISBOA, 17 -20 October 2021

Faculdade de Ciências
Universidade de Lisboa, Portugal

ciencias.ulisboa.pt

Contacts: Carlos Cordeiro
cacordeiro@fc.ul.pt

Marta Sousa Silva
mfsilva@fc.ul.pt

EU FT-ICR MS · Ciências ULisboa · FCiências

Course overview

This course will cover the analysis and mapping of protein post-translational modifications using FT-ICR mass spectrometry

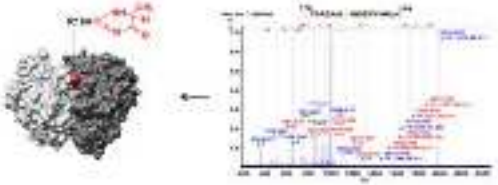

Specific topics include:

Sample preparation
Ionization
Top-down MS
Fragmentation methods
Sequence analysis

NO PARTICIPATION FEE!
Travel, accommodation, meals and social program included

Up to 20 applicants will be selected by the Scientific Committee

Tutorial lectures
Instrument demos
Hands-on exercises
Computational data analysis

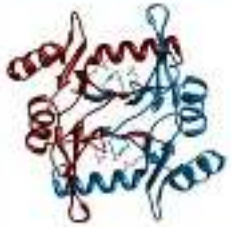

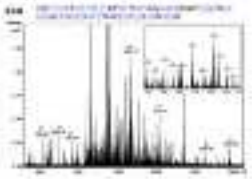

Faculty

Carlos CORDEIRO

Peter O'CONNOR

Petr NOVAK

Roman ZUBAREV

Application: www.eu-fticr-ms.eu

DEADLINE FOR APPLICATIONS:
June 31st 2021

This project has received funding from the European Union's Horizon 2020 research and innovation programme under grant agreement No 731077

THE TEAM

MARE

Ciências ULisboa

U LISBOA

FCT Fundação para a Ciência e a Tecnologia

EU FT-ICR MS

RNEM Portuguese Mass Spectrometry Network

Combination of FT-ICR mass spectrometry and spectroscopy for the characterization of ion structures

Guillaume van der Rest
Institut de Chimie Physique
Université Paris-Saclay

Outline

1. Advantages and limitations of FT-ICR cells for ion spectroscopy
2. Single photon processes
3. Multiple photon processes

WHY USE FT-ICR FOR ION PHOTODISSOCIATION ?

Ion storage in ICR cells

Dates back to before FT was introduced.

Photodissociation of the CH_3Cl^+ and N_2O^+ Cations

Robert C. Dunbar*

Contribution from the Department of Chemistry, Stanford University, Stanford, California 94305. *Received October 2, 1970*

Abstract: The ion cyclotron resonance technique was used to observe the photodissociation of the cations CH_3Cl^+ and N_2O^+ in the gas phase. Ions were trapped in the icr cell for periods of the order of seconds, which permitted the photodissociation process to be observed with wavelength-selected light. A cyclotron resonance ejection technique was employed to show that CH_3Cl^+ ions were being dissociated rather than the CH_2ClH^+ ions which were also present. The photodissociation cross section for N_2O^+ was found to be roughly 0.25×10^{-18} cm² without strong wavelength dependence between 4000 and 6500 Å. The cross section for CH_3Cl^+ showed a large peak at 3150 Å, having a value at that wavelength of 7.8×10^{-18} cm². Possible assignments of this peak are considered, and it is suggested that photodissociation occurs through an ion excitation involving a change in occupation of the bonding or antibonding orbitals of the C–Cl bond.

R.C. Dunbar, J. Am. Chem. Soc. **93**, 4354 (1971)

Ion storage in ICR cells

At low field, FT-ICR allowed **long storage times** for the ions.

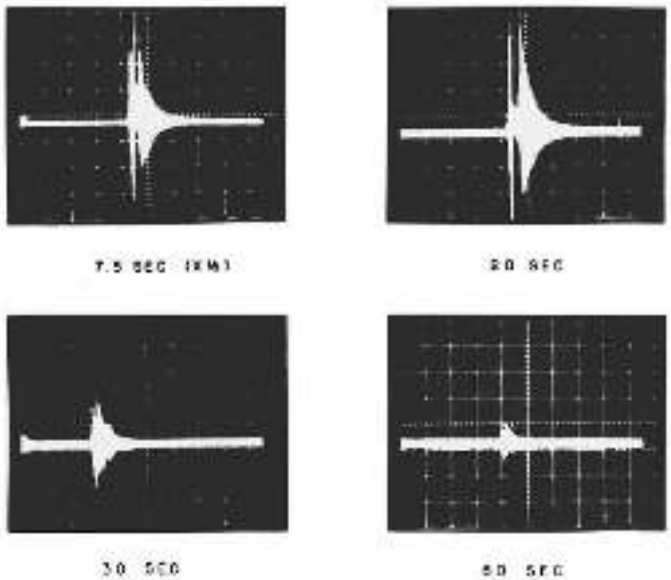

Figure 2. Ion trapping. The trapping of H_2O^+ ions under conditions of extremely long trapping is shown. The traces shown indicate a trapping time of about 30 sec for H_2O^+.

Wavelength tunability allows recording of an **action spectrum** of the CH_3Cl^+ ion.

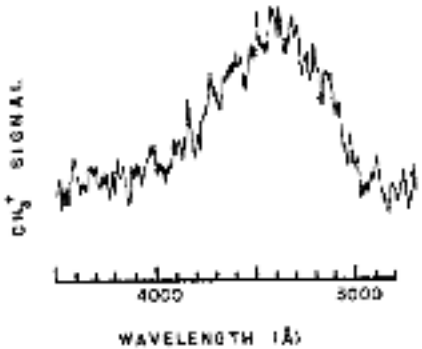

Figure 1. Production of CH_3^+ by photodissociation of CH_3Cl^+. The concentration of CH_3^+ in the icr cell is continuously monitored while the wavelength of the irradiating light from the monochromator is swept. The wavelength resolution (FWHM of the irradiating light) is 140 Å.

Ion beam and irradiation overlap

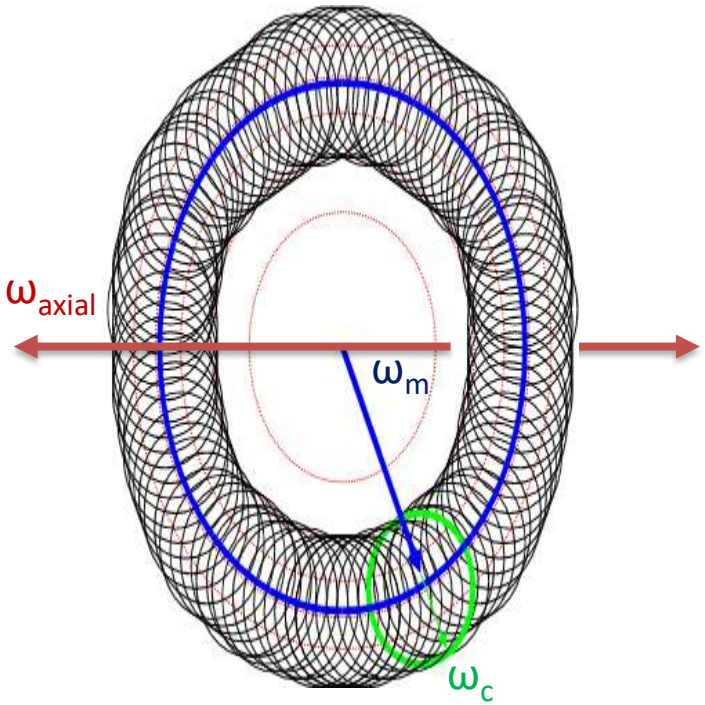

- Radiation needs to intersect the ion trajectory both in space and in time.
- Irradiation along the cell axis is the most usual setup.

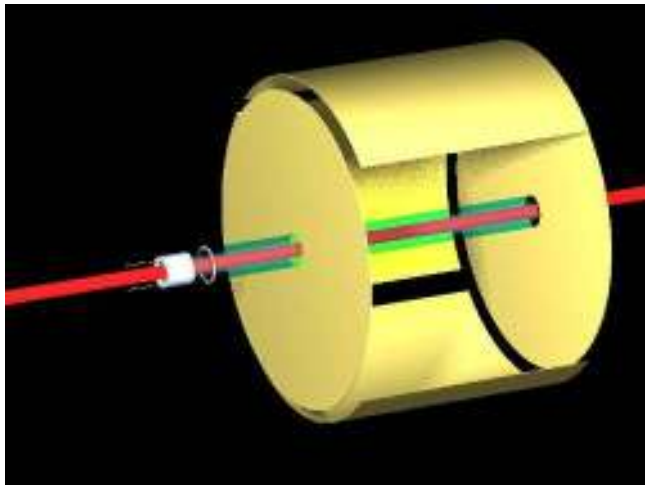

Ion beam and irradiation overlap

- On permanent magnet based instrument, irradiation can also be performed orthogonaly to the magnetic field.

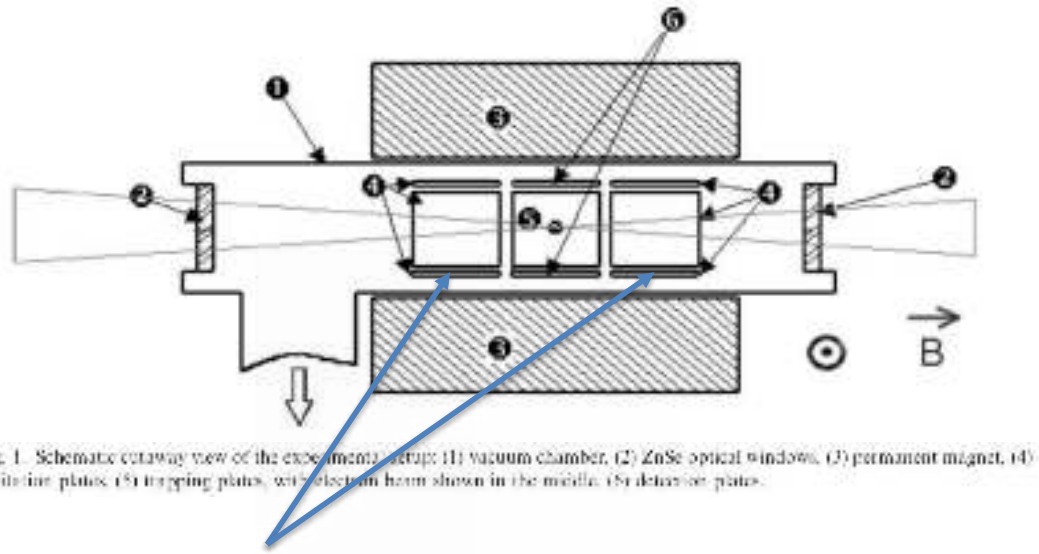

Open ended excitation electrodes

*P. Maître et al. Nucl. Instrum. and Meth. Phys. Res. A **507** 541 (2003)*

Ion beam and irradation overlap

- Issues with overlapping beams :
  - Highest power densities are achieved with tightly focused pulsed photon sources
  - FT-ICR is not optimal for this :
    - Axial motion is generally on the order of centimeters : requires very good on axis alignement of the light beam in order to cover the complete cloud.
    - Radial (magnetron / cyclotron) motions radius depends on the magnetic field, initial ion velocities but also alignment and centering of the cell axis and ion injection path. Order of magnitude: millimiter.
    - 3D ion traps perform much better (overall volume on the order of 1 mm^3)
  - Solutions :
    - Higher irradiation power with an unfocused beam (use of beam expanders in IRMPD for instance)
    - **(Pseudo) Continuous irradiation** : increase the irradiation time to average over ion positions (but beware that some ions might remain out of the beam).
    - **Pulsed irradiation :** timing and delay effects might dramatically change the results with a focused beam as the ion cloud sample will change over time.

Action spectrscopy vs absorption spectroscopy

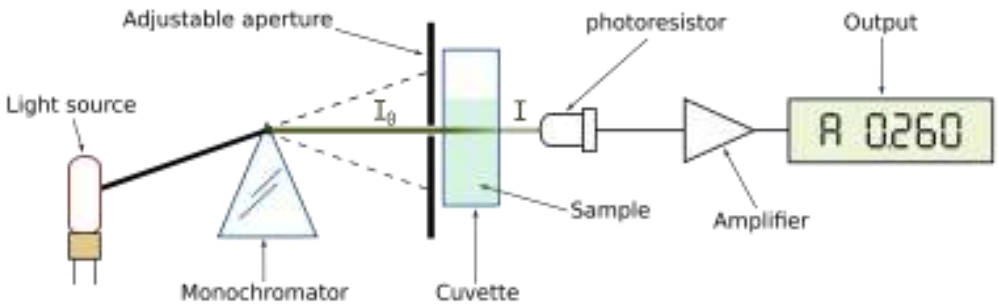

Standard spectrophotometer setup (source wikipedia)

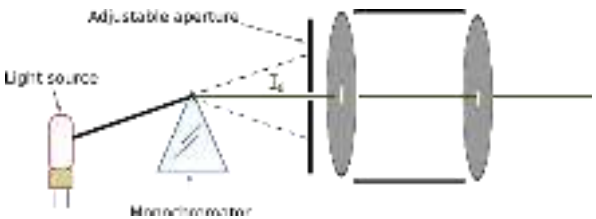

$$Eff = \frac{I_{frag}}{I_{prec} + I_{frag}}$$

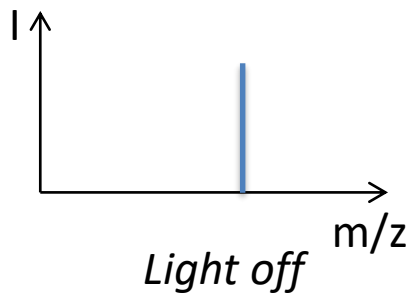

Light off

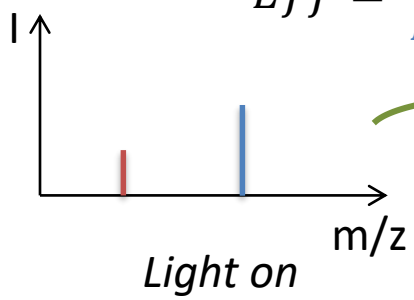

Light on

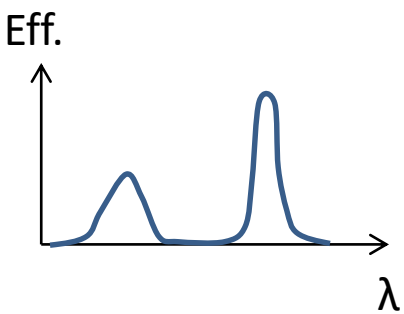

Pros and cons of FT-ICR vs ion traps for spectroscopy

- Cons :
  - Ion cloud overlap is more difficult to achieve compared to a 3D ion trap.
- Pros :
  - High resolution which can be achieved in the detection of product ions
  - Low pressure of the gas background : reduced thermalization effects.
    - Action spectroscopy assumes that absorption of a photon is related to fragmentation efficiency.

$$\text{Precursor} \underset{k_{-1}}{\overset{k_1(\lambda,I)}{\rightleftharpoons}} [\text{Precursor}]^* \xrightarrow{k_{uni}(E)} \text{Fragment}$$

k_{-1} is composed of a collisional and a radiative component. Minimization of the collisional component improves the result.
This is even more the case for multiple photon processes.

SINGLE PHOTON PROCESSES

Photon activation (UV – Visible)

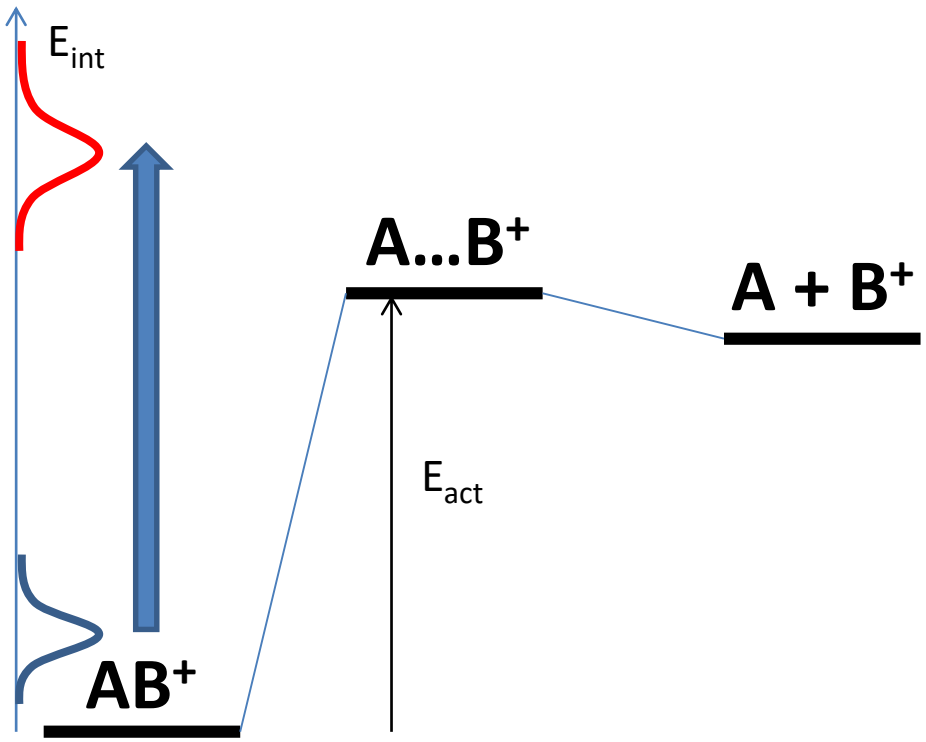

Single photon activation :

- Requires a photon with sufficient energy : ~ eV
- Requires an absorption band
- Proceeds through an electronic excited state, which can either directly dissociate or redistribute energy through intersystem crossing.

Tunable UV and FT-ICR

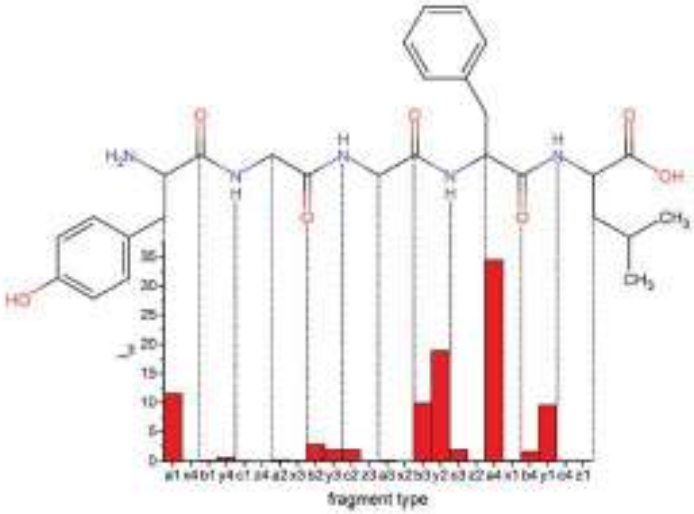

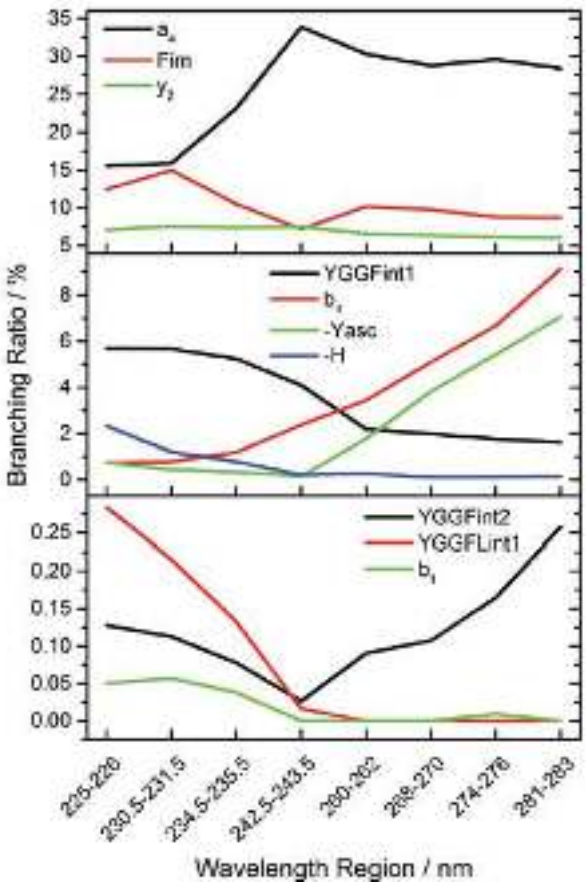

- Fragmentation favored close to the aromatic residues.
- Some dependence of the pathways on the laser wavelength.

A. Herburger, C. van der Linde, M. Beyer, Phys. Chem. Chem. Phys. **19** 10786 (2017)

Tunable UV-PD

- FT-ICR trap is quite ideal for alignment with a laser and long activation periods due to a low photon flux.

Validation on small systems: flavin co-factors of flavoproteins

OPO UV-Vis laser @ Ecole Polytechnique

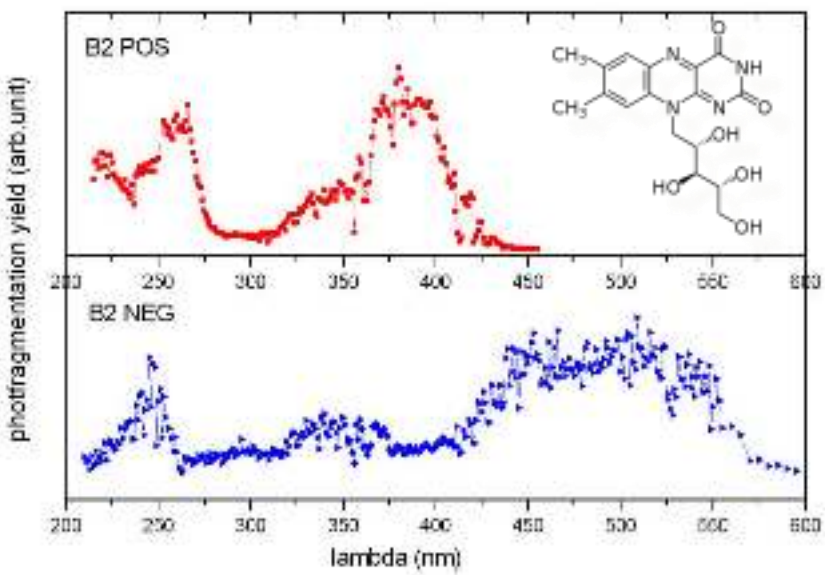

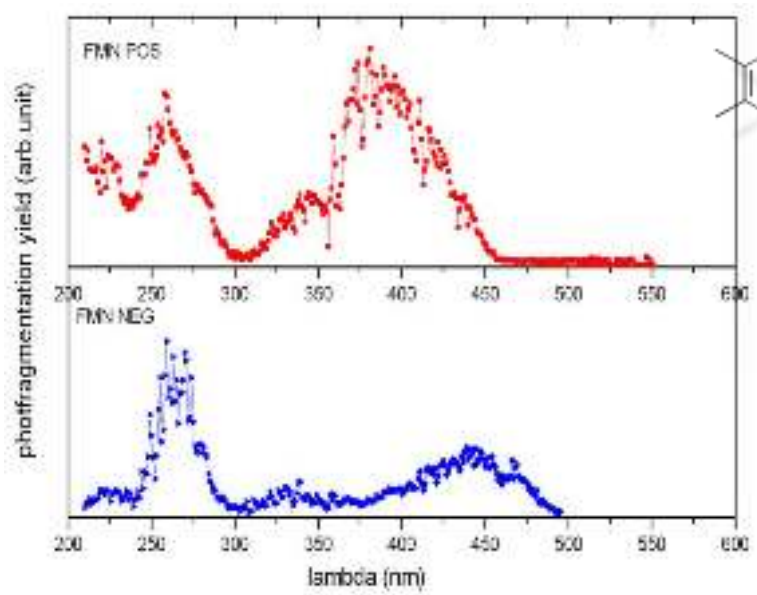

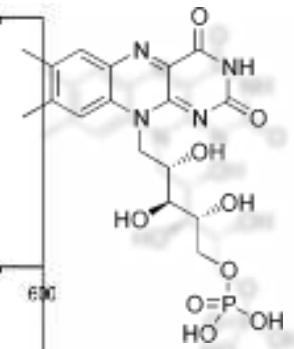

The optical response depends on the **chemical environment**

The optical response depends on the **charge environment**

UVPD at 213 nm

The Ups and Downs of Repeated Cleavage and Internal Fragment Production in Top-Down Proteomics

Yana A. Lyon,[1] Dylan Riggs,[1] Luca Fornelli,[2] Philip D. Compton,[2] Ryan R. Julian[1]

[1]Department of Chemistry, University of California, Riverside, 501 Big Springs Road, Riverside, CA 92521, USA
[2]Departments of Chemistry and Molecular Biosciences, and the Proteomics Center of Excellence, Northwestern University, N. Sheridan Road, Evanston, IL 60208, USA

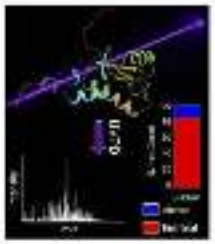

Abstract. Analysis of whole proteins by mass spectrometry, or top-down proteomics, has several advantages over methods relying on proteolysis. For example, proteoforms can be unambiguously identified and examined. However, from a gas-phase ion-chemistry perspective, proteins are enormous molecules that present novel challenges relative to peptide analysis. Herein, the statistics of cleaving the peptide backbone multiple times are examined to evaluate the inherent propensity for generating internal versus terminal ions. The raw statistics reveal an inherent bias favoring production of terminal ions, which holds true regardless of protein size. Importantly, even if the full suite of internal ions is generated by statistical dissociation, terminal ions are predicted to account for at least 50% of the total ion current, regardless of protein size, if there are three backbone dissociations or fewer. Top-down analysis should therefore be a viable approach for examining proteins of significant size. Comparison of the purely statistical analysis with actual top-down data derived from ultraviolet photodissociation (UVPD) and higher-energy collisional dissociation (HCD) reveals that terminal ions account for much of the total ion current in both experiments. Terminal ion production is more favored in UVPD relative to HCD, which is likely due to differences in the mechanisms controlling fragmentation. Importantly, internal ions are not found to dominate from either the theoretical or experimental point of view.

Keywords: UVPD, HCD, Statistical analysis, Internal ion

- Nd-YAG 5th harmonic
- Commercial device by Thermo
- Applied for top-down proteomics on Orbitrap systems

Femto-second laser induced dissociation

Technique introduced by G.E. Reid in 2009 for peptide fragmentation analysis, using an activation in a rf ion trap device.

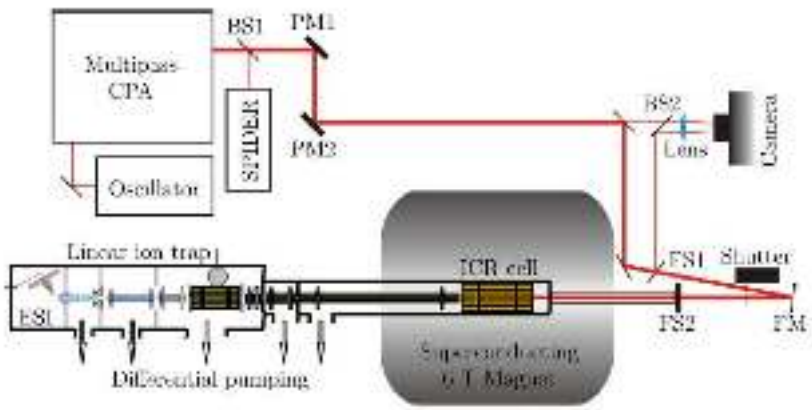

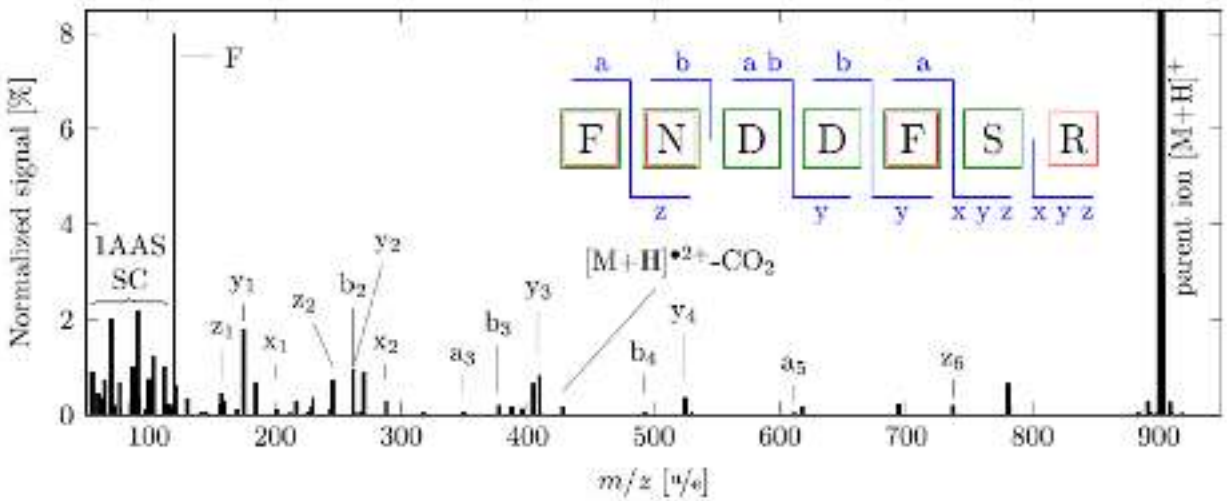

C. Neidel et al. Chem. Phys. (2018)

MULTIPLE PHOTON PROCESSES

Infra-red Multiphoton dissociation

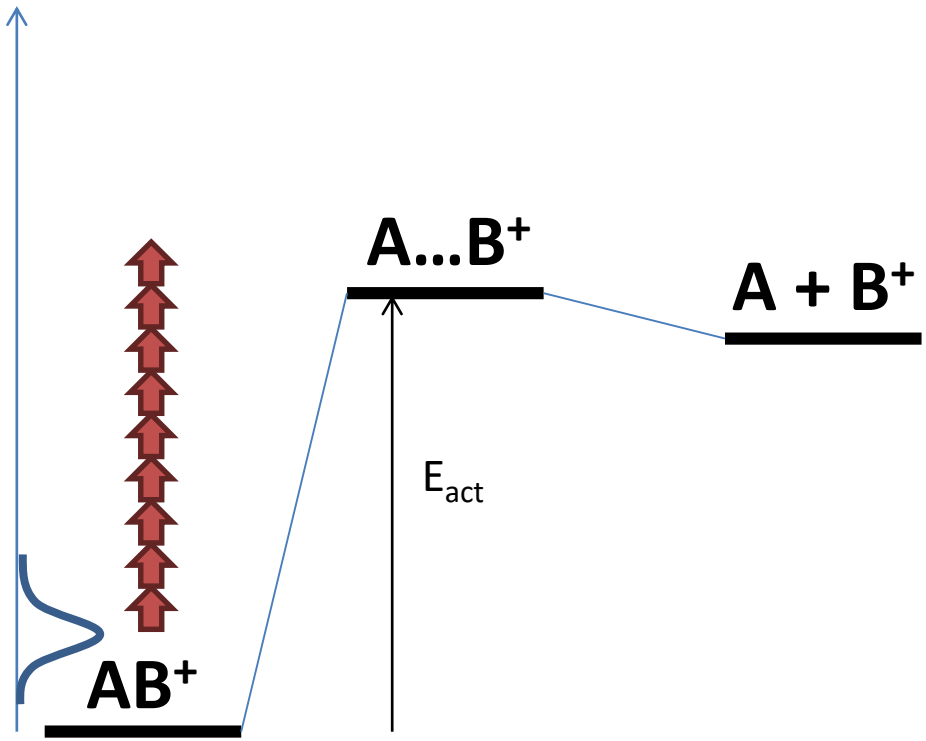

Multiple photon activation:

- IR photon ~ 0,1 eV
- Absorption of a number of photons is required to lead to fragmentation ***I**nfra-**R**ed **M**ulti-**P**hoton **D**issociation (IRMPD)*
- As for UVPD, an absorption band is required to observe fragmentation.

Wavelength ranges in IR spectroscopy

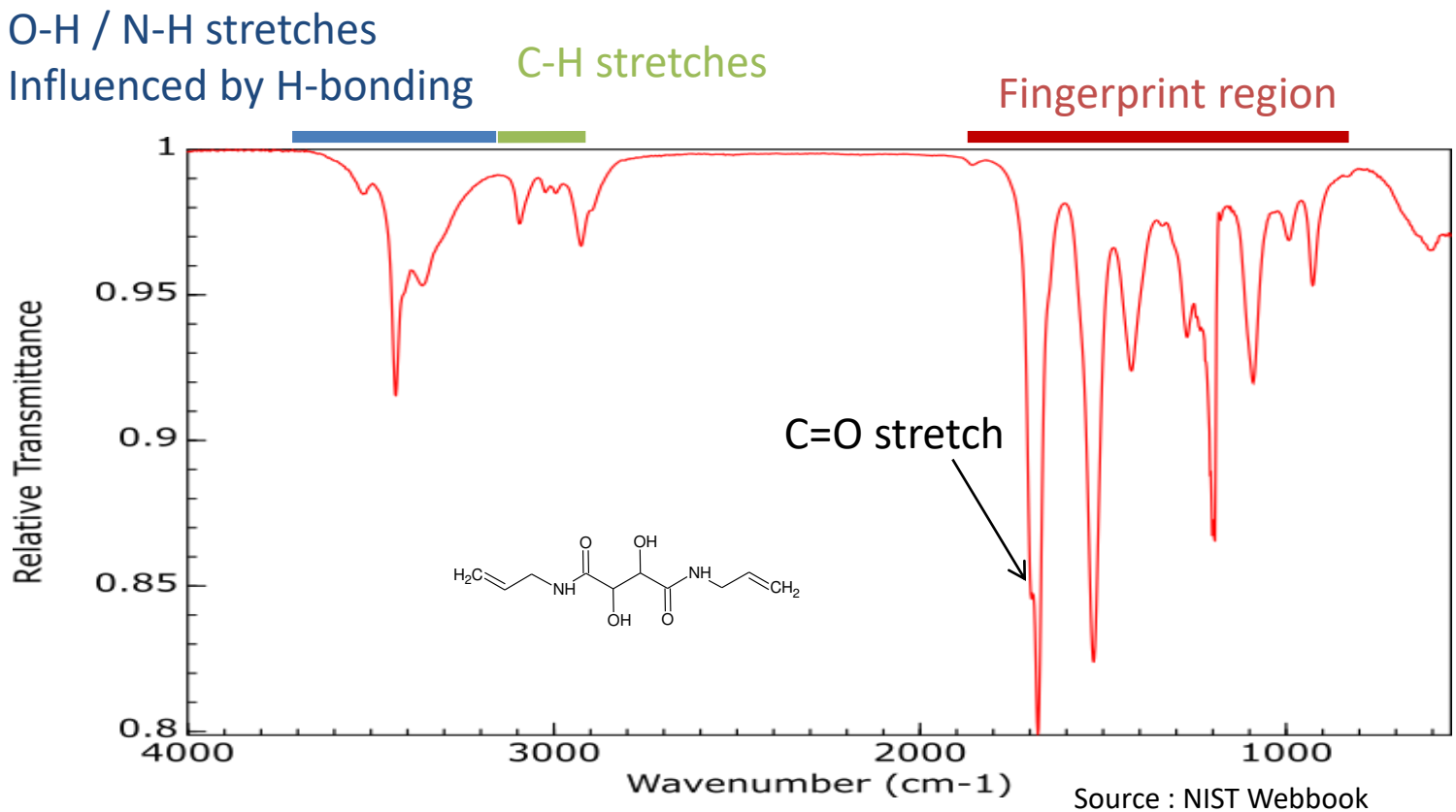

Source : NIST Webbook

Photon sources for IRMPD

- Tunable lasers – Free Electron lasers

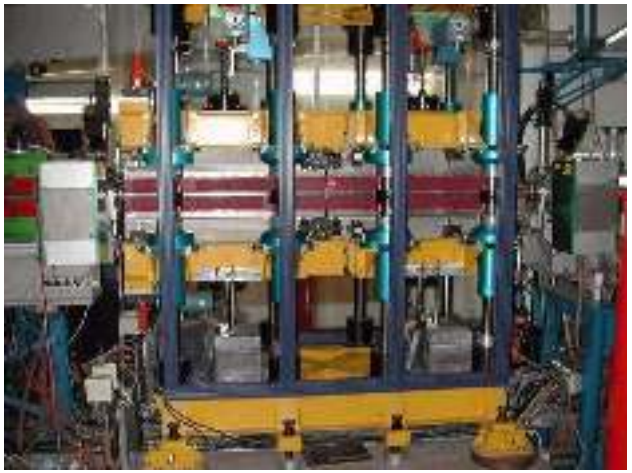

Based on an electron accelerator (16-48 MeV)
IR beam is generated within the undulator placed in the optical cavity.

Tuning of the wavelength by adjusting the gap between two sets of magnets in the undulator.

At 40 MeV : access to the 800-2000 cm-1 band (Fingerprint region) with ~1 W of power.

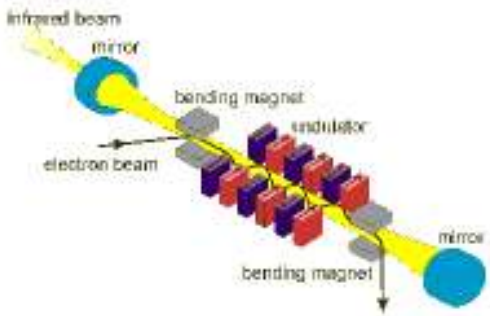

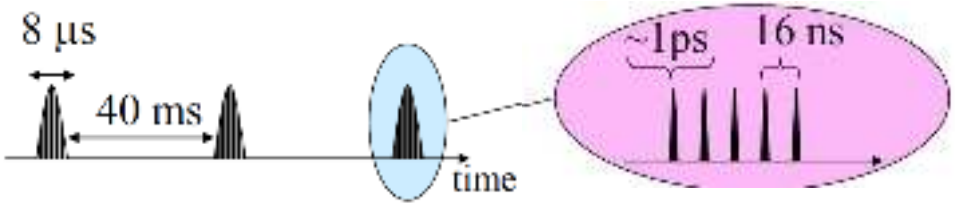

Photon sources for IRMPD

- Tunable lasers : table-top OPO-OPA lasers

  Based on the non-linear optical properties of crystal materials (such as KTP potassium titanyl phosphate)

  Repetition rate: 10 – 25 Hz, Power: ~10 mJ.

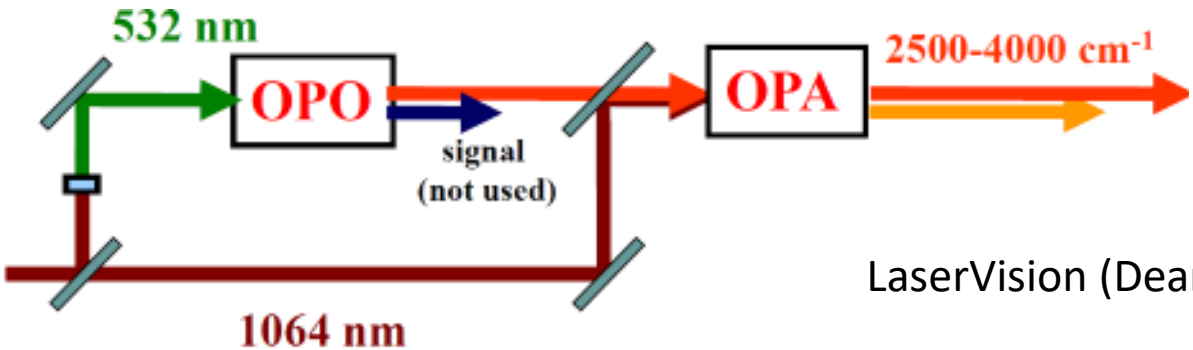

LaserVision (Dean Guyer)

Optical Parametric Oscillator Generates signal

Optical Parametric Amplifier Boosts signal (single pass)

Photon sources for IRMPD

- CO_2 laser

- Electric discharge in a N_2 / CO_2 / He gas mixture
- High power conversion efficiency (up to 20%)
- High power (50 W or more can be purchased readily)
- Fixed wavelength (some are tunable) between 10.6 µm and 9.4 µm.

Principles of IRMPD

IVR : statistical redistribution of energy in several vibration modes of the molecule

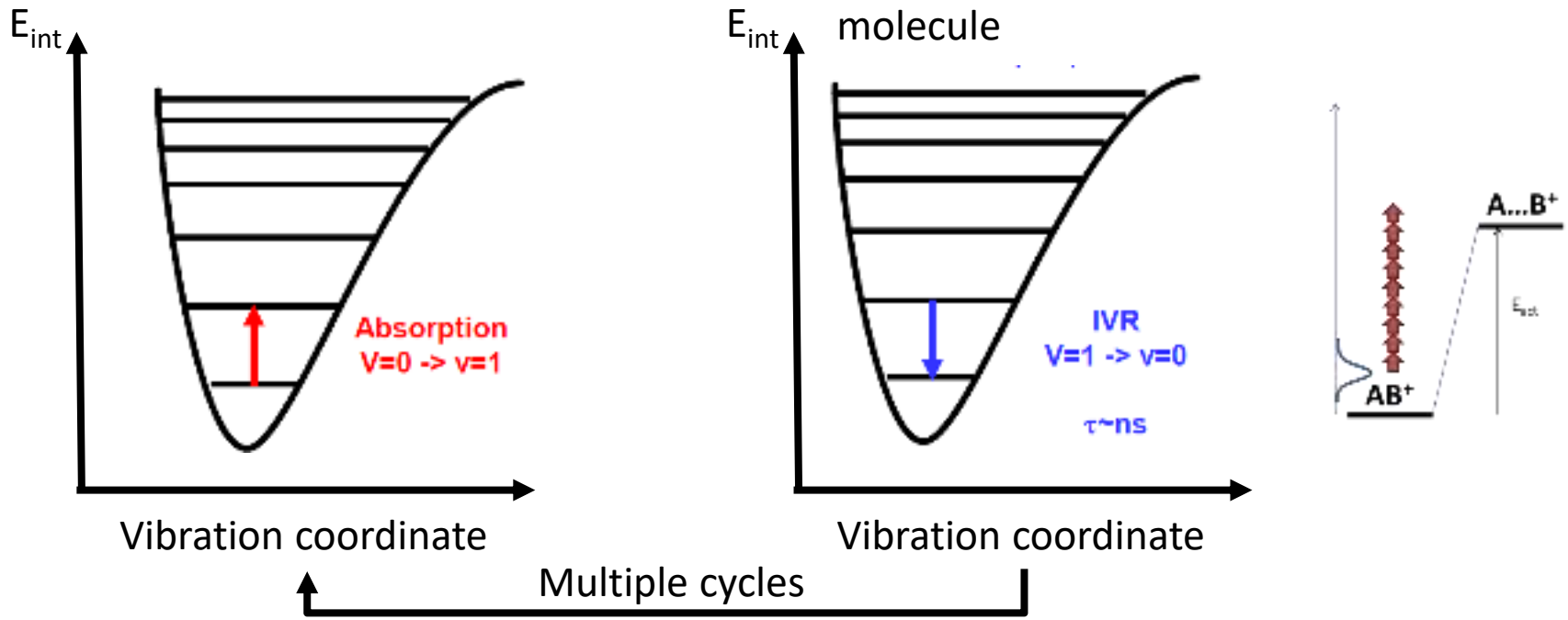

Referring to IRMPD : « This method employs an intense infrared laser to resonantly pump vibrational energy into the molecule in a **noncoherent** fashion, until it has sufficient energy to dissociate. »

R. C. Dunbar, D. T. Moore, J. Oomens, *J. Phys. Chem. A* **110**, 8316-8326 (2006)

Advantages of FT-ICR for IRMPD spectroscopy

- Multiphoton process can be inhibited by collisional relaxation.
  - In ion traps, relaxation occurs within 10 ms (P.M. Remes, G.L. Glish J. Am. Soc. Mass Spectrom. **20**, 1801 (2009)) which is shorter than the time between two OPO laser pulses or two FEL macropulses.
  - FT-ICR vacuum is thus better suited for IRMPD when a single pulse is not sufficient to accumulate sufficient amount of energy in an ion trap.
    - Many benefits for :
      - Large molecular systems (increased kinetic shift)
      - Strongly bound systems
      - Low intensity bands (but requires multiple passes and spectrum stiching).
    - Ion trap present the option of ion tagging as a subtitute for this limitation. But ion tagging can induce molecular structure shifts.

IRMPD spectroscopy in practice

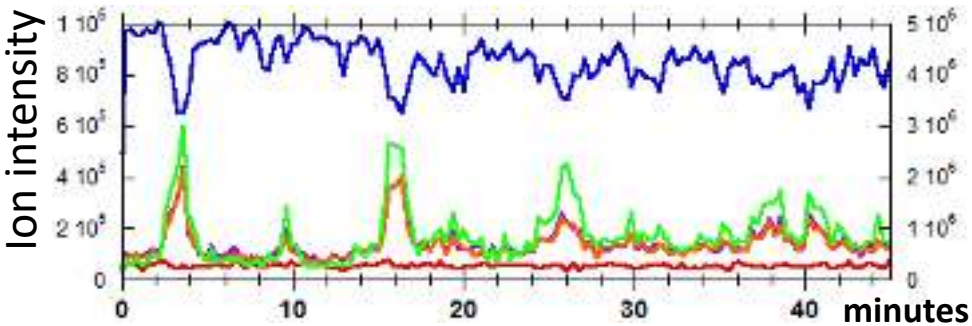

Spectrum recorded as an MS/MS chromatogram where each data point corresponds to one wavelength. Synchronisation through instrument / laser TTL exchanges.

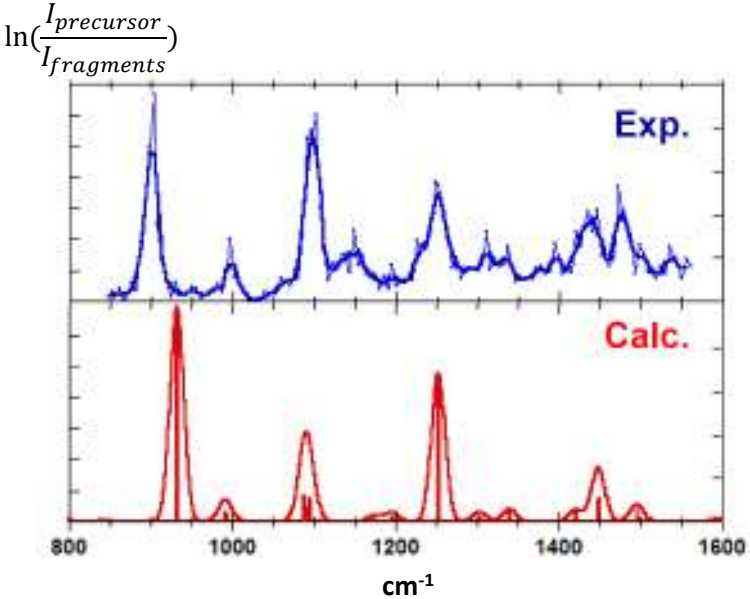

Comparison with calculated spectra

- Geometry optimization, mostly carried out with a standard basis set (6-31+G**)
  - Search for conformers with the lowest energy.
  - Harmonic bands are calculated from a frequency calculation and convoluted with a Gaussian profile (FWHM 10 or 20 cm^{-1})
- Scaling factors :
  - Multiple scaling factors have been proposed in the litterature depending on the method and basis set.
  - Issue is that most of the time the scaling factors differ between the fingerprint and harmonic regions (0.98 for fingerprint, 0.955 for X-H stretching region.

Scaling factors for IRMPD

- In 2017, we introduced the use of a linear scaling factor based on a series of 68 experimental values in the fingerprint region for which frequency assignment was structurally and spectrally unambiguous.
- The publication also introduces a measurement for similarity (similar to a Fisher test) which relies on the observed correlation for individual spectra.

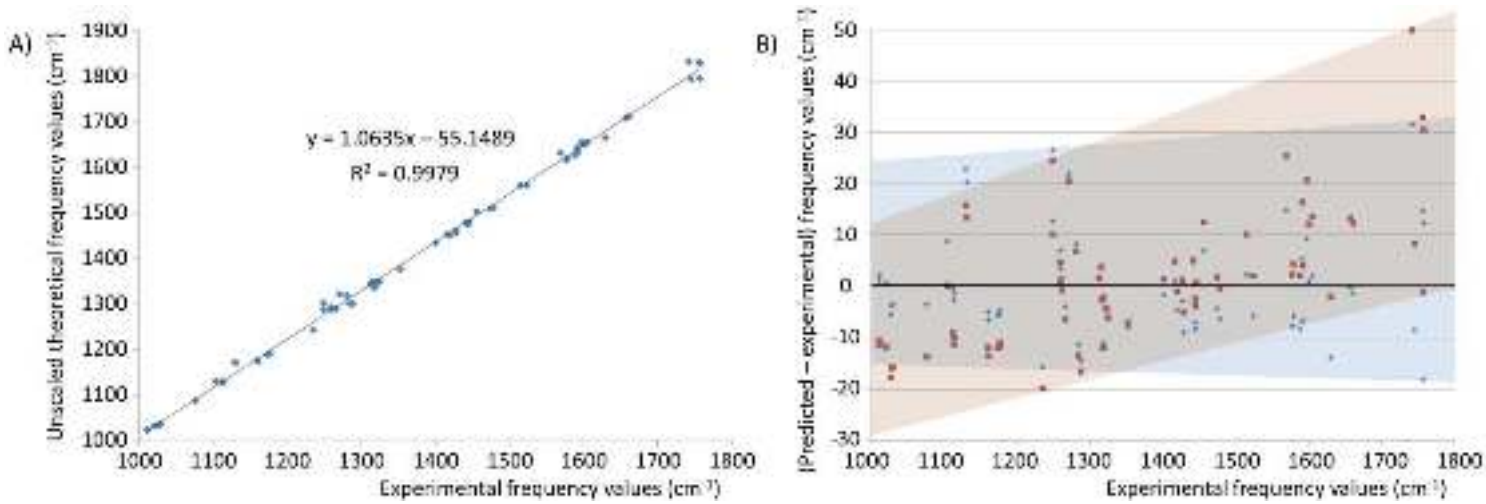

K. Madanakhrishna et al. Chem. Eur. J. **23**, 8414 (2017)

Improving OPO dissociation using CO_2 laser

- Low power of OPO laser can lead to situation in which radiative cooling exceeds resonant photoexcitation.
- CO_2 laser is synchronized with the OPO and irradiation time needs to be optimized for each system to set irradiation time just below the dissociation threshold.

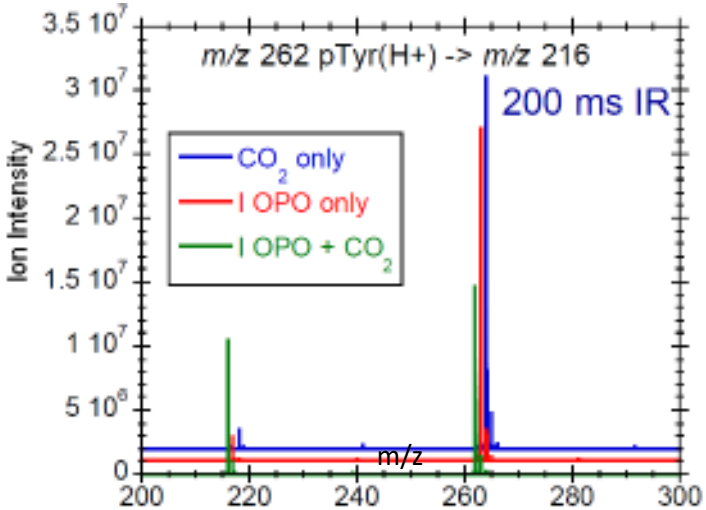

Phosphotyrosine+H⁺ : [pTyr+H]⁺

OPO, on resonance with an O-H band

OPO+CO_2: significant amplification

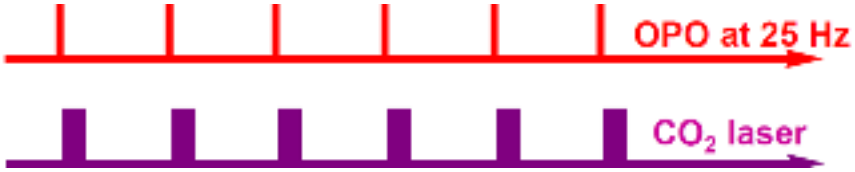

IRMPD at fixed wavelength

- Usually low intensity absorption bands in the fingerprint region at 943 cm^{-1}.
- High laser power (high photon density) compensates for the low intensity of the bands.

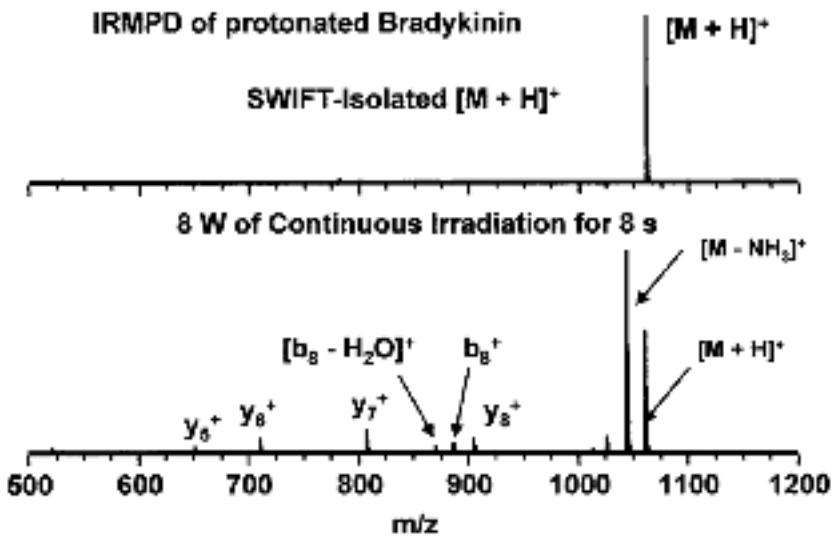

Figure 1. Infrared multiphoton dissociation (IRMPD) of protonated bradykinin, $[M+H]^+$. Protonated bradykinin was SWIFT-isolated (top) and irradiated with the IR laser for 8 s at 8 W (bottom).

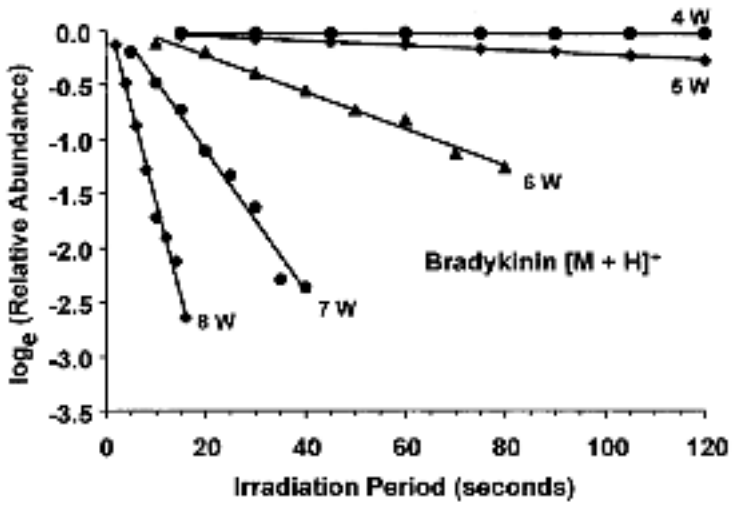

Figure 2. Plot of the natural logarithm of the relative abundance of protonated bradykinin, $[M+H]^+$, vs. time for unimolecular dissociation at each of five indicated laser powers. Note the highly linear behavior, showing that ions remain within the cross-section of the laser beam throughout the experiment.

M.A. Freitas et al. Rapid Comm. Mass Spectrom. **13**, 1639 (1999)

Resonant IRMPD with CO_2 laser

- Brodbelt and coworkers introduced the use of resonant IRMPD for phosphorylated peptides.

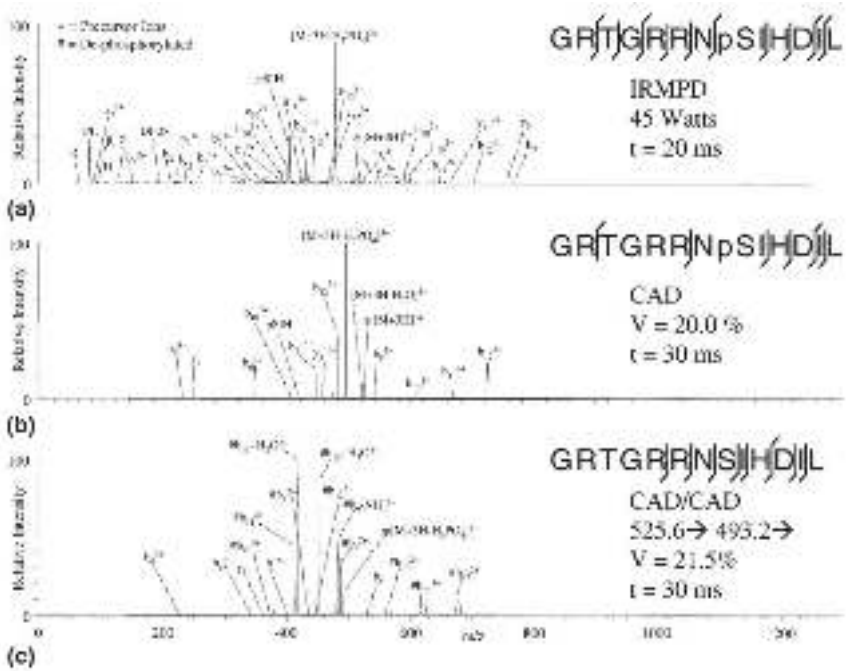

Figure 5. (a) IRMPD, (b) CAD MS², and (c) CAD MS³ mass spectra of triply protonated GRTGRRNpSIHDIL.

M.C. Crowe and J.S. Brodbelt, *J. Am. Soc. Mass Spectrom.* **15**, 1581 (2004)

Resonant IRMPD with CO_2 laser

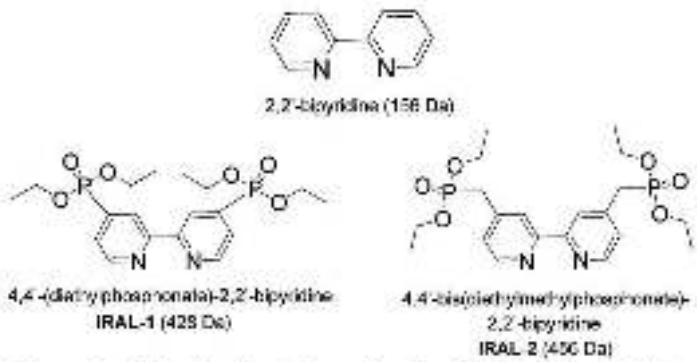

Figure 1. IR-active ligands based on the 2,2'-bipyridine skeleton synthesized and used in the study. Molecular weight is shown in parentheses.

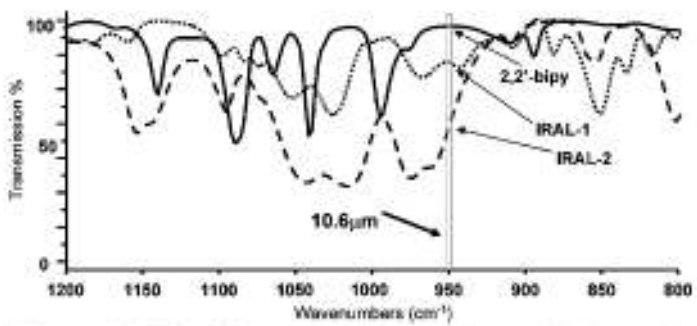

Figure 6. FTIR ATR spectra of the ligands used in the study, showing the enhanced absorption of the IR-active ligands, IRAL-1 and IRAL-2, at 10.6 μm as compared to 2,2'-bipyridine.

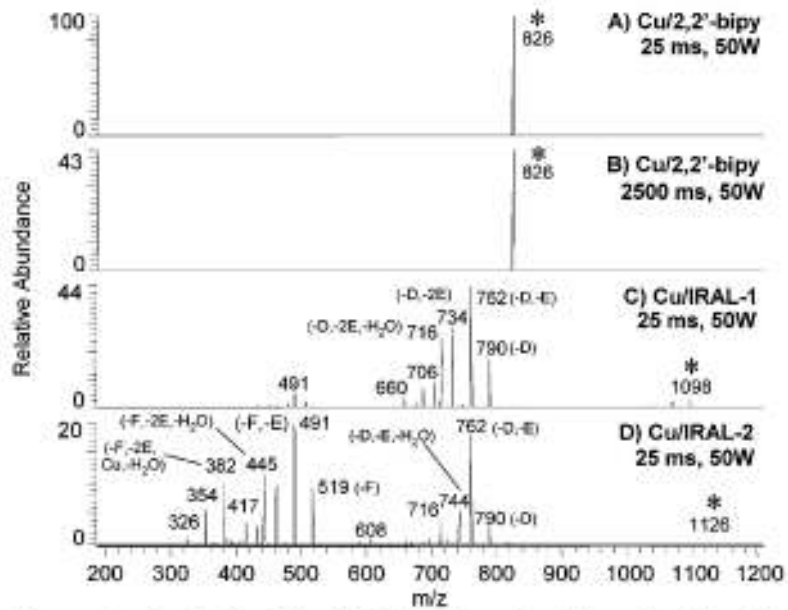

Figure 4. Irradiation of the $[Cu^{2+}(\text{neodiosmin} - H)\text{auxiliary ligand}]^+$ complexes containing different ligands: (A) $[Cu^{2+}(\text{neodiosmin} - H)2,2\text{-bipy}]^+$, 50 W for 25 ms; (B) $[Cu^{2+}(\text{neodiosmin} - H)2,2\text{-bipy}]^+$, 50 W for 2500 ms; (C) $[Cu^{2+}(\text{neodiosmin} - H)\text{IRAL-1}]^+$, 50 W for 25 ms; (D) $[Cu^{2+}(\text{neodiosmin} - H)\text{IRAL-2}]^+$, 50 W for 25 ms.

M. Pikulski et al. *Anal. Chem.* **78**, 8512 (2006)

Resonant excitation with tunable IR laser

- Peptide fragmentation has been abundantly studied using IRMPD spectroscopy.

b and a type ions have electrophilic and nucleophilic groups : cyclisation during the fragmentation process is an option.

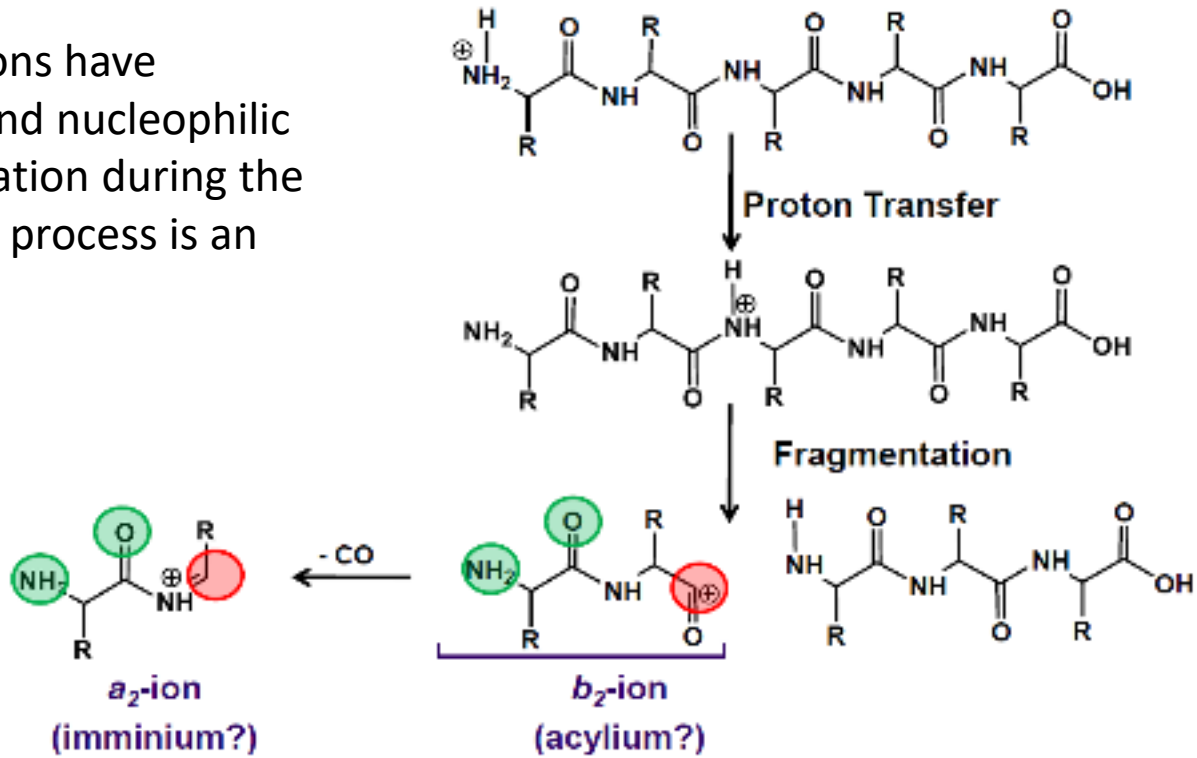

Peptide structures solved through tunable IRMPD

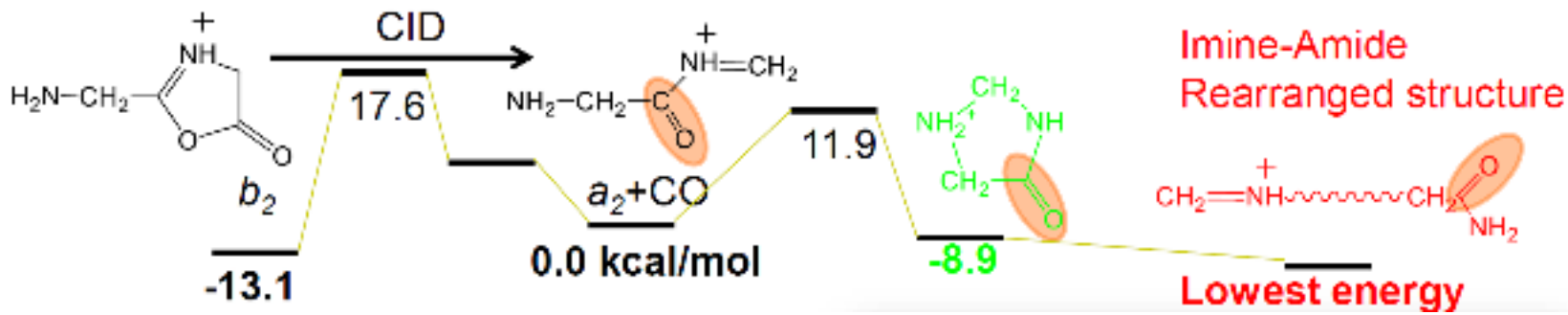

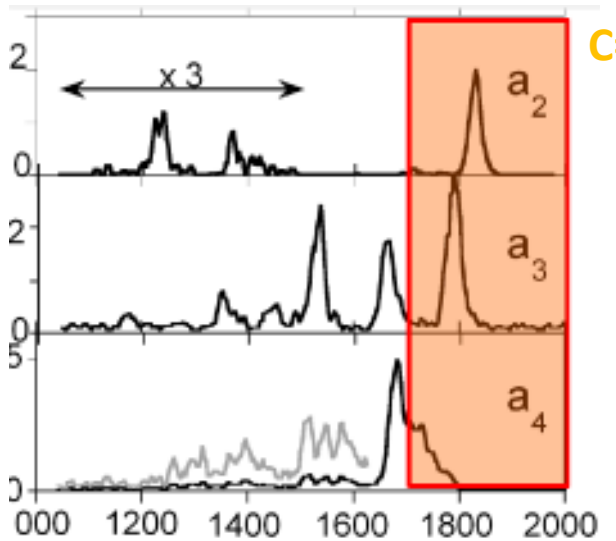

C=O stretch region

Oligoglycine a_2, a_3 and a_4 ions display strongly different C=O stretches.
Rearrangement of the an ions is kinetically controlled.

B. Bythell et al. J. Am. Chem. Soc **132**, 14766 (2010)

Peptide structures solved through IRMPD spectroscopy

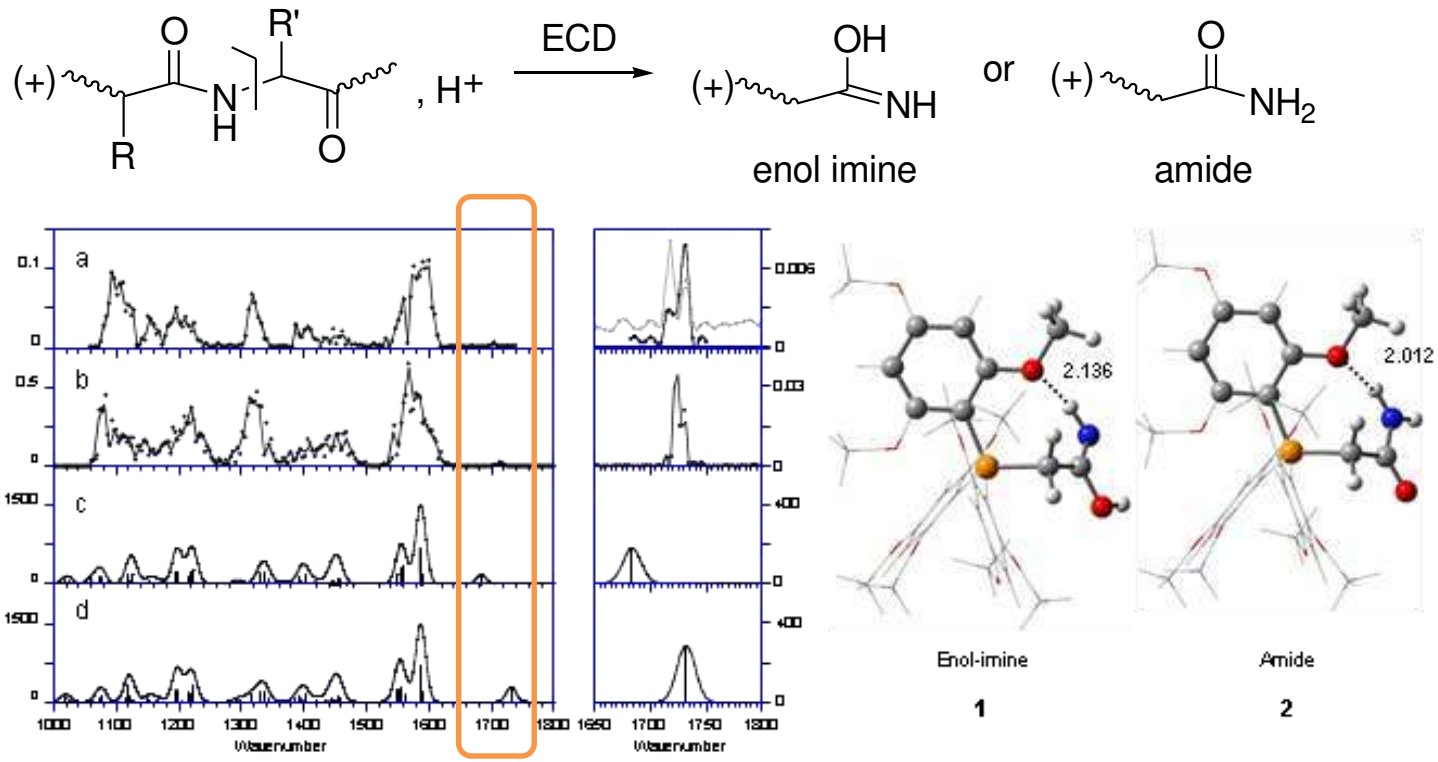

G. Frison et al. *J. Am. Chem. Soc.* ***130,*** 14916 (2008)

BIRD

- Radiative equilibrium between ions and cell walls.

Presure ~10^{-6}-10^{-8} mbar
t ~ 10s of seconds

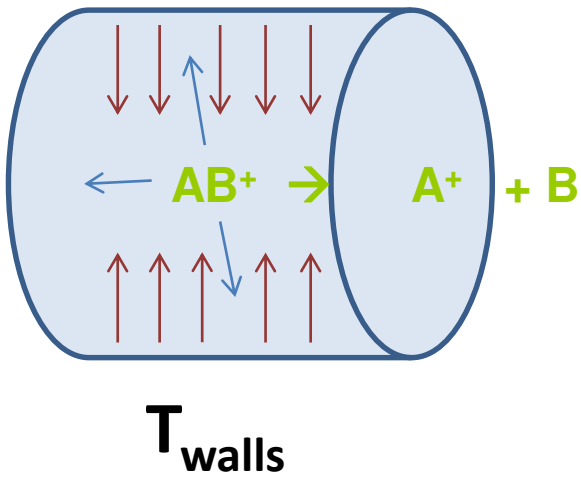

Measurement of fragmentation kinetics at variable temperatures:

$$k(T) = A\, e^{-\frac{E_a}{RT}}$$

Access to kinetic parameters (A and E_a)

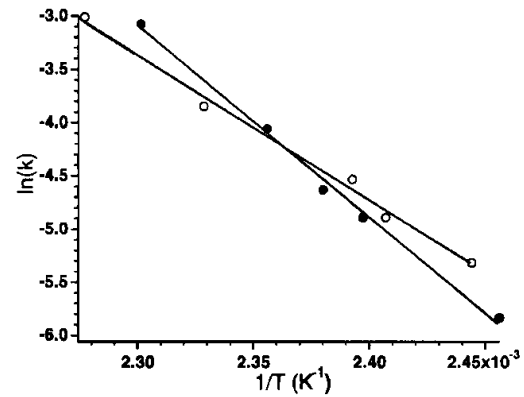

Figure 2. Arrhenius plot for dissociation of ubiquitin 5+ (○) (E_a = 1.2 eV; $A = 10^{12}$ s^{-1}) and 11+ (●) (E_a = 1.6 eV; $A = 10^{17}$ s^{-1}).

Application to a protein – ligand system

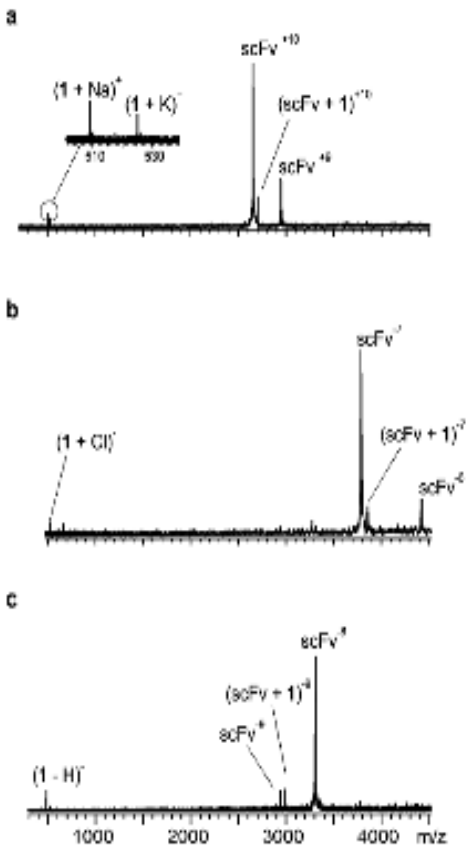

Figure 4. BIRD mass spectra obtained for protonated and deprotonated (scFv +1)$^{n\pm}$ ions (a) $n = +10$, 151 °C, 6 s; (b) $n = -8$, 147 °C, 5 s; (c) $n = -9$, 147 °C, 5 s.

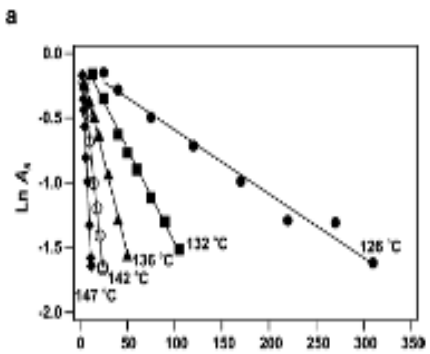

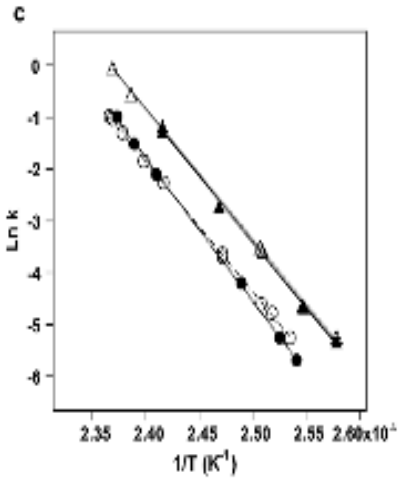

Figure 6. Arrhenius plots obtained for the loss of neutral L from the (P + L)$^{n\pm}$ ions: (a) L = 1, P = scFv, +6 (◆), +7 (◇), +8 (△), +9 (▲), +10 (●), +11 (■), +12 (○), +13 (×), (b) L = 1, P = scFv, −6 (□), −7 (▼), −8 (▽); (c) $n = +10$, L = 1, P = scFv (●), L = 1, P = His$^{H(0)}$Ala (○), L = 4, P = scFv (▲), L = 4, P = His$^{H(0)}$Ala (△).

E.N. Kitova et al, J. Am. Chem. Soc ***130****, 1214 (2008)*

EU FT-ICR MS

AUS2- Prague, 26-30 September 2021

Exploring the intrinsic properties of bioinorganic complexes by Ion-Molecule Reactions

SAPIENZA
UNIVERSITÀ DI ROMA

Maria Elisa Crestoni

Dipartimento di Chimica e Tecnologie del Farmaco,
Sapienza Università di Roma, P.le A. Moro 5, I-00185, Roma (Italy)

Ion-Molecule Reactions

- First observation (Thomson, 1913)
- Chemical Ionization Source (Munson and Field, 1966)
- Multiple-stage Mass Spectrometers (ion isolation + reactions with specific gaseous reagent under low-energy, controlled conditions)
- High degree of experimental flexibility

The Gas Phase, in the absence of solvent and counterions, allows to elucidate the **intrinsic behavior in ionic reactions** and expose the role of the environment.

M.S.B. Munson, F. H. Field, J. Am. Chem. Soc. 1966;
J. I. Brauman, Science 1998

IMPACT of IMR

fundamentals

Thermodynamic properties
Reaction mechanisms

applications

Identification of functional group
Fine structural elucidation
Biochemistry, astrochemistry,…

J. S. Brodbelt, Mass Spectrom. Rev. 1997; M. Eberlin, J.Mass Spectrom. 2006;
S. Gronert, Chem. Rev. 2001; V. Ryzhov, Anal. Chem. 2013;
H. I. Kenttamaa, Mass Spectrom. Rev. 2021

IMR by FT-ICR

Pros

- sensitivity
- specificity
- speed
- efficiency
- numerous reaction-based strategies
- no extensive purification/sample preparation
- (indirect) structural information

Cons

- inferred information on neutral products
- volatile neutrals (b.p. < 200 °C)

Gas phase ion molecule reactions

- **General aspects** (reaction efficiency; double-well potential energy surface)
- **Instrumentation**
- **IMR** (functional group-selective reactions; structurally diagnostic reactions)
- **Applications of IMR**

General aspects

Collision rate
the greatest possible reaction rate

number of charges in the ion

dipole moment and polarizability of the neutral

$$A^+ + B \underset{k_{-1}}{\overset{k_1}{\rightleftharpoons}} [AB]^+ \xrightarrow{k_2} C^+ + D$$

collision complex

Capture/collision rate : k_{coll} ~ 1×10^{-9} cm^3 molecule^{-1} s^{-1}

One or two order of magnitude larger than molecule-molecule reactions

E. Uggerud, *Fundamentals and Applications of Gas Phase Ion Chemistry* 1999

How to calculate the k_{coll}

Calculations of collision rate constant

- Ion/induced dipole potential: **Langevin** theory
- Average dipole orientation (**ADO**) : Su & Bowers
- Angular momentum conserved ADO (**AADO**) : Su & Chesnavich

$$k_L = 2\pi e \left(\frac{\alpha}{\mu}\right)^{1/2}$$

capture rate coefficient

Langevin theory

α= polarizability

μ= the reduced mass of the pair

Interaction: ion-induced dipole

P. Langevin, *Ann. Chim. Phys. Ser.* 1905;
G. Giomousis, D. P. Stevenson, *J. Chem. Phys.* 1958

ADO theory

ADO: averaged dipole orientation

$$k_{ADO} = \frac{2\pi q}{\sqrt{\mu}} \left\{ \sqrt{\alpha} + C\mu_D \left(\frac{2}{\pi k_B T} \right)^{1/2} \right\}$$

the first term is the Langevin contribution

Interaction: ion- dipole

μ is the reduced mass; μ_D is the permanent dipole;
C is a correction factor depending on $\mu_D / \alpha^{1/2}$;
k_B is Boltzmann's constant
The dipole orientation is not considered

k_{ADO} predicts accurate Proton Transfer rate constants

T. Su, . T. Bowers, *J. Chem. Phys.* 1973; *Int. J. Mass Spectrom. Ion Phys.* 1973

k_{AADO} Theory

AADO: angular momentum conserved ADO

parametrized trajectory theory

- there is a net angular momentum transfer between the rotating molecule and the ion-molecule orbital motion.
- the AADO theory yields capture rate constants larger than ADO theory
- the AADO equation represents the best means to obtain an estimated capture rate for comparison with experimental reaction rate constants (± 10%) .

$$k_{AADO} = k_L\, G(x)$$

$$G(x) = \frac{(x+0.509)^2}{10.526} + 0.9754 \qquad x < 2$$

$$G(x) = (x+0.509)^2 + 0.9754 \qquad x \geq 2$$

empirical parametrization

$$x = \frac{\mu_D}{(8\pi\varepsilon_0\alpha k_B T)^{1/2}}$$

This equation makes it possible to approximate k_{coll} within ± 10%.

T. Su, . W. J. Chesnavich, *J. Chem. Phys.* 1982

Reaction Rates

$$R^+ + N \longrightarrow P^+ + \text{neutral products}$$

$$-\frac{dR(t)}{dt} = k\, n\, R(t)$$ **bimolecular reaction**

n = number density of neutral N

In a conventional bimolecular process the number density of neutral reactant would decrease with time. Here, it does not.

$$I_{(t)} = I_0\, e^{-nkt}$$ pseudo-first order reaction

$$\ln \frac{I_{(t)}}{I_0} = -\, n\, k\, t$$ $k = k_{exp}$

The total signal intensity is used to normalize the data and avoid errors from slight variations in the number of ions.

The signal intensity of $I_{(t)}$ can be monitored as a function of time and the rate constants for the disappearance of reactant ions and the appearance of product ions are obtained.

- The semilog plot of the decrease of the parent ion abundance with time is linearly interpolated and the **pseudo-first order rate constant** is obtained.
- The bimolecular rate constant (k_{exp}) at 300 K is gained from the ratio between the negative slope and ***n***, the number density of the neutral.
- ***n*** is calculated from the ideal gas equation and allows to convert the measured value of the neutral pressure (mbar) in molecule cm^{-3} at 300 K.

- $$k_{exp} = \frac{-\,\text{slope}\ (s^{-1})}{n\ (\text{molecule cm}^{-3})} = \ldots.\ cm^3\ \text{molecule}^{-1}\ s^{-1}$$

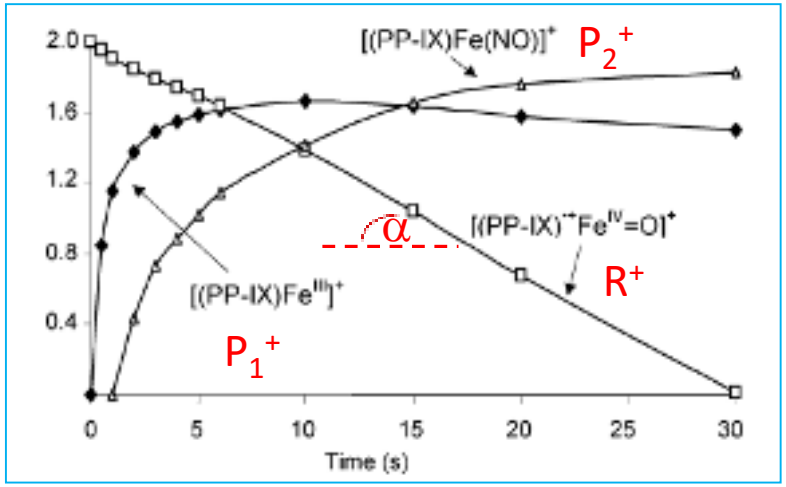

Figure 2. Plot of the logarithm of the relative ion abundances (%) versus time for the reaction of $(PP\text{-}IX)^{\bullet+}Fe^{IV}{=}O$ with NO at 3.0×10^{-8} mbar.

$$R^+ + NO \xrightarrow{OAT} P_1^+ + NO_2$$

$$P_1^+ + NO \xrightarrow{Add} P_2^+$$

Two consecutive reactions

Typically, the reproducibility of k_{exp} values is within 10%;

while the error in the absolute rate constants is estimated to be ± 30%.

It is mainly due to uncertainty in pressure measurements.

calibration of cold cathode gauge

$$CH_4^{+\cdot} + CH_4 \longrightarrow CH_5^+ + CH_3$$

$k_{CH4} = 1{,}1 \times 10^{-9}\ cm^3\ molecule\ s^{-1}$

time	I% m/z 16	I% m/z 17	ln 16
0	100.00	0.00	4.605
0.01	84.00	15.00	4.431
0.02	79.00	22.00	4.369
0.03	71.00	29.00	4.263
0.04	66.00	34.00	4.190
0.05	62.00	38.00	4.127
0.06	57.00	43.00	4.043
0.08	50.00	50.00	3.912
0.1	42.00	58.00	3.738
0.12	37.00	63.00	3.611
0.14	30.00	70.00	3.401
0.16	25.00	75.00	3.219
0.18	20.00	80.00	2.996
0.2	16.00	84.00	2.773
0.25	9.00	91.00	2.197
0.3	6.00	94.00	1.792
0.4	0.00	100.00	

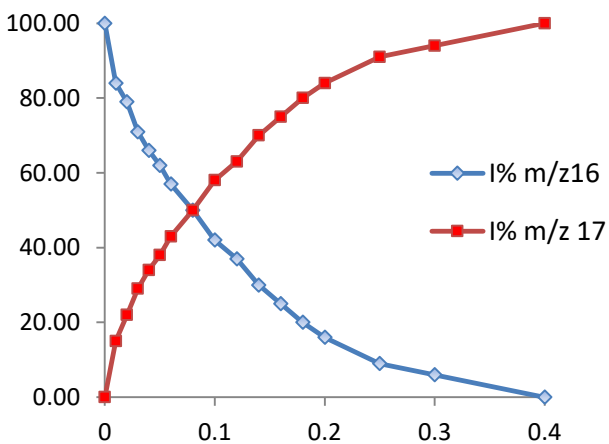

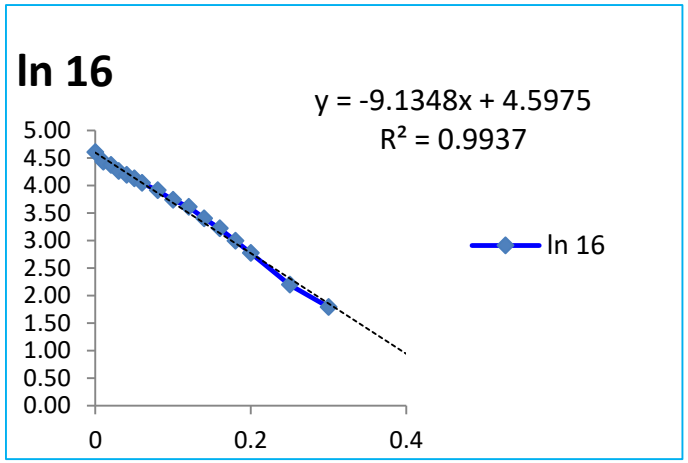

-slope

$$k_{exp} = \frac{9{,}13}{\underbrace{2{,}4 \times 10^{16} \times 1{,}1\times10^{-7}}_{\text{number density at } 1.1\times10^{-7} \text{ mbar}}}\ cm^3\ molecule^{-1}\ s^{-1}$$

$K_{exp} / k_{CH4} = f$ (calibration factor)

The efficiency (Φ) of an ion molecule reaction can be determined by comparing the experimental rate constant (k_{exp}) with a theoretical estimate of the capture rate constant as percentages of the collision rate constant (k_{coll}).

$$\Phi = \frac{k_{exp}}{k_{coll}}$$

measure of reaction probability per collision
(number of events that bring to reaction)

Many exothermic reactions exhibit unit reaction probability at room T;

others proceed with reaction efficiency much less than unity.

Brauman double-well model

Many exothermic IMR have unit efficiency (fast reactions), others present very low efficiency (slow reactions)

Capture is a necessary but not sufficient condition for reaction…

slow means that most of the collisions simply return back to reactants

$$A^+ + B \underset{k_{-1}}{\overset{k_1}{\rightleftharpoons}} \underset{\text{collision complex}}{[AB]^+} \xrightarrow{k_2} C^+ + D$$

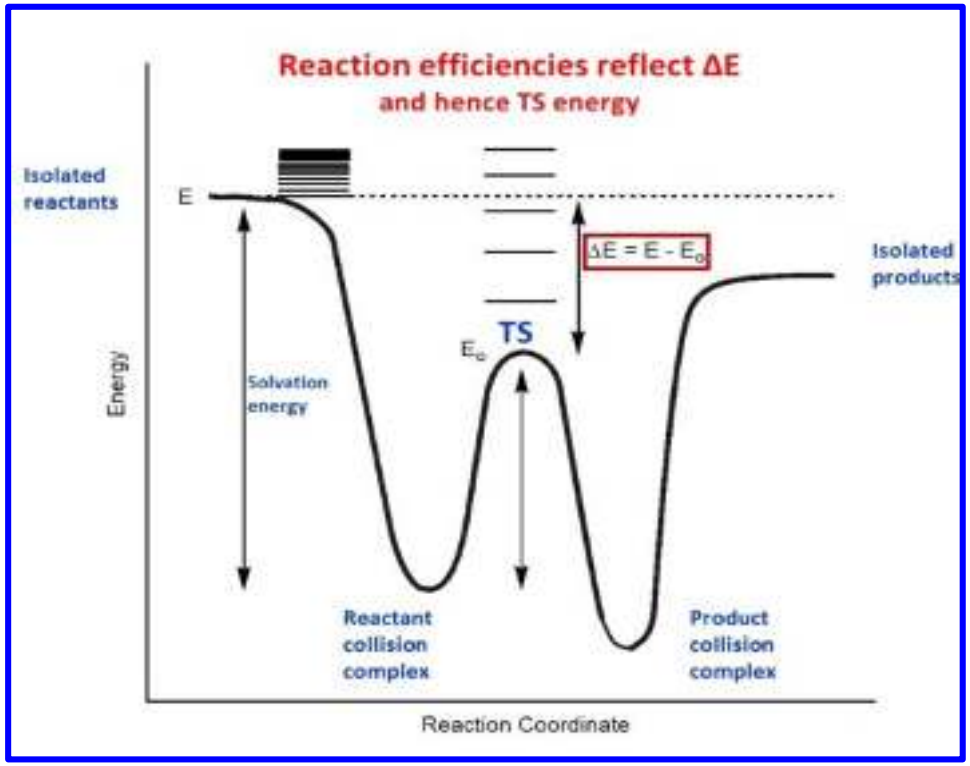

Only exothermic IMR with all barriers below the total energy level can proceed fast.

W. N. Olmstead, J. I. Brauman, *J. Am. Chem. Soc.* 1977

Overall, the efficiency depends on the height of the central barrier and the entropic constraints at the transition state.

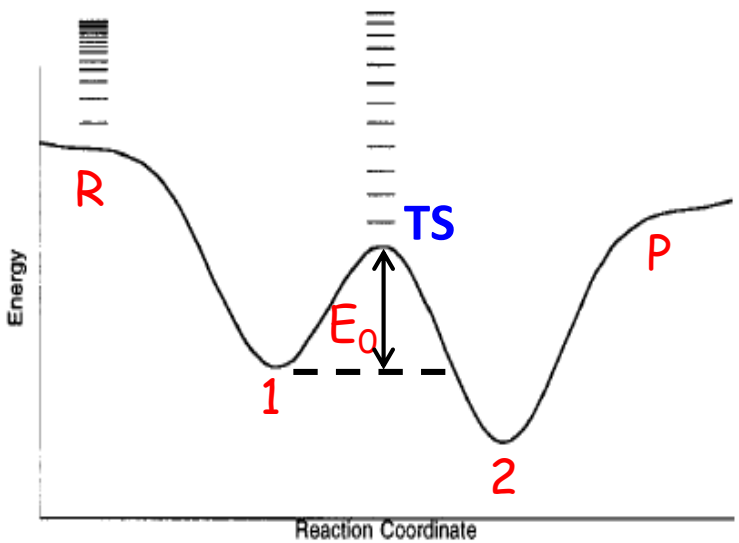

under the collisionless condition of FT-ICR, the intermediate complexes 1 and 2 are chemically activated

k_2: unimolecular isomerization with a *tight* (highy organized) TS (low A pre-exponential factor);
k_{-1} : fragmentation reaction with a *loose* (with many degrees of freedom) TS (high A pre-exponential factor)

TS may correspond to an entropic bottle-neck

competition takes place between one pathway that is energetically favored and another that is entropically favored.

energy favors k_2; entropy favors k_{-1}

At low E_0 a fast reaction will occur

S. Gronert, Chem. Rev. 2001

At high E_0 : (very) slow reaction

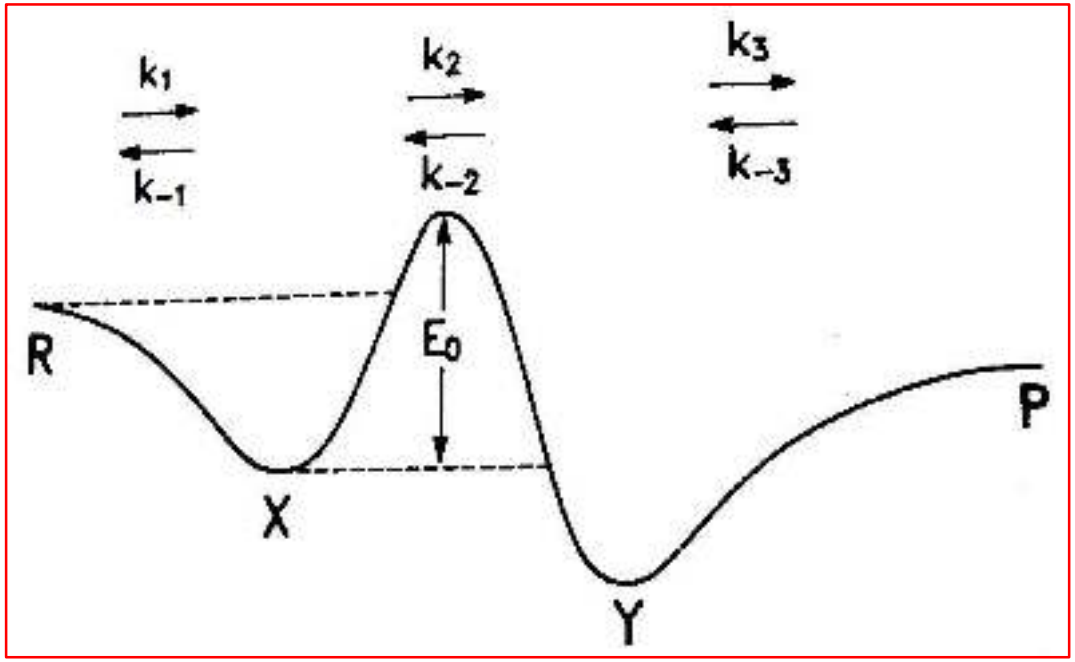

Slow reactions

k_{-1} will always be larger than k_2

At low pressure, double-minimum potential surface with TS lying above the reactants in energy : dissociation is energetically and entropically favored

For **long-lived** initial complexes, the energy can be removed *via* emission of a photon (**radiative stabilization**) and a slow reaction will be observed

S. Gronert, Chem. Rev. 2001

Instrumental aspects

Where to perform IMR:

- Chemical ionization ion source
- Atmospheric pressure ion source
- rf-only quadrupole of a triple quadrupole
- Ion-trapping instruments: linear quadrupole ion-trap and FT-ICR (the most versatile MS)

In FT-ICR:

- low pressure measurements (10^{-5}-10^{-8} torr)
- reagent introduction with variable leak valves and/or pulsed valves
- time and energy control of reactions
- mass selection of reactant and product ions
- structural characterization by CID, ECD, IRMPD
- multistep MS^n sequences
- high resolution, high mass accuracy mode of operation

Multichannel Pulsed-Valves Inlet System

analytical chemistry

Article

pubs.acs.org/ac

Integration of a Multichannel Pulsed-Valve Inlet System to a Linear Quadrupole Ion Trap Mass Spectrometer for the Rapid Consecutive Introduction of Nine Reagents for Diagnostic Ion/Molecule Reactions

John Y. Kong, Ryan T. Hilger, Chunfen Jin, Ravikiran Yerabolu, James R. Zimmerman, Randall W. Replogle, Tiffany M. Jarrell, Leah Easterling, Rashmi Kumar, and Hilkka I. Kenttämaa*

- rapid consecutive introduction of up 9 reagents
- automatic triggering allows to perform IMR on the HLPC time scale
- each component of a complex mixture: eluted, ionized, isolated, exposed to 9 different reagents

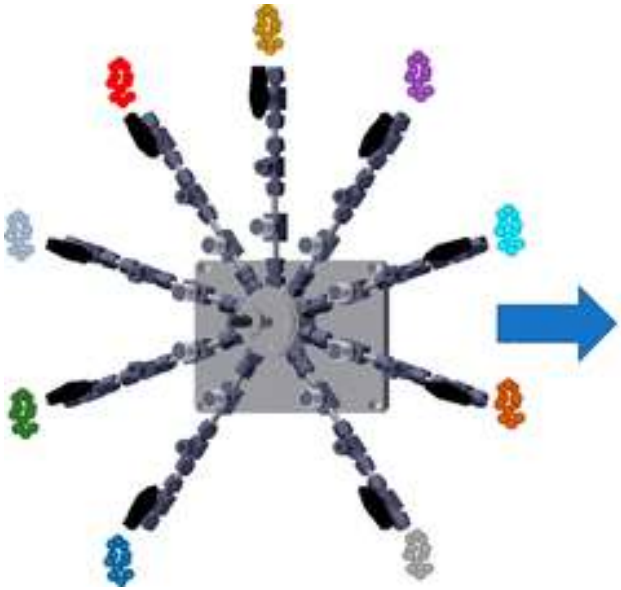

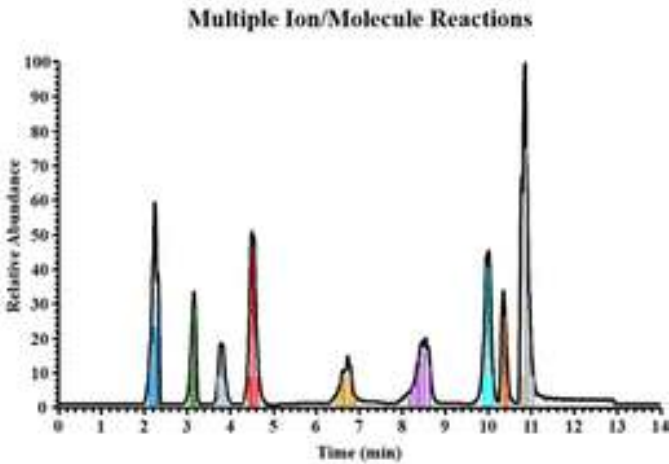

H. I. Kenttämaa, Anal. Chem. 2019

Bruker Apex II, 4.7T FT-ICR MS

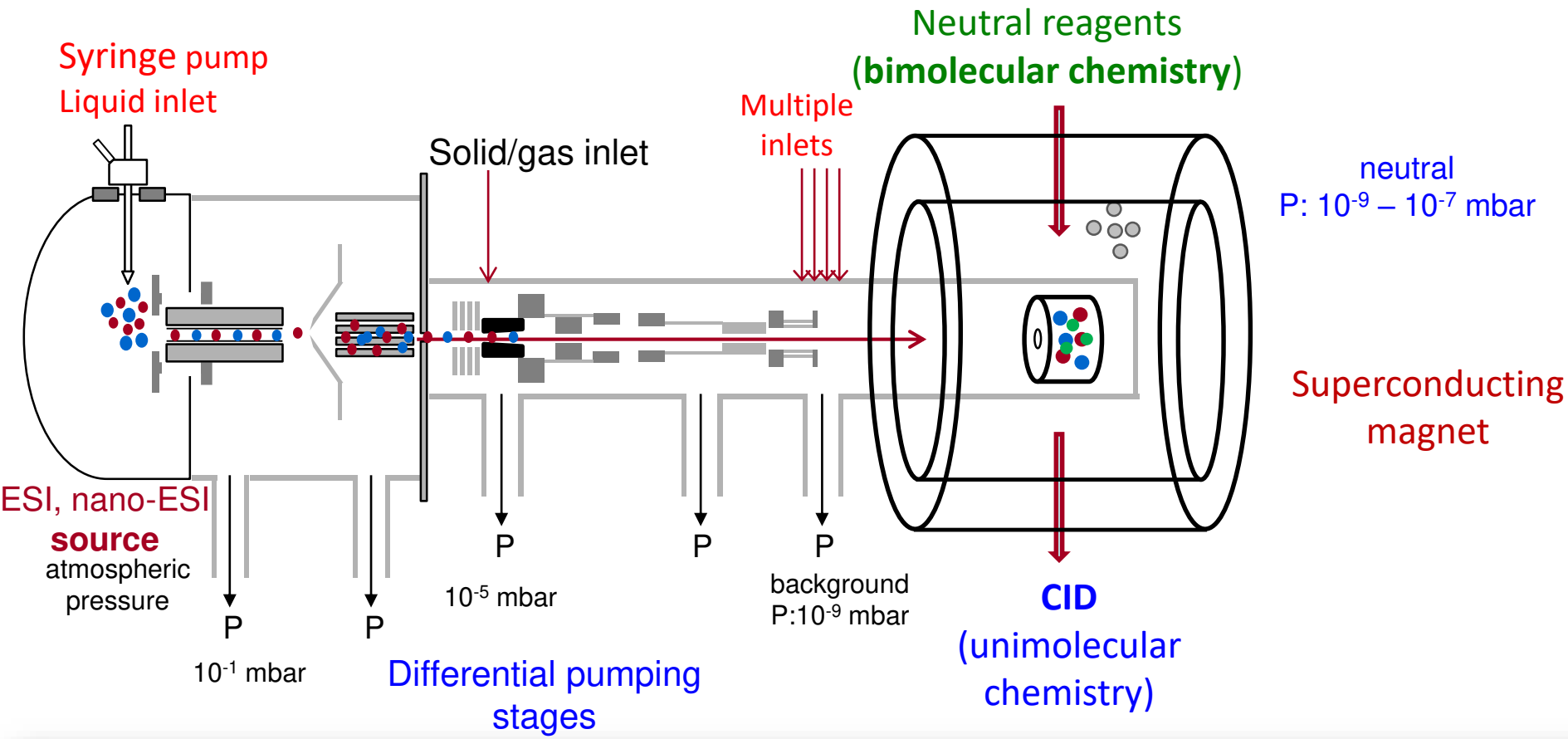

mass range extends in the low mass region down to 14.5 Da

Equipment for TNA in Roma

https://www.eu-fticr-ms.eu/

https://web.uniroma1.it/dip_ctf/

Types of Ion-Molecule Reactions

- Electron-Transfer
- Proton transfer
- H-atom/ O-atom transfer
- H/D exchange
- Functional-group selective
- Nucleophilic displacement
- Radiative association

V. Ryzhov, *Anal. Chem.* 2013; H. I. Kenttämaa, *Mass Spectrom. Rev.* 2021

Electron-Transfer Reactions

HNO^+ is more stable than HON^+ by 16.7 kcal/mol; isomerization requires 55.7 kcal/mol.

decomposition of hydroxylamine phosphate salt

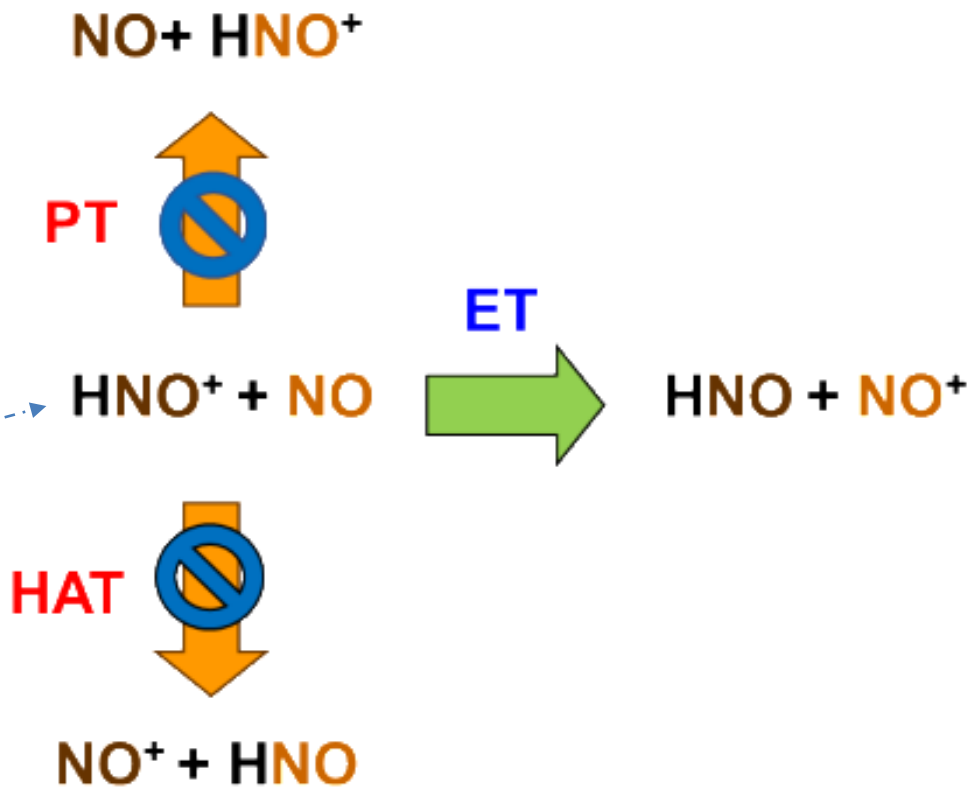

calculations at the CCSD(T)/augccpVTZ//B3LYP/def2-TZVP level of theory

U. Dandamudi, M.E. Crestoni, S. Fornarini, 2021, *submitted*

Proton-Transfer Reactions

$$AH^+ + B \rightleftharpoons BH^+ + A$$

$$A^- + BH \rightleftharpoons AH + B^-$$

base A of unknown GB (PA)

base B of known GB (PA)

by using several reference bases B, **the GB (PA) of A can be determined**

Bracketing method: **kinetics**

$$AH^+ + B \longrightarrow BH^+ + A$$

- measurement of k_{exp}
- presence of gaseous B

Equilibrium method: **equilibrium**

$$AH^+ + B \rightleftharpoons BH^+ + A$$

- measurement of K_{eq}
- presence of gaseous A and B

$$K_{eq} = \frac{[BH]^+ [A]}{[AH]^+ [B]} \qquad \ln K_{eq} = \frac{-\Delta G°}{RT}$$

G. Bouchoux, Int. J. Mass Spectrom. Ion Processes 1996

Chiral recognition in deprotonation reactions

J. Am. Chem. Soc. **1996**, *118*, 8751−8752

Chiral Recognition Is Observed in the Deprotonation Reaction of Cytochrome *c* by (2*R*)- and (2*S*)-2-Butylamine

Elvira Camara, M. Kirk Green, Sharron G. Penn, and Carlito B. Lebrilla*

Department of Chemistry, University of California Davis, California 95616

cyt c + (2R)/(2S)-2-butylamine
(9+, 8+, 7+)

- (2R)- <u>10 times</u> greater than (2S)-
- one reacting species for 9^+ and two for 8^+ and 7^+ : different conformers

chiral probes of gas-phase structures provide :
- indirect information on protein structures (intermediates of defined structures) and
- thermochemical data about individual sites in large (bio)molecules

C. B. Lebrilla et al., J. Am. Chem. Soc. 1996; J. Am. Chem. Soc. 1998; M. Speranza et al. Chiral. 2009

OAT from the naked core of Cpd I

$$(heme)FeCl \xrightarrow{ESI} [(heme)Fe^{III}]^+ \xrightarrow{[O_3/O_2]} [(heme)^{+\cdot}Fe^{IV}{=}O]^+ \xrightarrow[cell]{FT\text{-}ICR} \text{OAT Products}$$

solution — *gas phase* — *gas phase*

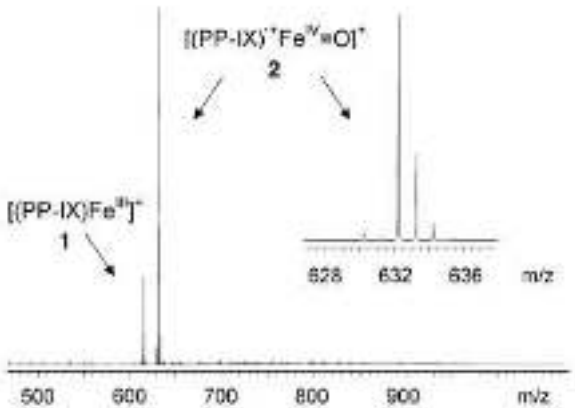

Figure 1. ESI FT-ICR mass spectrum from a methanol solution of (PP-IX)FeCl (10 μM), admitting O_3/O_2 in the capillary/skimmer interface of the ESI source. The inset is an enlargement of the spectrum displaying signals characteristic of $(PP\text{-}IX)^{\cdot+}Fe^{IV}{=}O$ ions (2).

Oxophylic Character

C

N

S

P

Ion-molecule reactions of $[(heme)^{+\cdot}Fe^{IV}{=}O]^+$

Table 1. Gas-Phase Reactivity of Selected Substrates (L) with $(PP\text{-}IX)^{\cdot+}Fe^{IV}(O)^+$ (**2**) Formed by the Reaction of $Fe(PP\text{-}IX)^+$ (**1**) with O_3

L	k_{exp}[a]	Φ[b]	product ions 1/(PP-IX)Fe(O)(L)$^+$
NO	3.0	4.2	100/0
NO_2	1.9	2.9	100/0
propyne	0.036	0.027	100/0
Me_2S	1.7	1.3	80/20
Me_2S_2	2.8	2.4	90/10
pyridine	2.4	1.7	100/0
$P(OMe)_3$	8.6	7.3	95/5

M. E. Crestoni, S. Fornarini, *Inorg. Chem.* **2007**

OAT by Mn(V)-Oxo porphyrin complex

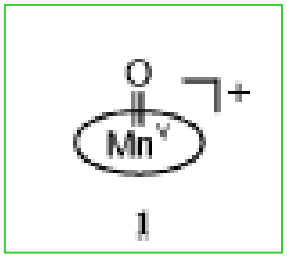

Mn^{V}-oxo-porphyrin complexes prepared in aqueous solution: diamagnetic d^2 low-spin ground state

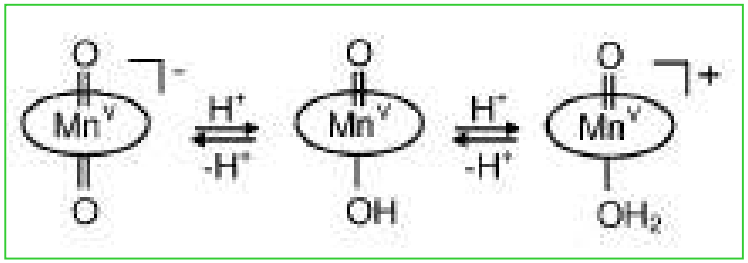

high pH low pH

The OAT reactivity in water is found to be strongly pH-dependent: prototropic equilibria

$$[(TPFPP)MnCl]^+ + PhIO \xrightarrow{ESI} [(TPFPP)Mn^{V}O]^+ + L \xrightarrow{FT\text{-}ICR} [(TPFPP)Mn^{III}]^+ + LO$$

solution, -20°C *gas phase*

L = propene, (E)-2-butene, (Z)-2-butene, styrene, cyclohexene, 1,3,5-CHT, (+)-camphene, indene, β-pinene, (R)-(+)-limonene. OAT reactivty increases with the olefin's IE value

M. E. Crestoni, et al. *Chem. Eur. J. 2009*

Properties of biomimetic models of enzymatic reaction intermediates by IMR

J|A|C|S
ARTICLES
Published on Web 02/16/2008

Probing the Compound I-like Reactivity of a Bare High-Valent Oxo Iron Porphyrin Complex: The Oxidation of Tertiary Amines

Barbara Chiavarino,† Romano Cipollini,† Maria Elisa Crestoni,† Simonetta Fornarini,*,† Francesco Lanucara,† and Andrea Lapi‡

Chemical Science
EDGE ARTICLE

A comprehensive test set of epoxidation rate constants for iron(IV)–oxo porphyrin cation radical complexes†

Mala A. Sainna,* Suresh Kumar,[b] Devesh Kumar,*[b] Simonetta Fornarini,* Maria Elisa Crestoni* and Sam P. de Visser*

high-valent iron(IV)-oxo porphyrin radical cation complex

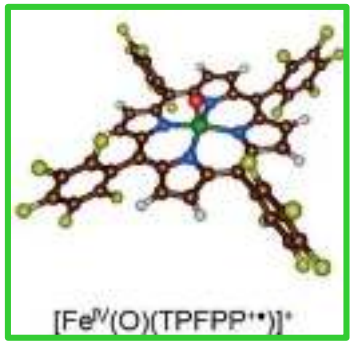

ChemPubSoc Europe
DOI: 10.1002/chem.201604361
CHEMISTRY A European Journal
Full Paper

Reaction Mechanisms

A Systematic Account on Aromatic Hydroxylation by a Cytochrome P450 Model Compound I: A Low-Pressure Mass Spectrometry and Computational Study

Fabián G. Cantú Reinhard,[a] Mala A. Sainna,[a] Pranav Upadhyay,[b] G. Alex Balan,[a] Devesh Kumar,[b] Simonetta Fornarini,*[a] Maria Elisa Crestoni,*[a] and Sam P. de Visser*[a]

ChemPubSoc Europe
DOI: 10.1002/ejic.201800273
EurJIC
Full Paper

Enzyme Models

Hydrogen Atom vs. Hydride Transfer in Cytochrome P450 Oxidations: A Combined Mass Spectrometry and Computational Study

Fabián G. Cantú Reinhard,[a] Simonetta Fornarini*[a] Maria Elisa Crestoni*[a] and Sam P. de Visser*[a]

M. E. Crestoni, S. Fornarini, *J.Am.Chem.Soc.* 2008; S. Fornarini, M. E. Crestoni, S. De Visser, *Chem. Science* 2015; *Chem Eur. J.* 2016; *EurJIC* 2018

Functional-group selective IMR

Anal. Chem. 2004, 76, 964−978

Ion−Molecule Reactions for Mass Spectrometric Identification of Functional Groups in Protonated Oxygen-Containing Monofunctional Compounds

Michael A. Watkins,[†] Jason M. Price,[†,‡] Brian E. Winger,[§] and Hilkka I. Kenttämaa*,[†]

1) ethyl vinyl ether
2) diethylmethoxyborane

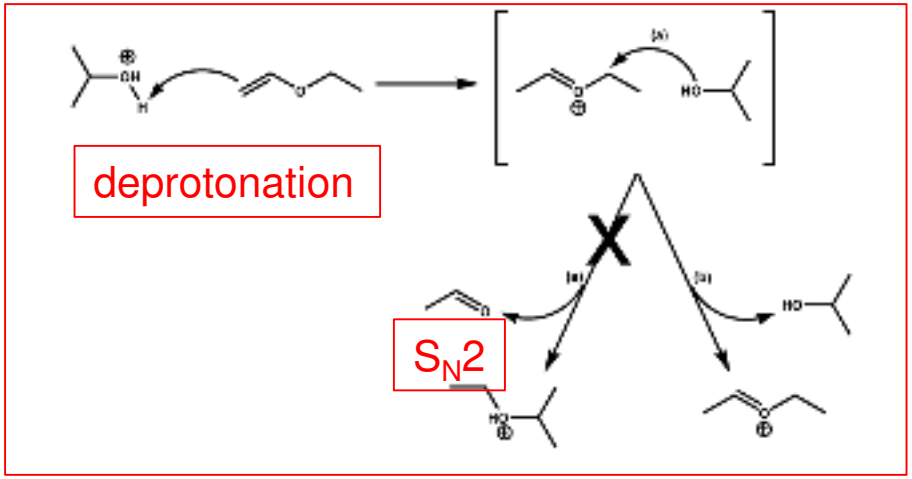

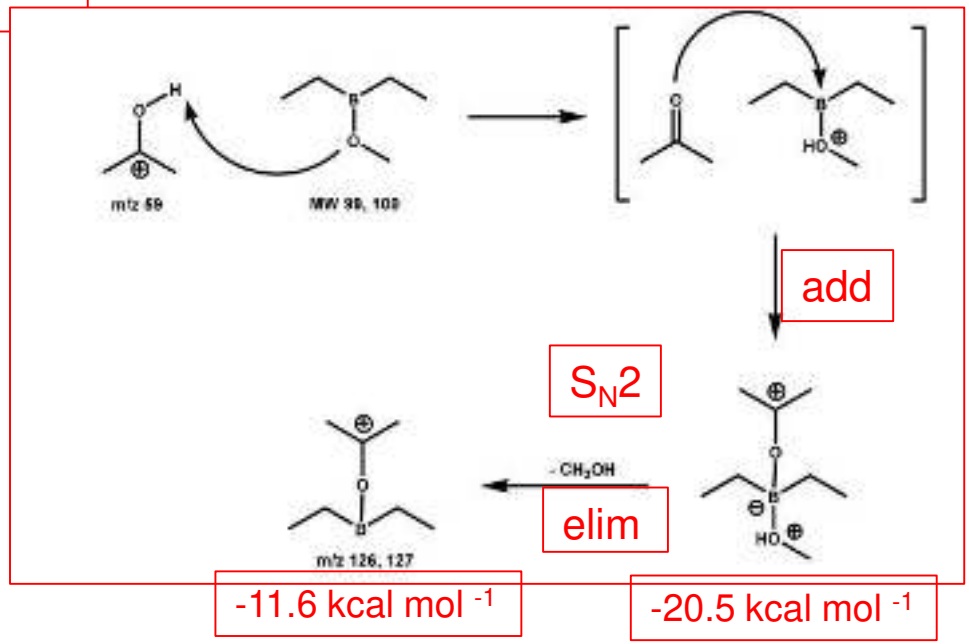

diethylmethoxyborane reacts with protonated monofunctional oxygen-containing analytes (**alcohols, ketones, aldehydes, esters, ethers, carboxylic acids, amides**) by deprotonation followed by substitution of methanol: provides structure elucidation for unknown mixture components

H. I. Kenttamaa, *Anal. Chem. 2004;* M. N. Eberlin, *J. Mass Spectrom.* 2006; H. I. Kenttämaa, *Mass Spectrom. Rev.* 2021

Identification of N-oxide and sulfoxide functionalities in protonated drug metabolites by using IMR

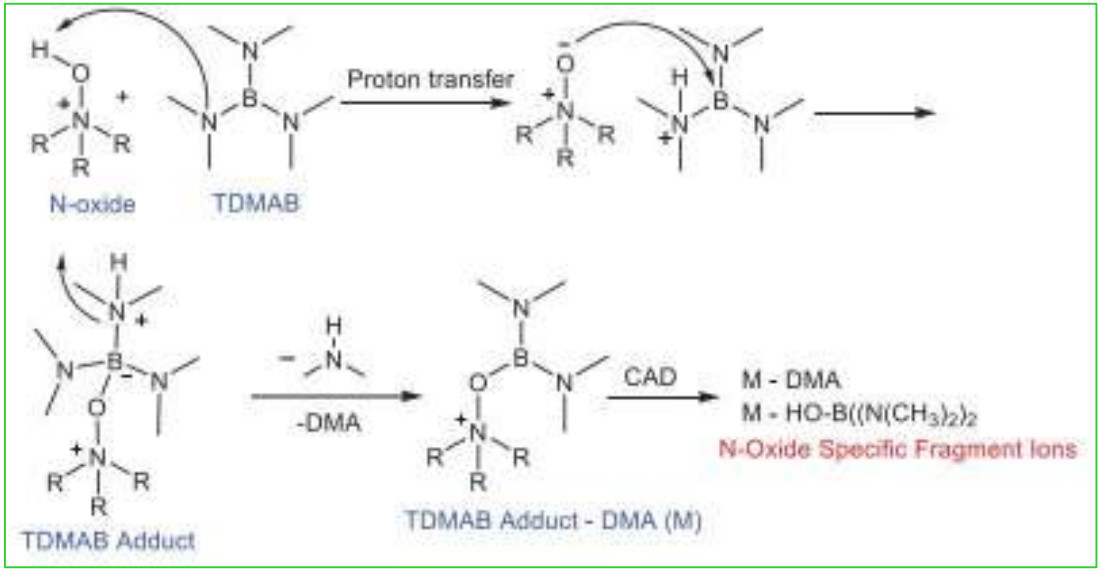

PA (TDMAB) = 230 kcal/mol
PA (N-oxides) = 220-240 kcal/mol
PA (sulfoxides) = 215-220 kcal/mol

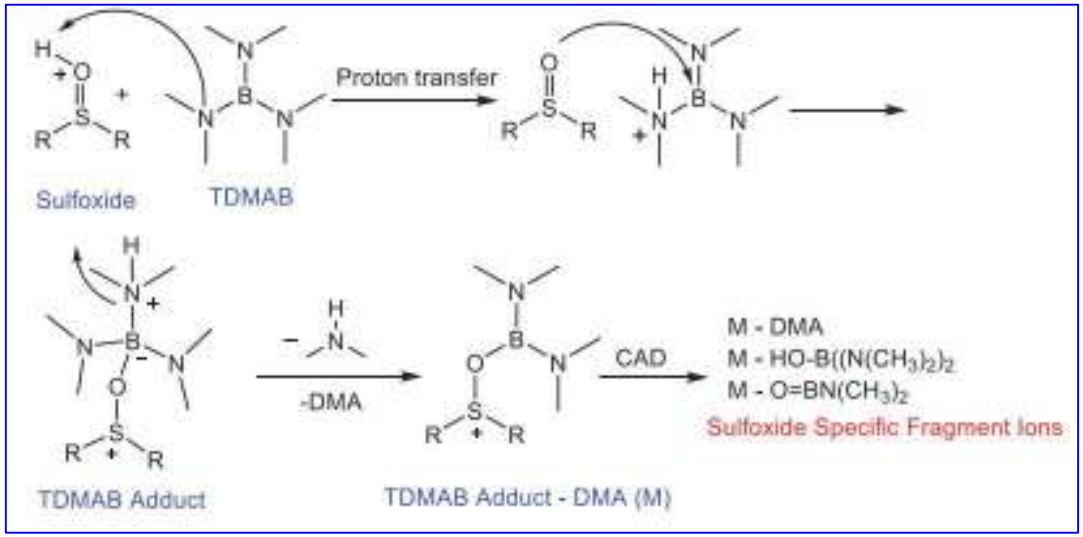

H. I. Kenttämaa, *J. Org. Chem.* 2016

Application to antipsychotics drug metabolites

Journal of Pharmaceutical and Biomedical Analysis 51 (2010) 805–811

Contents lists available at ScienceDirect

Journal of Pharmaceutical and Biomedical Analysis

journal homepage: www.elsevier.com/locate/jpba

Liquid chromatography/tandem mass spectrometry utilizing ion-molecule reactions and collision-activated dissociation for the identification of N-oxide drug metabolites

Steven C. Habicht, Penggao Duan[1], Nelson R. Vinueza, Mingkun Fu, Hilkka I. Kenttämaa*

Department of Chemistry, Purdue University, West Lafayette, IN 47907, USA

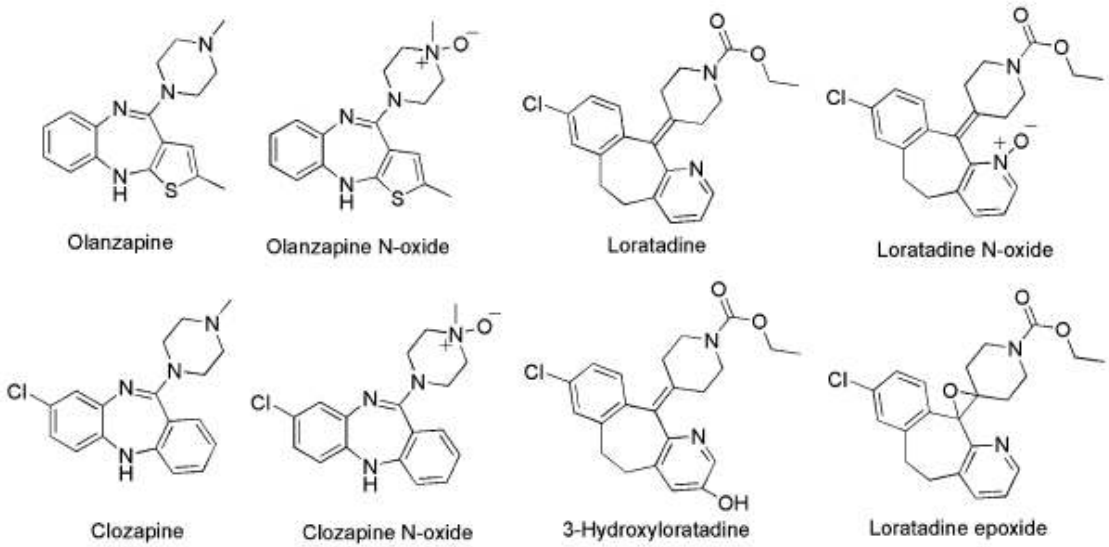

Fig. 1. Drugs and derivatives used to demonstrate the feasibility of the method.

H. I. Kenttämaa, *J. Org. Chem.* 2016

Functional-group selective IMR

Research Article

Received: 25 January 2014 Revised: 27 February 2014 Accepted: 27 February 2014 Published online in Wiley Online Library

Rapid Commun. Mass Spectrom. **2014**, *28*, 1107–1116
(wileyonlinelibrary.com) DOI: 10.1002/rcm.6884

Probing the exposure of the phosphate group in modified amino acids and peptides by ion-molecule reactions with triethoxyborane in Fourier transform ion cyclotron resonance mass spectrometry

Francesco Lanucara[1,2*], Simonetta Fornarini[3], Claire E. Eyers[2] and Maria Elisa Crestoni[3]

$$[\text{Peptide-O-P(O)(OH)}_2\text{+nH}]^{n+} + \text{B(OR)}_3 \rightarrow [\text{Peptide-O-PO(OH)OB(OR)}_2\text{+nH}]^{n+} + \text{ROH}$$

Scheme 1. Addition-elimination reaction of phosphorylated amino acids and peptides with alkoxyboranes $B(OR)_3$.

Potential to measure the effect of local environment, the exposure and accessibility of a phosphate moiety on the surface of a biomolecule and to distinguish positional phosphorylated peptide isomers

The reaction efficiency allows to explore the accessibility of phosphate groups in biomolecules

Lanucara et al., *Rapid Commun. Mass Spectrom.* 2014

Hydrolysis of cis and transplatin

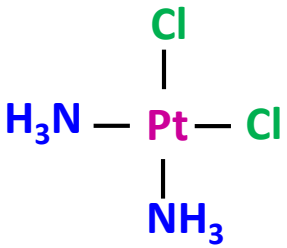

cis-platin

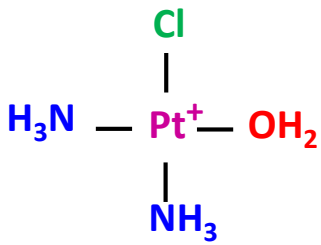

cis-$[PtCl(NH_3)_2(H_2O)]^+$

singly aquated

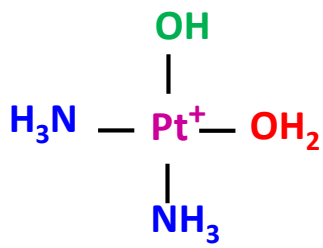

cis-$[PtOH(NH_3)_2(H_2O)]^+$

deprotonated form of doubly aquated

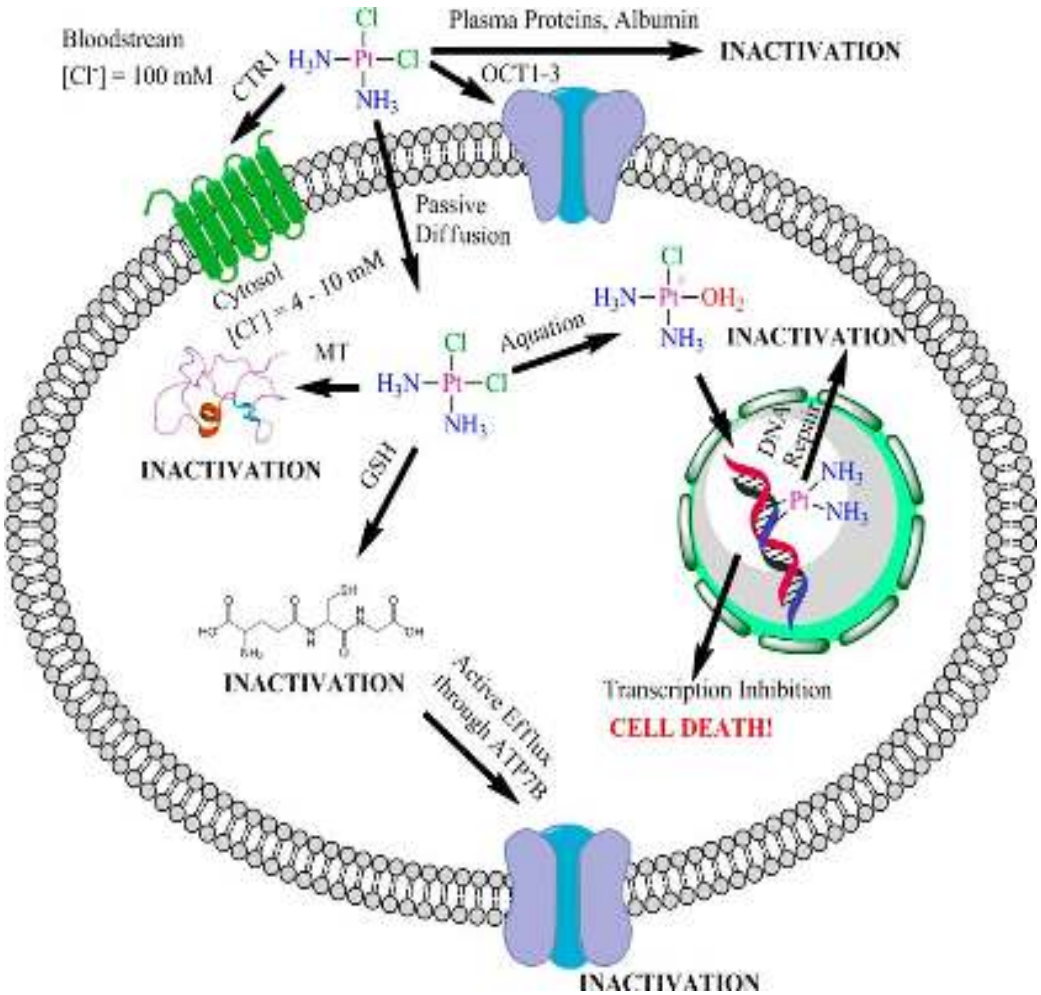

in solution it is not easy to separate the influence of the nature of the incoming and leaving ligands

S. Fornarini et al., RSC Adv. 2017

$$cis/trans\text{-}[PtX(NH_3)_2(H_2O)]^+ + L \longrightarrow cis/trans\text{-}[PtX(NH_3)_2(L)]^+ + H_2O$$

(X=Cl, OH)

In solution, formation of hydroxo-bridged polynuclear complexes.

Table 2 Reactivity of $[PtX(NH_3)_2(H_2O)]^+$ (X = Cl, OH; *cis* and *trans* isomers) with simple molecules in the gas-phase

Reagent ion	Neutral	k_{exp}[a]	Eff[b] (%)
cis-$[PtCl(NH_3)_2(H_2O)]^+$	TMP	3.7	2.5[b]
	Pyridine	0.6	0.41[b,c]
	Thioanisole	1.4	1.1[b]
	Dimethylsulfide	0.034	0.026
trans-$[PtCl(NH_3)_2(H_2O)]^+$	TMP	3.3	2.3
	Pyridine	1.4	0.93[d]
	Thioanisole	7.7	6.3
	Dimethylsulfide	2.4	1.7
cis-$[Pt(OH)(NH_3)_2(H_2O)]^+$	TMP	0.96	0.66
	Pyridine	0.46	0.31[e]
	Thioanisole	0.1	0.08
	Dimethylsulfide	n. r.[f]	
trans-$[Pt(OH)(NH_3)_2(H_2O)]^+$	TMP	1.1	0.78
	Pyridine	0.05	0.03[g]
	Thioanisole	0.46	0.37
	Dimethylsulfide	n. r.[f]	

[a] Second order rate constant in units of 10^{-11} cm^3 s^{-1} at 298 K, estimated error ±30%. Other sampled compounds proved to be

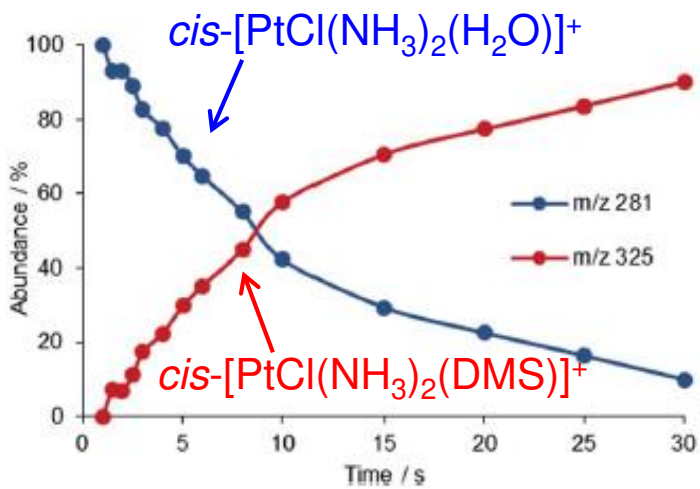

- ligand exchange; low efficiencies
- Cl complexes more reactive than OH
- TMP more reactive than TA
- *trans*Pt more reactive than *cis*Pt vs S ligands

S. Fornarini et al., RSC Adv. 2017

The ligand exchange is a stepwise process

$$[PtX(NH_3)_2(H_2O)]^+ + L \rightleftharpoons \underset{RC}{[PtX(NH_3)_2(H_2O)]^+ \bullet L} \overset{TS}{\rightleftharpoons}$$

$$\underset{PC}{[PtX(NH_3)_2(L)]^+} \bullet H_2O \longrightarrow [PtX(NH_3)_2(L)]^+ + H_2O$$

The Φ of the overall process depends on the branching of RC

S. Fornarini et al., RSC Adv. 2017

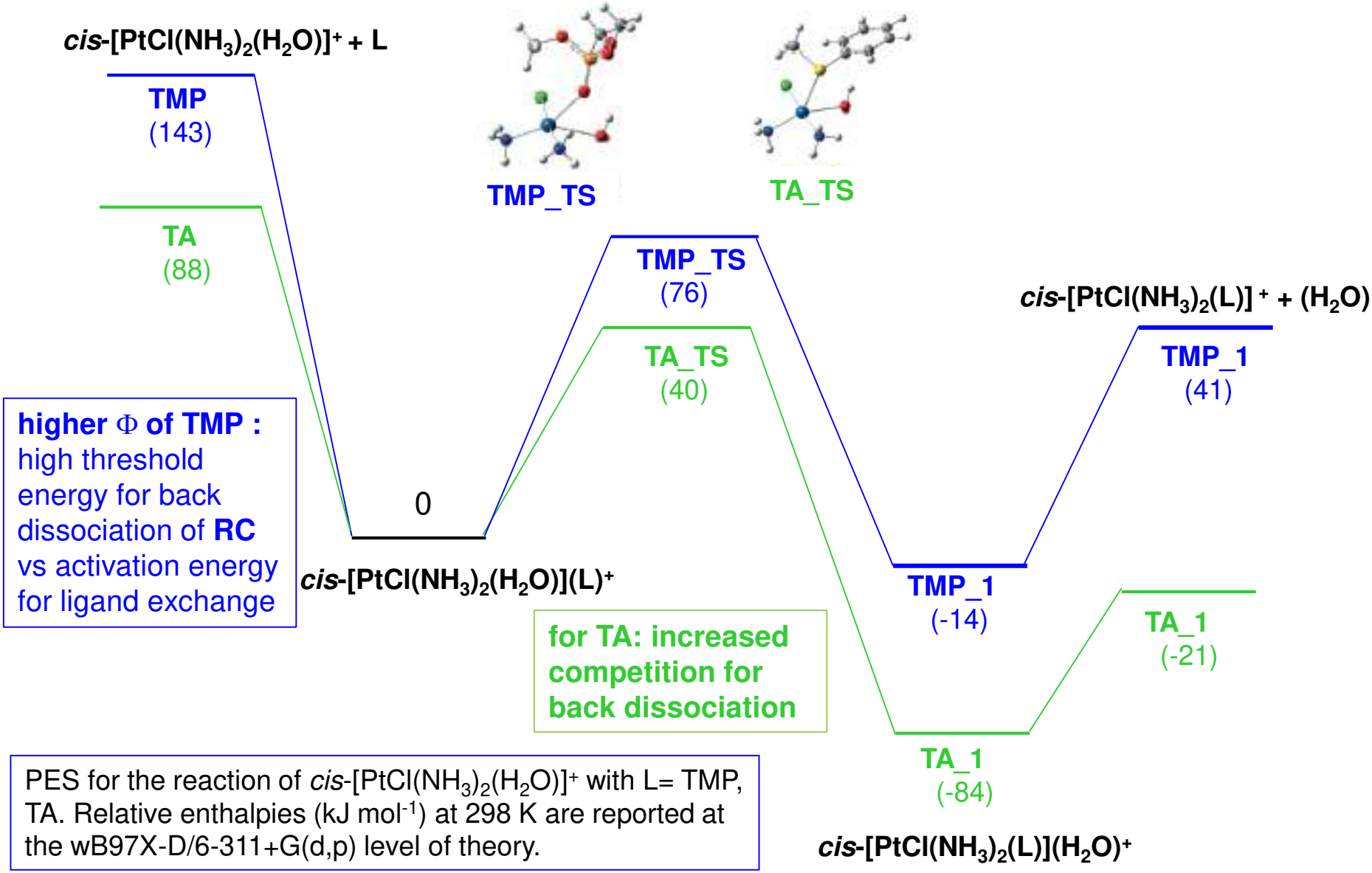

PES for the reaction of *cis*-[PtCl(NH$_3$)$_2$(H$_2$O)]$^+$ with L= TMP, TA. Relative enthalpies (kJ mol^{-1}) at 298 K are reported at the wB97X-D/6-311+G(d,p) level of theory.

S. Fornarini et al., RSC Adv. 2017

Ligand exchange of water by TA is kinetically more favored in the *trans*- with respect to the *cis*-isomers

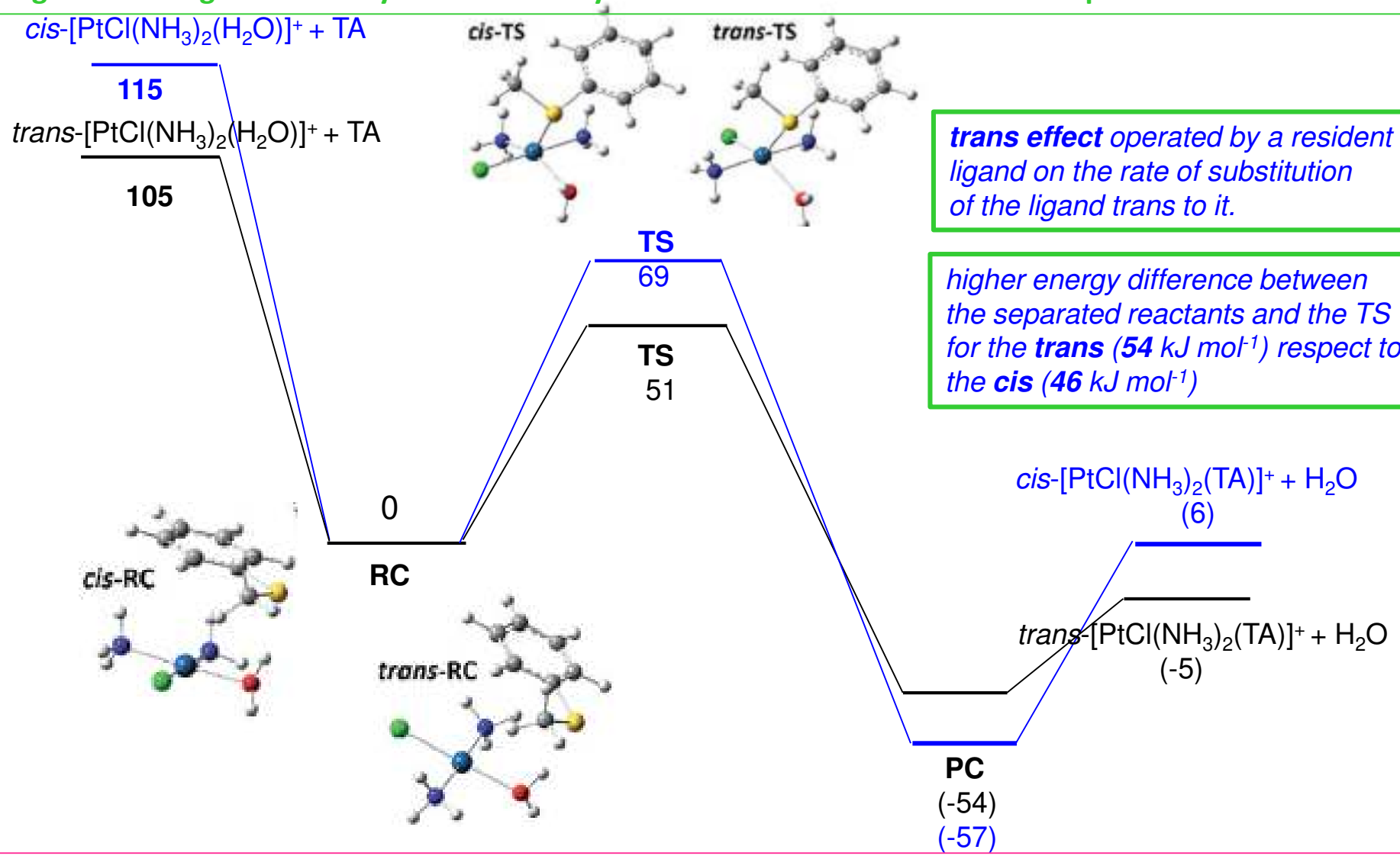

trans effect *operated by a resident ligand on the rate of substitution of the ligand trans to it.*

higher energy difference between the separated reactants and the TS for the ***trans*** *(**54** kJ mol^{-1}) respect to the* ***cis*** *(**46** kJ mol^{-1})*

water is displaced by TA more easily when the trans-site is occupied by a Cl than by NH_3, according to *trans*-directing sequence $Cl^- > NH_3$

S. Fornarini et al., RSC Adv. 2017

Association Reactions

- solvation of an ion by weak electrostatic forces or hydrogen bonding;
- ion ligation involving bonds of intermediate strength;
- strong chemical bond formation

$$A^{\pm} + B \rightleftharpoons (AB)^{\pm *}$$

$$(AB)^{\pm *} \longrightarrow AB^{\pm} + h\nu$$ ---------- FT-ICR

$$(AB)^{\pm *} + M \longrightarrow AB^{\pm} + M$$ ---------- Ion-trap

at the low operating pressures of the FT-ICR cell: thermal equilibration of the adduct ion via IR radiative emission

The rate of radiative emission is expected to increase with increasing size of the ion

F.W. Mc Lafferty et al., *J. Am. Chem. Soc. 2001*

Functional-group selective IMR

J Biol Inorg Chem (2007) 12:22–35
DOI 10.1007/s00775-006-0159-9

ORIGINAL PAPER

Heme-peptide/protein ions and phosphorous ligands: search for site-specific addition reactions

Maria Elisa Crestoni · Simonetta Fornarini

- **Fe(III)-heme$^+$**
- **MP11**
- **cyt c**
- **myoglobin**

+ $OP(OMe)_3$ (GB: 206 kcal/mol)
+ $P(OMe)_3$ (GB: 215.3 kcal/mol)

the addition of phosphite is limited to just one molecule, irrespective of charge state, in contrast with a charge-dependent number of added phosphate ligands

- **$OP(OMe)_3$ is engaged in H bonding to protonated sites**
- **$P(OMe)_3$ is sampling the protein prosthetic group**

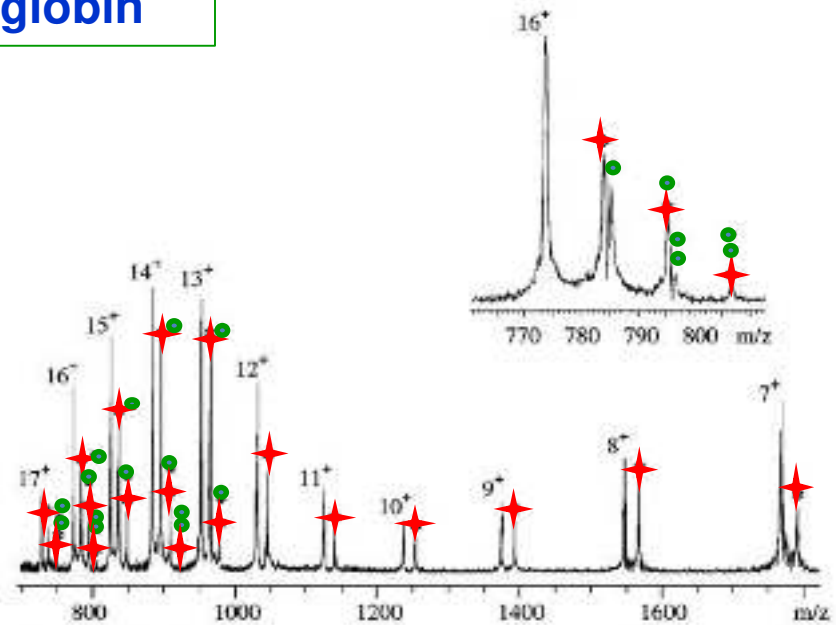

Fig. 9 FT-ICR mass spectrum of cyt *c* allowed to react with a 70:30 mixture of triethylphosphite, $P(OEt)_3$, and triethylphosphate, $OP(OEt)_3$, at 2.4×10^{-8} mbar for 3 s. *Numbers* denote the charge states of cyt *c* ions. Each charge state forms adducts with a single $P(OEt)_3$ molecule (represented by a *star*). The high charge states add up to four $OP(OEt)_3$ molecules; each $OP(OMe)_3$ molecule is represented by a *circle*

Crestoni, Fornarini, *J. Biol. Inorg. Chem.* 2007

(J Am Soc Mass Spectrom 2005, 16, 589–598)

Binding of Gaseous Fe(III)-Heme Cation to Model Biological Molecules: Direct Association and Ligand Transfer Reactions

Fausto Angelelli, Barbara Chiavarino, Maria Elisa Crestoni, and Simonetta Fornarini
Department of Studies on Chemistry and Technology of Biologically Active Substances, University of Rome, "La Sapienza," Rome, Italy

Ligand association equilibrium

$$\text{Fe(III)-heme}^+ + \text{L} \underset{k_{-1}}{\overset{k_1}{\rightleftarrows}} \text{Fe(III)-heme(L)}^+$$

L= NO, amines, carbonyl compounds, ethers, nitriles, sulfides, phosphoryl compounds

$$HCB(L) = -\Delta G° = -RT\ln K_{eq}$$

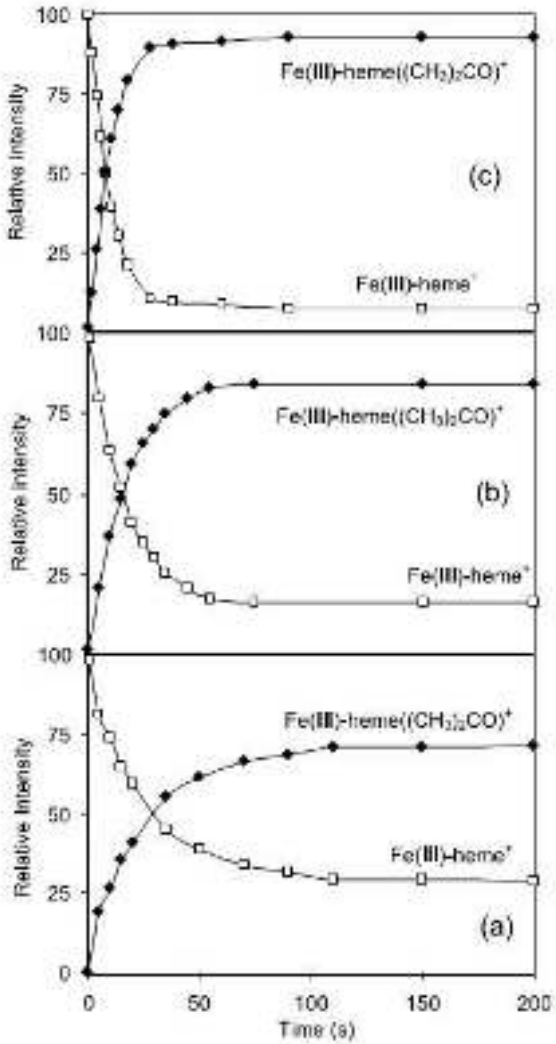

Figure 5. Time dependence of ion abundances for the Fe(III)-heme$^+$ ion reaction with acetone at 5.2×10^{-8} mbar (a), 8.7×10^{-8} mbar (b), 2.1×10^{-7} mbar (c).

S. Fornarini et al. JASMS 2005

Ligand transfer equilibria

$$Fe(III)\text{-heme}(L_1)^+ + L_2 \rightleftarrows Fe(III)\text{-heme}(L_2)^+ + L_1$$

$$HCB(L_1) - HCB(L_2) = -\Delta G^\circ = -RT\ln K_{eq}$$

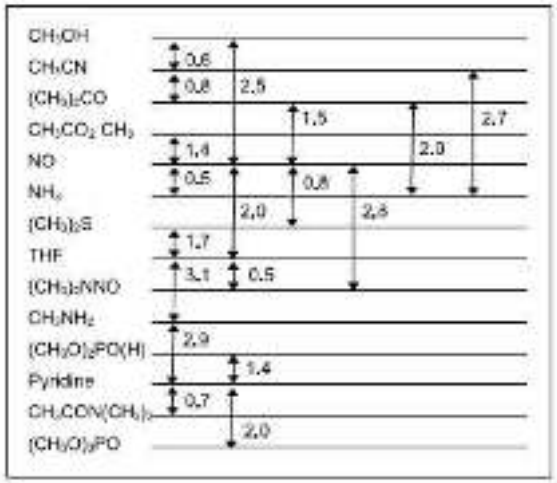

Figure 7. ΔG_a° (kcal mol^{-1}, 300 K) ladder for the Fe(III)-heme transfer reactions between selected pairs of ligands. The values in the ladder correspond to HCB differences for each couple of ligands.

Table 6. Free energy changes for gas-phase ligand binding toward H^+ and Fe(III)-heme[a]

L	GB[a]	HCB[b]
CH_3OH	173.2	13.1
CH_3CN	179.0	13.7
$(CH_3)_2CO$	186.9	14.6
$CH_3CO_2CH_3$	189.0	14.8
NO	120.8	16.1
NH_3	195.7	16.6
$(CH_3)_2S$	191.5	16.9
Tetrahydrofuran	189.9	18.1
$(CH_3)_2N$-NO	203.0[c]	18.9
CH_3NH_2	206.6	21.2
$(CH_3O)_2PO(H)$	206.1	22.7
Pyridine	214.7	24.1
$CH_3CONCH_3)_2$	209.6	24.8
$(CH_3O)_3PO$	205.7	26.1

NO stands out as a superior ligand

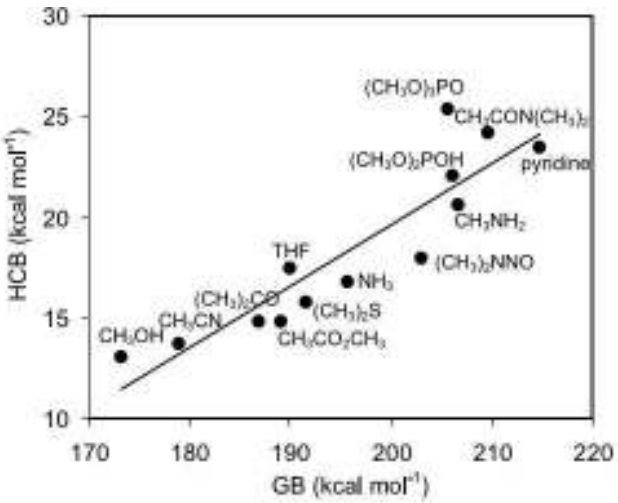

Figure 9. General correlation between Fe(III)-heme$^+$ cation b sicities (HCB, equal to $-\Delta G_1^\circ$ for the ligand association reactio and gas phase basicity toward the proton (GB) values.

A linear correlation between HCBs and ΔGBs of the ligands suggests that similar effects play a role when a lone pair donor binds to a proton or to Fe(III)heme$^+$

S. Fornarini et al. JASMS 2005

SAPIENZA
UNIVERSITÀ DI ROMA

Dip. CTF

Simonetta Fornarini

Barbara Chiavarino

Davide Corinti

Alessandro Maccelli

Alba Lasalvia

Valentina Lilla

SAPIENZA
UNIVERSITÀ DI ROMA

EU FT-ICR MS

Thank you for the kind attention

Universität Rostock HelmholtzZentrum münchen
JOINT MASS SPECTROMETRY CENTRE

EU FT-ICR MS

Ionization schemes and techniques in FT- ICR MS: From commercial towards customized solutions

EU_FT-ICR_MS
2nd Advanced User School
Prague, 26 - 30 September 2021

Christopher P. Rüger

Group Leader High-Resolution Mass Spectrometry
University of Rostock, Institute of Chemistry, Division of Analytical Chemistry

Outline

- **Introduction and Motivation**
  - Chemical Space, Selectivity of Ionization Techniques, Overview of Schemes and Concepts
- **Vacuum Ionization**
  - Electron Impact and Photoionization
  - Laser Desorption Ionization and Allied Techniques
- **Atmospheric Pressure Ionization**
  - Electrospray Ionization, Atmospheric Pressure Chemical/Photo/Laser Ionization
  - Other Concepts and Combination, Applications
- **Summary**

Complexity of organic mixtures – The chemical space

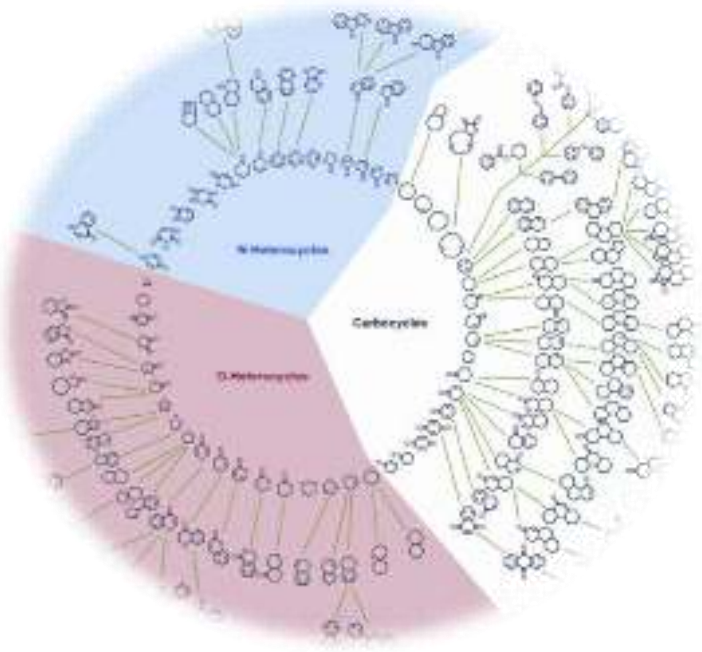

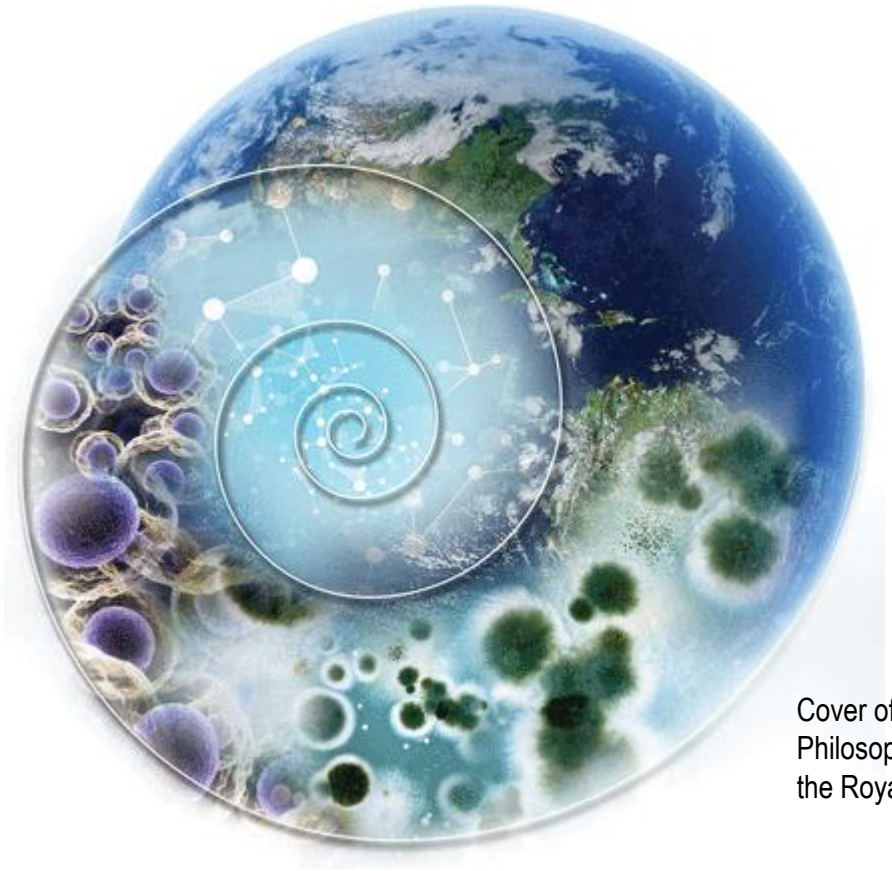

Cover of Vol. 375, 2109, Philosophical Transactions of the Royal Society A, Dec. 2017

Estimated number of organic molecules with MW < 500: 10^{62}

Bohacek, R. S., McMartin, C., and Guida, W. C. (1996), Med. Res. Rev. 16, 3−50

What are Complex Mixtures?

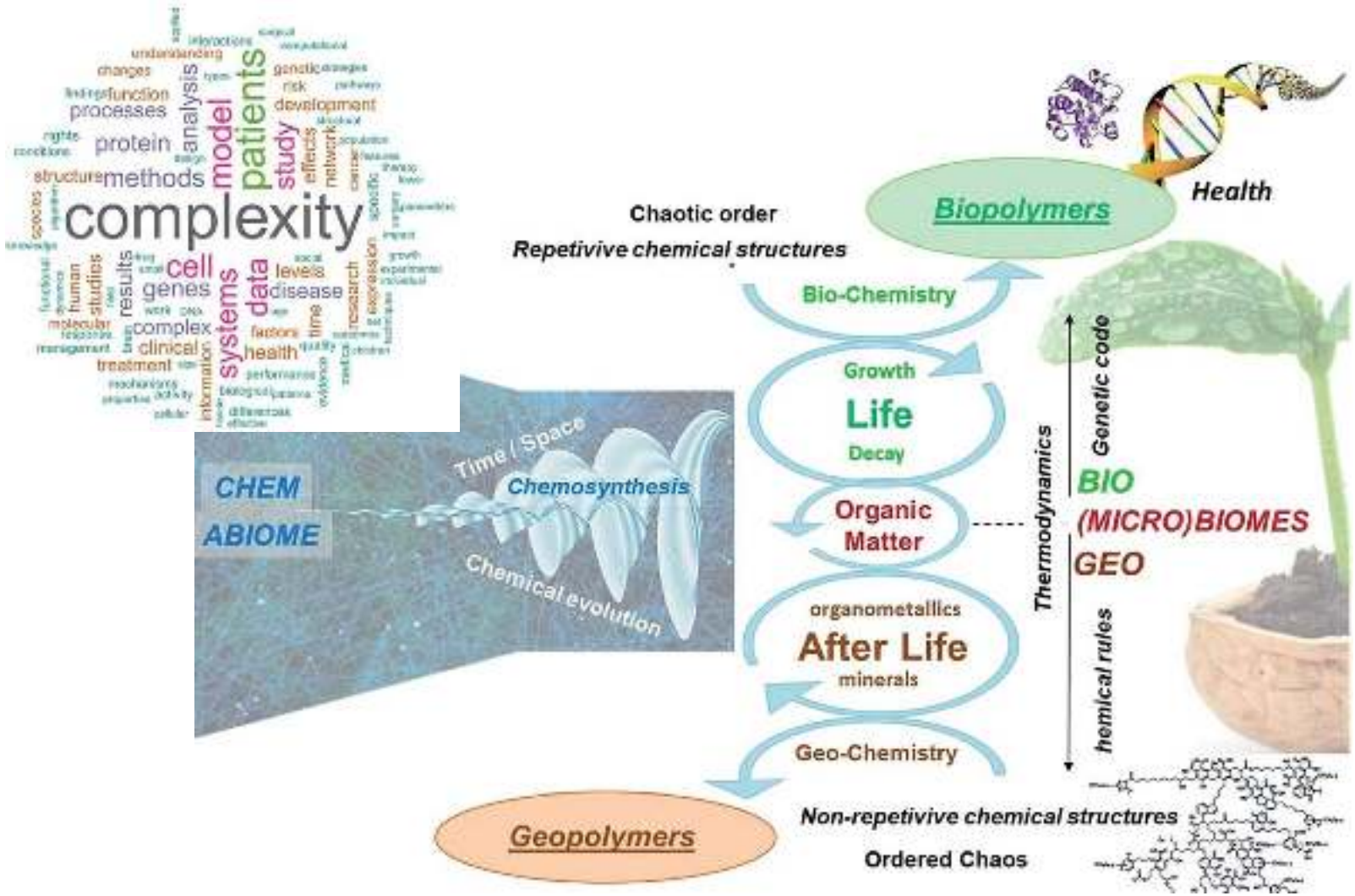

Schmitt-Kopplin et al., *Faraday Discussions*, **2019**, *218, 9-28*

Chemical Complexity

"Universal" Complexity Scale

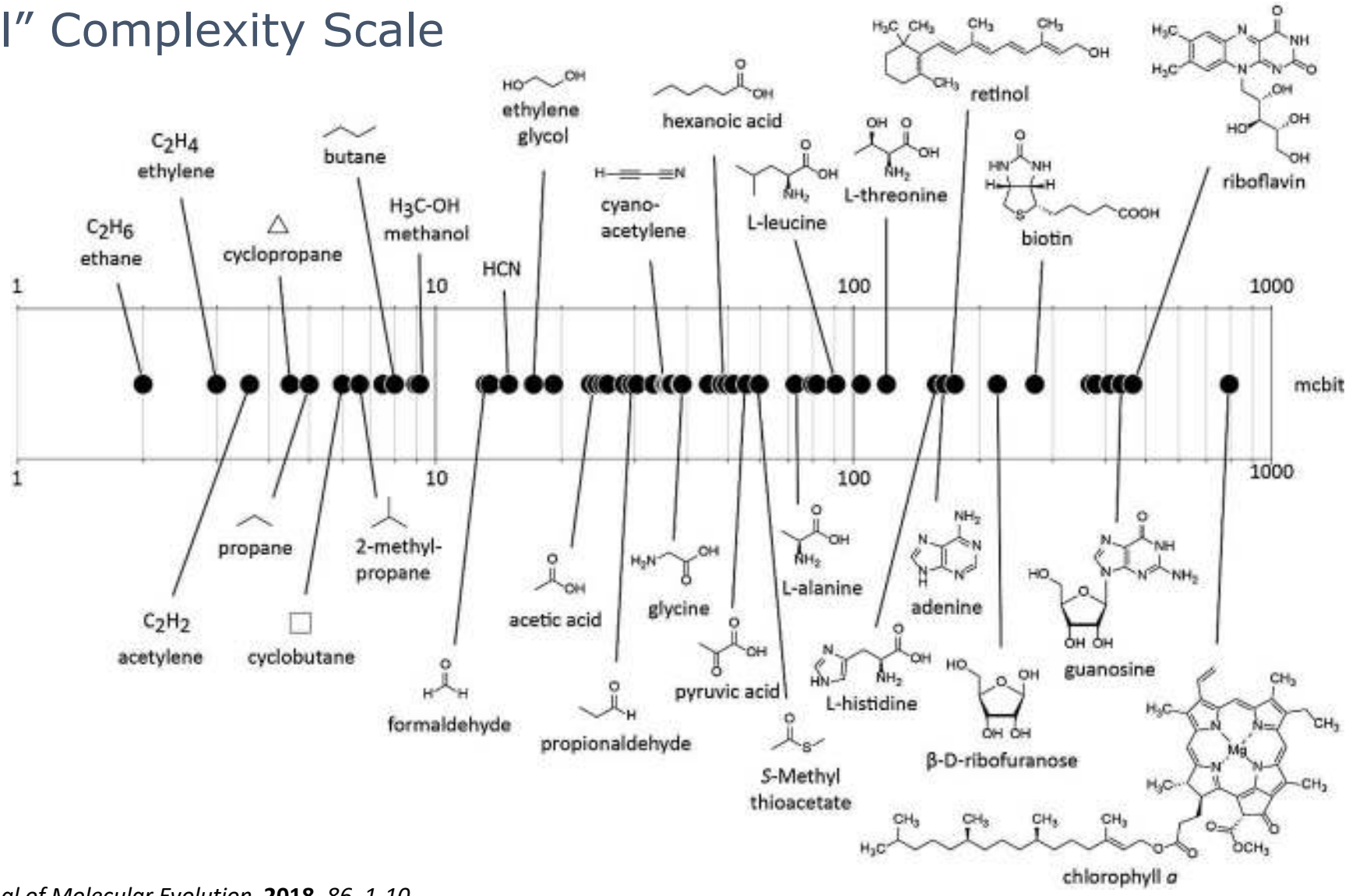

Thomas Böttcher, *Journal of Molecular Evolution*, **2018**, *86, 1-10*

Why High-Resolution Mass Spectrometry?

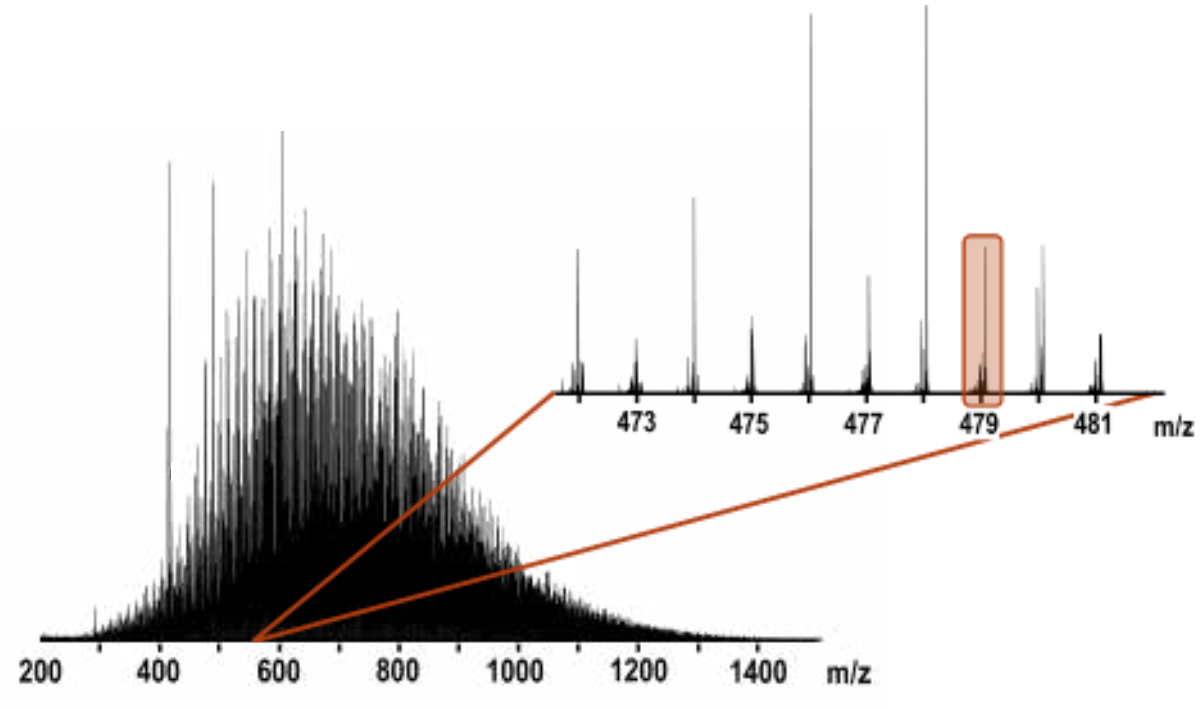

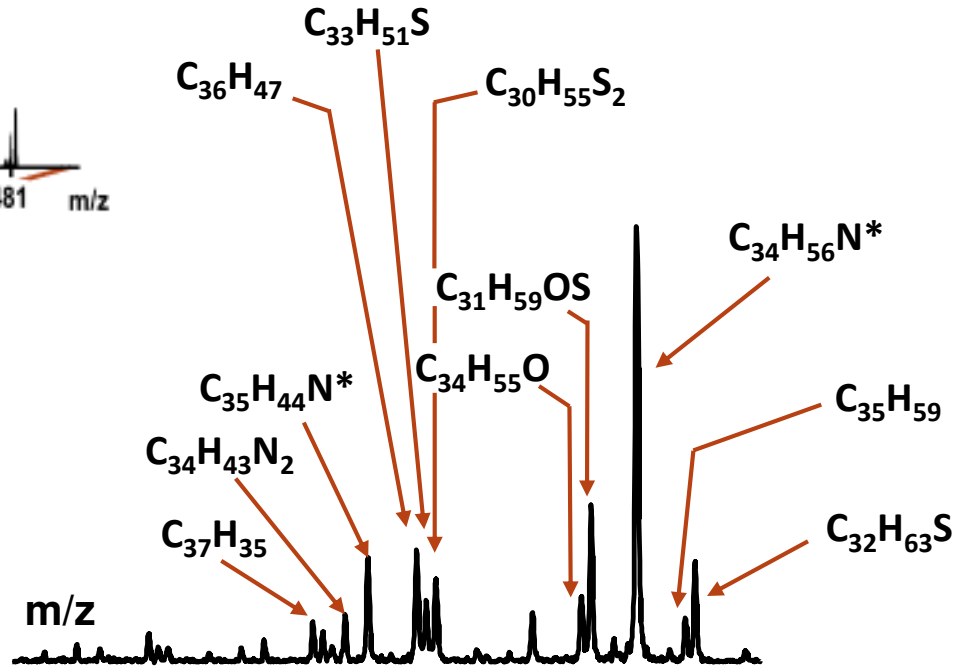

Every $C_cH_hN_nO_oS_s$ mass is unique!

Mass defect =
Atom mass – nearest integer mass

What can high-resolution mass spectrometry do for us?

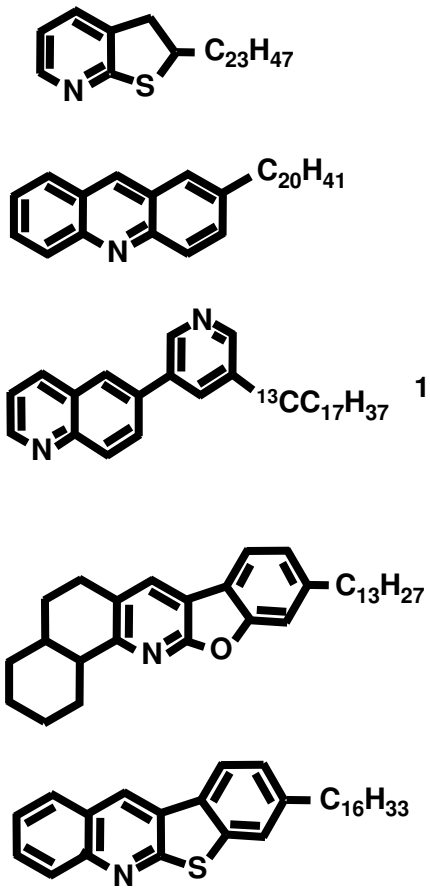

459.3899
$C_{30}H_{53}NS$

459.3865
$C_{33}H_{49}N$

459.3695
$^{13}CC_{31}H_{46}N_2$

459.3501
$C_{32}H_{45}NO$

459.2960
$C_{31}H_{41}NS$

Doublet	m_2-m_1	$\frac{m_2}{m_2-m_1}$
SH_4/C_3	3.4 mDa	135,000
$C_2H_3/^{13}CN$	17.0 mDa	27,000
O/CH_4	36.4 mDa	13,000
H_{12}/C	93.9 mDa	5,000

Rodgers, R., Presentation at Mag Lab Summer School 2009

Complex Mixtures – Example: Petroleum

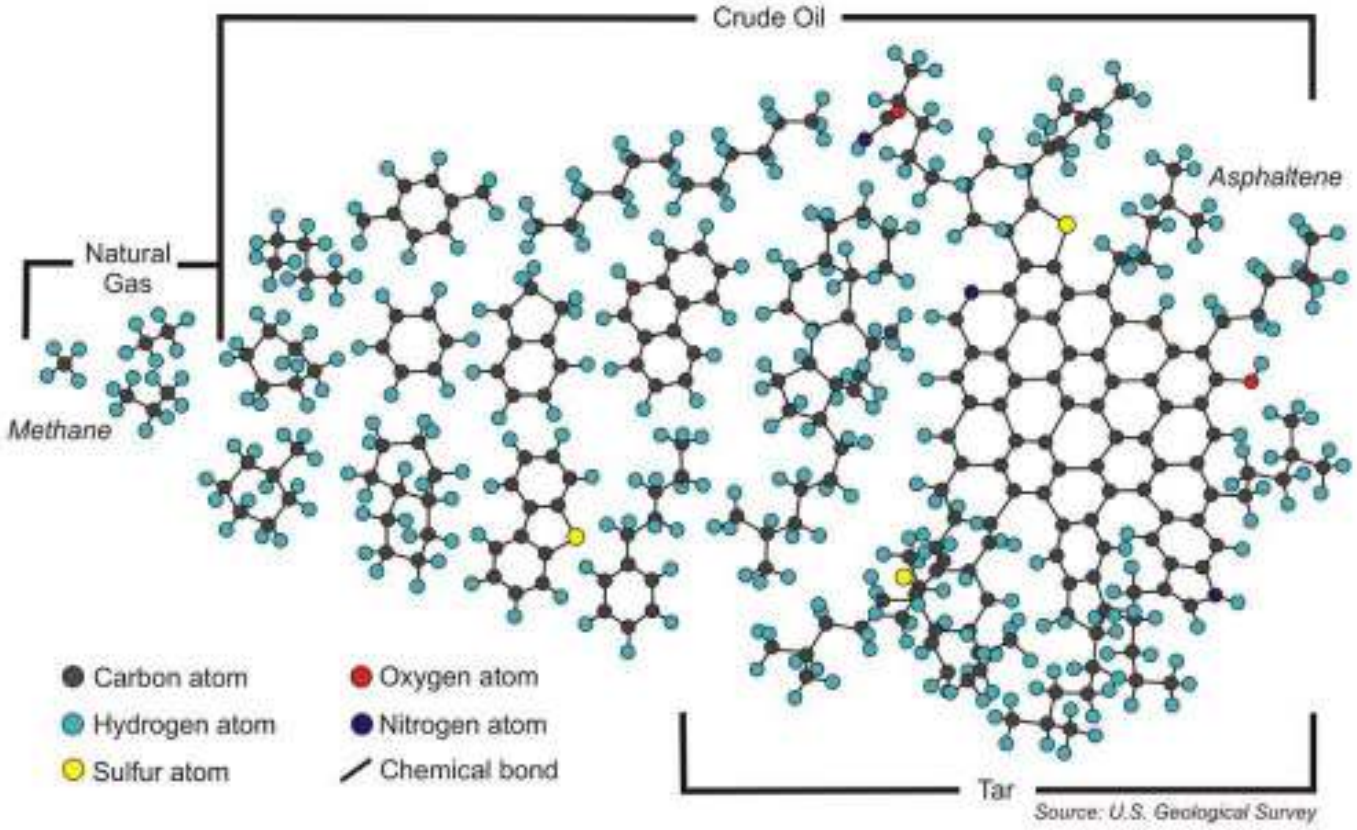

Boduszynski continuum

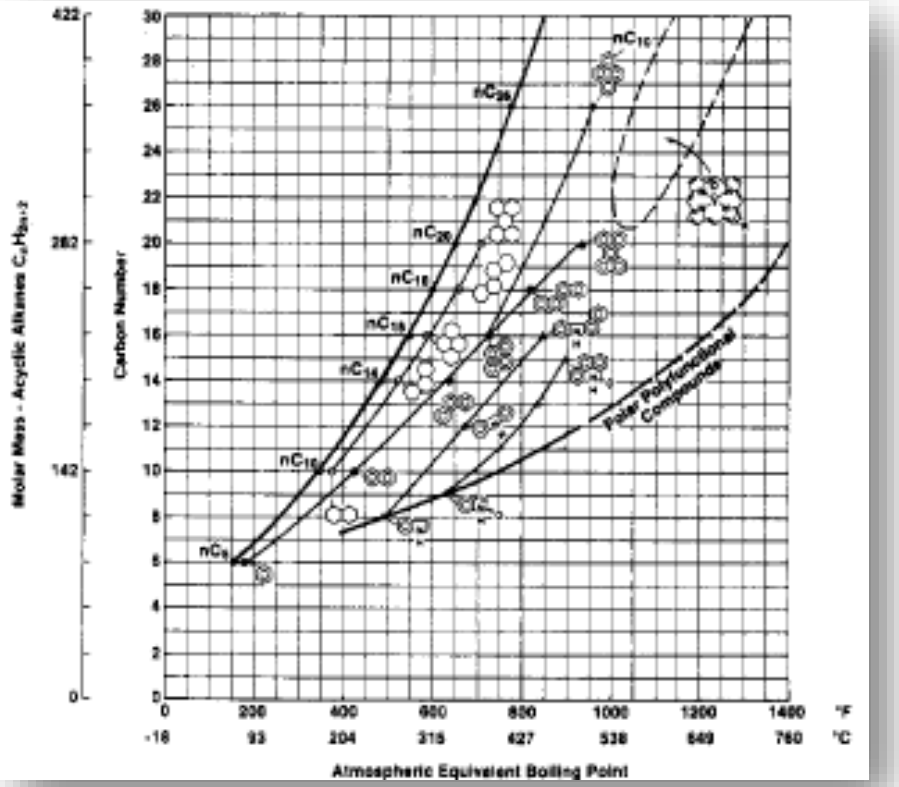

- Petroleum (fossil/**biomass/pyrolysis**): an complex mixture with continuum of chemical functionalities

Complex Mixtures – Example: Petroleum

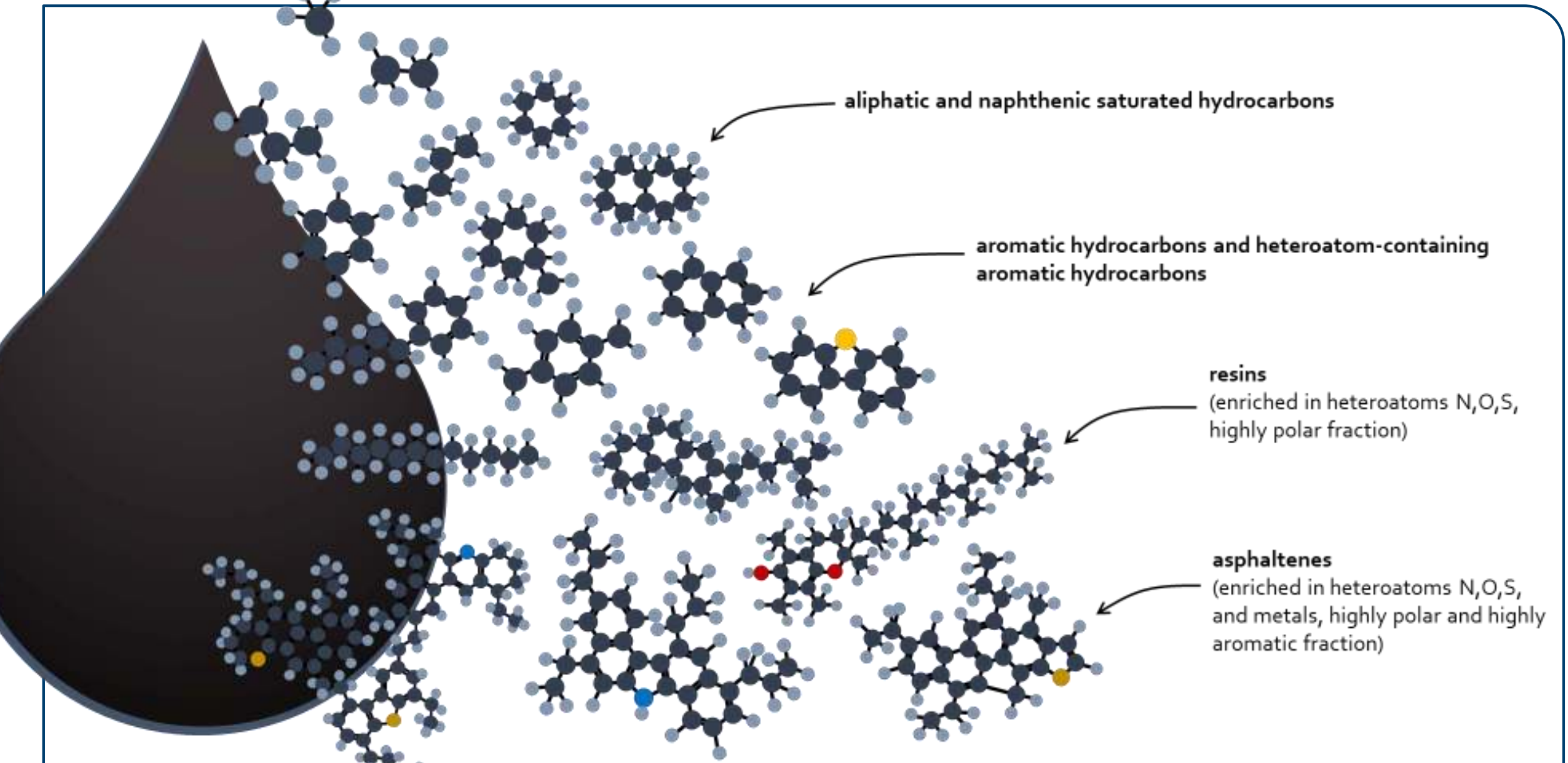

The many Facets of Mass Spectrometry

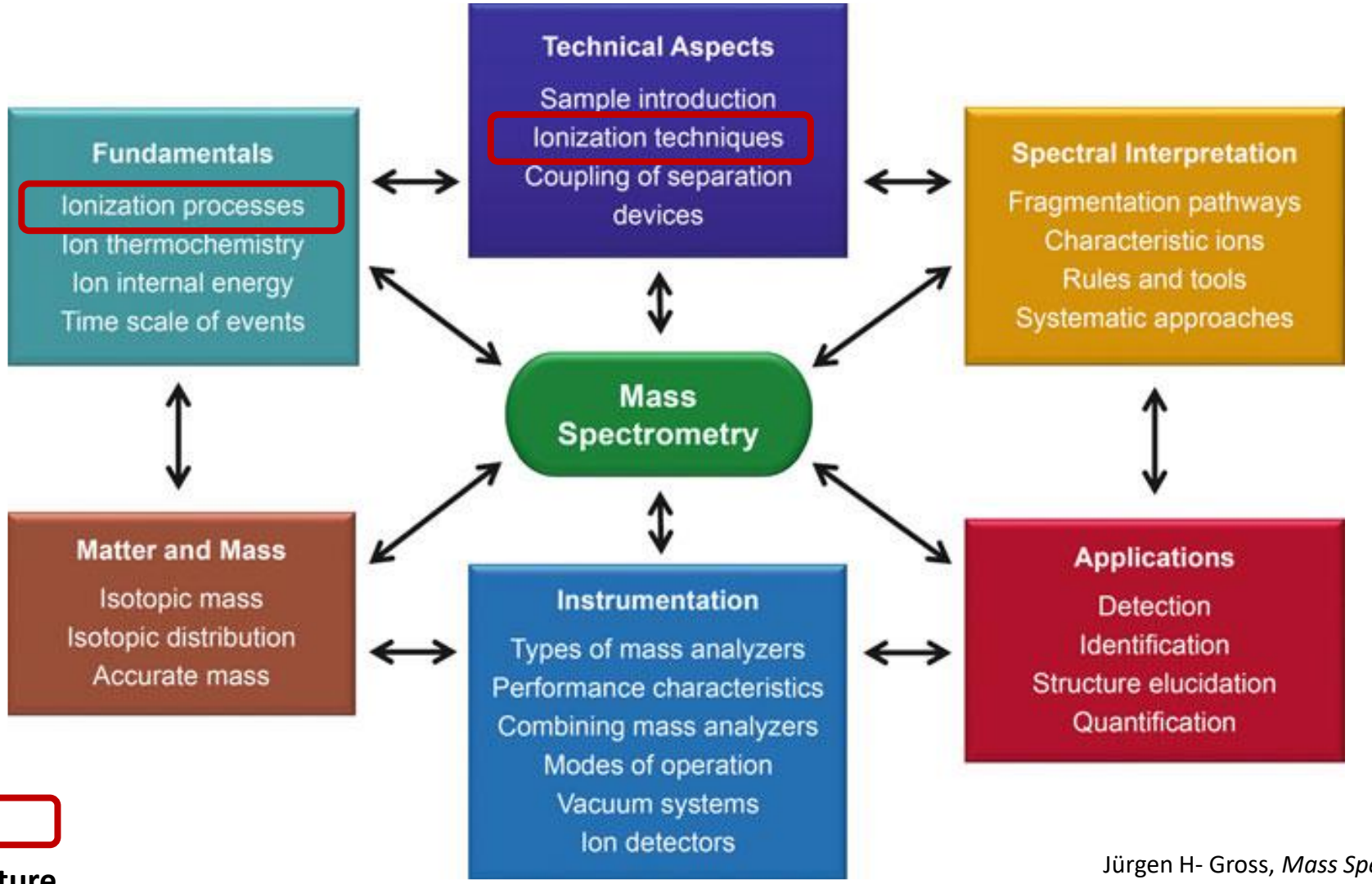

covered in this lecture

Jürgen H- Gross, *Mass Spectrometry – A Textbook*, **2017**, Spinger, ISBN *978-3-319-54398-7*

FT-ICR MS Instrumentation

Manufactures 2005…

Bruker Daltonics

Varian

Thermo

slide original from Peter O'Connor, adapted

Manufactures today

Bruker Daltonics

solariX / solariXR

scimaX

Non-commercial Platforms

21 T FT-ICR MS system at Pacific Northwest National Laboratory – PNNL (Washington, USA)

21 T FT-ICR MS system at National High Magnetic Field Laboratory – MagLab (Florida, USA)

Creating Ions – Main Physicochemical Pathways

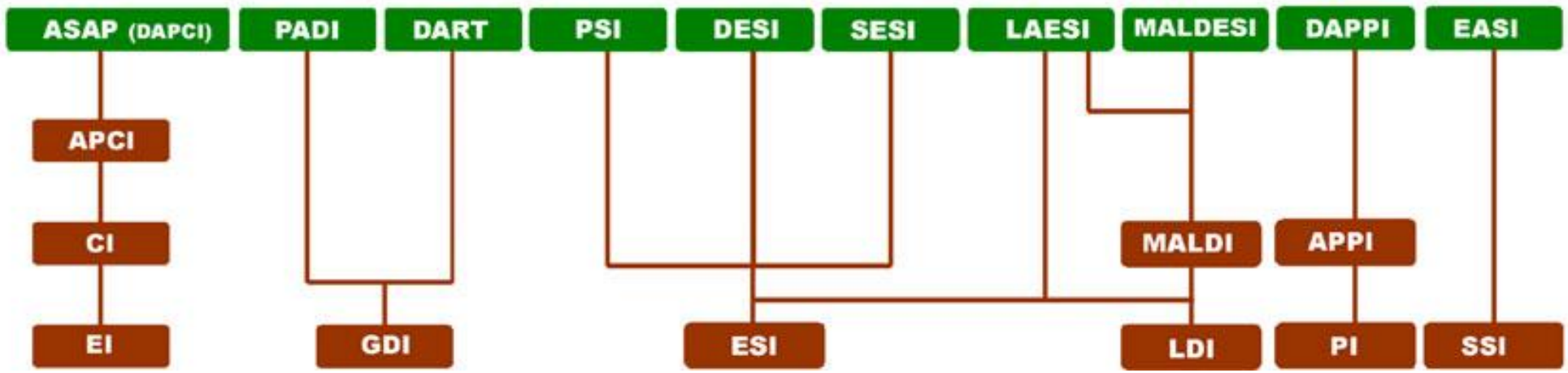

Simplified “ionization tree” – “root” technique given in brown and selected concepts based on them in green

Alberici et al., *Anal Bionanal Chem*, **2010**, 398:265–294

Primary Requirement for MS - Ions

Creating Ions – Main Physicochemical Pathways

	Molecular Ionization		
Atomic Ionization	Sample Phase	Mode	Pressure[a]
Thermal ionization	Gas phase	Electron ionization	HV
Spark source		Chemical ionization (CI)	IV
Glow discharge		Photoionization (PI)	HV
Inductively coupled plasma		Field ionization	HV
Resonance ionization		Metastable atom bombardment	HV
	Solution phase	Thermospray	LV
		Atmospheric-pressure CI	AP
		Atmospheric-pressure PI	AP
		Electrospray	AP
	Solid phase	Plasma desorption	HV
		Field desorption	HV
		Secondary-ion MS	HV
		Fast atom bombardment	HV
		Matrix assisted laser desorption	HV

[a] HV, high vacuum; IV, intermediate vacuum; LV, low vacuum; AP, atmospheric pressure.

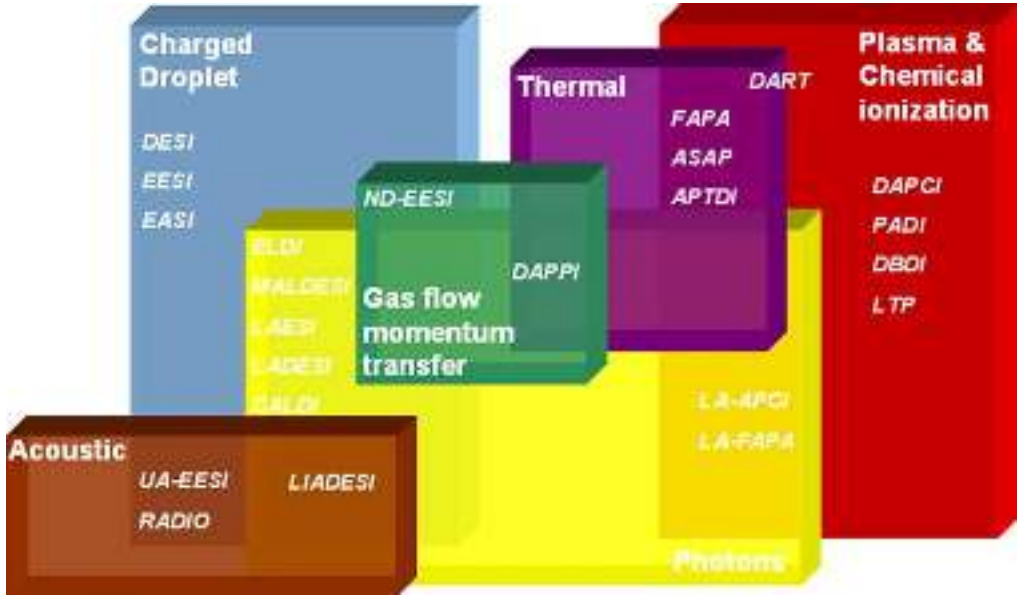

Structuring ionization concepts in MS with main physicochemical background

Chen et al., *JASMS*, **209**, 1947-1963

Basic Physical Concepts and Schemes for Ionization

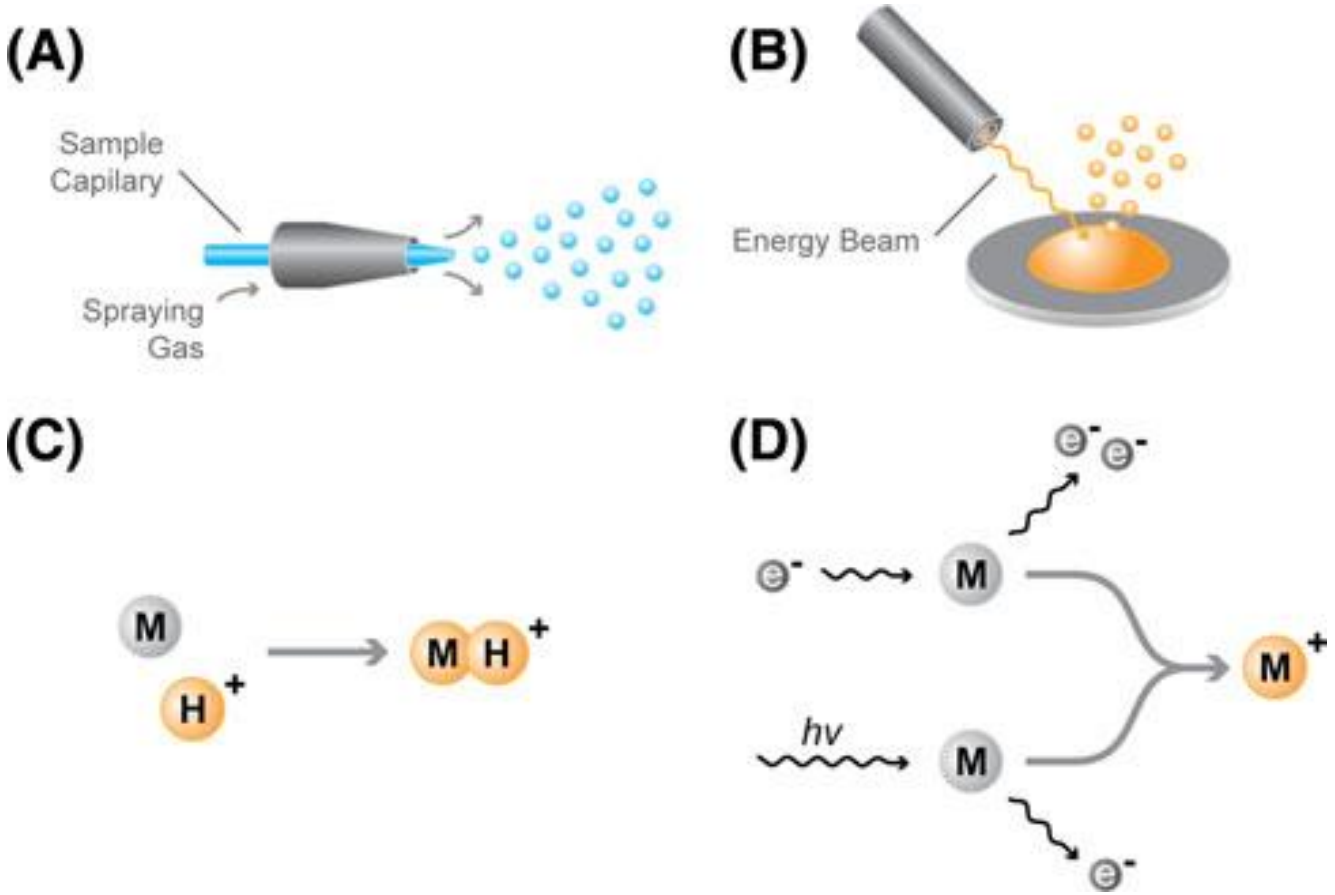

A) Spray Ionization

B) Desorption Ionization

C) Chemical Ionization

D) Electron/Photon Ionization

Pól et al., *Histochem Cell Biol*, **2010**, 134:423–443

Ionization Techniques

Timeline and the Ambient Ionization Techniques "Zoo"

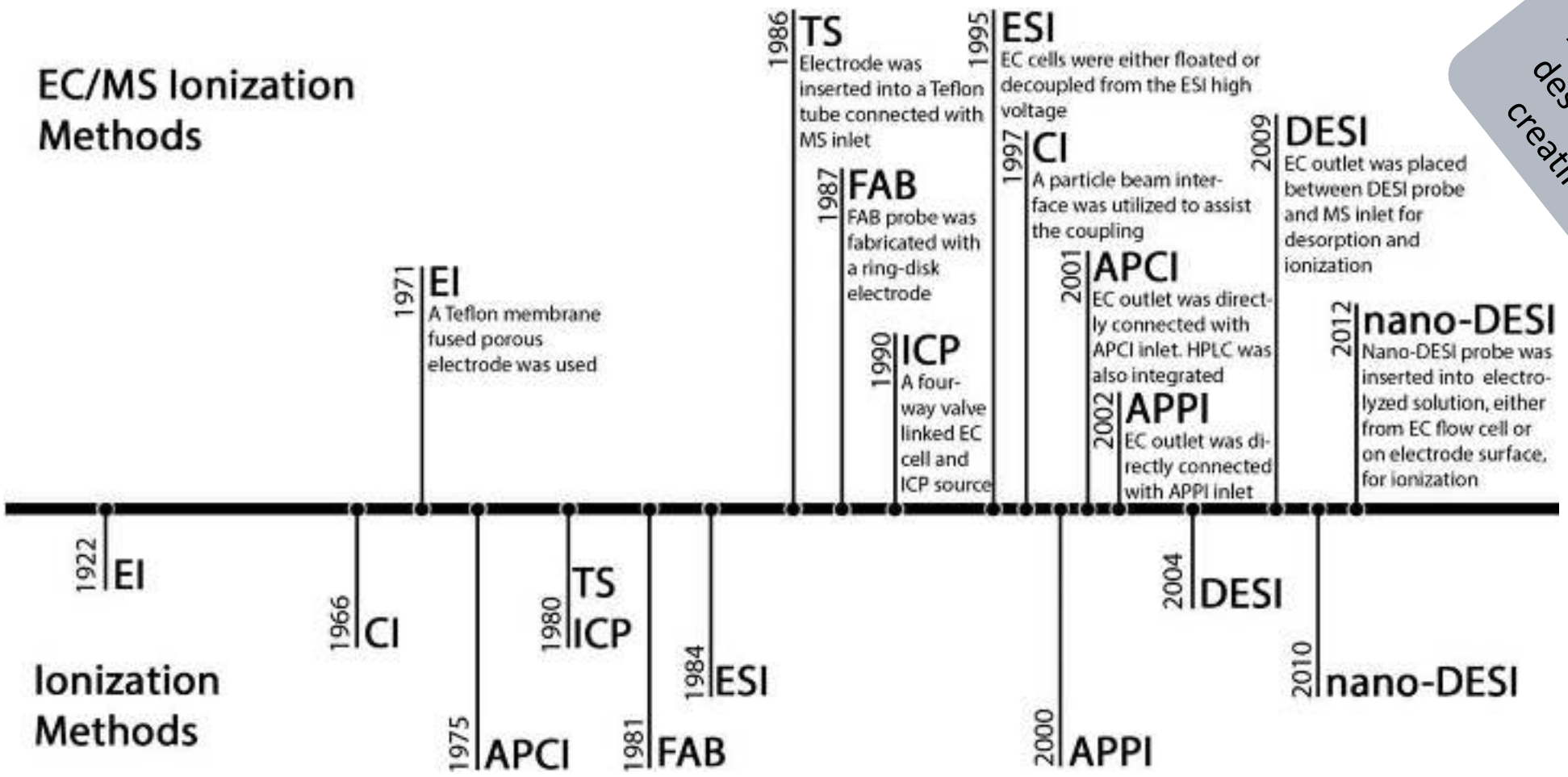

After ~2013 endless variations of desorption and spray techniques creating an abbreviation „zoo"

Liu et al., *The Analyst*, **2013**, 138, 5519

Trying to get an overview of existing ionization concepts and schemes…

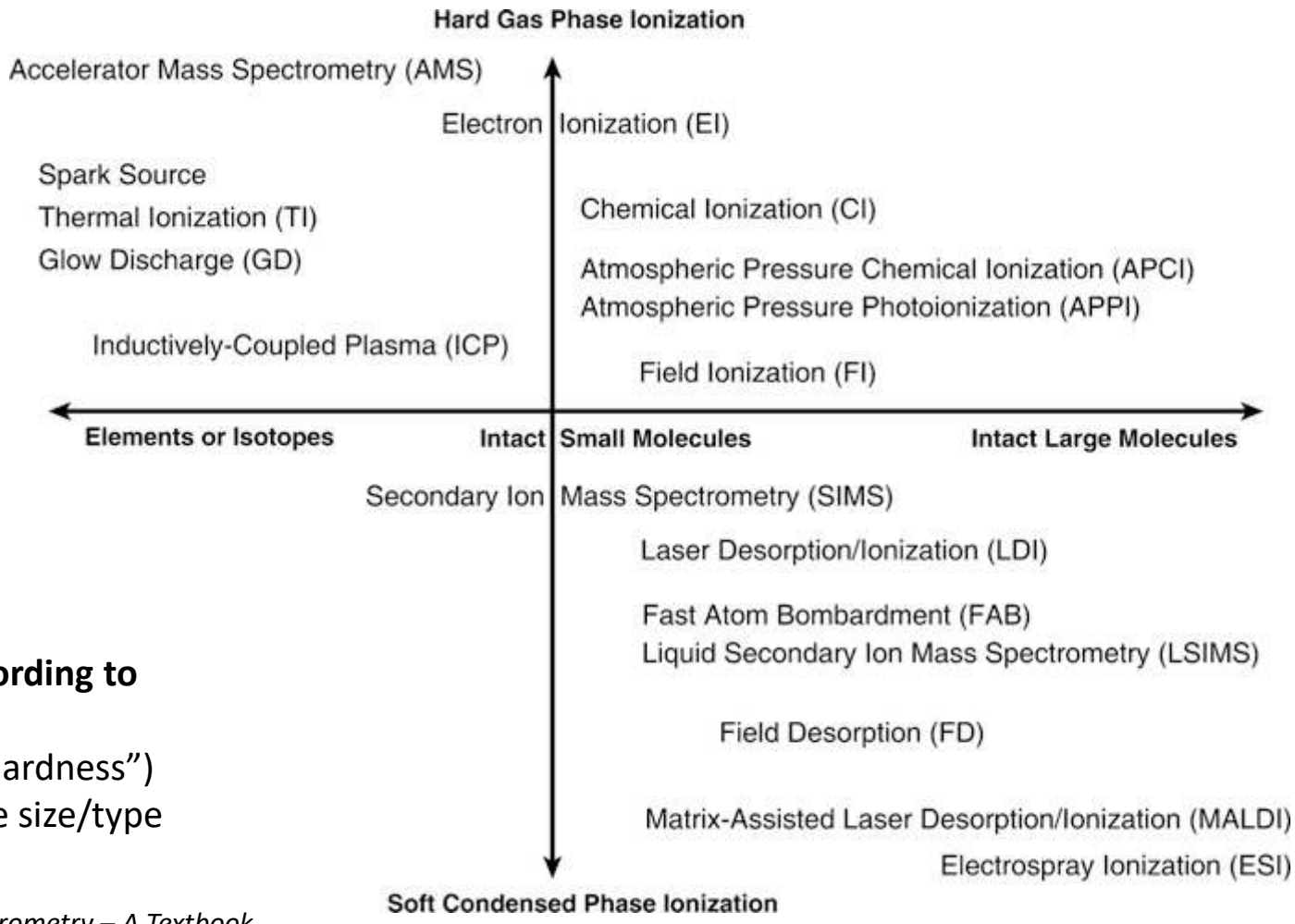

Structuring here according to

- energy uptake ("hardness")
- molecular/analyte size/type

Jürgen H- Gross, *Mass Spectrometry – A Textbook*, **2017**, Spinger, ISBN *978-3-319-54398-7*

Selectivity of Ionization in Mass Spectrometry – "Analytical Glasses"

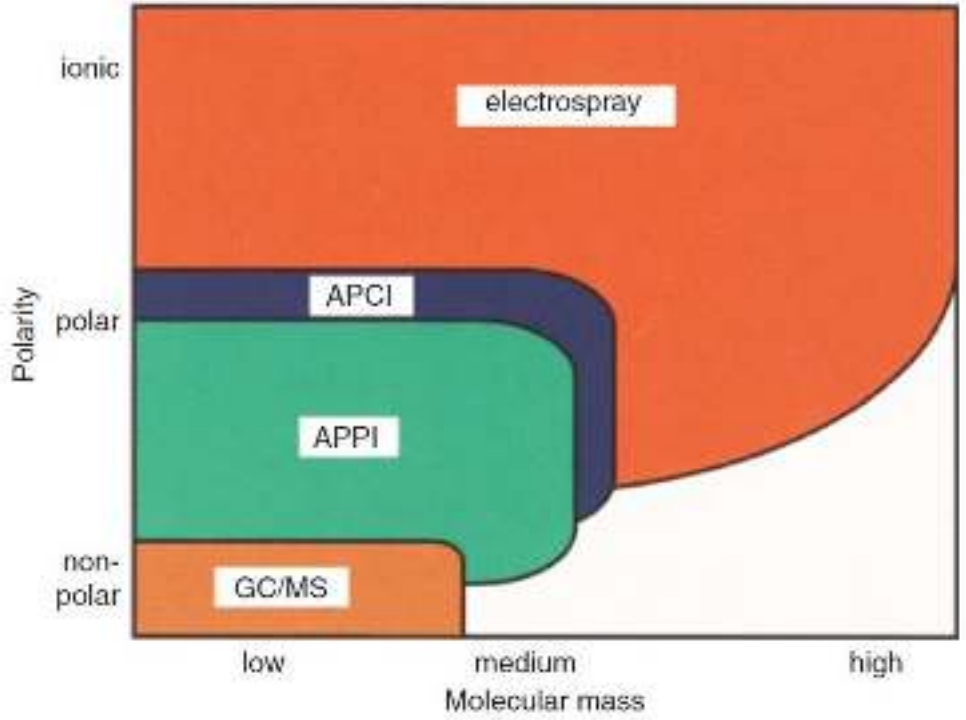

Cover of *Anal. Bioanal. Chem.*, **2004**, 378(4)

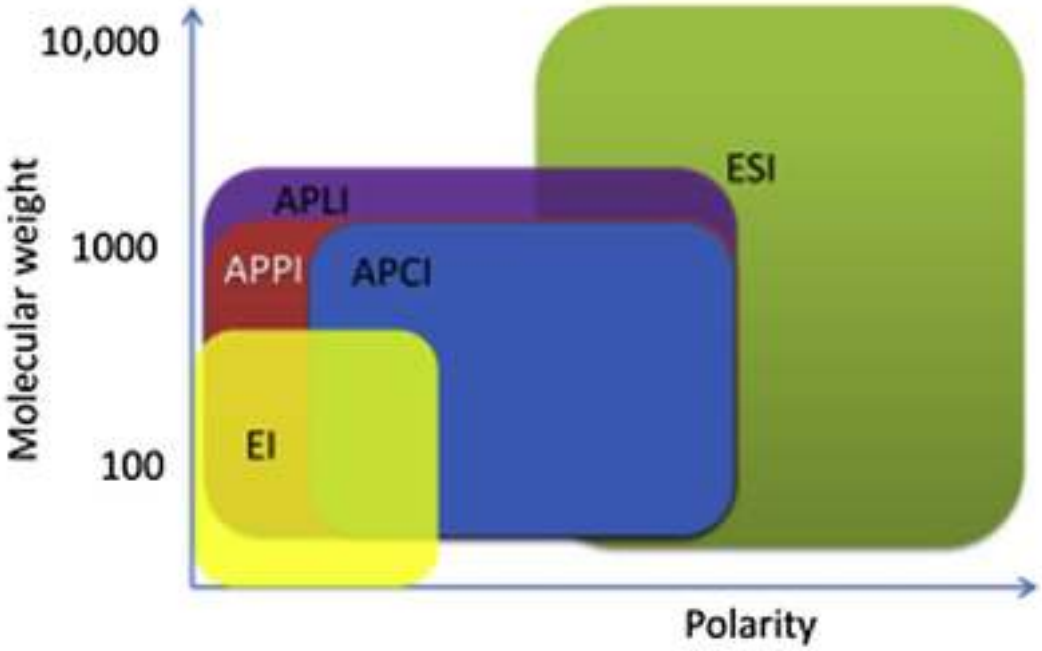

Li et al., *Analytica Chimica Acta*, **2015**, *43-61*

Selectivity of Ionization in Mass Spectrometry – "Analytical Glasses"

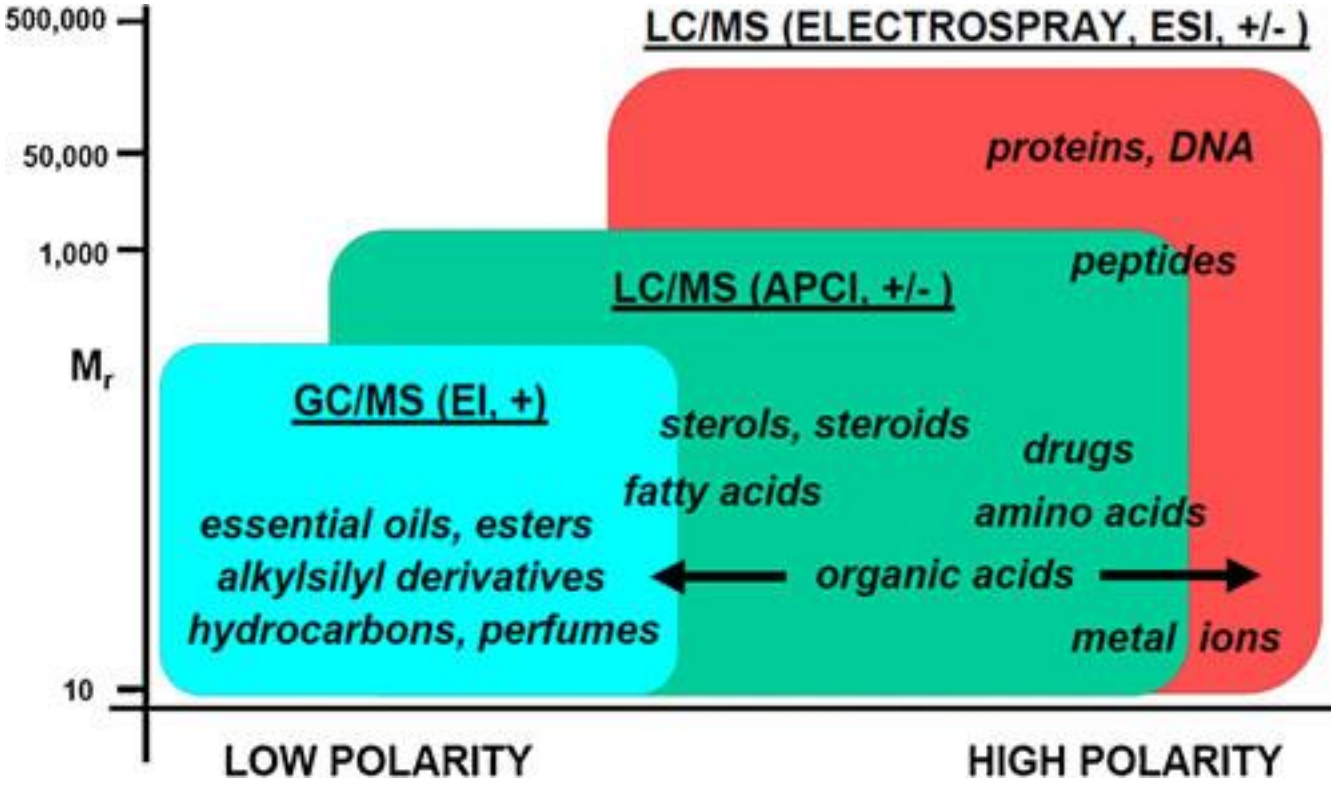

Halket et al., *J. Exp. Bot.*, **2005**, *56(410):219–243*

Outline

- **Introduction and Motivation**
  - Chemical Space, Selectivity of Ionization Techniques, Overview of Schemes and Concepts
- **Vacuum Ionization**
  - Electron Impact, Chemical Ionization and Photoionization
  - Laser Desorption Ionization and Allied Techniques
- **Atmospheric Pressure Ionization**
  - Electrospray Ionization, Atmospheric Pressure Chemical/Photo/Laser Ionization
  - Other Concepts and Combination, Applications
- **Summary**

Vacuum Ionization Concepts

Is this of relevance for the FT-ICR MS community?

Yes and No!

State-of-the-art FT-ICR MS comes with

- ESI/MALDI
- Optional: APPI, APCI, GC-APCI, nanoESI, DIP…

Electron and chemical ionization source

+ self-build and customized solutions

+ small specialized companies offering solutions

Electron (Impact) Ionization - EI

Basics and Technical Aspects

$$M + e^- \rightarrow M^{+\bullet} + 2e^-$$

neutral hit by energetic electron – effective collision exceed ionization energy (IE) and ejection of an electron forming a radical cation

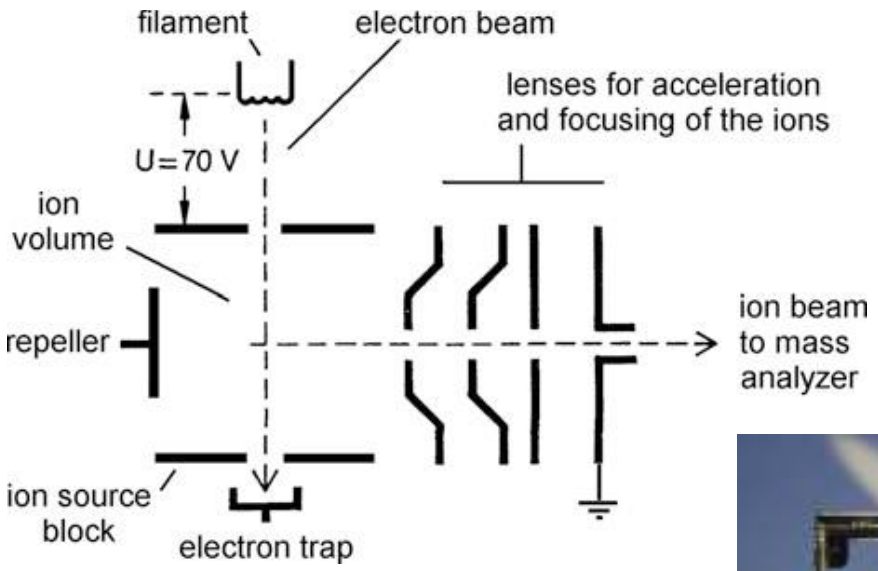

Principle layout of an EI source with photography of filaments

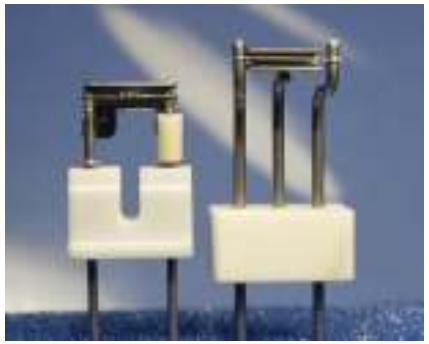

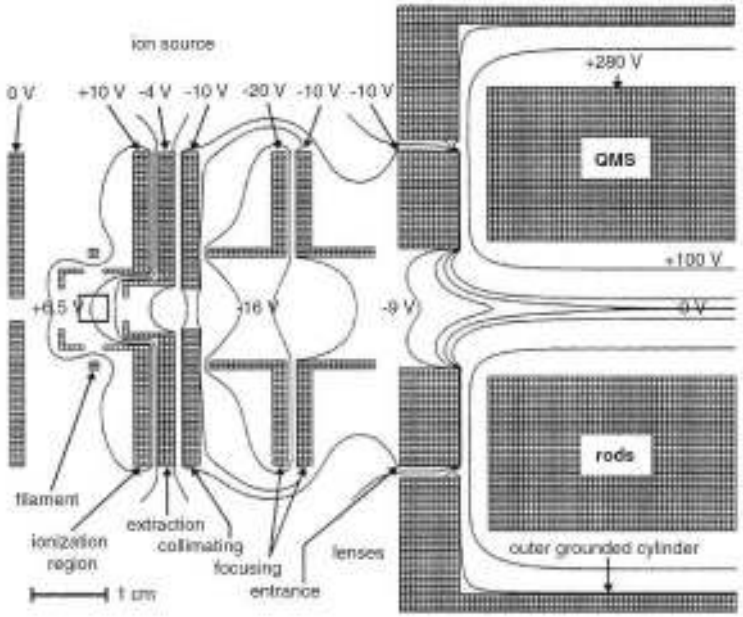

SIMION field simulation of a EI source of a quadrupole MS

Schröder (1991), Massenspektrometrie – Begriffe und Definitionen, Heidelberg

Blaum et al., *Int J Mass Spectrom*, **1998**, 181:67-87

Electron (Impact) Ionization - EI

The concept of ionization energy (IE)

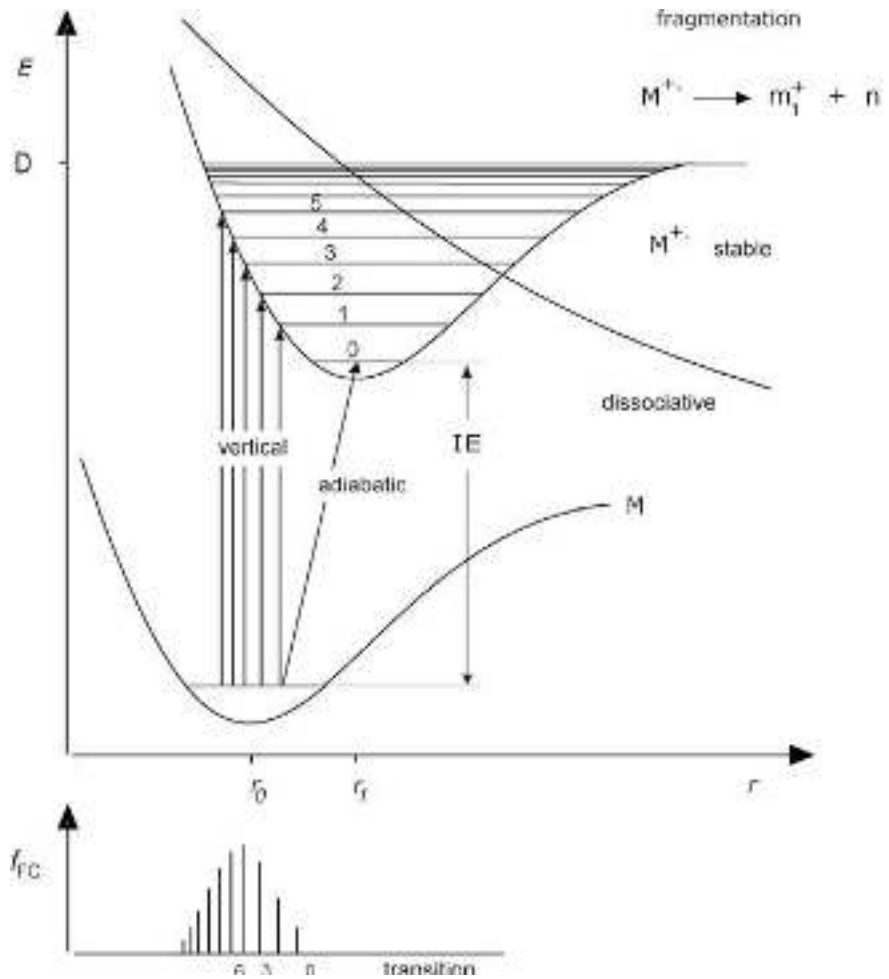

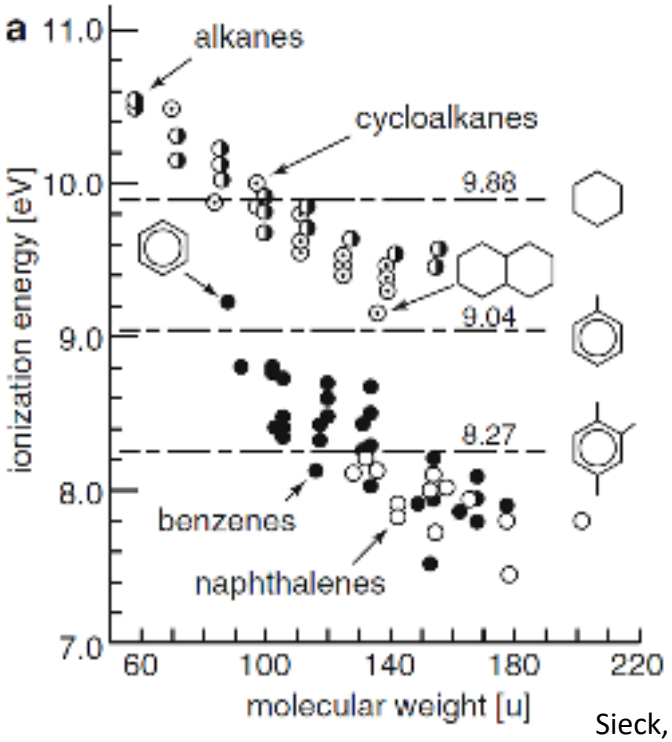

Sieck, *Anal Chem*, **1983**, 55:38-41

- fast process → vertical transition (Franck-Condon principle)
- e^- from the highest occupied molecular orbital (HOMO) is removed (IE ~ negative energy of the HOMO (Koopman's theorem)
- ionization energy of most organic molecules range from 7-15 eV

Stability of Ions – Stable, Metastable and Unstable Ions

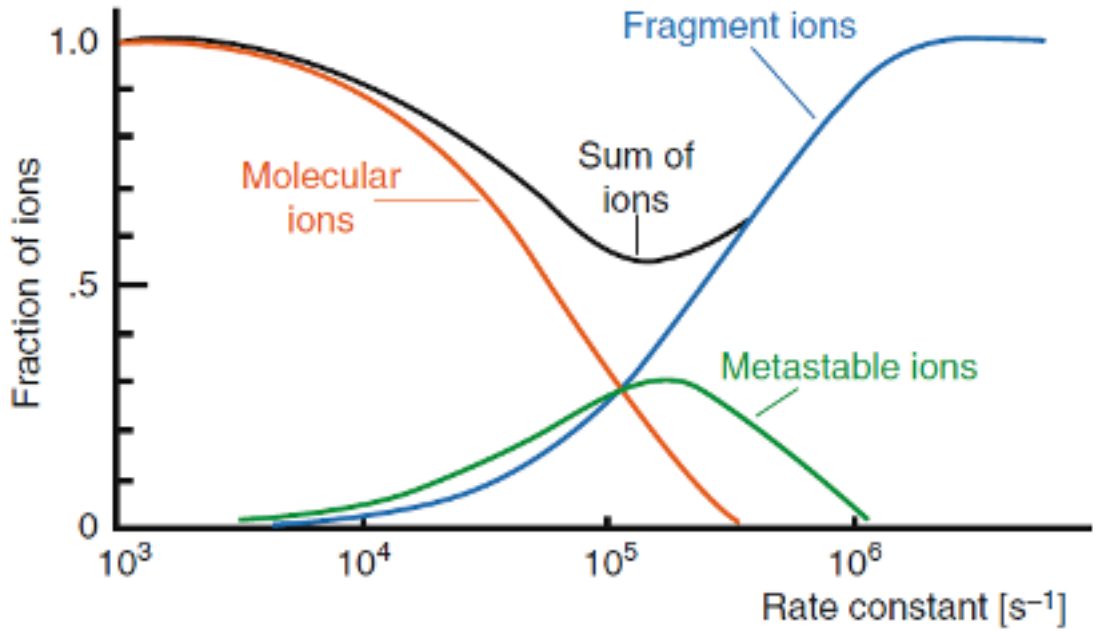

Chupka, *J Chem Phys*, **1959**, 30:191-211

stable ions: $k < 10^5\ s^{-1}$
metastable ions: $10^5\ s^{-1} < k < 10^6\ s^{-1}$
unstable ions: $k > 10^6\ s^{-1}$

- needs to be considered for all ionization techniques
- in particular for mass storing devices in the mass spectrometric setup (ion traps or other ion accumulation)

"Do my ion arrive at the mass analyzer without further reactions and if not how does these reactions look like?"

Ionization Cross Sections – a Measure for Ionization Efficiency

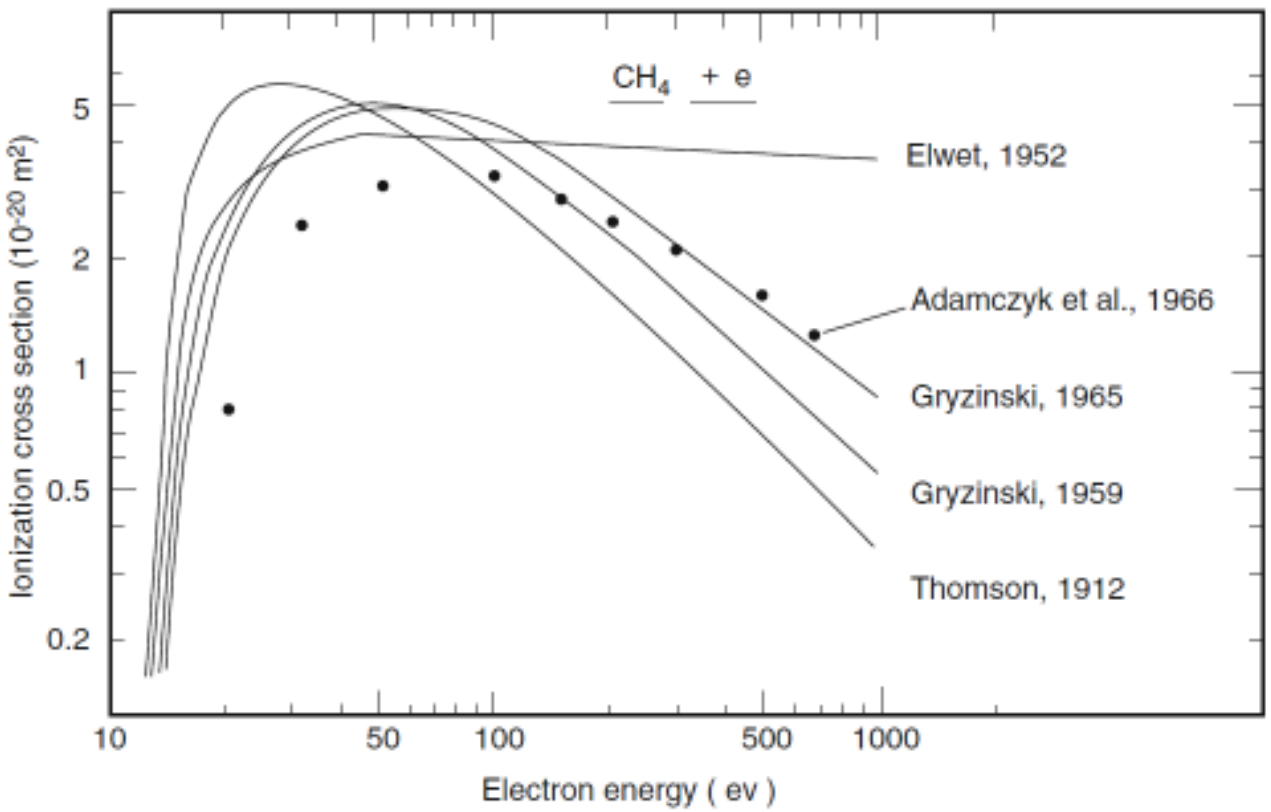

- ionization cross section within on-order-of-magnitude
- universal + no matrix effects → quantification possible
- high ionization efficiency + highly reproducible

Märk, *Electron impact ionization. In: Futrell JH (ed) Gaseous Ion Chemistry and Mass Spectrometry.*, **1986**

Problems and Limitations of EI

Fragmentation: Benefit and drawback at the same time

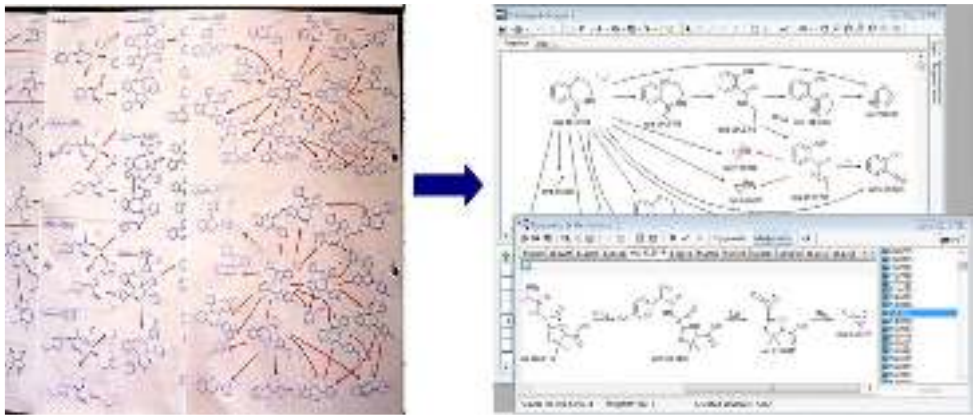

Highly complex fragmentation pattern are a problem for complex mixture analysis – particularly for comprehensive analysis of unknowns

Kind and Fiehn, *Bioanal Rev*, **2010**, 2:23-60

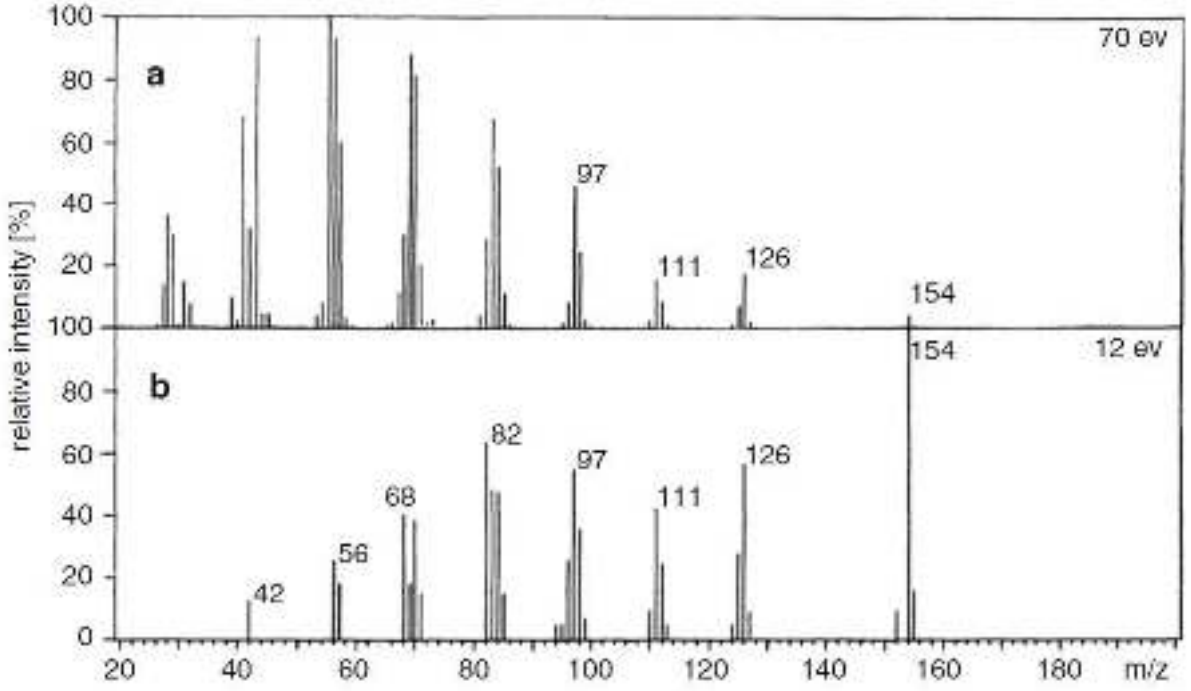

Comparison of the fragmentation pattern of Undecan-1-ol of EI at 70 and 12 eV (significant loss in sensitivity for low eV EI!)

Brophy et al. , *Org Mass Spectrom*, **1988**, 23:659-662

Problems and Limitations of EI – Coupling of LC to vacuum ionization

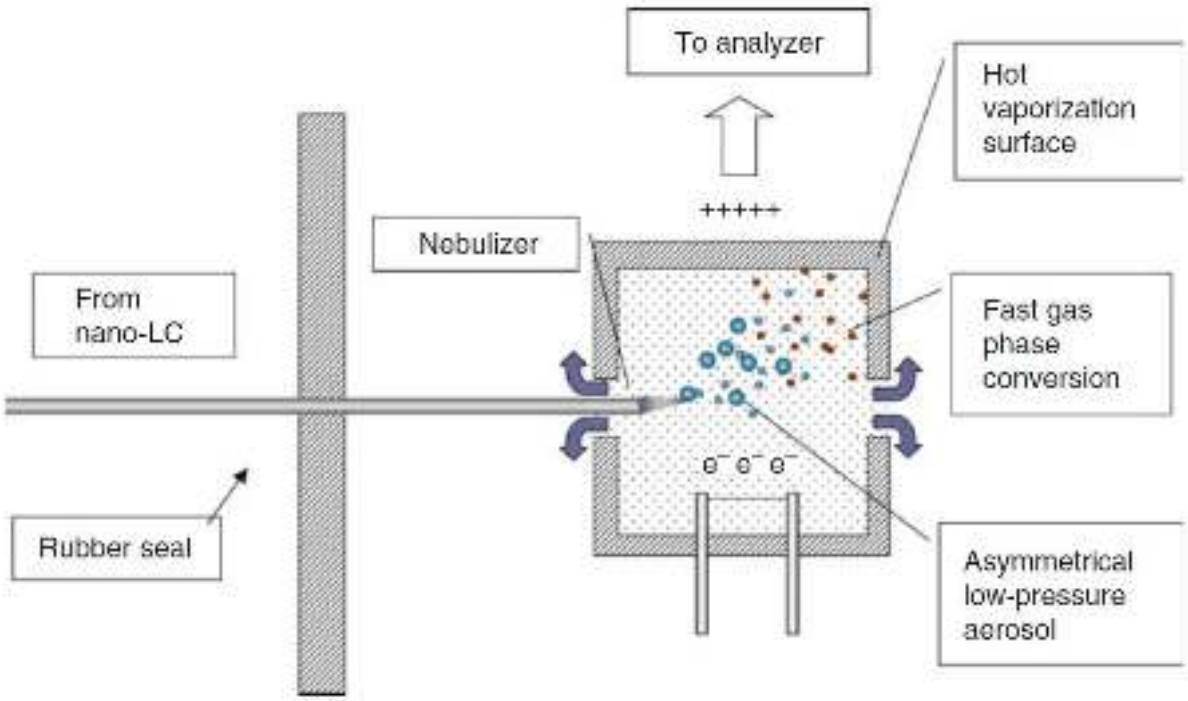

Nano-LC-EI interface with direct connection of LC effluent into the vacuum ionization chamber

LC coupling to vacuum ionization technically difficult due to 1) challenge in maintaining the vacuum (high **pumping requirements**, potential discharge for pressure spikes, etc.), and 2) adiabatic expansion caused by the pressure drop leads to **freezing out** the solvent blocking the inlet capillary easily.

Käfer et al., *Talanta*, **2019**, 309-316

Direct Inlet Probe as Sample Introduction Technique

inlet technique for solid and high-viscous materials, a temperature program is applied to evaporate and consequently ionize the analytes in the ionization source

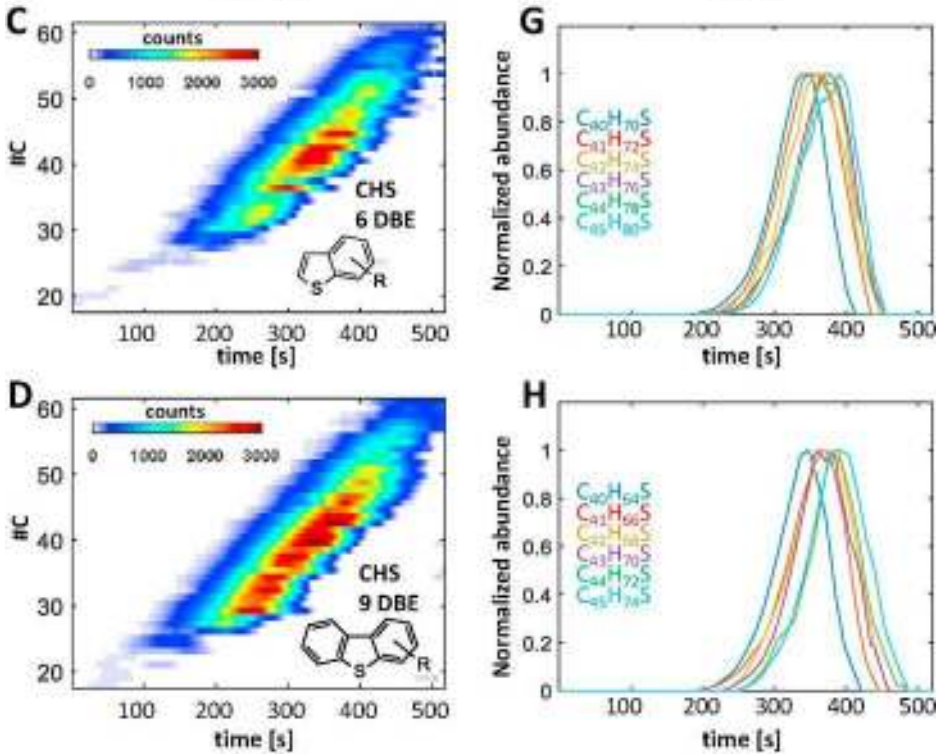

analysis of bitumen by DIP-EI high-resolution time-of-flight mass spectrometry

Käfer et al., *Talanta*, **2019**, 309-316

Electron (Impact) Ionization - EI

Application of EI in FT-ICR MS

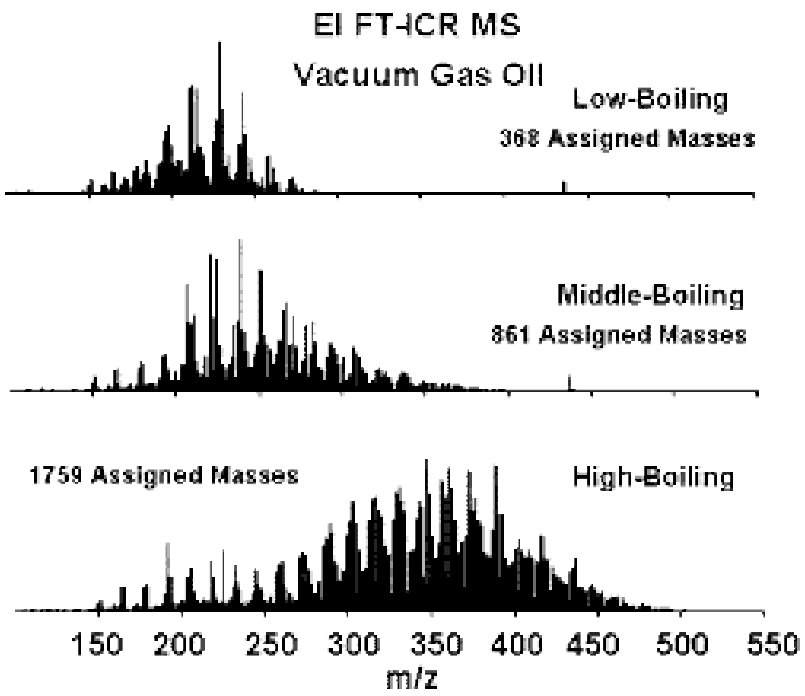

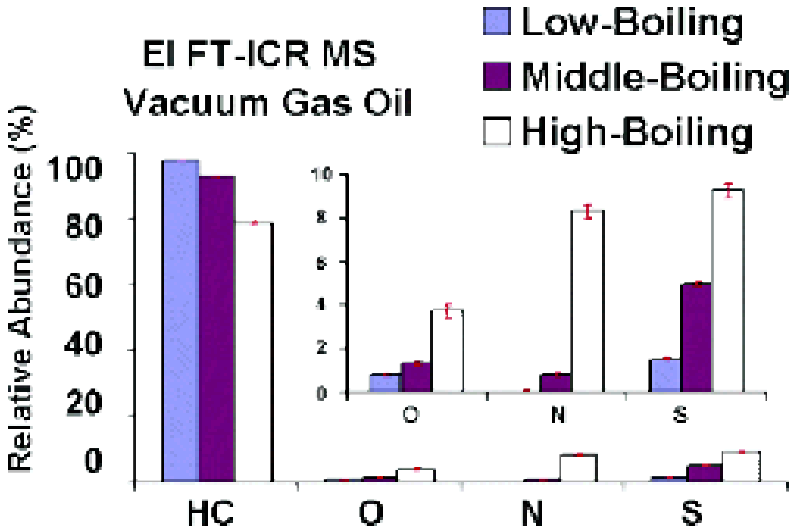

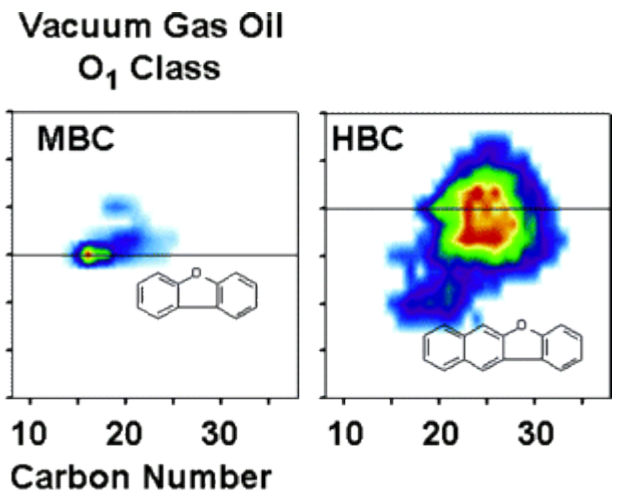

EI FT-ICR MS of vacuum gas oil distillation fractions – aromatic constituents show less fragmentation and the molecular analysis advantageous for spectral analysis in complex mixtures (but limited)

Fu et al., *Energy and Fuels*, **2006**, 661-667

but EI almost not featured anymore as a consequence of the drawbacks and manufacturer orientation

Brief Basics and Variations

- gaseous molecules react with ions → ion-molecule reactions (bimolecular processes)
- may involve transfer of an electron, proton, or other ions between the reactants
- low mbar vacuum in the source increasing dwell time and collisions
- formation of quasi-molecular ions, *e.g.*, $[M+H]^+$ and $[M-H]^+$

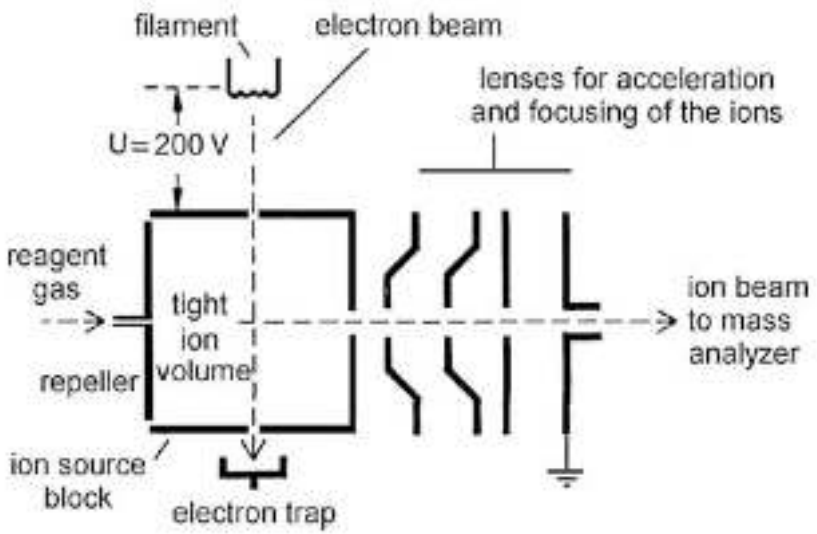

Layout of a chemical ionization source

Schröder (1991), Massenspektrometrie – Begriffe und Definitionen, Heidelberg

Reagent gas	Reagent ions	Neutral from reagent ions	*PA* of neutral product [kJ mol^{-1}]	Analyte ions and relative analyte ion masses
H_2	H_3^+	H_2	424	$[M+H]^+$, $[M-H]^+$ [M+1], [M−1]
CH_4	CH_5^+ ($C_2H_5^+$ and $C_3H_5^+$)	CH_4	552	$[M+H]^+$, also $[M+C_2H_5]^+$ and $[M+C_3H_5]^+$ [M+1], [M+29], [M+41]
i-C_4H_{10}	t-$C_4H_9^+$	i-C_4H_8	820	$[M+H]^+$, also $[M+C_4H_9]^+$, (eventually $[M+C_3H_3]^+$, $[M+C_3H_5]^+$ and $[M+C_3H_7]^+$), [M+1], [M+57]
NH_3	NH_4^+	NH_3	854	$[M+H]^+$, $[M+NH_4]^+$, [M+1], [M+18]

Common positive chemical ionization reagent gases

Field Desorption (FD) Ionization FT-ICR MS Example Study

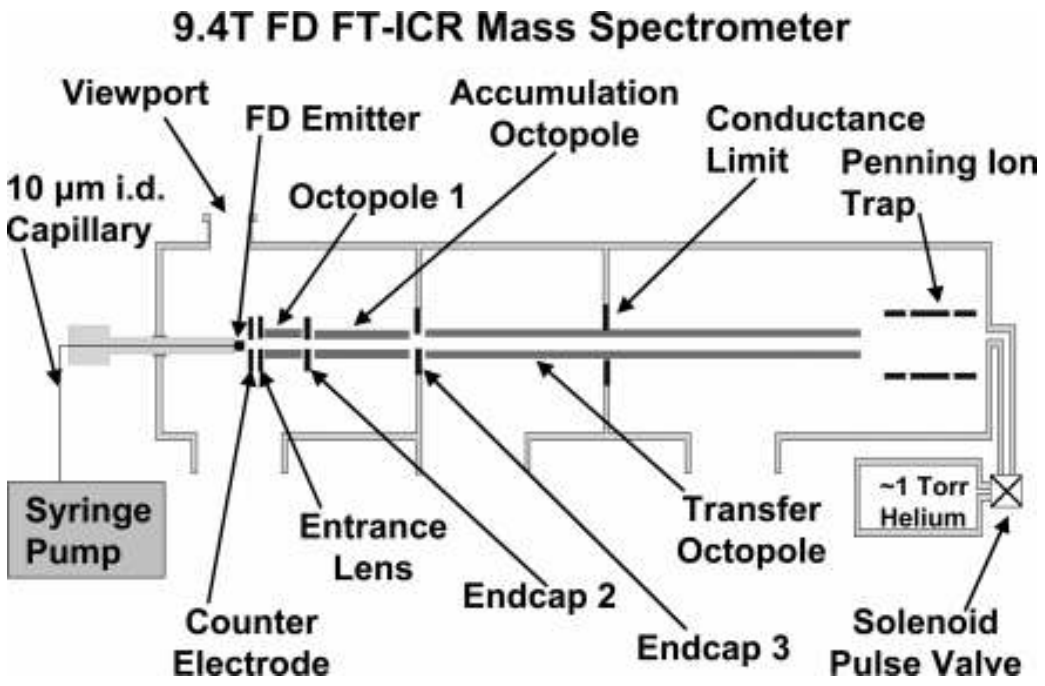

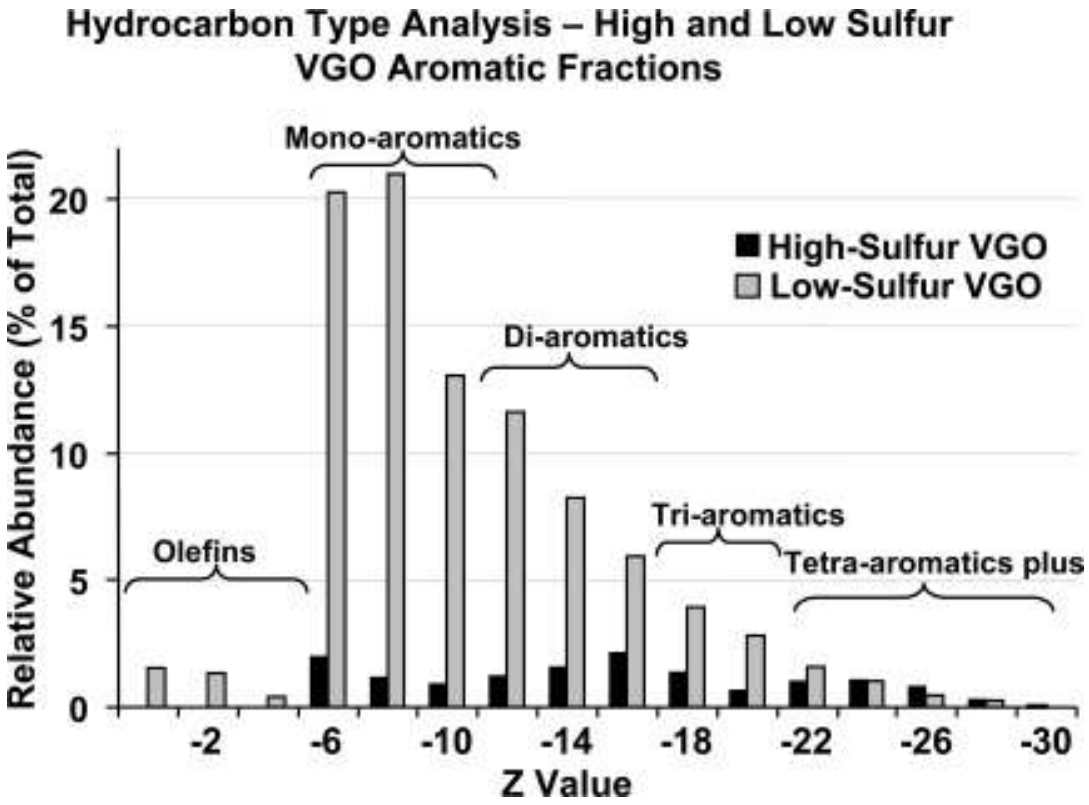

Schaub et al., *Energy and Fuels*, **2005**, 1566-1573

Ionization – Photoionization

Soft ionization of analytes by photon irradiation

at atmospheric pressure

Most often divided in:

- **a**tmospheric **p**ressure **p**hoto **i**onization utilizing rare gas discharge lamps (APPI using Krypton lamps, 10/10.6 eV)
- **a**tmospheric **p**ressure **l**aser **i**onization (APLI, most often 248/266 nm)

NdYag-Laser (266nm)
2 x 4,66eV – 9,3eV

at reduced pressure / vacuum

Most often divided in:

- **s**ingle-**p**hoton **i**onization (SPI) using VUV laser, synchrotron radiation or discharge lamps
- **r**esonance-**e**nhanced **m**ulti**p**hoton **i**onization (REMPI)

no matrix effects

almost no fragmentation

F2-Laser (157nm)
7.9eV

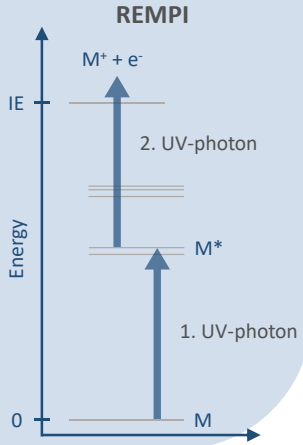

General Concept and Light Sources - REMPI

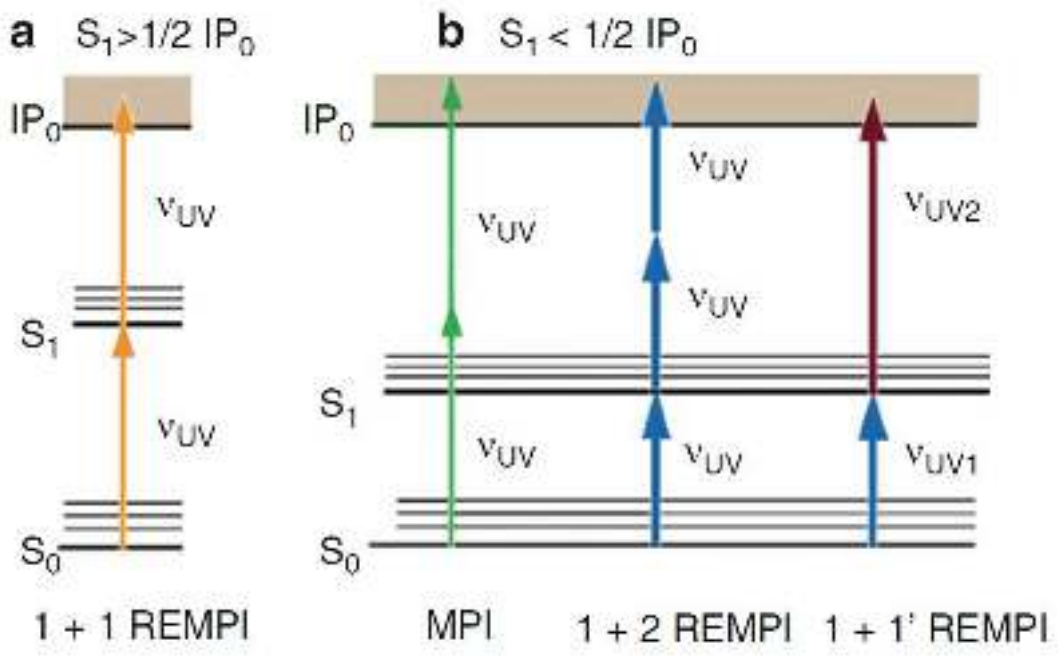

Multiphoton ionization schemes, a) Resonant 1+1 process, b) multicolor less frequently used multiphoton ionization schemes

Matsumoto et al., *Shinku*, **2007**, 50:241-245

Light source	Wavelength range		Lowest molecular absorption	Typ. transitions
Two-photon absorption $\lambda_{exc} = 1/2\ \lambda_{UV}$	150 nm / 8.3 eV	Vacuum UV	Alkanes	$\sigma^* \leftarrow \sigma$
	200 nm / 6.2 eV		Alkenes, Alkines, Alcohols, HCN, NH_3, OCS	$\sigma^* \leftarrow n$, $\pi^* \leftarrow \pi$
Frequency doubling $\lambda_{exc} = 1/2\ \lambda_{laser}$	250 nm / 5.0 eV		Aromatics, H_2S	$\pi^* \leftarrow n$
	300 nm / 4.1 eV	UV		
Tunable laser wavelength $\lambda_{exc} = \lambda_{laser}$	350 nm / 3.5 eV		Aldehydes	$\pi^* \leftarrow \pi$ conjug. syst.
	400 nm / 3.1 eV		SO_2	
	450 nm / 2.8 eV	VIS		$\pi^* \leftarrow n$ conjug. syst.
	500 nm / 2.5 eV		NO_2	

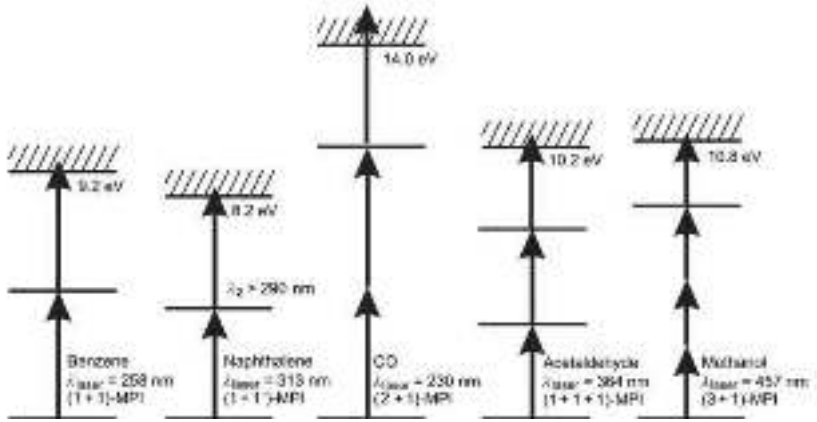

Photoionization and Photo-Induced Processes in Mass Spectrometry, Ralf Zimmermann and Luke Hanley, 2021 WILEY-VCH GmbH

General Concept and Light Sources - REMPI

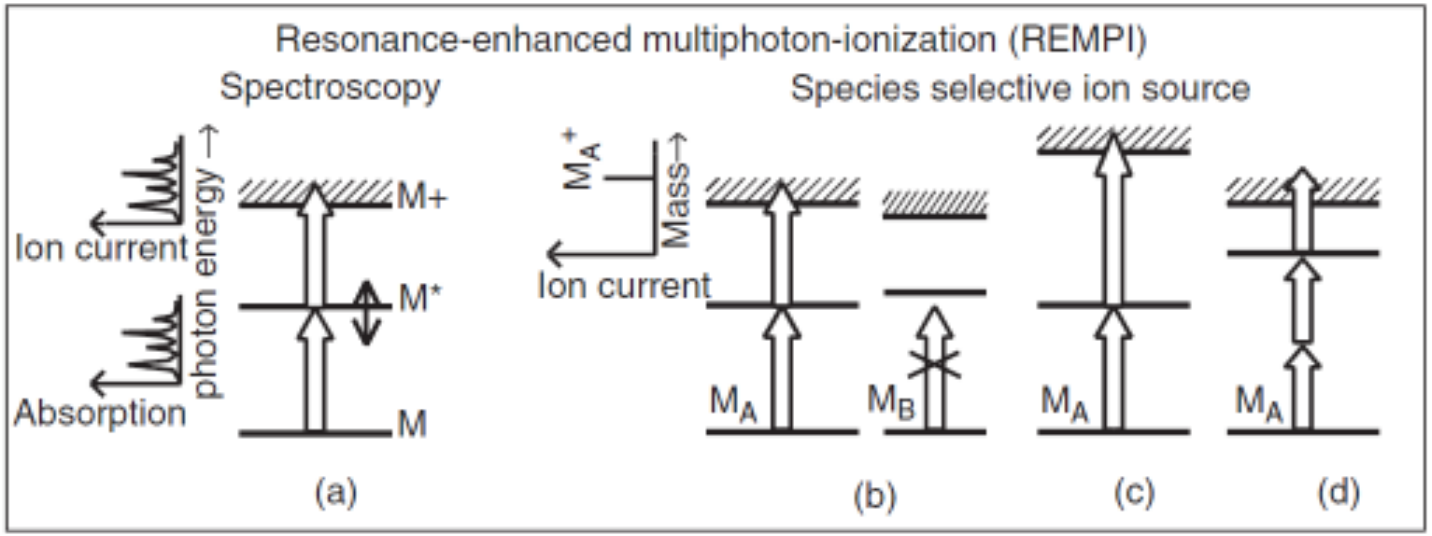

Figure 2.1 Schematic representation of the different possibilities of REMPI: (a) tuning the wavelength of the ionizing laser: the ion current (REMPI signal) reflects the gas-phase UV spectrum; (b) resonance-enhanced, two-photon ionization with photons of same energy (one-color REMPI) and illustration of selective ionization; (c) resonance-enhanced, two-photon ionization with photons of different energies (two-color REMPI); and (d) resonance-enhanced, three-photon ionization of higher order, here the example of (2 + 1)-REMPI.

Photoionization and Photo-Induced Processes in Mass Spectrometry, Ralf Zimmermann and Luke Hanley, 2021 WILEY-VCH GmbH

Ionization Cross Sections

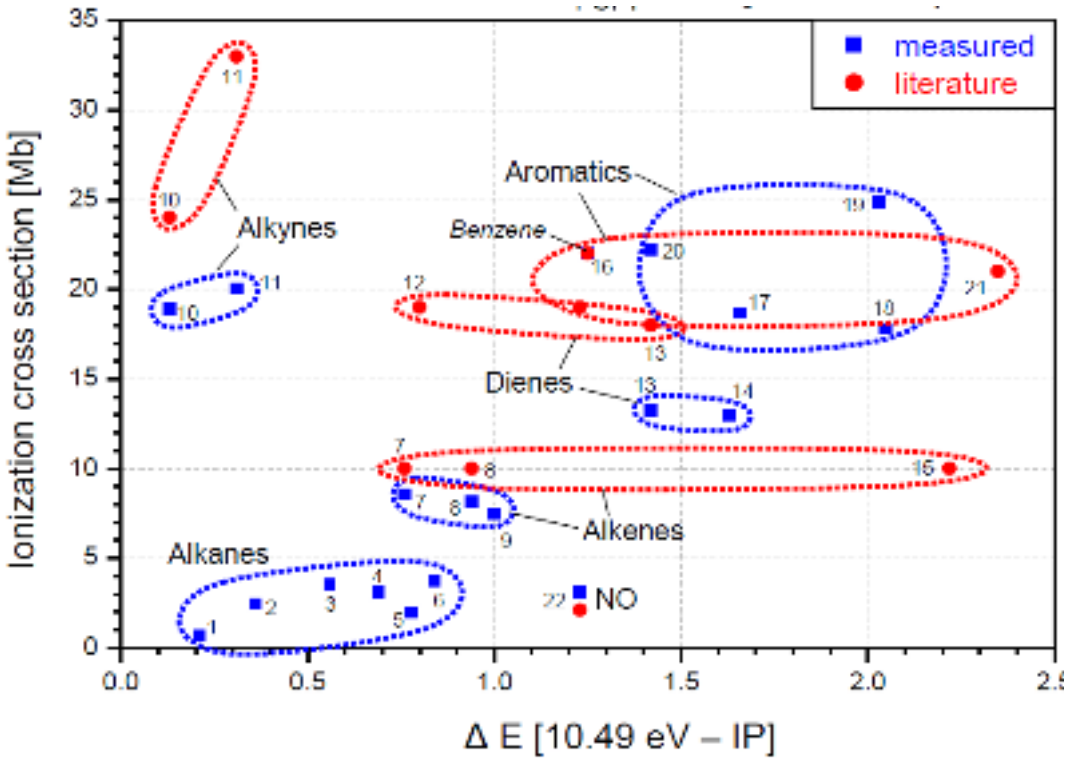

Adam et al., *Anal Bioanal Chem*, **2007**

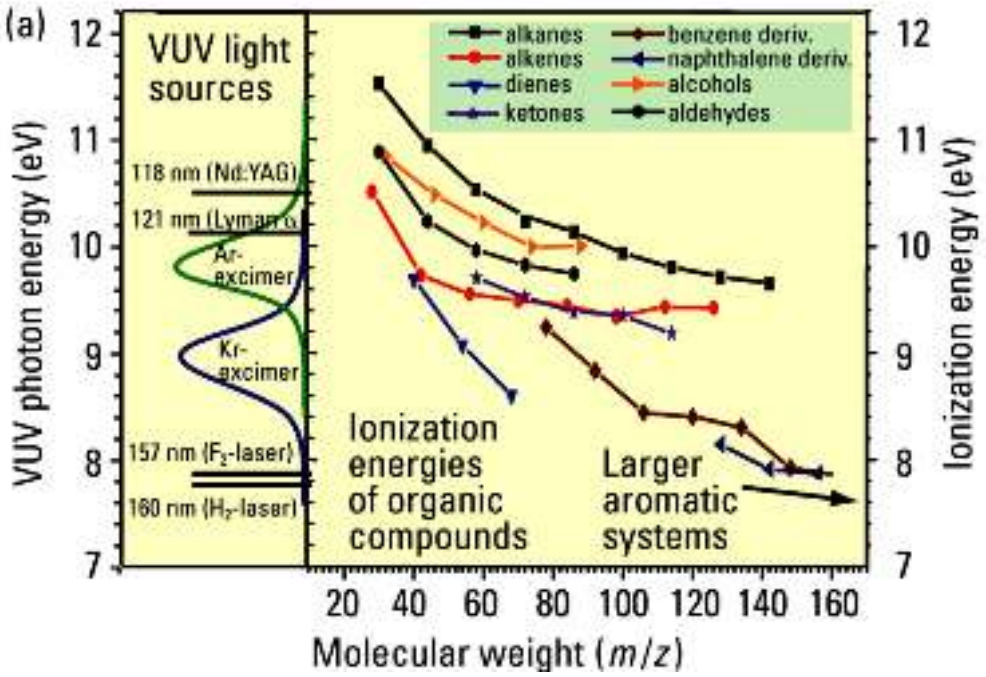

Hanley, L.; Zimmermann, R. *Analytical Chemistry* **2009**

- single photon ionization ion yield ~ concentration x VUV intensity x cross section
- variability of cross section in single photon ionization roughly one order of magnitude
- quantification feasible!

VUV Light Sources in Single Photon Ionization

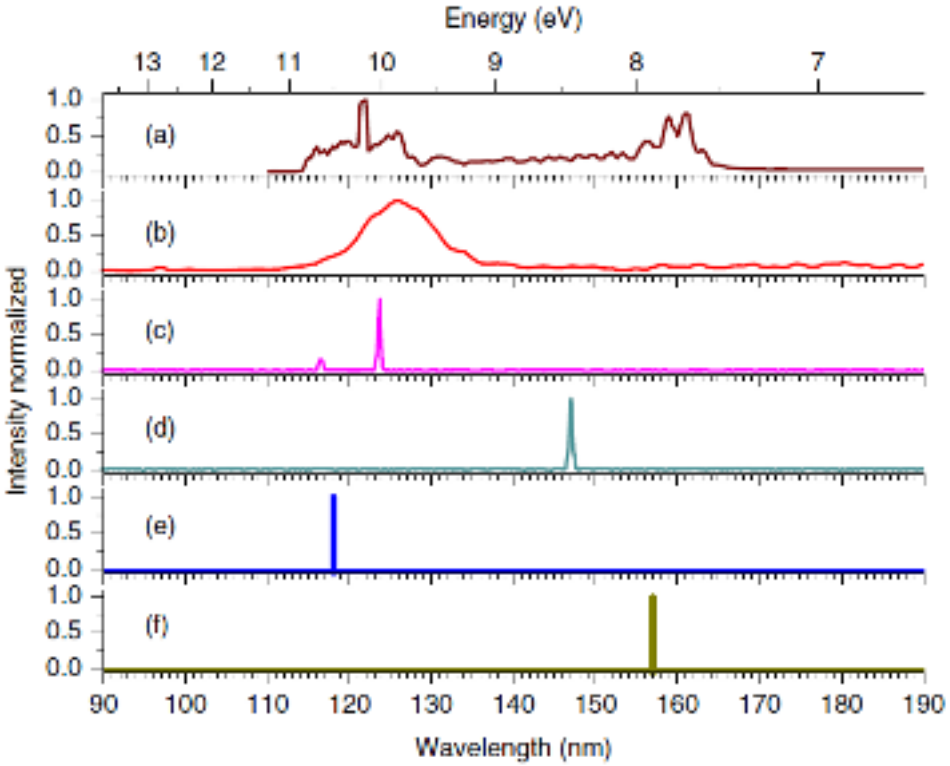

Figure 3.1 Measured emission spectra of different VUV light sources in the wavelength range between 90 and 190 nm, corresponding to photon energies from 6.5 to 13.75 eV (VUV spectrometer with low resolution monochromator): (a) D_2-Lamp (McPherson), (b) Ar-Electron beam-pumped lamp, (c) Kr-discharge lamp (PID), (d) Xe-discharge lamp (PID), (e) ninth harmonic frequency of the Nd:YAG laser line (sketched), and (f) F_2-Excimer laser line (sketched).

Photoionization and Photo-Induced Processes in Mass Spectrometry, Ralf Zimmermann and Luke Hanley, 2021 WILEY-VCH GmbH

Single Photon Ionization – Example and Cross Section Correction

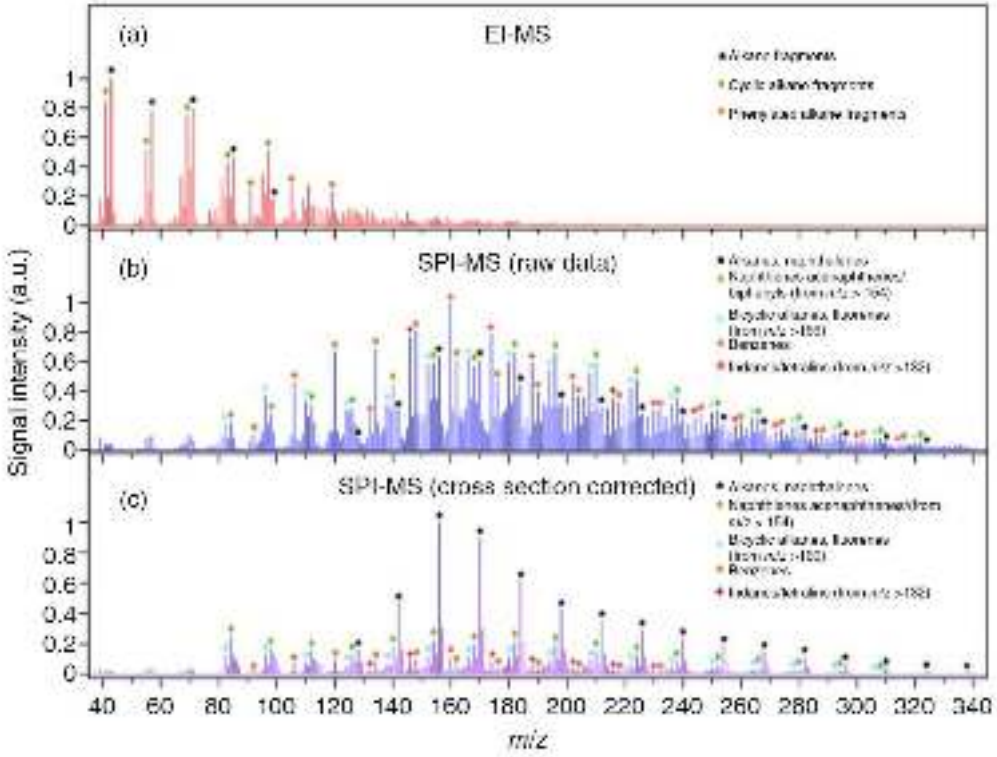

Figure 3.3 Three mass spectra of a mineral oil-type fuel (diesel fuel, fully vaporized). (a) 70 eV EI mass spectrum obtained by summing up over the total gas chromatographic run. (b) SPI mass spectrum (raw data) obtained by summing up over the total gas chromatographic run. (c) Cross section corrected SPI mass spectrum (averaged cross sections for compound classes) approximating the molar concentration profile of the mineral oil distillate sample. Source: Modified from Eschner et al. (2011b).

Photoionization and Photo-Induced Processes in Mass Spectrometry, Ralf Zimmermann and Luke Hanley, 2021 WILEY-VCH GmbH

Single Photon Ionization – Examples

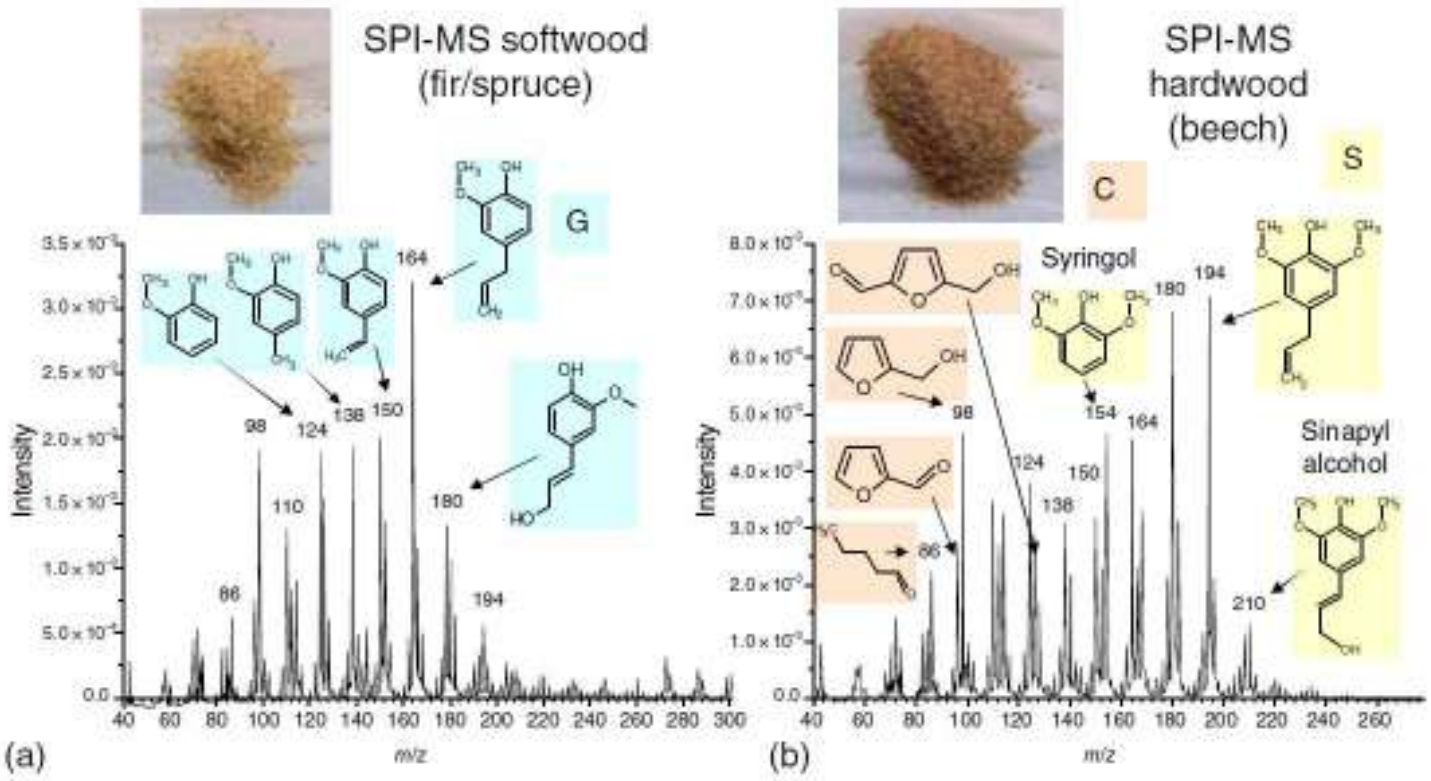

Figure 3.7 Emerging gas-phase products from wood pyrolysis recorded by real-time SPI-ToFMS depicting differences between softwood (a) and hardwood (b) via the respective patterns of phenolic and furanoic species. G stands for guaiacol derivatives, S for syringol derivatives, and C for cellulose decomposition products. See also: Fendt et al. (2012).

Photoionization and Photo-Induced Processes in Mass Spectrometry, Ralf Zimmermann and Luke Hanley, 2021 WILEY-VCH GmbH

Single Photon Ionization – Examples

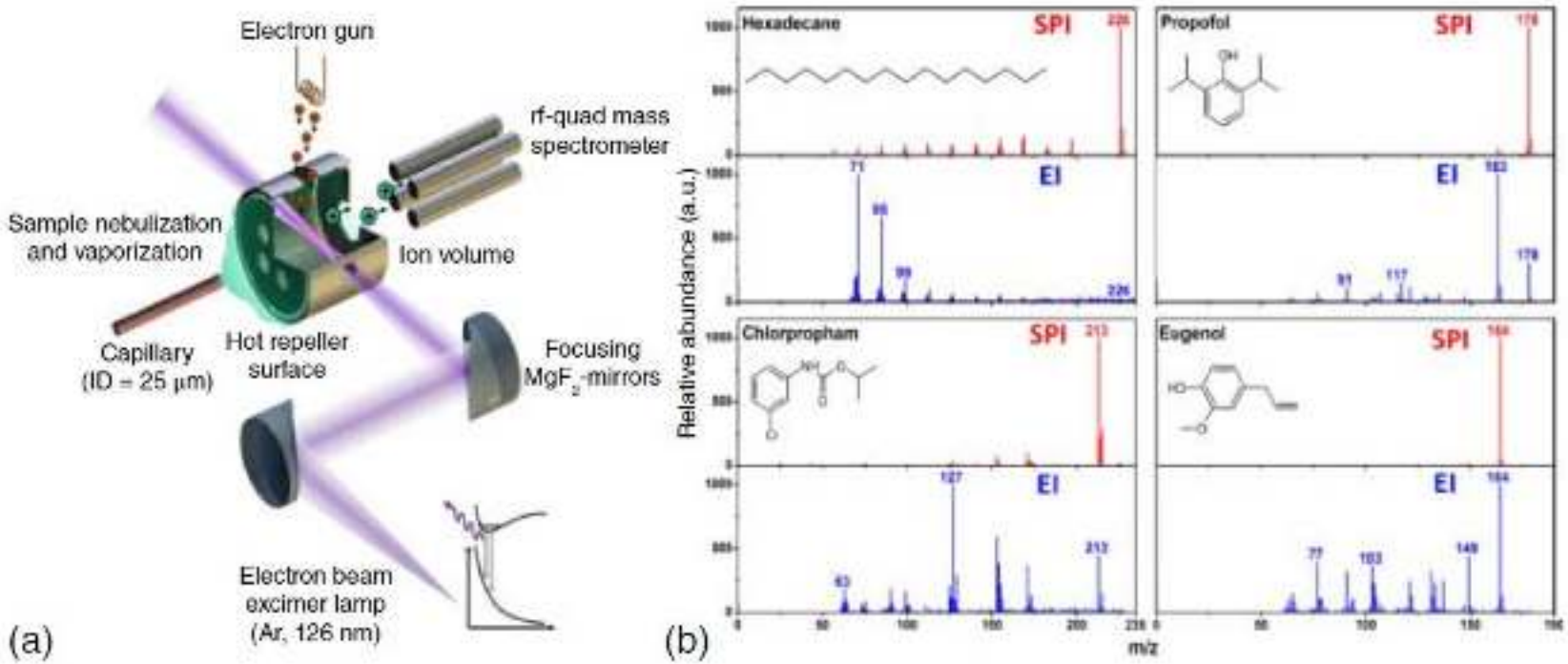

Figure 3.14 (a) Setup of a direct inlet for liquid samples with photoionization and electron ionization. (b) Corrected SPI (top) and EI (bottom) spectra and the respective NIST spectra (inset) for hexadecane, propofol, chlorpropham, and eugenol: the EI fragment mass spectra depict the fragmentation pattern in good agreement, whereas the SPI spectra are dominated by the molecular ions. Source: From Schepler et al. (2013).

Photoionization and Photo-Induced Processes in Mass Spectrometry, Ralf Zimmermann and Luke Hanley, 2021 WILEY-VCH GmbH

Goal: Vacuum photoionization on an Orbitrap mass analyzer

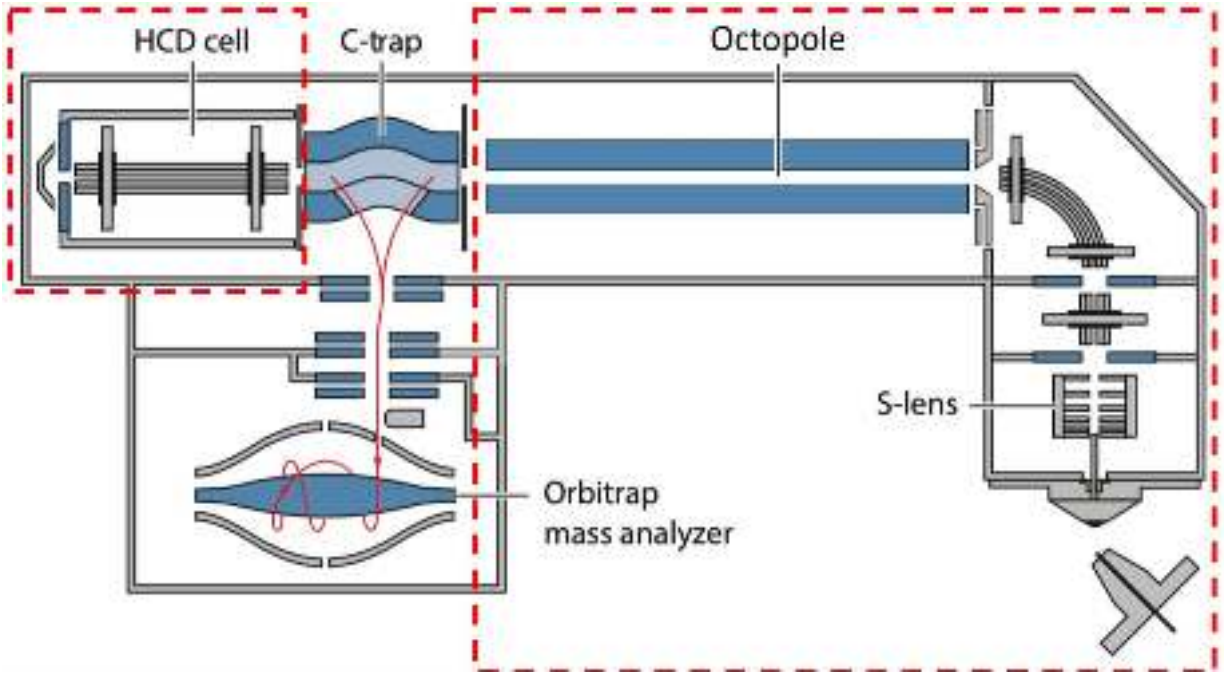

Idea of the so-called "naked" Orbitrap

- removing the ion transmission optics and components for the atmospheric pressure inlet
- adaption of the vacuum system allowing direct sampling of the evolved gas mixture

→ compact and robust instrumentation for field usage at the emissions site maintaining high-resolving power and high mass accuracy

Schematic setup of the Orbitrap Exactive™ mass spectrometer used as a basis for the novel photoionization platform. Components in the dashed red boxes are removed. Adapted based on (1).

(1) Eliuk, S.; Makarov, A. *Annual review of analytical chemistry* **2015.** "Evolution of Orbitrap Mass Spectrometry Instrumentation", DOI: 10.1146/annurev-anchem-071114-040325.

Particulate Matter and Carbonaceous Aerosols

carbon cores

lung depos., inflamm.

Janssen et al. WHO, 2012, wedocs.unep.org/handle/20.500.11822/8699

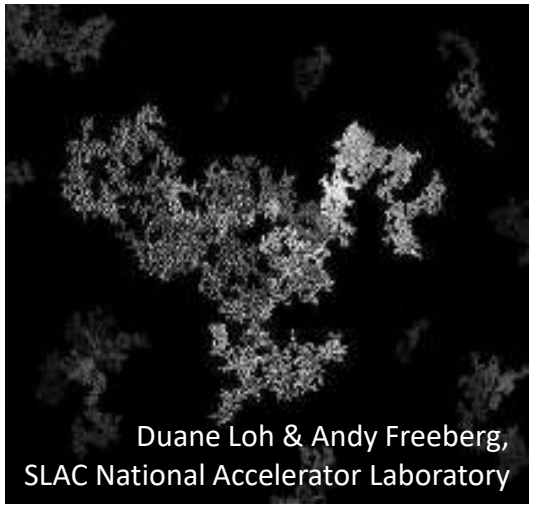

Duane Loh & Andy Freeberg, SLAC National Accelerator Laboratory

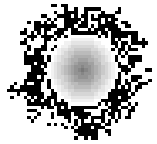

organic coatings

carcinogenic PAHs

Kim, K.-H. et al. *Environ. Int.* **60**, 71-80, **2013**
Boström, C.-E. et al. *Environ. Health Perspect.* **110**, Suppl 3, 451-488, **2002**

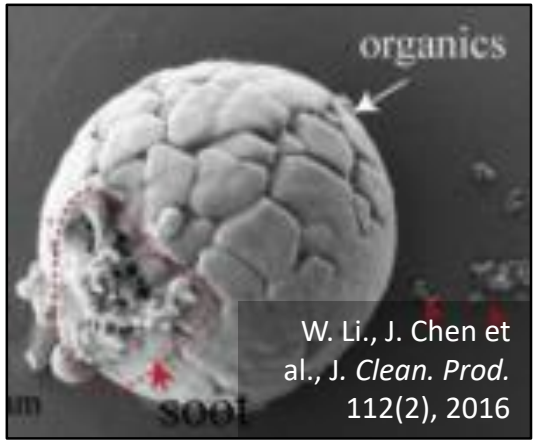

W. Li., J. Chen et al., J. *Clean. Prod.* 112(2), 2016

Polycyclic aromatic hydrocarbons (PAHs)

- formation in combustion processes
- absorption of UV-light
- some with carcinogenic, mutagenic, genotoxic potential

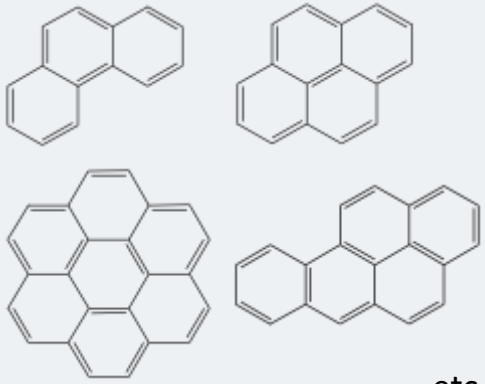

etc.

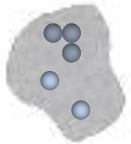

metal oxides

cardiov. desease

Fang, T. et al. *Environ. Sci. Technol.* **51**, 2611-2620, **2017**
Ye, D. et al. *Environ. Health Perspect.* **126**, 2, 27007, **2018**

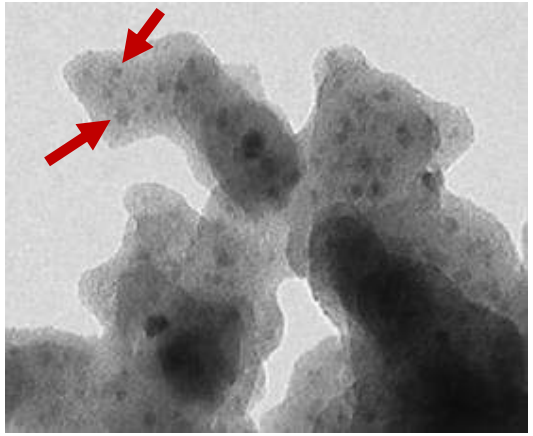

Vacuum laser ionization on an Orbitrap mass analyzer – A not very new idea…

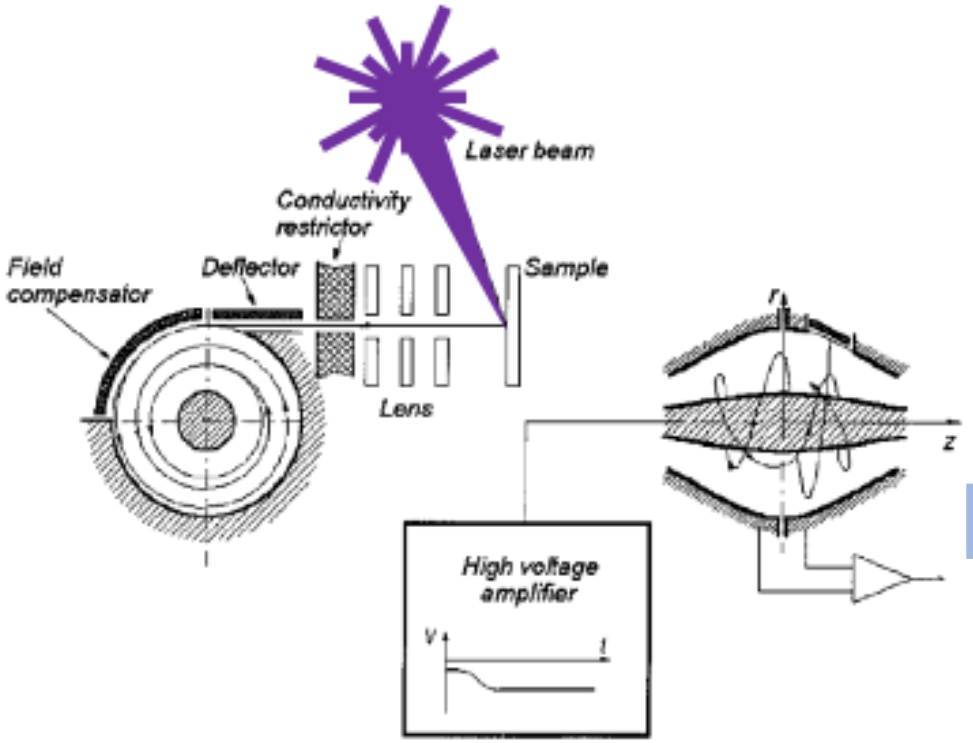

Transfer to modern Orbitrap platform

First theoretical conception

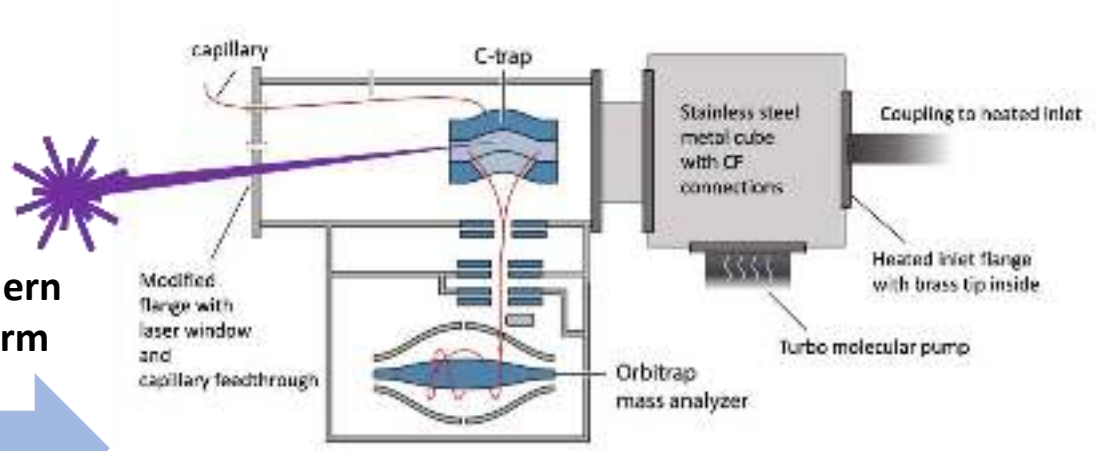

… **but** not realized in C-trap so far and various problems might occur due to

- restricted ionization volume and space
- difficult sample introduction
- vacuum requirements …

Adapted based on Makarov, A. Analytical Chemistry 2000. "Electrostatic axially harmonic orbital trapping: a high-performance technique of mass analysis", DOI: 10.1021/ac991131p.

Vacuum Photoionization Orbitrap

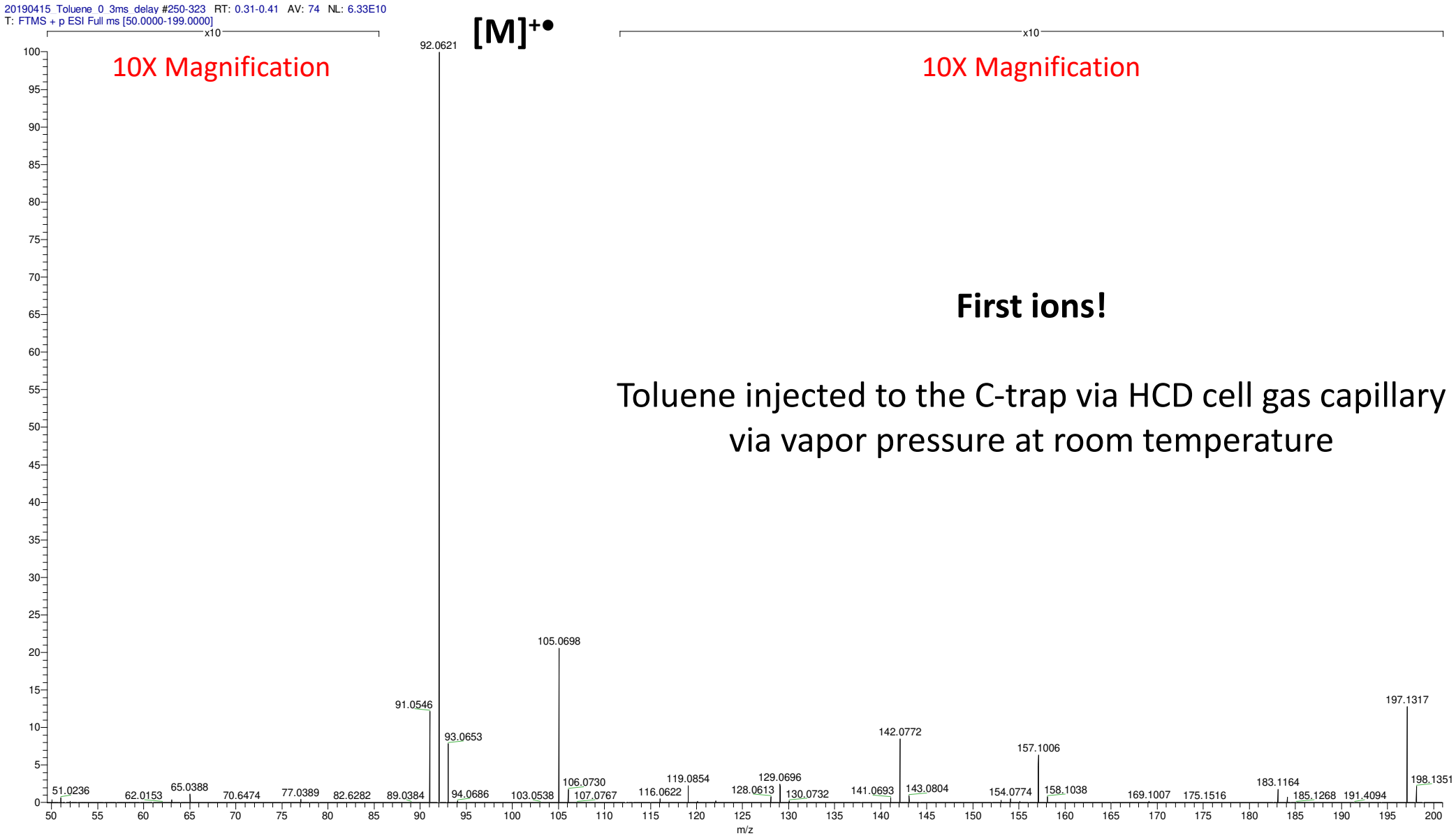

First ions!

Toluene injected to the C-trap via HCD cell gas capillary via vapor pressure at room temperature

Vacuum Photoionization Orbitrap

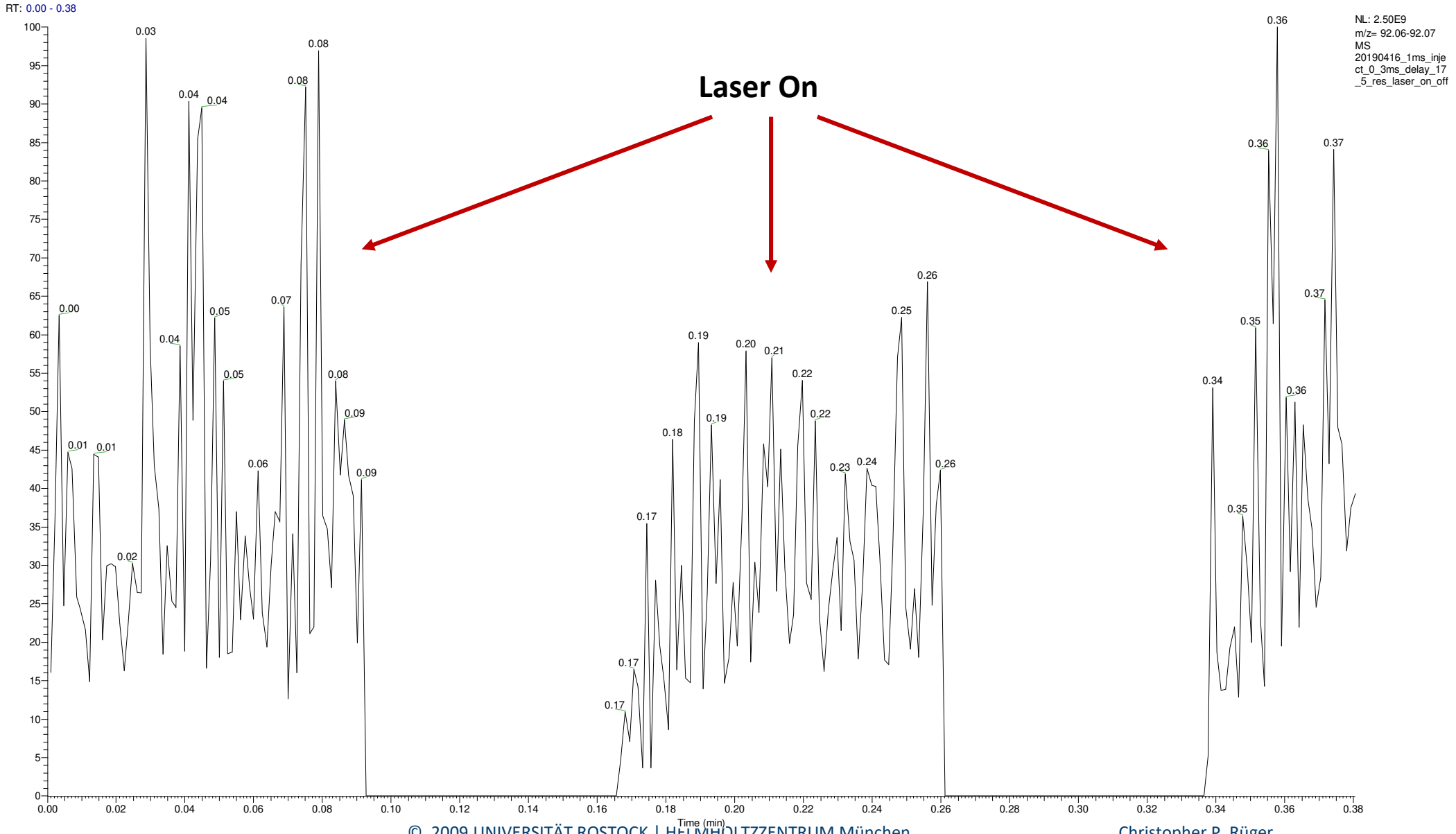

Setting-up the Photoionization Prototype

Hardware changes and reconstruction

→ physical removement (before just electronic unplugging) of the components related to the atmospheric pressure inlet

→ design of heated inlet system with introduction volume for additional turbo molecular pumping

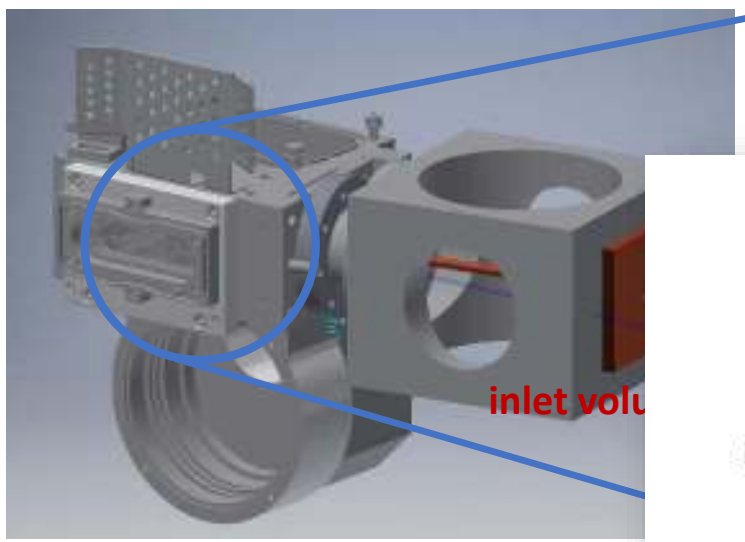

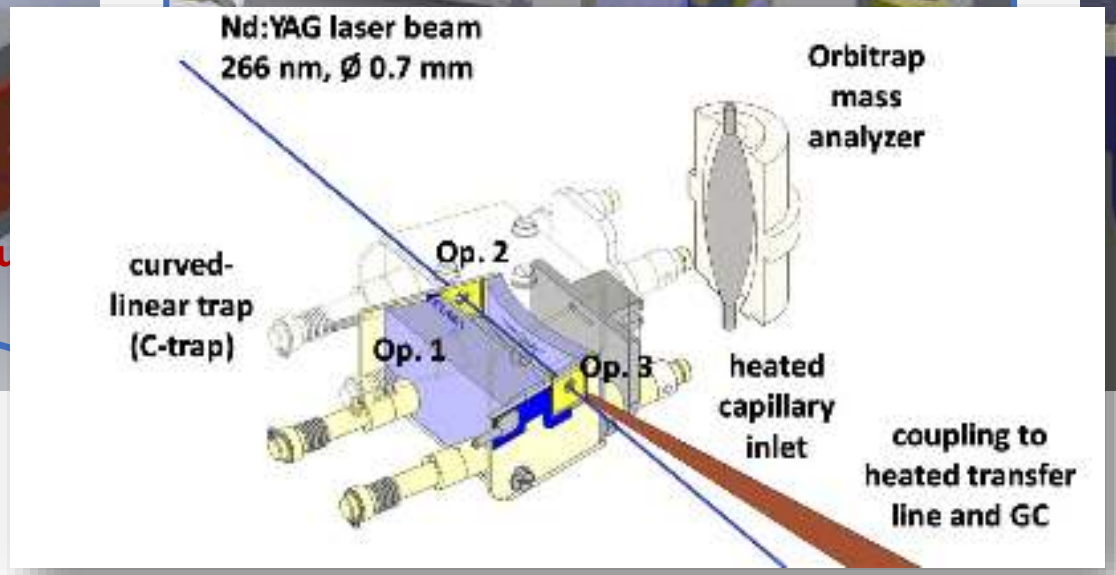

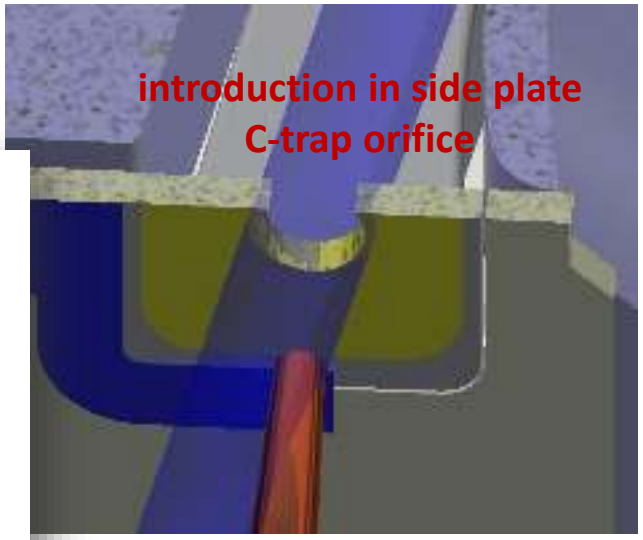

Benzene, Toluene, p-Xylene and 1,2,4-trimethylbenzene (BTX)

→ sensitivity, stability, mass accuracy and other figures of merit

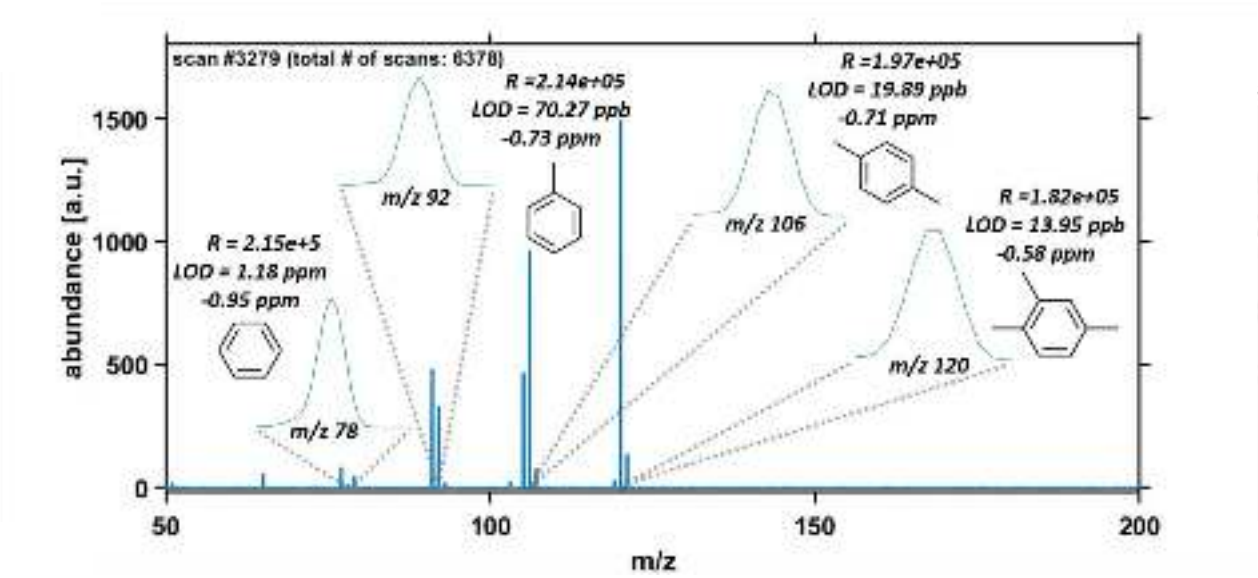

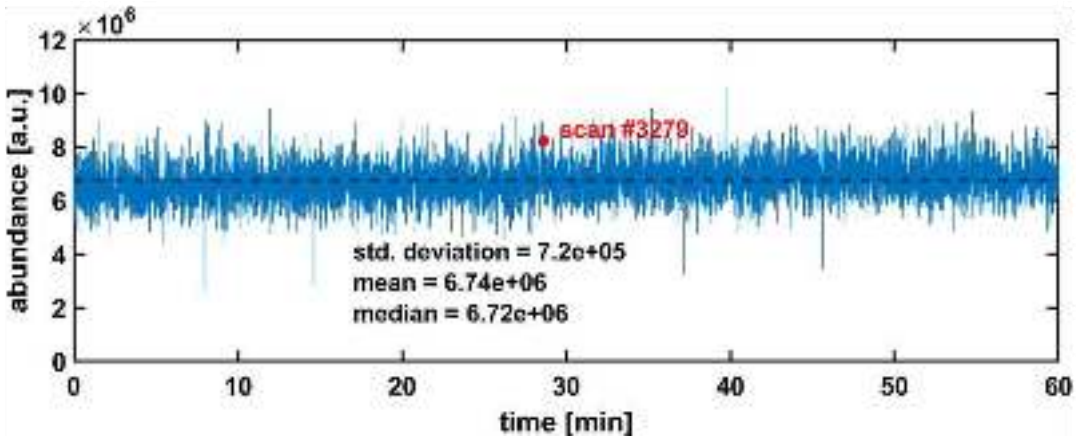

- high resolution and sub-ppm mass accuracy could be retained
- signal stability for hours (mainly effects due to laser energy drift)
- sensitivity in low ppm/ppb-range comparable to time-of-flight MS solutions

Evaluation of the platform with higher boiling point constituents

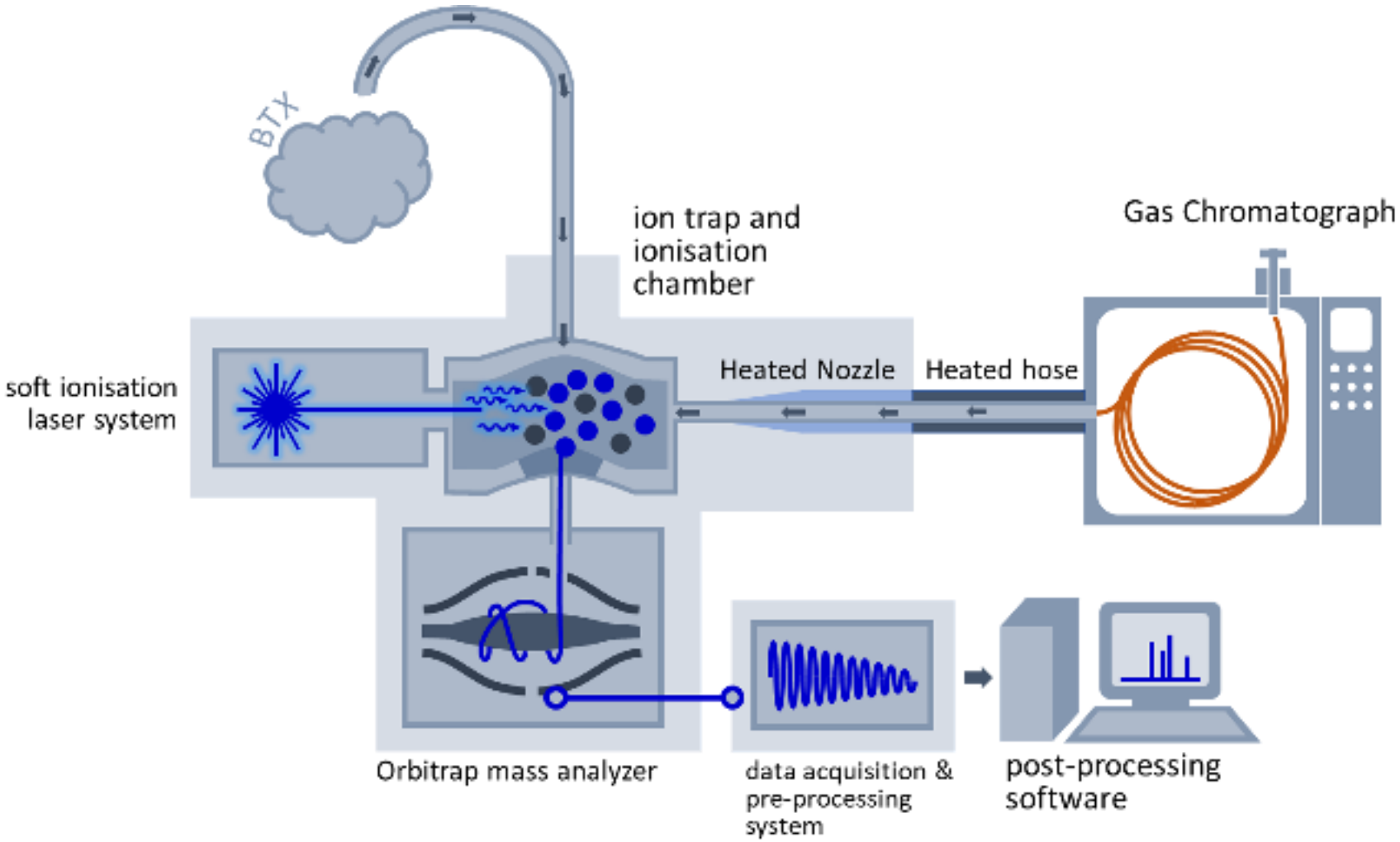

Petroleomics sample material introduced via gas chromatography hyphenation

Heavy fuel oil (HFO) as petrochemical feed fuel for ship diesel engines → precursor for aerosol emissions

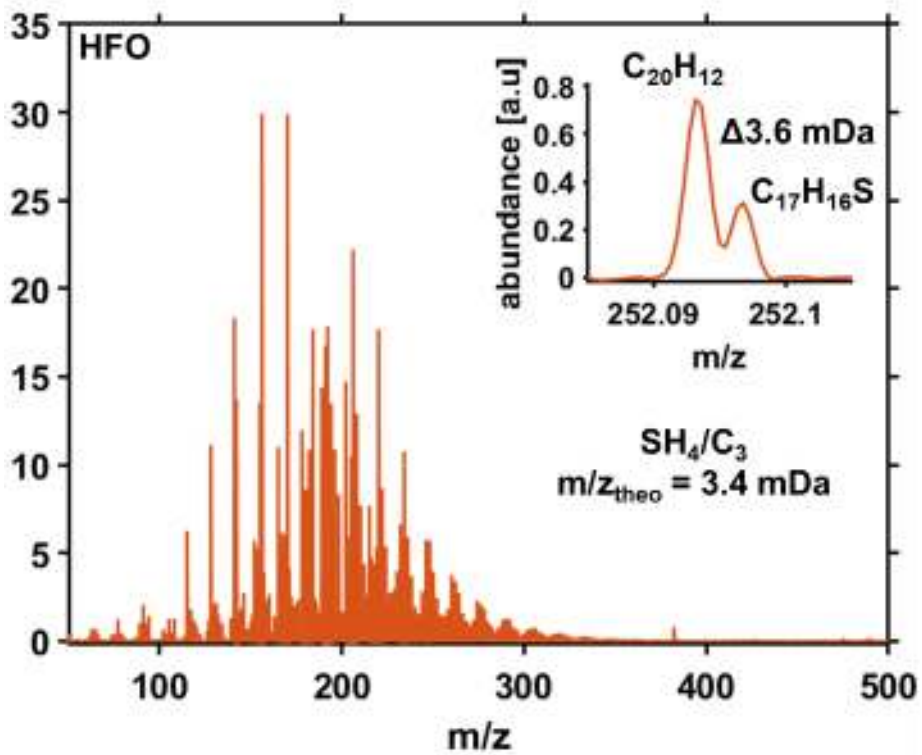

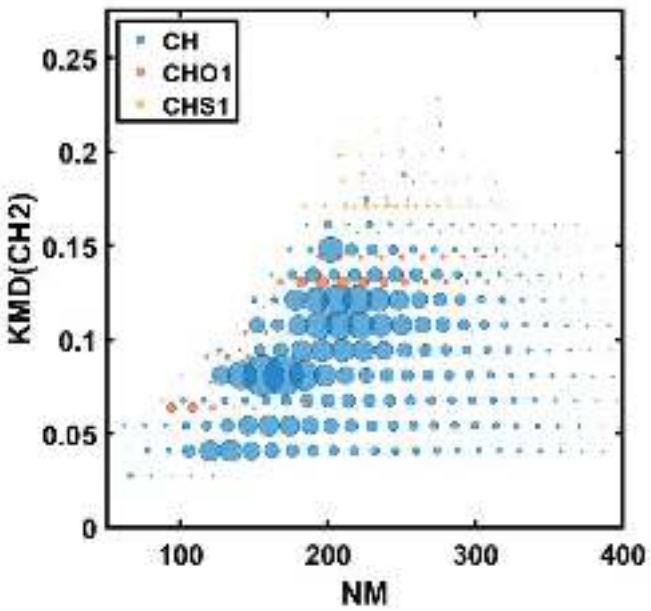

Kendrick mass defect plot
Horizontal lines – alkylation

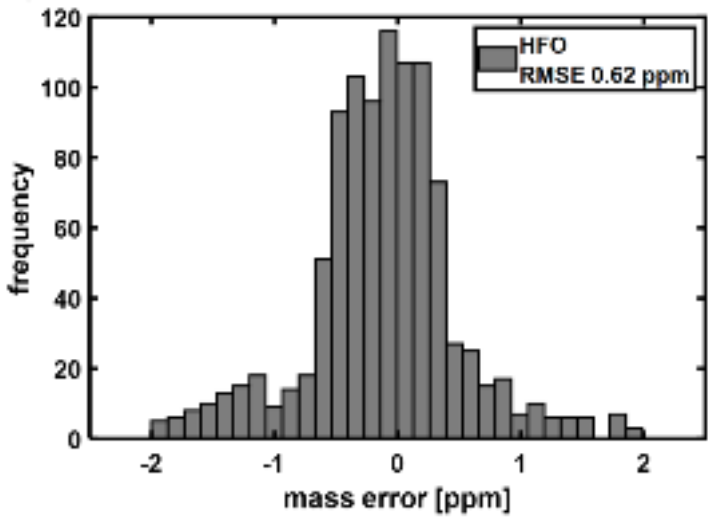

Attribution error histogram
with < 1 ppm RMSE

Analytical Chemistry, **2021**, 93, 27, 9418–9427
DOI: 10.1021/acs.analchem.0c04740

→ preserving the molecular complexity of alkylated PAHs
→ high mass resolving power and mass accuracy allows to separate isobaric interferences

Concept and Basics

- pulsed laser light as a source of energy for desorption and ionization
- ion formation from thin solid layers
- matrix assistance as a key to soft desorption/ionization
- vacuum and atmospheric pressure sources for MALDI
- MALDI imaging techniques as one important application

Simplistic ion source for LDI design

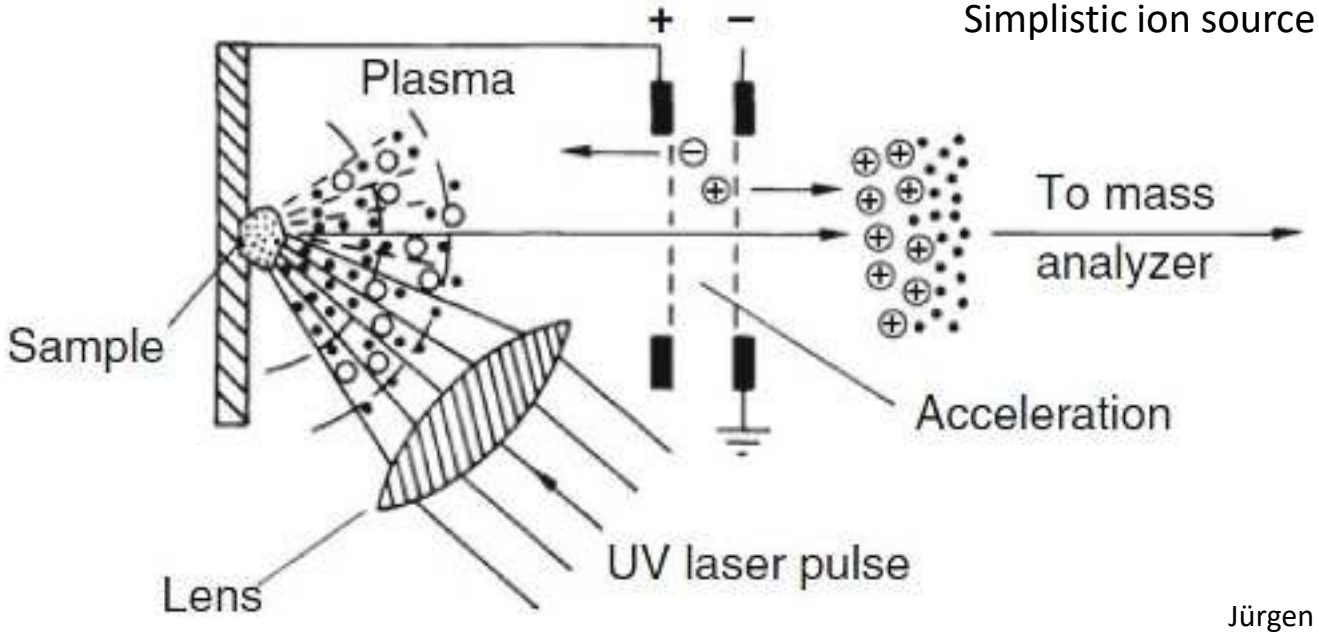

Jürgen H- Gross, *Mass Spectrometry – A Textbook*, **2017**, Spinger, ISBN *978-3-319-54398-7*

Laser Usage and Imaging Concept

Spectral range	Wavelength	Photon energy	Laser type
UV	193 nm	6.4 eV	ArF Excimer laser
UV	248 nm	5.0 eV	KrF Excimer laser
UV	266 nm	4.7 eV	Frequency-quadrupled Nd:YAG laser
UV	308 nm	3.8 eV	XeCl Excimer laser
UV	337 nm	3.7 eV	Nitrogen laser[a]
UV	355 nm	3.5 eV	Frequency-tripled Nd:YAG laser[a]
IR	1.06 μm	1.2 eV	Nd:YAG laser[b]
IR	2.94 μm	0.4 eV	Er:YAG laser[b]
IR	1.7–2.5 μm	0.7–0.5 eV	Optical parametric oscillator (OPO) laser
IR	10.6 μm	0.1 eV	CO_2 laser

[a]most frequently used UV lasers
[b]most frequently used IR lasers

Common laser types for laser desorption ionization

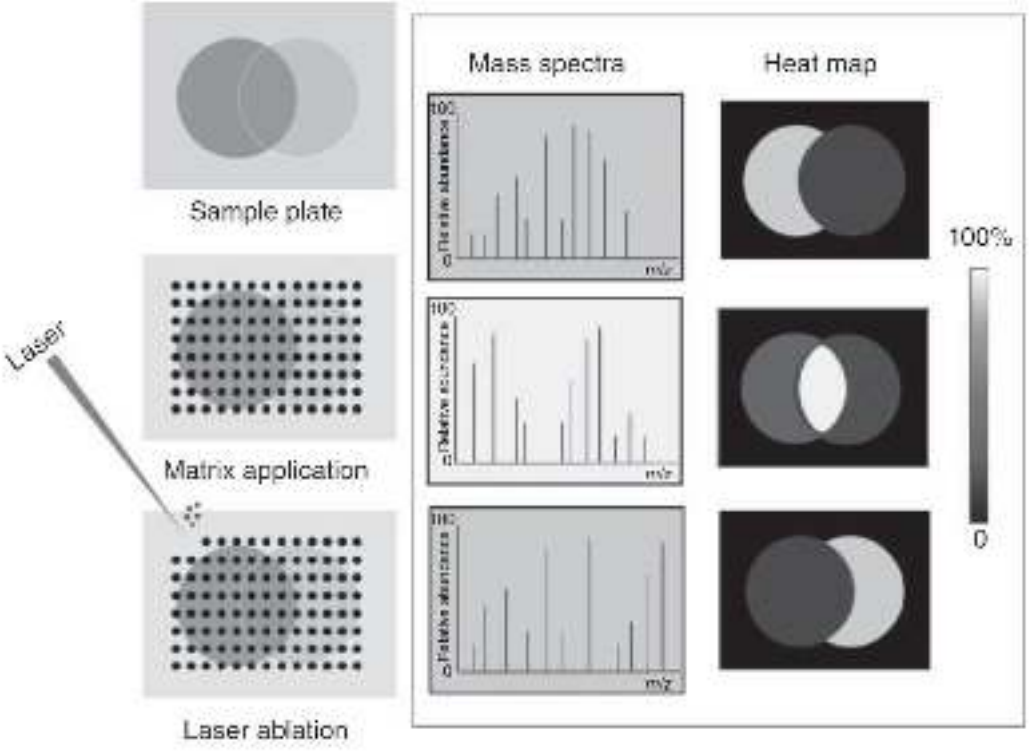

General concept for (MA)LDI imaging creating three-dimensional information from the lateral distributed spectral data

Matsumoto et al., *Shinku*, **2007**, 50:241-245

Laser Desorption Ionization – LDI

Approximate timescales of nanosecond and femtosecond energy absorption and laser ablation (in atmosphere)

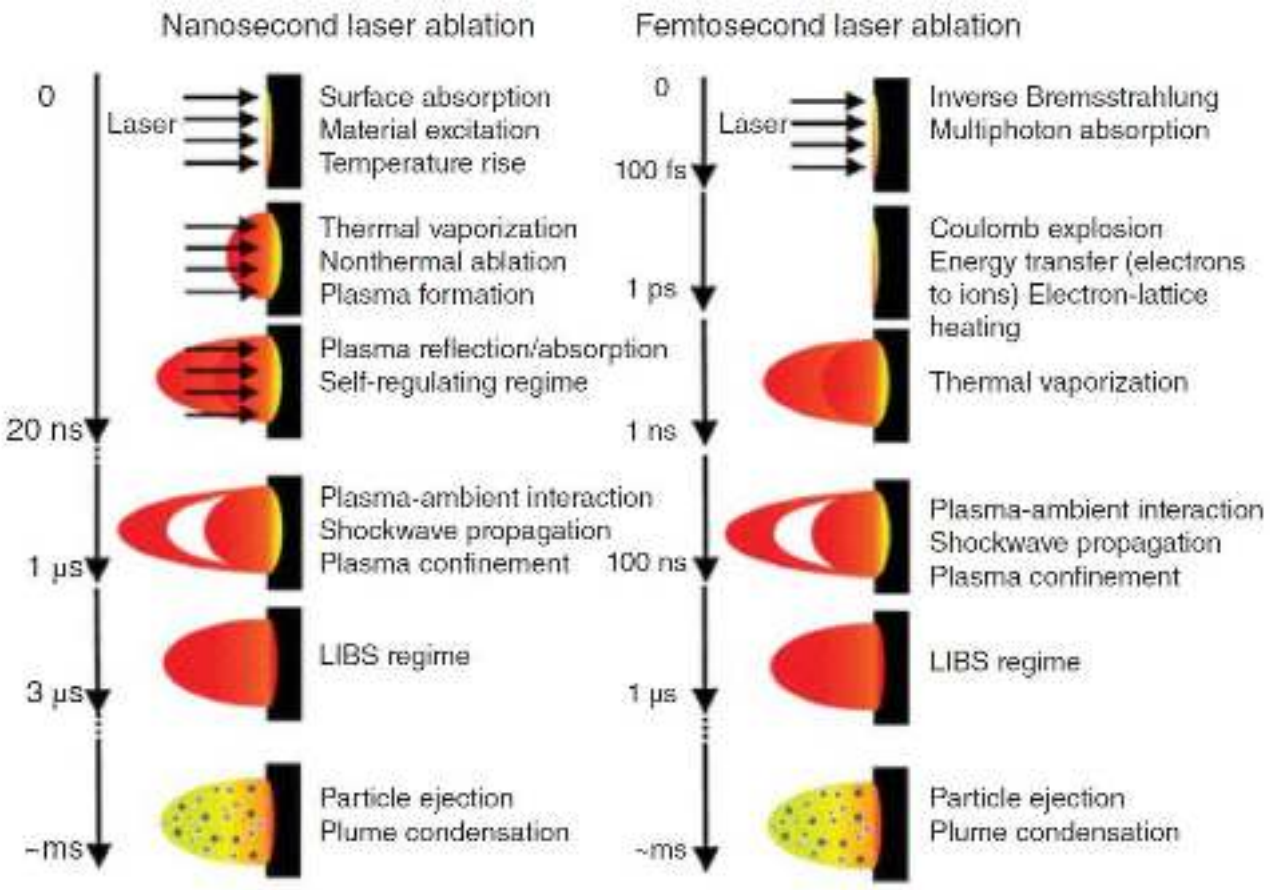

Photoionization and Photo-Induced Processes in Mass Spectrometry, Ralf Zimmermann and Luke Hanley, 2021 WILEY-VCH GmbH

Harila et al., **2014**

Laser Desorption Ionization – LDI

Laser Ablation Process

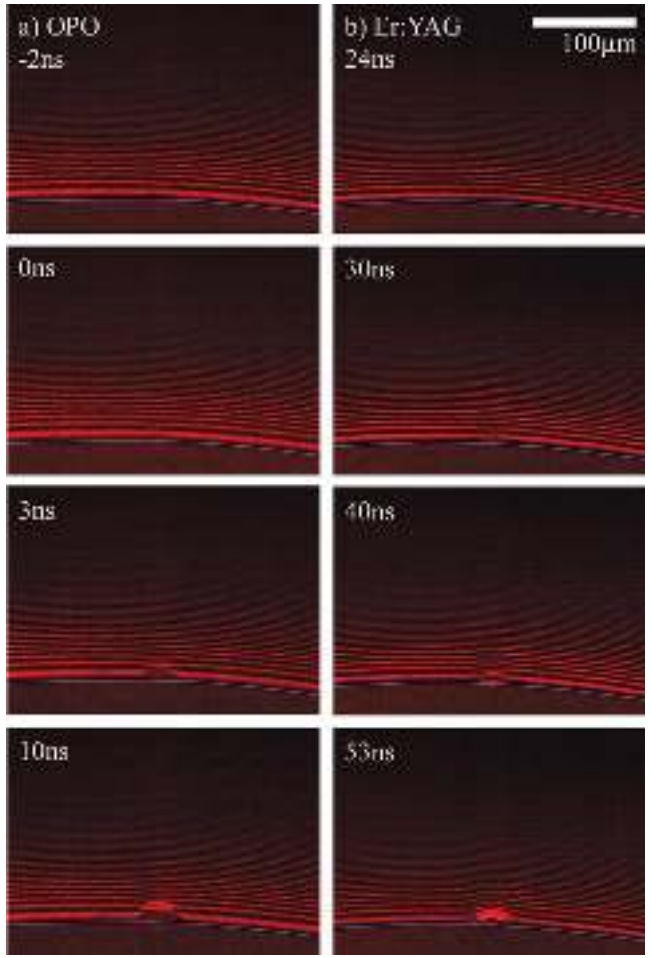

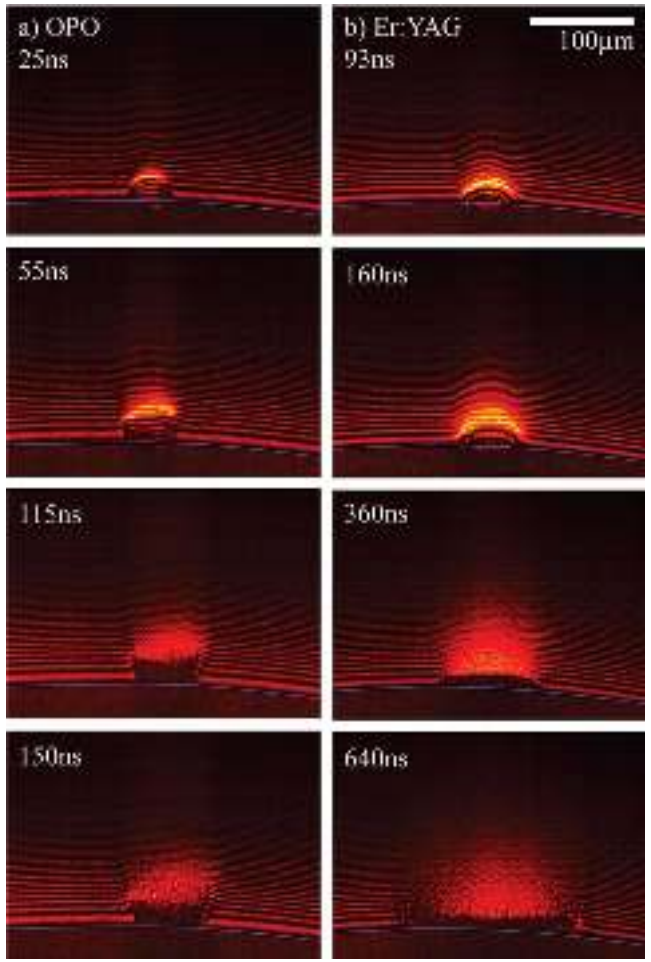

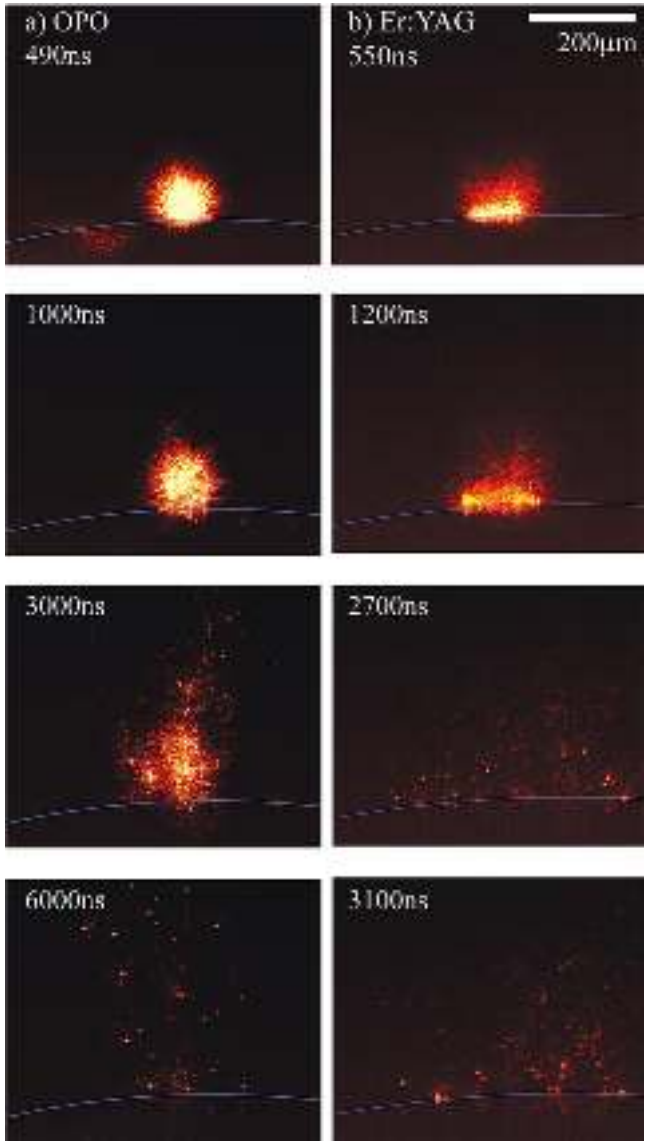

Leisner et al., *J. Phys. Chem. B,* **2005**, 11661-11666

Laser Profile and the Ablation Process

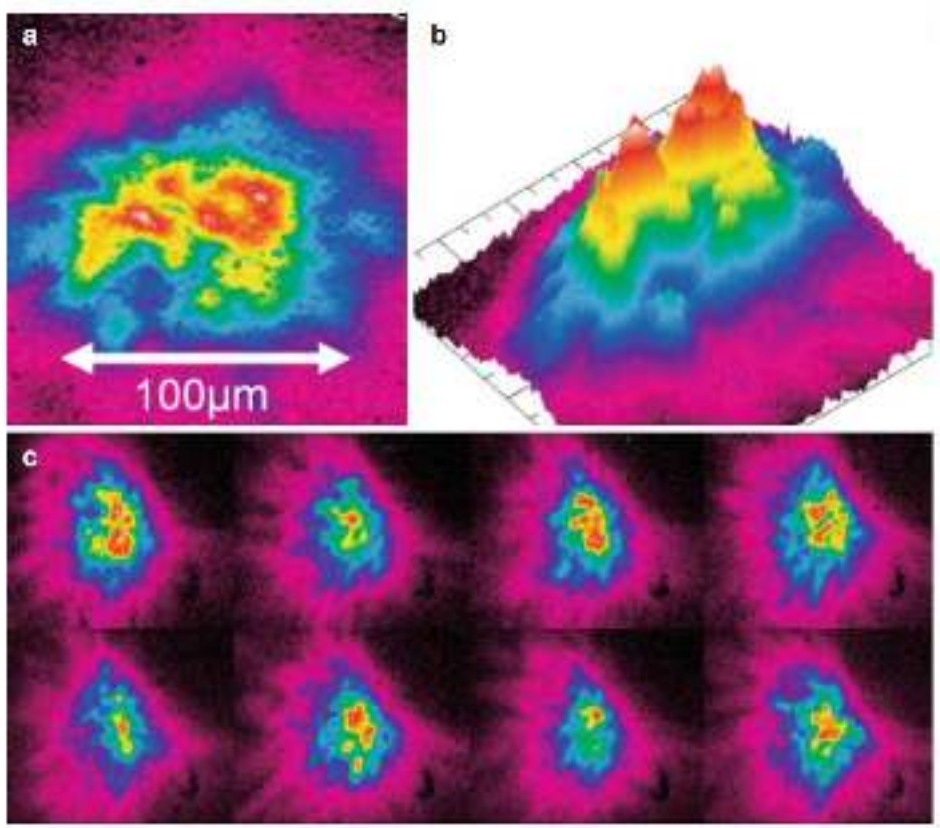

Nitrogen laser beam profile

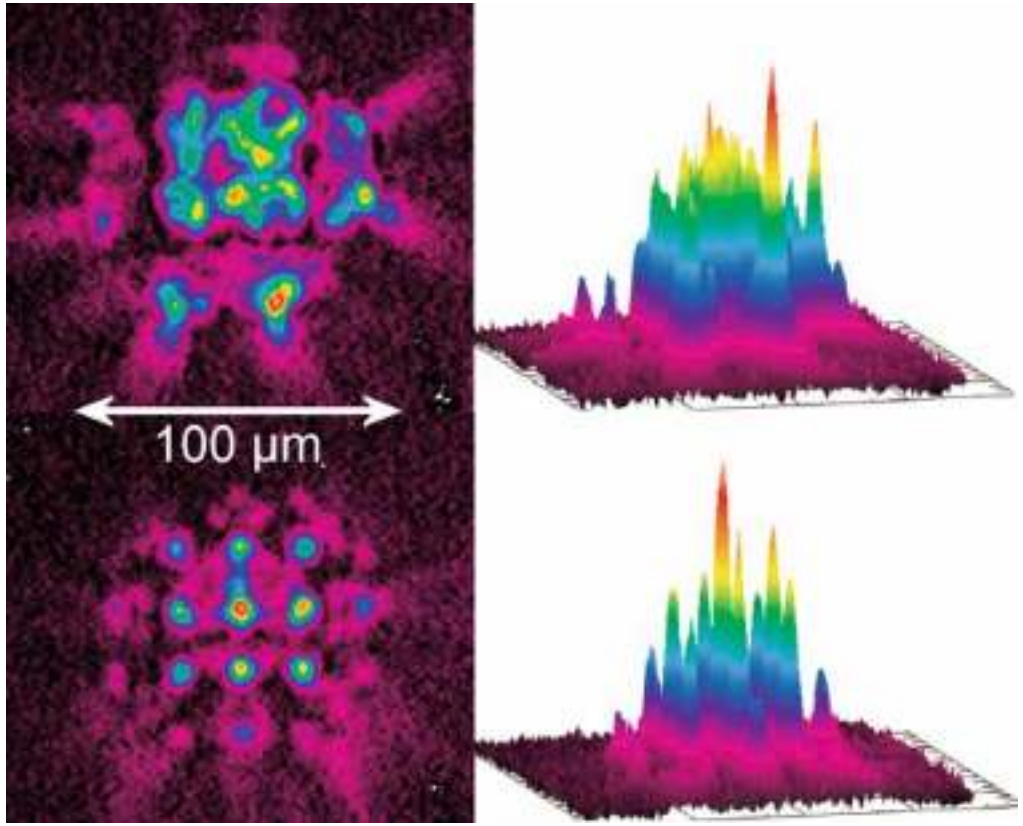

Nd:YAG Bruker Smartbeam laser beam profile

Nitrogen laser beam profile, the non-homogenous energy distribution has to be considered for imaging aspects

Holle et al., *J Mass Spec*, **2006**, 41:705–716

The Use of Matrices for Energy Uptake and Adapting Ionization Behavior

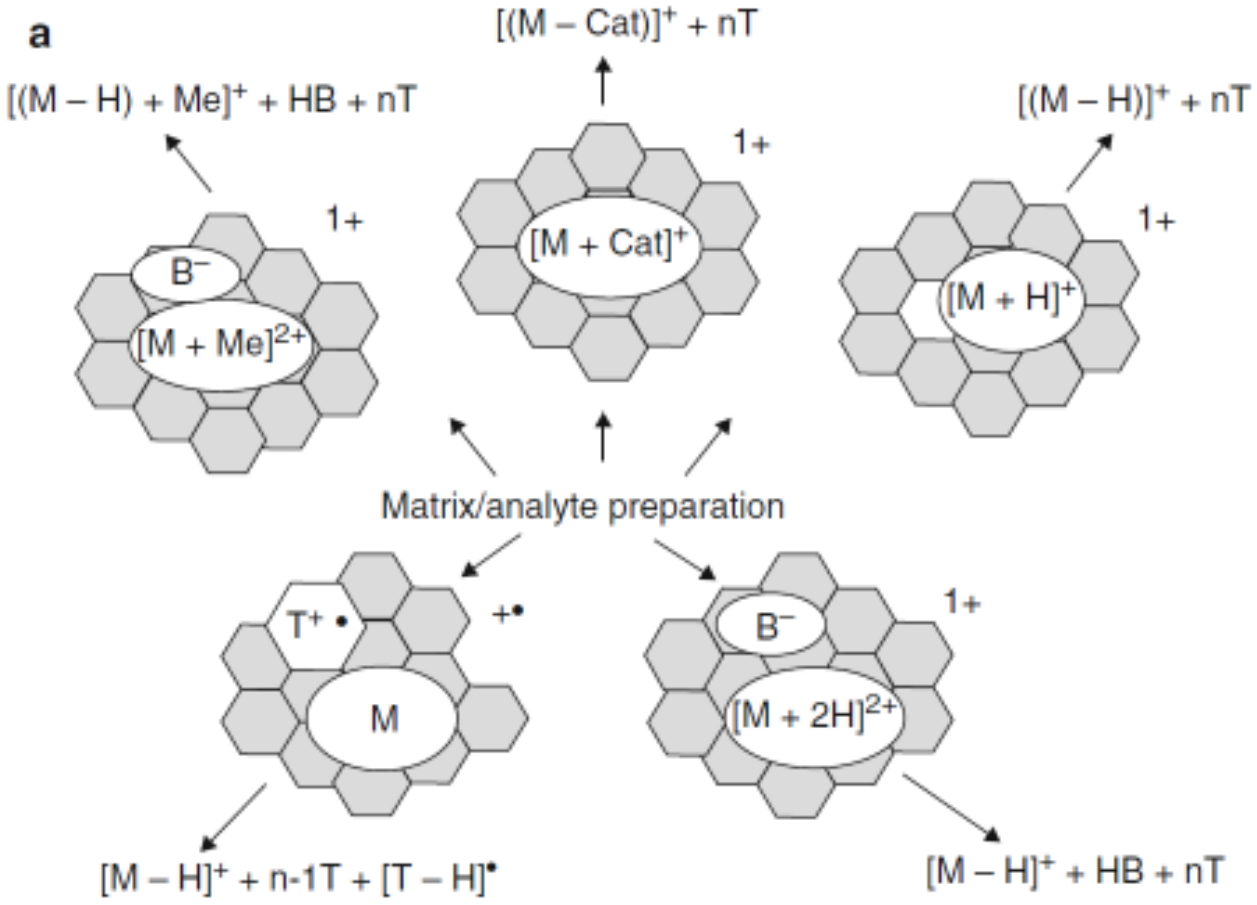

Pathways of formation of singly charged ions from sample–matrix preparations according to the lucky survivor model.

M: analyte molecule
T: matrix molecule
Cat: small cation
Me: metal^{2+}
B: base

Karas et al., *J Mass Spectrom*, **2000**, 35:1–12

Laser Desorption Ionization – LDI

The Use of Matrices for Energy Uptake and Adapting Ionization Behavior

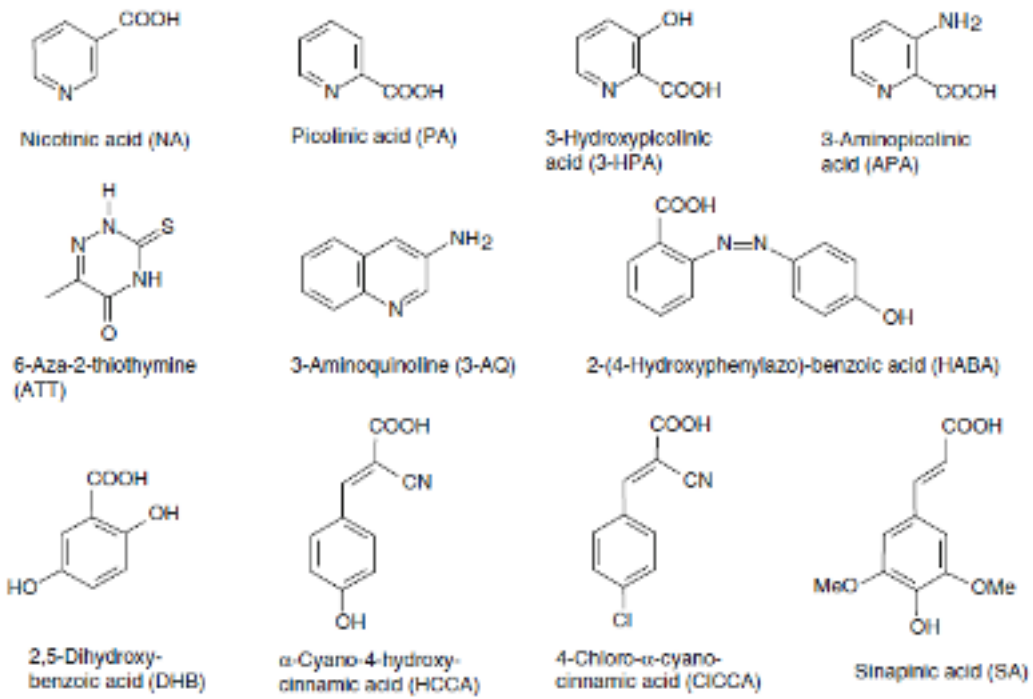

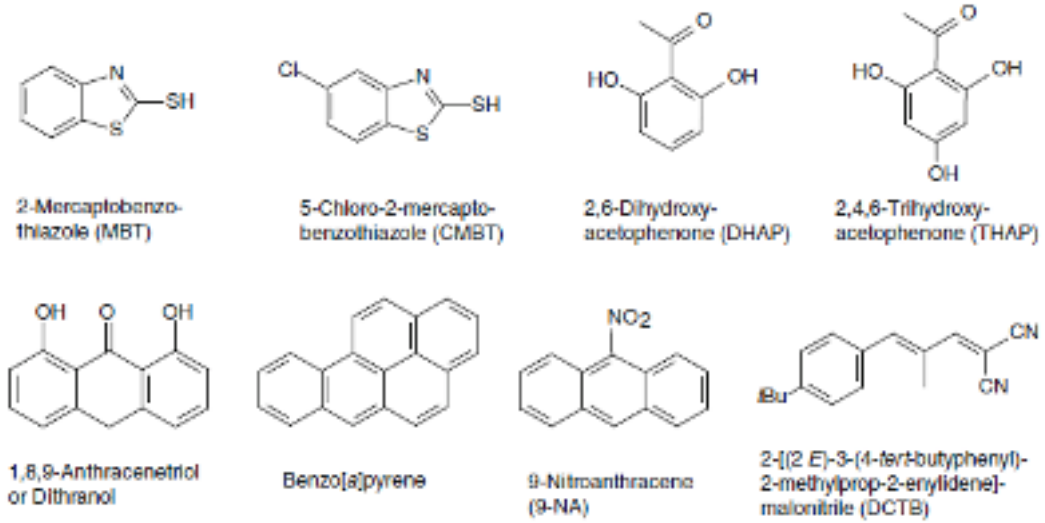

Common UV-MALDI matrices

Jürgen H- Gross, *Mass Spectrometry – A Textbook*, **2017**, Spinger, ISBN *978-3-319-54398-7*

Application – Ship Aerosol Emissions by LDI FT-ICR MS

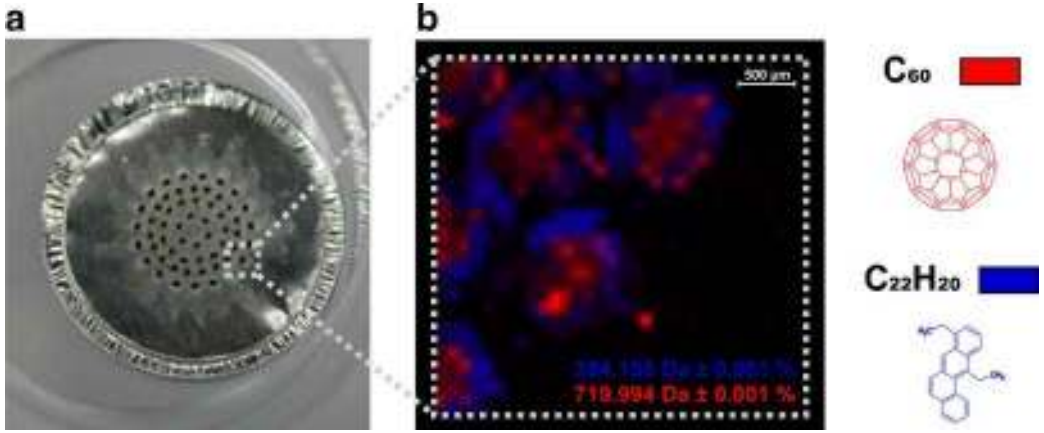

Imaging of the ship diesel aerosol particles by (GA)LDI FT-ICR MS, LDI parameters (spot size and energy) have to be carefully adjusted to prevent ionization artifacts

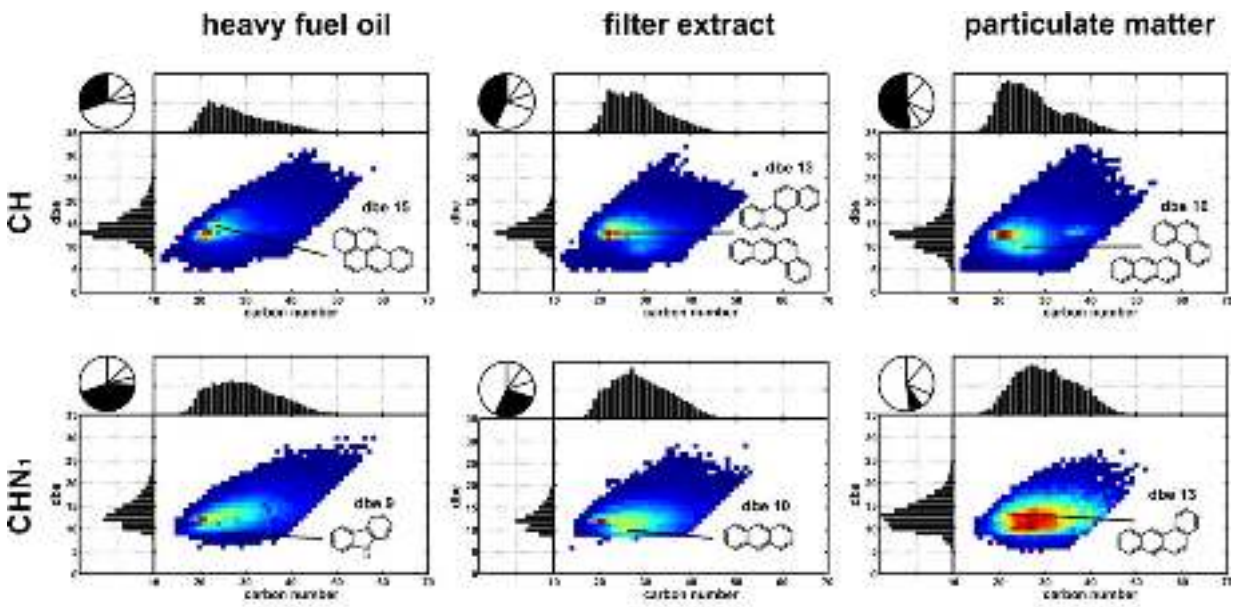

Cartographic visualization using carbon number versus double bond equivalent diagrams comparing the heavy fuel oil feed with aerosol emission, (+)LDI shows a high sensitivity towards Nitrogen-containing aromatics

Rüger et al., *Anal Bioanal Chem*, **2015**, 5923–5937

Application – Cigarette Smoke Analysis by LDI FT-ICR MS

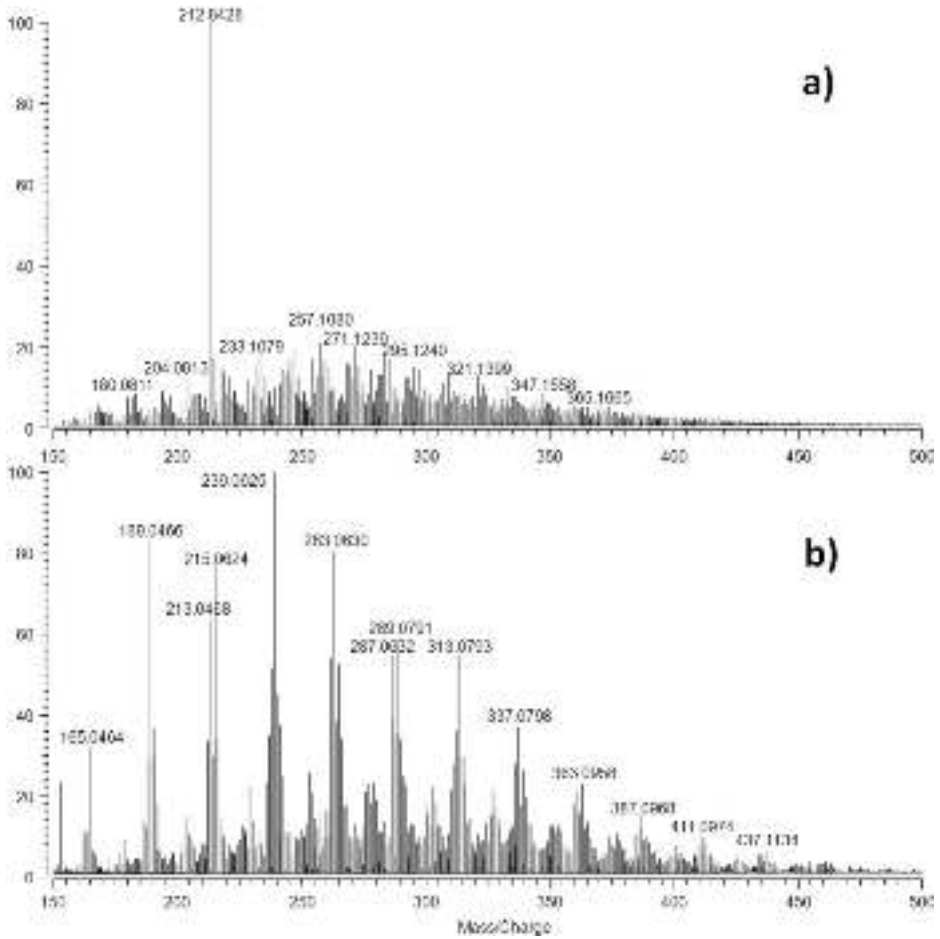

Positive and negative LDI mass spectra of smoke aerosol after inhalation

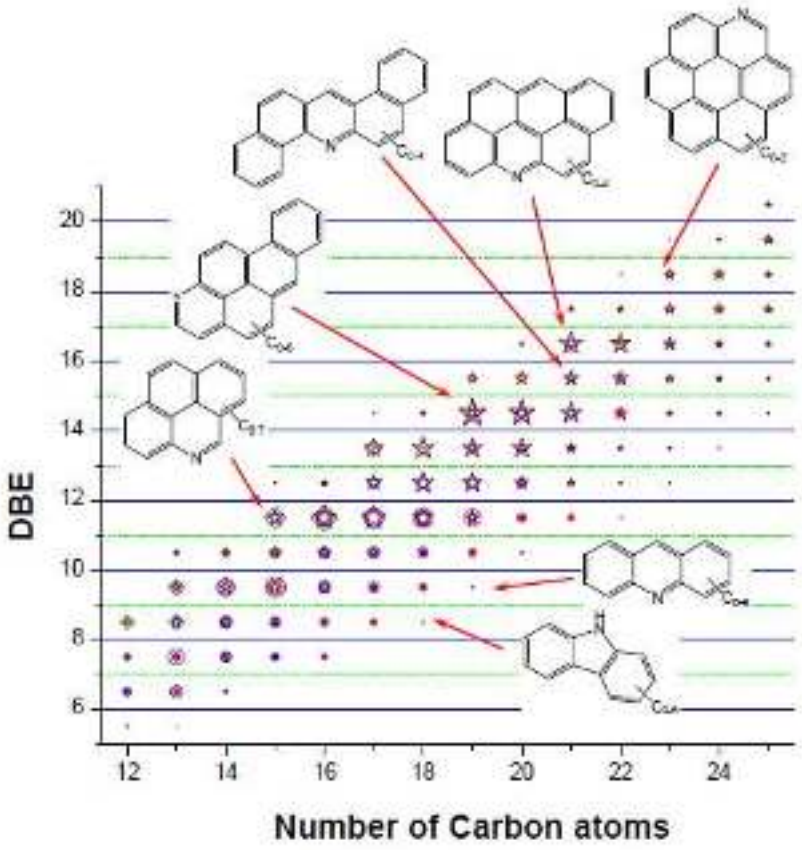

Fig. 8. Distribution of aza-arenes and alkyl-aza-arenes detected as $[M+H]^+$ in respect with the number of carbon and the double bound equivalent (DBE) in MSS ○, SSS ○ and, EXS for smoker F ☆ and smoker V ◇. The size of the symbol is associated to its relative abundance on the mass spectrum. For MSS and SSS, the relative abundance is multiple by a factor of 5.

Schramm et al., *Atmospheric Environment*, **2014**, 411-420

Application – Coal Analysis by GALDI FT-ICR MS

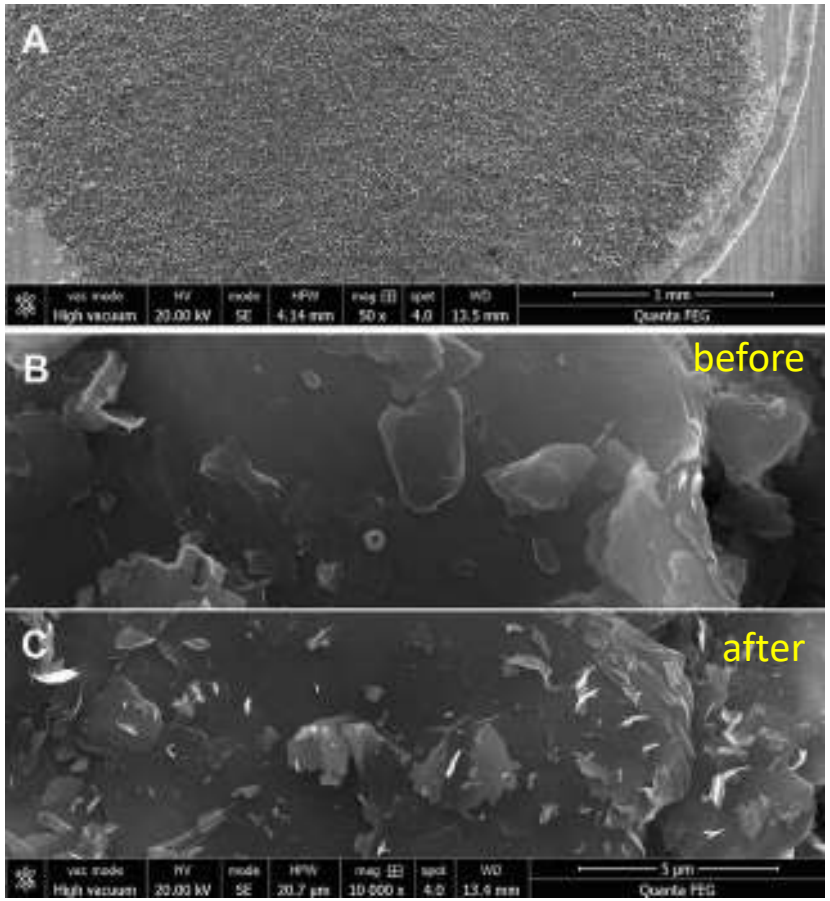

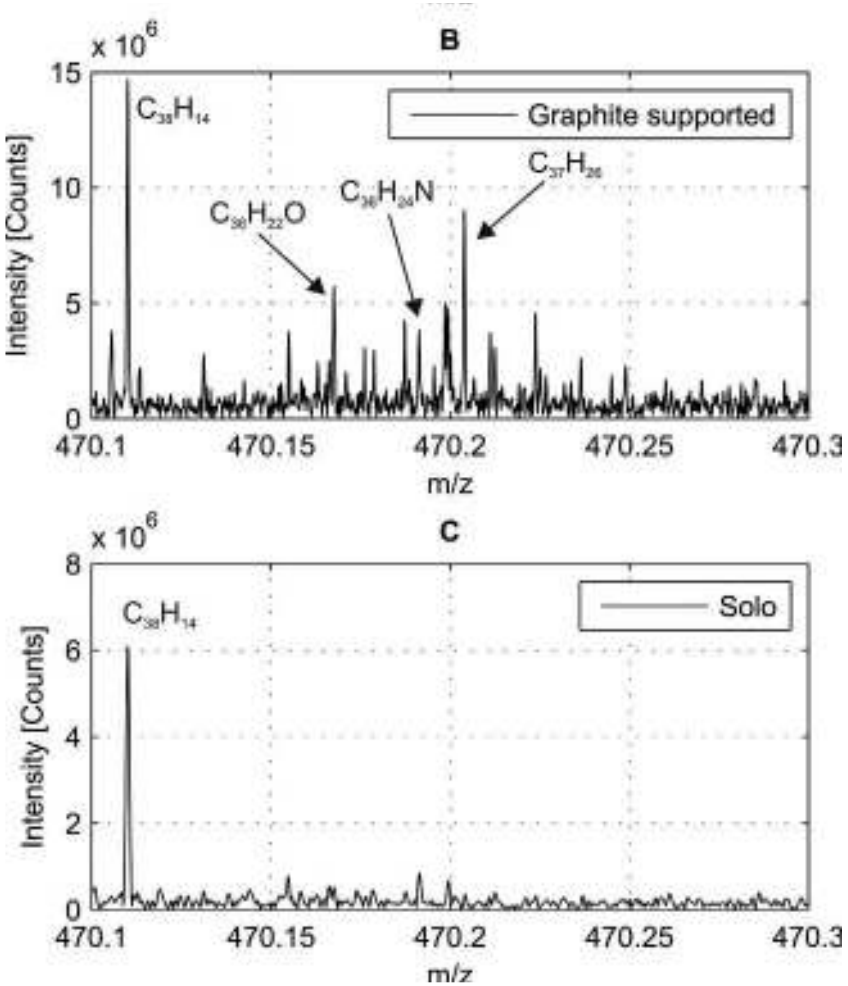

Rathsack et al., *Journal of Analytical and Applied Pyrolysis,* **2014**, 142–149

Laser Desorption Ionization – LDI

Application – Petroporpyhrin Analysis from Cruse Oils

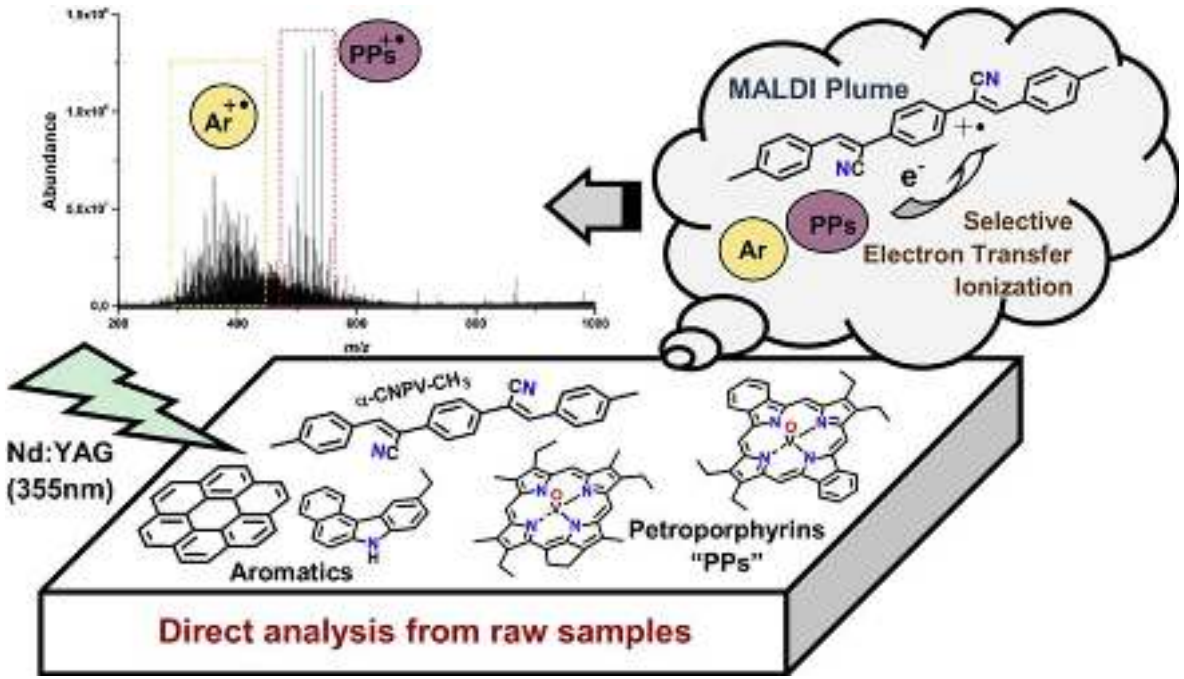

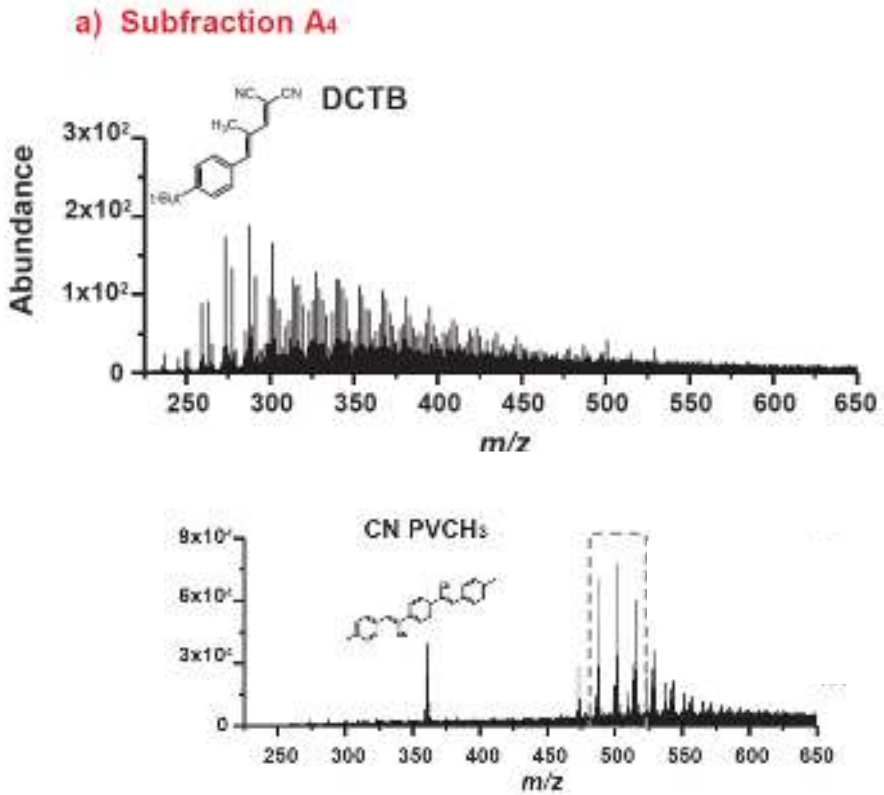

Giraldo-Dávila et al., *Fuel*, **2018**, 103-111

Outlook: Two-Step Laser Desorption Photo Ionization – the timsTOF flex

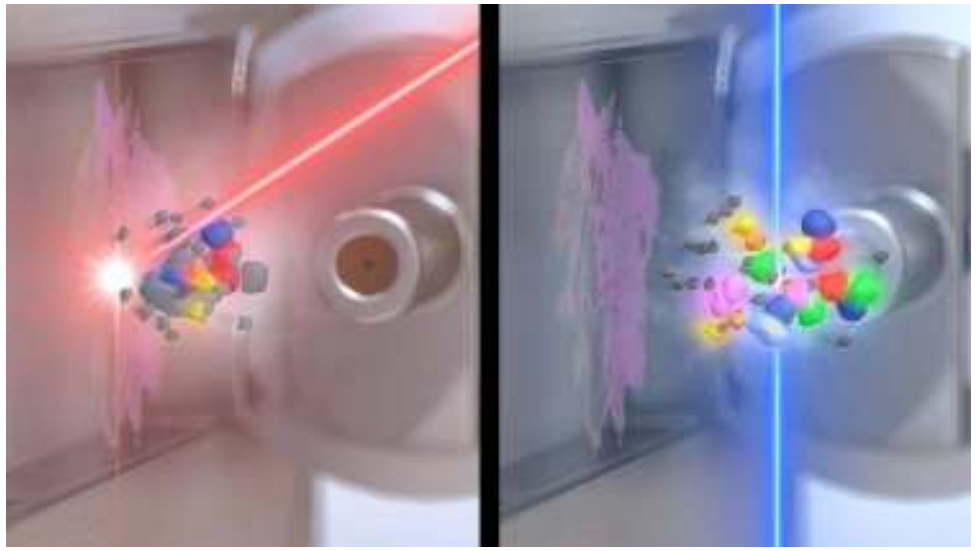

Two-Step Process: 1) Laser Desorption event creating an energetic plume, and 2) ionization of the plume analytes by a second UV laser.

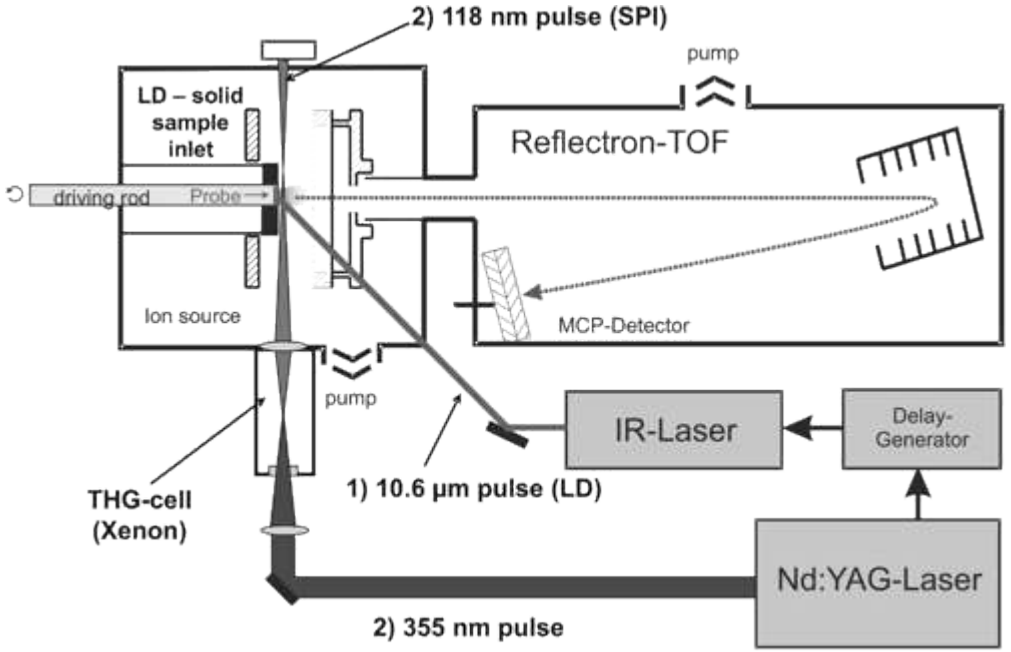

Two-Step Laser Desorption Ionization (L2MS) – actually a very old and heavily used technique on time-of-flight mass analyzers

Ferge et al., *Analytical Chemistry*, **2005**, 4528–4538

Commercialization might be realized in the next FT-ICR MS systems and become broadly available!

Outlook: Two-Step Laser Desorption Photo Ionization

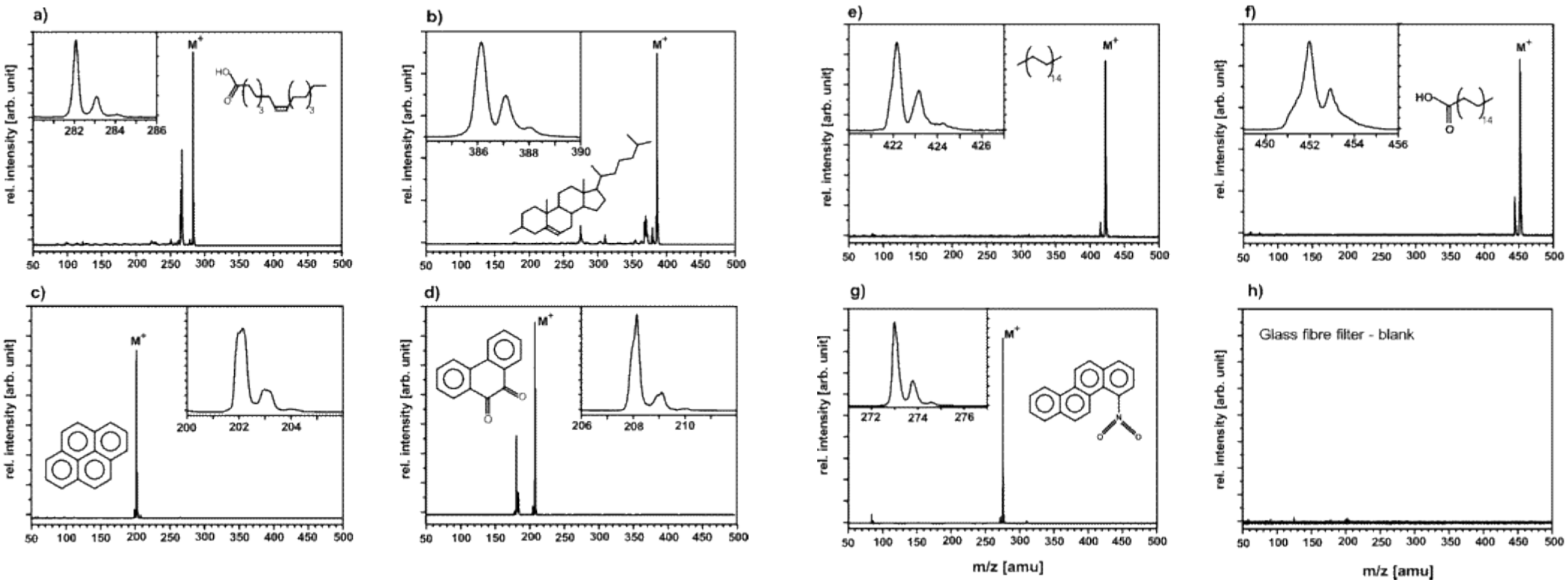

Infrared laser desorption with UV laser post ionization mass spectrometry for aerosol analysis

Ferge et al., *Analytical Chemistry*, **2005**, 4528–4538

Outline

- **Introduction and Motivation**
  - Chemical Space, Selectivity of Ionization Techniques, Overview of Schemes and Concepts
- **Vacuum Ionization**
  - Electron Impact, Chemical Ionization and Photoionization
  - Laser Desorption Ionization and Allied Techniques
- **Atmospheric Pressure Ionization**
  - Electrospray Ionization, Atmospheric Pressure Chemical/Photo/Laser Ionization
  - Other Concepts and Combination, Applications
- **Summary**

Selectivity of Ionization in Mass Spectrometry – "Analytical Glasses"

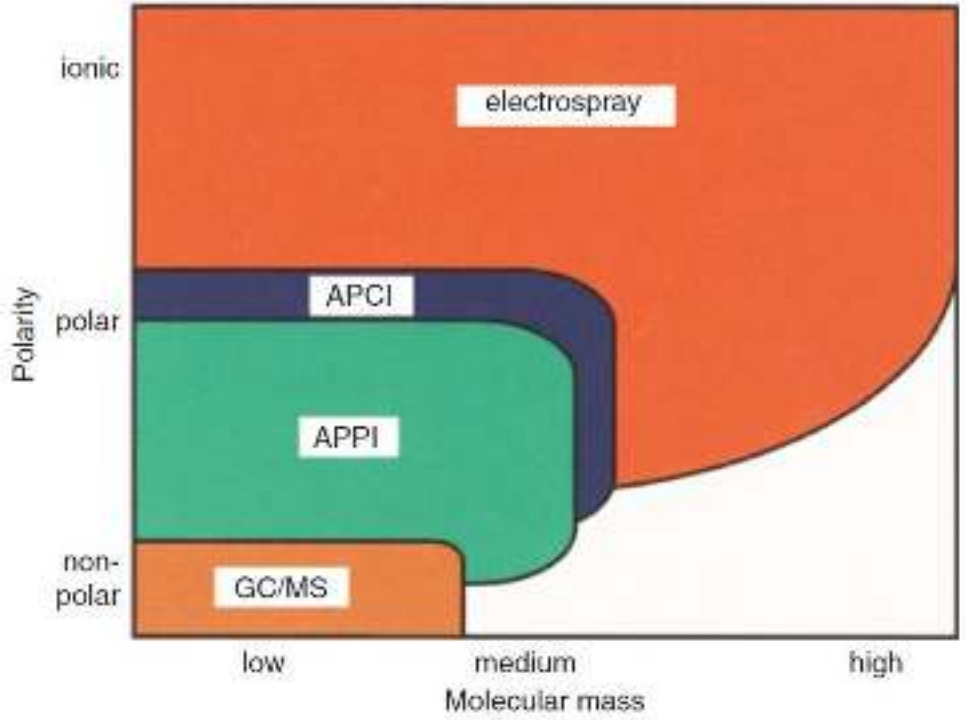

Cover of *Anal. Bioanal. Chem.*, **2004**, 378(4)

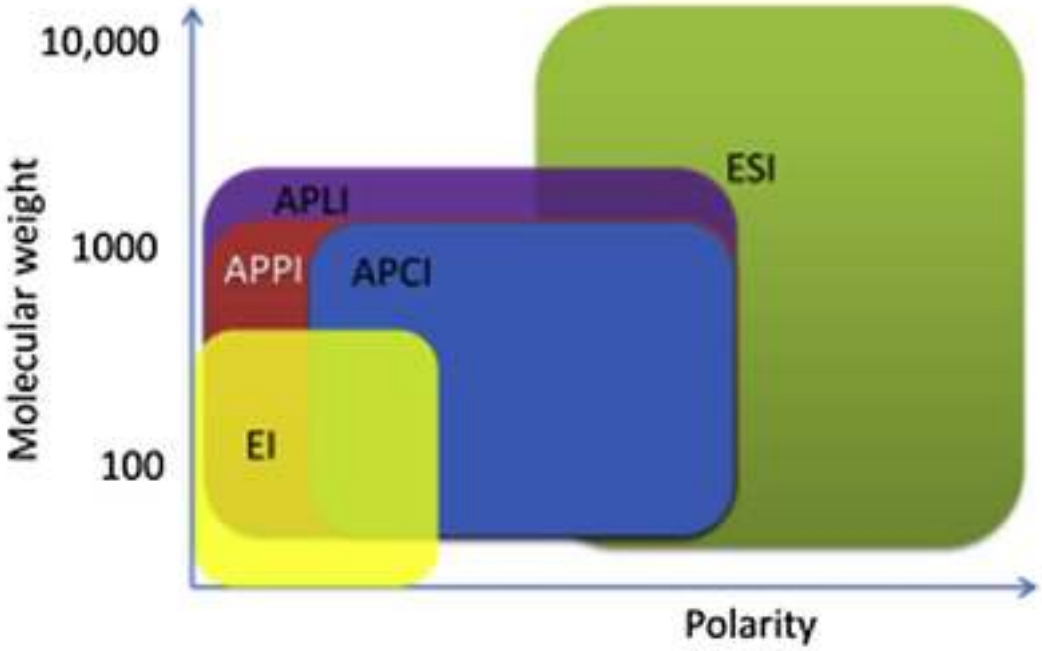

Li et al., *Analytica Chimica Acta*, **2015**, *43-61*

Brief History and Importance

- most prominent technique in the realm of atmospheric pressure ionization schemes
- “wings for molecular elephants” [1]
- ESI was <u>not</u> a straight-forward development – many predecessors
  - thermospray (solution + volatile buffer evaporated from heated capillary)
  - electrohydrodynamic ionization (spraying electrolyte solution with low volatility)
  - …

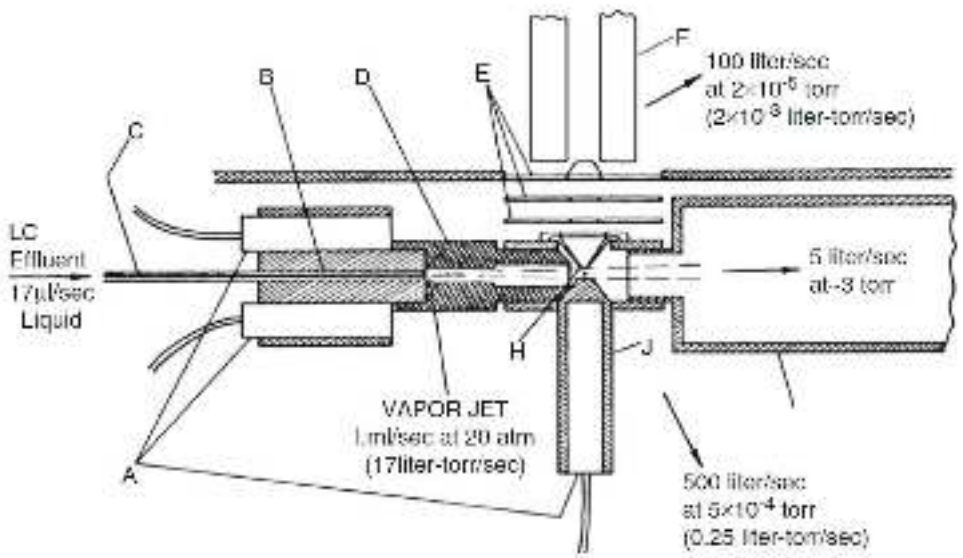

Jürgen H- Gross, *Mass Spectrometry – A Textbook*, **2017**, Spinger, ISBN *978-3-319-54398-7*

Thermospray interface.
A cartridge heater
B copper block brazed to stainless steel capillary
C capillary
D copper tube
E ion lenses
F quadrupole mass analyser
G line to rotary vane pump
H ion exit aperture
J source heater

Concept and Basics

- mist of µm-sized electrically charged droplets is generated from almost any standard solvent
- repetitive shrinking and droplet disintegration
- droplets would freeze on their transition from atmosphere to vacuum (adiabatic expansion) → heated counter gas stream or heated capillary (common to all ESI sources)
- contrast to vacuum ionization → differential pumping needed to remove the concomitant gas

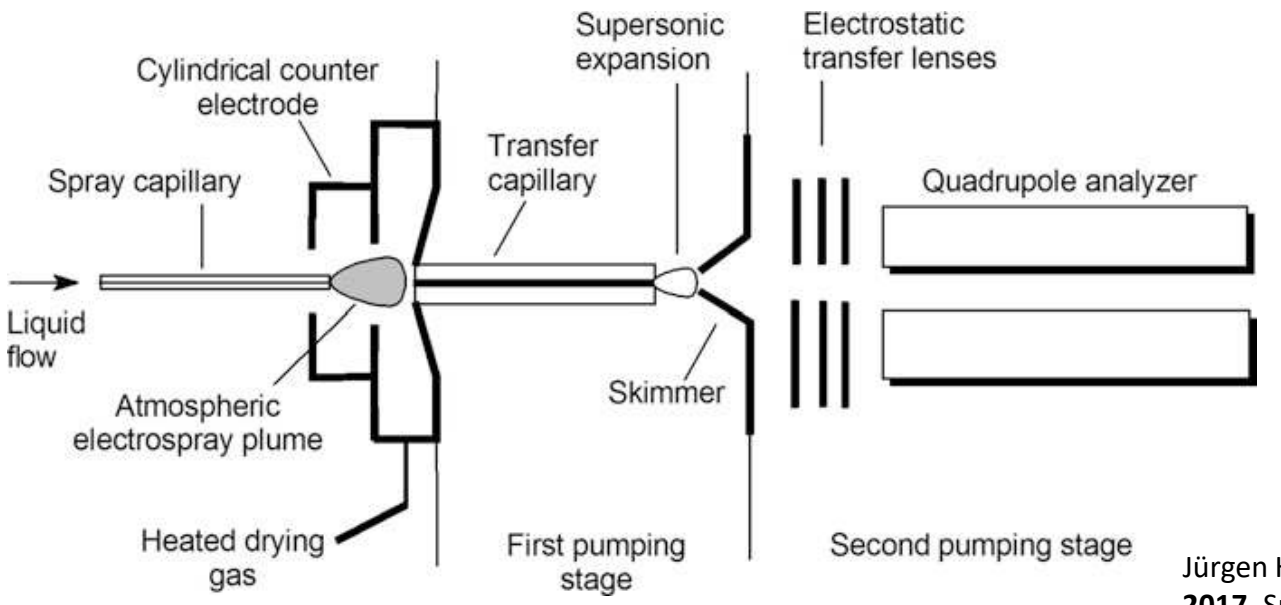

Jürgen H- Gross, *Mass Spectrometry – A Textbook*, **2017**, Spinger, ISBN *978-3-319-54398-7*

Electrospray Ionization – ESI

Concept and Basics

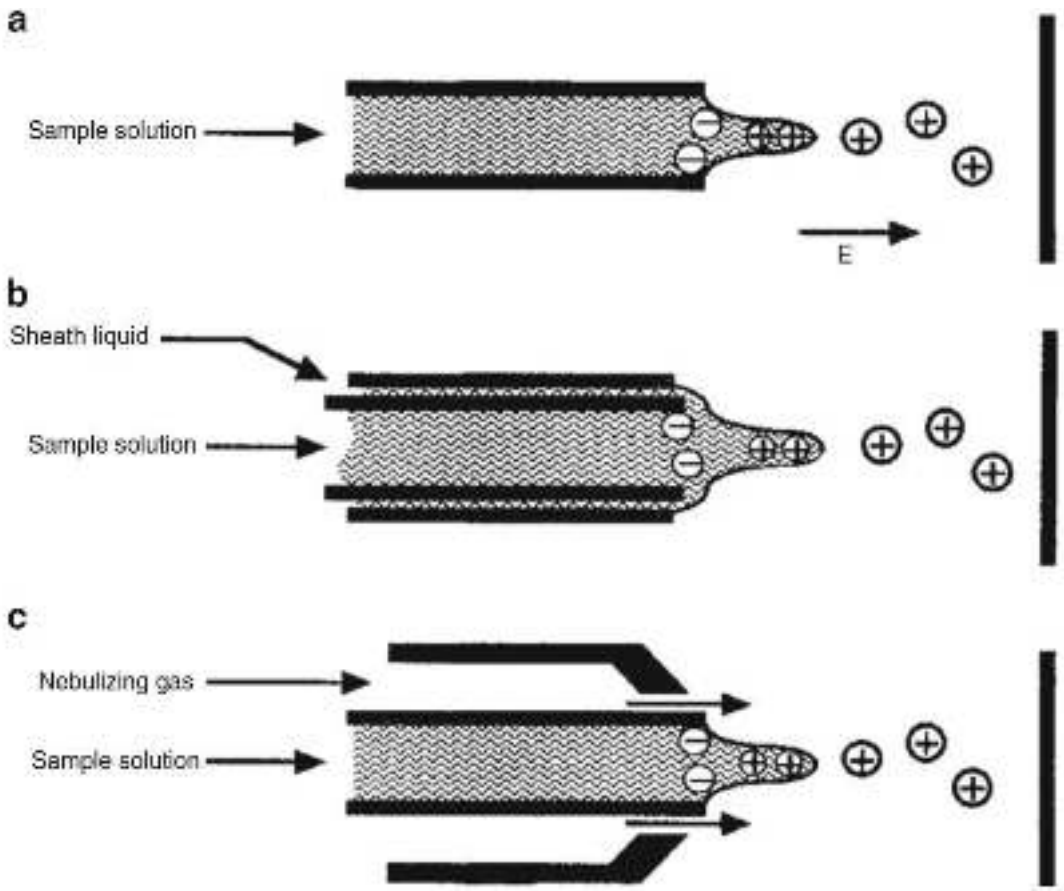

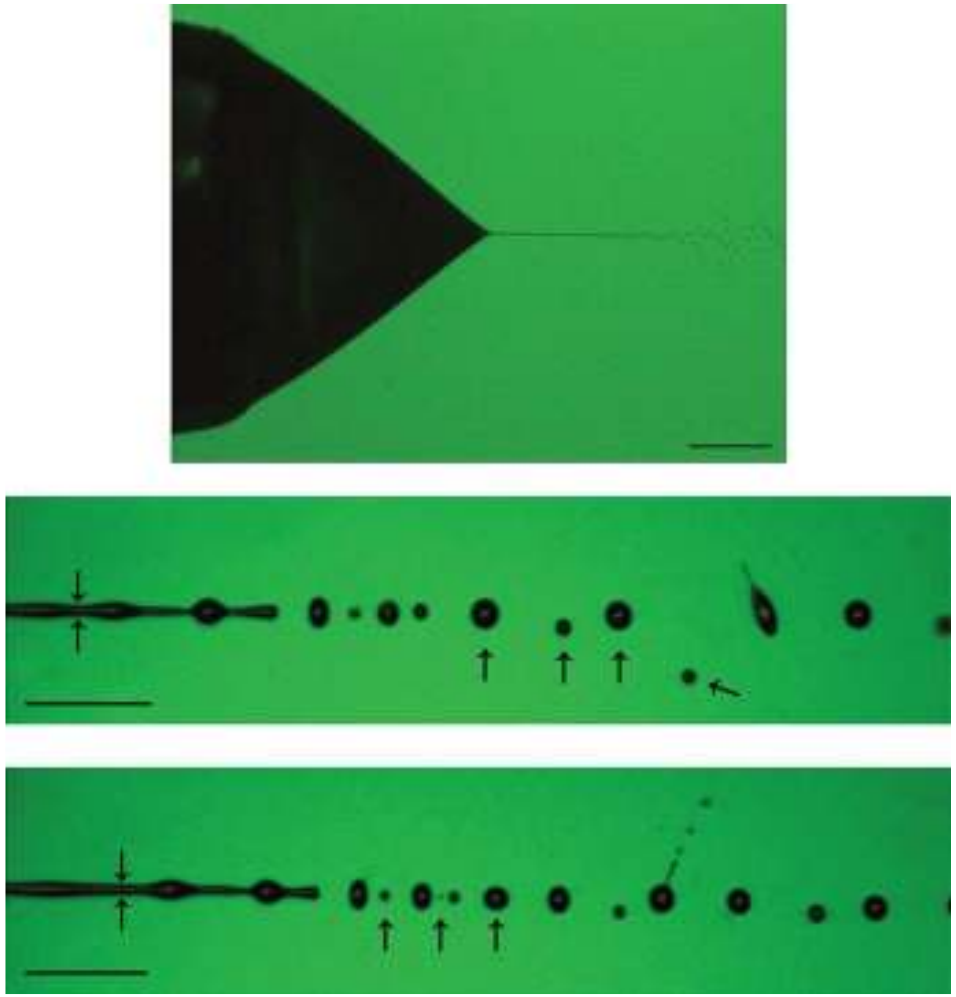

Jürgen H- Gross, *Mass Spectrometry – A Textbook*, **2017**, Spinger, ISBN *978-3-319-54398-7*

Overview Ion Formation in Electrospray Ionization

Table 12.1 Ions formed by ESI

Analytes	Positive ions	Negative ions
Low polarity	$[M+H]^+$, $[M+cat]^+$ if any at all[a]	$[M-H]^-$, $[M+an]^-$ if any at all[a]
Medium polarity	$[M+H]^+$, $[M+cat]^+$, $[M+alkali]^{+a}$	$[M-H]^-$, $[M+an]^{-a}$
Medium to high polarity	$[M+H]^+$, $[M+cat]^+$, $[M+alkali]^{+a}$ *exchange* $[M-H_n+alkali_{n+1}]^+$ {*clusters* $[2M+H]^+$, $[2M+alkali]^+$, *adducts* $[M+solv+H]^+$, $[M+solv+alkali]^+$}[c]	$[M-H]^-$, $[M+an]^{-a}$ *exchange* $[M-H_n+alkali_{n-1}]^-$ {*clusters* $[2M-H]^-$ *adducts* $[M+solv-H]^-$}[c]
Ionic[b]	C^+, $[C_n+A_{n-1}]^+$	A^-, $[C_{n-1}+A_n]^-$

[a]Some cation cat^+ or anion an^- incidentally present
[b]Comprising analyte cation C^+ and analyte anion A^-
[c]Braces denote less abundant species

Jürgen H- Gross, *Mass Spectrometry – A Textbook*, **2017**, Spinger, ISBN *978-3-319-54398-7*

Geometry and Designs

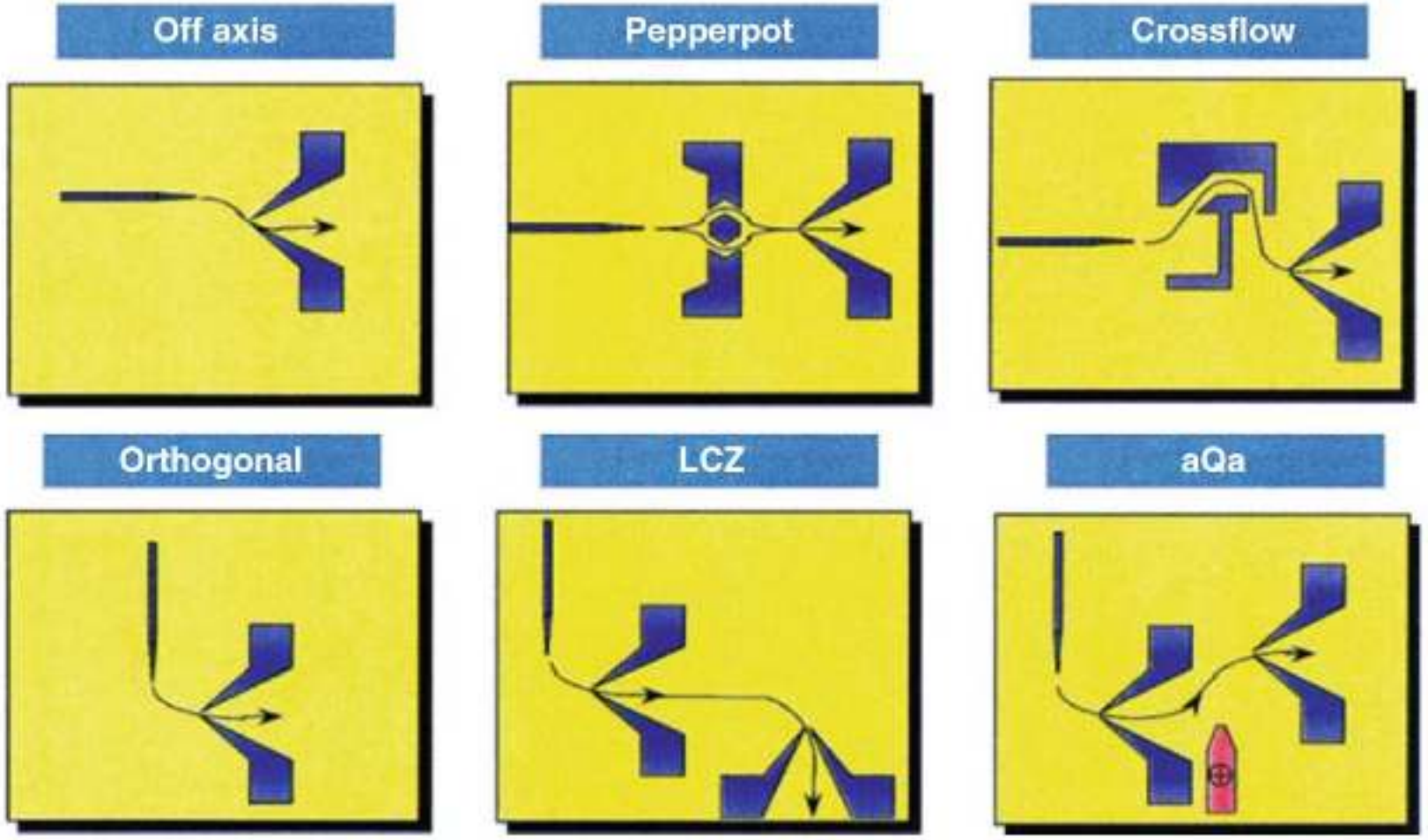

Jürgen H- Gross, *Mass Spectrometry – A Textbook*, **2017**, Spinger, ISBN *978-3-319-54398-7*

Electrospray Ionization – ESI

Geometry and Construction

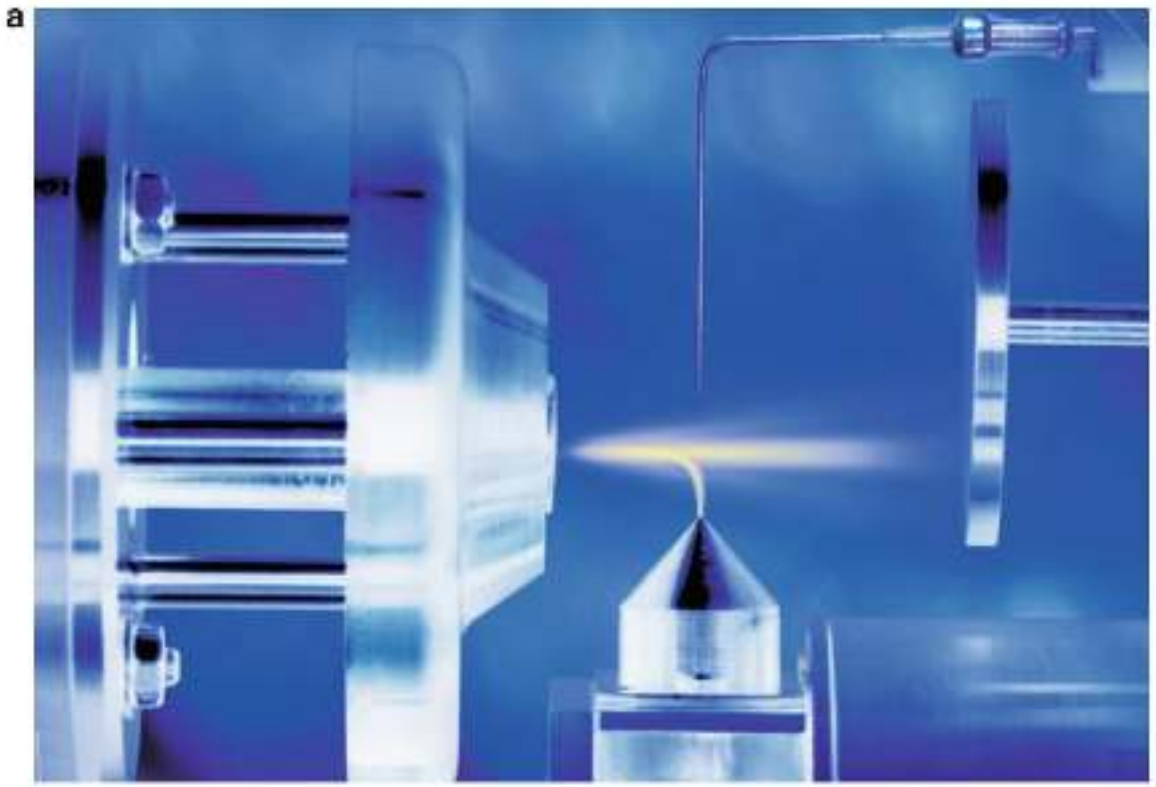

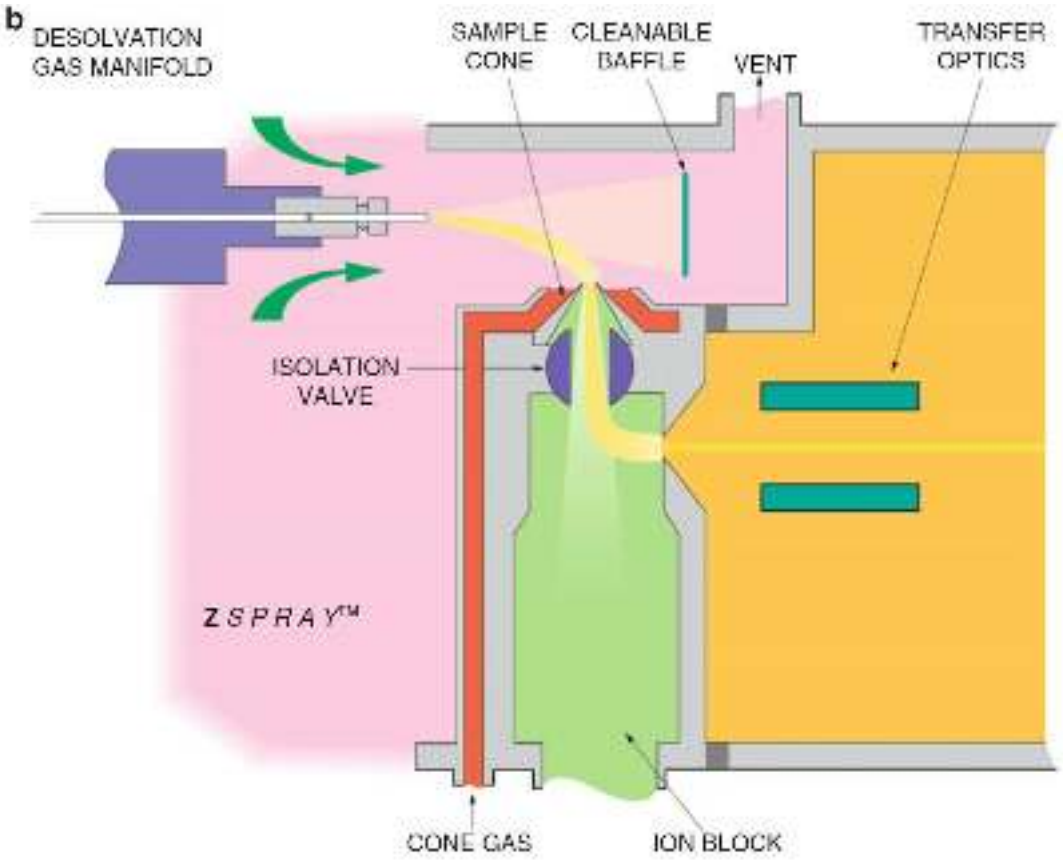

Jürgen H- Gross, *Mass Spectrometry – A Textbook*, **2017**, Spinger, ISBN *978-3-319-54398-7*

Electrospray Ionization – ESI

Common Bruker ESI source in FT-ICR MS

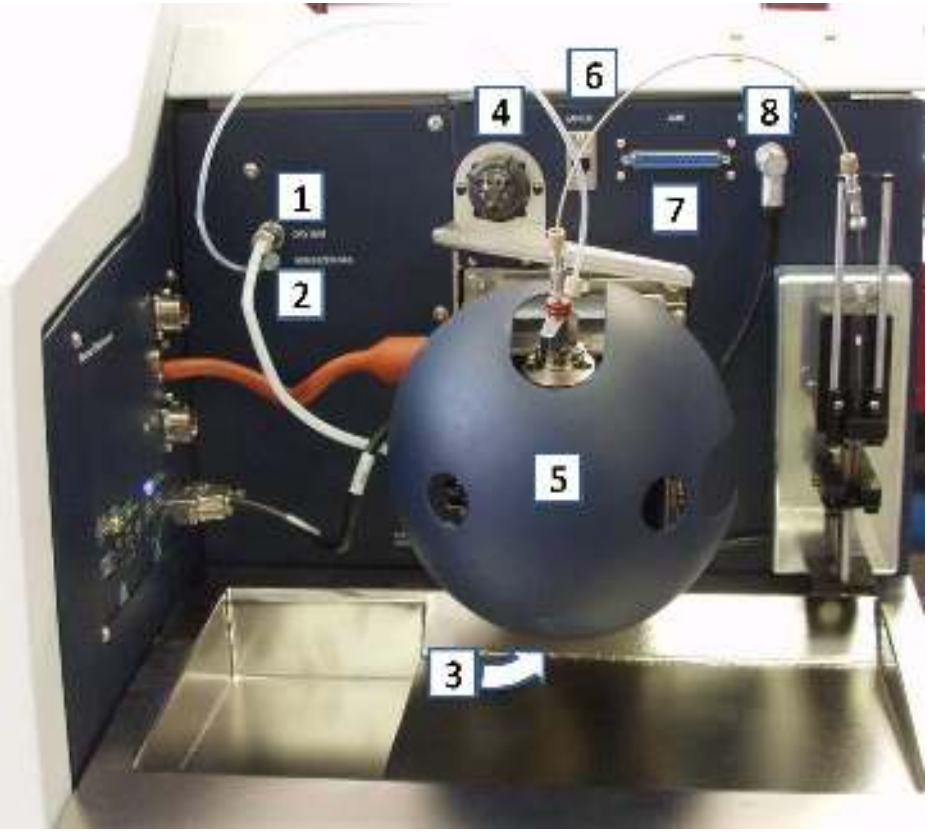

Bruker Daltonics ESI source at a solariX MRMS equipped with a Apollo II interface

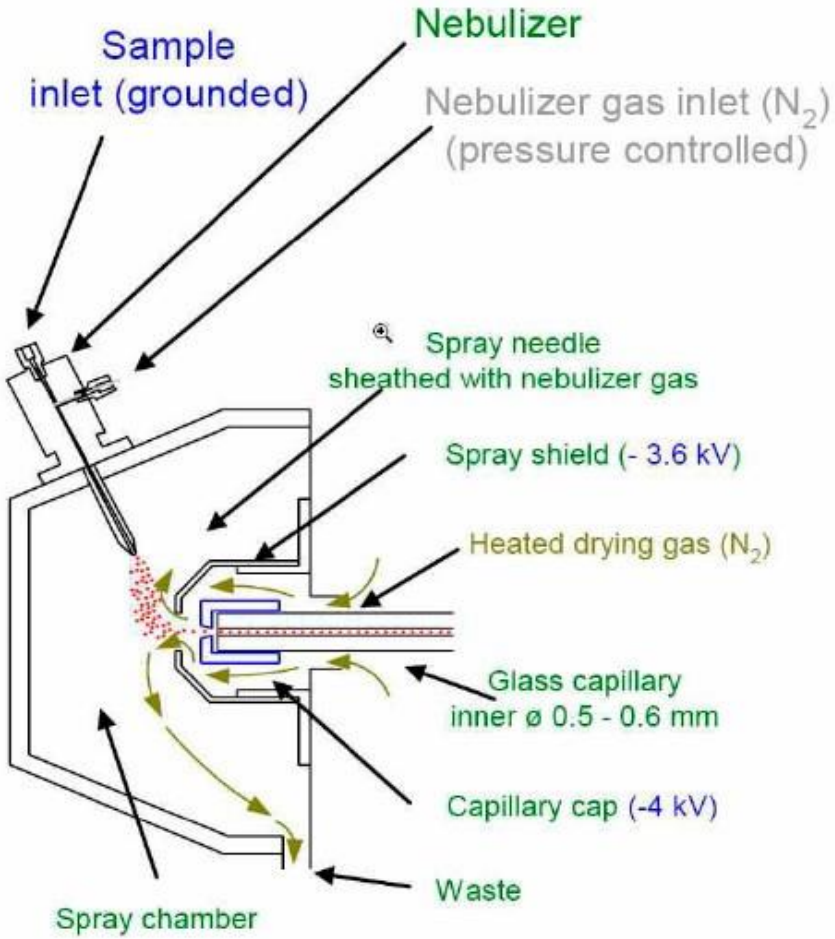

Scheme of the Bruker ESI general construction

Bruker Daltonics Tutorial Material

Common Bruker ESI source in FT-ICR MS - Atmospheric Pressure Interface

Bruker Apollo II API interface found at almost all Bruker FT-ICR MS

Collision Induced Dissociation in AP Ionization Interfaces – Do we want that?

- weekly bonded substituents can cleave of even at low collision energies
- Bruker Apollo II source common in FT-ICR MS features dual ion funnel setup
  - first funnel: 3-4 mbar, directly collecting the ions after supersonic expansion from AP to the vacuum
  - second funnel prior RF hexapol to guide/collect ions (~0.1 mbar)
- in-source CID (Bruker terminology!): shifting DC potential to have large drop from first to second funnel

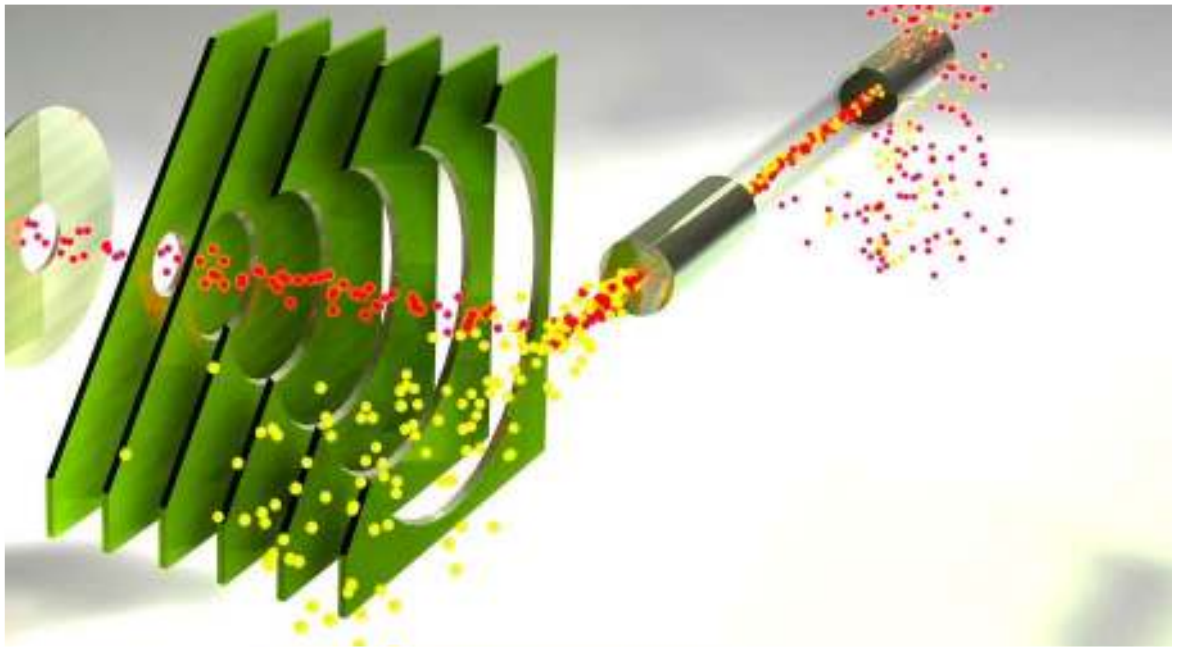

Scheme of the atmospheric pressure interface: Glass-capillary inlet coupling atmospheric pressure to first vacuum stage ~mbar

Collision Induced Dissociation in AP Ionization Interfaces – Do we want that?

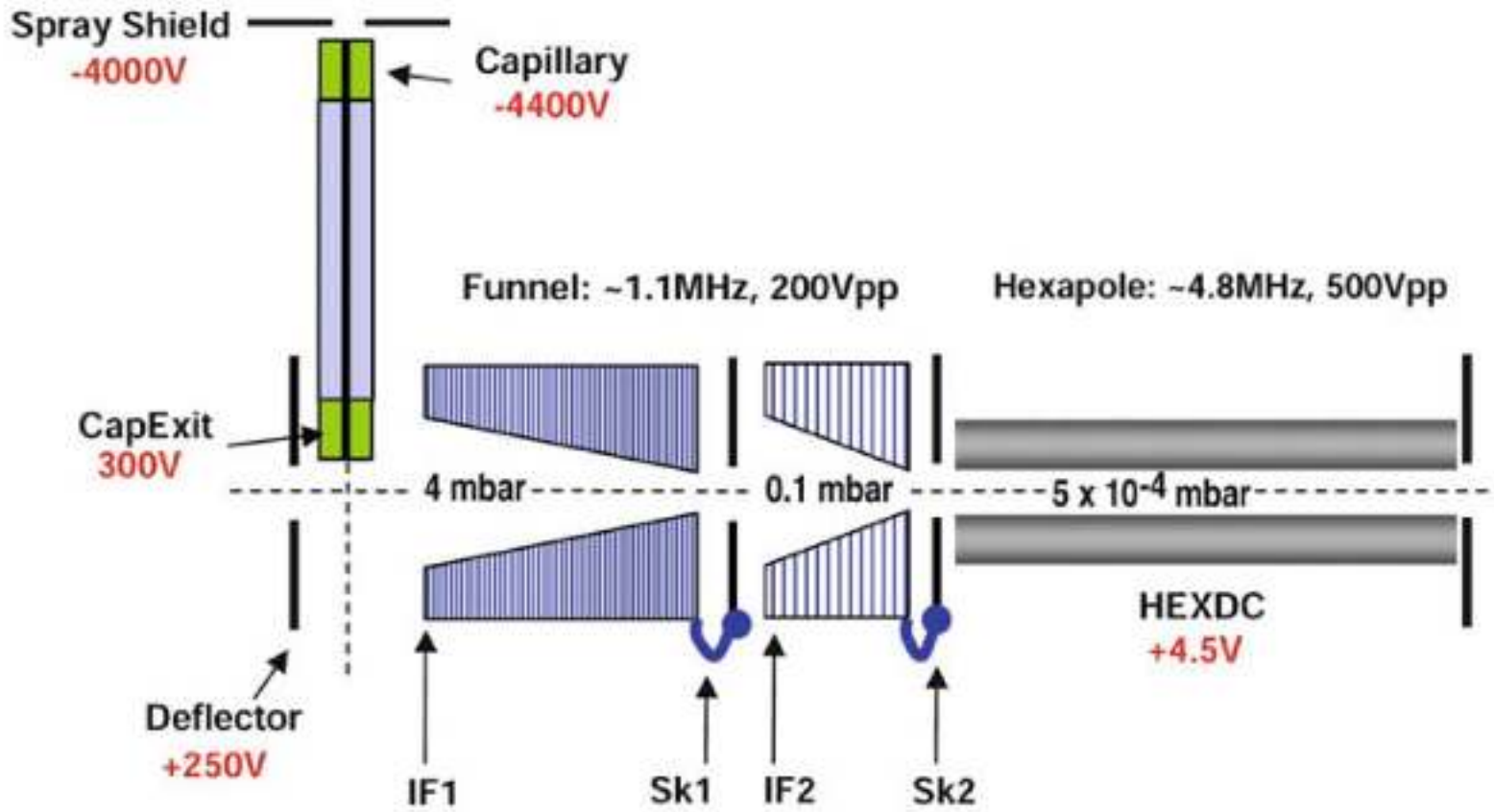

	IF1	Sk1	IF2	Sk2
Normal ESI operation:	+ 150 V	+ 15 V	+ 7 V	+ 5 V
In-source CID @ 50 V:	+ 150 V	+ 65 V	+ 7 V	+ 5 V

Bruker Daltonics Tutorial Material

Charge State Distribution

Influencing parameters:

- pH of the sprayed solution,
- flow of sample solution,
- flow (or pressure) of nebulizing gas
- flow and temperature of the desolvation gas
- temperature of the heated desolvation capillary
- …

ESI: Broadband Spectrum of BSA (66kDa)

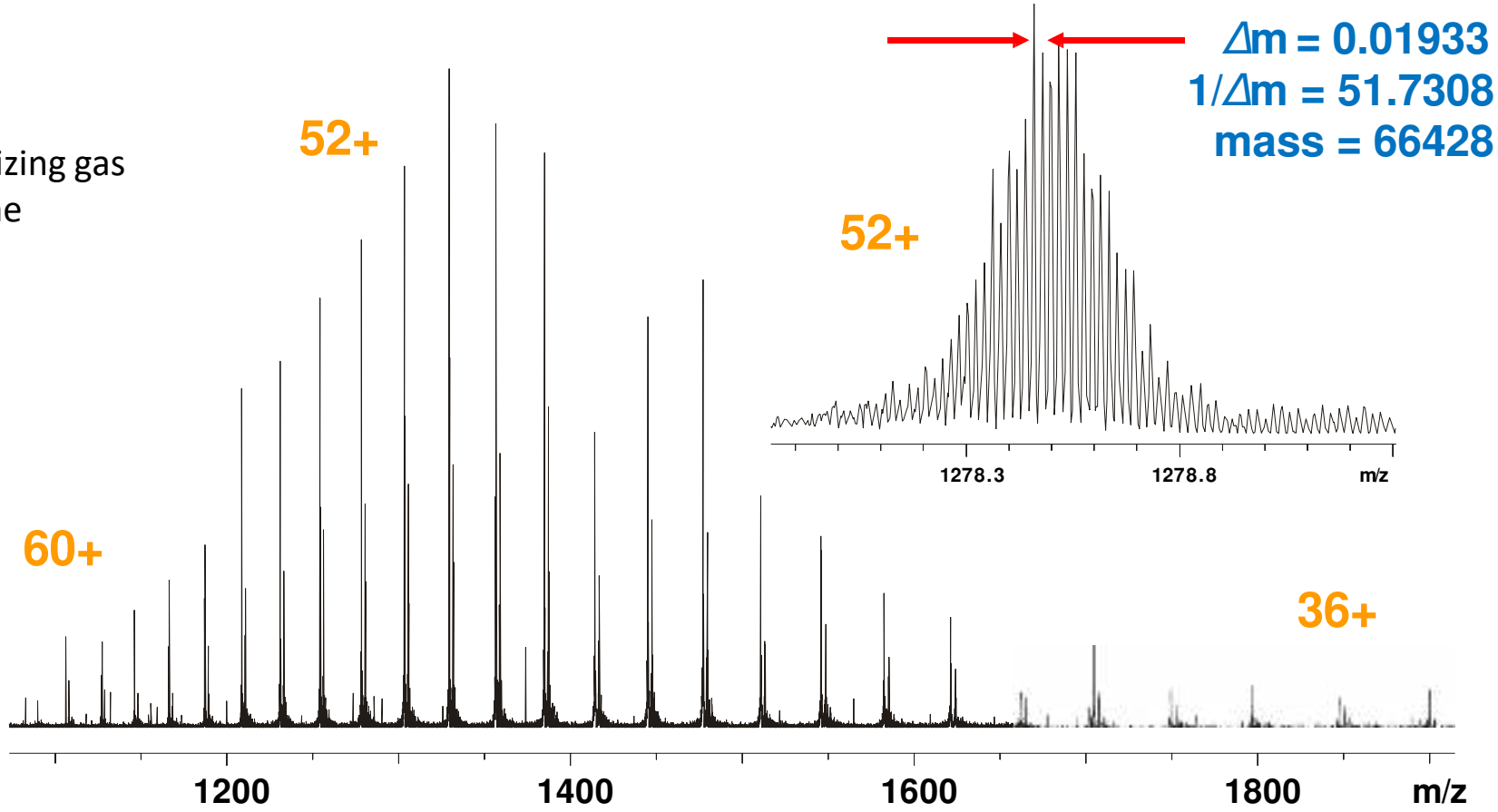

Bruker Daltonics Tutorial Material

Charge State Distribution and How to Influence it

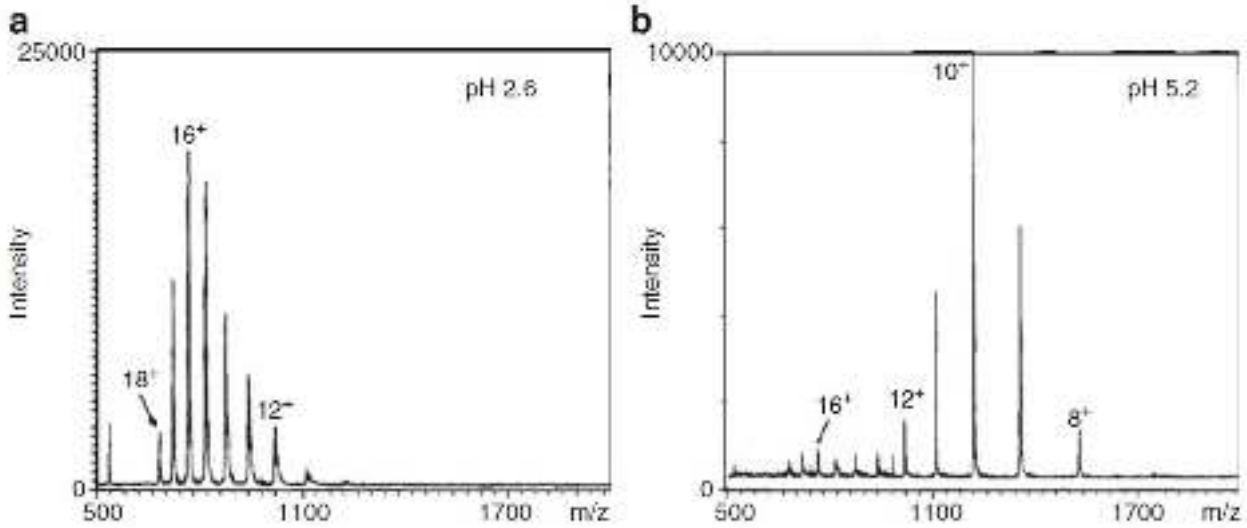

Fig. 12.21 Positive-ion ESI mass spectra of cytochrome c at different pH of the sprayed solution: (a) at pH 2.6, (b) at pH 5.2 (Adapted from Ref. [107] by permission. © American Chemical Society, 1990)

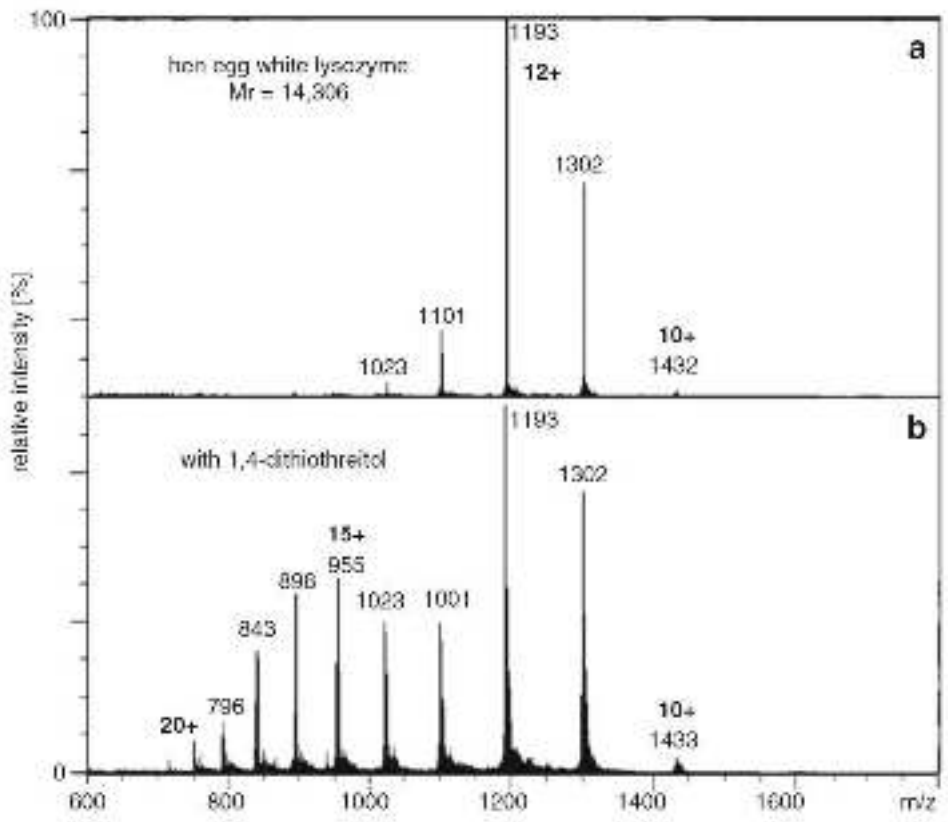

Charge state can be influenced by pH and reduction agent!

Jürgen H- Gross, *Mass Spectrometry – A Textbook*, **2017**, Spinger, ISBN *978-3-319-54398-7*

Charge Deconvolution and the Benefit of Ultrahigh Resolving Power

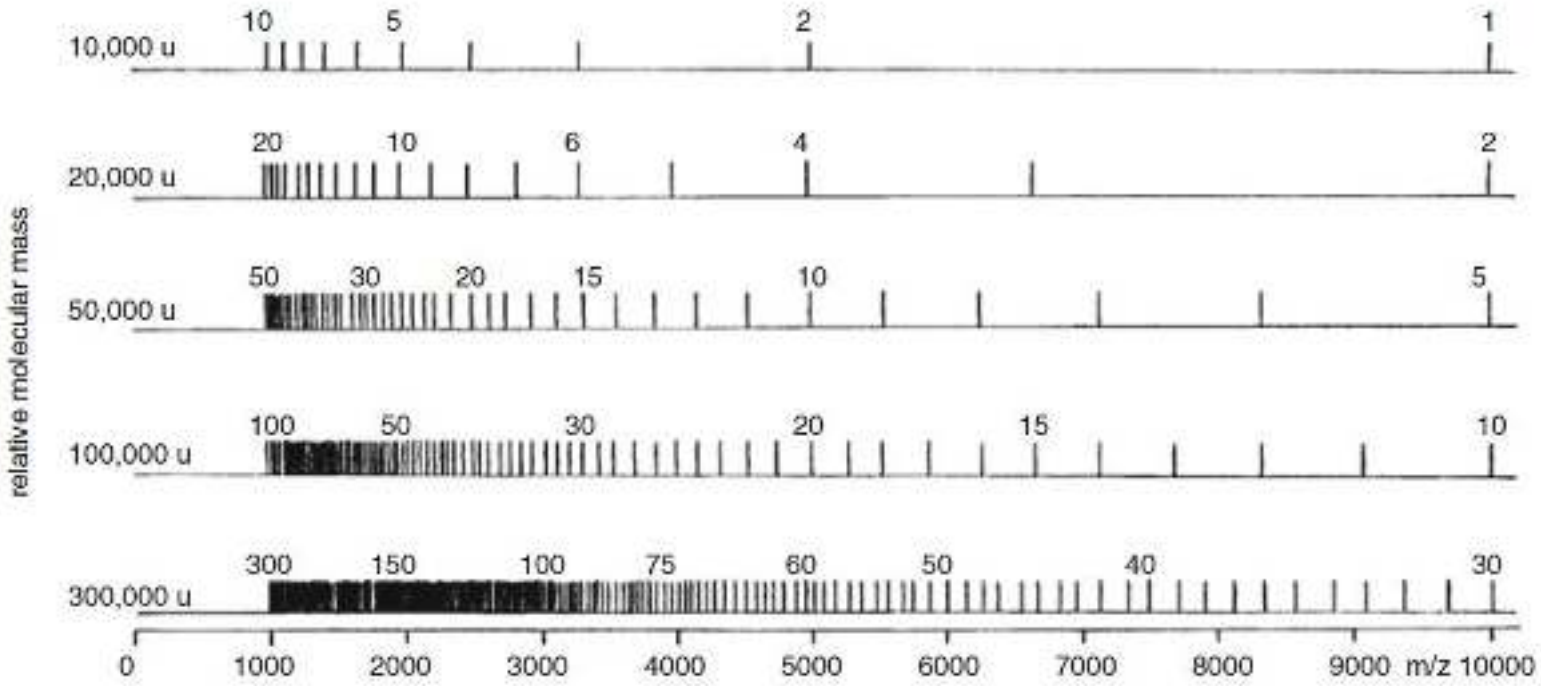

Fig. 12.24 Calculated *m/z* values for the different charge states of molecules of different molecular weight. Representative peaks are labeled with their corresponding charge state (Adapted from Ref. [116] by permission. © John Wiley & Sons, 1992)

Jürgen H- Gross, *Mass Spectrometry – A Textbook*, **2017**, Spinger, ISBN *978-3-319-54398-7*

Charge Deconvolution and the Benefit of Ultrahigh Resolving Power

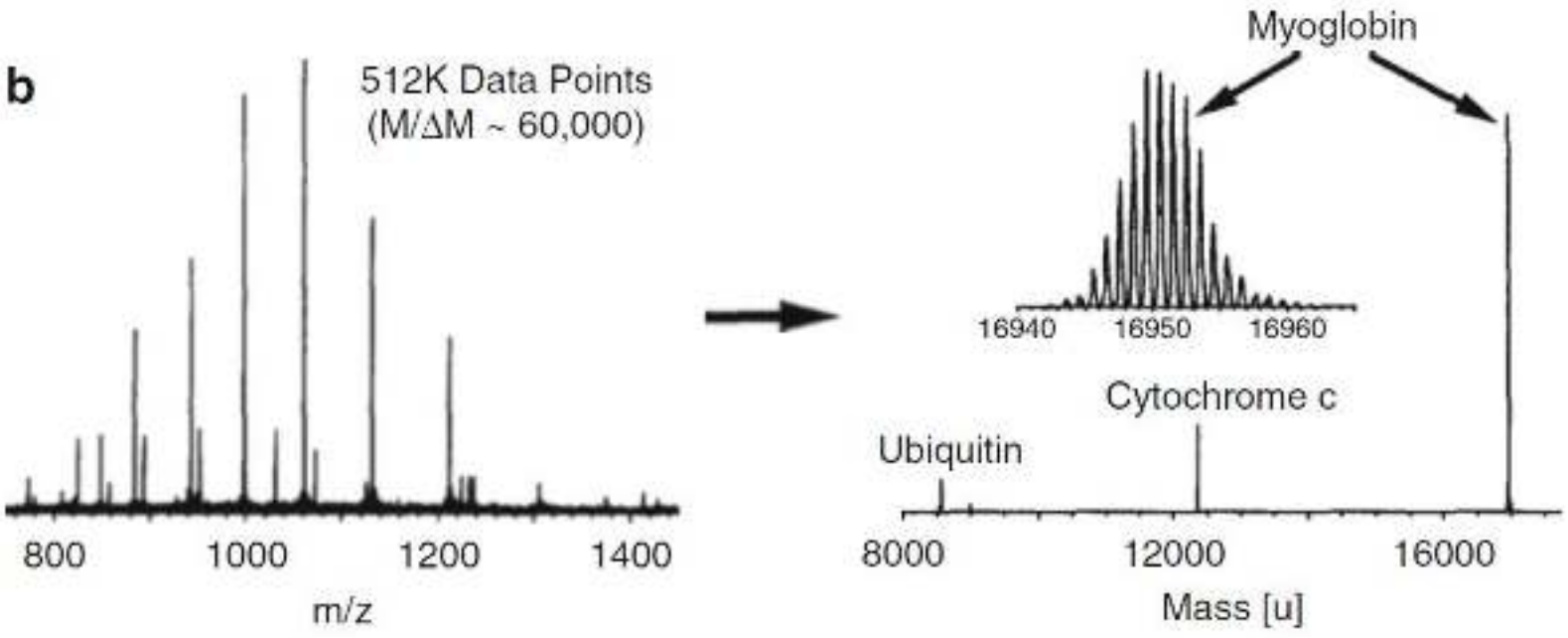

Fig. 12.27 Charge deconvolution of (**a**) LR and (**b**) HR positive-ion ESI spectra of an artificial protein mixture. The "zero-charge" peak of myoglobin is also shown in expanded view to reveal the delineation of the isotopic pattern (Adapted from Ref. [123] by permission. © Elsevier, 1998)

Jürgen H- Gross, *Mass Spectrometry – A Textbook*, **2017**, Spinger, ISBN *978-3-319-54398-7*

Charge Deconvolution and the Benefit of Ultrahigh Resolving Power

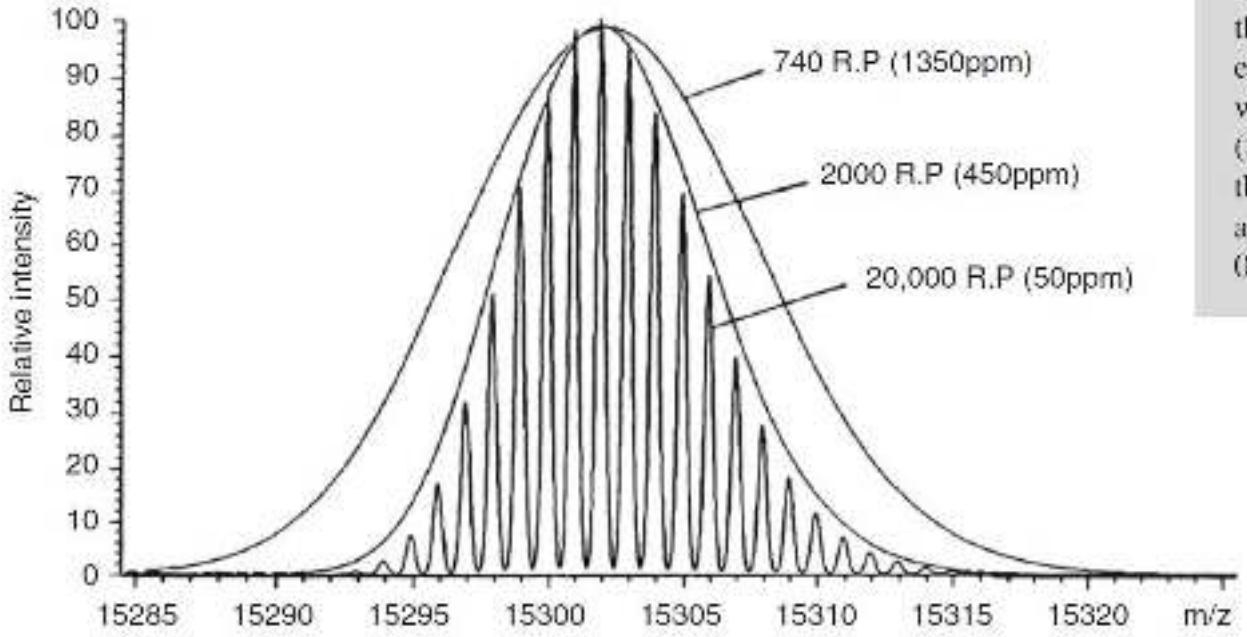

Fig. 12.28 Theoretical peak shape for a hypothetical singly charged protein ion of $M_r = 15{,}300$ u at different settings of resolution (Reproduced from Ref. [116] by permission. © John Wiley & Sons, 1992)

Rule for minimum resolving power: The mass resolving power to achieve full separation of isotopic peaks only depends on the molecular weight, M_r, of the analyte, but it is independent of the number of charges, z, of the ions. For example, the isotope peaks of the $[M+H]^+$ ion of thioredoxin (Fig. 12.1) would appear at m/z 11674 and be spaced at $\Delta(m/z) = 1$. Using $R = m/\Delta m$ (Sect. 3.4) we calculate the minimum value $R_{min} = 11674 / 1 = 11674$. For the $[M+8H]^{8+}$ ion of this protein ($z = 8$), the signals are centered at m/z 1459 and spaced at $\Delta(m/z) = 0.125$. Thus, we calculate $R_{min} = m/\Delta m = 1459 / 0.125 = 11674$. In brief, the numerical value of M_r directly reflects R_{min}.

Jürgen H- Gross, *Mass Spectrometry – A Textbook*, **2017**, Spinger, ISBN *978-3-319-54398-7*

Selectivity of Ionization in Mass Spectrometry – "Analytical Glasses"

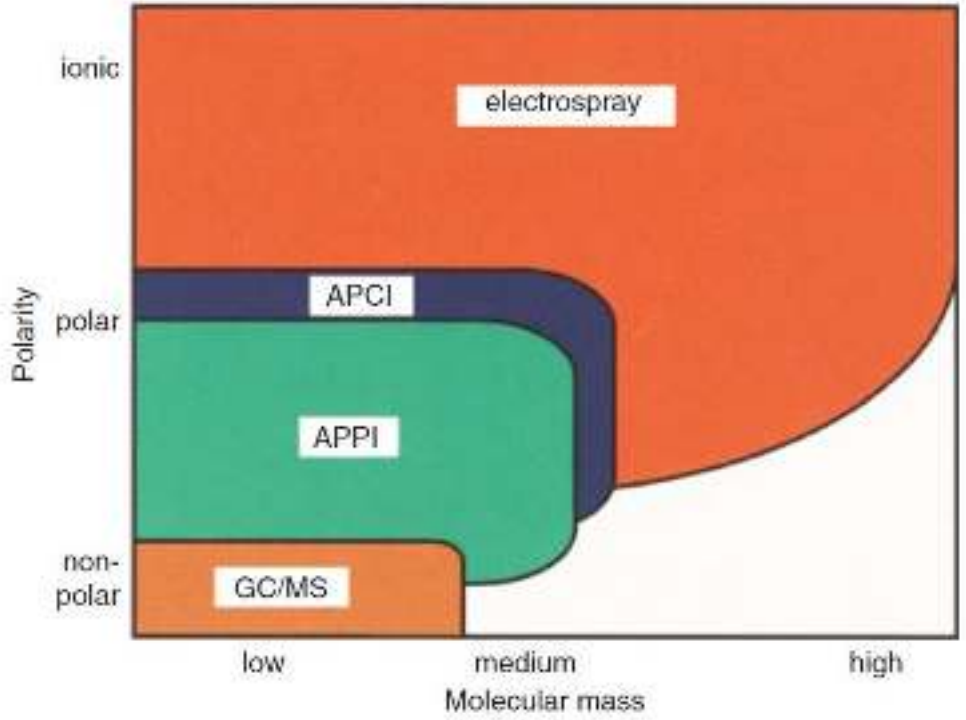

Cover of *Anal. Bioanal. Chem.*, **2004**, 378(4)

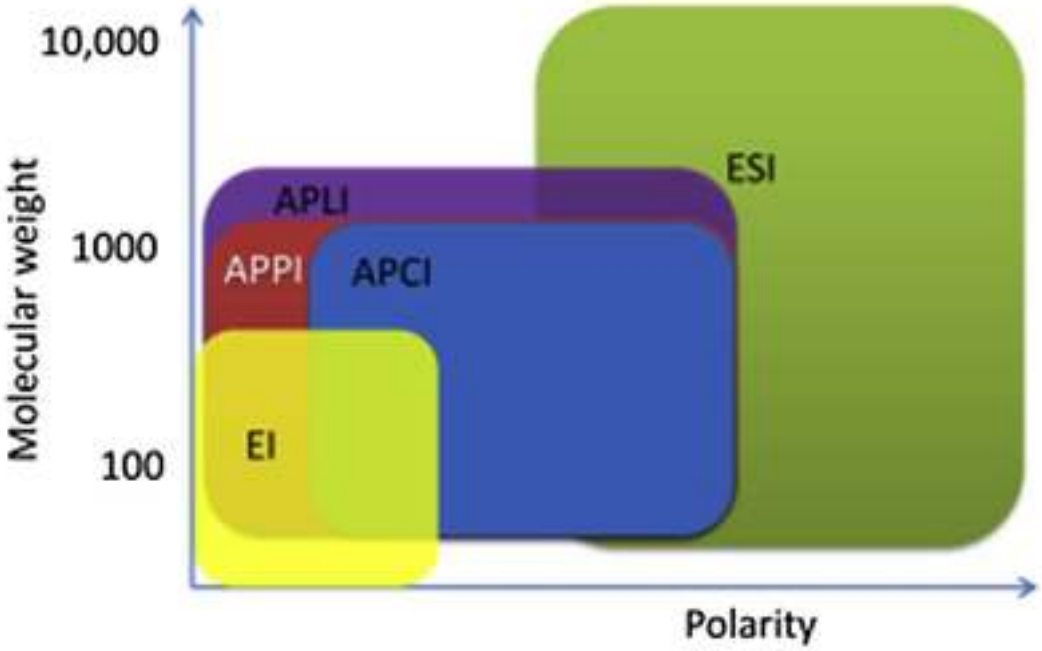

Li et al., *Analytica Chimica Acta*, **2015**, *43-61*

Historic Background – Atmospheric Pressure Ionization

- first technique combining solution liquid introduction with mass spectrometry
- diluted solution of the analyte is sprayed into a hot Nitrogen gas stream (~200 °C)
- vapor is guided into an ionization chamber containing a β emitter (^{63}Ni foil) followed by complex reaction cascade – finally leading to protonated water clusters acting as ionization reagent

$$N_2 + e^- \rightarrow N_2^{+\bullet} + 2e^-$$

$$N_2^{+\bullet} + N_2 + N_{2(3rd\ body)} \rightarrow N_4^{+\bullet} + N_{2(3rd\ body)}$$

$$N_4^{+\bullet} + H_2O \rightarrow H_2O^{+\bullet} + 2N_2$$

$$H_2O^{+\bullet} + H_2O \rightarrow H_3O^+ + OH^\bullet$$

$$H_3O^+ + H_2O \rightarrow [(H_2O)_2 + H]^+$$

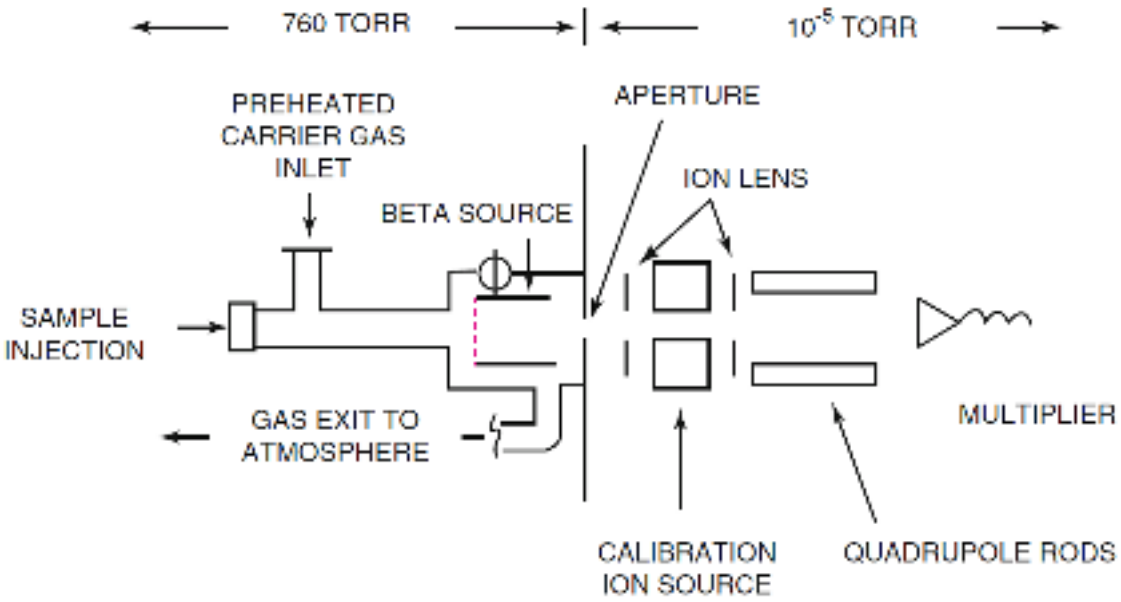

→ <u>but</u> radioactive source not suitable for common laboratories

Jürgen H- Gross, *Mass Spectrometry – A Textbook*, **2017**, Spinger, ISBN *978-3-319-54398-7*

Modern Version commonly named APCI

- introduced by Horning et al. by changing the β emitter to a corona discharge plasma
- reagent ion plasma is maintained by a current applied between the sharp tip of the corona needle and the counter electrode (spray inlet)
- basically atmospheric pressure analogous of classical vacuum chemical ionization <u>but</u> at atmospheric pressure higher number of collisions and probability of subsequent reactions

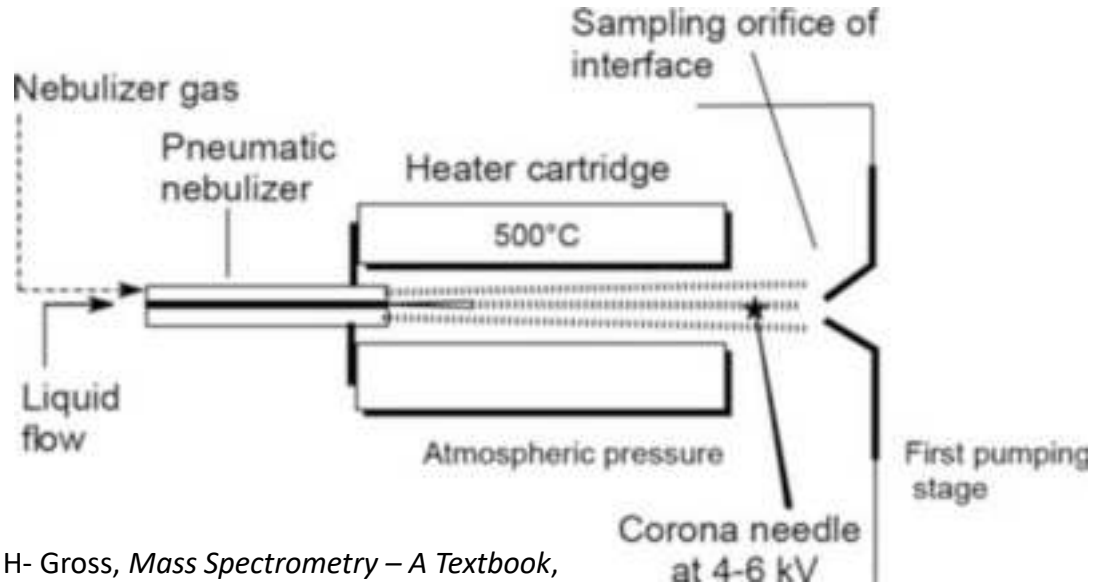

Jürgen H- Gross, *Mass Spectrometry – A Textbook*, **2017**, Spinger, ISBN *978-3-319-54398-7*

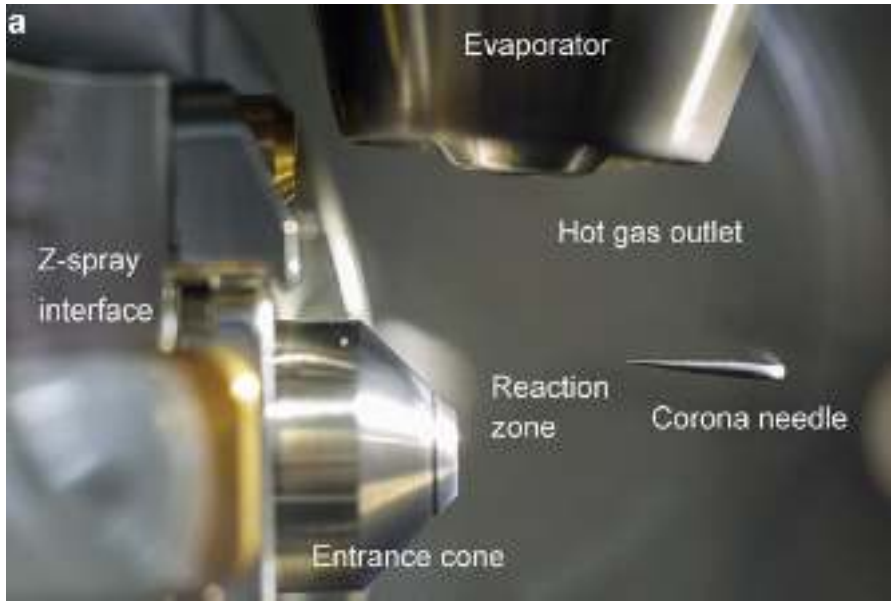

Ion Formation in Positive and Negative Polarity

- complex reaction cascade comparable the API scheme
- strongly influenced by water and oxygen concentration and dwell time in the reagent zone → ionization source parameter (flow rates of dry and nebulizer gas, source and gas temperatures, etc.) have a significant effect on the ionization conditions!

positive polarity

$$\text{corona discharge} + N_2 \rightarrow N_2^{+\bullet} + e^-$$

$$N_2^{+\bullet} + N_2 + N_{2(\text{3rd body})} \rightarrow N_4^{+\bullet} + N_{2(\text{3rd body})}$$

$$N_4^{+\bullet} + H_2O \rightarrow 2N_2 + H_2O^{+\bullet}$$

$$H_2O^{+\bullet} + H_2O \rightarrow H_3O^+ + OH^\bullet$$

$$H_3O^+ + nH_2O \rightarrow [(H_2O)_n + H]^+$$

$$M + [(H_2O)_n + H]^+ \rightarrow [M + H]^+ + nH_2O$$

negative polarity

$$O_2 + e^- \rightarrow O_2^{-\bullet}$$

$$O_2^{-\bullet} + M \rightarrow [M + O_2]^{-\bullet}$$

$$M^{-\bullet} + O_2 \rightarrow [M + O_2]^{-\bullet}$$

$$[M + O_2]^{-\bullet} \rightarrow M^{-\bullet} + O_2$$

$$[M + O_2]^{-\bullet} \rightarrow [M - H]^- + HOO^\bullet$$

Jürgen H- Gross, *Mass Spectrometry – A Textbook*, **2017**, Spinger, ISBN *978-3-319-54398-7*

Nebulizer temperature commonly >350 °C – does this cause problems?

Yes and No!

- very labile molecules might degrade and fragment **but** the majority of organic molecules is softly ionized (even "softer" compared to classical vacuum CI)

Why?

- temperature of the aerosol droplet stays low as the energy is taken to evaporate the solvent
- at the end of the vaporization process only 150-200 °C
  - 150-200 °C ~ 0.1-02. eV but bond braking starts commonly > 2 eV
- thermal cooling – Millions of collisions per Second at atmospheric pressure dissipating the excess energy efficiently

Problems and Disadvantages

- frequent formation of ionization artifacts (adducts and additional reaction pathways)
  - ammonium adducts in pos. mode (mostly delivered by the sample, *e.g.*, buffer solution)
  - halogenide adducts in negative mode or less common CO_3^-, NO_2^-, or OH^-
  - oxidation (strongly depending on oxygen and water concentration)
  - …

$$M + [NH_4]^+ \rightarrow [M + NH_4]^+$$

$$M + Hal^- \rightarrow [M + Hal]^-$$

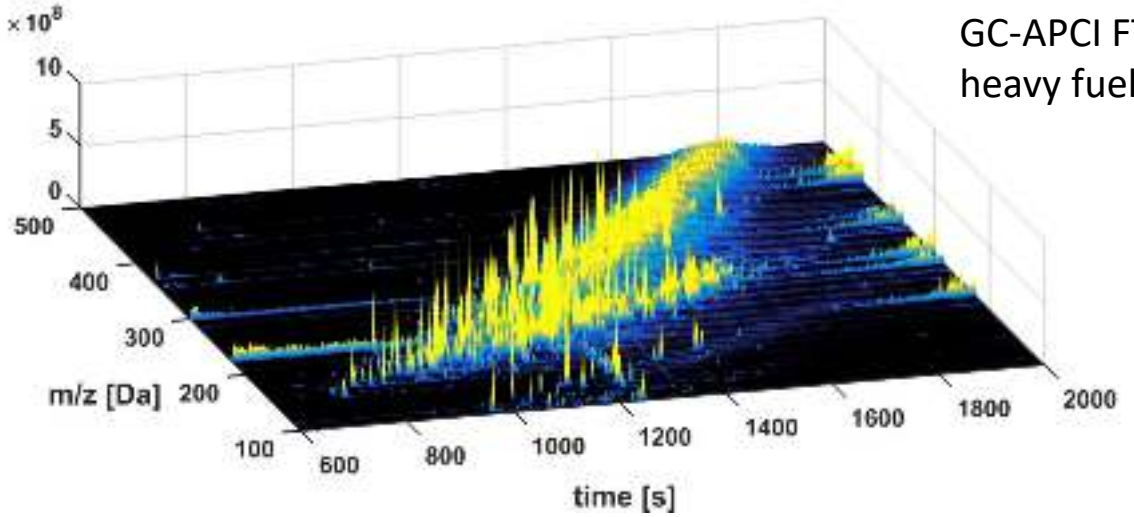

GC-APCI FT-ICR MS of heavy fuel oil

Artifact correction concepts

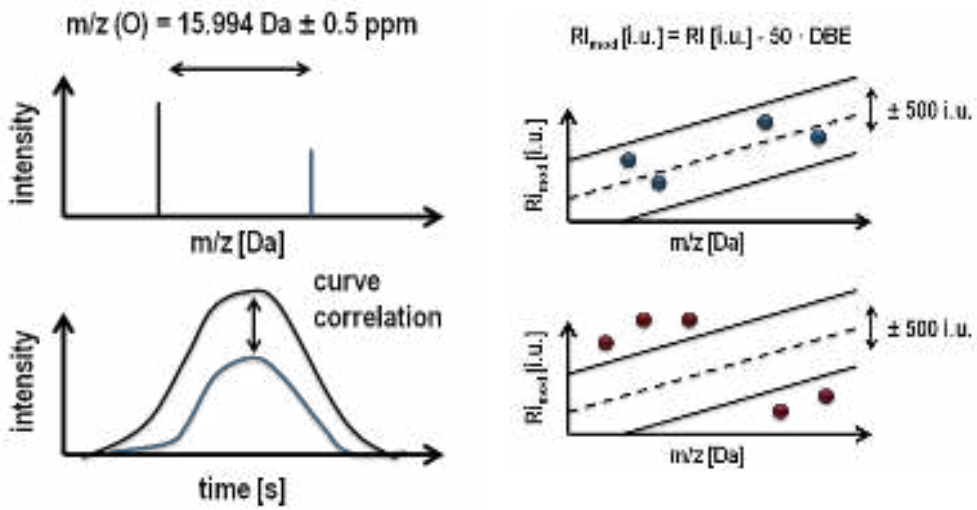

Schwemer et al., *Analytical Chemistry,* **2015**, 11957–11961
Rüger et al., *EJMS*, **2017**, 28–39

Selectivity of Ionization in Mass Spectrometry – "Analytical Glasses"

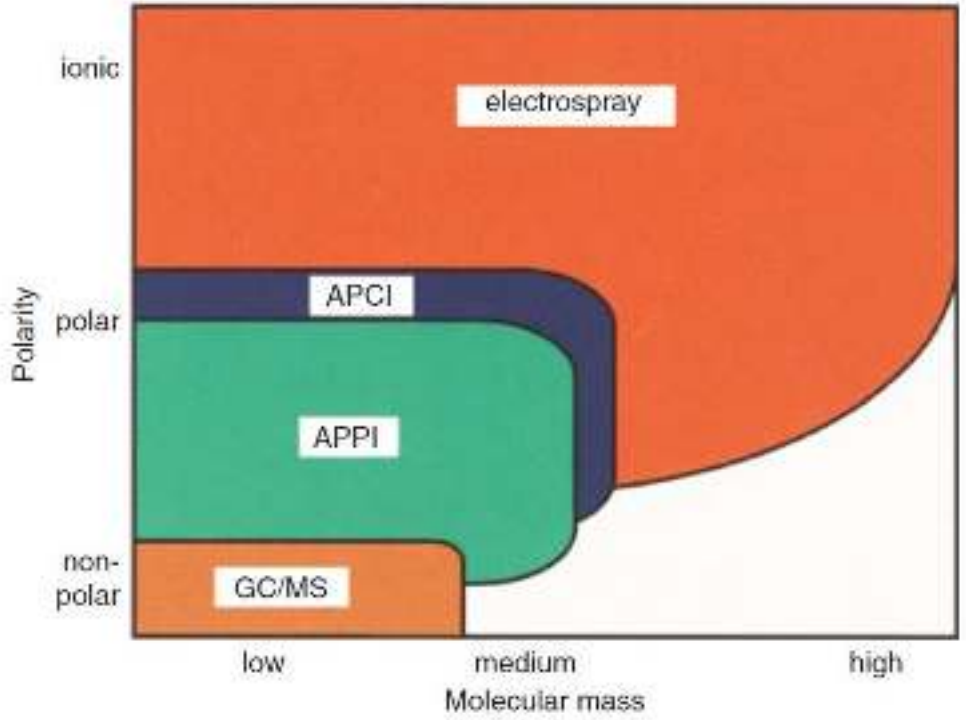

Cover of *Anal. Bioanal. Chem.*, **2004**, 378(4)

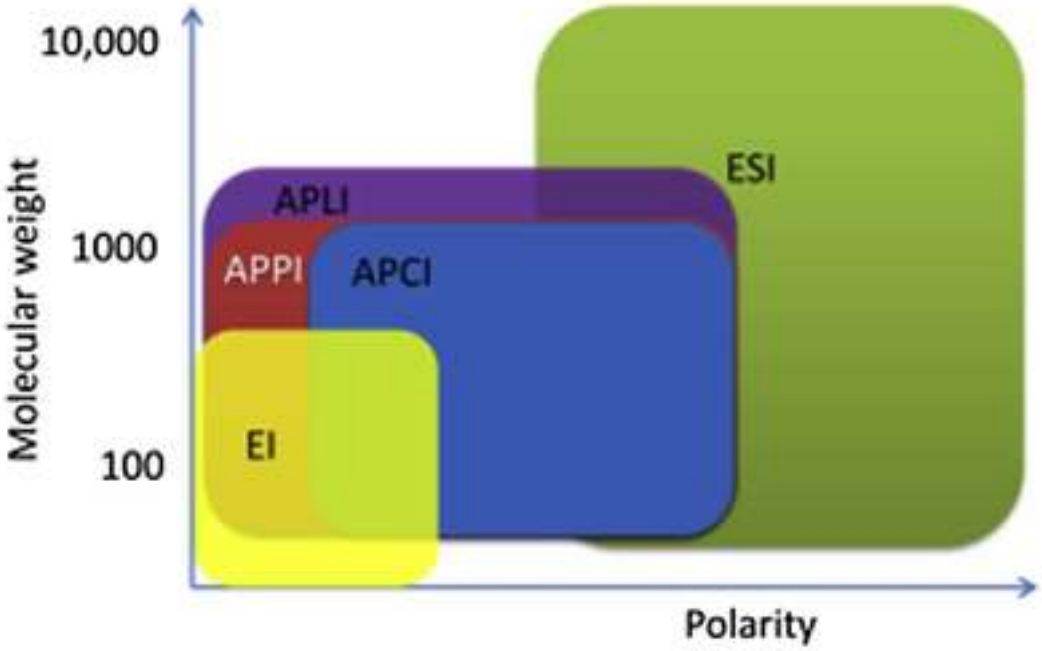

Li et al., *Analytica Chimica Acta*, **2015**, *43-61*

Atmospheric Pressure PI – APPI

Basics and Geometry

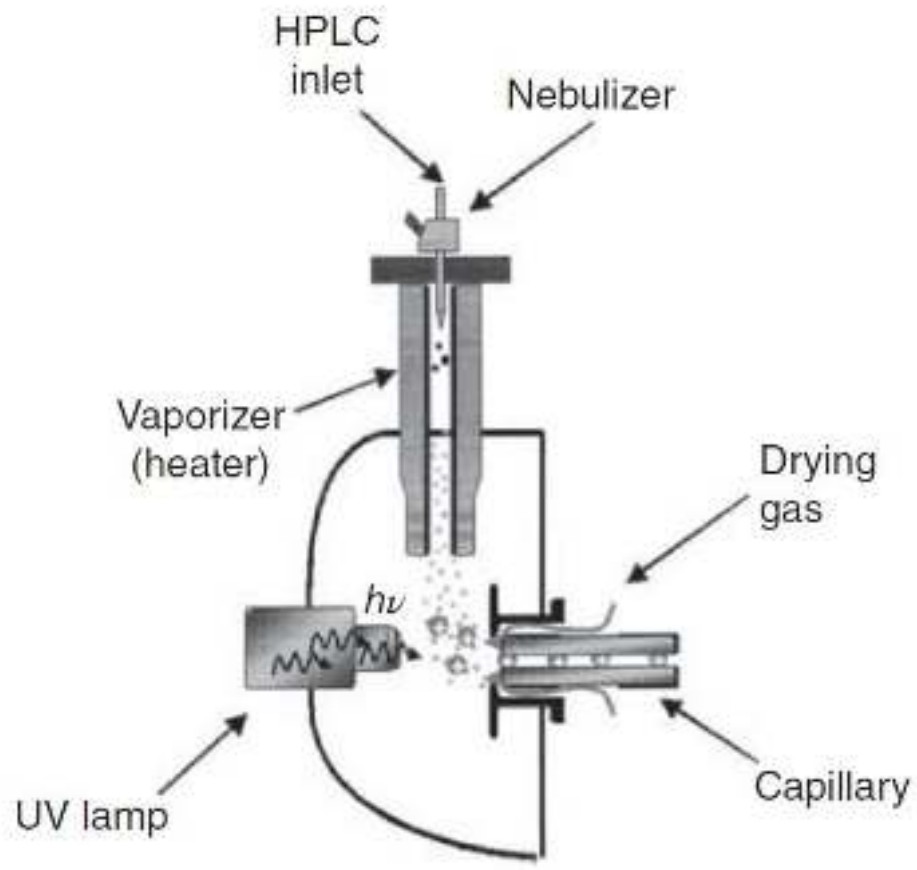

Photoionization and Photo-Induced Processes in Mass Spectrometry, Ralf Zimmermann and Luke Hanley, 2021 WILEY-VCH GmbH

$M + h\nu$	$\rightarrow$	$M^{+\cdot} + e^-$,	if IE (M) < 10 eV	(1)
$S + h\nu$	$\rightarrow$	$S^{+\cdot} + e^-$,	if IE (S) < 10 eV	(2)
D (dopant) $+ h\nu$	$\rightarrow$	$D^{+\cdot} + e^-$		(3)
$D^{+\cdot} + M$	$\rightarrow$	$M^{+\cdot} + D$,	if IE (M) < IE (D)	(4)
$D^{+\cdot} + nH_2O$	$\rightarrow$	$[D^{+\cdot}(H_2O)_n]$		(5)
$D^{+\cdot} + nS$	$\rightarrow$	$[D^{+\cdot}(S)_n]$		(6)
$[D^{+\cdot}(H_2O)_n]$	$\rightarrow$	$[(H_2O)_n+H]^+ + [D-H]^\cdot$		(7)
$[D^{+\cdot}(H_2O)_n]$	$\rightarrow$	$(H_2O)_n^{+\cdot} + D^\cdot$		(8)
$[(H_2O)_n+H]^+ + M$	$\rightarrow$	$[M+(H_2O)_n+H]^+ + H_2O$		(9)
$[(H_2O)_n+H]^+ + M$	$\rightarrow$	$[M+(H_2O)_n+H]^+$		(10)
$[M+(H_2O)_n+H^+]$	$\rightarrow$	$[M+H]^+ + nH_2O$		(11)

Scheme 8.1 Ionization reactions in APPI (Kauppila et al. 2002; Syage 2004; Klee et al. 2013).

Adjusting the Ionization Properties – The Use of Dopants

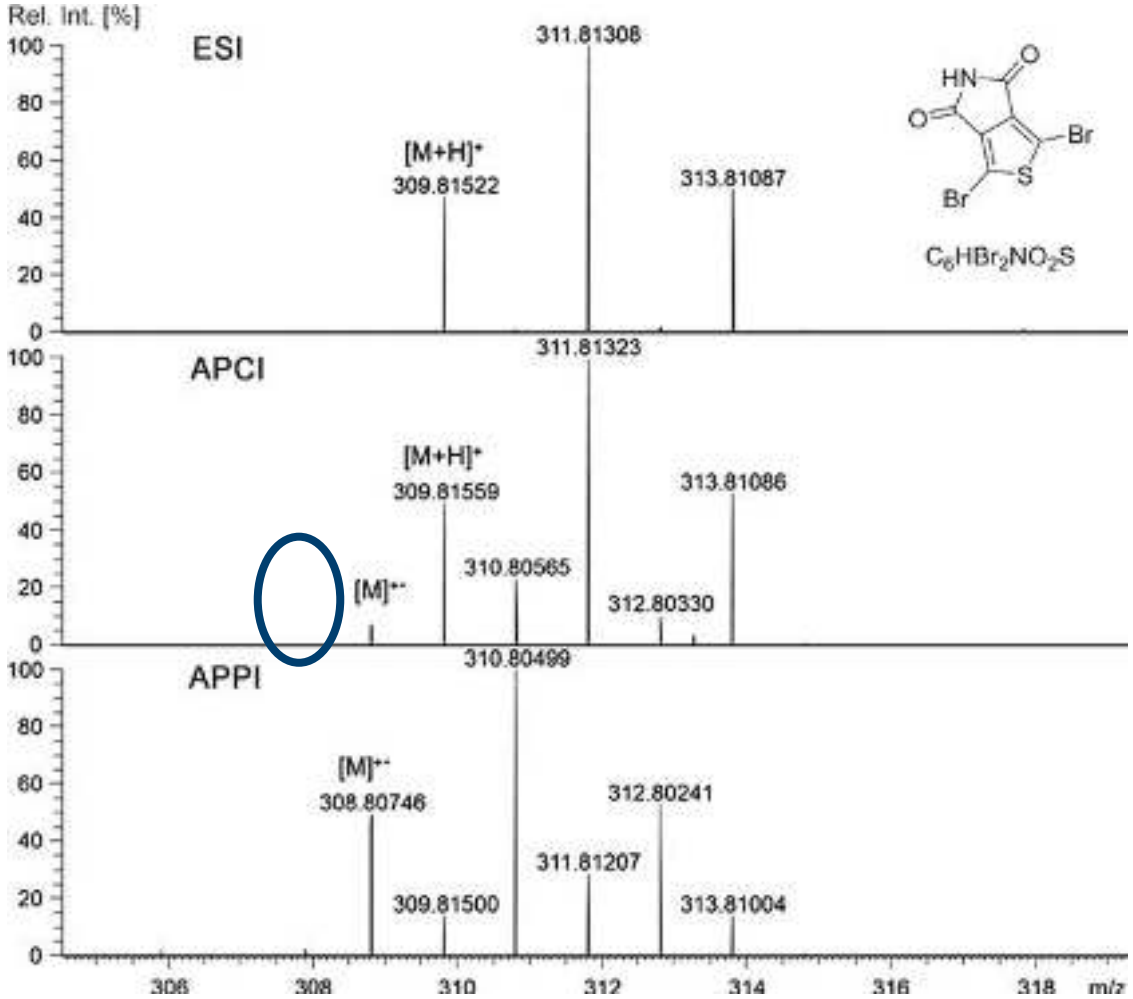

Table 8.1 Properties of the most typical dopants.

Dopant	IE (eV)	PA (kJ/mol)
Toluene	8.83	784.0
Anisole	8.20	839.6
Chlorobenzene	9.07	753.1
Acetone	9.70	812.0

IE = ionization energy, PA = proton affinity
Source: From Linstrom and Mallard (2015).

Jürgen H- Gross, *Mass Spectrometry – A Textbook*, **2017**, Spinger, ISBN *978-3-319-54398-7*

GC-APPI Interface Designs

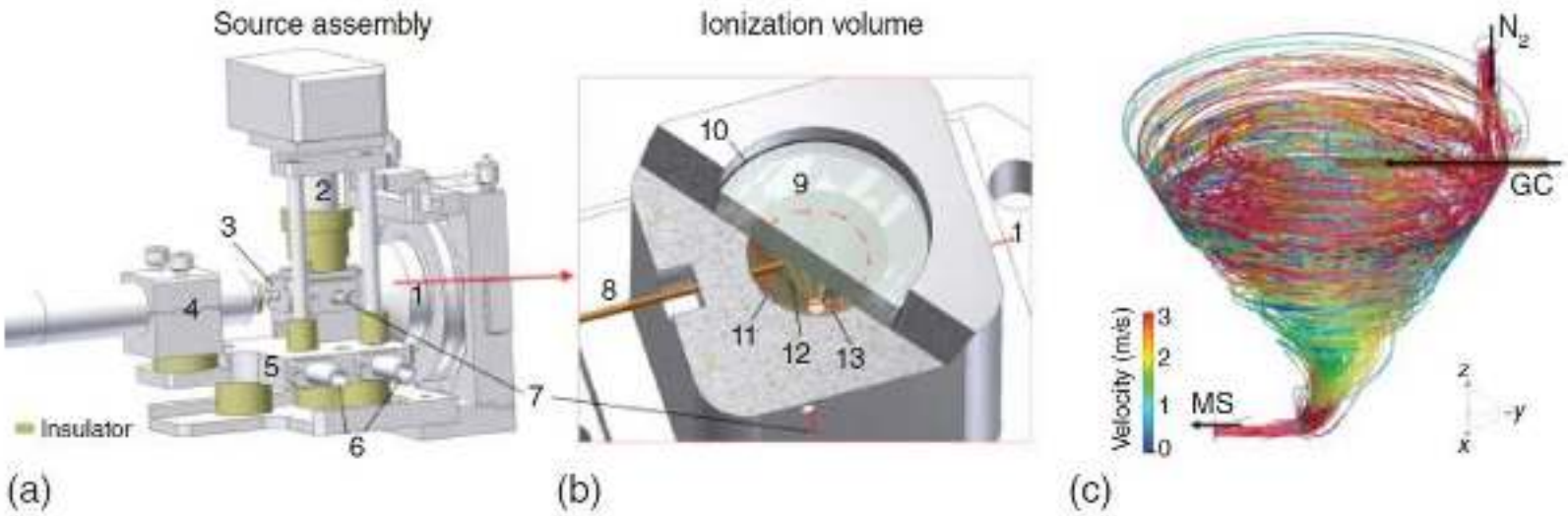

Figure 8.5 Schematic of the GC-APPI-Orbitrap interface by Kersten et al. (a) 1. MS, 2. VUV lamp, 3. GC column adapter, 4. GC transfer line assembly, 5. heater table, 6. heater cartridges, 7. makeup gas adapter, 8. GC column, 9. MgF_2 window; (b) 10. sealing with cement and inorganic coating, 11. makeup gas inlet, 12. conical ionization volume, 13. exit to MS, (c) massless particle trace simulation of the makeup gas inside the conical ionization volume. Source: Kersten et al. (2016). Copyright 2016, Reprinted with permission of Springer Nature.

Photoionization and Photo-Induced Processes in Mass Spectrometry, Ralf Zimmermann and Luke Hanley, 2021 WILEY-VCH GmbH

Desorption-APPI Interface Designs

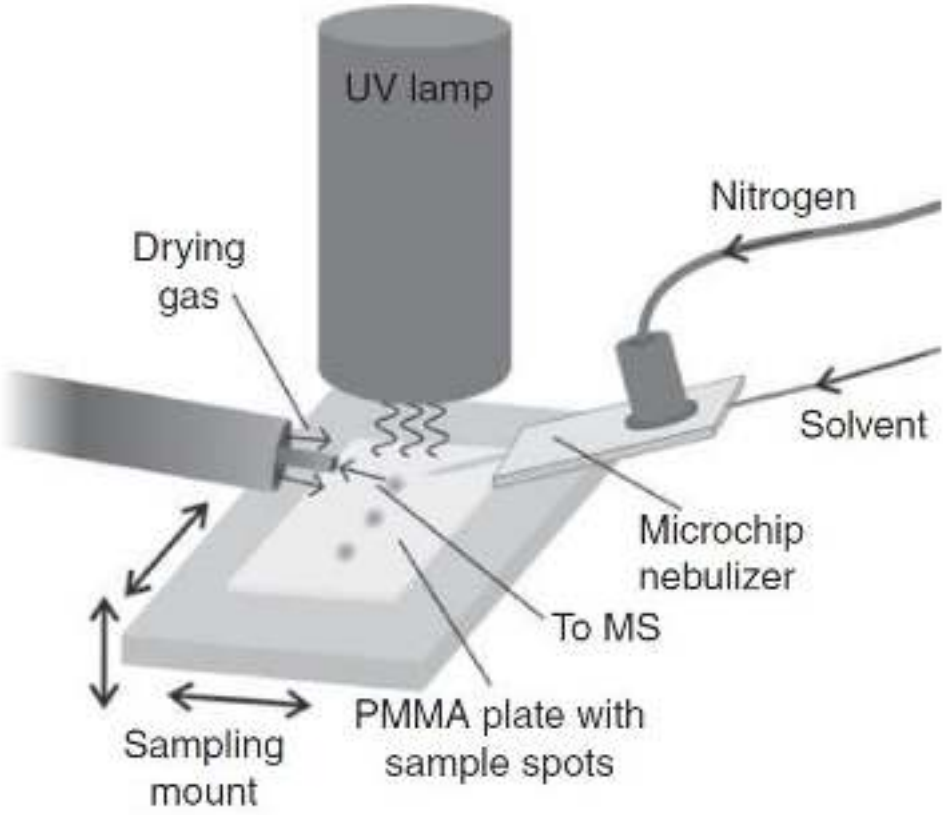

Figure 8.7 Schematic of the desorption atmospheric pressure ionization (DAPPI) source. Source: Haapala et al. (2007b). Copyright 2007, Reprinted with permission of American Chemical Society.

Photoionization and Photo-Induced Processes in Mass Spectrometry, Ralf Zimmermann and Luke Hanley, 2021 WILEY-VCH GmbH

Mass Spectrometric Platform – FT-ICR MS

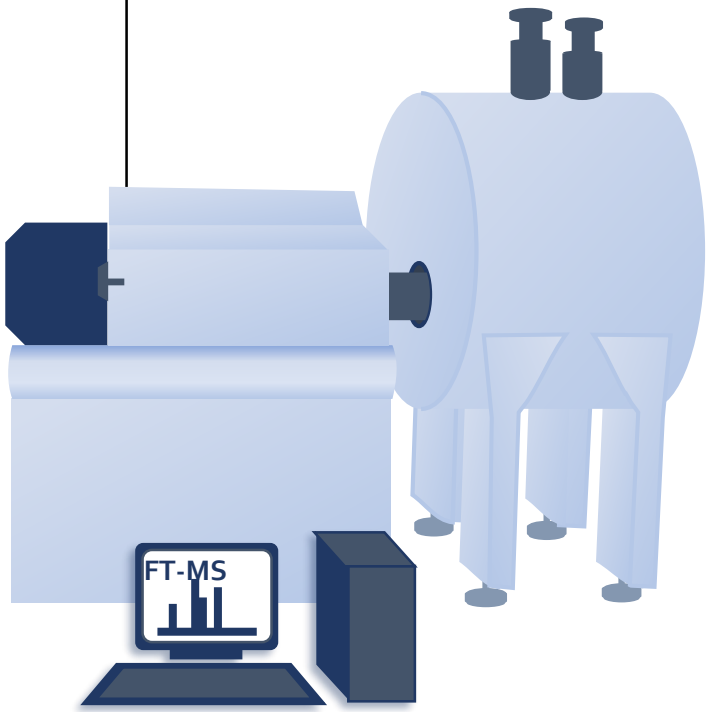

Limitations:
especially for high complex mixtures, ion suppression is a critical issue

→ **reduction of matrix effects by prior separation or novel ionization schemes**

Mass Spectrometric Platform – FT-ICR MS

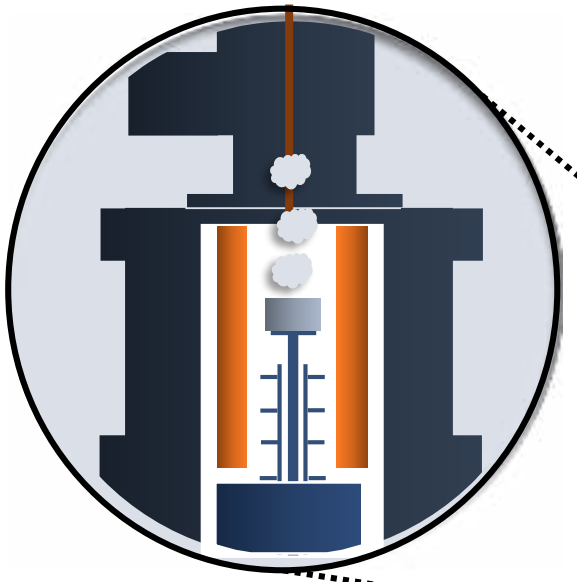

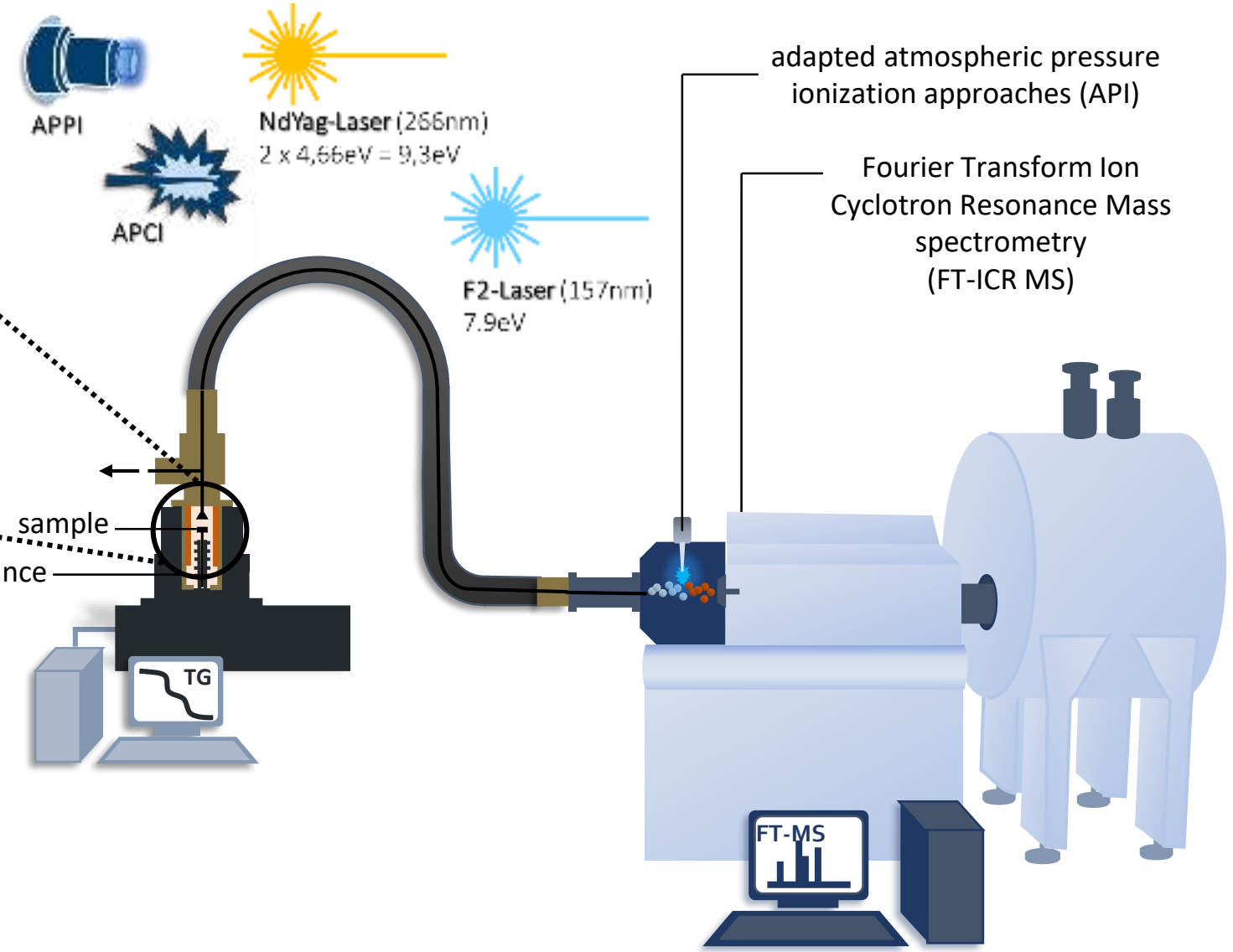

- thermal separation by a defined heating ramp leading to less matrix effects
- tracing mass loss during the heating process

Rüger et al., *Anal. Chem.* 2015, 87, 13, 6493–6499
Rüger et al., *Anal. Chem*. 2021, 93, 8, 3691–3697

Thermogravimetric Processes

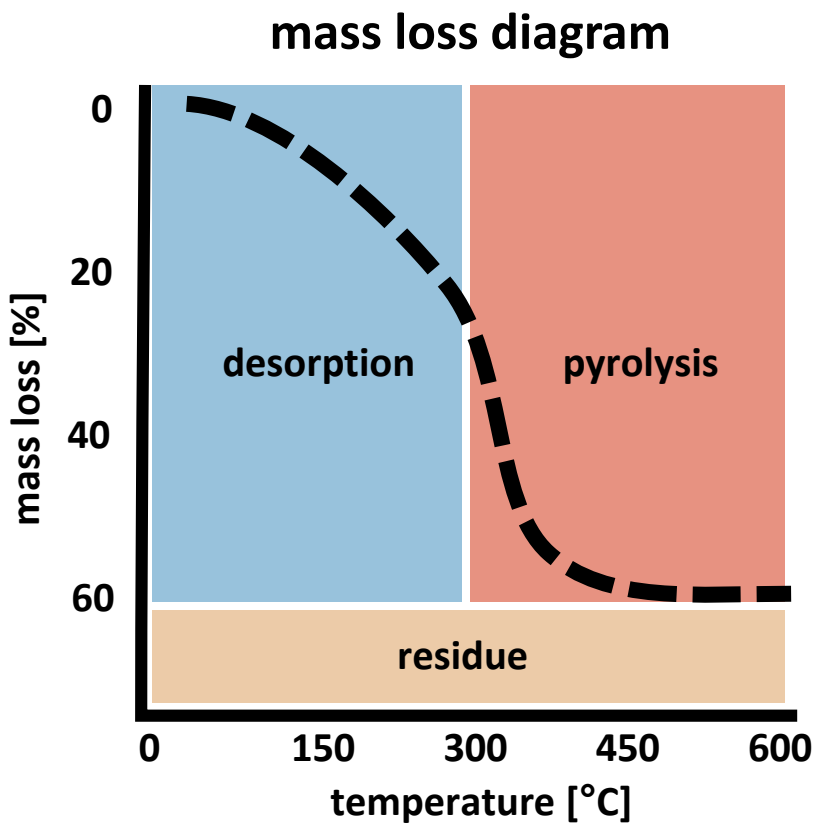

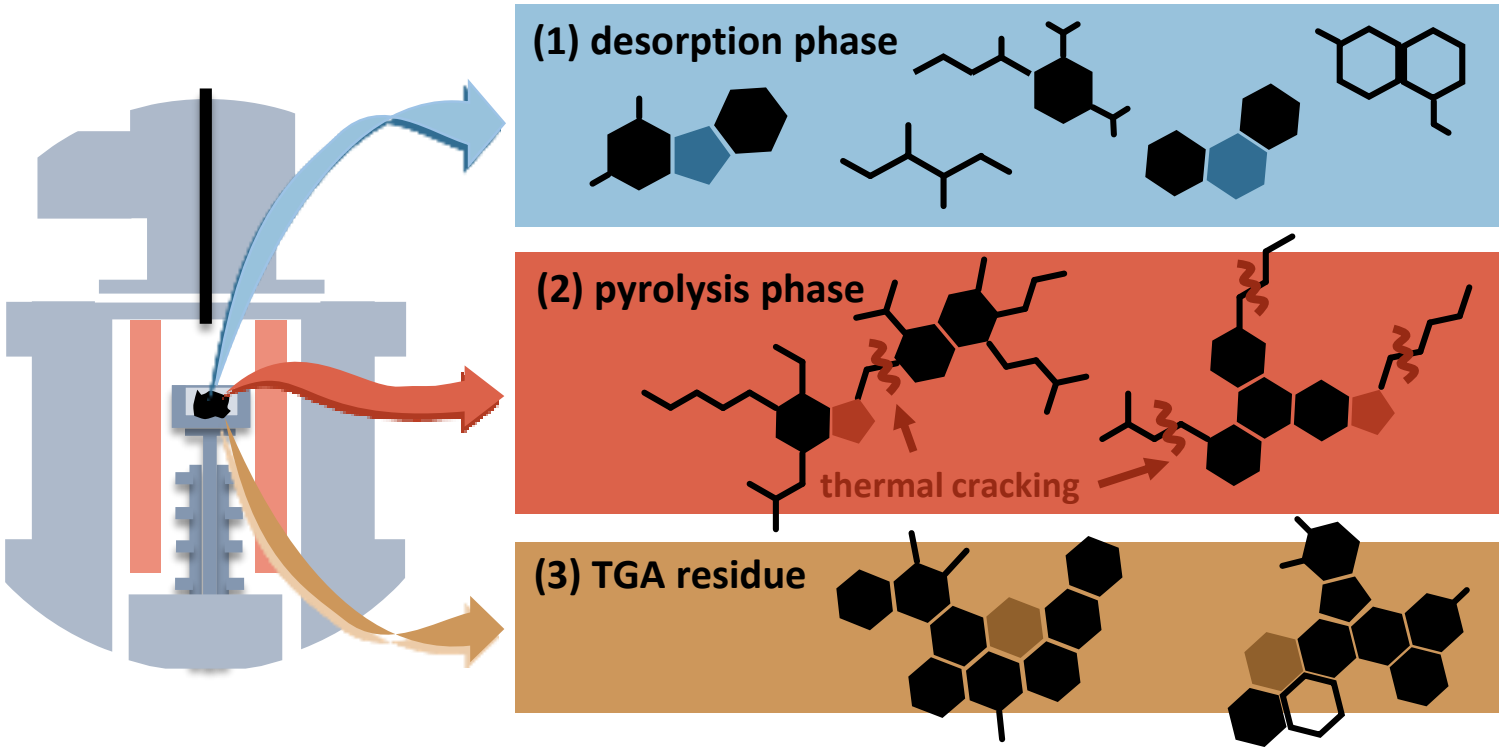

Three processes occur during the thermogravimetric heating process:

(1) Desorption: mostly evaporation of intact compounds
(2) Pyrolysis: thermal decomposition of high molecular weight species (starting at 300-350 °C)
(3) Residue: coke formation of high aromatic compounds and highly stable aggregates

Chemical description of plastic pyrolysis coke residues for improved recycling

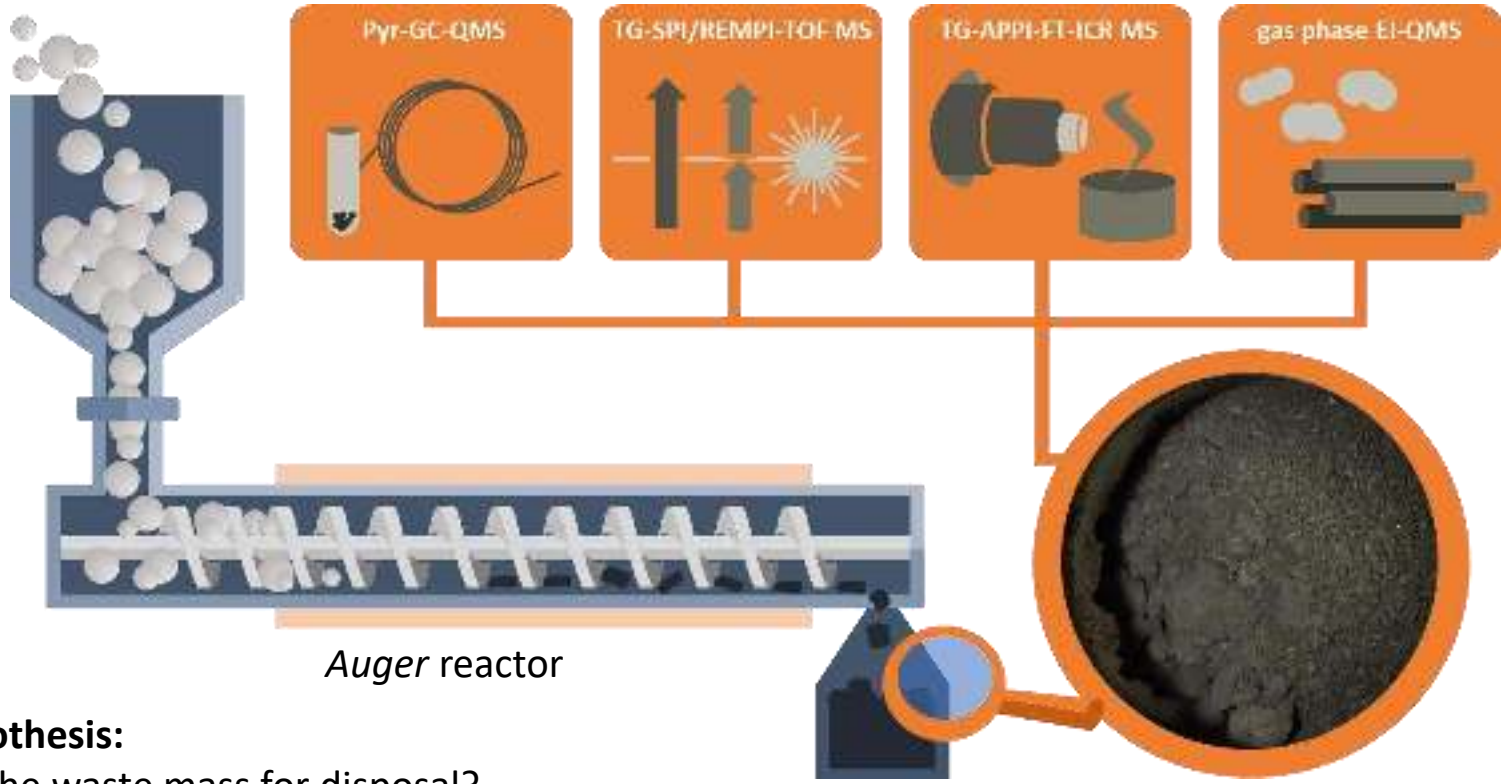

Auger reactor

Main research hypothesis:

- Can we reduce the waste mass for disposal?
- Can we examine the quality and purity/toxicity of the coke?
- Are valuable chemicals be accessible based on a second pyrolysis step?
- Is there a potential for usage of the residue in material science?

TotalEnergies

Plastic Pyrolysis Coke

Unique thermogravimetric behavior with several distinct mass loss events

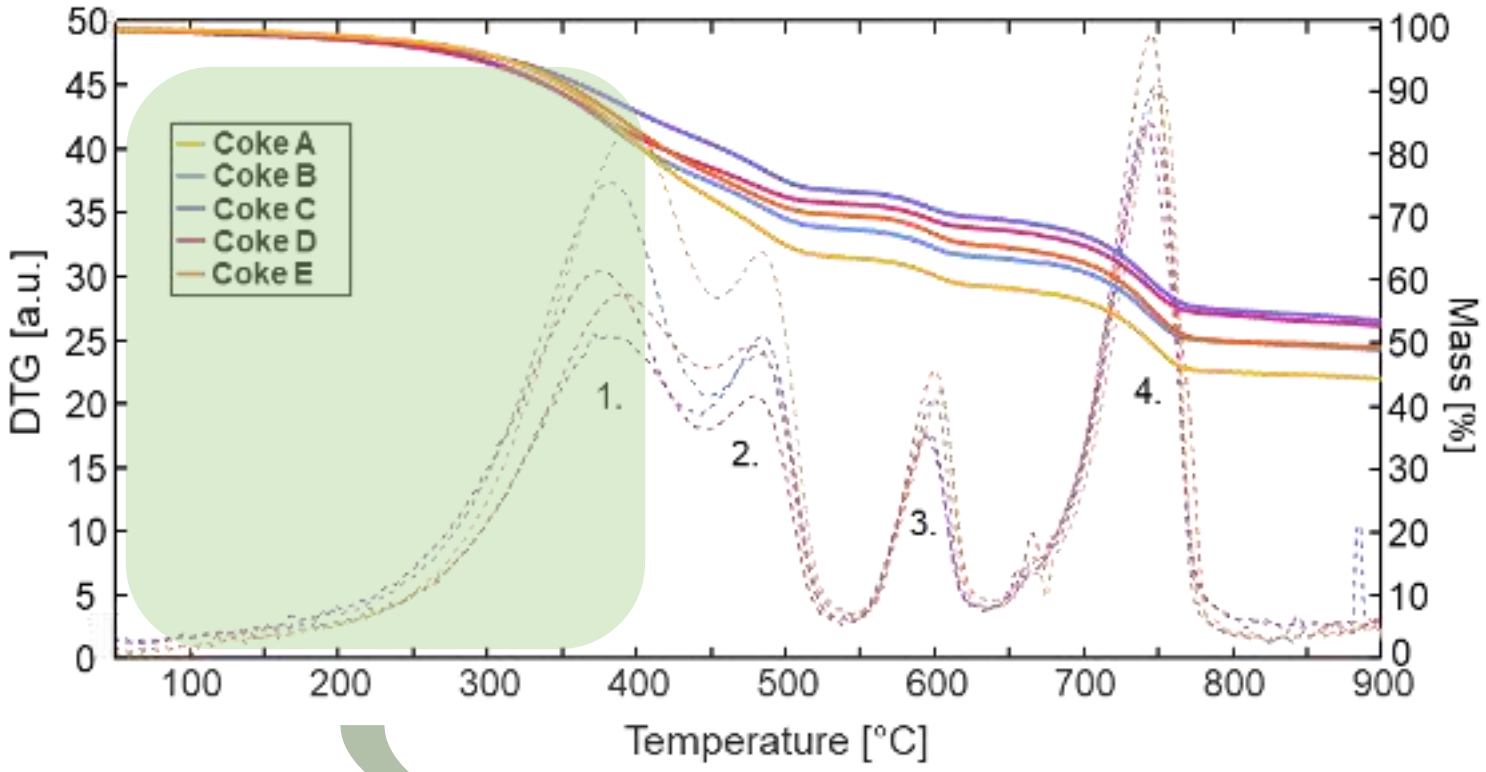

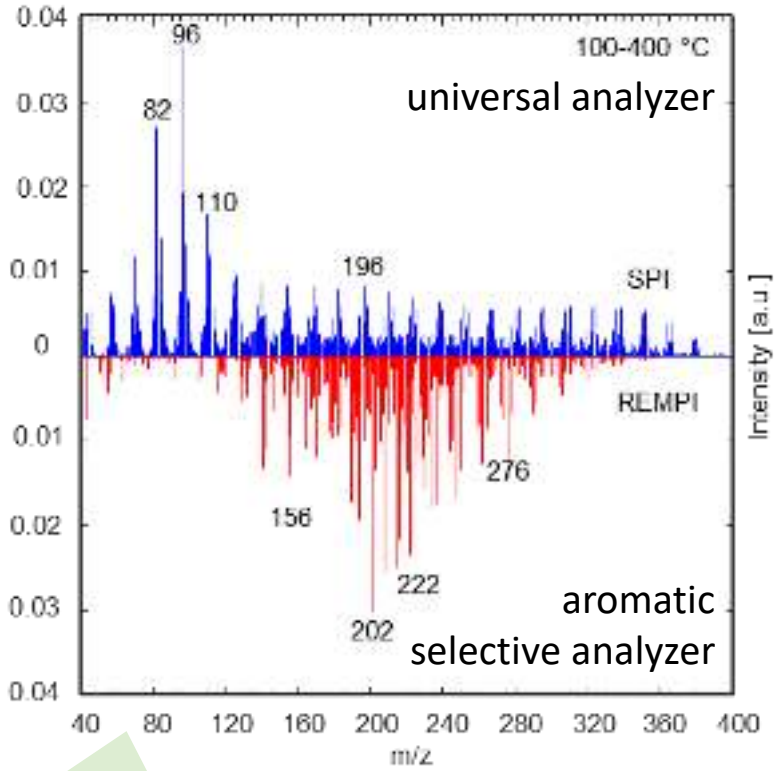

Plastic pyrolysis - coke

Polymer additives and plasticizers cause unique pyrolysis chemistry

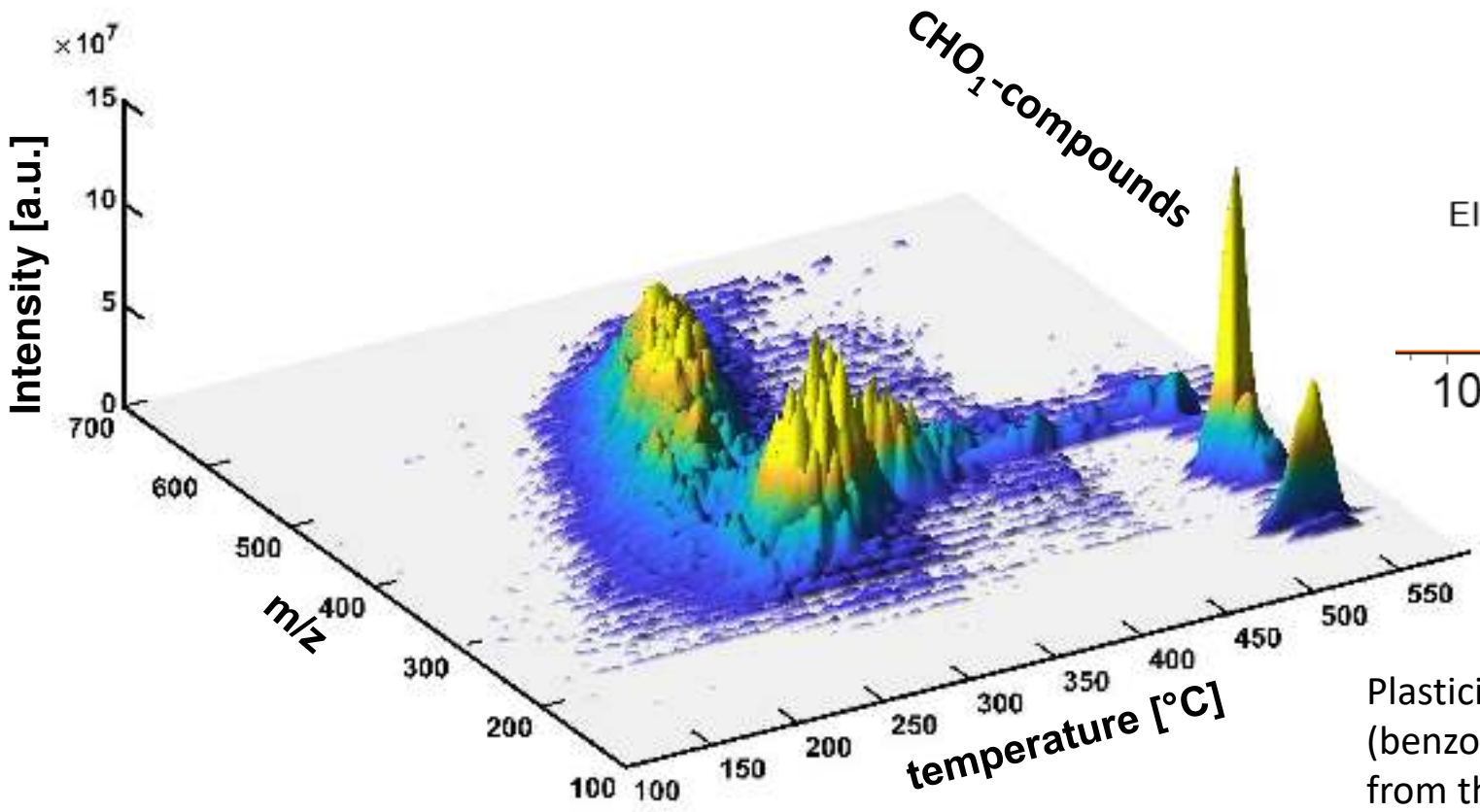

Survey view of the thermal analysis high-resolution mass spectrometric data

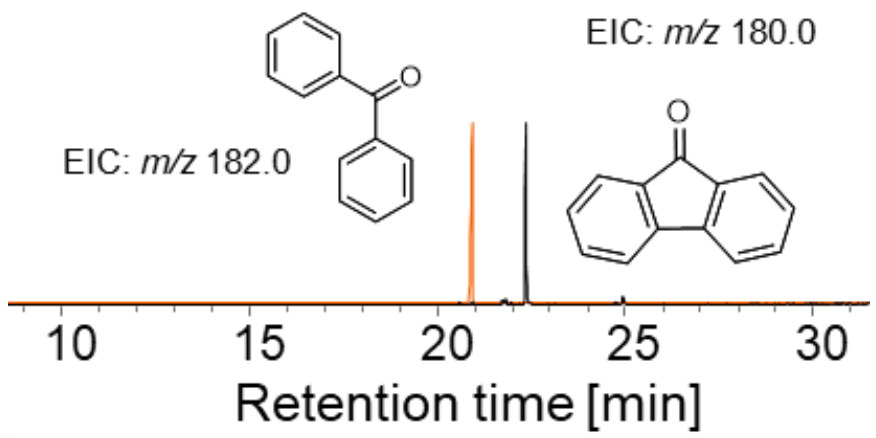

Plasticizer derivatives, such as UV-stabilizers (benzophenones) released at elevated temperatures from the char network (strongly bound and/or integrated in the macromolecular structure.

Plastic pyrolysis - coke

Island/Archipelago-type structural motives with low heteroatom count

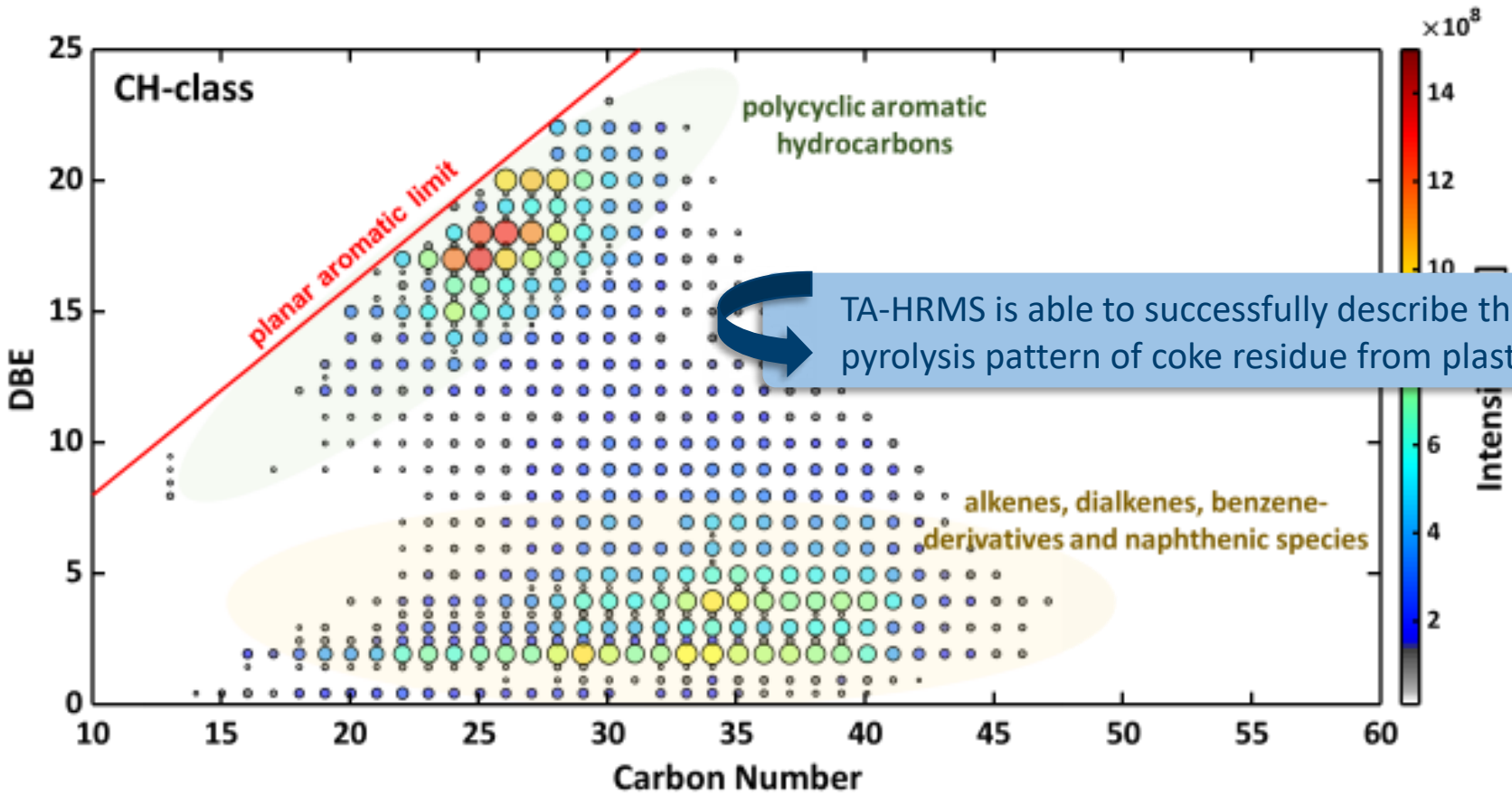

TA-HRMS is able to successfully describe the complex pyrolysis pattern of coke residue from plastic recycling

Comprehensive Chemical Description of Pyrolysis Chars from Low-Density Polyethylene by Thermal Analysis Hyphenated to Different Mass Spectrometric Approaches, Friederici et al., *Energy and Fuels*, 2021, DOI 10.1021/acs.energyfuels.1c01994

Atmospheric Pressure Laser Ionization (APLI)

Novel Concepts for APLI – Deploying < 200 nm radiation for ionization

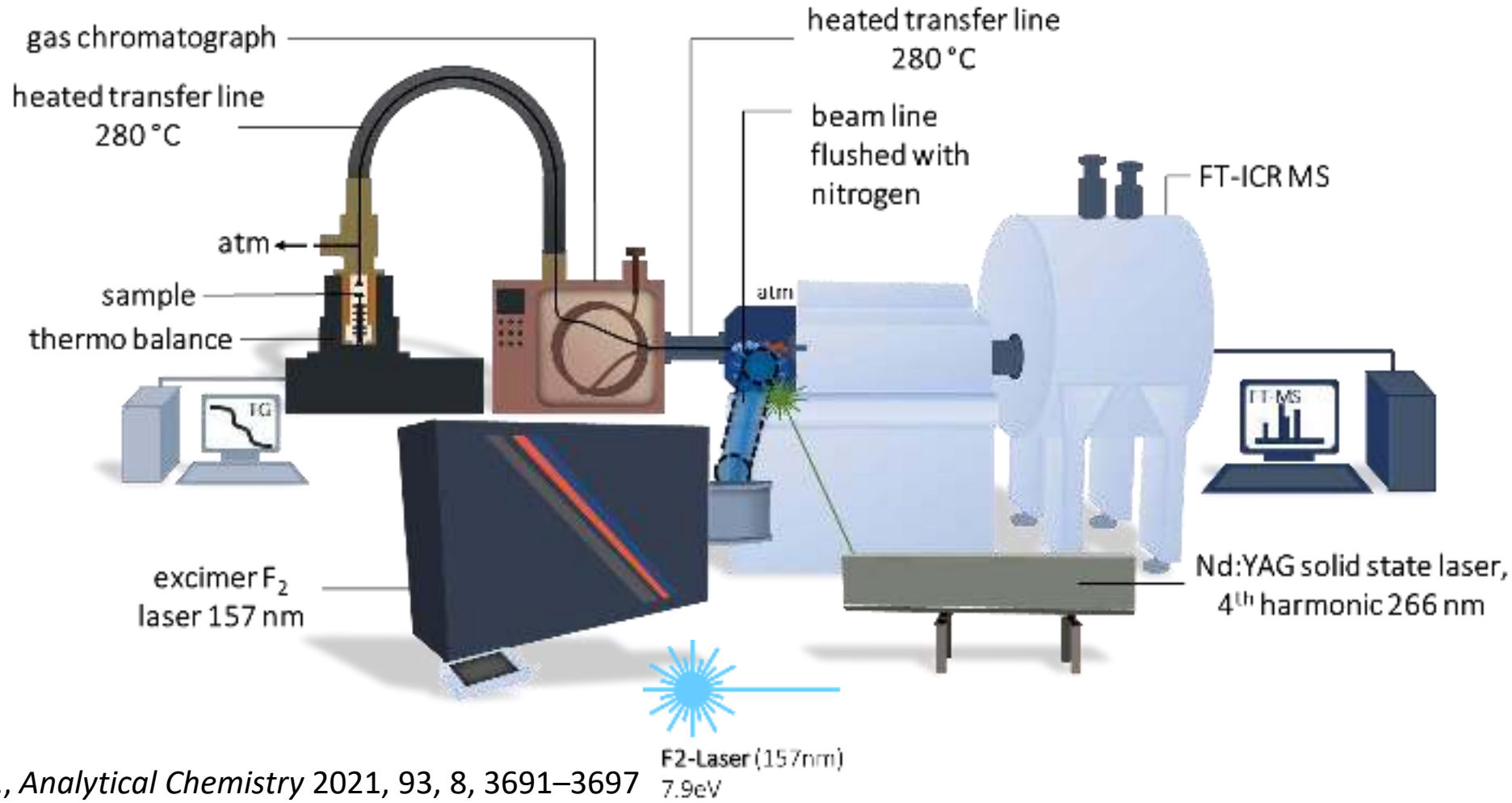

Rüger et al., *Analytical Chemistry* 2021, 93, 8, 3691–3697

Gas chromatographic investigation of PAH mixtures

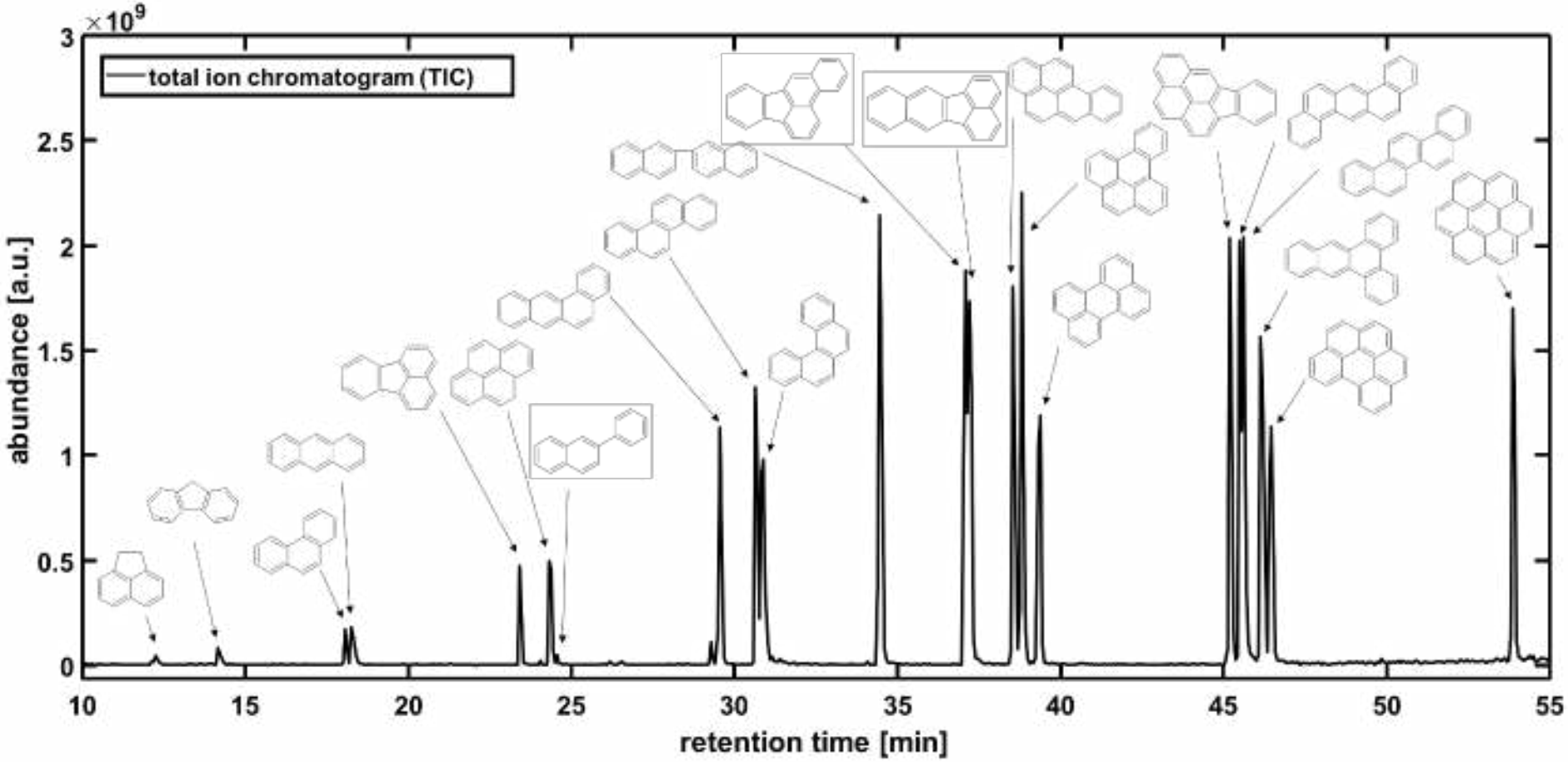

Rüger et al., *Analytical Chemistry* 2021, 93, 8, 3691–3697

Atmospheric Pressure Laser Ionization (APLI)

Application towards complex mixtures – additional chemical space addressed

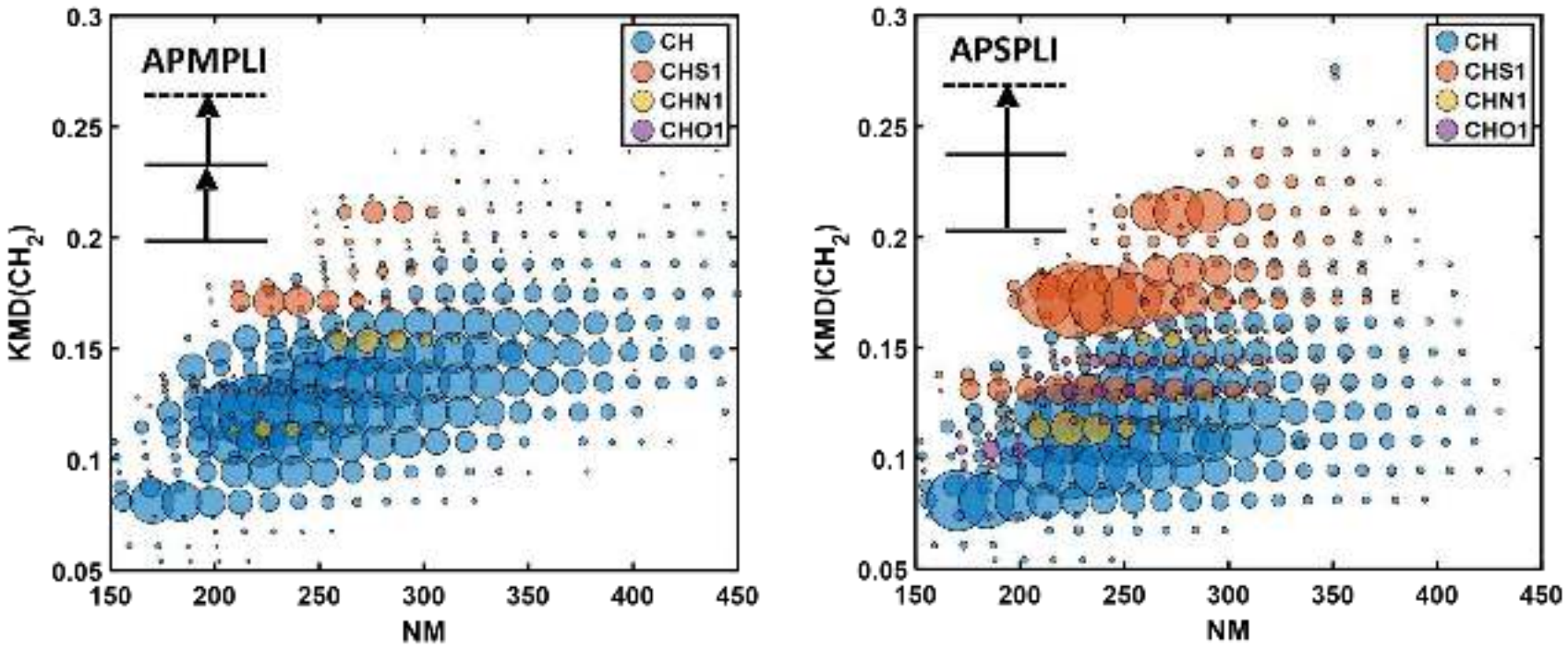

APLI at 157 nm allows to target a broader chemical space compared to APLI at 266 nm – sensitive detection of heteroatom containing aromatics

Customized photoionization concepts allow for novel analytical approaches with unique capabilities

Rüger et al., *Analytical Chemistry* 2021, 93, 8, 3691–3697

Selected Comparison Studies of Ionization Techniques

Direct insertion probe APCI (blue) and APPI (red) analysis of lignocellulosic biomass

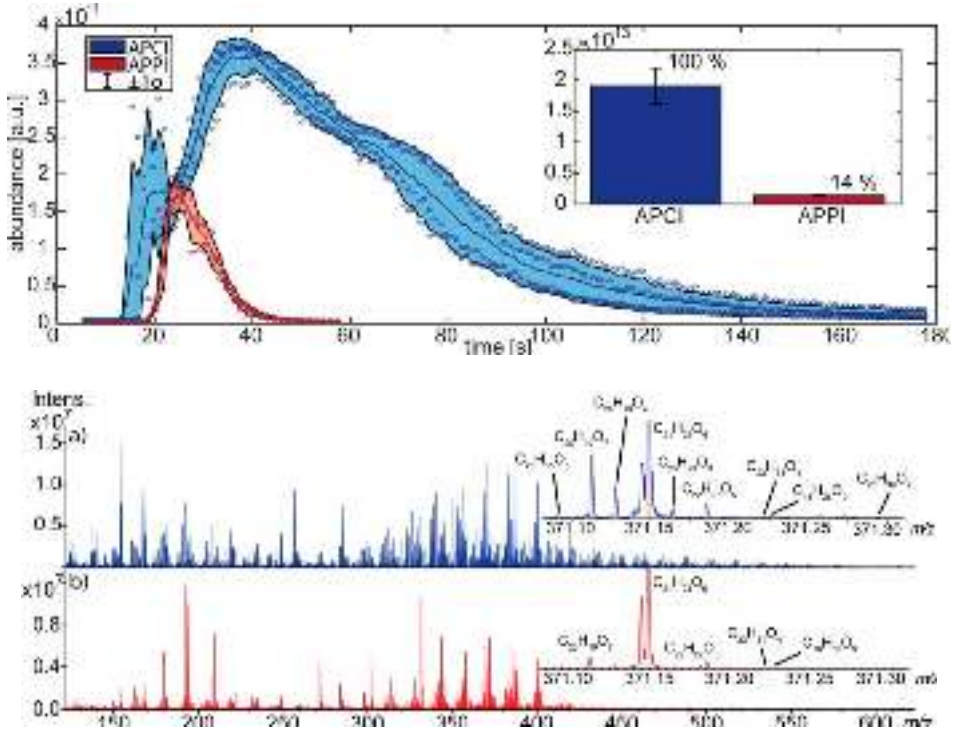

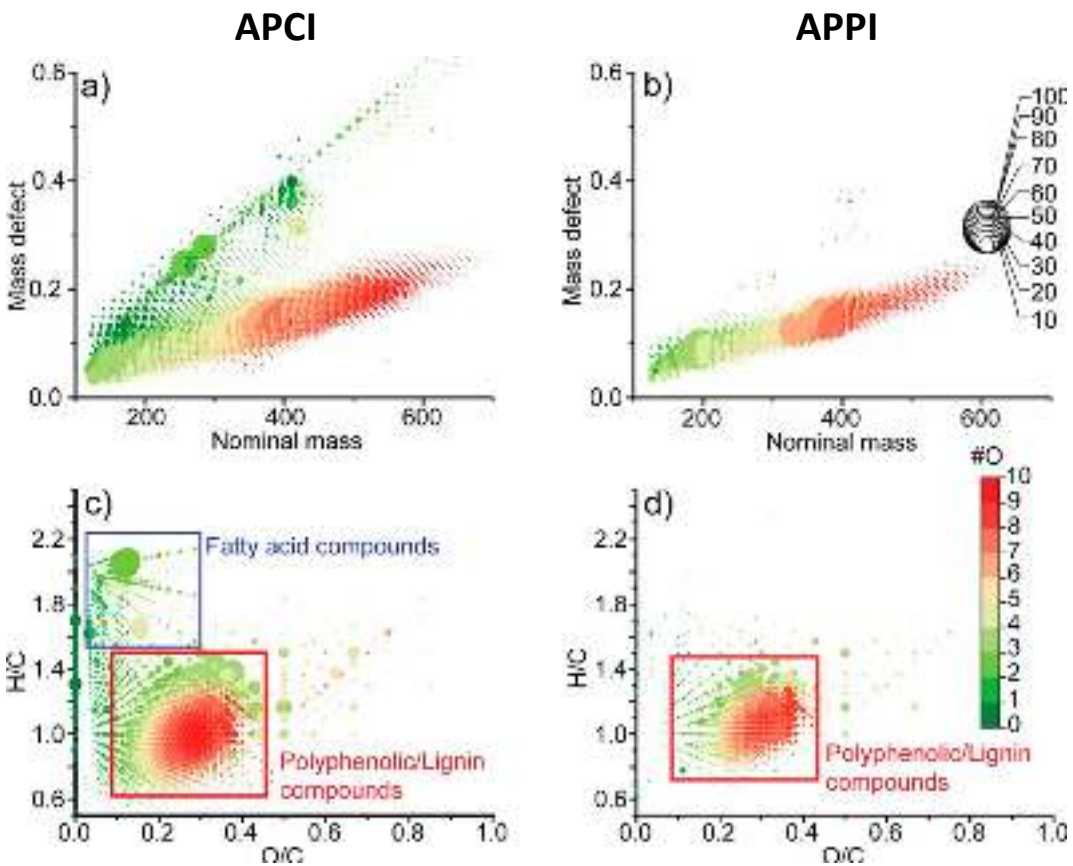

Castilla et al., *JASMS*, **2020**, 822-831

Selected Comparison Studies of Ionization Techniques

Heavy petroleum fractions analyzed by high-resolution time of flight mass spectrometry (HR-TOF)

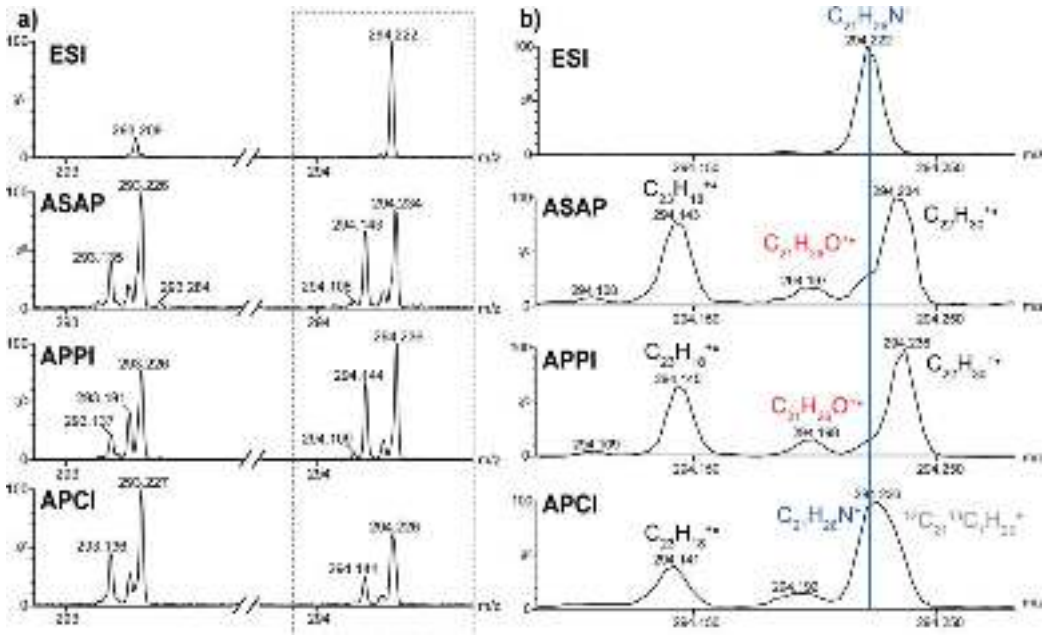

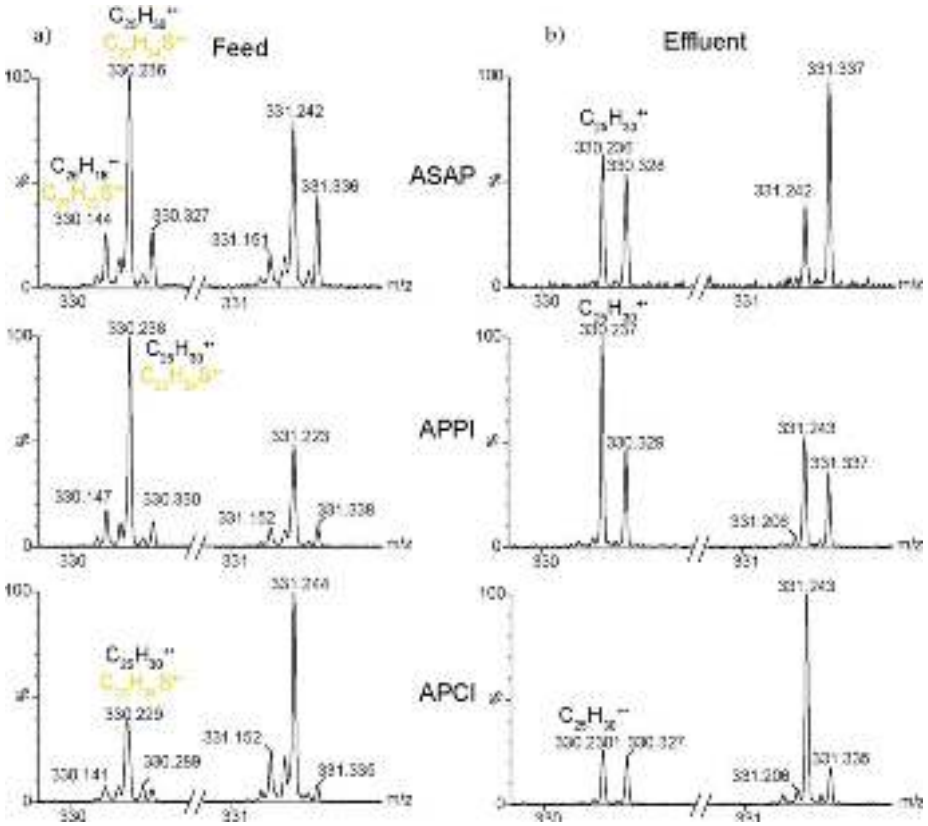

HR-TOF cannot resolved the isobaric complexity but the different selectivity of ionization is nicely visible, *e.g.*, CH-species absent in ESI spectra

Farenc et al., *Energy and Fuels*, **2016**, 8896-8903

Asphaltenes – Study on the Combination of Information retrieved from Different Ionization Techniques

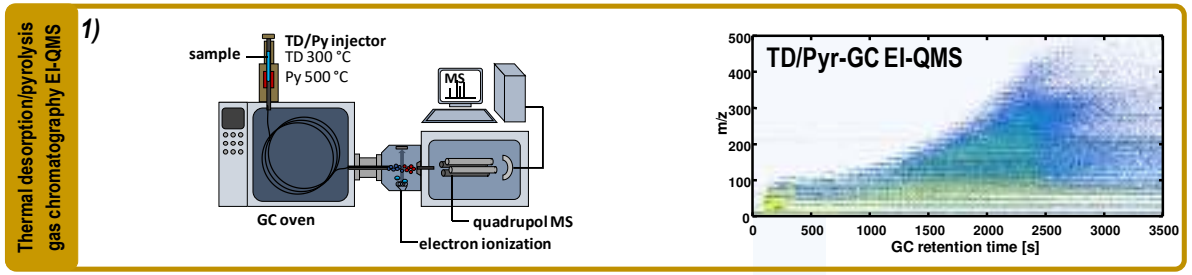

Rüger et al., *Energy and Fuels*, **2016**, 2699-2711

Asphaltenes – Study on the Combination of Information retrieved from Different Ionization Techniques

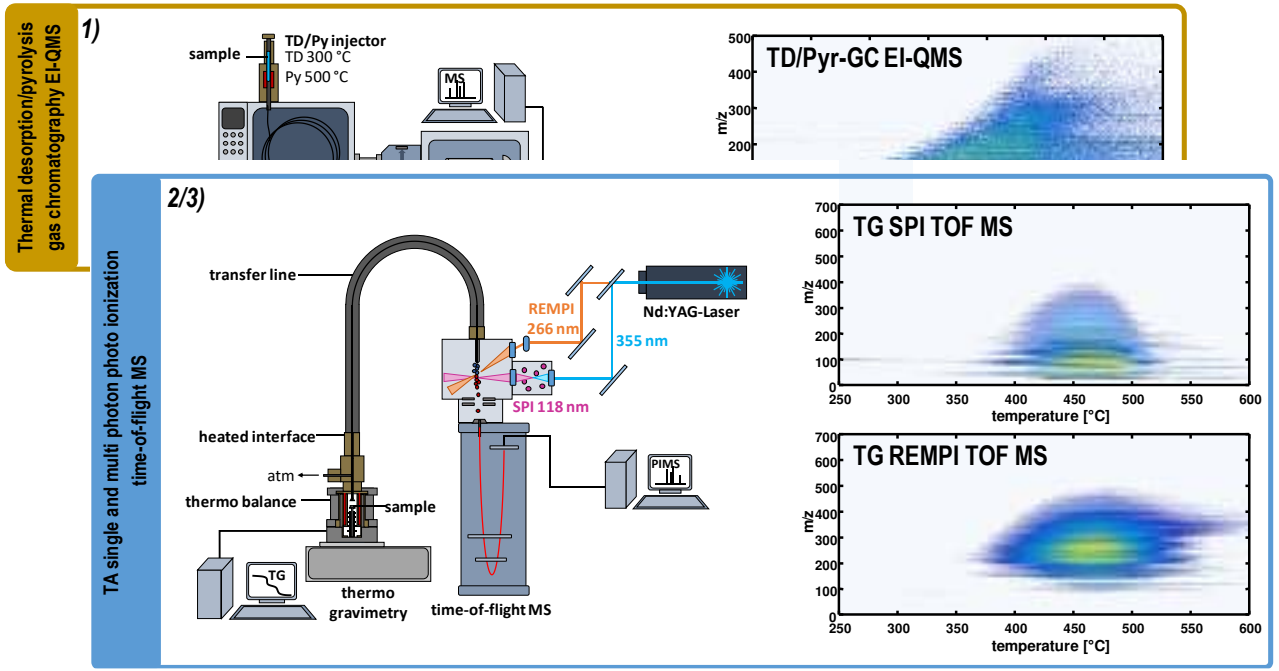

Rüger et al., *Energy and Fuels*, **2016**, 2699-2711

Asphaltenes – Study on the Combination of Information retrieved from Different Ionization Techniques

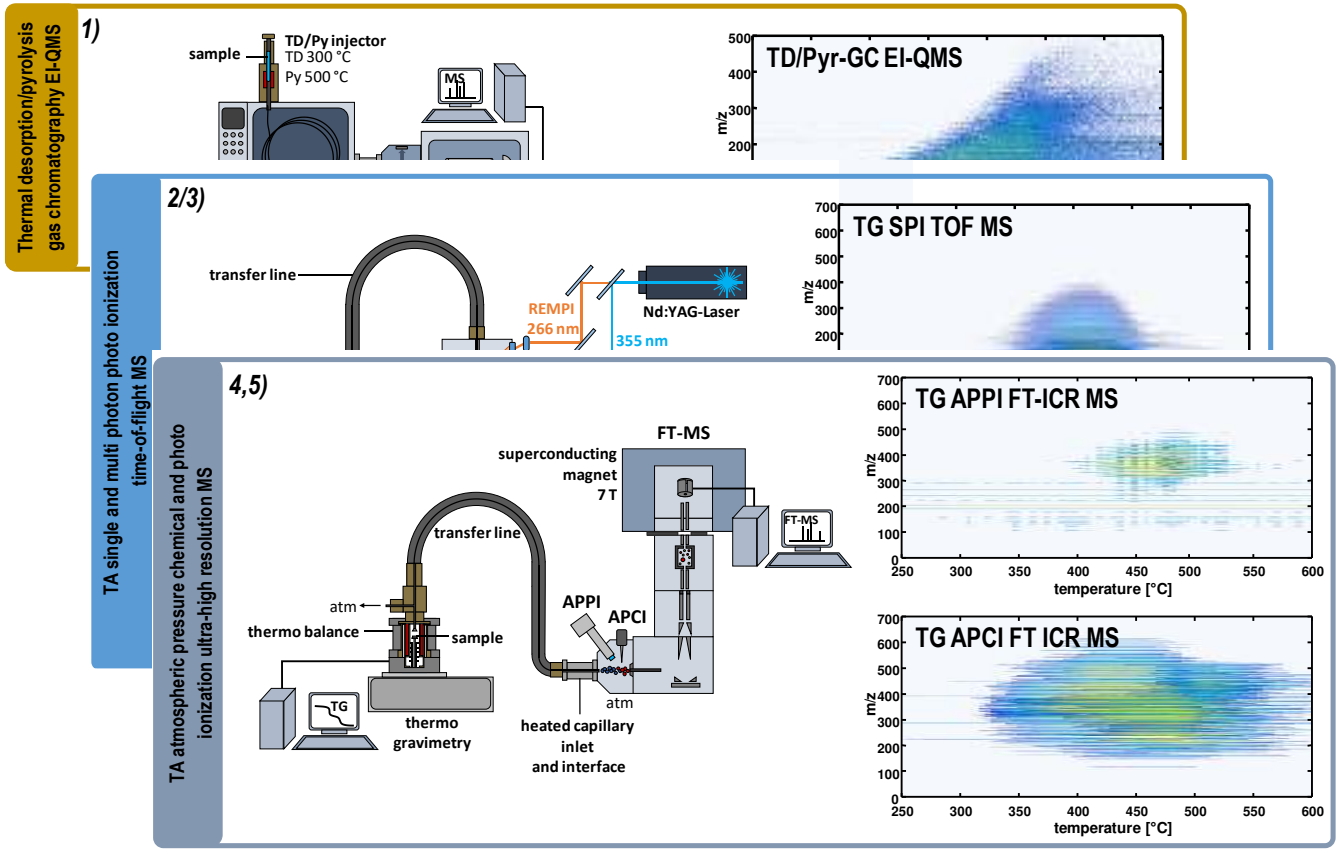

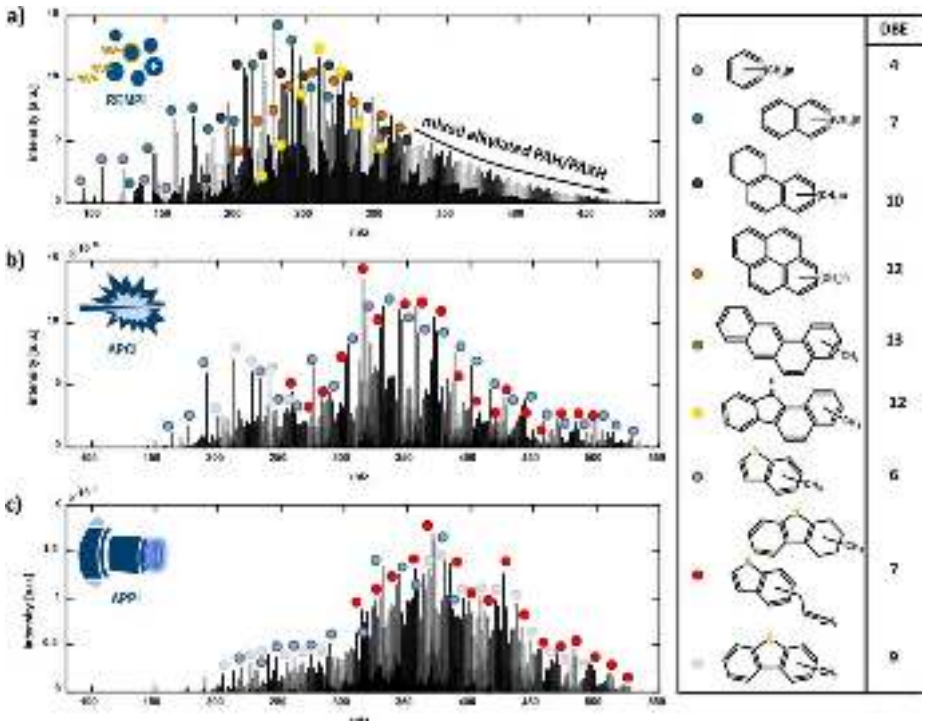

Rüger et al., *Energy and Fuels*, **2016**, 2699-2711

Asphaltenes – Study on the Combination of Information retrieved from Different Ionization Techniques

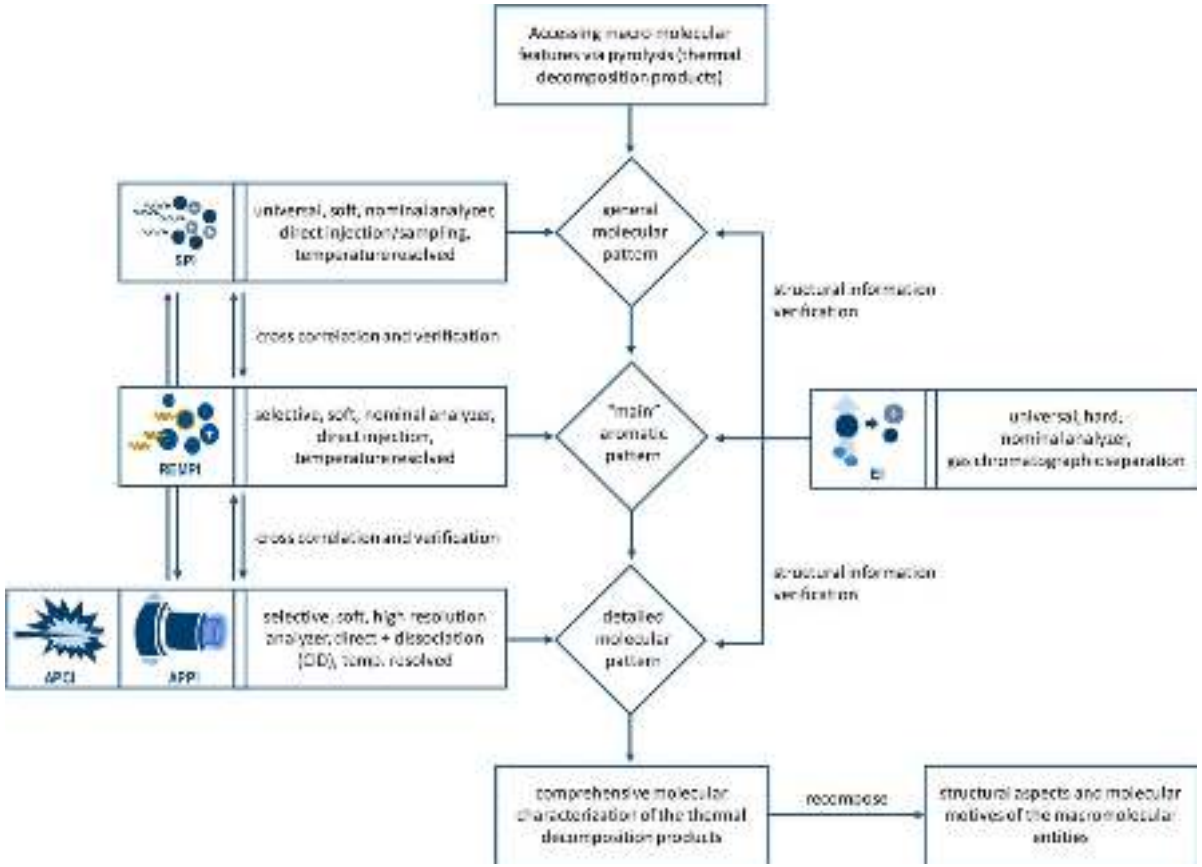

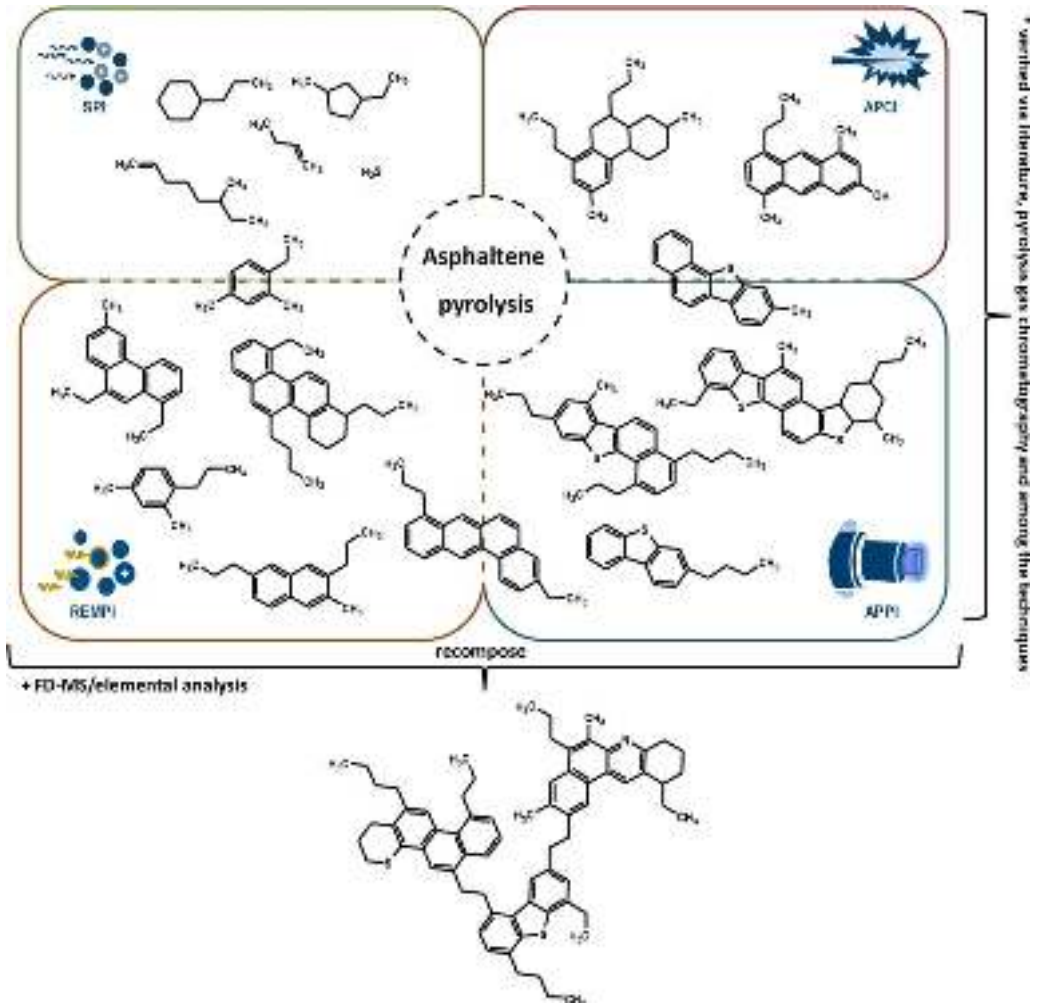

Rüger et al., *Energy and Fuels*, **2016**, 2699-2711

Summary

Atmospheric pressure versus vacuum ionization

Parameter or reaction	API methods	Vacuum ionization
Pressure	1000 mbar	10^{-6} mbar
Mean free molecular path	100 nm	100 m
Hard sphere collision number	10^{9} s^{-1}	1 s^{-1}
Number density of O_2	10^{14}–10^{18} molecules cm^{-3}	10^{4}–10^{7} molecules cm^{-3}
Number density of H_2O	10^{13}–10^{16} molecules cm^{-3}	10^{3}–10^{6} molecules cm^{-3}
Source residence time of ions	10 ms to 1 s	1 µs
Unimolecular decay of ions	None to rarely	Yes
Bimolecular reactions	Yes	No
Termolecular reactions	Yes	No

Typical conditions and occurrence of elementary processes in atmospheric pressure ionization and vacuum ionization techniques

Jürgen H- Gross, *Mass Spectrometry – A Textbook*, **2017**, Spinger, ISBN *978-3-319-54398-7*

Ionization Concepts Frequently Found in Applied FT-ICR MS Studies

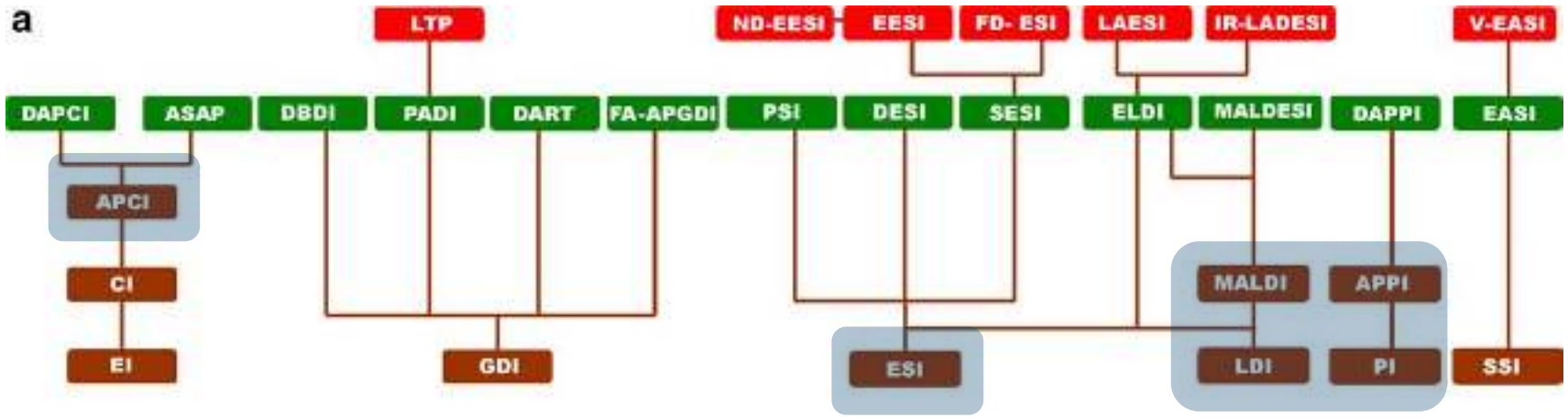

but many other research grade or customized solutions available, *e.g.*, laser ionization concepts, numerous variations of desorption/spray solutions

Alberici et al., *Anal Bionanal Chem*, **2010**, 398:265–294

Ionization Concepts Found in Applied FT-ICR MS Studies

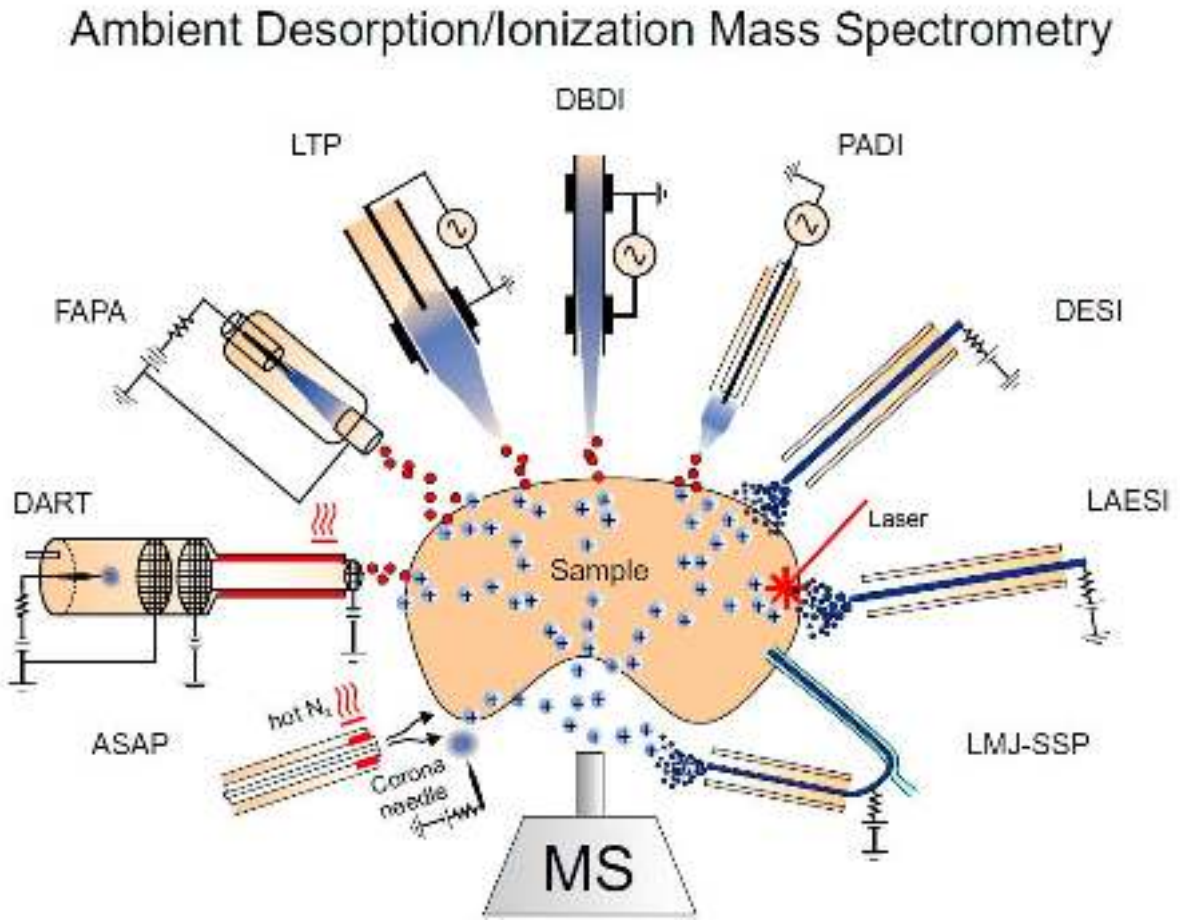

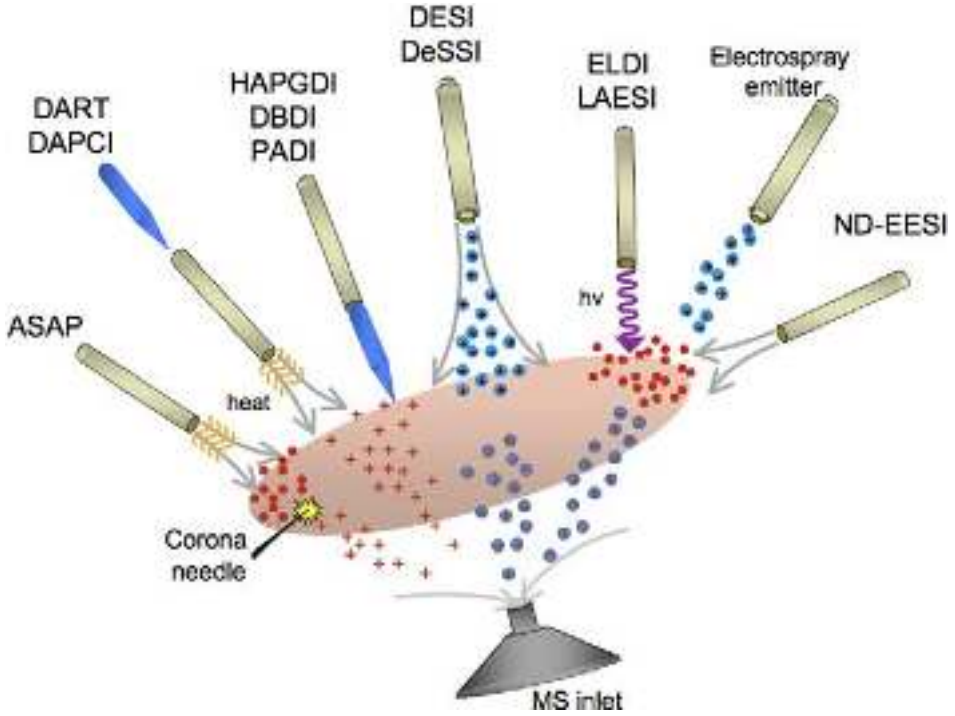

Shelley et al., *Anal Bioanal Chem*, **2018**, 410:4061–4076

Venter et al., *Trends in Analytical Chemistry,* Vol. 27, No. 4, **2008**

The Potential of Light Based Ionization Techniques

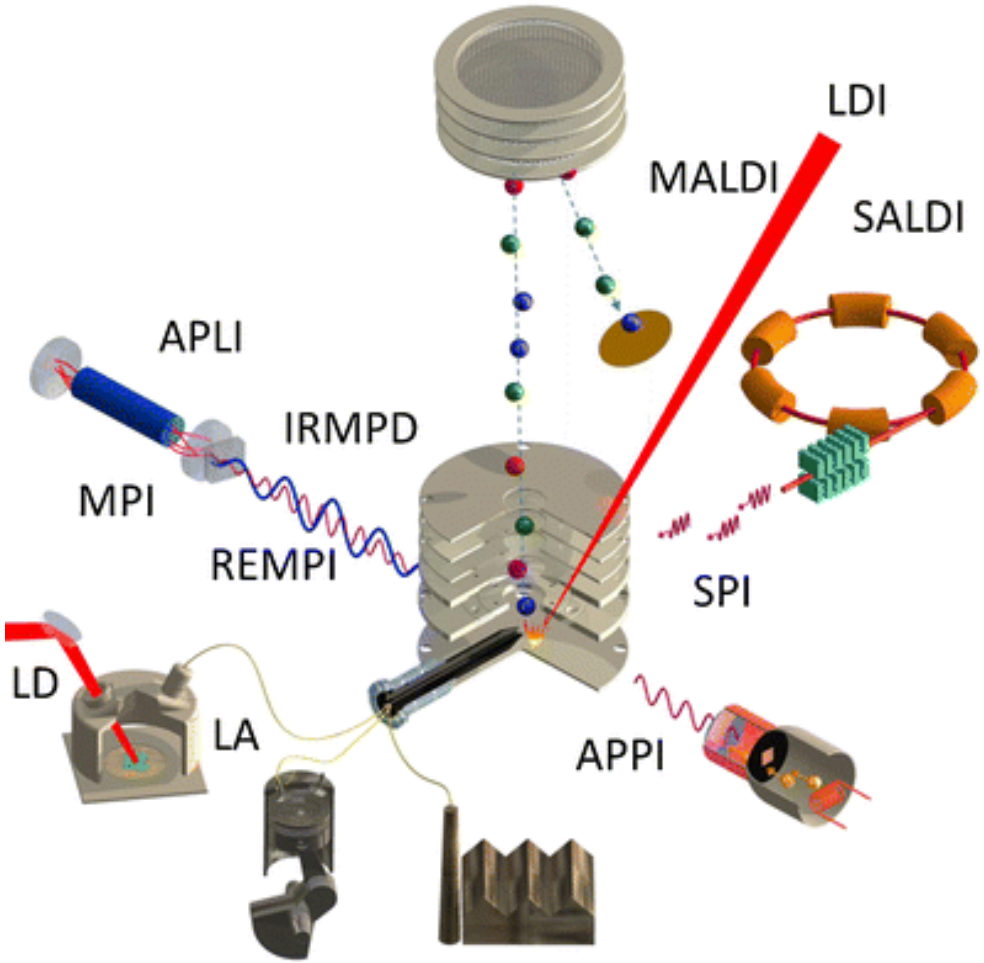

Zimmermann et al., *Anal Bioanal Chem*, **2013**, 6901–6905

Take Home Messages

Summary

- **choosing the right ionization scheme** for the given research questions is an early and highly important step
- EI, FD/FI and SPI as only true universal ionization techniques but FT-ICR MS dominated by atmospheric pressure ionization concepts and laser desorption ionization
- common atmospheric pressure techniques are not universal and strongly favor certain chemical functionalities
  - **selectivity** has always taken into account analyzing complex mixtures → What can I "see" in theory?
  - ionization might suffer from strong charge competition – **matrix effects** → What can I "see" in my real-world complex sample?
  - **sample preparation** and ionization **parameters** have significant effect on spectral pattern and behavior
    → Am I doing everything "correctly" for my given problem?
- **hyphenation techniques** (gas/liquid chromatography, thermal analysis) for pre-separation overcoming some API limitations (ion mobility occurs after ionization process and does not help with ionization aspects!)
- **combination** of the information from several **ionization schemes** can be beneficial for complex mixtures analysis

Acknowledgment

Thank you for the kind attention!

christopher.rueger@uni-rostock.de

Questions and Discussion!?

Monday

(short)

2nd Advanced User School

EU FT-ICR MS

Pushing the capacity of the FT-ICR MS for the analysis of biooils to a higher level

Presented by : Anthony ABOU DIB

2nd year PhD student

Supervisors : Frédéric AUBRIET

Vincent CARRE

LCP-A2MC

Laboratoire de Chimie et Physique

Approche Multi-échelle des Milieux Complexes

Presentation Plan

General context

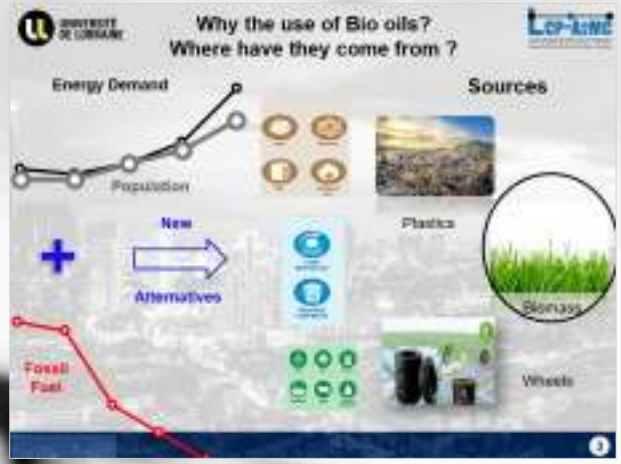

Experimental part

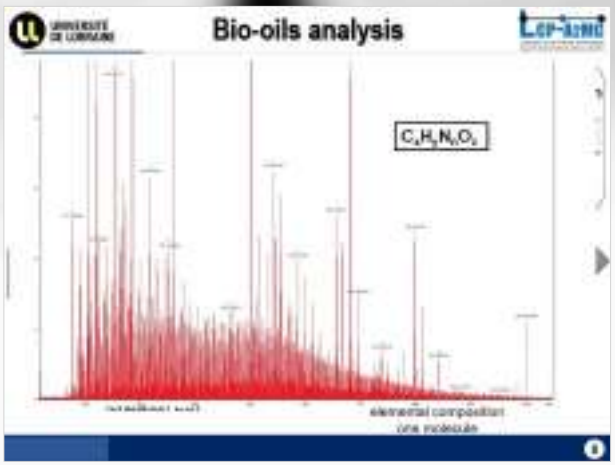

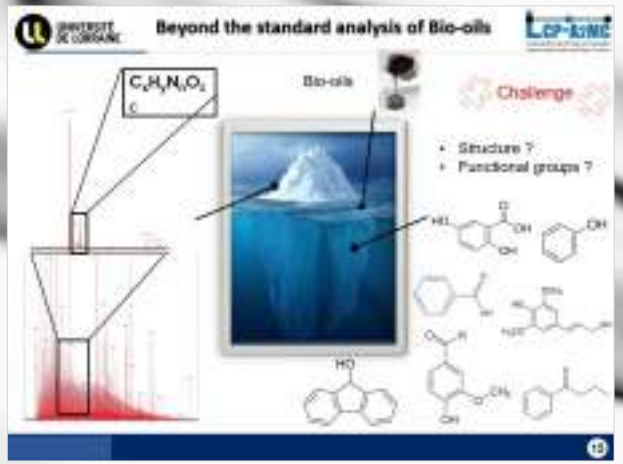

Experimental part

Conclusion and perspectives

Why the use of Bio oils?
Where have they come from ?

Energy Demand

Population

New

Alternatives

Fossil Fuel

Sources

Plastics

Biomass

Wheels

What is lignocellulosic biomass?

Animal Feed

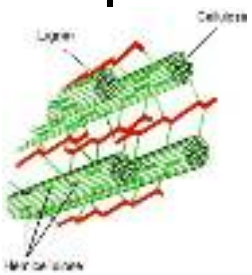

Human Feed

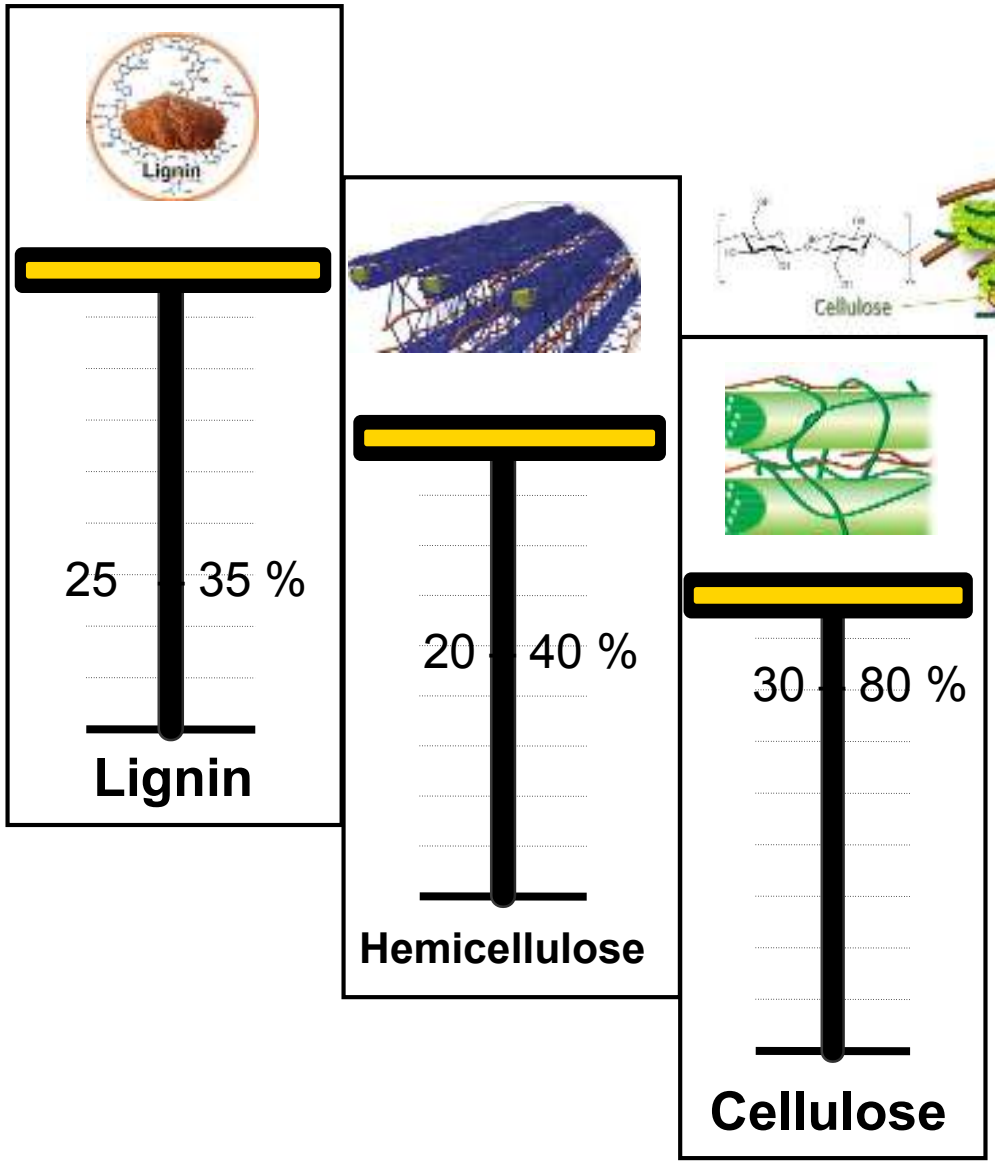

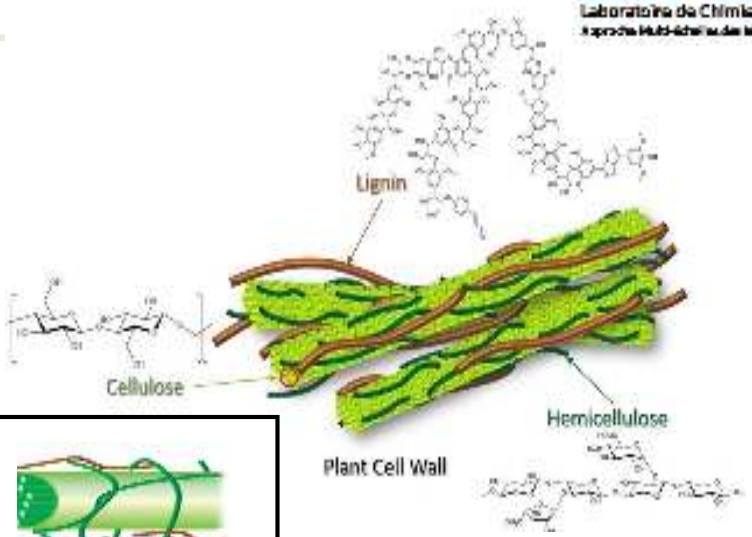

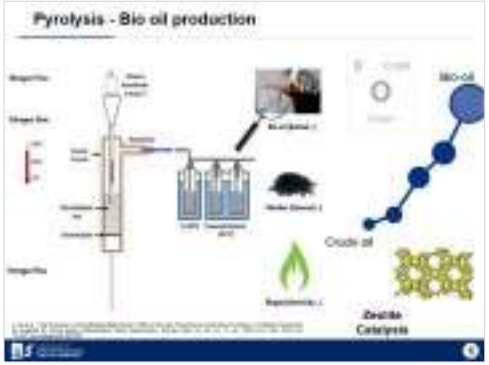

Pyrolysis - Bio oil production

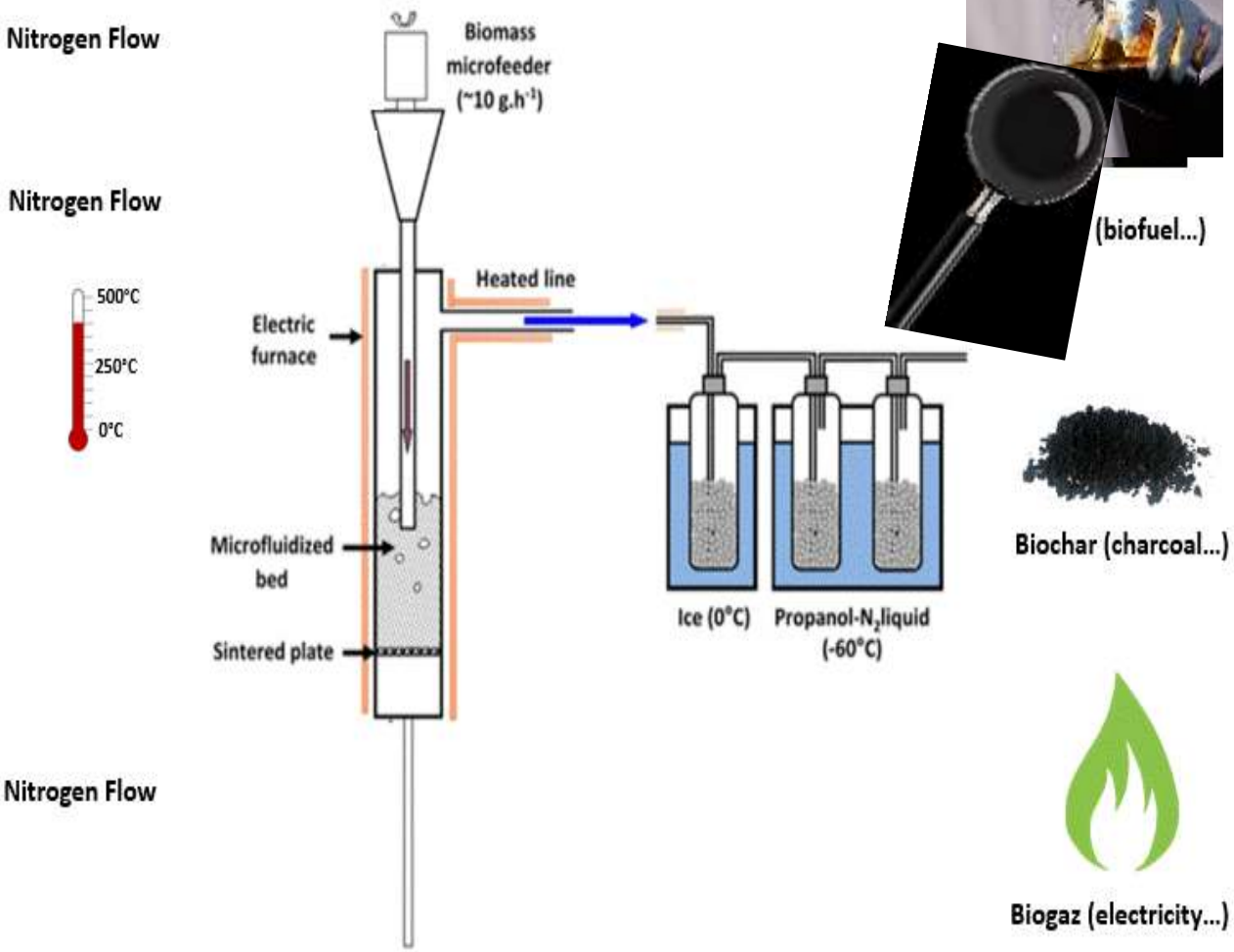

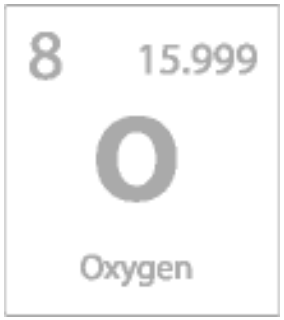

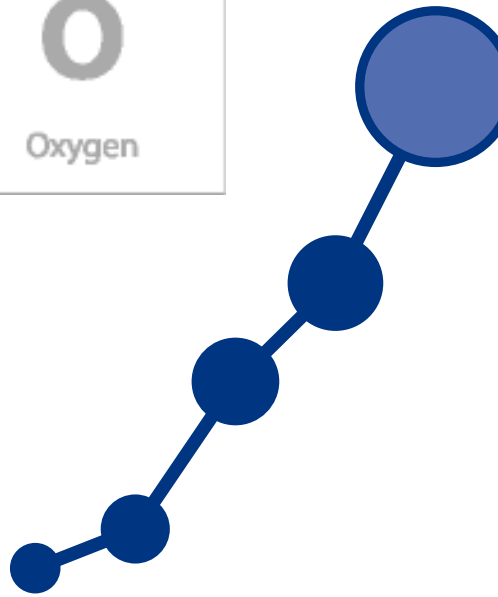

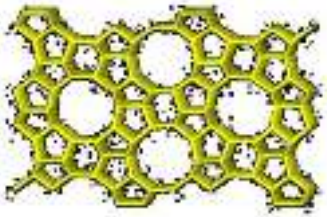

Zeolite Catalysis

L. Jia et al., 'Fast Pyrolysis in a Microfluidized Bed Reactor: Effect of Biomass Properties and Operating Conditions on Volatiles Composition as Analyzed by Online Single Photoionization Mass Spectrometry', Energy Fuels, vol. 29, no. 11, pp. 7364–7374, Nov. 2015, doi: 10.1021/acs.energyfuels.5b01803.

Type of bio-oils produced

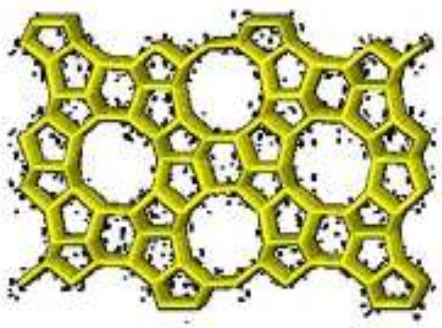

Zeolite Socony Mobil-5
ZSM-5

→ ✗ Raw bio-oil

→ Parental zeolite → Parental HZSM-5 bio-oil

→ Hierarchical zeolite → Hierarchical HZSM-5 bio-oil

Parental

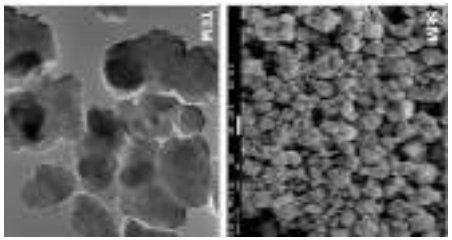

Hierarchical

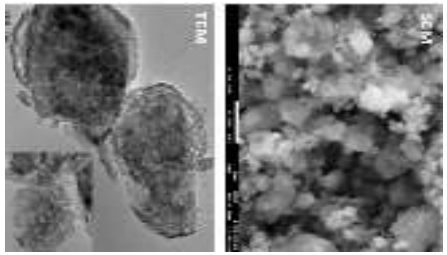

≠

Structural (micropores and mesopores)

Jacobson, K., Maheria, K. C. & Kumar Dalai, A. Bio-oil valorization: A review. Renew. Sustain. Energy Rev. 23, 91–106 (2013).

FT-ICR MS – 7 Tesla 2w
Bruker SolariX

Ionization source

Ion guide

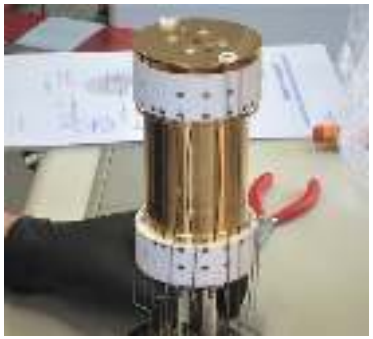

Paracell

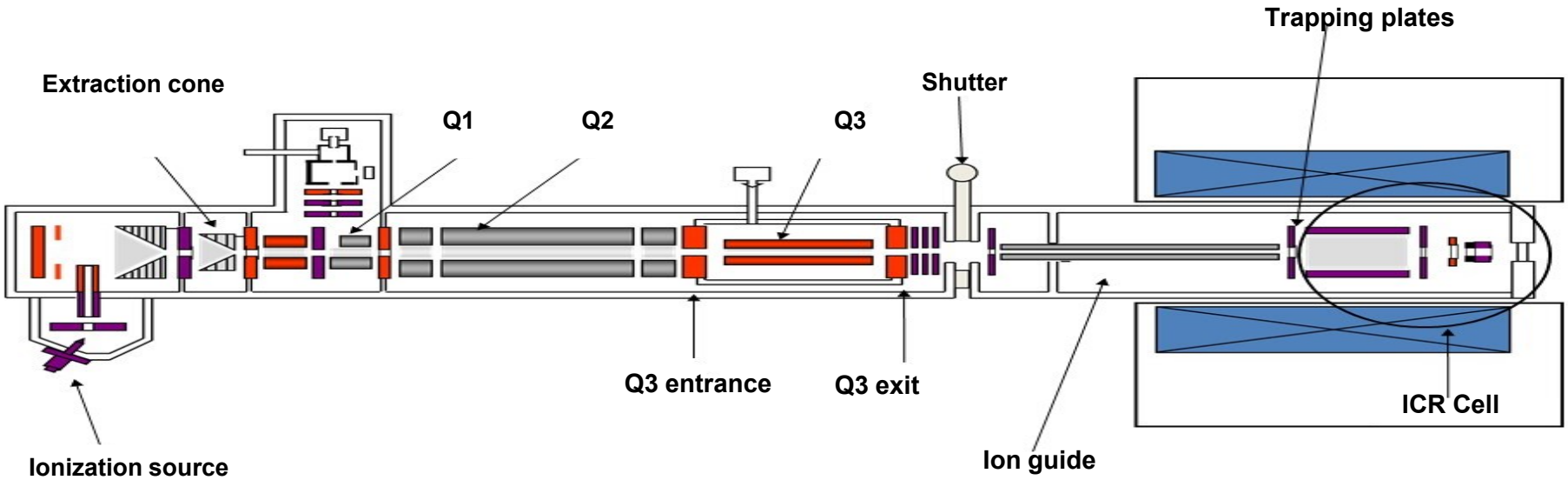

Bio-oils analysis

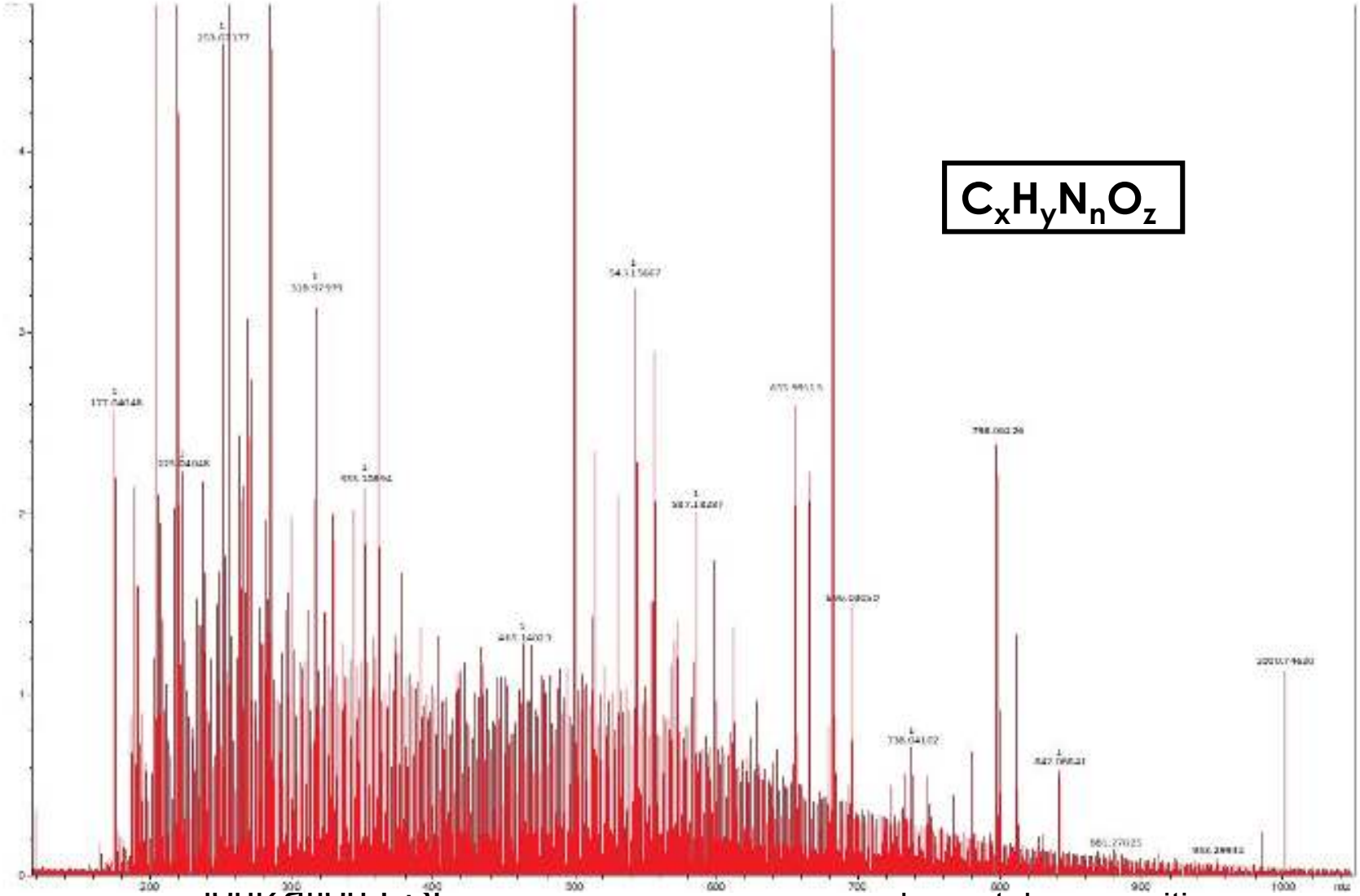

ionization ESI

elemental composition
one molecule

Graphic representation of the results

Kendrick maps

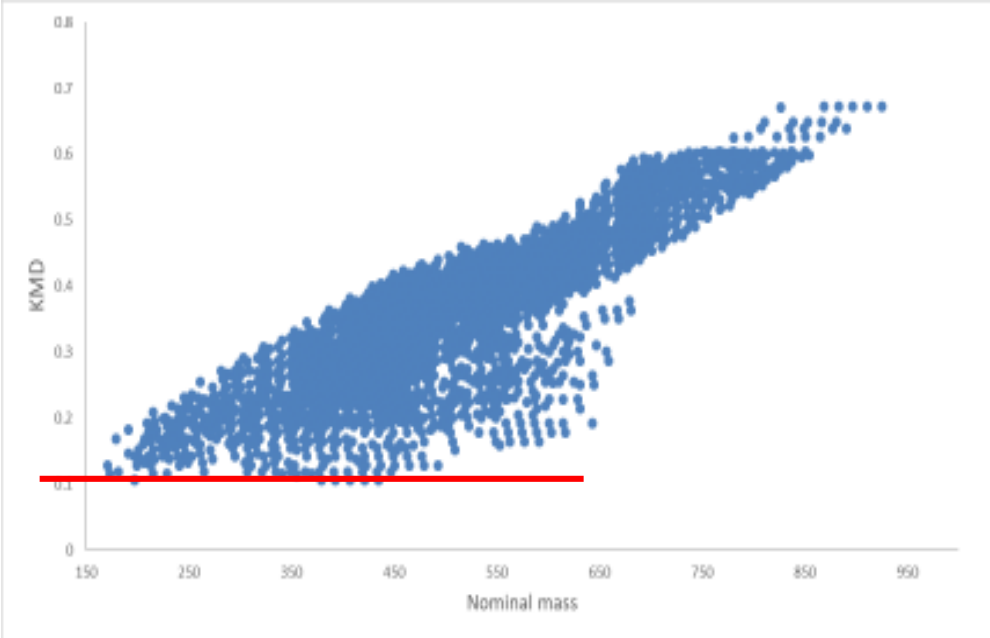

Van Krevlen

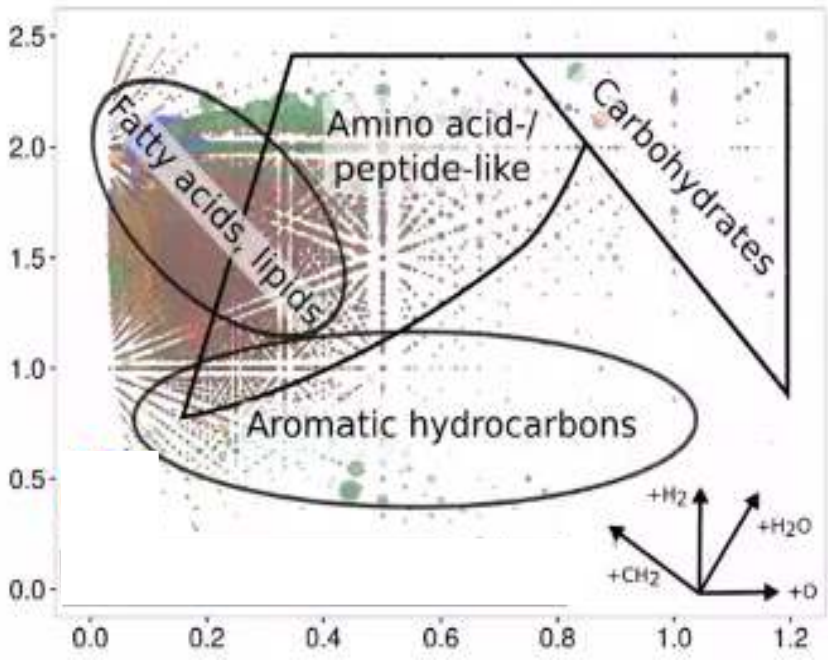

A. Ruf, L. L. S. D'Hendecourt, and P. Schmitt-Kopplin, 'Data-Driven Astrochemistry: One Step Further within the Origin of Life Puzzle', Life, vol. 8, no. 2, Art. no. 2, Jun. 2018, doi: 10.3390/life8020018

KMD Kendrick's mass defect :

KMD = masse nominale – KM

KM Kendrick's Mass :

KM = masse exacte mesurée x $\frac{14.00000}{14.01565}$

Results : Resolution and precision

- In absorption mode
- Correction of the baseline

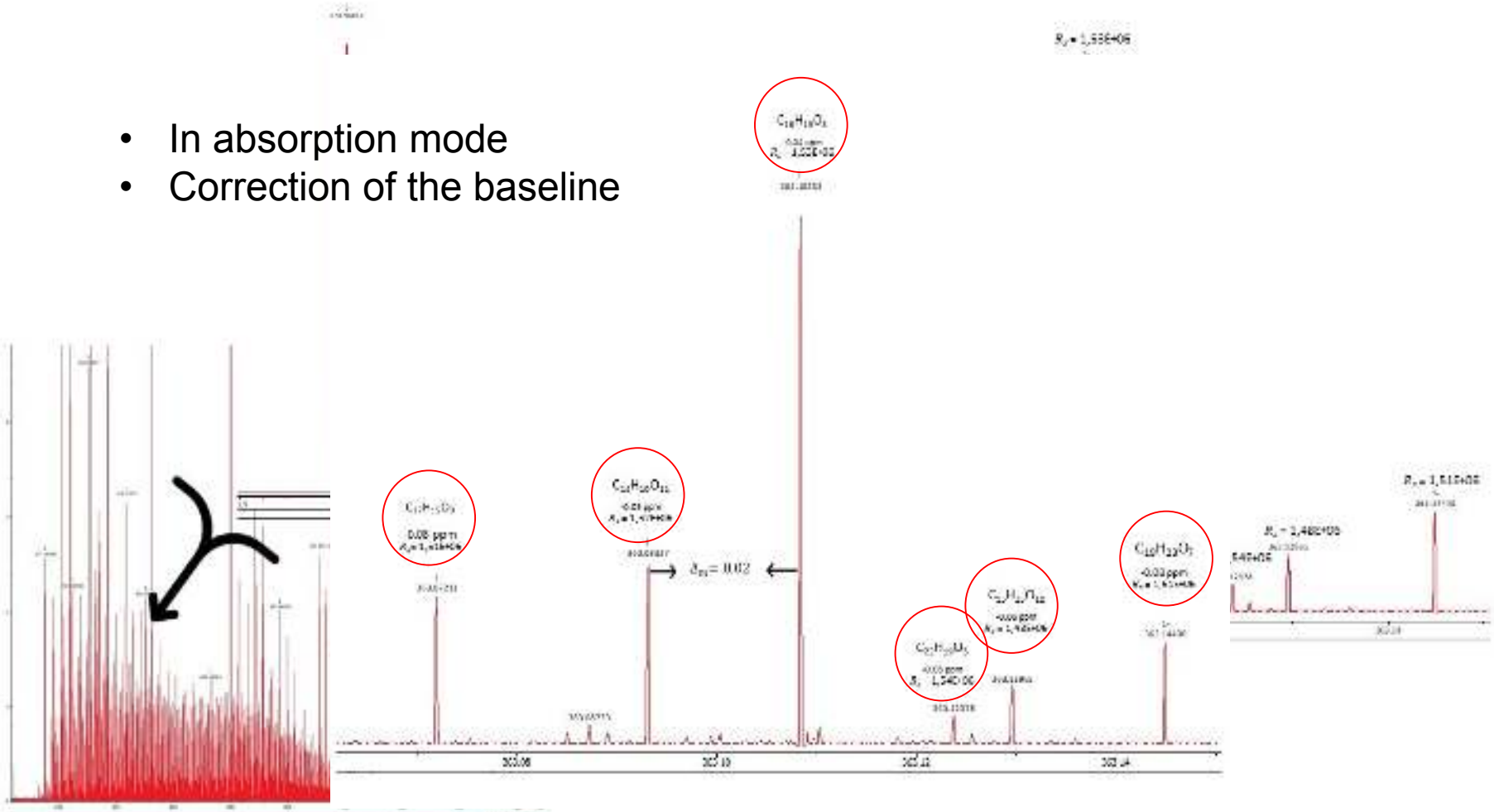

Results : graphic representation

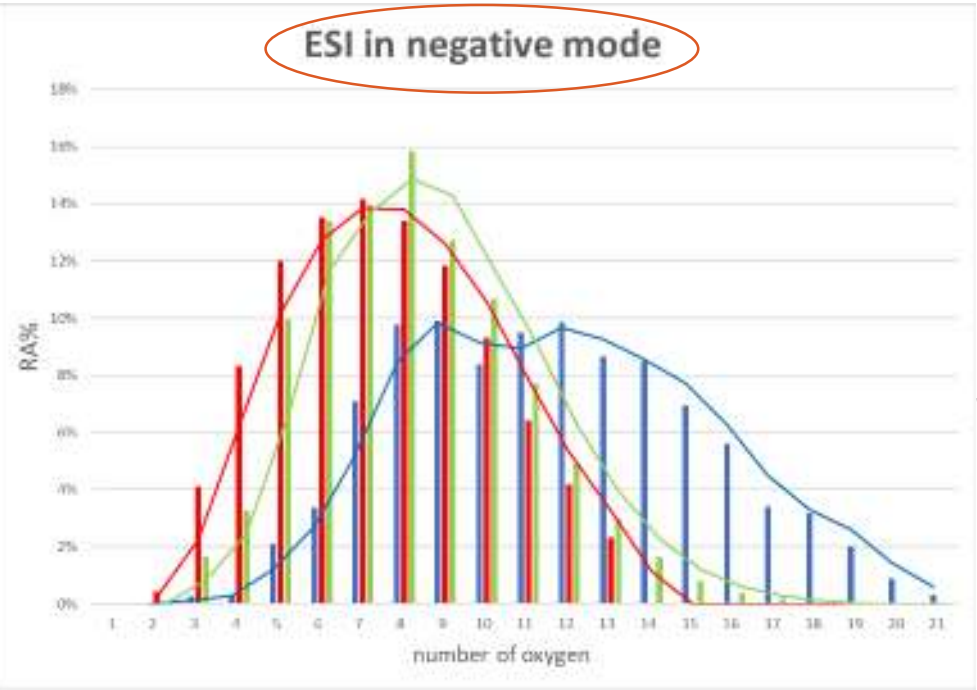

Intensity

Ameliorated BO

Raw BO

Hierarchical Bio-oil

Parental Bio-oil

Raw Bio-oil

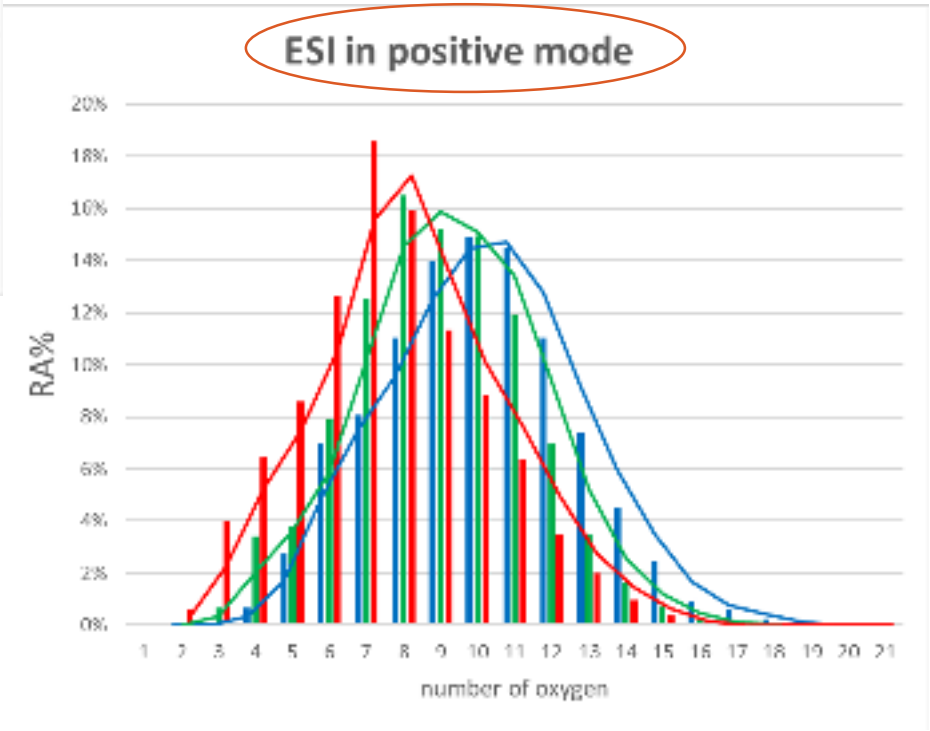

Results : graphic representation

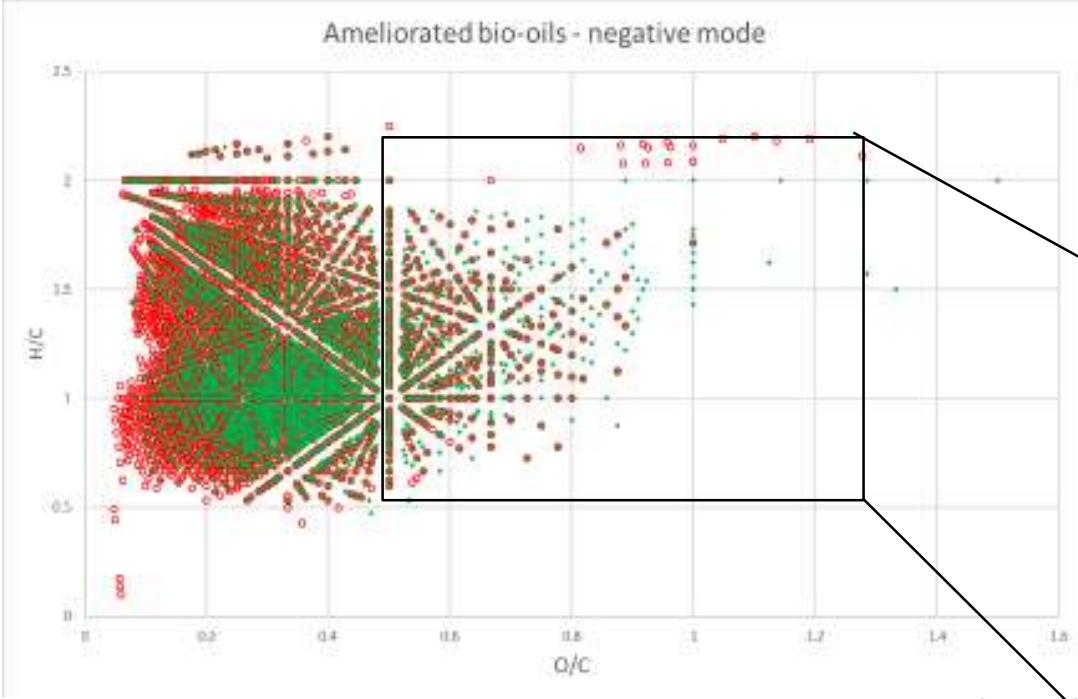

Cellulose and Hemicellulose

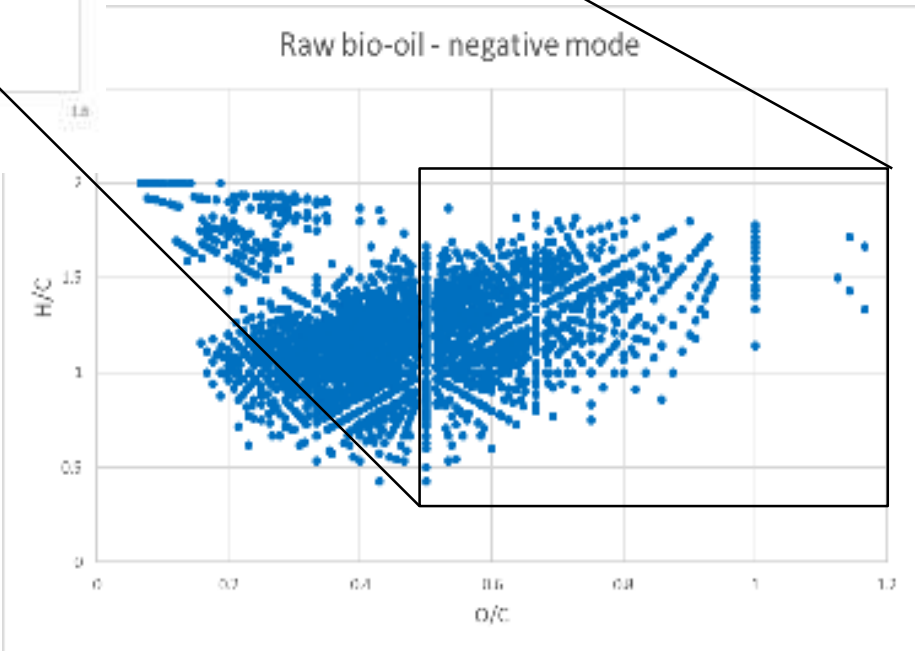

- Hierarchical Bio-oil
- Parental Bio-oil
- Raw Bio-oil

Results : graphic representation

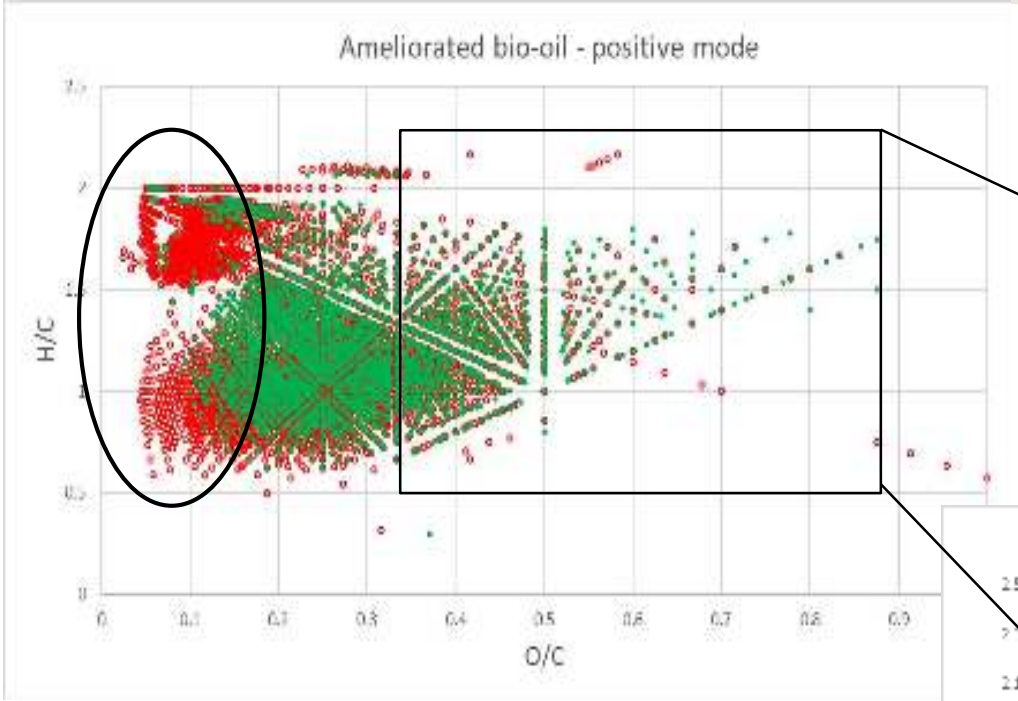

Cellulose and Hemicellulose

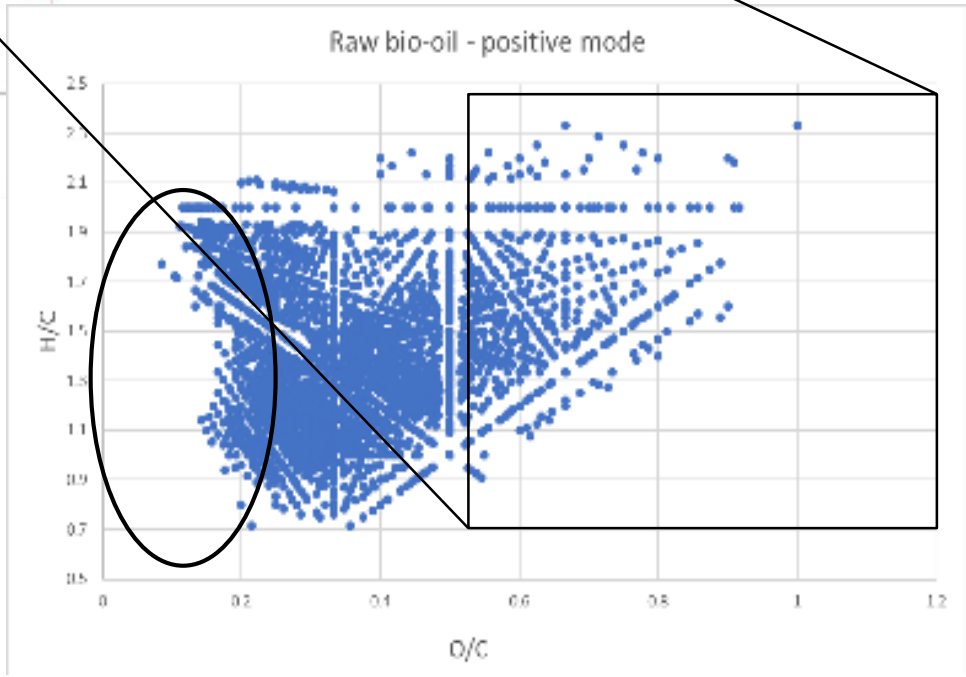

Hierarchical Bio-oil

Parental Bio-oil

Raw Bio-oil

Polyaromatic compounds

ULTRA-HIGH RESOLUTION

HIGH ACCURACY OF MASS MEASUREMENT AND SENSIBILITY

REQUIREMENT FOR A HIGH-FIELD SUPERCONDUCTING MAGNET

SHORT ANALYSIS TIME FOR HIGHLY COMPLEXE MIXTURES

HIGH COSTS OF OPERATION AND MAINTENANCE

HIGH CAPACITY OF THE NEW 2W TECHNOLOGY

Advantage and disadvantage of FT ICR-MS 7T

Beyond the standard analysis of Bio-oils

$C_xH_yN_nO_z$

c

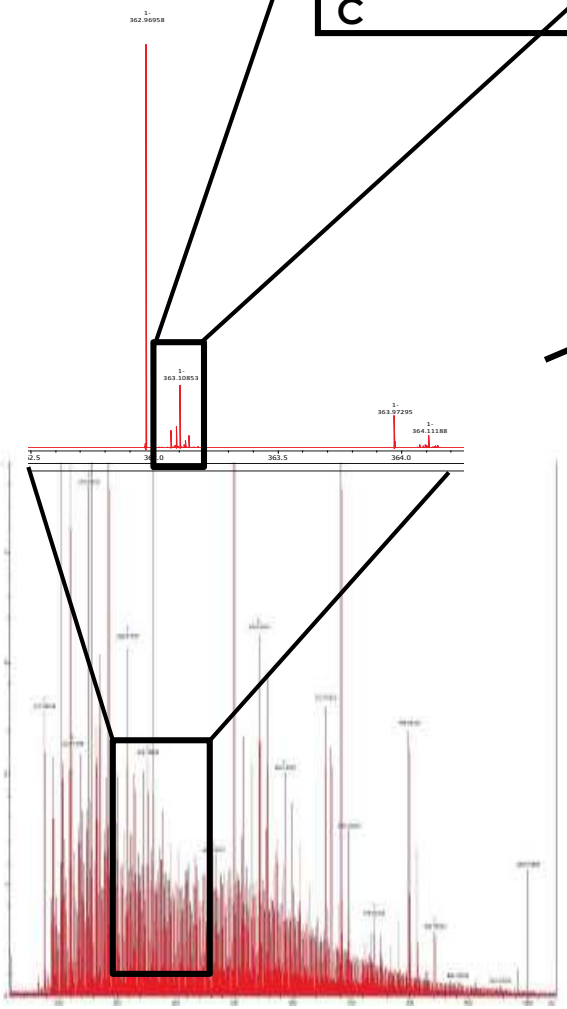

Bio-oils

Challenge

- Structure ?
- Functional groups ?

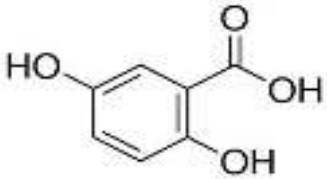

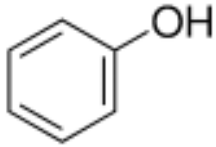

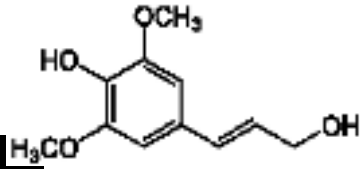

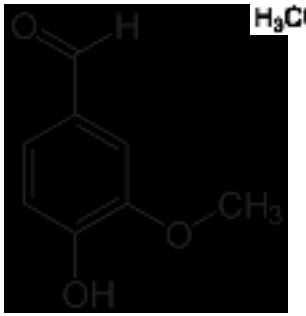

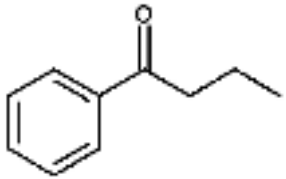

Beyond the standard analysis of Bio-oils

Derivatization

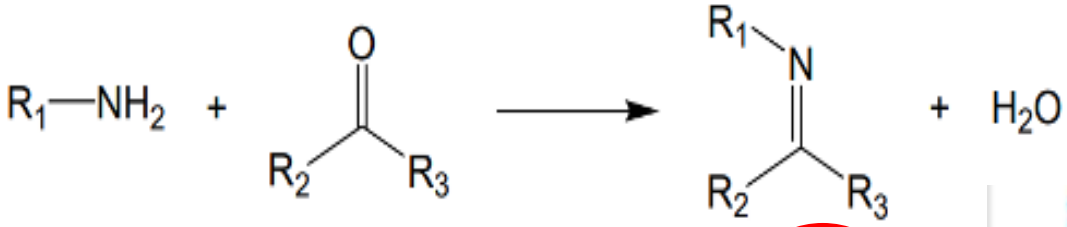

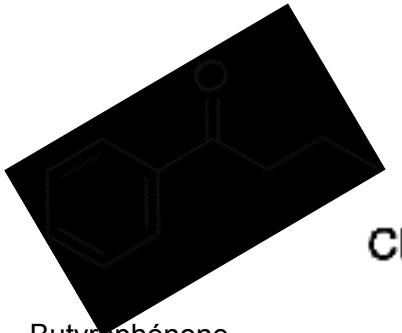

Butyrophénone

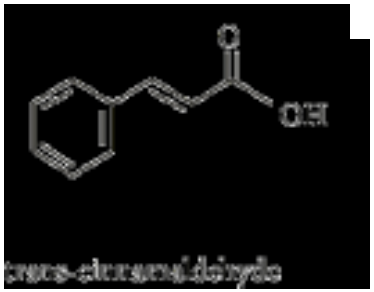

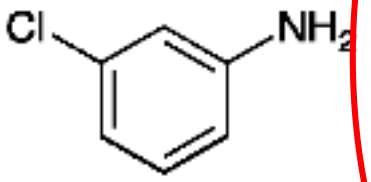

3-chloroaniline

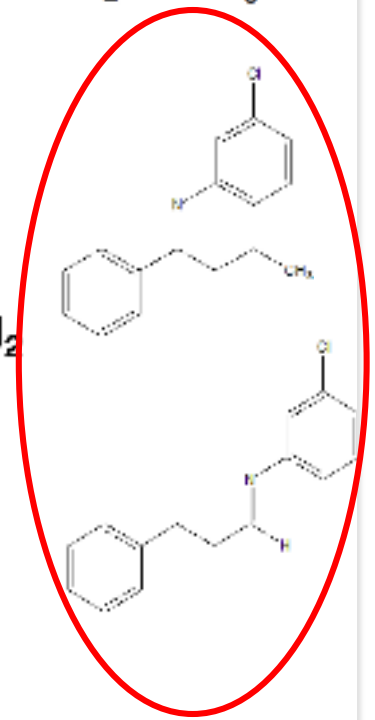

Iminiums

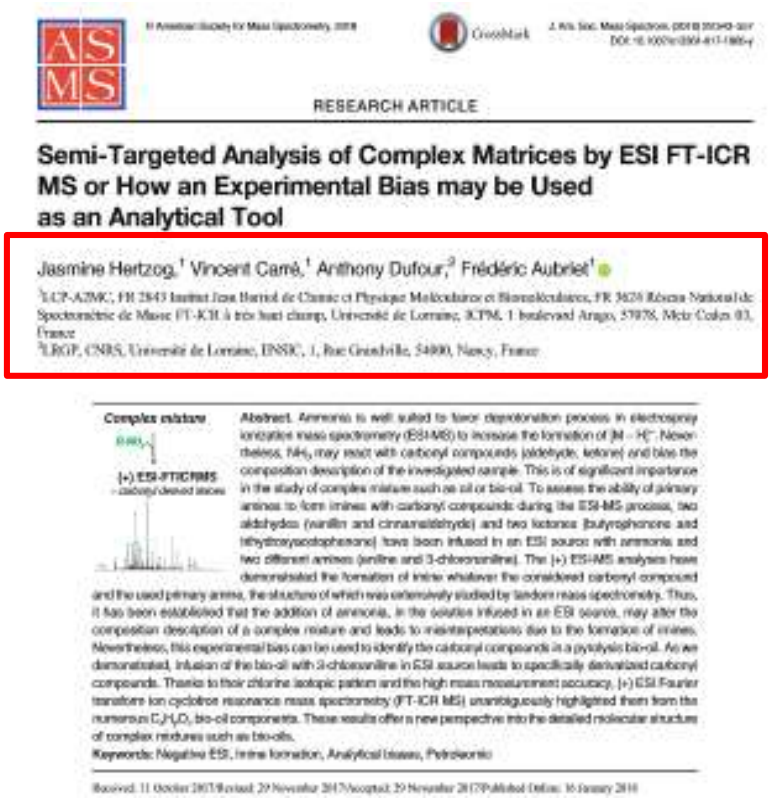

RESEARCH ARTICLE

Semi-Targeted Analysis of Complex Matrices by ESI FT-ICR MS or How an Experimental Bias may be Used as an Analytical Tool

Jasmine Hertzog,[1] Vincent Carré,[1] Anthony Dufour,[2] Frédéric Aubriet[1]

[1]LCP-A2MC, FR 2843 Institut Jean Barriol de Chimie et Physique Moléculaire et Biomoléculaires, FR 3624 Réseau National de Spectrométrie de Masse FT-ICR à très haut champ, Université de Lorraine, ICPM, 1 boulevard Arago, 57078, Metz Cedex 03, France
[2]LRGP, CNRS, Université de Lorraine, ENSIC, 1, Rue Grandville, 54000, Nancy, France

Complex mixture

(+) ESI-FTICRMS

Abstract. Ammonia is well suited to favor deprotonation process in electrospray ionization mass spectrometry (ESI-MS) to increase the formation of $[M-H]^-$. Nevertheless, NH_3 may react with carbonyl compounds (aldehyde, ketone) and bias the composition description of the investigated sample. This is of significant importance in the study of complex mixture such as oil or bio-oil. To assess the ability of primary amines to form imines with carbonyl compounds during the ESI-MS process, two aldehydes (vanillin and cinnamaldehyde) and two ketones (butyrophenone and trihydroxyacetophenone) have been infused in an ESI source with ammonia and two different amines (aniline and 3-chloroaniline). The (+) ESI-MS analyses have demonstrated the formation of imine whatever the considered carbonyl compound and the used primary amine, the structure of which was extensively studied by tandem mass spectrometry. Thus, it has been established that the addition of ammonia, in the solution infused in an ESI source, may alter the composition description of a complex mixture and leads to misinterpretations due to the formation of imines. Nevertheless, this experimental bias can be used to identify the carbonyl compounds in a pyrolysis bio-oil. As we demonstrated, infusion of the bio-oil with 3-chloroaniline in ESI source leads to specifically derivatized carbonyl compounds. Thanks to their chlorine isotopic pattern and the high mass measurement accuracy, (+) ESI Fourier transform ion cyclotron resonance mass spectrometry (FT-ICR MS) unambiguously highlighted them from the numerous $C_xH_yO_z$ bio-oil components. These results offer a new perspective into the detailed molecular structure of complex mixtures such as bio-oils.

Keywords: Negative ESI, Imine formation, Analytical biases, Petroleomic

Received: 11 October 2017/Revised: 29 November 2017/Accepted: 29 November 2017/Published Online: 16 January 2018

Conclusions and Perspectives

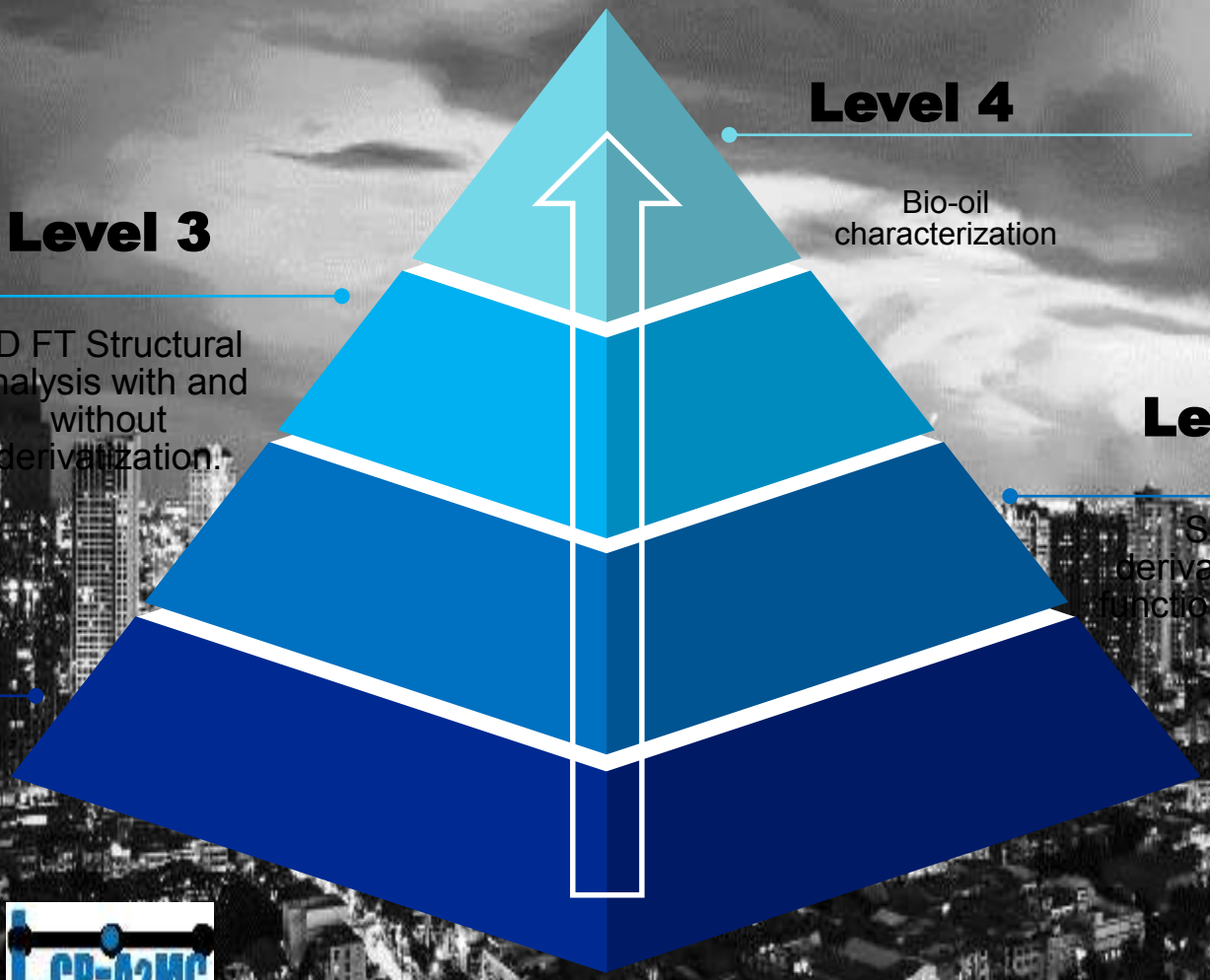

Level 4

Bio-oil characterization

Level 3

2D FT Structural analysis with and without derivatization.

Level 2

Specific derivatization of functional groups.

Level 1

FT-ICR MS 7T performance in the analysis of raw and ameliorated bio-oils and the effect of the catalyst

Thank you for your attention! ☺

EU FT-ICR MS

LAB COLLEAGUES:

FRÉDÉRIC AUBRIET

VINCENT CARRE

SÉBASTIEN SCHRAMM

PATRICK CHAIMBAULT

LIONEL VERNEX-LOSSET

JULIEN COMEL

CLARISSE GOSSET-ERRAD

THEO VOELLINGER

PIERRE PACHOLSKI

Sponsors of the Project: ResEx Program

- Feder (Europe)
- Metz Métropole
- Conseil Général 57 (Moselle)
- Région Grand EST

This project has received funding from the European Union's Horizon 2020 research and innovation programme under grant agreement No 731077.

Super-resolution in FT-ICR MS by non-Fourier Transform genetic evolution signal processing

Marc HAEGELIN

Miniaturization for Synthesis, Analysis & Proteomics, USR 3290

EU FT-ICR Prague 2021

Recall plan

1 What is an evolutionary algorithm ?

2 Sinus_it

3 Results

Evolutionary algorithms (EAs)

- Bio-inspired algorithms that simulate evolution by natural selection in order to solve optimization problems or find innovative solutions

- We create a virtual population of individuals that are candidate solutions to the problem we want to solve

- Used in artificial creation, travel salesman problem, signal processing

Evolutionary algorithm (example : onemax)

- An individual is a combination of N bits : ...1001011100010110...
- A mutation corresponds to the modification of a bit (0 switches to 1 or the inverse)
- The crossover function consists in cutting the individual into two and exchange the first/second part of each individual
  - ...10010111 00010110...
  - ...00110010 11011010...

  become

  ...10010111 11011010…
  ...00110010 00010110...
- Evaluation function is to count the number of 1's
- Stopping criteria : the maximal value was found (only 1's).

Plotting onemax results (N=100 bits / ≈10^30 combinations !)

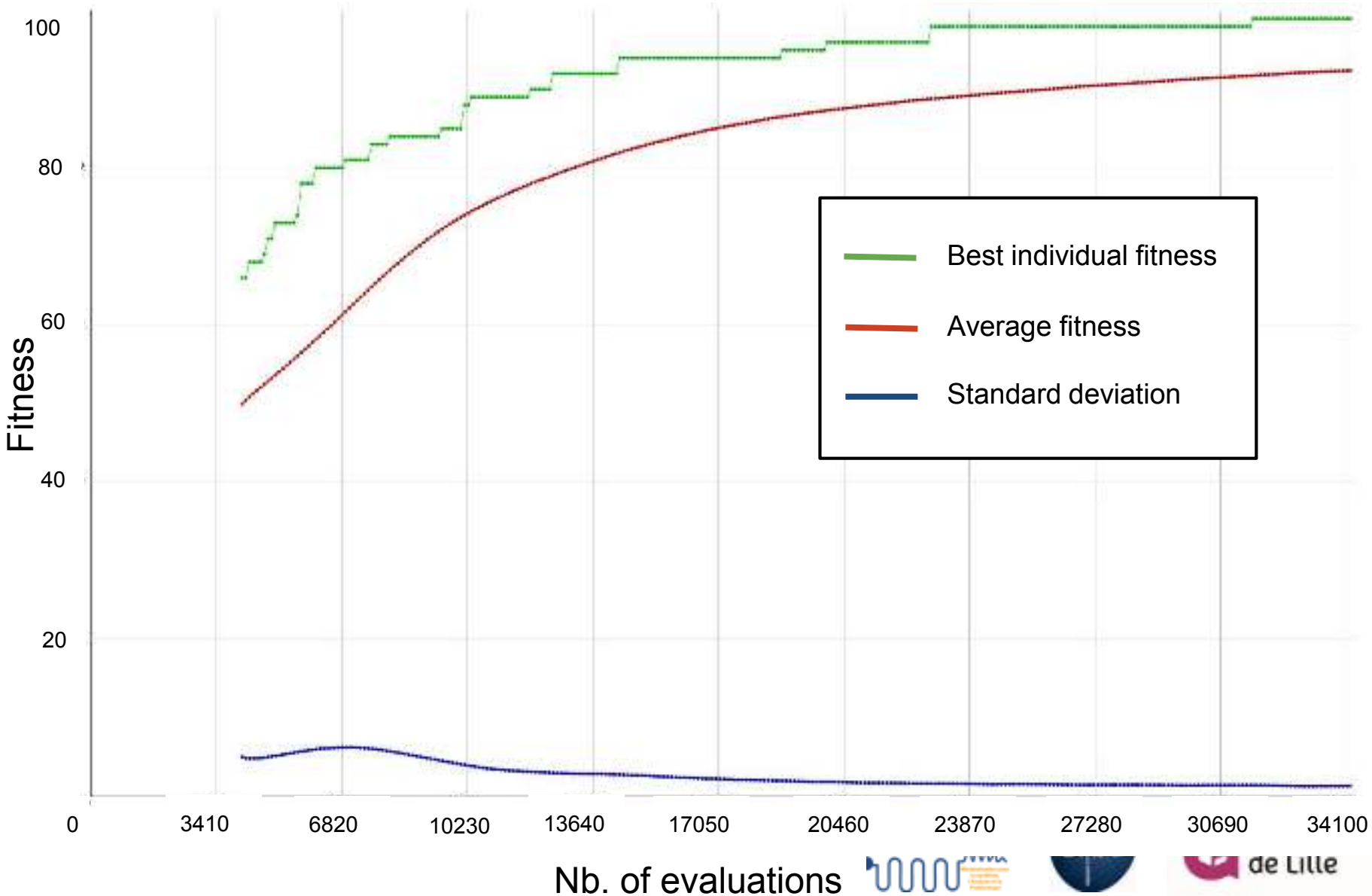

Recall plan

1 What is an evolutionary algorithm ?

2 Sinus_it

3 Results

Implementation

- Sinus_it is an evolutionary algorithm implemented with EASENA from CSTB, Strasbourg University

- The program is in C++/CUDA in order to have high control over the hardware and to benefit from the speed of the C++ langage.

NVIDIA RTX 2080 TI

- The program was run on a 2 × 16 cores 2.1 Ghz Intel Xeon server with one GPU Nvidia RTX 2080 Ti card

State of the art

- **Filter diagonalization** to achieve super-resolution

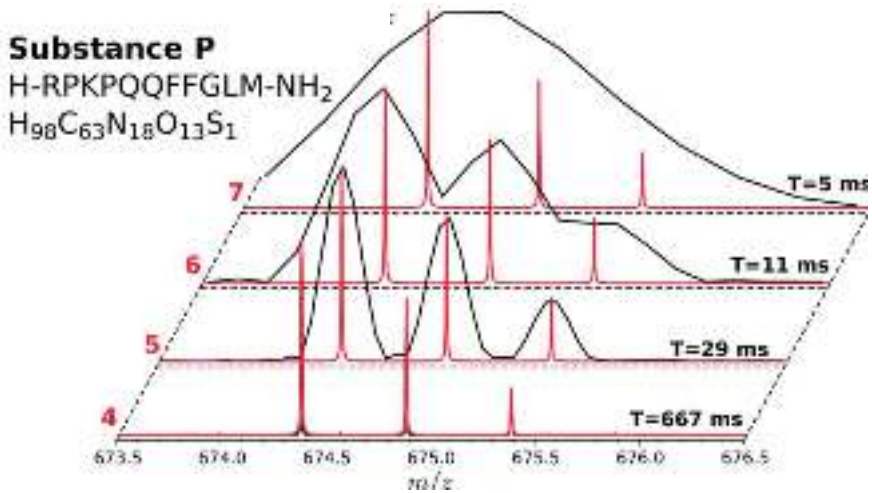

KOZHINOV, Anton N. et TSYBIN, Yury O. Filter diagonalization method-based mass spectrometry for molecular and macromolecular structure analysis. *Analytical chemistry*, 2012, 84, 2850-2856.

- Or having correct **mass isotopic ratios**

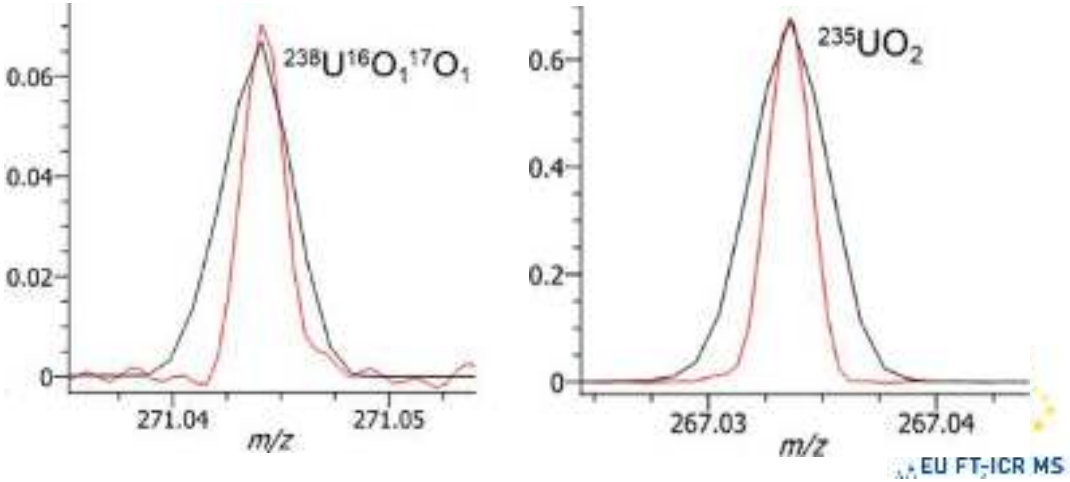

BILLS, Jacob R., NAGORNOV, Konstantin O., KOZHINOV, Anton N., *et al.* Improved Uranium Isotope Ratio Analysis in Liquid Sampling–Atmospheric Pressure Glow Discharge/Orbitrap FTMS Coupling through the Use of an External Data Acquisition System. *Journal of the American Society for Mass Spectrometry*, 2021, 32, 1224-1236.

Workflow

TRANSIENT

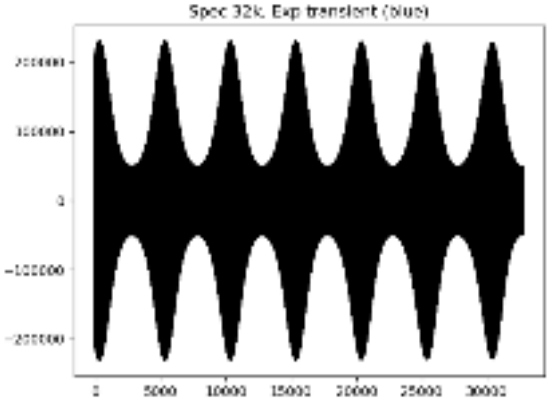

1) Fourier transform

2) Butterworth filter

3) Butterworth filter

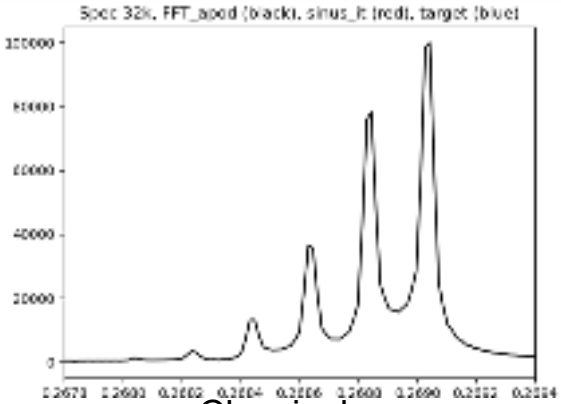

Classical FFT

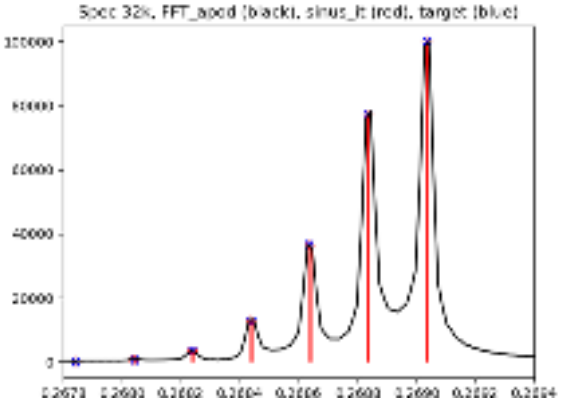

Sinus_it coarse isotopic

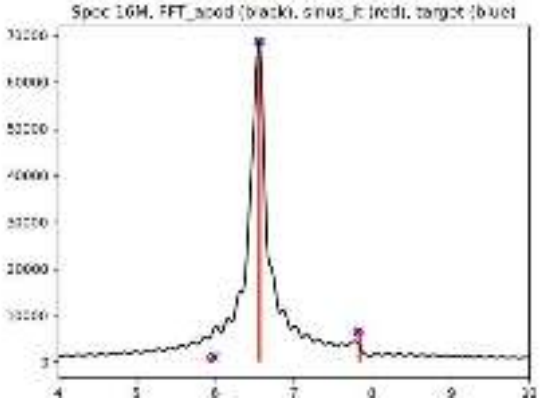

Sinus_it fine isotopic

Signal fitting

- Sinus_it tries to approach/fit the decaying sinusoidal signal
  - e.g. With an individual
    - sine1 = 6578.95 * sin(2*pi*0.2688379 + 1.40878)
    - sine2 = 68232.5 * sin(2*pi*0.2688365 + 1.41167)
    - sine3 = 1142.58 * sin(2*pi*0.2608350 + 1.41348)
  - The real signal is
    - sine1 = 6575.94 * sin(2*pi*0.2688378 + 1.40905)
    - sine2 = 68139.09 * sin(2*pi*0.2688365 + 1.41165)
    - sine3 = 1150.13 * sin(2*pi*0.2688359 + 1.41284)

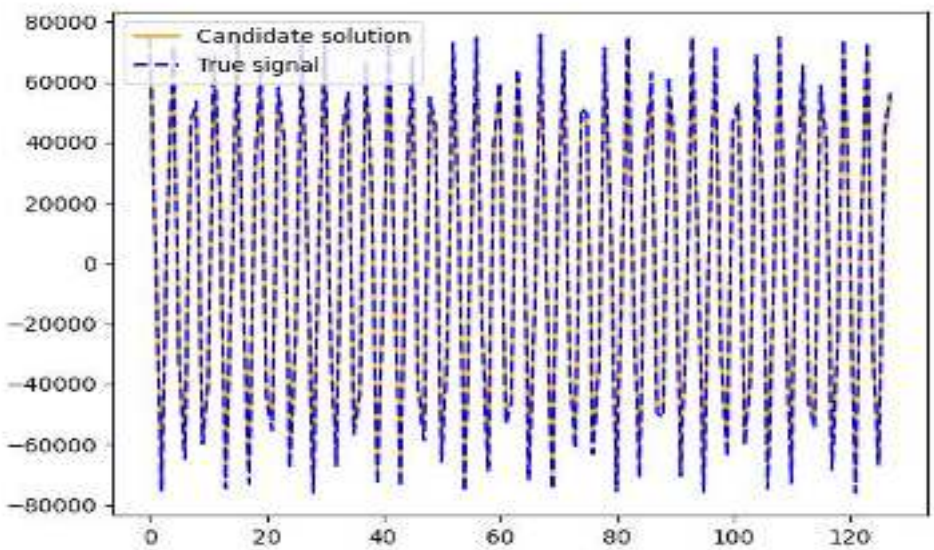

Comparison of the real signal (blue dash) and the candidate solution (orange line)

Recall plan

1 What is an evolutionary algorithm ?

2 Sinus_it

3 Results

Coarse isotopic graph (Substance P simulated / 7 peaks)

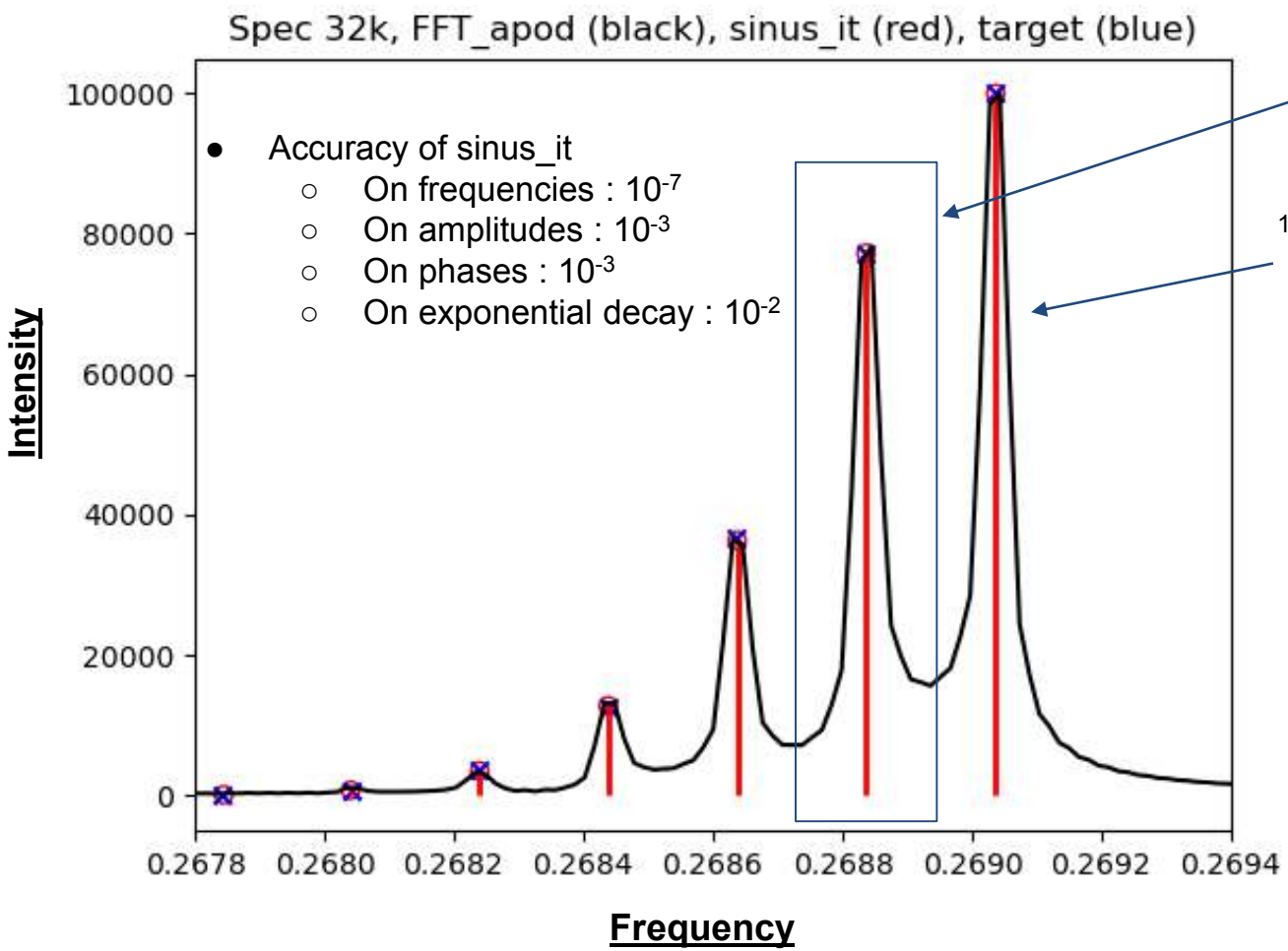

First isotopic distribution

$^{12}C_{63}{}^{1}H_{100}{}^{14}N_{18}{}^{16}O_{13}{}^{32}S$

Coarse isotopic graph (Substance P simulated / 7 peaks)

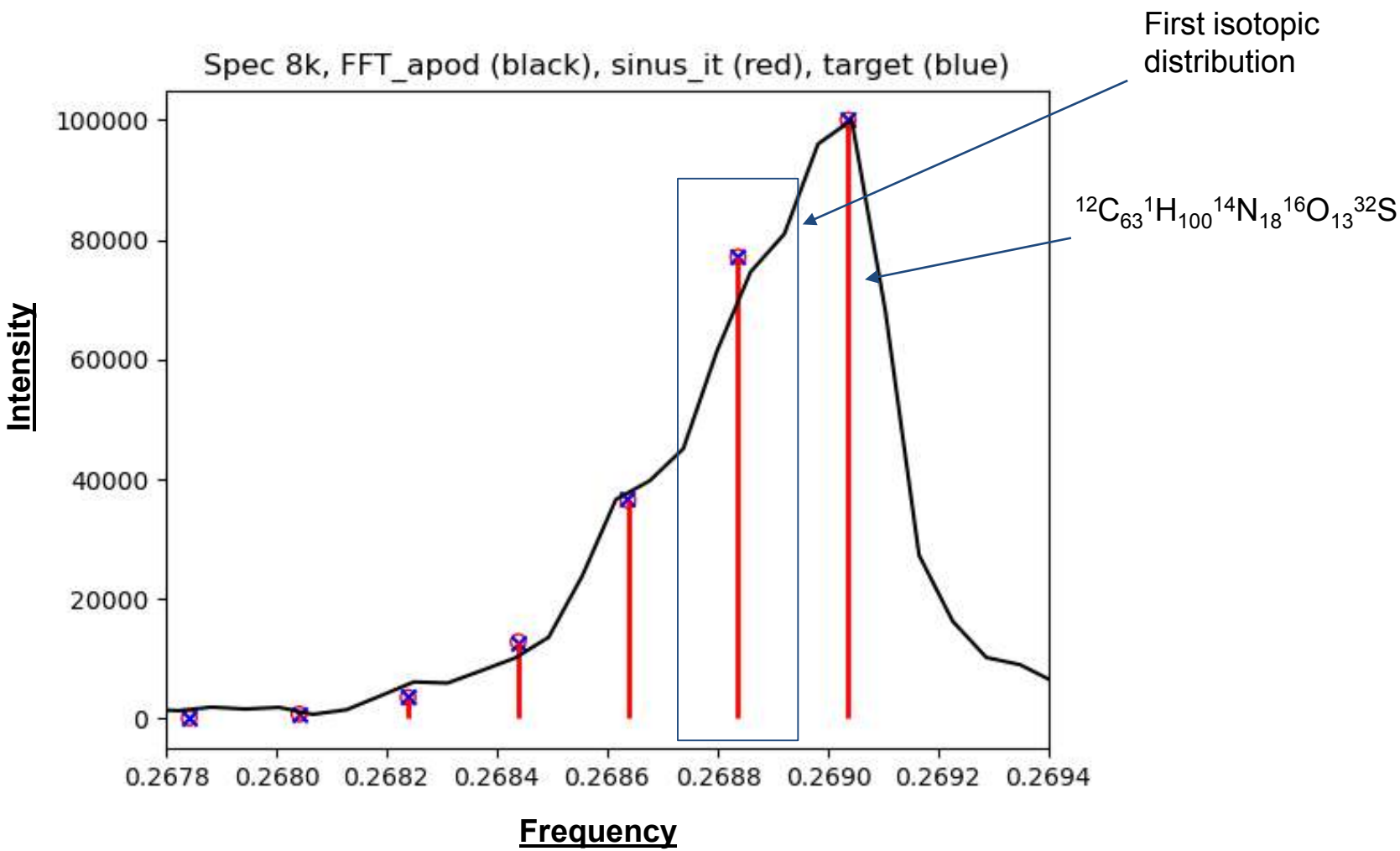

Fine isotopic graph (Substance P simulated / 1st isotope)

FFT_apod 16 Mpoints (black), **sinus_it 1 Mpoints (red)**, target (blue)

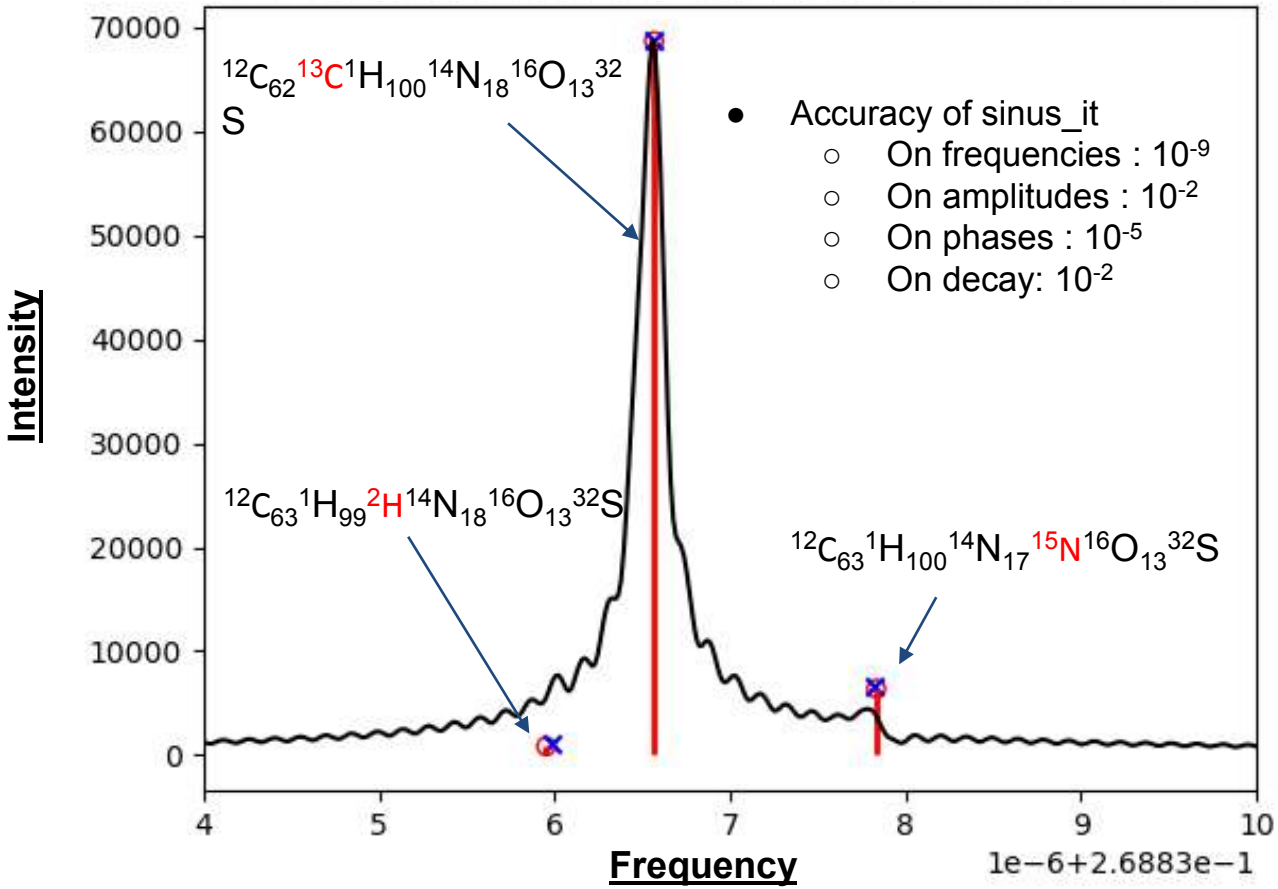

- Accuracy of sinus_it
  - On frequencies : 10^{-9}
  - On amplitudes : 10^{-2}
  - On phases : 10^{-5}
  - On decay: 10^{-2}

Coarse isotopic distribution (Substance P real signal / 5 peaks)

FFT_apod 128 Kpoints (black), **sinus_it 32 Kpoints (red)**, target (blue)

First isotopic distribution

$^{12}C_{63}{}^{1}H_{100}{}^{14}N_{18}{}^{16}O_{13}{}^{32}S$

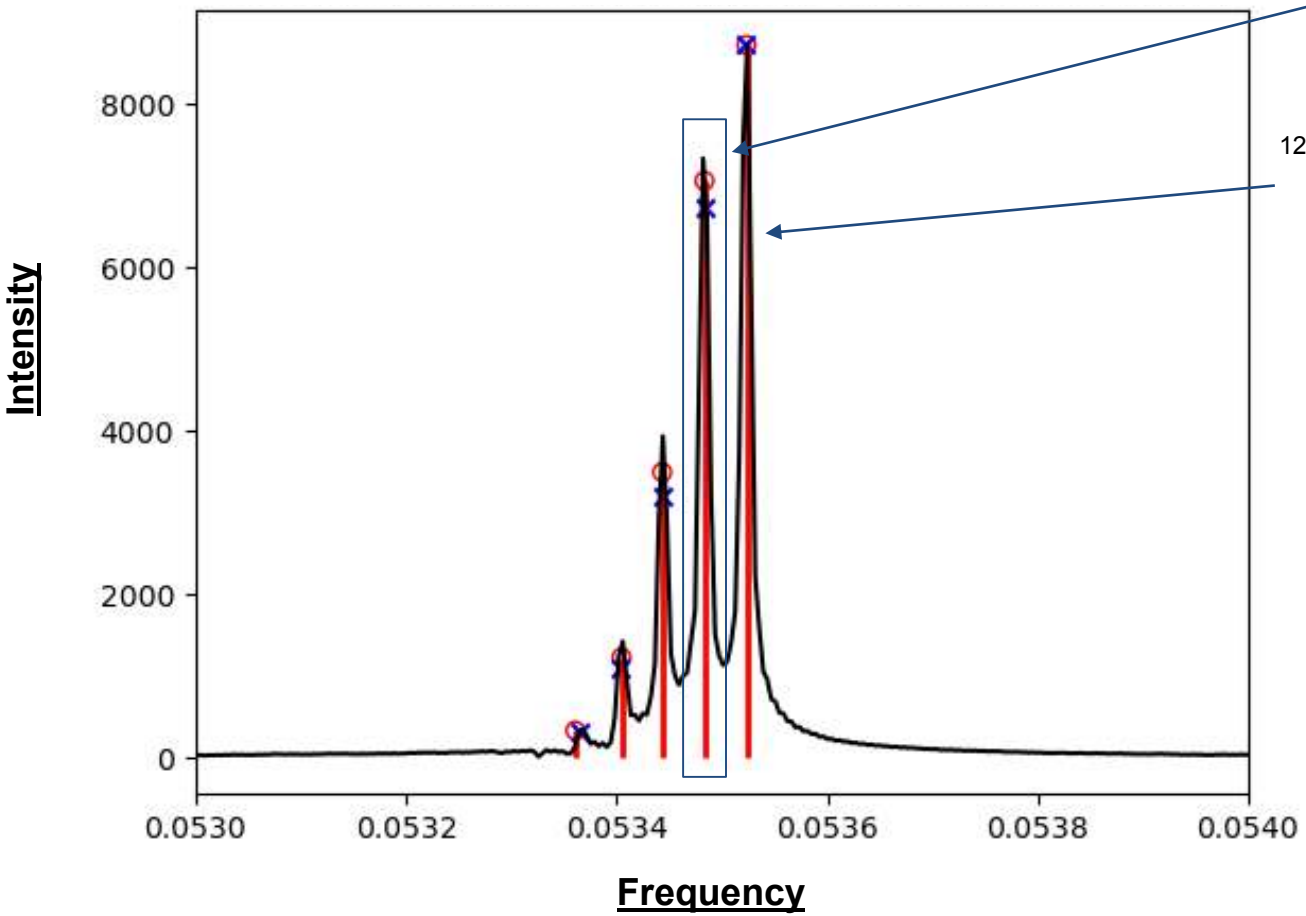

Coarse isotopic distribution (Gluthation real signal narrow band)

Sinus_it with dynamic number of sine

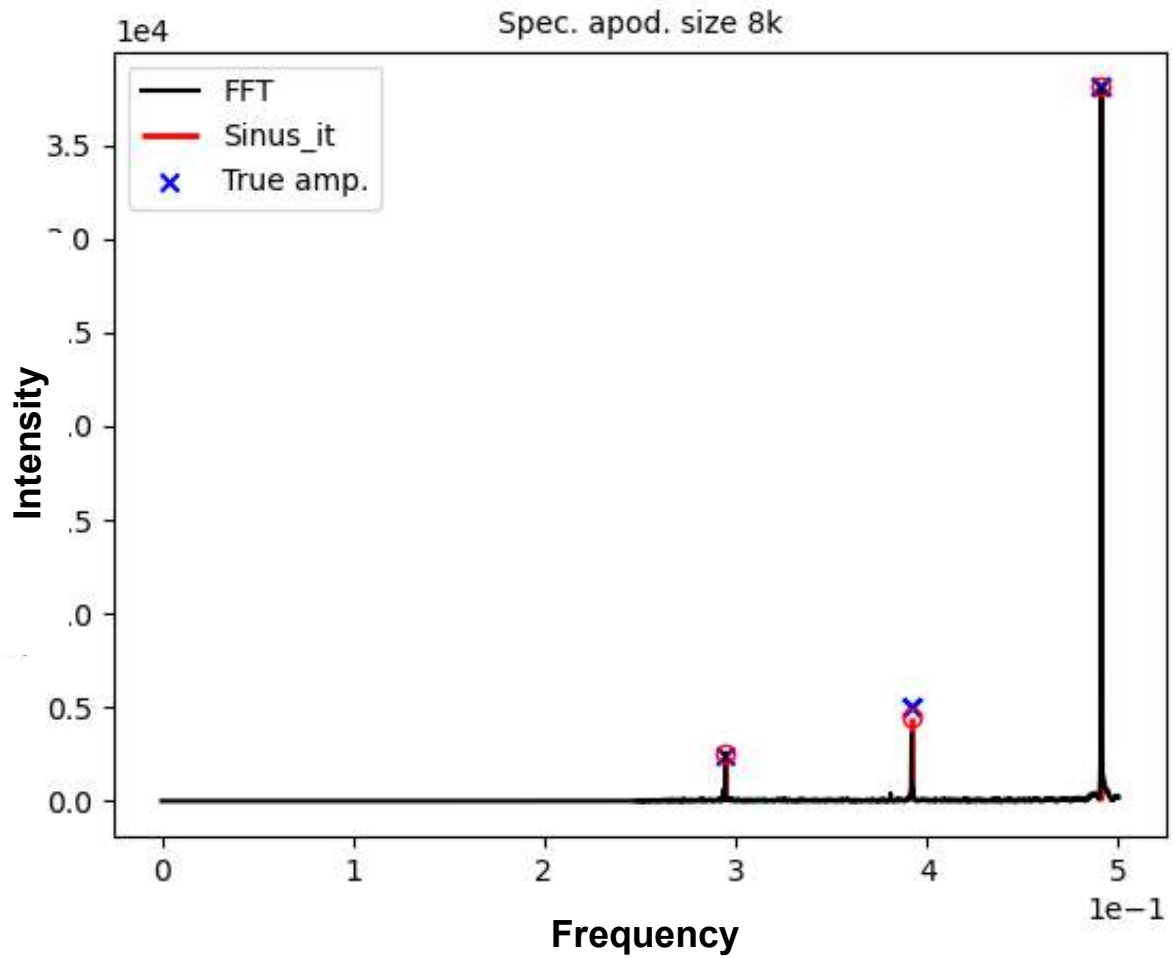

Glutathione (broad band) frequency, phase vs time

- Glutathione (broad band, sampling frequency 1 MHz), monoisotopic peak
- 32k transients sliced on 16M transient at different time (kpoints = 1.024 ms)

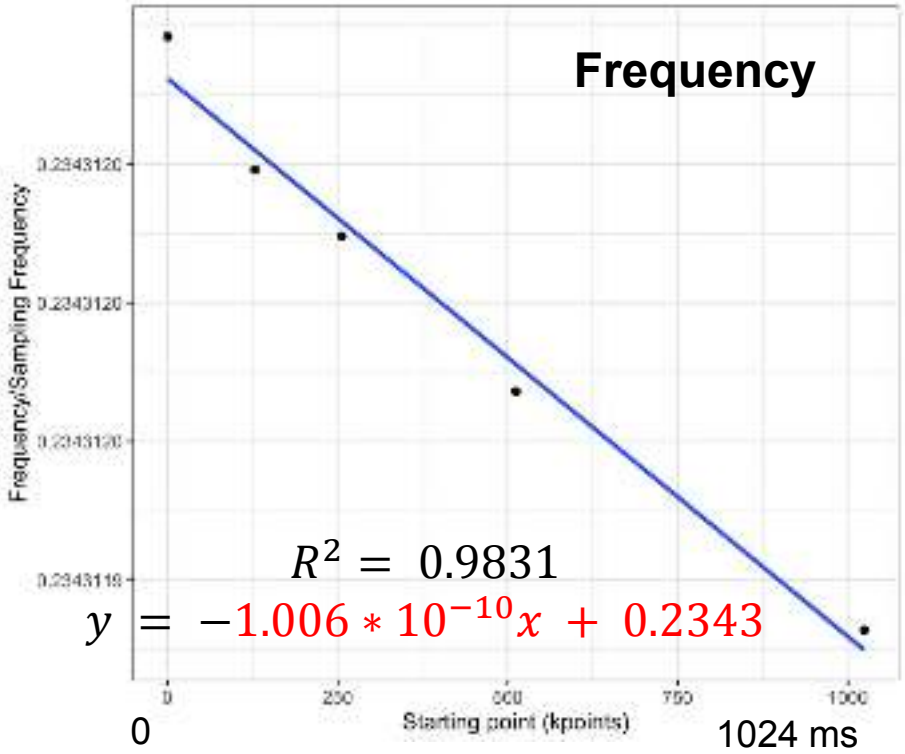

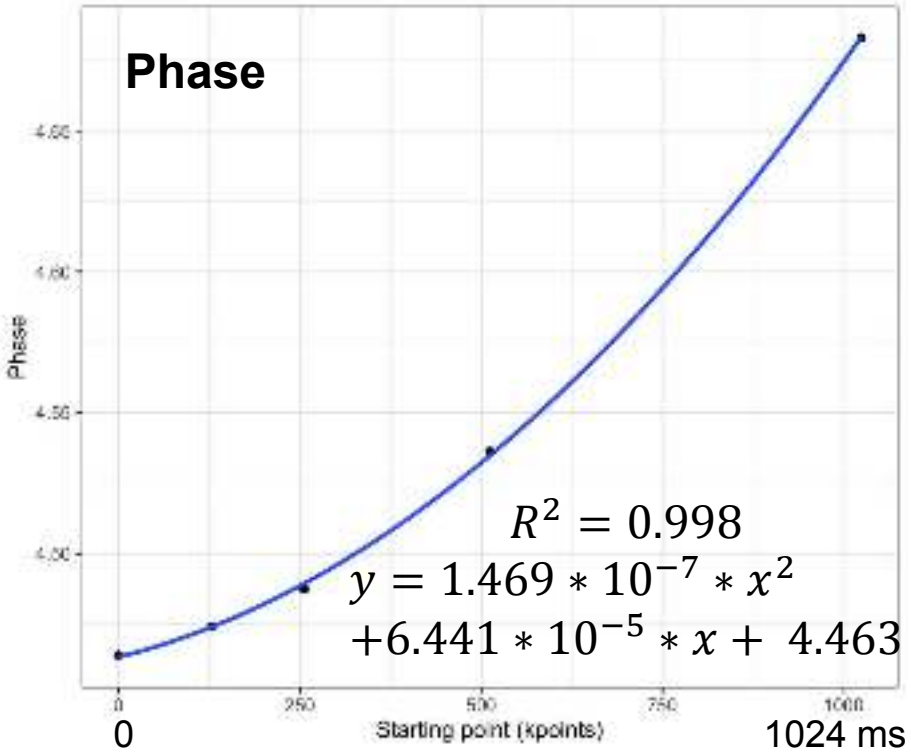

- Phases and frequencies **varie along the transient** and are correlated

EU FT-ICR MS MSAP cnrs Université de Lille

Speed and complexity

Sinus_it execution time

Arbitrary units

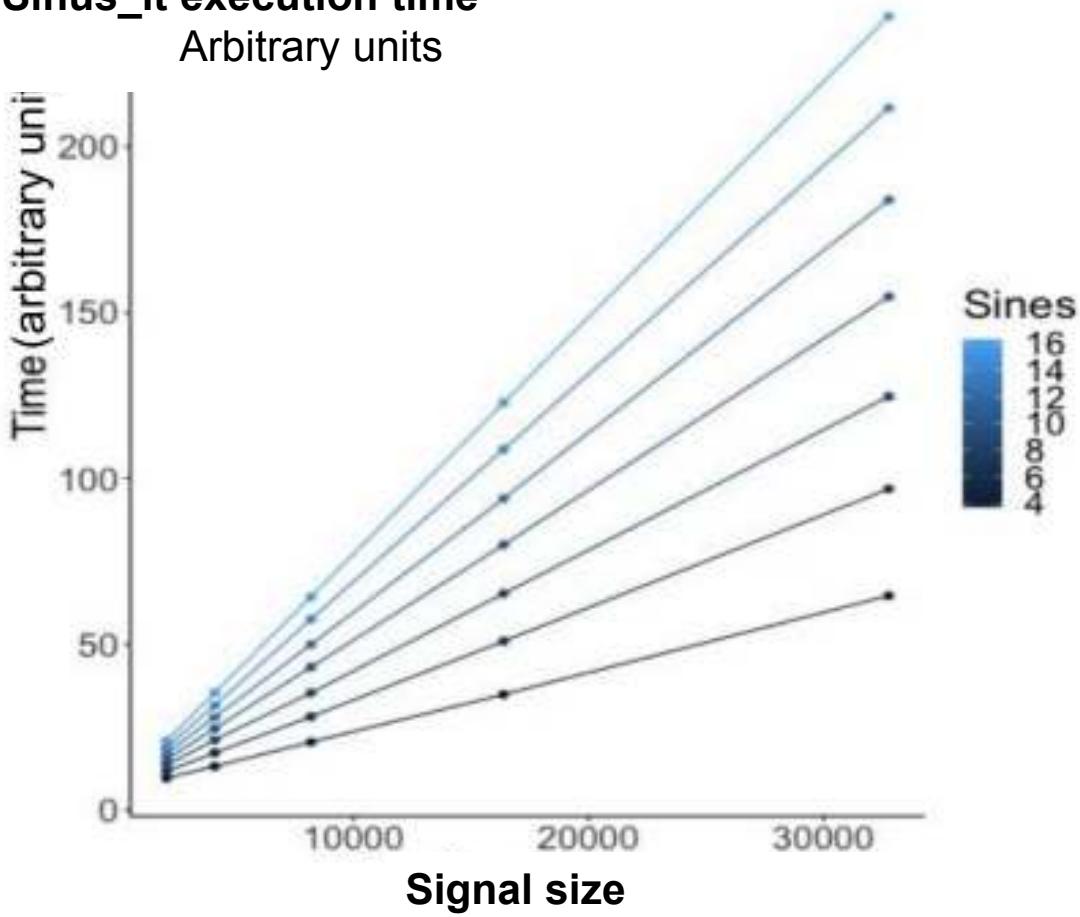

Sinus_it execution time propotionnal to:

- **Sine**
- **Generations**
- Coarse isotopic: **~2-3 hours**
- Fine isotopic: **~4 hours**

Conclusion

- FFT has many drawbacks
  - limited resolving power,
  - Shannon-Nyquist limit,
  - damping, apodization ...

- Sinus_it is a genetic algorithm that achieves harmonic inversion of exponentially damped sine without these drawbacks and is close to the theoretical maximum resolution (super-resolution).

  CANDÈS, Emmanuel J. et FERNANDEZ-GRANDA, Carlos. Super-resolution from noisy data. *Journal of Fourier Analysis and Applications*, 2013, 19, 1229-1254.

- Sinus_it can find the right amplitude for quantification, or the decay constant as well as the correct phase.

Acknowledgements

MSAP (Lille)

Dr. Christian ROLANDO
Dr. Fabrice BRAY
Stéphanie FLAMANT
Ziad MAHMOUD
Marie YAMMINE
Caterina BORDIN

ICube (Strasbourg & Baku)

Pr. Pierre COLLET

Dr. Ulviya ABDULKARIMOVA

EU FT-ICR MS MSAP cnrs Université de Lille

EU FT-ICR MS

Sulfur compounds characterization using FT-ICR MS: towards a better comprehension of vacuum gas oils hydrodesulfurization process

Julie Guillemant[1], Alexandra Berlioz-Barbier[1], Luis Pereira de Oliveira[1], Marion Lacoue-Nègre[1], Ludovic Duponchel[2] and Jean-François Joly[1]

[1]IFP Energies Nouvelles, Solaize, France
[2]LASIRE, Univ. Lille, France
julie.guillemant@univ-pau.fr

PETROLEUM CUTS

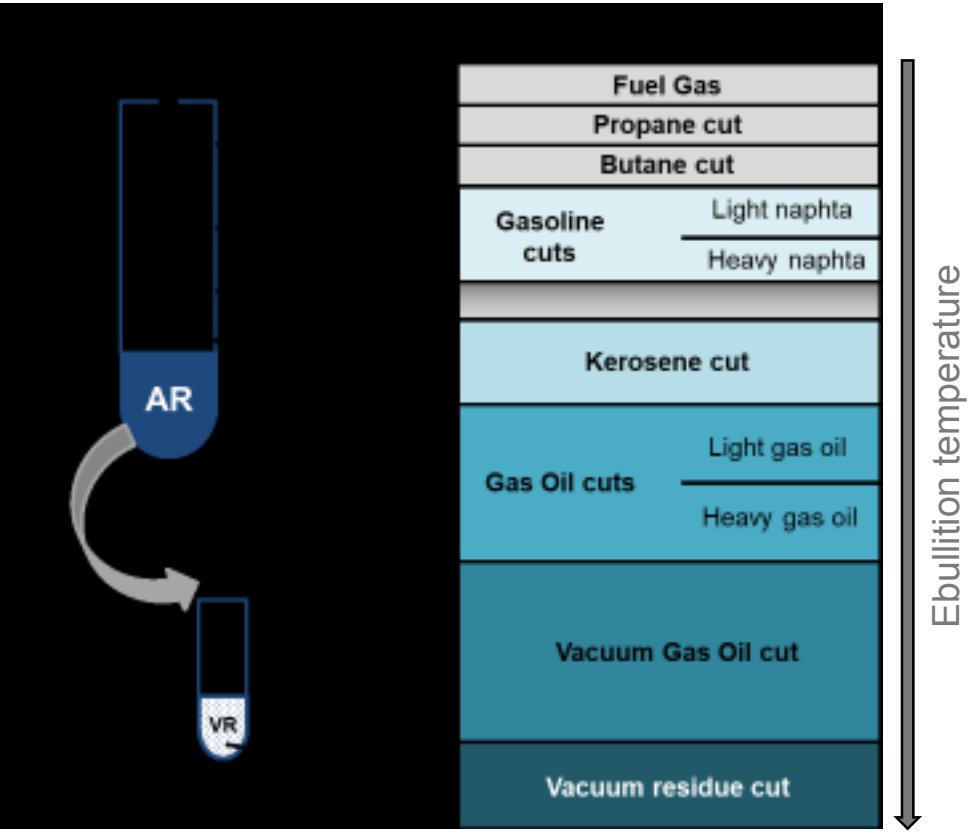

Depending on crude oil origin, up to 100% can contain **heavy cuts** that have a lower commercial value than light products

- **How can we valorize these heavy cuts ?**

VGO **conversion** into lighter cuts thanks to several **processes** using **catalysts** that might be **deactivated** by heteroatomic compounds[1] (N, O, **S**…).

- **How can we improve conversion processes ?**

Removal of sulfur compounds using **hydrodesulfurization** process prior to conversion processes to **improve conversion efficiency**[2]

[1] Effects of organic nitrogen compounds on hydrotreating and hydrocracking reactions. Sau, M, *Catalysis Today* , **2005**
[2] Hydrodesulfurization Reactivities of Various Sulfur Compounds in Vacuum Gas Oil, Ma, X, . *Ind. Eng. Chem. Res.* **1996**

HYDRODESULFURIZATION PROCESS

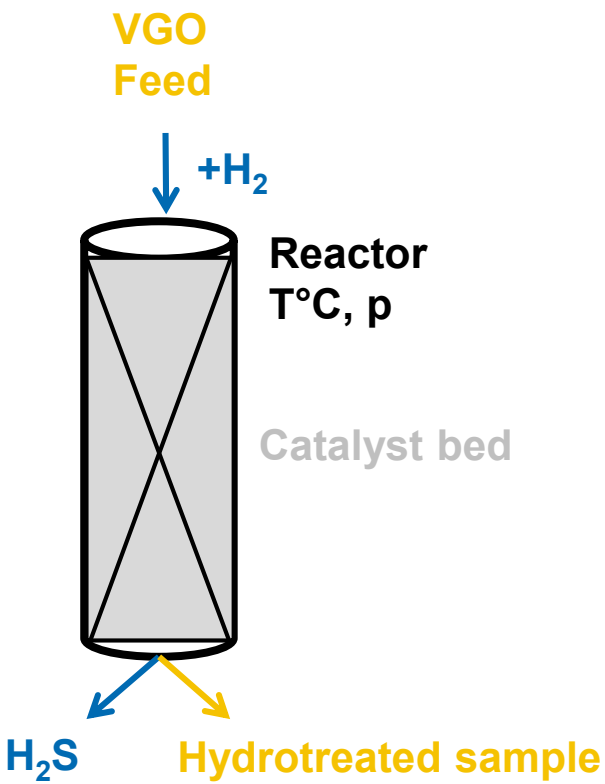

Main objectives: **Removing sulfur compounds** from the feed by **mixing the feed with H_2** into a closed reactor at high **T°C** and **pressure** conditions with a **catalyst**

Main parameters to be changed:

- Temperature
- Pressure
- Catalyst: improve reaction efficiency
- H_2/HC ratio: ratio between H_2 introduced and HC content
- LHSV (liquid hourly space velocity): volumic ratio between the quantity of feed and catalyst

HDS efficiency evaluated over the **total S content**
Not enough to explain **reactivity behaviors**
Need to monitor HDS efficiency at the **molecular level**

Ultra-high resolution mass spectrometry: FT-ICR MS

Sulfur compounds characterization using FT-ICR MS: towards a better comprehension of vacuum gas oils hydrodesulfurization process, Guillemant J. et al., *Fuel Processing Technology*, **2020**

SAMPLES CHARACTERISTICS

One feedstock and 6 hydrotreated samples produced using:

- Two different **catalysts**: A and B → evaluation of catalyst efficiency
- Three different **temperatures**: 1 < 2 < 3 → evaluation of temperature impact

Sample	S content (ppm)	Catalyst	LHSV ($^{-1}$)	Pressure (bars)	Temperature (°C)	H_2/HC (NL/L)
Feed	18921	-	-	-	-	-
A-1	1251	A	1	a	1	a
A-2	693	A	1	a	2	a
A-3	334	A	1	a	3	a
B-1	949	B	1	a	1	a
B-2	483	B	1	a	2	a
B-3	200	B	1	a	3	a

FT-ICR MS sample preparation

- The feed and the hydrotreated samples were first solubilized in Toluene to 1% w/w
- The samples were diluted to 0.05% v/v in a 90%-10% Toluene-Methanol
- 6 technical replicates were prepared and analyzed in the same experimental conditions

INSTRUMENTAL SET-UP

FT-ICR MS

Thermo LTQ FT Ultra 7T

- APPI ion source operated in (+) mode
- *m/z* 98 to 1000
- R=200,000 at *m/z* 500
- 70 scans, 4 µ-scans, 1.6s transient
- Focus on S1 class ($M^{+\bullet}$)

Data processing

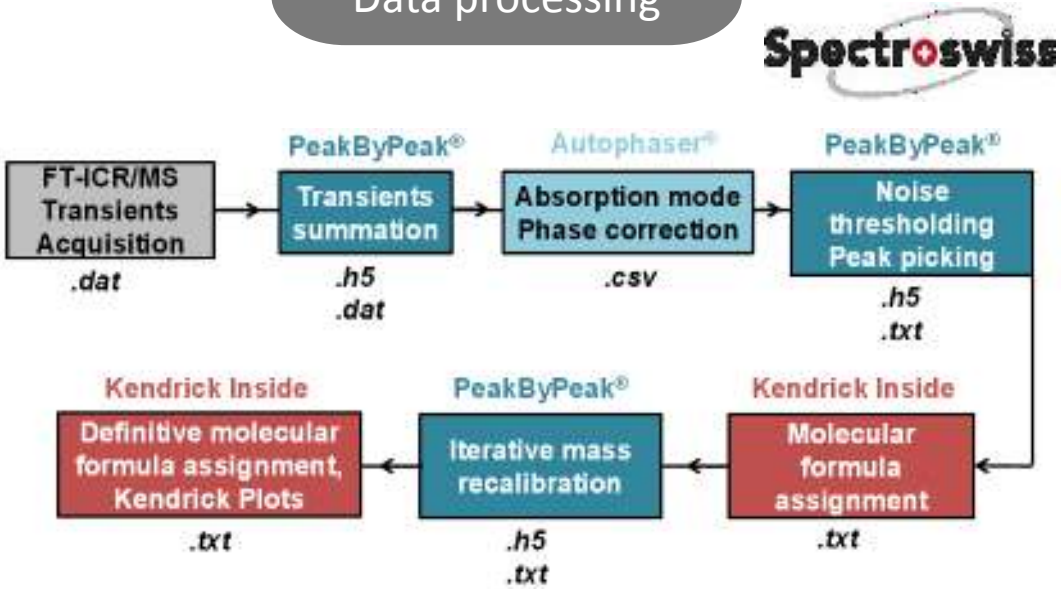

- Increased resolution of about **2.5%** for VGO samples up to **700,000**
- Mass error below **800 ppb**
- Pseudo-concentration: Relative intensity × Sulfur content (ppm)

COMPARISON OF ALL SAMPLES

- **DBE=f(#C) plots:** Fast evaluation of **temperature** and **catalyst effects** on the **aromaticity** and **alkylation** levels of the sulfur compounds

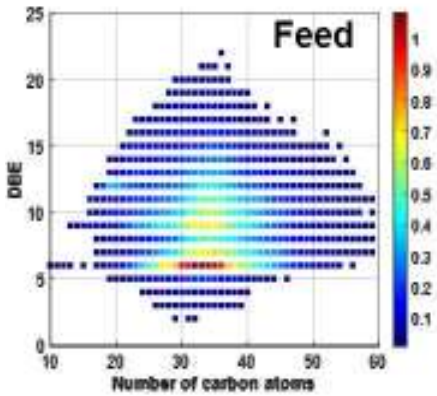

DBE: Number of rings + Double bonds

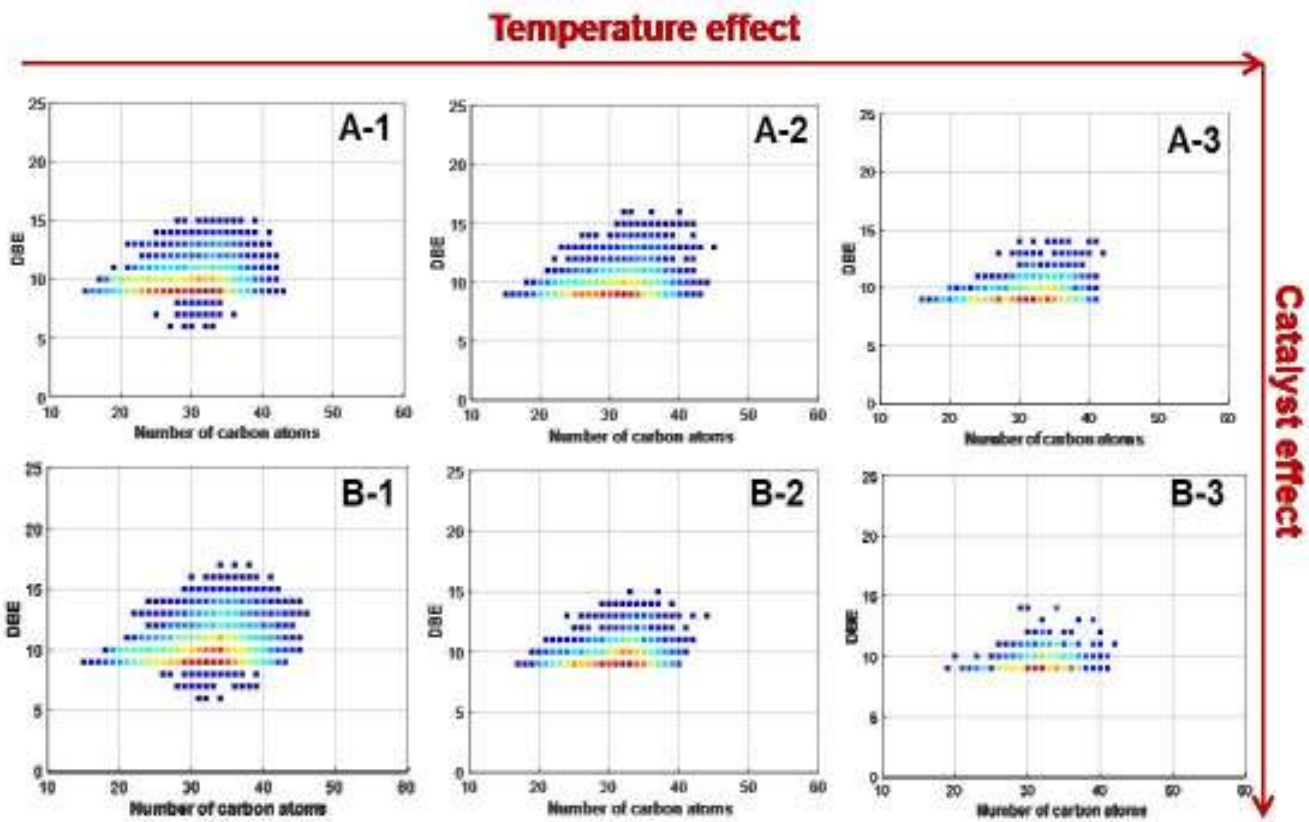

COMPARISON OF ALL SAMPLES

- FT-ICR MS data processing for **chemometrics**: unfolding on the DBE=f(#C)

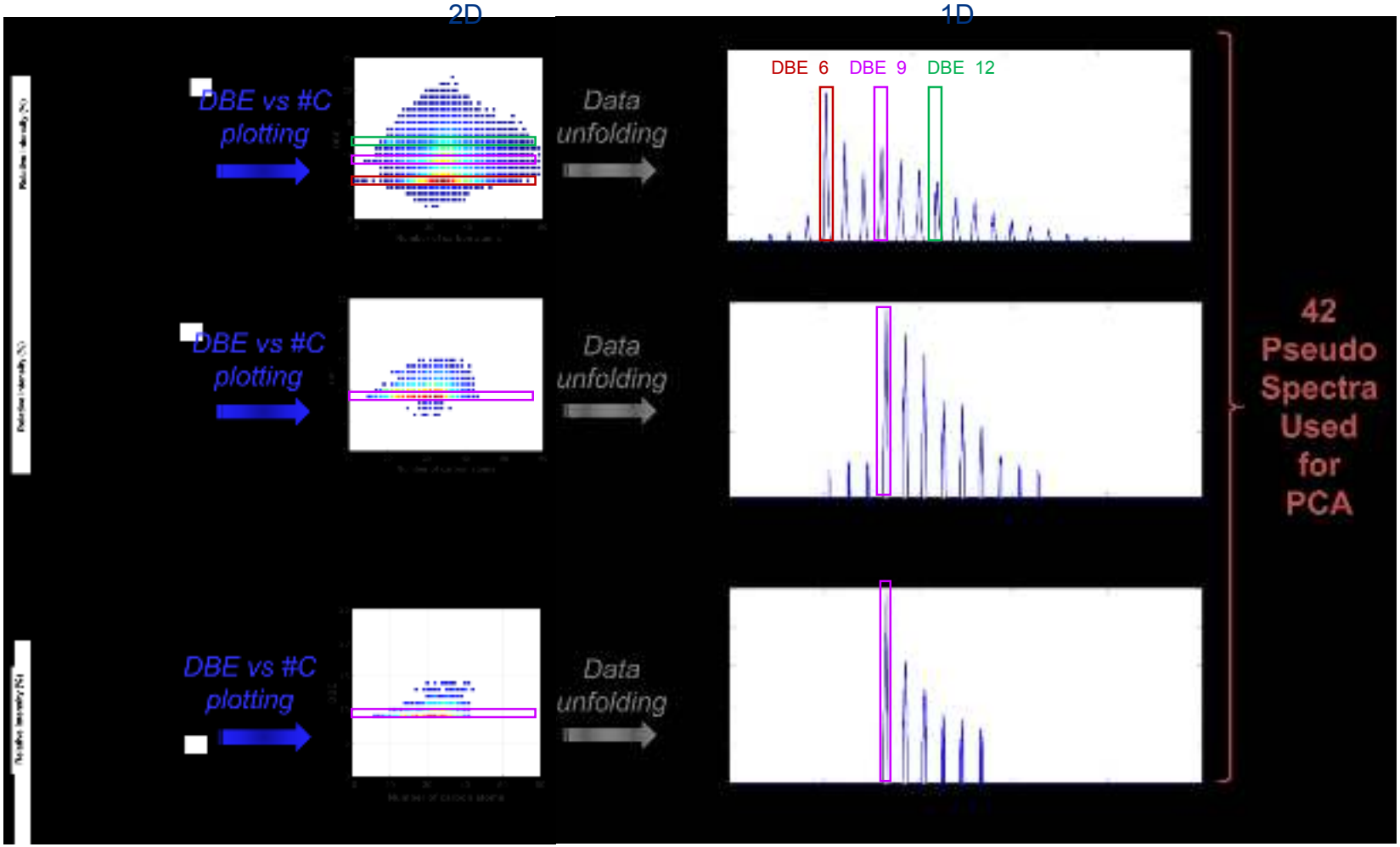

COMPARISON OF ALL SAMPLES

Score plot

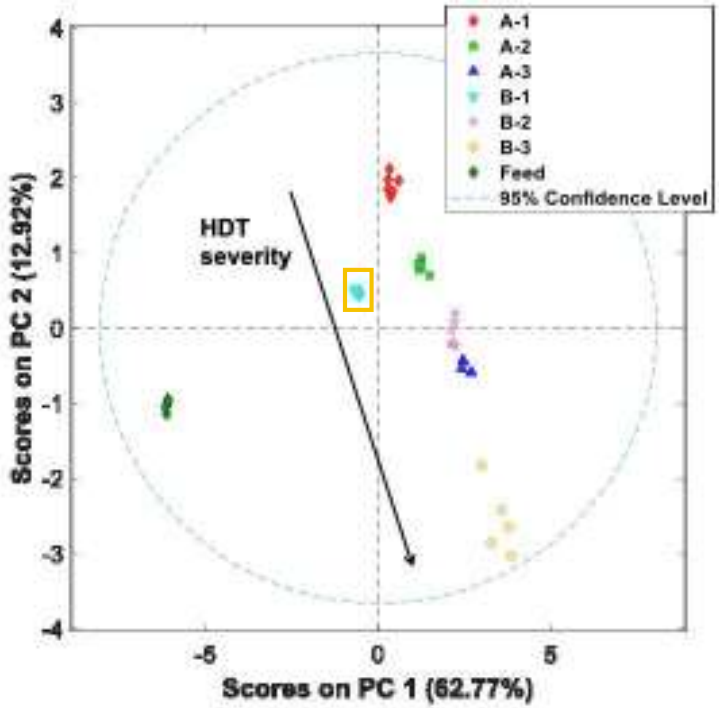

Loadings plots

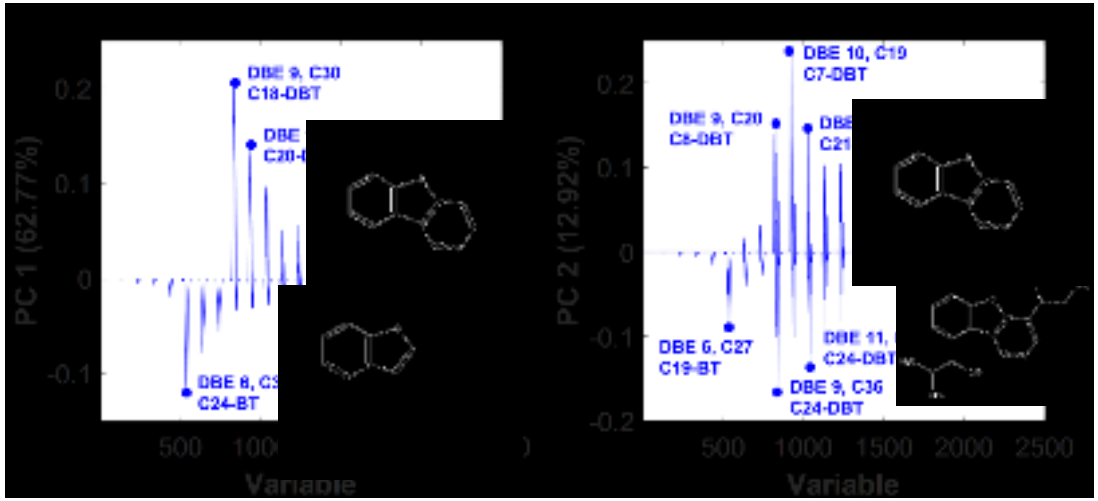

- Separation of the **feed from the effluents** on PC1: linked to BT and DBT contents
- Separation of the effluents depending on the **HDT severity** on PC2: more alkylated species at high HDS efficiency
- **Atypical** projection for sample B-1 compared to A-1 ?

COMPARISON OF ALL SAMPLES

Low temperature case: A-1 and B-1

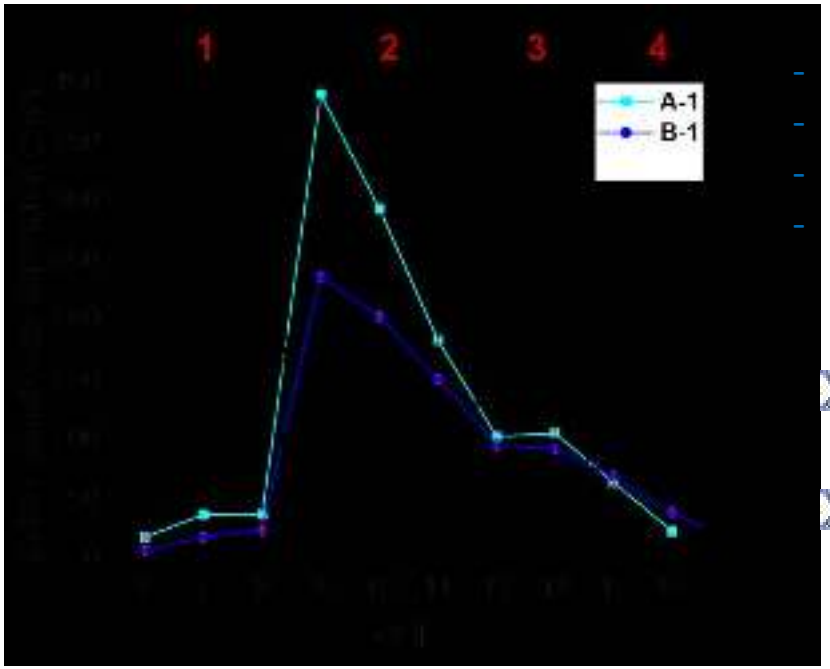

Activity of catalyst B is separated into **4 phases:**

- Phase 1: both catalysts A and B have similar activity
- Phase 2: catalyst B is by far more efficient than catalyst
- Phase 3: both catalysts A and B have similar activity
- Phase 4: catalyst A is slightly more efficient than catalyst B

Catalyst B is more selective towards DBT compounds (DBE 9-10-11)

Catalyst A is a little bit more selective towards very aromatic compounds (DBE >14)

Two possible hydrodesulfurization mechanisms ?

COMPARISON OF ALL SAMPLES

DBE 9 case:

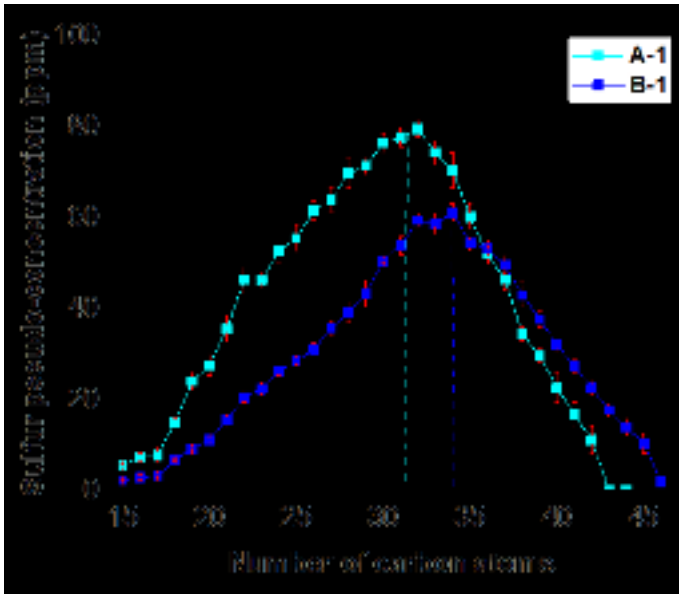

- DBT in sample A-1 are **less alkylated** than DBT in sample A-2
- Catalyst A: **change in alkylation level** compared to feed → catalyst A more efficient to remove very alkylated species
- Catalyst B: **no change in alkylation level** compared to feed → catalyst B more efficient to remove less alkylated species

Two possible hydrodesulfurization mechanisms ?

CONCLUSIONS AND PERSPECTIVES

Global comparison

- FT-ICR MS is a very powerful tool to **monitor the hydrodesulfurization mechanism**
- The effects of **temperature** and **catalyst** over the global HDS efficiency were studied
- The main **refractory** compounds were identified: **dibenzothiophenes** family

Aromaticity

- The DBT with a **DBE equal to 9** were shown to be the **most refractory** compounds
- At the lowest HDS severity, both catalysts were shown to present **different selectivity**

Alkylation

- The carbon atoms distribution of the DBE 9 compounds was relatively large (**C15-C42**)
- The hydrogenation of poorly alkylated species was **slower at low temperature**
- At the lowest HDS severity, both catalysts were shown to present **different selectivity**

→ **Perspectives: ion mobility analysis to identify the most refractory isomers, DBT ?**

Thank you!

- **PhD supervisors:** Alexandra Berlioz-Barbier, Florian Albrieux, Luis Pereira de Oliveira, Marion Lacoue-Nègre, Jean-François Joly, Ludovic Duponchel and Jérémie Ponthus
- **IFPEN MS team**
- **Brice Bouyssiere**
- **EU FT-ICR MS committee**

Thank you for your attention !

@ julie.guillemant@univ-pau.fr

EU FT-ICR MS

This project has received funding from the European Union's Horizon 2020 research and innovation programme under grant agreement No 731077.

Untargeted metabolomic profiling of Goji berries and leaves (Lycium barbarum L.) by FT-ICR MS

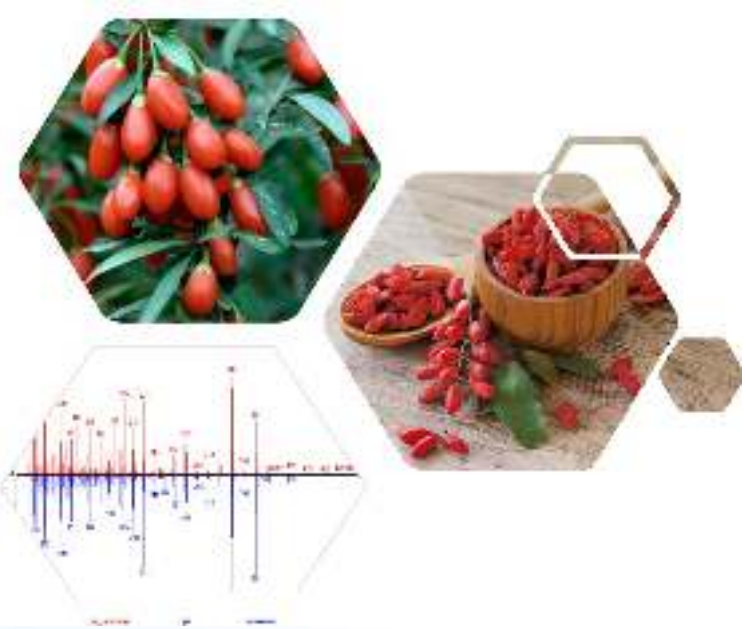

Alessandro Maccelli, Alba Lasalvia, Cinzia Ingallina, Luisa Mannina and Maria Elisa Crestoni

The super fruit: Goji berries

Goji berry (*Lycium* species) have gained enormously importance in western world becoming one of the *"superfood"* due to their beneficial properties for health or well-being.

Choose of samples

EU FT-ICR MS

Unripe

Ripe

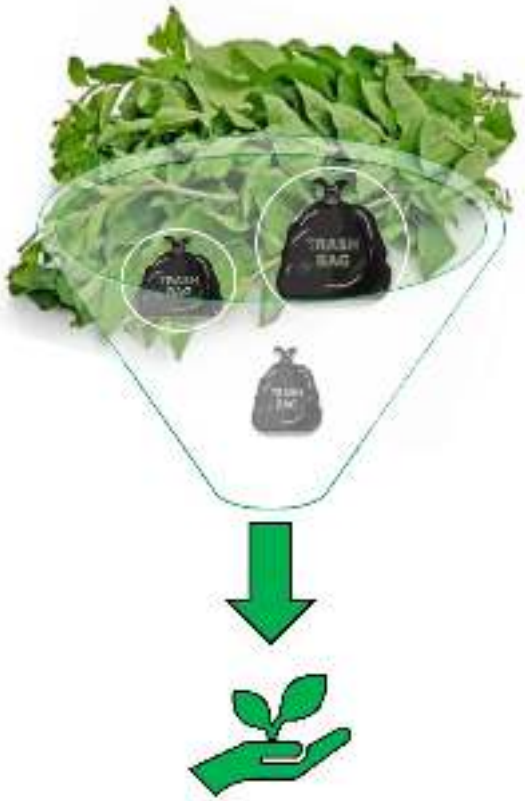

The high versatility of FT-ICR MS in metabolomics

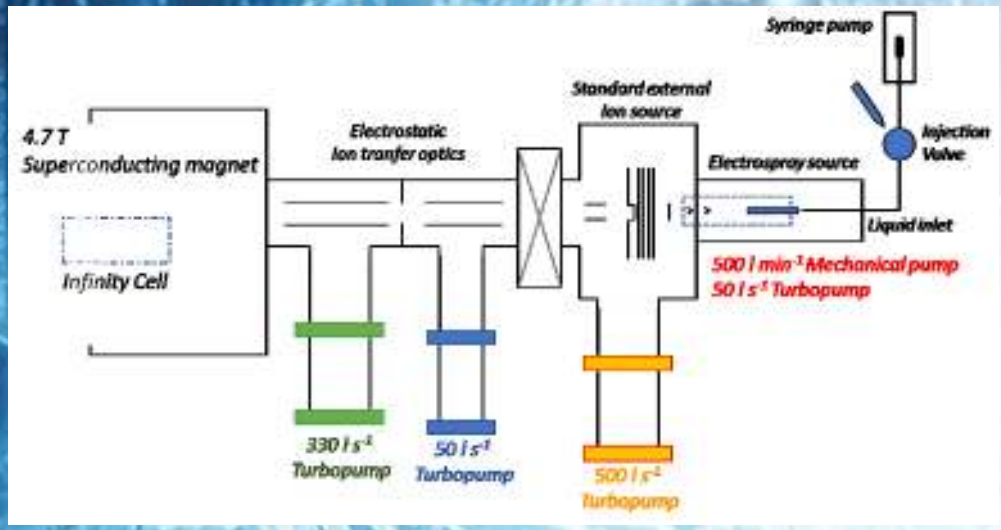

EU FT-ICR MS

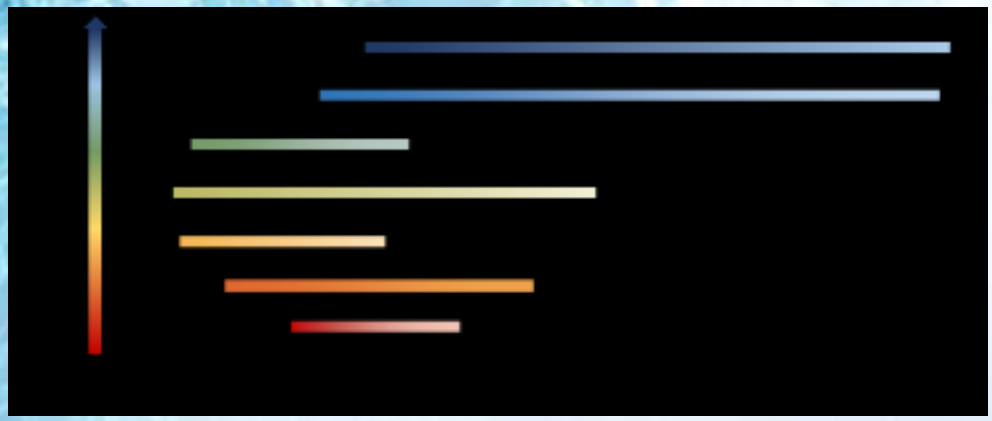

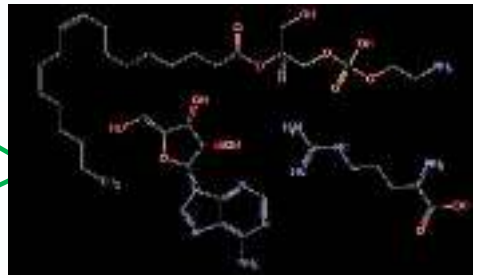

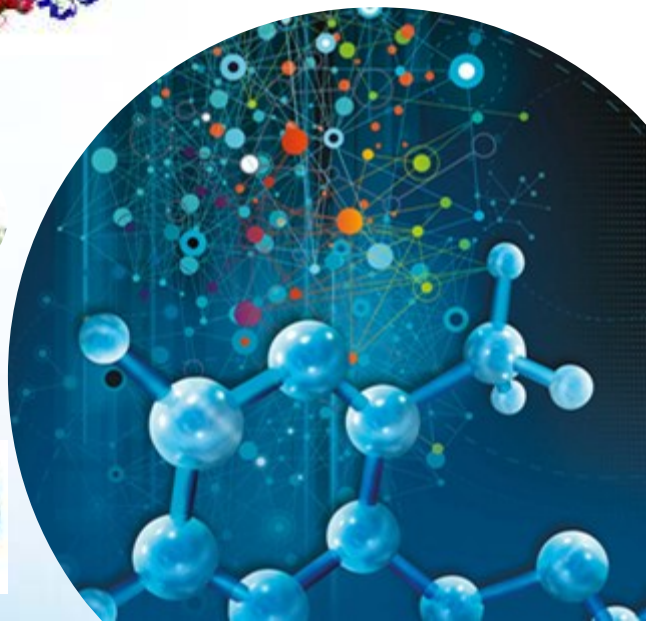

Analytical Workflow

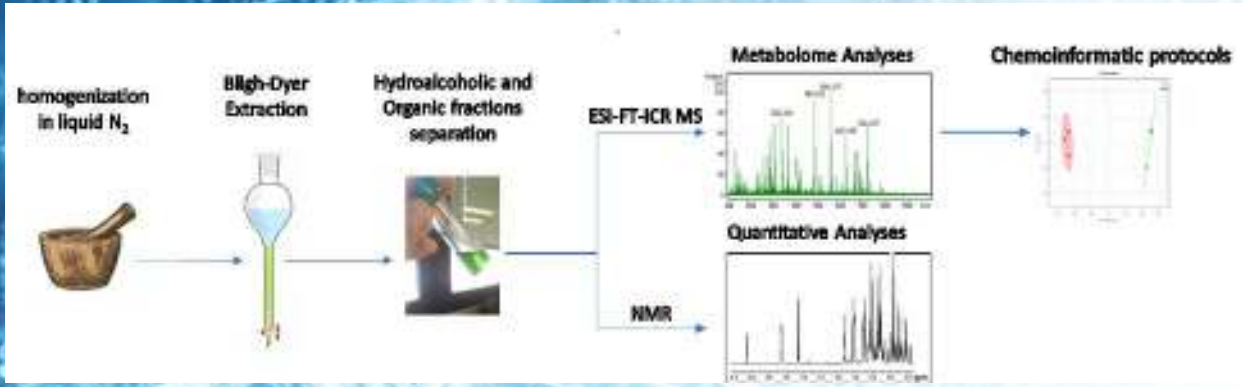

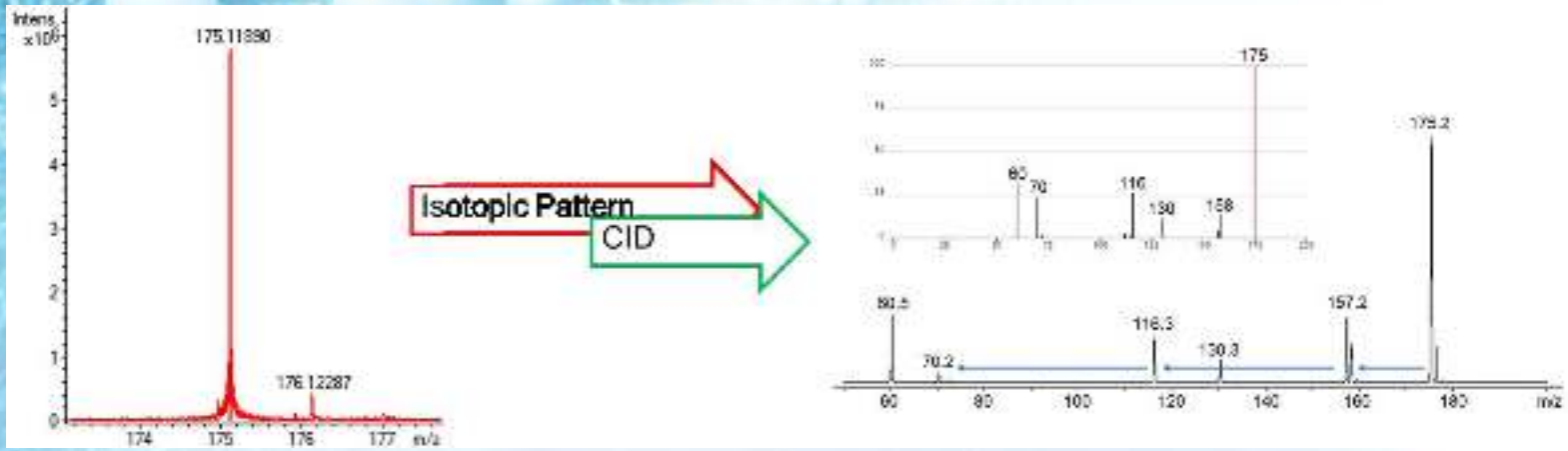

Qualitative composition of Goji berries

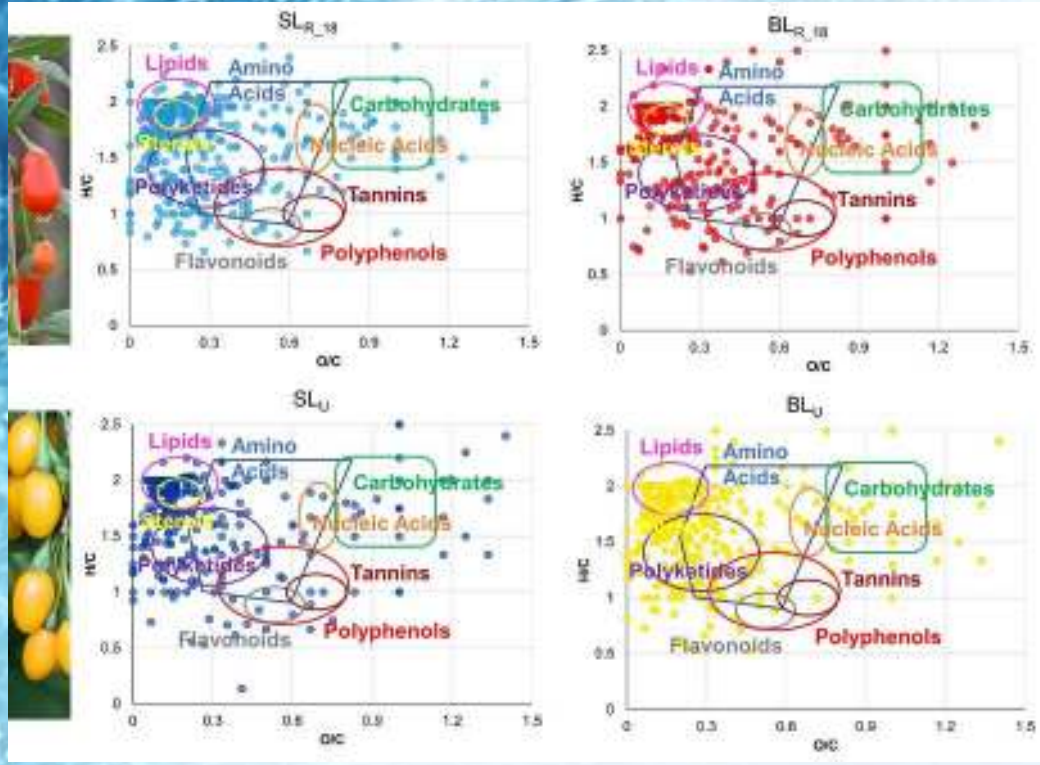

Extract	Hydroalcoholic[a]			Organic[b]		
	Ion Mode	Identified MF		Ion Mode	Identified MF	
BL_R_17	ESI(+)	119	219	ESI(+)	72	105
	ESI(-)	121		ESI(-)	38	
BL_R_18	ESI(+)	93	191	ESI(+)	55	110
	ESI(-)	115		ESI(-)	66	
BL_U_18	ESI(+)	212	243	ESI(+)	77	117
	ESI(-)	74		ESI(-)	48	
BL_{LF}_18	ESI(+)	116	161	ESI(+)	74	127
	ESI(-)	65		ESI(-)	62	
SR_R_17	ESI(+)	93	138	ESI(+)	112	170
	ESI(-)	56		ESI(-)	99	
SR_R_18	ESI(+)	168	273	ESI(+)	115	150
	ESI(-)	117		ESI(-)	40	
SR_U_18	ESI(+)	90	159	ESI(+)	104	144
	ESI(-)	83		ESI(-)	53	
Leaves	ESI(+)	286	364	ESI(+)	202	244
	ESI(-)	100		ESI(-)	84	

[a] Investigated by means of ESI FT-ICR MS.

[b] Investigated by means of ESI ion trap MS.

Qualitative composition of Goji berries

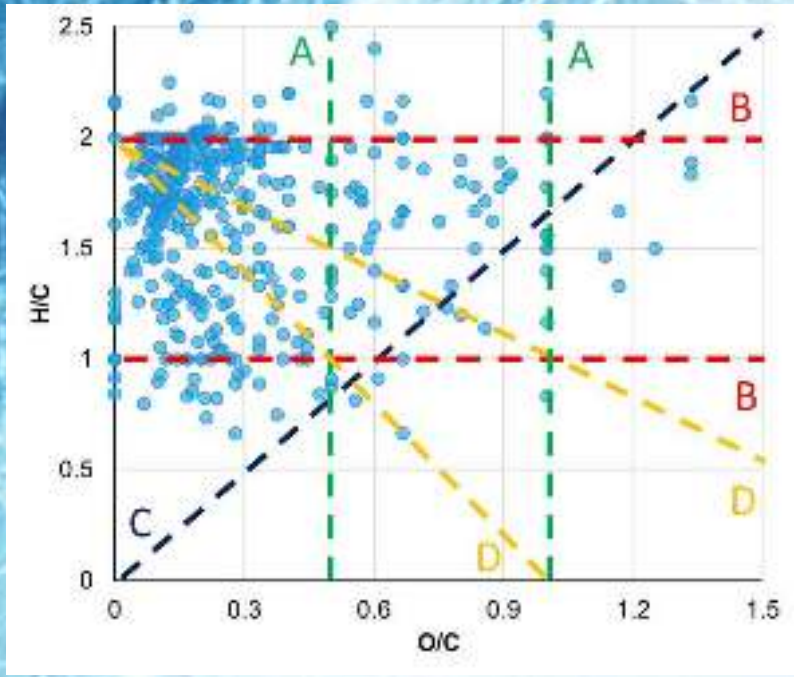

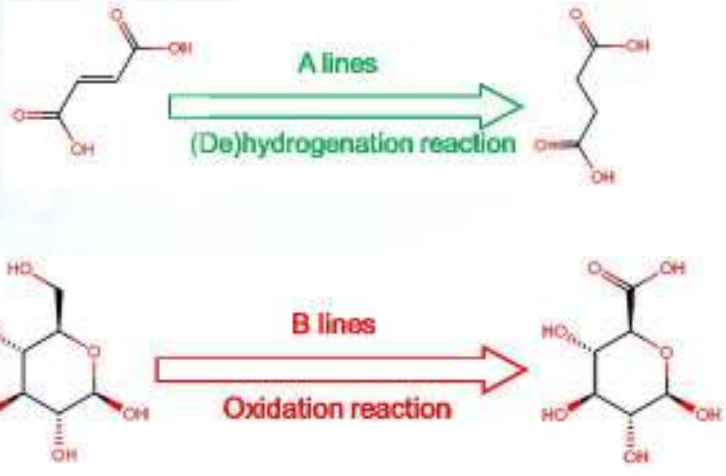

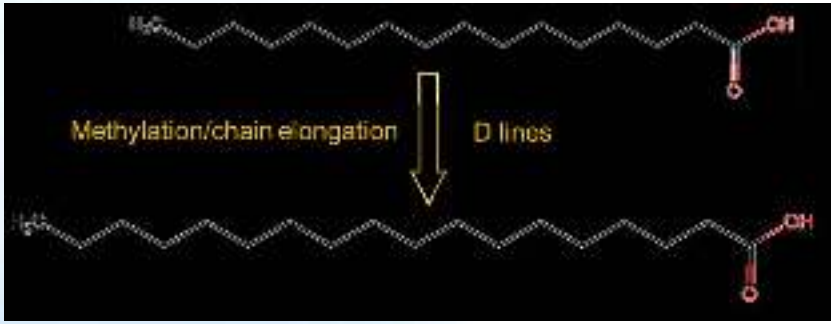

Clusterization of results

EU FT-ICR MS

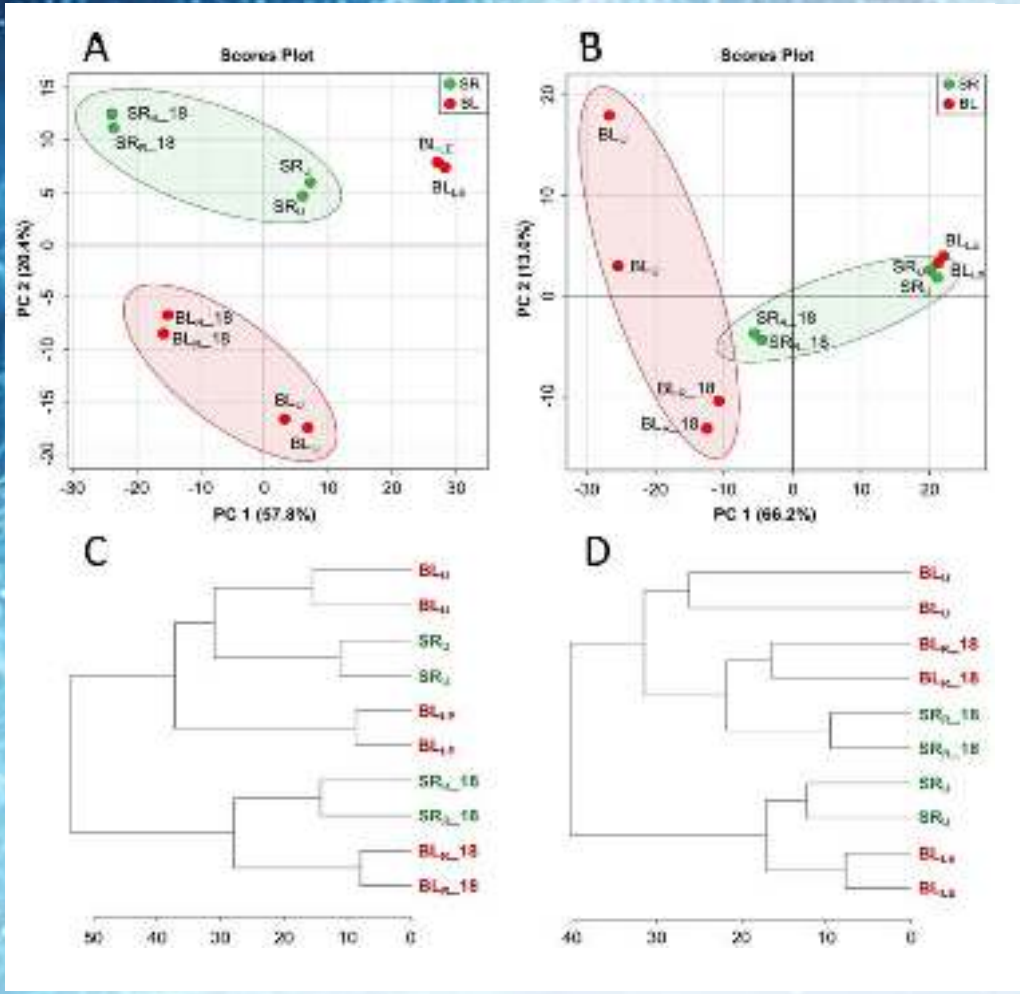

Effect of ripeness

i)

ii)

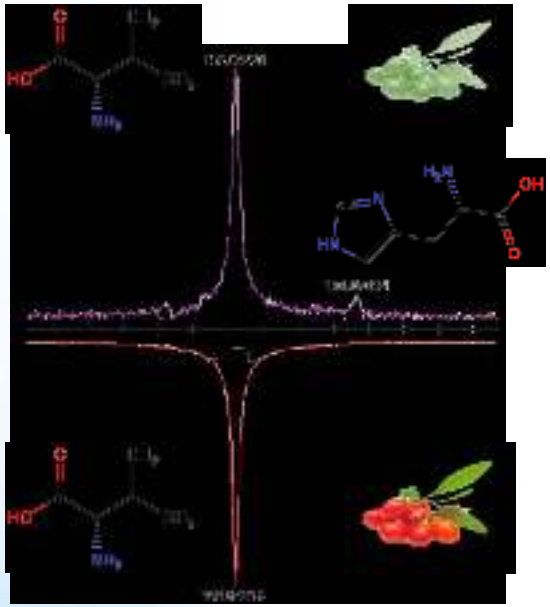

… and finally, leaves!!!!

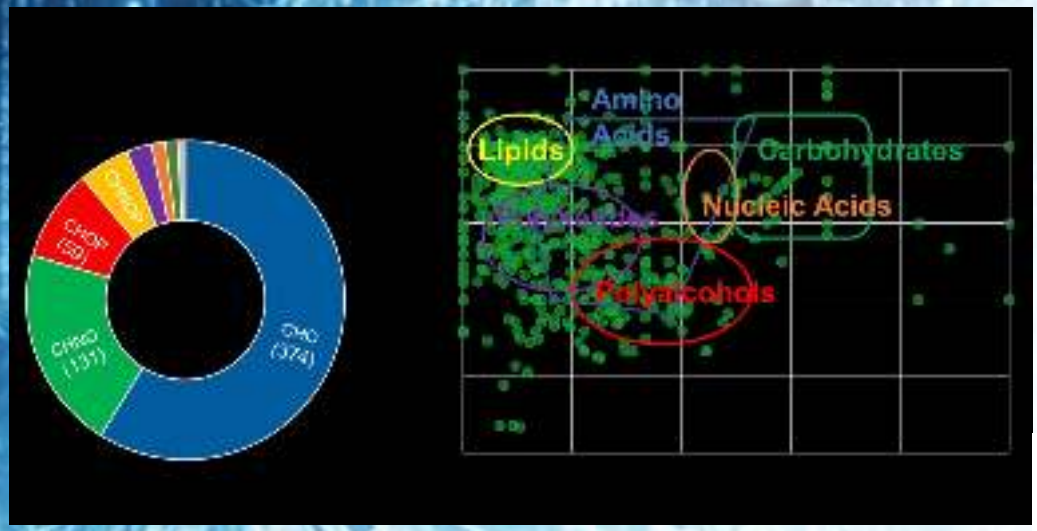

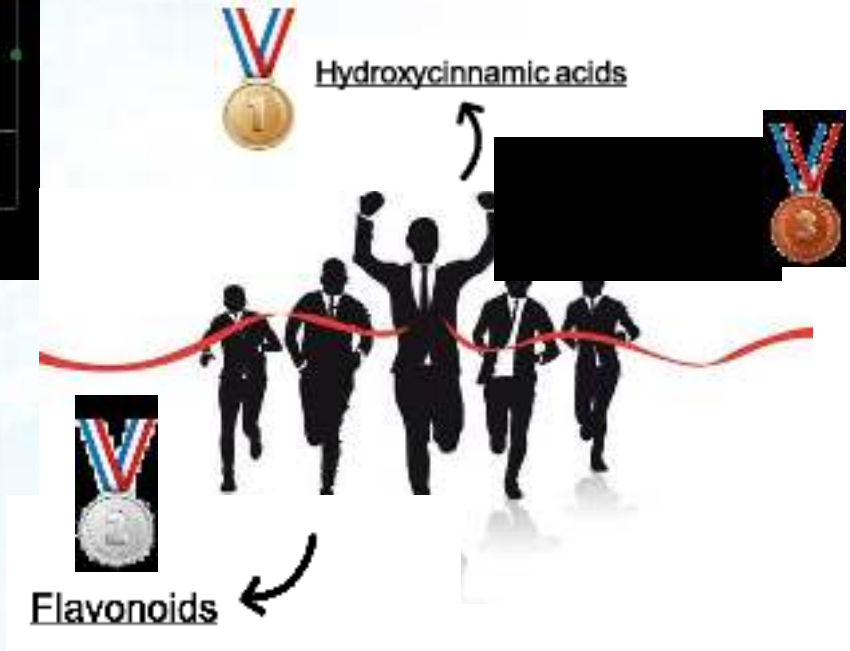

Polyalcohols

- [redacted] Radical scavenging
- [redacted] UV protective
- [redacted] Anti-inflammatory

Conclusion

EU FT-ICR MS

molecules MDPI

Article

Metabolomic Profiling of Fresh Goji (*Lycium barbarum* L.) Berries from Two Cultivars Grown in Central Italy: A Multi-Methodological Approach

Mattia Spano [1,†], Alessandro Maccelli [1,†], Giacomo Di Matteo [1], Cinzia Ingallina [1], Mariangela Biava [1], Maria Elisa Crestoni [1,*], Jean-Xavier Bardaud [2], Anna Maria Giusti [3], Alessia Mariano [4], Anna Scotto D'Abusco [4], Anatoly P. Sobolev [5,*], Alba Lasalvia [1], Simonetta Fornarini [1] and Luisa Mannina [1]

Molecules 2021, 26, 5412. https://doi.org/10.3390/molecules26175412

Don't forget to read our last article!!!

- ESI FT-ICR MS has been exploited offering a fast, sensitive, and reproducible assay without the usage of any chromatographic method.
- The obtained results confirmed the rich composition in bioactive compounds (carotenoids, polyphenols, etc.) of Goji berries who give them beneficial properties for health or well-being.
- The study highlights the presence of antioxidant compounds in Goji leaves making them a promising source in the pharmaceutical, food, and cosmetic fields.

Acknowledgement

EU FT-ICR MS

SAPIENZA
UNIVERSITÀ DI ROMA

Dipartimento di Chimica e Tecnologie del Farmaco

Prof. Maria Elisa Crestoni

Prof. Simonetta Fornarini

Prof. Luisa Mannina

Dr. Davide Corinti

Alba Lasalvia

Valentina Lilla

...and thank you all for the attention!!!

This project has received funding from the European Union's Horizon 2020 research and innovation programme under grant agreement No 731077.

ANALYSIS OF SOLID AND LIQUID SAMPLES IN THE CONTEXT OF SWIM USING LDI FT-ICR MS

EU_FT-ICR_MS – 2nd Advanced User School

NATHANIEL TERRA TELLES SOUZA [a,b,e], Leticia M. Ligiero [b,e], Nicolas Agenet [b], Marie Hubert-Roux [c,e], Carlos Afonso [c,e], Ryan Rodgers [a,d,e]

[a] *Université de Pau et des Pays de L'Adour, IPREM*
[b] *Pôle d'Études et de Recherche de Lacq (PERL) - TotalEnergies*
[c] *Normandie Université, COBRA*
[d] *Florida State University, NHMFL*
[e] *International Joint Laboratory iC2MC : Complex Matrices Molecular Characterization*

Introduction

SMART water = low salinity water
(or water with a controlled composition)

SWIM effects: wettability changes and increase in oil recovery rate

Determining mechanism: unknown, despite the several proposed mechanisms found in literature

Need of a better characterization of organic species adsorbed onto the rock surface and their influence on wettability changes during SMART waterflooding

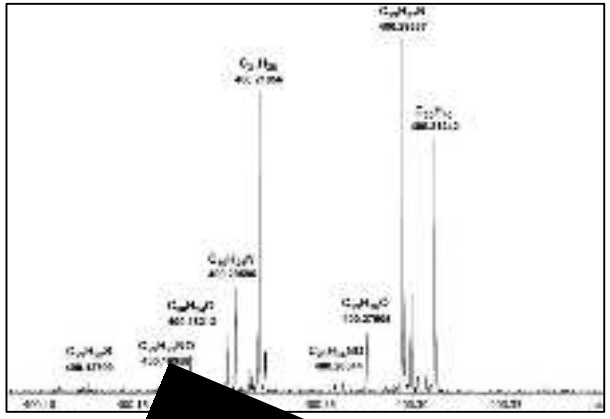

Intensity	m/z	Error (ppm)	Formula
2686100	400.12799	0.092	$C_{29}H_{20}S$
3966114	400.16958	0.022	$C_{29}H_{22}NO$
8365222	400.18213	0.083	$C_{30}H_{24}O$
23188654	400.20596	0.035	$C_{30}H_{26}N$
66491568	400.21856	0.019	$C_{31}H_{28}$

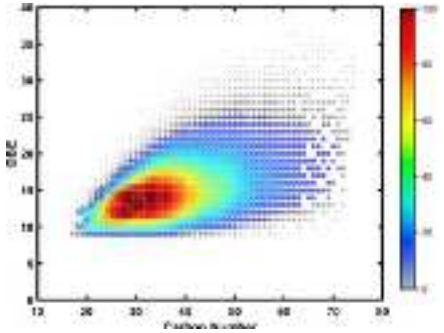

$$DBE = c - \frac{h}{2} + \frac{n}{2} + 1$$

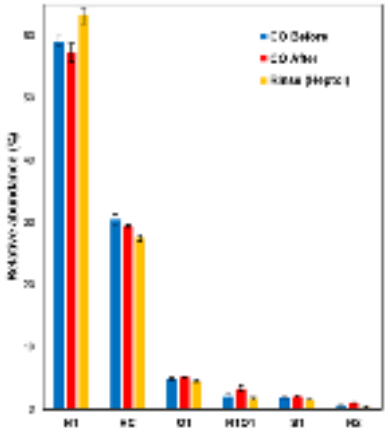

Experimental Methods

SWIM at lab scale

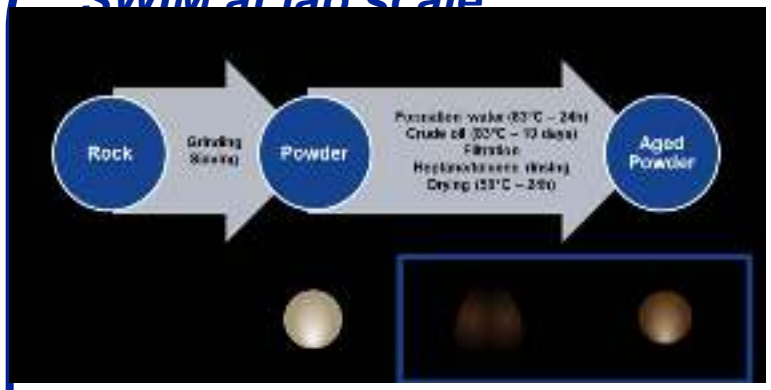

How to analyze (and to compare) crude oil and aged powder samples?

Laser Desorption Ionization (LDI)

Frequency-tripled Nd:YAG laser (355 nm)

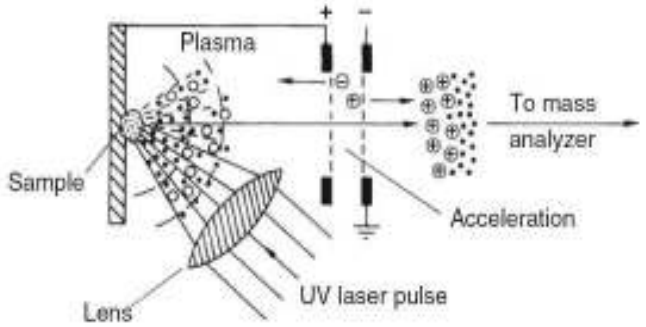

Mamyrin BA (1994) Laser Assisted Reflectron Time-of-Flight Mass Spectrometry. Int J Mass Spectrom Ion Proc 131:1–19. doi:10.1016/0168-1176(93)03891-O

Laser Power Optimization

- Ion production threshold
- Artifact formation and fragmentation

Solid samples require higher laser power

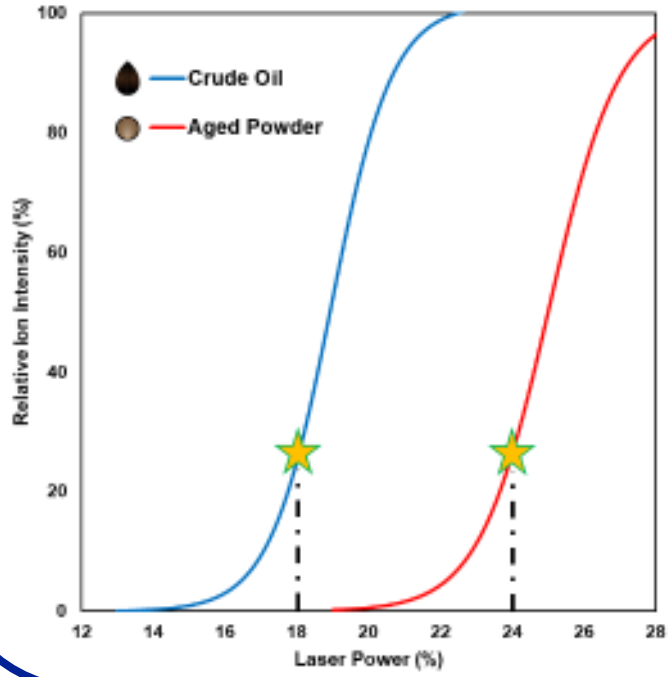

Sample deposit on the target

- Dry droplet method for crude oil samples
- Powder samples deposited with the help of a pestle

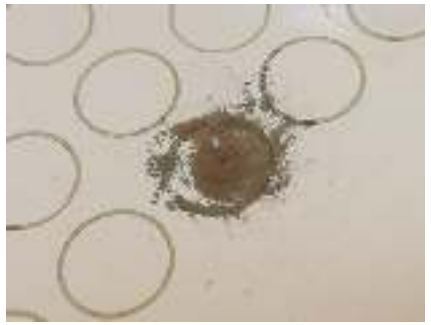

(+) LDI FT-ICR MS

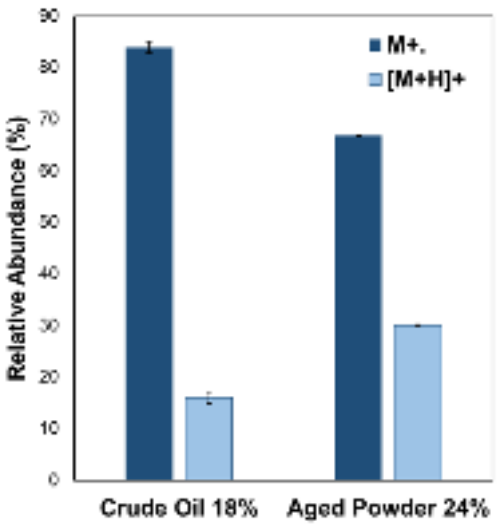

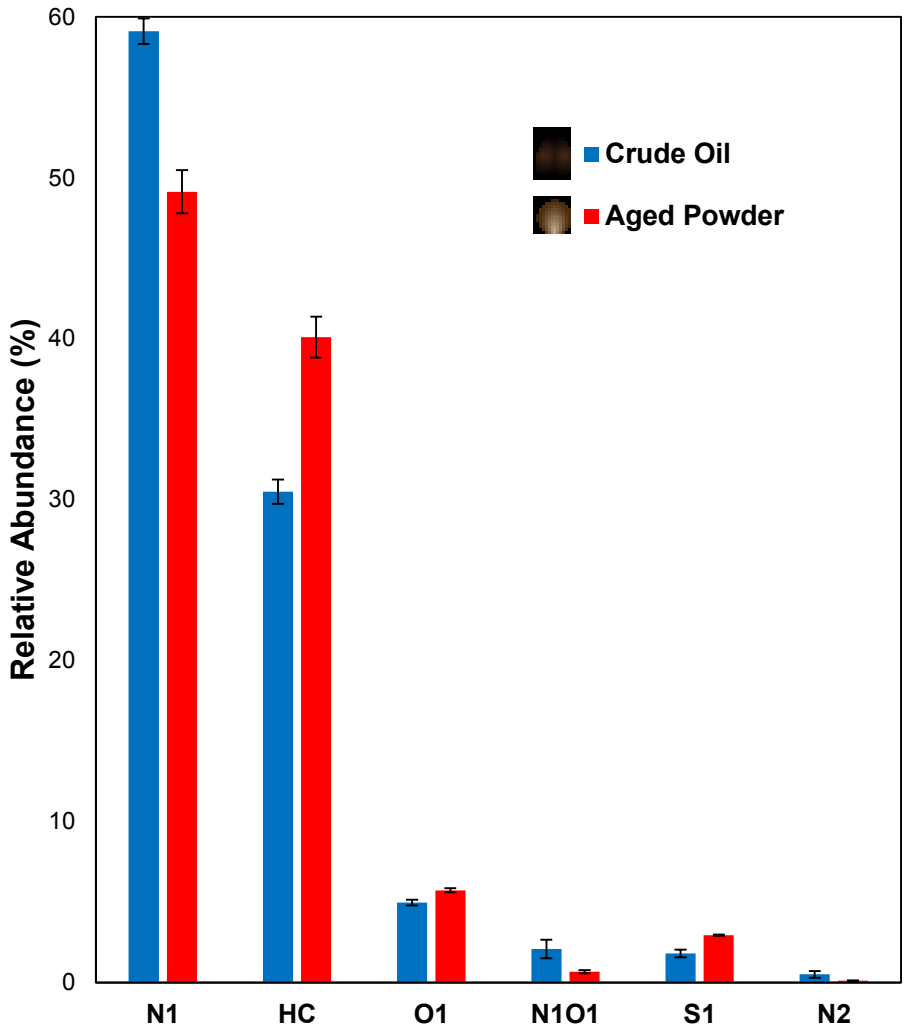

- Odd-electron ions are dominant in positive mode
- Higher laser power (24%) increase the formation of even-electron ions
- N1 and HC classes represent ~ 90% of the detected ions
- Decrease of N1 for aged powder

(+) LDI FT-ICR MS – DBE vs C#

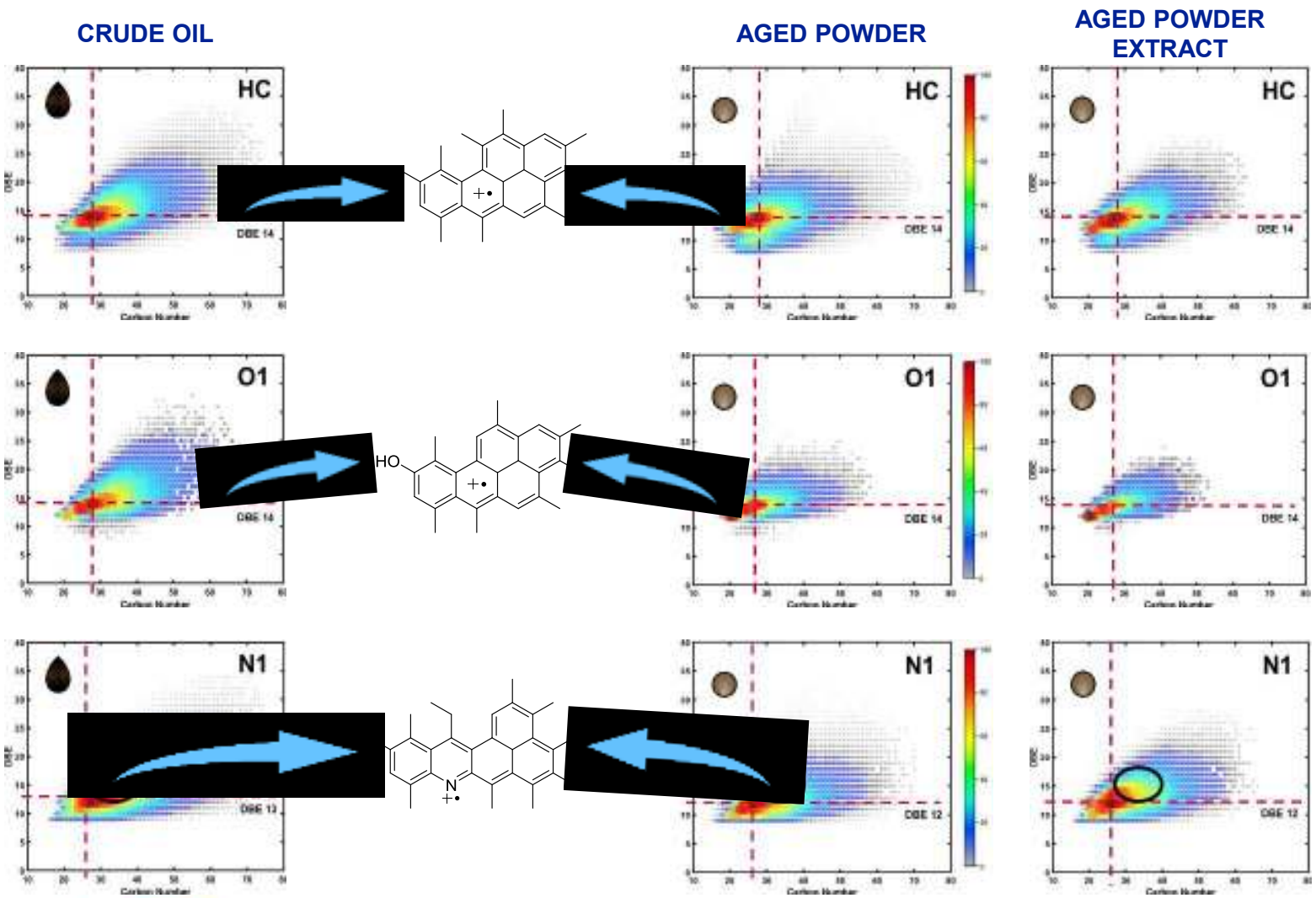

- No significant differences are observed between crude oil and aged powder for HC and O1 species. Same thing happens to even-electron ions
- Depletion of high DBE N1 species is observed in aged powder
- Direct and indirect (solvent extract) analysis of aged powder present similar results

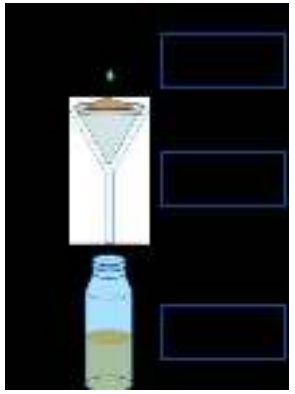

(-) LDI FT-ICR MS

No signal was obtained durin the direct analysis of so samples in (-) LDI

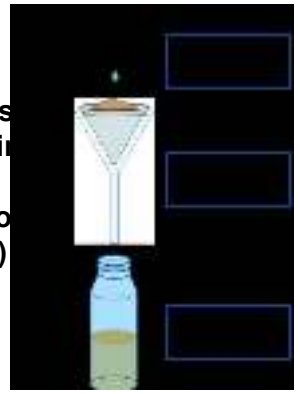

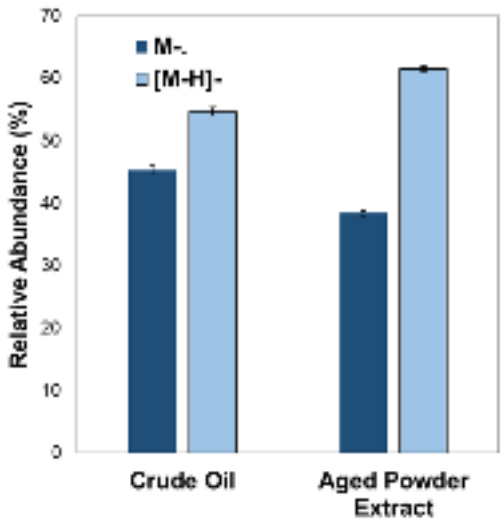

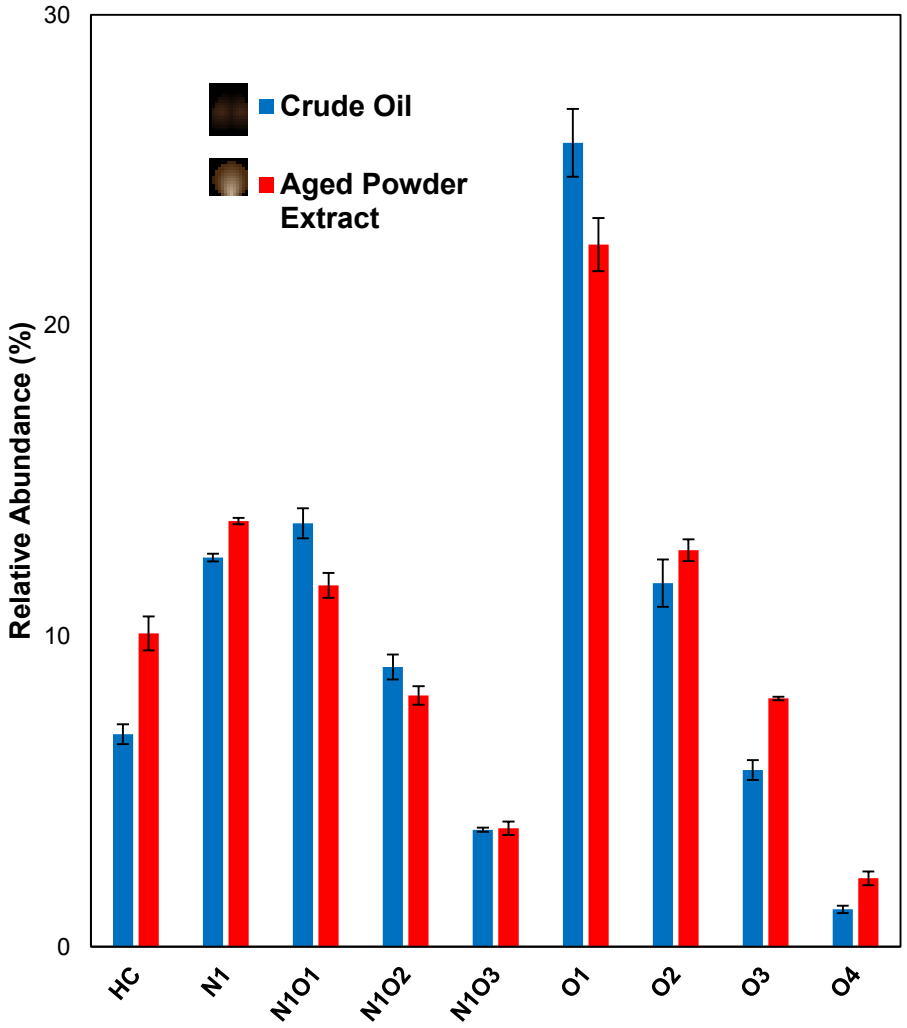

- Even-electron (deprotonated) ions are dominant in negative mode
- Bigger diversity of chemical classes than in positive mode
- Aged powder extract enriched with HC, N1, O3 and O4 compounds

(-) LDI FT-ICR MS – DBE vs C#

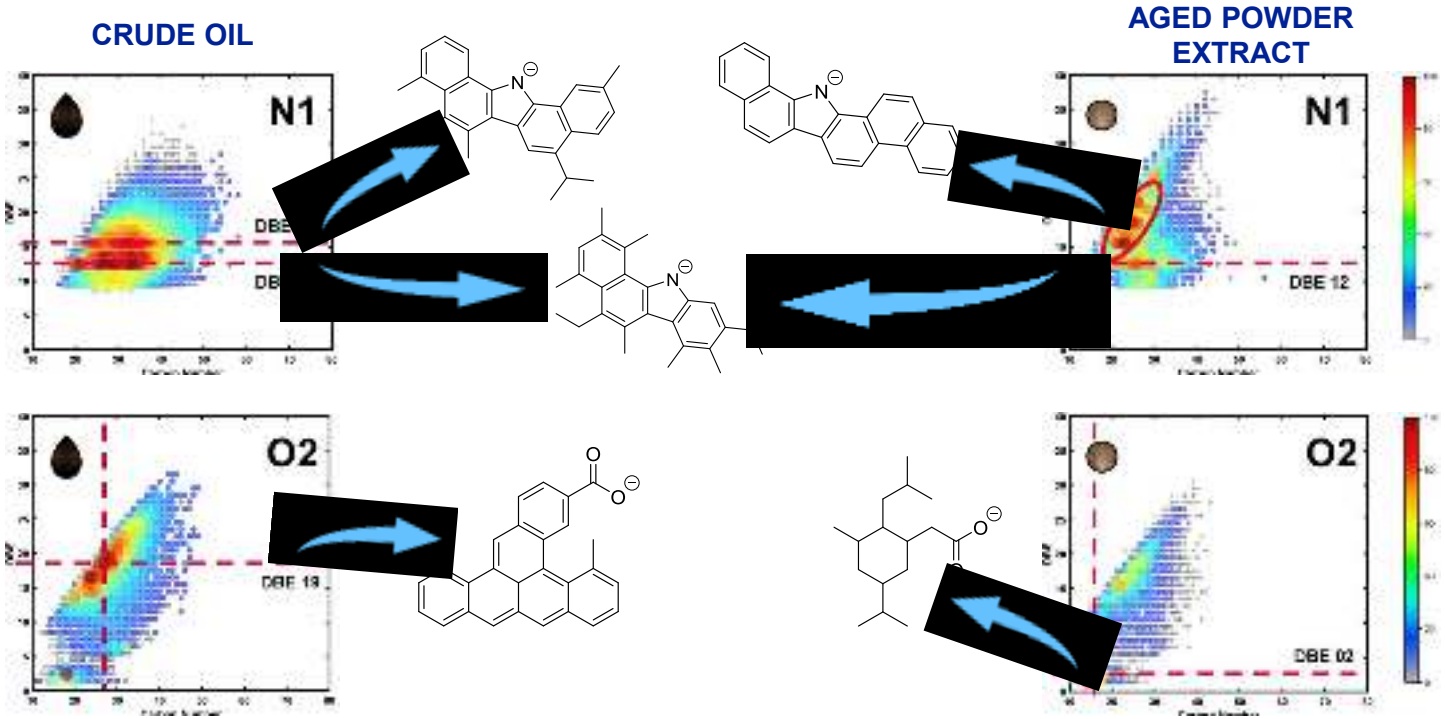

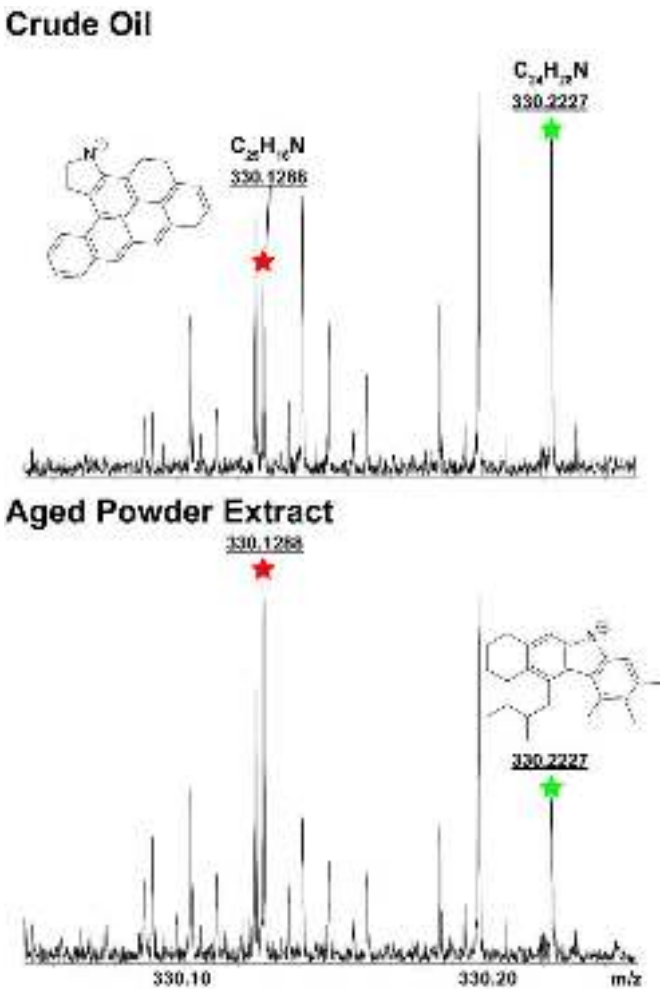

- Decrease of bigger N1 ions (bigger C#)
- Decrease of highly aromatic carboxylic acids

Conclusions

- Solid samples demand higher laser power for ionization to happen in positive mode, because the organic species are adsorbed and maybe chemically bound to the powder surface
- Direct and indirect (solvent extract) analysis of aged powder present very similar results in positive mode
- (-) LDI detects a bigger number of chemical classes than (+) LDI
- Aged powder extract is enriched with acidic N1 species with high DBE and small C#. Bigger molecules might remain adsorbed/bound to the powder surface

EU FT-ICR MS

TotalEnergies

iC2MC
INTERNATIONAL – COMPLEX MATRICES MOLECULAR CHARACTERIZATION

IPREM

Cobra
Chimie organique, Bioorganique, Réactivité et Analyse.

Thank you

This project has received funding from the European Union's Horizon 2020 research and innovation program under grant agreement No 731077.

Tuesday

Structural Proteomics – From protein stable covalent labeling to chemical cross-linking

Petr Novák

2nd Advanced User School

Institute of Microbiology, Czech Republic, September 28th, 2021

Six Blind Men and the Protein of Unknown Structure

"It was six men of Indostan
To learning much inclined,
Who went to see the Elephant
(Though all of them were blind)
That each by observation
Might satisfy his mind..."
John Godfrey Saxe
(1816-1887)

Structural Mass Spectrometry…

Protein covalent labeling

Chemical cross-linking

H/D exchange

Disulfide bonds mapping

Native mass spectrometry and Ion mobility

Fast photochemical oxidation of proteins

ETD/ECD fragmentation

Limited proteolysis

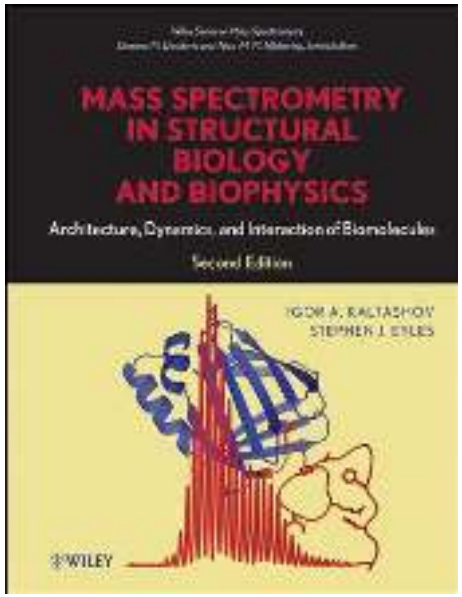

Special Issue on Mass Spectrometry in Structural Biology (2015) Protein Science *24*, 1173-1332

Mass Spectrometry: Goal in Protein Structure Characterization

EU FT-ICR MS

Bottom-Up

Protein sample

↑

Purification of Monomer (Gel, Size Exclusion Column)

↑

Digest

↑

Mass Measurement of Peptides

↑

Data Analysis, Identify modified fragments, put it all back together

Top-Down

Protein sample

↓

Sample Cleanup (Protein Trap)

↓

Gas-Phase "Purification" of crosslinked species

↓

Gas-Phase "Digest", CID, IRMPD, ECD

↓

Data Analysis, Identify fragments containing modification, put it all back together

Footprinting

Assay examining higher structures of biomacromolecules by monitoring solvent accessibility of their regions

- Single molecule conformation / Conformational changes
- Ligand binding / biomacromolecular interactions

Different techniques

- Enzymatic / chemical cleavage
- Covalent labeling

Covalent labeling

- Hydrogen-deuterium Exchange
- Stable covalent labeling – Chemical or Radical footprinting and cross-linking

Enzymatic cleavage – Limited proteolysis

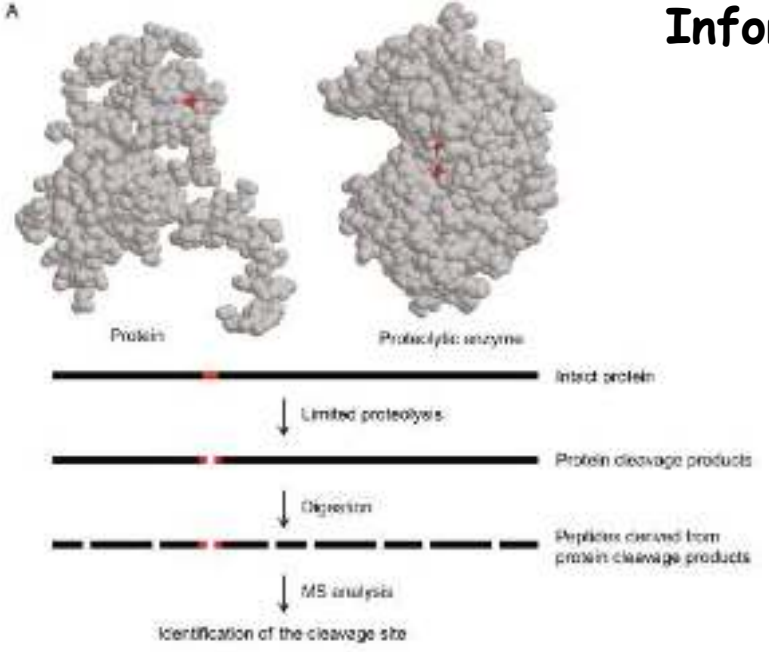

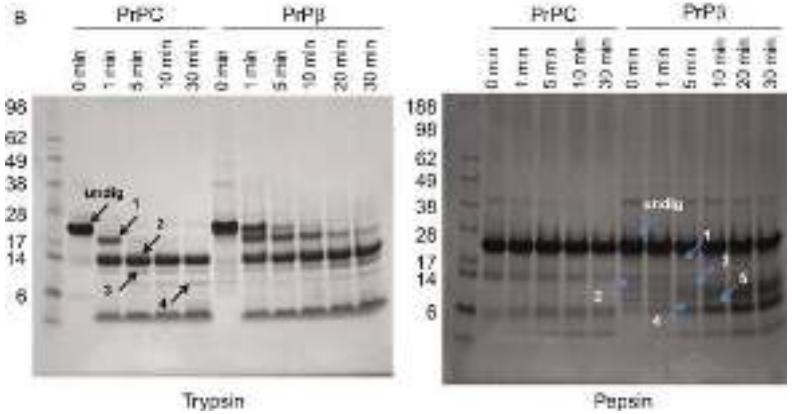

Information about the surface accessible area

Several available proteases

Native conditions

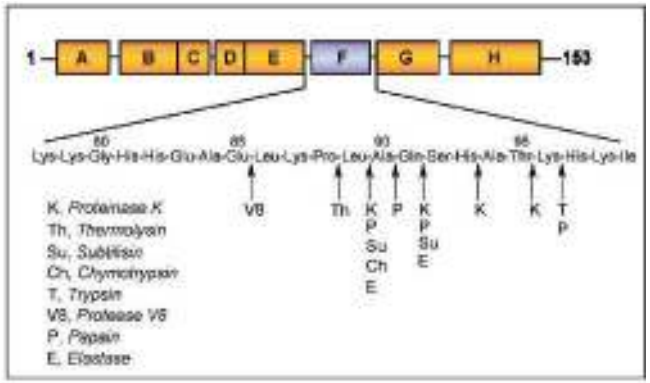

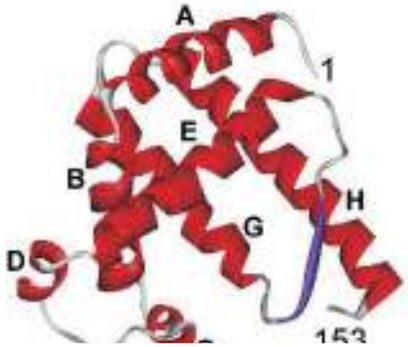

Limited proteolysis – identification of fragments ("Top down")

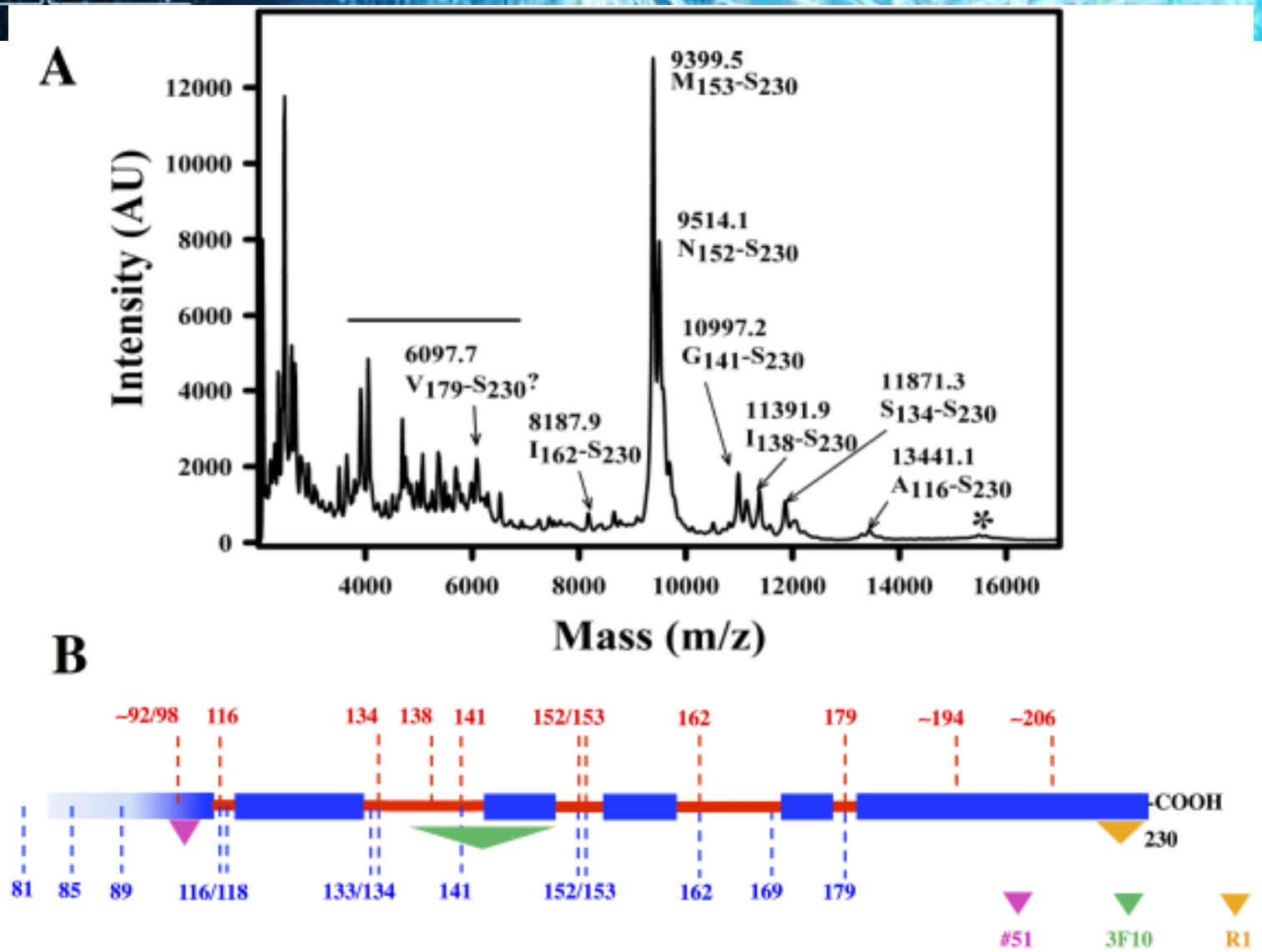

Limited proteolysis – identification of fragments ("Bottom up")

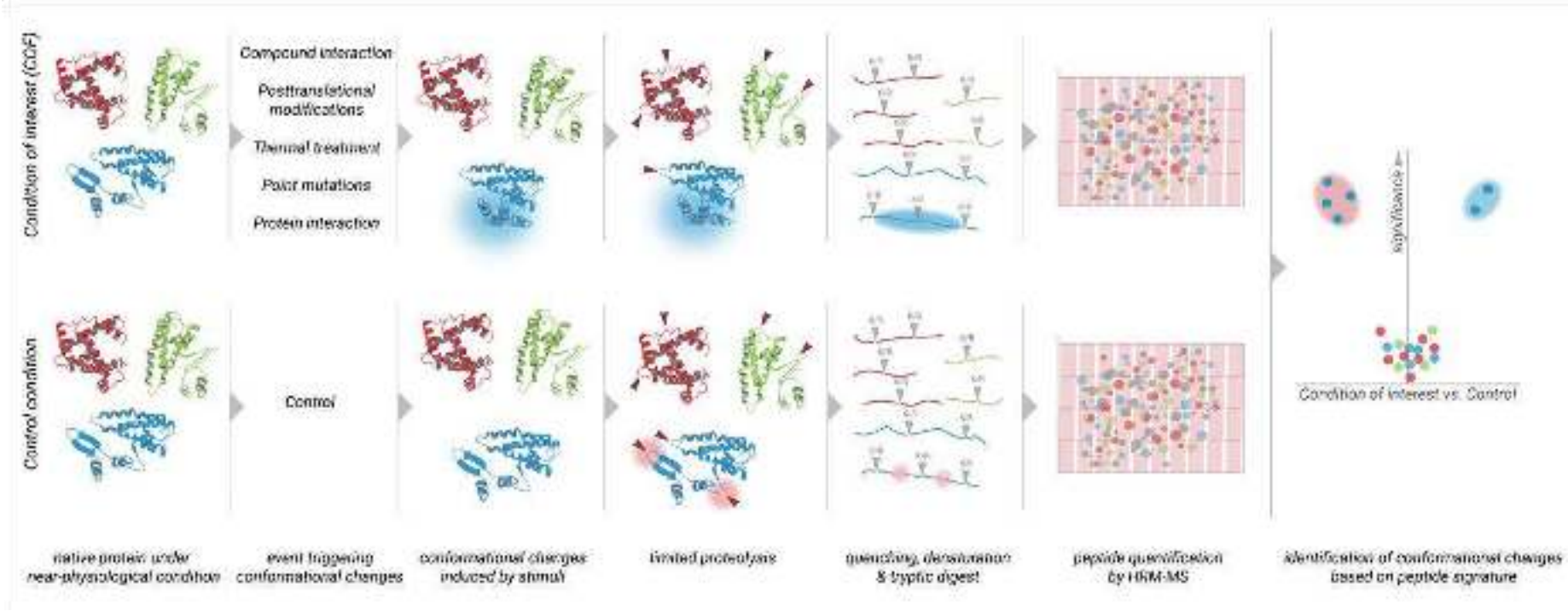

Schopper S, Kahraman A, Leuenberger P, et al. Measuring protein structural changes on a proteome-wide scale using limited proteolysis-coupled mass spectrometry. Nat Protoc. 2017;12(11):2391-2410. doi:10.1038/nprot.2017.100

Limited proteolysis – identification of fragments ("Chip set up")

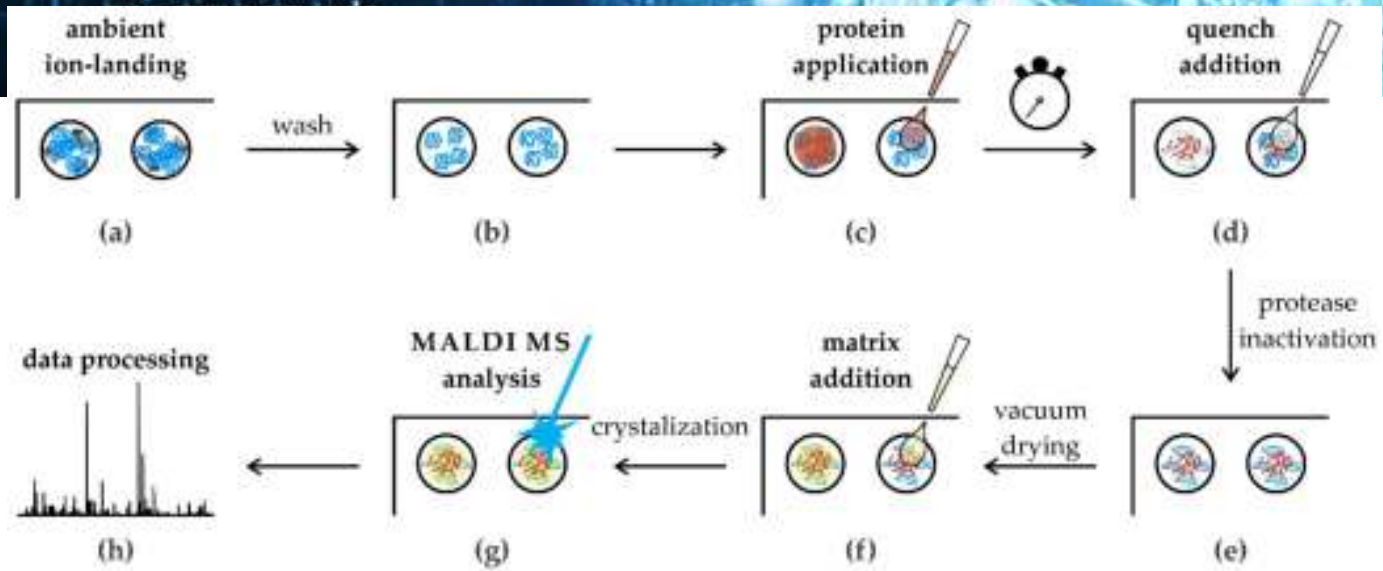

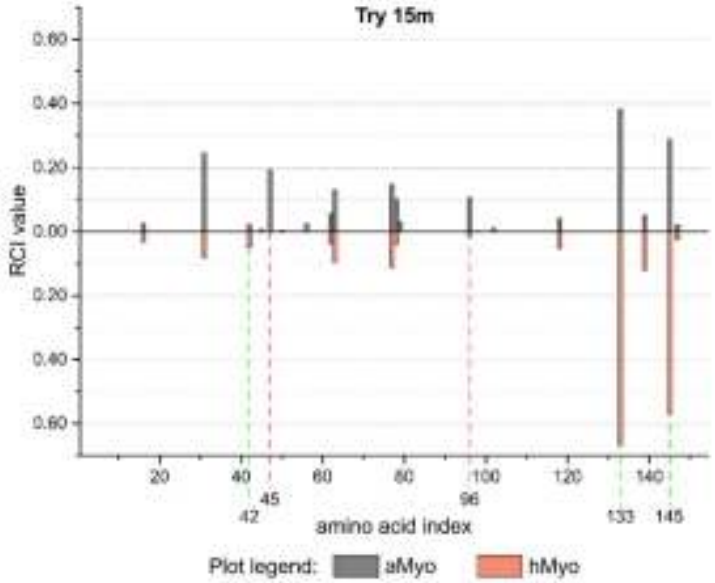

(a)

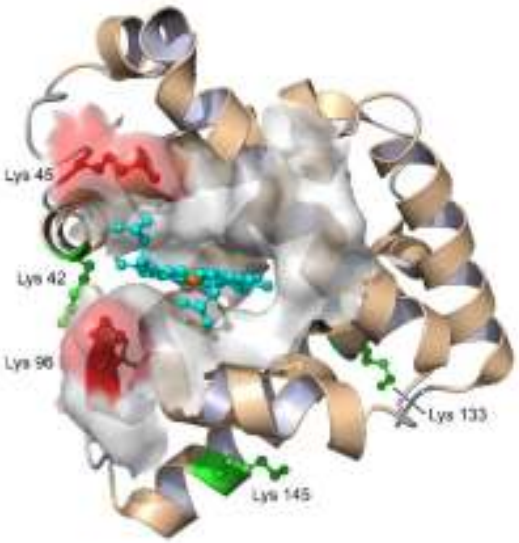

(b)

Protein covalent labeling and chemical cross-linking

EU FT-ICR MS

Available amino acid sidechains for covalent modification

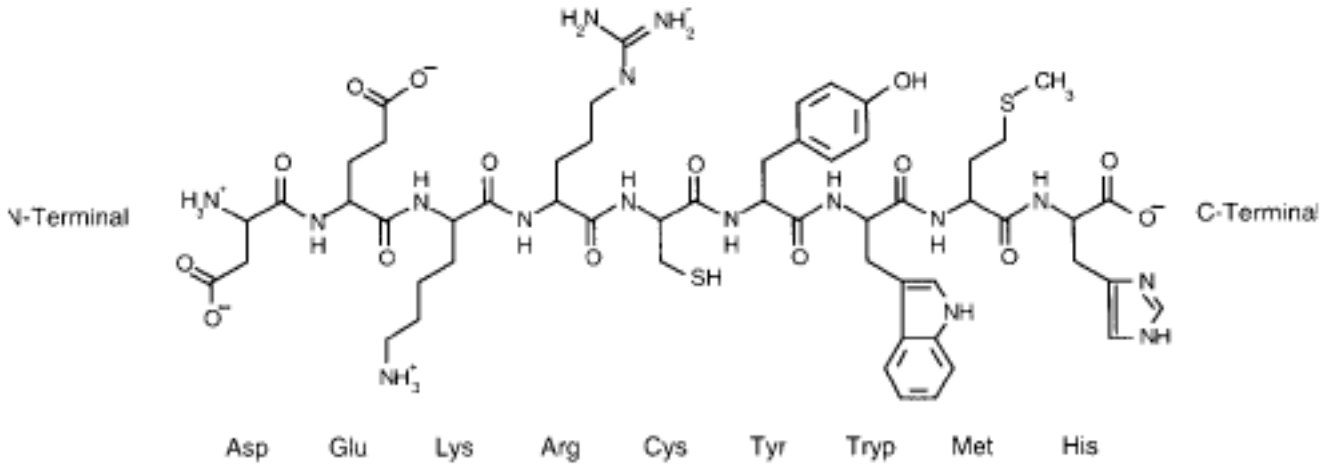

Carboxy groups – Asp, Glu, C-term, pKa (3.8, 4.3, 2.3) pH≥7 » deprotonation

Amino groups – Lys, Arg, His, N-term, pKa (9.4, 12, 6.8, 7.8) 7≥pH » protonation

Sulfhydryl groups - Cys . pKa 8.9 pH≥7 » -SH

Aromatic groups– Trp (indol), Tyr (hydroxyfenyl, pKa 9.9)

~ 23% of amino acid can be covalently modified

Klapper et. al. Biochem. Biophys. Res. Commun. 1977, 78, 1018.

Covalent modification of amino acid side chains

Acetylation
(N-hydroxysuccinimide esters)

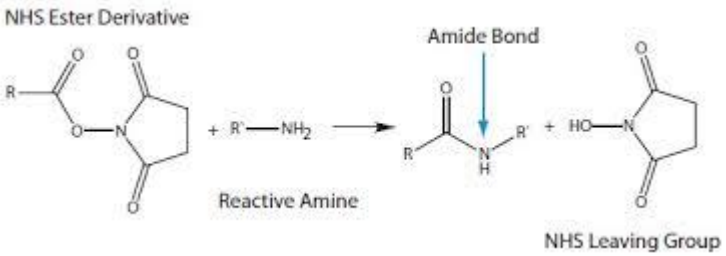

Acetylation
(Anhydrides)

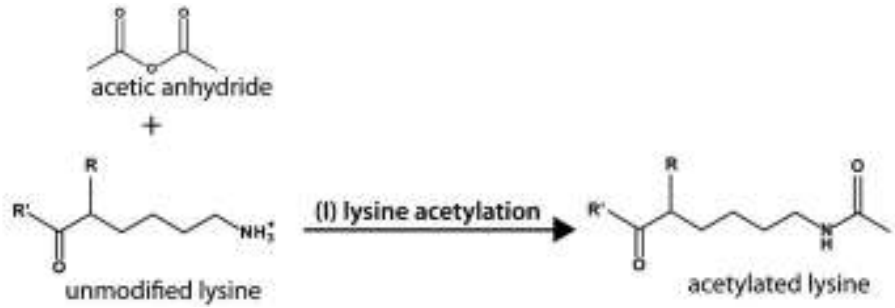

Modification of carboxylic acids
(1-Ethyl-3-(3-dimethylaminopropyl) carbodiimide and glycine ethyl ester)

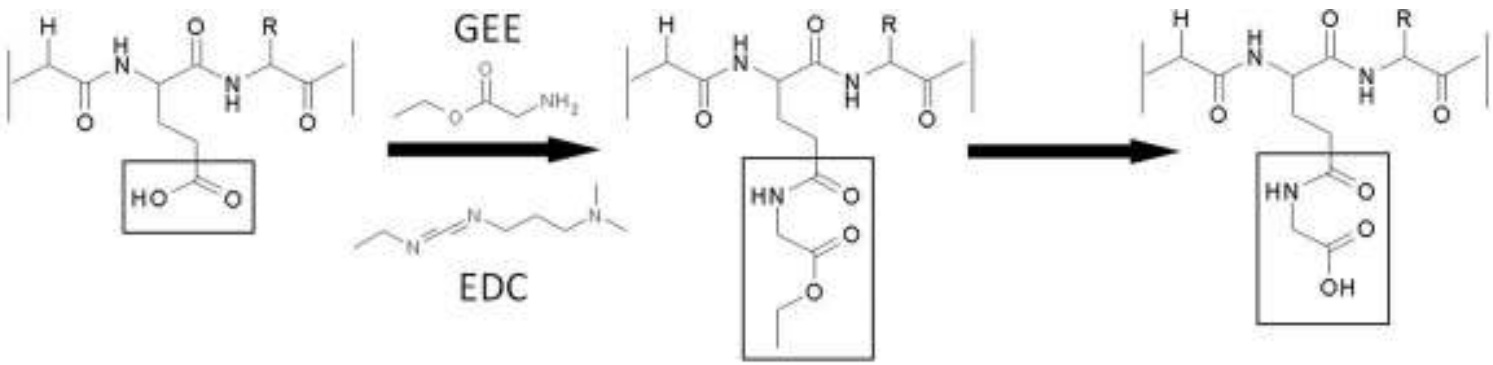

Covalent modification of amino acid side chains

Modification of arginine
(diketones)

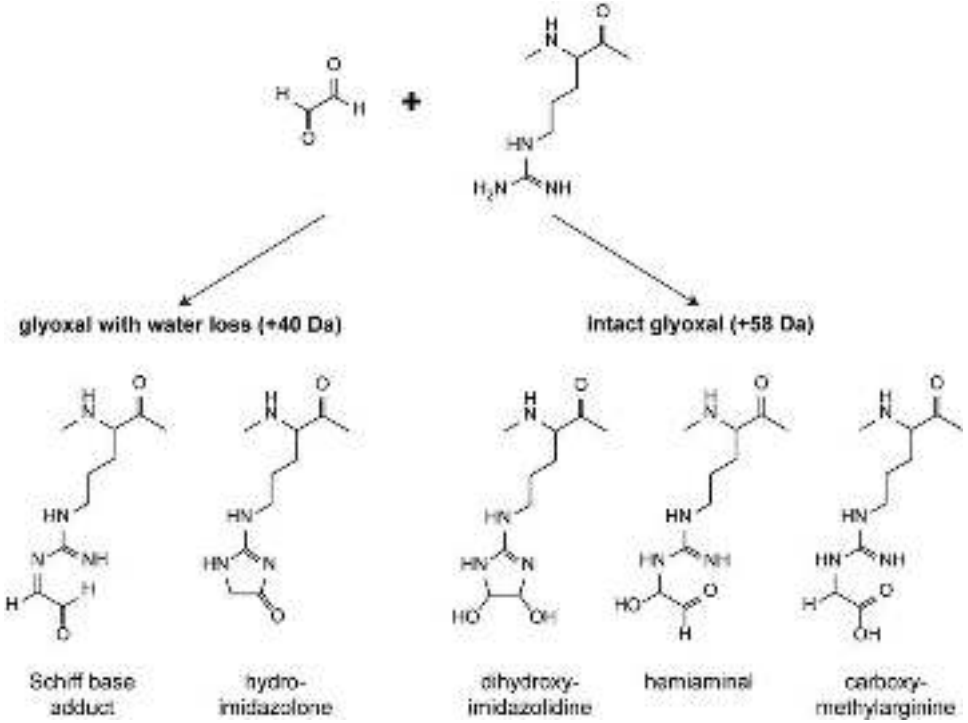

Nitration
(tetranitromethane)

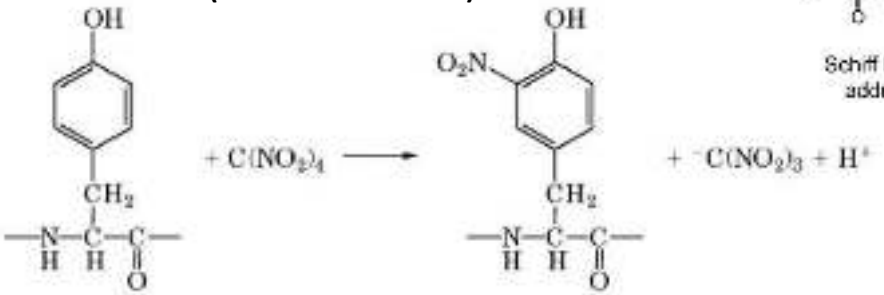

Tyrosine [I] Tetranitromethane [II] 3-Nitrotyrosine

Protein covalent labeling: Lys, Tyr, Arg

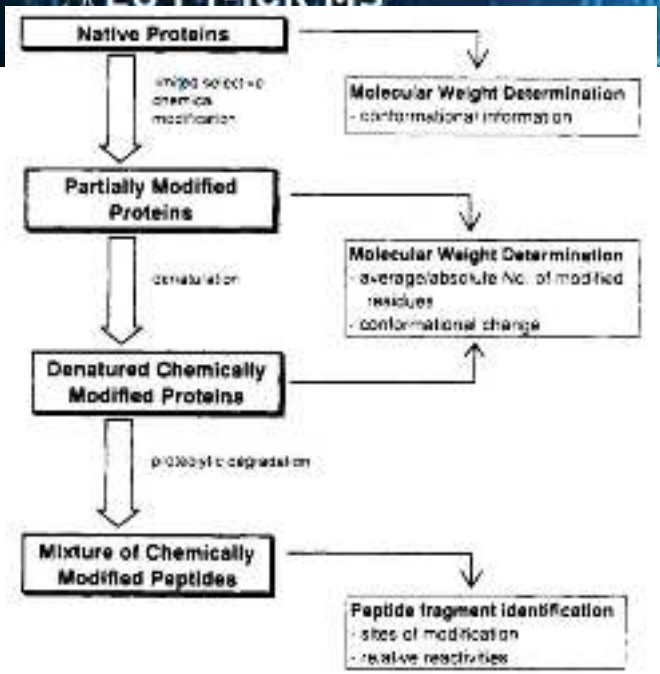

relative reactivity NH_2 groups[a]	lysine residues, ε-amino groups		
	RNAse A	HEL	myoglobin
	α-NH_2		α-NH_2
1	41, 104	97, 33 α-NH_2	45, 63, 77, 79, 145, 147
2	1, 7, 37	1	16, 42, 87
3	31, 61, 91	13, 116	56, 50, 62, 78, 102
4	66, 98	96	96, 47, 87, 133,[b] 118[b]

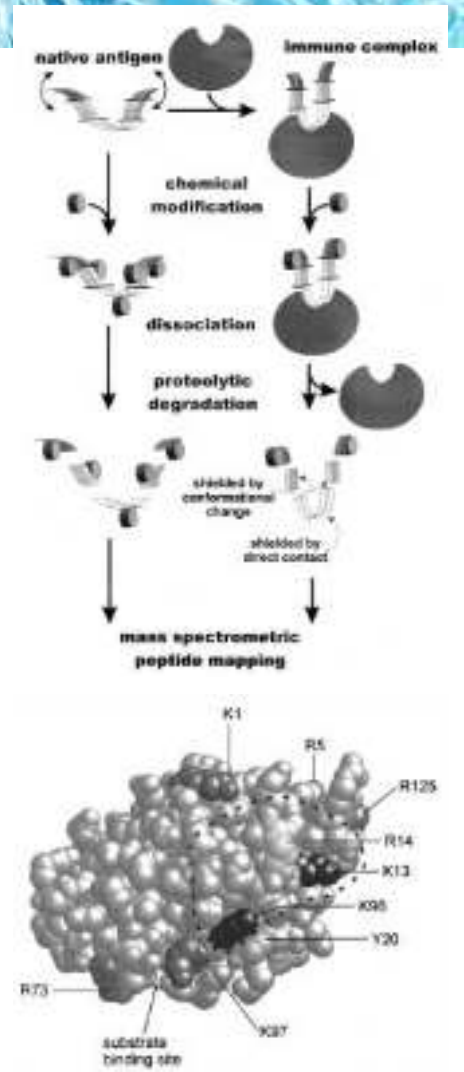

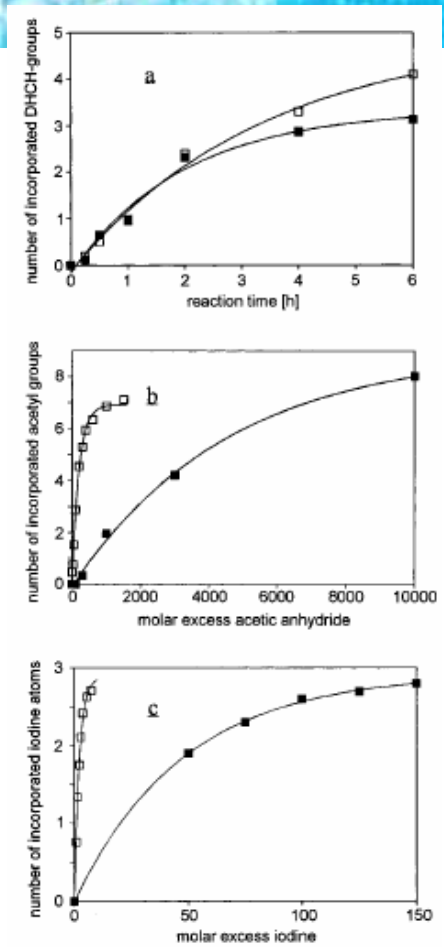

Suckau et. al. *PNAS 1992, 89, 5630*
and ***Glocker et. al.*** *Bioconj. Chem. 1994, 5, 583*

Fiedler et. al. *Bioconj. Chem. 1998, 9, 236*

Protein covalent labeling: Top down

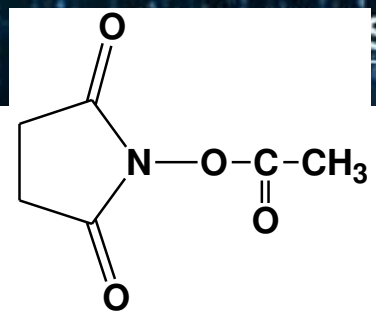

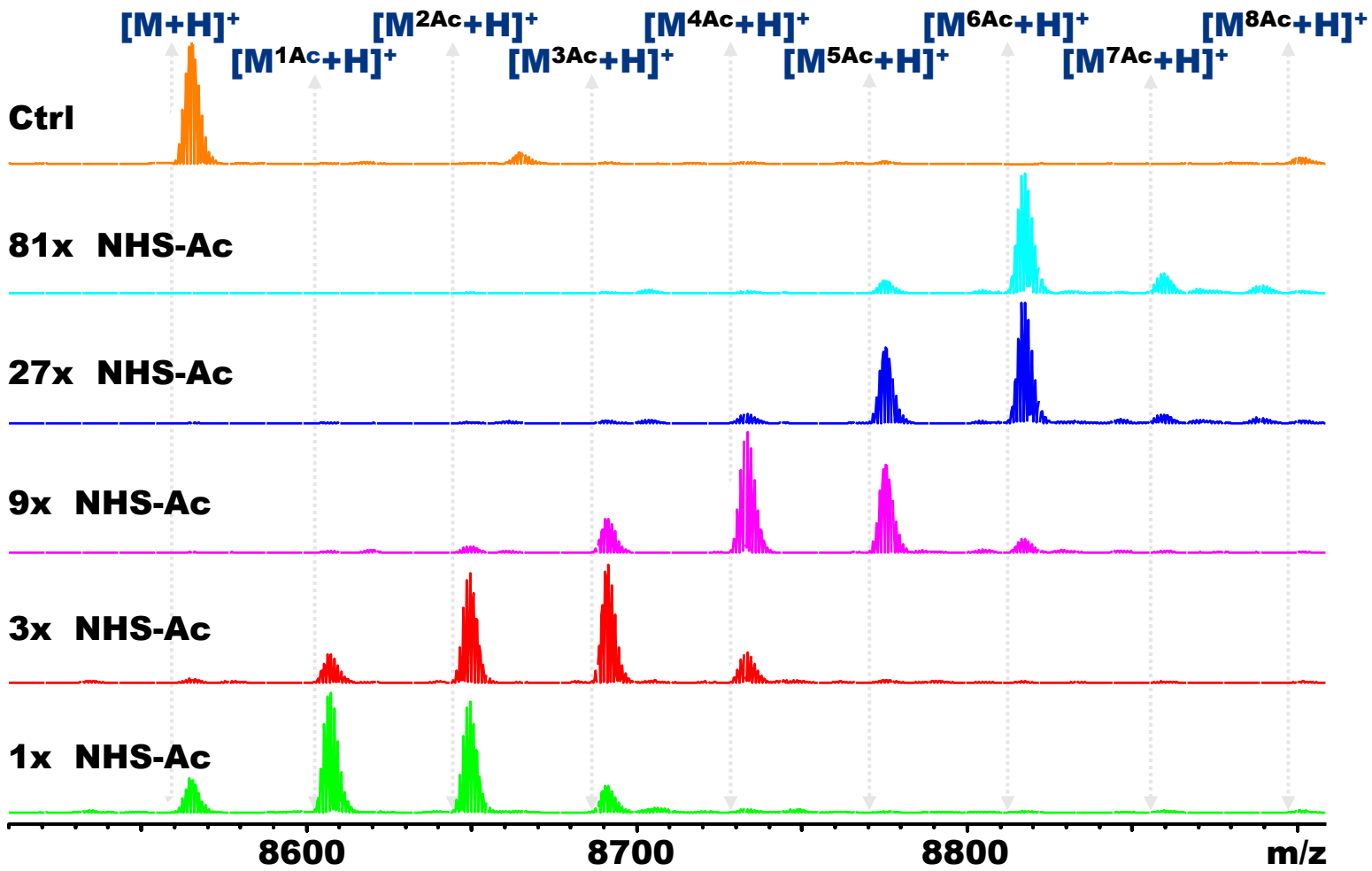

Protein covalent labeling: Top down

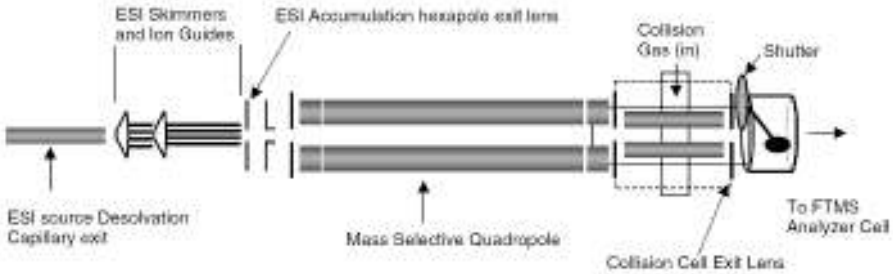

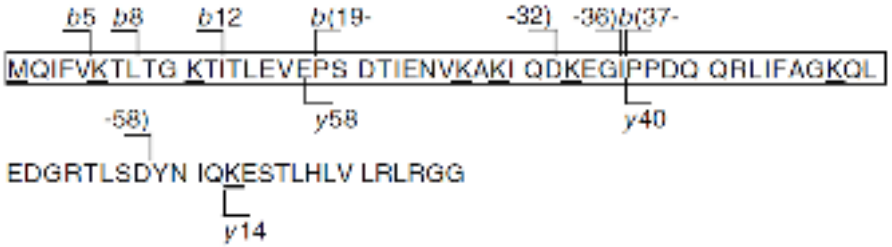

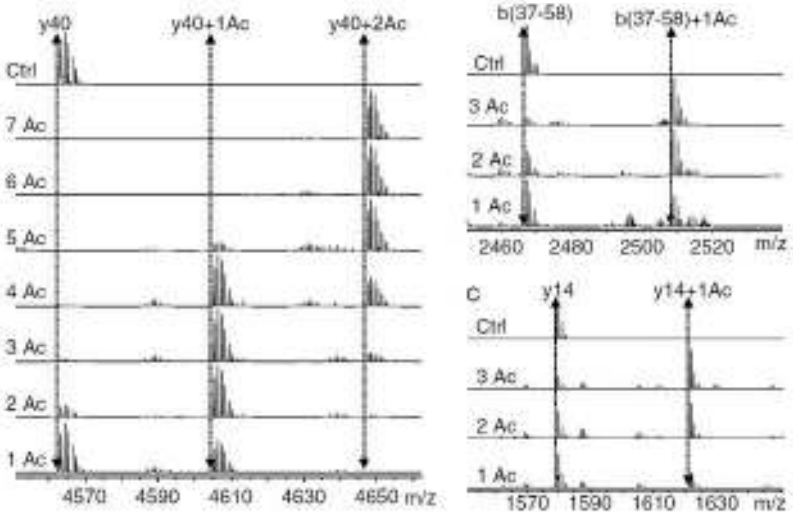

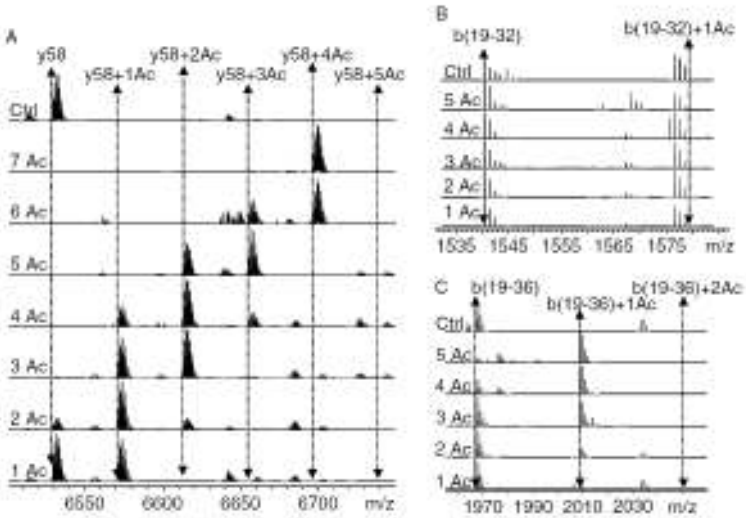

Protein covalent labeling: a reactivity of lysine in an issue

^{1}MQIFVKTLTG ^{11}KTITLEVEPS ^{21}DTIENVKAKI ^{31}QDKEGIPPDQ
^{41}QRLIFAGKQL ^{51}EDGRTLSDYN ^{61}IQKESTLHLV ^{71}LRLRGG

(^{1}M~K6~K48~K63) > K33 > K11 > (K27,K29)

- In agreement with NMR data, which shows.
  - K11 interacts with E34; K29 interacts with D21
- Crystal structure indicates K27 H-bonds to D52.
- More reactive lysines don't H-bond (K63) or H-bond to backbone carbonyls (K48, K33).
- K48 and K63 participate in formation of polyubiquitin.

Novak et. al. *J. Mass Spectrom. 2004, 39, 322*

Protein covalent labeling: Asp, Glu

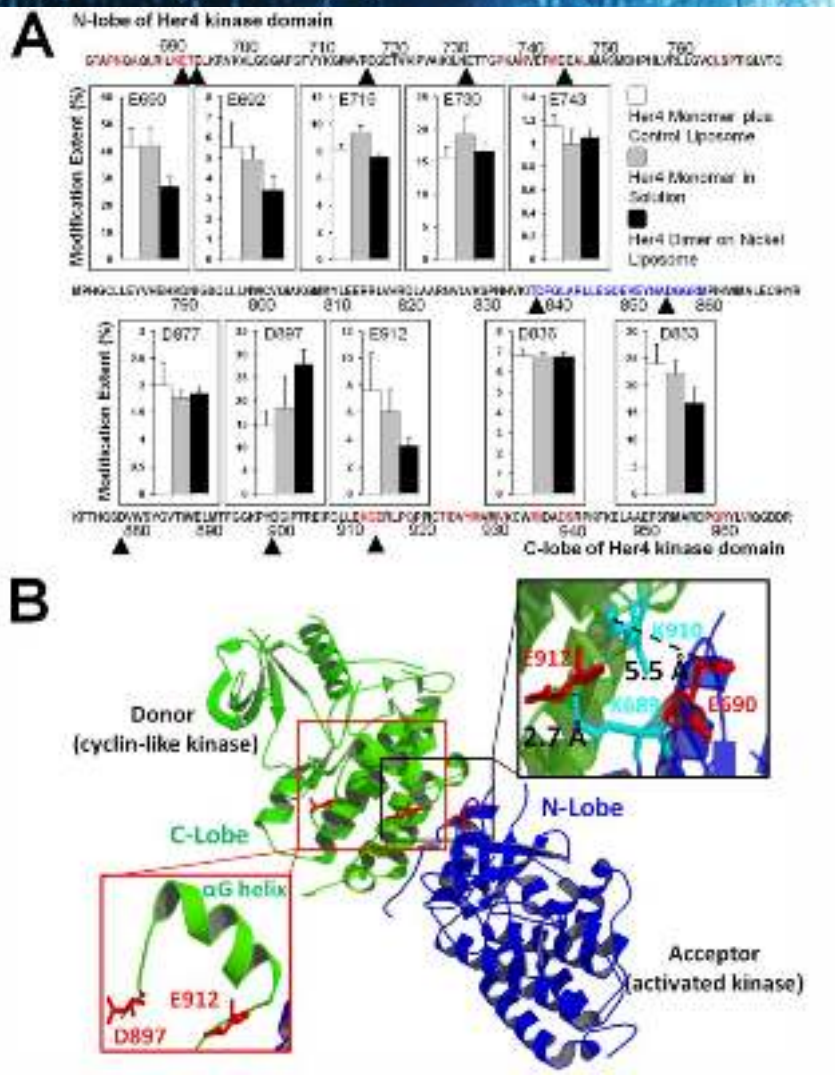

Zhang H. et al. MCP 2011

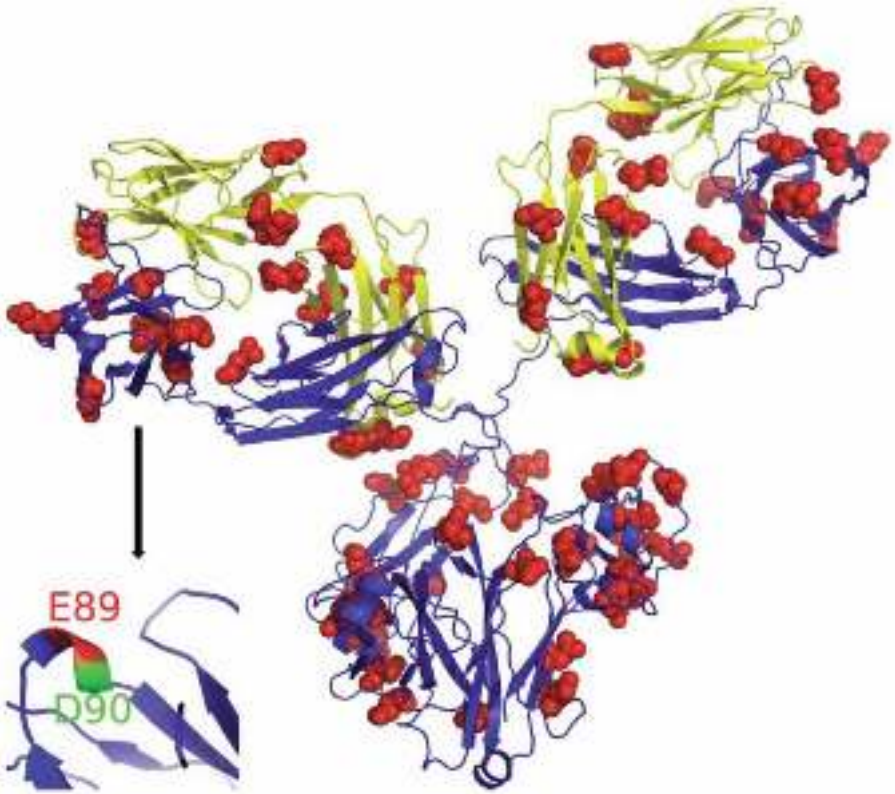

Kaur P. et al. mAb 2015

Hydroxyl Radical Footprinting

Products of water or hydrogen peroxide molecule homolytic bond cleavage

Hydroxyl radicals can be generated by various means:

- **Fenton reaction**
- **Irradiation of water by x-rays or electron beams**
- **Photolysis of hydrogen peroxide FPOP (fast photochemical oxidation of proteins)**
- **Other radicals available • OH, • I, • CF3**

The relative reactivity of the amino acid side chains

Cysteine, Methionine, Tryptophan

Tyr > Phe > His > Leu ~ Ile > Arg ~ Lys ~ Val > Ser ~ Thr ~ Pro > Gln ~ Glu > Asp

Alanine, Glycine

- **Reactive species**
- **React efficiently with most AA side chains**
- **Form STABLE oxidation products**

Takamoto K . et al. *Annu Rev Biophys Biomol Struct.* 2006, 35, 251-276

Conditions for radical labeling

- Electron pulse radiolysis:
  - reproducible 1-100 ns pulses; MeV energy range on linear accelerator

- Synchrotron radiolysis:
  - X-ray; 3-30 keV @ beam current ~ 250 mA

- Laser H_2O_2 photolysis:

  1% - 0,04% H_2O_2 (mixing by stopped-flow device or just before irradiation); quench and removal of residual peroxide is vital
  - Nd:YAG; 2 mJ/pulse @ 266 nm; 3-5 ns pulse; 1-100 shots
  - 17 ns KrF excimer laser; 50 mJ/pulse @ 248 nm
  - 18 ns KrF excimer laser; 62,5 mJ/pulse @ 248 nm; 16 Hz

Fast photochemical oxidation of proteins

- **Covalent modification preserves the primary sequence of modified residues**

- **High reactivity of •OH the modifications of more than half of amino acid side-chains, providing a higher coverage**

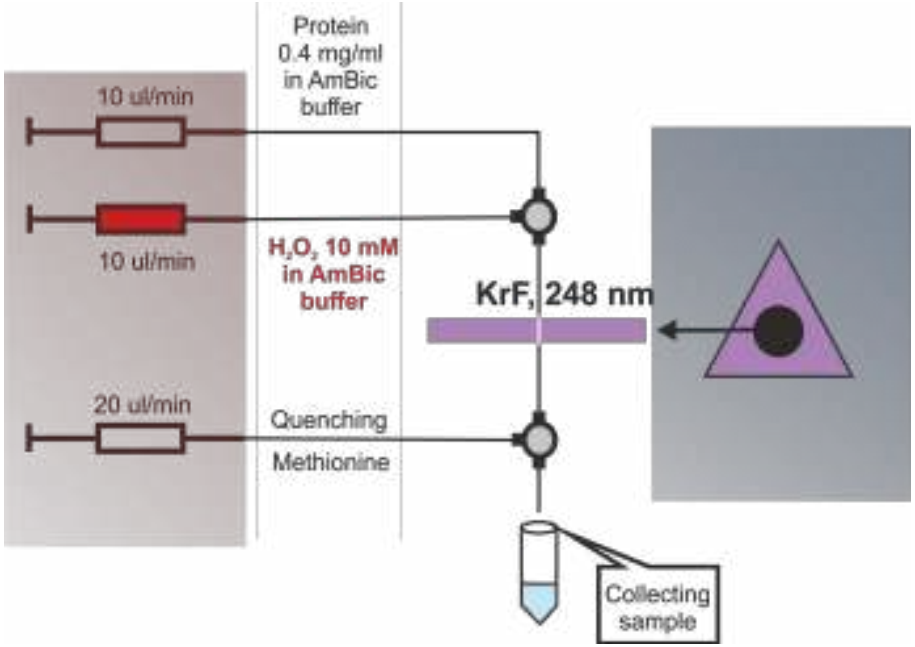

Experimental setup

- Sample mixed and irradiated in
  - **µtubes** (sample volume ~ 15 µl) or in
  - **stopped-flow microfluidic mixing device** - essential for folding / kinetic studies (capillary flow ~ 20 µl.min^{-1})

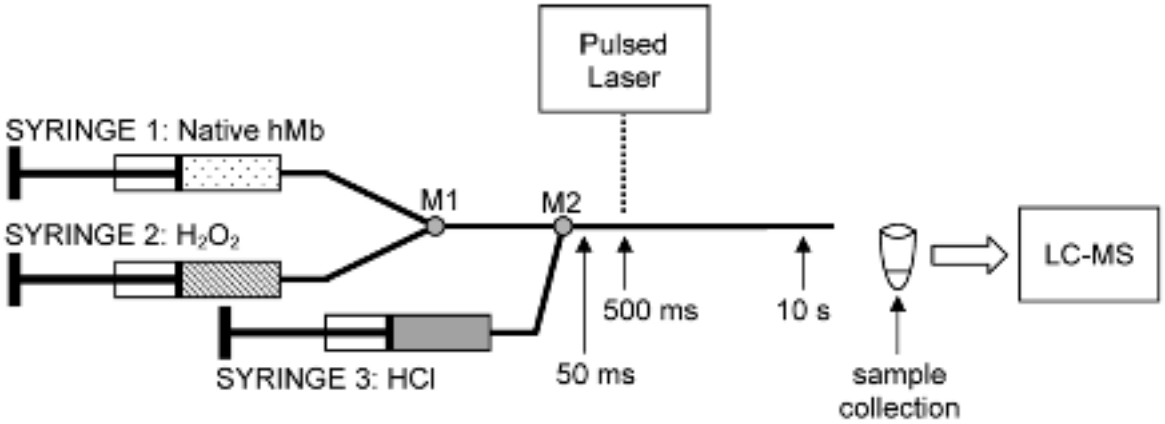

• Short pulses with high energy are needed to create sufficient concentration of radicals on very short (sub-microsecond) timescales to avoid conformational changes of protein during labeling.
• Possible protein conformational changes occur mostly on a longer than milisecond timescale.

Hydroxyl radical footprinting – work-flow

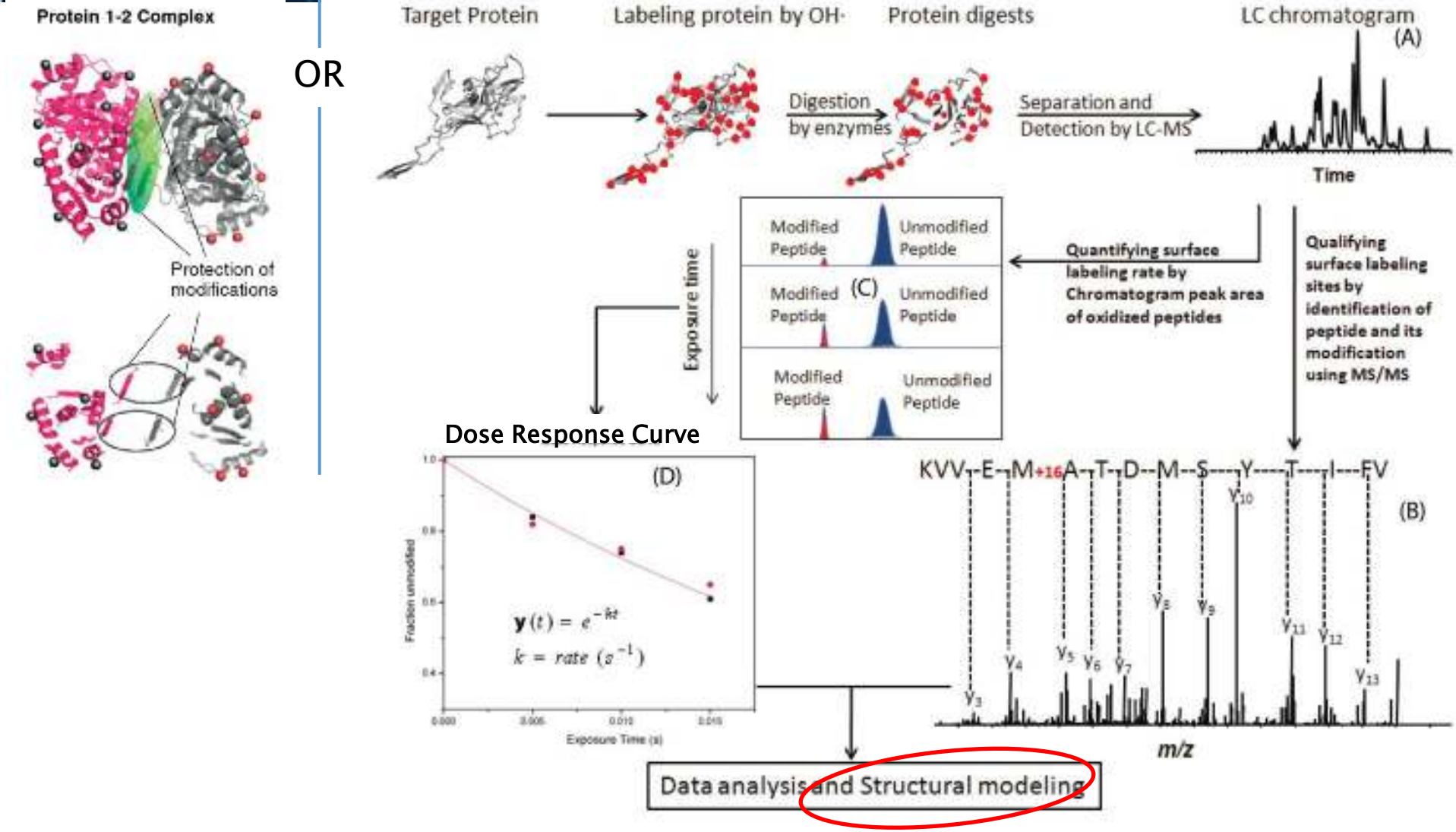

Some (recent) results

- Protein-protein interaction
  - Actin – coffilin interaction:

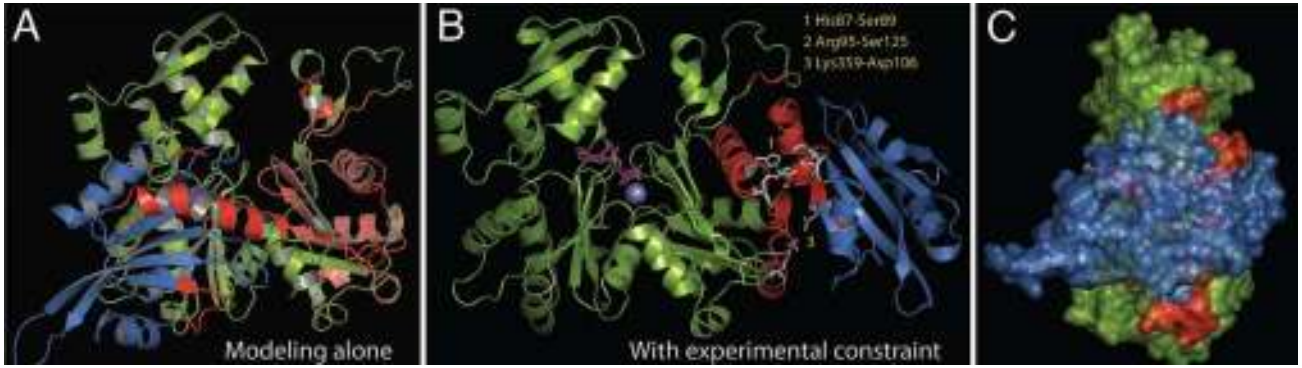

Kamal JK et al. PNAS, 104, 19, 7910-7915 (2007)

  - Dimerization interface of galectin-1:

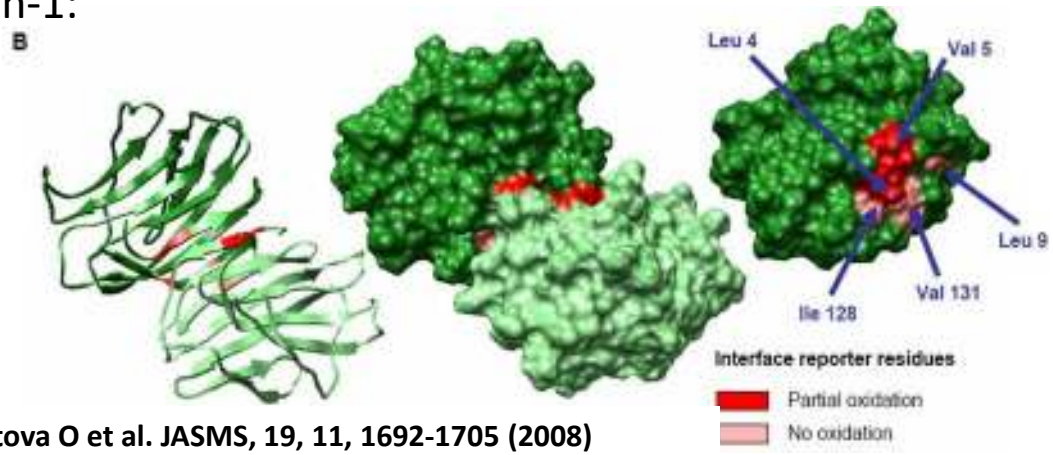

Charvatova O et al. JASMS, 19, 11, 1692-1705 (2008)

More recent results

- Protein structure
  - Integral membrane protein (BR) structure in its natural lipid environment

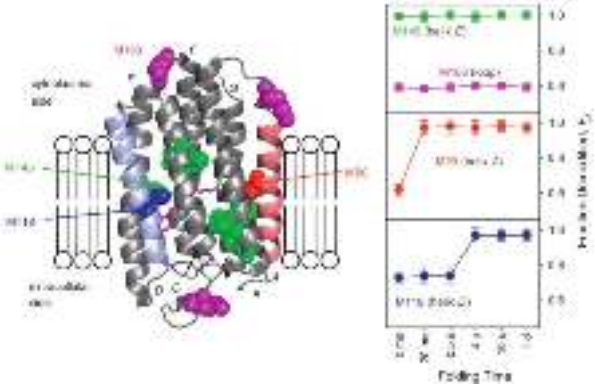

Pan Y et al. J Mol Biol, 410, 146-158 (2011)

- Protein folding kinetics
  - Time-resolved folding and dimerization changes in Ca-binding protein

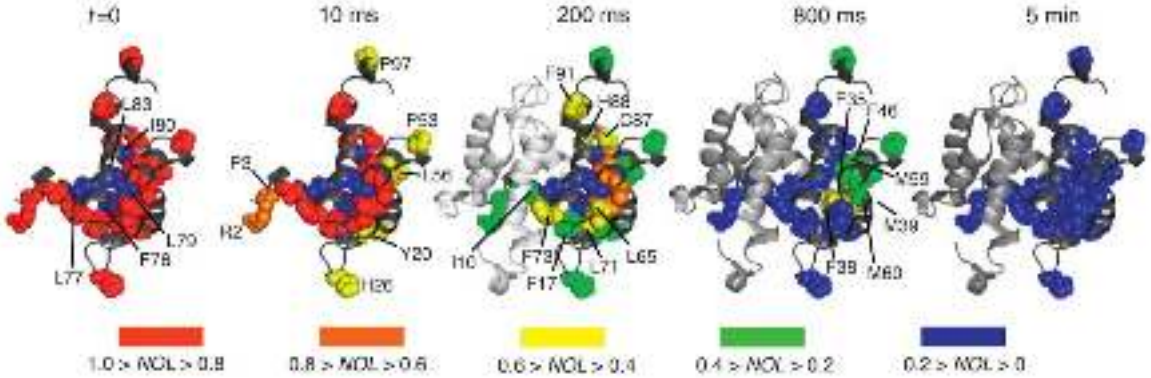

Stocks BB et al. J Mol Biol, 409, 669-679 (2011)

Fast Photochemical Iodination and Top down

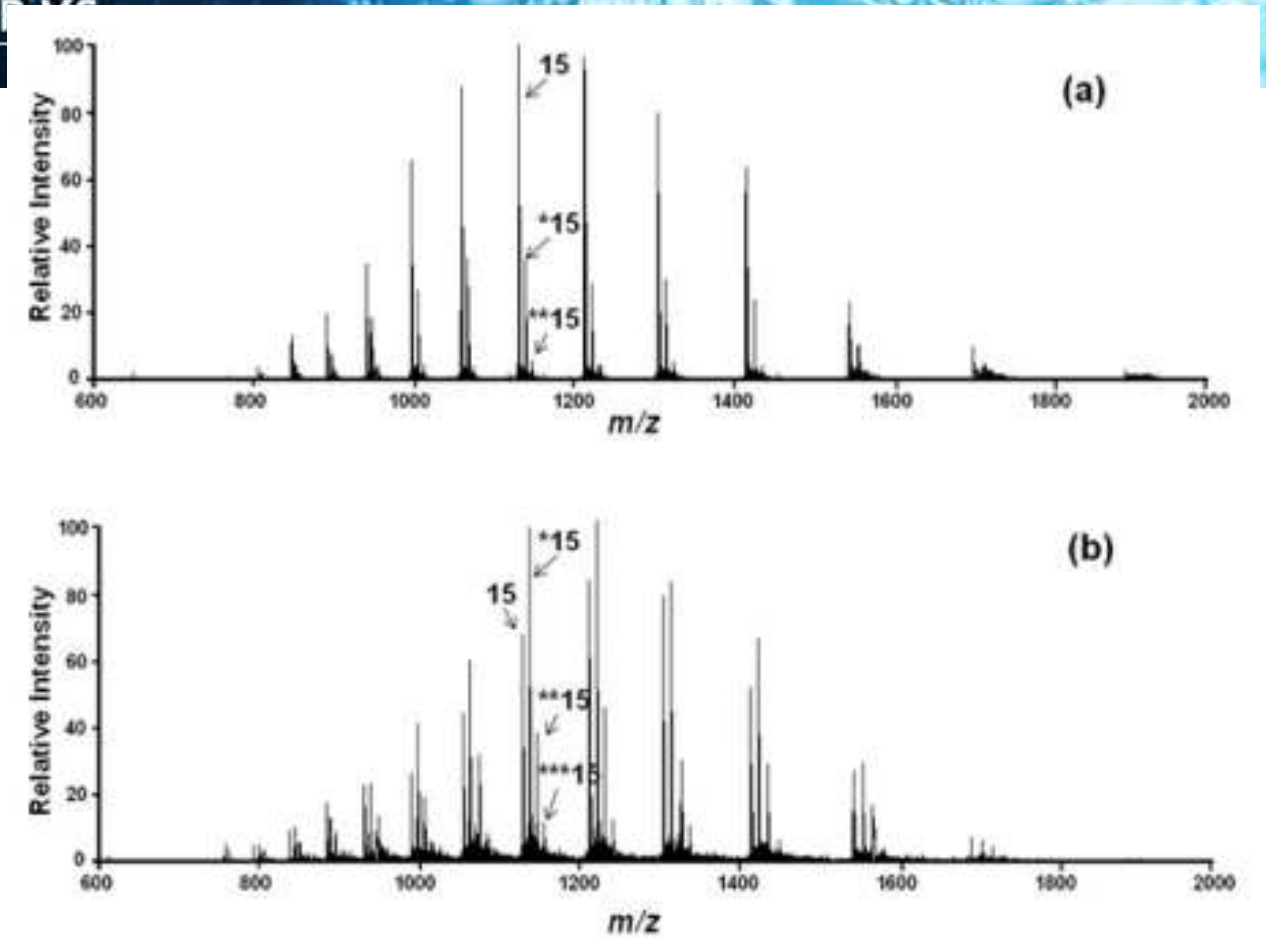

Figure 1.
(a) Full ESI mass spectrum of iodinated myoglobin (Mb). (b) Full ESI mass spectrum of iodinated apomyoglobin (aMb). The unmodified, mono-, di- and tri-iodinated species of the 15th charge state are indicated by the number of stars.

Chen J, Cui W, Giblin D, Gross ML. New protein footprinting: fast photochemical iodination combined with top-down and bottom-up mass spectrometry. J Am Soc Mass Spectrom. 2012;23(8):1306-1318. doi:10.1007/s13361-012-0403-1

Fast Photochemical Iodination and Top down

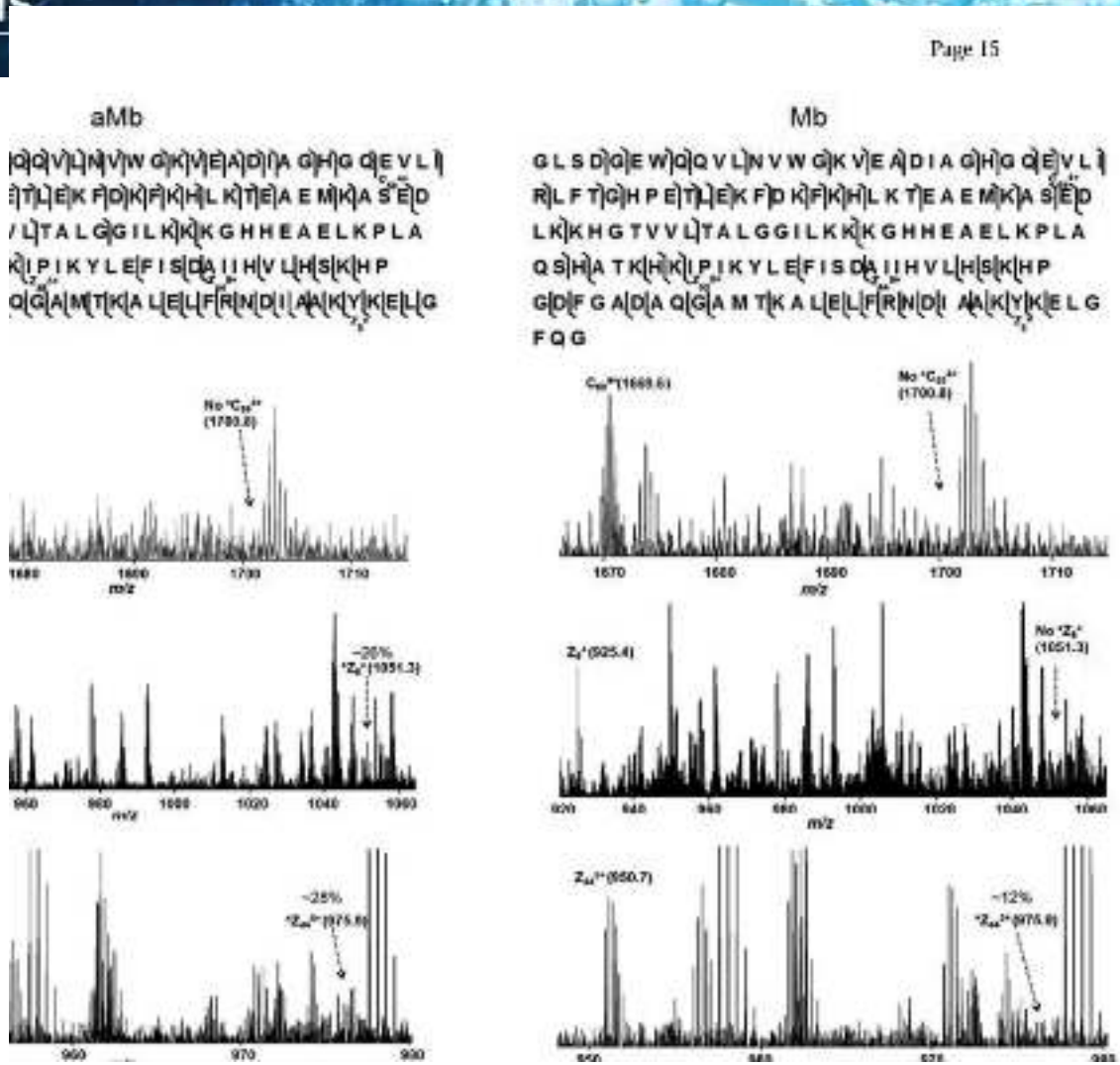

Chen J, Cui W, Giblin D, Gross ML. New protein footprinting: fast photochemical iodination combined with top-down and bottom-up mass spectrometry. J Am Soc Mass Spectrom. 2012;23(8):1306-1318. doi:10.1007/s13361-012-0403-1

Fast Photochemical Iodination and Bottom up

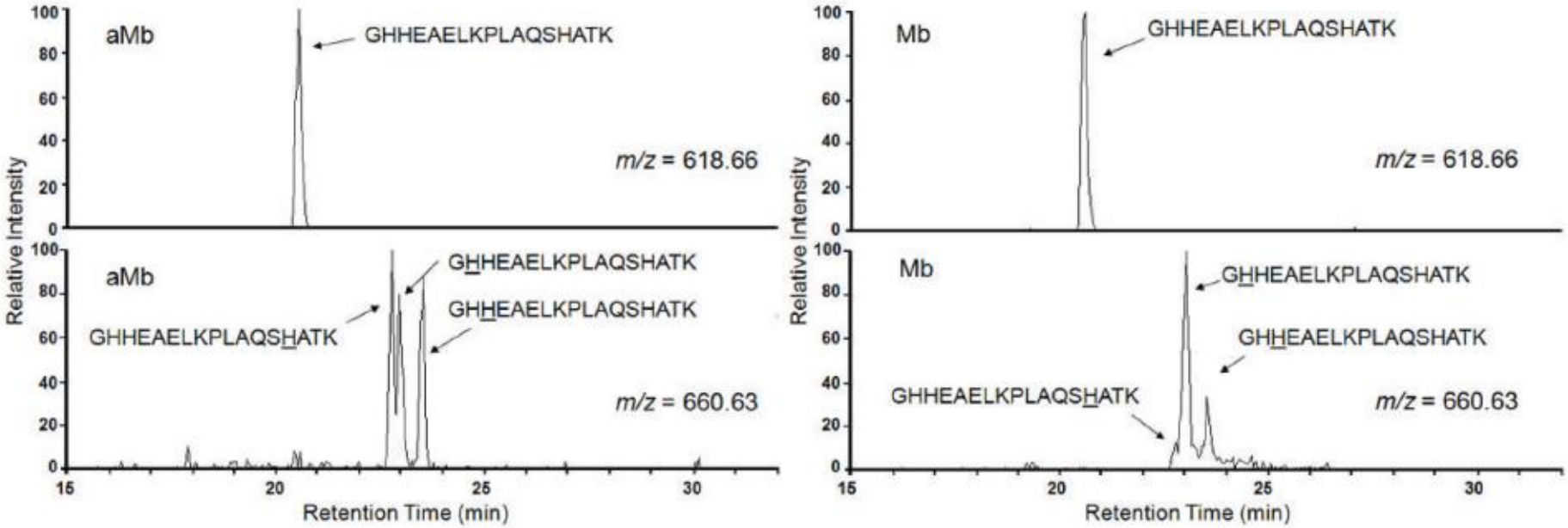

Figure 3.
Extracted ion chromatograms of doubly charged peptide 80-96 of aMb (top left) and Mb (top right), monoiodinated peptide 80-96 of aMb (bottom left) and aMb (bottom right). The assigned modification sites are underlined.

Chen J, Cui W, Giblin D, Gross ML. New protein footprinting: fast photochemical iodination combined with top-down and bottom-up mass spectrometry. J Am Soc Mass Spectrom. 2012;23(8):1306-1318. doi:10.1007/s13361-012-0403-1

Fast Photochemical Iodination: Data visualization

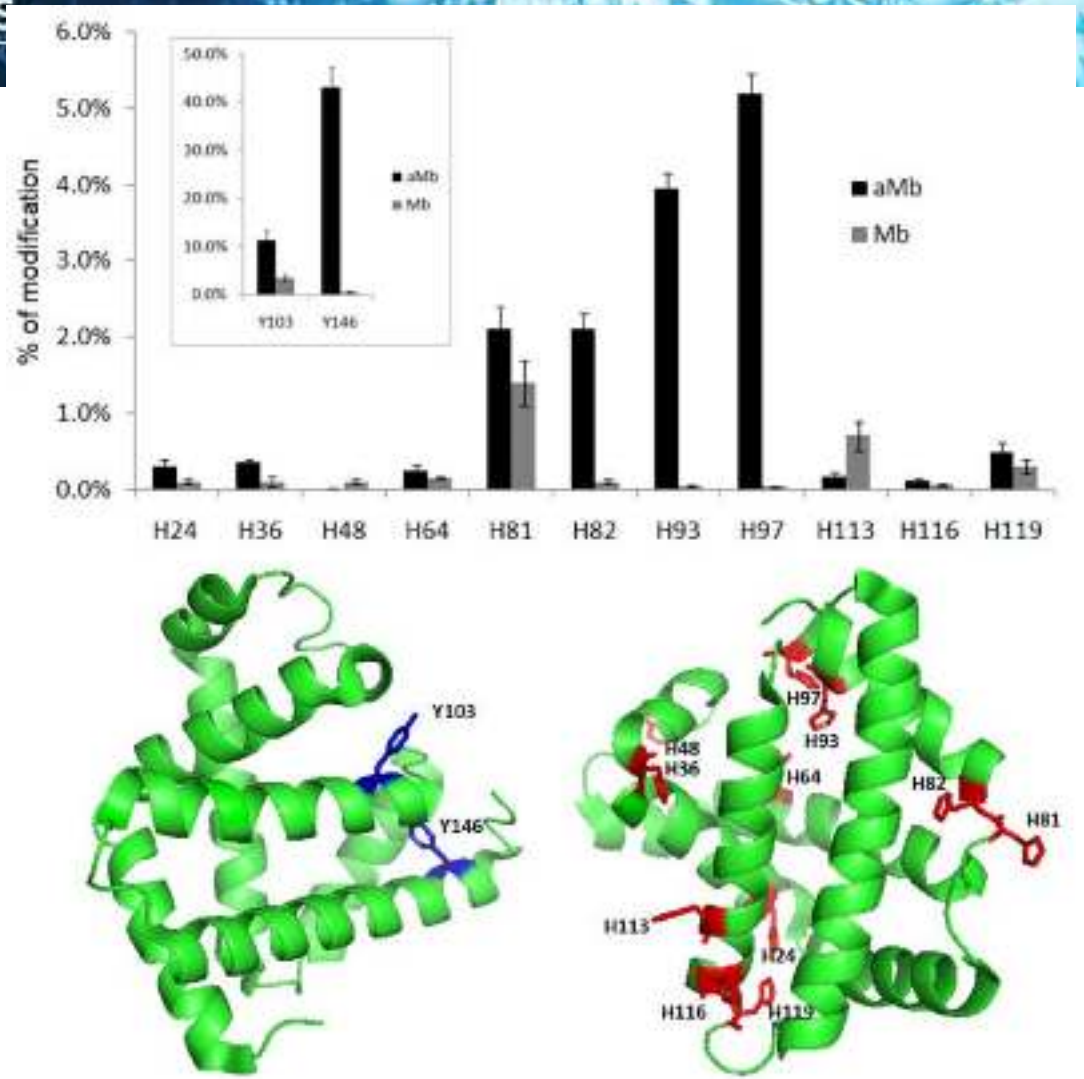

Chen J, Cui W, Giblin D, Gross ML. New protein footprinting: fast photochemical iodination combined with top-down and bottom-up mass spectrometry. J Am Soc Mass Spectrom. 2012;23(8):1306-1318. doi:10.1007/s13361-012-0403-1

Chemical cross-linking

Chemical cross-linking combined with MS has been proposed as a method to obtain distance constraints (MS3D)

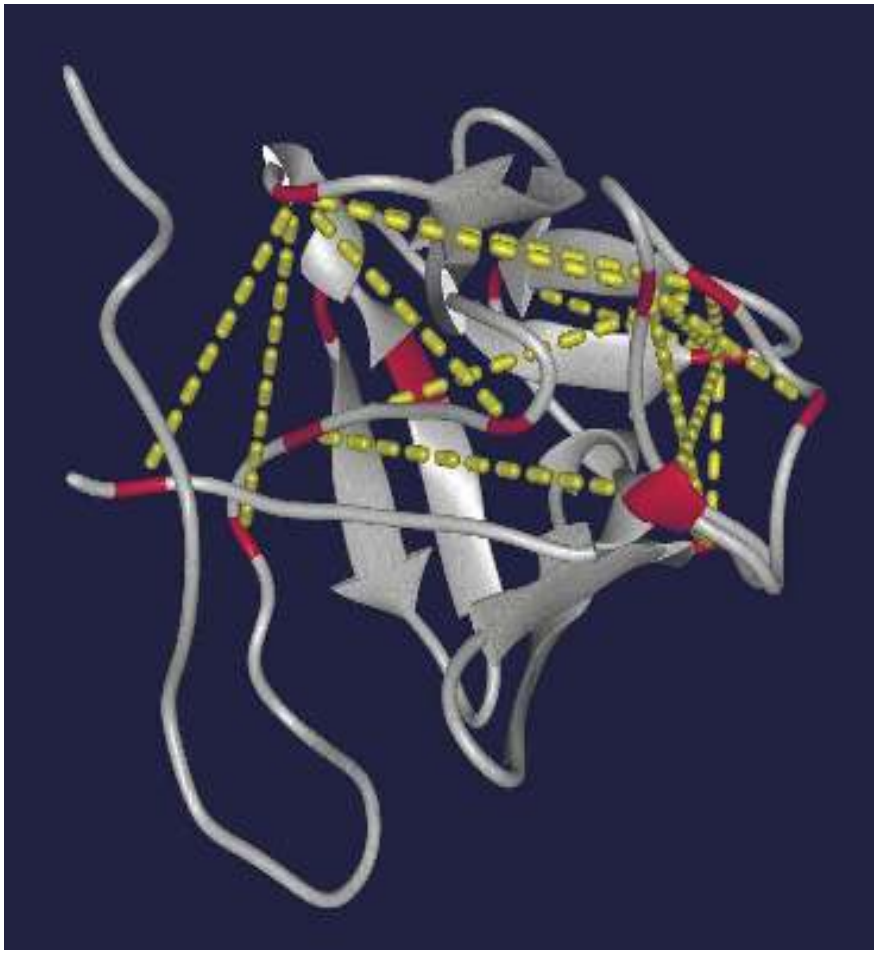

Young, Tang et al. *PNAS* 97(11):5802-6. 2000.

Chemical cross-linking: the first 3-D structure

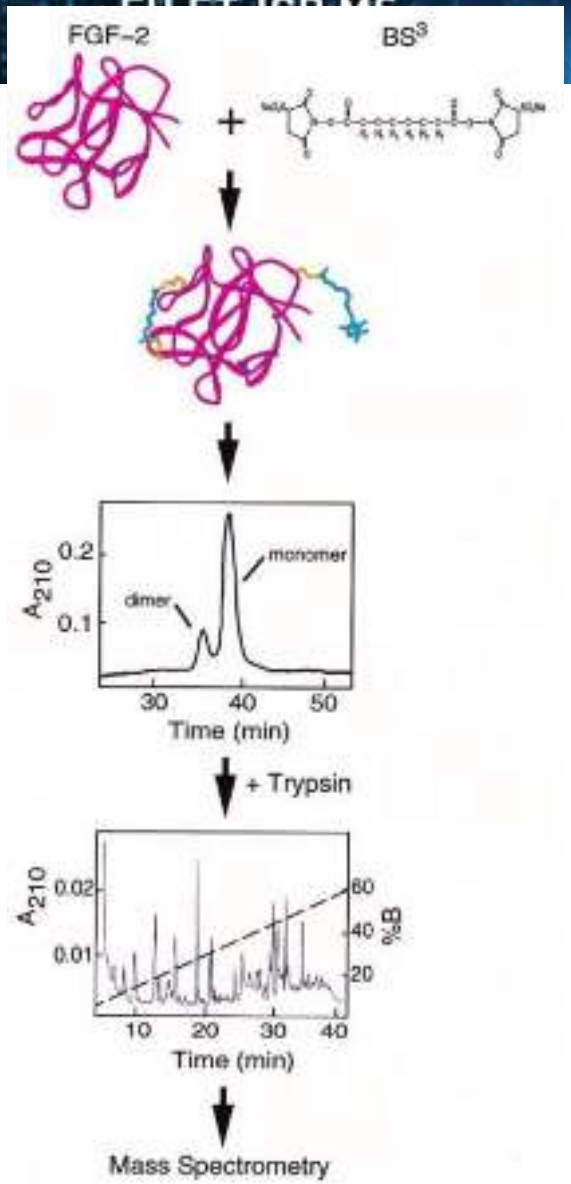

Fibroblast grow factor 2

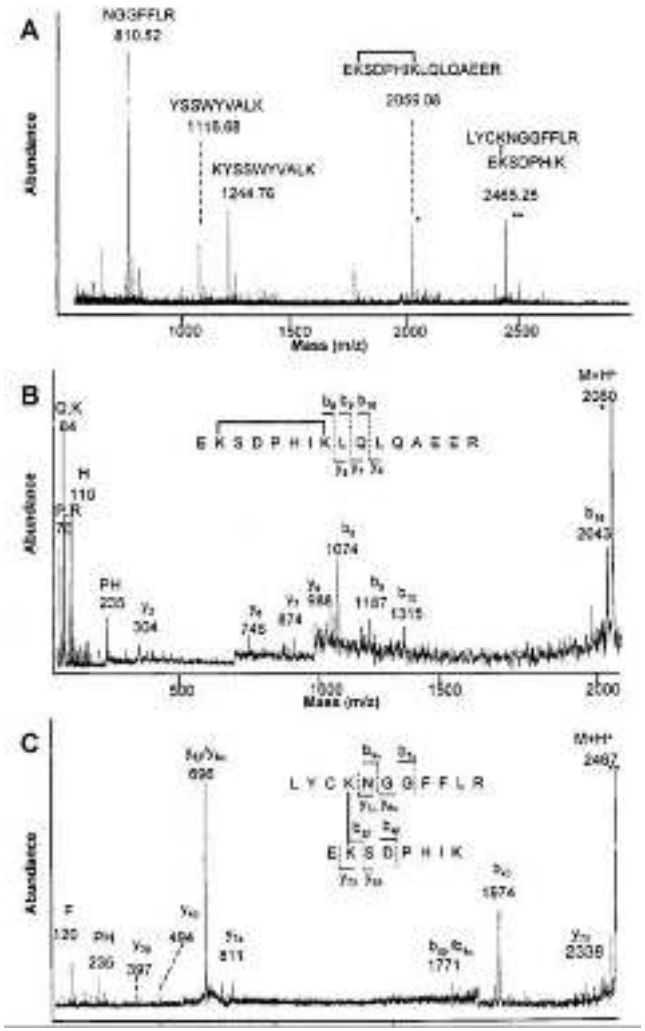

Top 20 threading models ranked by constraint error

Name	Fold family	% Sequence identity	Threading rank	Constraint error, Å²	Number of violations
FGF-2	α-Helical	38.0	1	0.0	0
IL-12	α-Helical	12.1	3	1.0	0
Gastrotropin	Globular	1.1	4	2.0	1
Bovine pancreatic trypsin inhibitor	α-Helical	8.4	10	3.5	1
Scorpion toxin	β-Sheet	11.4	5	1.4	0
6-N-phosphohexylsuccinoyl-cAMP	NAD-binding Rossmann fold	5.1	6	14.0	1
Glucoamylase saccharidase	Thioesterase	11.1	14	16.0	1
Retinol binding protein	Lipocalin	6.1	18	11.1	1
Nucleoside diphosphokinase	Periplasmic fold	8.8	20	18.0	2
Cytochrome c_3	Cytochrome c	12.5	11	21.0	5
Aspartate carbamoyltransferase	Periplasmic fold	9.8	12	23.0	3
S-100 Protein	S-100s	7.8	2	27.1	7
Disulfide bond formation protein	Thioredoxin	8.4	15	28.1	8
Alb Interferon	Albumin based fold	7.8	16	30.0	3
Endoglucanase C	Galactose binding	11.6	9	32.0	6
TATA box binding protein	TATA box binding protein fold	10.1	7	40.0	8
Phospholipase A2	Phospholipase A2	2.1	45	50.4	7
PAX paired domain	3 Helix bundle	13.1	11	100.4	8

Young et. al. PNAS 2000, 97, 5802

Chemical cross-linking: the chemistry behind…

EU FT-ICR MS

Primary amine reactive cross-linker

Disuccinimidyl Suberate (DSS)
Cross-linker "arm length"

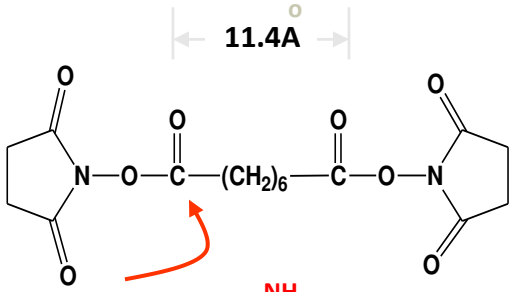

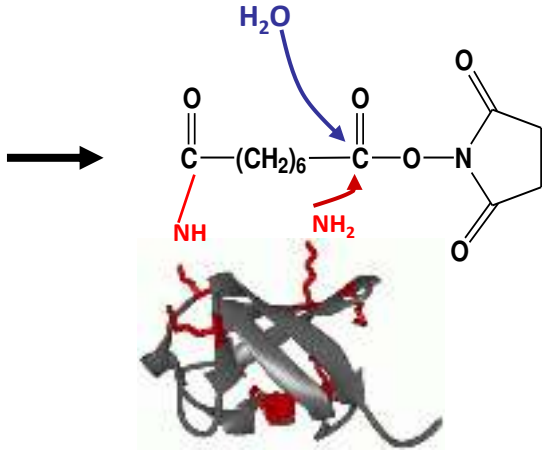

"Hanging" Cross-link
Add $C_8H_{12}O_3$,
Δm = 156.0786

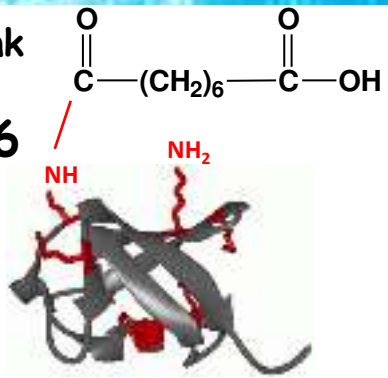

"Internal" Cross-link
Add $C_8H_{10}O_2$,
Δm = 138.0861

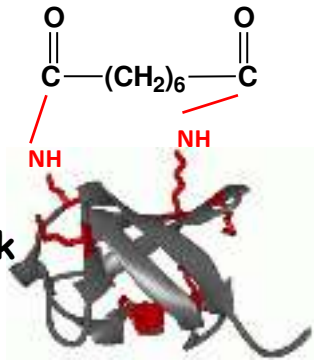

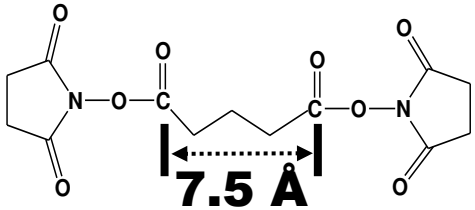

DSG

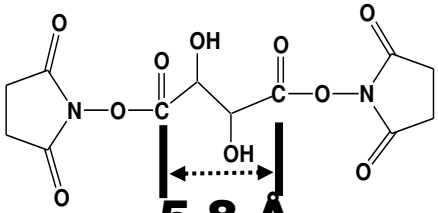

DST

CXMS experiment

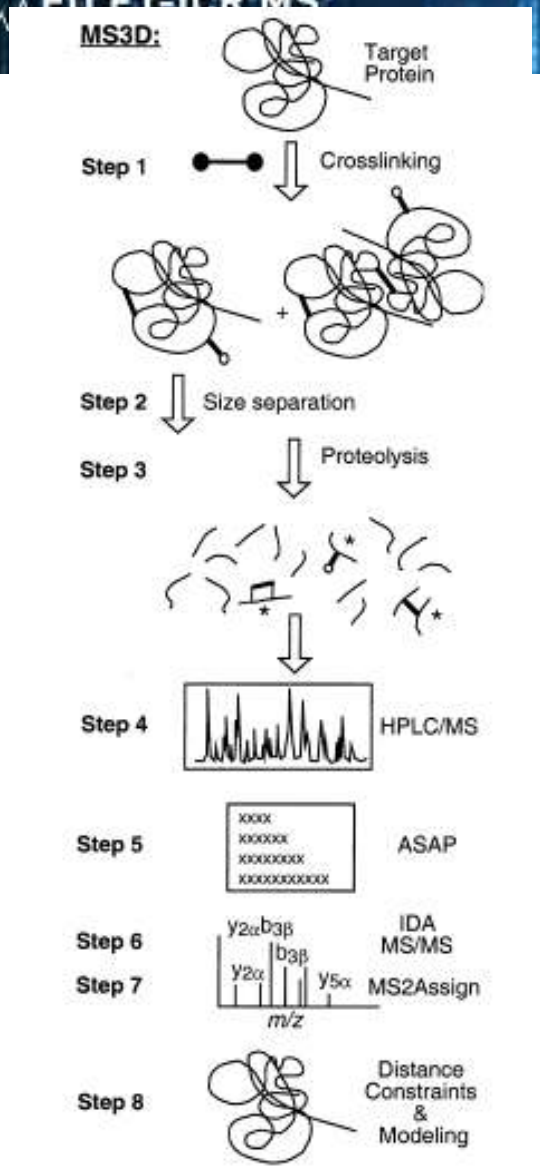

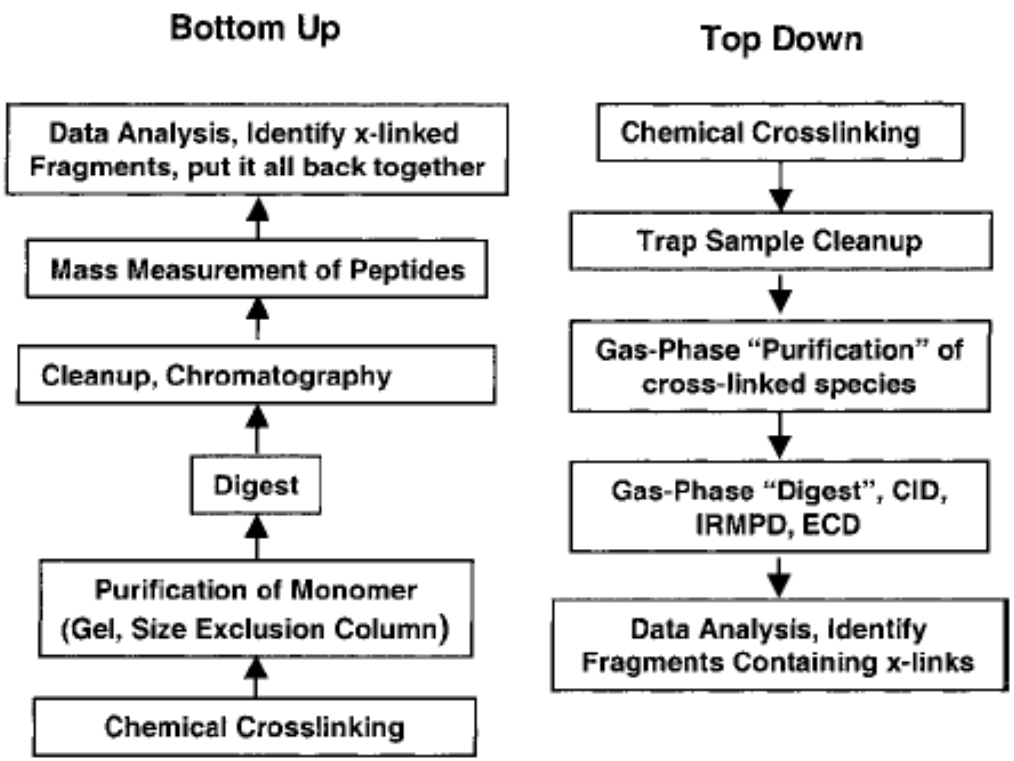

Nomenclature of peptide cross-linked fragments

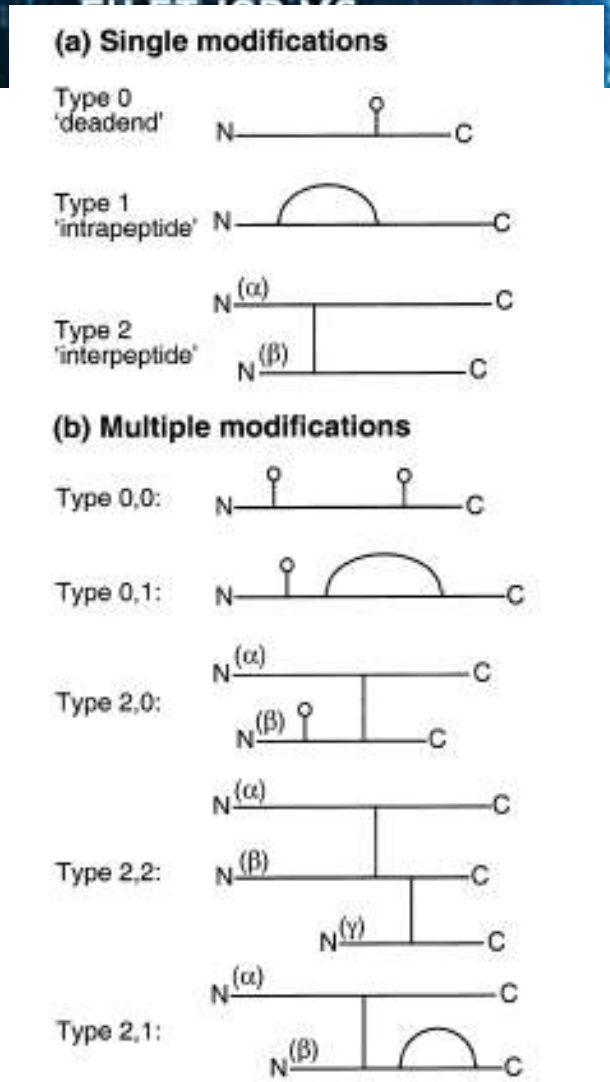

Type 1

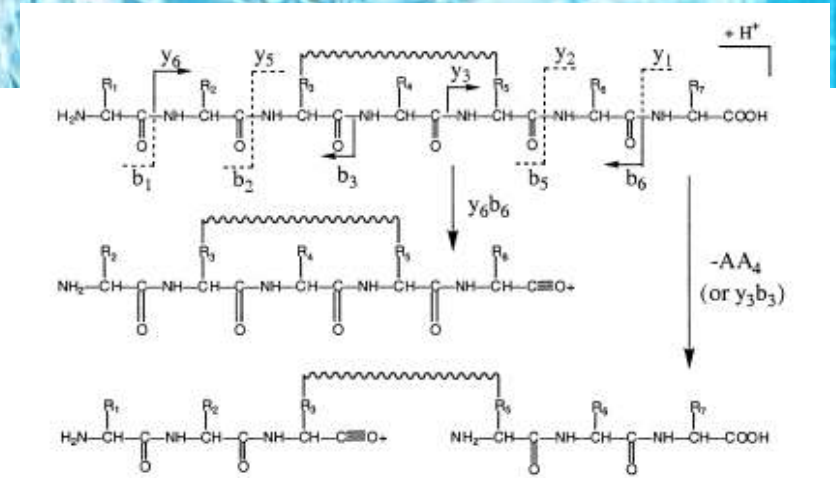

Type 2

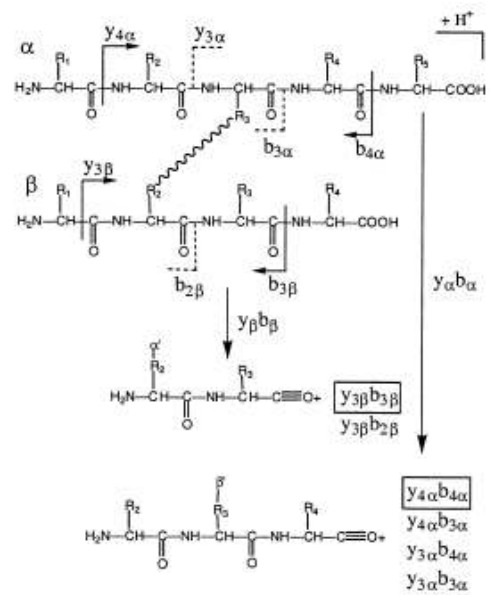

Schilling B, Row RH, Gibson BW, Guo X, Young MM. MS2Assign, automated assignment and nomenclature of tandem mass spectra of chemically crosslinked peptides. J Am Soc Mass Spectrom. 2003;14(8):834-850.

Data analysis: STAVROX

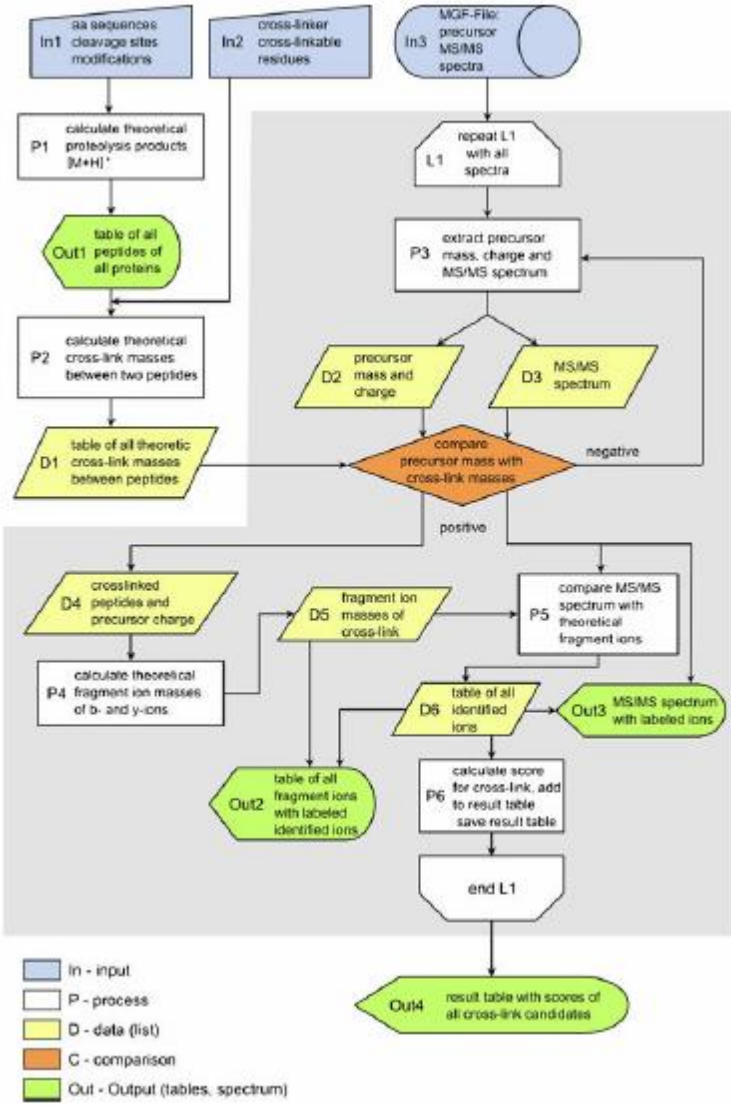

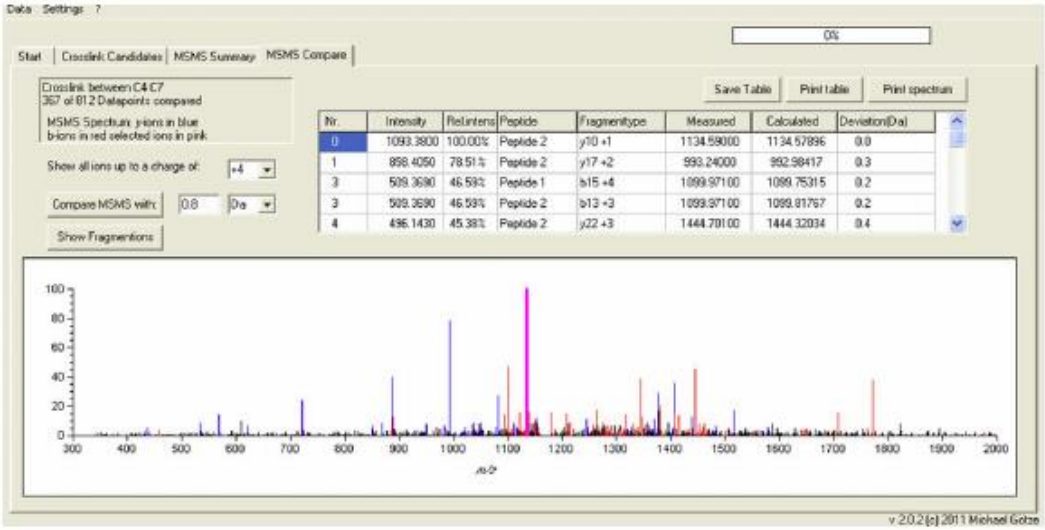

Gotze M. et al. JASMS 2012

Middle down - *Rhodopsin*

Rhodopsin has open structure/function questions

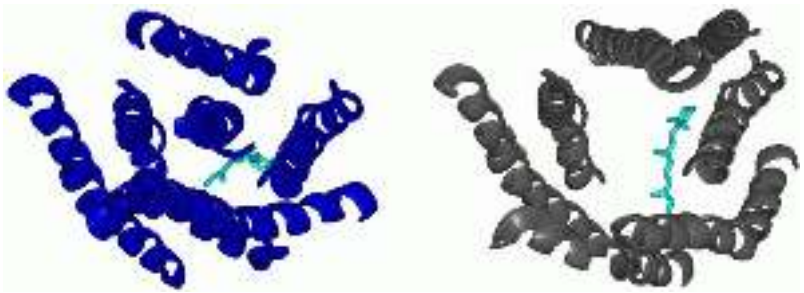

- **What is the conformational change that occurs upon light activation?**
- **What is the configuration of loops involved in Gi binding (not visible on X-ray)?**

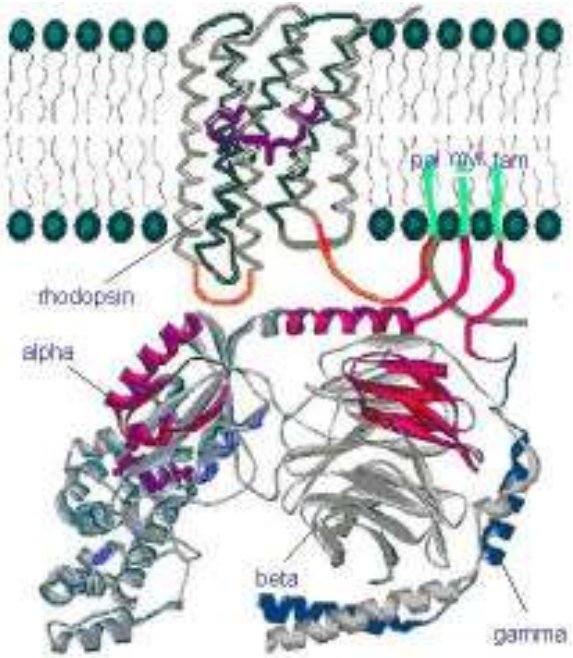

Rhodopsin Has Many Potential Targets for Cross-linking

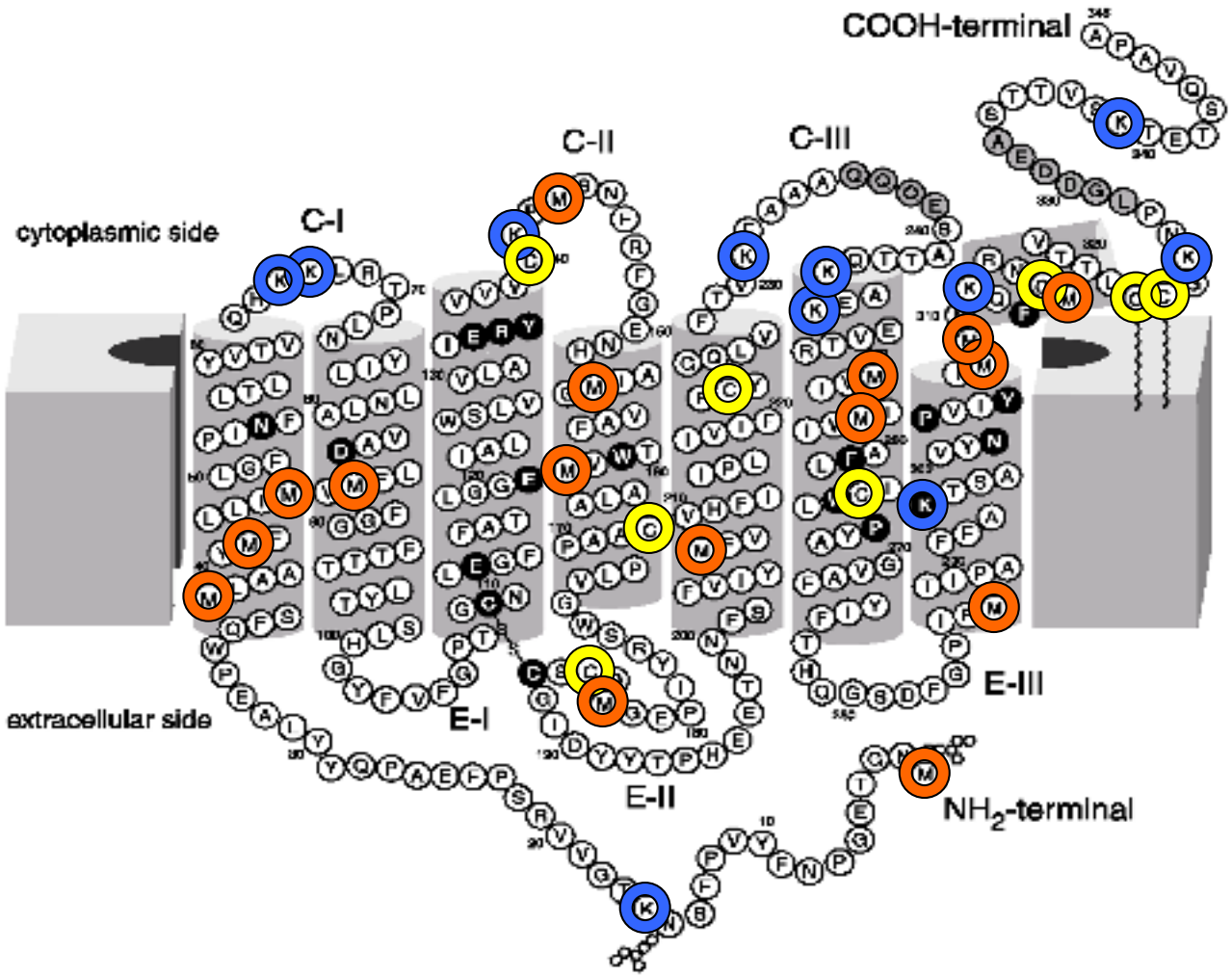

Proteoliposomes/Detergent

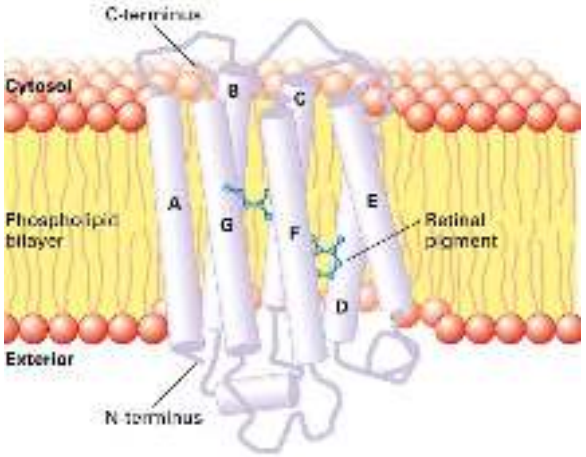

Crosslink Protein

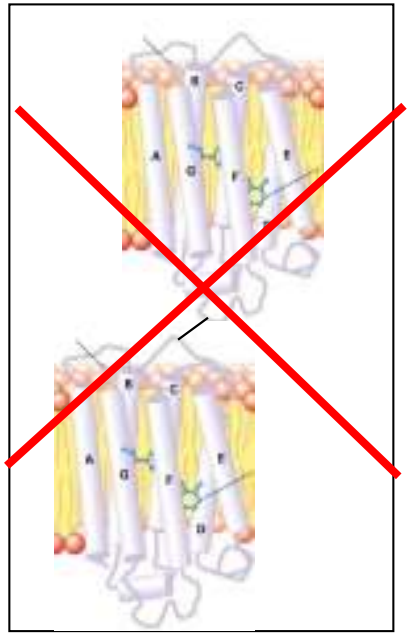

Purify Monomer

Protein Digestion

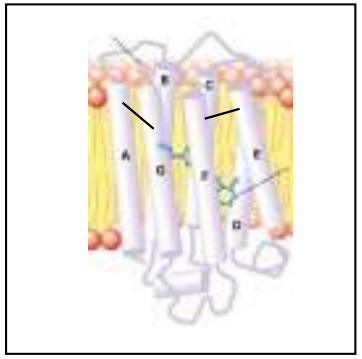

LC/MS Analysis

Data Analysis

LCMS analysis of Rhodopsine CNBr digest

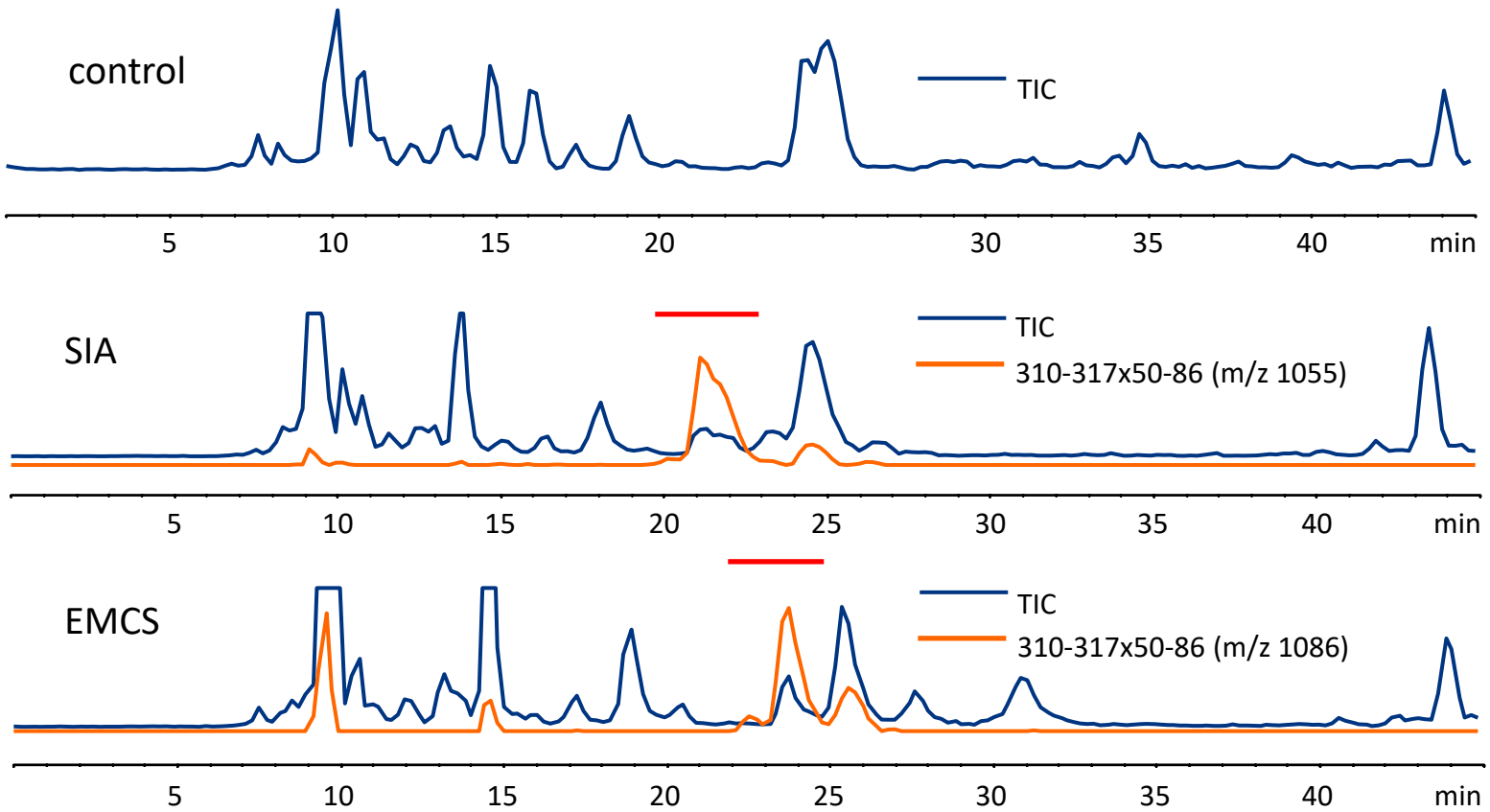

Red line corresponds to extracted ion chromatograms of selected cross-linked peptides.

What's wrong? Too many possibilities….

α - ^{50}LGFPINFLTLYVTVQH**KK**LRTPLNYILLNLAVADLFM^{86}

?

β1 - ^{310}NKQFRN**C**M^{317}

α - ^{50}LGFPINFLTLYVTVQH**KK**LRTPLNYILLNLAVADLFM^{86}

? ?

β2 - ^{318}VTTLCCG**K**NPLGDDEASTTVS**K**TETSQVAPA^{348}

Can We Resolve the Cross-link at K66/K67?

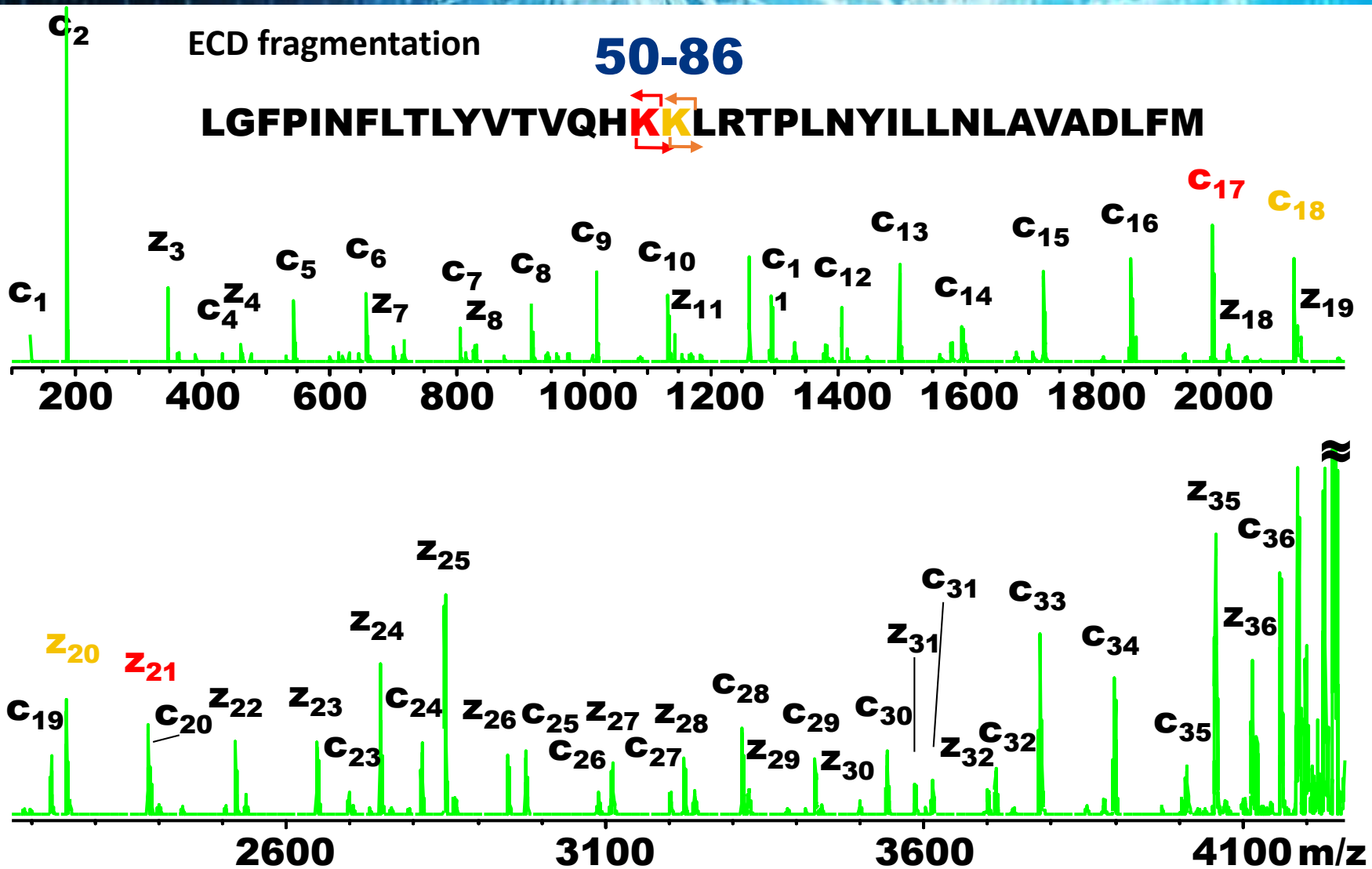

ECD fragmentation of cross-linked peptides

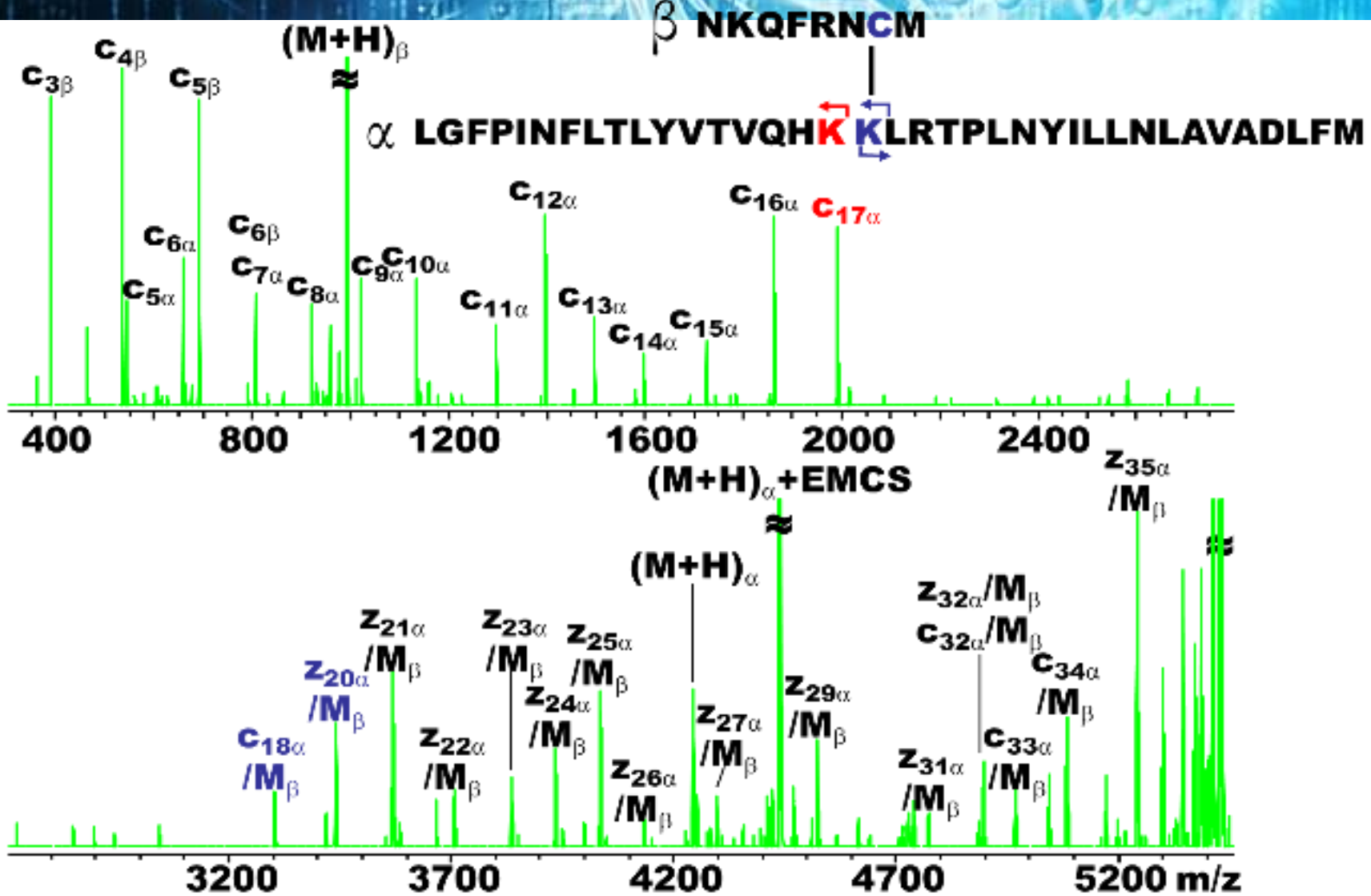

ECD enables single residue resolution!

α - ^{50}LGFPINFLTLYVTVQH**KK**LRTPLNYILLNLAVADLFM^{86}

β1 - ^{310}NKQFRN**C**M^{317}

α - ^{50}LGFPINFLTLYVTVQH**KK**LRTPLNYILLNLAVADLFM^{86}

β2 - ^{318}VTTLCCG**K**NPLGDDEASTTVS**K**TETSQVAPA^{348}

Novak P, Haskins WE, Ayson MJ, et al. Unambiguous assignment of intramolecular chemical cross-links in modified mammalian membrane proteins by Fourier transform-tandem mass spectrometry. Anal Chem. 2005;77(16):5101-5106. doi:10.1021/ac040194r

The Cytoplasmic Face of Rhodopsin

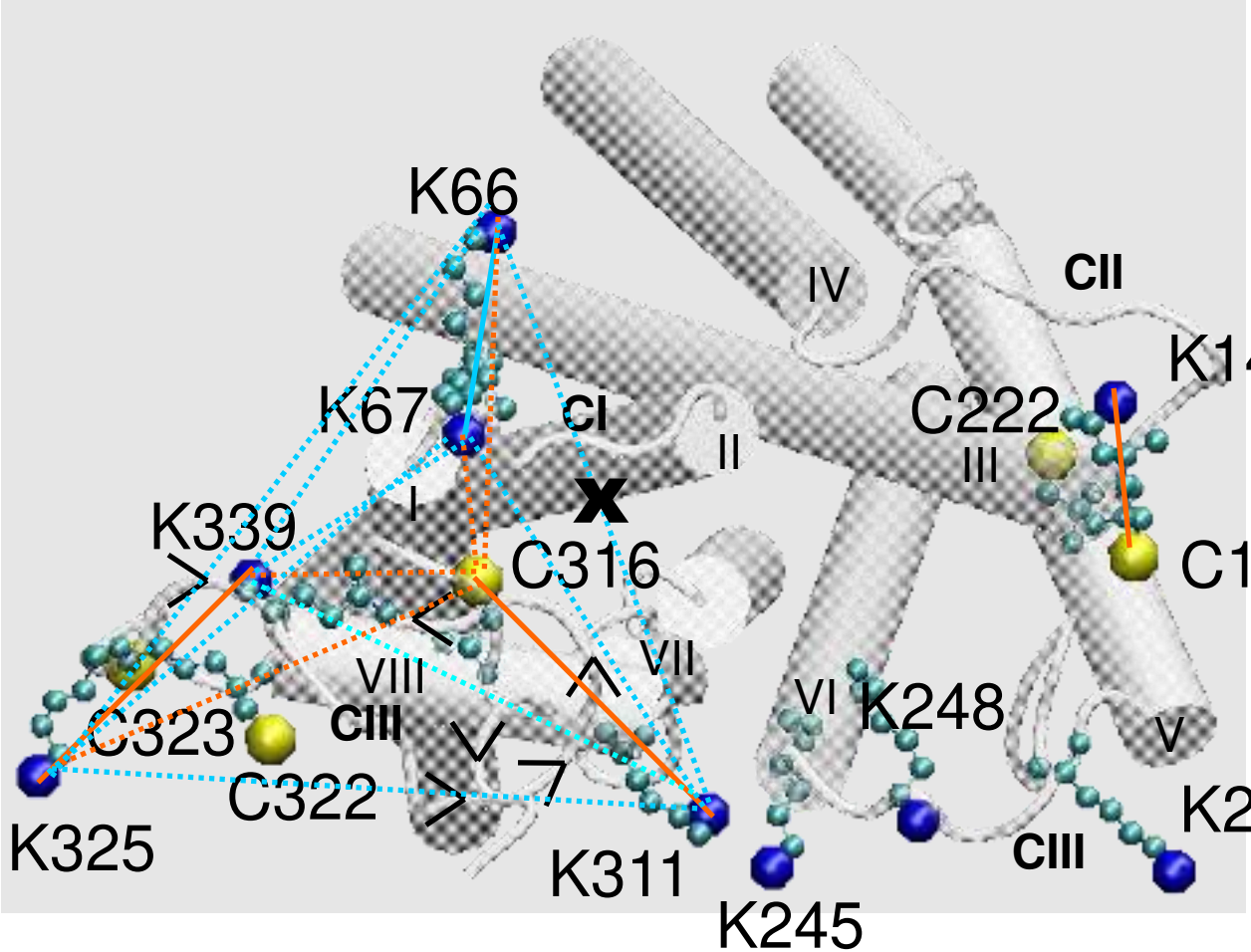

Jacobsen RB, Sale KL, Ayson MJ, et al. Structure and dynamics of dark-state bovine rhodopsin revealed by chemical cross-linking and high-resolution mass spectrometry. Protein Sci. 2006;15(6):1303-1317. doi:10.1110/ps.052040406

CXMS experiment: Topdown approach

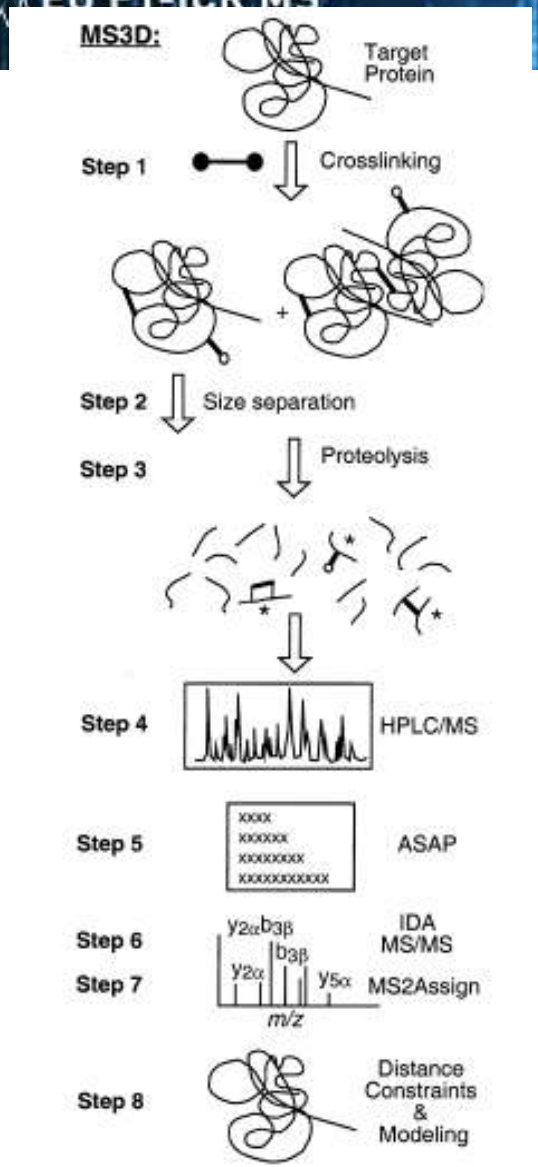

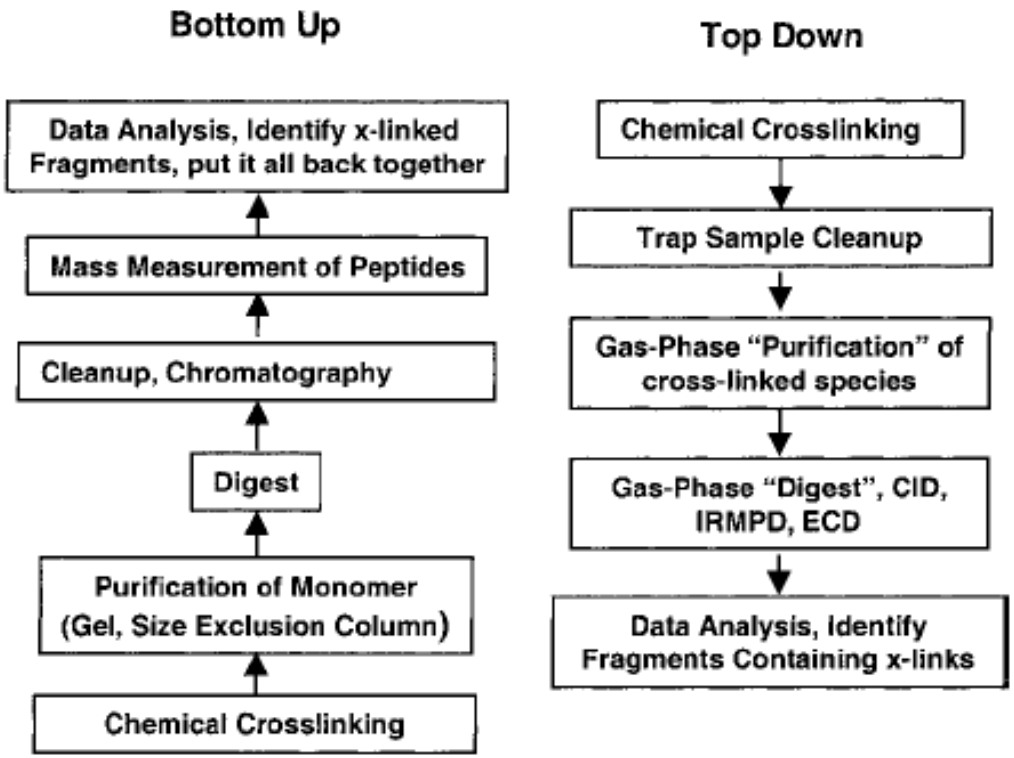

Top down: Cross-linked Ubiquitin with a Series of Cross-linkers

Varying Arm Length

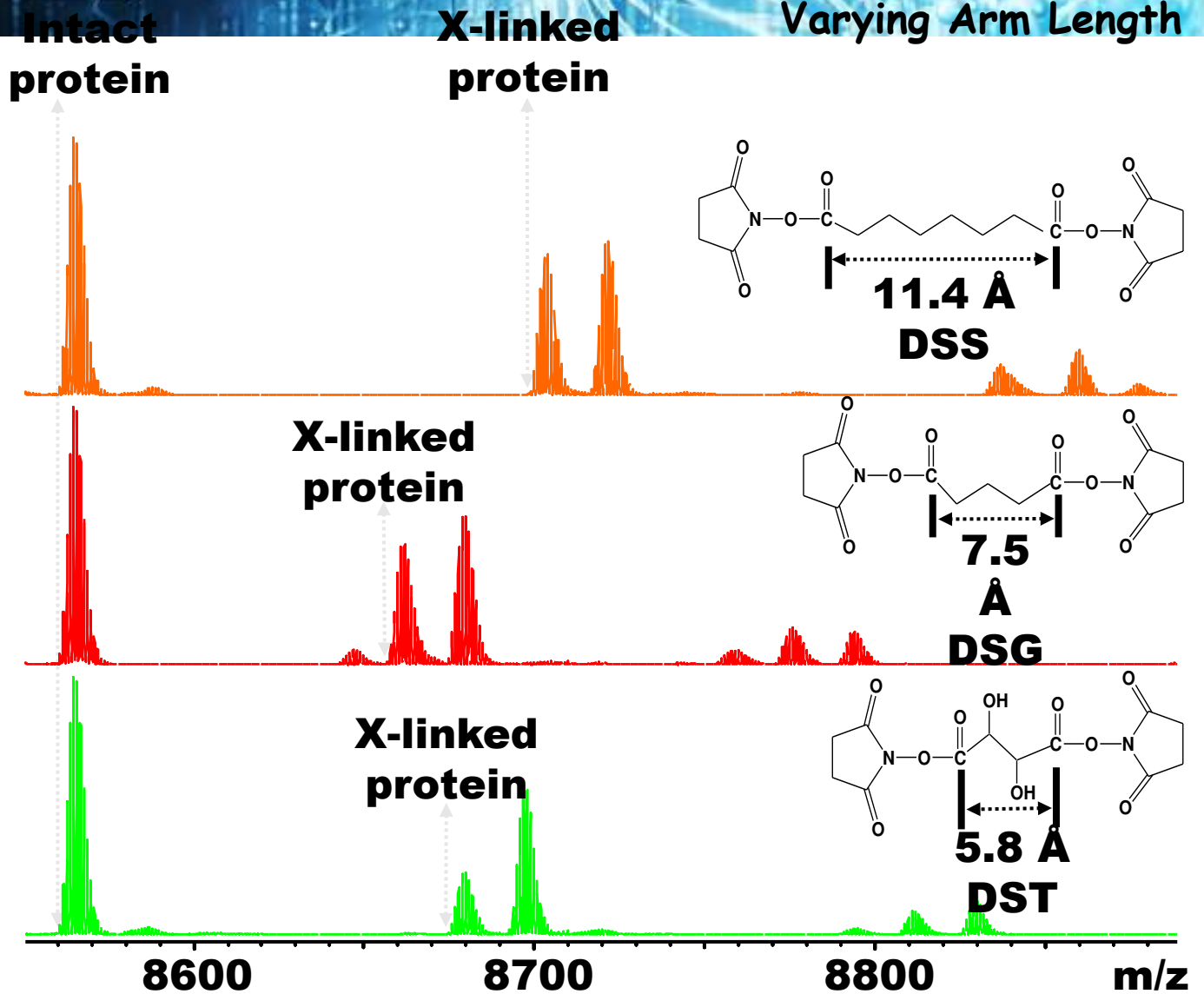

Chemical cross-linking: the identification of cross-link

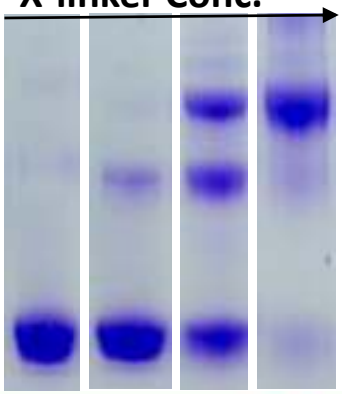

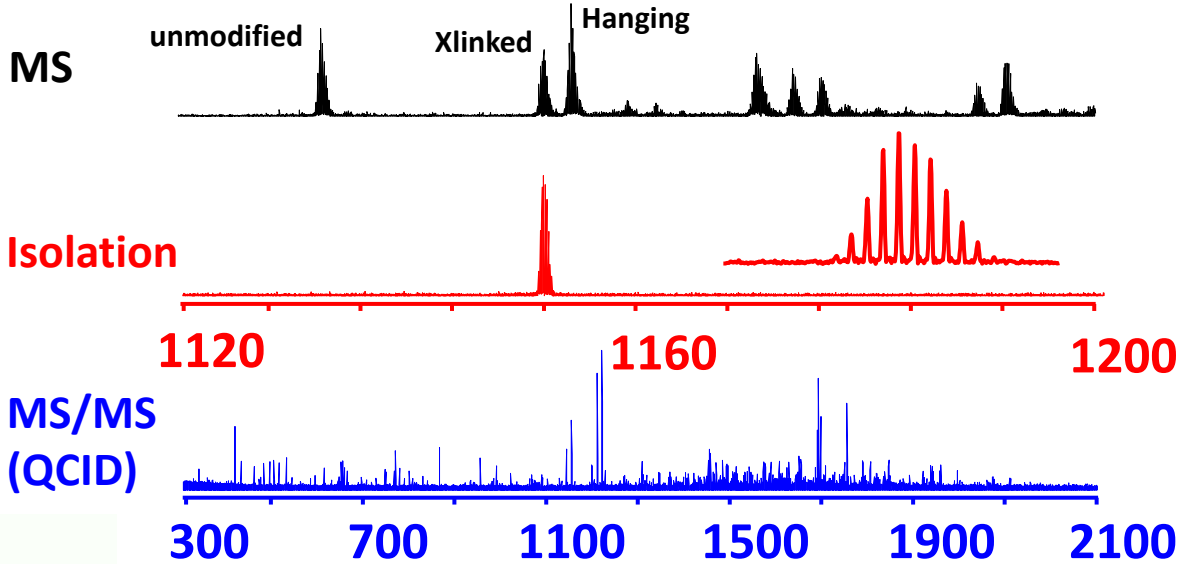

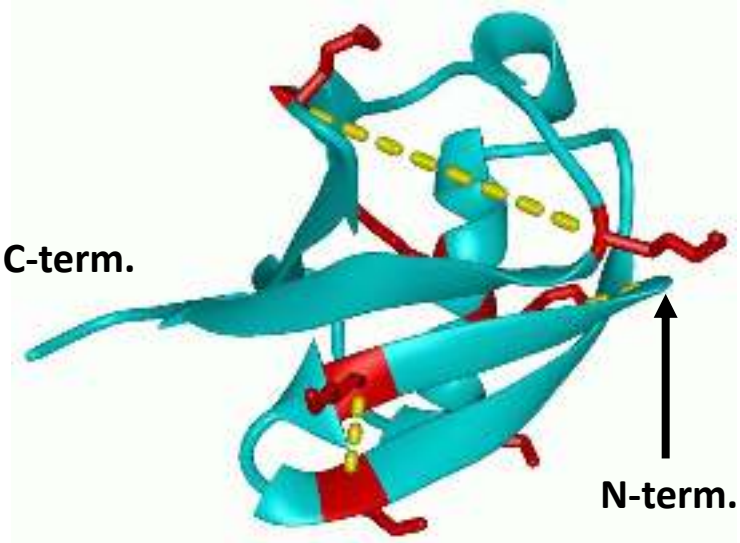

Cross-Link	DSS	DSG	DST	Constraint (N_e-N_e)
M1 – K6	Yes	Yes	Yes	Distance < 5.8 Å
K6-K11	Yes	Yes	Yes	Distance < 5.8 Å
K48-K63	Yes	Yes	No	5.8 Å < Distance < 7.5 Å

Novak et. al. *Eur. J. Mass Spectrom. 2003, 9, 623*

Zero-Length and Carboxy-Carboxy Cross-linking

- "Zero-Length" Cross-linking
  - **No cross-linker used.**
  - **Activate carboxylic acid groups with EDC.**
  - **Activated acid side-chains react with primary amine side-chains (DEO-XK).**
  - **Cross-link formed via new amide linkage.**

- EDC activation can also be used to cross-link acidic side-chains to each other (DEO-DEO)
  - **Use dihydrazides as the cross-linking reagent.**

Chemical cross-linking: an alternative chemistry

Carboxylic group reactive cross-linkers

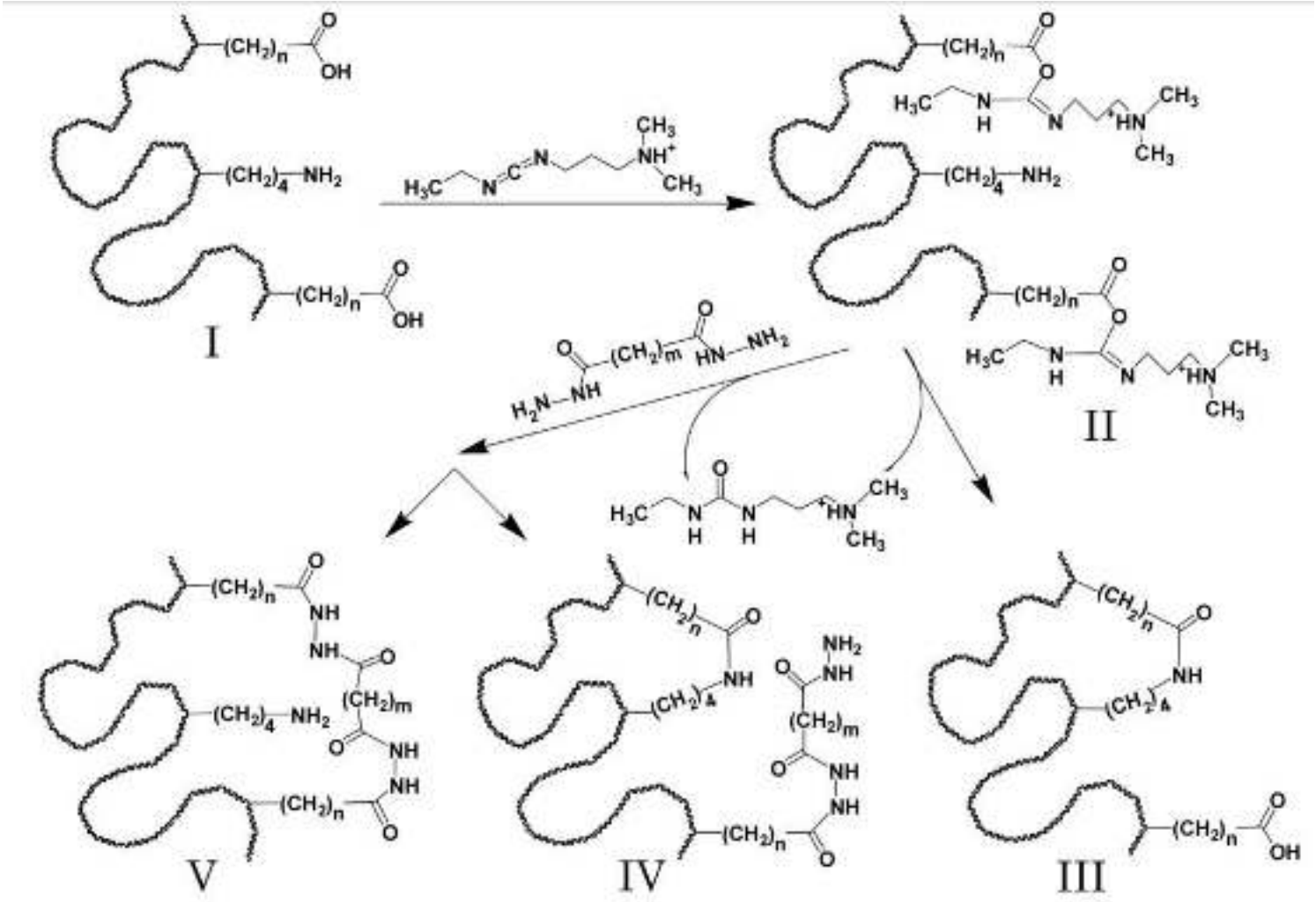

Zero-Length Cross-linking

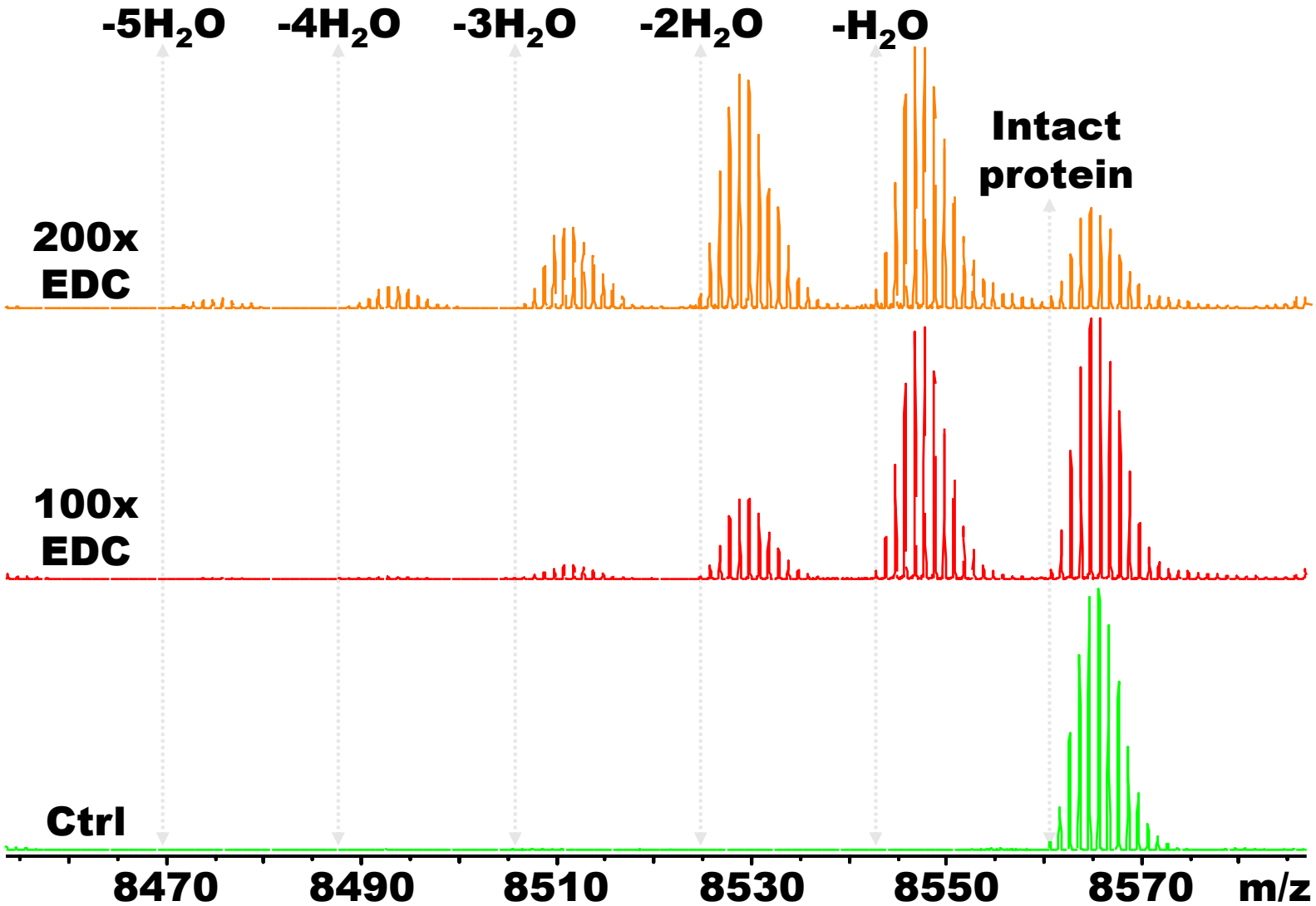

Carboxy-Carboxy Cross-linking

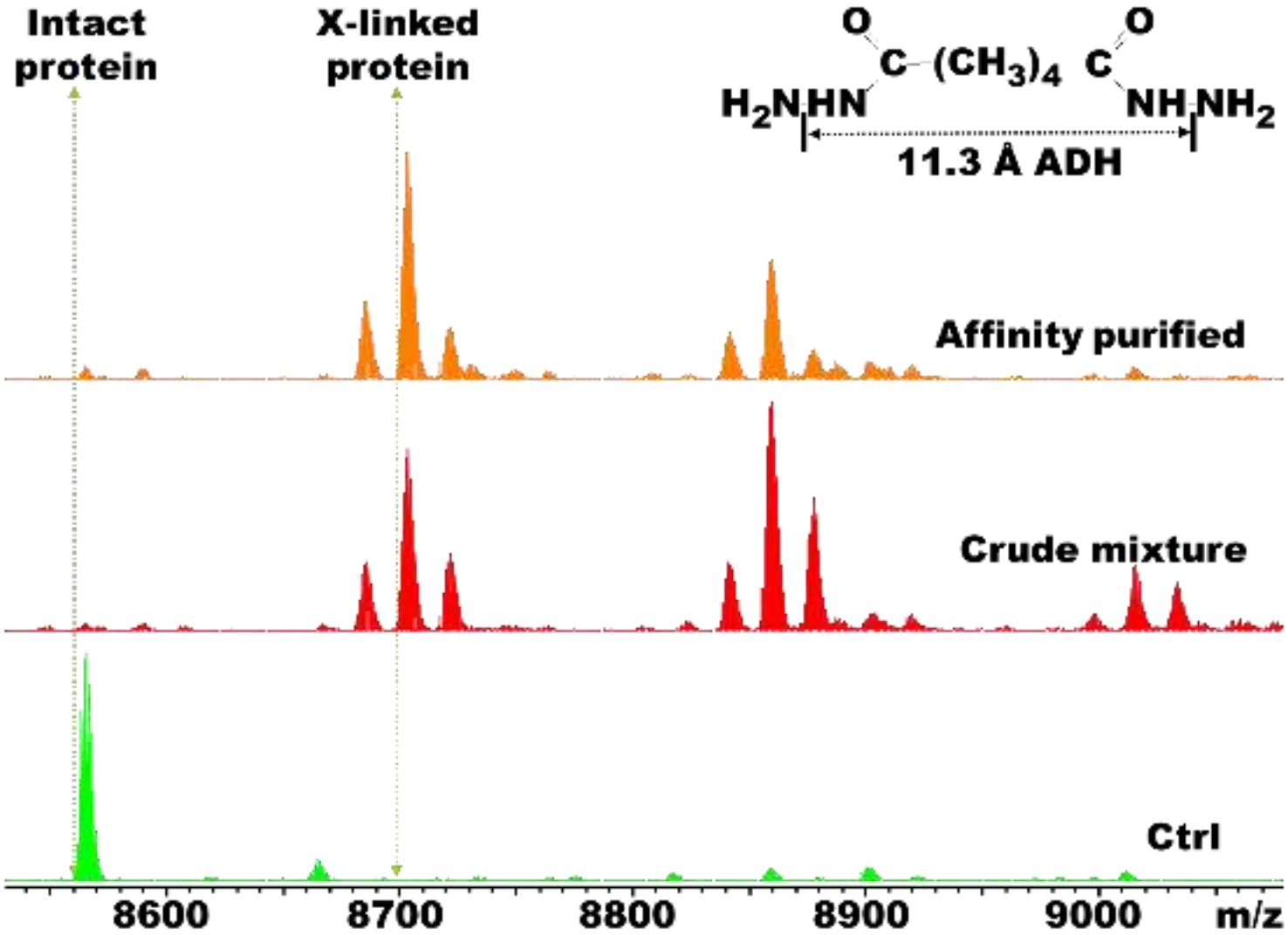

Chemical cross-linking: an alternative chemistry

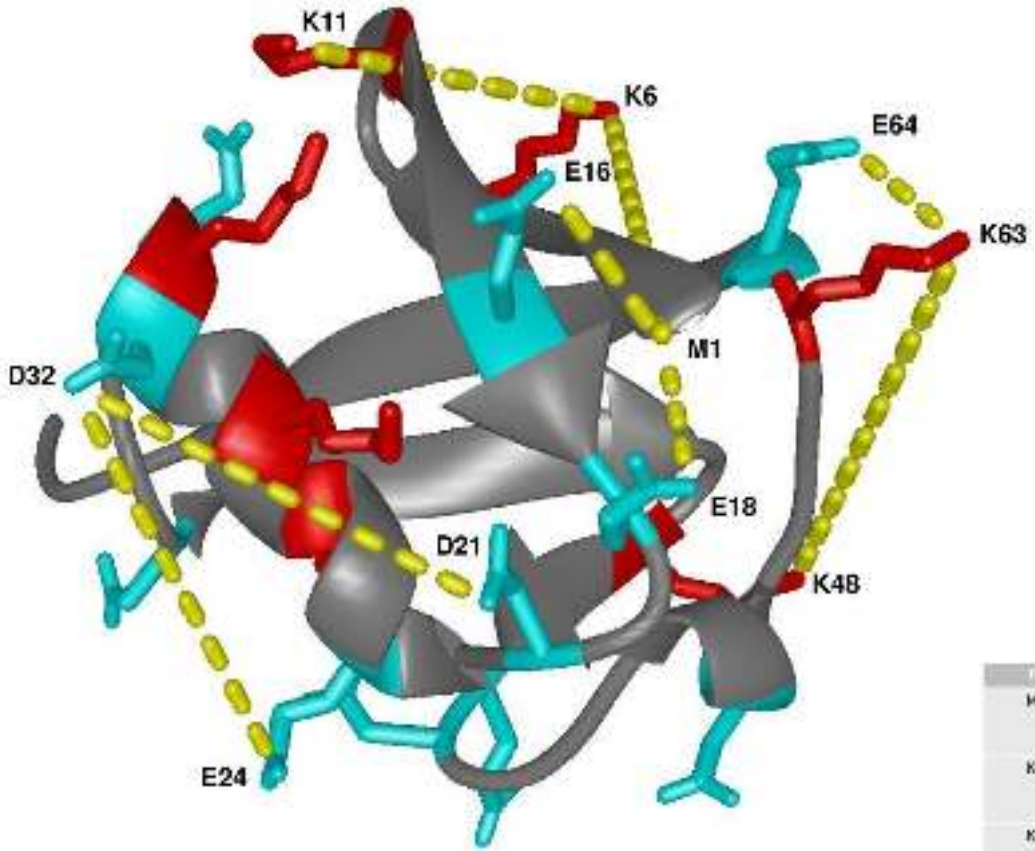

Residue	Cross-linker	Cross-link	Distance (X-ray structure)	Type
M1-K6	DSS	Yes	5.8Å<Distance<15Å (10.1Å)	N_α-N_ε
	DSG	Yes		
	DST	No		
K6-K11	DSS	Yes	Distance<5.8Å (4.0Å)	N_ε-N_ε
	DSG	Yes		
	DST	Yes		
K48-K63	DSS	Yes	5.8Å<Distance<15Å (9.6Å)	N_ε-N_ε
	DSG	Yes		
	DST	No		
M1-E16	EDC	Yes	Distance<15Å (6.3Å)	N_α-C_δ
M1-E18	EDC	Yes	Distance<15Å (6.4Å)	N_α-C_δ
K63-E64	EDC	Yes	Distance<15Å (6.8Å)	N_ε-C_δ
E21-D32	ADH	Yes	5.8Å<Distance<15Å (12.5Å)	C_γ-C_γ
	SDH	No		
E24-D32	ADH	Yes	5.8Å<Distance<15Å (14.0Å)	C_δ-C_γ
	SDH	No		

Novak et. al. *Eur. J. Mass Spectrom. 2008, 14, 355*

Bottom up/Top down

TOP DOWN MS3D WORKS WELL FOR:

- Characterizing new cross-linking chemistry on small model proteins (< 20 kDa).
- Small proteins with unknown or partially known structures.
- Reactivity studies.

BOTTOM UP APPROACH WITH DIGEST FOR LARGER PROTEINS

- Localizing cross-links with digests alone is difficult
- Combined bottom up/top down approach
  - Digest protein with a single protease
  - Analyze the large cross-linked fragments with top down methods

Introduction of isotopically labeled probes

Incorporation of stable isotopes (deuterium) to the linker

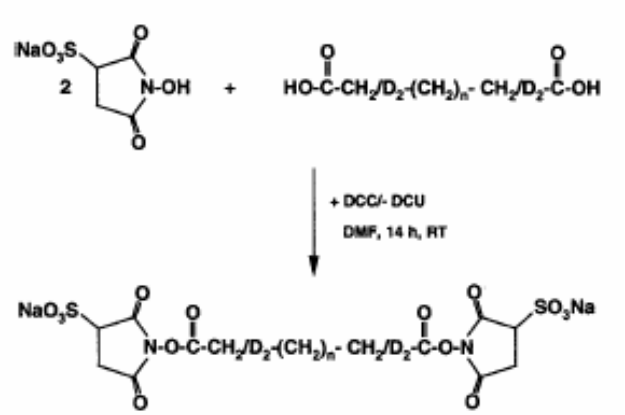

^{13}C available as well

Muller DR. et al. Anal. Chem. 2001

Incorporation of stable isotopes (oxygen, ^{18}O) to the linker

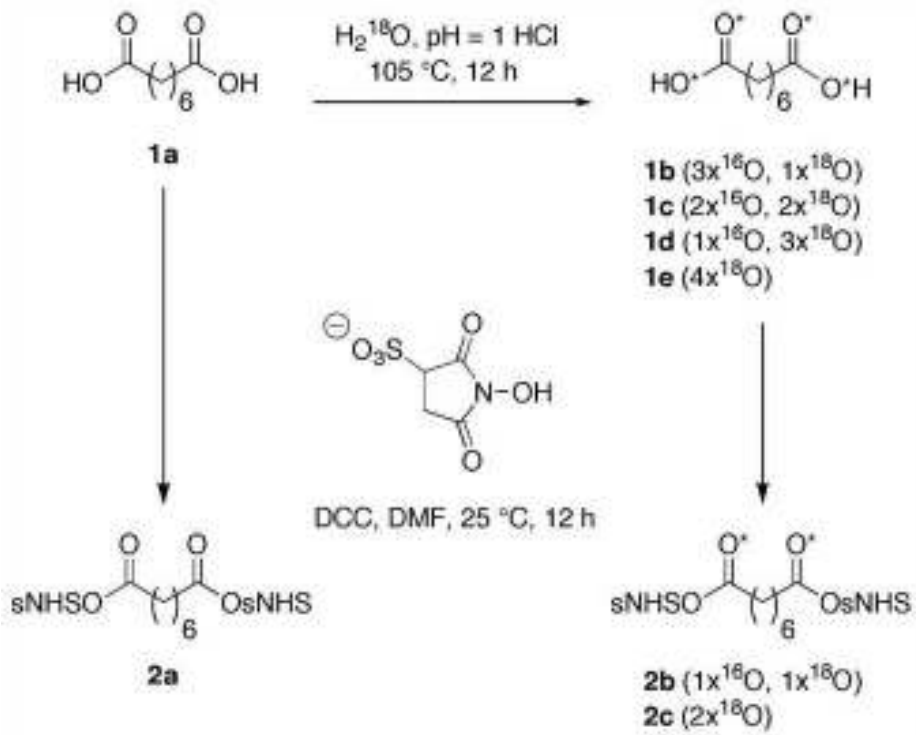

Collins CJ. et al. Bioorg. Med. Chem. Lett. 2003

Introduction of isotopically labeled probes

EU FT-ICR MS

Simplifies data analysis

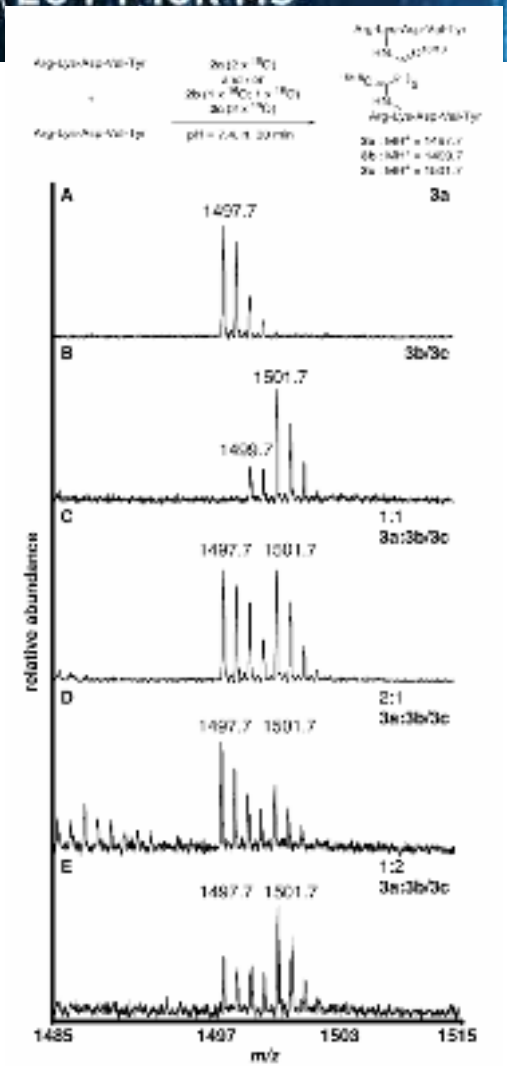

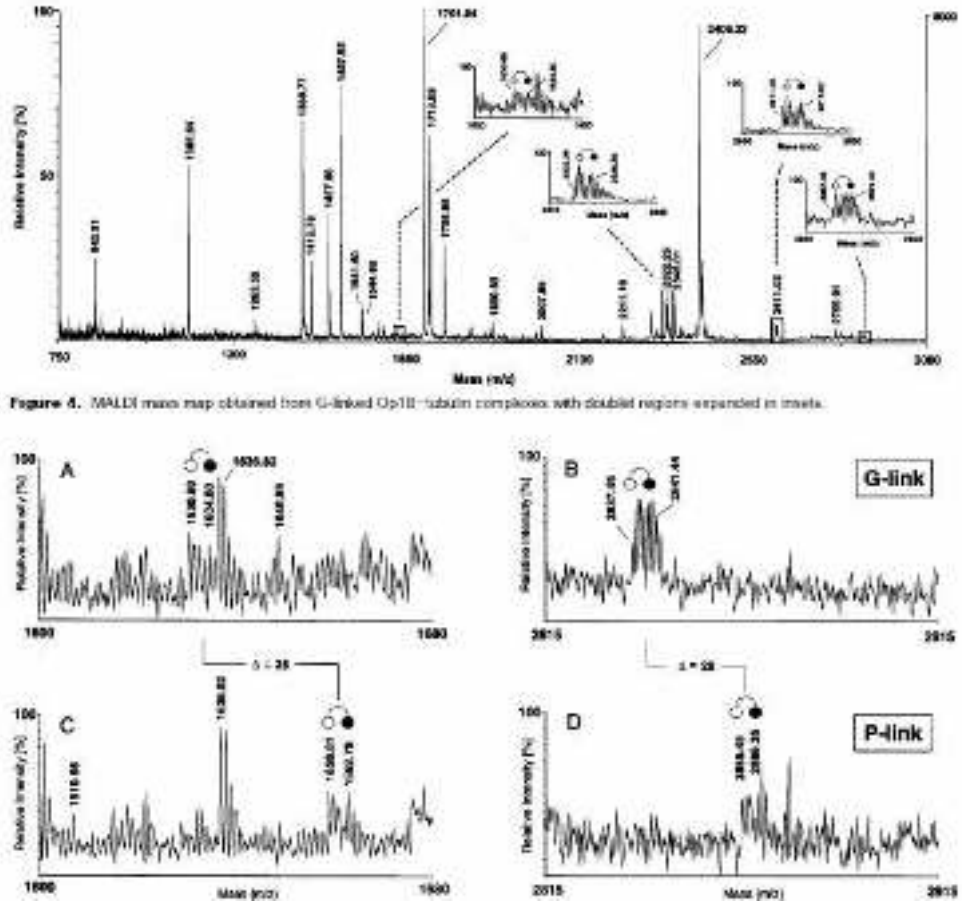

Figure 4. MALDI mass map obtained from G-linked Op18–tubulin complexes with doublet regions expanded in insets.

Collins CJ. et al. Bioorg. Med. Chem. Lett. 2003

Muller DR. et al. Anal. Chem. 2001

Quantitative chemical cross-linking

Protein dynamics and conformationa

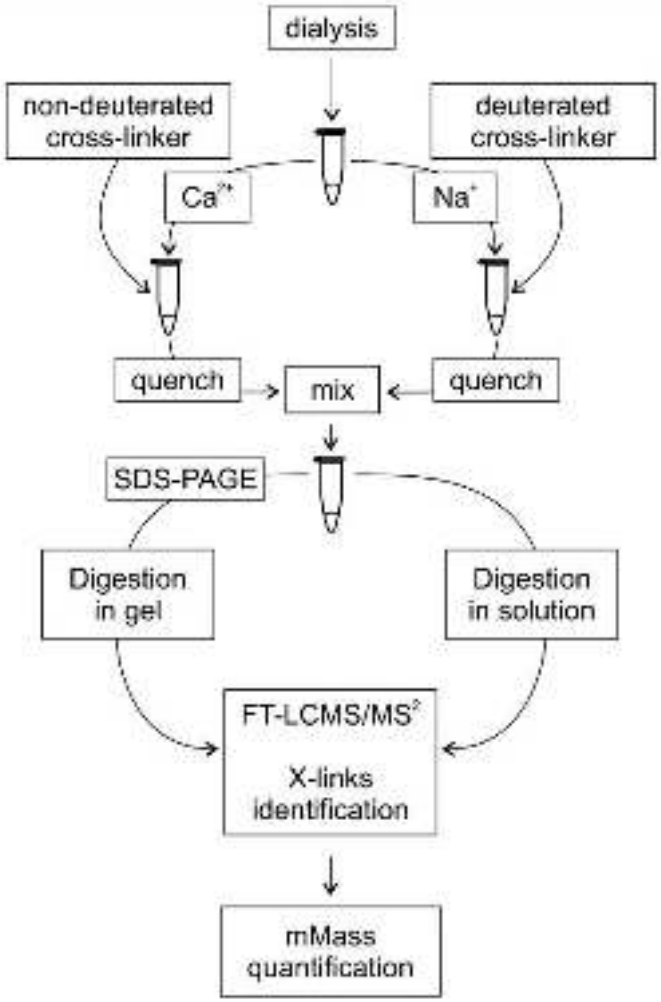

Kukacka Z. et al. Methods 2015

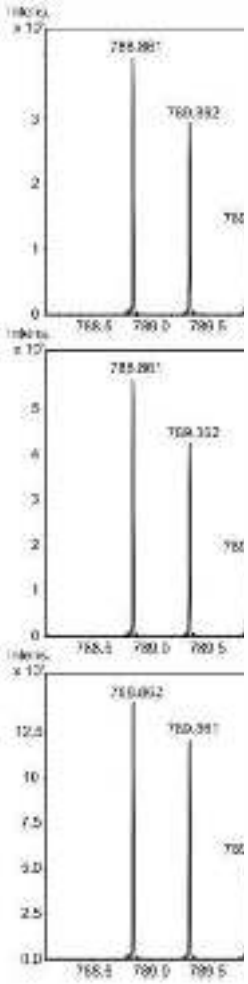

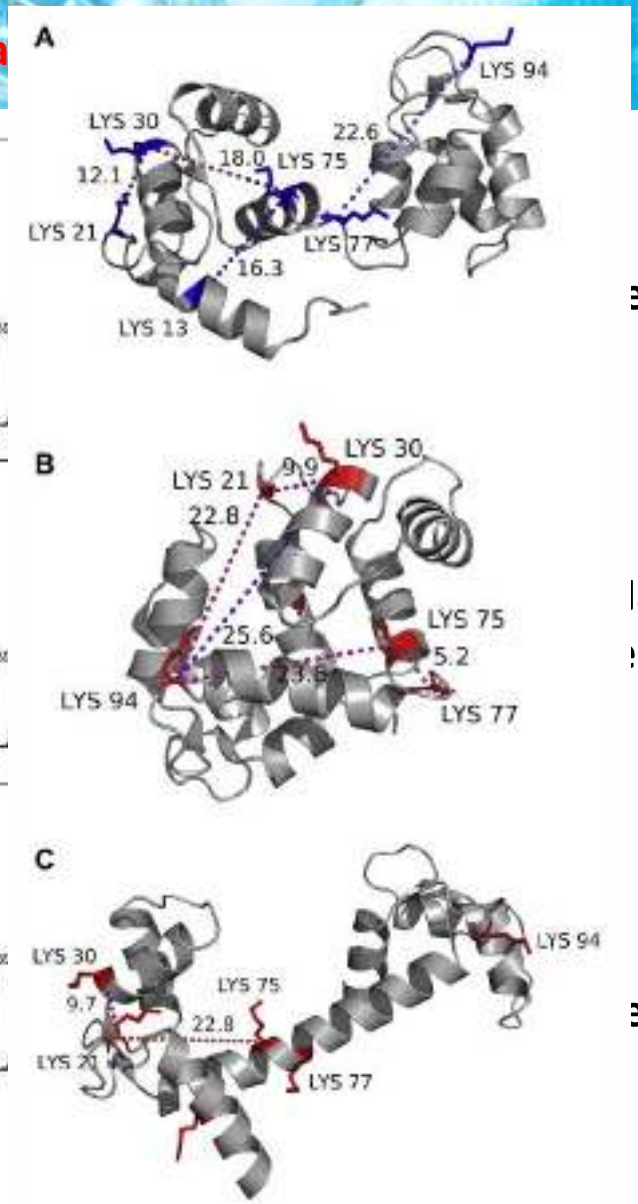

Novel cross-linker design

- Affinity tag for purification
- Gas phase cleavable linker for easy data analysis

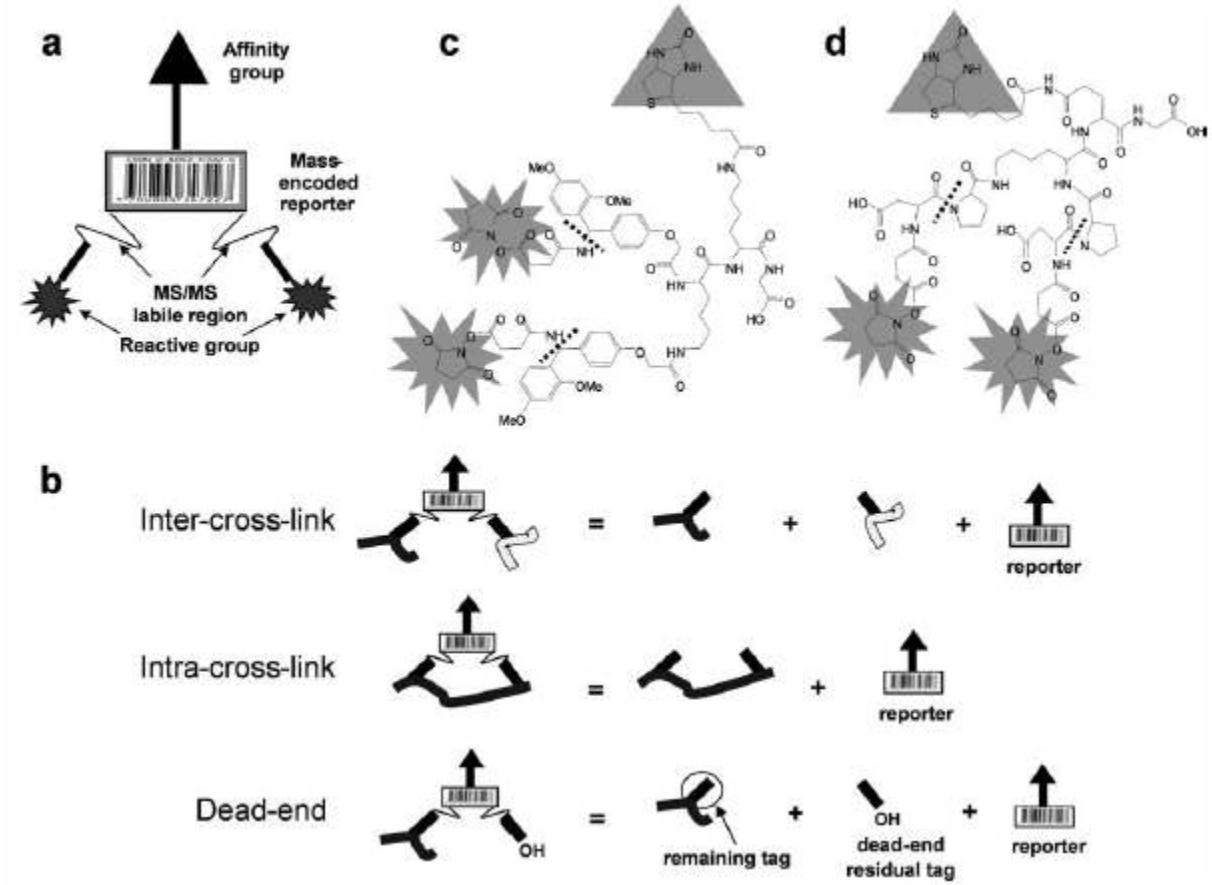

Tang X. et al. Anal. Chem. 2005

Smart design enables in vivo cross-linking

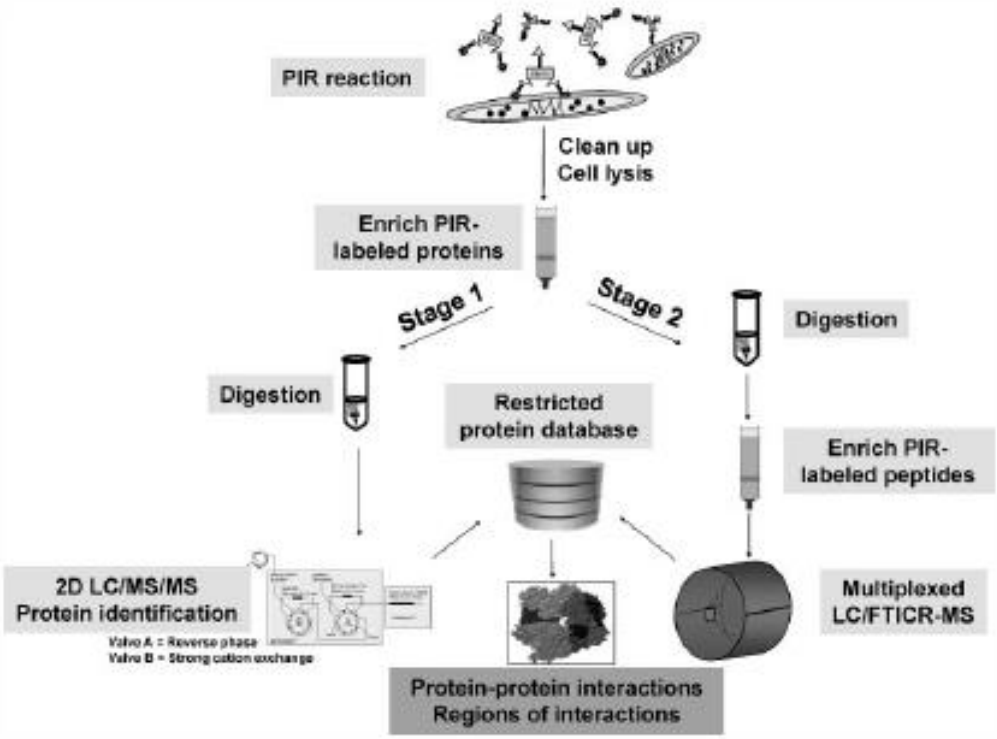

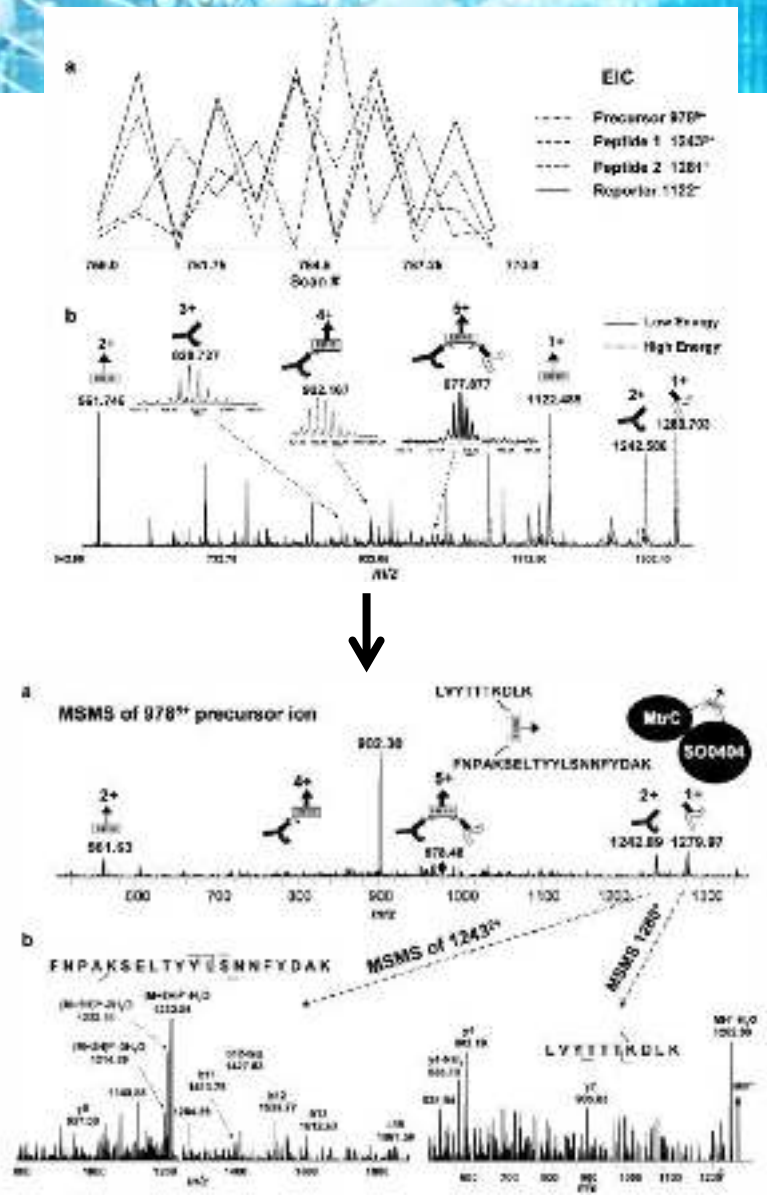

New generation of cleavable cross-linkers

DSSO

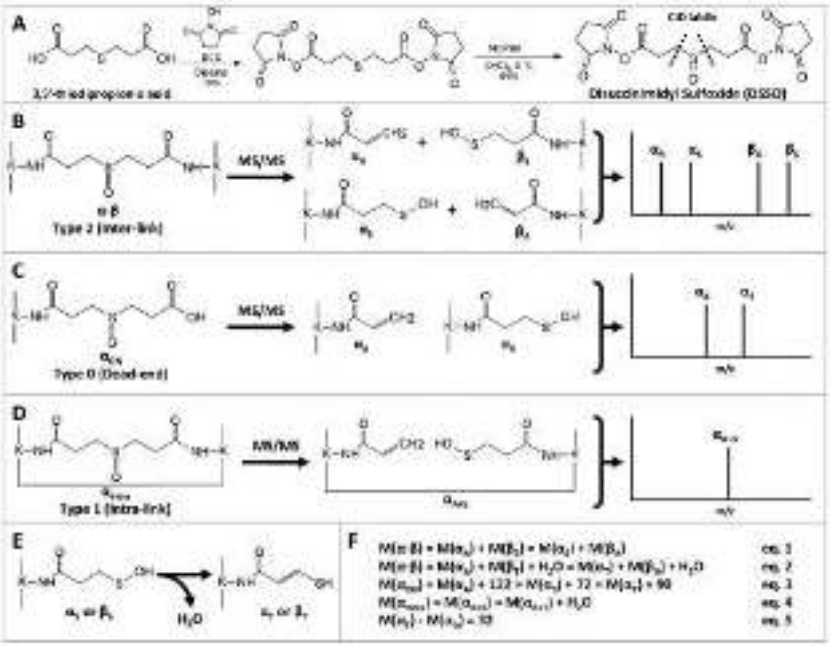

Kao MQ. et al. Mol. Cell Prot. 2010

DSSBu

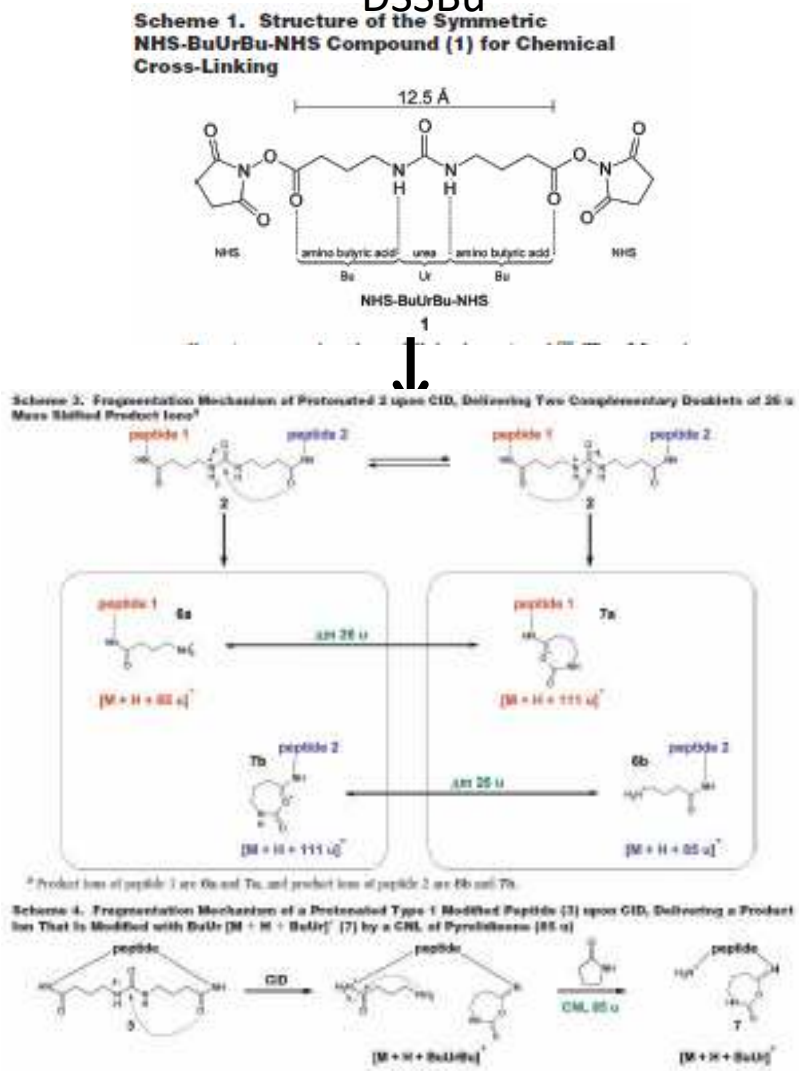

Muller A. et al. Anal. Chem. 2011

Data analysis: MEROX

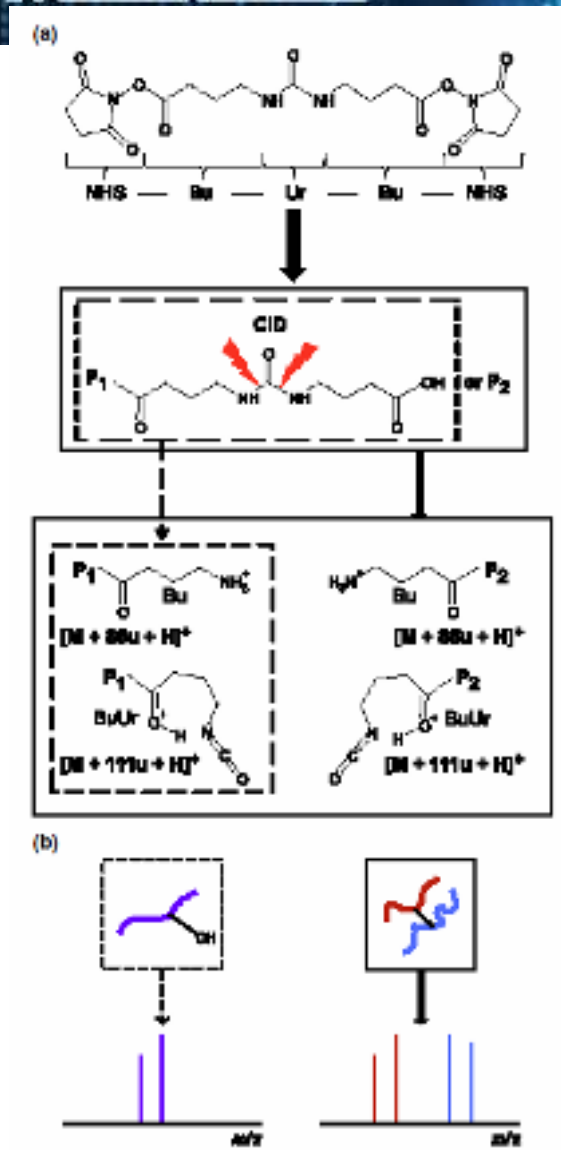

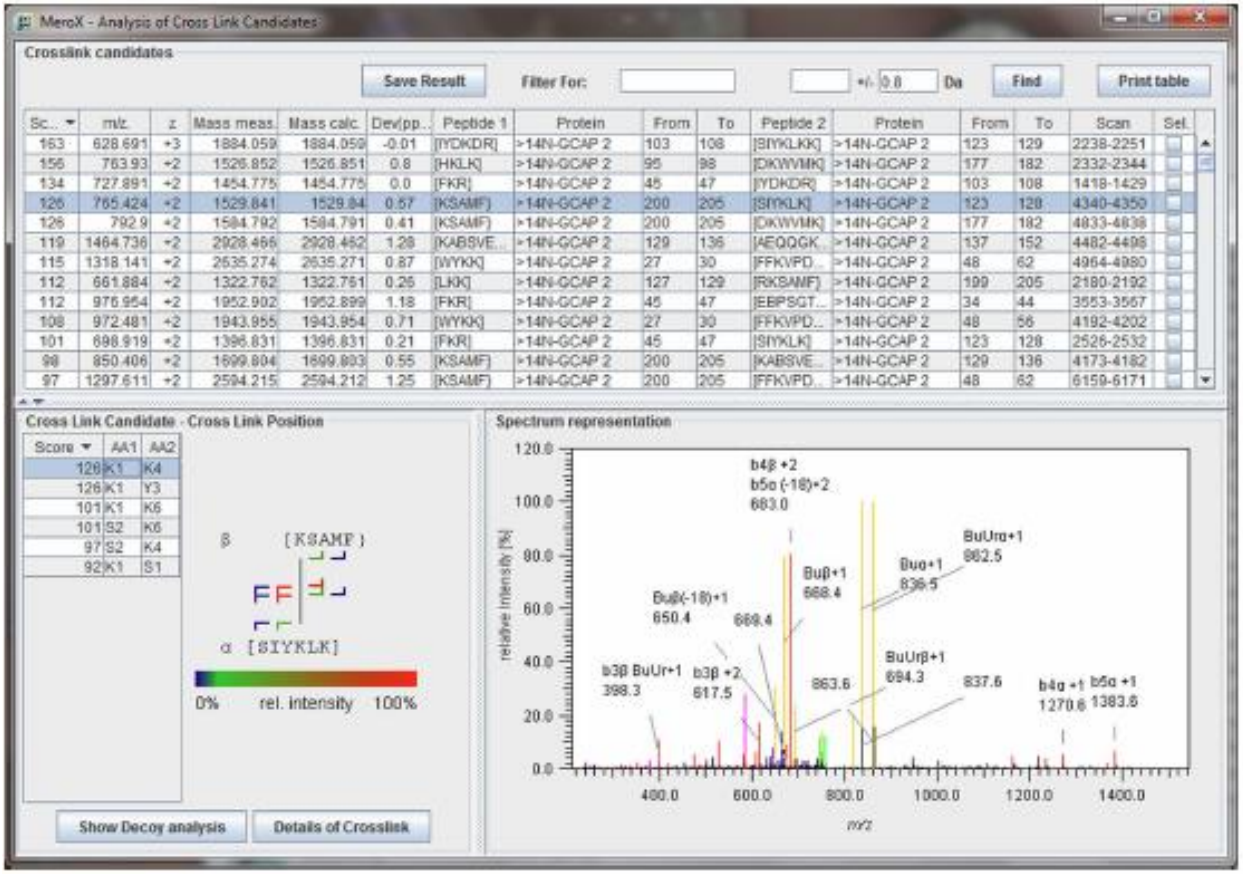

Gotze M. et al. JASMS 2015

Protein-nucleic acid cross-linking

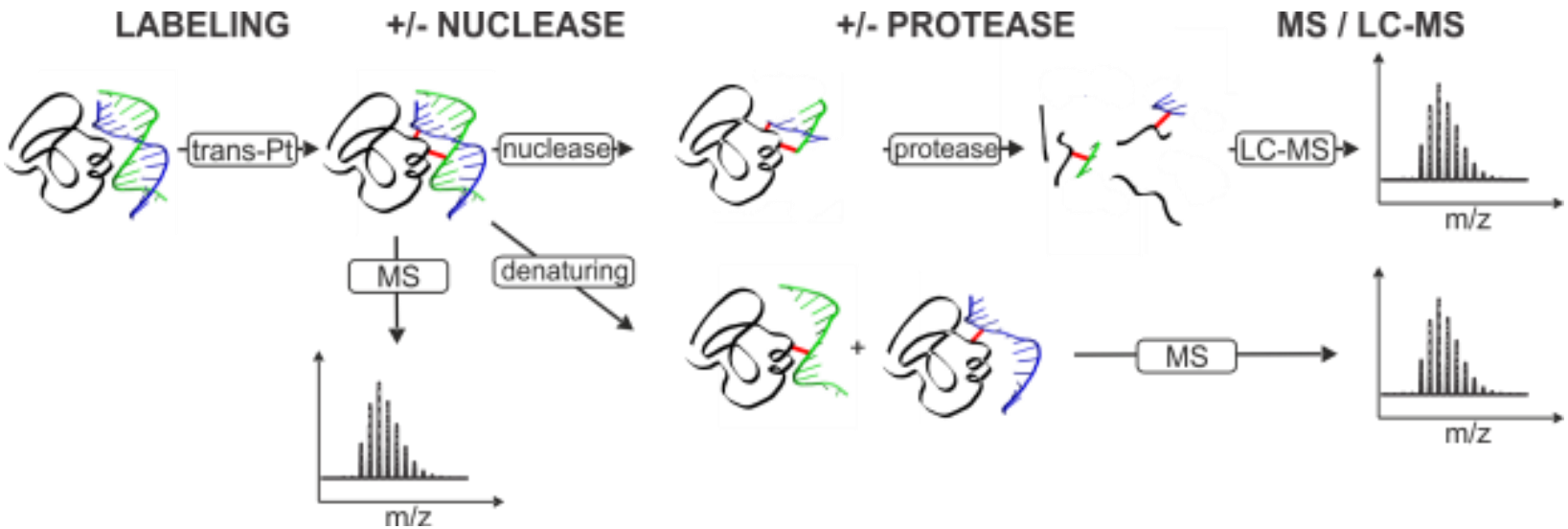

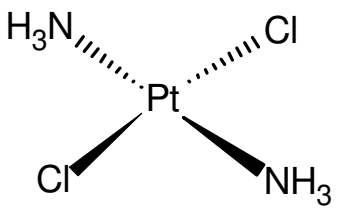

Trans-platinum

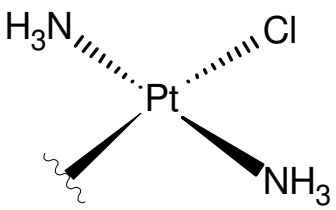

Trans-platinum (monofunctional)

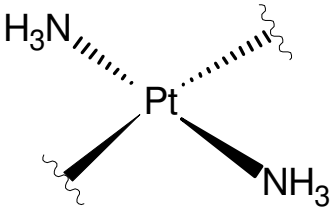

Trans-platinum (bifunctional)

Slavata, L. et al Biomolecules 2019, 9(10), 535

Protein – DNA cross-links

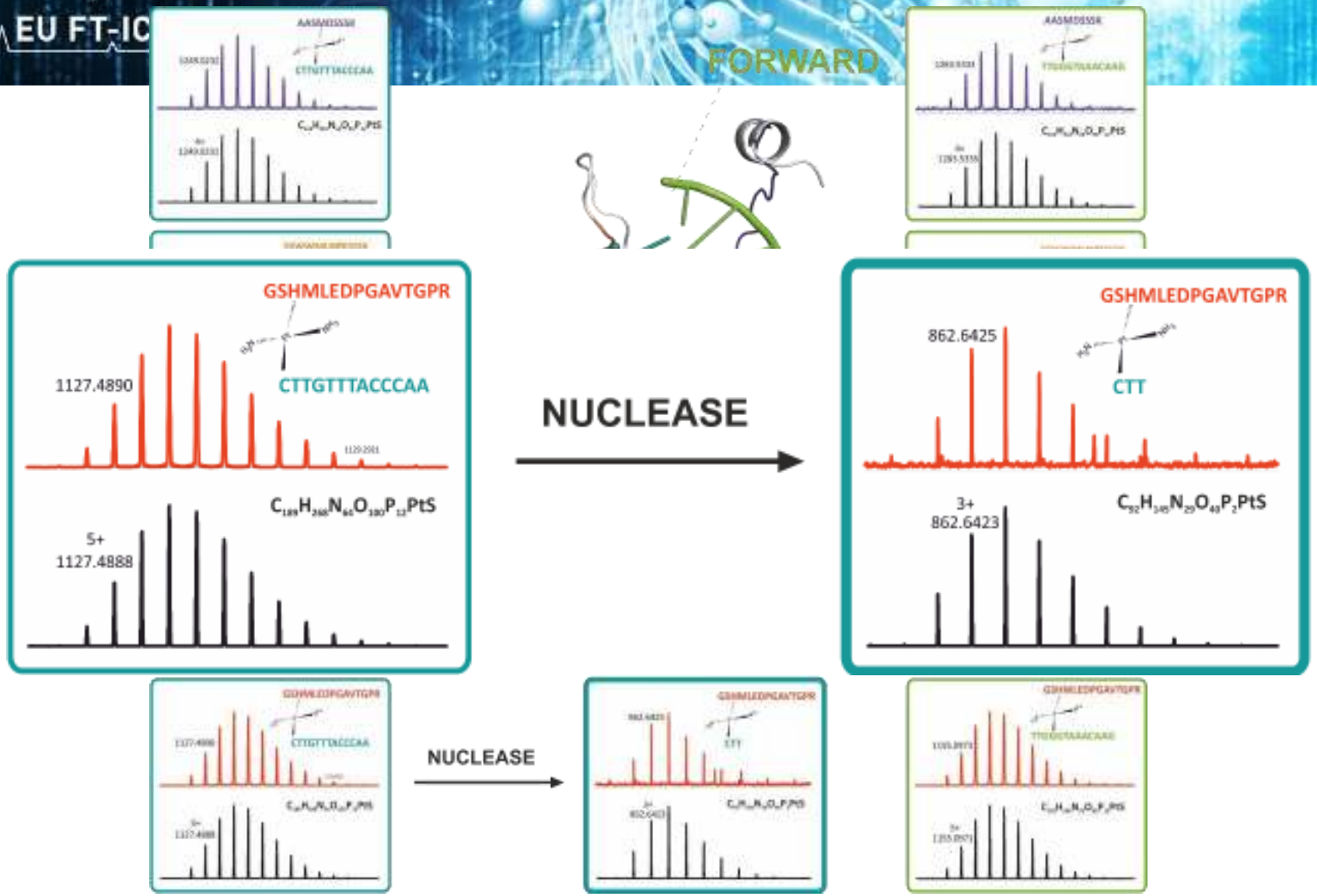

Kukačka Z et al J Proteome Res. 2021 Apr 2;20(4):2021-2027

Thanks for your attention!

EU FT-ICR MS

H2020 EUROPEAN NETWORK OF FOURIER-TRANSFORM ION-CYCLOTRON-RESONANCE MASS SPECTROMETRY CENTERS - PROJECT AGREEMENT NO.731077

EU FT-ICR MS

Structural Proteomics

Hydrogen/deuterium exchange

Petr Man

IMIC

Hydrogen/deuterium exchange…

…is good for what?

Conformational characterization

protein fold (structured regions)
comparability of proteins (biosimilars)
stability
influence of pH, ionic strength, temperature, mutation

Protein-ligand interactions

lipids / membranes
nucleic acids
small molecules, cofactors, ions
proteins (epitope mapping)

Hydrogen/deuterium exchange

How it works?

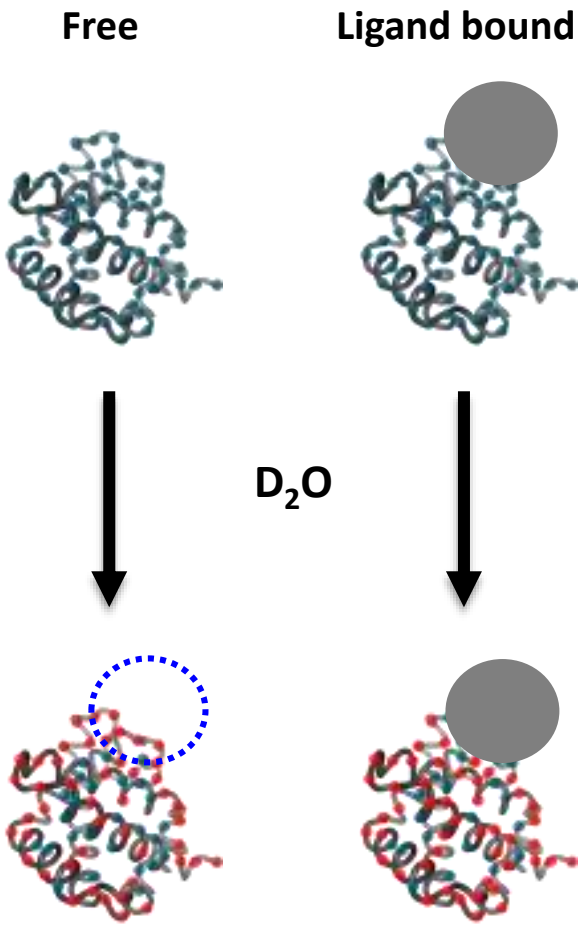

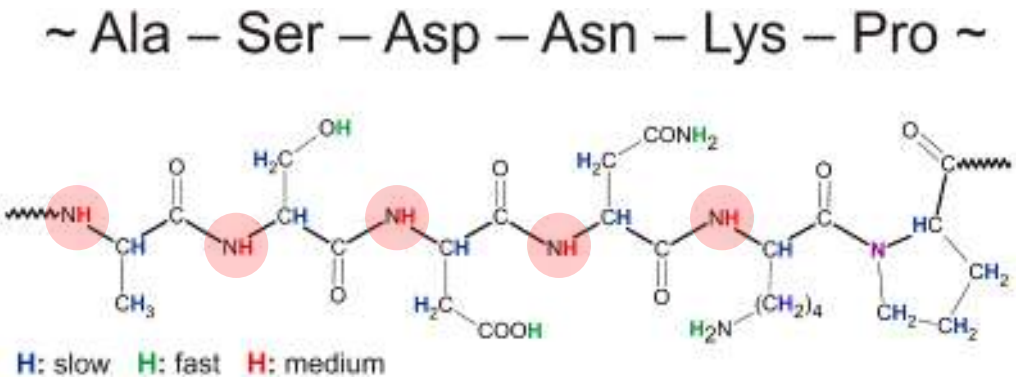

Factors affecting H/D exchange

~ Ala – Ser – Asp – Asn – Lys – Pro ~

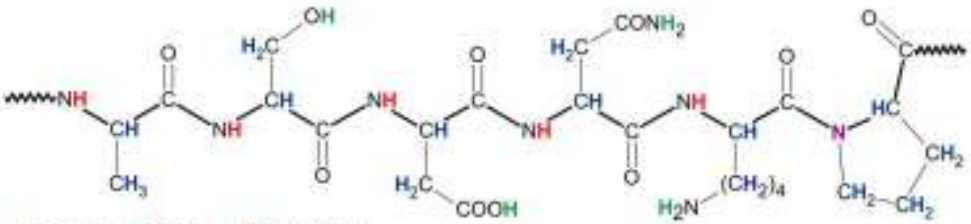

H: slow H: fast H: medium

Changes in **hydrogen bonding** and **solvent accessibility** accessed through **H/D exchange of protein backbone amide hydrogens.**

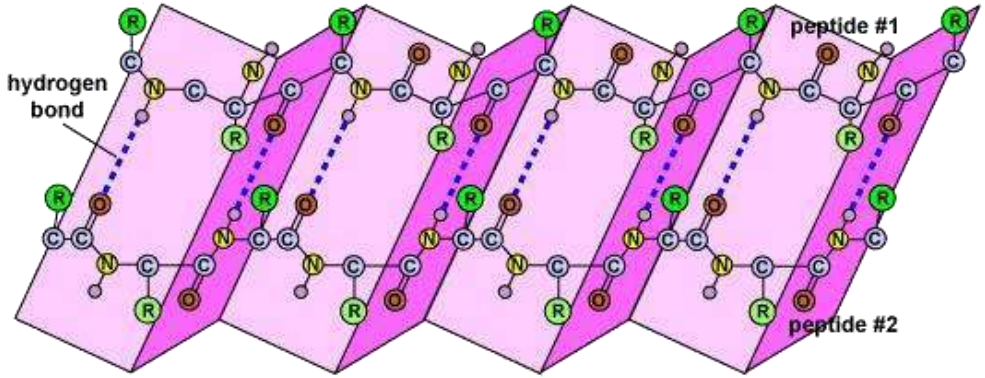

beta pleated sheet

alpha helix

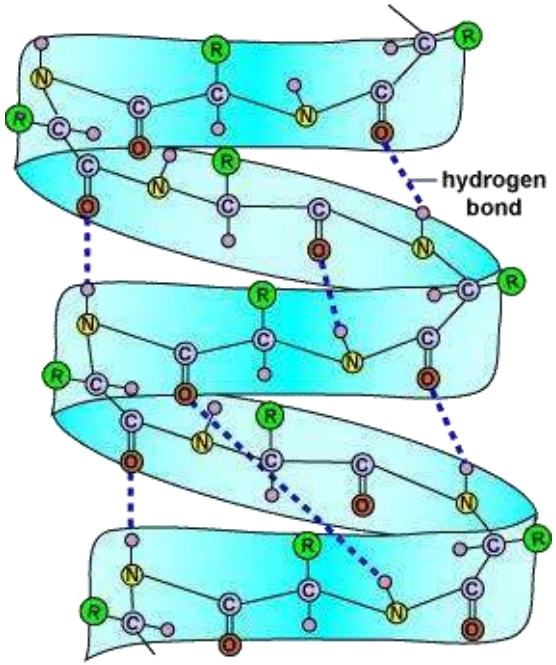

H/D exchange mechanism / kinetics

$$F_H \underset{k_{-1}}{\overset{k_1}{\rightleftharpoons}} U_H \xrightarrow[D_2O]{k_2} U_D \underset{k_1}{\overset{k_{-1}}{\rightleftharpoons}} F_D$$

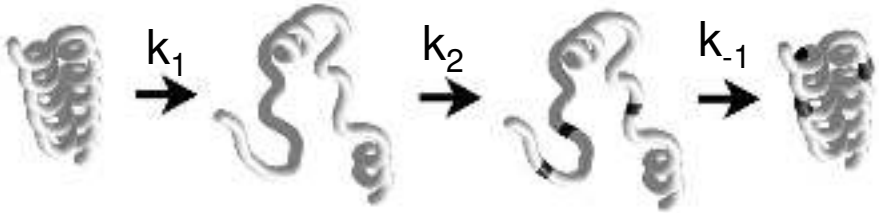

EX2

$k_{-1} >> k_2$

uncorrelated

EX1

$k_{-1} << k_2$

correlated

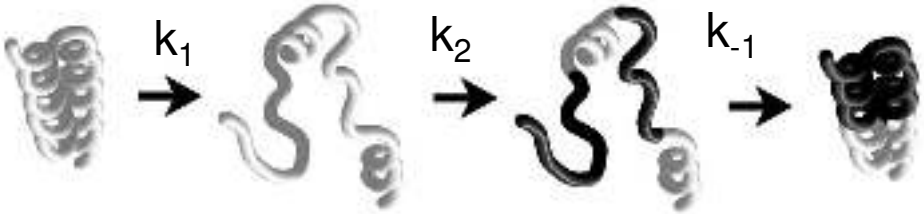

Factors affecting H/D exchange

Temperature

$$k(T_2) = k(T_1)exp^{-\frac{E_a}{R}\left(\frac{1}{T_2}-\frac{1}{T_1}\right)}$$

pH

$$pD = pH_{read} + 0.4$$

1 ΔpH ... 10×
10°C ... 3×

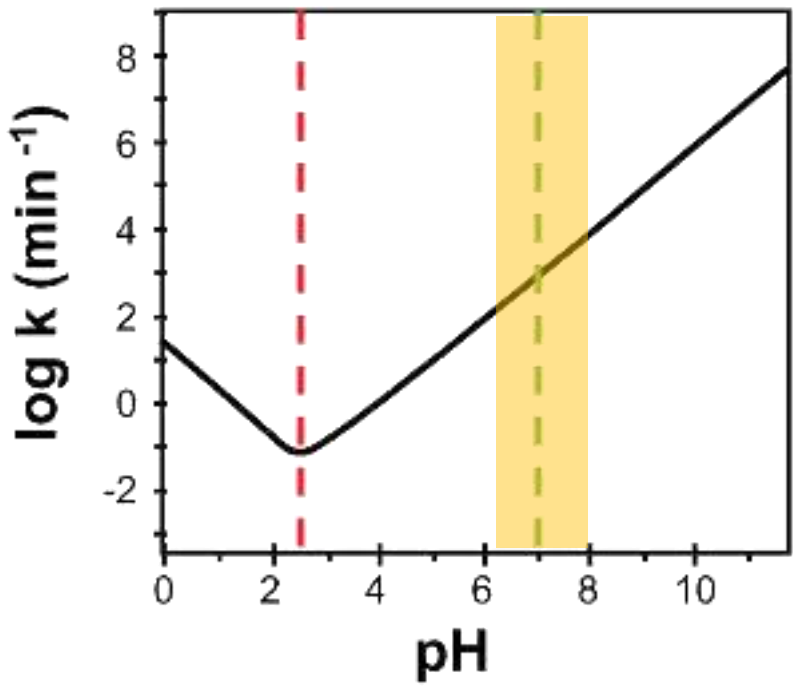

Bai *et al.*: Proteins (1993)

Glasoe, Long: J. Phys. Chem. (1960)

Factors affecting H/D exchange

Side chains

(acidity, steric shielding)

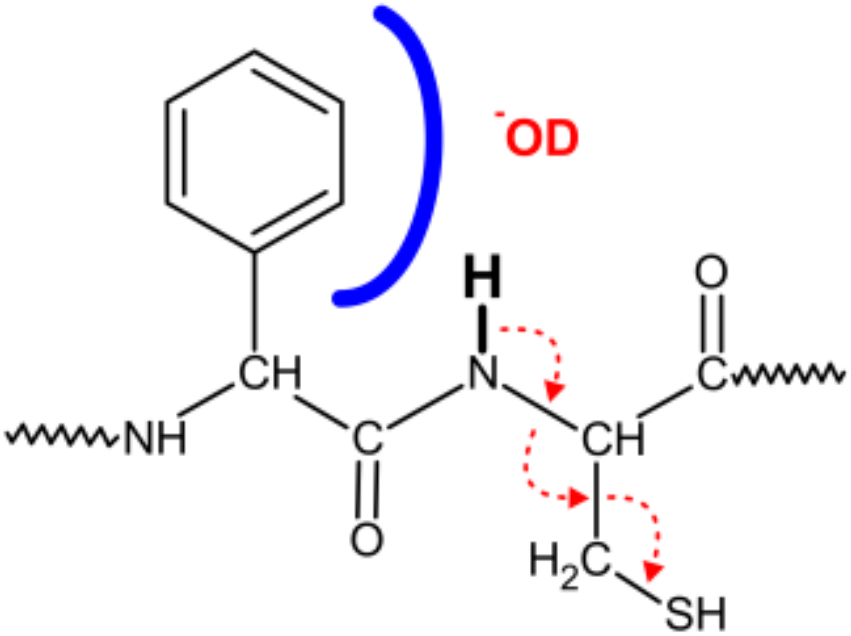

Bai *et al.*: Proteins (1993)

Factors affecting H/D exchange – side chain effects

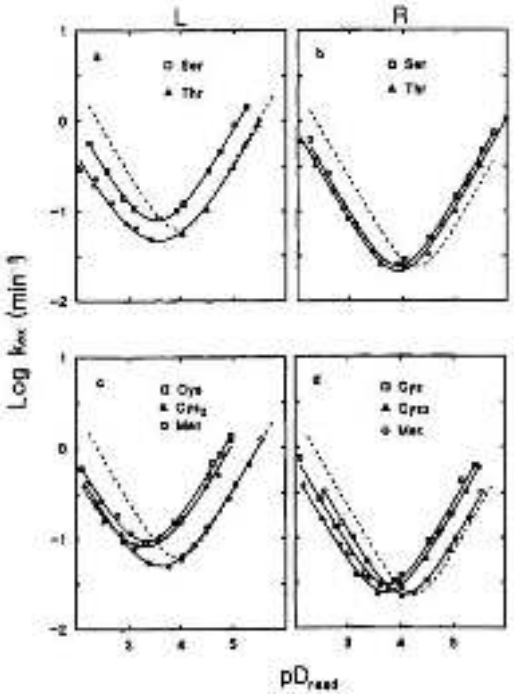

Inductive effect – electron density is withdrawn from peptide bond (S, O). Increasing base catalyzed and decreasing acid catalyzed rates

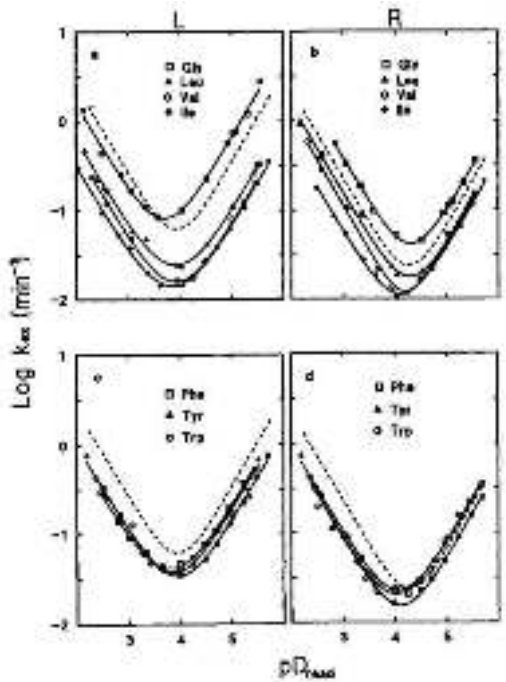

Downward shift due to steric hindrance effect of aliphatic and aromartic side chains. Aromatics also shows inductive effect

TABLE II. Effects of Amino Acid Side Chains on the HX Rates of Neighboring Peptides*

	$Log k_{ex}(X) - Log k_{ex}(Ala)$			
	Acid catalysis		Base catalysis	
Side chain (X)	L	R	L	R
Ala	0.00	0.00	0.00	0.00
Arg	−0.59	−0.32	0.08	0.22
Asn	−0.58	−0.13	0.49	0.32
Asp(COO⁻)	(0.9)	0.58	−0.30	−0.18
Asp(COOH)	(−0.9)	−0.12	0.69	(0.6)
Cys	−0.54	−0.46	0.62	0.55
Cys_2	−0.74	−0.58	0.55	0.46
Gly	−0.22	0.22	0.27	0.17
Gln	−0.47	−0.27	0.06	0.20
Glu(COO⁻)	(−0.9)	0.31	−0.51	−0.15
Glu(COOH)	(−0.6)	−0.27	0.24	0.39
His			−0.10	0.14
His^+	(−0.8)	−0.51	(0.8)	0.83
Ile	−0.91	−0.59	−0.73	−0.23
Leu	−0.57	−0.13	−0.58	−0.21
Lys	−0.56	−0.29	−0.04	0.12
Met	−0.64	−0.28	−0.01	0.11
Phe	−0.52	−0.43	−0.24	0.06
Pro(*trans*)		−0.19		−0.24
Pro(*cis*)		−0.85		0.60
Ser	−0.44	−0.39	0.37	0.30
Thr	−0.79	−0.47	−0.07	0.20
Trp	−0.40	−0.44	−0.41	−0.11
Tyr	−0.41	−0.37	−0.27	0.06
Val	−0.74	−0.30	−0.70	−0.14
N-term (NH_3^+)		−1.32		1.62
C-term (COO⁻)	0.96		(−1.8)	
C-term (COOH)	(0.05)			

*L and R refer to peptide groups to the left and right, respectively, of the side chain indicated (replacing the λ and ρ terminology of Molday et al.[6]). Values are listed in logarithmic form for use with Eq. (2). Values in parentheses are less well determined.

Bai *et al.*: Proteins (1993)

H/D exchange workflow

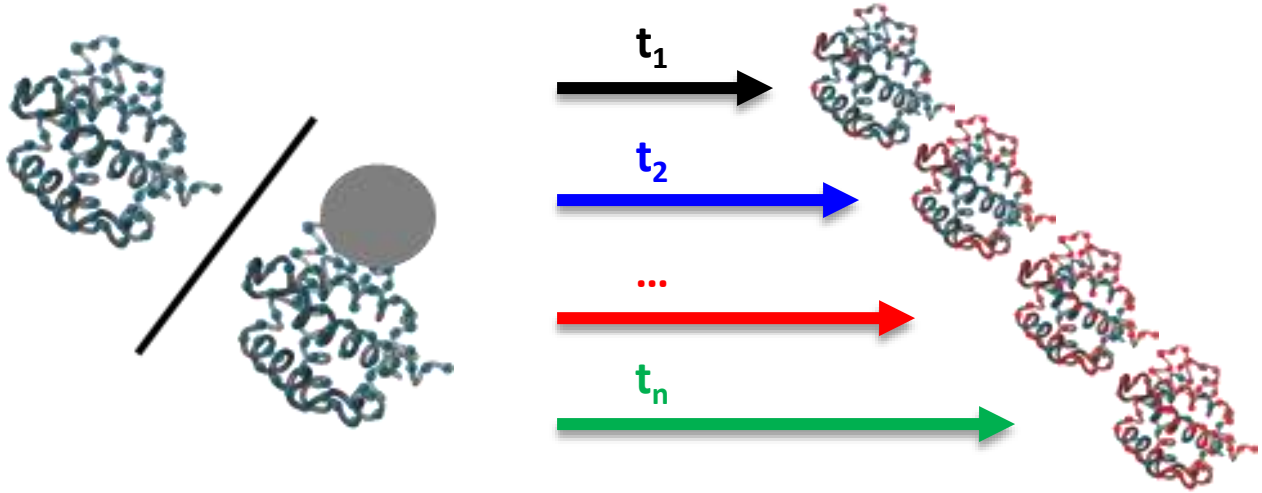

Stop the exchange

?

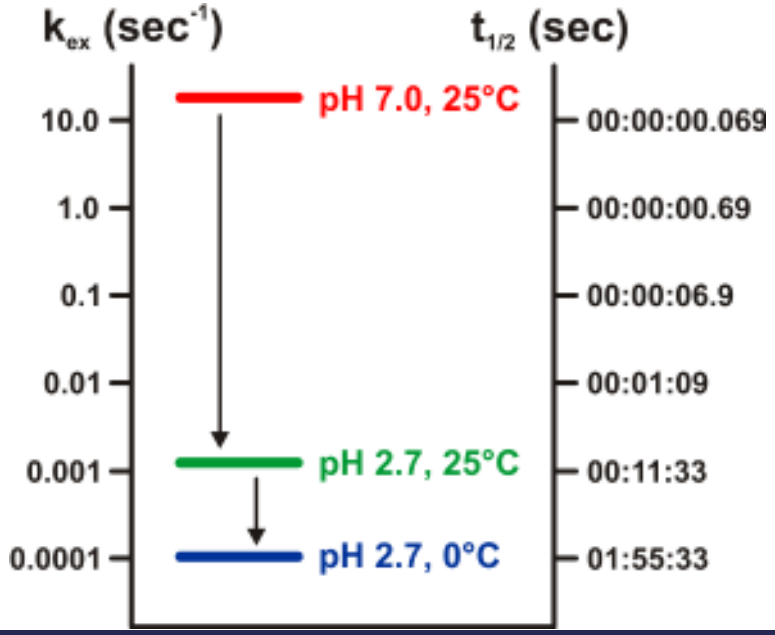

H/D exchange workflow

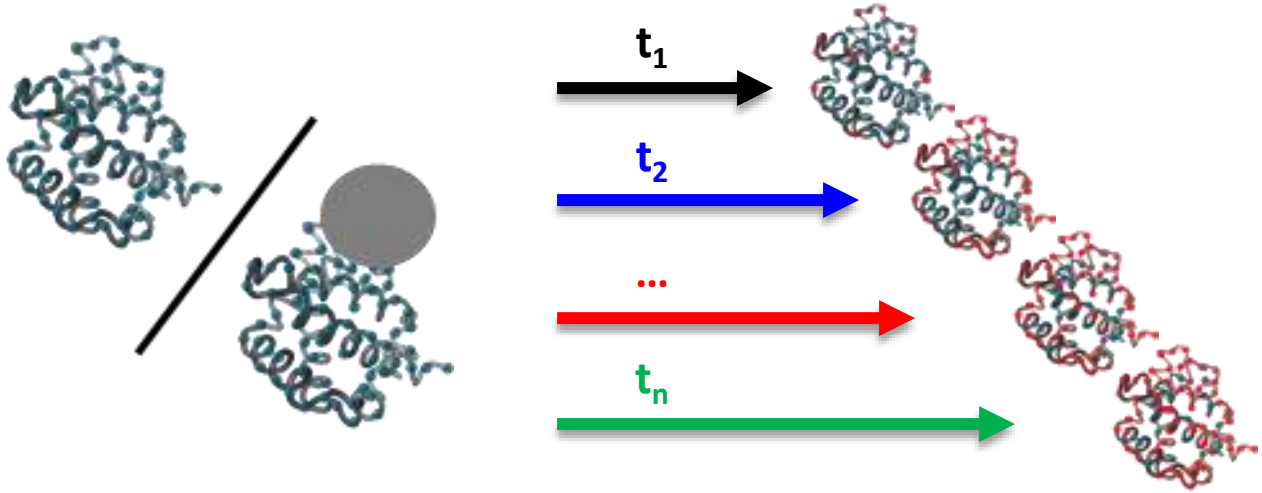

Stop the exchange
pH (2,5)
T (0°C)

MS analysis
?

Interpretation

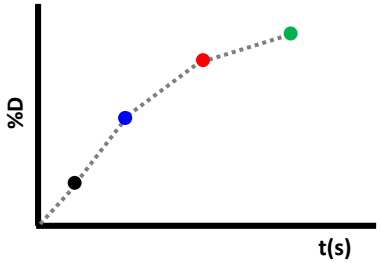

LC-MS

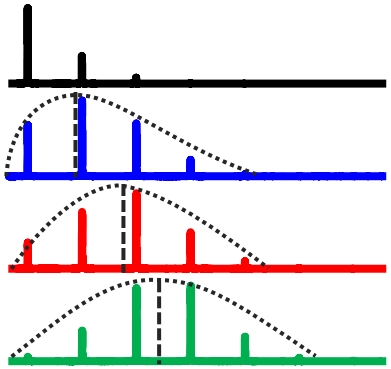

H/D exchange affects MS spectrum – isotopic pattern

Mass spectrum

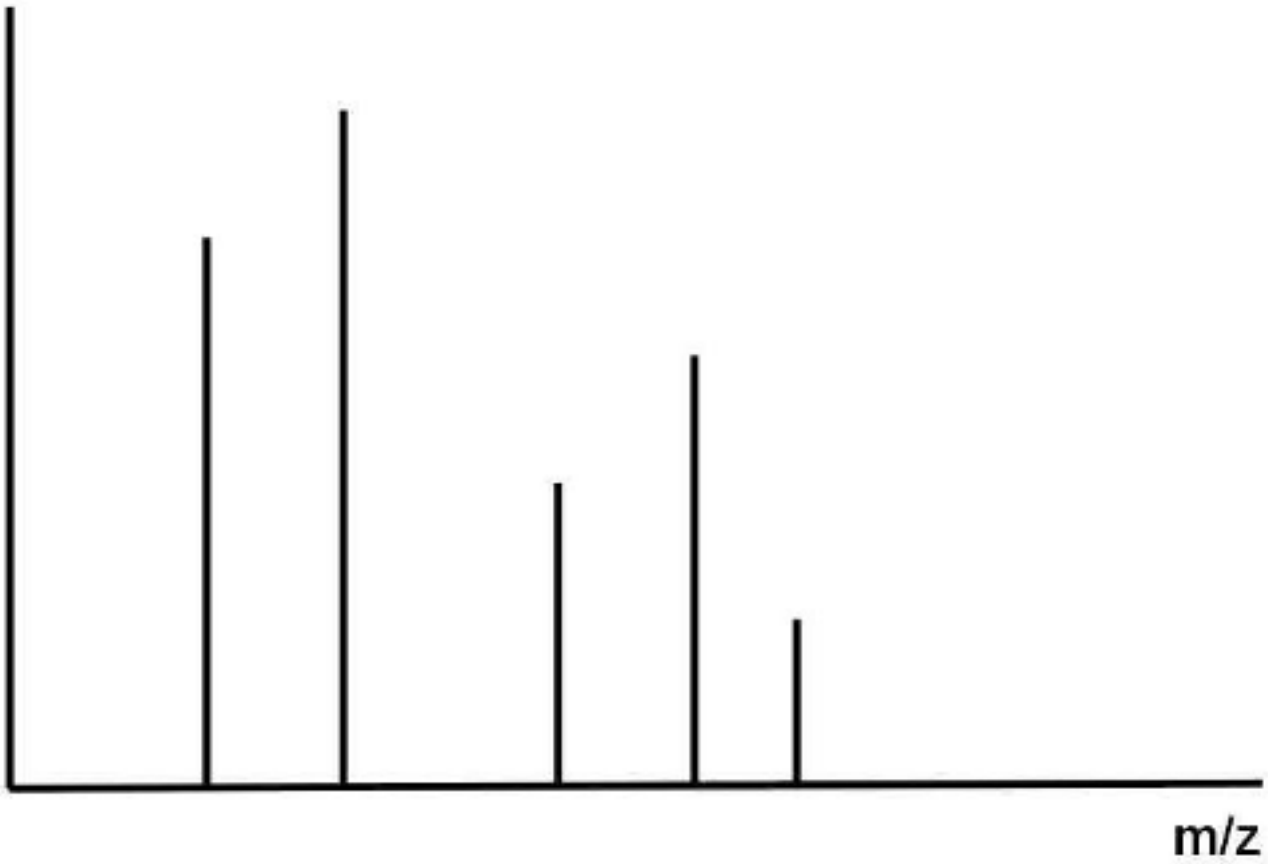

H/D exchange affects MS spectrum – isotopic pattern

Mass spectrum in detail

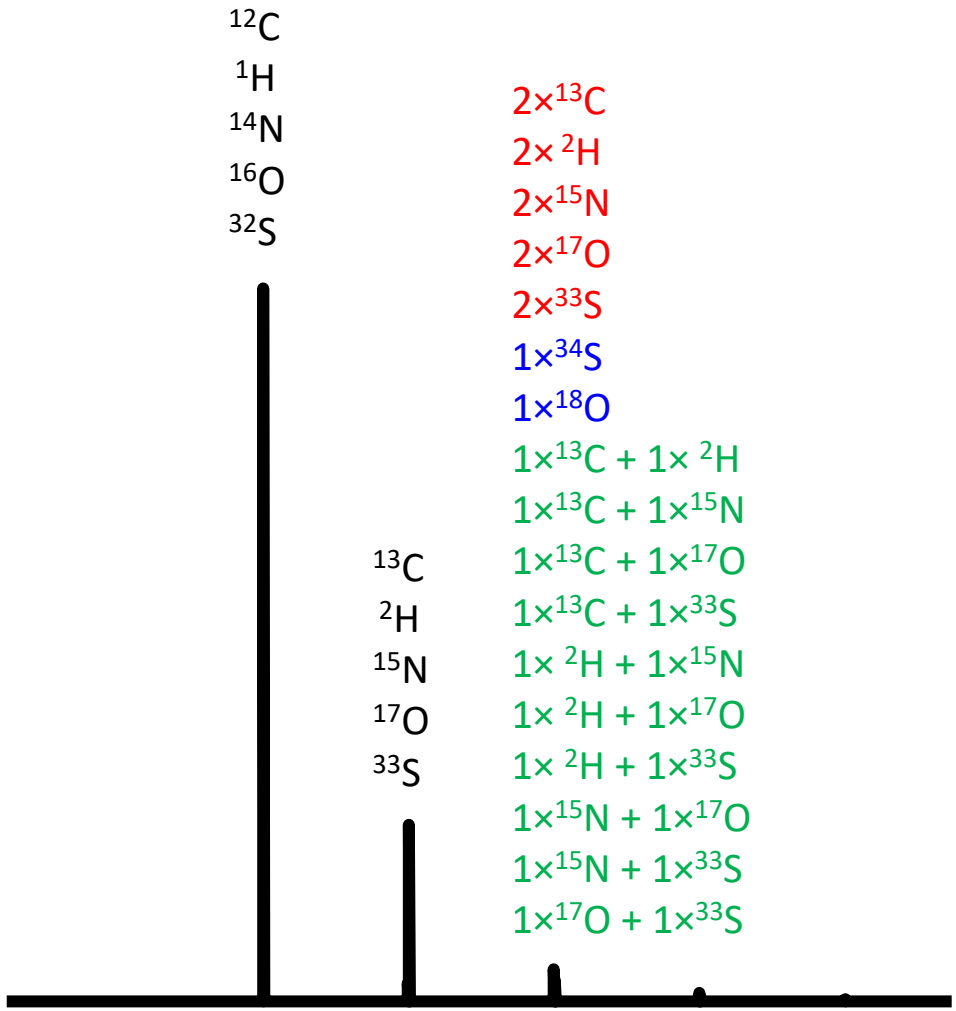

Symbol	M_{nom}	M_{mono}	%
C	12	12.00000	98.9300
	13	13.00336	1.0700
H	1	1.00783	99.9885
	2	2.01411	0.1150
N	14	14.00307	99.6320
	15	15.00011	0.3680
O	16	15.99492	99.7570
	17	16.99913	0.0380
	18	17.99916	0.2050
S	32	31.97207	94.9300
	33	32.97146	0.7600
	34	33.96787	4.2900
	36	35.96708	0.0200
P	31	30.97376	100.0000

Isotope pattern at increasing mass

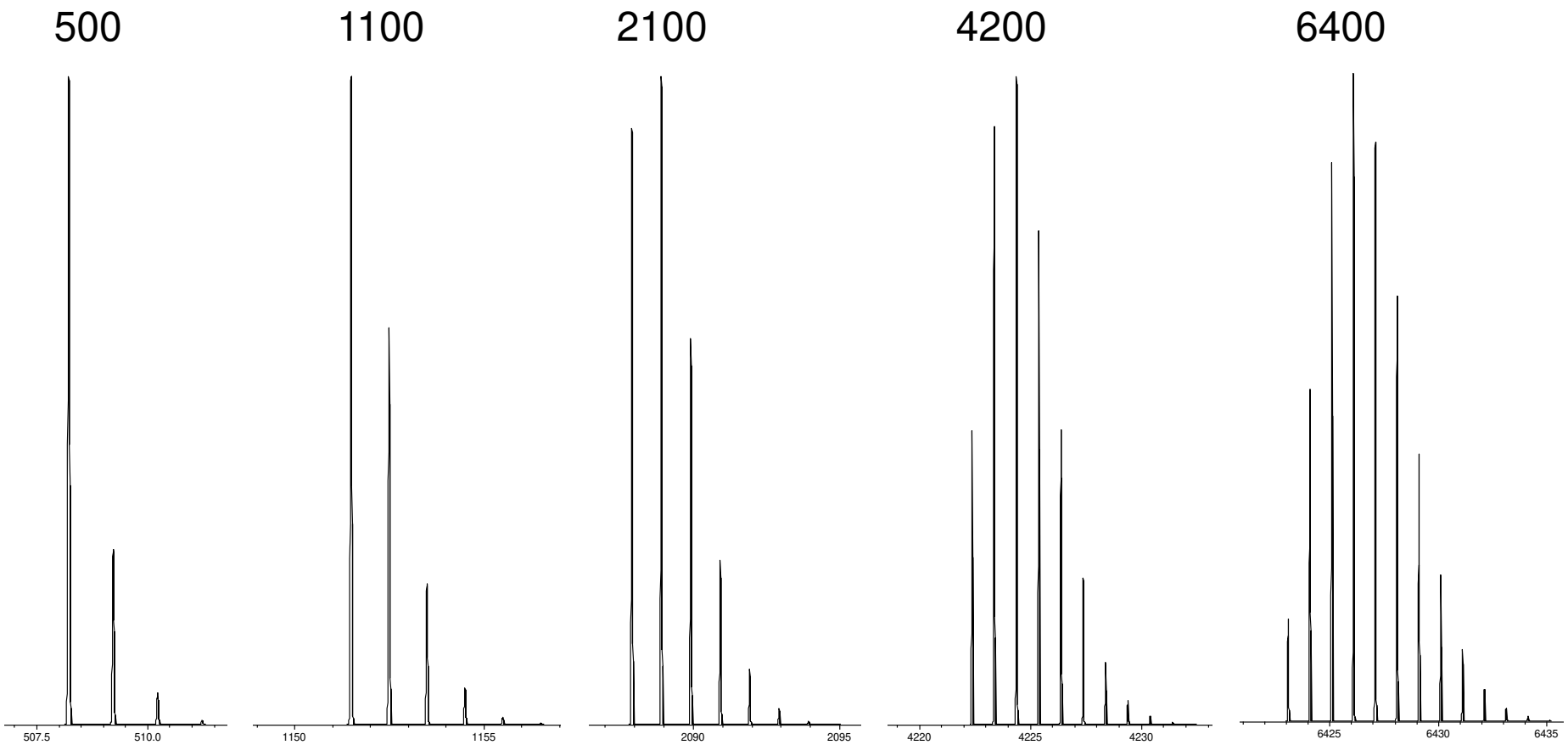

Isotope pattern changes through isotope exchange

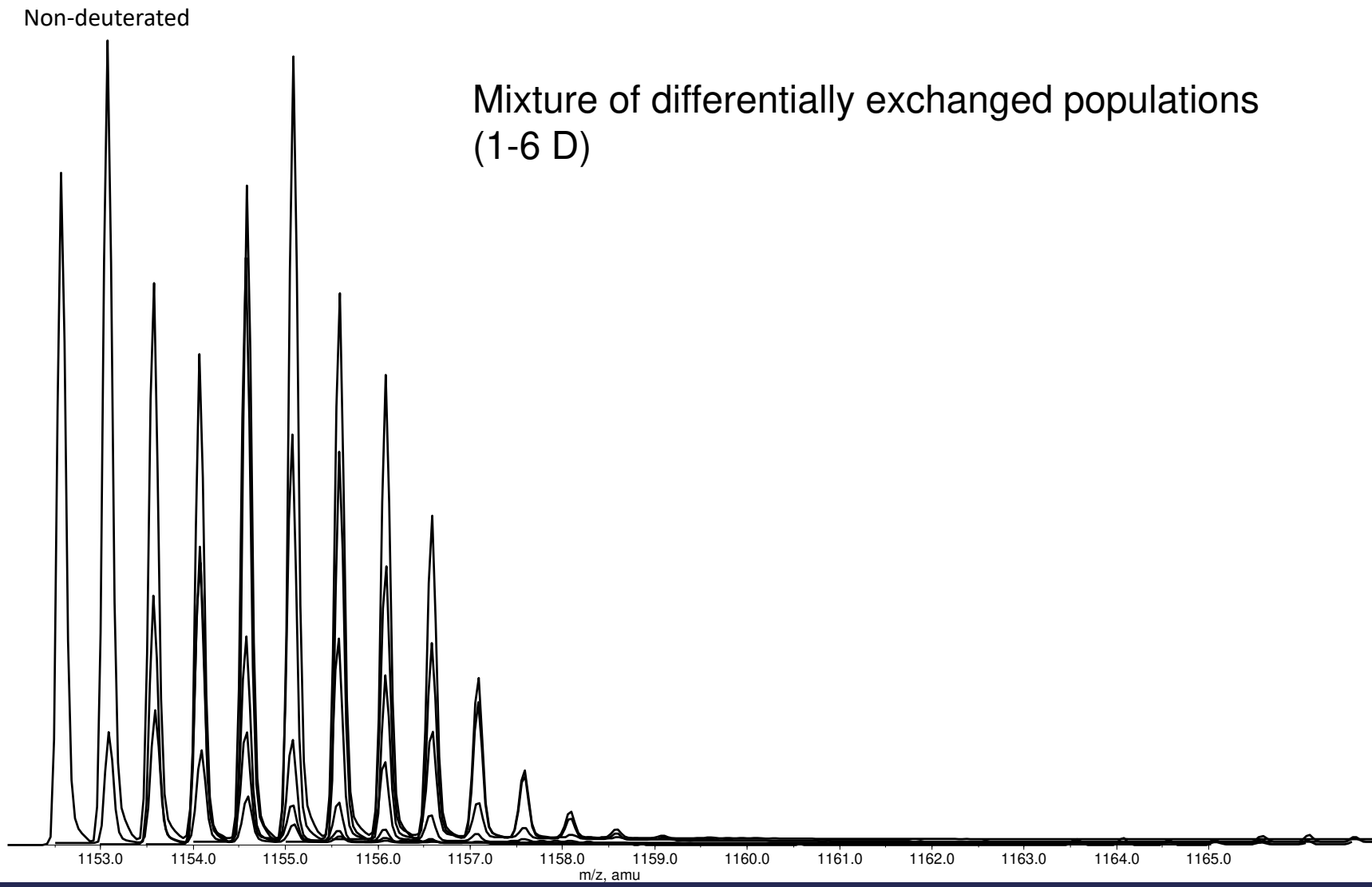

Time resolved deuteration changes

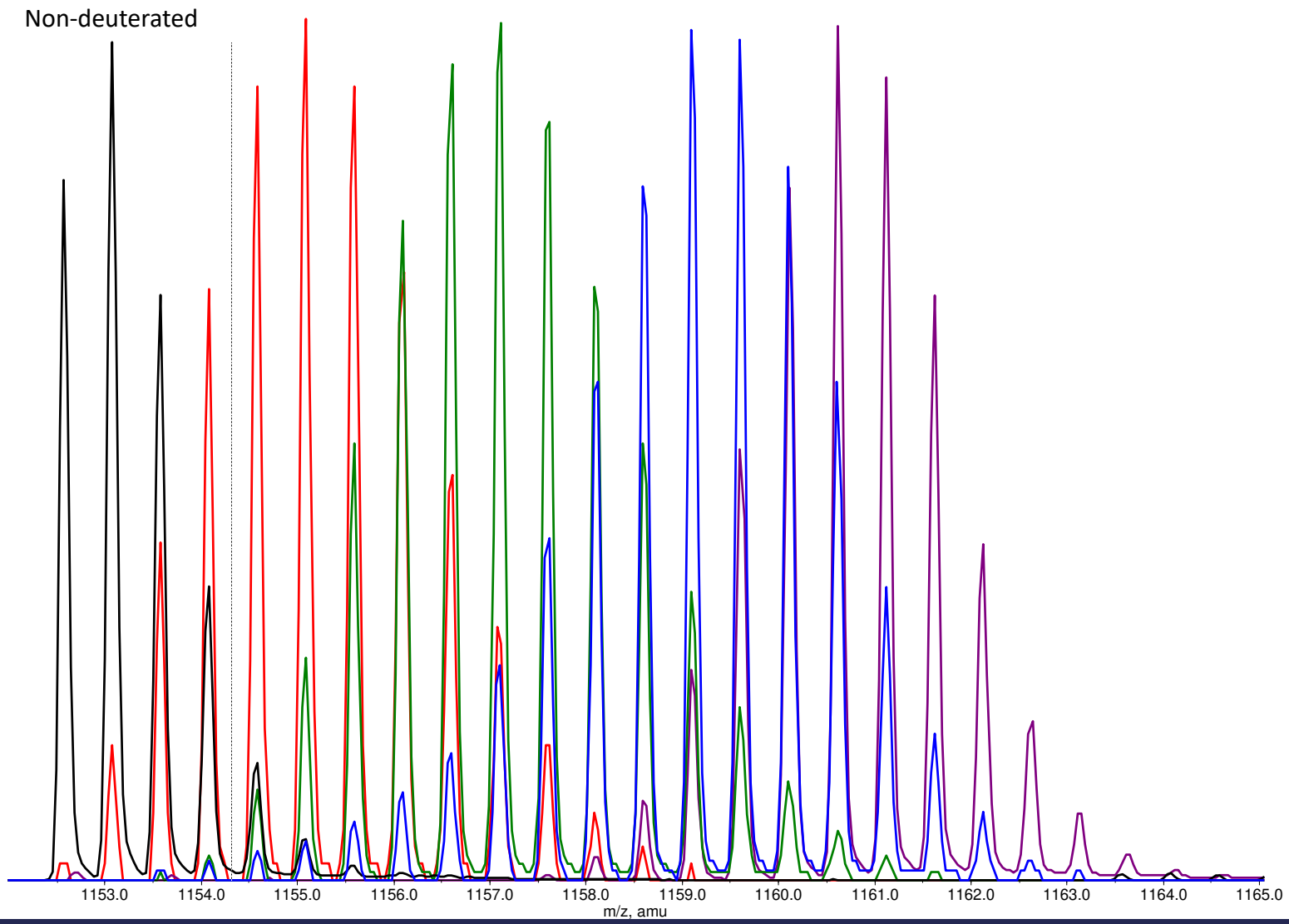

Comparison of free vs ligated protein state

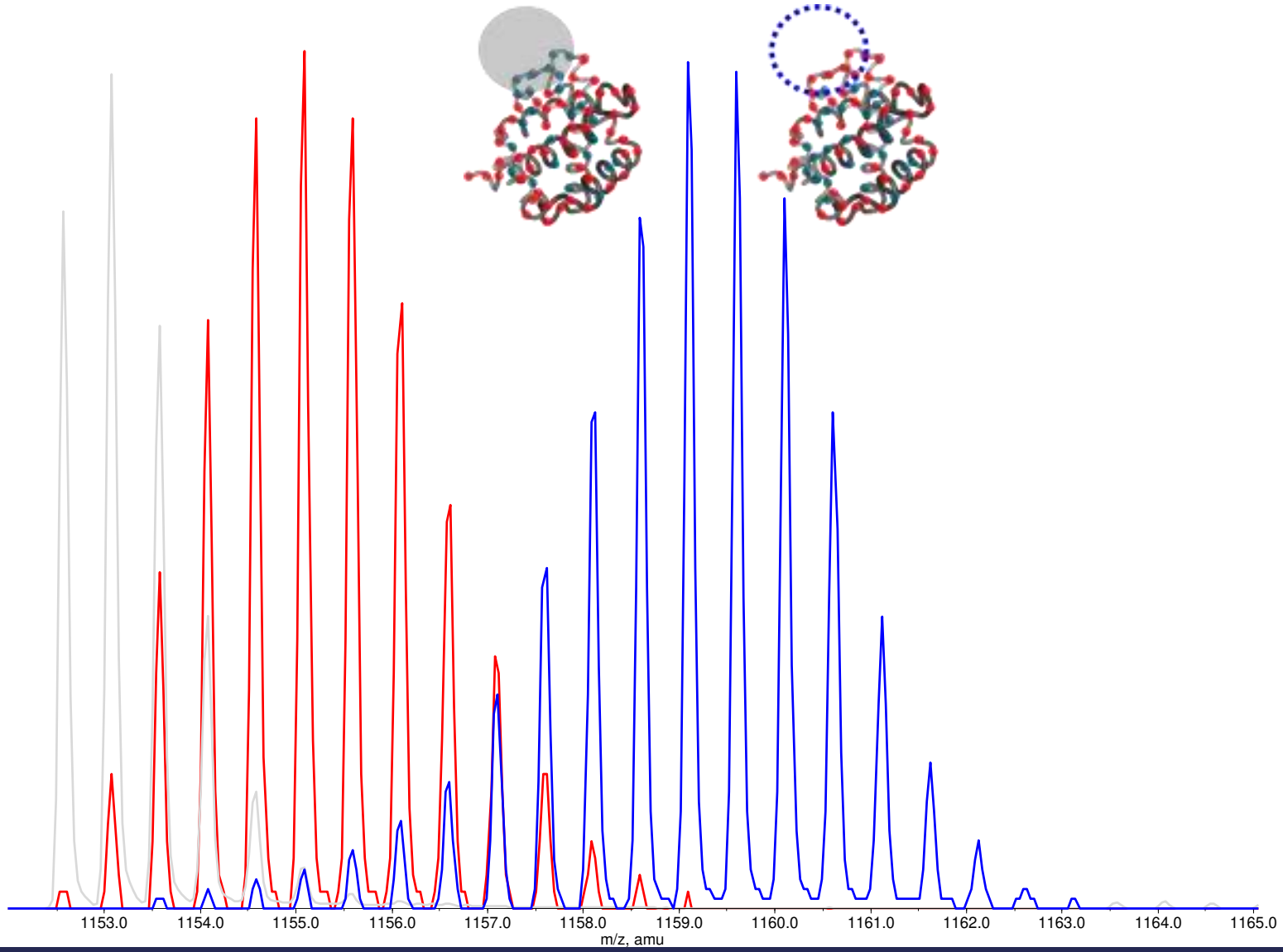

Back-exchange!

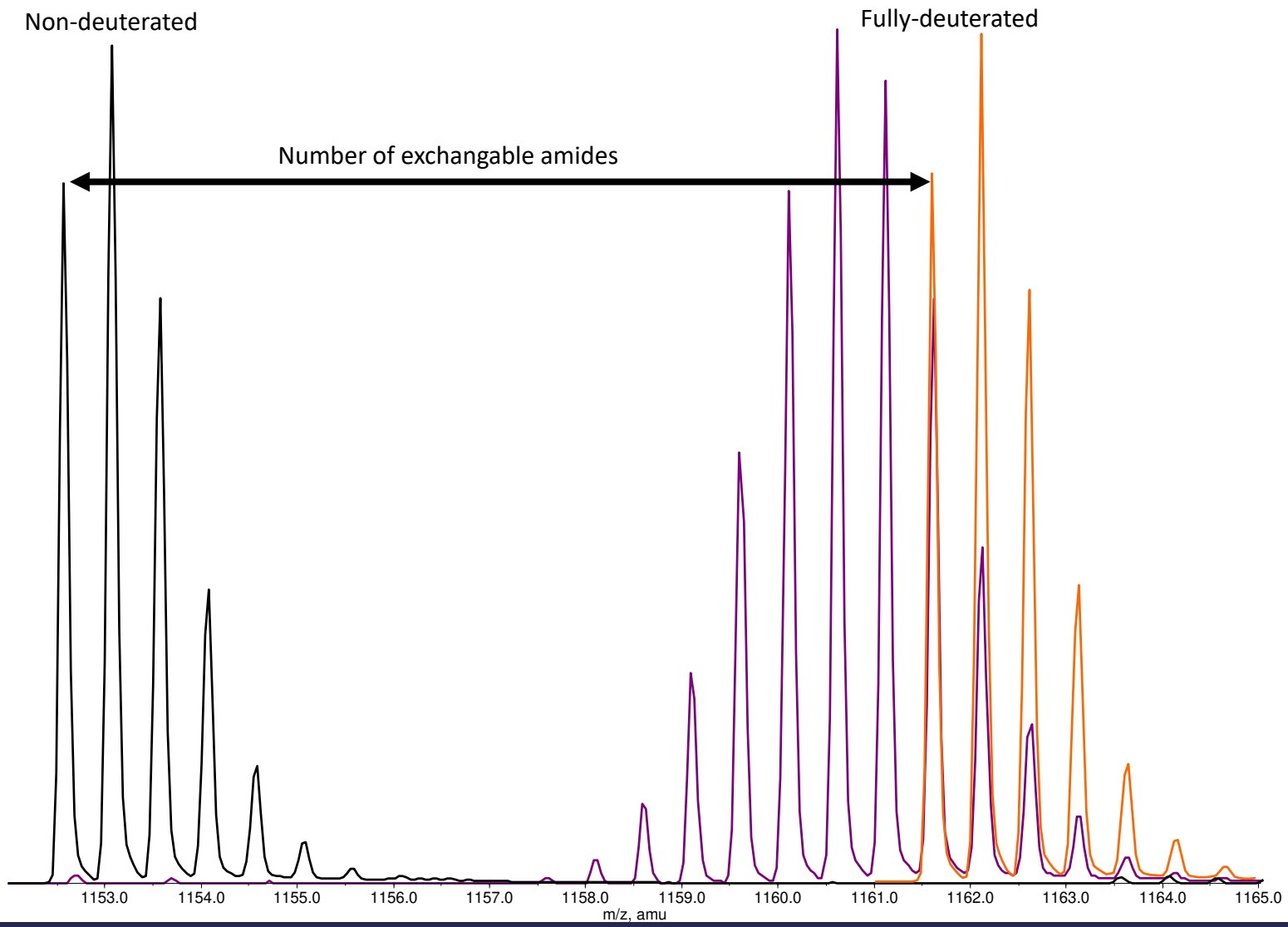

H/D exchange mechanism / kinetics

$$\text{prot - H}_{\text{closed}} \underset{k_{cl}}{\overset{k_{op}}{\rightleftharpoons}} \text{prot - H}_{\text{open}} \xrightarrow[D_2O]{k_{ex}} \text{prot - D}$$

EX2: $k_{cl} >> k_{ex}$

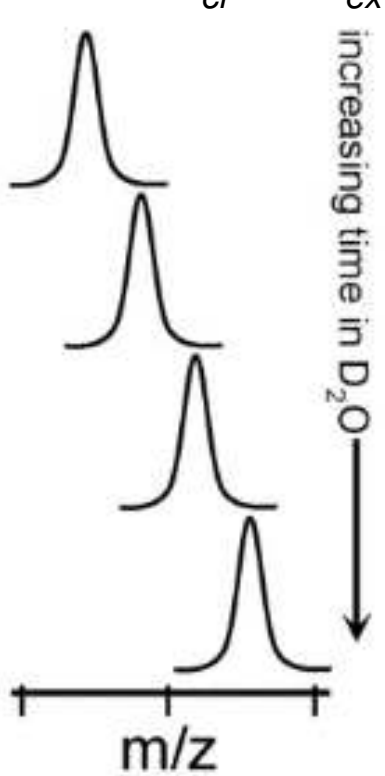

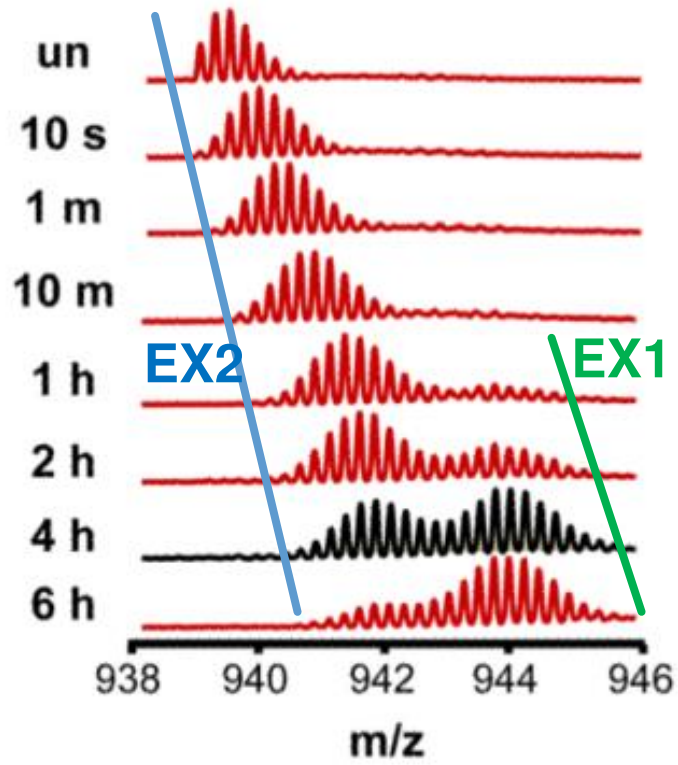

EX1: $k_{cl} << k_{ex}$

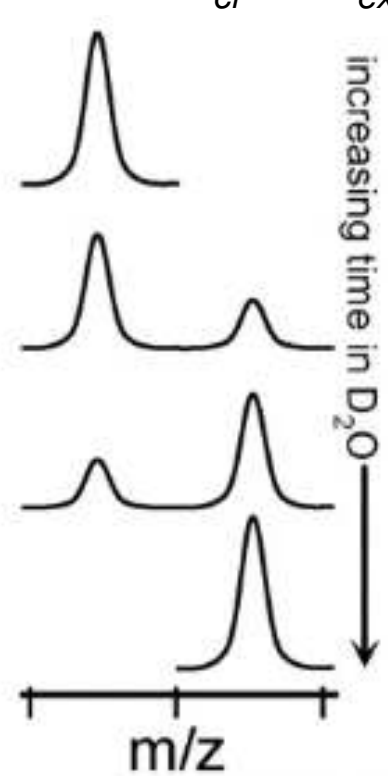

Weis DD *et al.*: J. Am. Soc. Mass Spectrom. (2006) Fang J *et al.*: Biochemistry (2011)

Isotope pattern at increasing resolving power

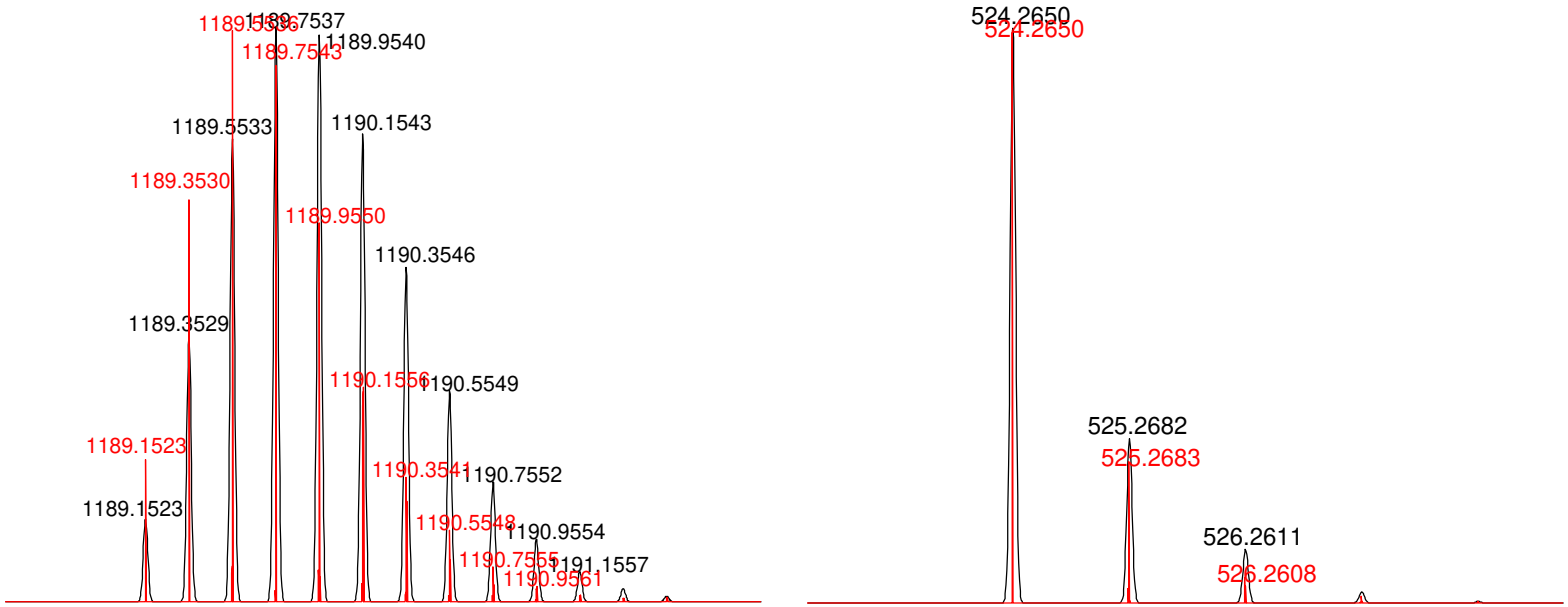

Theoretical models for 5+ insulin and 1+ MFRA @ 50.000 vs 5.000.000

Fine isotopic structure

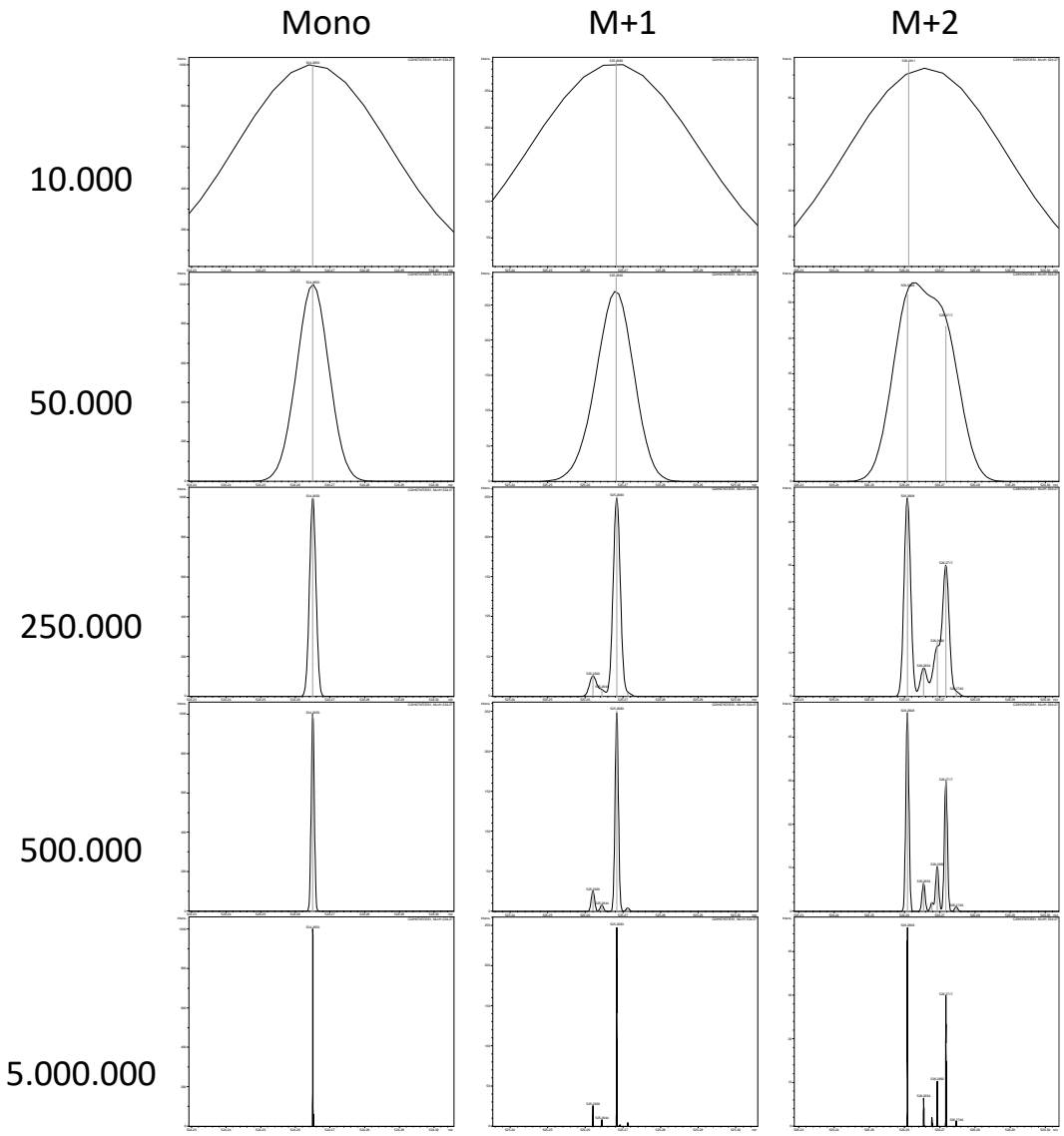

Fine isotopic structure

MRFA
M+1

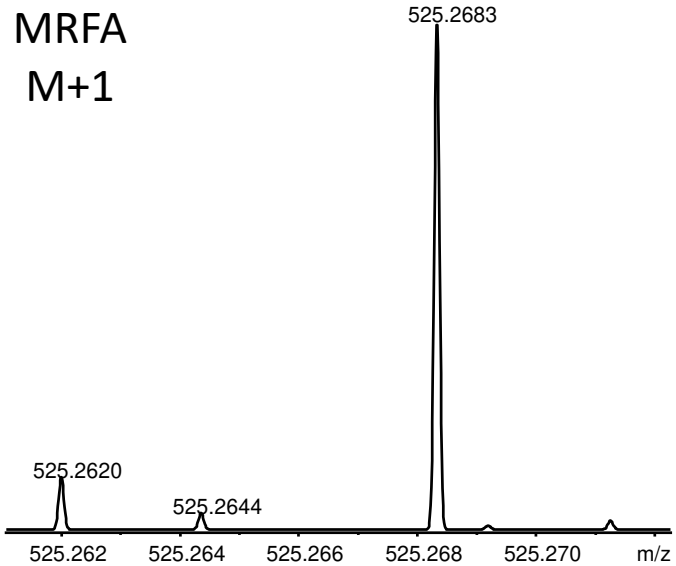

Distance between isotopes

^{13}C-^{12}C	1,003355
^{2}H- ^{1}H	1,006280
^{15}N-^{14}N	0,997035
^{17}O-^{16}O	1,004217
^{33}S-^{32}S	0,999387

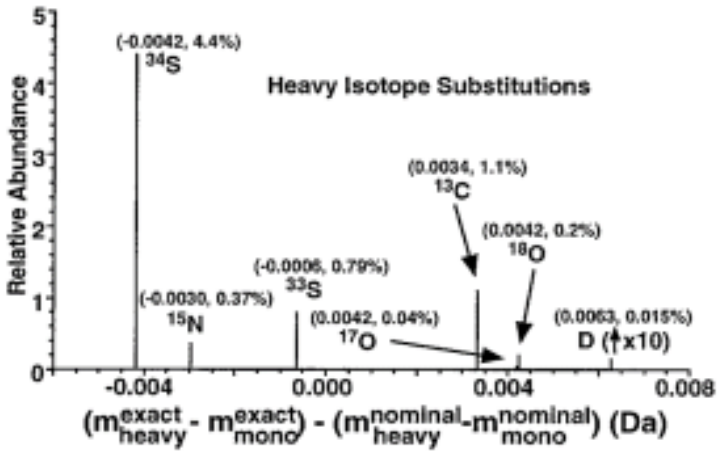

Shi DH et al Proc. Natl. Acad. Sci USA 1998, 95, 11532.

MRFA
M+2

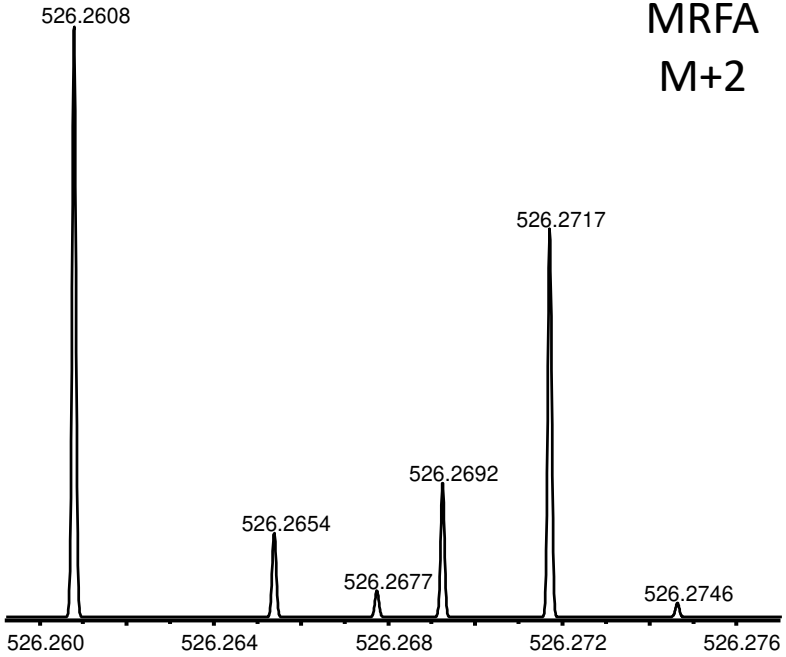

Fine isotopic structure

MRFA
M+1

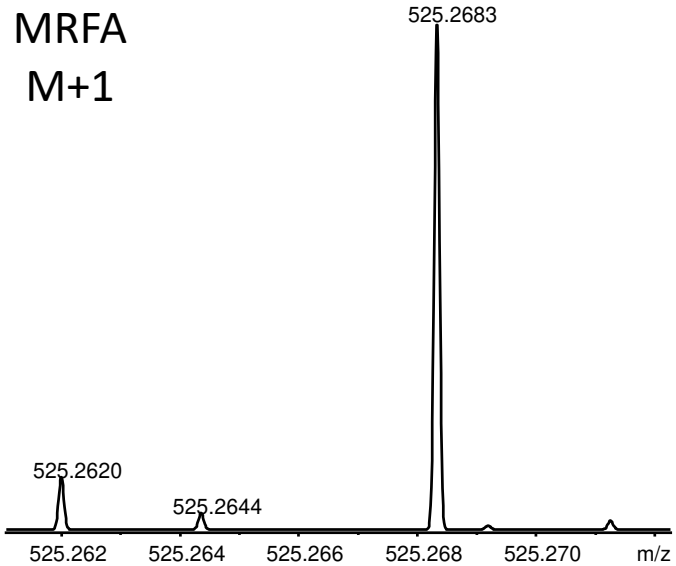

Distance from nominal mass +1

525.2620 = −0.0030 ~ ^{15}N

525.2644 = −0.0006 ~ ^{33}S

525.2683 = +0.0033 ~ ^{13}C

525.2692 = +0.0042 ~ ^{17}O

525.2713 = +0.0063 ~ ^{2}H

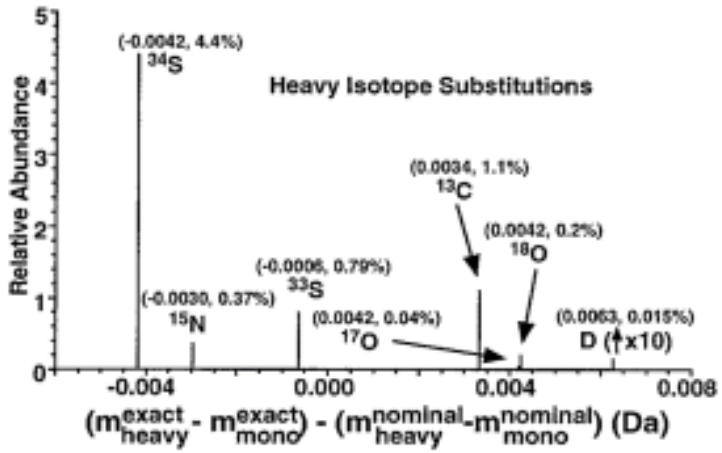

Shi DH et al Proc. Natl. Acad. Sci USA 1998, 95, 11532.

MRFA
M+2

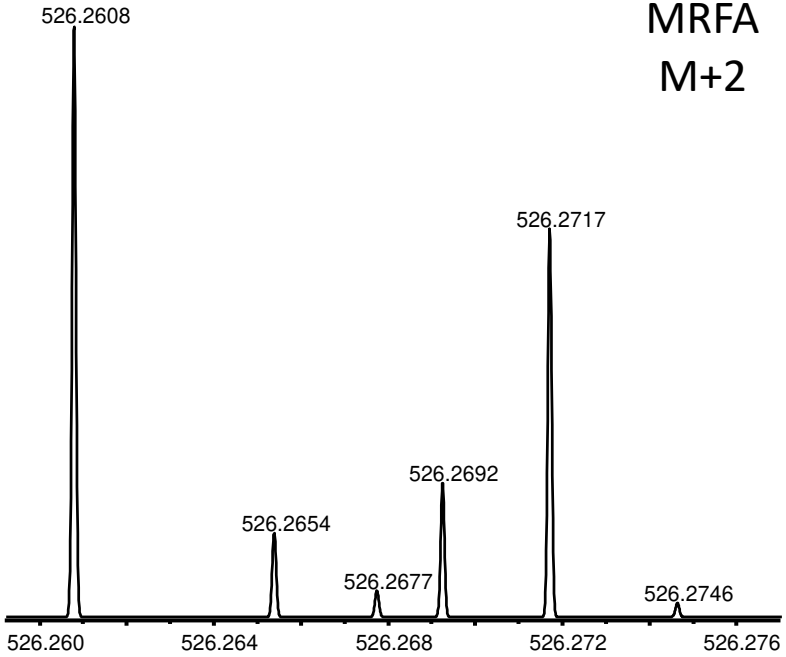

Utility of fine isotopic structure in HDX

Ultra high resolution required! ^{12}C-^{13}C vs ^{1}H-^{2}H ~ 3mDa

Direct readout of the deuteration level (ND spectrum not needed) + “deconvolution” of differentially deuterated species – exchangeomer distribution

Pseudomonoisotopic peak is defined – monoisotopic undergoing just H/D exchanges. No other isotopes.

Claimed to be more accurate…

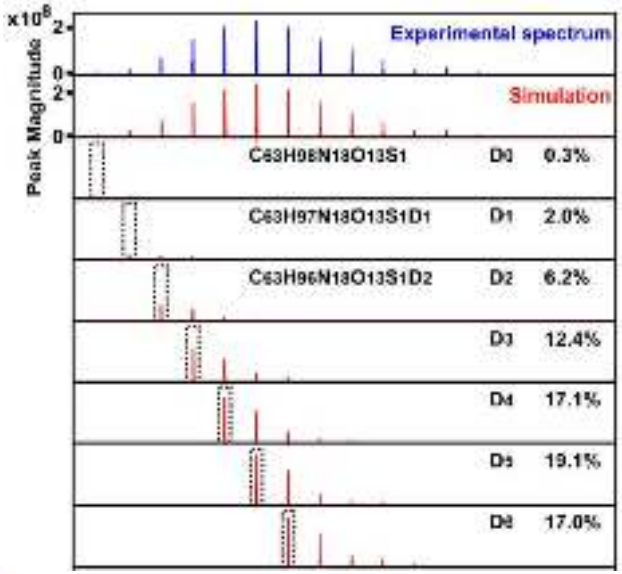

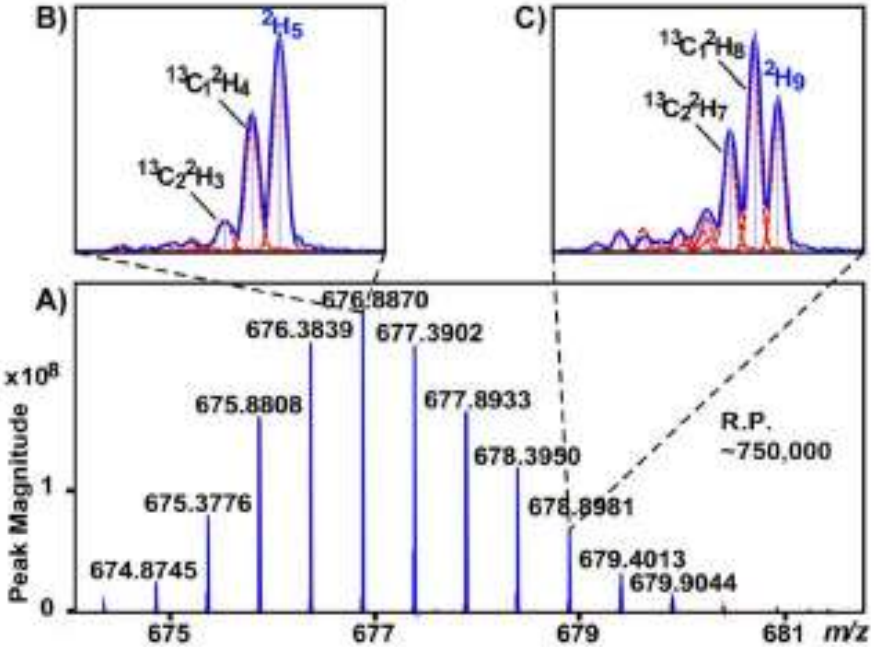

Global exchange

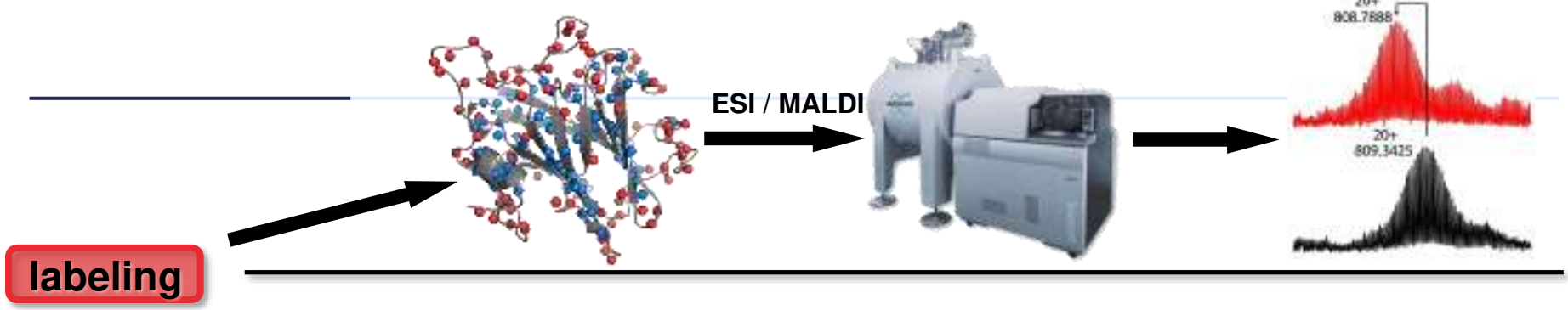

doi:10.1016/j.jmb.2007.02.014 J. Mol. Biol. (2007) 366, 464–472

JMB

Available online at www.sciencedirect.com
ScienceDirect
ELSEVIER

Defining the Interacting Regions between Apomyoglobin and Lipid Membrane by Hydrogen/ Deuterium Exchange Coupled to Mass Spectrometry

Petr Man[1], Caroline Montagner[2], Grégory Vernier[2], Bernard Dublet[1] Alexandre Chenal[2], Eric Forest[1]* and Vincent Forge[2]*

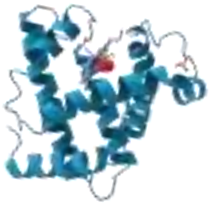

D/H exchange (to diminish effect of side-chains) using MALDI-TOF

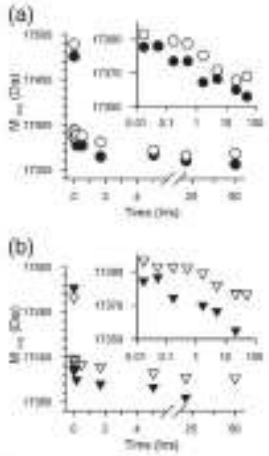

aMb free (black) / + membrane (white)

pH 5.5

pH 4.0

Bigger protection @ pH 4.0
Stronger interaction

Comparison at different pH values (correction by $10^{1.5}$)
aMb free (black) / + membrane (white)

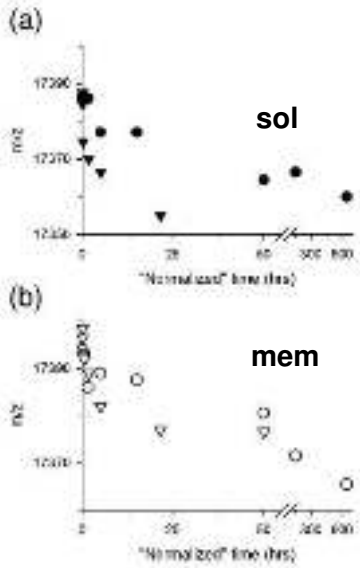

Faster exchange at pH 4.0
=
protein opens (molten globule)

Faster exchange at pH 4.0
but stops at certain moment
=
protein opens (molten globule)
but is protected by the membrane

Global exchange

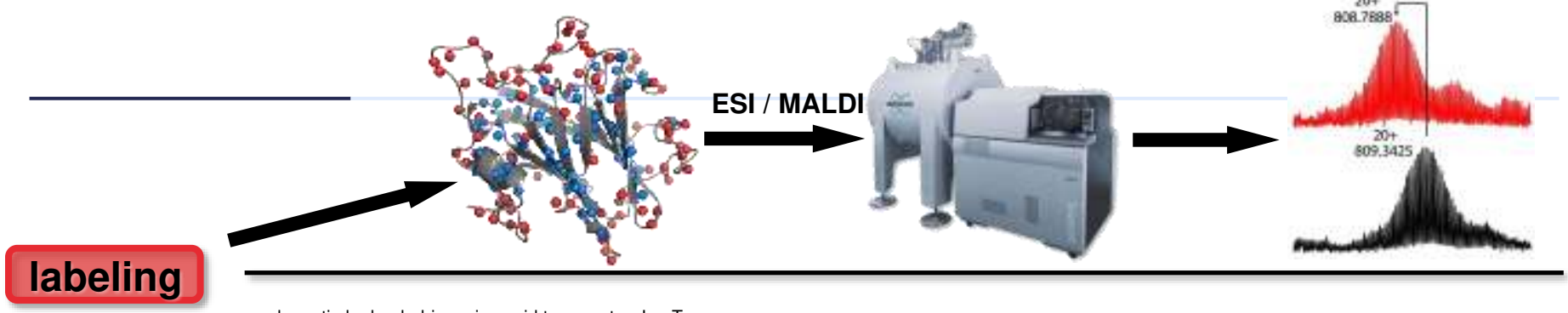

prokaryotic hydrophobic amino acid transporter, LeuT

Moeller *et al.*: J Proteomics (2020)

Probing the conformational impact of detergents on the integral membrane protein LeuT by global HDX-MS

Detergent DM/LMNG and ions K+/Na+

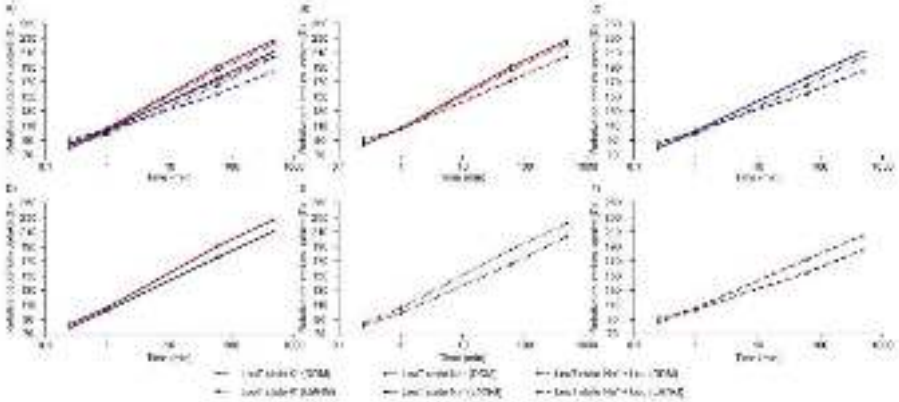

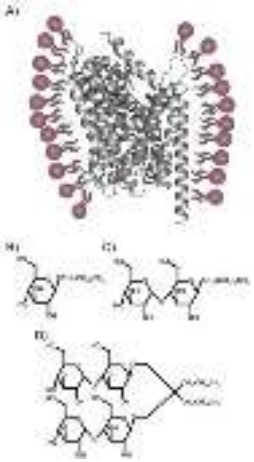

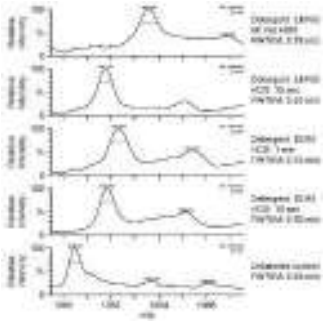

Protein dynamics (EX1/EX2) assessed through peak width

Global exchange

labeling

Local exchange

Rand *et al.*: Acc. Chem. Res. (2014)

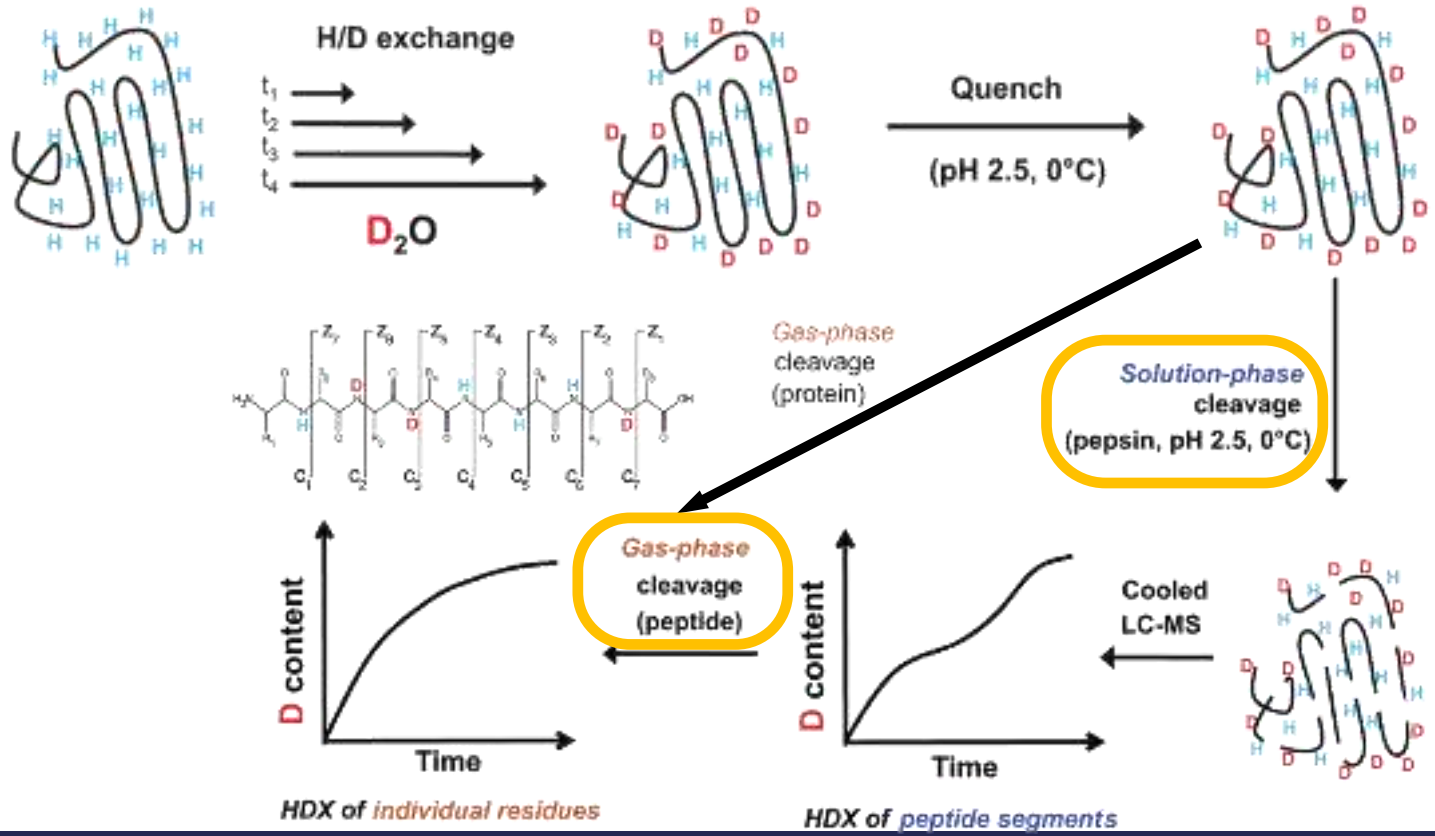

CID vs Electron Capture/Transfer Dissociation (ECD/ETD)

CID – collision-induced dissociation

Slow, leads to H/D movement = scrambling

Spatial information is lost

ECD / ETD – electron capture/transfer dissociation

Capture of electron or transfer from radical anions

Faster fragmentation, no scrambling!

Side effect – poor yield, charge neutralization (needs multiply charged precursors)

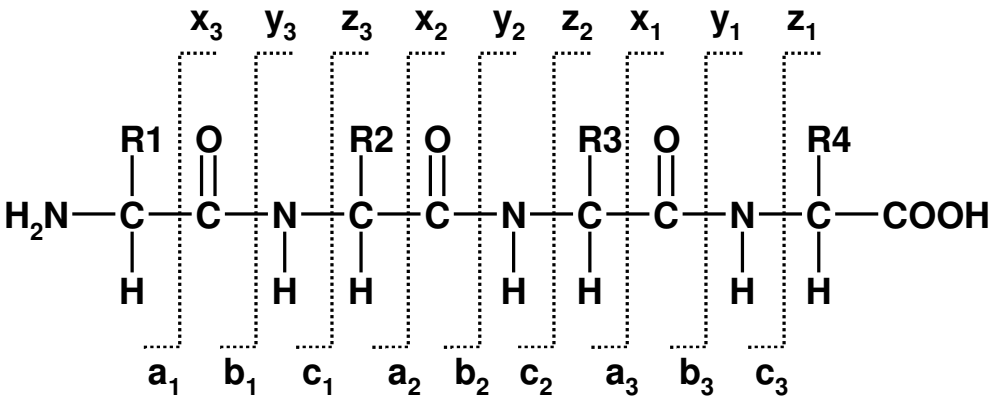

UltraViolet PhotoDissociation (UVPD)

UV lasers – Nd:YAG a excimer ArF, KrF,..

wavelength: 157nm, 193nm (peptide bond), 213nm, 266nm,…
wavelength close to 280nm – fragmentation close to aromatics

Very fast fragmentation – no/minimal scrambling

a/x, c/z, but also b/y ions and side chain fragments

UVPD

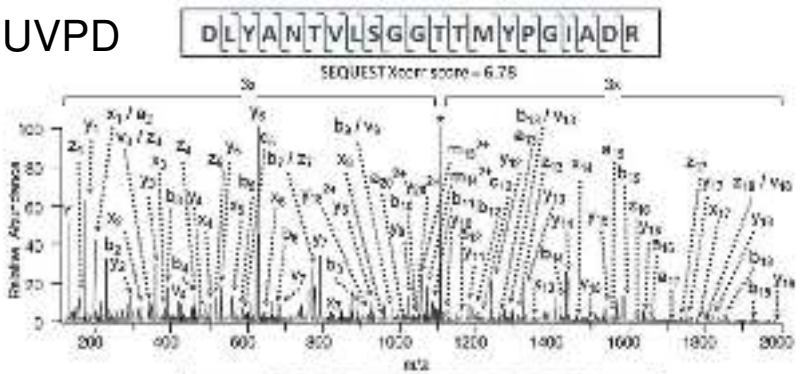

CID

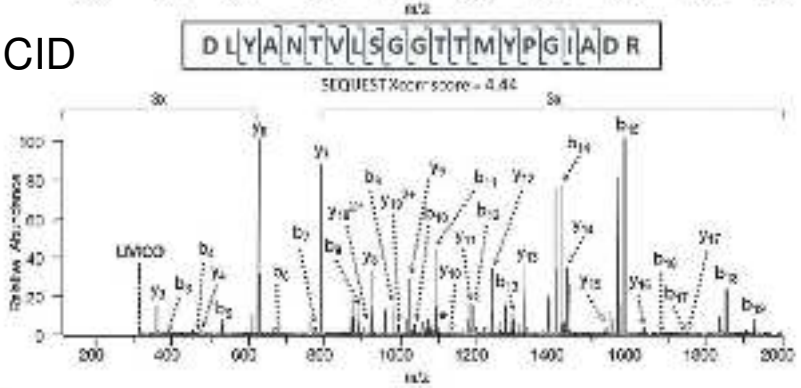

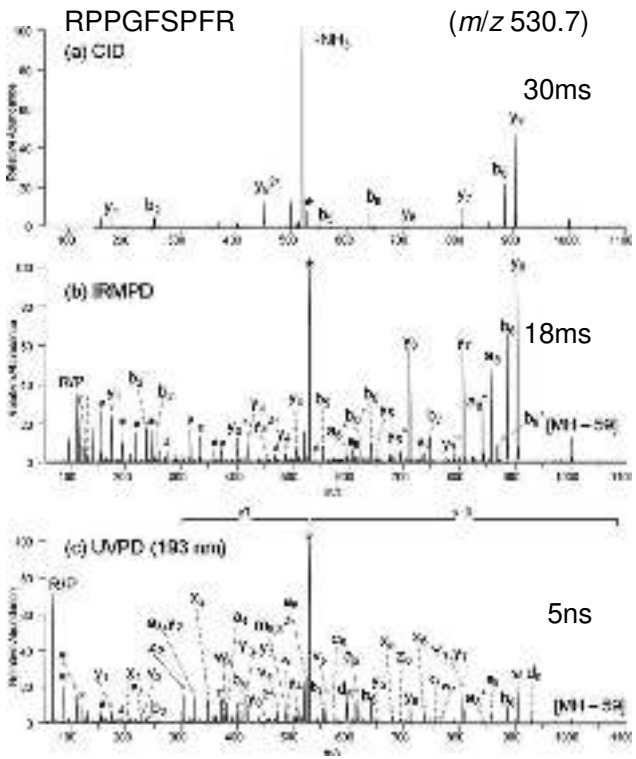

Scrambling test

Kaltashov, Eyles: J. Mass Spectrom. (2002)
Rand *et al.*: Acc. Chem. Res. (2014)

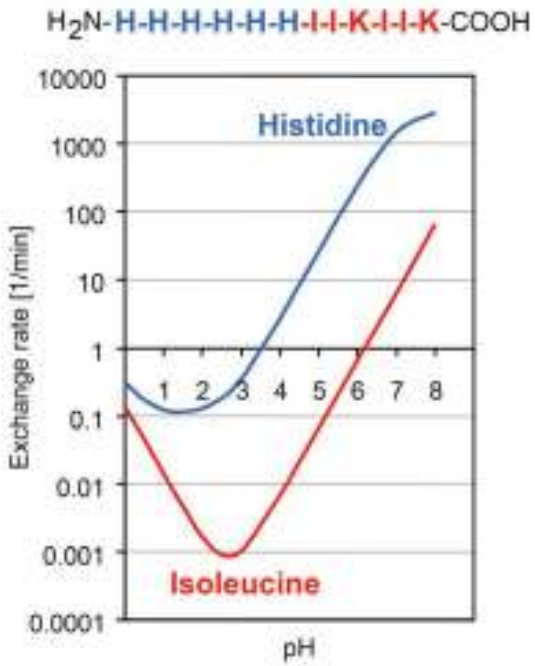

HHHHHHIIKIIK

Fully deuterate

⬇

Quench

⬇

Infuse

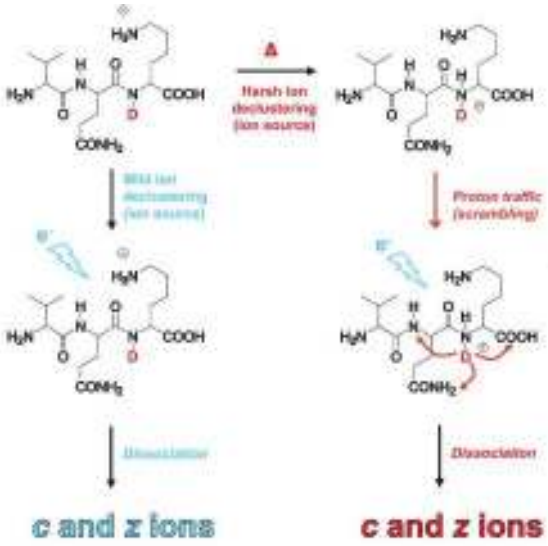

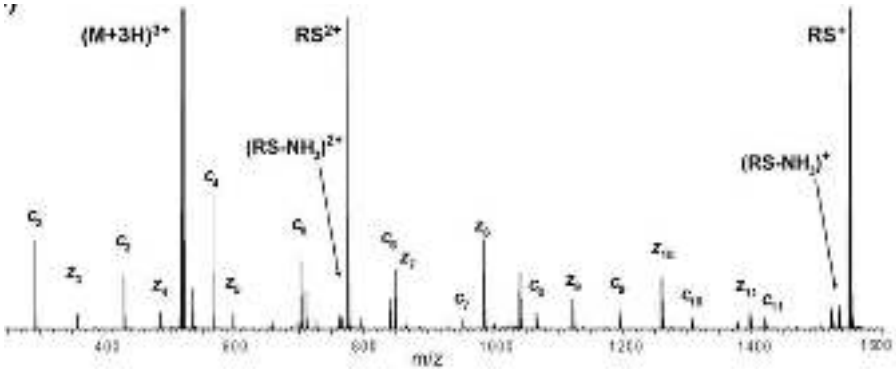

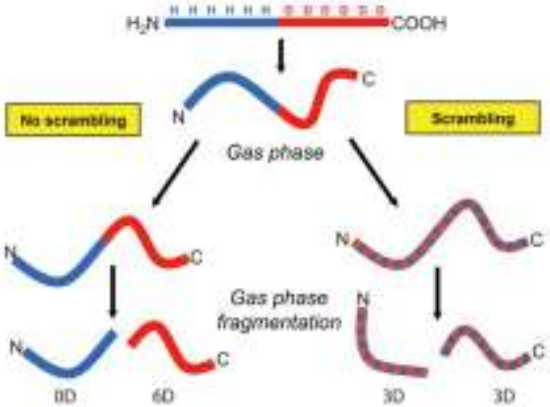

Scrambling – ETD/ECD

Kaltashov, Eyles: J. Mass Spectrom. (2002)
Rand *et al.*: Acc. Chem. Res. (2014)

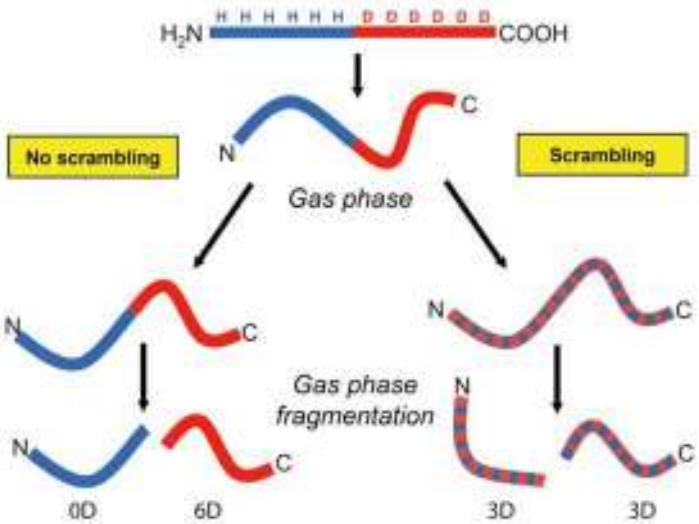

Activation via dissociation but also during ionization and ion transfer

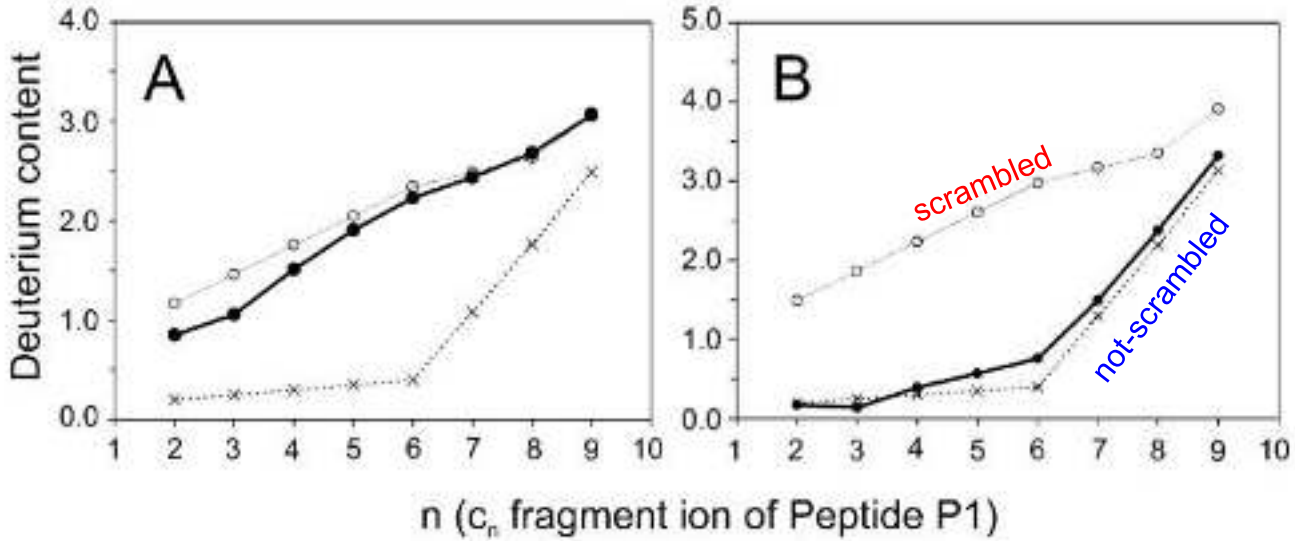

Scrambling - UVPD

Mistraz U.H. et al Anal Chem 2018
Brodie N.I. et al Anal Chem 2018

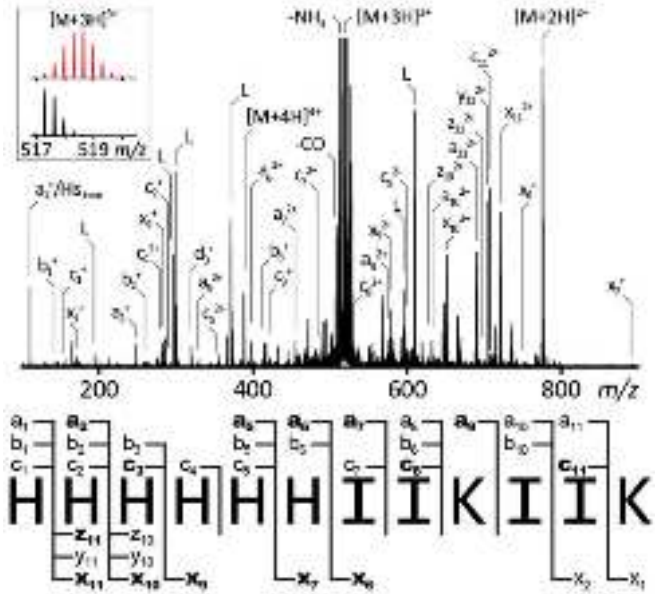

UVPD is applicable (similarly to ExD)

More fragments produced (P1 on the *left* and Mb top-down *bottom*)

ETD

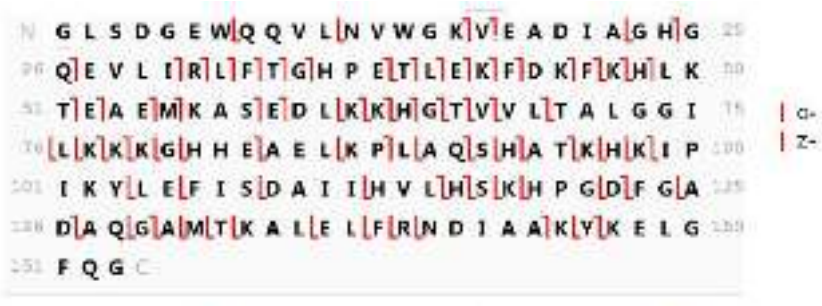

UVPD

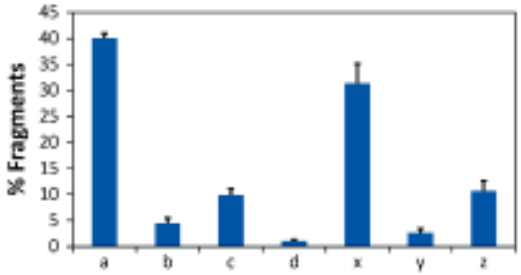

Figure 5-2. Abundance of fragment ion types observed during 213 ms UVPD of peptide P1.

Top-Down HDX-MS

Number of reports rather limited (C.H. Borchers, L. Konermann, I.A. Kaltashov,…).

Mostly on smaller, well behaving, well characterized proteins – e.g. Mb folding, histones,…

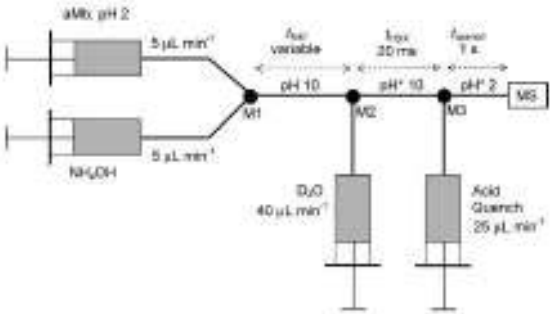

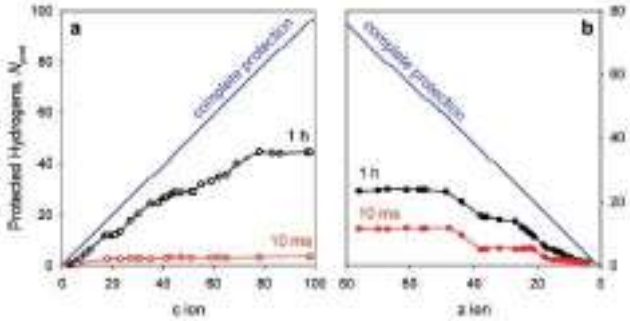

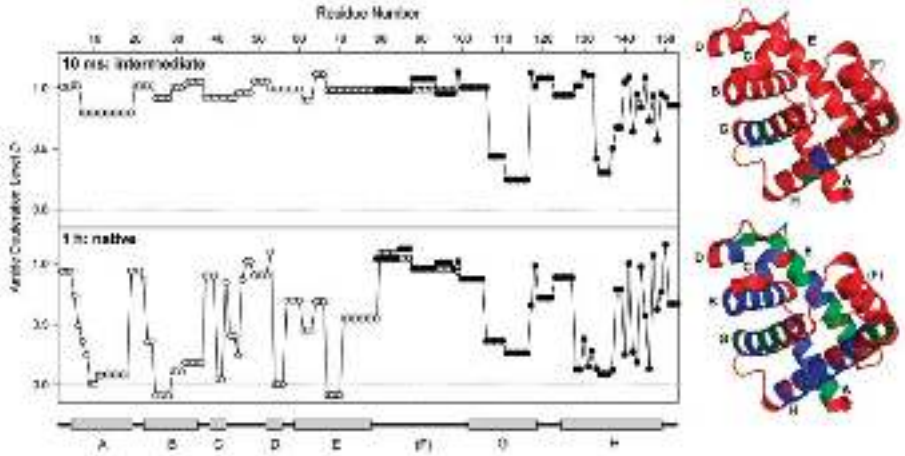

Pan J et al Anal Chem 2010
c ions (open)
z ions (closed)

Top-Down HDX-MS

Number of reports still limited (C.H. Borchers, L. Konermann, I.A. Kaltashov,…).

Mostly on smaller, well behaving, well characterized proteins – e.g. CaM

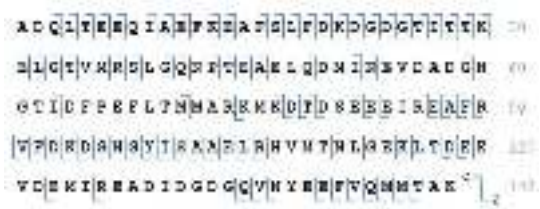

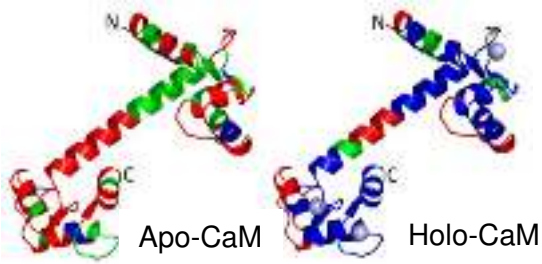

D-level
<0.33
0.33-0.66
>0.66

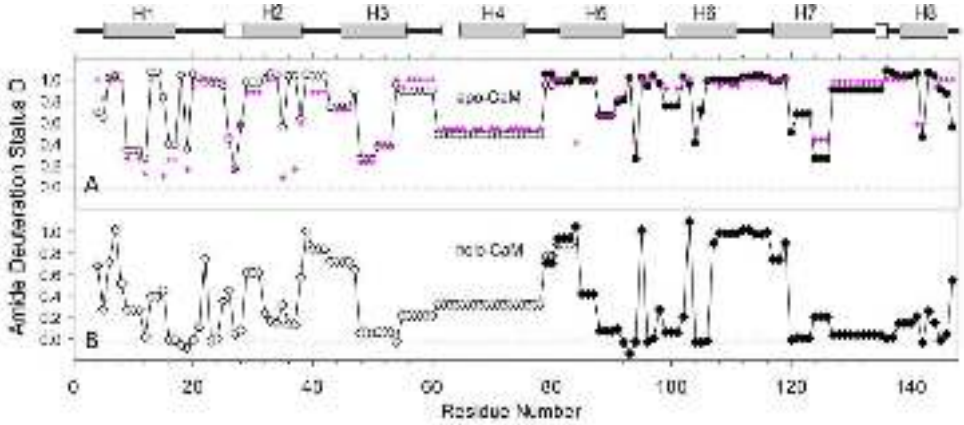

Pan J et al JACS 2014
c ions (open)
z ions (closed)

Top-Down HDX-MS

Ab studies also reported, however, Ab (150kDa) is in fact composed of 50kDa and 25kDa proteins (HC and LC, respectively) + HC is “not interesting”

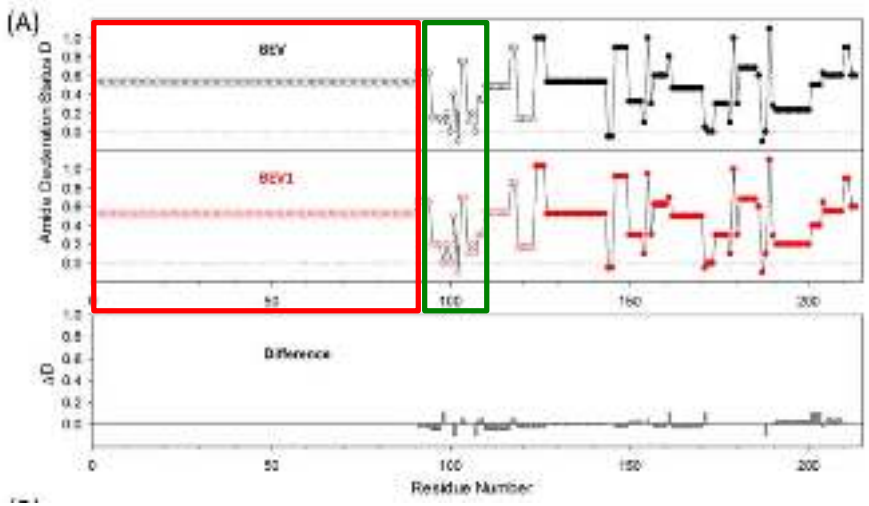

Fragmentation can go to “residue level” but has also spans over large portion of the protein – BEV = Bevacizumab (Avastin) = Ab against VEGF – light chain shown here

Pan J et al BBA 2016
c ions (open)
z ions (closed)

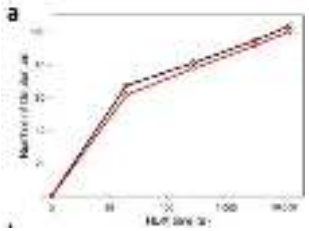

Pan J et al JACS 2014
c ions (open)
z ions (closed)

LC

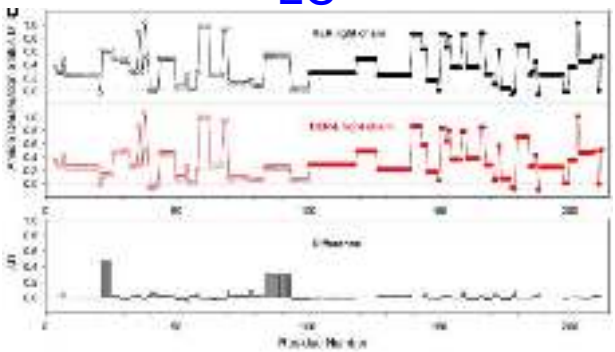

HC – 1-132 + 328-449

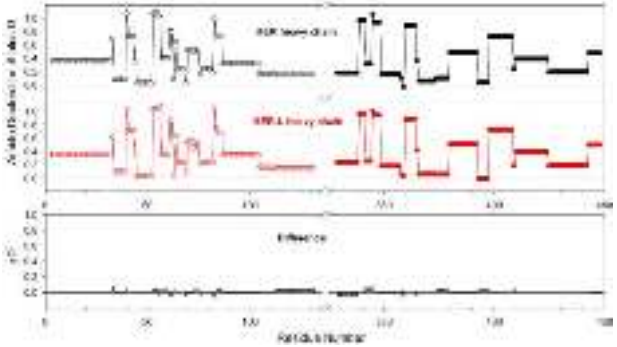

Top-Down HDX-MS

Problem with ionization/fragmentation of some/larger proteins, not likely applicable (yet) to complexes.

Poor fragmentation yield - coverage/resolution. Fragments mostly at the termini.

Motivation/advantages – sequence coverage sometimes not complete – already two complementary fragment ions do the job!

Digestion is often not easy, more handling=bigger D-loss (BE in bottom-up 15-35%, in top-down approx 2% using sub-zero LC – Pan J et al. JACS 2014)

H/D exchange setup for online digestion and LC

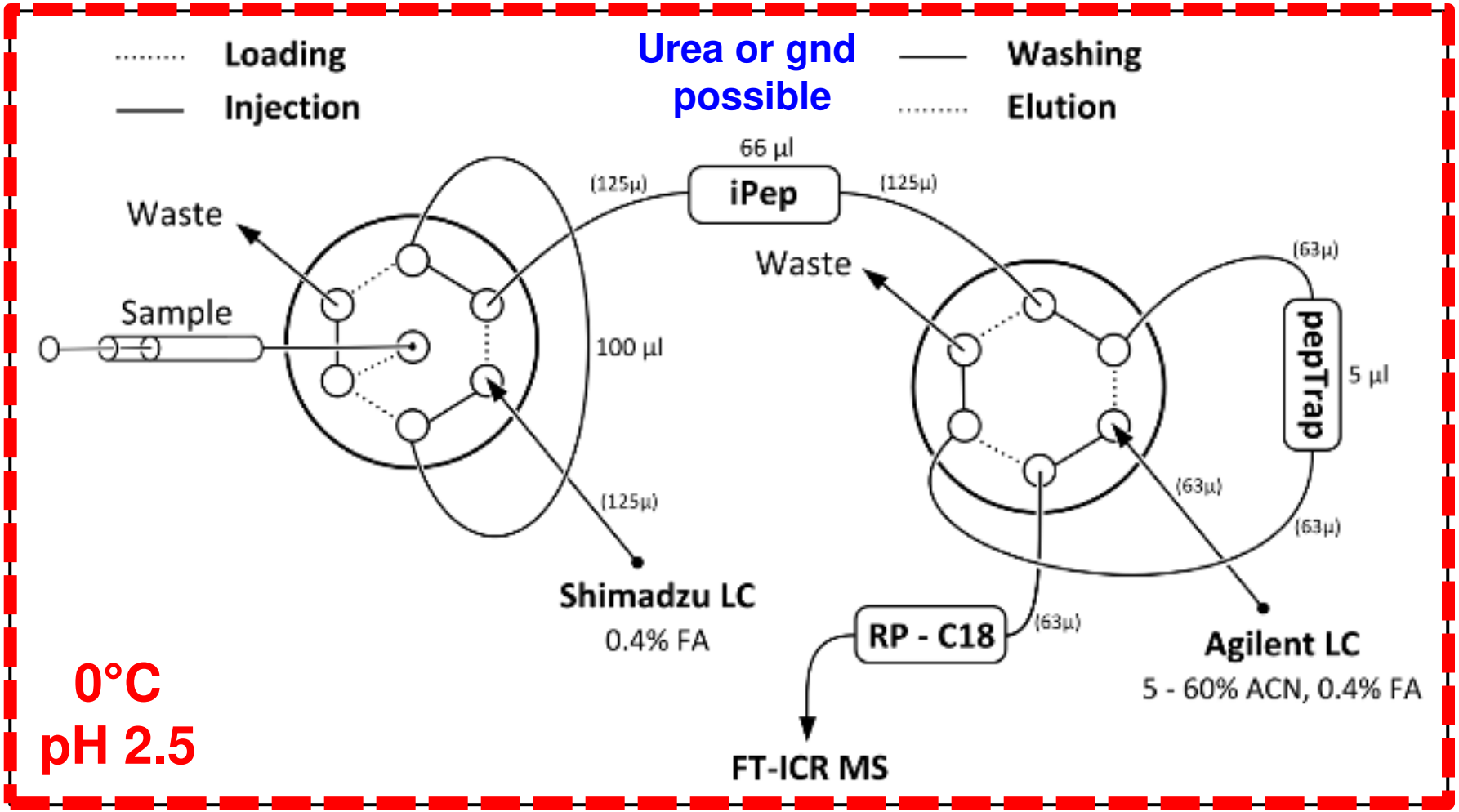

H/D exchange setup for online digestion and LC

Bottom-up HDX - proteolysis

- defines spatial resolution of the method / full sequence coverage wanted

- Golden standard – porcine pepsin A
  not all proteins can be efficiently by pepsin digested under HDX-MS conditions

- poor choice of commercial proteases suitable for HDX-MS
  type XIII – Aspergillopepsin, type XVIII – Rhizopuspepsin
  – both not very well defined crude extracts

- *Immobilized protease – high local protein-enzyme ratio, tunable via column size, flow, pressure, temperature*

Bottom-up HDX - proteolysis

Proteolysis

- defines spatial resolution of the method
- not all proteins can be efficiently by pepsin digested under HX-MS conditions

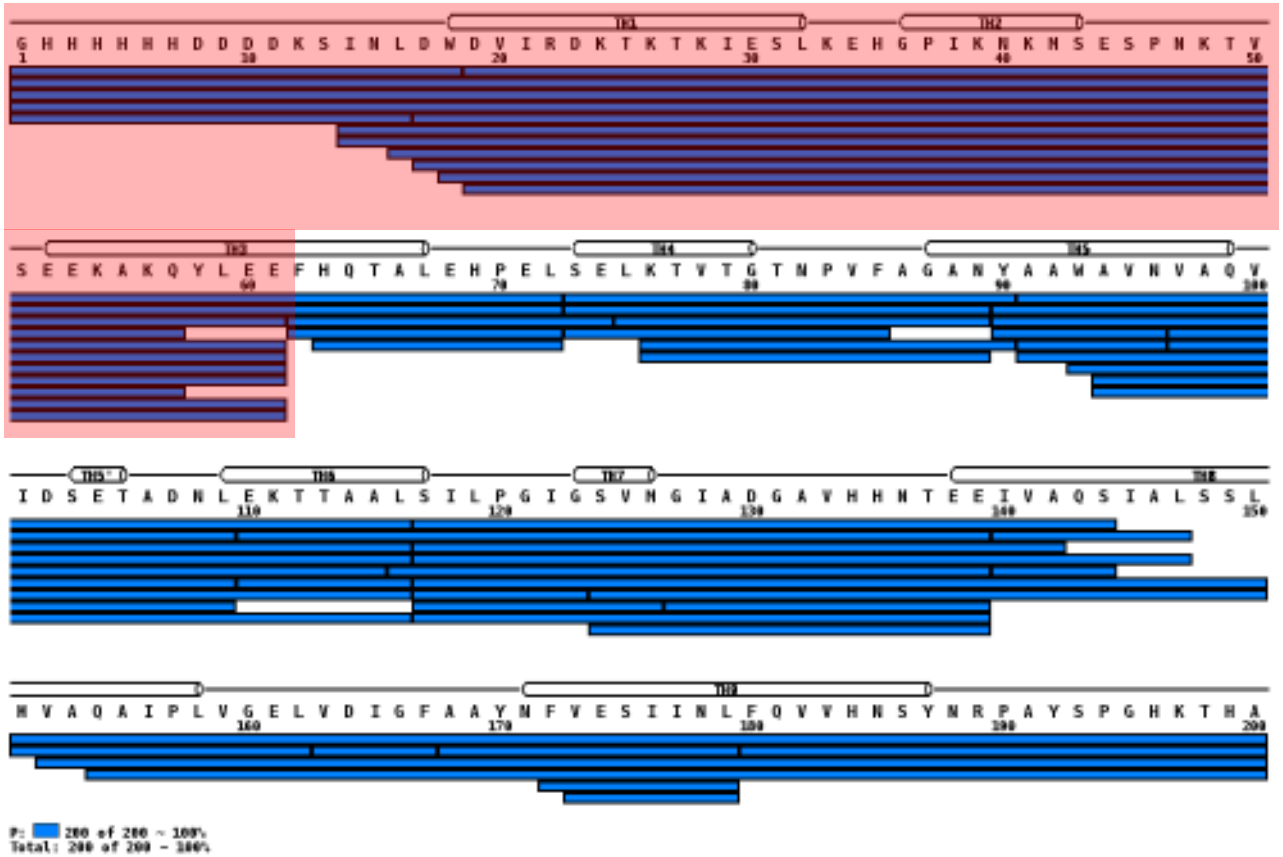

Bottom-up HDX - proteolysis

Try different proteases (commercial extracts – protease type XIII, type XVIII)

Digestion by pepsin+rhizopuspepsin (type XVIII)

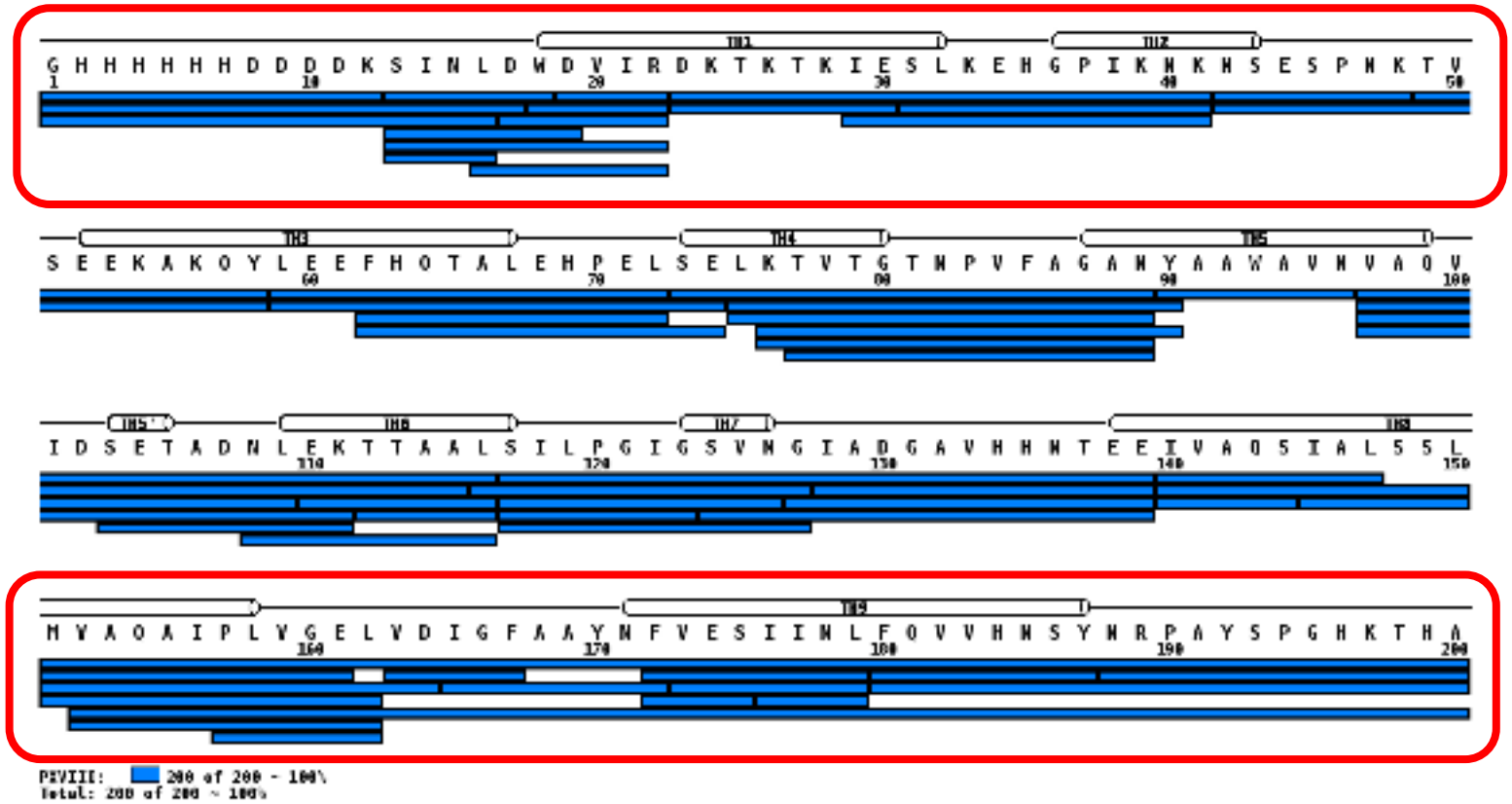

Acidic proteases in HDX – overview

- 2017 – Tsiatsiani et al – An-PEP + Nirudodhi et al – dual proteases (XIII+pepsin)
- 2016 – Rey et al – neprosin (not yet for H/D)
- 2015 – Yang et al – nepenthesin-2
- 2014 – Kadek et al – nepenthesin-1
- 2013 – Ahn et al – rice field eel
  2013 – Rey et al – nepenthes pitcher fluid
- 2010 – Marcoux et al – plasmepsin 2
- 2009 – Rey et al – recombinant rhizopuspepsin
  (protease type XVIII)
- 2007 – Brier et al – pepsins from Antarctic rock cod
- 2003 – Cravello et al – protease type XIII and XVIII
  Dykstra et al – endothiapepsin
- 2002 – Wang et al – pepsin immobilization
- 1993 – Zhang&Smith – MS + protein digestion (pepsin)
- 1979 - Rosa&Richards – protein digestion (pepsin, rhizopuspepsin)

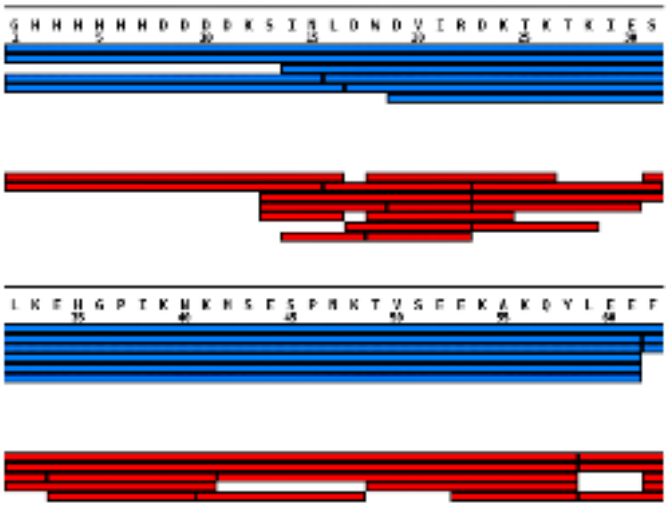

Proteases – what is available

Nepenthesin-1
Nepenthesin-2
Rhizopuspepsin (XVIII)
Aspergillopepsin (XIII)
Pepsin
AN-PEP
Orzyasin
Neprosin

Comparisons of peptide maps

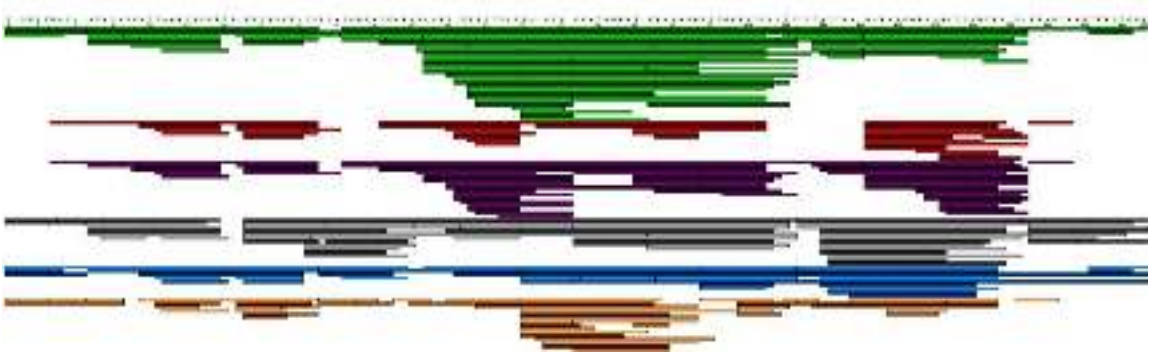

Cleavage after…

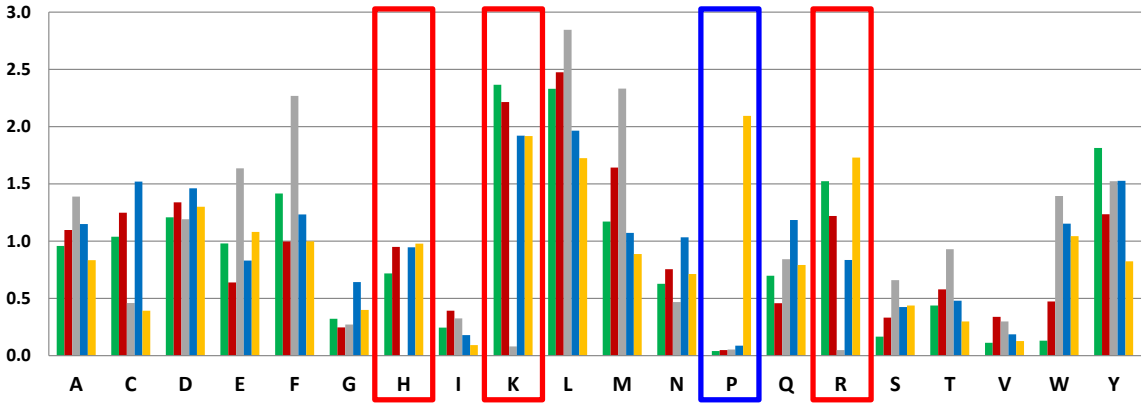

GOALS

Digest every protein

Care about average peptide length, redundancy, reproducibility, suitability for ETD,…

Output and data presentation – uptake plots

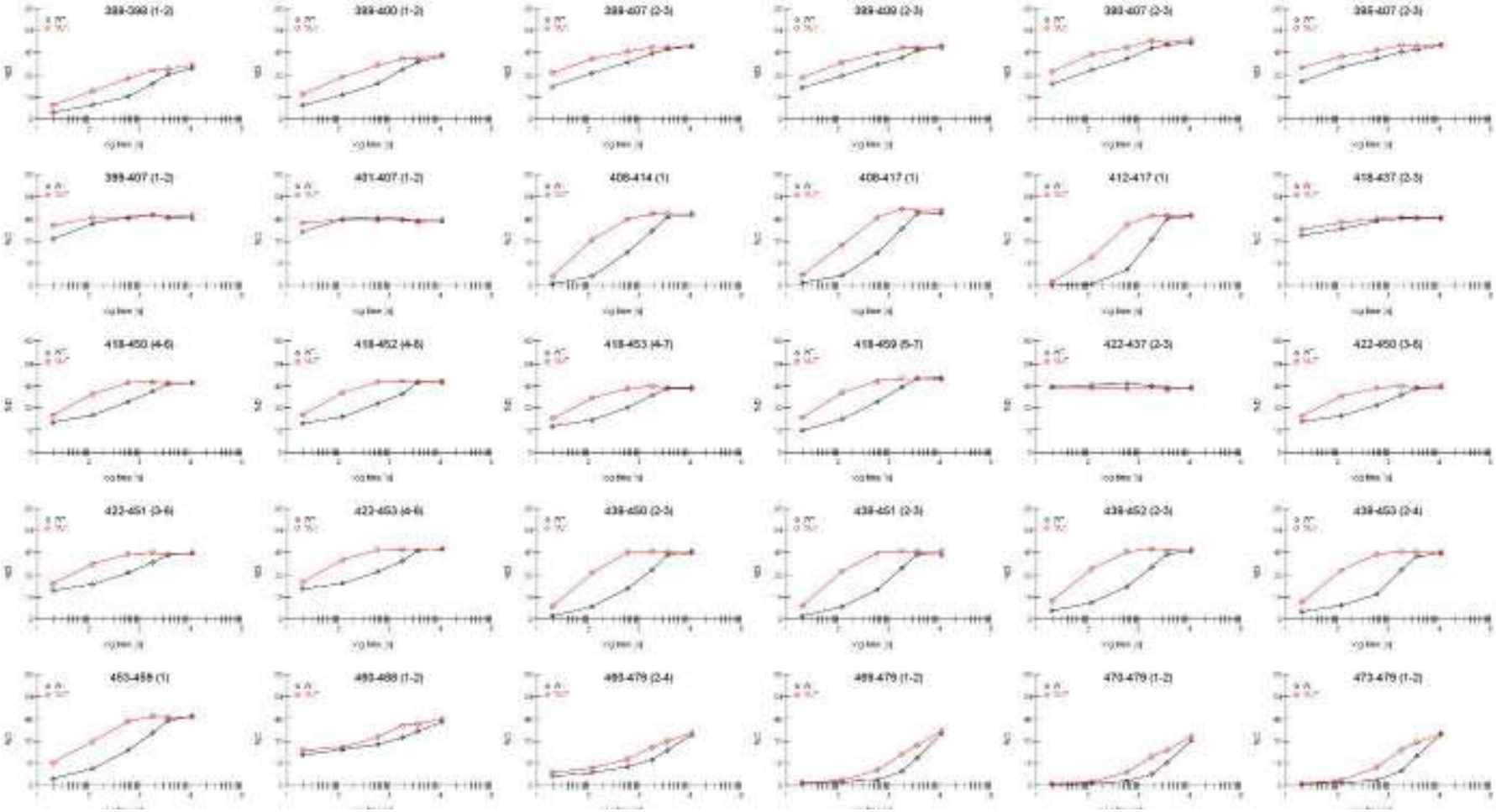

Output and data presentation – uptake plots

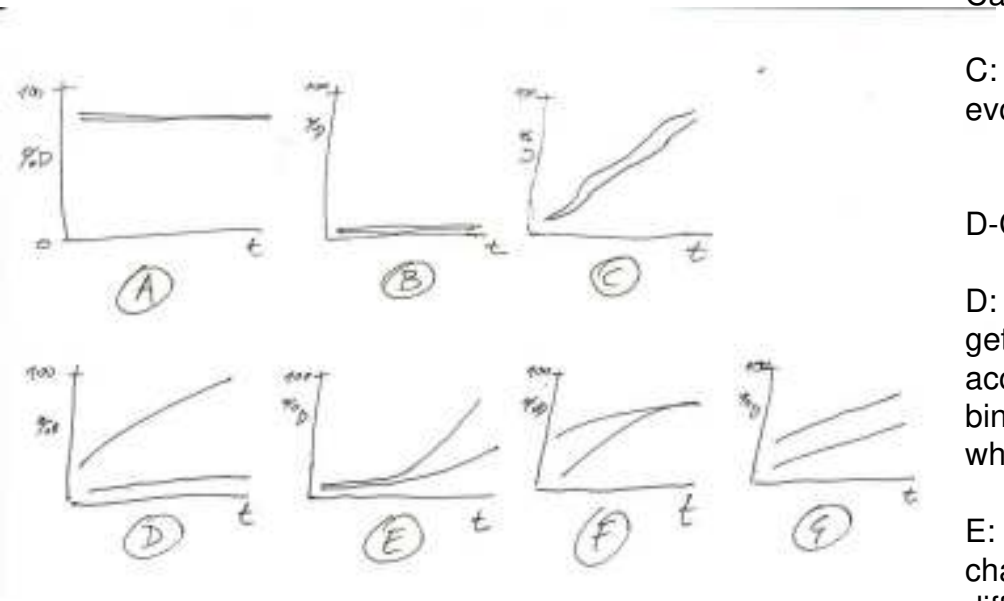

A: fast deuteration and remains constant - fast exchanging region, most likely no secondary structure

B: most probably deep in the structure - virtually no exchange. Can be also fast exchanger

C: structured region - deuterium uptake plots are somehow evolving

D-G: Various types of differences in deuteration

D: huge difference that appears already in the beginning and is getting even bigger during the exchange - clear difference is accessibility and H-bonding + signature of extremely stable binding of a ligand - the lower curve simply does not change while the upper one (for free protein) evolves

E: in contrast to D, this is poorly exchanging region with stable change upon ligand binding - it takes some time for the differences to appear but once they are there, the curves are separating

F: ligand binding occurs but is not so stable. so during the time of exchange we can observe dissociation events during which the protein has chance to gets deuterated.

G: stable change, similar to D

Back-exchange correction

Correction for back-exchange

$$\text{Corr \%D} = \frac{Mp - Mn}{Mf - Mn} * 100$$

$$\text{Corr No D} = \frac{Mp - Mn}{Mf - Mn} * Ns$$

Mp - MW partially deuterated
Mn - MW nondeuterated
Mf - MW fully deuterated (equilibrium)
Ns - number of exchangeable sites (Σamide bonds-Pro)

Important for comparison of different sequences, mutants

Not needed in typical comparison experiment

Needed when conclusions about protein folding or fold are made – helps to distinguish fast exchanging (in- as well as out- exchangers) and poor accessibility/strong hydrogen bodning

Protein incubated in D2O (under denaturing, heating,… conditions) and analyzed like the samples. Alternative – pre-digestion and deuteration of peptides!

In general between 15-25%

Back-exchange correction

Correction for back-exchange

$$\text{Corr \%D} = \frac{Mp - Mn}{Mf - Mn} * 100$$

$$\text{Corr No D} = \frac{Mp - Mn}{Mf - Mn} * Ns$$

Mp - MW partially deuterated
Mn - MW nondeuterated
Mf - MW fully deuterated (equilibrium)
Ns - number of exchangeable sites (Σamide bonds-Pro)

Examples – before (left) and after (right) correction to BE – overall level raises + difference is slightly bigger (due to bigger y-scale)

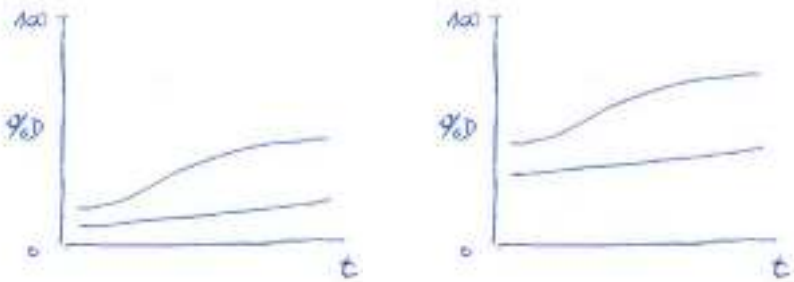

Examples – slow and fast exchanger
left – before BE correction hard to judge; middle – slow exchanger (deep in the structure) after correction; right – fast exchanger – e.g. HisTag - after correction

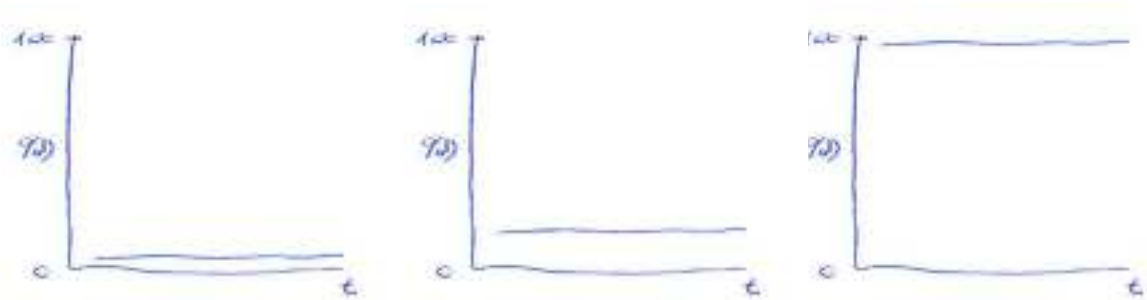

Datamining

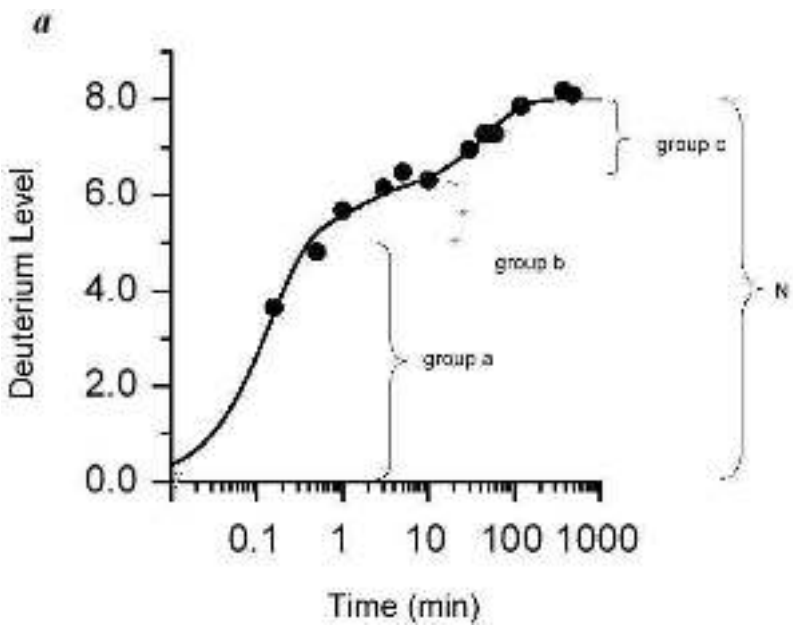

If fine sampling in HDX is used, the curve can be fitted and number of fast, slow and intermediate exchanging amides can be deduced

b

$$D = N - \sum_{i=1}^{N} \exp^{-k_i t}$$

c

$$D = 8 - \left[\underbrace{(5\,(e^{-(m1)\cdot t}))}_{\substack{\text{group a} \\ m1=7.21 \pm 0.82\ \text{min}^{-1} \\ t_{1/2}=0.096\ \text{min}}} + \underbrace{(1\,(e^{-(m2)\cdot t}))}_{\substack{\text{group b} \\ m2=0.77 \pm 0.32\ \text{min}^{-1} \\ t_{1/2}=0.90\ \text{min}}} + \underbrace{(2\,(e^{-(m3)\cdot t}))}_{\substack{\text{group c} \\ m3=0.021 \pm 0.003\ \text{min}^{-1} \\ t_{1/2}=33.0\ \text{min}}} \right]$$

Data presentation

http://peterslab.org/MSTools/

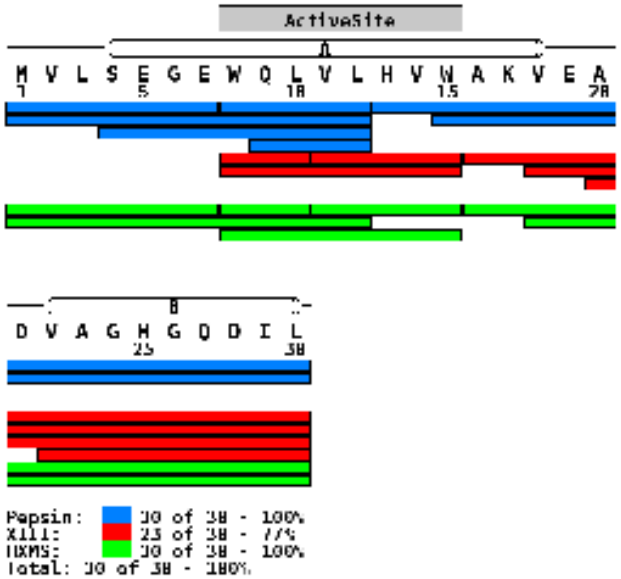

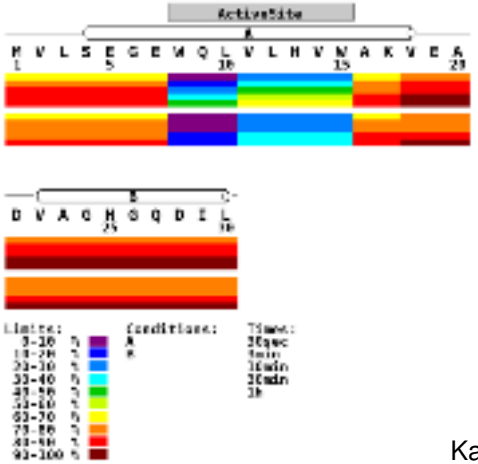

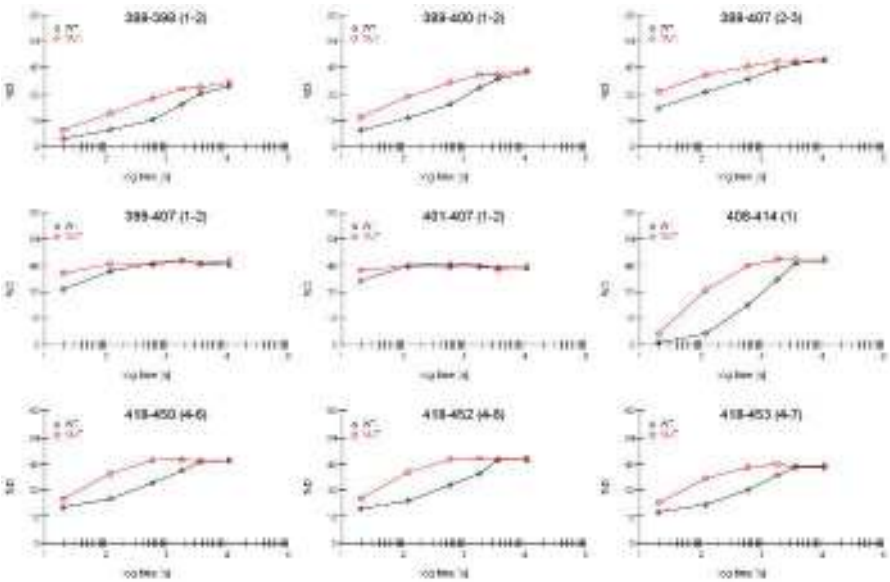

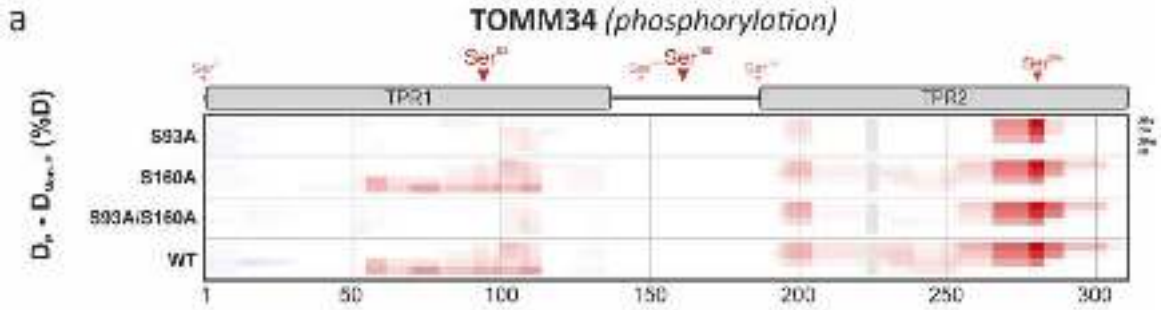

Kavan, D. and Man, P. Int. J. Mass Spectrom. 2011, 302: 53-58. http://dx.doi.org/10.1016/j.ijms.2010.07.030.

Data presentation

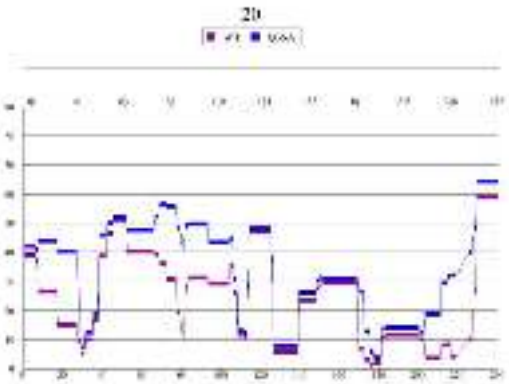

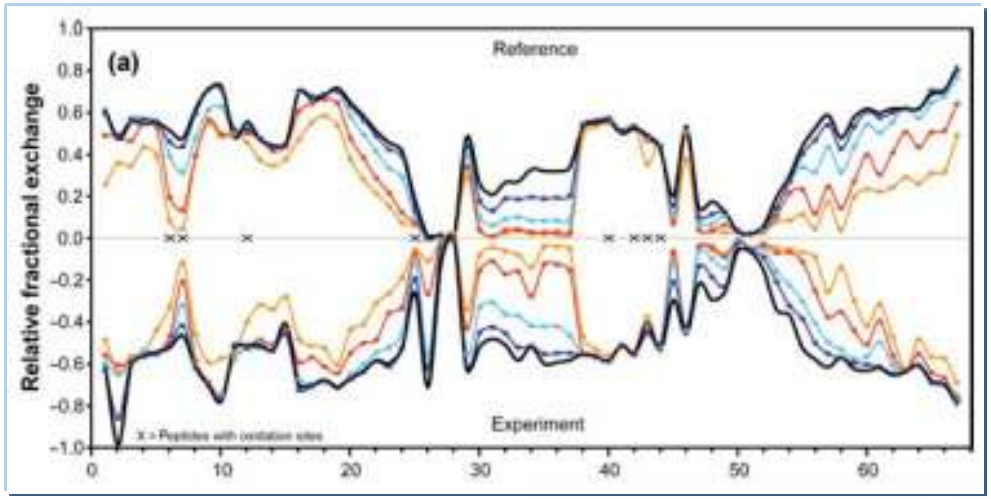

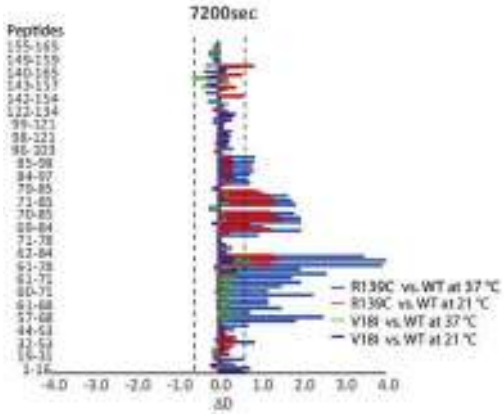

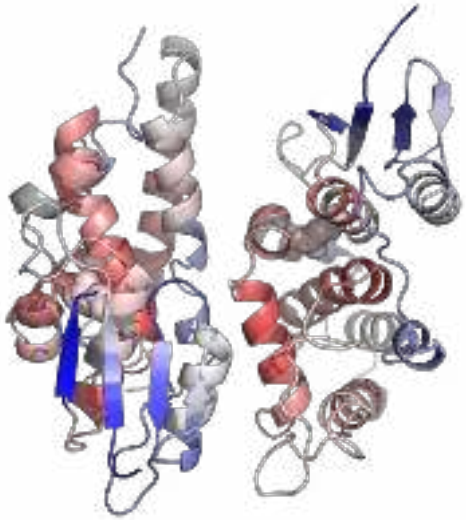

What is it good for?

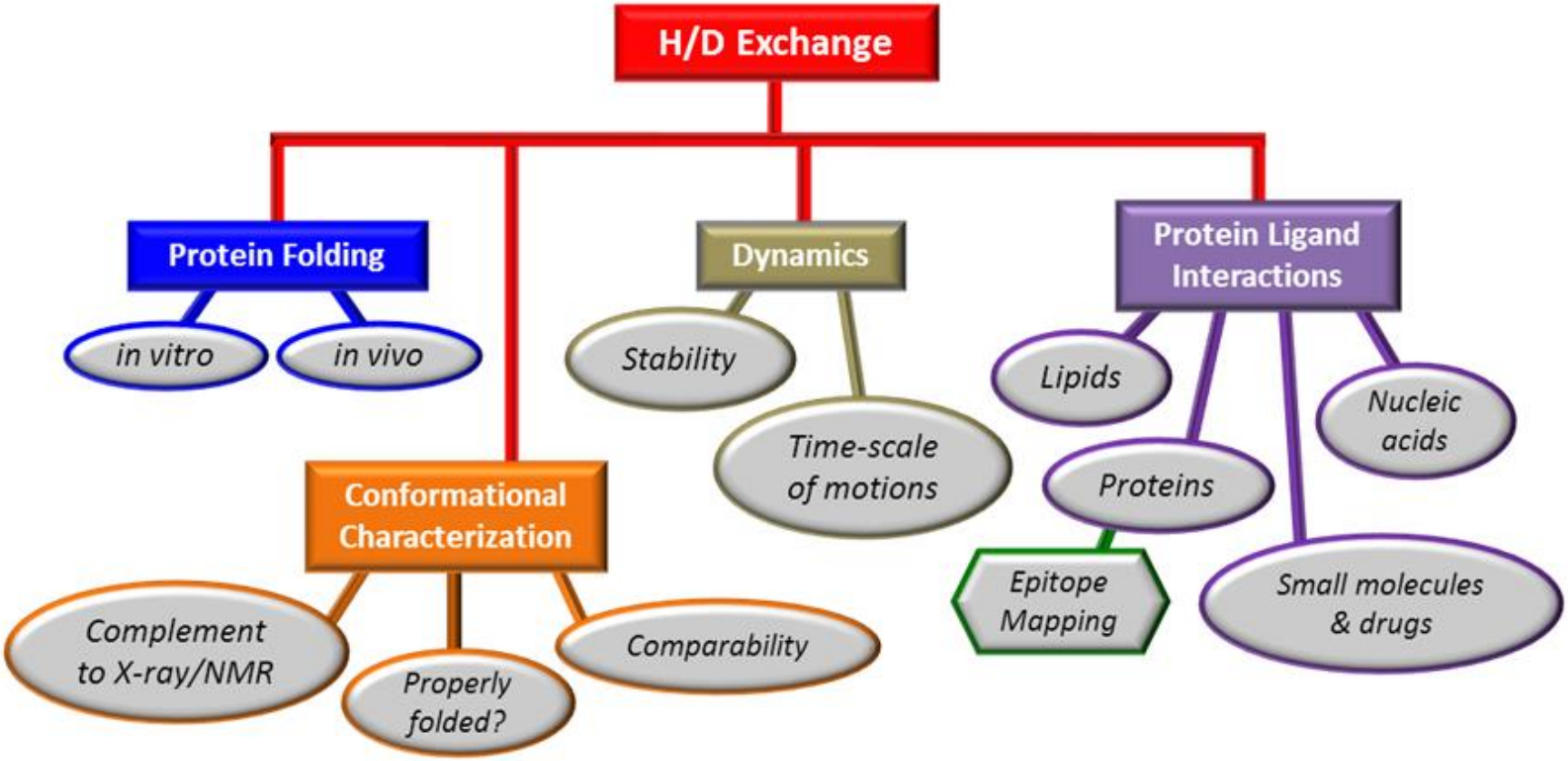

Engen et al. (2011). *Ency. Anal. Chem.* ISBN 978-04-700-2731.

Biologicals, anitbodies, epitope mapping

EPITOPE MAPPING

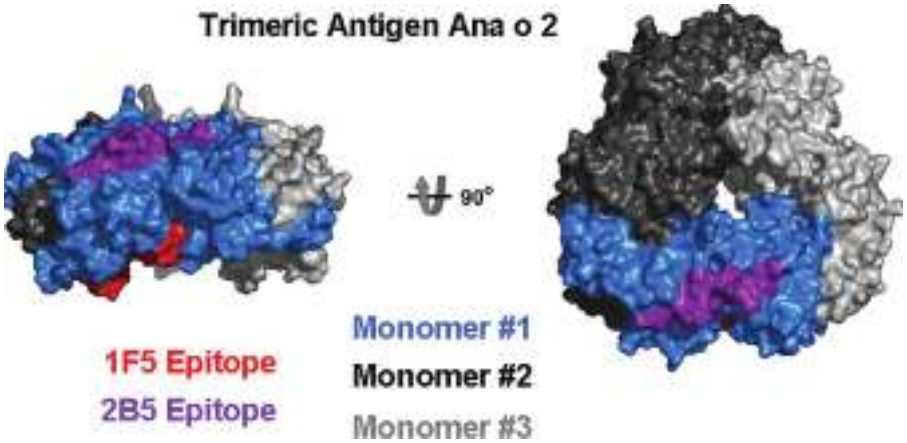

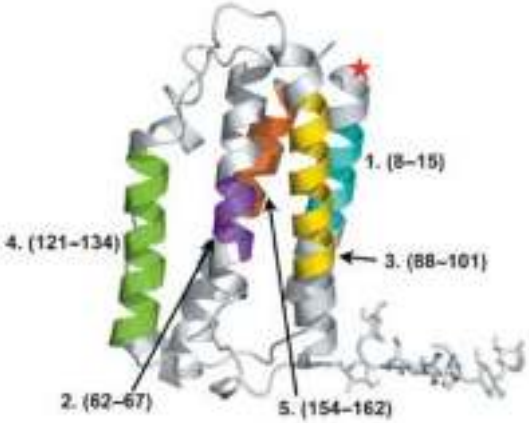

BIOSIMILARS

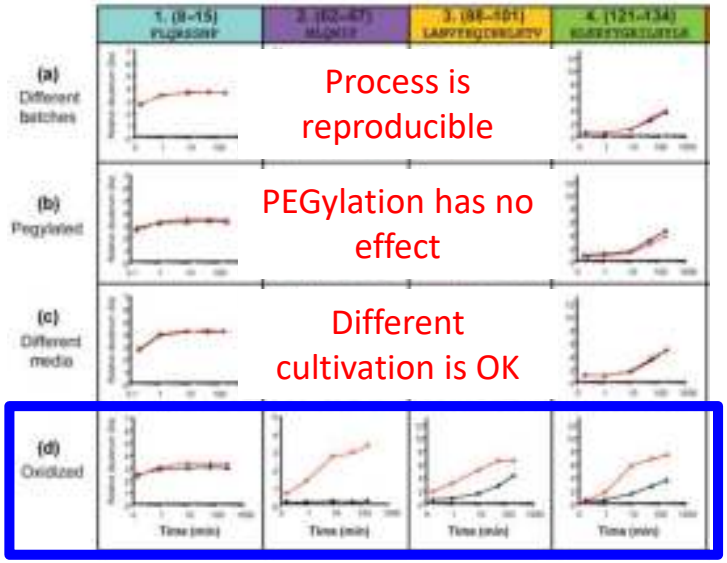

!oxidation!

Zhang *et al.*: Anal. Chem. (2011) Houde *et al.*: J. Pharm. Sci. (2011)

Protein structuration

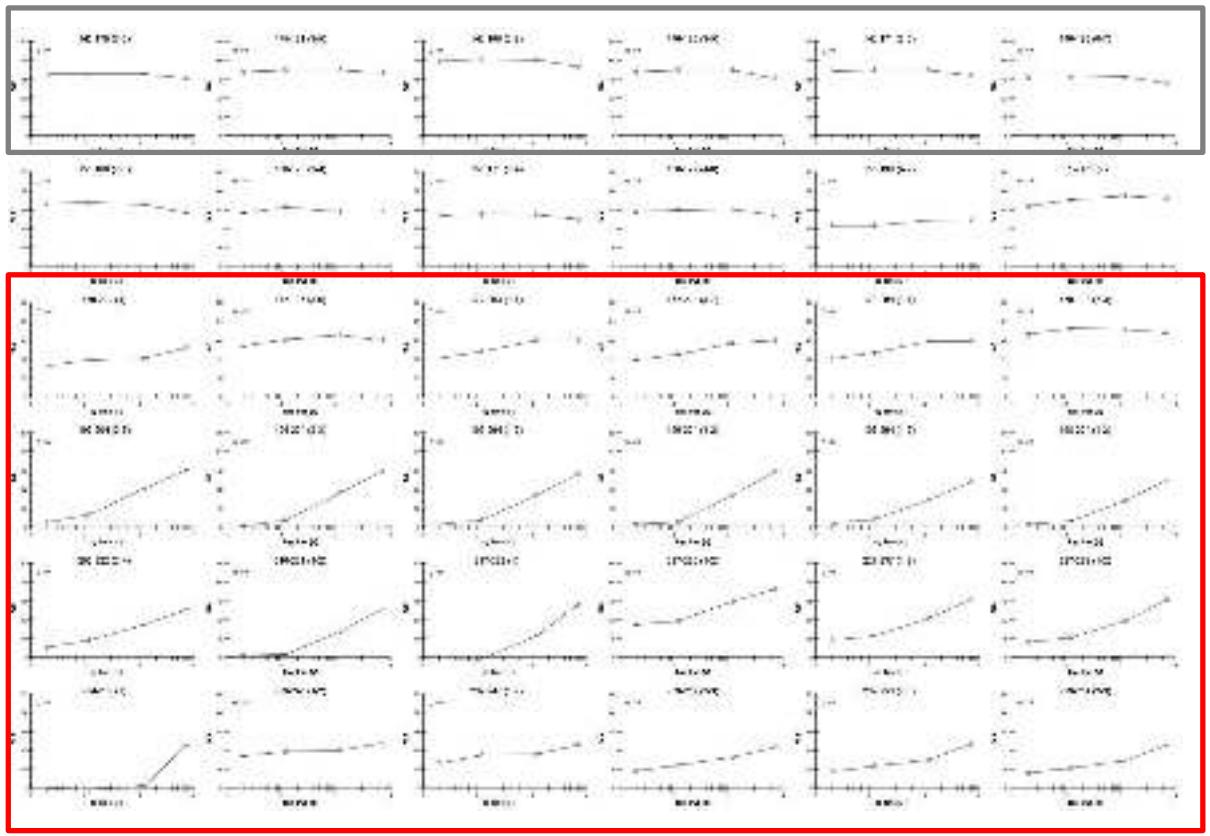

The easiest and simplest setup + data interpretation – HDX profile of a single protein

Tomm34 – structured vs unstructured regions

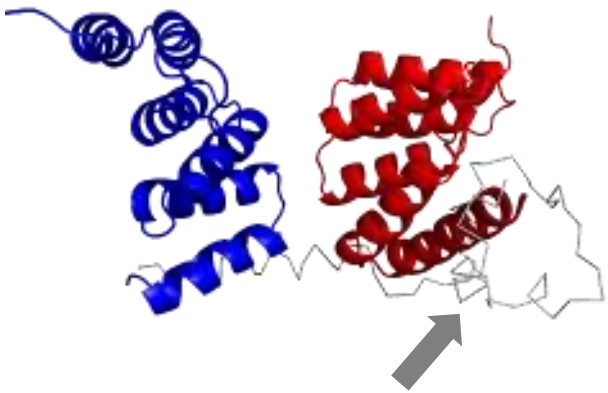

Protein:protein interactions + effect of modifications

Phosphorylated TOMM34 interacts with 14-3-3 through its unstructured linker (no change in HDX detected) but it leads to overall structure “opening”. Weak protection is observed on14-3-3.

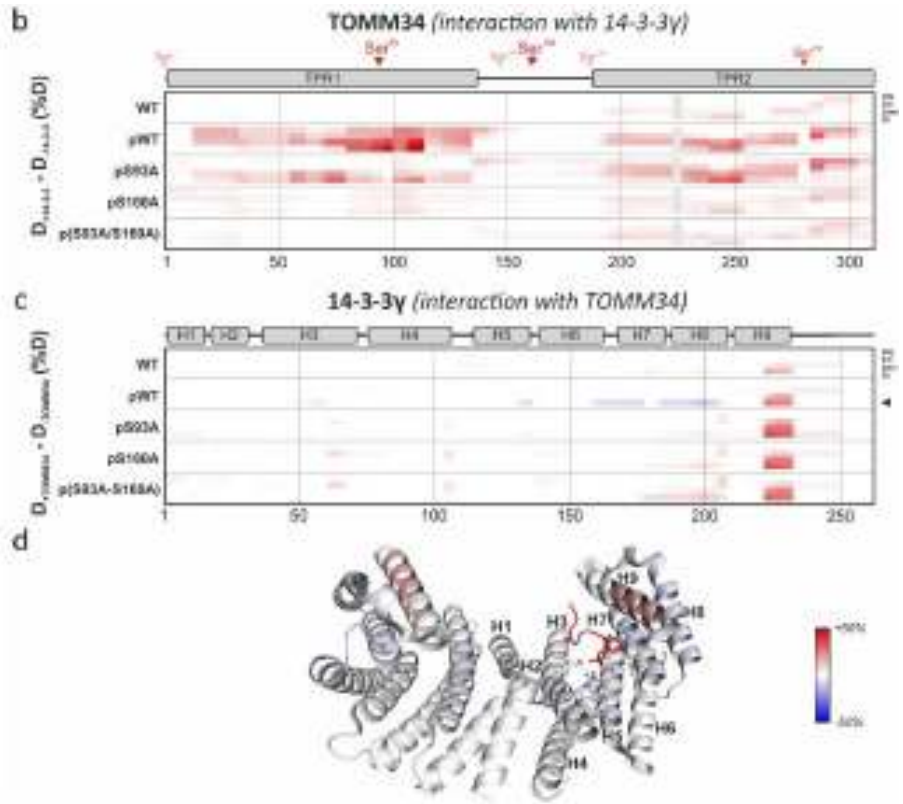

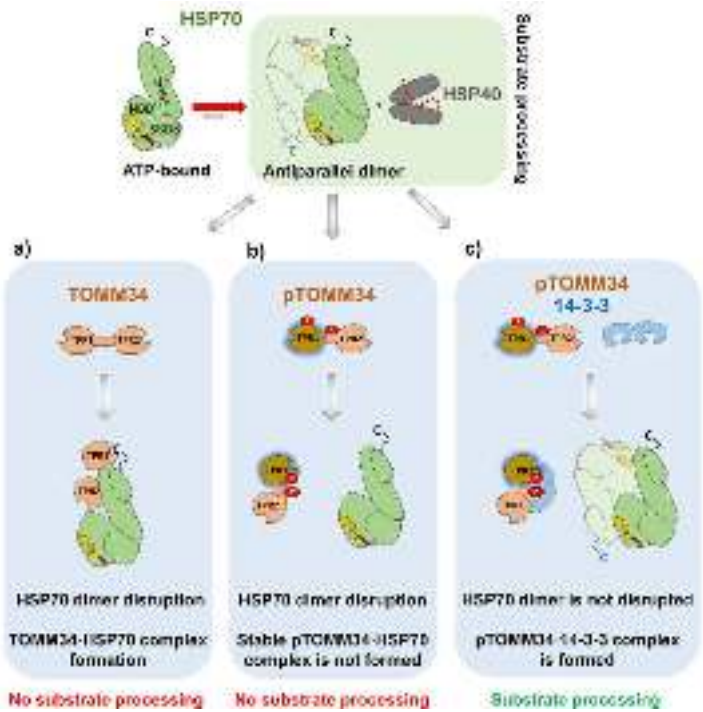

Intraprotein interaction

Cellobiose dehydrogenase – pH dependent intraprotein domain-domain interaction = protection. But it is all different!

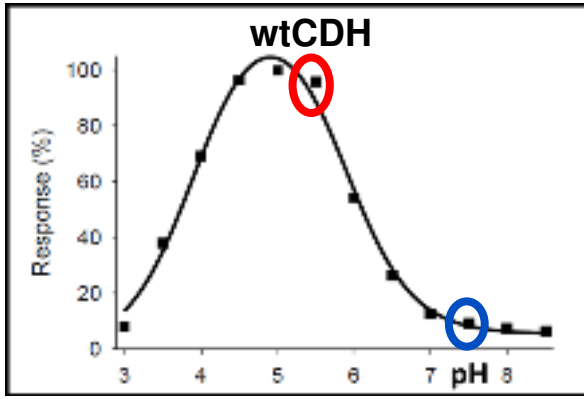

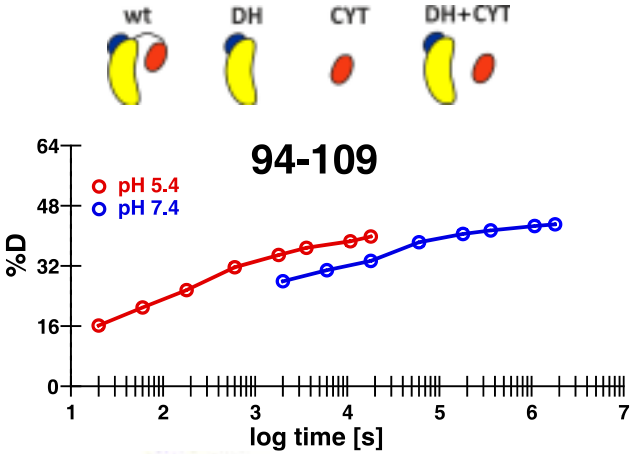

No protection upon the interaction

Deprotection around the proposed interacting surfaces

Protonation (charge neutralization) enables the interaction…

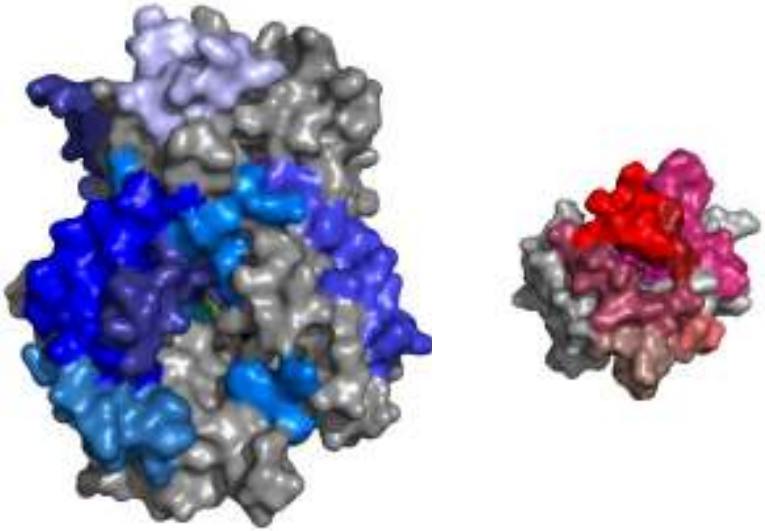

Kadek A et al BBA 2017

Membrane proteins

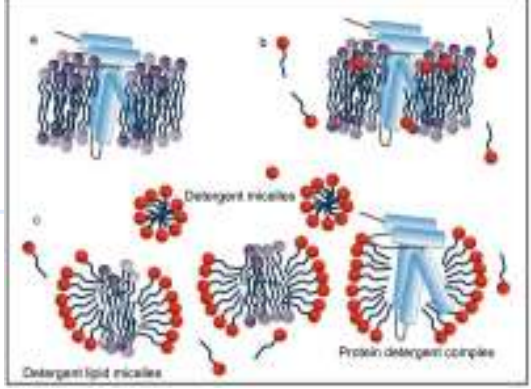

Detergent solubilized
- not all detergents are MS-friendly (CHAPS, cholate, SDS)
- not all detergents can be removed prior to the MS
- fancy detergents with very low CMC likely have “issues”

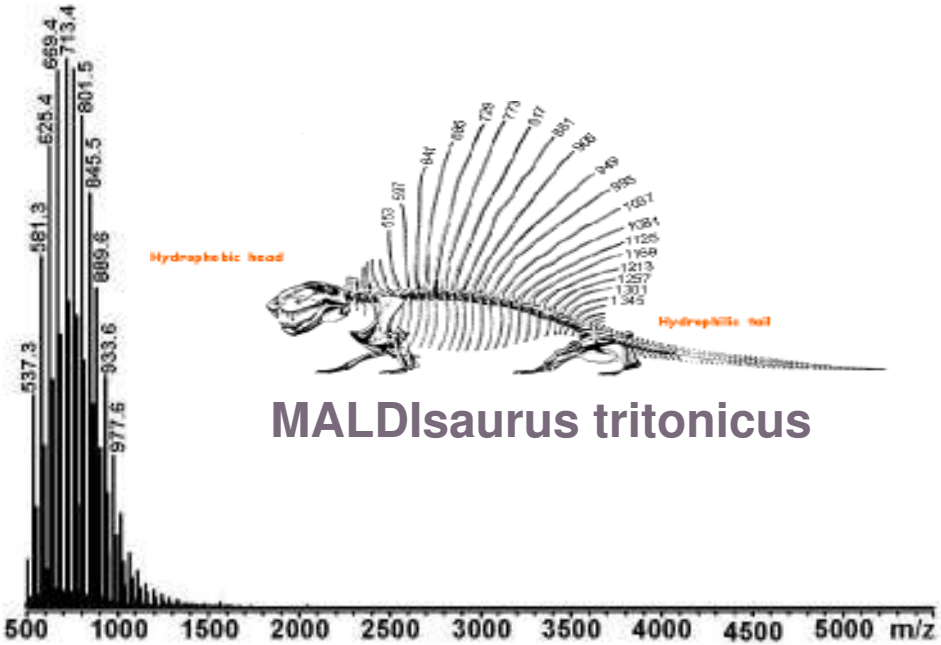

Rey M. et al. Anal. Chem. 2010

Membrane proteins

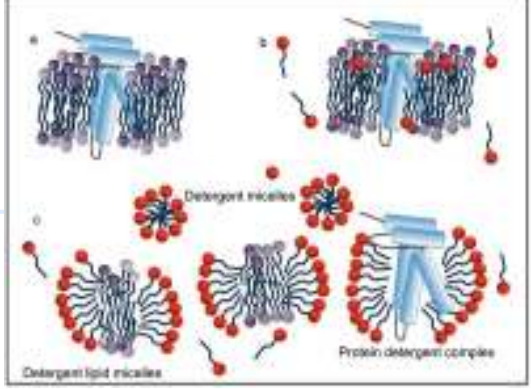

Detergent solubilized

- not all detergents are MS-friendly (CHAPS, cholate, SDS)
- not all detergents can be removed prior to the MS
- fancy detergents with very low CMC likely have “issues”

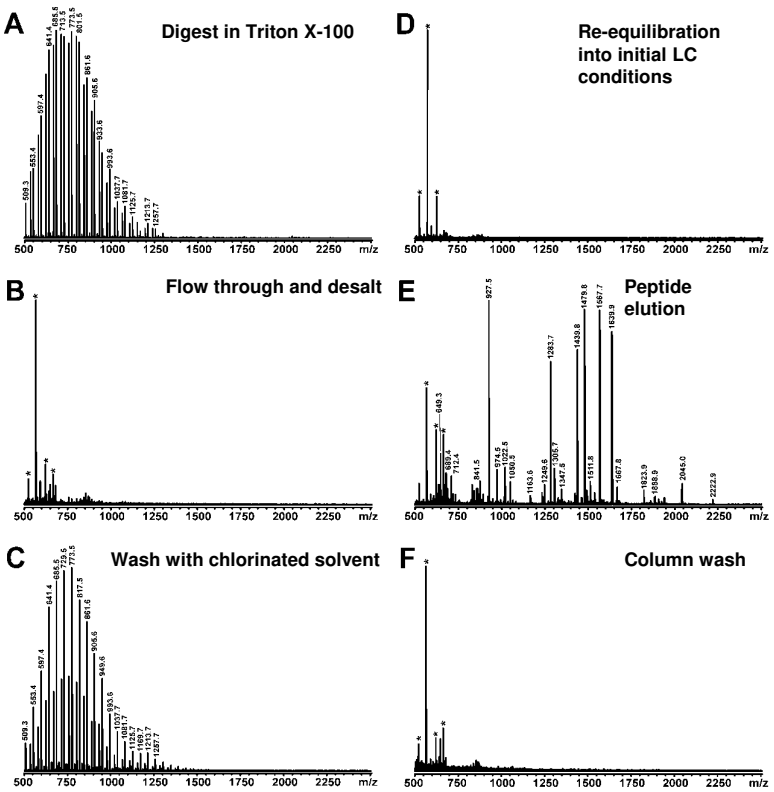

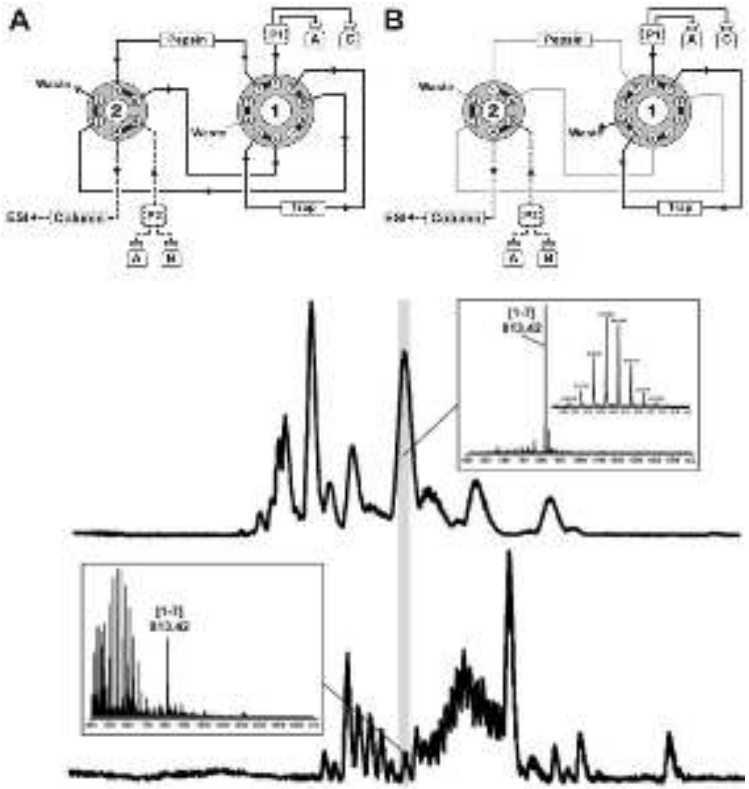

Rey M. et al. Anal. Chem. 2010

Membrane proteins

Nanodiscs – membrane scaffolding protein + lipids

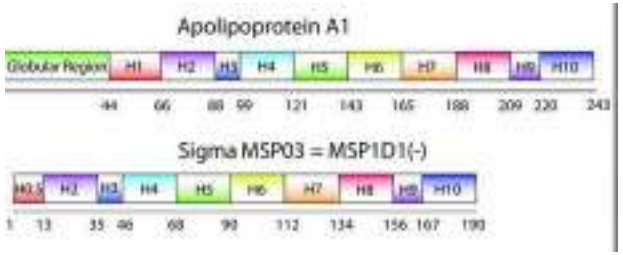

Many different (size/no of repeats) MSPs, various lipid compositions

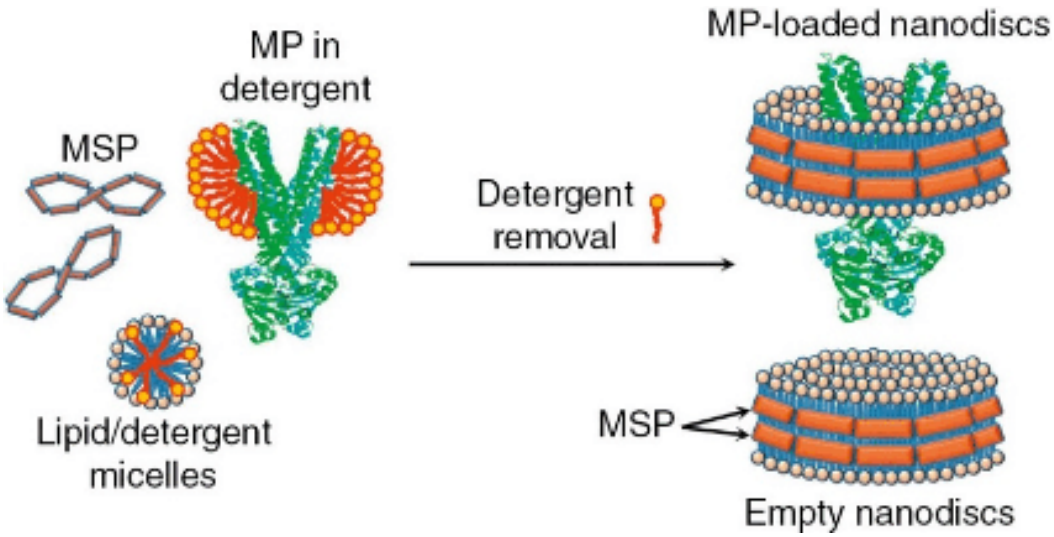

Alternatives to MSP

SMALP (styrene maleic acid/anhydride copolymer)

SaposinA

Hebling CM et al Anal Chem 2010
Harrison RA et al Curr Opin Struct Biol 2016
Martens C et al Nat Protocols 2019

Membrane proteins

Nanodiscs – protocol *(Martens C et al Nat Protocols 2019)*

- Quench + disassembly (detergent)
- Lipid removal by ZrO2 coated resin
- ZrO2 particles filtering
- Digestions (eventually done during lipid removal)

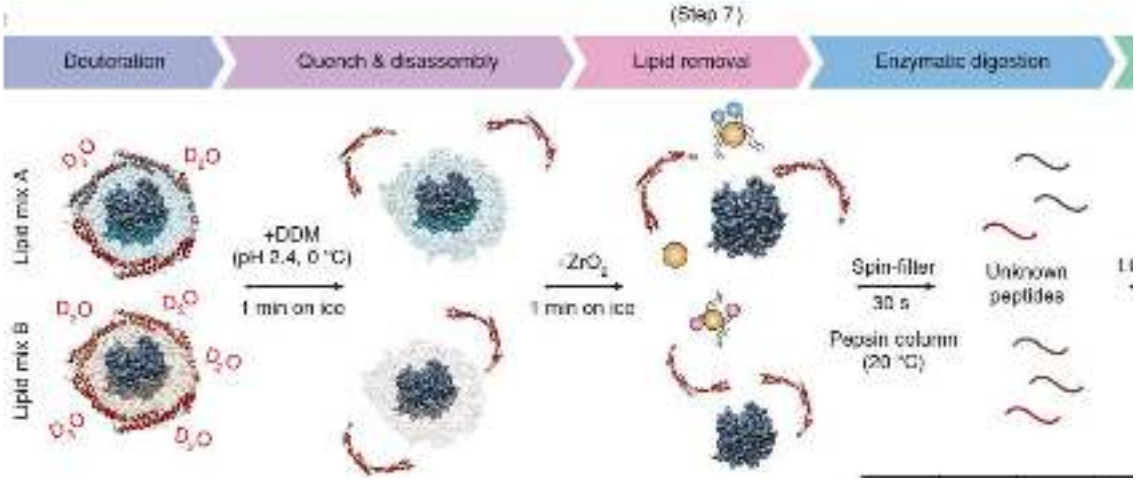

Pros and cons of HDX-MS

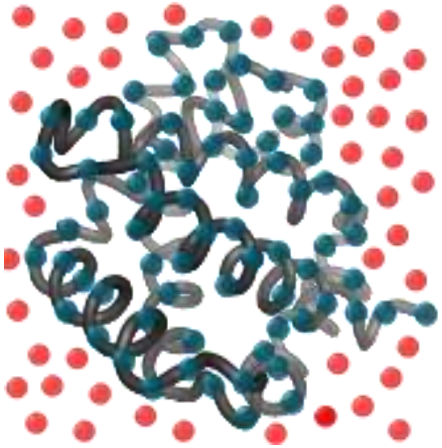

D_2O buffer

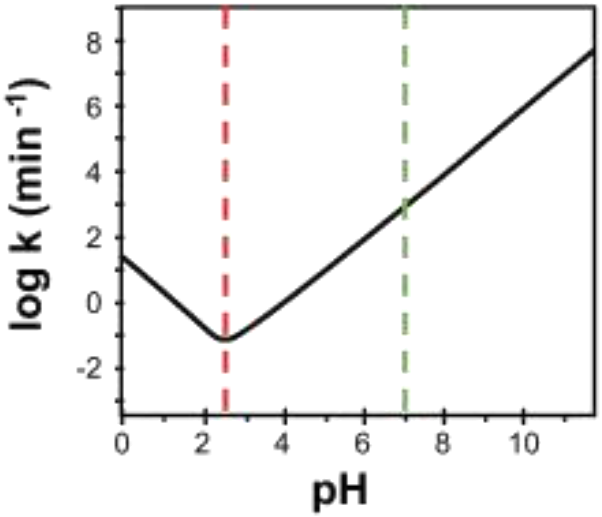

$$k(T_2) = k(T_1)exp^{-\frac{E_a}{R}\left(\frac{1}{T_2}-\frac{1}{T_1}\right)}$$

1 ΔpH … 10×
10°C … 3×

Buffer – can be whatever
Protein size – does not matter
Protein concentration – can be very low
Mixture compatible – many proteins
Temperature or pH – can be whatever
(correction must be done - H/D depends on pH and T)
Commercial solutions available

Dilutions – into D_2O and to lower the pH
Protein concentration – not all complexes are formed at given concentration (K_D)
Comparison – at least two states required

H2020

EUROPEAN NETWORK OF FOURIER-TRANSFORM ION-CYCLOTRON-RESONANCE MASS SPECTROMETRY CENTERS

PROJECT AGREEMENT NO.731077

EU FT-ICR MS

Sample preparation
FT-ICR MS sample analysis
Top down of proteins
Data interpretation

Petr Novák, Zdeněk Kukačka, Petr Man, Jan Fiala & Tereza Kadavá

IMIC

EU FT-ICR MS

Sample preparation
FT-ICR MS sample analysis
Top down of proteins
Data interpretation

Petr Novák, Zdeněk Kukačka, Petr Man

IMIC

Protein desalting under denaturing conditions

Protein MicroTrap

https://www.optimizetech.com/opti-trap-cartridges/

Manual trap holder

https://www.optimizetech.com/opti-trap-manual-holder-kit/

https://www.optimizetech.com/opti-trap-loop-trap-holder-kit-micro-and-macro/

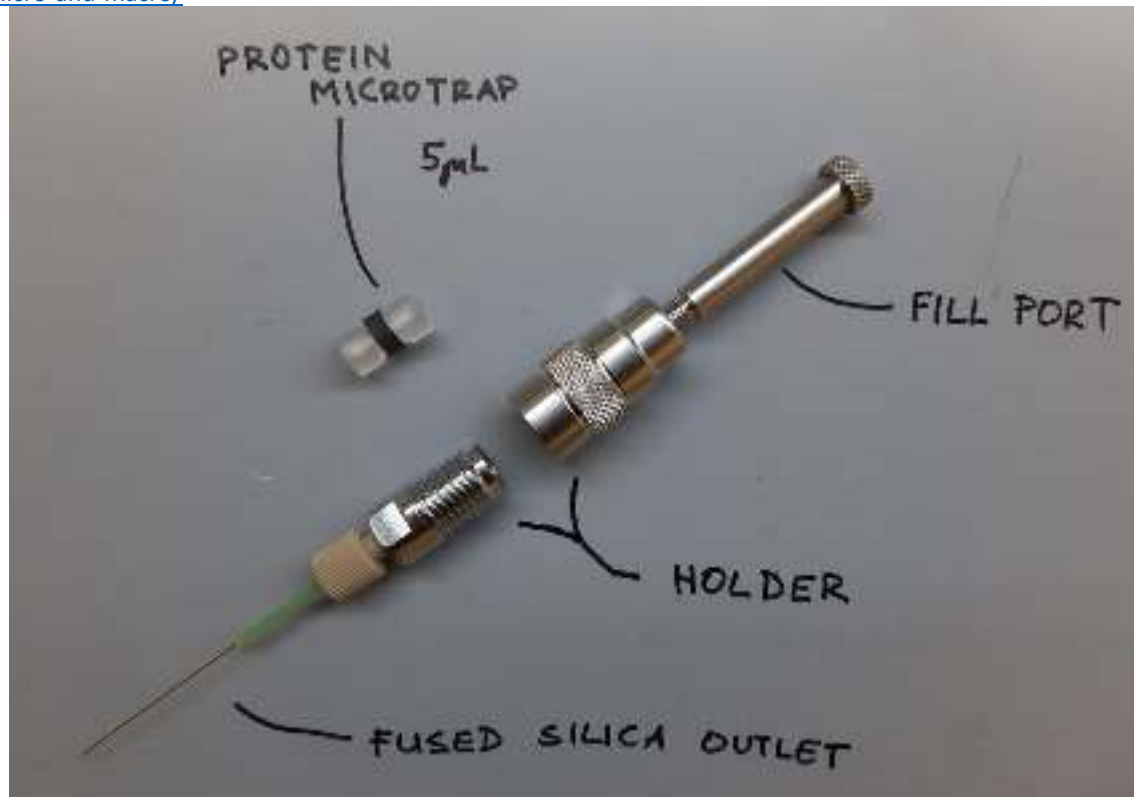

Protein desalting under denaturing conditions

Solvents A 0.4 % formic acid in water

B 70% acetonitrile / 0.4% formic acid

C water / MeOH / iPrOH / ACN / FA

Hamilton (gas tight) syringes – 100 and 25uL

Kim Wipe

Protein solution

Microtube (Eppendorf)

Protein desalting under denaturing conditions

Solvents	A	0.4 % formic acid in water
	B	70% acetonitrile / 0.4% formic acid
	C	water / MeOH / iPrOH / ACN / FA

1. Clean trap with solvent C
2. Wash with solvent B and equilibrate to A
3. Dilute sample with A
4. Slowly load onto the trap
5. Desalt with A
6. Elute with B into a clean tube
7. Go to 1.

Native Mb desalting – Zeba Spin columns

150mM Amonium Acetate, pH set to 7.4

Zeba Spin columns (7K MWCO, 75uL)

Protein sample

Pipettes and tips

Collection and wash tubes
(Eppendorf tube 2 and 1.5mL)

Native Mb desalting – Zeba Spin columns

Making nESI tips

Laser puller P-2000 (Sutter Instruments)

https://www.sutter.com/MICROPIPETTE/p-2000.html

Quartz glass capillaries – Q-100-70-7.5

https://www.sutter.com/MICROPIPETTE/glass.html

Petri dish for nESI tips

Plastic (silicon covered) forceps

Making nESI tips

Loading nESI tip

Long gel loader tips (20uL) + pipette (5-10uL)

nESI tips and 3D printed nESI tip holders

Desalted protein solution (1-10uM)

Desktop centrifuge set to
- 15sec
- 150 x g

Plastic (silicon covered) forceps

Small screw-driver

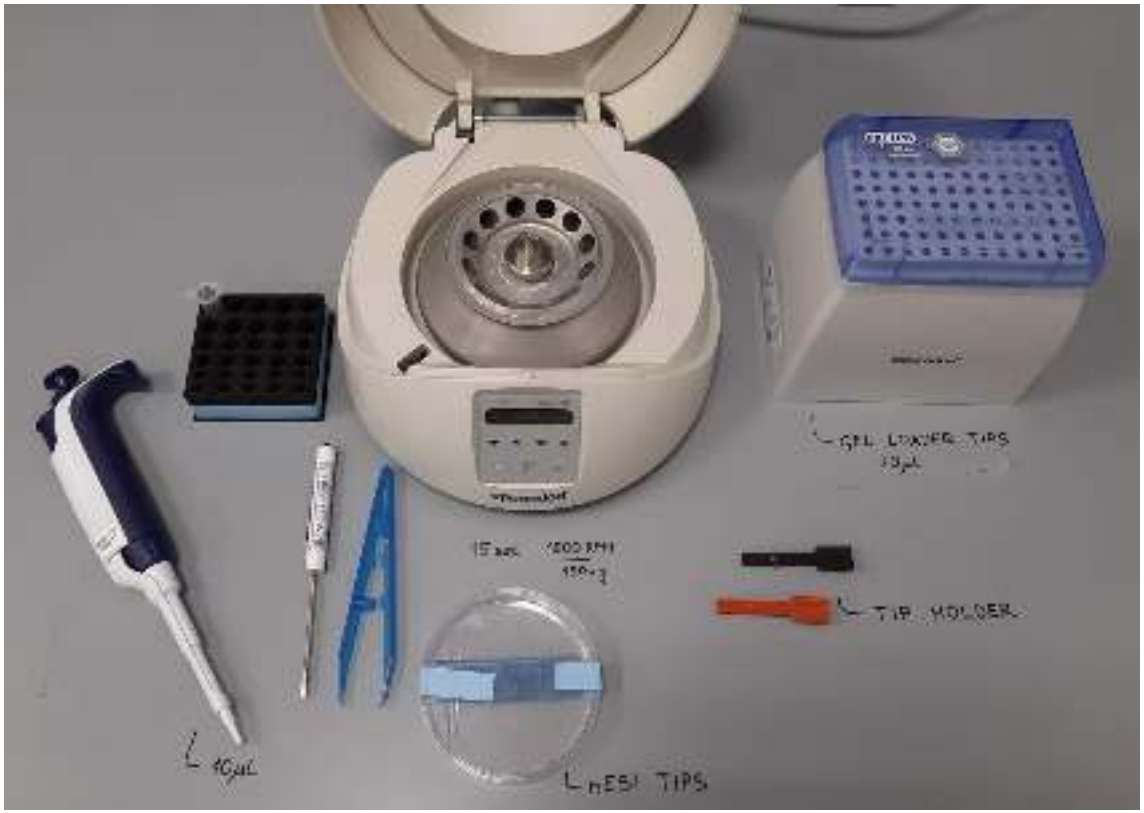

Loading nESI tip

nESI setup

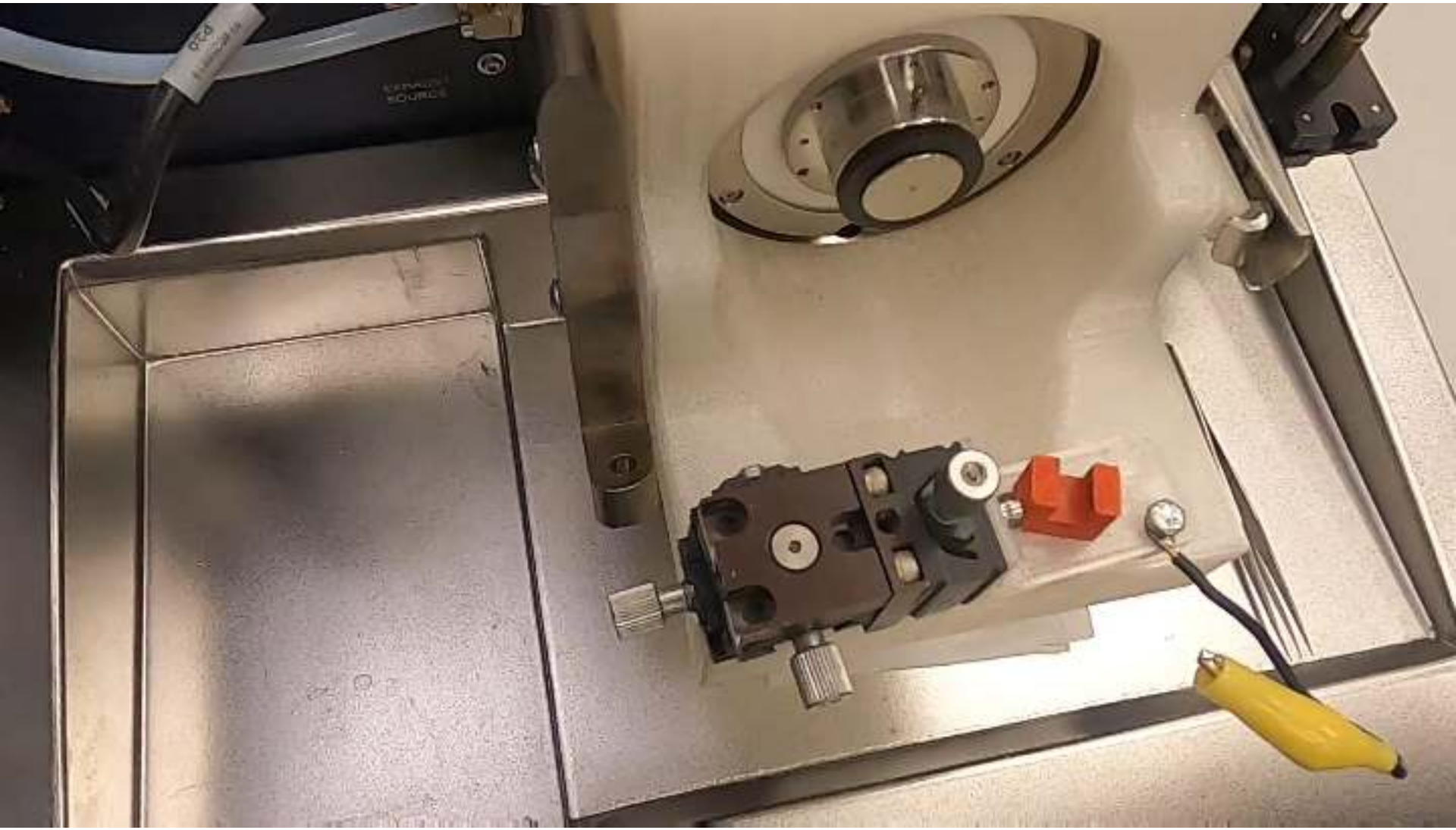

MS analysis - direct infusion - under denaturing conditions

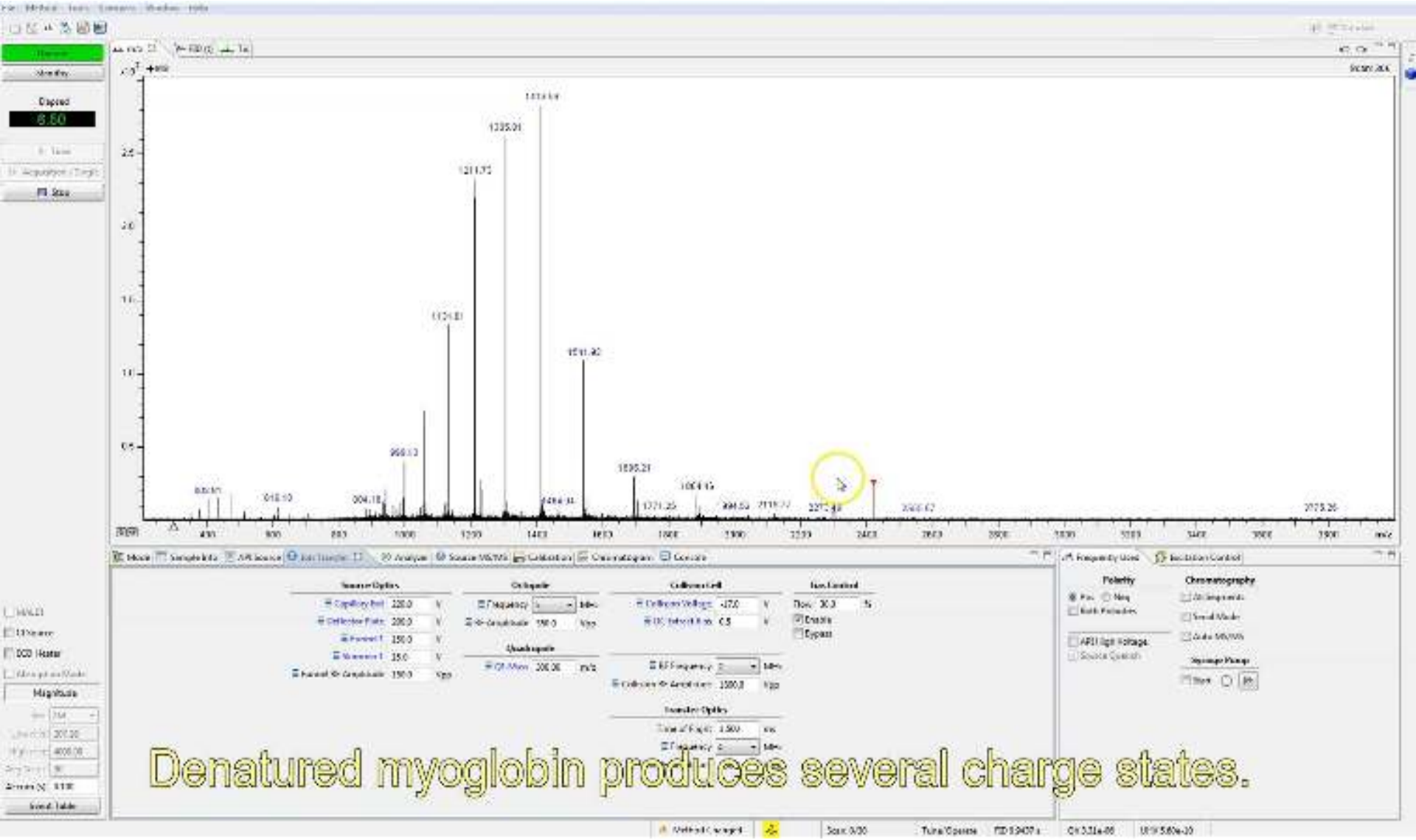

MS analysis - multiCASI

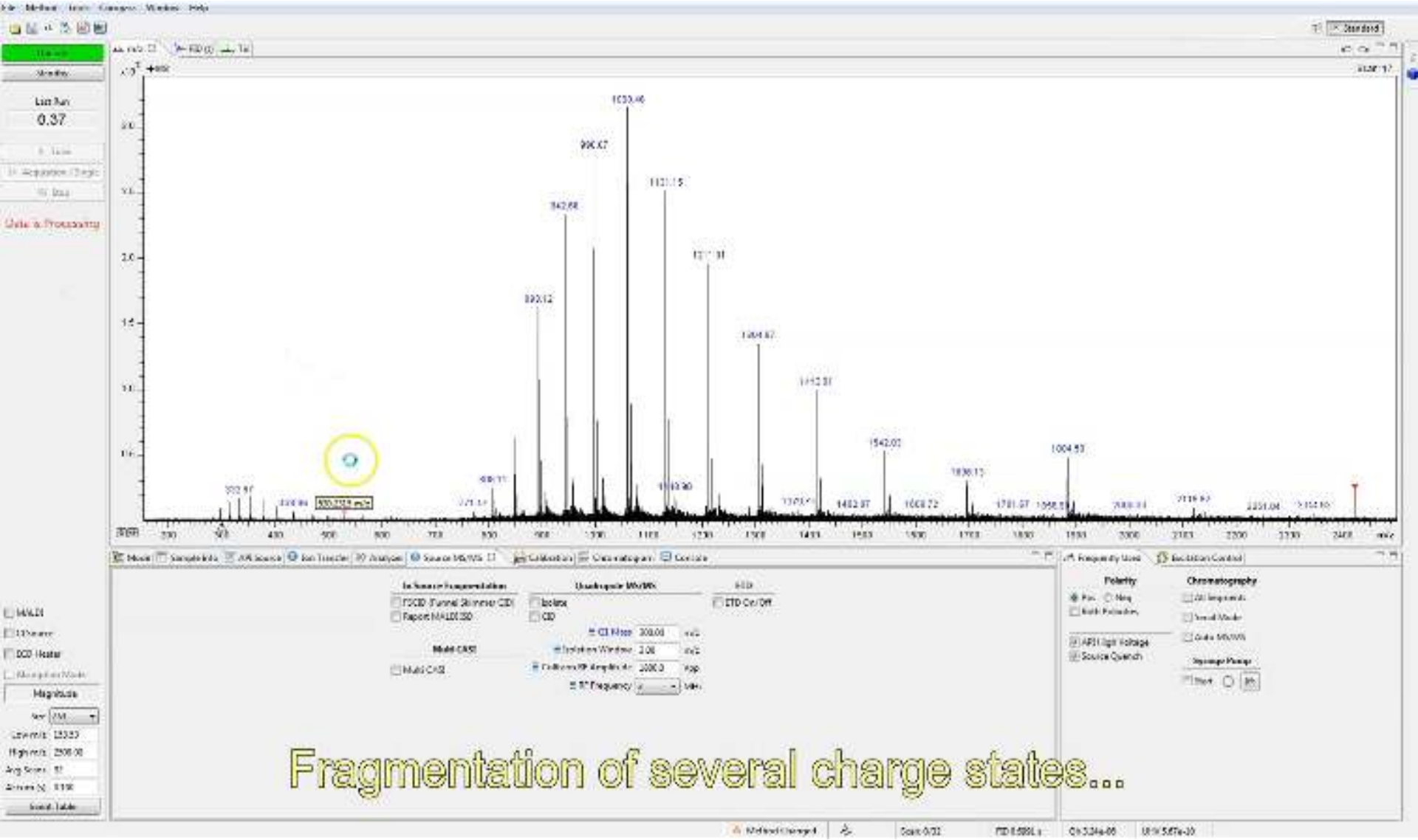

MS analysis – native Mb (and its activation)

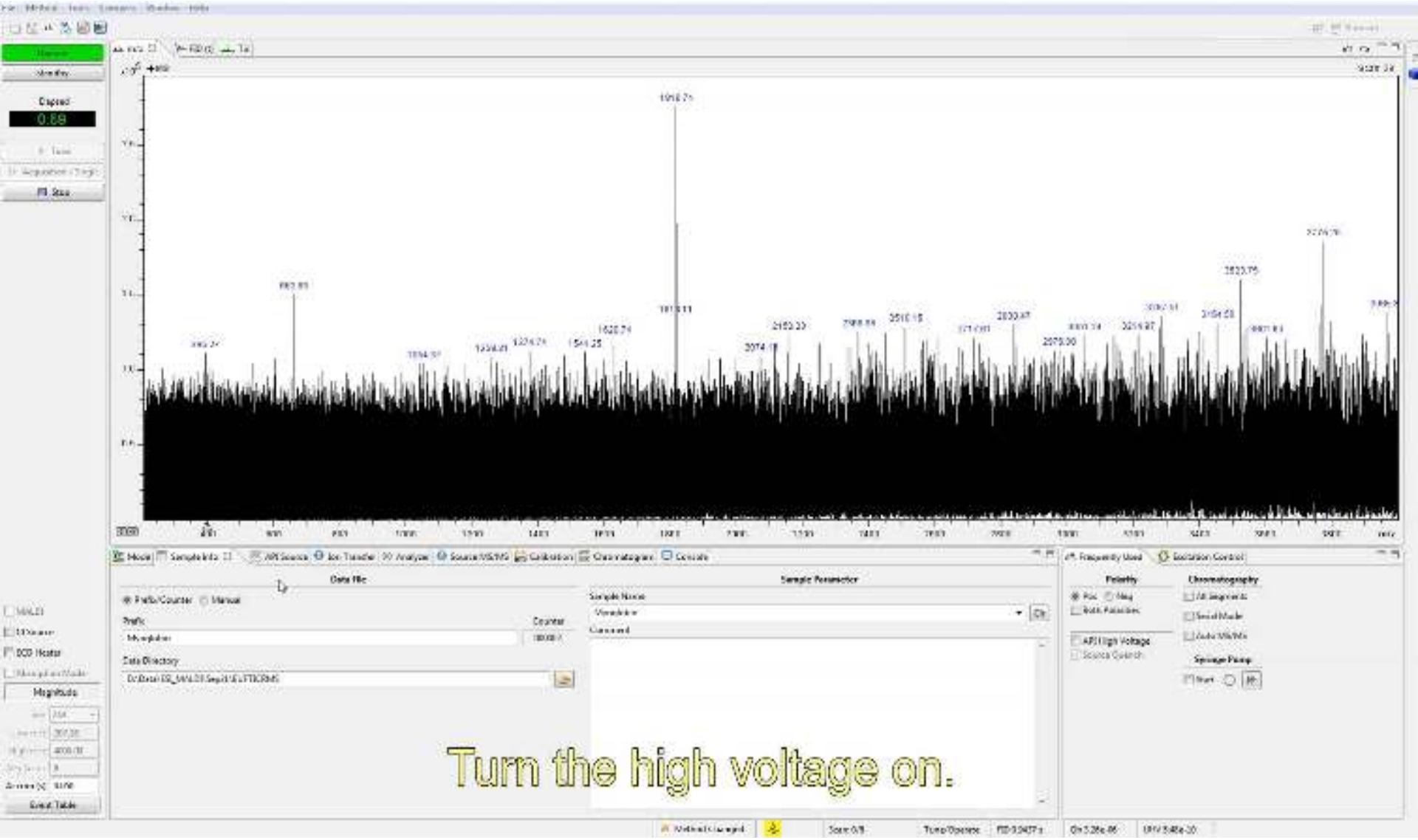

MS analysis – native Mb (resolution)

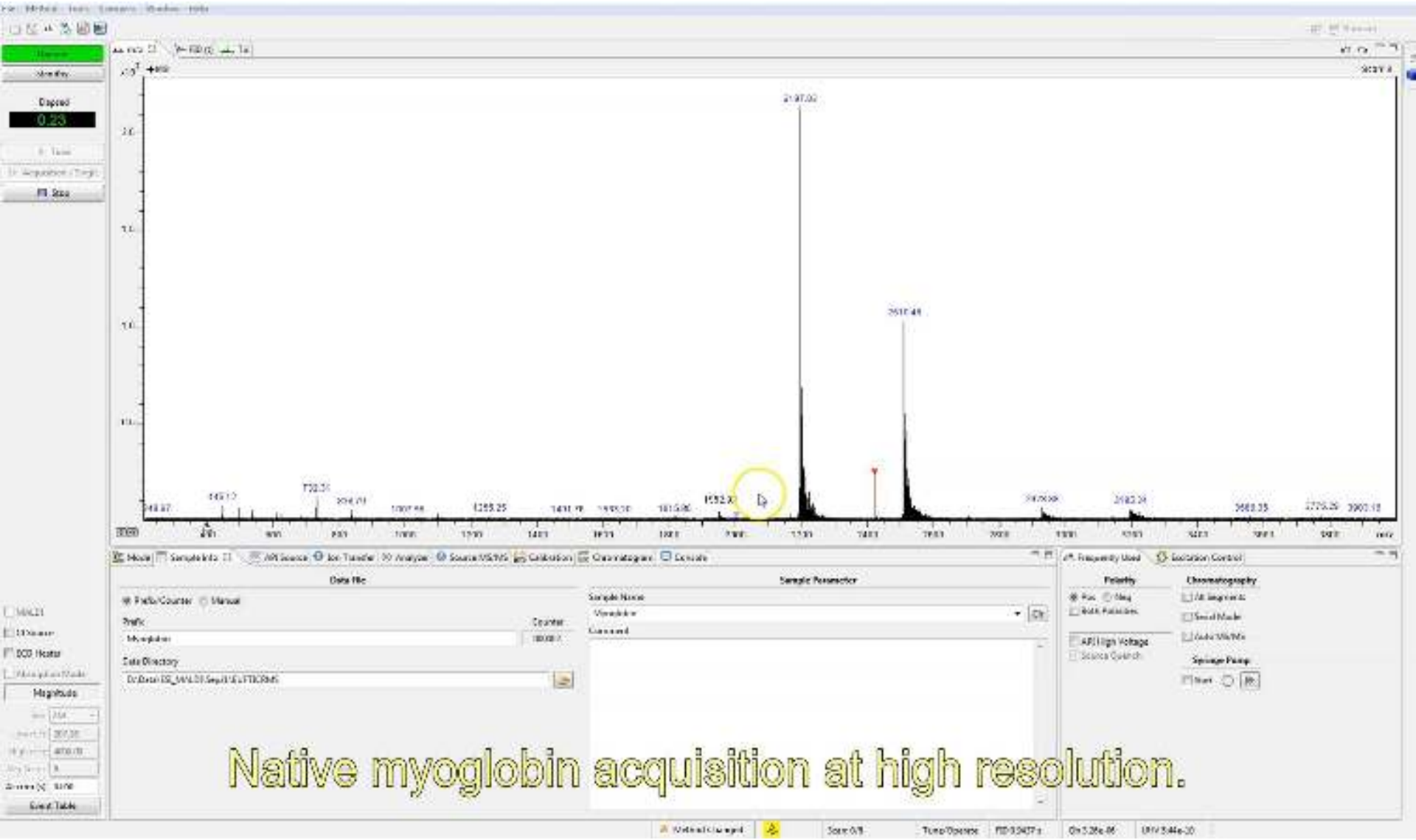

EU FT-ICR MS

Sample preparation
FT-ICR MS sample analysis
Top down of proteins
Data interpretation

Petr Novák, **Zdeněk Kukačka**, Petr Man

IMIC

EU FT-ICR MS

Sample preparation
FT-ICR MS sample analysis
Top down of proteins
Data interpretation

Petr Novák, **Zdeněk Kukačka**, Petr Man

IMIC

ProSight Lite – freely available

http://prosightlite.northwestern.edu/

- Groups of Neil L. Kelleher and Paul M. Thoms
- Windows operating systems

ProSight Lite – Manual and software description

ProSight Lite: Graphical Software to Analyze Top-Down Mass Spectrometry Data

Ryan T. Fellers, Joseph B. Greer, Bryan P. Early, Xiang Yu, Richard D. LeDuc, Neil L. Kelleher*, and Paul M. Thomas*
Departments of Chemistry, Molecular Biosciences and the Proteomics Center of Excellence Northwestern University, 2145 N. Sheridan Road, Evanston, IL 60208

Abstract

Many top-down proteomics experiments focus on identifying and localizing post-translational modifications and other potential sources of "mass shift" on a known protein sequence. A simple application to match ion masses and facilitate the iterative hypothesis testing of PTM presence and location would assist with the data analysis in these experiments. ProSight Lite is a free software tool for matching a single candidate sequence against a set of mass spectrometric observations. Fixed or variable modification, including both post-translational modifications and a select number of glycosylations, can be applied to the amino acid sequence. The application reports multiple scores and a matching fragment list. Fragmentation maps can be exported for publication in either PNG or SVG format. ProSight Lite can be freely downloaded from http://prosightlite.northwestern.edu, installs and updates from the web, and requires Windows 7 or higher.

Keywords

Top-down proteomics; proteomics software; MS Analysis; proteoform characterization

Top-down proteomics describes the study of intact proteins with mass spectrometry [1, 2]. Traditional bottom-up proteomics experiments are marked by the use of an enzyme, typically trypsin, to proteolyze intact proteins into more analytically manageable peptides (0.5-3 kDa)[3]. This proteolysis effects a loss of information between the ribosomally-expressed pro-protein, which in eukaryotes often contains RNA splice variants, and the post-translationally modified intact protein (termed a "proteoform")[4]. If a modification has been identified on two separate peptides, a typical bottom-up proteomics experiment cannot know whether those modification existed singly on two separate proteoforms or in tandem on a single proteoform. While more analytically challenging, top-down proteomics provides that full information[5].

Bioinformatics Analysis of Top-Down Mass Spectrometry Data with ProSight Lite

Caroline J. DeHart, Ryan T. Fellers, Luca Fornelli, Neil L. Kelleher, and Paul M. Thomas

Abstract

Traditional bottom-up mass spectrometry-based proteomics relies on the use of an enzyme, often trypsin, to generate small peptides (typically < 25 amino acids long). In top-down proteomics, proteins remain intact and are directly measured within the mass spectrometer. This technique, while inherently simpler than bottom-up proteomics, generates data which must be processed and analyzed using software tools "purpose-built" for the job. In this chapter, we will show the analysis of intact protein species through deconvolution, deisotoping, and searching with ProSight Lite, a free, vendor agnostic tool for the analysis of top-down mass spectrometry data. We will illustrate with two examples of intact protein fragmentation spectra and discuss the iterative use of the software to characterize proteoforms and discover the sites of post-translational modifications.

Key words Top-down, Mass spectrometry, Proteomics, ProSight Lite, Intact protein, Bioinformatics

1 Introduction

Complementing the speed and sensitivity of bottom-up proteomics [1, 2], top-down proteomics [3] offers a comprehensive view of proteoforms present in the sample (for a more detailed description of a proteoform, see **Note 1**) [4]. It is important to distinguish between top-down mass spectrometry and top-down proteomics. In top-down mass spectrometry, one or a few proteoforms are isolated and studied. This technique is typified by studies of histones [5–7] and immunoglobulins [8–10], among others, including the routine analysis of small (< 40 kDa) proteins. In top-down proteomics, a whole, unknown proteome is typically isolated, fractionated, and analyzed by mass spectrometry [11–13]. The tools used for the study of top-down mass spectrometry and top-down proteomics are related, but fundamentally different. Top-down proteomics requires searching tandem MS data against a database of known proteins and proteoforms [14, 15], while top-down mass

Cathy H. Wu et al. (eds.), Protein Bioinformatics: From Protein Modifications and Networks to Proteomics, Methods in Molecular Biology, vol. 1558, DOI 10.1007/978-1-4939-6783-4_16, © Springer Science+Business Media LLC 2017

ProSight Lite – User interface

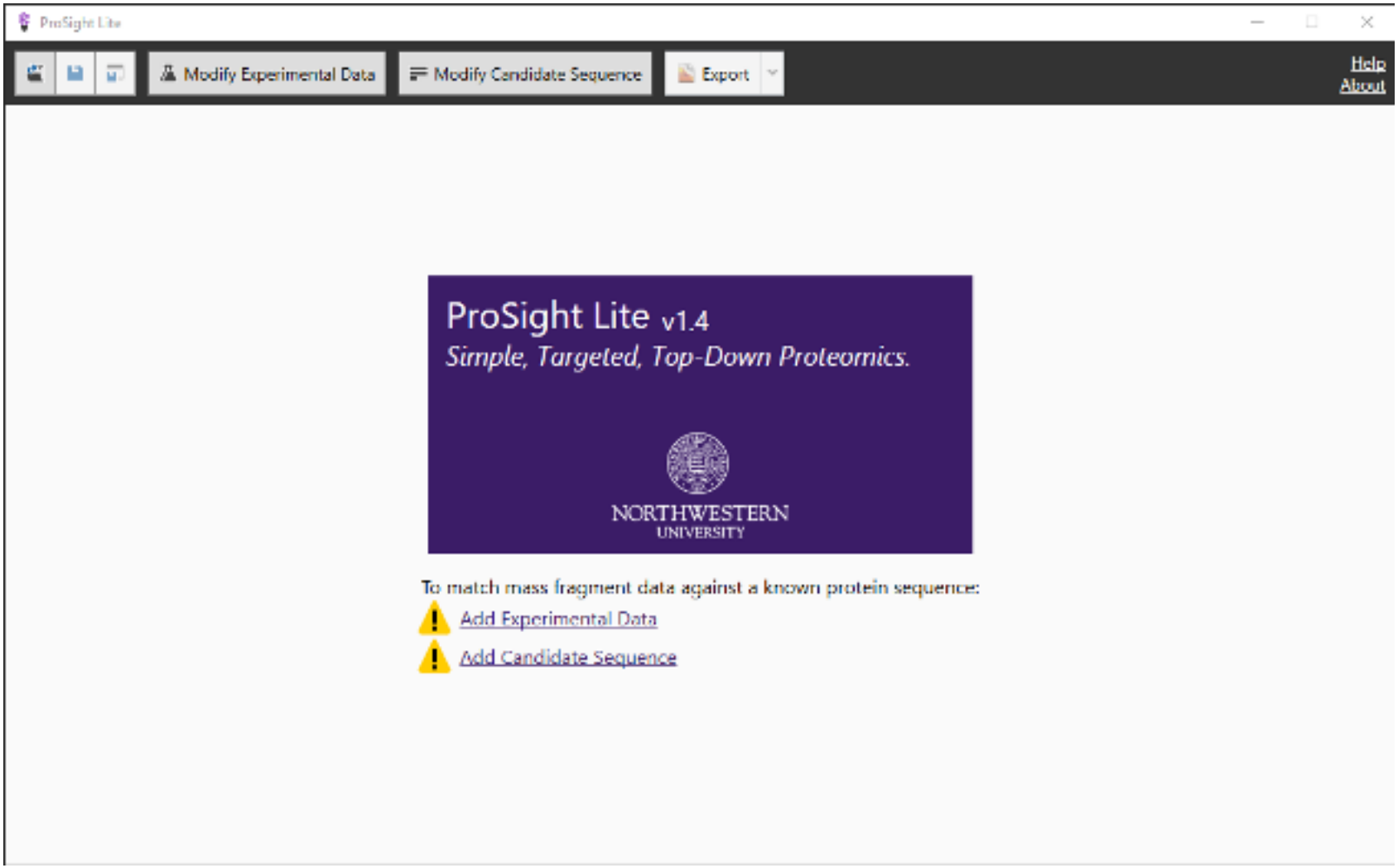

ProSight Lite – Sequence Uniprot/fasta

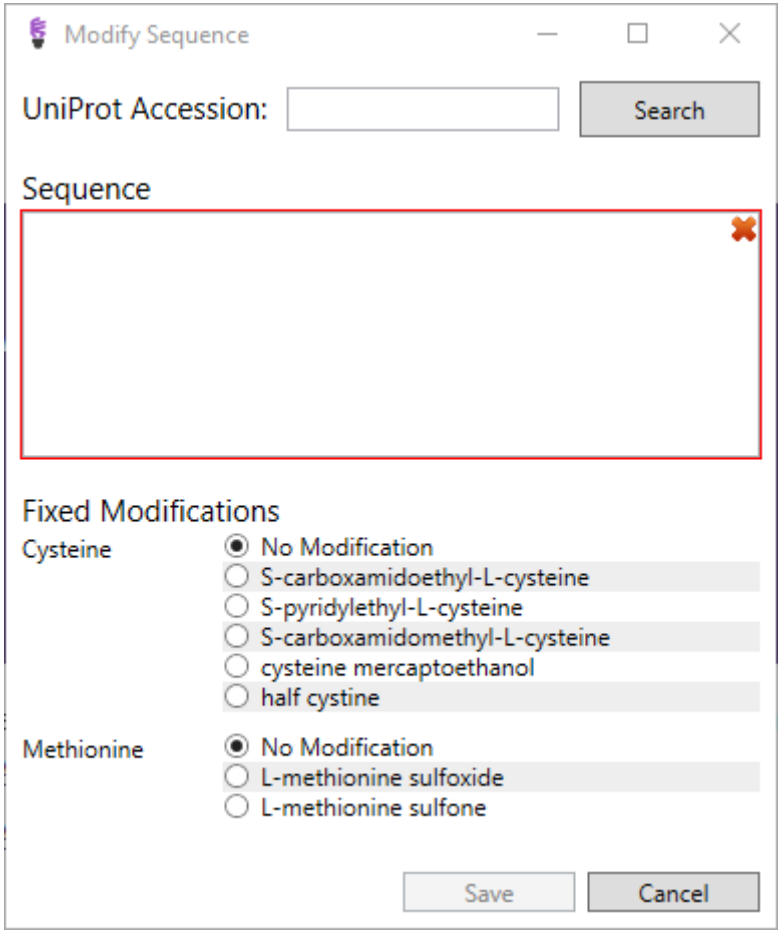

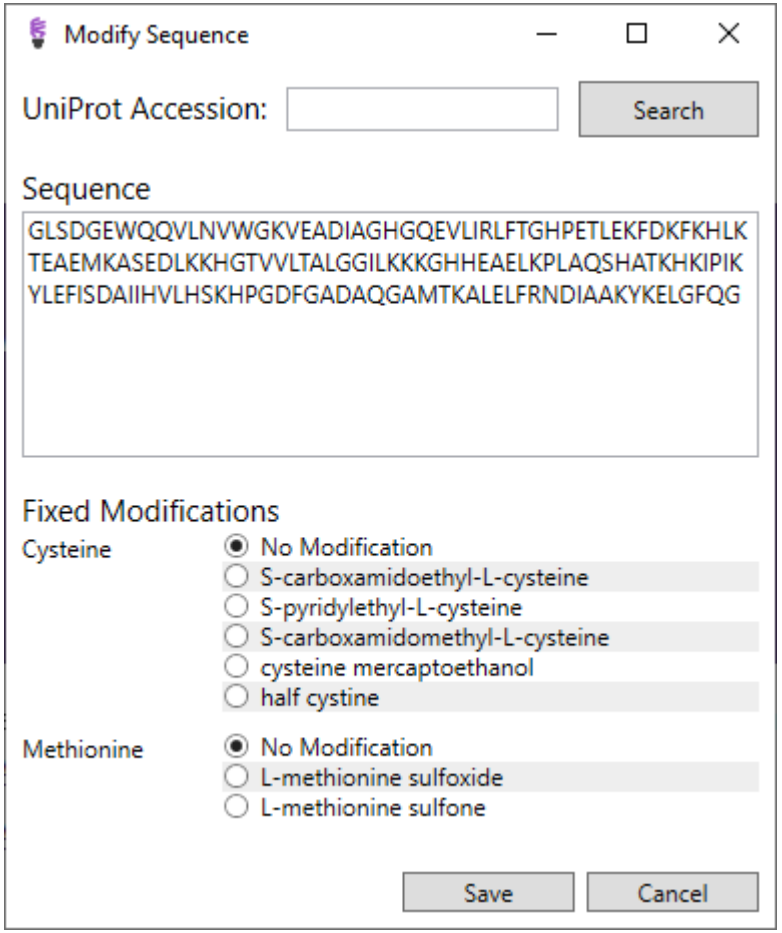

ProSight Lite – Experimental data

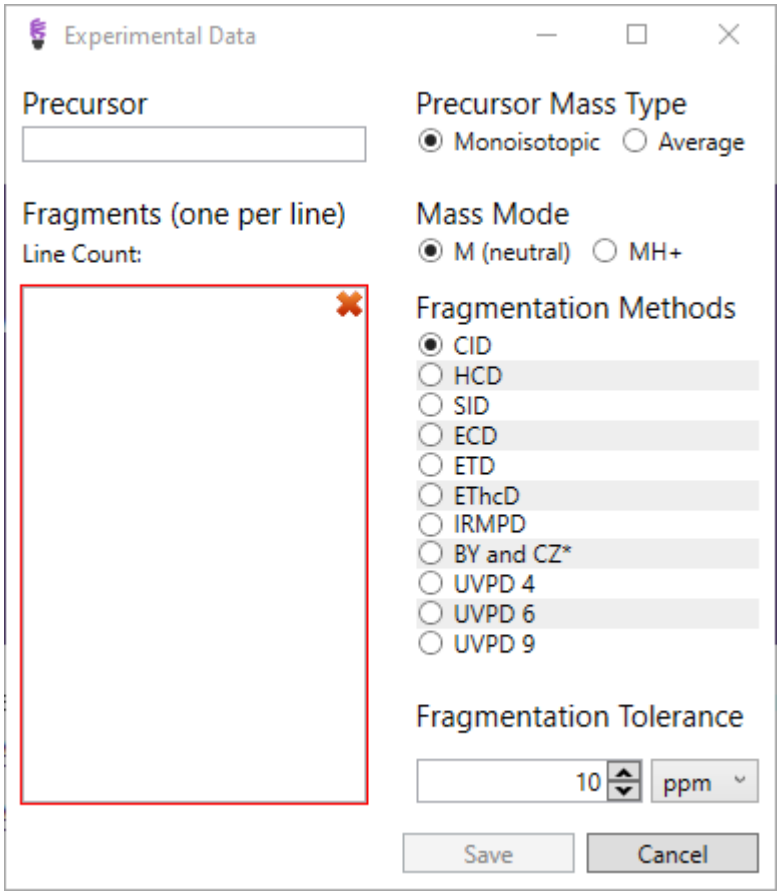

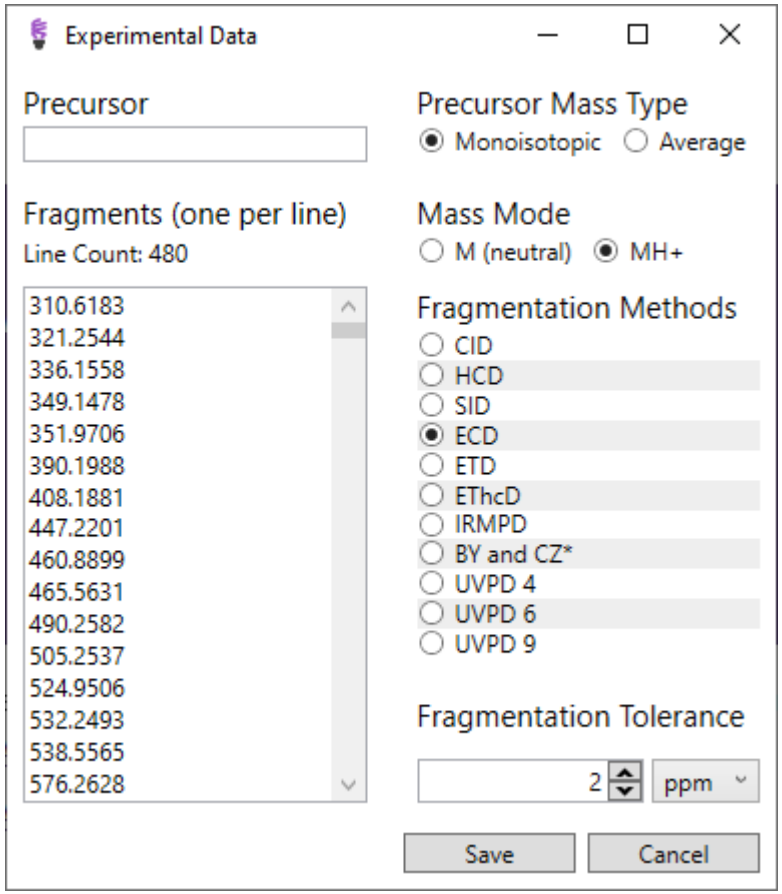

First Example

Myoglobin – modification by NHS-propionate (mass shift 56.026)

ECD – fragmentation of singly modified protein

ProSight Lite – Experimental data from mgf file

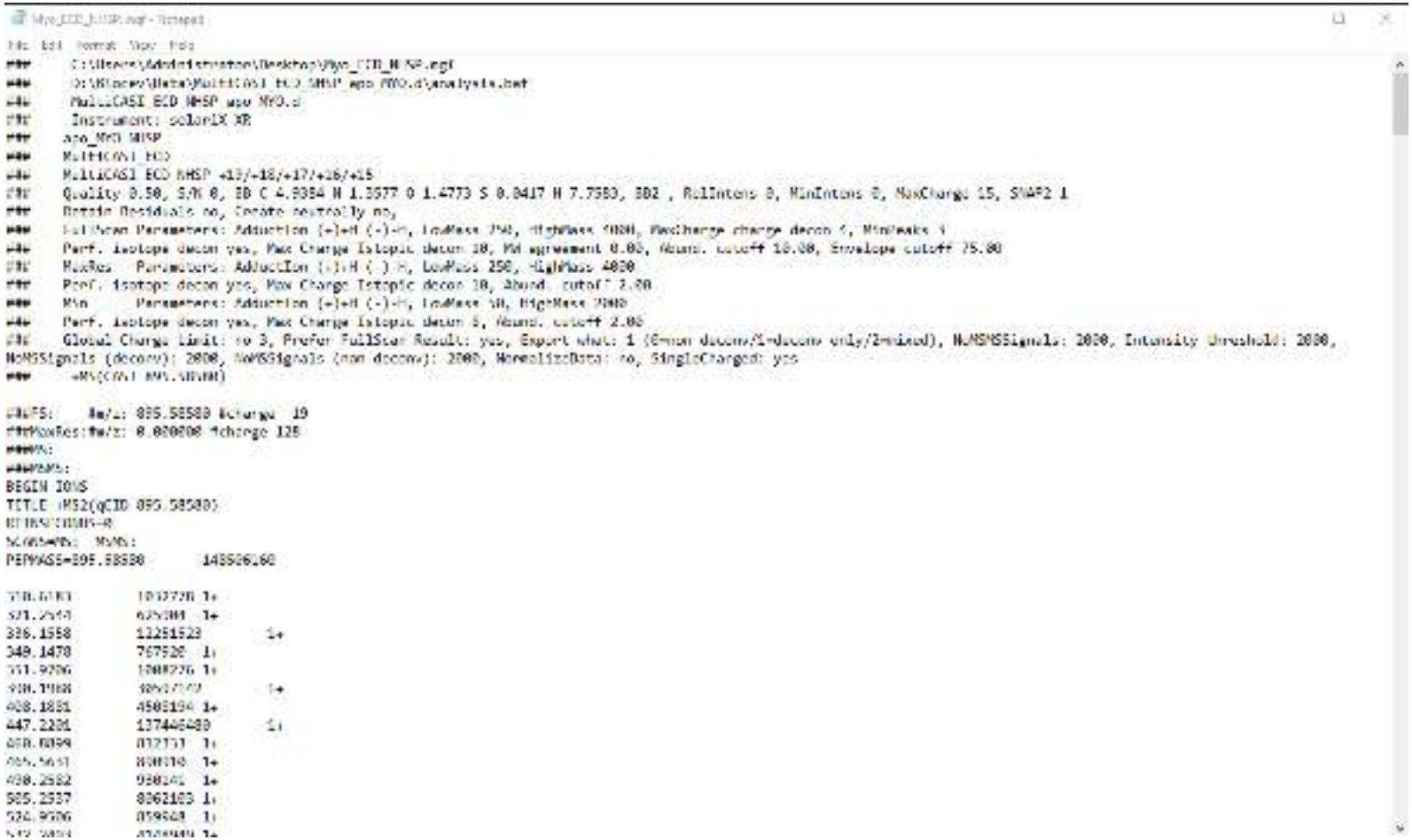

ProSight Lite – Results window

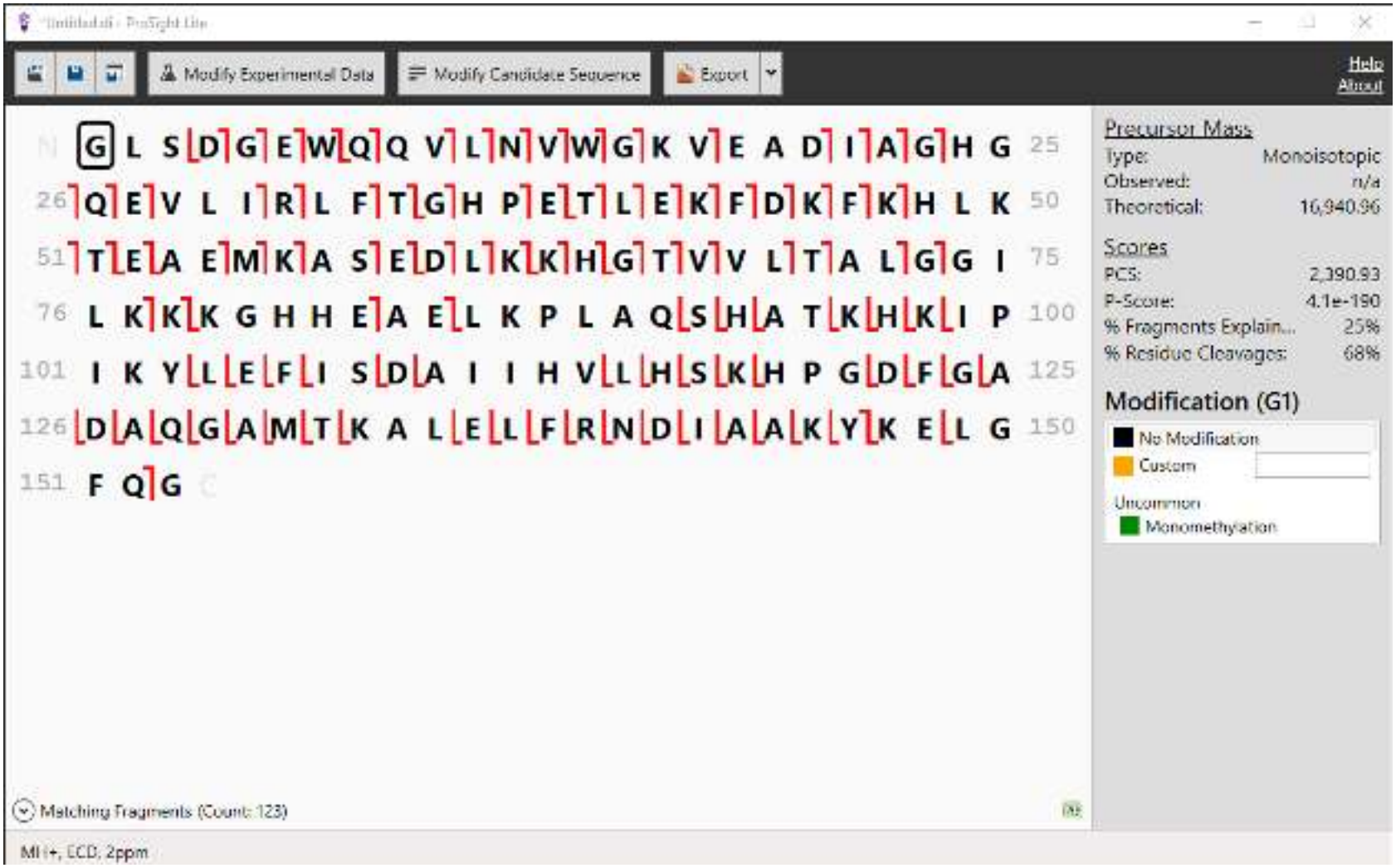

ProSight Lite – List of matching fragments

*Untitled.di - ProSight Lite

Modify Experimental Data | Modify Candidate Sequence | Export | Help | About

G L S D G E W Q Q V L N V W G K V E A D I A G H G 25
26 Q E V L I R L F T G H P E T L E K F D K F K H L K 50
51 T E A E M K A S E D L K K H G T V V L T A L G G I 75
76 L K K K G H H E A E L K P L A Q S H A T K H K I P 100
101 I K Y L L E F I S D A I I H V L H S K H P G D F G A 125
126 D A Q G A M T K A L E L L F R N D I A A K Y K E L G 150
151 F Q G C

Precursor Mass

Type:	Monoisotopic
Observed:	n/a
Theoretical:	16,940.96

Scores

PCS:	2,390.93
P-Score:	4.1e-190
% Fragments Explain...	25%
% Residue Cleavages:	68%

Modification (G1)

No Modification
Custom
Uncommon
Monomethylation

Matching Fragments (Count: 123)

Name	Ion Type	Ion Number	Theoretical Mass	Observed Mass	Mass Difference (Da)	Mass Difference (ppm)
C4	C	4	389.19	389.19	0.001	1.88
C5	C	5	446.21	446.21	0.001	1.29
C6	C	6	575.25	575.26	0.001	1.19
C7	C	7	761.33	761.34	0.001	1.15
C8	C	8	889.39	889.39	0.001	0.89
C10	C	10	1,116.52	1,116.52	0.001	0.54

MI (+, ECD, 2ppm

ProSight Lite – Modification of N-terminus

Modify Experimental Data | Modify Candidate Sequence | Export | Help | About

N G L S D G E W Q Q V L N V W G K V E A D I A G H G 25
26 Q E V L I R L F T G H P E T L E K F D K F K H L K 50
51 T E A E M K A S E D L K K H G T V V L T A L G G I 75
76 L K K K G H H E A E L K P L A Q S H A T K H K I P 100
101 I K Y L E F I S D A I I H V L H S K H P G D F G A 125
126 D A Q G A M T K A L E L F R N D I A A K Y K E L G 150
151 F Q G C

Precursor Mass

Type:	Monoisotopic
Observed:	n/a
Theoretical:	16,996.99

Scores

PCS:	1,169.56
P-Score:	7.8e-98
% Fragments Explaine...	15%
% Residue Cleavages:	38%

Modification (G1)

- No Modification
- Custom 56.026

Uncommon
- Monomethylation

Matching Fragments (Count: 72)

Name	Ion Type	Ion Number	Theoretical Mass	Observed Mass	Mass Difference (Da)	Mass Difference (ppm)
C90	C	90	10,013.36	10,013.36	-0.001	-0.11
C92	C	92	10,228.45	10,228.45	0.006	0.62
C93	C	93	10,365.51	10,365.51	0.003	0.26
C97	C	97	10,802.74	10,802.75	0.002	0.16
C98	C	98	10,990.84	10,990.84	0.003	0.27
C109	C	109	12,249.56	12,249.56	0.005	0.37

MH+, ECD, 2ppm

ProSight Lite – Modification of K16

*Untitled.di - ProSight Lite

Modify Experimental Data | Modify Candidate Sequence | Export | Help | About

```
N  G L S D G E W Q Q V L N V W G K V E A D I A G H G  25
26 Q E V L I R L F T G H P E T L E K F D K F K H L K  50
51 T E A E M K A S E D L K K H G T V V L T A L G G I  75
76 L K K K G H H E A E L K P L A Q S H A T K H K I P  100
101 I K Y L L E F I S D A I I H V L H S K H P G D F G A  125
126 D A Q G A M T K A L E L L F R N D I A A K Y K E L G  150
151 F Q G C
```

Precursor Mass

Type:	Monoisotopic
Observed:	n/a
Theoretical:	16,996.99

Scores

PCS:	1,415.87
P-Score:	1.5e-116
% Fragments Explain...	17%
% Residue Cleavages:	44%

Modification (K16)

- No Modification
- Custom 56.026

Common
- Acetylation
- Monomethylation
- Dimethylation
- Trimethylation

Uncommon
- Phosphorylation

Matching Fragments (Count: 81)

Name	Ion Type	Ion Number	Theoretical Mass	Observed Mass	Mass Difference (Da)	Mass Difference (ppm)
C4	C	4	389.19	389.19	0.001	1.88
C5	C	5	446.21	446.21	0.001	1.29
C6	C	6	575.25	575.26	0.001	1.19
C7	C	7	761.33	761.34	0.001	1.15
C8	C	8	889.39	889.39	0.001	0.89
C10	C	10	1,116.52	1,116.52	0.001	0.54

MH+, ECD, 2ppm

ProSight Lite – Modification of K87

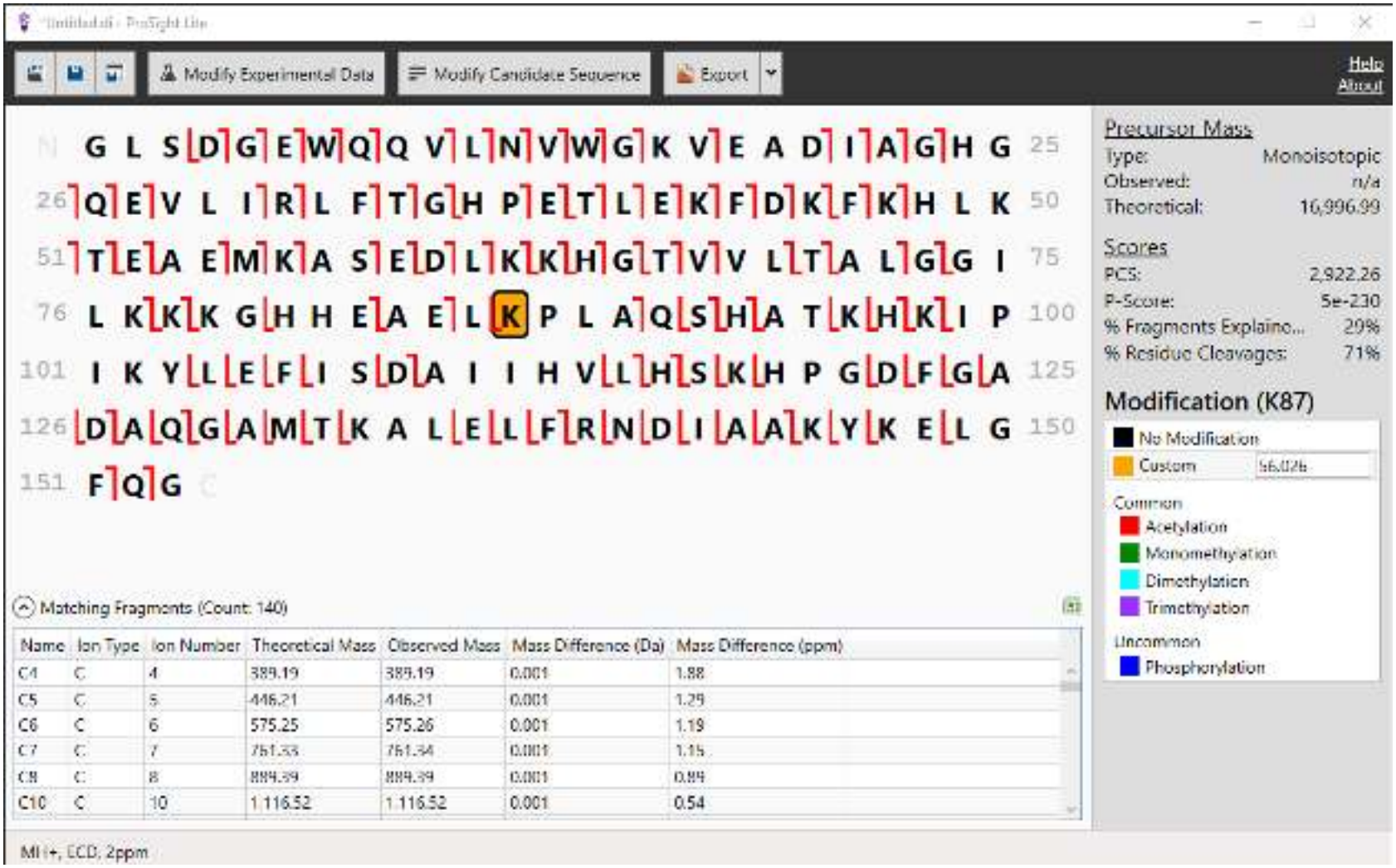

Second Example

Ubiquitin – modification by NHS-propionate (mass shift 56.026)

CID – fragmentation of singly modified protein

ProSight Lite – Experimental data

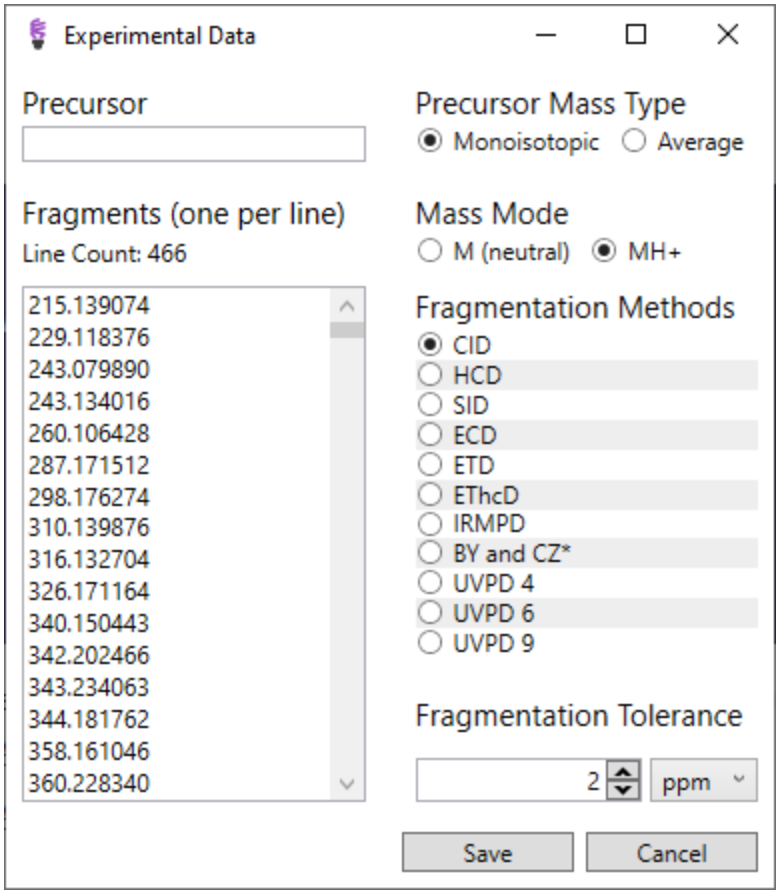

ProSight Lite – Result window

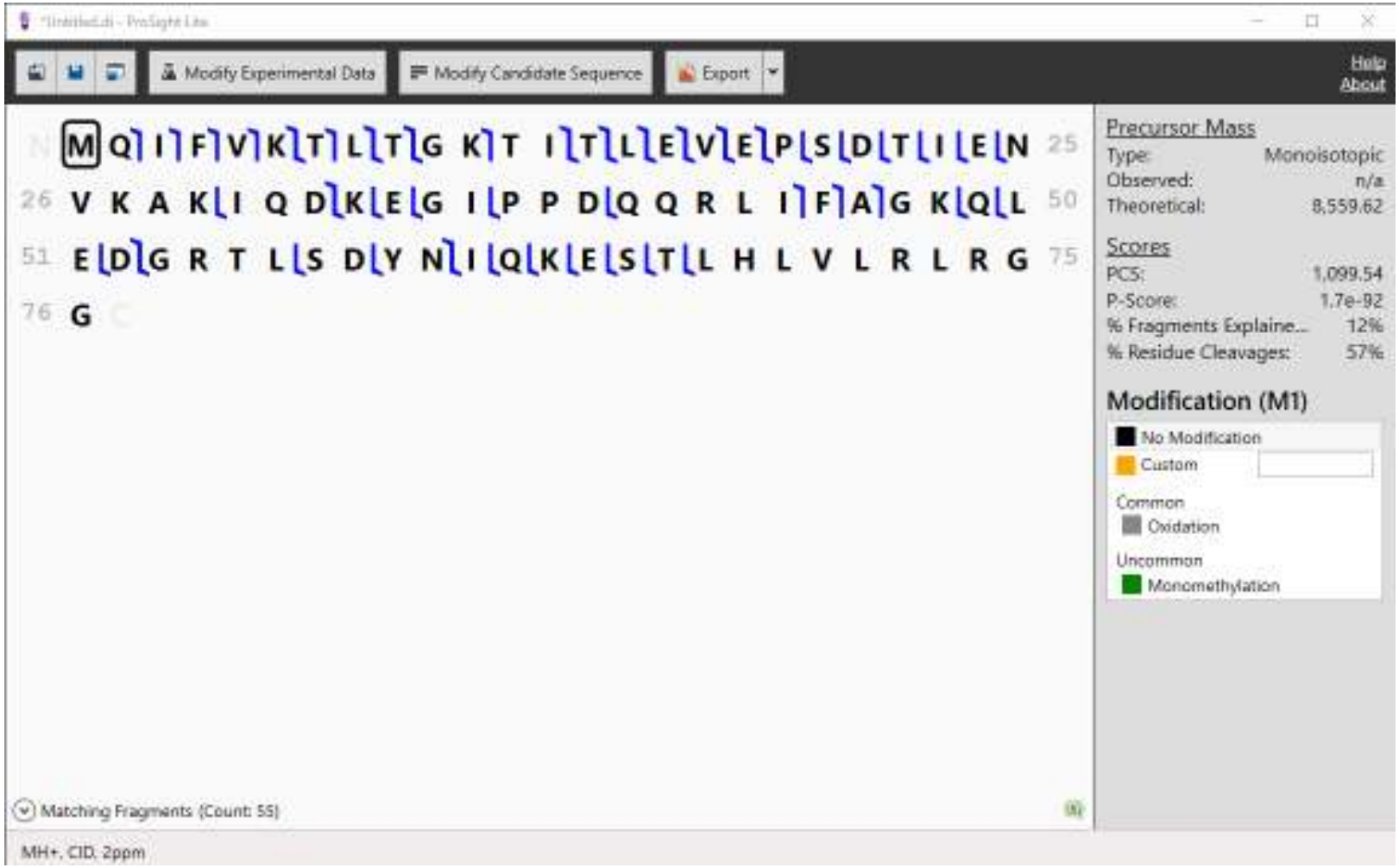

ProSight Lite – Matching fragments

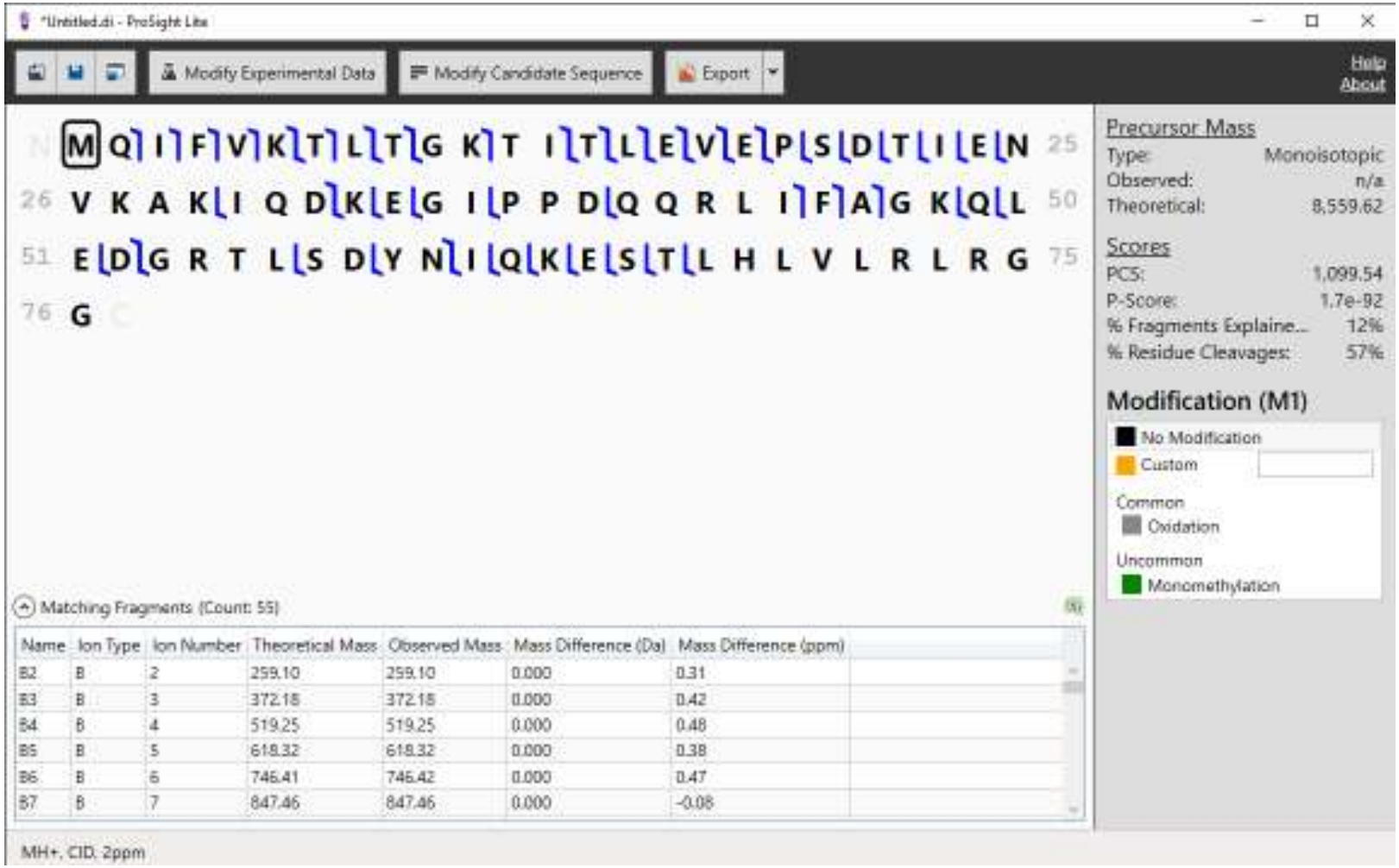

ProSight Lite – Modification of N-terminus

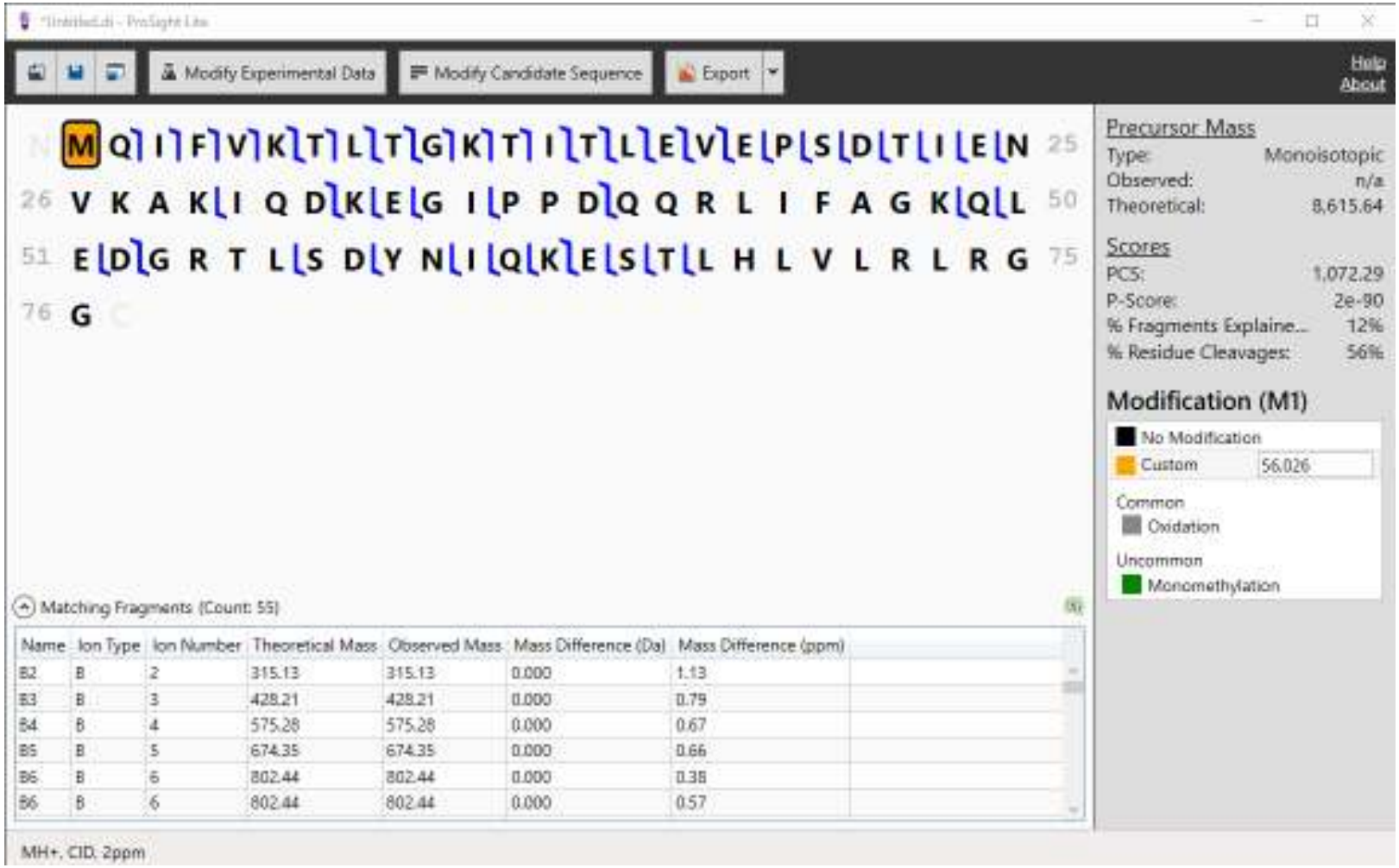

ProSight Lite – Modification of K6

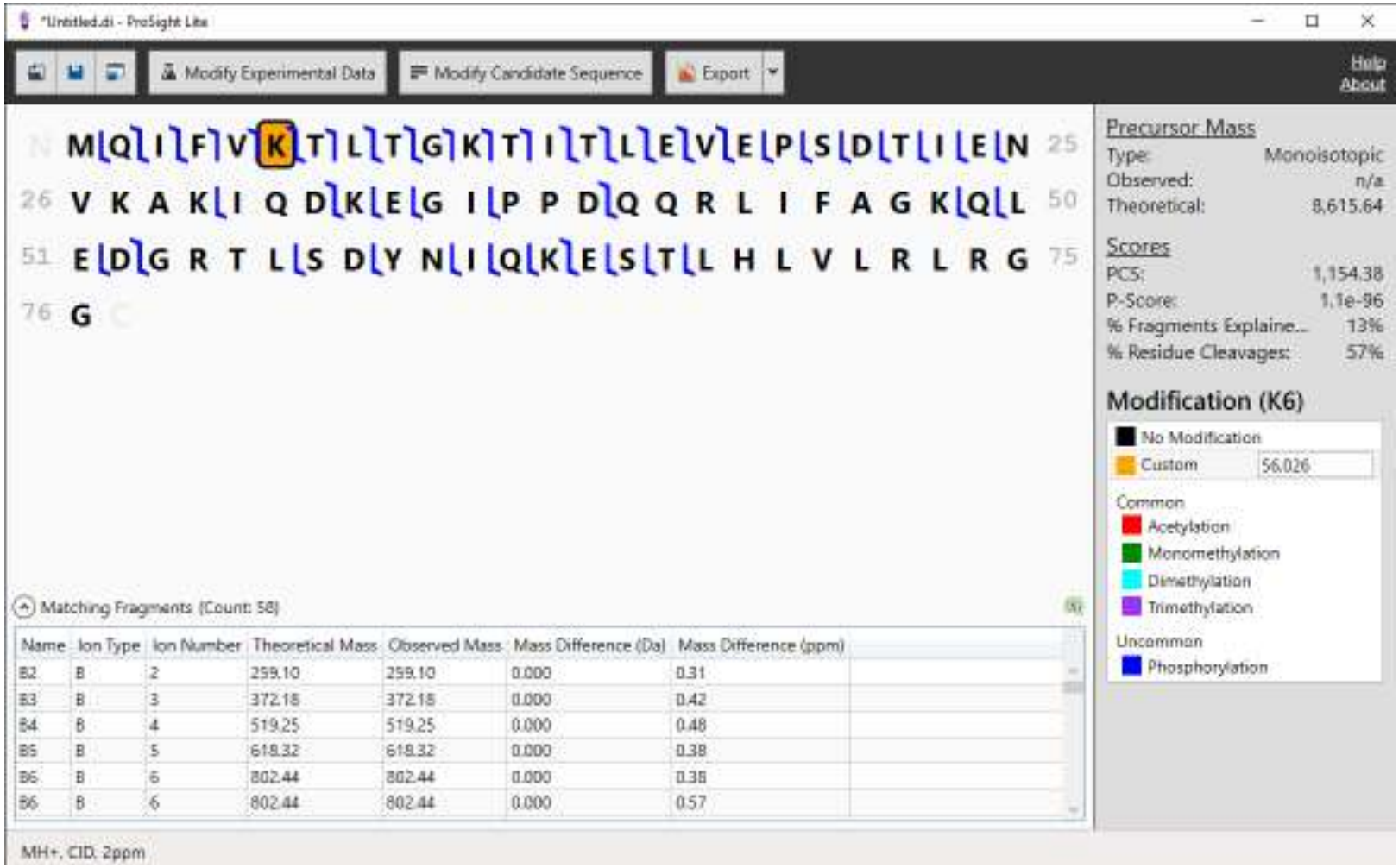

ProSight Lite – Modification of K63

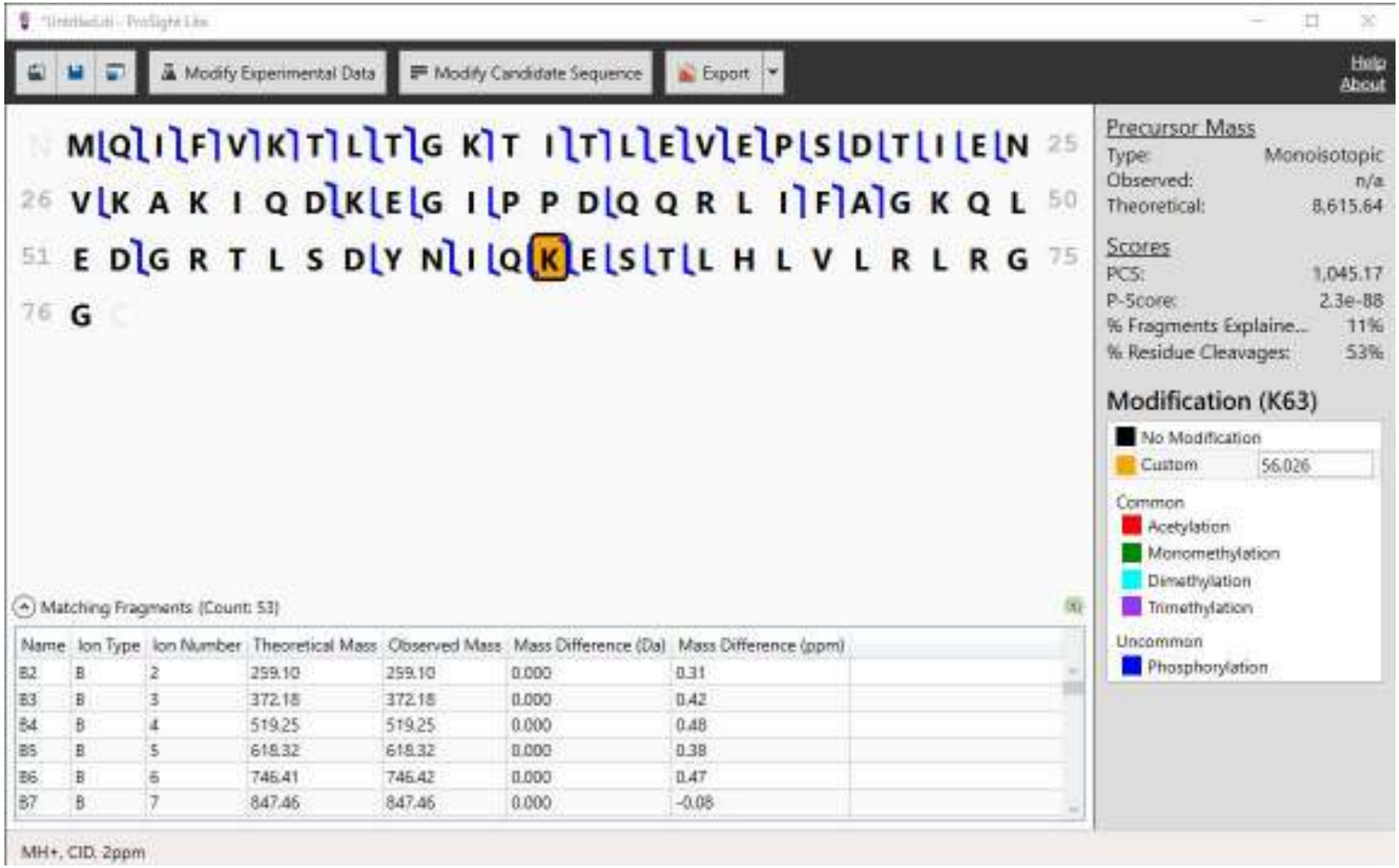

EU FT-ICR MS

Sample preparation
FT-ICR MS sample analysis
Top down of proteins
Data interpretation

Petr Novák, Zdeněk Kukačka, **Petr Man**

IMIC

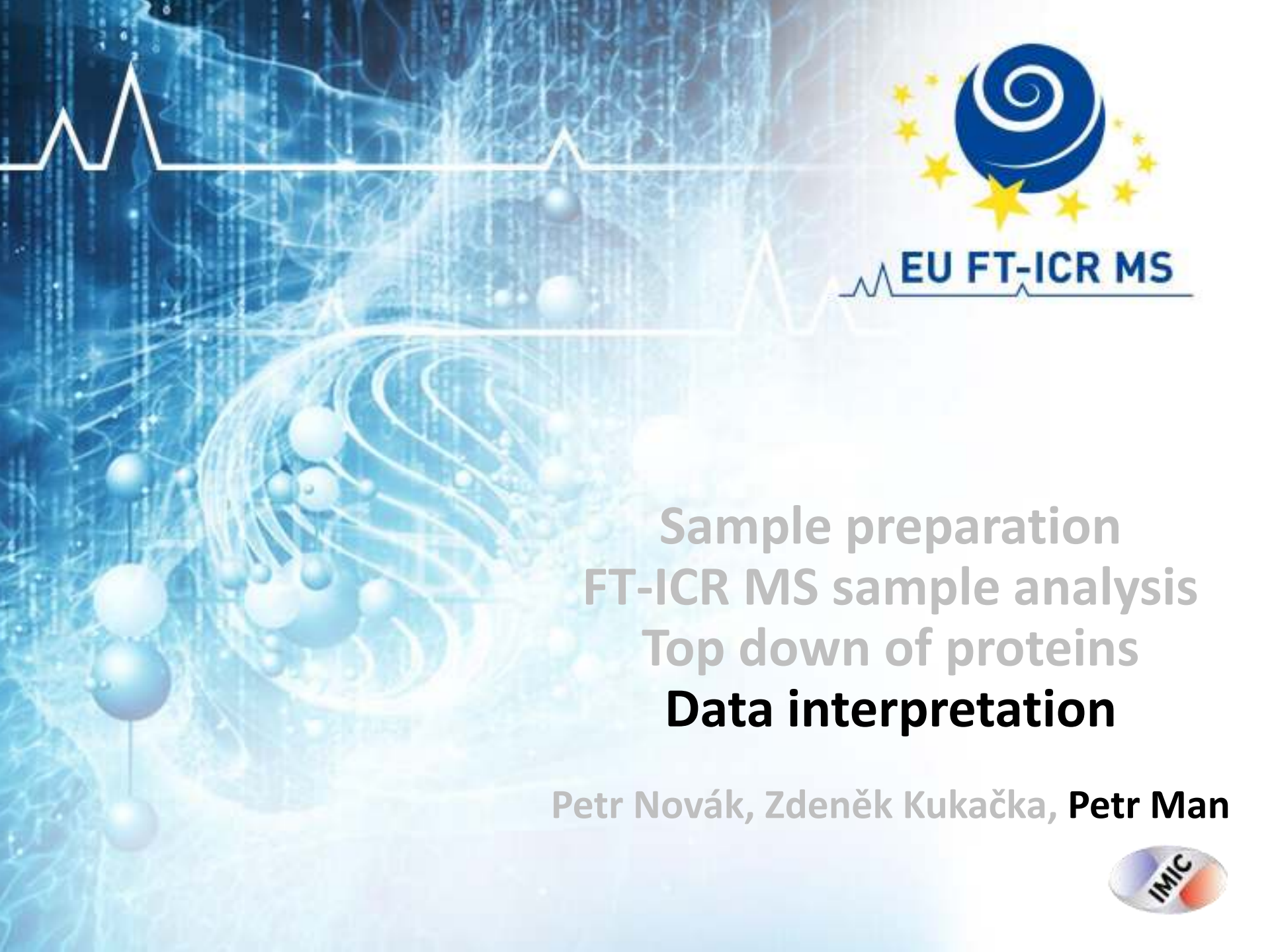

Sample preparation
FT-ICR MS sample analysis
Top down of proteins
Data interpretation

Petr Novák, Zdeněk Kukačka, **Petr Man**

mMass – freely available

http://mmass.org/

- Works with open format data
- Direct import of Bruker data
  (if the CompassXport is installed)
- Platform independent + no installation required
- Manual + YouTube videos
  (https://www.youtube.com/user/martinstrohalm/videos)
- Configuration in easily editable *.xml files

aminoacids	xml
compounds	xml
config	xml
elements	xml
enzymes	xml
fragments	xml
mascot	xml
modifications	xml
monomers	xml
presets	xml
references	xml

```
<?xml version="1.0" encoding="utf-8" ?>
<mspyModifications version="1.0">
  <modification name="-NH3">
    <description>NH3 loss</description>
    <formula gain="" loss="N1H3" />
    <specifity amino="QN" terminus="N" />
  </modification>
  <modification name="-Ntern Met">
    <description>loss of Ntern Methionine</description>
    <formula gain="" loss="C5H9N1O1S1" />
    <specifity amino="" terminus="N" />
  </modification>
```

Strohalm M et al. *Anal Chem* 82 (11), 4648-4651 (2010).

mMass – import, peak picking (ctrl+F)

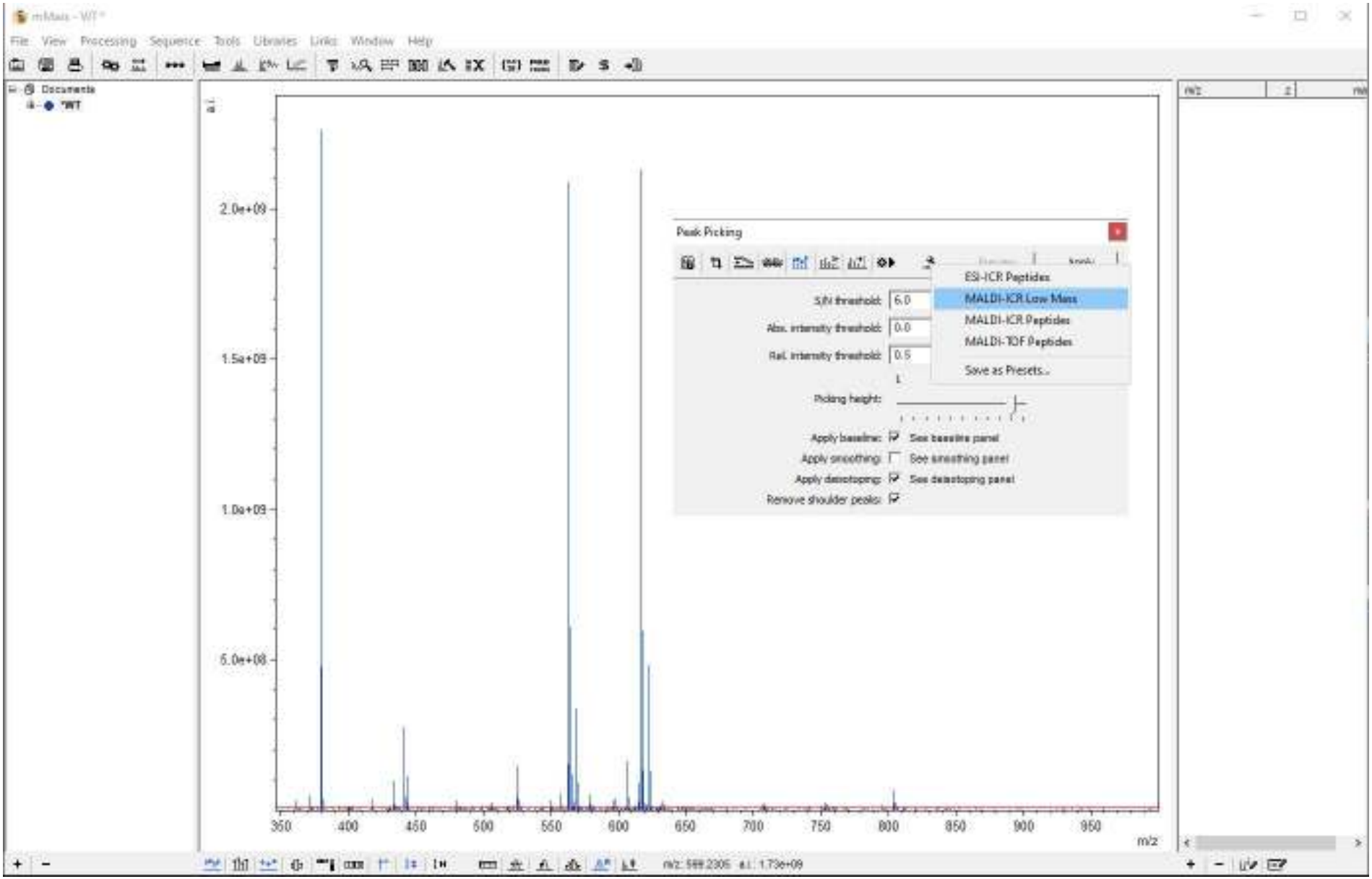

mMass – import, peak picking (ctrl+F)

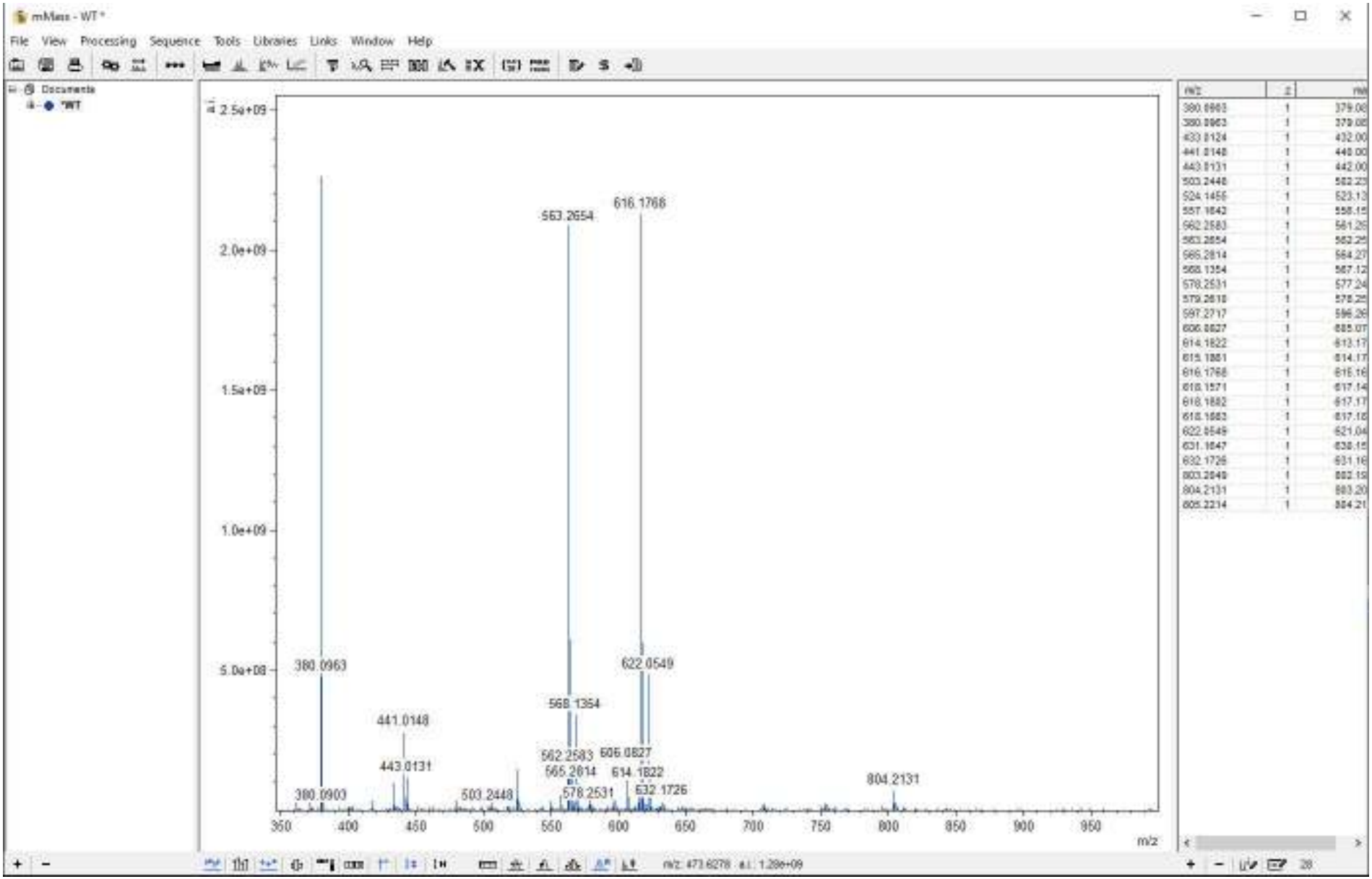

mMass – import, peak picking (manual editing)

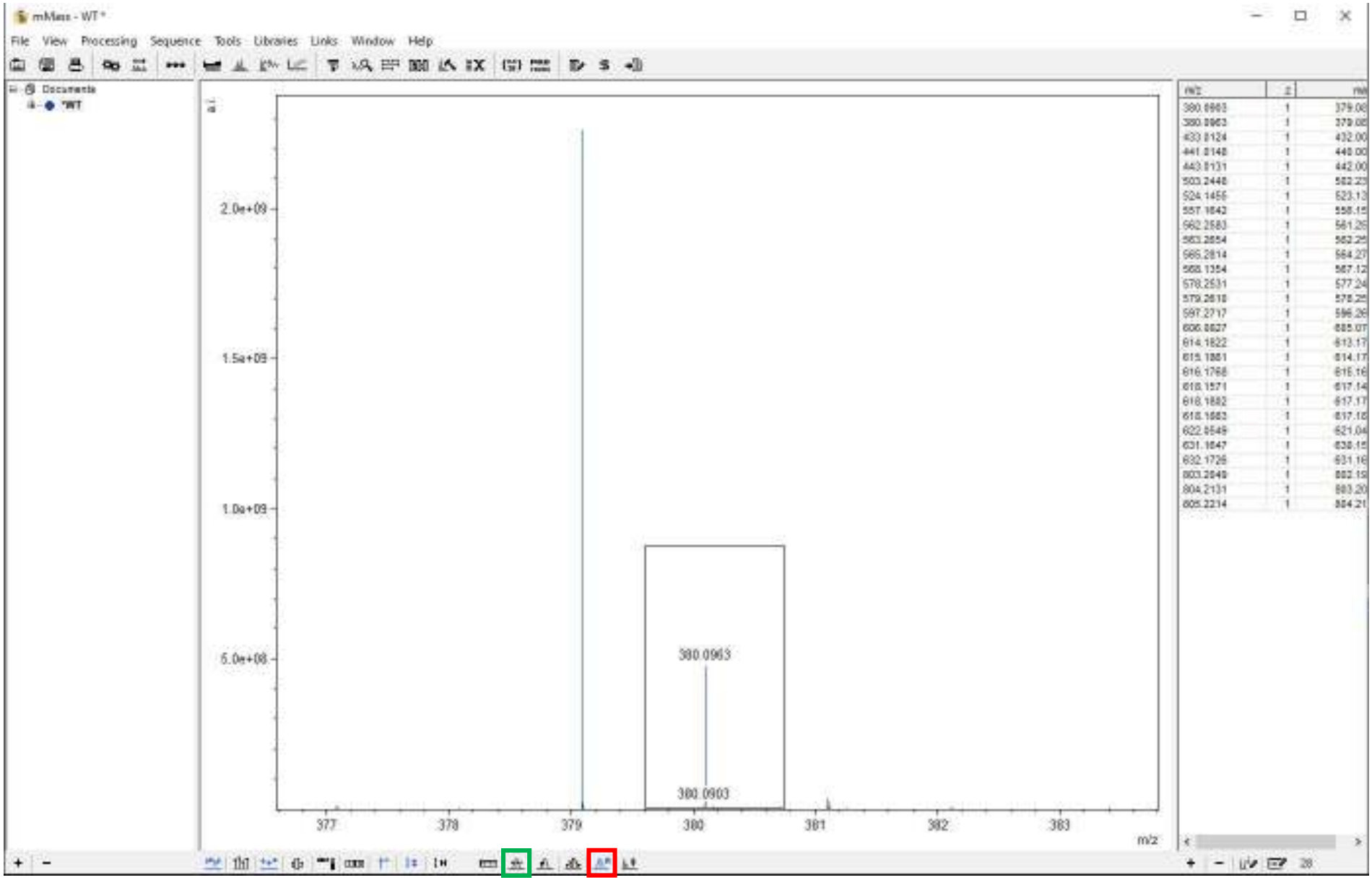

mMass – import, peak picking (manual editing)

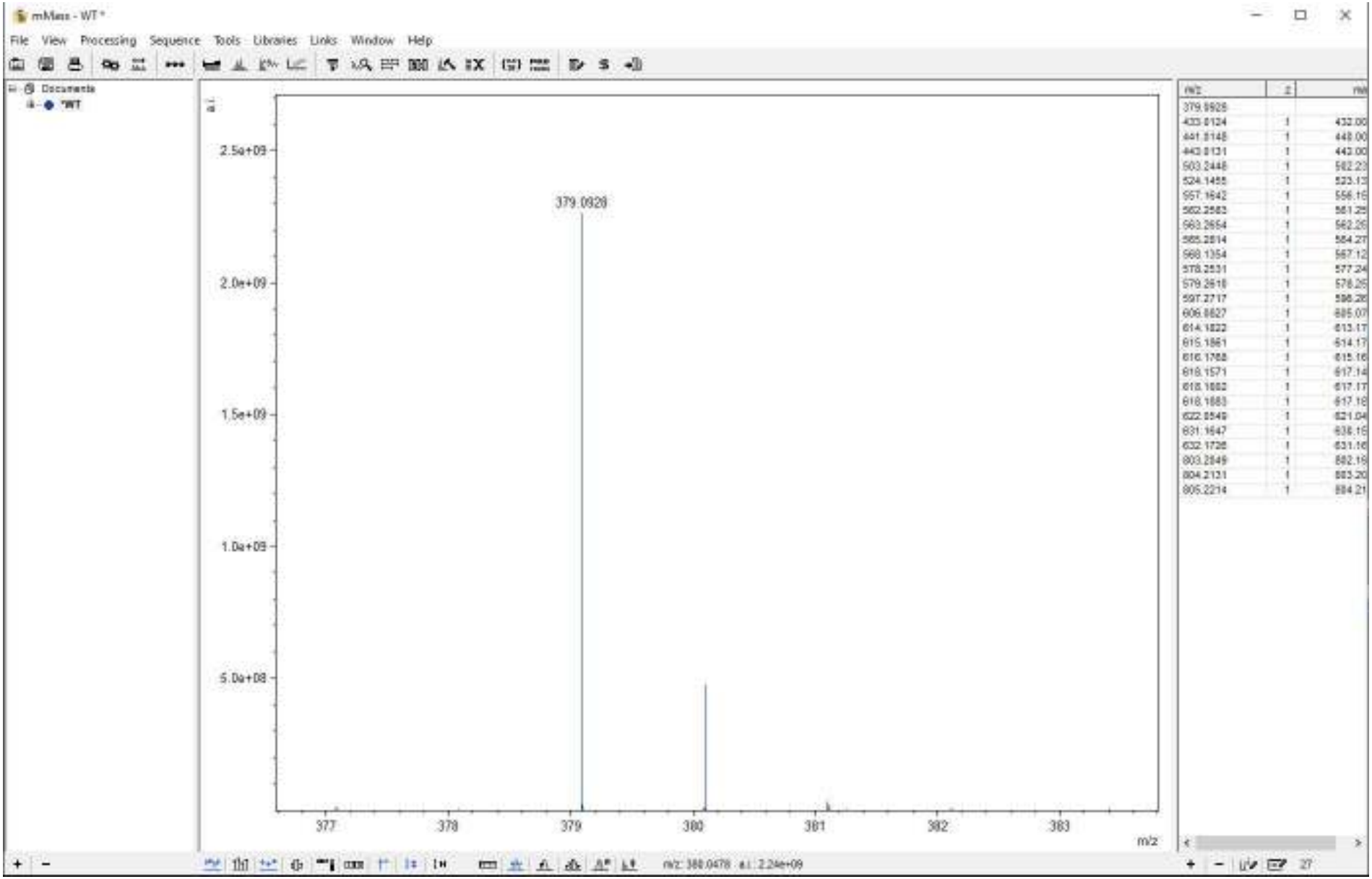

mMass – heme compounds

Heme **C34H32N4O4Fe1**

- isotopes of iron: ^{54}Fe 5.85%
  ^{56}Fe 91.75%
  ^{57}Fe 2.12%
  ^{58}Fe 0.28%

- Fe^{3+} / 2 x COO^- (M+)
- Fe^{2+} / 2 x COO^- (M+H+)

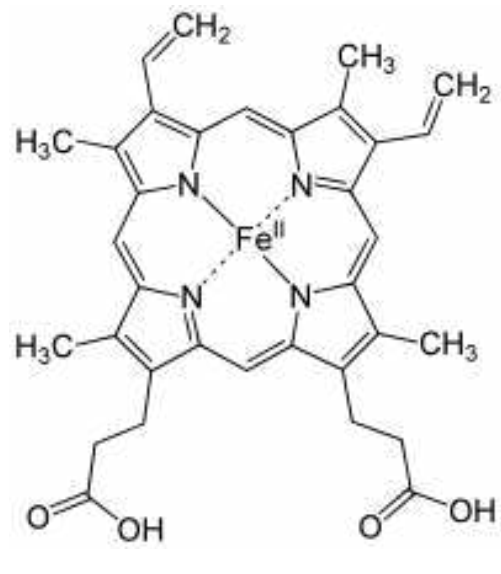

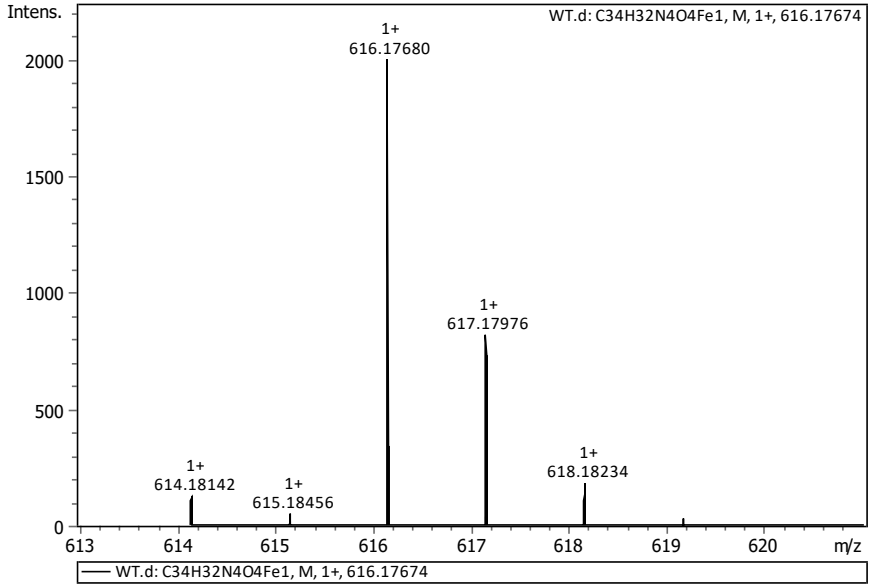

mMass – editing compounds or references

Compounds *vs* references

```
<group name="HCCA Clusters - MALDI Pos Mo">
  <reference name="HCCA [M+H-H2O]+" mass="172.039304" />
  <reference name="HCCA [M+H]+" mass="190.049869" />
  <reference name="HCCA [M+Na-H2O]+" mass="194.021249" />
  <reference name="HCCA [M+Na]+" mass="212.031814" />
  <reference name="HCCA [M+K-H2O]+" mass="209.995186" />
  <reference name="HCCA [M+K]+" mass="228.005751" />
  <reference name="HCCA [2M+H-H2O]+" mass="361.081897" />
  <reference name="HCCA [2M+H]+" mass="379.092462" />
  <reference name="HCCA [2M+Na-H2O]+" mass="383.063842" />
  <reference name="HCCA [2M+Na]+" mass="401.074407" />
  <reference name="HCCA [2M+K-H2O]+" mass="399.037779" />
  <reference name="HCCA [2M+K]+" mass="417.048344" />
  <reference name="HCCA [2M+K+Na-H2O]+" mass="422.027000" />
```

Definition by:
mass vs by elemental composition

- Has to enter Na+ or K+ etc. or can be calculated by mMass (see later)
- Formula can be directly submitted to peak modelling

```
<mMassCompounds version="1.0">

  <group name="LIPID MAPS Fatty Acyls [FA]">
    <compound name="LMFA00000001" formula="C40H66O5">Fatty Acyls [FA] with formula: C40H66O5</compound>
    <compound name="LMFA00000002 (Serratamic acid)" formula="C13H25NO5">Fatty Acyls [FA] with formula: C13H25NO5</compound>
    <compound name="LMFA00000003" formula="C38H74N2O5">Fatty Acyls [FA] with formula: C38H74N2O5</compound>
    <compound name="LMFA00000004 (N-linolenoyl-glutamine)" formula="C23H38N2O4">Fatty Acyls [FA] with formula: C23H38N2O4</compound>
    <compound name="LMFA00000005" formula="C37H71NO6">Fatty Acyls [FA] with formula: C37H71NO6</compound>
```

mMass – editing compounds or references

Prepare template in Excel

```
<group name="Heme-like">
        <reference name="Heme(M+)" mass="616.177300" />
        …
        …
</group>
```

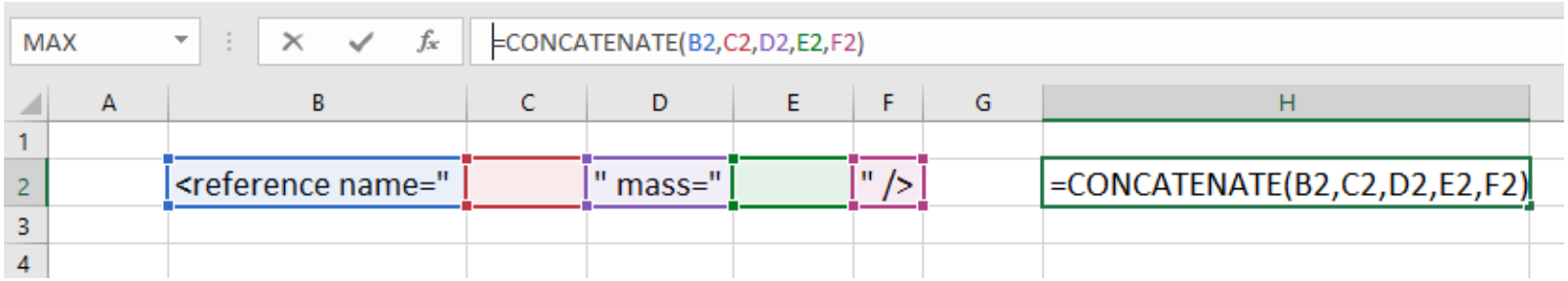

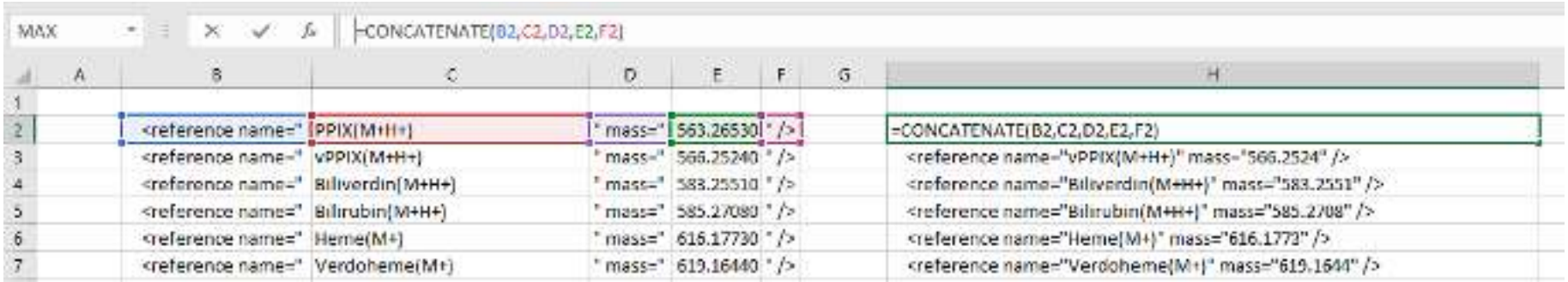

mMass – assigning references / compounds

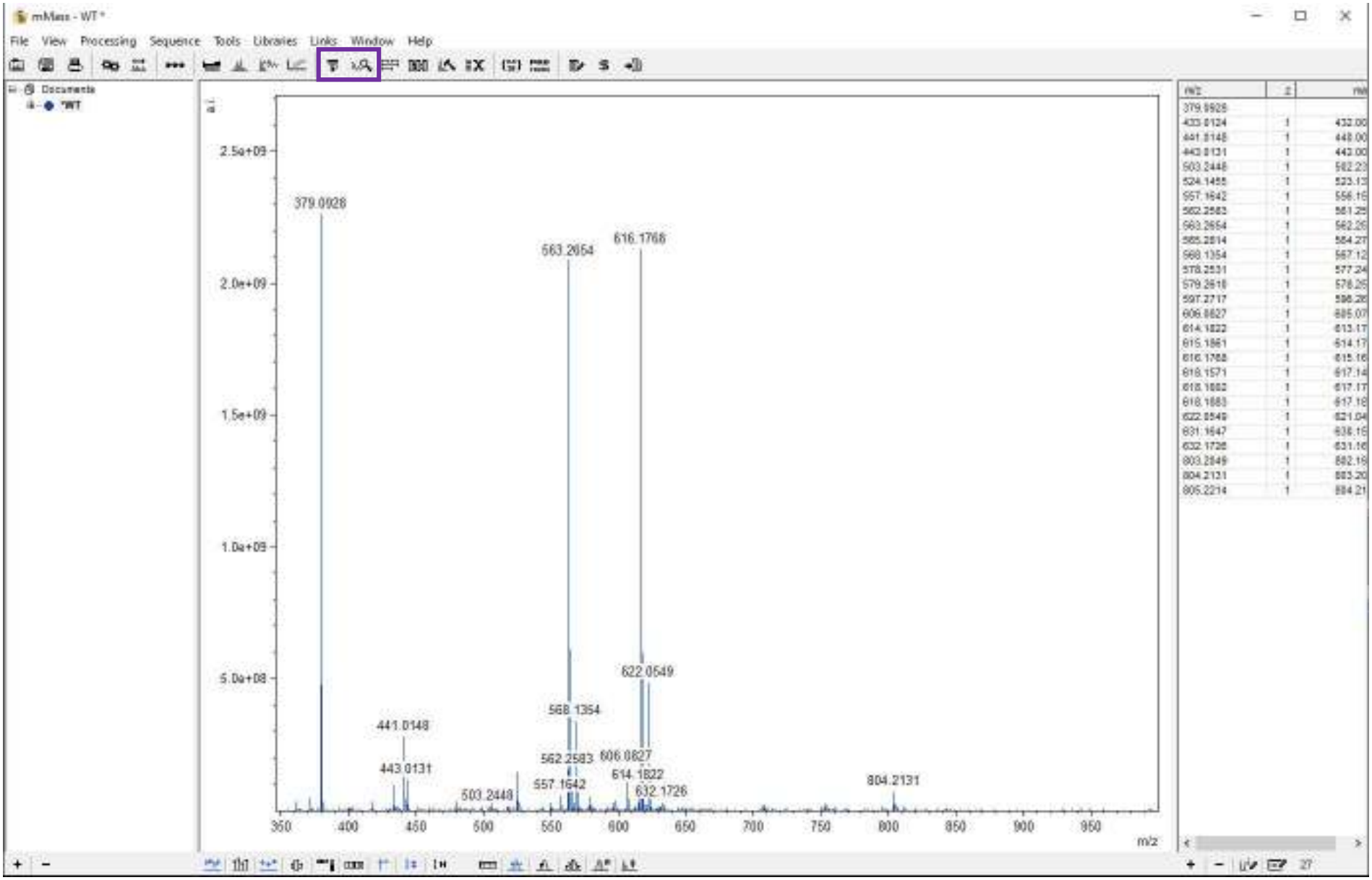

mMass – assigning references / compounds

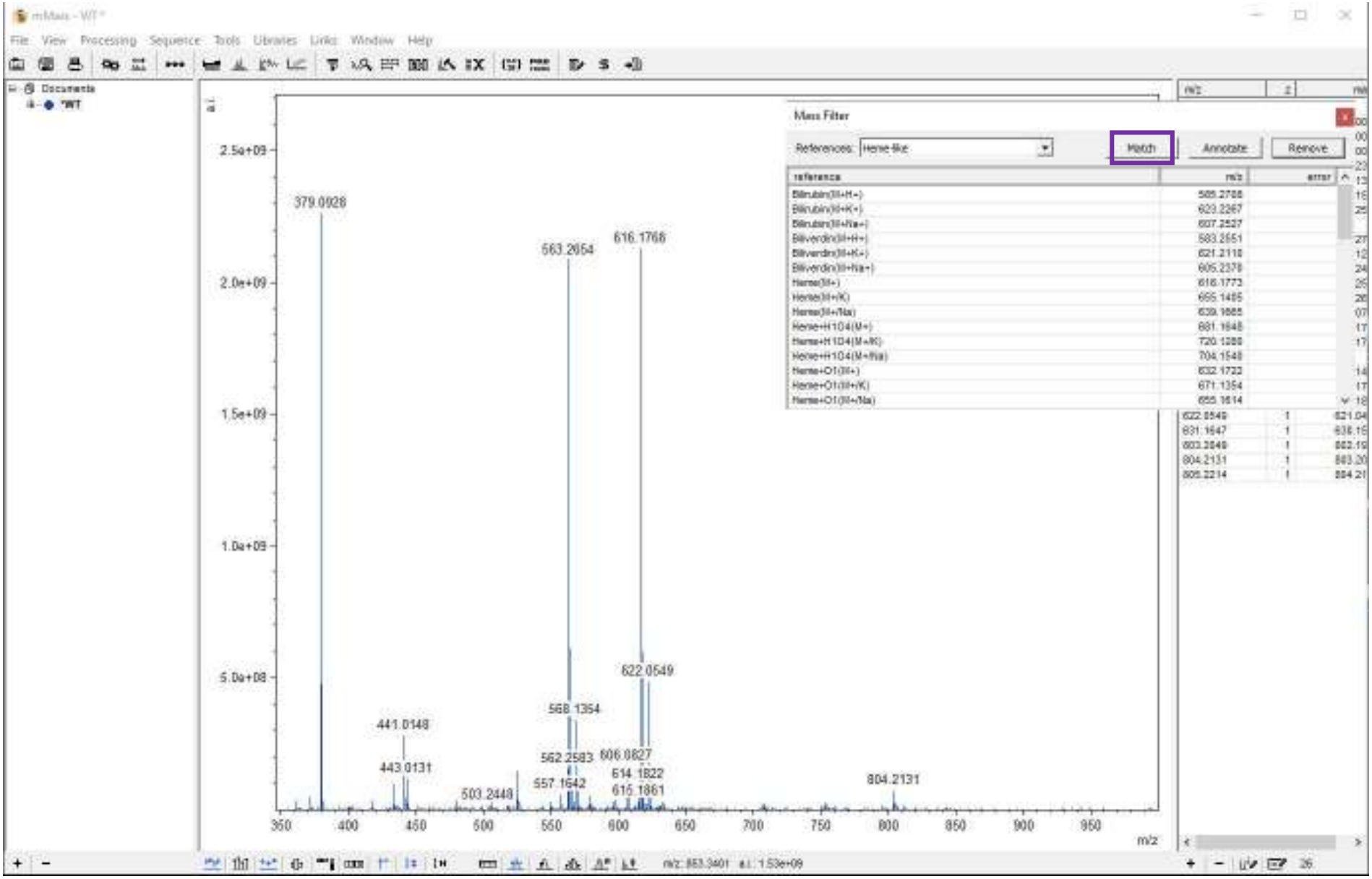

mMass – assigning references / compounds

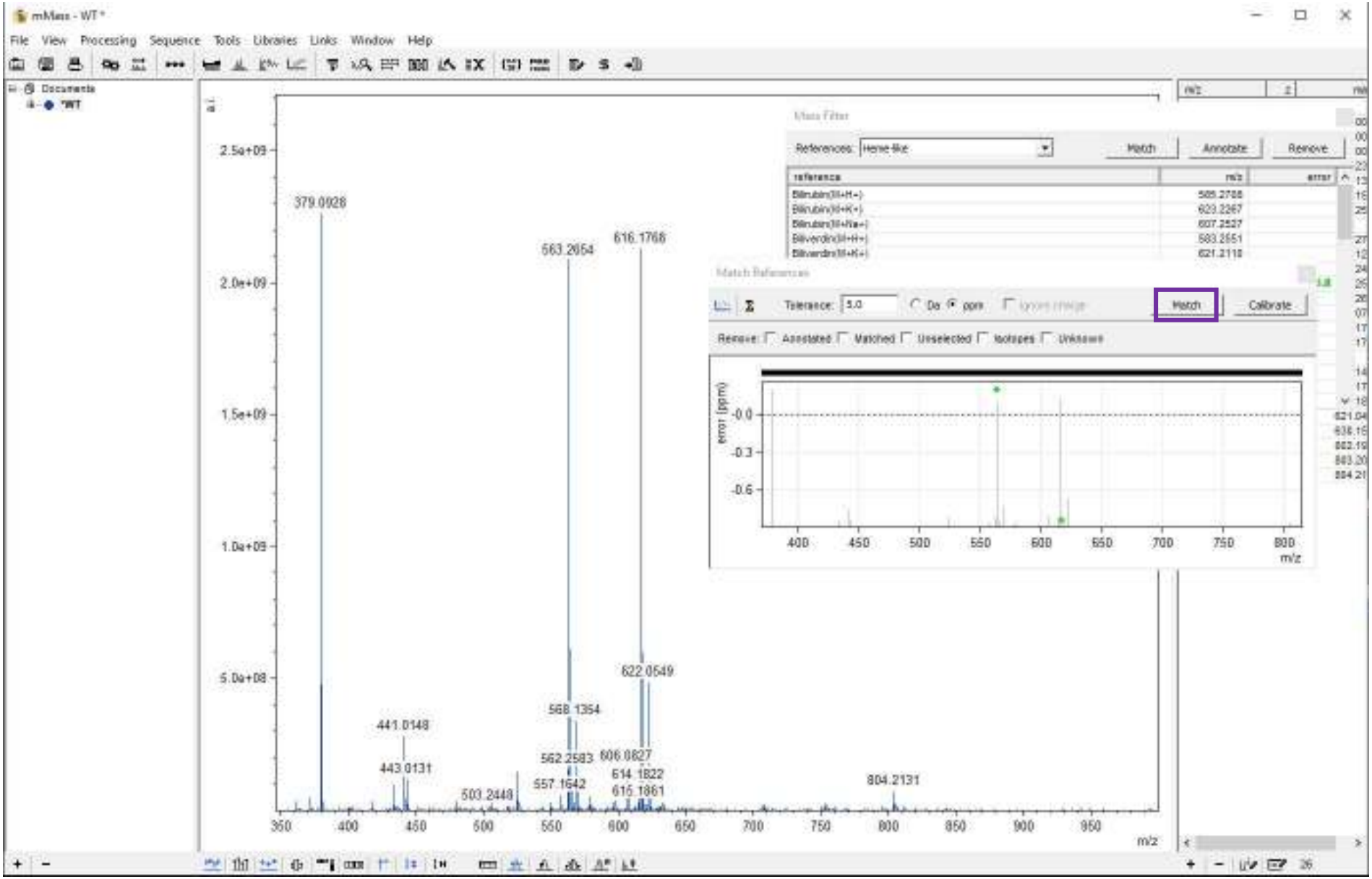

mMass – assigning references / compounds

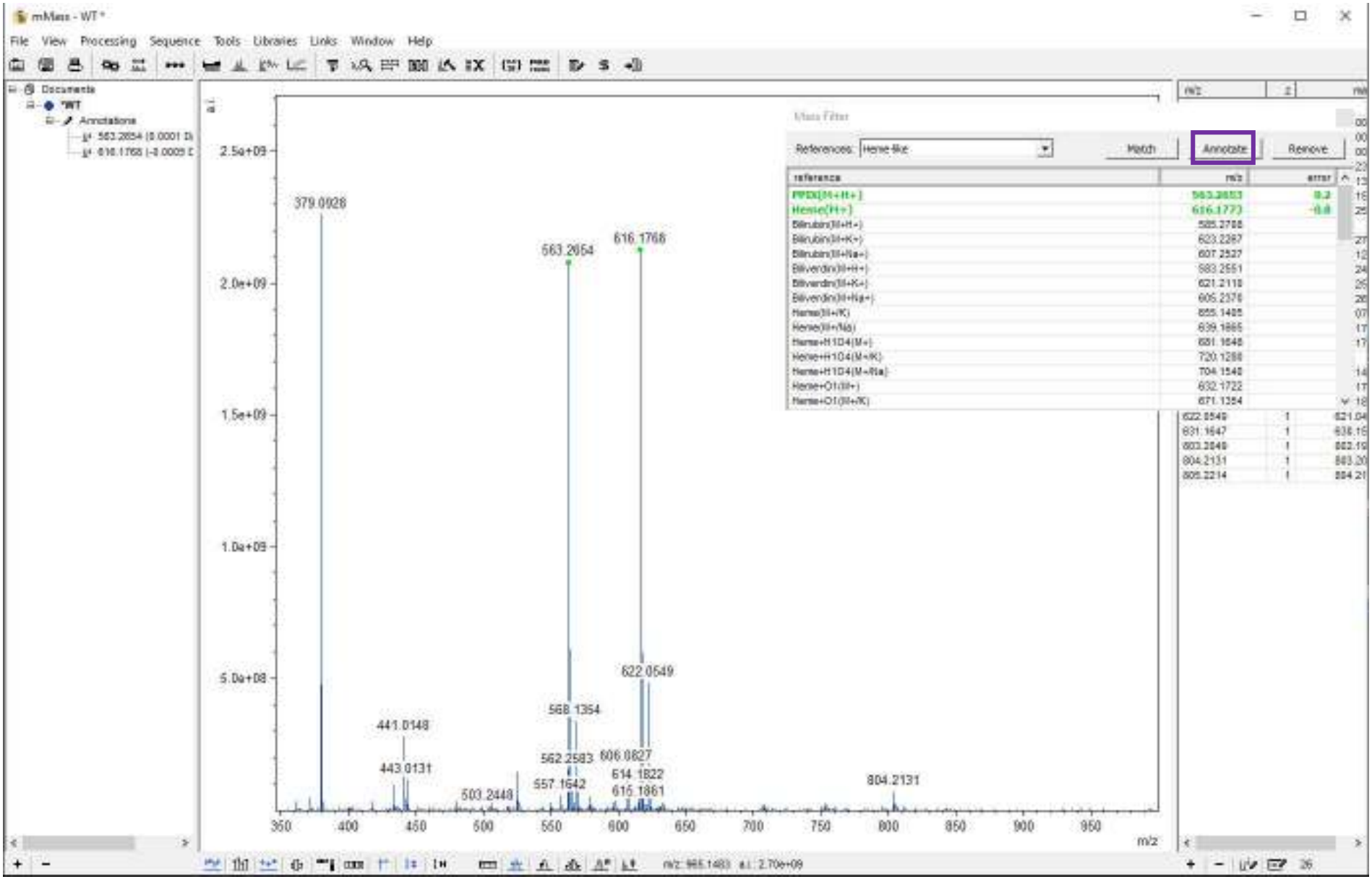

mMass – assigning references / compounds

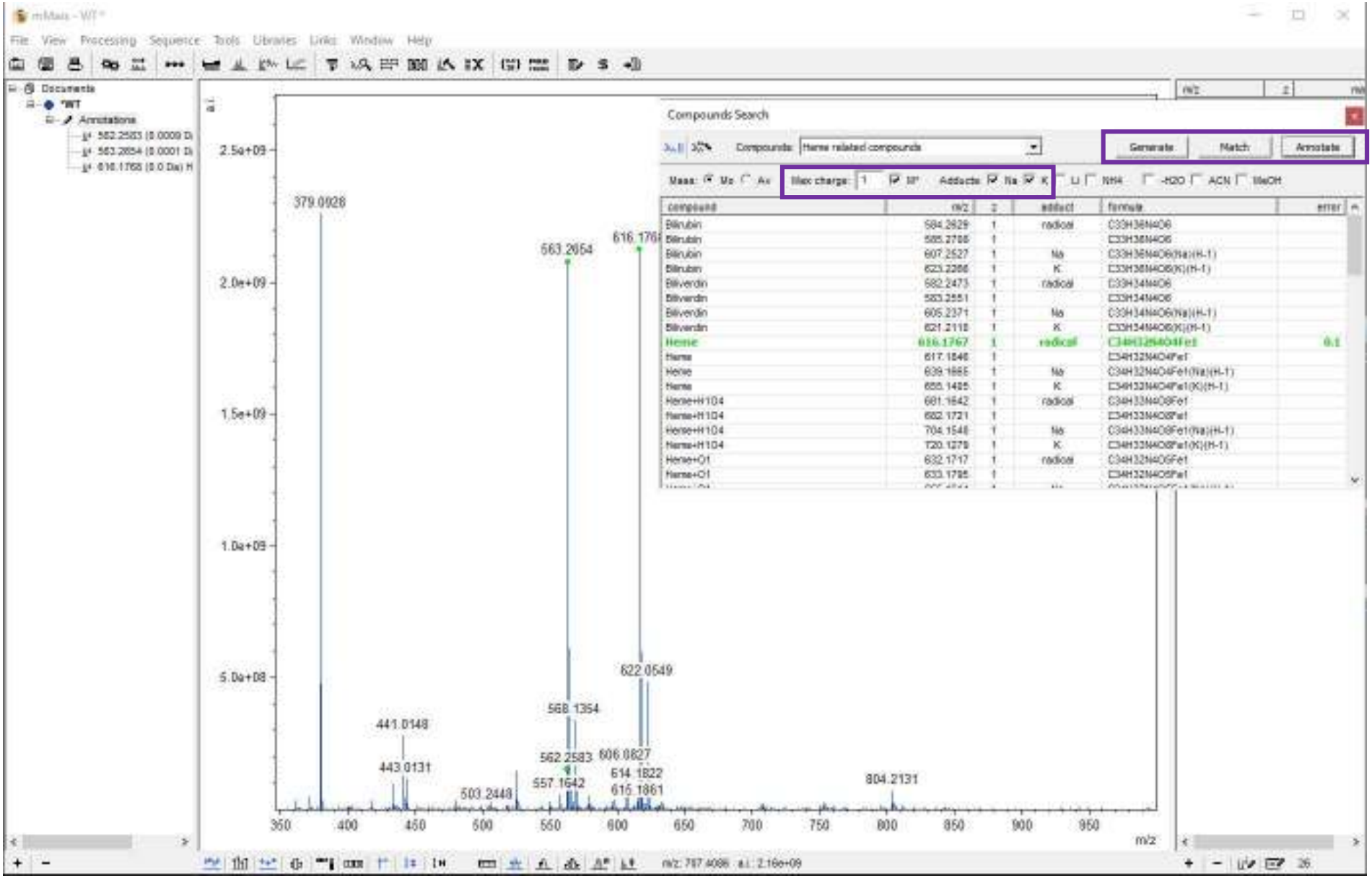

mMass – envelope fit

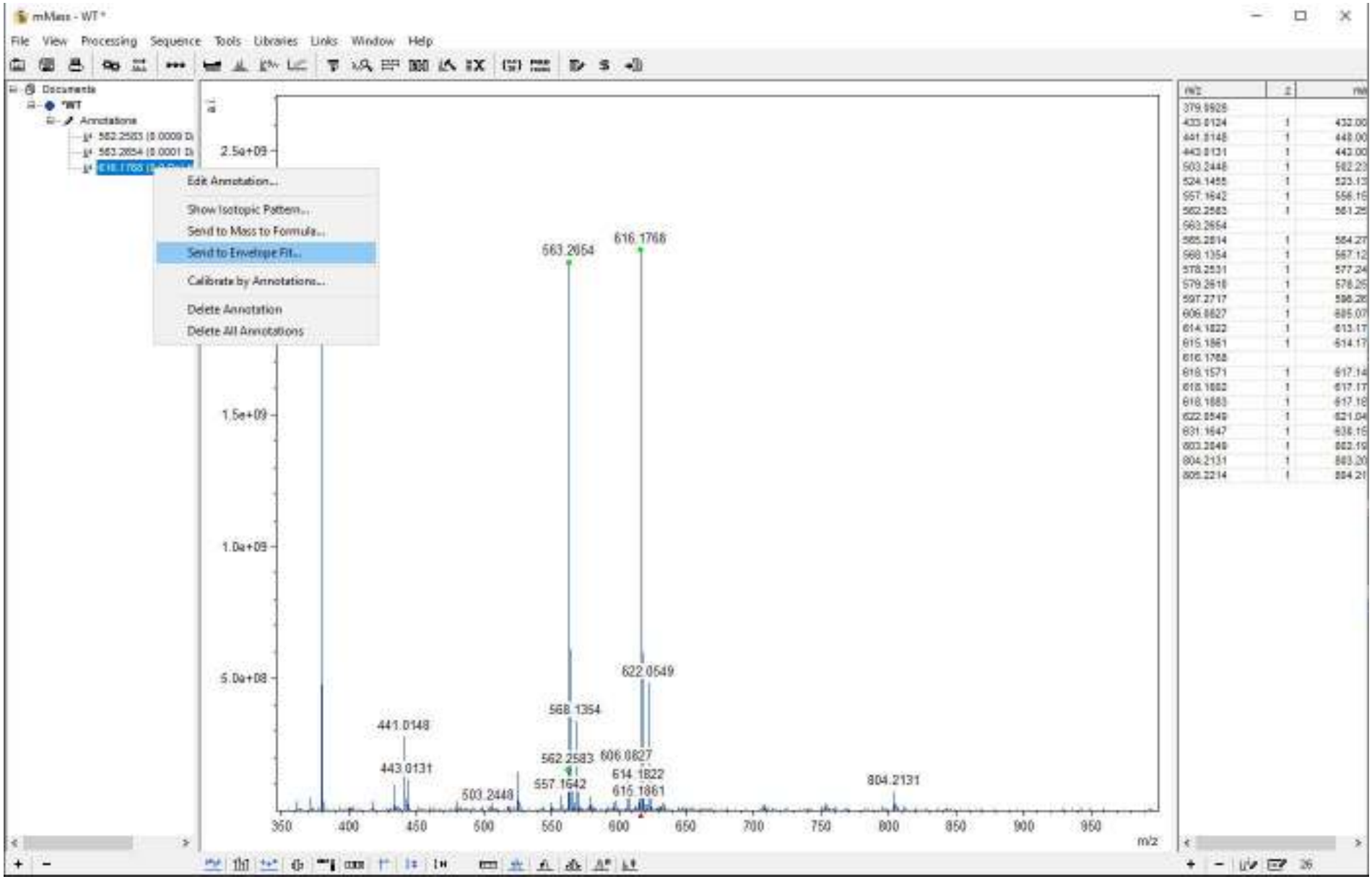

mMass – envelope fit

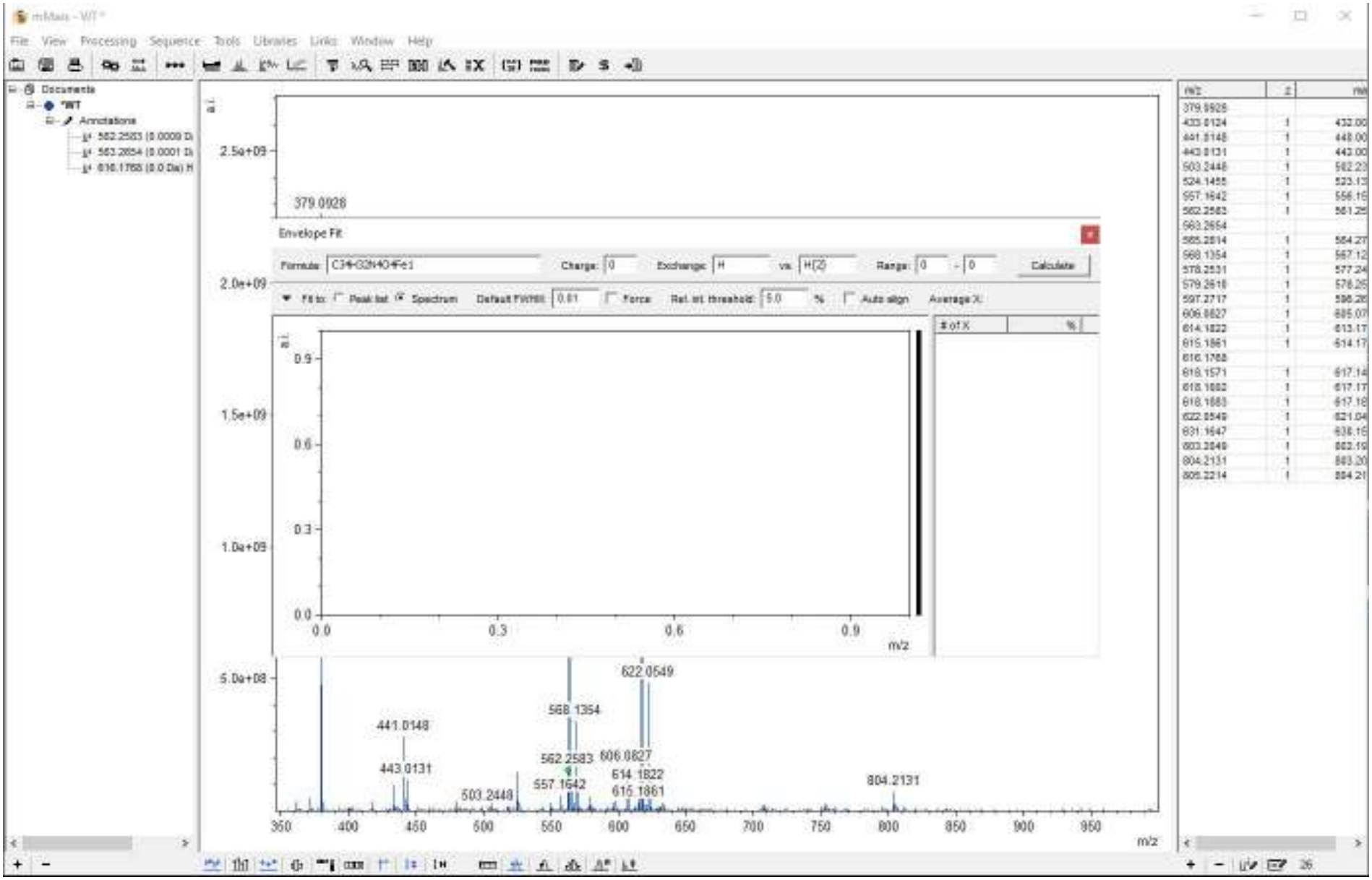

mMass – envelope fit

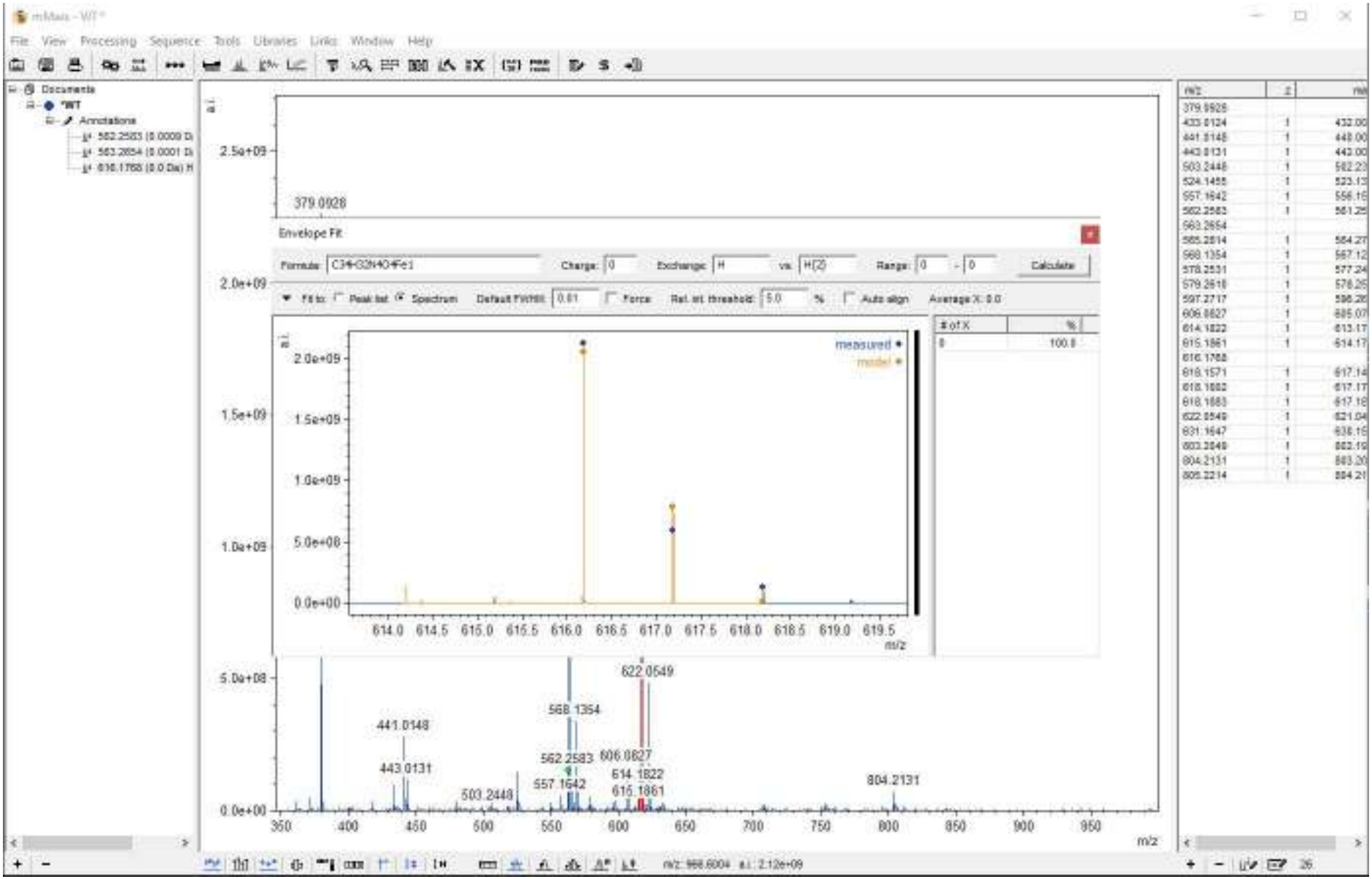

mMass – envelope fit

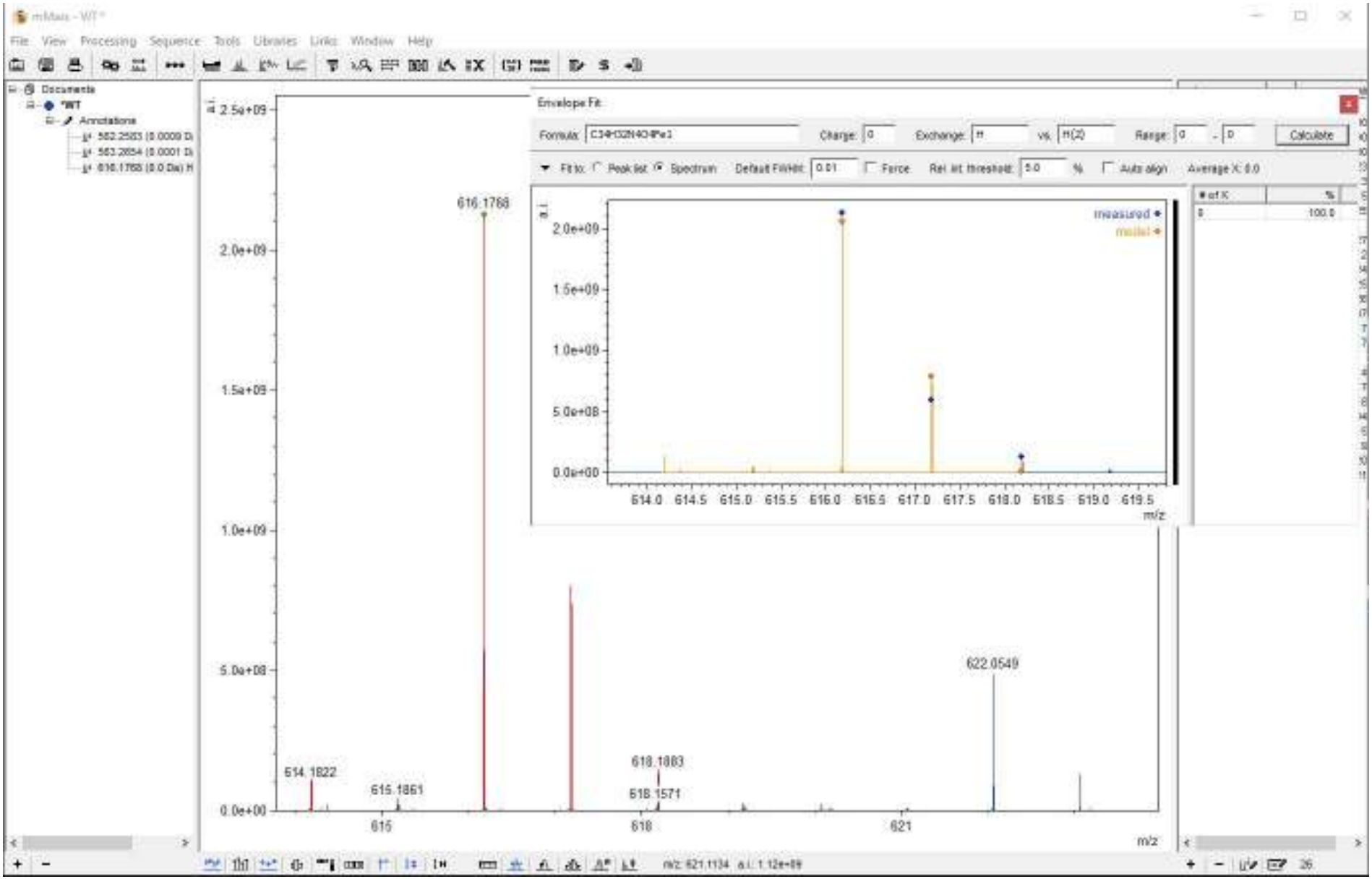

mMass – heme oxidation/degradation

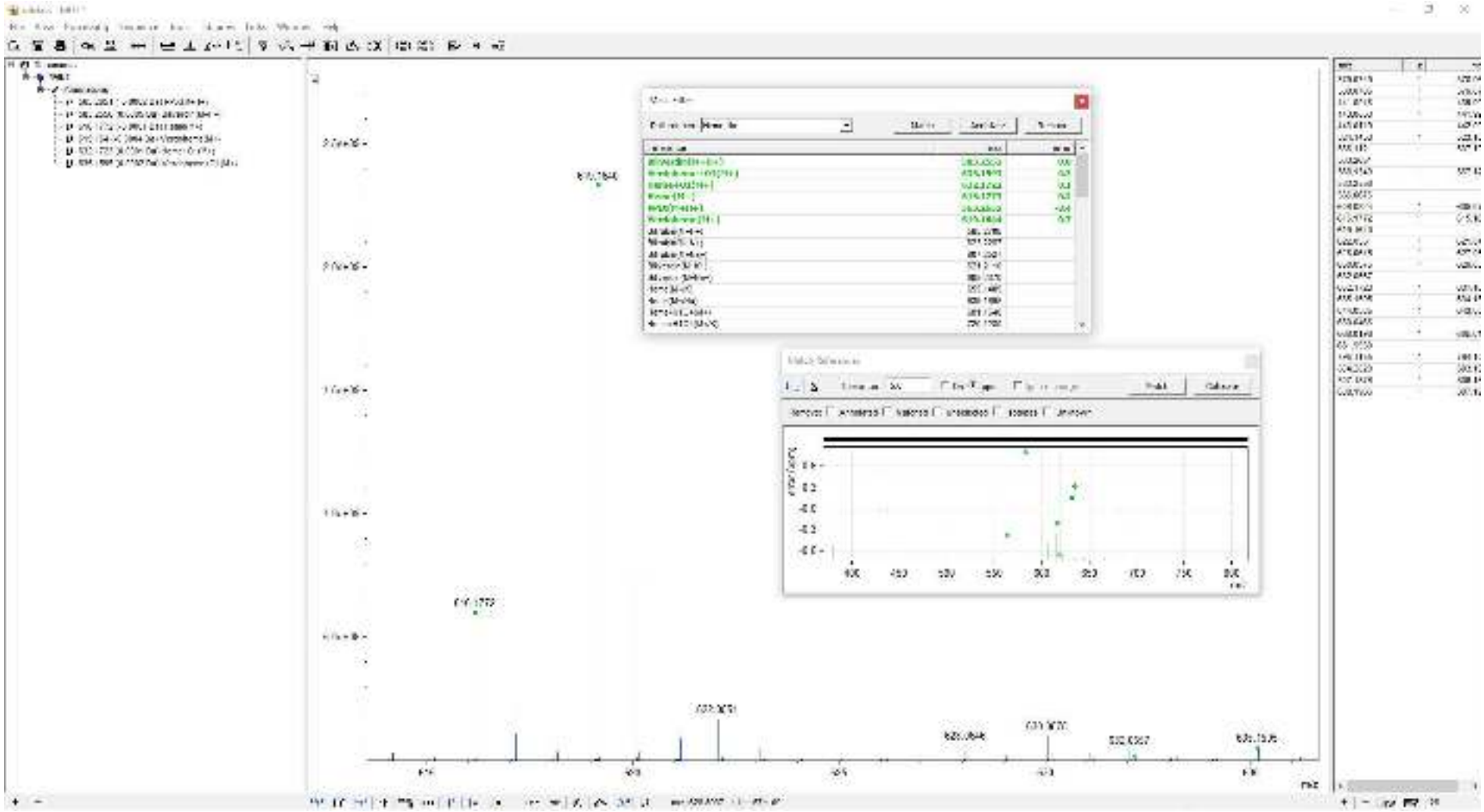

mMass – contaminated peptide mixture (find actin)

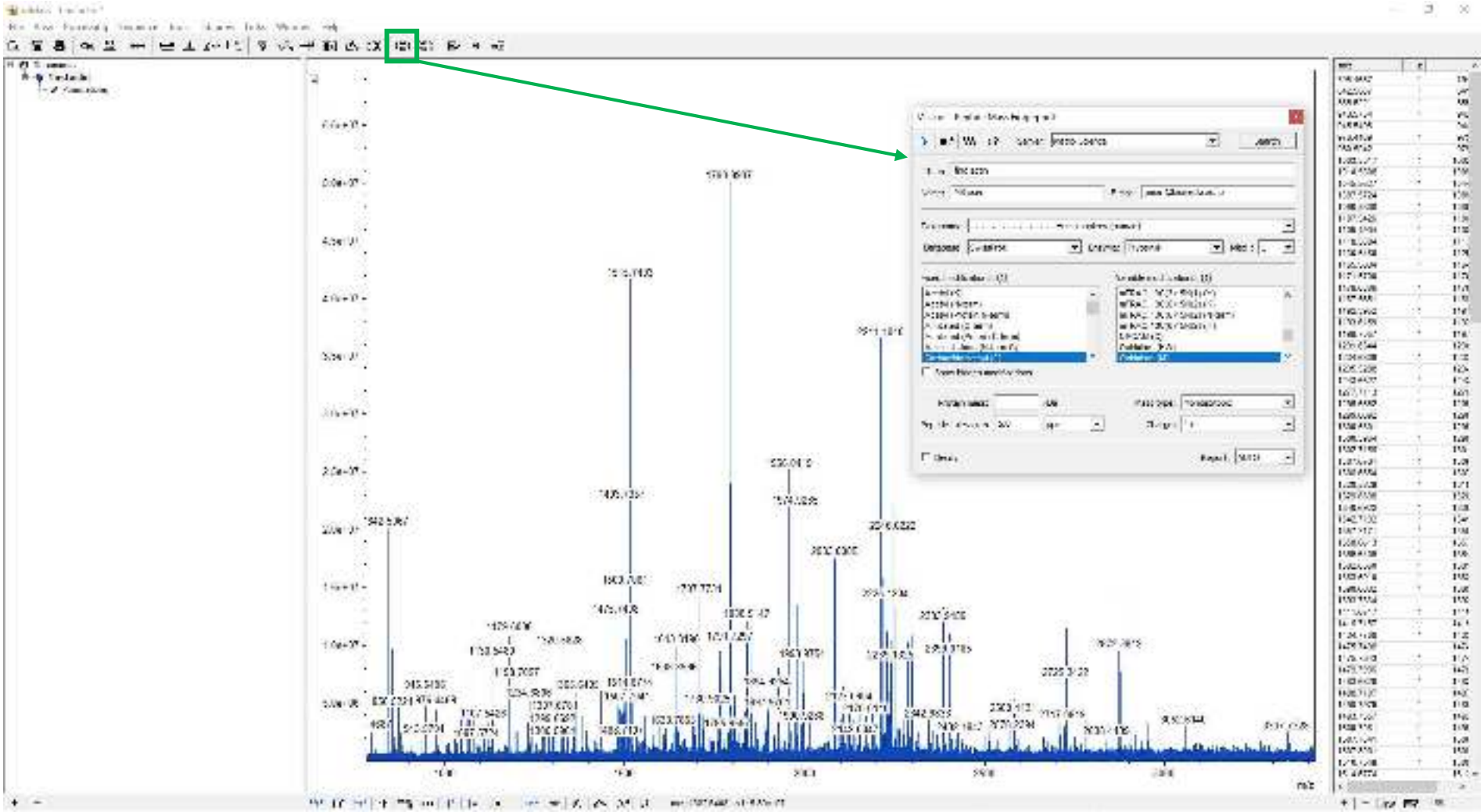

mMass – contaminated peptide mixture (find actin)

not very optimistic search result

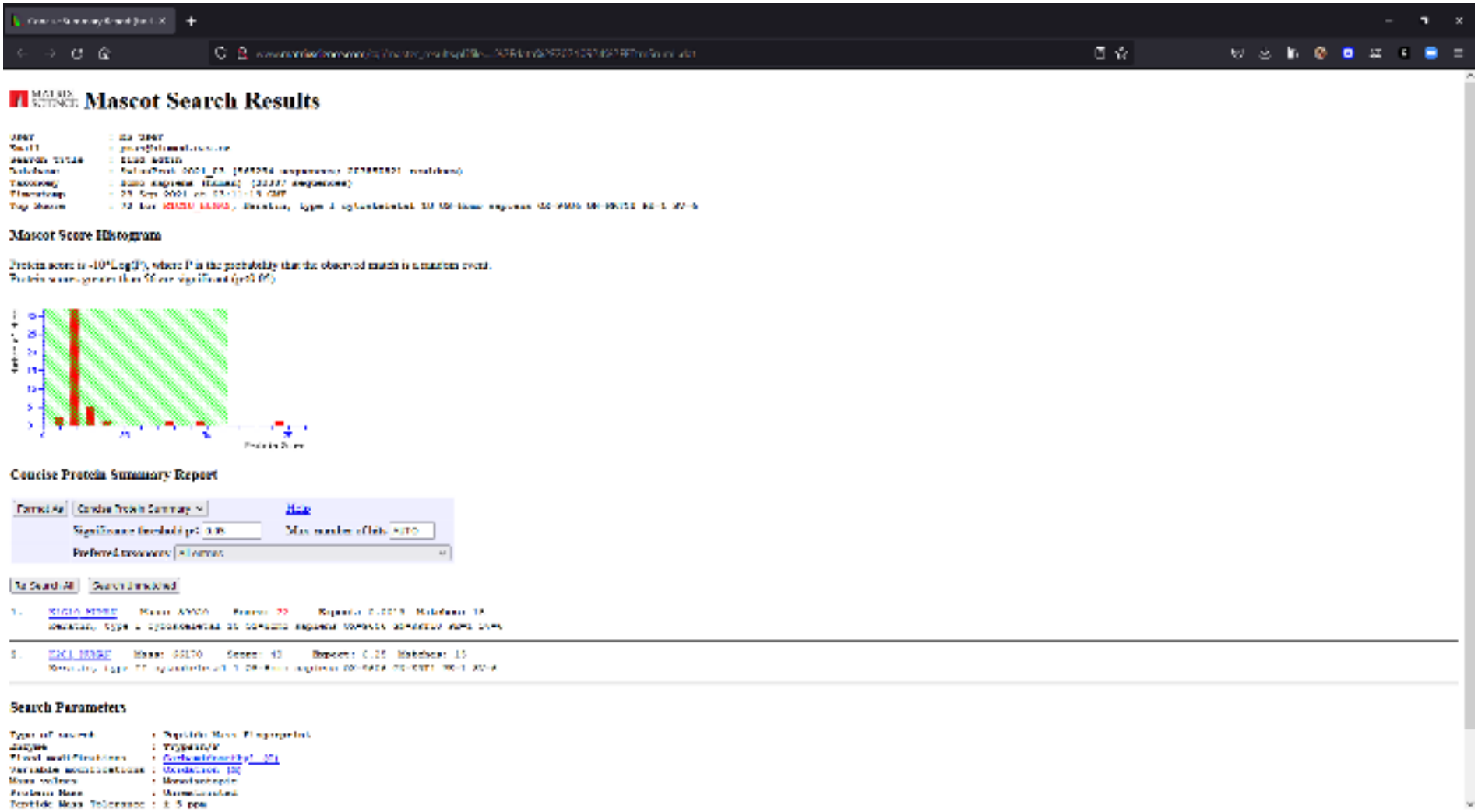

mMass – contaminated peptide mixture (find actin)

filter out contaminations

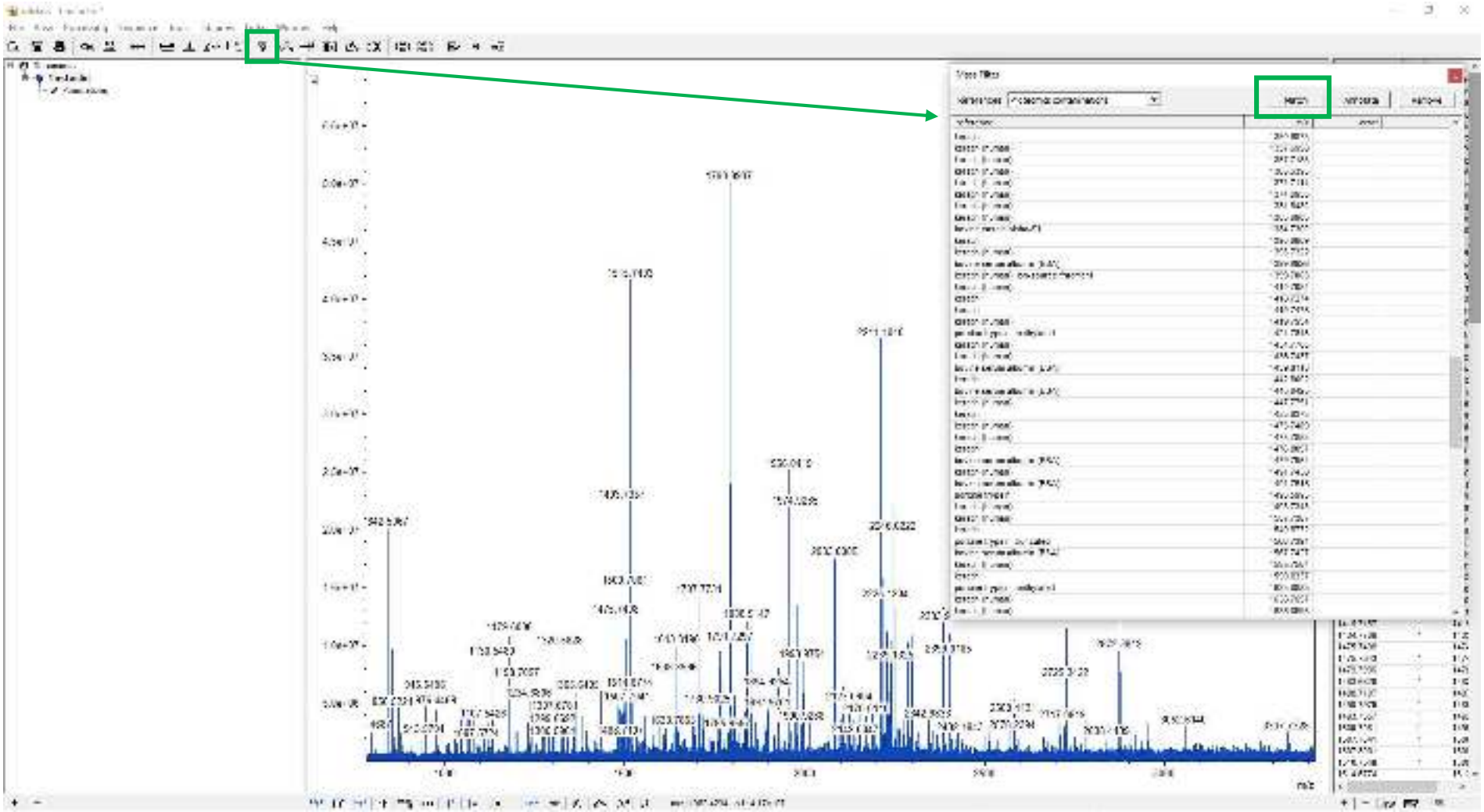

Interferences and contaminants encountered in modern mass spectrometry.
Keller BO et al. Anal Chim Acta 627(1):71-81 (2008).

mMass – contaminated peptide mixture (find actin)

match and annotate

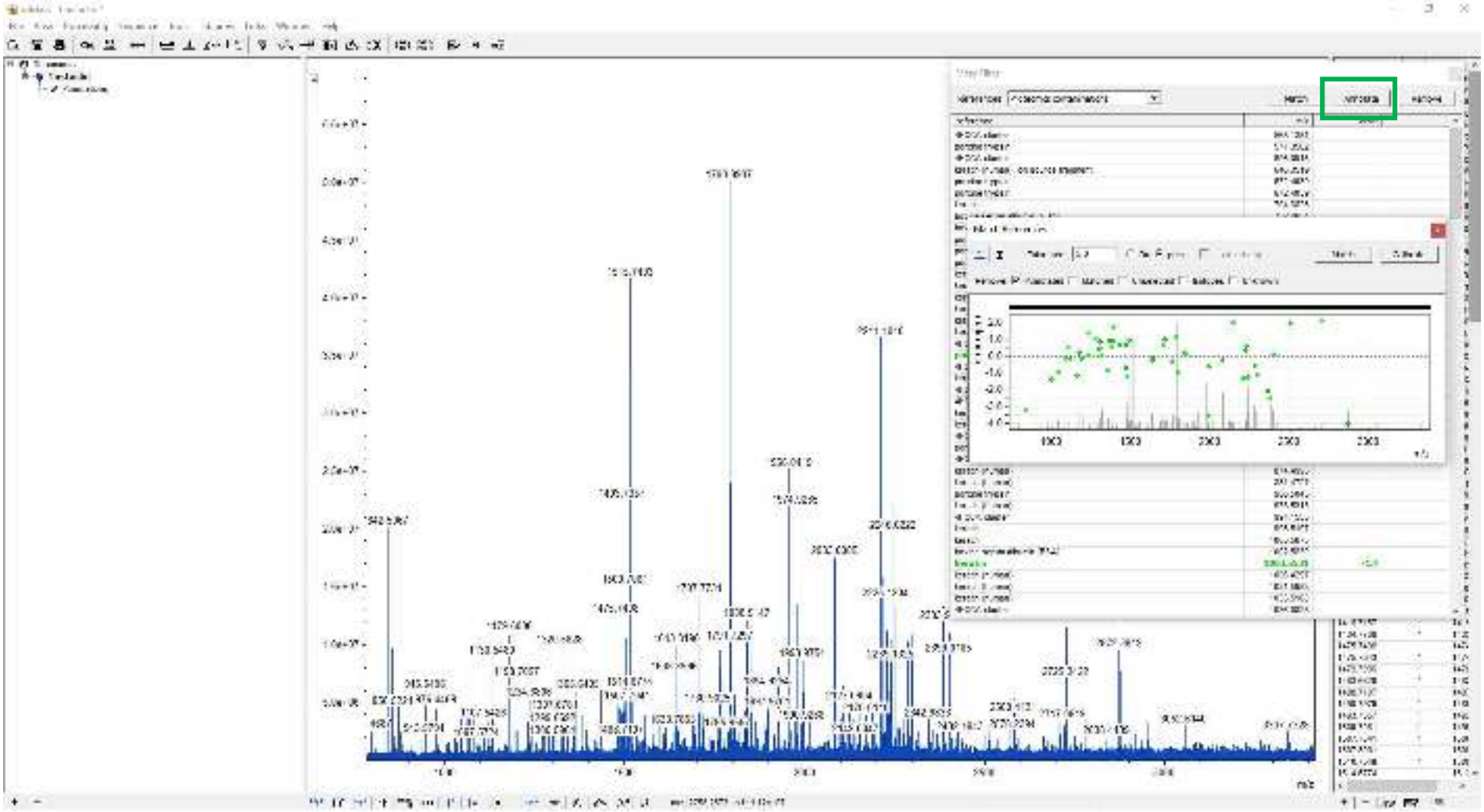

mMass – contaminated peptide mixture (find actin)

green dots mark the contaminations

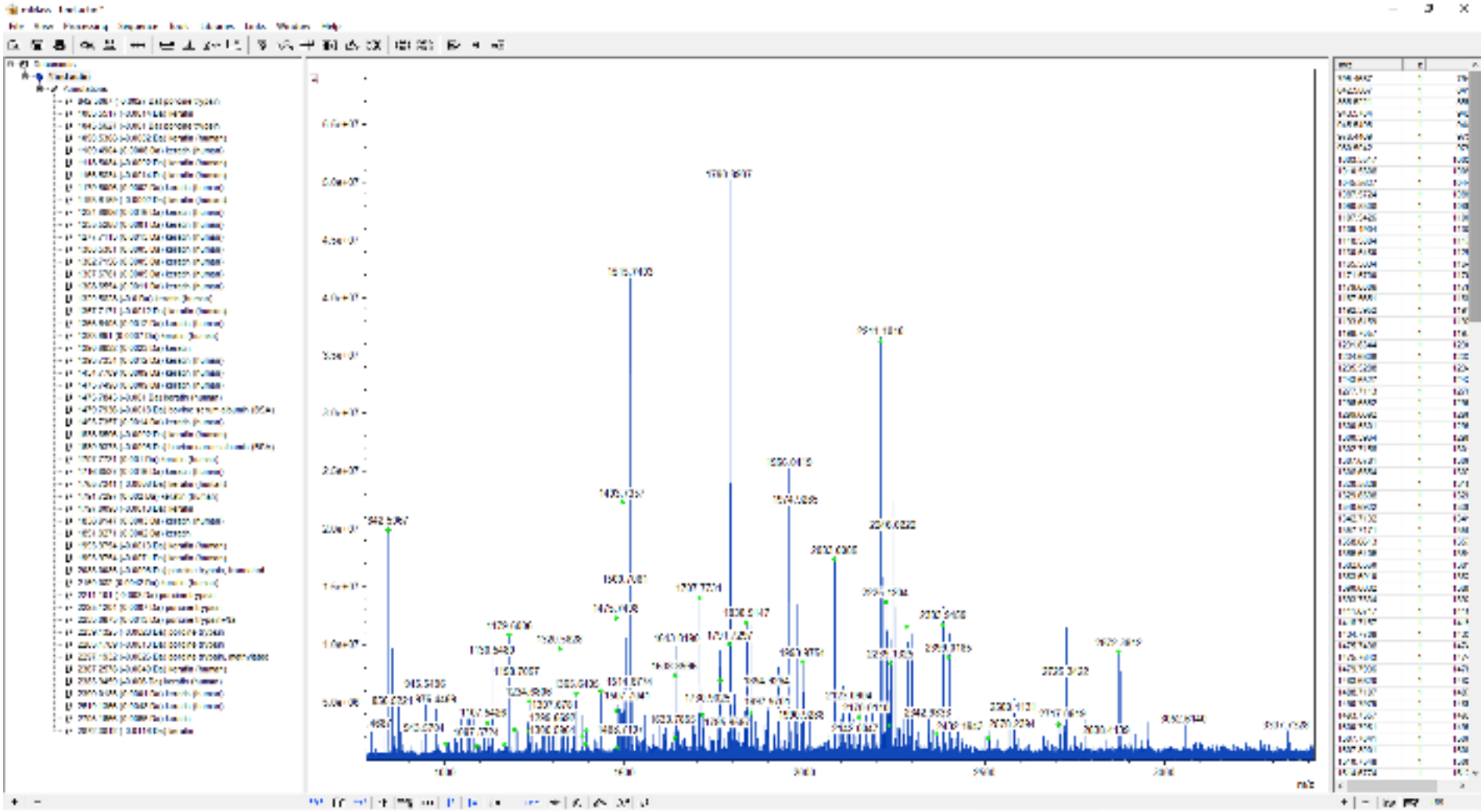

mMass – contaminated peptide mixture (find actin)

running the search again, now filtering out the contaminants

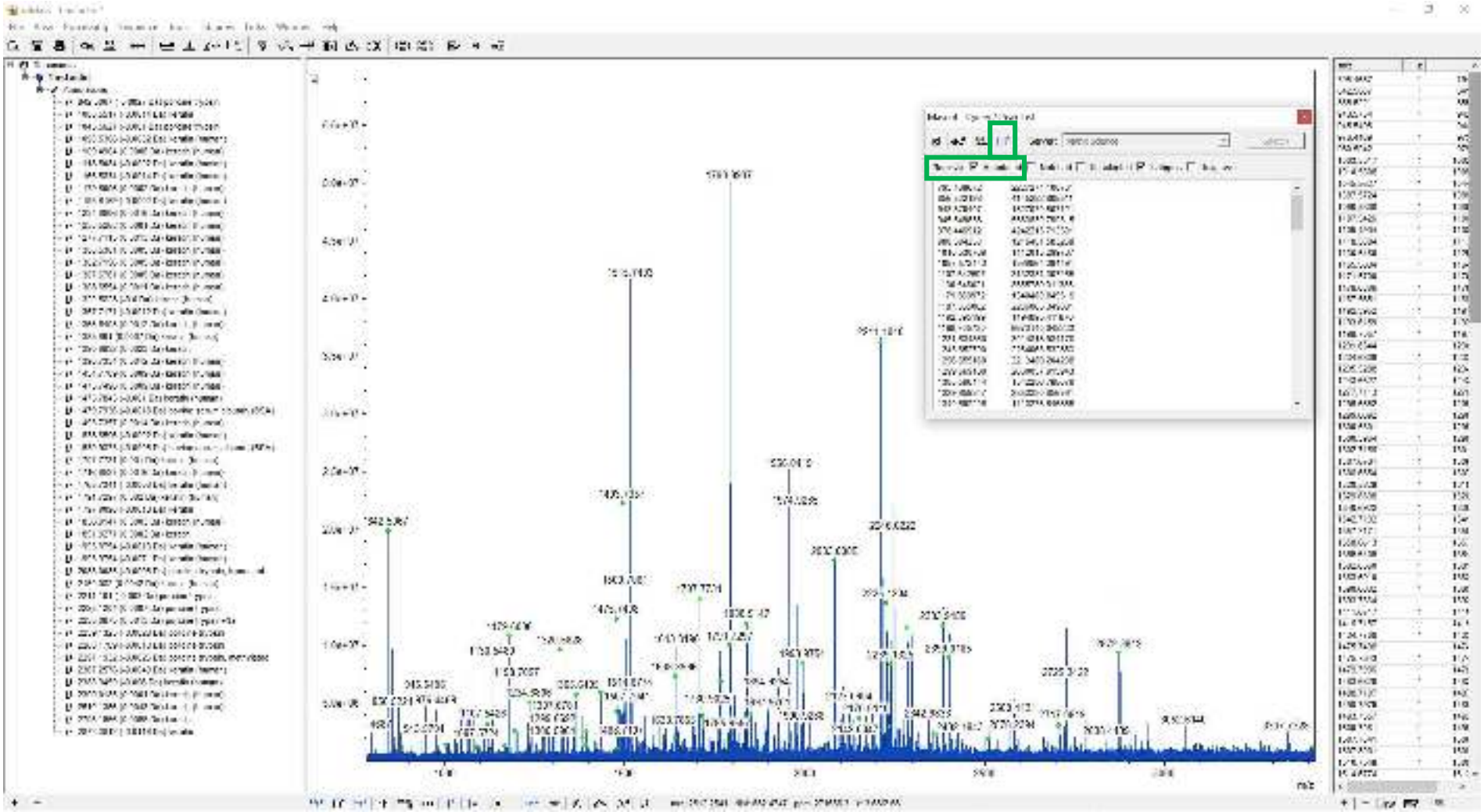

mMass – contaminated peptide mixture (find actin)

now actin is identified

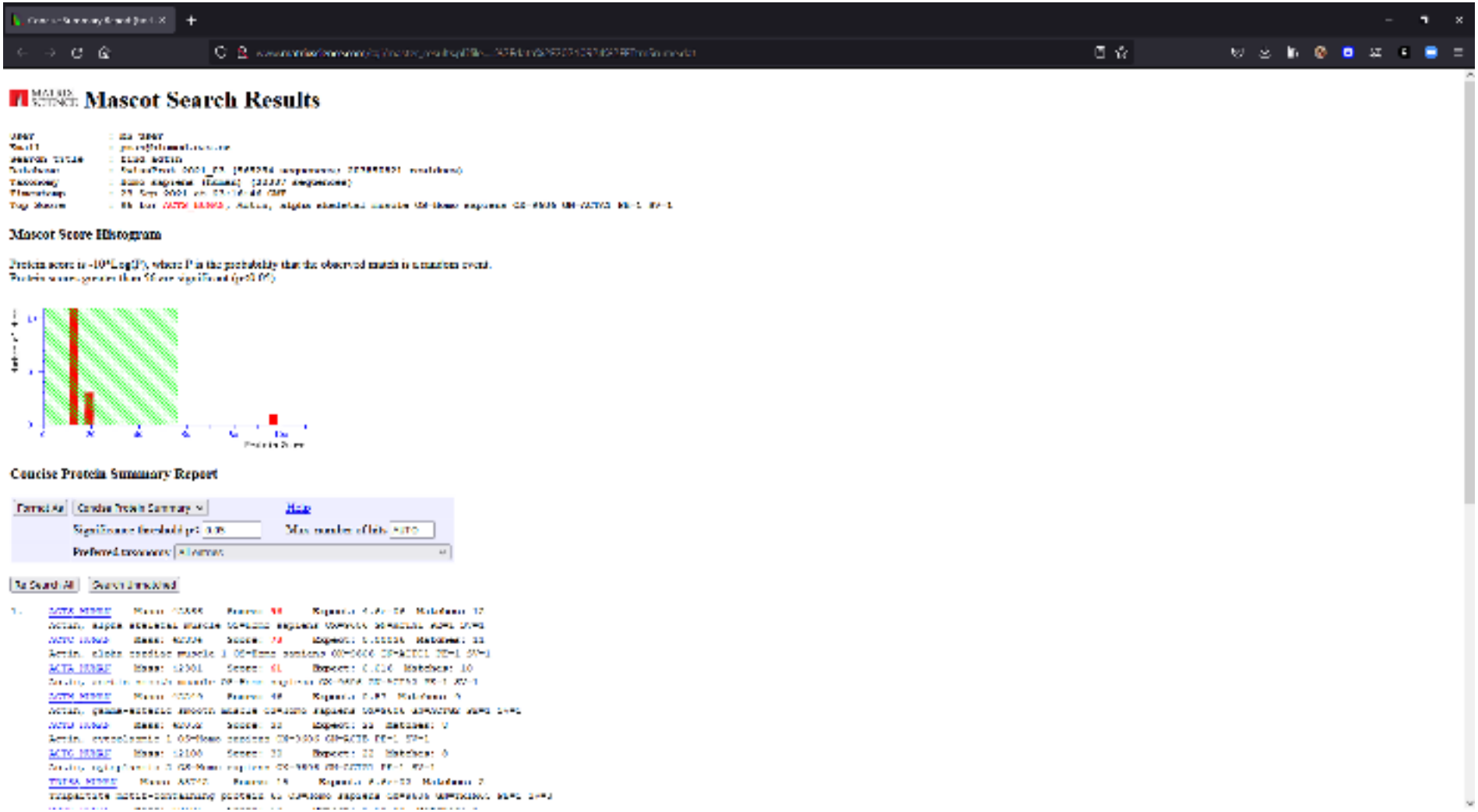

mMass – contaminated peptide mixture (find actin)

details of the identification + copy-paste the sequence for mMass

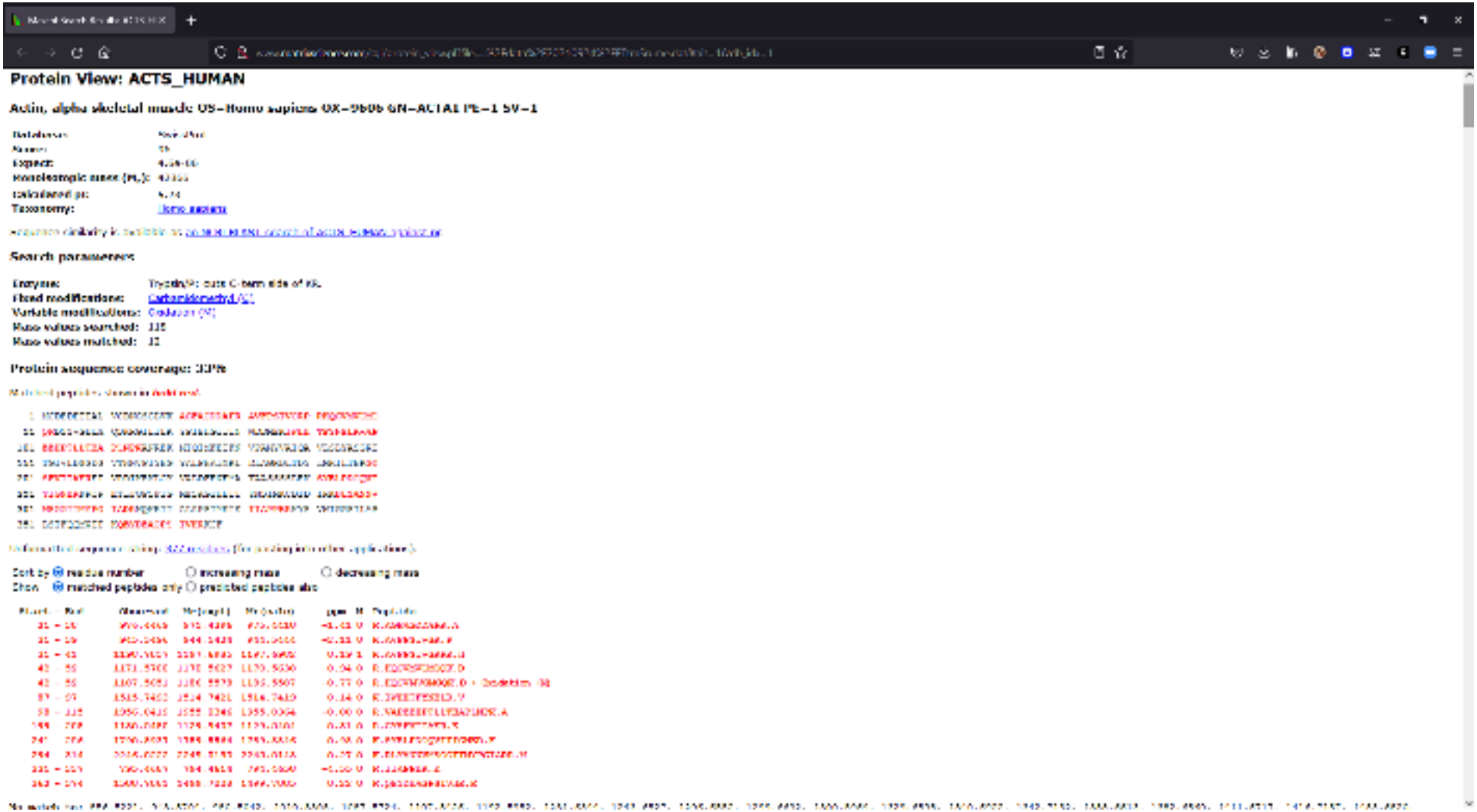

mMass – contaminated peptide mixture (find actin)

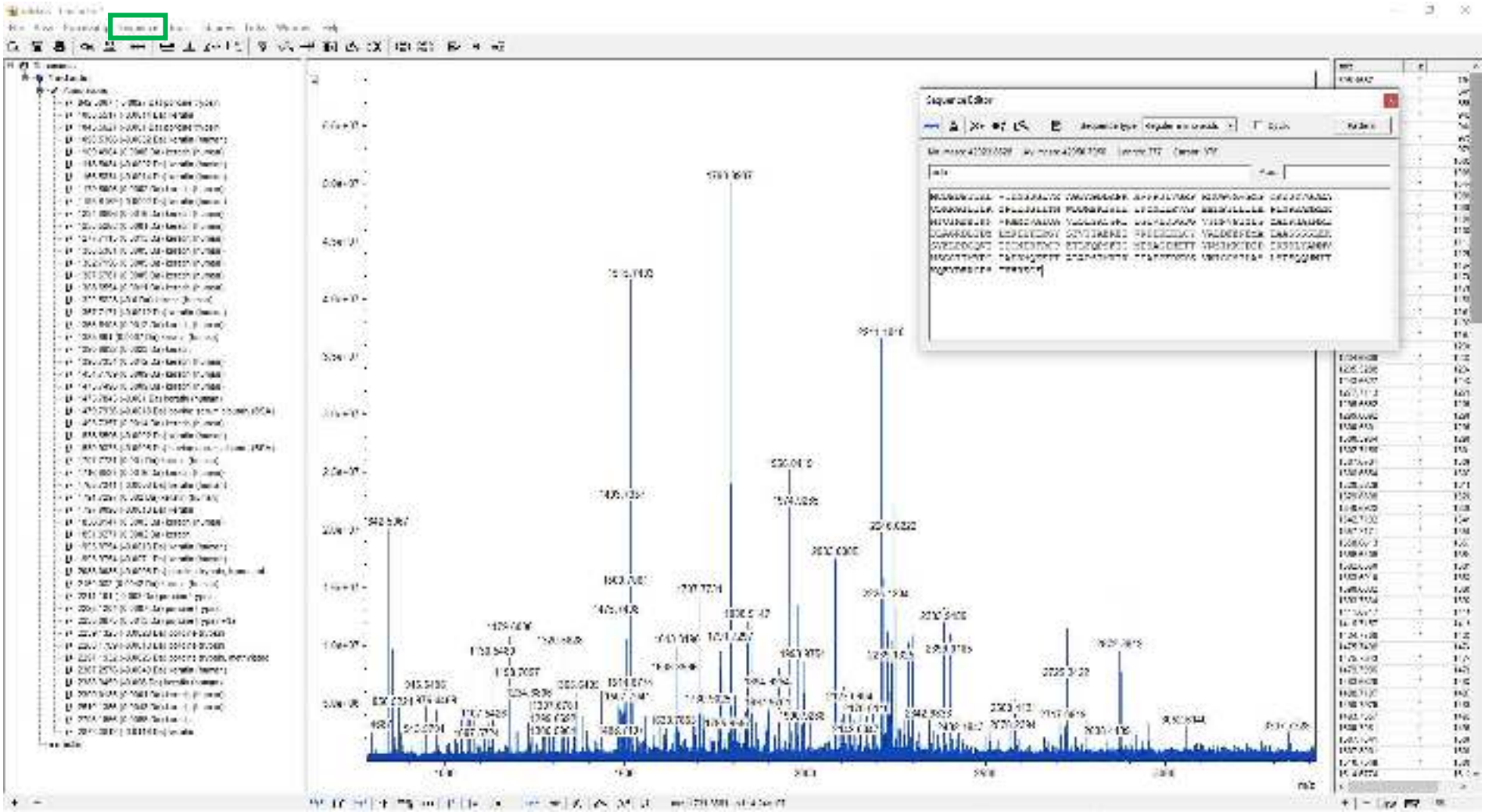

mMass – contaminated peptide mixture (find actin)

add modifications (can use pre-sets)

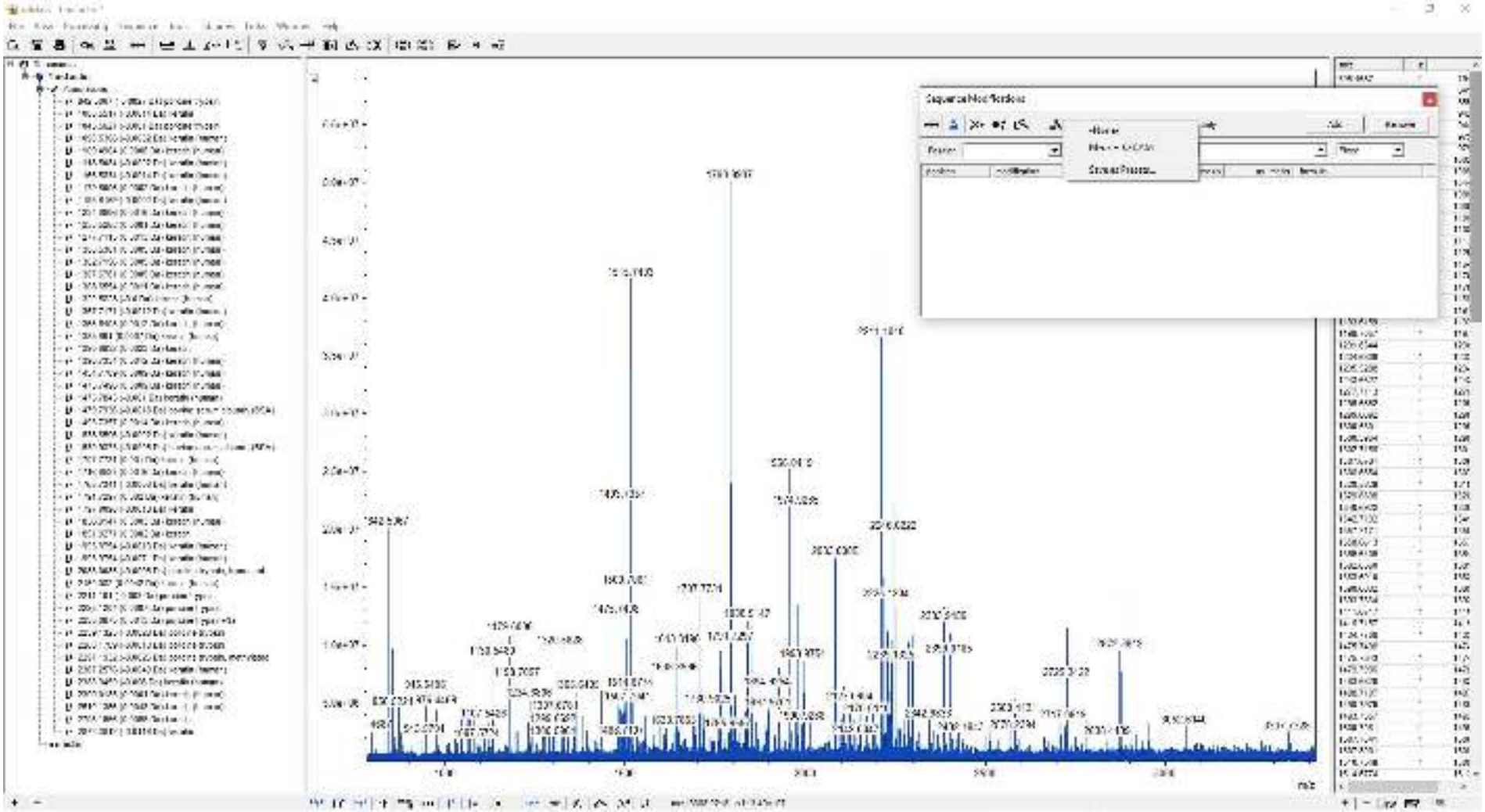

mMass – contaminated peptide mixture (find actin)

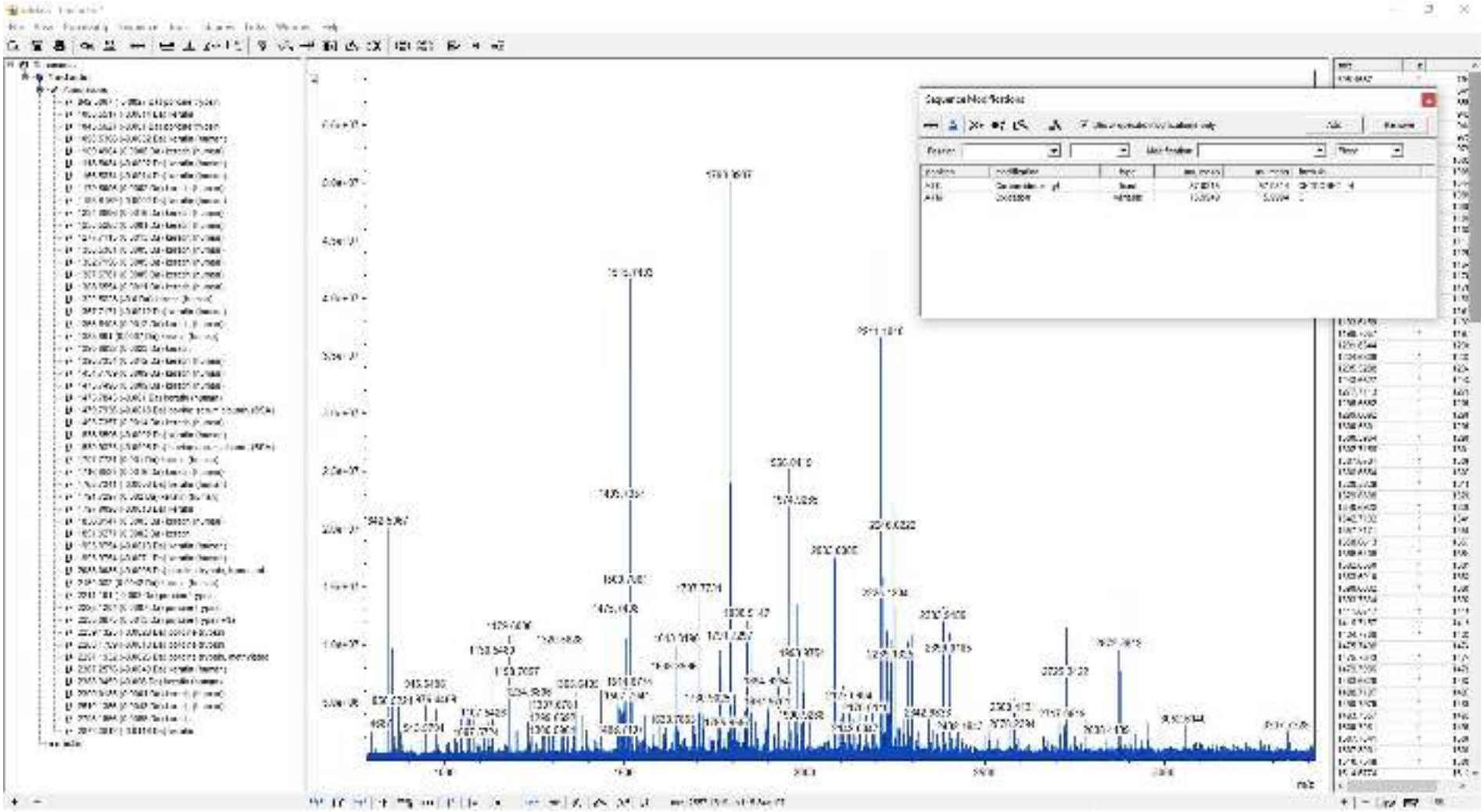

mMass – contaminated peptide mixture (find actin)

in silico digestion…

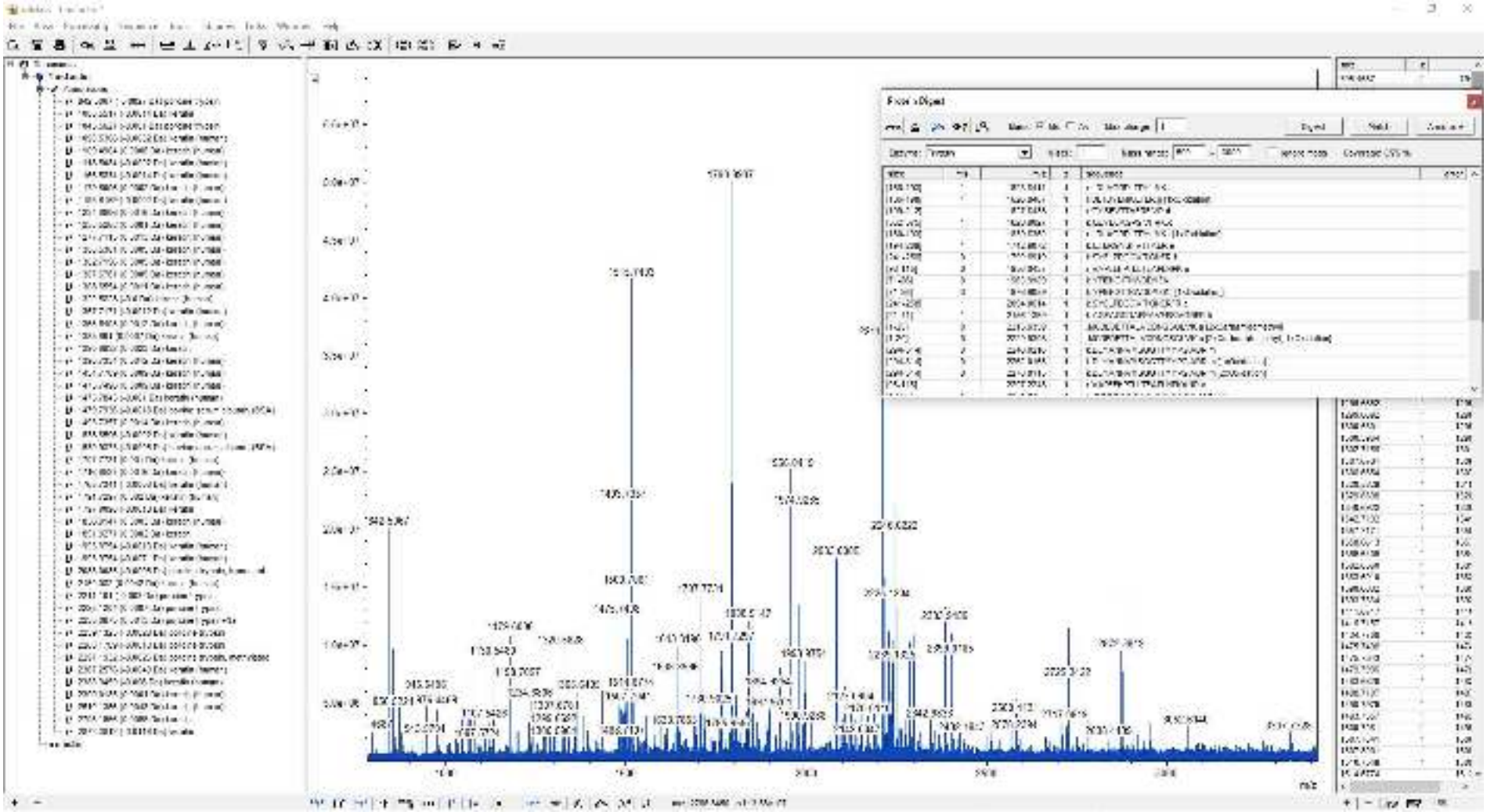

mMass – contaminated peptide mixture (find actin)

…and its assignment

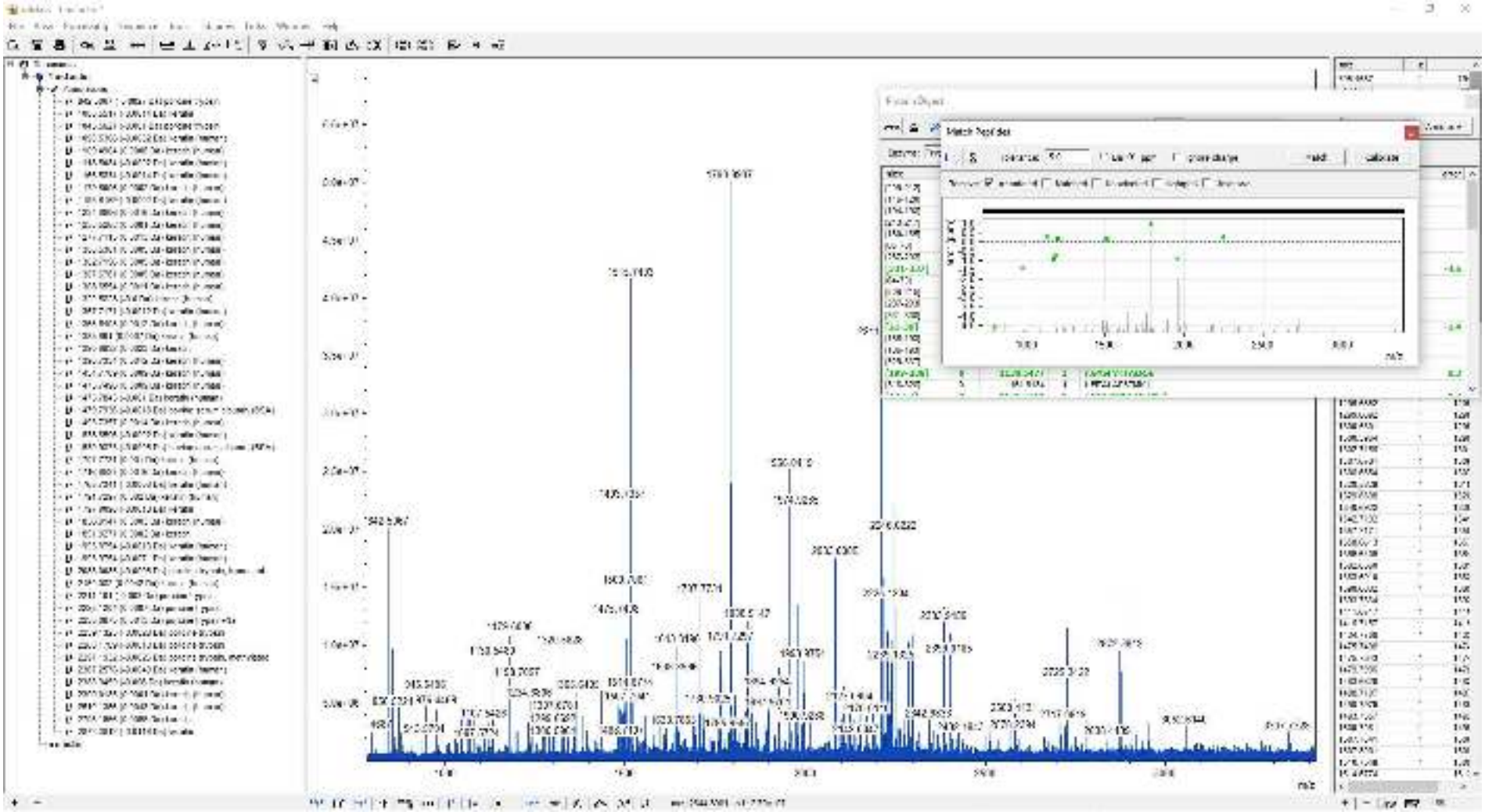

mMass – contaminated peptide mixture (find actin)

fully annotated spectrum

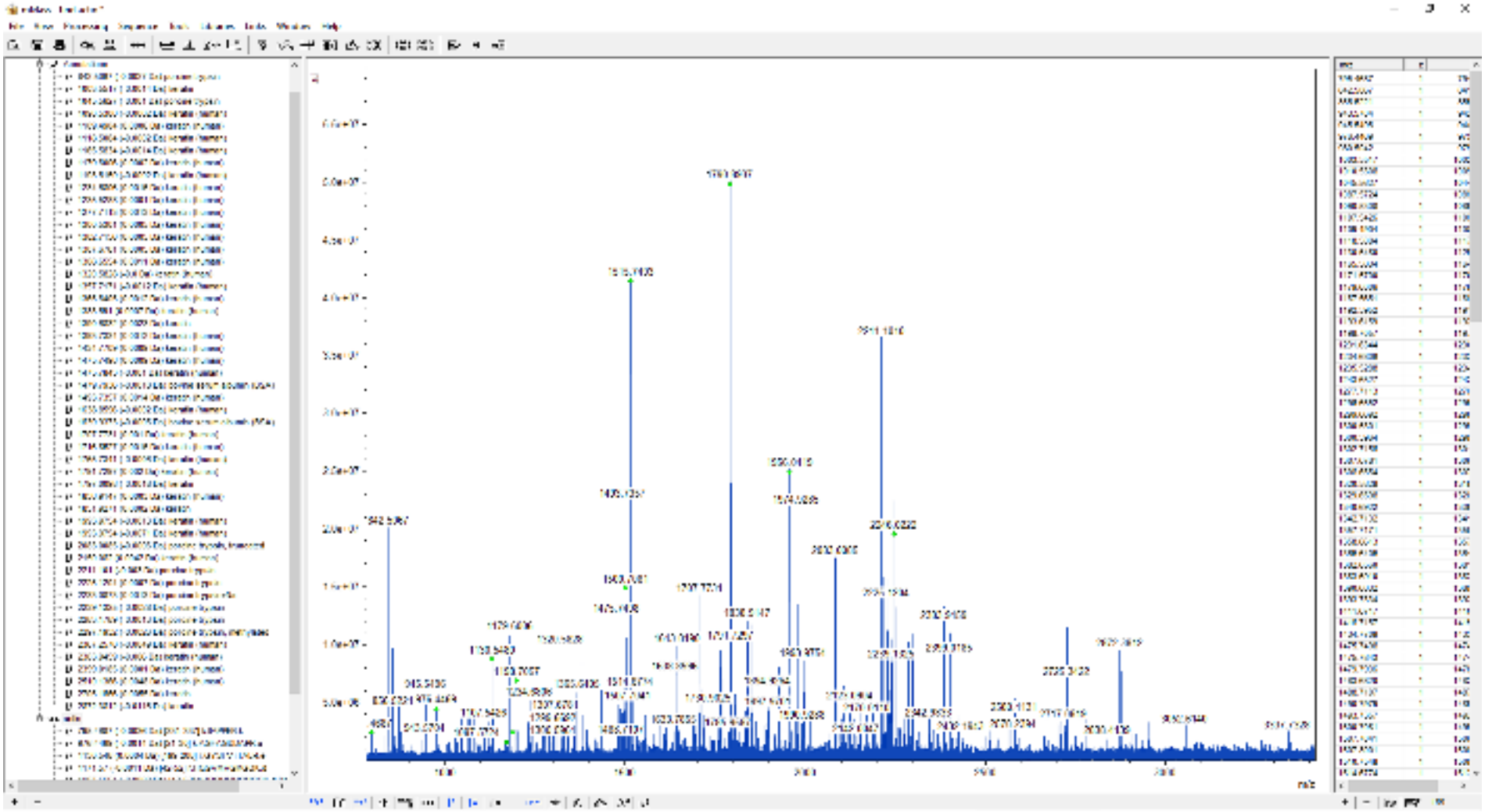

mMass – the power of high resolution

peptide mass fingerprinting - plectin

Plectin – huge cytoskeletal protein (530kDa, 4900 AAs, various splice variants)

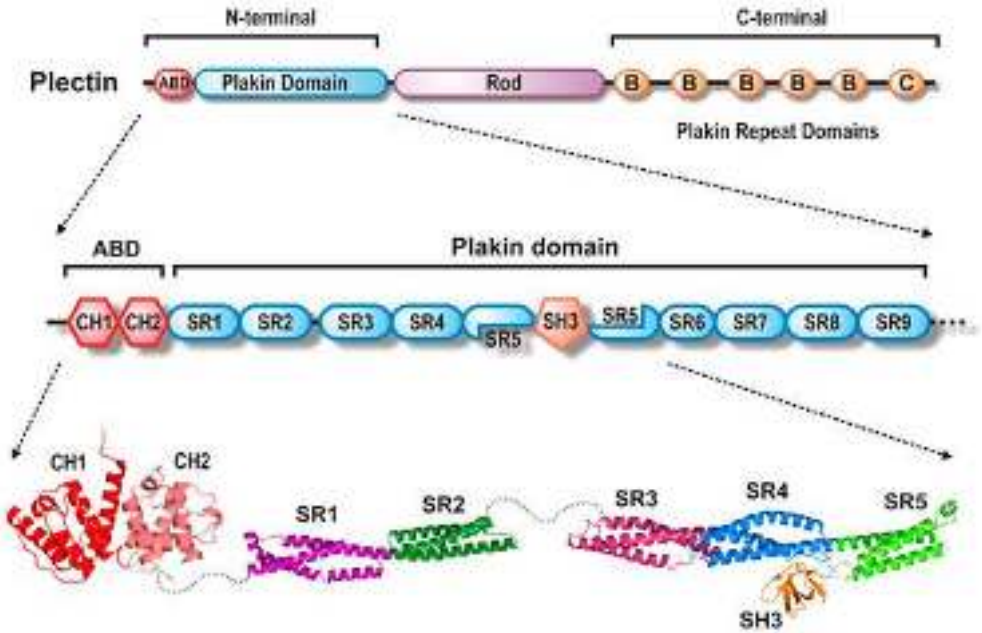

MVAGMLMPRDQLRAIYEVLFREGVMVAKKDRRPRSLHPHVPGVTNLQVMRAMASLRARGLVRETFAWCHFYWYLTNEGIAHLRQYL
HLPPEIVPASLQRVRRPVAMVMPARRTPHVQAVQGPLGSPPKRGPLPTEEQRVYRRKELEEVSPETPVVPATTQRTLARPGPEPAP
ATDERDRVQKKTFTKWVNKHLIKAQRHISDLYEDLRDGHNLISLLEVLSGDSLPREKGRMRFHKLQNVQIALDYLRHRQVKLVNIRND
DIADGNPKLTLGLIWTIILHFQISDIQVSGQSEDMTAKEKLLLWSQRMVEGYQGLRCDNFTSSWRDGRLFNAIIHRHKPLLIDMNKVYRQ
TNLENLDQAFSVAERDLGVTRLLDPEDVDVPQPDEKSIITYVSSLYDAMPRVPDVQDGVRANELQLRWQEYRELVLLLLQWMRHHTA
AFEERRFPSSFEEIEILWSQFLKFKEMELPAKEADKNRSKGIYQSLEGAVQAGQLKVPPGYHPLDVEKEWGKLHVAILEREKQLRSEF
ERLECLQRIVTKLQMEAGLCEEQLNQADALLQSDVRLLAAGKVPQRAGEVERDLDKADSMIRLLFNDVQTLKDGRHPQGEQMYRRV
YRLHERLVAIRTEYNLRLKAGVAAPATQVAQVTLQSVQRRPELEDSTLRYLQDLLAWVEENQHRVDGAEWGVDLPSVEAQLGSHRG
LHQSIEEFRAKIERARSDEGQLSPATRGAYRDCLGRLDLQYAKLLNSSKARLRSLESLHSFVAAATKELMWLNEKEEEEVGFDWSDR
NTNMTAKKESYSALMRELELKEKKIKELQNAGDRLLREDHPARPTVESFQAALQTQWSWMLQLCCCIEAHLKENAAYFQFFSDVREA
EGQLQKLQEALRRKYSCDRSATVTRLEDLLQDAQDEKEQLNEYKGHLSGLAKRAKAVVQLKPRHPAHPMRGRLPLLAVCDYKQVEV
TVHKGDECQLVGPAQPSHWKVLSSSGSEAAVPSVCFLVPPPNQEAQEAVTRLEAQHQALVTLWHQLHVDMKSLLAWQSLRRDVQL
IRSWSLATFRTLKPEEQRQALHSLELHYQAFLRDSQDAGGFGPEDRLMAEREYGSCSHHYQQLLQSLEQGAQEESRCQRCISELKDI
RLQLEACETRTVHRLRLPLDKEPARECAQRIAEQQKAQAEVEGLGKGVARLSAEAEKVLALPEPSPAAPTLRSELELTLGKLEQVRSL
SAIYLEKLKTISLVIRGTQGAEEVLRAHEEQLKEAQAVPATLPELEATKASLKKLRAQAEAQQPTFDALRDELRGAQEVGERLQQRHG
ERDVEVERWRERVAQLLERWQAVLAQTDVRQRELEQLGRQLRYYRESADPLGAWLQDARRRQEQIQAMPLADSQAVREQLRQEQ
ALLEEIERHGEKVEECQRFAKQYINAIKDYELQLVTYKAQLEPVASPAKKPKVQSGSESVIQEYVDLRTHYSELTTLTSQYIKFISETLRR
MEEEERLAEQQRAEERERLAEVEAALEKQRQLAEAHAQAKAQAEREAKELQQRMQEEVVRREEAAVDAQQQKRSIQEELQQLRQS
SEAEIQAKARQAEAAERSRLRIEEEIRVVRLQLEATERQRGGAEGELQALRARAEEAEAQKRQAQEEAERLRRQVQDESQRKRQAE
VELASRVKAEAEAAREKQRALQALEELRLQAEEAERRLRQAEVERARQVQVALETAQRSAEAELQSKRASFAEKTAQLERSLQEEH
VAVAQLREEAERRAQQQAEAERAREEAERELERWQLKANEALRLRLQAEEVAQQKSLAQAEAEKQKEEAEREARRRGKAEEQAVR
QRELAEQELEKQRQLAEGTAQQRLAAEQELIRLRAETEQGEQQRQLLEEELARLQREAAAATQKRQELEAELAKVRAEMEVLLASKA
RAEEESRSTSEKSKQRLEAEAGRFRELAEEAARLRALAEEAKRQRQLAEEDAARQRAEAERVLAEKLAAIGEATRLKTEAEIALKEKE
AENERLRRLAEDEAFQRRRLEEQAAQHKADIEERLAQLRKASDSELERQKGLVEDTLRQRRQVEEEILALKASFEKAAAGKAELELEL
GRIRSNAEDTLRSKEQAELEAARQRQLAAEEERRRREAEERVQKSLAAEEEAARQRKAALEEVERLKAKVEEARRLRERAEQESAR
QLQLAQEAAQKRLQAEEKAHAFAVQQKEQELQQTLQQEQSVLDQLRGEAEAARRAAEEAEEARVQAEREAAQSRRQVEEAERLKQ
SAEEQAQARAQAQAAAEKLRKEAEQEAARRAQAEQAALRQKQAADAEMEKHKKFAEQTLRQKAQVEQELTTLRLQLEETDHQKNLL
DEELQRLKAEATEAARQRSQVEEELFSVRVQMEELSKLKARIEAENRALILRDKDNTQRFLQEEAEKMKQVAEEAARLSVAAQEAAR
LRQLAEEDLAQQRALAEKMLKEKMQAVQEATRLKAEAELLQQQKELAQEQARRLQEDKEQMAQQLAEETQGFQRTLEAERQRQLE
MSAEAERLKLRVAEMSRAQARAEEDAQRFRKQAEEIGEKLHRTELATQEKVTLVQTLEIQRQQSDHDAERLREAIAELEREKEKLQQ
EAKLLQLKSEEMQTVQQEQLLQETQALQQSFLSEKDSLLQRERFIEQEKAKLEQLFQDEVAKAQQLREEQQRQQQQMEQERQRLVA
SMEEARRRQHEAEEGVRRKQEELQQLEQQRRQQEELLAEENQRLREQLQLLEEQHRAALAHSEEVTASQVAATKTLPNGRDALDG
PAAEAEPEHSFDGLRRKVSAQRLQEAGILSAEELQRLAQGHTTVDELARREDVRHYLQGRSSIAGLLLKATNEKLSVYAALQRQLLSP
GTALILLEAQAASGFLLDPVRNRRLTVNEAVKEGVVGPELHHKLLSAERAVTGYKDPYTGQQISLFQAMQKGLIVREHGIRLLEAQIAT
GGVIDPVHSHRVPVDVAYRRGYFDEEMNRVLADPSDDTKGFFDPNTHENLTYLQLLERCVEDPETGLCLLPLTDKAAKGGELVYTDS
EARDVFEKATVSAPFGKFQGKTVTIWEIINSEYFTAEQRRDLLRQFRTGRITVEKIIKIIITVVEEQEQKGRLCFEGLRSLVPAAELLESRV
IDRELYQQLQRGERSVRDVAEVDTVRRALRGANVIAGVWLEEAGQKLSIYNALKKDLLPSDMAVALLEAQAGTGHIIDPATSARLTVD
EAVRAGLVGPEFHEKLLSAEKAVTGYRDPYTGQSVSLFQALKKGLIPREQGLRLLDAQLSTGGIVDPSKSHRVPLDVACARGCLDEET
SRALSAPRADAKAYSDPSTGEPATYGELQQRCRPDQLTGLSLLPLSEKAARARQEELYSELQARETFEKTPVEVPVGGFKGRTVTV
WELISSEYFTAEQRQELLRQFRTGKVTVEKVIKILITIVEEVETLRQERLSFSGLRAPVPASELLASGVLSRAQFEQLKDGKTTVKDLSEL
GSVRTLLQGSGCLAGIYLEDTKEKVSIYEAMRRGLLRATTAALLLEAQAATGFLVDPVRNQRLYVHEAVKAGVVGPELHEQLLSAEKA
VTGYRDPYSGSTISLFQAMQKGLVLRQHGIRLLEAQIATGGIIDPVHSHRVPVDVAYQRGYFSEEMNRVLADPSDDTKGFFDPNTHEN
LTYRQLLERCVEDPETGLRLLPLKGAEKAEVVETTQVYTEEETRRAFEETQIDIPGGGSHGGSTMSLWEVMQSDLIPEEQRAQLMAD
FQAGRVTKERMIIIIIEIIEKTEIIRQQGLASYDYVRRRLTAEDLFEARIISLETYNLLREGTRSLREALEAESAWCYLYGTGSVAGVYLPGS
RQTLSIYQALKKGLLSAEVARLLLEAQAATGFLLDPVKGERLTVDEAVRKGLVGPELHDRLLSAERAVTGYRDPYTEQTISLFQAMKKE
LIPTEEALRLLDAQLATGGIVDPRLGFHLPLEVAYQRGYLNKDTHDQLSEPSEVRSYVDPSTDERLSYTQLLRRCRRDDGTGQLLLPLS
DARKLTFRGLRKQITMEELVRSQVMDEATALQLREGLTSIEEVTKNLQKFLEGTSCIAGVFVDATKERLSVYQAMKKGIIRPGTAFELLE
AQAATGYVIDPIKGLKLTVEEAVRMGIVGPEFKDKLLSAERAVTGYKDPYSGKLISLFQAMKKGLILKDHGIRLLEAQIATGGIIDPEESH
RLPVEVAYKRGLFDEEMNEILTDPSDDTKGFFDPNTEENLTYLQLMERCITDPQTGLCLLPLKEKKRERKTSSKSSVRKRRVVIVDPET
GKEMSVYEAYRKGLIDHQTYLELSEQECEWEEITISSSDGVVKSMIIDRRSGRQYDIDDAIAKNLIDRSALDQYRAGTLSITEFADMLSG
NAGGFRSRSSSVGSSSSYPISPAVSRTQLASWSDPTEETGPVAGILDTETLEKVSITEAMHRNLVDNITGQRLLEAQACTGGIIDPSTG
ERFPVTDAVNKGLVDKIMVDRINLAQKAFCGFEDPRTKTKMSAAQALKKGWLYYEAGQRFLEVQYLTGGLIEPDTPGRVPLDEALQR
GTVDARTAQKLRDVGAYSKYLTCPKTKLKISYKDALDRSMVEEGTGLRLLEAAAQSTKGYYSPYSVSGSGSTAGSRTGSRTGSRAG
SRRGSFDATGSGFSMTFSSSSYSSSGYGRRYASGSSASLGGPESAVA

mMass – the power of high resolution

Analytical challenge

trypsin digestion (500-3000, Met-ox, Cys-CAM, 1 missed cleavage)
yields 1171 theoretical peptides, 102 are isobaric

significant number of repetitive sequences

[1745-1749]	0	633.28385	EEAER
[1762-1766]	0	633.28385	EEAER
[1804-1808]	0	633.28385	EEAER
[2122-2126]	0	633.28385	EAEER

[1493-1498]	1	789.38496	AEERER
[1745-1750]	1	789.38496	EEAERR
[2121-2126]	1	789.38496	REAEER

PAAEAEPEHSFDGLRRKVSAQRLQEAGILSAEELQRLAQGHTTVDELARREDVRHYLQGRSSIAGLLLKATNEKLSV
YAALQRQLLSPGTALILLEAQAASGFLLDPVRNRRLTVNEAVKEGVVGPELHHKLLSAERAVTGYKDPYTGQQISLF
QAMQKGLIVREHGIRLLEAQIATGGVIDPVHSHRVPVDVAYRRGYFDEEMNRVLADPSDDTKGFFDPNTHENLTYLQ
LLERCVEDPETGLCLLPLTDKAAKGGELVYTDSEARDVFEKATVSAPFGKFQGKTVTIWEIINSEYFTAEQRRDLLR
QFRTGRITVEKIIKIIITVVEEQEQKGRLCFEGLRSLVPAARLLESRVIDRELYQQLQRGERSVRDVAEVDTVRRAL
RGANVTAGVWLEEAGQKLSTYNALKKDLLPSDMAVALLEAQAGTGHIIDPATSARLTVDEAVRAGLVGPEFHRKLLS
AEKAVTGYRDPYTGQSVSLFQALKKGLIPREQGLRLLDAQLSTGGIVDPSKSHRVPLDVACARGCLDEETSRALSAP
RADAKAYSDPSTGEPATYGELQQRCRPDQLTGLSLLPLSEKAARARQEELYSELQARETFEKTFVEVPVGGFKGRTV
TVWELISSEYFTAEQRQELLRQFRTGKVTVEKVIKILITIVEEVETLRQERLSFSGLRAPVPASELLASGVLSRAQF
RQLKDGKTTVKDLSELGSVRTILQGSGCLAGIYLEDTKEKVSIYEAMRRGLIRATTAALLLEAQAATGFLVDPVRNQ
RLYVHEAVKAGVVGPELHEQLLSAEKAVTCYRDPYSGSTISLFQAMQKGLVLRQHGIRLLEAQIATGGIIDPVHSHR
VPVDVAYQRGYFSEEMNRVLADPSDDTKGFFDPNTHENLTYRQLLERCVEDPETGLRLLPLKGAEKAEVVETTQVYT
EEETRRAFEETQIDIPGGGSHGGSTMSLWEVMQSDLIPEEQRAQLMADFQAGRVTKERMIIIIIEIIEKTEIIRQQG
LASYDYVRRRLTAEDLFEARIISLETYNLLREGTRSLREALEAESAWCYLYGTGSVAGVYLPGSRQTLSIYQALKKG
LLSAEVARLLLEAQAATGFLLDPVKGERLTVDEAVRKGLVGPELHDRLLSAERAVTGYRDPYTEQTISLFQAMKKEL
IPTEEALRLLDAQLATGGIVDPRLGFHLPLEVAYQRGYLNKDTHDQLSEPSEVRSYVDPSTDERLSYTQLLRRCRRD
DGTGQLLLPLSDARKLTFRGLRKQITMEELVRSQVMDEATALQLREGLTSIEEVTKNLQKFLEGTSCIAGVFVDATK
ERLSVYQAMKKGIIRPGTAFELLEAQAATGYVIDPIKGLKLTVEEAVRMGIVGPEFKDKLLSAERAVTGYKDPYSGK
LISLFQAMKKGLILKDHGIRLLEAQIATGGIIDPEESHRLPVEVAYKRGLFDEEMNEILTDPSDDTKGFFDPNTEEN
LTYLQLMERCITDPQTGLCLLPLKEKKRERKTSSKSSVRKRRVVIVDPETGKEMSVYEAYRKGLIDHQTYLELSEQE

mMass – the power of high resolution

MALDI-TOF vs MALDI-FT-ICR

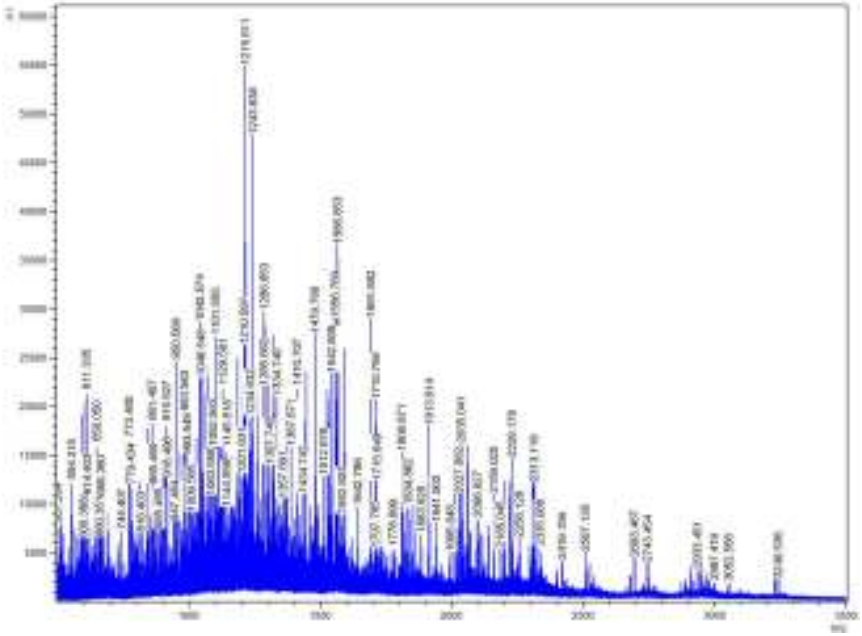

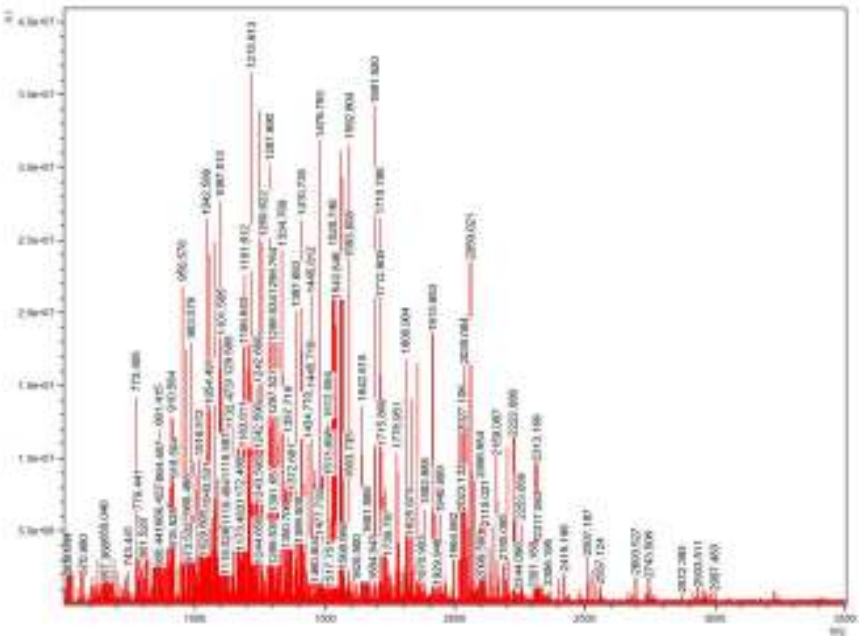

mMass – the power of high resolution

Only FT-ICR data are reliable

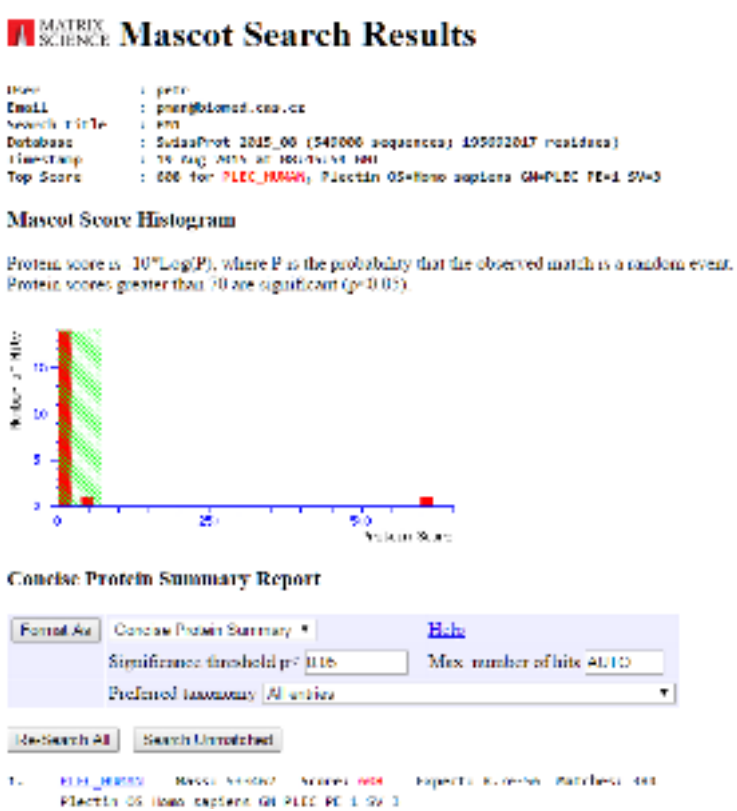

nearly 400 peptides assigned and seq. cov ~70%

TOF **ICR**

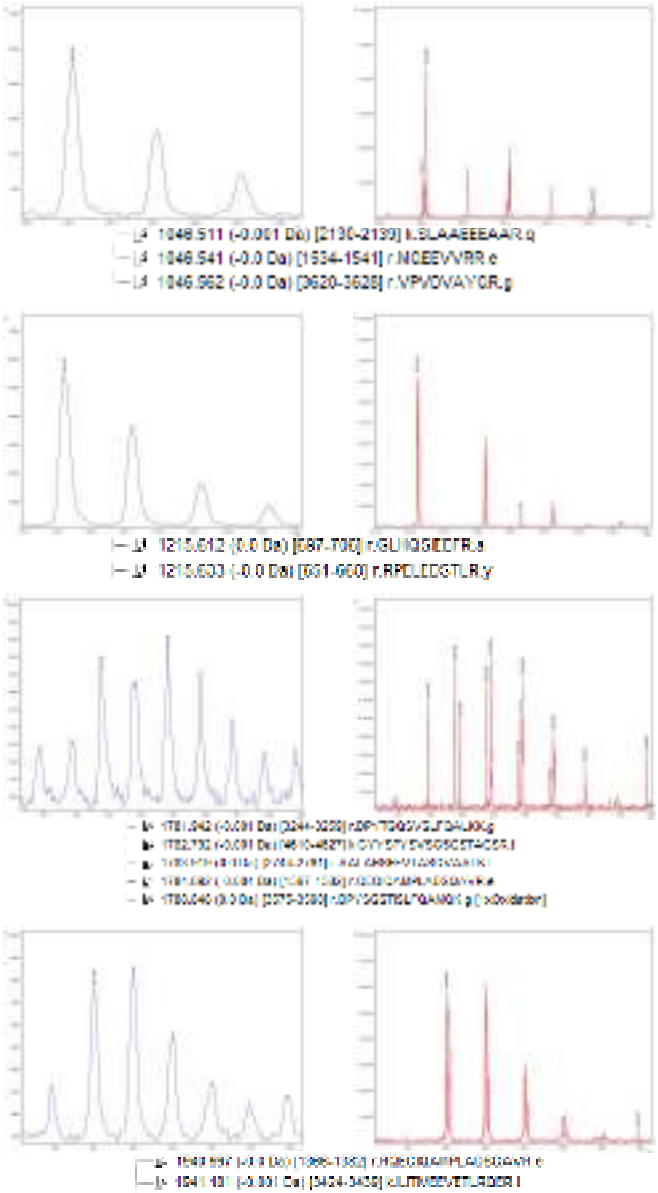

mMass – the power of high resolution

Only FT-ICR data are reliable

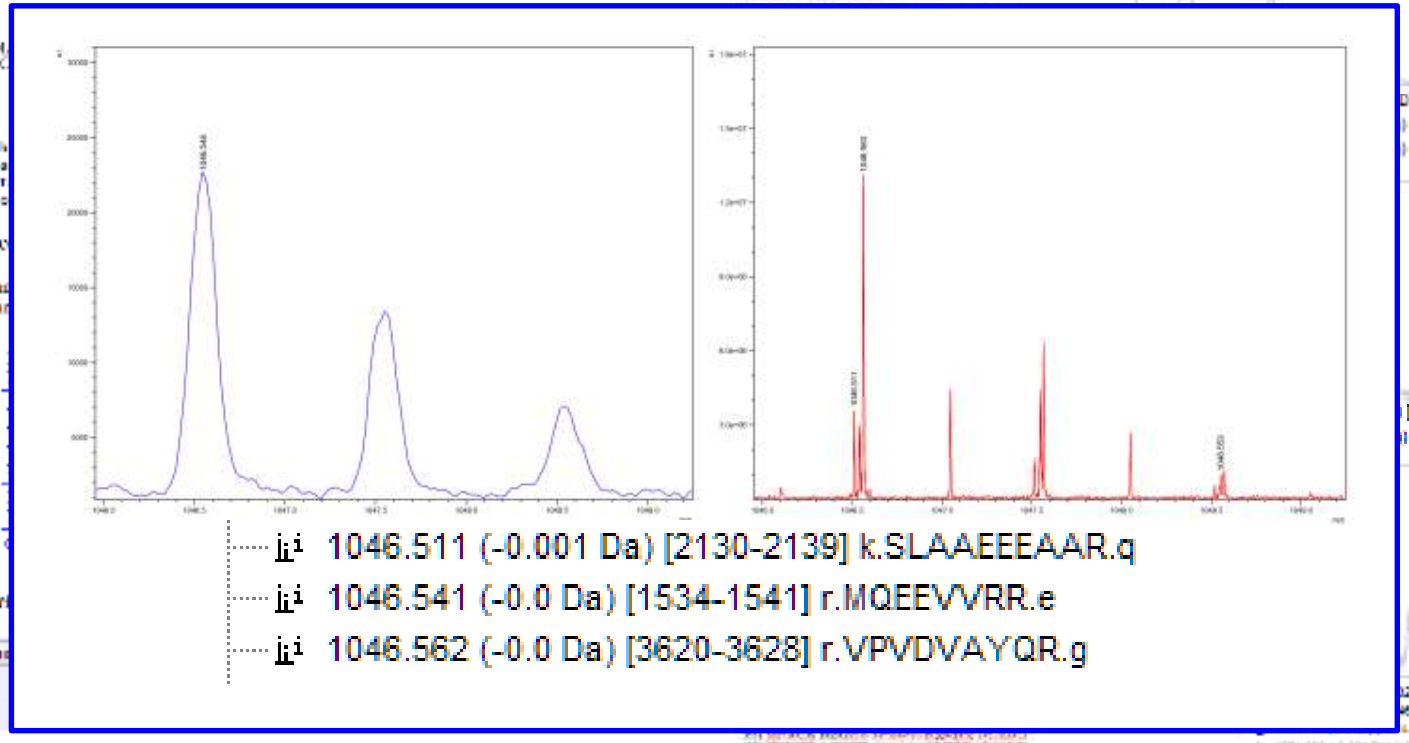

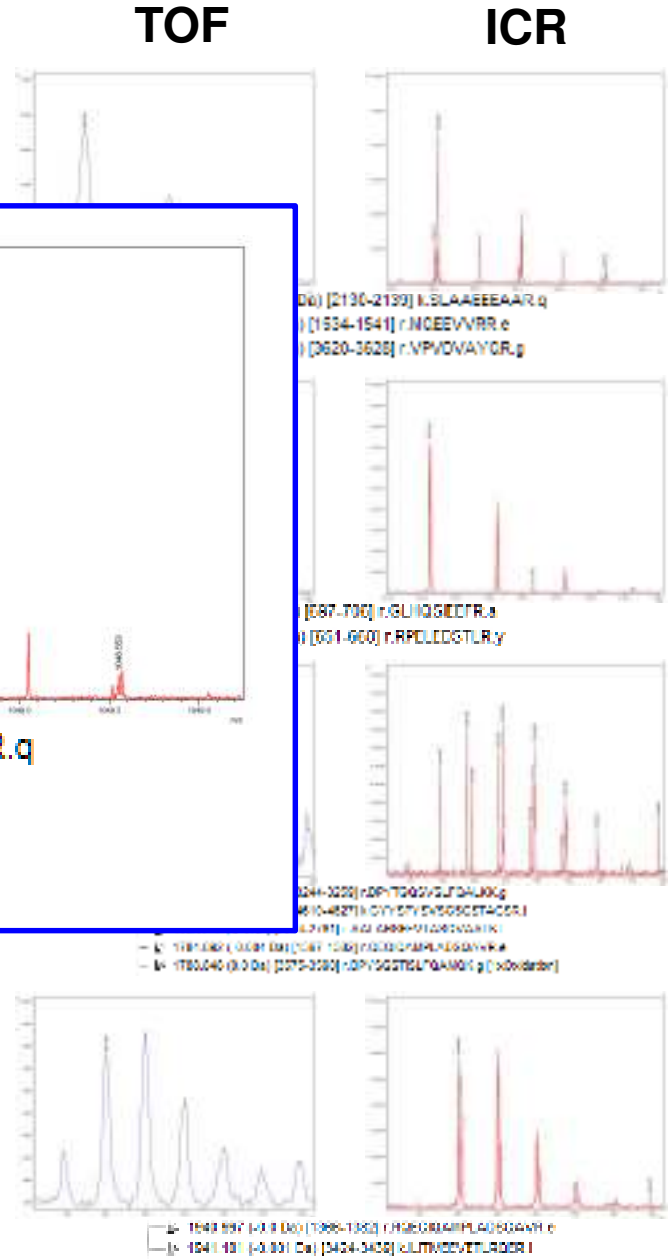

nearly 400 peptides assigned and seq. cov ~70%

mMass – the power of high resolution

Only FT-ICR data are reliable

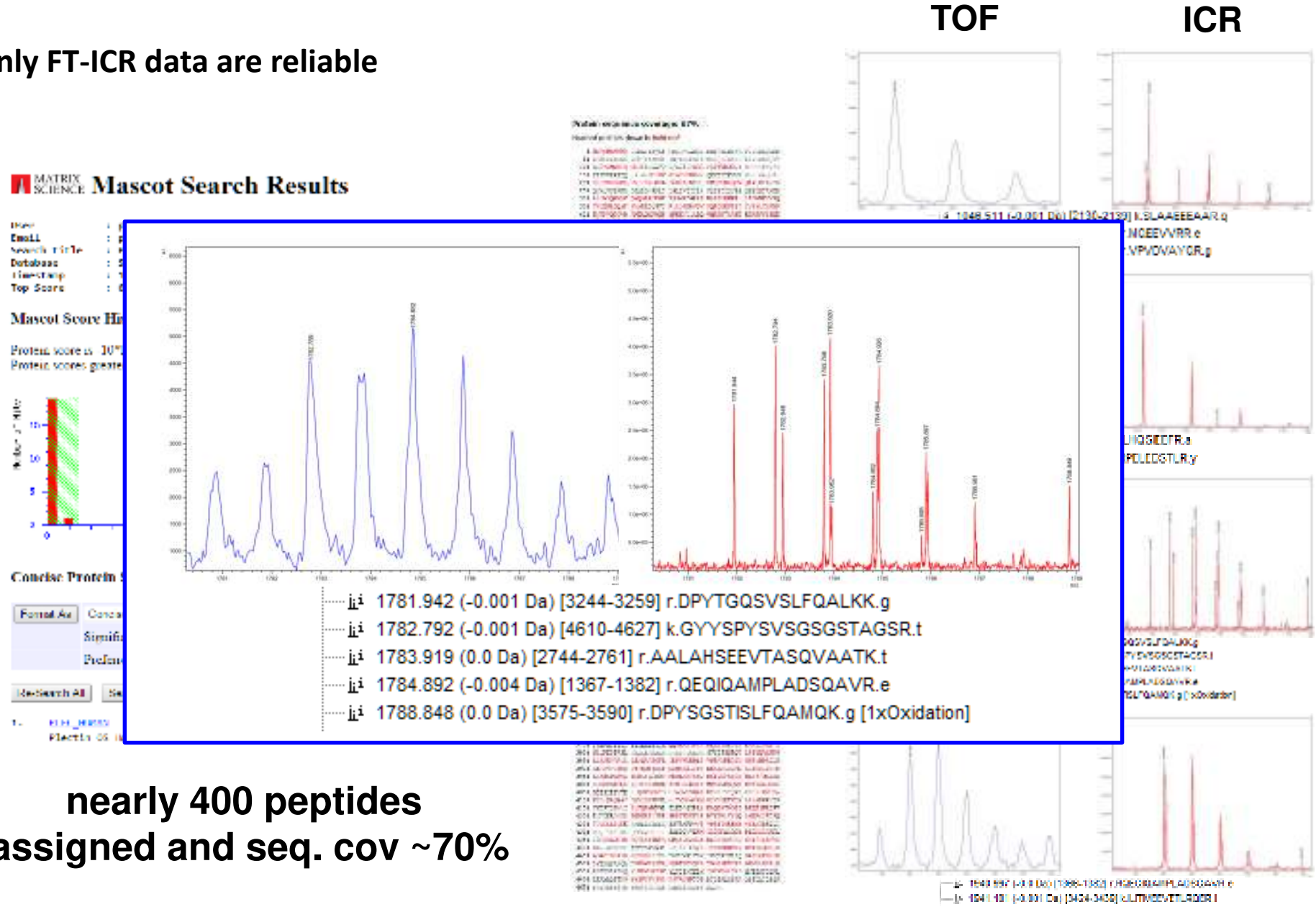

nearly 400 peptides assigned and seq. cov ~70%

mMass – the power of high resolution

using envelope fit to validate the assignments

C81H128N20O25
1781.942, 3244-3259

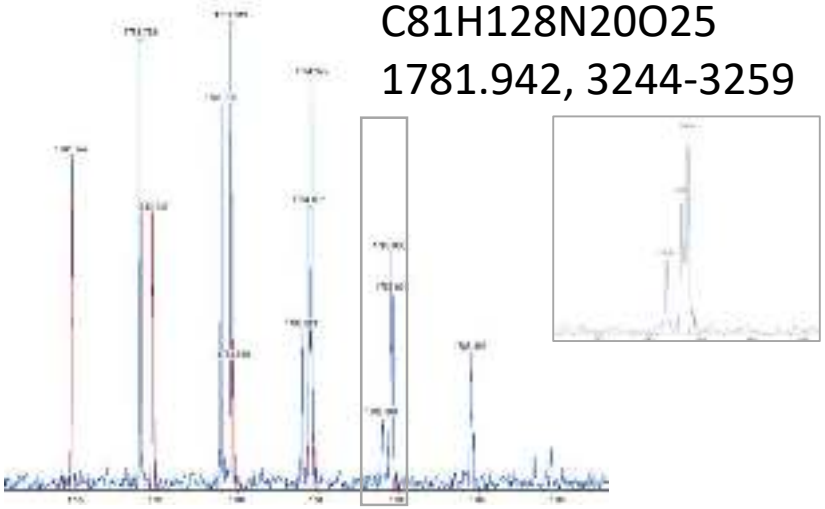

C75H126N22O28
1783.919, 2744-2761

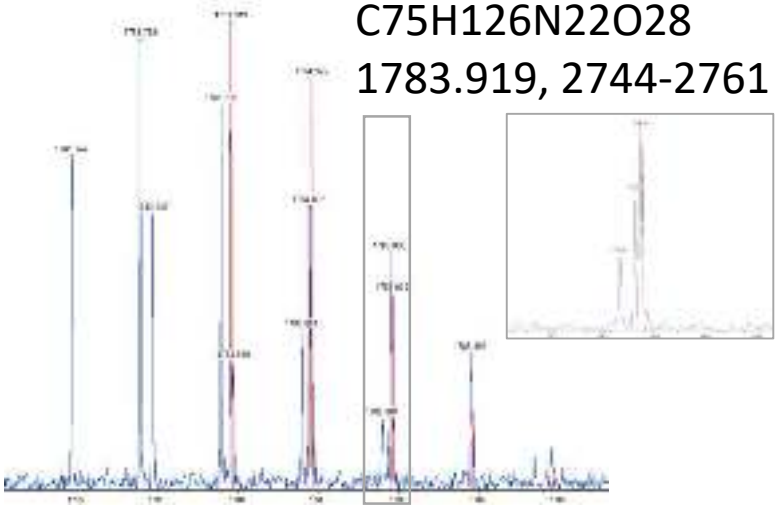

C76H111N21O29
1782.792, 4610-4627

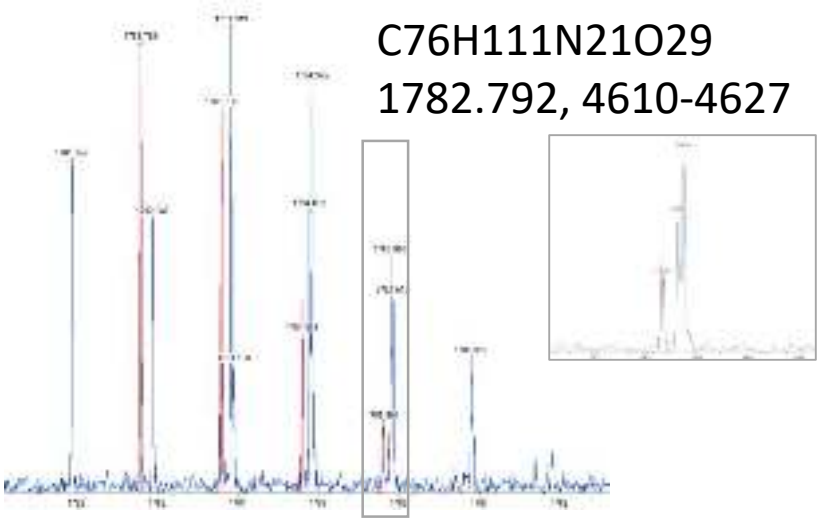

C74H125N23O26S
1784.892, 1367-1382

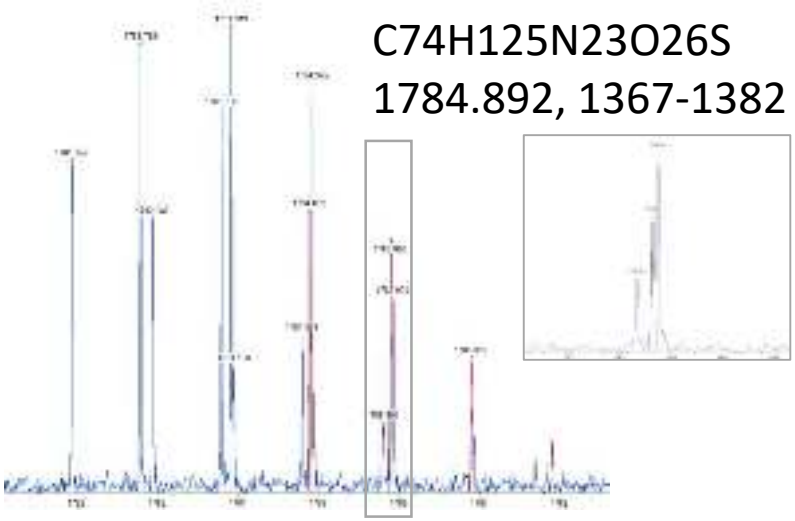

EU FT-ICR MS

H2020

EUROPEAN NETWORK OF FOURIER-TRANSFORM ION-CYCLOTRON-RESONANCE MASS SPECTROMETRY CENTERS

PROJECT AGREEMENT NO.731077

IMIC

Wednesday

Current capabilities in 2DMS on FTICR mass spectrometers

Pui Yiu (Yuko) Lam, Chris Wootton, Johanna Paris, Tomos Morgan, Bryan Marzullo, Maria van Agthoven, Alina Theissen,

Peter B. O'Connor

University of Warwick, Coventry, United Kingdom

EU_FT-ICR_MS 2nd Advanced Users School
Prague, 26 - 30 September 2021

This project has received funding from the European Union's Horizon 2020 research and innovation programme under grant agreement No 731077.

Current capabilities in 2DMS on FTICR mass spectrometers

Pui Yiu (Yuko) Lam, Chris Wootton, Johanna Paris, Tomos Morgan, Bryan Marzullo, Maria van Agthoven, Alina Theissen,

Peter B. O'Connor

EU_FT-ICR_MS 2nd Advanced Users School
Prague, 26 - 30 September 2021

THE UNIVERSITY OF WARWICK

Fourier Transform Ion Cyclotron Resonance Mass Spectrometry

- Extremely high resolving power
- Many (new) types of MS^n
- New instrumentation

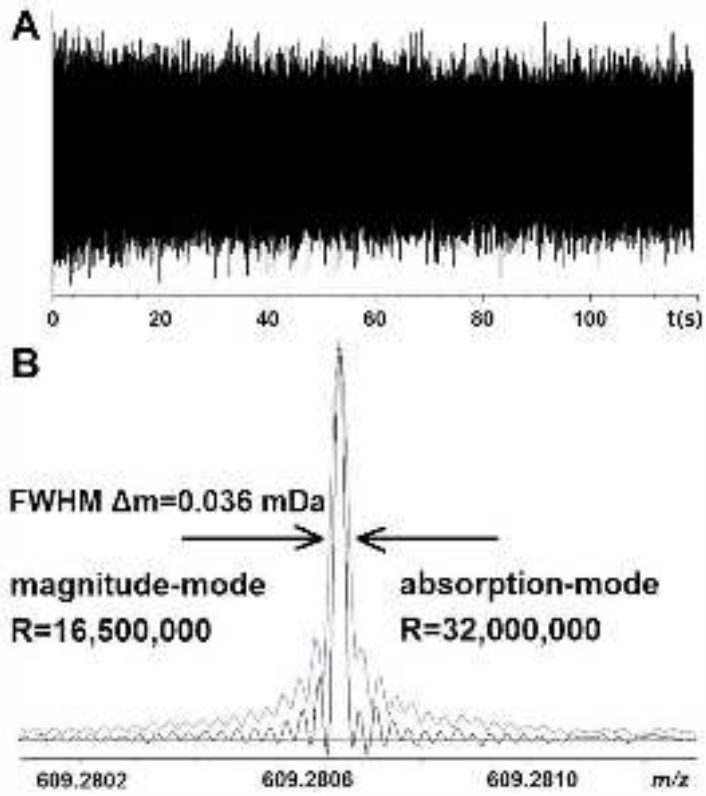

Figure 1. (A) Time-domain transient of the resperine $[M+H]^+$ ion in heterodyne mode, acquired for 2 min. (B) Spectrum in both magnitude- (grey) and absorption-mode (black), the peak width of the magnitude-mode is labelled.

THE UNIVERSITY OF WARWICK

Qi, Y.; Witt, M.; Jertz, R.; Baykut, G.; Barrow, M. P.; Nikolaev, E. N.; O'Connor, P. B., Absorption-mode spectra on the dynamically harmonized Fourier transform ion cyclotron resonance cell. *Rapid Commun. Mass Spectrom. 26 (17),(**2012**) 2021-2026.*

Tandem Mass Spectrometry or MS/MS

CID/CAD, IRMPD
ECD, ETC, EID, EDD, EIEIO
UVPD (193 nm, 213 nm, 266 nm)

Isolation
Fragmentation
Isolation
Fragmentation

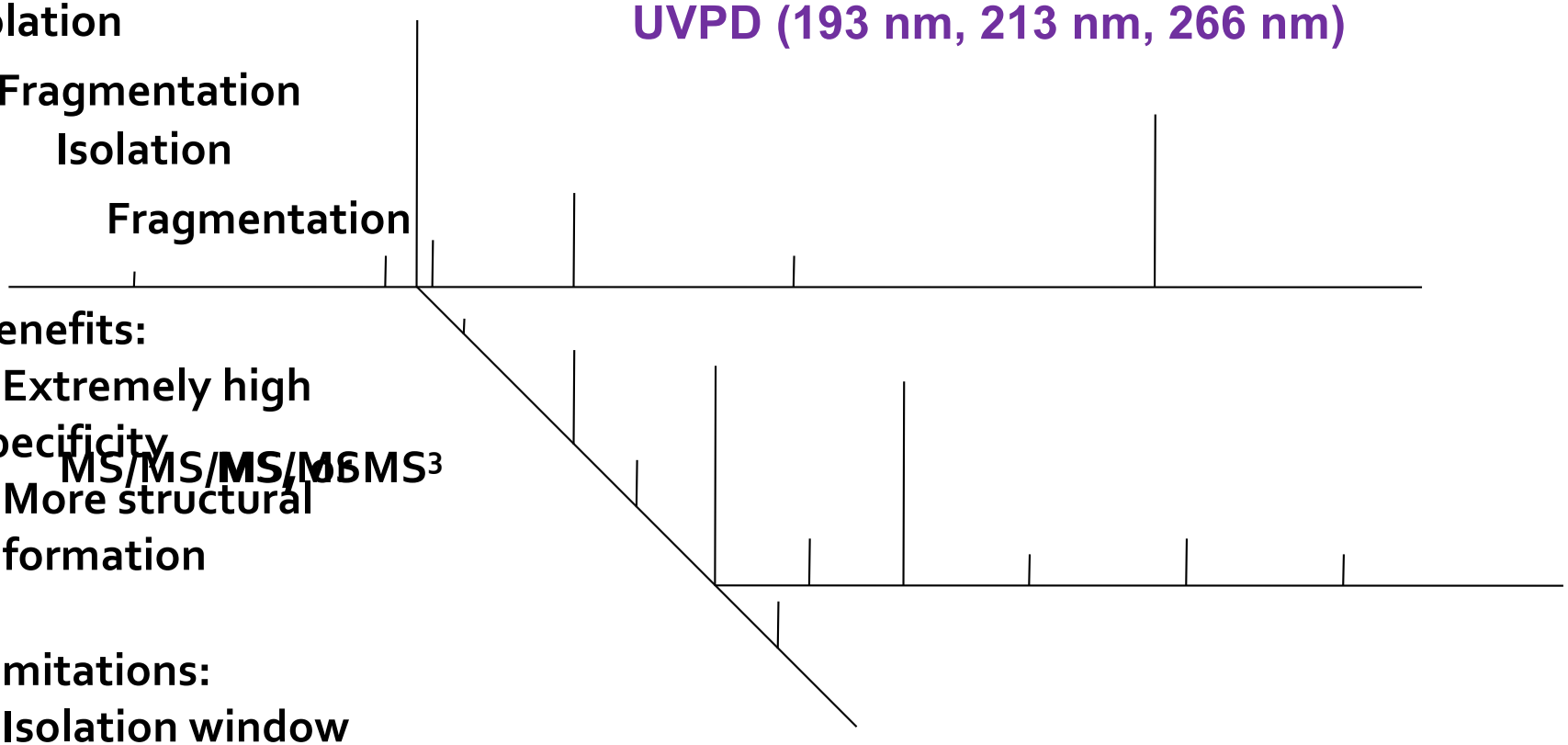

MS/MS/MS/MS^3

Benefits:
1. Extremely high specificity
2. More structural information

Limitations:
1. Isolation window
2. Fragmentation efficiency
3. Ion Losses

UVPD spectrum of carbonic anhydrase (34+) and its sequence map

259 residues (29 kDa)

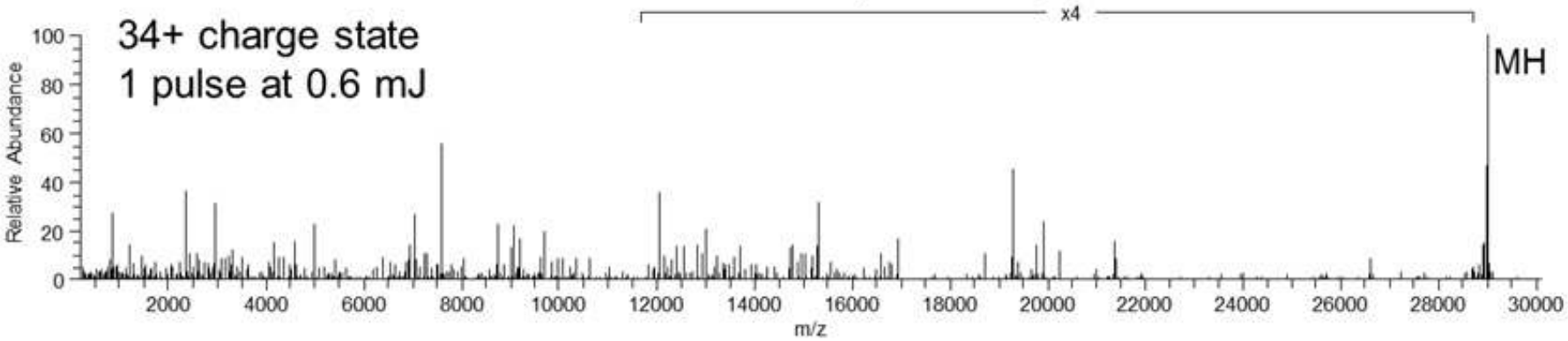

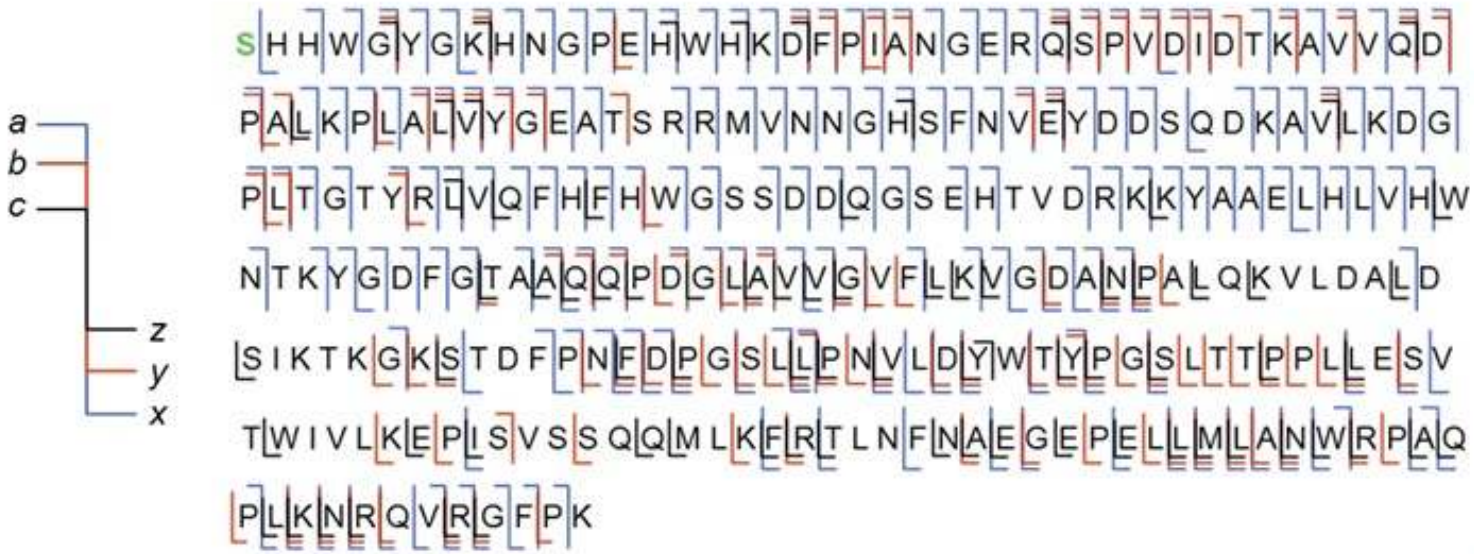

Ions Series	Number Observed
a	150
b	38
c	14
x	54
y	71
z	64

Shaw, J. B.; ….; Brodbelt, J. S., Complete Protein Characterization Using Top-Down Mass Spectrometry and Ultraviolet Photodissociation. *J Am Chem Soc 2013, 135 (34), 12646-12651.*

But, what if we don't need to isolate prior to fragmentation?

J. Am. Chem. Soc. **1988**, *110*, 5625–5628 5625

Broad-Band Two-Dimensional Fourier Transform Ion Cyclotron Resonance

Peter Pfändler,[†] Geoffrey Bodenhausen,*[†] Jacques Rapin,[‡] Marc-Etienne Walser,[‡] and Tino Gäumann*[‡]

Contribution from the Institut de Chimie Organique, Université de Lausanne, Rue de la Barre 2, CH-1005 Lausanne, Switzerland, and Institut de Chimie Physique, Ecole Polytechnique Fédérale, CH-1015 Lausanne, Switzerland. *Received December 17, 1987*

Abstract: Two-dimensional Fourier transform ion cyclotron resonance (2D FT-ICR) allows one to obtain direct evidence for the occurrence of ion–molecule reactions. In 2D FT-ICR spectra, one observes resonances with two distinct frequency coordinates ω_1 and ω_2 that correspond to the mass-to-charge ratios of the ions that participate as reactants and products, respectively. It is possible to monitor a manifold of distinct reactions in one single 2D spectrum. Spectral ranges of the order of several MHz can be covered by using frequency-swept ("chirped") radio-frequency pulses.

Two-dimensional Mass Spectrometry

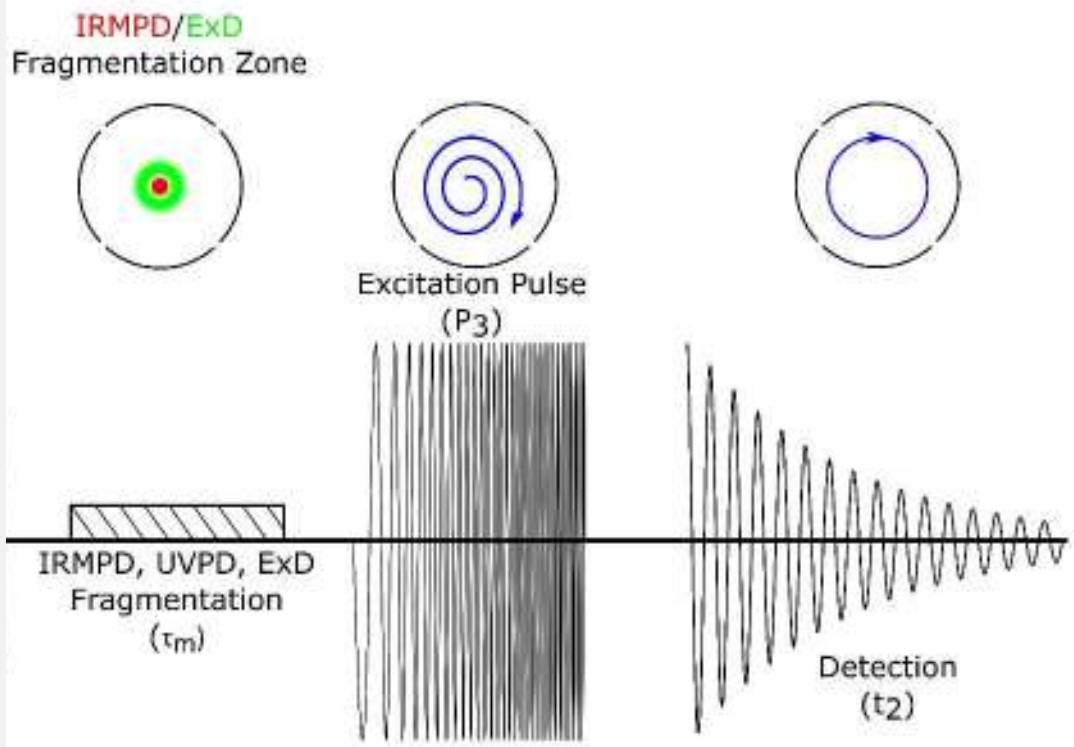

Principle of 2D FT-ICR MS: Modulation

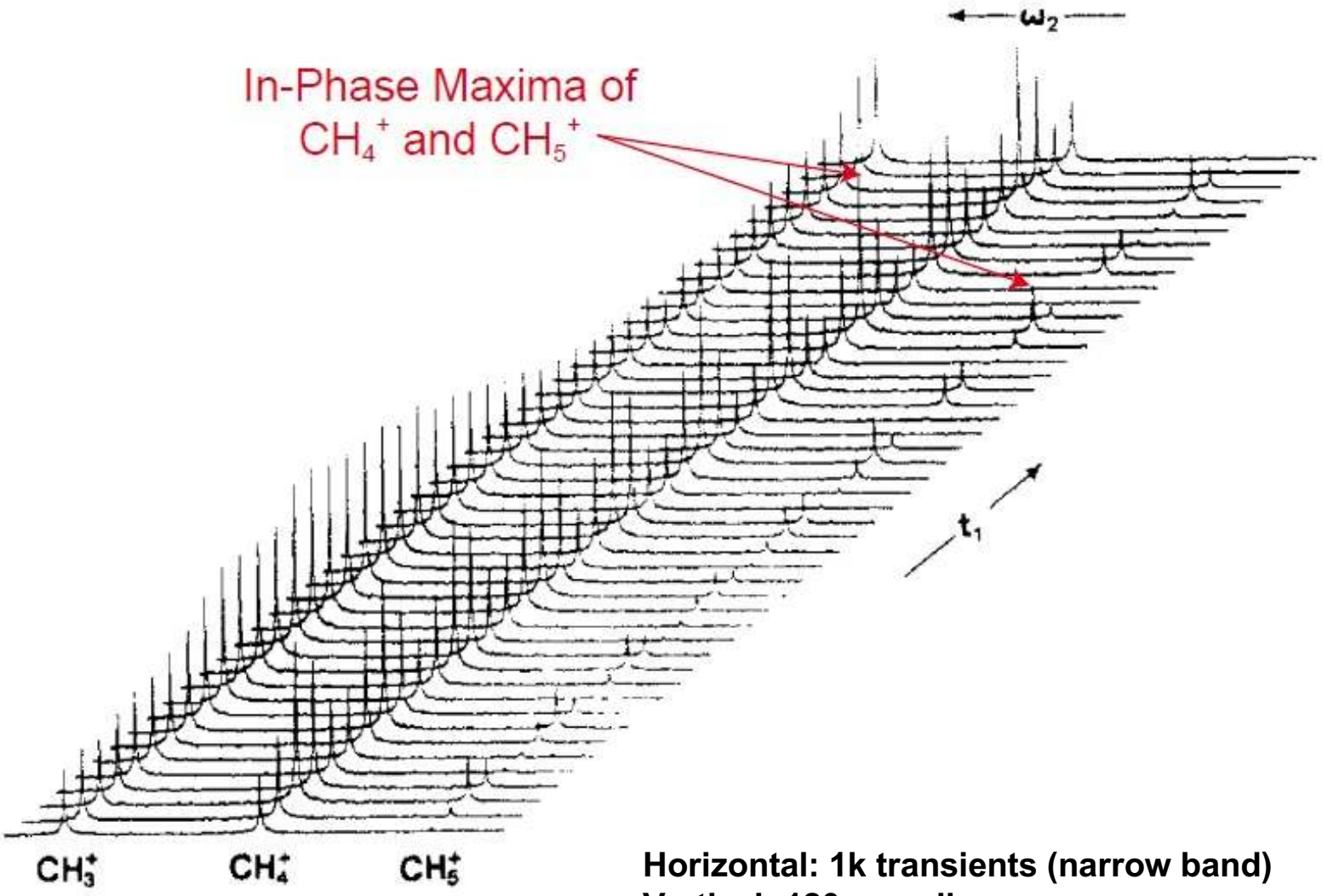

Horizontal: 1k transients (narrow band)
Vertical: 120 scan lines.
Total: 120,000 data points

P. Pfändler, G. Bodenhausen, J. Rapin, M.-E. Walser, T. Gäumann, *J. Am. Chem. Soc.* 110 (1988) 5625-5628.

Lecture overview

- 2DMS for agrichemical analysis.
- 2DMS for polymer analysis.
- 2DMS for monoclonal antibodies.
- Distinguishing phosphopeptides using 2DMS
- 2DMS – UVPD
- 2DMS on a linear ion trap

Case study of 2DMS with Syngenta UK

syngenta

Agrochemical and pesticide analysis

Pesticides degrade and react with their local environment to produce many potentially dangerous compounds:

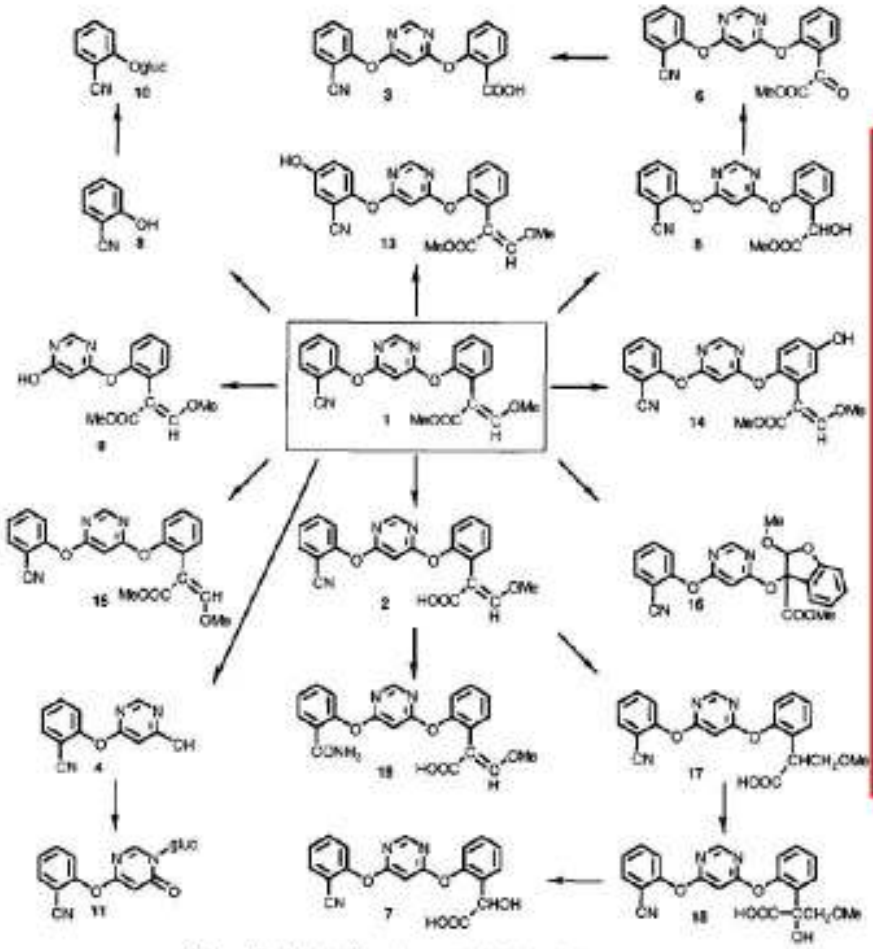

Scheme 2 Metabolism of azoxystrobin in plants.

We need methods to detect all of these species in real, complex samples to identify toxic compounds. Like 2DMS

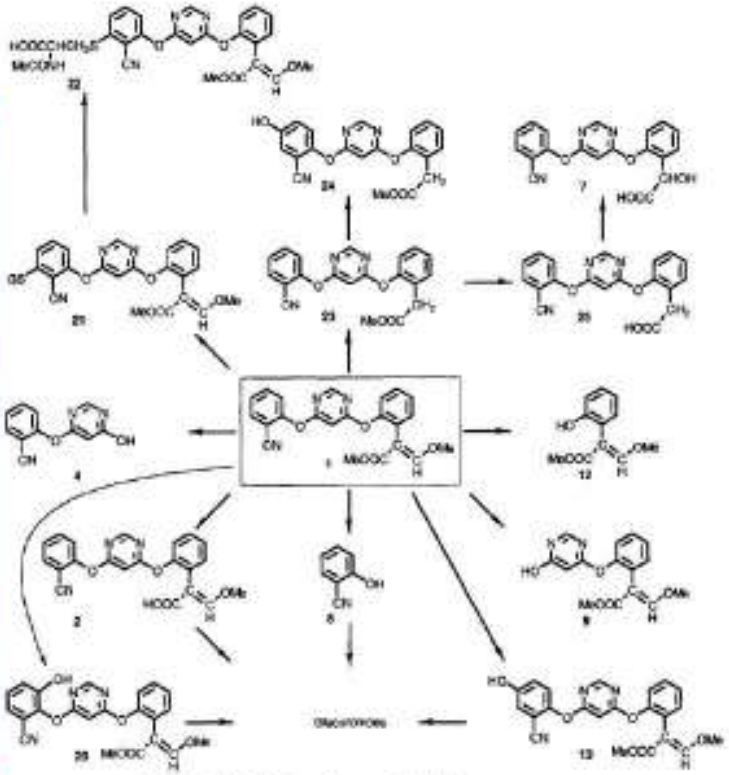

Scheme 3 Metabolism of azoxystrobin in the rat.

Copping, Leonard G. "Metabolic pathways of agrochemicals: part two–insecticides and fungicides, eds-in-chief T Roberts and D Hutson, Royal Society of Chemistry, Cambridge, 1999, 1475 pp, ISBN 085404 499 X." *Pest Management Science: formerly Pesticide Science* 56.1 (2000): 103-104.

2D IRMPD MS

2DMS provides a wealth of information in a single plot:

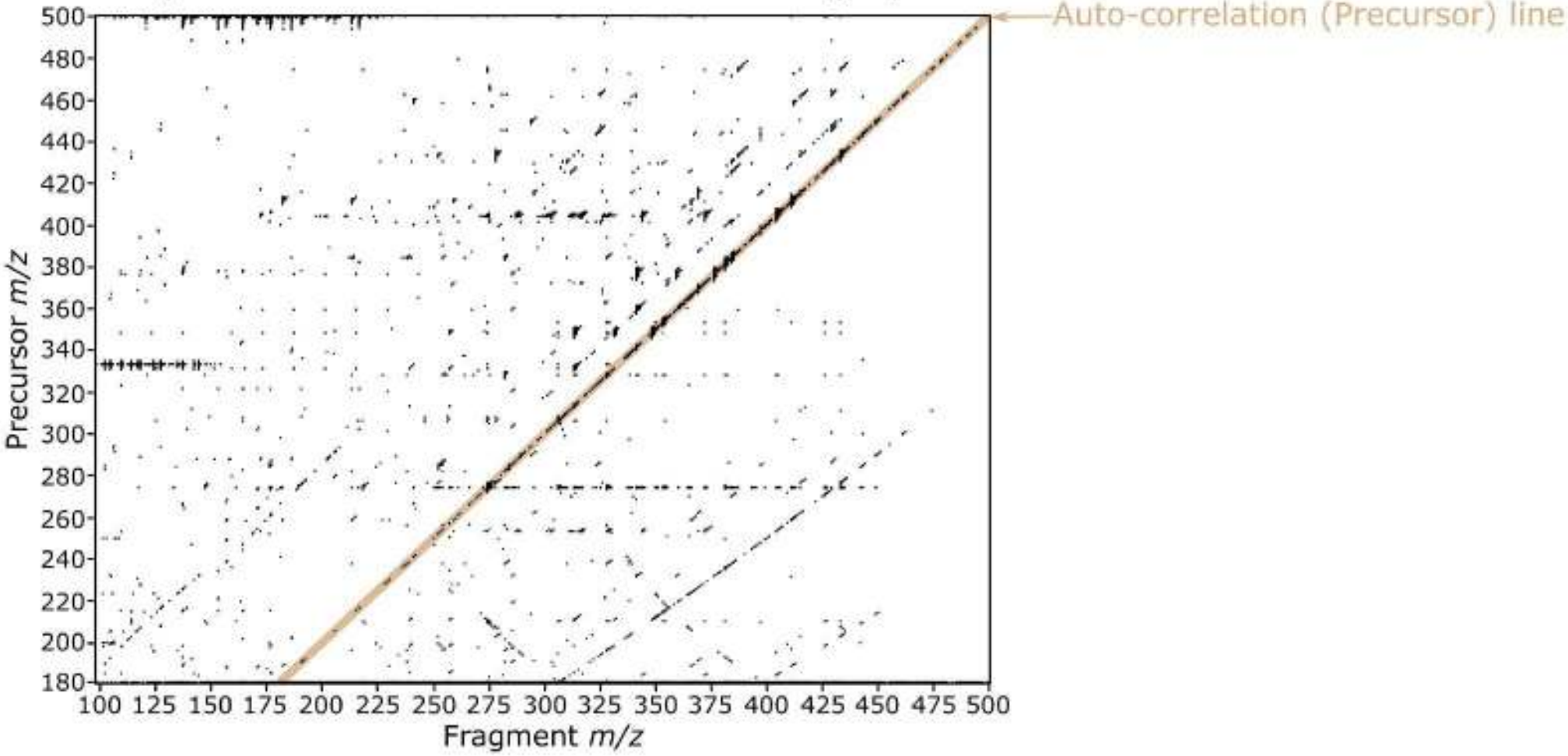

2D IRMPD MS – autocorrelation (precursor) line

Pesticides are often used in mixtures of active components

Creating complex samples for analysis:

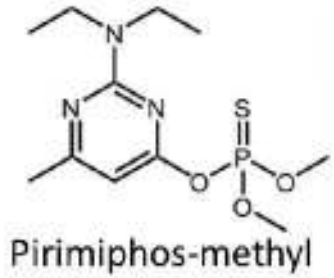

Pirimiphos-methyl

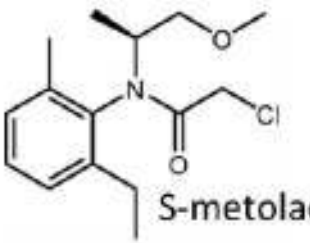

S-metolachlor

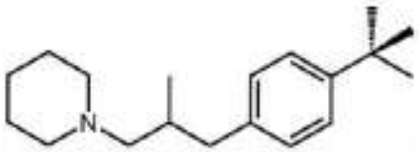

Fenpropridin

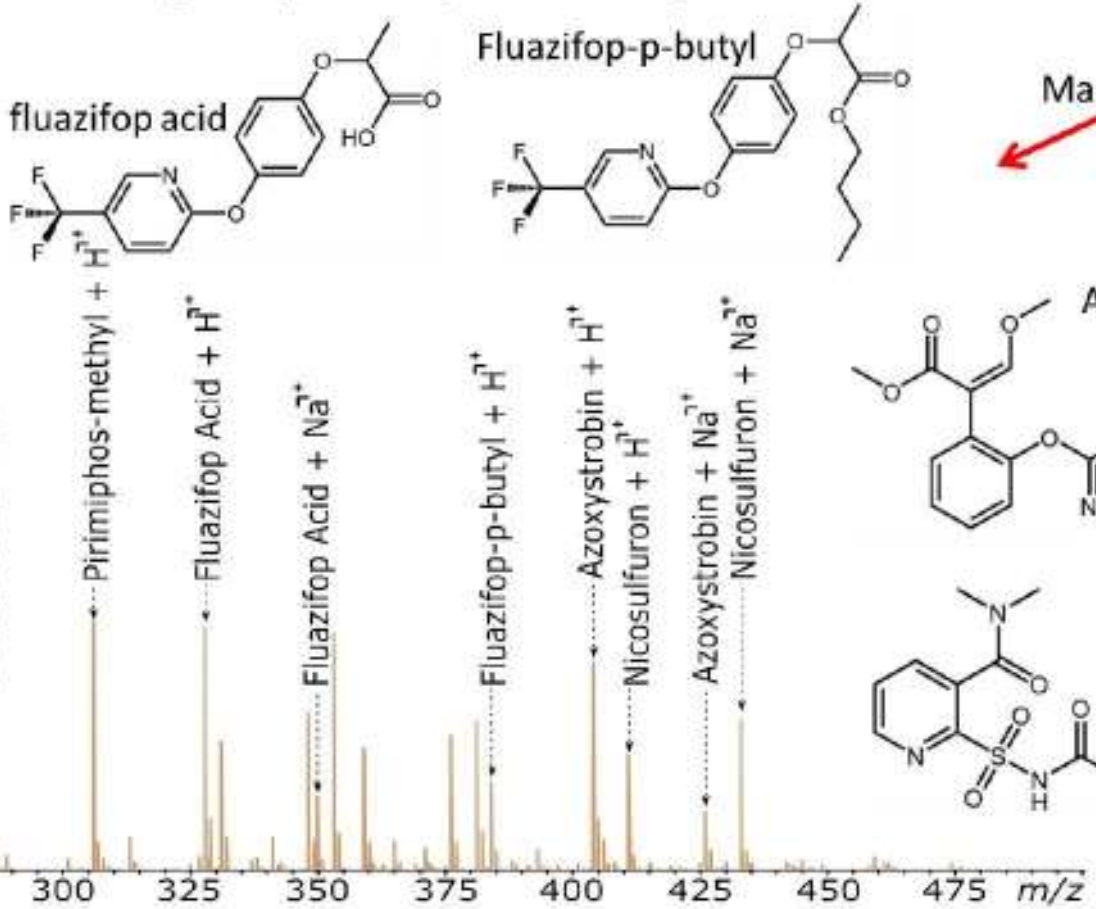

fluazifop acid

Fluazifop-p-butyl

Many pesticides detected

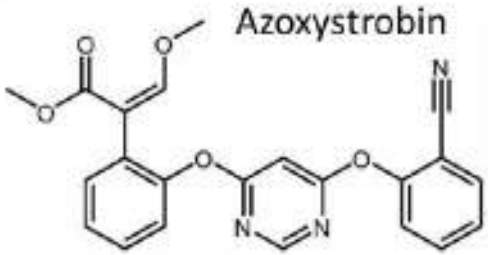

Azoxystrobin

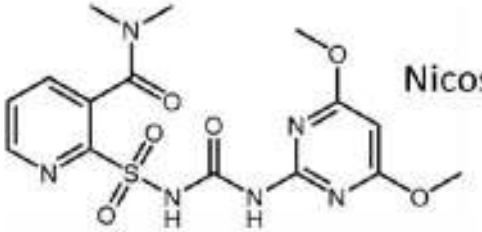

Nicosulfuron

2D IRMPD MS

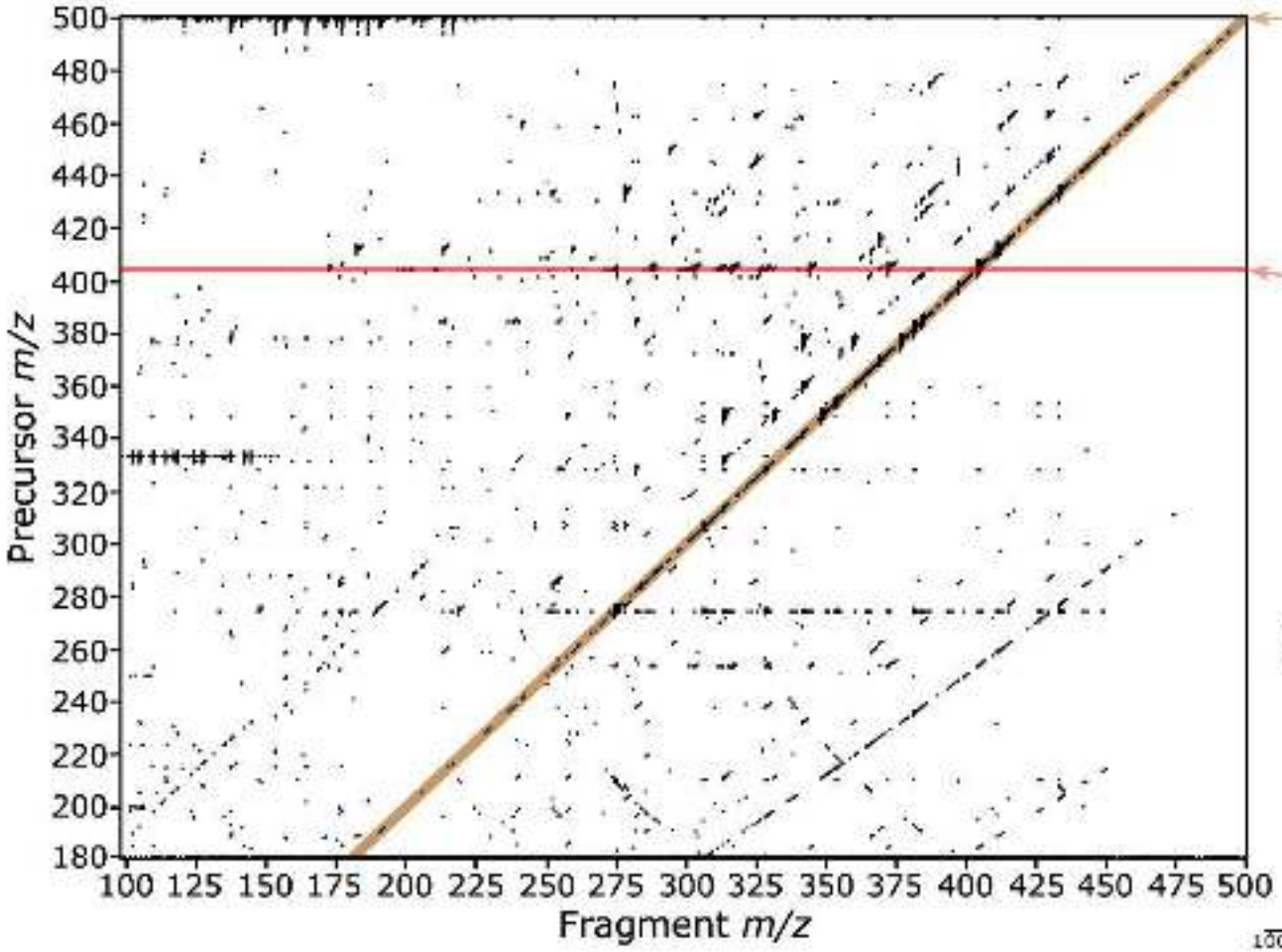

Auto-correlation (Precursor) line

Each chemical presents as a line in the spectrum
Each line provide unique information about the chemical species:

Azoxystrobin (404.124 *m/z*)

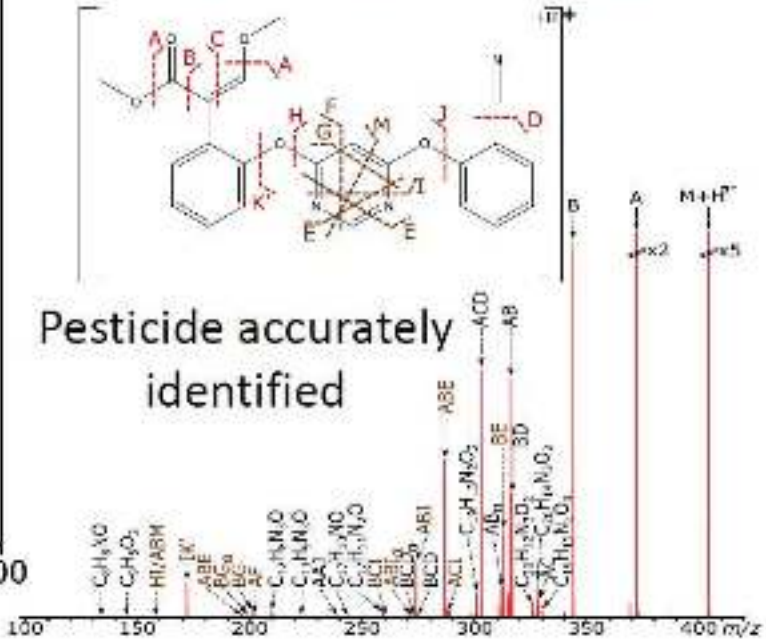

Pesticide accurately identified

2D EID MS

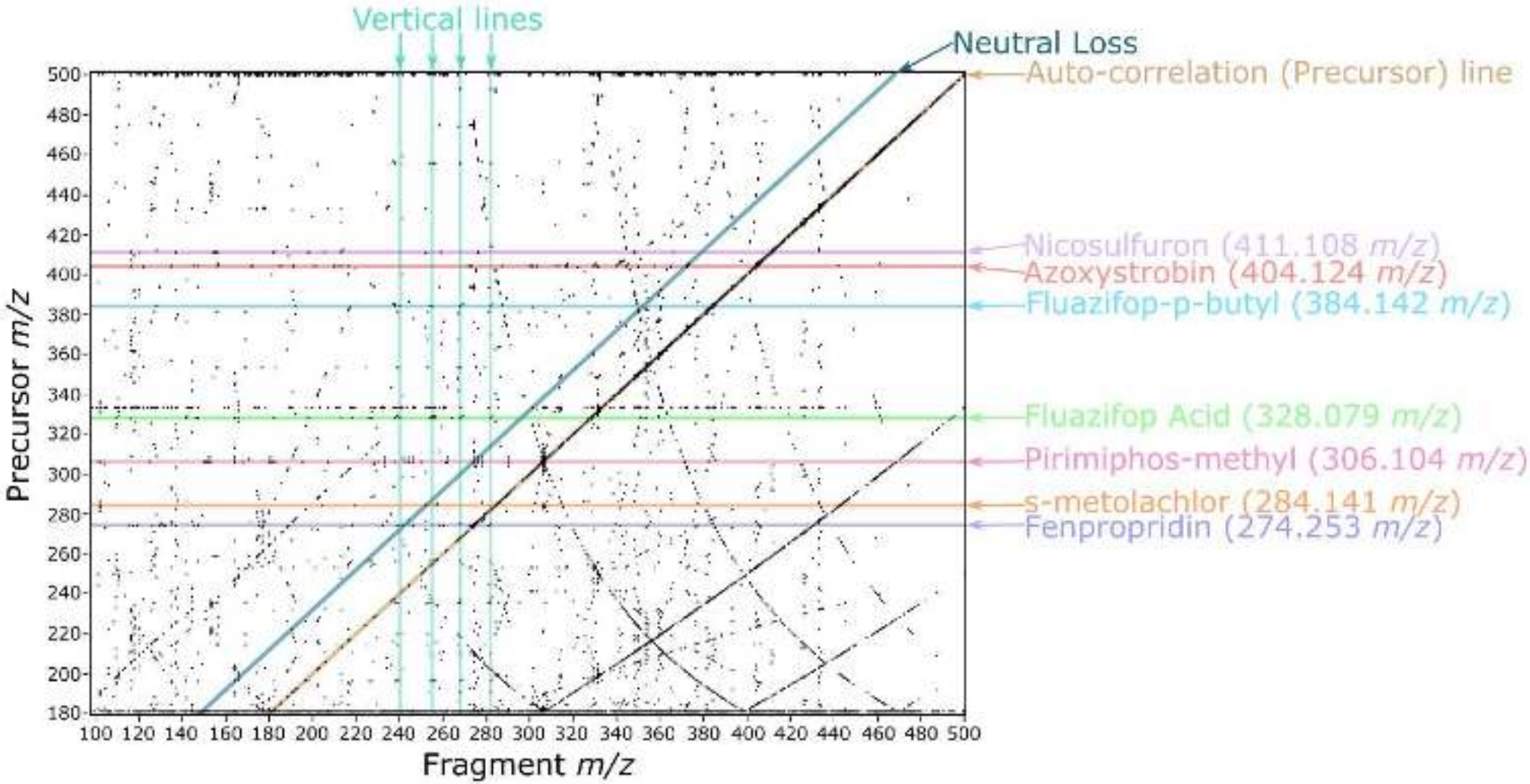
Vertical lines
Neutral Loss
Auto-correlation (Precursor) line
Nicosulfuron (411.108 m/z)
Azoxystrobin (404.124 m/z)
Fluazifop-p-butyl (384.142 m/z)
Fluazifop Acid (328.079 m/z)
Pirimiphos-methyl (306.104 m/z)
s-metolachlor (284.141 m/z)
Fenpropridin (274.253 m/z)
Precursor m/z
Fragment m/z
500
480
460
440
420
400
380
360
340
320
300
280
260
240
220
200
180
100 120 140 160 180 200 220 240 260 280 300 320 340 360 380 400 420 440 460 480 500

2D EID MS

EID

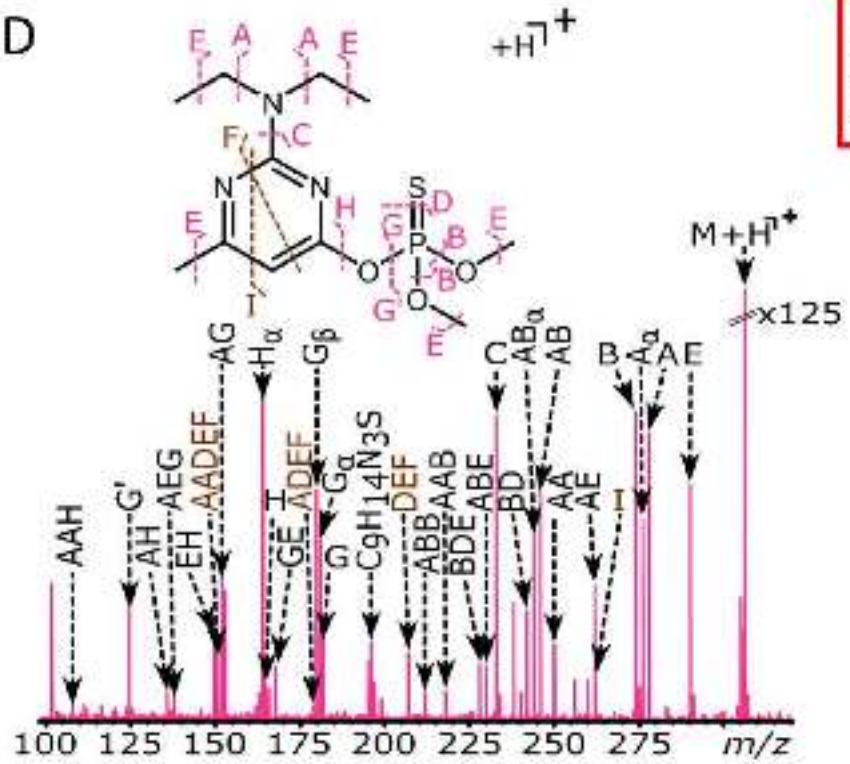

Extensive characterisation
Of every species
Allows upmost confidence of assignments

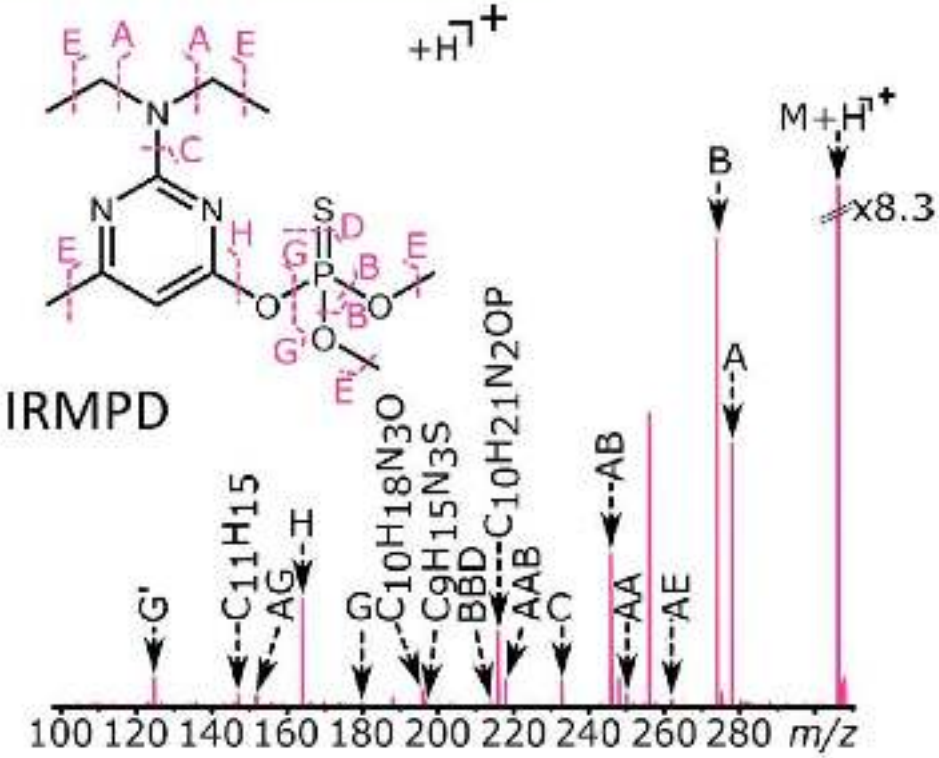

Allows both identification of known products / toxins
And characterisation of unknowns easily and accurately
Can use multiple types of analysis (EID or IRMPD shown)

Pirimiphos-methyl assignments

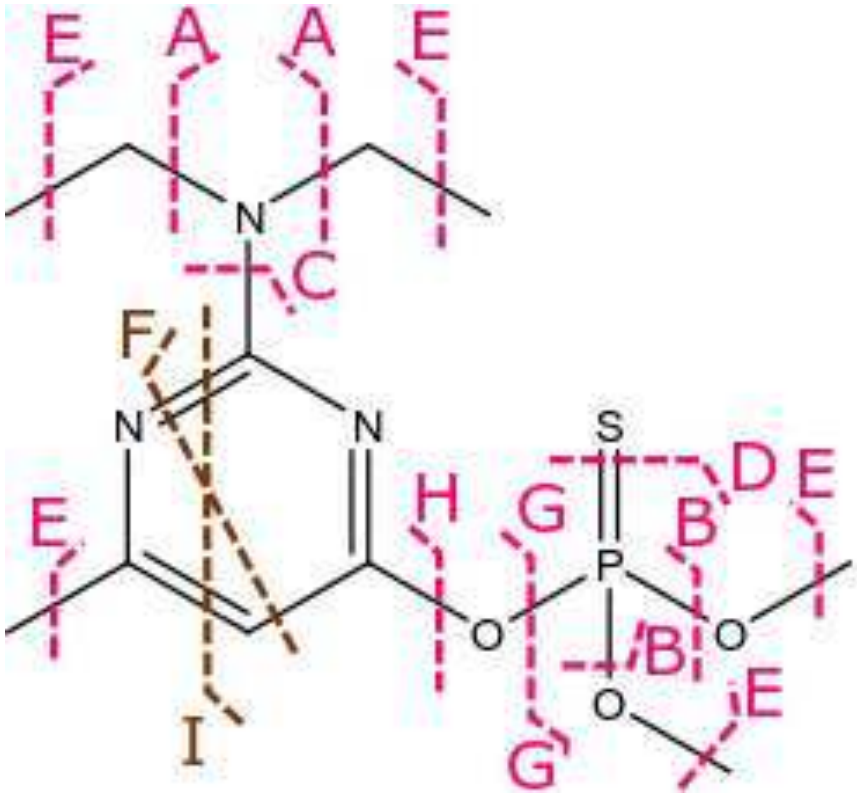

$+\overline{H}^{+}$

m/z	Relative Intensity	Description	Theoretical Mass	Error
290.07239	0.47	C10H17N3O3PS	290.07228	0.411
278.07227	0.57	C9H16N3O3PSH	278.07228	-0.009
276.05665	0.39	C9H15N3O3PS	276.05663	0.075
274.13167	0.41	C11H21N3O3P	274.13150	0.596
274.07733	0.60	C10H16N3O2PSH	274.07736	-0.128
262.05342	0.09	C9H15N2O3PS	262.05355	-0.493
262.04083	0.27	C8H13N3O3PS	262.04098	-0.556
250.04110	0.15	C7H13N3O3PS	250.04098	0.489
246.04608	0.45	C8H13N3O2PS	246.04606	0.059
244.03039	0.37	C8H11N3O2PS	244.03041	-0.088
242.10537	0.22	C10H17N3O2P	242.10529	0.325
233.01443	0.59	C7H10N2O3PS	233.01443	0.012
230.01457	0.11	C7H9N3O2PS	230.01476	-0.825
228.08968	0.12	C9H15N3O2P	228.08964	0.165
218.01495	0.06	C6H9N3O2PS	218.01476	0.872
212.00441	0.06	C7H7N3OPS	212.00420	0.991
207.08940	0.14	C7H16N2O3P	207.08931	0.465
197.09803	0.08	C9H15N3S	197.09812	-0.459
196.14446	0.16	C10H18N3O	196.14444	0.124
196.09034	0.14	C9H14N3S	196.09029	0.226
195.13652	0.12	C10H17N3O	195.13661	-0.491
182.12885	0.16	C9H16N3O	182.12879	0.332
182.07458	0.08	C8H12N3S	182.07464	-0.349
181.12101	0.35	C9H15N3O	181.12096	0.255
180.11315	0.46	C9H14N3O	180.11314	0.070
179.05809	0.03	C5H12N2O3P	179.05801	0.488
168.11314	0.11	C8H14N3O	168.11314	-0.004
168.05902	0.11	C7H10N3S	168.05899	0.155
166.09747	0.07	C8H12N3O	166.09749	-0.098
166.04342	0.02	C7H8N3S	166.04334	0.480
165.12605	0.07	C9H15N3	165.12605	0.033
164.11825	0.62	C9H14N3	164.11822	0.172
163.11050	0.06	C9H13N3	163.11040	0.643
152.08186	0.28	C7H10N3O	152.08184	0.170
151.02672	0.13	C3H8N2O3P	151.02671	0.097
150.10263	0.18	C8H12N3	150.10257	0.368
138.06627	0.05	C6H8N3O	138.06619	0.617
136.08691	0.06	C7H10N3	136.08692	-0.090
124.98209	0.22	C2H6O2PS	124.98206	0.218
108.05562	0.04	C5H6N3	108.05562	0.000

Absolute Average: 0.312 ppm
Standard Deviation: 0.385 ppm

Assignments - 2D IRMPD

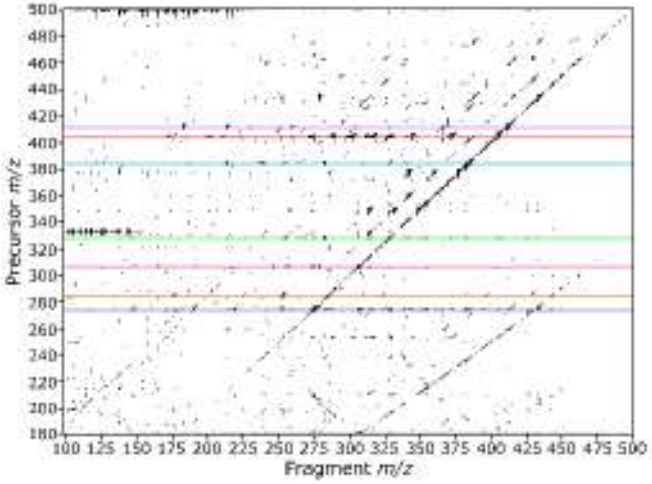

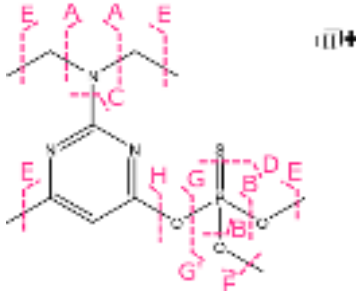

IRMPD

Abs. Ave. Std. Dev.

0.29 ppm 0.49 ppm

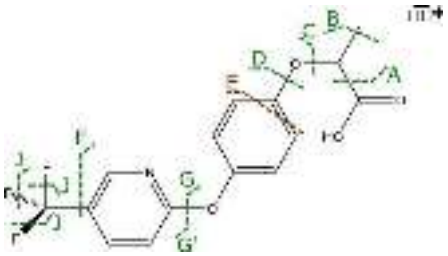

IRMPD

Abs. Ave. Std. Dev.

0.23 ppm 0.26 ppm

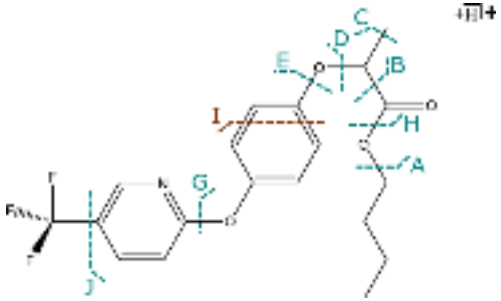

IRMPD

Abs. Ave. Std. Dev.

0.20 ppm 0.24 ppm

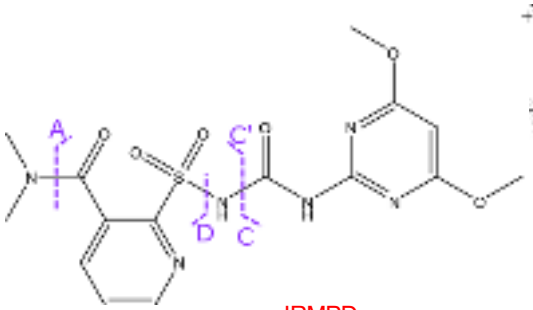

IRMPD

Abs. Ave. Std. Dev.

0.15 ppm 0.26 ppm

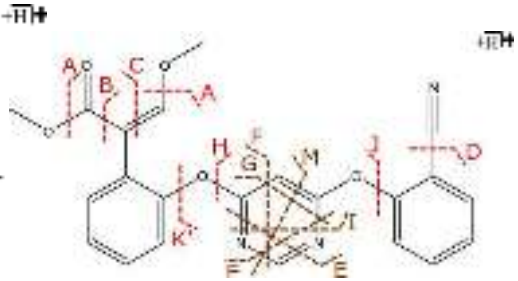

IRMPD

Abs. Ave. Std. Dev.

0.19 ppm 0.36 ppm

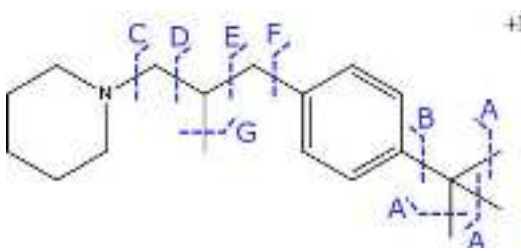

IRMPD

Abs. Ave. Std. Dev.

0.22 ppm 0.32 ppm

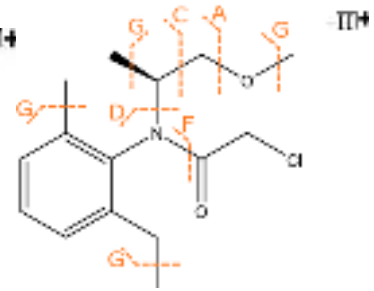

IRMPD

Abs. Ave. Std. Dev.

0.42 ppm 0.30 ppm

Assignments - 2D EID

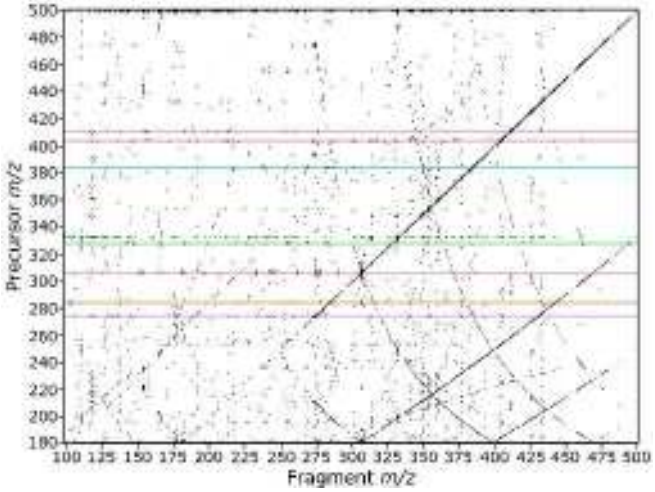

EID

Abs. Ave.	Std. Dev.
0.31 ppm	0.39 ppm

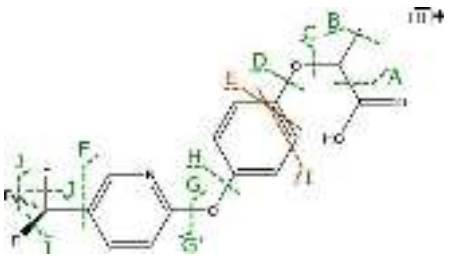

EID

Abs. Ave.	Std. Dev.
0.55 ppm	0.77 ppm

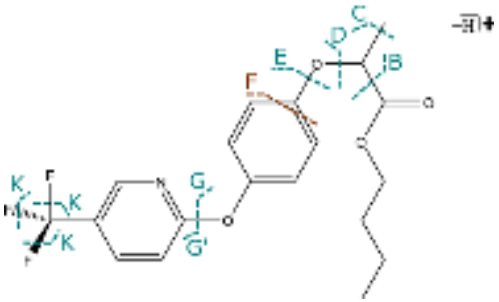

EID

Abs. Ave.	Std. Dev.
0.15 ppm	0.17 ppm

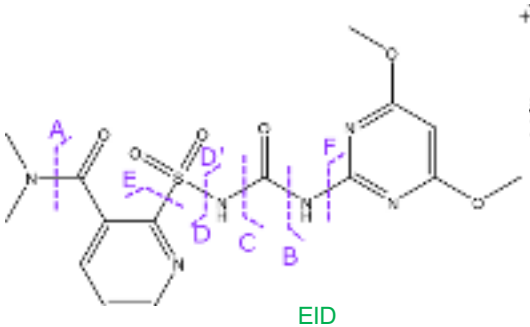

EID

Abs. Ave.	Std. Dev.
0.50 ppm	0.54 ppm

EID

Abs. Ave.	Std. Dev.
0.52 ppm	0.96 ppm

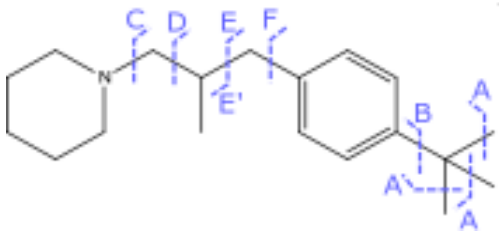

EID

Abs. Ave.	Std. Dev.
0.91 ppm	1.16 ppm

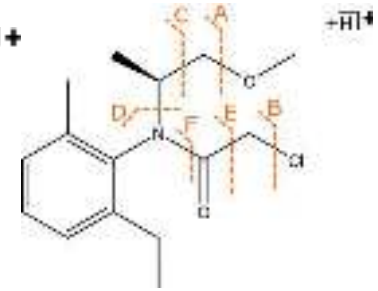

EID

Abs. Ave.	Std. Dev.
0.09 ppm	0.19 ppm

Case study of 2DMS with Syngenta UK

Agrochemical and pesticide analysis

Issues with current analysis:

- Unique method required for certain compounds – no one-size-fits-all
- LC-MS/MS based – fails to scale with complexity, induces bias in LC
- Restricted solvent systems makes certain compounds "off-limits" or require separate methods
- Large optimisations needed for each question, no future proofing for later questions – very long and expensive

What we achieved:

- Parallel analysis of all pesticide and degradation products in one run
- Extensive fragmentation patterns for each unique species – enables accurate identification
- Data independent analysis which is future-proof for unknown questions
- Less bias analysis, not reliant on solvent systems or LC compatibility

Lecture overview

- 2DMS for agrichemical analysis.
- 2DMS for polymer analysis.
- 2DMS for monoclonal antibodies.
- Distinguishing phosphopeptides using 2DMS
- 2DMS – UVPD
- 2DMS on a linear ion trap

Case study of 2DMS with Astra Zeneca UK

AstraZeneca

Biologically relevant polymer analysis

Polymer analysis by mass spectrometry

- Increased use of polymeric species as therapeutic agents
- Movement away from PEG due to chemical modification
- Focus on primary chemical structure and how this varies properties
- Presence of sample complexity as well as need to understand primary structure

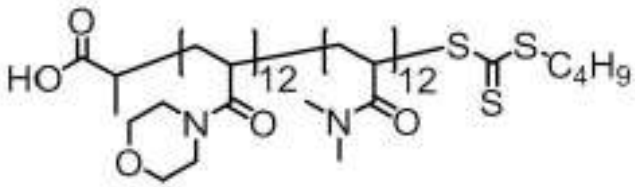

Acrylamide copolymers

Polyoxazoline homopolymers

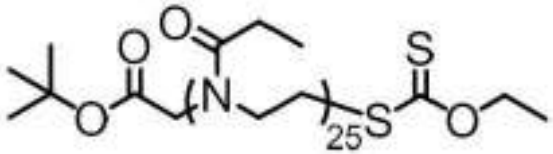

Self-assembly peptide polymer conjugates

Cyclic-peptide polymer conjugates

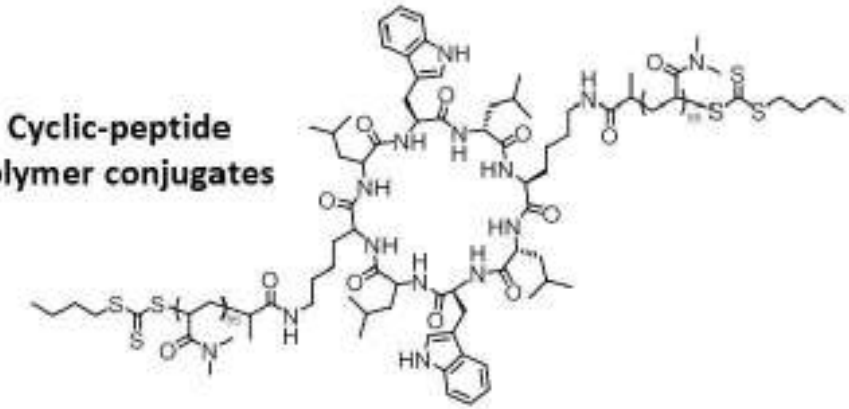

Polymer analysis by 2D ECD

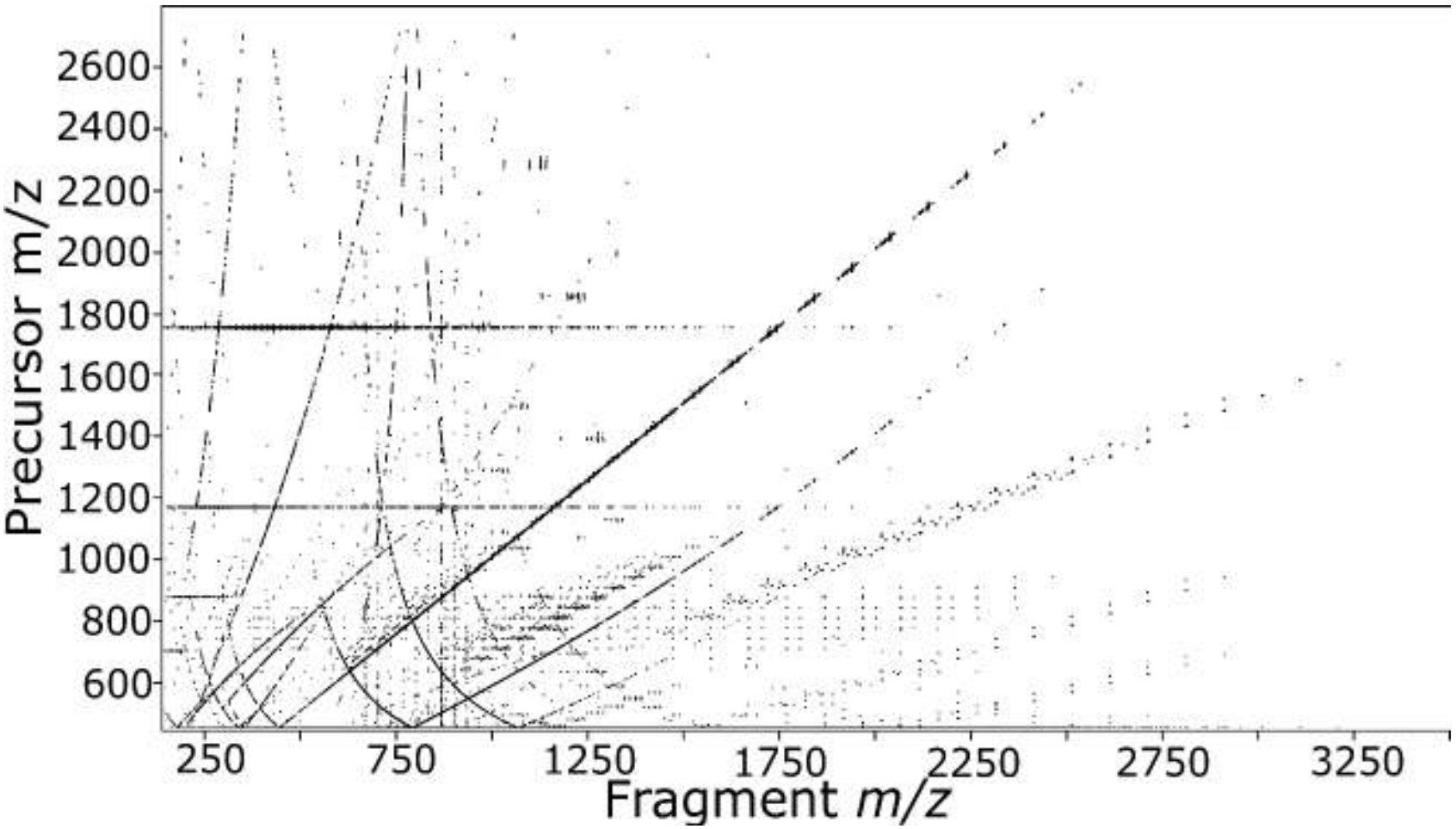

- Information dense 2D spectrum

Polymer analysis by 2D ECD

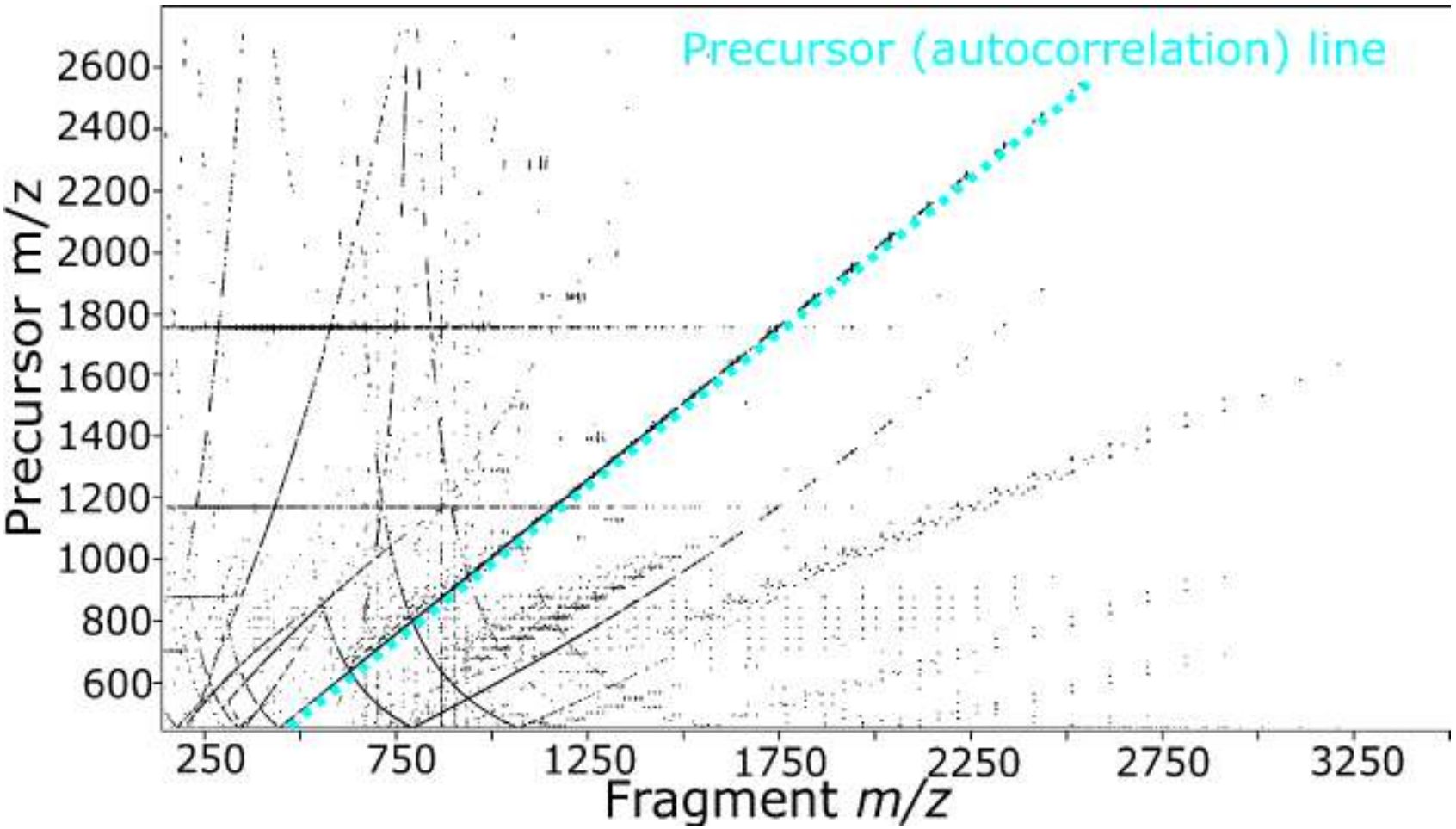

Polymer analysis by 2D ECD

Autocorrelation line

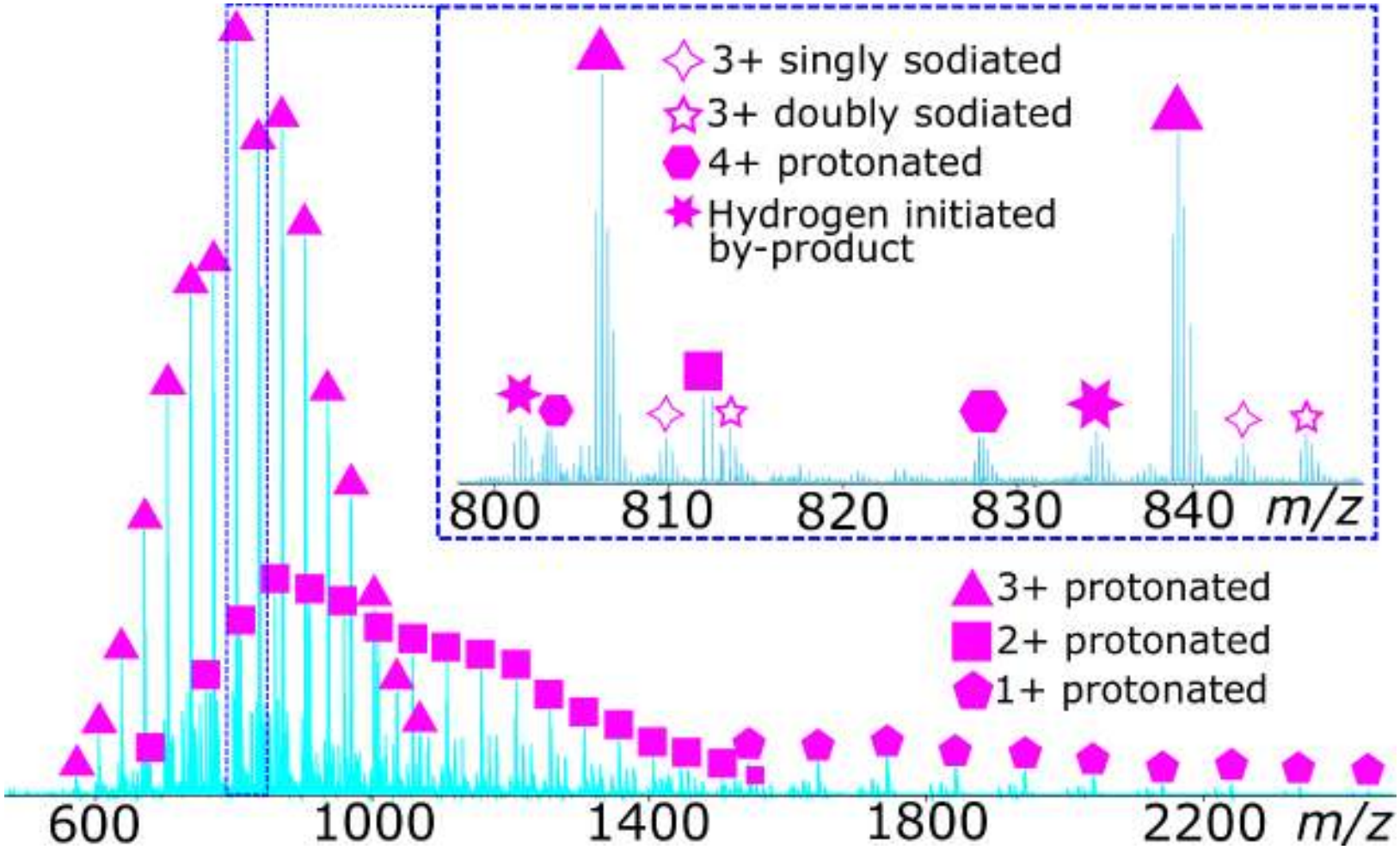

Polymer analysis by 2D ECD

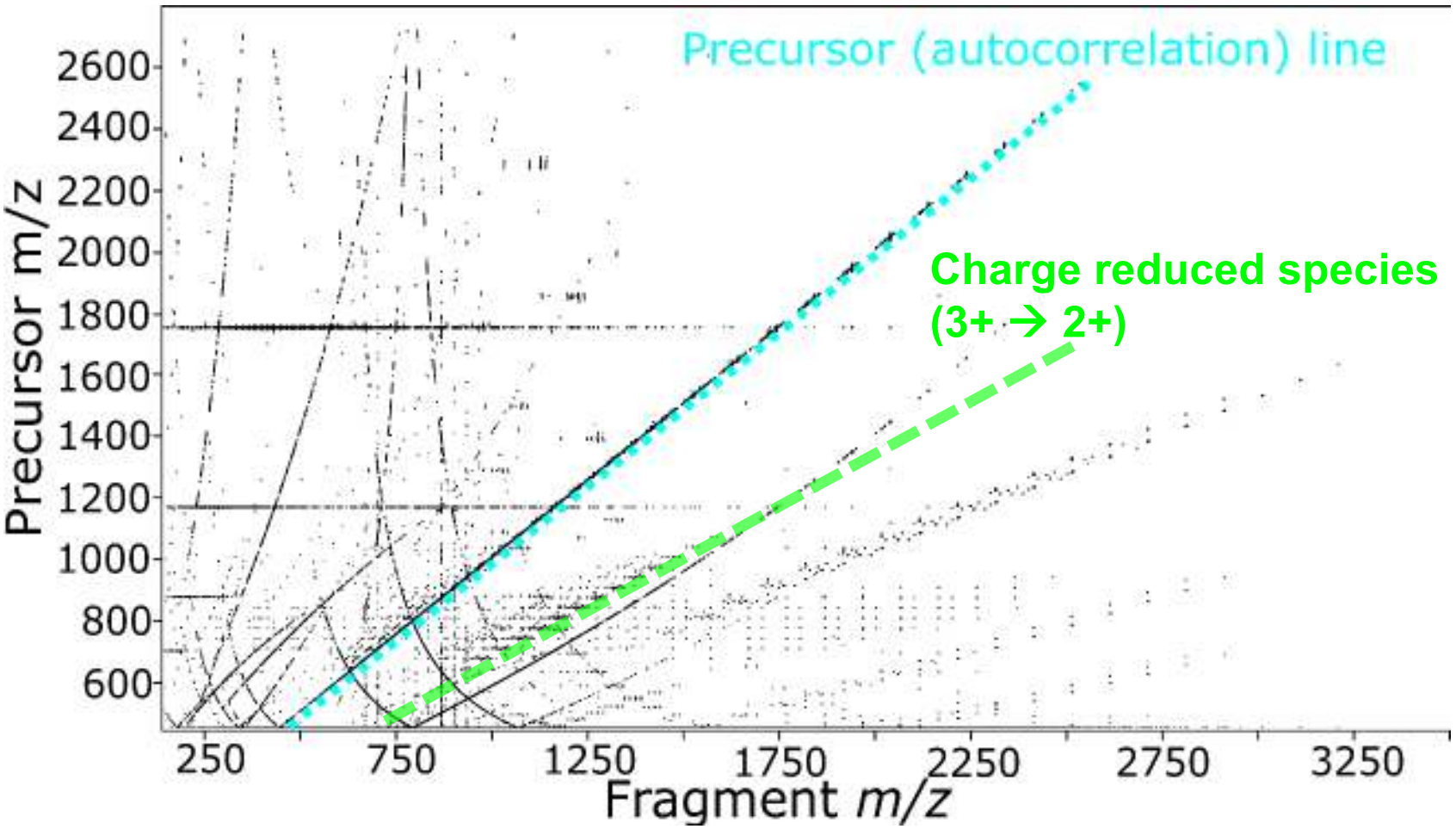

Polymer analysis by 2D ECD

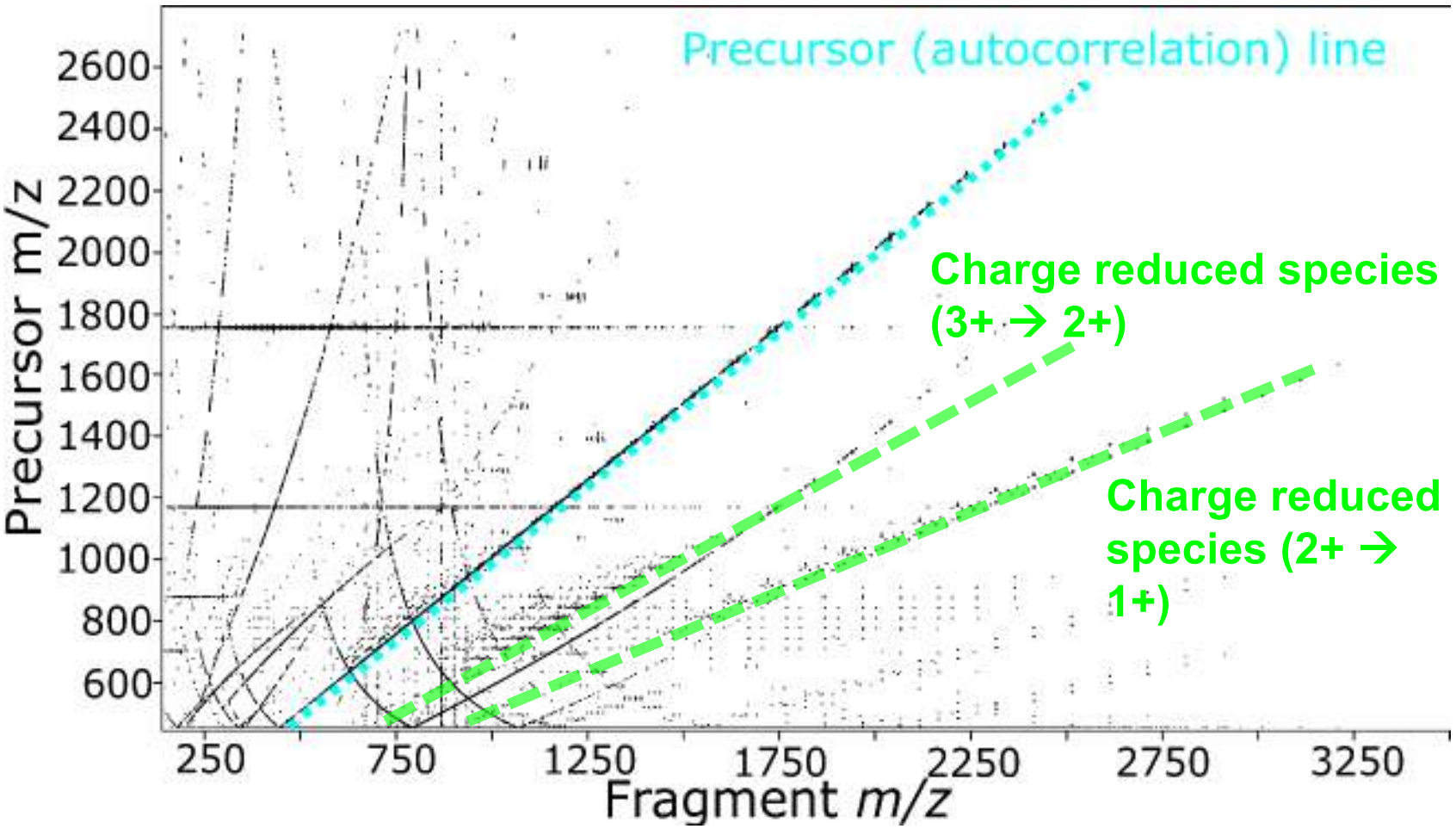

Polymer analysis by 2D ECD

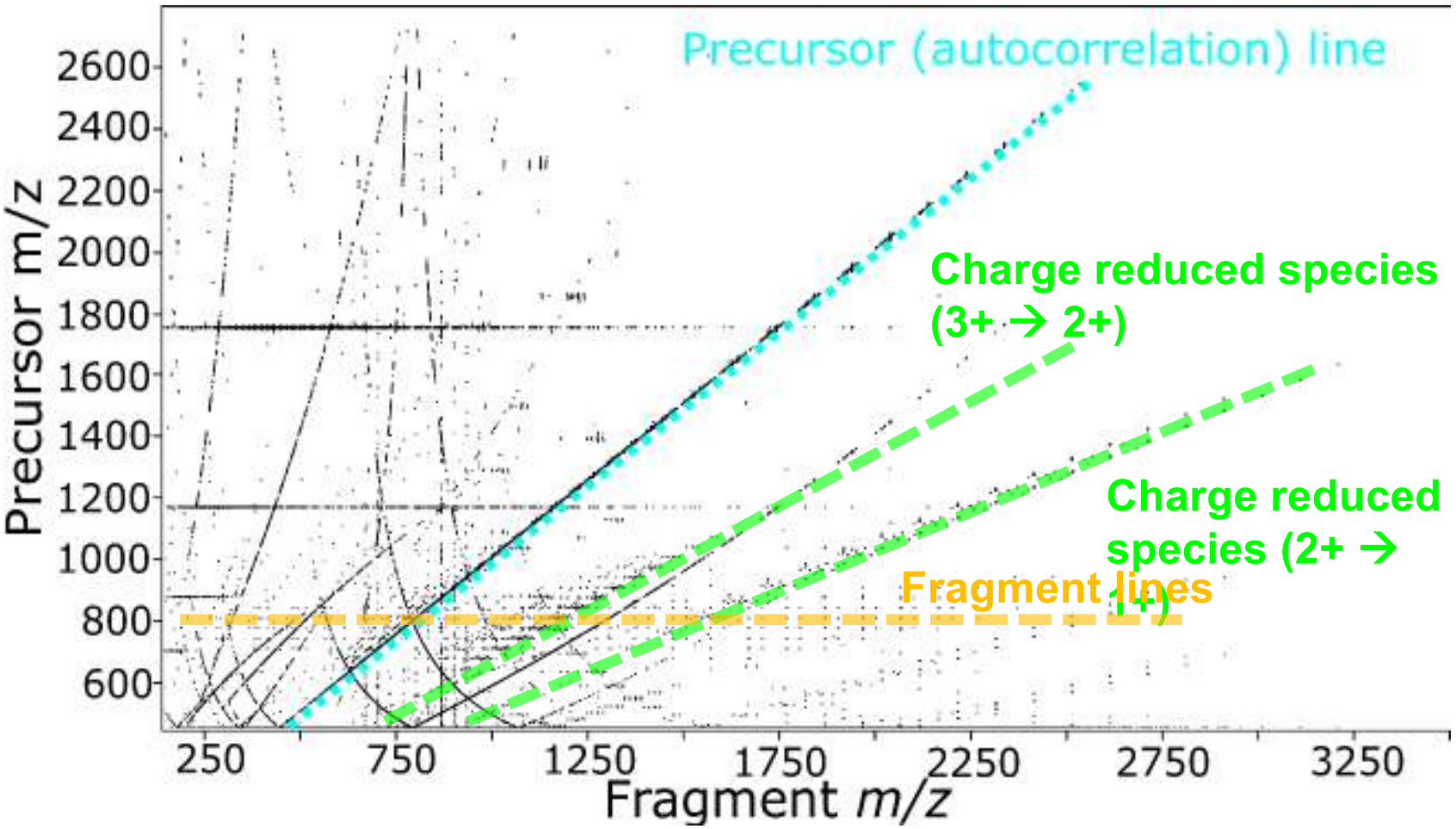

Polymer analysis by 2D ECD

Fragment ion scans

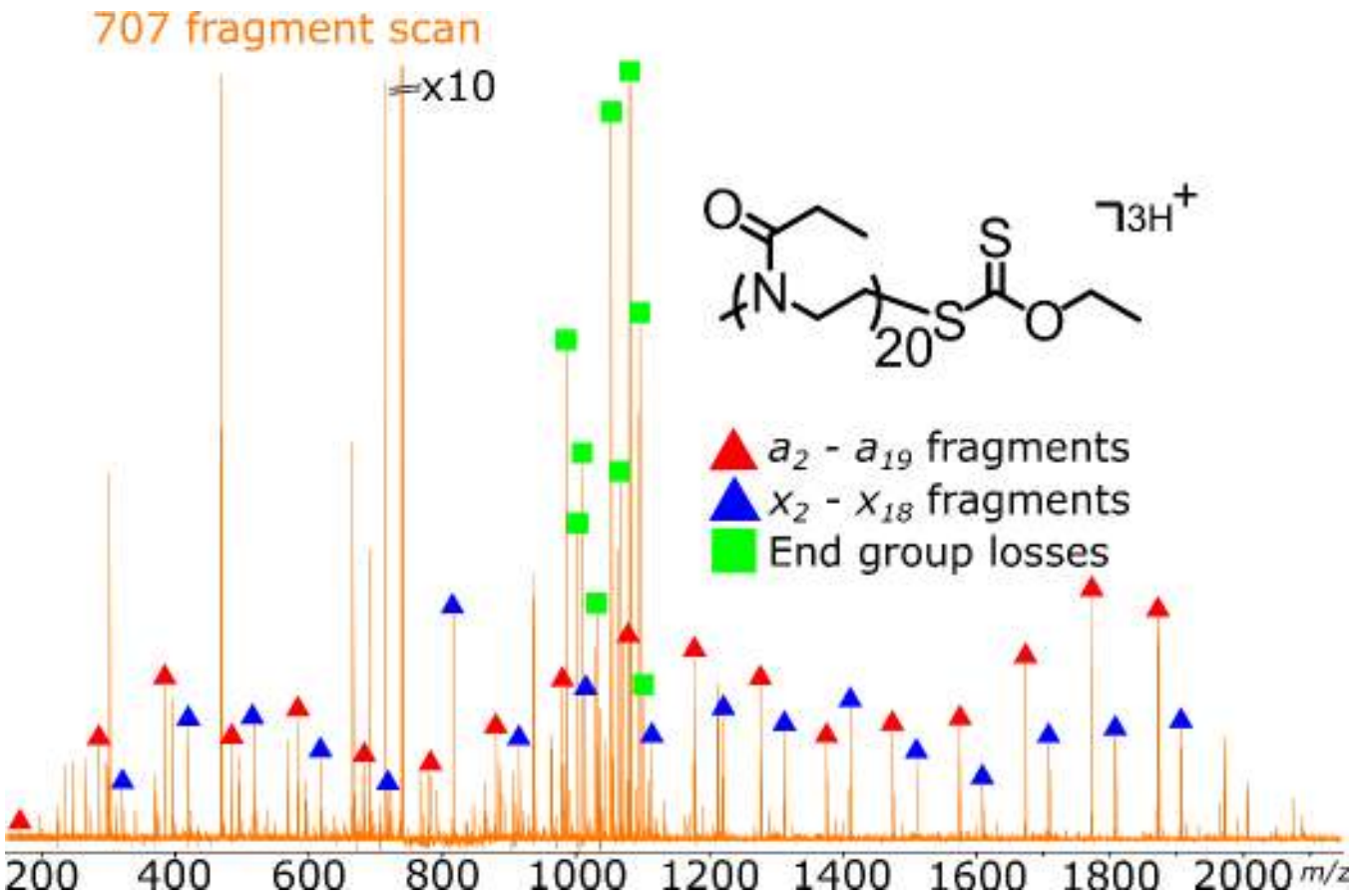

Polymer analysis by 2D ECD

Fragment ion scans

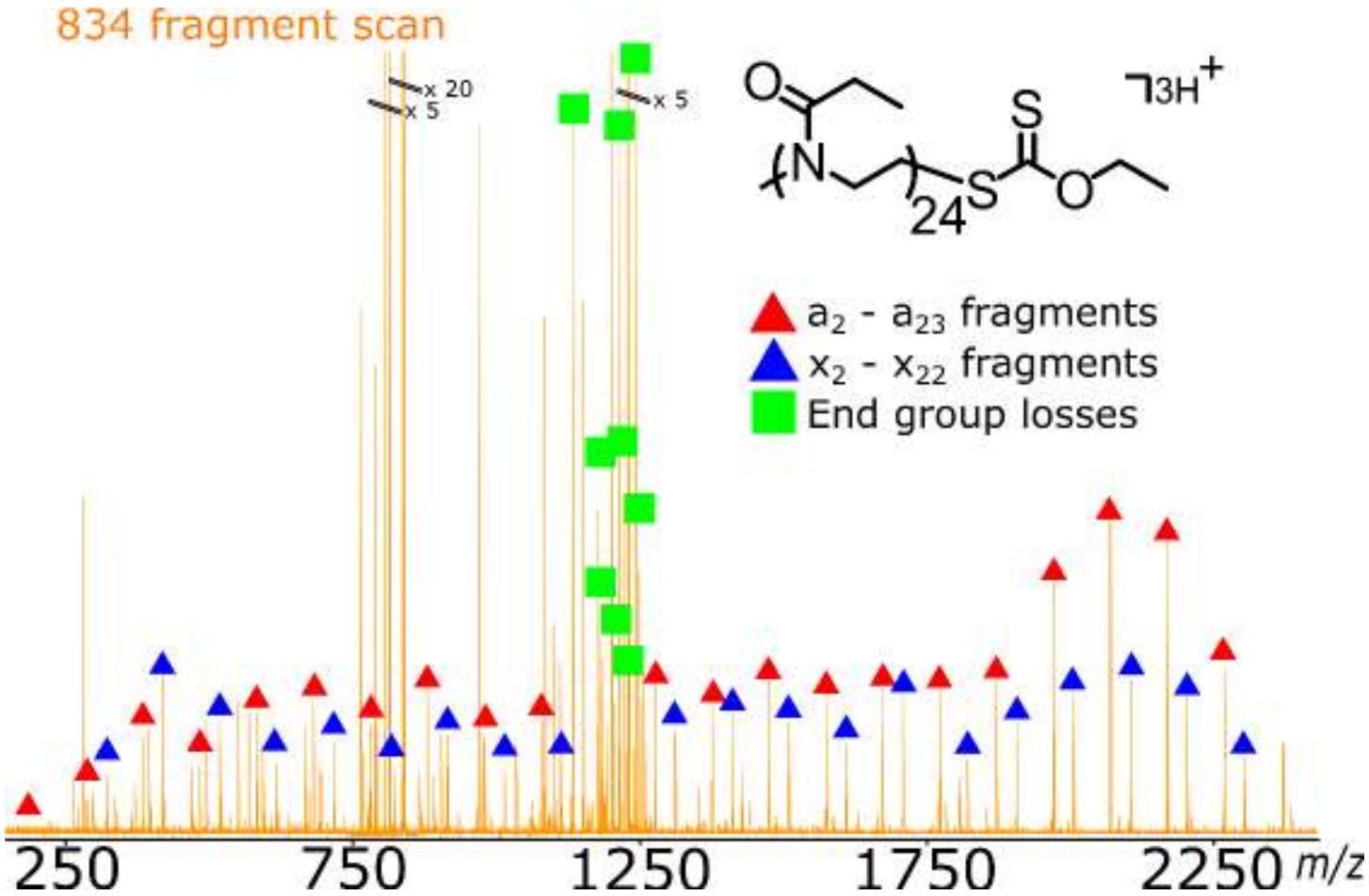

Polymer analysis by 2D ECD

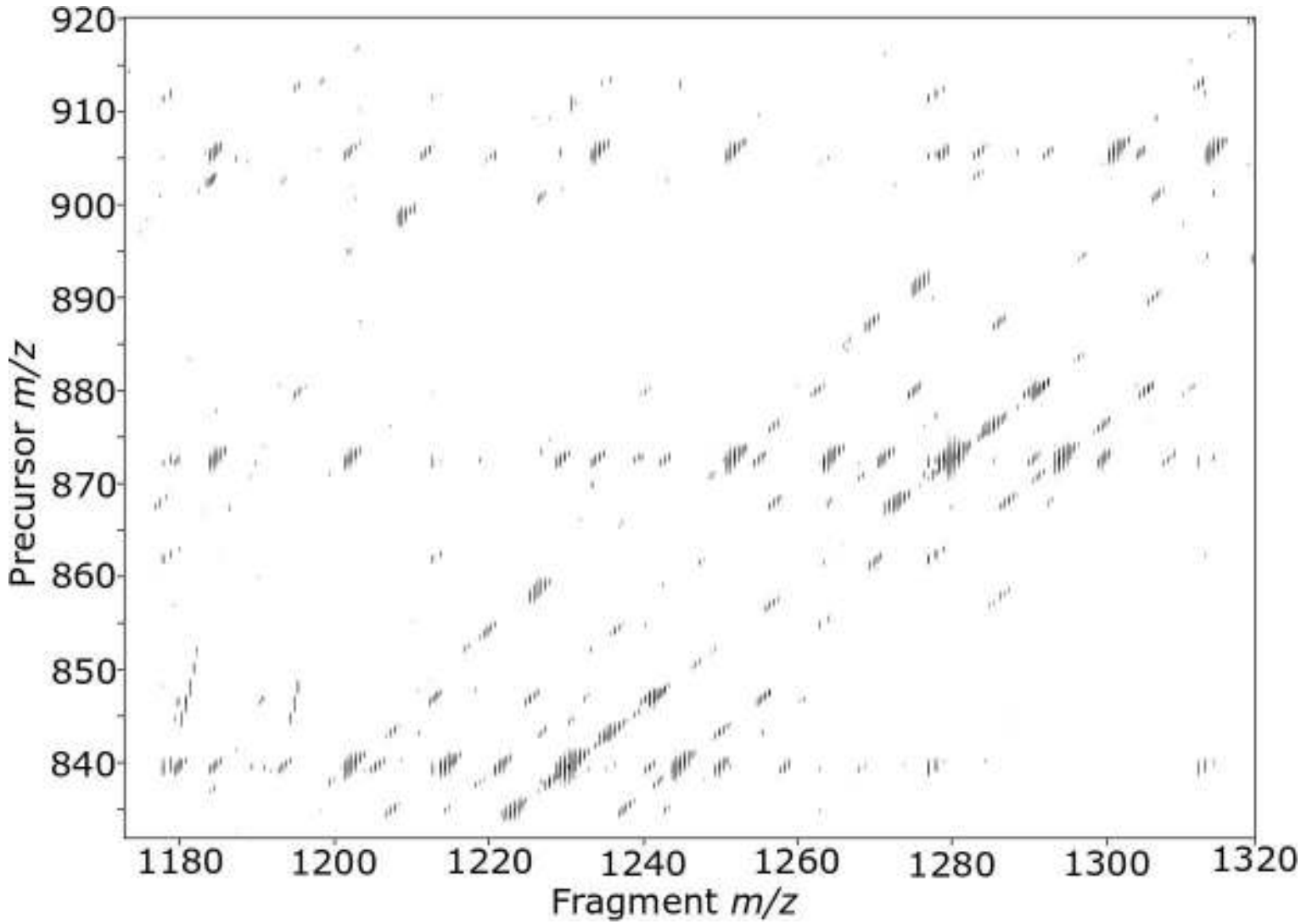

- Zoom in of region shows isotopic distribution

Polymer analysis by 2D ECD

Combined R = 435,000,000

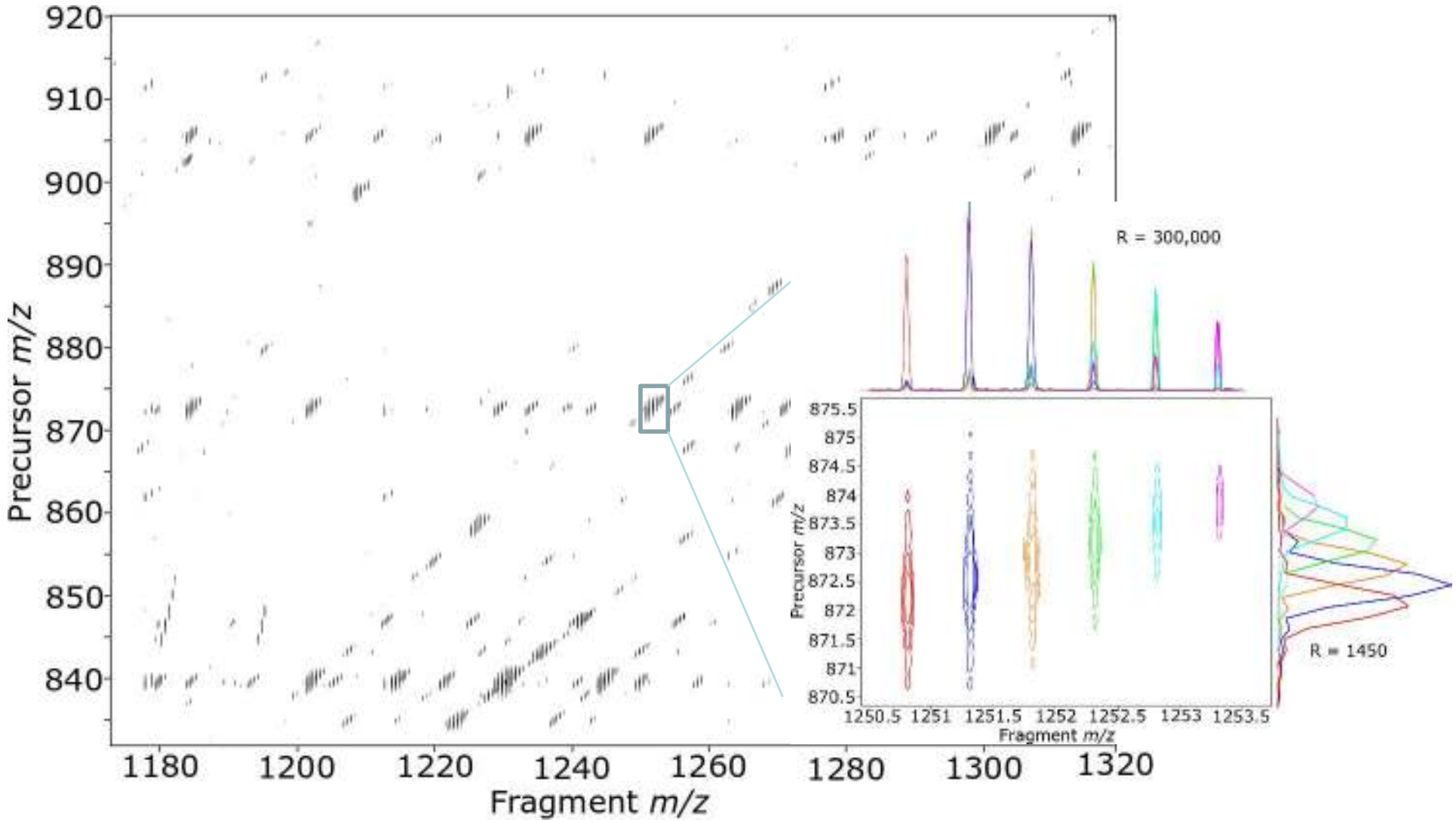

Polymer analysis by 2D ECD

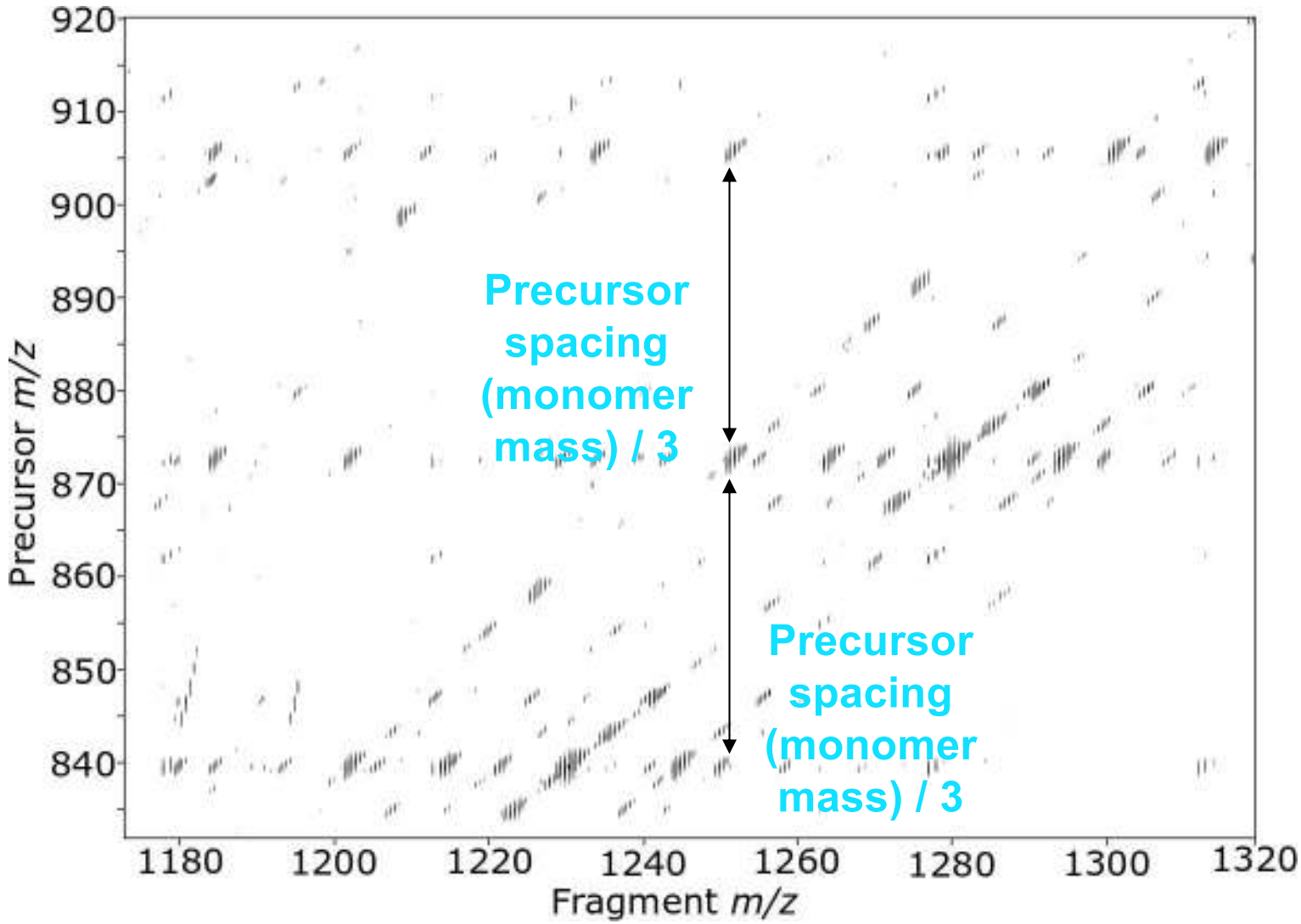

- Spacing of lines is equal to that of (monomer mass)/3 due to charge

Polymer analysis by 2D ECD

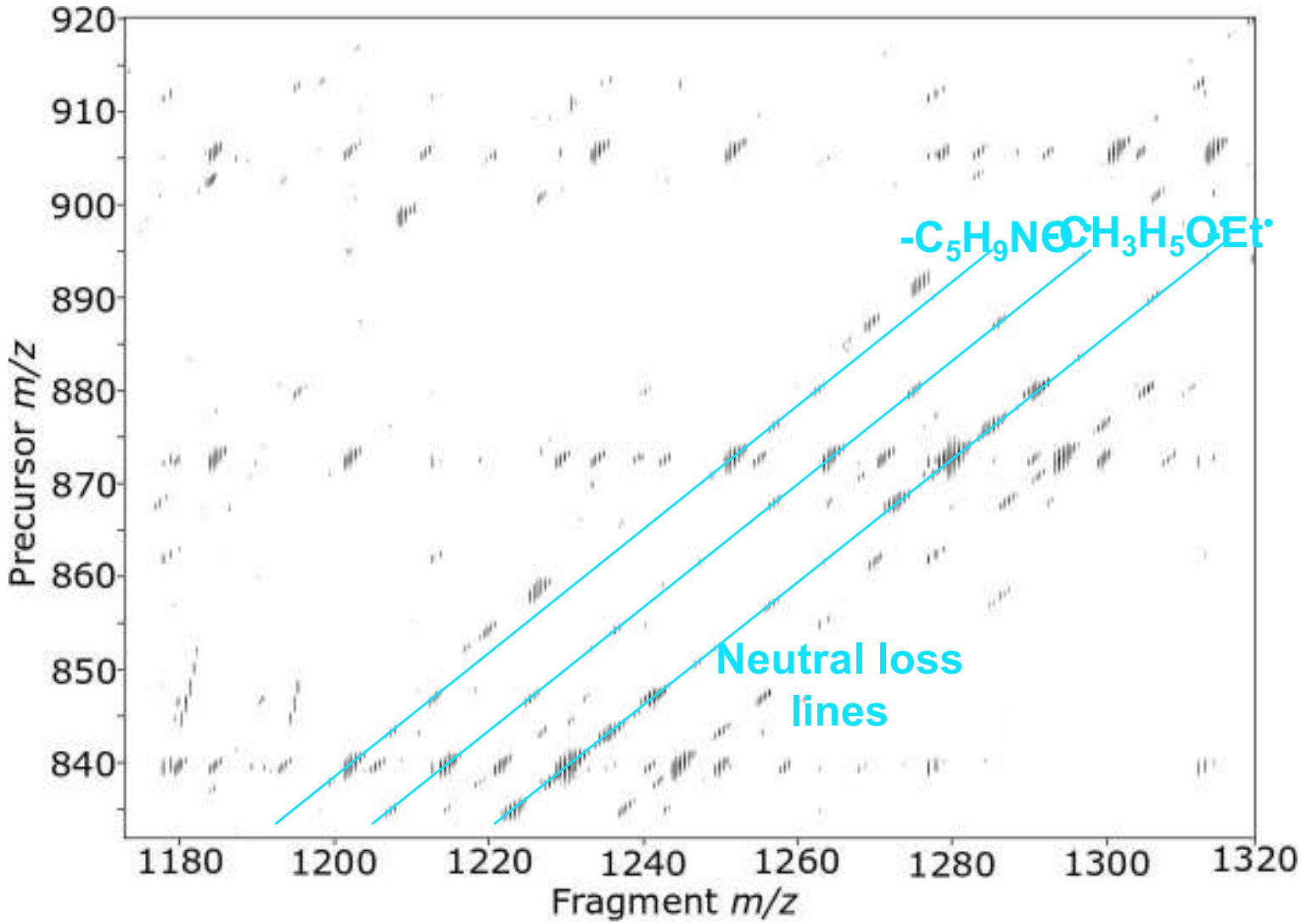

- Neutral losses from charged reduced species
- Fragments on the same intercept means the loss is equal from the charged reduced species

Polymer analysis by 2D ECD

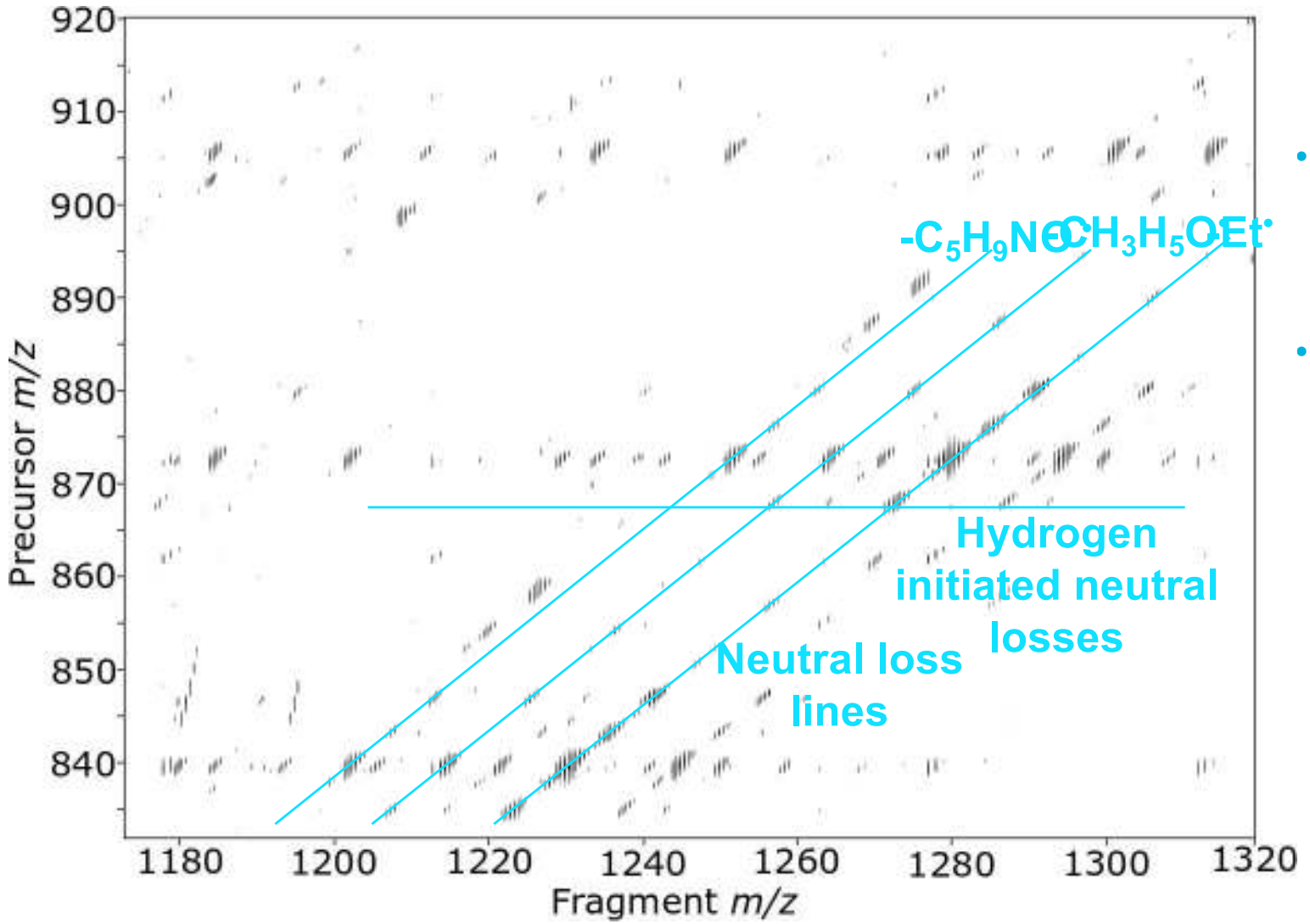

- Neutral losses from charged reduced species
- Fragments on the same intercept means the loss is equal from the charged reduced species

Conclusions

- ECD fragmentation can be used to analyze a polyoxazoline
- 2D mass analysis gives significant fragment information

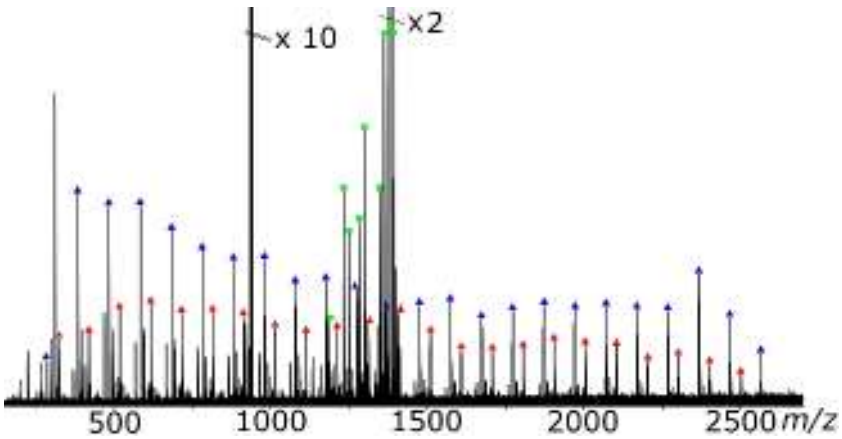

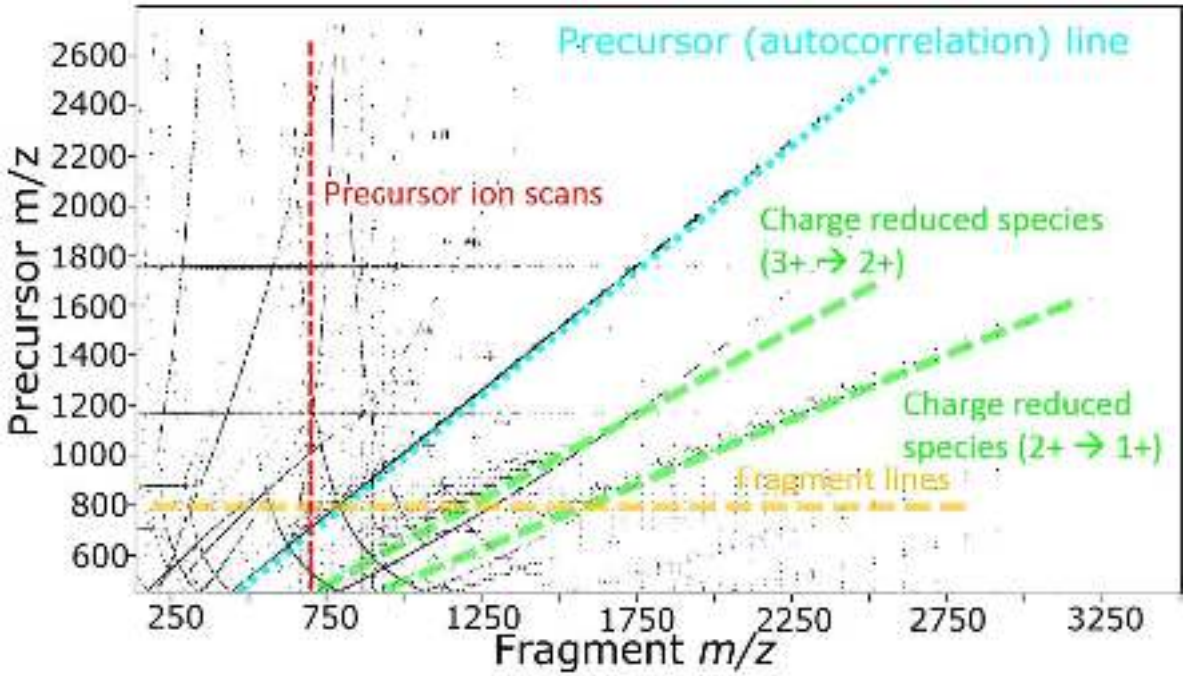

Lecture overview

- 2DMS for agrichemical analysis.
- 2DMS for polymer analysis.
- 2DMS for monoclonal antibodies.
- Distinguishing phosphopeptides using 2DMS
- 2DMS – UVPD
- 2DMS on a linear ion trap

Case study of 2DMS with UCB

Antibody modification analysis

Antibody 2DMS

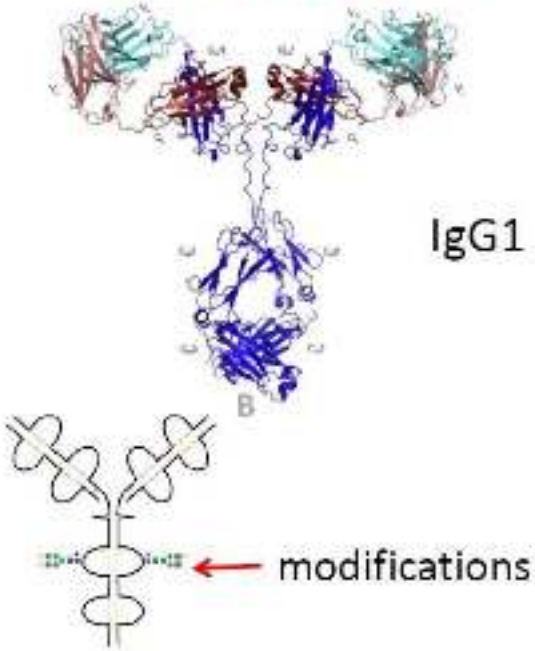

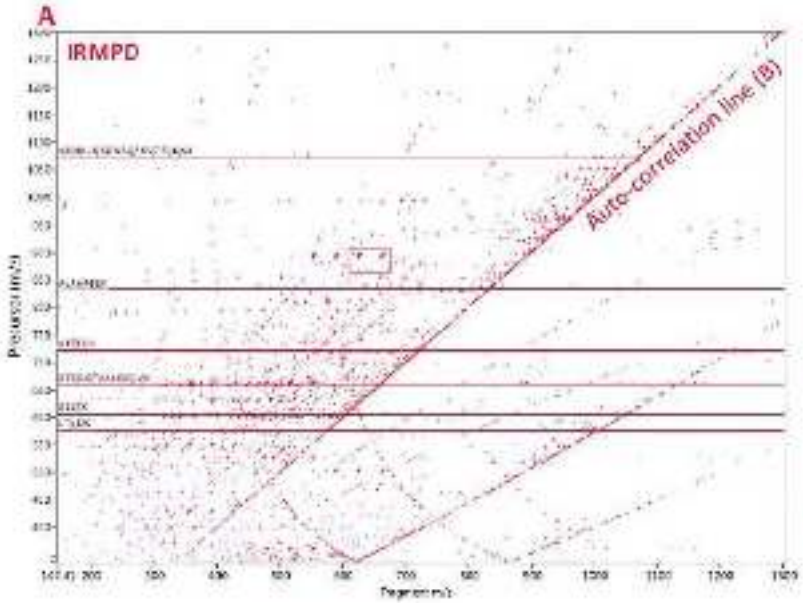

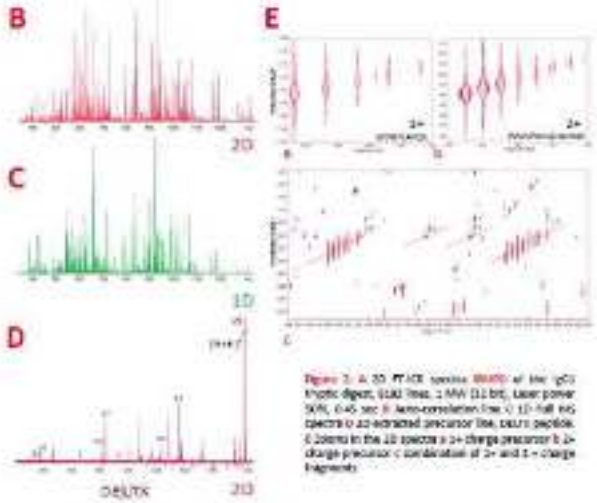

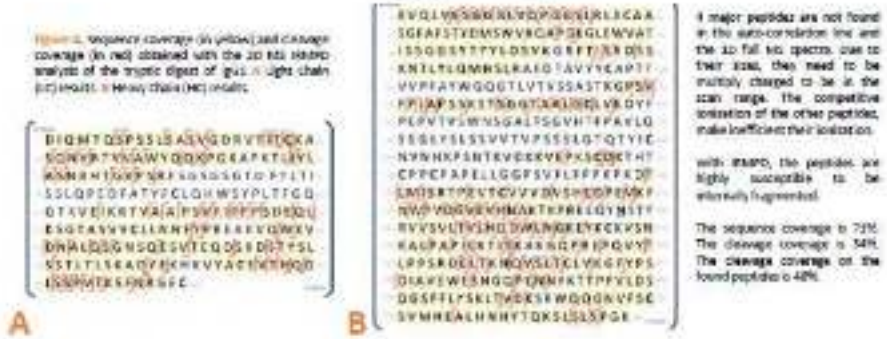

Antibodies are large, complex biomolecules which are often biologically modified for function (good).
But also get modified/degrade during bio-production, leading to either little/no change (good)
Loss of function (bad)
Or different function (possibly very bad)
2DMS can handle complex samples where LC often fails

Extracted Lines Resolution

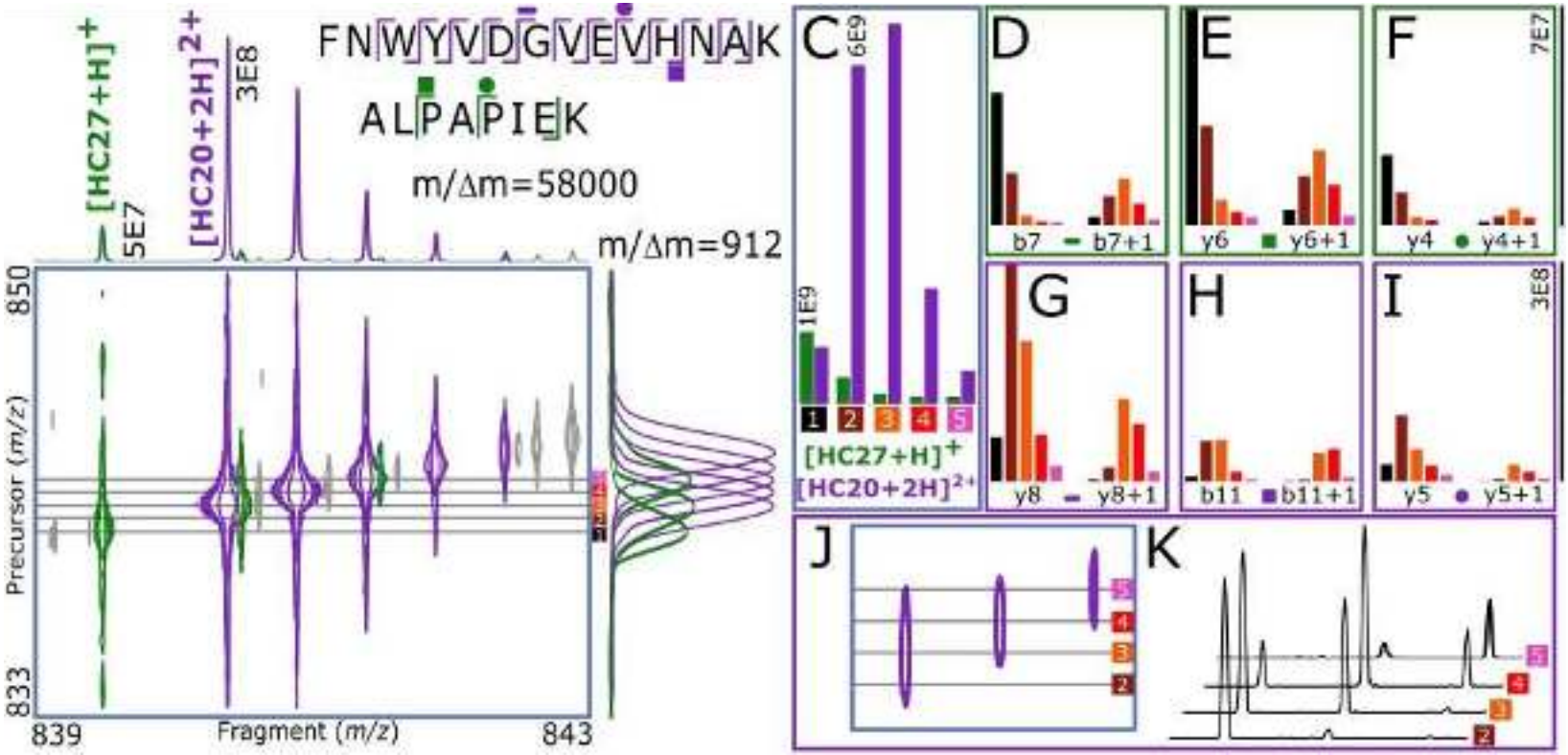

Peak Picking Resolution

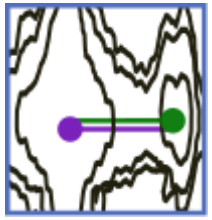

- Δx: 0.094 *m/z*
- Δy: 0.089 *m/z*

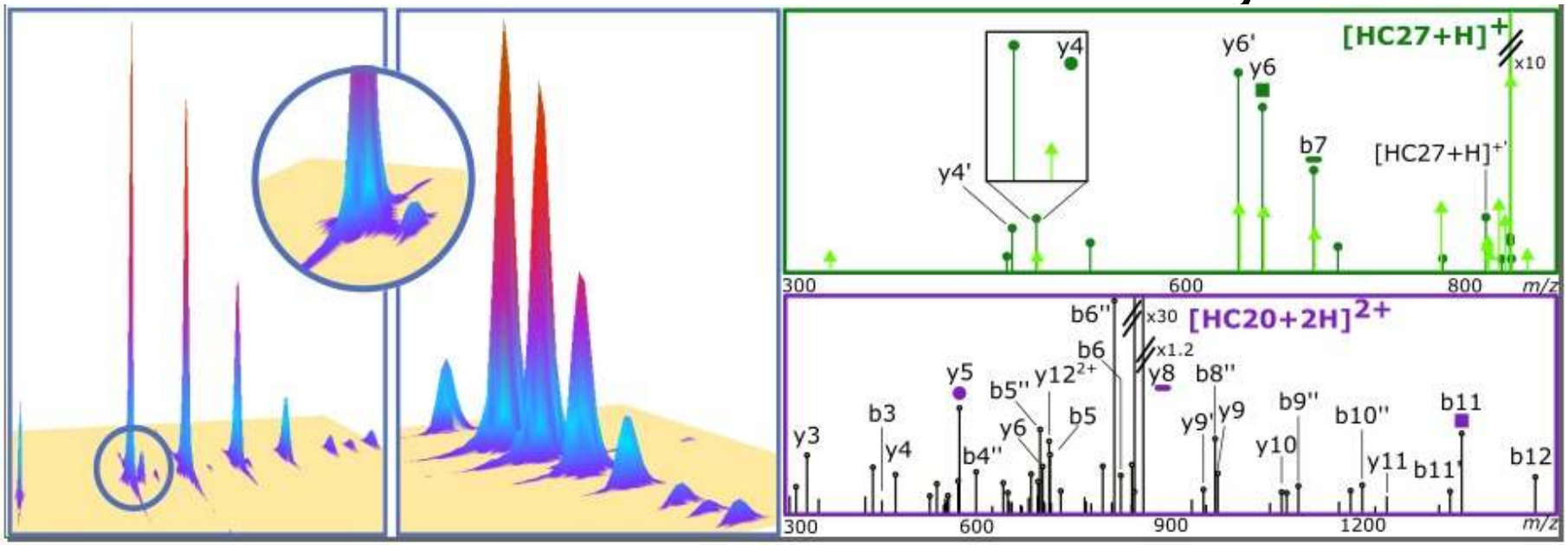

PTM Detection -Antibody

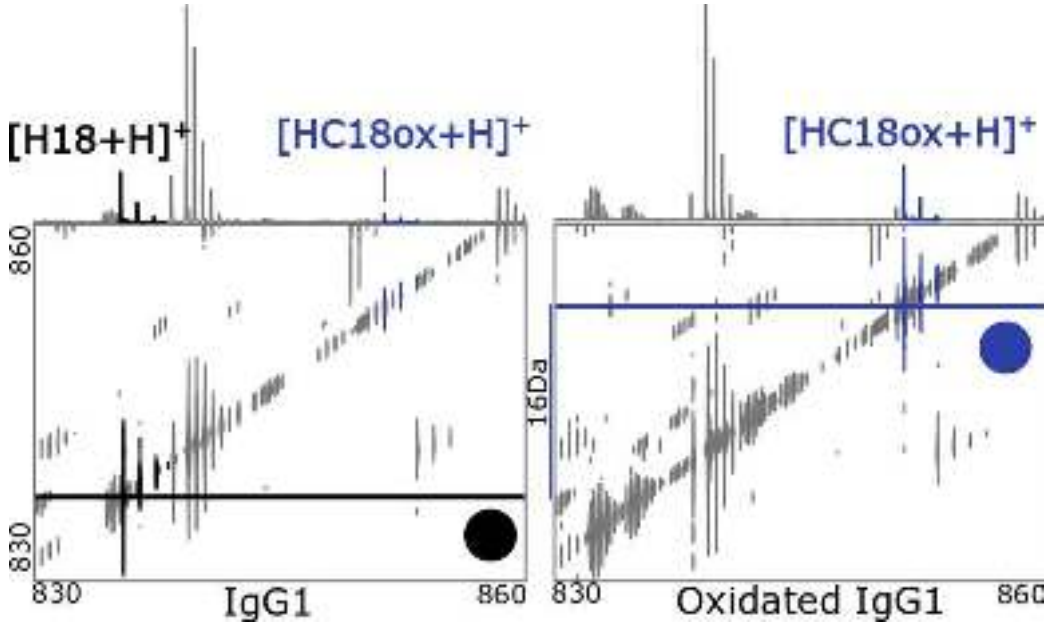

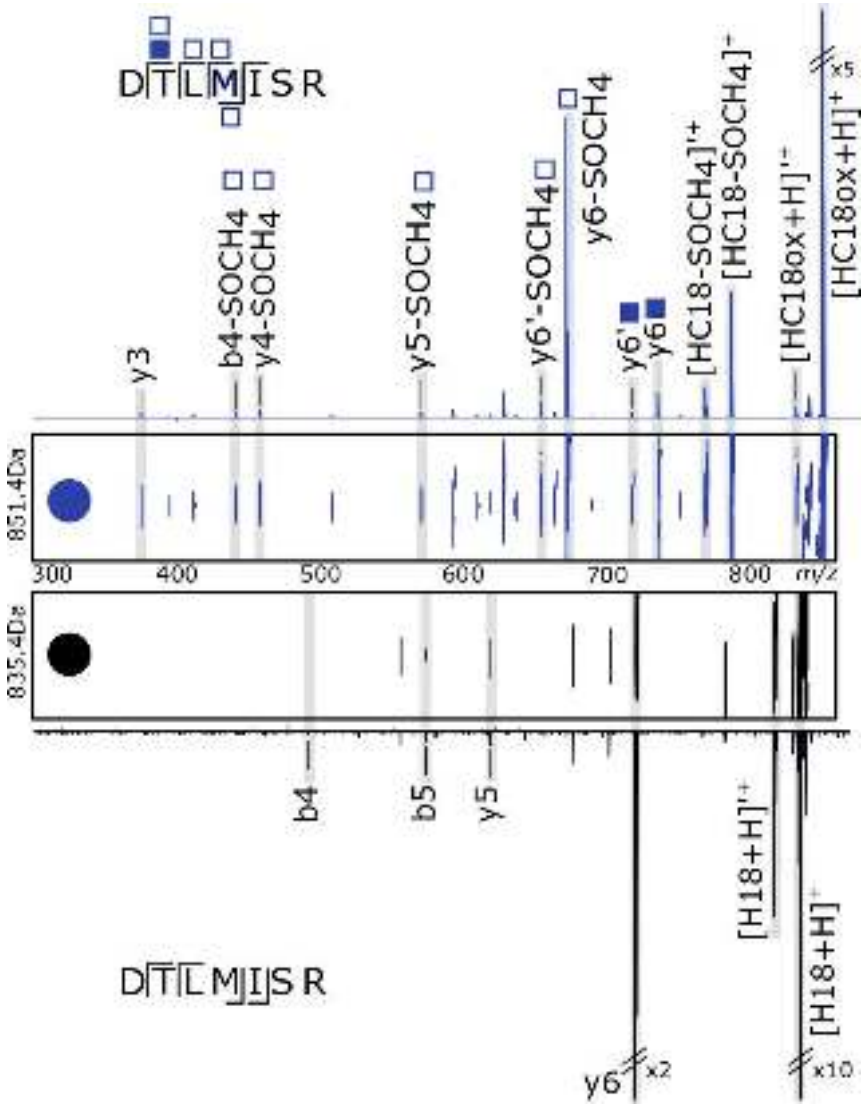

Lecture overview

- 2DMS for agrichemical analysis.
- 2DMS for polymer analysis.
- 2DMS for monoclonal antibodies.
- Distinguishing phosphopeptides using 2DMS
- 2DMS – UVPD
- 2DMS on a linear ion trap

Phosphorylation

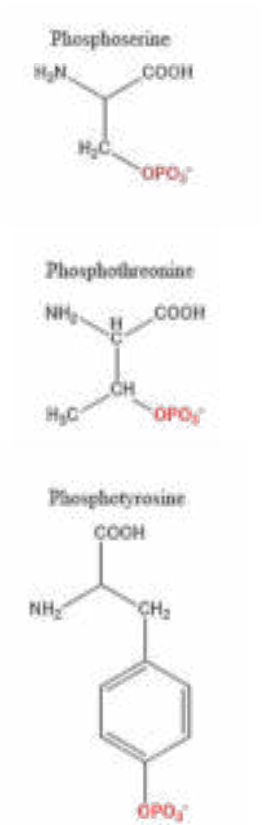

- Serine, Threonine or Tyrosine
- Phosphoester linkage.
- Regulation of intercellular processes
- Cell signalling pathway
- Change activity, subcellular location, degradation and interaction with other proteins
- Limit of RP-LC: the phosphopeptide loss during the sample preparation or the liquid chromatography

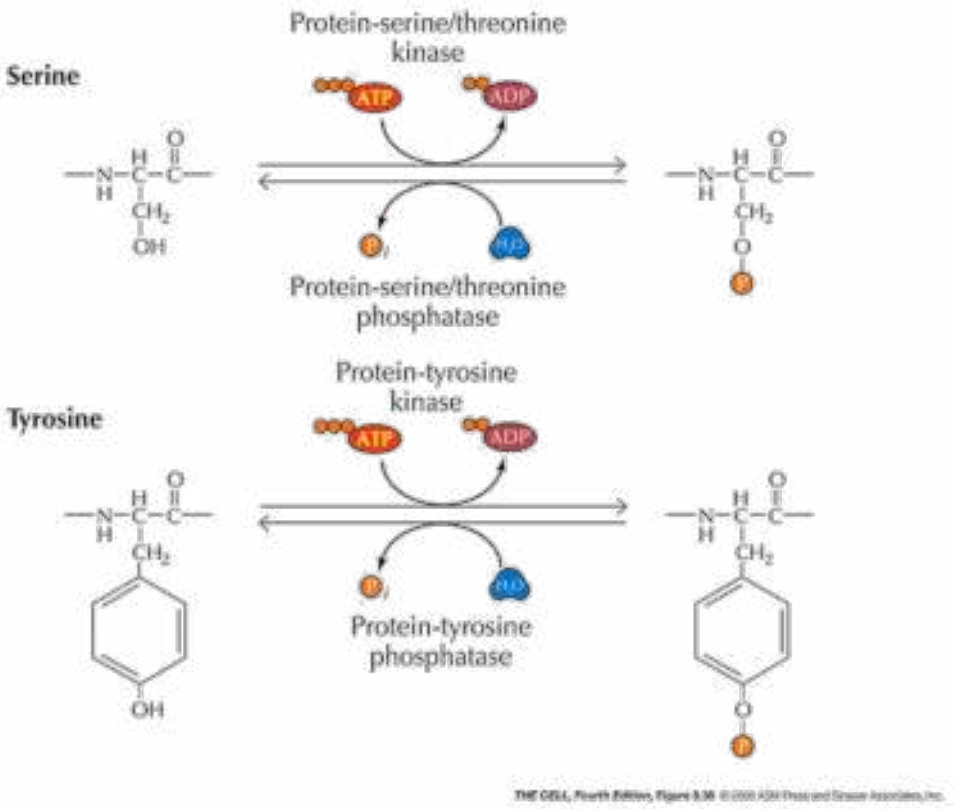

InfraRed Multi-Photon Dissociation

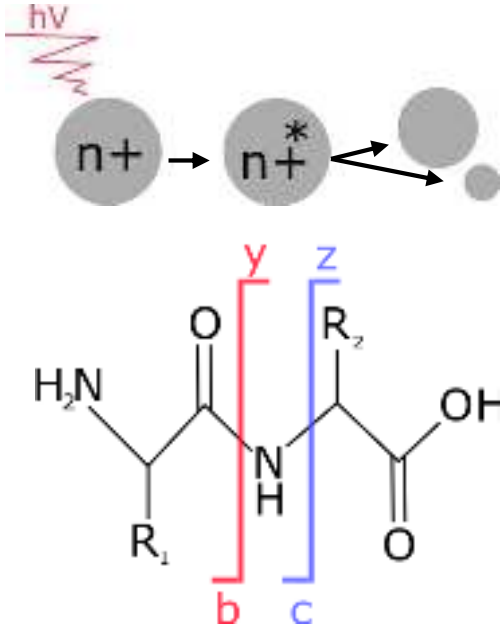

- CO_2 laser (10.6 µm photons)
- Resonance with the P-O stretch of the phosphate (9.6-11 µm)

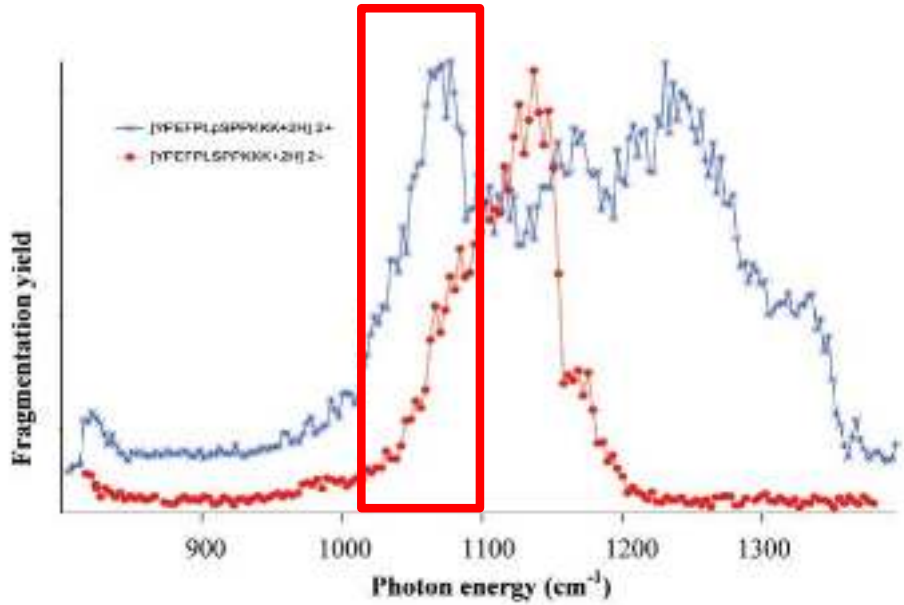

Figure. IRMPD spectra. Fragmentation efficiencies defined as -ln(P/F + P), with F being the sum of fragment abundances and P the abundance of the intact precursor.

Correia, C. F.; Balaj, P. O.; Scuderi, D.; Maitre, P.; Ohanessian, G. *J. Am. Chem. Soc.* 2008, *130*, 3359-3370.

2D MS IRMPD Analysis of Phosphopeptides

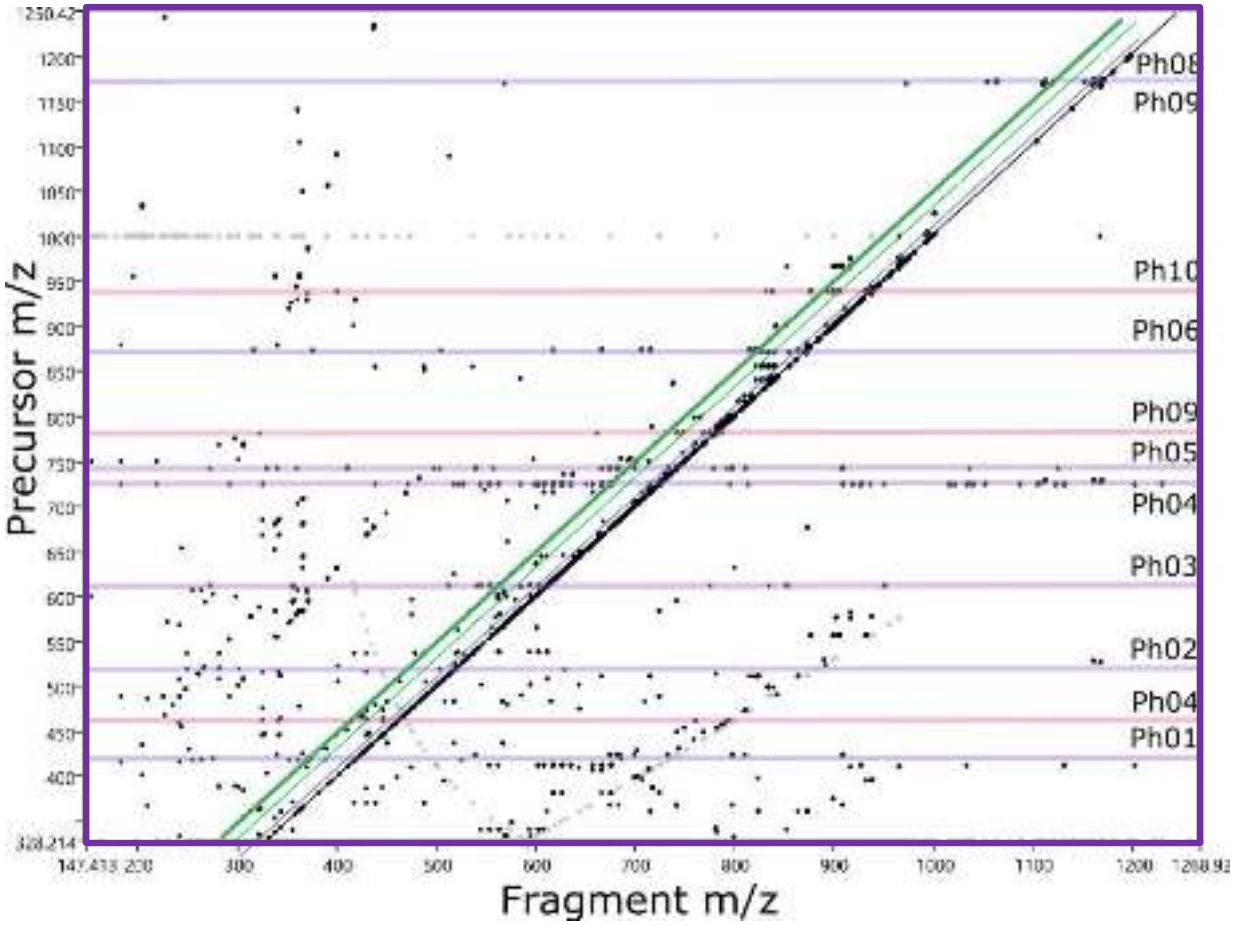

Figure. 2D FT-ICR spectra IRMPD of the Phosphomix, y: 8192 lines, x: 1 megapoints

Direct infusion.
10 Phosphopeptides.
No prior separation.

In pink and purple, precursor lines.
In black, auto-correlation line.
In blue and green, neutral loss lines.

Horizontal: 1,048,576k transients (broadband)
Vertical: 8,192 scan lines.
Total: 8,589,934,592 data points

Comparison 1D/2D Full MS

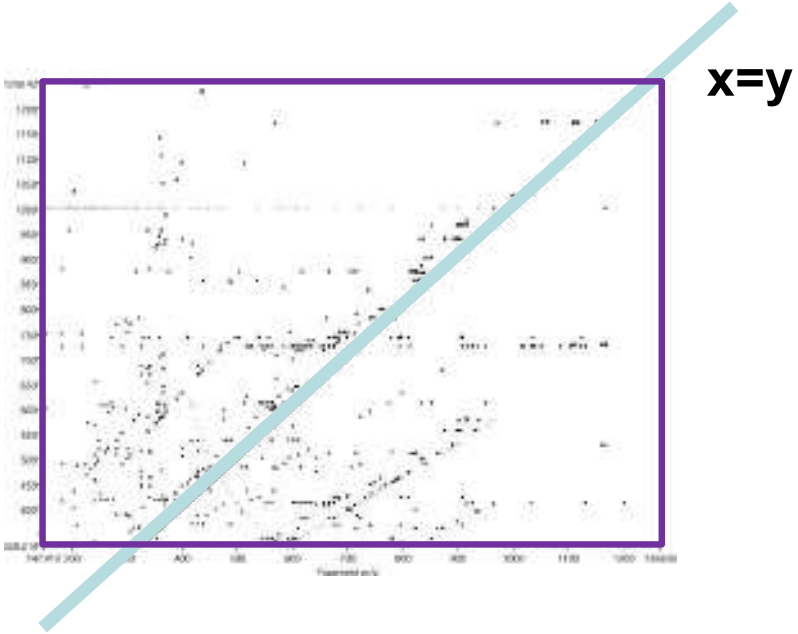

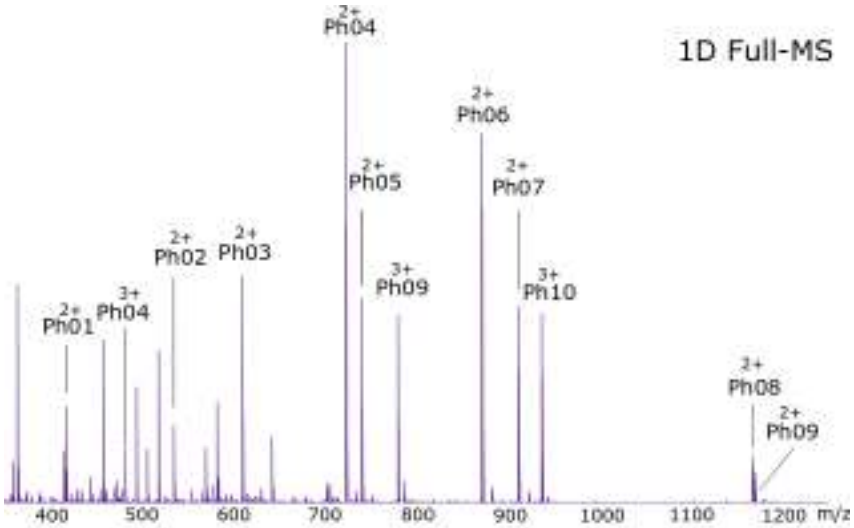

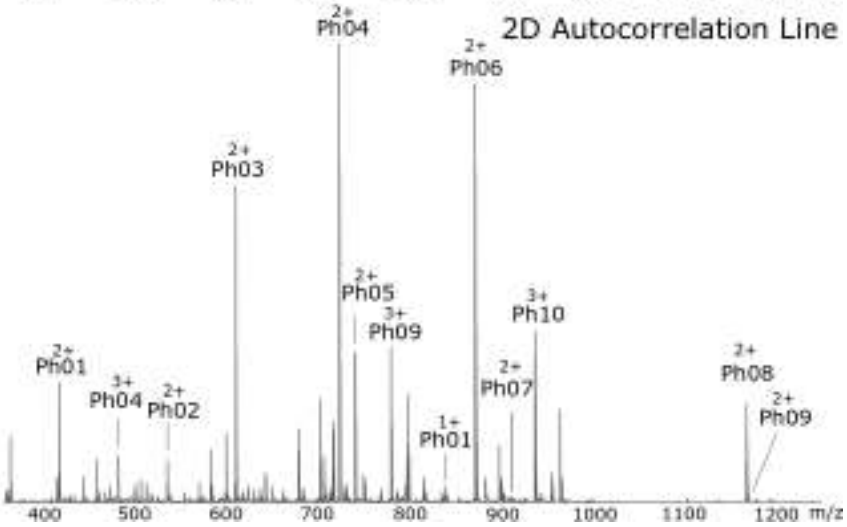

Loss of Ph07
Hydrophobic peptide

Zoom into a region

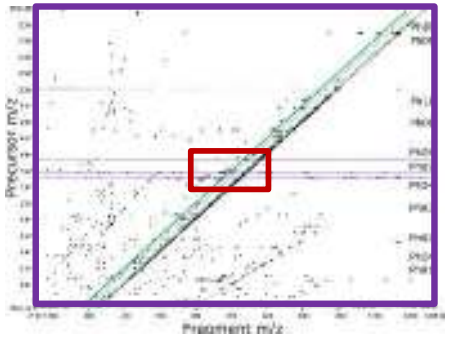

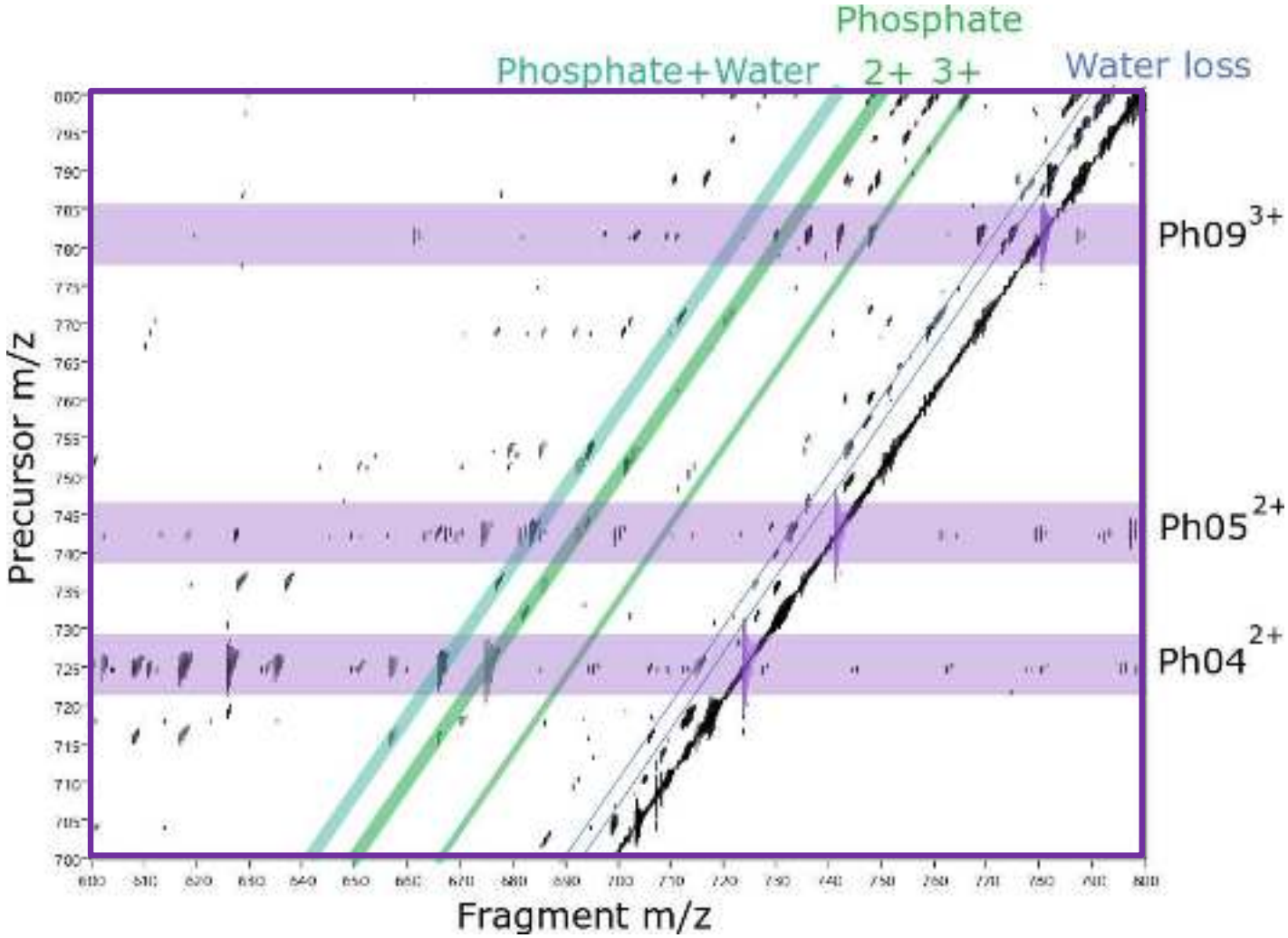

Zoom into a region

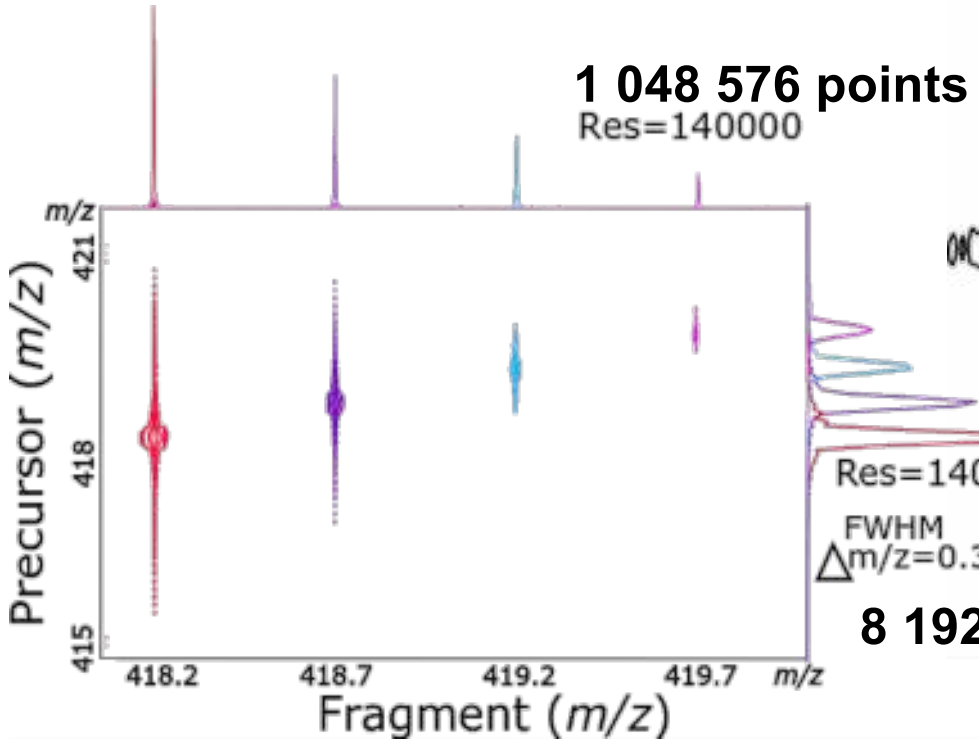

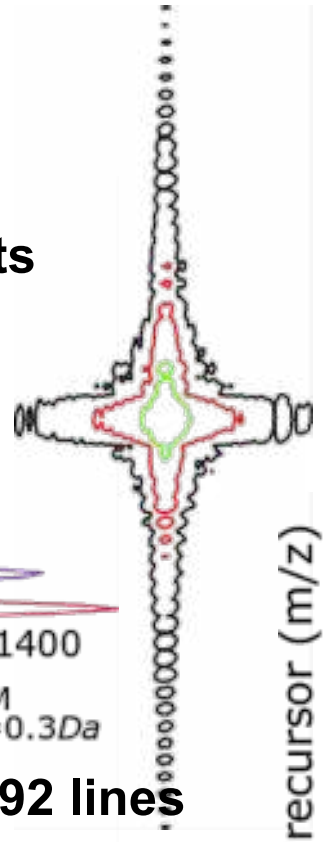

Black 1E6
Red 1E7
Green 1E8
Threshold

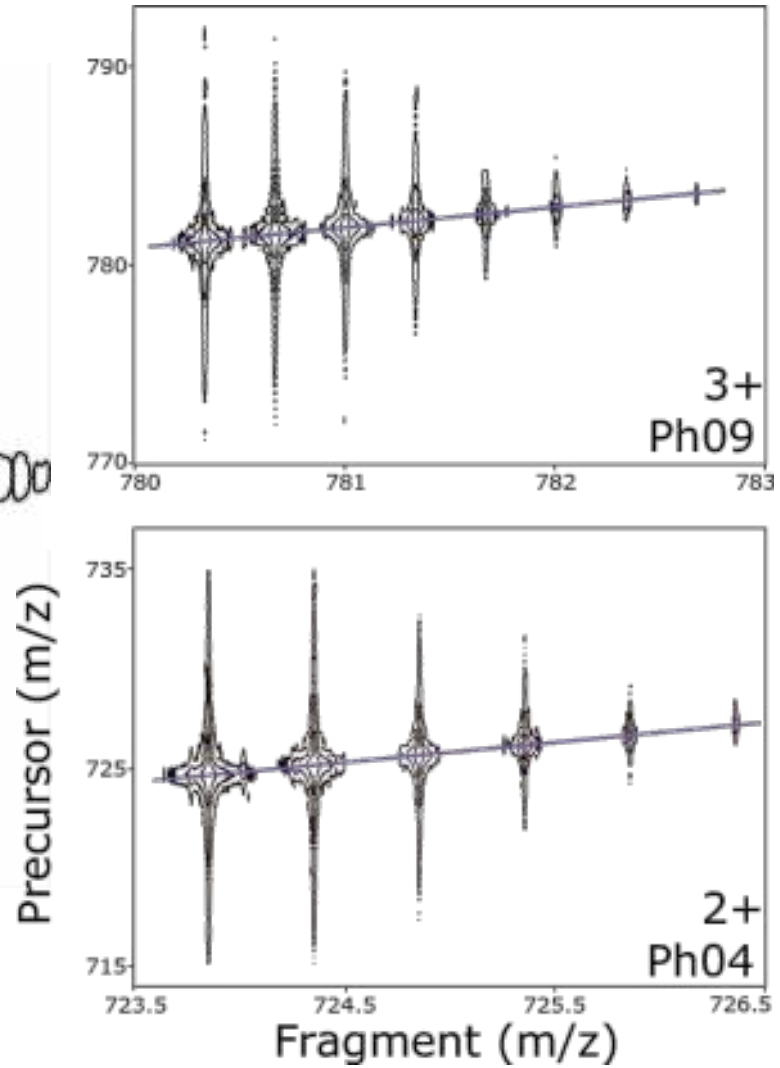

Horizontal: 1,048,576k transients (broadband)
Vertical: 8,192 scan lines.
Total: 8,589,934,592 data points

Phosphate Neutral Losses

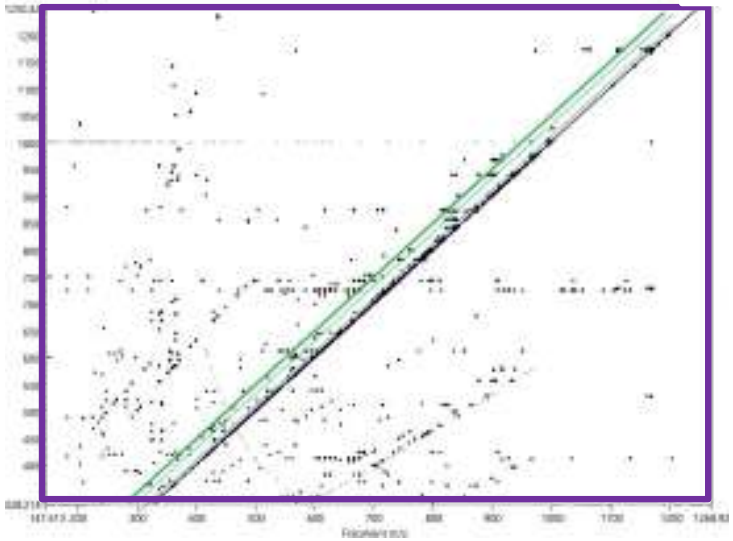

Detection of the Phosphopeptides

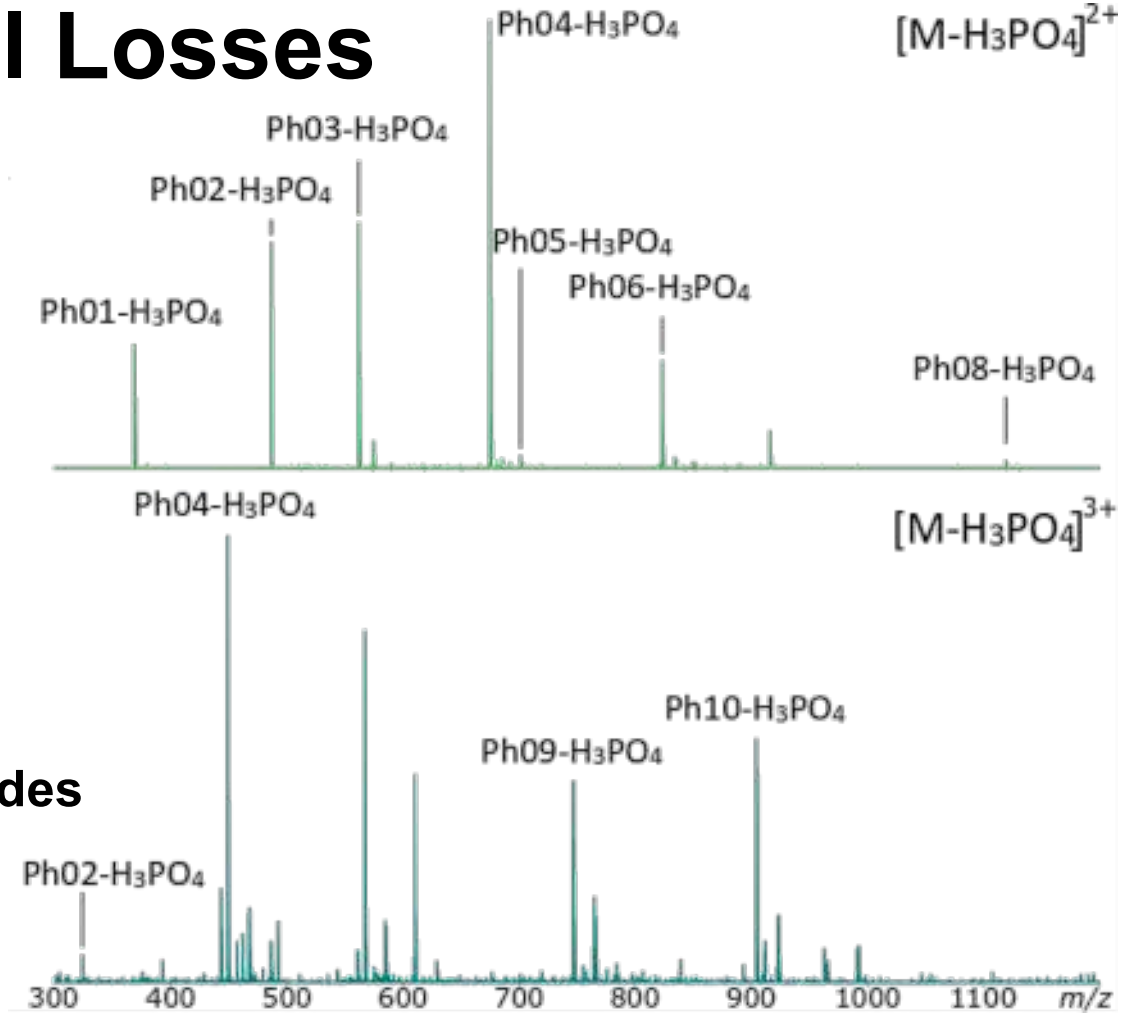

Extracted fragment Line of Ph06

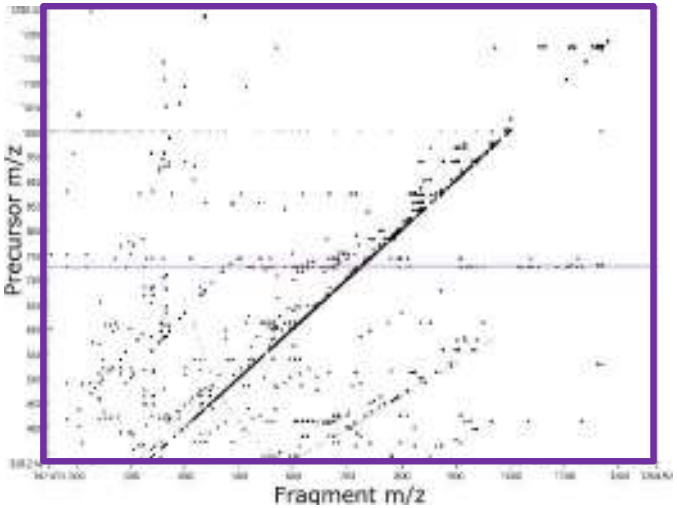

A D E P pS S E E S D L E I D

In red: fragments without Phosphate
In green: fragments with Phosphate

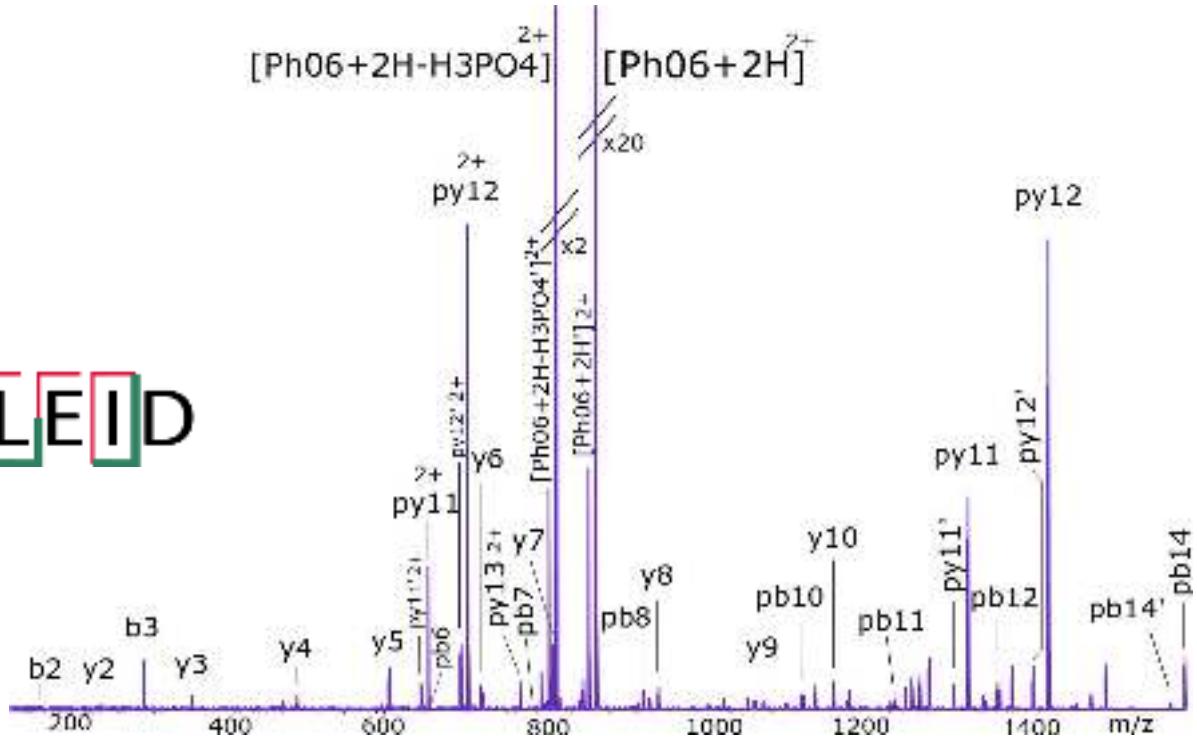

All Results

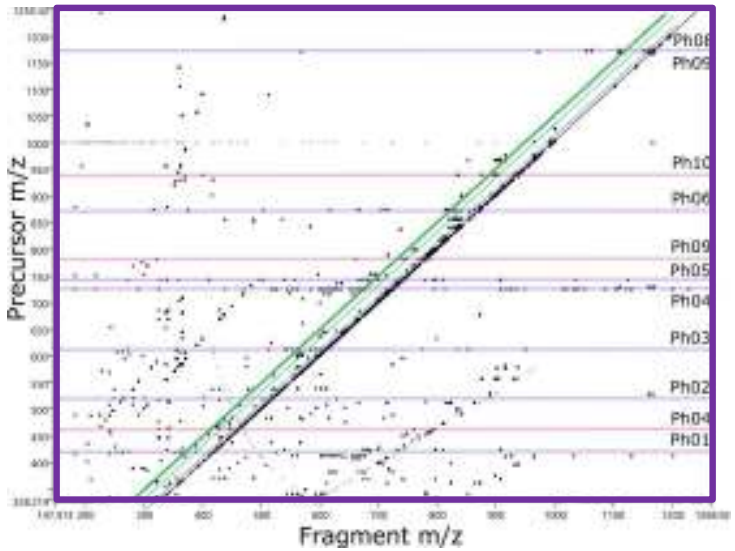

Advantages of 2DMS strategy:

Direct infusion

Quick identification with neutral loss lines

IRMPD selectively fragment phosphopeptides

Fragmentation of the Phosphopeptides

In red fragment without Phosphate

In green fragment with Phosphate

Ph01 V L H S G pS R

Ph02 R S pY pS R S R

Ph03 R D S L G pT Y S S R

Ph04 pT K L I pT Q L R D A K

Ph05 E V Q A E Q P S S pS S P R

Ph06 A D E P pS S E E S D L E I D K

Ph08 F E D E G A G F E E S pS E T G D Y E E K

Ph09 E L S N pS P L R E N S F G pS P L E F R

Ph10 S P T E Y H E P V pY A N P F Y R P T pT P Q R

Lecture overview

- 2DMS for agrichemical analysis.
- 2DMS for polymer analysis.
- 2DMS for monoclonal antibodies.
- Distinguishing phosphopeptides using 2DMS
- 2DMS – UVPD
- 2DMS on a linear ion trap

solariX – Laser Setup

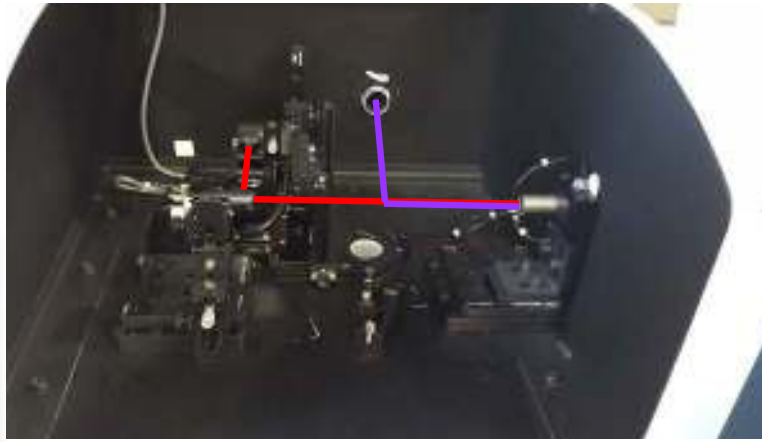

Dichroic mirror allows co-alignment of UV and IR beams

Coherent ExciStar XS, 193 nm
Synrad 48-2, 10.6 µm

UVPD-2DMS: Ubiquitin

8192 lines x 1 MW (just under 4 hours)

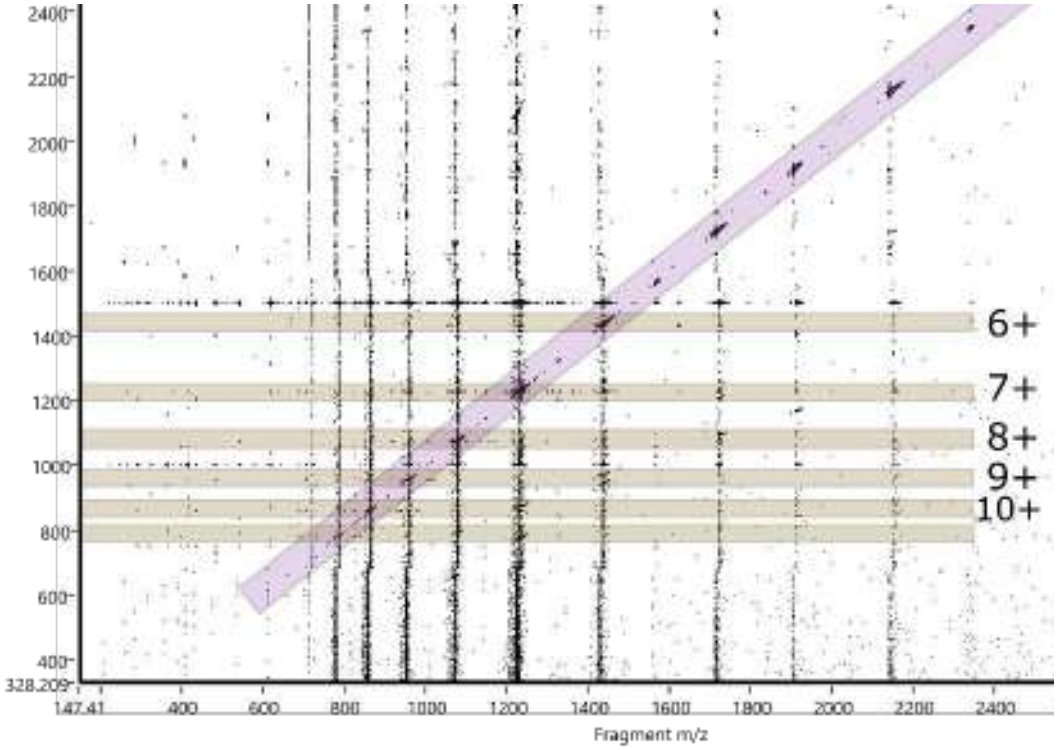

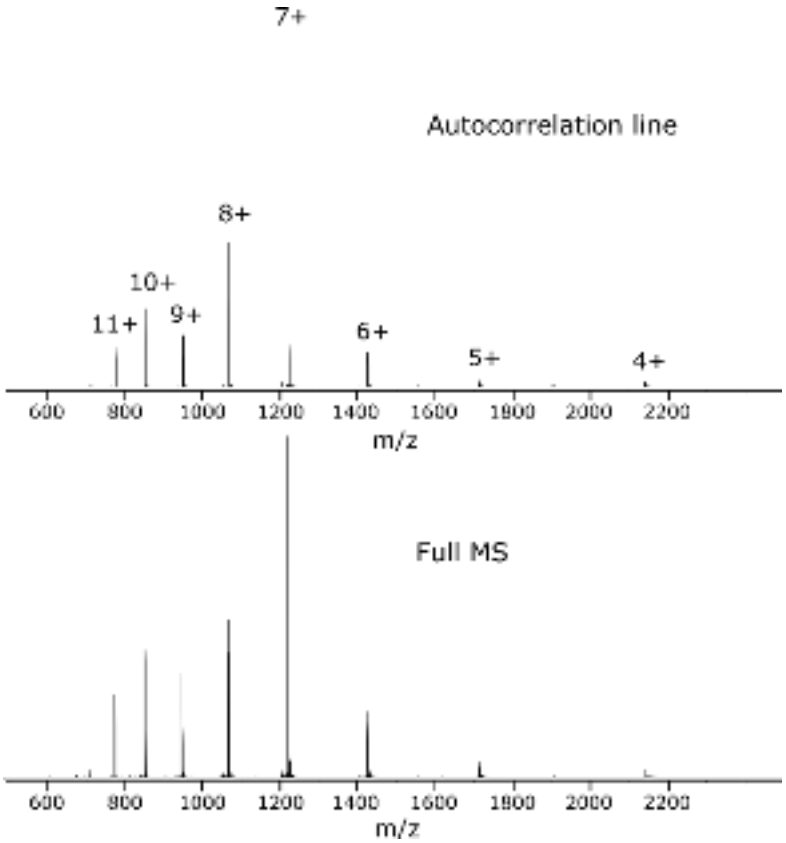

UVPD: 193 nm, 4 shots @ 6 mJ (~0.4 mJ in cell)

Horizontal lines

★ Scintillation noise
★ Precursor

6+

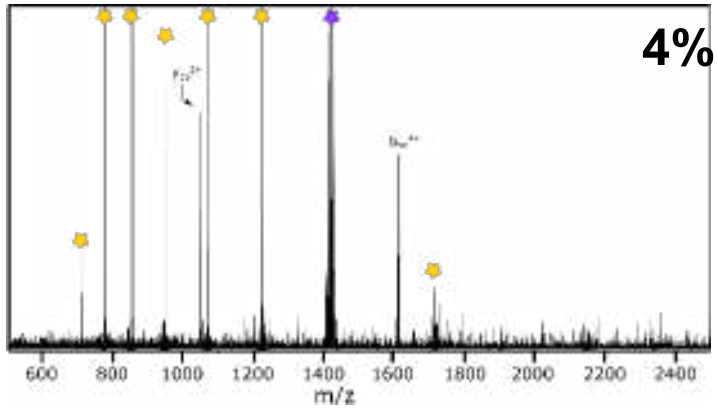

7+

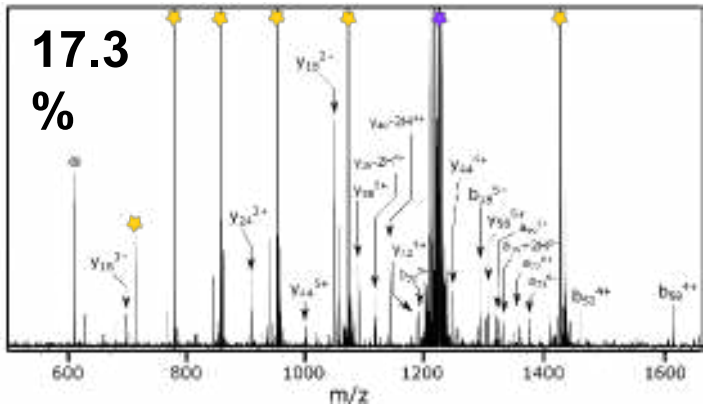

8+

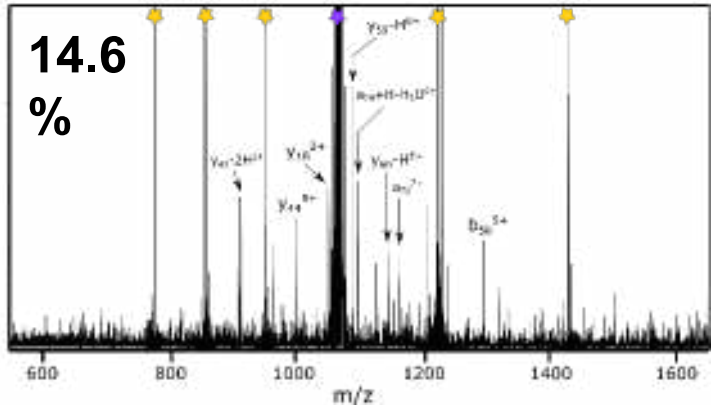

9+

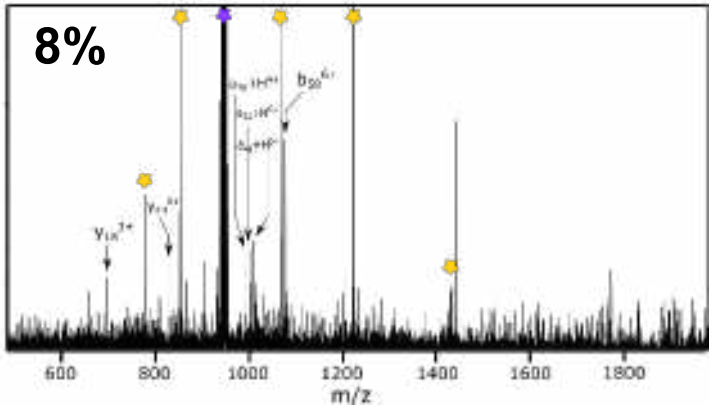

10+ : 9%

Lecture overview

- 2DMS for agrichemical analysis.
- 2DMS for polymer analysis.
- 2DMS for monoclonal antibodies.
- Distinguishing phosphopeptides using 2DMS
- 2DMS – UVPD
- 2DMS on a linear ion trap

Linear Ion Trap Geometry

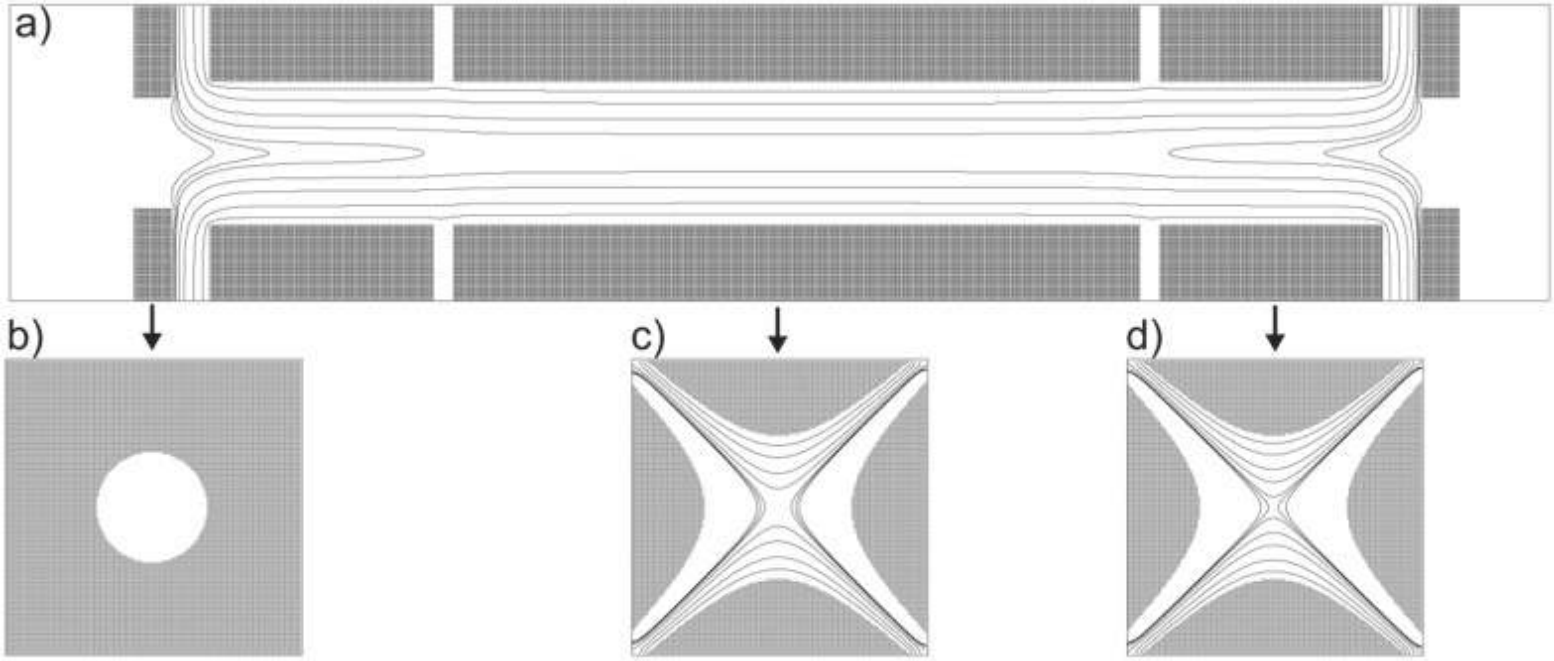

Figure 1. SIMION model of the linear ion trap with equipotential lines. a) Horizontal cut. b) Vertical cut of trapping electrode. c) Vertical cut of center quadrupole. d) Vertical cut of side quadrupole. The voltages applied on the LIT electrodes in this instance are +10.0 V_{DC} on the end-cap electrodes, +5.0 V_{DC} on the outer quadrupole rods, +/- 100.0 V_{RF} on the quadrupole rods. The equipotential lines are for: -100.0 V, -75.0 V, -50.0 V, -25.0 V, -10.0 V, 0.0 V, +2.5 V, 5.0 V, and 10.0 V.

1. Maria van Agthoven, Peter B. O'Connor, 2 Dimensional Mass Spectrometry in a Linear Ion Trap UK Patent GB1615469, 2016.
2. Maria van Agthoven and Peter B. O'Connor, Rapid Communications in Mass Spectrometry 2017, 31 (8), 674-684

2D MS in a Linear Ion Trap with SWIM

- Simion ion trajectory simulations show that 2DMS can be done on a linear ion trap.
- We have built a LIT-2DMS system and are in the process of testing the prototype.
- If coupled to a TOF mass analyzer, a LIT-TOF instrument could allow full 2DMS experiments in less than 10 seconds.

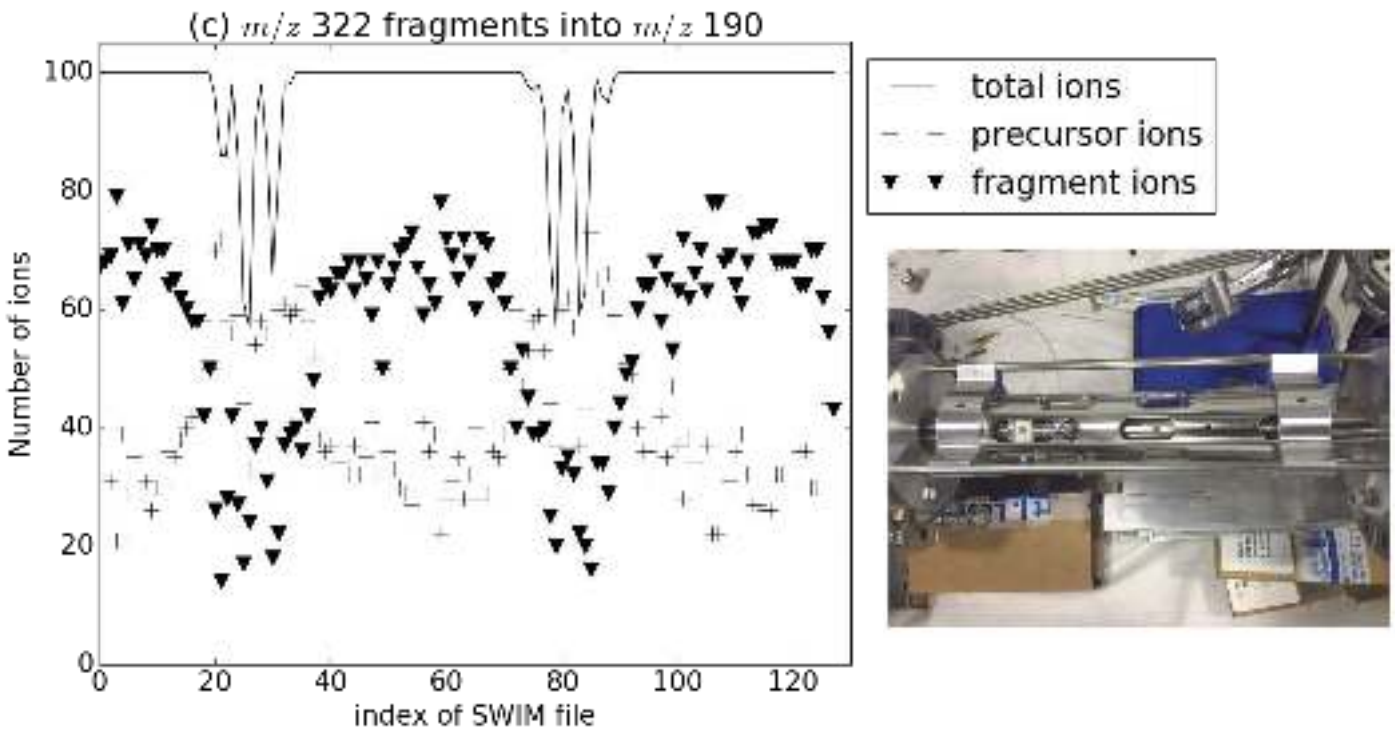

1. Maria van Agthoven, Peter B. O'Connor, 2 Dimensional Mass Spectrometry in a Linear Ion Trap UK Patent GB1615469, 2016.
2. Maria van Agthoven and Peter B. O'Connor, Rapid Communications in Mass Spectrometry 2017, 31 (8), 674-684

Tailored excitation for Fourier transform ion cyclotron mass spectrometry

Alan G. Marshall, Tao Chin Lin Wang, and Tom L. Ricca

Cite this: *J. Am. Chem. Soc.* 1985, 107, 26, 7893–7897
Publication Date: December 1, 1985
https://doi.org/10.1021/ja00312a015

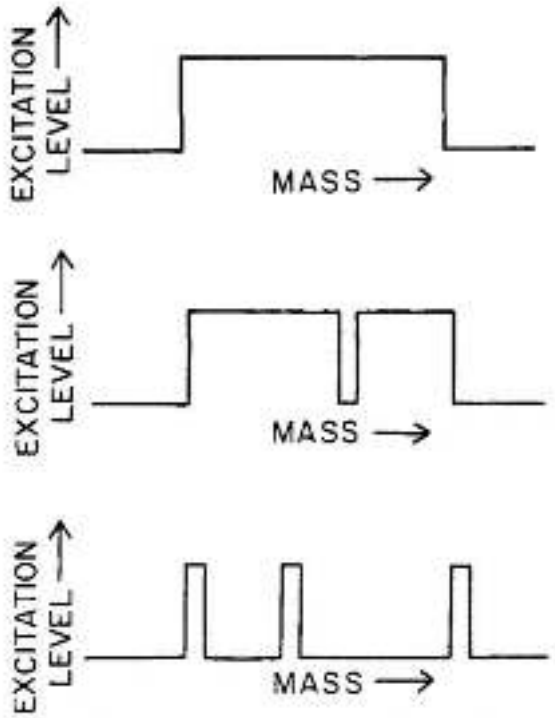

Figure 1. Desired excitation power spectra for Fourier transform ion cyclotron resonance mass spectrometry (FT/ICR). Top: Flat power over a specified mass range, for ordinary detection and/or isotope-ratio measurements. Middle: Flat excitation with a zero-power window, for use in the first stage of MS/MS experiments. Bottom: Multiple-frequency excitation for use in multiple-ion monitoring.

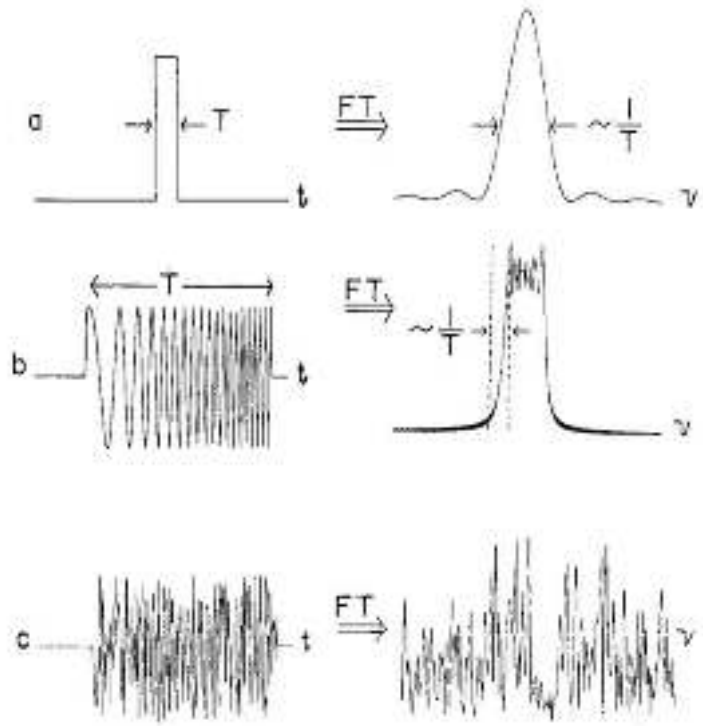

Figure 2. Previously employed time-domain excitation waveforms and their corresponding frequency-domain magnitude-mode spectra. Top: Single-pulse excitation (1). Middle: Frequency-sweep excitation (2, 12). Bottom: Pseudorandom noise excitation (13). Note the nonflat power and broad cutoff shoulders.

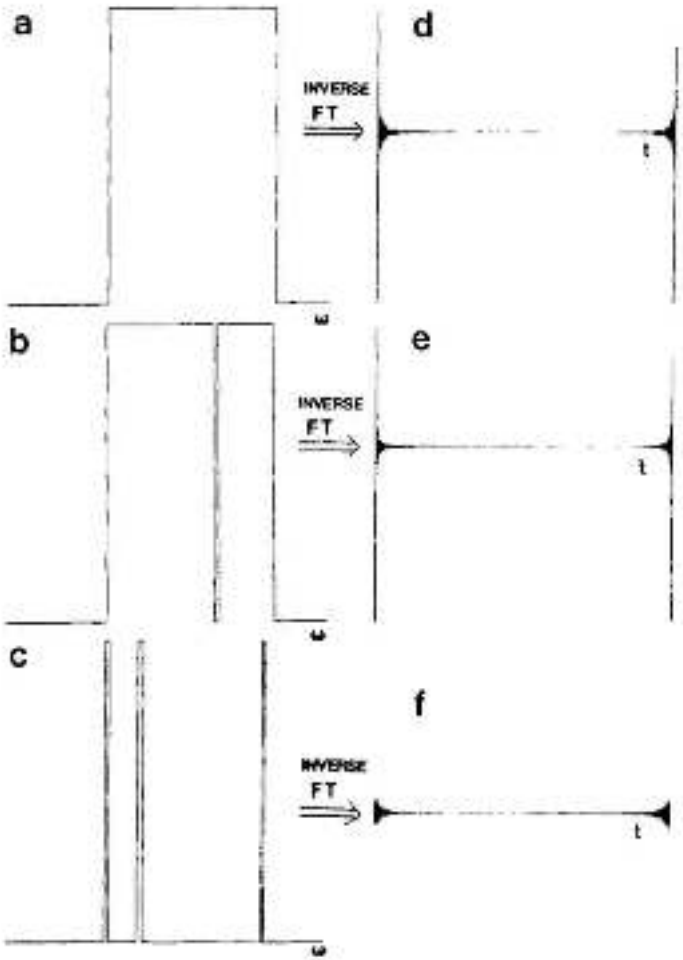

Figure 5. Time-domain excitation waveforms (right) generated by inverse Fourier transformation of the desired frequency-domain excitation spectra (left). Because mass and frequency are inversely related in ICR, the desired excitation mass spectra of Figure 1 are readily converted to those shown at the left in this figure.

J. Am. Chem. Soc. **1993**, *115*, 7854–7861

Two-Dimensional Fourier Transform Ion Cyclotron Resonance Mass Spectrometry/Mass Spectrometry with Stored-Waveform Ion Radius Modulation

Charles W. Ross, III, Shenheng Guan, Peter B. Grosshans,[†] Tom L. Ricca,[‡] and Alan G. Marshall*[,§]

Contribution from the Department of Chemistry, The Ohio State University, 120 West Eighteenth Avenue, Columbus, Ohio 43210

Received March 4, 1993

Abstract: A fundamentally new two-dimensional Fourier transform ion cyclotron resonance mass spectrometry experiment, SWIM ("stored-waveform ion modulation") 2D-FT/ICR MS/MS, is described. Prior encodement of the second dimension by use of two identical excitation waveforms separated by a variable delay period (analogous to 2D-NOESY NMR) is replaced by a new encodement in which each row of the two-dimensional data array is obtained by use of a single stored excitation waveform whose frequency-domain magnitude spectrum is a sinusoid whose frequency increases from one row to the next. In the two-dimensional mass spectrum, the conventional one-dimensional FT/ICR mass spectrum appears along the diagonal, and each off-diagonal peak corresponds to an ion-neutral reaction whose ionic components may be identified by horizontal and vertical projections to the diagonal spectrum. Fragmentation due to (e.g.) collision-induced dissociation results in peaks on only one side of the diagonal, whereas bidirectional ion–molecule reactions result in peaks on both sides of the diagonal. All ion–molecule reactions in a gaseous mixture may be identified from a single 2D-FT/ICR MS/MS experiment, without any prior knowledge of the system.

The fundamental concept of SWIM:

Through each of the succeeding scans, calculate a SWIFT pulse with steadily incrementing cycles of a sine wave.

This will have the effect of modulating ion radius rapidly on the right end of the spectrum and slowly on the left end, and linearly varying modulation frequencies in between.

When combined with a radius-dependent fragmentation method, to create a 'fragmentation zone', this allows 2DMS.

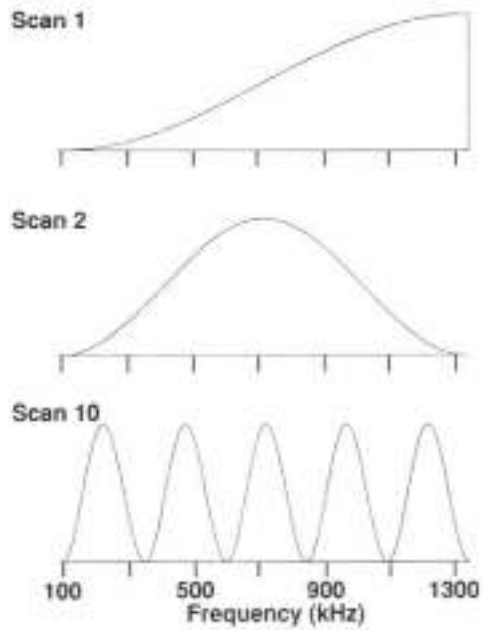

Figure 2. SWIFT magnitude-mode spectra (see eq. 3) of several parent ion modulation waveforms, for $j = 1, 2$, and 10. Note that the excitation amplitude for ions of the highest cyclotron frequency, 1333.0 kHz, is modulated the fastest in proceeding from one waveform to the next, whereas the excitation amplitude for ions of the lowest cyclotron frequency, 100 kHz, is not modulated at all from one waveform to the next. The mass-to-charge ratio range corresponding to these ion cyclotron frequencies is $34.8 < m/z < 463$ ($B = 3.02$ T).

Anal. Chem. **2002**, *74*, 4625−4633

Application of Stored Waveform Ion Modulation 2D-FTICR MS/MS to the Analysis of Complex Mixtures

Charles W. Ross, III,*,† William J. Simonsick, Jr.,‡ and David J. Aaserud‡

DuPont Marshall R & D Laboratory, Philadelphia, Pennsylvania 19146, and Merck Research Labs, Merck & Co. Inc., West Point, Pennsylvania 19486

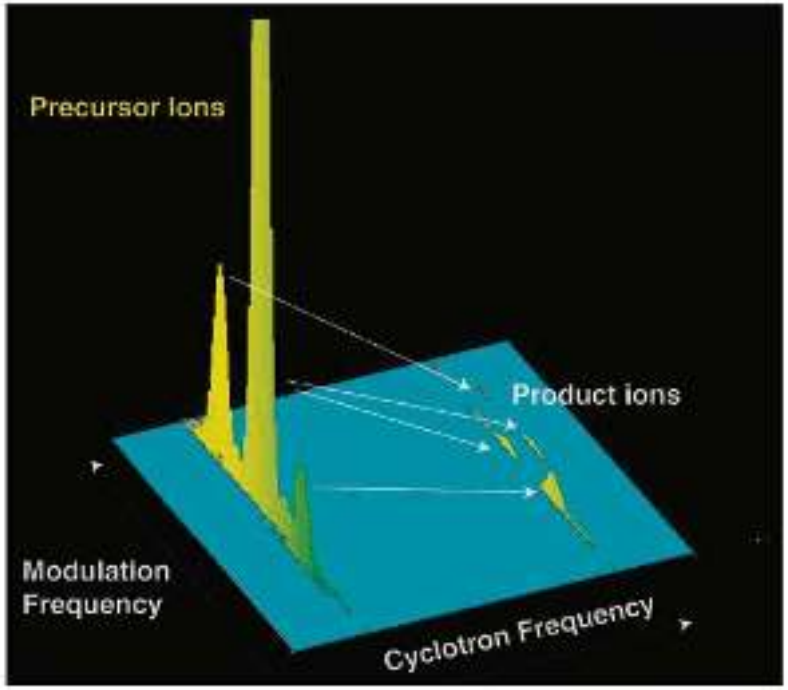

Figure 3. Power plot of the SWIM two-dimensional Fourier transform mass spectrum of the reactive oligomer intermediate.

Horizontal: 16k transients (narrow band)
Vertical: 128 scan lines.
Total: 2,097,152 data points

Verdel Instruments: 2DMS using UVPD on a Q-TOF

UV laser and beam optics

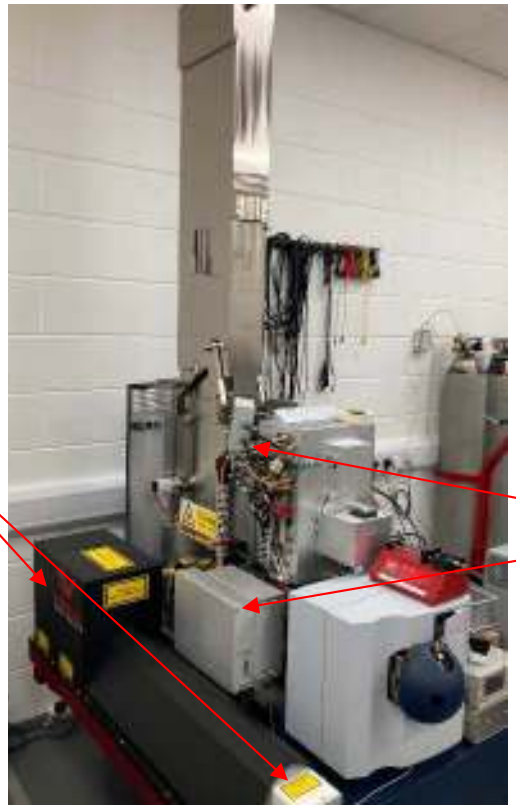

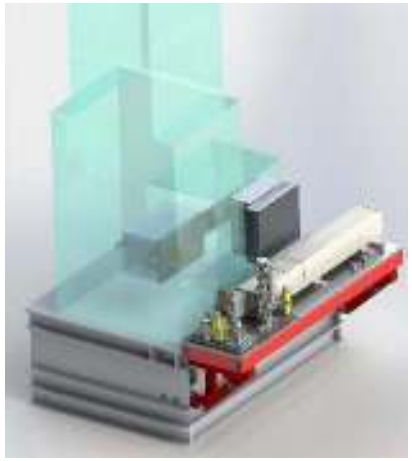

Quadrupole and lens control systems

MaXis ETD II Q-TOF

VERDEL INSTRUMENTS LTD

Slide from Dr. Nathan Cassidy, Verdel Instruments Ltd.

Instrument Modifications

- Transformed quadrupole to linear ion trap (LIT).

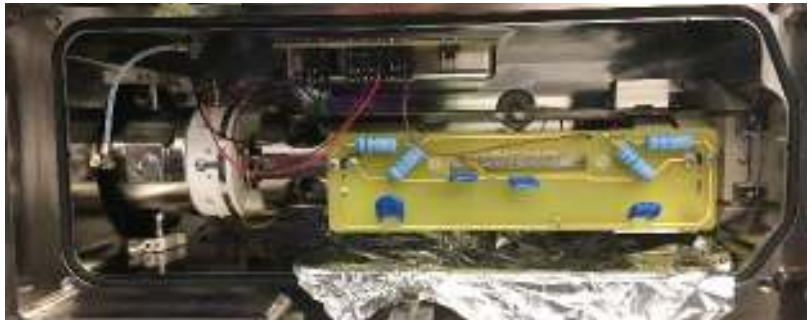

- Drive the RF with our own tank circuit amplifier.

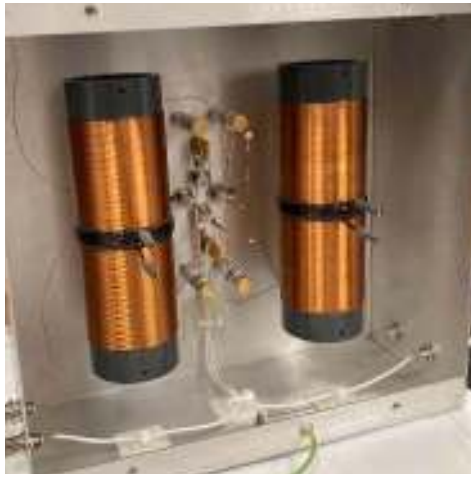

- Control of LIT lenses with DC trapping amp.

VERDEL INSTRUMENTS LTD

Slide from Dr. Nathan Cassidy, Verdel Instruments Ltd.

Excitation of Ions

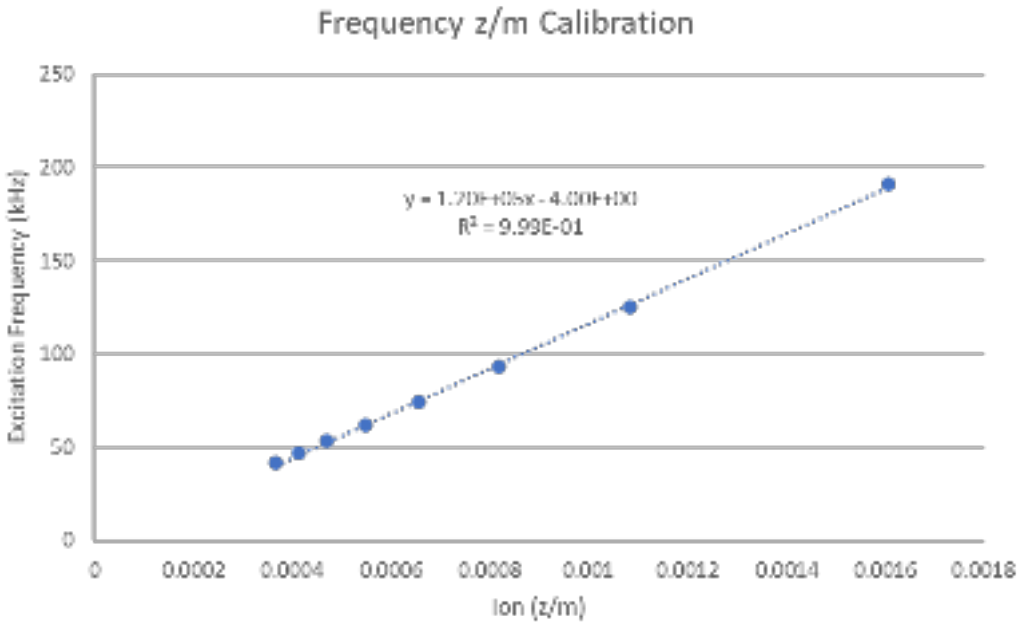

- **Linear relation between excitation frequency and z/m of ejected ion**

$$\omega = \frac{6}{\sqrt{2}} \frac{z}{m} \frac{V_{RF}}{r^2 \Omega}$$

Stability of V_{RF} and Ω are critical for stability of the secular frequency

constant

Mass/charge

fixed

fixed

VERDEL INSTRUMENTS LTD

Slide from Dr. Nathan Cassidy, Verdel Instruments Ltd.

Substance P: 449.9 m/z isotope pattern

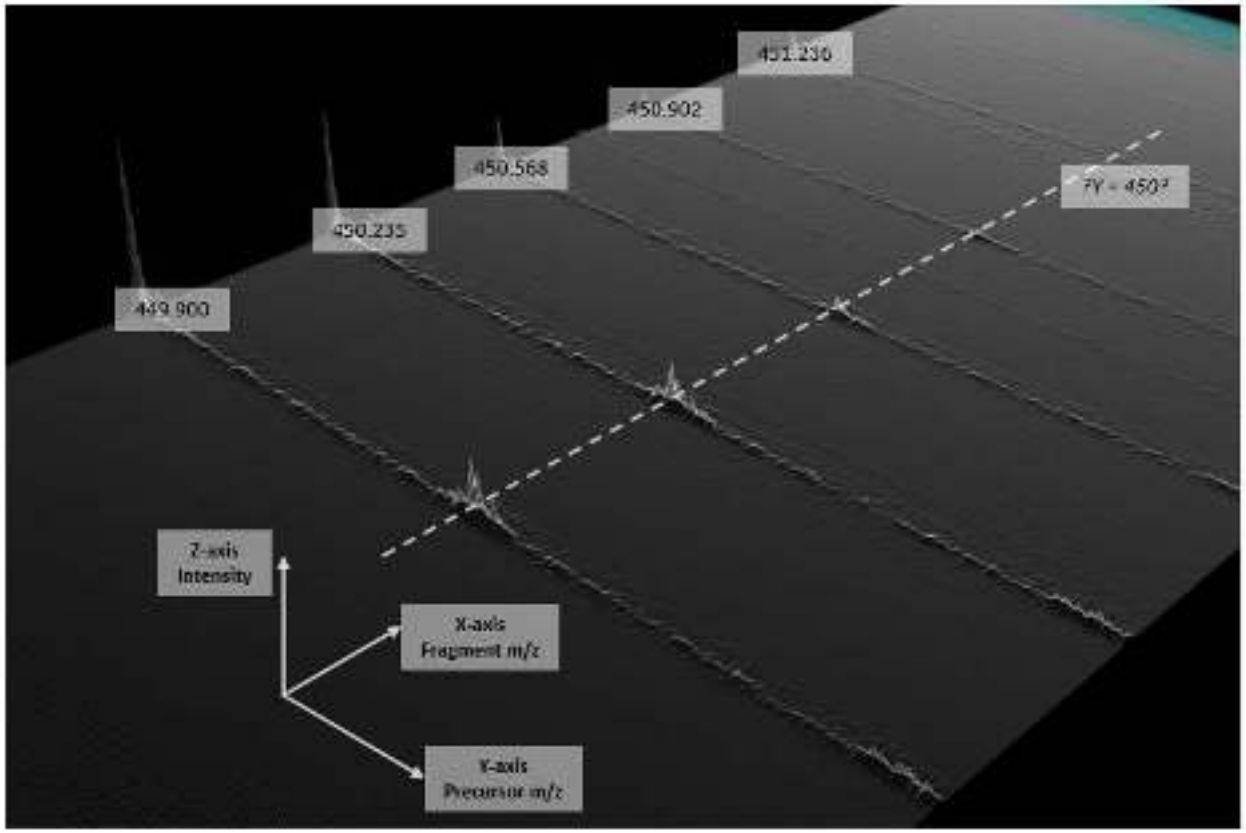

VERDEL
INSTRUMENTS LTD

Slide from Dr. Nathan Cassidy, Verdel Instruments Ltd.

LEADING INNOVATION IN TOC-MS™

TOTAL CORRELATION MASS SPECTROMETRY™

The Next Generation of Mass Spectrometry

Compatible with any mass spectrometer that uses linear ion trap technology.

VERDEL
INSTRUMENTS LTD

2-Dimensional mass spectrometry

- 2-dimensional mass spectrometry (2DMS) is now feasible, and bordering on the routine, for a wide range of samples in FTICR mass spectrometry.

- 2DMS can be achieved by modulating ions through a fragmentation zone (with frequencies dependent on m/z) using the Gaumann pulse sequence or the SWIM methods. Fragments will appear at the modulation frequencies thus correlating fragments with their precursors. The Fourier transform can extract those frequencies.

- 2DMS requires large data sets, currently up to 2B data points or more, which wasn't really feasible to process in the 1990's, but it now can be done.

- 2DMS can be done with a range of fragmentation methods, including IRMPD, ExD, and UVPD.

- 2DMS can be done on a linear ion trap, and we've spun out Verdel Instruments to achieve this commercially.

Acknowledgements

Funding

- EPSRC (J003022, N021630, N033191)
- BBSRC (P021875, R022399)
- Royal Society Translation Award
- Innovate UK iCure award
- H2020 EU-FT-ICR-MS Network
- Innovate UK / Verdel Instruments Ltd

This project has received funding from the European Union's Horizon 2020 research and innovation programme under grant agreement No 731077.

EU FT-ICR MS

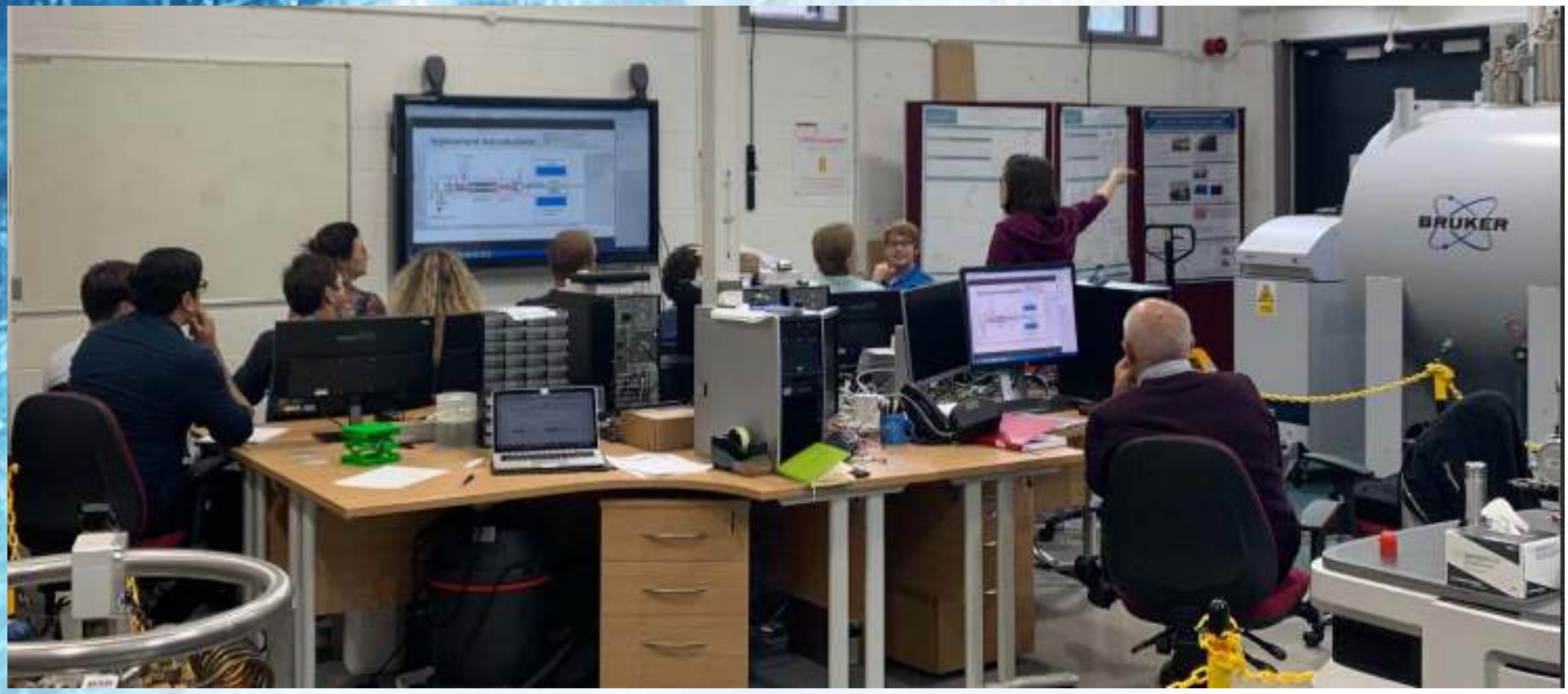

This project has received funding from the European Union's Horizon 2020 research and innovation programme under grant agreement No 731077.

This project has received funding from the European Union's Horizon 2020 research and innovation programme under grant agreement No 731077.

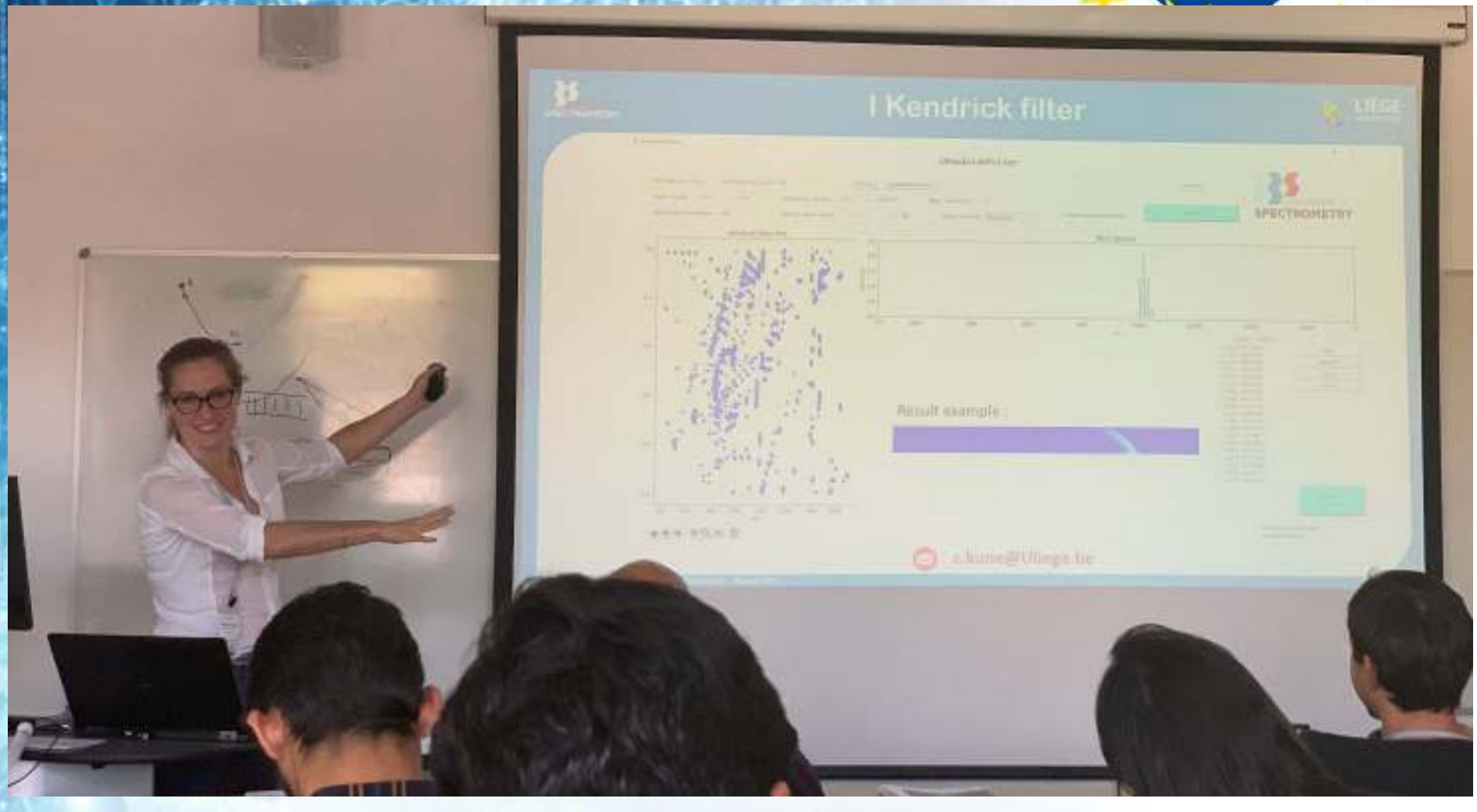

This project has received funding from the European Union's Horizon 2020 research and innovation programme under grant agreement No 731077.

This project has received funding from the European Union's Horizon 2020 research and innovation programme under grant agreement No 731077.

This project has received funding from the European Union's Horizon 2020 research and innovation programme under grant agreement No 731077.

This project has received funding from the European Union's Horizon 2020 research and innovation programme under grant agreement No 731077.

This project has received funding from the European Union's Horizon 2020 research and innovation programme under grant agreement No 731077.

This project has received funding from the European Union's Horizon 2020 research and innovation programme under grant agreement No 731077.

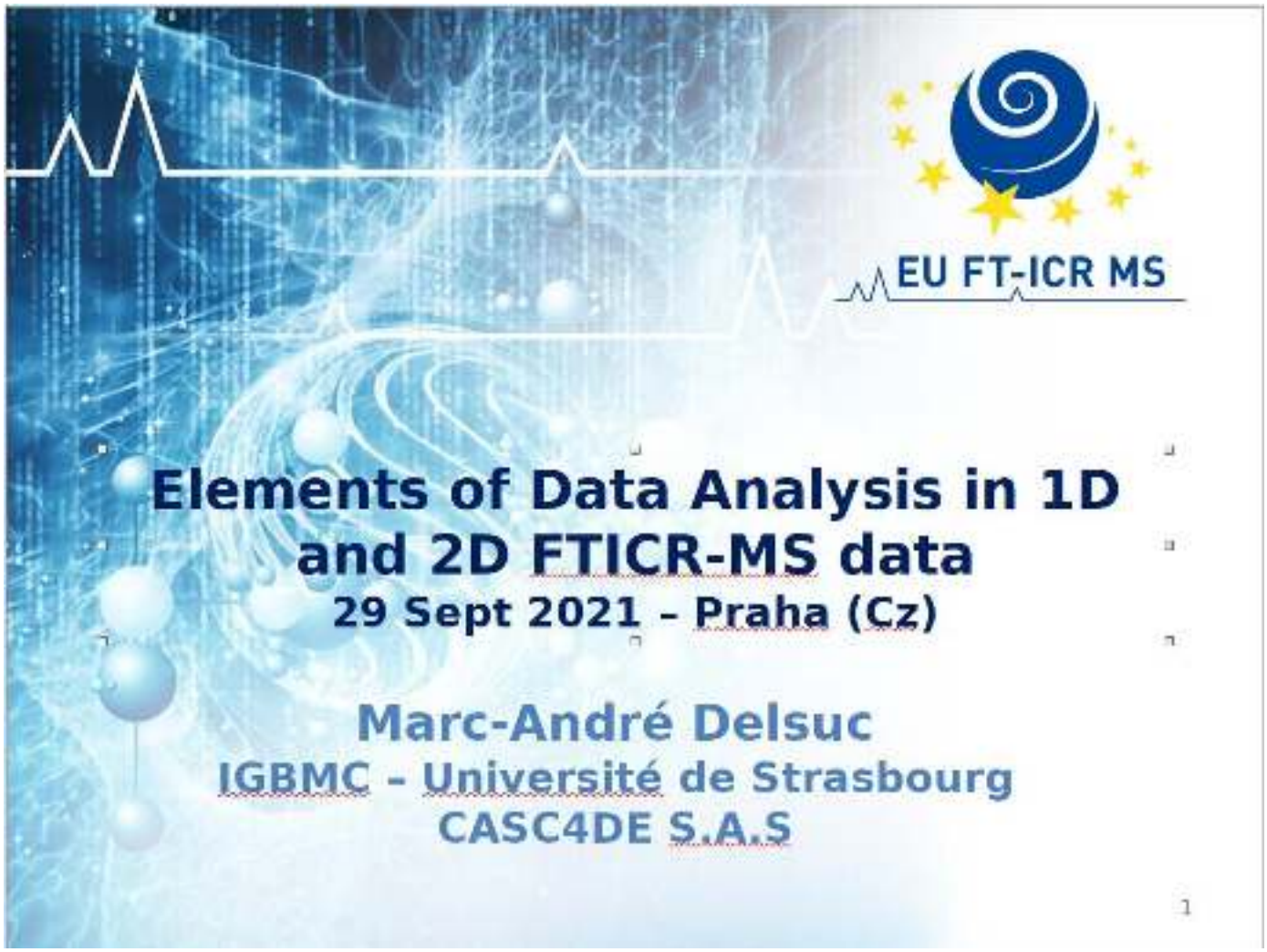

This presentation relies on several tools and set-up available in jupyter notebooks

- a complex scientific python stack
- the spike processing library installed
- choosing to view the cell slideshow support will help
- the "Hide imput" nb extension to hide the python code
- the RISE nbextension to run the slideshow

In [1]:

```
%matplotlib inline
%autosave 60
```

executed in 512ms, finished 09:41:32 2021-09-30

```
Autosaving every 60 seconds
```

In [2]:

```
#import spike
#from spike.Interactive import INTER as I
#I.hidecode(message="")
import matplotlib
import matplotlib.pyplot as plt
from matplotlib.pyplot import scatter, plot, figure, text, title, xlabel, ylabe
import numpy as np
from numpy import exp, cos, sin, arctan2, pi, linspace, arange

from ipywidgets import Button, interactive
import ipywidgets as widgets
from IPython.display import display, HTML, Javascript, Markdown, Image

matplotlib.style.use("fivethirtyeight")
for i in ('font.size','axes.labelsize','legend.fontsize','legend.title_fontsize
    matplotlib.rcParams[i]=24
for i in ('xtick.labelsize', 'ytick.labelsize'):
    matplotlib.rcParams[i]=18

#matplotlib.style.available
```

executed in 108ms, finished 09:41:32 2021-09-30

Elements of Data Analysis in 1D

and 2D FTICR-MS data

Marc-André Delsuc - 2nd Advanced User School, Prague, Sept 2021

---

3 parts

- **The Fourier Transform - the basic aspects**
  - some theory
- **The basic FT-ICR experiment**
  - playing with real data
  - some more theory
- **more advanced aspects**
  - big datasets
  - even more theory

The slides presented during this meeting are available under a CC BY-SA licence at `github.com/delsuc/2nd-AUS-FTICR`

1. The Fourier Transform - the basic aspects

2nd-AUS-FTICR

Marc-André Delsuc - Prague 26-30 Sept 2021

This work is licensed under CC BY-SA 4.0 (https://creativecommons.org/licenses/by-sa/4.0/)

a developed content of this part can be found on github.com/delsuc (https://github.com/delsuc/Fourier_Transform/blob/master/Definition_Properties.ipynb)

FT-MS - Fourier Transform Mass Spectrometry

You know it !

FT-ICR - indeed

Orbitrap - of course

also Charge Detection MS

and other more "exotic" approaches

they have in common

- very high resolving power
- slow...

BUT what is Fourier transform ?

Fourier Transform Definition

Fourier Transform is defined on continuous functions:

for a function $f(x)$ $x \in \mathbb{R} \rightarrow f(x) \in \mathbb{C}$

the **Fourier transform** of f is another function F

$F(X)$ $X \in \mathbb{R} \rightarrow F(X) \in \mathbb{C}$

$$f \xrightarrow{FT} F$$

$$F(X) = \int_{-\infty}^{+\infty} f(x) e^{-2i\pi x X} dx$$

❓

😭 **or** 🤣

Time vs Frequency - One example

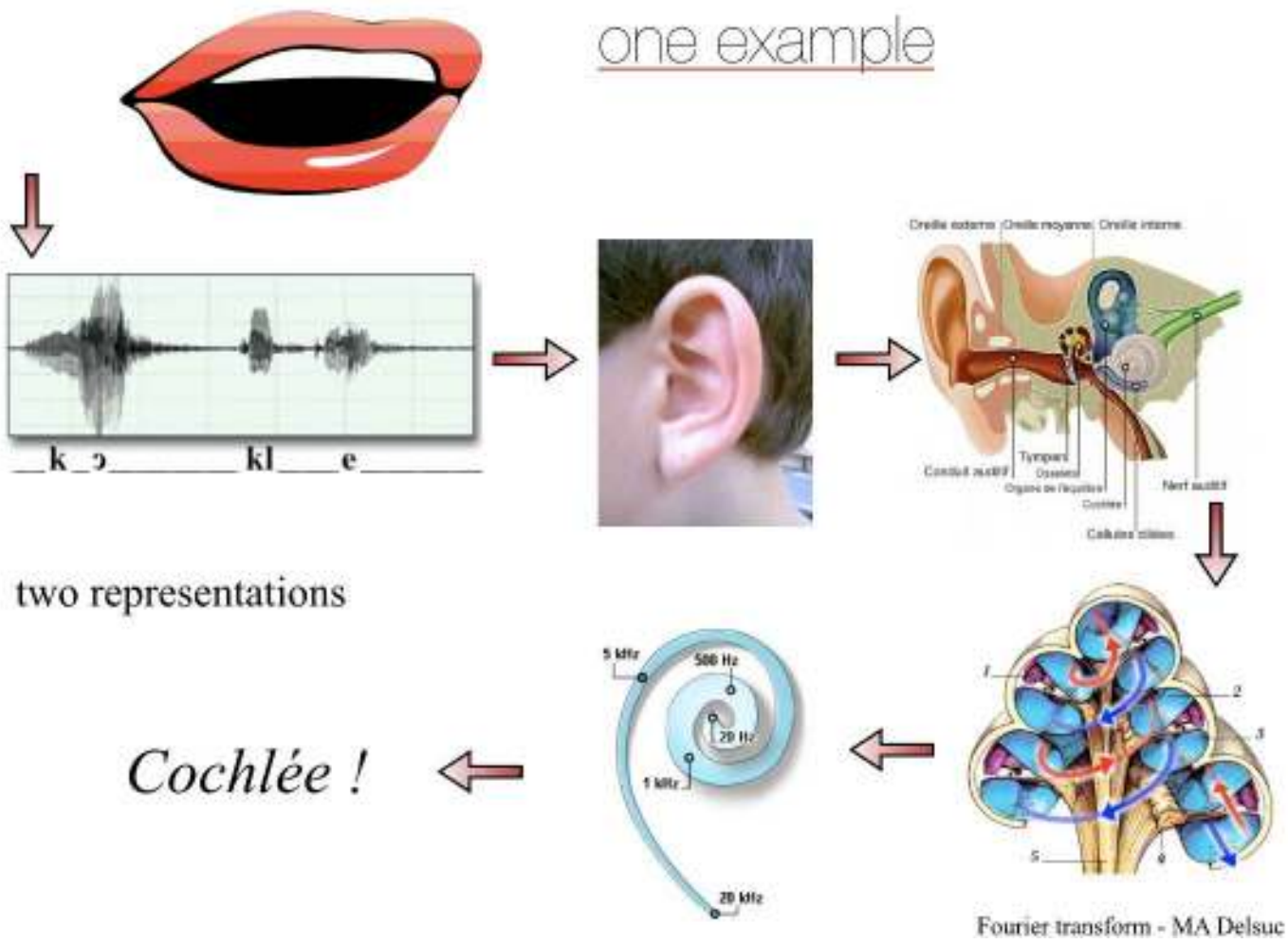

Time vs Frequency - One example

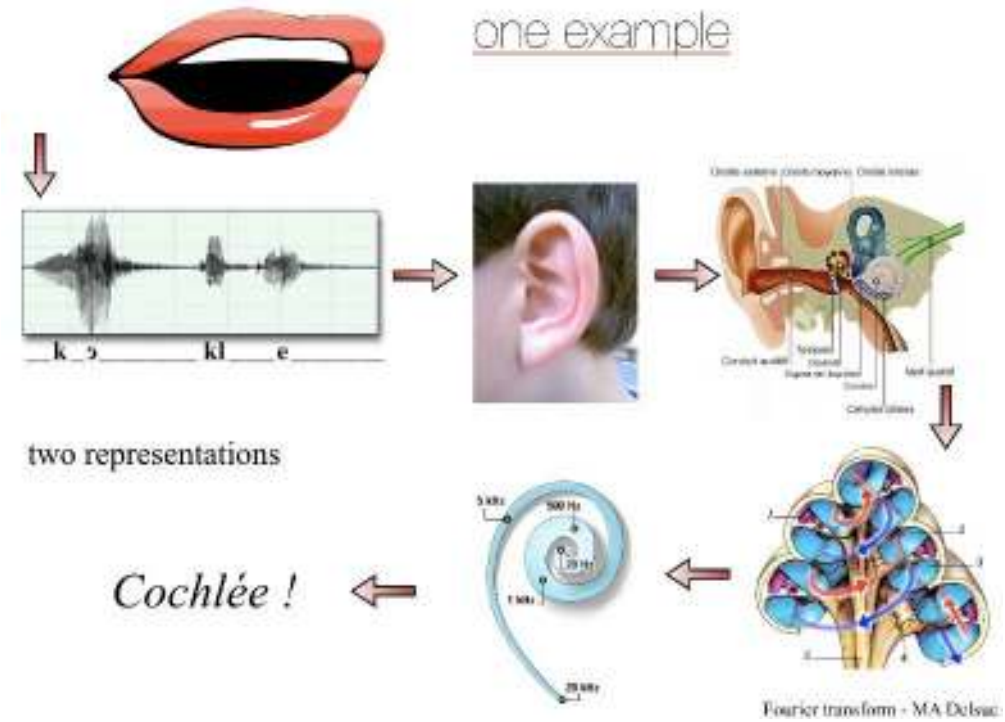

- $f(t)$ pressure wave / function of time.

- ear-drum vibrate with the same pattern → standing wave in the cochlea → *position F(frequency)*
  - ⇒ a mechanical Fourier transform !
- phonetic pattern is somehow the time-dependent **Fourier transform** of the inital pressure wave.
- They both carry somehow the same information, but in a very different way.
- 2 point of views for the same information

Fourier Transform Definition (2)

using $x \rightarrow t$ as time

and $X \rightarrow \omega$ as frequency

$$\text{the expression} \qquad \int_{-\infty}^{+\infty} f(t) e^{-2i\pi\omega t} dt$$

is just a way to **weigh** in $f(t)$ the presence of a given frequency ω : $e^{-2i\pi\omega t}$

x and X represent two different reciproqual quantitites, and can be found in many domains

x	X
t : time (sec)	ω : frequency (Hz)
x : space (Å)	k : spatial frequency (Å^{-1})
λ : wavelength (cm)	k : spatial frequency (cm^{-1})
etc...	

exemple on a real data-set !

ECD fragmentation of a mixture of 4 histone peptides with various PTM *from M. van Agthoven - Innsbruck*

In [3]:

```
import spike
from spike.File import BrukerMS as bkMS
d = bkMS.Import_1D("files/histonepeptide_ms2_000002.d/fid")
```

executed in 3.75s, finished 09:41:36 2021-09-30

```
    ========================
          SPIKE
    ========================
    Version     : 0.99.29
    Date        : 20-09-2021
    Revision Id : 529
    ========================
*** zoom3D not loaded ***
plugins loaded:
Fitter,  Linear_prediction,  Peaks,  bcorr,  fastclean,  gaussenh,  re
m_ridge,  sane,  sg,  test,  urQRd,
plugins loaded:
msapmin,

spike.plugins.report() for a short description of each plugins
spike.plugins.report('module_name') for complete documentation on one
plugin
plugins loaded:
FTMS_calib,  PhaseMS,  diagonal_2DMS,
*** PALMA not loaded ***
plugins loaded:
Bruker_NMR_FT,  Bucketing,  Integrate,  apmin,
Using 3 parameters calibration,  Warning calibB is -ML2
```

In [4]:

```
figure(figsize=(16, 3))
d.display(new_fig=False)
```

executed in 325ms, finished 09:41:36 2021-09-30

Out[4]:

```
FTICR data-set
Bo: 7.05
Single Spectrum data-set
FT-ICR axis at 535.714286 kHz,  524288 real points,  from physical mz
=  202.203   to m/z = 1450.000  R max (M=400) = 265036
```

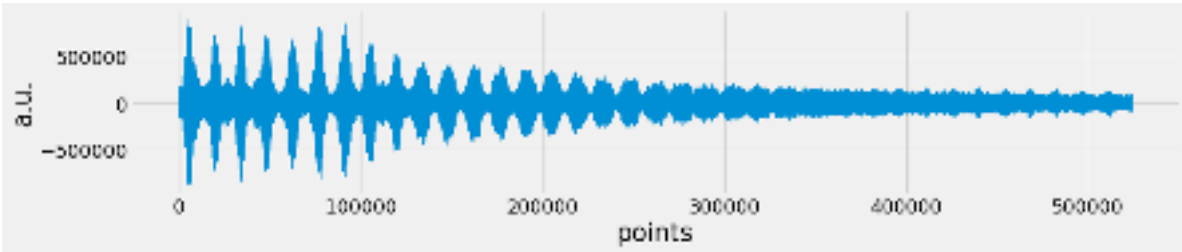

In [5]:

```
figure(figsize=(16,4))
D = d.copy().center().kaiser(4).zf(2).rfft().modulus()
D.set_unit('m/z').display(zoom=(400,750),new_fig=False);
```

executed in 332ms, finished 09:41:37 2021-09-30

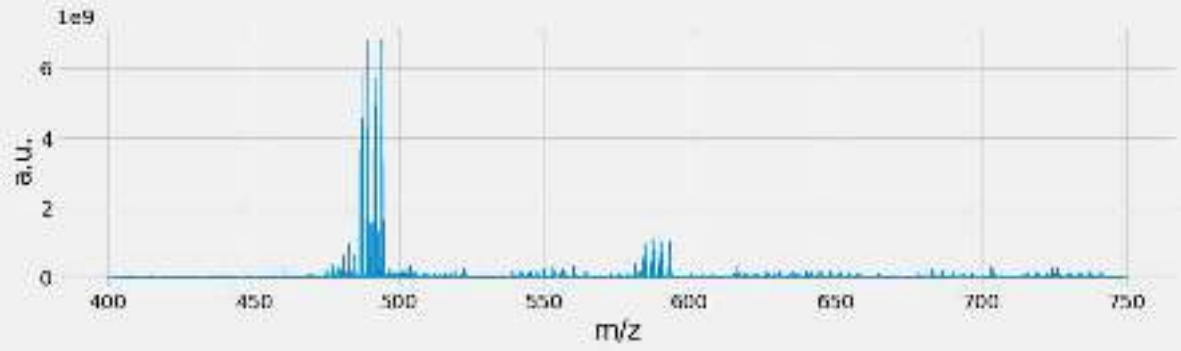

In [6]:

```
display(Markdown("**zooming on the main peptides** *(10 Thomson wide)*"))
figure(figsize=(16,4))
D.display(zoom=(486, 496),new_fig=False);
```

executed in 148ms, finished 09:41:37 2021-09-30

zooming on the main peptides *(10 Thomson wide)*

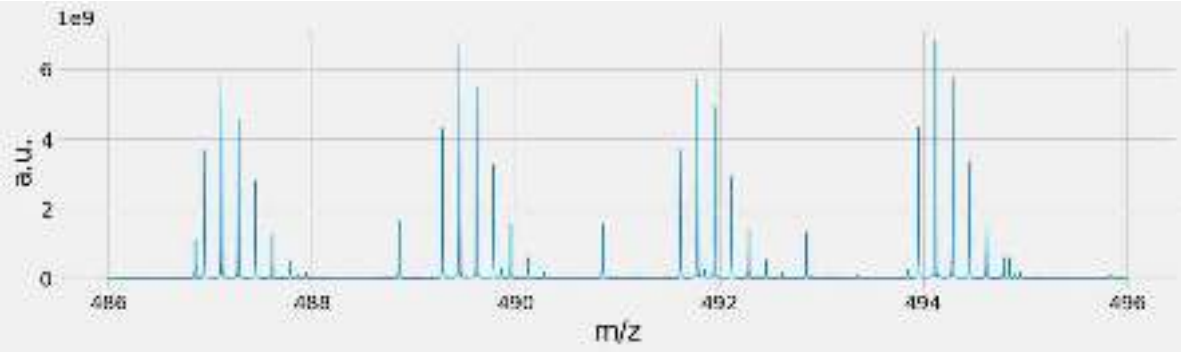

In [7]:

```
display(Markdown(r"**zooming on smaller fragments** *( 5 Thomson wide - $\times
figure(figsize=(16,4))
D.display(zoom=(554, 559),scale=50,new_fig=False);
```

executed in 147ms, finished 09:41:37 2021-09-30

zooming on smaller fragments *(5 Thomson wide - $\times 50$)*

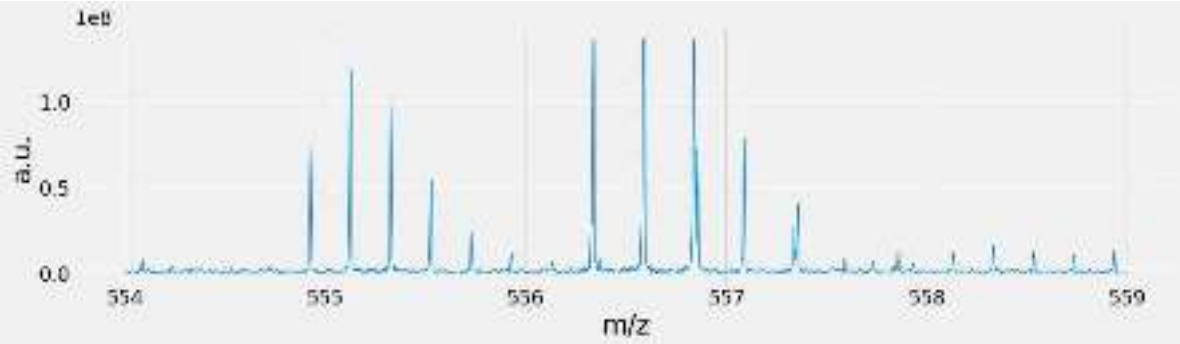

a brief reminder on complex numbers.

- *complex numbers are central to Fourier analysis, and their understanding is needed to fully comprehend the beauty of Fourier analysis*

Real numbers are *regular* numbers, going from $-\infty$ to $+\infty$.

- They belong to $\mathbb{R}$, the set of all real numbers
- $\mathbb{R}$ can be seen as a line, going from $-\infty$ to $+\infty$.

If Reals are on a line, Complex numbers are on a plane.

As any plane, the coordinates are defined on two axes, the horizontal axis is the $\mathbb{R}$ line, the vertical one is the *Imaginary* axis, also holding real numbers, and labeled with i. This plane is called $\mathbb{C}$ the complex plane.

A complex number z (a point in this plane) is thus described with two numbers, a and b:

$$z = a + ib$$

a is the real part, and b the imaginary part.

In [8]:

```
# let's draw this
figure(figsize=(8,8))
plot([-3,3],[0,0],':k') # the real axis
plot([0,0],[-3,3],':k') # the imaginary axis
scatter([1,0,-1,0],[0,1,0,-1], 100)
text(1,0.15,'1')
text(-1,0.15,'-1')
text(0.15,1,'i')
text(0.15,-1,'-i')
title('the complex plane $\mathbb{C}$')
a = 2
b = 1.5
z = a + 1j*b             #  i is noted j in python
scatter(z.real, z.imag, 100)
plot([0,z.real],[0,z.imag],'--k')
plot([z.real,z.real],[0,z.imag],':k')
plot([0,z.real],[z.imag,z.imag],':k')
xlabel("Real")
ylabel("Imaginary")

text(a, -0.3, '$a$')
text(-0.3, b,'$b$')
text(a-0.3,b+0.2,'$z = a +ib$');

```

executed in 416ms, finished 09:41:37 2021-09-30

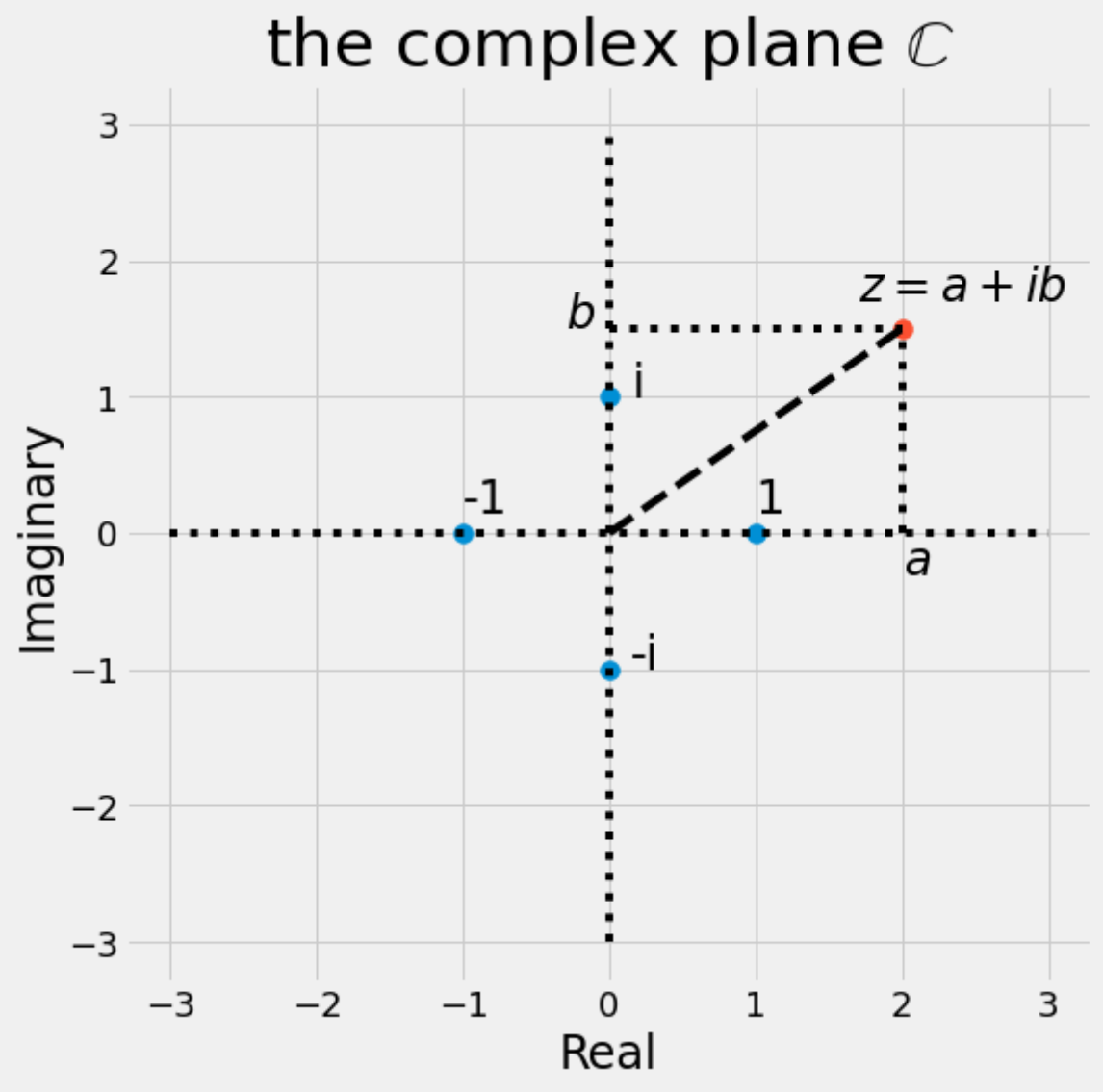

modulus

$$|z| = R = \sqrt{a^2 + b^2}$$

argument (*usually noted with a greek letter*)

$$arg(z) = \arctan\left(\frac{b}{a}\right) = \theta$$

This is noted using the *Euler* notation:

$$z = a + ib$$
$$z = Re^{i\,\arg(z)} = Re^{i\theta}$$

In [9]:

```
# let's draw this
figure(figsize=(8,8))
plot([-3,3],[0,0],':k') # the real axis
plot([0,0],[-3,3],':k') # the imaginary axis
title('the complex plane $\mathbb{C}$')
a = 2
b = 1.5
z = a + 1j*b              #  i is noted j in python
scatter(z.real, z.imag, 100)
plot([0,z.real],[0,z.imag],'--k')

xlabel("Real")
ylabel("Imaginary")

text(a-0.3,b+0.2,r'$z = R e^{i \theta}$');

t = linspace(0, np.arctan2(b,a),30)
plot(cos(t),sin(t))
text(a-0.5, b/2+0.1, '$R$')

text(1,0.5, r'$\theta$');
```

executed in 223ms, finished 09:41:37 2021-09-30

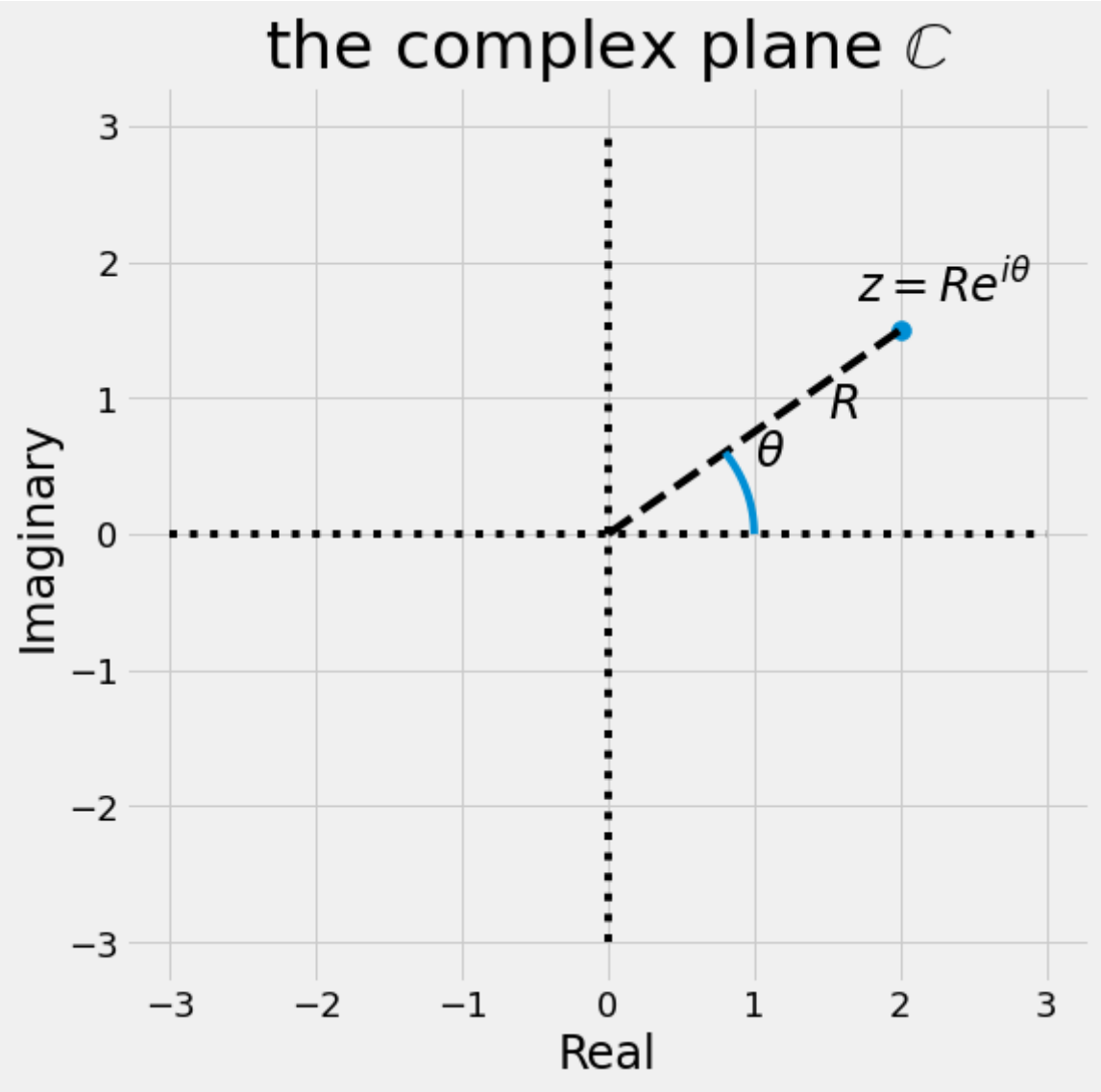

Complex numbers can be added and multiplied, they form an **algebra**.

The Euler Notation stresses the multiplicative rules, where **modulus** are multiplied, and **angles** are added.

$$z_1 . z_2 = R_1 e^{i\theta_1} . R_2 e^{i\theta_2}$$
$$z_1 . z_2 = R_1 R_2 e^{i(\theta_1 + \theta_2)}$$

In [10]:

```
# let's draw this
figure(figsize=(8,8))
plot([-3,3],[0,0],':k') # the real axis
plot([0,0],[-3,3],':k') # the imaginary axis
title('Multiplication on the complex plane $\mathbb{C}$')
z1 = a + 1j*b                              #  i is noted j in python
c = cos(pi/3)
d = sin(pi/3)
z2 = c + 1j*d
xp = (z1*z2).real
yp = (z1*z2).imag
scatter(a, b, 100)
scatter(c, d, 100)
scatter(xp, yp, 100)

plot([0,a],[0,b],'--k')
plot([0,c],[0,d],'--k')
plot([0,xp],[0,yp],'--k')

xlabel("Real")
ylabel("Imaginary")

text(a-0.3,b+0.2,r'$z1 = R e^{i \theta_1}$');
text(c-0.3,d+0.2,r'$z2 = e^{i \pi / 3}$');
text(xp-1.2, yp+0.2, r'$z3 = z1 . z2 = R e^{i (\theta_1 + \pi/3)}$');

text(a-0.5, b/2+0.1, '$R$')

t1 = linspace(0, arctan2(b,a),30)
plot(1.2*cos(t1), 1.2*sin(t1))

t2 = linspace(0, pi/3,30)
plot(cos(t2), sin(t2))

t3 = linspace(0, arctan2(yp,xp),30)
plot(0.8*cos(t3), 0.8*sin(t3));

```

executed in 374ms, finished 09:41:38 2021-09-30

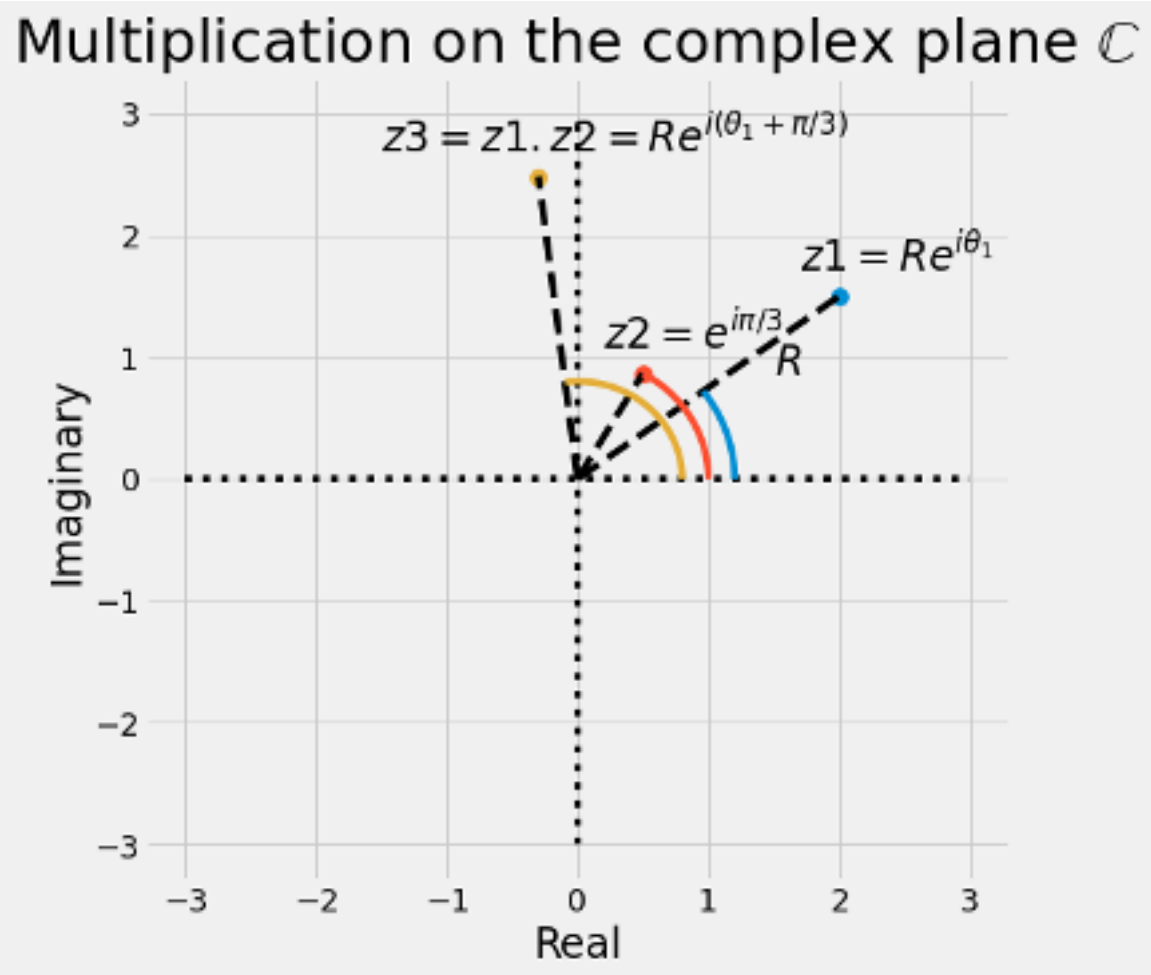

You have a more detailed (in interactive) presentation in [the complex_reminder (https://github.com/delsuc/Fourier_Transform/blob/master/Definition_Properties.ipynb)](https://github.com/delsuc/Fourier_Transform/blob/master/Definition_Properties.ipynb) on `github`
see also: [Wikipedia:Complex_plane (https://en.wikipedia.org/wiki/Complex_plane)](https://en.wikipedia.org/wiki/Complex_plane)

some useful properties of FT

Linearity

- $FT(A+B) = FT(A) + FT(B)$ FT of sum = sum of FT
- $\Rightarrow$ FT of a composite signal is just the sum of the FT of each component

Invertible

- $f \xrightarrow{FT} F \qquad F \xrightarrow{FT^{-1}} f$
- actually $F^{-1} = F^3$
- 2 different points of view of the SAME information ! *(~ rotating by 90° in information space)*

Unitary

- *if F is the FT of f* $\int |f(t)|^2 dt = \int |F(\omega)|^2 d\omega$ $\Rightarrow$ signal power is conserved

some useful properties of FT *(2)*

integrals

$F_o = \int f(t)dt \qquad f_o = \int F(\omega)d\omega$

compaction theorem

convolution theorem

- both are central !
- so important we shall see them later on !

FT vs DFT

Fourier Transform

- This Fourier transform is analytic, defined on continuous, infinite functions

Digital Fourier Transform

- the counter part for **regularly** sampled data $\quad x_n \rightarrow X_n \quad$ (with $n \in \{1 \cdots N\}$)

$$X_n = \sum_{k=1}^{N} x_k e^{-2\pi \frac{kn}{N}}$$

This is the operation which is used *nearly* everywhere - and in particular in most FT-ICR processing.

The elements

$$e^{\frac{2\pi k}{N}}$$

are the k roots of 1 of order N

so

$$e^{\frac{2\pi kn}{N}} = (e^{\frac{2\pi k}{N}})^n$$

are these roots at the power n

In [11]:

```
# let's make it interactive
def Nroot(k=1,N=8):
    f,(ax) = subplots(figsize=(7,7))
    t = linspace(0, 2*pi,100)
    ax.plot([-1.3,1.3],[0,0],':k') # the real axis
    ax.plot([0,0],[-1.3,1.3],':k') # the imaginary axis
    ax.plot(np.cos(t), np.sin(t),':k')   # the unity circle
    scatter([1,0,-1,0],[0,1,0,-1], 100)
    text(1,0.15,'1')
    text(-1,0.15,'-1')
    text(0.15,1,'i')
    text(0.15,-1,'-i')

    z = exp(2j * pi /N)         # e^(2 i pi / N)
    zk = z**k
    ax.scatter(zk.real, zk.imag, 200, c='r',edgecolors='r')   # draw roots
    ax.plot([0,zk.real],[0,zk.imag],'r')
    ax.text(1.3*zk.real-0.1, 1.2*zk.imag, r"$e^{2 i \pi \frac{%d}{%d}}$"%(k,N),
    ax.set_axis_off()
    ax.set_title(r'showing $e^{2i\pi %d/%d}$ on the unity circle'%(k,N));
interactive(Nroot, k=(0,16), N=(2,16))
```

executed in 179ms, finished 09:41:38 2021-09-30

k 1

N 8

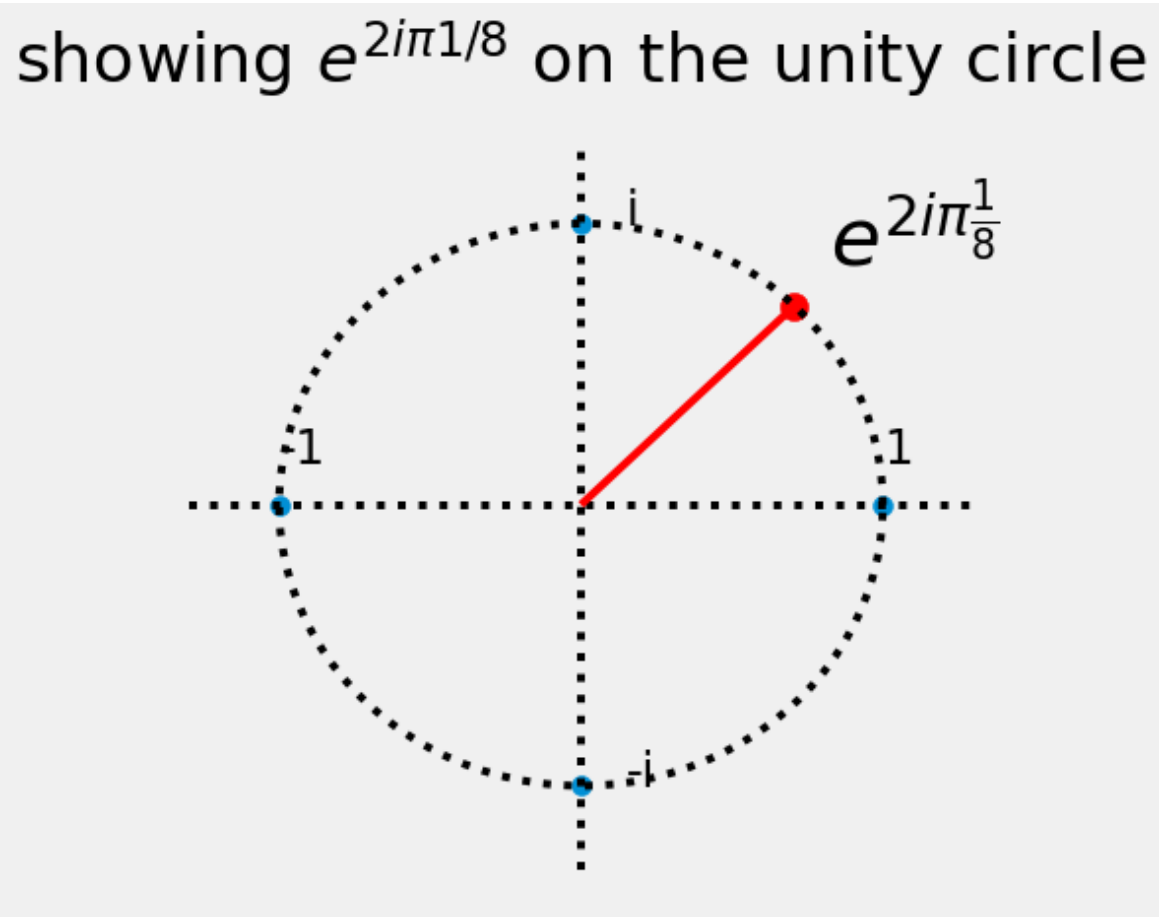

DFT / FT fundamental difference

analytical Fourier	digital Fourier
infinite signal	finite signal
	time bounded signal
continuous signal	sampled signal
	missing information
infinite spectrum	finite spectrum
	frequency bounded signal
continuous spectrum	sampled spectrum
	missing information

Nyquist relation

$$\Delta t = \frac{1}{2F_{max}} \qquad \text{or} \qquad F_{max} = \frac{1}{2\Delta t}$$

sampling = 0.01 => Fmax = 50 Hz

- F1 (blue) = 45 Hz
- F2 (red) = 55 Hz

In [12]:

```
deltat = 0.01   # 10 msec => Fmax = 50Hz
t = 0.1*deltat * np.arange(100)   # oversampling x10 to draw
F1 = 45
F2 = 55
figure(figsize=(12,4))
plot(t, np.cos(2*pi*F1*t))
plot(t, np.cos(2*pi*F2*t))
for i in range(10):
    scatter(i*deltat, 0, 200, 'g', marker="|")
    scatter(i*deltat, np.cos(2*pi*F1*i*deltat), 200, 'g')

```

executed in 294ms, finished 09:41:38 2021-09-30

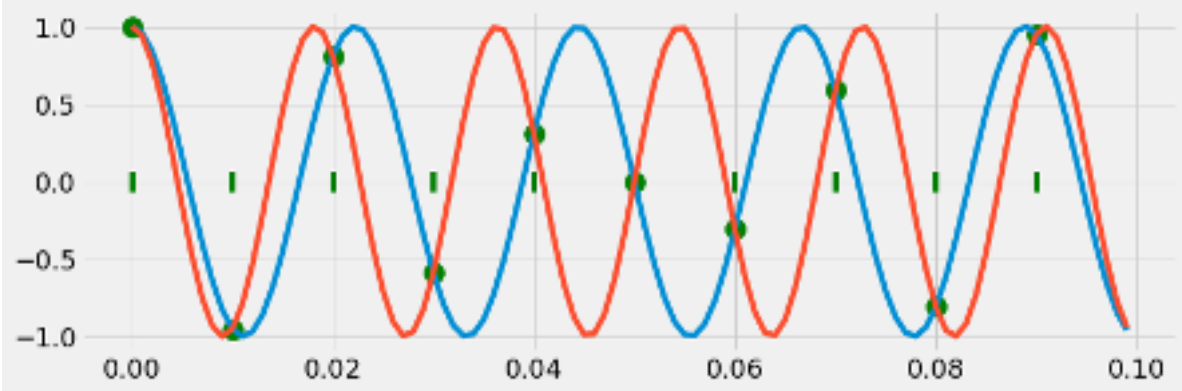

aliasing

sampling ⇒ periodisation of the reciprocal space

- time sampling ⇒ frequency periodisation
  - aliasing / folding
- frequency sampling ⇒ time periodisation
  - time shifting

fundamental relationships

N points, acquired at sampling rate Δt ⇒ N point spectrum sampled at ΔF.

Time domain

- Δt
- $t_{max} = N\Delta t$
- $\Delta t = \frac{1}{2F_{max}}$
- $t_{max} = \frac{1}{2\Delta F}$

Frequency domain

- ΔF
- $F_{max} = N\Delta F$
- $\Delta F = \frac{1}{2t_{max}}$
- $F_{max} = \frac{1}{2\Delta t}$

And a general relation: $N = 2F_{max}t_{max} \quad = \frac{1}{2\Delta t \Delta F}$

fundamental relationships

N points, acquired at sampling rate $\Delta t \Rightarrow N$ point spectrum sampled at ΔF.

Time domain

- Δt
- $t_{max} = N\Delta t$
- $\Delta t = \frac{1}{2F_{max}}$ Nyquist-Shanon theorem
- $t_{max} = \frac{1}{2\Delta F}$

Frequency domain

- ΔF
- $F_{max} = N\Delta F$
- $\Delta F = \frac{1}{2t_{max}}$ Heisenberg uncertainty
- $F_{max} = \frac{1}{2\Delta t}$

And a general relation: $N = 2F_{max}t_{max} \quad = \frac{1}{2\Delta t \Delta F} \quad \Delta t \Delta F = \frac{2}{N}$ Gabor theorem

	Time domain	Frequency domain
	Δt	ΔF
$t_{max} = N\Delta t$		$F_{max} = N\Delta F$
	$\Delta t = \frac{1}{2F_{max}}$	$\Delta F = \frac{1}{2t_{max}}$
	$t_{max} = \frac{1}{2\Delta F}$	$F_{max} = \frac{1}{2\Delta t}$

some algorithmic

DFT can be seen as the product of the signal series $\mathbf{x} = x_n$ of length N, by a $N \times N$ square matrix $\mathcal{M}$:

$$\mathbf{X} = \mathcal{M}\mathbf{x}$$

$$X_n = \sum_{k=1}^{N} x_k e^{2\pi \frac{kn}{N}}$$

so $\mathcal{M}_{ij} = e^{2\pi \frac{ij}{N}}$ is the matrix of the power of the N roots of 1 we have seen earlier.

As a matrix product, we expect the processing time to be $\propto N^2$.

HOWEVER, there is a fast algorithm, (*Cooley & Tuckey 1965*) called **FFT**

- $\propto N \log_2(N)$ *much* faster for large data-sets.
- does not require matrix expression (*a* $512k \times 512k$ *matrix is not easy to handle on a computer*)
- faster if N used

Comparing FFT and DFT

In [13]:

```
figure(figsize=(12,8))
P = np.arange(1,20)                # power of 2
N = 1024*(2**P)                  # size of vectors, starting at 1k points
base = 1e-6/(N[0]**2)            # assume 1µsec processing for 1k vector ( my la
DFT = base*(N**2)
plt.loglog(N, DFT, label='DFT')          # draw both
text(N[-1], DFT[-1], 'DFT')
FFT = 2*1024*base*N*P
plt.loglog(N, FFT, label='FFT')
text(N[-1], FFT[-1], 'FFT')
# some annotations
plt.title('processing time simulation')
plt.xlabel('Size of vector')
plt.ylabel('processing time in sec')
#plt.legend(loc=4)
plt.plot(N, [1E-3]*19, '--k'); plt.text(2*1024, 2E-3, '1 msec')
plt.plot(N, [1]*19, '--k');    plt.text(2*1024, 2, '1 sec')
plt.plot(N, [60]*19, '--k');   plt.text(2*1024, 120, '1 min')
plt.plot(N, [3600]*19, '--k'); plt.text(2*1024, 2*3600, '1 hour')
plt.plot(N, [24*3600]*19, '--k'); plt.text(2*1024, 50*3600, '1 day');
```

executed in 636ms, finished 09:41:39 2021-09-30

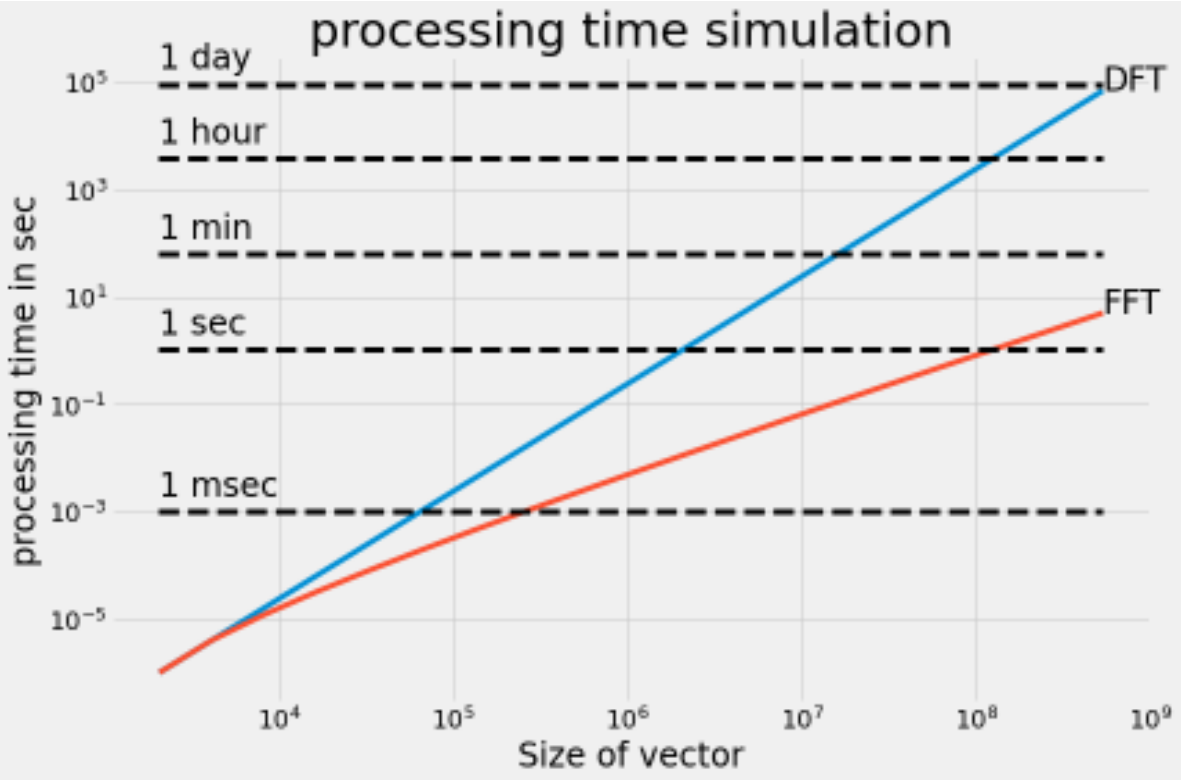

26 slides

In [ ]:

```

```

In [1]:

```
%matplotlib inline
%autosave 60
```

executed in 333ms, finished 07:03:59 2021-09-29

```
Autosaving every 60 seconds
```

In [2]:

```
#import spike
#from spike.Interactive import INTER as I
#I.hidecode(message="")
import matplotlib
import matplotlib.pyplot as plt
from matplotlib.pyplot import scatter, plot, figure, text, title, xlabel, ylabel,
import numpy as np
from numpy import exp, cos, sin, arctan2, pi, linspace, arange

import spike
from spike.File import BrukerMS as bkMS

from ipywidgets import Button, interactive, interact, FloatSlider, IntSlider
import ipywidgets as widgets
from IPython.display import display, HTML, Javascript, Markdown, Image

matplotlib.style.use("fivethirtyeight")
for i in ('font.size','axes.labelsize','legend.fontsize','legend.title_fontsize')
    matplotlib.rcParams[i]=24
for i in ('xtick.labelsize', 'ytick.labelsize'):
    matplotlib.rcParams[i]=18

#matplotlib.style.available
```

executed in 3.40s, finished 07:04:02 2021-09-29

```
    ========================
          SPIKE
    ========================
    Version     : 0.99.29
    Date        : 20-09-2021
    Revision Id : 529
    ========================
*** zoom3D not loaded ***
plugins loaded:
Fitter,  Linear_prediction,  Peaks,  bcorr,  fastclean,  gaussenh,  re
m_ridge,  sane,  sg,  test,  urQRd,
plugins loaded:
msapmin,

spike.plugins.report() for a short description of each plugins
spike.plugins.report('module_name') for complete documentation on one
plugin
plugins loaded:
FTMS_calib,  PhaseMS,  diagonal_2DMS,
*** PALMA not loaded ***
plugins loaded:
Bruker_NMR_FT,  Bucketing,  Integrate,  apmin,
```

2. The basic FTICR experiment

2nd-AUS-FTICR

Marc-André Delsuc - Prague 26-30 Sept 2021

This work is licensed under CC BY-SA 4.0 (https://creativecommons.org/licenses/by-sa/4.0/)

a developed content of this part can be found on github.com/delsuc (https://github.com/delsuc/Fourier_Transform/blob/master/Definition_Properties.ipynb)

classical processing

We are going to go slowly through the steps that produced that nice spectrum earlier.

We will use `SPIKE` a processing library written in python, able to handle all sorts of FT spectrometries

`SPIKE` is freely available on github : github.com/spike-project/spike (https://github.com/spike-project/spike)

Check a deeper presentation (https://github.com/delsuc/Spike_in_MS_2021) of `SPIKE` done in Prof P.O'Connor lab in April 2021

The process that run on the previous slide

Actually, just a few lines of python

```
import spike
from spike.File import BrukerMS
d = BrukerMS.Import_1D("files/histonepeptide_ms2_000002.d/fid")
figure(figsize=(16, 3))
d.display(new_fig=False)
D = d.copy().center().kaiser(4).zf(2).rfft().modulus()
figure(figsize=(16,4))
D.set_unit('m/z').display(zoom=(400,750),new_fig=False);
```

Let's go through them slowly...

First get rid of the syntax problems !

First, load the `SPIKE` environment into this presentation - which is in fact a python program presenting its results in a browser *(amazing if you ask me)* and load the specific tool for reading Bruker FT-ICR files.

```
import spike
from spike.File import BrukerMS
```

Then, import the raw data-set from the instrument and create `d` a python object - and display.
The program takes care of handling all the acquisition parameters.

```
d = BrukerMS.Import_1D("files/histonepeptide_ms2_000002.d/fid")
figure(figsize=(16, 3))
d.display(new_fig=False)
```

Then do the processing - *this is where everything takes place*

```
D = d.copy().center().kaiser(4).zf(2).rfft().modulus()
```

Finally, display the spectrum with a given zoom window

```
figure(figsize=(16,4))
D.set_unit('m/z').display(zoom=(400,750),new_fig=False);
```

let's explore the processing

D = d. **copy()** .center().kaiser(4).zf(2).rfft().modulus()

Actions are applied to the object by the mean of the dot "`.`"

in `SPIKE` spectroscopic objects are modified in-place, in order to optimize speed and memory.

`d` has been created in memory, we do not want to loose it while doing transformations, so we just `copy()` it and create a new object on which the following actions are applied

D = d.copy().**center().kaiser(4).zf(2).rfft().modulus()**

actions are chained, the whole expression evaluates as the final spectrum.

The processing is done in 5 steps !! ... not just one ❓

let's explore the processing - 1 -

D = d.copy(). **center()** .kaiser(4).zf(2).rfft().modulus()

Remember one of the relationships presented in first part:

integrals

$$F_o = \int f(t)dt \qquad f_o = \int F(\omega)d\omega$$

So, if a slight miss-adjustment of the 0 of the detector is present, there might be a small continuous constant value added to all measured points.

Added over the whole `fid` this value will show up as a strong spike at F_o the null frequency.

Even if it corresponds to $m/z = \infty$ *(but only in Broad-Band mode)* it might creates round-off errors in the processing because of a very strong dynamics.

So we just compute a **centering** of the data-set to remove this artefact.

let's explore the processing - 2 -

D = d.copy().center(). **kaiser(4)** .zf(2).rfft().modulus()

This is the very important **Apodisation** step.

It consists in pre-multiplying the `fid` with some shape, with a strong impact on the lineshape, resolution and noise level in the final spectrum.

It is deeply related to the convolution theorem - which we will go through now...

Convolution

We have seen that Linearity means that **FT of sum** is the **sum of FT**

if linearity is for addition, convolution is for multiplication.

Convolution of two functions f and g is defined as: (noted it here $*$)

$$(f * g)(t') = \int_{-\infty}^{\infty} f(t)g(t - t')dt$$

Then the convolution theorem states that **FT of product** is the **convolution of FT**

This is a symmetric operation for f and g, and can be described as f and g sharing their shapes.

Difficult to apprehend, Let see it in action:

In [22]:

```
def ftcv(frequency = 3.0, broadening=2.0, truncating_to=30):
    "showing convolution"
    freq = frequency
    N = truncating_to
    br = broadening
    x = np.linspace(0,10,1000)    # a vector of 1000 points equi distant from 0.0
    y = np.cos(2*np.pi*freq*x)
    g = np.zeros_like(x)
    g[0:N] = 1.0
    apod = g*np.exp(-br*x**2)
    y = y*apod
    YY = np.fft.rfft(y,n=1000)
    yax = np.linspace(0,50,501)
    f, (ax1,ax2) = plt.subplots(nrows=2, figsize=(16,8))
    ax1.plot(apod, ':k', lw=2)
    ax1.plot(y.real)
    ax1.set_ylim(ymin=-1.1, ymax=1.1)
    ax1.set_xlim(xmax=400)
    ax2.plot(yax, abs(YY))
    ax2.set_xlim(xmax=20)
display(Markdown("""## Toy Convolution"""))
interact(ftcv,
        frequency=FloatSlider(min=0, max=20, value=8, continuous_update=False),
        broadening=FloatSlider(min=0,max=5, value=0, continuous_update=False),
        truncating_to=IntSlider(min=20, max=1000, value=1000, continuous_update=F
#interactive( ftcv, frequency=(0.0,50.0), truncating_to=(4,500), broadening=(0,30
```

executed in 375ms, finished 07:14:47 2021-09-29

Toy Convolution

frequency 8.00

broadening 0.00

truncating_to 1000

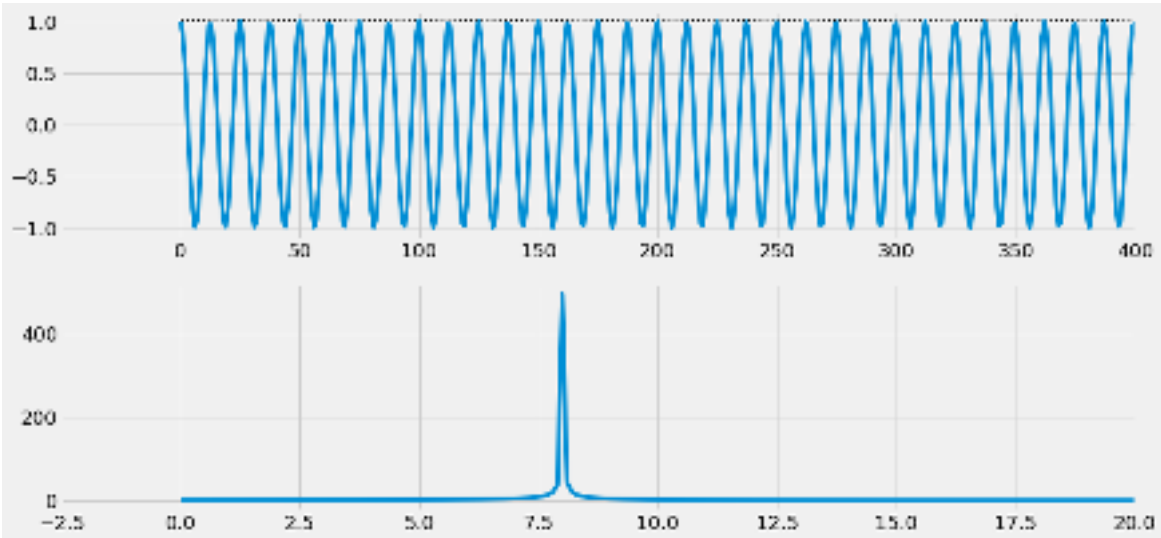

- the broadening exemplify the *Gabor principle* which states that
  - $\sigma_f \sigma_F \geq \frac{1}{4\pi}$ where σ is the standard deviation (the spreading) of each signals
  - $\Rightarrow f$ and F cannot be slim (or fat) at the same time, if one is fat, the other is slim.

- the truncation shows the same but the FT of the truncature function is the *cardinal sine* :

$$\mathrm{sinc}(x) = \frac{\sin(x)}{x}$$

Classical apodisation functions

chosen to limit the truncation effect, while keeping narrow lines

In [4]:

```
from numpy import blackman, hamming, hanning, bartlett, kaiser  # these are pre-d
def sine_bell(N):                                               # this one is missing
    "defines the sine-bell apodisation window"
    return np.sin( np.linspace(0,np.pi,N) )
figure(figsize=(10,8))
for apod in ("sine_bell", "bartlett", "hamming", "hanning", "blackman"):
    y = eval("%s(100)"%(apod))
    plt.plot(y,label=apod)
plt.legend();
```

executed in 245ms, finished 07:04:03 2021-09-29

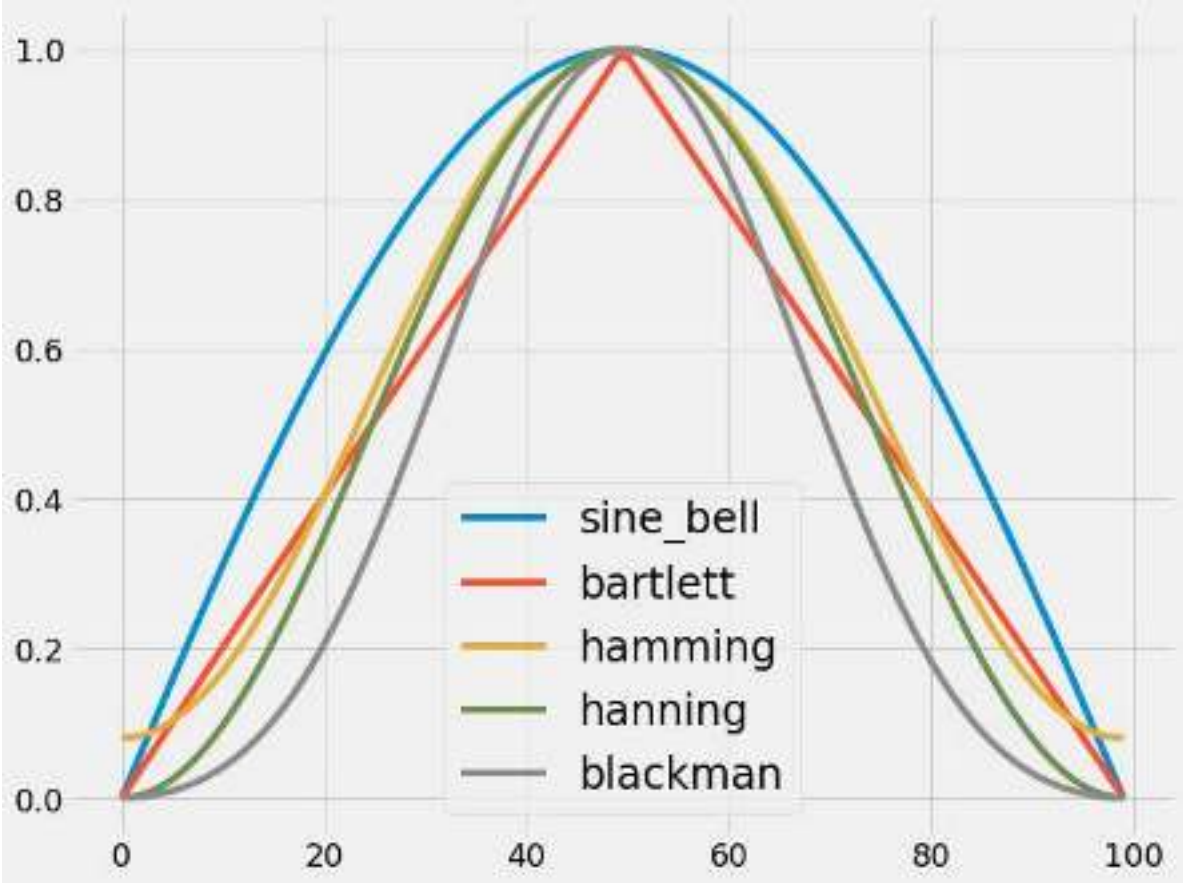

The **kaiser** function is also very usefull as a generic/tunable apodisation function.

```
kaiser(β=...)
```

In [5]:

```
plt.figure(figsize=(10,8))
for beta in range(1,11):
    plt.plot(kaiser(100, beta), label=r"$\beta=%.1f$"%beta)
#plt.legend()
plt.text(2,0.9,r"$\beta=1$",fontsize=18)
plt.text(5,0.68,r"$\beta=2$",fontsize=18)
plt.text(6,0.5,r"$\beta=3$",fontsize=18)
plt.text(30,0.4,r"$\beta=10$",fontsize=18);
#plt.title(r'The Kaiser($\beta$) apodisation');
```

executed in 414ms, finished 07:04:04 2021-09-29

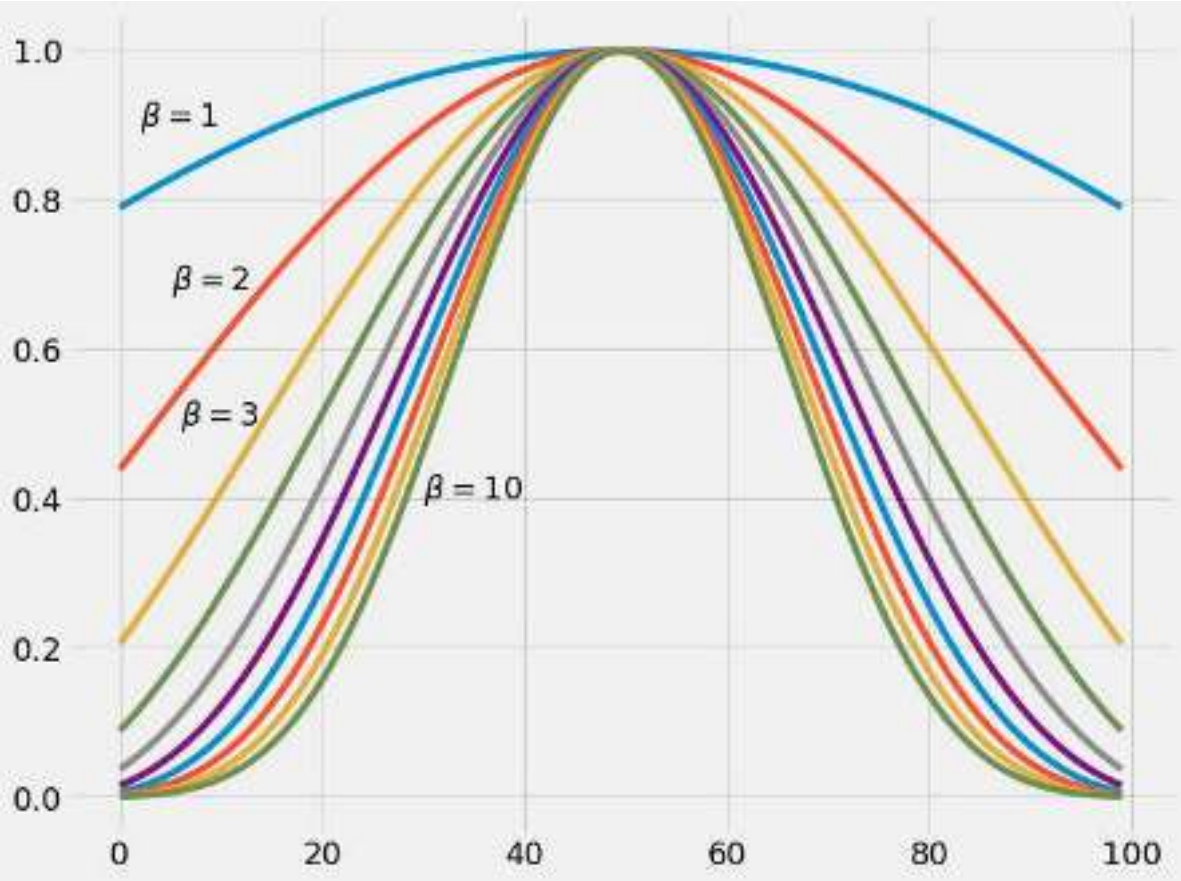

In [6]:

```
apodlist = ["None", "sine_bell", "bartlett", "hamming", "hanning", "blackman", "k
def ftapod(freq1 = 10.0, freq2 = 20.0, br=0.5, N=150, apod="empty", beta=3.0, noi
    "showing convolution"
    x = np.linspace(0,10,1000)    # a vector of 1000 points equi distant from 0.0
    y = np.cos(2*pi*freq1*x) + np.cos(2*pi*freq2*x)
    g = np.zeros_like(x)
    if apod == 'None':
        g[0:N] = 1.0
    elif apod == 'kaiser':
        g[0:N] = eval("%s(%d,%f)"%(apod,N,beta))
    elif apod != 'None':
        g[0:N] = eval("%s(%d)"%(apod,N))
    y *= np.exp(-br*x**2)
    if noise>0:
        y += noise*np.random.randn(1000)
    ymax = max(y)
    YY = np.fft.rfft(y*g,n=1000)
    yax = np.linspace(0,50,501)
    f, (ax1,ax2) = plt.subplots(nrows=2, figsize=(12,6))
    ax1.plot(ymax*g, ':k', lw=2)
    ax1.plot(y*g)
    ax1.set_ylim(ymin=-1.1*ymax, ymax=1.1*ymax)
    ax1.set_xlim(xmax=400)
    ax2.plot(yax, abs(YY))
    ax2.set_xlim(xmax=20)
display(Markdown("""## Exploring a slightly more realistic signal"""))

from ipywidgets import interactive_output, Dropdown, HBox, VBox, Label
freq1 = FloatSlider(description='Freq1',min=0, max=20, value=13, continuous_updat
freq2 = FloatSlider(description='Freq2',min=0, max=20, value=14, continuous_updat
beta = FloatSlider(description='β',min=1.0, max=10.0, value=4, continuous_update=
truncating_to = IntSlider(description='Truncation to',min=2,max=1000, value=1000,
broadening = FloatSlider(description='Broadening',min=0,max=1, value=0, continuou
noise = FloatSlider(description='added noise',min=0, max=3, value=0, continuous_u
apodisation = Dropdown(description='Apodisation',options=apodlist)
uibox = VBox([HBox([freq1, freq2]),
              HBox([truncating_to, broadening, noise]),
              HBox([apodisation, beta, Label('(β used by Kaiser only)')])])
out = interactive_output( ftapod,
    {'freq1':freq1, 'freq2':freq2, 'br':broadening, 'N':truncating_to, 'apod':apo
display(uibox, out)
```

executed in 341ms, finished 07:04:04 2021-09-29

Exploring a slightly more realistic signal

Freq1 13.00 Freq2 14.00

Truncation to 1000 Broadening 0.00 added noise 0.00

Apodisation None β 4.00 (β used by Kais…

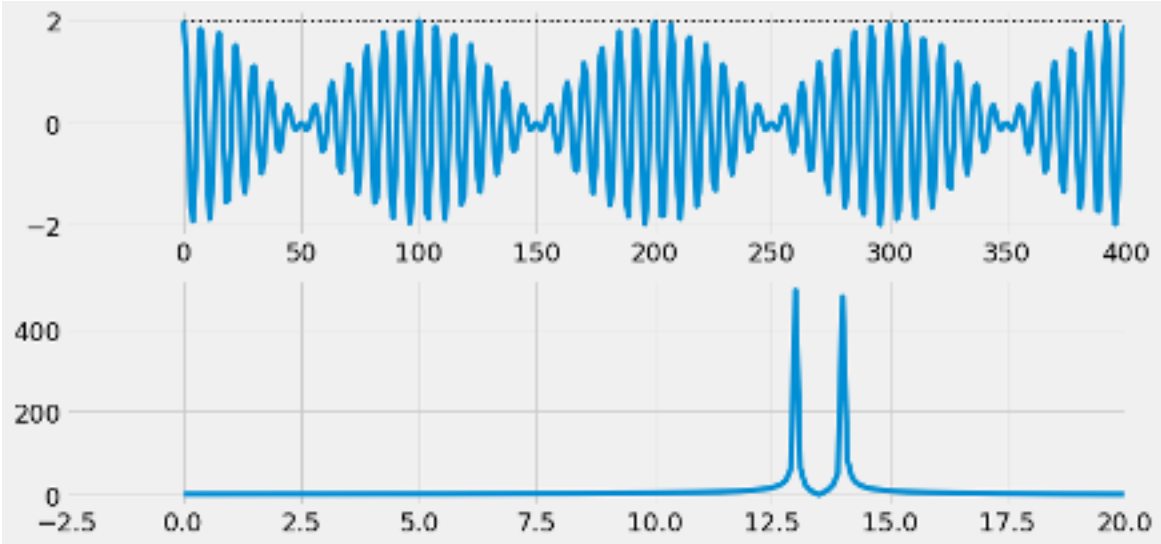

- Explore the effect of truncation and apodisation with respect to signal life-time (broadening) and noise level.
- explore how apodisation may improve the resolving power
- and how it degrades the SNR in the same time

let's explore the processing - 3 & 4-

D = d.copy().center().kaiser(4). **zf(2)** .rfft().modulus()

- **zerofilling** consists in adding zeros to the data-set *before* FT.
- what we've seen about truncation is an example
- improves numerical resolution - here doubling the number of points
- Finally, as in take the modulus (in step **5**) which halves the amount of information, it is actually a requisite !
  - *always zerofill at least once*

D = d.copy().center().kaiser(4).zf(2). **rfft()** .modulus()

- This is the Fourier step - this is actually the simpler step -
- `rfft()` **r** is for **real** - we use here an optimized FT - whichs knows that the imaginary part is null
- there are some other subtilities here that we will not discussed *(check `SPIKE` source code !)*

let's explore the processing - 5 -

D = d.copy().center().kaiser(4).rfft().zf(2). **modulus()**

This step replaces the complex series X_i produced by FT (even `rfft()`) by its modulus $|X_i|$

What happens if we don't do that ?

```
d = bkMS.Import_1D("files/histonepeptide_ms2_000002.d/fid")
figure(figsize=(16, 3))
d.display(new_fig=False)

D = d.copy().center().kaiser(4).zf(2).rfft()

figure(figsize=(16,4))
D.set_unit('m/z').display(zoom=(400,750),new_fig=False);
```

we get this

In [23]:

```
d = bkMS.Import_1D("files/histonepeptide_ms2_000002.d/fid")

D = d.copy().center().kaiser(4).zf(2).rfft()
```

executed in 228ms, finished 07:16:45 2021-09-29

```
Using 3 parameters calibration,  Warning calibB is -ML2
```

In [24]:

```
figure(figsize=(16,4))
D.set_unit('m/z').display(zoom=(400,750),new_fig=False);
```

executed in 311ms, finished 07:16:46 2021-09-29

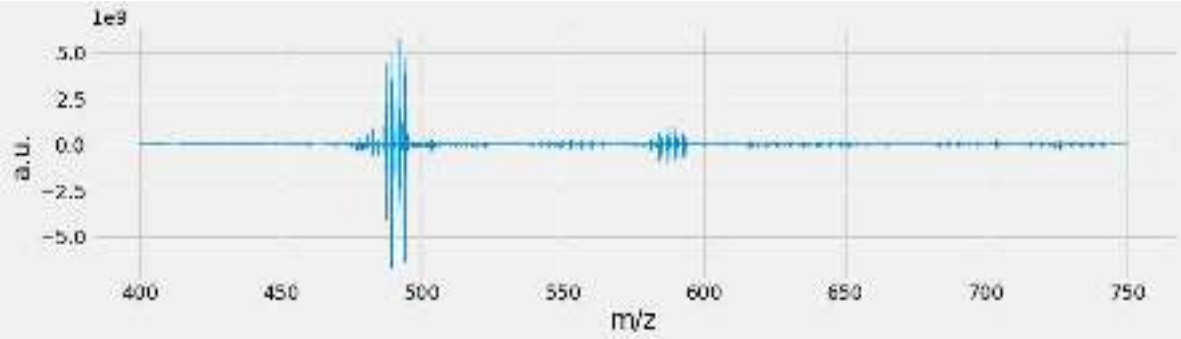

What's going on ?

To find out, we zoom on a peptide pattern

In [8]:

```
figure(figsize=(16,4))
D.display(zoom=(489.2, 490),linewidth=2, new_fig=False);
```

executed in 206ms, finished 07:04:05 2021-09-29

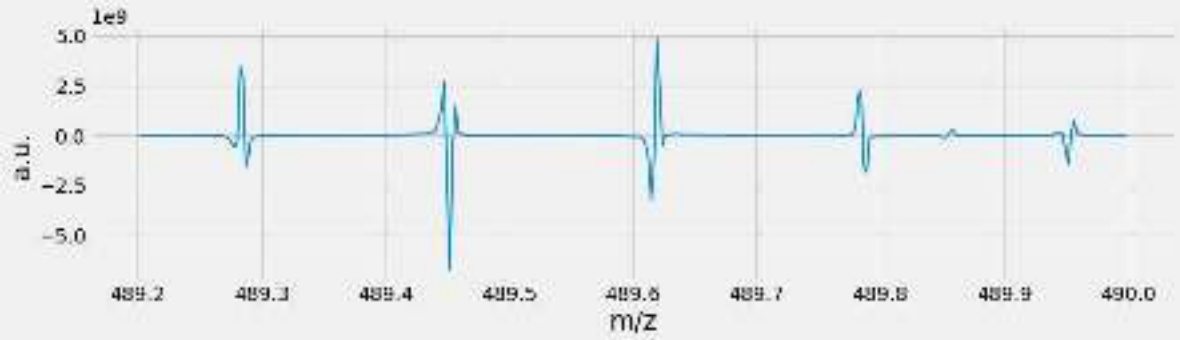

to make clearer - let's change the apodisation, for a much smoother one *(that conserves the beginning of the `fid`)*

In [9]:

```
figure(figsize=(16,4))
Dph = d.copy().center().apod_sin(0).zf(2).rfft().set_unit('m/z').display(zoom=(48
```

executed in 241ms, finished 07:04:05 2021-09-29

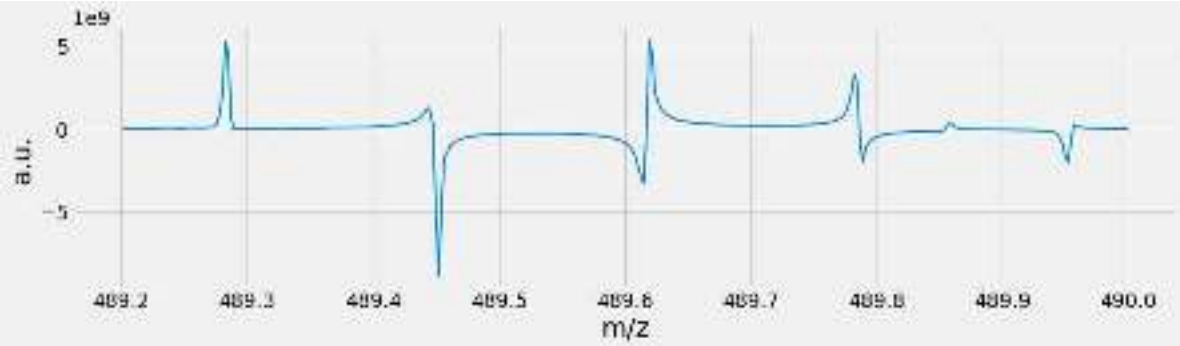

FT of a *Causal* signal

It all comes from the fact that the signal of the `fid` comes from a pulse

- $\Rightarrow$ signal for $t < 0$ is null
- signal is said *Causal*
- its real part is **Absorptive** and decay rapidly
- its real part is **Dispertive** and decay more slowly *(is null for a stationary signal)*

Here is a simulation

In [10]:

```
freq = 20
t = linspace(0,10,10000)
y = cos(2*np.pi*freq*t)*exp(-3*t)
YY = np.fft.rfft(y)
figure(figsize=(16,4))
yax = linspace(0,500,len(YY))
plot(yax, YY.real, label='real part - Absorptive')
plot(yax, YY.imag, label='imaginary part - Dispersive')
plt.xlim(xmin=15, xmax=28)
plt.legend();
```

executed in 168ms, finished 07:04:05 2021-09-29

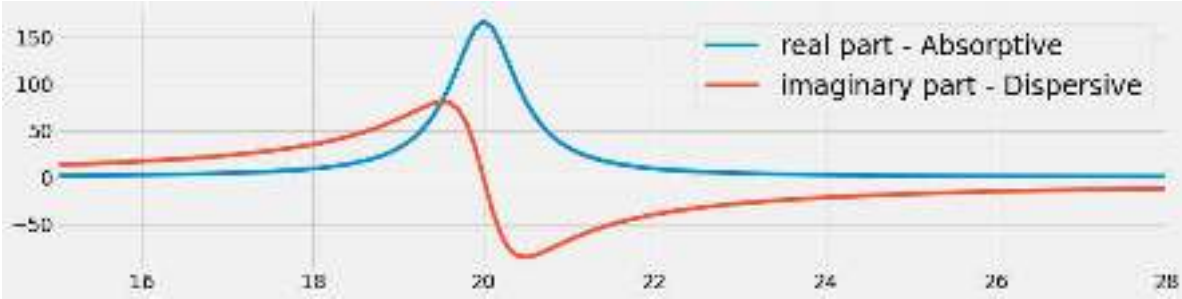

dephasing

However, if there is an error on the *t=0* position, the phase of the time signal is $\neq 0$ Then the signal get dephased
here with an error of 70°...

In [11]:

```
freq = 20
t = linspace(0,10,10000)
y = cos(2*np.pi*freq*t+(7/9)*pi/2)*exp(-3*t)
YY = np.fft.rfft(y)
figure(figsize=(16,4))
yax = linspace(0,500,len(YY))
plot(yax, YY.real, label='real part')
plot(yax, YY.imag, label='imaginary part')
plt.xlim(xmin=15, xmax=28)
plt.legend();
```

executed in 249ms, finished 07:04:05 2021-09-29

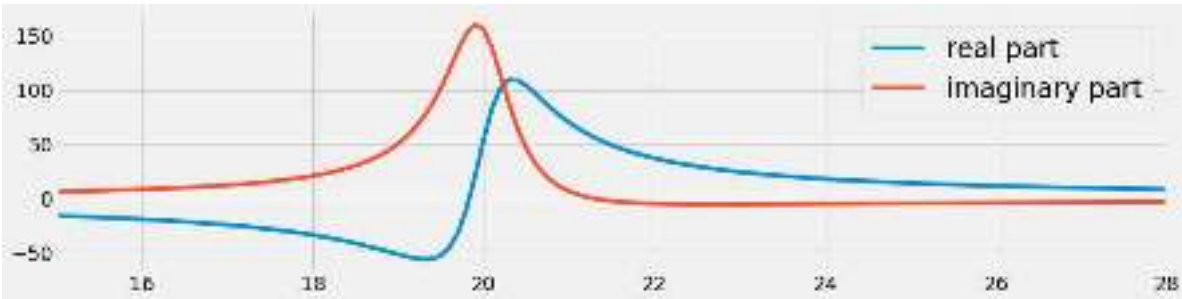

This is exactly what we see here - with each line has a different phase.
Line at $m/z = 489.28$ is in absorption - Line at $m/z = 489.61$ is in dispersion - other are mixed

In [12]:

```
figure(figsize=(16,4))
Dph.display(zoom=(489.2, 490),linewidth=2,new_fig=False);
Dph.phase(90,0).display(zoom=(489.2, 490),linewidth=2,new_fig=False);
```

executed in 201ms, finished 07:04:05 2021-09-29

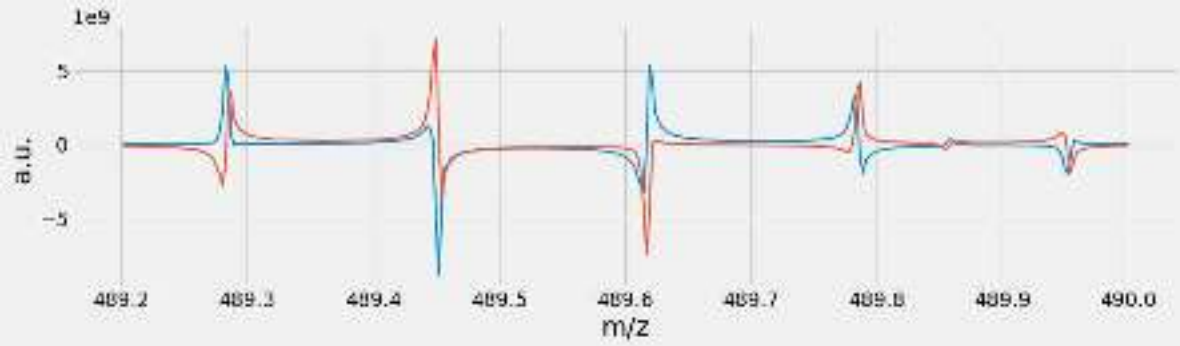

Usual solution is to take the modulus

But then line are as broad as the Dispersive lineshape

In [13]:

```
figure(figsize=(16,4))
Dph.modulus().display(zoom=(489.2, 490),linewidth=2,new_fig=False);
```

executed in 173ms, finished 07:04:06 2021-09-29

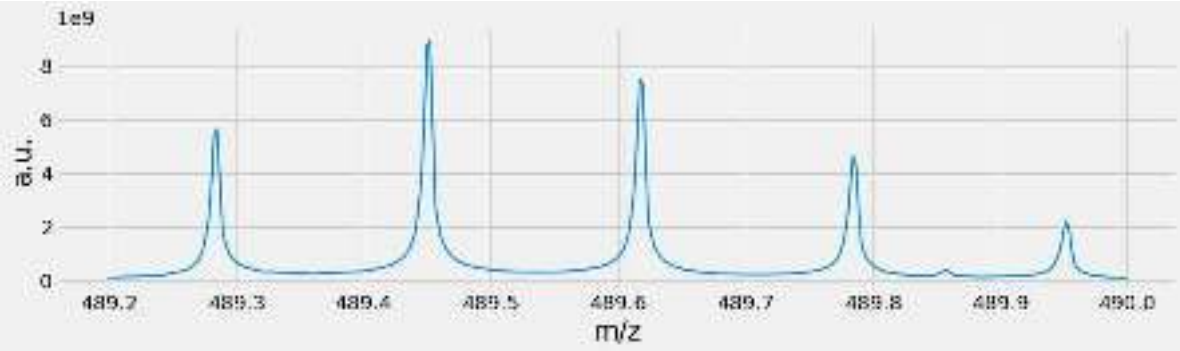

and compared to the previous version, strongly apodised - which "compresses" the line to the detriment of SNR

In [14]:

```
figure(figsize=(16,4))
Dph.display(zoom=(489.2, 490),linewidth=2,new_fig=False)
D.modulus().display(zoom=(489.2, 490),linewidth=2,new_fig=False);
```

executed in 196ms, finished 07:04:06 2021-09-29

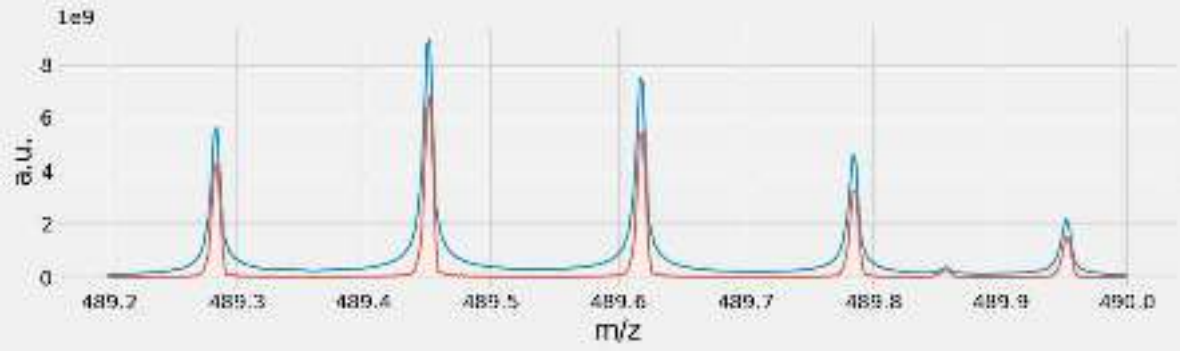

Absorption mode

- Of course we would prefer to have all lines in absorption, to do that we need to know/find the dependence of phase with peak position.

$$\phi(\omega) = \phi_o + \phi_1\omega + \phi_2\omega^2$$

	cause	effect	oder
ϕ_o	error on 0 of phase ref.	phase error common to all signals	0th order
ϕ_1	error on t=0 postion	phase error proportional to frequency	1st order
ϕ_2	error on ion excitation time	phase error proportional to frequency²	2nd order

- ϕ_o : trivial to correct
- ϕ_1 : can be estimated, easy to correct - as variation $\frac{d\phi}{d\omega}$ is constant
  - created by a delay after excitation
- ϕ_2 : can be estimated, difficult to correct - as variation $\frac{d\phi}{d\omega}$ is unbound
  - created by "*chirp*" frequency swept excitation pulses !

Examples of phase error

In [15]:

```
sw = 200000
omega = linspace(0,sw,10000) # freq axis
mz = np.random.randint(5000,10000,300)
ph0=123
phase = ph0*np.ones(10000)
figure(figsize=(16,3))
plot(omega, phase, 'k', lw=2, alpha=0.2)
scatter(omega[mz], phase[mz], 200,'r')
plt.title("0th order phase error    123° phase error")
plt.xlim(xmin=100000, xmax=200000);
plt.ylim(ymin=-180, ymax=+180);
```

executed in 149ms, finished 07:04:06 2021-09-29

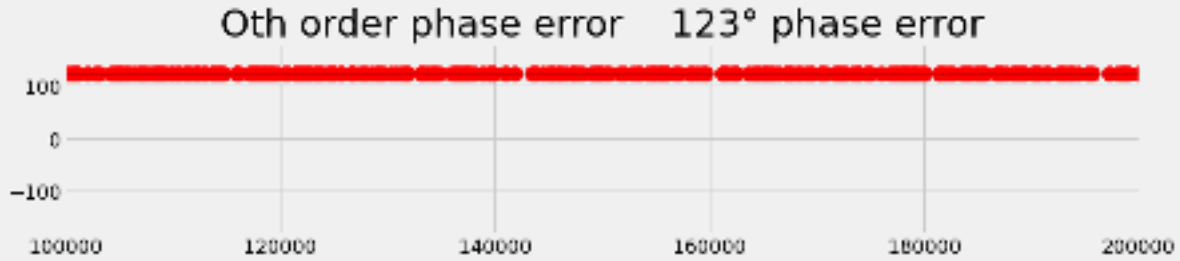

In [16]:

```
# 200kHz - 400kH Nyq - 2.5 µs sampl - 250µs error = 100 points = 50 turns
ph1 = 50*360/sw
phase = (ph0 + ph1*omega )%360 - 180
figure(figsize=(16,3))
plot(omega, phase, 'k', lw=2, alpha=0.2)
scatter(omega[mz], phase[mz], 200,'r')
plt.title("1st order phase error    250µsec error on t0")
plt.xlim(xmin=100000, xmax=200000)
plt.ylim(ymin=-180, ymax=+180);
```

executed in 155ms, finished 07:04:06 2021-09-29

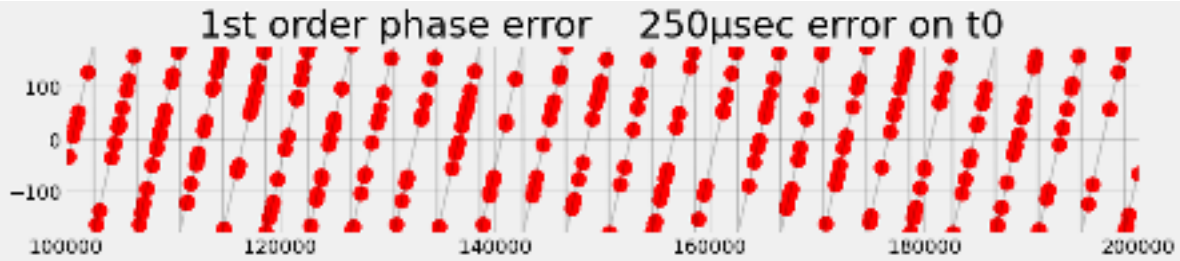

In [17]:

```
# 1ms pulse
ph1 = -100*360/sw
ph2 = 200*360/sw/sw
phase = (ph0 + ph1*omega +ph2*omega**2)%360 - 180
figure(figsize=(16,3))
plot(omega, phase, 'k', lw=2, alpha=0.2)
scatter(omega[mz], phase[mz], 200,'r')
plt.title("2nd order phase error    1msec freq. swept pulse")

plt.xlim(xmin=100000, xmax=200000);
plt.ylim(ymin=-180, ymax=+180);
```

executed in 160ms, finished 07:04:06 2021-09-29

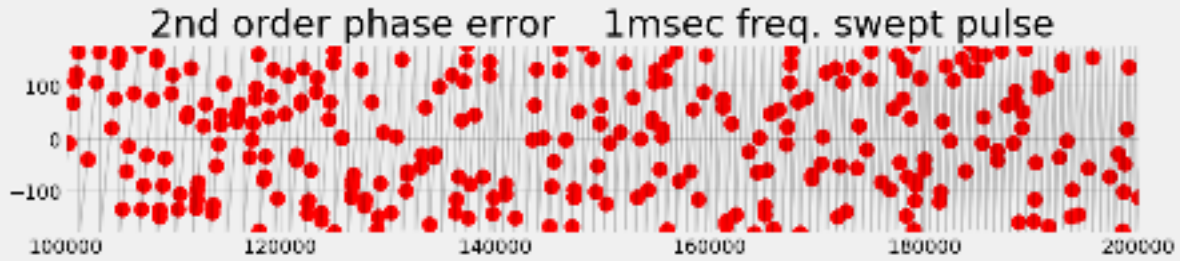

phase is random-like

Getting an absorption spectrum

- use swift excitation to generate 1st order only correction
  - if you can
- adapt the processing (special apodisation for instance)
- use ad-hoc phase correction
  - optimising the excitation pulse - the shorter the better
    - phase rotation induces some artefacts that cannot be corrected
  - compute and apply a phase correction

2 methods for finding the phase correction

Automatic approach

Anal Chem. 2013 April 16; 85(8): 3903–3911. doi:10.1021/ac303289c.

Autophaser: An Algorithm for Automated Generation of Absorption Mode Spectra for FT-ICR MS

David P.A. Kilgour[1,*], **Rebecca Wills**[1], **Yulin Qi**[1], and **Peter B. O'Connor**[1]
[1]Department of Chemistry, University of Warwick, Coventry, CV4 7AL, UK

1. Peak Detection
2. Initial fitting to a reduced m/z range (Followed by the Iterative Tune procedure)
3. Extension of the initial fit (Followed by the Iterative Tune procedure)

4. Fitting of the complete spectrum (Followed by the Iterative Tune procedure)
5. Peak symmetry adjustment
6. Baseline correction- detect peaks on magnitude spectrum

Works well if a high density of peaks....

Apply a manual approach

- determine ϕ_o and ϕ_1 locally
- use the fact that locally $\phi_1 = \frac{d\phi}{dt}$ is not bounded

In [18]:

```
# 1ms pulse
ph1 = -100*360/sw
ph2 = 200*360/sw/sw
phase = (ph0 + ph1*omega +ph2*omega**2)%360 - 180
dphi = sw*(ph1 + 2*ph2*omega)
mz = np.random.randint(5000,10000,30)

figure(figsize=(16,3))
plot(omega, phase, 'k', lw=2, alpha=0.2)
scatter(omega[mz], phase[mz], 200,'r')
plt.title("2nd order phase error    1msec freq. swept pulse")
plt.xlim(xmin=100000, xmax=200000);
plt.ylim(ymin=-180, ymax=+180);

figure(figsize=(16,5))
plot(omega, dphi, 'k', lw=2, alpha=0.2)
scatter(omega[mz], dphi[mz], 200,'r')
plt.title("$\phi_1$     1msec freq. swept pulse")
plt.xlim(xmin=100000, xmax=200000);
plt.ylim(ymin=20000);
```

executed in 321ms, finished 07:04:07 2021-09-29

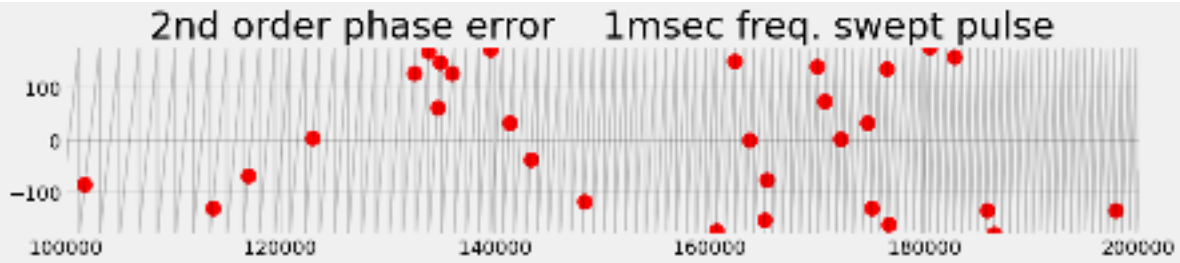

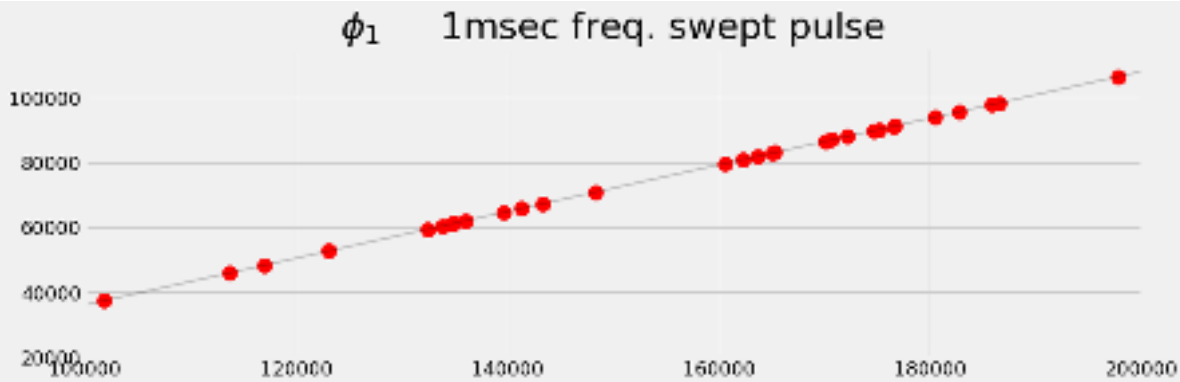

do a linear fit of ϕ_1 , integrate to get $\phi_2 \rightarrow \phi_o$ is left to do !

works also on sparse spectra

Phase sensitive FTICR-MS

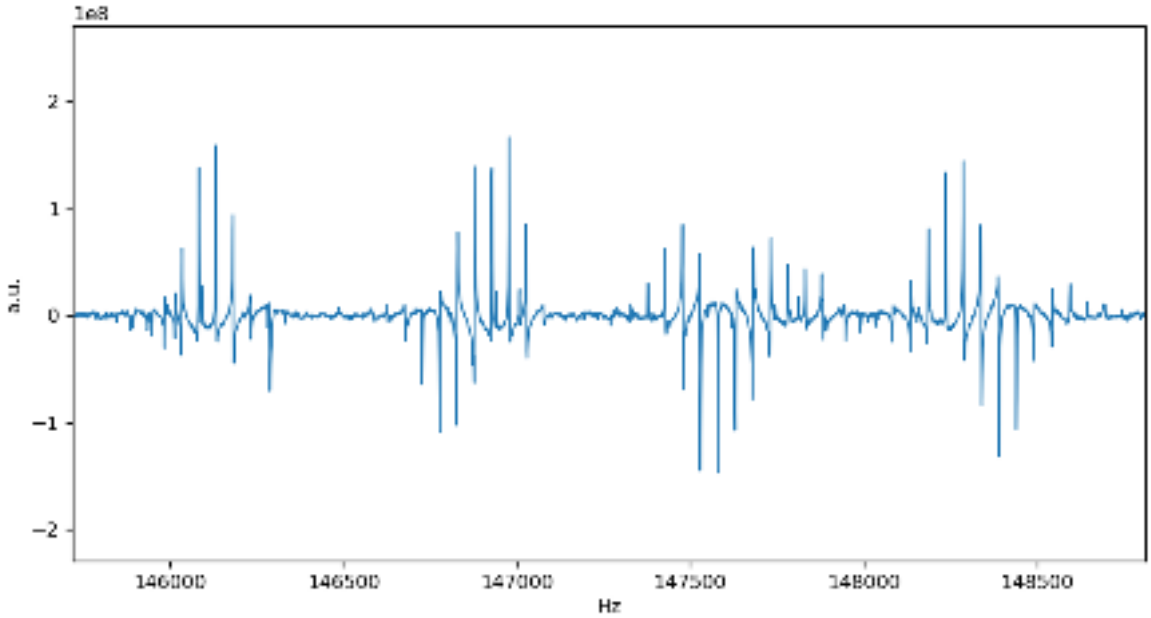

- The phase mix the absorption and dispersion linesphapes
- We see a strong linear dependence of phase (here a small spectral window)

Phase sensitive FTICR-MS

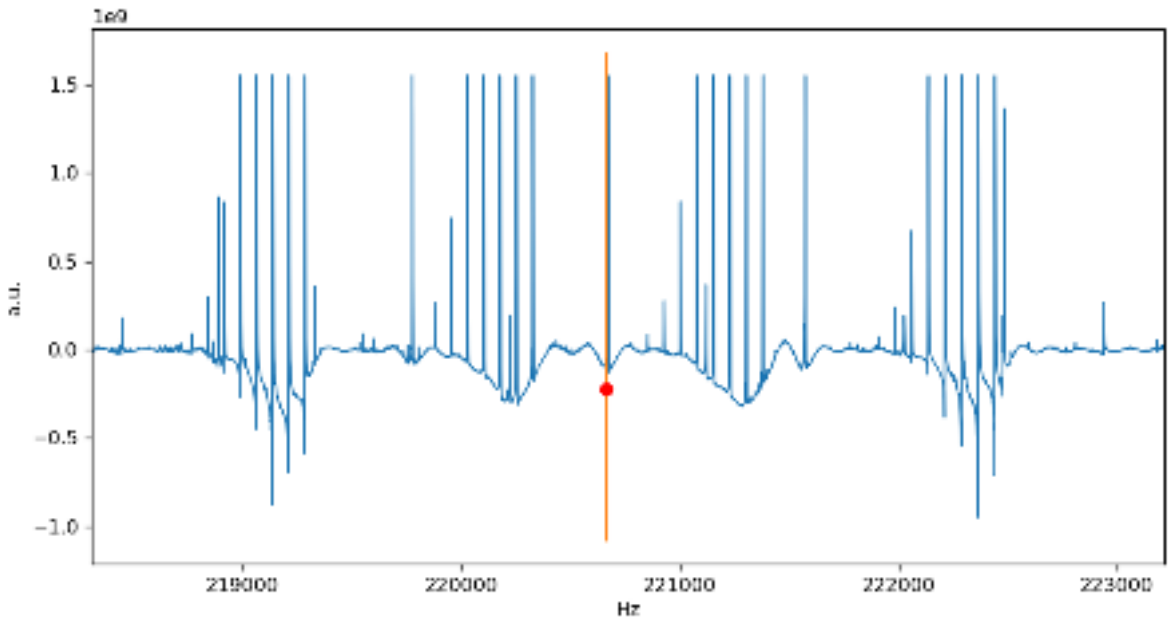

linear phase correction in not enough

⇒ quadratic phase correction

Phase sensitive FTICR-MS

interactive/automatic module for FTICR phasing in Spike (not finished yet, but available)

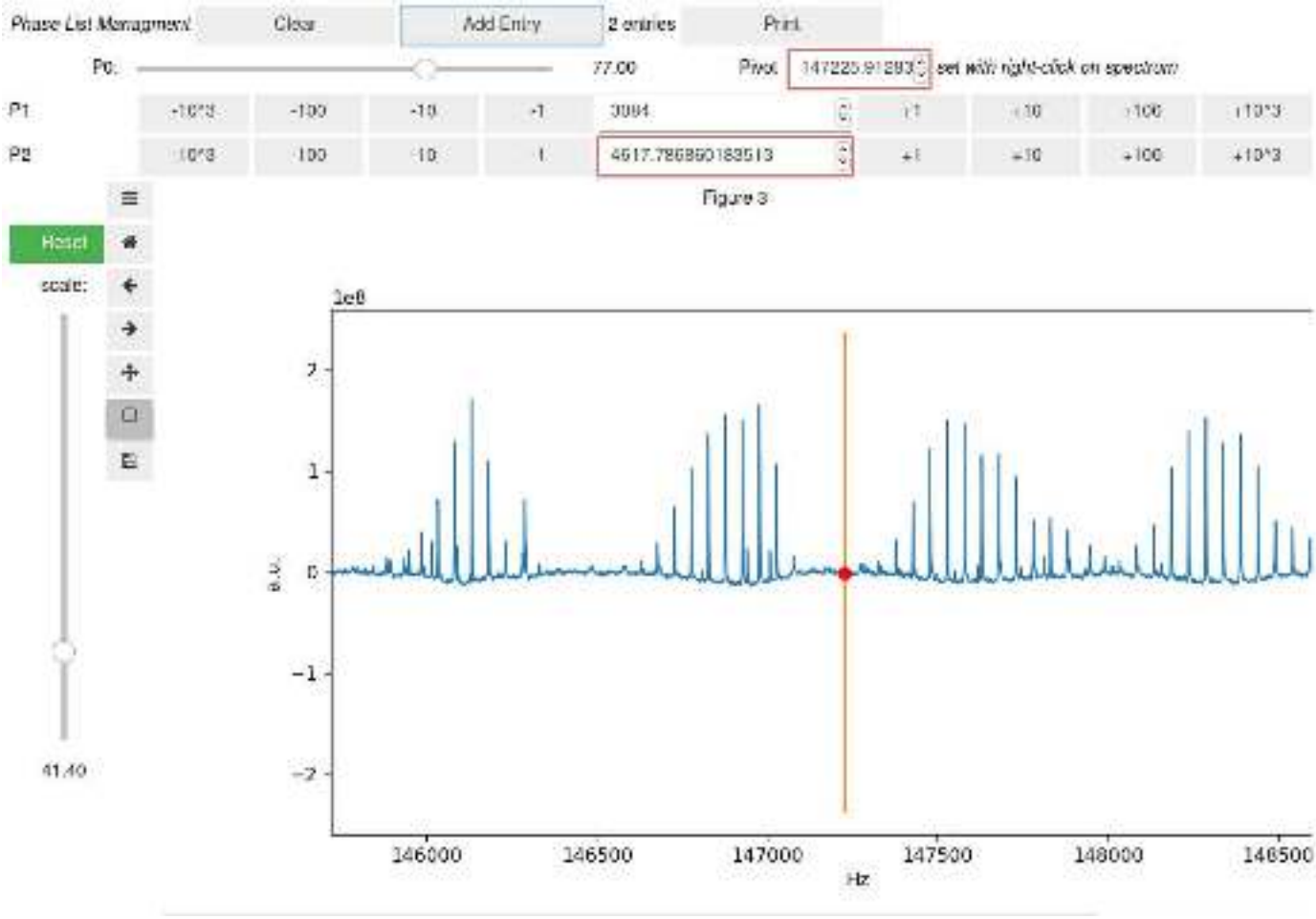

Phase sensitive FTICR-MS

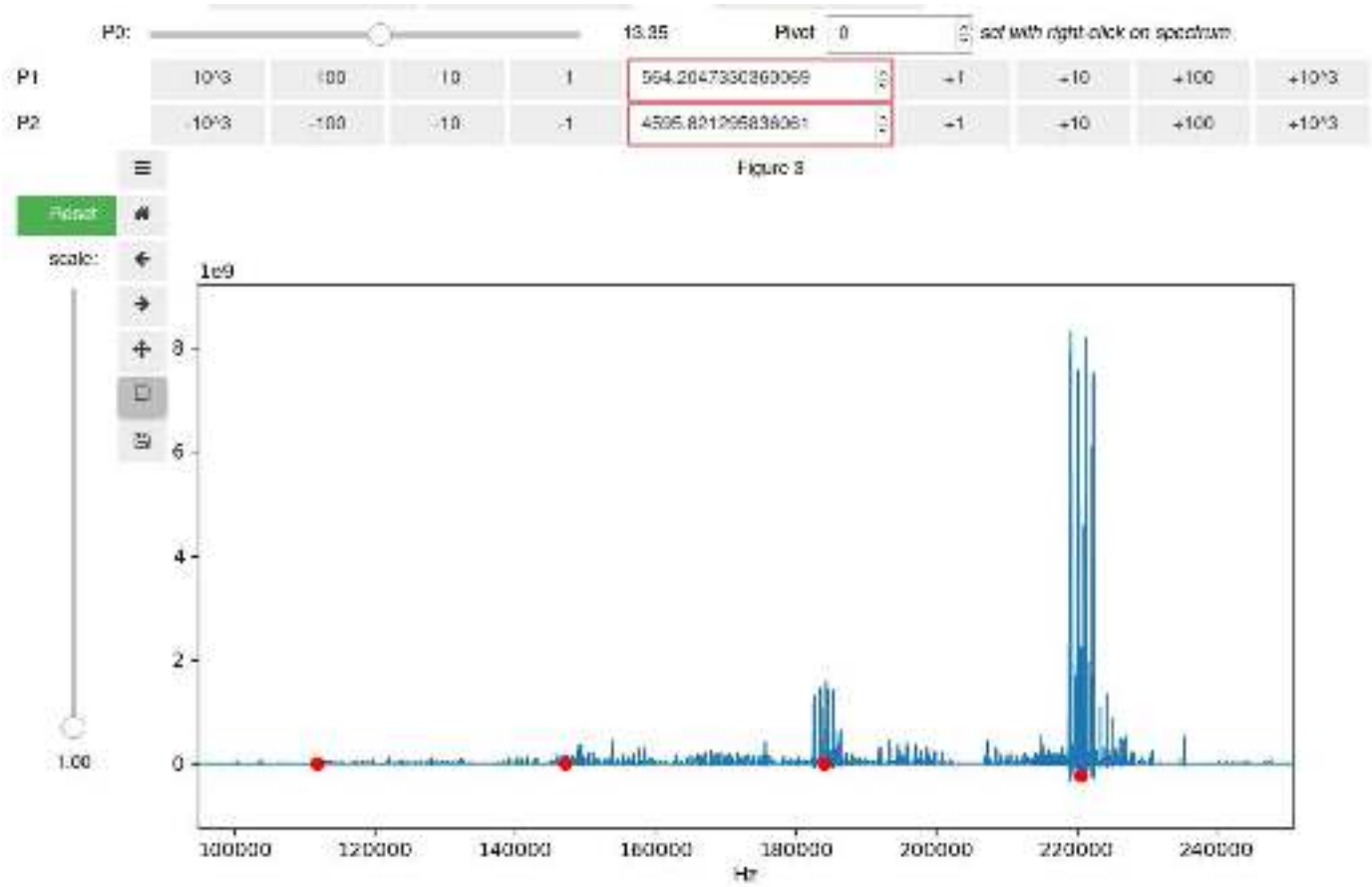

Phase sensitive FTICR-MS

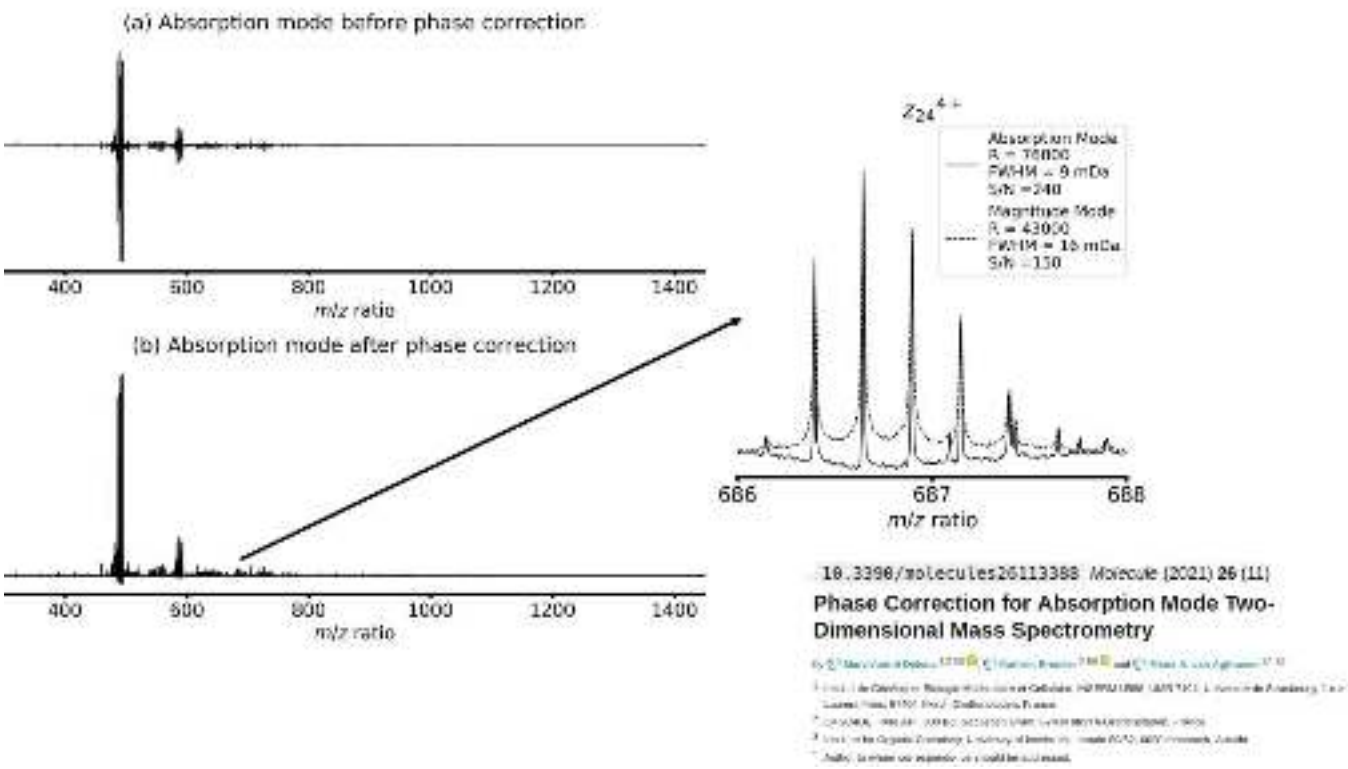

notice the baseline distortion

the Hilbert transform

relates the *Absorptive* and *Dispersive* shape

- complex: real / imaginary
  - and time/freq asymmetry
    - due topoint 0 => odd number
  - 3 DFT
    - fft - rfft - fftr
  - causal signal
  - KK
  - Hilbert transform

29 slides

Beyond Fourier transform

There are MANY alternative to the DFT *(i.e. the numerical handling of the Fourier Transform)*

some general principles

- ALL methods are based on **assumptions** on the signal, and ask a **question** to the data
  Important to know them to interpret the answers (and the problems)
- there is no difference between a **spectral method** and a **noise reduction** method.

There are **Three** famillies of approaches, which differ fundamentaly,
depending how many parameters P are extracted from the N experimental points (the `fid`)

Some are known in this community (FDM), some less, some are old (Burg mem 1975), some are very recent...

transform methods are trendy (ML, NN, images ...)

many have advantages ... and defaults !

- not the place to present them
  - give you some hints of useful methods / what they are good for
  - mostly give you the big principles...

3 different famillies

N experimental points / P parameters

- $\mathbf{N > P}$ - **parametric** methods
  - an analytical **model** of the signal is assumed *(sum of damped sinusoids)*
  - the model parameters are **fitted** to the data using some kind of **target function** (usually Mean Squared Error or Maximum Likelihood)
  - the method produces the list of the parameter values
  - **Sinus-it** is an example, (there are many others, FDM, HSVD, Burg,...)
- $\mathbf{P > N}$ - **transform** methods *(my naming)*
  - assumptions are introduces indirectly by modeling the **measurement** process,
  - these assumptions are generally introduced by a **regularisation function**
  - the method produces a graphic / (a spectrum / an image)
  - there are many examples: **FISTA**, **MaxEnt**, **wavelet**, urODd, ...

- $\mathbf{P} = \mathbf{N}$ - the **Fourier transform**
  - FT is invertible $\Rightarrow$ just changing of point of view *(no assumption ?)*

Fourier Transform

which assumptions ?

- the signal is zero when I did not measure it
- there is no noise - everything is data
- the spectrum is modeled as a sum of oscillators, regularly placed along the frequency axis
- DFT is the least square solution - and MSE = 0

Advantages

- Very fast
- Very stable
- Very well known

Drawbacks

- data as a whole $\Rightarrow$ cannot do varying frequency!

- Nyquist - Heisenberg - Gabor

Nyquist - Heisenberg - Gabor ???

Here - 2 signals differing by 0.1 Hz over 10sec :

$$0.1\frac{1}{2t_{max}}$$

In [19]:

```
t = linspace(0,10,1000)
f1 = 2
f2 = 2.005
y1 = cos(2*pi*f1*t)
y2 = cos(2*pi*f2*t)
figure(figsize=(16,6))
plot(t, y1)
plot(t, y2)
for io in (258, 508, 858):
    xo = t[io]
    plot([xo,xo],[-1,1],':k',lw=3)
    scatter(xo,y1[io],200)
    scatter(xo,y2[io],200)
```

executed in 248ms, finished 07:04:07 2021-09-29

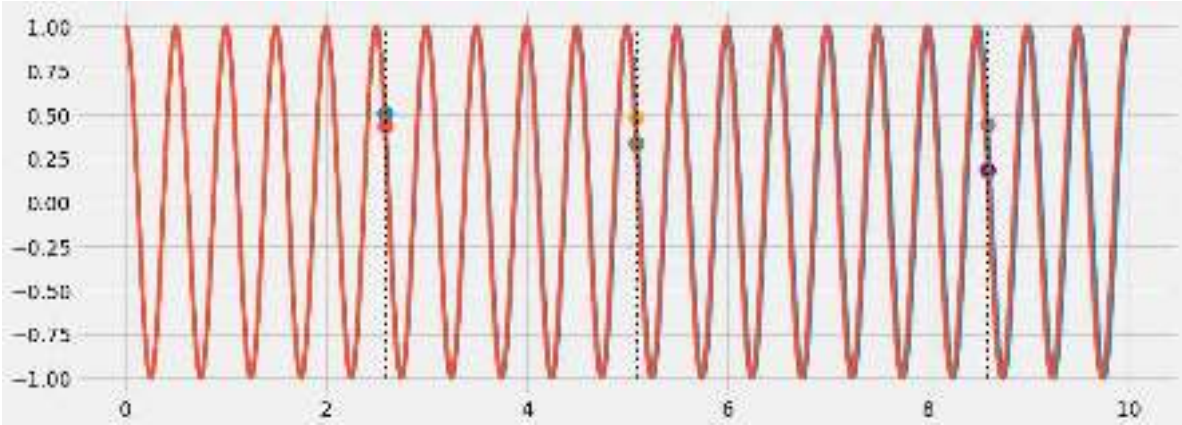

it seems that a clever analysis, in high SNR , is able to extract this information

parametric

- **Advantages**
  - very precise
  - go beyond Gabor and Nyquist limits (continuity assumption)
  - ⇒ can do instantaneous frequency!
  - can adapt the model to signal specificities
- **Drawbacks**
  - noise is not in the model *(by definition)* / cannot hardly be handled - in particular complex noise
  - problems with non-standard line-shapes
  - always present nice looking results coherent with the model *(check your statistics !)*
  - usually slow to very slow *(no Cooley-Tuckey algo !)*
  - non convex problem ⇒ MANY methods ⇒ which one to choose ?

transforms

- **Advantages**
  - Very stable - Very well known
  - go beyond Gabor and Nyquist limits ⇒ can do instantaneous frequency! (wavelet)
  - strong theoretical background (ℓ_1 norm and compressed sensing theorem (Candès - Donoho))
  - noise is in the model ⇒ can be used as de-noising

  - can be used along FT (de-noising, deconvolution, NUS, ...)
  - (near) convex problem ⇒ MANY methods ⇒ all equivalent in the end ! *(except for the regularisation function)*
- **Drawbacks**
  - not so fast
  - not very well known
  - MANY methods

Noise reduction - urQRd[1] (2014)

An Linear Algebra approach *(known since the `80s)*, based on a new sort of *fast SVD* ...

- Truncate $\mathbf{H}$ first, thanks to *random projection* theorem urQRd
- use **QR** to estimate **SVD** from truncated $\mathbf{H}$ urQRd
- from **QR** decomposition, rebuild $\mathbf{H}$ then S urQRd
- iterate

plus...

- use FFT trick to compute all matrix products. urQRd

1.Chiron L., van Agthoven M. A., Kieffer B., Rolando C., Delsuc M-A. *Proc Natl Acad Sci USA*, **111** (4) :1385–1390, (2014)

example in FT-ICR

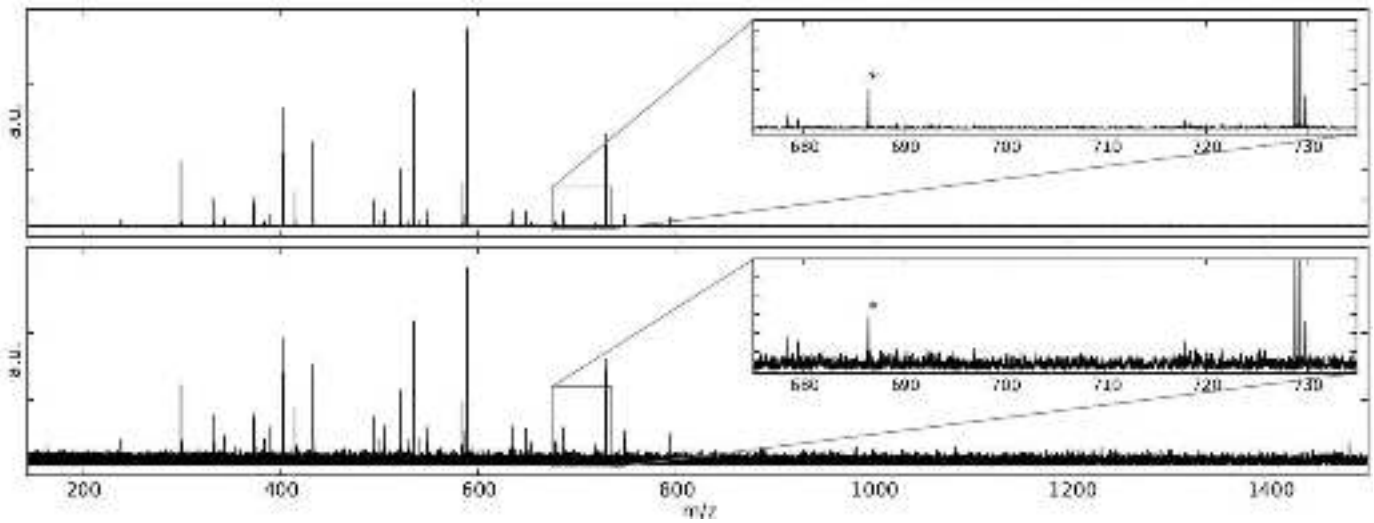

urQRd - speed and robustness compared to Cadzow

on a synthetic dataset

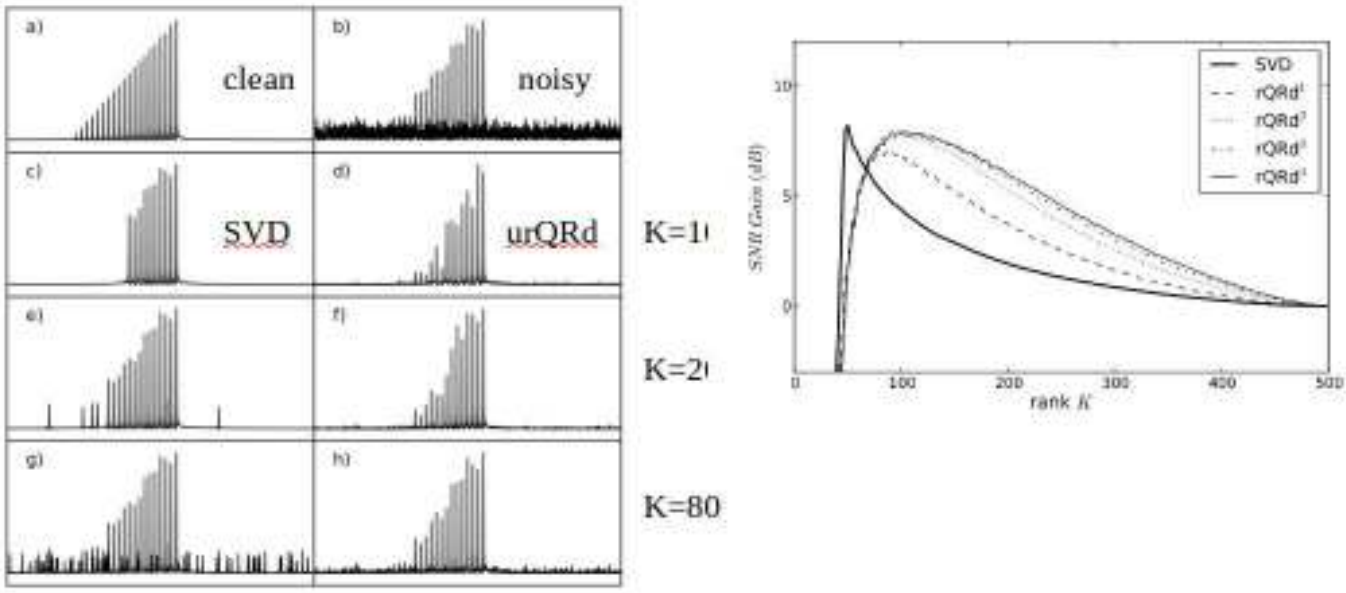

compressed sensing

Here, standard FISTA analysis

example on 64k / 75msec acquisition of ubiquitine

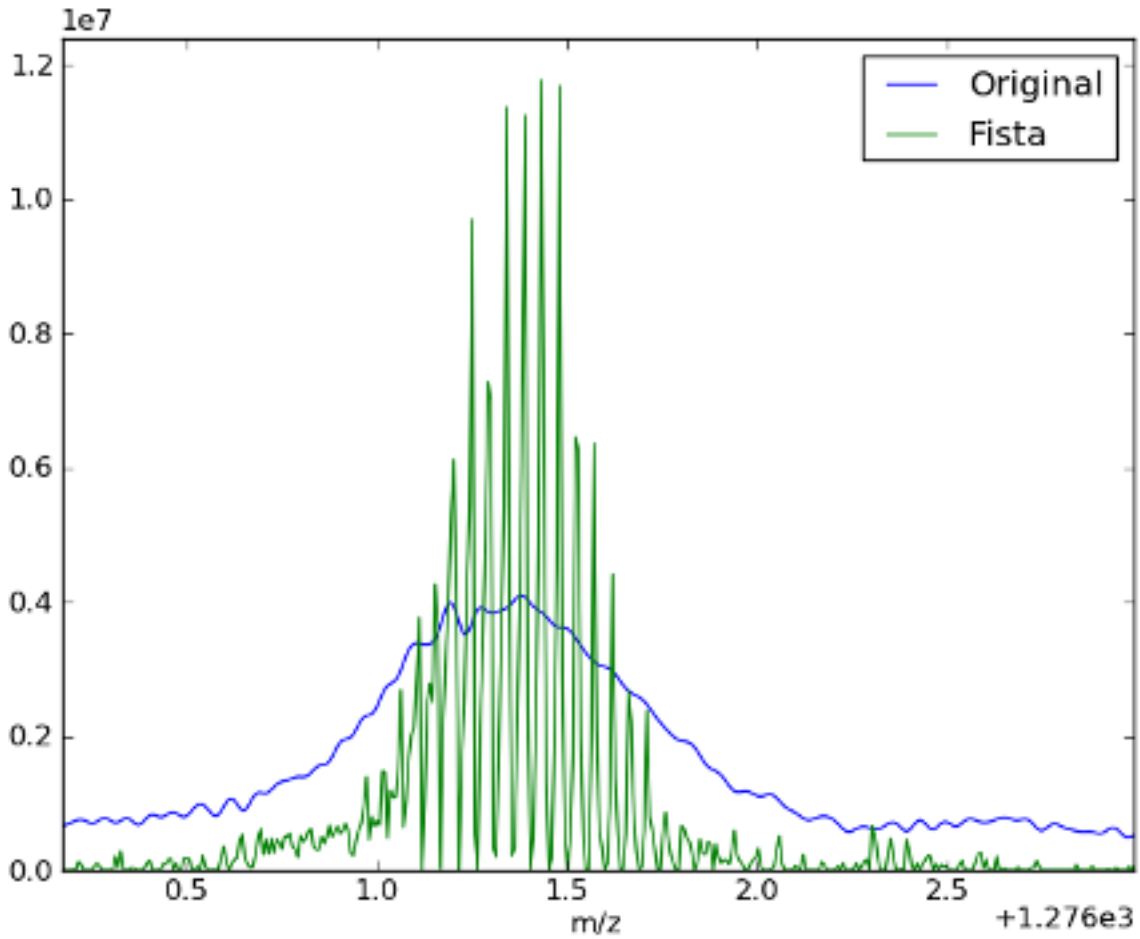

- ion cloud dynamic

    - and line-shape
- beyond FT
    - FT has many drawbacks
- many advantages
- hidden hypothesis
- noise
    - instantaneous freq
        - FT
        - FDM
        - genetic
            - signal modeling
            - noise handling
            - N>P P>N
        - FISTA
        - ...

In [ ]:

```
Autosaving every 60 seconds
```

3. more advanced aspects

2nd-AUS-FTICR

Marc-André Delsuc - Prague 26-30 Sept 2021

This work is licensed under CC BY-SA 4.0 (https://creativecommons.org/licenses/by-sa/4.0/)

a developed content of this part can be found on github.com/delsuc (https://github.com/delsuc/Fourier_Transform/blob/master/Definition_Properties.ipynb)

Time resolved MS

All the steps presented so far are producing a final spectrum.

is outside of the presentation:

- peak picking
  - detection
  - filtering
  - centroid fit ⇒ precise position and width estimate
- calibration
- interpretation ...

what about Time resolved MS ?

problems with

- loss of information
- artefact cannot be explored
- instanteneous variation lost, improved - slower - method, ...)
- choices made during processing cannot be revisited

One example

2 years ago Matthias W. sent me some data-sets from Asphaltene samples

I processed them - every thing is normal !

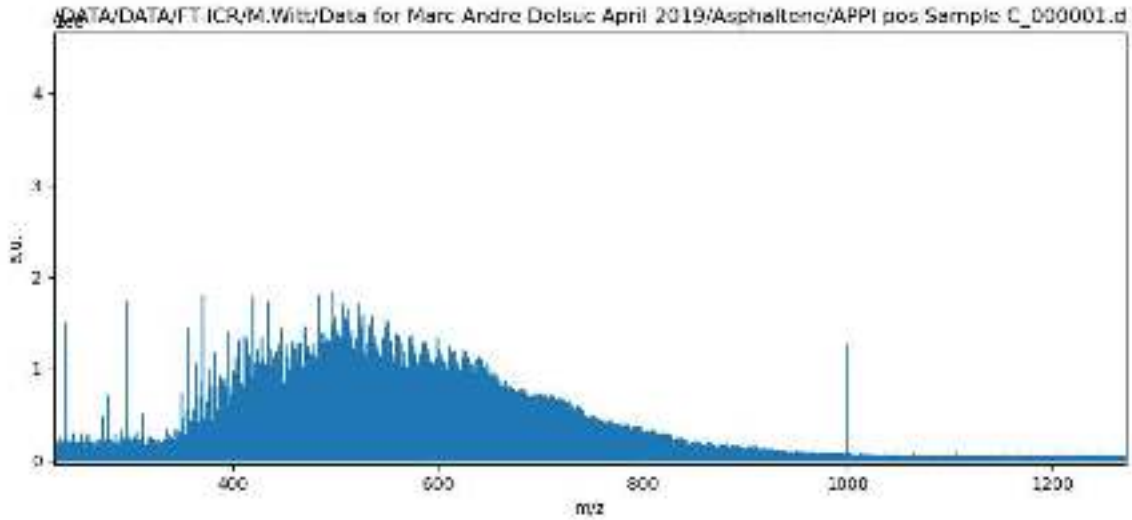

very normal !

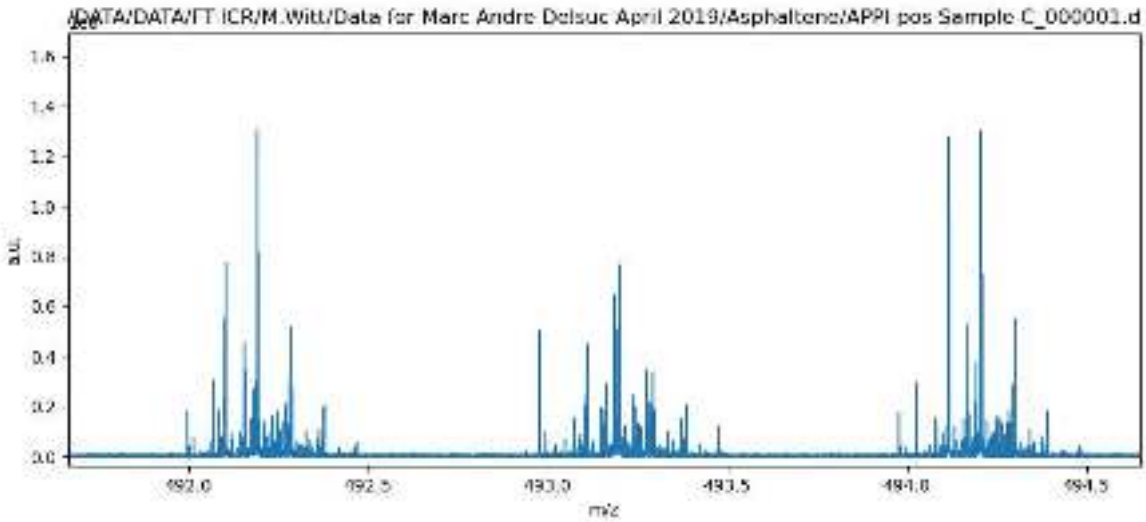

Really ?

looking at the time domain data-set

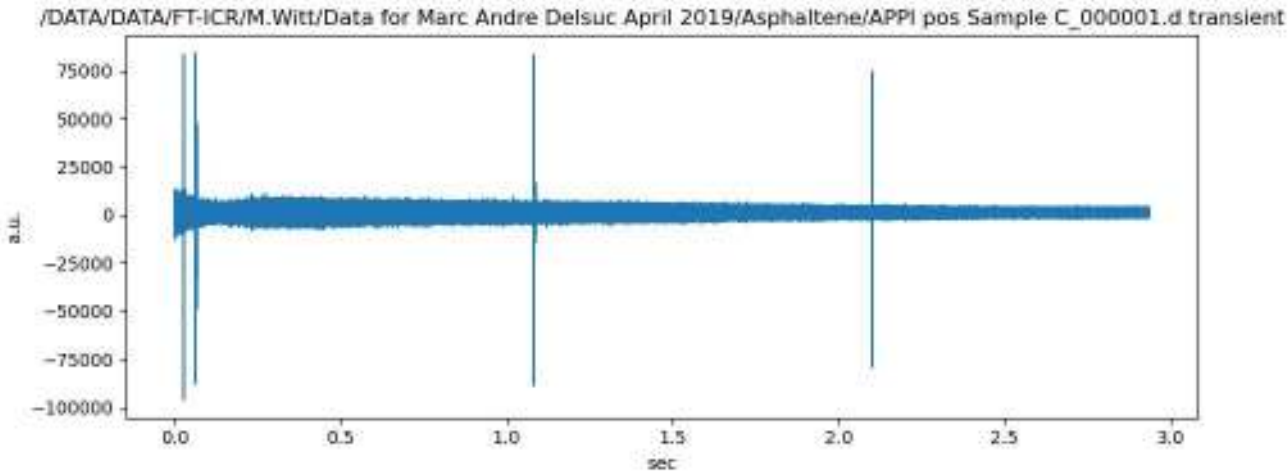

Really ?

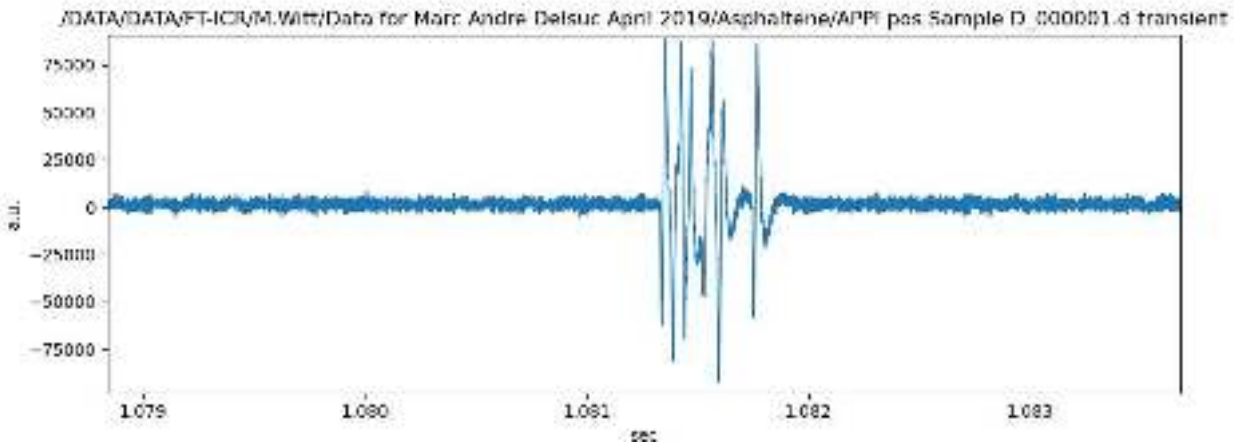

FT stability !

Open-Science trend

Open Science - Open source softwares - Open data

save raw / time domain / data

as early as possible in the analysis pipeline:

- for later (re)-analysis
  - eventually with a newer approach, not available at acquisition time
- for transverse data-mining
- needs to be F.A.I.R.
  - **F**indable
  - **A**ccessible
  - **I**nteroperable
  - **R**eusable

developping every where

- Genomic data !
- many biological data
- official administration data
- XRay data (Cambridge database / PDB database)
  - similar to MS

enforced by many provider

in particular within EU-FTICR-MS Network

But is it feasible ???

Out[8]:

```
(1535611.754328803, 42.1875)
```

Volume of data to store

standard pipeline

`fid` *(big)* → spectrum *(very big)* → parameter lists *(smaller)* → further analysis *(may grow again)*

how big ?

one example

- 15T (or 7T 2XR) - *m/z* 150 ≈ 1.5 MHz ⇒ 3 MHz sampling
- 4 bytes per point ⇒ 12 MB per second ⇒ **42 GB per hour**
- depends on resolving power - but whatever you you, there is only 3600 seconds per hour !
- big ! **but**
  - doable
  - not *much* bigger than NetFlix ! - and much more informational !!

efficient large data-set storage

on example

- HDF5 storage developped at CERN for fast access to huge data-sets
- random access along all axes
  - useful in LC-MS / mandatory in 2D-MS
- loss-less compression possibilities on the fly

compression

- spectra are *very* easy to compress efficiently
- time domain are more tricky, and usually poorly compressible
- there are loss-less compression methods for periodic datasets - not used yet -
- only noise is uncompressible

tentative implementation in EU FT-ICR MS network

- alternative analysis pipeline independent of manufacturer software, down to peak-list.
- possibility to display and analyze data-sets
- FAIR **public dataset** deposited and available at [data.eu-fticr-ms.eu/ (https://data.eu-fticr-ms.eu/)](https://data.eu-fticr-ms.eu/)

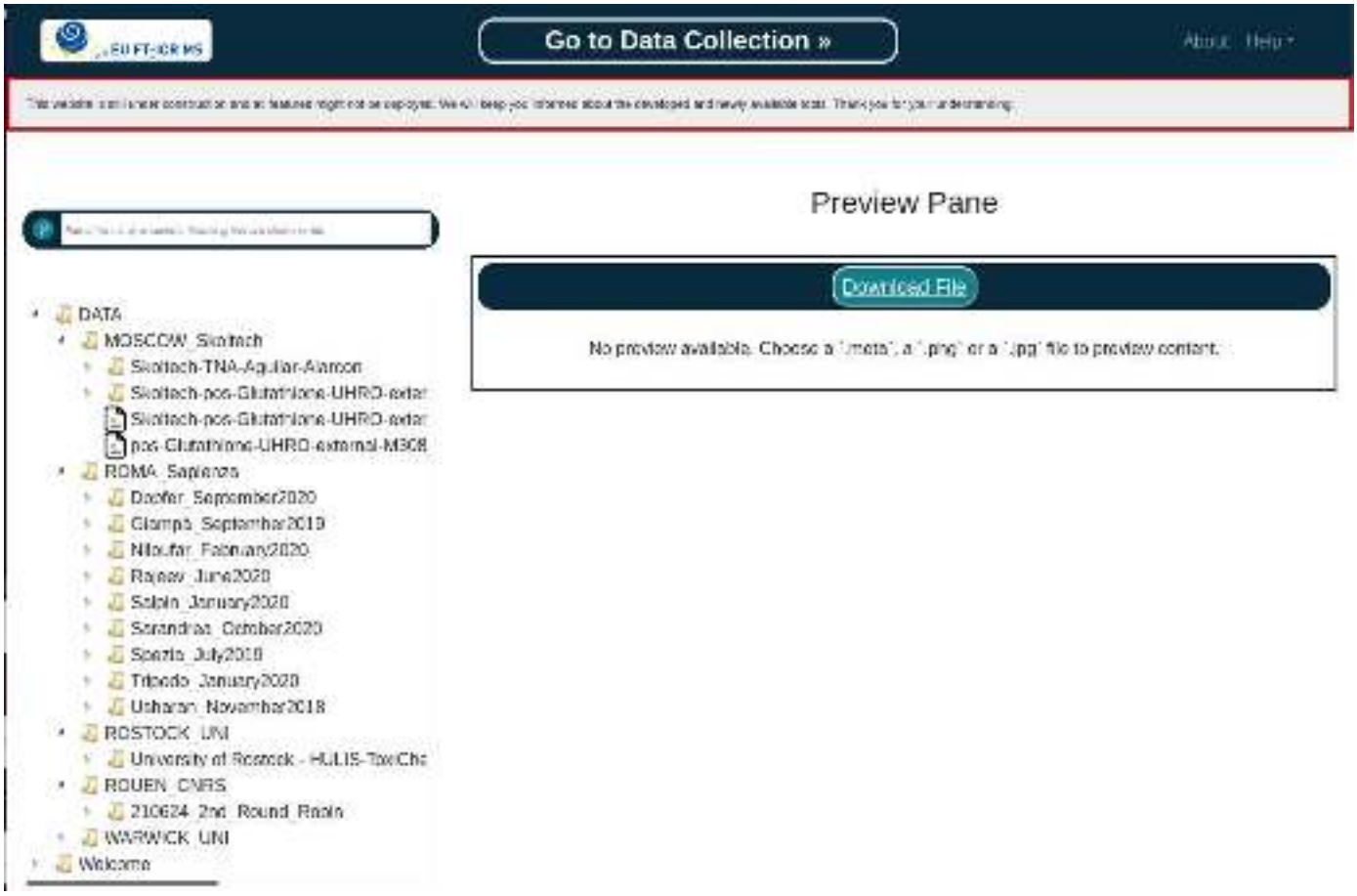

2D experiments

Thematic of the day.

Actually, there is a just a few things which are really special in 2D

2D basic principles

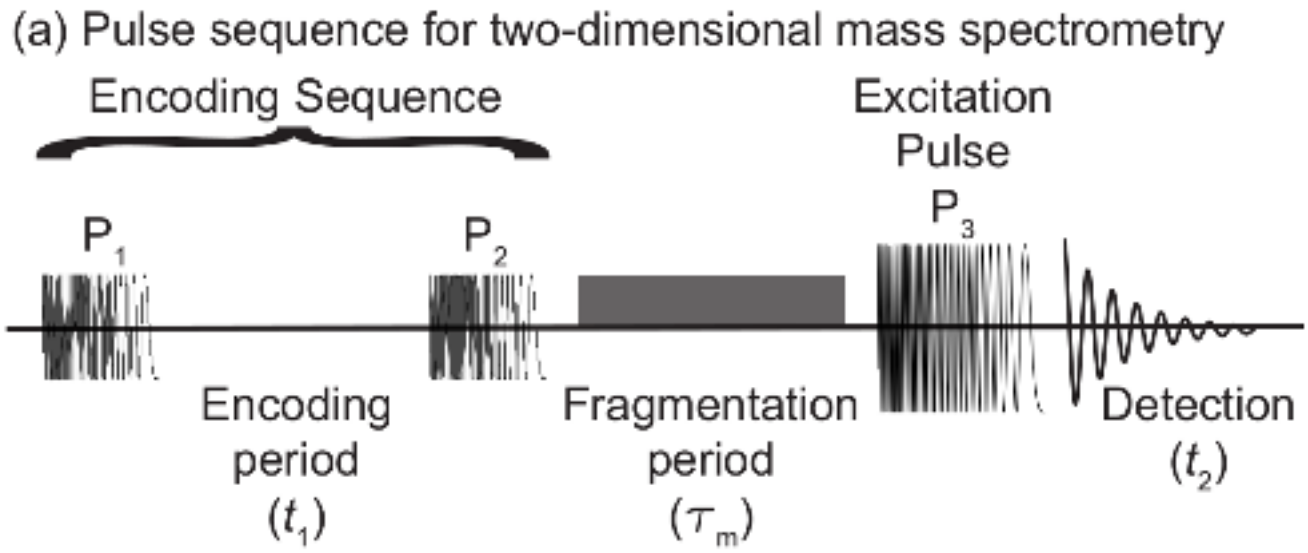

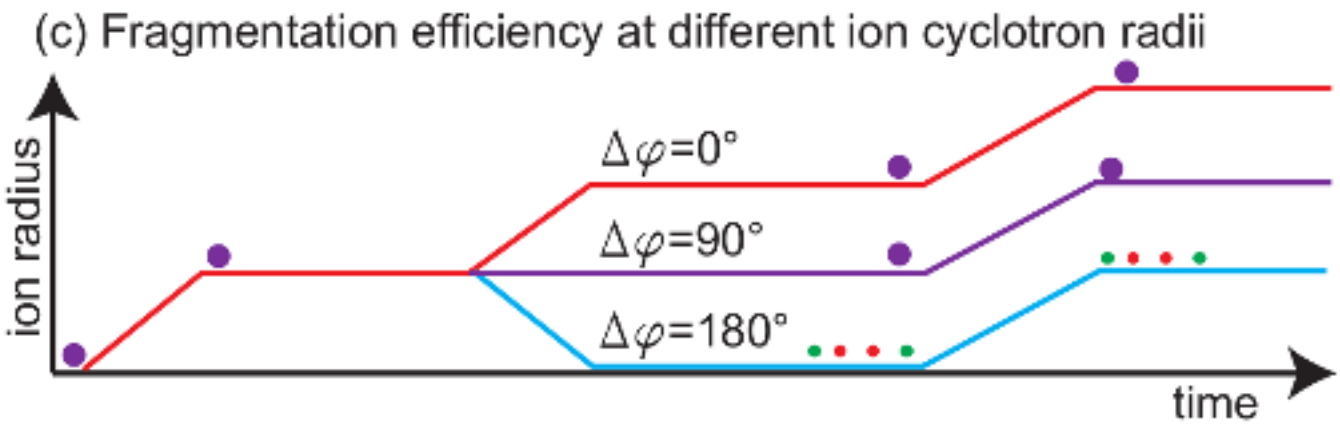

The 3 pulses have different roles

- P_1 excites ions to a first orbit at a given radius,
- P_2 similar to P_1 stops this first evolution
- P_3 is the read pulse which generates the signal that will be acquired

The 3 periods have very different properties

- t_1 is a delay, which will be incremented throughout the experiment
- τ_m is a fixed delay during which fragmentation takes place
- t_2 is a regular acquisition

t1

t_1 is a delay which samples the evolution of the ions between the two pulses P_1 and P_2

- we repeat several time the whole experiment, while incrementing t_1
- we use a constant increment Δt_1 applying Nyquist rule to this period

$$\Delta t_1 = \frac{1}{2F_1^{max}}$$

- the intensition of the fragment ions measure during t_2 is modulated by the evolution of the precursor during t_1

$$S(t_1) \propto \sqrt{1 + \cos(\omega_1 t_1)}$$

experimental protocol

Using a setup with a constant (as constant as possible) source of invariant sample

- start with a given t_1 (usually close to 0)
- repeat many time:
  - run the sequence above
  - store the resulting `fid`
  - increment t_1 by Δt_1
  - redo

Then we have a surface $S(t_1, t_2)$ - considered as a big matrix S_{ij}

- process all the `fid` in t_2 :

    - center - apodisation - zerofilling - FT
- process all the column of the data matrix - doing independently real and imaginary parts
    - apodisation - zerofilling - FT
    - combine real and imaginary to compute modulus

specificities of this *t1* modulation

the $S(t_1) \propto \sqrt{1+\cos(\omega_1 t_1)}$ modulation

- is periodic $\Rightarrow$ FT
- is not pure $\Rightarrow$ strong harmonics
- the signal along t_1 can be very noisy $\Rightarrow$ need for a (fast) denoising tool
- because of the frequency generator continuous phase, there is an additional frequency in the t_1 signal which has to be "demodulated"

One additional remark

We have: $S(t_1, t_2) \propto \cos(\omega_2 t_2)\sqrt{1+\cos(\omega_1 t_1)}$

there 2 ways to do a 2D modulation

amplitude modulation : $S(t_1, t_2) \propto \cos(\omega_2 t_2)\cos(\omega_1 t_1)$

- this is the classical modulation in image processing (MRI, Xray, ...)

phase modulation : $S(t_1, t_2) \propto \cos(\omega_2 t_2 + \omega_1 t_1)$

- is specific to spectrometry (2D-NMR - 2D-MS - ...)
- requires special algebra !

Hypercomplex Algebra

you cannot do that in $\mathbb{C}$, we have "only" one phase, one j

We posit a hypercomplex algebra $\mathbb{H}$, a 4 dimensionnal, commutative, non-invertible algebra.

$$z = a + ib + jc + kd \tag{1}$$
$$i^2 = -1 \quad j^2 = -1 \quad k^2 = 1$$
$$ij = ji = k \quad ik = ki = -j \quad jk = kj = -i$$

in $\mathbb{H}$ you can define independent phases: $e^{i\theta}$ and $e^{j\phi}$

and you can write (for a sub class of the element of $\mathbb{H}$) :

$$z = Ae^{i\theta}e^{j\phi} \tag{2}$$

$\Rightarrow \quad |z| = \sqrt{a^2+b^2+c^2+d^2}$

$\Rightarrow$ phases in F1 and in F2 are independent

Absorption mode 2D MS

We will use this this mathematics to phase correct both dimensions and generate 2D peaks in absorption mode in both dimensions

However one thing is simpler

- F2 (horizontal - classical) requires a 2nd order correction
- F1 (vertical - indirect) requires a 1st order correction

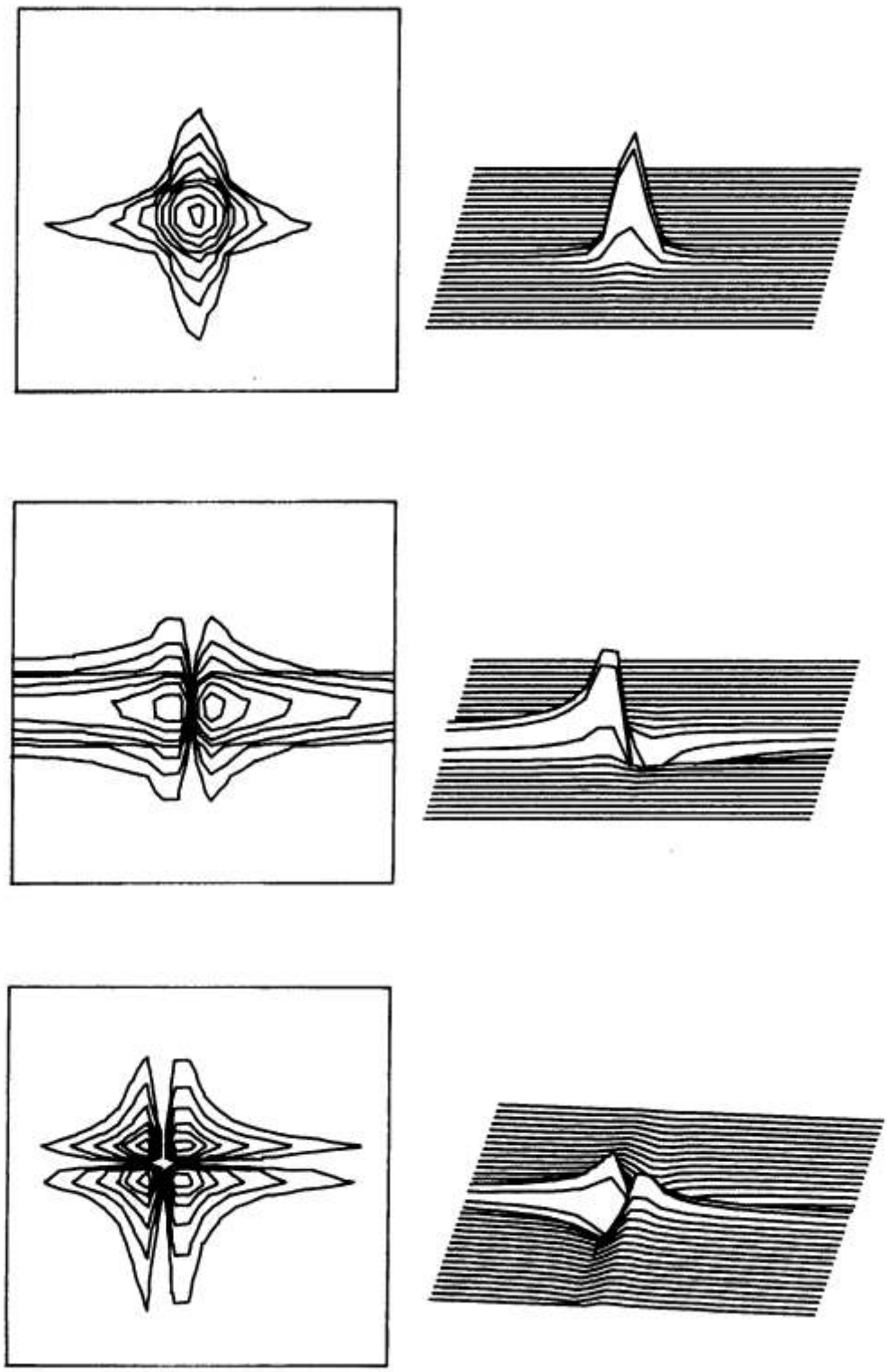

Non-linear Sampling

Many thanks

- Christian Rolando
- Peter O'Connor
- Maria van Agthoven
- Kathrin Breuker

but also

- The CASC4DE team
  - Camille Marin; Lionel Chiron; Laura Duciel; Luis Baptista; Anne Briot Dietsch; Do Manh Dung
- the IGMBC team
  - Bruno Kieffer; Jocelyn Céraline; Celia Deville; Claude Ling; ...

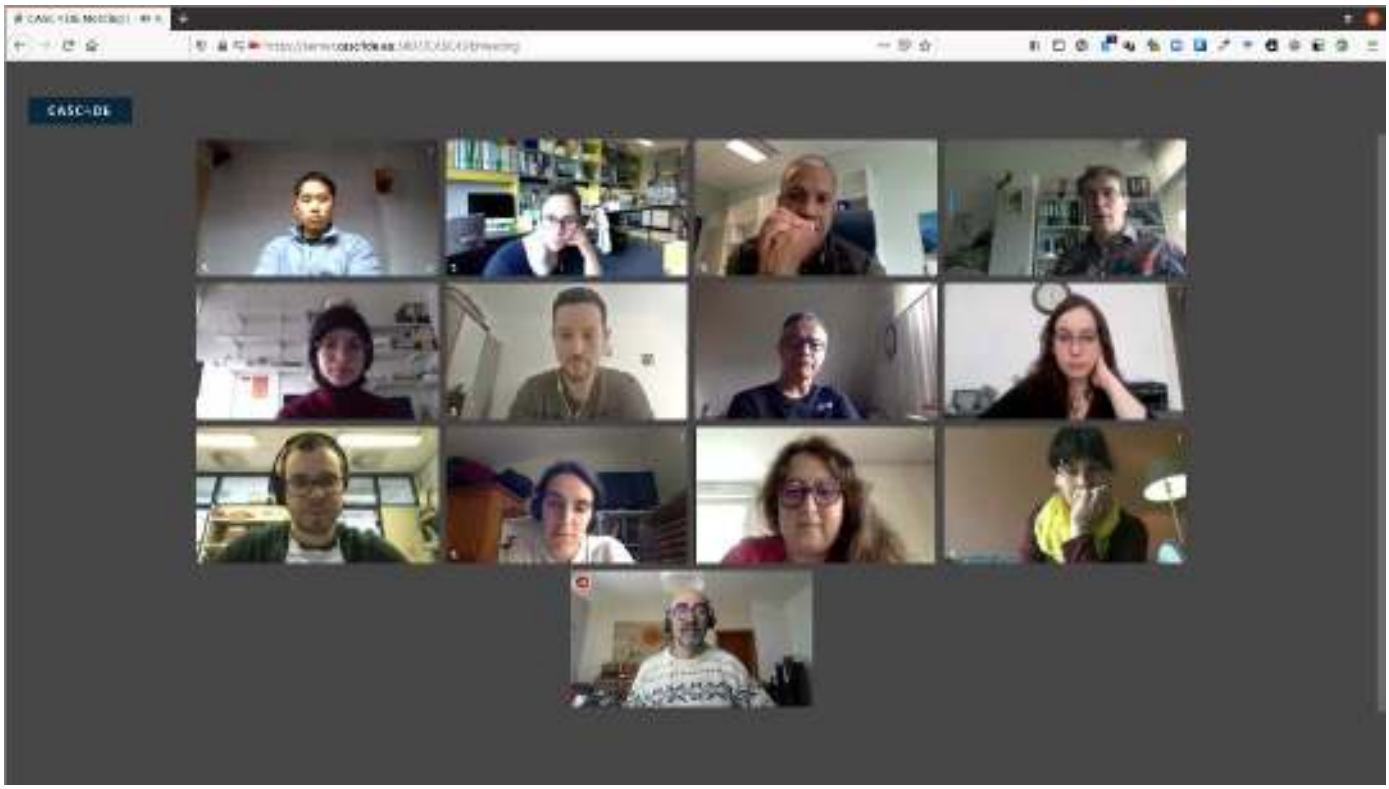

Thank you !

The Benefits of 2D-Mass Spectrometry for Protein Structural Characterization

Maria van Agthoven

Institute of Organic Chemistry, University of Innsbruck, Austria

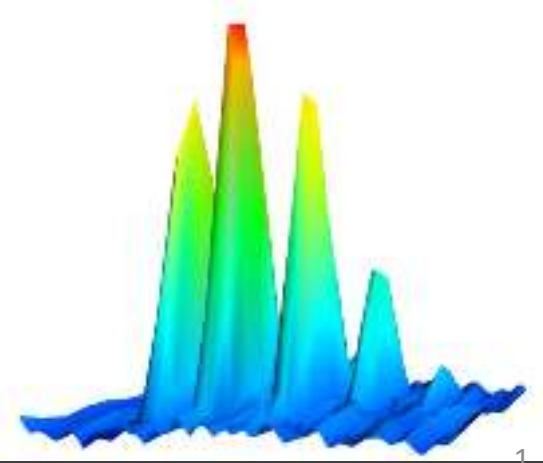

- Protein or RNA sequencing
- Modifications:
  - Identification
  - Location
  - Relative quantification

Two-dimensional FT-ICR MS

- All ions in a complex sample fragmented and visualised on one spectrum
- NO isolation ✗
- YES fragmentation ✓
- Horizontal axis: fragment *m/z*
- Vertical axis: precursor *m/z*
- Each peak corresponds to one fragmentation

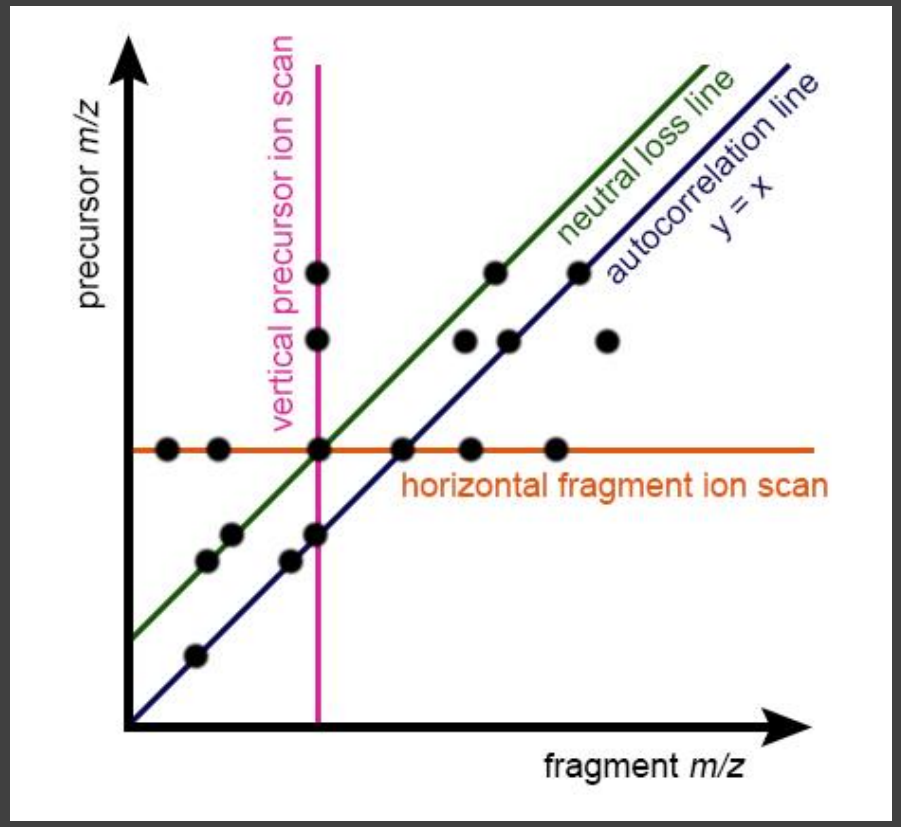

M. van Agthoven et al., *Anal. Bioanal. Chem.* 405 (2013) 51.
M. van Agthoven et al., *Eur. Biophys. J.* 48 (2019) 213.

Back to basics: Original Ion De-excitation Experiment

Coherent excitation in the ICR cell

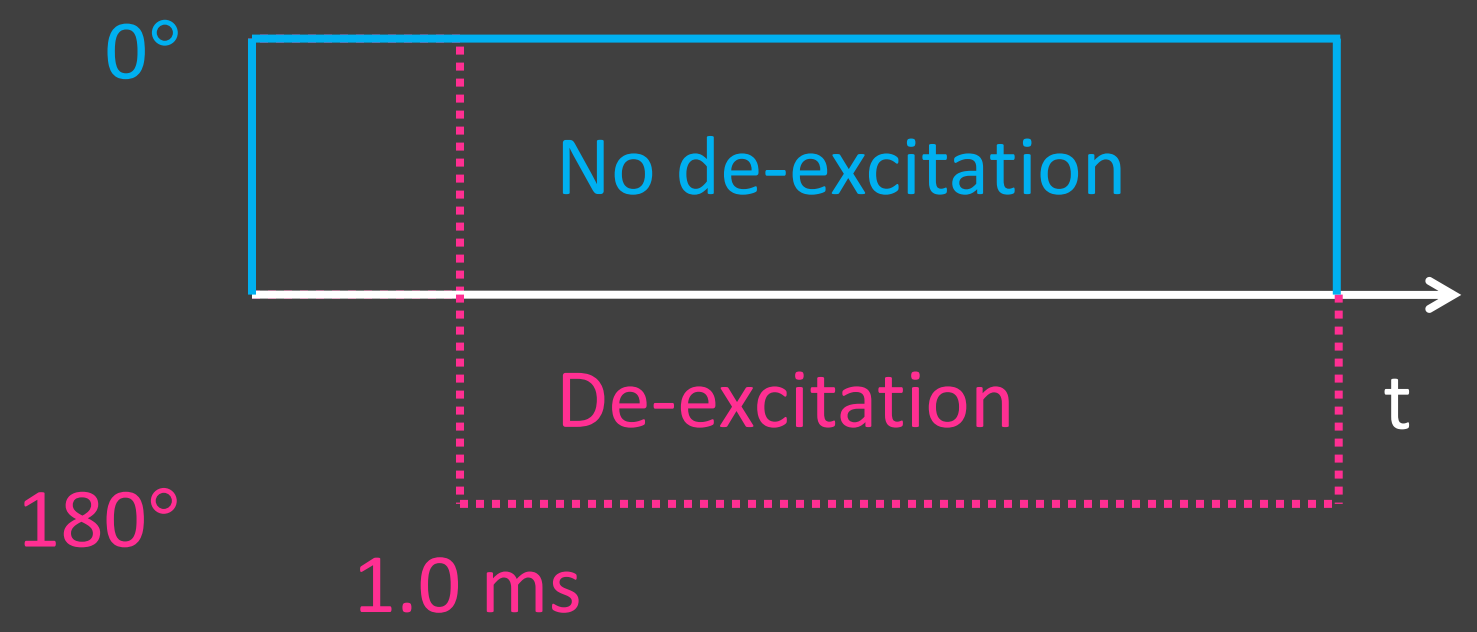

A.G. Marshall, T.C. Lin Wang, T. Lebatuan Ricca, *Chem. Phys. Letts.* 105 (1984) 233-236.

Original Ion De-excitation Experiment

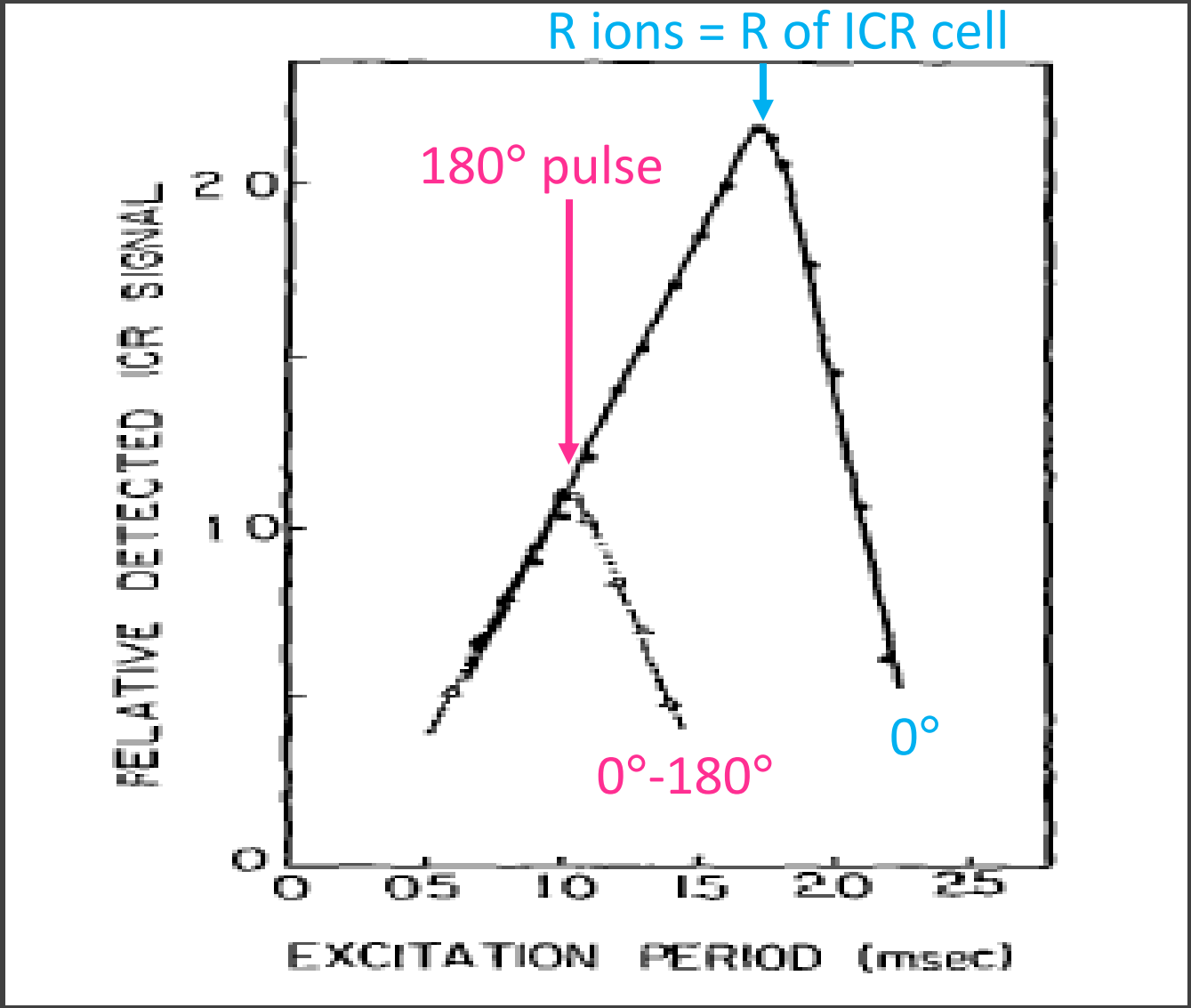

A.G. Marshall, T.C. Lin Wang, T. Lebatuan Ricca, *Chem. Phys. Letts.* 105 (1984) 233-236.

Original Ion De-excitation Experiment

Excitation voltage ***in phase with*** ion motion: ions excited to higher radius

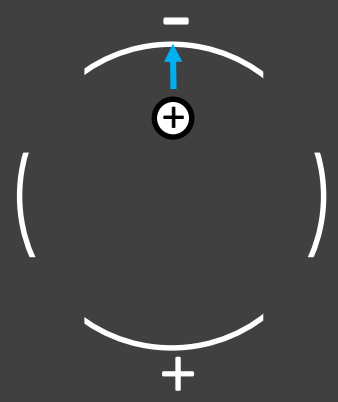

Excitation voltage ***in phase opposition with*** ion motion: ions de-excited to center of ICR cell.

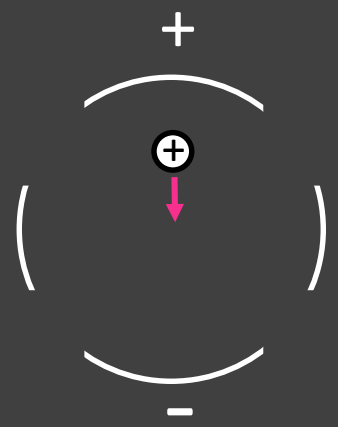

A.G. Marshall, T.C. Lin Wang, T. Lebatuan Ricca, *Chem. Phys. Letts.* 105 (1984) 233-236.

2D MS Pulse Sequence

P. Pfändler, G. Bodenhausen, J. Rapin, M.-E. Walser, T. Gäumann, *J. Am. Chem. Soc.* 110 (1988) 5625-5628.
M. Bensimon, G. Zhao, T. Gäumann, *Chem. Phys. Letts.* 157 (1989) 97-100.
S. Guan, P.R. Jones, *J. Chem. Phys.* 91 (1989) 5291-5295.

Radius Modulation

$$\text{Phase} = \text{Frequency} \times \text{Delay}$$

P. Pfändler, G. Bodenhausen, J. Rapin, M.-E. Walser, T. Gäumann, *J. Am. Chem. Soc.* 110 (1988) 5625-5628.
M. Bensimon, G. Zhao, T. Gäumann, *Chem. Phys. Letts.* 157 (1989) 97-100.
S. Guan, P.R. Jones, *J. Chem. Phys.* 91 (1989) 5291-5295.

Radius Modulation

$$radius \propto \sqrt{2\left(1 + cos(Frequency \times Delay)\right)}$$

P. Pfändler, G. Bodenhausen, J. Rapin, M.-E. Walser, T. Gäumann, *J. Am. Chem. Soc.* 110 (1988) 5625-5628.
M. Bensimon, G. Zhao, T. Gäumann, *Chem. Phys. Letts.* 157 (1989) 97-100.
S. Guan, P.R. Jones, *J. Chem. Phys.* 91 (1989) 5291-5295.

2D MS Pulse Sequence

Fragmentation

P. Pfändler, G. Bodenhausen, J. Rapin, M.-E. Walser, T. Gäumann, *J. Am. Chem. Soc.* 110 (1988) 5625-5628.
M. Bensimon, G. Zhao, T. Gäumann, *Chem. Phys. Letts.* 157 (1989) 97-100.
S. Guan, P.R. Jones, *J. Chem. Phys.* 91 (1989) 5291-5295.

Phase = 180°

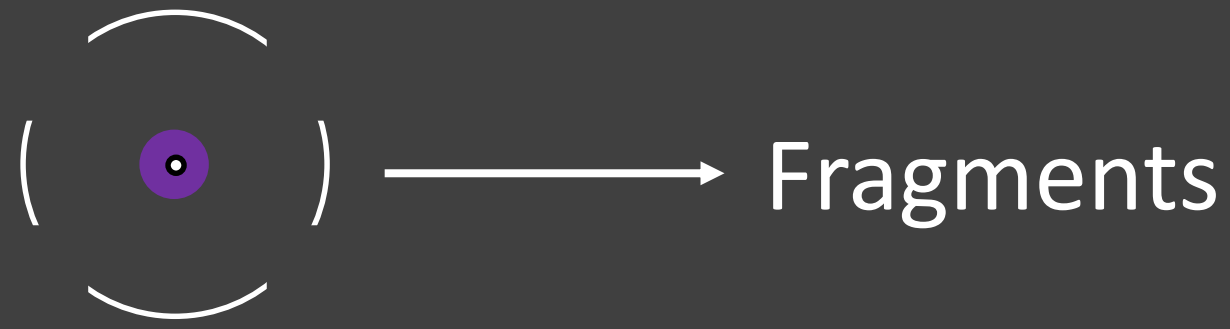

P. Pfändler, G. Bodenhausen, J. Rapin, M.-E. Walser, T. Gäumann, *J. Am. Chem. Soc.* 110 (1988) 5625-5628.
M. Bensimon, G. Zhao, T. Gäumann, *Chem. Phys. Letts.* 157 (1989) 97-100.
S. Guan, P.R. Jones, *J. Chem. Phys.* 91 (1989) 5291-5295.

Phase = 360°

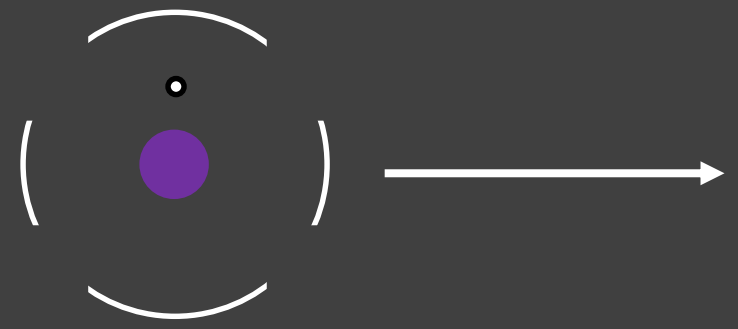

No Fragments

P. Pfändler, G. Bodenhausen, J. Rapin, M.-E. Walser, T. Gäumann, *J. Am. Chem. Soc.* 110 (1988) 5625-5628.
M. Bensimon, G. Zhao, T. Gäumann, *Chem. Phys. Letts.* 157 (1989) 97-100.
S. Guan, P.R. Jones, *J. Chem. Phys.* 91 (1989) 5291-5295.

Fragment abundance ∝ Precursor radius

Fragment abundance modulation = Precursor radius modulation

P. Pfändler, G. Bodenhausen, J. Rapin, M.-E. Walser, T. Gäumann, *J. Am. Chem. Soc.* 110 (1988) 5625-5628.
M. Bensimon, G. Zhao, T. Gäumann, *Chem. Phys. Letts.* 157 (1989) 97-100.
S. Guan, P.R. Jones, *J. Chem. Phys.* 91 (1989) 5291-5295.

2D MS Pulse Sequence

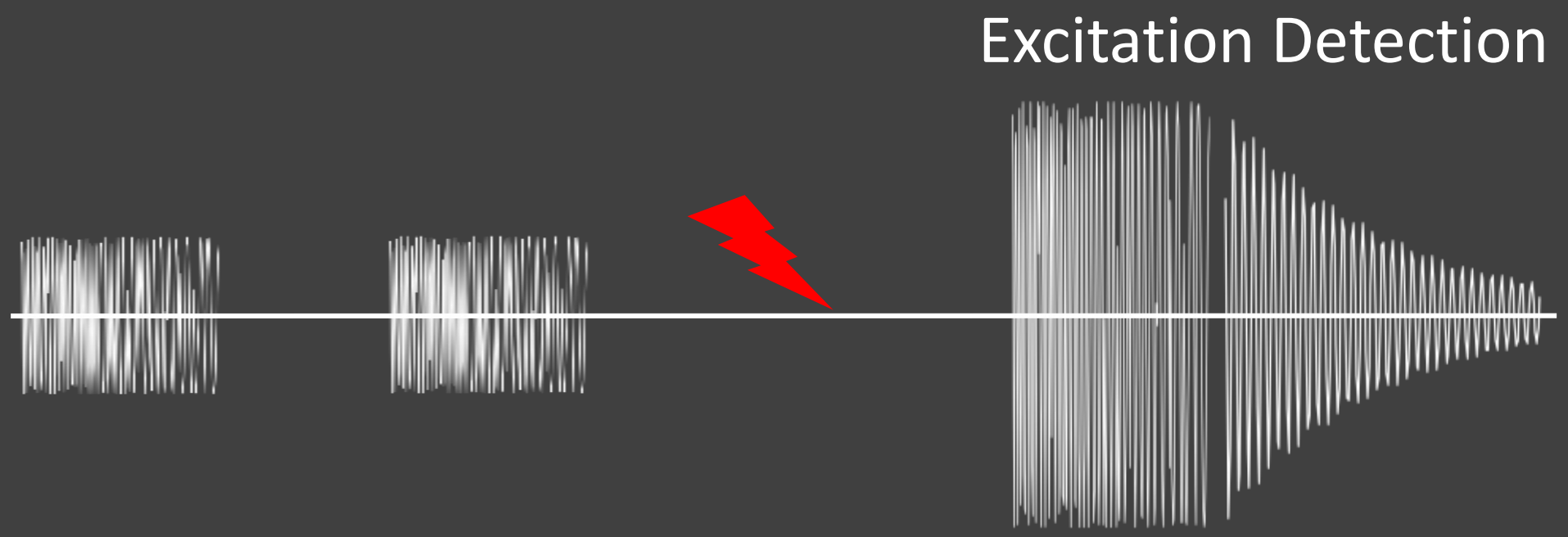

P. Pfändler, G. Bodenhausen, J. Rapin, M.-E. Walser, T. Gäumann, *J. Am. Chem. Soc.* 110 (1988) 5625-5628.
M. Bensimon, G. Zhao, T. Gäumann, *Chem. Phys. Letts.* 157 (1989) 97-100.
S. Guan, P.R. Jones, *J. Chem. Phys.* 91 (1989) 5291-5295.

Precursor-Fragment correlation

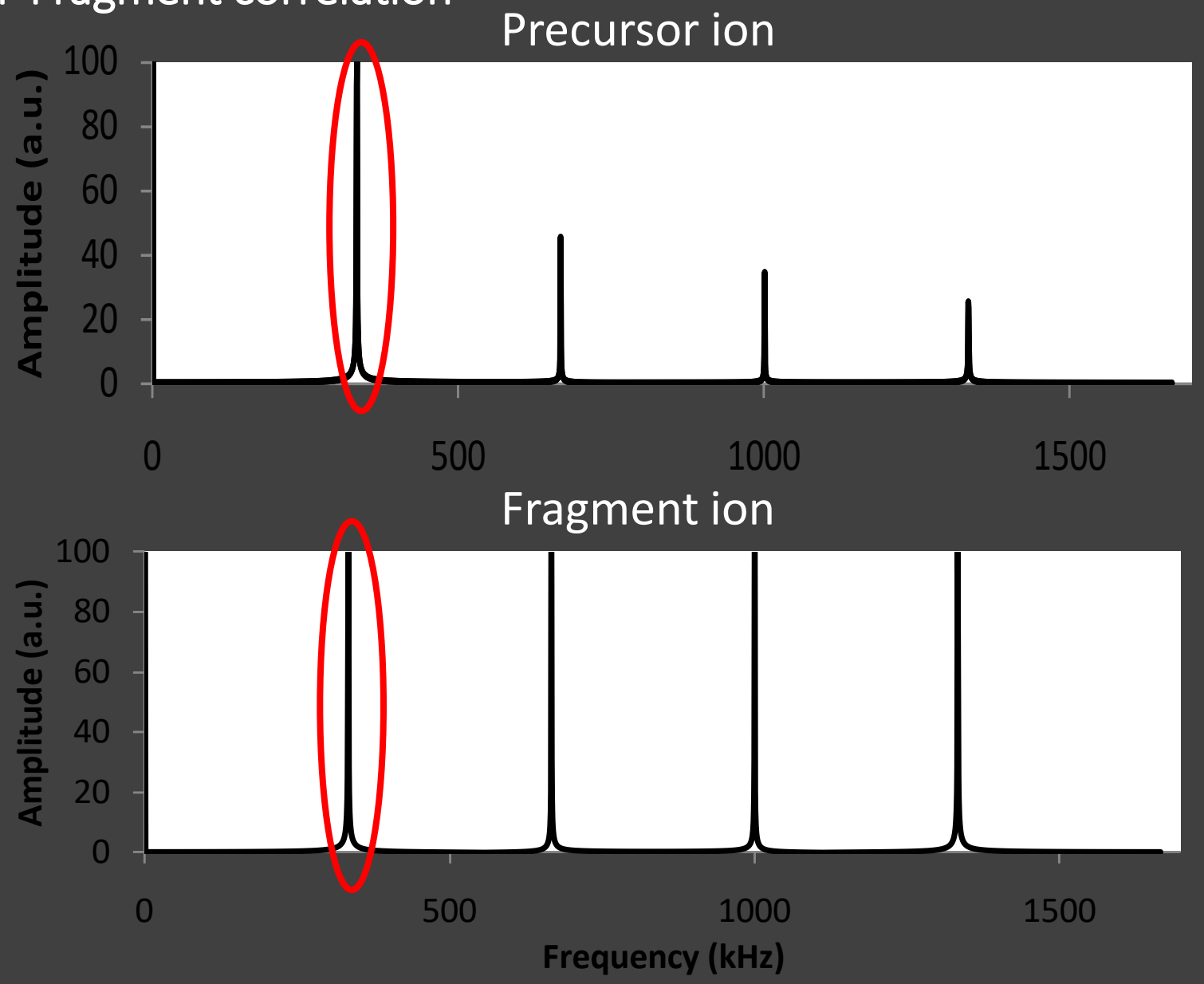

P. Pfändler, G. Bodenhausen, J. Rapin, M.-E. Walser, T. Gäumann, *J. Am. Chem. Soc.* 110 (1988) 5625-5628.
M. Bensimon, G. Zhao, T. Gäumann, *Chem. Phys. Letts.* 157 (1989) 97-100.
S. Guan, P.R. Jones, *J. Chem. Phys.* 91 (1989) 5291-5295.

First 2D FT-ICR Spectra
Ion-Molecule Reactions of CH_4^+

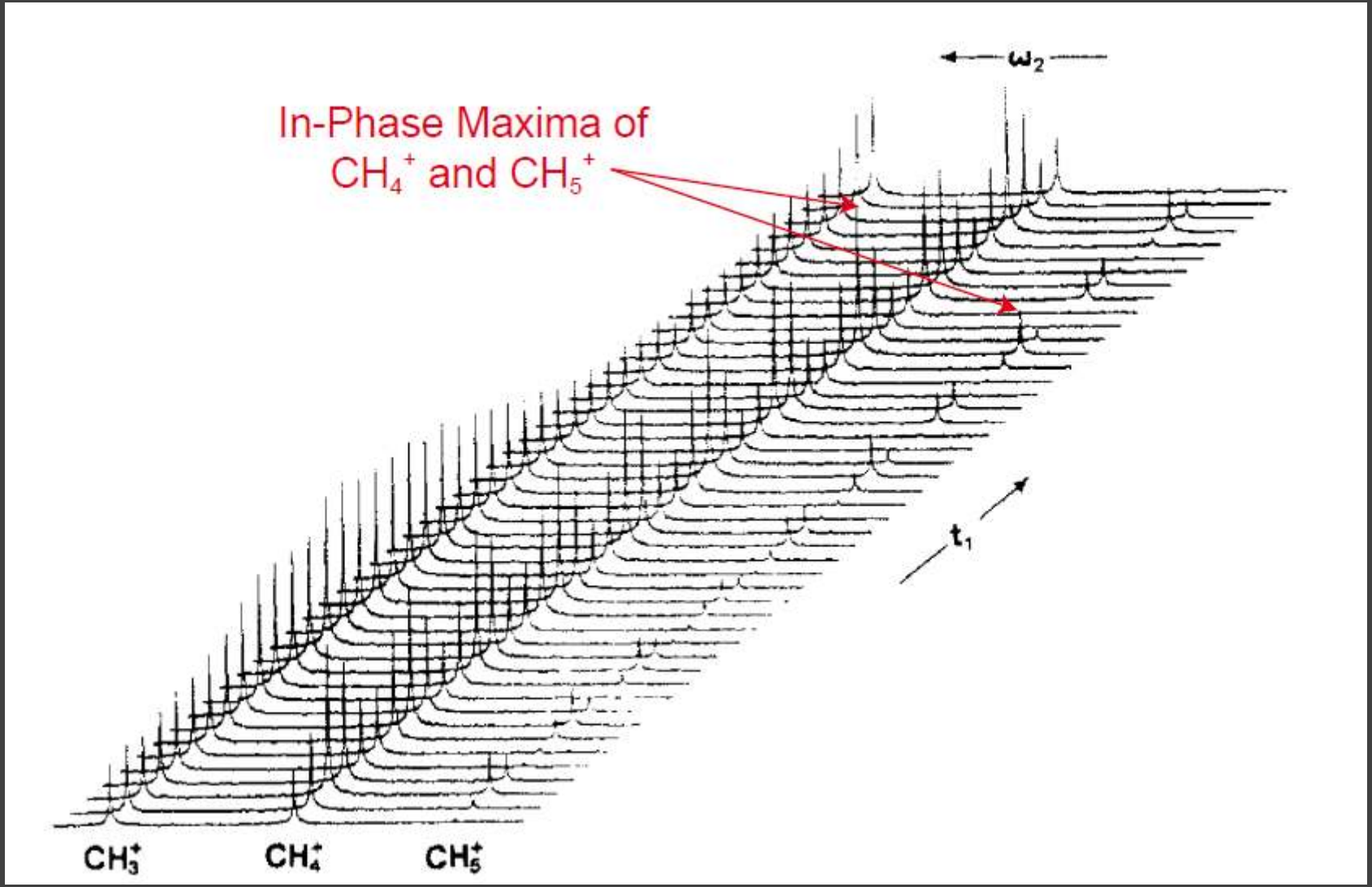

P. Pfändler, G. Bodenhausen, J. Rapin, M.-E. Walser, T. Gäumann, *J. Am. Chem. Soc.* 110 (1988) 5625-5628.

First 2D FT-ICR Spectra
Ion-molecule reactions of CH_4^+ (120×1k data points)

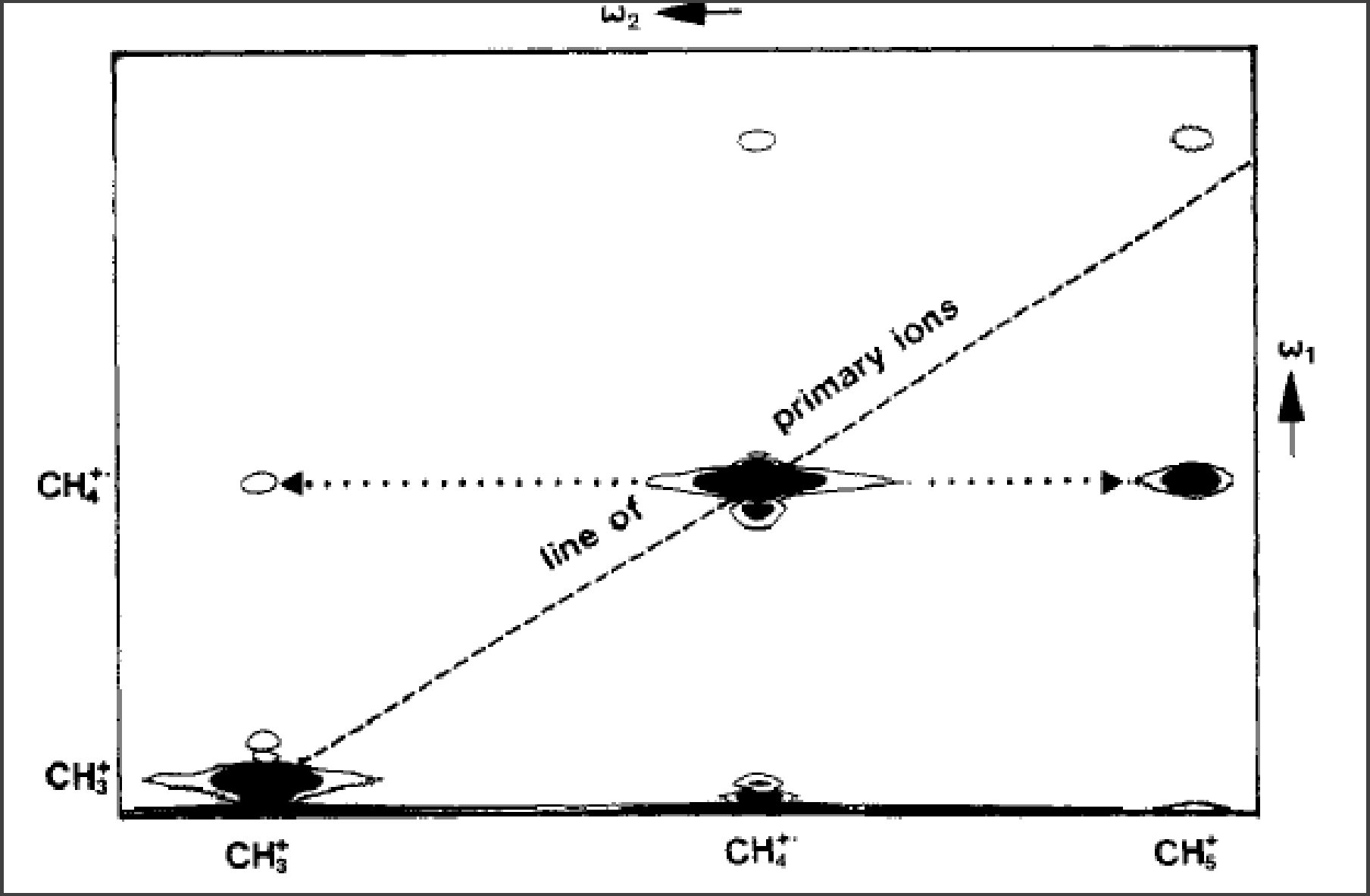

P. Pfändler et al., *J. Am. Chem. Soc.* 110 (1988) 5625-5628.

First 2D FT-ICR Spectra
Ion-molecule reactions of CHD_3 (256×1k data points)

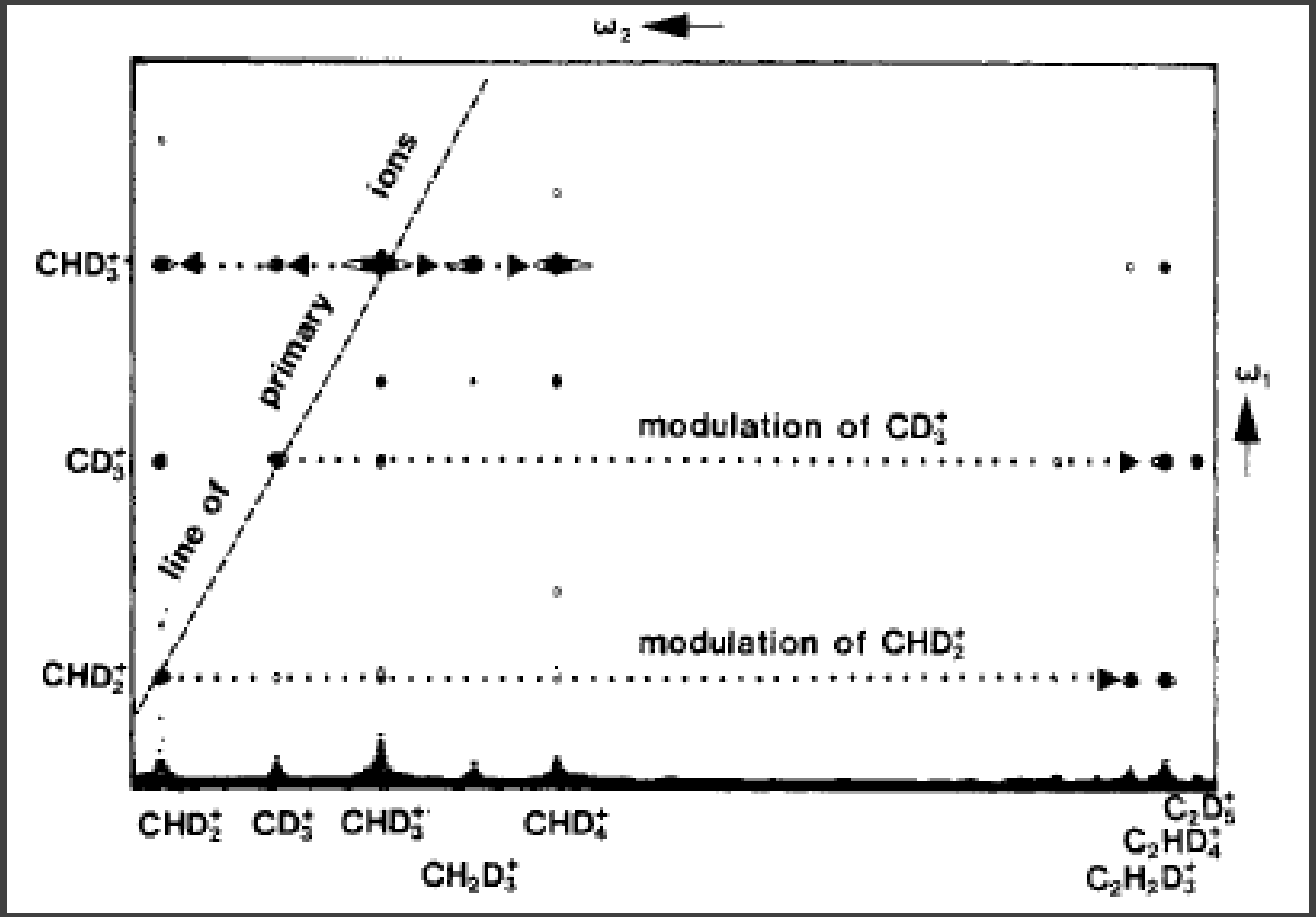

P. Pfändler et al., *J. Am. Chem. Soc.* 110 (1988) 5625-5628.

Further 2D FT-ICR MS Studies

A theory for two-dimensional Fourier-transform ion cyclotron resonance mass spectrometry

Shenheng Guan and Patrick R. Jones
University of the Pacific, Chemistry Department, Stockton, California 95211

(Received 8 March 1989; accepted 27 July 1989)

A theoretical model, based on the Lorentz equations for ion motion and the mass action law, is developed for two-dimensional Fourier-transform mass spectrometry known as 2D FT–ICR or 2D FTMS. The theory illustrates that the modulation of 2D FT–ICR ion signals in the additional time dimension comes from the modulation of the primary ion speed by the 2D excitation pulses. The modulation of the primary ion speed is found not to be sinusoidal and the modulation of the ion signals in 2D FT–ICR spectra is found to be complicated even in the simplest chemical system. The complex modulation creates higher harmonic components in the spectra. Based on the model, a data processing algorithm is proposed. The results show that the Fourier transformation should be performed stepwise in order to obtain complete information, and that the phase portion of the frequency domain generated by the second Fourier transformation should not be discarded since it contains useful information.

Noise analysis for 2D tandem Fourier transform ion cyclotron resonance mass spectrometry

Guillaume van der Rest, Alan G. Marshall*

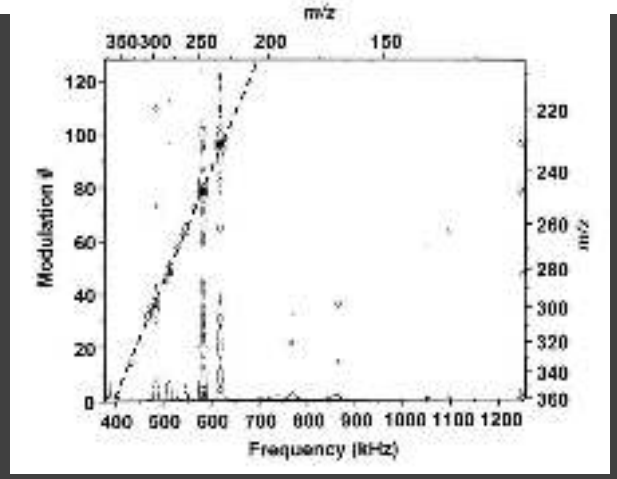

Two-Dimensional Fourier Transform Ion Cyclotron Resonance Mass Spectrometry/Mass Spectrometry with Stored-Waveform Ion Radius Modulation

Charles W. Ross, III, Shenheng Guan, Peter B. Grosshans,[1] Tom L. Ricca,[2] and Alan G. Marshall*[3]
Contribution from the Department of Chemistry, The Ohio State University, 120 West Eighteenth Avenue, Columbus, Ohio 43210

Received March 4, 1993

Abstract: A fundamentally new two-dimensional Fourier transform ion cyclotron resonance mass spectrometry experiment, SWIM ("stored-waveform ion modulation") 2D-FT/ICR MS/MS, is described. Prior encodement of the second dimension by use of two identical excitation waveforms separated by a variable delay period (analogous to 2D-NOESY NMR) is replaced by a new encodement in which each row of the two-dimensional data array is obtained by use of a single stored excitation waveform whose frequency-domain magnitude spectrum is a sinusoid whose frequency increases from one row to the next. In the two-dimensional mass spectrum, the conventional one-dimensional FT/ICR mass spectrum appears along the diagonal, and each off-diagonal peak corresponds to an ion-neutral reaction whose ionic components may be identified by horizontal and vertical projections to the diagonal spectrum. Fragmentation due to (e.g.) collision-induced dissociation results in peaks only on one side of the diagonal, whereas bidirectional ion-molecule reactions result in peaks on both sides of the diagonal. All ion-molecule reactions in a gaseous mixture may be identified from a single 2D-FT/ICR MS/MS experiment, without any prior knowledge of the system.

Anal. Chem. 2002, 74, 4625–4633

Application of Stored Waveform Ion Modulation 2D-FTICR MS/MS to the Analysis of Complex Mixtures

Charles W. Ross, III,[*,†] William J. Simonsick, Jr.,[‡] and David J. Aaserud[†]
DuPont Marshall R & D Laboratory, Philadelphia, Pennsylvania 19145, and Merck Research Labs, Merck & Co. Inc., West Point, Pennsylvania 19486

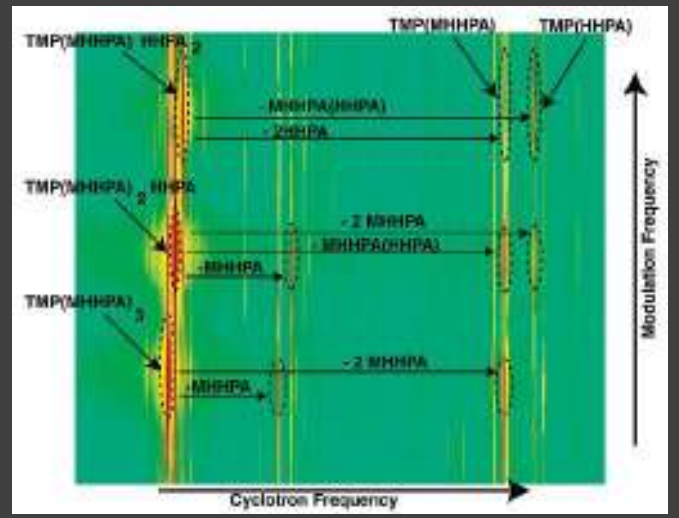

Guan et al. J. Chem. Phys. 91 (1989) 5291-5295.
Ross et al. J. Am. Chem. Soc. 115 (1993) 7854-7861.
van der Rest et al. Int. J. Mass Spectrom. 210/211 (2001) 101-111.
Ross et al. Anal. Chem. 74 (2002) 4625-4633.

2D FT-ICR MS Renewal: Adaptation to IRMPD and ECD

Two-dimensional FT-ICR/MS with IRMPD as fragmentation mode

Maria A. van Agthoven[a], Marc-André Delsuc[b], Christian Rolando[a,*]

[a] USR CNRS 3290 Miniaturisation de Systèmes d'Analyse et de Protéomique and FR CNRS 2638 Institut Michel-Eugène Chevreul, Université de Lille 1, Sciences et Technologie, Villeneuve d'Ascq, France
[b] Institut de Génétique et de Biologie Moléculaire et Cellulaire, Illkirch-Graffenstaden, France

ARTICLE INFO

Article history:
Received 27 August 2010
Received in revised form 22 October 2010
Accepted 27 October 2010
Available online xxx

Keywords:
FT-ICR
2-Dimensional
IRMPD
FTMS
Pulse sequence
Double-frequency

ABSTRACT

In 1988, Gäumann et al. introduced a pulse sequence for two-dimensional FT-ICR/MS correlating parent ions and fragment ions without the need for ion isolation. The improvement in computer technology makes this pulse sequence analytically useful in order to obtain structural information on complex samples. The pulse sequence can be applied to all cyclotron radius-dependent fragmentation modes, including gas free fragmentation modes like IRMPD, which do not affect sensitivity and resolving power like the pulsing of a gas into the ICR cell does. This study shows the feasibility of 2D FT-ICR/MS and lays the groundwork to turn this method into a viable analytical tool.

© 2010 Elsevier B.V. All rights reserved.

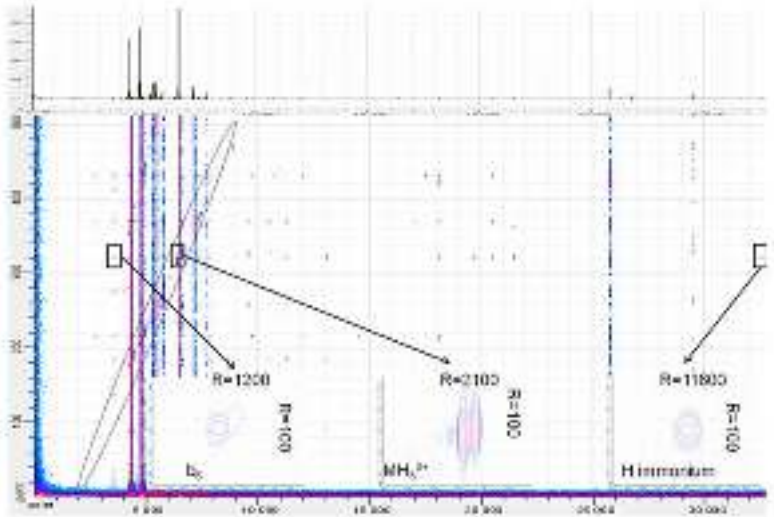

Fig. 2. 2D IRMPD mass spectrum of angiotensin I (1 pmol/μL in MeOH/water with 0.1% formic acid) using IRMPD (30% for 0.1 s). Cyclotron frequencies are represented horizontally (f_{sample} = 1667 kHz = 32,768 a.u., corresponding to a m/z 88–2000 mass range) and correlation frequencies are represented vertically (f_{sample} = 1667 kHz = 2048 a.u., corresponding to a m/z 66–2000 mass range). Although the size of the data file is 32,768 × 2048, we chose to represent 32,768 × 512 for better visibility. Inserts: Self-correlation peak of MH_2^{2+} (m/z 403) with its ^{13}C isotopes and resolution of the peak in both directions. Correlation peaks of MH_2^{2+} and b_3 (m/z 764) and H immonium (m/z 110) and resolution of the peaks in both dimensions.

Two-Dimensional ECD FT-ICR Mass Spectrometry of Peptides and Glycopeptides

Maria A. van Agthoven,[†] Lionel Chiron,[‡] Marie-Aude Coutouly,[§] Marc-André Delsuc,[‡,§] and Christian Rolando[*,†]

[†] Miniaturisation pour la Synthèse, l'Analyse & la Protéomique (MSAP), USR CNRS 3290, and Protéomique, Modifications Post-traductionnelles et Glycobiologie, IFR 147 and Institut Eugène-Michel Chevreul, FR CNRS 2638, Université de Lille 1 Sciences et Technologies, 59655 Villeneuve d'Ascq Cedex, France
[‡] Institut de Génétique et de Biologie Moléculaire et Cellulaire, INSERM, U596, CNRS, UMR7104, Université de Strasbourg, 1 rue Laurent Fries, 67404 Illkirch-Graffenstaden, France
[§] NMRTEC, Bld. Sébastien Brandt, Biopare-Bat. B, 67400 Illkirch-Graffenstaden, France

Supporting Information

ABSTRACT: 2D FT-ICR MS allows the correlation between precursor and fragment ions by modulating ion cyclotron radii for fragmentation modes with radius-dependent efficiency in the ICR cell without the need for prior ion isolation. This technique has been successfully applied to ion–molecule reactions, Collision-induced dissociation and infrared multiphoton dissociation. In this study, we used electron capture dissociation for 2D FT-ICR MS for the first time, and we recorded two-dimensional mass spectra of peptides and a mixture of glycopeptides that showed fragments that are characteristic of ECD for each of the precursor ions in the sample. We compare the sequence coverage obtained with 2D ECD FT-ICR MS with the sequence coverage obtained with ECD MS/MS and compare the sensitivities of both techniques. We demonstrate how 2D ECD FT-ICR MS can be implemented to identify peptides and glycopeptides for proteomics analysis.

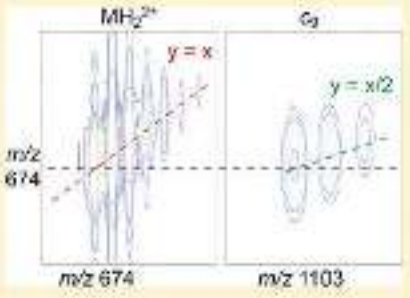

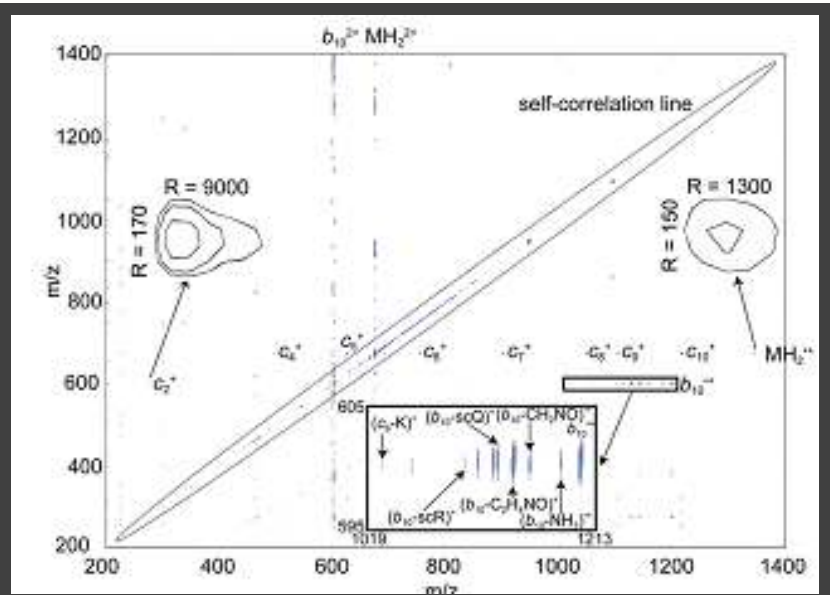

van Agthoven et al. Int. J. Mass Spectrom. 306 (2011) 196-203.
van Agthoven et al. Anal. Chem. 84 (2012) 5589-5595.
SPIKE: http://www.bitbucket.org/delsuc/spike
Chiron et al. arXiv.org, e-Print Arch., Phys., 1-13 (2016).

2D FT-ICR MS Renewal: Adaptation to IR-ECD

analytical chemistry

Article

Cite This: Anal. Chem. 2018, 90, 3496−3504

pubs.acs.org/ac

Can Two-Dimensional IR-ECD Mass Spectrometry Improve Peptide de Novo Sequencing?

Maria A. van Agthoven,[§] Alice M. Lynch,[§] Tomos E. Morgan,[§] Christopher A. Wootton,[§] Yuko P.Y. Lam,[§] Lionel Chiron,[⊥] Mark P. Barrow,[§] Marc-André Delsuc,[#,+] and Peter B. O'Connor*[,§]

[§]Department of Chemistry, University of Warwick, Gibbet Hill Road, Coventry CV4 7AL, United Kingdom

[+]CASCADE, Le Lodge, 20 av. du Neuhof, 67100 Strasbourg, France

[#]Institut de Génétique et de Biologie Moléculaire et Cellulaire, INSERM, U596; CNRS, UMR7104, Université de Strasbourg, 1 rue Laurent Fries, 67404 Illkirch-Graffenstaden, France

Supporting Information

ABSTRACT: Two-dimensional mass spectrometry (2D MS) correlates precursor and fragment ions without ion isolation in a Fourier transform ion cyclotron resonance mass spectrometer (FTICR MS) for tandem mass spectrometry. Infrared activated electron capture dissociation (IR-ECD), using a hollow cathode configuration, generally yields more information for peptide sequencing in tandem mass spectrometry than ECD (electron capture dissociation) alone. The effects of the fragmentation zone on the 2D mass spectrum are investigated as well as the structural information that can be derived from it. The enhanced structural information gathered from the 2D mass spectrum is discussed in terms of how de novo peptide sequencing can be performed with increased confidence. 2D IR-ECD MS is shown to sequence peptides, to distinguish between leucine and isoleucine residues through the production of *w* ions as well as between C-terminal (*b*/*c*) and N-terminal (*y*/*z*) fragments through the use of higher harmonics, and to assign and locate peptide modifications.

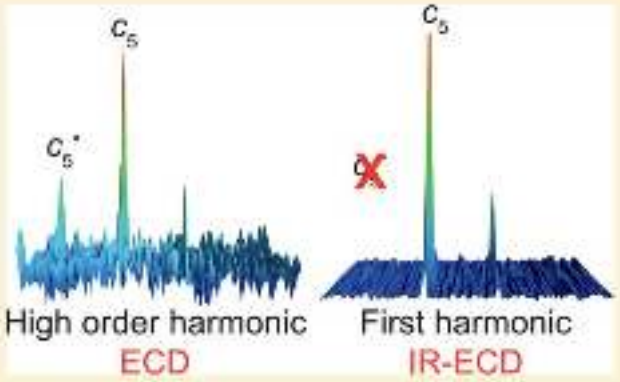

van Agthoven et al. Anal. Chem. 90 (2018) 3496-3504.

2D FT-ICR MS Renewal: Adaptation to EID

analytical chemistry

pubs.acs.org/ac

Article

Advantages of Two-Dimensional Electron-Induced Dissociation and Infrared Multiphoton Dissociation Mass Spectrometry for the Analysis of Agrochemicals

Bryan P. Marzullo, Tomos E. Morgan, Christopher A. Wootton, Simon J. Perry, Mansoor Saeed, Mark P. Barrow, and Peter B. O'Connor*

Cite This: Anal. Chem. 2020, 92, 11687−11695

Read Online

ACCESS | Metrics & More | Article Recommendations | Supporting Information

ABSTRACT: Analysis of agrochemicals in an environmental matrix is challenging because these samples contain multiple agrochemicals, their metabolites, degradation products, and endogenous compounds. The analysis of such complex samples is achieved using chromatographic separation techniques coupled to mass spectrometry. Herein, we demonstrate a two-dimensional mass spectrometry (2DMS) technique on a 12 T Fourier transform ion cyclotron resonance mass spectrometer that can analyze a mixture of agrochemicals without using chromatography or quadrupole isolation in a single experiment. The resulting 2DMS contour plot contains abundant tandem MS information for each component in the sample and correlates product ions to their corresponding precursor ions. Two different fragmentation methods are employed, infrared multiphoton dissociation (IRMPD) and electron-induced dissociation (EID), with 2DMS to analyze the mixture of singly charged agrochemicals. The product ions of one of the agrochemicals, pirimiphos-methyl, present in the sample was used to internally calibrate the entire 2DMS spectrum, achieving sub part per million (ppm) to part per billion (ppb) mass accuracies for all species analyzed. The work described in this study will show the advantages of the 2DMS approach, by grouping species with common fragments/core structure and mutual functional groups, using precursor lines and neutral loss lines. In addition, the rich spectral information obtained from IRMPD and EID 2DMS contour plots can accurately identify and characterize agrochemicals.

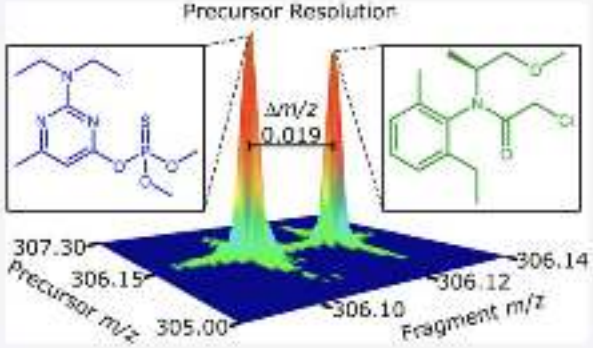

Marzullo et al. Anal. Chem. 92 (2020) 11687-11695.

2D FT-ICR MS Renewal: Pulse Sequence Optimisation and Data Processing

Optimization of the discrete pulse sequence for two-dimensional FT-ICR mass spectrometry using infrared multiphoton dissociation

Maria A. van Agthoven[a,1], Lionel Chiron[b], Marie-Aude Coutouly[c], Akansha Ashvani Sehgal[d], Philippe Pelupessy[d], Marc-André Delsuc[b,c], Christian Rolando[a,*]

ARTICLE INFO

Article history:
Received 15 March 2014
Received in revised form 9 June 2014
Accepted 25 June 2014
Available online xxx

Keywords:
FT-ICR
2-dimensional
FTMS
Pulse sequence
Optimization

ABSTRACT

2D FT-ICR MS, introduced by Pfändler et al. (Chem. Phys. Lett. 138 (1987) 195), allows one to correlate precursor and fragment ions in complex samples without requiring ion isolation. Recent advances in electronics, computer capacities, and gas-free in-cell fragmentation techniques open up new perspectives for 2D FT-ICR MS as an analytical technique. The pulse sequence consists of two encoding pulses separated by an incremental delay, followed by an observe pulse. In our previous 2D FT-ICR MS work we used three pulses of equal duration and amplitude. However, signal intensity was low because it was distributed over a series of intense harmonics. Using a simple theoretical model to analytically express ion fragmentation and 2D FT-ICR MS ion trajectories, we obtained a nearly pure signal when the maximum radius of the ions during the encoding pulses is within the laser beam. By adjusting the experimental parameters of the encoding pulses according to the calculation on the same cyclotron radius, we strongly decrease the intensity of harmonic peaks. We also discuss the effect of increasing the amplitude of the observe pulse, which affects precursor and fragment ion peaks differently in terms of signal-to-noise ratio. The 2D mass spectra obtained with the optimized pulse sequence show a much higher signal-to-noise ratio, even without using denoising algorithms.

© 2014 Elsevier B.V. All rights reserved.

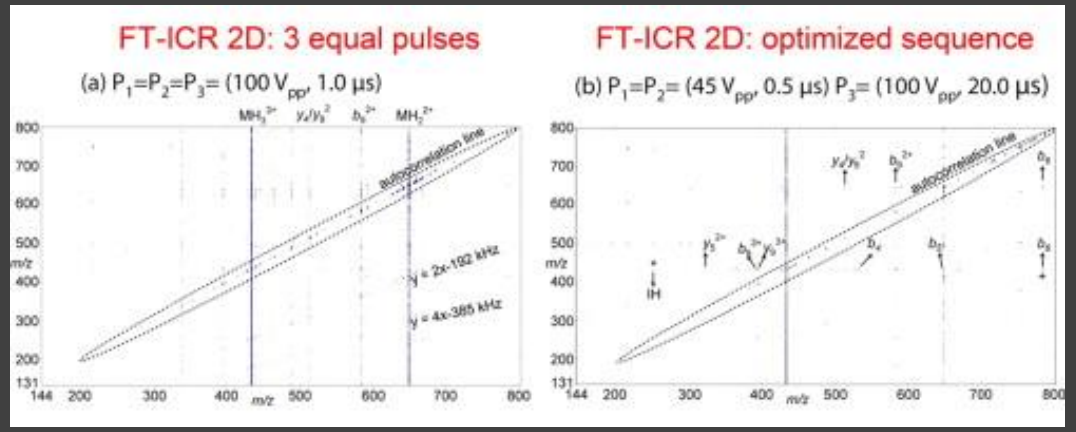

Two-dimensional Fourier transform ion cyclotron resonance mass spectrometry: reduction of scintillation noise using Cadzow data processing

Maria A. van Agthoven[1*], Marie-Aude Coutouly[2], Christian Rolando[1] and Marc-André Delsuc[2,3]

[1]Miniaturisation pour la Synthèse l'Analyse et la Protéomique, USR CNRS 3290, Institut Michel-Eugène Chevreul, FR CNRS 2638 and Protéomique, Modifications Post-Traductionnelles et Glycobiologie, IFR 147 Université de Lille 1, Sciences et Technologie, 59655 Villeneuve d'Ascq cedex, France
[2]NMRTEC, Bld. Sébastien Brandt, Bioparc – Bat. B, 67400 Illkirch-Graffenstaden, France
[3]Institut de Génétique et de Biologie Moléculaire et Cellulaire, INSERM, U 596 and, UMR CNRS 7104, Université de Strasbourg, 1 rue Laurent Fries, 67404 Illkirch-Graffenstaden, France

In two-dimensional Fourier transform ion cyclotron resonance mass spectrometry (2D FTICR-MS), scintillation noise, caused mostly by fluctuations in the number of ions in the ICR cell, is the leading cause for errors in spectrum interpretation. In this study, we adapted an algorithm based on singular value decomposition and first introduced by Cadzow *et al.* (*IEE Proceedings Pt. F* 1987, 134, 69) to 2D FTICR-MS and we measured its performance in terms of noise reduction without losing signal information in the 2D mass spectrum. Copyright © 2011 John Wiley & Sons, Ltd.

Efficient denoising algorithms for large experimental datasets and their applications in Fourier transform ion cyclotron resonance mass spectrometry

Lionel Chiron[a], Maria A. van Agthoven[b], Bruno Kieffer[a], Christian Rolando[b], and Marc-André Delsuc[a,1]

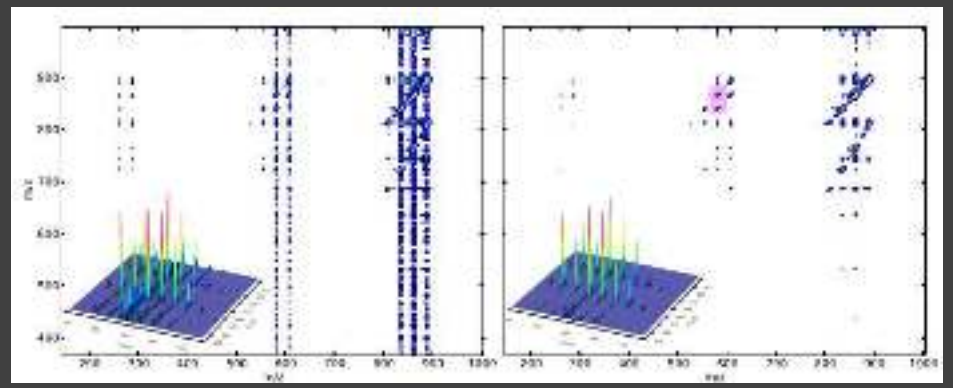

van Agthoven et al. Int. J. Mass Spectrom. 370 (2014) 114-124.
van Agthoven et al. Rapid Comm. Mass Spectrom. 25 (2011) 1609-1616.
Chiron et al. Proc. Nat. Acac. Sci. 111 (2014) 1385-1390.

2D FT-ICR MS Renewal: Non-Uniform Sampling

analytical chemistry

Letter

pubs.acs.org/ac

Nonuniform Sampling Acquisition of Two-Dimensional Fourier Transform Ion Cyclotron Resonance Mass Spectrometry for Increased Mass Resolution of Tandem Mass Spectrometry Precursor Ions

Fabrice Bray,[†] Julien Bouclon,[†,‡] Lionel Chiron,[§] Matthias Witt,[∥] Marc-André Delsuc,[⊥] and Christian Rolando[*,†]

[†]Univ. Lille, CNRS, MSAP USR 3290, FR 3688 FRABIO, FR 2638 Institut Eugène-Michel Chevreul, F-59000 Lille, France

[‡]École Normale Supérieure, PSL Research University, Département de Chimie, 24, Rue Lhomond, F-75005 Paris, France

[§]CASC4DE, Le Lodge, 20, Avenue du Neuhof, F-67100 Strasbourg, France

[∥]Bruker Daltonik, FTMS Applications, Fahrenheitstrasse 4, D-28359 Bremen, Germany

[⊥]Univ. Strasbourg, INSERM U596, CNRS UMR 7104, F-67404 Illkirch-Graffenstaden, France

Supporting Information

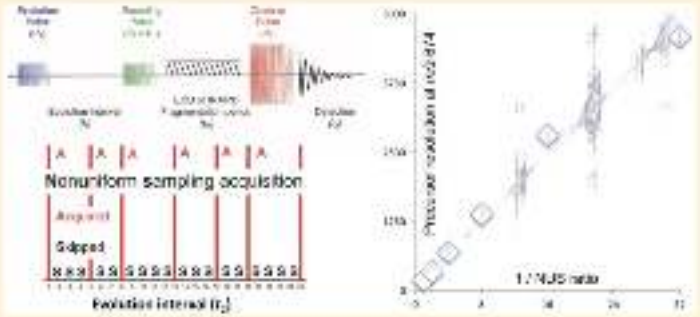

ABSTRACT: Obtaining the full MS/MS map for fragments and precursors of complex mixtures without hyphenation with chromatographic separation by a data-independent acquisition is a challenge in mass spectrometry which is solved by two-dimensional (2D) Fourier transform ion cyclotron resonance mass spectrometry (FTICR MS). Until now 2D FTICR MS afforded only a moderate resolution for precursor ion since this resolution is limited by the number of evolution interval steps to which the number of scans, the acquisition time, and the sample consumption are proportional. An overnight acquisition is already required to reach a quadrupole mass filter-like unit mass resolution. Here, we report that 2D FTICR MS using nonuniform sampling (NUS) obtained by randomly skipping points in the first dimension corresponding to the precursor selection gives access, after data processing, to the same structural information contained in a complex mixture. The resolution increases roughly as the inverse of the NUS ratio, up to 26 times at NUS 1/32, leading to an acquisition time reduced in the same ratio compared to a classical acquisition at the same resolution. As an example, the analysis of a natural oil is presented.

Bray et al. Ana. Chem. 89 (2017) 8589-8593.

2D FT-ICR MS Renewal: Narrowband Modulation

This is an open access article published under a Creative Commons Attribution (CC-BY) License, which permits unrestricted use, distribution and reproduction in any medium, provided the author and source are cited.

analytical chemistry

pubs.acs.org/ac

Article

Narrowband Modulation Two-Dimensional Mass Spectrometry and Label-Free Relative Quantification of Histone Peptides

Matthias Halper, Marc-André Delsuc, Kathrin Breuker, and Maria A. van Agthoven*

Cite This: https://dx.doi.org/10.1021/acs.analchem.0c02843

Read Online

ACCESS | Metrics & More | Article Recommendations | Supporting Information

ABSTRACT: Two-dimensional mass spectrometry (2D MS) on a Fourier transform ion cyclotron resonance (FT-ICR) mass analyzer allows for tandem mass spectrometry without requiring ion isolation. In the ICR cell, the precursor ion radii are modulated before fragmentation, which results in modulation of the abundance of their fragments. The resulting 2D mass spectrum enables a correlation between the precursor and fragment ions. In a standard broadband 2D MS, the range of precursor ion cyclotron frequencies is determined by the lowest mass-to-charge (m/z) ratio to be fragmented in the 2D MS experiment, which leads to precursor ion m/z ranges that are much wider than necessary, thereby limiting the resolving power for precursor ions and the accuracy of the correlation between the precursor and fragment ions. We present narrowband modulation 2D MS, which increases the precursor ion resolving power by reducing the precursor ion m/z range, with the aim of resolving the fragment ion patterns of overlapping isotopic distributions. In this proof-of-concept study, we compare broadband and narrowband modulation 2D mass spectra of an equimolar mixture of histone peptide isoforms. In narrowband modulation 2D MS, we were able to separate the fragment ion patterns of all ^{13}C isotopes of the different histone peptide forms. We further demonstrate the potential of narrowband 2D MS for label-free quantification of peptides.

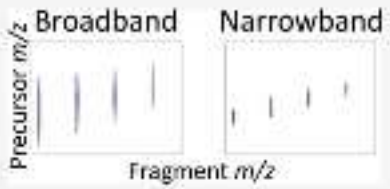

Halper et al. Ana. Chem. 92 (2020), 13945–13952

2D FT-ICR MS Renewal: Phase correction for Absorption Mode 2D MS

molecules

MDPI

Article

Phase Correction for Absorption Mode Two-Dimensional Mass Spectrometry

Marc-André Delsuc [1,2], Kathrin Breuker [3] and Maria A. van Agthoven [3,*]

[1] Institut de Génétique, Biologie Moléculaire et Cellulaire, INSERM U596, UMR 7104, Université de Strasbourg, 1 rue Laurent Fries, 67404 Illkirch-Graffenstaden, France; madelsuc@unistra.fr
[2] CASC4DE, Pôle API, 300 Bd. Sébastien Grant, 67400 Illkirch-Graffenstaden, France
[3] Institute for Organic Chemistry, University of Innsbruck, Innrain 80/82, 6020 Innsbruck, Austria; kathrin.breuker@uibk.ac.at
* Correspondence: maria.van-agthoven@uibk.ac.at

Abstract: Two-dimensional mass spectrometry (2D MS) is a tandem mass spectrometry method that relies on manipulating ion motions to correlate precursor and fragment ion signals. 2D mass spectra are obtained by performing a Fourier transform in both the precursor ion mass-to-charge ratio (m/z) dimension and the fragment ion m/z dimension. The phase of the ion signals evolves linearly in the precursor m/z dimension and quadratically in the fragment m/z dimension. This study demonstrates that phase-corrected absorption mode 2D mass spectrometry improves signal-to-noise ratios by a factor of 2 and resolving power by a factor of 2 in each dimension compared to magnitude mode. Furthermore, phase correction leads to an easier differentiation between ion signals and artefacts, and therefore easier data interpretation.

Halper et al. Molecules 26 (2021), 3388–3402

2D Mass Spectra

- Autocorrelation line = MS
- Fragment ion scan = MS/MS
- Precursor ion scan = all precursors that have the same fragment
  ABBA → ABB
  ABBC→ ABB
- Neutral loss line = all precursors that lose the same neutral
  ABBA → BA
  ABBC→ BC

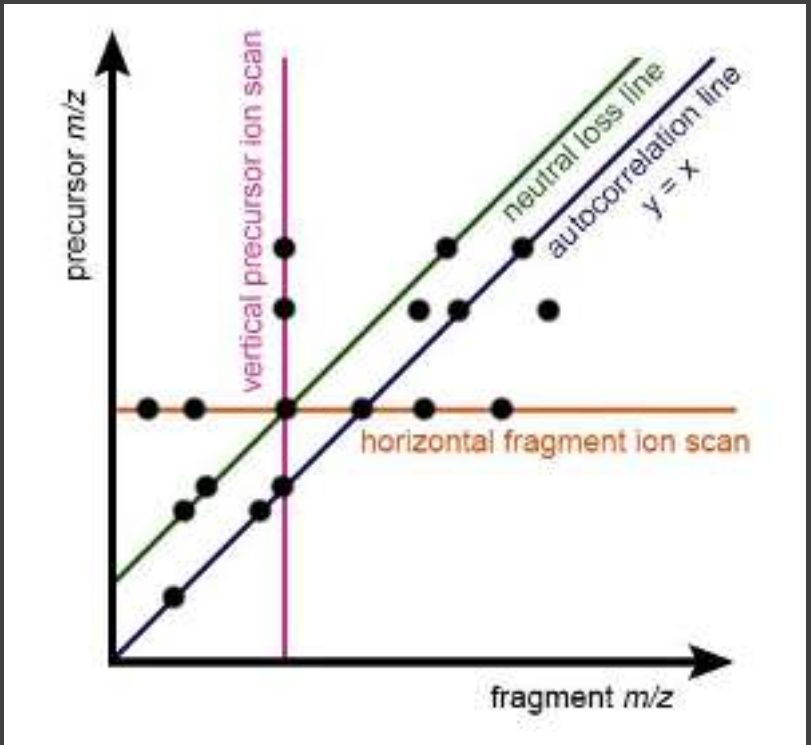

M. van Agthoven et al., *Anal. Bioanal. Chem.* 405 (2013) 51.
M. van Agthoven et al., *Eur. Biophys. J.* 48 (2019) 213.

Dissociation Lines in 2D Mass Spectra

- Precursors of same charge state
- Lose the same charge
- Lose the same mass

M. van Agthoven et al., *Anal Chem.* 88 (2016) 4409-4417.

Fragment charge

Neutral loss

$$(m/z)_{precursor} = \frac{p}{n}(m/z)_{fragment} + \frac{m_n}{n}$$

Precursor charge

Precursor charge

M. van Agthoven et al., *Anal Chem.* 88 (2016) 4409-4417.

Dissociation Lines in 2D Mass Spectra

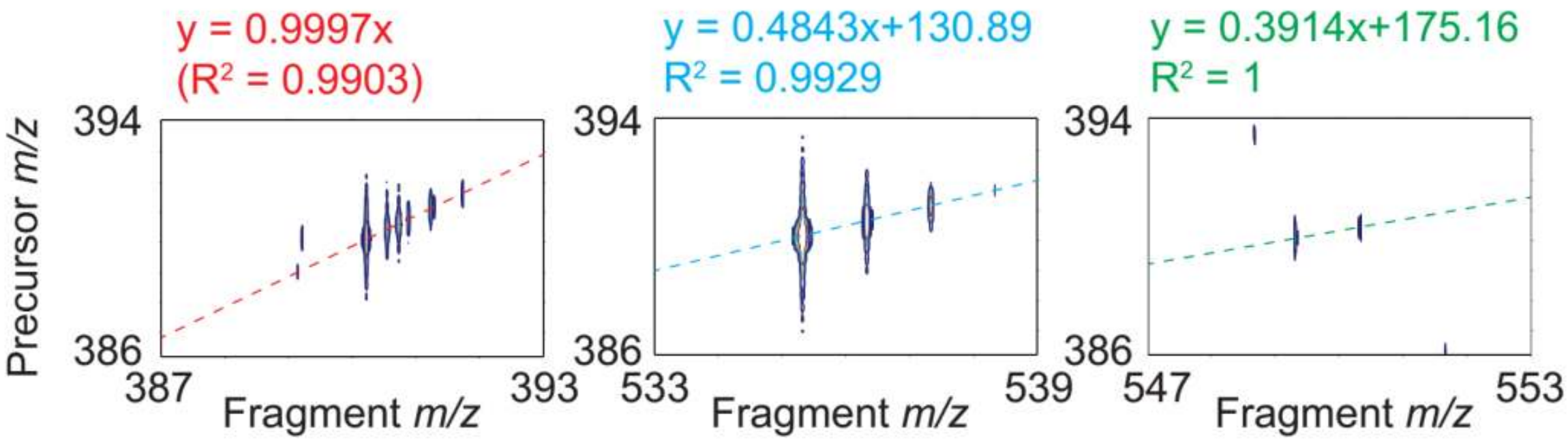

(a) Autocorrelation peaks for $(MIFAGIK)^{2+}$ and $(TGPNLHGLFGR)^{3+}$

(b) Isotopic distribution for y_5 fragment of $(MIFAGIK)^{2+}$

(c) Isotopic distribution for y_5 fragment of $(TGPNLHGLFGR)^{3+}$

M. van Agthoven et al., *Anal Chem.* 88 (2016) 4409-4417.

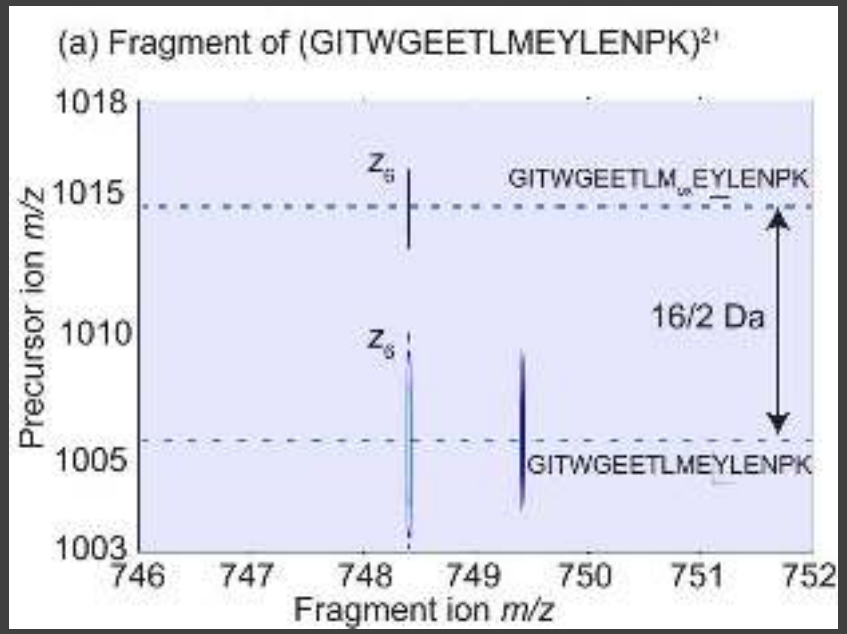

Fragment without the modification: vertical

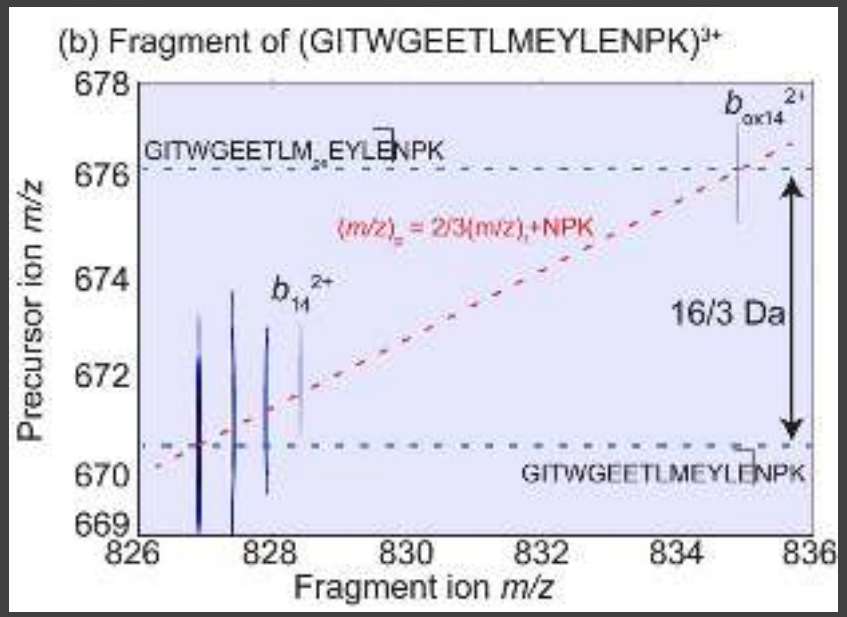

Fragment with the modification: on the same dissociation line

Easy method for assignment and location of peptide modifications!

M. van Agthoven et al., *Anal Chem.* 90 (2018) 3496-3504.

nanoESI 2D (IRMPD) FT-ICR Mass Spectrum of Bovine Serum Albumin Digest

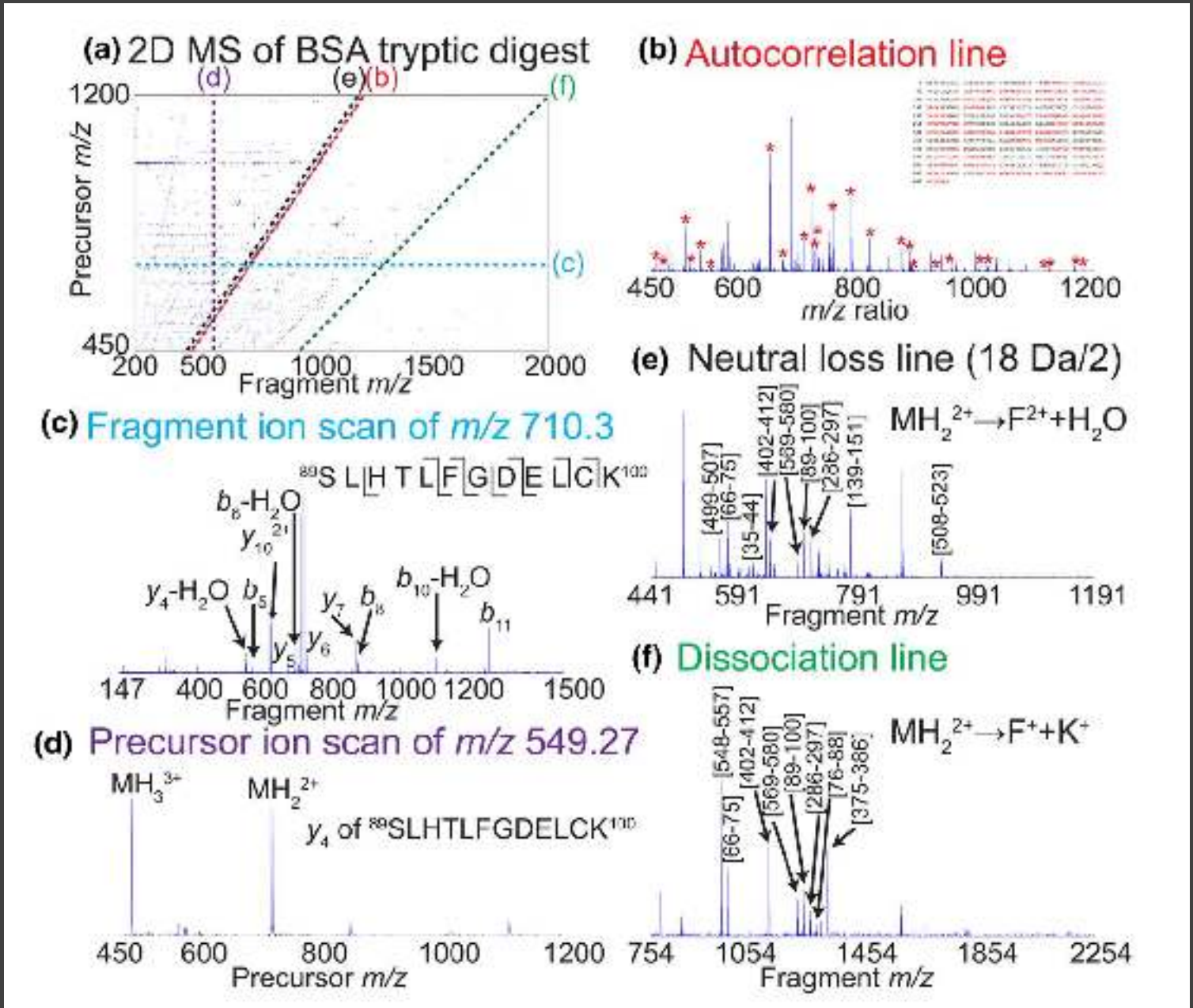

M.A. van Agthoven, Y.P.Y. Lam, P.B. O'Connor, C. Rolando, M.-A. Delsuc, *Eur. Biophys. J.* 48 (2019) 213-229.

2D ECD MS of histone H4:

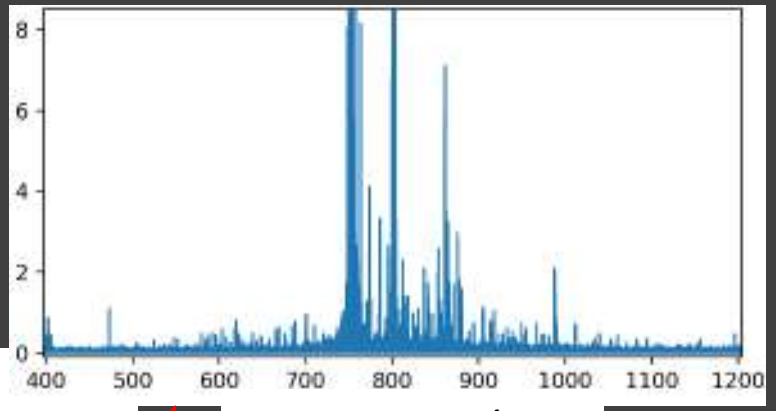

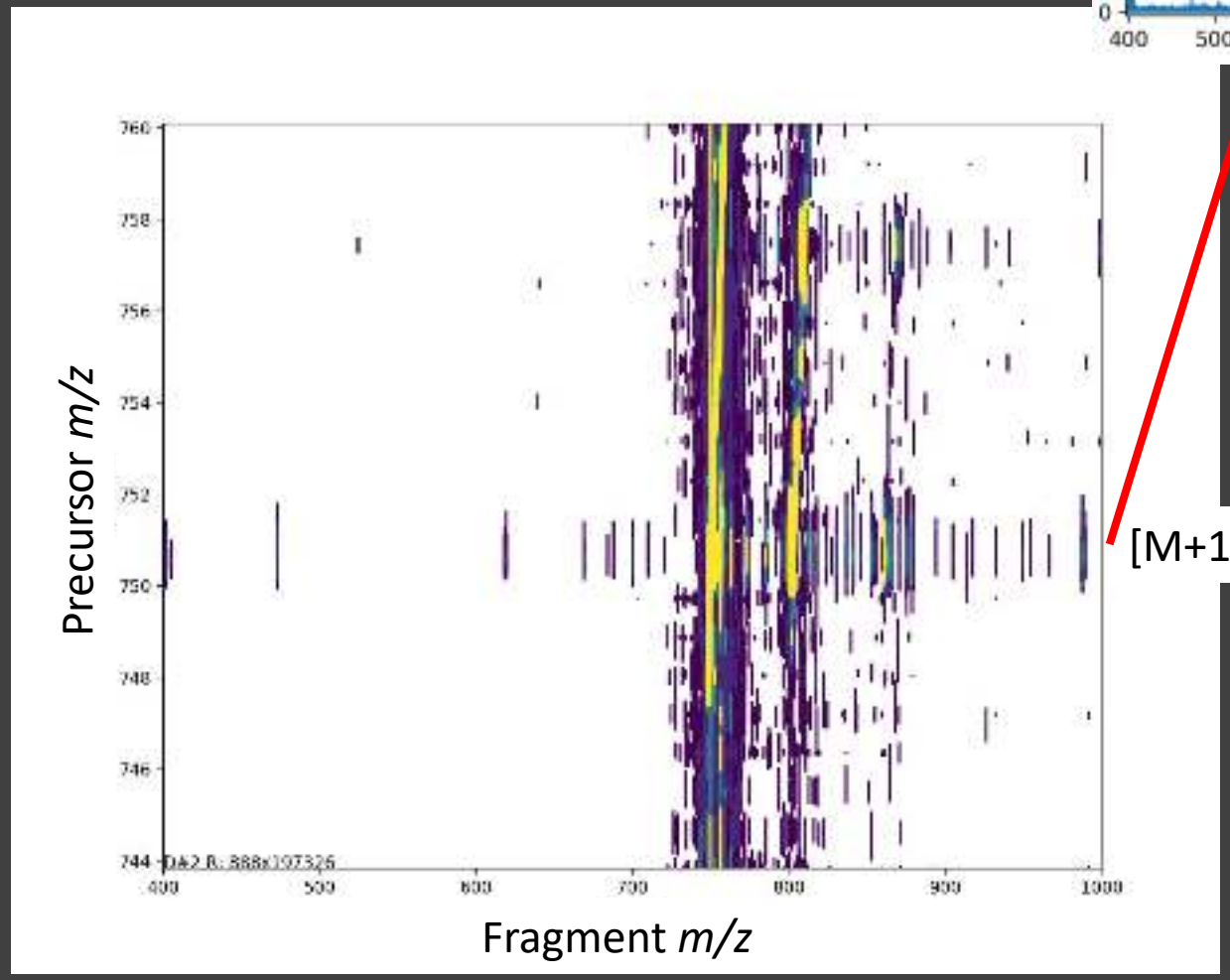

$[M+15H]^{15+}$

Vertical FWHM:
m/z 0.8 @ *m/z* 750

- Optimal signal-to-noise ratio
- Maximum precursor-fragment correlation

- Narrowband mode 2D MS
- Phase correction for absorption mode 2DMS

Narrowband 2D MS: Principle

Maximum frequency foldover!

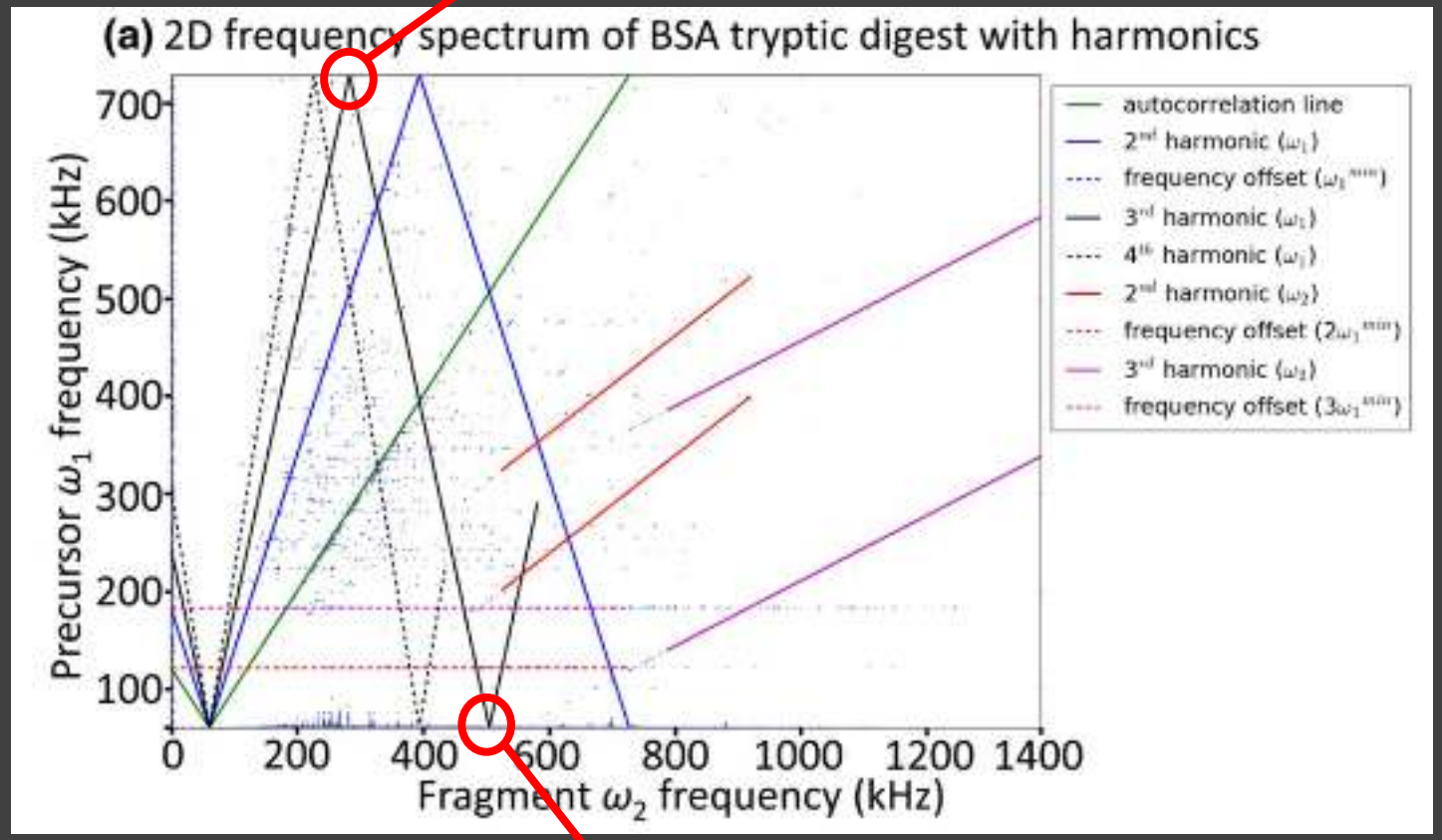

Zero frequency foldover!

Signals can be folded over at the borders of the spectrum!

M. van Agthoven et al., *Eur. Biophys. J.* 48 (2019) 213.

Narrowband 2D MS: Principle

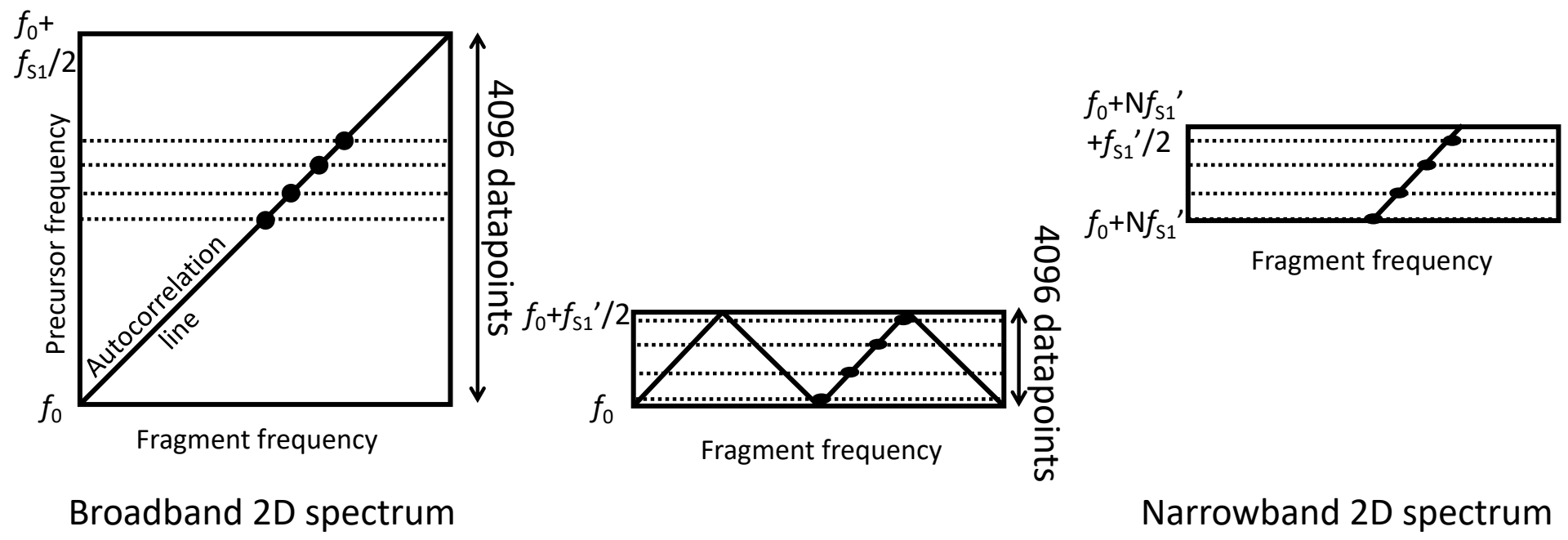

- Maximum frequency reduced to fold over autocorrelation line
- Same number of datapoints over smaller mass range
- Increase in resolving power/precursor-fragment correlation

M. Halper et al., *Anal Chem.* 92 (2020) 13945-13952.

Narrowband 2D MS: Experimental Conditions

- C-terminal GK-biotinylated histone H3 sequences (residues 21 to 44)
- Modified at K7 (1, 2, 3 methylations)
- Equimolar mixture

- 7 T ApexQE FT-ICR MS
- ECD fragmentation
- 2D MS maximum frequency: 250 kHz (broadband) and 62.5 kHz (narrowband)
- 2 x foldover in narrowband

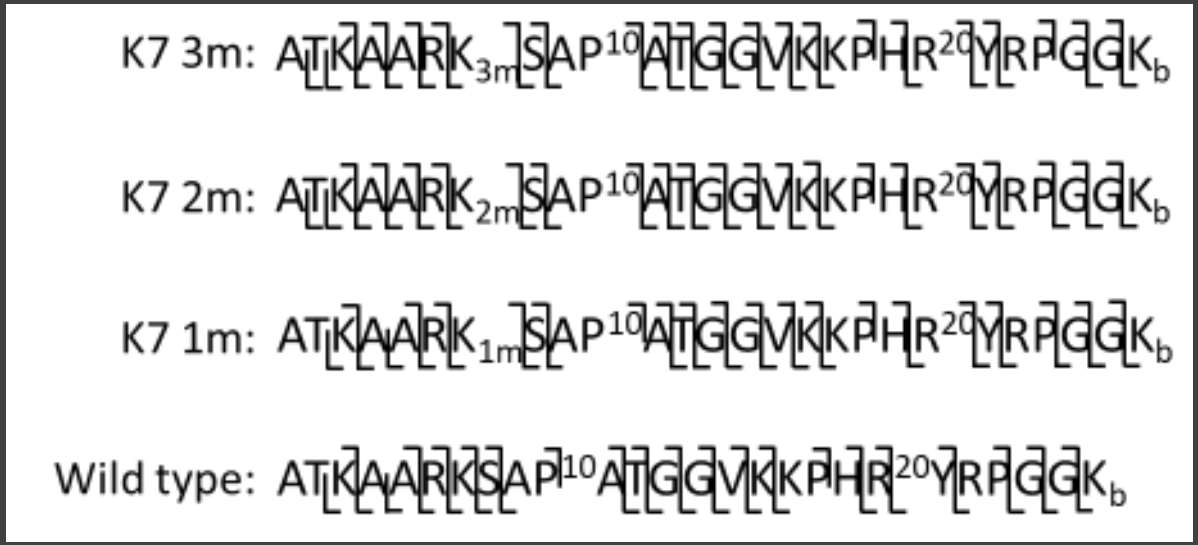

M. Halper et al., *Anal Chem.* 92 (2020) 13945-13952.

Broadband vs. Narrowband 2D MS

Broadband 2D mass spectrum

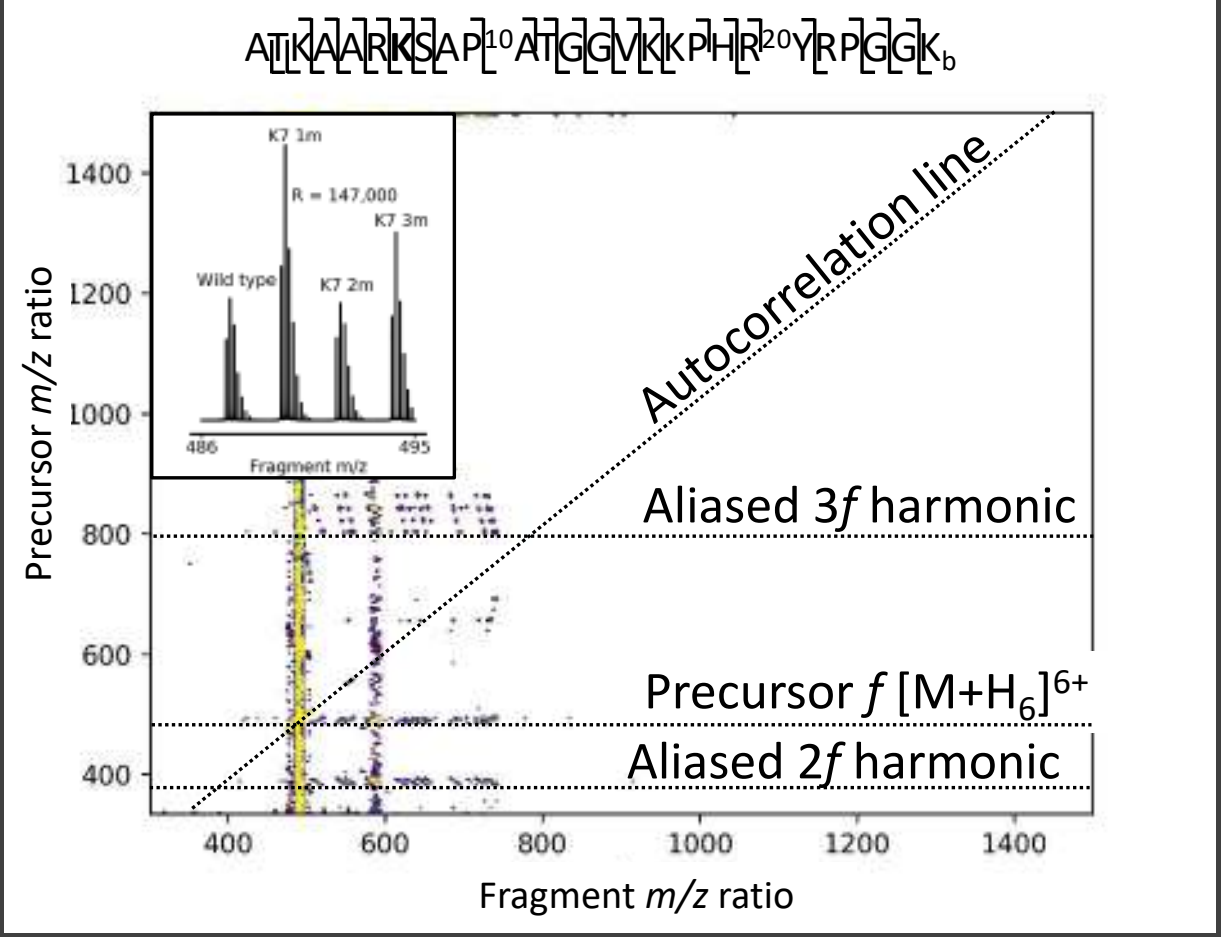

Narrowband 2D mass spectrum

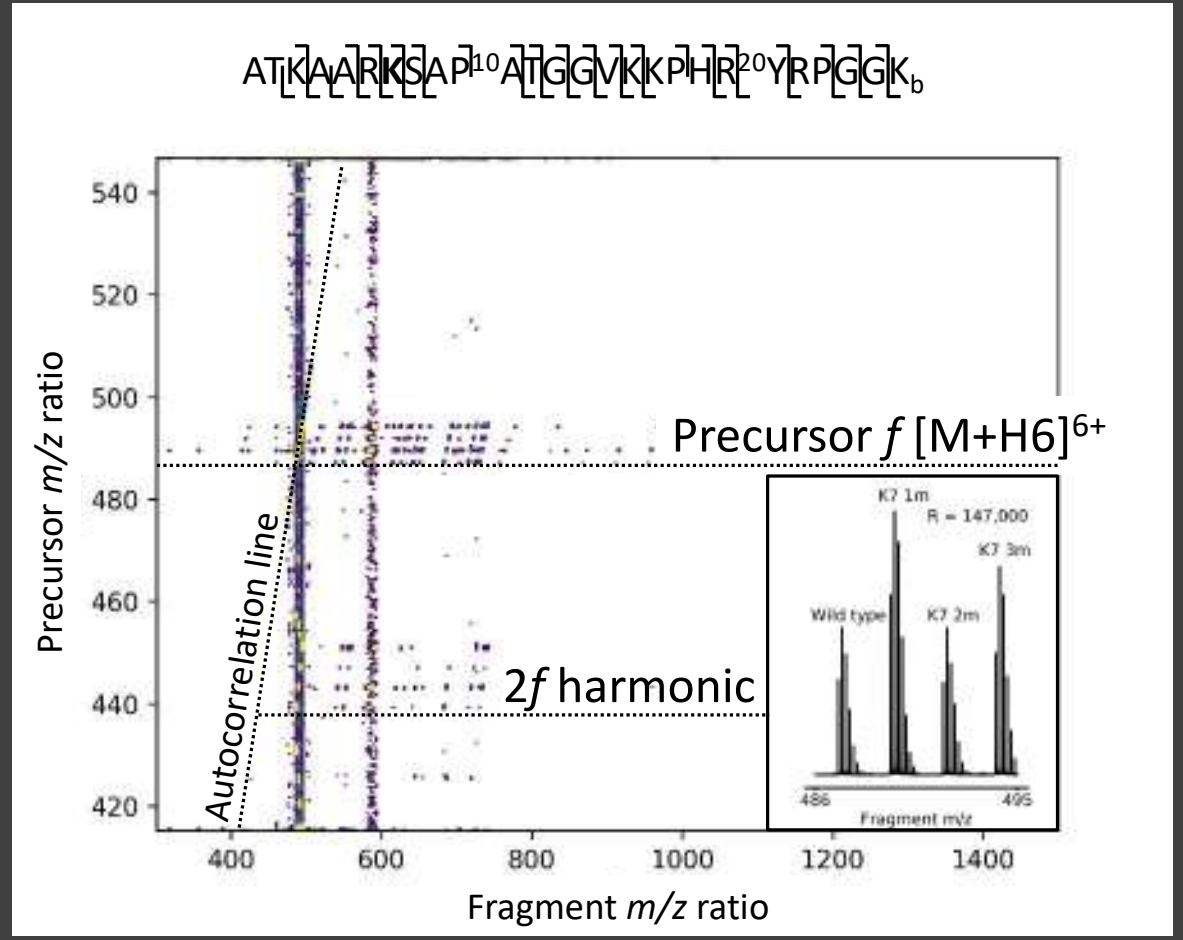

M. Halper et al., *Anal Chem.* 92 (2020) 13945-13952.

Broadband vs. Narrowband 2D MS

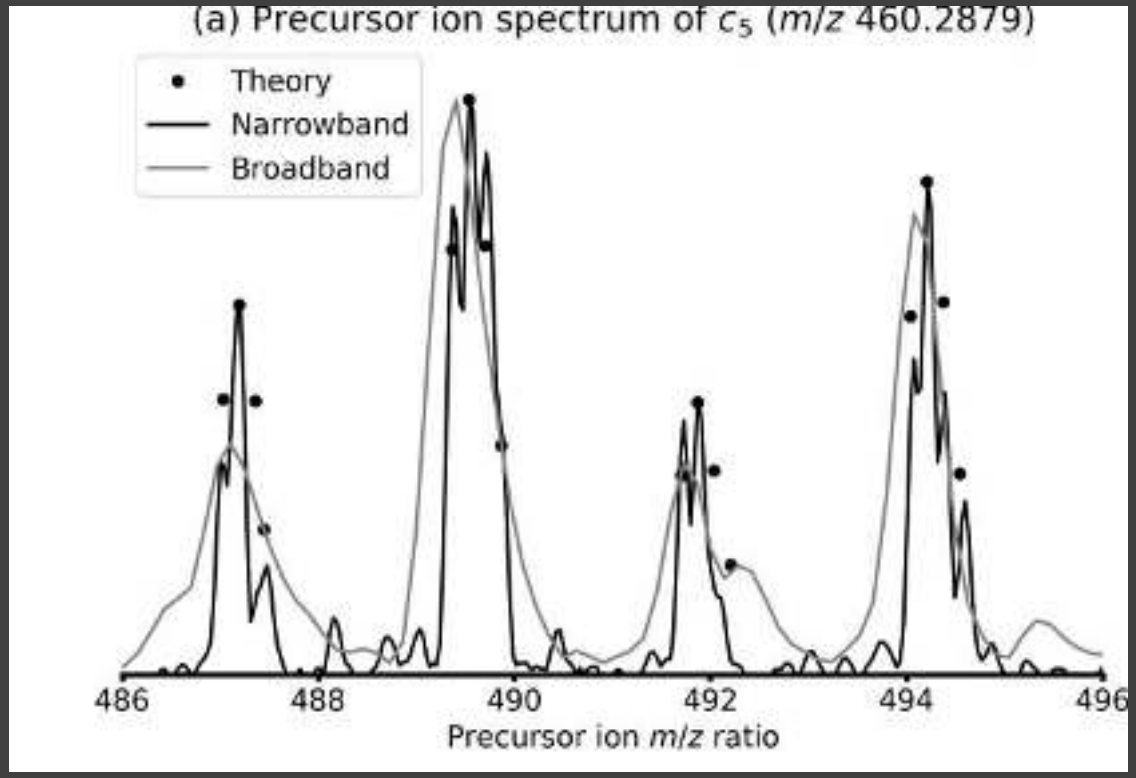

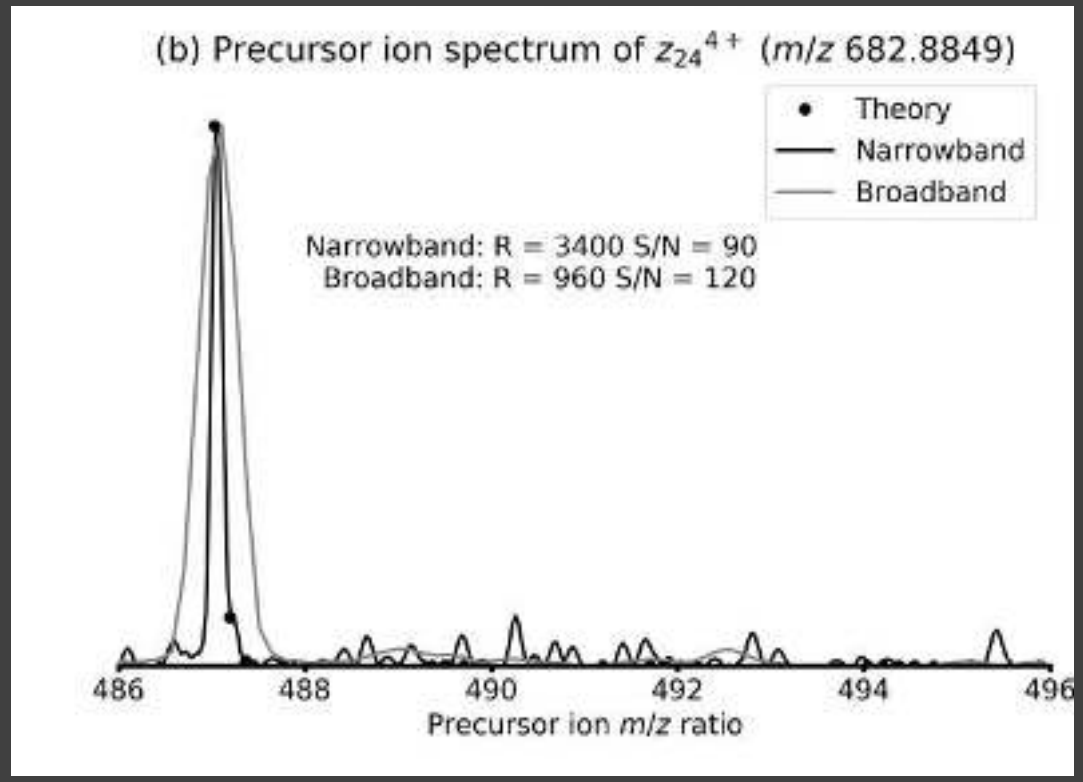

M. Halper et al., *Anal Chem.* 92 (2020) 13945-13952.

Isotopic Distributions in Narrowband 2D Mass Spectrum

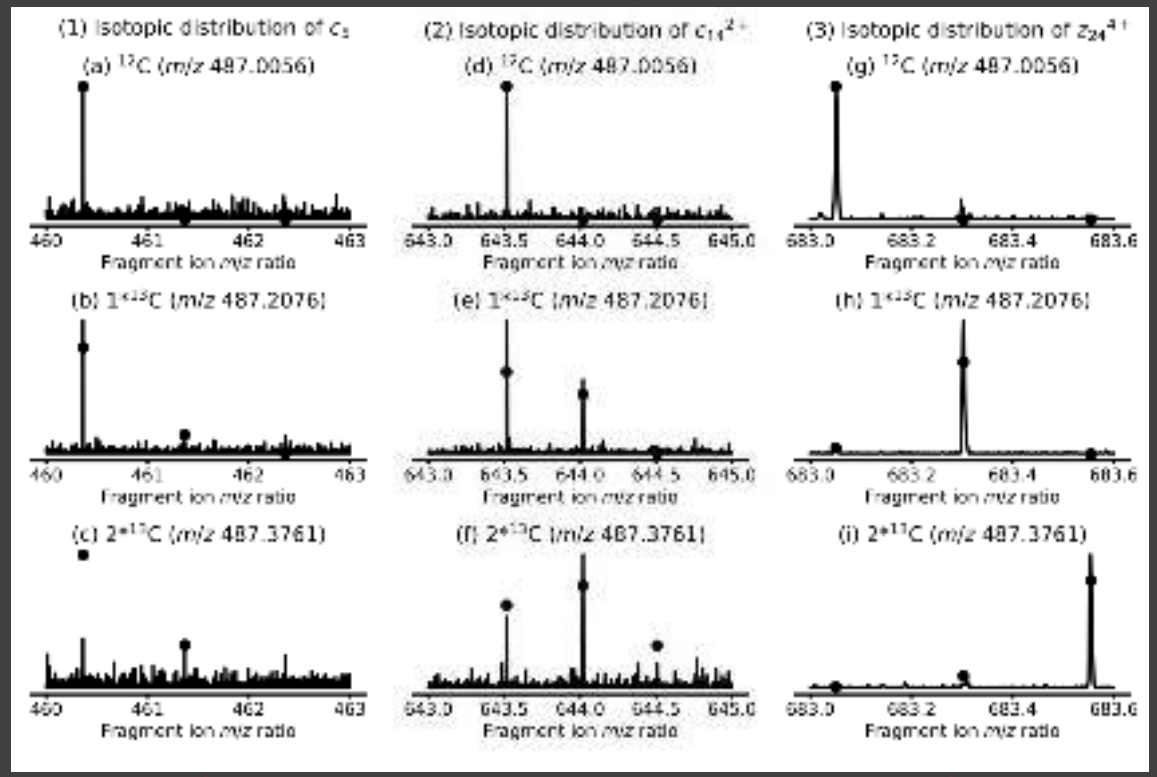

Small fragment: most ^{13}C isotopes in complement

Medium fragment: ^{13}C isotopes evenly distributed between fragment and complement

Big fragment: most ^{13}C isotopes in fragment

M. Halper et al., *Anal Chem.* 92 (2020) 13945-13952.

Narrowband 2D MS: Identification and Location of PTM

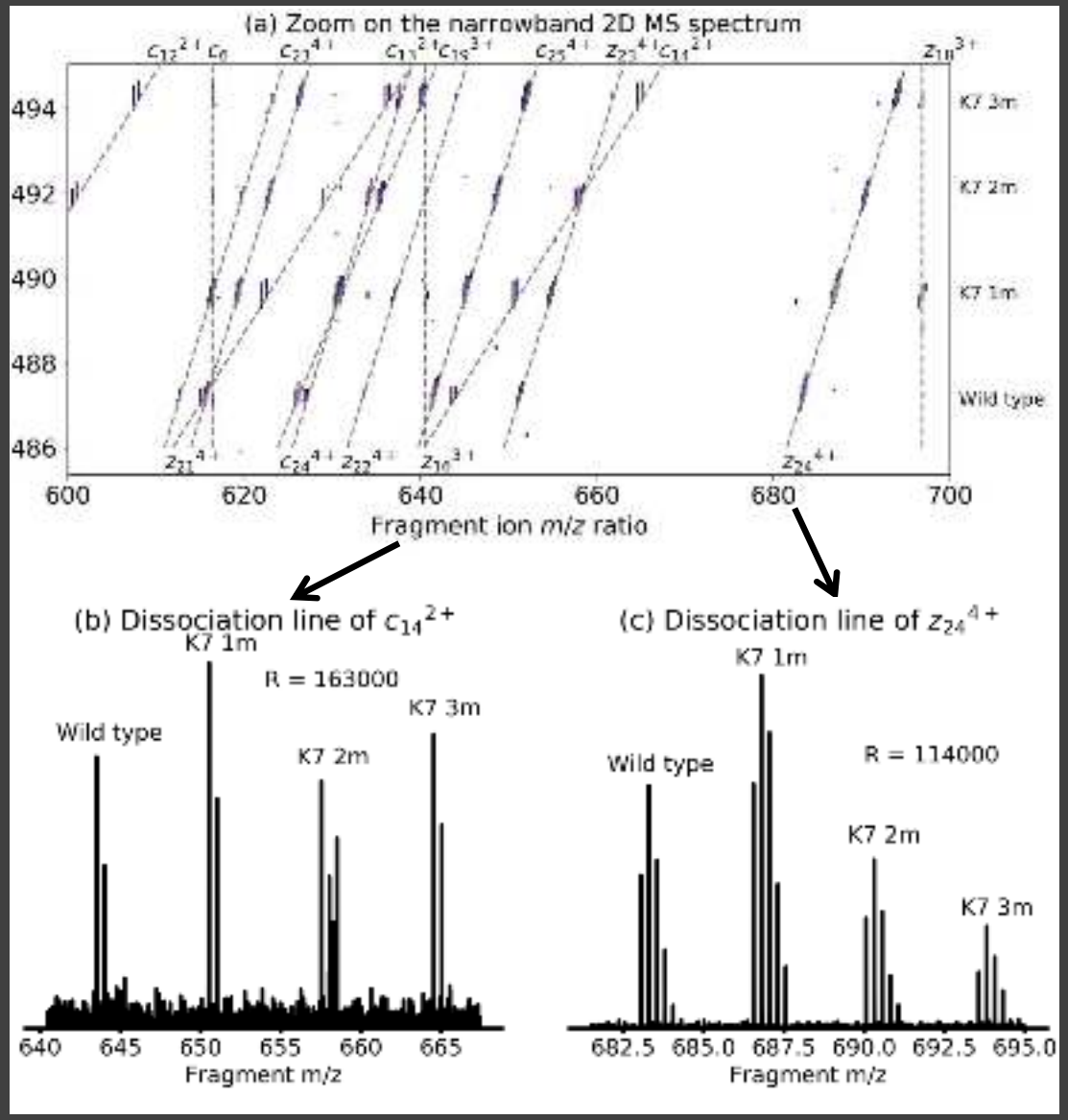

- Dissociation lines: slopes 0.33, 0.5, 0.67
  $\Longrightarrow$ confirm ID and location of PTM
- m/z difference: 14.0157 Da
  $\Longrightarrow$ methylations
- c_6 and z_{18}^{3+}: vertical precursor ion scans
  $\Longrightarrow$ PTMs on 7th residue

M. Halper et al., *Anal Chem.* 92 (2020) 13945-13952.

Narrowband 2D MS: Label-free relative quantification

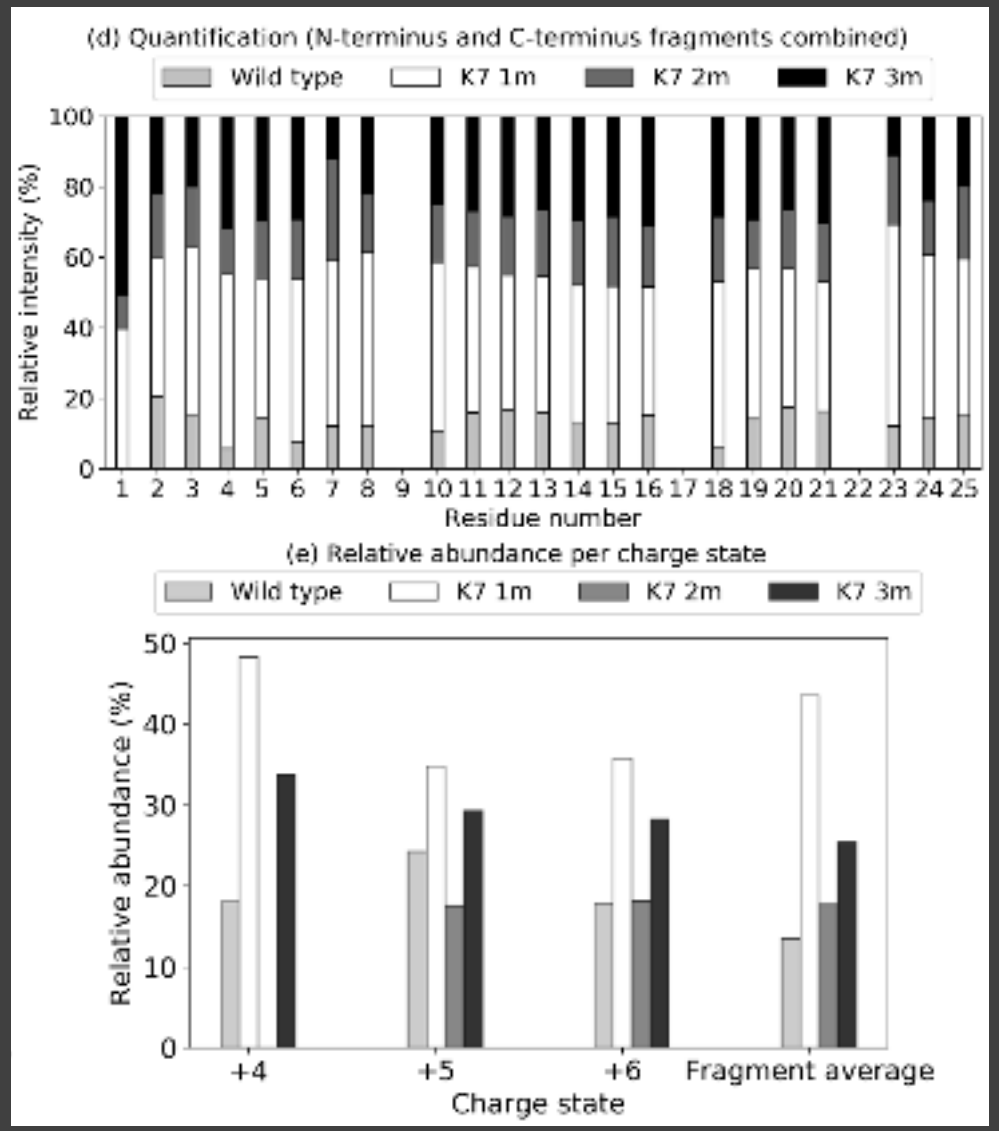

- PTM location achieved visually
  ⟹ relative intensities plotted without distinguishing fragment *m/z*

- Comparable results from intensities of precursor ions, charge-reduced species, and fragment ions
  ⟹ 2D MS can be used for label-free relative quantification

M. Halper et al., *Anal Chem.* 92 (2020) 13945-13952.

Phase correction in 1D FT-ICR MS

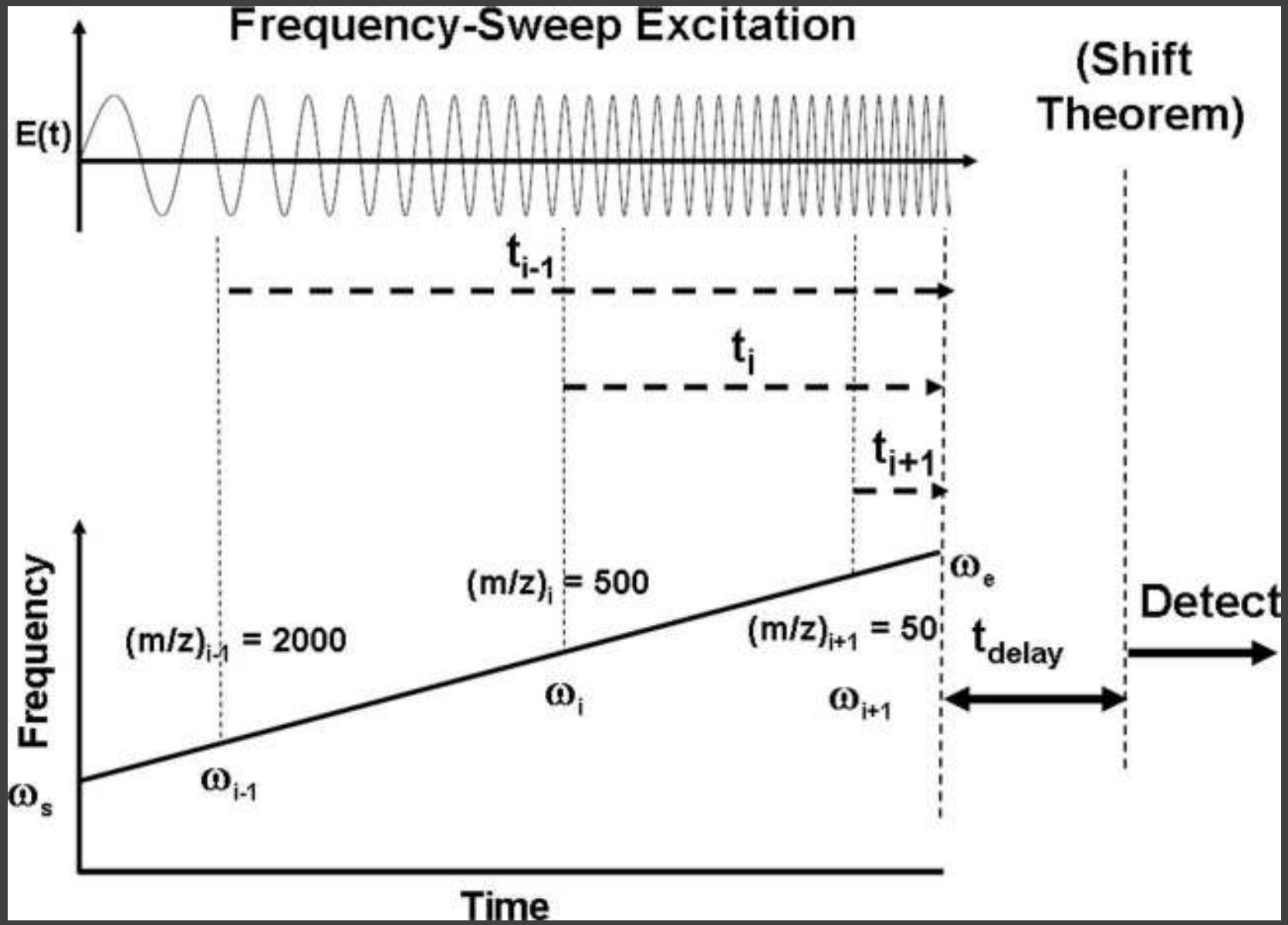

Feng Xian et al., *Anal Chem.* 82 (2010) 8807-8812.

Phase correction in 1D FT-ICR MS

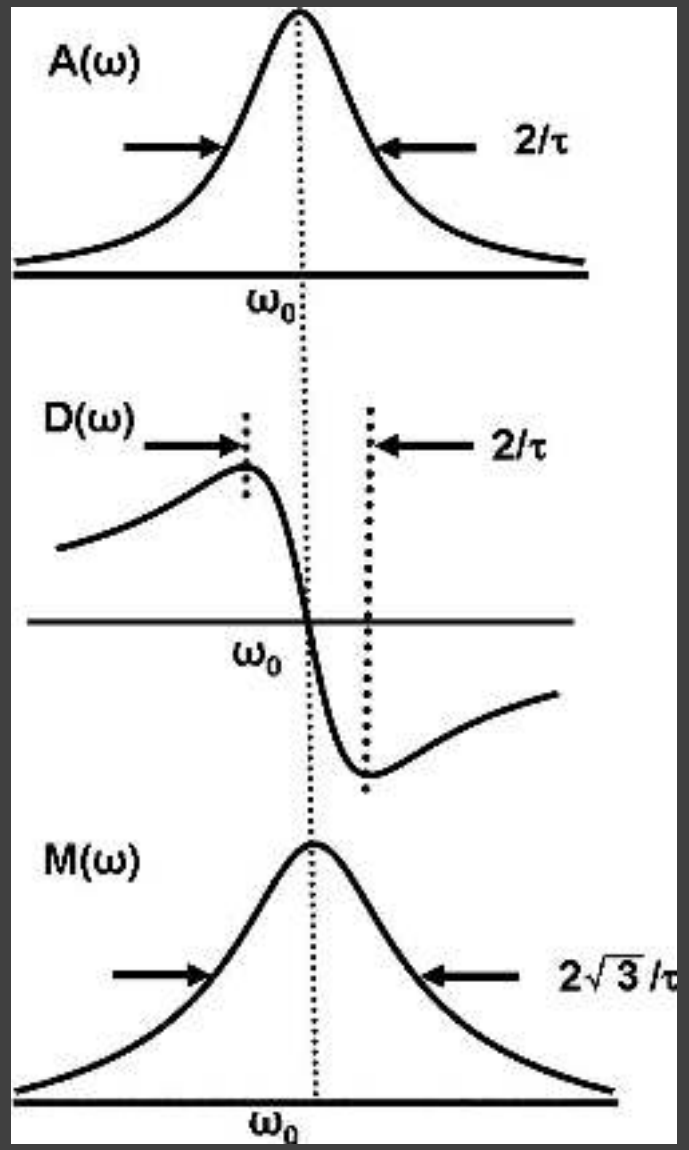

Absorption mode:
Gain in S/N and resolving power
Need to know phase of peak

Dispersion mode

Magnitude mode:
No need to know phase of peak

Feng Xian et al., *Anal Chem.* 82 (2010) 8807-8812.

Phase correction in 1D FT-ICR MS

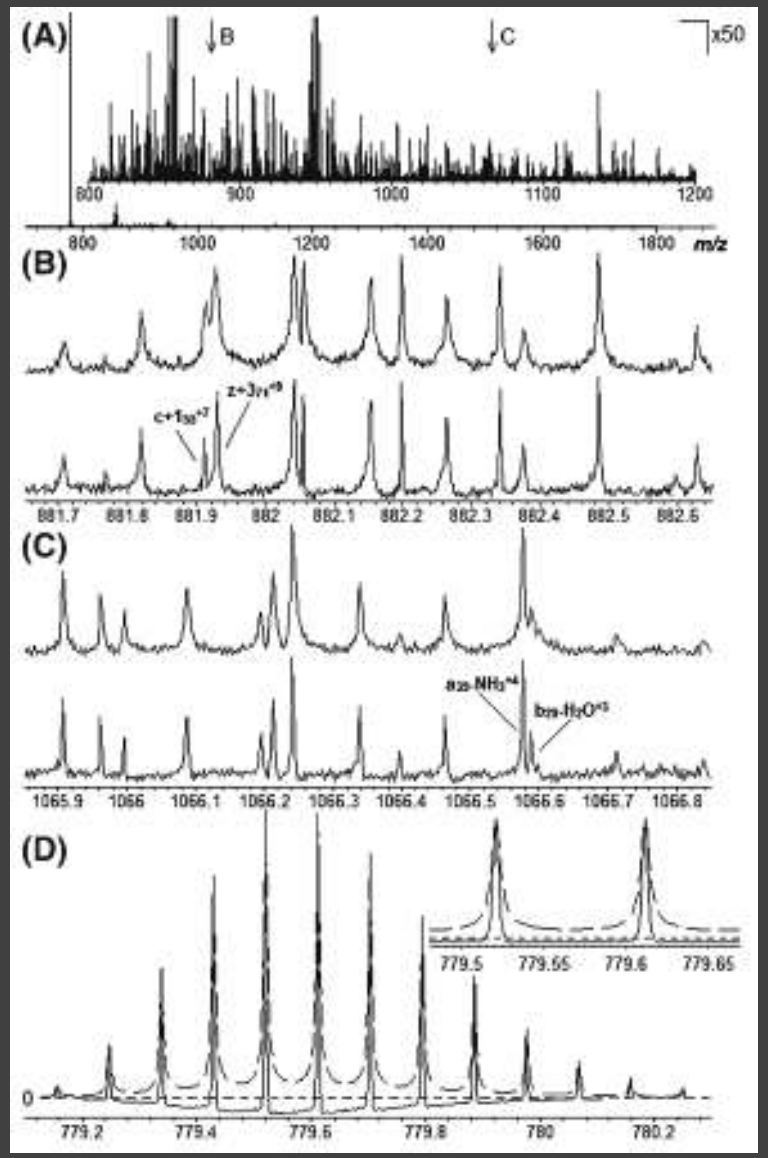

ECD MS/MS of ubiquitin

Zoom on *m/z* 882

Zoom on *m/z* 1066

Zoom on precursor ion

Yulin Qi et al., *J. Am. Soc. Mass Spectrom.* 22 (2011) 138-147.

Phase correction in 2D FT-ICR MS

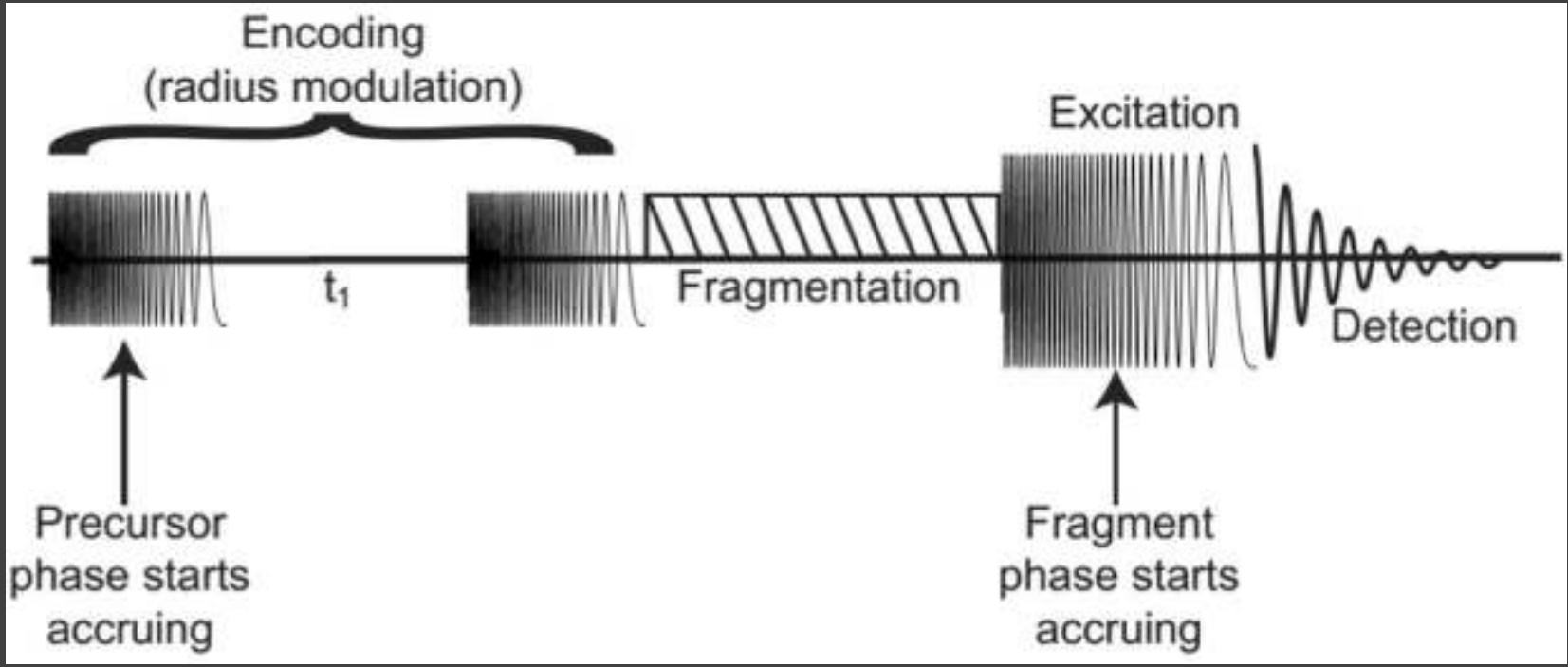

M. van Agthoven et al., *J. Am. Soc. Mass Spectrom.* 30 (2019) 2594-2607.

Phase correction in 2D FT-ICR MS

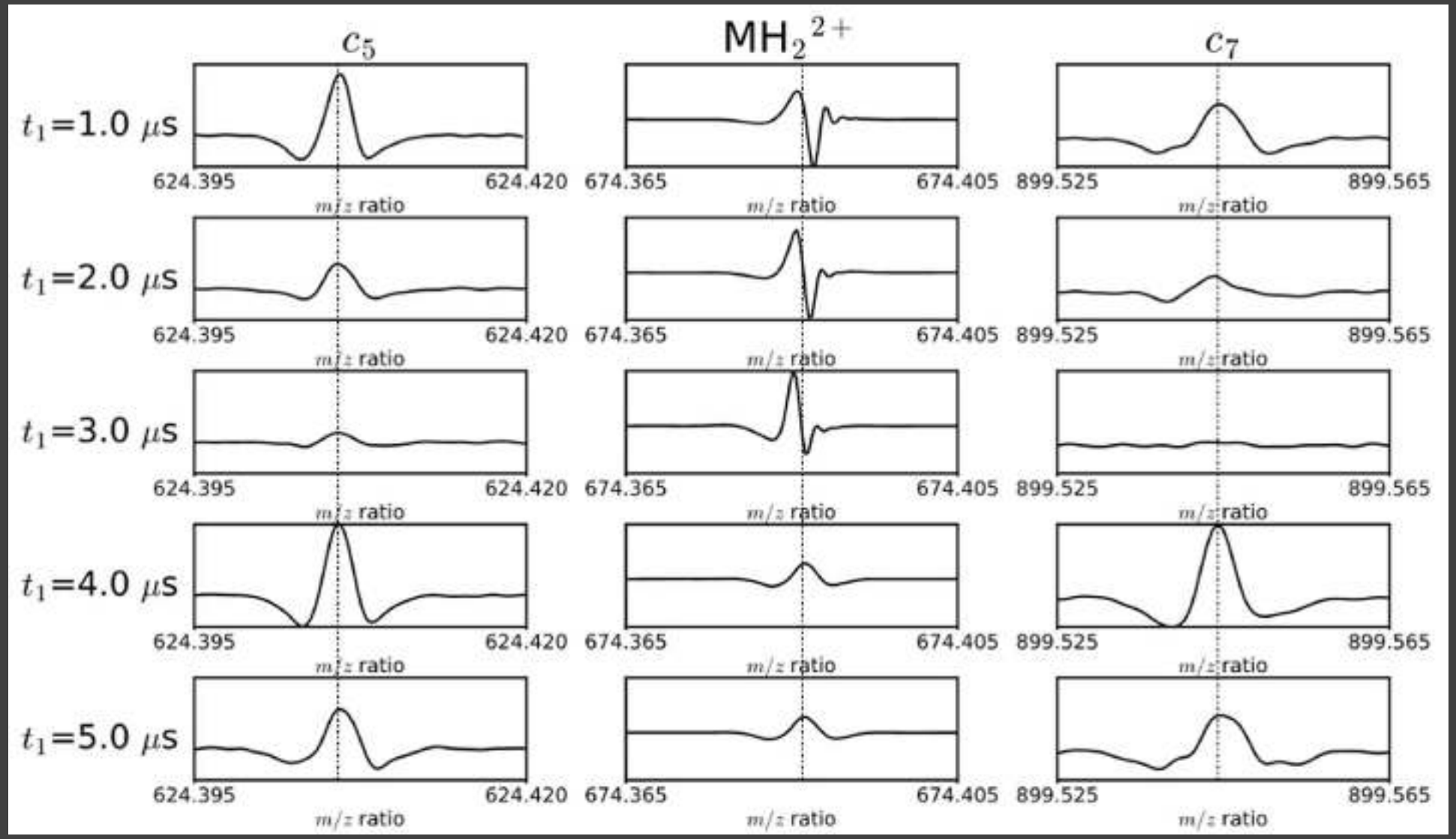

M. van Agthoven et al., *J. Am. Soc. Mass Spectrom.* 30 (2019) 2594-2607.

Phase correction in 2D FT-ICR MS

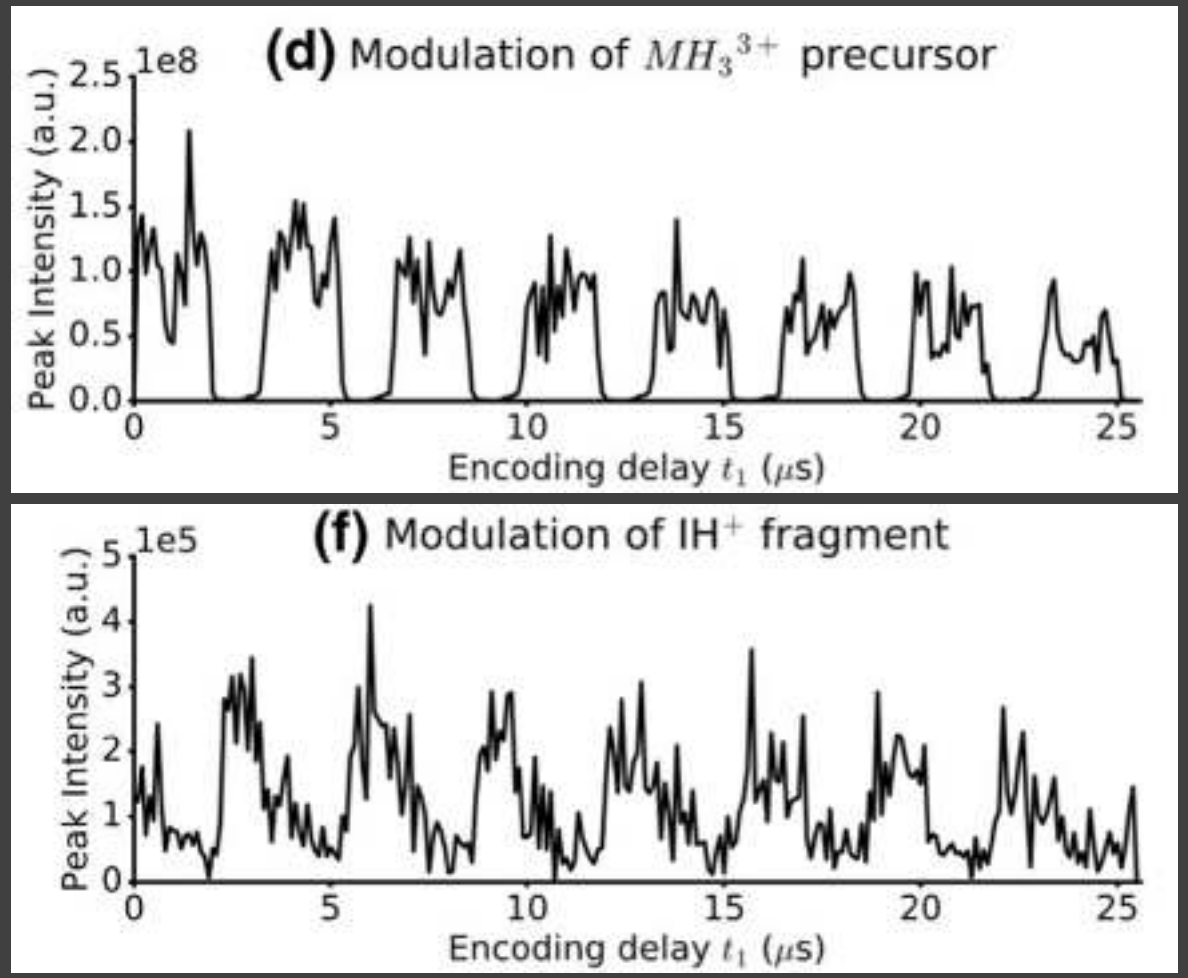

M. van Agthoven et al., *J. Am. Soc. Mass Spectrom.* 30 (2019) 2594-2607.

Phase correction in 2D FT-ICR MS

- Fragment ion (horizontal) dimension: quadratic phase correction
- Precursor ion (vertical) dimension: linear phase correction
- Resolving power expected x2
- Signal-to-noise expected x2

M. van Agthoven et al., *J. Am. Soc. Mass Spectrom.* 30 (2019) 2594-2607.

Phase correction in 2D FT-ICR MS:
Horizontal Phase correction Determined by Phasing MS/MS spectrum

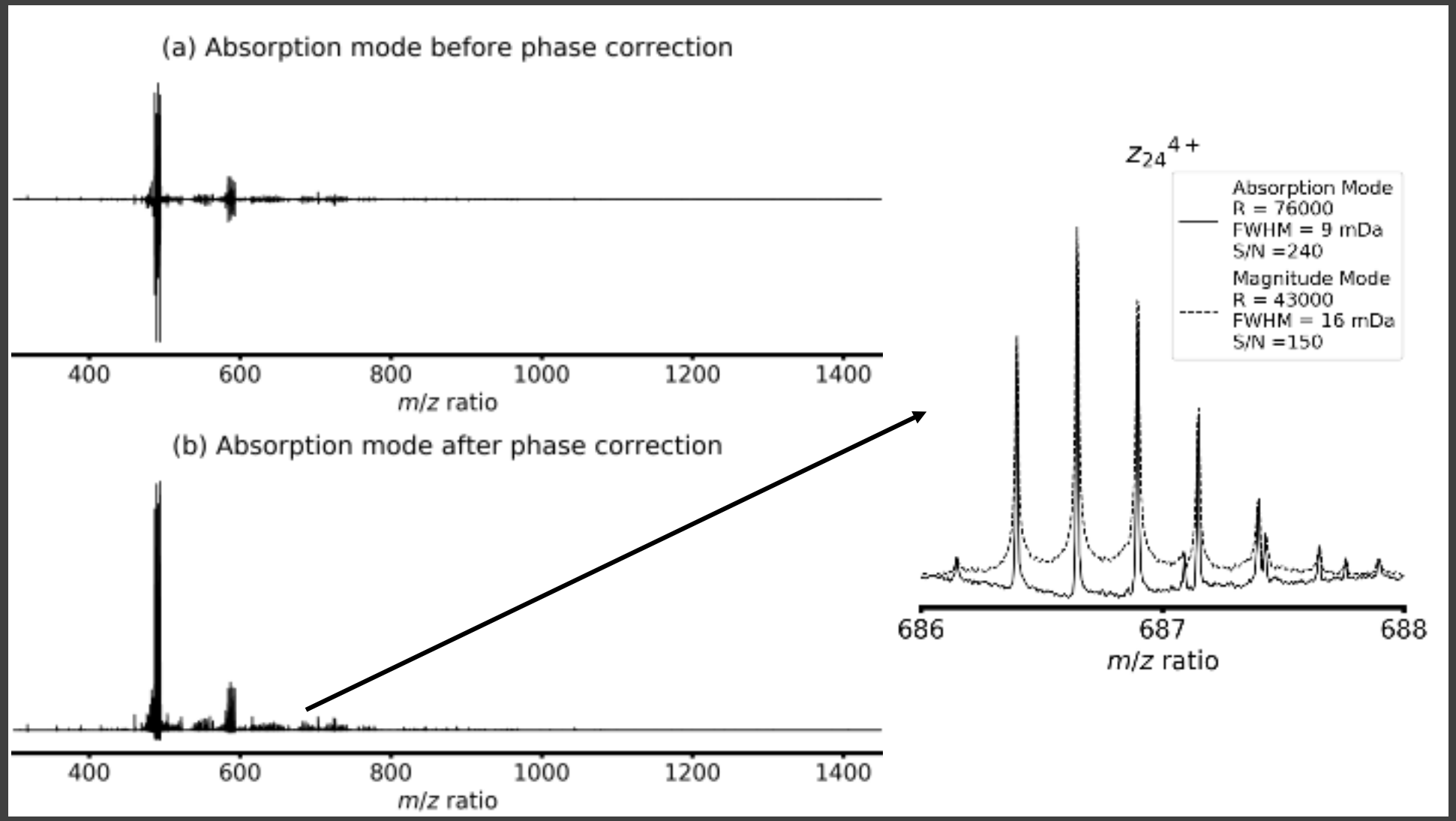

M.-A. Delsuc et al., *Molecules* 26 (2021) 3388.

Phase correction in 2D FT-ICR MS

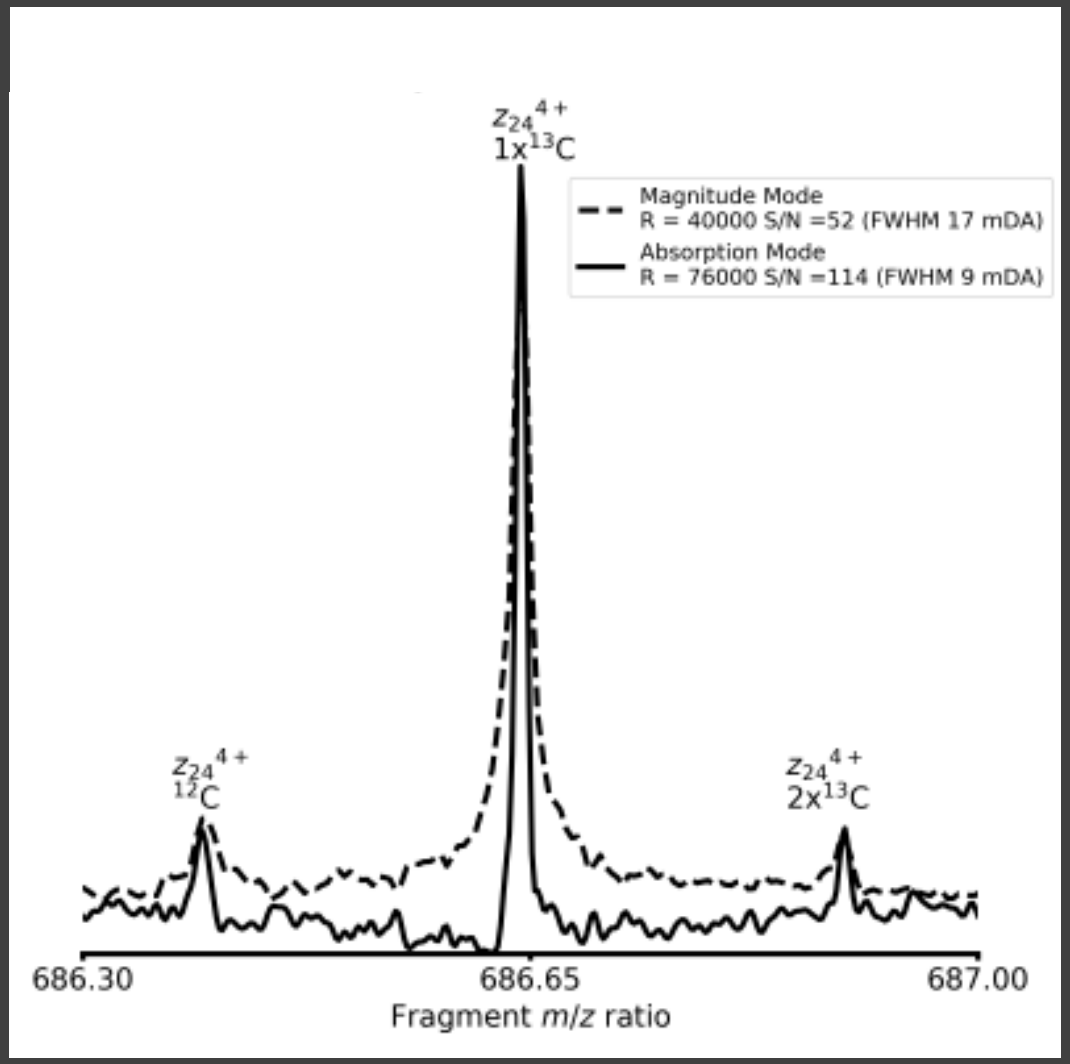

M.-A. Delsuc et al., *Molecules* 26 (2021) 3388.

Phase correction in 2D FT-ICR MS: Vertical Linear Phase Correction

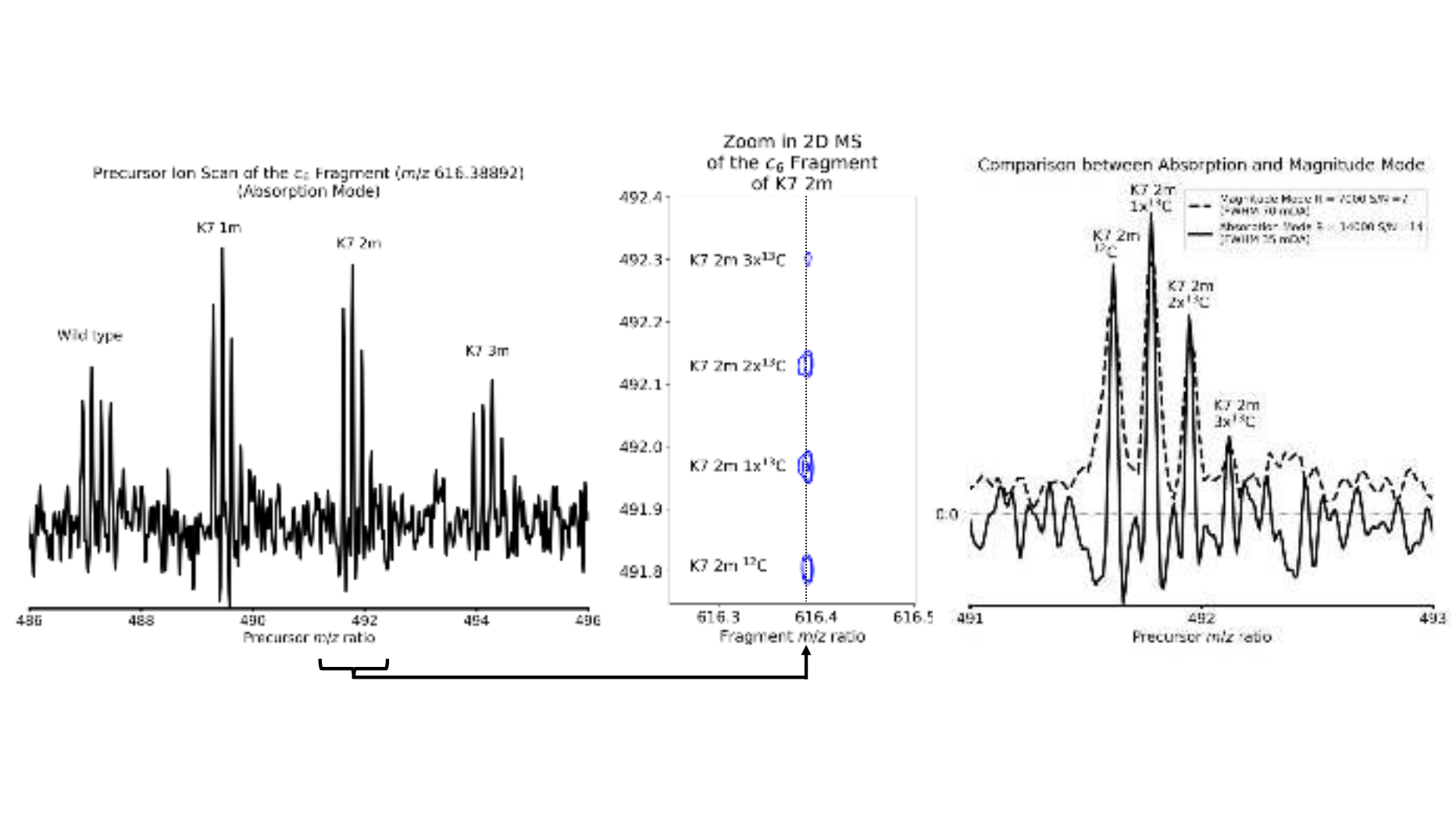

M.-A. Delsuc et al., *Molecules* 26 (2021) 3388.

Phase correction in 2D FT-ICR MS

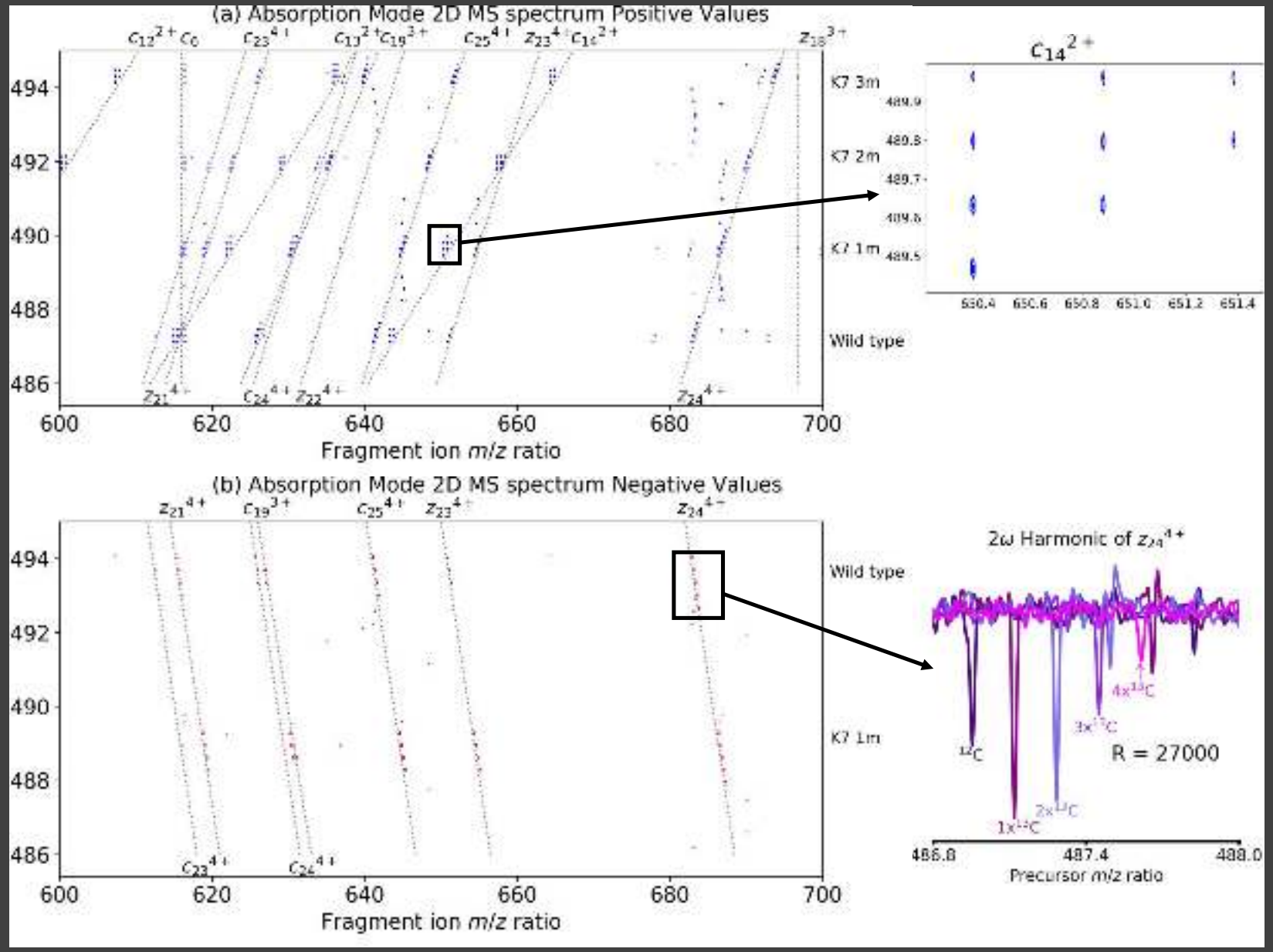

M.-A. Delsuc et al., *Molecules* 26 (2021) 3388.

Can we separate a trimethylated and an acetylated histone peptide?

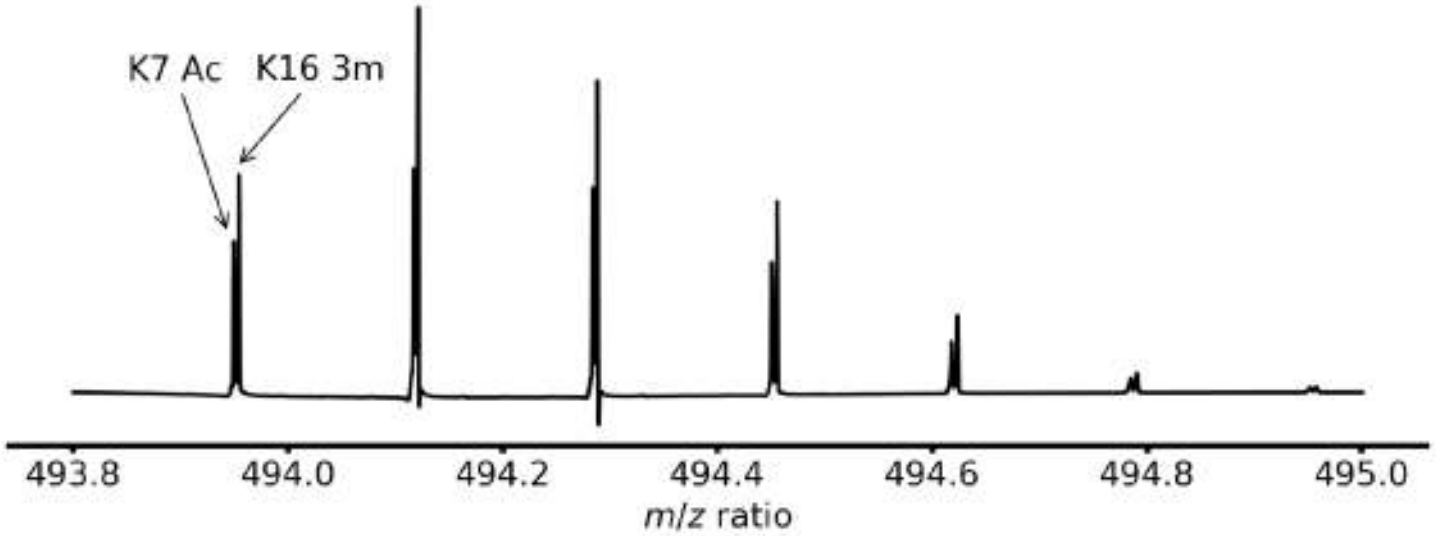

m/z(K7 Ac)	493.944715	f_{ICR} = 219173.83 Hz
m/z(K16 3m)	493.950779	f_{ICR} = 219171.14 Hz
$\Delta m/z$	0.006064	Δf_{ICR}= 2.69 Hz

ATKAARK_{Ac}SAP^{10} ATGGVKK PHR^{20} YRPGGK$_{biotin}$

ATKAARK SAP^{10} ATGGVKK_{3m}PHR^{20} YRPGGK$_{biotin}$

$c_{1\rightarrow6}$: Δm = 0	$c_{7\rightarrow15}$: Δm = 42.010564	$c_{16\rightarrow25}$: Δm = 0.0364
$z_{20\rightarrow25}$: Δm = -0.0364	$z_{11\rightarrow19}$: Δm = -42.046950	$z_{1\rightarrow10}$: Δm = 0

Can we separate a trimethylated and an acetylated histone peptide?

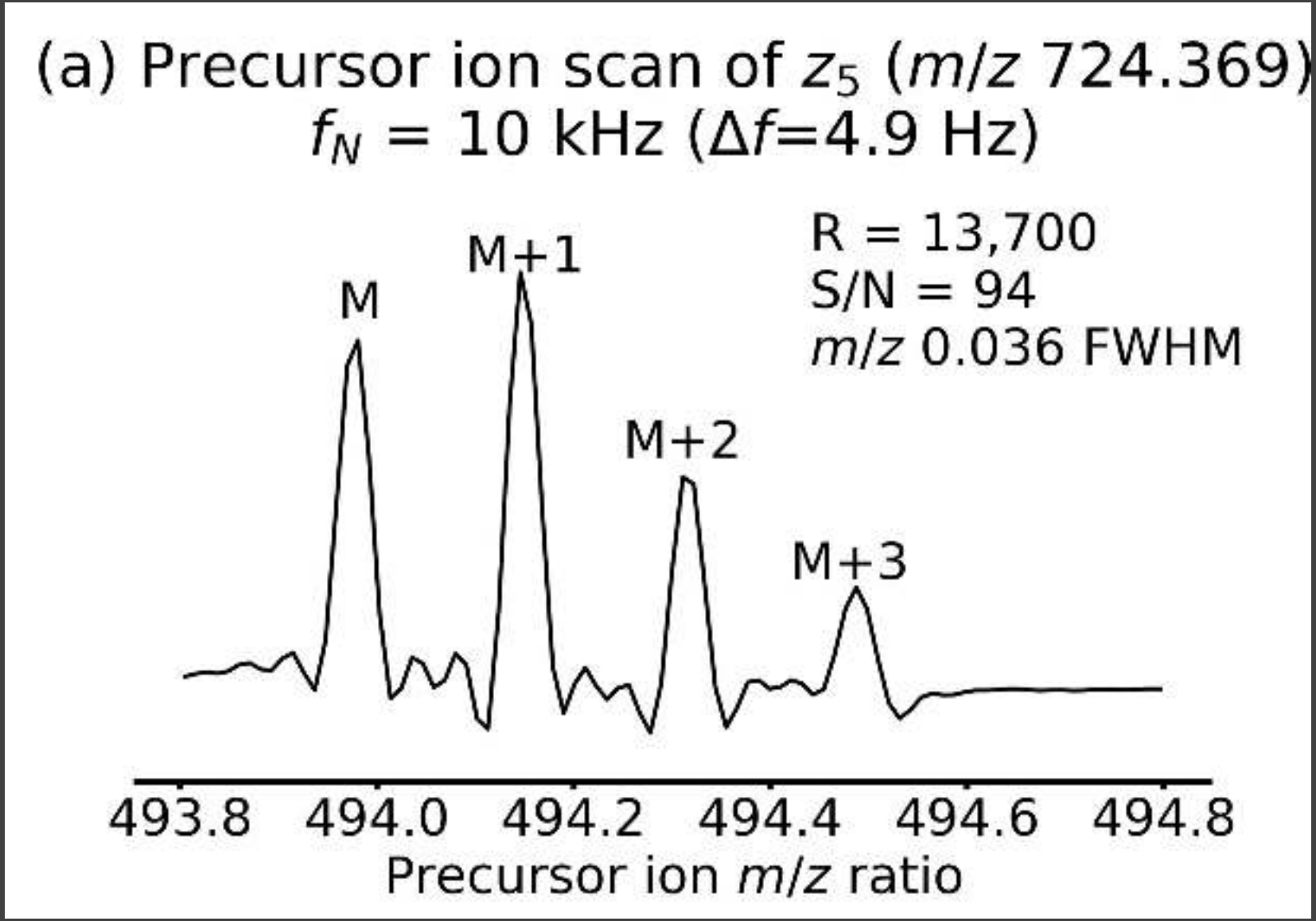

Can we separate a trimethylated and an acetylated histone peptide?

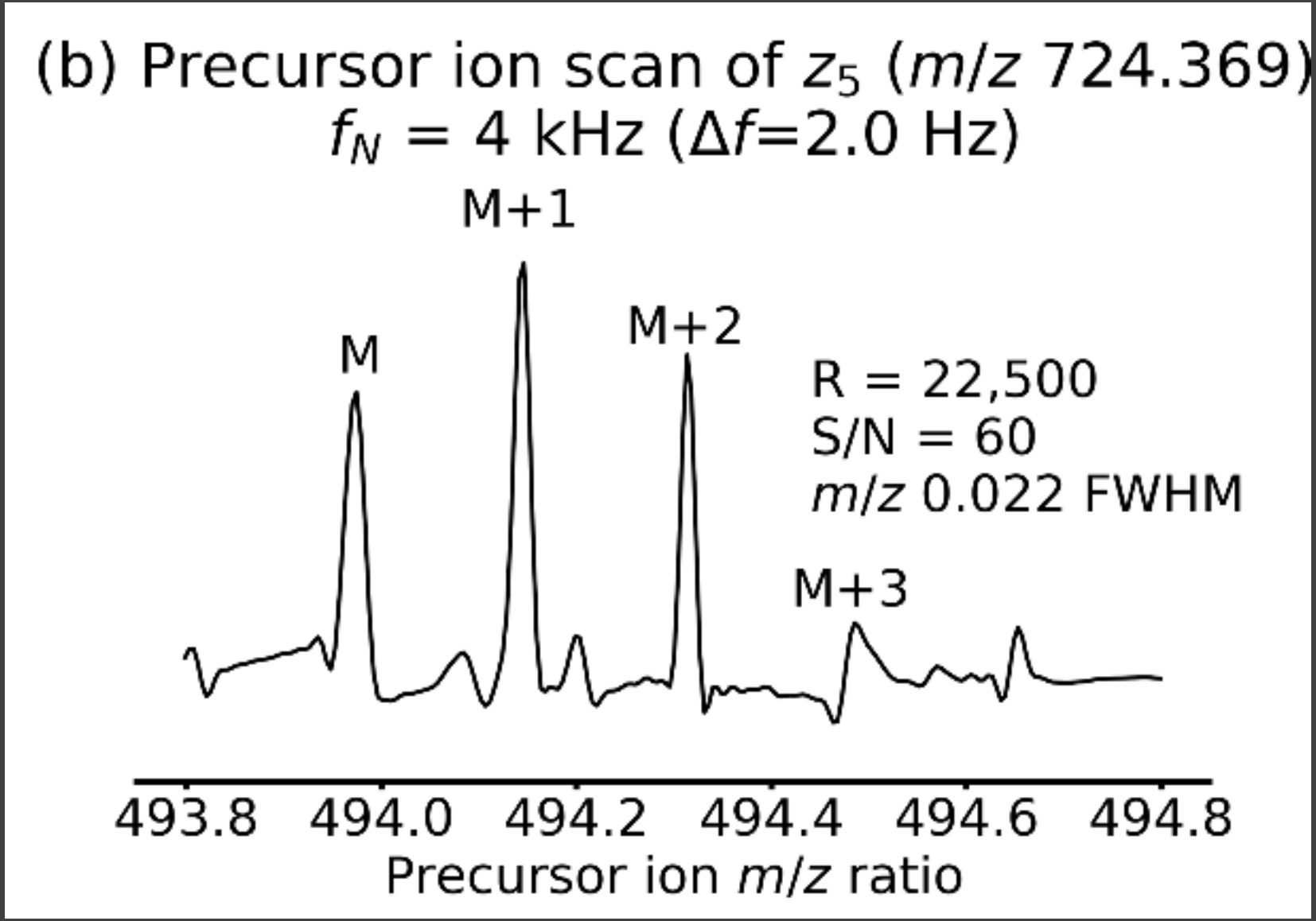

Can we separate a trimethylated and an acetylated histone peptide?

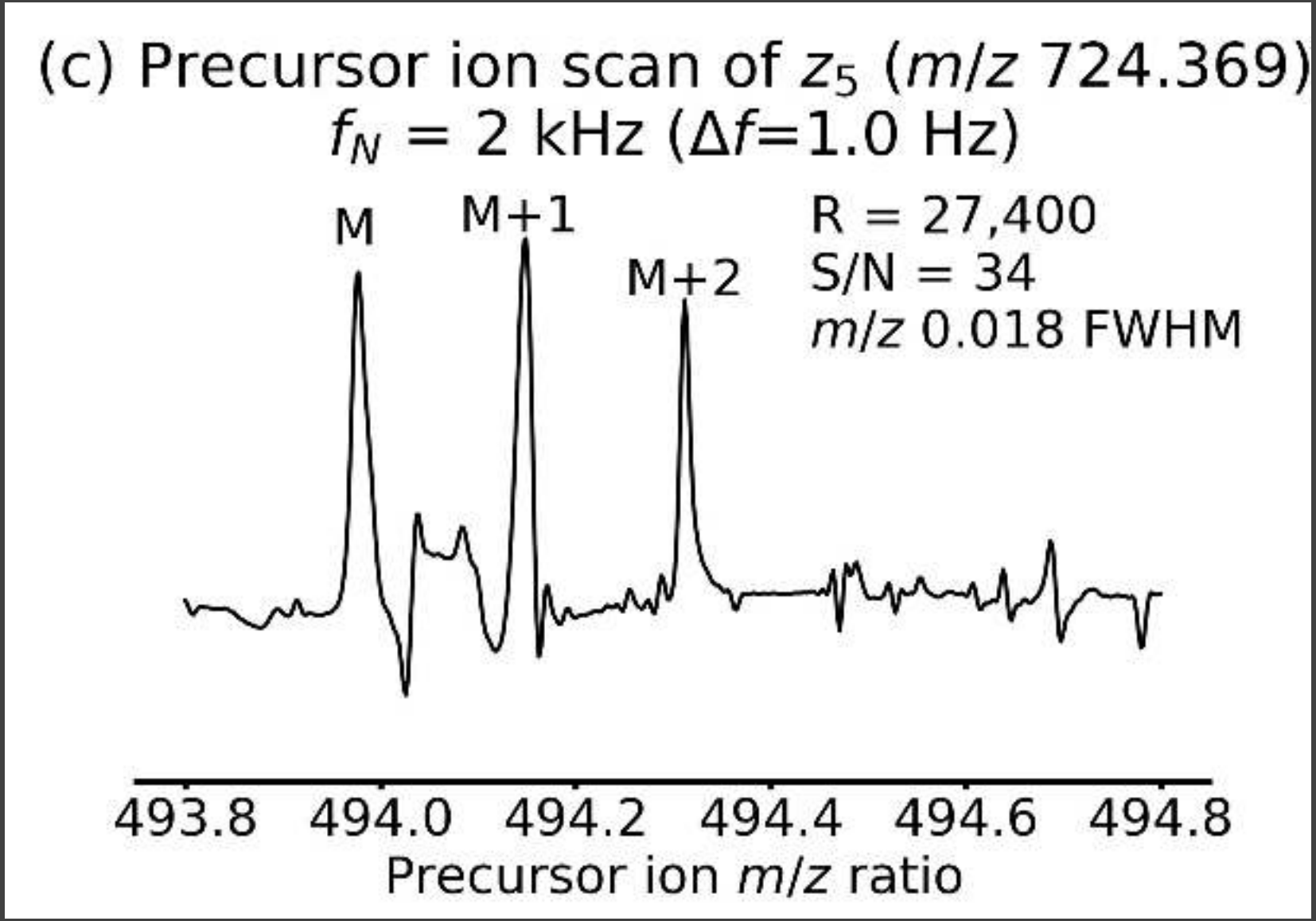

Can we separate a trimethylated and an acetylated histone peptide?

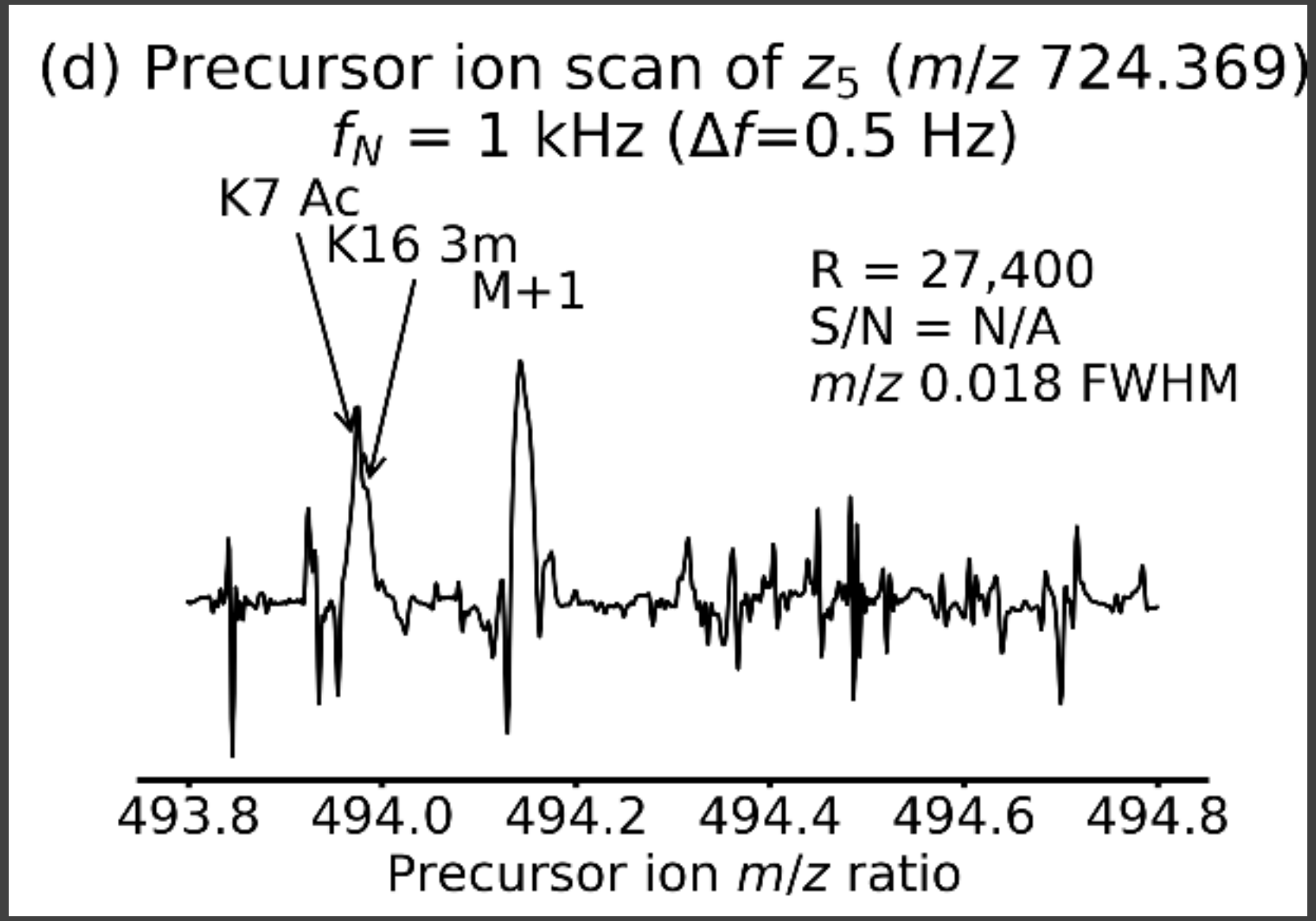

Can we separate a trimethylated and an acetylated histone peptide?

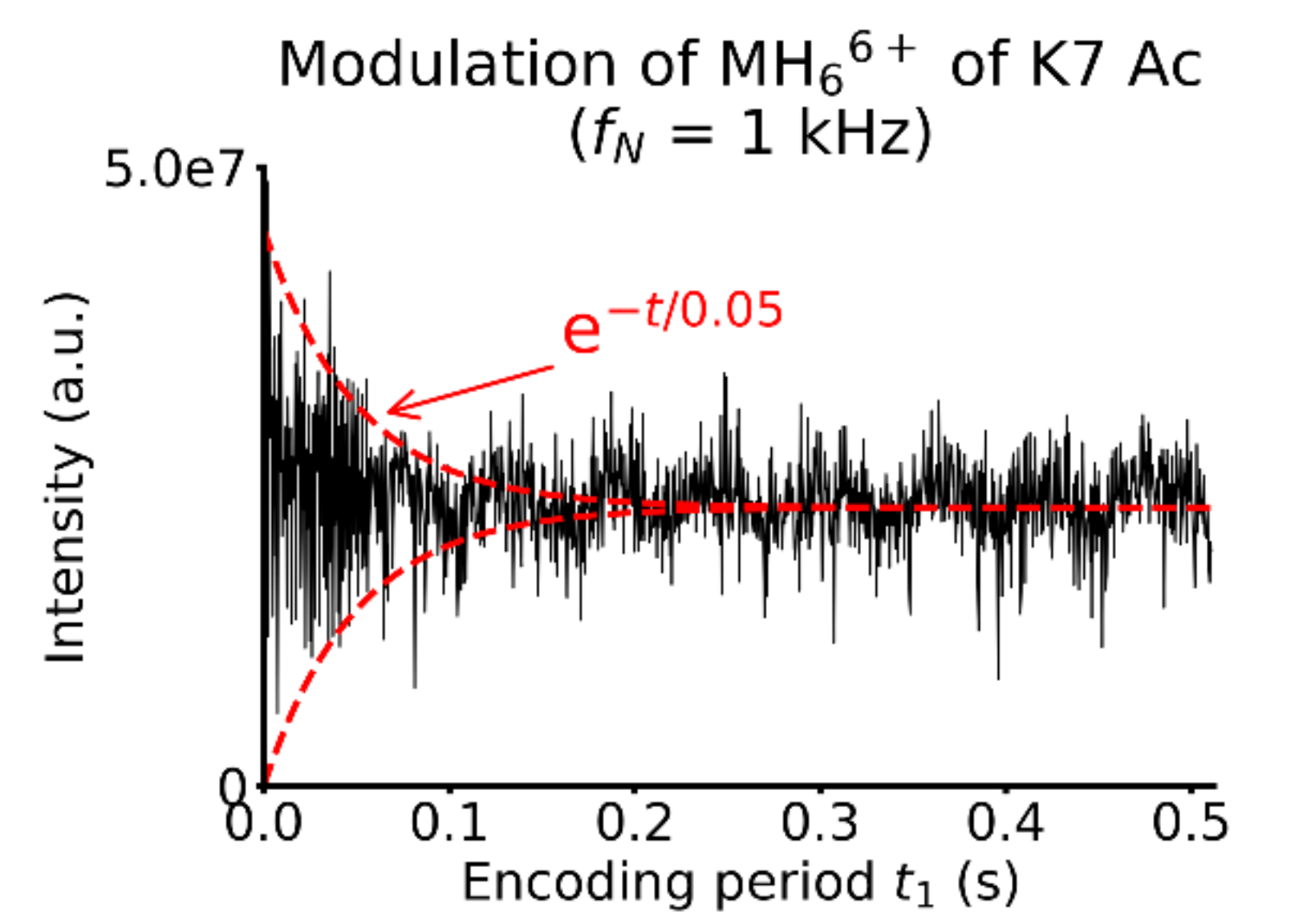

Can we separate a trimethylated and an acetylated histone peptide?

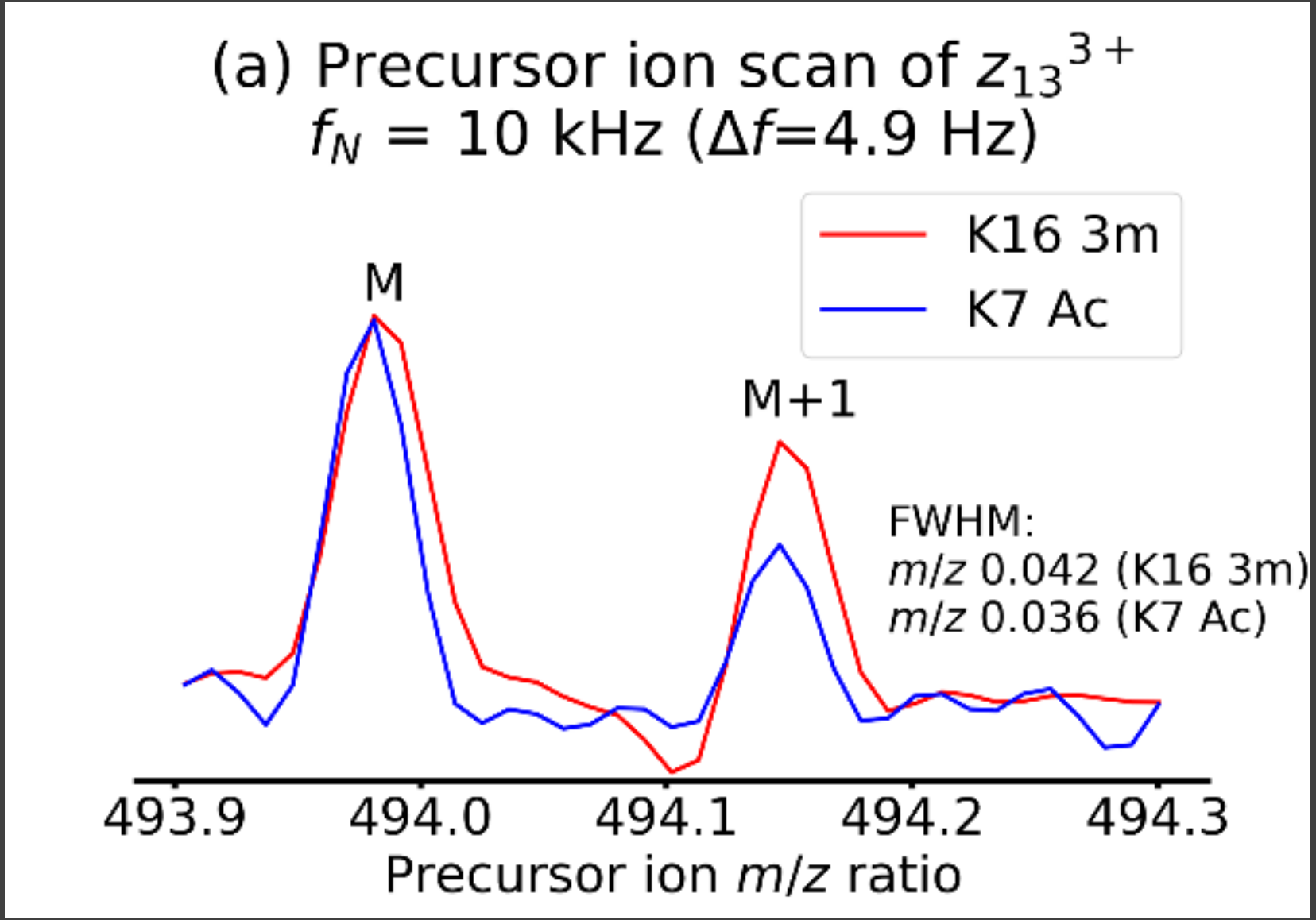

Can we separate a trimethylated and an acetylated histone peptide?

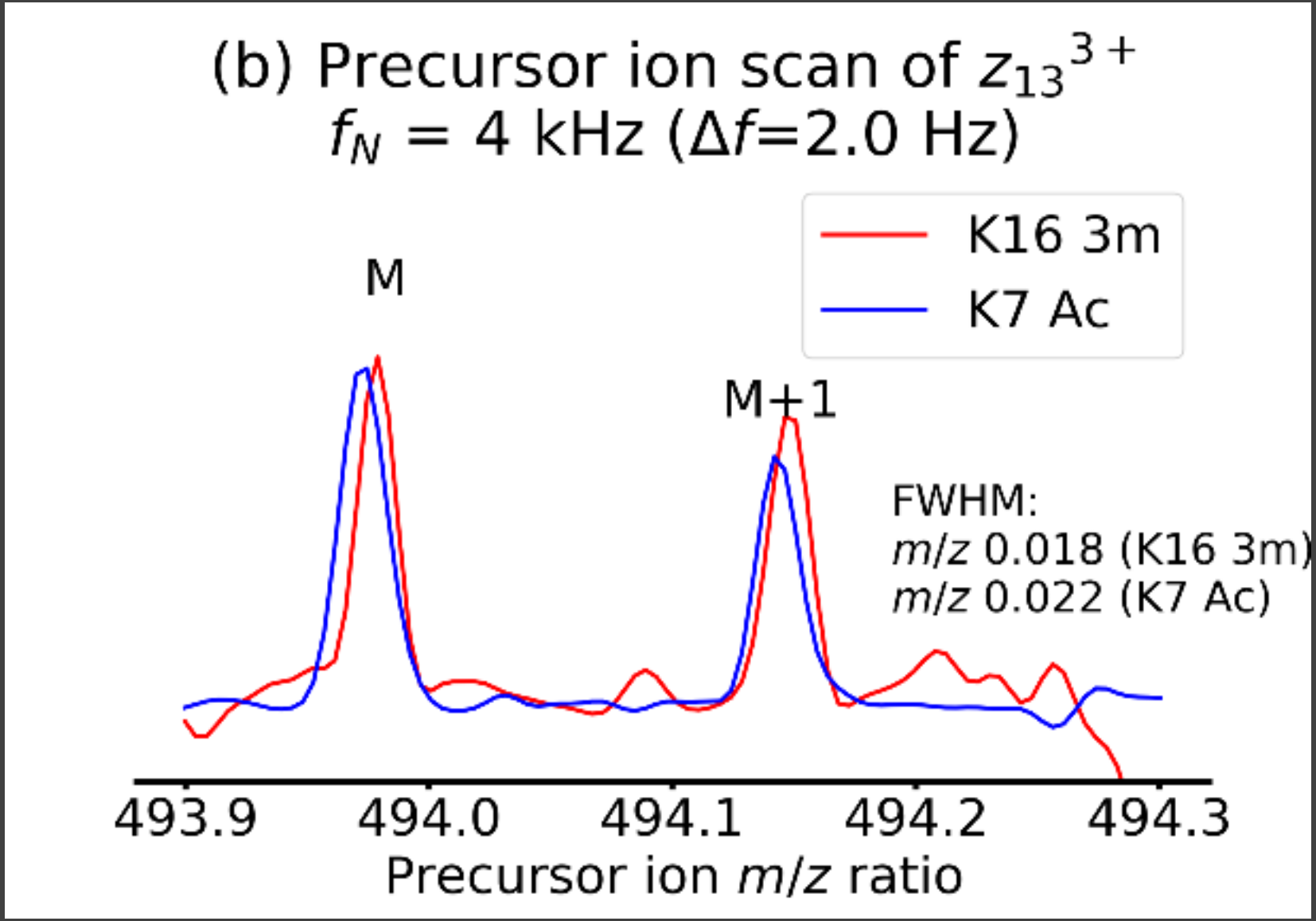

Can we separate a trimethylated and an acetylated histone peptide?

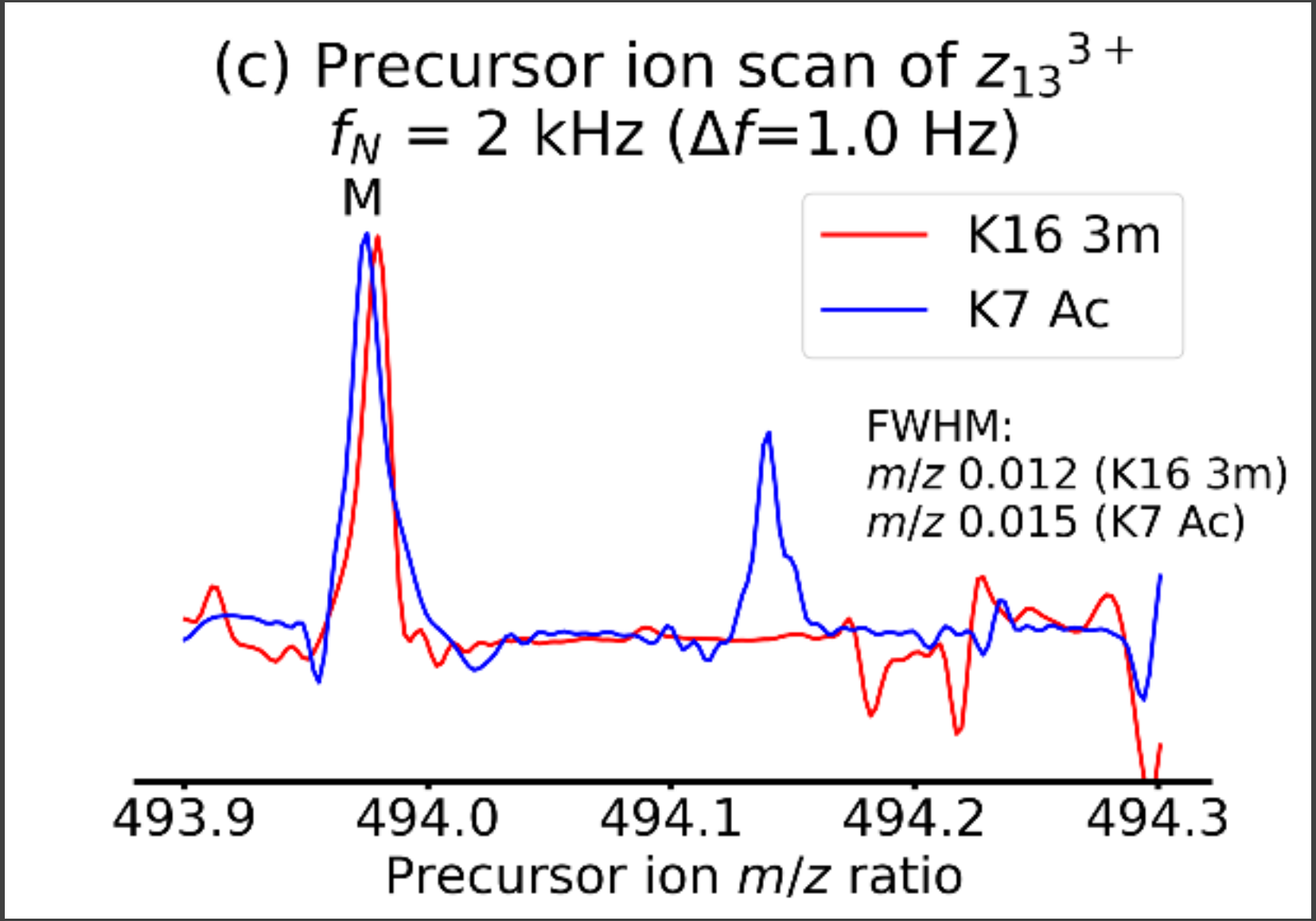

Can we separate a trimethylated and an acetylated histone peptide?

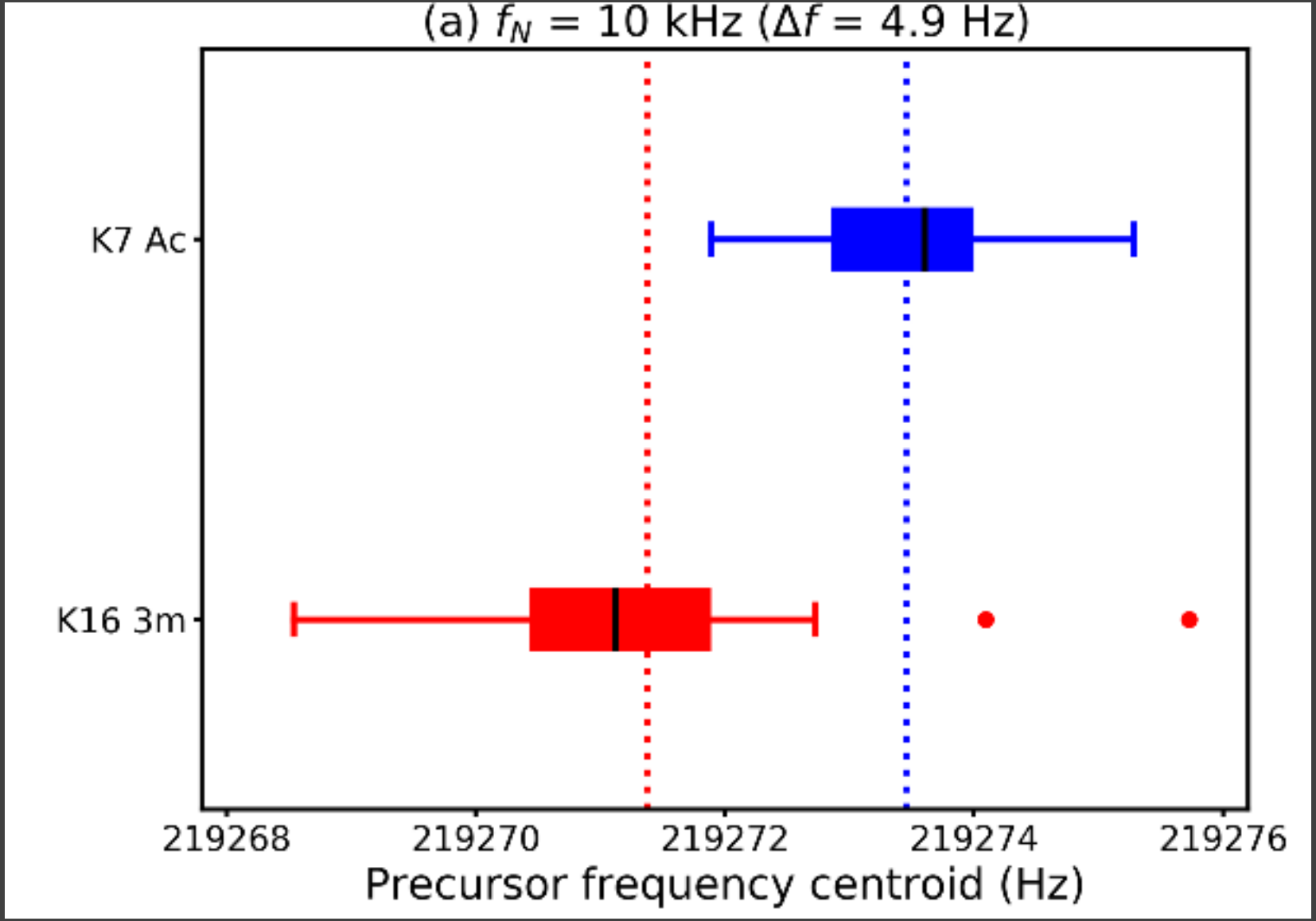

Can we separate a trimethylated and an acetylated histone peptide?

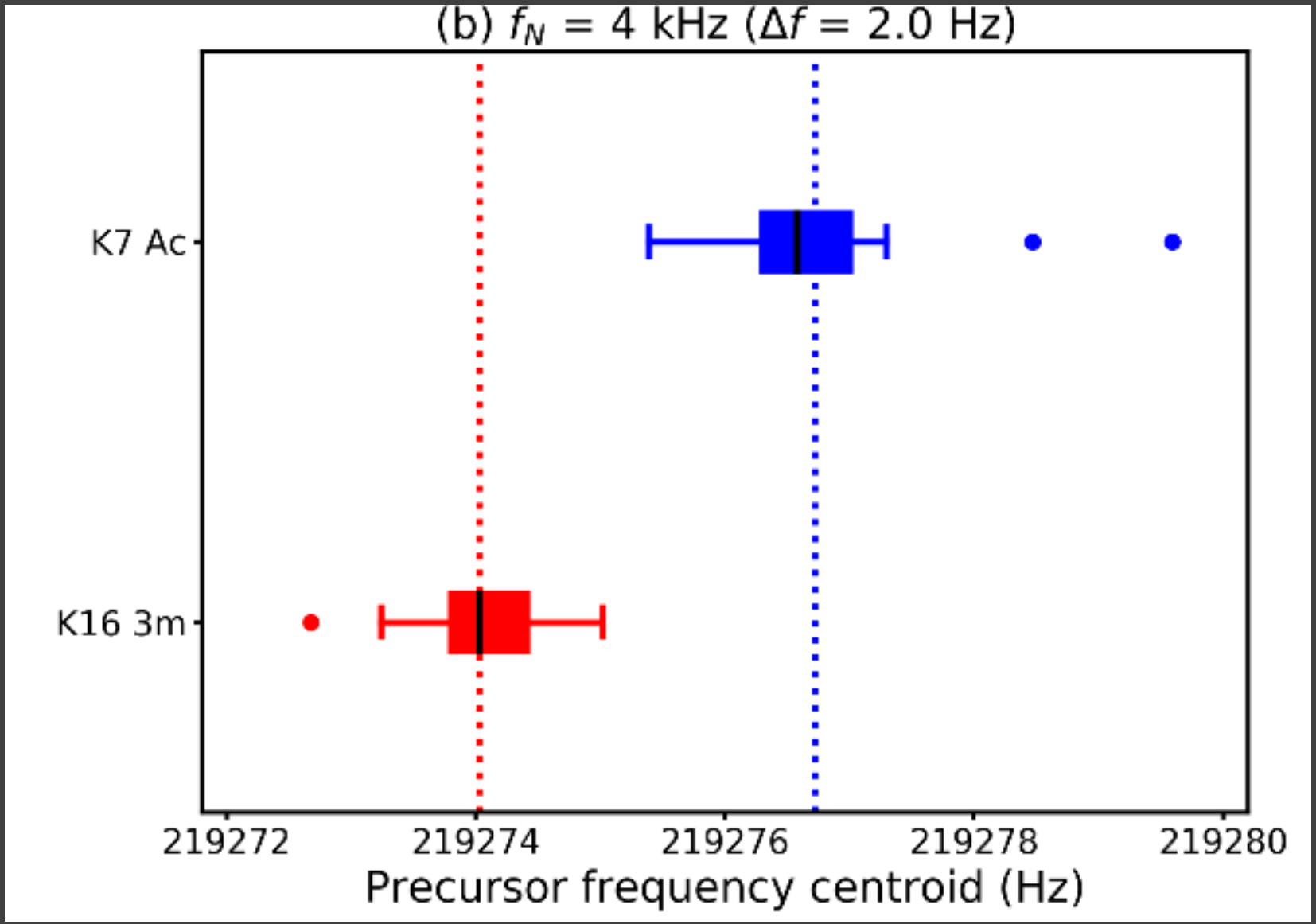

Can we separate a trimethylated and an acetylated histone peptide?

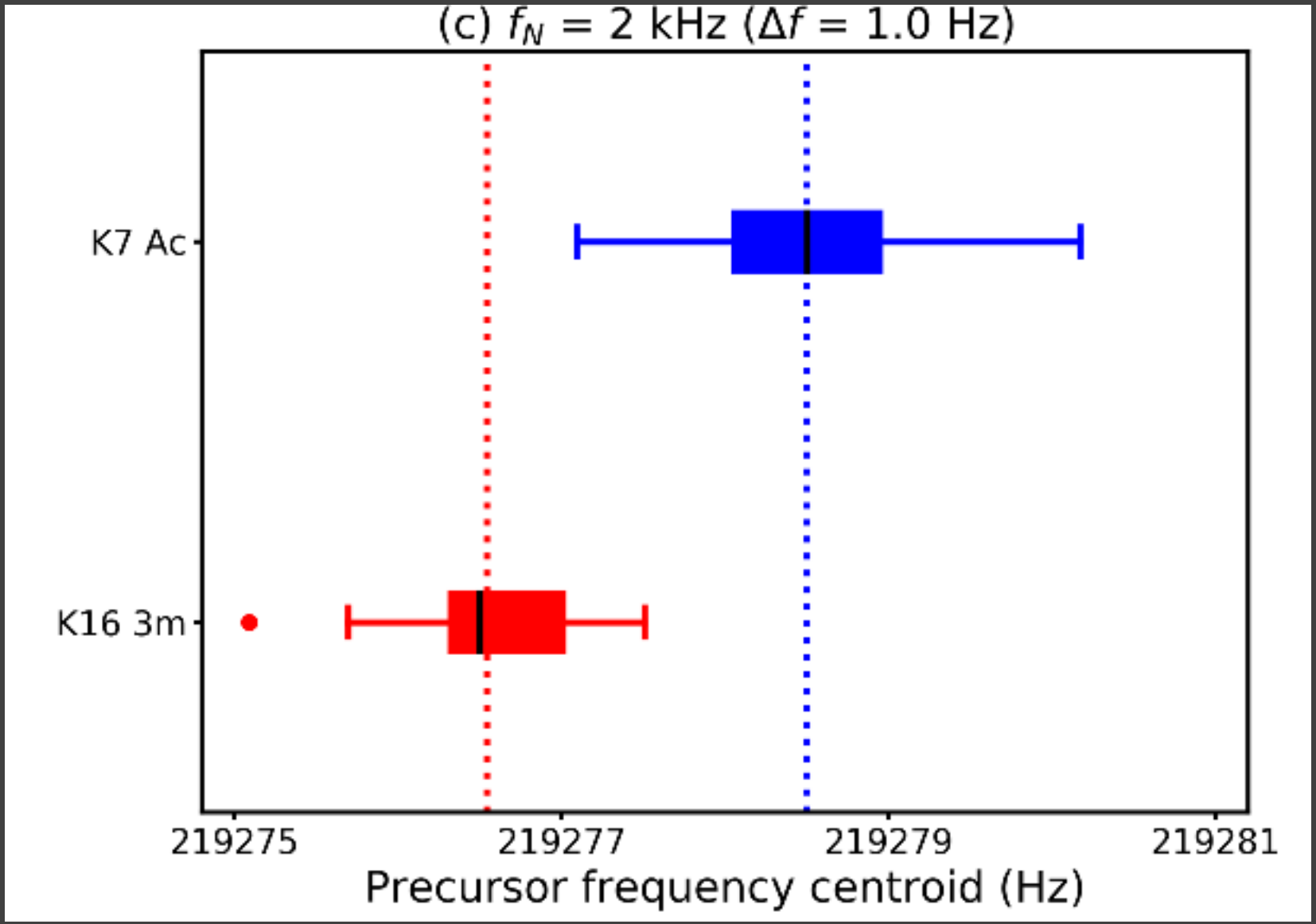

Conclusion

- Narrowband 2D MS: increased resolving power
- Absorption mode 2D MS: increased S/N and resolving power
- Application to top-down analysis of histones and RNA for modifications (identification, location, relative quantification)
- Separation in 2D MS goes beyond resolving power
- Further methods to increase resolving power: non-uniform sampling (NUS)

Acknowledgements

University of Warwick:
Prof. Peter O'Connor
Dr. Mark Barrow
Prof. Alex Jones
Dr. Federico Floris
Dr. Hayley Simon
Dr. Christopher Wootton
Dr. Yuko Lam
Alice Lynch
Dr. Tomos Morgan
Bryan Marzullo
Dr. Georgina Charlton

University of Innsbruck:
Prof. Kathrin Breuker
Dr. Giovanni Calderisi
Matthias Halper
Michael Palasser
Sarah Heel

Université Lille 1:
Dr. Christian Rolando
Dr. Olga Plechakova
Dr. Fabrice Bray

IGBMC, CASC4DE, NMRTEC:
Dr. Marc-André Delsuc
Dr. Lionel Chiron
Dr. Marie-Aude Coutouly

Funding:
- Région Nord Pas-de-Calais
- Agence Nationale de la Recherche
- TGE FT-ICR
- University of Warwick
- Engineering and Physical Sciences Research Council
- Biotechnology and Biological Sciences Research Council
- Warwick Ventures
- ICURe Programme
- Austrian Science Fund

Lise Meitner Fellowship Project M-2757

- EU FT-ICR Network

Thank you for your attention!

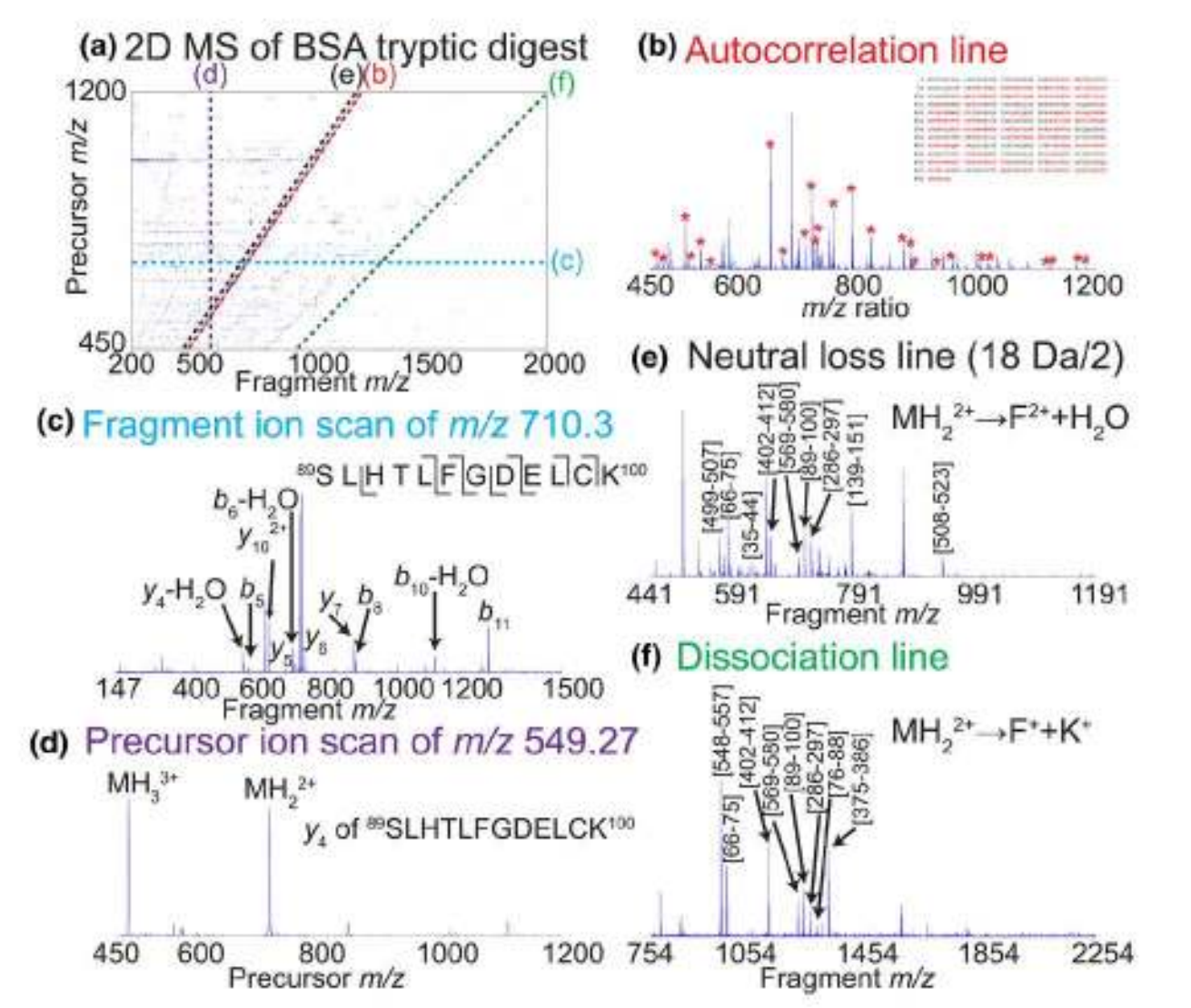

Tutorial review:

M.A. van Agthoven, Y.P.Y. Lam, P.B. O'Connor, C. Rolando, M.-A. Delsuc, *Eur. Biophys. J.* 48 (2019) 213-229.

In open access!

EU FT-ICR MS

Principle and practise of native mass spectrometry

Janne Jänis

University of Eastern Finland
Department of Chemistry

2nd Advanced User School (AUS)
Prague, 26–29.9.2021

EU FT-ICR MS

[redacted]

"Electrospray Wings for Molecular Elephants"
John B. Fenn (1917-2010), Nobel lecture ***2002***

EU FT-ICR MS

[redacted]

© The Author(s), 2016. This article is published with open access at Springerlink.com

J. Am. Soc. Mass Spectrom. (2016)
DOI: 10.1007/s13361-016-1545-3

FOCUS: 31st ASILOMAR CONFERENCE,
NATIVE MS-BASED STRUCTURAL BIOLOGY: ACCOUNT & PERSPECTIVE

Native Mass Spectrometry: What is in the Name?

Aneika C. Leney,[1,2] Albert J. R. Heck[1,2]

[1]Biomolecular Mass Spectrometry and Proteomics, Bijvoet Center for Biomolecular Research and Utrecht Institute for Pharmaceutical Sciences, Utrecht University, Padualaan 8, 3584CH, Utrecht, The Netherlands
[2]Netherlands Proteomics Center, Padualaan 8, 3584CH, Utrecht, The Netherlands

"Native MS is a particular approach based on electrospray ionization, whereby the biological <u>analytes are sprayed from a nondenaturing solvent</u>"

The term describes the biological status of the analytes in solution, <u>prior</u> to the ionization event analytes in solution."

[redacted]

- Levels of protein structure:
  - Primary, secondary, tertiary, quaternary, (quinary)
- Conventional ”denaturing” mass spectrometry
- Native mass spectrometry

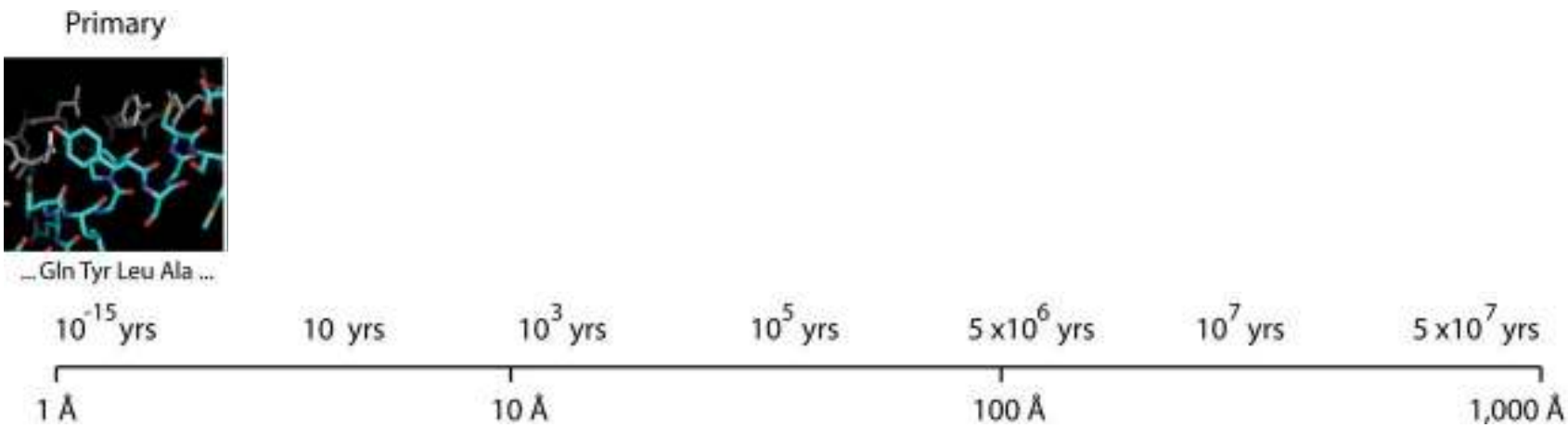

[redacted]

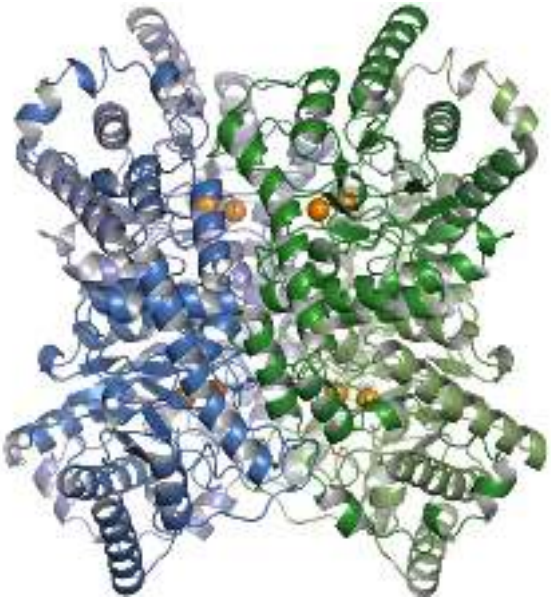

Xylose isomerase tetramer:
Exp. 173 129 ± 12 Da
Calc. 173 104 Da for
4 × monomer + 8 × Mg^{2+}

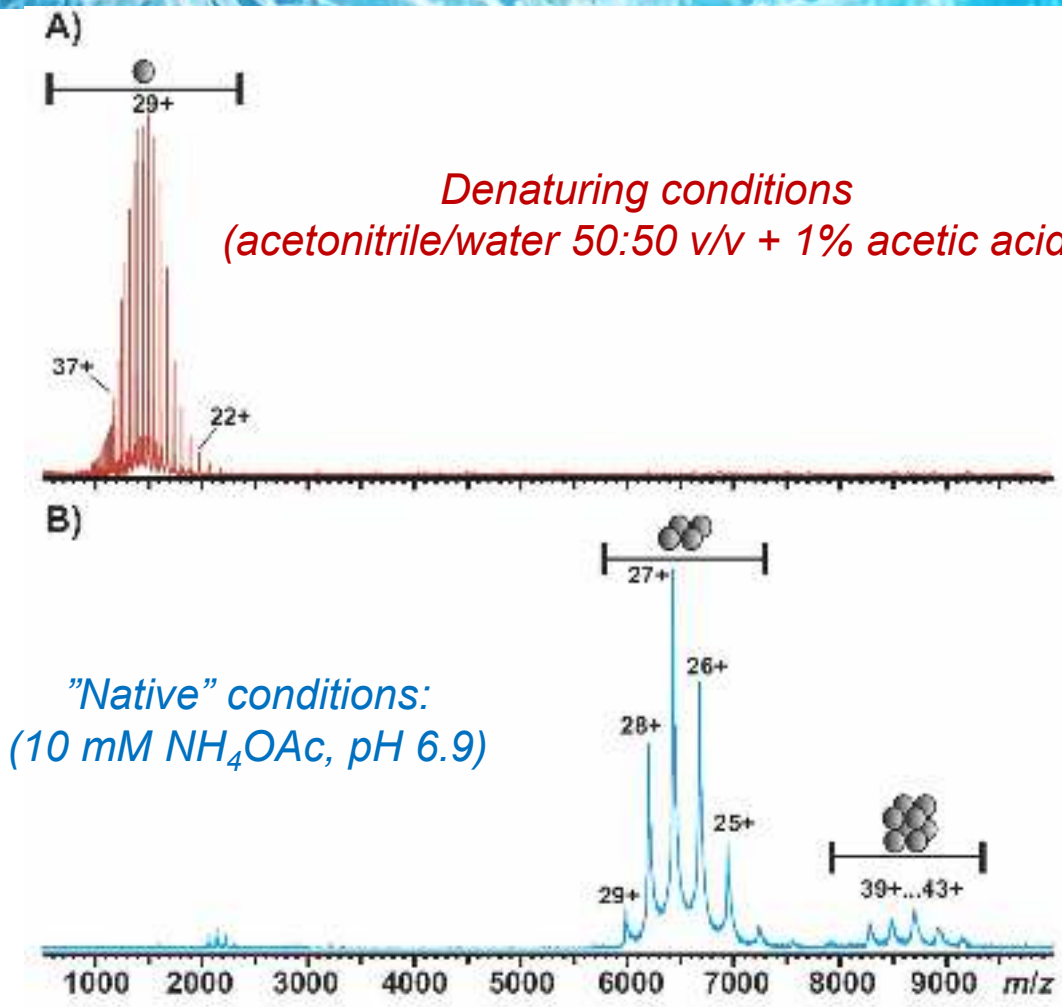

Jänis, J et al. *J. Mass Spectrom.* 2008, 43: 1376-1380.

[redacted]

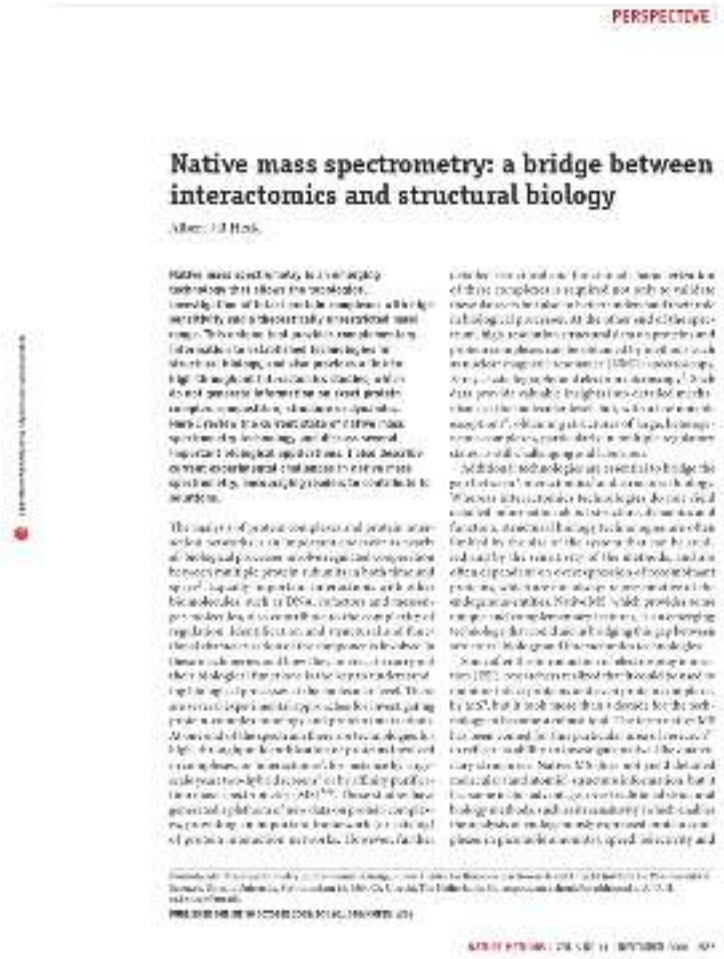

PERSPECTIVE

Native mass spectrometry: a bridge between interactomics and structural biology

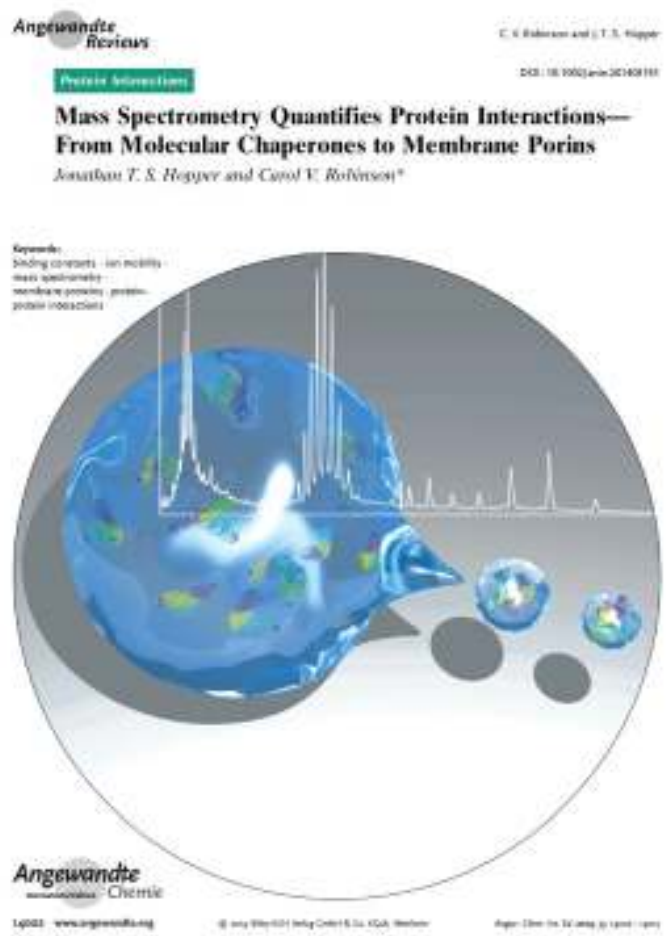

Angewandte Reviews

Protein Interactions

Mass Spectrometry Quantifies Protein Interactions—From Molecular Chaperones to Membrane Porins

*Jonathan T. S. Hopper and Carol V. Robinson**

Angewandte Chemie

Heck AJR, Nature Methods 2008, 5:927

Hopper JTS & Robinson CV, ACIE 2014, 53:14002

EU FT-ICR MS

Electrospray ionization (ESI)

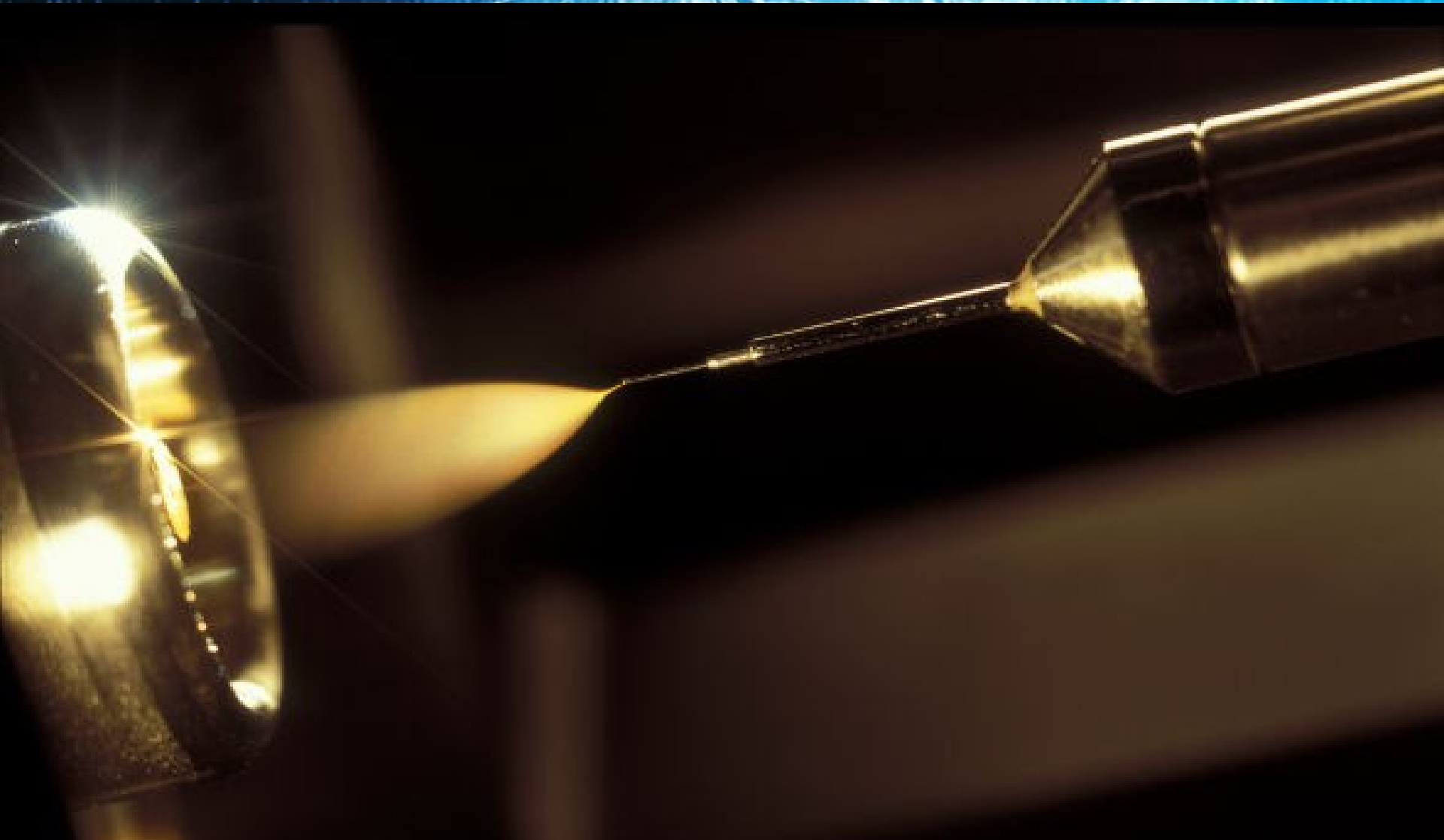

Charge residue model for large protein ions in ESI

- Complicated, multi-phased process
  - A droplet srinkage by evaporation, until the electric field exceeds surface tension (a Rayleigh limit);

$$q^2 \leq 8\ \pi^2 \varepsilon_0 \gamma R^3,$$

q = droplet charge, ε_0 = solvent permittivity, γ = surface tension

R = droplet radius

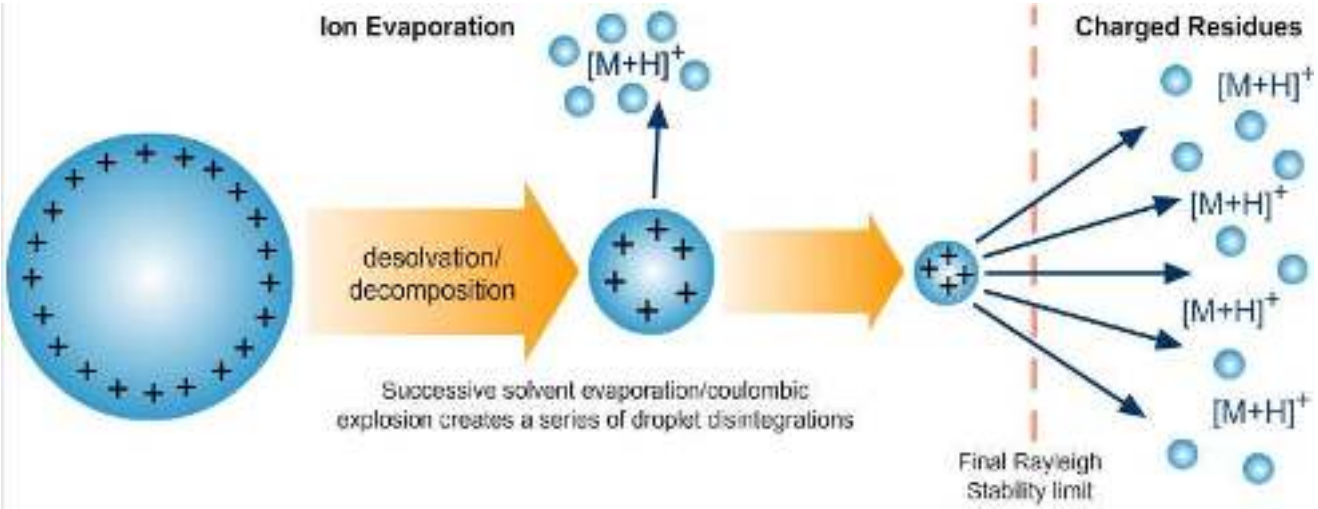

Kebarle P & Verkerk UH, *Mass Spectrom. Rev.* **2009**, 28: 898–917.

Electrospray ionization (ESI)

Electrospray Ionization for Mass Spectrometry of Large Biomolecules

John B. Fenn, Matthias Mann, Chin Kai Meng, Shek Fu Wong, Craig M. Whitehouse

Electrospray ionization has recently emerged as a powerful technique for producing intact ions in vacuo from large and complex species in solution. To an extent greater than has previously been possible with the more familiar "soft" ionization methods, this technique makes the power and elegance of mass spectrometric analysis applicable to the large and fragile polar molecules that play such vital roles in biological systems. The distinguishing features of electrospray spectra for large molecules are coherent sequences of peaks whose component ions are multiply charged, the ions of each peak differing by one charge from those of adjacent neighbors in the sequence. Spectra have been obtained for biopolymers including oligonucleotides and proteins, the latter having molecular weights up to 130,000, with as yet no evidence of an upper limit.

Mass spectrometry consists of "weighing" individual molecules by transforming them into ions in vacuo and then measuring the sequence of their trajectories in electric and magnetic fields or both. Attempts to extend the sensitivity and accuracy of mass spectrometric methods to the analysis of large polar organic molecules of interest in biology and medicine have long been frustrated by the difficulties of transforming such molecules into gas phase ions. They cannot be vaporized without extensive, even catastrophic, decomposition. Consequently, one cannot apply the classical methods of ionization that are based on gas phase encounters of the molecule to be ionized with electrons in electron ionization, photons in photo ionization, other ions in chemical ionization, or electrically excited atoms or molecules in Penning ionization. Such encounters can remove a negatively or positively charged entity from a neutral molecule, or sometimes attach one, thus transforming it into an ion.

In the last 20 years intrepid experimenters have developed a number of so-called "soft" ionization methods that have been used with varying degrees of success to produce intact ions from molecular species of ever-increasing size and decreasing volatility. One class of such methods is based on very rapid deposition of energy on a surface over which the species to be analyzed (analyte) has been dispersed. The underlying idea, first proposed by Beuhler et al., is that sufficiently rapid energy input may bring about vaporization before decomposition has a chance to take place (1). The several methods differ in the way that rapid energy deposition is brought about. In plasma desorption (PD) it results from the impact of a fission product of a radioactive isotope, usually californium-252. So-called secondary ionization mass spectrometry (SIMS) makes use of an incident beam of high-energy ions, such as 40 keV Cs^+ and will therefore be referred to here as fast ion bombardment (FIB). If the ions are neutralized by charge exchange before they strike the surface, FIB becomes FAB (for fast atom bombardment). In laser desorption (LD), photons are the vehicle for energy deposition. These "energy-additive" techniques have been able to produce intact ions from remarkably large analyte species, even though in an overall sense the processes involved are highly irreversible. Striking improvements have resulted from dispersing the analyte not on a bare surface but in a layer of suitable matrix, for example, thioglycerol for FAB or FIB, nitrocellulose for PD, and nicotinic acid for LD. At this writing the highest molecular weights of ions that have been produced are with LD 210,000 (2), with FAB (or FIB) 24,000 (3), and with PD 45,000 (4). However, product ion currents are usually very small and, except in the case of LD, decrease rapidly with increasing molecular weight of the analyte. When the ions are very large, their detection with multiplier requires postacceleration voltages that are sometimes awkwardly high. Furthermore, the ions often have high levels of internal excitation that can cause substantial peak broadening as a result of postionization.

Quite different in practice and principle from these "violent" ionization methods are techniques that use strong electrostatic fields to extract ions from a substrate. In so-called field desorption (FD) ionization, the analyte molecules are applied to a fine wire on whose surface is deposited an array of sharp pointed needles or "whiskers." When the wire is placed in a vacuum system and a high voltage is applied while it is carefully heated, the analyte molecules desorb as ions from the tips of the needles where the field strength is very high (5). Even though it can transform highly nonvolatile analytes into ions in vacuo, FD has not been widely used because sample preparation is arduous. Finding and maintaining the combination of temperature and voltage that is right for a particular species requires both luck and the right touch. Finally, the desorbed ions have such high energies that relatively expensive magnetic sector analyzers must be used for their analysis. In electrohydrodynamic (EH) ionization, the analyte is dissolved in a nonvolatile liquid (for example, glycerol) and injected into an evacuated chamber through a small capillary tube that is maintained at high voltage (6). The

The authors are in the Chemical Engineering Department, Yale University, New Haven, CT 06520.

Downloaded from www.sciencemag.org on March 28, 2016

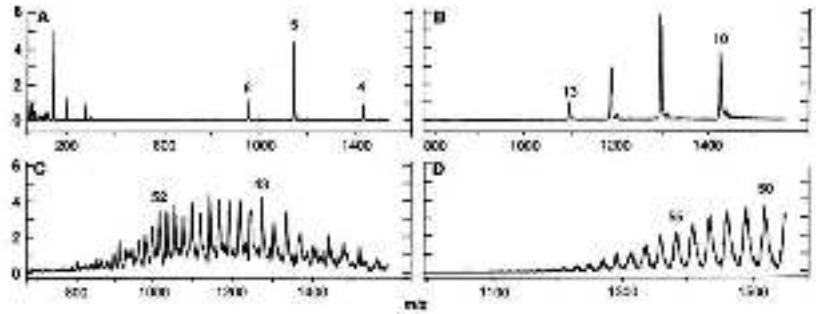

Fig. 6. Representative electrospray mass spectra for protein samples in acid/fed mixtures of water and methanol. The adduct ions were protons, and the infusion flow rate was 1 to 2 μl/min. The spectra are the results of single, 30-s scans. Approximate molecular weight and amount of samples used in the spectrum are as follows: (A) insulin, 5,730, 1.7 pmol; (B) lysozyme, 14,300, 175 fmol; (C) α-amylase, 84,700, 1.7 pmol; and (D) conalbumin, 76,000, 300 fmol. See Table 1 for more data.

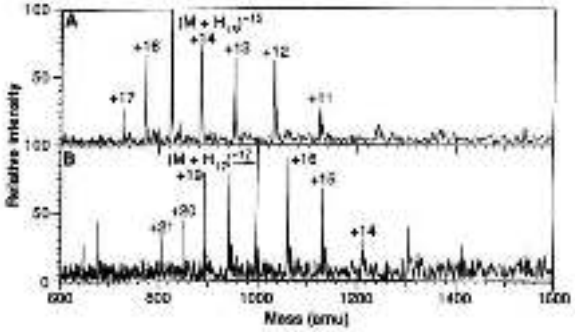

Fig. 8. Electrospray mass spectra obtained by coupling an ES source to a Fourier transform mass spectrometer (24): (A) cytochrome c (equine); calculated average molecular weight, 12,360.1; measured molecular weight, 12,356.9 ± 0.9, (B) myoglobin (equine skeletal muscle); calculated average molecular weight, 16,950.7; measured molecular weight, 16,947.5 ± 1.4.

[redacted]

EU FT-ICR MS

The advent of native MS

8534 *J. Am. Chem. Soc.* **1991**, *113*, 8534–8535

Observation of the Heme–Globin Complex in Native Myoglobin by Electrospray-Ionization Mass Spectrometry

Viswanatham Katta and Brian T. Chait*

The Rockefeller University, New York, New York 10021

Received May 8, 1991

In their native state, globular proteins are tightly folded, compact structures, certain of which may be characterized by the association of the globin with small, noncovalently bound cofactors and prosthetic groups. These proteins can be denatured and caused to unfold by subjecting them to high temperatures, extremes of pH, detergents, and solutions containing high concentrations of compounds like urea, guanidinium chloride, and organic solvents.[1] As the severity of the denaturing conditions is increased, the interaction between the globin and the cofactor can be weakened, with possible separation of the cofactor from the globin. For example, the oxygen-carrying protein myoglobin contains a noncovalently bound heme group in the hydrophobic pocket of the native globin chain that can be induced to unfold under acidic conditions, thus weakening the heme–globin interaction. Under these conditions, the heme moiety can be readily extracted into an organic phase, and this phenomenon forms the basis of widely used procedures for preparing apomyoglobin from the native proteins.[2,3]

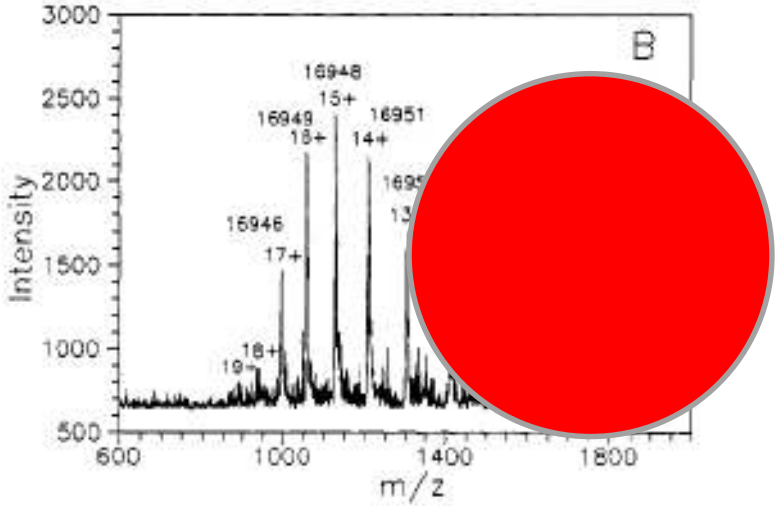

Figure 1. Electrospray-ionization mass spectra of equine skeletal muscle myoglobin obtained from aqueous solutions at different pH values: (A) 3.35; (B) 3.90. The protein concentration is 20–40 μM. The peaks are labeled with the protonation state, *n*+, and the number of protons, *n*, attached to the protein molecule. The circled protonation states designate the peaks corresponding to the intact heme–globin complex in myoglobin. The most intense peaks are also labeled with the molecular masses determinated from the measured *m/z* values.

EU FT-ICR MS

The advent of native MS

Detection of Noncovalent Receptor–Ligand Complexes by Mass Spectrometry

Bruce Ganem*

Department of Chemistry, Baker Laboratory
Cornell University, Ithaca, New York 14853

Yu-Tsyr Li and Jack D. Henion*

Drug Testing and Toxicology
New York State College of Veterinary Medicine
Cornell University, 925 Warren Drive
Ithaca, New York 14850

Received April 24, 1991

Few methods are known for detecting and identifying enzyme–substrate, receptor–ligand, and antibody–antigen complexes, whose weak noncovalent interactions constitute the essential basis of molecular recognition in the biological world. With newer ionization techniques, mass spectrometry (MS) can be applied to problems of biological interest;[1] however, efforts to date have focused on sequencing carbohydrates,[2] oligonucleotides,[3] peptides, and proteins[4] and detecting other macromolecules.[5]

The newly developed technique of ion-spray (pneumatically assisted electrospray) MS forms gas-phase macromolecular ions directly from solution at atmospheric pressure via protonation and ion evaporation.[6,7] In contrast to electrospray, ion-spray MS can be performed in water without cosolvent, which is ideal for most biological systems. Multiple charging produces a family of molecular ions and dramatically reduces the mass-to-charge ratio, so that even quadrupole mass spectrometers having a typical mass range of 1000–2000 daltons (Da) can determine high MW species with unit mass resolution.

Since ionization of the targeted molecular species occurs under very mild conditions, fragmentation is usually not observed in ion-spray MS experiments, thus suggesting that noncovalent molecular association complexes might be detectable under conditions of real-time[8] reaction monitoring. Here we describe the first successful application of such a technique to a problem of considerable contemporary interest. The method should prove useful in probing a wide variety of macromolecular host–guest interactions.

The macrolides FK506 1 (MW 804 Da, Figure 1) and rapamycin 2 (RM, MW 913 Da) are promising new immunosuppressive agents with approximately 100-fold better activity than the widely used immunosuppressant cyclosporin A.[9] Both 1 and 2 inhibit T-cell activation in a complex series of events triggered by binding of the drugs to their naturally occurring cytoplasmic receptor FKBP, a member of the immunophilin family of im-

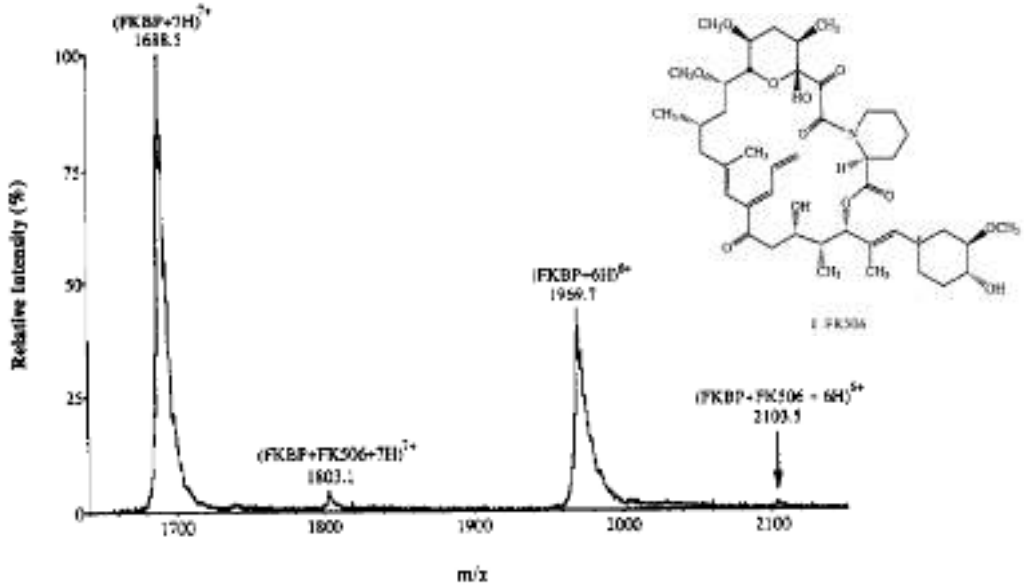

Figure 3. Ion-spray mass spectrum of FKBP + FK506 at pH 7.5.

"The newly developed technique of ion-spray (pneumatically assisted electrospray) MS forms gas-phase macromolecular ions directly from solution…
… suggesting that <u>noncovalent molecular association complexes might be detectable</u>.

Ganem B, *JACS* **1991**, 113, 6294-6296

EU FT-ICR MS

Largest native MS complex todate

The largest biomolecular assembly recorded to date with native MS: An 18-MDa viral capsid of the bacteriophage HK97

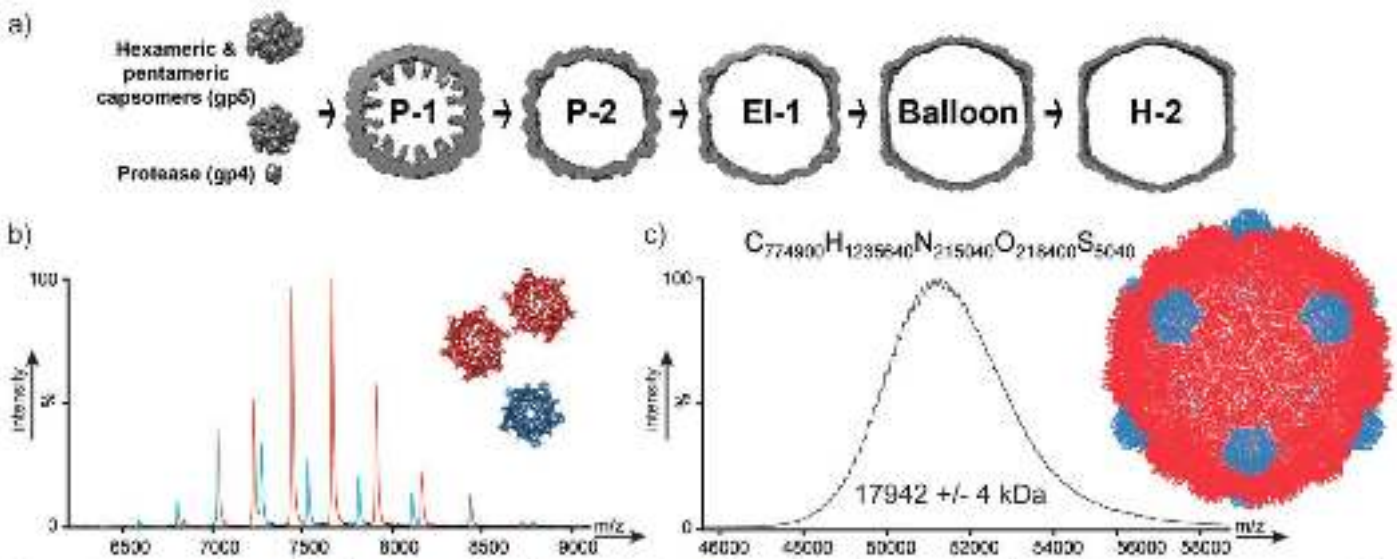

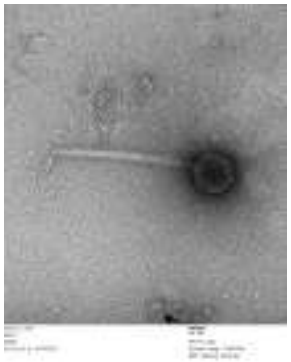

Figure 1. Monitoring the assembly of HK97 capsids with native ESI-MS. a) Assembly and maturation pathway of HK97. b) Free capsomers with penton signal in blue and hexon signal in red. c) Intact Prohead-1 particle. A well-resolved series of charge states is observed allowing the accurate mass calculation.

Intact HK97 capsids measured in 12.5 mM ammonium acetate (pH 7) having a collision voltage of 500 V in the desolvation region of the ESI source with Xe as the collision gas.

Snijder et al, *Angewandte Chem. Int. Ed.* **2013**, 52: 1–5

EU FT-ICR MS

Charge state distribution (CSD)

Small protein, average mass 8285 Da

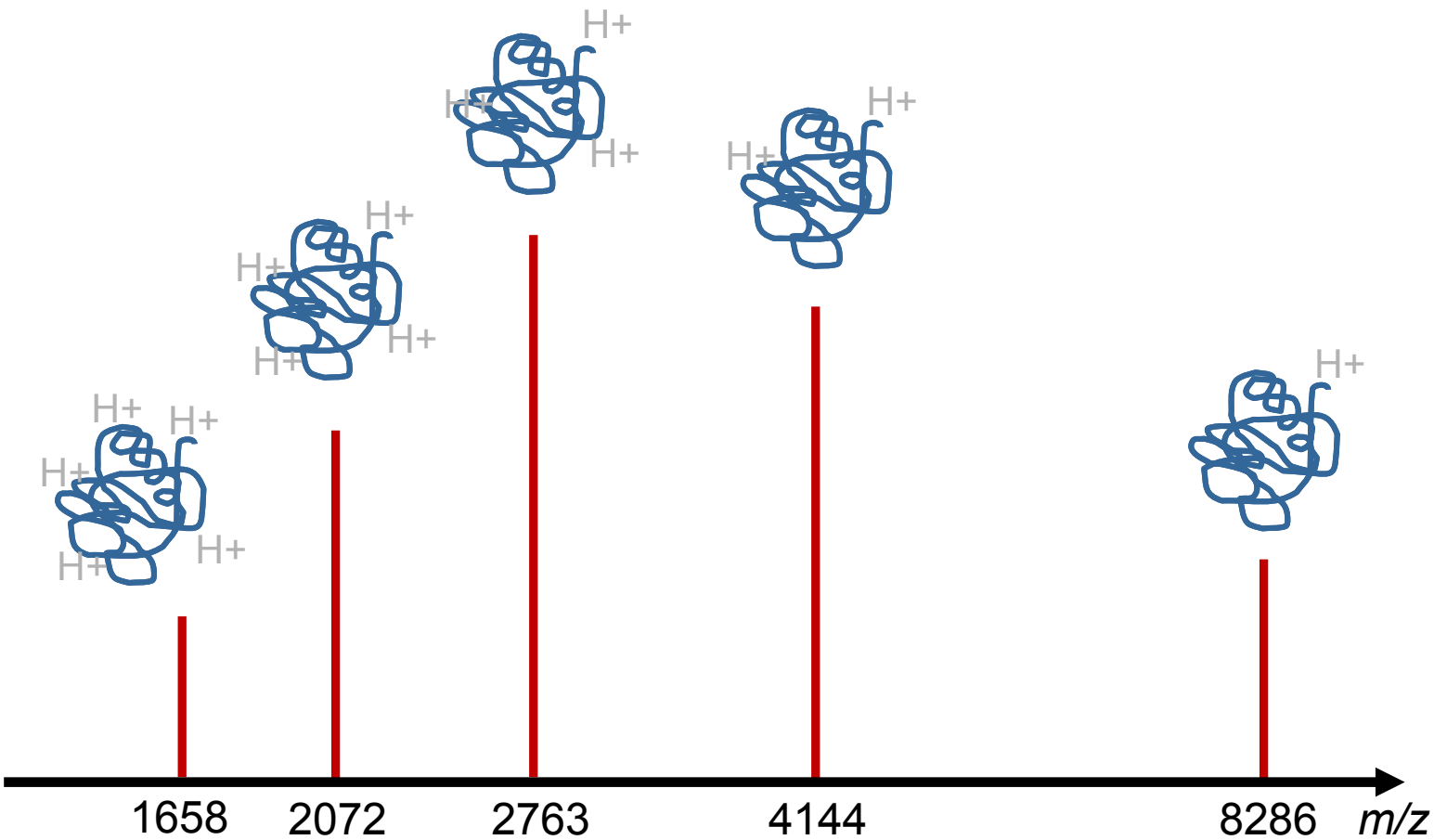

Charge state distribution (CSD)

- ESI of polypeptides gives rise to multiply-charged ions $[M + nH]^+$, where n = 1,2,3…
  - Average <n> depends on polypeptide sequence & conformation
  - CSD is dependent on *relative proton affinities* of amino acid residues; thus, it is not easy to predict max. and av. charge state

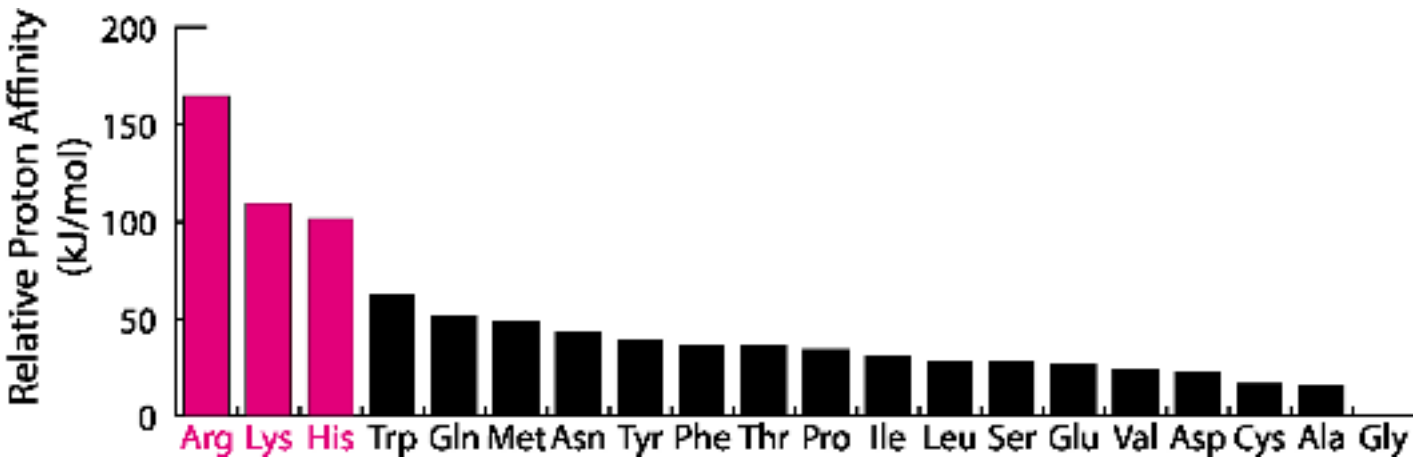

EU FT-ICR MS

Protein ion CSD: a probe for polypeptide conformation

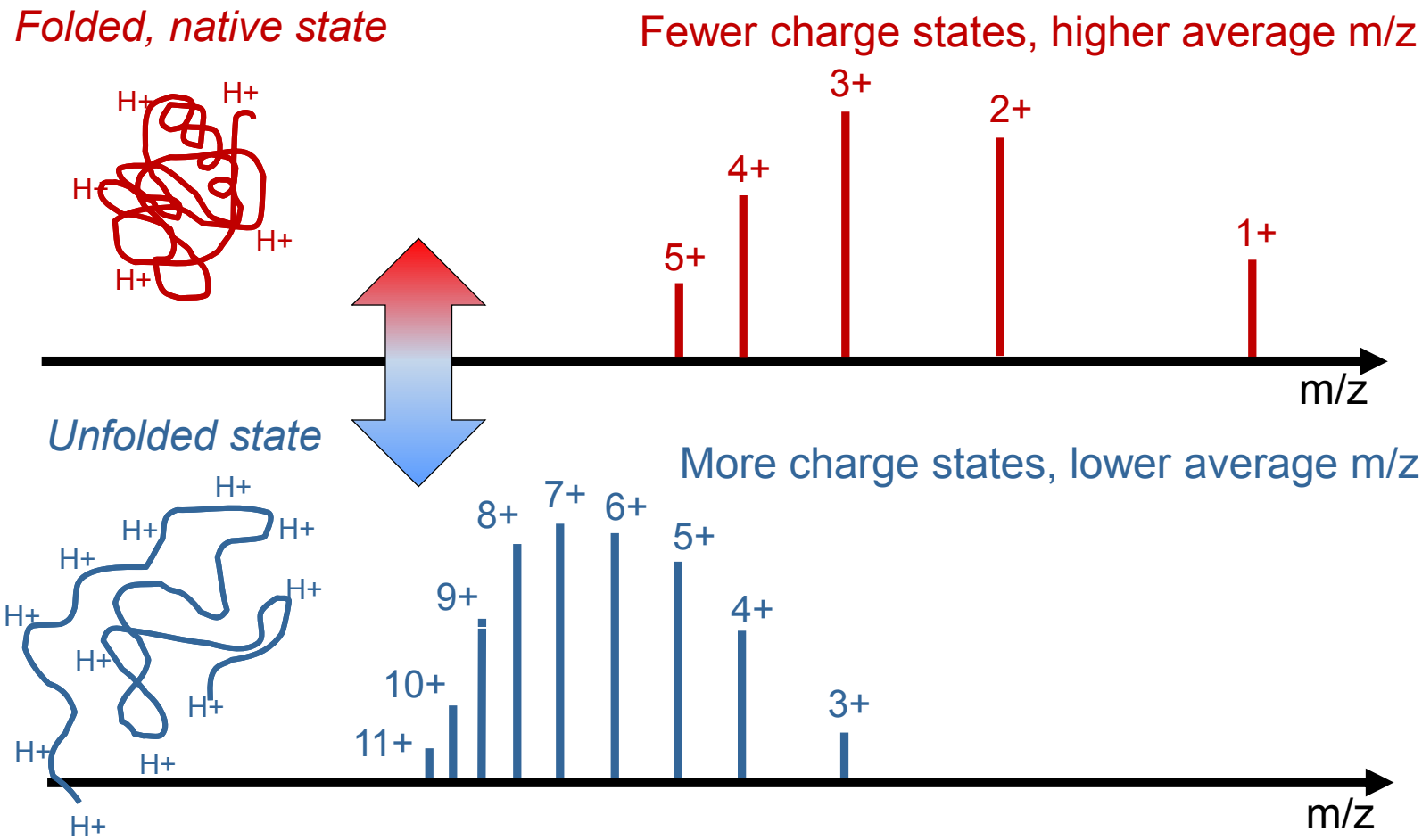

EU FT-ICR MS

Protein ion CSD: a probe for polypeptide conformation

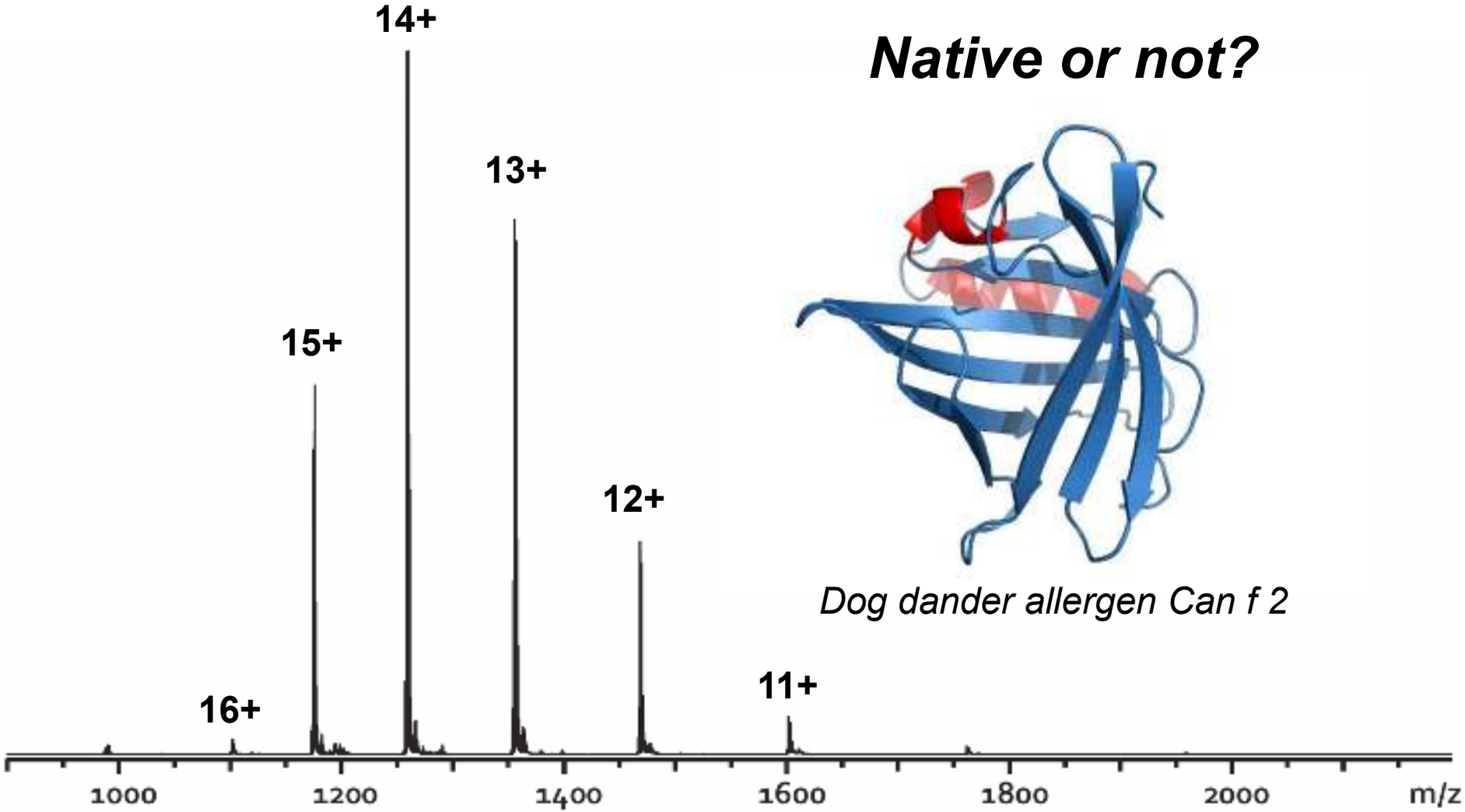

Native or not?

Dog dander allergen Can f 2

Charge state distribution (CSD)

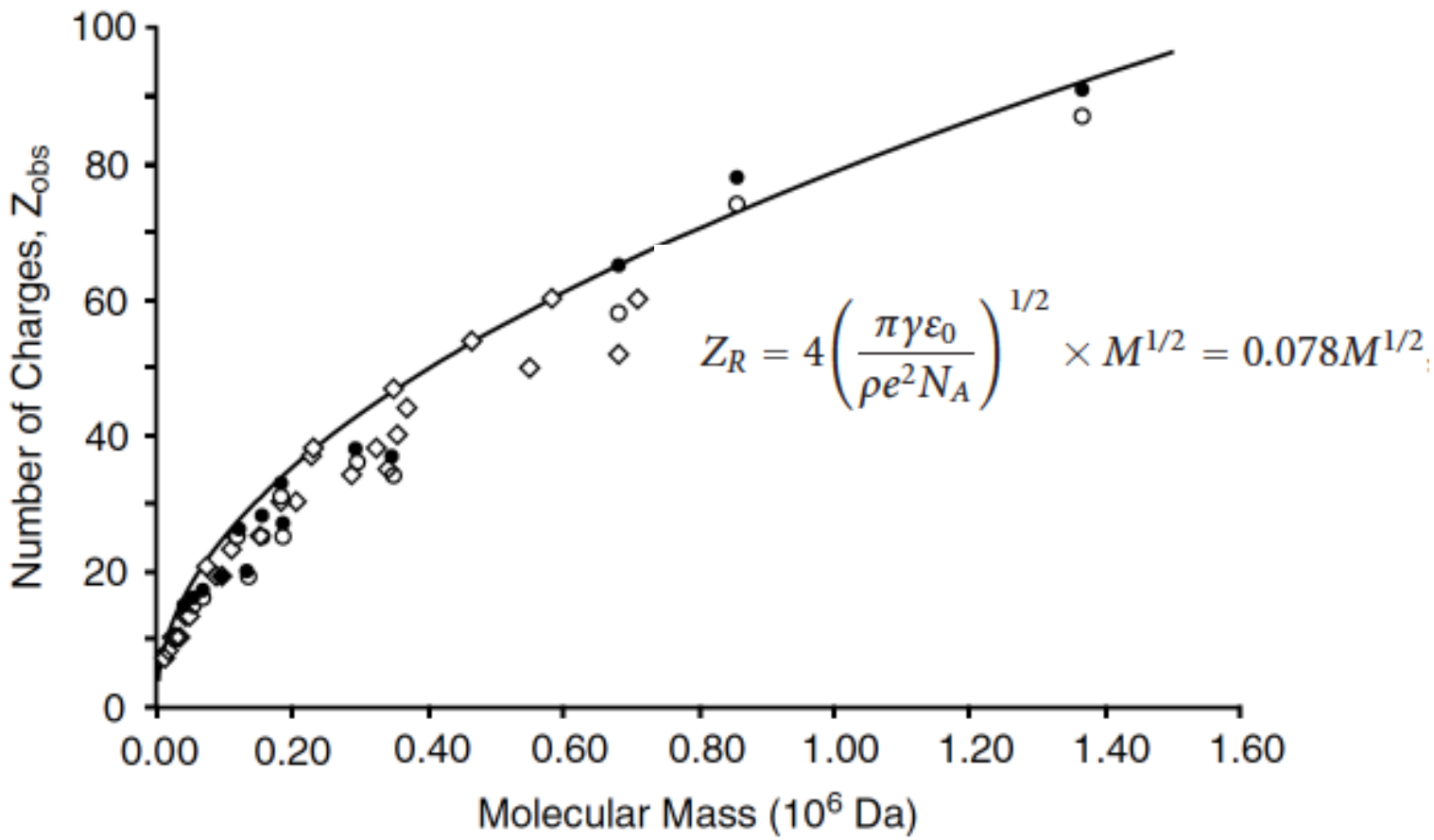

De La Mora, F. *Anal. Chim. Acta*, **2000**, 406: 93-104.

Charge state distribution (CSD)

Table 1. Proteins Used To Obtain a Charge–Surface Correlation Shown in Figure 2

protein	PDB id	no. of basic residues (R, K, H)	no. of acidic residues (D, E)	av charge of protein ions	surface area (Å^2) (crystal structure)
insulin (bovine)	1APH	1, 1, 2	0, 4	4.4	3396
chymotrypsin inhibitor II	1CIQ	4, 6, 0	4, 6	5.42	4052
ubiquitin (human)	1UBQ	4, 7, 1	5, 6	5.9	4758
cytochrome C (equine)	1HRC	2, 19, 3	3, 9	7.2	6232
cellular retinoic acid binding protein I (mice)	1CBI	9, 9, 2	8, 14	8.13	7341
β-lactoglobulin A (bovine)	1BSY	3, 15, 2	11, 16	8.65	8321
myoglobin (equine)	1WLA	2, 19, 11	8, 13	8.7	8017
H-chain of ferritin (human)	2FHA	7, 12, 10	15, 16	9.33	9816
α1 chymotrypsinogen (bovine)	1EX3	4, 14, 2	9, 5	10.56	10317
ligand binding domain of retinoic acid receptor (human)	3LBD	16, 13, 10	15, 20	11.17	11230
carbonic anhydrase I (human)	2CAB	7, 18, 11	14, 13	10.54	10997
pepsin (porcine)	5PEP	2, 1, 1	28, 13	10.74	13351
β-lactoglobulin dimer (bovine)	1BEB	6, 30, 4	22, 32	12.9	14698
apotransferrin, N-lobe (human)	1BTJ	12, 27, 9	25, 17	13.1	14970
holotransferrin, N-lobe (human)	1A8E	12, 27, 9	25, 17	12.93	13973
ovalbumin (hen egg)	1OVA	15, 20, 7	14, 33	13.89	15586
serum albumin (human)	1AO6	24, 59, 16	36, 62	17.2	28103
hemoglobin (human)	1A3N	12, 44, 38	30, 24	17.8	24548
transferrin (rabbit)	1JNF	26, 57, 18	43, 46	19.8	27395
soluble transferrin receptor (human)	1CX8	48, 88, 24	74, 72	27.2	46530
transferrin–transferrin receptor complex (human)	1SUV[a]	100, 202, 62	166, 154	40.5	91258
H-chain ferritin 24-mer (human)	2FHA	168, 288, 240	360, 384	62.16	141541

[a] Cryo-EM structure of the assembly is refined using X-ray structures of individual subunits.

Kaltashov I. A. and Mohimen, A. *Anal. Chem.* **2005**, 77: 5370-5379

Charge state distribution (CSD)

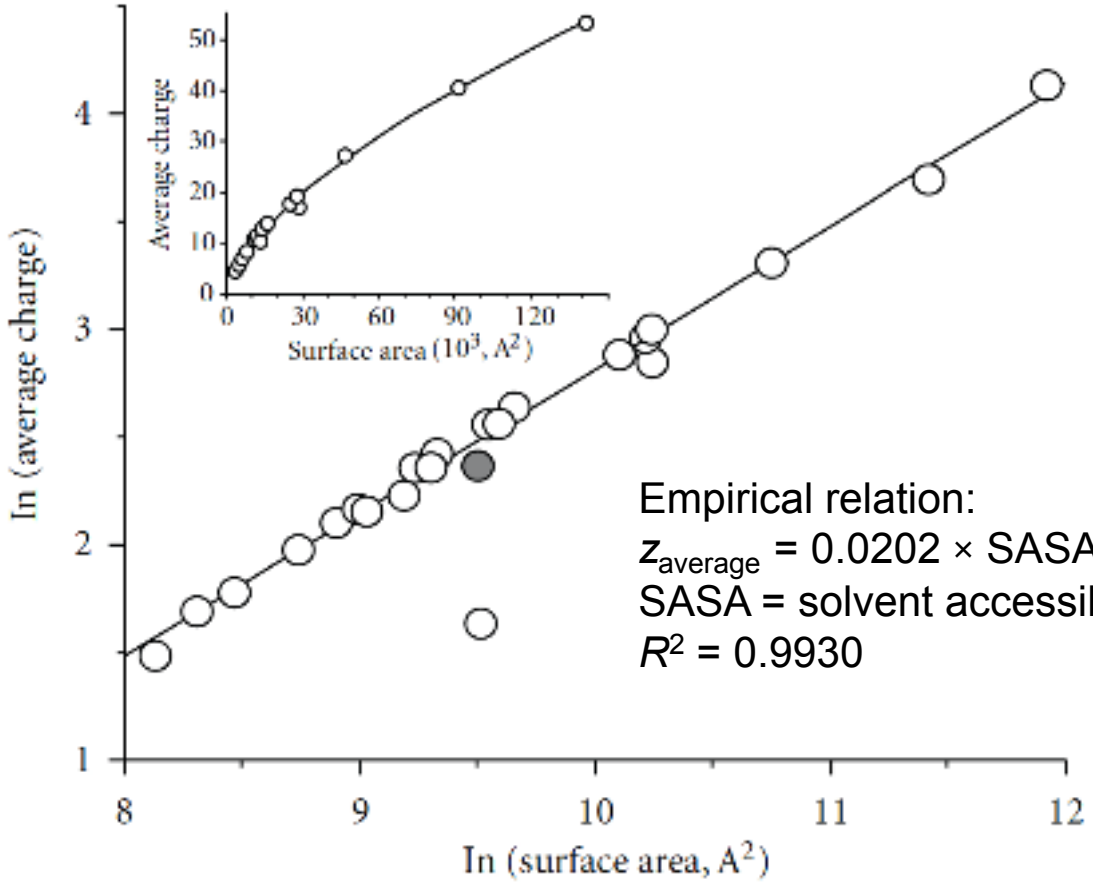

Empirical relation:

$z_{average} = 0.0202 \times SASA\ (Å^2)^{0.6715}$

SASA = solvent accessible surface area

$R^2 = 0.9930$

Kaltashov I. A. and Mohimen, A. *Anal. Chem.* **2005**, 77: 5370-5379

EU FT-ICR MS

Monitoring conformational changes by CSD analysis

Acid-induced unfolding of myoglobin:
A–E, holo-Mb; F–J: apo-Mb

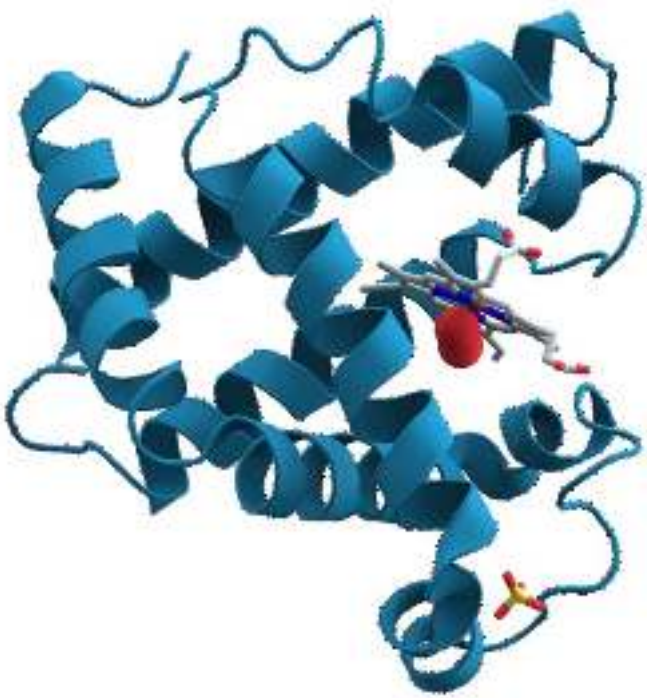

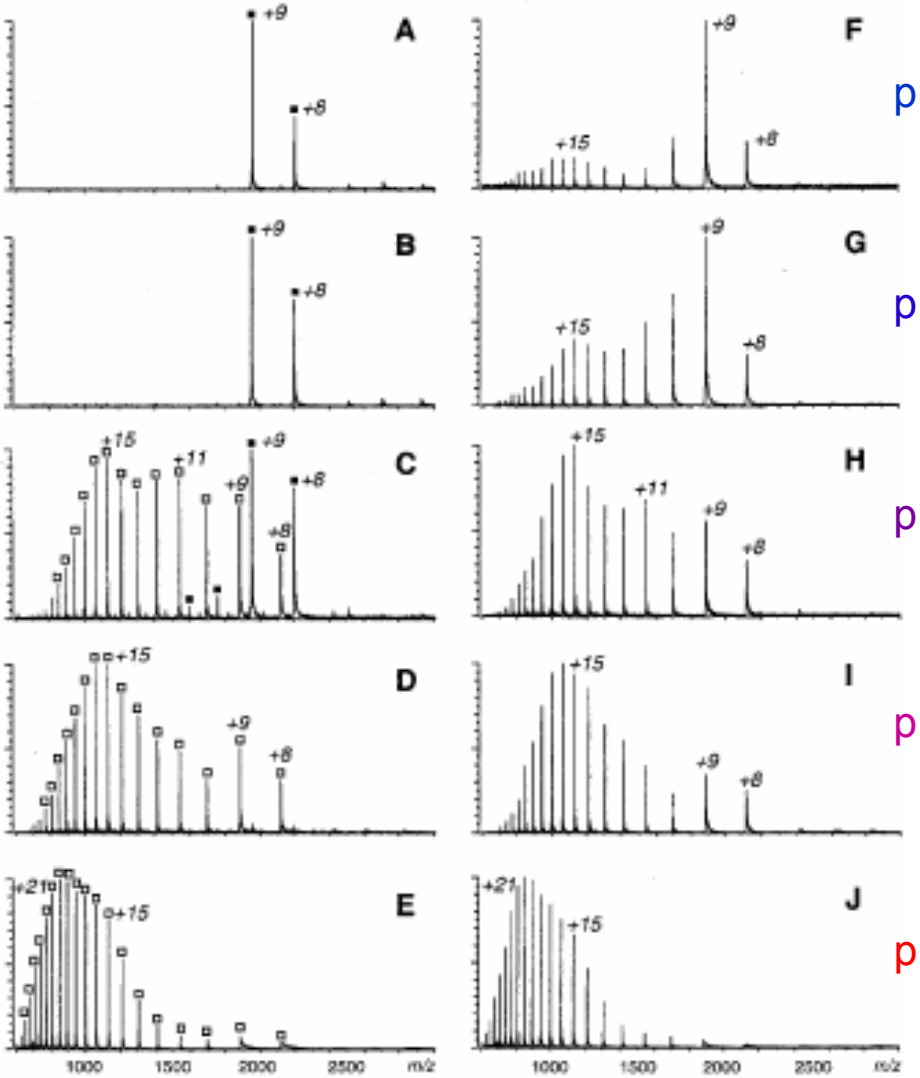

pH 7.4

pH 4.5

pH 4.0

pH 3.5

pH 2.5

Konermann *et al.* JASMS 1995

[redacted]

Geobacillus sp. deoxyribose-phosphate aldolase (DERA)
Different structural states of DERA are resolvable

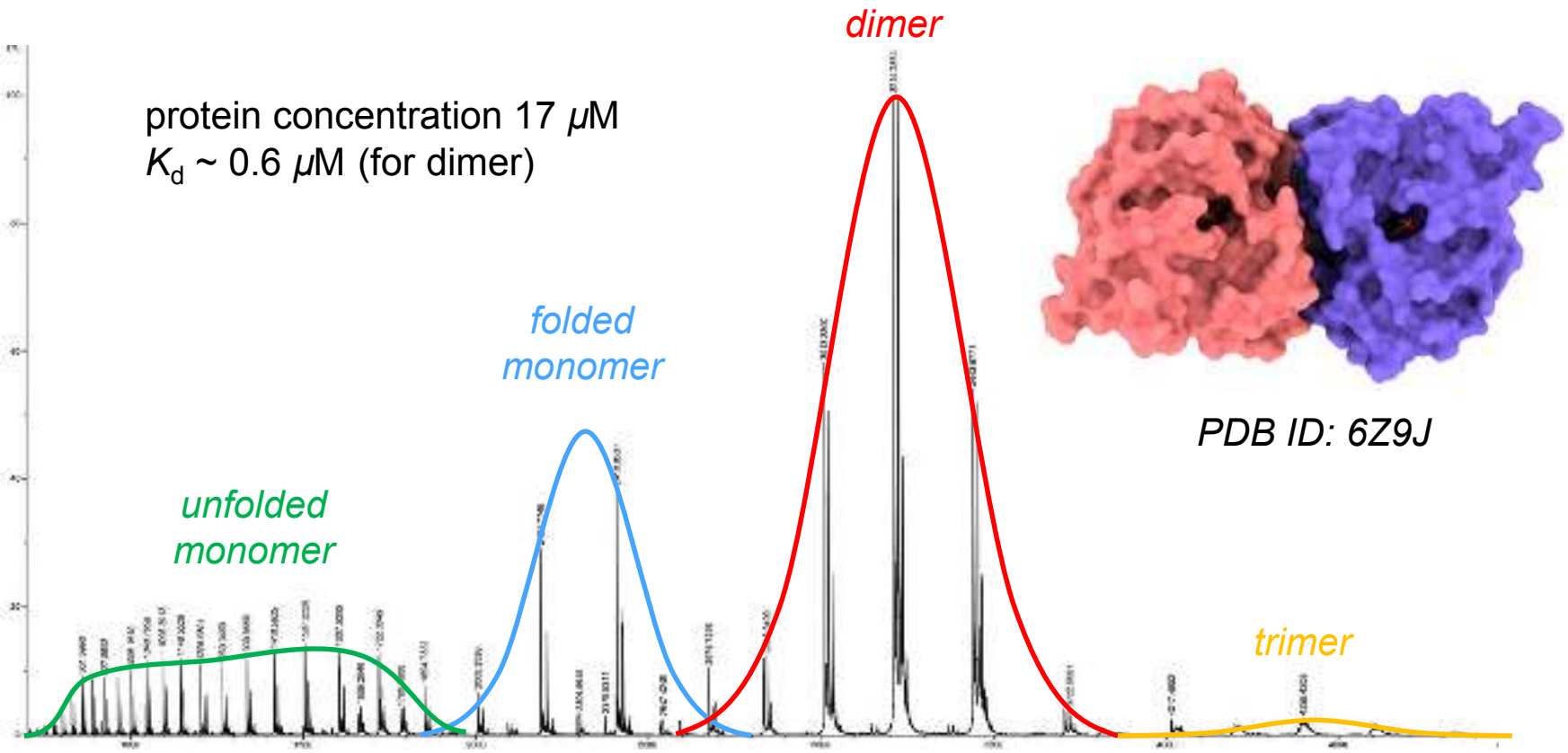

Courtesy of Johan Pääkkönen

EU FT-ICR MS

Metalloproteins: SAP30L zinc finger domain

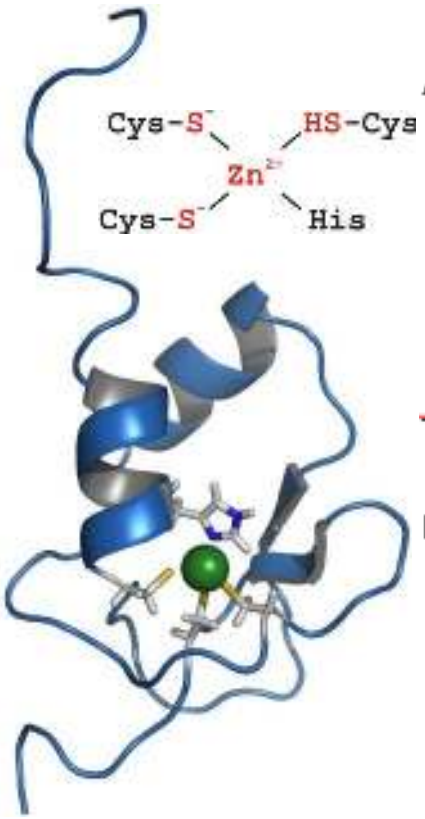

Solution NMR structure, PDB: 2N1U

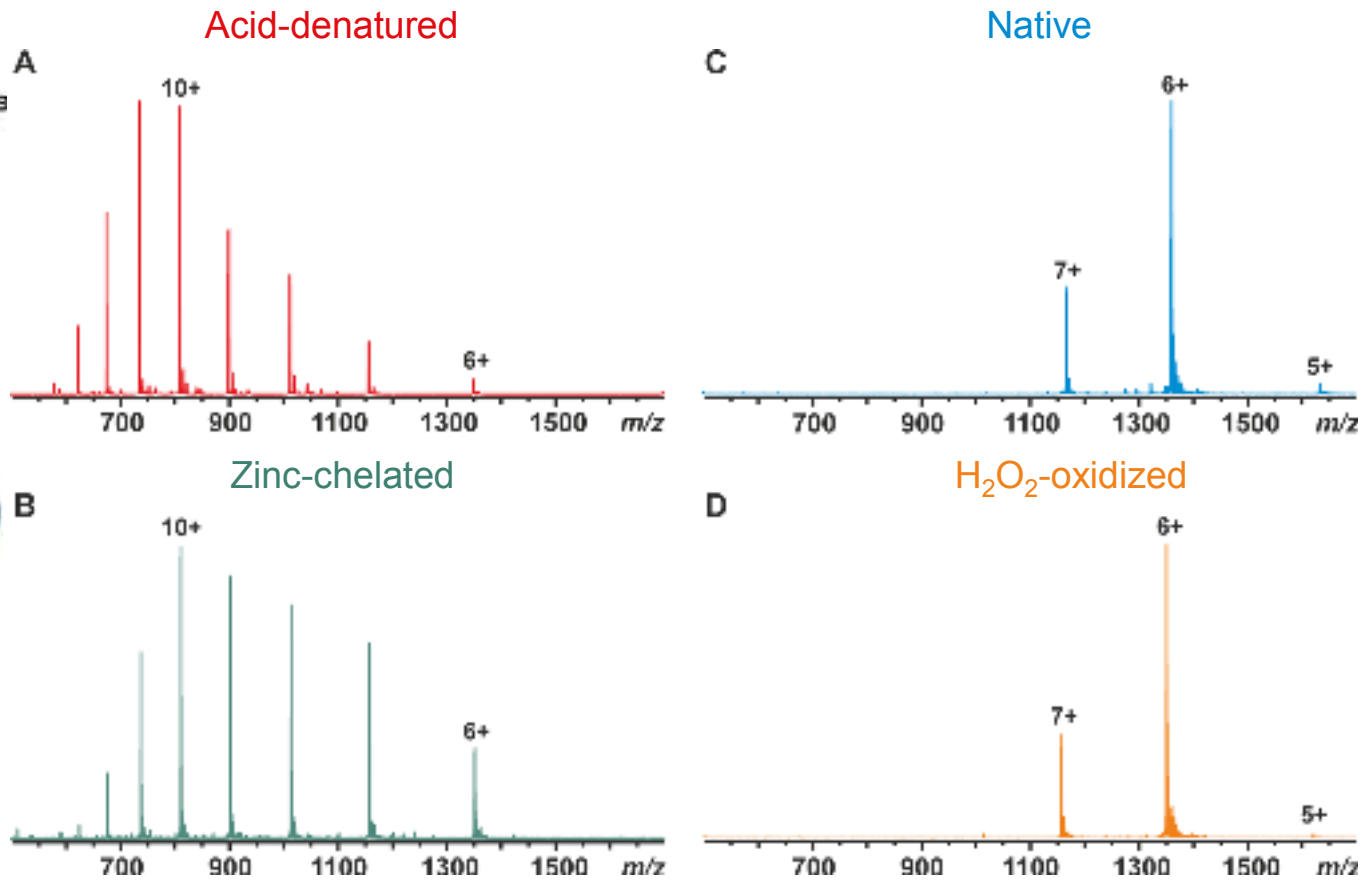

Laitaoja M, et al. *Protein Sci.* **2016**, 25: 572-586.

EU FT-ICR MS

Metalloproteins: ESI FT-ICR MS of SAP30L

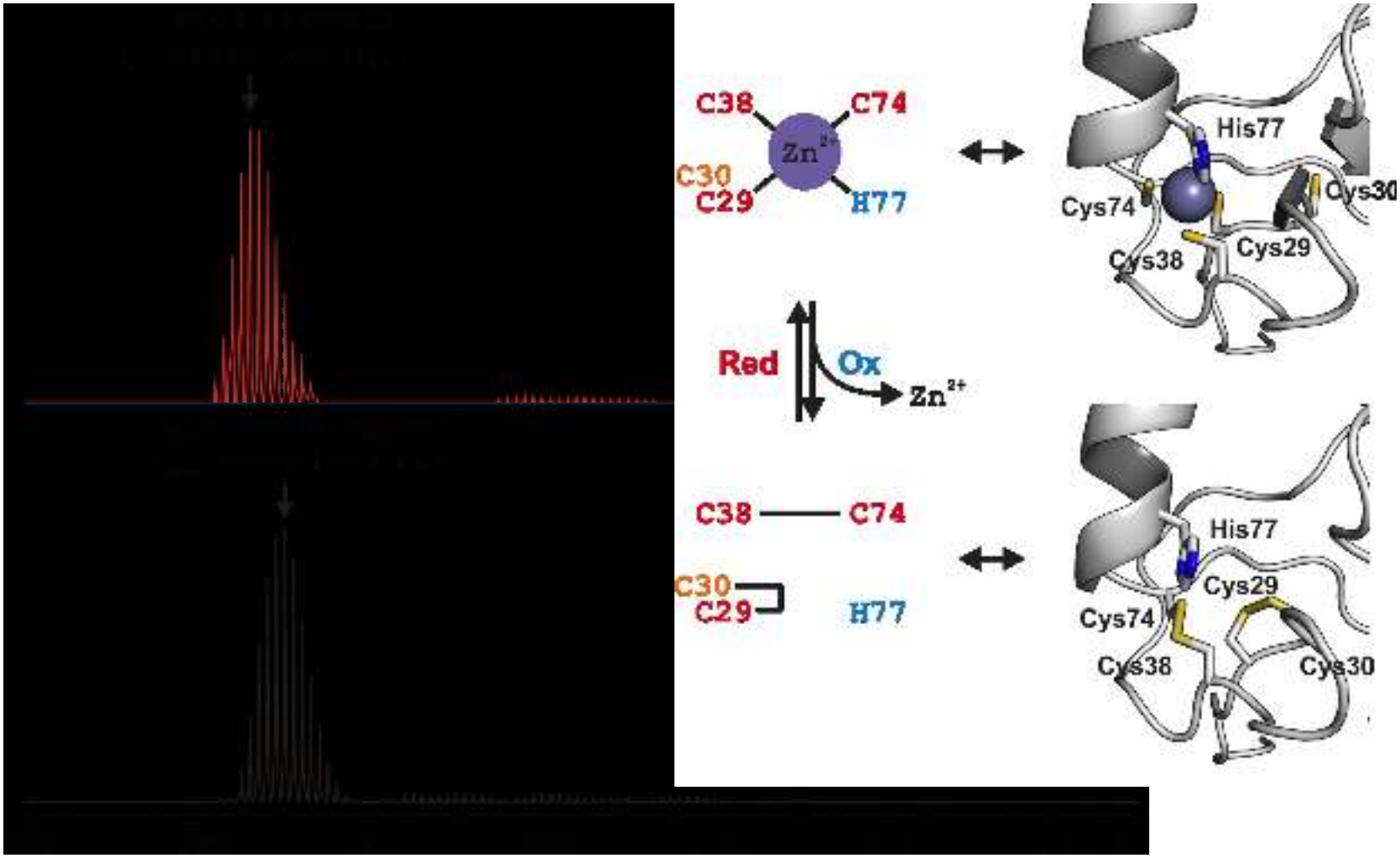

Laitaoja M, et al. *Protein Sci.* **2016**, 25: 572-586.

Metalloproteins: rabbit liver metallothionein

Desalted rabbit liver extract MT-Zn_7 measured in 20 mM NH_4AOc (pH 7) + 20 mM DTT shows broad peak distribution of several overlapping species

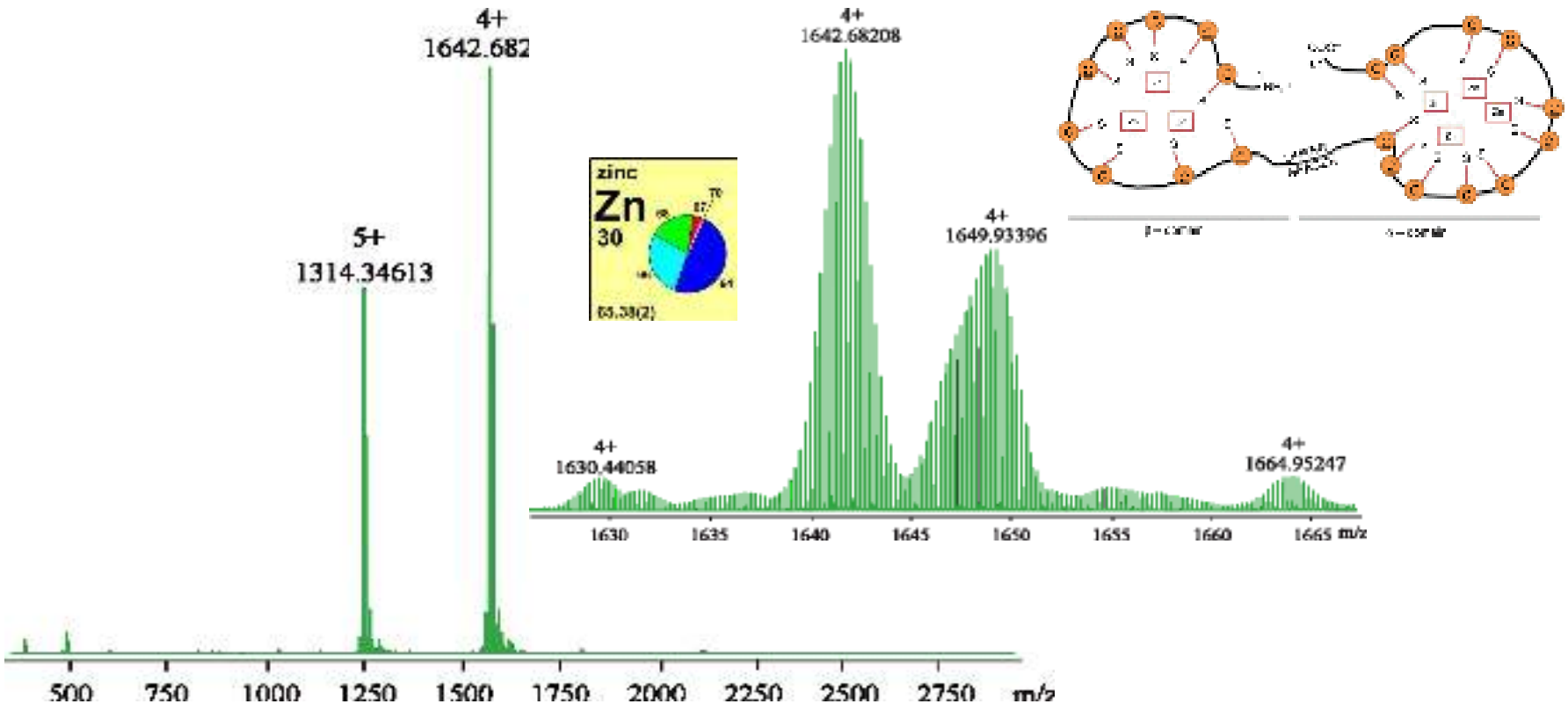

Metalloproteins: rabbit liver metallothionein

Fully demetallated (1 mM 1,10-FEN) rabbit MT shows presence of 9 different proteoforms!

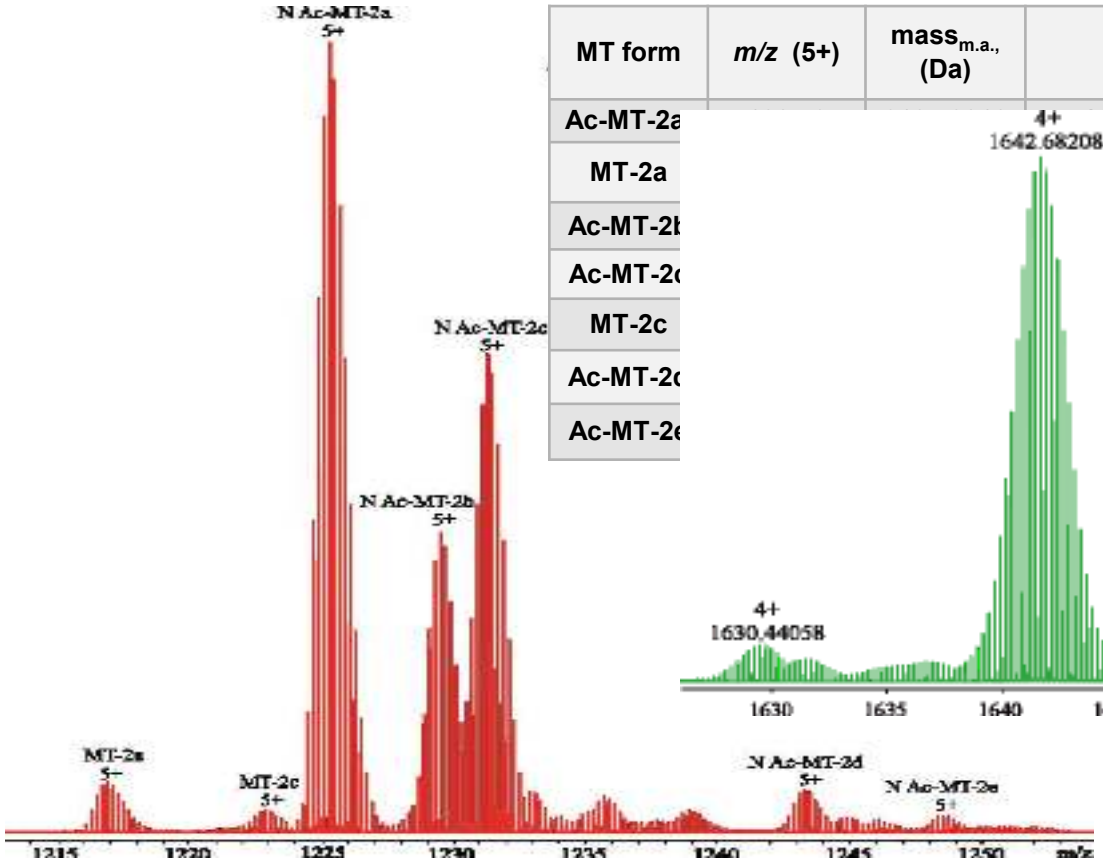

MT form	*m/z* (5+)	$mass_{m.a.,}$ (Da)	Amino acid Composition	Molecular Formula
Ac-MT-2a				$_{32}N_{72}O_{84}S_{21}$
MT-2a				$_{30}N_{72}O_{83}S_{21}$
Ac-MT-2b				$_{35}N_{71}O_{86}S_{21}$
Ac-MT-2c				$_{34}N_{72}O_{85}S_{21}$
MT-2c				$_{32}N_{72}O_{84}S_{21}$
Ac-MT-2d				$_{92}N_{74}O_{85}S_{21}$
Ac-MT-2e				$_{98}N_{74}O_{84}S_{21}$

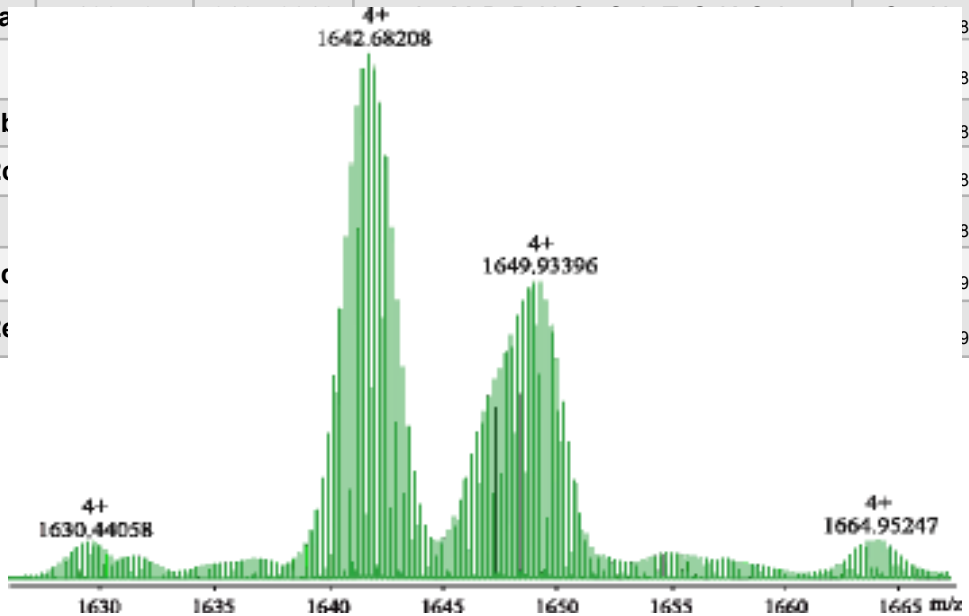

Manuscript in preparation

Protein–ligand interactions: Bidning affinity by ESI-MS

- Example: Determination of binding constants for antibody fragment–trisaccharide complexes by direct ESI-MS analysis

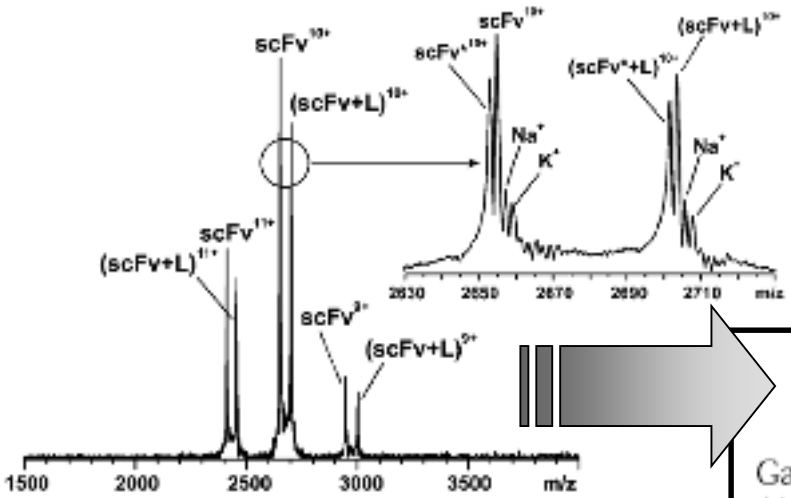

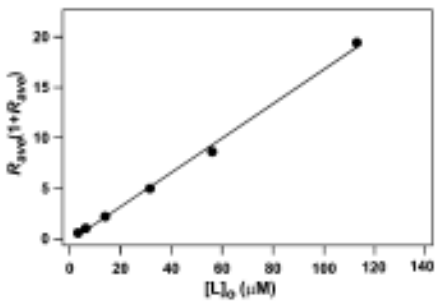

$$K_{assoc} = \frac{[PL]_{equil}}{[P]_{equil}[L]_{equil}} = \frac{R}{[L]_{equil}} = \frac{R(1+R)}{[P]_0}$$

$$R = \frac{[PL]_{equil}}{[P]_{equil}} = \frac{\sum_n (I_{[PL]_n^{z+}}/n)}{\sum_n (I_{[P]_n^{z+}}/n)}$$

ligand	$K_{assoc} \times 10^{-5}$ M^{-1} (MS)	$K_{assoc} \times 10^{-5}$ M^{-1} (ITC)[a]
Galα[Abe]Man	1.70 ± 0.05	1.6 ± 0.2
Abe(2-O–CH_3–Man)	1.50 ± 0.20	1.43 ± 0.05
Glcβ[Abe]Man	0.15 ± 0.04	0.30 ± 0.14
GlcGlcGalα[Abe]Man	5.30 ± 0.50	3.81 ± 0.13

Good agreement between ESI-MS (gas-phase) and ITC (solution)!

W. Wang, E.N. Kitova and J.S. Klassen. *Methods Enzymol.* **2003**, 362

Protein–ligand interactions: Bidning affinity by ESI-MS

Ligand binding preference and cross-reactivity of anti-thyroxine antibody Fab fragment

T4

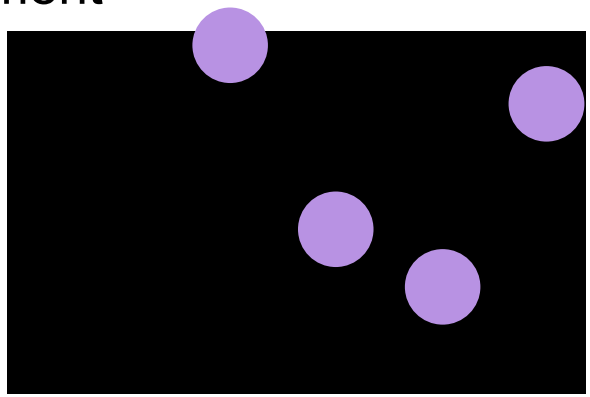

T2

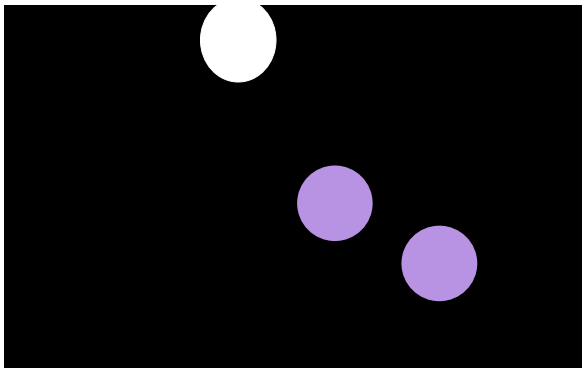

T3

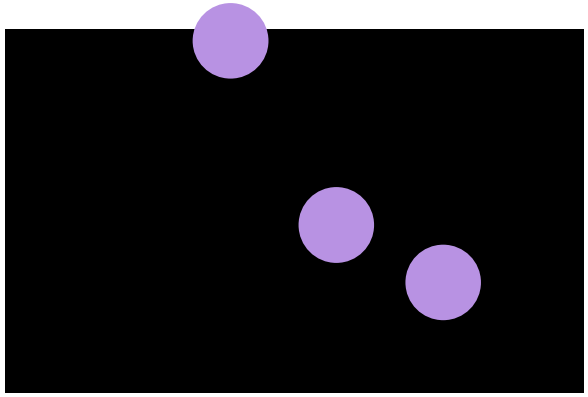

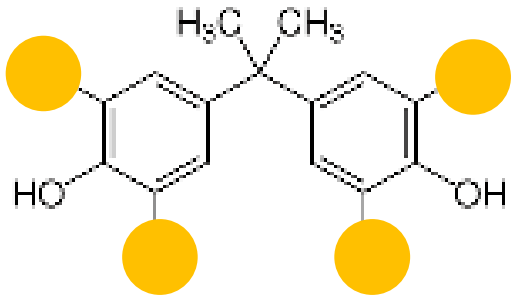

Bisphenols

TXB,
X = Cl, Br, I

Thangaraj S *et al* Quantitation of thyroid hormone binding to anti-thyroxine antibody Fab fragment by native mass spectrometry. *ACS Omega* 4 (2019) 18718-18724.

Protein–ligand interactions: Bidning affinity by ESI-MS

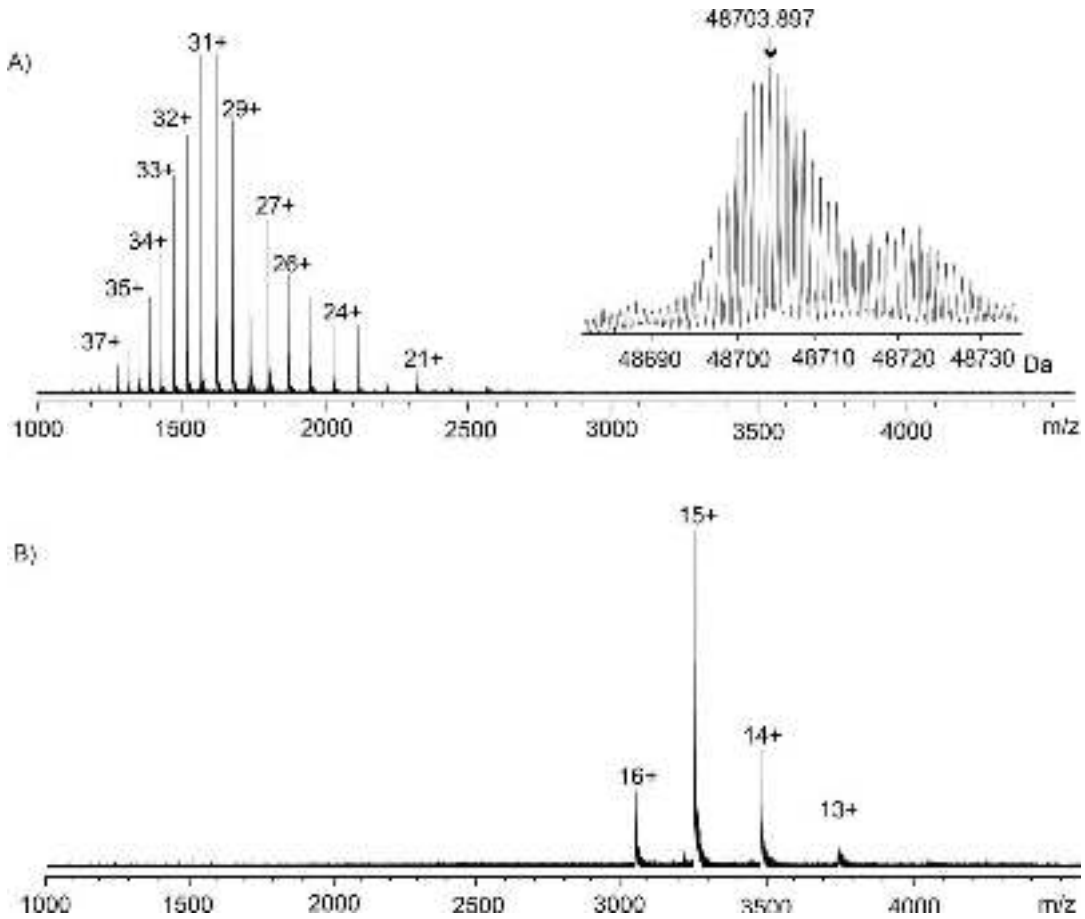

Thangaraj S *et al* Quantitation of thyroid hormone binding to anti-thyroxine antibody Fab fragment by native mass spectrometry. *ACS Omega* 4 (2019) 18718-18724.

EU FT-ICR MS

Protein–ligand interactions: Anti-T4 Fab fragment

Direct ligand titration of anti-thyroxine antibody Fab fragment with 3,3'-diodo-L-thyronine (T2) – *a reference ligand*

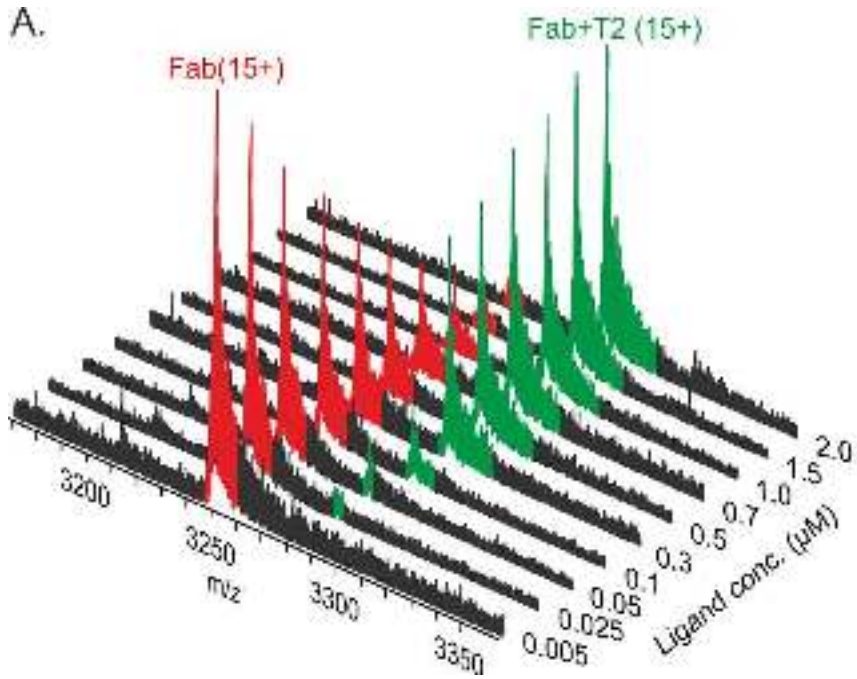

Thangaraj S *et al* Quantitation of thyroid hormone binding to anti-thyroxine antibody Fab fragment by native mass spectrometry. *ACS Omega* 4 (2019) 18718-18724.

Protein–ligand interactions: Anti-T4 Fab fragment

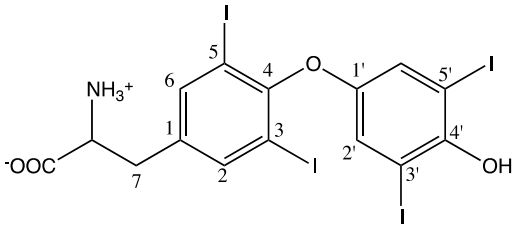

Thyroxine (T4)

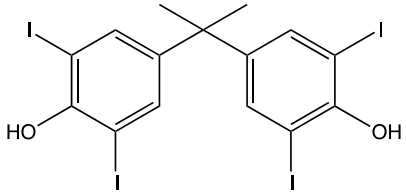

Tetraiodobisphenol A

Ligand competition experiments

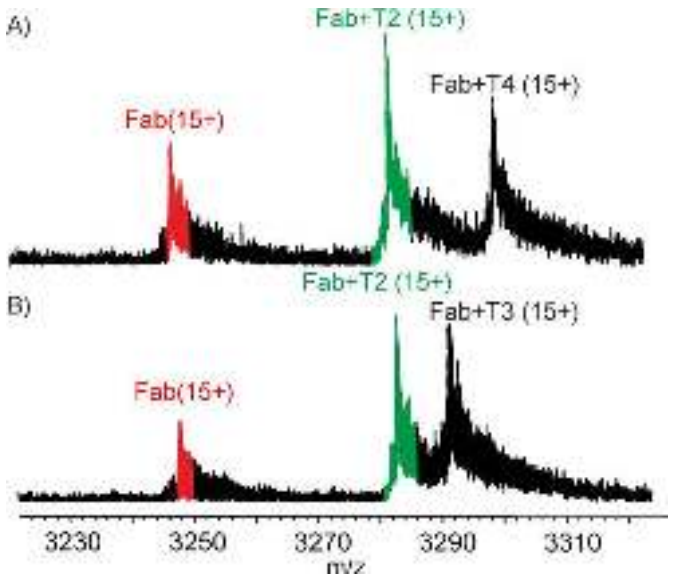

Ligand	Ligand conc. (μM)	Ref. ligand (T_2) conc. (μM)	K_d (nM)
T_4	0.07	0.5	29 ± 4
T_3	0.05	0.5	3.4 ± 0.7
T_2	0.005 to 2.0	–	260 ± 20
T_0	12	0.07	130000 ± 10000
TIB	0.1	0.7	11 ± 1
TBB	0.5	1.2	87 ± 5
TCB	10	0.4	7800 ± 500

Thangaraj S *et al* Quantitation of thyroid hormone binding to anti-thyroxine antibody Fab fragment by native mass spectrometry. *ACS Omega* 4 (2019) 18718-18724.

Transient homodimerization – β-lactoglobulin (Bos d 5)

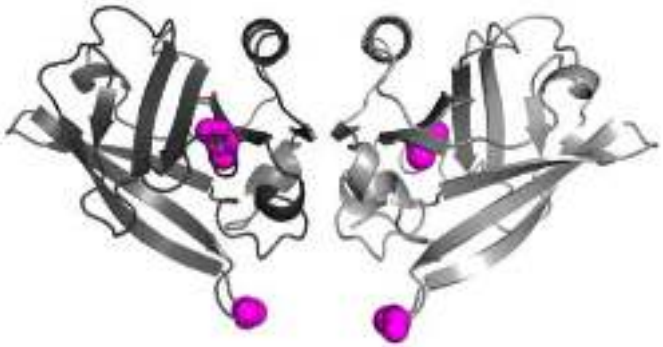

BLG dimer (X-ray structure)

Native-MS of bovine beta-lactoglobulin at two concentrations: blue = monomer, red = dimer

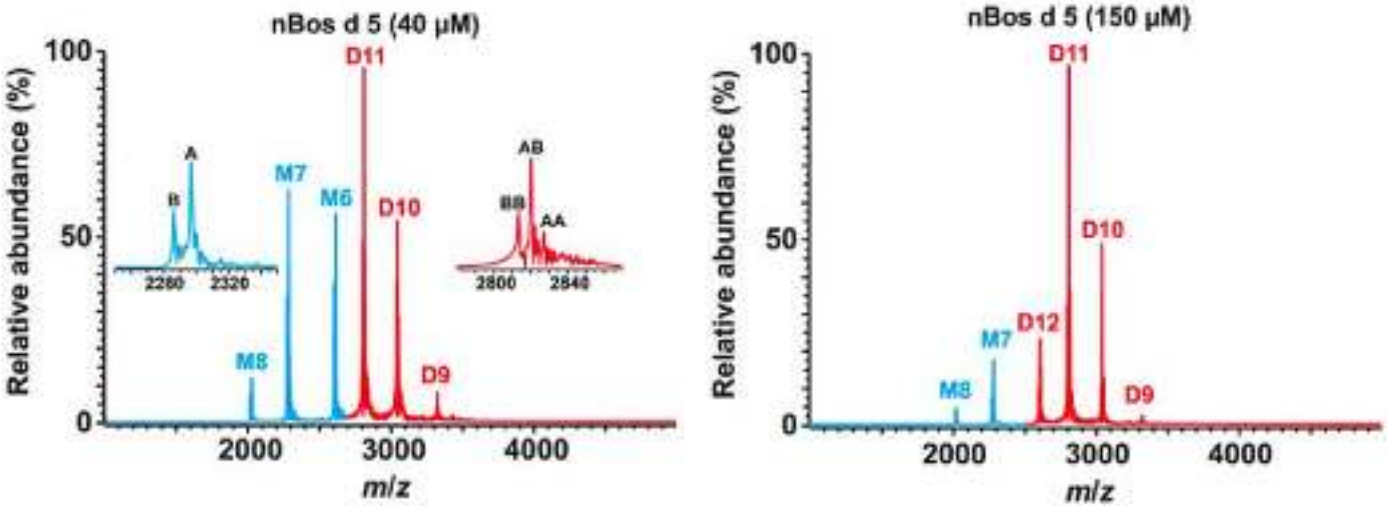

Rouvinen, J., Jänis J., et al. *PLoS ONE* 5 (**2010**) e9037.

Transient oligomerization – zebrafish avidin

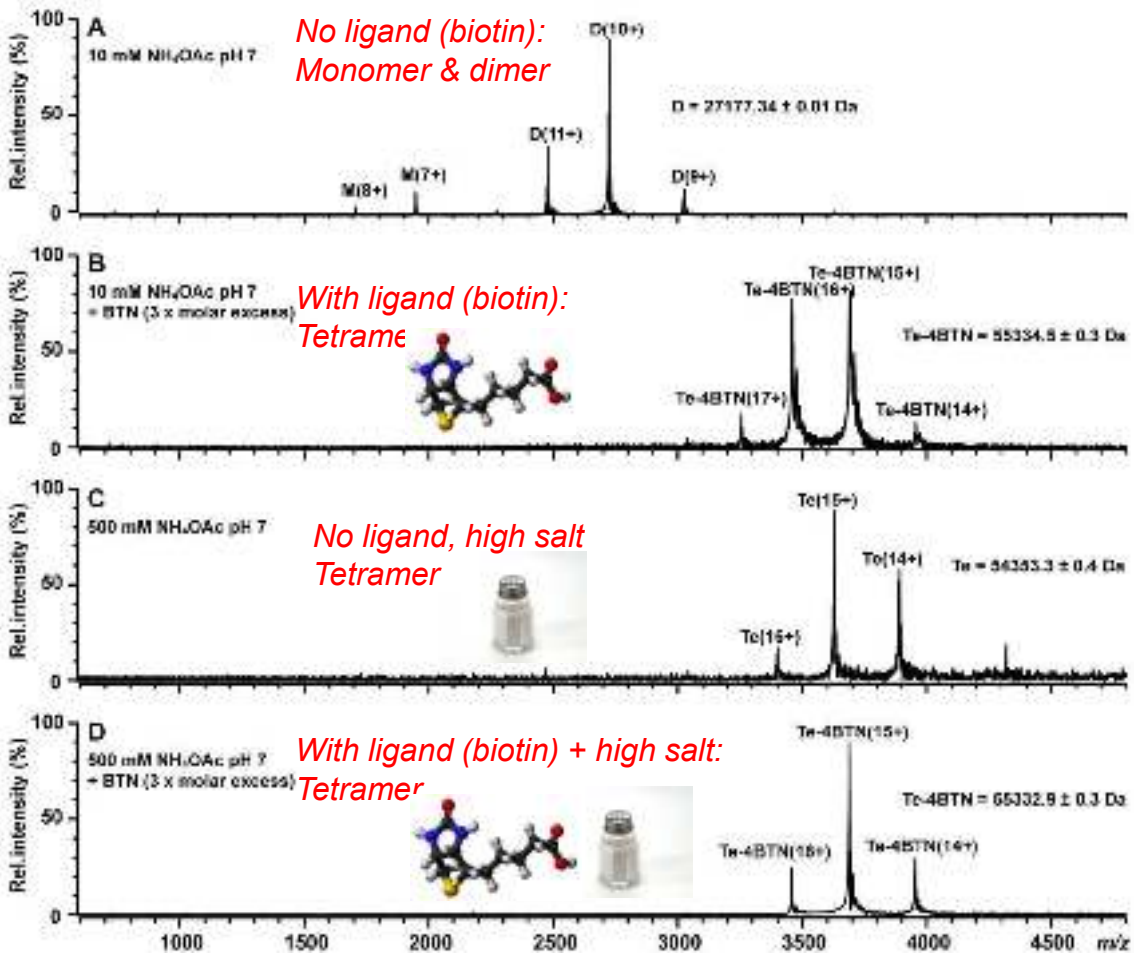

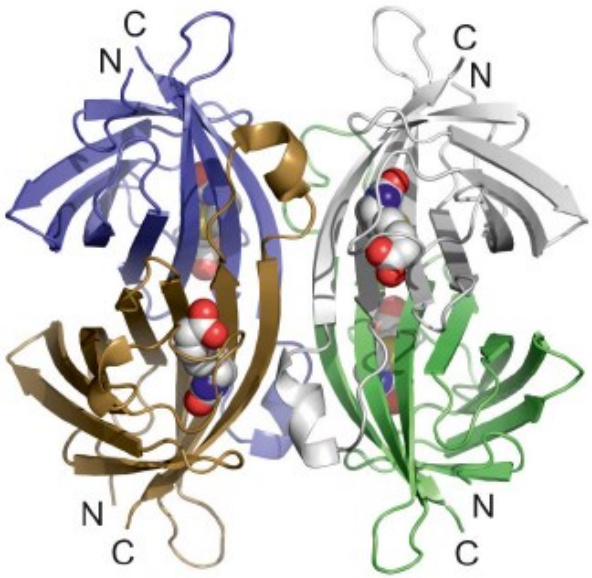

X-ray structure of zebavidin tetramer (PDB entry 2UYW)

Taskinen B., et al. *PLoS ONE* 8 (**2013**) e77207.

Transient oligomerization – hydrophobin

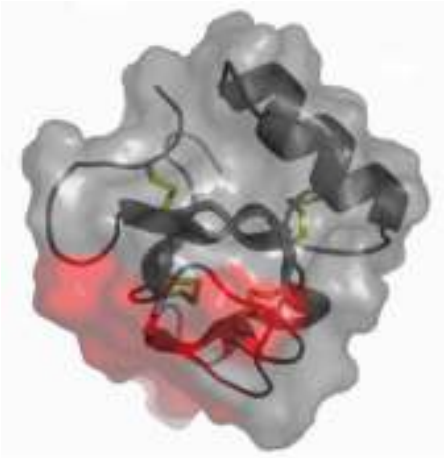

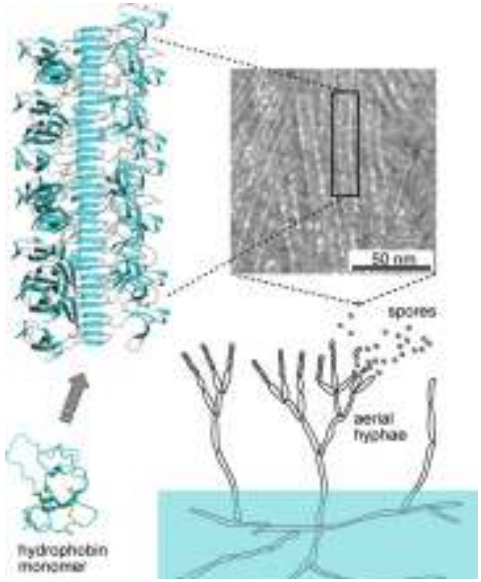

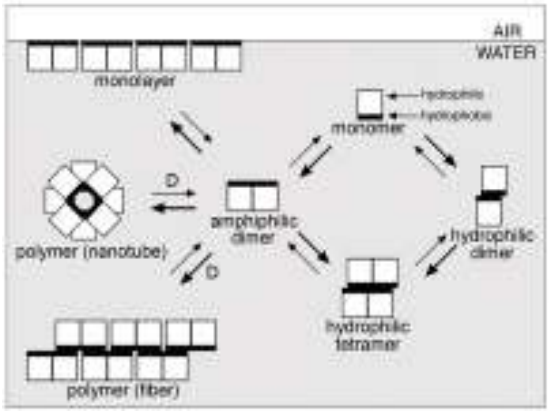

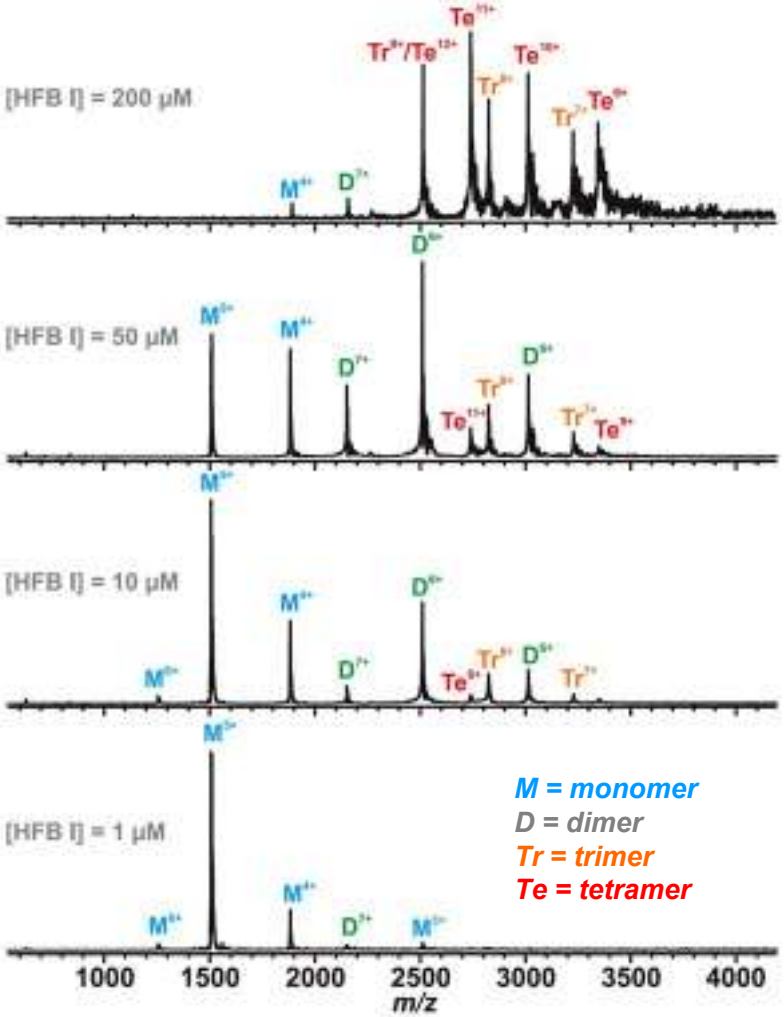

Kallio JM *et al.*, *Chem. Commun.* **2011**, 47, 9843-9845

Larger protein complexes with native ESI FT-ICR MS

Native MS of light-sensitive plant phytochrome

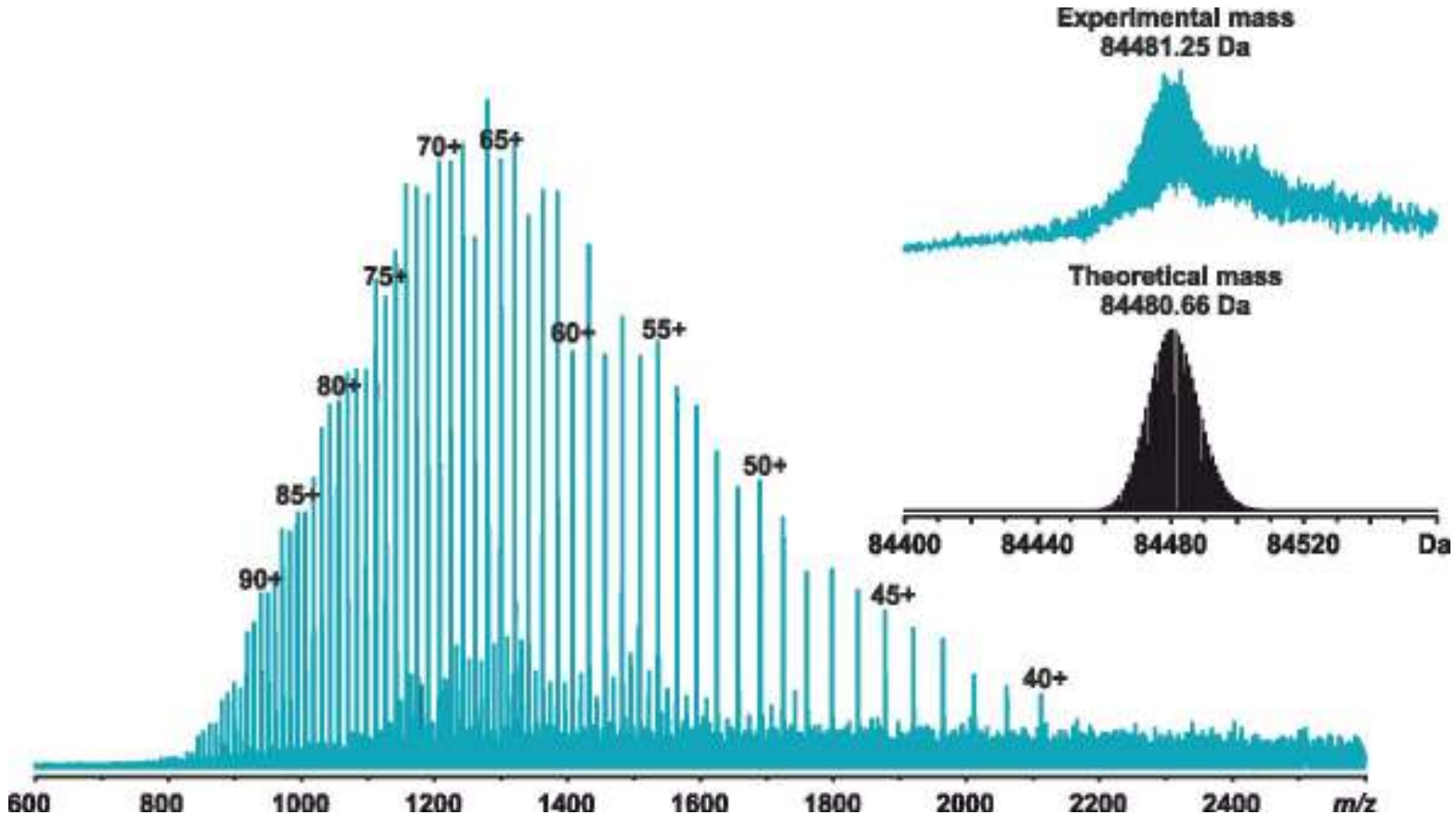

Larger protein complexes with native ESI FT-ICR MS

Native MS of light-sensitive plant phytochrome

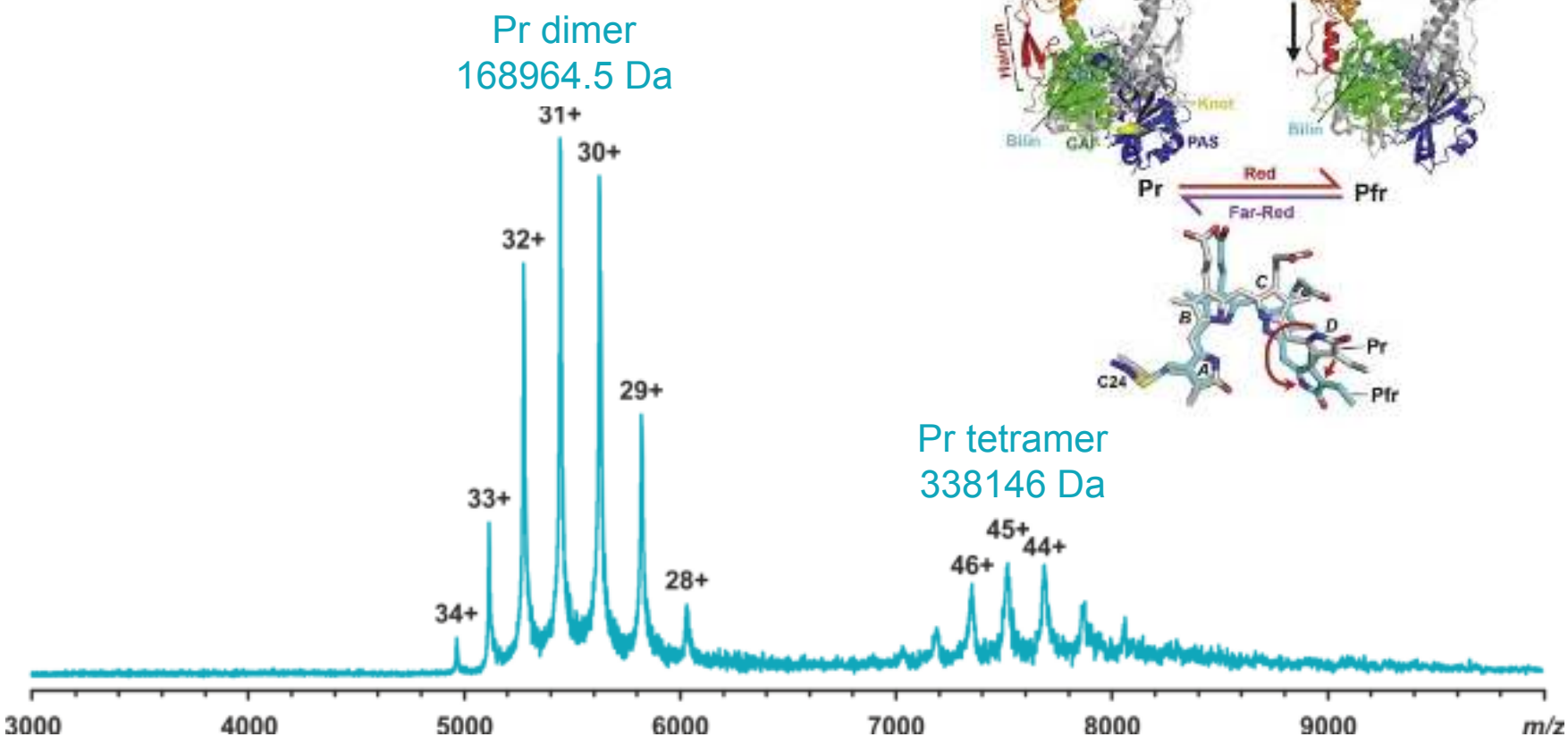

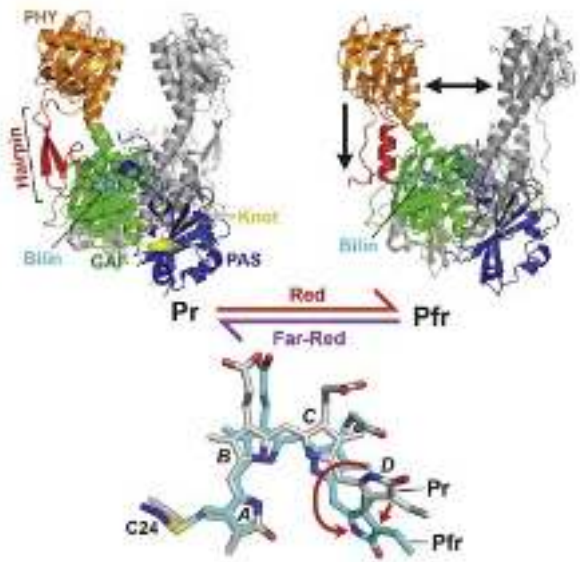

Largest macromolecular complexes with native ESI FT-ICR MS

nature chemistry
ARTICLES
PUBLISHED ONLINE: 1 JANUARY 2018 | DOI: 10.1038/NCHEM.2908

An integrated native mass spectrometry and top-down proteomics method that connects sequence to structure and function of macromolecular complexes

Huilin Li[1]*, Hong Hanh Nguyen[1], Rachel R. Ogorzalek Loo[2], Iain D. G. Campuzano[1] and Joseph A. Loo[1,2]*

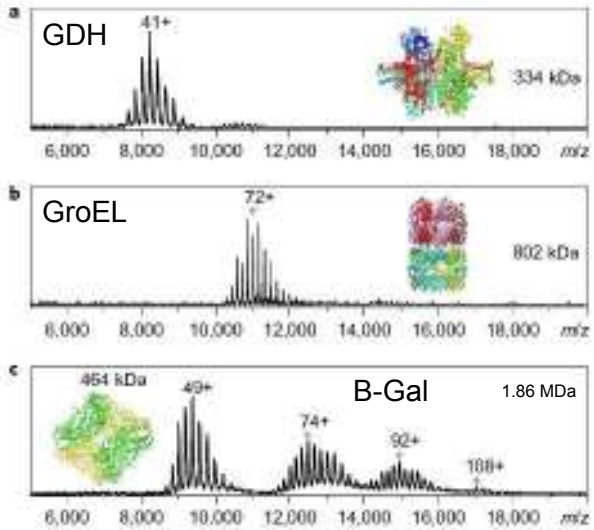

$m_{critical} = 1.20607 \times 10^7\, zB^2d^2/(V_{trap}\alpha)$

Since B = 15 T, a = 0.06 m, α = 2.8404, for V_{trap} = 1.0 V, $m_{critical}$ ~3.43 MDa (If z_{CRM} = 144, ion is detected at m/z 24,000)

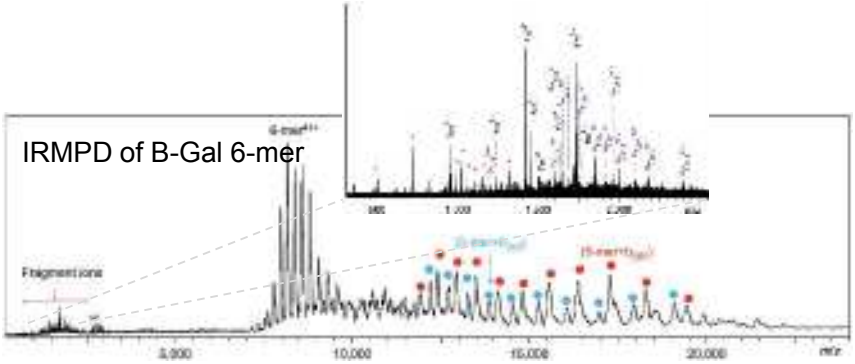

Combining ion mobility with native MS

Native TIMS-TOF bovine b-lactoglobulin

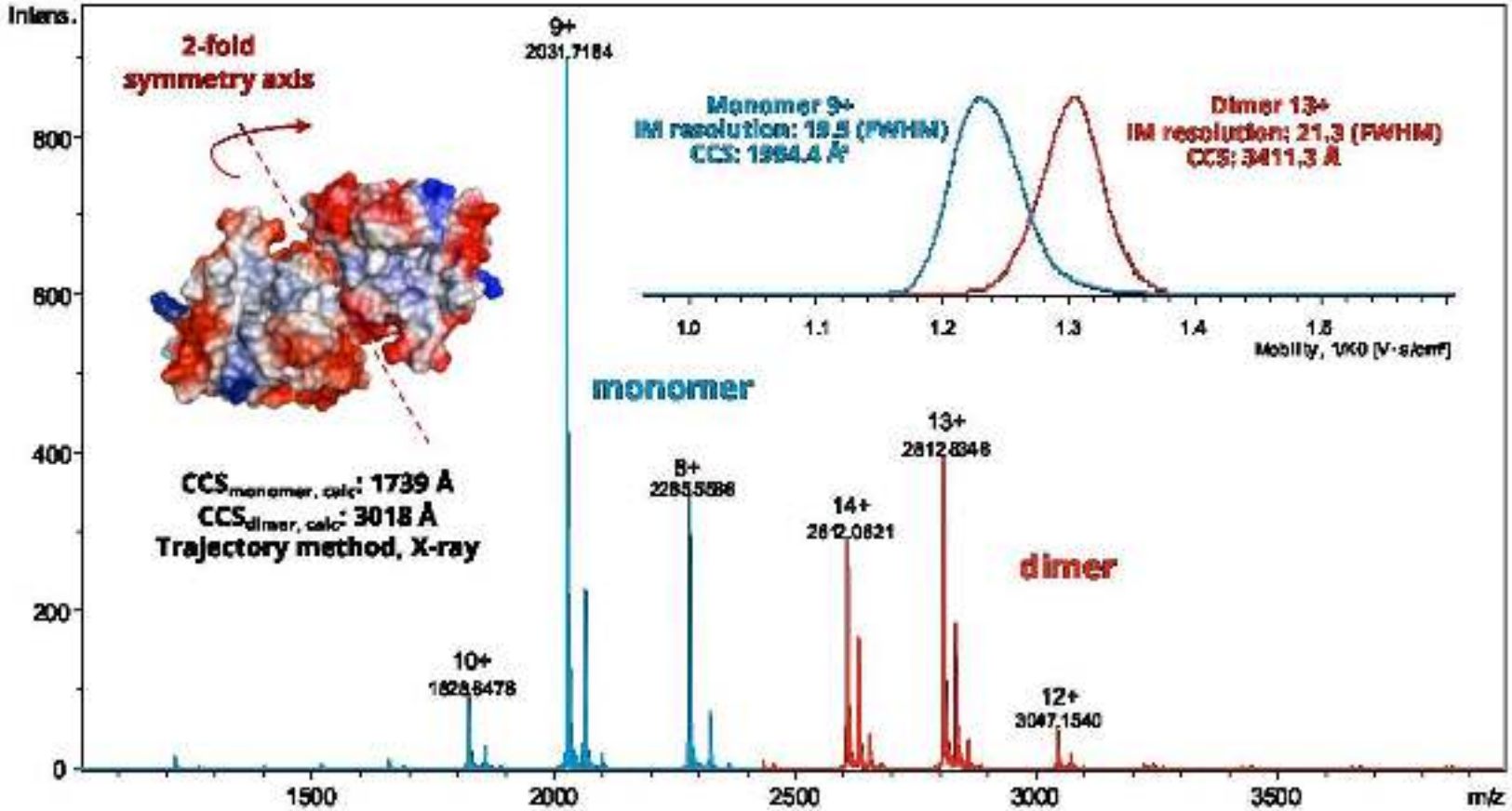

Unpublished results

Combining ion mobility with native MS

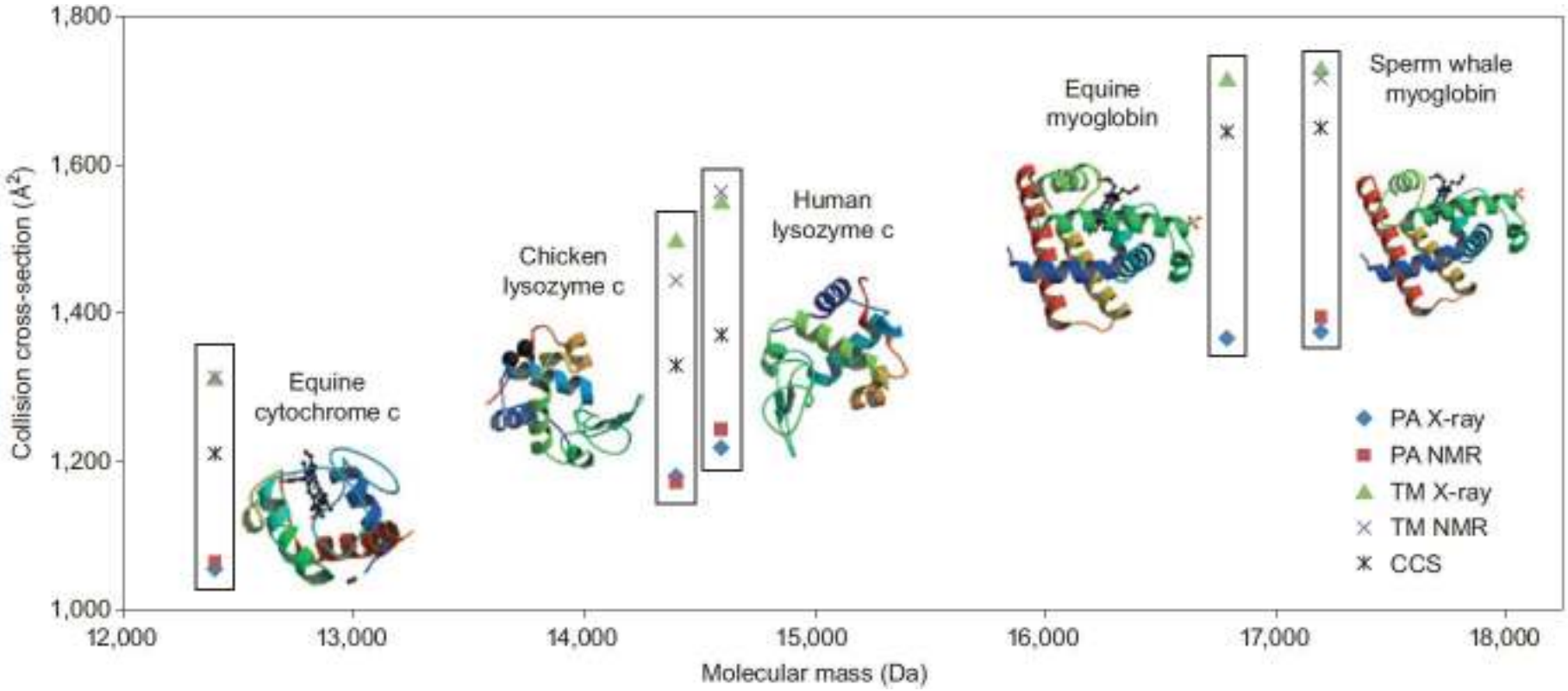

Lanucara F *et al.* The power of ion mobility-mass spectrometry for structural characterization and the study of conformational dynamics, *Nature Chem* **2014**, 6: 281–294

How to perform native MS?

- Important considerations
  - Volatile buffers only (1-1000 mM ammonium acetate or ammonium bicarbonate, pH by formic/acetic acid or ammonia)
  - Extensive desalting and detergent removal needed
  - Fine tuning of instrument parameters to avoid unfolding/complex dissociation and to maintain efficient desolvation, on the other hand
  - Designing experiments: appropriate protein/ligand concentrations

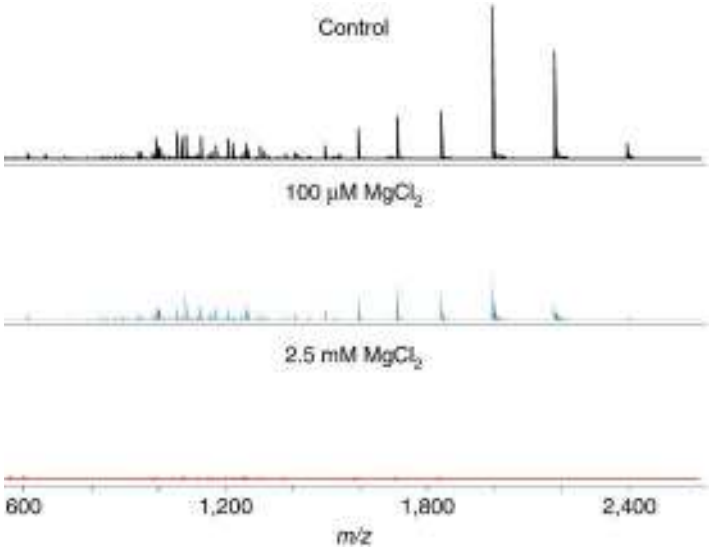

EU FT-ICR MS

Native MS on Bruker Solarix FT-ICR instrument

solarix

Critical parameters to tune
- Transfer optics RF frequencies & amplitudes
- Time-of-flight (P2)

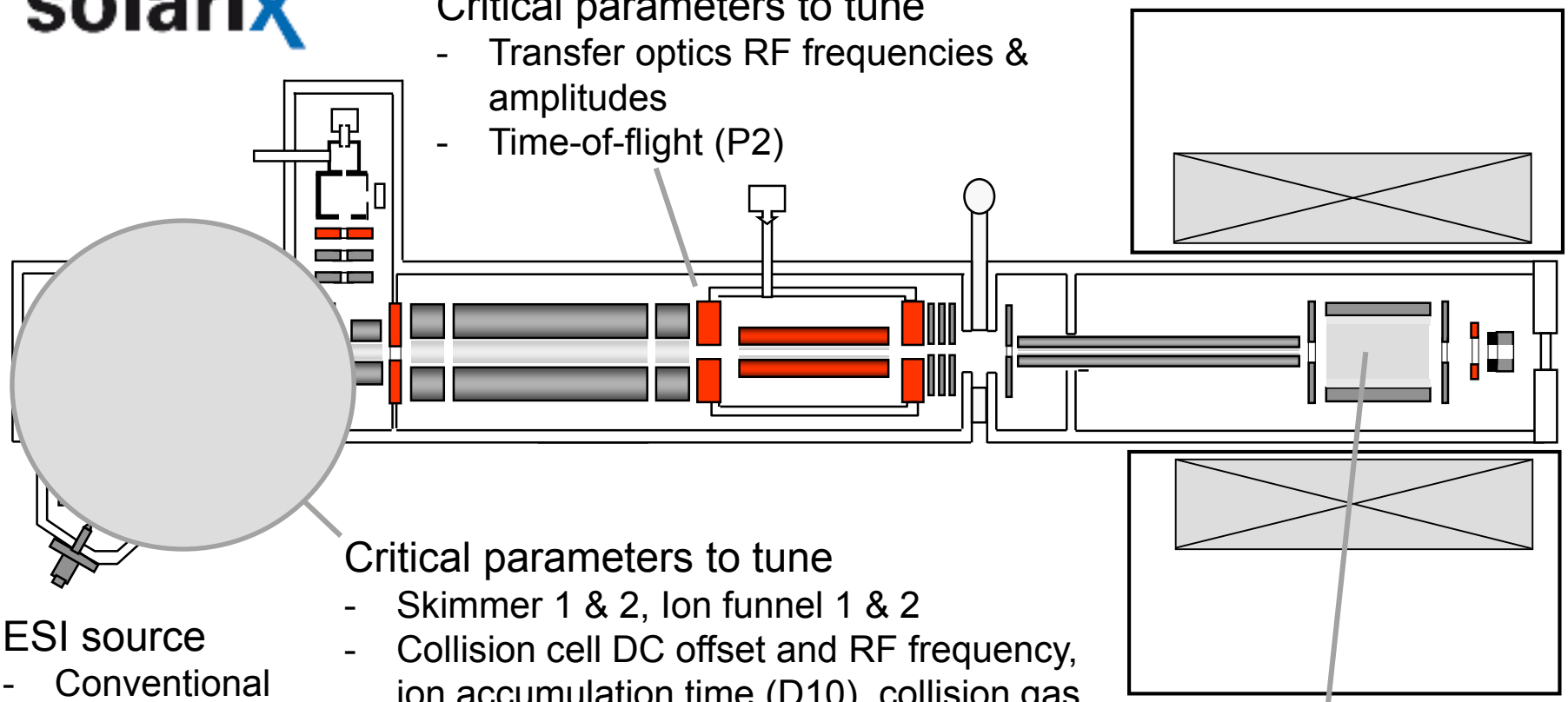

ESI source
- Conventional
- NanoESI
- Microchip

Critical parameters to tune
- Skimmer 1 & 2, Ion funnel 1 & 2
- Collision cell DC offset and RF frequency, ion accumulation time (D10), collision gas
- Drying gas temperature & pressures
- Capillary exit

Critical parameters to tune
- Trapping voltage
- Excitation power

EU FT-ICR MS

Agreement between solution and gas-phase?

THE JOURNAL OF PHYSICAL CHEMISTRY B

ARTICLE

pubs.acs.org/JPCB

Structural Stability from Solution to the Gas Phase: Native Solution Structure of Ubiquitin Survives Analysis in a Solvent-Free Ion Mobility–Mass Spectrometry Environment

Thomas Wyttenbach and Michael T. Bowers*

Department of Chemistry and Biochemistry, University of California Santa Barbara, Santa Barbara, California 93106, United States

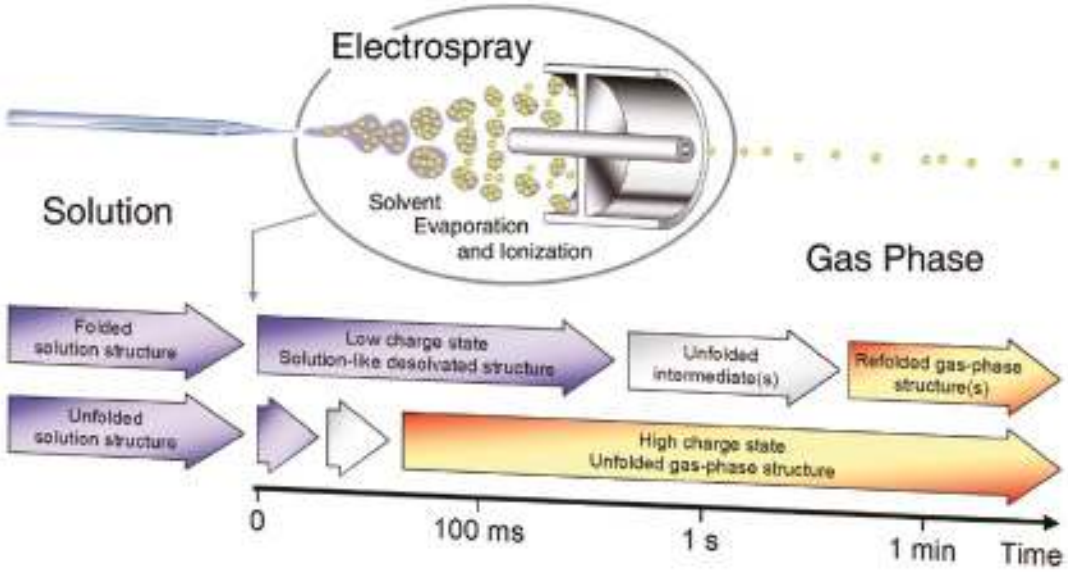

Wyttenbach & Bowers, *J. Phys. Chem. B* **2011**, 115, 12266–12275

European Union
European Regional Development Fund

BF
Biocenter Finland

bck

EU FT-ICR MS

HORIZON 2020

EU FT-ICR MS

The info in this presentation reflects the views only of the author, and the Commission cannot be held responsible for any use which may be made of the info contained therein.

This project has received funding from the European Union's Horizon 2020 research and innovation programme under grant agreement No 731077

Wednesday

(short)

EU FT-ICR MS

Acylation dictates the extent of activation of bacterial RTX toxins

David Jurnečka

Bordetella pertussis

- exclusively human pathogen and the causative agent of whooping cough
- one of the world least controlled vaccine-preventable diseases
- accounting for more than 40 million cases and close to 200,000 deaths every year
- severe symptoms are common in young unvaccinated infants
- whole-cell vaccine introduced in 1950s
- exchanged by acellular vaccine in most of the developed countries in early 2000s
    - associated with waning immunity of vaccinated individuals linked to pertussis resurgence
    - contains up to 5 purified antigens

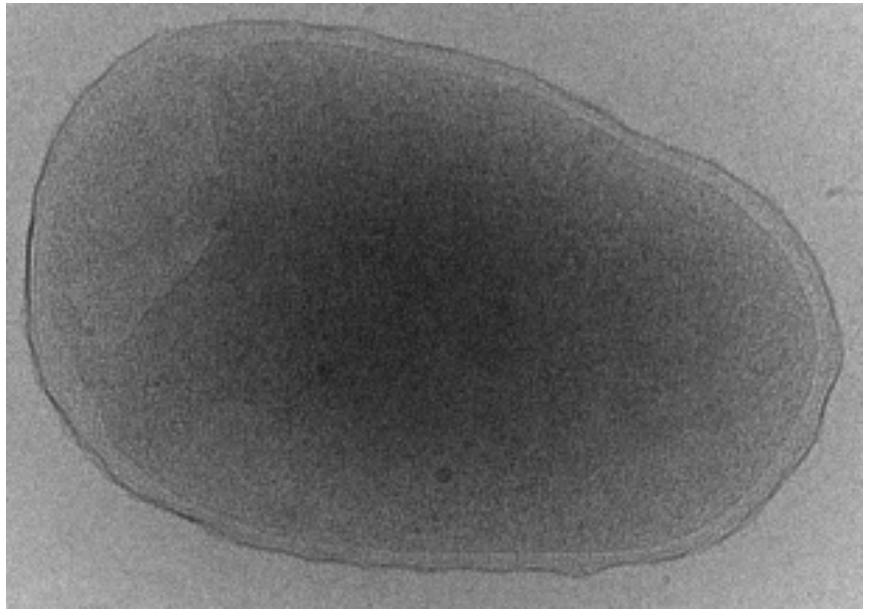

(SEM-Benada O., TEM-Nováček J.)

Virulence factors of *Bordetellae*

Adhesins/Autotransporters
Filamentous hemagglutinin (FHA)
Fimbriae (Fim2, Fim3)
Pertactin
BrkA
Vag8

Toxins
Pertussis toxin (PTX)
Adenylate cyclase toxin (CyaA)
Tracheal cytotoxin (TCT)
Dermonecrotic toxin (DNT)
Endotoxin (LOS)

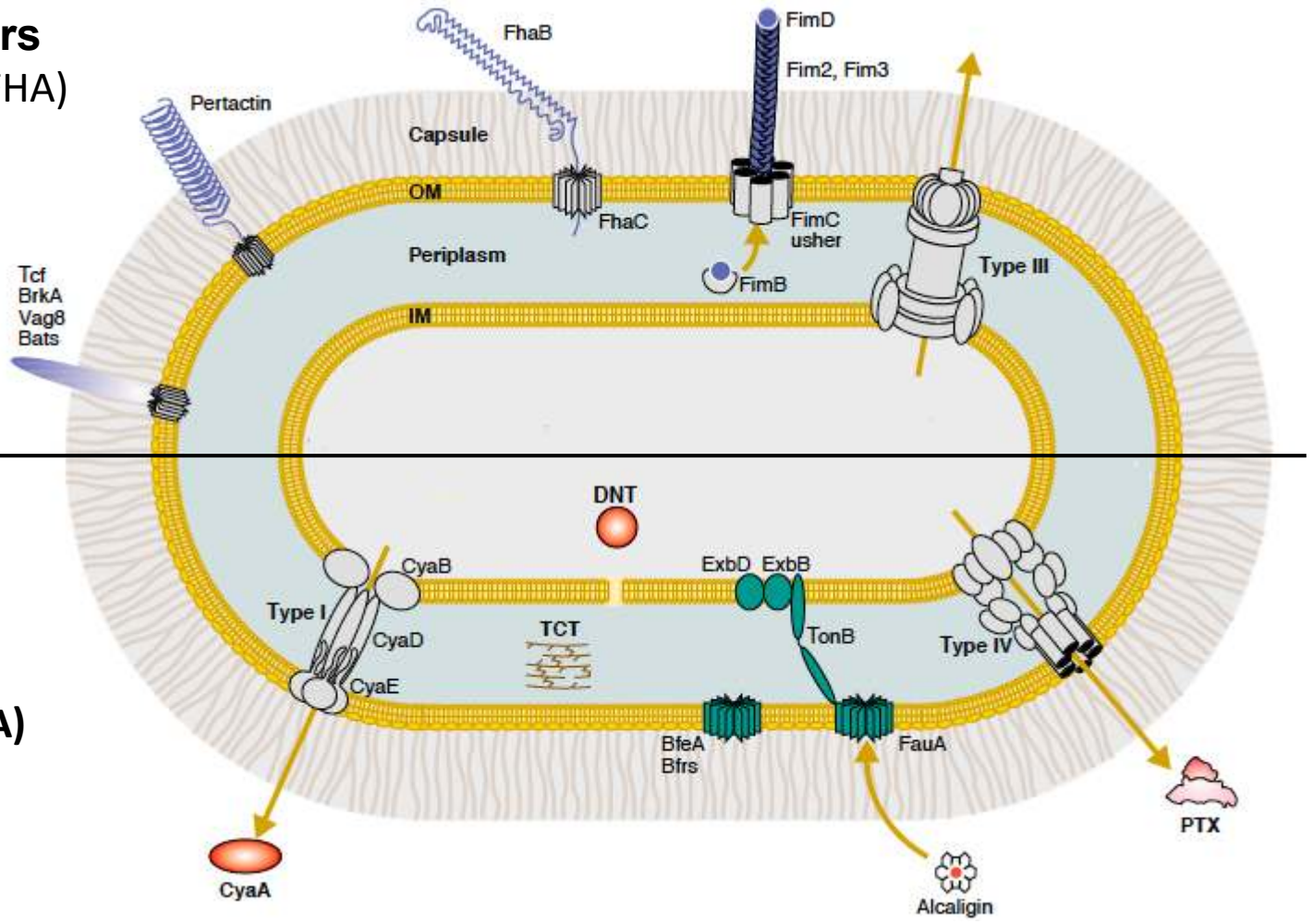

(adapted from Carrof et al, 1990)

Repeats in ToXin (RTX) cytolysins from various bacterial species

Bordetellae
CyaA

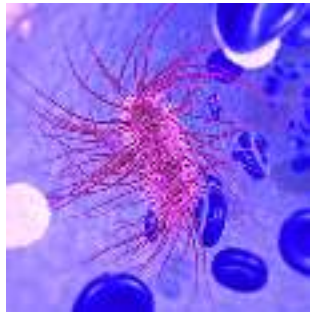

Uropathogenic *Escherichia coli*
HlyA

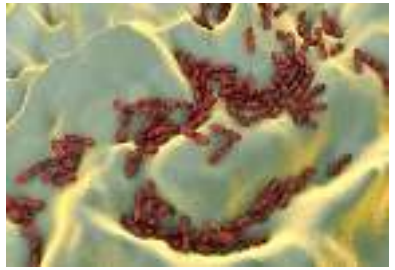

Kingella kingae
RtxA

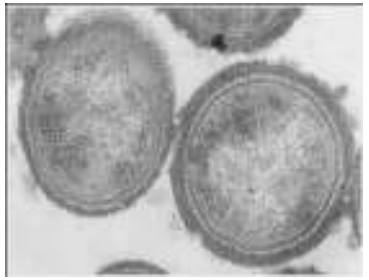

Actinobacillus pleuropneumoniae
ApxI-IVA

Vibrio, Aggregatibacter, Morganella . . .

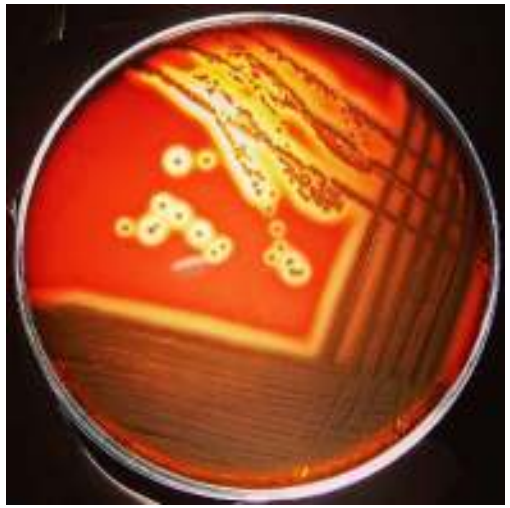

Overall characteristics of RTX toxins

```
CyaA 850-EEQRRRTKTGKSEFTTFVEIV-870 ... 973-GVATQTTAYGKRTENVQYRHV-993
HlyA 554-EEIRERRQSGKYEYITELLVK-574 ... 680-VVKEQEVSVGKRTEKTQYRSY-700
RtxA 548-TETRERVQNGKYSYINQLKFN-568 ... 679-VIKRQTTQVGKRTETLEYRDF-699
```

N-terminal pore-forming hydrophobic domain

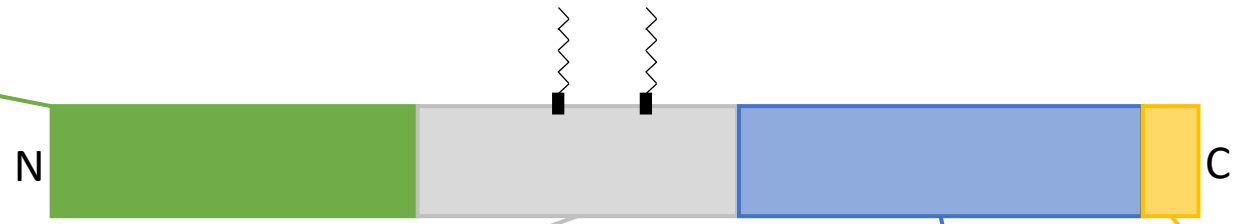

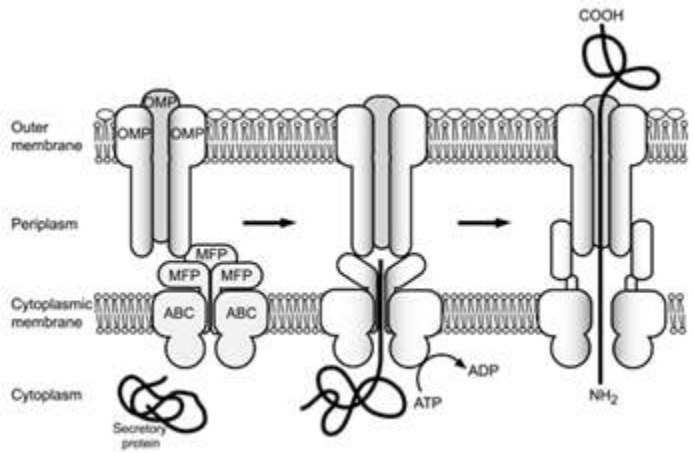

non-cleavable C-terminal secretion signal for the Type I secretion system (T1SS)

central segment harboring post-translationally acylated lysine residues activated by a cognate acyltransferase

Ca^{2+}-binding domain comprising tandem gly- and asp-rich nonapeptide repeats

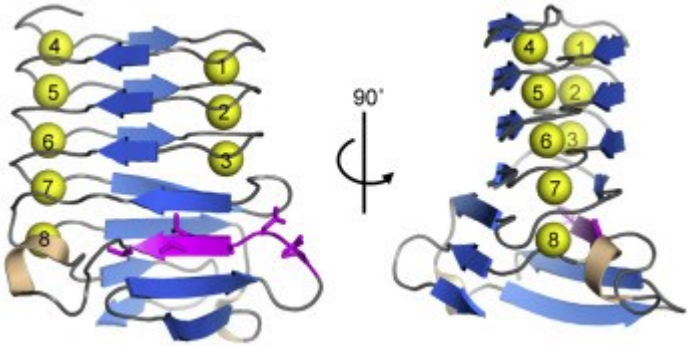

(adapted from Bumba et al., 2016; Linhartova et al., 2010)

Biological activity of RTX toxins depends on their acylation status

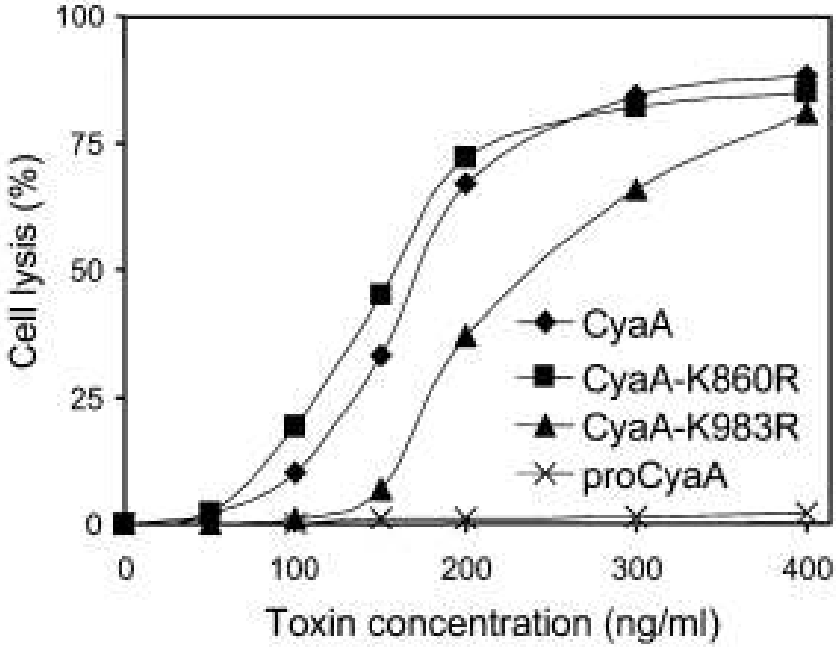

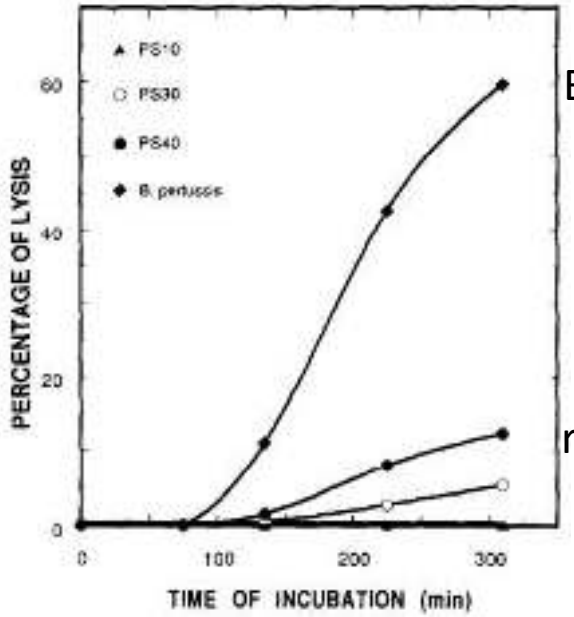

Bp CyaA-C16:0

recombinant CyaA-C16:0/C16:1

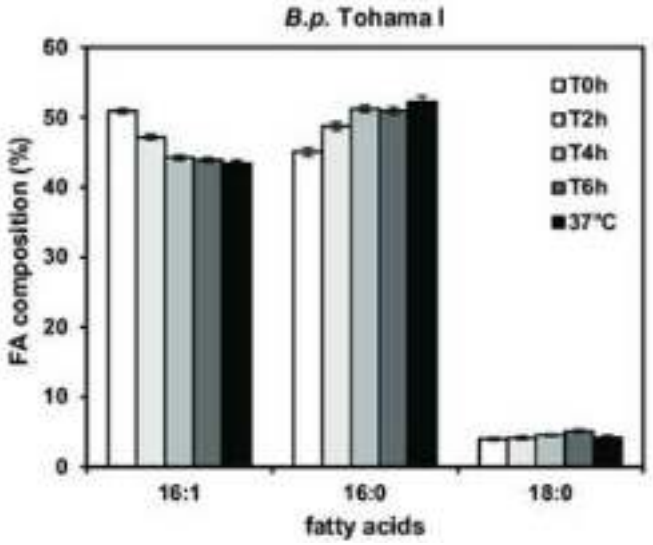

(Sebo et al., 1999; Basar et al., 2001, Masin et al. 2005)

Strategy for purification of recombinant RTX toxins

Transformed *E. coli* BL21/pMM100
cultured at 37°C in MDO medium
3h post IPTG induction

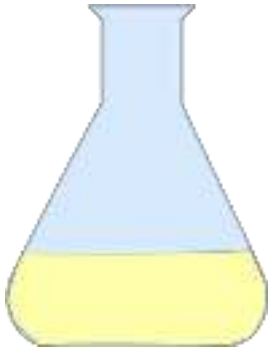

harvesting
sonication
centrifugation

The cleared urea extracts
of inclusion bodies

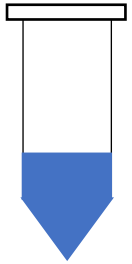

load at room temperature

Affinity chromatography - **Ni-NTA agarose**
Ion Exchange chromatography – **DEAE sepharose**

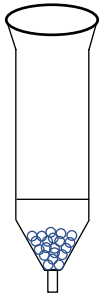

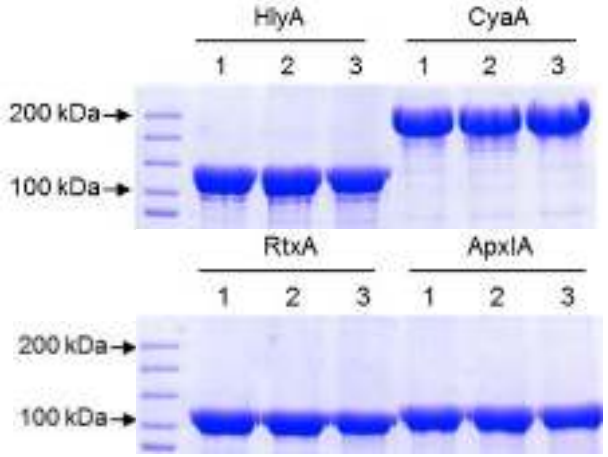

dilution in 50 mM ammonium
bicarbonate buffer (pH 8.2) to
reach 4 M urea concentration

Trypsin
30°C
12h

LC system
desalting and separation

Acylation of RtxA peptide QTTQVGKR

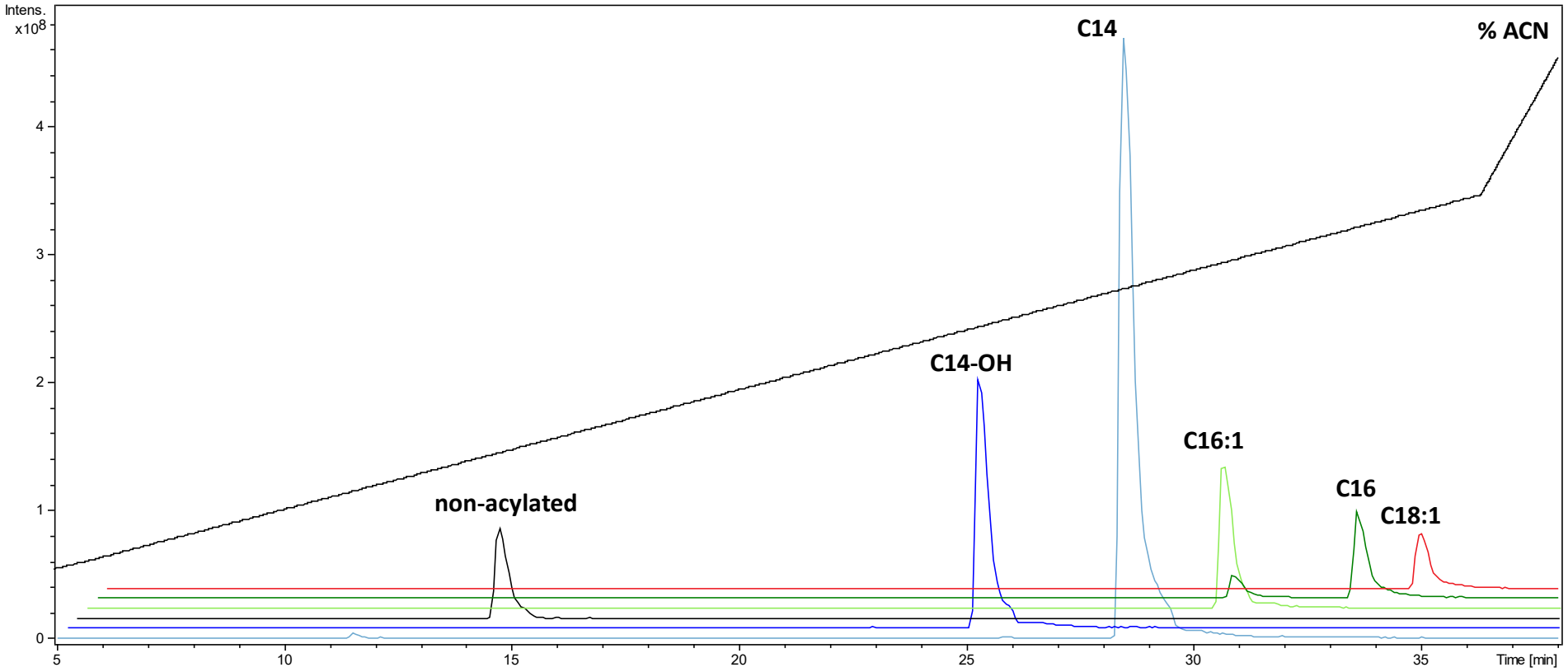

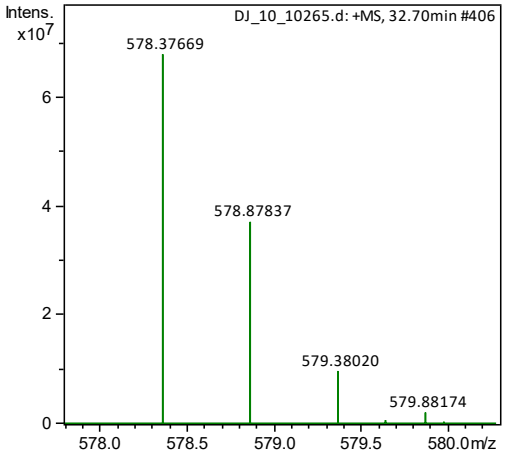

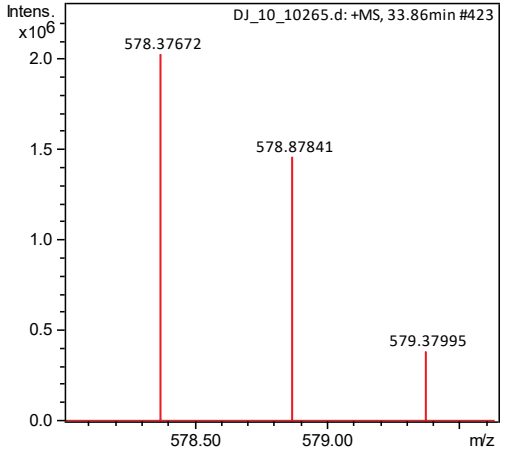

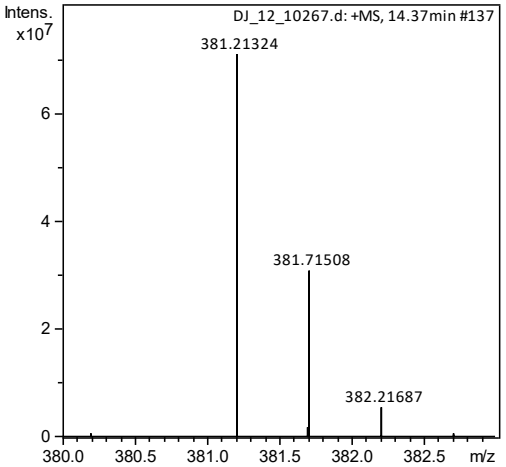

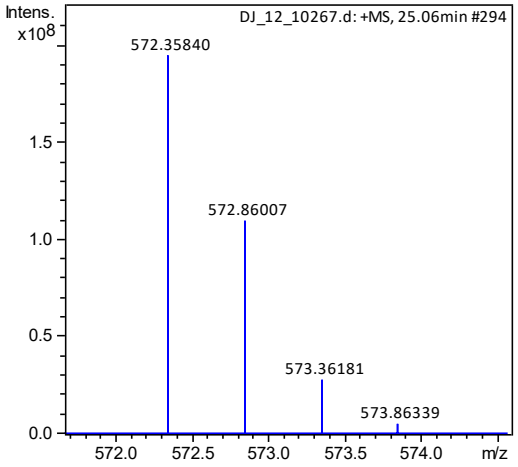

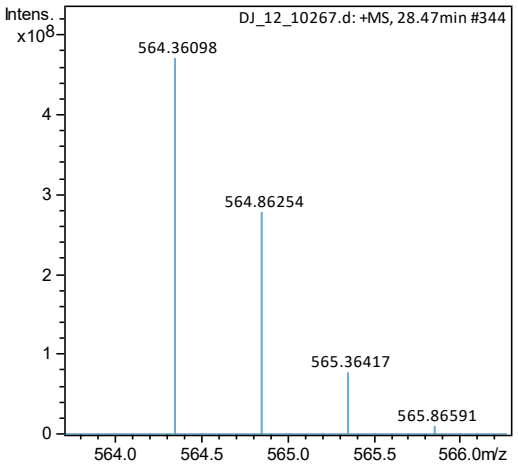

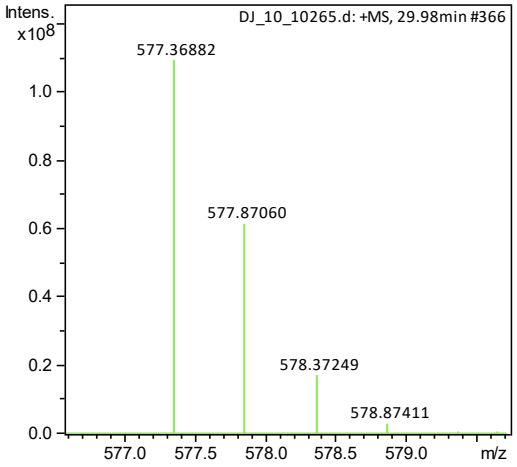

Acylation status and cytolytic activity of RTX toxins activated by cognate acyltransferases

Protein	1st Lysine	2nd Lysine
CyaA	C16:0/C16:1	C16:0/C16:1
HlyA	C14:0/C14:0-OH	C14:0/C14:0-OH
RtxA	-	C14:0/C14:0-OH
ApxIA	C14:0/C14:0-OH	C14:0/C14:0-OH

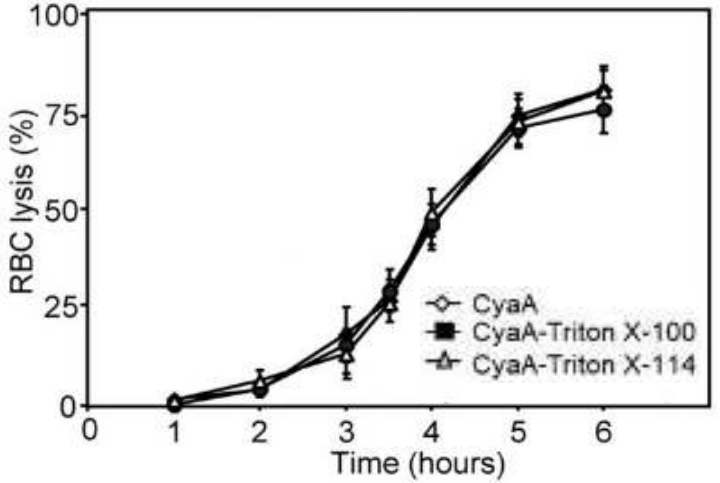

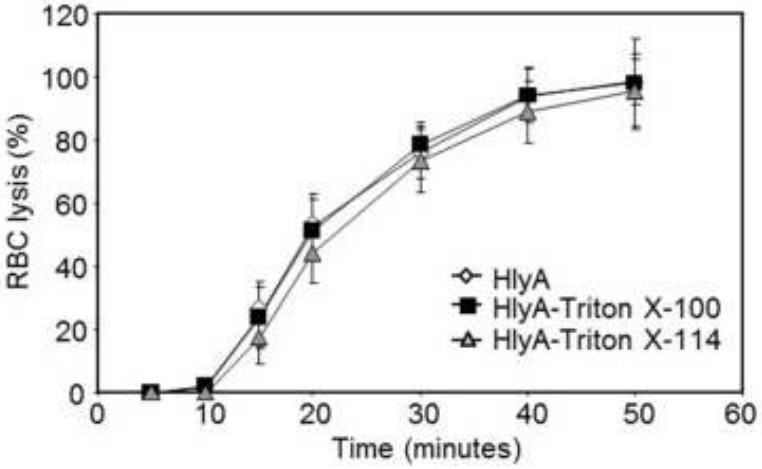

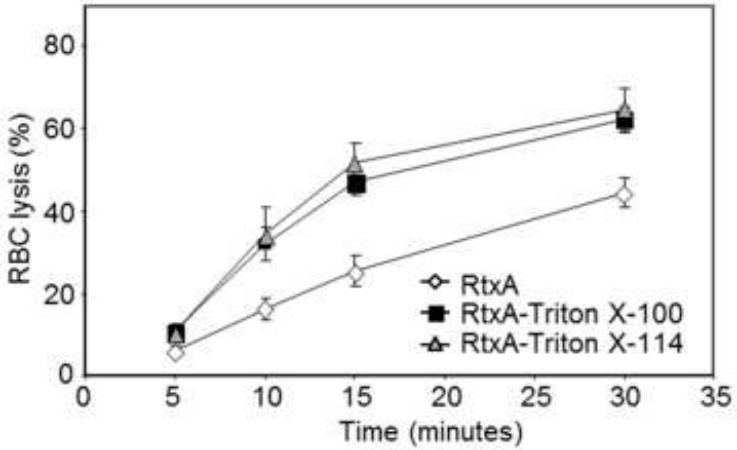

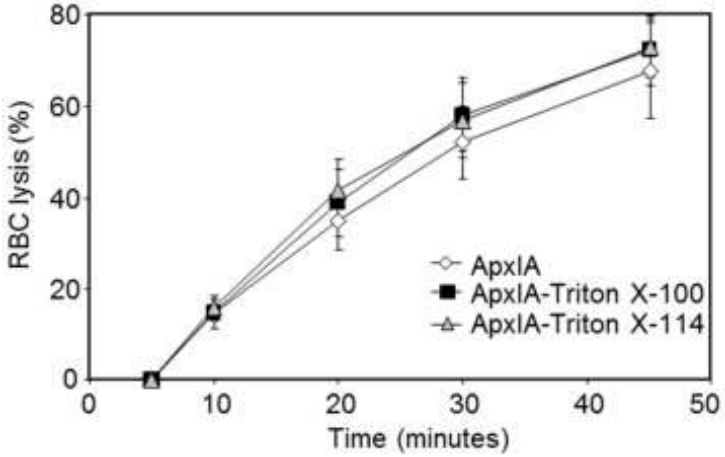

Determination of acylation status of RTX toxins

Acyltransferase		RTX toxin
CyaC		CyaA
HlyC	X	HlyA
RtxC		RtxA

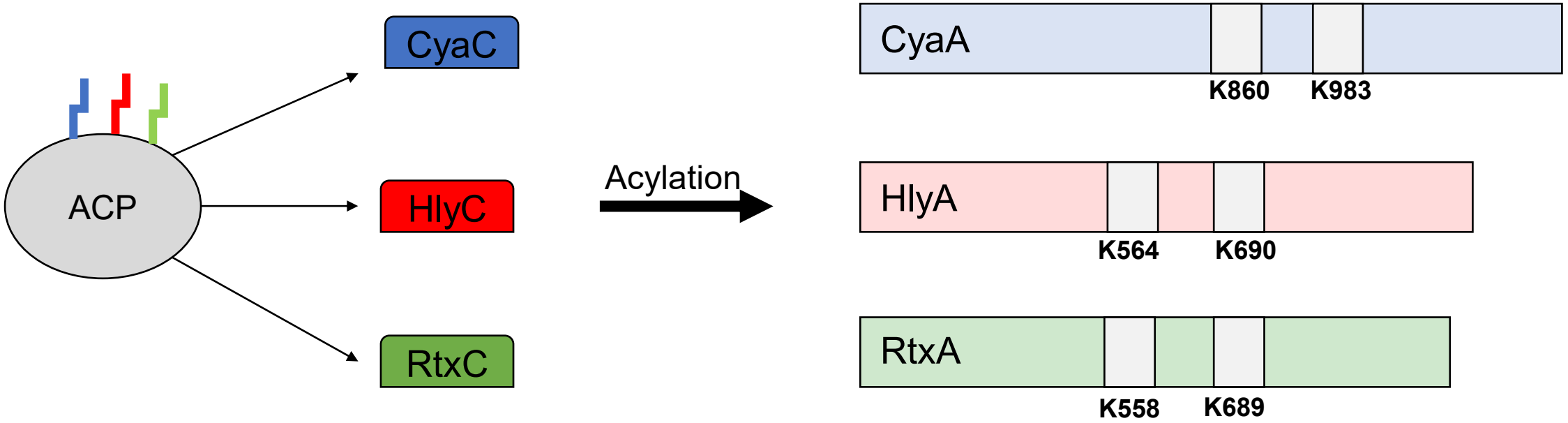

(Osickova et al., 2020)

Determination of acylation status of RTX toxins

Acyltransferase		RTX toxin
CyaC		CyaA
HlyC	X	HlyA
RtxC		RtxA

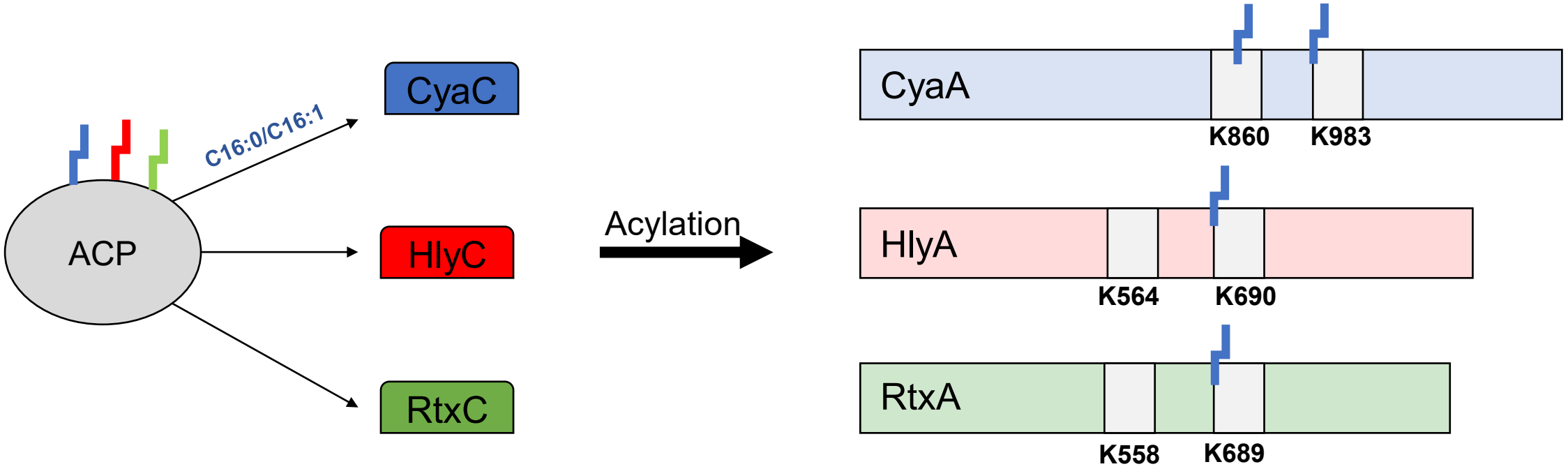

(Osickova et al., 2020)

Determination of acylation status of RTX toxins

Acyltransferase		RTX toxin
CyaC		CyaA
HlyC	X	HlyA
RtxC		RtxA

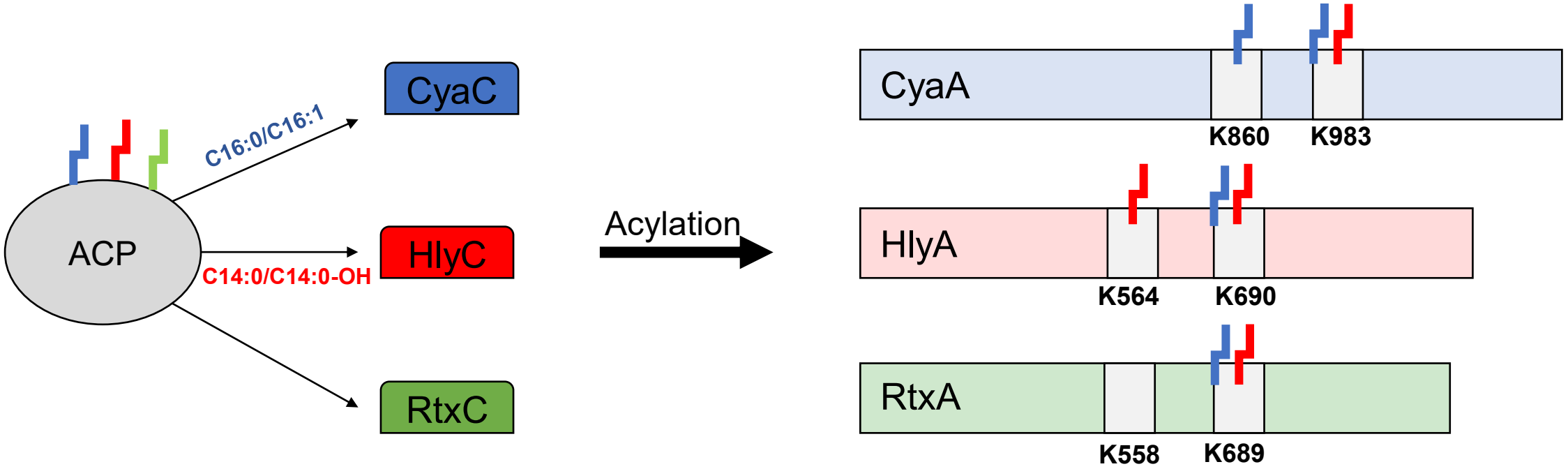

(Osickova et al., 2020)

Determination of acylation status of RTX toxins

Acyltransferase		RTX toxin
CyaC		CyaA
HlyC	X	HlyA
RtxC		RtxA

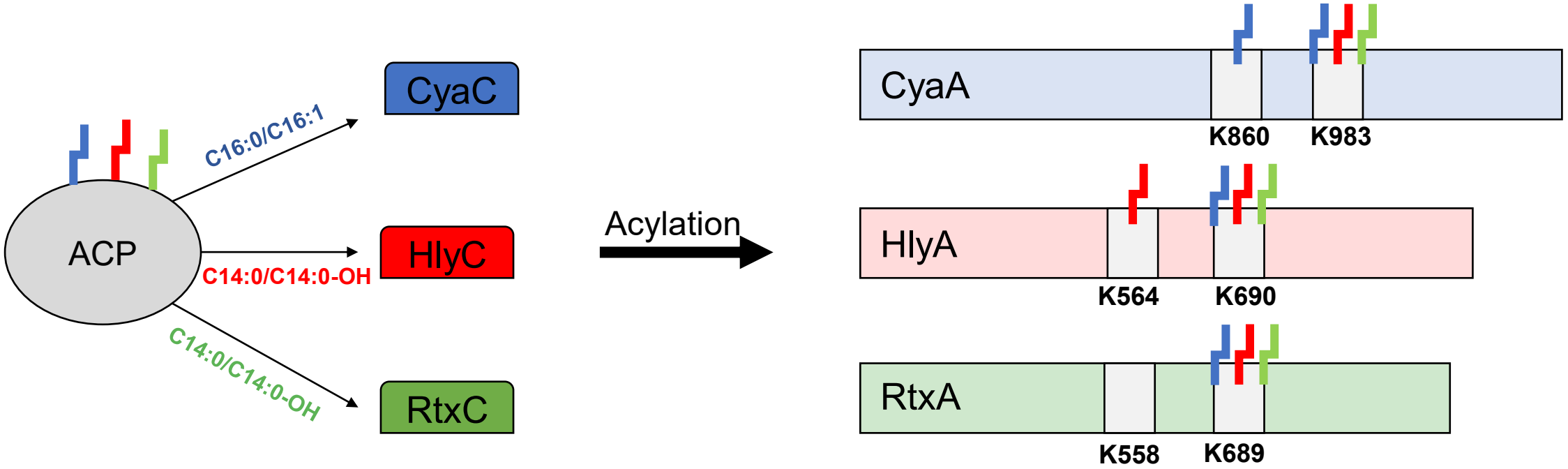

(Osickova et al., 2020)

Biological activity of differently acylated RTXA toxins

CyaA
C16/C16:1

RtxA
C14/C14:0-OH

HlyA
C16/C16:1
C14/C14:0-OH

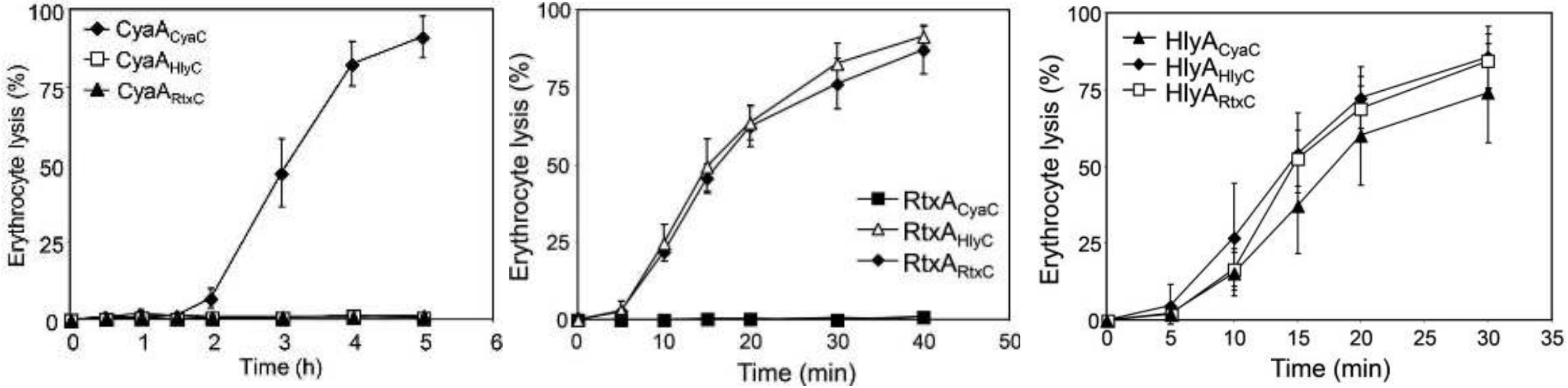

(Osickova et al., 2020)

EU FT-ICR MS

Acknowledgement

Members of Laboratory of Molecular Biology of Bacterial Pathogens

Petr Novák
Petr Pompach

Thank you for your attention !

EU FT-ICR MS

Michael Palasser, Maria A. van Agthoven, Kathrin Breuker

Institute of Organic Chemistry and

Center for Molecular Biosciences Innsbruck (CMBI)
University of Innsbruck, Austria

FAST MS:

An open-source software for automated and quantitative analysis of top-down mass spectra

Data Processing and Analysis in FTMS

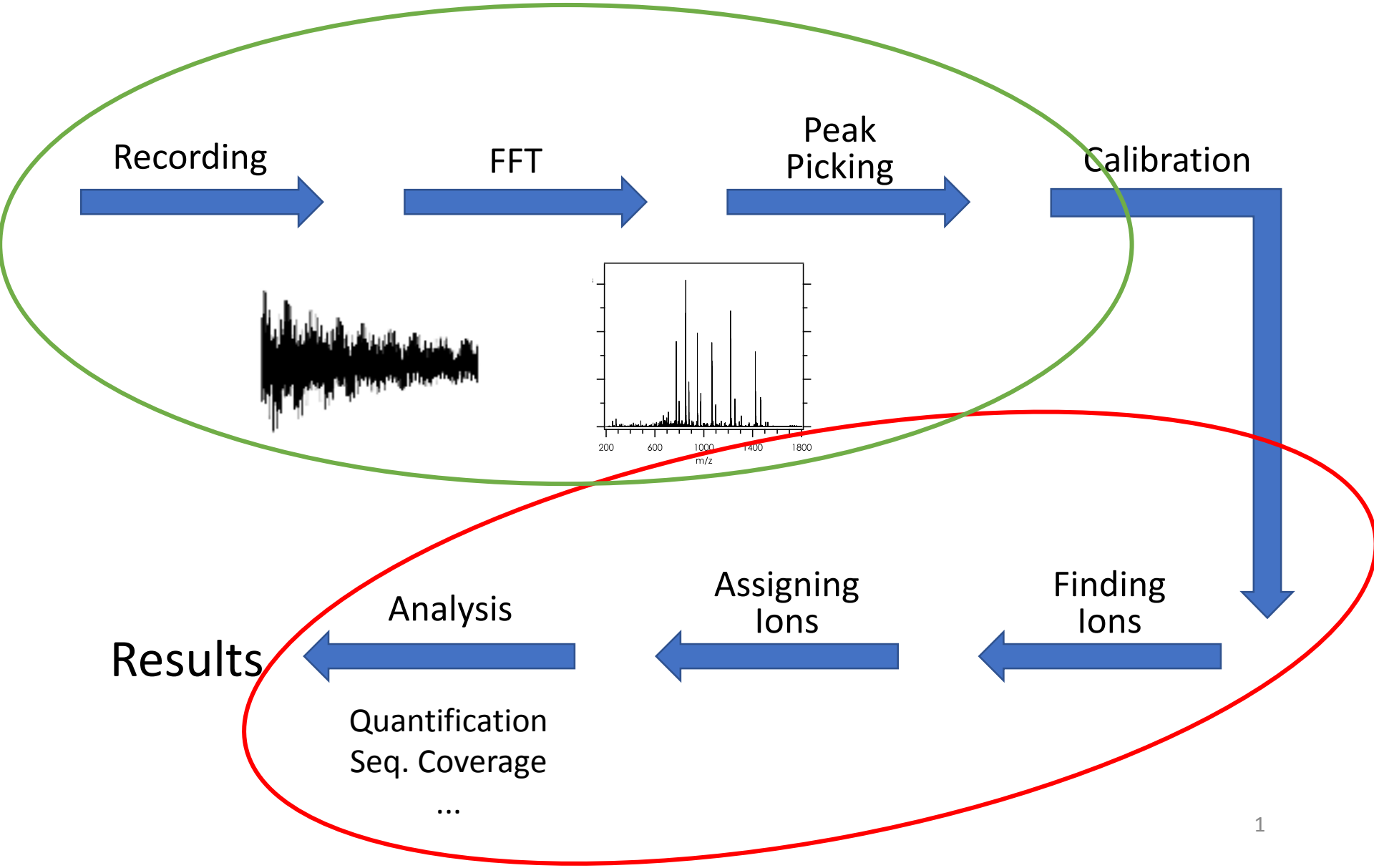

Data Analysis ?

SNAP?

- Great for de-novo sequencing
- Misses many ions → Problem for:
  - Characterisation of PTMs, ligand binding sites, ...
  - Spectra with low S/N
  - Larger molecules

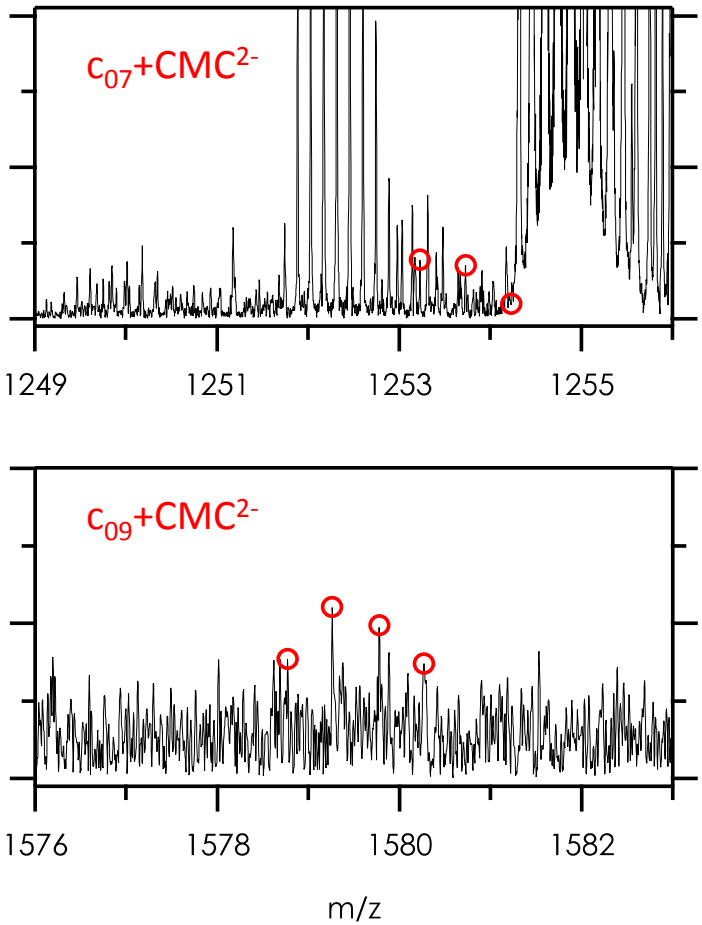

Data Analysis ?

- SNAP?
- Other software tools?
  - just for proteins
- Finding ions manually?
  - Quantification
  - Reproducibility?
  - Very tedious

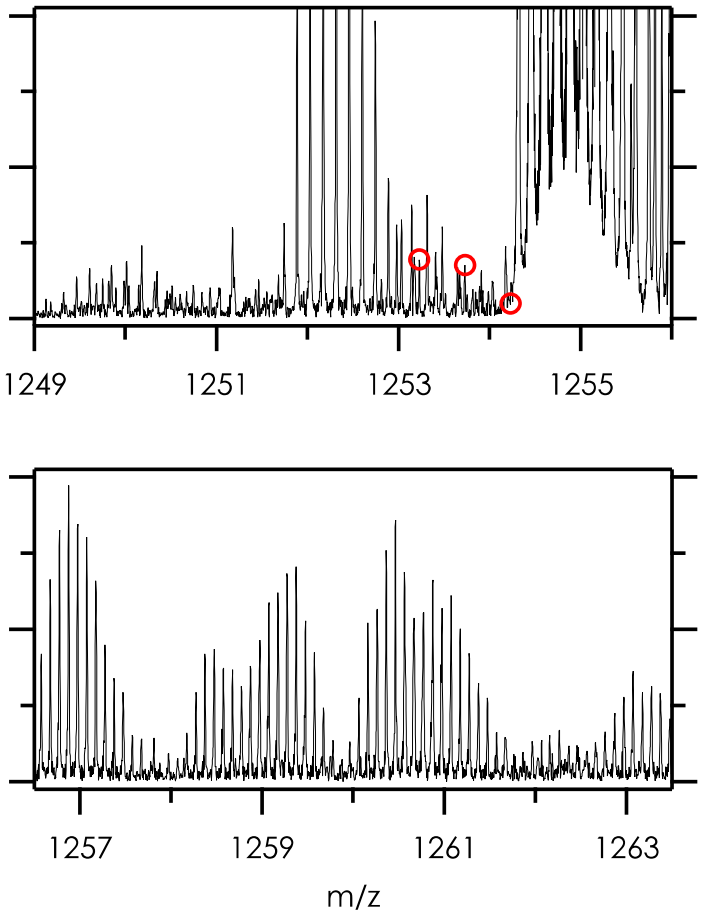

Data Analysis: FAST MS

Free **A**nalysis **S**oftware for **T**op-down **M**ass **S**pectrometry

- Written in Python (open-source)
- Cross platform
- Full GUI support
- For analysis of top-down <u>and</u> mass spectra of intact ions (known sequence)
- RNA, DNA, proteins, ...

FAST MS: Top-Down MS

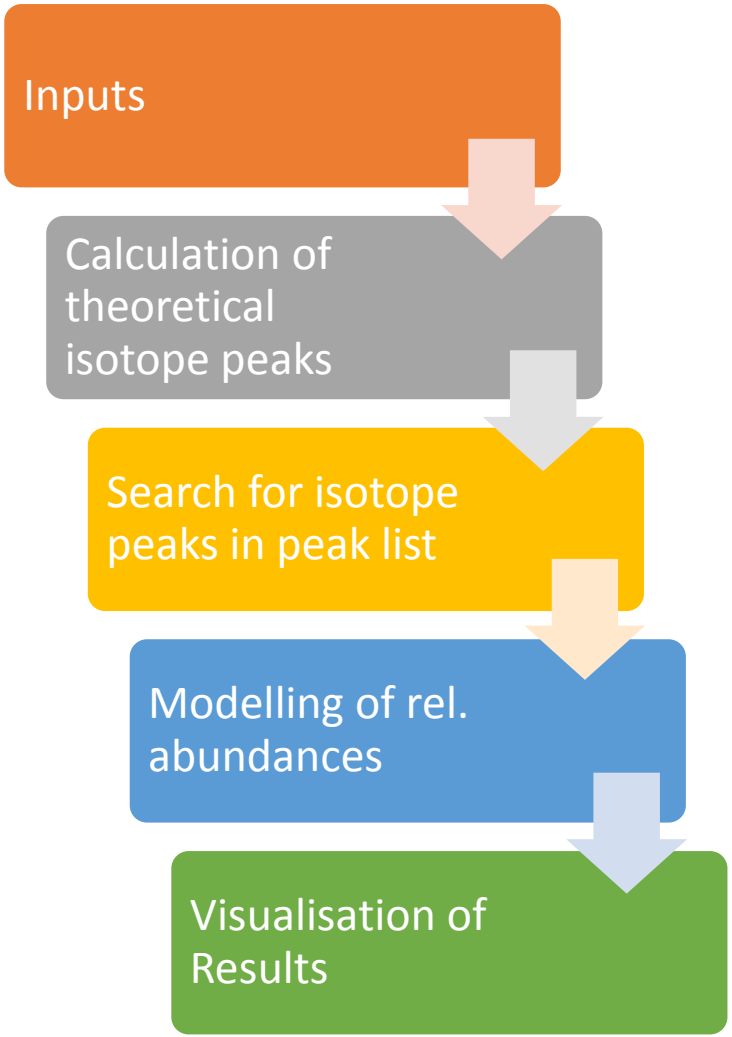

FAST MS: Top-Down MS

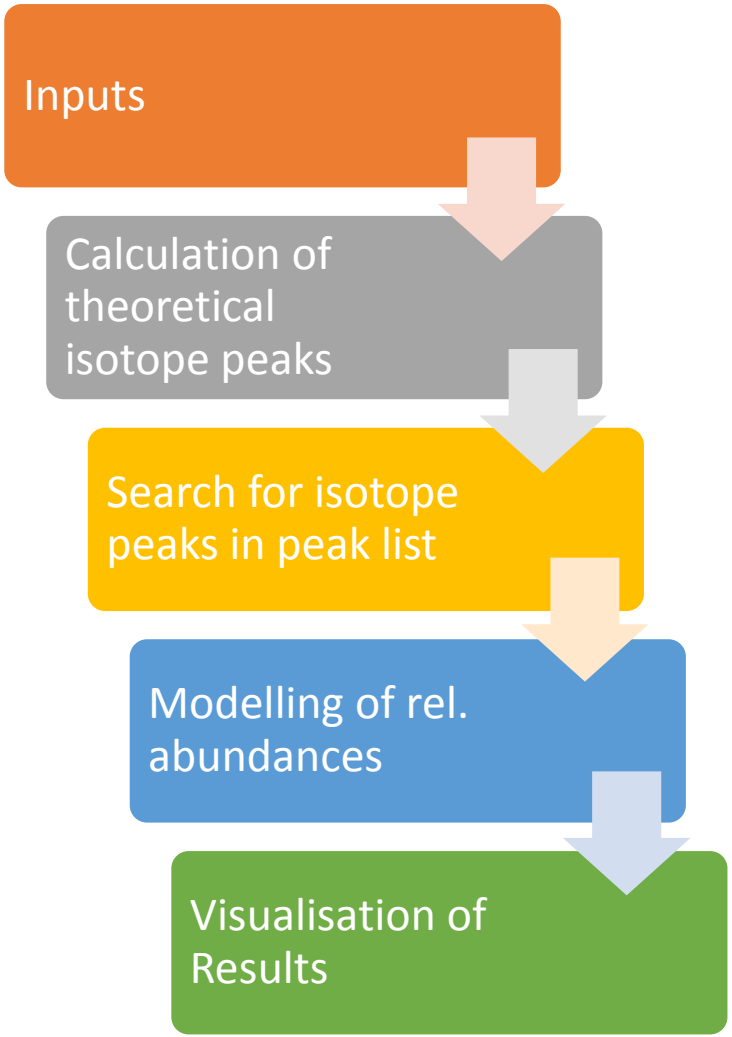

- Peak list
- Sequence
- Charge of precursor
- Modifications, ligands, ...

FAST MS: Top-Down MS

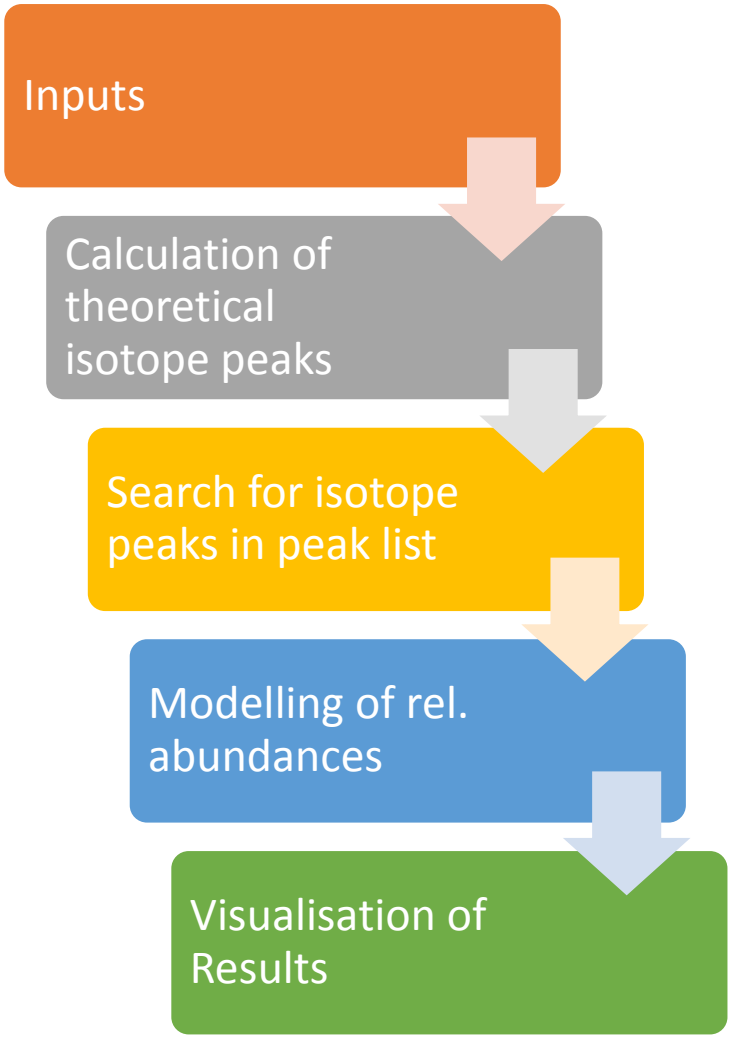

FAST MS: Top-Down MS

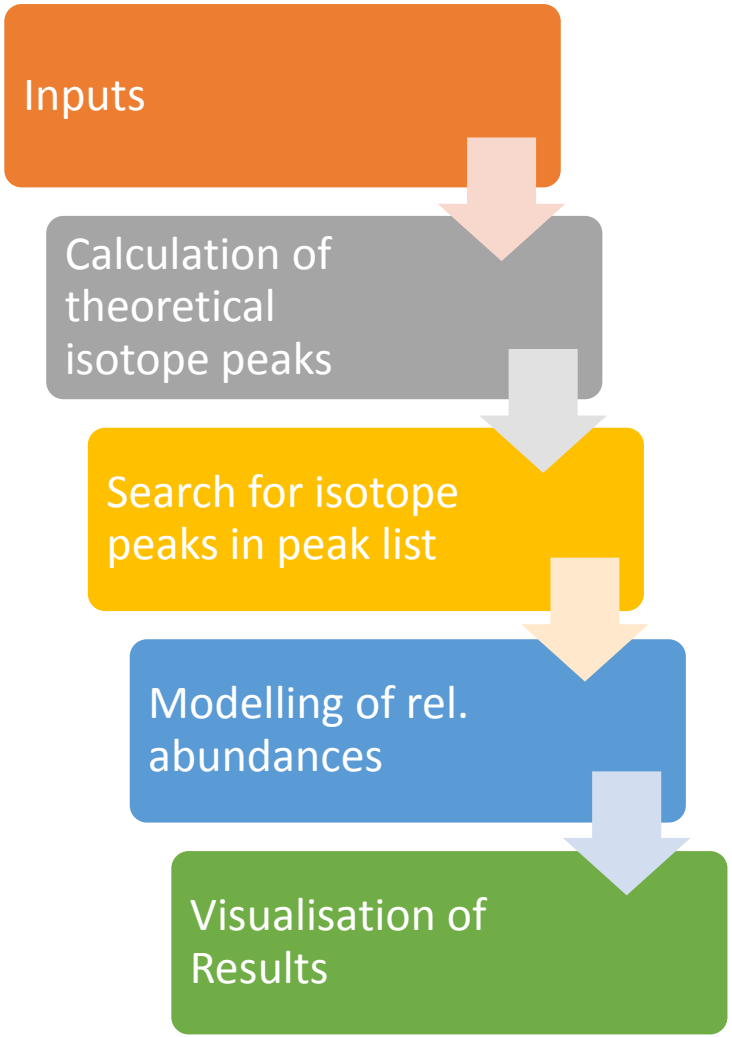

Charge state estimation

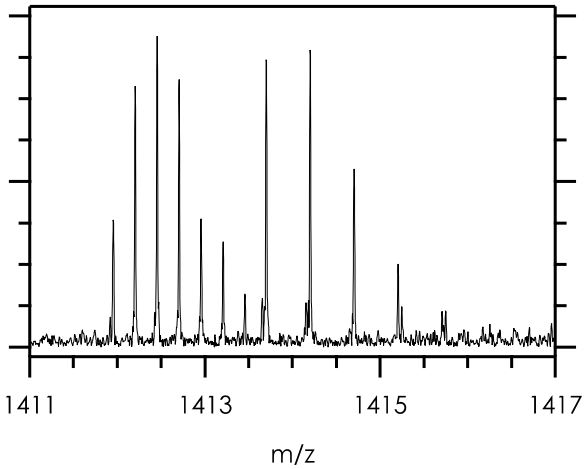

FAST MS: Top-Down MS

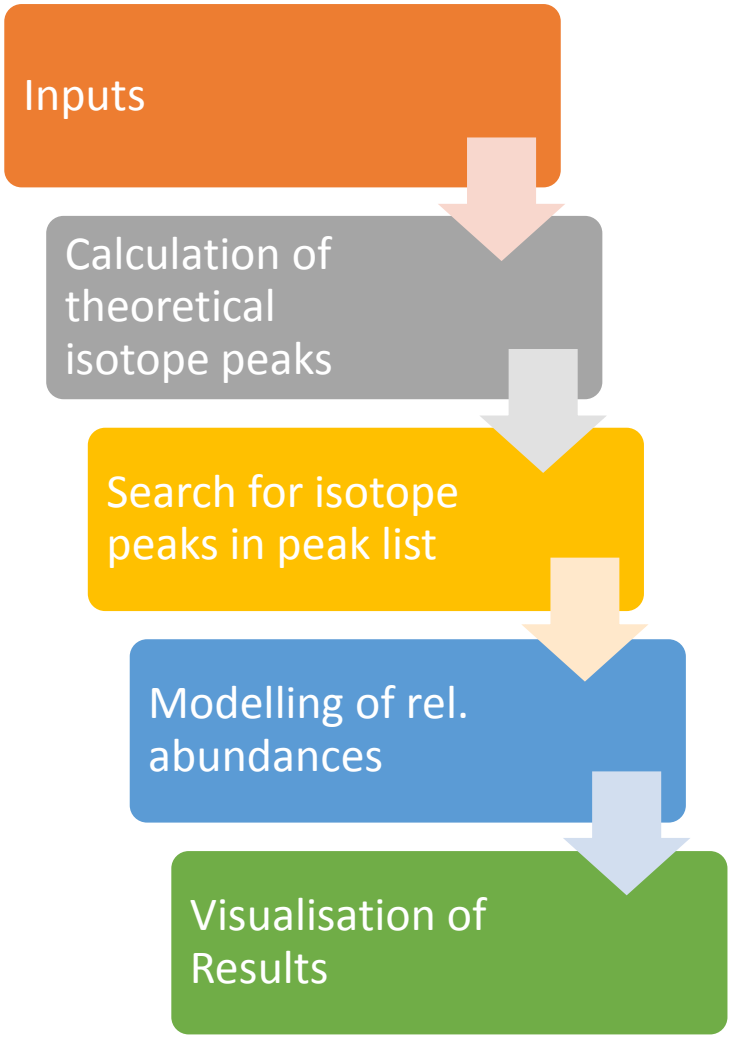

Charge state estimation

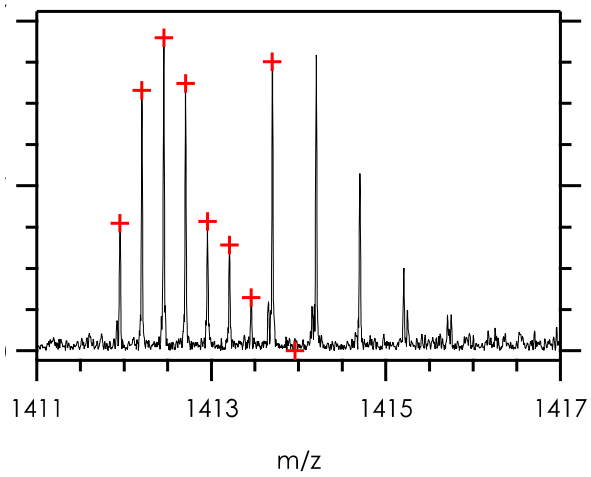

FAST MS: Top-Down MS

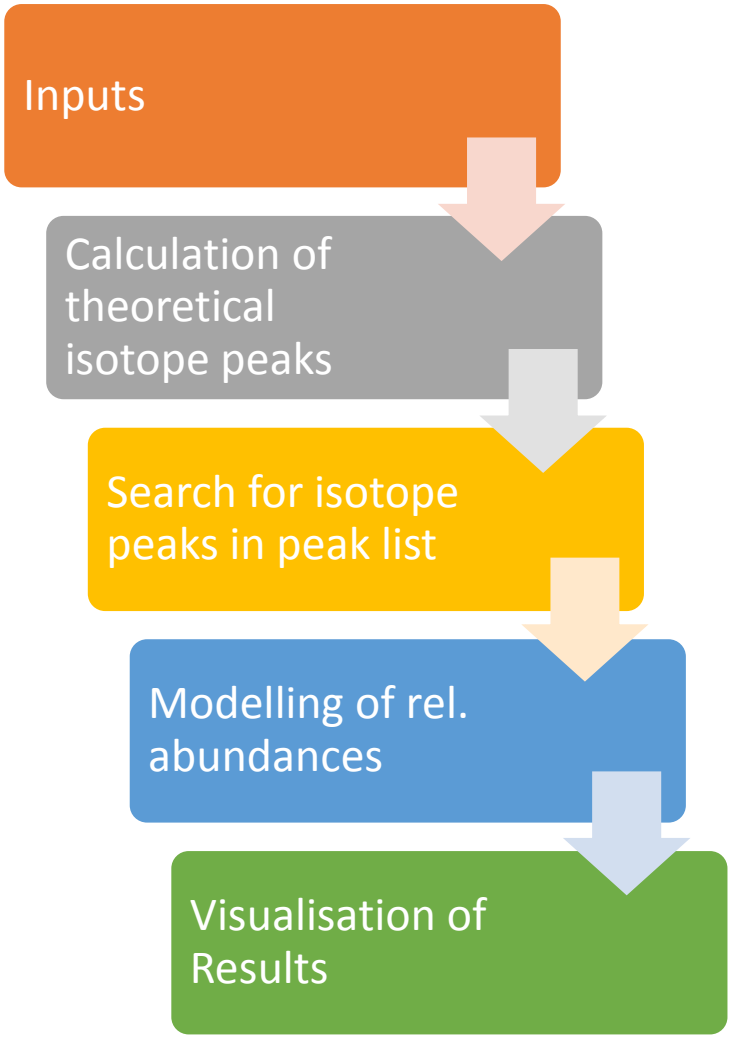

- Least-square fit
- Outlier detection

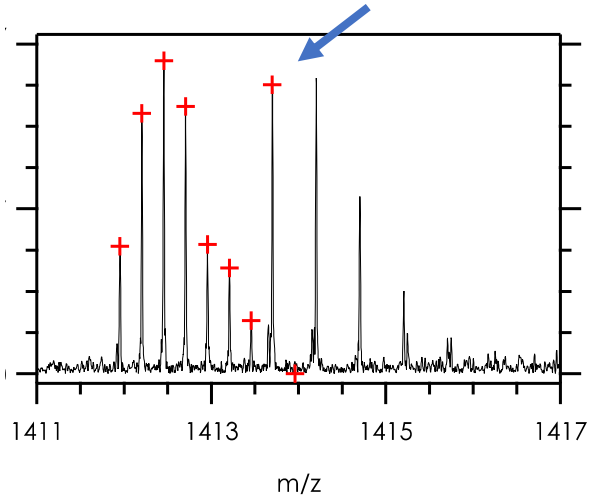

FAST MS: Top-Down MS

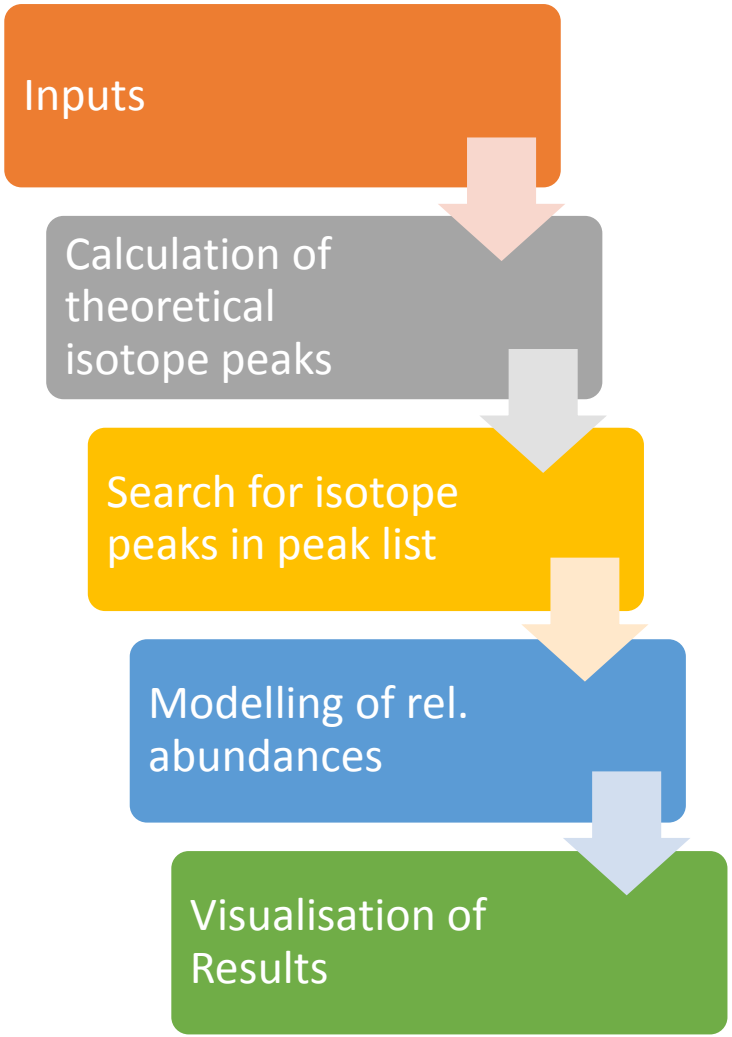

- Least-square fit
- Outlier detection

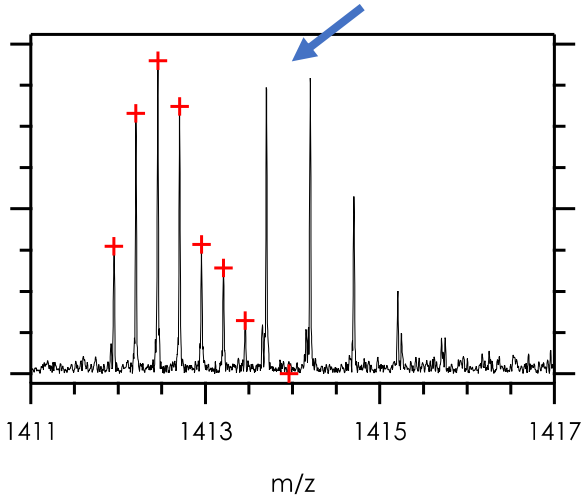

FAST MS: Top-Down MS

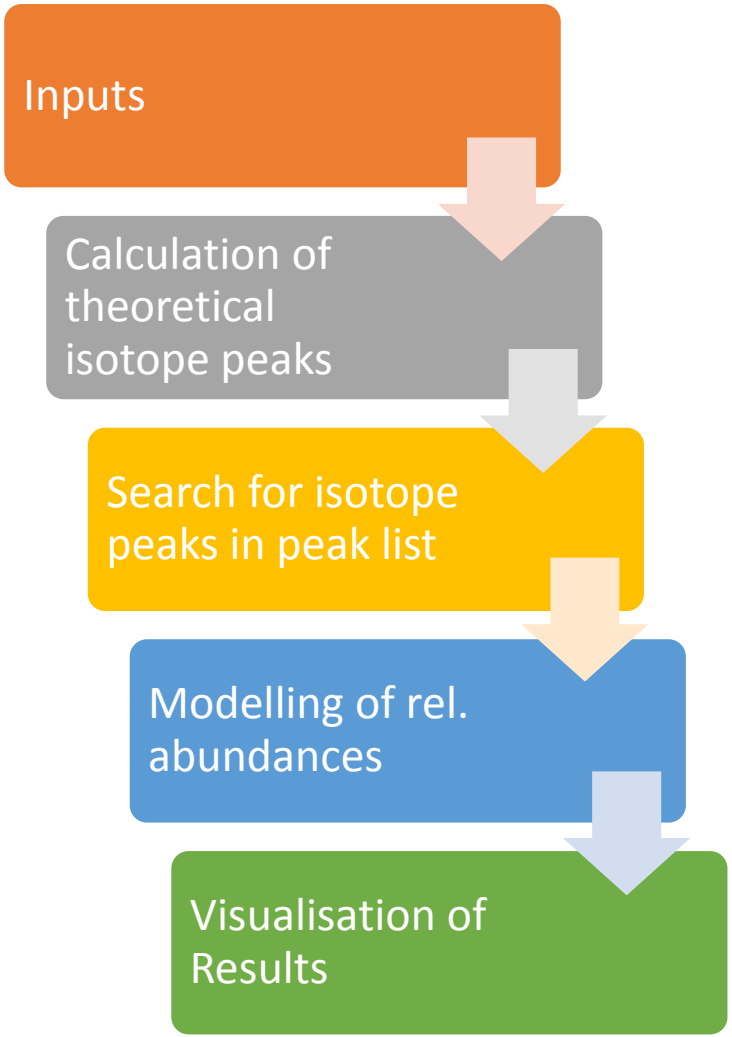

- Least-square fit
- Outlier detection
- Evaluation

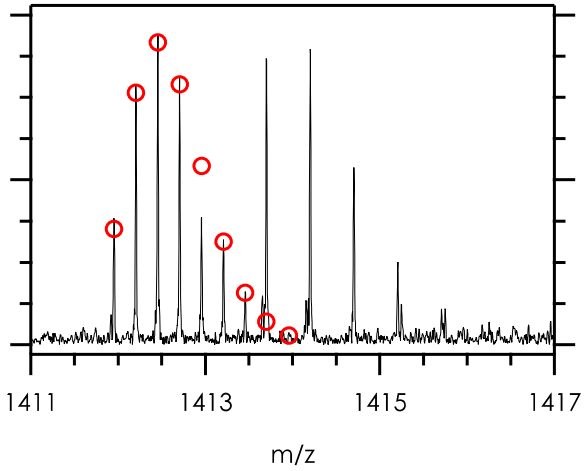

FAST MS: Top-Down MS

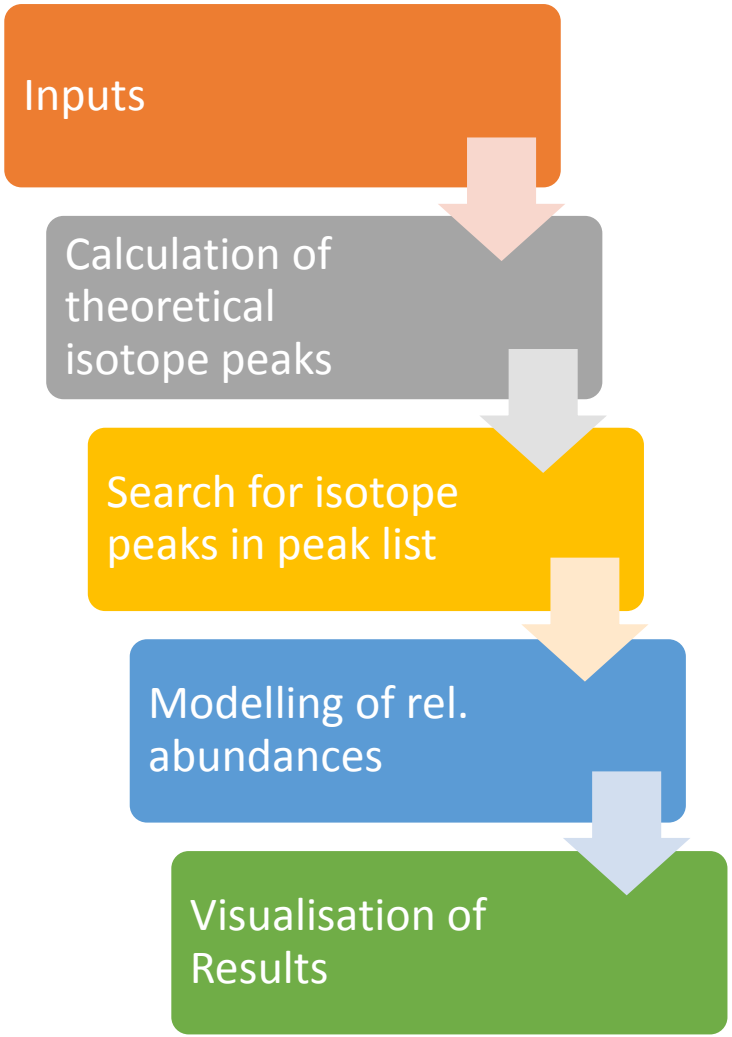

- Least-square fit
- Outlier detection
- Evaluation
- Overlapping ions

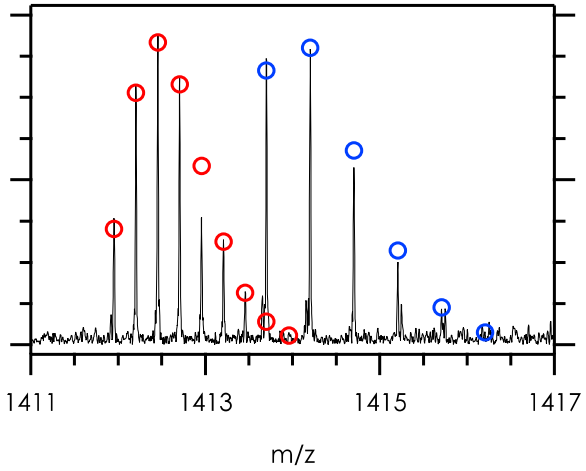

FAST MS: Top-Down MS

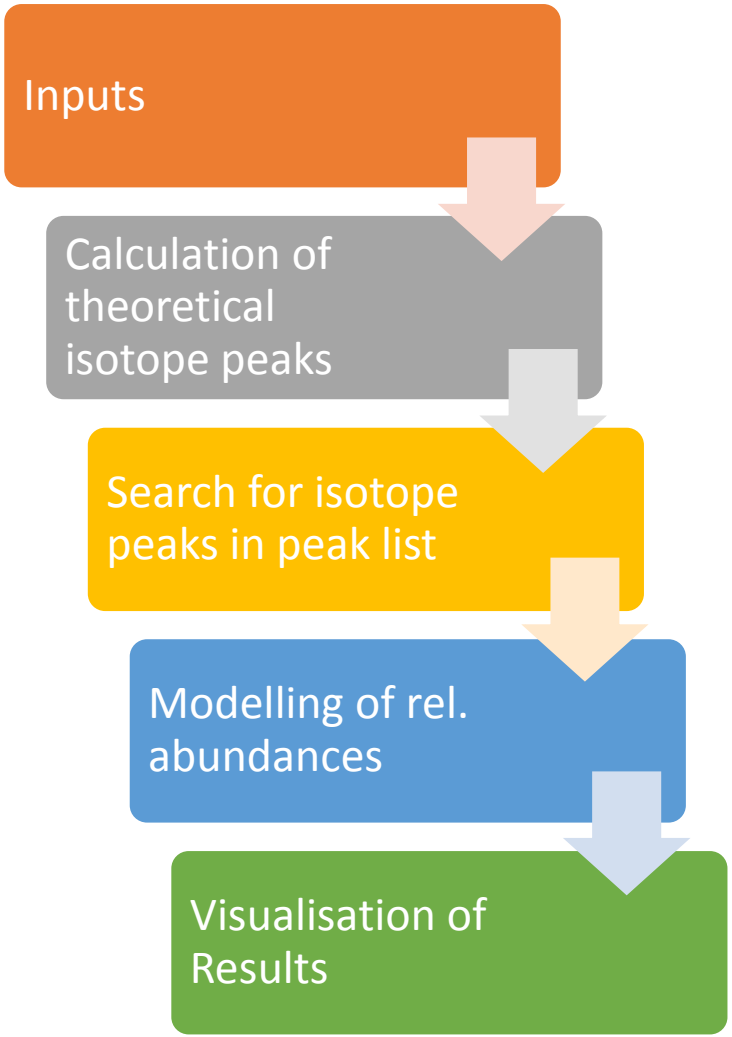

- Least-square fit
- Outlier detection
- Evaluation
- Overlapping ions

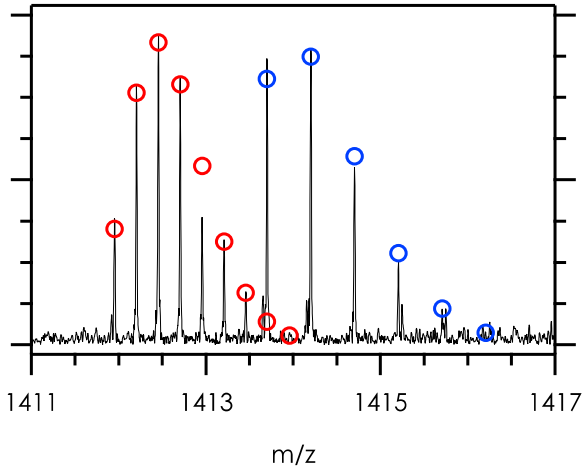

FAST MS: Top-Down MS

Inputs

Calculation of theoretical isotope peaks

Search for isotope peaks in peak list

Modelling of rel. abundances

Visualisation of Results

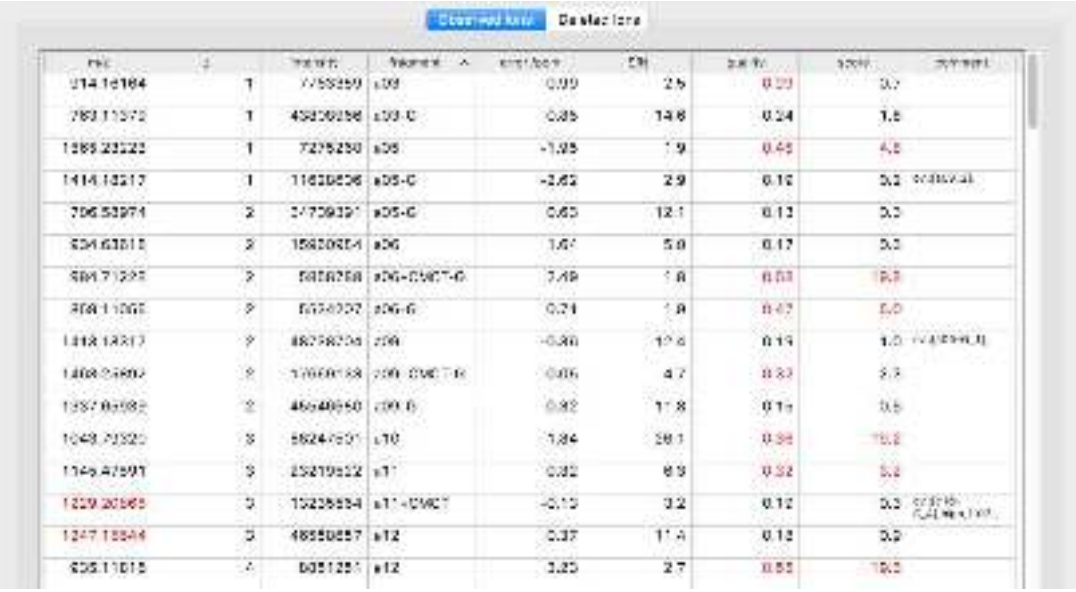

FAST MS: Visualisation of Results

- Manual editing, deleting, restoring, adding of ions possible
- Visualisation of spectrum
- Protocol
- Analysis tools

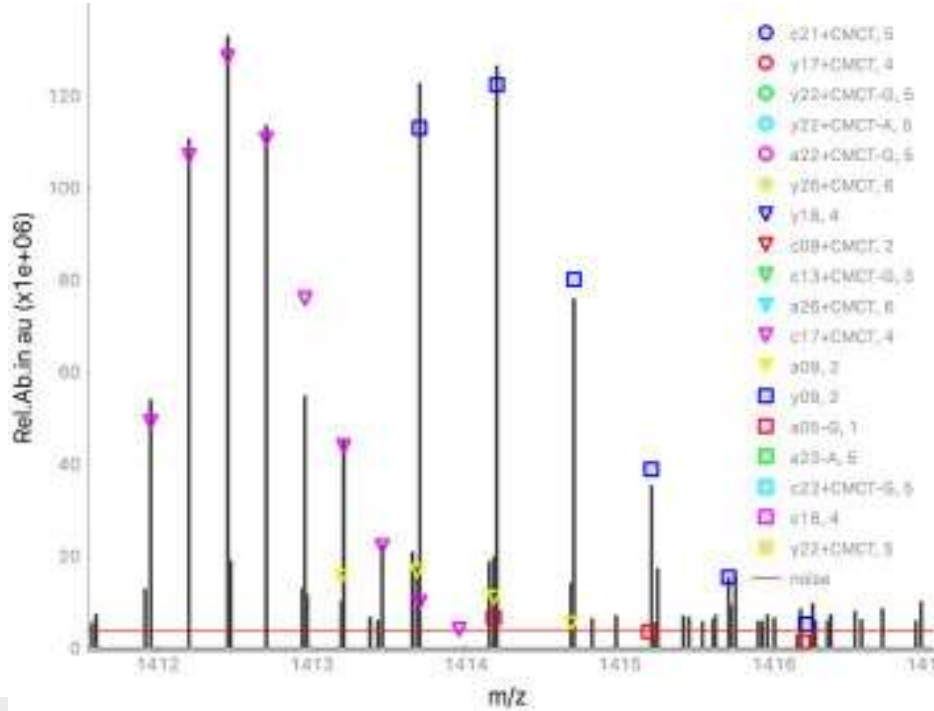

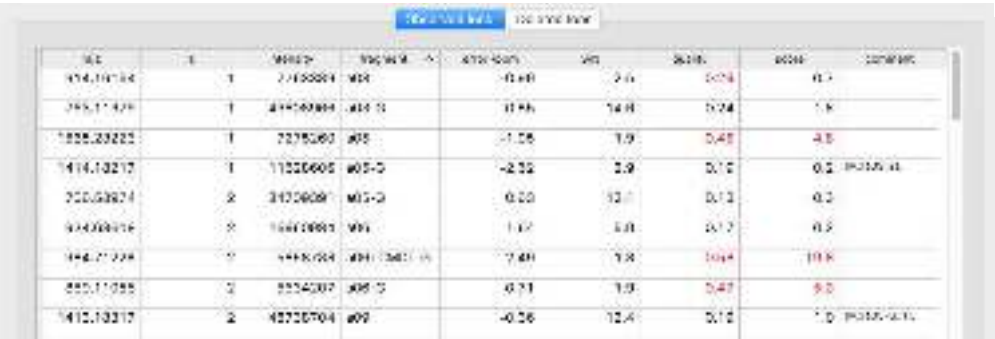

FAST MS: Visualisation of Results

Analysis:

- Fragmentation efficiencies

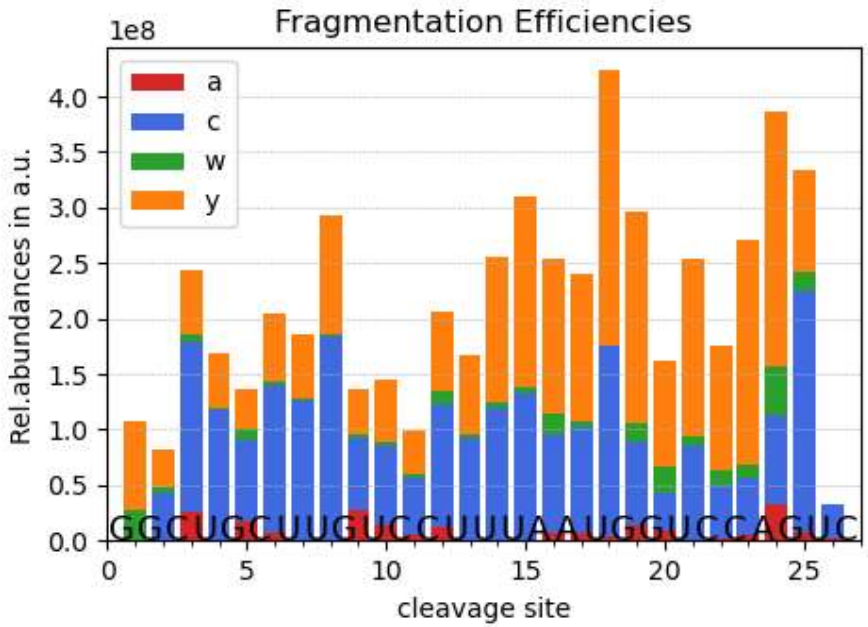

type	rel.proportion
neoRibo	0.762
a	0.009
c	0.105
w	0.011
y	0.114

sequ. (f)	cleav.site (f)	a	c	w	y	cleav.site (b)	sequ. (b)
G	1	0	0	26941802	80804486	26	G
G	2	0	42693262	4713574	34853025	25	C
C	3	25786178	153220090	6869211	58460113	24	U
U	4	0	118445190	1750776	49280631	23	G
G	5	18129281	72844497	9667250	35673648	22	C
C	6	6838495	132896376	3127108	62327208	21	U
U	7	0	125863821	2016989	57450035	20	U

FAST MS: Visualisation of Results

Analysis:

- Fragmentation efficiencies
- Charge distributions

sequ. (f)	cleav.site (f)	c	y	cleav.site (b)	sequ. (b)
G	1		6.1	26	G
G	2	1.0	6.0	25	C
C	3	1.0	6.0	24	U
U	4	1.5	5.5	23	G
G	5	2.0	5.0	22	C
C	6	2.0	5.0	21	U
U	7	2.0	5.0	20	U
U	8	2.1	4.9	19	G
G	9	2.4	4.7	18	U
U	10	2.8	4.2	17	C
C	11		4.2	16	C
C	12	3.0	4.0	15	U
U	13	3.1	3.8	14	U
U	14	3.2	3.6	13	U
U	15	3.6	3.4	12	A
A	16	3.9	3.0	11	A
A	17	4.0	2.9	10	U

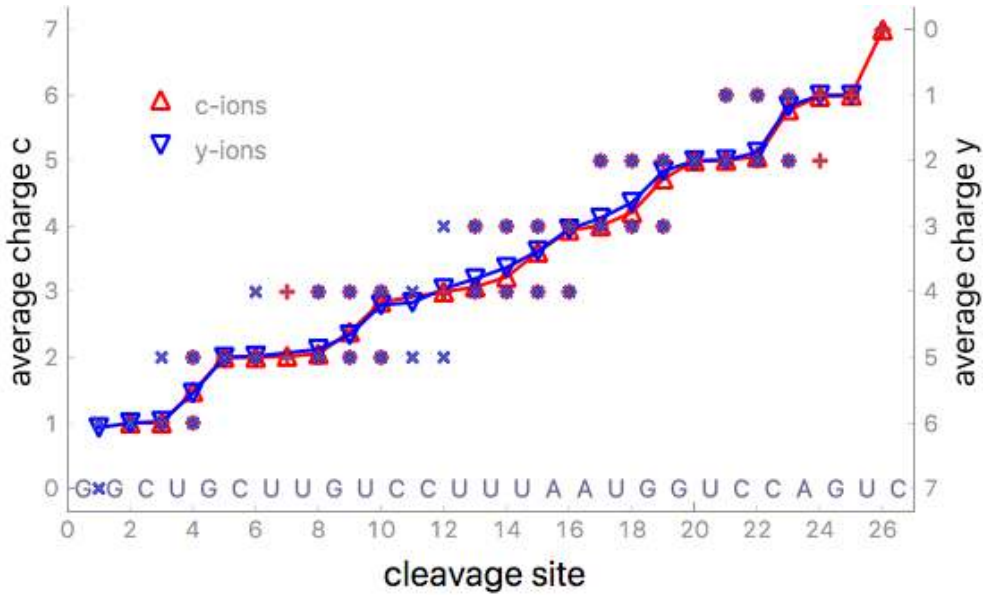

FAST MS: Visualisation of Results

Analysis:

- Fragmentation efficiencies
- Charge distributions
- Sequence coverage

FAST MS: Visualisation of Results

Analysis:

- Fragmentation efficiencies
- Charge distributions
- Sequence coverage
- Locating & quantification of modifications / ligands

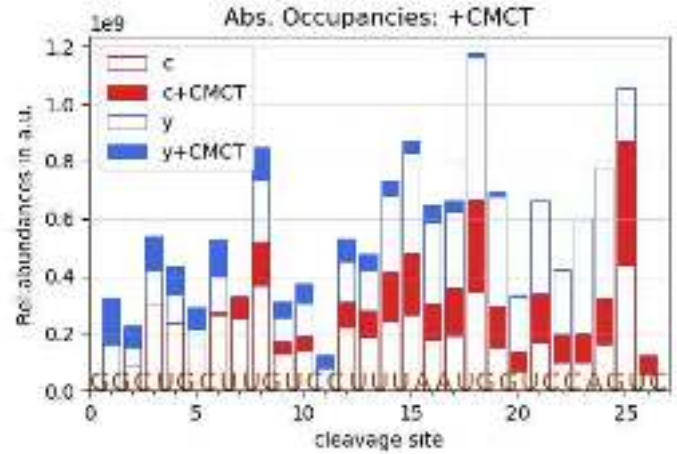

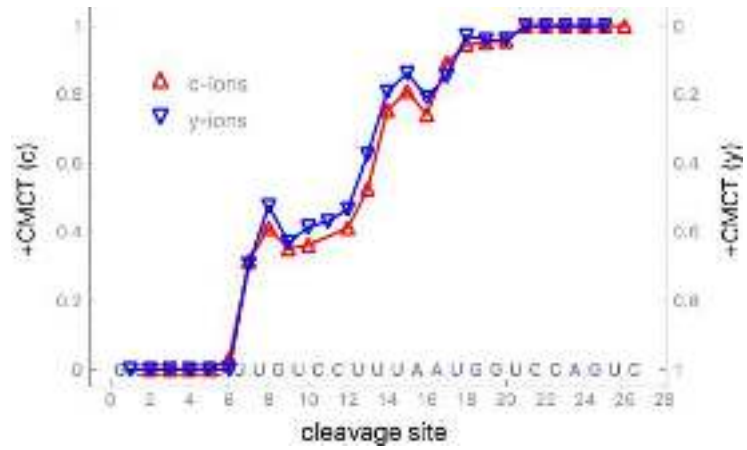

prec. mod. loss: 0.6 %

sequ. (f)	cleav.side (f)	c	y	cleav.side (b)	sequ. (b)
G	1		1.000	26	G
G	2	0.000	1.000	25	C
C	3	0.000	1.000	24	U
U	4	0.000	1.000	23	G
G	5	0.000	1.000	22	C
C	6	0.031	1.000	21	U
U	7	0.317	0.694	20	U

sequ. (f)	cleav.side (f)	c	c+CMCT	y	y+CMCT
G	1	0.0	0.0	161606891.8	18160898
G	2	86286524.0	0.0	69706060.5	8970605
C	3	306440180.0	0.0	116920226.8	11682022
U	4	236090380.5	0.0	98581261.7	9856126
G	5	146688994.5	0.0	71347295.2	7134725

FAST MS: Top-Down MS

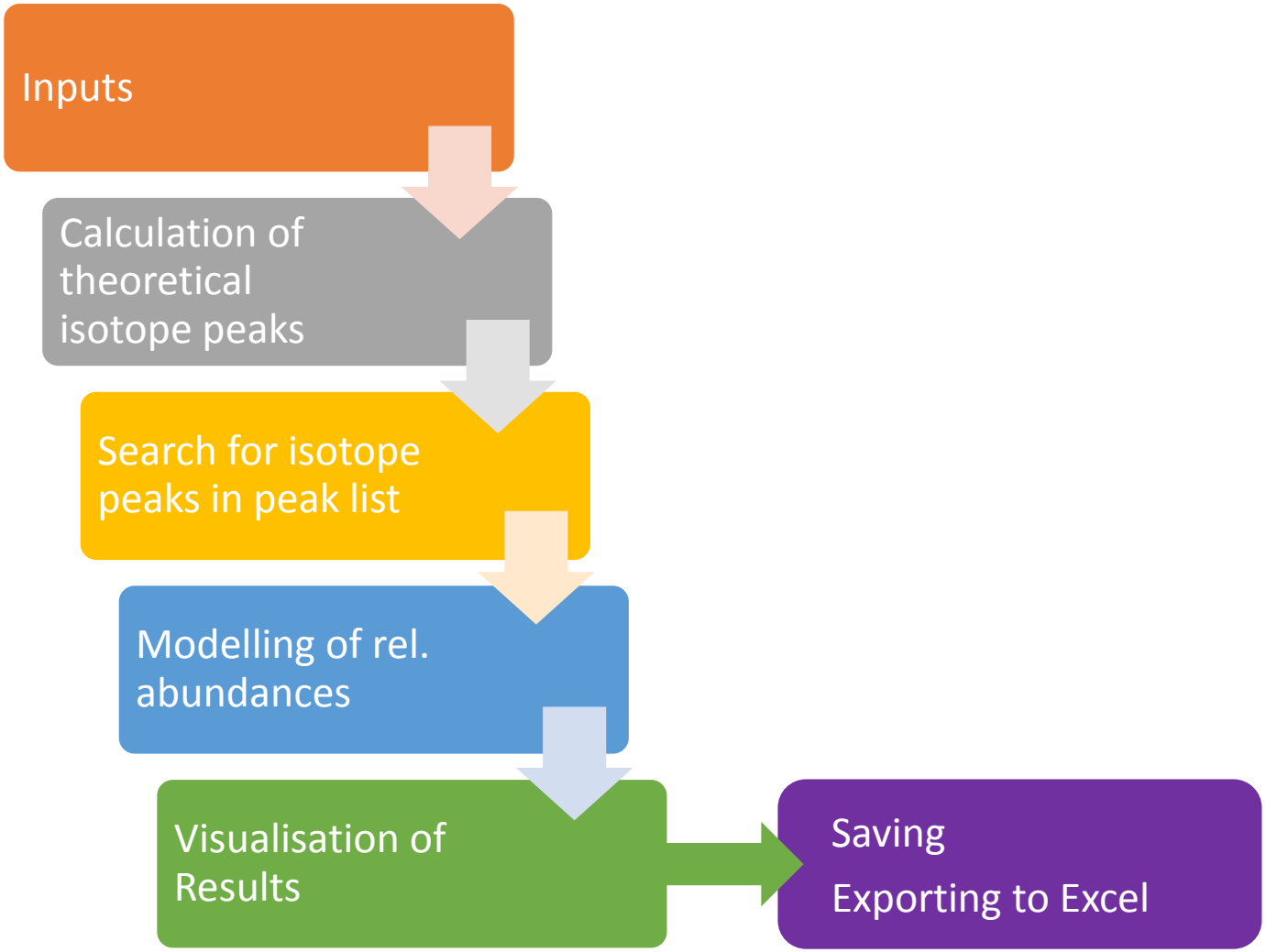

FAST MS: Evaluation

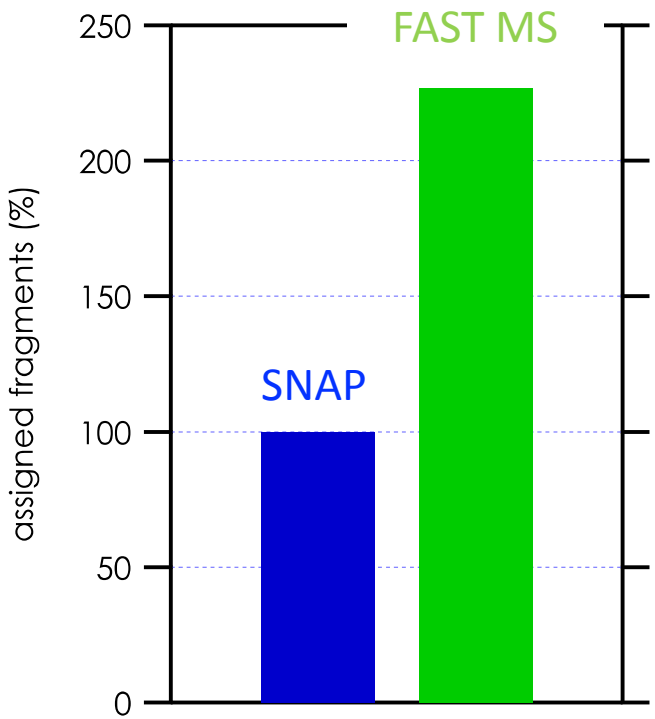

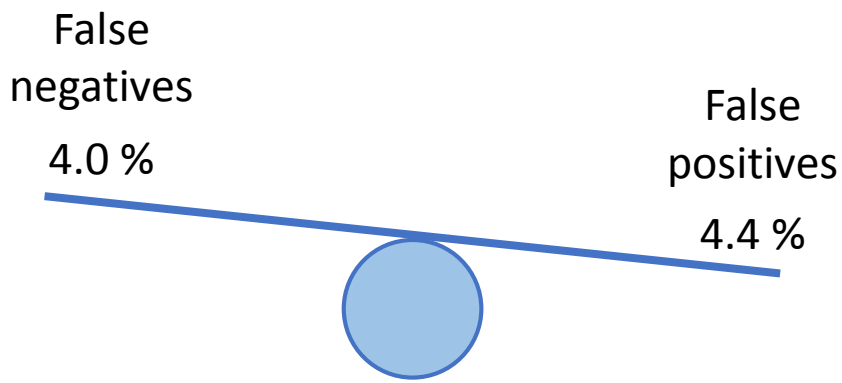

Other Tools

- Analyse ESI spectra with intact ions
  - Ion Assignment and Analysis
  - Autocalibration
- Tool to model isotope patterns
- Tool to compare ion lists of different spectra

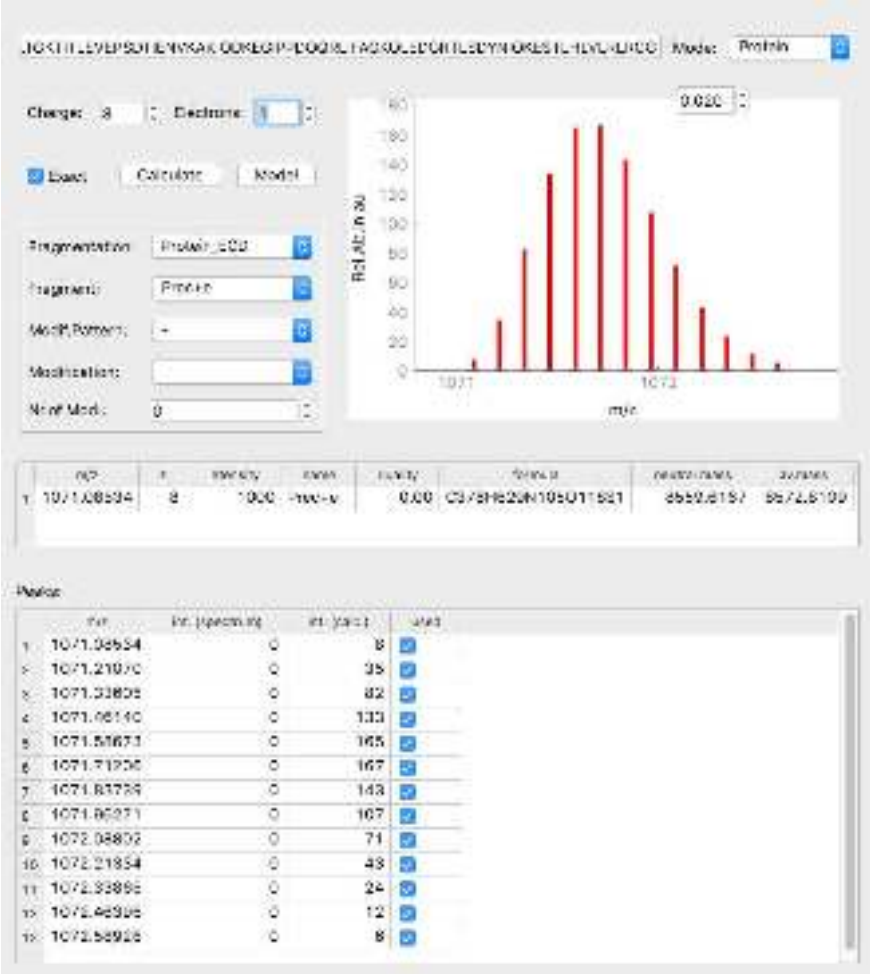

Conclusion

- Robust:
  - Beta-Version(s) User-tested for > 1 year
  - Unit-tested
- Universal:
  - All kinds of polymers
  - Isotopically depleted/enriched molecules
  - User-defined building blocks
  - dissociation methods
  - Positive and negative spray mode
  - 2D MS
- User-friendly

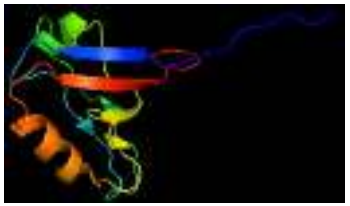

^{12}C ^{13}C

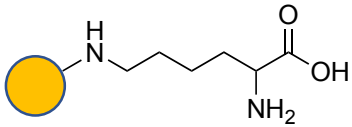

EDD UVPD
CAD IRMPD ECD
EDD

- +

Outlook

- Coming soon: Autocalibration for top-down mass spectra

- ASMS 2021:
  Utilizing the power of mass spectrometry for chemical probing of RNA

Acknowledgements

EU FT-ICR MS

Kathrin Breuker
Maria van Agthoven
Sarah Heel

FWF
Der Wissenschaftsfonds.

This project has received funding from the European Union's Horizon 2020 research and innovation programme under grant agreement No 731077.

Faculty of Science

LABORATORY OF MOLECULAR STRUCTURE CHARACTERIZATION

EU FT-ICR MS

Visualization of Polyamines and Amino Acids Alterations in Neonatal Brain Hypoxic-Ischemic Injury in Rats by Mass Spectrometry Imaging

MSc. Hynek Mácha

Department of Analytical Chemistry
Faculty of Science
Palacký University Olomouc

Laboratory of Molecular Structure Characterization
Institute of Microbiology
Academy of Sciences of the Czech Republic

Hypoxic-ischemic neonatal brain injury

EU FT-ICR MS

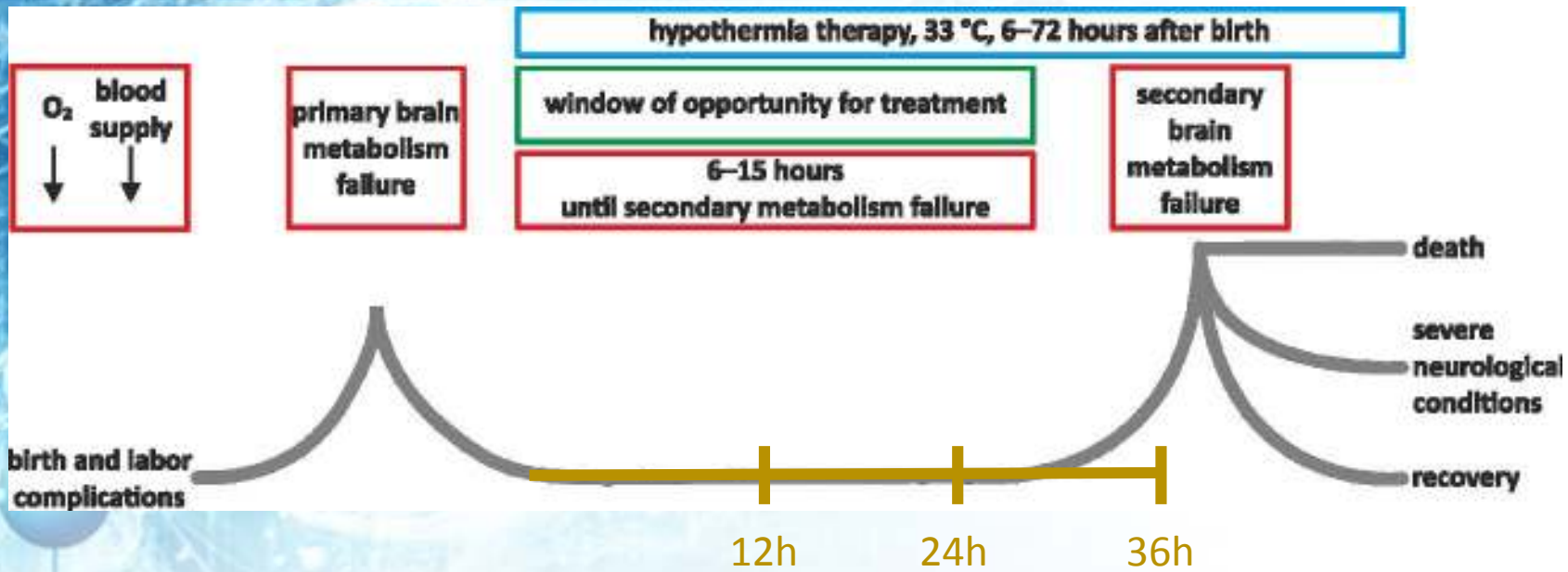

Aims

1) **MALDI-MSI** analysis **of small molecules**
2) **Time-dependent** alterations in a brain
3) Description of **post-primary brain metabolism failure**

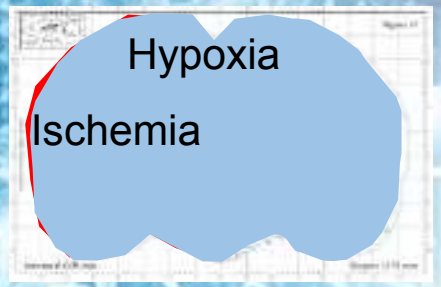

Methods

Rice-Vannucci model of hypoxic-ischemic neonatal rat brain injury

EU FT-ICR MS

FMP-10 derivatization

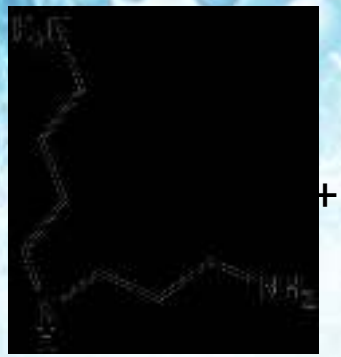

+

→ HF

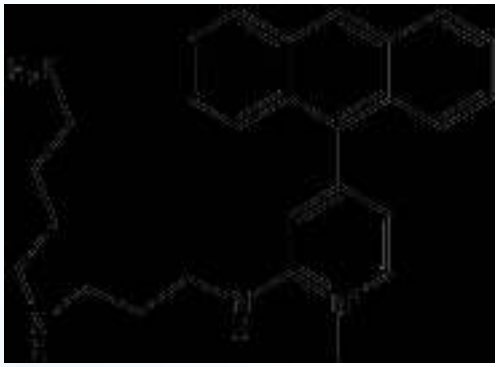

Spermidine | FMP-10 | Single derivatized spermidine

Shariatgorji, M. et al., Nature Methods 2019

Molecules of interest

1) **Aminoacids**

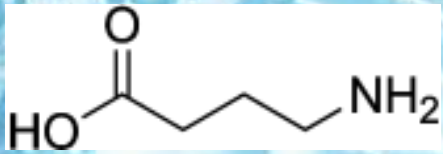

γ-aminobutyric acid (GABA)

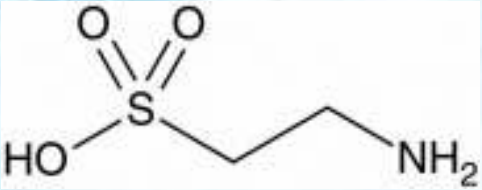

Taurine

2) **Polyamines**

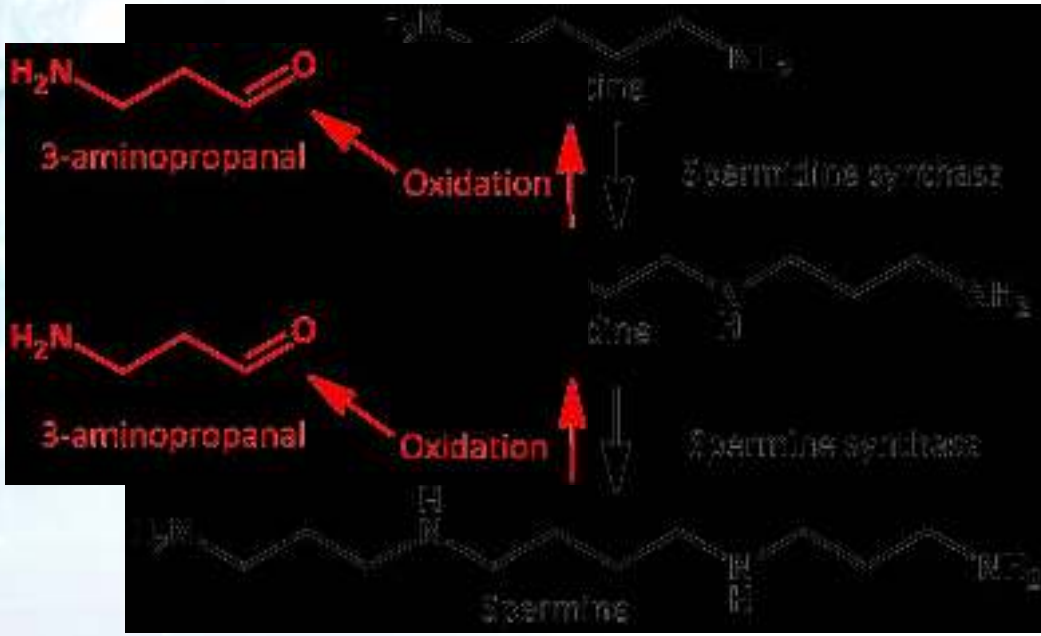

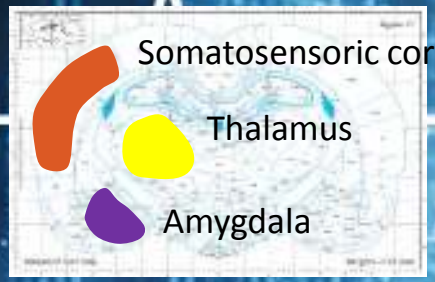

Polyamines changes

EU FT-ICR MS

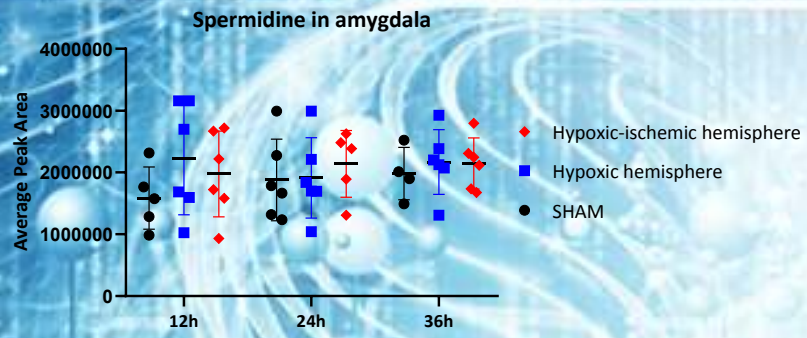

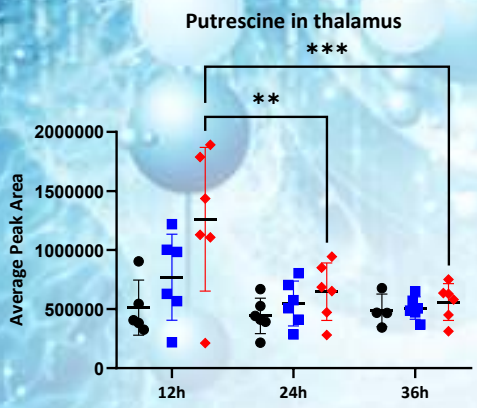

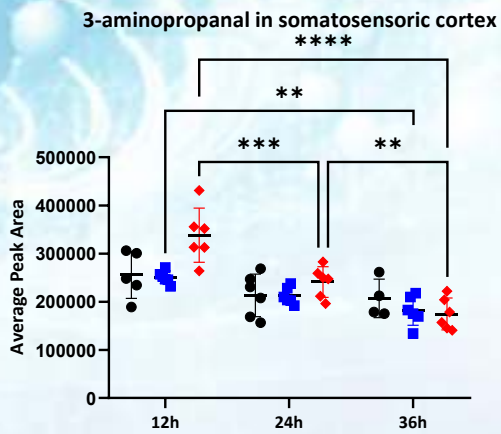

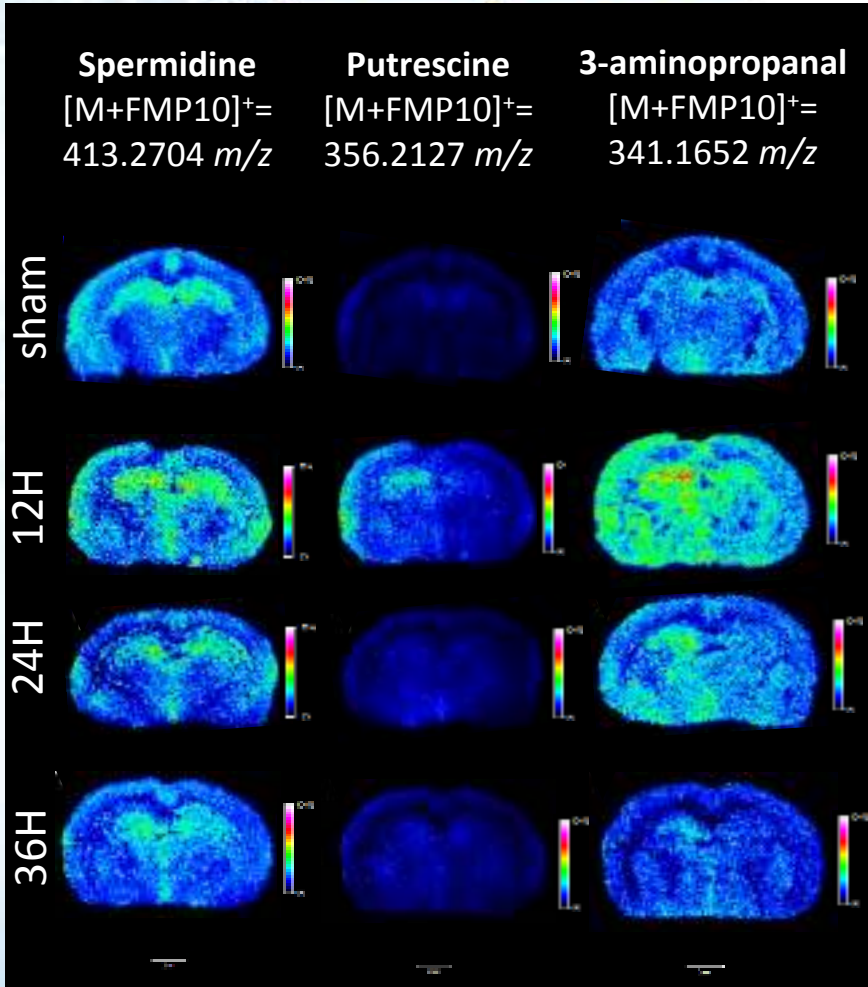

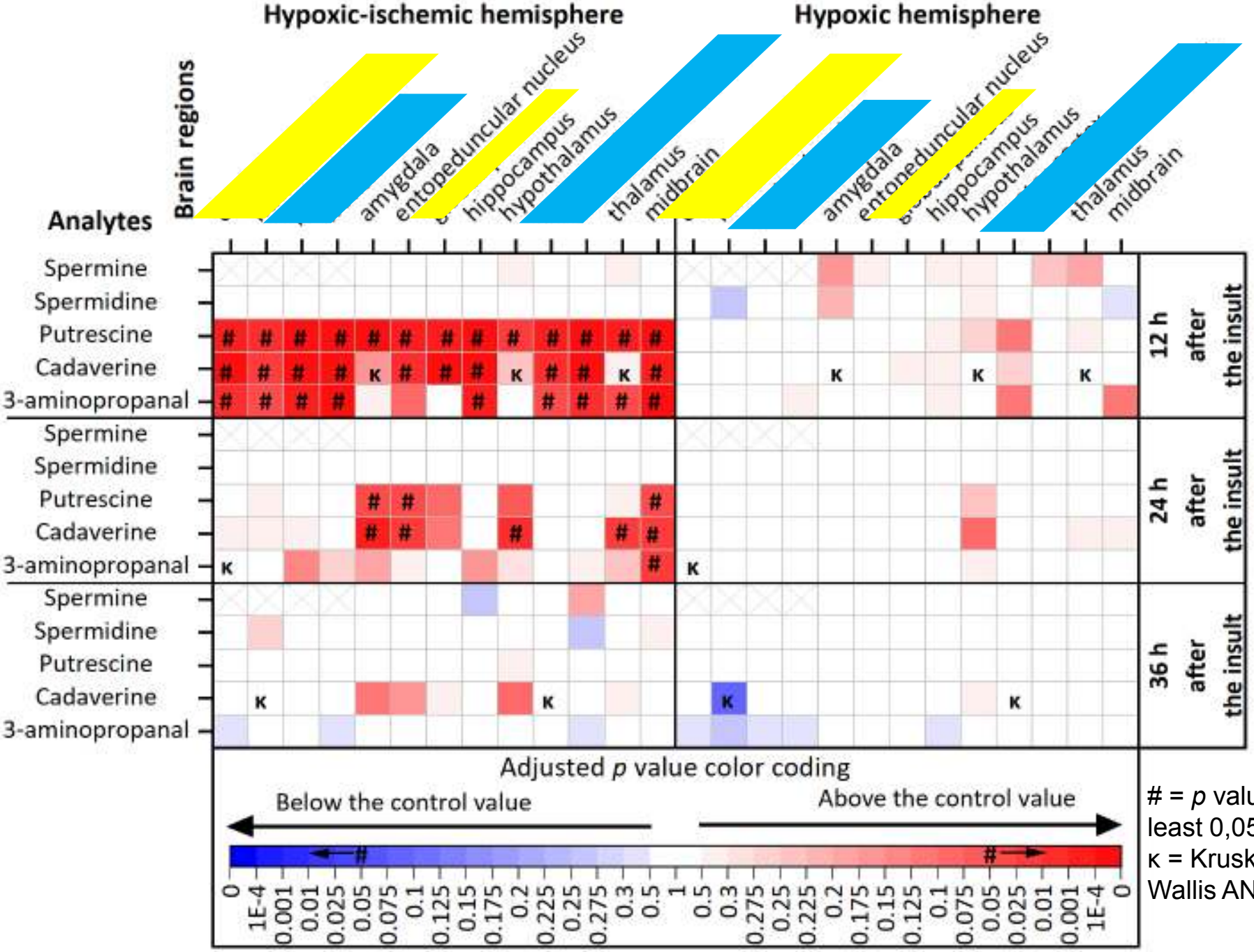
Hypoxic-ischemic hemisphere
Hypoxic hemisphere
Brain regions
Analytes
amygdala
entopeduncular nucleus
hippocampus
hypothalamus
thalamus
midbrain
Spermine
Spermidine
Putrescine
Cadaverine
3-aminopropanal
12 h after the insult
24 h after the insult
36 h after the insult
Adjusted p value color coding
Below the control value
Above the control value
0
1E-4
0.001
0.01
0.025
0.05
0.075
0.1
0.125
0.15
0.175
0.2
0.225
0.25
0.275
0.3
0.5
1
0.5
0.3
0.275
0.25
0.225
0.2
0.175
0.15
0.125
0.1
0.075
0.05
0.025
0.01
0.001
1E-4
0
= p value at least 0,05
κ = Kruskal-Wallis ANOVA

- **Increased level of putrescine, cadaverine, and 3-aminopropanal in the hypoxic-ischemic hemisphere 12 hours** after the insult
  - Putrescine and cadaverine could reflect the severity of ischemic cells injury (*Paschen, W. et al., Neurochemical Pathology, 1988; Shin, T. et al., Stem Cells Int., 2016*)
  - 3-aminopropanal generated from spermidine during ischemia leads to apoptosis (*Li, W. et al., Biochem J., 2003*)

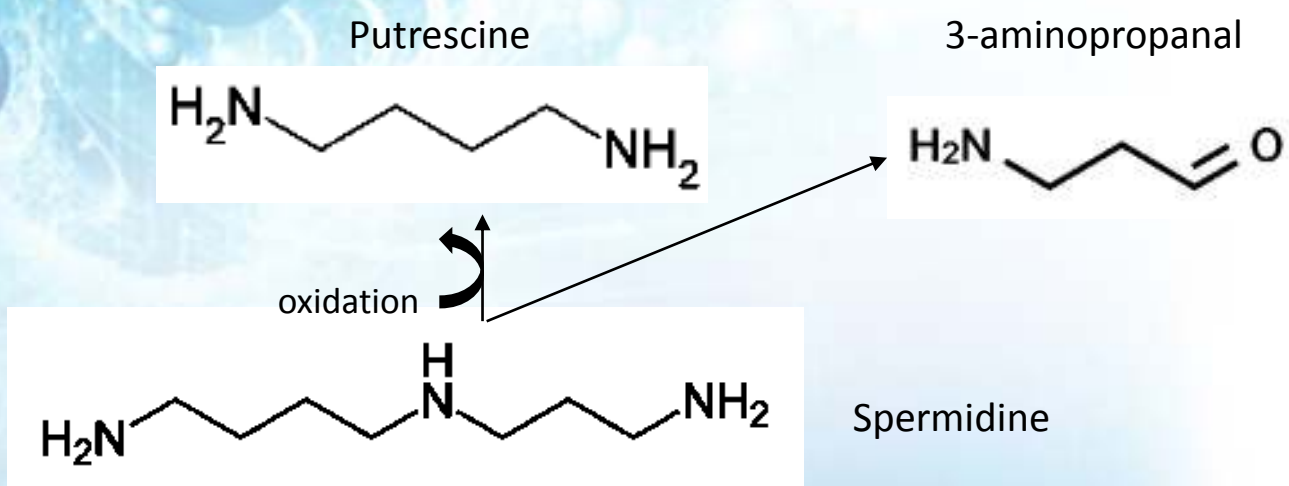

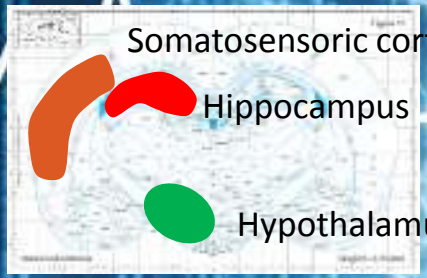

Aminoacids changes

EU FT-ICR MS

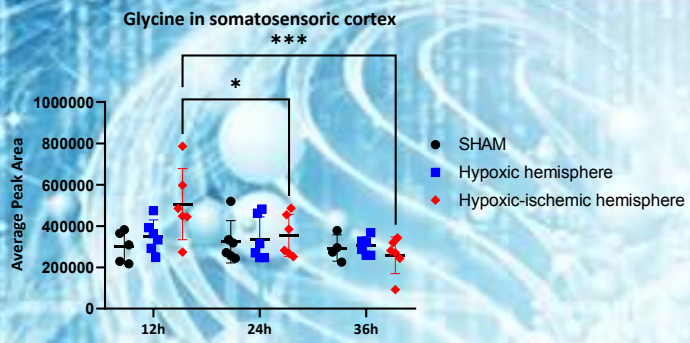

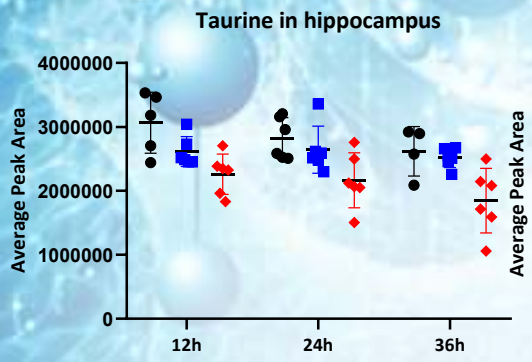

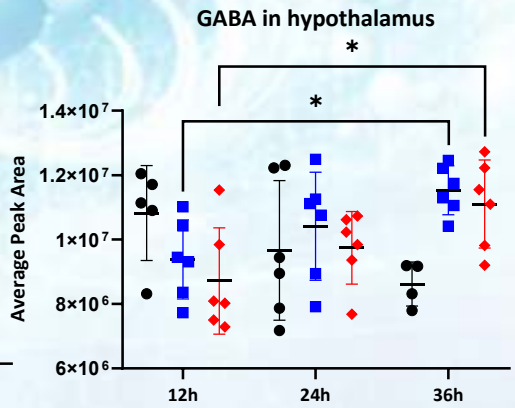

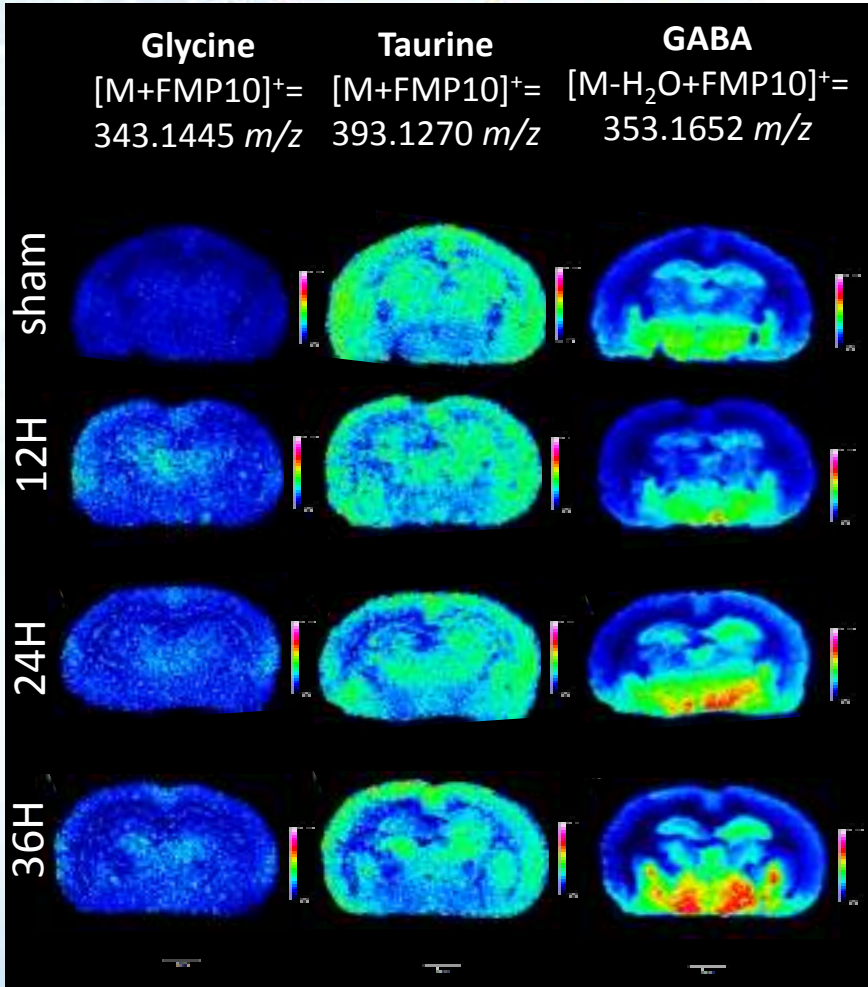

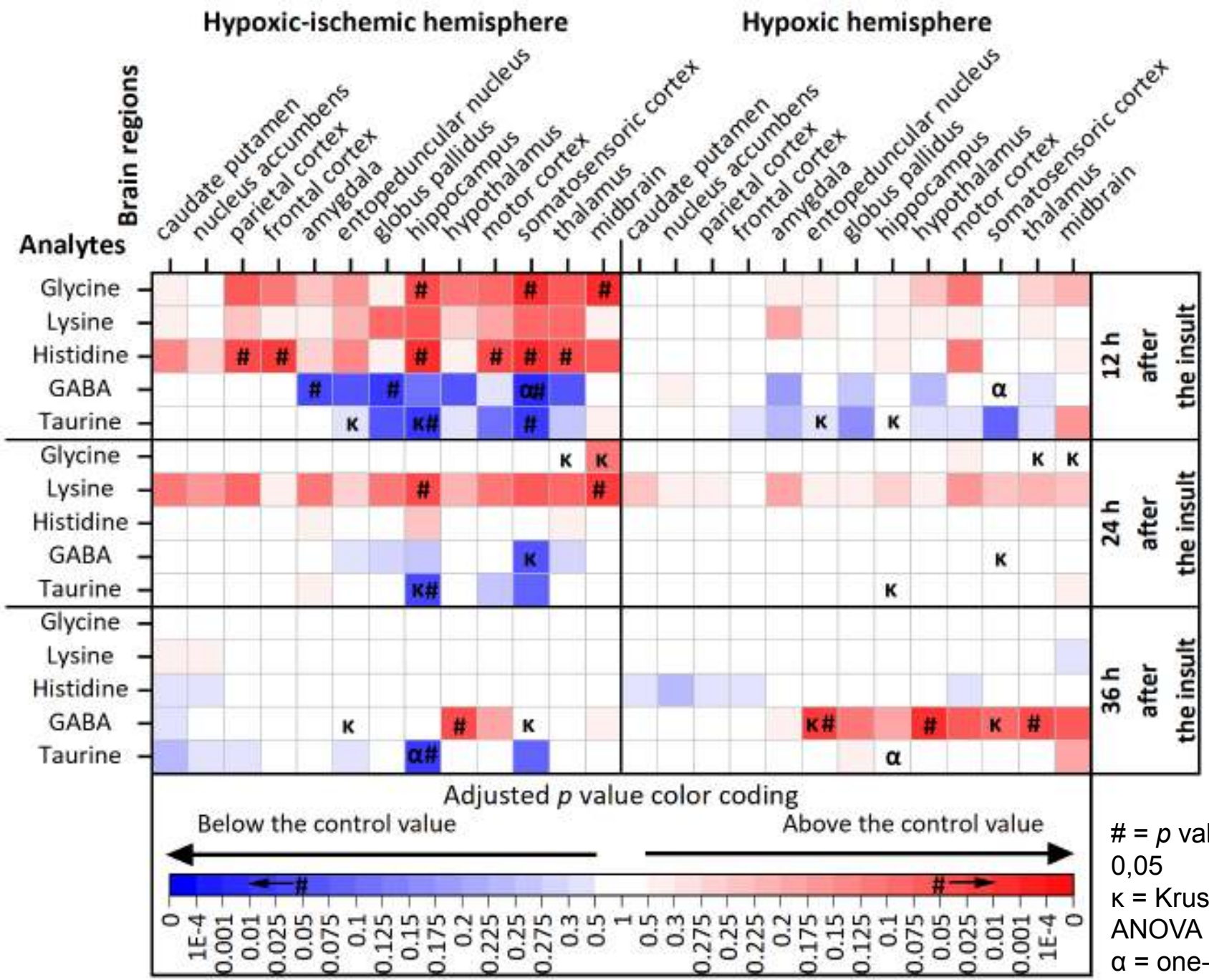

= *p* value at least 0,05
κ = Kruskal-Wallis ANOVA
α = one-way ANOVA

- Aminoacids **histidine** and **glycine** were significantly **higher in the hypoxic-ischemic hemisphere 12h** after the insult
  - Both aminoacids could play a role in neuroprotection as they could lower ischemic damage (*Adachi, N., Brain Research Reviews, 2005; Liu, R. et al, J Immunol, 2019*)

- **Taurine** showed **decreased** intensity trend **in all time points in the hypoxic-ischemic hemisphere,** which may worsen ischemic injury *(Menzie, J. et al, Brain Sci., 2013)*

- **GABA decreased** in the **hypoxic-ischemic hemisphere 12h** and **increased 36h** after the injury in the **hypoxic** only **hemisphere**

Summary

1) We spatialy visualized aminoacids and polyamines by MALDI-MSI
2) We found time-dependent alteration following HI injury
3) Most highlighted changes were seen 12 hours after HI injury

Acknowledgment

prof. Vladimír Havlíček
Dominika Luptáková, PhD

Laboratory of Molecular Structure Characterization
Institute of Microbiology, Academy of Sciences of the Czech Republic

Department of Analytical Chemistry, Faculty of Science, Palacký University Olomouc

prof. Per E. Andrén
Medical Mass Spectrometry Imaging, Department of Pharmaceutical Biosciences
Uppsala University, Sweden

Ivo Juránek, DrSc
Center of Experimental Medicine, Slovak Academy of Sciences, Slovakia

And all lab members

This project has received funding from the European Union's Horizon 2020 research and innovation programme under grant agreement No 731077.

EU FT-ICR MS

Open-shell Pt(III)-containing complexes characterized by IRMPD spectroscopy and quantum chemical calculations

Davide Corinti

Dipartimento di Chimica e Tecnologie del Farmaco, Sapienza- Università di Roma

Prodrug activation,

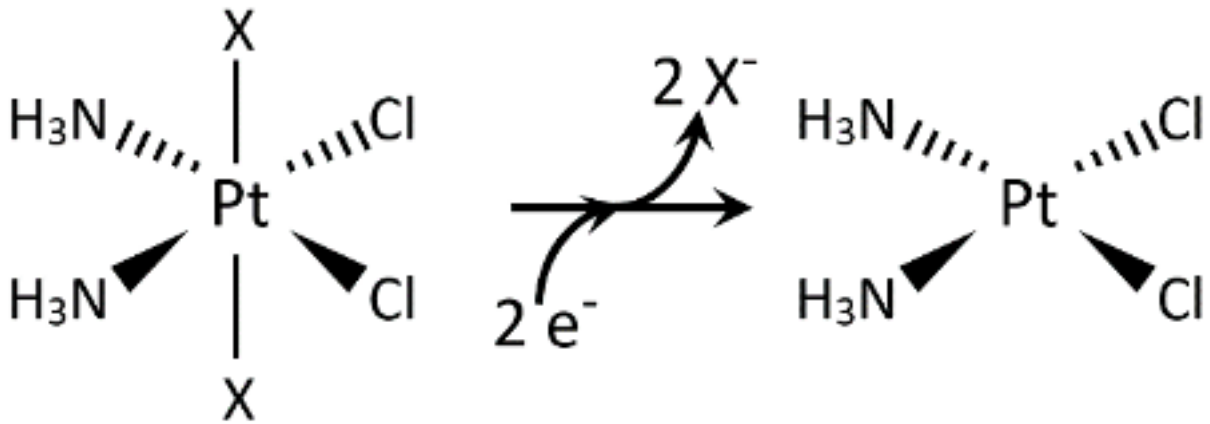

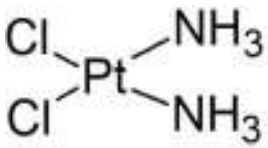

Cisplatin

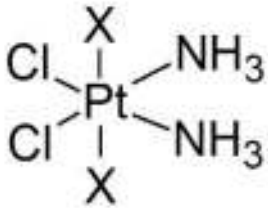

1 X=OH

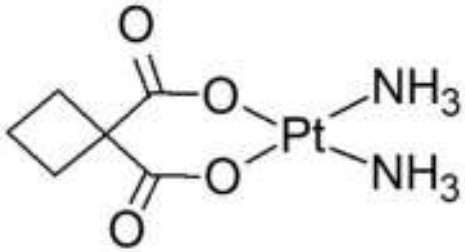

Carboplatin

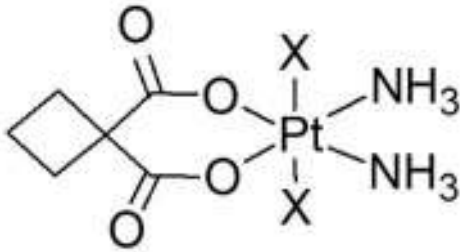

2 X=OH
3 X=CH_3COO

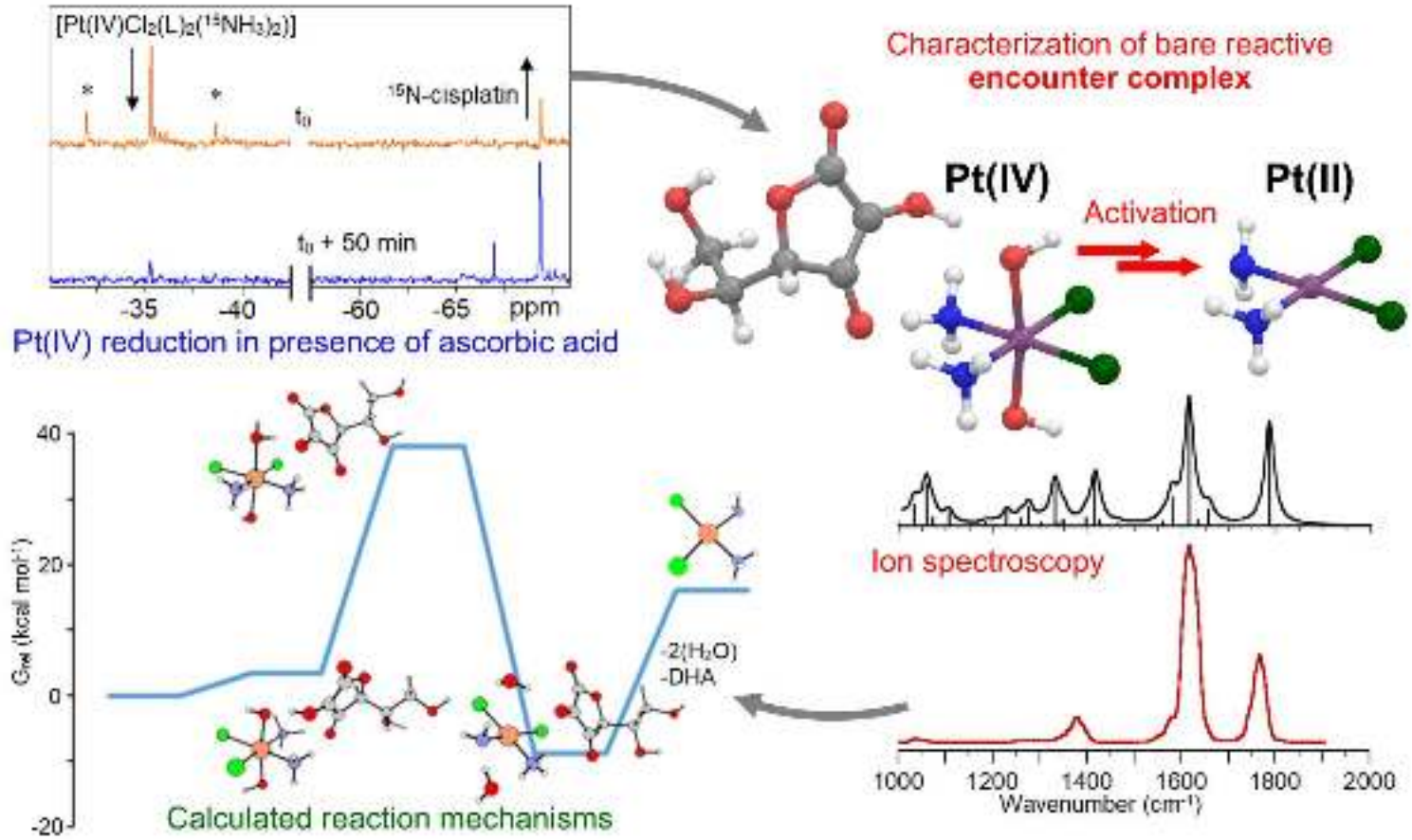

D. Corinti et al. JBIC J. Biol. Inorg. Chem. 25 (2020) 655–670

CID mass spectrum of [**1**-H]$^-$ (*m/z* 331-337)

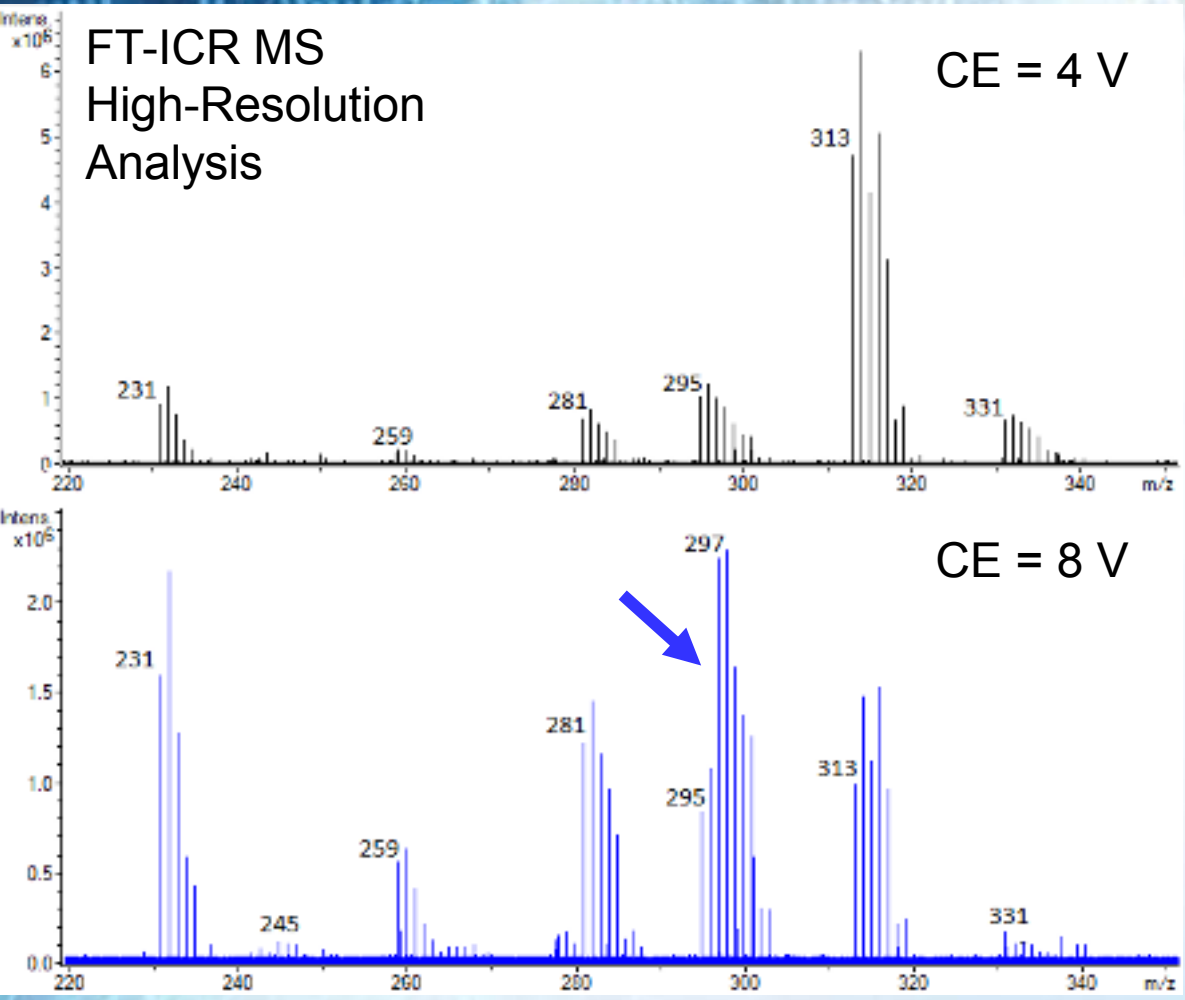

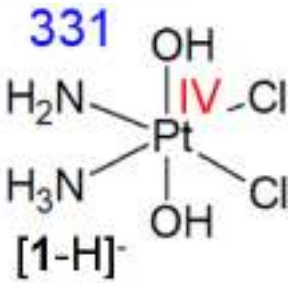

D. Corinti et al., J. Am. Soc. Mass Spectrom. 30 (2019) 1881–1894

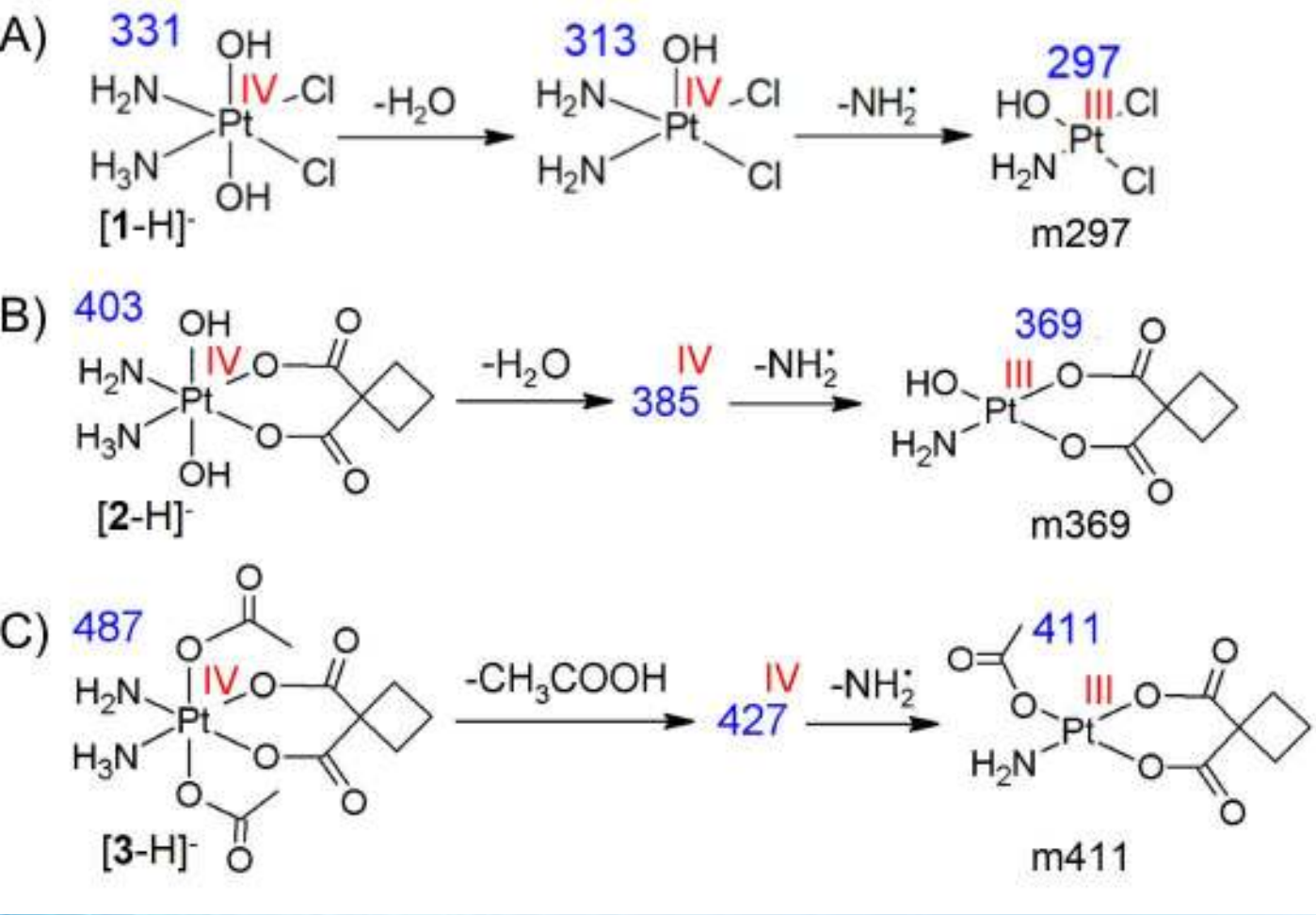

The *m/z* ratio of each species is indicated in **blue** and the formal oxidation state of platinum in **red**.

Each complex is negatively charged; charges are not made explicit

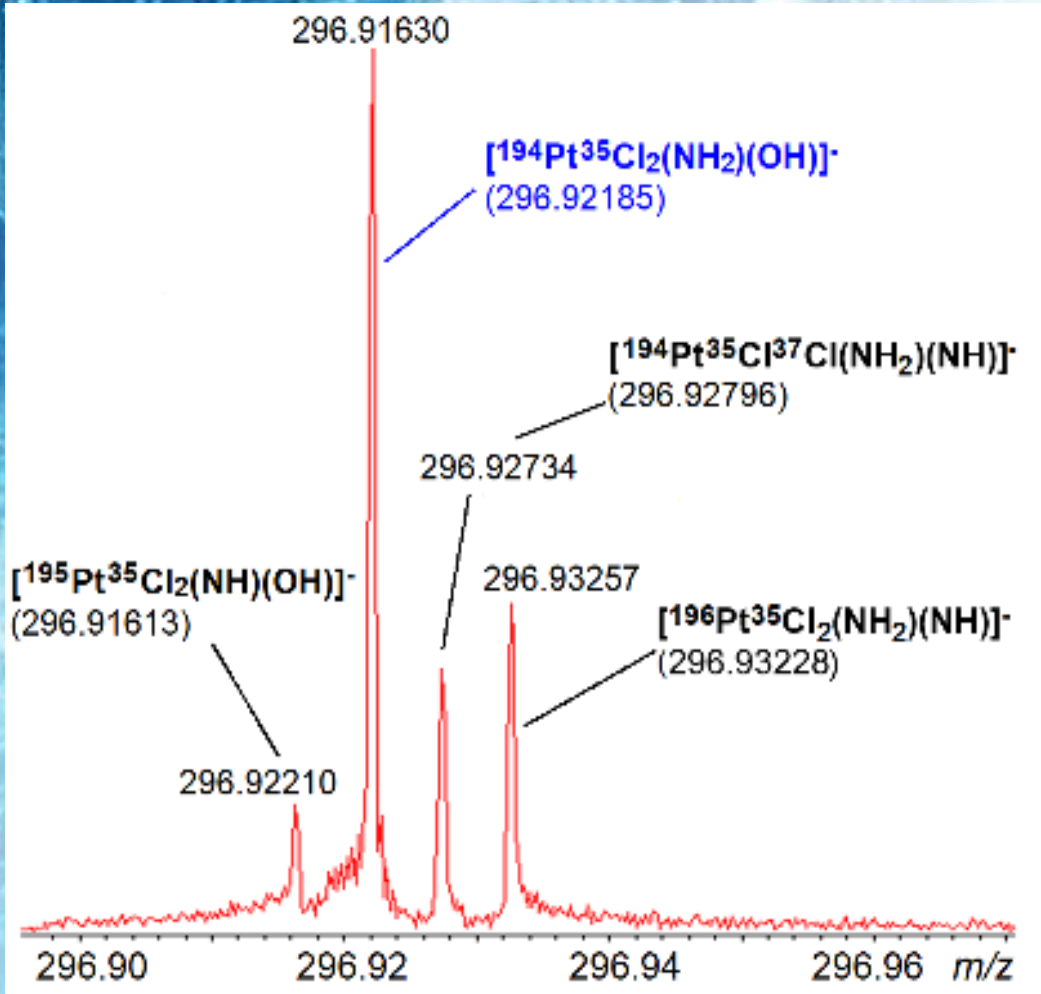

Excerpt of the CID mass spectrum of [**1**-H]$^-$. The assigned elemental composition is reported for each ion together with the corresponding calculated exact mass in Da (in brackets).

The ion corresponding to the Pt(III) containing complex is reported in **blue** while all other species are formal Pt(IV) complexes.

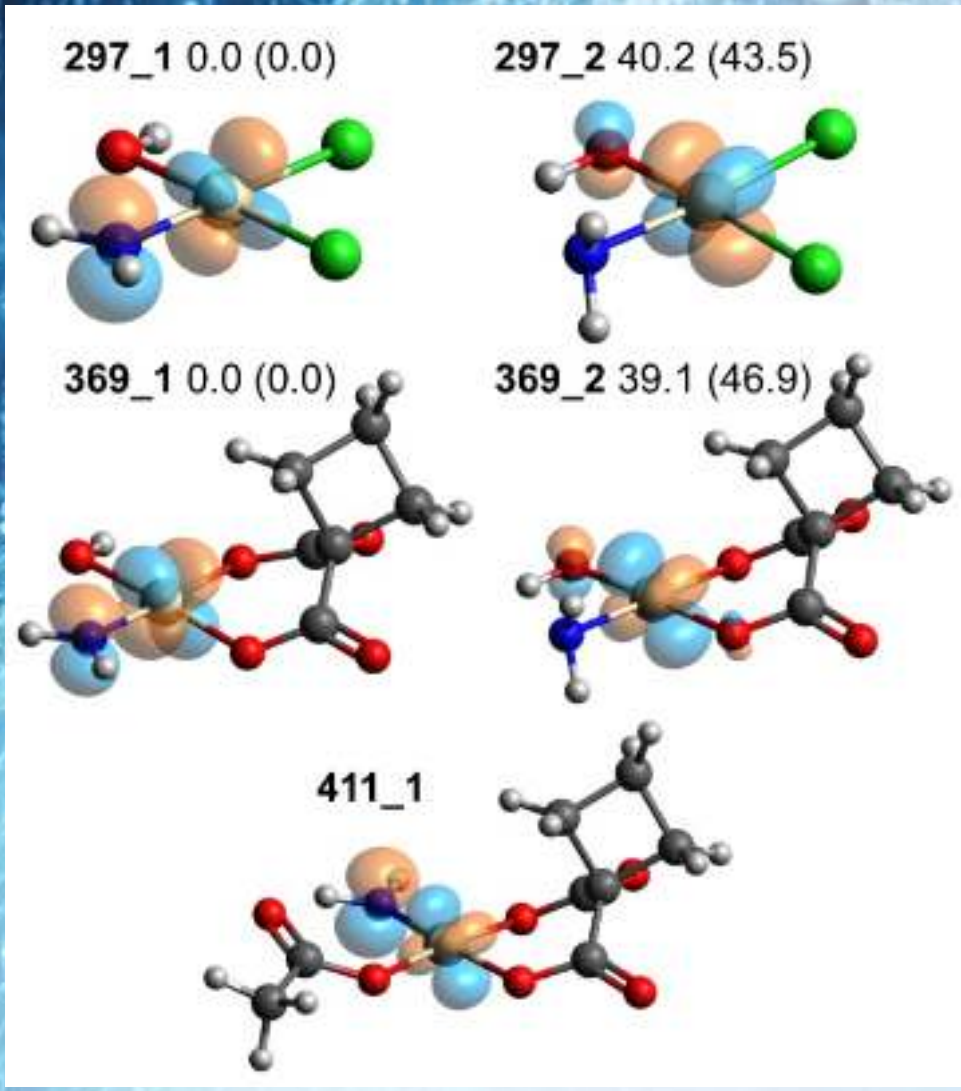

Optimized geometries at the MP2/6-311++G(d,p) (Pt = def2-TZVP) level. SNOs obtained at the MP2/6-311++G(d,p) (Pt = def2-TZVP) level are shown with an isovalue of 0.20.

Relative free energies in kJ mol^{-1} are reported at the B3LYP and MP2 (in brackets) levels.

D. Corinti et al. Angew. Chemie Int. Ed. 59 (2020) 15595-15598

Experimental IRMPD spectrum of a) **m297** compared with the calculated IR spectra of b) **297_1** and c) **297_2** (scaling factor = 0.974).

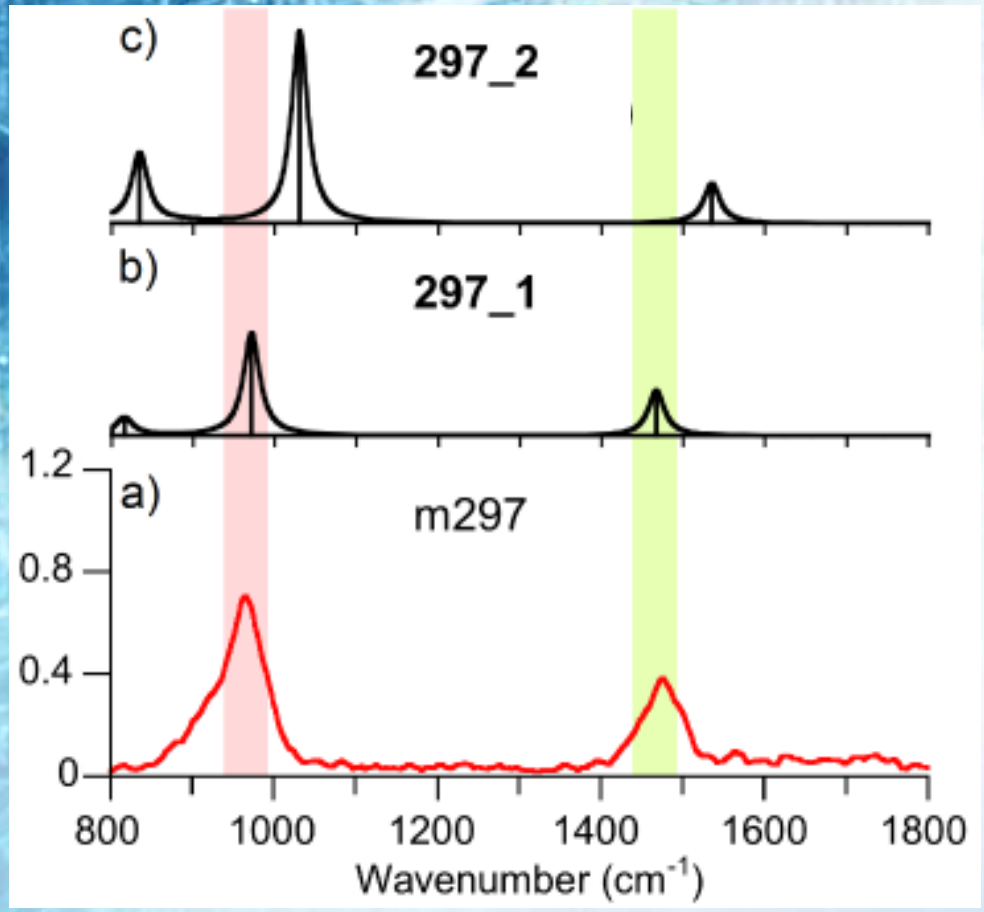

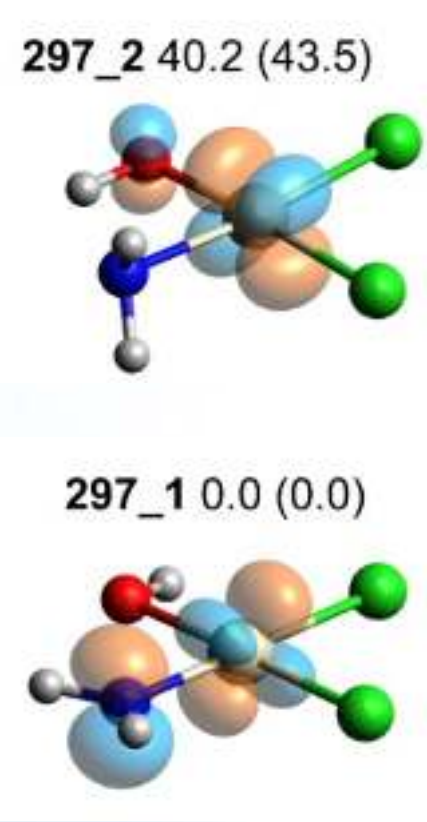

Experimental IRMPD spectra of a) **m369** compared with the calculated IR spectra of b) **369_1**, c) **369_2** (scaling factor = 0.974).

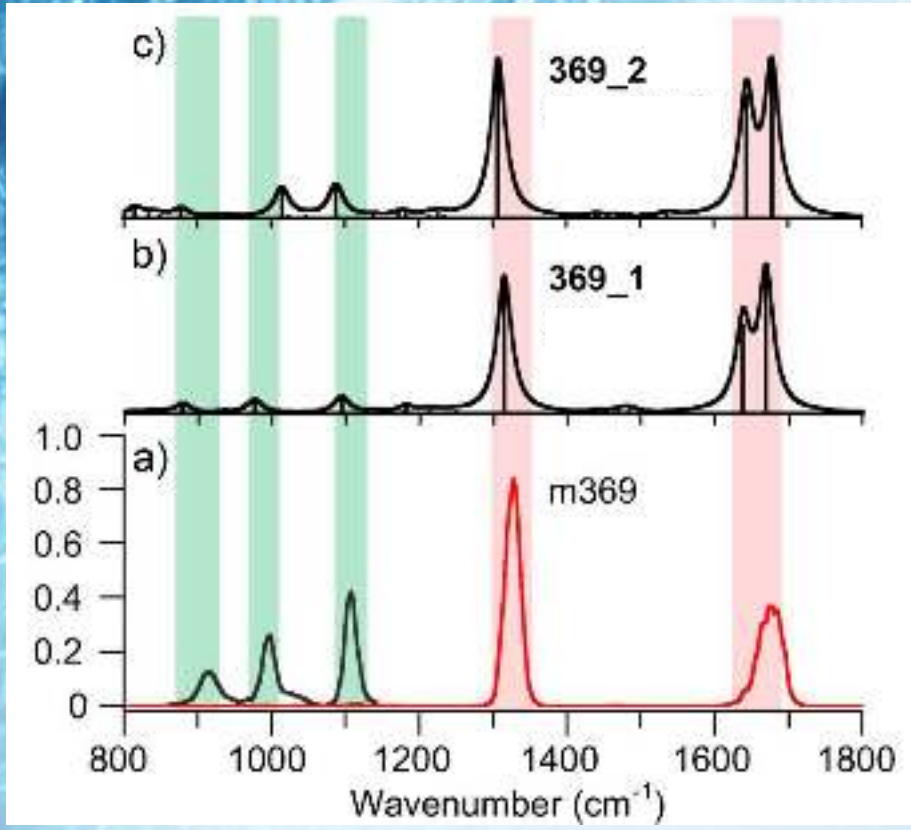

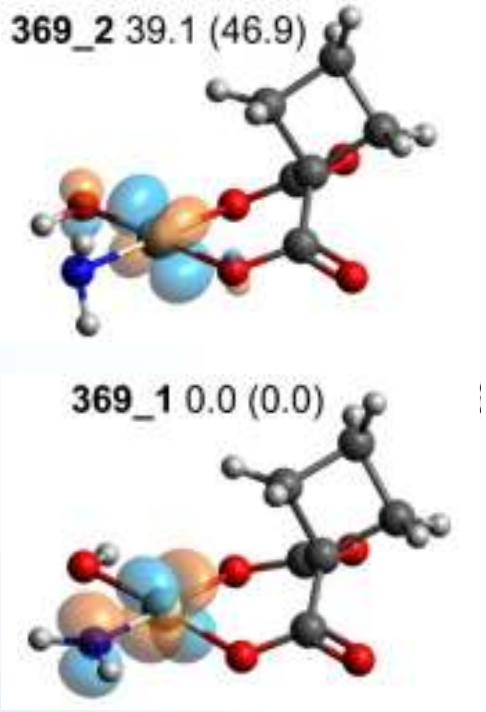

Conclusions

EU FT-ICR MS

- The gas-phase activation of [**1**-H]$^-$, [**2**-H]$^-$ and [**3**-H]$^-$ has permitted to isolate and characterize platinum complexes with **formal metal oxidation state of +3.**

- The participation of platinum in the spin-density of the assayed ions with its d_{xz} orbital is a sign of the presence of a **radical character on platinum**.

- The **noninnocence of the amino ligand**, expressed in the high degree of delocalization of the unpaired electron onto the amino ligand can be identified as the main reason behind the unexpected finding of platinum(III)-containing ions

Acknowledgement

EU FT-ICR MS

Sapienza – Università di Roma
Prof. Simonetta Fornarini
Prof. Maria Elisa Crestoni
Prof. Barbara Chiavarino

Centre Laser Infrarouge d'Orsay
Prof. Debora Scuderi
Prof. Philippe Maitre

Università del Piemonte Orientale
Prof. Domenico Osella
Dr. Elisabetta Gabano

Université Paris-Saclay
Dr. Gilles Frison

This project has received funding from the European Union's Horizon 2020 research and innovation programme under grant agreement No 731077.

Freeing *Aspergillus fumigatus* of polymycovirus infection renders it more resistant to competition with *Pseudomonas aeruginosa* due to altered iron-acquiring tactics

Rutuja H.Patil

Under the supervision of Prof. Vladimír Havlíček

Palacky University in Olomouc
Faculty of Science
Department of Analytical Chemistry

Invasive fungal infections

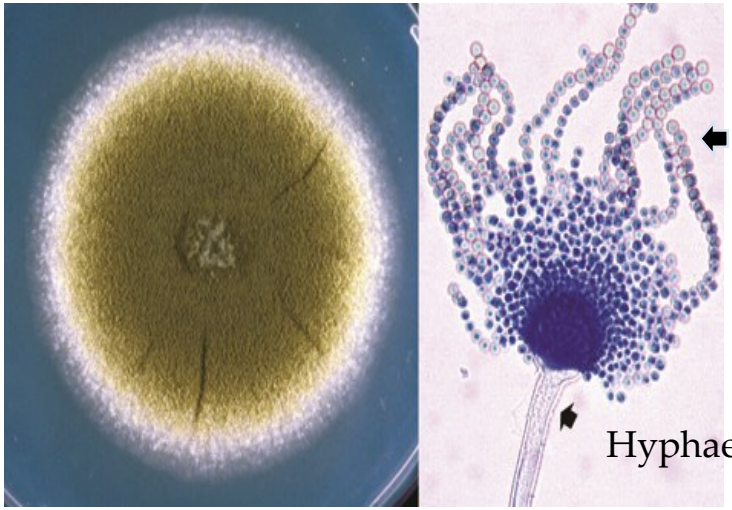

Disease (Most common species)	Location	Estimated life threatening infections/year	Mortality (%in infected populations)
Invasive aspergillosis (Aspergillus spp.)	Worldwide	>200,000	30-95%
Invasive candidiasis (Candida spp.)	Worldwide	>400,000	46-75%

- Common in the immunocompromised patients with AIDS, neutropenia and organ transplant
- If left untreated, invasive aspergillosis can have mortality approaching 95%

Dobiáš, Radim, and Vladimir Havlíček (2020). Microbial siderophores: Markers of infectious diseases. In *Microbial and Natural Macromolecules* (pp. 57-72). Academic Press.

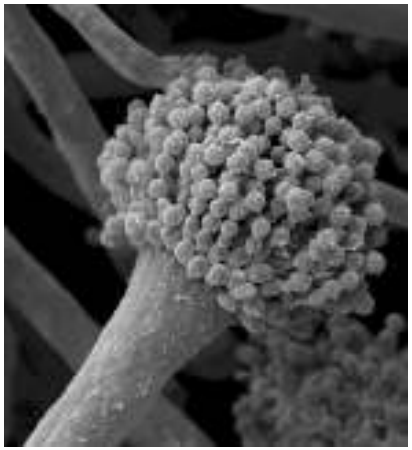

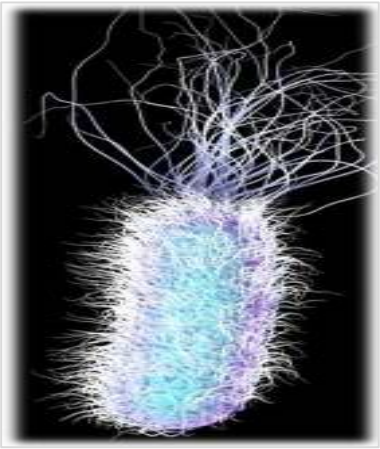

Aspergillus fumigatus *Pseudomonas aeruginosa*

Coexist in nature

- Intermicrobial competition in soil, water and also in the lungs of immunocompromised patients and persons with cystic fibrosis

What are Mycoviruses?

- Viruses that infect fungi
- Either double-stranded (ds) or single-stranded (ss) RNA genomes
- Can affect on fungal morphology, spore production, growth and virulence

How they affect *Aspergillus* physiology or virulence is unclear

Kotta-Loizou, Ioly. "Mycoviruses: past, present, and future." (2019): 361.

Purpose of the study

- *Aspergillus fumigatus* poly-mycovirus 1 (AfuPmV-1) was initially discovered in the *A. fumigatus*
- Virus free (VF) *A. fumigatus* reported to be more resistant in competition with *P. aeruginosa* compared to the virus infected (VI) isogenic lines
- The mycovirus infection weakens *A. fumigatus* via altering fungal stress responses by a mechanism somehow linked to iron metabolism

Nazik, Hasan, et al. "Aspergillus is inhibited by Pseudomonas aeruginosa volatiles." *Journal of Fungi* 6.3 (2020): 118.

Microbial siderophores based approach

- Small, high-affinity iron-chelating compounds secreted by microorganisms

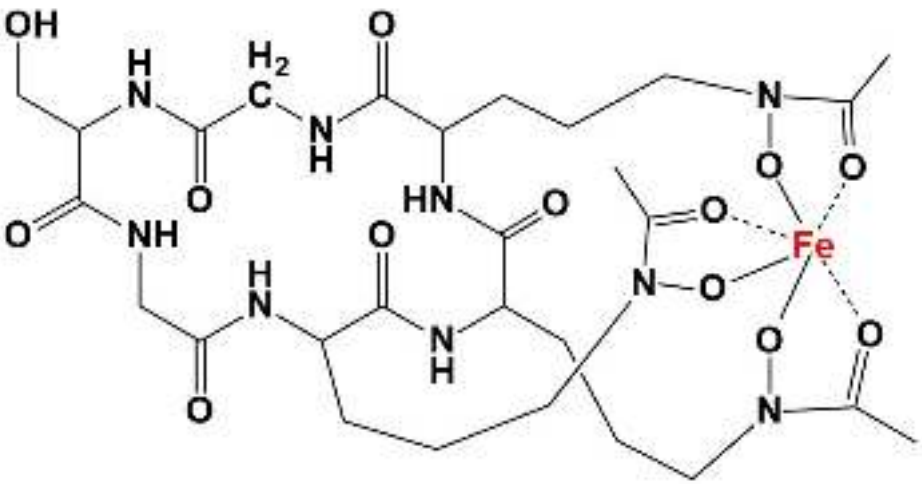

Ferricrocin (FC)

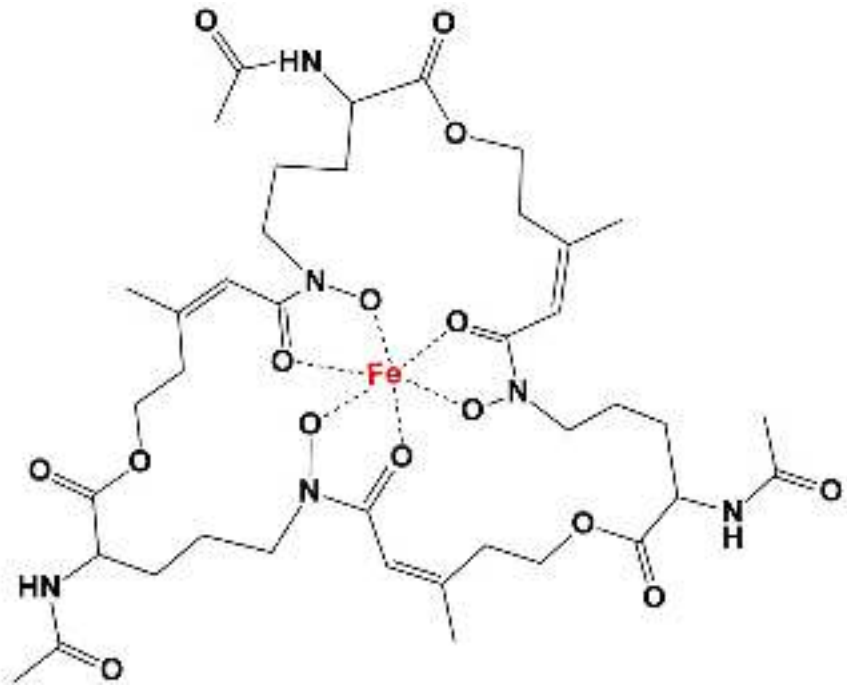

Triacetylfusarinine C (TAFC)

Experimental design

Growth of each strain in iron-limited medium

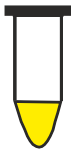

Extraction of siderophores

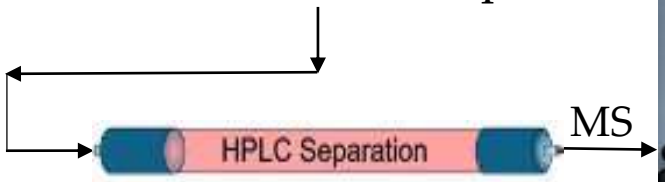

Strain	Designation
18-42 (VF)	UK Af293 cured from AfuPmV-1
18-95 (VI)	UK Af293 with AfuPmV-1
10-53 (VI)	USA Af293 with AfuPmV-1
19-40 (VI)	VF re-infected with AfuPmV-1
19-47 (VI)	VF re-infected with AfuPmV-1

SolariX 12T FT-ICR

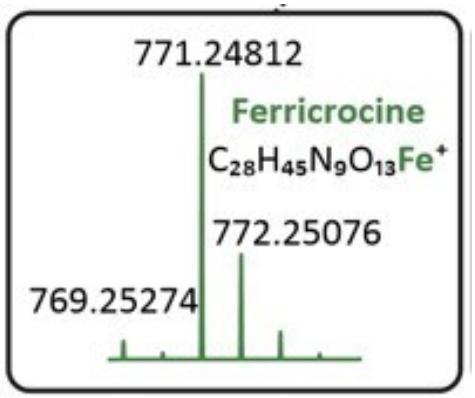

Isotope data filtration

Results

Extracellular secretion kinetics of TAFC

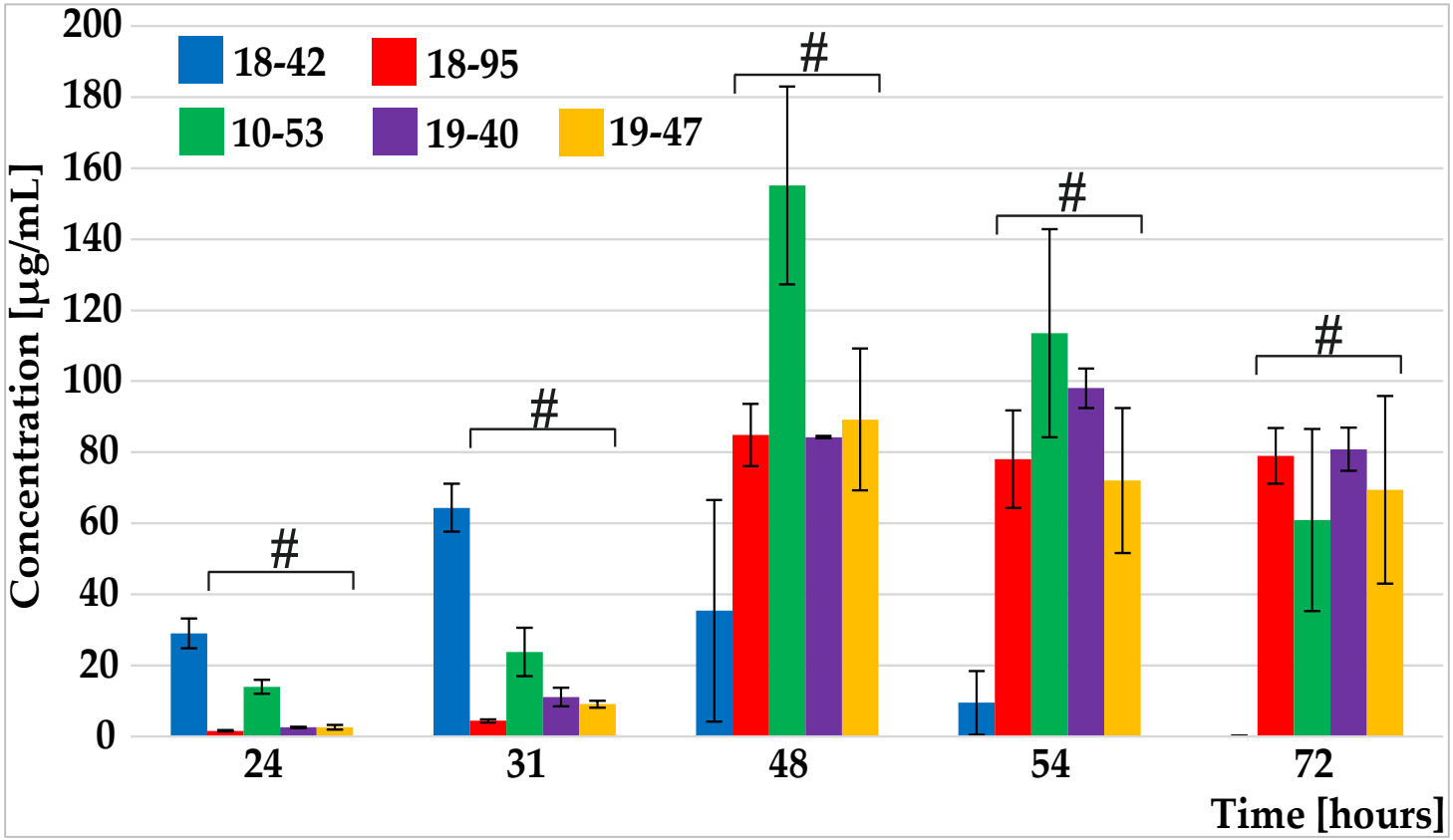

Virus infected strains indicated by an # symbol. The error bars indicate the standard error of the mean, n=9.

Content of **FC** in the stationary phase, i.e., **a) 48** and **b) 52** hours of cultivation

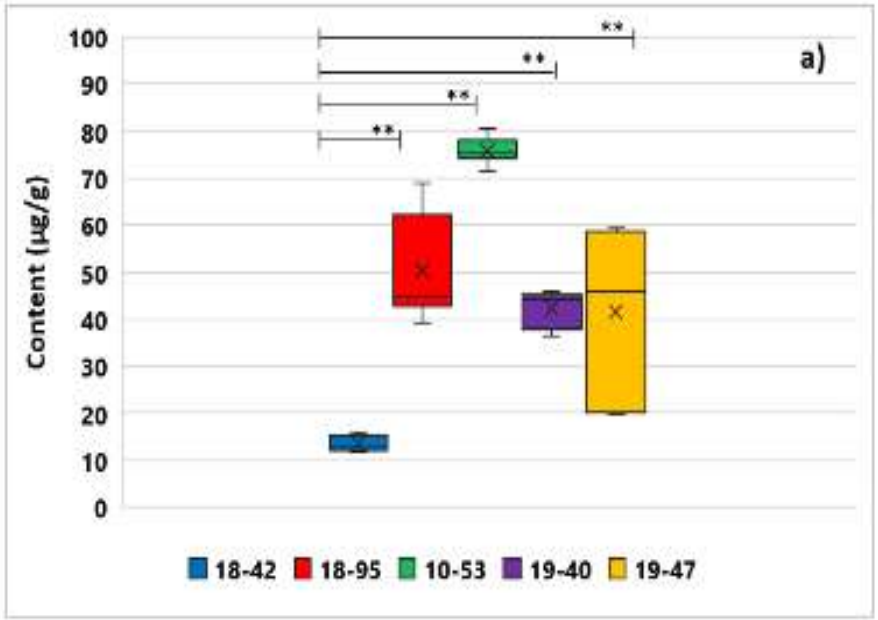

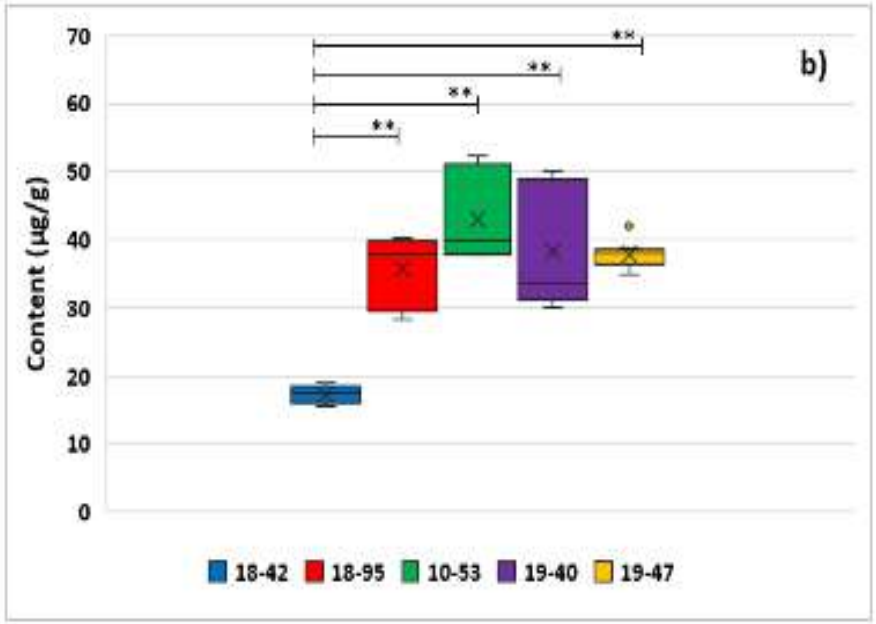

The Kruskal-Wallis One-Way ANOVA with Bonferroni Multiple Comparison results are represented by line segments marked by * * ($P < 0.01$), n=9.

The HFC/FC content variation in *A. fumigatus* conidia

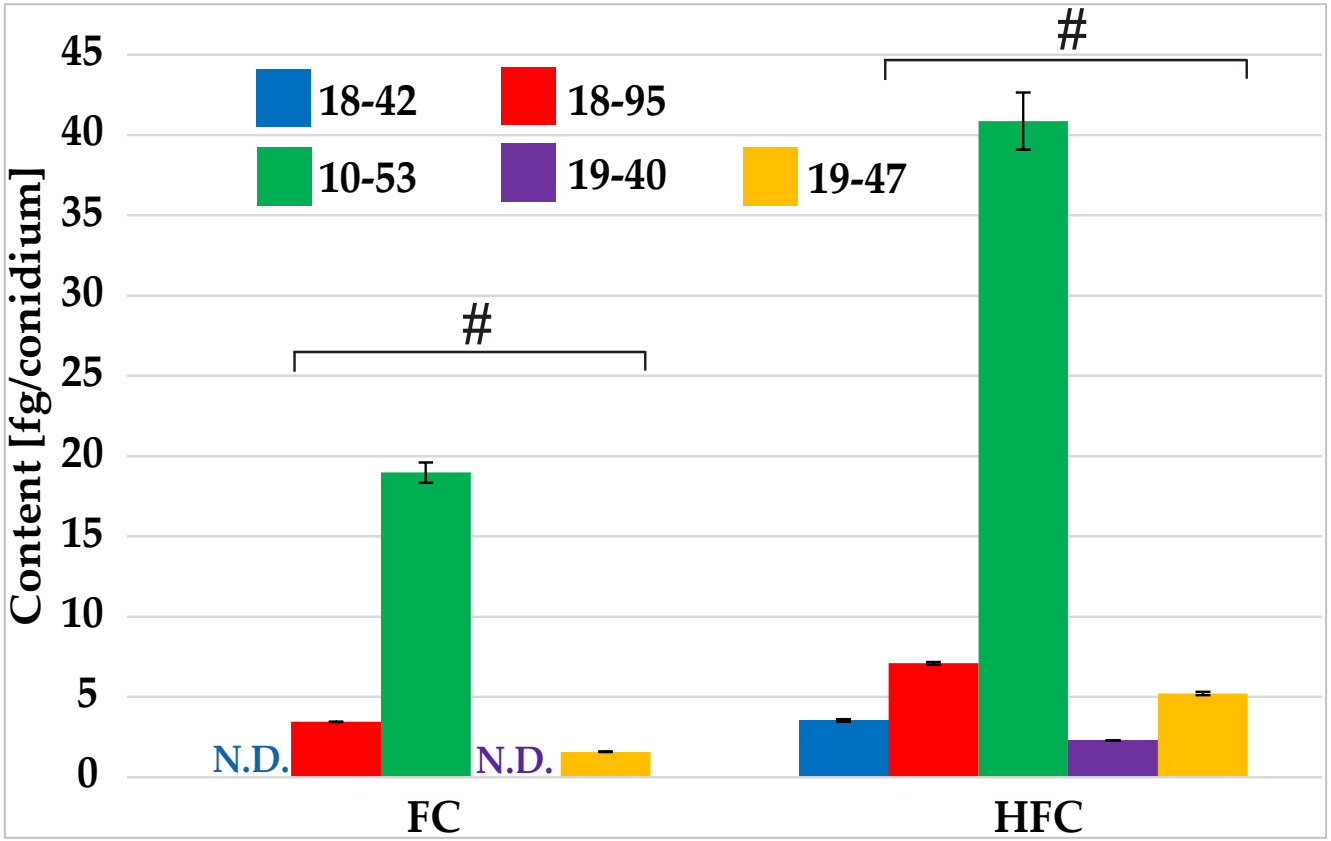

Virus infected strains indicated by an # symbol, N.D. denotes the FC content below limit of detection

Summary

- Mycoviruses interfere with host cell metabolism and, in so doing, alter production of fungal metabolites.

- Due to altered iron-acquiring tactics, the siderophore reservoir is consumed sooner by the VF *A. fumigatus* strain, which better withstood the competition for iron with *P. aeruginosa*.

- Viral proteins or RNA may interfere with non-ribosomal fungal siderophore synthesis and alter the fungal stress responses.

- Iron metabolism is a critical aspect of the competition between *A. fumigatus* and *P. aeruginosa*.
- Fungal virulence attenuation through transfection of Aspergillus with mycoviruses represents a promising experimental approach analogous to antibacterial phage therapy.

Acknowledgement

Support:
The Czech Science Foundation (21-17044S) and the internal grant agency of Palacký University (IGA_PrF_2021_021).

Supervisor: **Prof. Ing. Vladimír Havlíček, PhD**

Team: David A. Stevens, PhD
Ioly Kotta-Loizou, PhD
Andrea Palyzová, PhD
Tomáš Pluháček, PhD
Robert H. A. Coutts, PhD

California Institute for Medical Research

Palacký University Olomouc

Stanford MEDICINE

Imperial College London

Thank you

Siderophore-based differentiation of *Aspergillus fumigatus* colonization and invasion

Dominika Luptáková, Ph.D.

Institute of Microbiology of the Czech Academy of Sciences, Prague, Czech Republic
dominika.luptakova@biomed.cas.cz

Aspergillus fumigatus

- Omnipresent airborn pathogen
- In iron limited conditions – activation of iron acquisition strategies:
  - Reductive iron assimilation
  - **Siderophore-mediated iron acquisition**

Triacetylfusatinine C

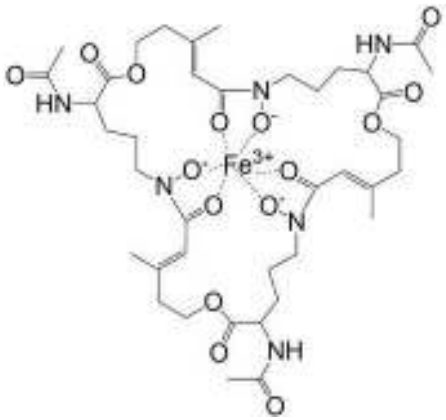

- **Siderophores:**
  - low molecular mass, **high-affinity ferric iron specific chelators** responsible for iron storage and acquisition
  - **Expression is regulated by actual fungal germination stage**

Ferricrocin

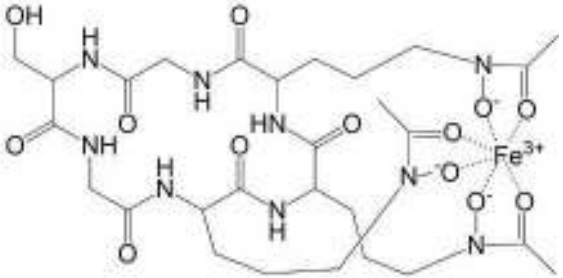

Invasive pulmonary aspergillosis in human

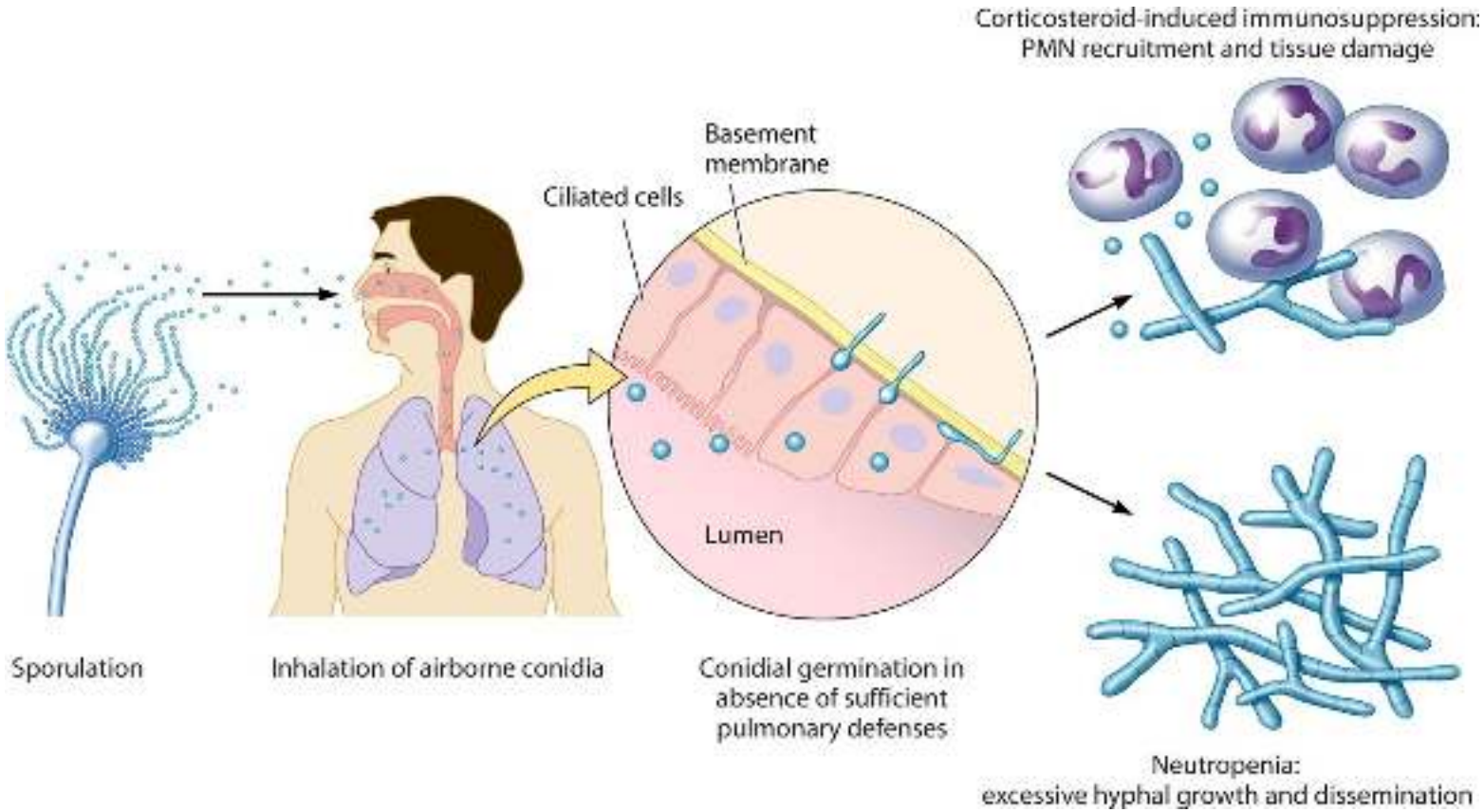

Dagenais, T. R. T.; Keller, N. P., *Clinical Microbiology Reviews* **2009,** *22* (3), 447-465

Aims of the study

- Detection of siderophores in invasive pulmonary aspergillosis animal model.
- Determination of *A. fumigatus*-produced siderophores in relation to its germination phase.
- Diagnosis of invasive pulmonary aspergillosis in critically ill patients.

From *in vitro* to *in vivo* study of invasive pulmonary aspergillosis

Animal study

Intratracheal application of *A. fumigatus* conidia (10^8 CFU)

Germination study

Cultivation of *A. fumigatus* conidia in iron-limited mineral medium at pH 7

Conidia
Pellet
Supernatant

LC-FT-ICR MS
FT-ICR MS Imaging

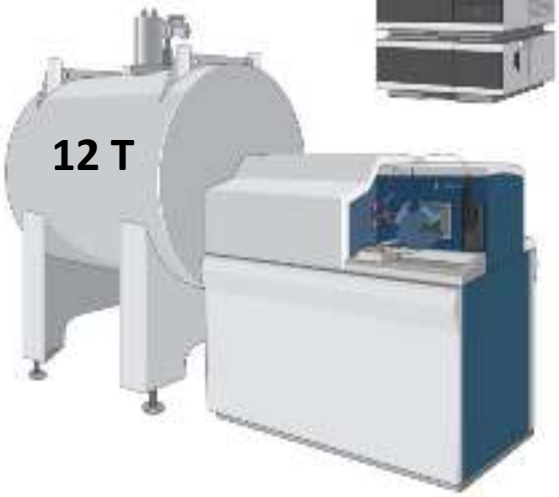

Clinical study

13 patients **diagnosed invasive pulmonary aspergillosis** and **22** patients **having other type of pulmonary disease**

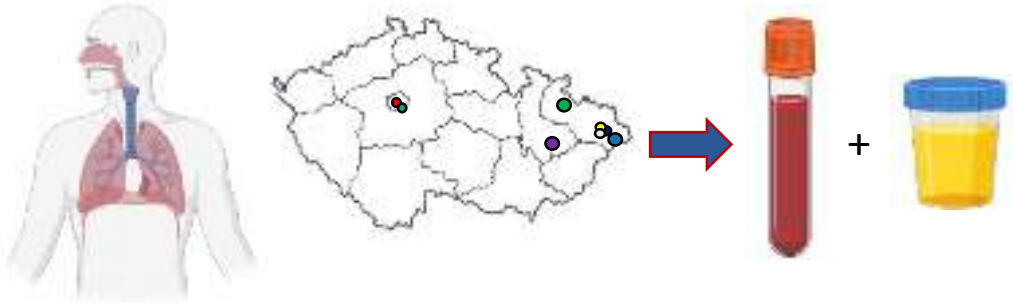

Infection metallomics

A tool based on the clinical **analysis of metal-containing microbial virulence factors**, specifically, analysis of metal-containing infection biomarkers **using a combination of elemental and molecular MS** that can be potentially applied in a wide range of pathogen-related functional studies

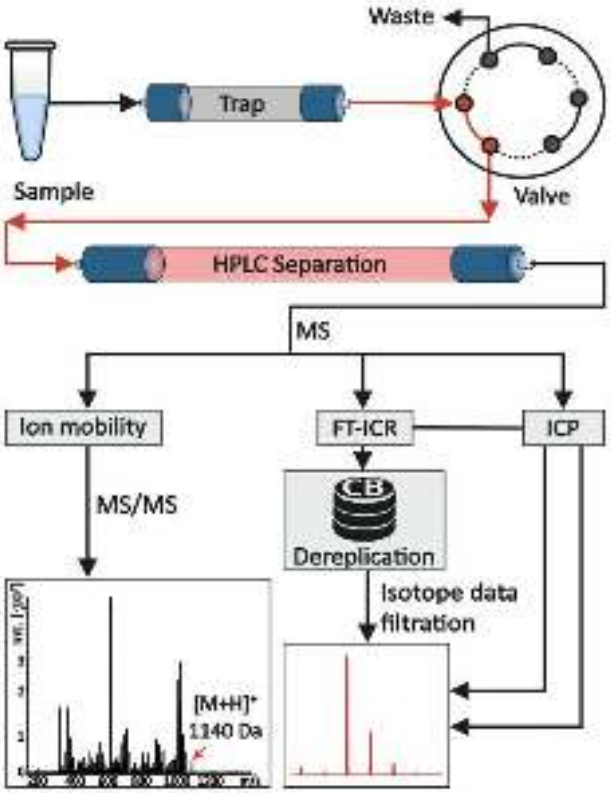

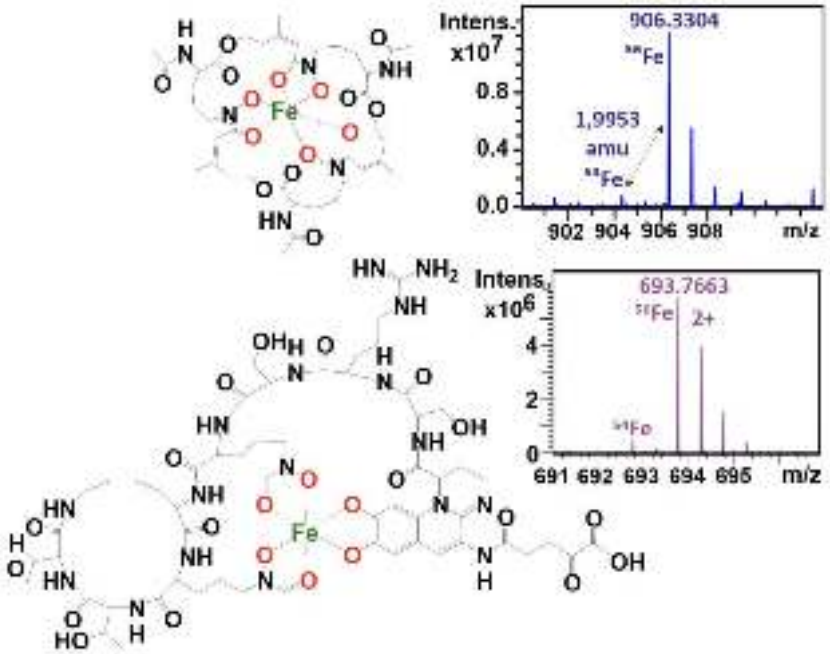

Patil, R.H., et al, 2021 (submitted)

Detection of siderophores in lung tissue

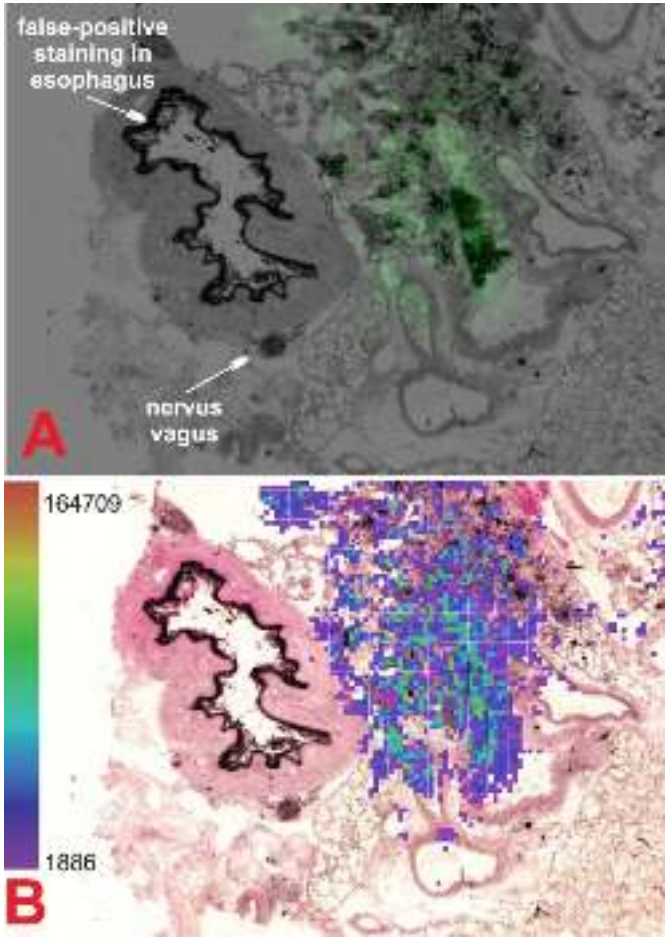

[Ferricrocin+Na]$^+$
m/z 740.3179

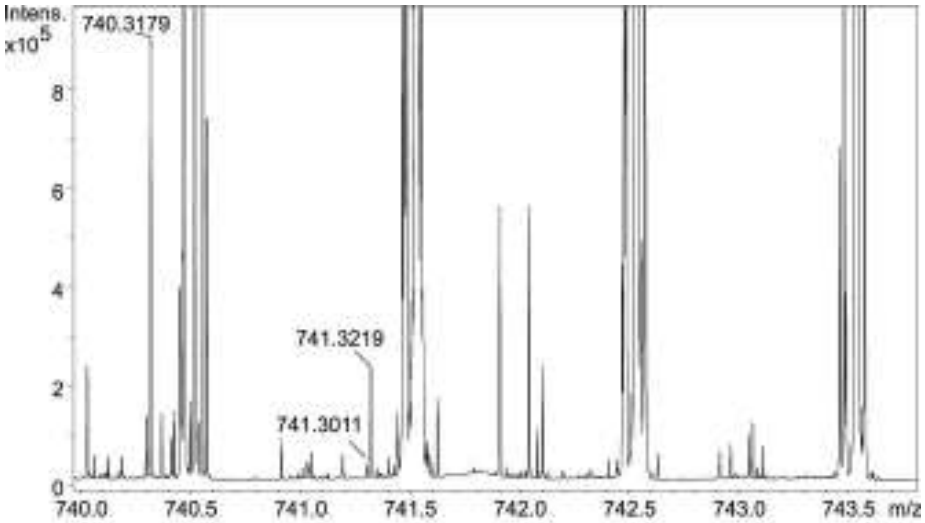

Luptáková, D., *Scientific Reports* **2017,** *7* (1), 16523.

Detection of siderophores in urine

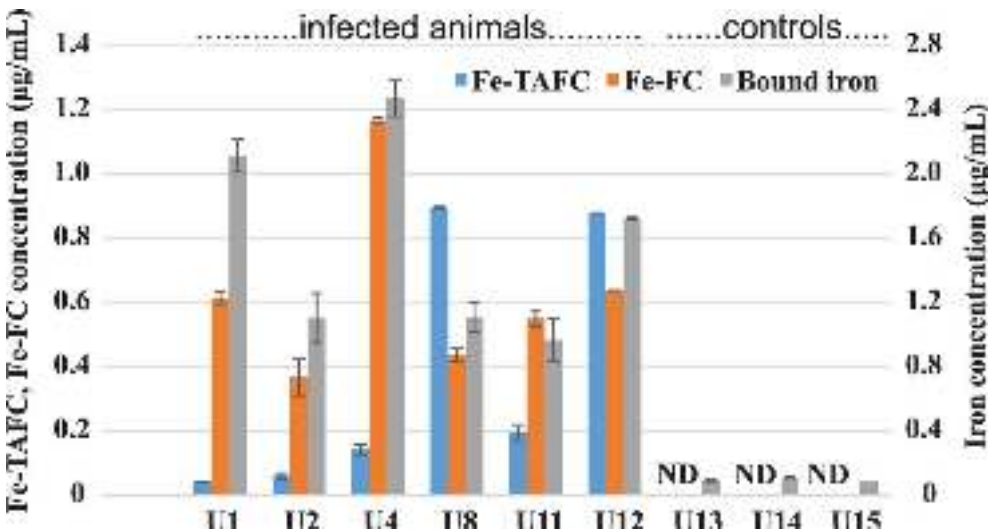

Triacetylfusatinine C

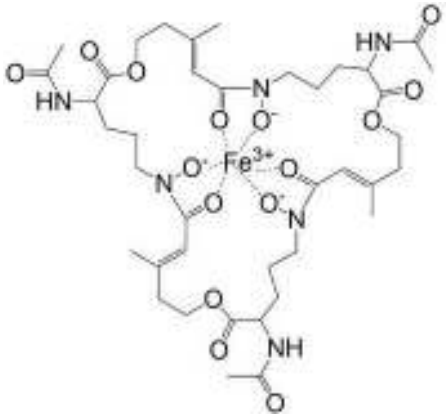

Ferricrocin

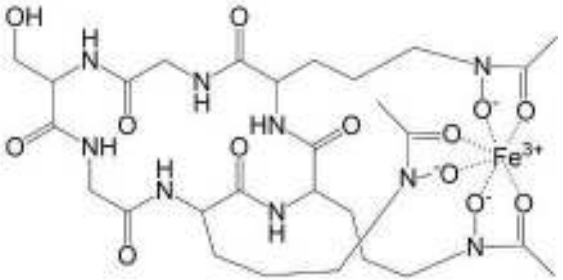

Luptáková, D., *Scientific Reports* **2017,** *7* (1), 16523.

In vitro screening of *A. fumigatus* germination – phase dependent production of siderophores

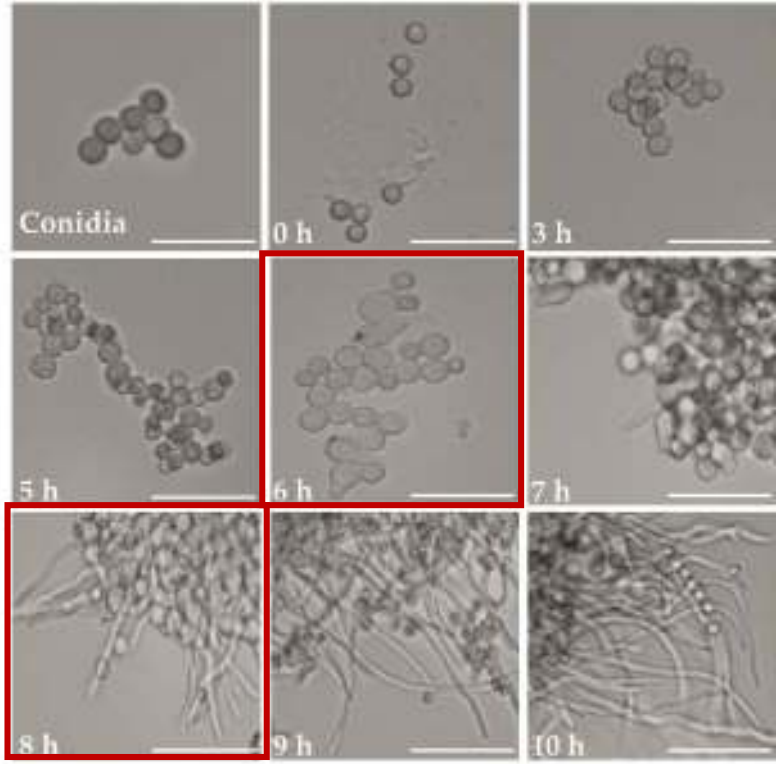

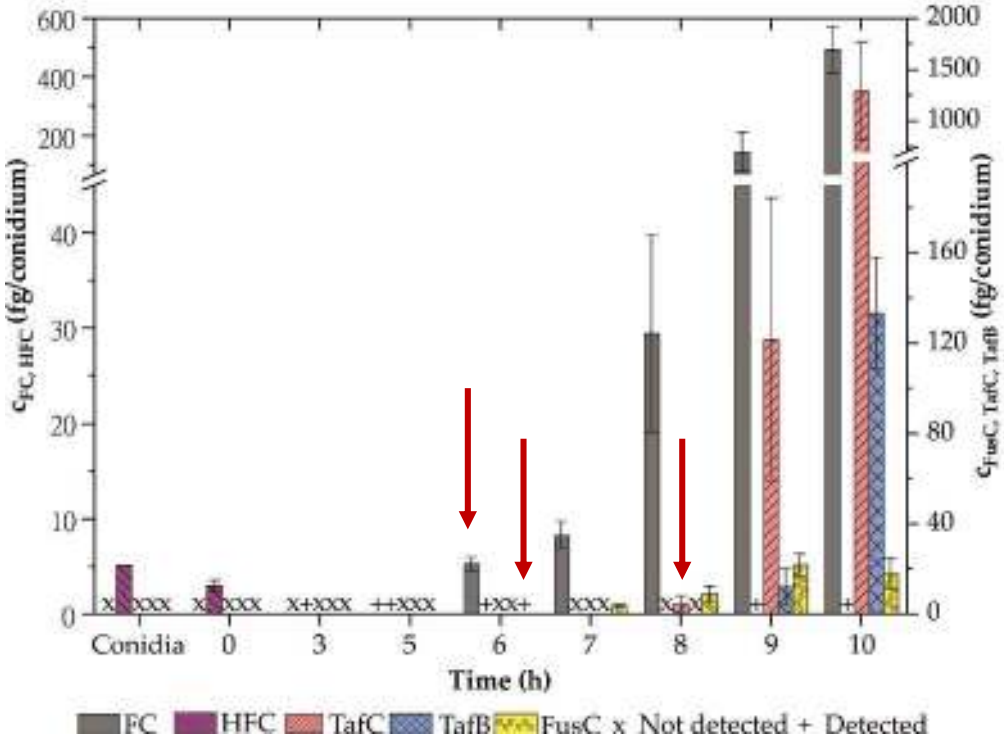

Monitoring of infection by *infection metallomics*

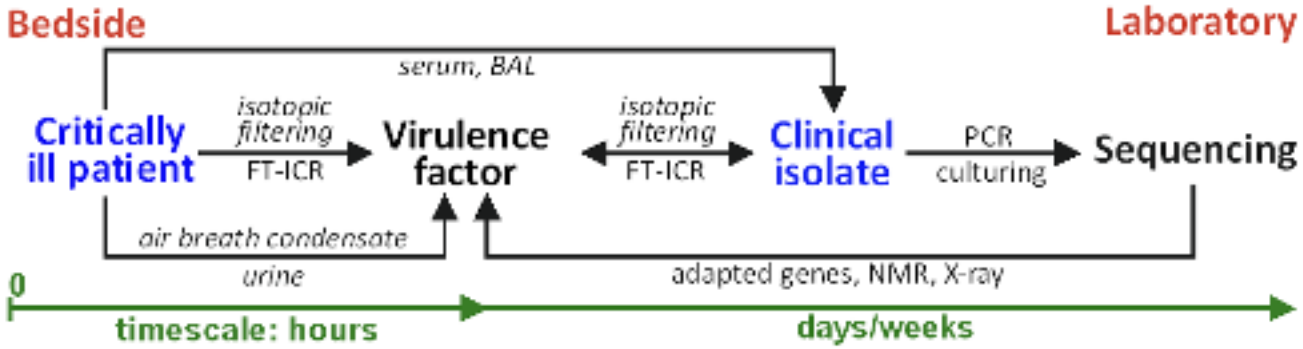

Non-invasive diagnostics of invasive pulmonary aspergillosis in urine

No.	GD	Age	Underlying disease	Risk factor	*Infection Metallomics*				Conventional clinical approach	
					uGtx/crea index*	uFC/crea index*	uTafC/crea index*	uTafB/crea index*	sGM (ODI)	sBG (pg/mL)
#1	M	50	Multiple myeloma	Neutropenia	15.8±1.0	1.5±0.3	17.2±0.2	0.4±0.0	1.56	501
#2	F	66	Cellular lymphoma	Neutropenia	2.8±0.2	nd	32.1±0.4	det	3.14	115
#3	M	79	Flu (H1N1)	Flu (H1N1)	85.2±3.7	8.3±0.7	82.9±1.5	5.4±0.1	5.9	276
#4	M	71	BB		nd	11.9±2.7	35.7±0.4	11.5±0.4	0.89	>523
#5	M	66	COPD, flu (H1N1)		nd	nd	1.7±0.1	nd	0.1	161
#6	M	50	BB	Diabetes mellitus II	33.8±1.4	4.2±0.5	2.3±0.1	0.4±0.0	0.26	155
#7	M	65	ARDS	Steroids	67.9±6.6	40.6±2.2	3117.4±78.2	59.6±3.0	7.9	>523
#8	M	59	Liver transplant	IST steroids	nd	nd	27.6±0.3	4.2±0.3	0.06	221
#9	M	61	BB	Sepsis**	nd	nd	12.9±0.3	nd	0.27	>523
#10	M	51	Polytrauma	Sepsis**	nd	nd	1.6±0.2	nd	0.24	75
#11	M	68	COPD, TBMA	Chronic ethylism	569.3±13.1	505.1±8.0	1071.1±5.6	251.3±2.2	0.126	>523
#12	M	63	Hepatopathy		nd	nd	det	nd	0.121	439
#13	M	75	Burns	Sepsis**	nd	nd	1.3±0.1	0.5±0.0	0.18	0
			Sensitivity (%)		**46.2**	**53.8**	**100**	**69.2**	**38.4**	**84.6**
			95% CI		17.6 - 71	25 - 81	66.1 – 99.8	39-91	12.7 - 65	57.2 - 98
			Specificity (%)		**100**	**100**	**100**	**100**	**73**	
			95% CI		76.8 - 100	76.8 - 100	76.8 - 100	76.8 - 100	39 - 94	

Summary

- Visualization of *A. fumigatus* infection in rat lung tissue.
- Detection of siderophores – ferricrocin and triacetylfusarinine C in rat plasma and urine.
- Activation of *A. fumigatus* excretome defines a borderline between colonization and invasion.
- **Triacetylfusarinine C**, triacetylfusarinine B, **ferricrocin**, and gliotoxin were markers of enhanced *A. fumigatus* proliferation and were detected non-invasively in urine of 13 patients with invasive pulmonary aspergillosis.

Thank you for your attention

EU FT-ICR MS

Acknowledgment

EUROPEAN UNION
European Structural and Investment Funds
Operational Programme Research, Development and Education

MINISTRY OF EDUCATION, YOUTH AND SPORTS

GAČR
GRANTOVÁ AGENTURA ČESKÉ REPUBLIKY

Prof. Vladimír Havlíček
Tomáš Pluháček, Ph.D.
MSc. Rutuja H. Patil
Andrea Palyzová, Ph.D.
Anton Škríba, Ph.D.
Jiří Novák, Ph.D.
Helena Marešová, Ph.D.
Radim Dobiáš, Ph.D.
Miloš Petřík, Ph.D.

And all lab/team members

This project has received funding from the European Union's Horizon 2020 research and innovation programme under grant agreement No 731077.

Oil paints in art: identifying and unravelling their reticulation by chemical depolymerization and ultrahigh resolution mass spectrometry

Caterina BORDIN

Miniaturization for Synthesis, Analysis & Proteomics USR 3290

EU FT-ICR MS, 2nd Advanced User School

Prague, 26th-30th September 2021

“Les secrets de Modigliani”

Corpus:

- All works by Amedeo Modigliani from French public collections: 25 paintings, 2 attributed and 3 sculptures

State of the art analyses:

- X-ray Fluorescence: analysis of the inorganic component only

Question:

- Is the paint in Amedeo Modigliani’s artworks Sennelier™ paint as according to historical sources?

Objective:

- Development of an analytical protocol for the analysis of the organic binder (siccative oil)

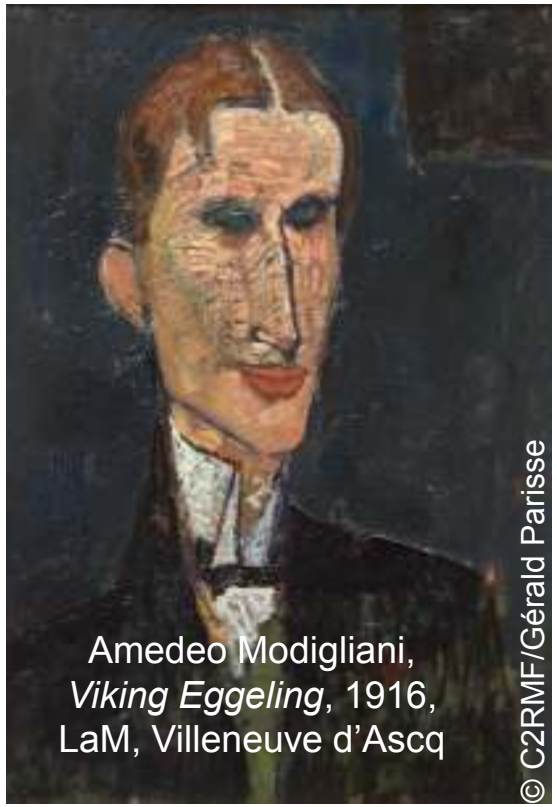

Amedeo Modigliani, *Viking Eggeling*, 1916, LaM, Villeneuve d’Ascq

- Dr Michel Menu
- Dr Anaïs Genty
- Marie-Amélie Sénot

Oil paint

- **Siccative** vegetable oils
- Siccativity: capability of forming a **solid film** upon exposition to light and air
- Common siccative oils: **linseed, poppy** and **nut** oils

Triglycerides in siccative oils

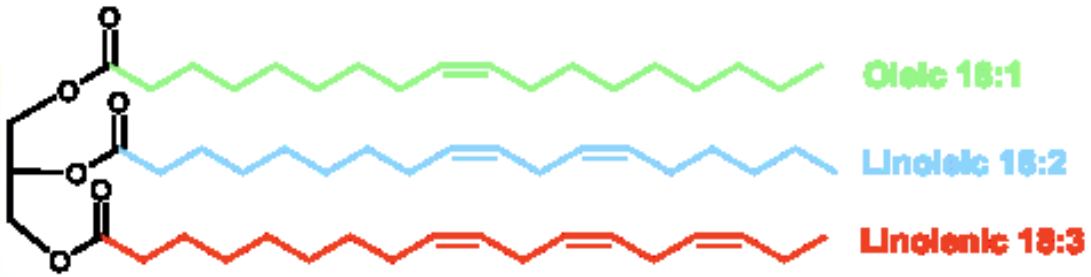

Unsaturated fatty acids

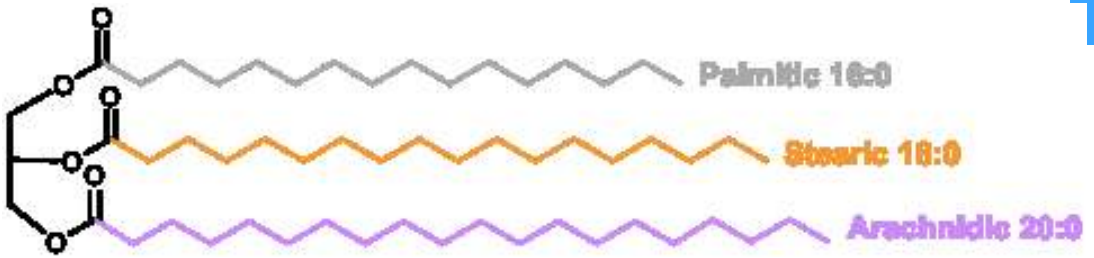

Saturated fatty acids

Oil	Palmic	Stearic	Oleic	Linoleic	Linolenic
Linseed	7%	4%	18-22%	14-17%	**52-55%**
Poppy	12%	2.3%	20%	**65%**	0.7%

EU FT-ICR MS MSAP cnrs Université de Lille

Oil siccativation

Initiation → Hydroperoxide formation → Hydroperoxide decomposition → Polymerization and cross-linking → Creation of a 3D insoluble network

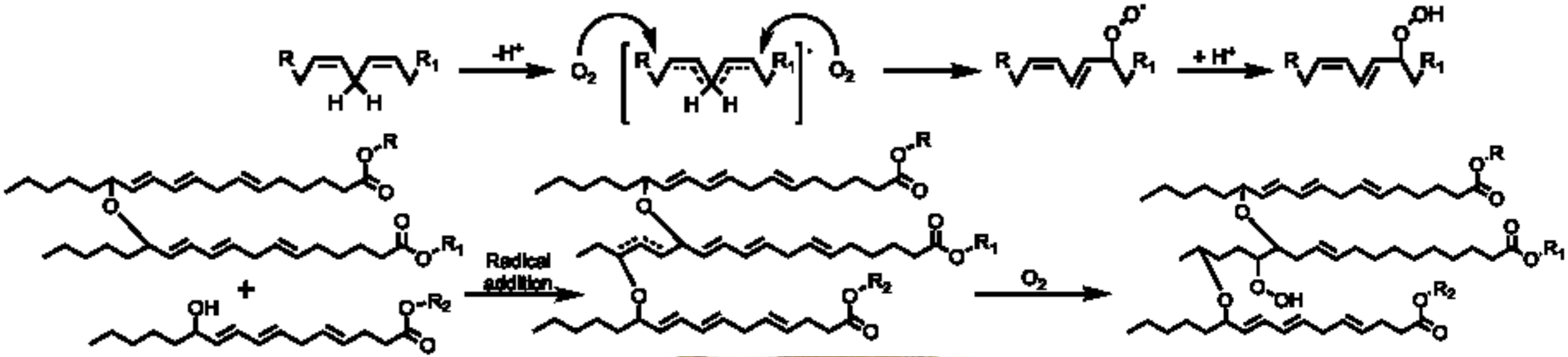

- Apolar environment required
- Catalyzed by added metal catalysts or pigment (Co, Cr, Fe, Mn, … salts)

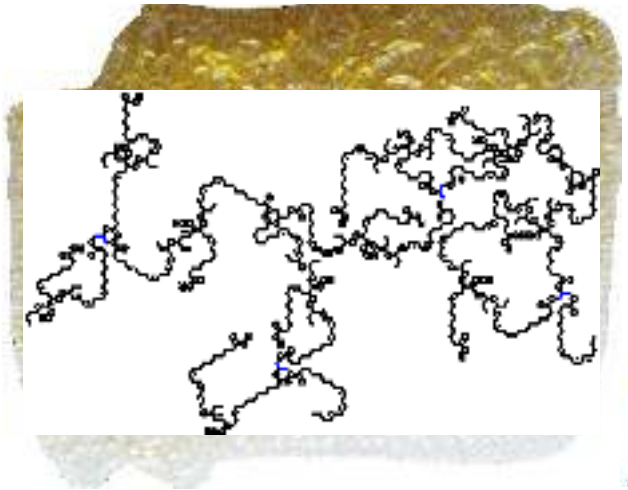

EU FT-ICR MS MSAP cnrs Université de Lille

State of the art techniques for the analyses of lipid binders

Py-GCMS

- **Harsh depolymerization conditions**
- **No information on cross-linking structures**
- **Unreliable quantificaiton**
- **Higher sample quantities required**

Temperature determines which products are obtained and their quantities!

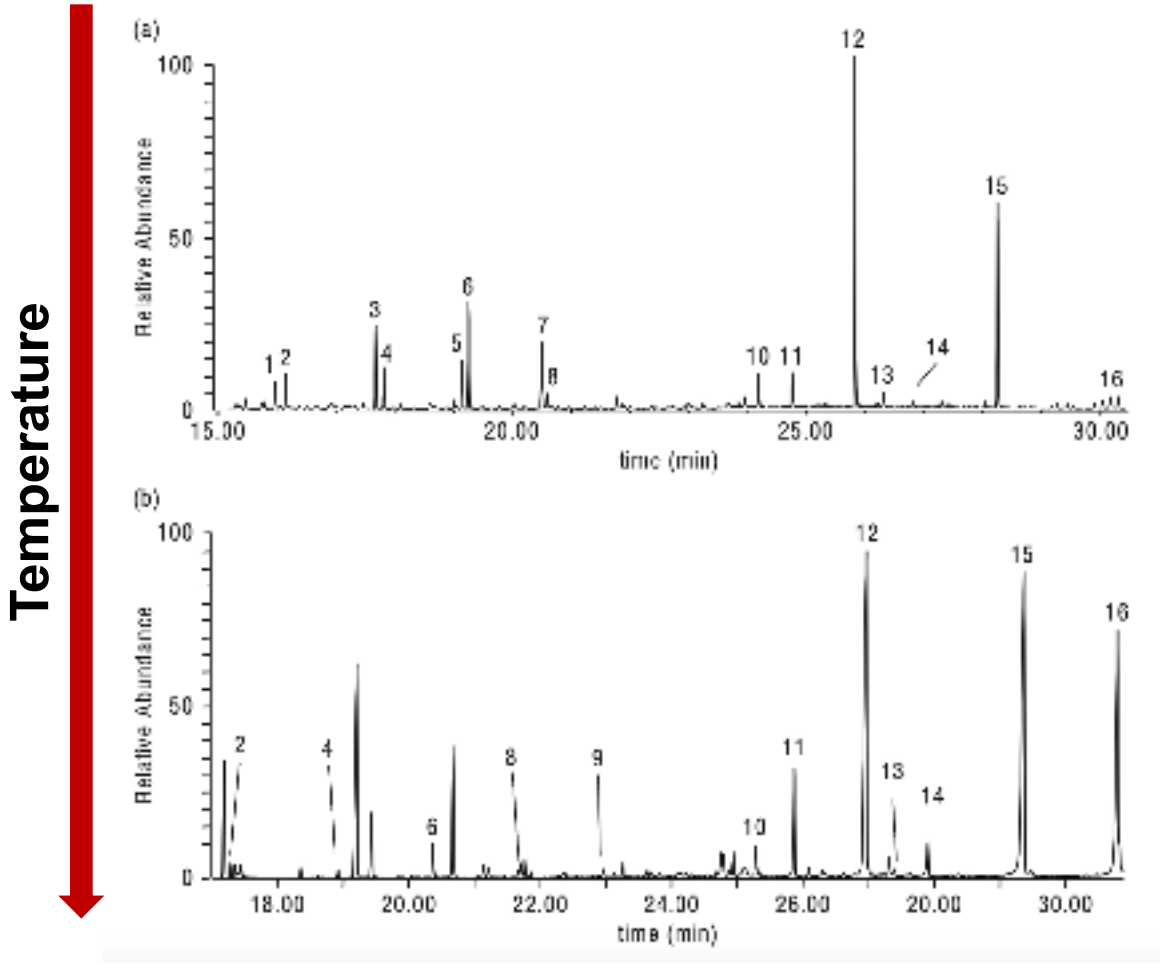

Bonaduce, I. (2009). Andreotti A. *Py–GC/MS of organic paint binders. In: Organic mass spectrometry in art and archaeology. Colombini MP, Modugno F, editors. John Wiley, Chinchester*, 303-326.

EU FT-ICR MS MSAP cnrs Université de Lille

Soft chemical depolymerization developed at MSAP

10 µg sample

58 samples from Amedeo Modigliani's artworks

Chemical depolymerization developed at MSAP

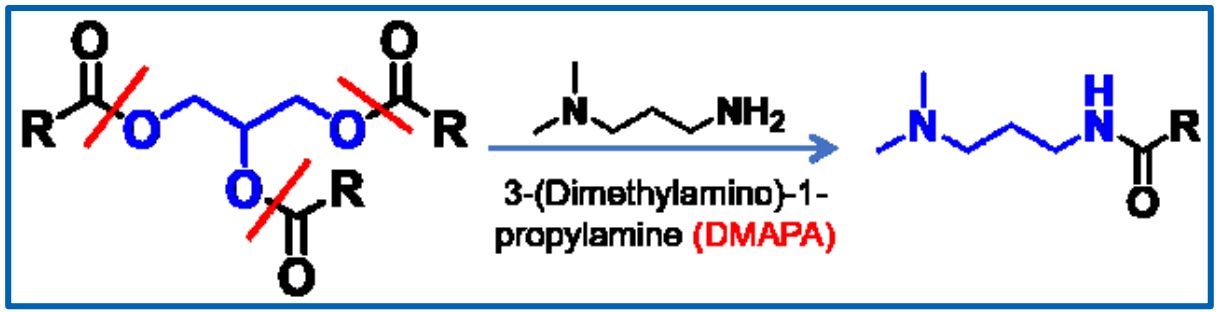

Quenching with 10 µL formic acid

Liquid-liquid extraction

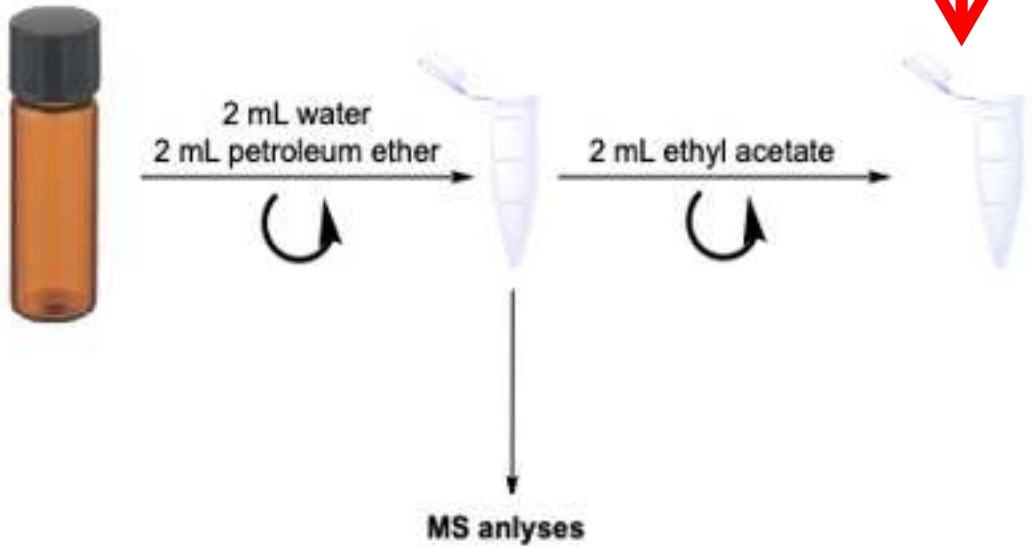

nanoESI source
8 Megapoints
Absorption mode

Strategies for the developement of oil paint analyses

Identification and classification

Fresh siccative oils

Polymerizatio and reticulation

transamidation

Protocol optimization

Painting on Sennelier™ canvas dated between WWI and WWII

58 samples from Amedeo Modigliani's artworks

EU FT-ICR MS MSAP cnrs Université de Lille

Oil analysis on modern and historical Sennelier™ paint tubes (nanoESI FTICR MS)

Modern Sennelier™ paint tubes

Historical Sennelier™ paint tubes

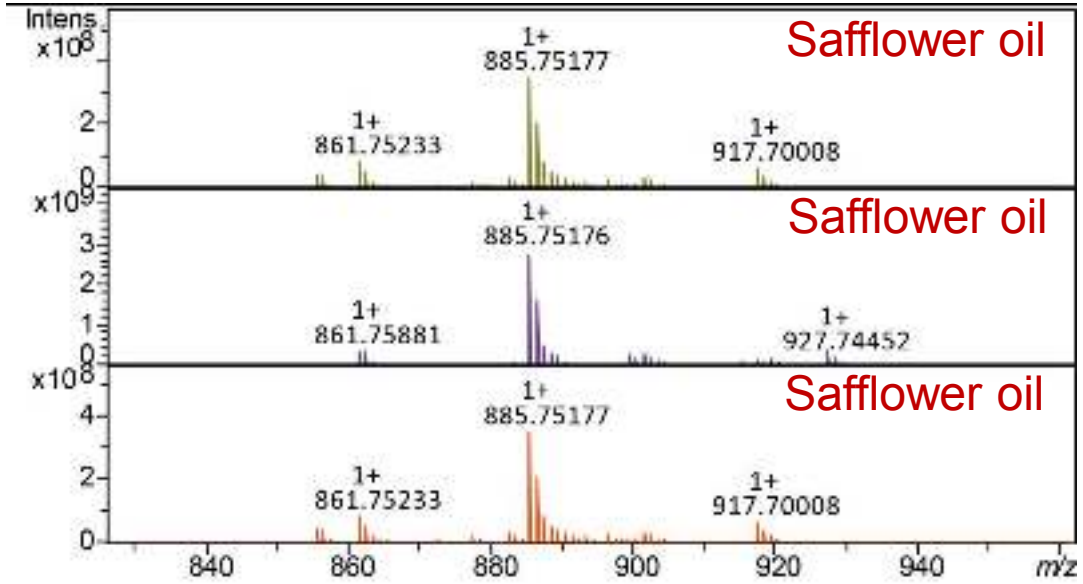

Yellow ochre

Burnt Sienna

Ivory Black

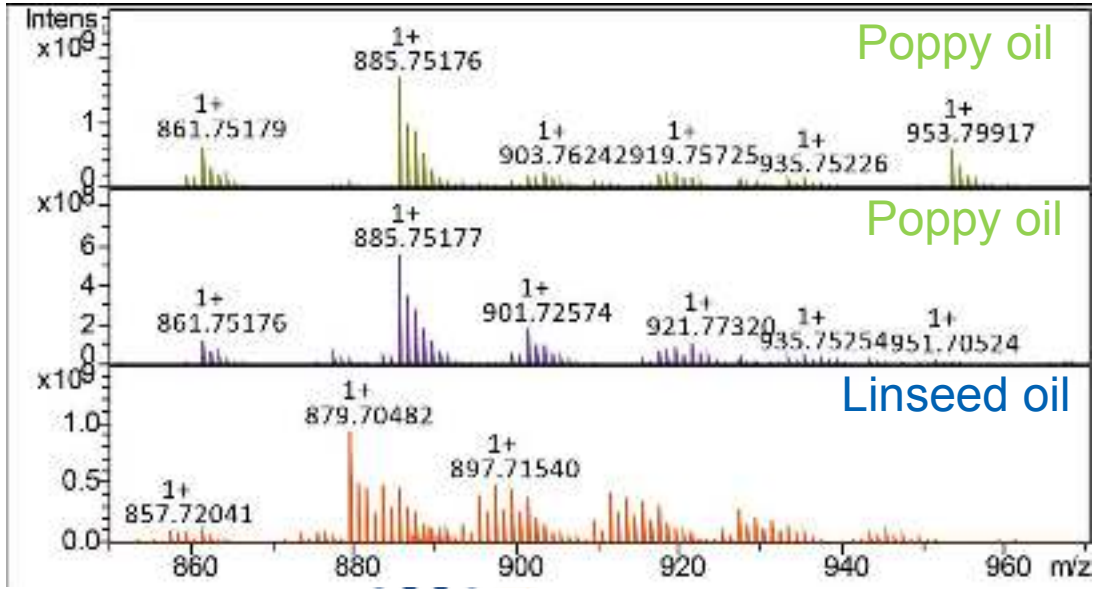

“Les secrets de Modigliani” – Polymerized organic binder analysis

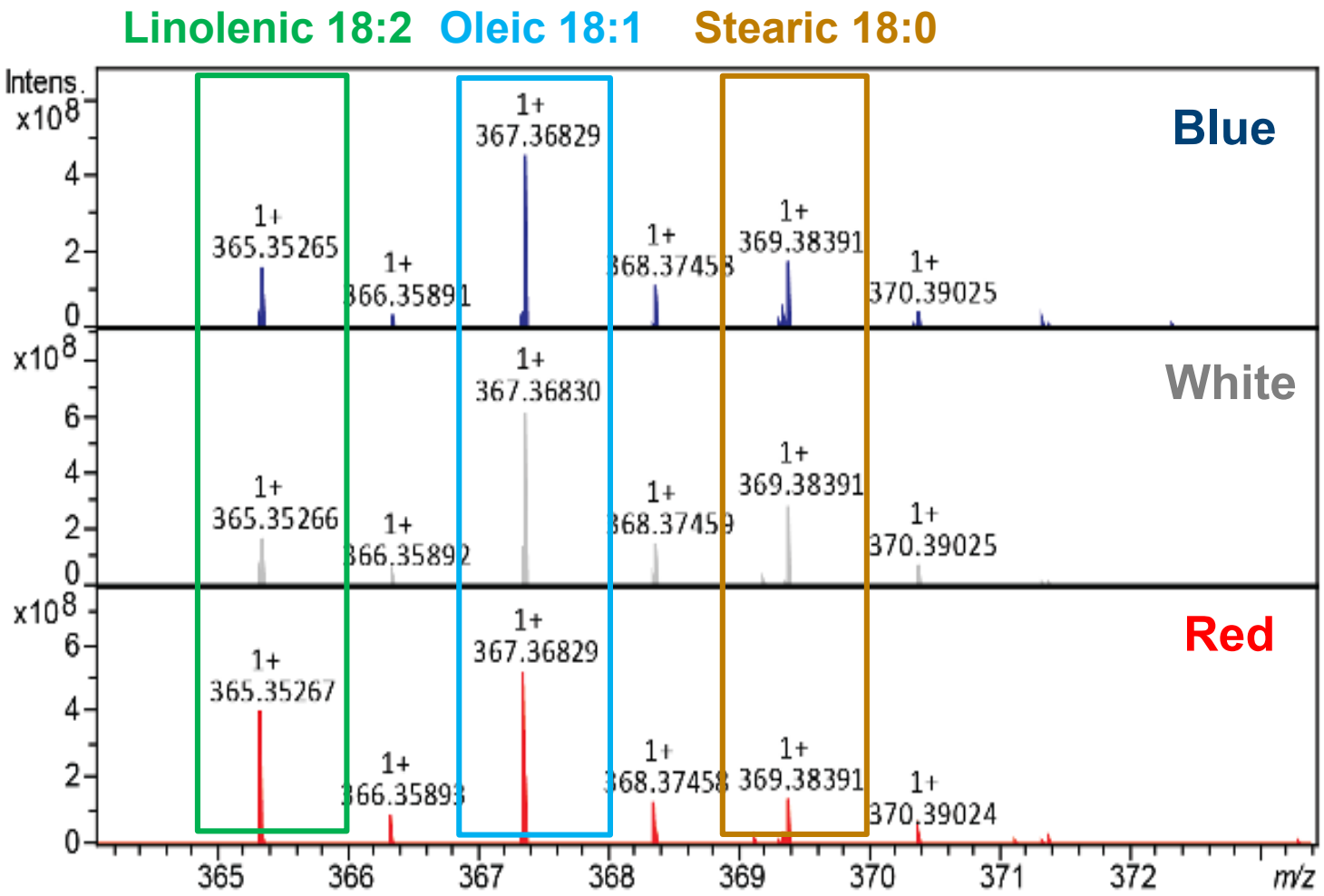

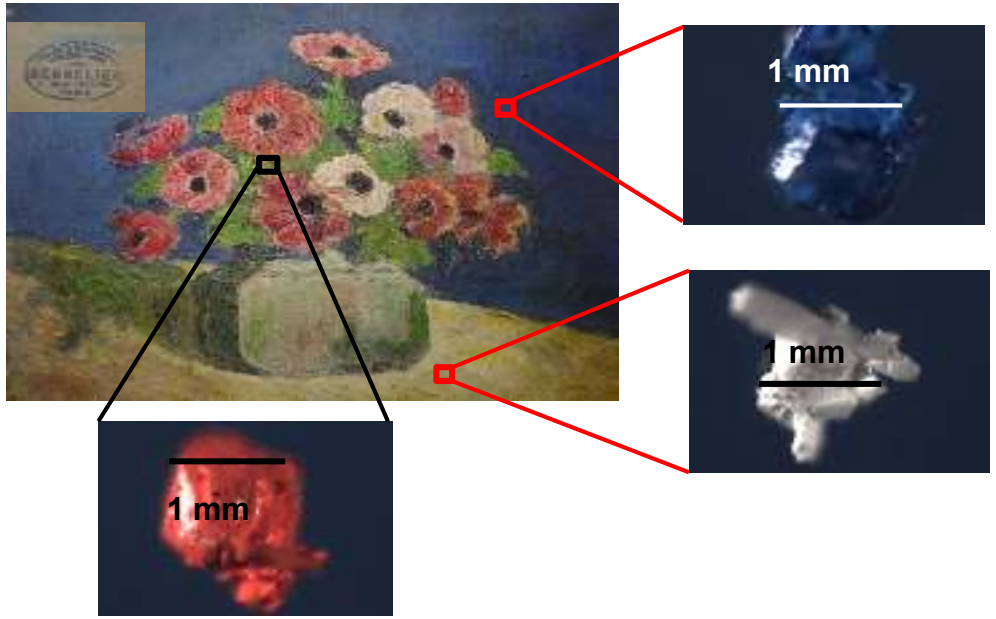

Triglyceride (TAG) molecule formed by one glycerol and three fatty acids (oleic, linoleic, linolenic)

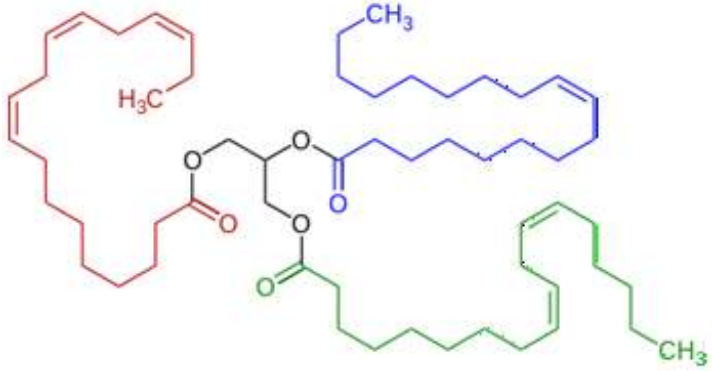

EU FT-ICR MS
MSAP
cnrs
Université de Lille

Winsor & Newton Griffin™ alkyd paint: depolymerized, derivatized fatty acids

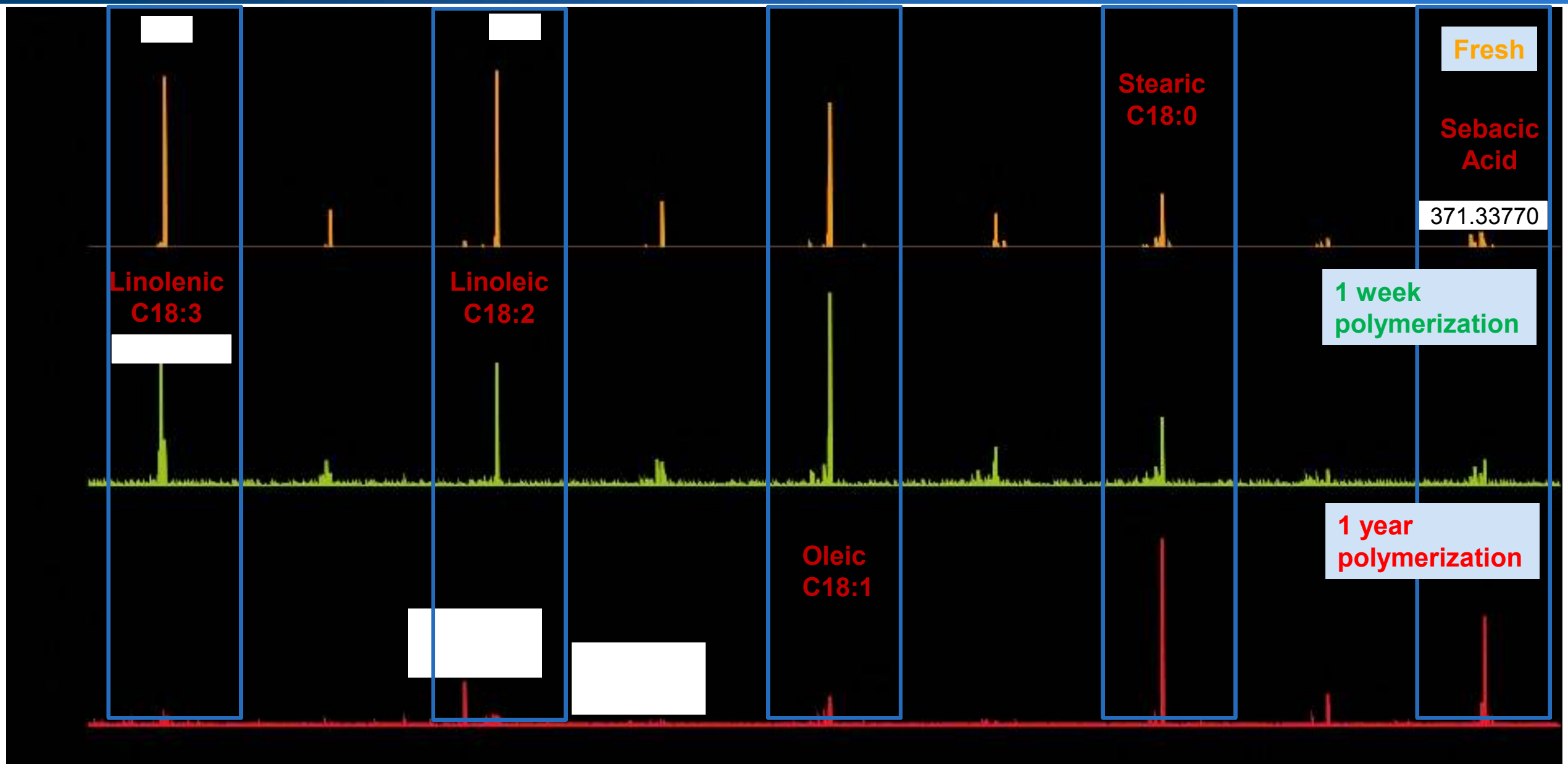

Winsor & Newton Griffin™ alkyd paint: effect of pigments, 1 week polymerization

Titanium white

Prussian blue

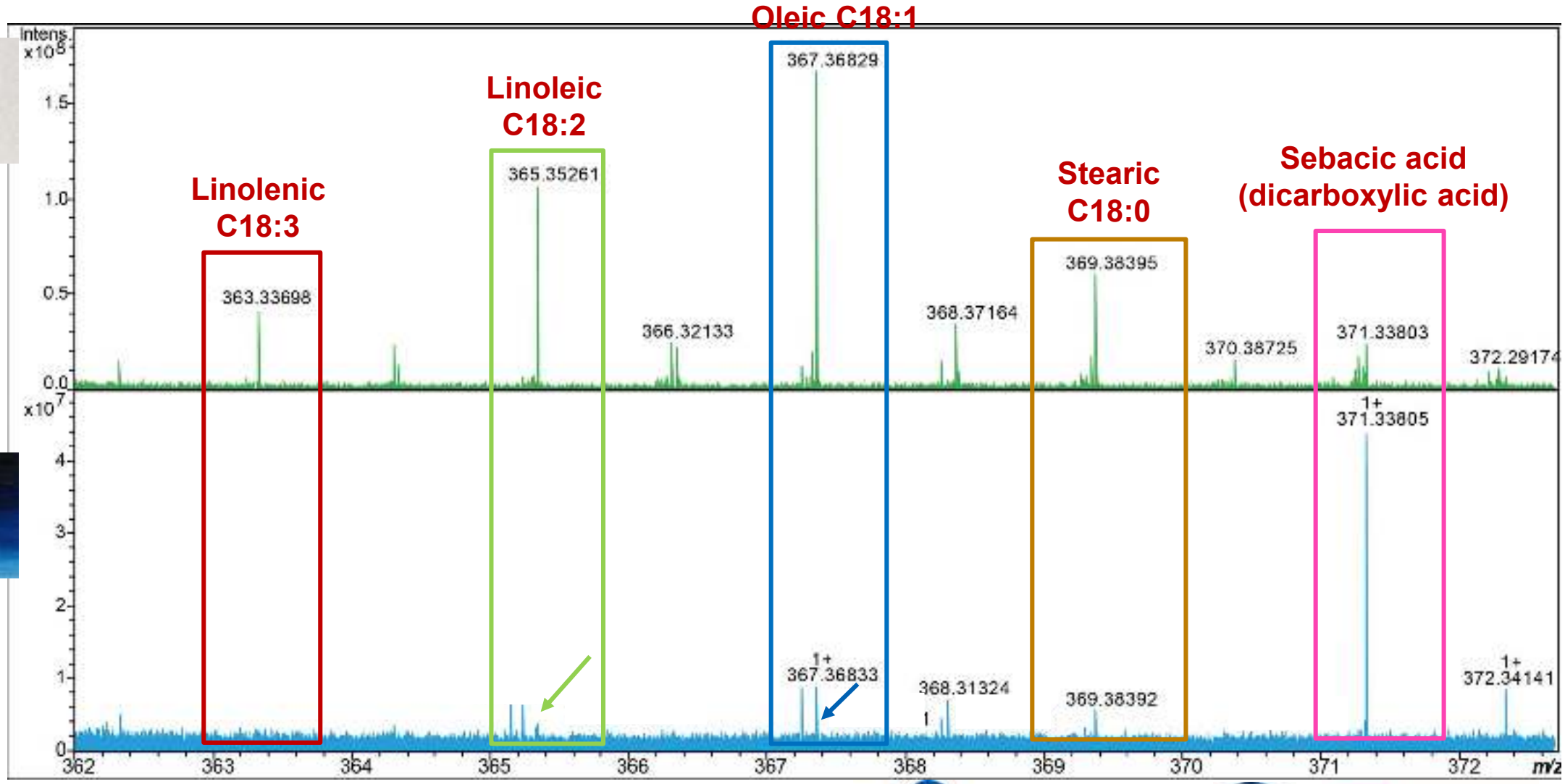

EU FT-ICR MS

MSAP

cnrs

Université de Lille

LTQ-Orbitrap analysis on historical canvas samples

Mass spectrometry analysis
nanoHPLC U 3000 (Thermo Scientific)
Column C18, 75 µm, 15 cm
Pre-column C18, 300 µm, 5 mm
Flow rate of 300 nL / min at 40 °C
Gradient duration = 65 min Injection 1 µL

Mass spectrometry
Nano électrospray
LTQ Orbitrap XL (Thermo Scientific)
Analyzer : FTMS
MS résolution 60 000
Scan ranges : 280-2000

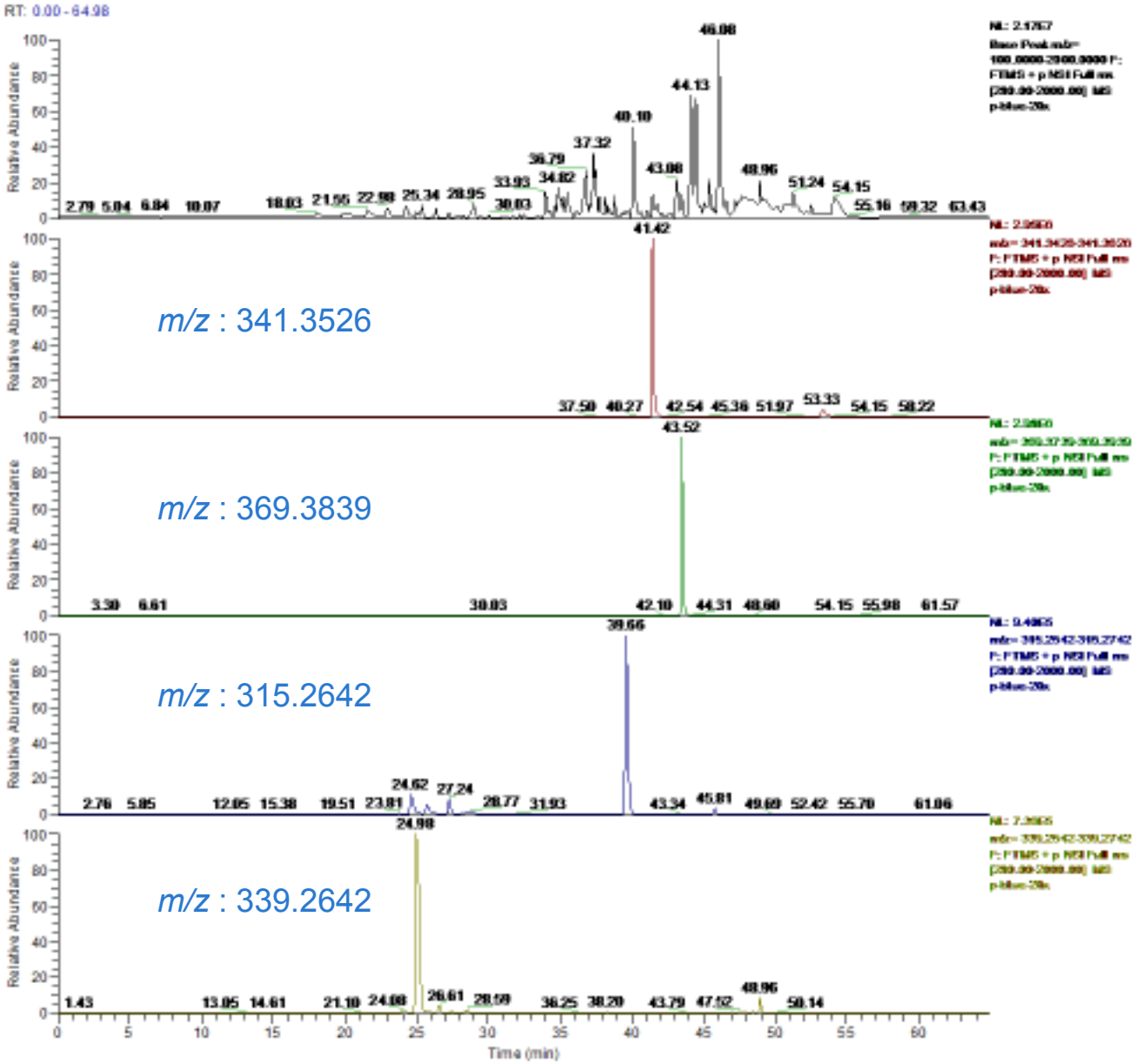

Modigliani F4010 (2)

Full spectrum

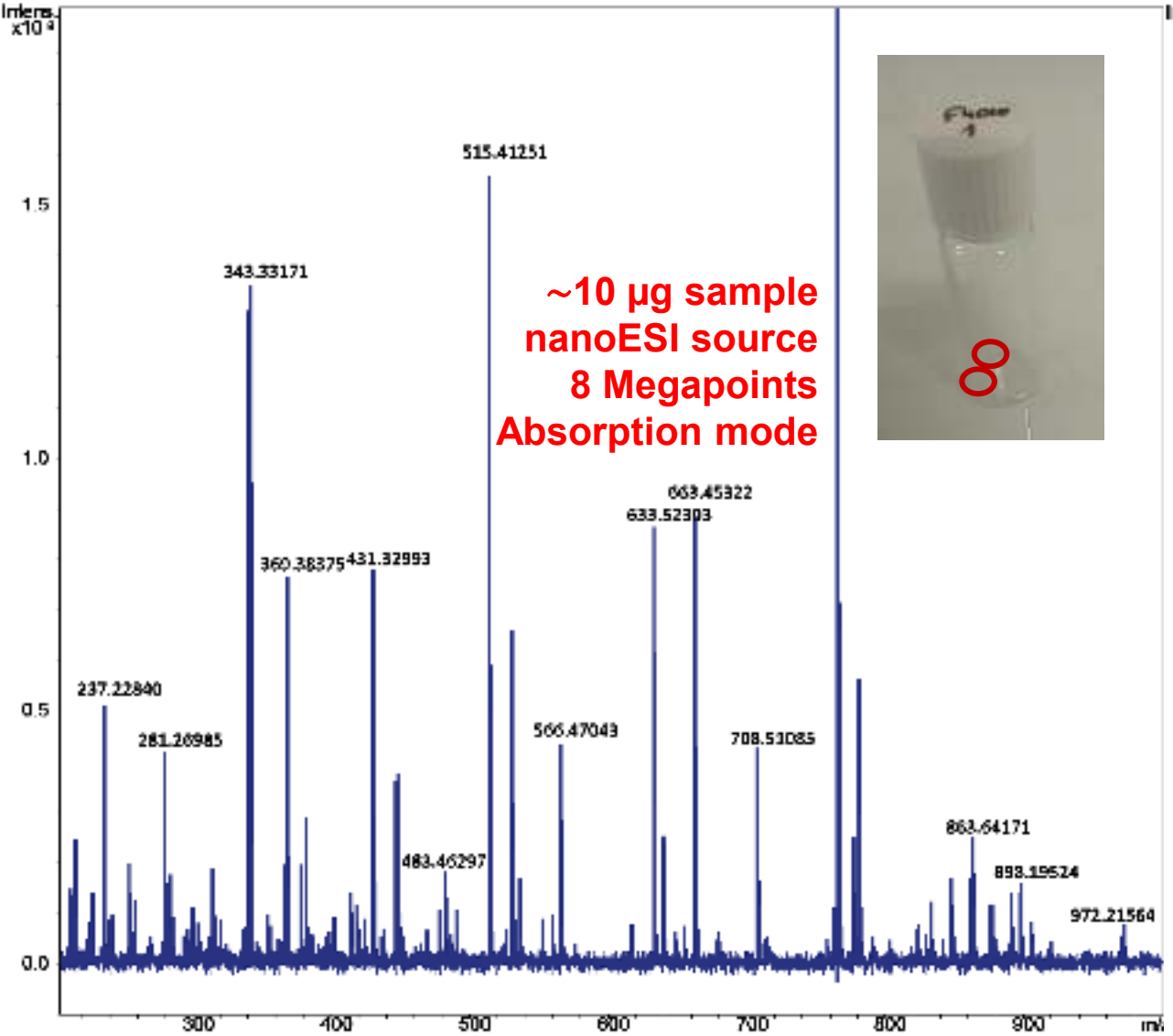

Fatty acids area close up

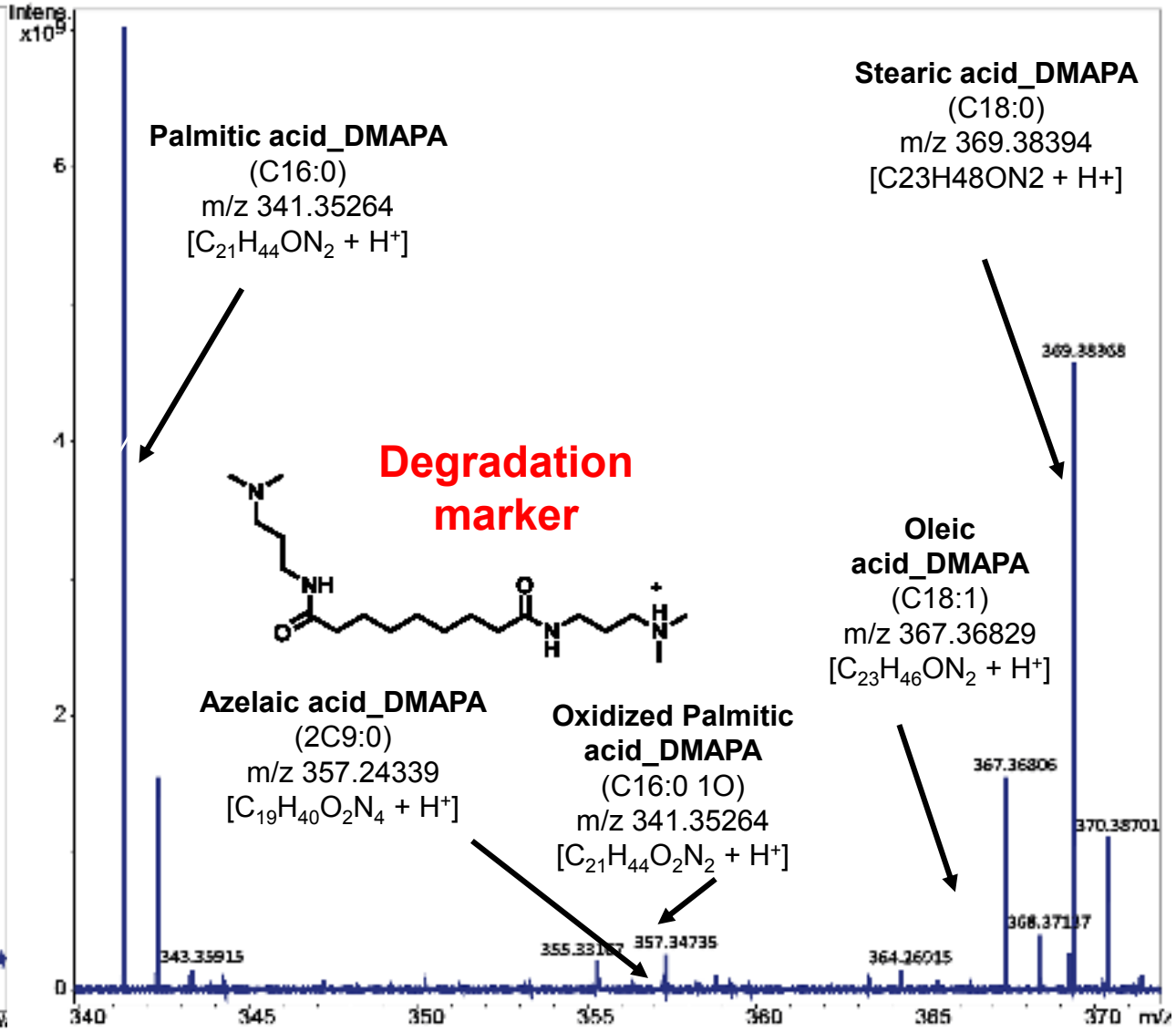

Modigliani F4010 (2)

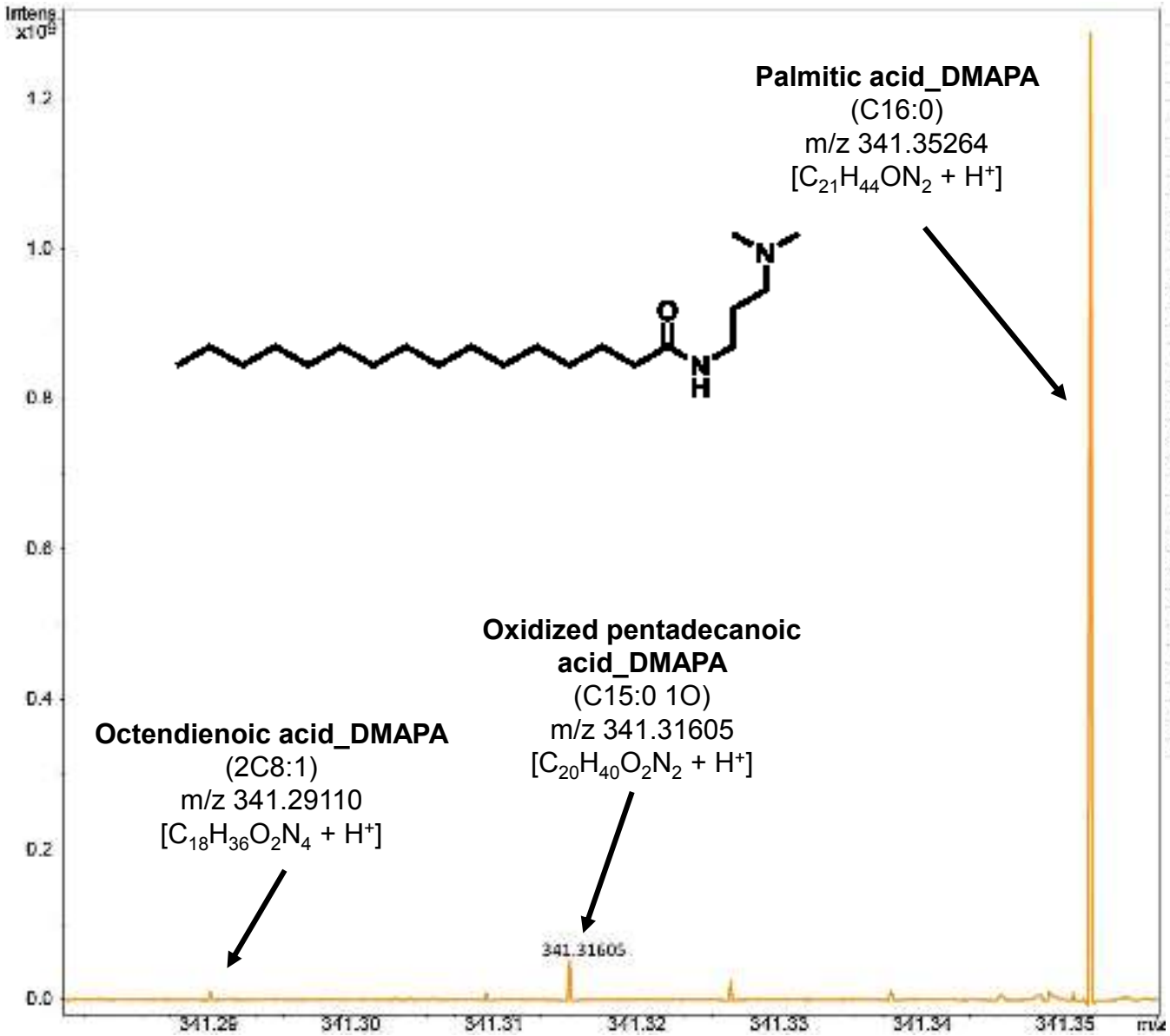

1	CN_5_u2_d1	183,149189	183,1492	0,00316632	3293324		0,25528346
2	CN_5_u1_d1	185,164839	185,1648	0,10488001	20821508		1,61598839
3	CN_5_s_d1	187,180489	187,1805	0,0565225	24385598		1,8902604
4	CN_6_u2_d1	197,164839	197,1649	0,05366022	5360630		0,4155316
5	CN_5_u2_o1_d1	199,144104	199,1441	0,13262523	5208973		0,40377577
6	CN_6_u1_d1	199,180489	199,1805	0,04729425	50660708		3,92698716
7	CN_5_u1_o1_d1	201,159754	201,1597	0,07168477	8291480		0,64271619
8	CN_6_s_d1	201,196139	201,1961	0,09652318	252658672		19,5849486
9	CN_5_s_o1_d1	203,175404	203,1754	0,02175505	145668864		11,2915884
10	CN_6_u2_o1_d1	213,159754	213,1598	0,02617712	3047901		0,23625939
11	CN_7_u1_d1	213,196139	213,1962	0,04962524	13824952		1,07164726
12	CN_6_u1_o1_d1	215,175404	215,1754	0,0205418	17759258		1,37661673
13	CN_7_s_d1	215,211789	215,2118	0,04327126	134156688		10,3991094
14	CN_6_s_o1_d1	211,116	###	CN_8_u1_d2	341,291102	341,2911	0,00709099	9295240	0,72052464
15	CN_5_s_o2_d1	21	###	CN_15_u1_o1_d1	341,316754	341,3163	0,10084516	48373216	3,74967121
16	CN_8_u2_d1	225	###	CN_16_s_d1	341,352639	341,3526	0,0861868	1,29E+09	100
17	CN_8_u1_d1	22							
18	CN_7_u1_o1_d1	229,197054	229,1971	0,01928562	7835772		0,60739833
19	CN_8_s_d1	229,237439	229,2375	0,04615484	140700064		10,9064276
20	CN_6_u1_o2_d1	231,170319	231,1703	0,04074957	5903505		0,4576128
21	CN_7_s_o1_d1	231,206704	231,2067	0,01911749	11850531		0,91859915
22	CN_6_s_o2_d1	233,185989	233,186	0,08328156	14118310		1,09438704
23	CN_9_u3_d1	237,196139	237,1962	0,08676325	12963331		1,00485833
24	CN_9_u2_d1	239,211789	239,2118	0,08603217	14872435		1,15284521
25	CN_9_u1_d1	241,227439	241,2274	0,08050632	28365904		2,19879558
26	CN_8_u1_o1_d1	243,206704	243,2067	0,0592915	9806233		0,76013448
27	CN_9_s_d1	243,243089	243,2431	0,04349521	97747200		7,57691739
28	CN_						
29	CN_						
30	CN_446	###	CN_23_u2_o3_d2	597,494947	597,4948	0,1797841	3547695	0,27500115
31	CN_447	###	CN_30_u2_o4_d1	597,520099	597,52	0,09944451	4295855	0,3329951
32	CN_						
33	CN_448	###	CN_31_u6_o4_d1	603,473149	603,4726	0,97671303	4486591	0,34778008
34	CN_449	###	CN_26_u4_o1_d2	603,520767	603,521	0,35223296	4254299	0,32977387
35	CN_						
36	CN_450	###	CN_25_u1_o2_d2	611,546982	611,5471	0,24132227	4607625	0,35716209
37	CN_451	###	CN_26_u3_o2_d2	621,531332	621,5315	0,25353494	4171607	0,32336396
38	CN_						
39	CN_452	###	CN_34_u2_o2_d1	621,592869	621,5929	0,08137144	9092748	0,70482838
	453	###	CN_26_u2_o2_d2	623,546982	623,5471	0,18856624	4617715	0,35794422
	454	###	CN_32_u2_o4_d1	625,551399	625,5514	0,04888473	3704033	0,28711975
	455	###	CN_26_u1_o2_d2	625,562632	625,5627	0,17197304	6784496	0,5259032
	456	###	CN_25_u4_o4_d2	637,489862	637,4902	0,5766051	4522301	0,35054816
	457	###	CN_27_u2_o2_d2	637,562632	637,5628	0,18442095	11351006	0,87987825
	458	###	CN_25_u3_o4_d2	639,505512	639,5057	0,21513483	7046968	0,54624884
	459	###	CN_36_u2_o2_d1	649,624169	649,6242	0,02989435	5741940	0,44508902
	460	###	CN_34_u2_o4_d1	653,582699	653,5827	0,01441301	3516498	0,2725829
	461	###	CN_27_u1_o3_d2	655,573197	655,5734	0,2632504	6147173	0,47650083
	462	###	CN_29_u2_o3_d2	681,588847	681,589	0,16517276	4136560	0,32064728

Δm/z = 0.02 Da

More than 400 identified peaks

Acknowledgements

MSAP, séminaire d'Unité, juillet 2020

"Les secrets de Modigliani" at LAM (**Lille Métropole Musée d'art moderne, d'art contemporain et d'art** brut) 19.02.21 > 20.02.22

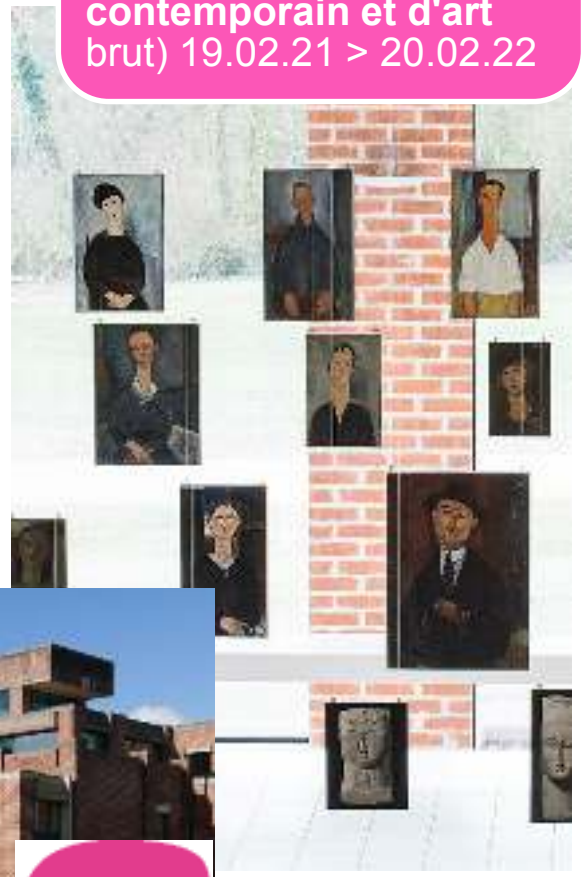

MSAP

§ Dr. Christian Rolando § Ziad Mahmoud

§ Dr. Fabrice Bray § Nathan Roy

And all the MSAP staff!

Application of MALDI-FT-ICR-MS for nanostructured thin films characterization

EU_FT-ICR-MS 2nd Advanced Users School

Bogdan Purcareanu[1], Alina Morosan[2], Adrian Costache[2], Alexia Popescu[2], Bogdan Mihaiescu[3], Rodica Cristescu[4], Daniela Istrati[2], Dan Eduard Mihaiescu[2]

1 - Biotehnos SA, Otopeni city,
2 - University Politehnica Bucharest - Faculty of Applied Chemistry and Material Science,
3 - University of Bucharest - Faculty of Biology,
4 - National Institute for Laser, Plasma and Radiation Physics, Magurele city.

SolariX-XR, QqqFT-ICR HR mass spectrometer with 15 T magnet

EU FT-ICR MS

Interfaces:
MALDI
GC
LC
Direct Probe
Infusion

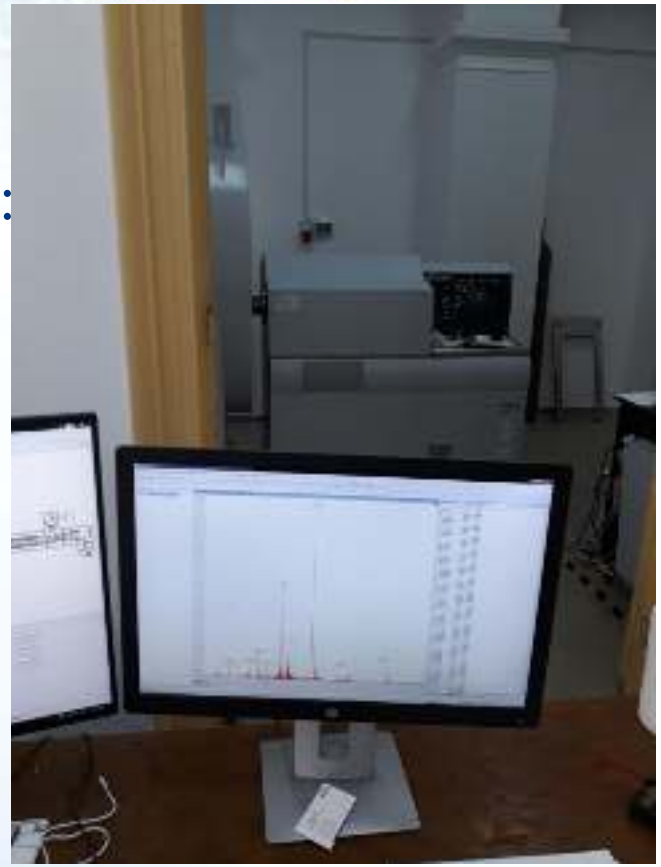

This project has received funding from the European Union's Horizon 2020 research and innovation programme under grant agreement No 731077.

Synthesis and caracterisation of magnetic core nanoparticles (Fe_3O_4/ PABA)

EU FT-ICR MS

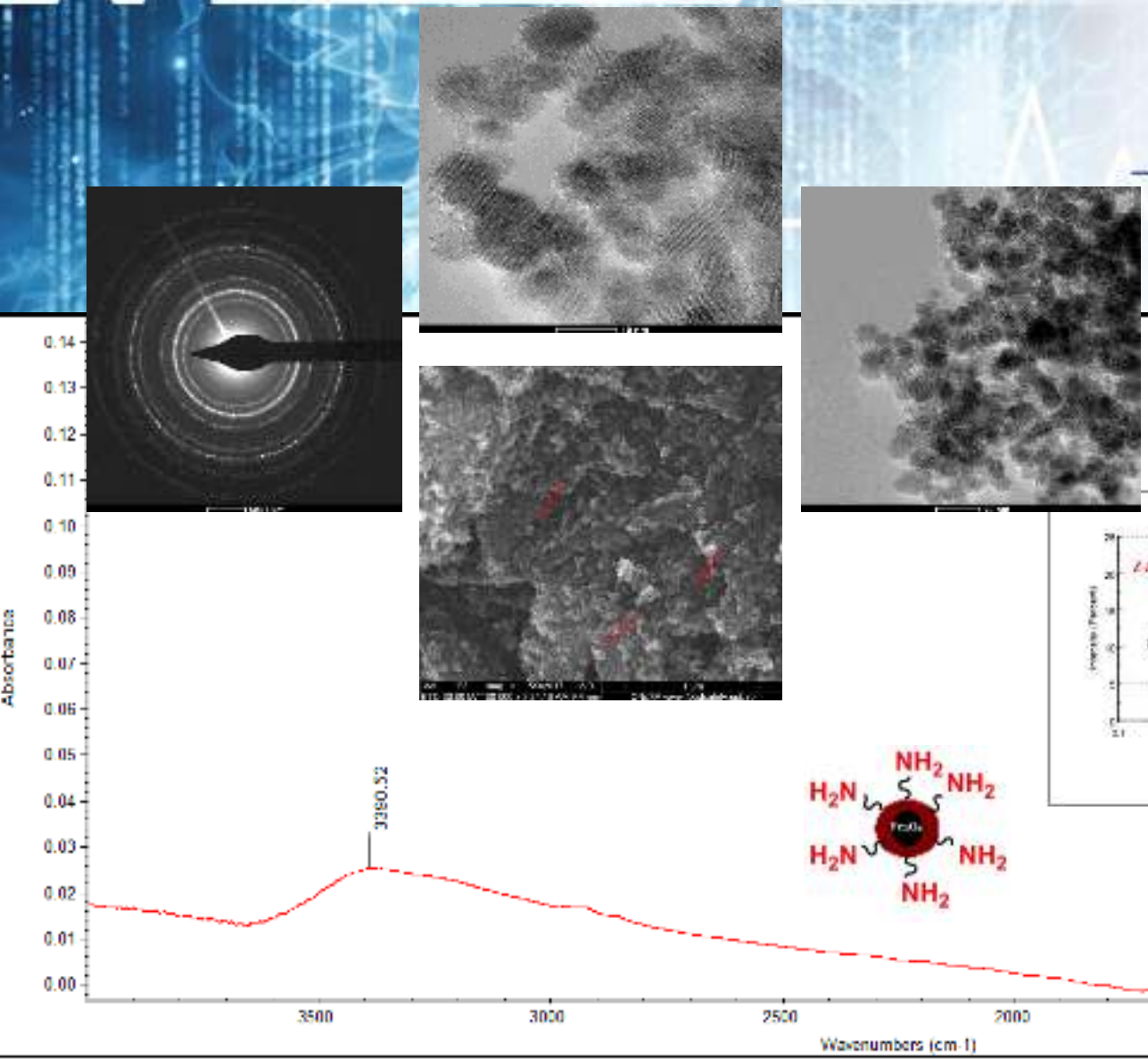

The synthesis and caracterisation of magnetite core-shell nanoparticles with secondary silica shell (Fe3O4/PABA/SiO2)

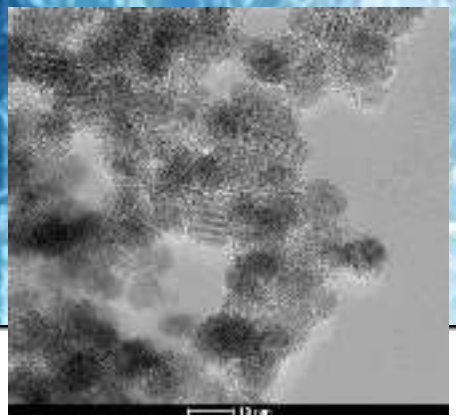

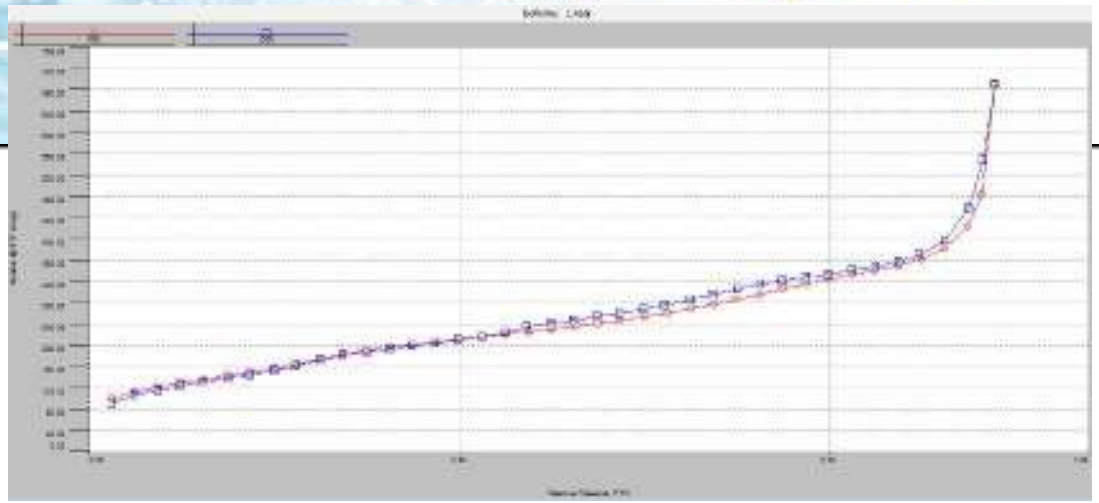

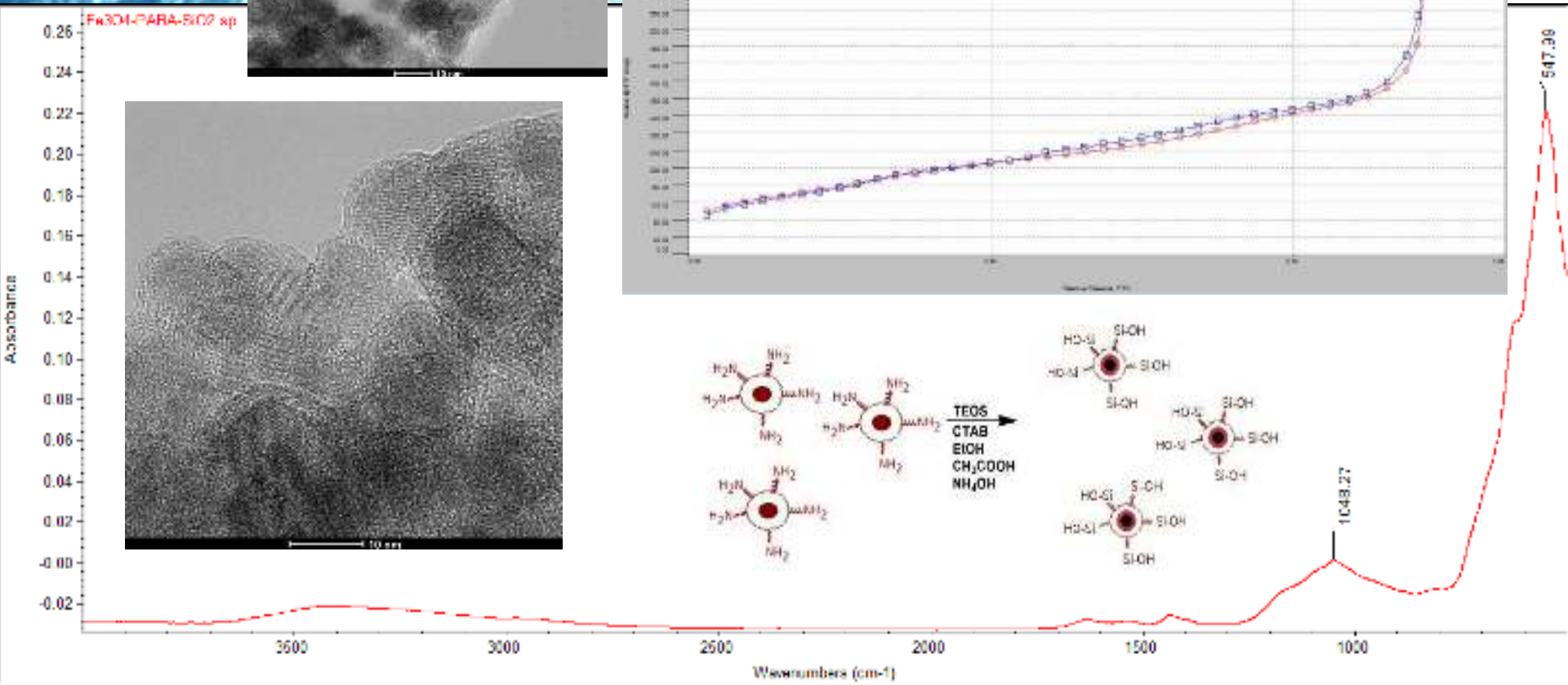

Dip-coating thin films

EU FT-ICR MS

Nanofilms obtained by dip-coating method from dispersions of core-shell magnetite nanoparticles with secondary silica shell (Fe_3O_4-PABA-SiO_2) loaded with DPPH radical

EU FT-ICR MS

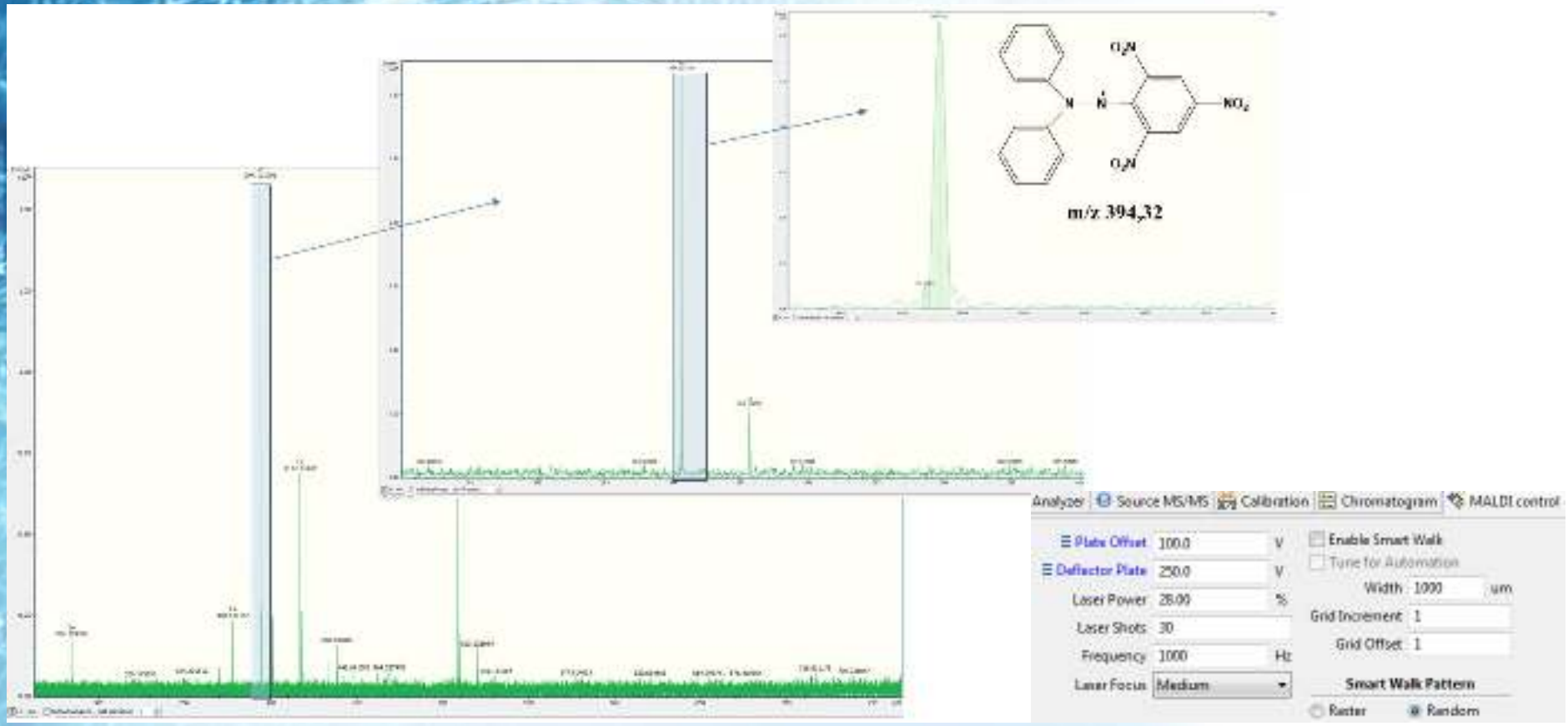

Nanofilms obtained by dip-coating method from dispersions of core-shell magnetite nanoparticles with secondary silica shell (Fe_3O_4-PABA-SiO_2) loaded with DPPH radical

EU FT-ICR MS

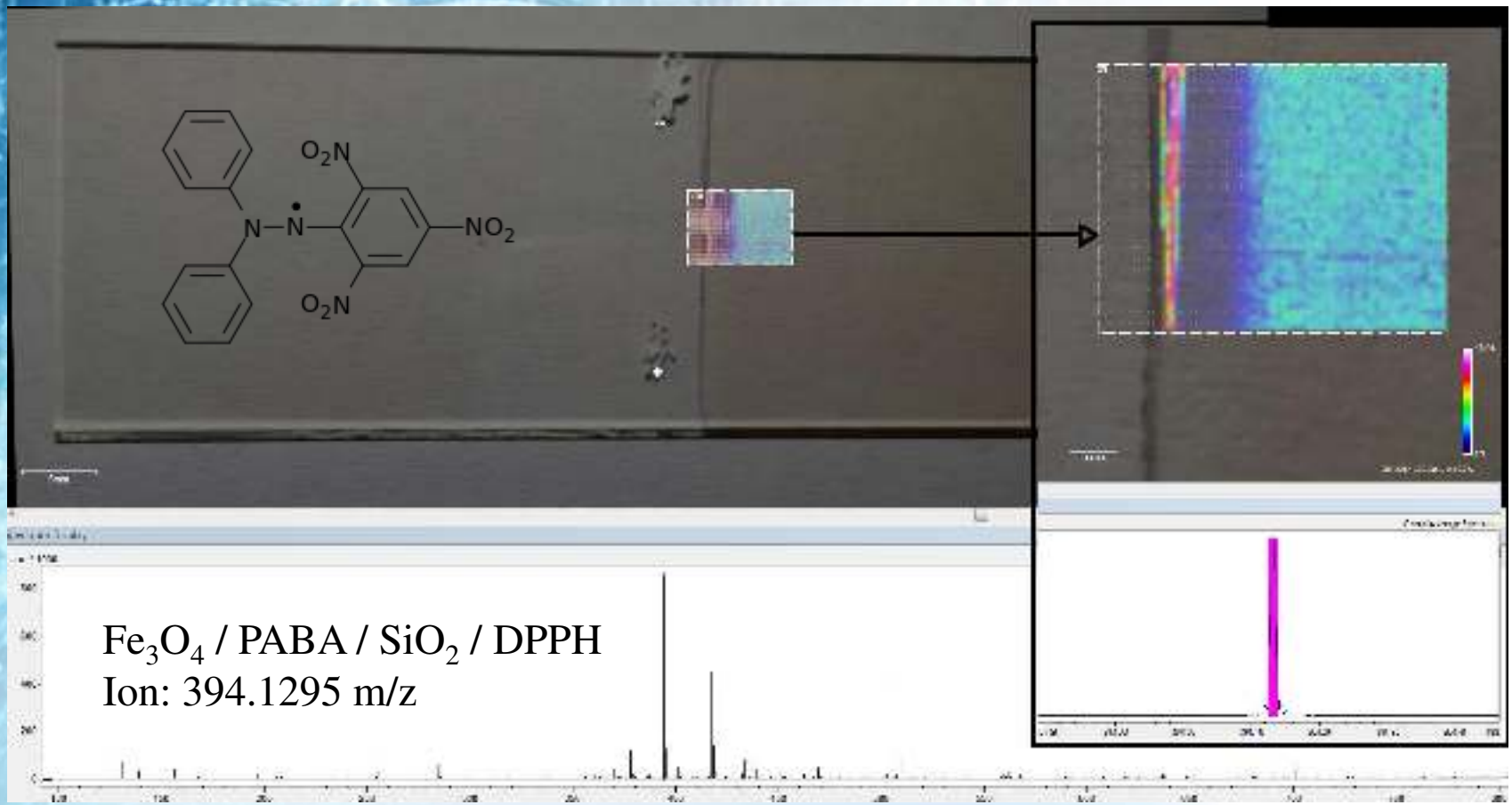

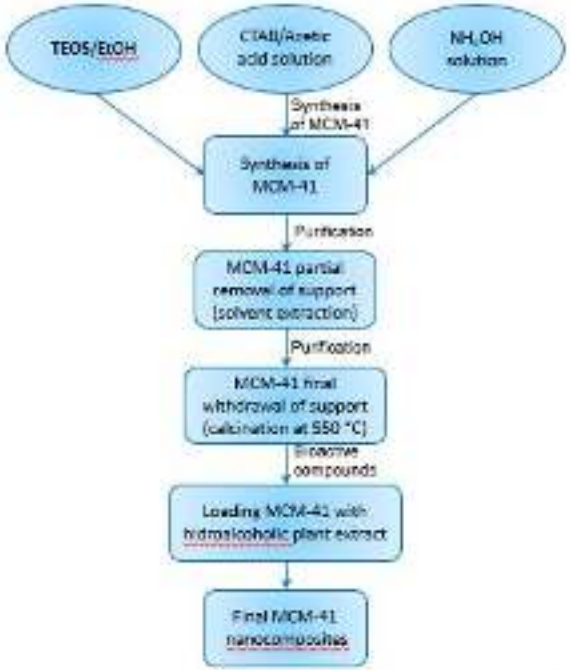

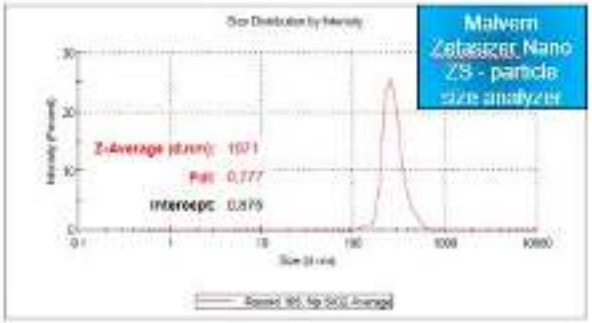

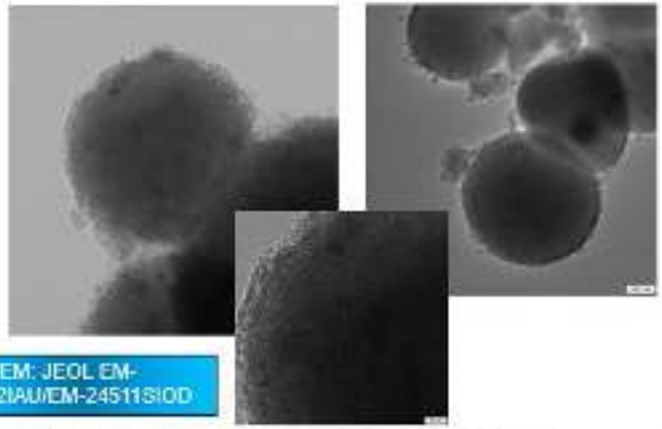

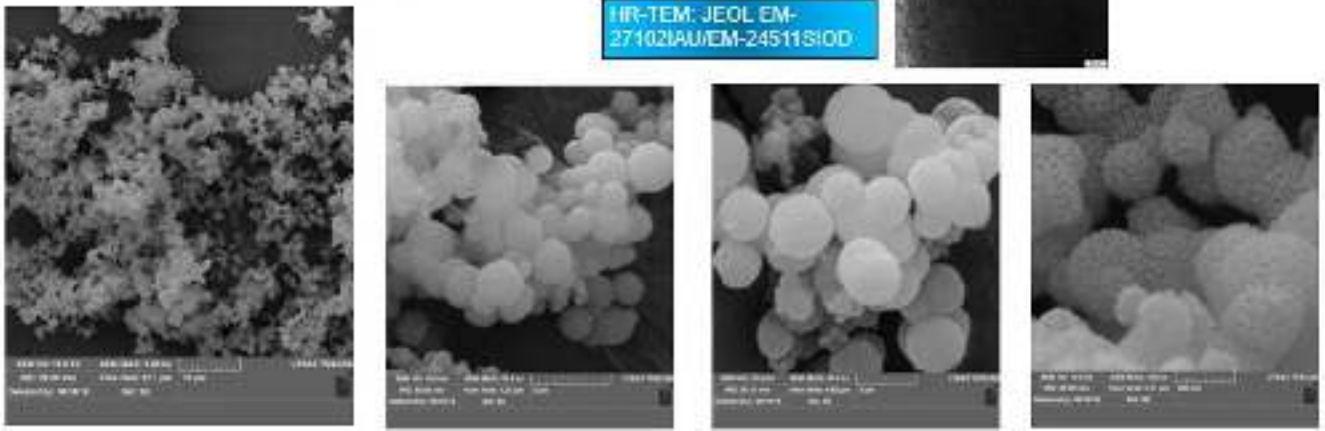

Synthesis and characterization of MCM-41

MCM - Mesoporous material loaded with Praziquantel

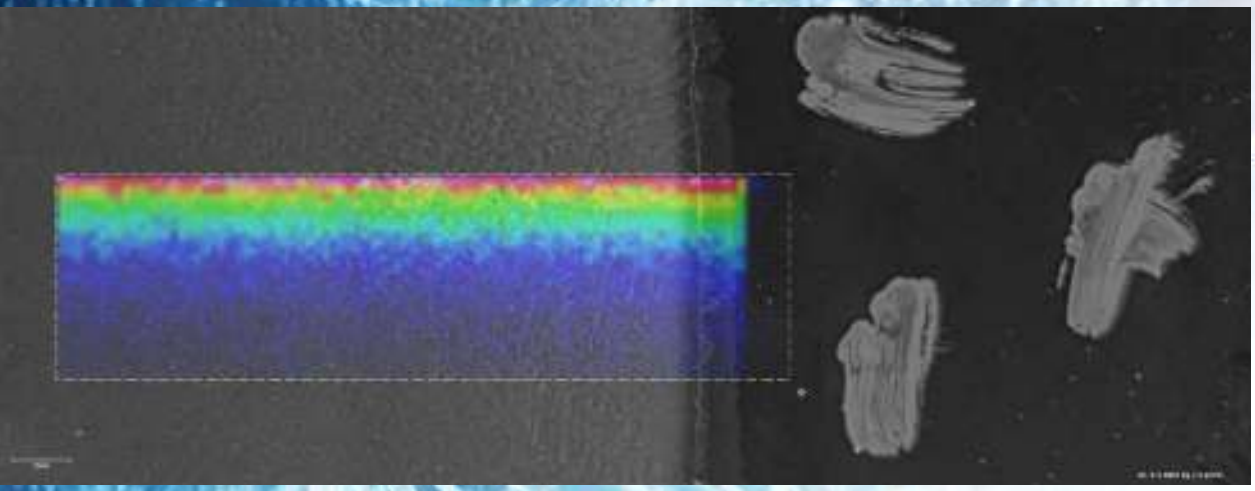

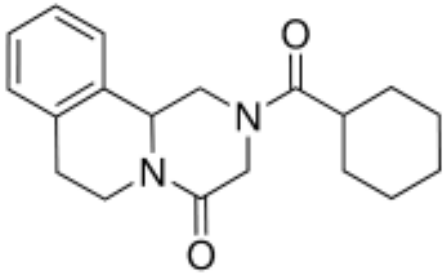

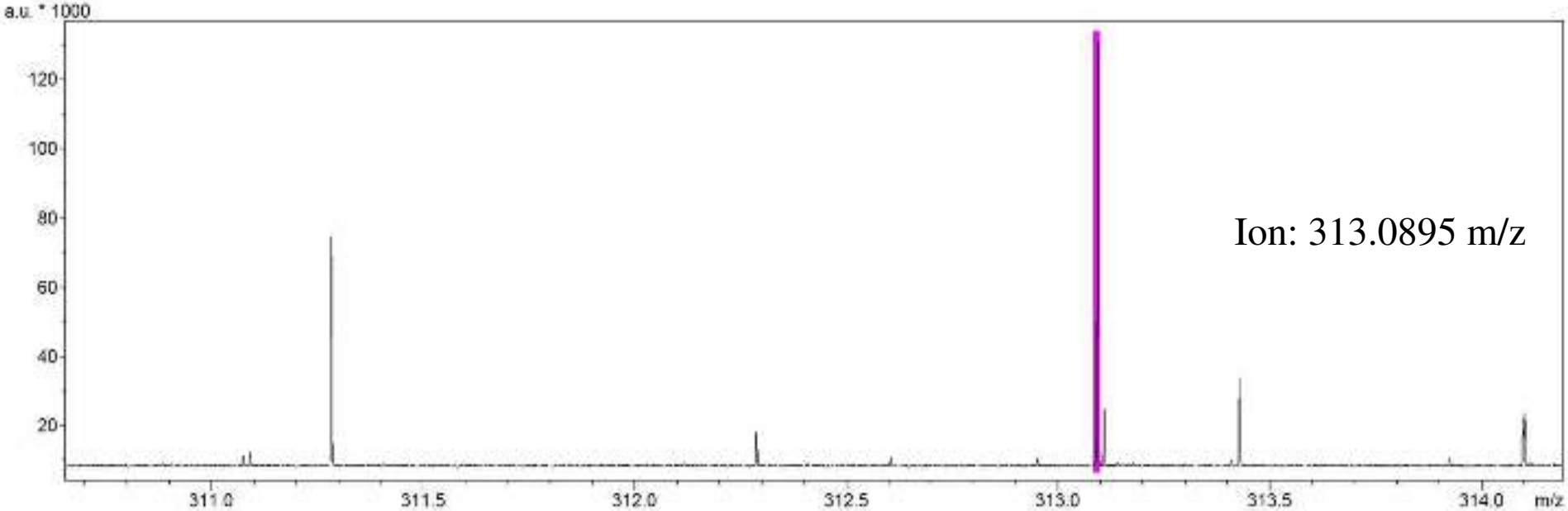

Thin films (dip coating) of biopolimer encapsulated MCM41 np's loaded with Harpagophitum extract

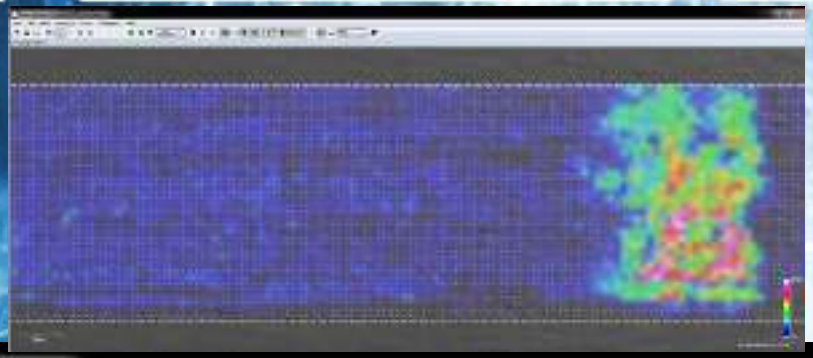

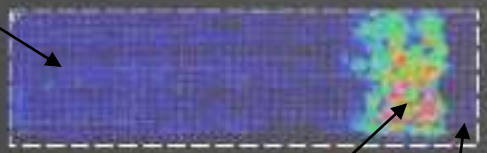

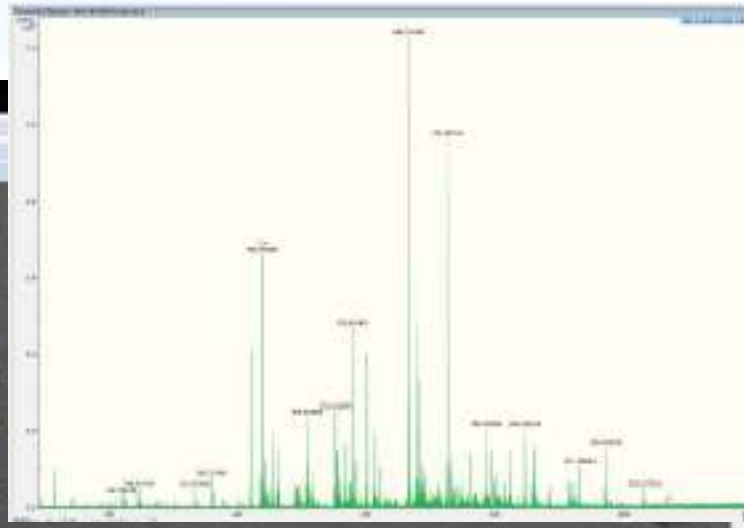

Higher thickness film

Deposition discontinuity

Low thickness film

ITO/glass slide

MAPLE: MATRIX Assisted Pulsed Laser Evaporation

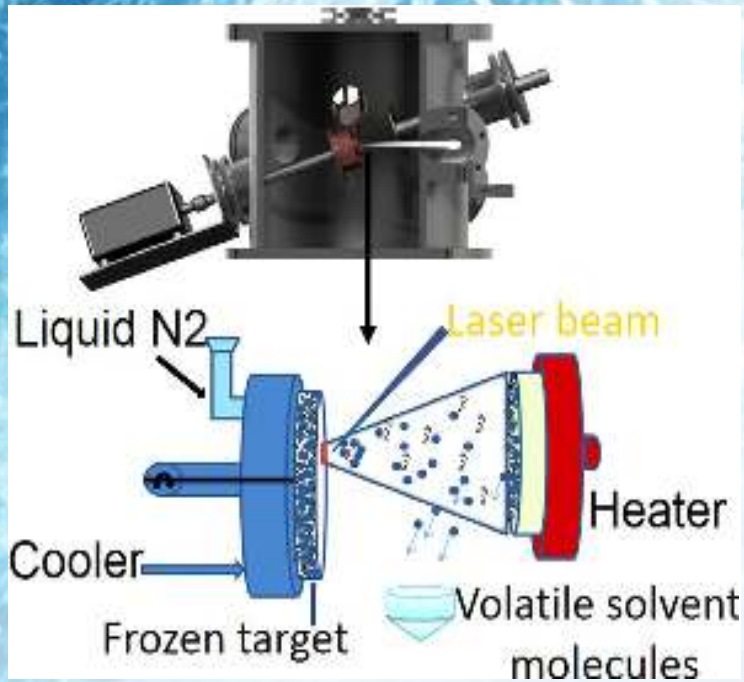

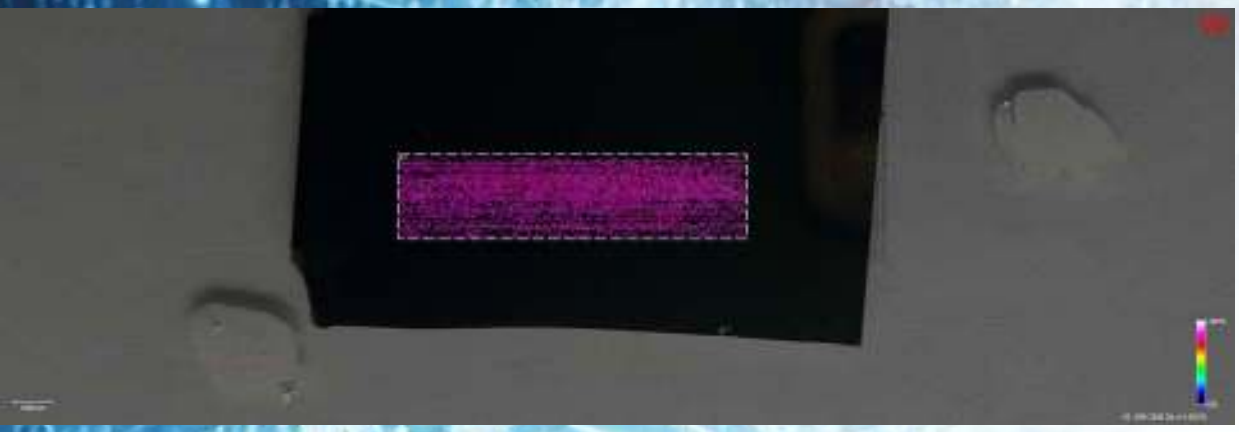

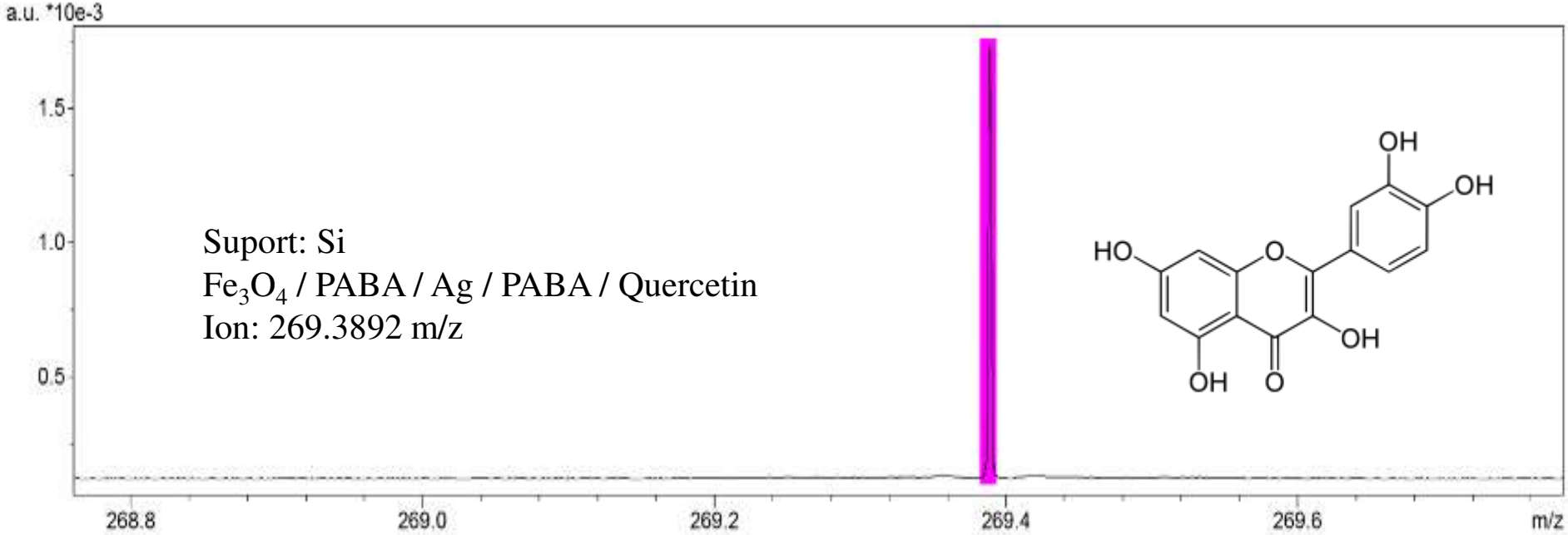
a.u. *10e-3
1.5
1.0
0.5
Suport: Si
Fe_3O_4 / PABA / Ag / PABA / Quercetin
Ion: 269.3892 m/z
OH
OH
HO
O
OH
OH
O
268.8
269.0
269.2
269.4
269.6
m/z

Suport: Si

Fe_3O_4 / PABA / Ag / PABA / Copper phthalocyanine

Ion: 576.6982 m/z

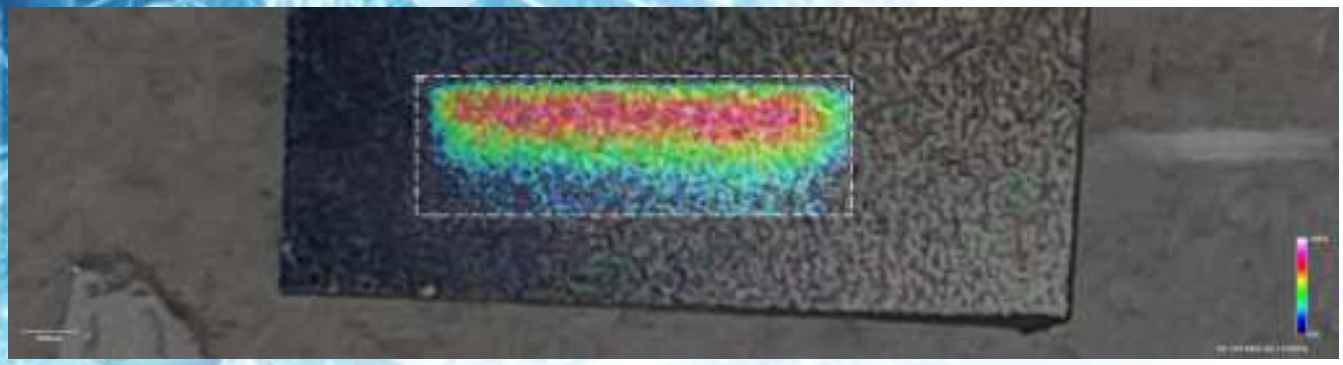

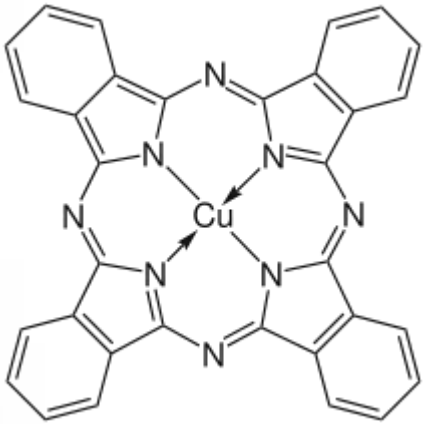

Acknowledgment

EU FT-ICR MS

THANK YOU FOR YOUR ATTENTION !

THIS RESEARCH WAS FUNDED BY THE PROJECTS:

- **EUROPEAN REGIONAL DEVELOPMENT FUND THROUGH COMPETITIVENESS OPERATIONAL PROGRAM 2014-2020, PRIORITY AXIS 1, PROJECT NO. P_36_611, MYSMIS CODE 107066, INNOVATIVE TECHNOLOGIES FOR MATERIALS QUALITY ASSURANCE IN HEALTH, ENERGY AND ENVIRONMENTAL - CENTER FOR INNOVATIVE MANUFACTURING SOLUTIONS OF SMART BIOMATERIALS AND BIOMEDICAL SURFACES – INOVABIOMED**

- **„COMPOZIT MULTIFUNCTIONAL PE BAZA DE MATRICE SILICA-ORGANICA TRANSPOZABILA PENTRU INOVATII DE PRODUSE SI FORMULARI PARTICULARIZATE IN INDUSTRIA ALIMENTARA SI FARMACEUTICA”, COD SMIS 122027, CONTRACT NO. 257/09.06.2020.**

Thursday

FT ICR cell: How to make the best

Evgeny Nikolaev
Skolkovo Institute of Science and Technology

Since introduction in 1974 FT ICR continue to be the best in resolving power and mass measurement accuracy!

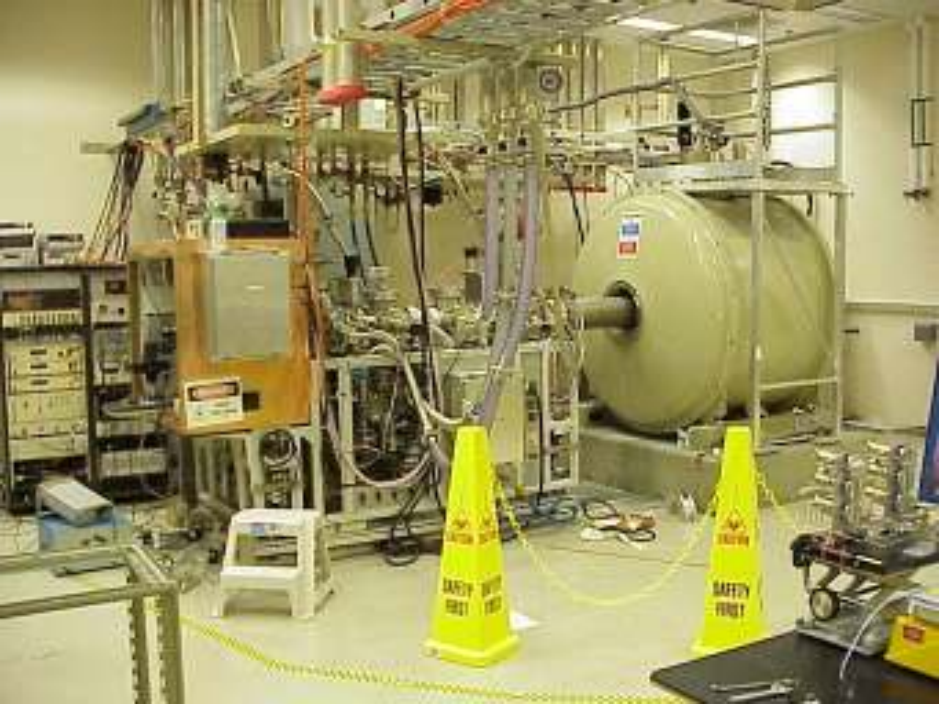
SAFETY FIRST
SAFETY FIRST

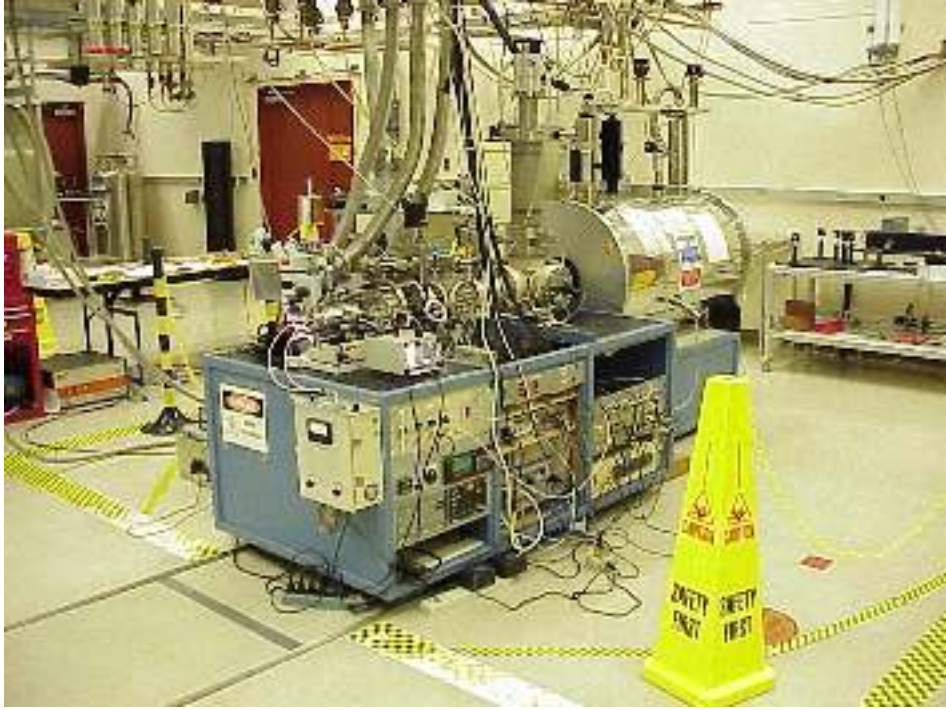
SAFETY FIRST
SAFETY FIRST

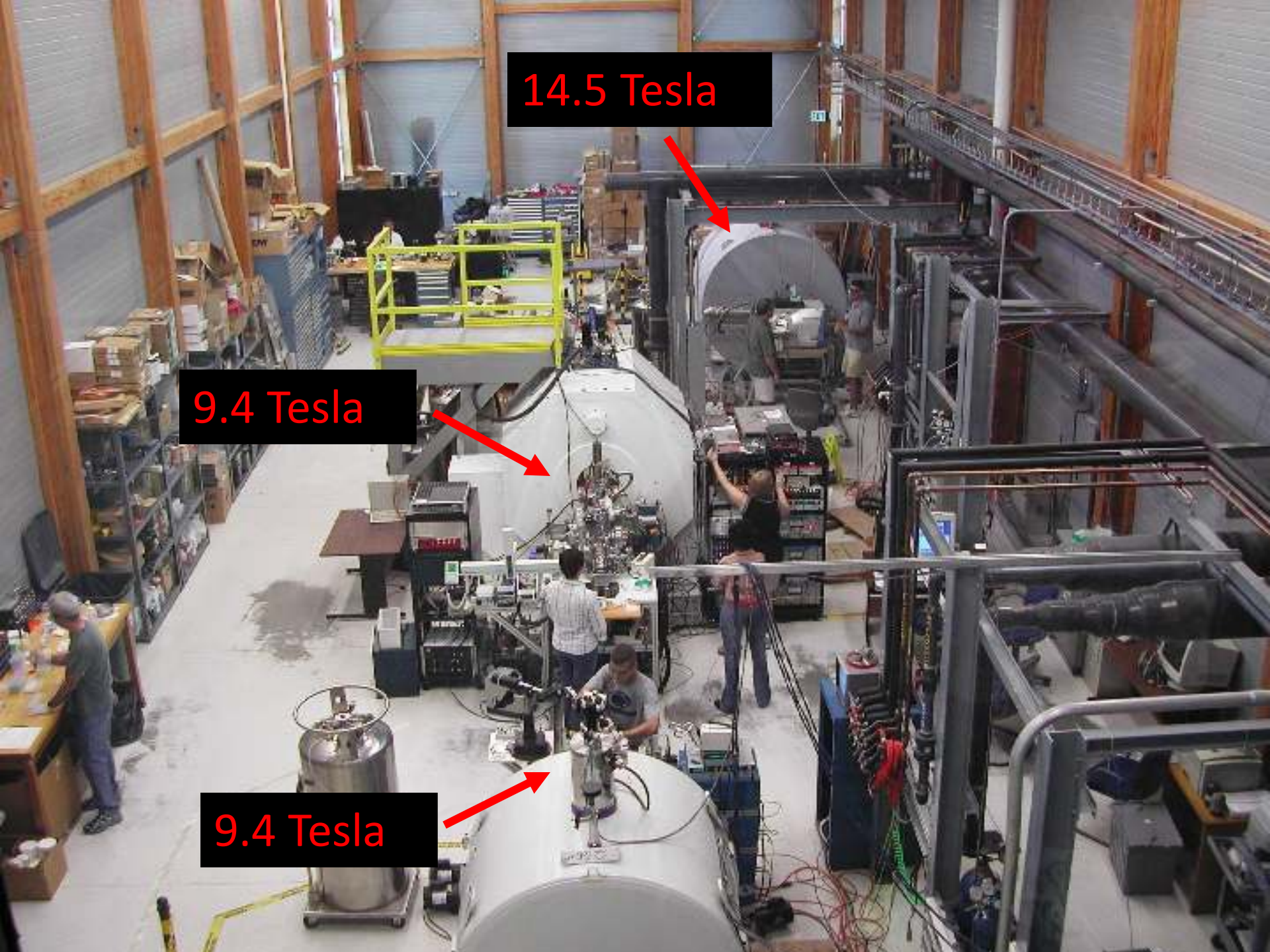
14.5 Tesla
9.4 Tesla
9.4 Tesla

National High Magnetic Field Laboratory NHMFL
(Tallahassee Florida)

From Alan Marshall 10th NA FTMS 21 T talk

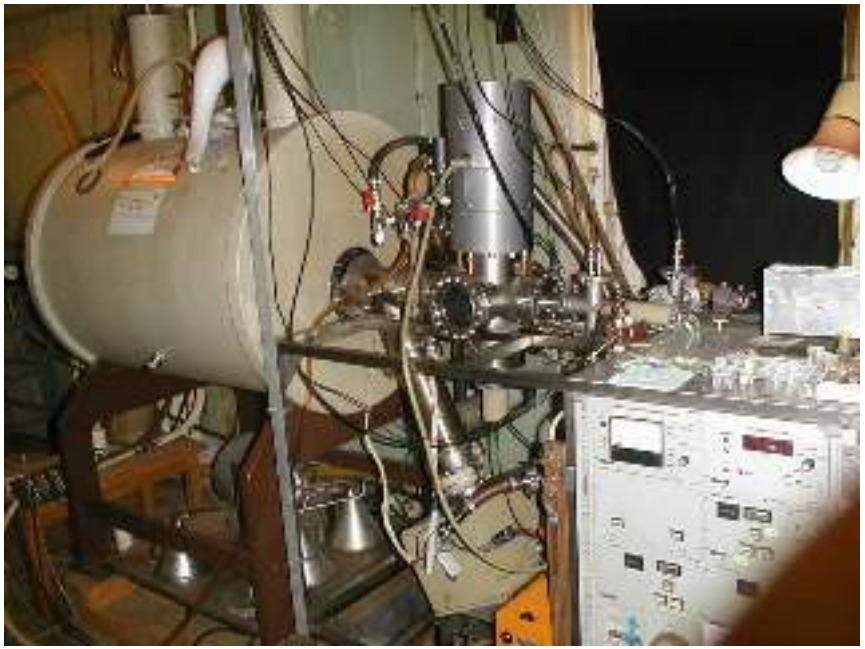

Moscow FT ICR instruments

After 47 years since introduction of FT ICR do we understand how it works?

Good!

Signals from same m/z ions

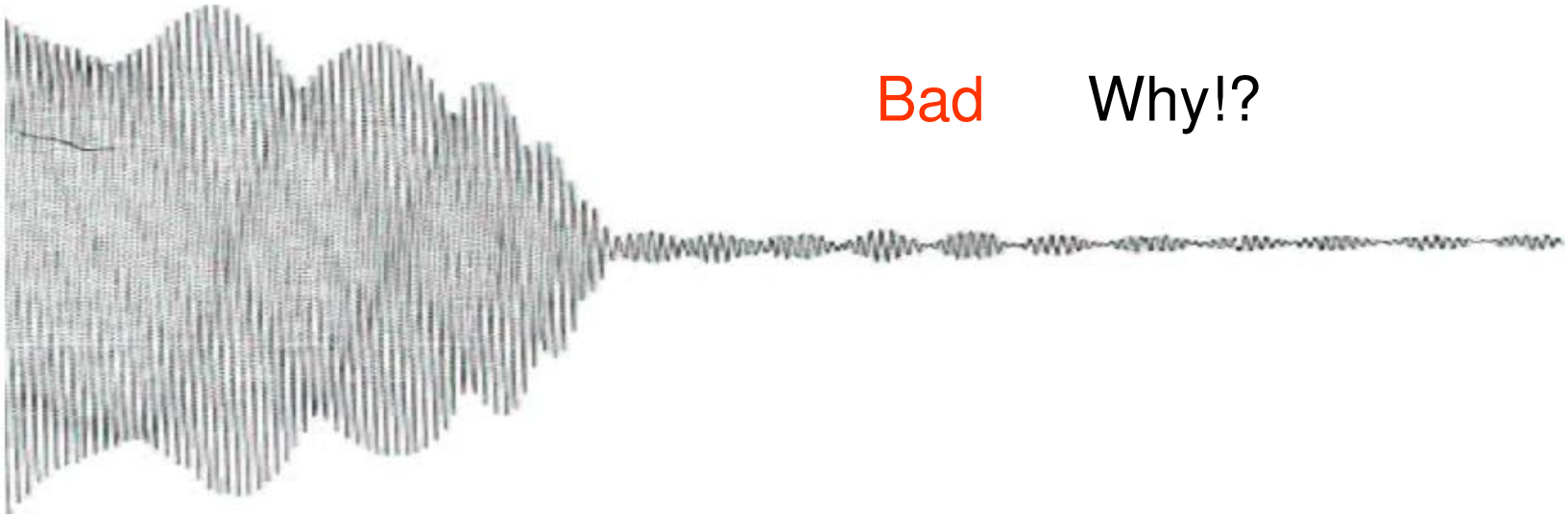

Bad Why!?

$\Omega(t)$ $\Omega(t+\Delta t)$

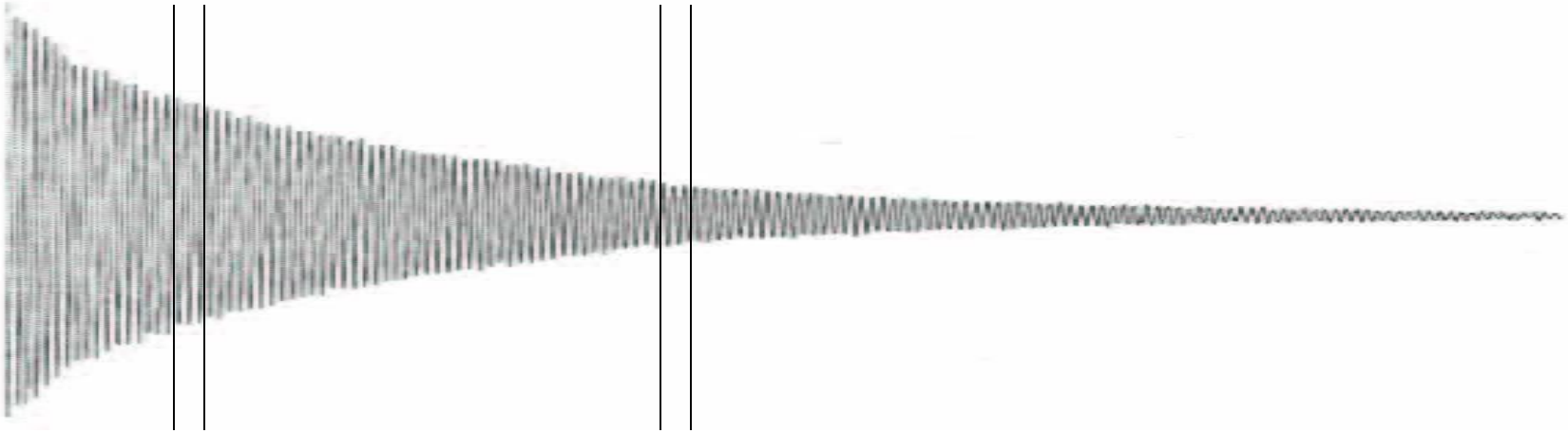

$\Omega(t+\Delta t) \neq \Omega(t)$ Why!?

Strange signal forms

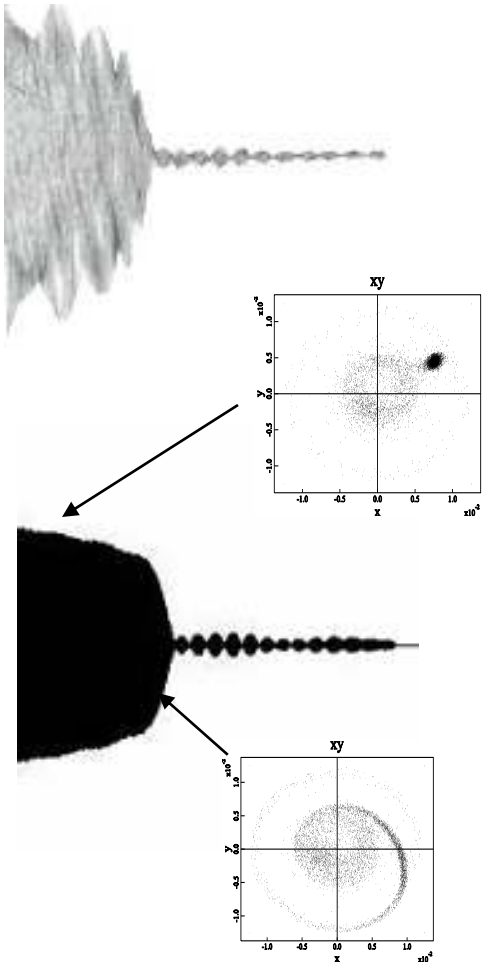

Experimental

Simulated

Charged particle in magnetic field

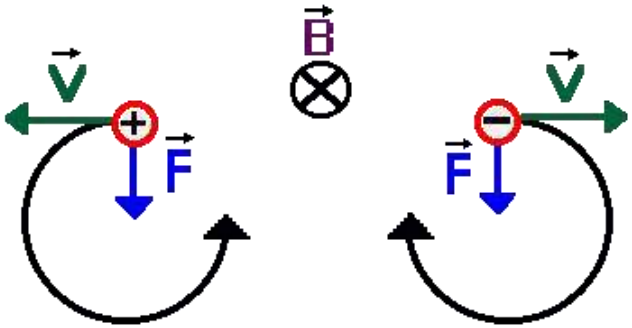

Lorentz force $F = ze^*v^*B = m^*v^2/r$

$v/r = 2\pi\omega$,

$ze^*B = m^*2\pi\omega$

$\omega = B^*ze/2\pi m$ (cyclotron frequency)

Cyclotron motion of ions

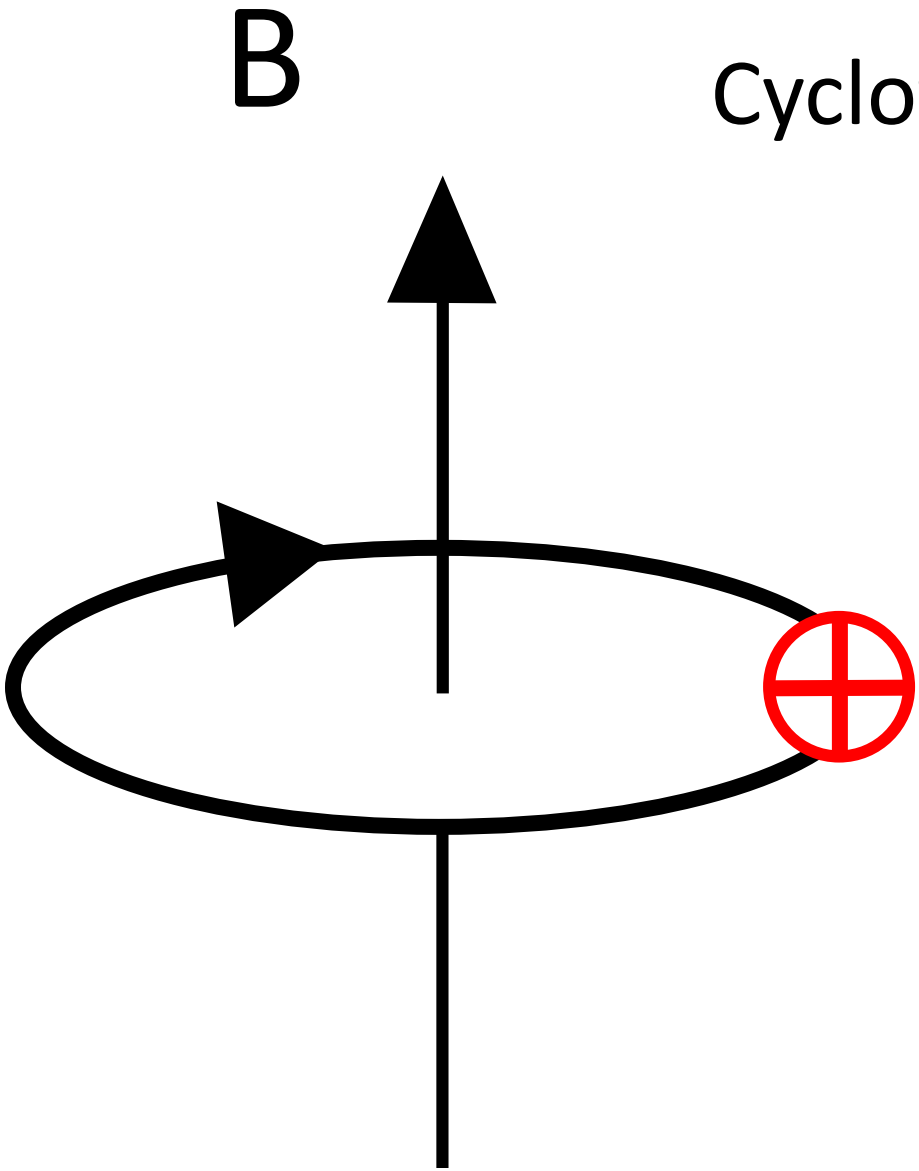

$$\omega = \frac{Z\,e\,B}{m}$$

Ion motion in electric field free space

$$\omega_c = \frac{|eB|}{mc}$$

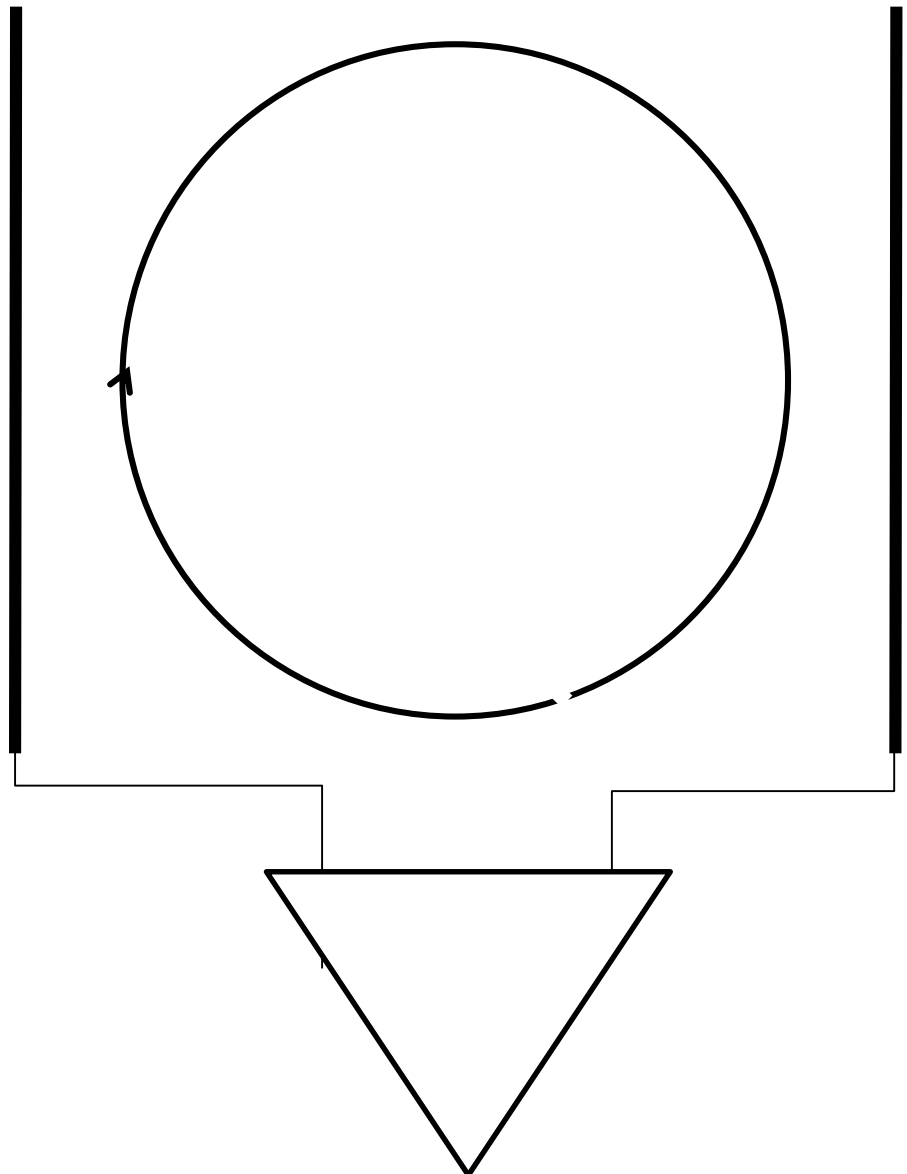

To excite cyclotron motion and detect the signal we need to trap ions

ICR Cells (Penning trap)

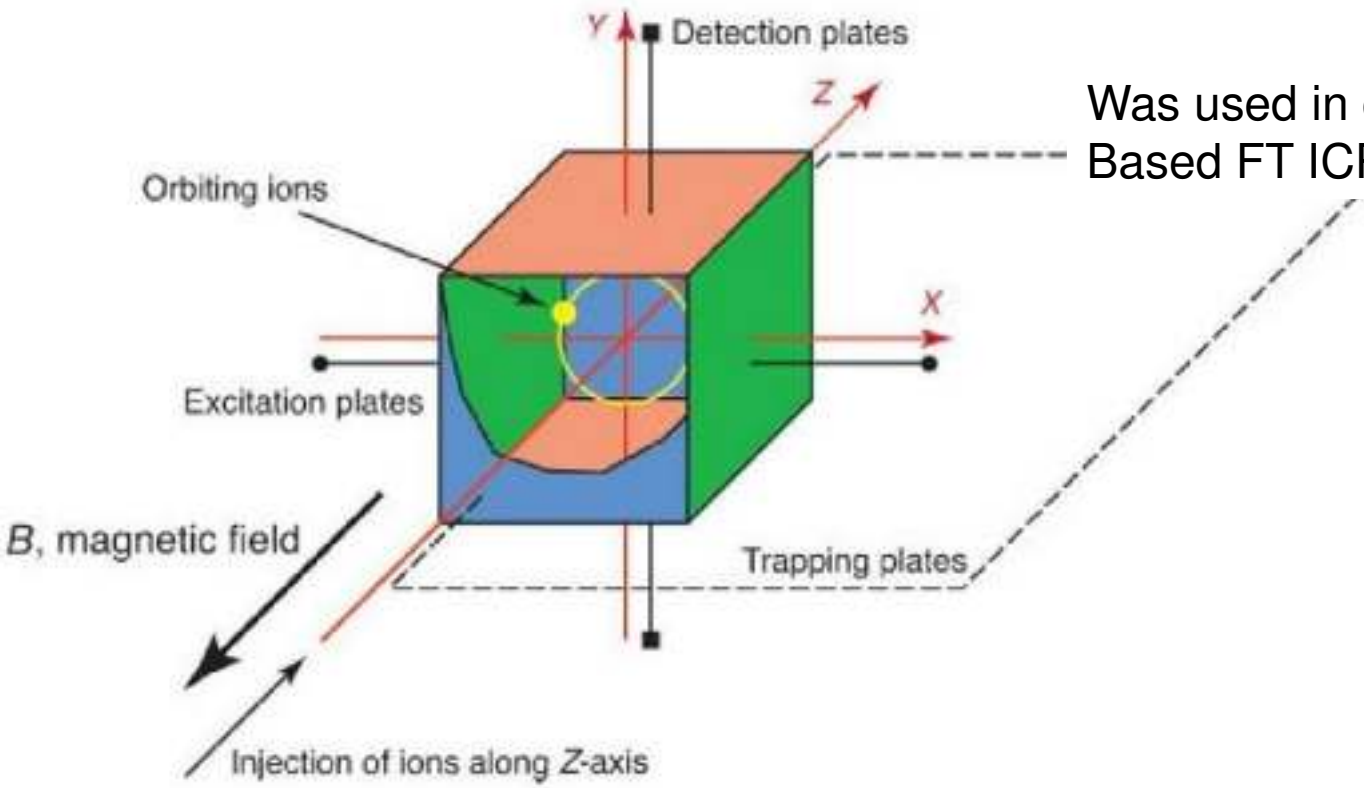

Was used in electromagnet
Based FT ICR instruments

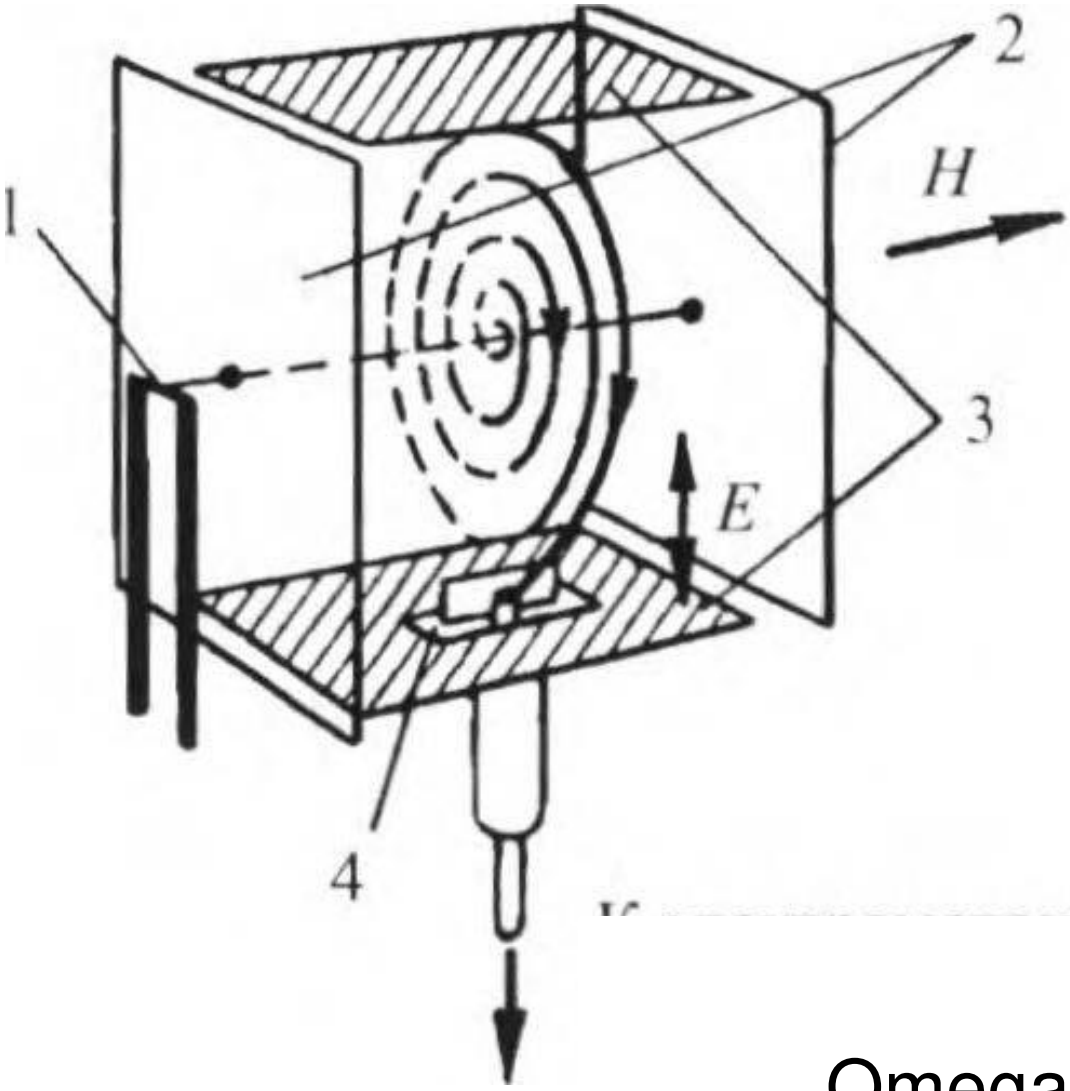

Omegatron

For superconductive magnets with cylindrical symmetry

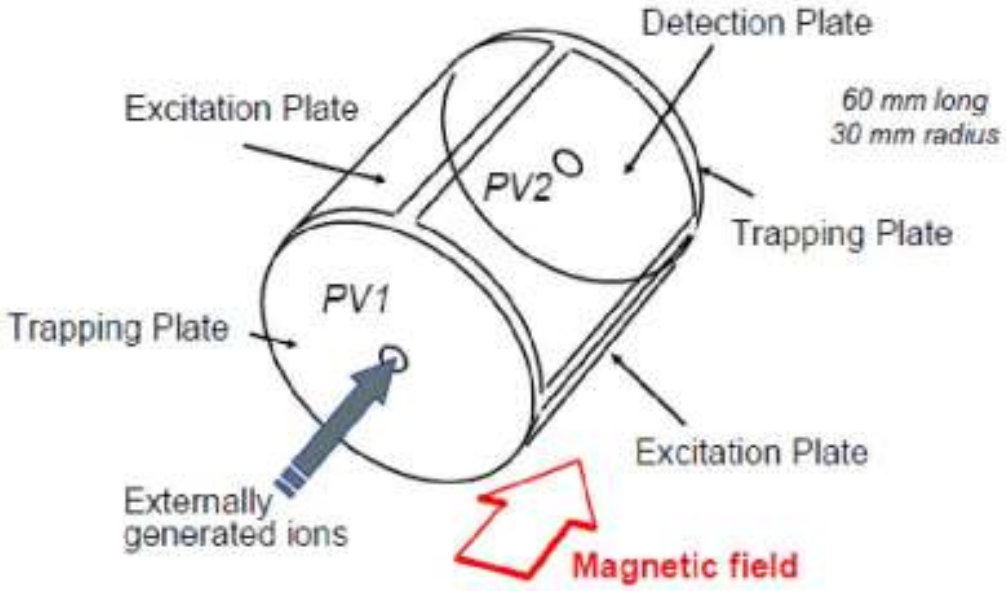

Most used cells

Bruker
Infinity cell
(until 2014)

Thermo
LTQ FT
(until 2006)

IonSpec Varian

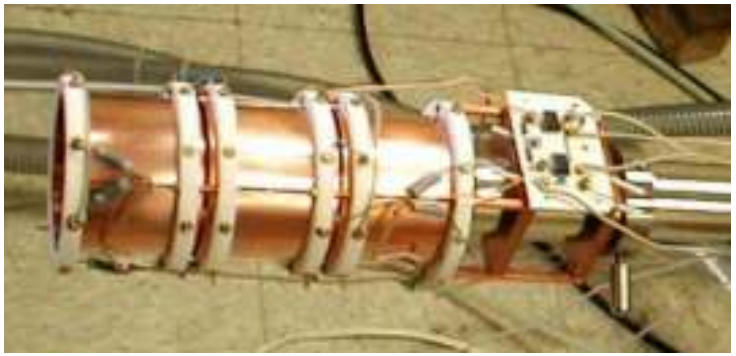

Compensated cells

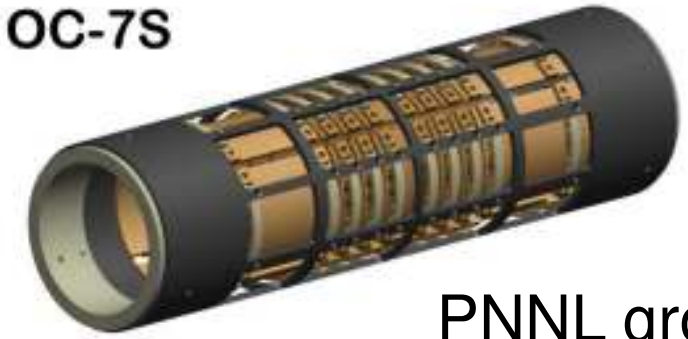

PNNL group

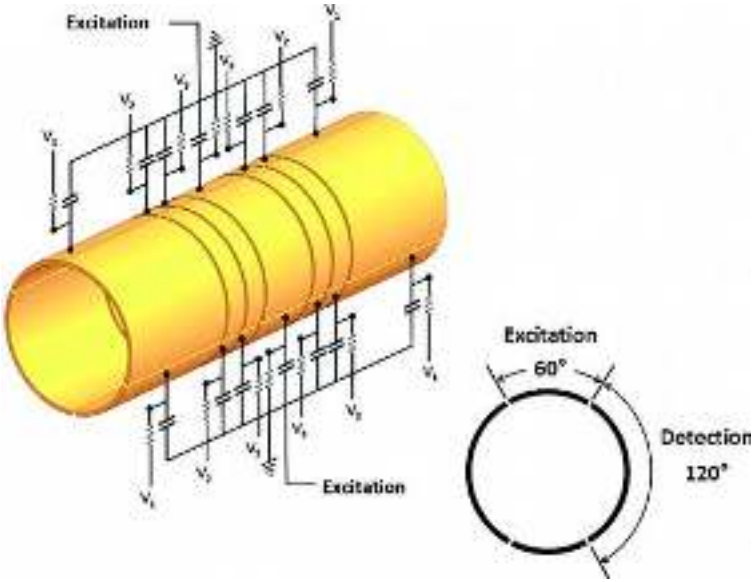

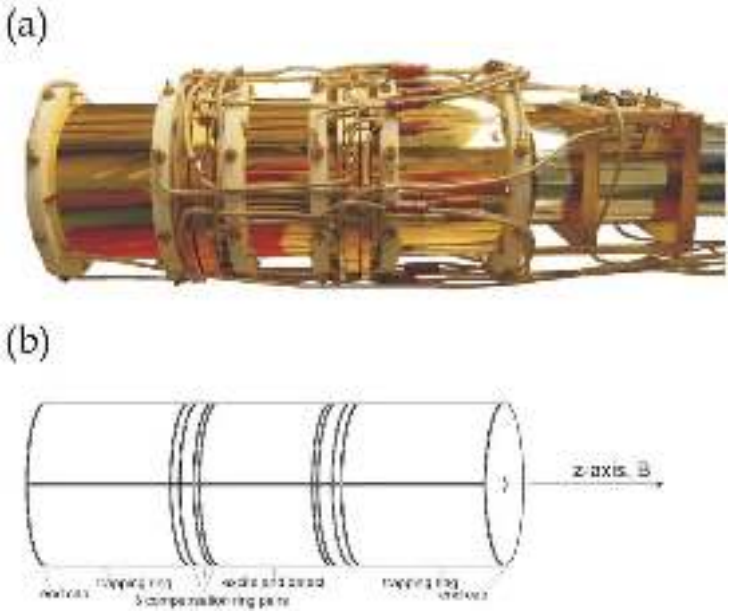

Marshall group

Gross group

Cells with trapping by pseudopotential

Nikolaev

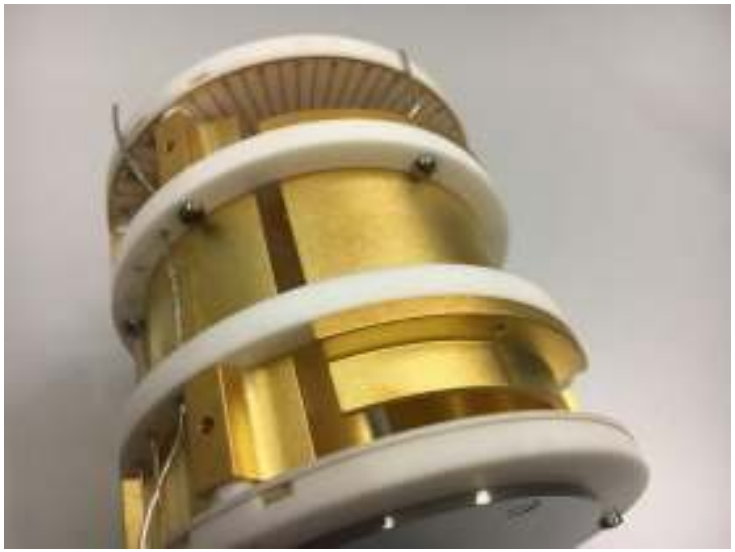

Bruker-Nikolaev

Cell with segmented trapping electrodes

Bruce

Fancy cells

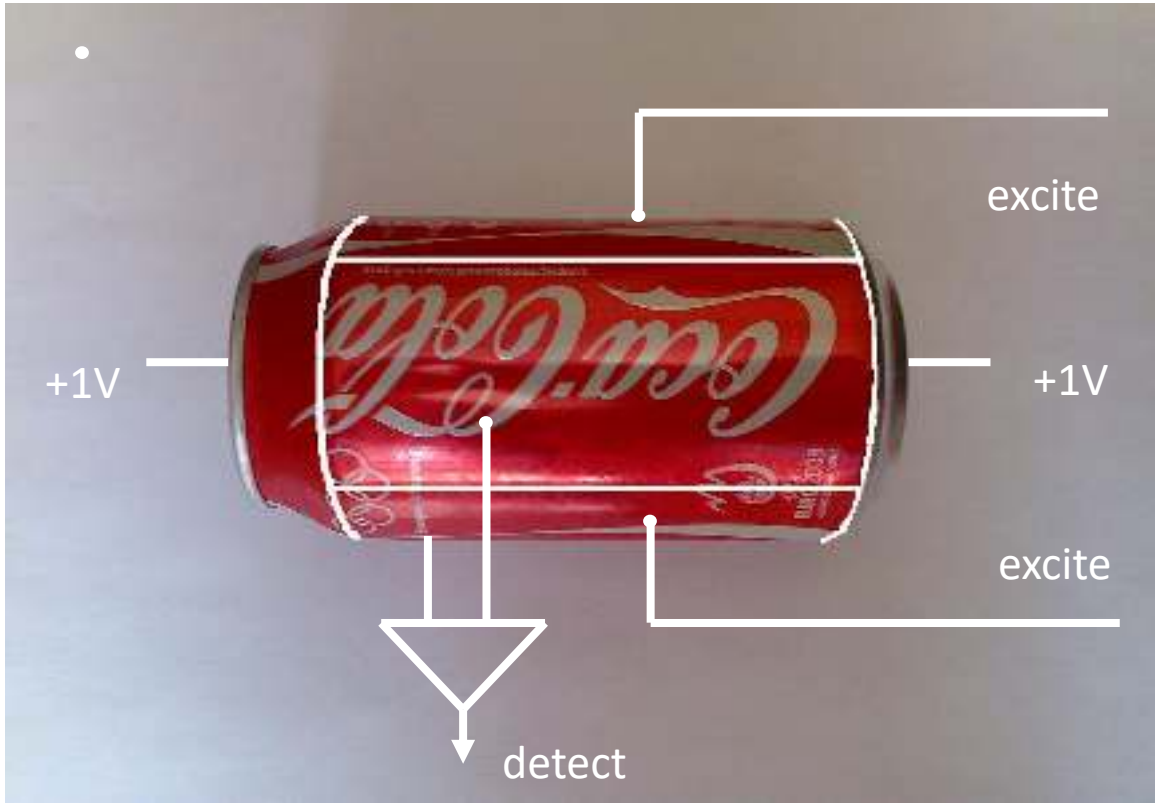

Coca-Cola cell

Spectroswiss NADEL cell

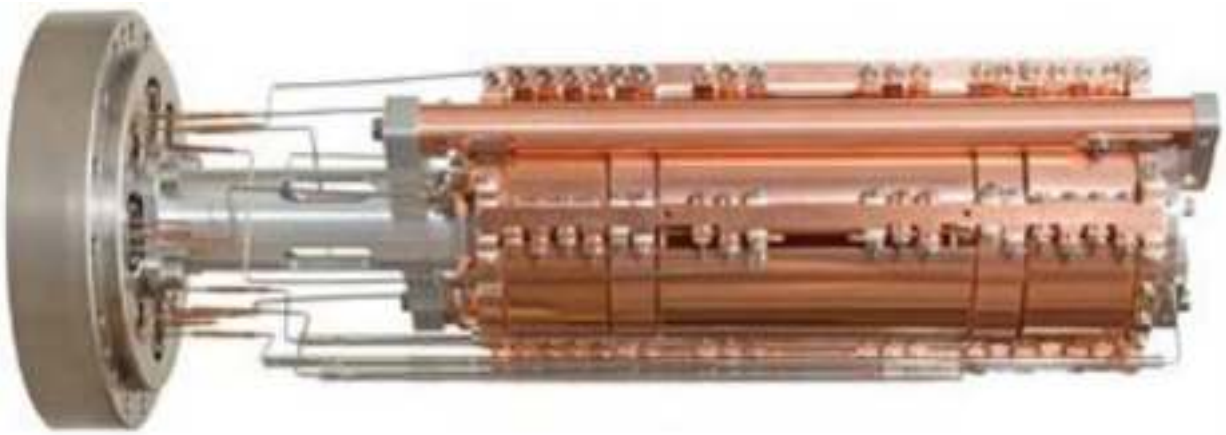

BIG
7 inches FT ICR cell

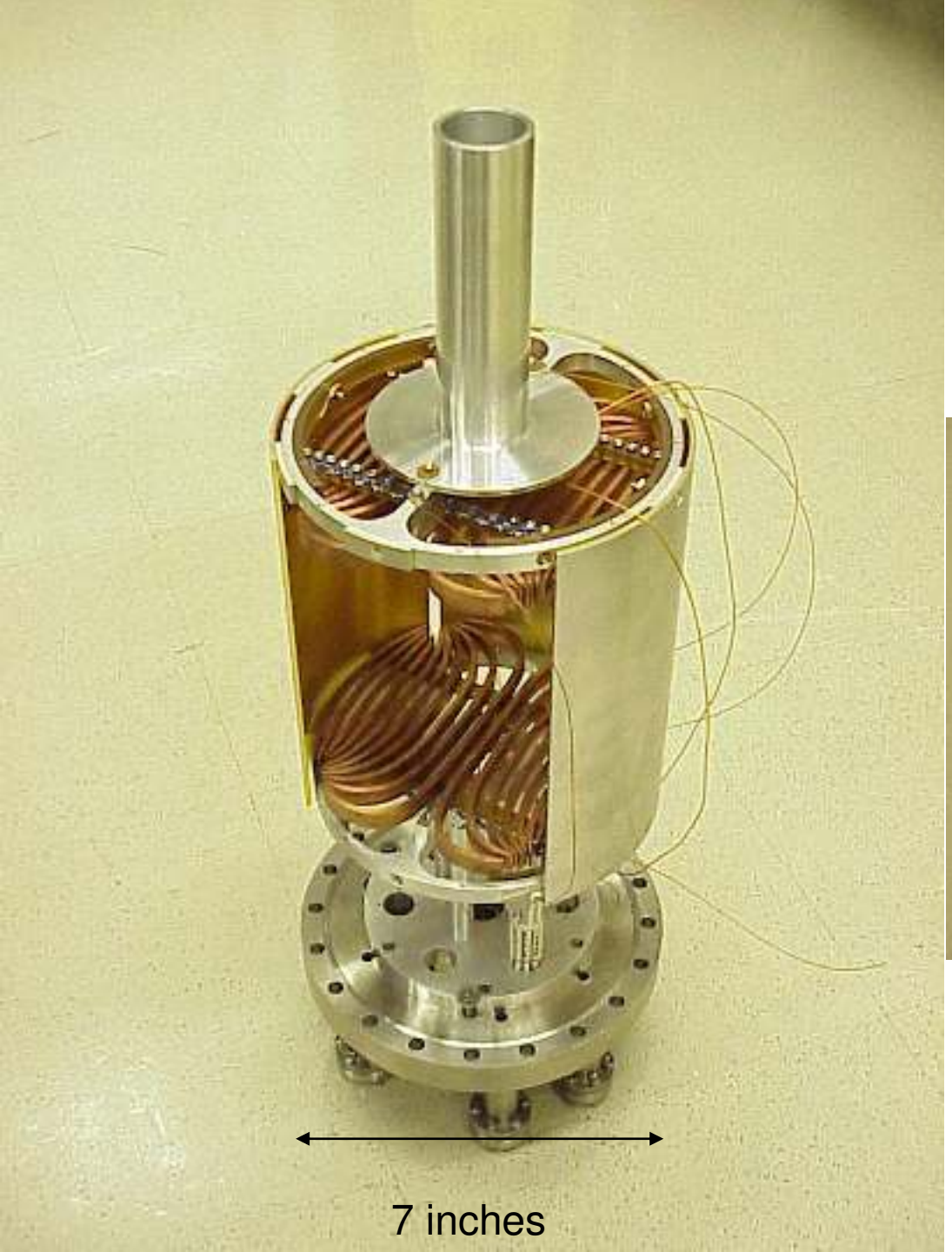

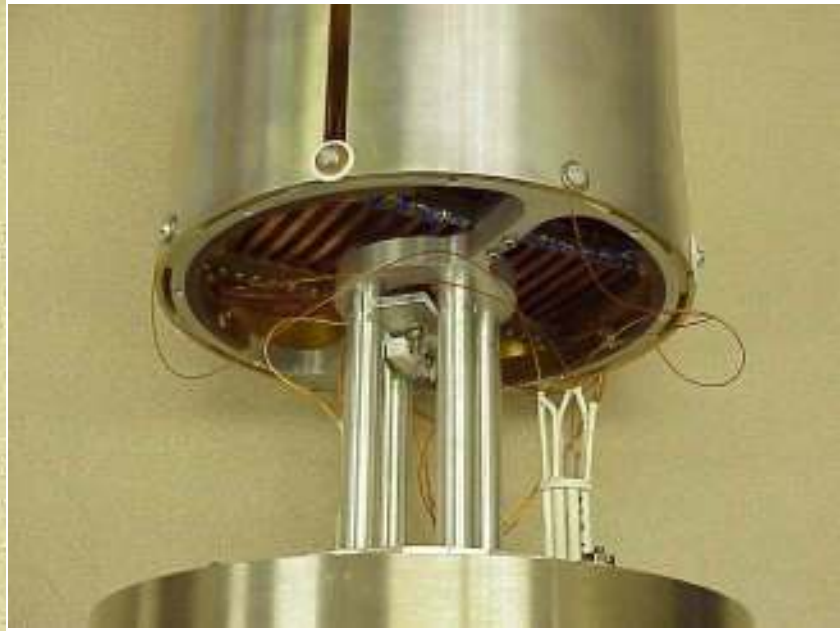

Dynamically harmonized cells

Bruker Solarix R&D

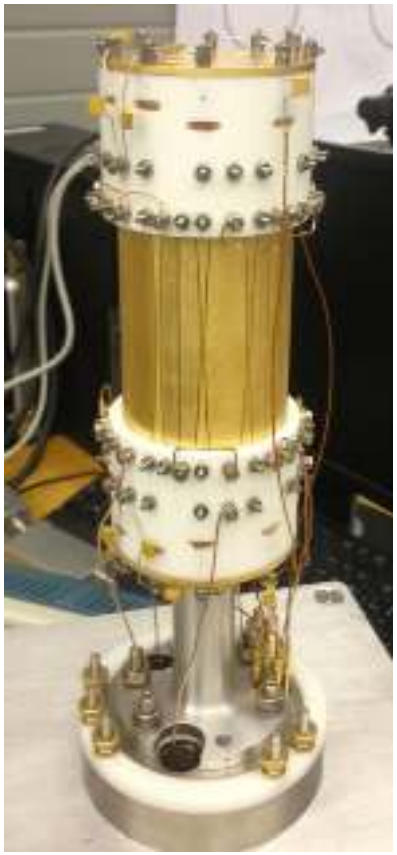

NHMFL cell From Alan Marshall 21 T talk

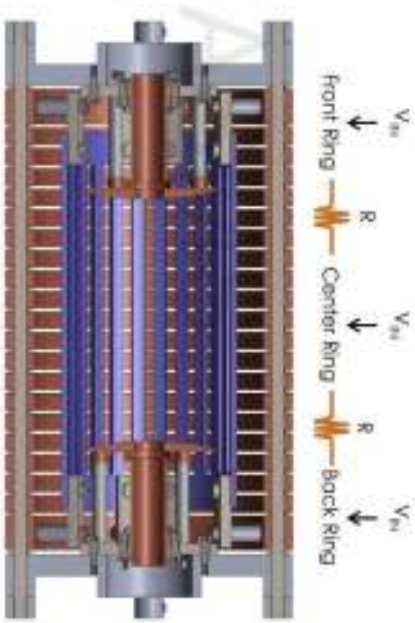

PNNL window cell

Dynamically harmonized
FT ICR cell for
Thermo LTQ FT

Why so many designs?

What is the problem?

The first problem was homogeneity of excitation
Field distribution

Cubic and cylindrical

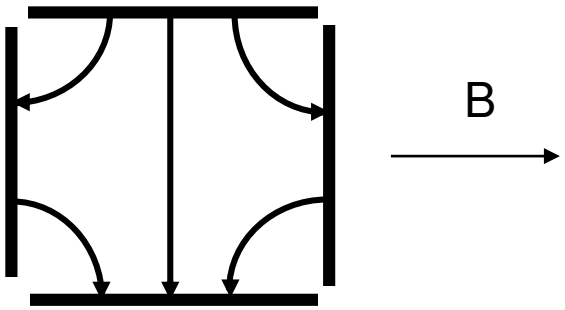

Elongated open cell

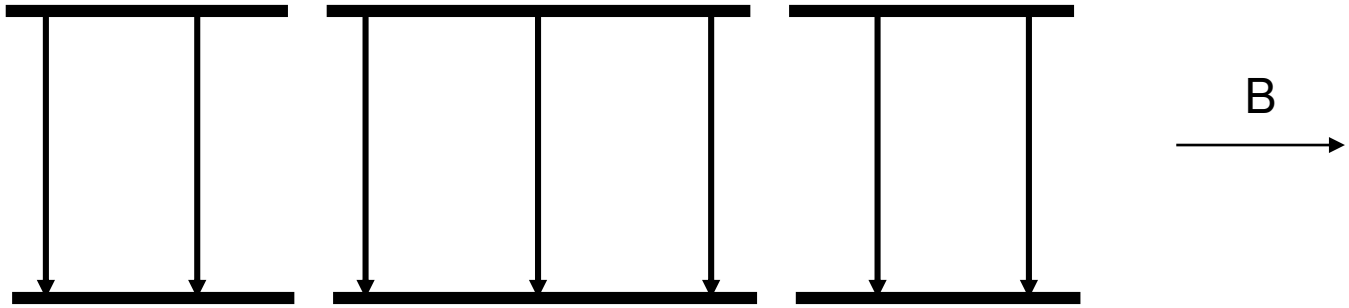

Elongated open cells

Thermo
LTQ FT
(until 2006)

IonSpec Varian

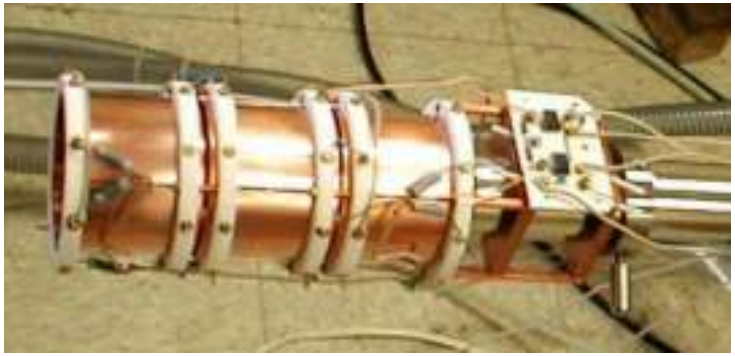

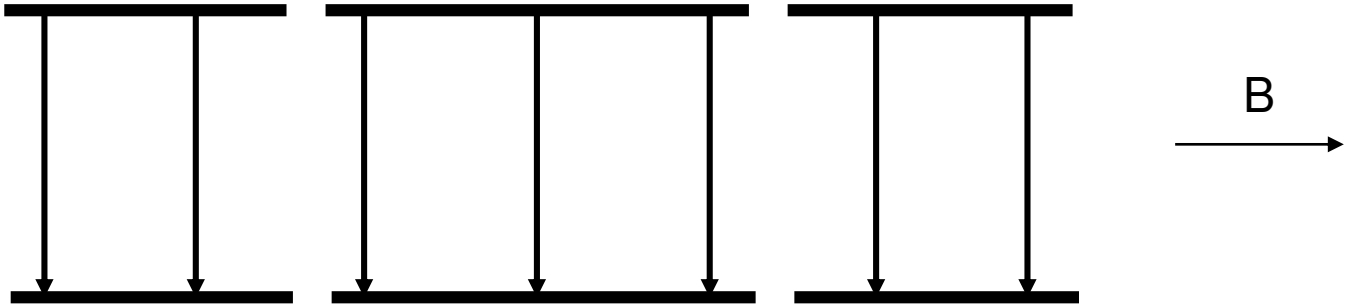

Infinity cell

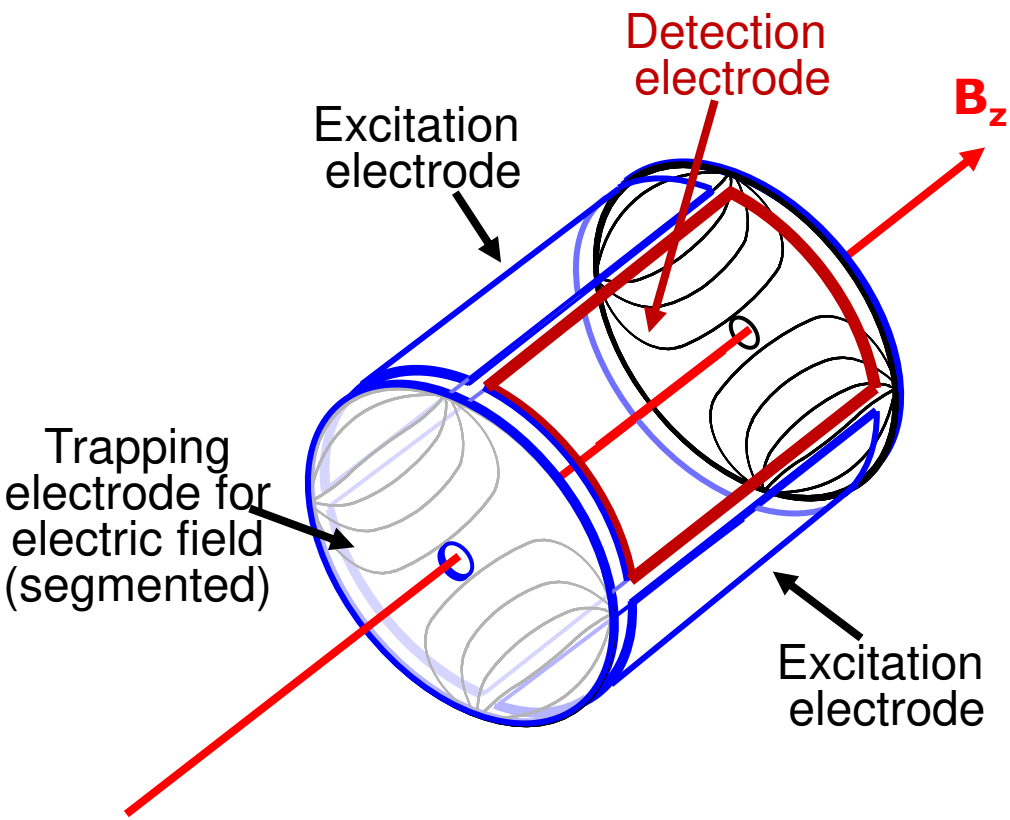

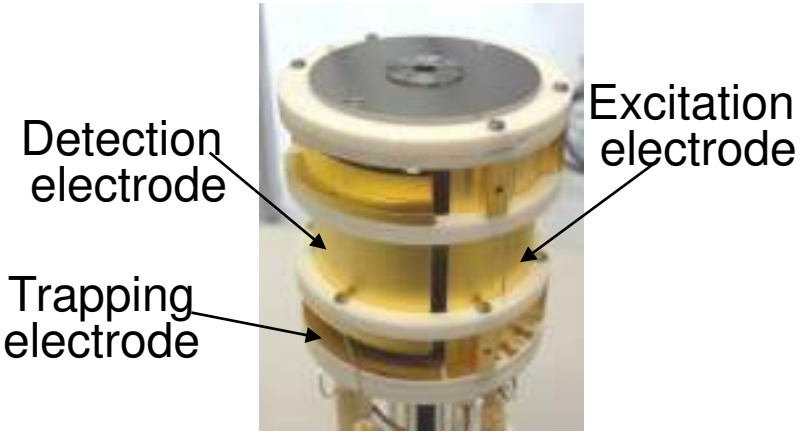

diameter: 60 mm
length: 60 mm

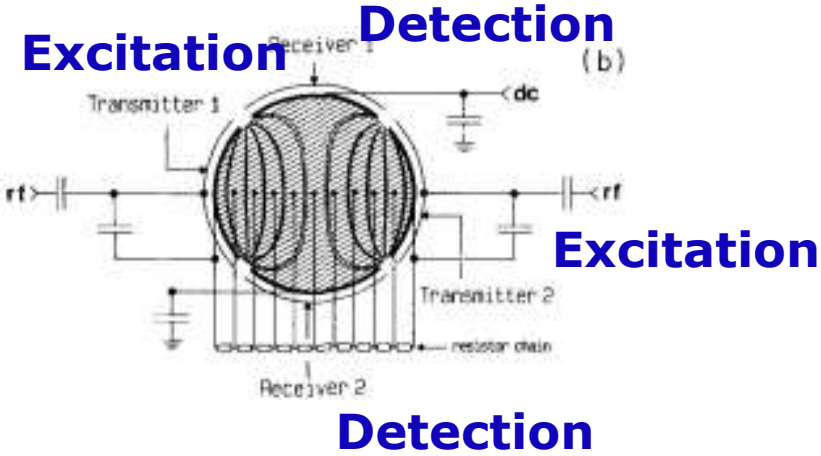

➔ Infinity trapping segments realize a dipolar excitation field, as if the ICR cell would be "infinitely" long.

BIG
7 inches FT ICR cell

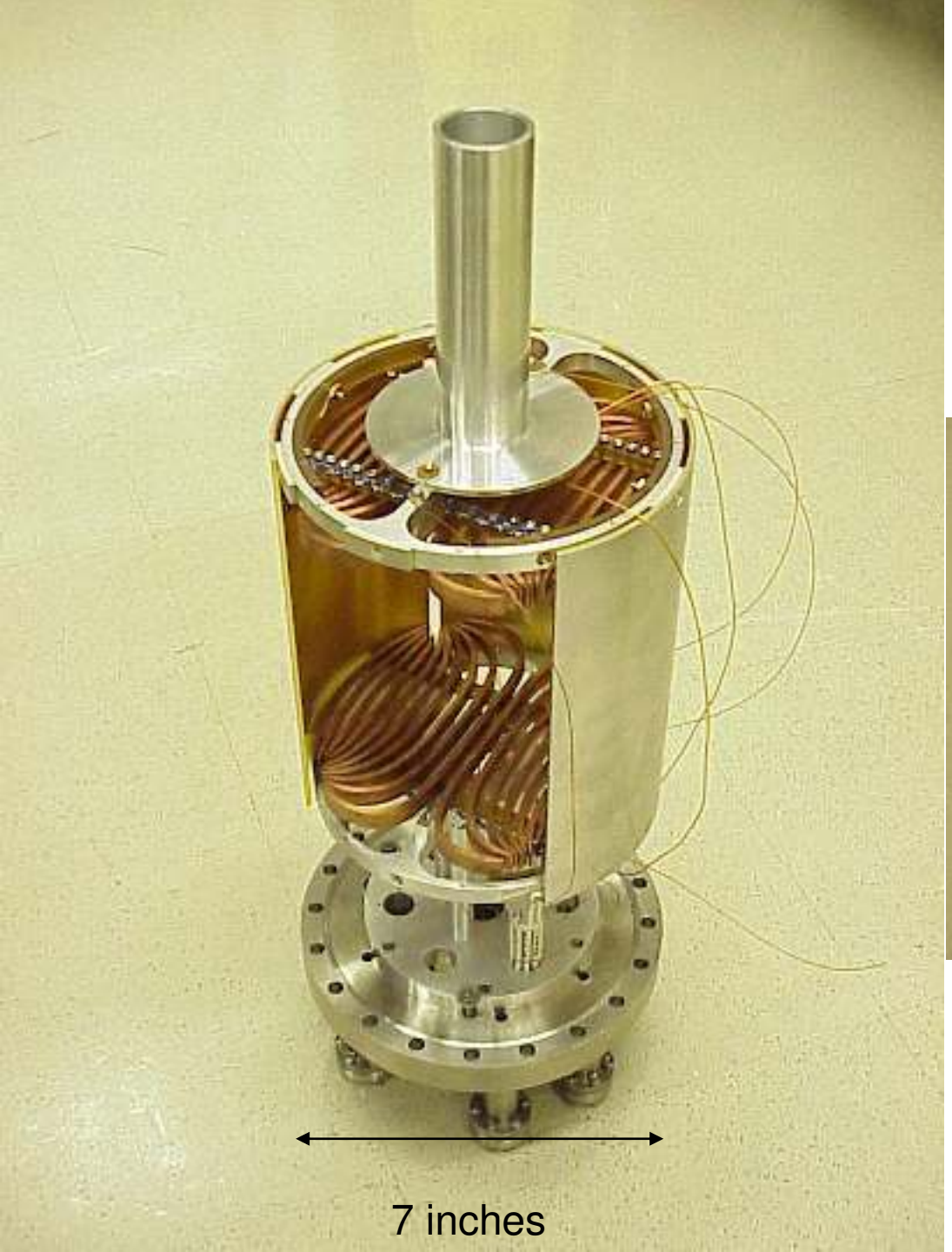

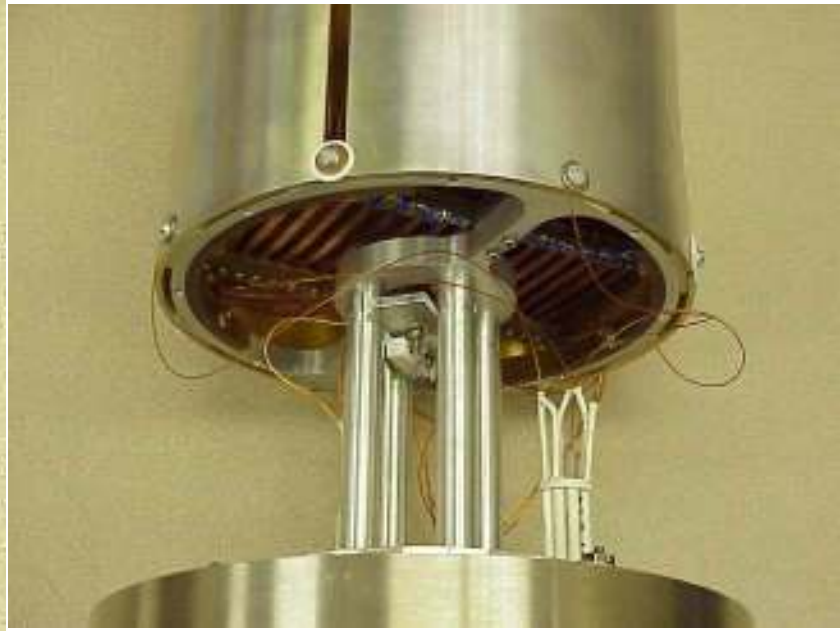

The second problem was:

Why we could not reach resolving power of more than 1 million at m/z close to 1000 Da?

Is it the vacuum problem?

Ion motion in electric field free space

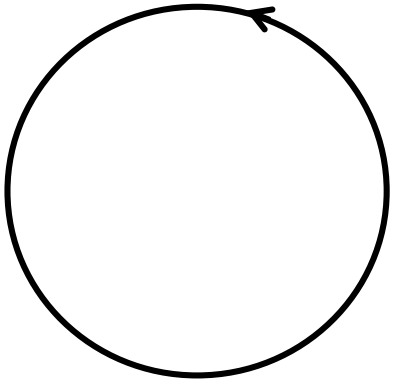

Cyclotron rotation

$$\omega_c = \frac{|eB|}{mc}$$

Distribution of potentials in rectangular or cylindrical FT ICR cells

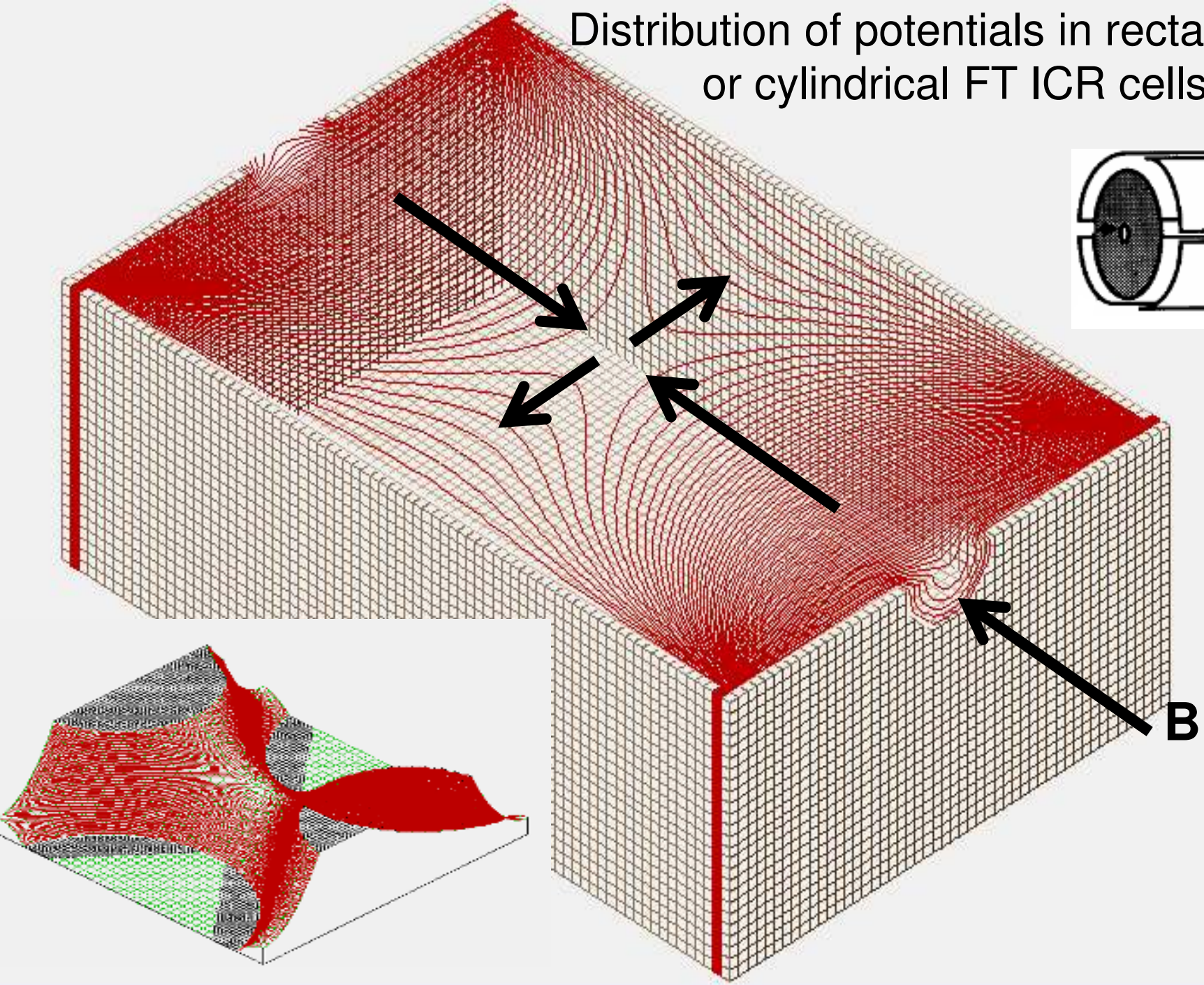

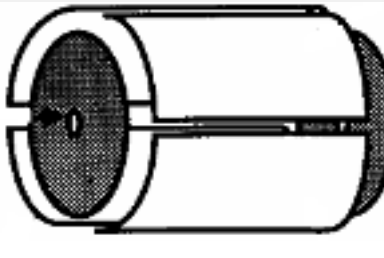

Motion of ions in crossed E/B fields

Cell potential plot in the xy plane of a cubic FT ICR cell.
3 V potential is applied to the trapping electrodes

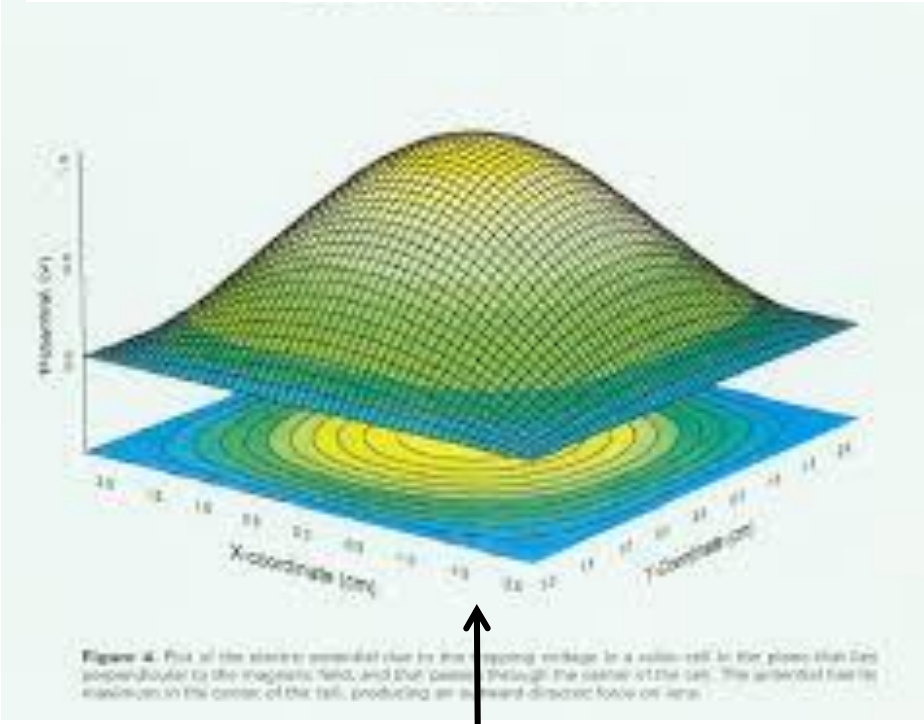

B

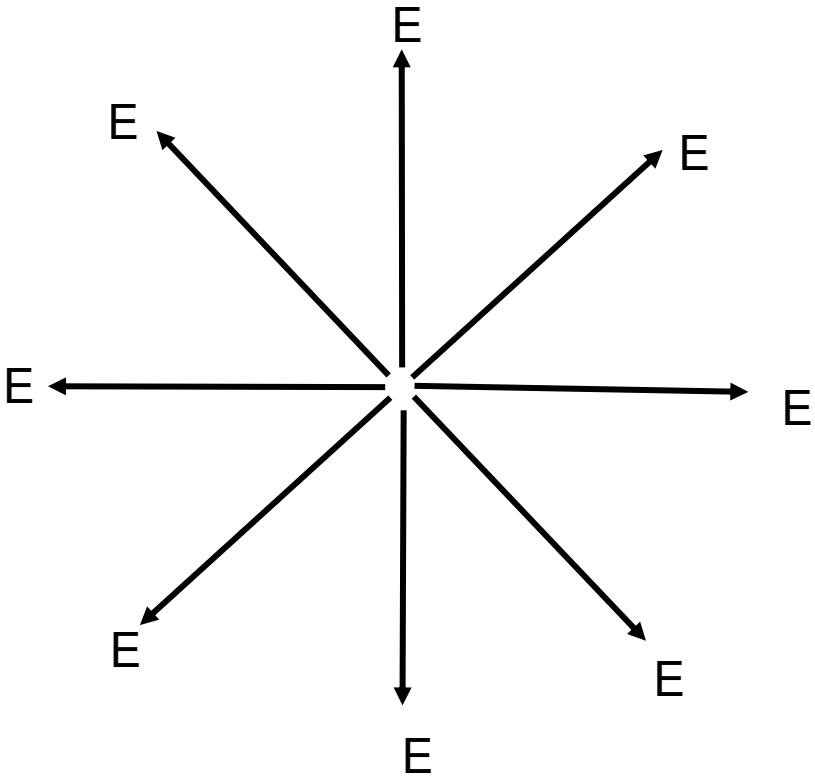

Motion of ions in crossed E/B fields

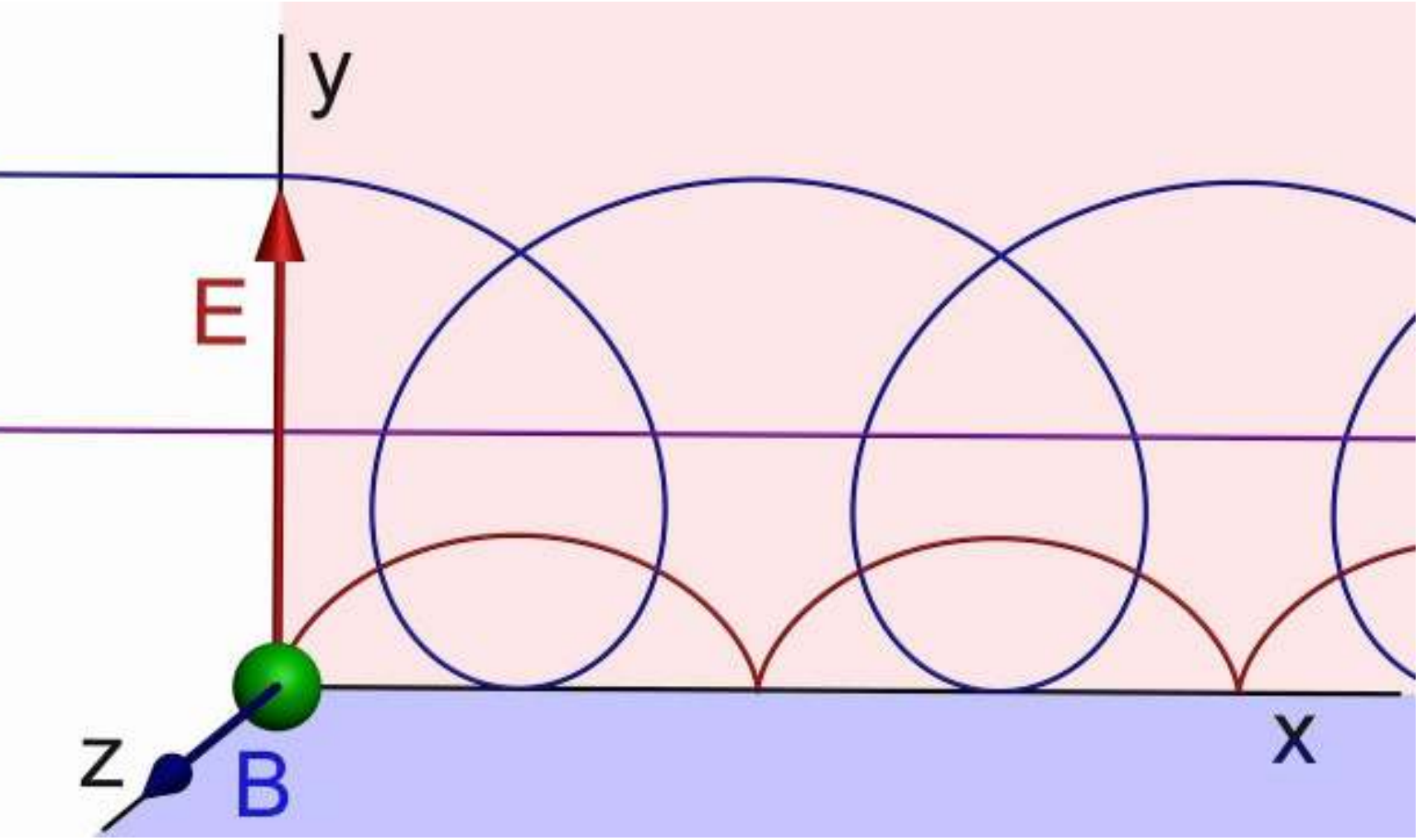

Magnetron motion. No excitation of cyclotron motion

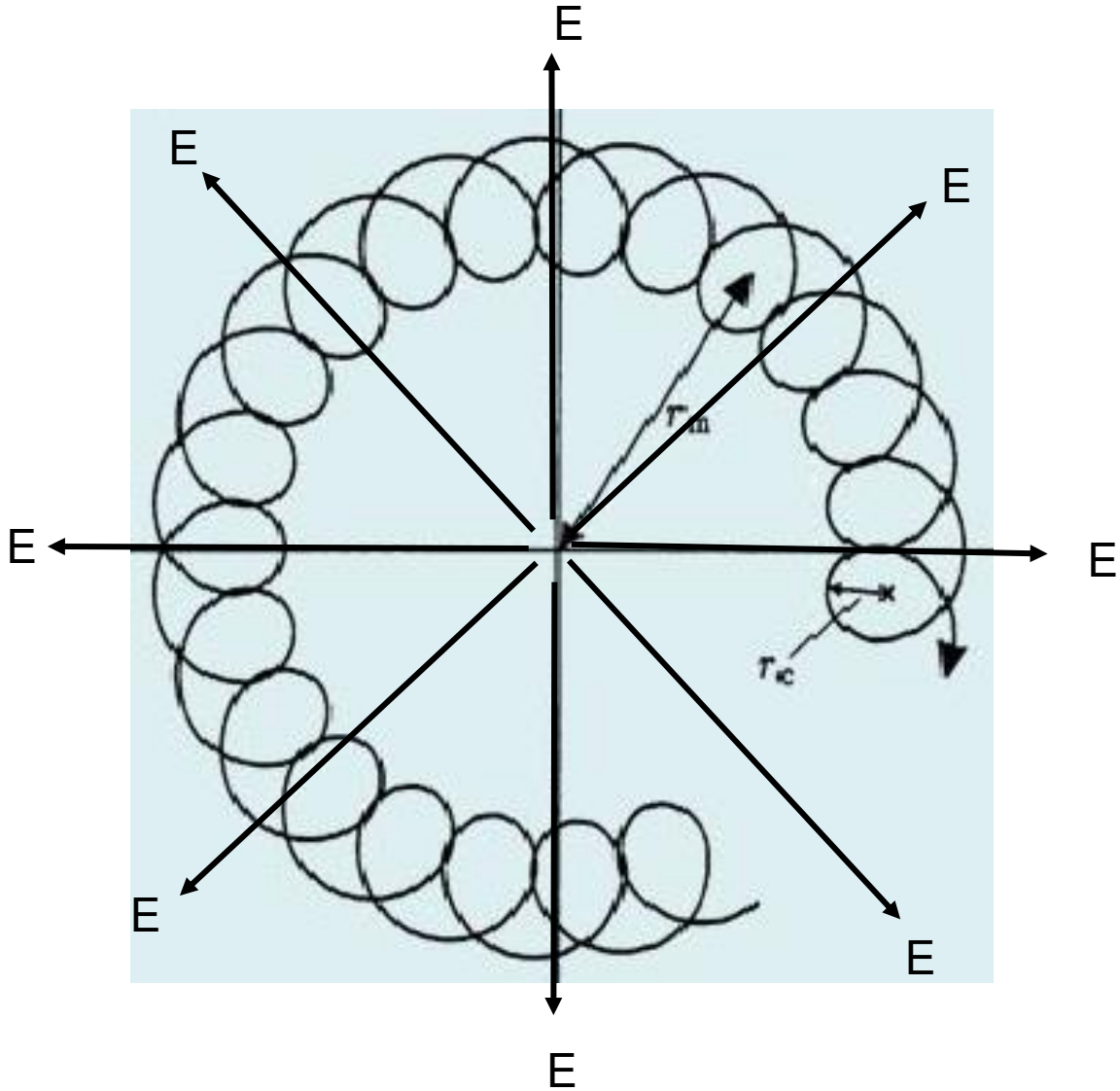

Ion motion in electric field free space

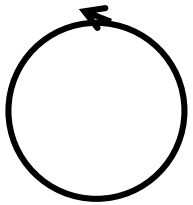

Cyclotron rotation

$$\omega_c = \frac{|eB|}{mc}$$

Ion motion in an electrostatic trap

Magnetron rotation

$$\omega_m = \omega_z^2 / 2\omega_c'$$

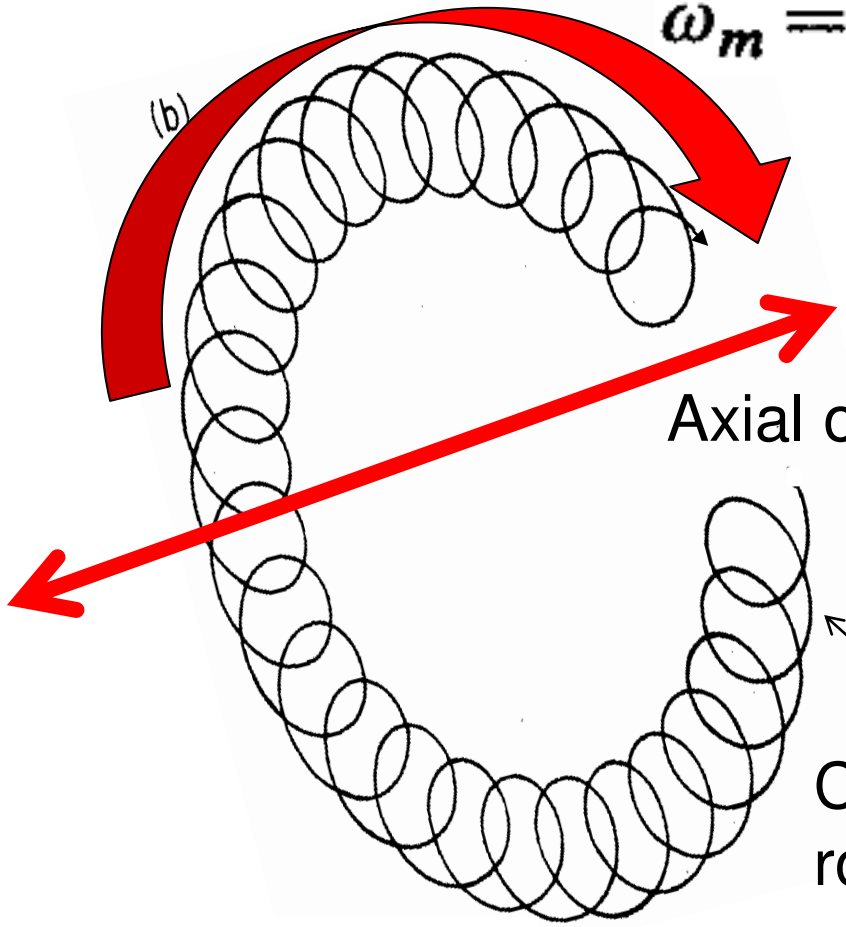

Axial oscillation

Cyclotron rotation

$$\omega_c' = \omega_c - \omega_m$$

Measured frequency

$$\omega_c = \frac{|eB|}{mc}$$

Hyperbolic cell

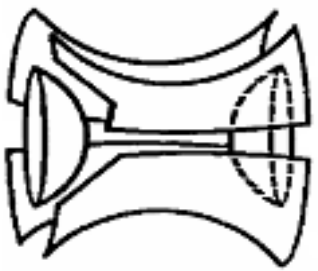

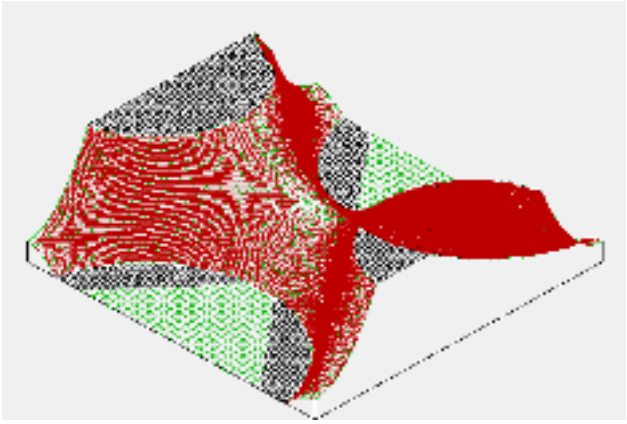

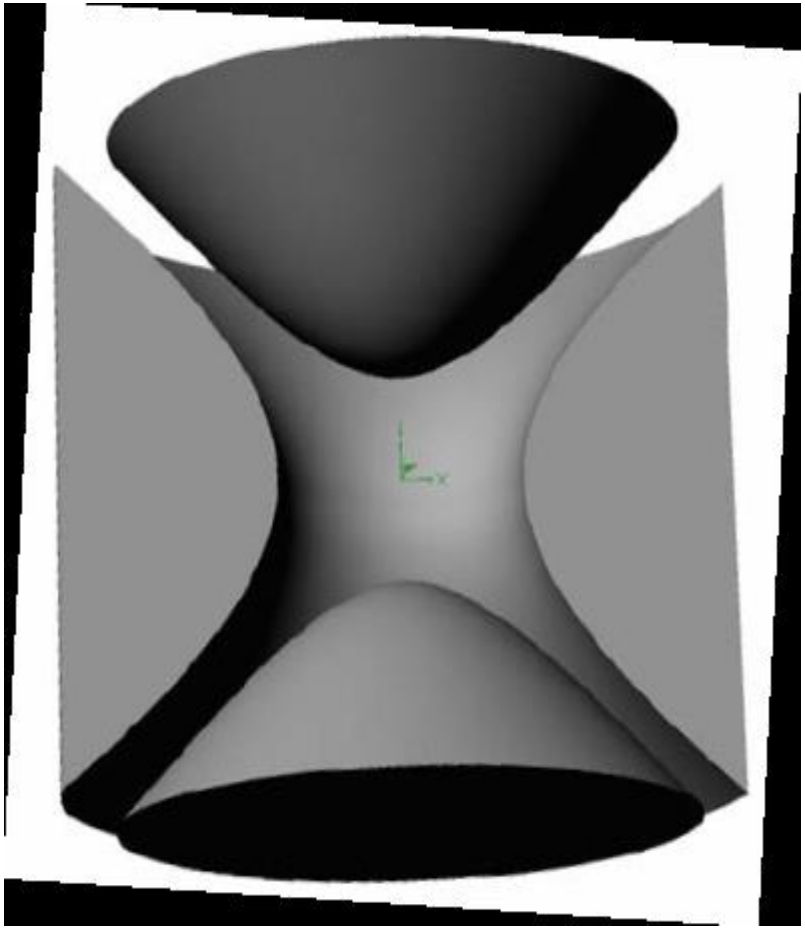

Hyperbolic Penning trap

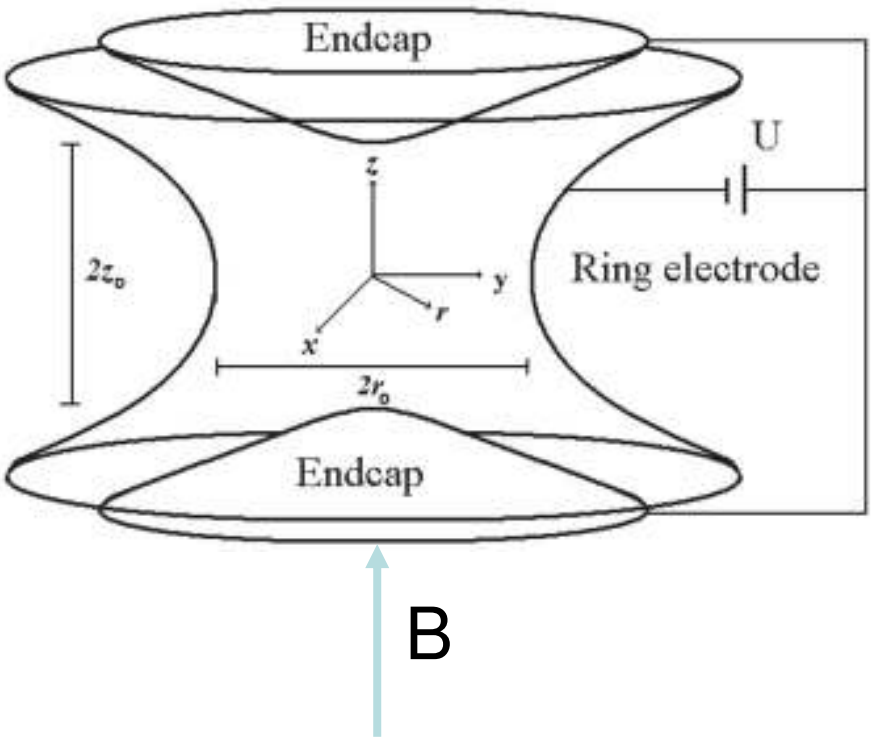

$$\phi(r,z) = \frac{U_0}{{R_0}^2}(r^2 - 2z^2)$$

$$R_0^2 = r_0^2 + 2z_0^2$$

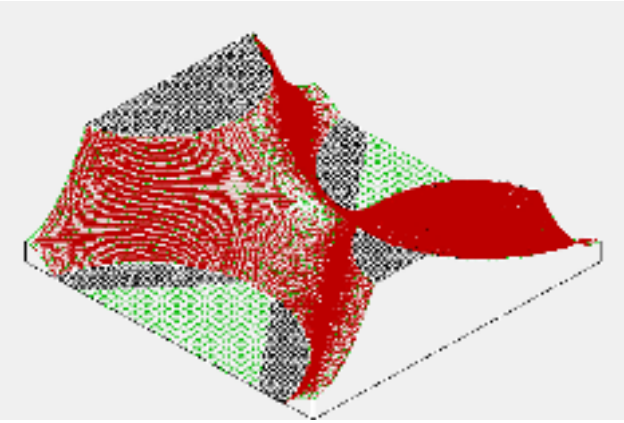

$$\vec{F} = q(\vec{E} + \vec{v} \times \vec{B})$$

Linear dependence of electric field on coordinates in hyperbolic ion trap

Electric field distribution

$$E_x = -\frac{\partial \phi(x,y,z)}{\partial x} = -\frac{2U_0}{R_0^2}x$$

$$E_y = -\frac{\partial \phi(x,y,z)}{\partial y} = -\frac{2U_0}{R_0^2}y$$

$$E_z = -\frac{\partial \phi(x,y,z)}{\partial z} = \frac{4U_0}{R_0^2}z$$

Potential distribution

$$\frac{\partial^2 x}{\partial t^2} = \frac{qB}{m}\frac{\partial y}{\partial t} - \frac{2qU_0}{mR_0^2}x$$

$$\frac{\partial^2 y}{\partial t^2} = -\frac{qB}{m}\frac{\partial x}{\partial t} - \frac{2qU_0}{mR_0^2}y$$

$$\frac{\partial^2 z}{\partial t^2} = \frac{4qU_0}{mR_0^2}z$$

$$\ddot{x} = \omega_c \dot{y} + \frac{\omega_z^2 x}{2} \qquad u = x + iy$$

$$\ddot{y} = -\omega_c \dot{x} + \frac{\omega_z^2 y}{2} \qquad \ddot{u} = -i\omega_c \dot{u} + \frac{1}{2}\omega_z^2 u$$

$$\ddot{z} = -\omega_z^2 z \qquad u = e^{-i\omega t}$$

$$\omega_c' = \frac{\omega_c + \sqrt{\omega_c^2 - 2\omega_z^2}}{2} \qquad \omega_m = \frac{\omega_c - \sqrt{\omega_c^2 - 2\omega_z^2}}{2}$$

$$\omega_c^2 > 2\omega_z^2 \qquad \omega_c' \approx \omega_c \gg \omega_z \gg \omega_m$$

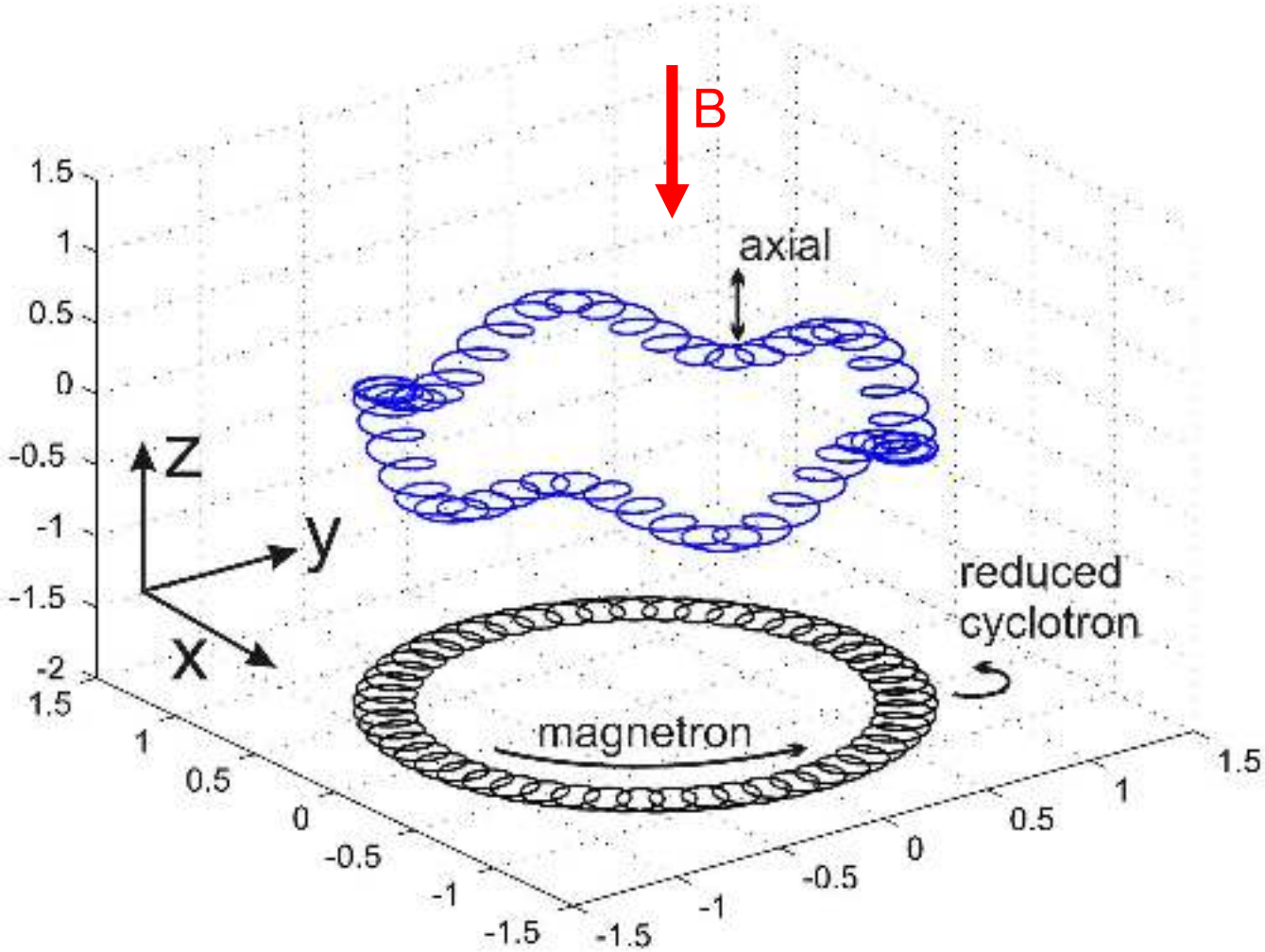

https://www.diva-portal.org/smash/get/diva2:413035/FULLTEXT01.pdf

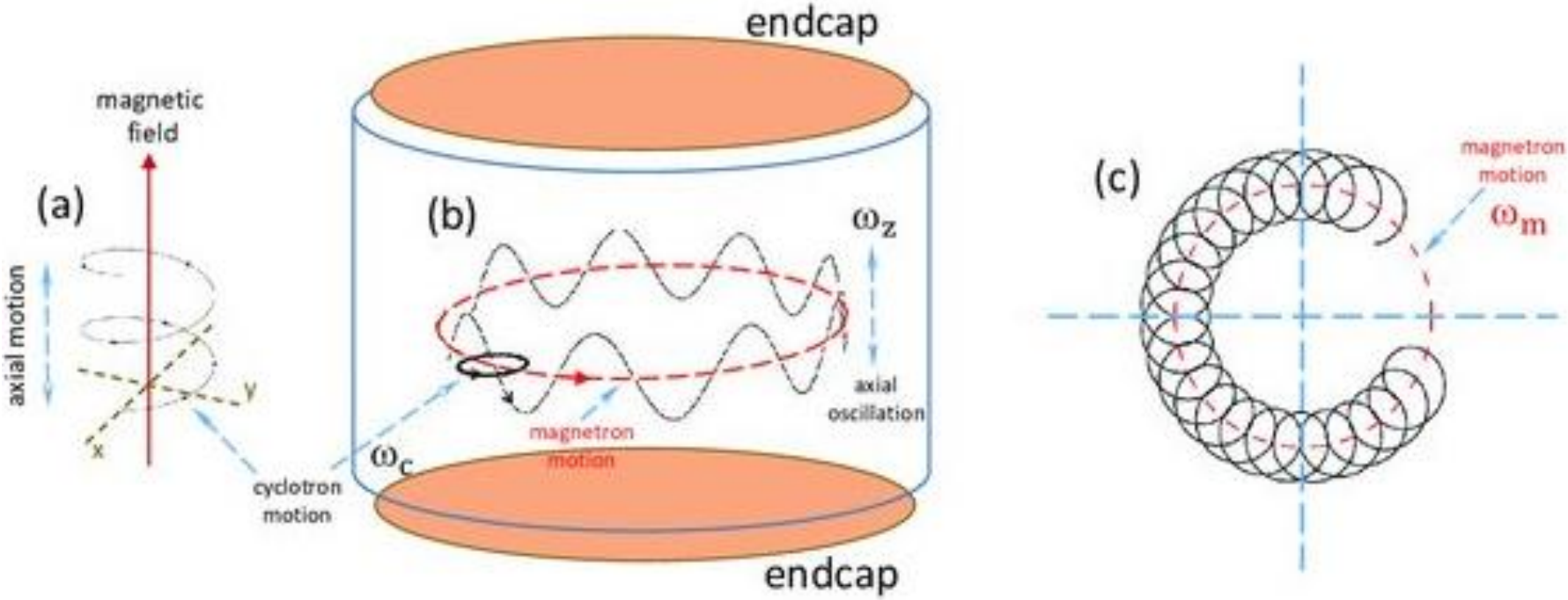
endcap
magnetic field
(a)
axial motion
y
x
(b)
ω_z
axial oscillation
magnetron motion
ω_c
cyclotron motion
endcap
(c)
magnetron motion
ω_m

In ideal hyperbolic trap all modes of ion motion are independent

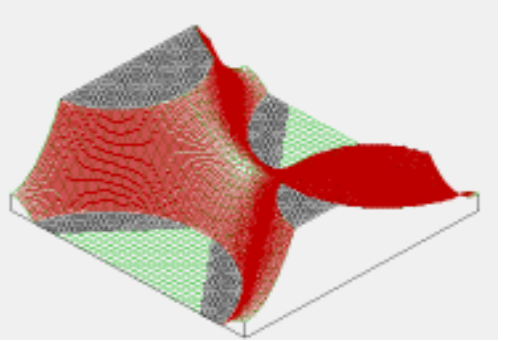

Magnetron rotation

$$\nu_- = \frac{\nu_c}{2} - \sqrt{\frac{\nu_c^2}{4} - \frac{\nu_T^2}{2}}.$$

Magnetron rotation center

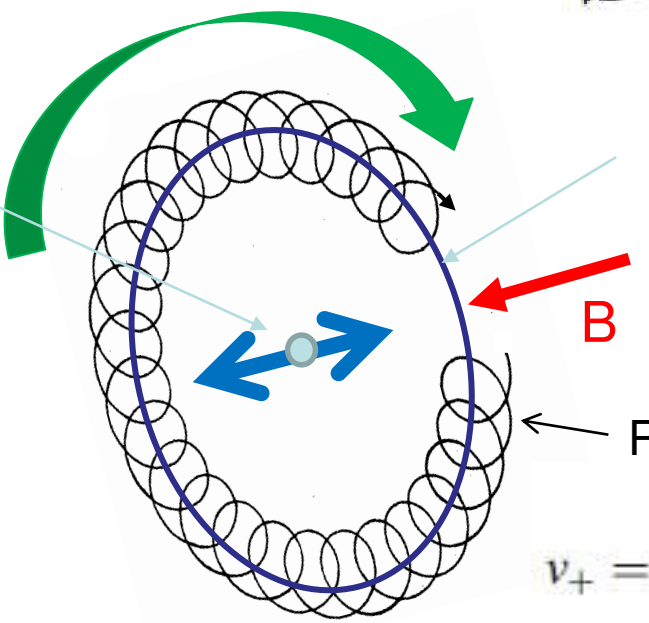

Equipotential of the trapping field

Axial oscillation

$$\nu_T = \frac{1}{2\pi}\sqrt{\frac{2\alpha z e V_T}{m a^2}}$$

Reduced cyclotron rotation

$$\nu_+ = \frac{\nu_c}{2} + \sqrt{\frac{\nu_c^2}{4} - \frac{\nu_T^2}{2}}.$$

Measured frequency

Distribution of potentials in rectangular or cylindrical FT ICR cells

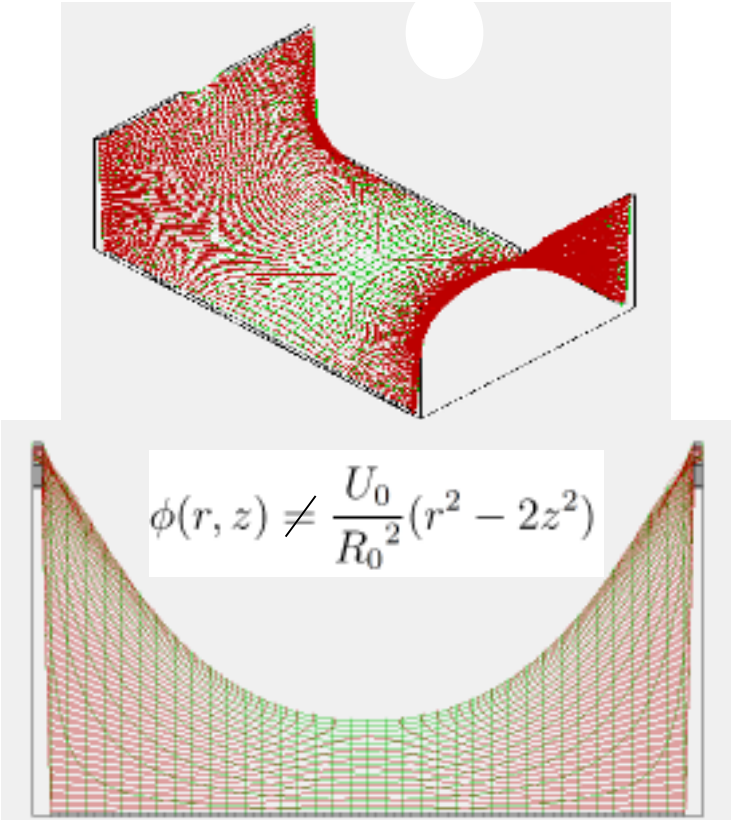

Axial and magnetron frequencies depend on axial oscillation amplitude

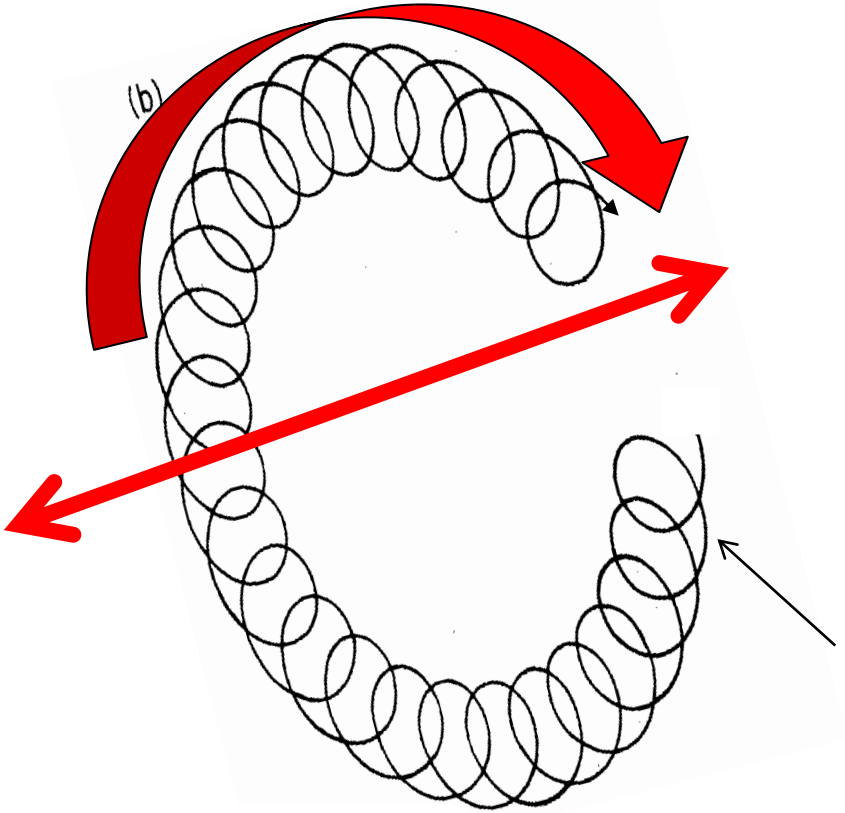

$$\omega_c' = \omega_c - \omega_m(z)$$

$$\omega_c = \frac{|eB|}{mc}$$

Measured frequency

The lost of phase coherence is a result of Inharmonicity of a regular FT ICR cell field

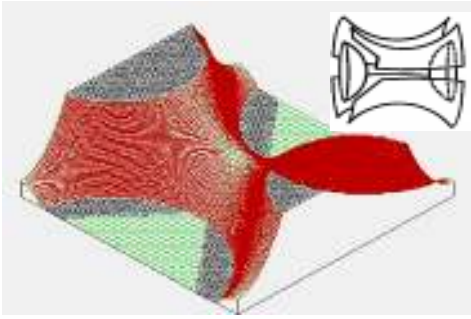

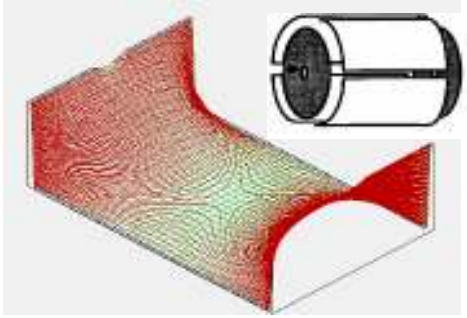

Distribution of potentials in hyperbolic (left) and rectangular or cylindrical FT ICR cells (right)

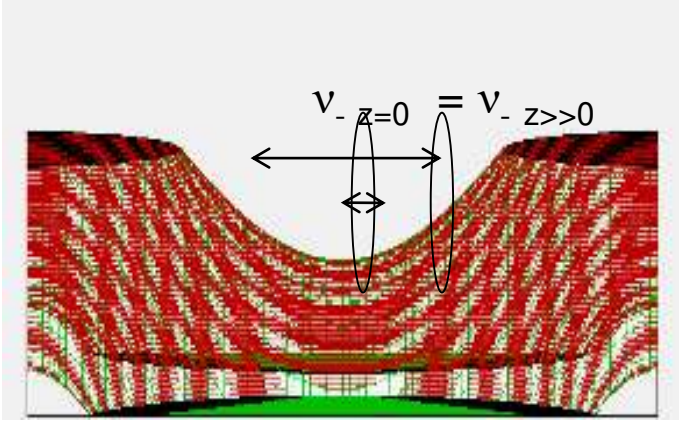

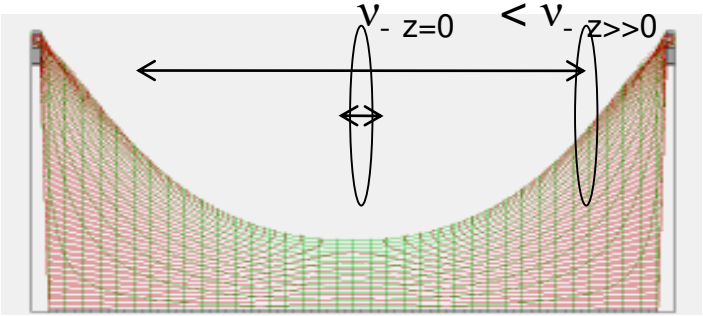

Cyclotron and magnetron frequencies are Independent on axial oscillation amplitude

Cyclotron and magnetron frequencies depend on axial oscillation amplitude

Comets in conventional FT ICR cell

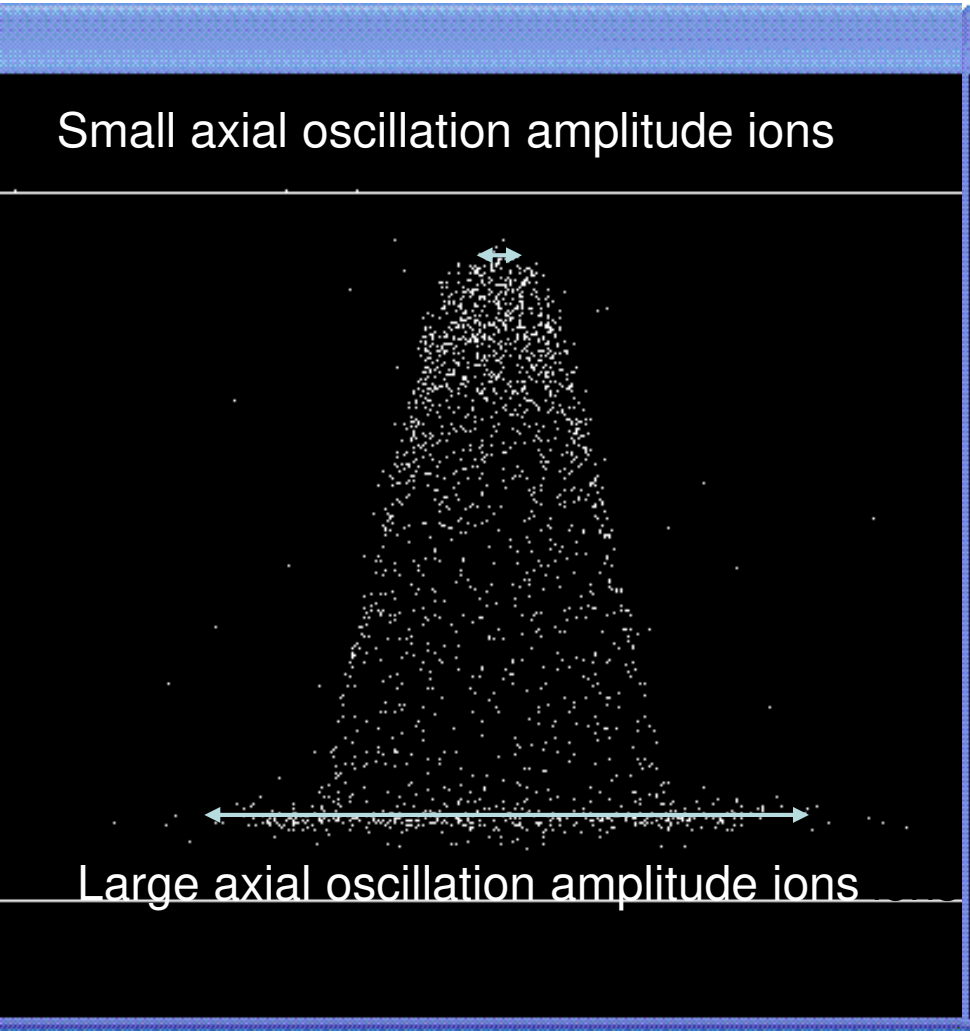

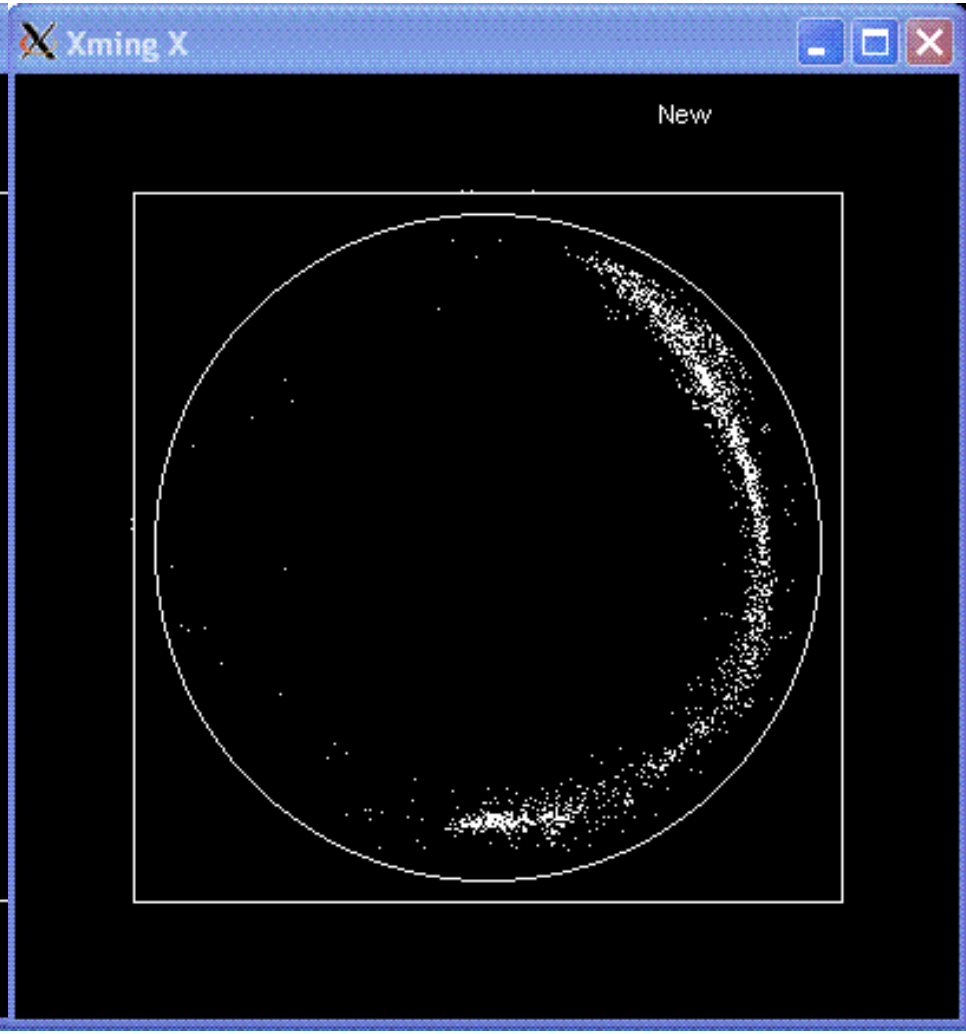

Comet in conventional
(cubic, cylindrical, “infinity”..)
FT ICR cells

$\omega_{t1} \neq \omega_{t2}$

Because ion-ion interaction inside comets is changing in time

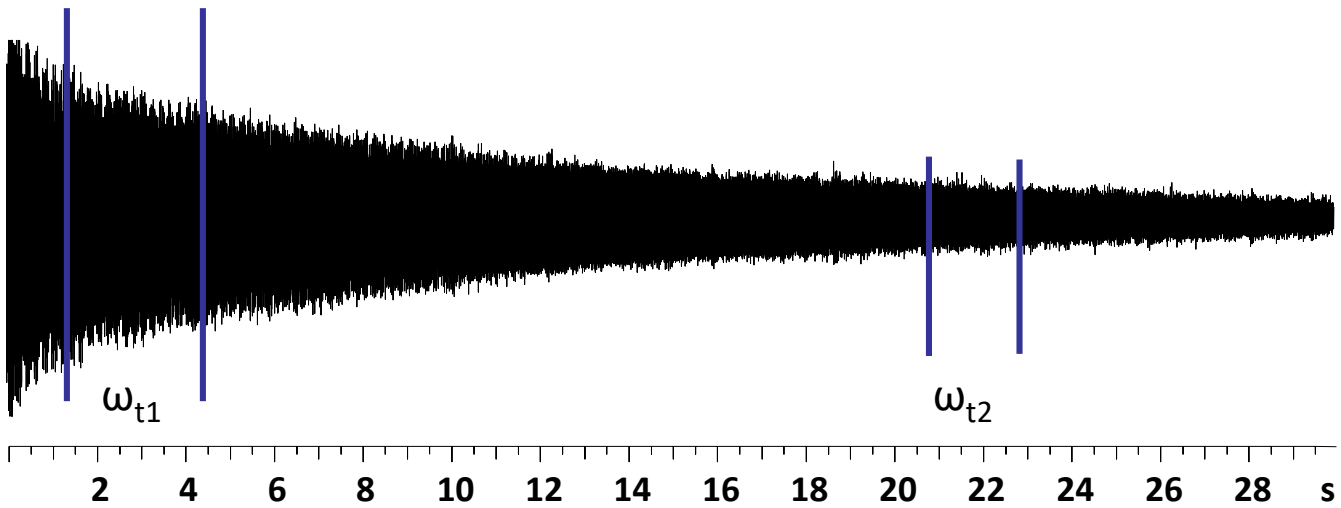

How do we know about comets?

Phase shift accumulation

(1) $$\varphi(t, z_0) = \int_0^t \omega_{eff}(\tau, z_0)\, d\tau$$

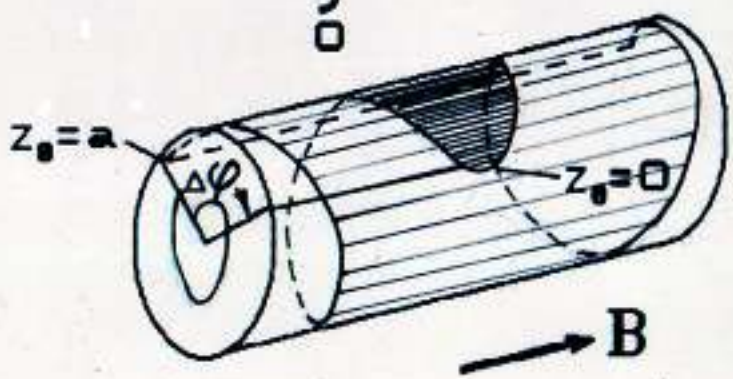

(2) $$G(\Omega) = Fur\langle\langle \cos(\varphi(t))\rangle\rangle$$

Nikolaev EN. 9th Asilomar Conference on Mass Spectrometry, Trapped Ions: Principle, Instrumentation and Applications, Sep 27–Oct 1, 1992

Two different approaches to simulation of ion cloud dynamics in FT ICR cell

1. Calculation of ion-ion and ion image charges interaction directly
2. Solving Poisson equation

ELSEVIER

International Journal of Mass Spectrometry and Ion Processes 148 (1995) 145–157

International Journal of Mass Spectrometry and Ion Processes

Evolution of an ion cloud in a Fourier transform ion cyclotron resonance mass spectrometer during signal detection: its influence on spectral line shape and position

Eugene N. Nikolaev[a], Nickolay V. Miluchihin[b,1], Masao Inoue[b,*]

[a]Institute for Energy Problems of Chemical Physics, Russian Academy of Sciences, Moscow 117829, Russian Federation
[b]Department of Applied Physics and Chemistry, University of Electro-Communications, Chofu-shi, Tokyo 182, Japan

Received 19 August 1994; accepted 31 May 1995

Simulation was carried out on a Fujitsu AP1000 parallel computer, which is a "multiple instruction multiple data" (MIMD) machine with 512 independent 25 MHz processors. **(One processor per ion)**

We were trying to explain:

Why ICR frequency is changing during detection?

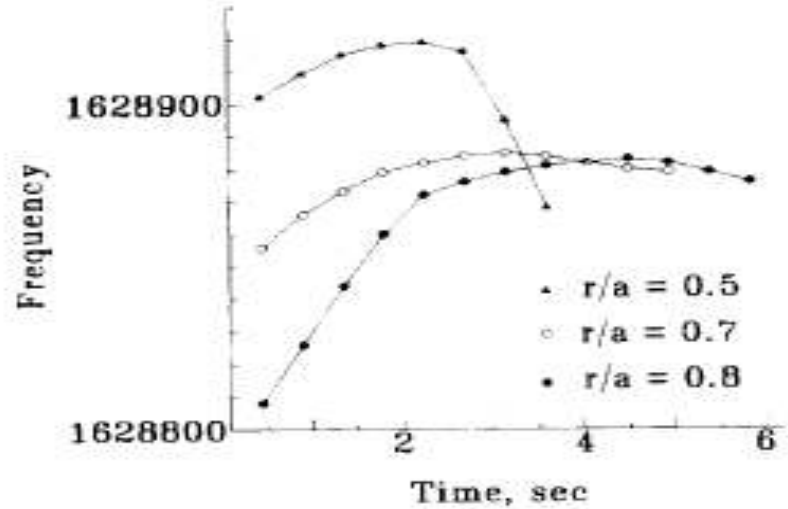

Fig. 1. Experimental ICR frequency of externally produced Cs^+ ions as a function of time. The three curves correspond to different ratios of cyclotron radius to cell radius.

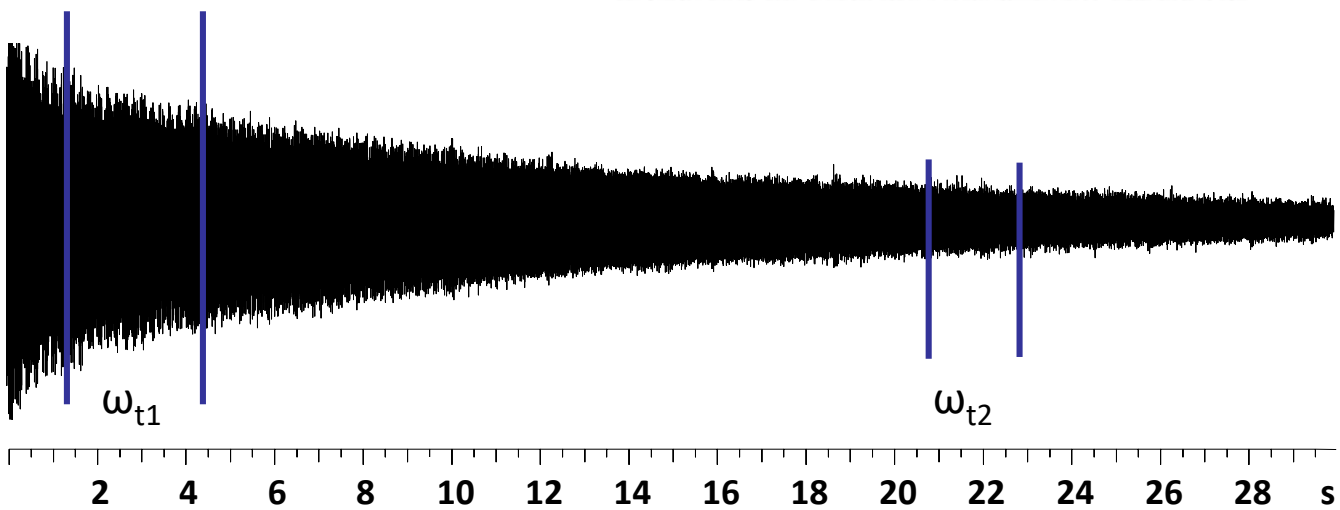

The Particle-Mesh Method

Dale Mitchell and Richard Smith
1996

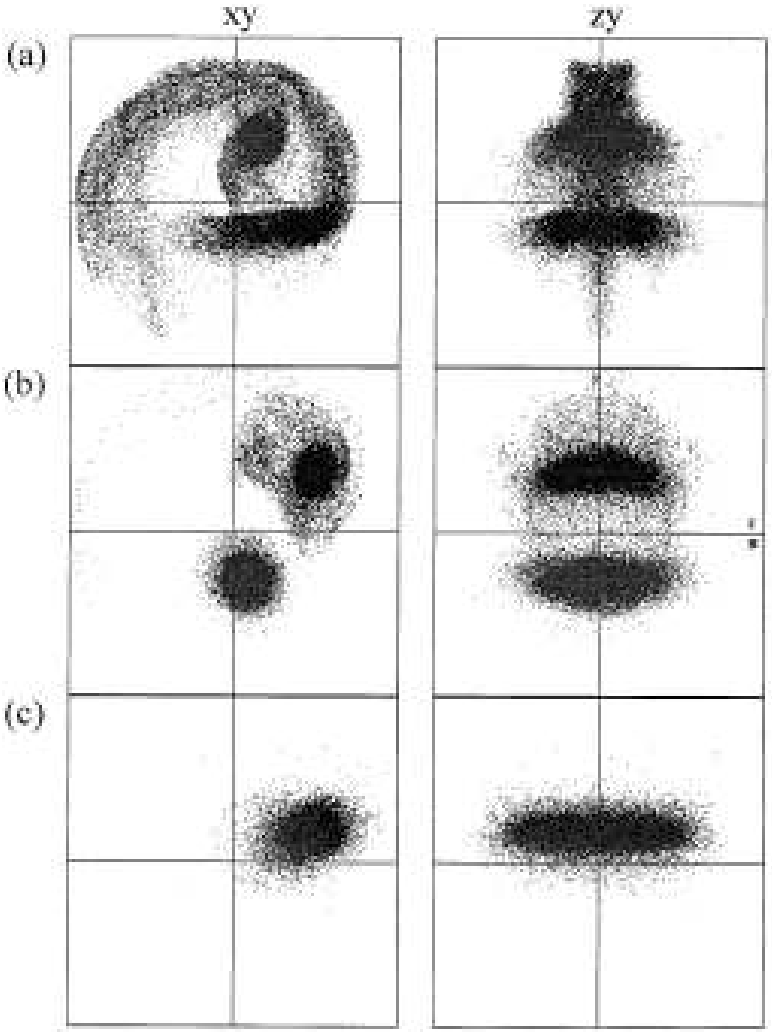

Snapshots in *xy* perspective (left) and *zy* perspective (right) at a late time during the detection period. **(a)** 50,000, **(b)**150,000, and **(c)** 350,000 ions.

Solving Poisson equation using supercomputer

Eugene N. Nikolaev; Ron M.A. Heeren; Alexander M. Popov;
Alexander V Pozdneev;
Konstantin S Chingin;

Realistic modeling of ion cloud motion in Fourier transform ion cyclotron resonance cell by use of a particle-in-cell approach

Rapid Commun. Mass Spectrom. 2007; 21,1-20

Particle-In-Cell Algorithm (first used to describe ion behavior in FT ICR cell by Dale Mitchell and Richard Smith)

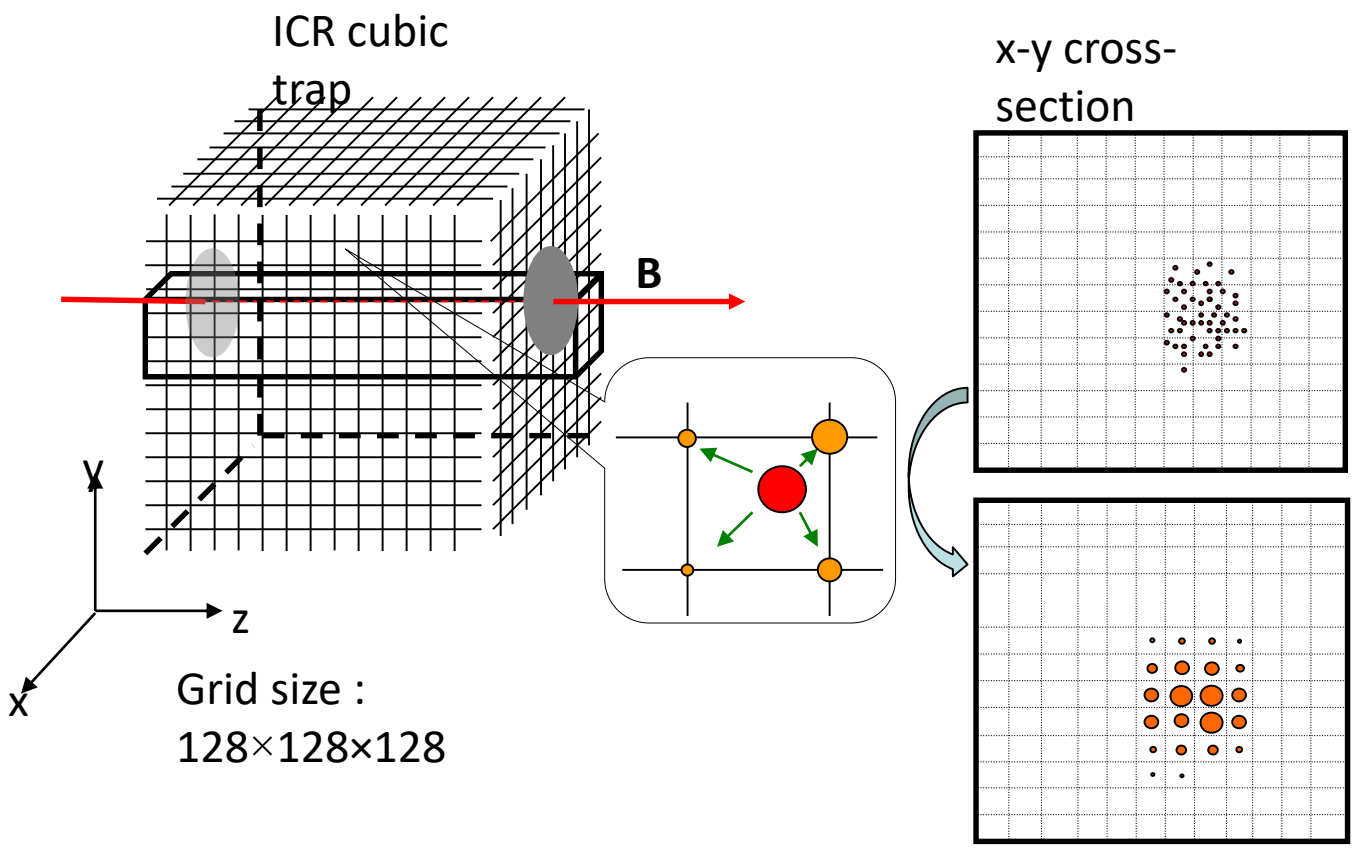

Solution for the electric field

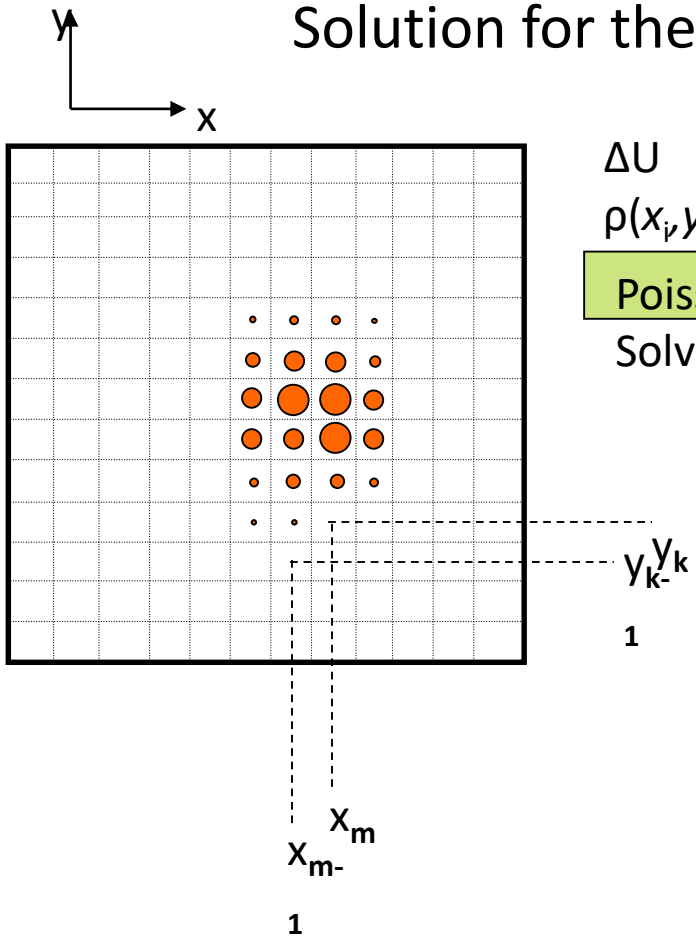

$\Delta U = -\rho(x_i,y_j,z_k)/\varepsilon_0$

Poisson Solver

$\mathbf{U}(x_i,y_j,z_k)$ *i, j, k=1-p*

$\mathbf{E}(x_i,y_j,z_k)$ *i, j, k=1-p*

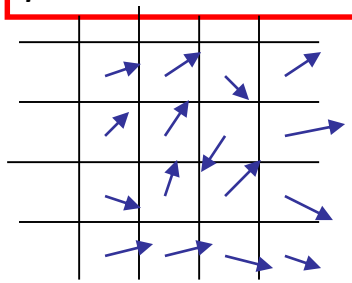

Integration the equation of motion

$$m\frac{d^2\vec{r}}{dt^2} = q\vec{E} + q\left(\frac{d\vec{r}}{dt}\times\vec{B}\right)$$

$\mathbf{E}(r_i)$

v_i , r_i

Boris integrator

new v_i , r_i

for every ion (i)

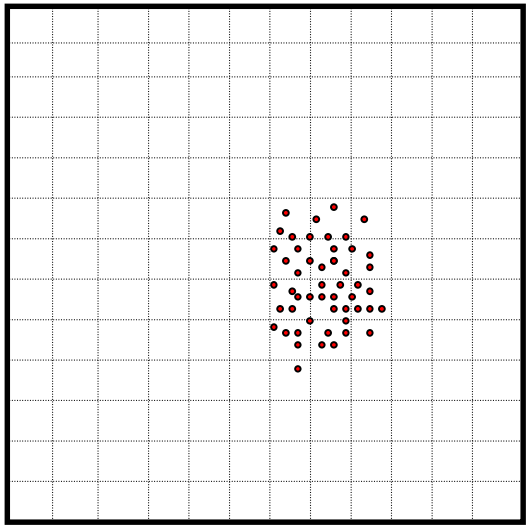

Next time step

Integration the equation of motion

$$m\frac{d^2\vec{r}}{dt^2} = q\vec{E} + q\left(\frac{d\vec{r}}{dt}\times\vec{B}\right)$$

$\mathbf{E}(r_i)$

v_i , r_i

Boris integrator

new v_i , r_i

for every ion (i)

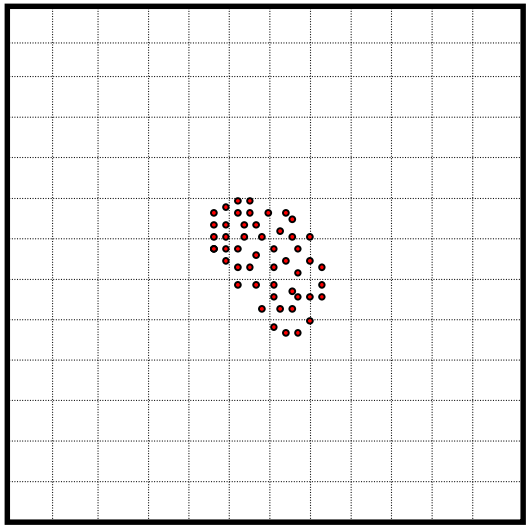

Next time step

Cloud of one m/z ions in a cylindrical geometry FT ICR cell

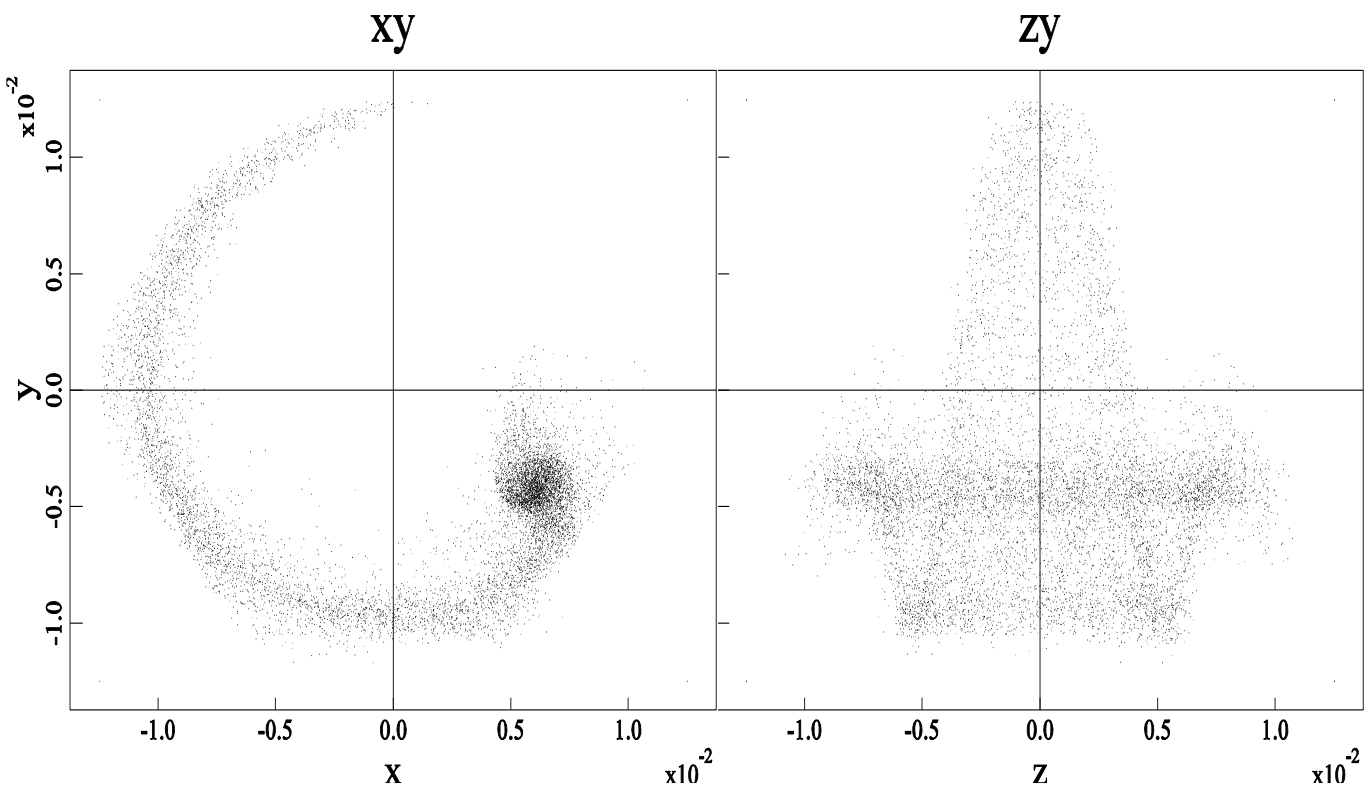

Evolution of ion clouds with different amount of ions in the cell

cloud initial radius 0.15 cm
cloud initial length 0.10 cm
T_{exc}= 0.07 ms , T_{detect}= 30 ms

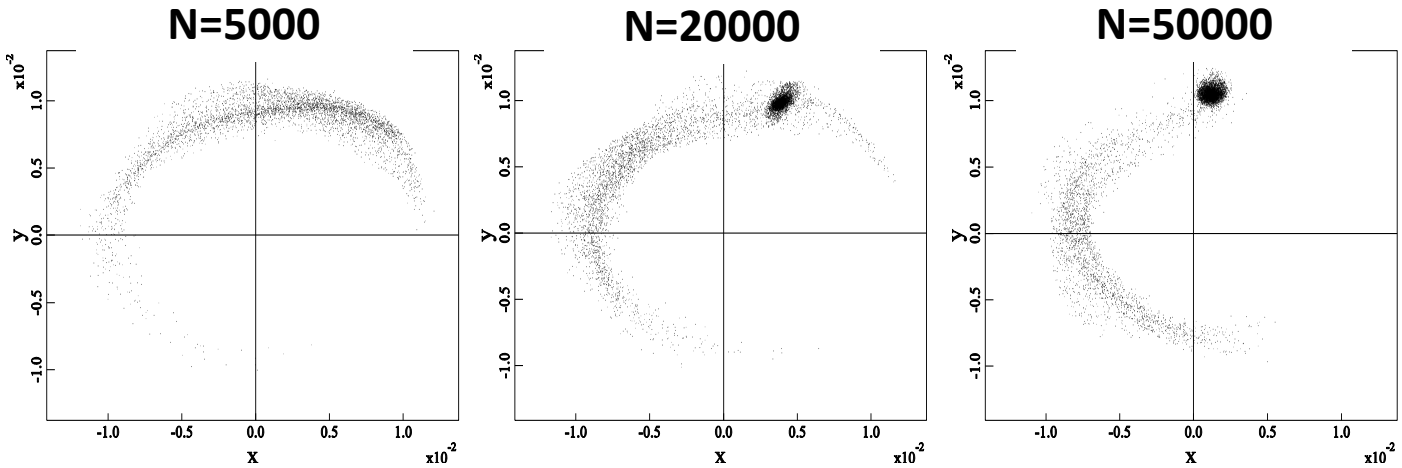

t = 3.24 ms

Comet in conventional
(cubic, cylindrical, “infinity”...)
FT ICR cells

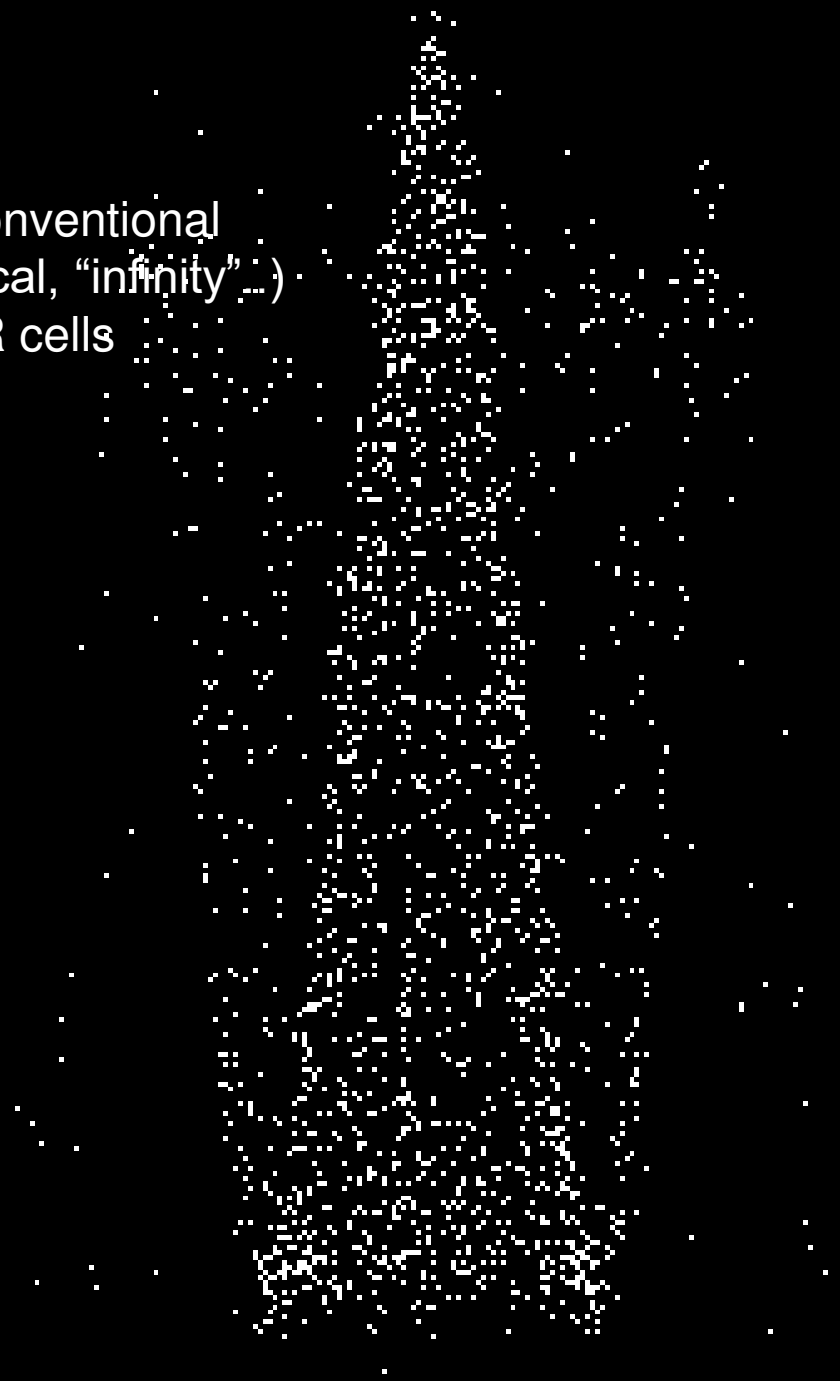

Ion clouds in harmonized cells have elliptical cigar like forms

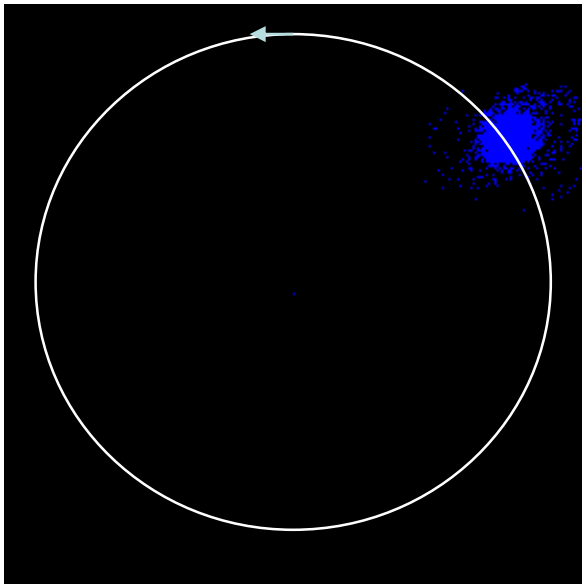

Projection on the plane
orthogonal to the magnetic field

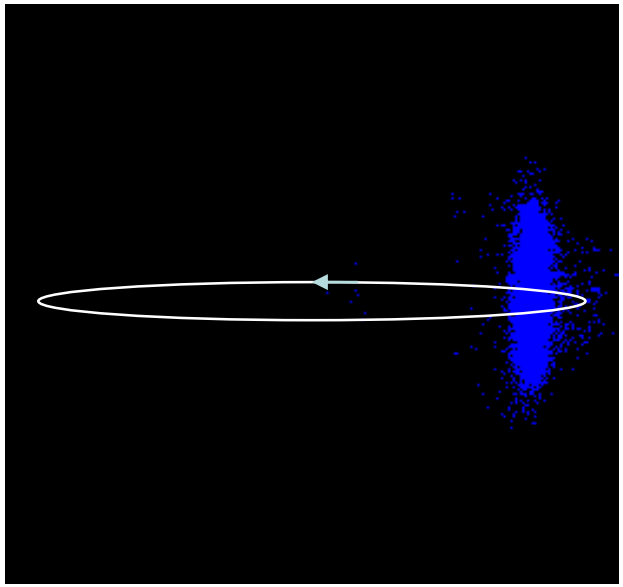

Projection on the plane almost
Parallel to the magnetic field

How to get rid of these comets?

The simple solution: use hyperbolic cell

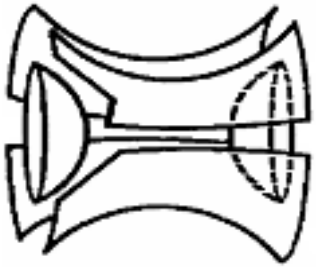

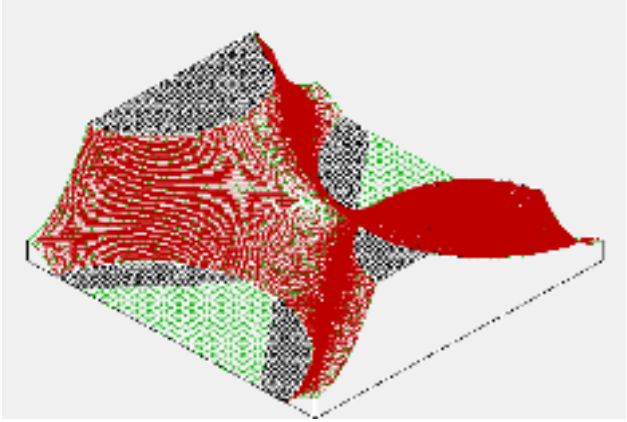

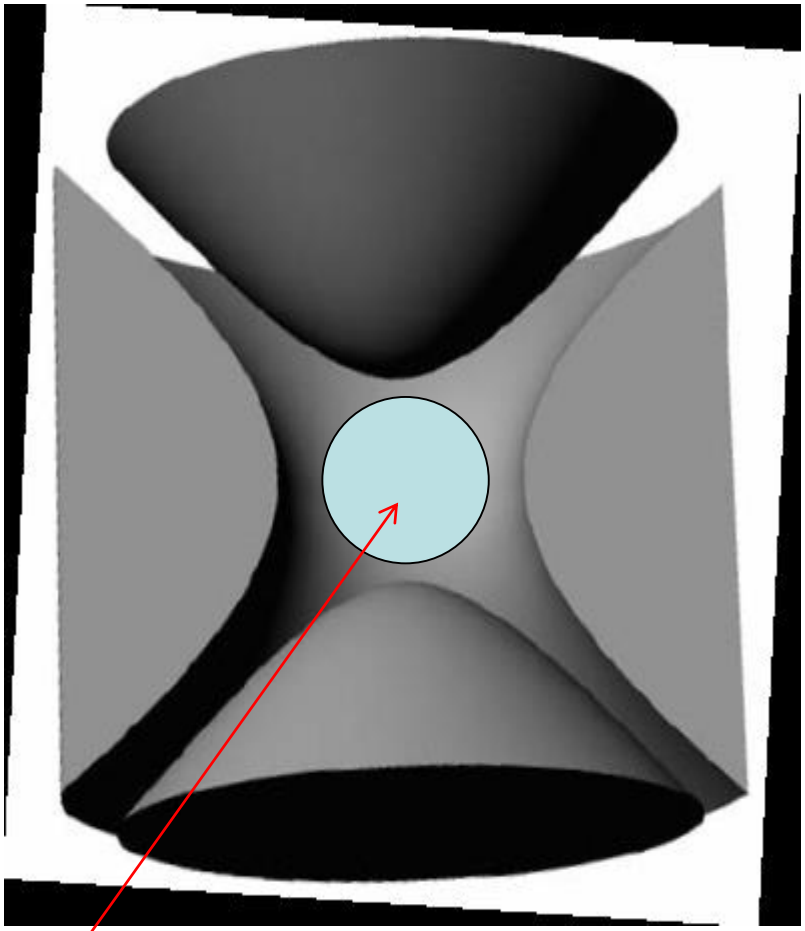

Used space

Other approaches

Flattering potential

Harmonization - making the field quadratic along z and r coordinates

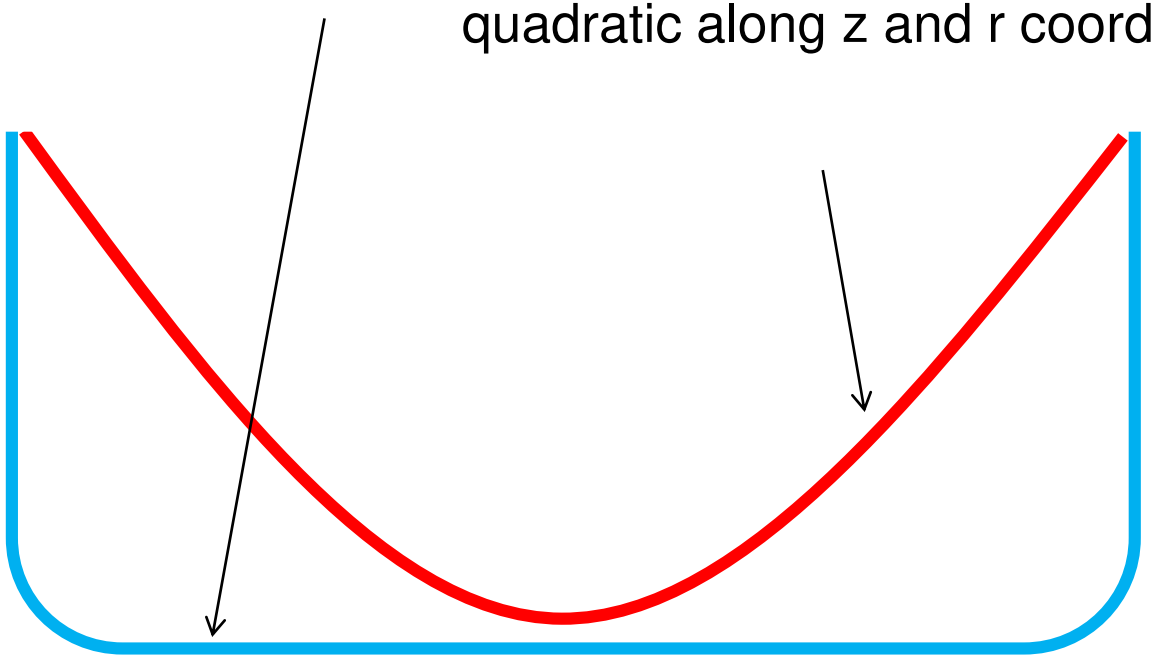

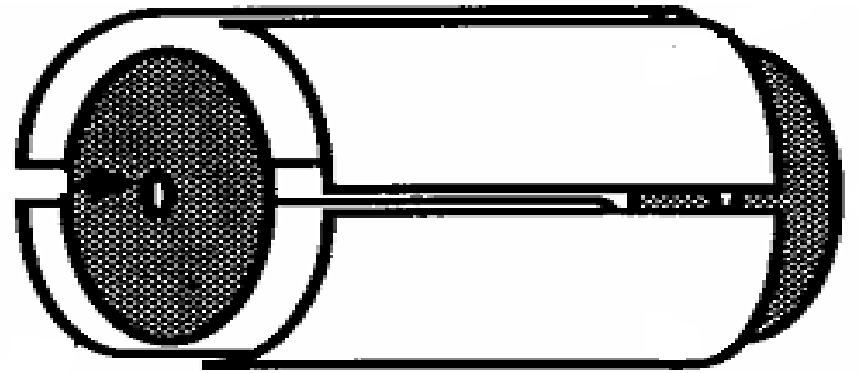

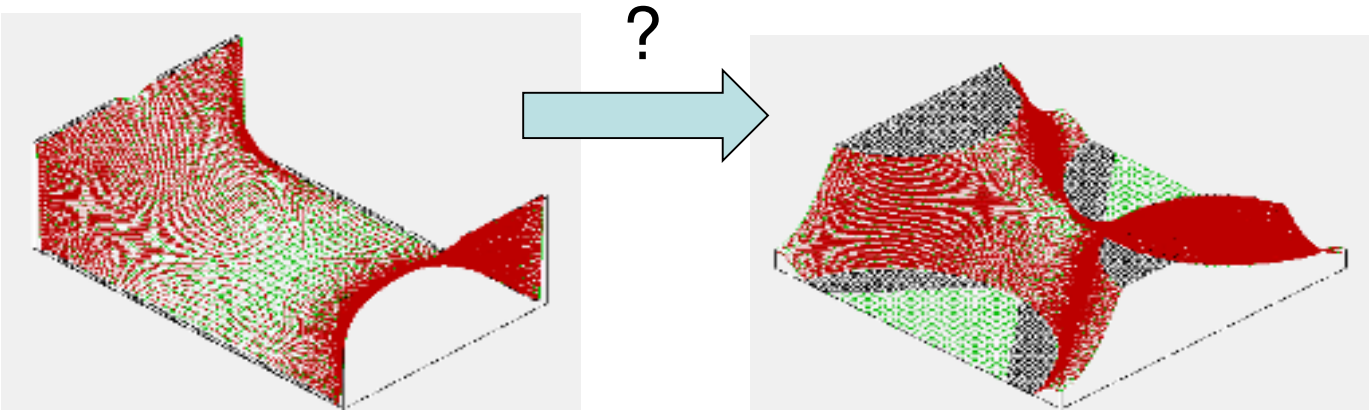

An instrument with a hyperbolic trap, however, suffers at least from inefficient use of the magnet bore and a relatively inaccessible trap interior.

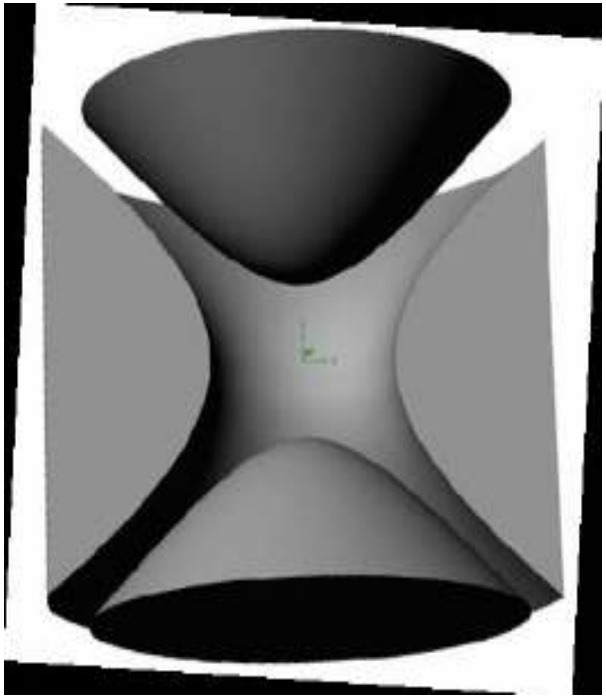

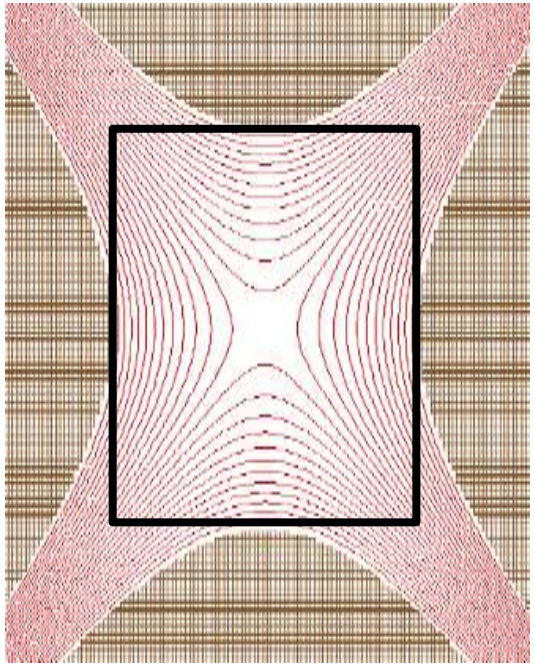

The quadrupolar potential well can also be approximated in a cylindrical or cubic trap by using simple electrode shapes and by optimizing the aspect ratio or by segmenting the electrodes

(Gerald Gabrielse)

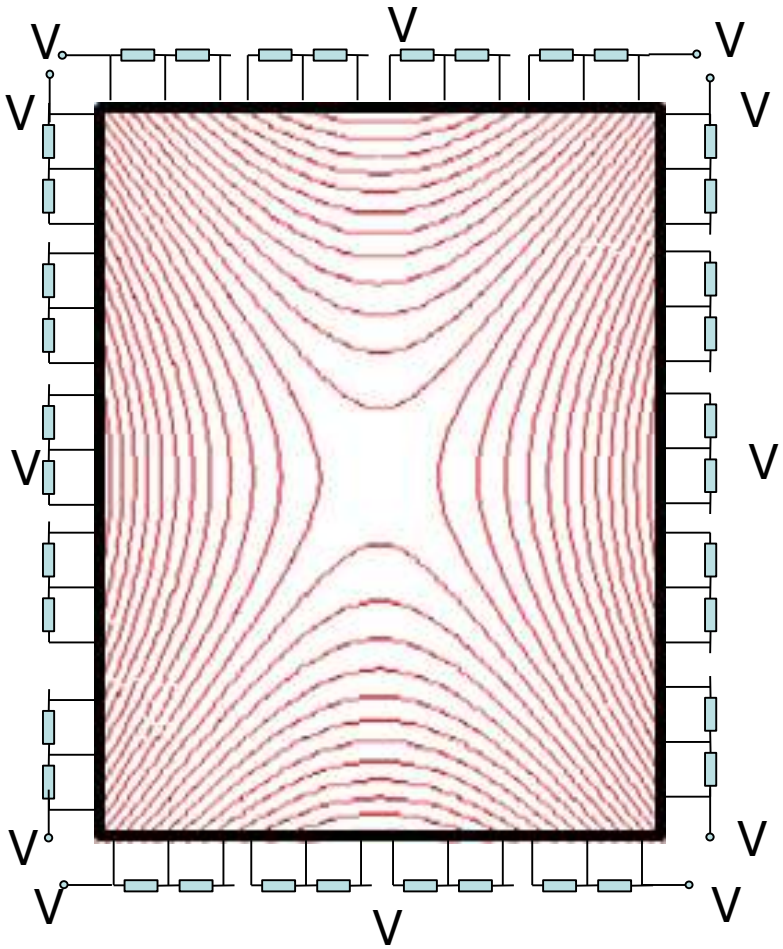
V
V
V
V
V
V
V
V
V
V
V
V

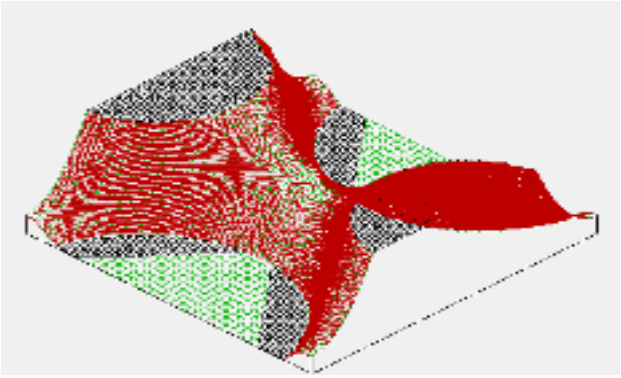

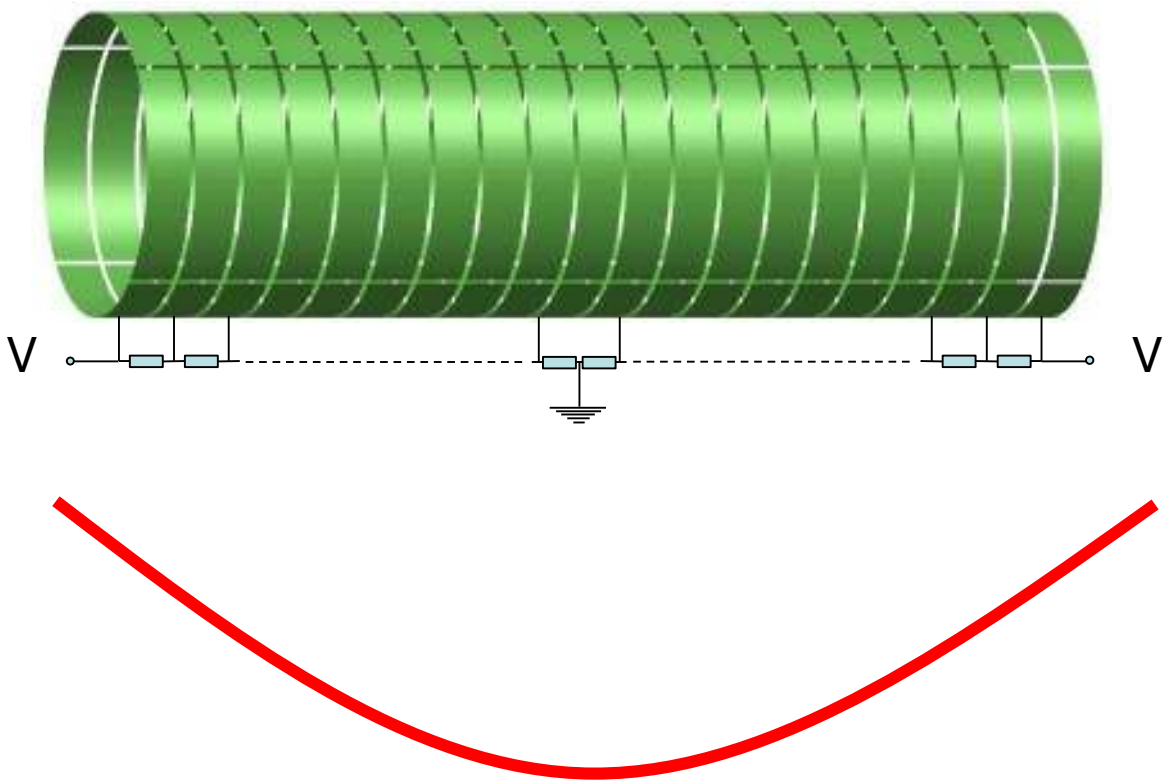
V
V

G. GABRIELSE, L. HAARSMA and S.L. ROLSTON

OPEN-ENDCAP PENNING TRAPS FOR HIGH PRECISION EXPERIMENTS

International Journal of Mass Spectrometry and Ion Processes, 88 (1989) 319–332

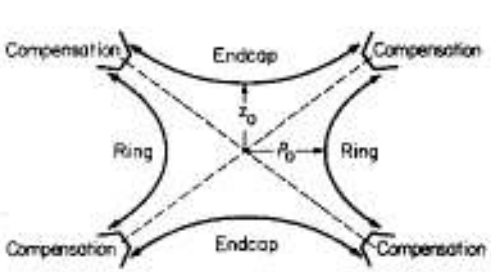

Hyperbolic Trap

(a)

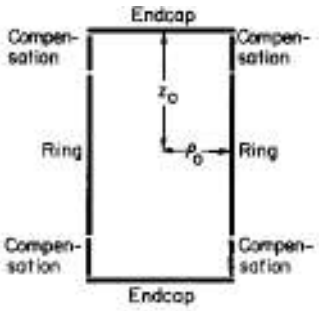

Flat-endcap Cylindrical Trap

(b)

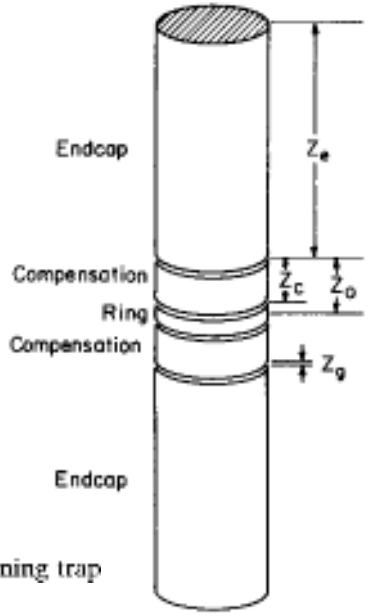

Open-endcap Penning trap

Harmonization of cell's electric potential (G.Gabrielse 1989)

Tolmachev, A. V.; Robinson, E. W.; Wu, S.; Kang, H.; Lourette, N. M.; Pasa-Tolic, L.; Smith, R. D. Trapped-Ion Cell with Improved DC Potential Harmonicity for FT-ICR MS

Brustkern A.M., Rempel D.L., Gross M.L. An Electrically Compensated Trap Designed to Eighth Order for FT-ICR Mass Spectrometry. J Am Soc Mass Spectrom 2008, 19, 1281–1285

Marshall's group,

Bruker……

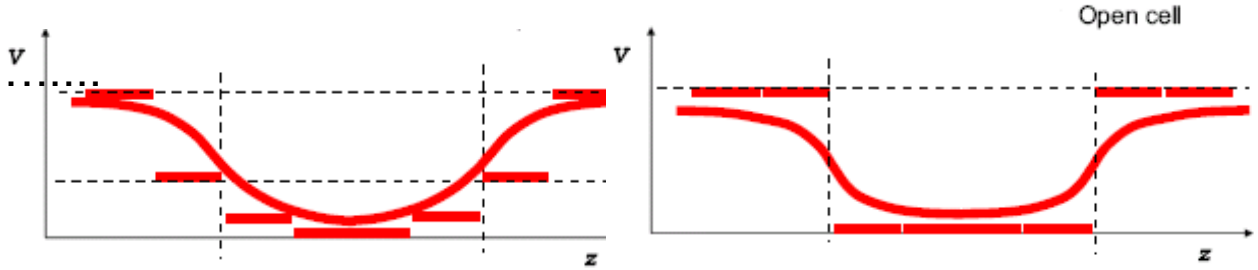

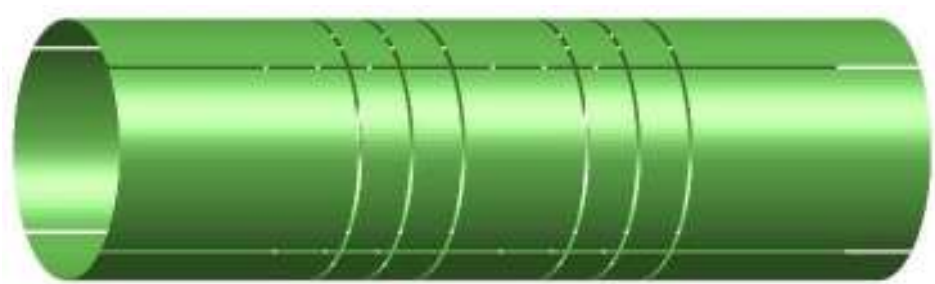

PNNL cell

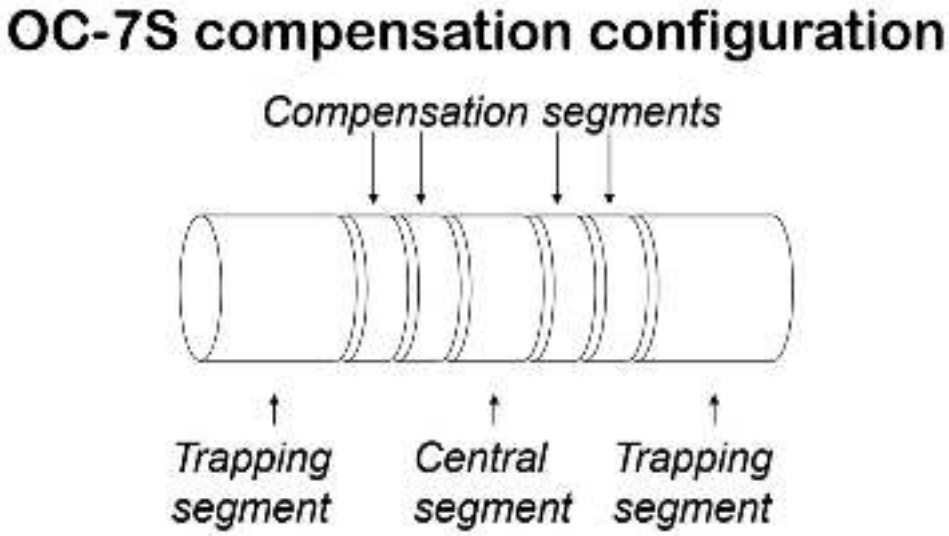
OC-7S compensation configuration
Compensation segments
Trapping segment
Central segment
Trapping segment

OC-7S

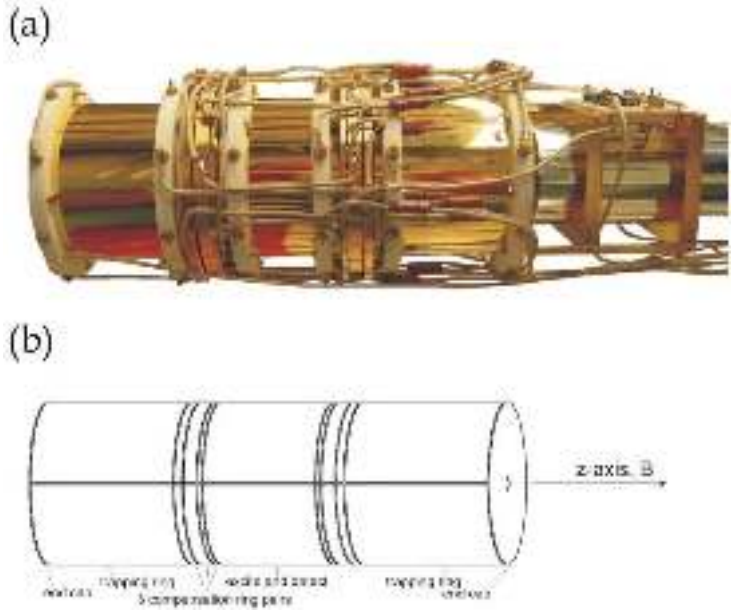

Gross group

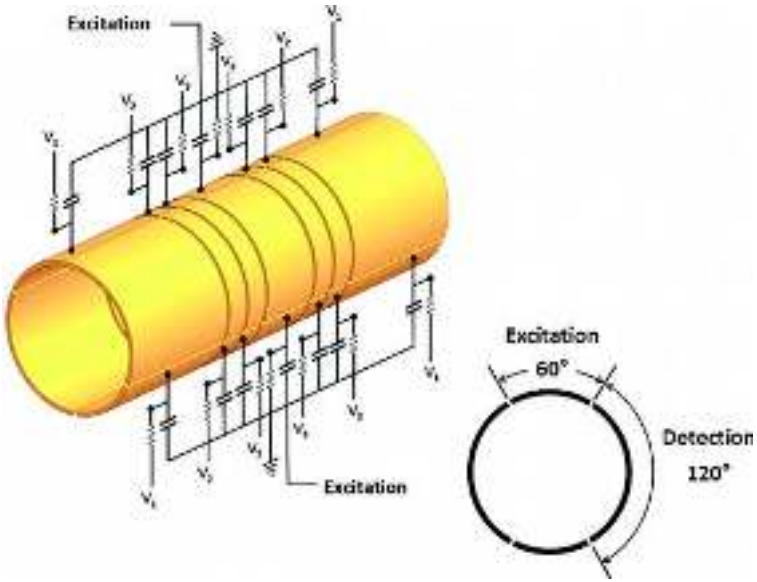

Marshall group

Two main approaches

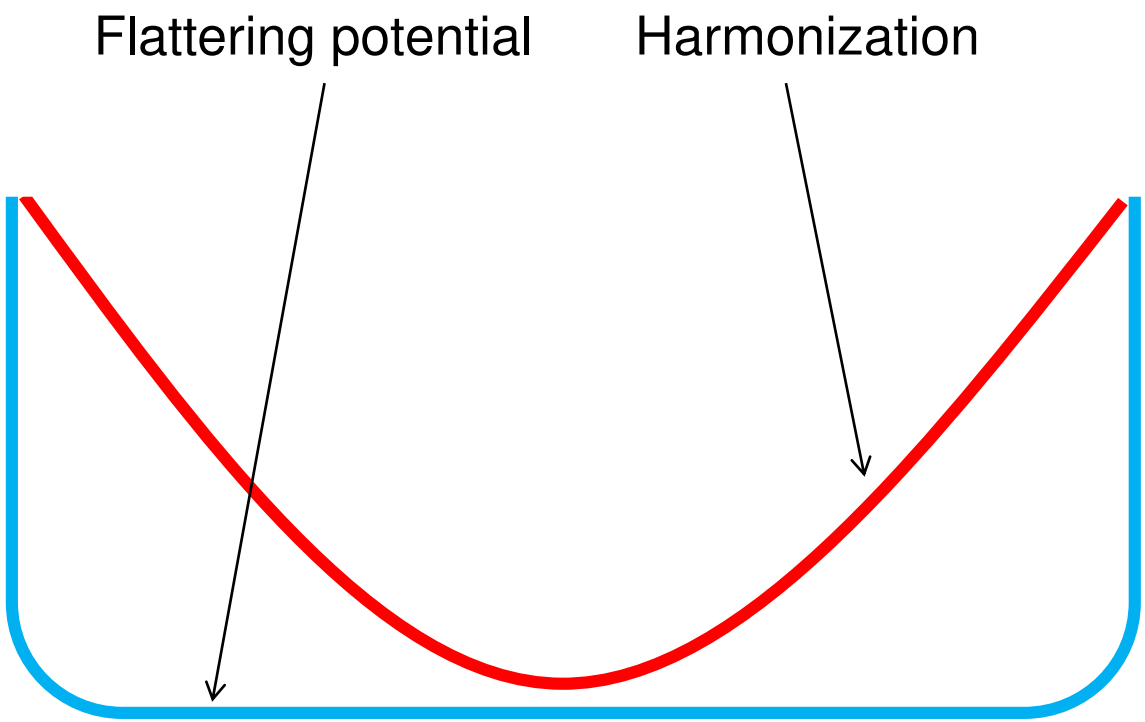

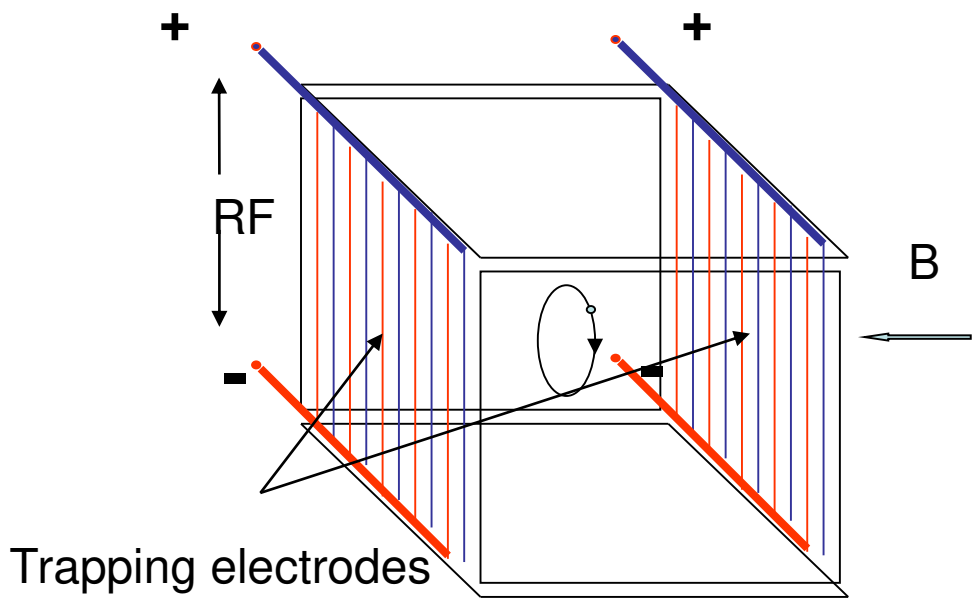
+
+
RF
B
-
-
Trapping electrodes

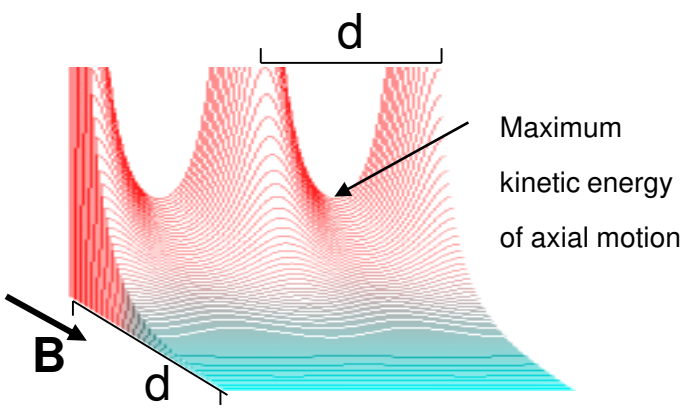
d
Maximum
kinetic energy
of axial motion
B
d

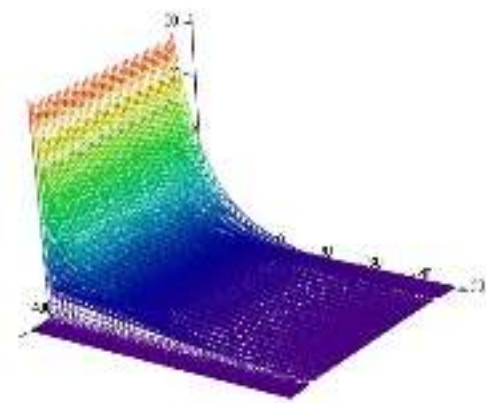

FT ICR cell with mesh trapping electrodes creating pseudopotential

Wire cell trapping electrode
(1 mm distance between adjacent wires)

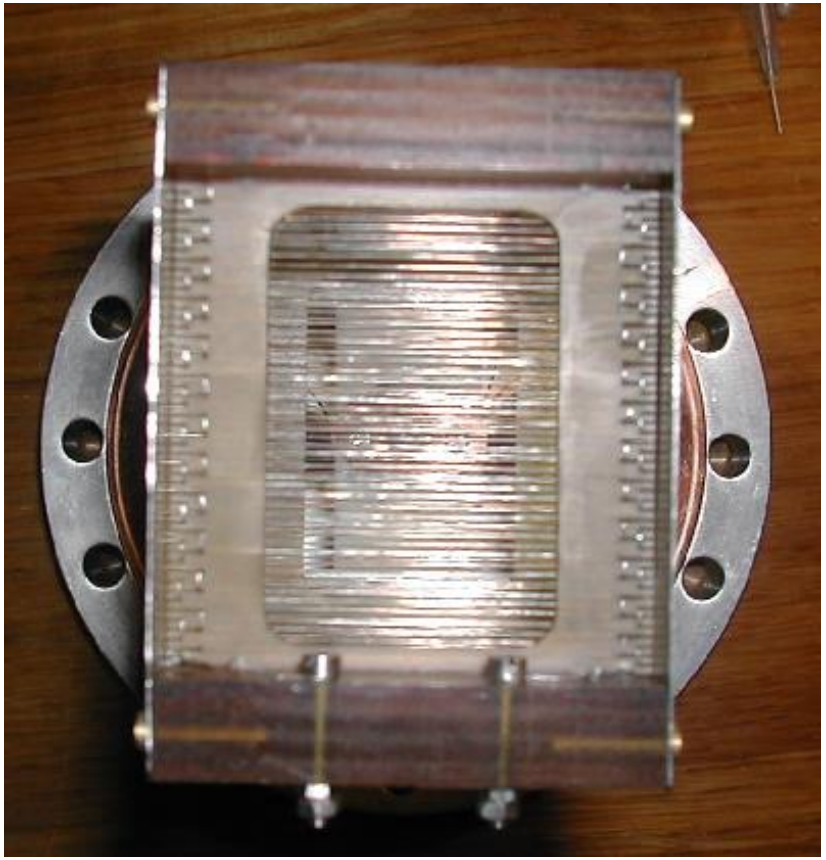

US 20050242280A1

(19) United States

(12) Patent Application Publication

(10) Pub. No.: US 2005/0242280 A1

(43) Pub. Date: Nov. 3, 2005

Nikolaev

(54) ION CYCLOTRON RESONANCE MASS SPECTROMETER

(75) Inventor: Evgenij Nikolaev, Moscow (RU)

Correspondence Address:
KUDIRKA & JOBSE, LLP
ONE STATE STREET
SUITE 800
BOSTON, MA 02109 (US)

(73) Assignee: Bruker Daltonik GMBH, Bremen (DE)

(21) Appl. No.: 10/833,938

(22) Filed: Apr. 28, 2004

Publication Classification

(51) Int. Cl.[7] H01J 49/38

(52) U.S. Cl. 250/291

(57) ABSTRACT

The invention describes an ion cyclotron resonance (ICR) mass spectrometer with an ICR trap, the ICR trap having as trapping electrodes two ion reflecting electrode structures operated by RF voltages without any DC voltage. The usual apertured ion trapping electrodes are replaced by multitudes of structural elements, electrically conducting, and repeating spatially in one or two directions of a surface, neighboring structure elements being connected each to different phases of an RF voltage. In the simplest case a grid of parallel wires can be used. The surface of such structures reflects ions of both polarities, if the mass-to-charge ratio of the ions is higher than a threshold.

(12) **United States Patent**
Franzen et al.

(10) **Patent No.: US 7,368,711 B2**
(45) **Date of Patent: May 6, 2008**

(54) **MEASURING CELL FOR ION CYCLOTRON RESONANCE MASS SPECTROMETER**

(75) Inventors: **Jochen Franzen**, Bremen (DE); **Evgenij Nikolaev**, Moscow (RU)

(73) Assignee: **Bruker Daltonik GmbH**, Bremen (DE)

5,019,706 A * 5/1991 Allemann et al. 250/291
5,572,035 A 11/1996 Franzen
6,403,955 B1 6/2002 Senko
7,223,965 B2 * 5/2007 Davis 250/283

FOREIGN PATENT DOCUMENTS

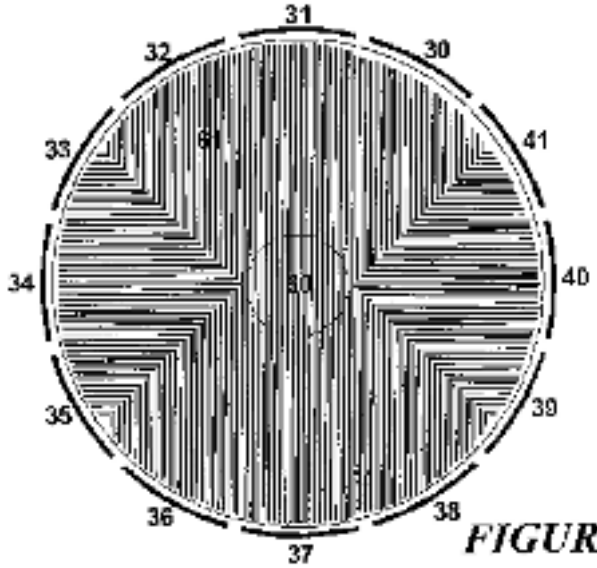

FIGURE 7

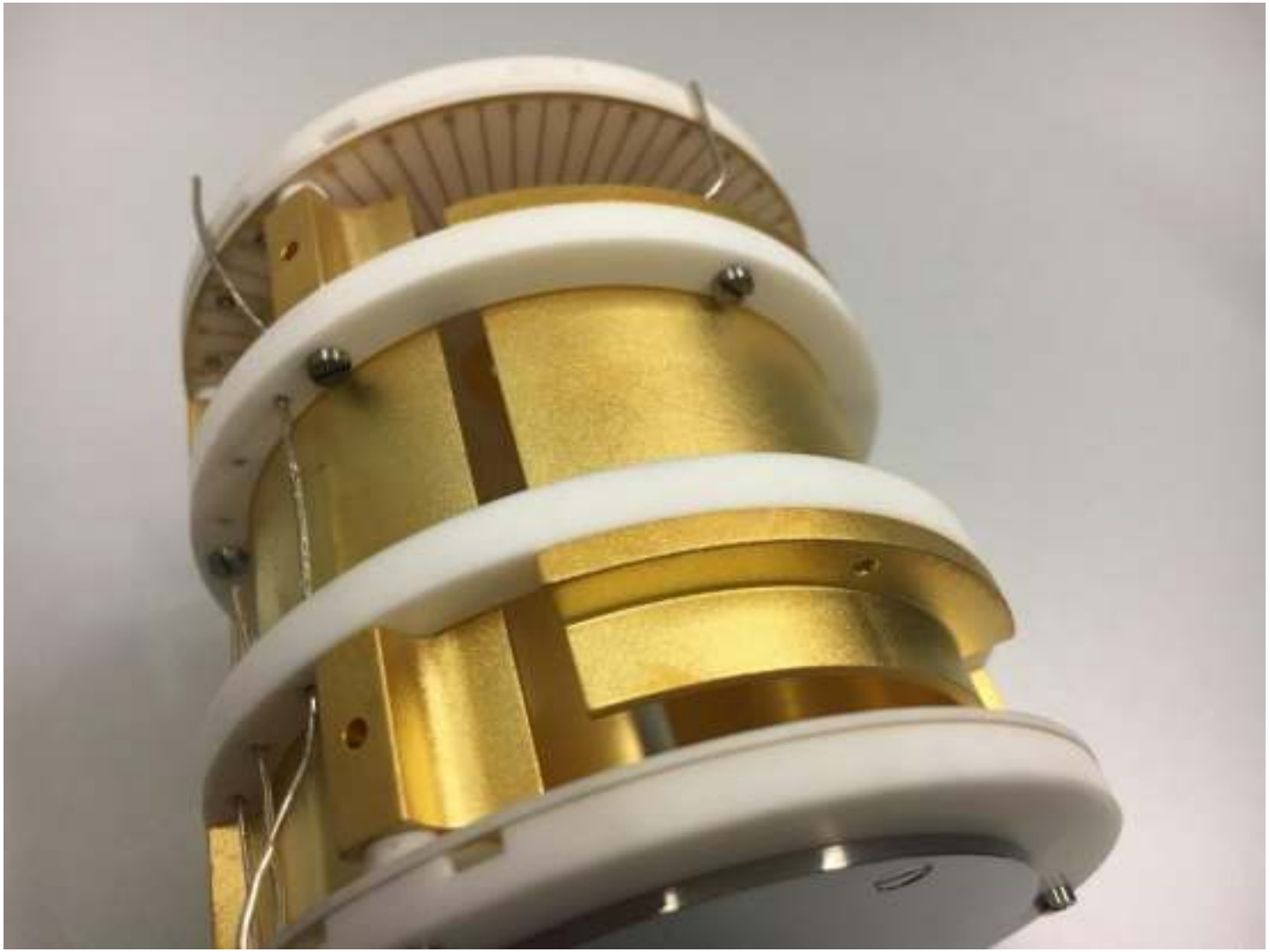

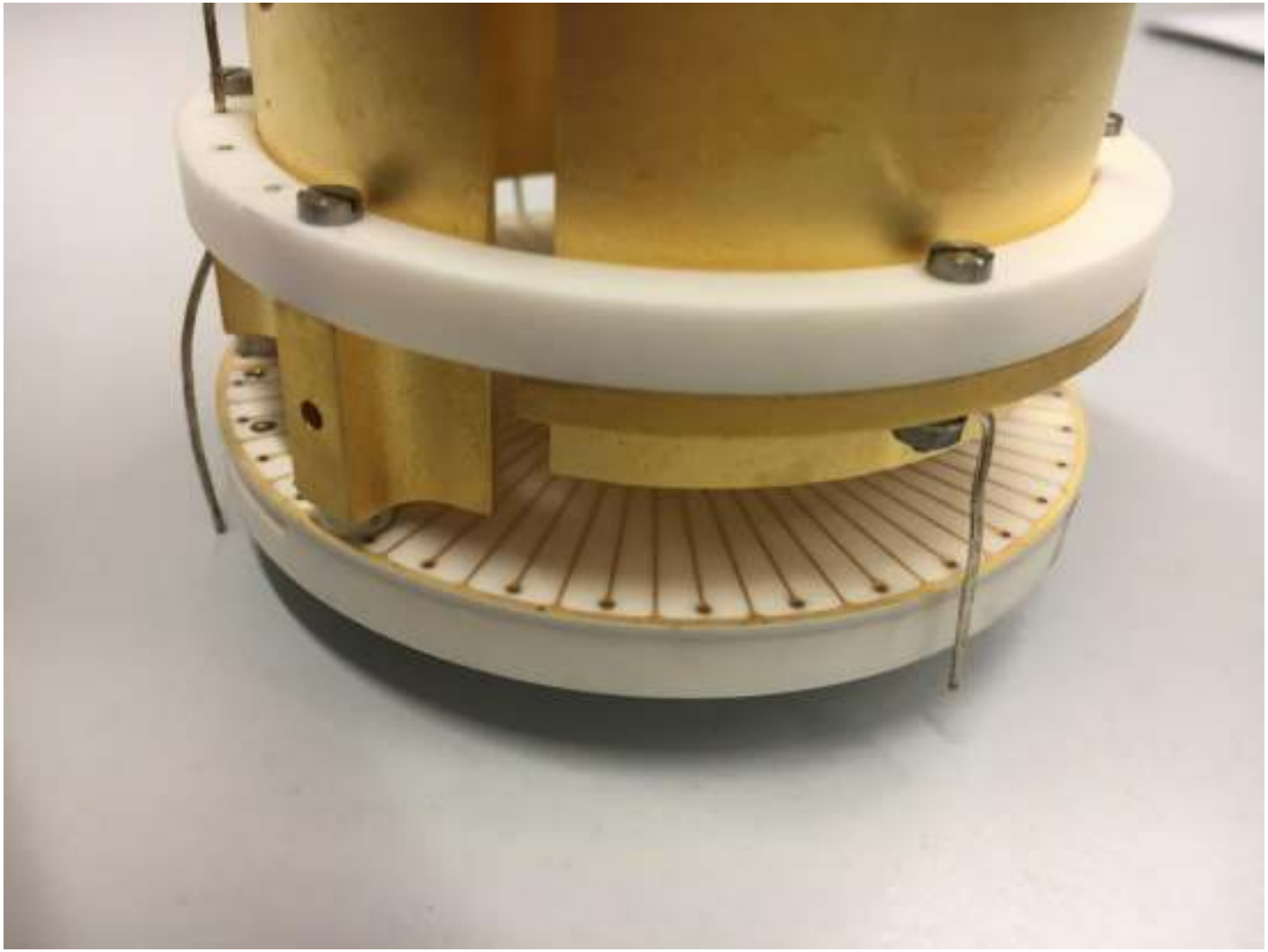

Cell with trapping electrodes segmented to rings

Chad R. Weisbrod, Nathan K. Kaiser, Gunnar E. Skulason, and James E. Bruce*
Trapping Ring Electrode Cell: A FTICR Mass Spectrometer Cell for Improved Signal-to-Noise and Resolving Power *Anal. Chem. 2008, 80, 6545–6553*

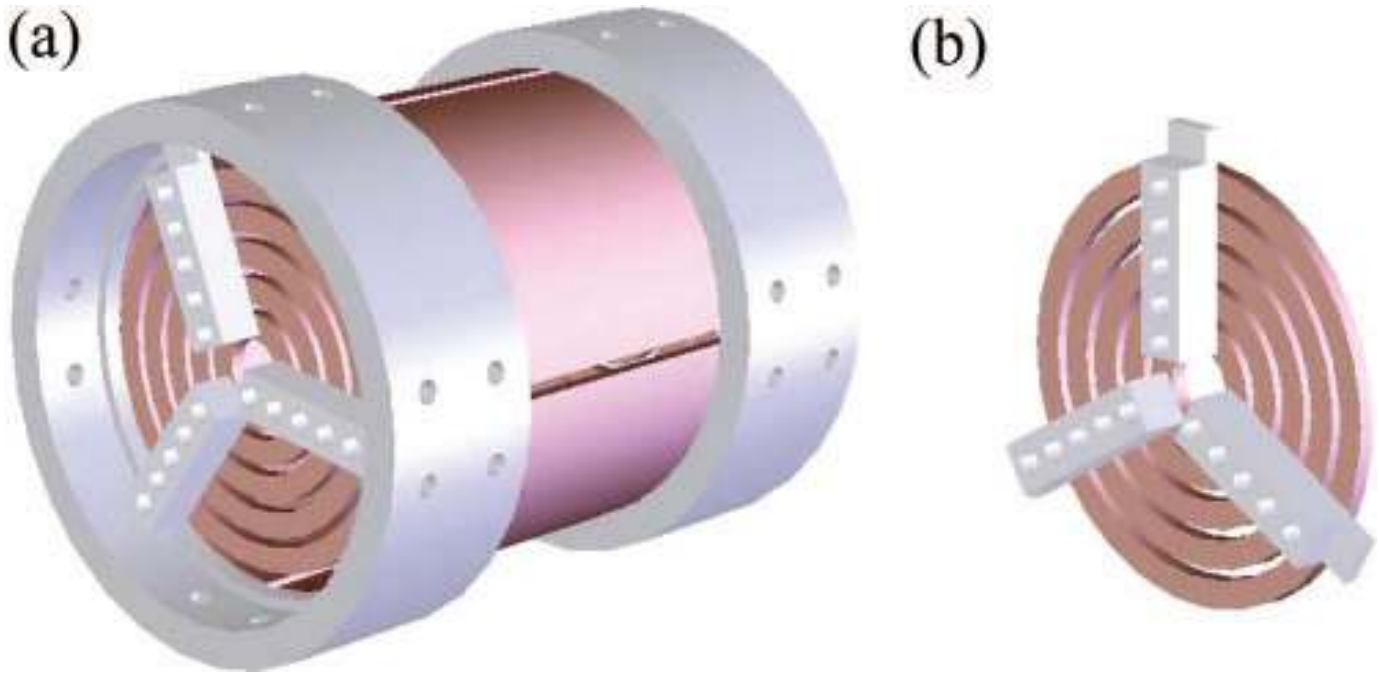

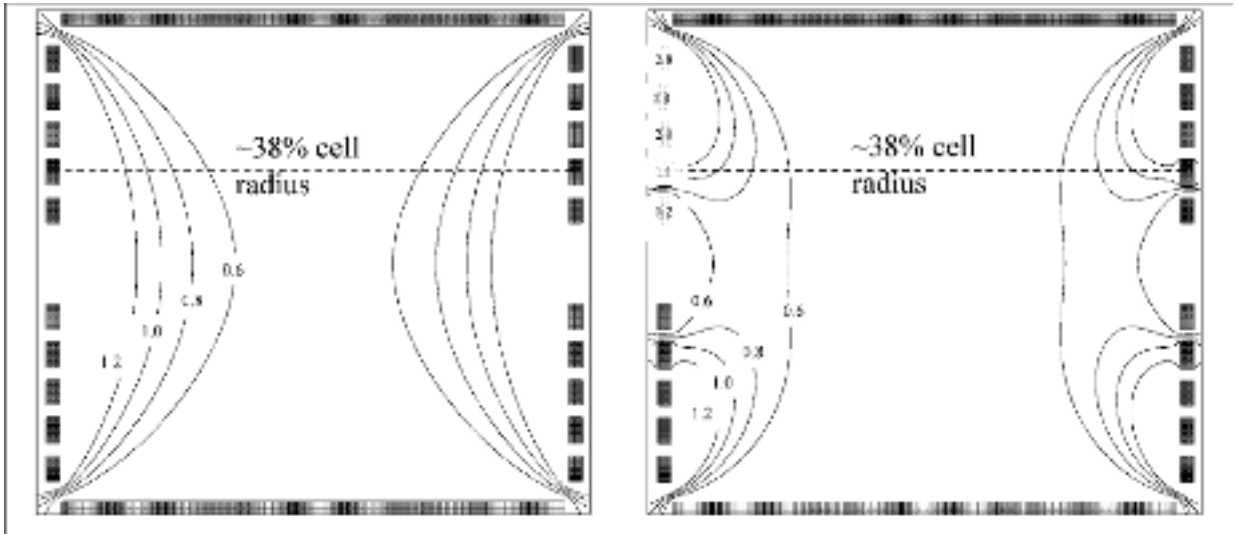

Figure 2. Equipotential contour plots are shown for (a) common 2.0 V trapping conditions and (b) the TREC trapping conditions. The voltages for the modulated (TREC) trapping conditions with increasing electrode radius are 0.2, 1.1, 2.0, 2.4, and 2.8 V respectively, as shown on the rings. A dashed line through the cell located at 38% cell radius is depicted.

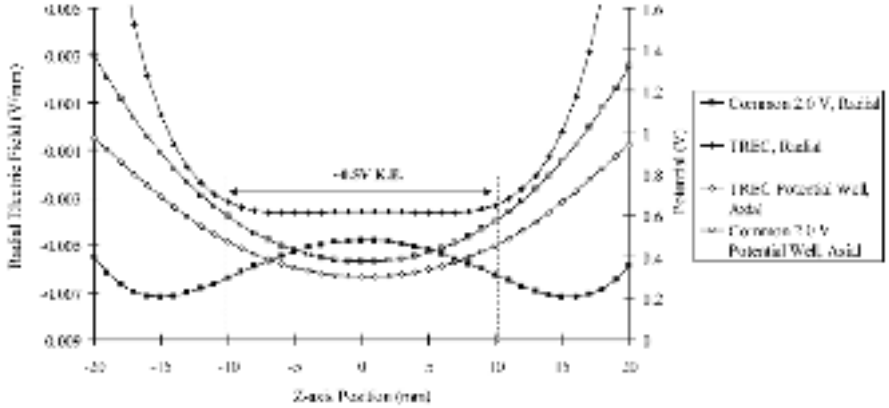

Figure 3. Radial electric field plots generated at 38% cell radius for both common 2.0 V trapping conditions and the TREC modulated conditions. A trapping potential well generated from the TREC conditions is overlaid to provide perspective.

The lost of phase coherence is a result of Unharmonicity of a regular FT ICR cell field

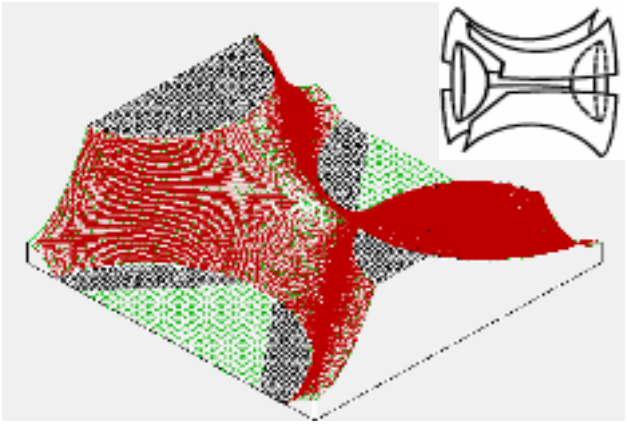

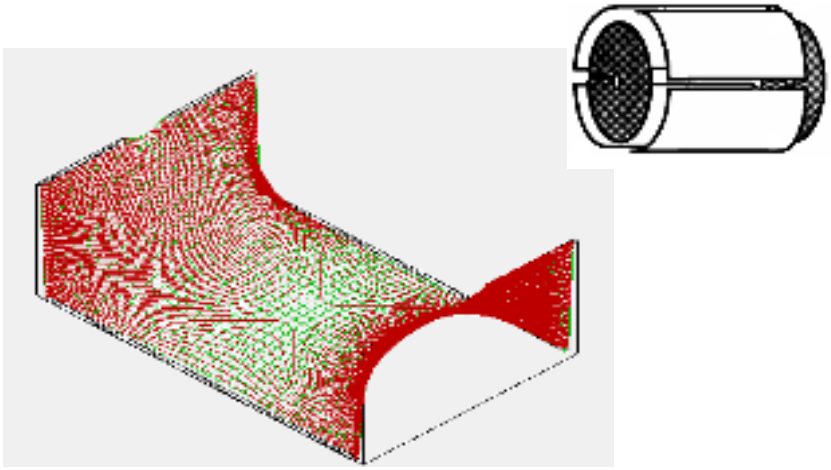

Distribution of potentials in hyperbolic (left) and rectangular or cylindrical FT ICR cells (right)

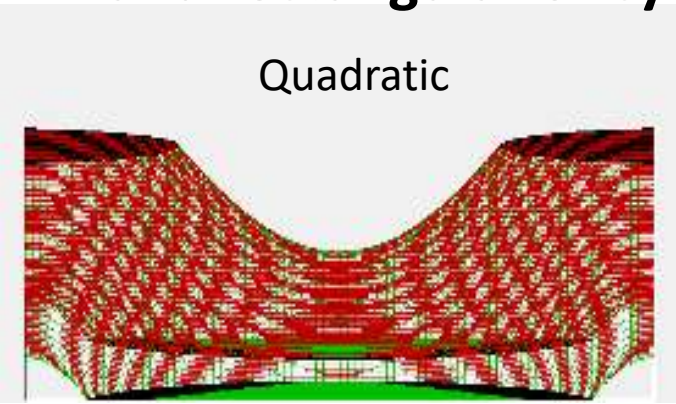

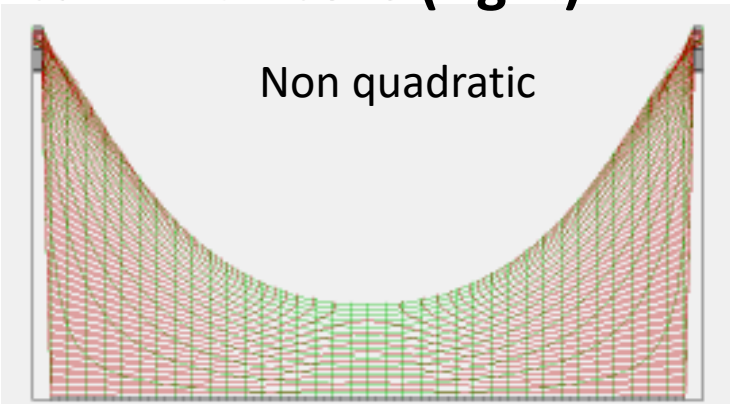

Axial and magnetron frequencies are Independent on axial oscillation amplitude

Axial and magnetron frequencies depend on axial oscillation amplitude

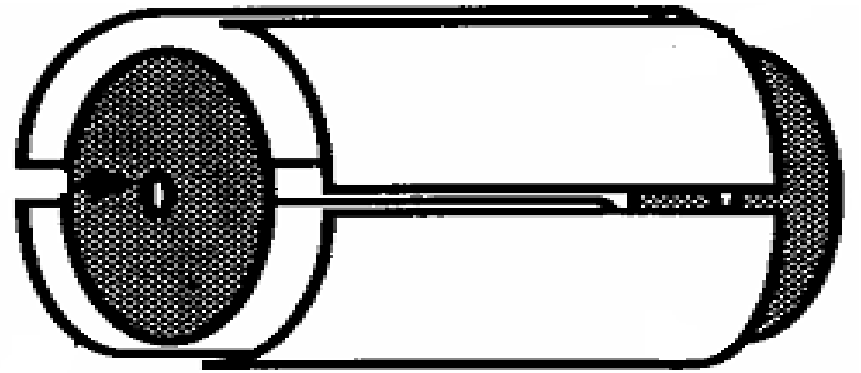

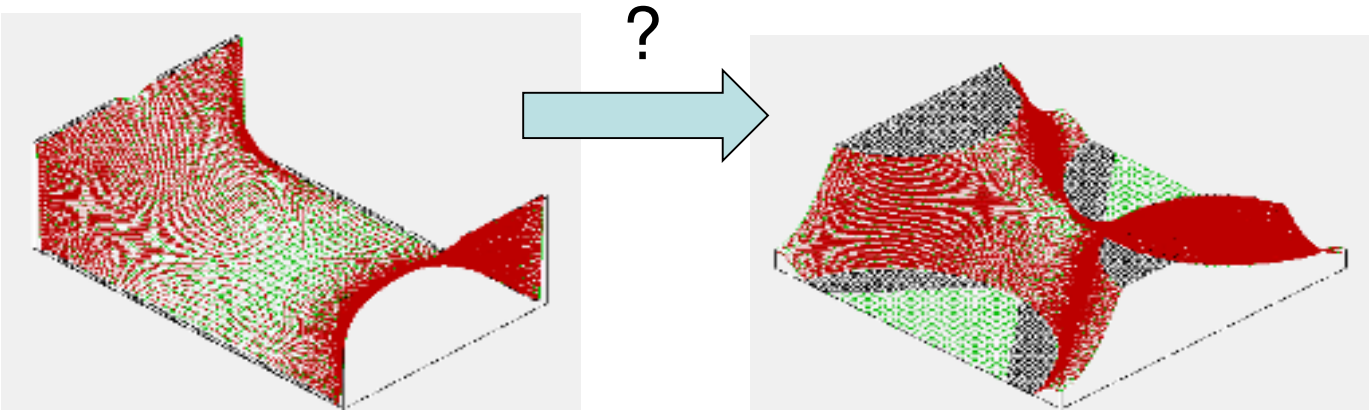

Averaging over cyclotron motion

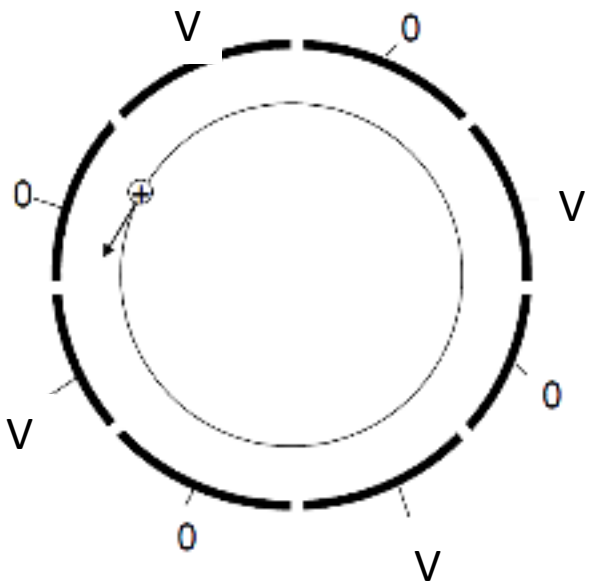

$$\langle \varphi \rangle = \frac{1}{2} V$$

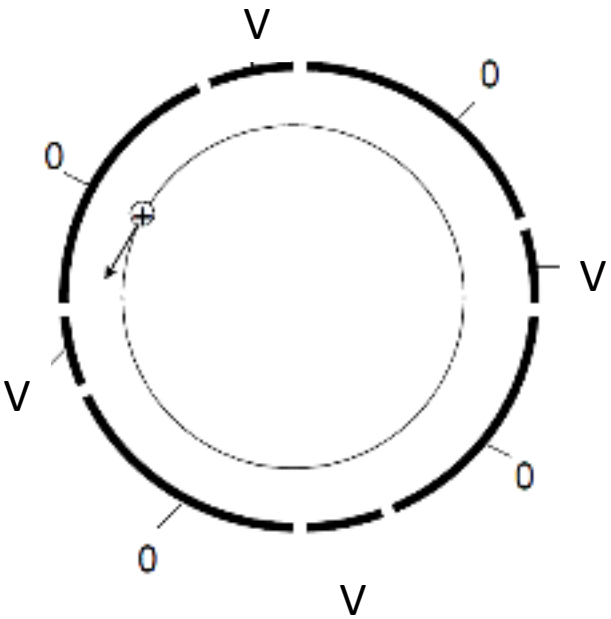

$$\langle \varphi \rangle = \frac{1}{4} V$$

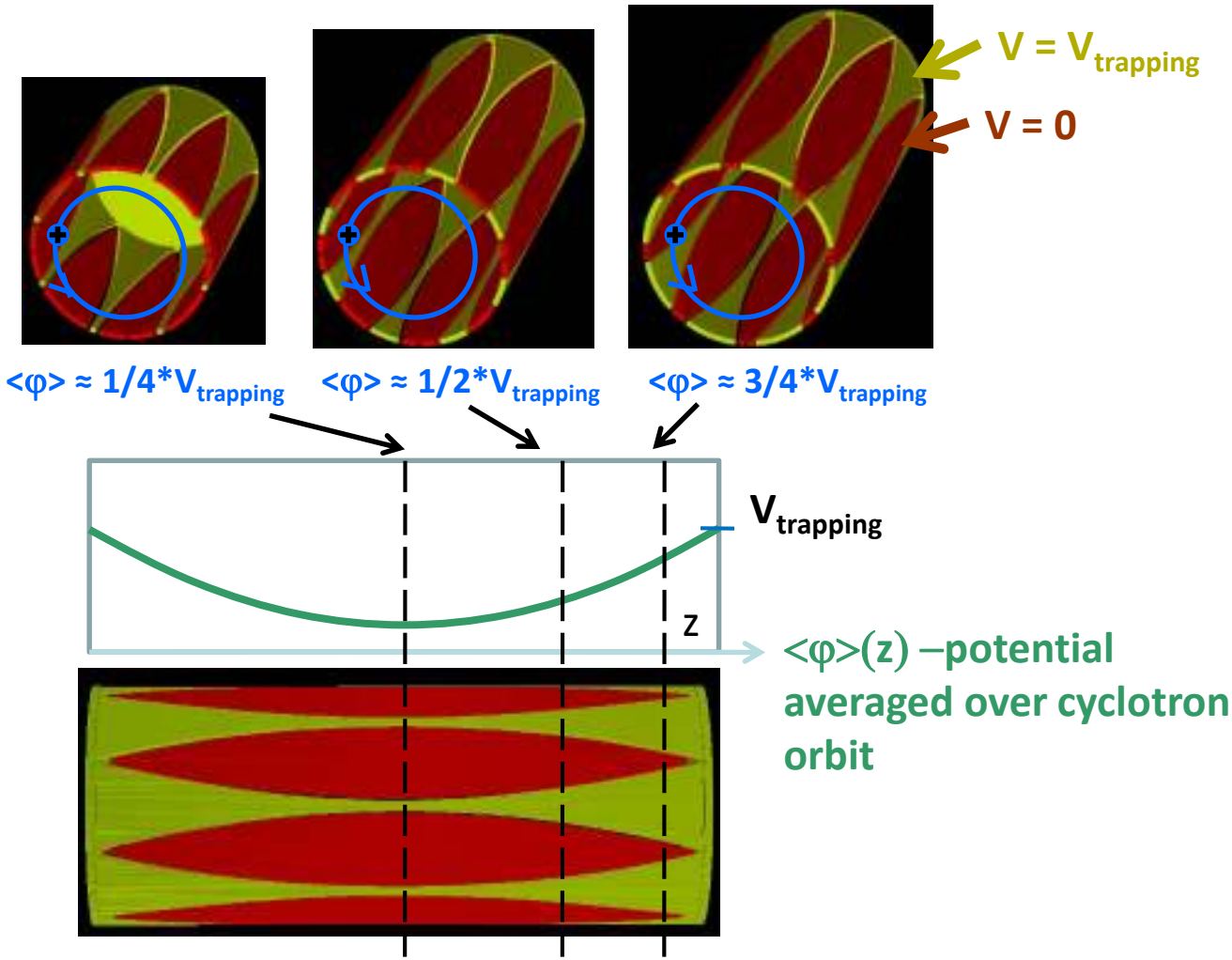
V = V_trapping
V = 0
<φ> ≈ 1/4*V_trapping
<φ> ≈ 1/2*V_trapping
<φ> ≈ 3/4*V_trapping
V_trapping
z
<φ>(z) –potential averaged over cyclotron orbit

Dynamically harmonized FT ICR cell

Parabolic shape gaps

$$\alpha = \frac{2\pi}{N} n \pm \alpha_0 \left(1 - \left(\frac{z}{a} \right)^2 \right)$$

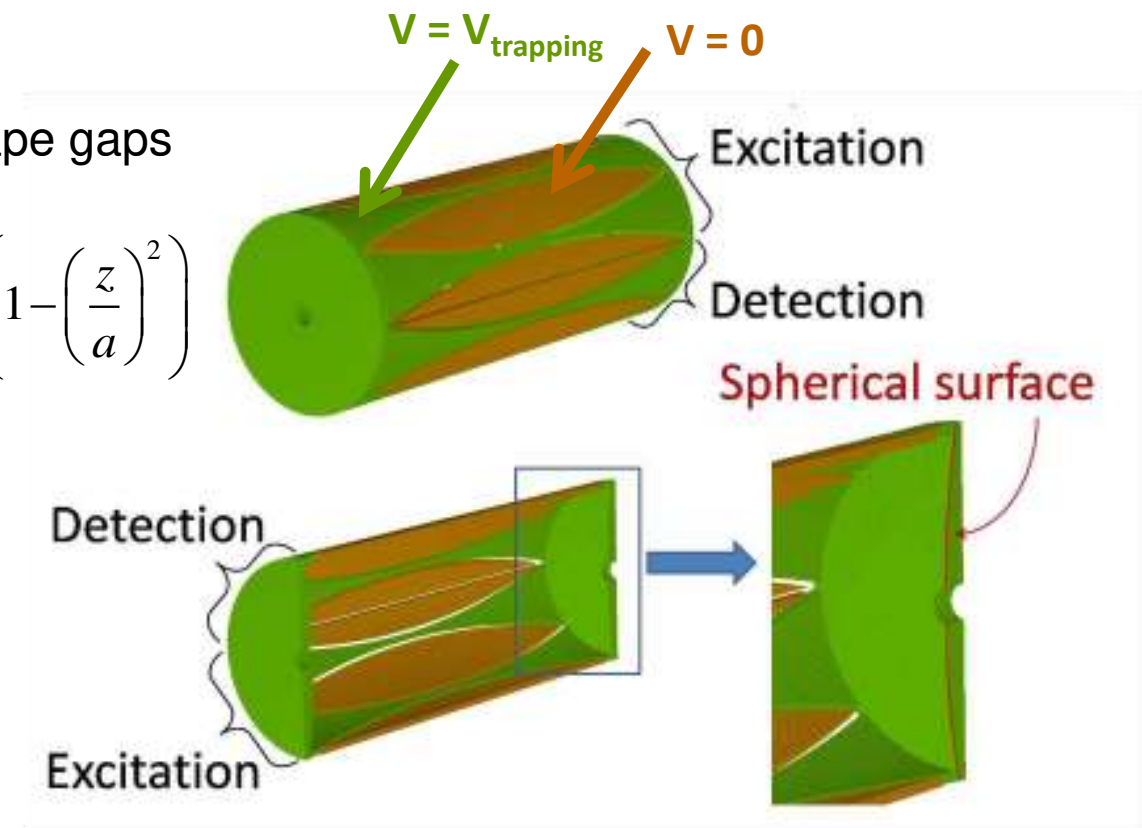

Evolution of ion cloud m/z = 500 Да, Z=1 in 7 T
0.5 s detection time.

Regular cubic cell

Hyperbolic cell

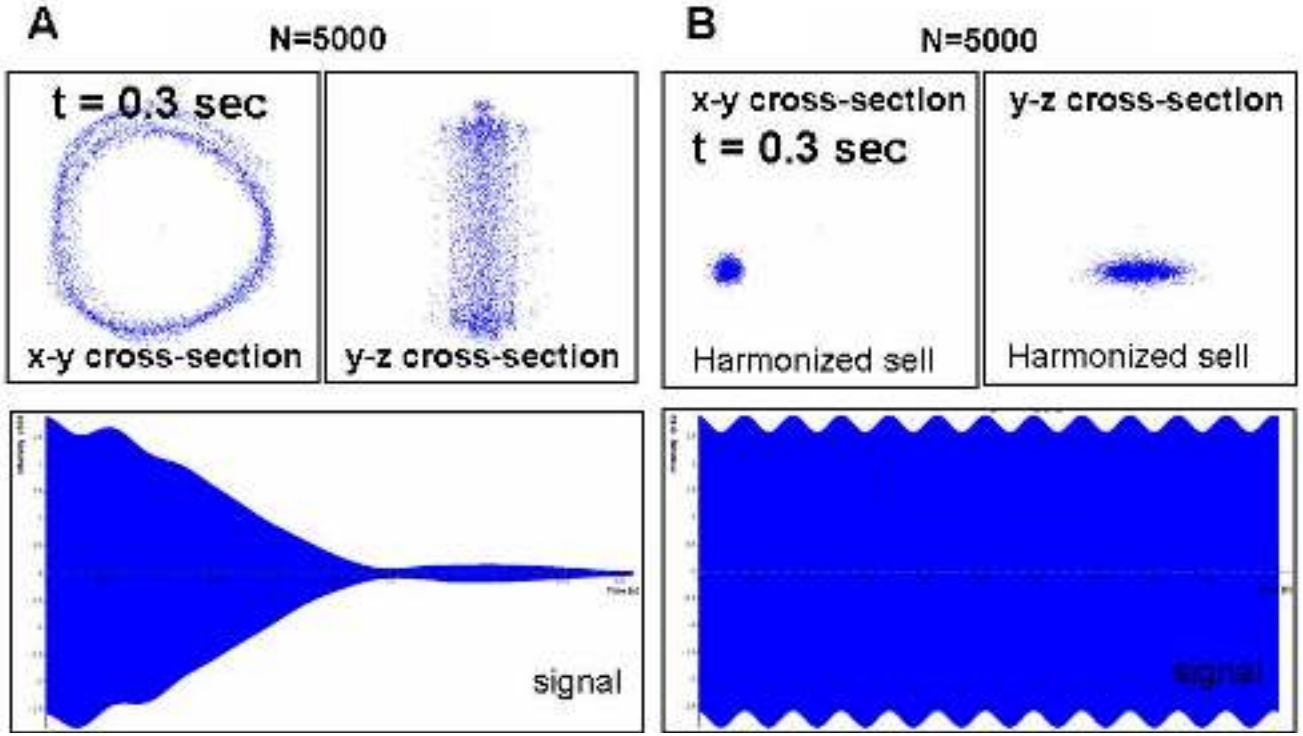

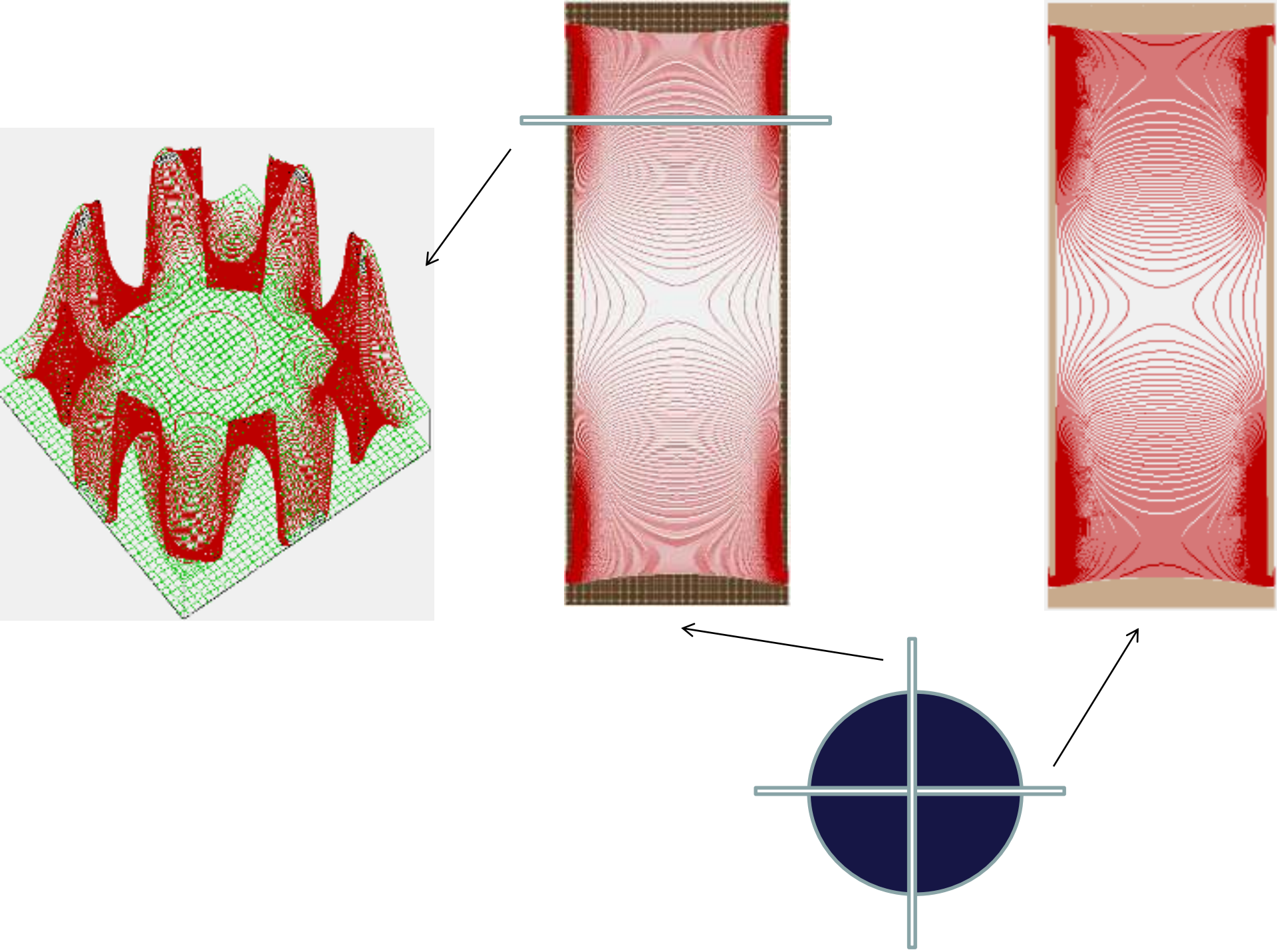

Comparison of averaged axial potential

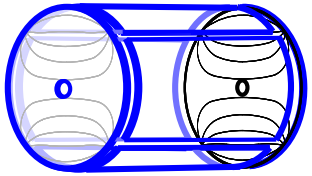

Infinity Cell

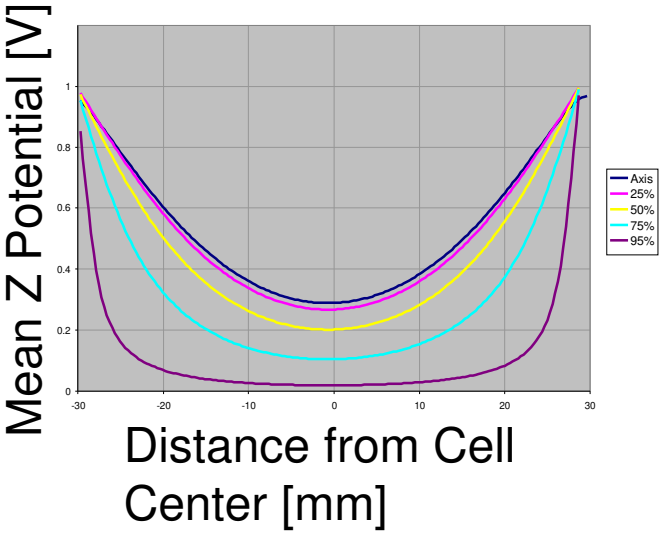

Dynamically Harmonized Cell

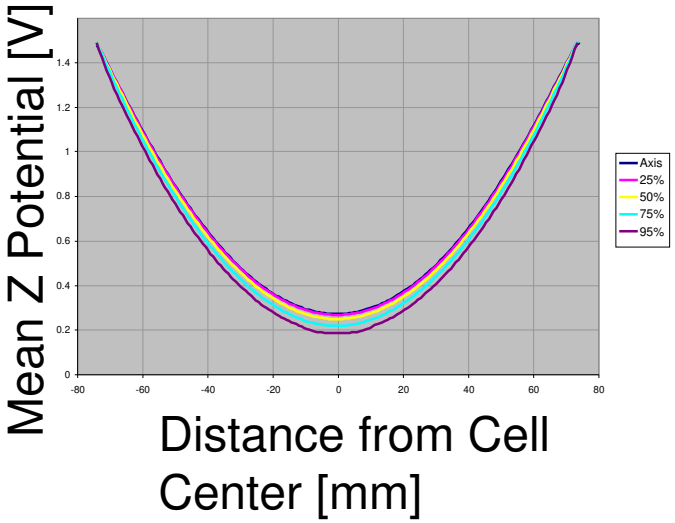

Near parabolic potential up to a cyclotron orbit of 50% of the cell radius.

Harmonic, parabolic potential at all cyclotron orbits.

Isotopic cluster of Cyt C (charge state Z=23)

Theoretical isotopic distribution

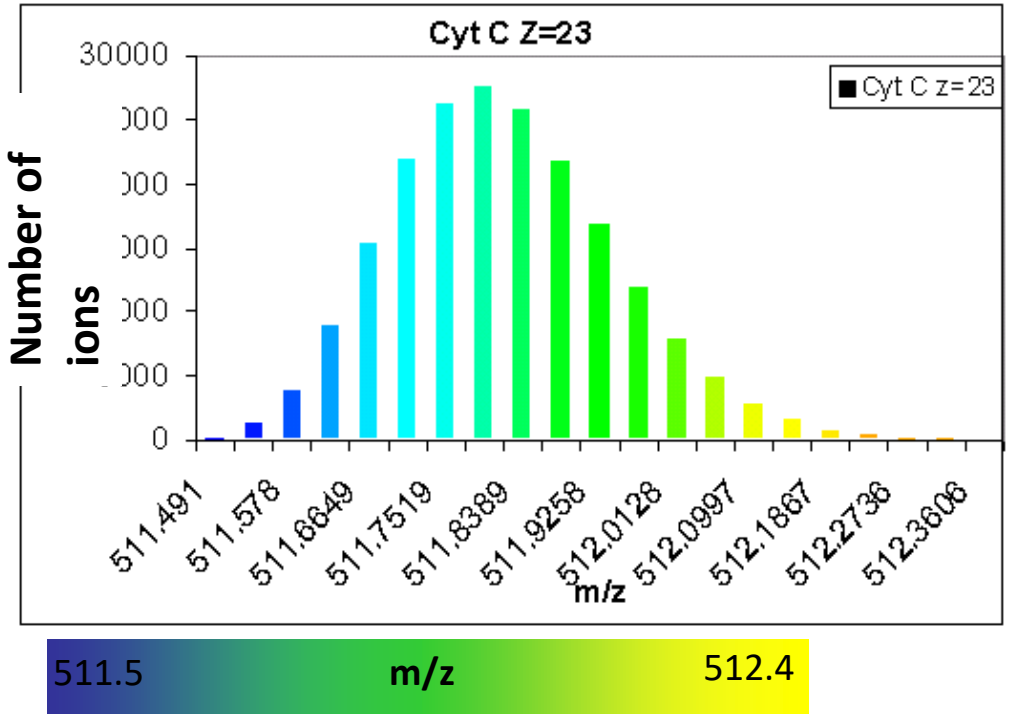

7T, 21T ; 0.3 sec detection; >100 steps per minimal cyclotron period;

0.0004 sec, 50V p-p excitation "chirp" excitation *; 5V trapping potential*

7T Cyt C 100000 charges

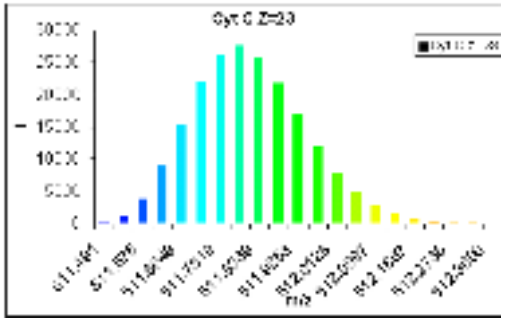

Cylindrical, cubic

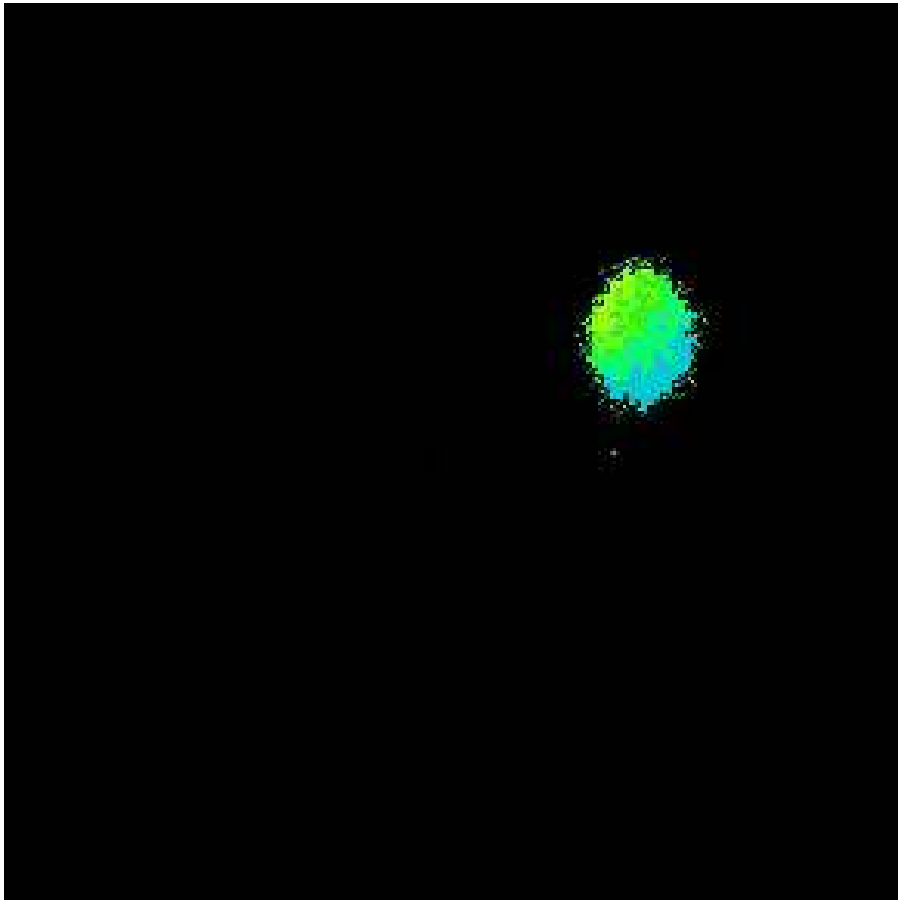

Hyperbolic, dynamically harmonized

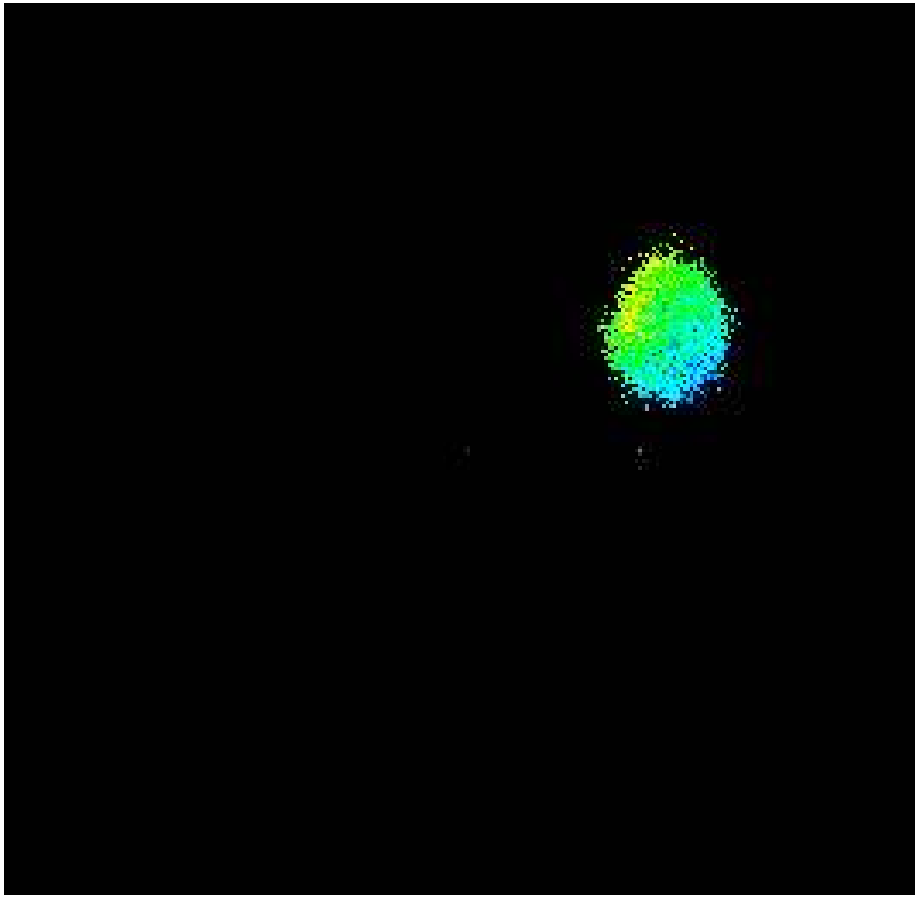

Reserpine. Lab Prototype , Solarix, 300s transient, RP 39,000,000 in magnitude mode

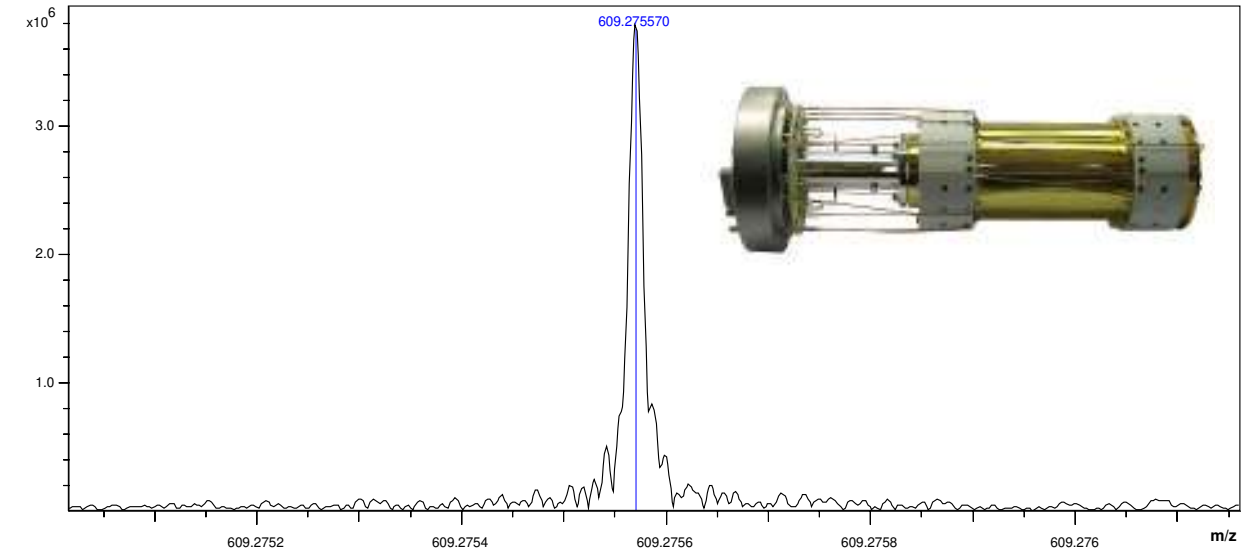

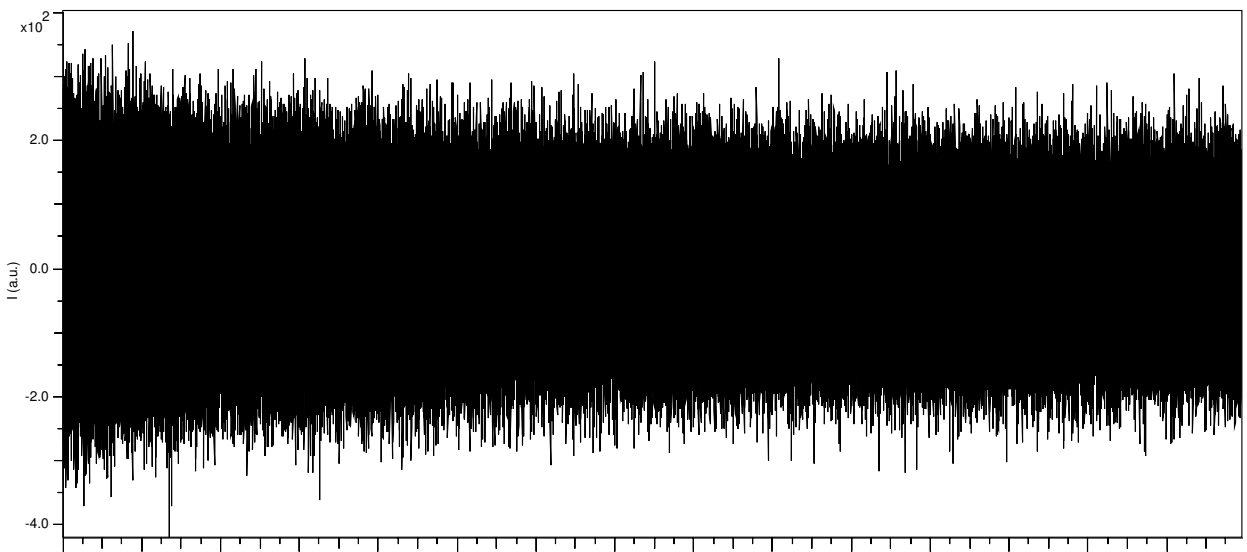

7T R&D, BSA, 51+, RP 1,700,000 28 s transient

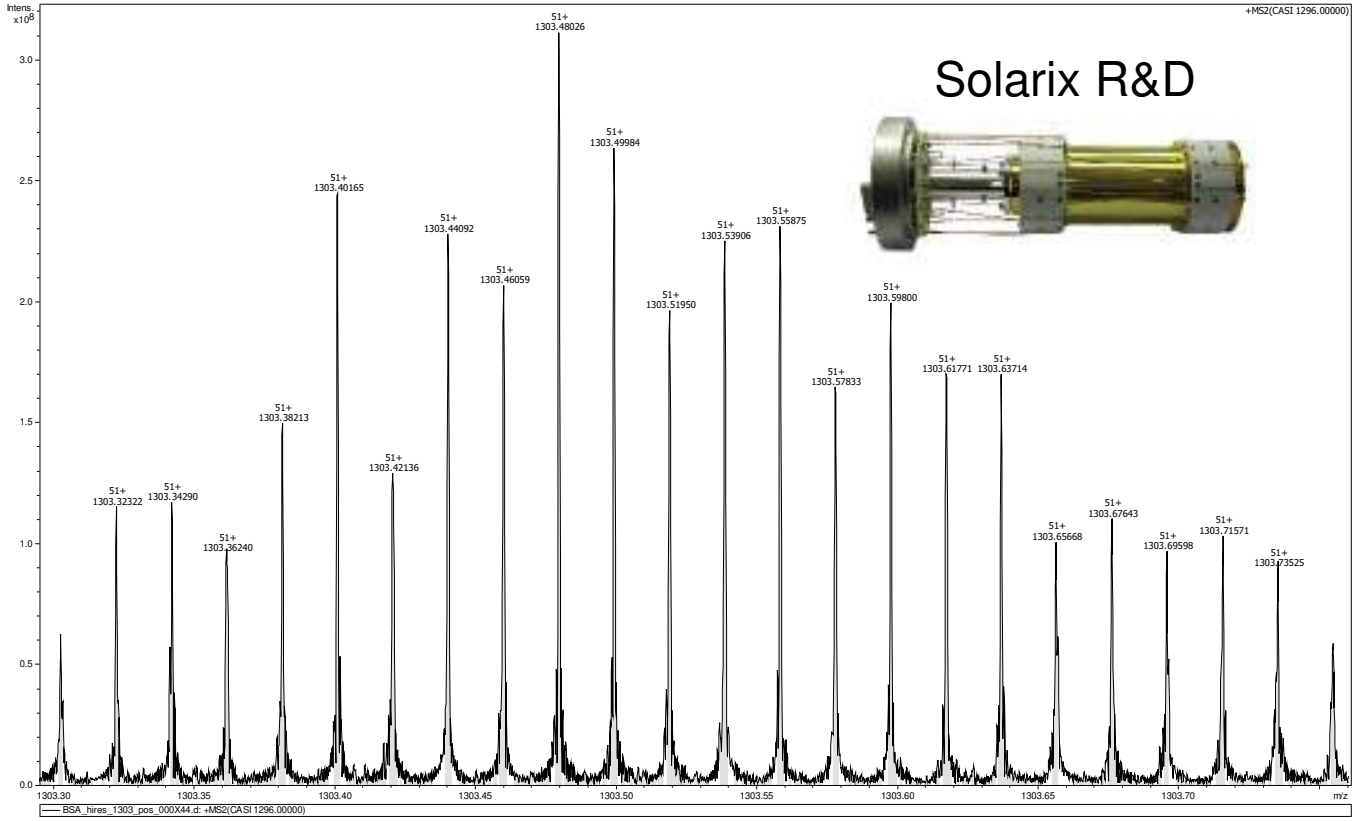

IgG1 (MW =147800 Da), 46+, RP 500 000

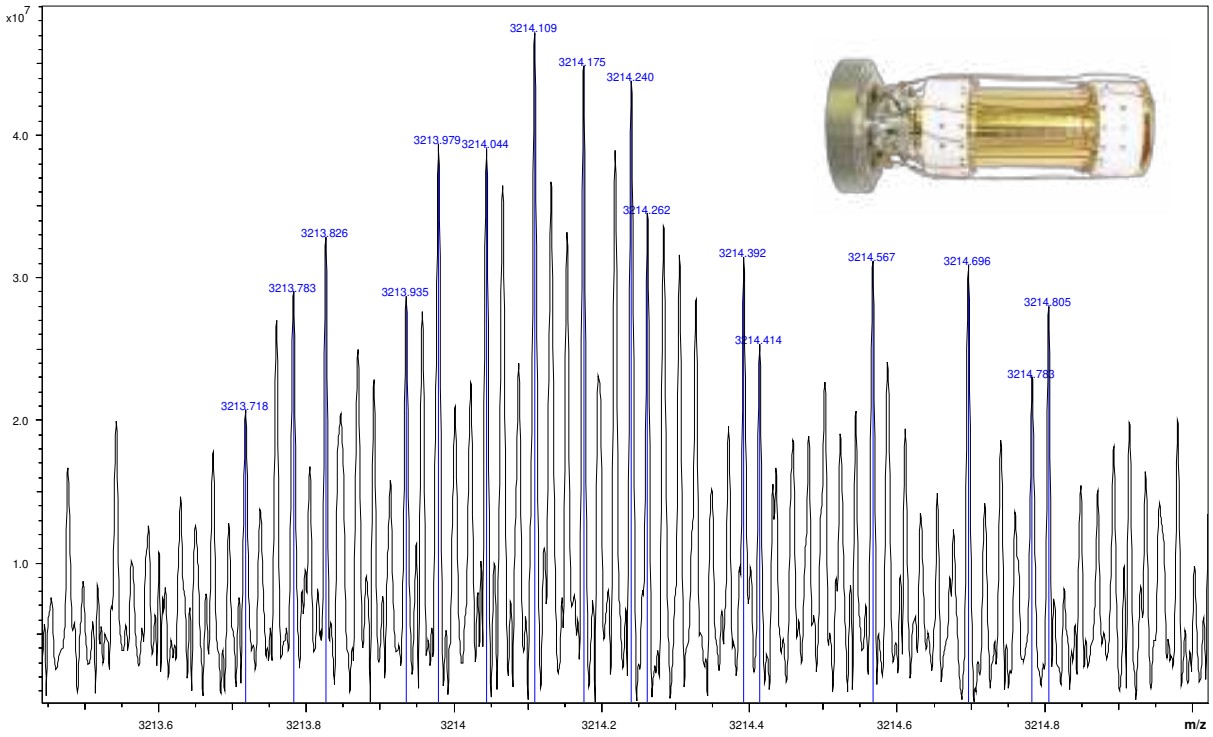

12T R&D, Enolase Tetramer, MW=**186713** Da, m/z=5835, (6мG/ml) , 32+, deconvoluted

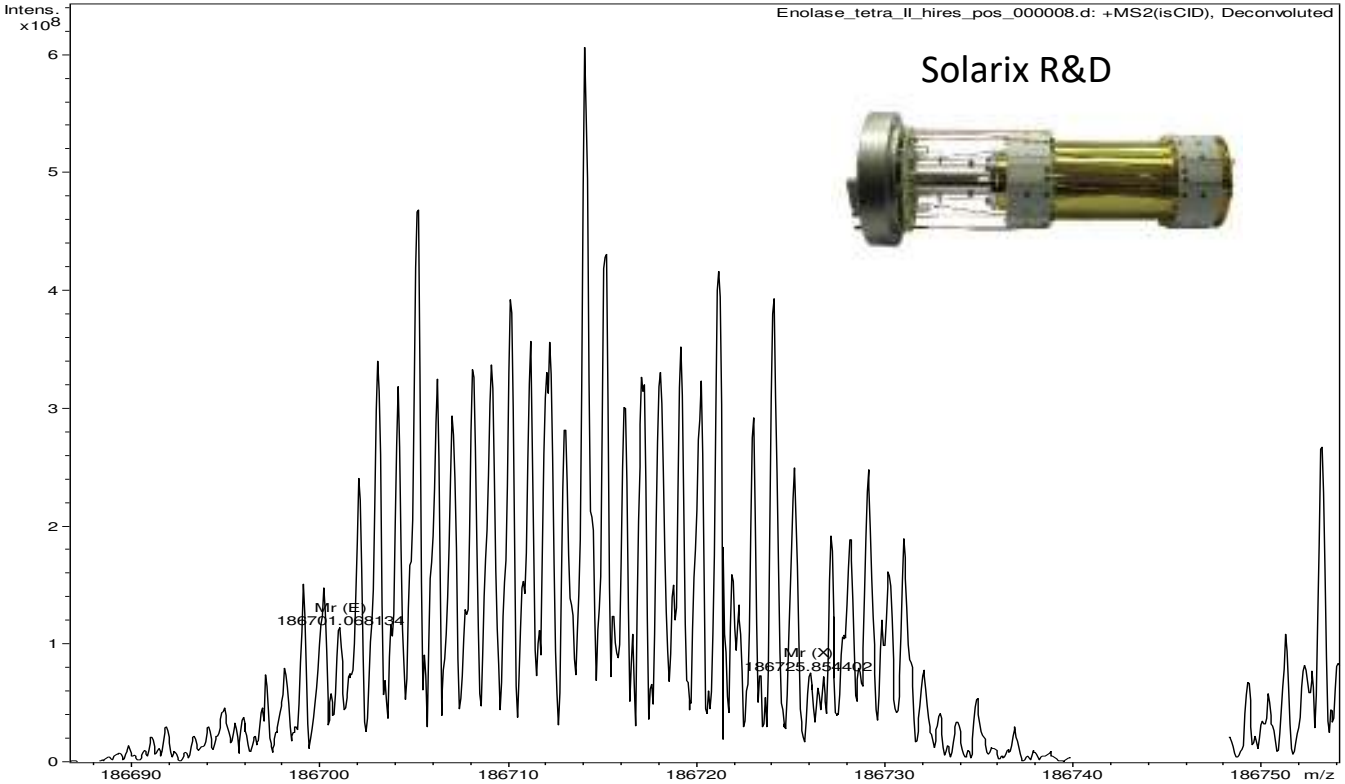

The highest mass protein complex isotopicaly resolved (2012)

Peptide spectra fine structure

Substance P, broadband spectrum

$C_{63}H_{100}N_{18}O_{13}S_1$

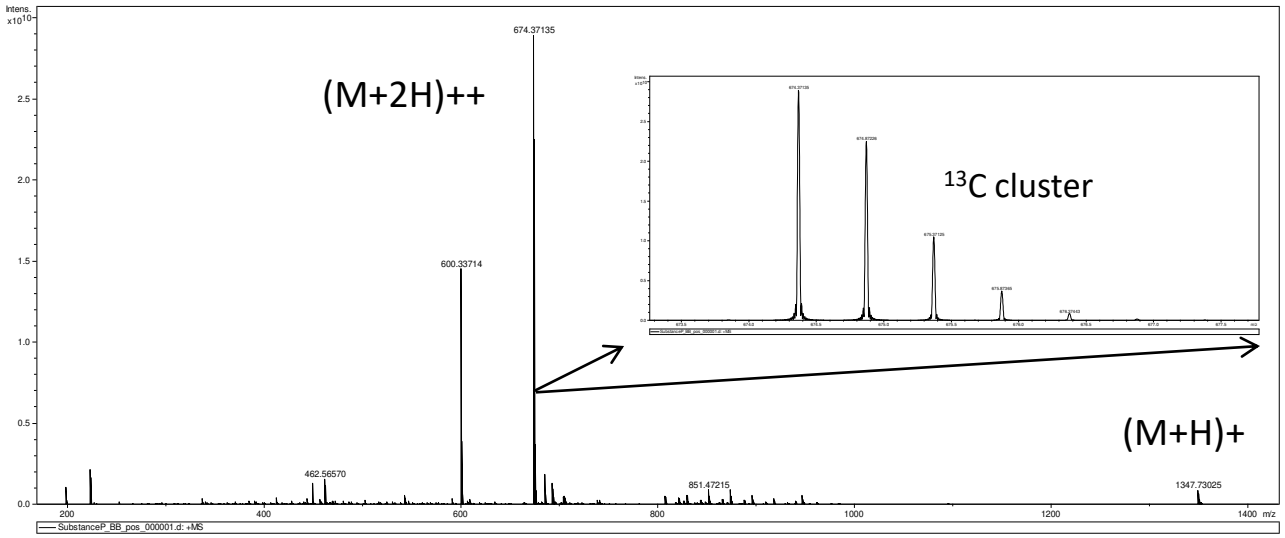

Substance P (M+ 2H$^+$) on 7 Tesla magnet

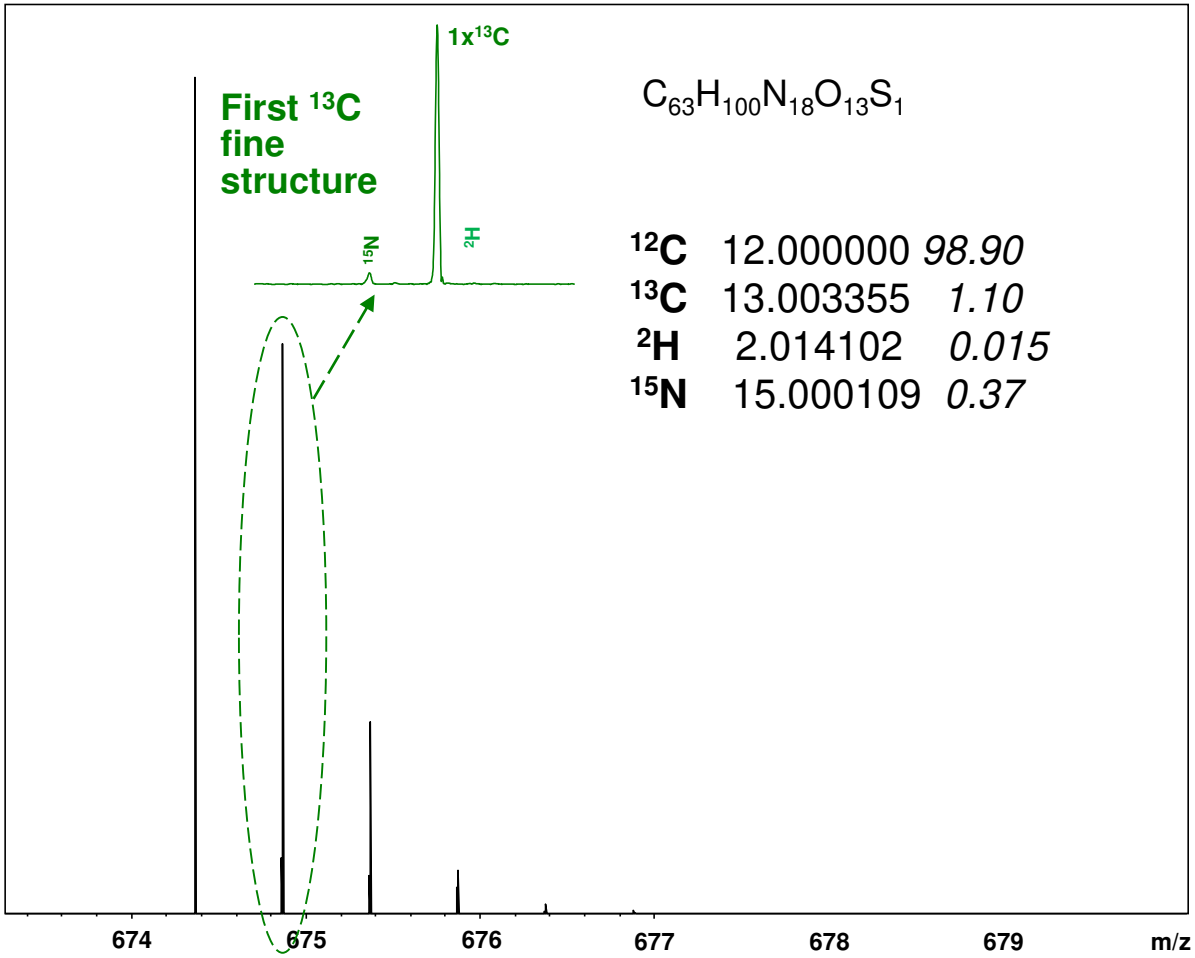

Substance P (M+ 2H$^+$) on 7 Tesla magnet

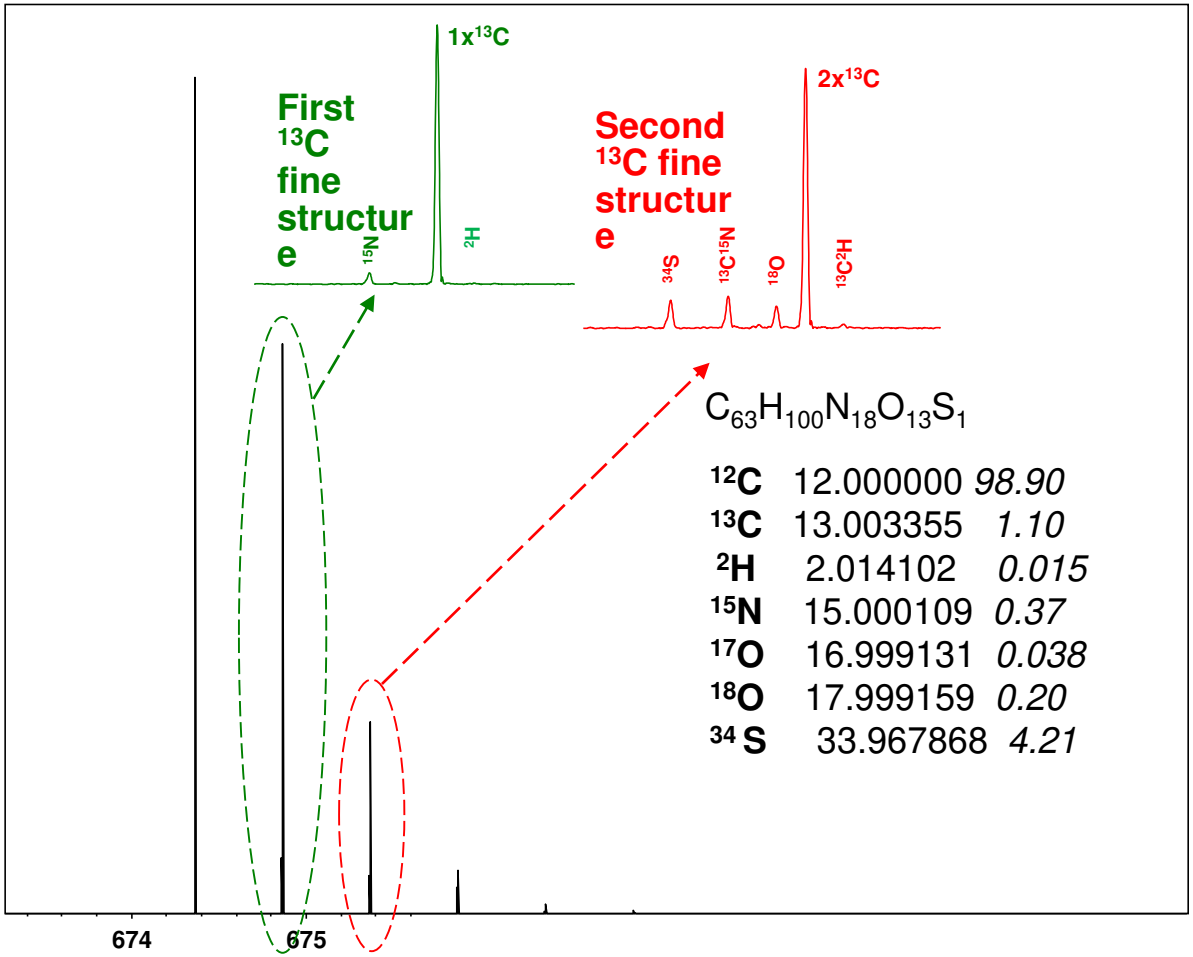

$C_{63}H_{100}N_{18}O_{13}S_1$

^{12}C	12.000000	*98.90*
^{13}C	13.003355	*1.10*
^{2}H	2.014102	*0.015*
^{15}N	15.000109	*0.37*
^{17}O	16.999131	*0.038*
^{18}O	17.999159	*0.20*
^{34}S	33.967868	*4.21*

Substance P (M+ 2H$^+$) on 7 Tesla magnet

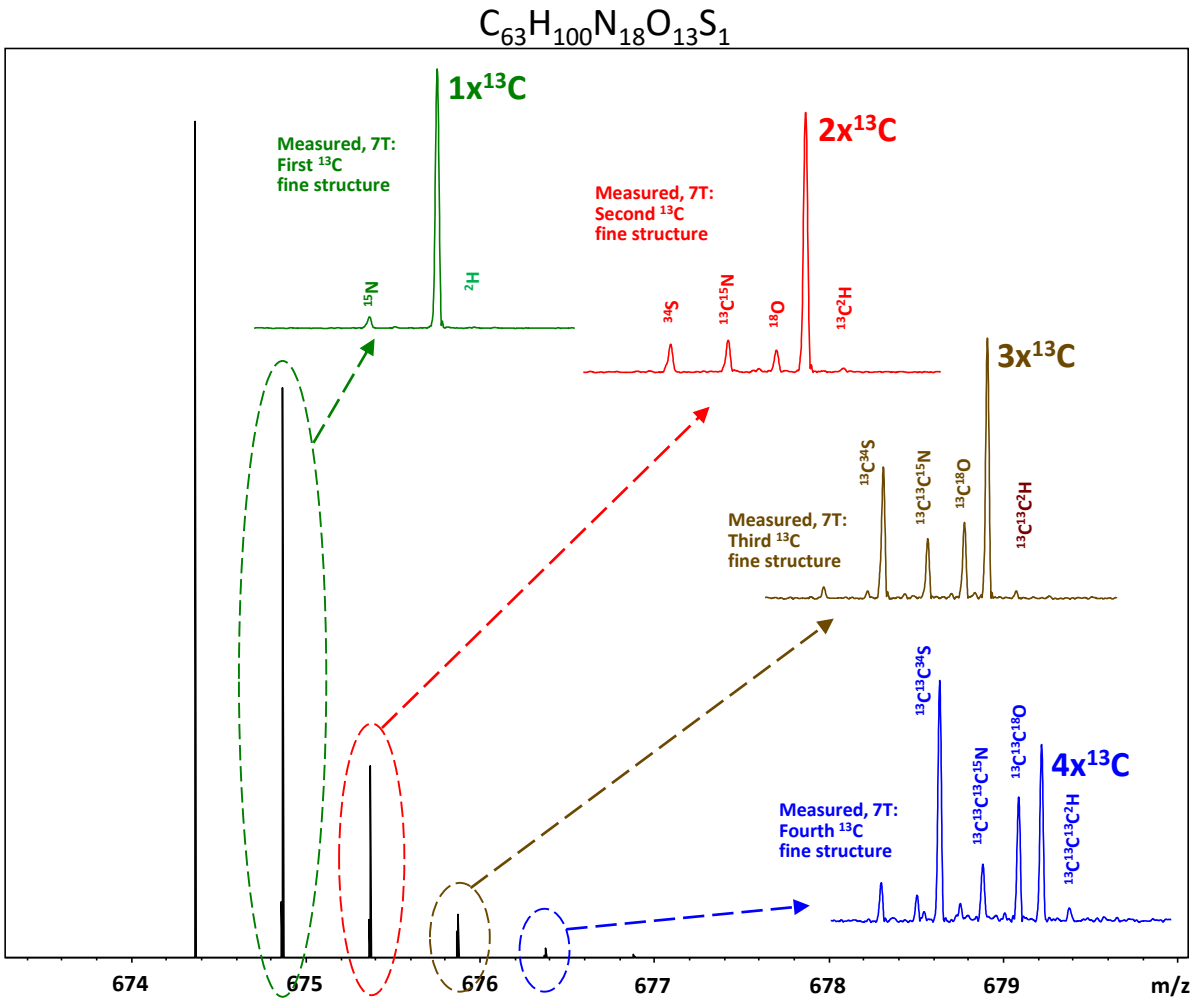

Substance P (M+ 2H^{+}) on 7 Tesla magnet

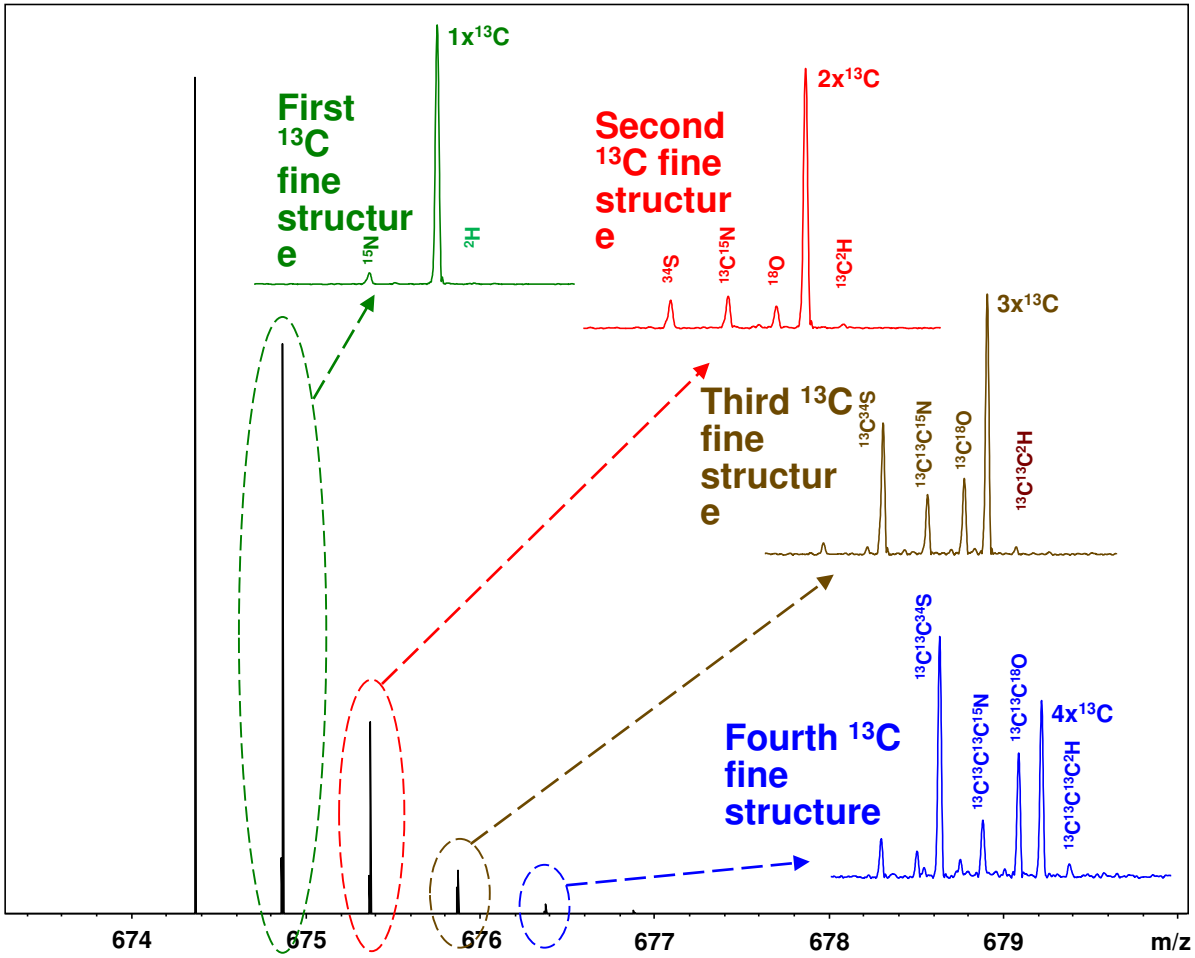

Substance P (M+ 2H$^+$) on 7 Tesla magnet

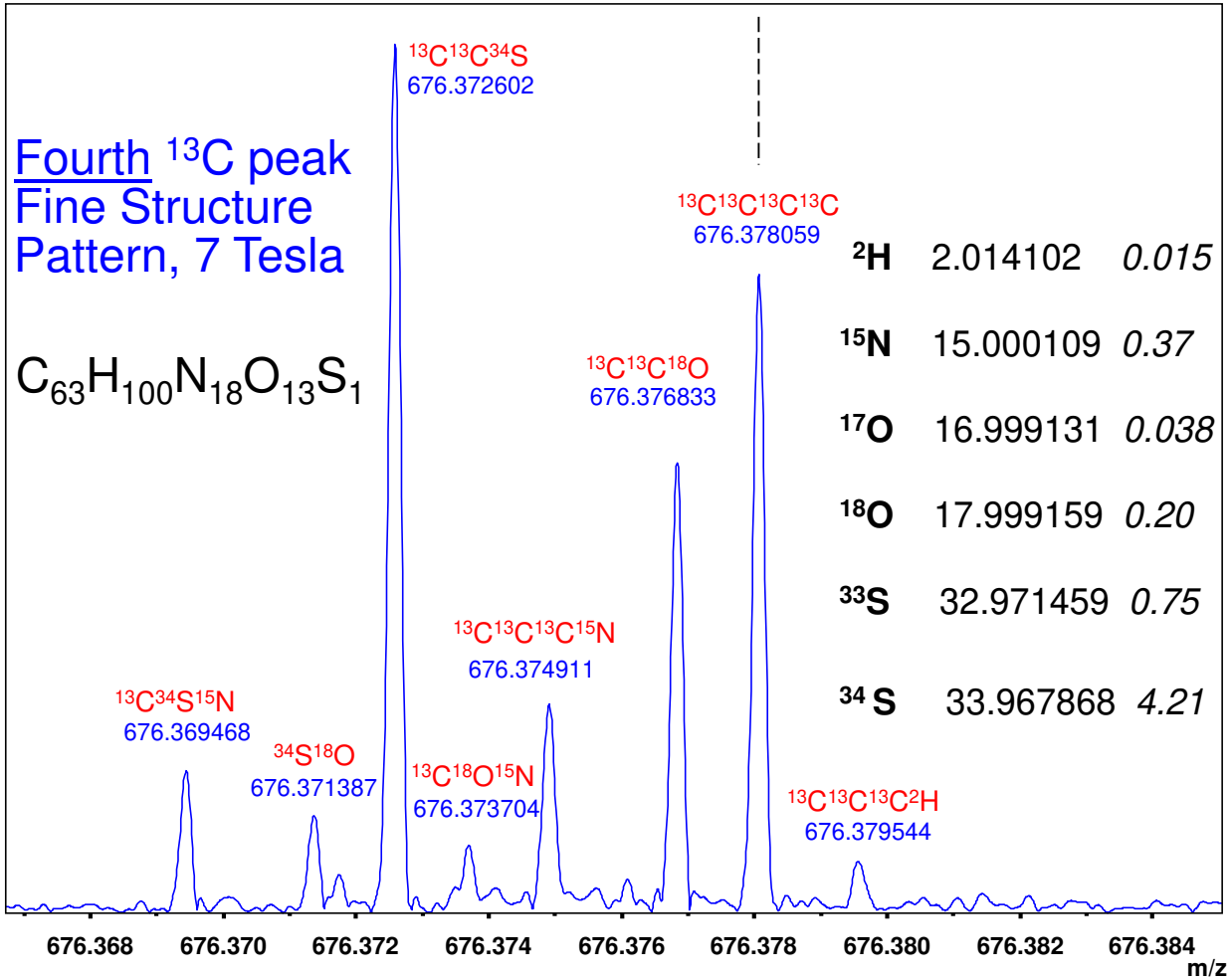

How to evaluate the cell quality?

E.Nikolaev, A.Lioznov
Evaluation of major historical ICR cell designs using electric field simulations
Mass Spec Rev. 2020;1–22

ers/e.nikolaev/Downloads/ThesisFinalReview2021%20-%20presentation_Lioznov.pdf

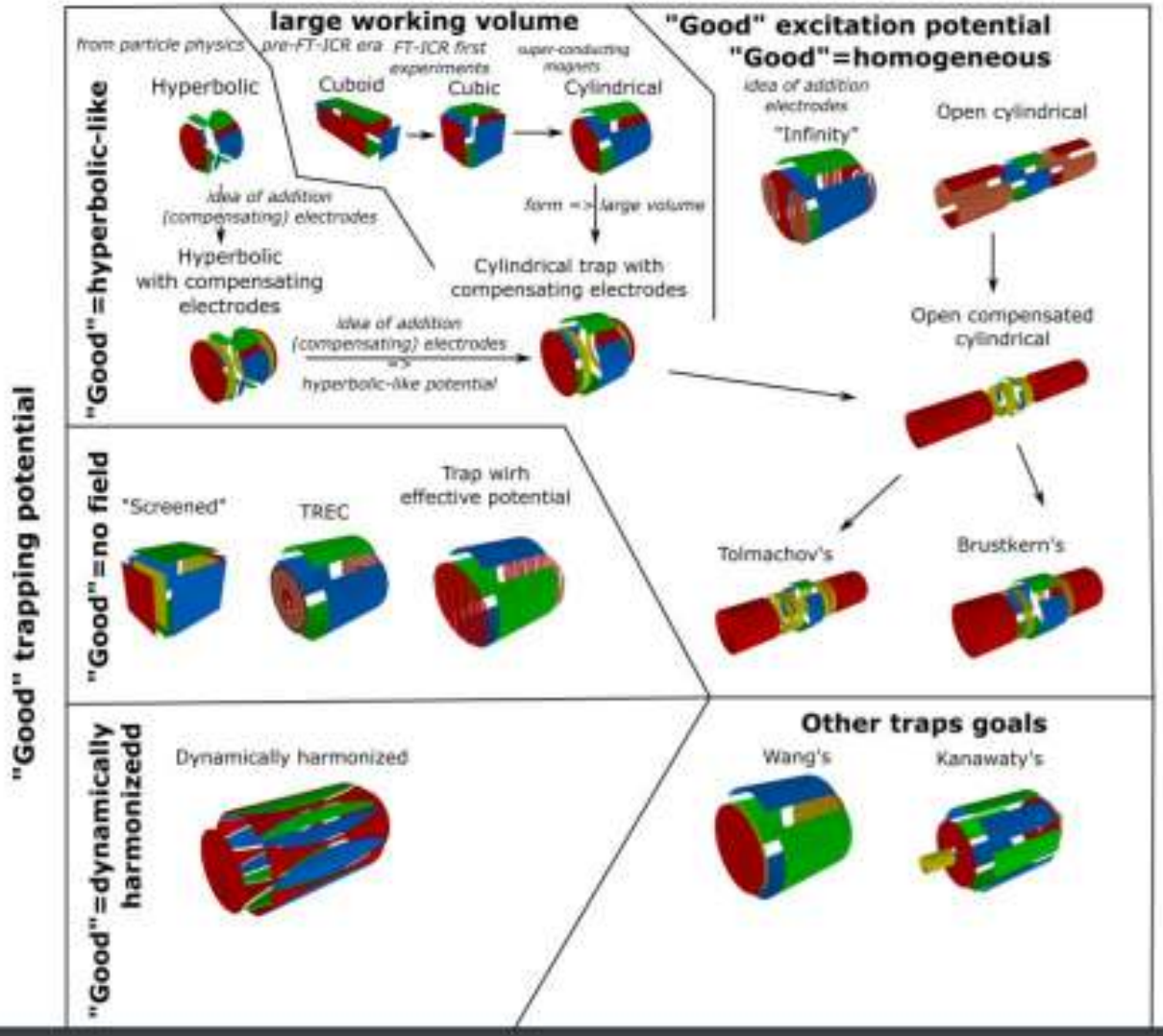

Skoltech

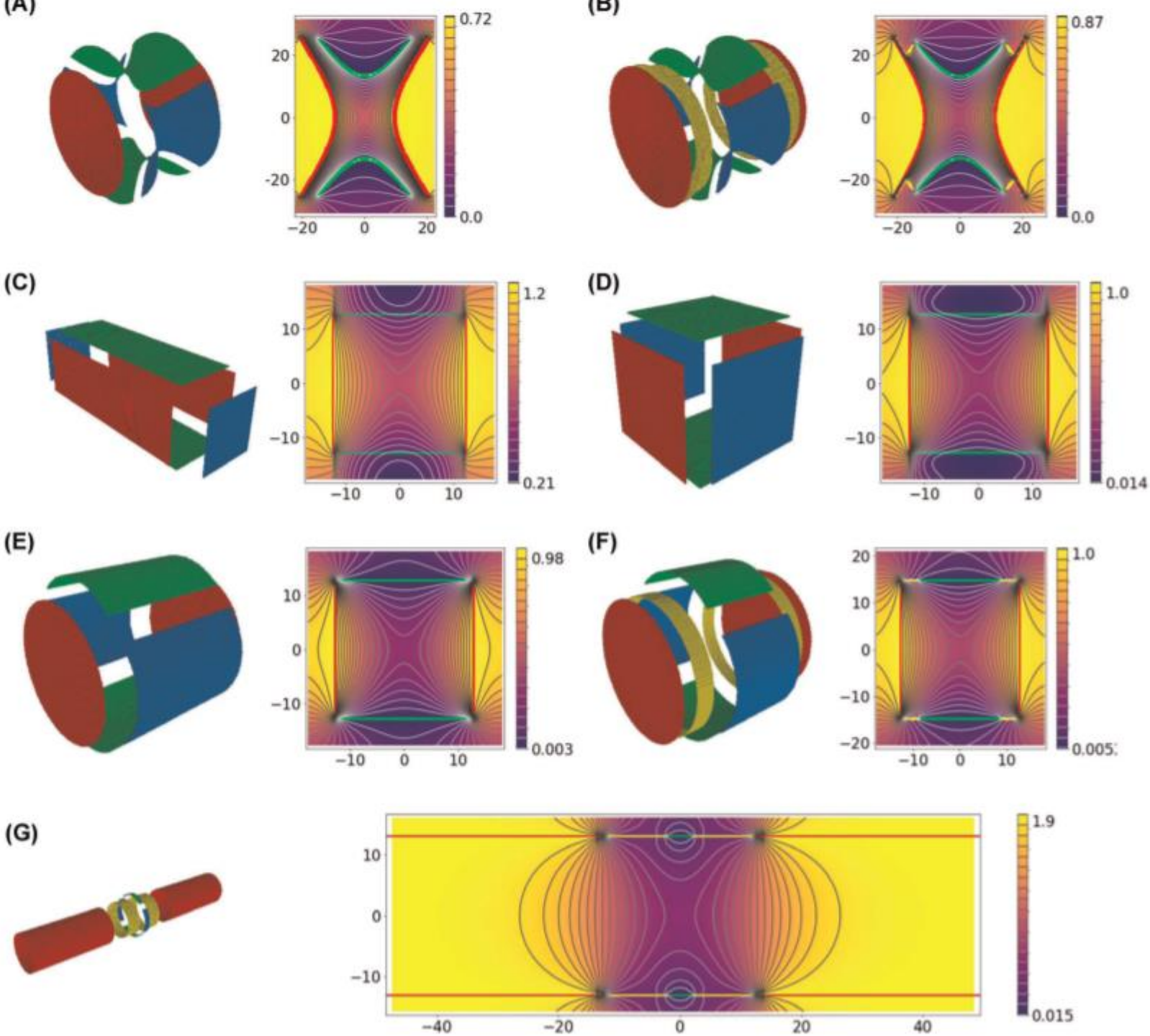
(A)
0.72
0.0
(B)
0.87
0.0
(C)
1.2
0.21
(D)
1.0
0.014
(E)
0.98
0.003
(F)
1.0
0.005
(G)
1.9
0.015

ntation_Lioznov.pdf 18 / 48 250%

(8)

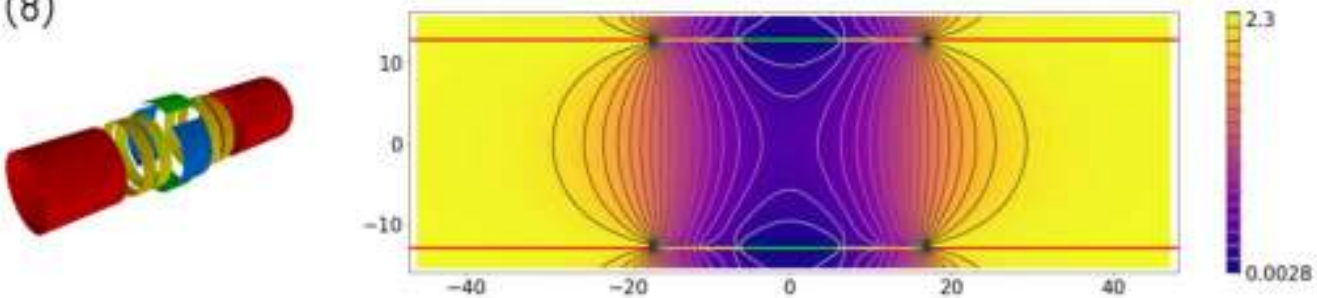

(9)

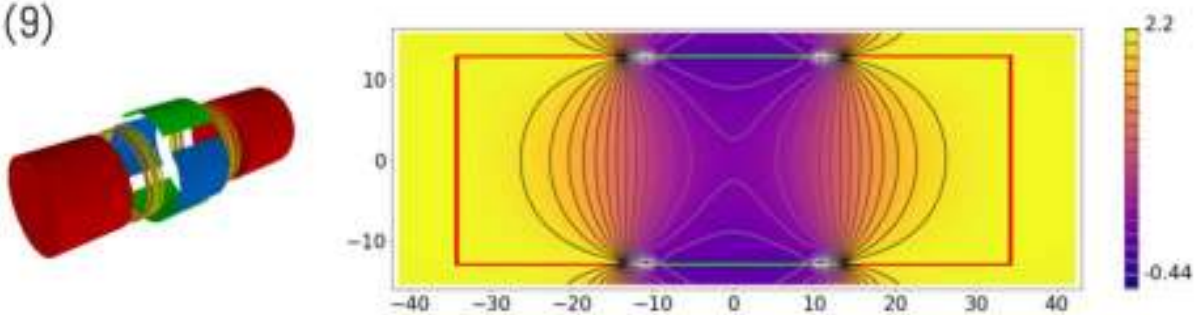

(10)

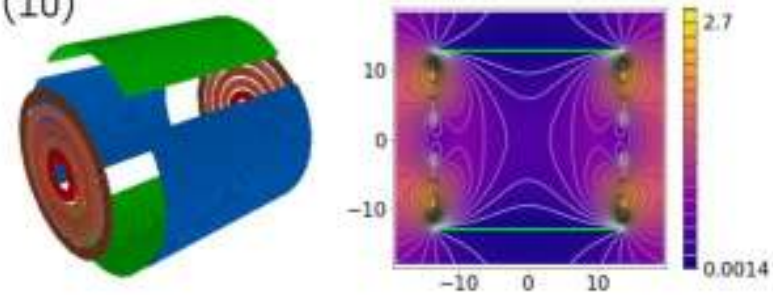

(11)

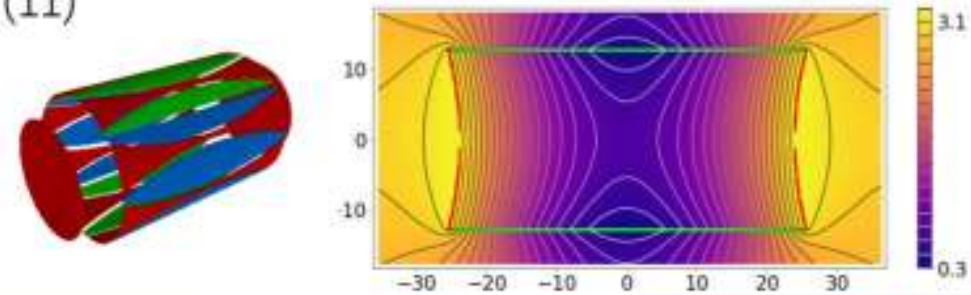

ENG 10:38 24.09.2021

The electric field inside any ion cell may be presented as Spherical Harmonic Decomposition

$$\phi(r,\theta,\varphi) = \sum_{l=0}^{\infty} \sum_{m=-l}^{l} A_{lm} Y_{lm}(\theta,\varphi) \cdot r^l$$

We take into account only first significant nonzero terms: $A_{20} r^2 Y_{20}$, $A_{40} r^4 Y_{40}$, $A_{60} r^6 Y_{60}$ and present the main mode of rotation ion frequency as

$$\omega_+(\rho,z) = \frac{qB}{2m} + \left[\left(\frac{qB}{2m}\right)^2 - \frac{q}{m}\{A_{20} + A_{40}(48z^2 - 12\rho^2) + \right.$$

$$\left. + A_{60}(240z^4 - 360z^2\rho^2 + 30\rho^4)\} \right]^{1/2}$$

sisFinalReview2021 - presentation_Lioznov.pdf 16 / 48 200%

The time of comet formation can be estimated as

$$T_{\text{comet formation}} = \frac{2\pi}{\max_{r,z}\omega_+ - \min_{r,z}\omega_+}$$

Relative time of synchronized motion of ions in different FT ICR cells

Trap name	A_{20}	A_{40}	A_{60}	t_{comet}, s
Hyperbolic trap	4.3e-01	-2.0e-05	4.5e-06	5.3e+00
Hyperbolic trap with compensating electrodes	4.3e-01	-1.9e-07	2.4e-06	1.8e+01
Cuboid cell	1.9e+00	-2.0e-02	-9.8e-02	3.2e-02
Cubic cell	5.2e-01	4.7e-03	-2.9e-03	2.4e-02
Cylindrical cell	5.3e-01	1.0e-02	-3.6e-03	1.4e-02
Cylindrical trap with compensating electrodes	5.8e-01	2.0e-06	-3.1e-03	3.3e-02
Open cylindrical cell with compensating electrodes	5.3e-01	2.4e-08	-5.9e-04	1.3e-01
Trap with compensating electrodes by Tolmachov	7.6e-01	7.2e-05	-1.3e-03	1.8e-01
Trap with compensating electrodes by Brustkern	5.8e-01	1.6e-02	-3.5e-03	1.3e-02
Dynamically Harmonized Cell or Paracell	1.6e+00	-4.4e-05	2.6e-04	7.0e+00

Dynamically harmonized cells are providing the highest resolving power

Bruker's cell

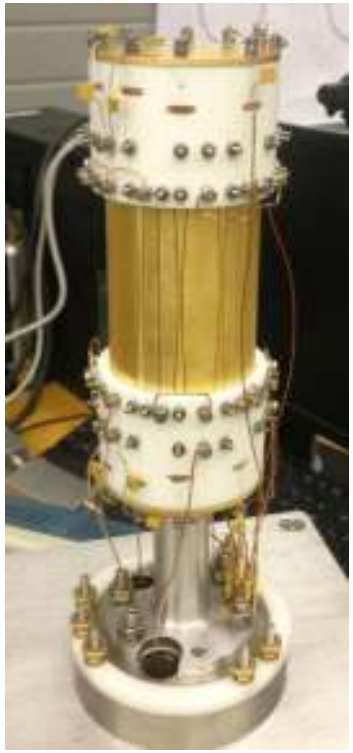

NHMFL cell

In 2015 we had Milestone events in FT ICR mass spectrometry

Launching two 21 tesla FT ICR mass Spectrometers

In National High Magnetic Field Laboratory NHMFL (Tallahassee Florida)

and in Pacific North West National Laboratory PNNL (Richland, Washington)

BRUKER
21T FT-ICR

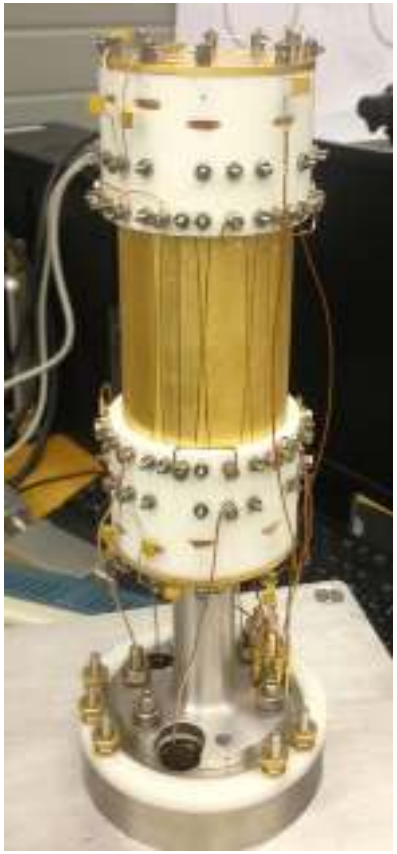

From Alan Marshall 10th NA FTMS 21 T talk

Solarix R&D

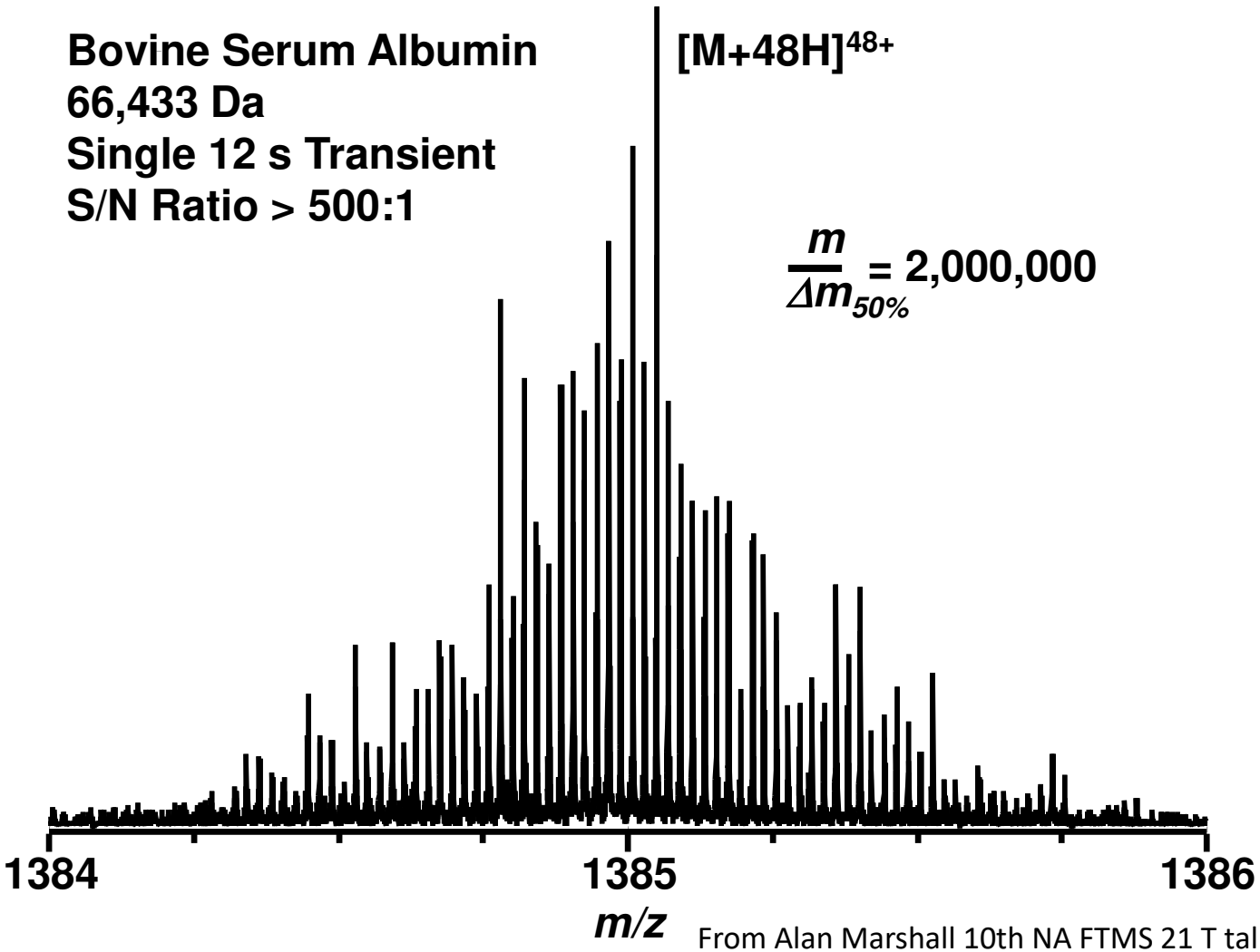

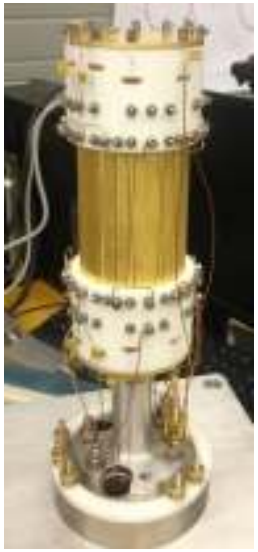

From Alan Marshall 10th NA FTMS 21 T talk

7T R&D, BSA, 51+, RP 1,700,000 28 s transient

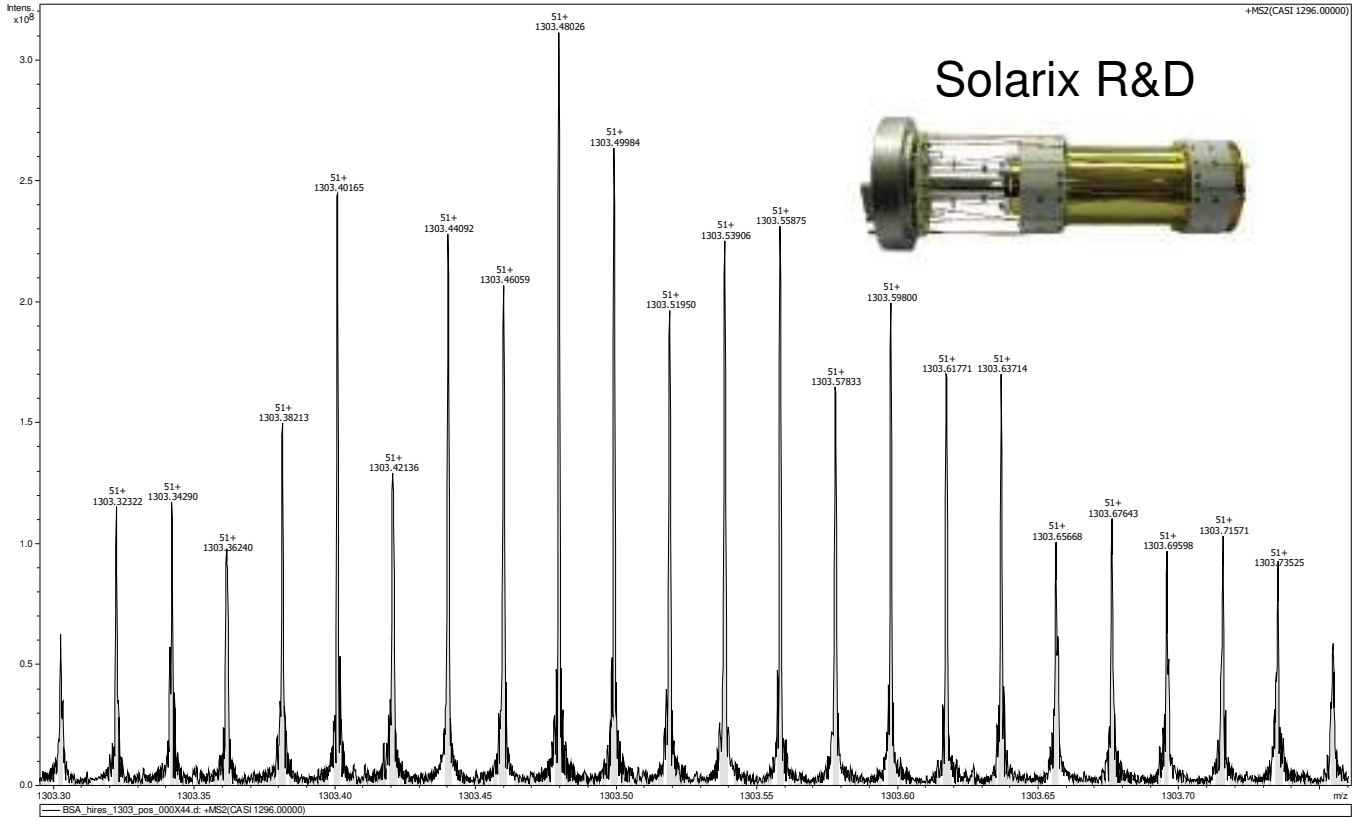

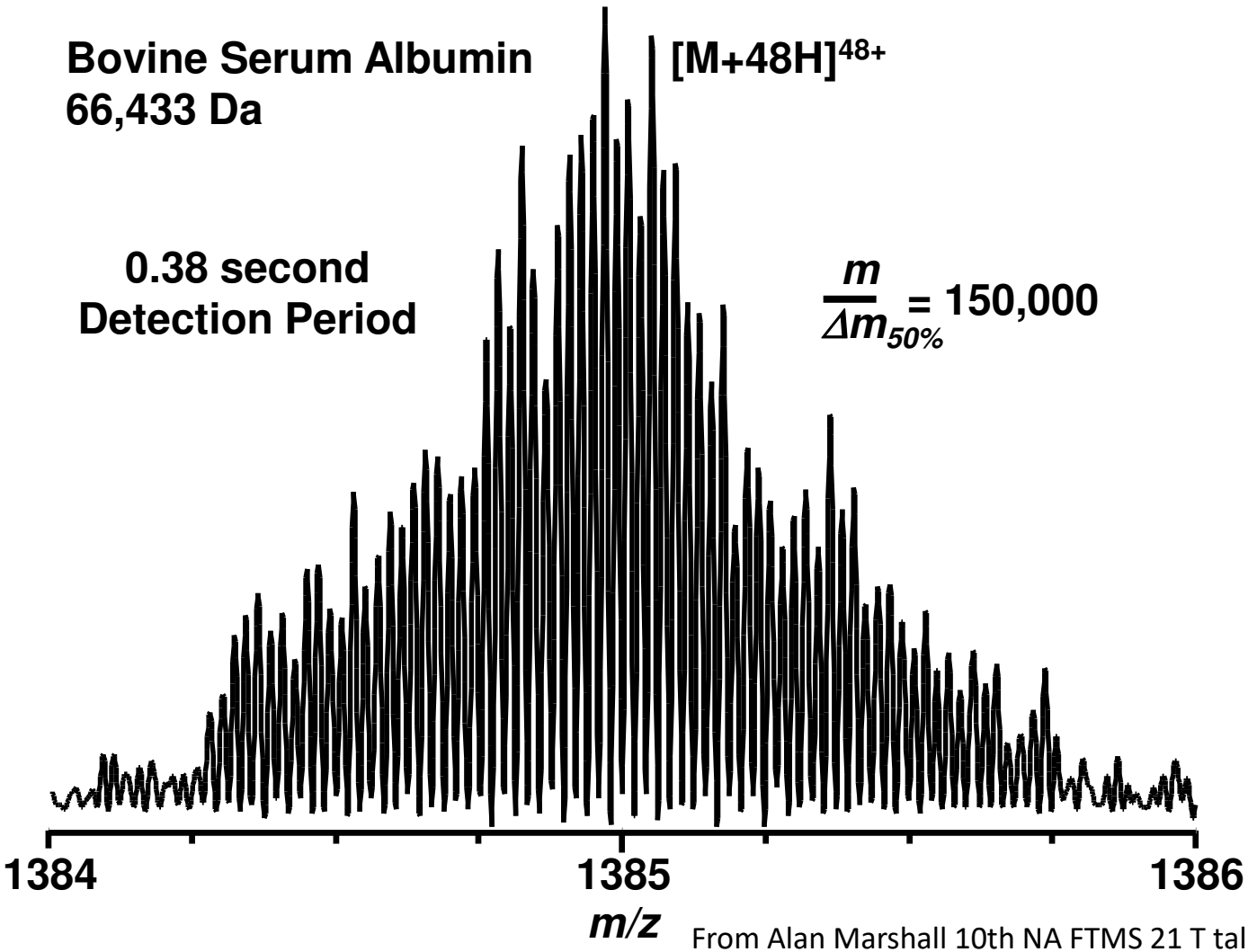

From Alan Marshall 10th NA FTMS 21 T talk

Highly developed surface with large «vacuum memory»

- Long pumping time;
- Not highest avalible final vacuum;
- Potential leakage in feedthroughs.
- Closed volume of the cell

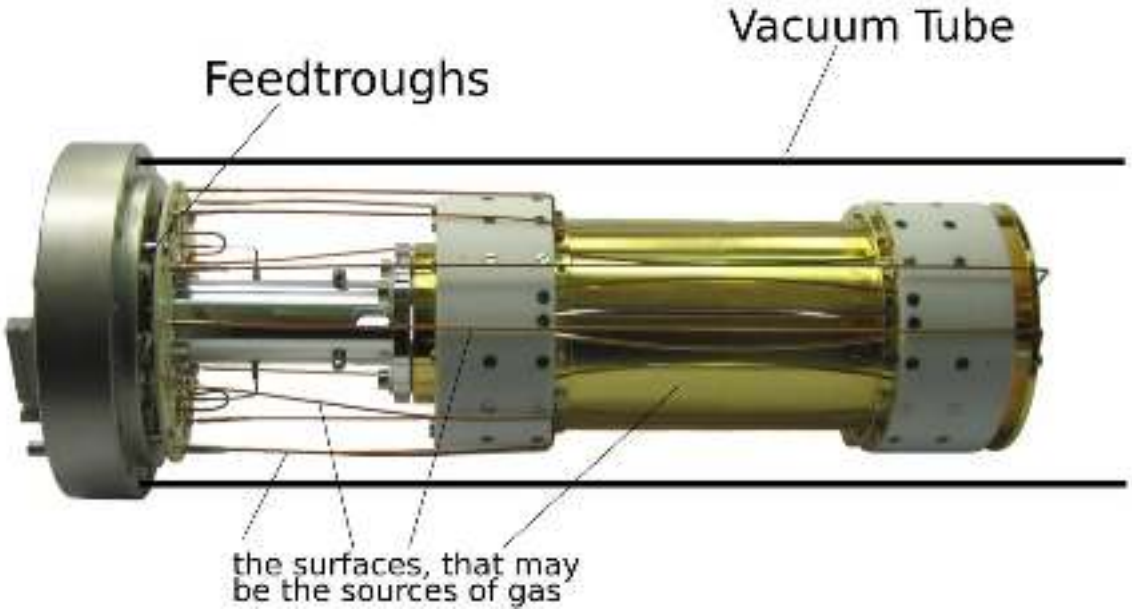

«Standard» (closed) DHC

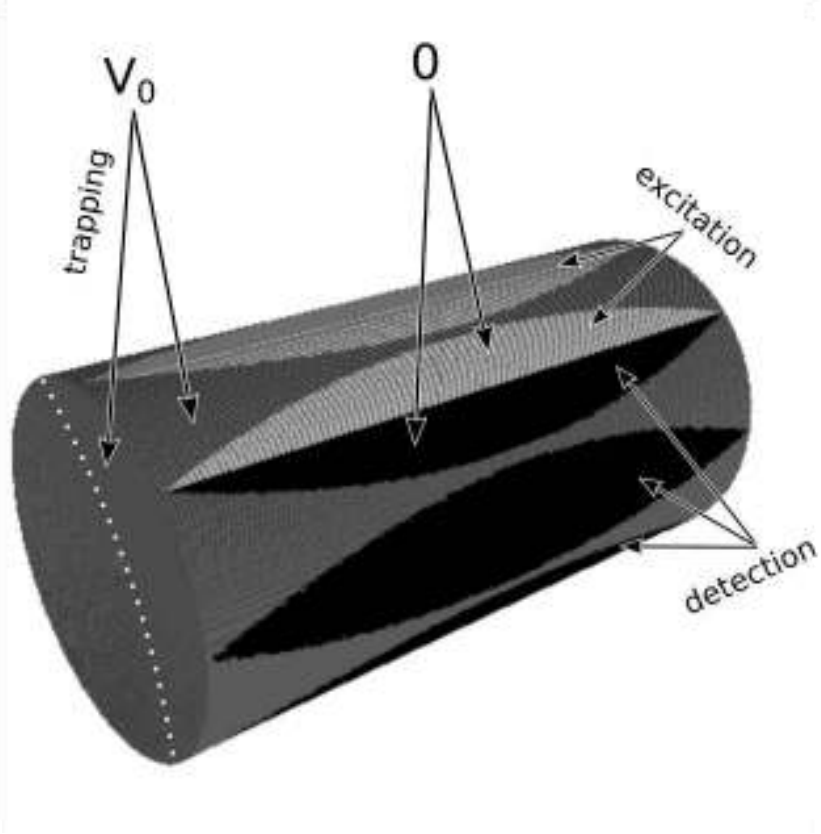

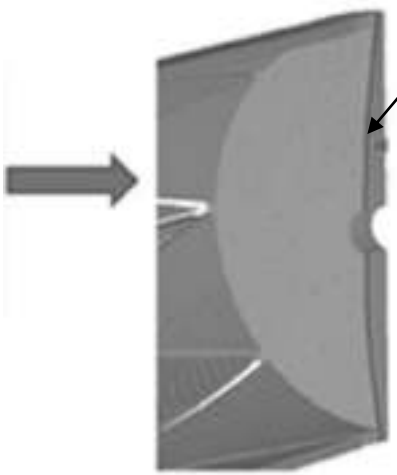

How to “open” dynamically harmonized cell?

It is easy to «Open» a simple Cylindrical Cell
Substituting flat trapping electrodes by cylinders

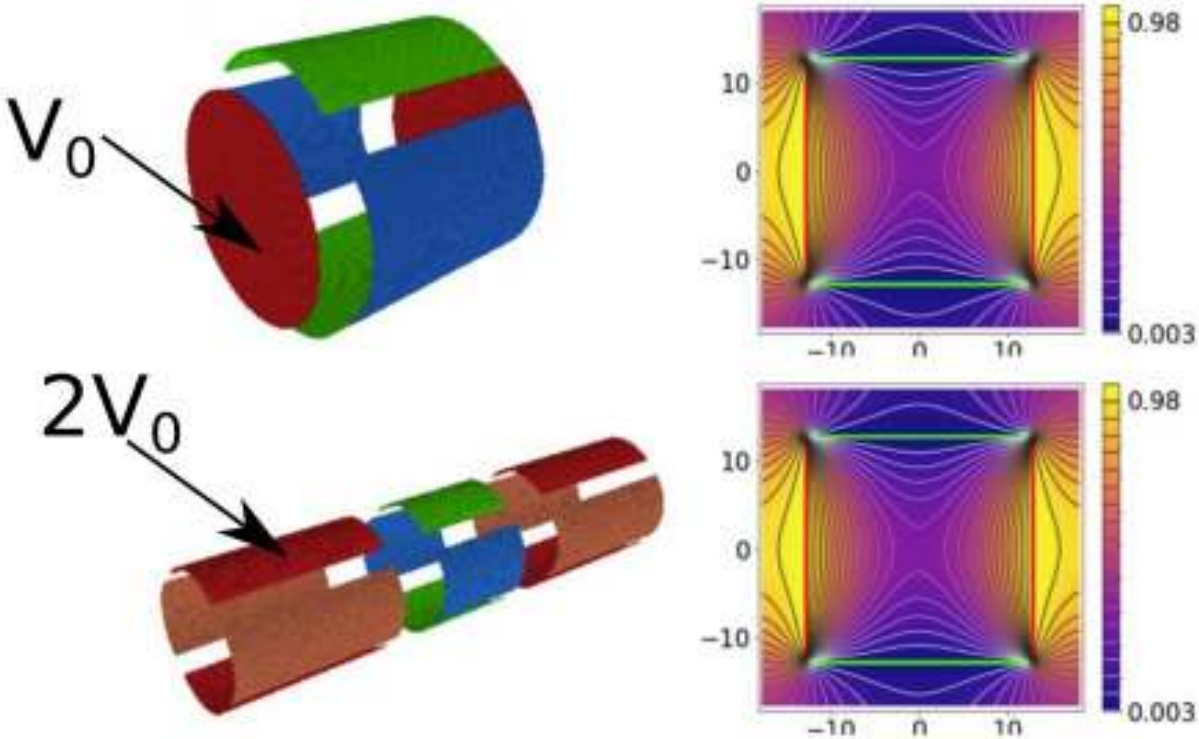

If we substitute in DHC the hyperbolic shape trapping electrodes by cylinders...

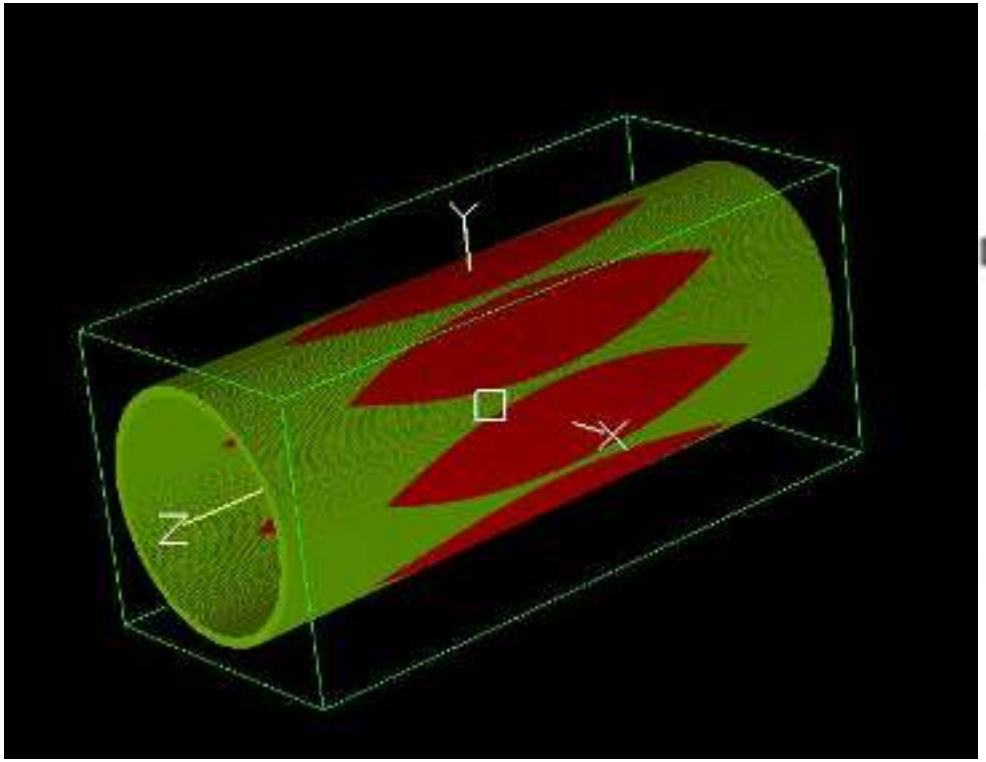

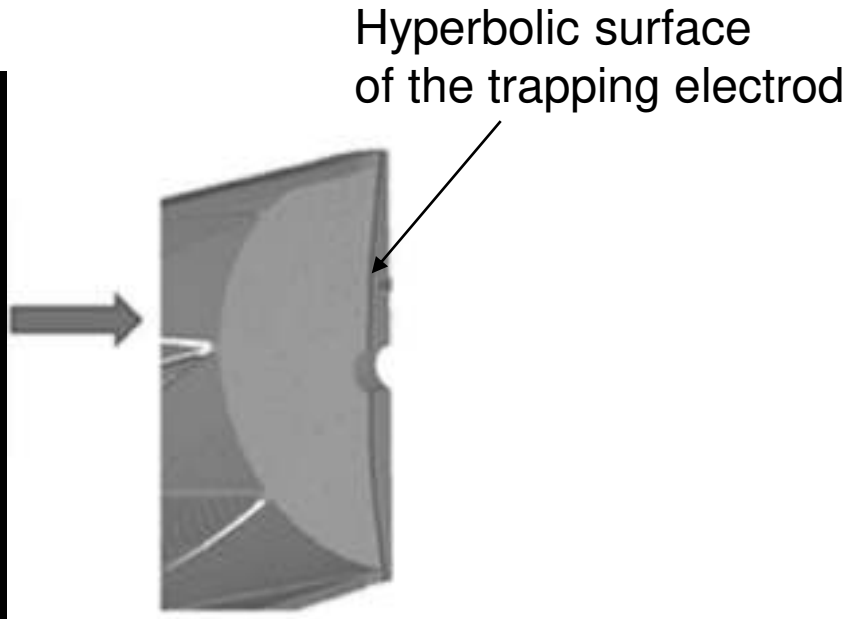

We will not obtain hyperbolic field inside the cell!

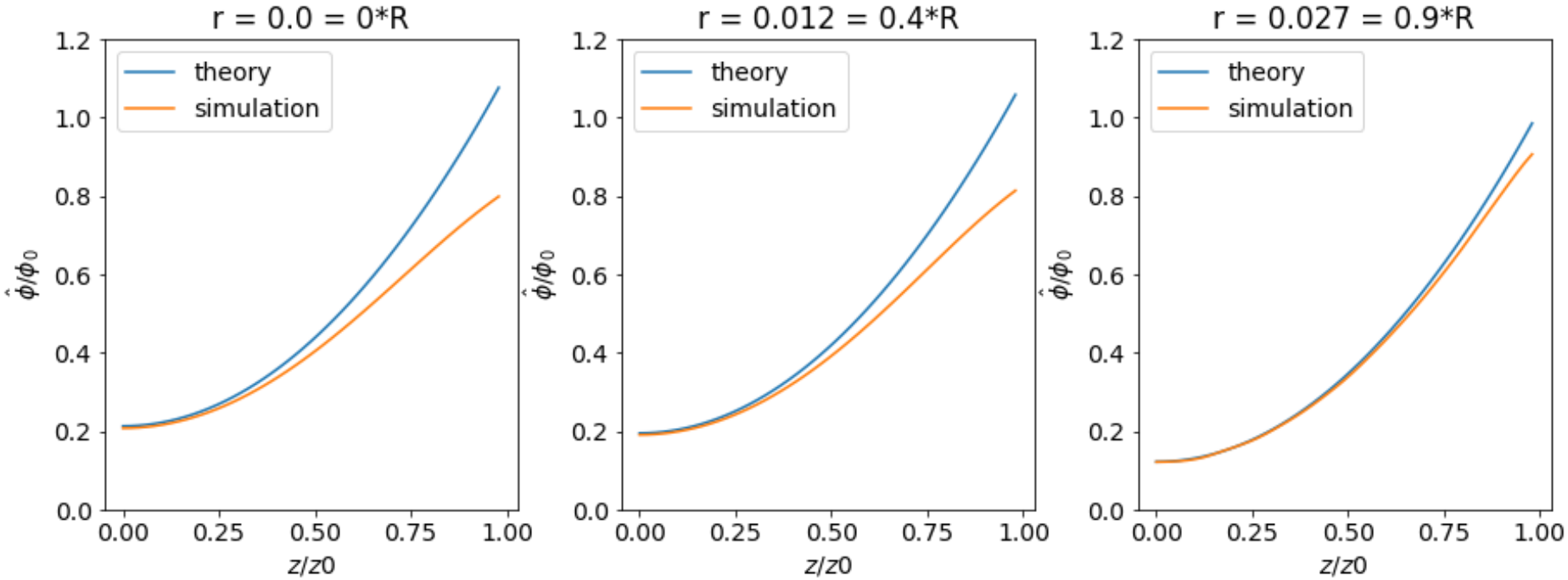

The 2D-unrolled electrode configuration for a closed DHC

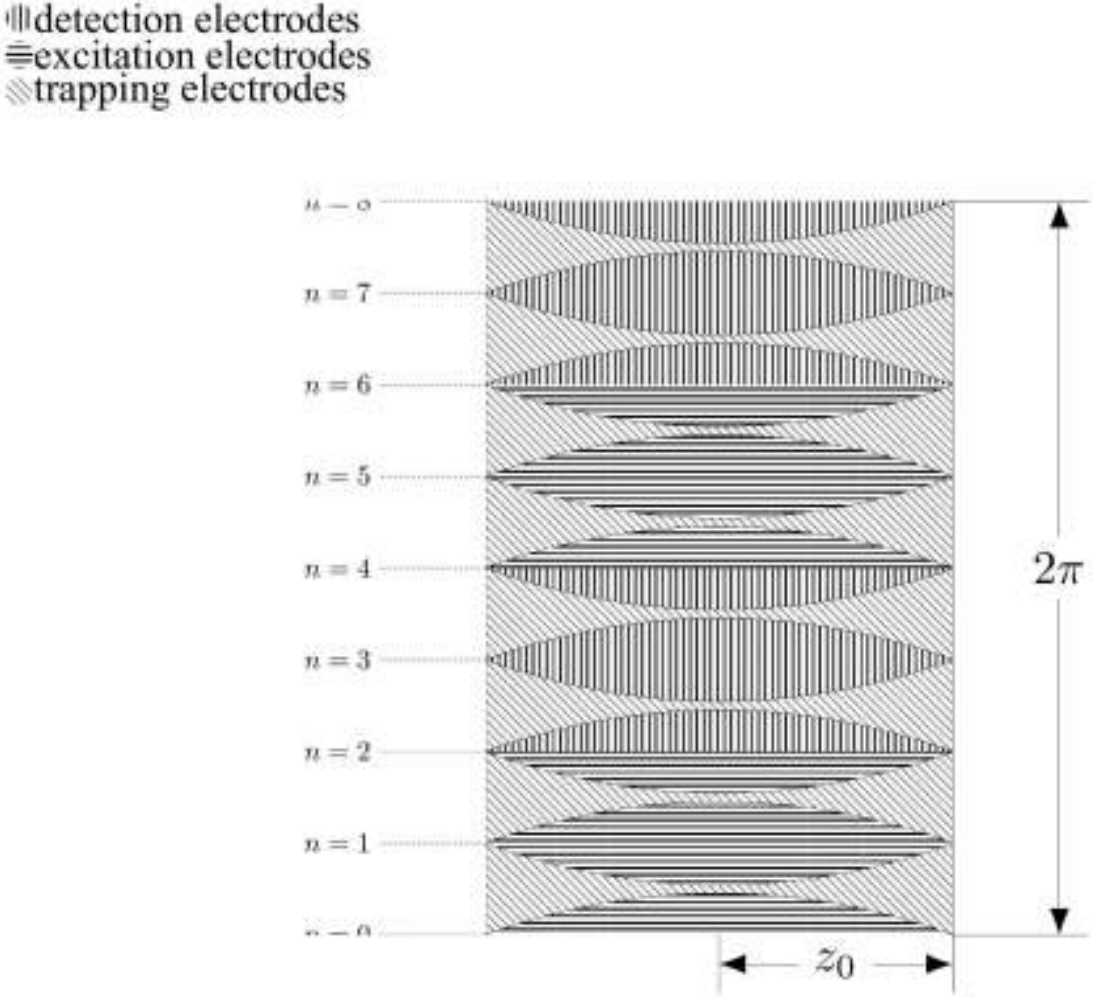

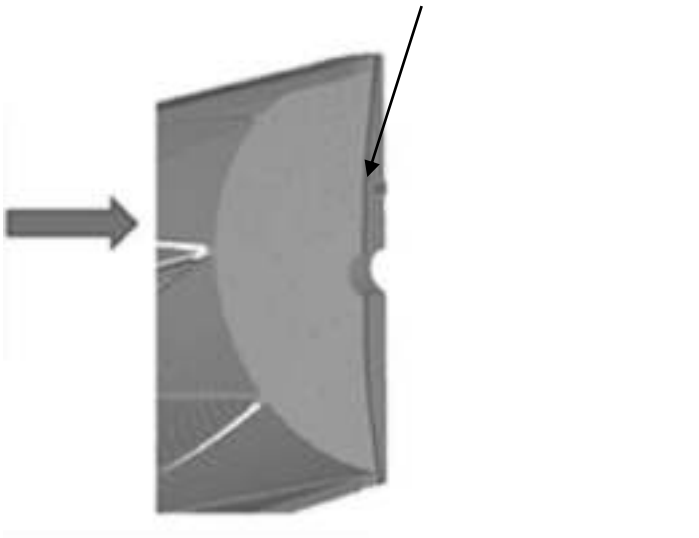

The 2D-unrolled electrode configuration for an ideal open DHC

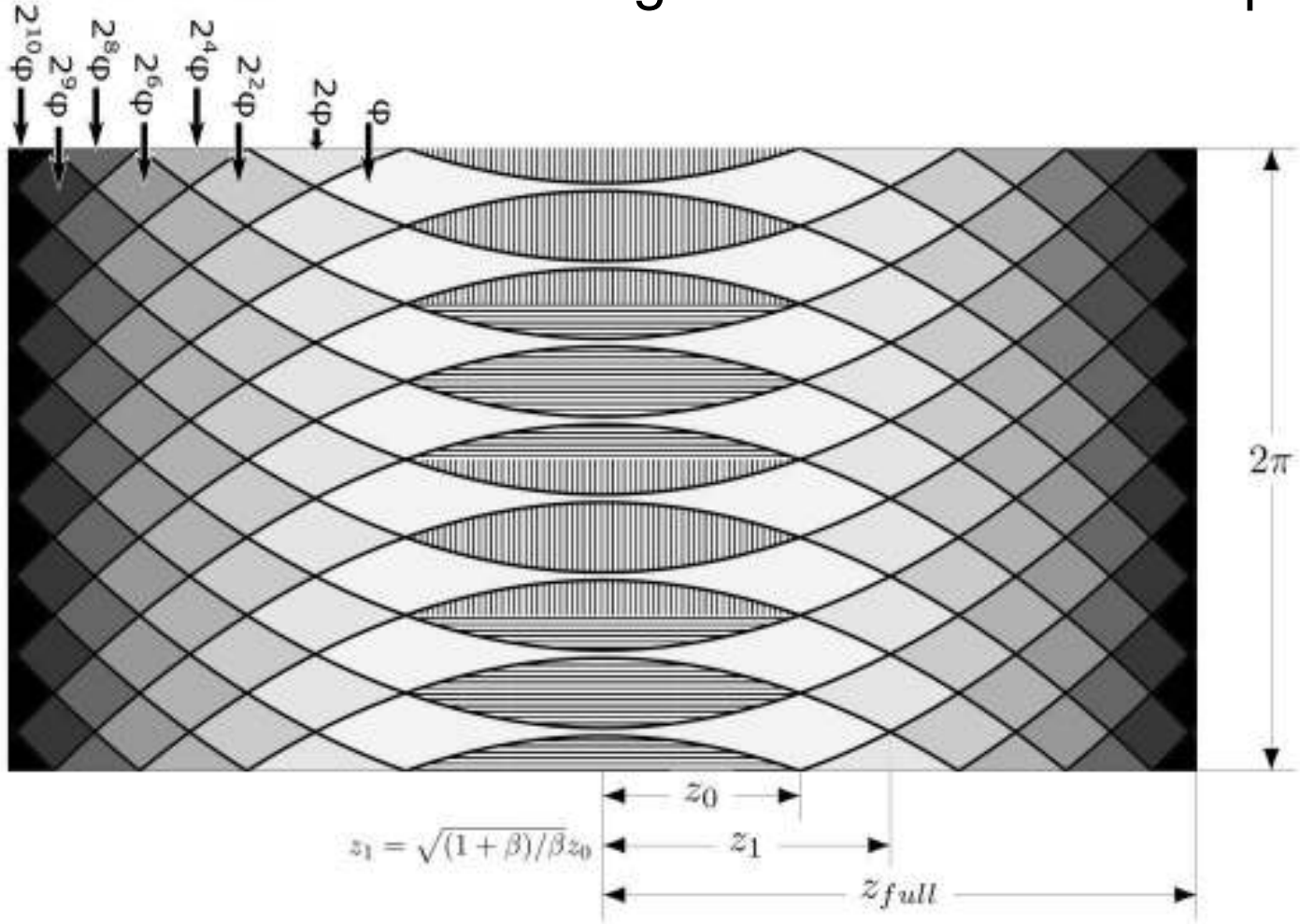

The 2D-unrolled electrode configuration for an ideal open DHC

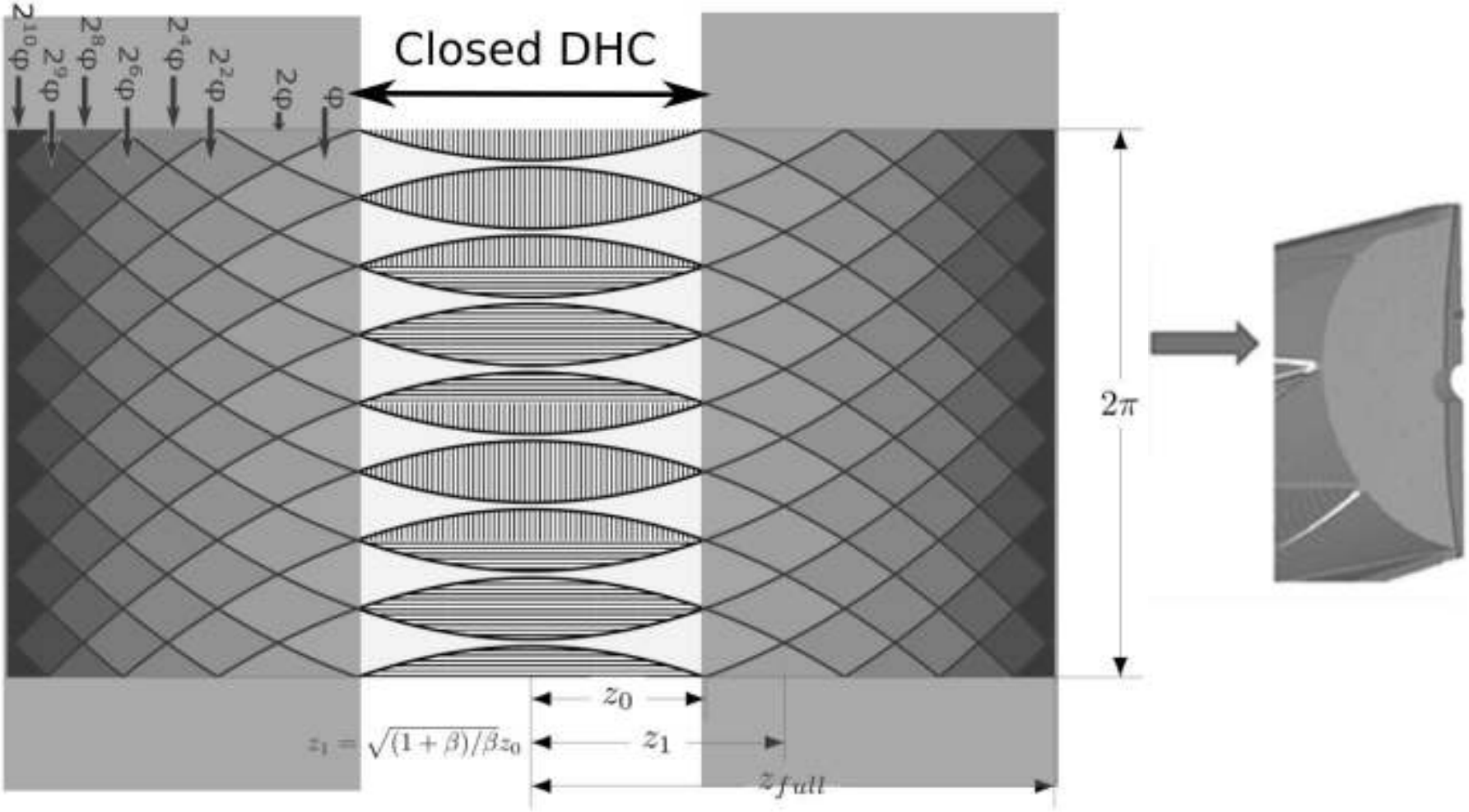

Reducing number of electrodes

- The set of electrodes shown above creates the needed field, but it is hard to build it.
- We have shown that the electrodes located far from the trap center has low effect on the field inside the working volume of the cell. Thus, we can merge all these electrodes into one.

The 2D-unrolled electrode configuration of realizable open DHC

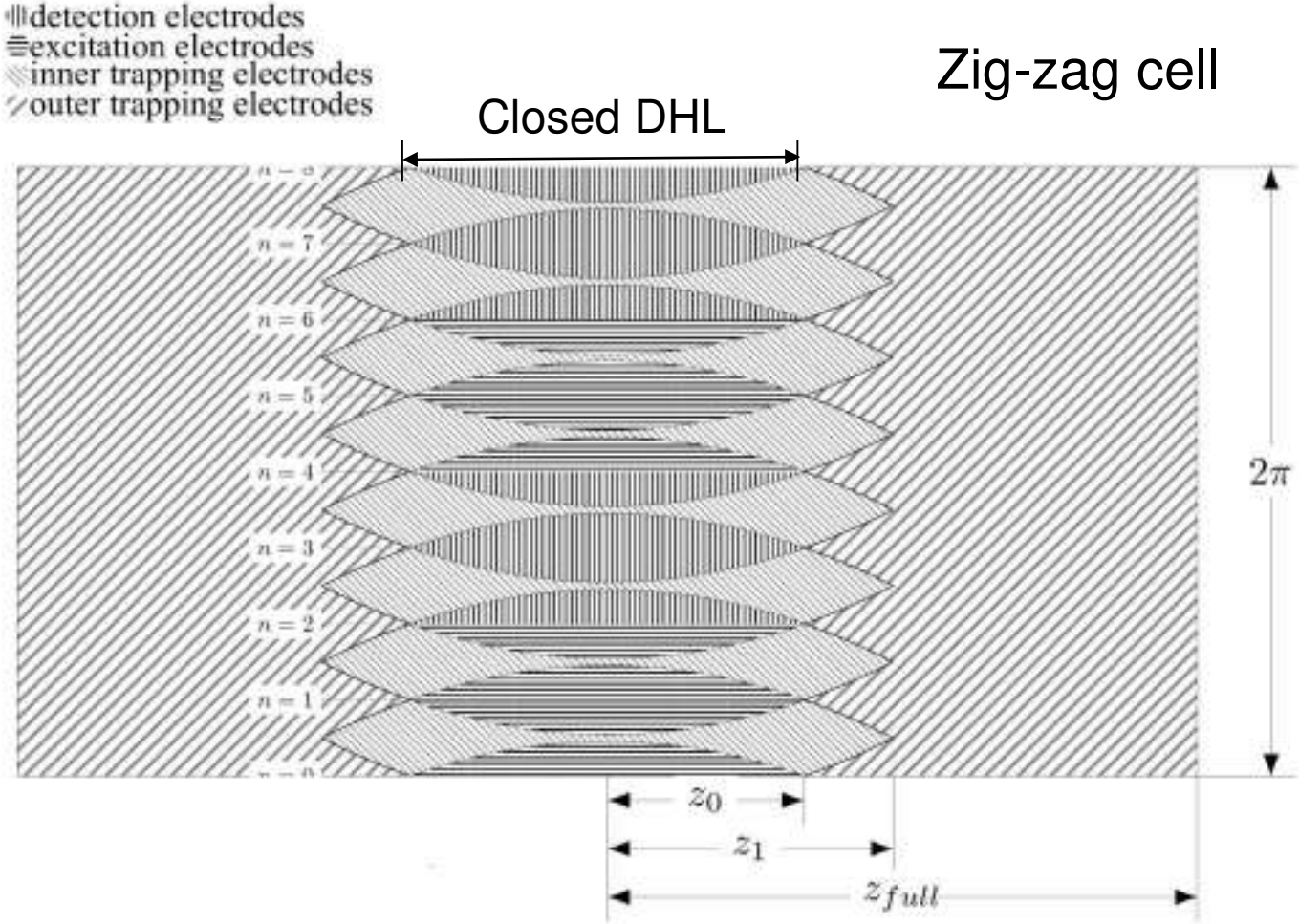

The ideal and simulated distribution of the electric potential inside the open DHC

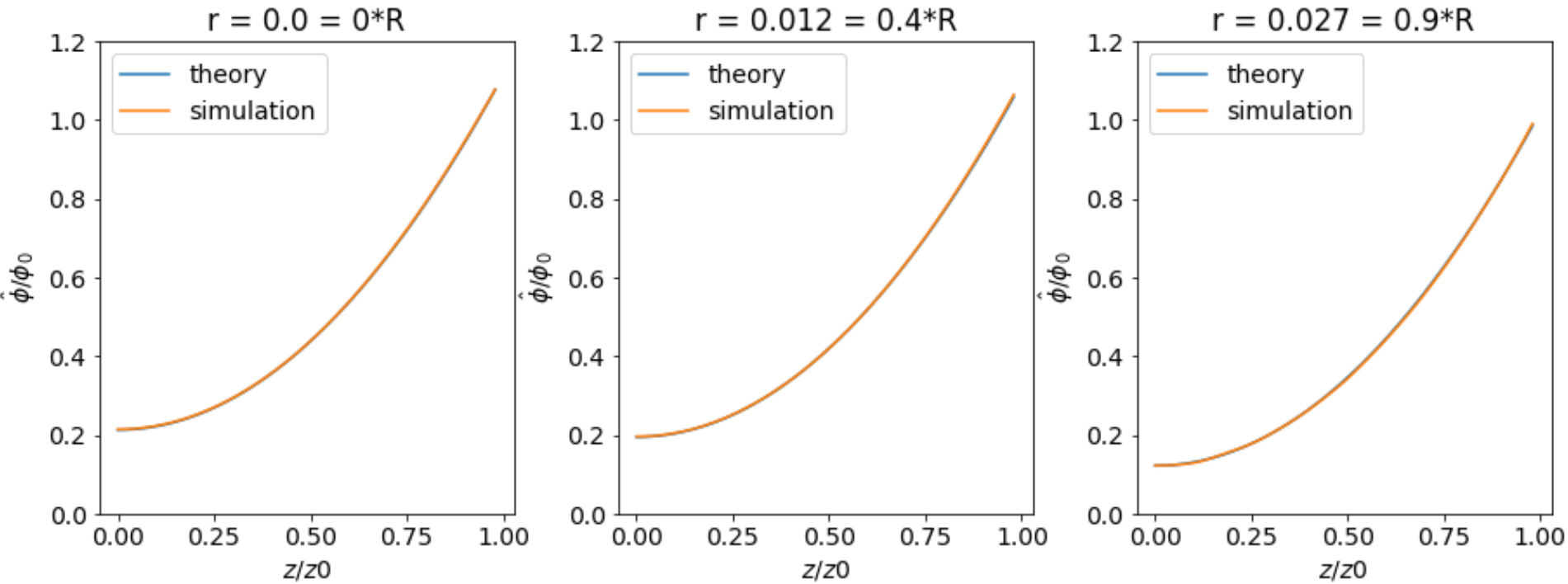

Z-component of electric field at different distance (r) from the cell axis

The deviations from the ideal field

The electric field distribution inside the Open Dynamically Harmonized «Zig-Zag» Cell is not absolutely ideal. But the field deviation is bellow numerical errors of simulations.

.

Tired of cells…

Is it possible to get rid of the cell as a **separate** element of FT ICR mass spectrometer?

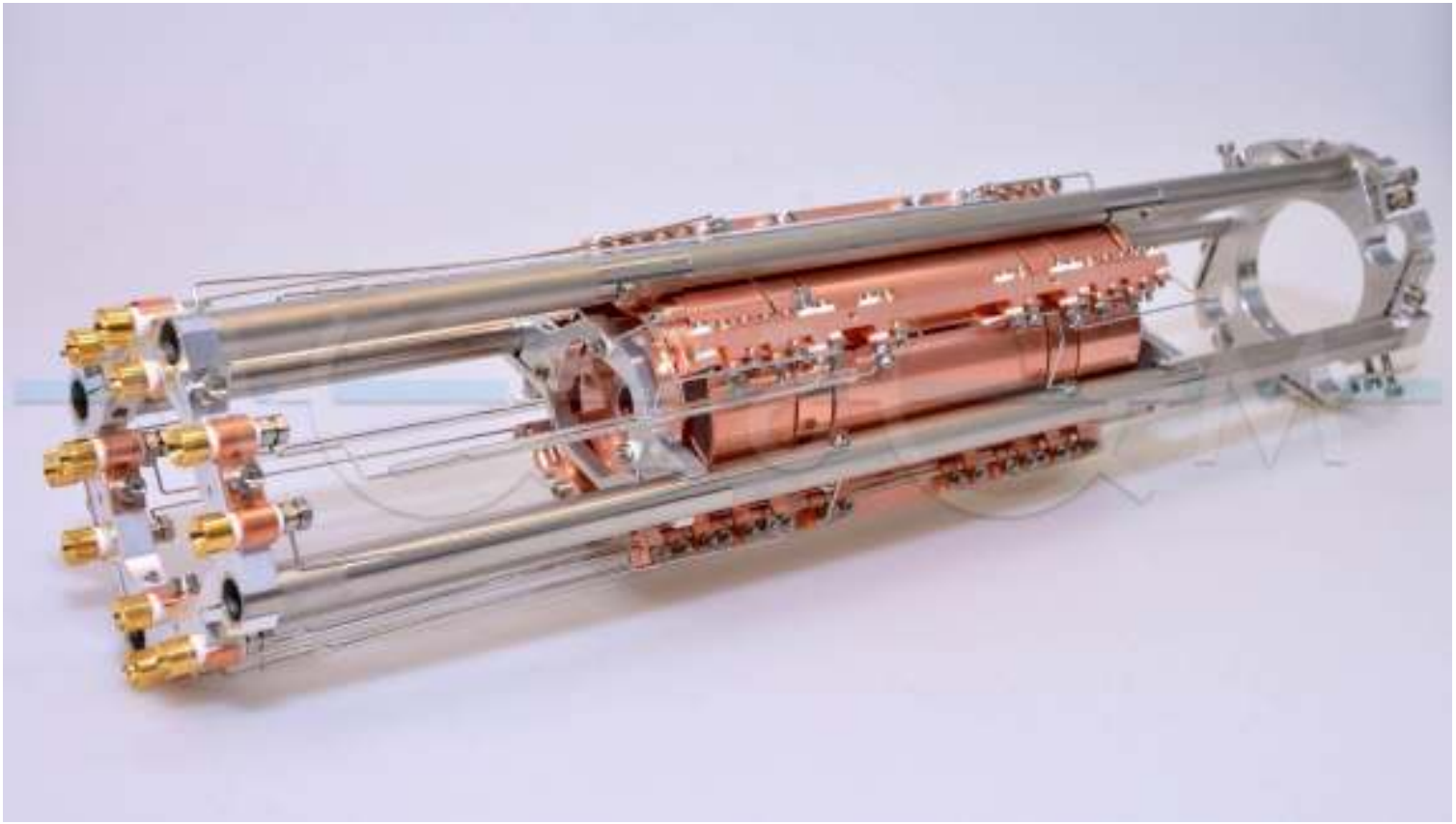

Trap walls are the walls of the vacuum chamber: Different geometries could be implemented

Open cylindrical cell

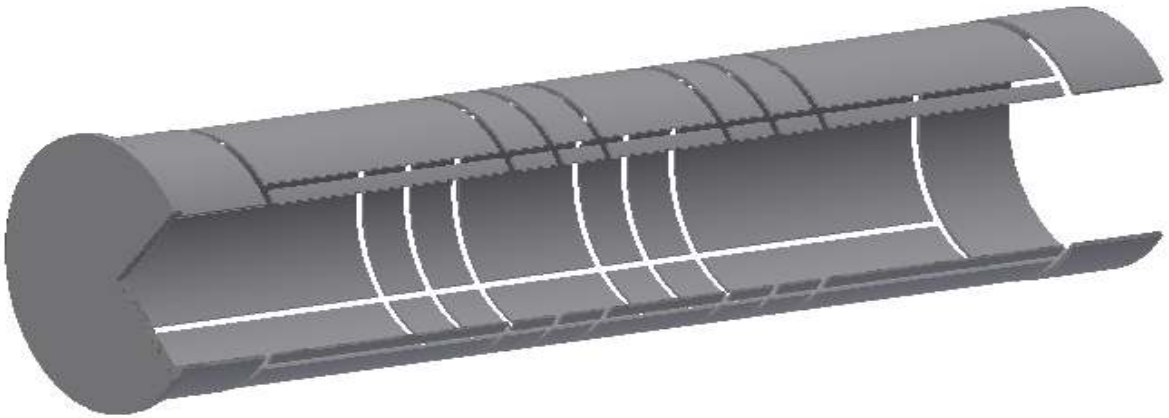

Open compensated cylindrical cell

Advantages of vacuum system wall imbedded cell

No feedthroughs (can apply voltages from outside)
No wires inside
Extremely low surface (only surfaces of the electrodes)
Easy to align to magnetic field
Low diameter of room temperature bore magnet could be used

Is it possible to incorporate an open DHC into the vacuum tube wall?

New Open DHC

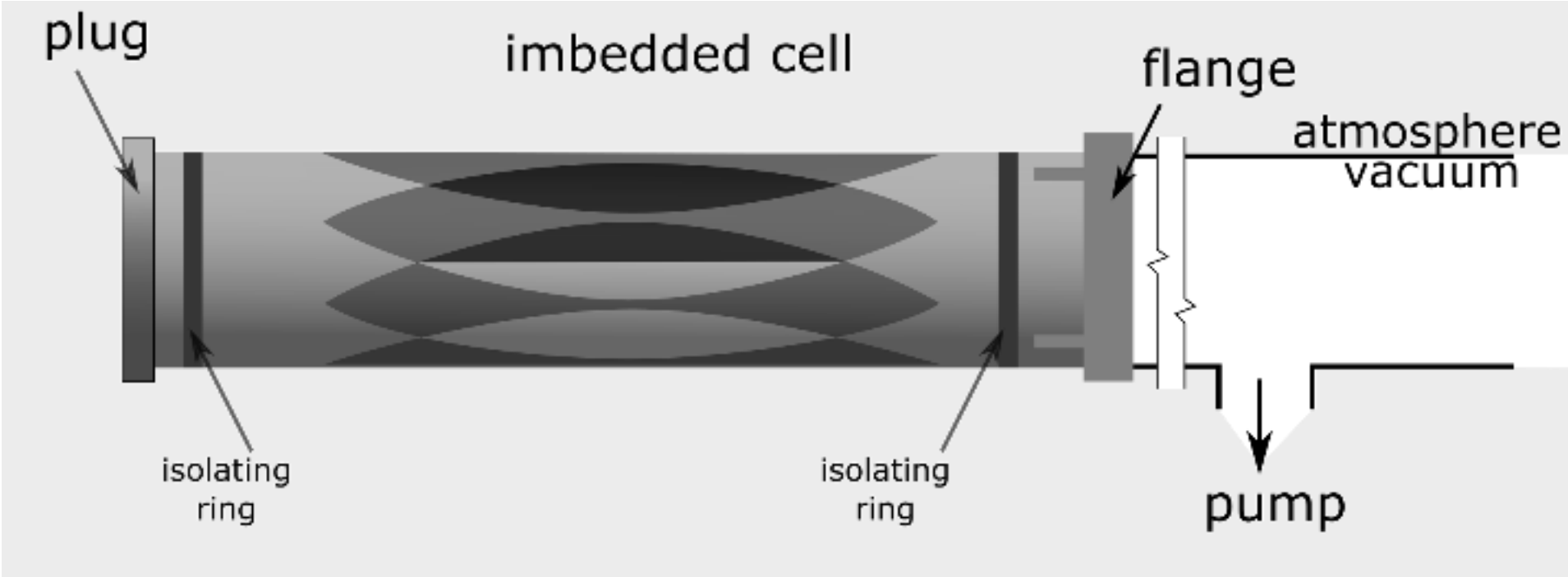
plug
imbedded cell
flange
atmosphere
vacuum
isolating
ring
isolating
ring
pump

The open dynamically harmonized cell could be made from a single cylinder

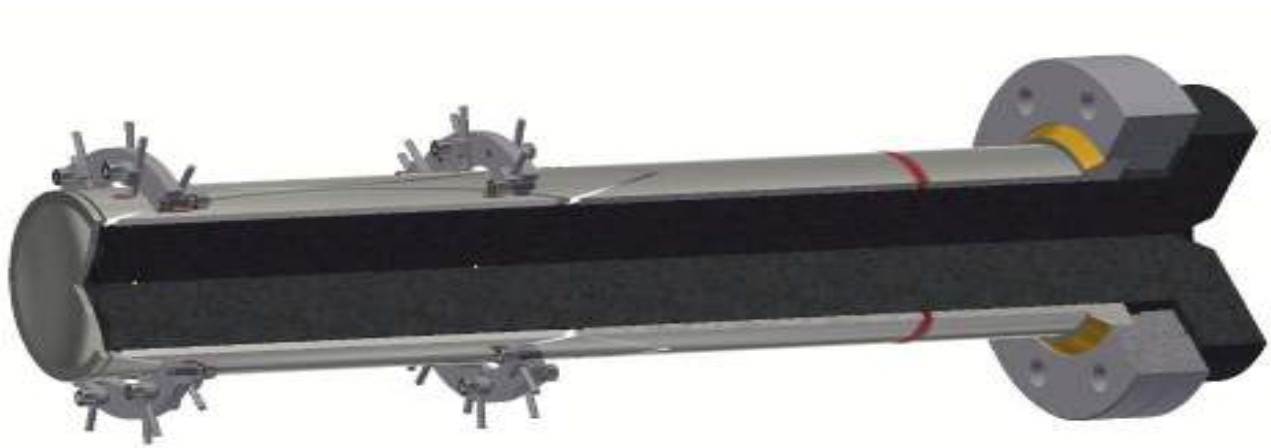

Spherical surface

The cell opened from one side

- Fabrication of ICR trap-vacuum chamber consists of the following steps
- 1) A titanium adapter for a CF63 flange is welded to a 62 mm diameter BT1-0 titanium tube
- 2) In certain places on the tube by means of contact welding, pieces of 2mm BT1-00cв titanium wire are welded
- 3) The pipe is cut into individual electrodes
- 4) Temporary fasteners are installed to hold the electrodes
- 5) A graphite insert is placed inside the pipe, and then the cut points are filled with a special ceramic powder. Then the billet is annealed in the furnace.

The voltage to the cell electrodes could be applied from outside

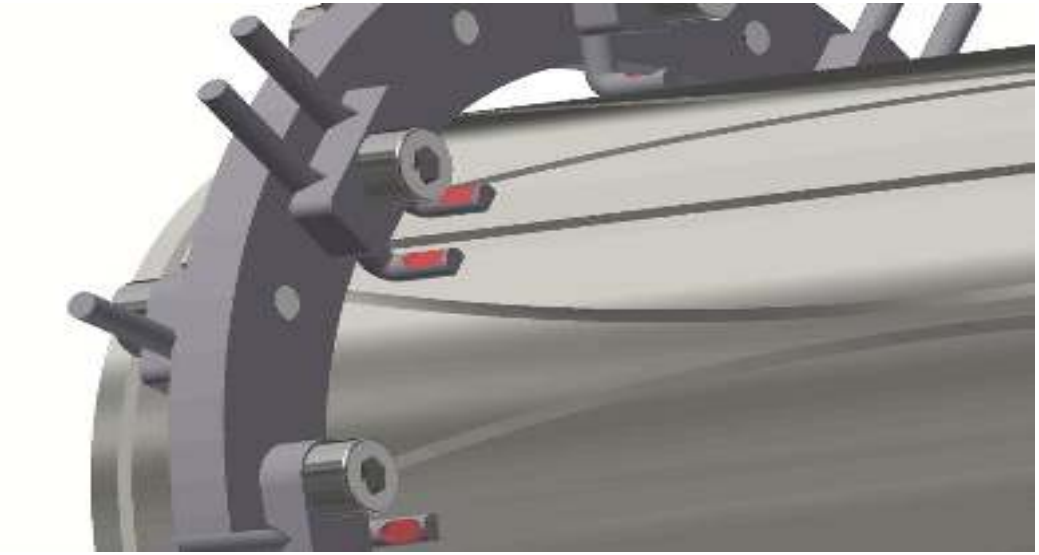

Amplifier could be installed directly on ICR trap using Flexible PCBs

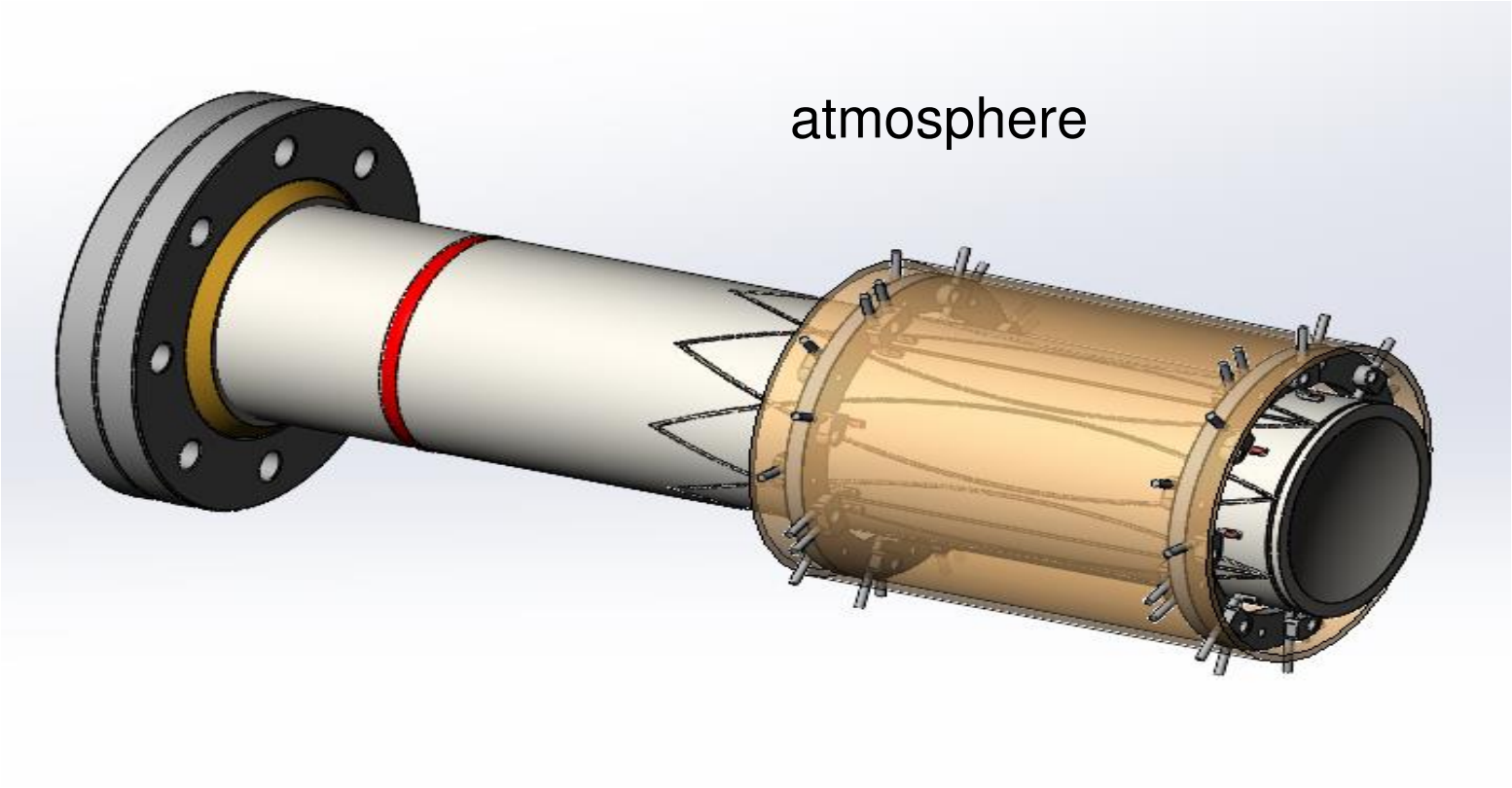

Open “atmospheric pressure” DHC

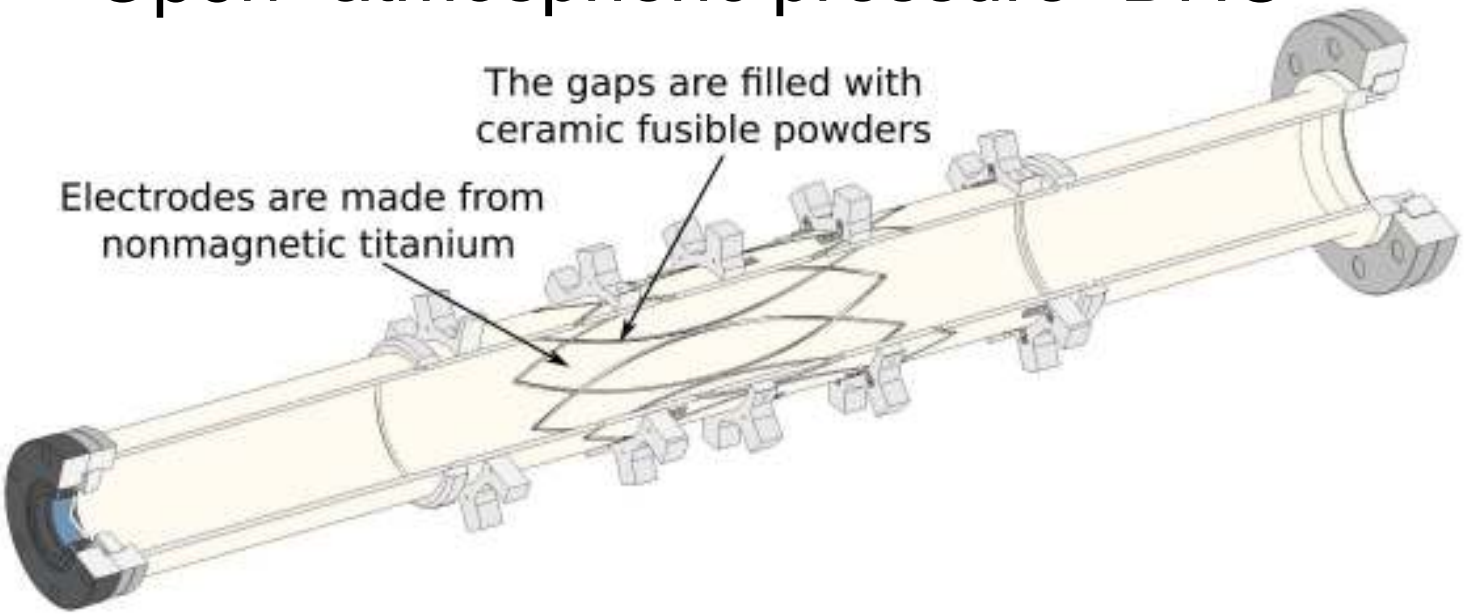

The titanium and the ceramics have the similar coefficient of thermal expansion, which allows annealing a vacuum system

Detection at multiple frequencies

Detection with more than two electrodes

4 electrode FT ICR cell dipolar detection

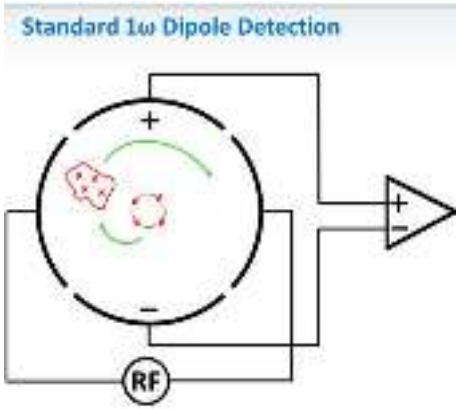

$\omega_{signal} = \omega_{cyclotron}$

4 electrode FT ICR cell quadrupolar detection

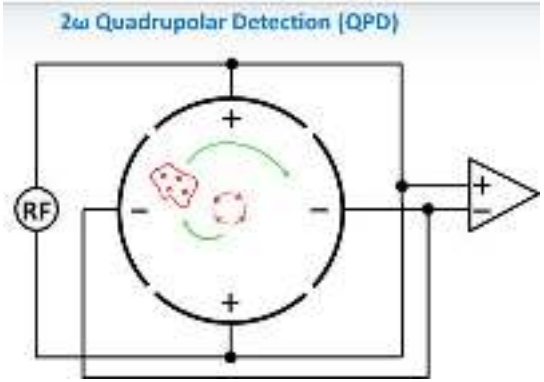

$\omega_{signal} = 2*\omega_{cyclotron}$

Double resolution or double speed

2N electrode FT ICR cell multipolar detection

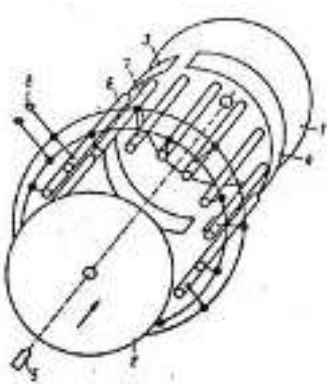

$\omega_{signal} = N*\omega_{cyclotron}$

N times higher resolution or speed

Detection on multiplied frequencies and on harmonics

$R = \omega / \Delta\omega$

$\Delta\omega \sim 1/T$

T is signal duration

If $\omega' = n * \omega$, $R' = n * R$

SU 1307492 A1

ОПИСАНИЕ ИЗОБРЕТЕНИЯ

К АВТОРСКОМУ СВИДЕТЕЛЬСТВУ

Soviet Union patent
Priority 05.07.1985
Nikolaev, Gorshkov, Mordehai, Talroze
Multi-electrode detection FT ICR cell

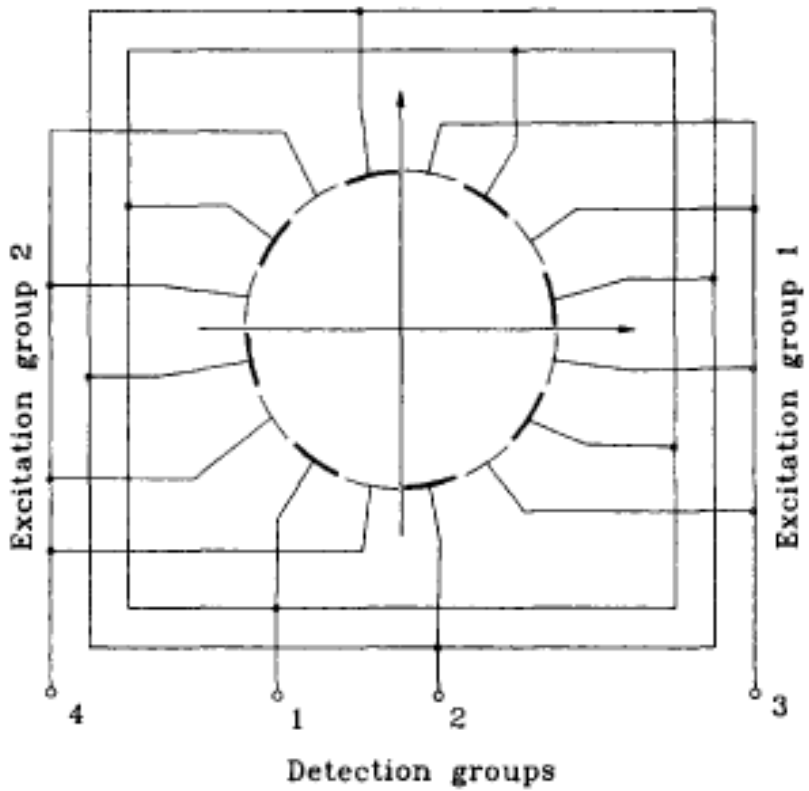

E.N. Nikolaev, M.V. Gorshkov, A.V. Mordehai and V.L. Talrose, Rapid Communications in Mass Spectrometry, 4 (1990) 144.

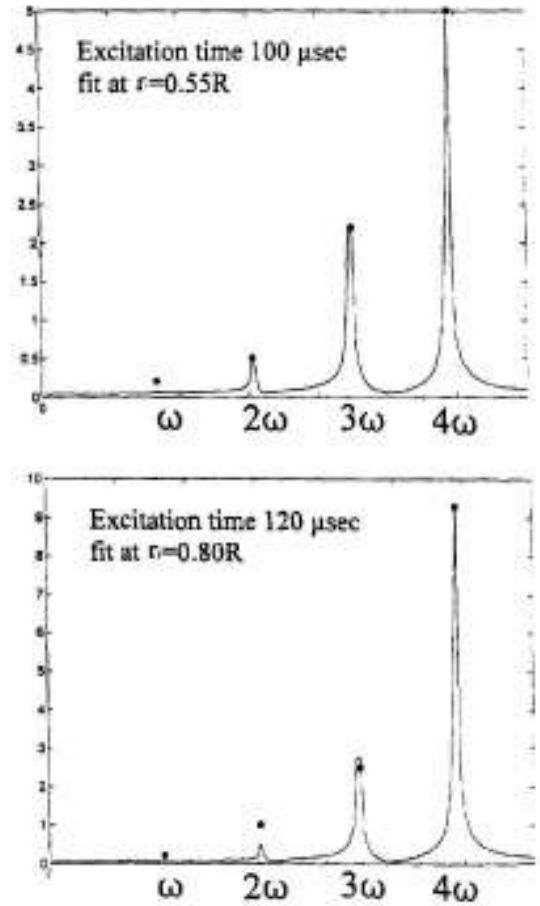

Fig. 11. Simulation for 16-electrode cell shown in . Cells radius $R = 1$. •, experimental amplitudes obtained in [7] for first four harmonics; ———, the result of computer simulation for fixed cyclotron radius, $\rho = 0.1$ and several magnetron radii. Correlation between excitation time and magnetron radius is pronounced.

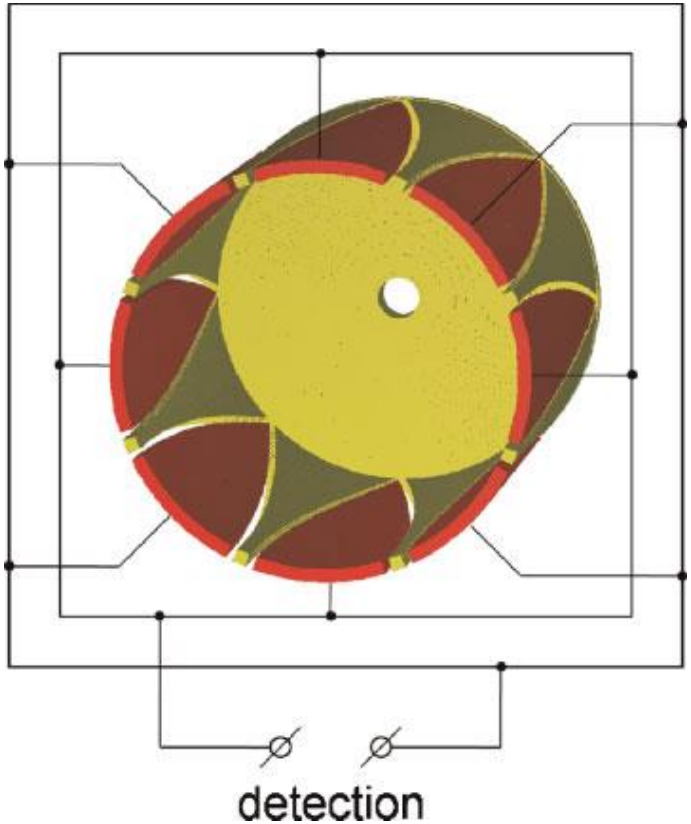

$$\omega_{signal} = 4^{*}\omega_{cyclotron}$$

Spectral Acquisition at 3Ω (14.5 T)

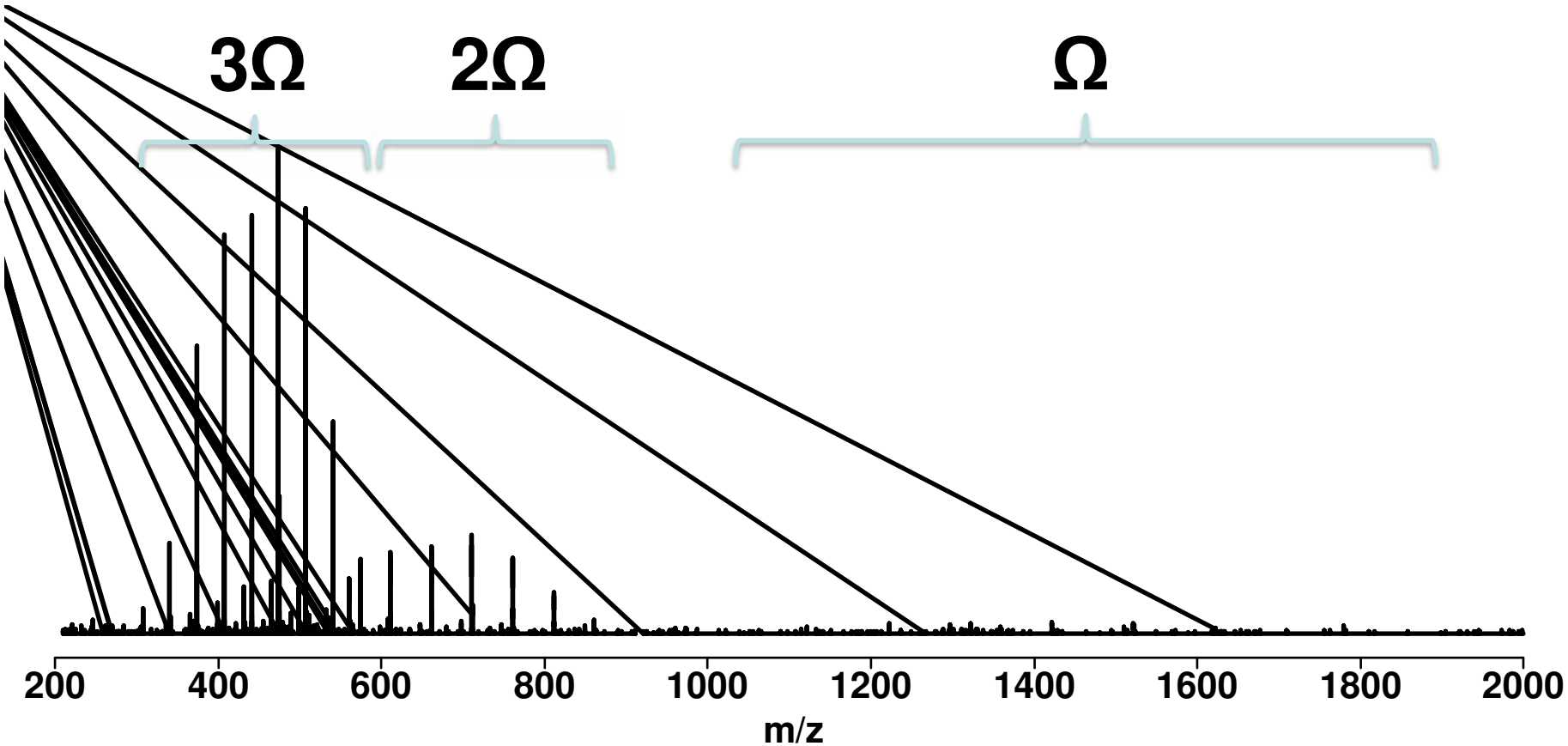

Alan Marshall 13th European FT MS Workshop (Freising)
26 April, 2018

3 Ω Detection Geometry

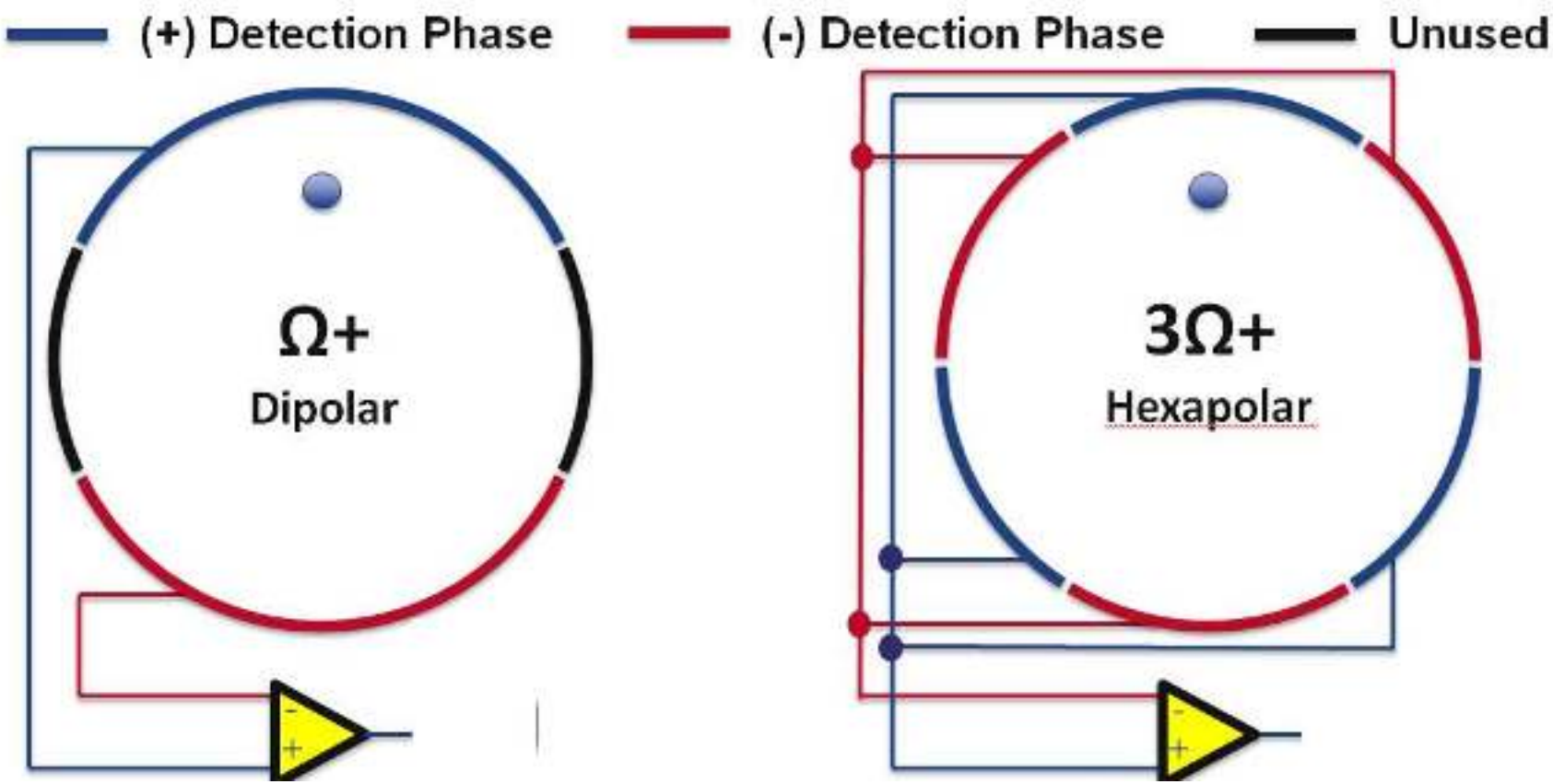

Alan Marshall 13th European FT MS Workshop (Freising) 26 April, 2018

Thank you!

Acknowledgement to

HORIZON 2020 FT ICR network programm

Petroleomics

From crude oil to asphaltenes

Dr. Matthias Witt, Senior Scientist MRMS, Bruker Daltonics GmbH & Co. KG, Bremen, Germany

Content

Content
Introduction
LDI in Petroleomics
Oil mixtures
Asphaltene fractions
Hydroprocessing
Continuum of Petroleum
Fractionation of Material
Structures of asphaltene molecules
Bio-oil analysis
Effect of Maturity
Improving S/N and mass resolution

Introduction

Introduction

Upstream, Midstream and Downstream

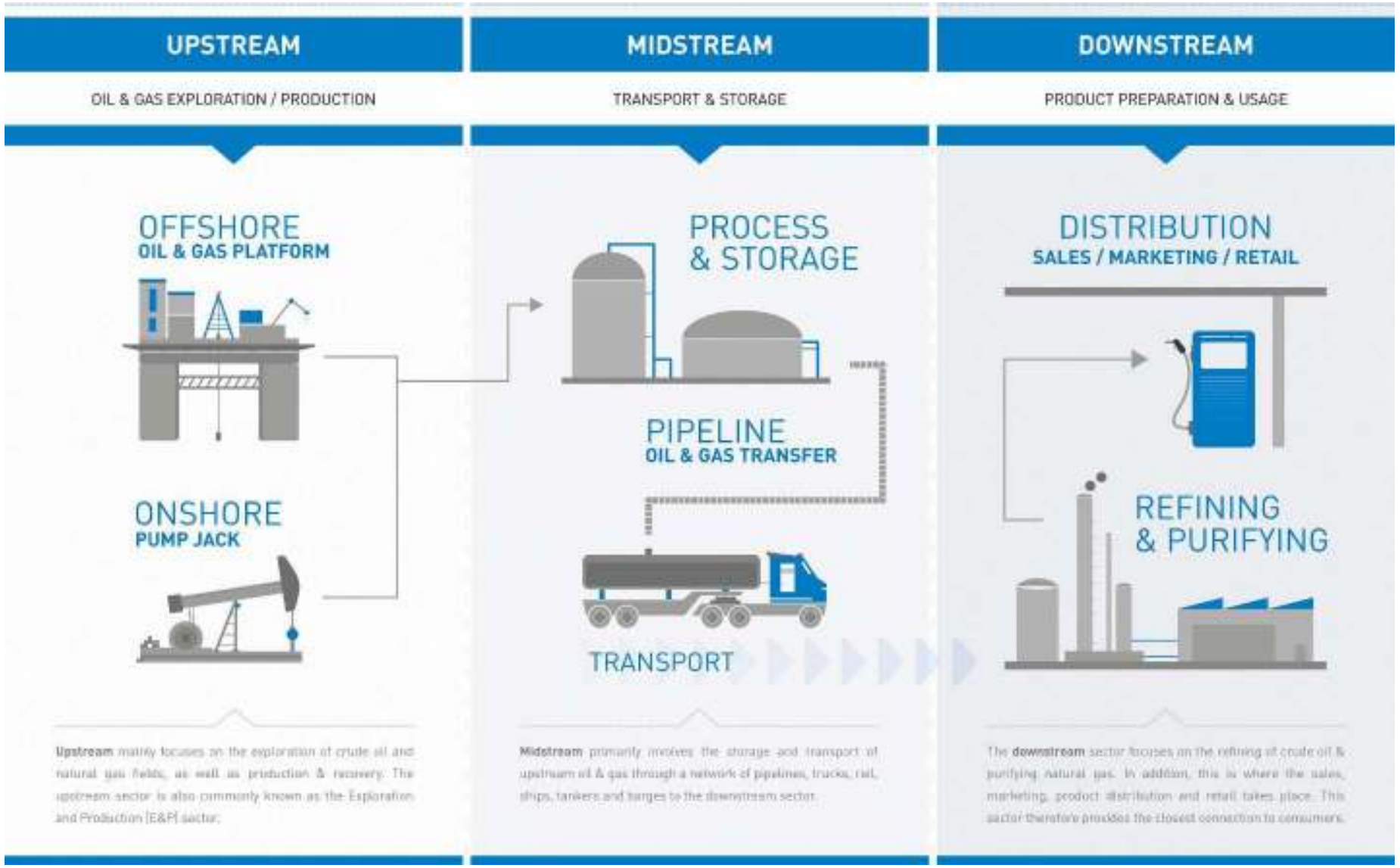

https://www.ecom-ex.com/de/loesungen/branchen/oel-und-gasindustrie/

Introduction

Petroleum products – different cuts

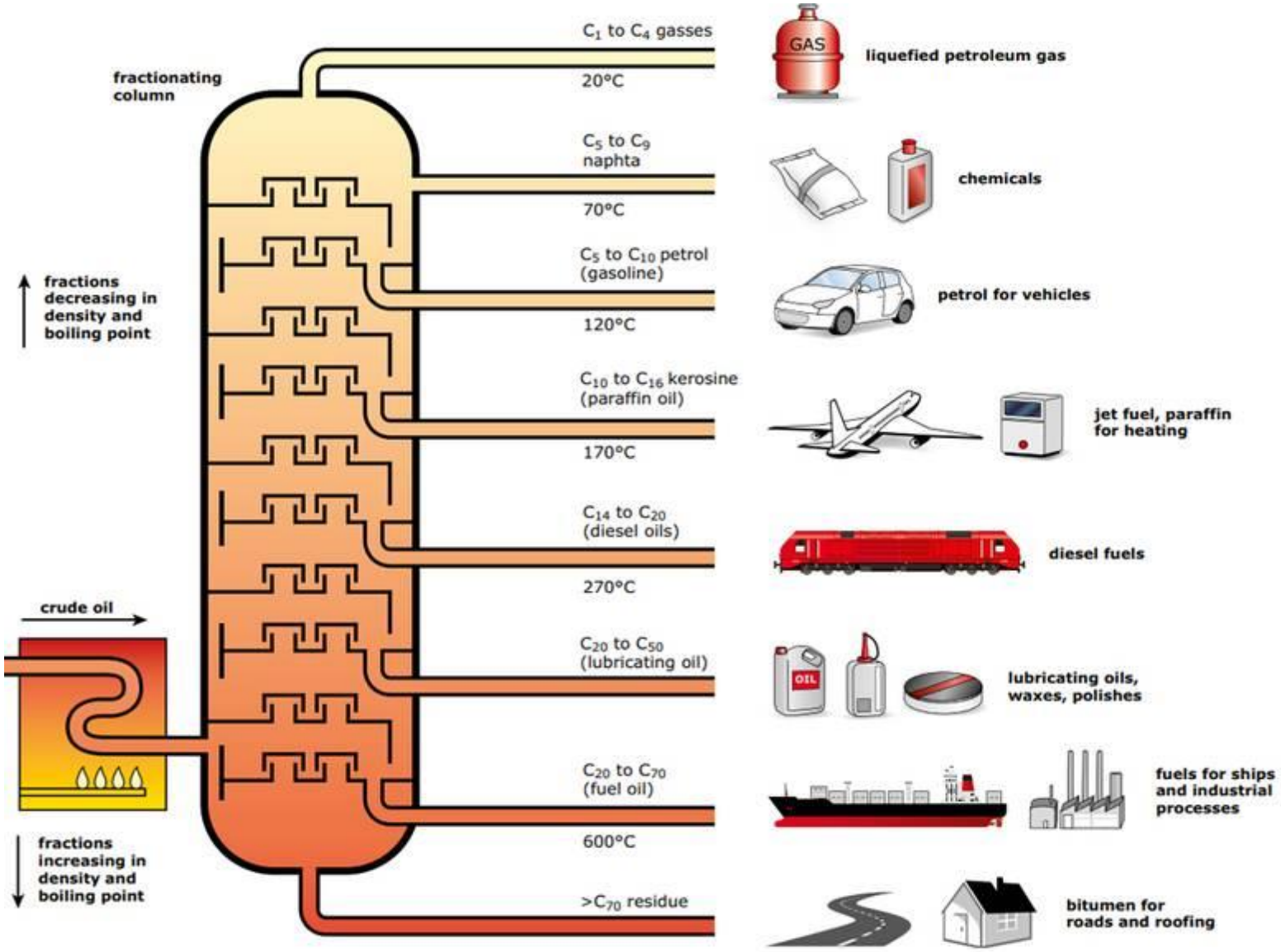

Introduction

Effect of molecular structure on boiling point

Boduszynski Continuum Model

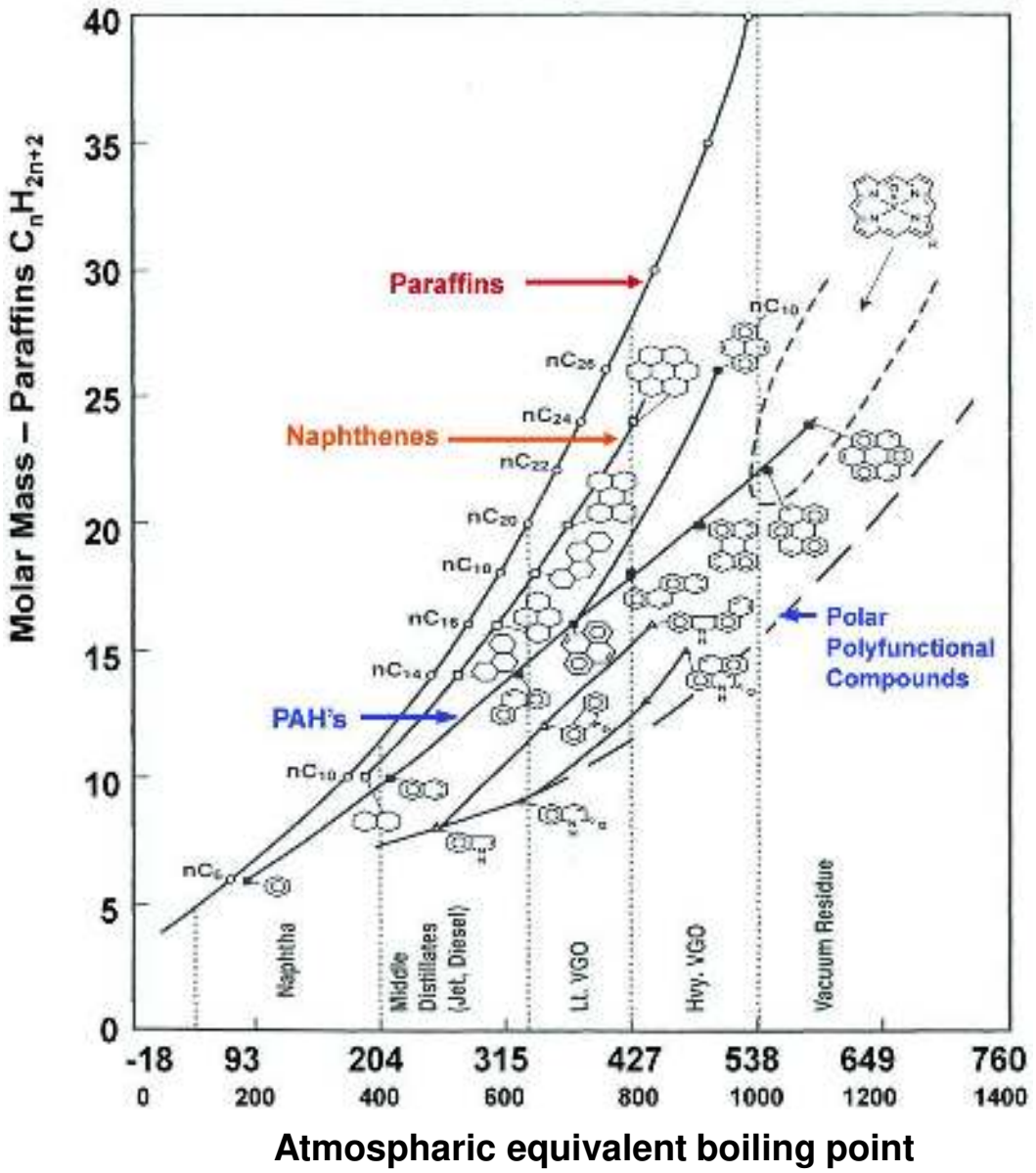

M. Boduszynski, Energy & Fuels 1987, 1, 2-11. *(1st paper in E&F)*

Introduction

SARA Fractionation

K. Akbarzadeh et al., Oilfield Review, Asphaltenes - Problematic but Rich in Potential, 2007.

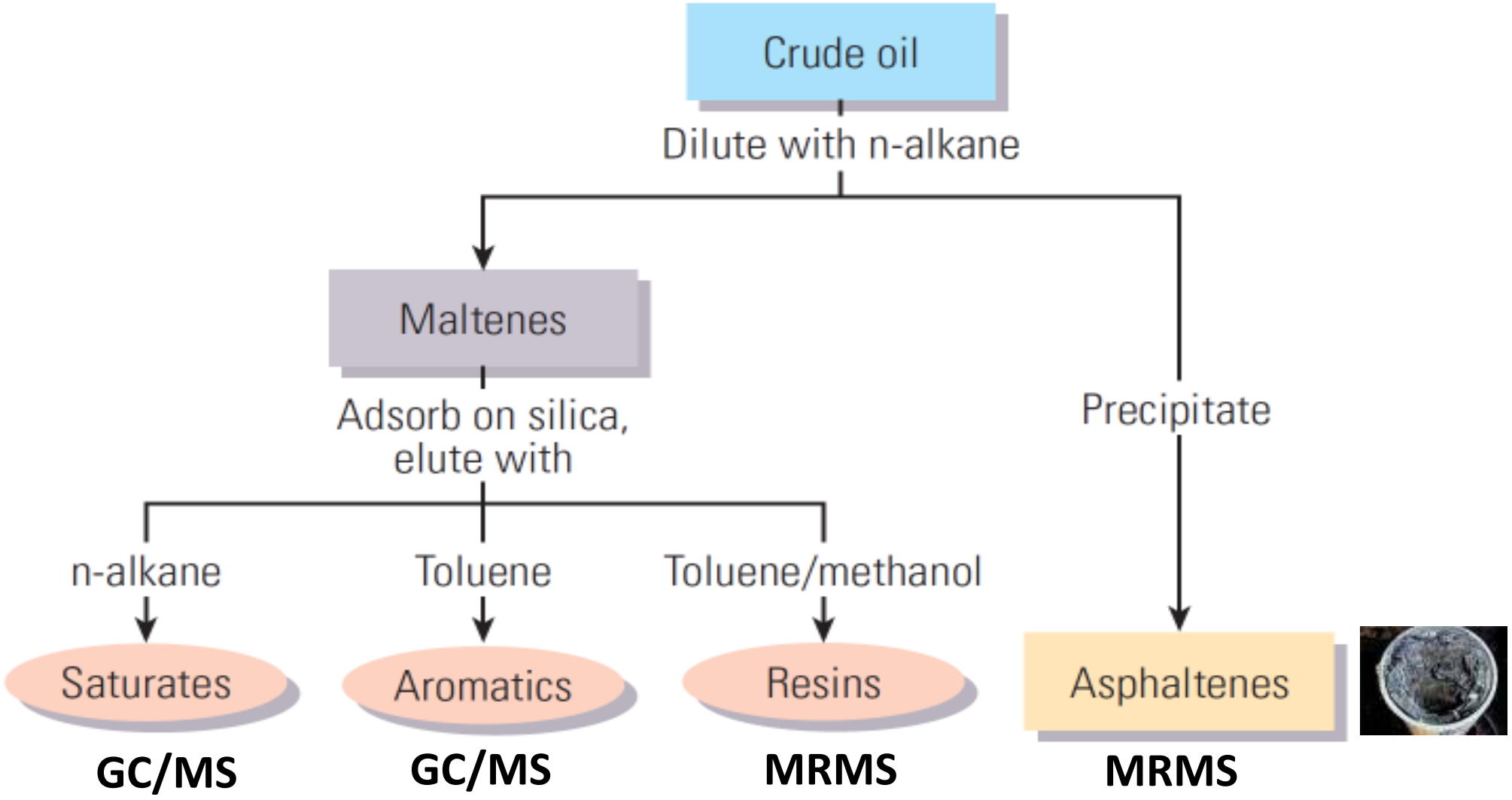

Introduction

Mass resolution and mass accuracy

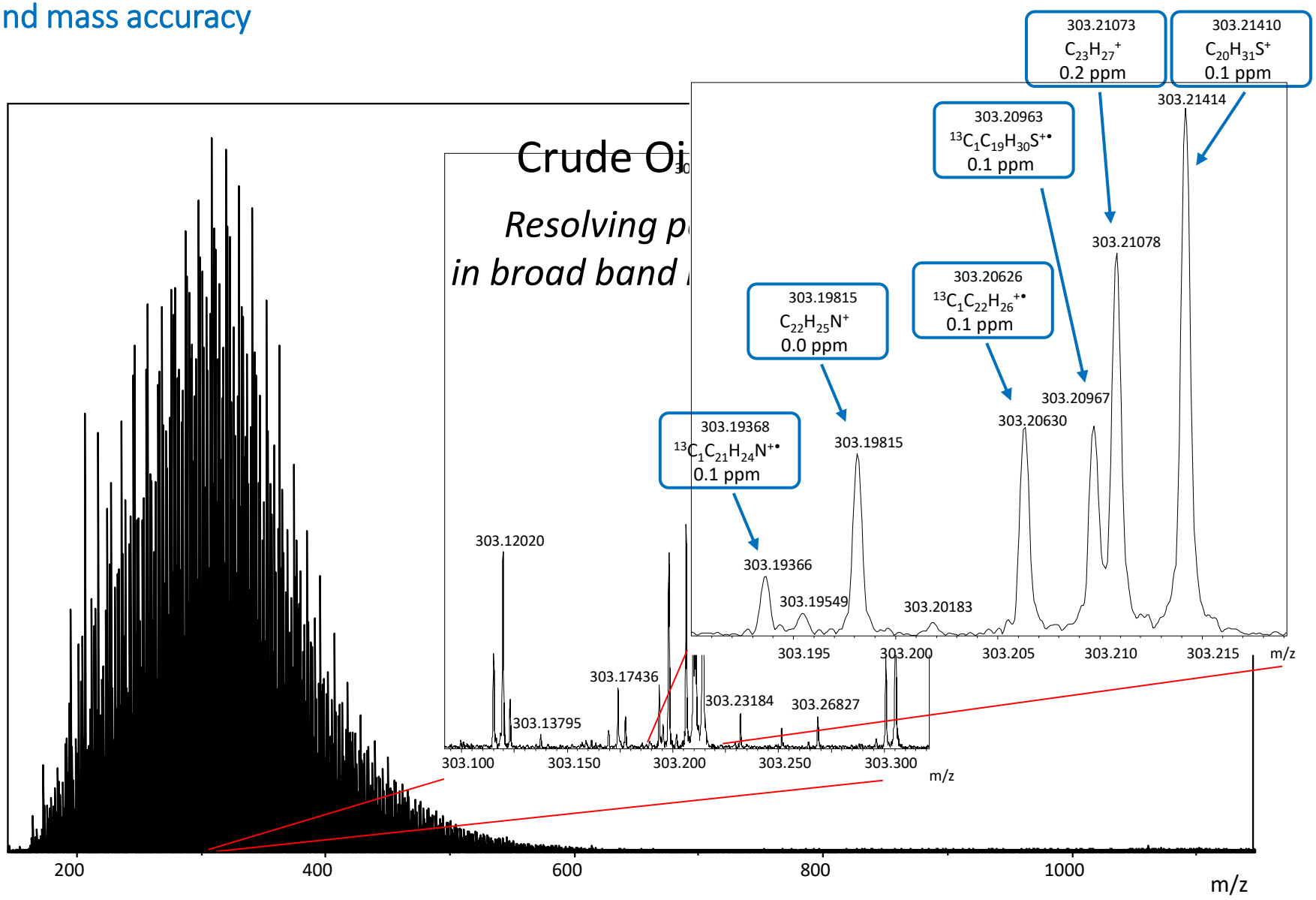

Introduction

Isotopic fine structure (IFS)

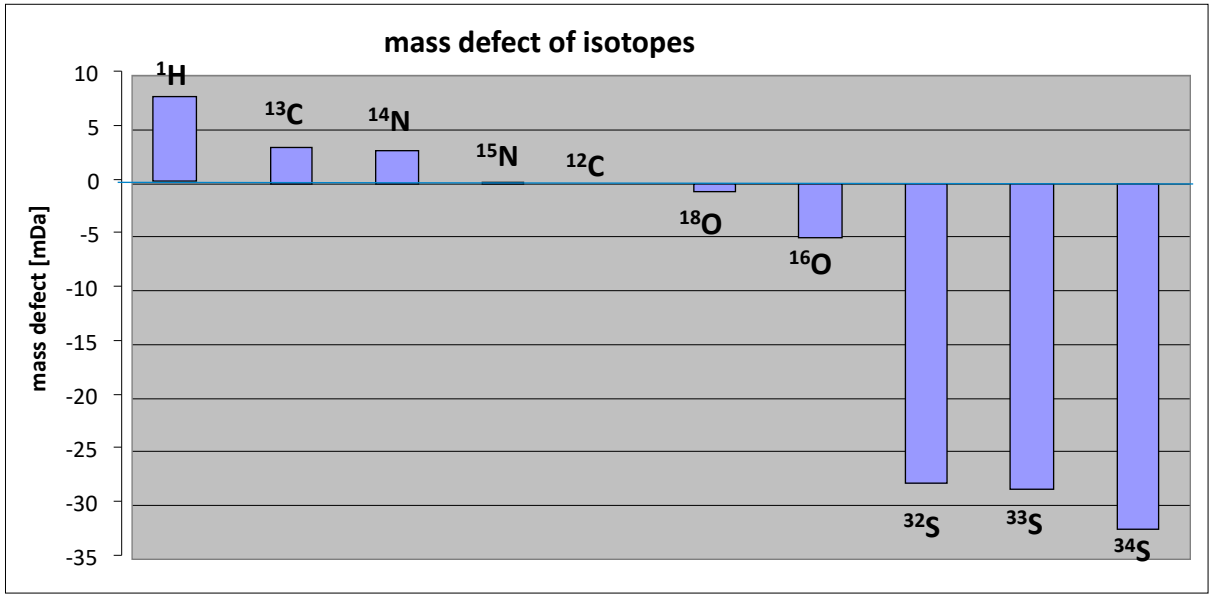

Δm (C_3;SH_4): 3.4 mDa

Δm ($^{13}C_2$;CN): 3.6 mDa

Δm (^{13}C;CH): 4.5 mDa

Δm (C_4H;$^{13}CSH_4$): 1.1 mDa

$\Delta m(^{32}S;^{34}S)$ = 1.9959 Da

$\Delta m(^{12}C_2;^{13}C_2)$ = 2.0067 Da

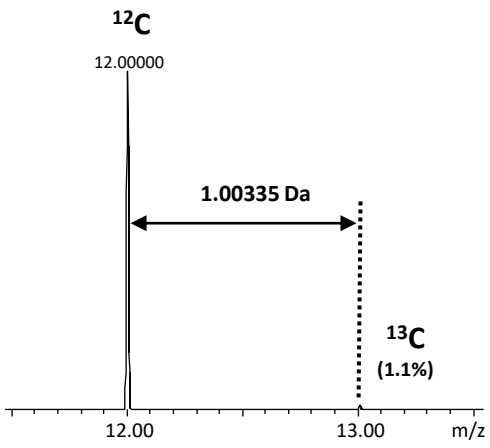

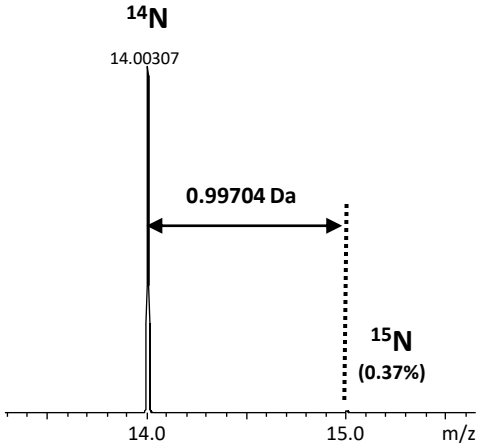

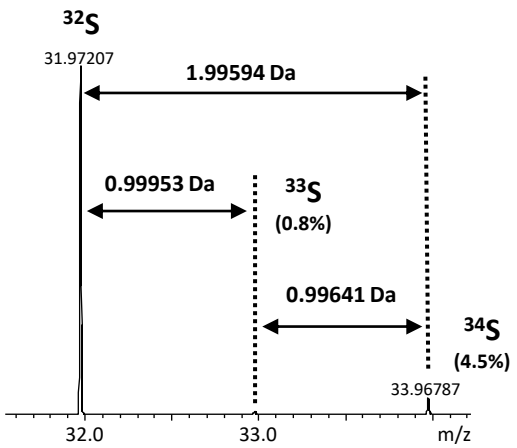

Introduction

Processing workflow in Petroleomics using PetroOrg

Internal recalibration

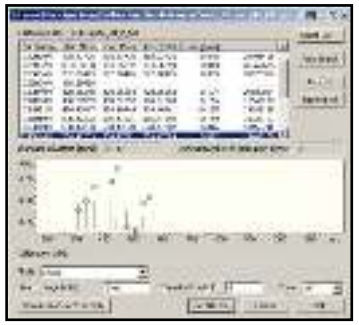

Export mass spectrum

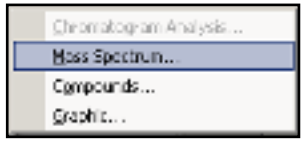

PetroOrg software
Molecular Formula calculation

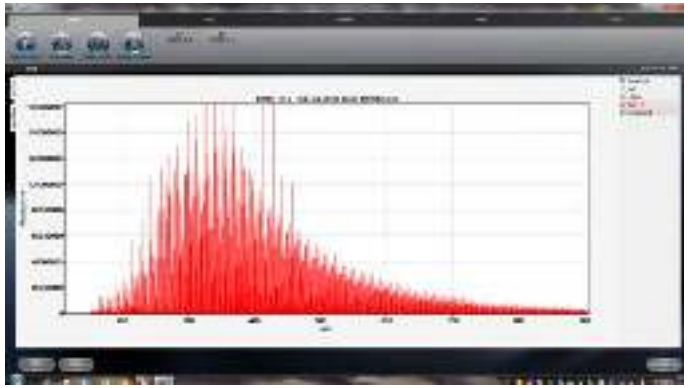

Mass spectrum

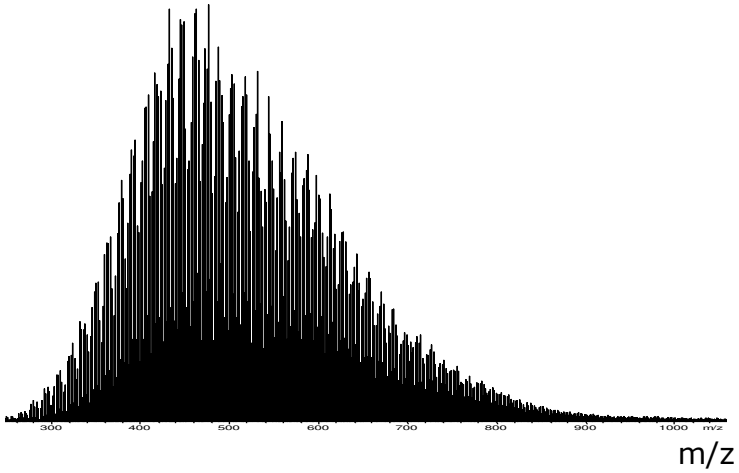

Class distribution plot

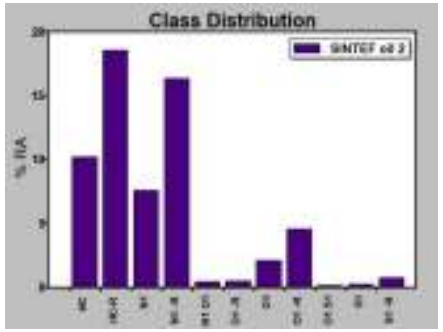

DBE vs. C plot

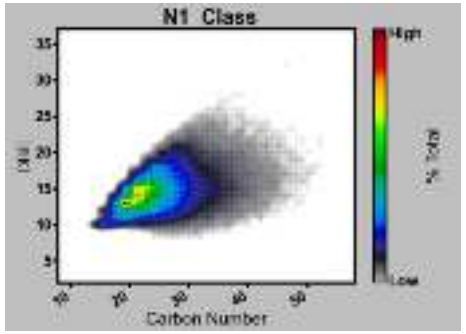

Introduction

Processing workflow in Petroleomics using PetroOrg

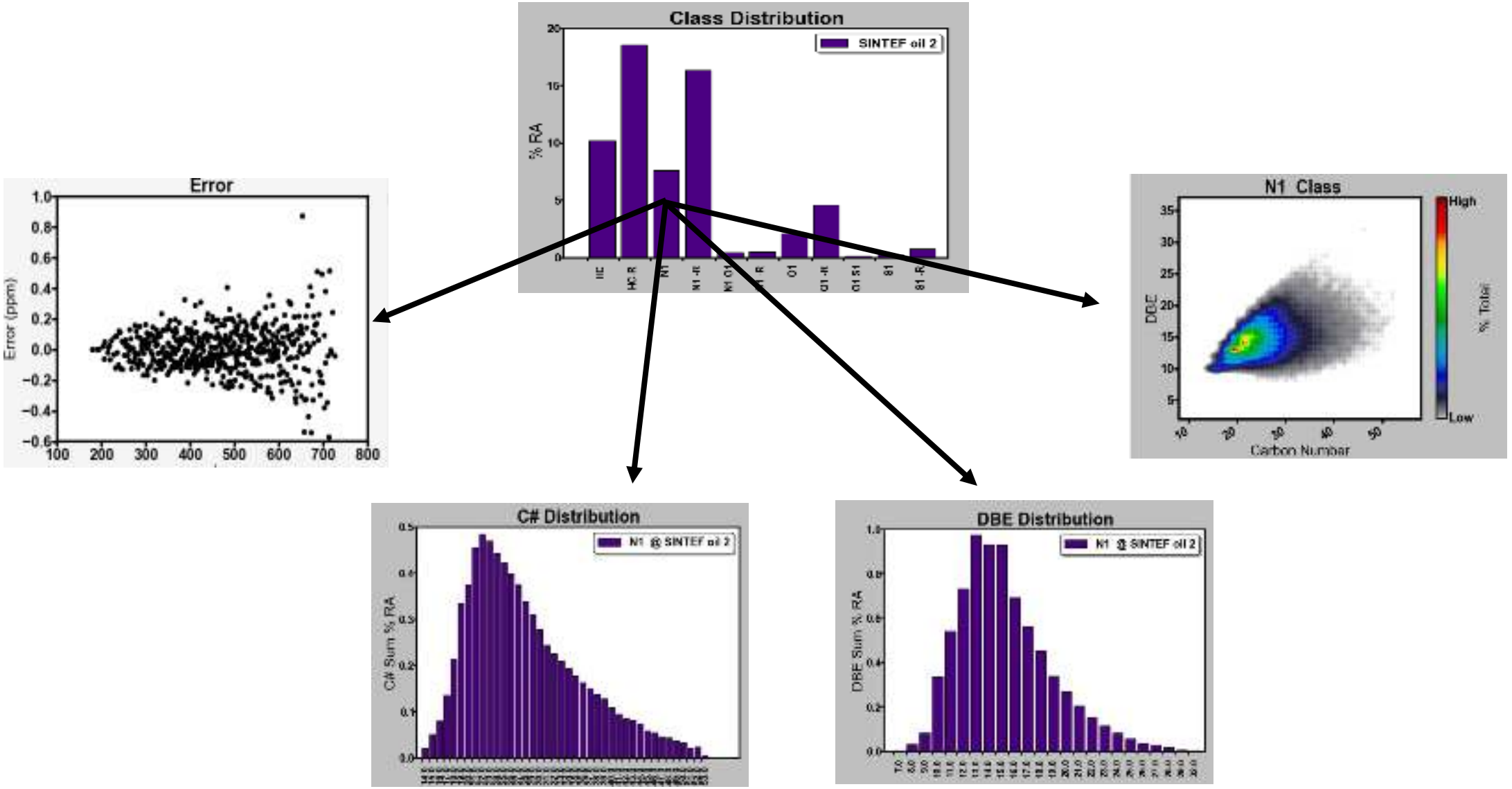

Introduction

Ionization methods for Petroleomics

ESI

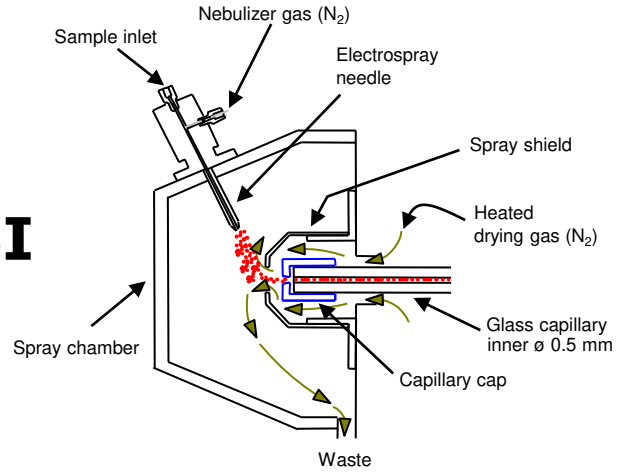

APCI

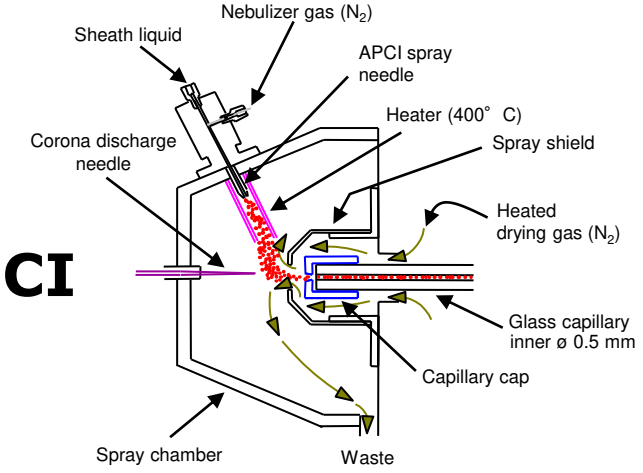

APPI

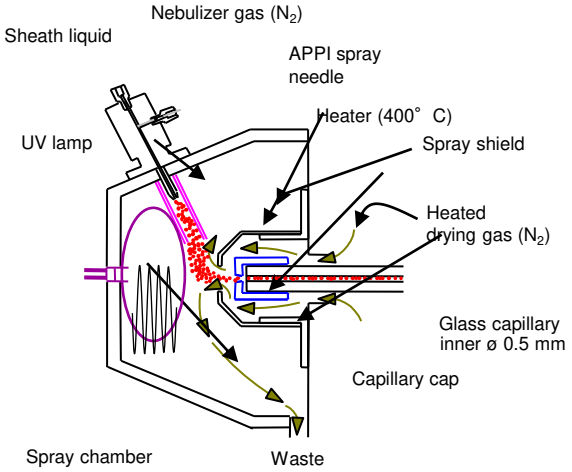

Introduction

Effect of Ionization methods – positive ion mode

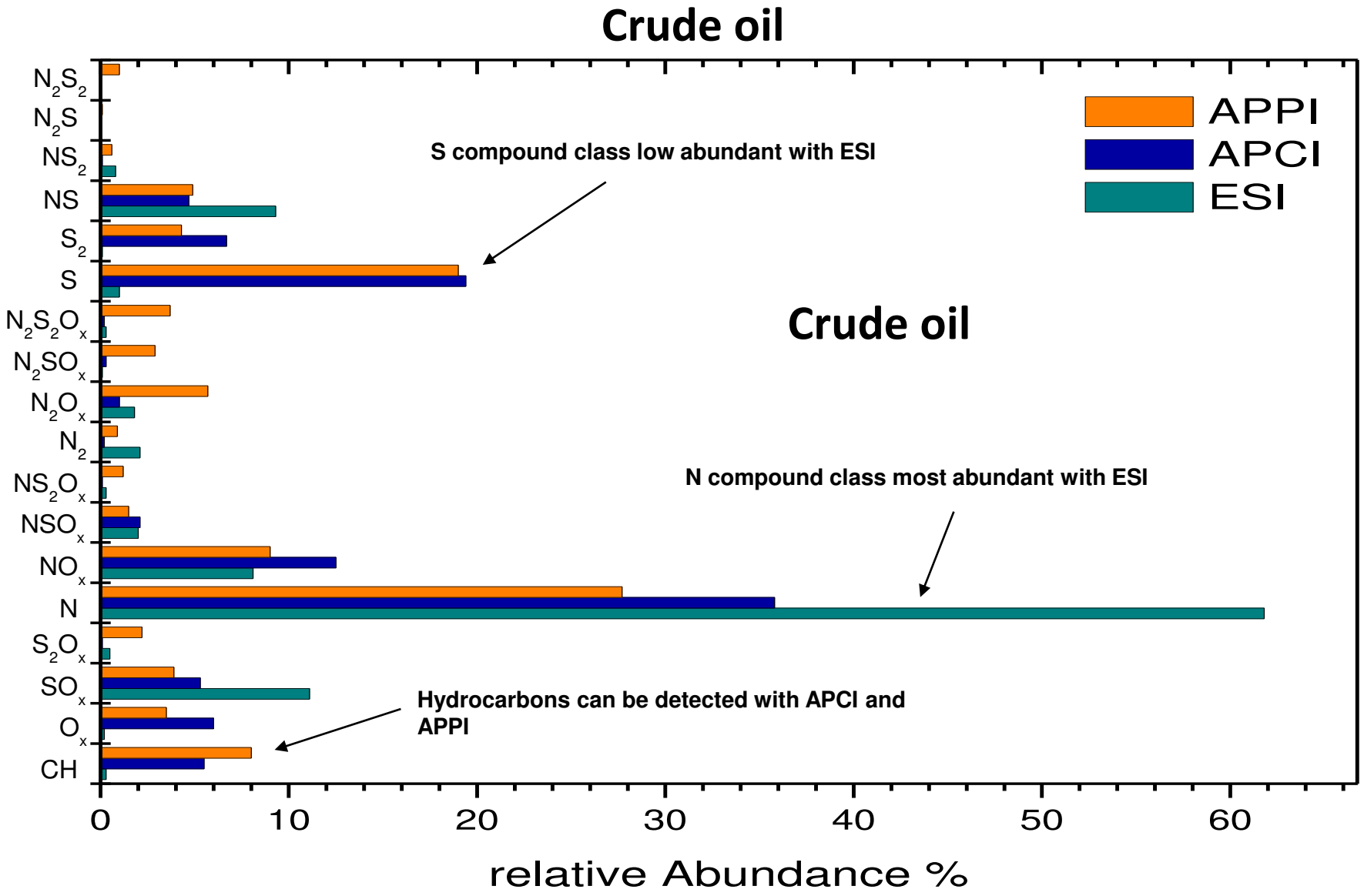

Introduction

Effect of Ionization methods – negative ion mode

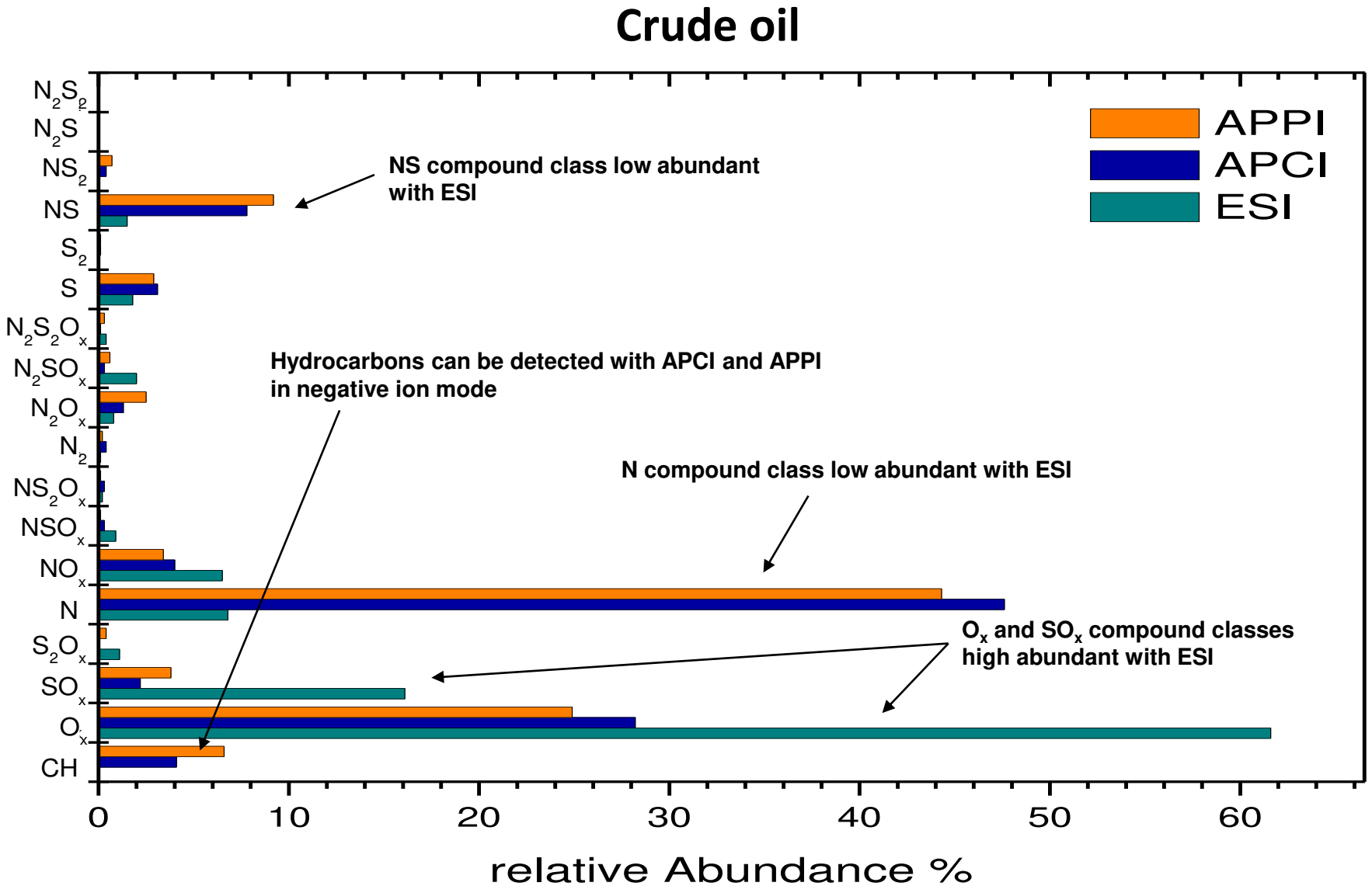

Introduction

Ionization method for Petroleomics

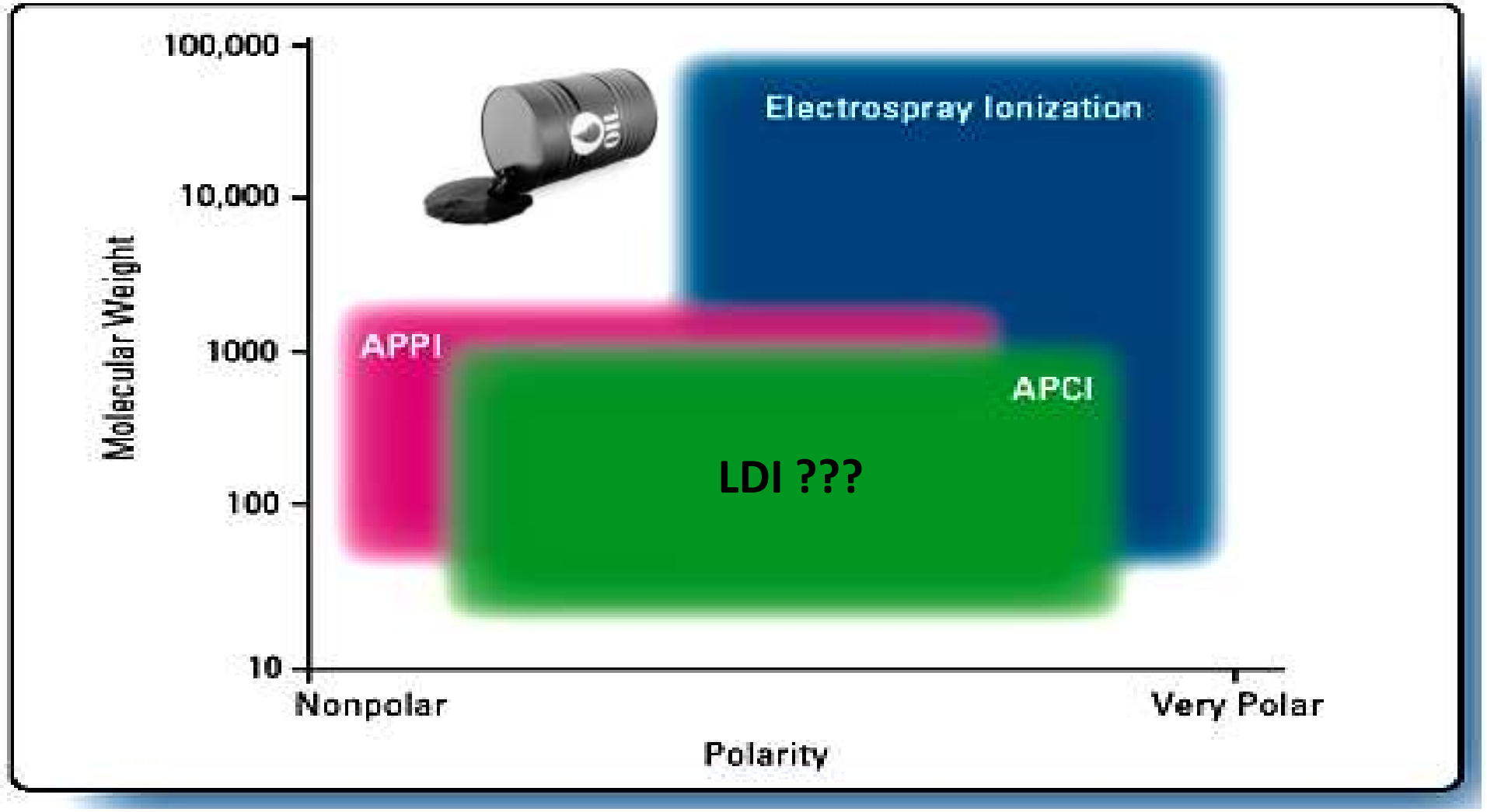

LDI in Petroleomics

LDI of Crude Oil

LDI at 355 nm with Nd:YAG laser

Properties of Crude Oils Used in This Study

	source	origin	S (ppm)[a]	N (ppm)[b]	TAN[c]
crude no. 1	Napo	Ecuador	20 100	4 011	0.18
crude no. 2	Qinhuangdao	China	2 500	4 405	3.15
crude no. 3	Doba	Congo	1 100	1 884	4.26

Correlation of oxygen containing classes (O_1 and O_2) with TAN in negative ion mode

Negative ion mode

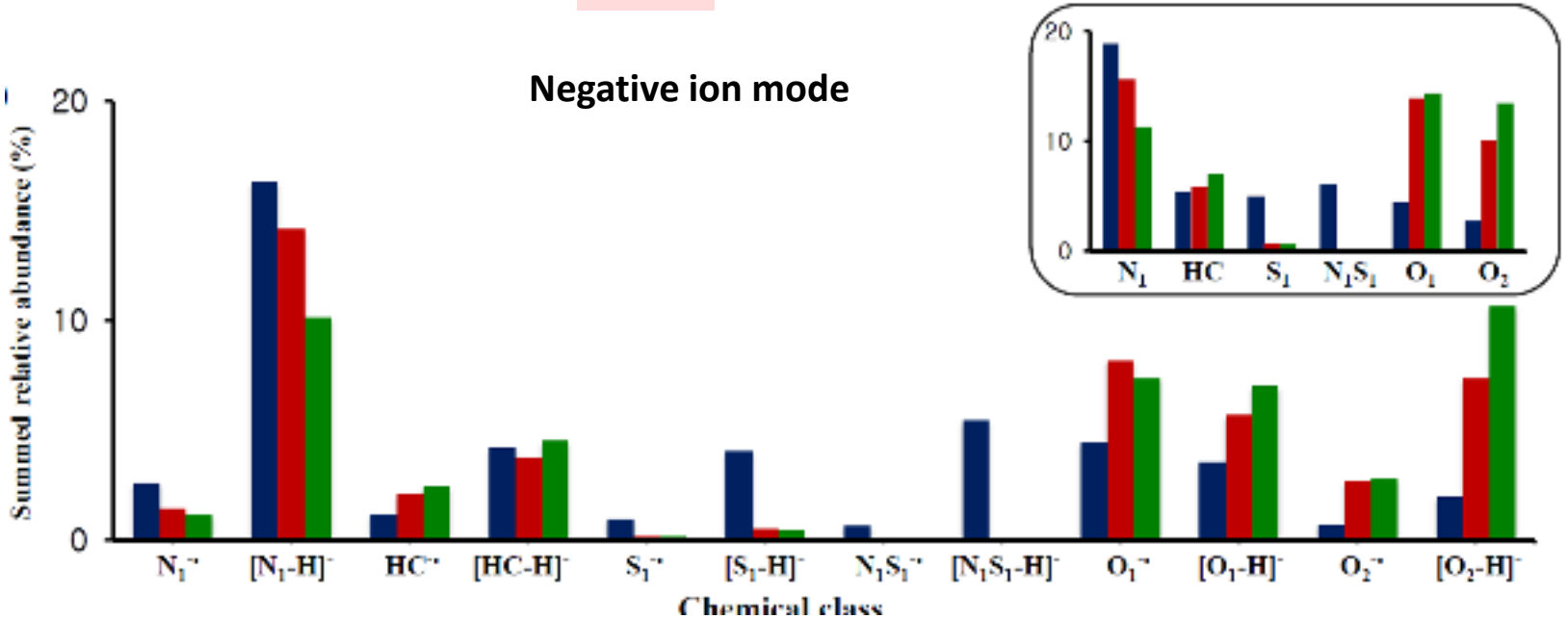

Cho, Y.; Witt, M.; Kim, H.K., Kim S. *Anal. Chem.* **2012**, *84*, 8587–8594.

LDI of Crude Oil

LDI at 355 nm with Nd:YAG laser

TAN: 0.18

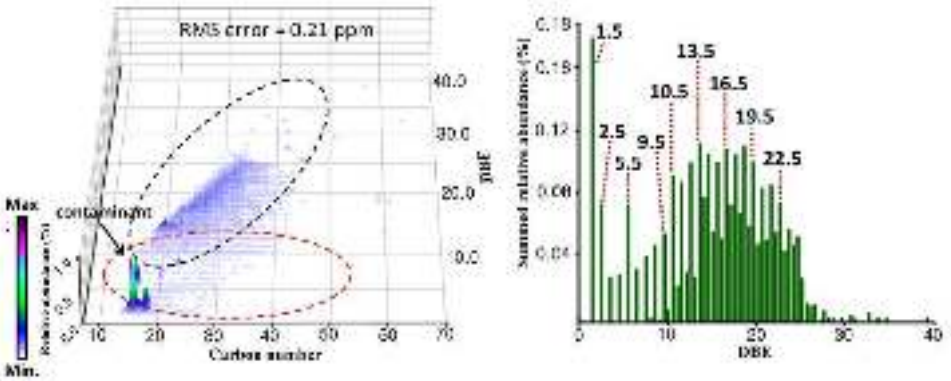

TAN: 3.15

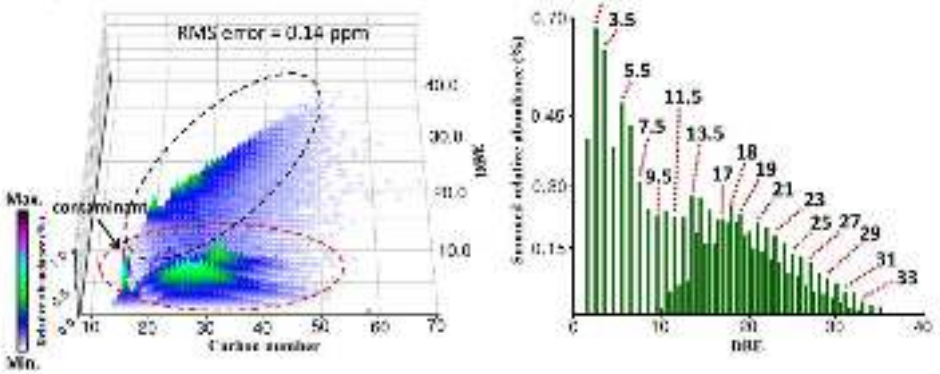

TAN: 4.26

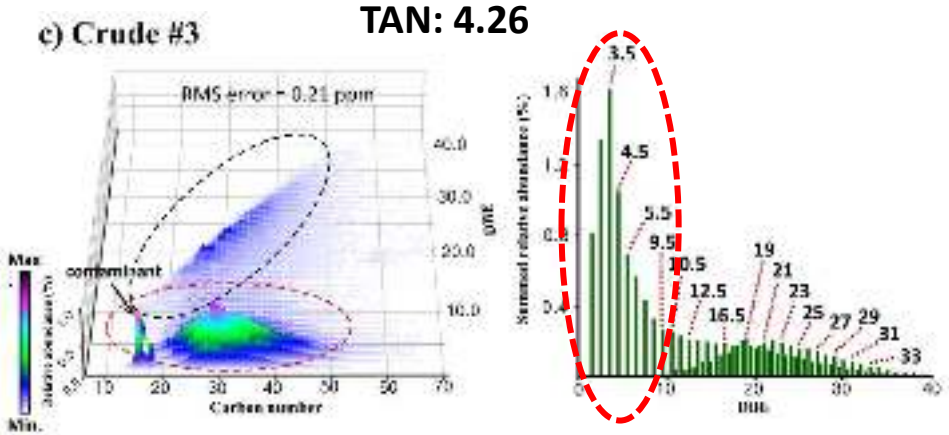

Cho, Y.; Witt, M.; Kim, H.K., Kim S. *Anal. Chem.* **2012**, *84*, 8587–8594.

Detection of Metalloporphyrins by LDI

LDI of crude oil on stainless steel target

Detection of vanadyl porphyrins

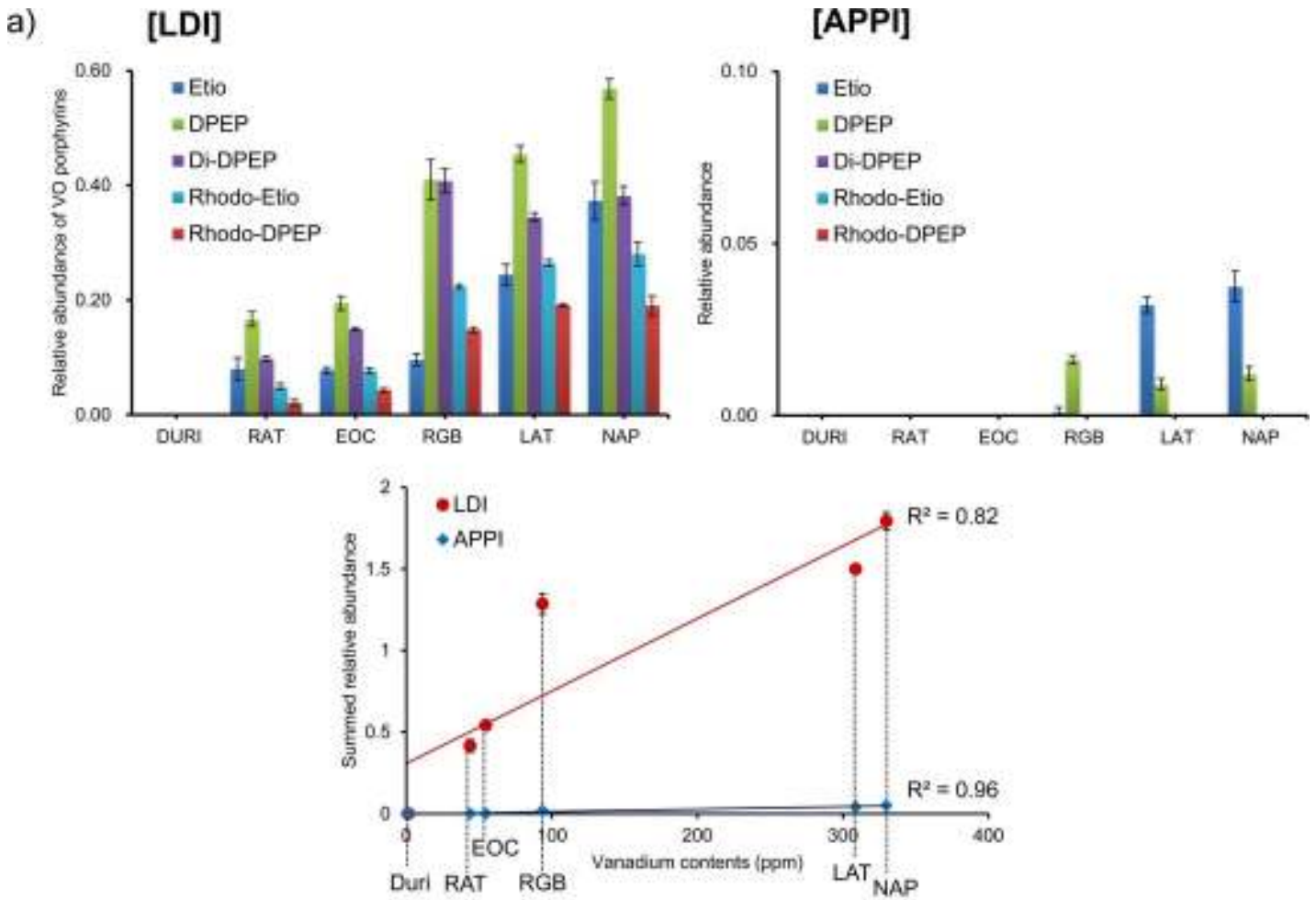

abbreviation	V (ppm)[e]	Ni (ppm)[f]
NAP	329.8	129.0
LAT	308.7	128.6
RGB	93.5	71.0
EOC	54.6	21.4
RAT	43.8	21.7
Duri	1.3	49.1

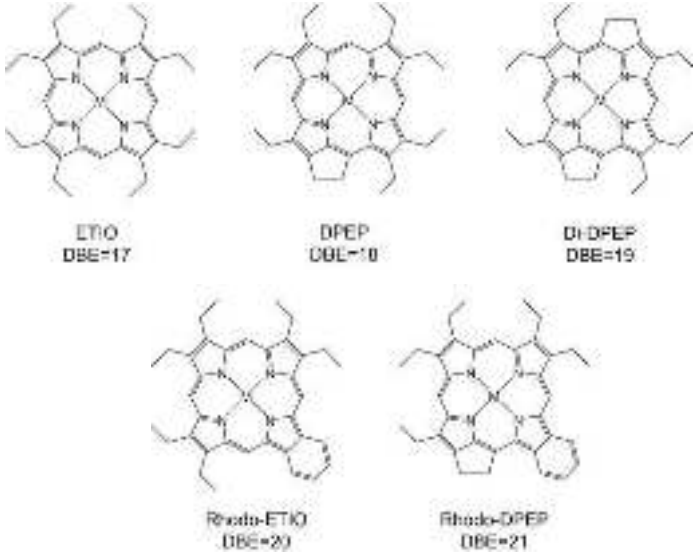

Vanadyl: M = V=O

Cho, Y.; Witt, M.; Jin, J.M., Kim, Y.H., Nho, N.-S., Kim; S. Energy Fuels 2014, 28, 6699-6706.

LDI *vs* APPI

Comparison of ionization methods

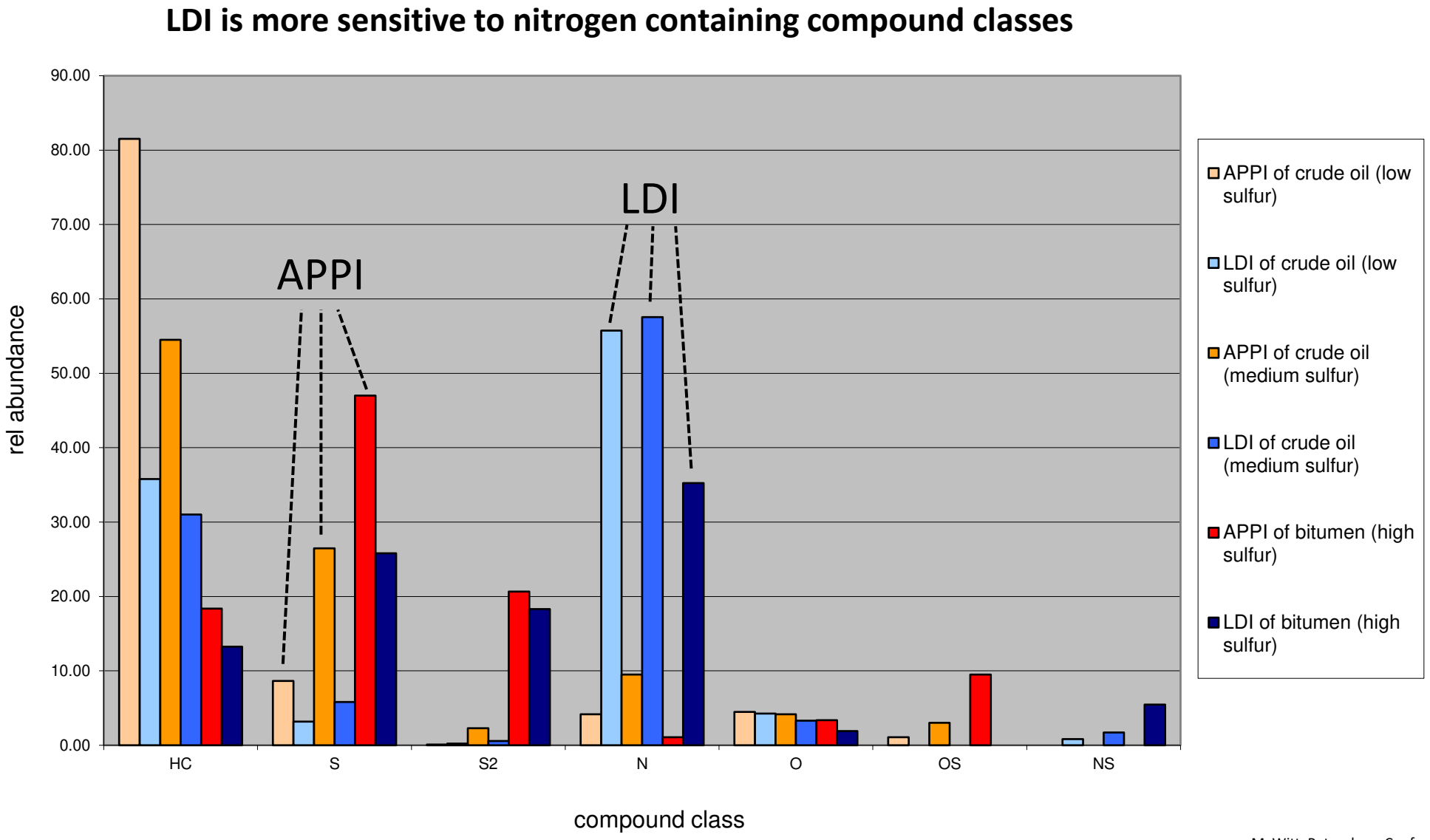

M. Witt, Petrophase Conference 2012.

LDI vs APPI

Comparison of ionization methods

Comparison of detected compounds in class S_1 in a crude oil by APPI and LDI

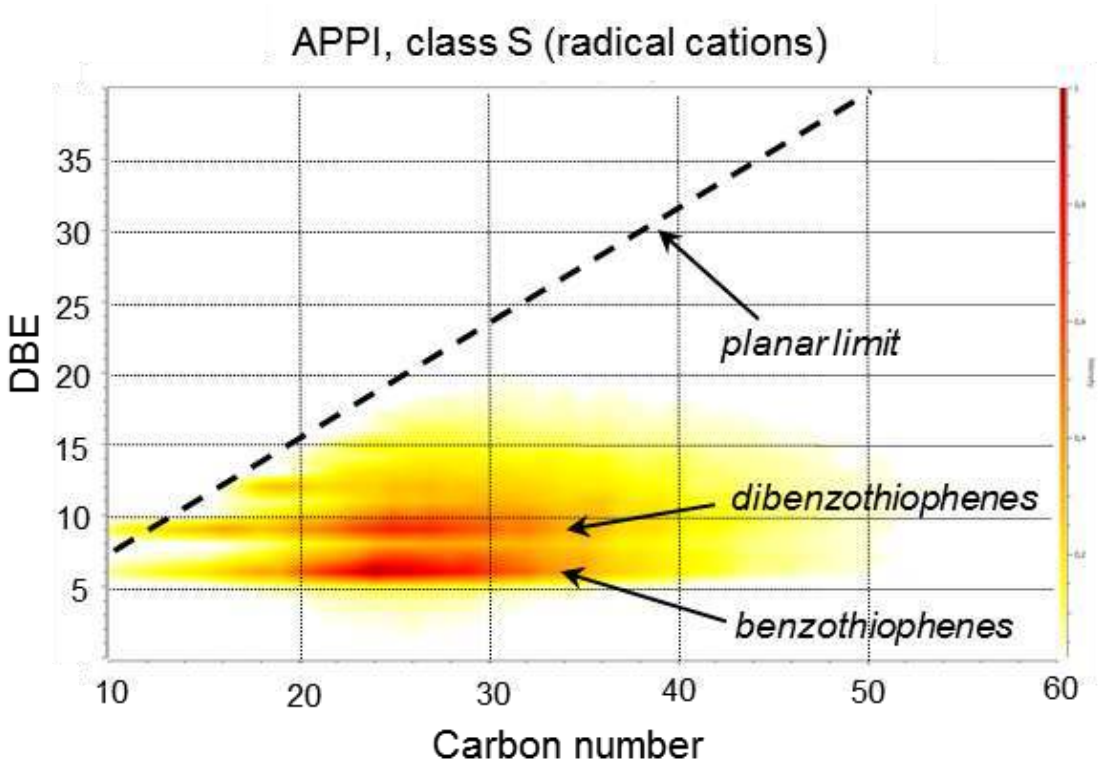

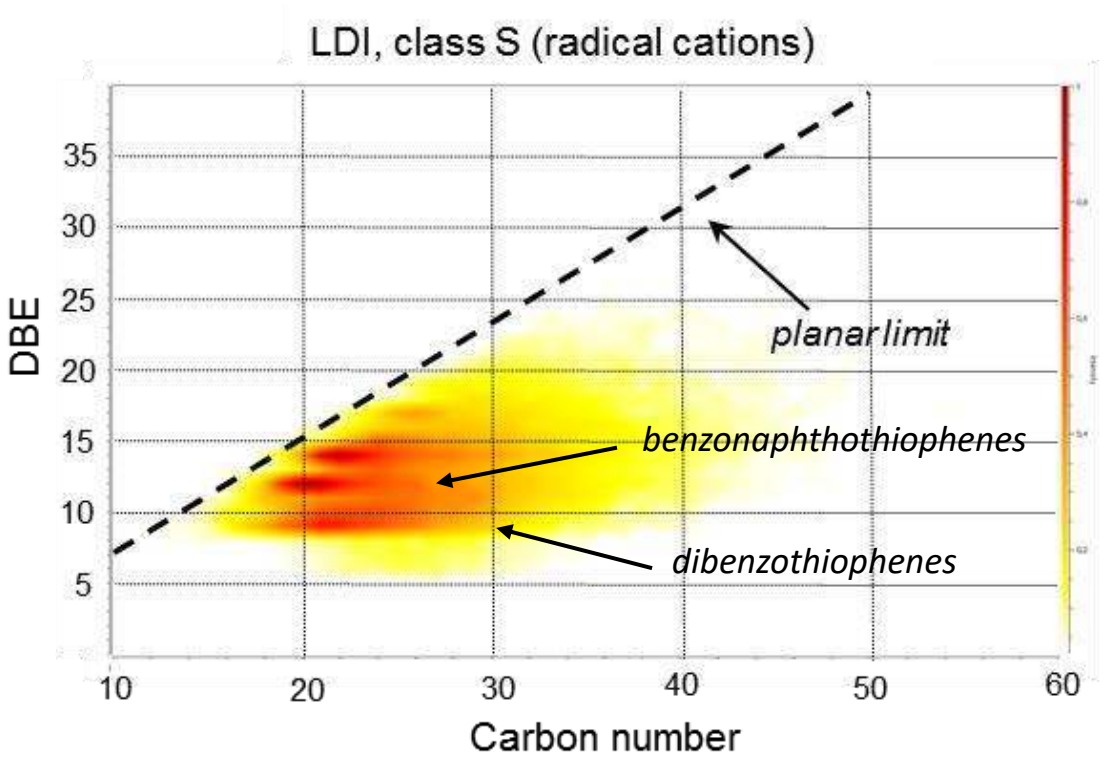

LDI is more sensitive to highly aromatic compounds!

M. Witt, Petrophase Conference 2012.

Thin Layer Chromatography

Experimental setup

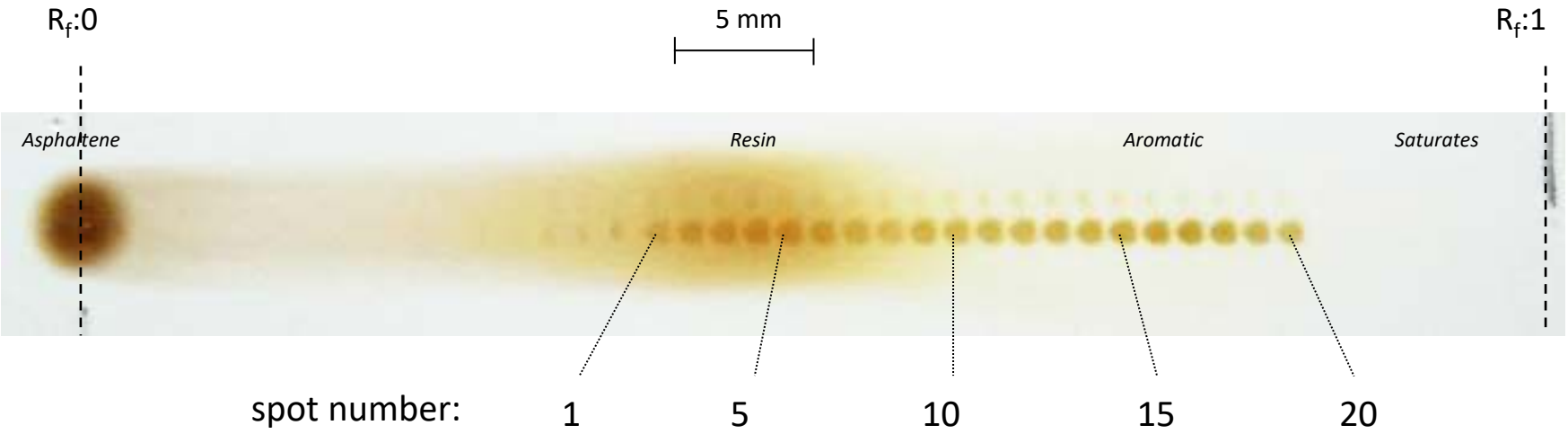

- Spot diameter: 1.0 mm
- Lateral difference between spots: 1.2 mm
- 3 µL of a 1:5 solution of crude oil dissolved in DCM deposited on the TLC plate
- mobile phase: n-heptane:i-propanol 95:5
- stationary phase: TLC silica 60 F254 (Merck 1.05539.00001) 5 × 7.5 cm sheet

Similar measurements were done by Smith et. al., Energy Fuels, 2014.

Thin Layer Chromatography

LDI spectra of different spot numbers

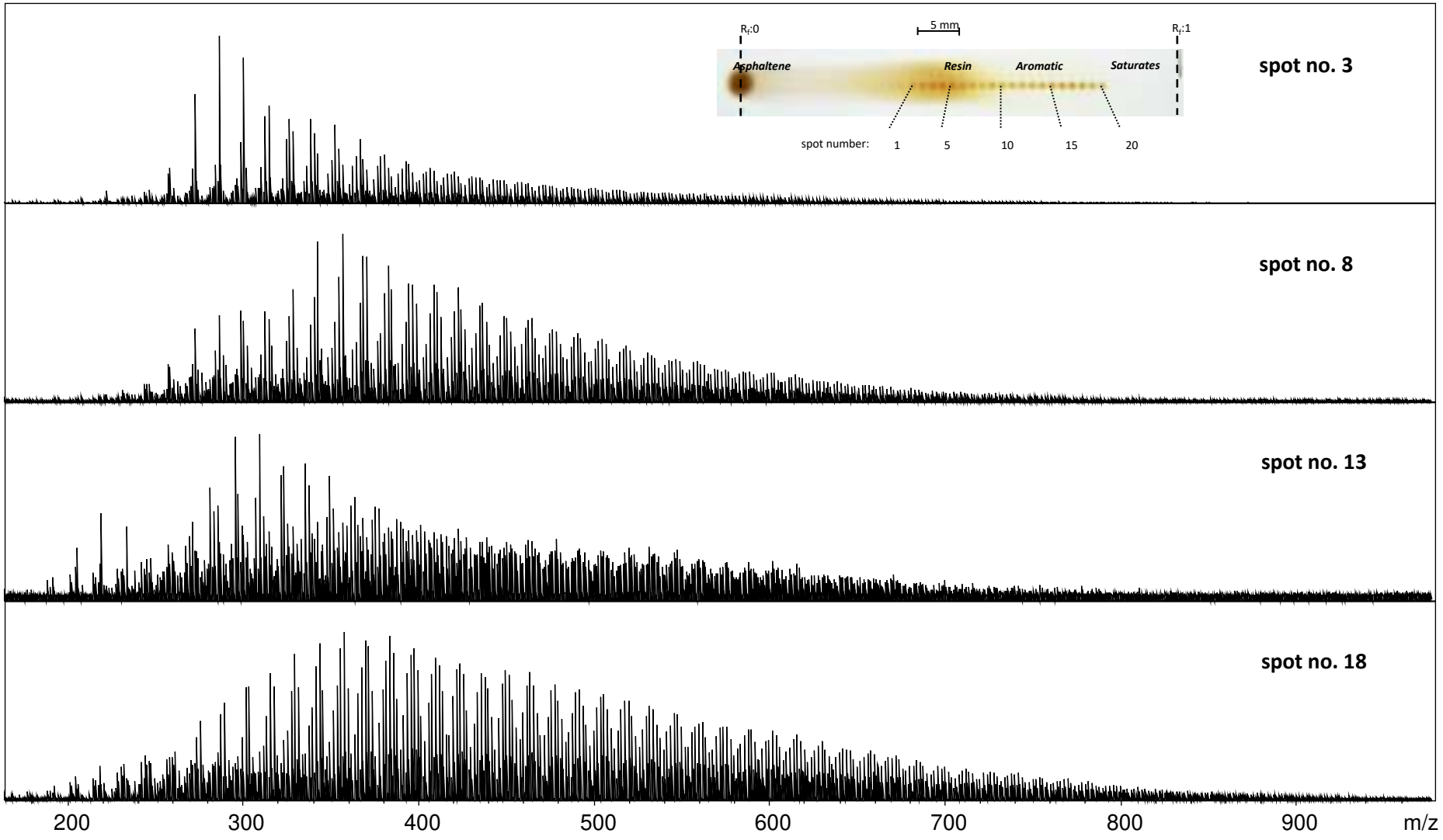

Thin Layer Chromatography

Relative abundance of compound classes

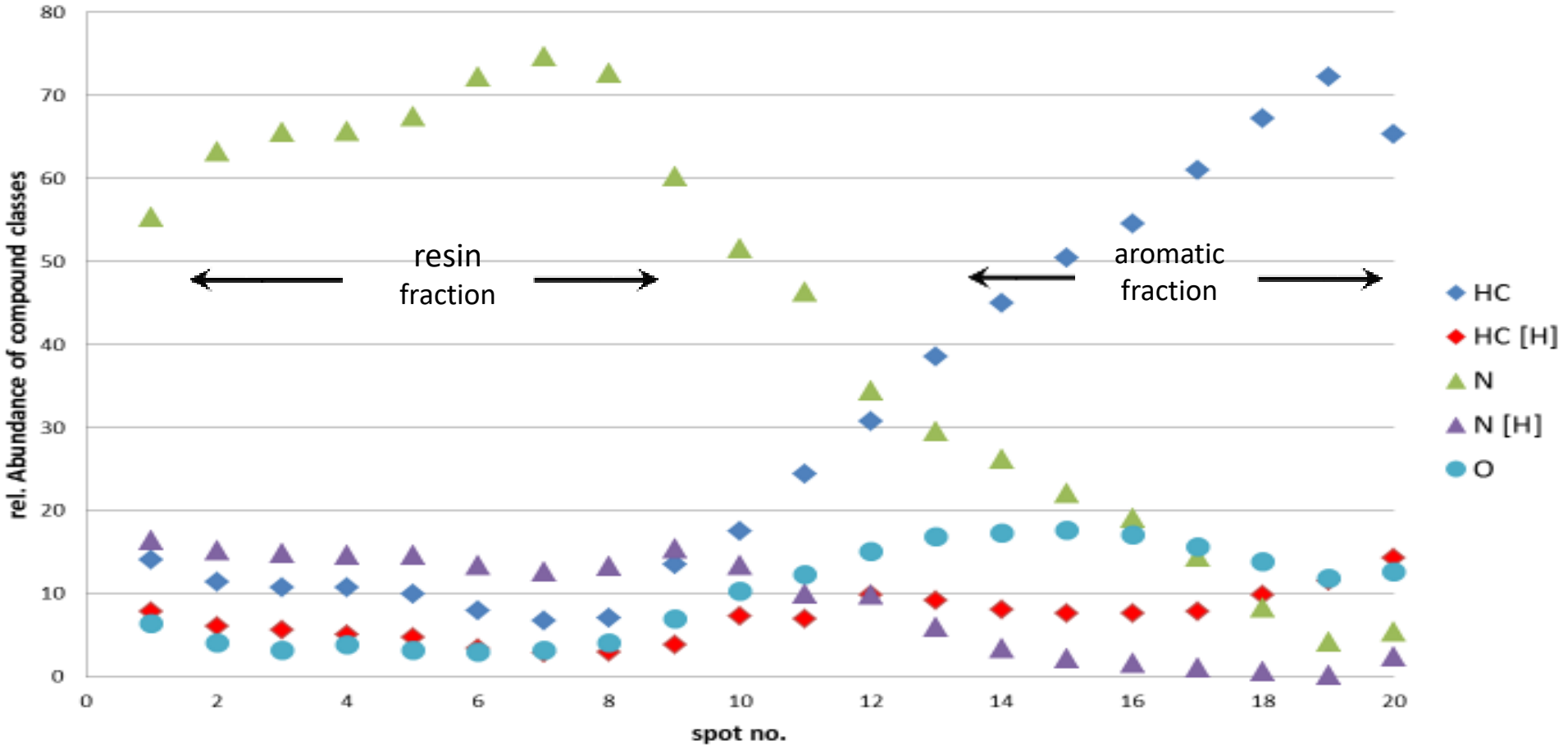

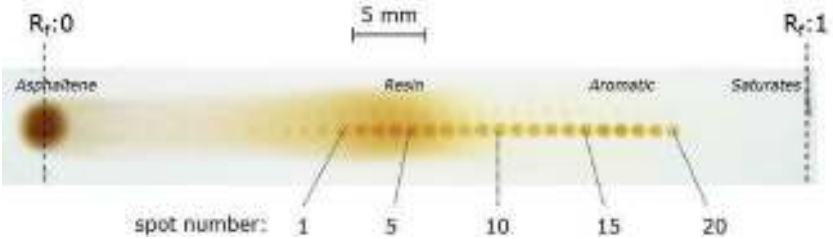

Thin Layer Chromatography

Aromaticity of resin fractions: class N_1

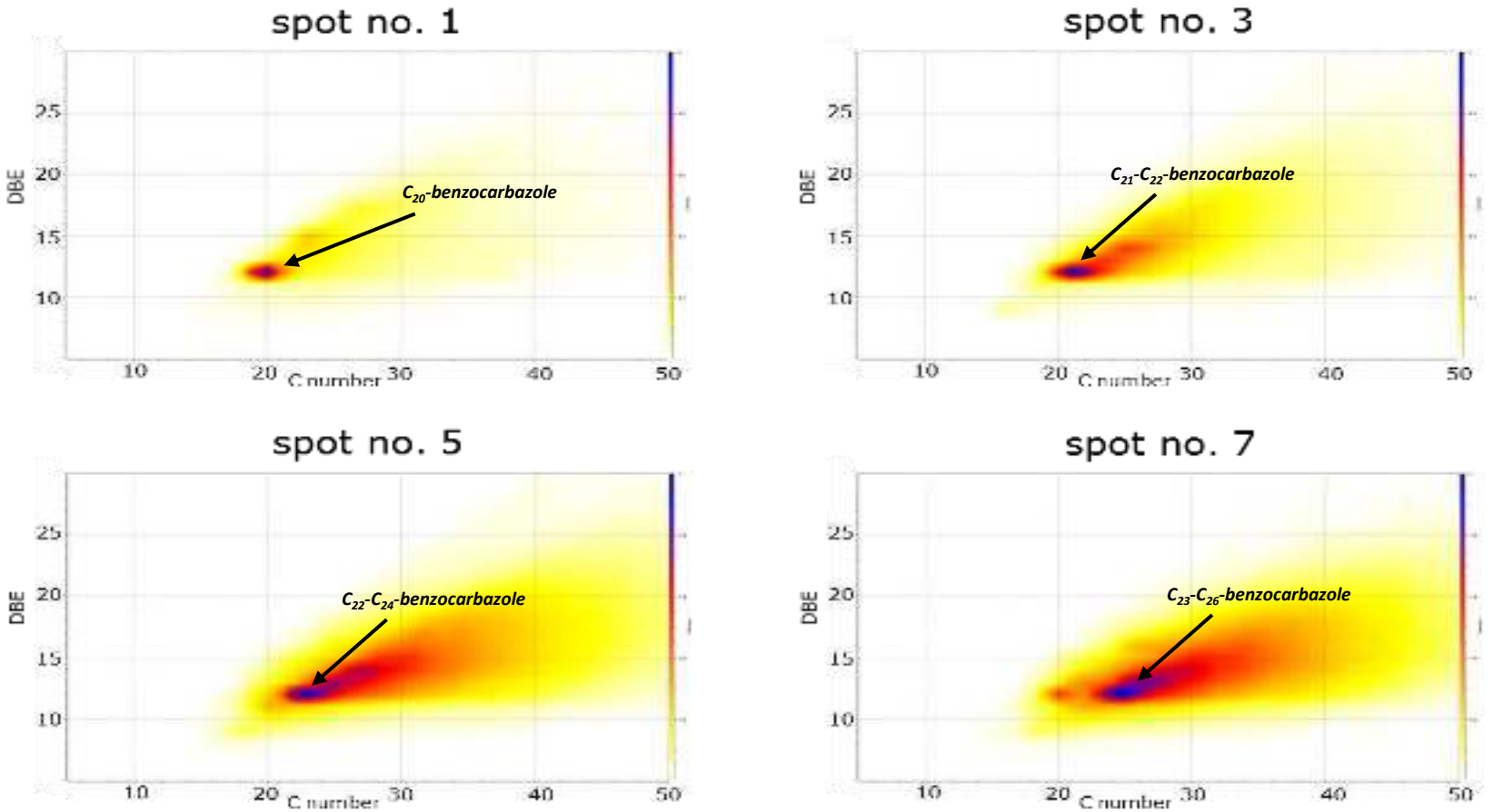

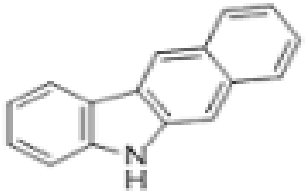

benzocarbazole

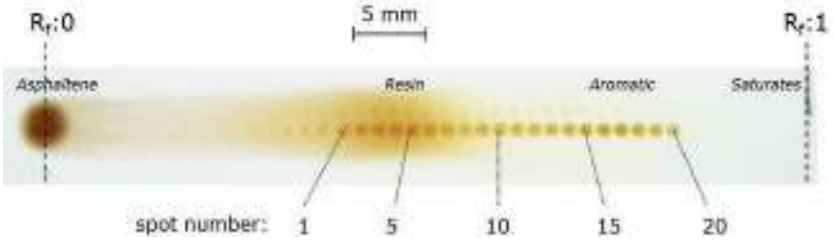

Can we quickly tell samples apart by LDI?

LDI of different crude oil samples

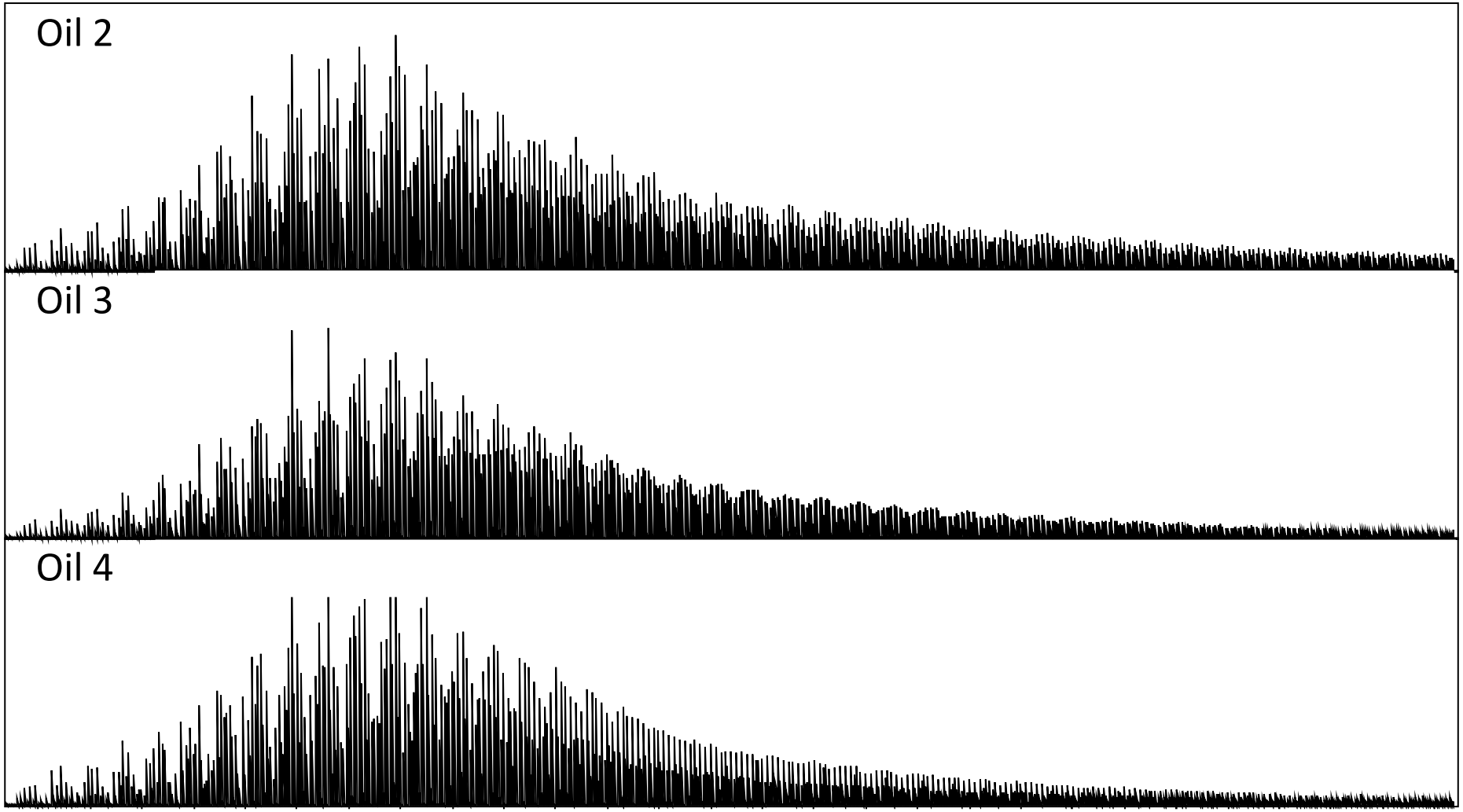

*Samples have been kindly provided by Dr. Kolbjørn (SINTEF, Trondheim, Norway)

Can we quickly tell samples apart by LDI?

LDI of different crude oil samples

Oil 8 and 8a: identical oils from different bottles
Oil 9a: Oil 9 one day in ion source at 3 mbar

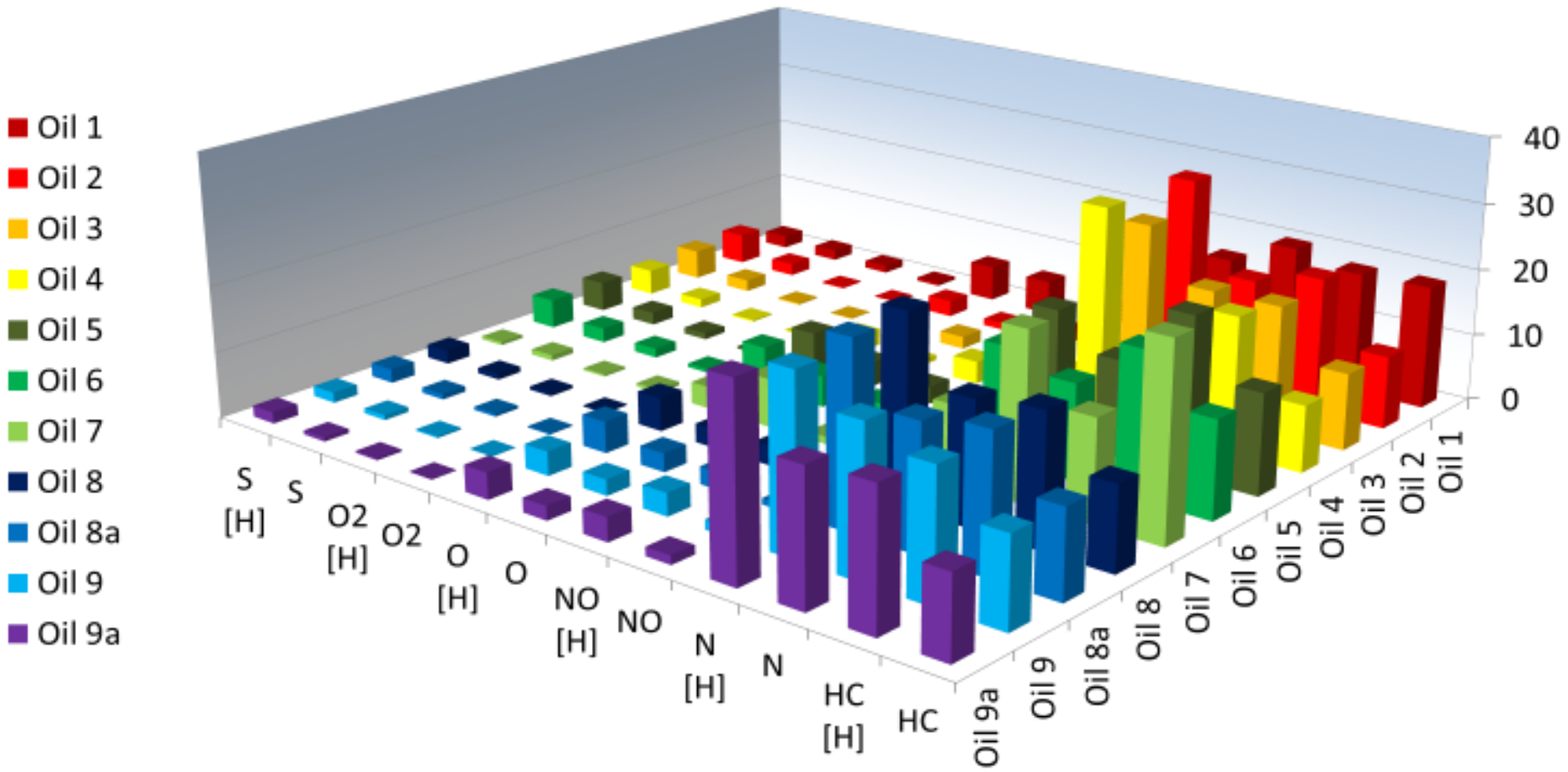

*Samples have been kindly provided by Dr. Kolbjørn (SINTEF, Trondheim, Norway)

Can we quickly tell samples apart by LDI?

Reproducibility of LDI measurements

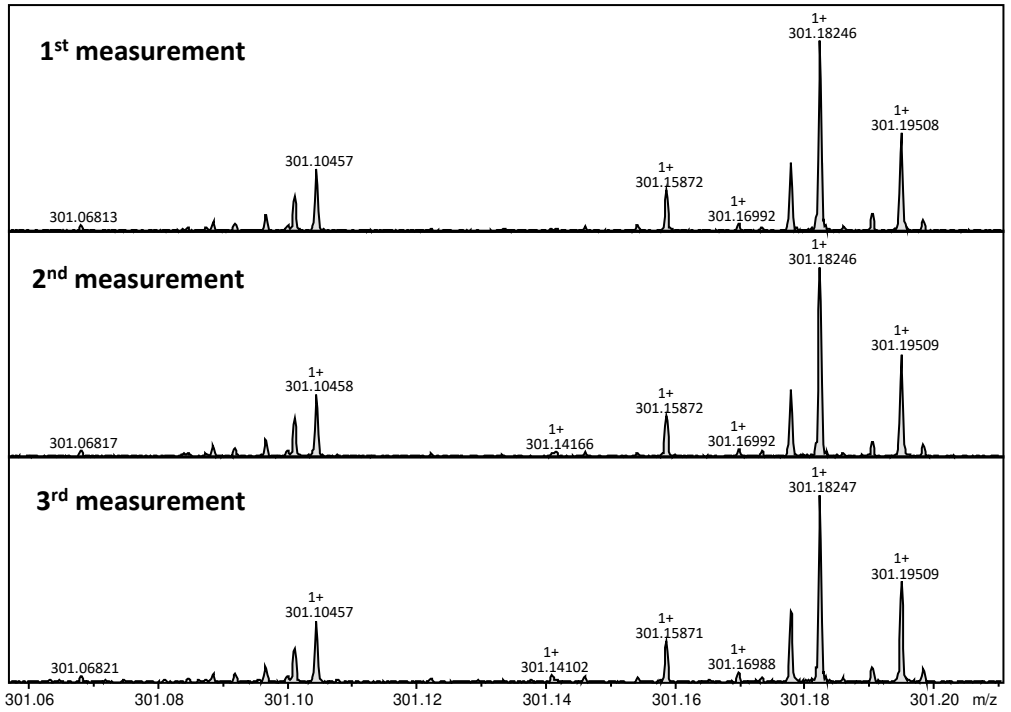

Class	Oil 8 rep1	Oil 8 rep2	Oil 8 rep3	Oil 8 rep4	Oil 8 rep5	Std. deviation [%]
HC	12.97	12.17	12.83	13.04	12.25	**3.3**
HC [H]	20.24	19.67	20.36	20.44	19.87	**1.6**
N	18.62	18.28	18.25	18.21	18.22	**0.9**
N [H]	27.27	28.74	27.47	27.24	28.56	**2.6**
O	2.82	2.62	2.76	2.71	2.61	**3.3**
O [H]	4.72	4.86	4.72	4.71	4.83	**1.5**
S [H]	2.14	2.08	2.15	2.14	2.11	**1.4**

*Samples have been kindly provided by Dr. Kolbjørn (SINTEF, Trondheim, Norway)

Principle Component Analysis

Reproducibility of LDI measurements

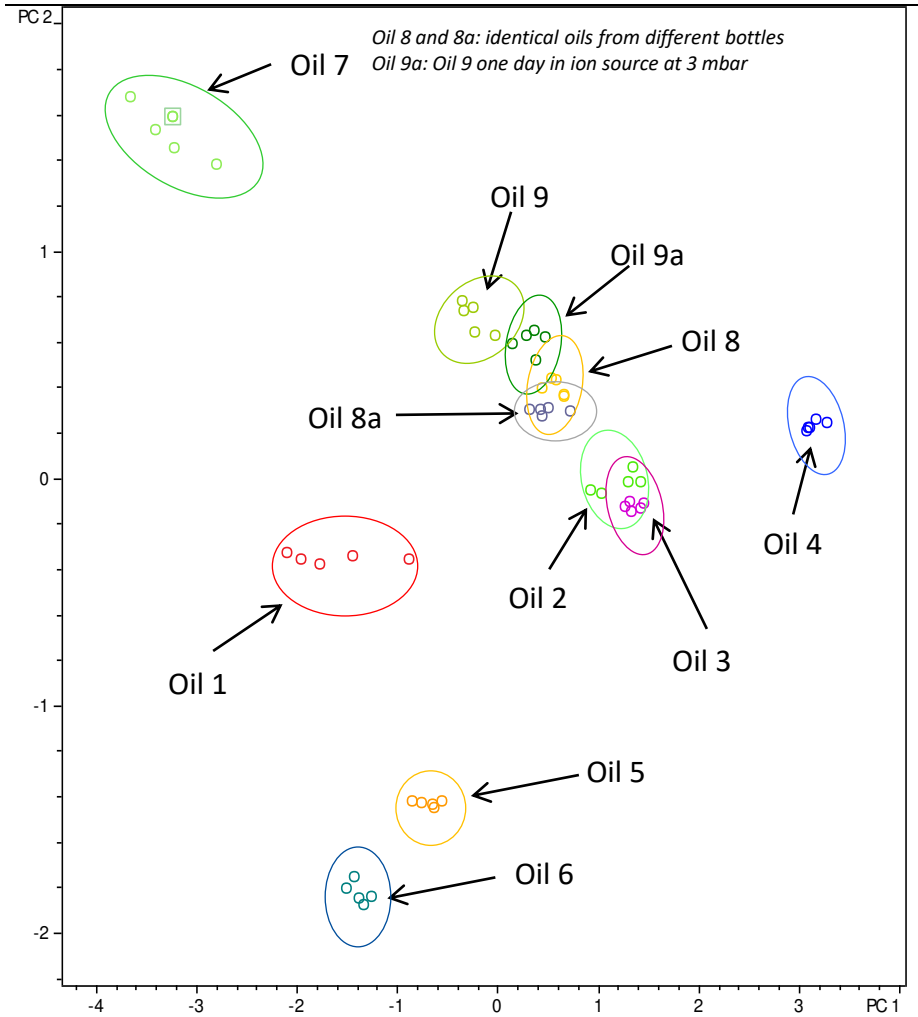

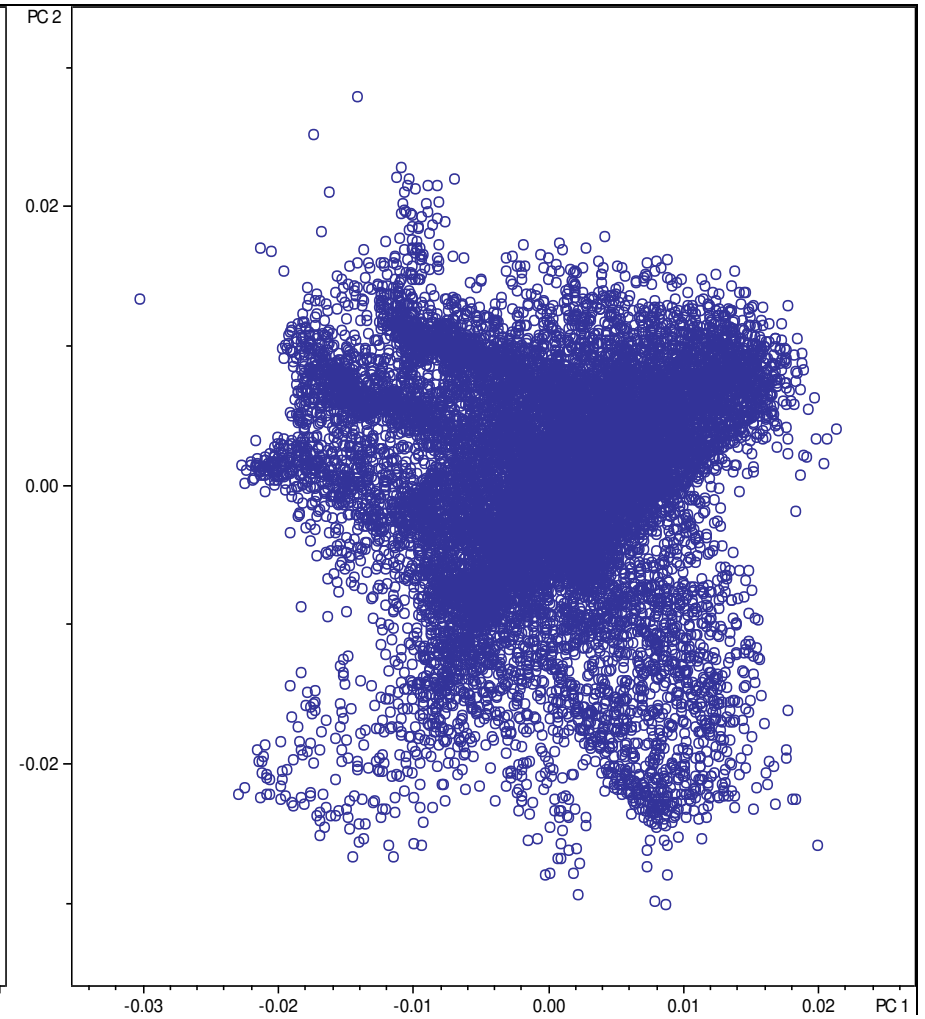

*Samples have been kindly provided by Dr. Kolbjørn (SINTEF, Trondheim, Norway)

Oil mixtures

Ternary Oil Mixtures

Compound classes of 3 different crude oils from North sea

M. Witt, W. Timm, *Energy Fuels 2016, 30, 5, 3707-3713.*

Compound classes plot

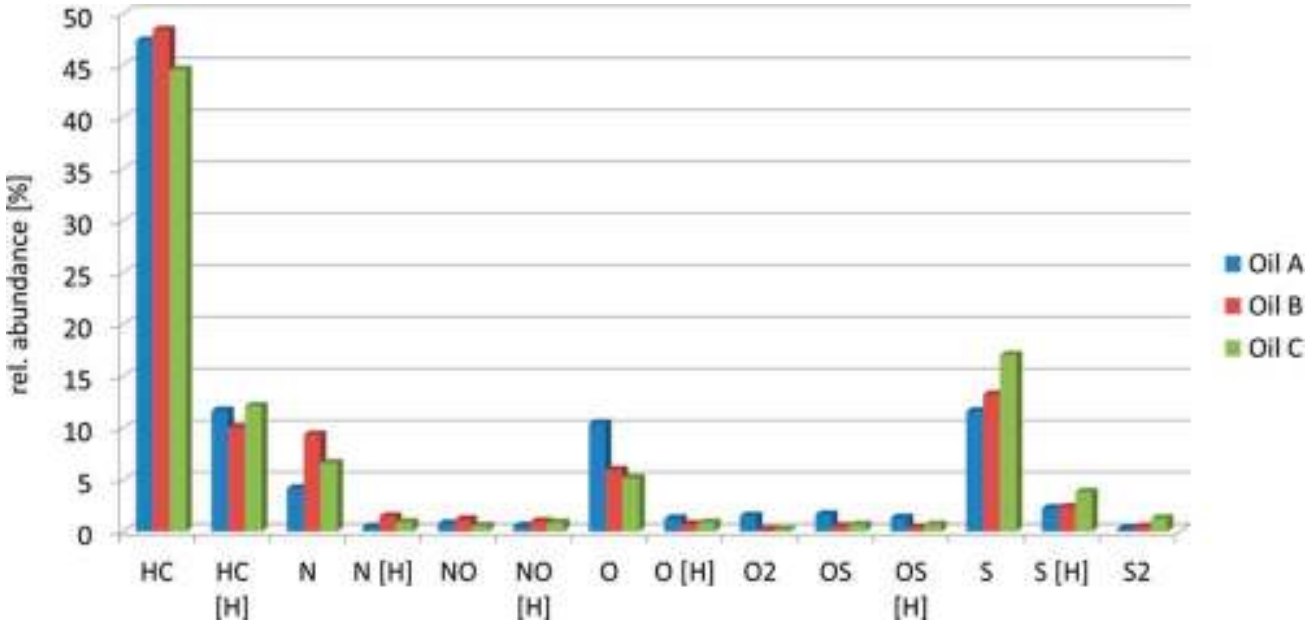

NNLS method

	measured (%)	actual (%)	relative error (%)
mixture 1: oil A	32.4	33.3	2.8
mixture 1: oil B	36.0	33.3	8.1
mixture 1: oil C	31.6	33.3	5.2
mixture 2: oil A	15.6	10.0	56.2
mixture 2: oil B	10.0	10.0	0.3
mixture 2: oil C	74.4	80.0	7.1
mixture 3: oil A	39.0	45.0	13.4
mixture 3: oil B	38.1	35.0	8.9
mixture 3: oil C	22.9	20.0	14.5

NNLS: non-negative least square

Ternary Oil Mixtures

Principle component analysis (PCA)

M. Witt, W. Timm, *Energy Fuels 2016, 30, 5, 3707-3713.*

Pure oils and defined mixtures

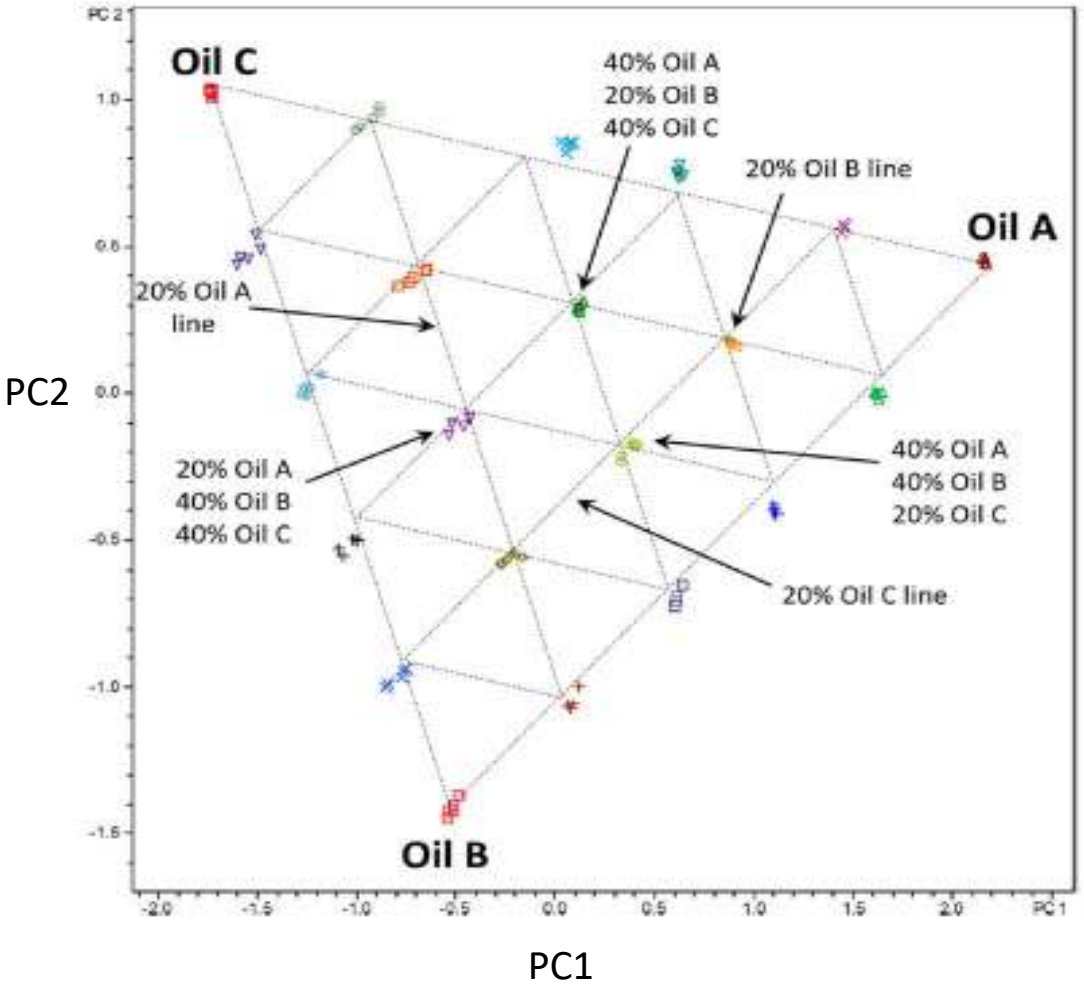

Calculation of mixtures based on PCA of defined mixtures

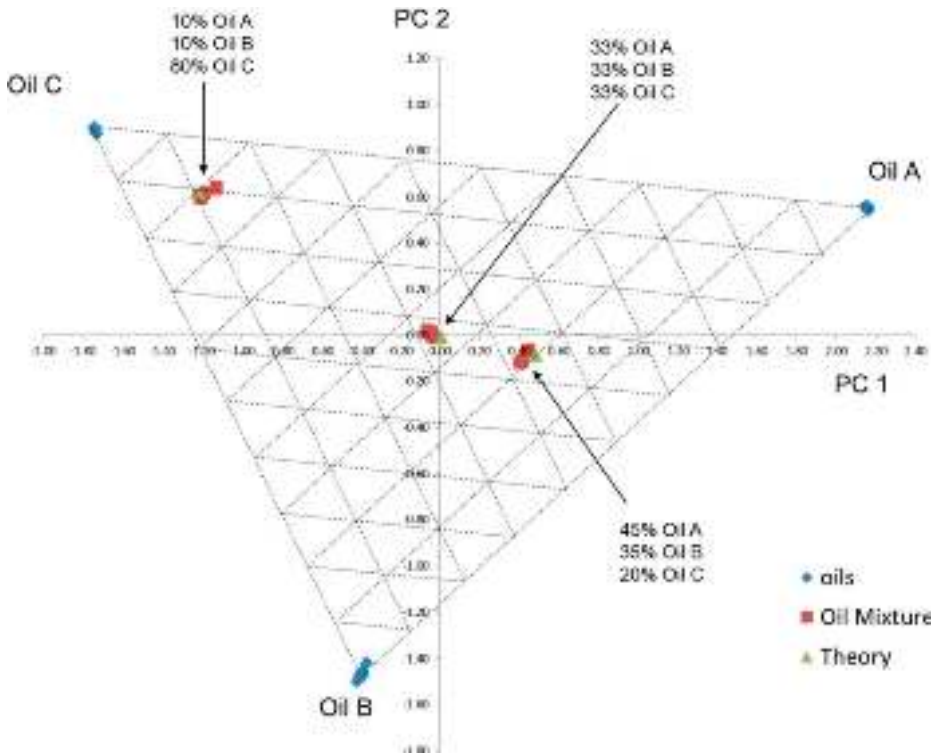

Ternary Oil Mixtures

Determination of mixture ratios using PCA and vector analysis

M. Witt, W. Timm, *Energy Fuels 2016, 30, 5, 3707-3713.*

Calculation of Relative Percentages of Three Ternary Oil Mixtures Using **Vector Analysis** of the Ternary Diagram Calculated with the PC1 versus PC2 of the **PCA Scoring Plot**

				PCA	**NNLS**
	measured (%)	actual (%)	absolute error (%)	relative error (%)	relative error (%)
mixture 1: oil A	32.1	33.3	1.2	3.5	2.8
mixture 1: oil B	32.9	33.3	0.4	1.3	8.1
mixture 1: oil C	34.9	33.3	1.6	4.7	5.2
mixture 2: oil A	11.1	10.0	1.1	10.7	56.2
mixture 2: oil B	9.8	10.0	0.2	1.6	0.3
mixture 2: oil C	79.1	80.0	0.9	1.1	7.1
mixture 3: oil A	43.2	45.0	1.8	3.9	13.4
mixture 3: oil B	35.5	35.0	0.5	1.5	8.9
mixture 3: oil C	21.2	20.0	1.2	6.2	14.5

Asphaltene fractions

Asphaltene fractions

Fractions based on solubility in different solvent

E. Rogel, M. Witt, *Energy & Fuels* 2016, 30, 915-923.

APPI positive ion mode

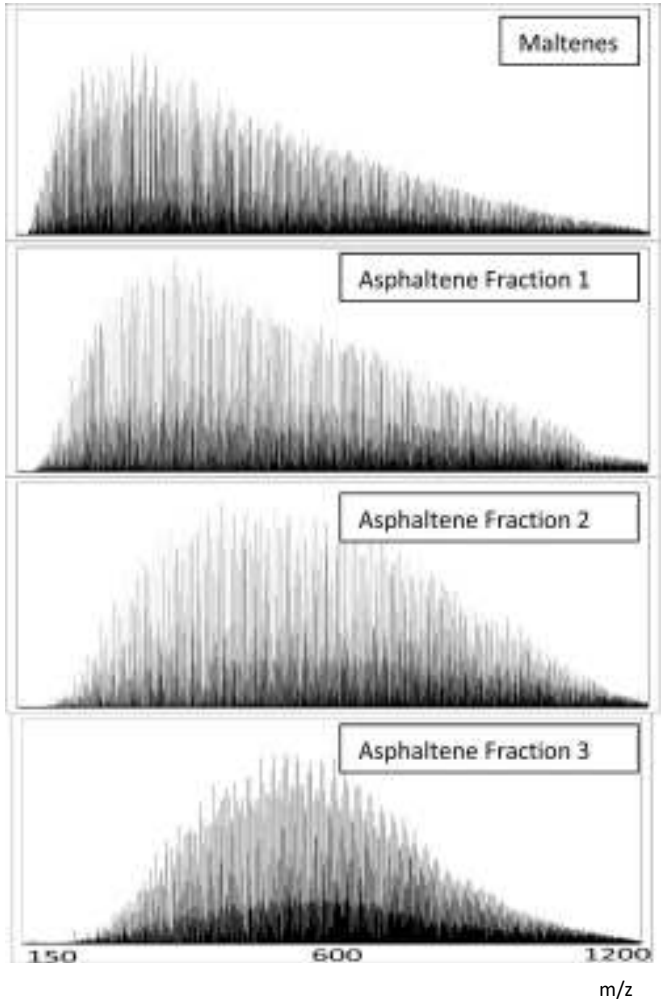

Maltene: Heptane solubles

Fraction 1: 15:85 CH_2Cl_2/n-heptane

Fraction 2: 30:70 CH_2Cl_2/n-heptane

Fraction 3: CH_2Cl_2 solubles

Asphaltene fractions

Fractions based on solubility in different solvent

E. Rogel, M. Witt, *Energy & Fuels* 2016, 30, 915-923.

Compound classes

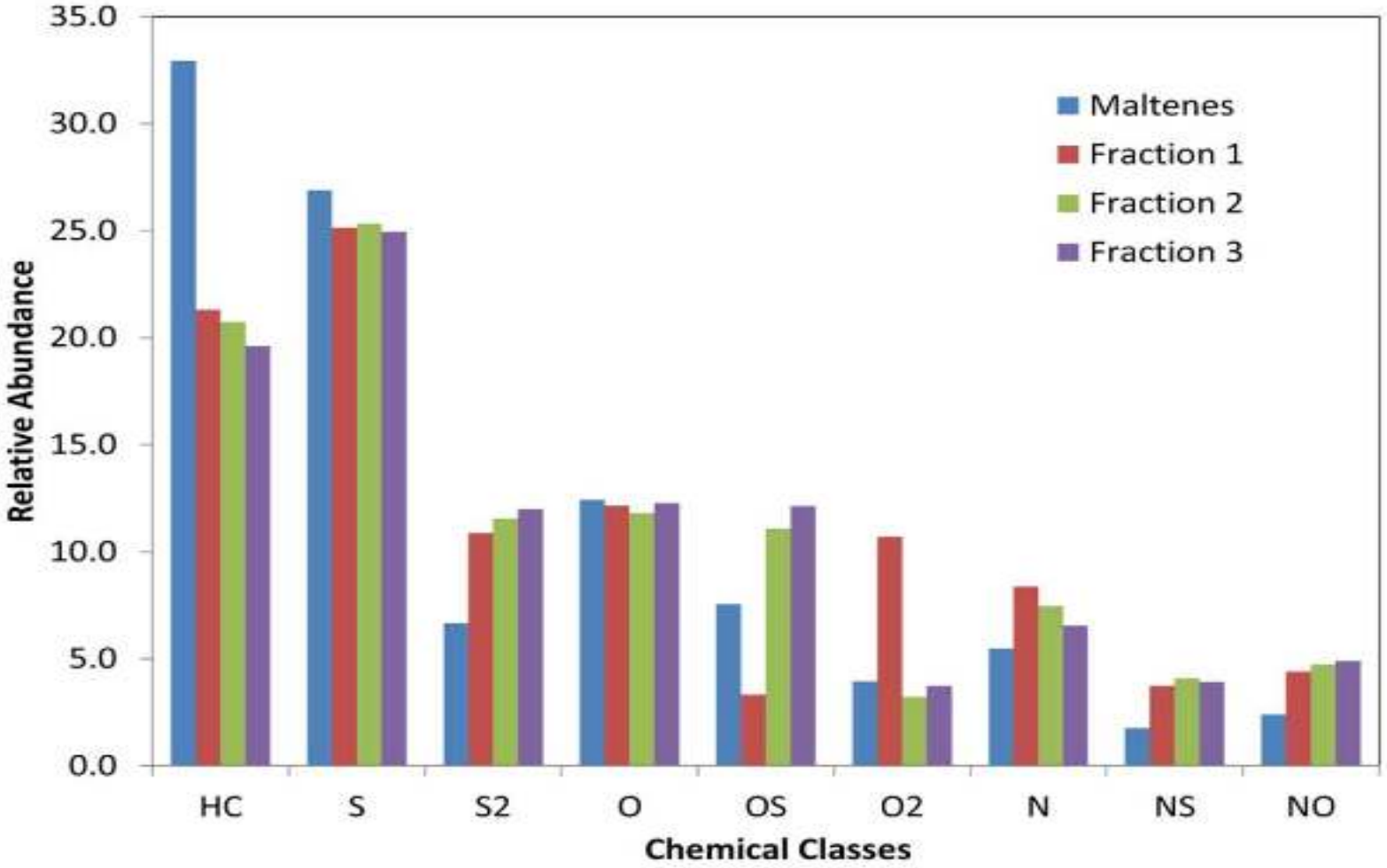

Asphaltene fractions

Fractions based on solubility in different solvent

E. Rogel, M. Witt, *Energy & Fuels* 2016, 30, 915-923.

Fractions: DBE and C number abundance plot

DBE

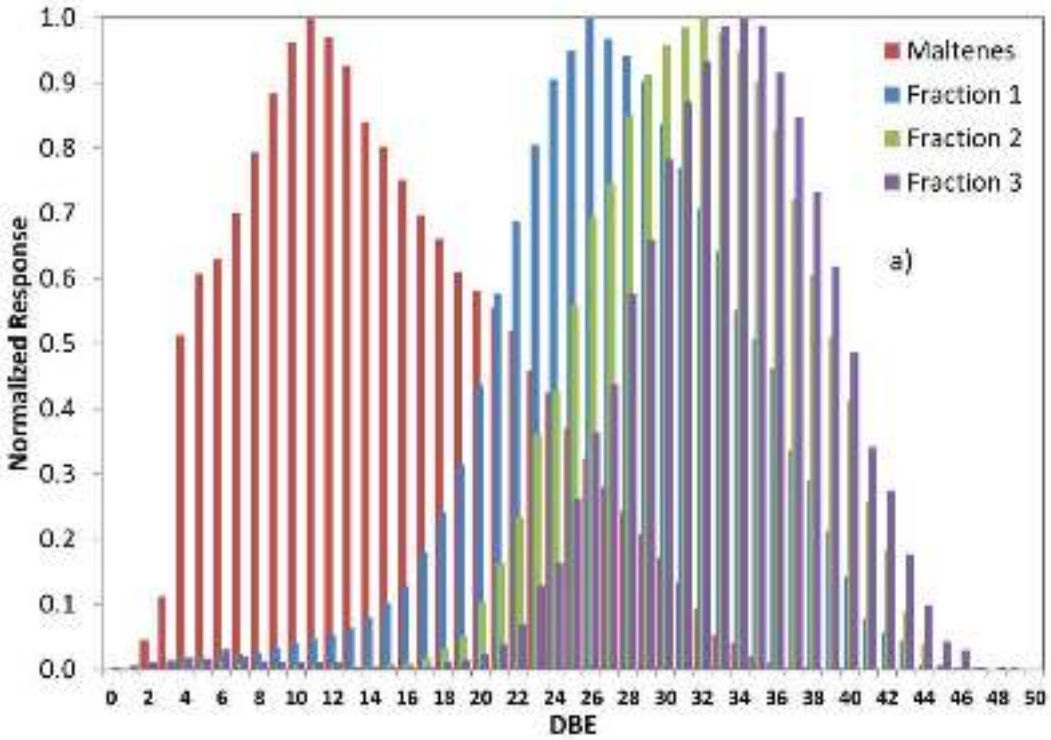

Carbon number

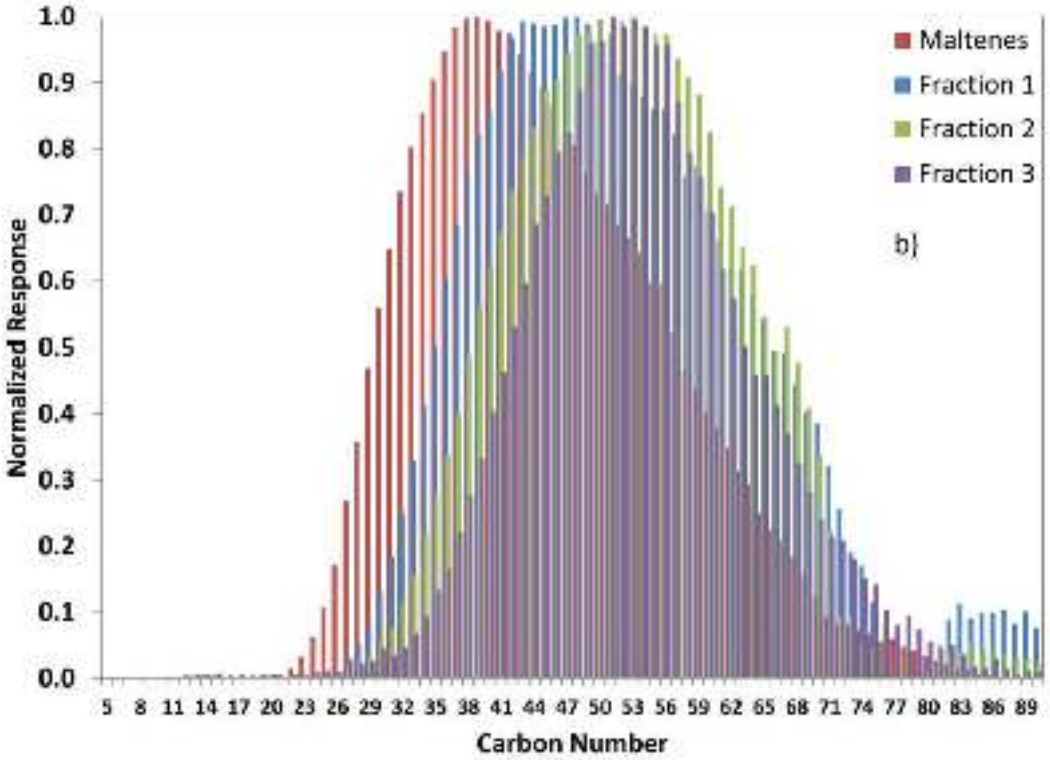

Asphaltene fractions

Fractions based on solubility in different solvent

E. Rogel, M. Witt, *Energy & Fuels* 2016, 30, 915-923.

Fraction 2

Compound classes: DBE and carbon number

DBE

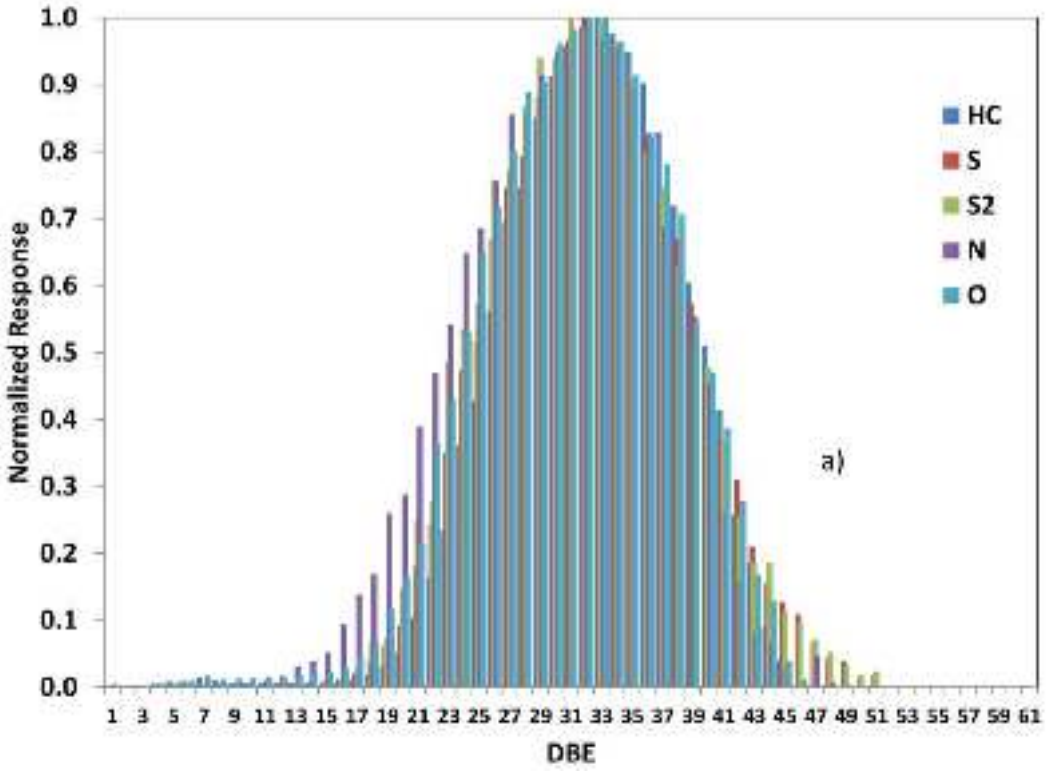

Carbon number

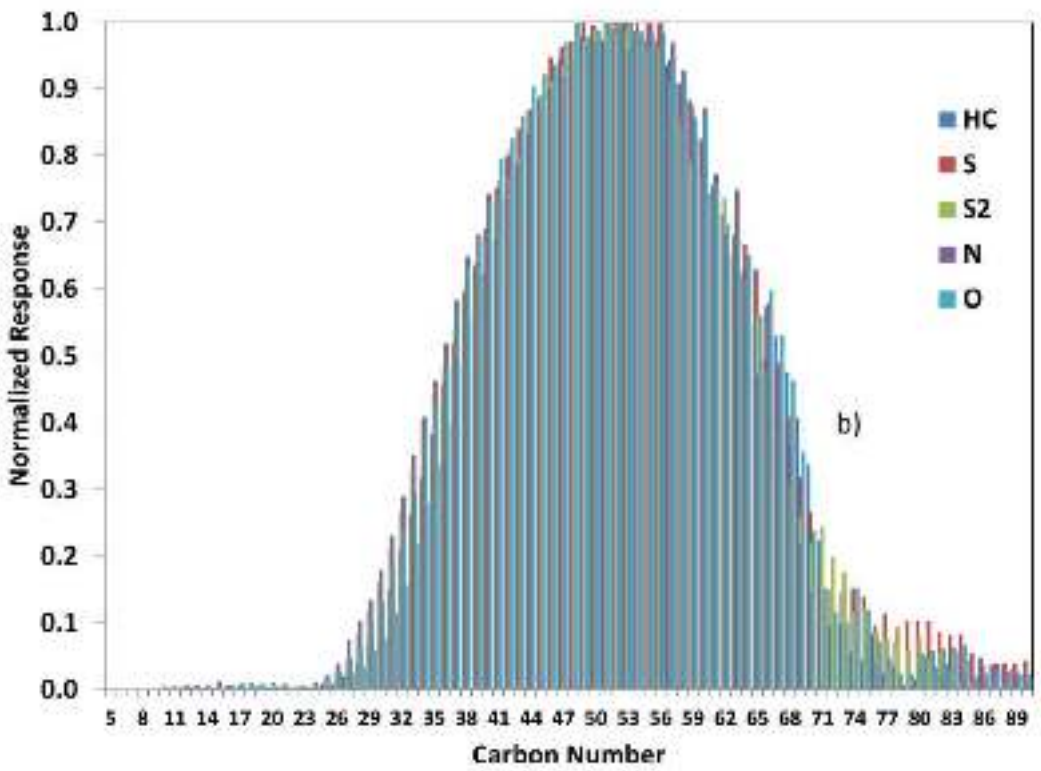

Asphaltene fractions

Precipitated at Different Solvent Power Conditions

E. Rogel, M. Witt, *Energy & Fuels* 2018, 32, 2653-2660.

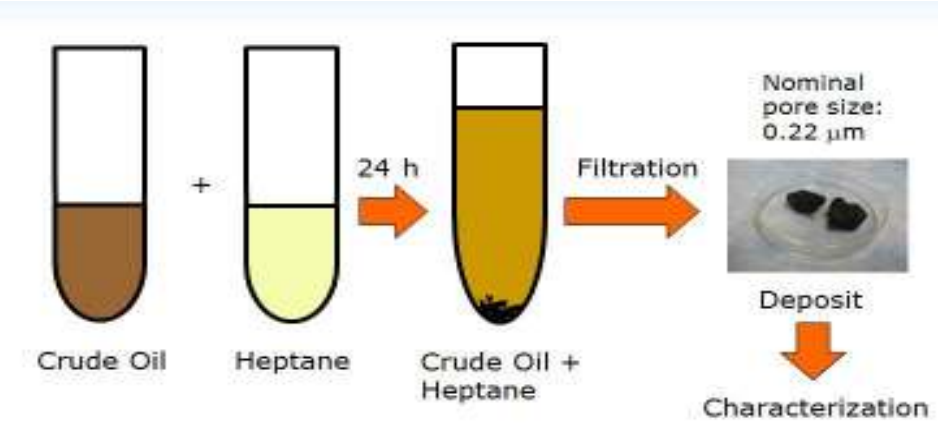

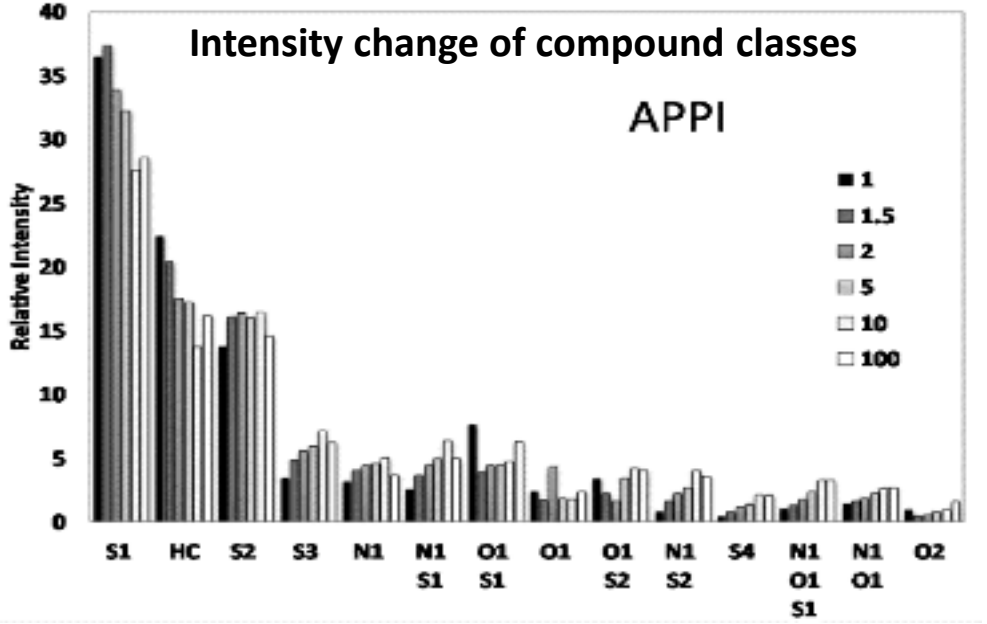

HCOR	C (wt %)	H (wt %)	H/C molar ratio
1	82.86	11.01	1.59
1.5	83.58	10.41	1.49
2	84.08	10.00	1.43
5	80.94	8.72	1.29
10	81.35	8.41	1.24
100	80.33	8.04	1.20

HCOR: heptane crude oil ratio

Asphaltene fractions

Precipitated at Different Solvent Power Conditions

E. Rogel, M. Witt, *Energy & Fuels* 2018, 32, 2653-2660.

Change of DBE and Aromaticity

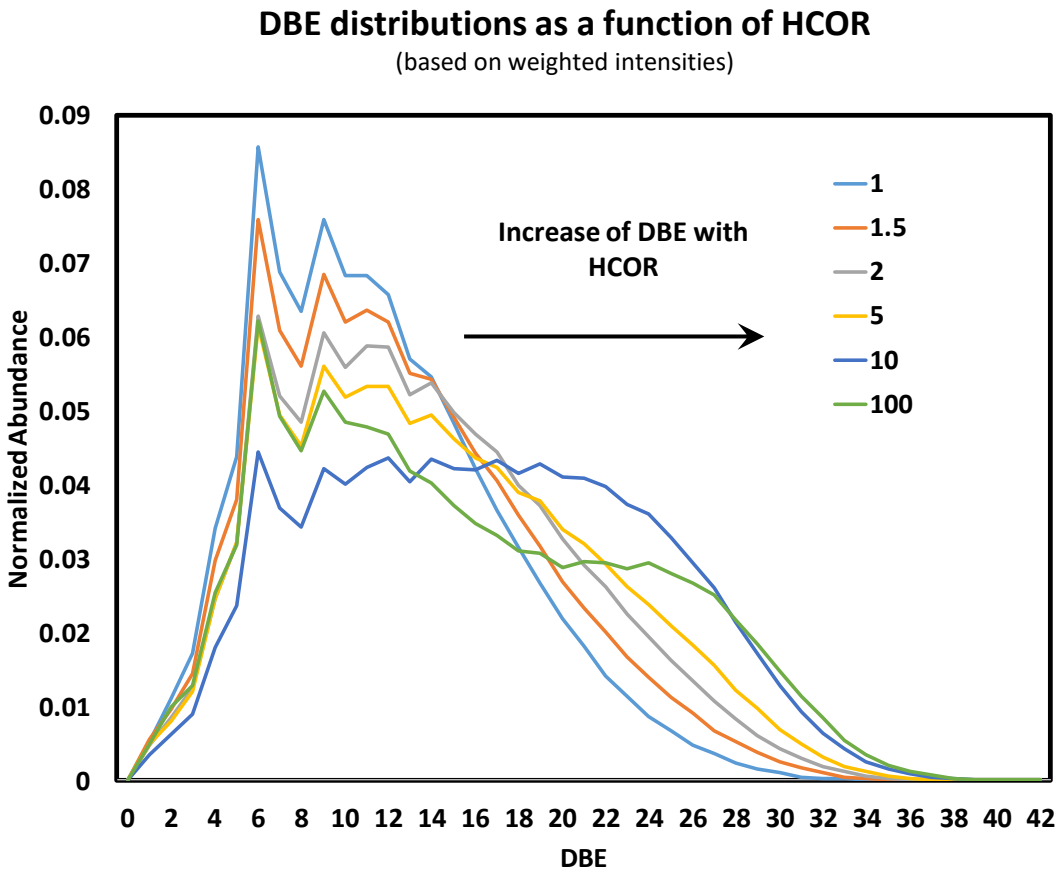

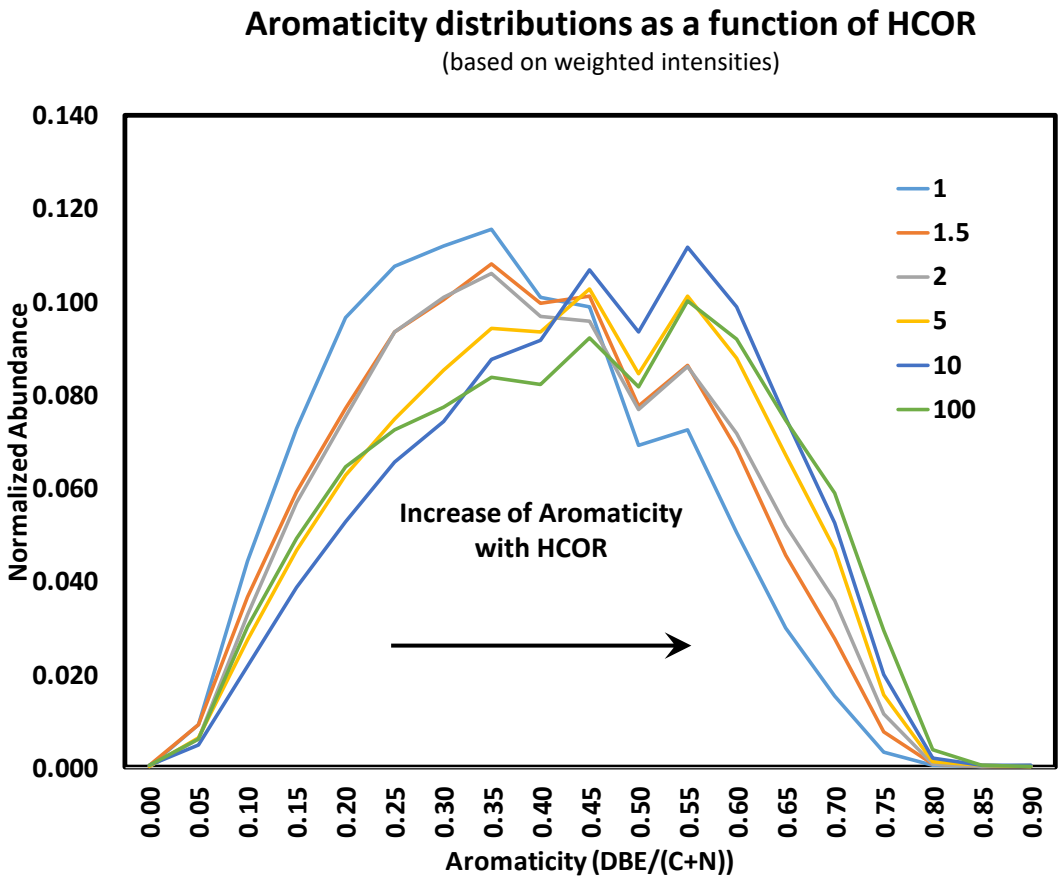

HCOR: heptane crude oil ratio

Asphaltene fractions

Precipitated at Different Solvent Power Conditions

E. Rogel, M. Witt, *Energy & Fuels* 2018, 32, 2653-2660.

DBE vs. C plots: Class HC

Distribution shifts with higher HCOR to higher DBE

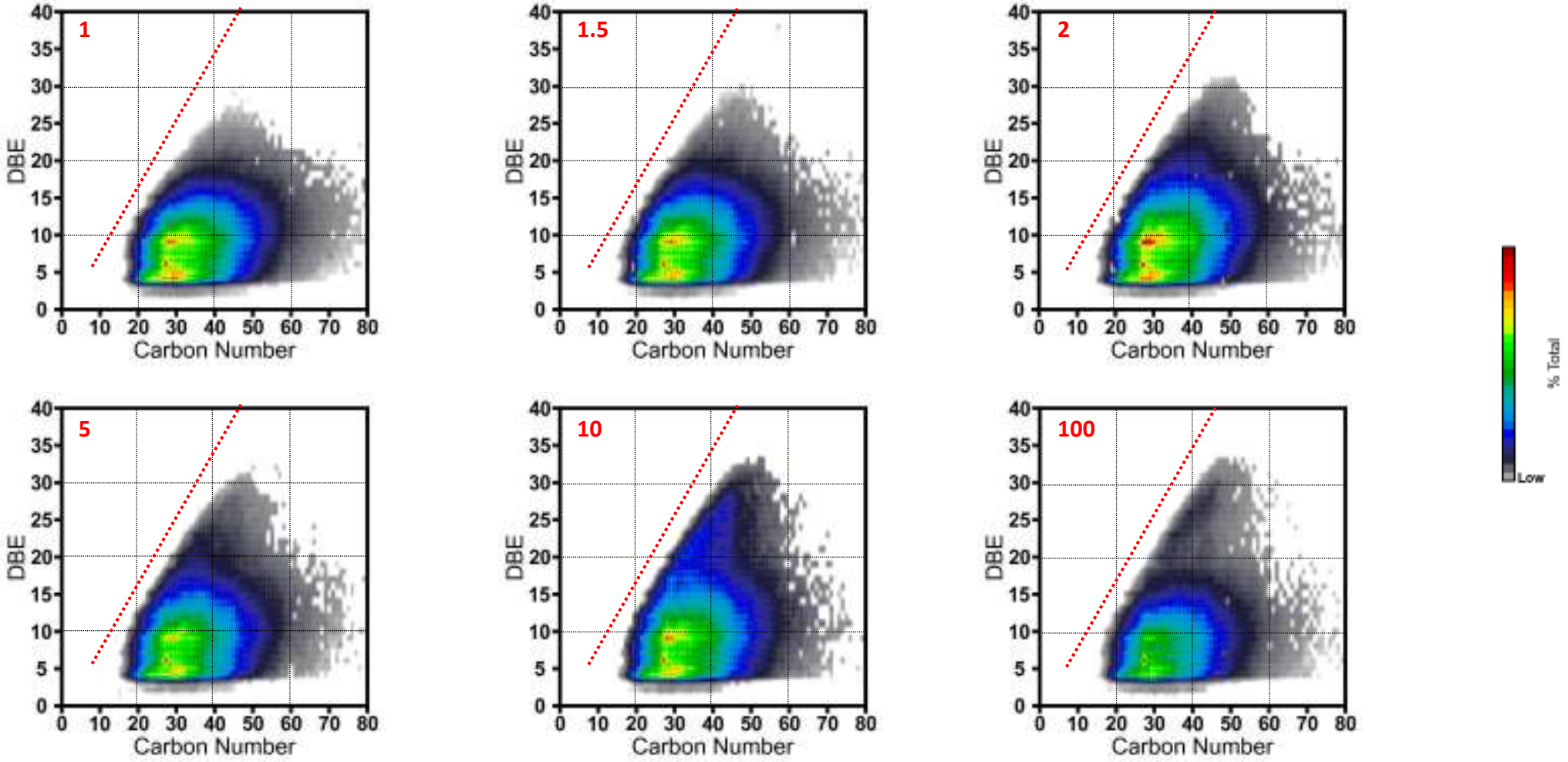

HCOR: heptane crude oil ratio

Asphaltene fractions

Precipitated at Different Solvent Power Conditions

E. Rogel, M. Witt, *Energy & Fuels* 2018, 32, 2653-2660.

DBE vs. C plots: Class S_1

Distribution shifts with higher HCOR to higher DBE

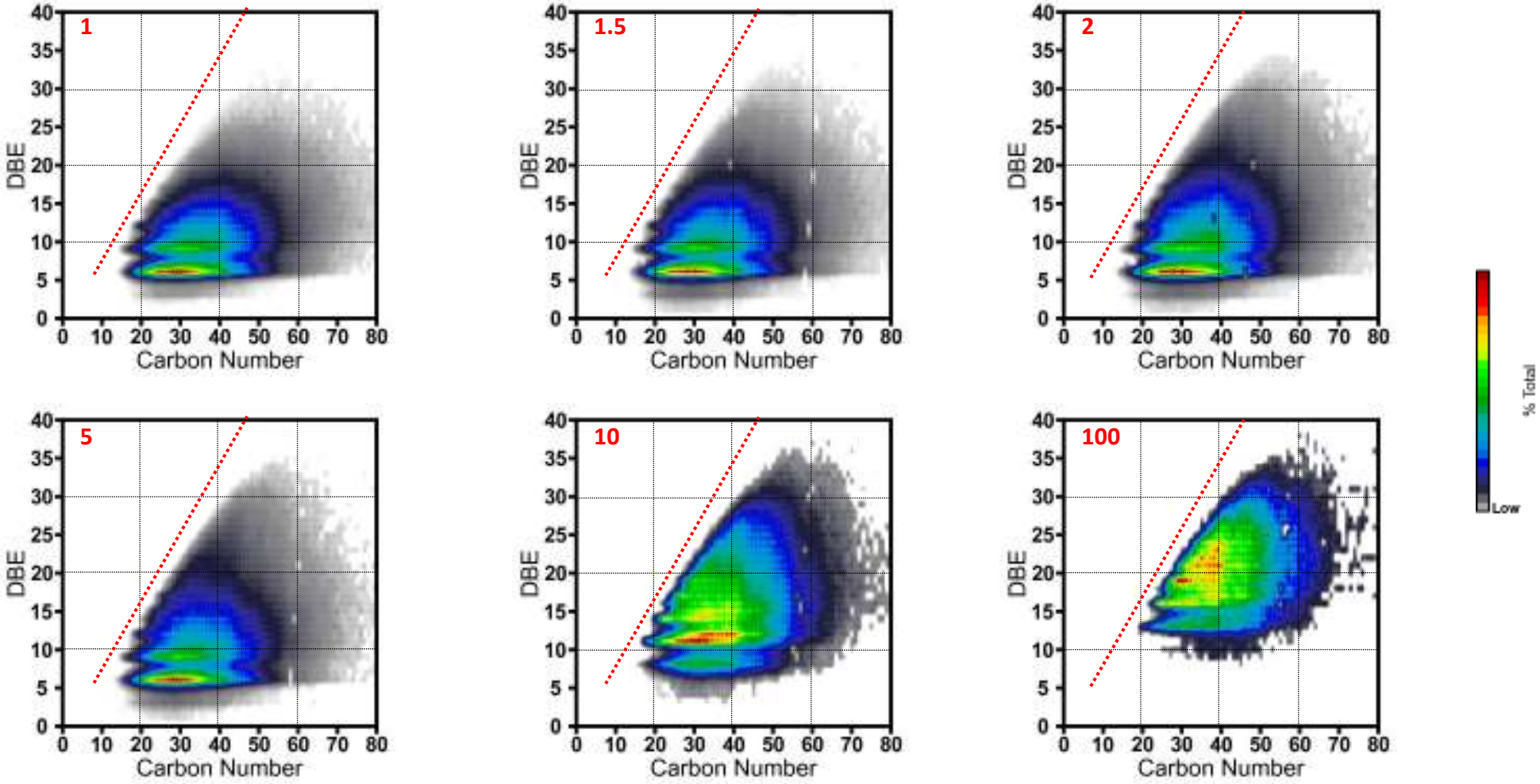

HCOR: heptane crude oil ratio

Asphaltene fractions

Precipitated at Different Solvent Power Conditions

E. Rogel, M. Witt, *Energy & Fuels* 2018, 32, 2653-2660.

No change in carbon distribution with HCOR

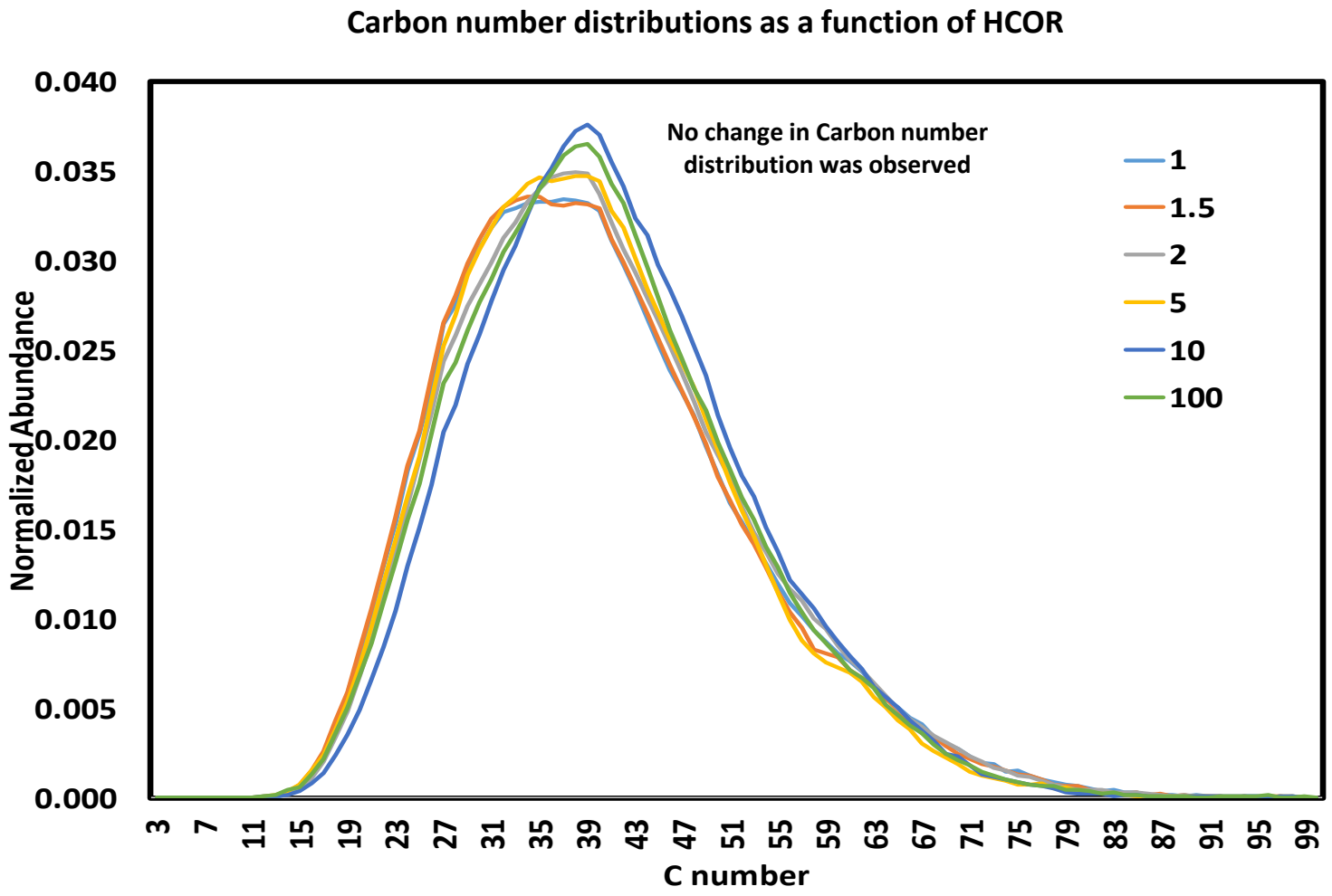

HCOR: heptane crude oil ratio

Asphaltene fractions

Precipitated at Different Solvent Power Conditions

E. Rogel, M. Witt, *Energy & Fuels* 2018, 32, 2653-2660.

Comparison of different aromaticity measurements: FT-IR, APPI FT-ICR MS and ^{1}H-NMR

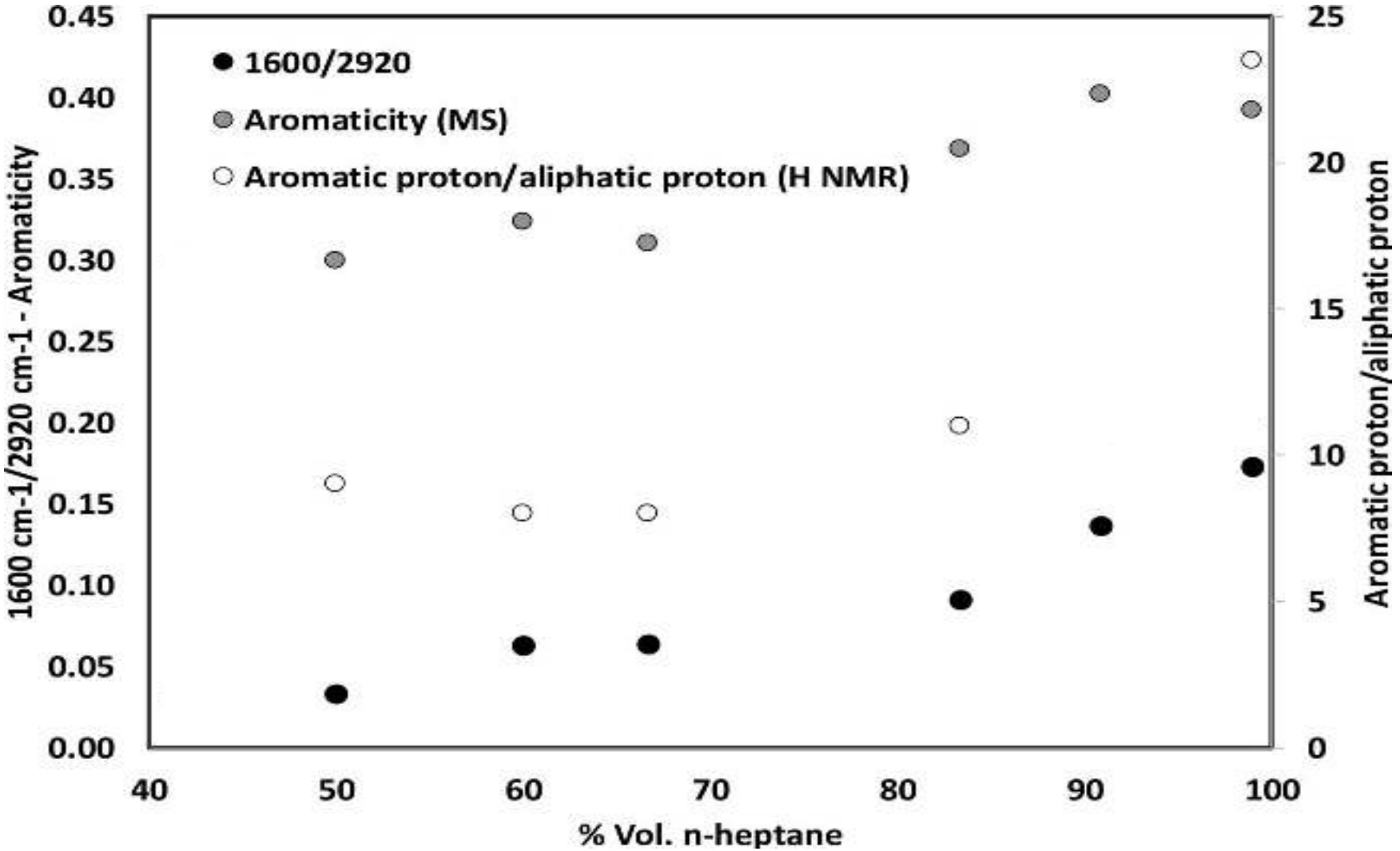

Asphaltene fractions

Precipitated at Different Solvent Power Conditions

E. Rogel, M. Witt, *Energy & Fuels* 2018, 32, 2653-2660.

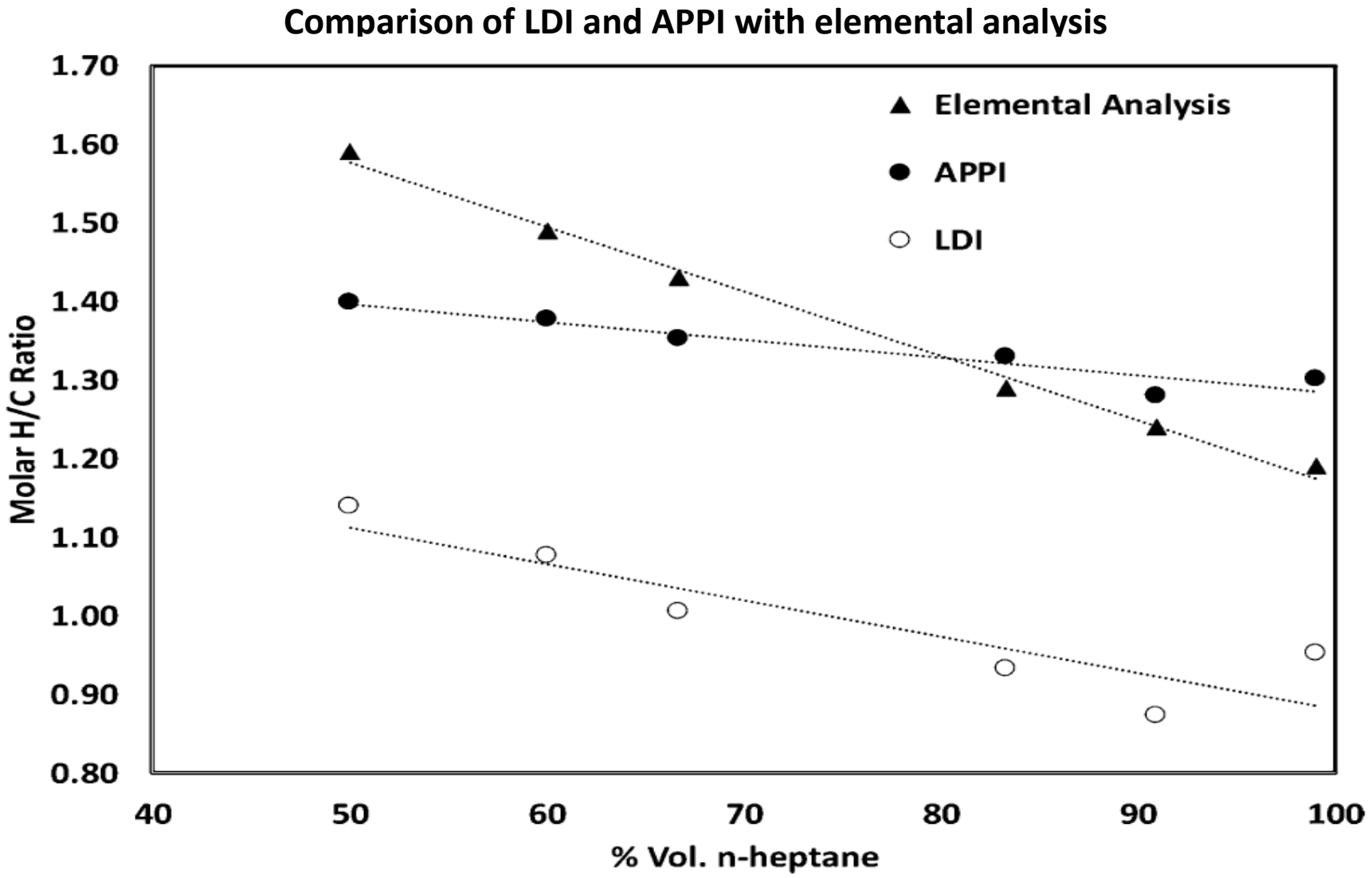

Asphaltene fractions

Precipitated at Different Solvent Power Conditions

E. Rogel, M. Witt, *Energy & Fuels* 2018, 32, 2653-2660.

Change of classes

Compositional distribution of unique species in the asphaltenes obtained at HCOR = 1 and 100

black: HCOR=1
grey: HCOR=100

a) DBE distribution

b) carbon distribution

c) hetero atom distribution

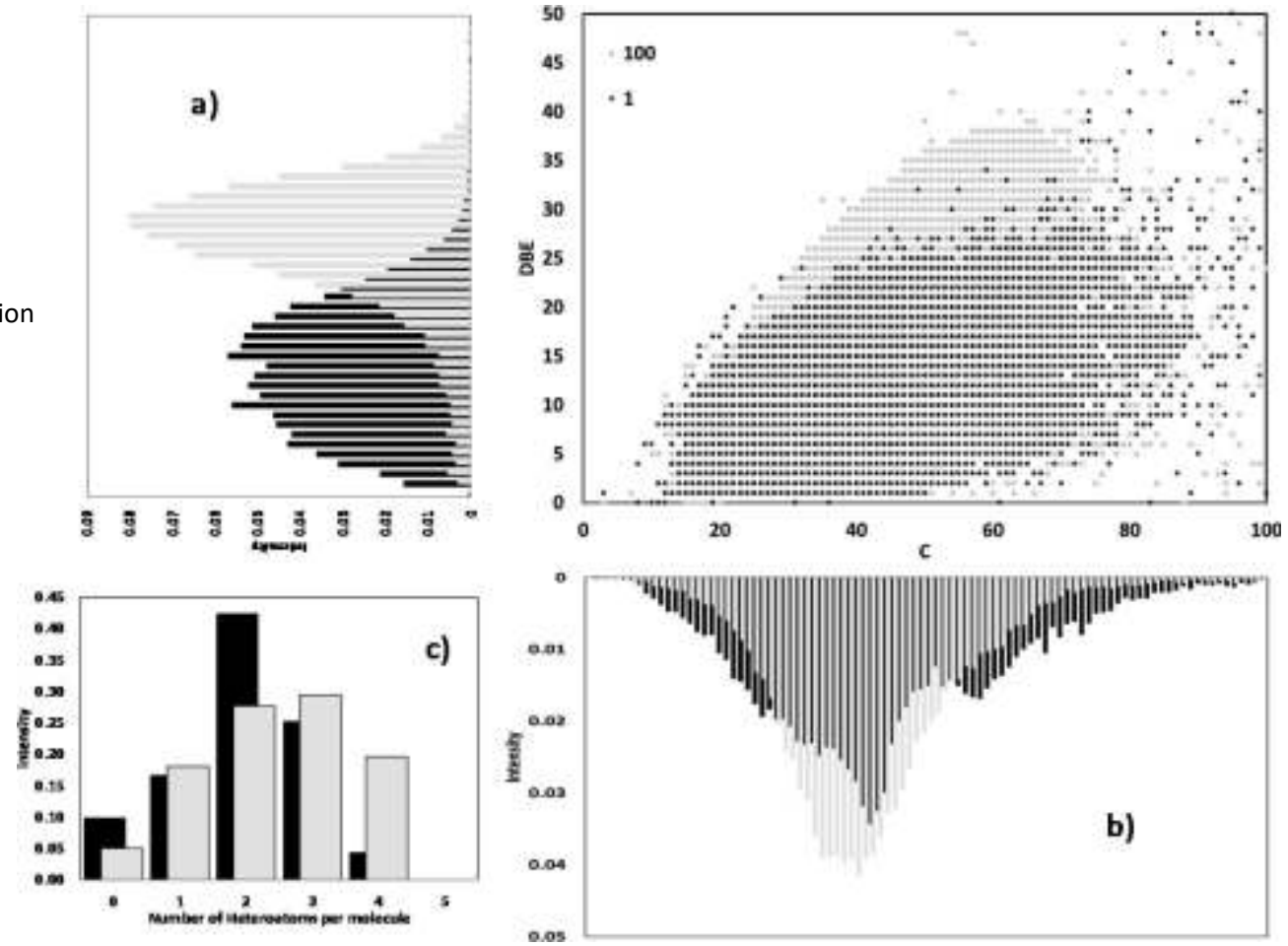

HCOR: heptane crude oil ratio

Asphaltene fractions

Time Effects on Precipitated Asphaltene

E. Rogel, M. Witt, *Energy & Fuels* 2019, 33, 9596−9603

Change of classes and hetero atom content

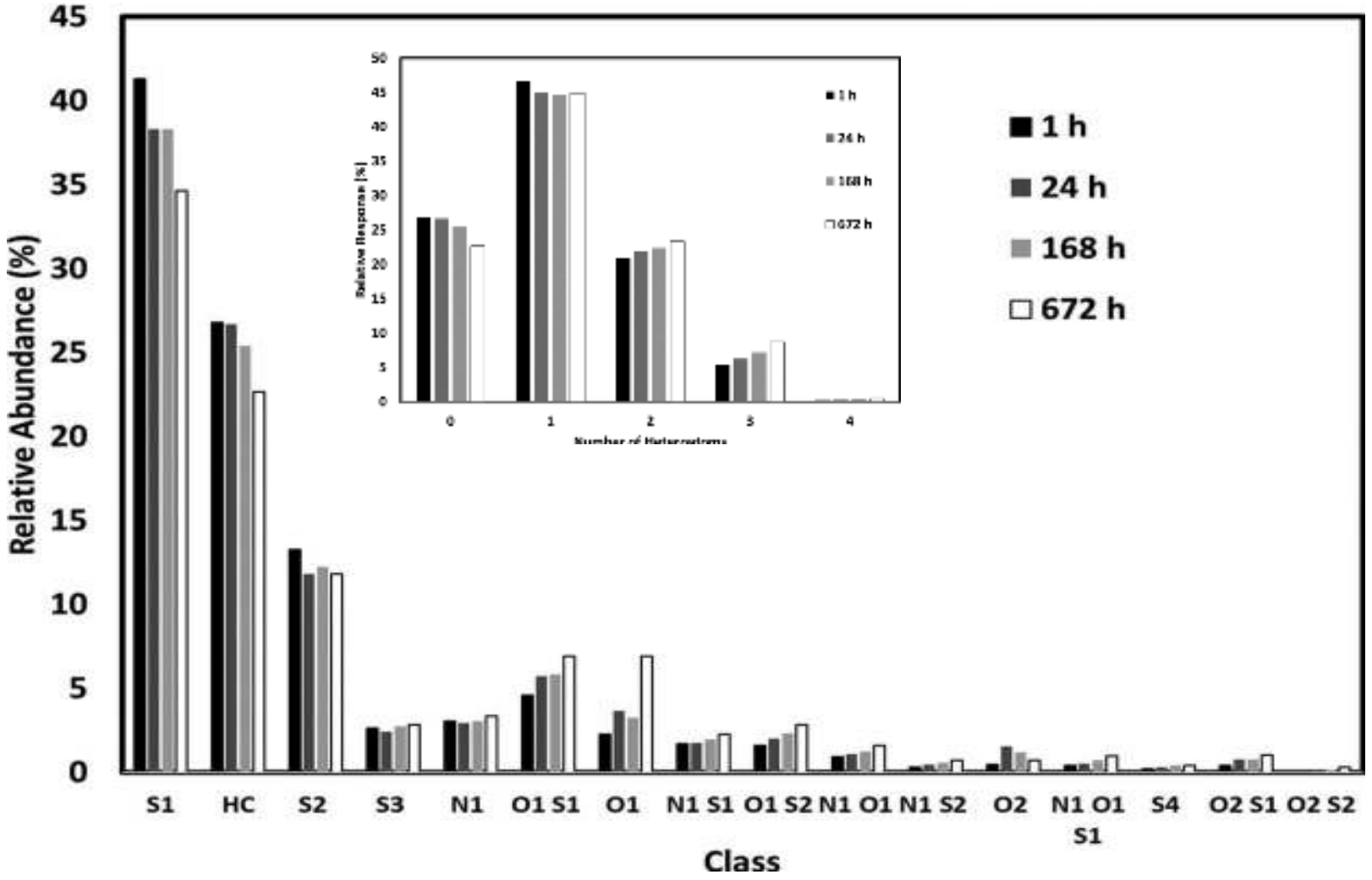

Time (h)	H/C ratio
1	1.54
24	1.43
168	1.42
672	1.38

heptane crude oil ratio 1:10

Asphaltene fractions

Time Effects on Precipitated Asphaltene

E. Rogel, M. Witt, *Energy & Fuels* 2019, 33, 9596−9603

Change in DBE

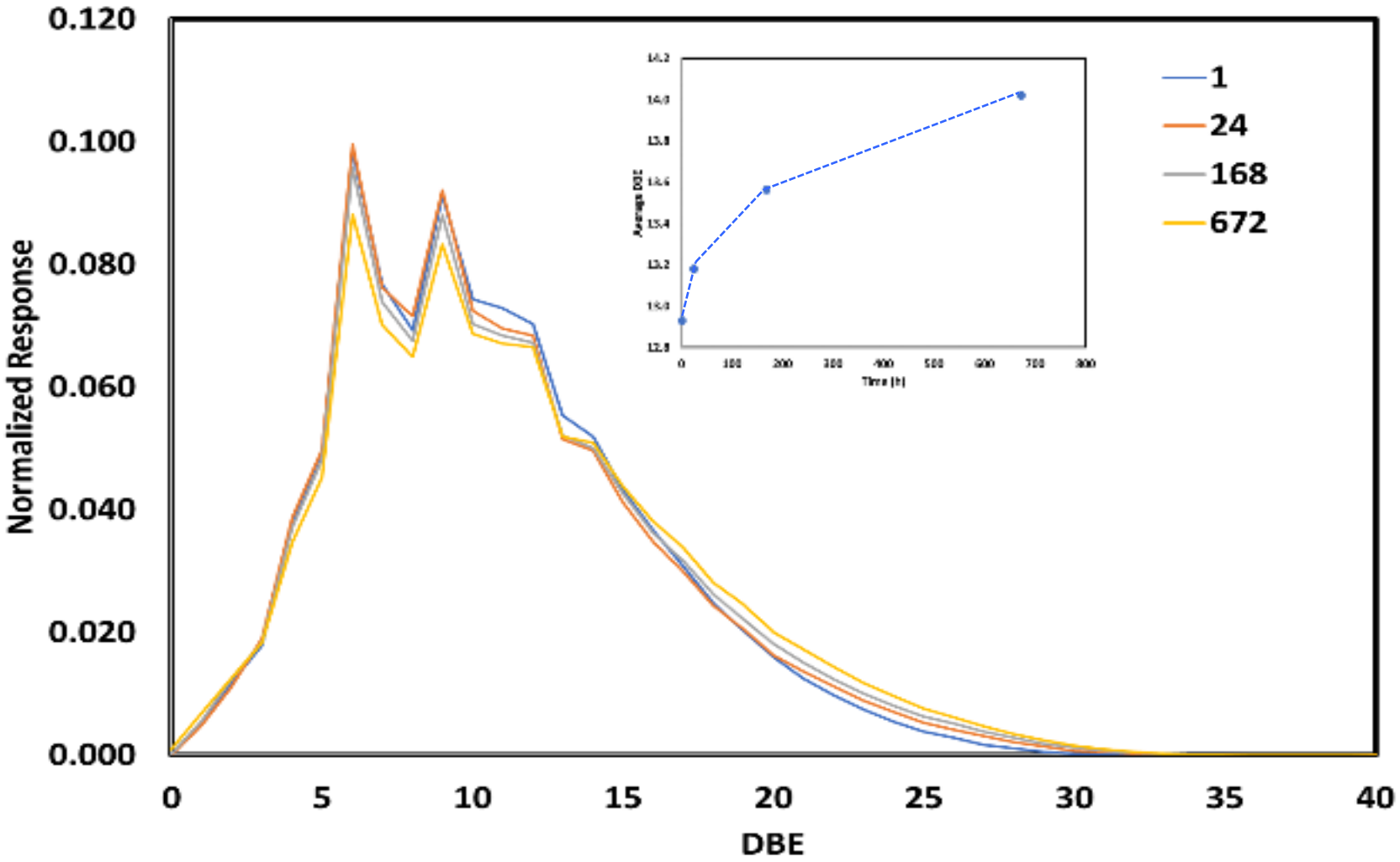

Time (h)	H/C ratio
1	1.54
24	1.43
168	1.42
672	1.38

heptane crude oil ratio 1:10

Asphaltene fractions

Time Effects on Precipitated Asphaltene

E. Rogel, M. Witt, *Energy & Fuels* 2019, 33, 9596−9603

Change in DBE

Class HC

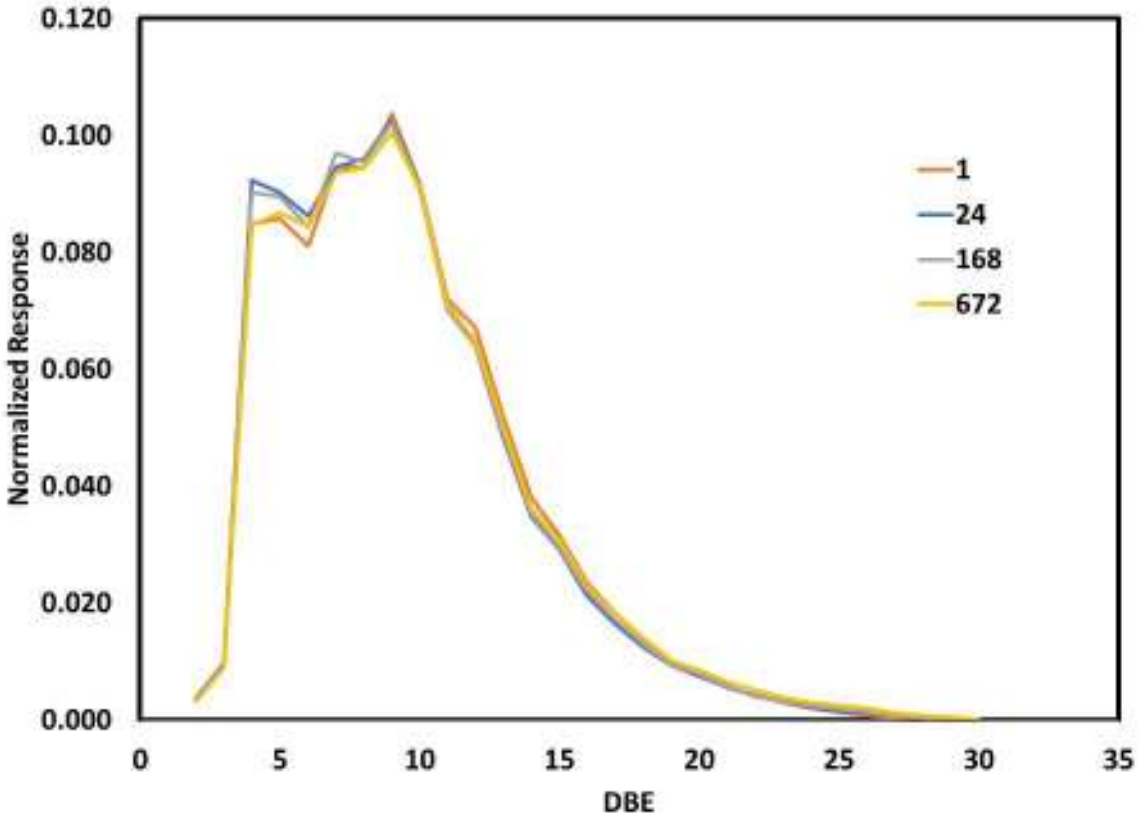

Class S_3

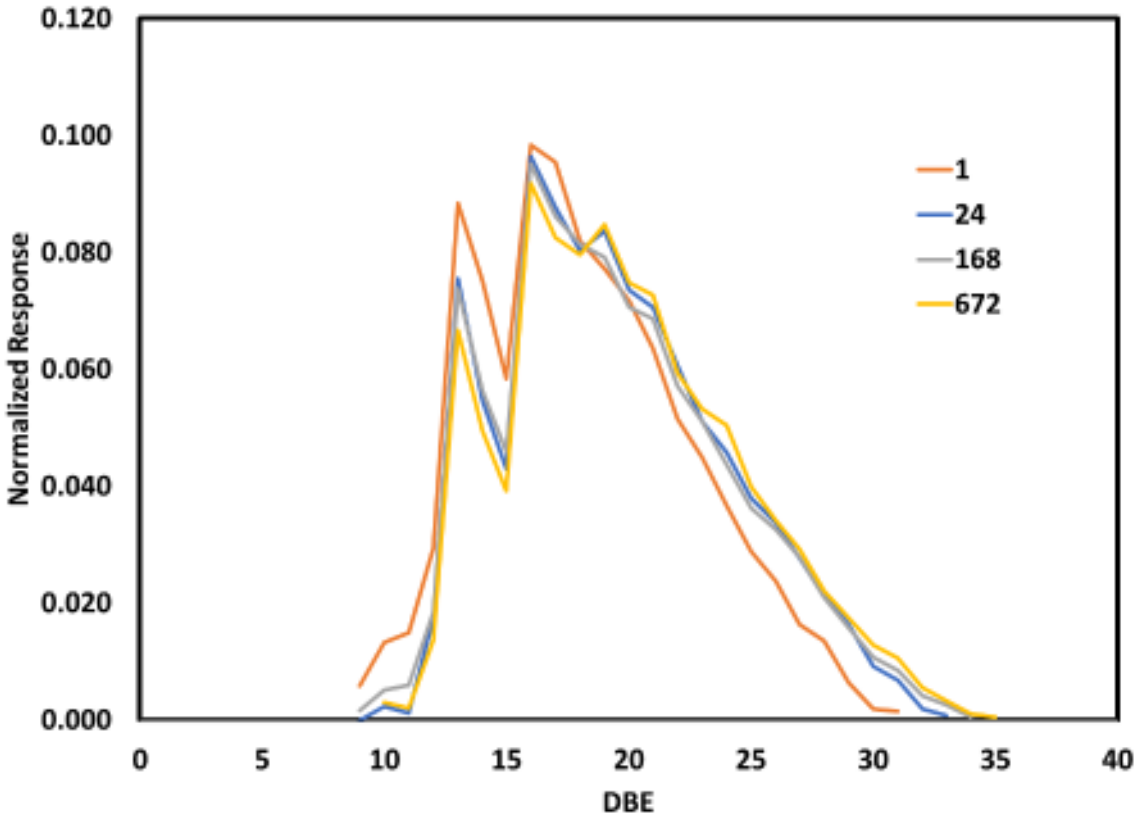

Asphaltene fractions

Time Effects on Precipitated Asphaltene

E. Rogel, M. Witt, *Energy & Fuels* 2019, 33, 9596−9603

Comparison of the compositional space for sulfur containing species that appear in the aged deposit (672 h) with the ones that go back to the fluid from the initially precipitated material (1 h)

▲ Dissolved species

○ Precipitated species

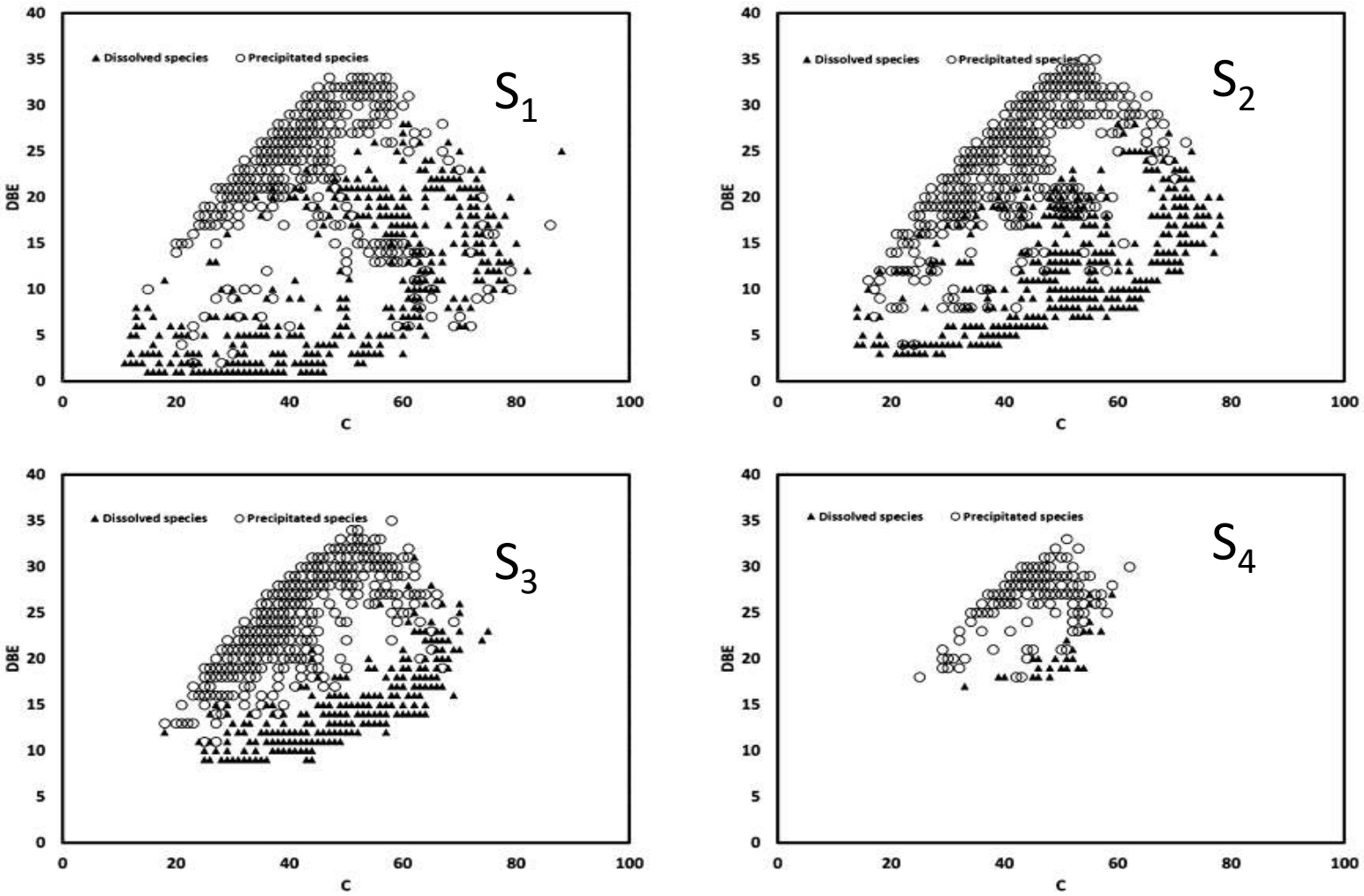

Hydroprocessing

Hydroprocessing

Effect on compound classes

E. Rogel, M. Witt, *Energy & Fuels* 2017, 31, 3409-3416.

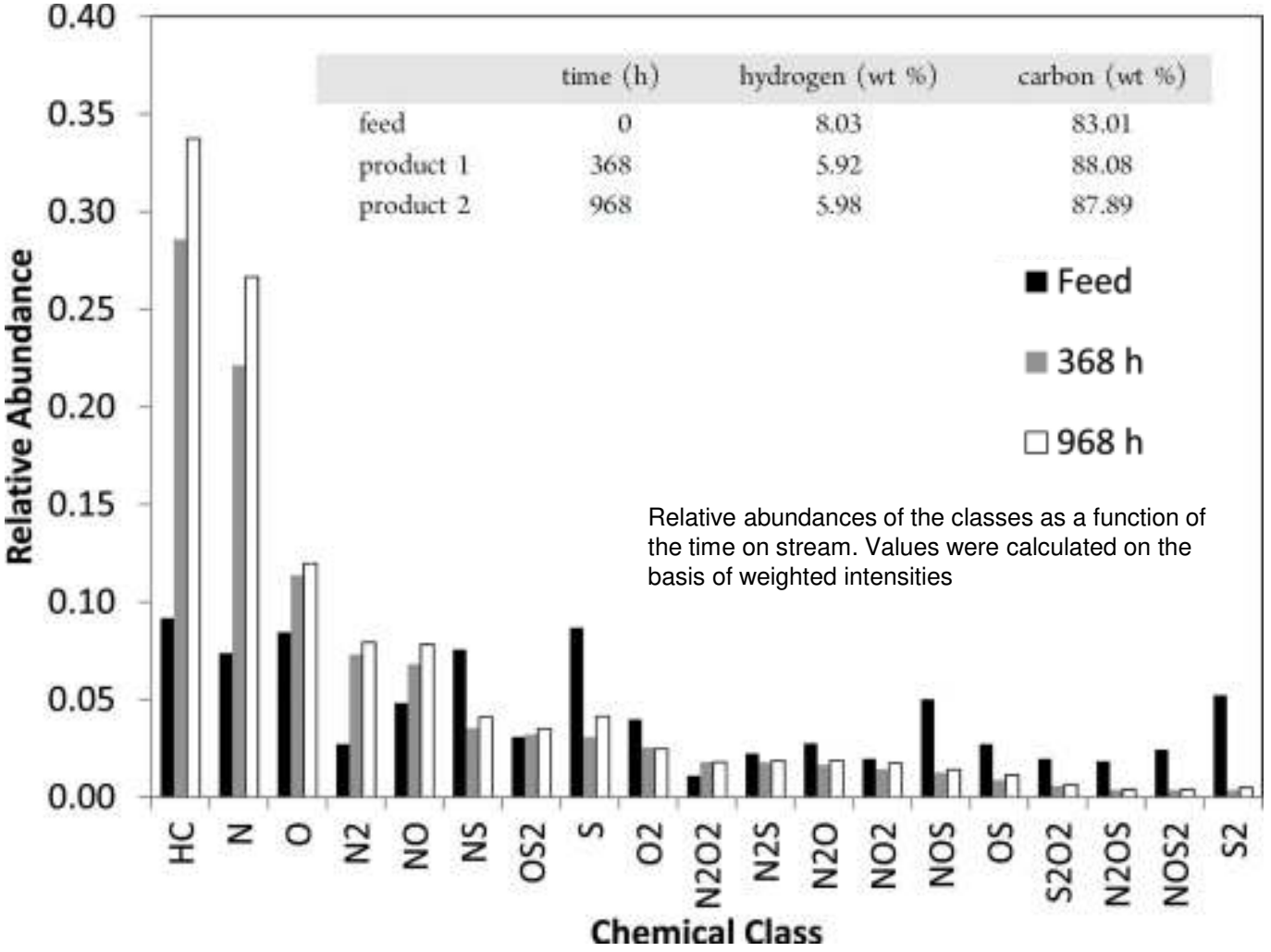

	time (h)	hydrogen (wt %)	carbon (wt %)
feed	0	8.03	83.01
product 1	368	5.92	88.08
product 2	968	5.98	87.89

Relative abundances of the classes as a function of the time on stream. Values were calculated on the basis of weighted intensities

Hydroprocessing

Effect on carbon distribution, aromaticity and hetero atom content

E. Rogel, M. Witt, *Energy & Fuels* 2017, 31, 3409-3416.

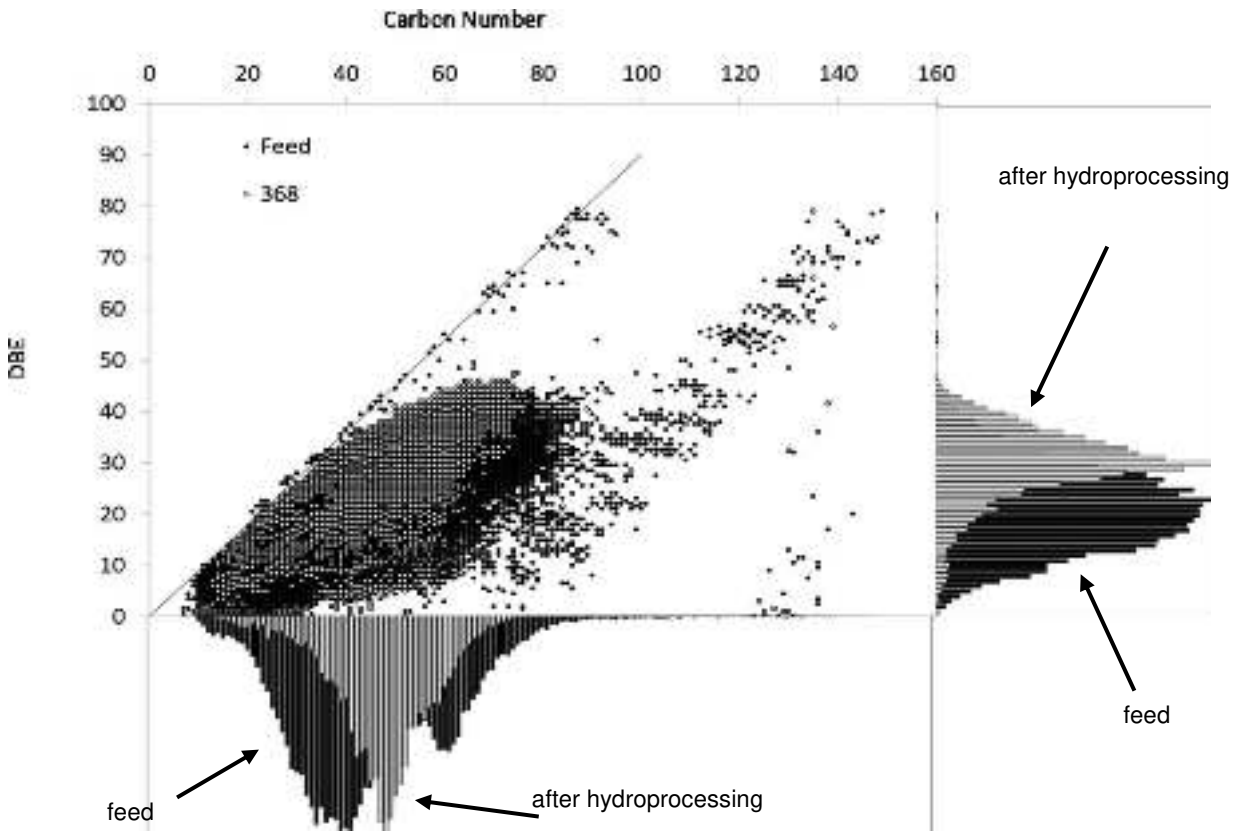

Heteroatom contents as a function of time on stream

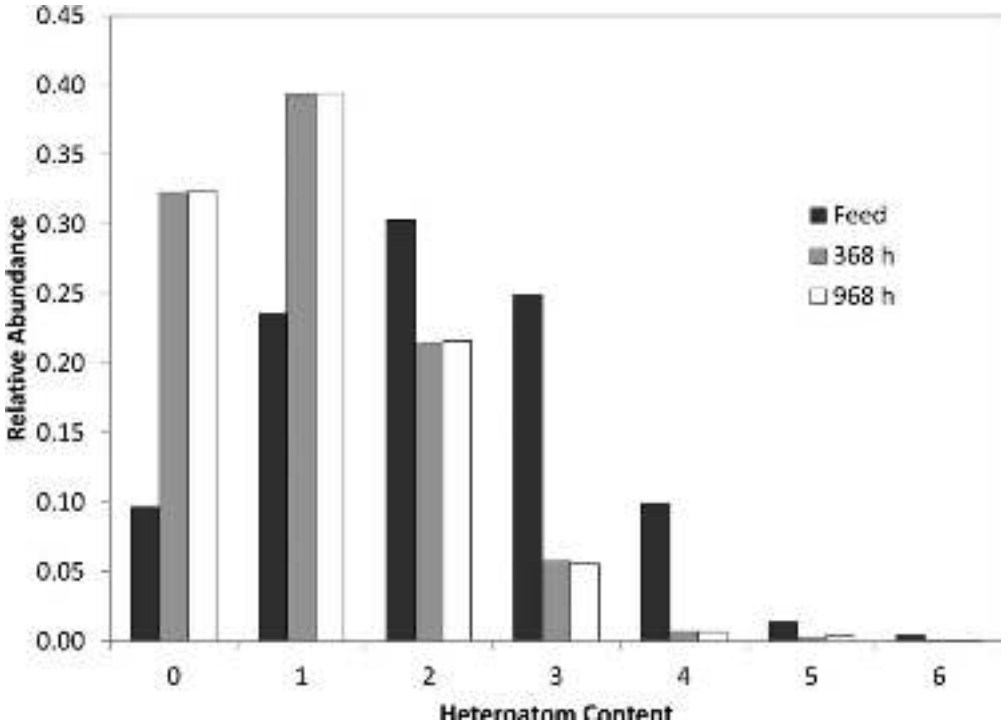

Comparison of the compositional space occupied by molecules that disappeared from the feed during processing to those that appeared in the products.

Hydroprocessing

Appearing and disappearing compound by hydroprocessing

E. Rogel, M. Witt, *Energy & Fuels* 2017, 31, 3409-3416.

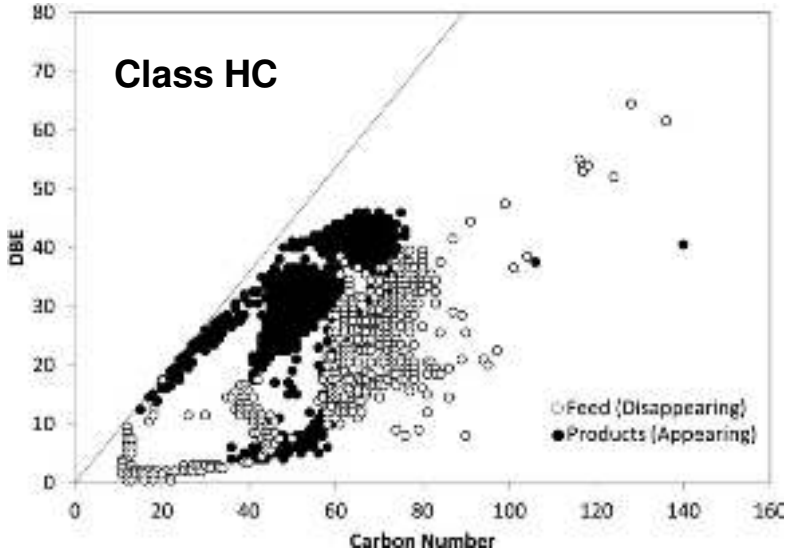

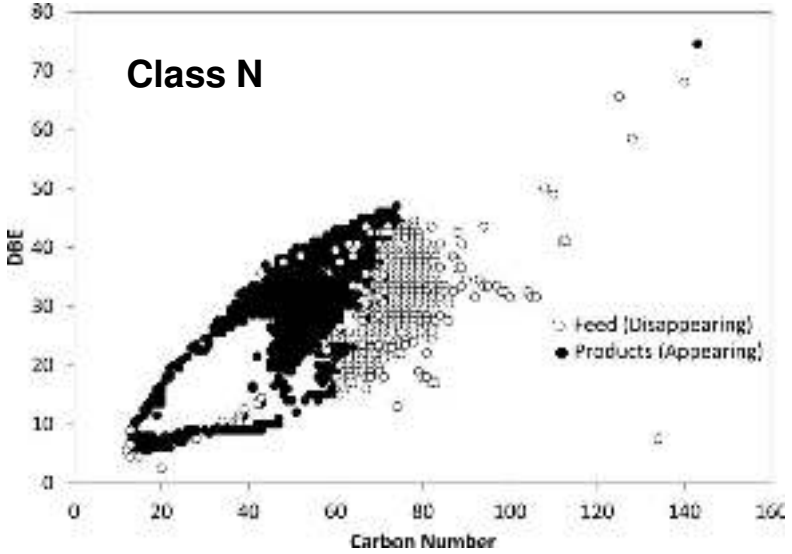

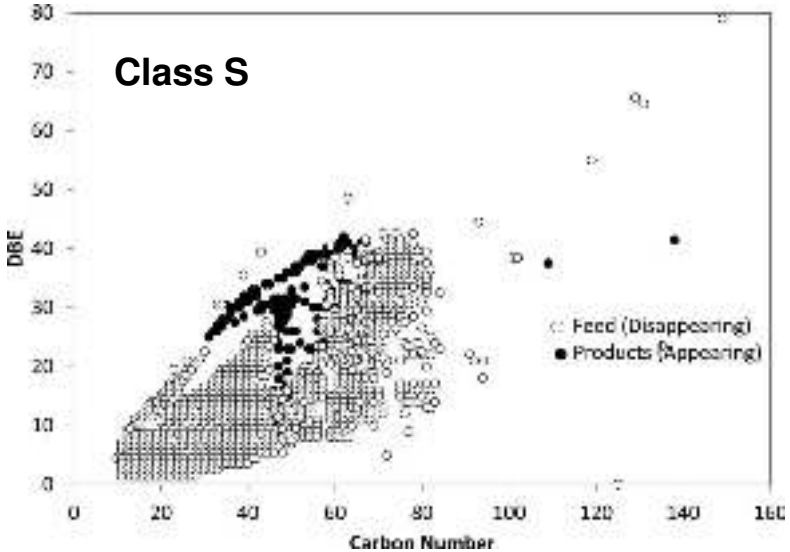

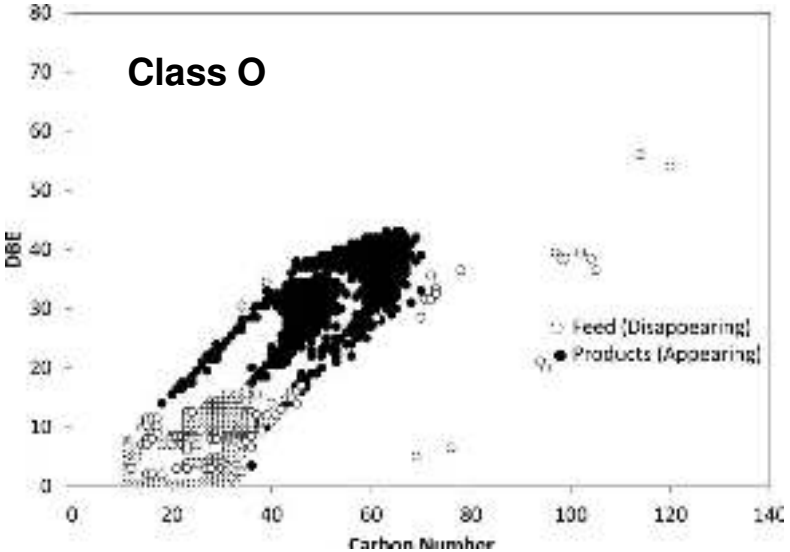

Compositional and Structural Continuum of Petroleum

Compositional and Structural Continuum of Petroleum

Distillation series

A. McKenna et al., *Energy Fuels 2010, 24 (5), 2929–2938.*

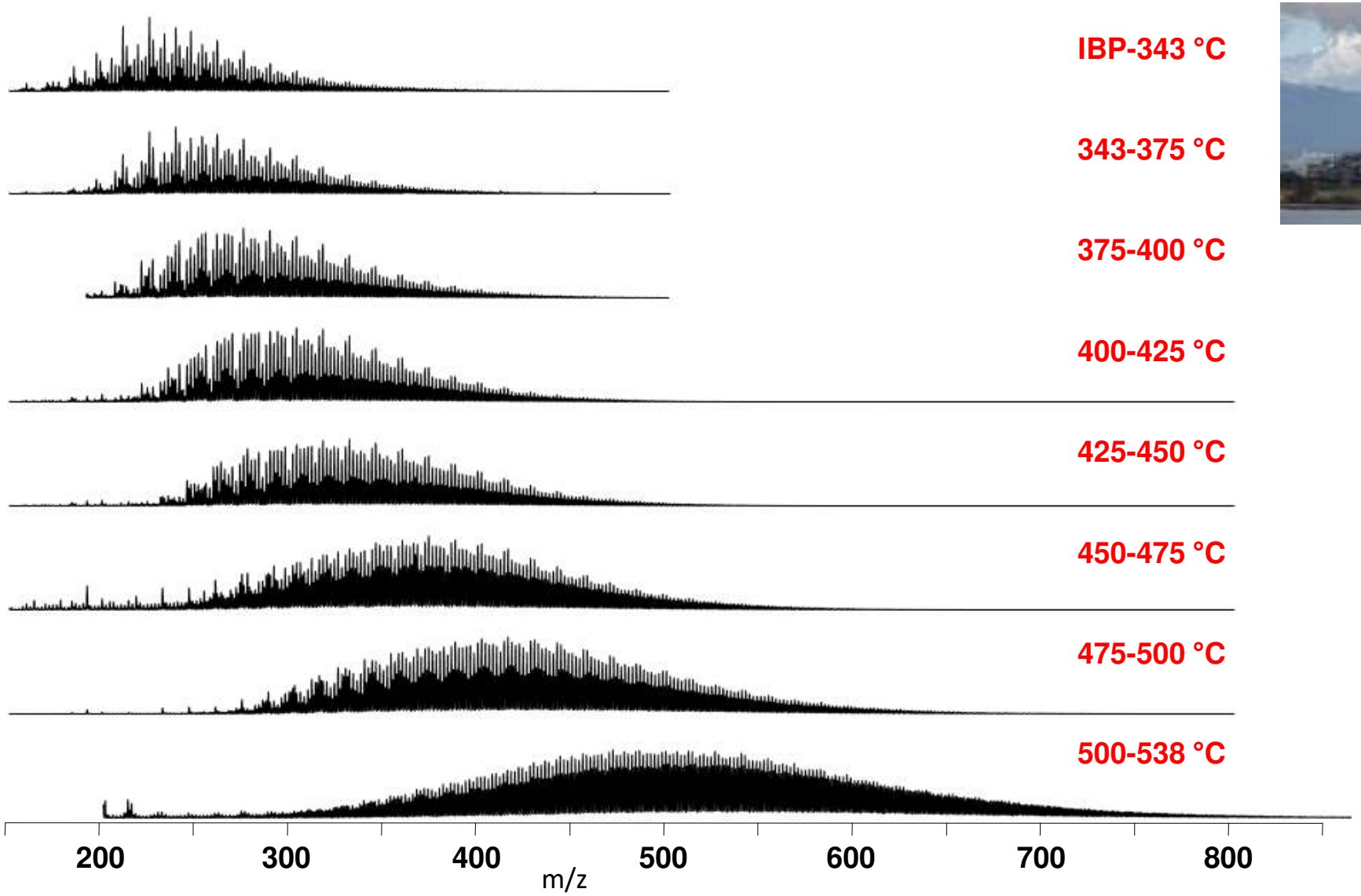

IBP: initial boiling point

Compositional and Structural Continuum of Petroleum

Distillation series – Boduszynski Continuum Model

A. McKenna et al., *Energy Fuels 2010, 24 (5), 2929–2938.*

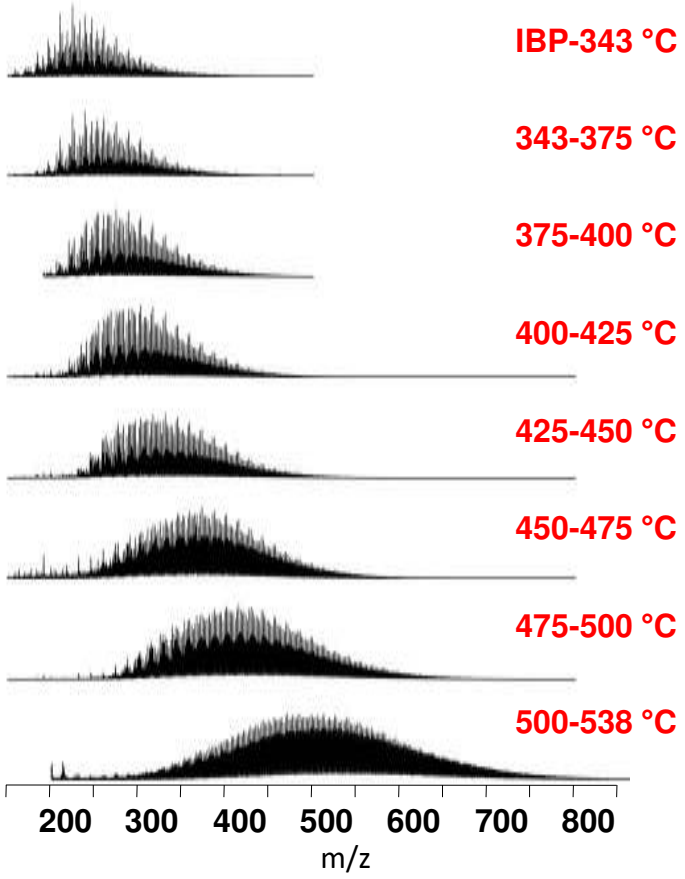

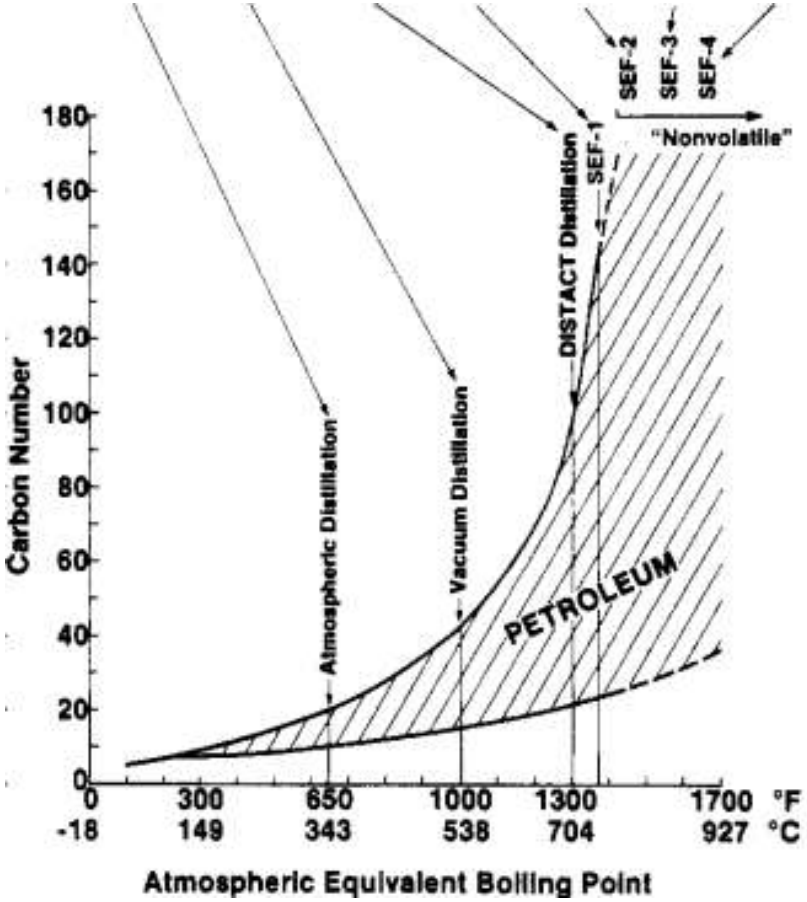

Boduszynski Continuum Model

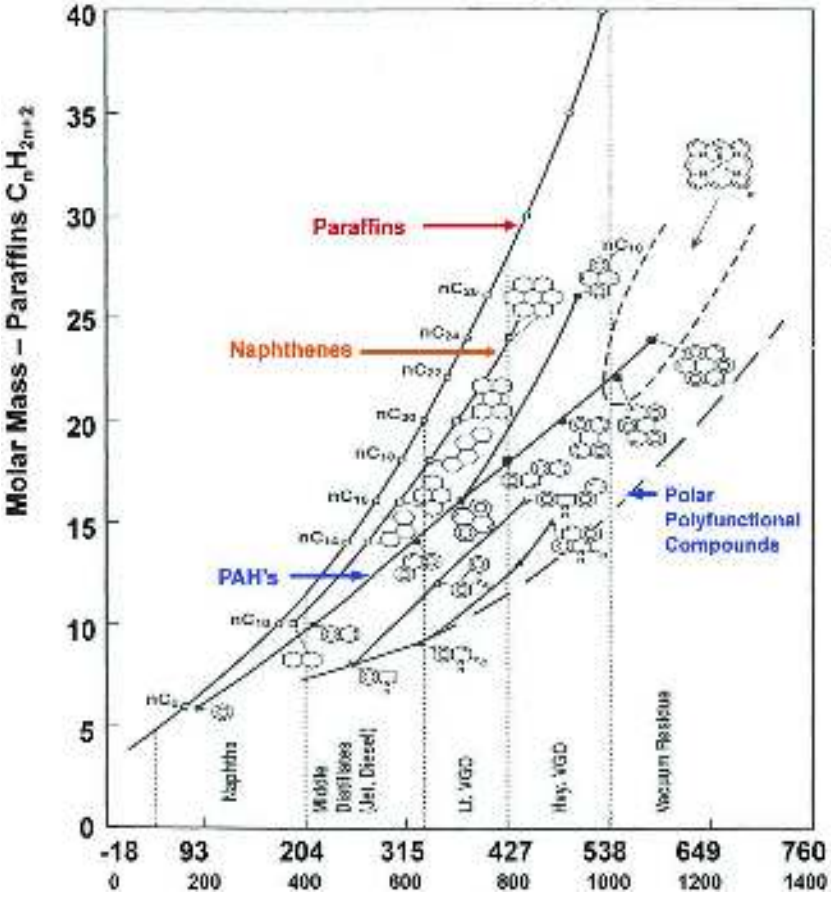

IBP: initial boiling point

Compositional and Structural Continuum of Petroleum

Distillation series

A. McKenna et al., *Energy Fuels 2010, 24 (5), 2929–2938.*

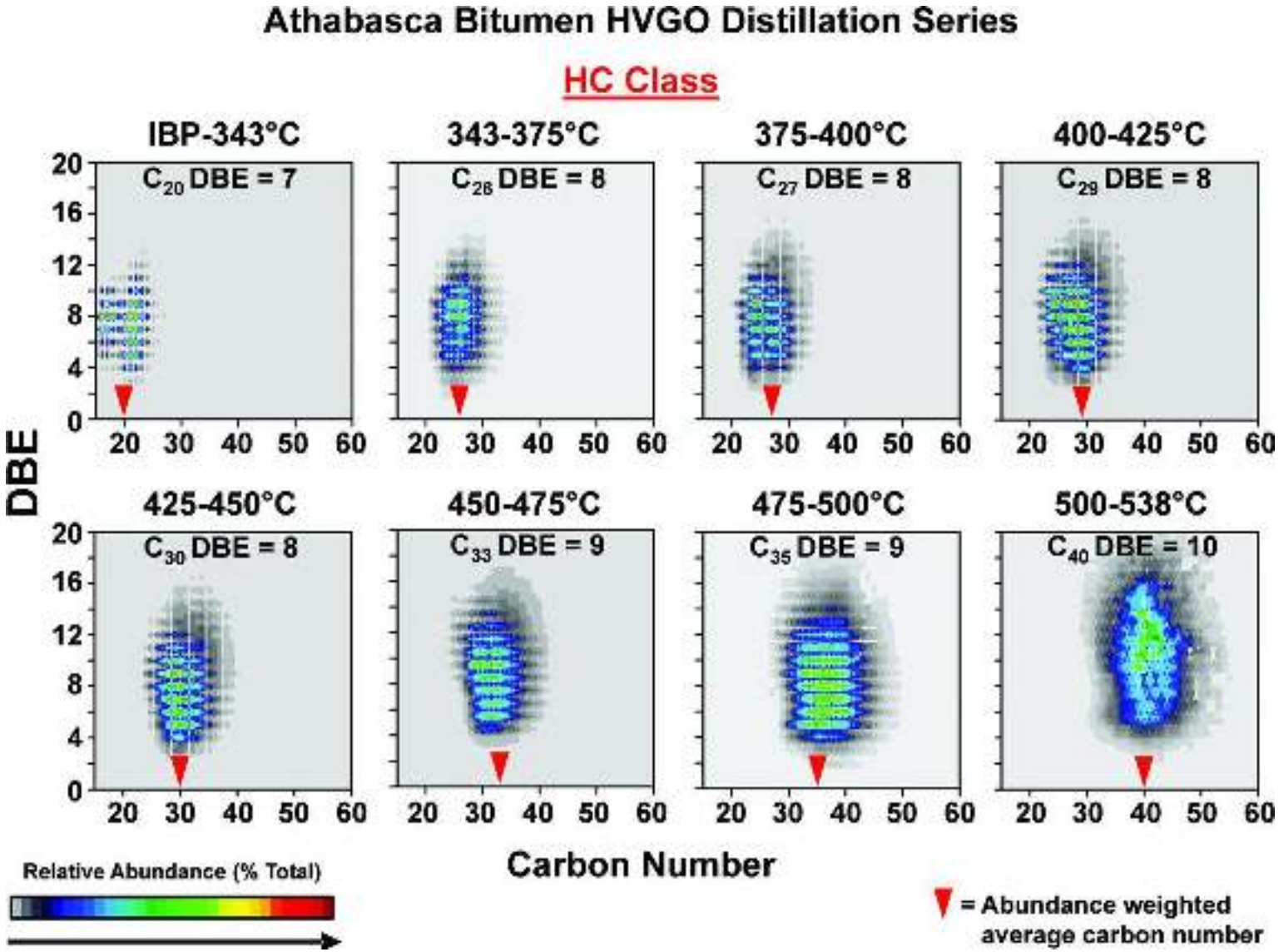

Compositional and Structural Continuum of Petroleum

Distillation series

A. McKenna et al., *Energy Fuels 2010, 24 (5), 2929–2938.*

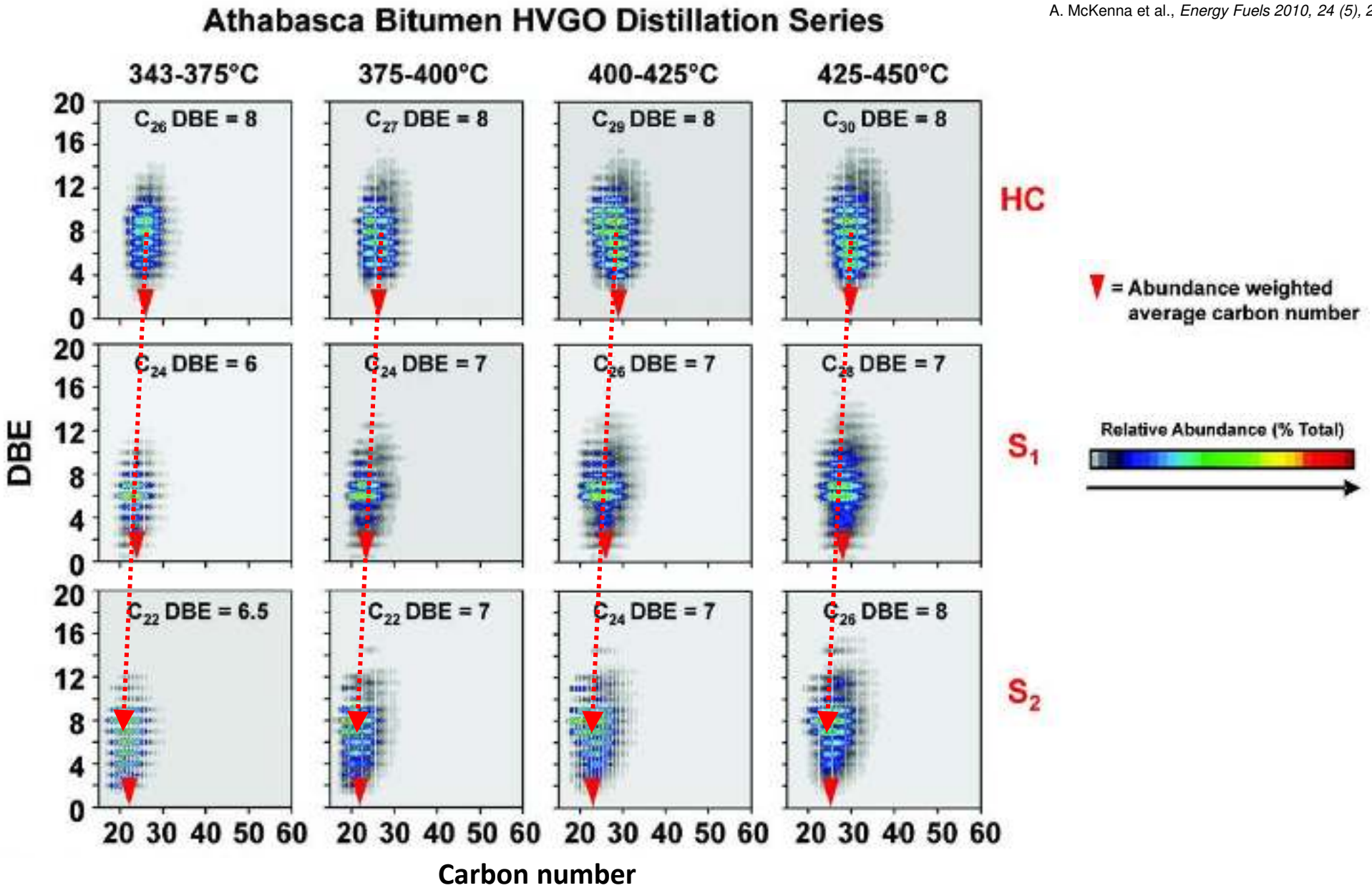

Compositional and Structural Continuum of Petroleum

Distillation series

A. McKenna et al., *Energy Fuels 2010, 24 (5), 2929–2938.*

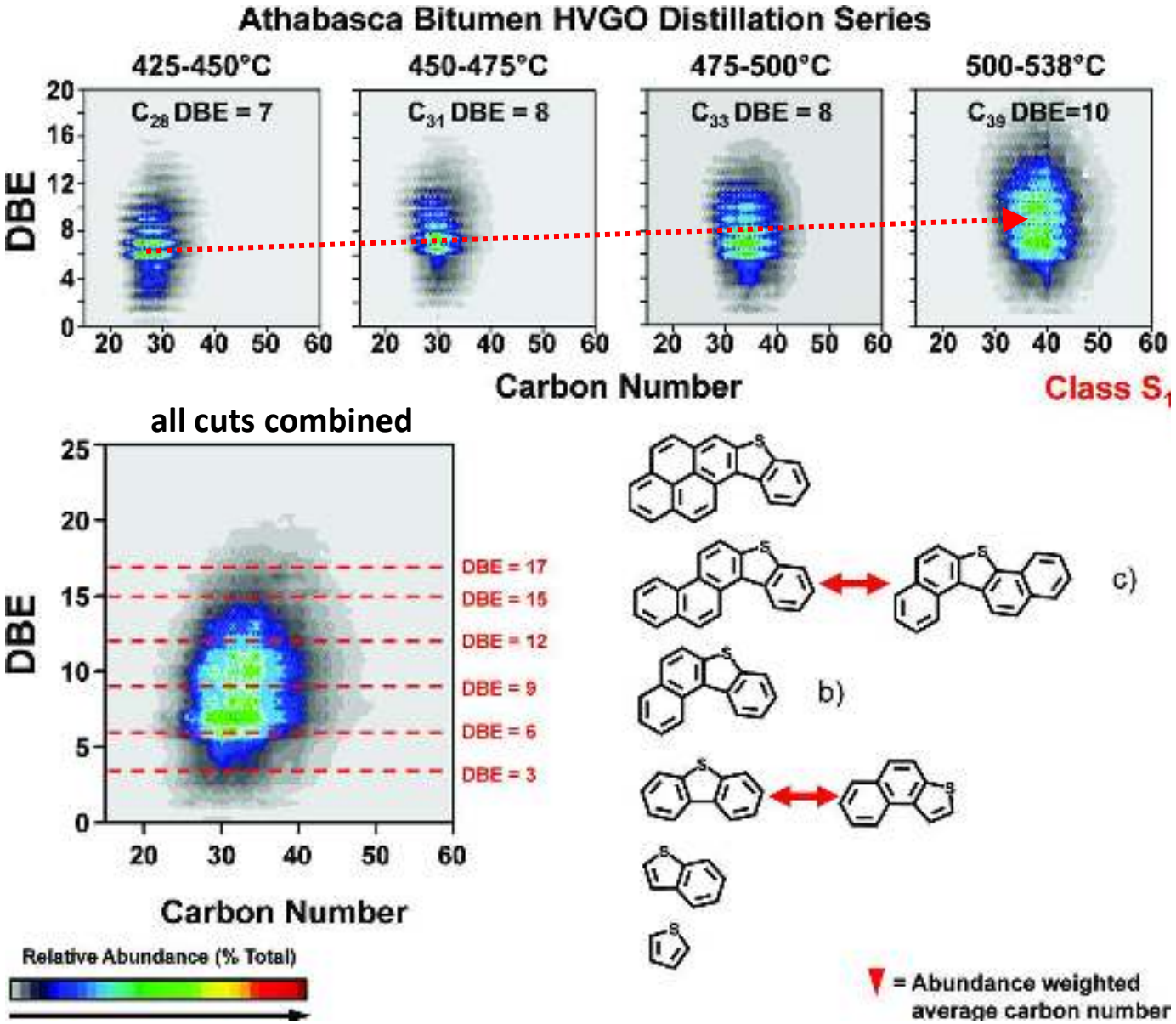

Compositional and Structural Continuum of Petroleum

Distillation series

A. McKenna et al., *Energy Fuels 2010, 24 (5), 2939–2946.*

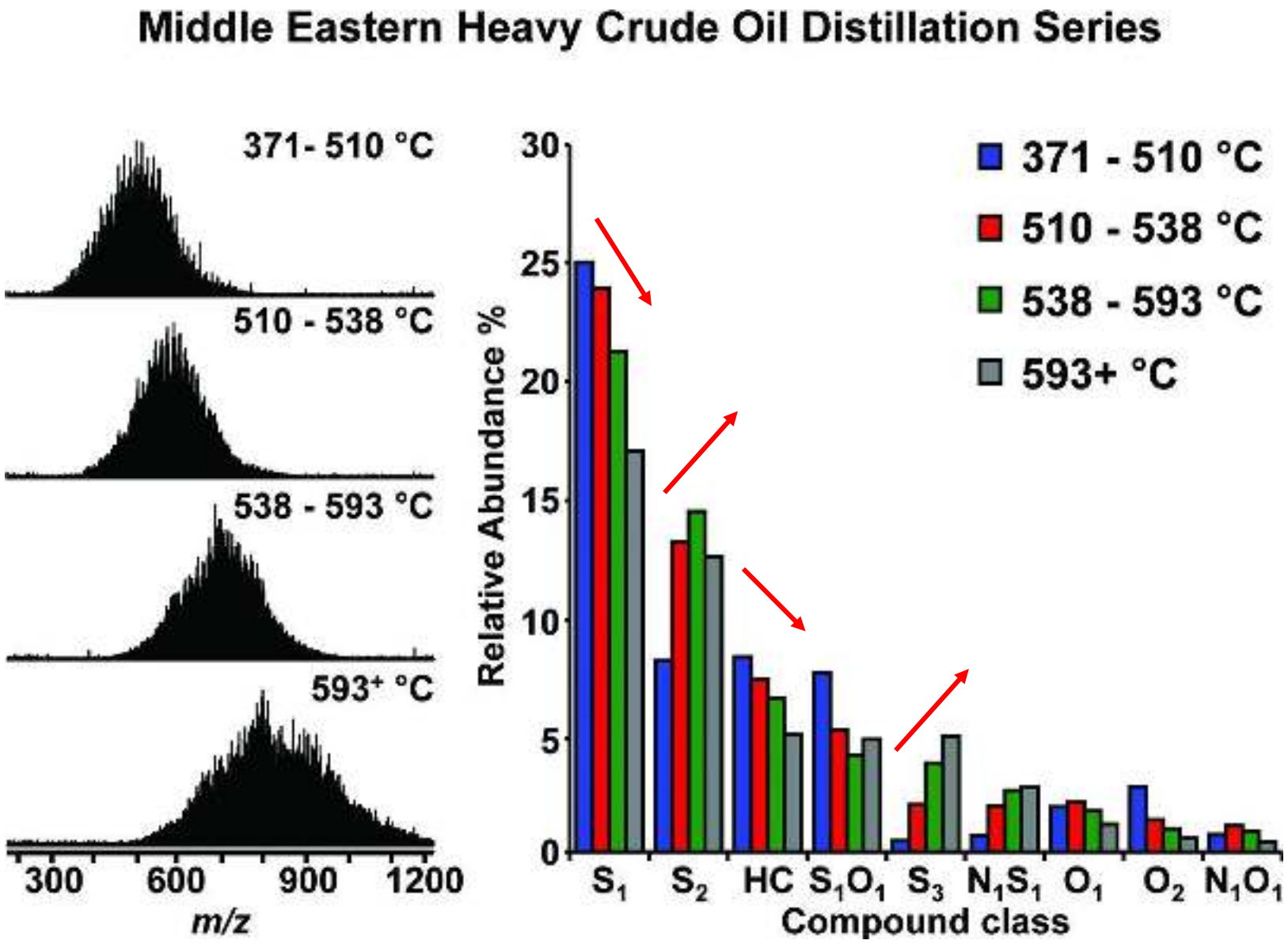

Fractionation of Material

Fractionation of Naphthenic acids

MAPS fractionation (MAPS: modified aminopropyl silica)

S. Rowland et al., *Energy Fuels 2014, 28, 5043−5048*

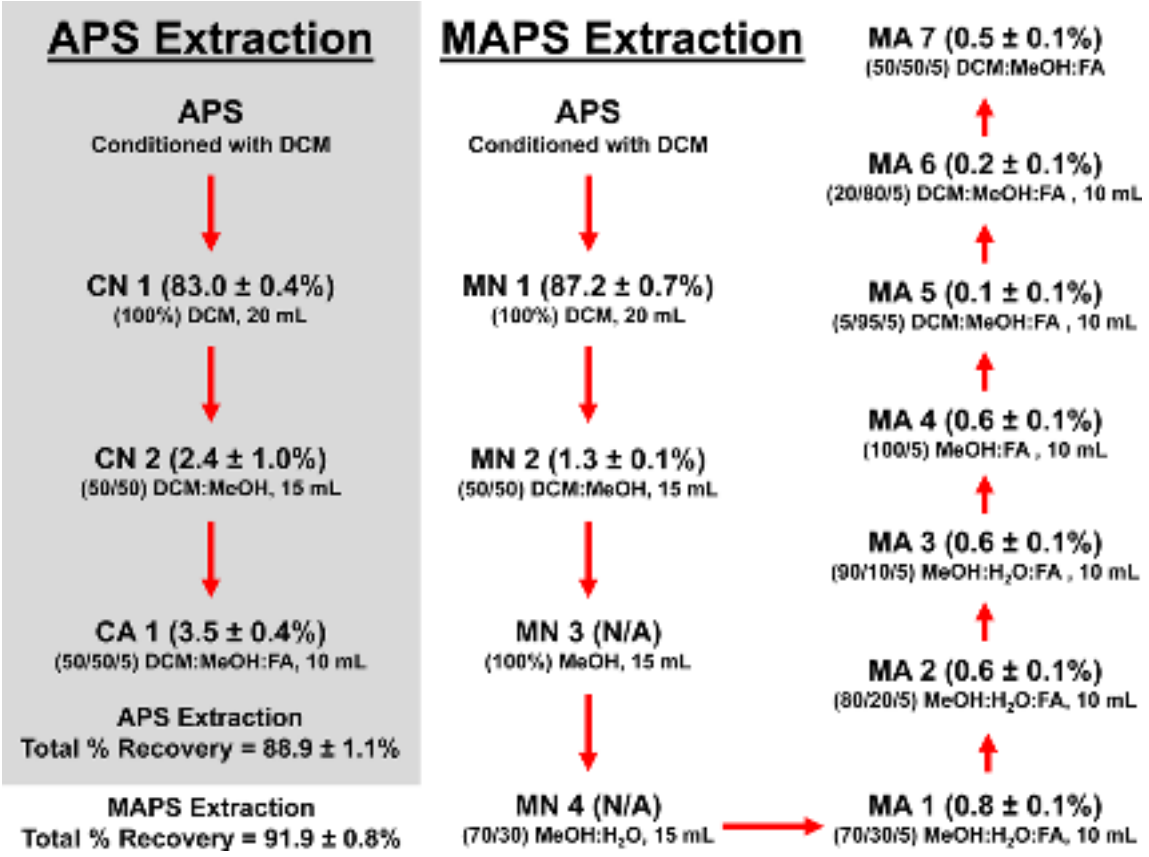

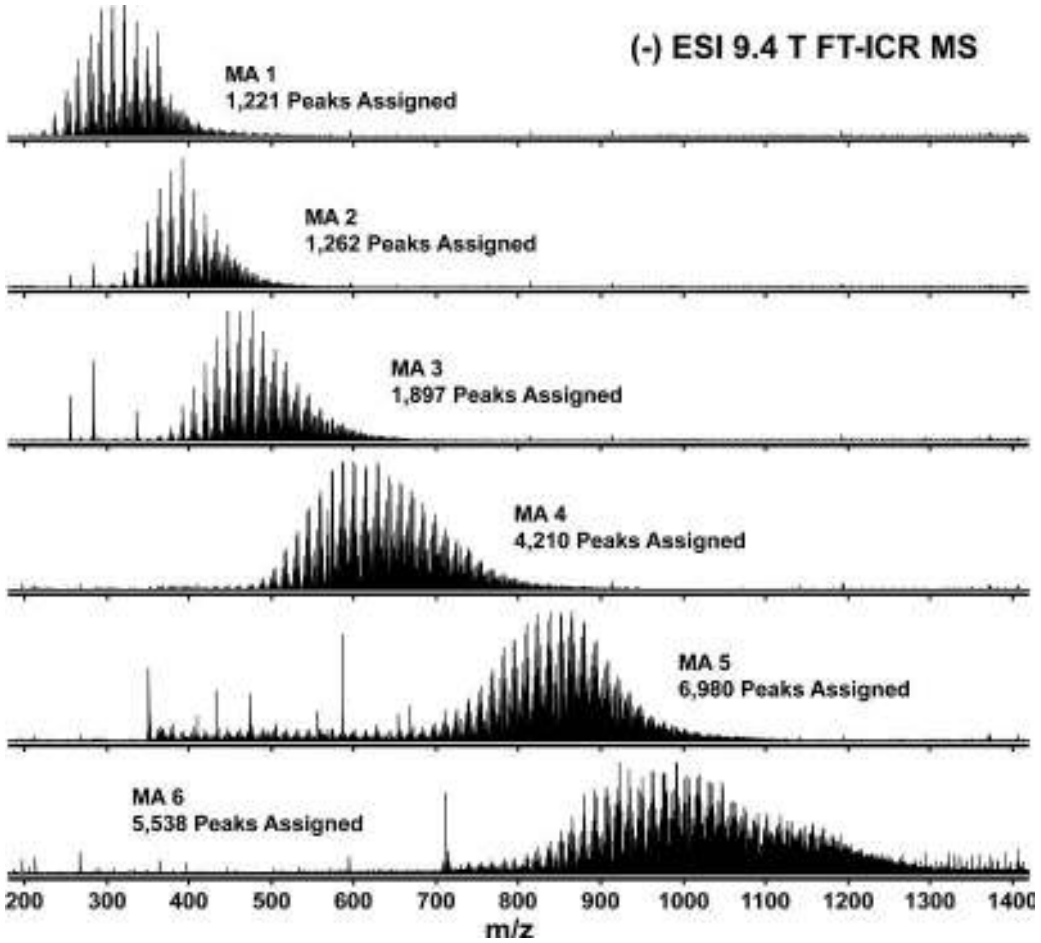

Fractionation of Naphthenic acids

MAPS fractionation (MAPS: modified aminopropyl silica)

S. Rowland et al., *Energy Fuels 2014, 28, 5043−5048*

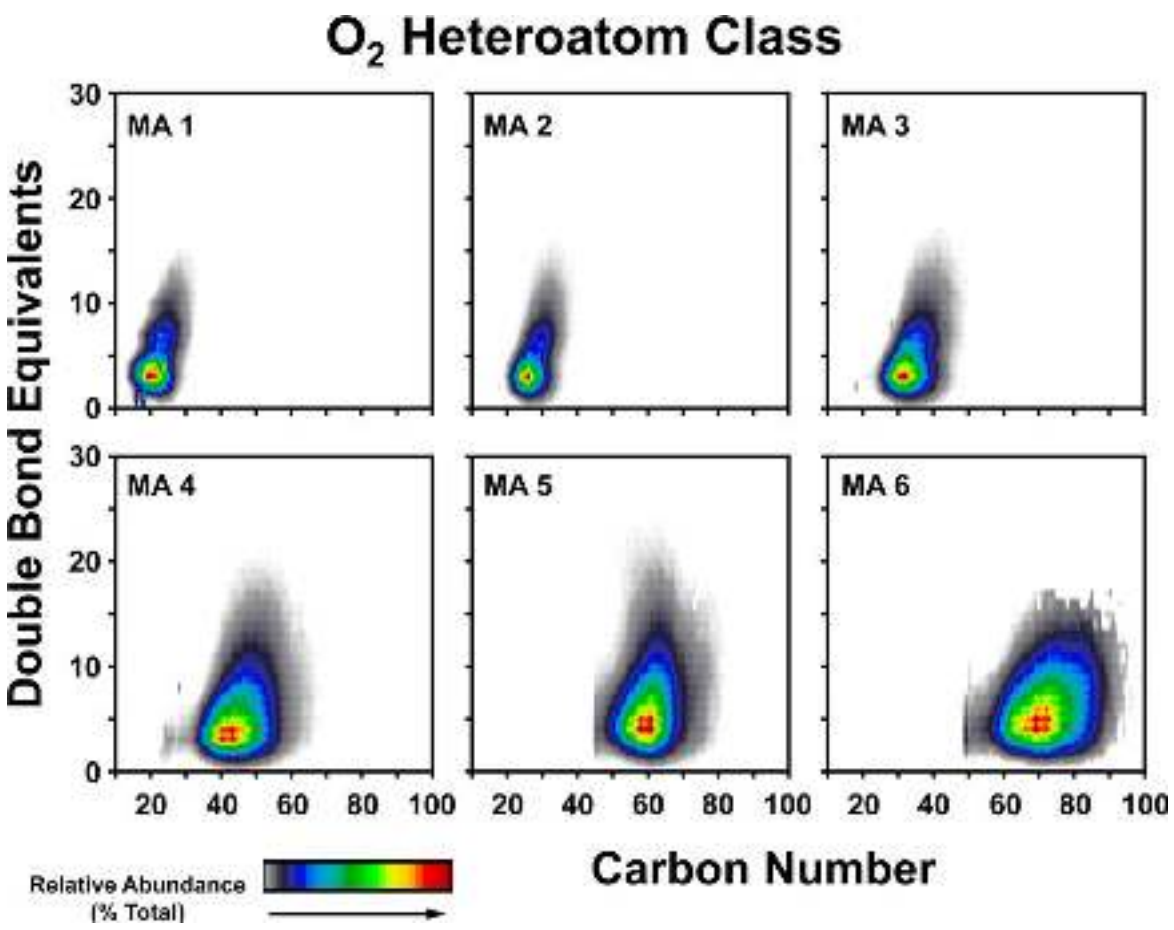

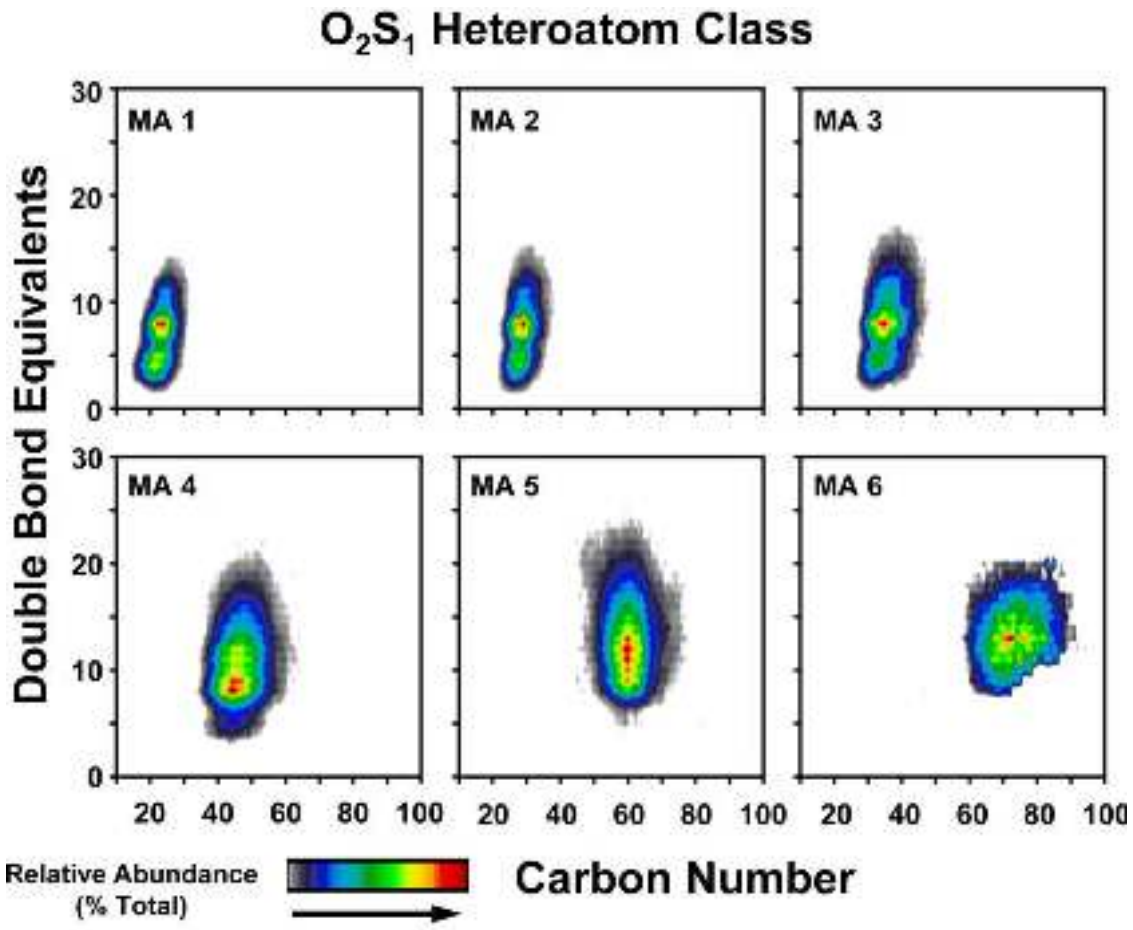

Fractionation of Interfacial Material

MAPS fractionation (MAPS: modified aminopropyl silica)

A. Klingenpeel et al., *Energy Fuels 2017, 31, 5933−5939.*

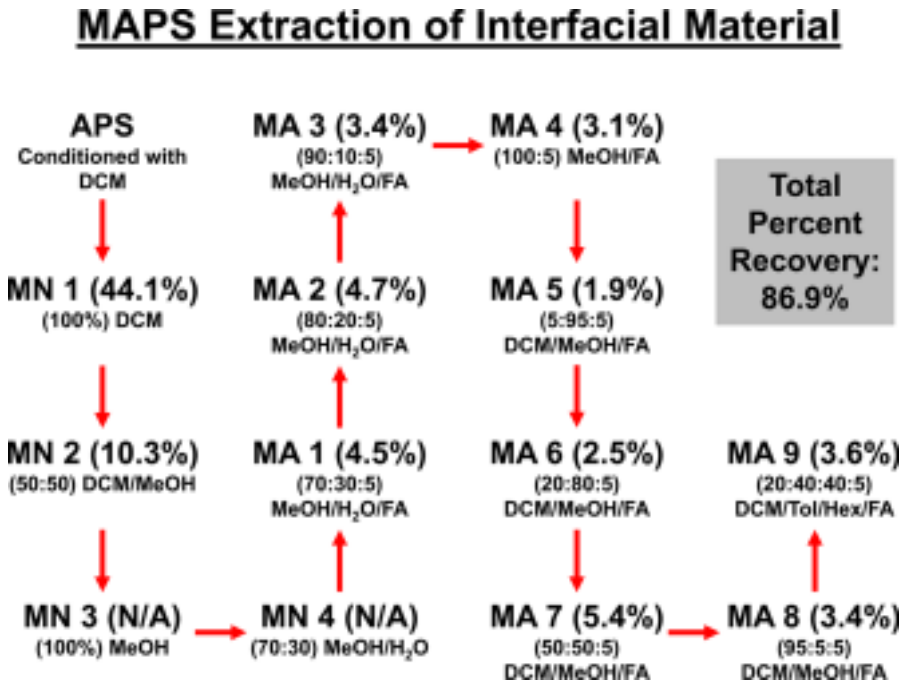

Emulsion test

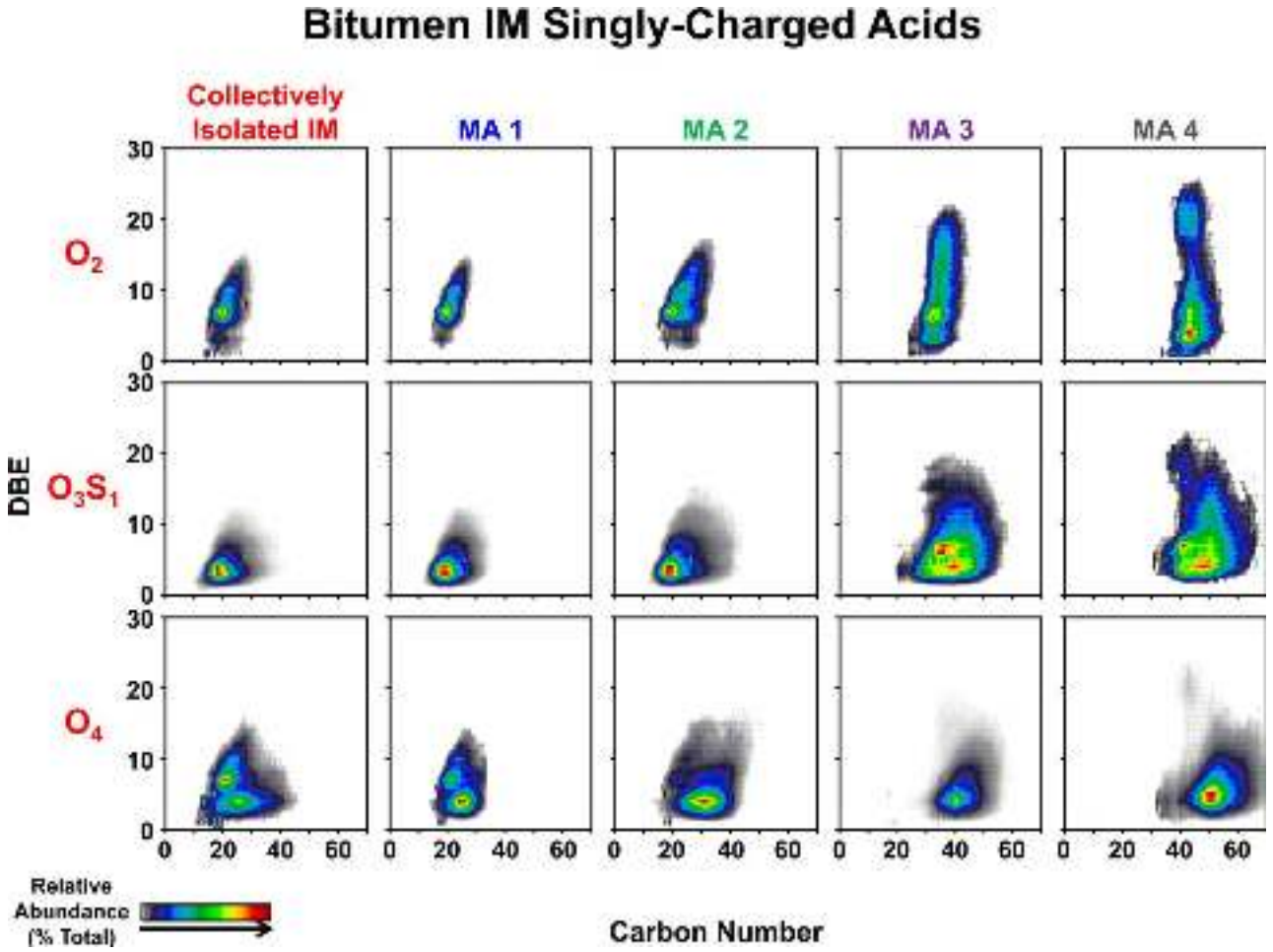

Island and archipelago structures of asphaltene molecules

Structure of Asphaltene molecules

CID of an Asphaltene fractions (APPI pos)

M. Witt et al., Petrophase 2018.

Q-isolation with a small mass window of **10 Da**.

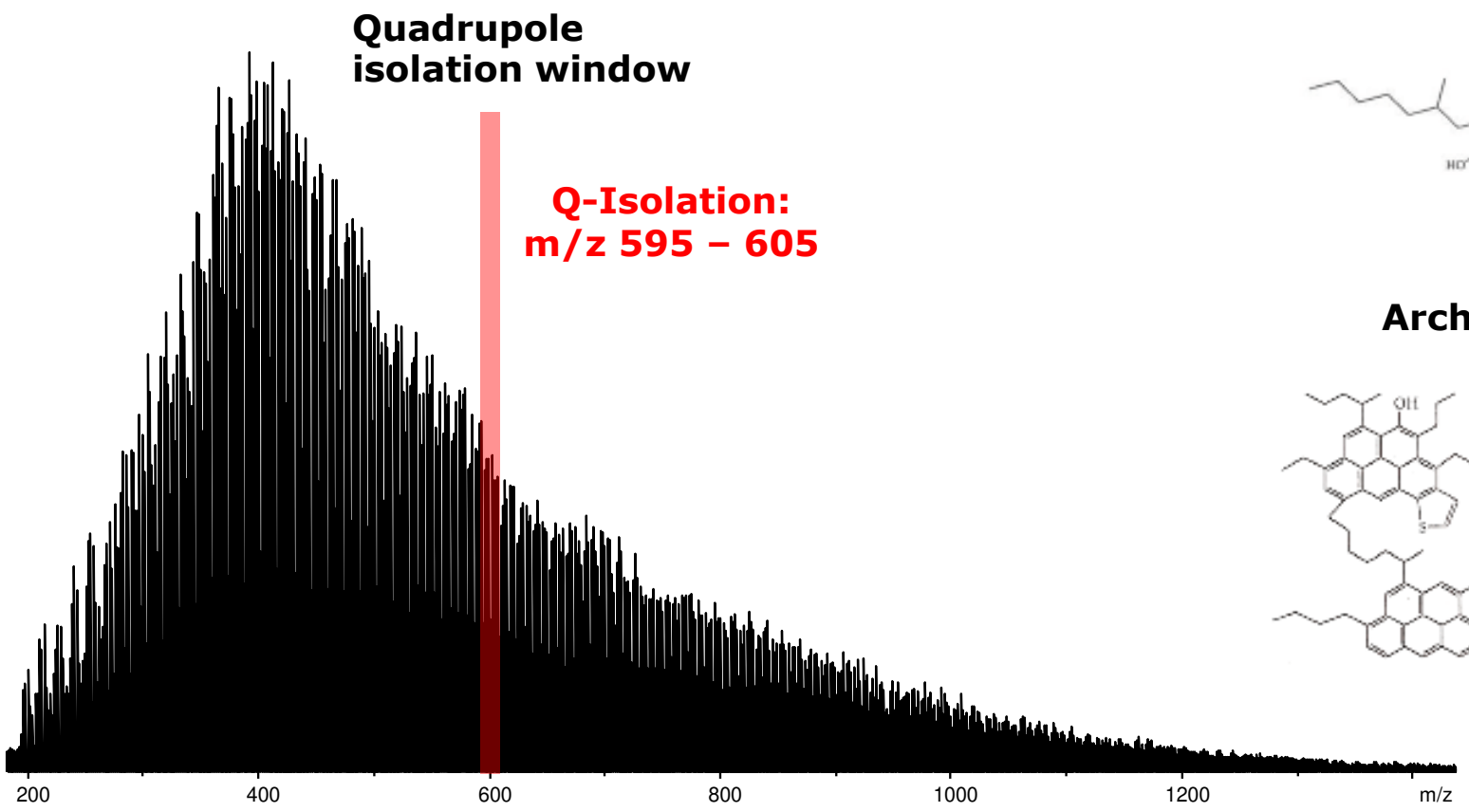

Island structurec

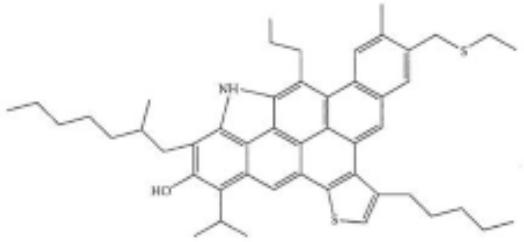

Archipelago structure

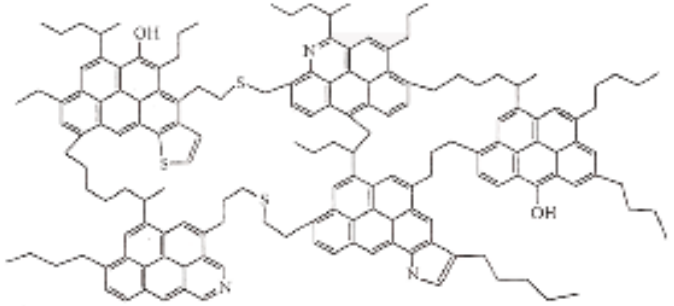

- confidential -

Structure of Asphaltene molecules

CID of an Asphaltene fractions (APPI pos)

M. Witt et al., Petrophase 2018.

Class S_1

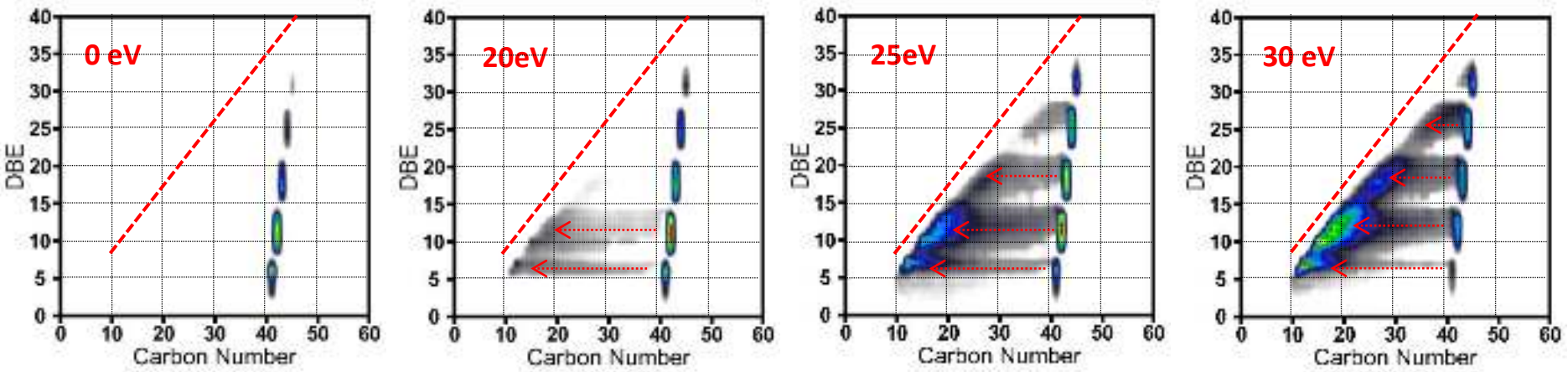

Class S_2

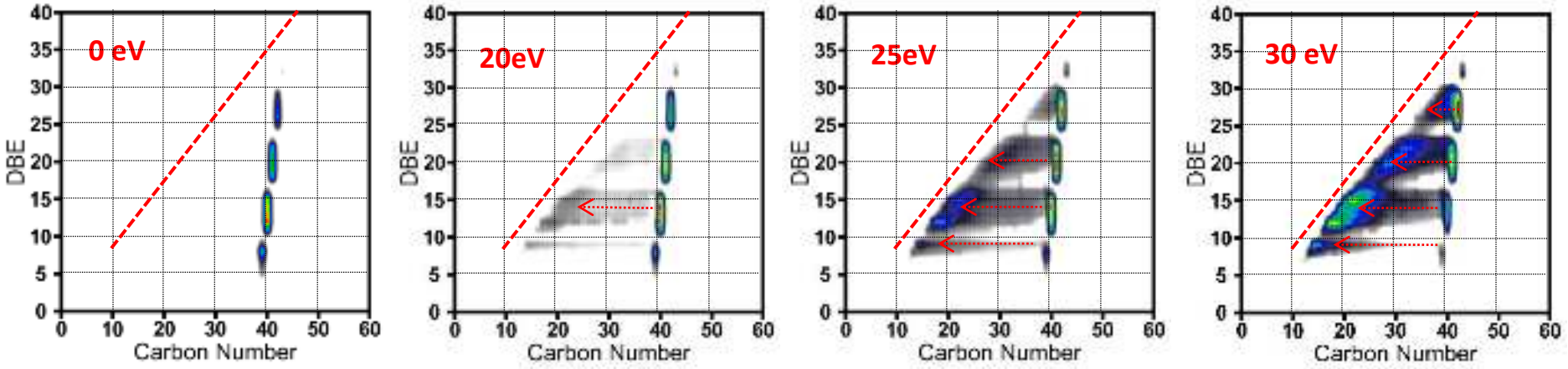

No loss is DBE ⇨ mainly island structures

- confidential -

Structure of Asphaltene molecules

Asphaltene fractions (APPI pos)

Martha L. Chacón-Patiño et al., *Energy & Fuels* 2018, 32, 314-328.

PetroPhase 2017 asphaltenes

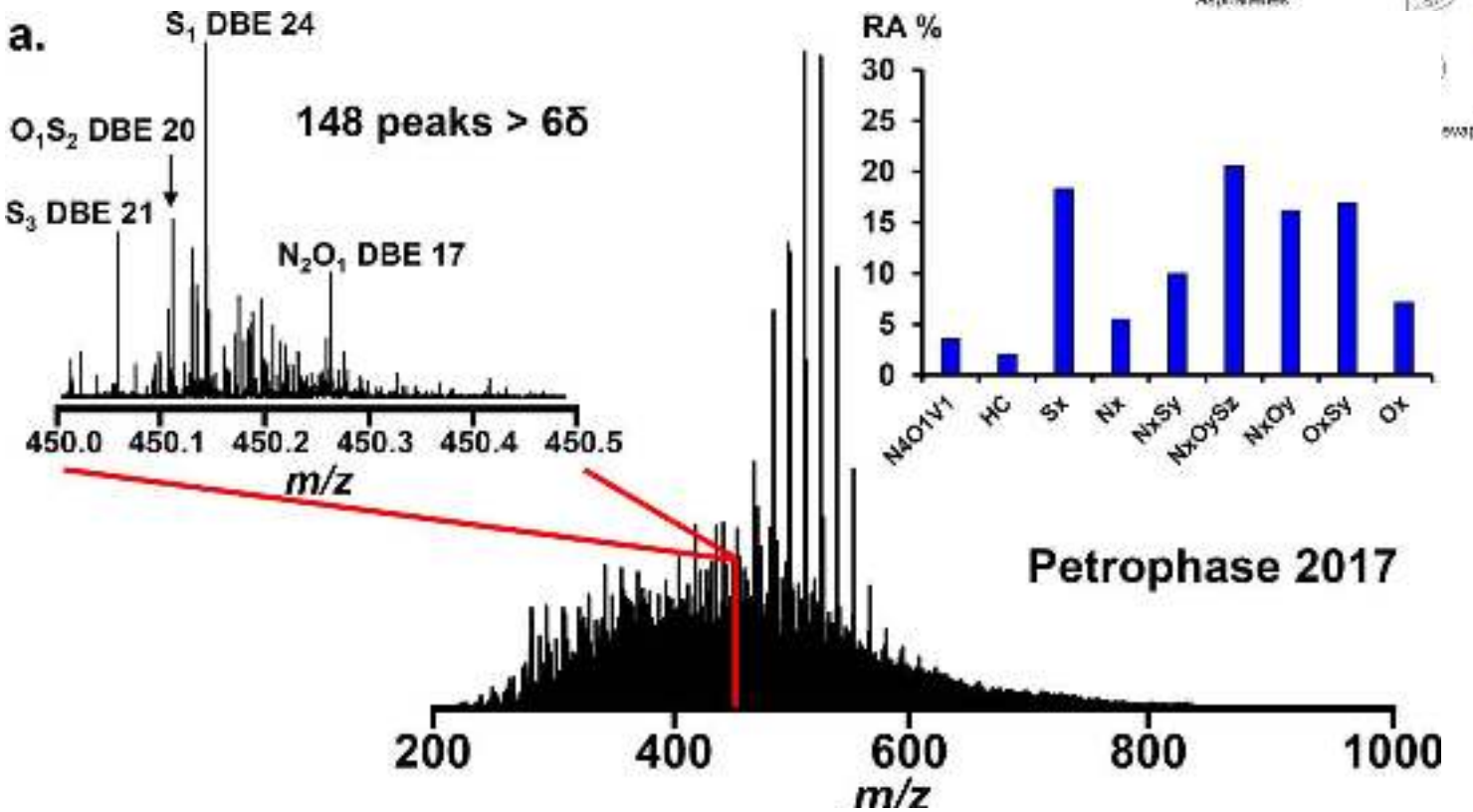

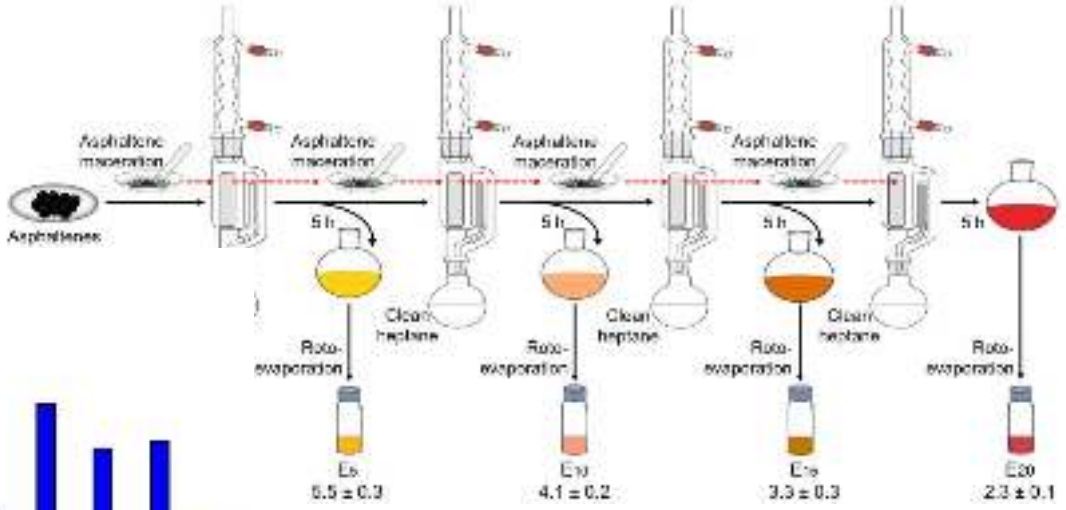

Structure of Asphaltene molecules

Asphaltene fractions (APPI pos)

Martha L. Chacón-Patiño et al., *Energy & Fuels* 2018, 32, 314-328.

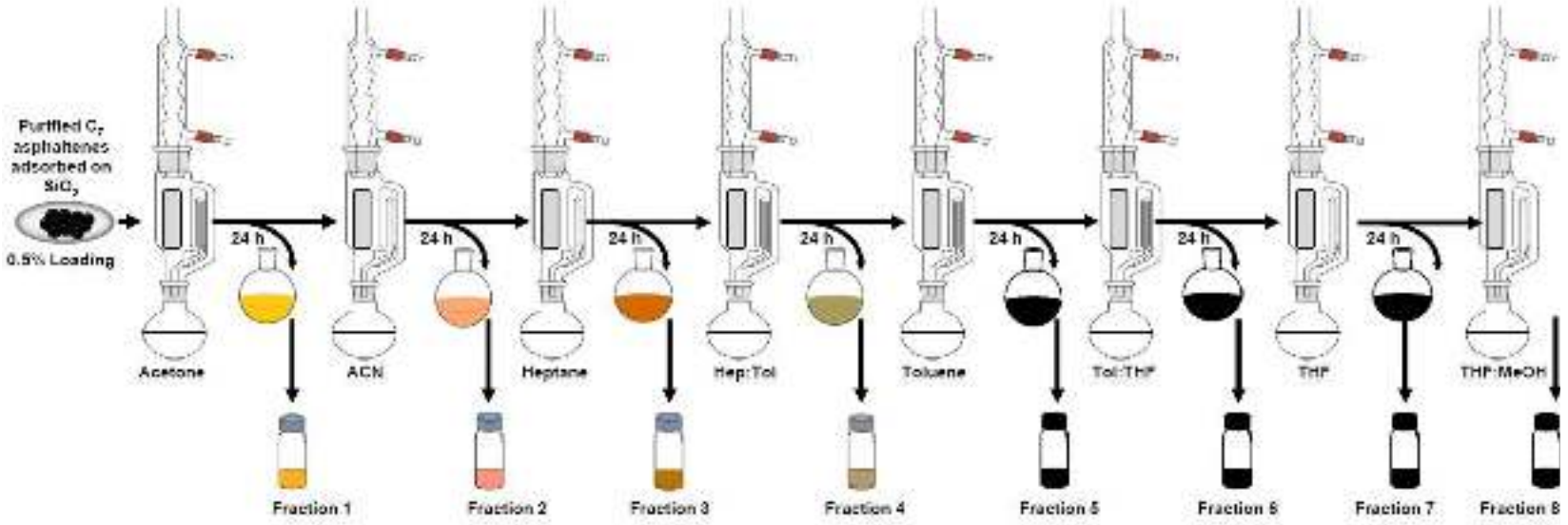

Petrophase 2017 wt.% Recovery 84.7%	17.4	0.2	6.9	11.3	8.7	19.7	7.5	13.0

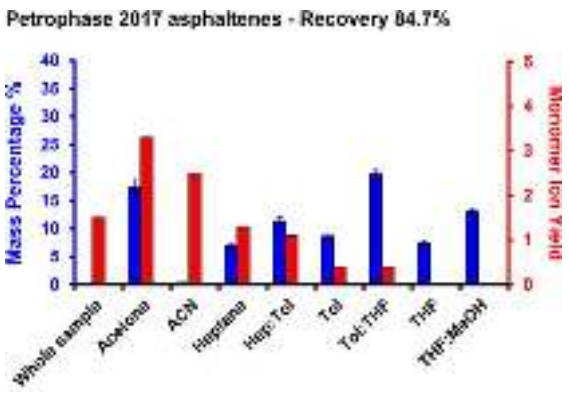

Structure of Asphaltene molecules

Asphaltene fractions (APPI pos)

Martha L. Chacón-Patiño et al., *Energy & Fuels* 2018, 32, 314-328.

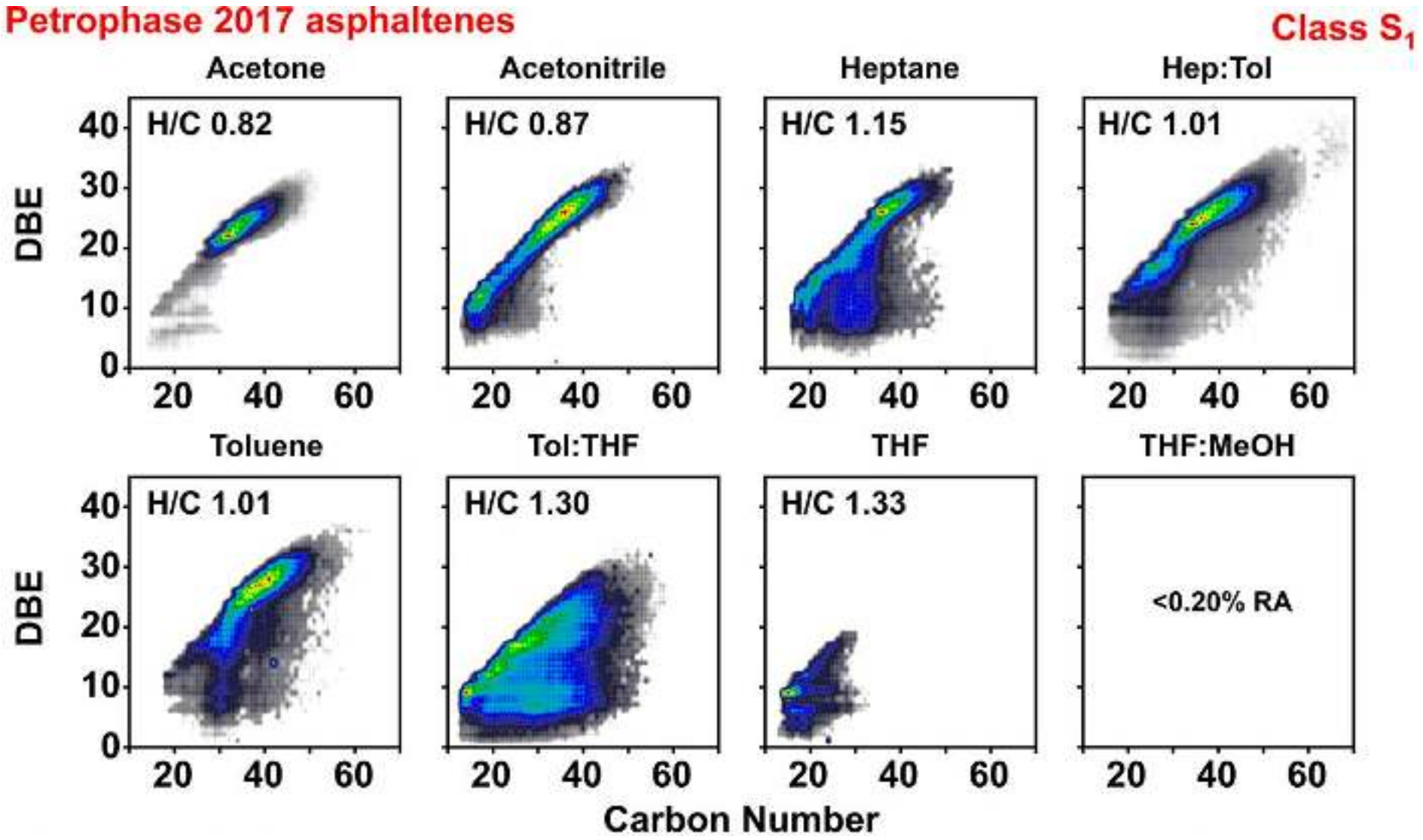

Structure of Asphaltene molecules

Asphaltene fractions (APPI pos)

Martha L. Chacón-Patiño et al., *Energy & Fuels* 2018, 32, 314-328.

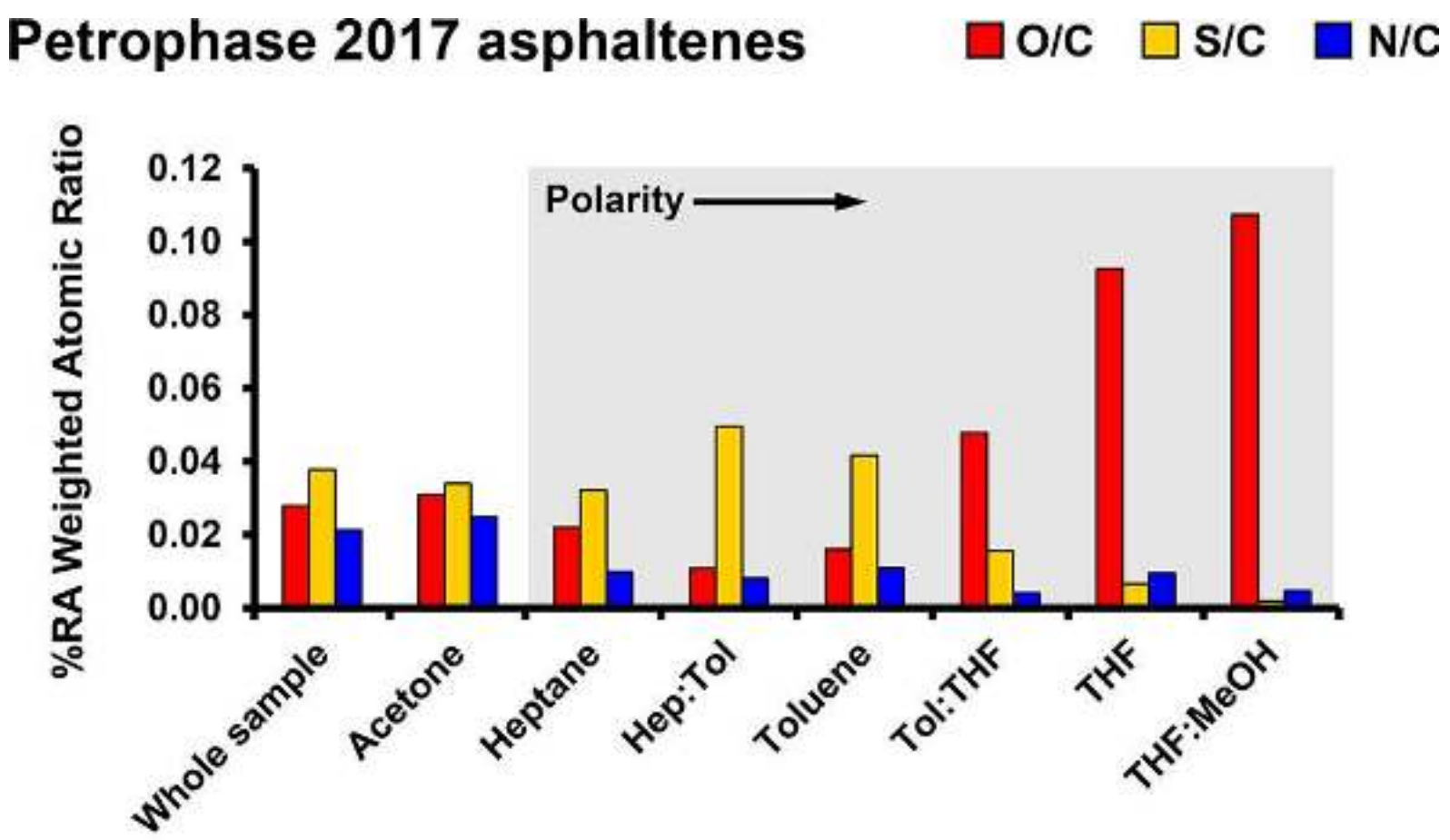

Structure of Asphaltene molecules

Asphaltene fractions (APPI pos)

Martha L. Chacón-Patiño et al., *Energy & Fuels* 2018, 32, 314-328.

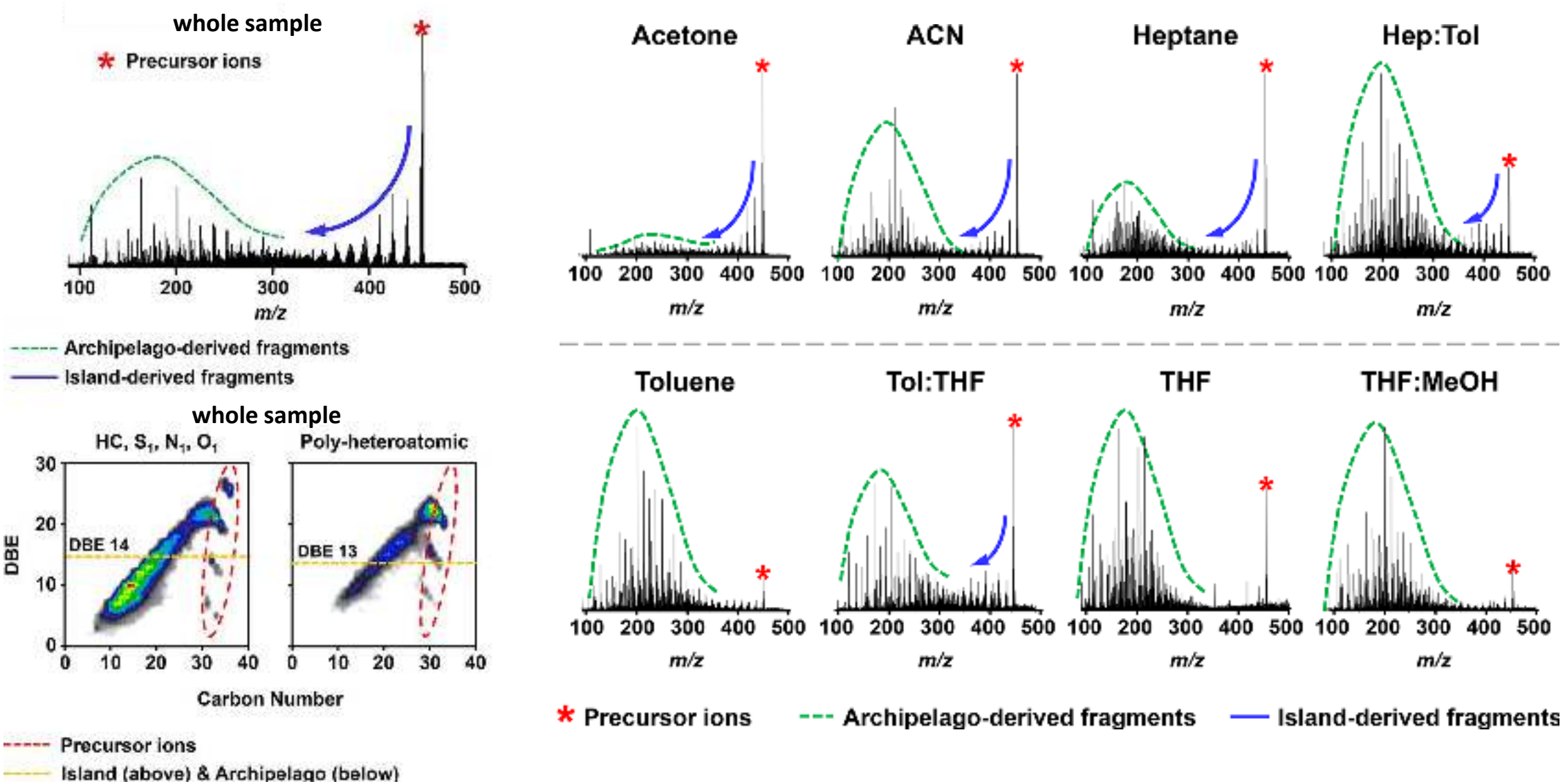

Structure of Asphaltene molecules

Asphaltene fractions (APPI pos)

Martha L. Chacón-Patiño et al., *Energy & Fuels* 2018, 32, 314-328.

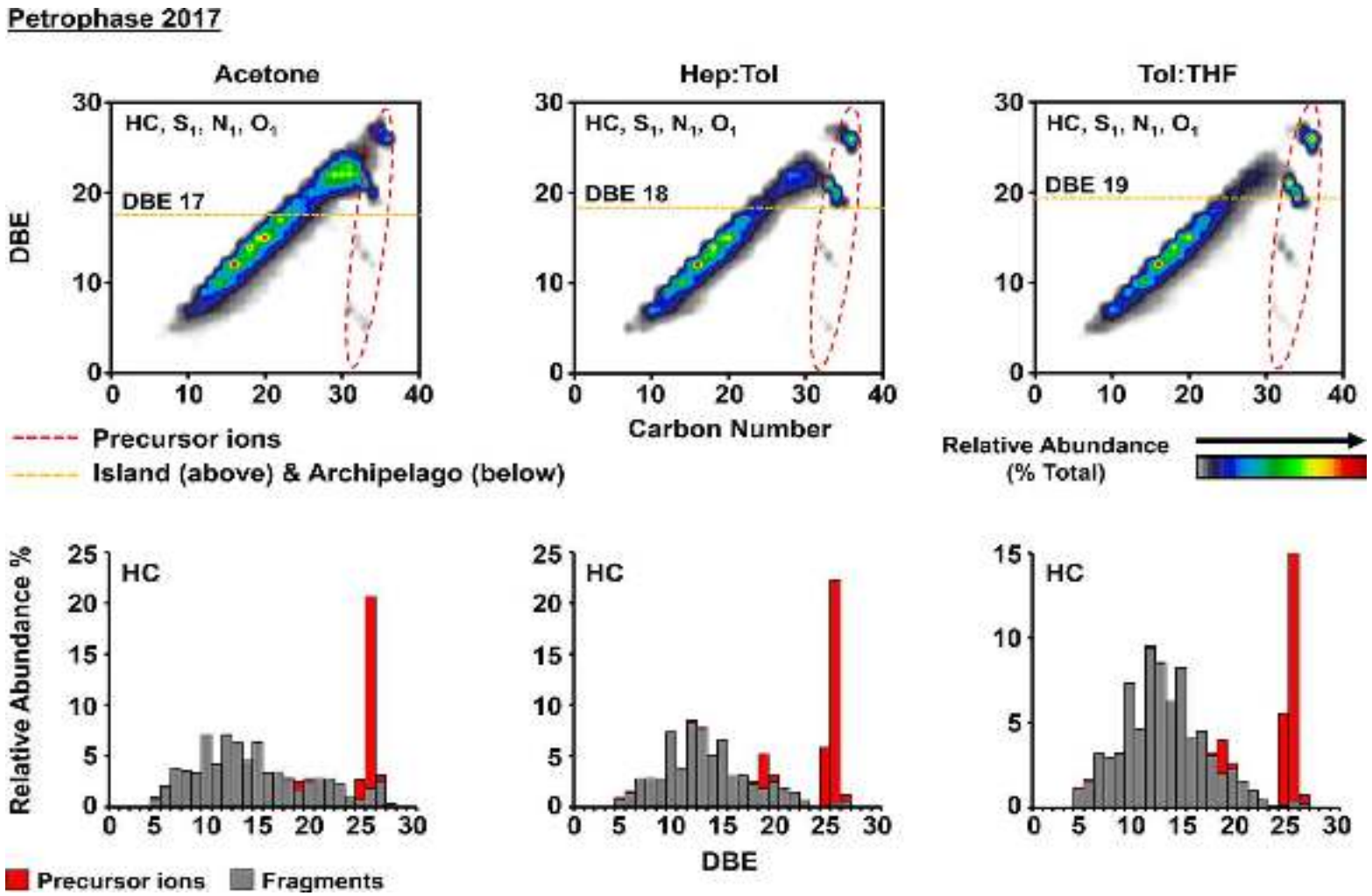

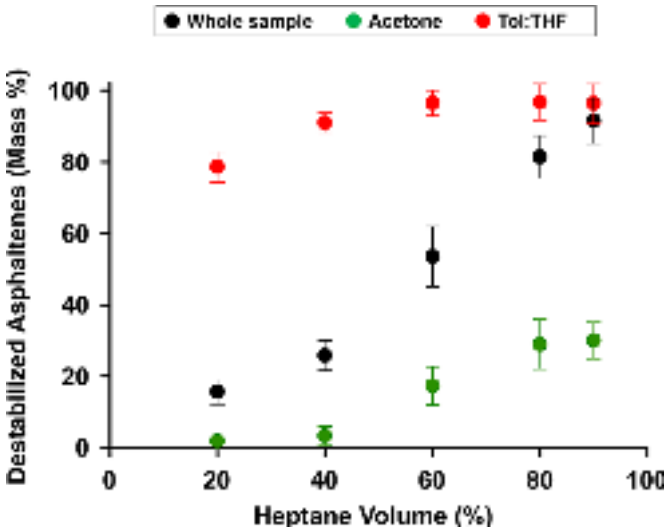

Structure of Asphaltene molecules

AFM – Atomic Force Microscopy

B. Schuler et al., *Energy Fuels* **2017**, *31*, 6856–6861

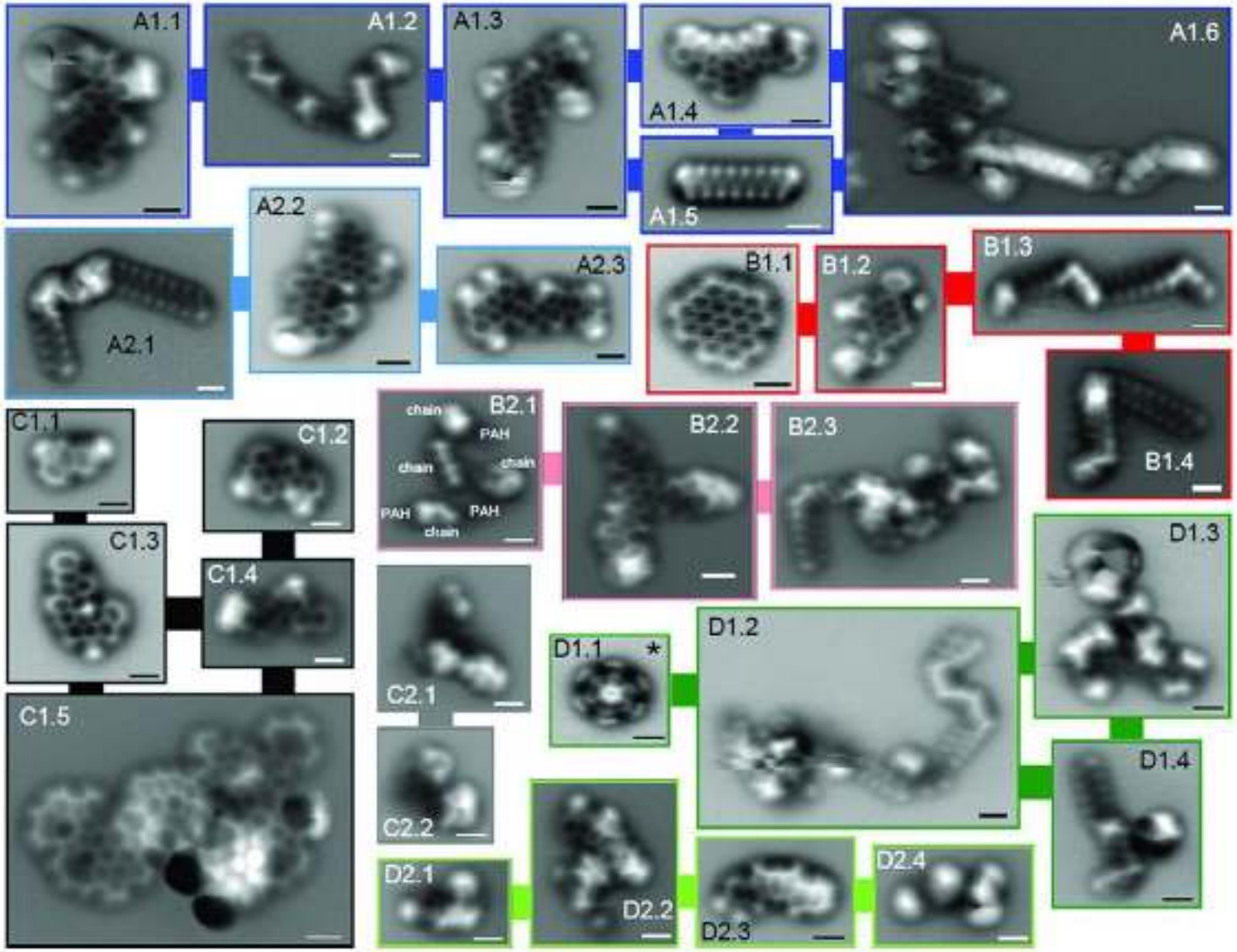

Bio-oil analysis

Bio-oil analysis

Pine pellet oily (red) and aqueous (blue) phase analysis

J. M. Jarvis et al., Energy Fuels 2012, 26, 3810−3815.

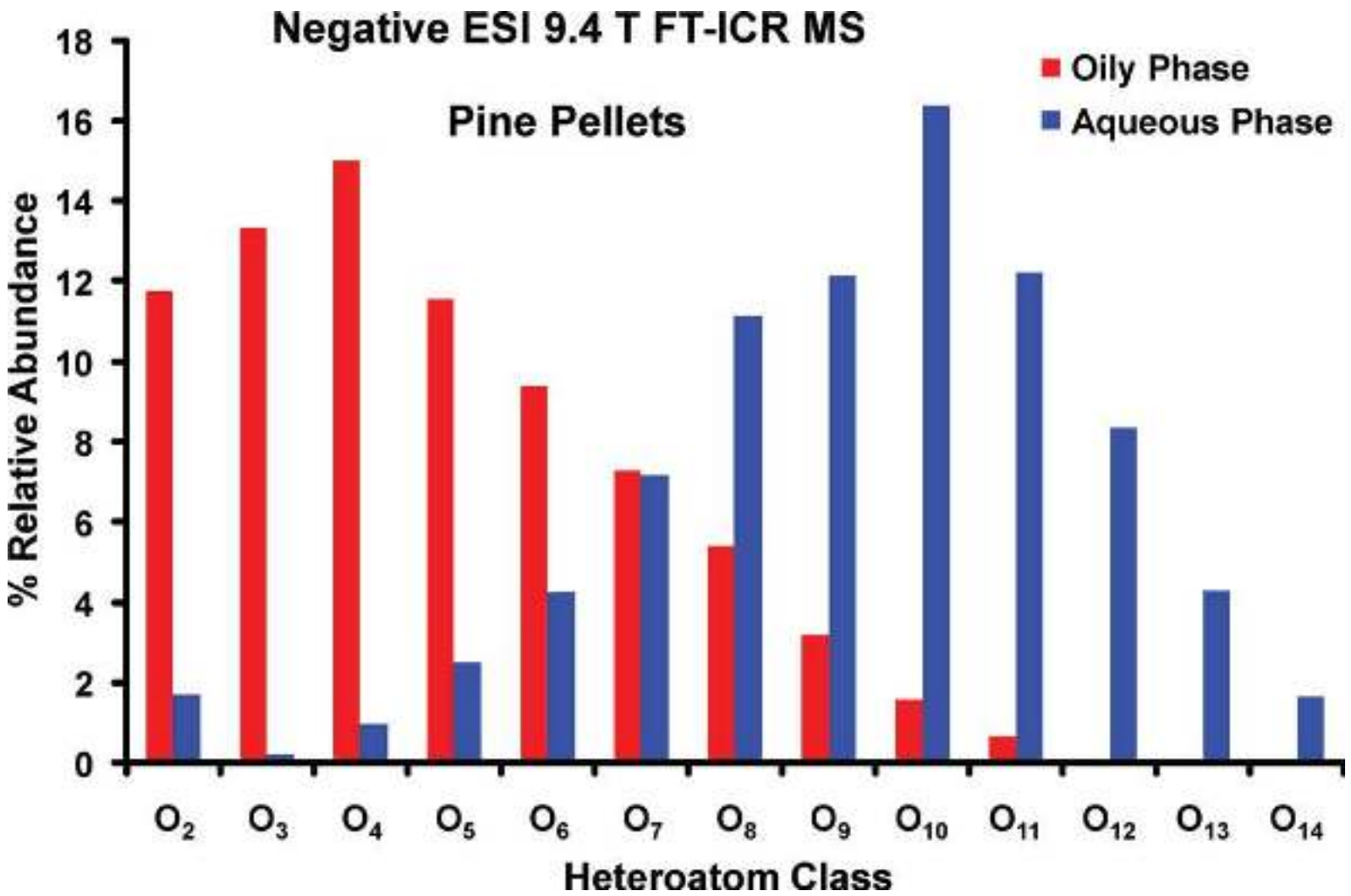

Bio-oil analysis

Pine pellet oily (red) and aqueous (blue) phase analysis

J. M. Jarvis et al., Energy Fuels 2012, 26, 3810−3815.

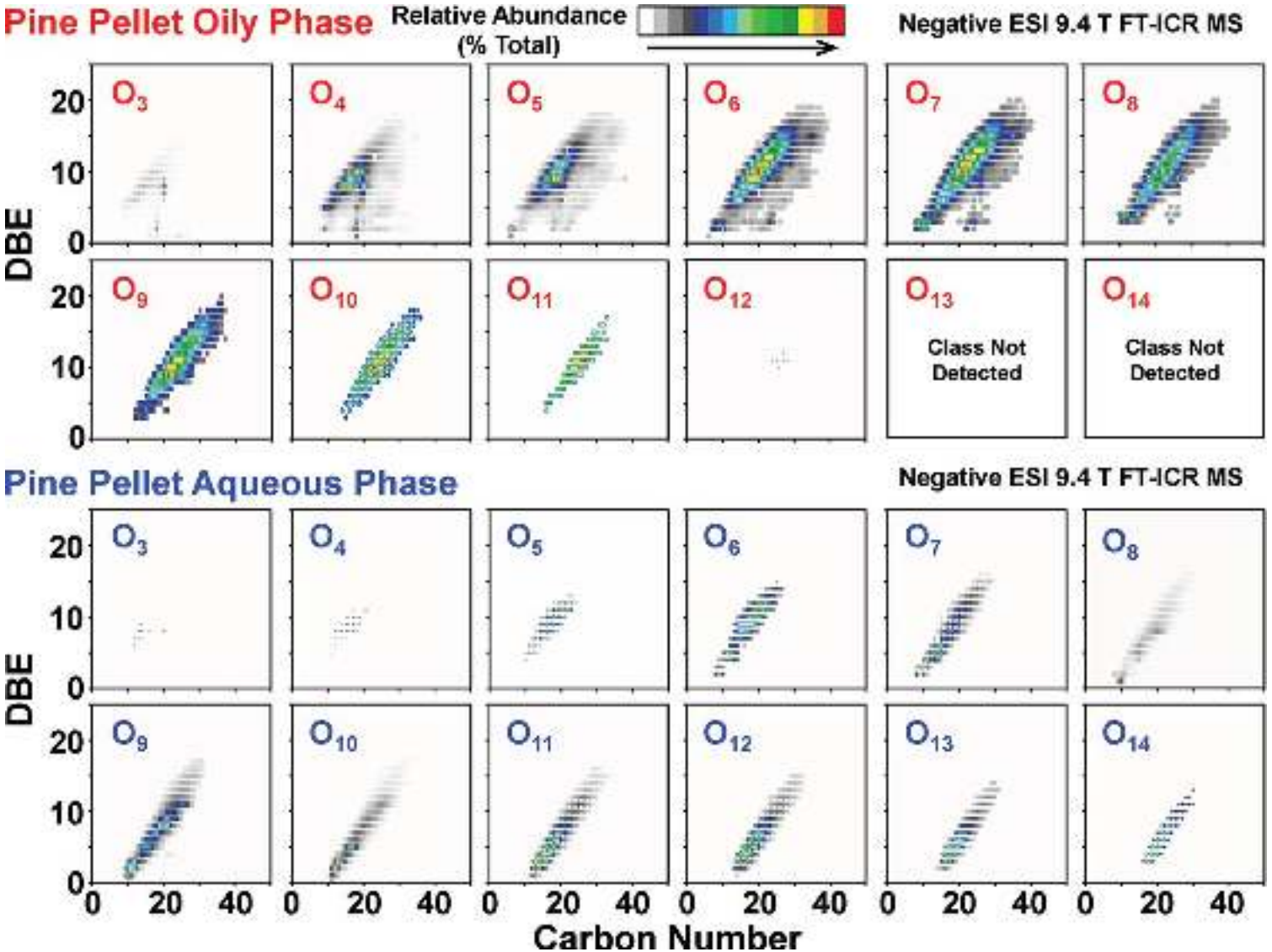

Effect of Maturity

Effect of Maturity

Effect of Maturity on oil composition

S. Poetz et al, *Energy Fuels* 2014, 28, 4877–4888.

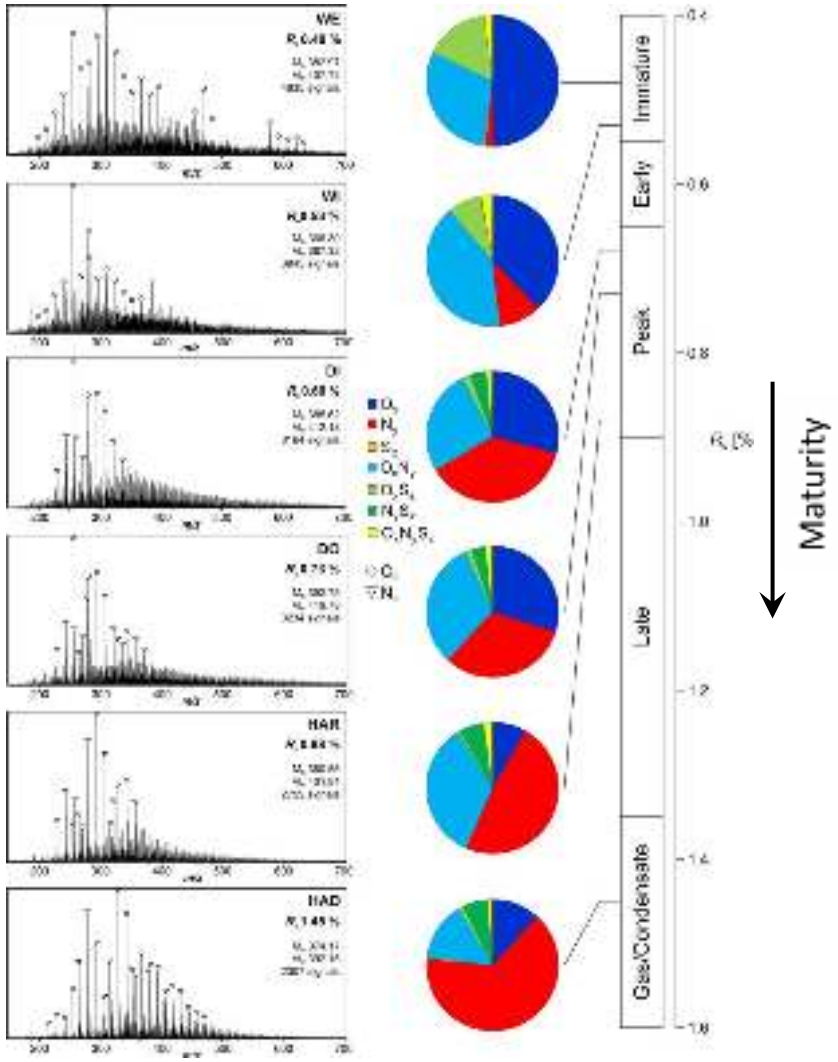

R_0: vitrinite reflectance

Transformation of Compounds in the Organic-Rich Posidonia Shale by Maturity

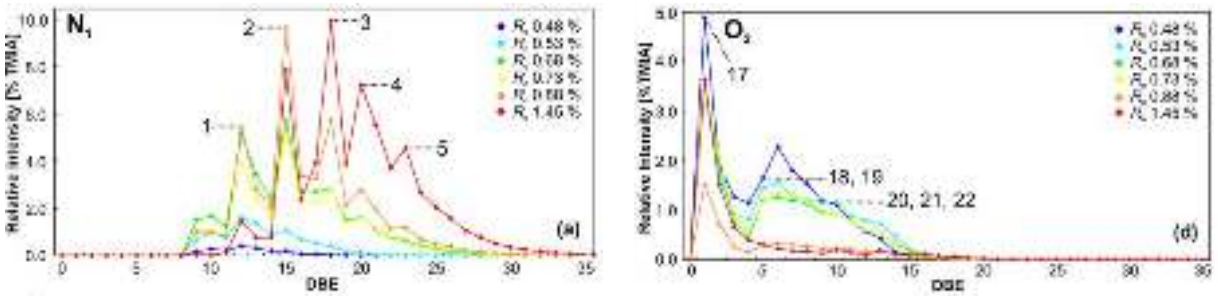

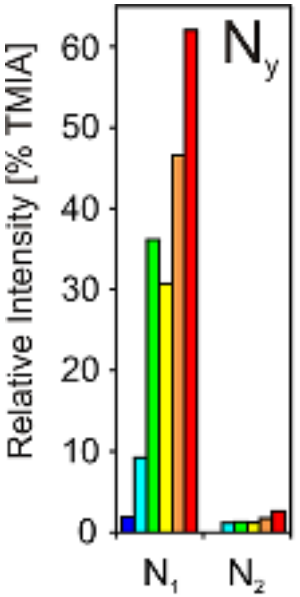

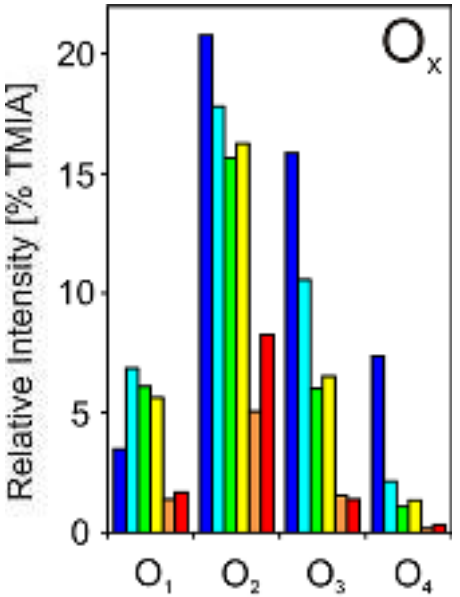

solariX 12T data, ESI(-)

Effect of Maturity

Effect of Maturity on oil composition

S. Poetz et al, *Energy Fuels* 2014, 28, 4877–4888.

Effect of Maturity of composition of N_1-containing compounds

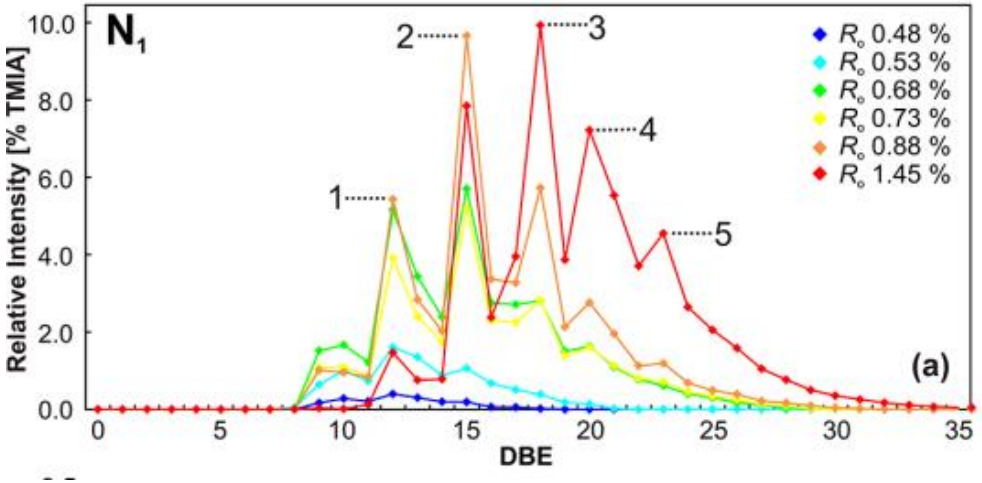

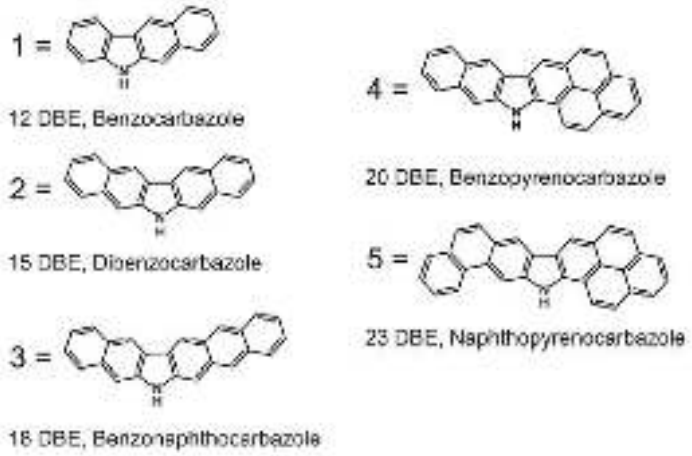

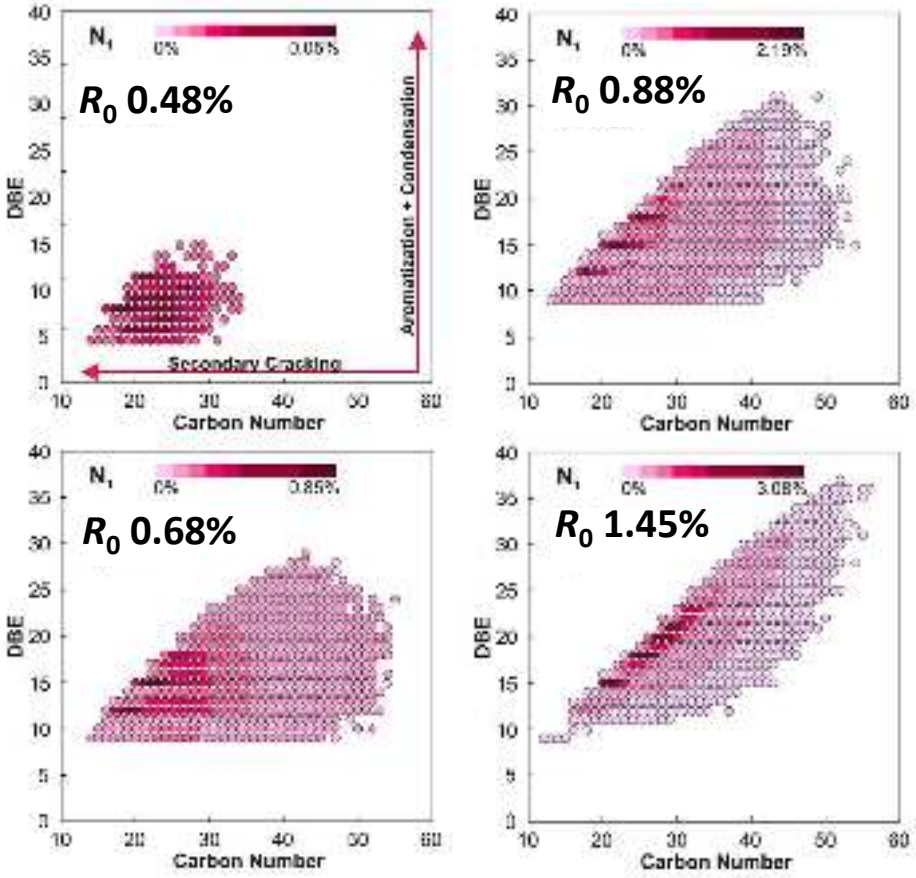

solariX 12T data, ESI(-)

Effect of Maturity

Effect of Maturity on oil composition

S. Poetz et al, *Energy Fuels* 2014, 28, 4877–4888.

Maturity-Driven Generation and Transformation of Compounds in the Organic-Rich Posidonia Shale

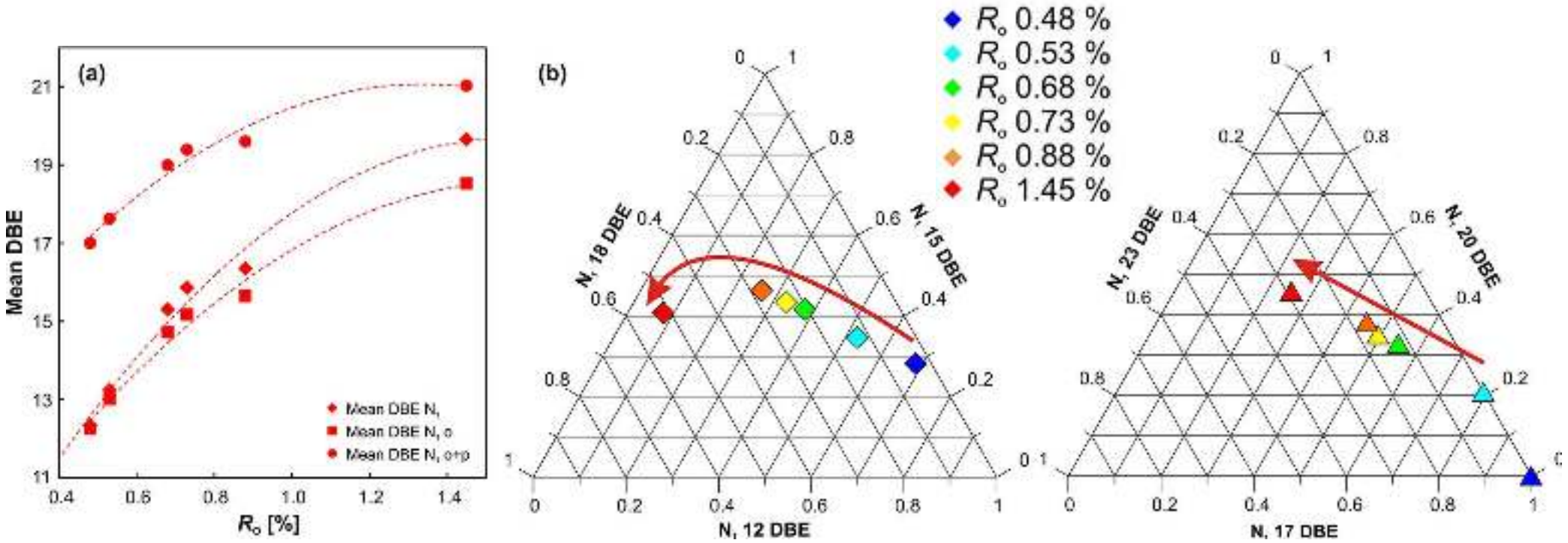

Possible Thermally-induced Reaction occurring during Maturation

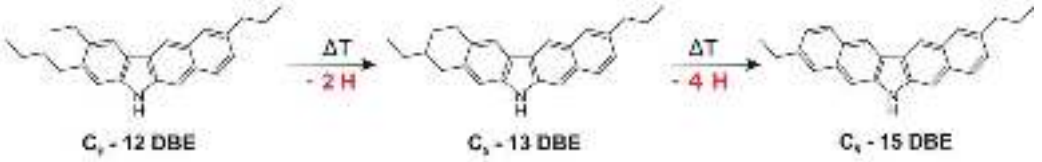

solariX 12T data, ESI(-)

Improving S/N and mass resolution

Improving S/N and mass resolution

Spectra stitching

L. C. Krajewski, Anal. Chem. 2017, 89, 21, 11318–11324.

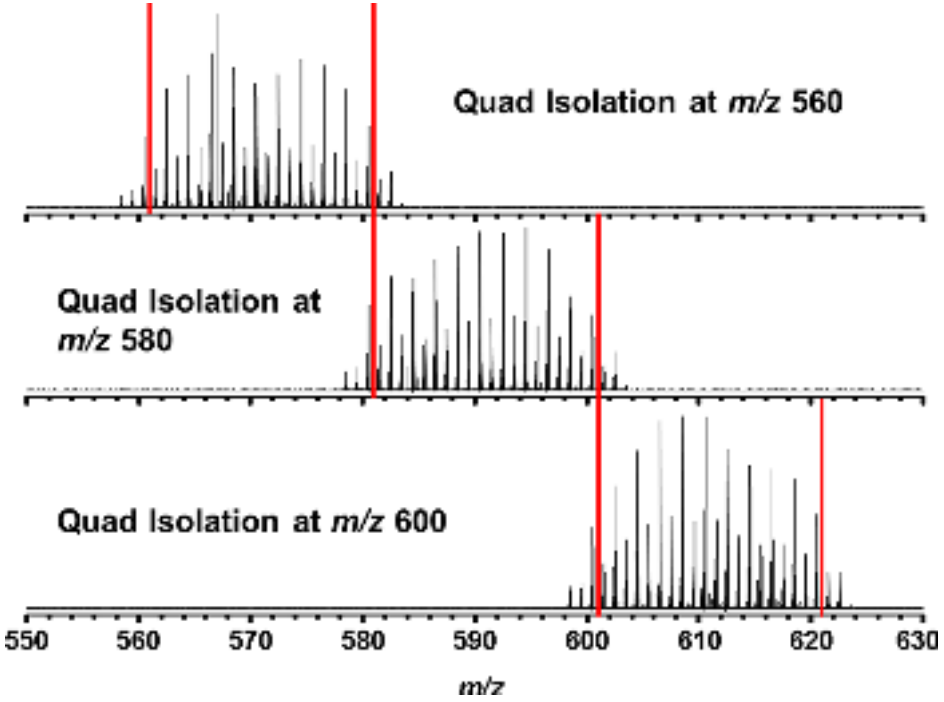

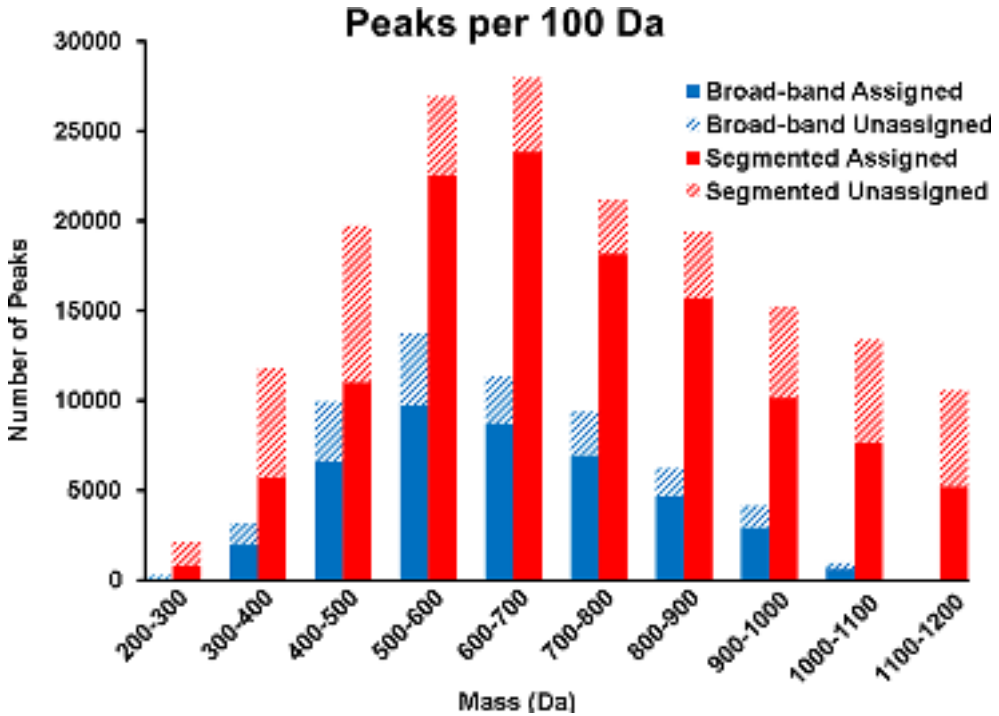

	broad band	segmented
no. of peaks	59 015	170 115
no. of assigned peaks/percentage of total	42 182 (71.5%)	126 264 (74.2%)
no. of monoisotopic peaks	23 946	67 237
rms mass error for assigned peaks (ppm)	0.19	0.13
number-average neutral mass (Da)	647.5	750.2
number-average carbon number	44.7	49.7
number-average neutral DBE	15.9	15.3
approximate total analysis time (s)	2000	37 500

Improving S/N and mass resolution

Spectra stitching and keeping mass resolution

D. C. Palacio Lozano, Chem. Sci., 2019, 10, 6966.

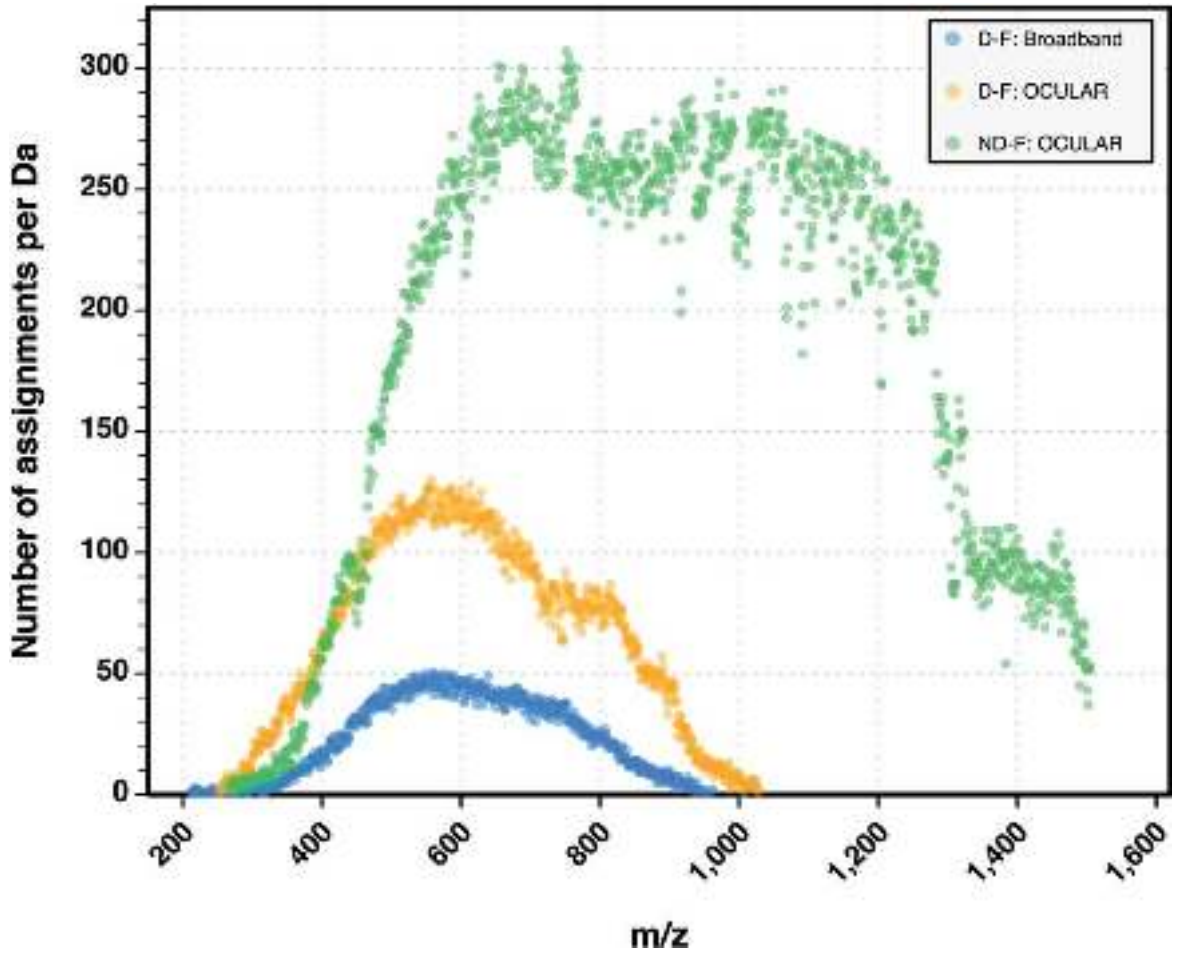

	Stitched
Average resolving power (m/z 260–1505)	3.12×10^6
Resolving power at m/z 400	3.07×10^6
Monoisotopic peaks assigned	106 871
Total peaks assigned	244 779
% Assigned	88.44%
RMS mass error for assigned peaks	0.11 ppm
Mean molecular weight	890.3 Da
Peaks with mass error ≤1 ppb	2305
Peaks with mass error ≤20 ppb	66 814
Peaks with mass error ≤50 ppb	122 911
Max. number of peaks assigned per Da	307

Improving S/N and mass resolution

Concept of dipolar and quadrupolar detection

Standard 1ω Dipole Detection

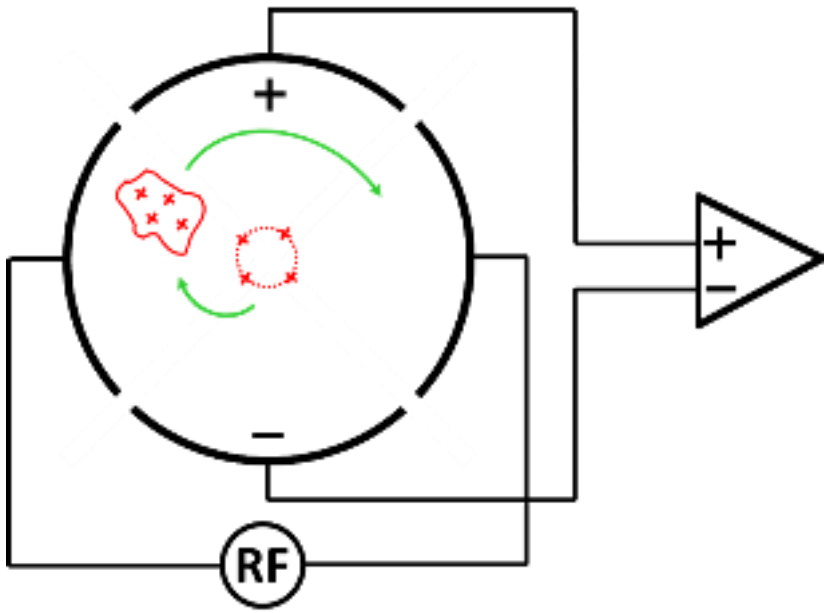

Direct detection of the cyclotron frequency ω_+

$$R_{Dipole} = \nu \cdot T$$

2ω Quadrupolar Detection (QPD)

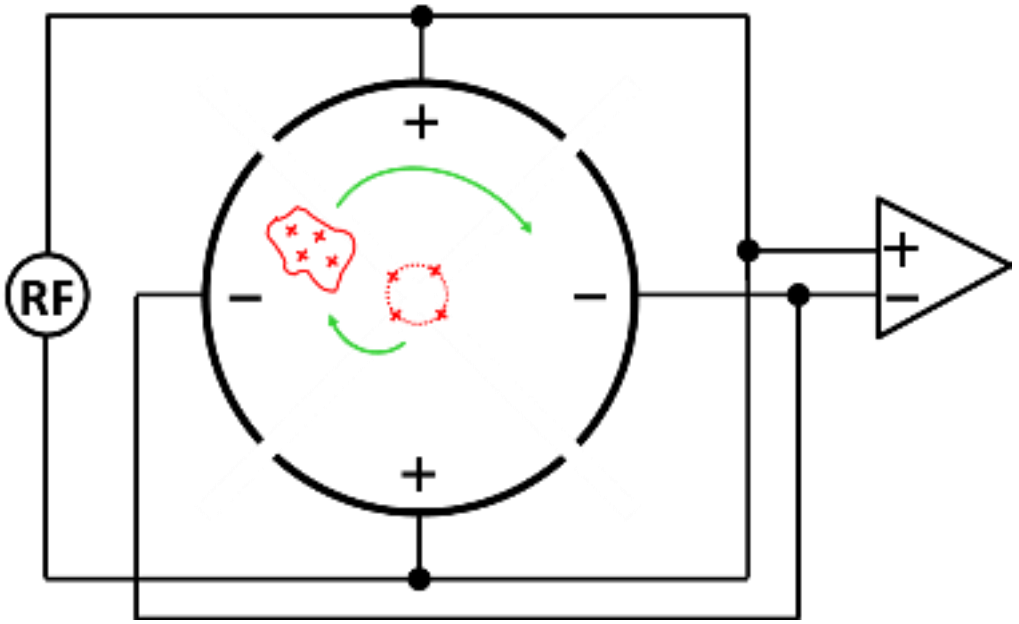

QUADRUPOLE-DETECTION FT-ICR MASS SPECTROMETRY*
L. SCHWEIKHARD, M. LINDINGER and H.-J. KUGE published 1990

Direct detection of the **double** cyclotron frequency $2\omega_+$

$$R_{QPD} = 2 \cdot \nu \cdot T = 2 \cdot R_{Dipole}$$

→ **Double mass resolution**

Improving S/N and mass resolution

12T 1ω measurement with AMP, APPI, Oil Residue, m/z 250-800

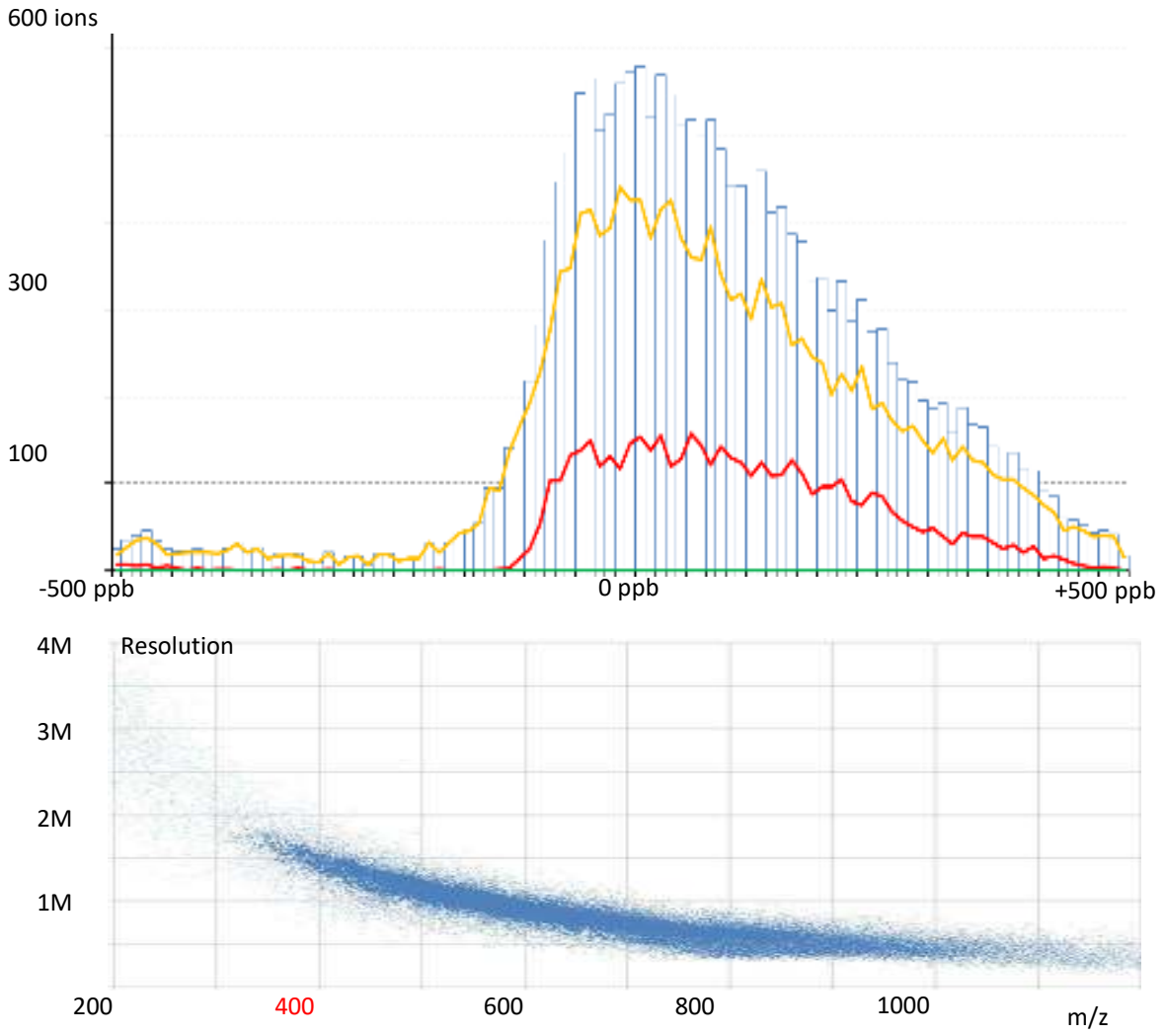

Mass resolution (m/z 400): **1,400,000**
Mass accuracy: **93 ± 161 ppb**
Compounds: **19847**

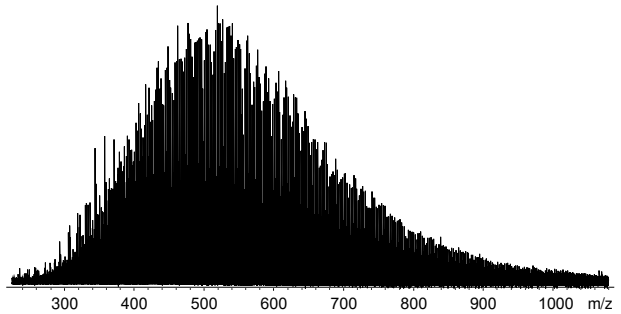

Improving S/N and mass resolution

7T 2ω measurement with AMP, APPI, Oil Residue, m/z 250-800

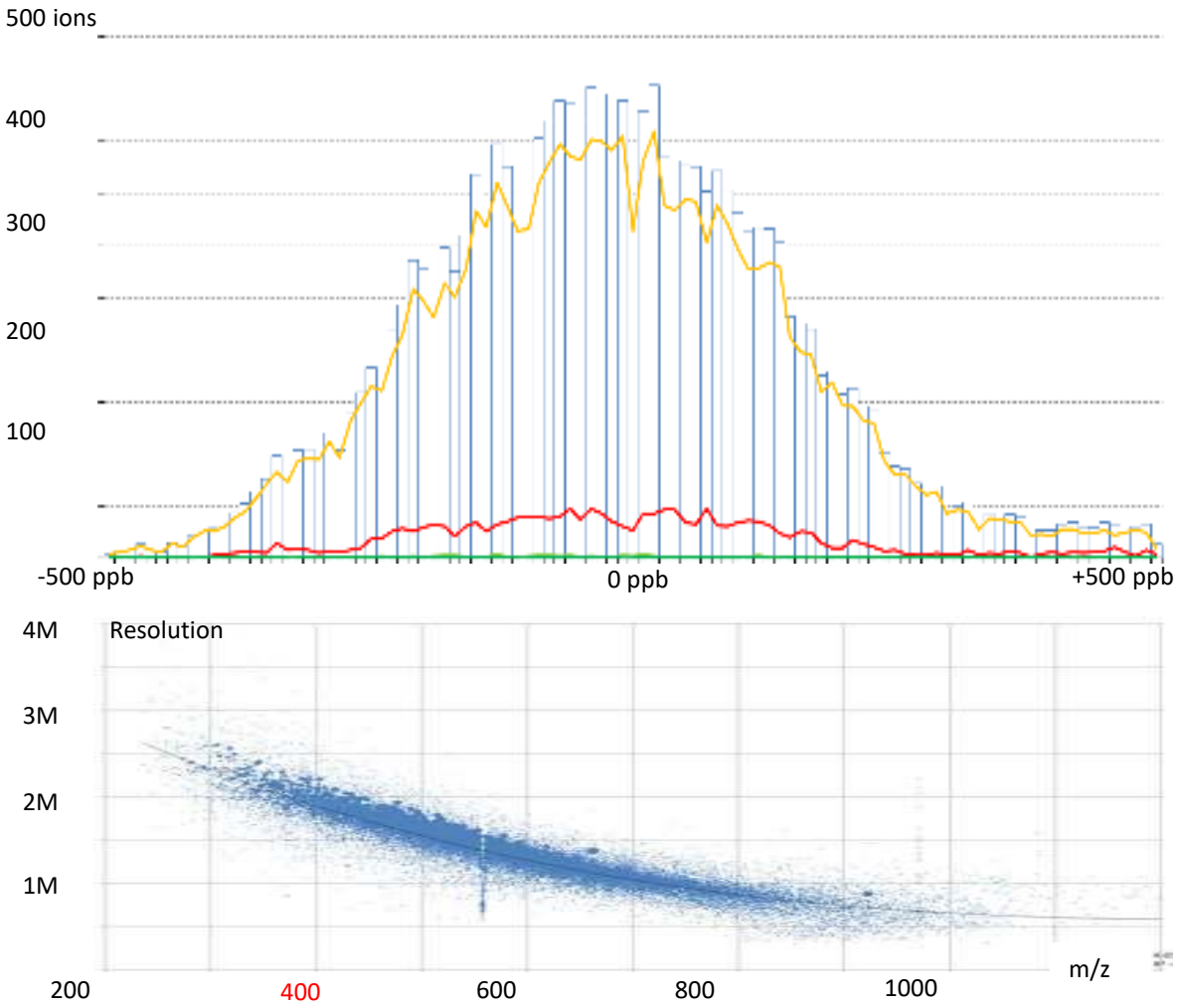

Mass resolution (m/z 400): **1,950,000**
Mass accuracy: **-20 ± 168 ppb**
Compounds: **18200**

m/z	Calc. Res.
300	2368970
400	1950080
500	1600250
600	1313480
700	1083770
800	905120
900	771530
1000	677000

Improving S/N and mass resolution

7T 2ω measurement with AMP, APPI, Oil Residue, m/z 200-800

CASI with 55 Da isolation windows

Isolation mass: m/z 325
Resolution at m/z 325: 3.300.000

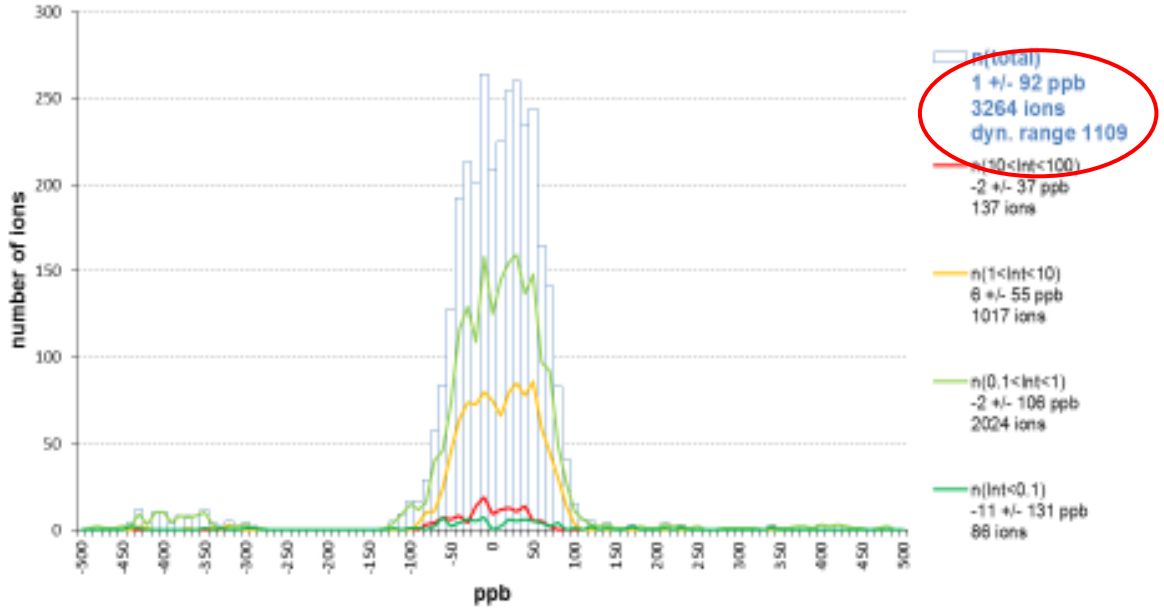

Isolation mass: m/z 525
Resolution at m/z 525: 2.100.000

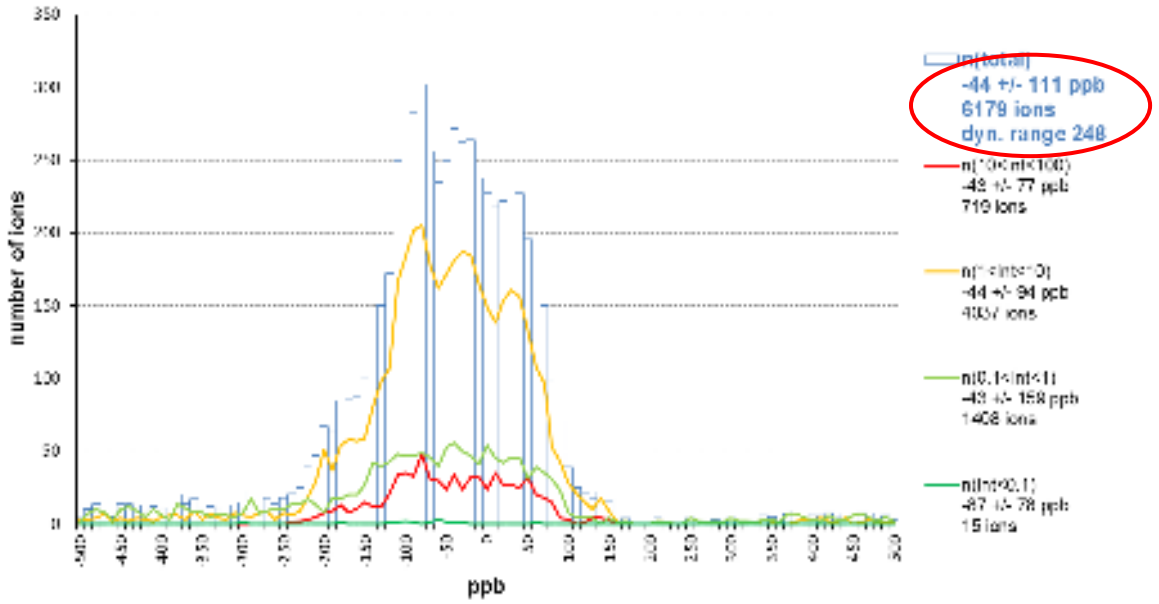

Improving S/N and mass resolution

7T 2ω measurement with AMP, APPI, Oil Residue, m/z 200-800

CASI with 55 Da isolation windows

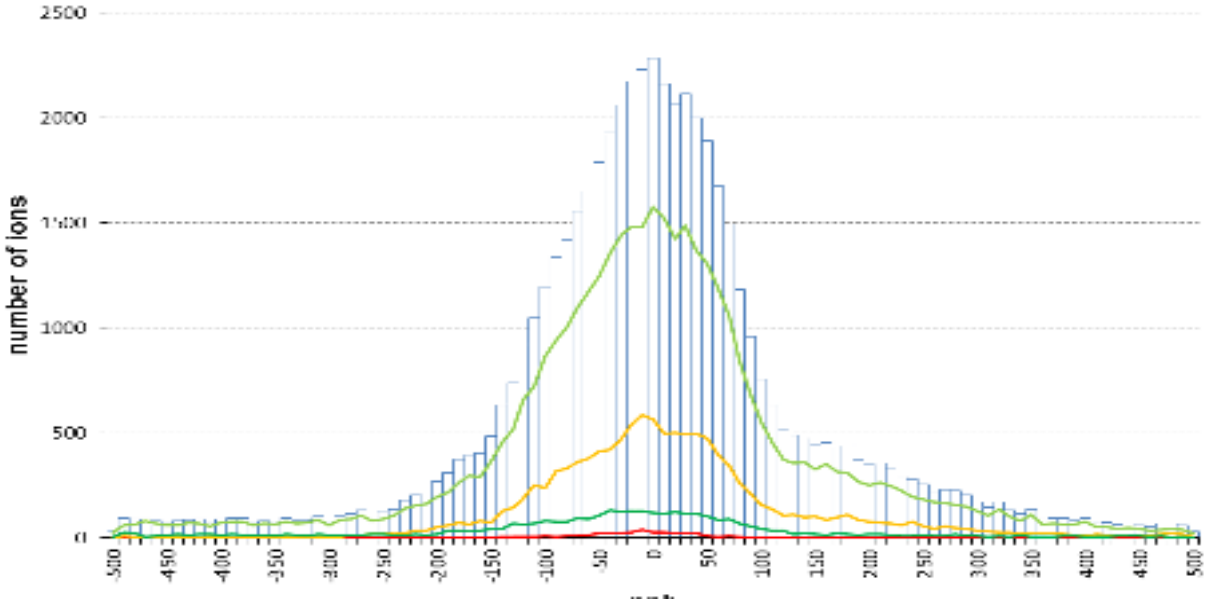

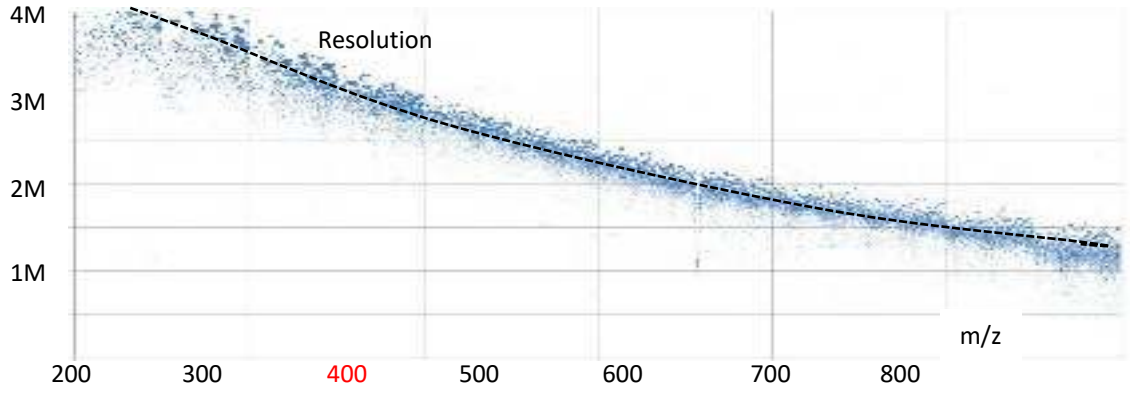

Resolution (m/z 400): **2,750,000**
Mass accuracy: **~~7± 138~~ ppb**
Compounds: **52370**

Petrophase 2017 asphaltene

7T solariX 2xR, quadrupolar detection, AMP

Compound classes plot

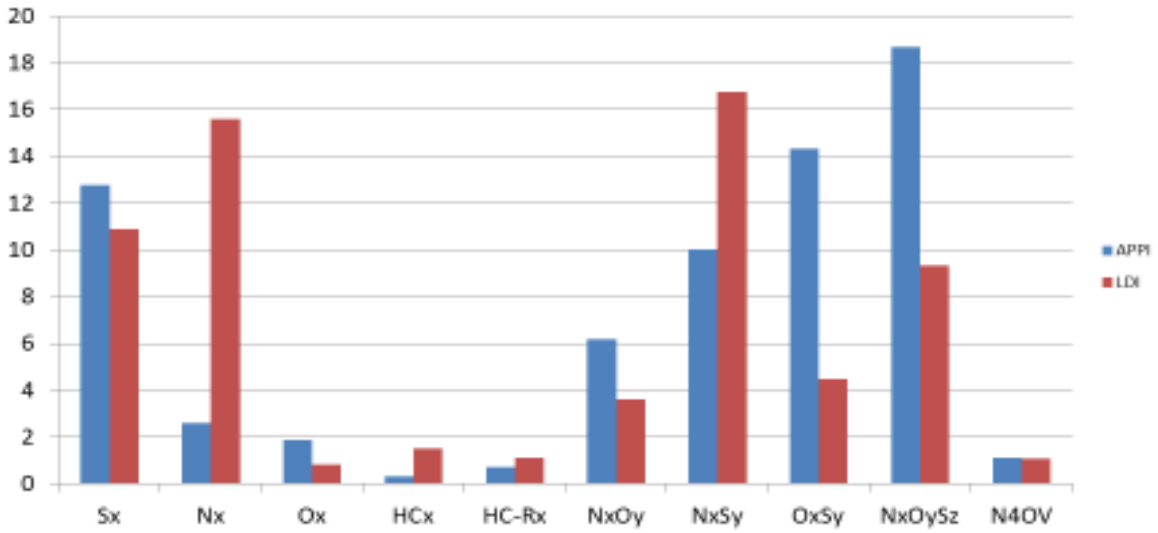

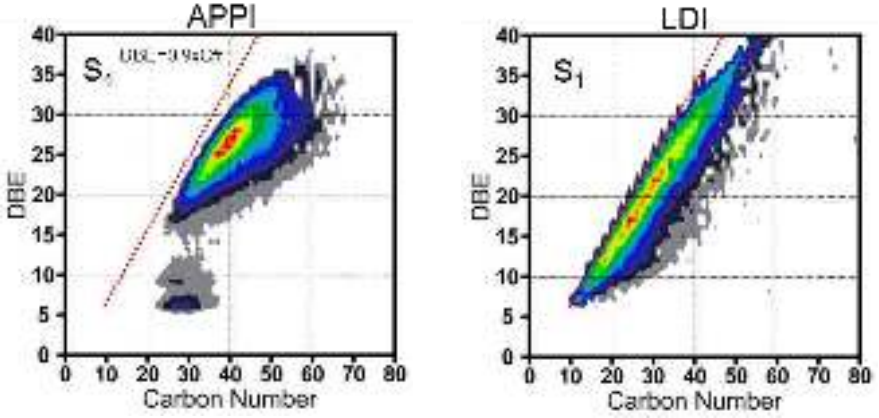

APPI: RMS mass error of 207 ppb (53000 molecular formulae)
LDI: RMS mass error of 248 ppb (42000 molecular formulae)

Resolving power: 1,200,000 @ m/z 400

C (wt. %)	H (wt. %)	N (wt. %)	S (wt. %)
81.78	7.06	1.17	6.82

Hetero atom content

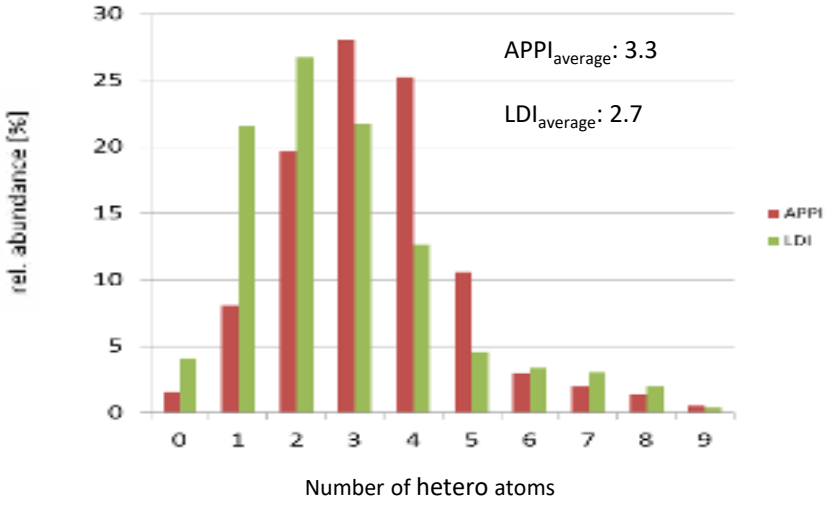

Petroleomics with scimaX

Petroleomics with scimaX

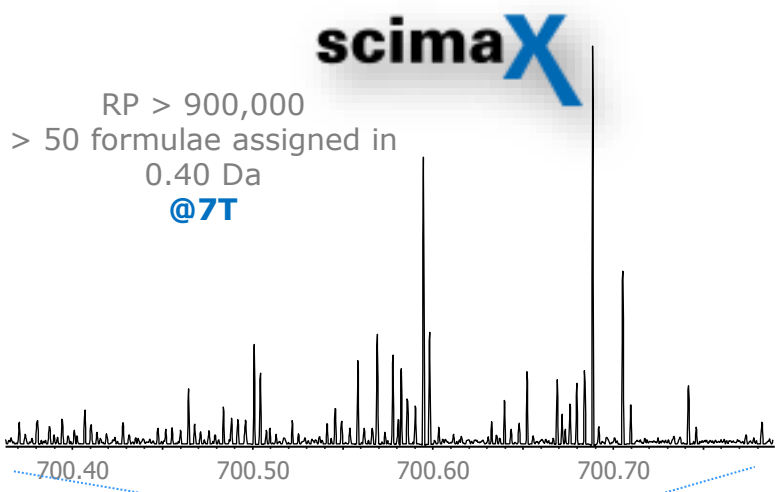

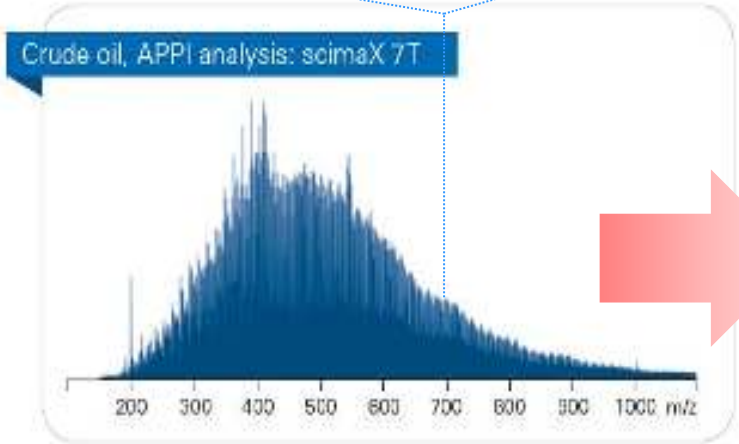

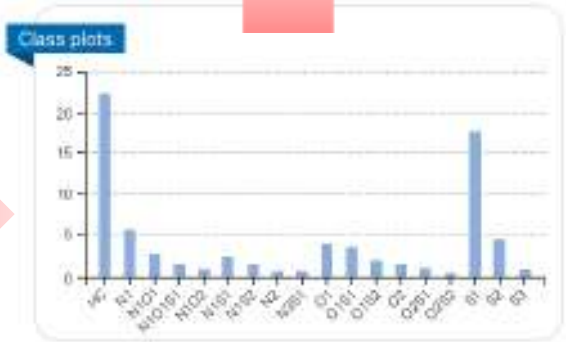

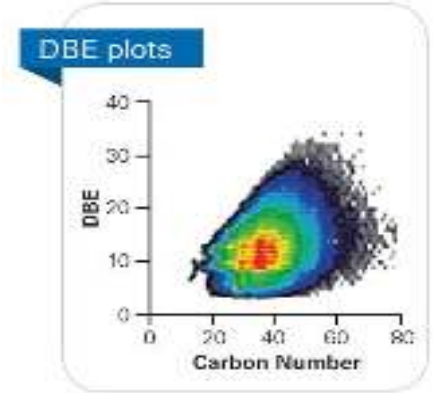

Petroleomics with scimaX

- Study of TAN, corrosion, fouling processes
- 2xR technology
- Easy import of data in Petroleomics software (PetroOrg/Composer) to generate classical plots
- compatible ionization sources to access different molecular species:
  - ESI for basic and acidic compounds
  - LDI, APCI and APPI to access aromatic and non-polar compounds

Summary and Acknowledgements

Summary

- LDI of crude oil, shale oil (correlation with acidity, detection of metallo porphyrins)
- Analysis of TLC fractions of crude oil by LDI
- Fingerprint of crude oils by LDI
- Analysis of oil mixtures
- Asphaltene fractions: - different solvent fractions
  - fractions at different solvent power
  - time effects on precipitation
  - island and archipelago structures
- Effect of hydroprocessing
- Continuum of Petroleum
- Fractionation of interfacial material and naphthenic acids
- Bio-oil analysis
- Effect of Maturity
- Improving data quality - Spectra stitching and quadrupolar detection

Acknowledgements

Kyungpook National University, Korea
Shungwan Kim
Yunju Cho

SINTEF, Norway
Kolbjørn Zahlsen
Anders Brunsvik

Chevron, Richmond, CA, USA
Estrella Rogel
Michael Moir

Bruker Daltonics
Jochen Friedrich
Roland Jertz

EU FT-ICR MS

Mass Spectrometry for **Cultural Heritage Science**

Christian ROLANDO

Miniaturization for Synthesis, Analysis & Proteomics USR 3290

EU_FT-ICR_MS, 2nd AUS, Prague

University of Lille, FST

Any analytical experience fits a class of Heritage Science samples!

- **Petroleomics** → bitumen
- **Proteomics** → paleontology, archaeology, Renaissance paint binder
- **Lipidomics**: → lipids in archaeological ceramic, oil paint
- **Metabomics**: → bee wax, glue, polyphenols from wine or beer
- **Glycomics**: stucco, watercolor
- **Polymer**: → amber, modern paints

Workflow for a new insoluble object in Heritage Science

- Mock samples
- Sample preparation
- Chemical or biological depolylmerization
- Mass spectrometry
- Data treatment

For valuable samples the quantity is always less than necessary to be confortable. Miniaturization is required.

For precious Heritage samples the quantities allow few trials only!

Similar well characterized samples from the Heritage Science point of view or modern for establishing the data bank.

Py-GC MS of modern paint varnishes

Identical pyrolysis conditions

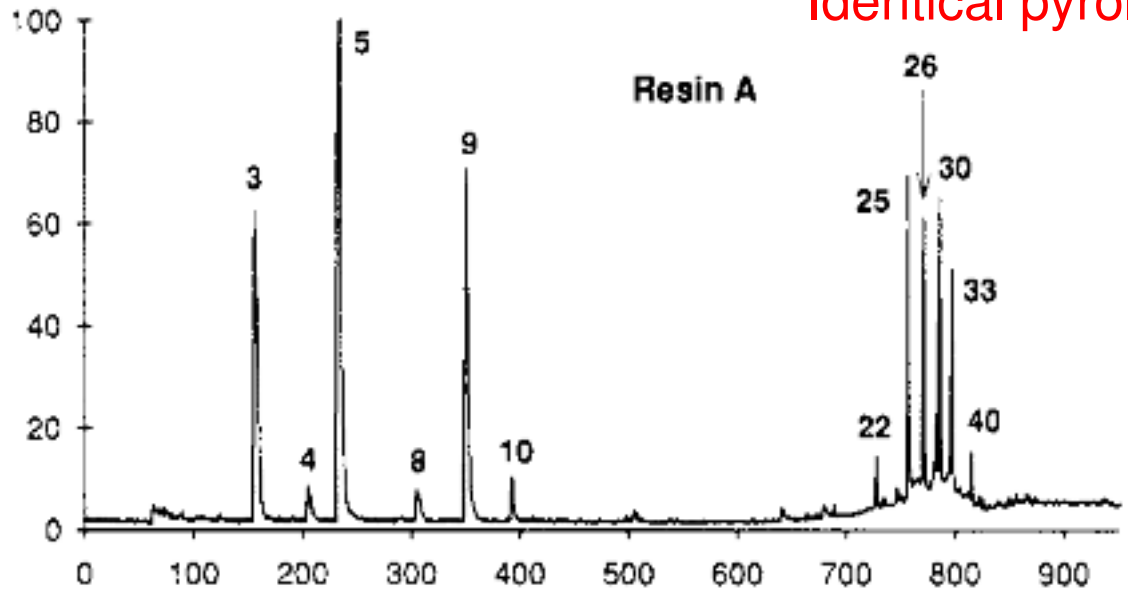

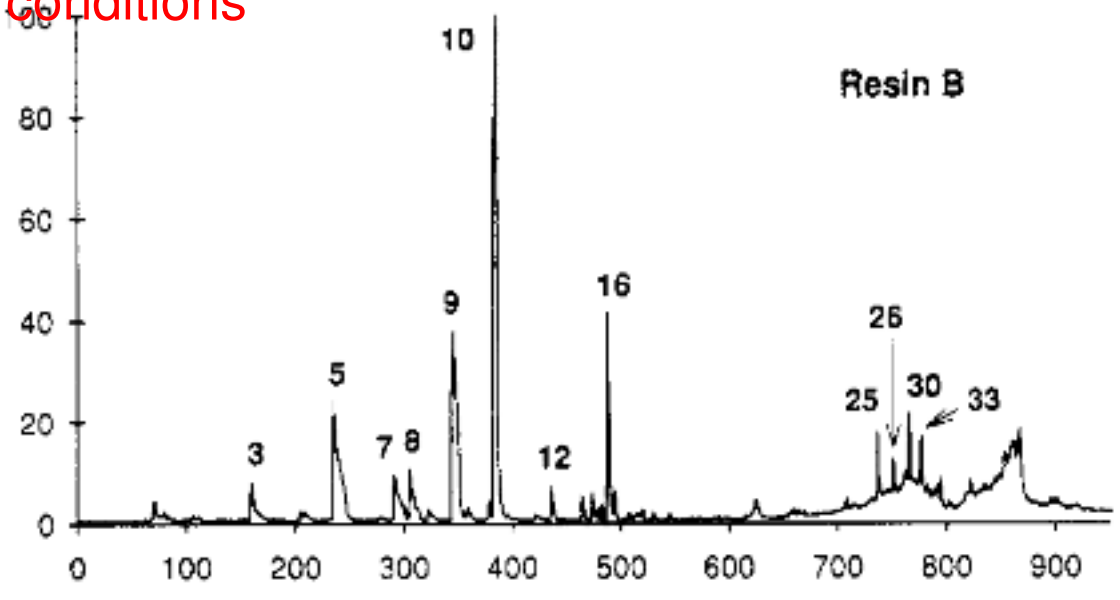

Resin A. To a mixture of cyclohexanone (9.8 g, 0.1 mol) and aqueous 5 M sodium hydroxide (50 mL) was added slowly formaldehyde trimer (6.0 g, 2 equiv of CH_2O), producing an exothermic reaction. The mixture was then refluxed for 30 min, yielding a gummy resin which was washed with water and dried in a vacuum dessicator.

Resin B was prepared in the same way, except for the amount of formaldehyde trimer (15 g, 5 equiv) and the reflux time (7 h).

Mestdagh, H., Rolando, C., Sablier, M., & Rioux, J. P. (1992). Characterization of ketone resins by pyrolysis/gas chromatography/mass spectrometry. *Analytical chemistry*, *64*, 2221-2226.

FTICR MS of bitumen from ancient Greek amphora

A,B—the ancient Greek Amphora full of bitumen.
C—The place of the discovery.

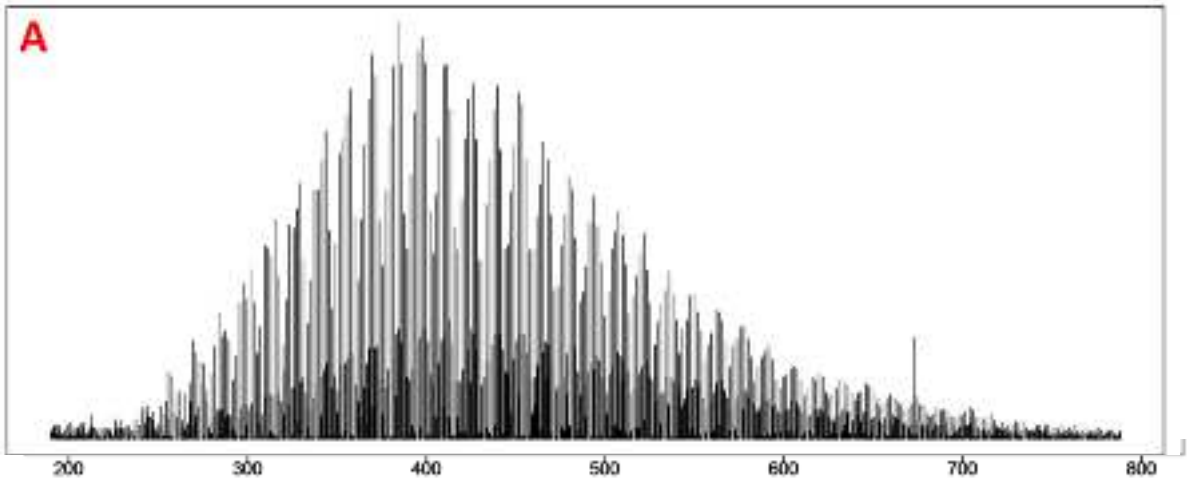

FT ICR spectrum of the bitumen from amphora, positive ESI mode,

Kostyukevich, Y., Solovyov, S., Kononikhin, A., Popov, I., & Nikolaev, E. (2016). The investigation of the bitumen from ancient Greek amphora using FT ICR MS, H/D exchange and novel spectrum reduction approach. *Journal of Mass Spectrometry*, *51*(6), 430-436.

Methodological developments applied to Cultural Heritage: protein identification

Usual approach

Sample → Extration combined with direct hydrolysis in aminoacids (acid or basic hydrolysis) → GC-MS analysis + comparison to models → Binder identification

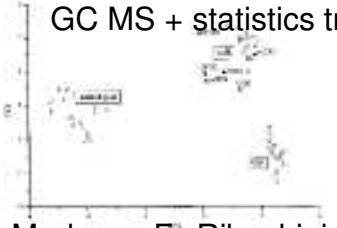

Identification of a binder using comparison to model

Colombini M. P., Andreotti A., Bonaduce I., Modugno F., Ribechini E. Acc. Chem. Res. 2010, 43, 715-727

Actual methodologies

Sample → Protein extraction → Enzymatic hydrolysis → Selective separation of peptides → MS analysis + Bio-informatics → Protein identification via peptides

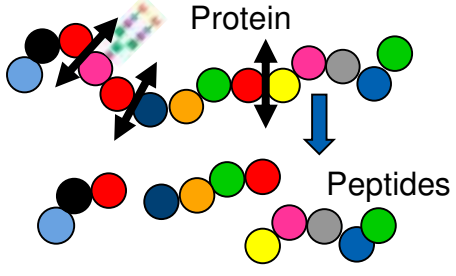

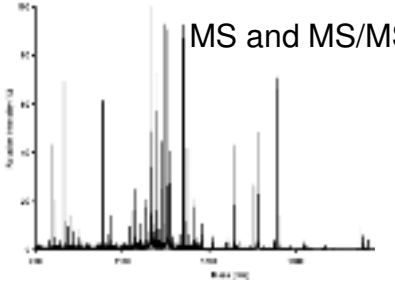

Sequence of the protein via peptides identification

Tokarski C.; Martin E.; Rolando C.; Cren-Olivé C. *Anal Chem* **2006,** 78, 1494-1502

New developments

Sample → Protein extraction → ~~Enzymatic hydrolysis~~ → Selective separation of peptides → MS analysis + Bio-informatics → Protein id. including modifications

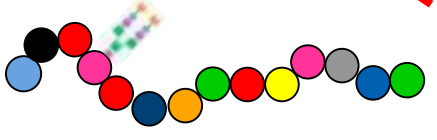

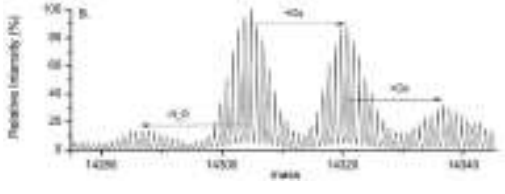

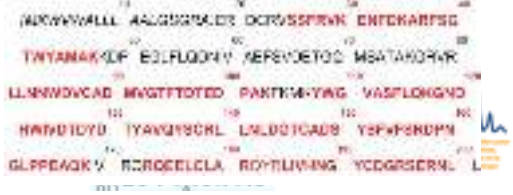

Methodological developments in proteomics applied to the analysis of cultural heritage samples

Sergui MANSOUR

Laboratory of Miniaturization for Synthesis, Analysis & Proteomics (MSAP), USR 3290

Archaeological sample

Collaboration with Dr Franca CIBBECCINI, DRASSM

Location of the shipwreck

- Studied ceramic samples were taken from a Dressel 14 amphora discovered in a shipwreck near the island of Tiboulen de Maïre, near Marseille
- The shipwreck is dated from 116 AD and it was found at 49-50 m deep

Various types of amphorae discovered in the shipwreck; on the right: Dressel 14

EU FT-ICR MS MSAP cnrs Université de Lille

Garum fish sauce

- Dressel-14 (Dr. 14) amphorae have been produced in south of Spain (Baetica) and Portugal (Lusitania) from the 1st century AD to the end of the 2nd century AD
- Tituli picti (inscriptions) found on Dr. 14 informs on their fish sauces contents (the studied Dr. 14 did not show titulus pictus)

Map of trade routes in Western Romain Empire for garum (from curtis 2005)

- Liquamen and garum sauces were obtained from fermented fishes (cuisine of Roman antiquity)
- Various recipes were used (e.g. small fishes versus bigger fishes and fish innards)
- Several fish species were used among which mackerels, sardines, tuna,...

Objective of the study: identification of protein remains trapped in the ceramic and identification of fish species

Current fish protein databases

	NCBI	TrEMBL	Swiss-Prot
Actinopterygii (Class)	3858321	1469565	5343
Clupeiformes (Order)	41668	3966	14
Perciformes (Order)	118224	67597	208
Clupeidae (Family)	36836	2274	13
Scombridae (Family)	9736	3425	68
Sardina (Genus)	1507	253	1
Clupea (Genus)	30480	703	16
Scomber (Genus)	1920	1635	22
Auxis (Genus)	605	191	1
Euthynnus (Genus)	271	133	-
Thunnus (Genus)	3188	1347	50
Sardina pilchardus (Species)	323	96	1
Scomber scombrus (Species)	694	207	4
Auxis thazard (Species)	261	6	-
Euthynnus alletteratus (Species)	131	-	-
Thunnus thynnus (Species)	687	325	16
Thunnus alalonga (Species)	436	109	2

- **The current fish protein databases have few entries**
- Informative entries for our study are missing
- An in house database with various fish species was build

Phylogenetic tree of the studied fish species

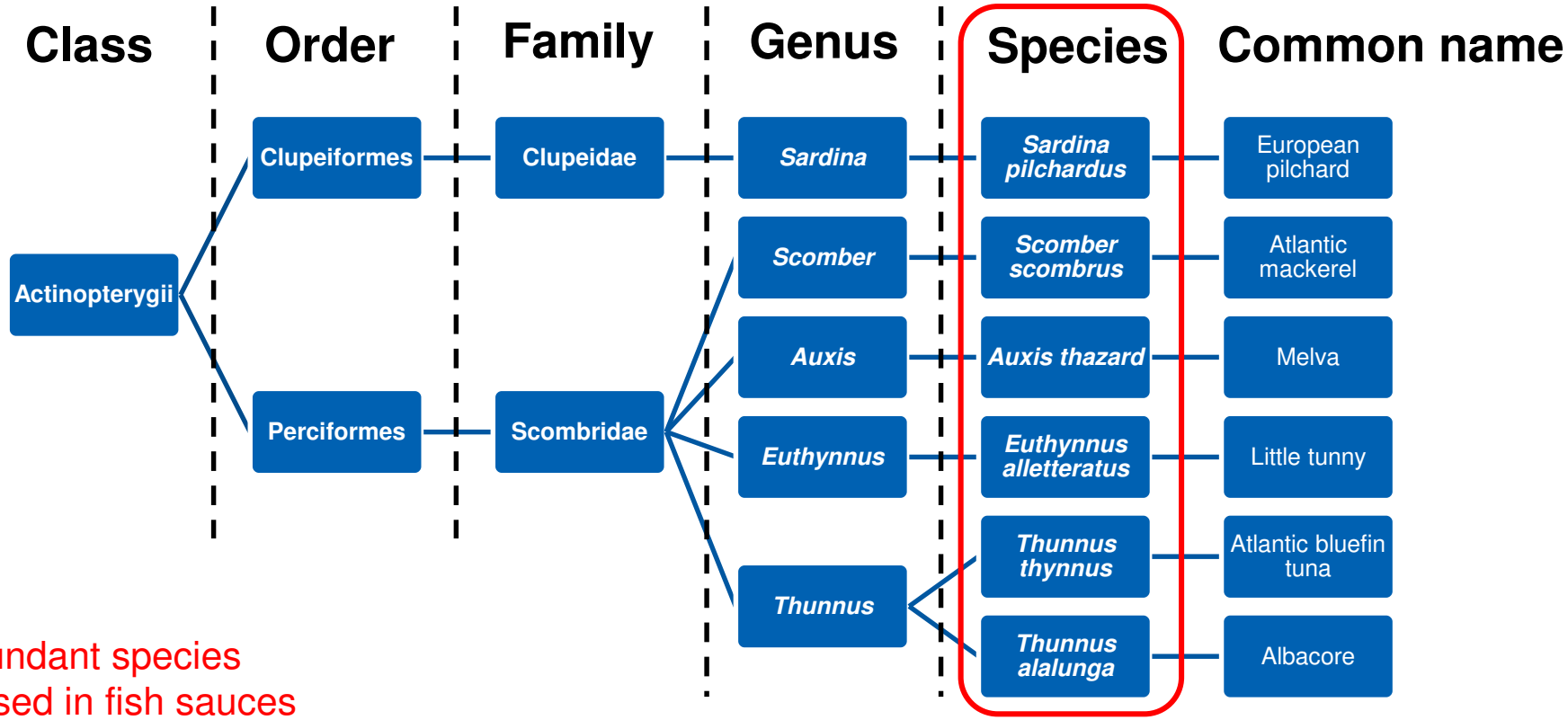

Focus on several abundant species described as being used in fish sauces

		Sardina pilchardus	*Scomber scombrus*	*Auxis thazard*	*Ehthynnus alletteratus*	*Thunnus thynnus*	*Thunnus alalunga*
Number of proteins	NCBI	323	694	261	131	687	436
	TrEMBL	96	207	6	-	325	109
	Swiss-Prot	1	4	-	-	16	2

Experimental procedure

I

Selection of 6 fish species to **build a database** (muscle and blood proteins)

II

Analysis of garum model sauces:

1. Sardines
2. Innards of mackerel

(Prepared with traditional recipes by Dr N. Garnier, and Dr E. Botte)

III

Analysis of archaeological ceramic

Extraction of proteins

↓

Digestion of proteins
(eFASP Protocol)

↓

Mass spectrometry analysis

↓

Raw data treatment

NanoLC NanoESI Orbitrap QExactivePlus

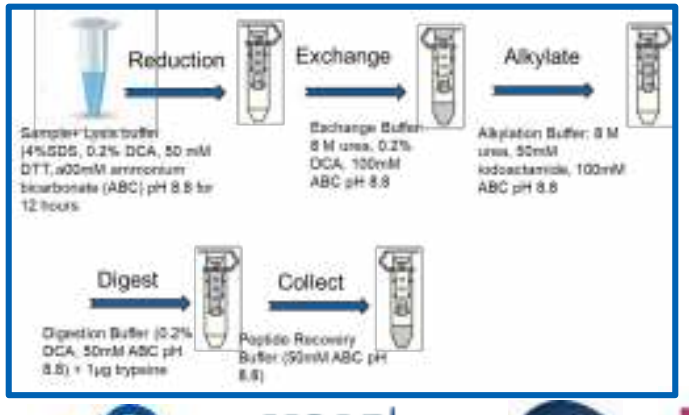

EU FT-ICR MS

MSAP

cnrs

Université de Lille

Workflow

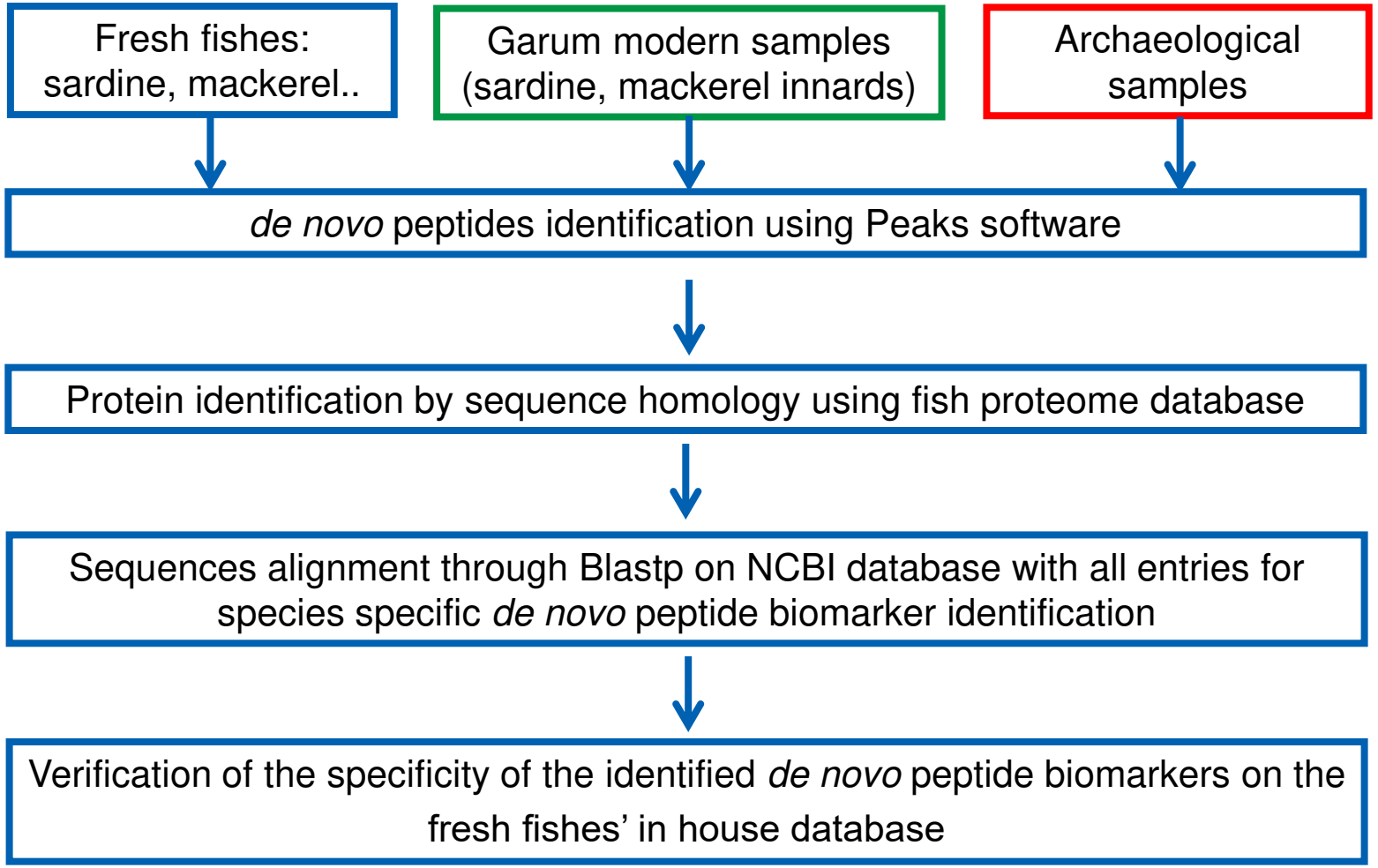
Fresh fishes: sardine, mackerel..
Garum modern samples (sardine, mackerel innards)
Archaeological samples
de novo peptides identification using Peaks software
Protein identification by sequence homology using fish proteome database
Sequences alignment through Blastp on NCBI database with all entries for species specific *de novo* peptide biomarker identification
Verification of the specificity of the identified *de novo* peptide biomarkers on the fresh fishes' in house database

De novo analysis of the fishes samples with Peaks software

	Sardina pilchardus	*Scomber scombrus*	*Auxis thazard*	*Ehthynnus alletteratus*	*Thunnus thynnus*	*Thunnus alalunga*
Number of MS	7729	7889	7664	8111	7584	7762
Number of MS/MS	49427	49329	49526	49144	49608	49526
Peptide-Spectrum Matches	18444	19388	18589	22700	24635	23454
Peptide sequences	9970	9804	9499	11596	12435	11068
Missed Cleavages = 0	6229	6711	6266	7493	8268	7405
Missed Cleavages = 1	2629	2394	2446	3013	3101	2780
Missed Cleavages = 2	834	575	660	890	869	741
Missed Cleavages = 3	242	112	117	179	173	131
Protein groups	521	490	441	522	609	428
Proteins	1388	1569	941	1240	1252	774
Proteins (>2 Unique Peptides)	**754**	**83**	**539**	**679**	**685**	**403**

- **Successful identification of proteins including muscle proteins and blood proteins**

Home-made database: identification fish specific peptides from fresh fishes

Example of Tropomyosin protein extracted from *Scomber scombrus* fish sample (identified by sequence homology to the *Thunnus thynnus)*

MEAIKKKMQM LKLDKENALD RAEQSESDKK AAEDRTKQLE DDLVDMQKRL KGTEDELEKY SGALKDVQEK LEVAEKQATD AEGDVASLNR RIQLVEEELD RAQERLATAL TKLEEAEKVA DESERGMKVI ENRNMKDEEK MEMQDVQLKE AKNIAEEADR KYEEVARKLV VIESDLERTE ERAELSETKC SELEEESKTV TNNLKSLEAQ AEKYTQKEDK YEEEIKVLTD KLKEAETRAE FAERSVAKLE KTIDDLEDEL YAQKQKFKSI SEELDHALND MTSI

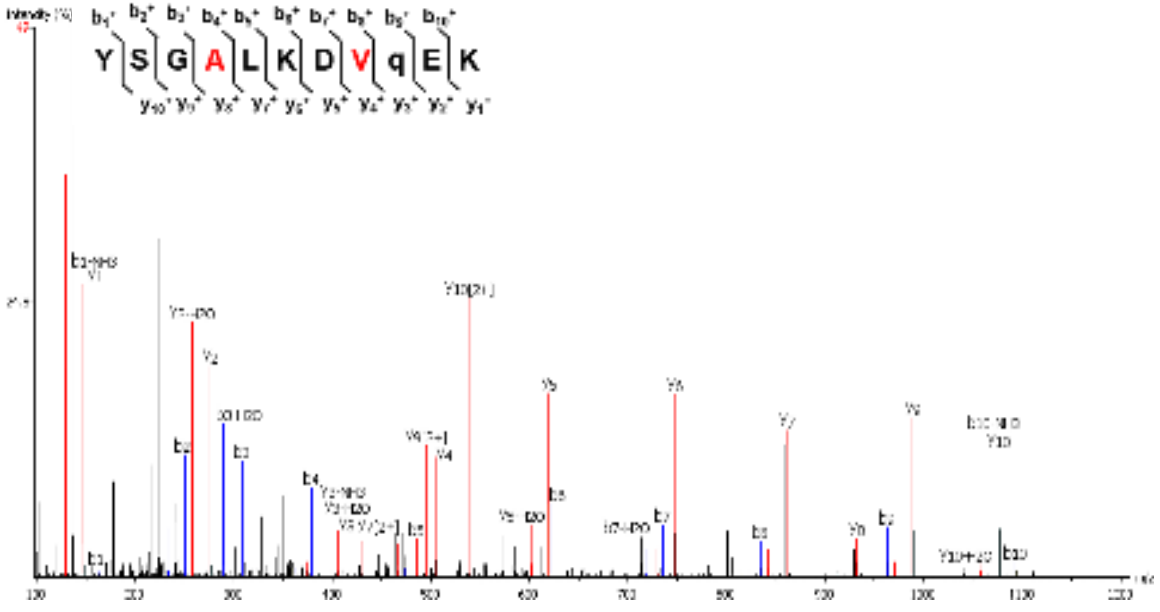

MS/MS spectrum of the doubly charged ion at *m/z* = 619.816 (Δm = 0.3 ppm)

- Several peptides (e.g. peptide in position 60-70) are showing amino acids substitutions and can be used to discriminate species

Home-made database: identification fish specific peptides from modern fishes

Example of Tropomyosin protein extracted from *Scomber scombrus* fish sample (identified by sequence homology to the *Thunnus thynnus)*

MEAIKKKMQM LKLDKENALD RAEQSESDKK AAEDRTKQLE DDLVDMQKRL KGTEDELEKY SGALKDVQEK LEVAEKQATD AEGDVASLNR RIQLVEEELD RAQERLATAL TKLEEAEKVA DESERGMKVI ENRNMKDEEK MEMQDVQLKE AKNIAEEADR KYEEVARKLV VIESDLERTE ERAELSETKC SELEEESKTV TNNLKSLEAQ AEKYTQKEDK YEEEIKVLTD KLKEAETRAE FAERSVAKLE KTIDDLEDEL YAQKQKFKSI SEELDHALND MTSI

***Scomber scombrus* Peptides**	**Species**
YSGALKDVQ(d)EK	*Scomber scombrus* (home-made database)
YSG**N**LKD**A**QEK	*Thunnus thynnus* (NCBI database)

- Specificity using Blastp on NCBI database (Identities 82%)

***Scomber scombrus* Peptides**	**Species**
YSGALKDVQ(d)EK	*Scomber scombrus* (home-made database)
YSEALKDAQEK	*Stegastes partitus* (NCBI database)

- Several peptides (e.g. peptide in position 60-70) are showing amino acids substitutions and can be used to discriminate species

Methodology development on model garum samples

Model garum sauce
(entire sardine)

Identification of 716 proteins

De novo peptides identification of muscle proteins

In house database

De novo peptides matching

Identification of *Sardina pilchardus* specific peptides

Model garum sauce
(mackerel innards)

Identification of 631 proteins

De novo peptides identification of blood proteins

In house database

De novo peptides matching

Identification of *Scomber scombrus* specific peptides

Université de Lille

Species specific peptide identified in garum sauce

- Muscle and blood proteins identified in the modern garum fishes sauces showed sequence matches and dissimilarities with several species present in the in house database

Example of garum modern sauce made from entire sardine

Sample	Protein	Specific peptide with amino acid substitution
Model garum sardine	myosin light chain 2	NLWAAFPPDVTGNVDYK
Sardina pilchardus in house data base	myosin light chain 2	NLWAAFPPDVTGNVDYK
Thunnus thynnus in house data base	myosin light chain 2	NMWAAFPPDVAGNVDYK
Sardinops melanostictus NCBI	myosin light chain 2	NLWAAFPPDVTGQVDYK

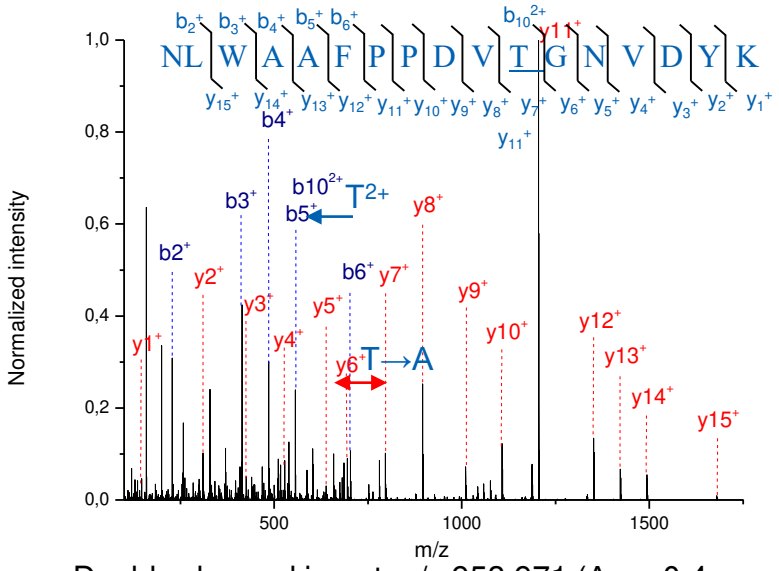

Doubly charged ion at m/z 953.971 (Δm= 0.4 ppm), Protein identified by sequence homology to the *Thynnus thynnus* species

Analysis of the archaeological sample

	Archaeological sample
Number of MS scans	25609
Number of MS/MS scans	33291
Peptide-spectrum matches	1721
Peptide sequence	701
Missed cleavages = 0	531
Missed cleavages = 1	152
Missed cleavages = 2	23
Missed cleavages = 3	1
Protein groups	39
Proteins	198
Proteins (>2 unique peptides)	**157**

50 mg of Dr. 14 archaeological ceramic used for analysis

Successful identification of 157 proteins among them 10 muscle proteins and 2 blood proteins contain specific peptides for fishes

Spectrum signal to noise ratio and sequence coverage

Archaeological Sample

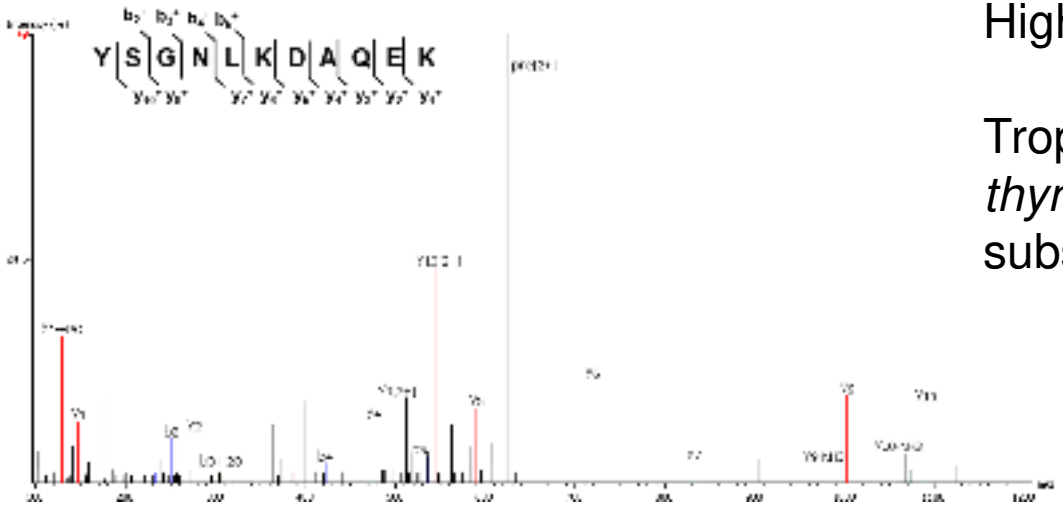

MS/MS spectrum of the doubly charged ion at m/z: 626.811 (Δm = 2.5 ppm)

High sequence coverage (61 %),

Tropomyosin protein identified *Thunnus thynnus* (NCBI database) whithout any substitution

MEAIKKKMQM LKLDKENALD RAEQSESDKK AAEDRTKQLE DDLVAMQKRL KGTEDELEKY SGNLKDAQEK
LEVAEKSATD AEGDVASLNR RIQLVEEELD RAQERLATAL TKLEEAEKAA DESERGMKVI ENRNMKDEEK
MEMQDVQLKE AKNIAEEADR KYEEVARKLV VIESDLERTE ERAELSESKC SELEEESKTV TNNLKSLEAQ
AEKYTQKEDK YEEEIKVLTD KLKEAETRAE FAERSVAKLE KTIDDLEDEL YAQKQKFKSI SEELDHALND MTSI

Grey: All sequenced peptides
Yellow: Considered peptide

Sequences alignments (tropomyosin protein)

>Analyzed sample: Archaeological sample
> Tropomyosin [*Thunnus thynnus*-NCBI]
MEAIKKKMQM LKLDKENALD RAEQSESDKK AAEDRTKQLE DDLVAMQKRL KGTEDELEKY SGNLKDAQEK LEVAEKSATD AEGDVASLNR RIQLVEEELD RAQERLATAL TKLEEAEKAA DESERGMKVI ENRNMKDEEK MEMQDVQLKE AKNIAEEADR KYEEVARKLV VIESDLERTE ERAELSESKC SELEEESKTV TNNLKSLEAQ AEKYTQKEDK YEEEIKVLTD KLKEAETRAE FAERSVAKLE KTIDDLEDEL YAQKQKFKSI SEELDHALND MTSI

> In house database *Thunnus alalunga*
> Tropomyosin [*Thunnus thynnus*-NCBI]
MEAIKKKMQM LKLDKENALD RAEQSESDKK AAEDRTKQLE DDLVAMQKRL KGTEDELEKY SGNLKDAQEK LEVAEKSATD AEGDVASLNR RIQLVEEELD RAQERLATAL TKLEEAEKAA DESERGMKVI ENRNMKDEEK MEMQDVQLKE AKNIAEEADR KYEEVARKLV VIESDLERTE ERAELSESKC SELEEESKTV TNNLKSLEAQ AEKYTQKEDK YEEEIKVLTD KLKEAETRAE FAERSVAKLE KTIDDLEDEL YAQKQKFKSI SEELDHALND MTSI
> In house database *Thunnus thynnus*
> Tropomyosin [*Thunnus thynnus*-NCBI]
MEAIKKKMQM LKLDKENALD RAEQSESDKK AAEDRTKQLE DDLVAMQKRL KGTEDELEKY SGNLKDAQEK LEVAEKSATD AEGDVASLNR RIQLVEEELD RAQERLATAL TKLEEAEKAA DESERGMKVI ENRNMKDEEK MEMQDVQLKE AKNIAEEADR KYEEVARKLV VIESDLERTE ERAELSESKC SELEEESKTV TNNLKSLEAQ AEKYTQKEDK YEEEIKVLTD KLKEAETRAE FAERSVAKLE KTIDDLEDEL YAQKQKFKSI SEELDHALND MTSI
> In house database *Scomber Scombrus*
> Tropomyosin [Thunnus thynnus-NCBI]
MEAIKKKMQM LKLDKENALD RAEQSESDKK AAEDRTKQLE DDLV**D**MQKRL KGTEDELEKY SG**A**LKD**V**QEK LEVAEK**Q**ATD AEGDVASLNR RIQLVEEELD RAQERLATAL TKLEEAEK**V**A DESERGMKVI ENRNMKDEEK MEMQDVQLKE AKNIAEEADR KYEEVARKLV VIESDLERTE ERAELSE**T**KC SELEEESKTV TNNLKSLEAQ AEKYTQKEDK YEEEIKVLTD KLKEAETRAE FAERSVAKLE KTIDDLEDEL YAQKQKFKSI SEELDHALND MTSI
> In house database *Auxis thazard*
> Tropomyosin [Thunnus thynnus-NCBI]
MEAIKKKMQM LKLDKENALD RAEQSESDKK AAEDRTKQLE DDLVAMQKRL KGTEDELEKY SG**A**LKDAQEK LEVAEKSATD AEGDVASLNR RIQLVEEELD RAQERLATAL TKLEEAEKAA DESERGMKVI ENRNMKDEEK MEMQDVQLKE AKNIAEEADR KYEEVARKLV VIESDLERTE ERAELSESKC SELEEESKTV TNNLKSLEAQ AEKYTQKEDK YEEEIKVLTD KLKEAETRAE FAERSVAKLE KTIDDLEDEL YAQKQKFKSI SEELDHALND MTSI
> In house database *Euthynnus alletteratus*
> Tropomyosin [*Thunnus thynnus-NCBI*]
MEAIKKKMQM LKLDKENALD RAEQSESDKK AAEDRTKQLE DDLVAMQKRL KGTEDELEKY SG**A**LKDAQEK LEVAEKSATD AEGDVASLNR RIQLVEEELD RAQERLATAL TKLEEAEKAA DESERGMKVI ENRNMKDEEK MEMQDVQLKE AKNIAEEADR KYEEVARKLV VIESDLERTE ERAELSESKC SELEEESKTV TNNLKSLEAQ AEKYTQKEDK YEEEIKVLTD KLKEAETRAE FAERSVAKLE KTIDDLEDEL YAQKQKFKSI SEELDHALND MTSI

Sequences matching(e.g. tropomyosin protein)

Archaeological Sample
(*Thunnus thynnus*)

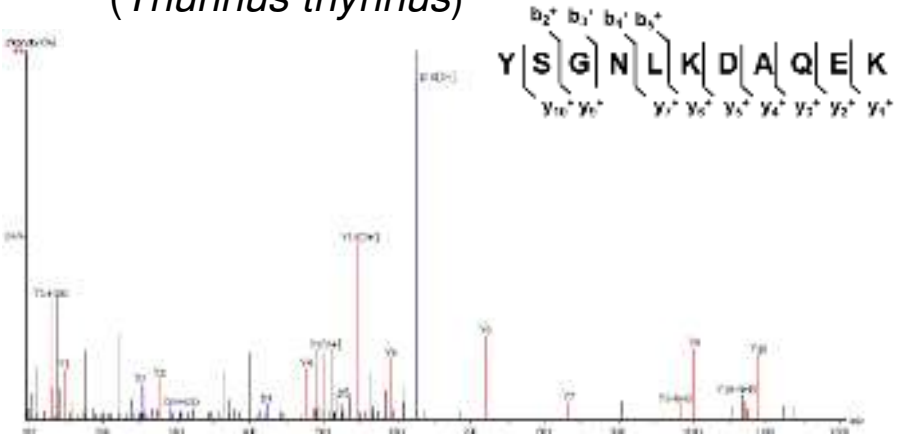

Auxis Thazard

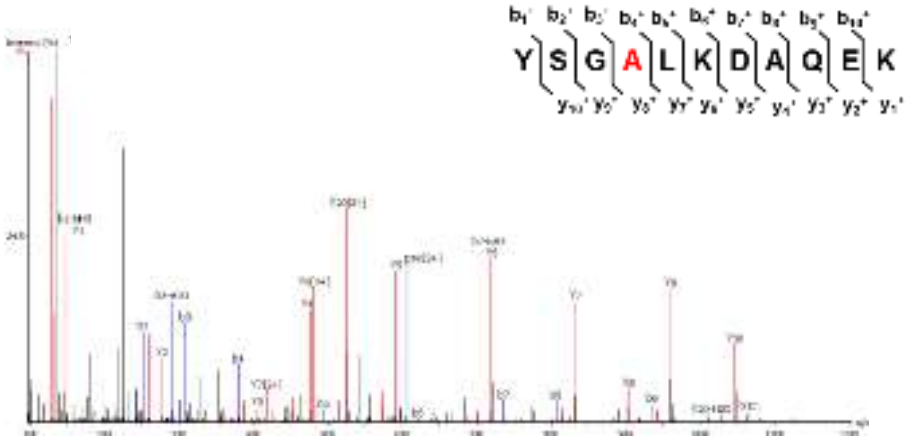

Thunnus alalunga

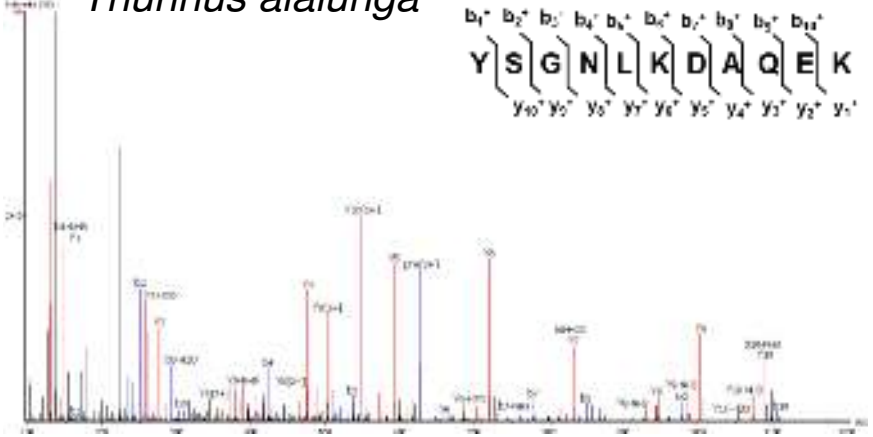

Scomber scombrus

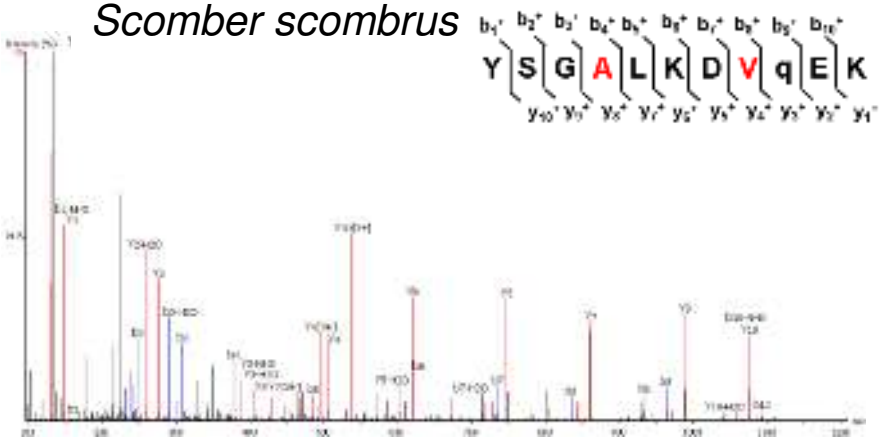

Sequence alignements were performed using public databases and our home-made databases; e.g. here an amino acid substitution is shown

Proteins identified in the archaeological sample

Among the 157 proteins (≥ 2 unique peptides):

10 muscle proteins:

- 32 peptides discriminant for fishes (comparison with the NCBI database)

2 blood proteins:

- 4 peptides discriminant for fishes

The peptides identified in the archaeological sample showed dissimilarities with several species studied in this work (e.g. *Sardina pilchardus, Scomber scombrus*)

No sequence dissimilarities were found with *Thunnus thynnus* and *Thunnus alalunga* species

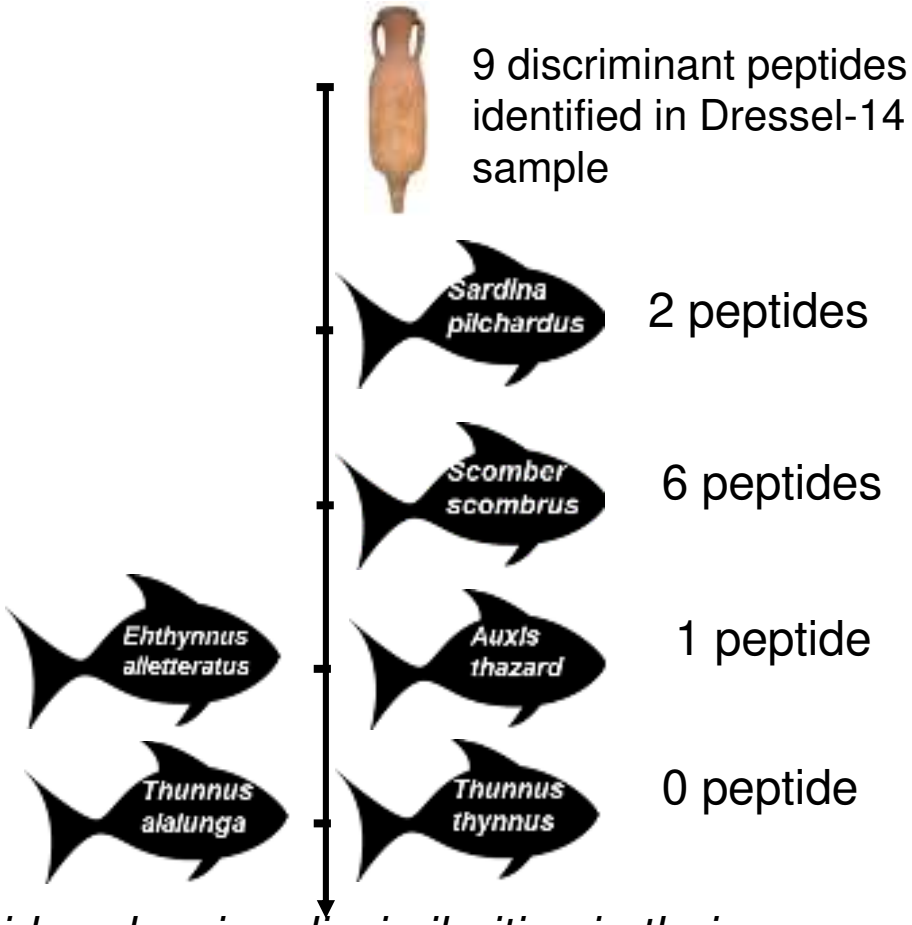

Peptides showing dissimilarities in their sequences

Université de Lille

Conclusion

- Proteins from Dressel 14 archaeological samples preserved in submarine context during two millenaries were identified
- Proteins from muscles and blood were identified
- Good protein sequence coverages were obtained allowing sequence alignment studies
- New peptides not referenced in the current databases have been identified by *de novo* sequencing (and sequence homology to referenced proteins)
- Proteins identified in the archaeological material showed sequence dissimilarities with several modern species studied in this work (e.g. *Sardina pilchardus, Scomber scombrus)*
- No sequence dissimilarities were identified with *Thunnus thynnus* and *Thunnus alalunga species* raising the question of the potential use of tuna in the studied amphorae.

Taxonomy and classification of Upper Pleistocene bones with ultrahigh resolution MALDI-FTICR Mass Spectrometry

Isabelle FABRIZI

Miniaturization for Synthesis, Analysis & Proteomics USR 3290

University of Lille, FST

Why

- Ancient preserved molecules give a **better knowledge** on the biological past
- Bones proteomic is a **good alternative to replace** ancient DNA analysis
- **Tiny fragments** are found in **large numbers** during paleontological excavations
- Analysis of fossils **must consume a low quantity of material** to avoid damaging samples
- Modifications post translationnal are **markers of degradation** of bones

ZooMS

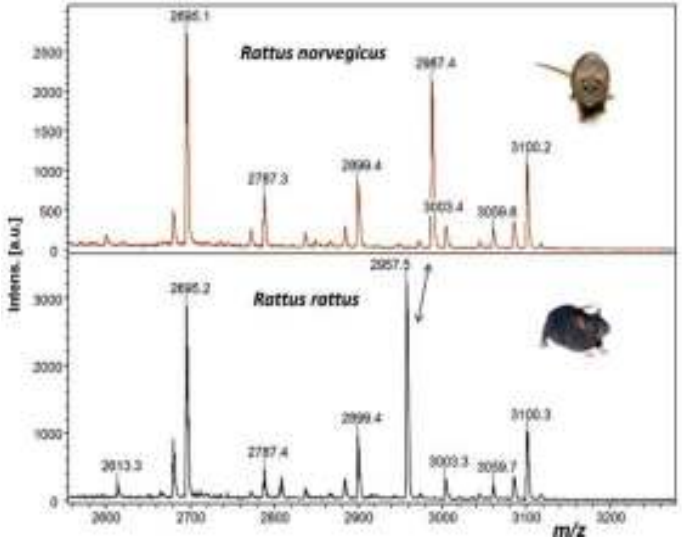

LC-MS/MS

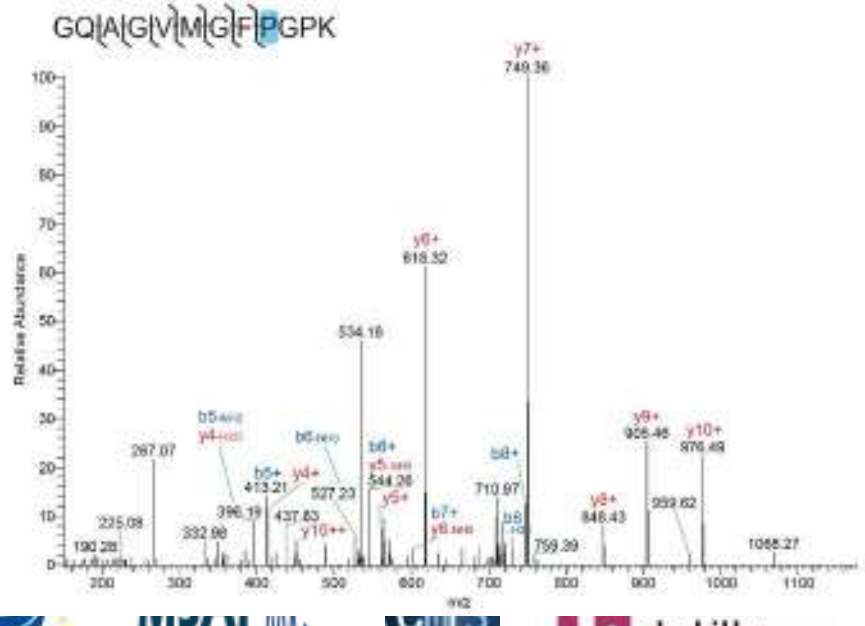

High throughput method using FT-ICR development

Sample preparation

Analysis

Bioinformatic without Data bank

Solarix XR 9.4 Tesla

Bones

500 µg

96-well plate digestion

Demineralisation
Denaturation
Digestion

MALDI FT ICR analysis
HCCA/ACN(10 mg/mL)

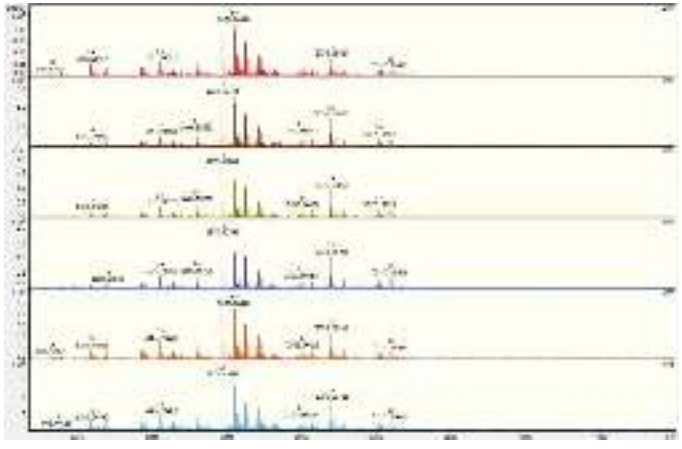

MALDI FT ICR spectra

Reference bones and paleontological bones from Caours and Waziers (130,000 – 110,000 years old, France) were given by Dr Patrick AUGUSTE, EEP laboratory.

EU FT-ICR MS

Workflow optimization on 96 well plate

- Reference bones

- eFASP (cellulose acetate)

- eFASP microplate 30 kDa (polyethersulfone)
- eFASP microplate 10 kDa (polyethersulfone)

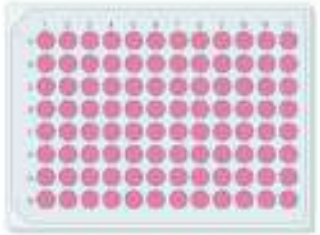

- eFASP microplate 0.45 µm (10 kDa) (PVDF)

MALDI FT ICR : detection limit from eFASP in 96 wells plates

Bos primigenus spectra from archeological site Caours (130,000 – 110,000 years old)

Resolution 2M, FID 5.0 sec, 15 accumulated spectra, laser shot: 1’30 s

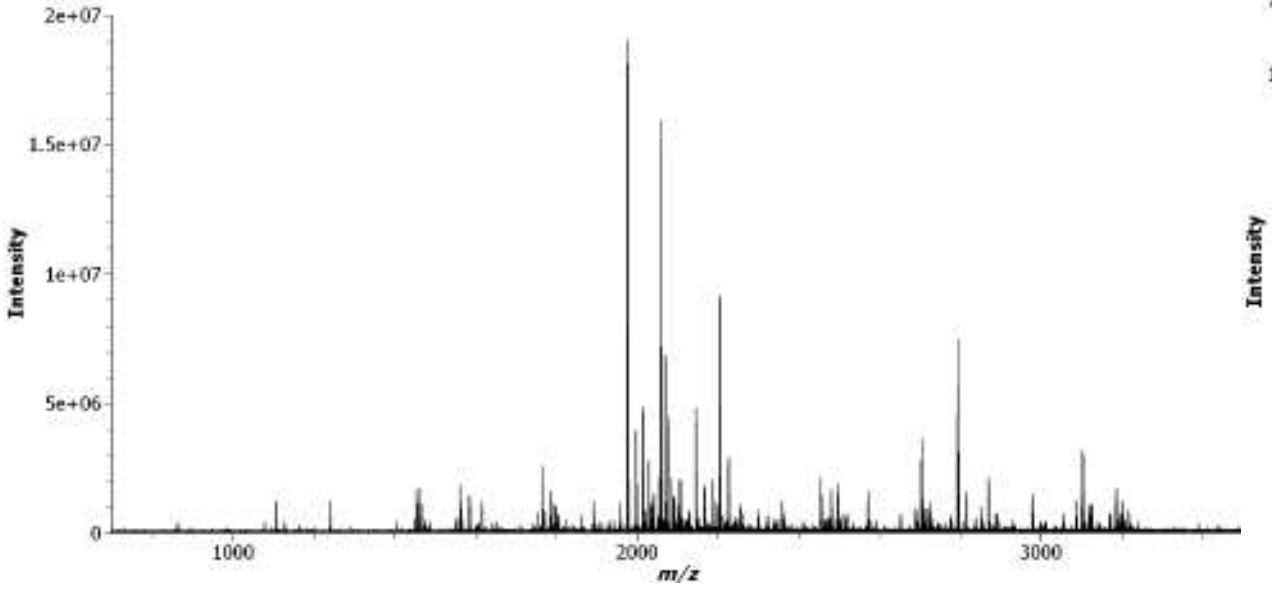

0.1 mg

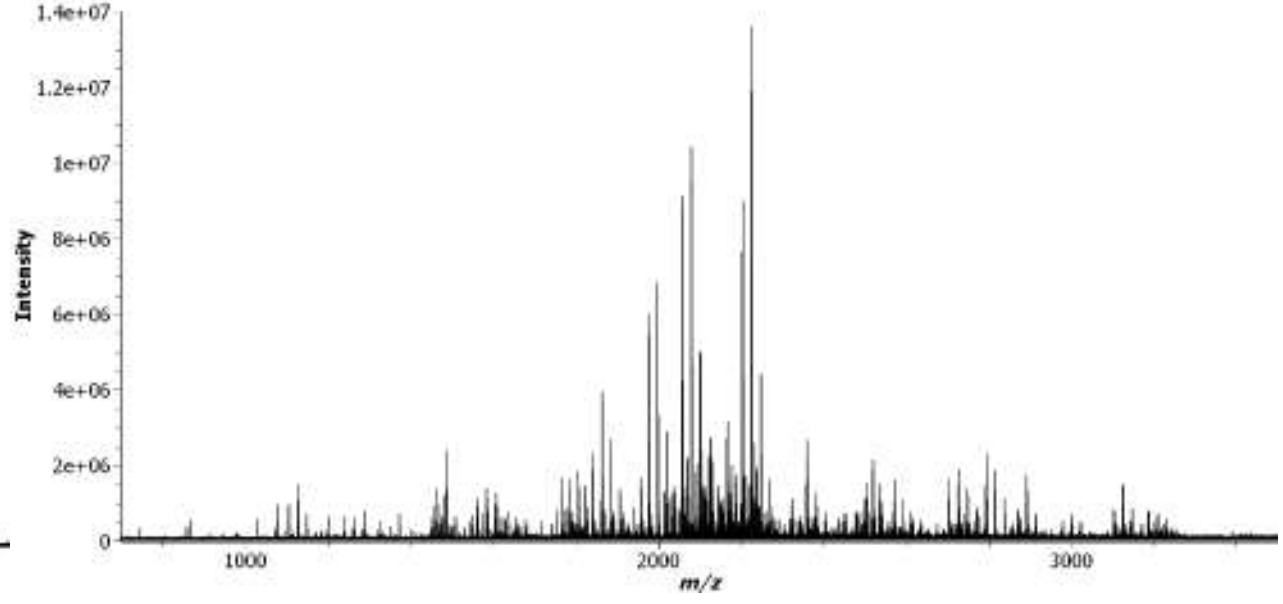

1 mg

Detection limit: 0.1 mg of bone

Depend on bone conservation & archaeological sites

Protocol reproductibility of 96 well plate digestion

Bos taurus (modern)
Bos primigenus (Aurochs, ancient)

6 peptidic digests from 1 mg of bones, analyzes in duplicate

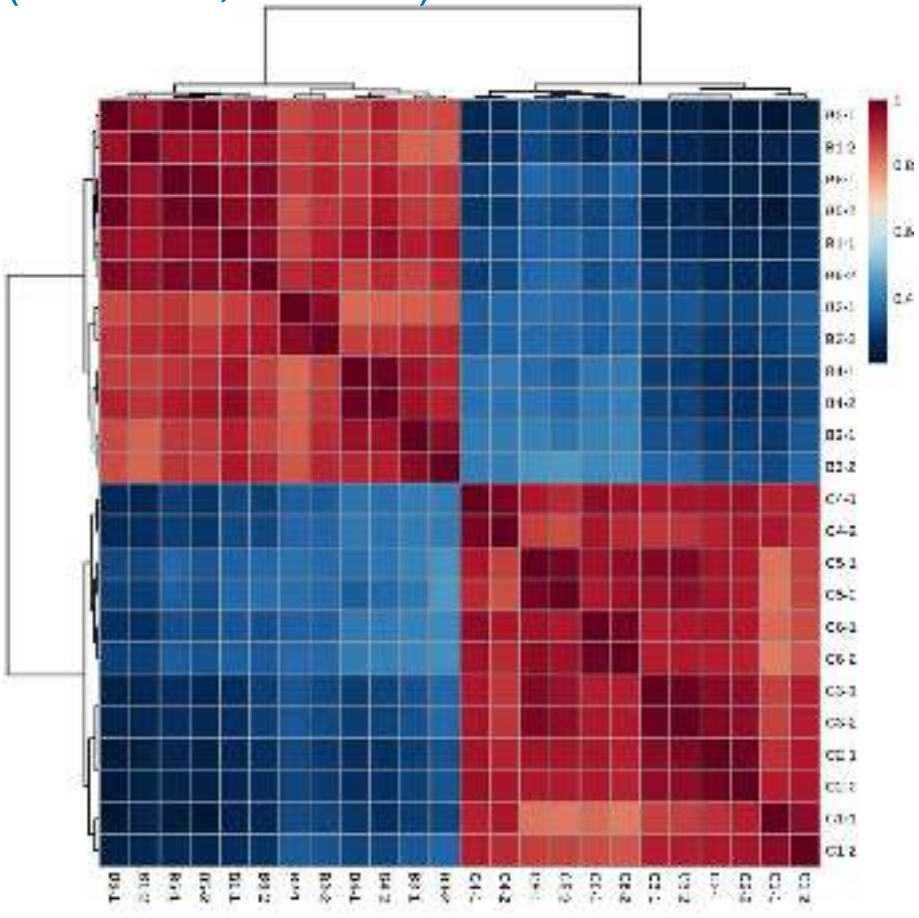

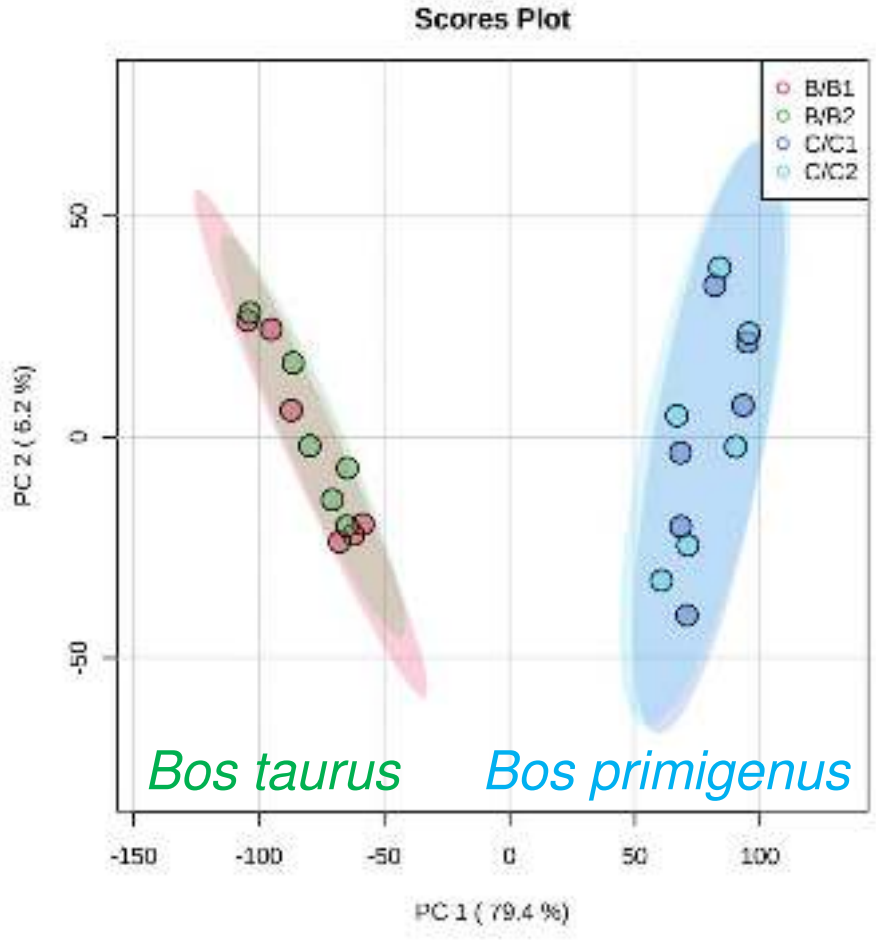

Modern and ancient species discrimation can be quickly discriminaated by PCA and Heatmap

Optimum resolution m/Δm for the identification of deamidation

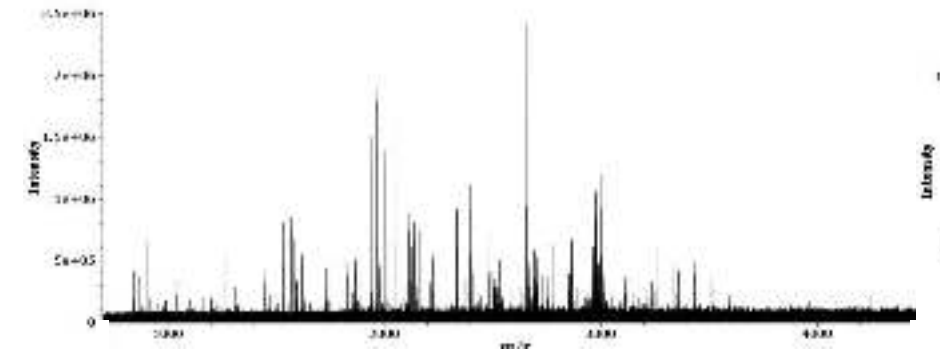

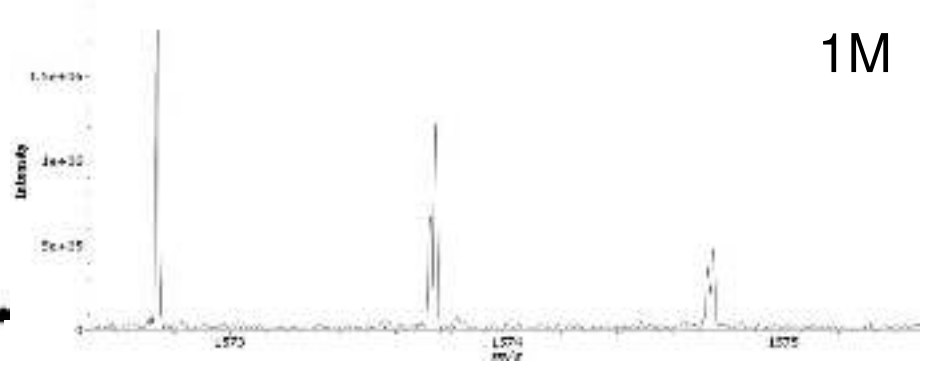

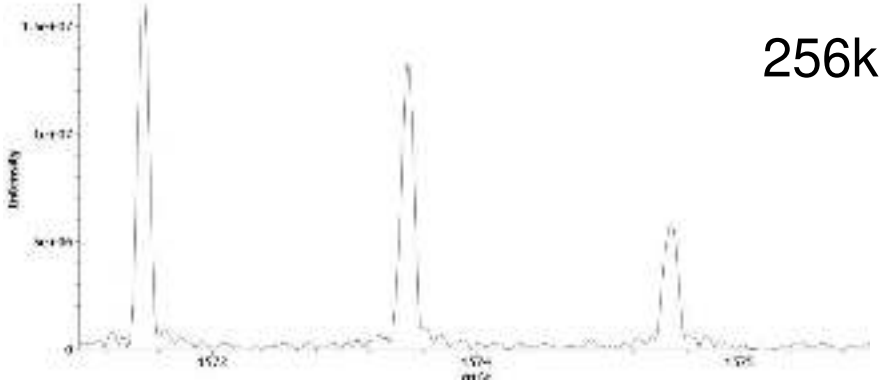

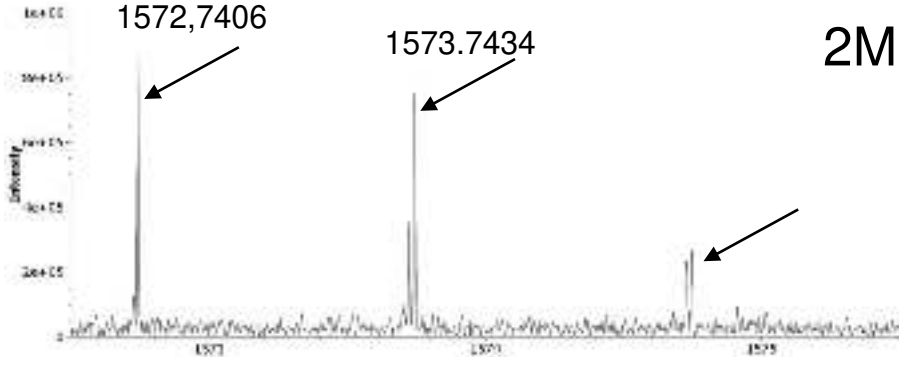

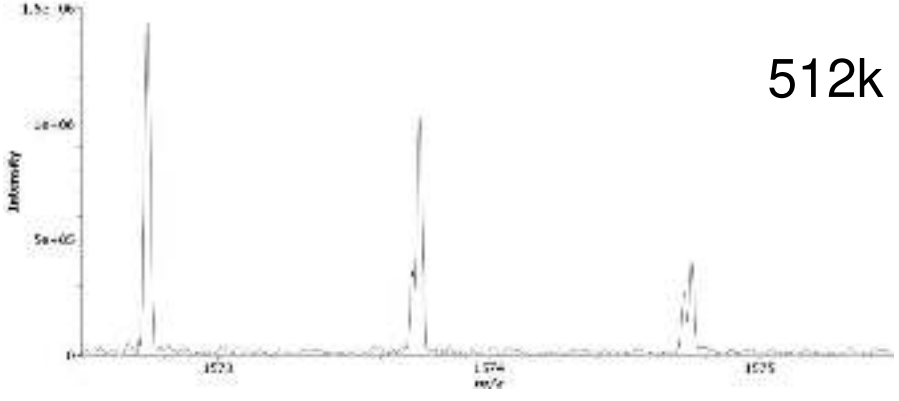

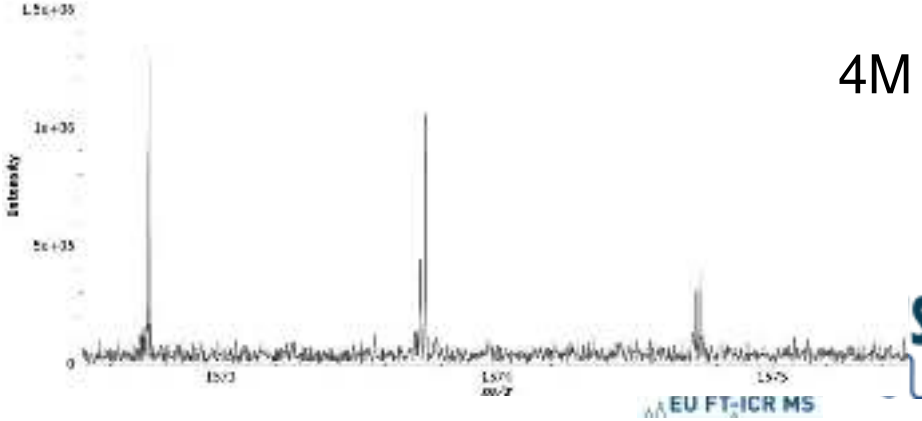

2M points: separation of deamidated isobaric peak

Zoom of deamidation on peptide of archaeological bone spectrum

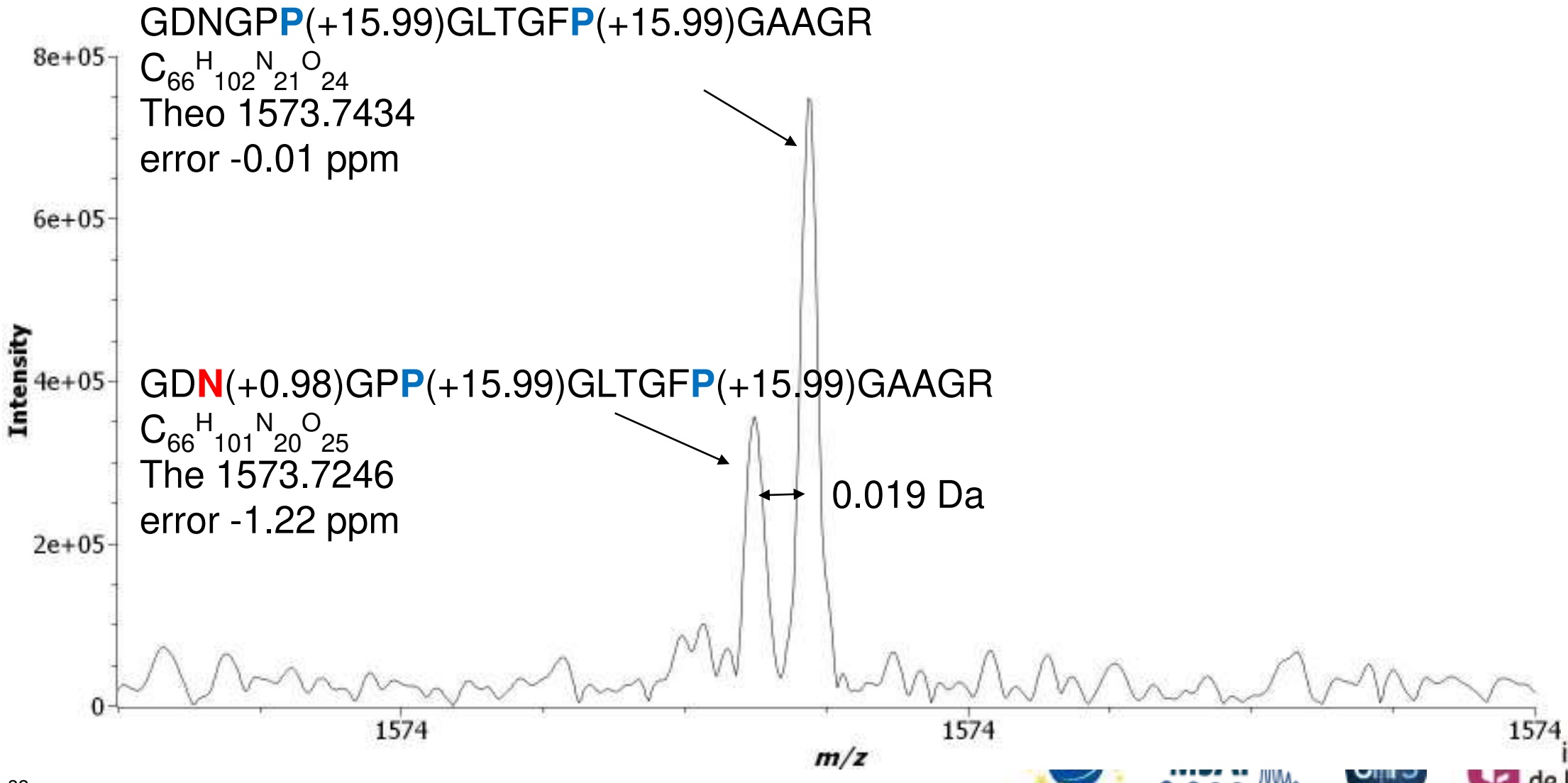

Analysis of archaeological bones from different sites

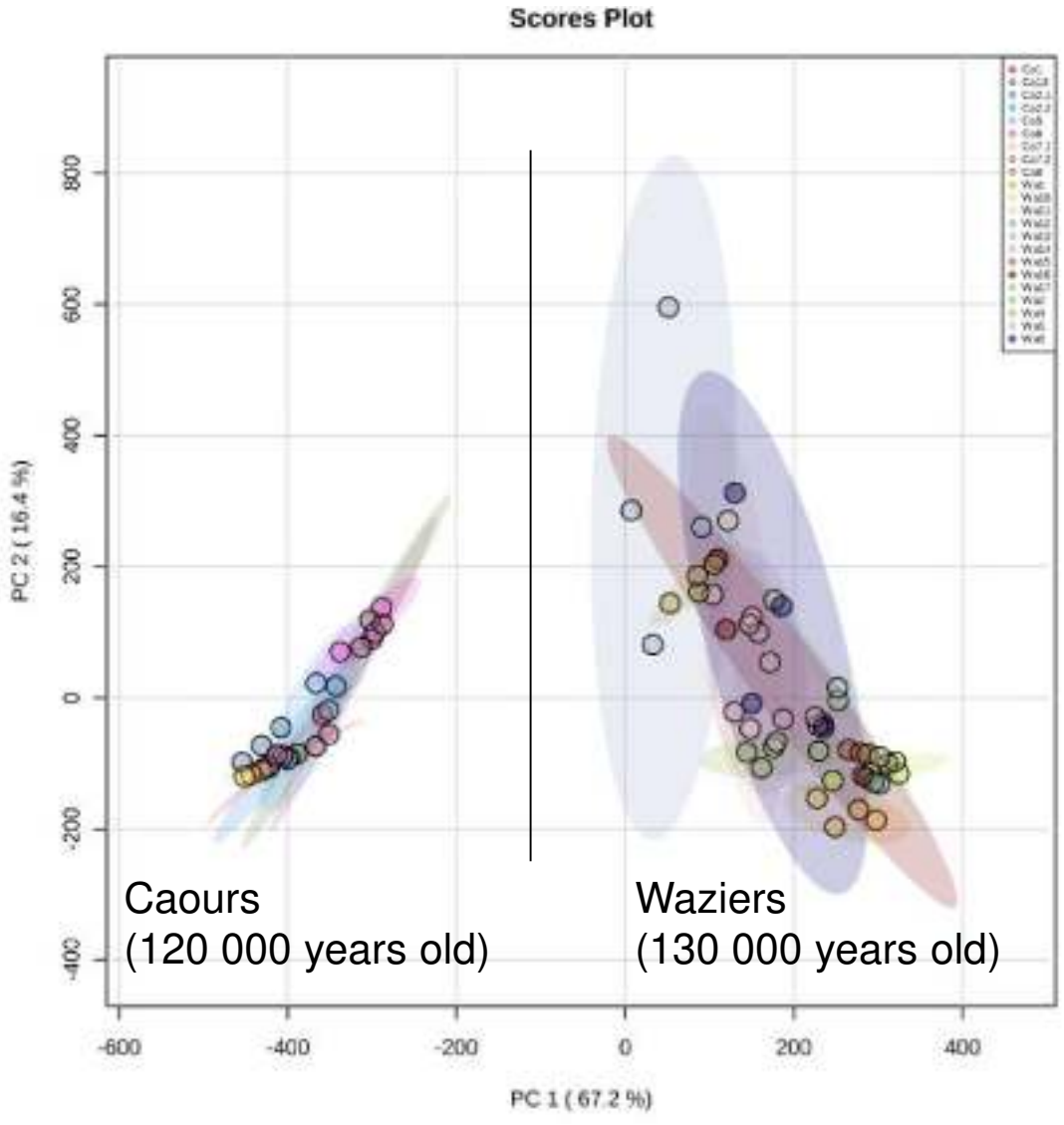

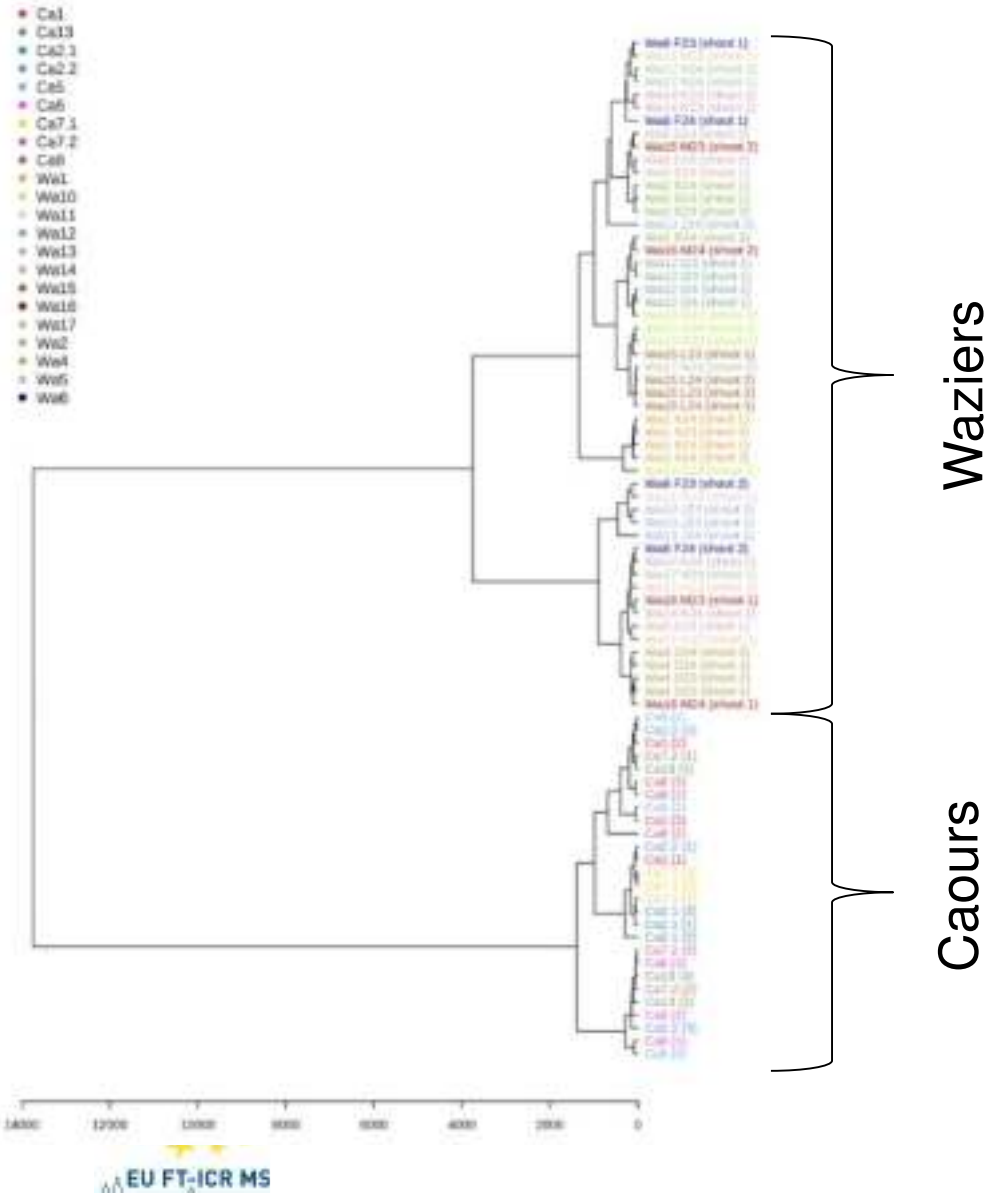

2 clusters are observed

Archaeological bones samples the Wazier site

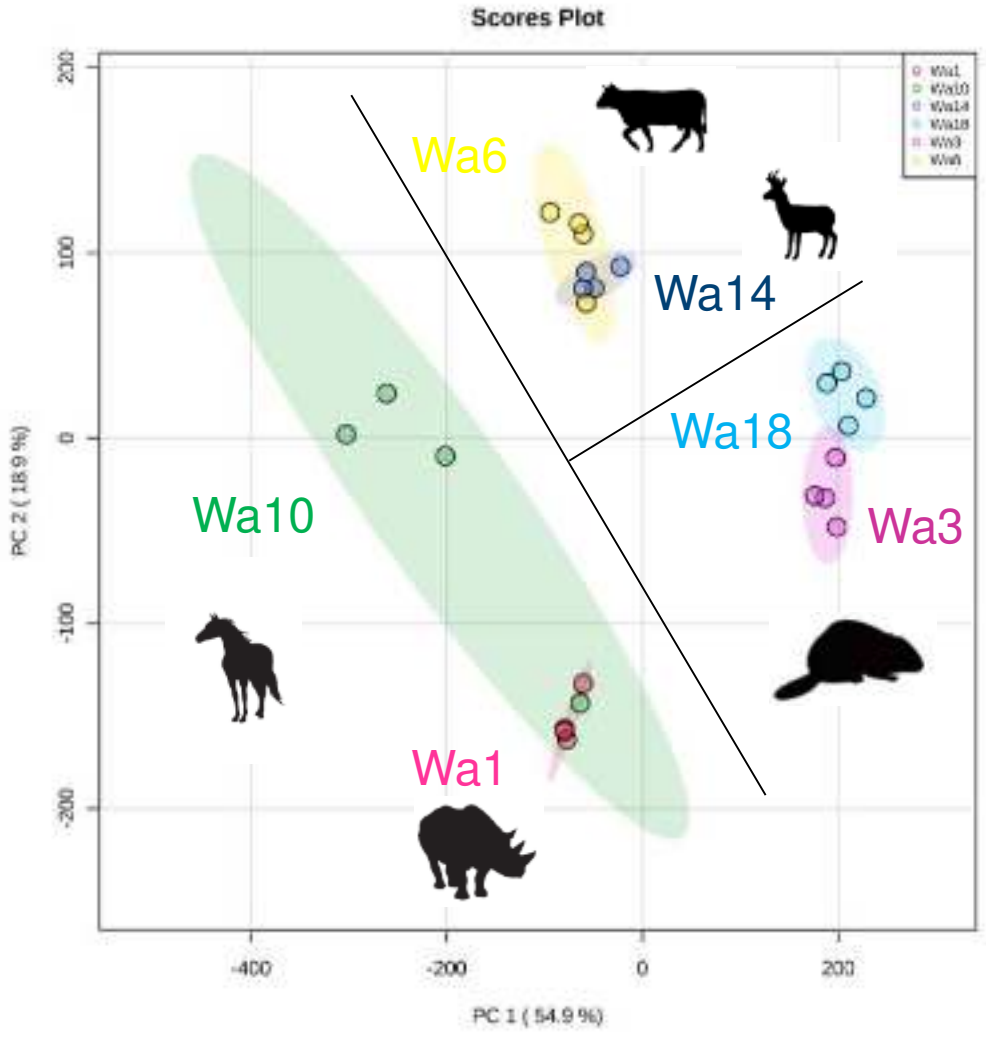

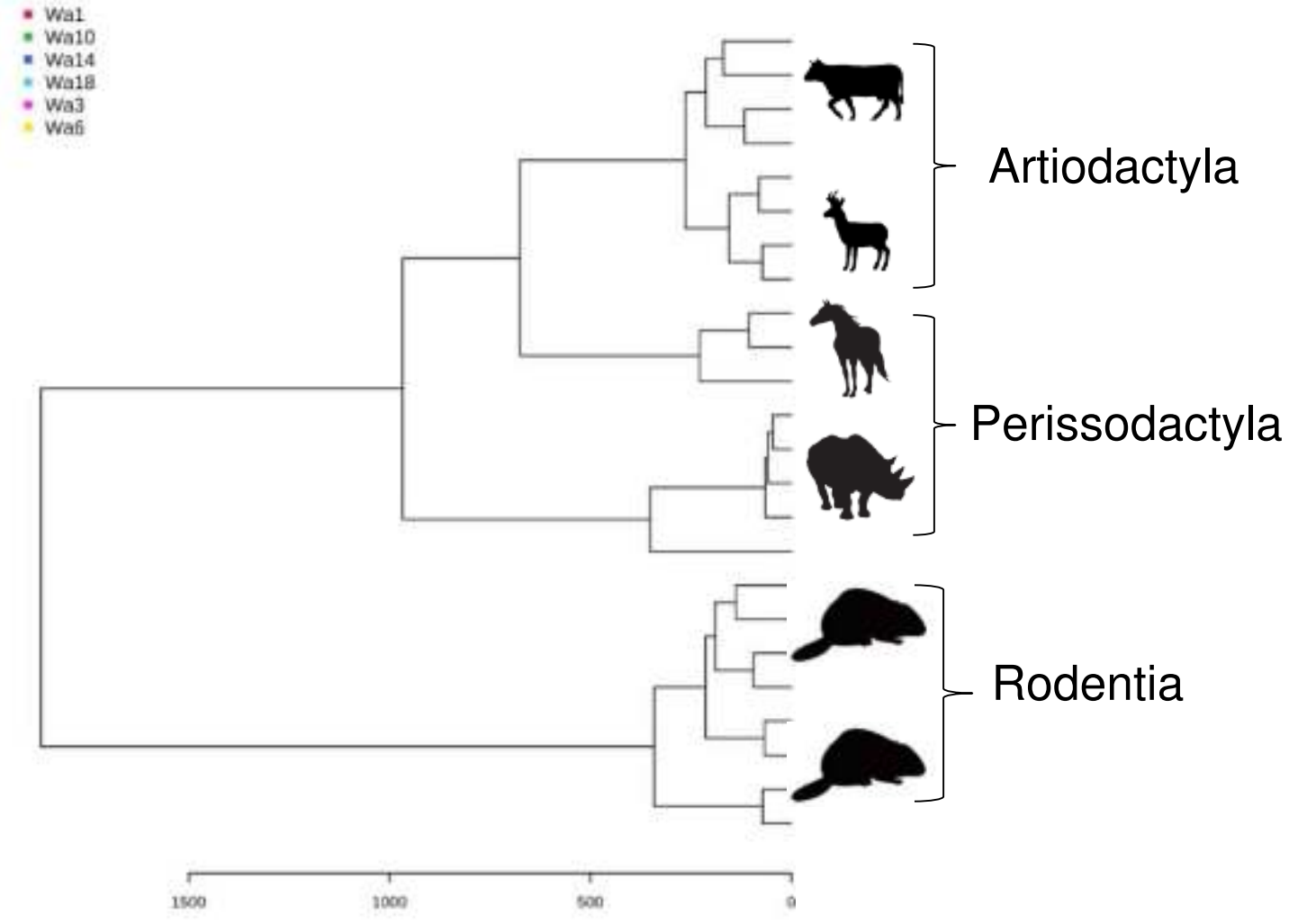

3 clusters observed

Correlation of % desamidation and datation of different sites

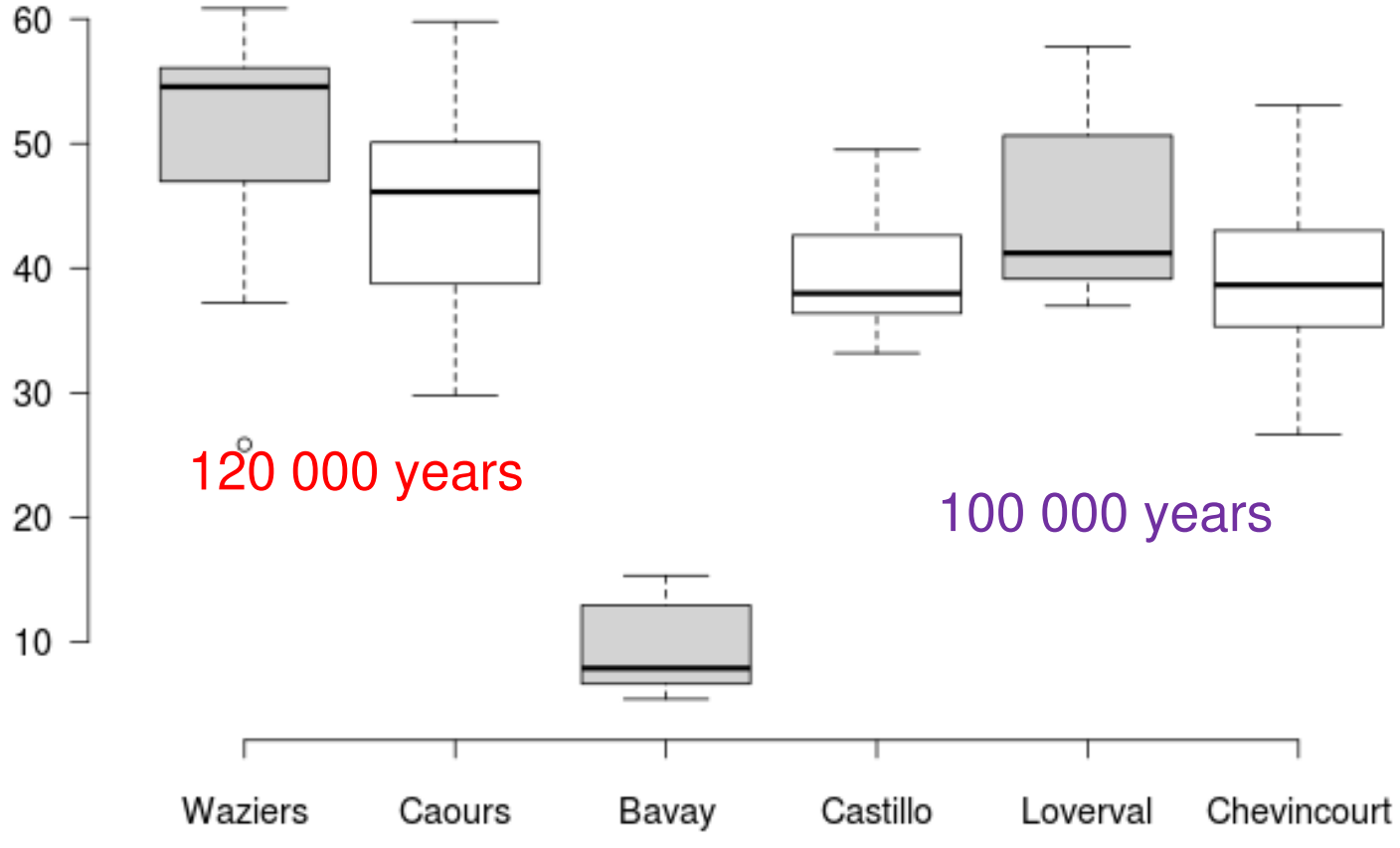

1000 - 3000 years

Study of plant gums polysaccharide moiety by sequential enzymatic hydrolysis

Clara GRANZOTTO

Miniaturisation pour la Synthèse, l'Analyse & la Protéomique USR 3290

Université Lille, CNRS

Plant gums: applications

Plant gums are naturally occurring polysaccharide materials exuded by several species of plants or extracted from the endosperm of some seeds.

gum arabic
fruit tree gums
gum tragacanth

karaya gum
locust bean gum
ghatti and guar gum

- **adhesive properties**
- **ability to form gels**
- **stabilize emulsion, foams and dispersions**

Plant gums: polysaccharides classification

Plant gum	Polysaccharide family
Arabic	Type II Arabinogalactan
Ghatti	Substituted glucuronomannan
Tragacanth	Mixture of type II arabinogalactan and galacturonan type
Karaya	Substituted rhamnogalacturonan
Guar/Locust bean	Galactomannan
Fruit tree (e.g. cherry)	Substituted arabinogalactan

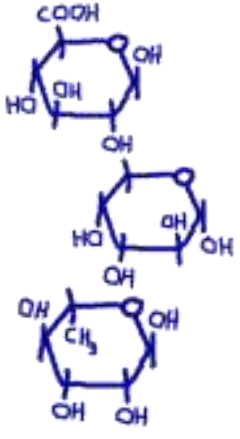

Arabinogalactan
arabinose, galactose

Galactomannan
galactose, mannose

Substituted Arabinogalactan
arabinose, galactose, galacturonic acid, xylose

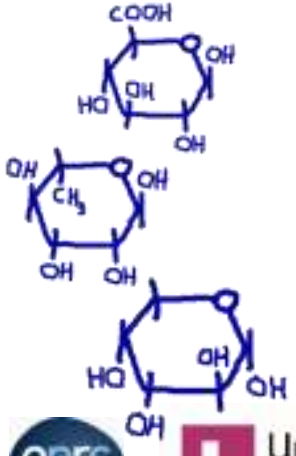

State of art and analytical approach

traditional technique: acid hydrolysis and monosaccharide composition by **GC-MS**.

cons: fairly limited and not specific if a mixture of polysaccharide materials is present

State of art and analytical approach

traditional technique: acid hydrolysis and monosaccharide composition by **GC-MS**.

cons: fairly limited and not specific if a mixture of polysaccharide materials is present

New analytical approach

(1) Gum solubilization

(2) Sequential enzymatic hydrolysis

(3) clean-up

(4) MALDI TOF of release oligosaccharides

State of art and analytical approach

traditional technique: acid hydrolysis and monosaccharide composition by **GC-MS**.

cons: fairly limited and not specific if a mixture of polysaccharide materials is present

New analytical approach

Different plant gums → **Polysaccharide fingerprint** → **Real art samples** → **Unique gum identification**

(4) MALDI TOF of release oligosaccharides

State of art and analytical approach

traditional technique: acid hydrolysis and monosaccharide composition by **GC-MS**.

cons: fairly limited and not specific if a mixture of polysaccharide materials is present

New analytical approach

(1) Gum solubilization

(2) Sequential enzymatic hydrolysis

(3) clean-up

(4) MALDI TOF of release oligosaccharides

Gum Arabic: arabinogalactan

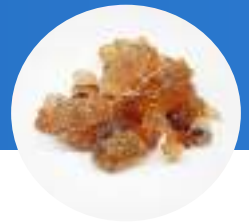

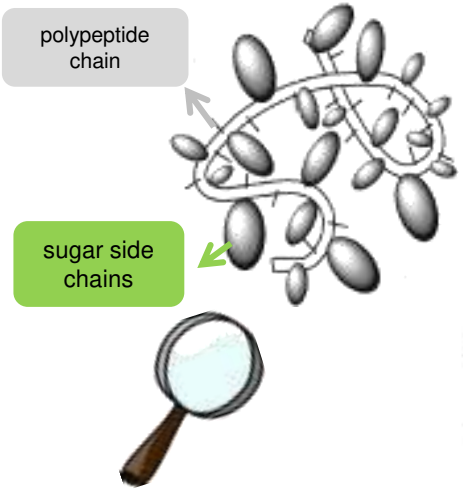

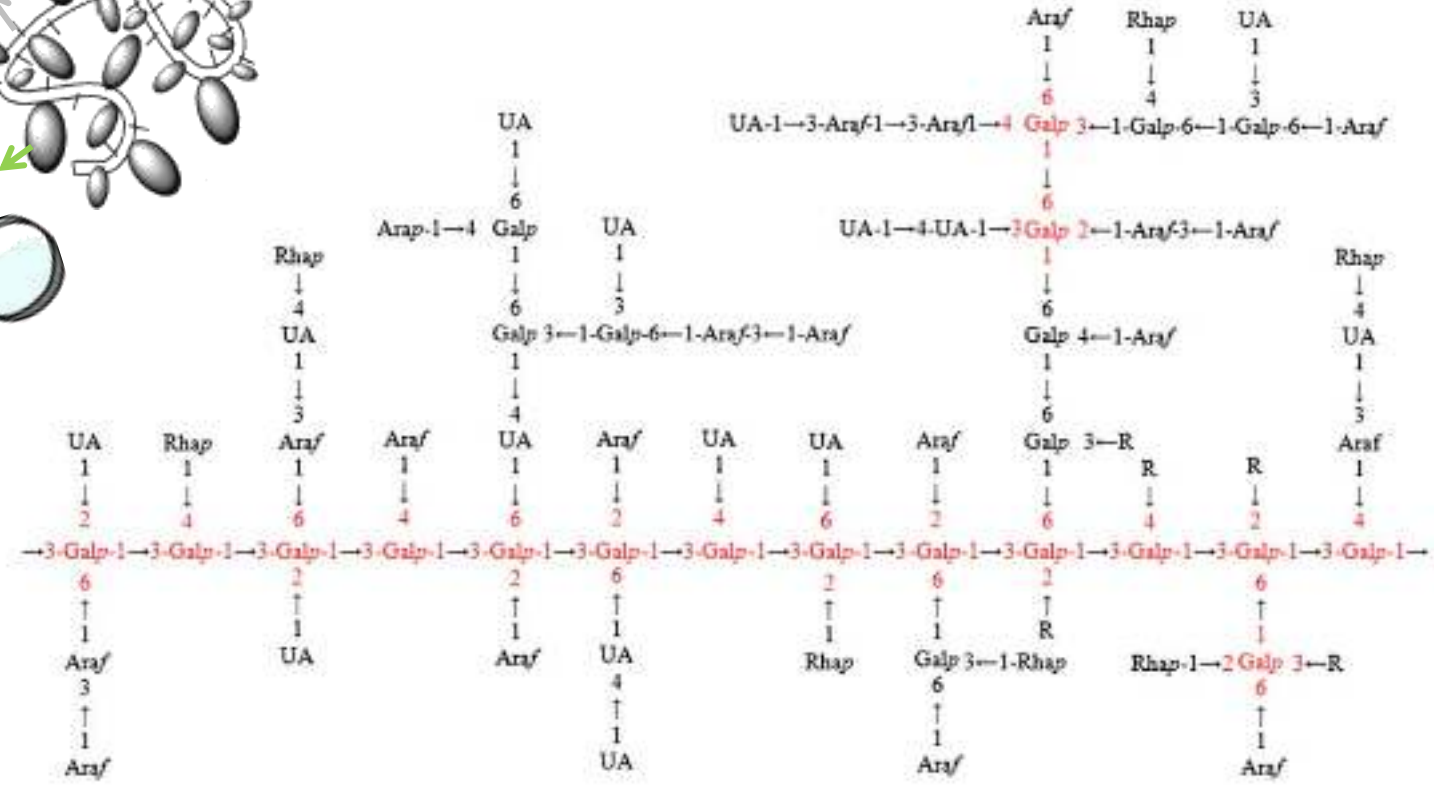

Nie S-P. A further amendment to the classical core structure of gum arabic (Acacia senegal). *Food Hydrocolloids* **2013**;31:42.

Gum Arabic: arabinogalactan

(1) α-L-Arabinofuranosidase

From side chains to main chain
→ access of enzyme

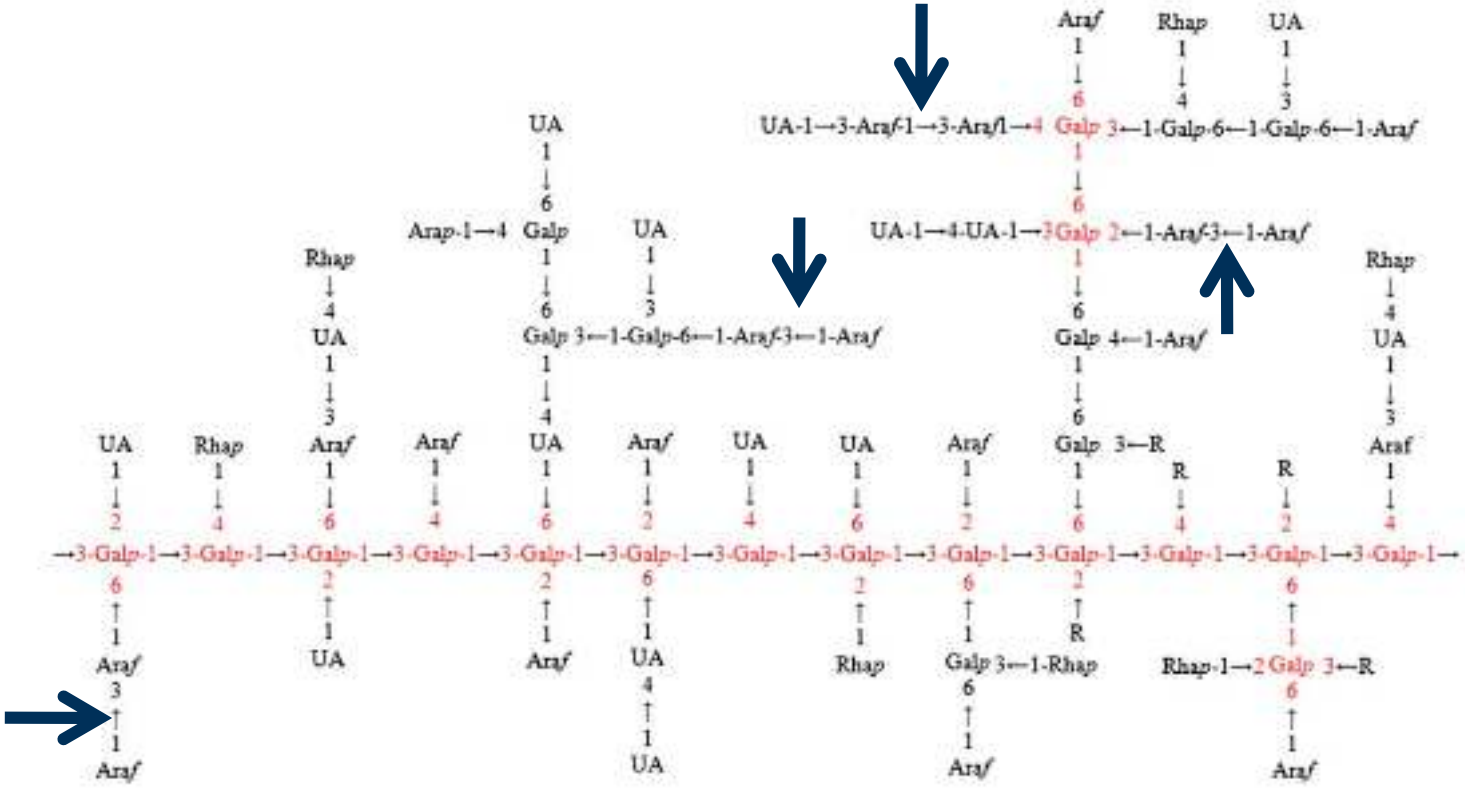

Nie S-P. A further amendment to the classical core structure of gum arabic (Acacia senegal). Food Hydrocolloids 2013;31:42.

Gum Arabic: arabinogalactan

(1) α-L-Arabinofuranosidase

(2) β-glucuronidase

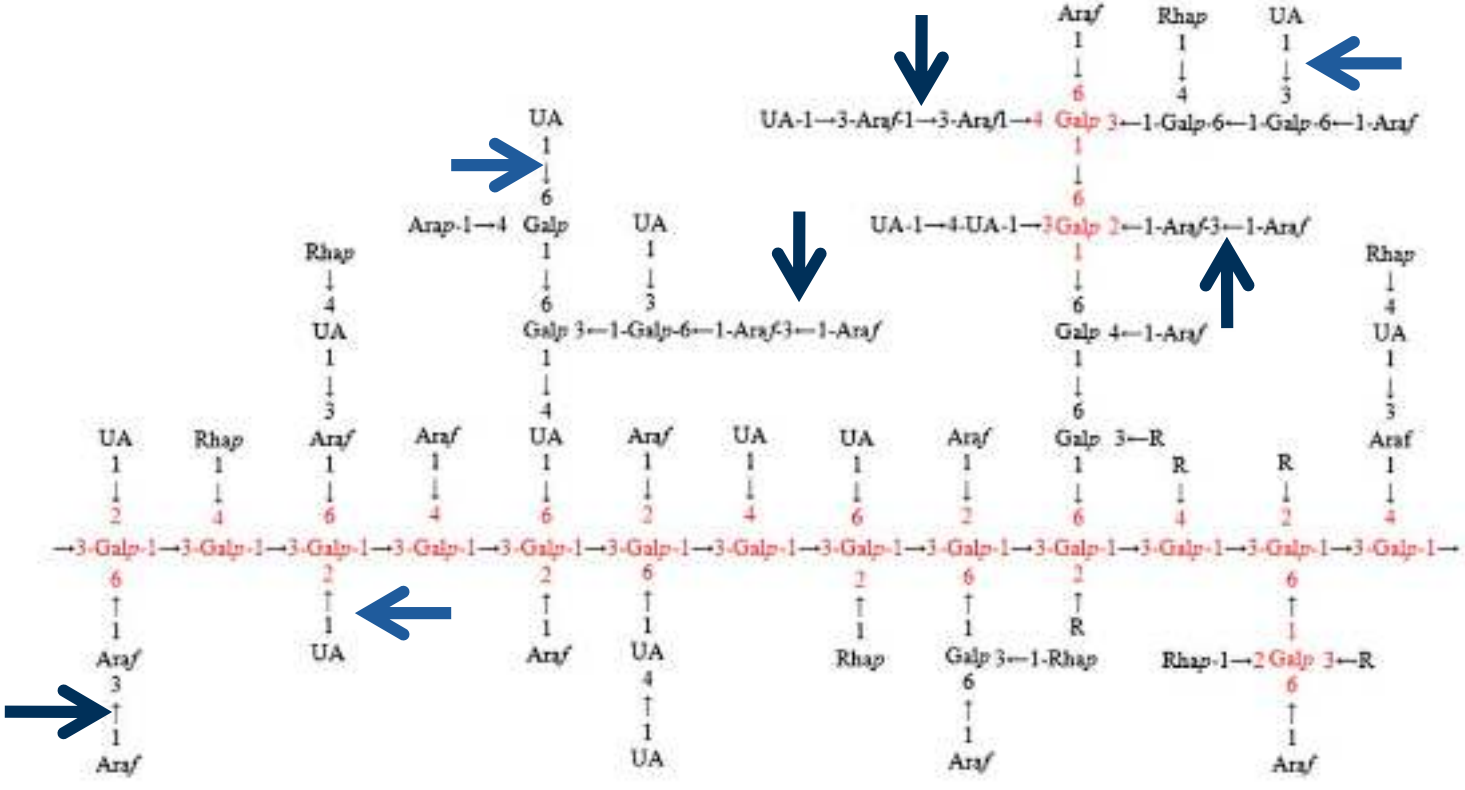

Nie S-P. A further amendment to the classical core structure of gum arabic (Acacia senegal). Food Hydrocolloids 2013;31:42.

Gum Arabic: arabinogalactan

(1) α-L-Arabinofuranosidase

(2) β-glucuronidase

(3) α-L-rhamnosidase

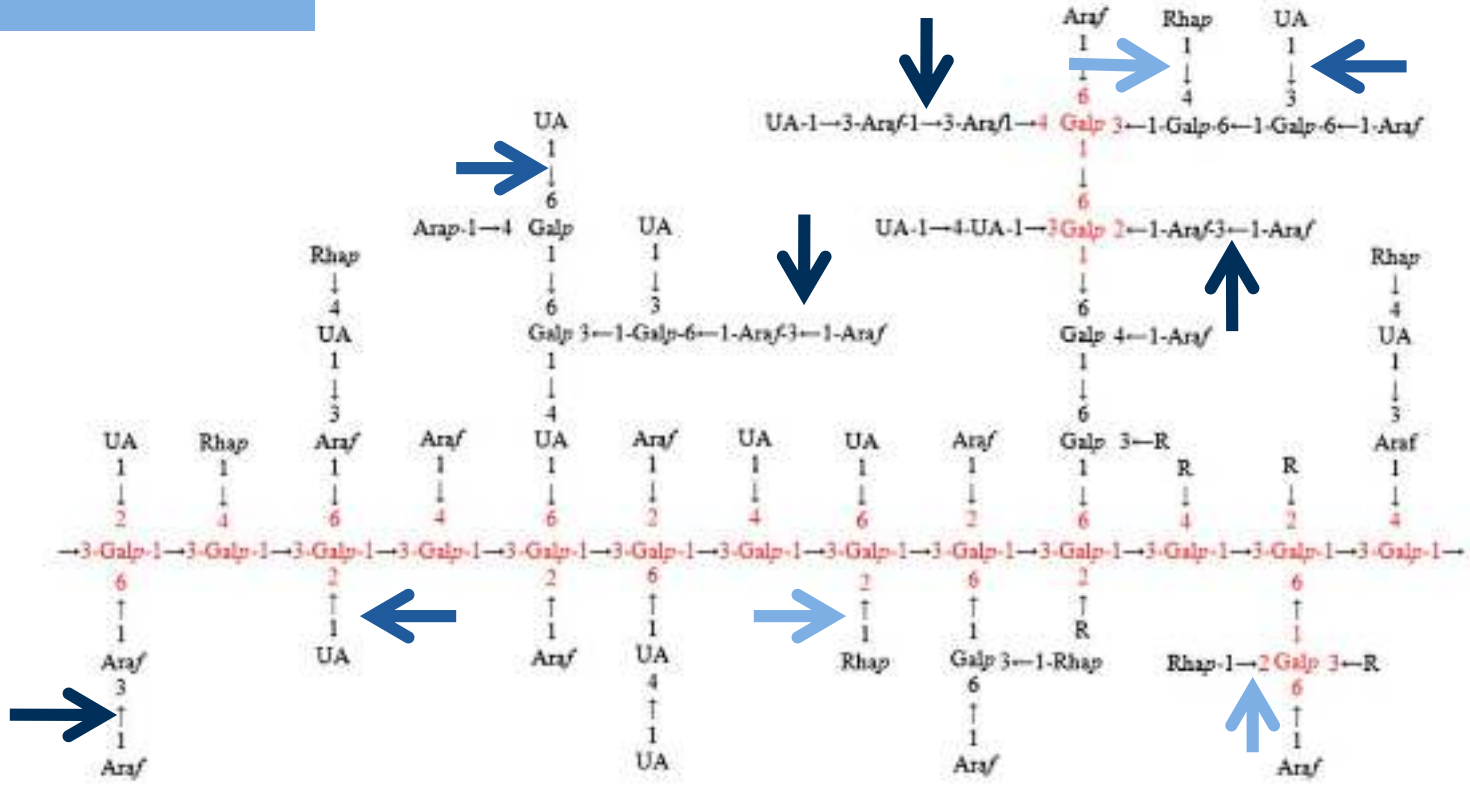

Nie S-P. A further amendment to the classical core structure of gum arabic (Acacia senegal). Food Hydrocolloids 2013;31:42.

Gum Arabic: arabinogalactan

(1) α-L-Arabinofuranosidase

(2) β-glucuronidase

(3) α-L-rhamnosidase

(4) β -Galactosidase

(5) exo--β- 1,3-galactanase

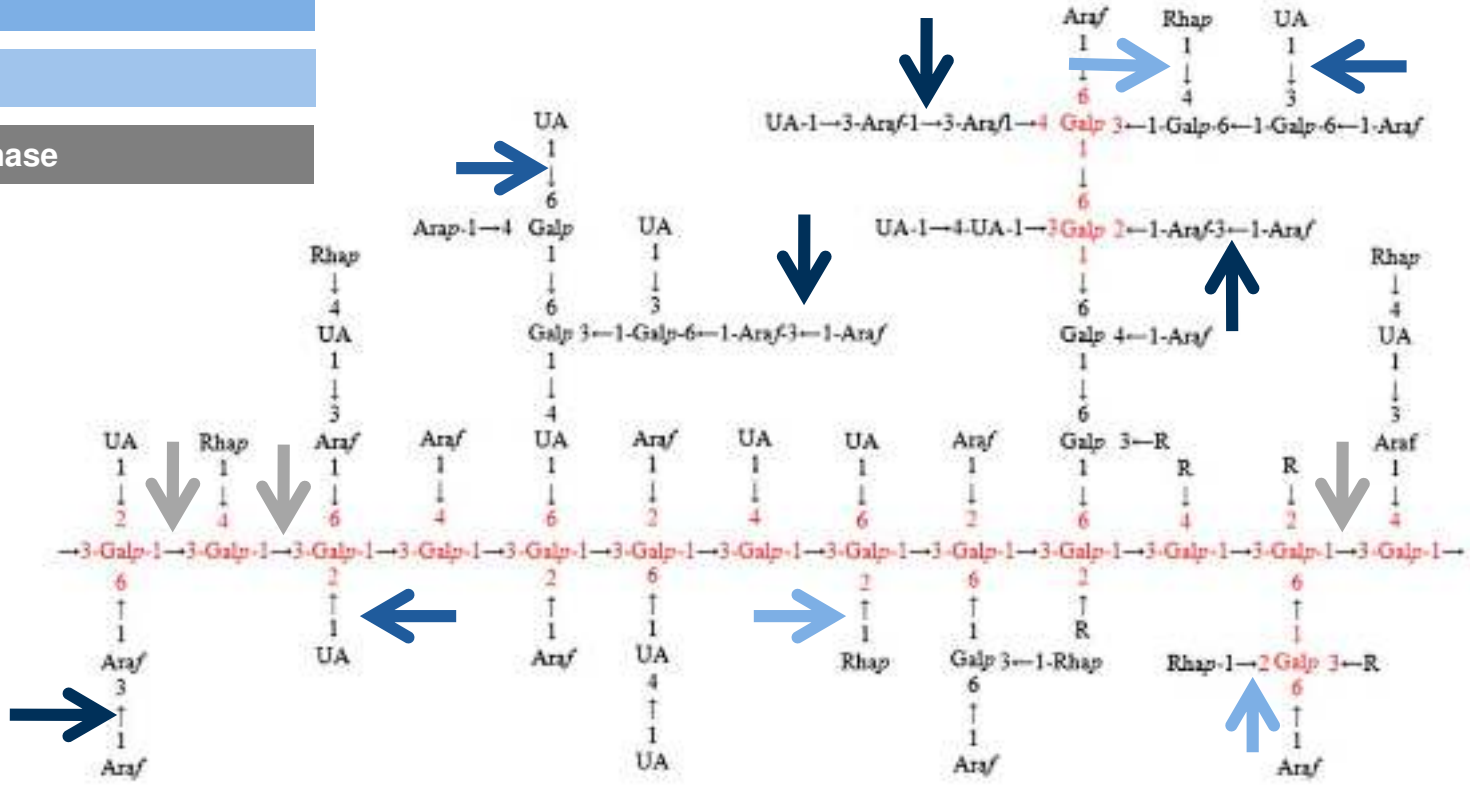

Nie S-P. A further amendment to the classical core structure of gum arabic (Acacia senegal). Food Hydrocolloids 2013;31:42.

Gum Arabic: arabinogalactan

- 100mU enzyme/1mg gum
- 24 h digesion each enzyme
- Specific T°, buffer and pH

(1) α-L-Arabinofuranosidase

(2) β-glucuronidase

(3) α-L-rhamnosidase

(4) β -Galactosidase

(5) exo--β- 1,3-galactanase

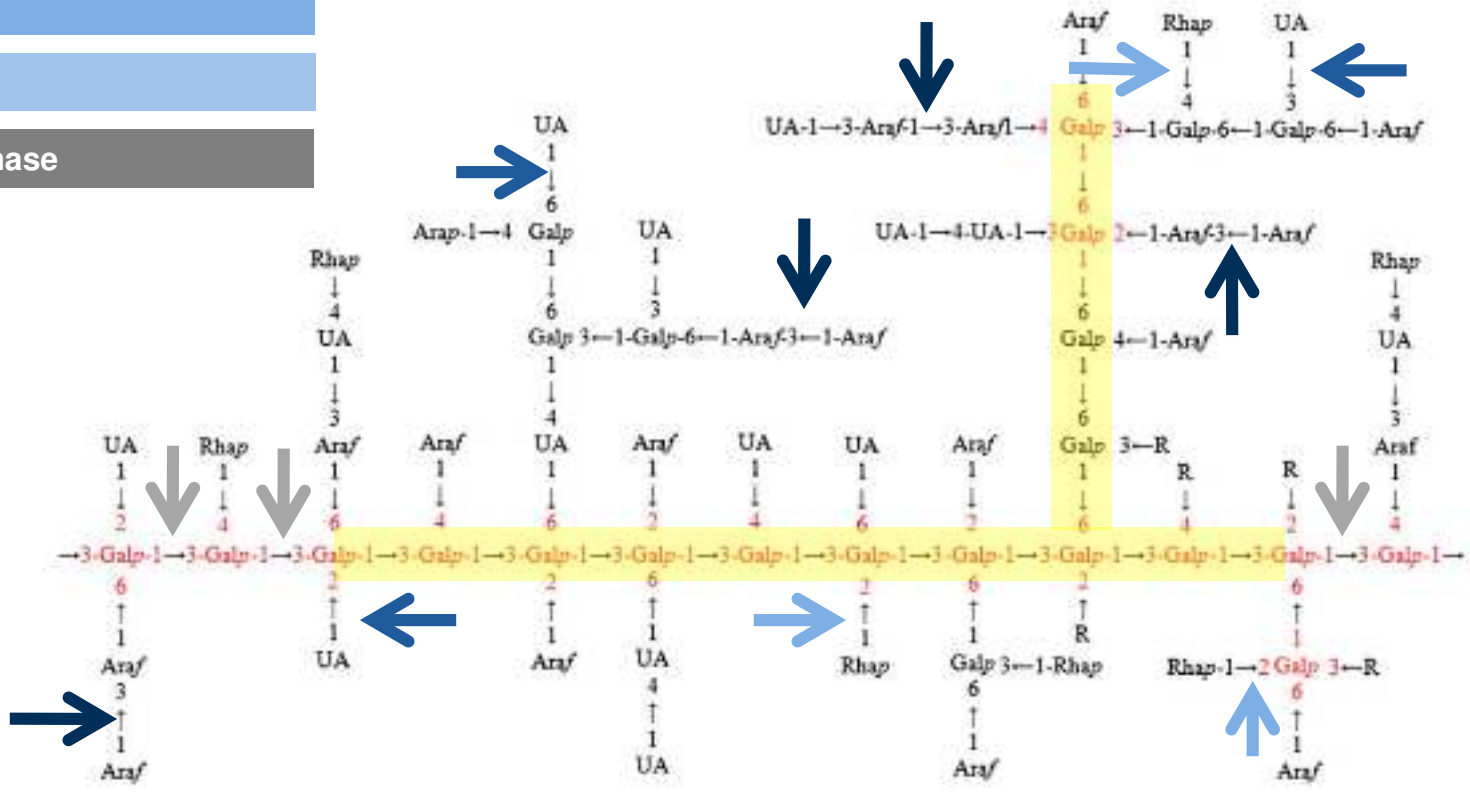

Nie S-P. A further amendment to the classical core structure of gum arabic (Acacia senegal). Food Hydrocolloids 2013;31:42.

Gum Arabic: MALDI

Methodology

- no clean-up procedure;
- 3AQ in ACN/H_2O
- reflector mode (50-3000 Da)

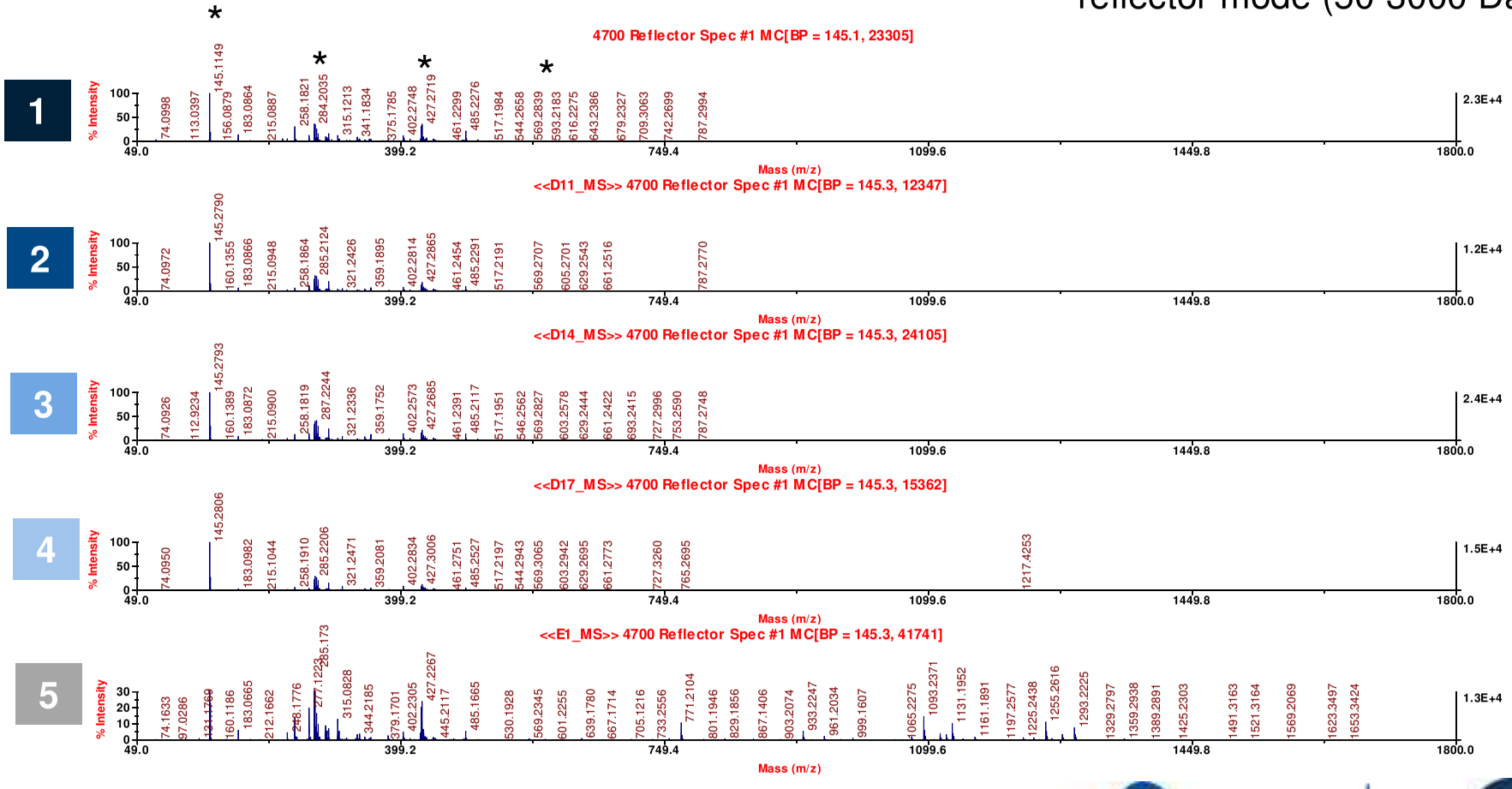

Gum Arabic: MALDI

Methodology

- no clean-up procedure;
- 3AQ in ACN/H_2O
- reflector mode (50-3000 Da)

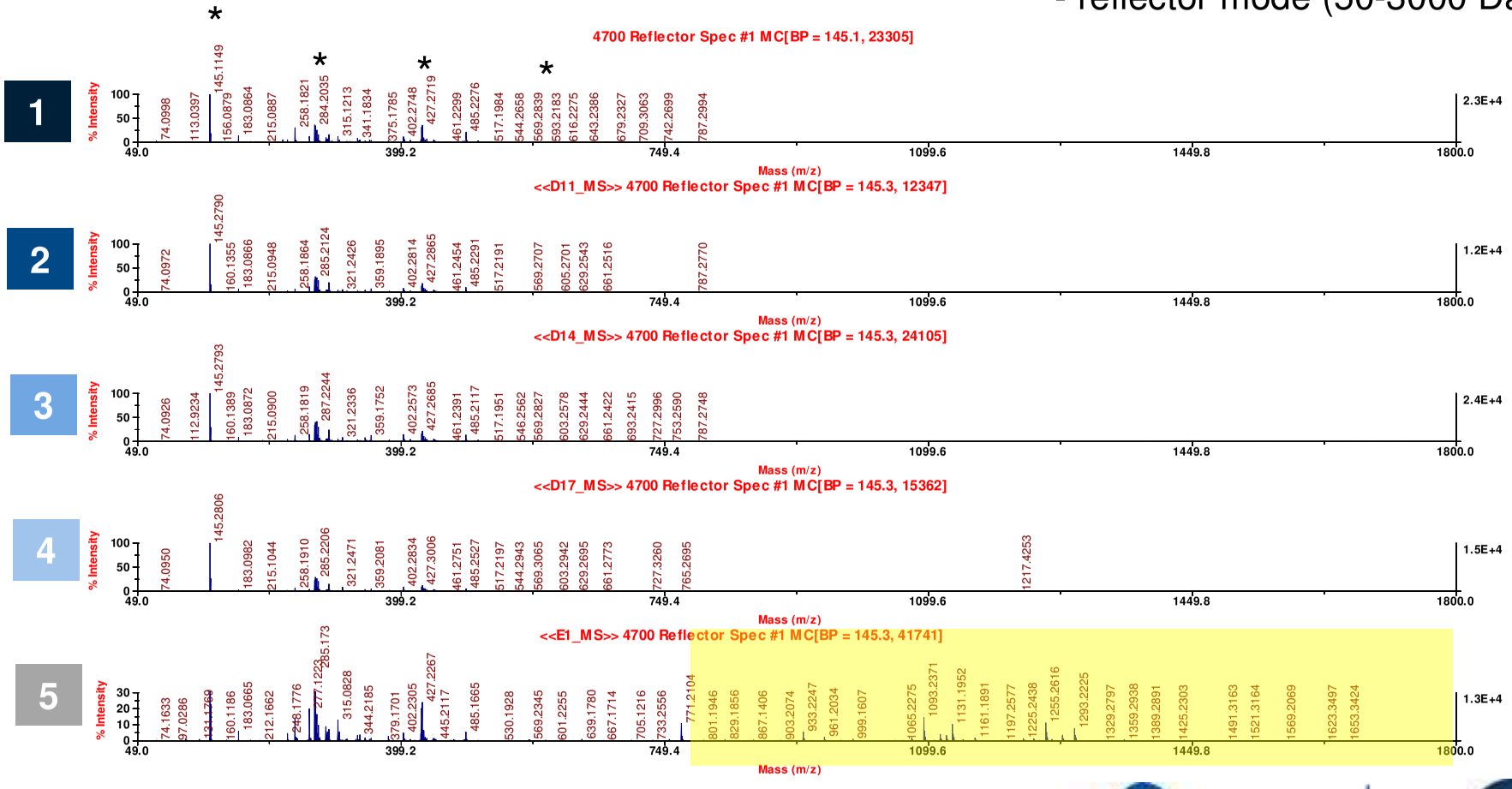

Gum Arabic: MALDI

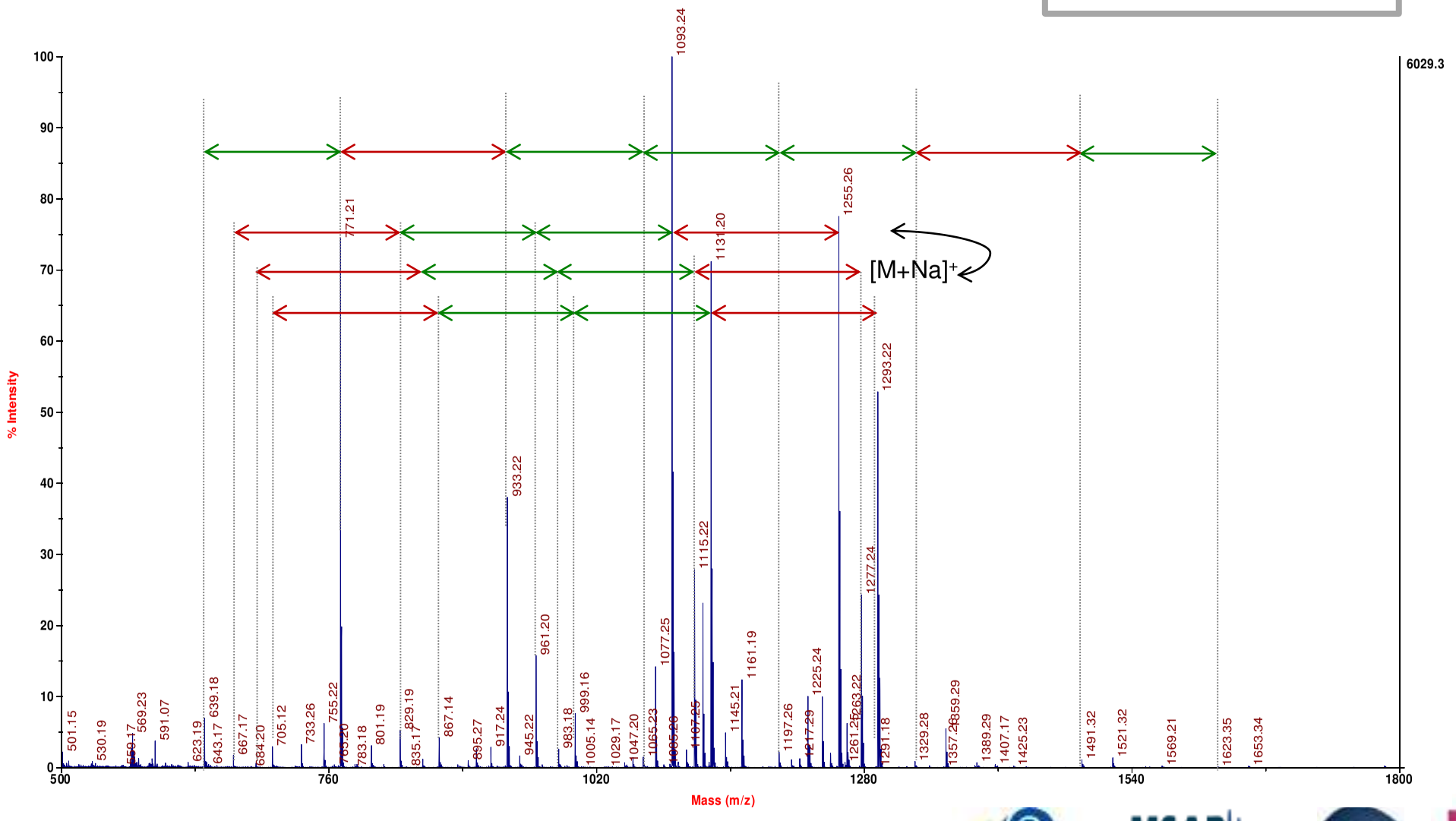

Summary

1 Plant gums: applications and polysaccharides families

2 Analytical approach and objectives

3 Methodological development and results: gum arabic

4 Methodological development and results: Locust Bean gum

5 Future perspectives

Locust Bean gum: galactomannan

(1) α-galactosidase

(2) Endo-1,4-beta-mannanase

Linear backbone of 1→4-linked β-D-mannose units attached by a single α-D-galactose residue at C-6 of mannose with 1→6 glycosidic bonds

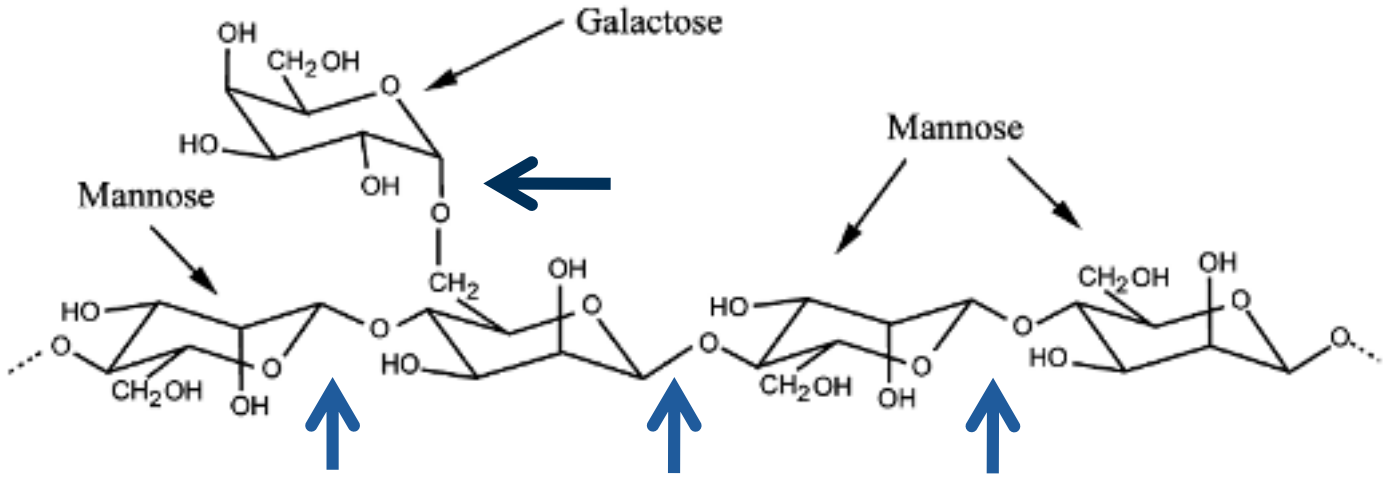

Moreira L.R.S. An overview of mannan structure and mannan-degrading enzyme systems. *Appl Microbiol Biotechnol* , **2008**, 79:165–178

Locust Bean gum : MALDI

Galactose or Mannose (Δm=162)

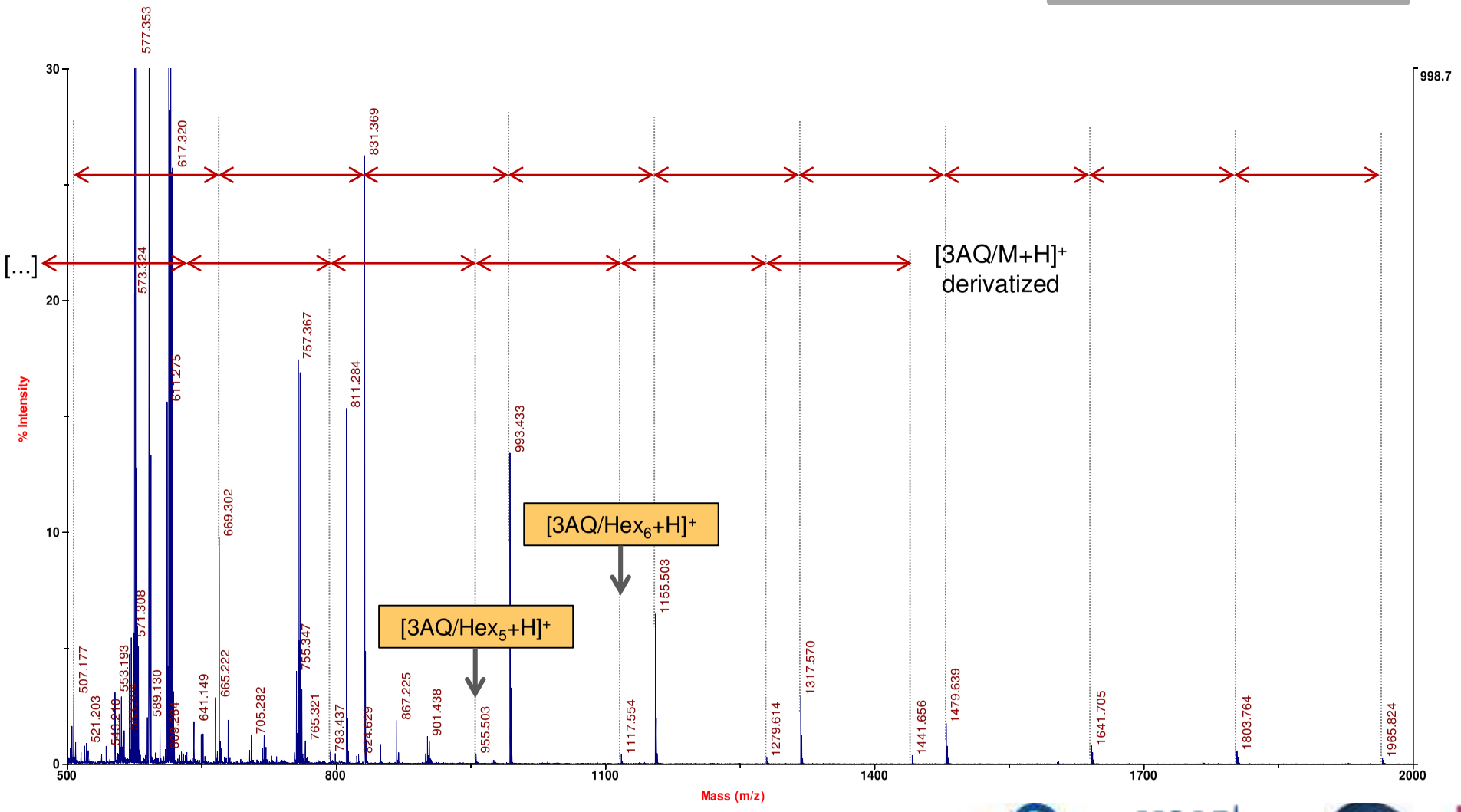

Identification of the binder of a watercolor paint

Wooden 'Colour Box Charles Roberson & Co' dating 1870s. Approximately 1 mg was sampled from the blue watercolor paint located on the left in the box

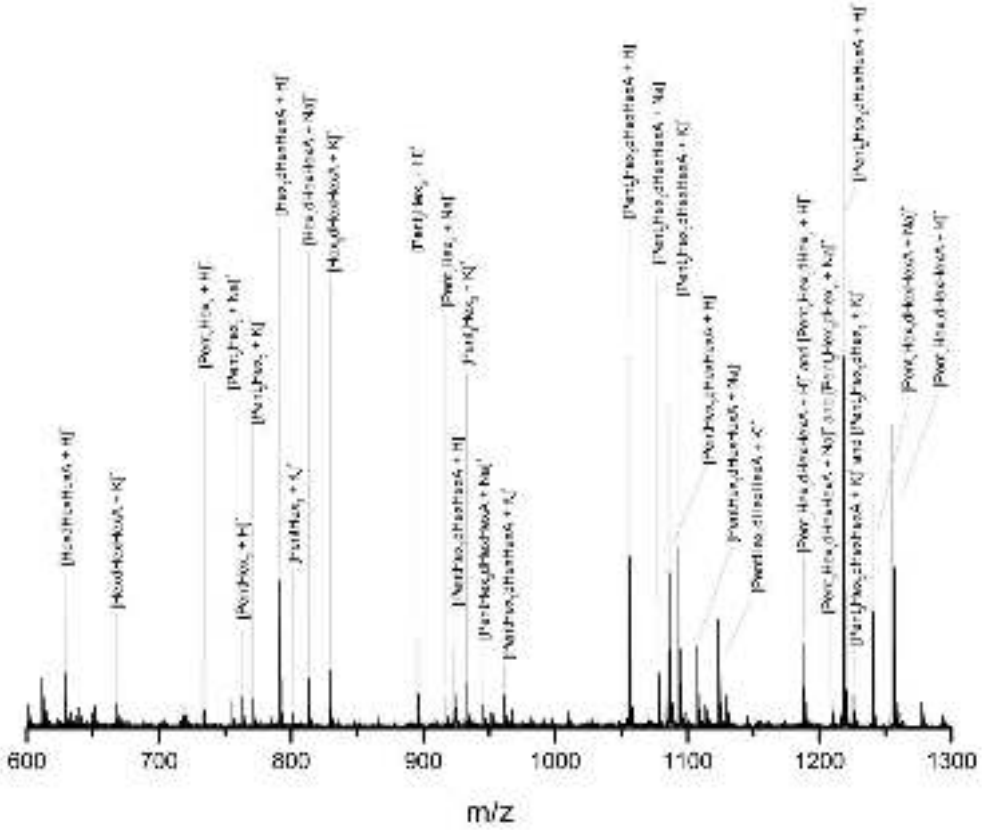

MALDI-TOF MS profile of the old watercolor sample dating 1870 with the related oligosaccharide attributions. The reported ions correspond to oligosaccharides derivatized with 3-aminoquinoline.

Granzotto, C., Arslanoglu, J., Rolando, C., Tokarski, C. (2017). Plant gum identification in historic artworks. *Scientific reports*, *7*, 1-15.

Identification of the origin of archaeological fat remains by triacylglycerols analysis using Li^+ cationization, nanoESI ionization, high resolution MS and IRMPD

Nicolas GARNIER

Miniaturization for Synthesis, Analysis & Proteomics USR 3290

Why and how studying archaeological object contents?

- **Why?**
  Historical, socio-economic, cultural precisions
  (knowledge of trades etc.) + analytical challenge
- **How?**
  - Typology (origin, content)
  - Epigraphy (stamp: potter, insurer; *Tituli picti*: owner, charterer; content and quality)
  - Coating (pitch = aqueous contents)
  - Chemical analysis based on fatty acid composition*

Port Vendres II (42-50 BC) shipwreck

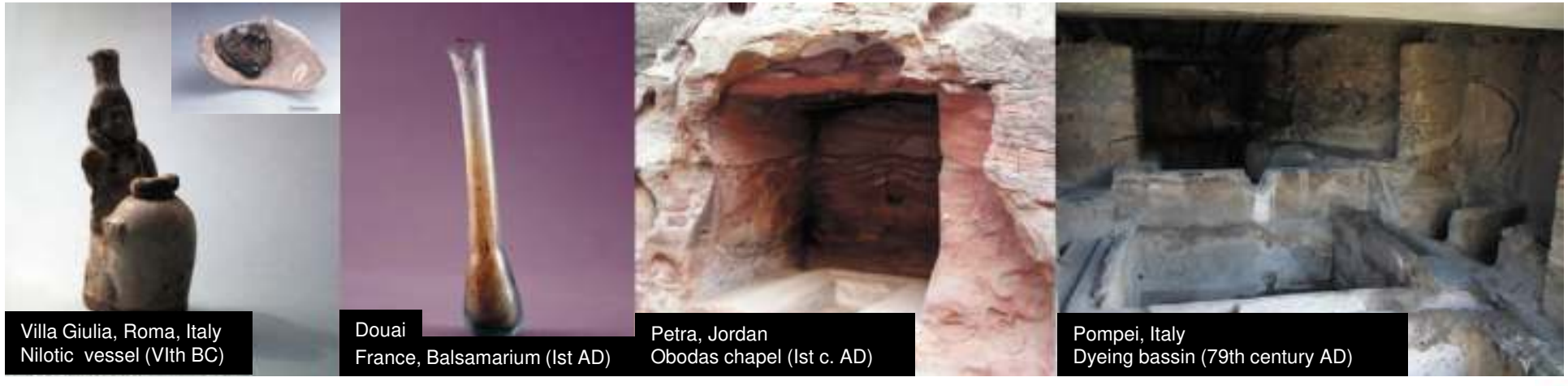

Villa Giulia, Roma, Italy
Nilotic vessel (VIth BC)

Douai
France, Balsamarium (Ist AD)

Petra, Jordan
Obodas chapel (Ist c. AD)

Pompei, Italy
Dyeing bassin (79th century AD)

* Evershed R.P. Archaeometry 2008, 50, 895–924.
Colombini M.P., Modugno F., Ribechini, E. 2009 GC/MS in the Characterization of Lipids, in Organic Mass Spectrometry in Art and Archaeology, Eds M. P. Colombini and F. Modugno, John Wiley & Sons, Ltd, Chichester, UK.

Triacylglycerols analysis: example of olive oil (cationized with Li^+)

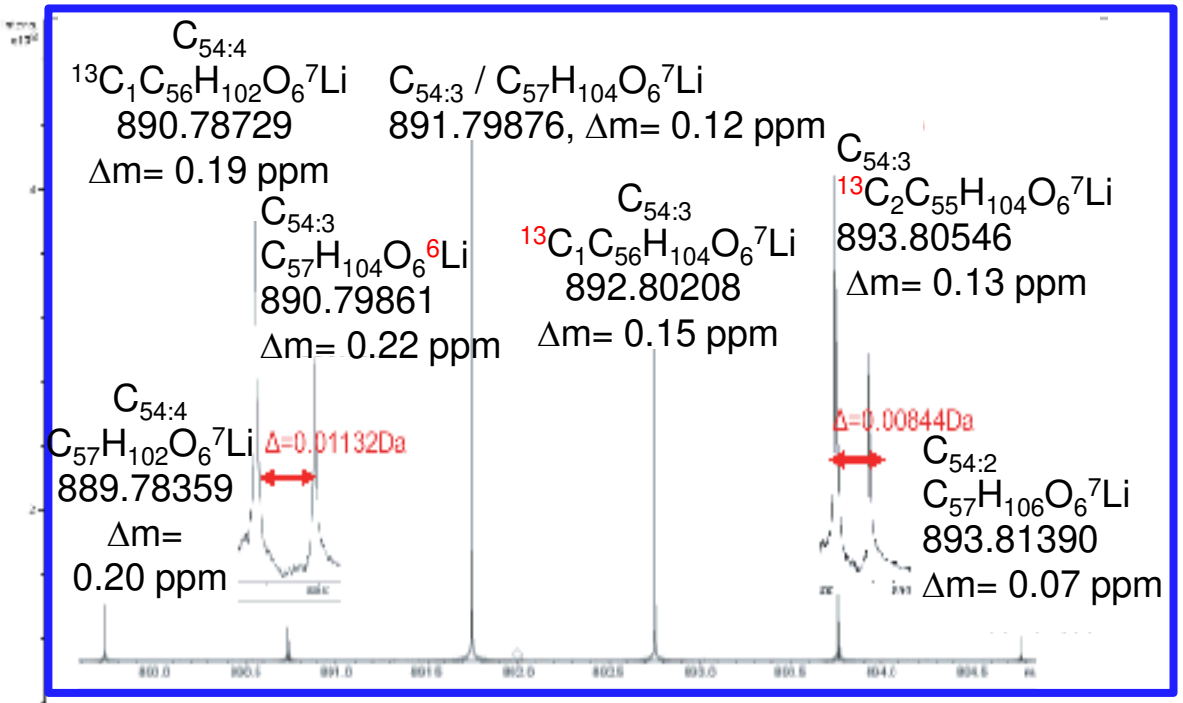

$C_{54:3}$
OOO
O: oleic fatty acid $C_{18}H_{34}O_2$

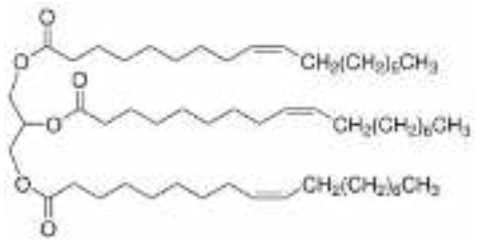

OPP, POP, MOS, MSO, OSM
M: myristic $C_{14}H_{28}O_2$
P: palmitic $C_{16}H_{32}O_2$
O: oleic $C_{18}H_{34}O_2$
S: stearic $C_{18}H_{36}O_2$

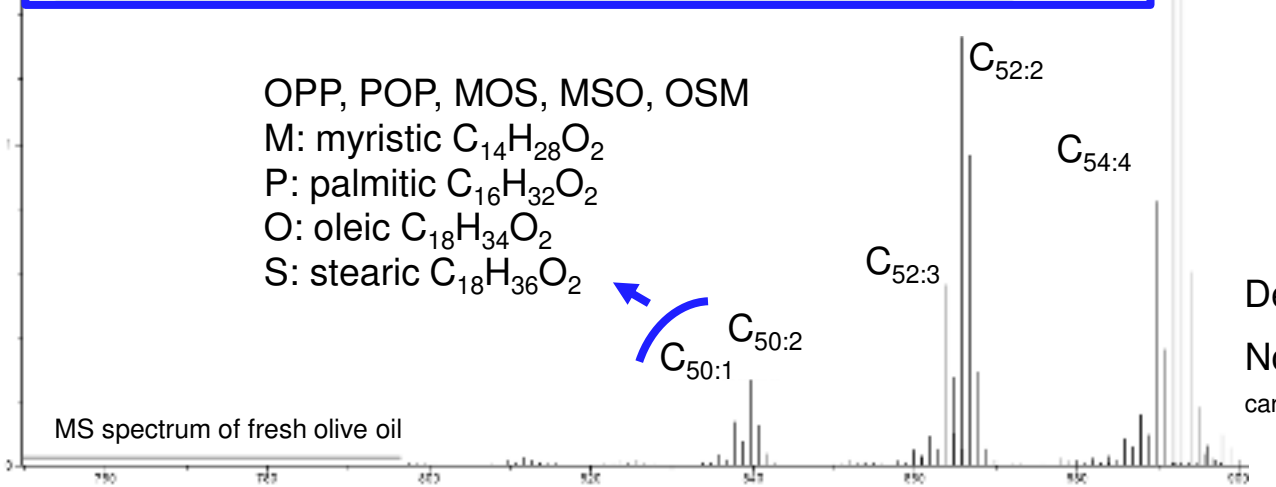

MS spectrum of fresh olive oil

Device: Apex Qe 9.4 T

Nomenclature: $C_{\text{sum of lateral chain carbons:insaturation number}}$

Université de Lille

TAGs purified on diol cartridge (elution: cyclohexane/dichloromethane/diethyl ether; 89/10/1; v/v/v)

MS spectra allow discrimination of oil origin: vegetal oils

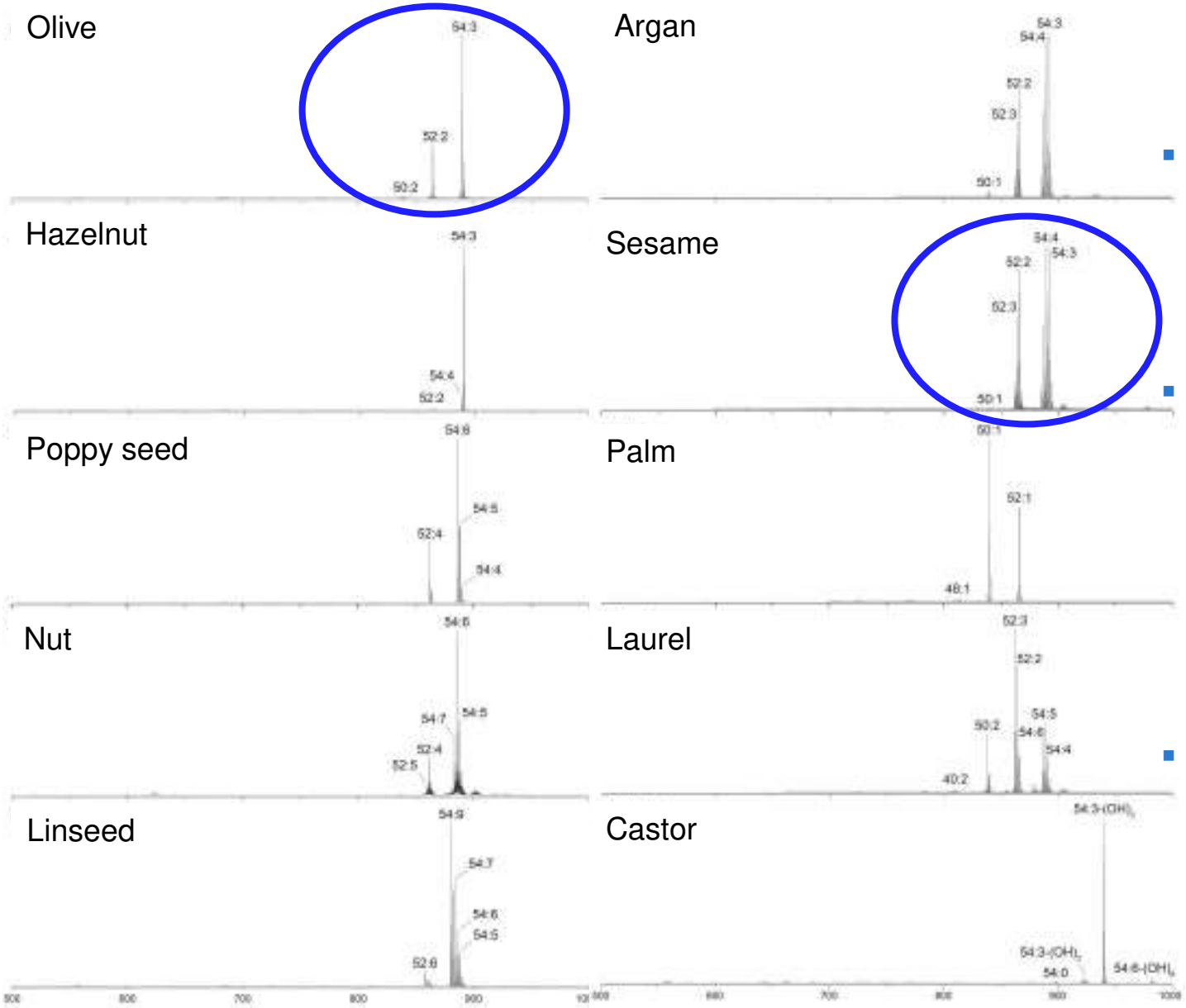

- TAGs purified on diol cartridge (elution: cyclohexane dichloromethane, diethyl ether; 89/10/1)
- Similar narrow distribution of TAGs from Equivalent Carbon Number (ECN) 50 to 54 with two or three patterns, each one separated by 26.01565 or 28.03130 amu
- MS/MS profiles for discrimination of oils with similar profiles

Université de Lille

MS/MS spectra allow discrimination of oil origin
InfraRed MultiPhoton Dissociation experiments ($C_{54:3}$ / $C_{57}H_{104}O_6Li$)

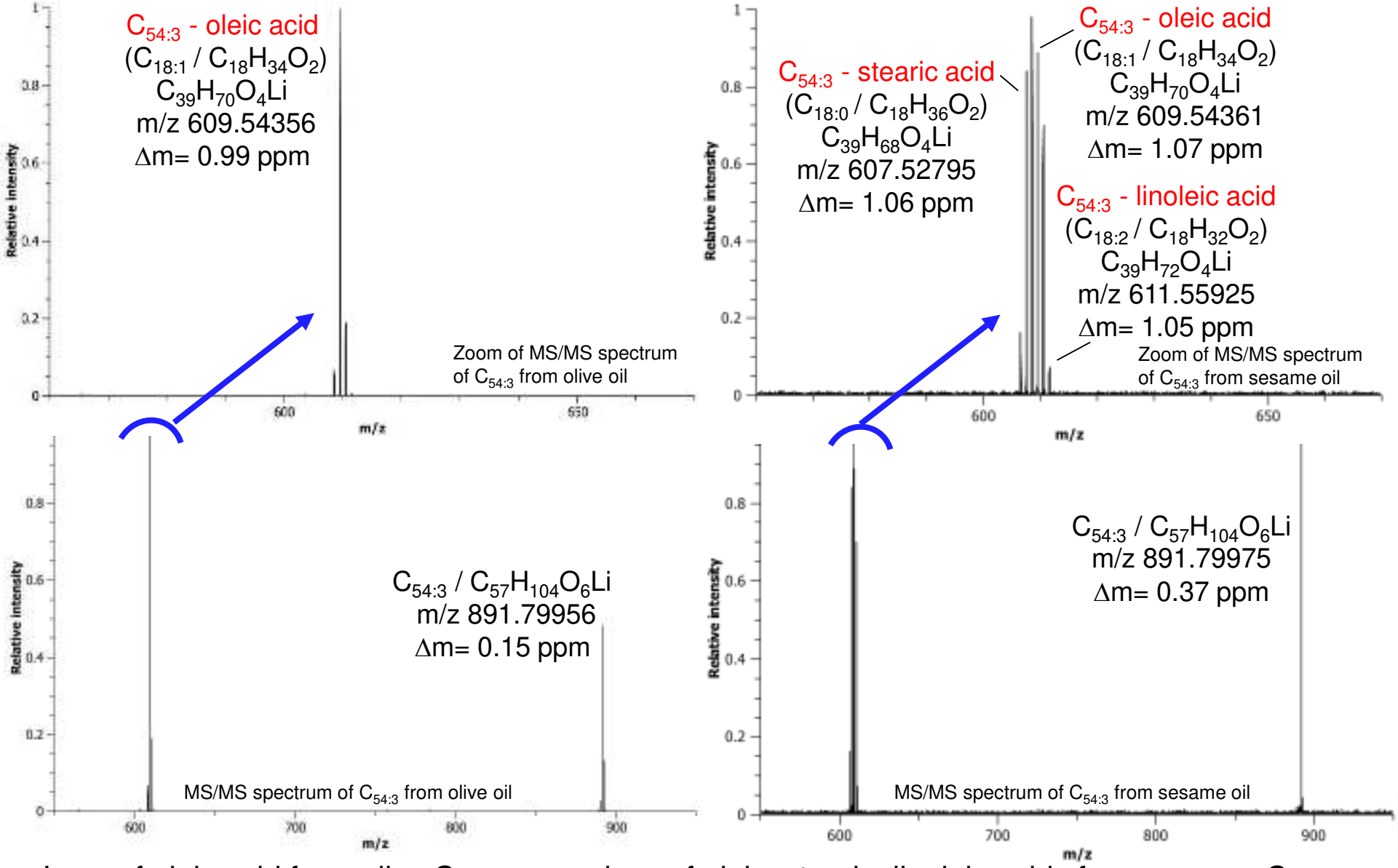

- Loss of oleic acid from olive $C_{54:3}$ versus loss of oleic, stearic, linoleic acids from sesame $C_{54:3}$

Université de Lille

MS spectra allow discrimination of oil origin: dairy products and animal fats

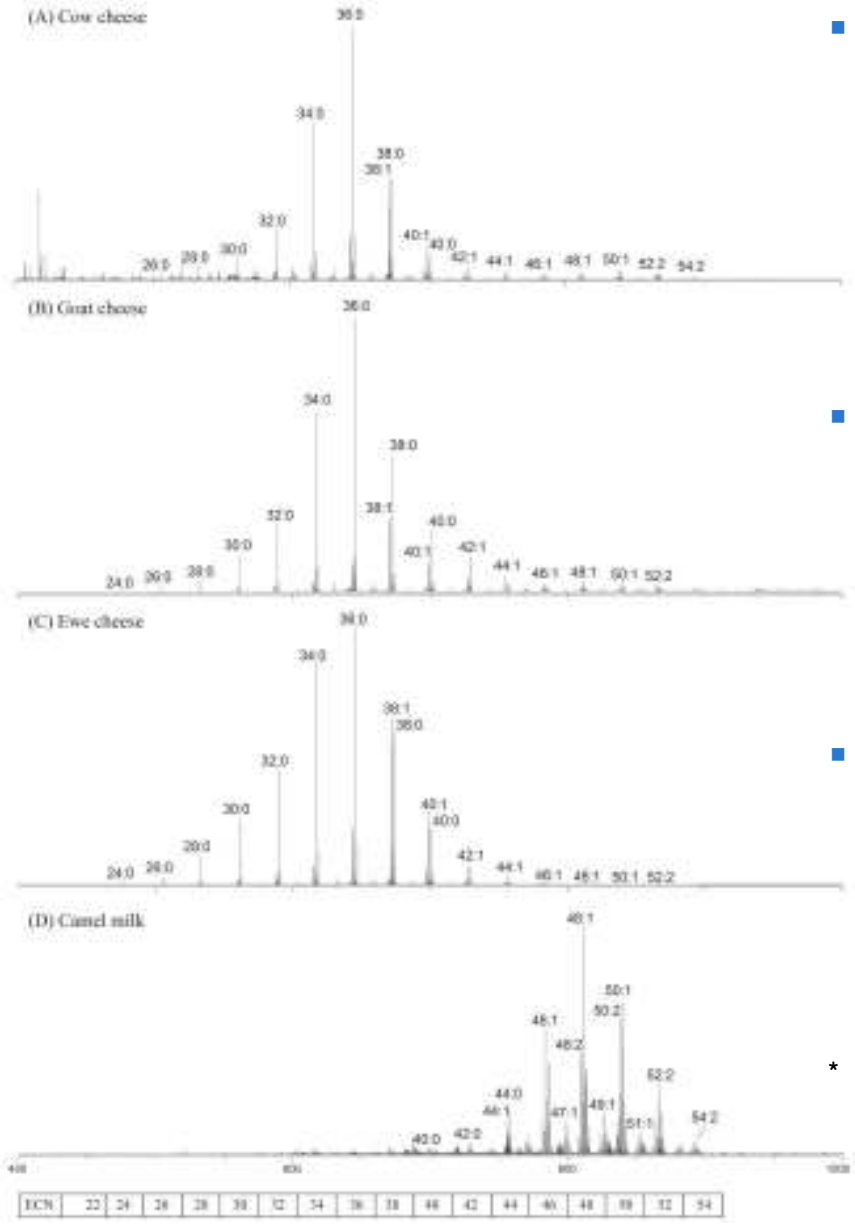

- Dairy products: rich in palmitic, oleic, stearic capric acids => large distribution from ECN 24 to 54 + Presence of TAG with 1 odd-number fatty acid.
- Animal fats: ECN from 46 to 54. Bovine and ovine profiles present even-number TAG + minor odd-number TAGs.
- Odd-number fatty acids: markers of ruminant species, mainly synthesized by bacteria present in the rumen*

* Vlaeminck B., Fievez V., Cabrita A.R.J., Fonseca A.J.M., Dewhurst R.J., An. Feed Sci. Technol. 2006, 131, 389–417

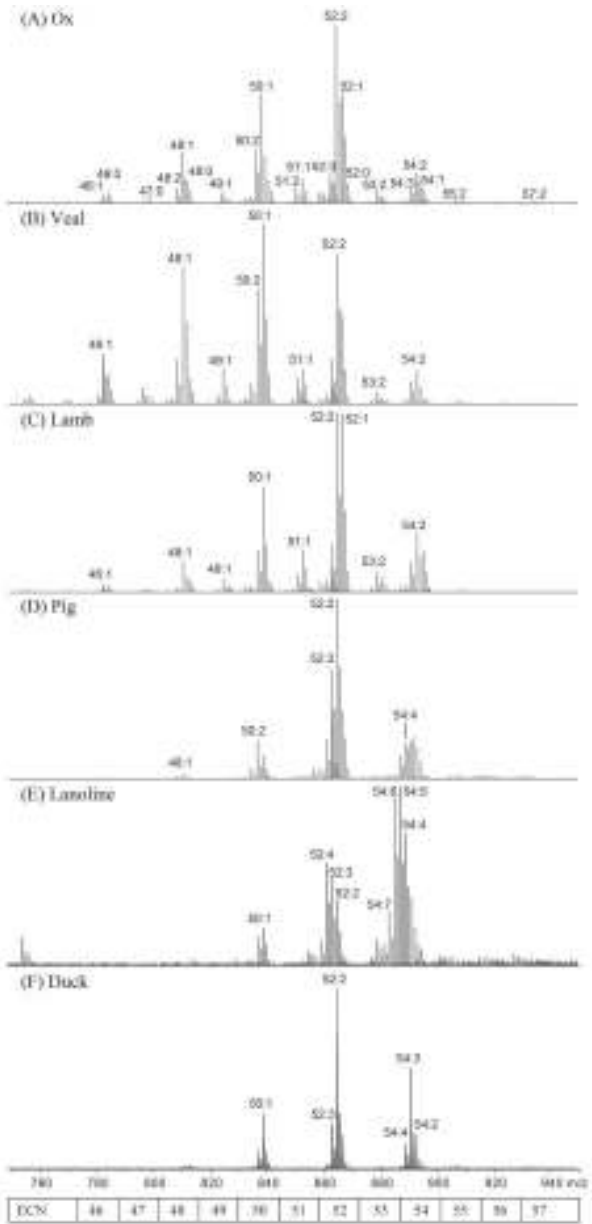

Université de Lille

Study of TAGs remains from 5th century BC–4th century AD archaeological lamps (Olbia, Ukraina)

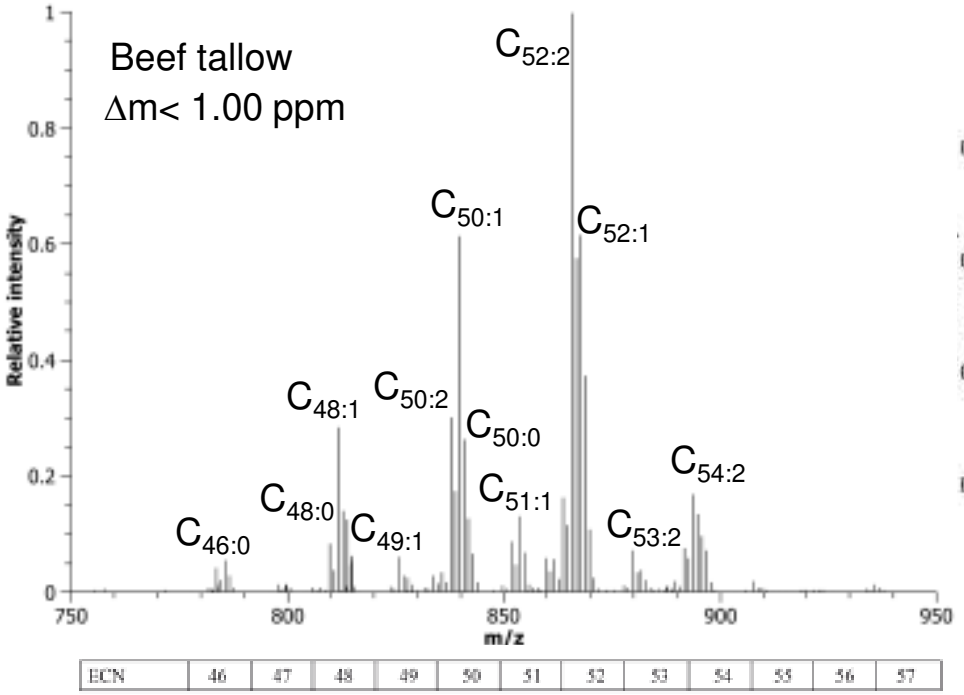

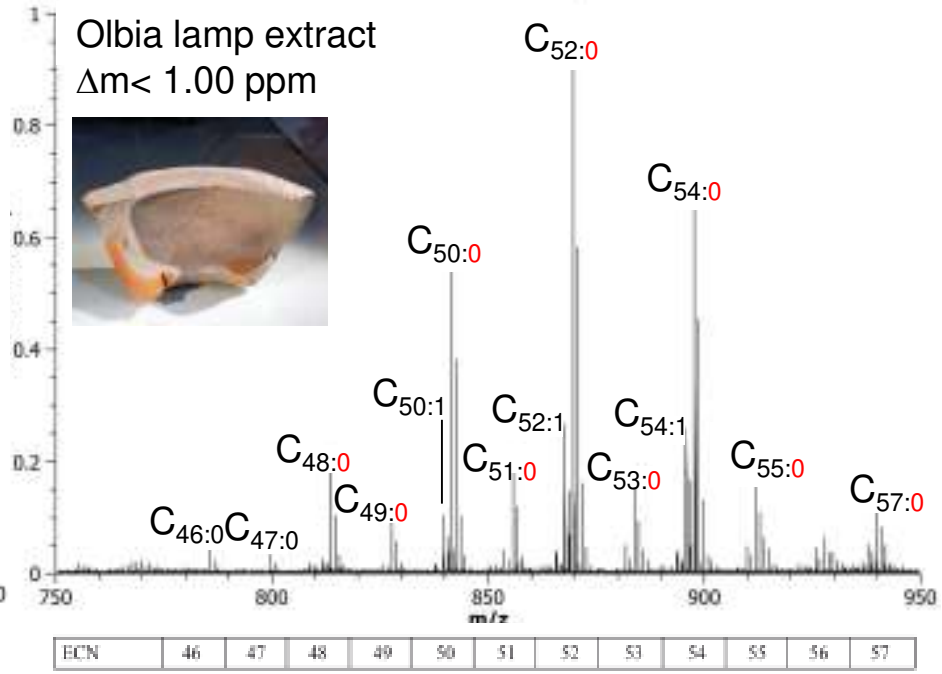

- Dichloromethane-methanol extraction + ultrasonic baths
- TAGs purified on diol cartridge (elution: cyclohexane dichloromethane, diethyl ether; 89/10/1)
- Strong dominance of saturated TAGs, a weak proportion of monounsaturated TAGs and few polyunsaturated TAGs (due to oxidation) in 6 analyzed lamps (9 lamps analyzed)
- Characteristic odd-C-numbered TAGs (not found in non-herbivore species) identifying ovine/bovine species

Garnier N., Rolando N., Høtje J.M., Tokarski C. Int. J. Mass Spectrom. 2009, 284, 47–56

Université de Lille

Study of TAGs remains from 5th century BC–4th century AD archaeological lamps (Olbia, Ukraina)

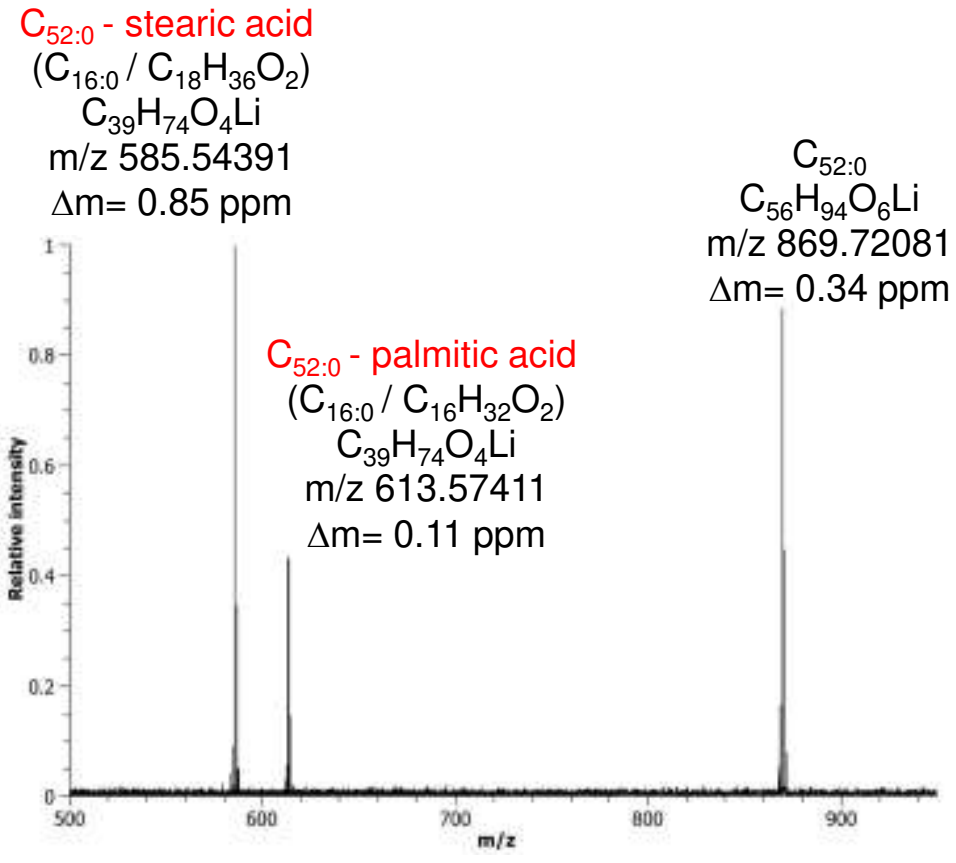

MS/MS spectrum of $C_{52:0}$ from Olbia lamp extract

- MS/MS profiles allow confirming each TAGs composition
- Here the $C_{52:0}$ TAG contains 2 stearic acid and 1 palmitic acid
- Precursor ion selection for MS/MS acquisition was made with higher Δm than Δm used for model oil analysis to increase the signal to noise
  (Δm 2 ppm for standard oils versus 5 ppm for ancient samples)

Garnier N., Rolando N., Høtje J.M., Tokarski C. Int. J. Mass Spectrom. 2009, 284, 47–56

EU FT-ICR MS MSAP cnrs Université de Lille

Analysis of fresh versus naturally aged olive oils

'Fresh' olive oil

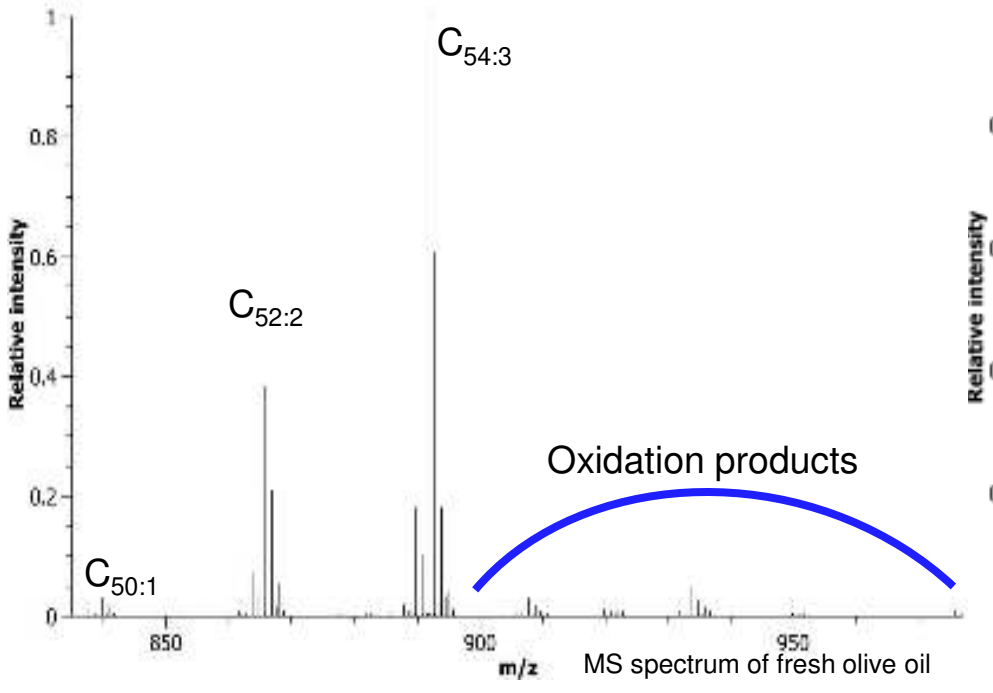

MS spectrum of fresh olive oil

Olive oil submitted to natural ageing during 10 years

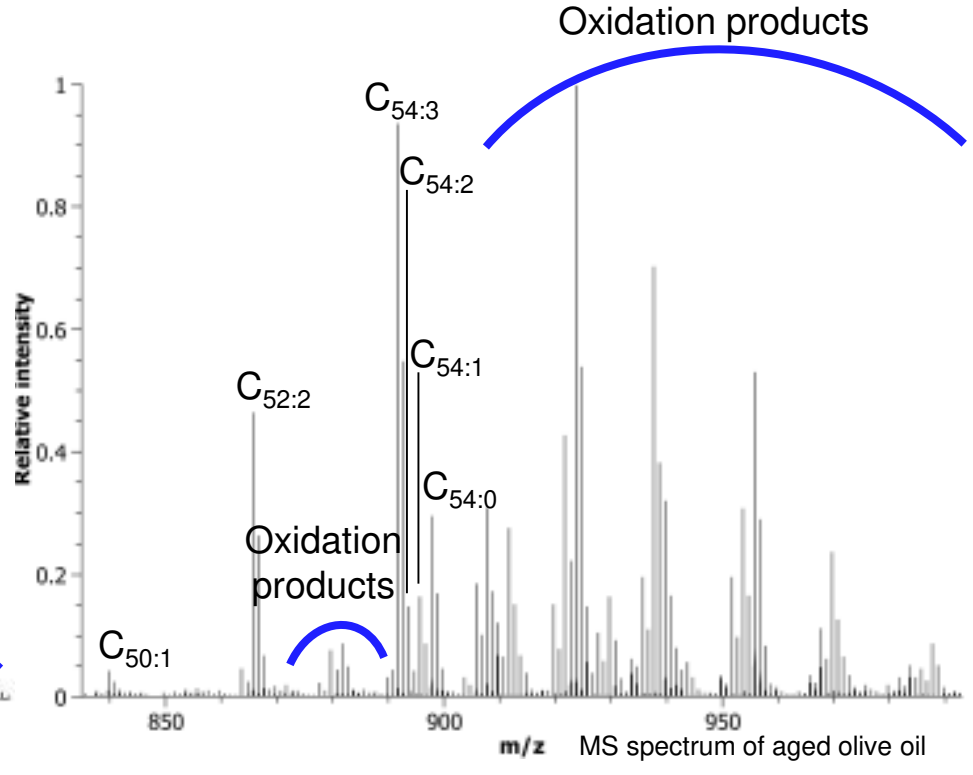

MS spectrum of aged olive oil

- Low intensity peaks related to oxidation in 'fresh' commercial olive oil
- Strong dominance of oxidized TAGs in 10 years-naturally aged olive oil

Université de Lille

Analysis of naturally aged olive oil (10 years)

- Detection of oxidation products of main olive oil unsaturated TAGs
- E.g., mass shift of 2 oxygen from $C_{52:2}$ TAG can be attributed to 2 epoxides or hydroperoxides or a combination

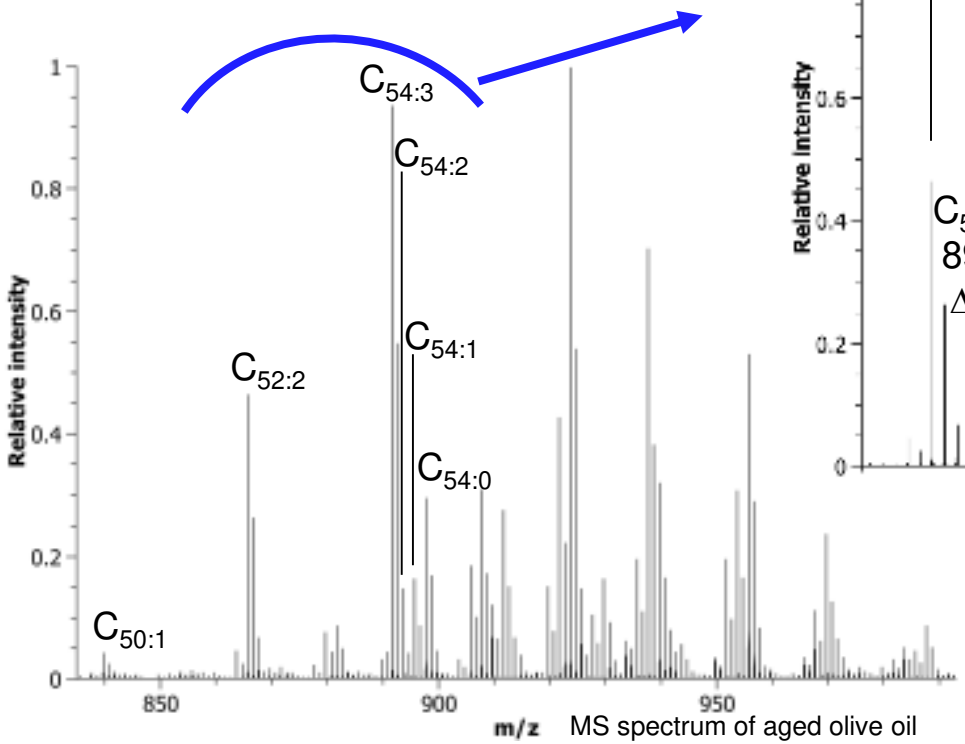

MS spectrum of aged olive oil

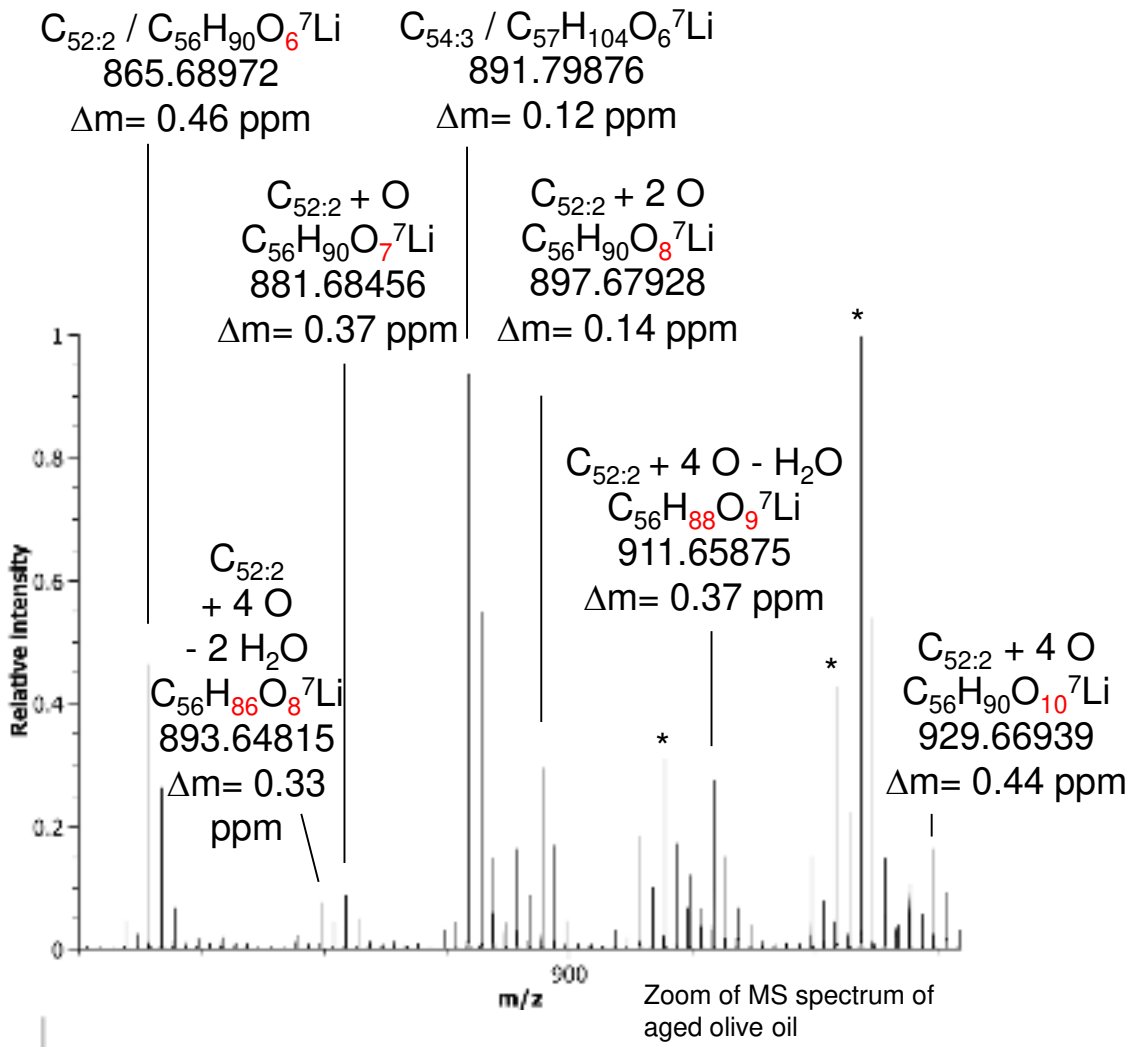

Zoom of MS spectrum of aged olive oil

* See next slide for attribution

Université de Lille

Analysis of naturally aged olive oil (10 years)

- Strong dominance of oxidized TAGs in 10 years-naturally aged olive oil
- Up to 6 oxidation products detected (potentially, hydroperoxides, epoxides, epidioxides)

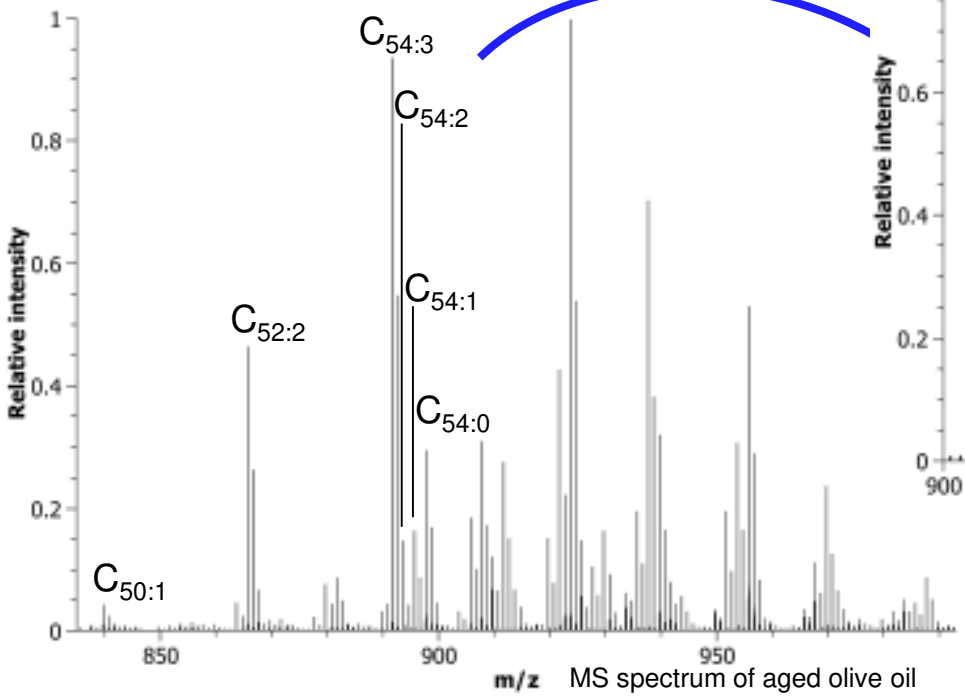

MS spectrum of aged olive oil

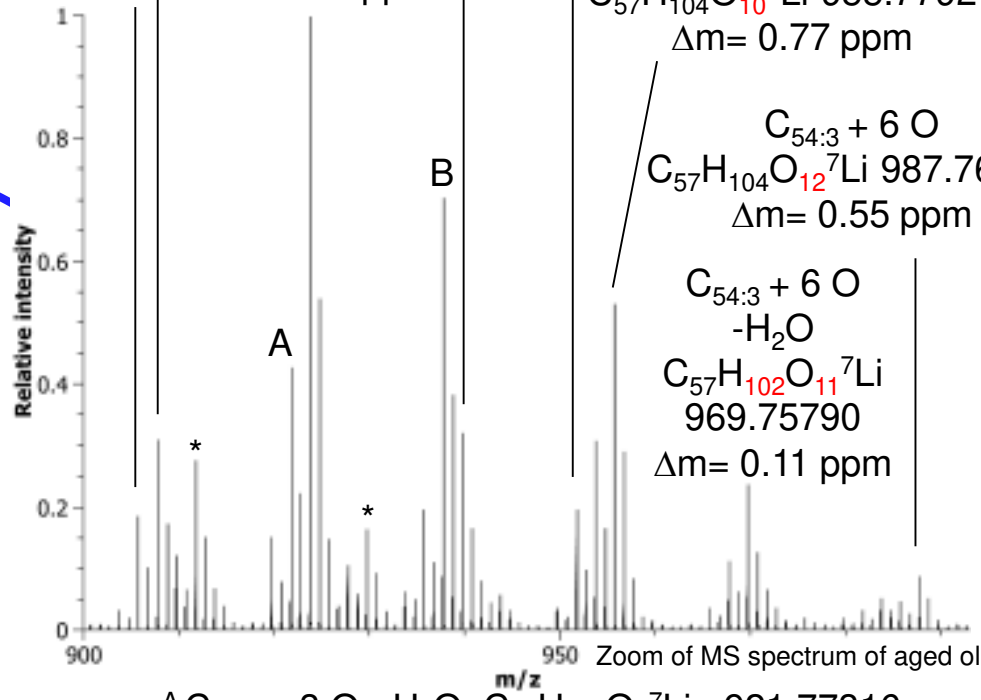

Zoom of MS spectrum of aged olive oil

[A] $C_{54:3}$ + 3 O - H_2O, $C_{57}H_{102}O_8{}^7Li$, 921.77316, Δm= 0.12 ppm; [B] $C_{54:3}$ + 4 O - H_2O, $C_{57}H_{102}O_9{}^7Li$ 939.76811, Δm= 0.15 ppm;

* Attributions presented on previous slide

Université de Lille

MS/MS (IRMPD) spectra of oxidized TAGs

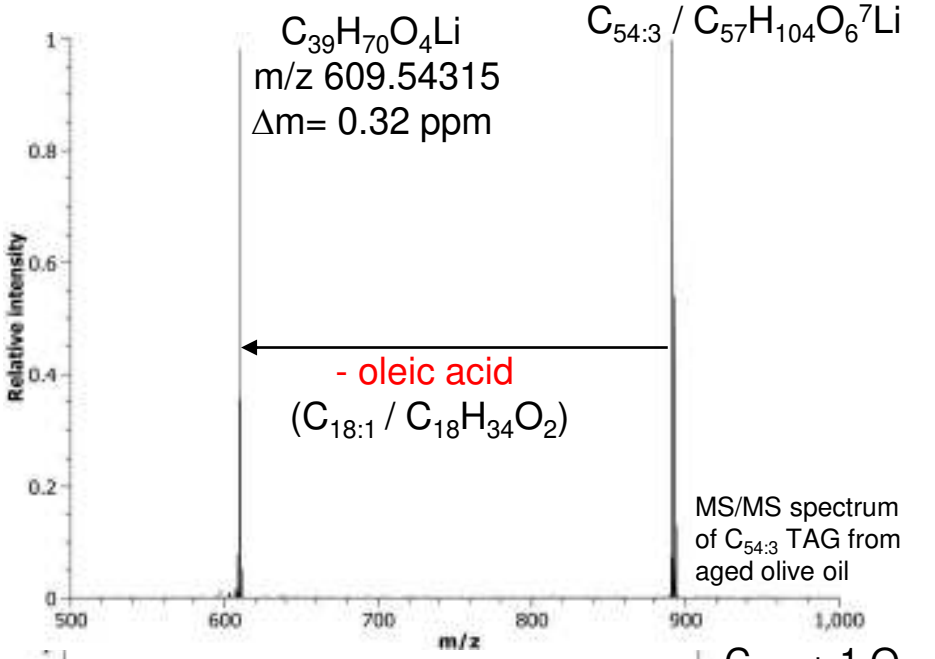

MS/MS spectrum of $C_{54:3}$ TAG from aged olive oil

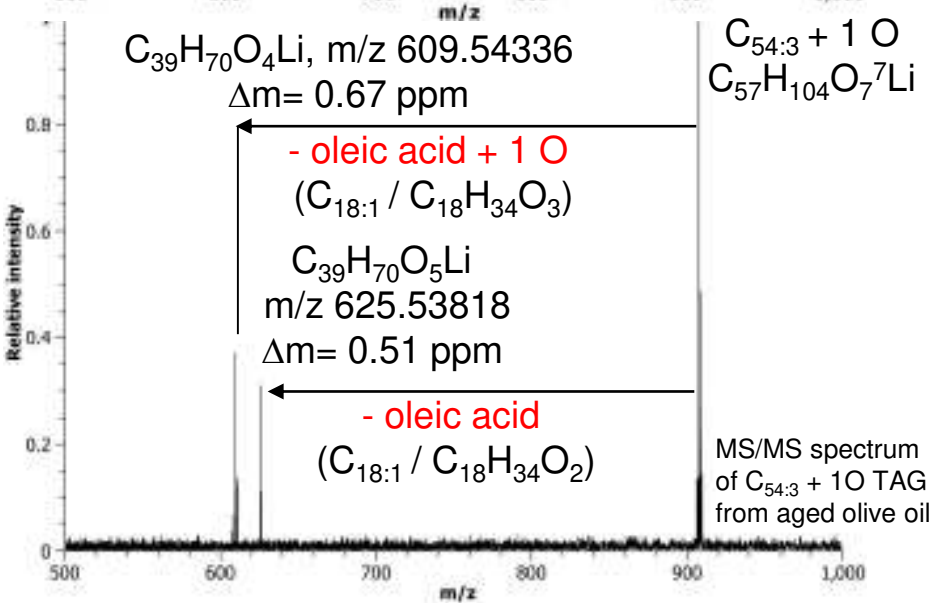

MS/MS spectrum of $C_{54:3}$ + 1O TAG from aged olive oil

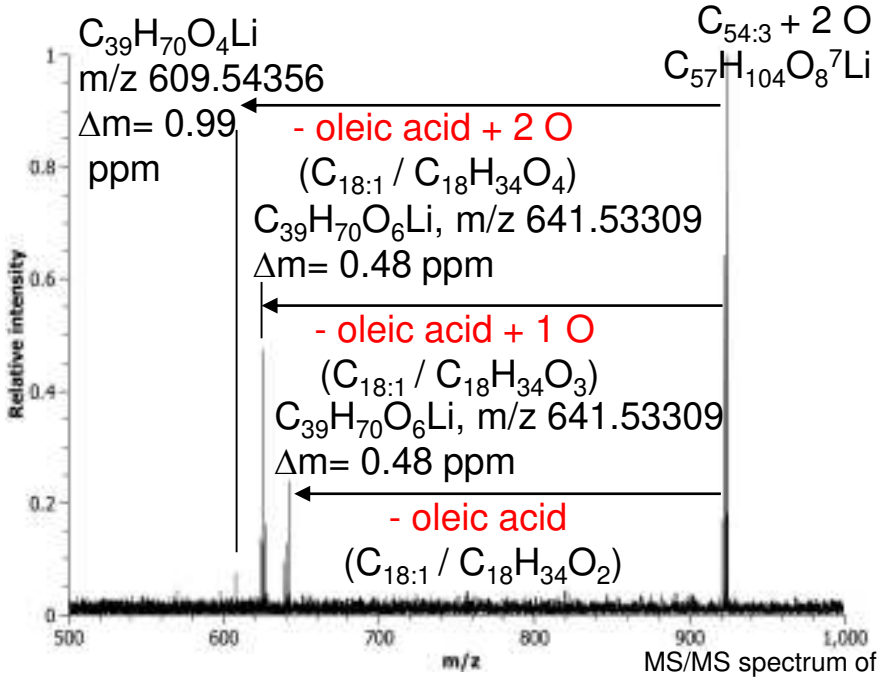

MS/MS spectrum of $C_{54:3}$ + 2O TAG from aged olive oil

- MS/MS spectra shows fatty acid moieties and their oxidized forms
- E.g. MS/MS spectrum of $C_{54:3}$ + 2 O shows the loss of oleic acid, monooxidized oleic acid and dioxidized oleic acid

Université de Lille

Analysis of Roman amphorae from Pisa San Rossore harbor (Ist century BC)

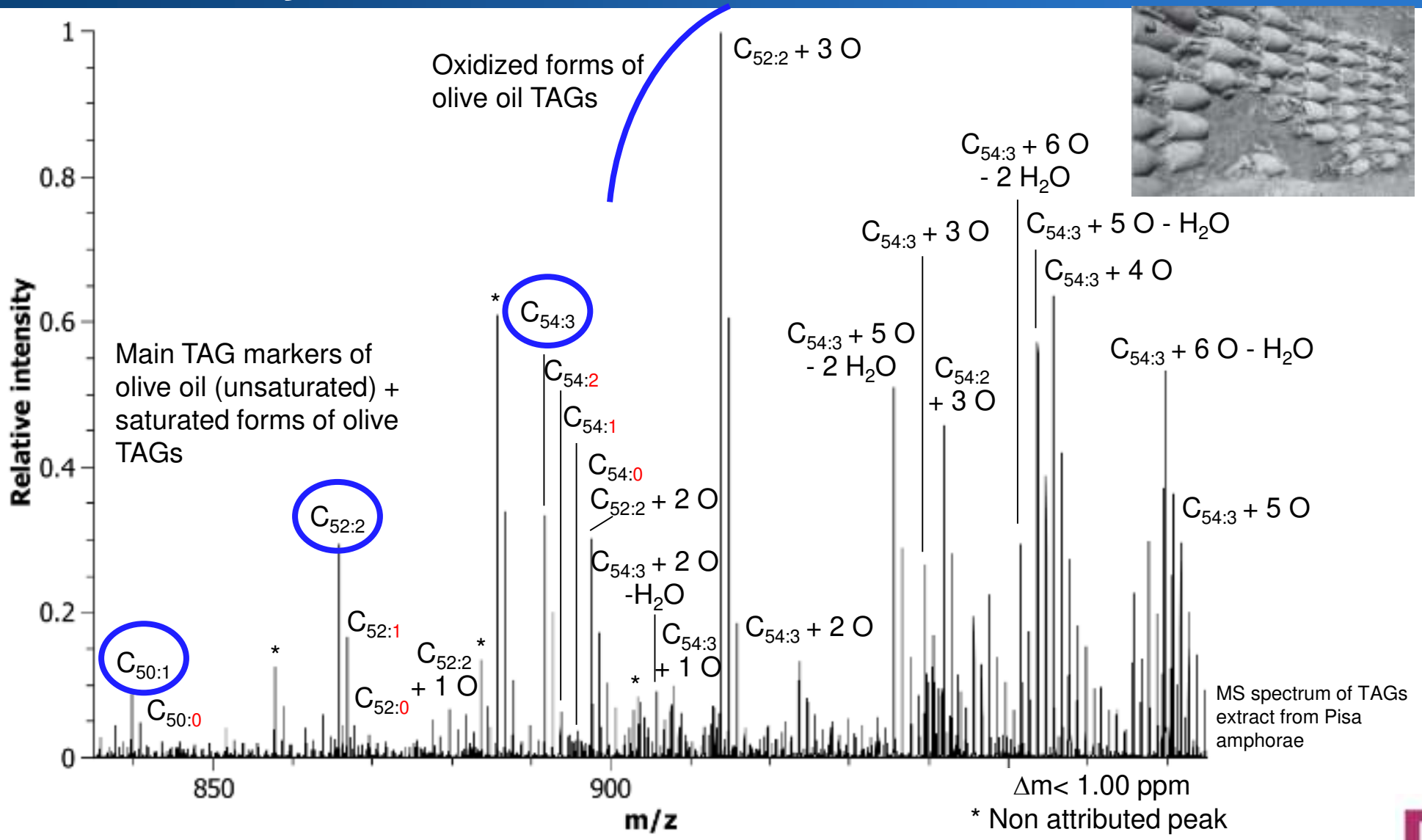

- In Pisa amphorae extract, main detection of olive oil TAGs (saturated and unsaturated forms) + their oxidized forms

Université de Lille

Analysis of Roman amphorae from Pisa San Rossore harbor (Ist century BC)

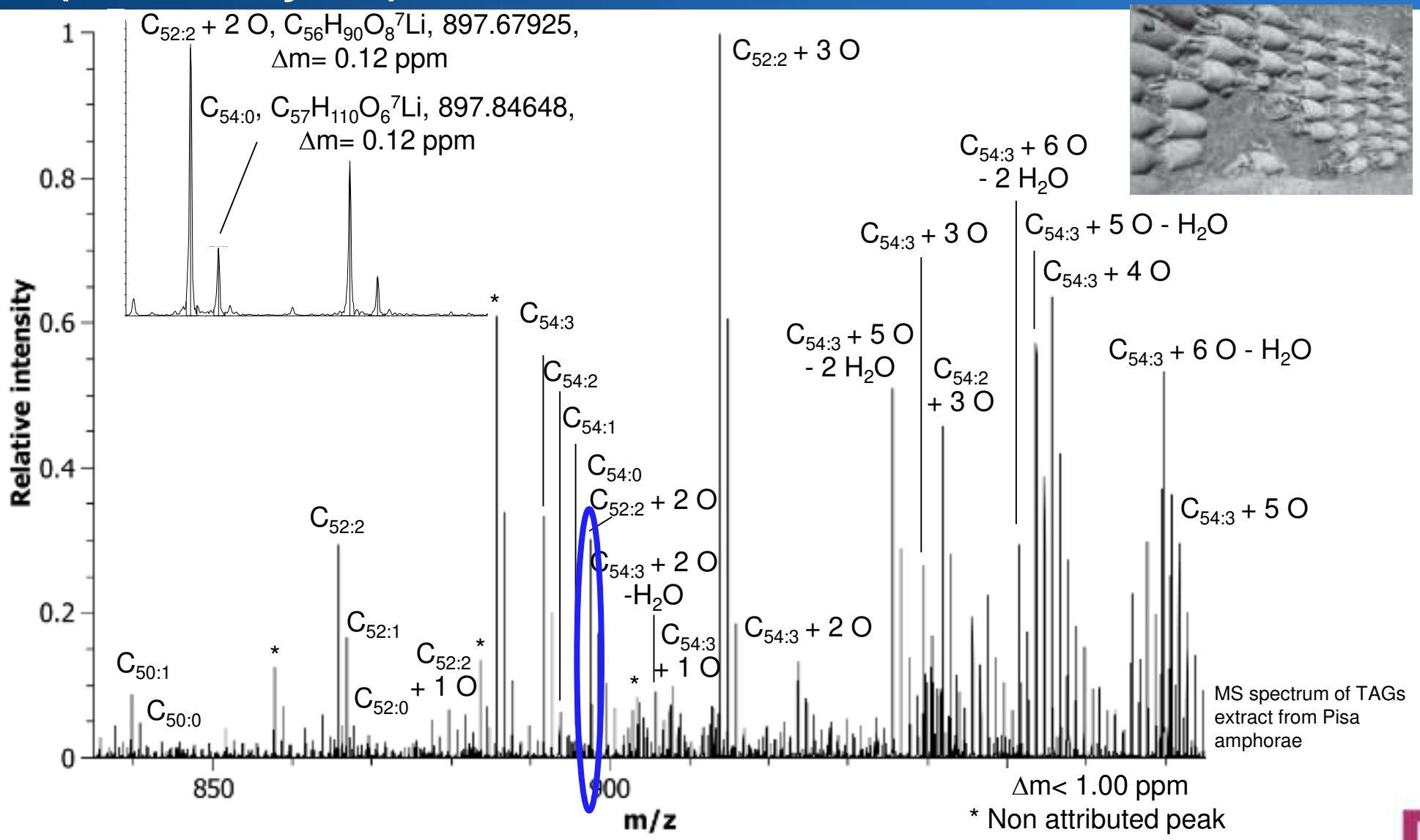

MS spectrum of TAGs extract from Pisa amphorae

- Despite spectrum complexity, separation of $C_{54:0}$ TAGs and $C_{52:2}$ + 2 O achieved

Université de Lille

Analysis of Roman amphorae from Pisa San Rossore harbor (Ist century BC)

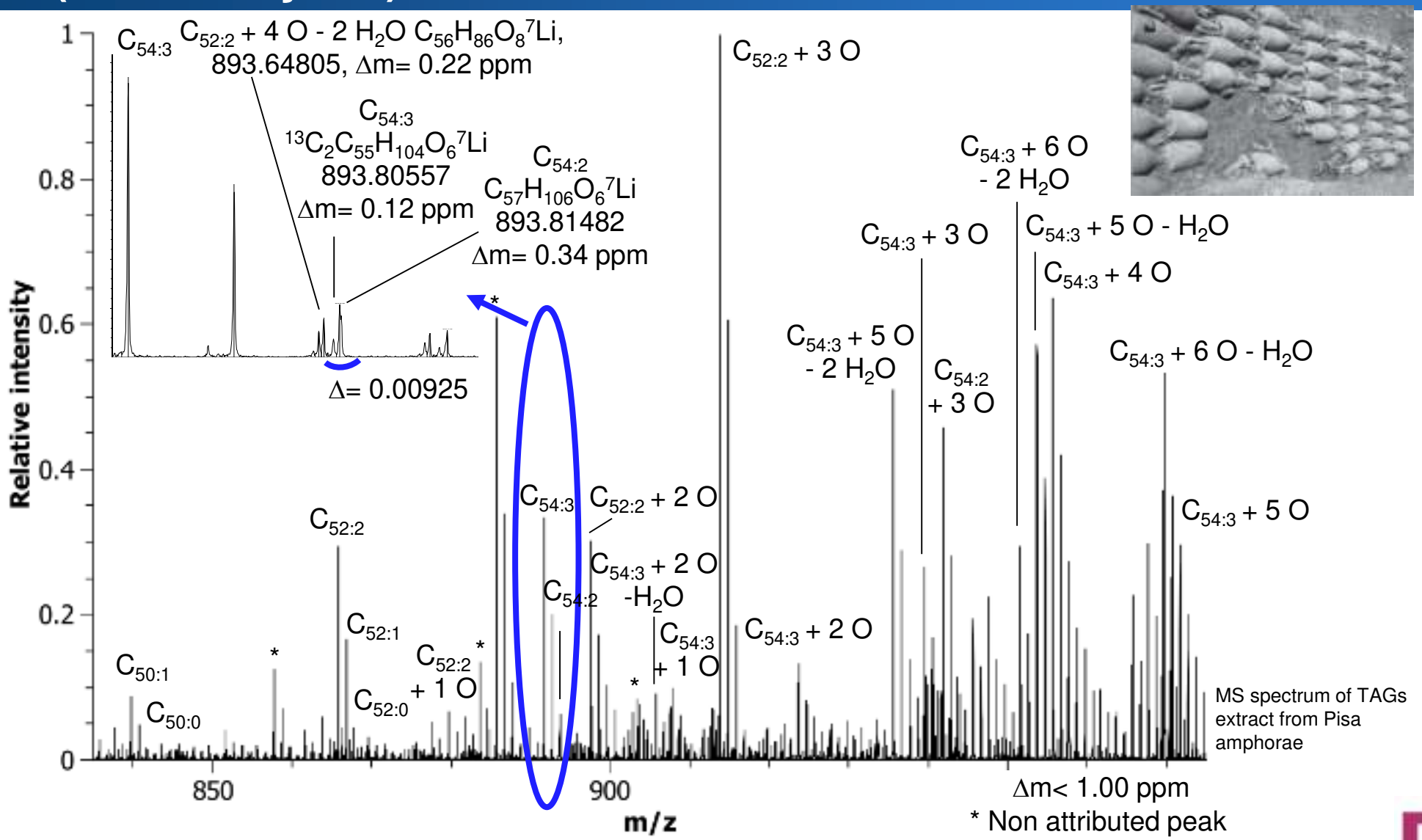

MS spectrum of TAGs extract from Pisa amphorae

- High resolution allows separating $C_{54:2}$ TAGs, second isotopic peak of $C_{54:3}$ TAGs and oxidized forms of $C_{52:2}$ TAGs

Université de Lille

Conclusion

Methodological developments based on MS and MS/MS profiles (IRMPD) allowed identification of archaeological triacylglycerols and their origins (from few micrograms of crushed sample)

- Study of TAGs remains from 5th century BC–4th century AD archaeological lamps (Olbia, Ukraina) showed characteristic odd-C-numbered TAGs (not found in non-herbivore species) identifying ovine/bovine species + strong dominance of saturated TAGs
- Analysis of Ist century BC Roman amphorae from Pisa San Rossore harbor (Italy) allowed identification of olive oil using marker TAGs and their oxidized forms (potentially hydroperoxides, epoxides, epidioxides)

Actually, studies on lipid (and protein) residues from amphorae preserved in marine context during 2 millenaries

Collaboration with the *Département des Recherches Archéologiques Subaquatiques et Sous-Marines* (DRASSM, Marseille, France; Dr Franca Cibecchini and Dr Michel L'Hour)

Spanish amphoras of Sud Perduto 2, 1st century AD

Université de Lille

Deciphering the structure of natural amber by chemical depolymerization and analysis by ultrahigh resolution FT-ICR mass spectrometry

Ziad MAHMOUD

Miniaturization for Synthesis, Analysis & Proteomics USR 3290

Amber

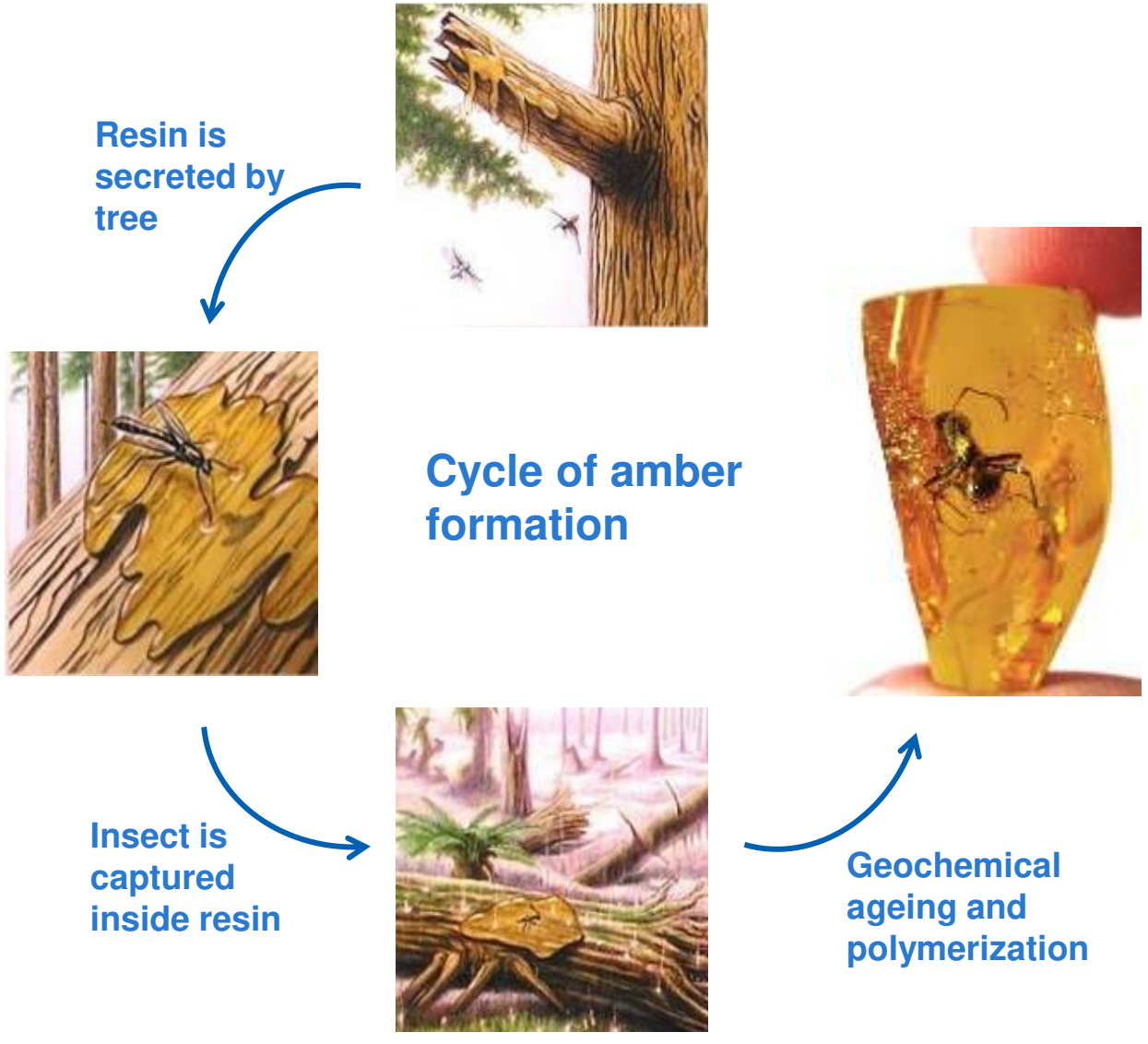

- Complex polymer
- Very insoluble
- Difficult to analyze
- Oldest amber: 320 million years ago
- Can contain fossilized animals or plants

Chemical composition of amber

^{13}C NMR AND IR ANALYSES OF STRUCTURE, AGING AND BOTANICAL ORIGIN OF DOMINICAN AND MEXICAN AMBERS

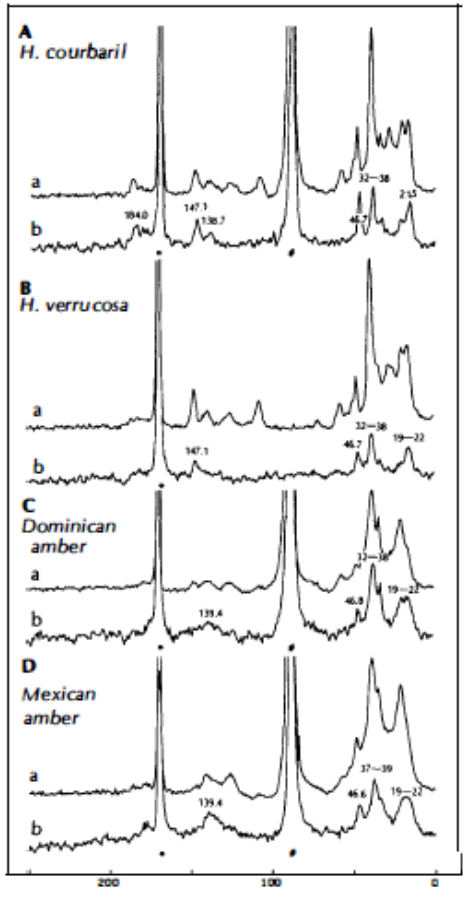

Thermal investigations of amber and copal

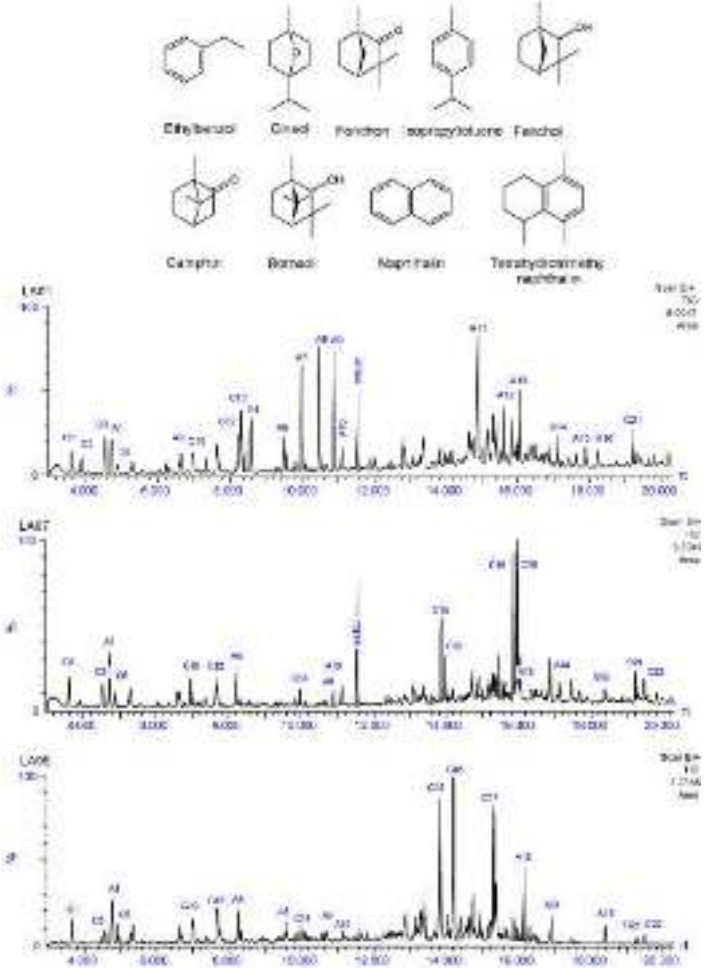

Non-destructive analysis of amber artefacts from the prehistoric Cioclovina hoard (Romania)

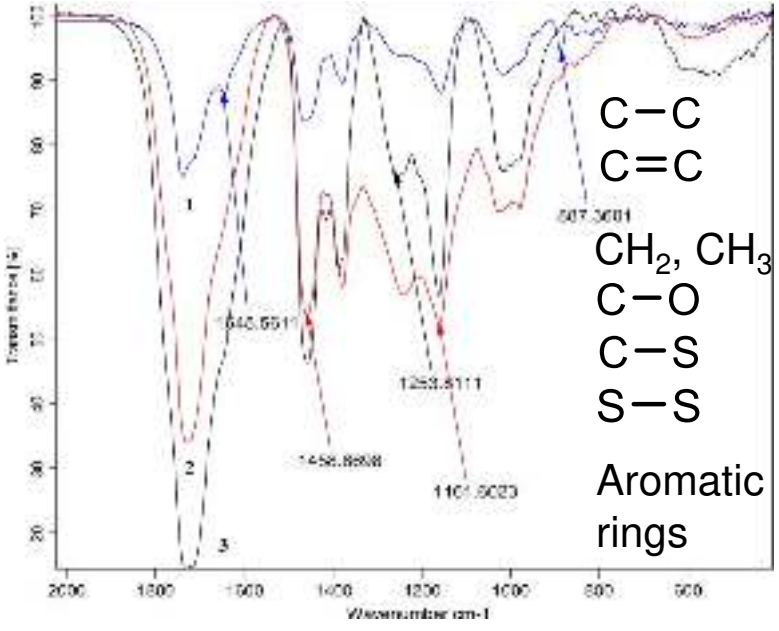

How to solubilize amber?
How to identify cross-linking products?

EU FT-ICR MS

MSAP

cnrs

Université de Lille

Chemical composition of amber

- Amber can be classified into classes from I to V
- Based on terpenoids formed of ring structures with isoprene (C_5H_8) units
- The formation of amber is the result of polymerization of one of its major compounds: communic acid

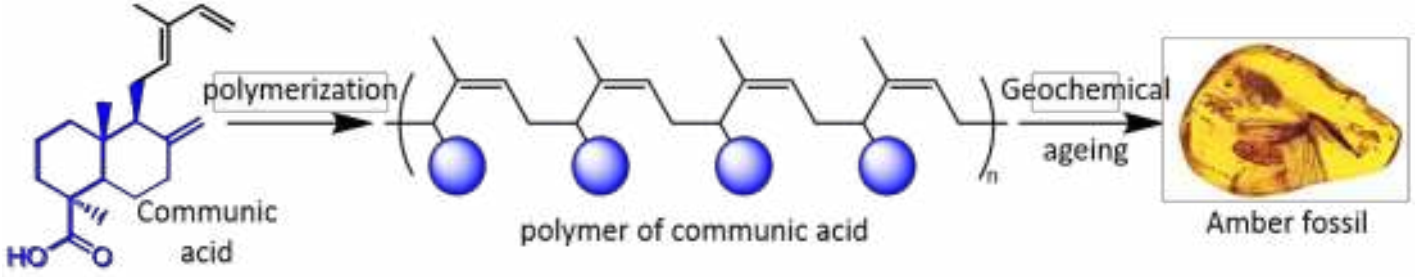

Cross-metathesis depolymerization of polybutadiene and polyisoprene

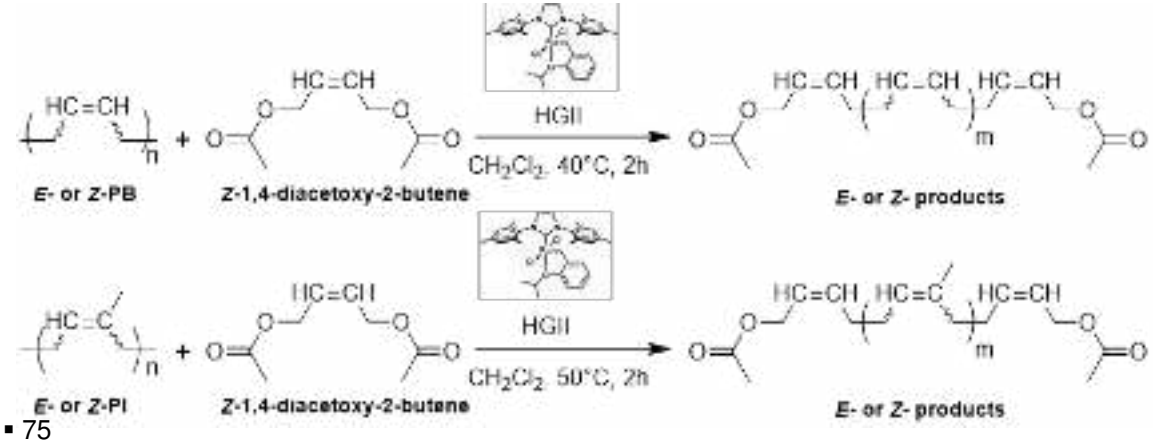

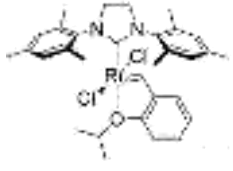

Hoveyda-Grubbs second generation catalyst

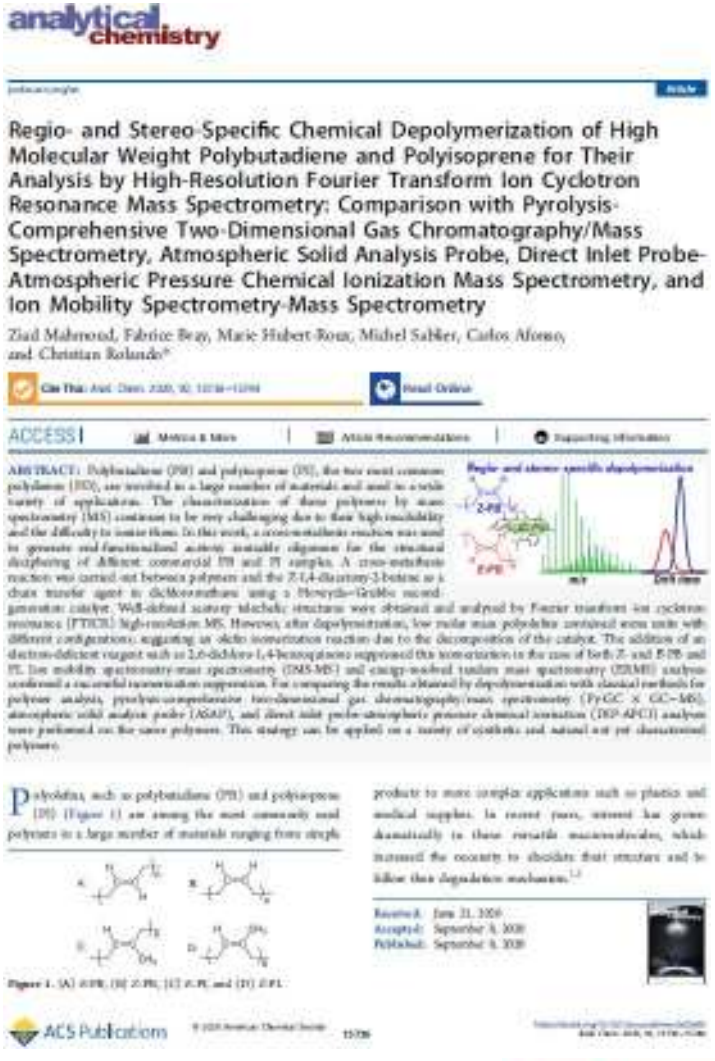

EU FT-ICR MS

Extraction and analysis of communic acid

- Communic acid was extracted from **cypress cones**, **purified** **and** **polymerized under UV**

- ***Analysis on SolarixXR 9.4 Tesla FT-ICR from Bruker Daltonis equipped with a nanoESI ionizzation source***

FT-ICR ESI(+) MS of communic acid

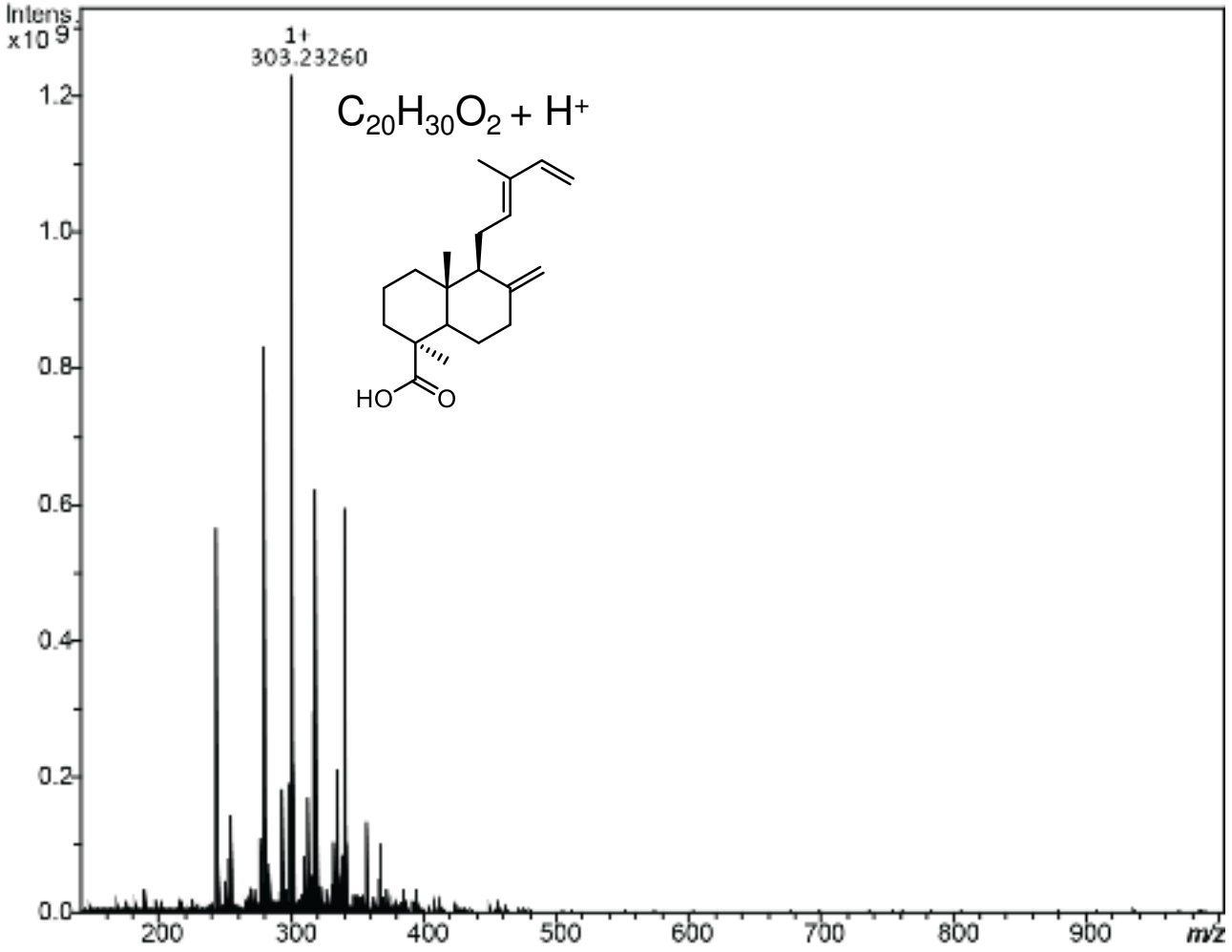

Extraction and analysis of communic acid

Communic acid polymerized under UV at 395 nm to mimic ageing and cross-linking in amber

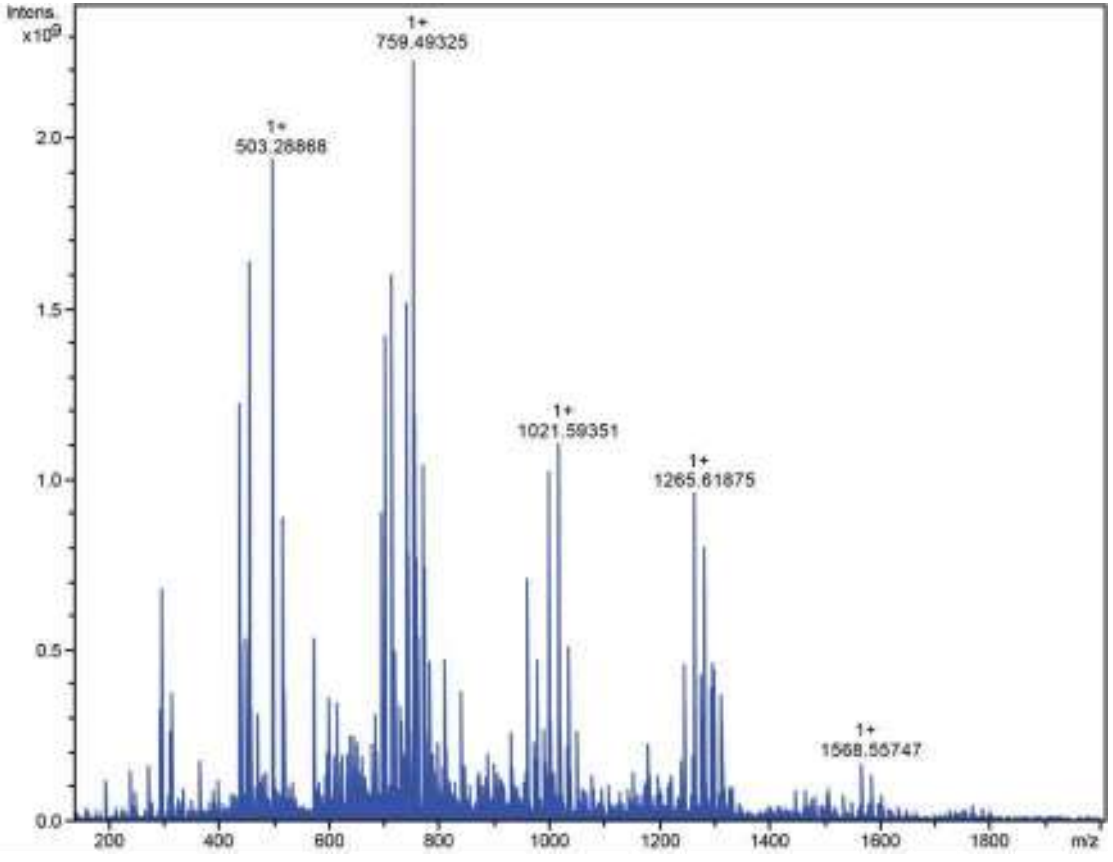

FT-ICR ESI(+) MS of depolymerized poly(communic acid)

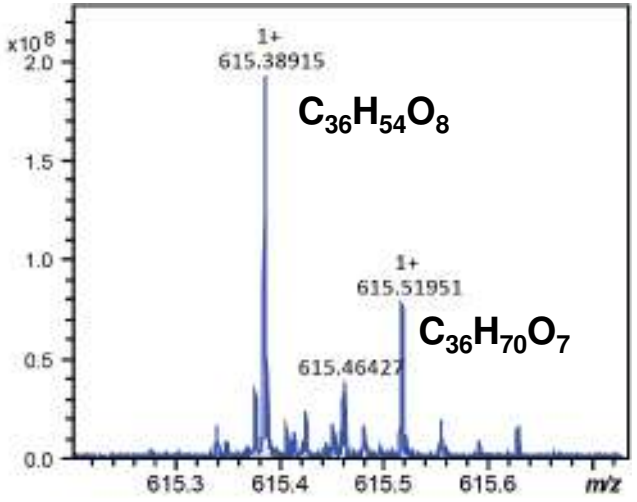

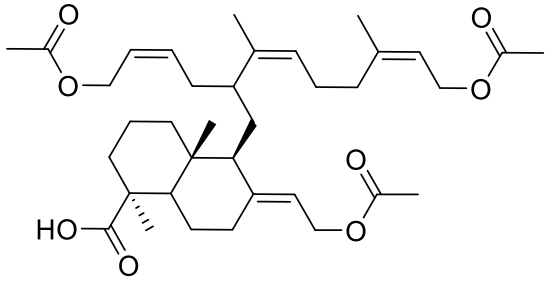

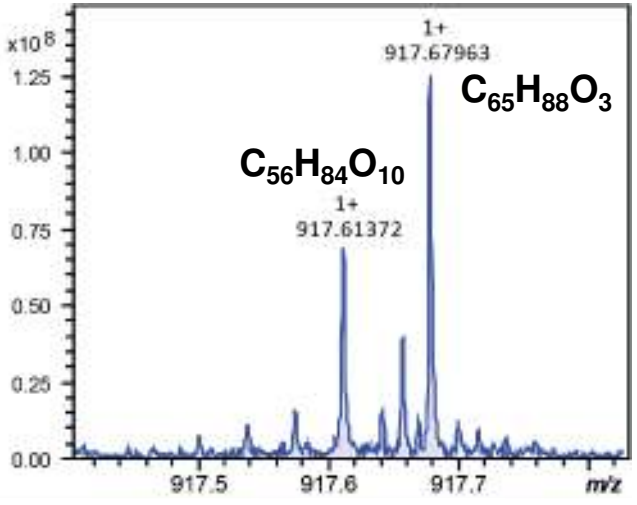

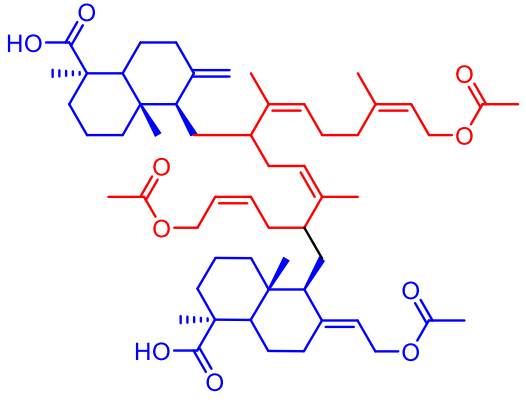

Amber samples

- Cross-metathesis with ruthenium catalyst was performed applied on the samples
- Disulfide bridges in act as poison to the catalyst and inhibit the depolymerization reaction

Development of alternative chemical pathway for the depolymerization and analysis of amber by high-resolution mass spectrometry

Samples provided by the National Museum of Natural History-Paris (MNHN)

Depolymerization and analysis of amber samples

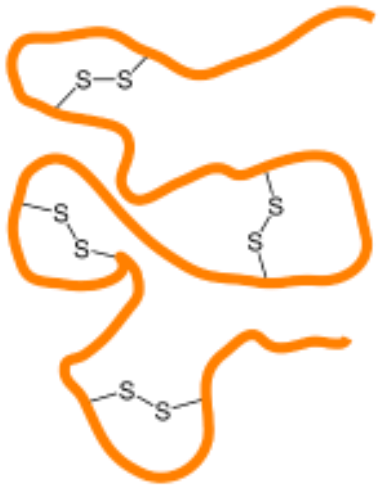

Amber polymer with disulfide bridges

Reduction

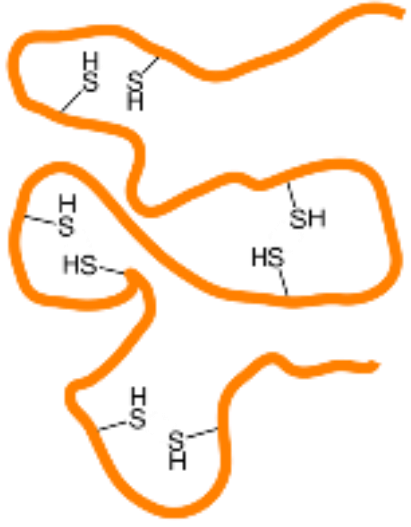

Cleavage of disulfide bridges

Raney Nickel

Desulfurization

Amber polymer free of sulfur and containing isoprenic units

TMSD methylation

Cross-metathesis

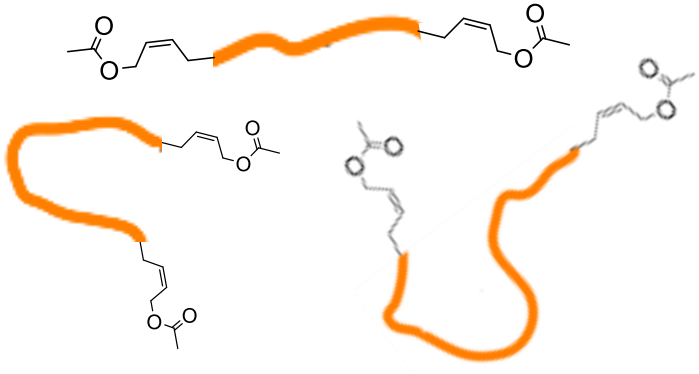

Functionalized solub. amber oligomers

Analysis by FT-ICR high resolution mass spectrometry

EU FT-ICR MS

MSAP

cnrs

Université de Lille

Analysis of amber by FT-ICR MS

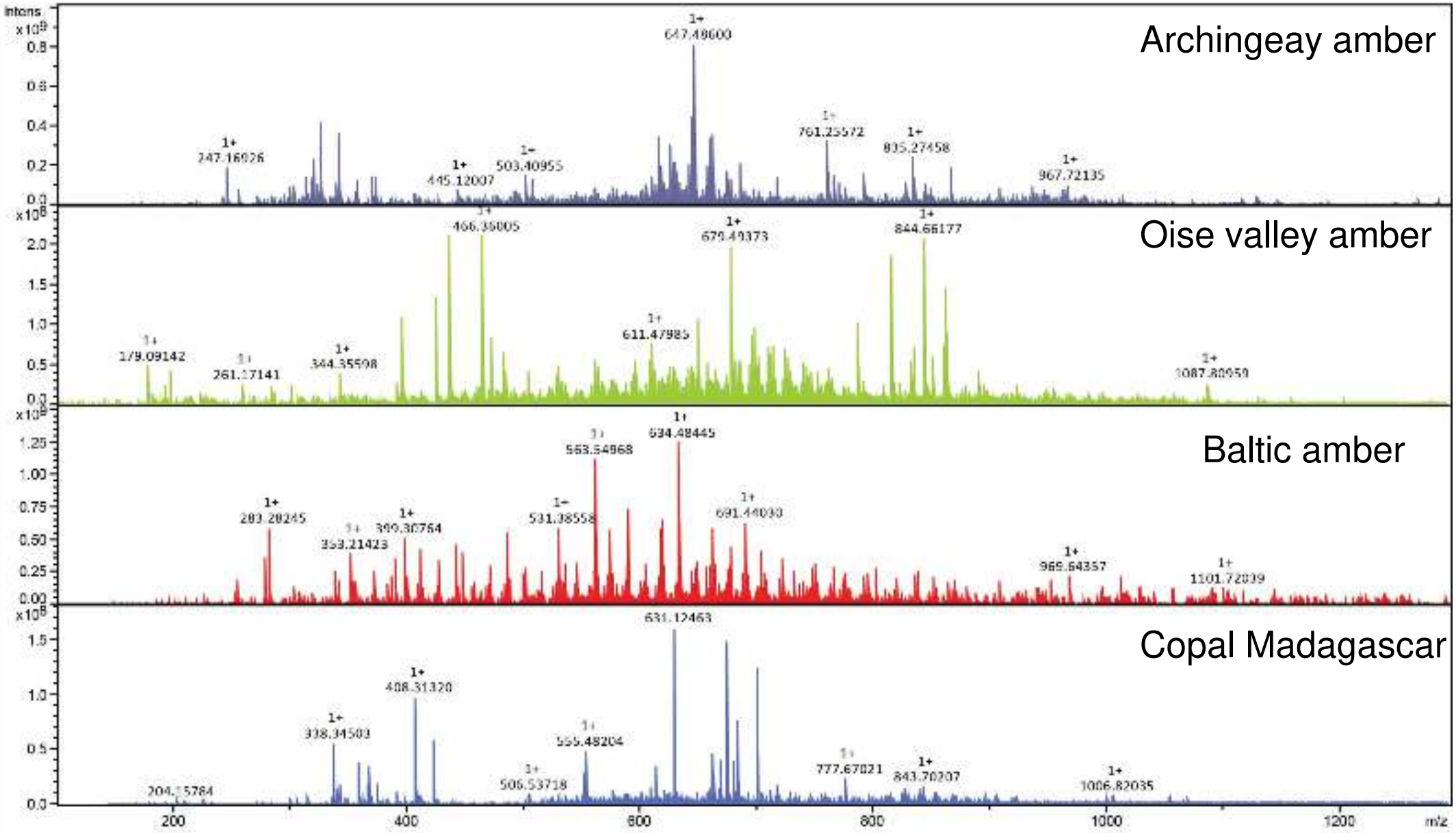

Analysis of amber samples by FT-ICR MS

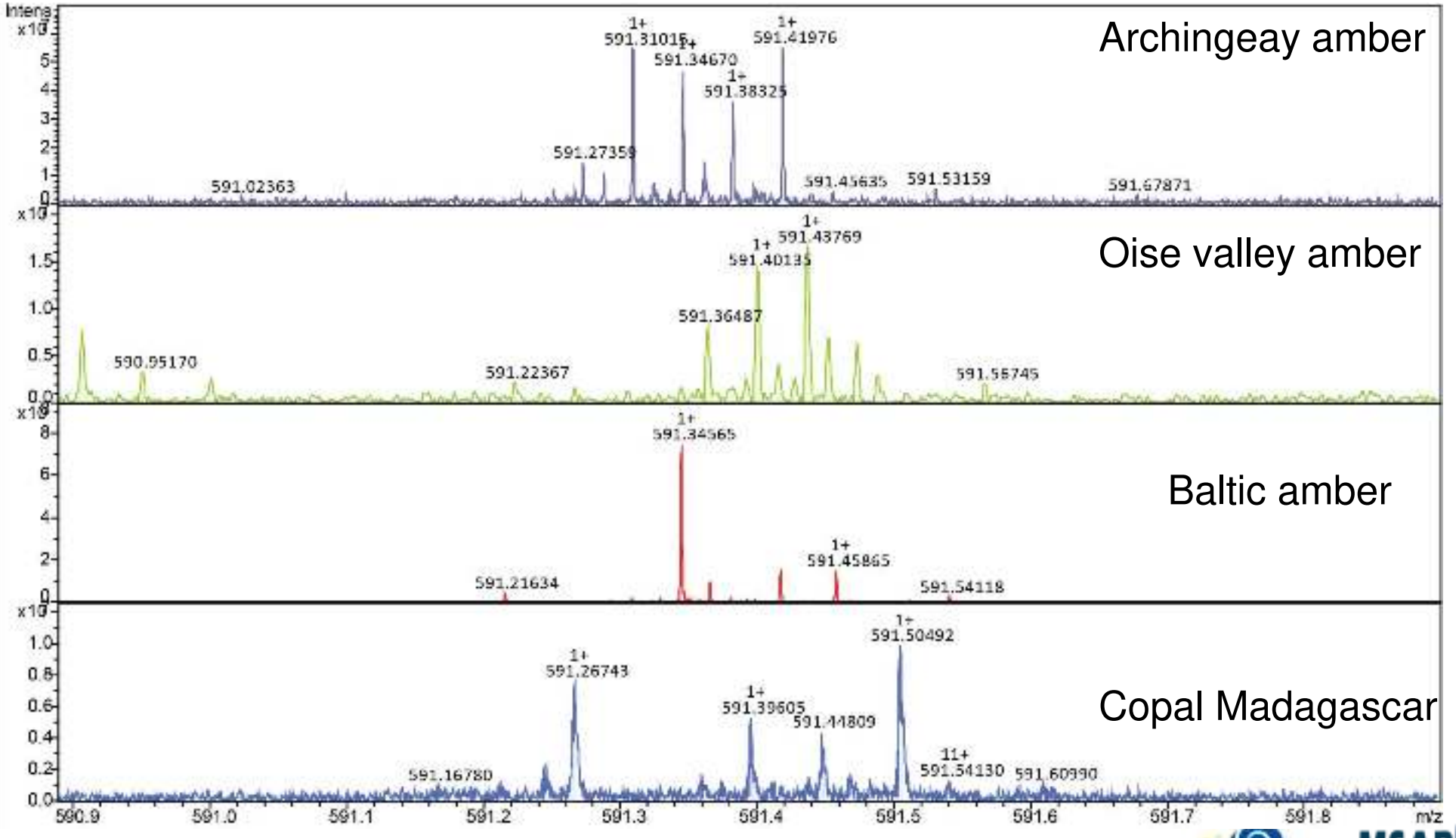

- Amber from different regions have specific chemical composition
- Possibility to determine the fingerprint of each sample

Analysis of amber by FT-ICR MS

Depolymerized Archingeay amber

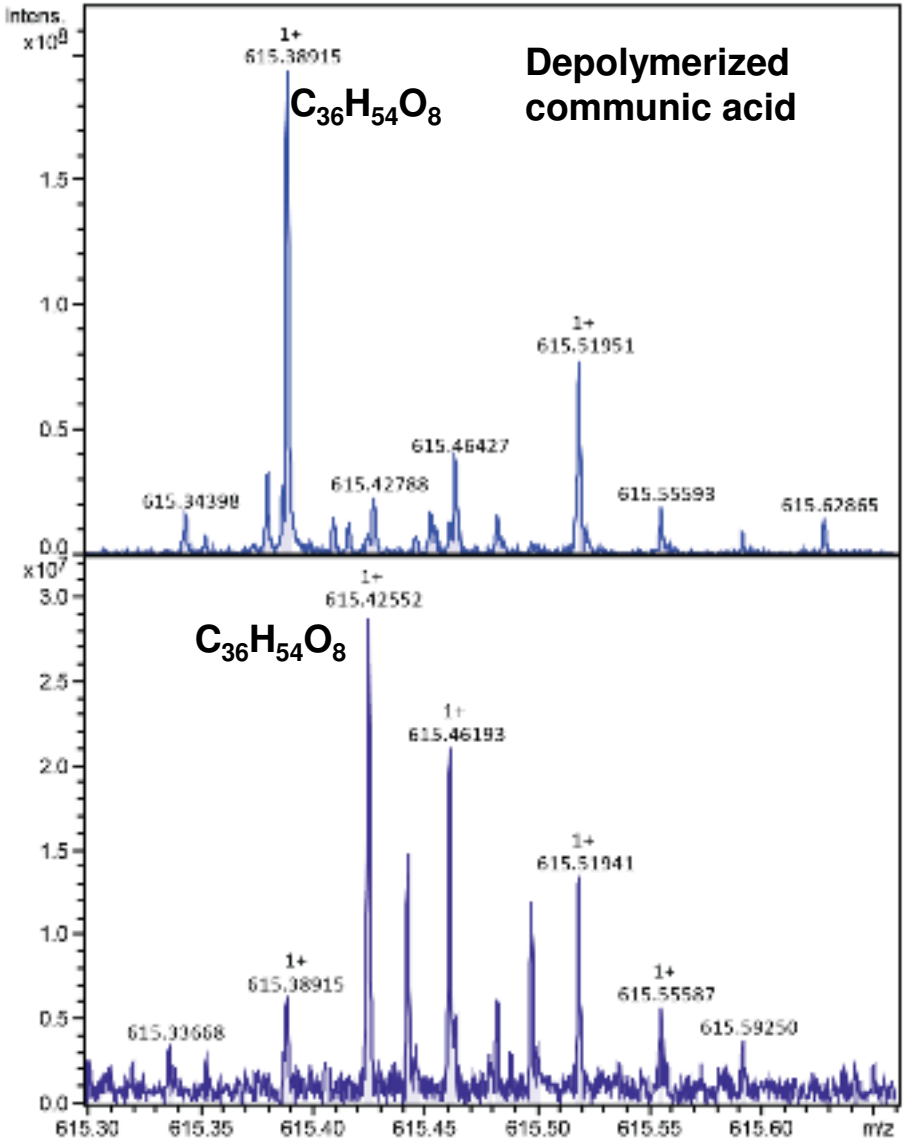

Depolymerized Baltic amber

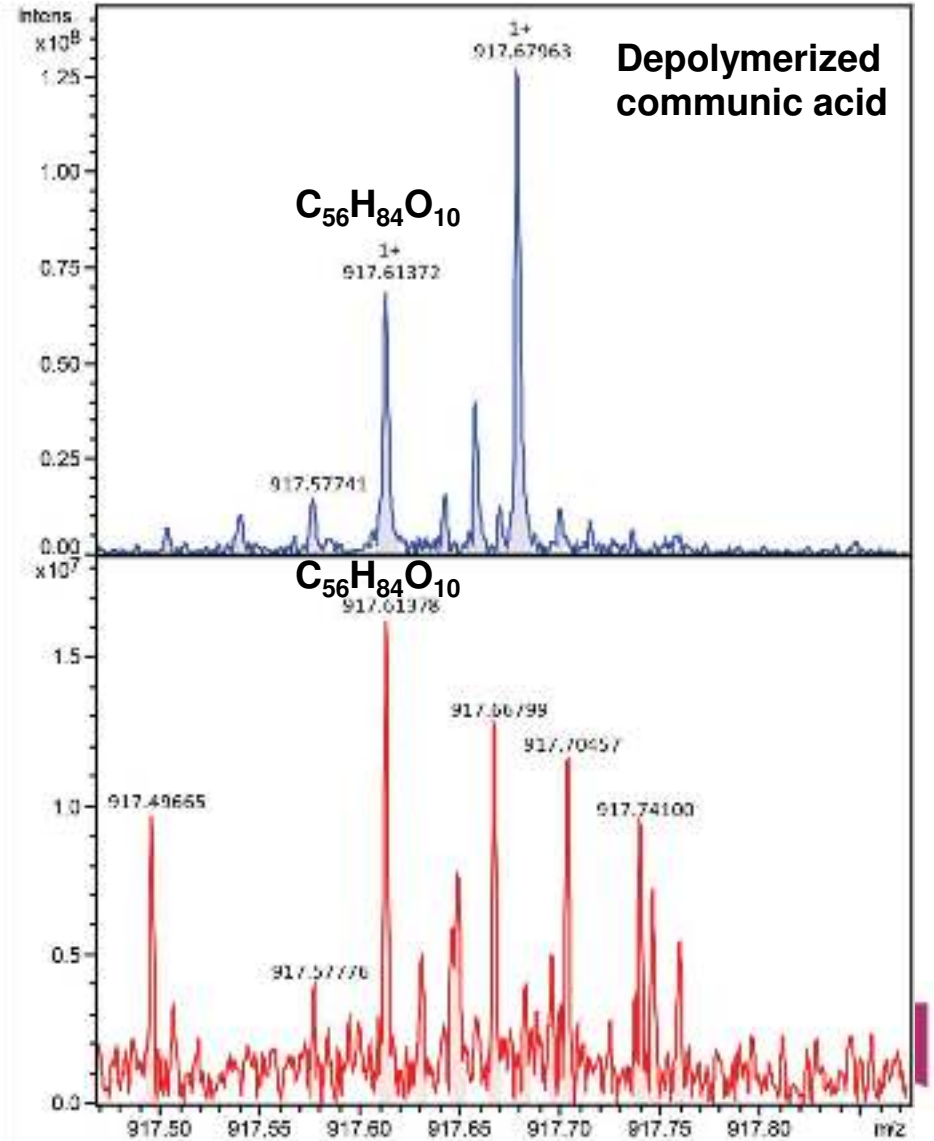

Université de Lille

Conclusions and perspectives

Conclusions:

- We developed a method for the analysis of natural amber based on desulfurization and depolymerization by olefin cross-metathesis using ruthenium catalysts
- Mass spectra showed the complexity of the amber after ageing and polymerization
- Analysis by high-resolution mass spectrometry revealed the fingerprint of ambers from different regions

Perspectives:

- Full characterization of products obtained from cross-linking after ageing
- Classification of amber samples according to their chemical composition
- Apply the same methodology on amber containing insects or plants

EU FT-ICR MS

Metabolomics of archaeological samples

- Funeral amphora discovered in a Gallic site at Cébazat (Auvergne, France)
- This amphora has been used as a wine container
- Traces of cannabis were guessed from GC-MS data by Dr Nicolas Garnier

Proof of cannabis presence in the archaeological amphora by FT-ICR MS

Extraction of compounds in amphora → Analysis by nanoESI FT-ICR SolariX XR 9.4 T

→ Identification of cannabis compounds

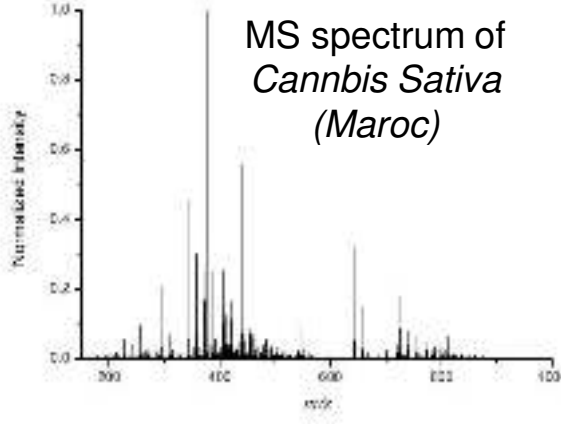

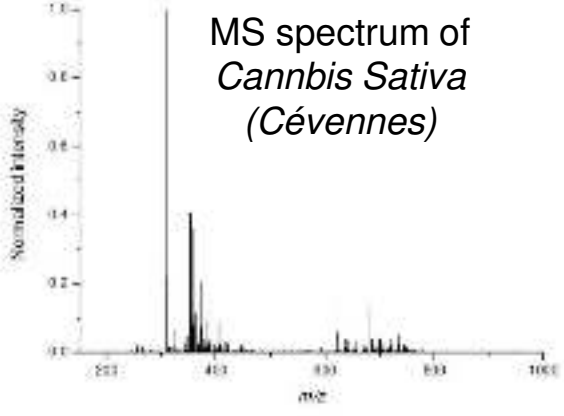

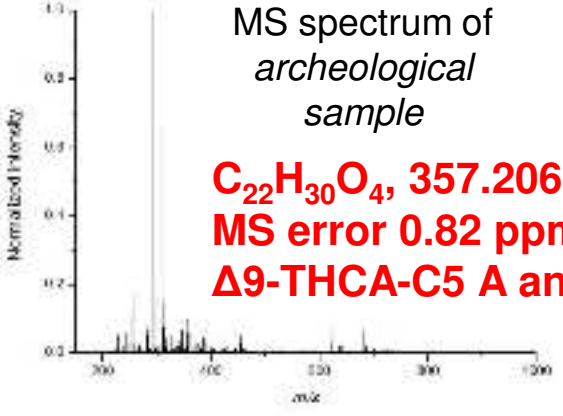

$C_{22}H_{30}O_4$, 357.206840
MS error 0.82 ppm
Δ9-THCA-C5 A and B

Nicolas GARNIER, LNG, Vic-le-Comte.
Exposition "Sorties de fouilles", Bargoin museum , Clermont-Ferrand

EU FT-ICR MS MSAP cnrs Université de Lille

Metabolomics of archaeological samples

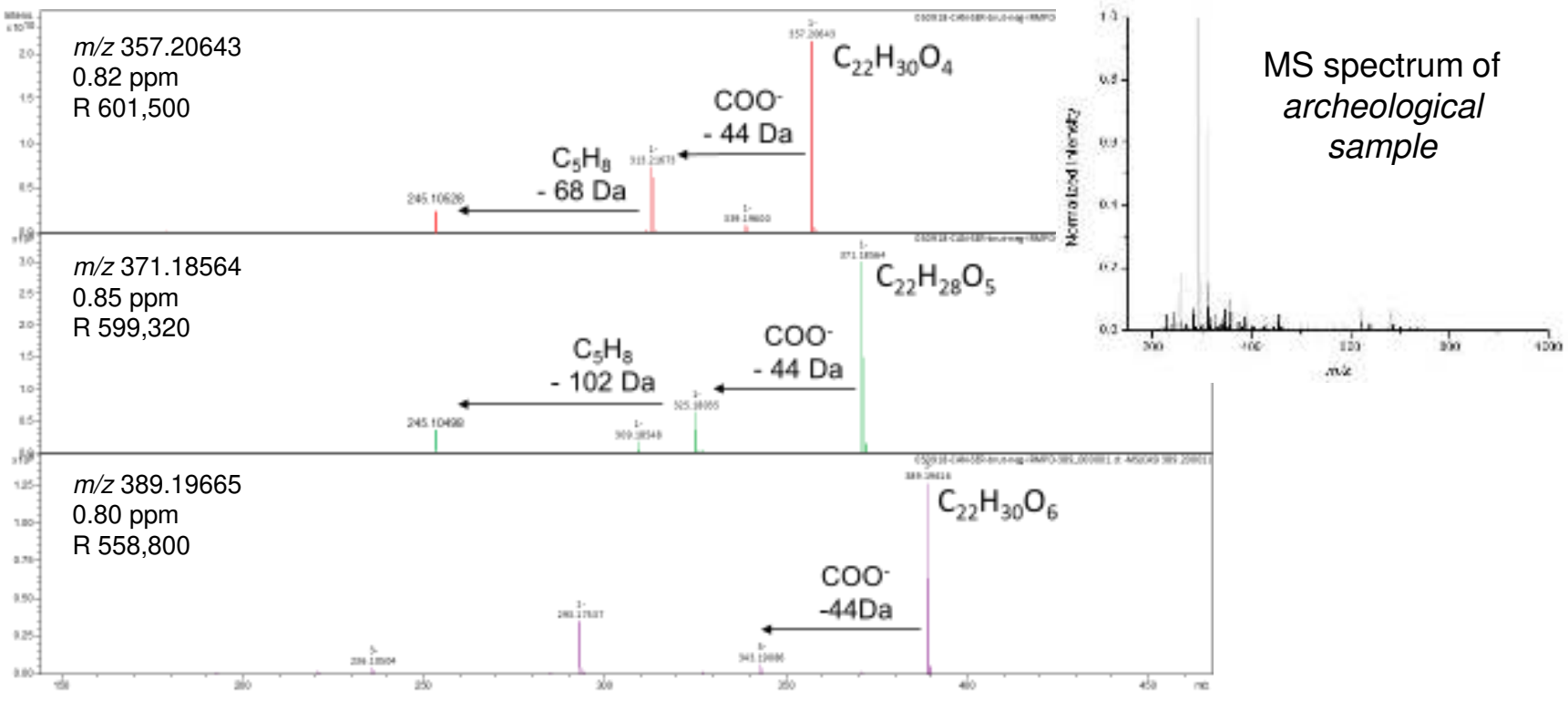

ESI(-)-FT-ICR IRMPD MS/MS allows to identify exact structure:

$C_{22}H_{30}O_4$ = Δ^9-THCA-C5 A and B

$C_{22}H_{28}O_5$ = Δ^9-THCA A-8-one

$C_{22}H_{30}O_6$ = 8β,11-Di-OH-Δ^9-THCA

Review

CHEMICAL REVIEWS

Proteins in Art, Archaeology, and Paleontology: From Detection to Identification

CONTENTS

Dallongeville, S., Garnier, N., Rolando, C., & Tokarski, C. (2016). Proteins in art, archaeology, and paleontology: from detection to identification. *Chemical reviews*, *116*(1), 2-79.

Acknowledgements

Dr Michel SABLIER
Dr Martine REGERT
Dr Nicolas GARNIER
Dr Cécile CREN-OLIVE
Dr Sigrid MIRABAUD

Pr Caroline TOKARSKI

Dr Clara GRANDZOTTO
Dr Sergui MANSOUR

Dr Fabrice BRAY

Ziad MAHMOUD
Isabelle FABRIZI
Caterina BORDIN